FEB - FRESENIUS ENVIRONMENTAL BULLETIN
Founded jointly by F. Korte and F. Coulston
Production by PSP - Vimy Str. 1e, 85354 Freising, Germany in
cooperation with PRT-Parlar Research & Technology
Vimy Str 1e, 85354 Freising

Printed in Germany-ISSN 1018-4619

Fresenius Environmental Bulletin is abstracted/indexed in:
Biology & Environmental Sciences, BIOSIS, CAB International, Cambridge Scientific abstracts, Chemical Abstracts, Current Awareness, Current Contents/Agriculture, CSA Civil Engineering Abstracts, CSA Mechanical & Transportation Engineering, IBIDS database, Information Ventures, NISC, Research Alert, Science Citation Index (SCI), Scisearch, Selected Water Resources Abstracts

CONTENTS

ORIGINAL PAPERS

© by PSP Volume 28 – No. 5/2019 pages 3607-3616 Fresenius Environmental Bulletin

CATTLE STOCKBREEDING AND NITRATE POLLUTION

Muge Erkan Can*

Çukurova University, Department of Agricultural Structures and Irrigation, Adana, Turkey

ABSTRACT

Nitrate has been accumulated in natural sources and soil and water have been contaminated as a result of uncontrolled applications conducted in the stages of storage of manure, processing and spreading it on the farms in stockbreeding enterprises. The purpose of the study is to search the effect of manure obtained from stockbreeding enterprises on the shallow ground water and emphasize the possible damages caused by this influence. Water samples were taken from the ground water observation wells and regular nitrate analysis were made in the experiments conducted in two different enterprises in one of which dairy farming is done and in the other livestock farming is conducted. In Farm 1, the highest nitrate value was measured as 54,63 mg/L in January and the lowest nitrate value was measured as 1.13 mg/L in July. In Farm 2, the highest nitrate value was measured as 52.24 mg/L again in January and the lowest value was measured as 1.35 mg/L in July. The accumulation of their waste on the soil causes the increase of nitrate concentration in shallow ground water. It has been detected that the increase in these concentrations exceeds the standard values especially after the rainy days and this issue has become a serious contamination factor for water resources.

KEYWORDS:
Cattle barns, manure management, nitrate, environmental pollution

INTRODUCTION

Spreading the manure on the farms in a way that it does not cause contamination in natural sources and accumulation in the soil and getting the utmost benefit from the nutrition elements of the plants will be possible due to the correct applications of waste management systems. Animal wastes includes not only nitrogen, phosphorus and potasium vital to the plants but also bacteria, virus, sediment, some microorganisms, salts, undissolved heavy metals and organic solid substances in amounts enough to cause contamination in water and soil. When these wastes mix up in water sources through leaking or direct discharge, they lower the quality of water by decreasing the quantity of dissolved oxygen and cause nonrecoverable damages such as the death of living things in the water.

In the stages of manure storage, processing and agronomic practice cause surface flows, washing out or contamination such as gas formation. While NO_3 formation during washing out causes coontamination, NH_3 is missing in the gas formation. Thus, precautions which do not derange the ecological balance must be predicated on during the time between cleaning out the manure from the barns to spreading it on the plants [1].

Organic wastes caused by humans and animals, warehose and barn leakage ultimately increase the nitrate rate in the soil due to their nitrogen content. Rain and snow, watering on the farms increase the nitrate movement getting through under ground water by leaking through earth stratums. Nitrate and nitrite components carried by the contaminated water whose content was altered and remains formed on the green leaves of the plants watered by these sources can directly cause acute and chronic poisoning in humans and animals contacting with these water sources

High proportion of nitrate in water, soil and vegetables has become a serious public health issue in developing and developed countries.

The detection of contaminaters with nitrogen and their effects have gained increasing importance and also detection of the content of so-called nitrogen components in surface and under ground waters and keeping the tracks of the contamination by assigning standard values to preserve environment and public health have been on the agenda of our country like European countries. The purpose of this study is to present the supervising levels of the enviromental circumstances in the shelters by detecting the levels of the nitrate contamination (pollution) in ground water in the land properties of cattle stock breeding enterprises and to help building modern facilities in accordance with the climate of the region.

MATERIALS AND METHODS

Based on the characteristics of regional stock breeding, two different barns-a nutrition stock breeding barn and a dairy farming barn-are taken as materials.

F1 (Farm 1) is a dairy farming facility which includes 4 barns with different capasities. There were totally 410 animals in the facility during the experiment period. There were 70 heifers, 100 calves and 240 cows. There are two semi-outdoor barns with free parlours for the cows and 2 free open barns for heifers and calves in the facility. There is one concrete embedded manure storage which was built indoor. The manure rubbed out daily from the barns. Firstly is accumulated in these manure storages and carried to manure separator in the facility when the storage is full, the manure separator decomposes.

The fertilizer separator separates the solid and liquid fertilizer and discharges the liquid part to the liquid fertilizer storage located next to it. The liquid manure is kept in reserves for long periods of time and spreaded on the farm when needed. The solid part is spreaded on farms after it has been kept in reserves for at least 6-7 months to 1 year on the landed property of the business.

F2 (Farm 2) is a stock breeding business which has 2 free open barns with altering capacities and it has a total capacity of 115 animals. Manure removal is carried out by manpower once in three months and there is not a manure storage in the facility. Manure is not accumulated but either sold or spreaded directly on the farm lands belonging to barn owner by tractors. The accumulated manure can be a threat for the environment because of the entire dirt surface in the barn and insufficient frequency of manure removal. The standards about the topic have been taken as basics for the design of experiment established in the chosen businesses and as indicated in [2] and [3], at least two observation wells are selected in the downstream direction of the shallow ground water and at least one well was selected around the well with maximum ground water level.

FIGURE 1
Management Plans And Design Of Experiments for F1

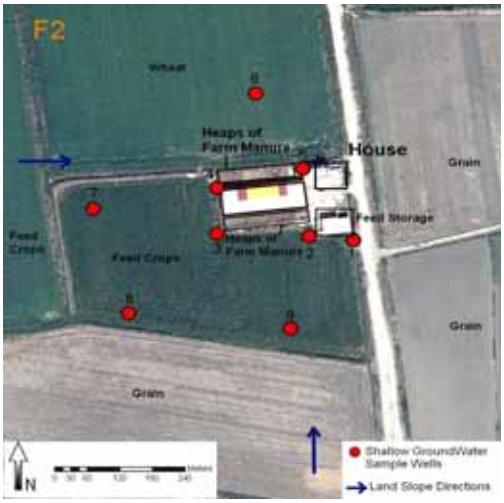

FIGURE 2
Management Plans And Design Of Experiments for F2

Wells have been digged around the manure droppings to make the spots where observation wells were digged to become the spots directly influenced by manure. Shallow ground water levels and flow directions and also the land slope and topography are tried to be determined and since shallow ground water flows from high to low places and the contamination will be increased in the direction of the flow. The highest point of contamination is tired to be confirmed by means of the observation wells digged in the different spots around the manure. Land slope and the ground level of the spots chosen to dig observation well have been found out by surface levelling.

The numbers and locations of observation wells show differences among themselves in case of the location of the buildings and the characteristics of the ground in the farm facility. The observation wells were digged with auger hole method and 3 m. auger hole was used for this purpose. Samples of ground water were taken from each well during the whole sampling periods. After reaching out the shallow ground water by auger hole, ground water in the well is kept in reserve to reach the static level and sampling process began. While taking samples, sampling conditions which were specified in Basic Water Analysis Techniques were implemented[4]. The texture analyze process used to detect the sand, silt and clay fractions of the soil was conducted according to hydrometer method indicated by [5] and according to the results of the analysis, the classification of the texture was determined by using the soil classification triangle [6]. The analysis of soil reaction are determined according to the rules of [7] and nitrate values of ground water samples were determined according to Kjeldahl method [8].

In the study, January, April, July and October are planned as the sampling periods based on the rain in the cities.

Bidirectional variant analysis was made and Repeated Randomized Blocks were implemented to make an evaluation appropriate to the experiment plan and to interpret the analysis results. After the diffference between the implicated variant analysis and the groups was detected the source of this difference was specified by Duncan Test.

RESULTS AND DISCUSSION

It has been determined that the soil of the two business facilities includes light alkali and neutral charcteristics and clay structure as a result of the samples made 0-30 cm intermittently starting from the surface into 3 m. depth.

Accumulation, deep seepage and surface flow conditions of solid and liquid wastes arising from cattle livestock operations are influential in determining the environmental impact of wastes. Because of this effect, the topography maps of the enterprises were taken out and the result of the evaluation of the maps was determined that both of the enterprises were established in a slight inclination land (Figure 3).

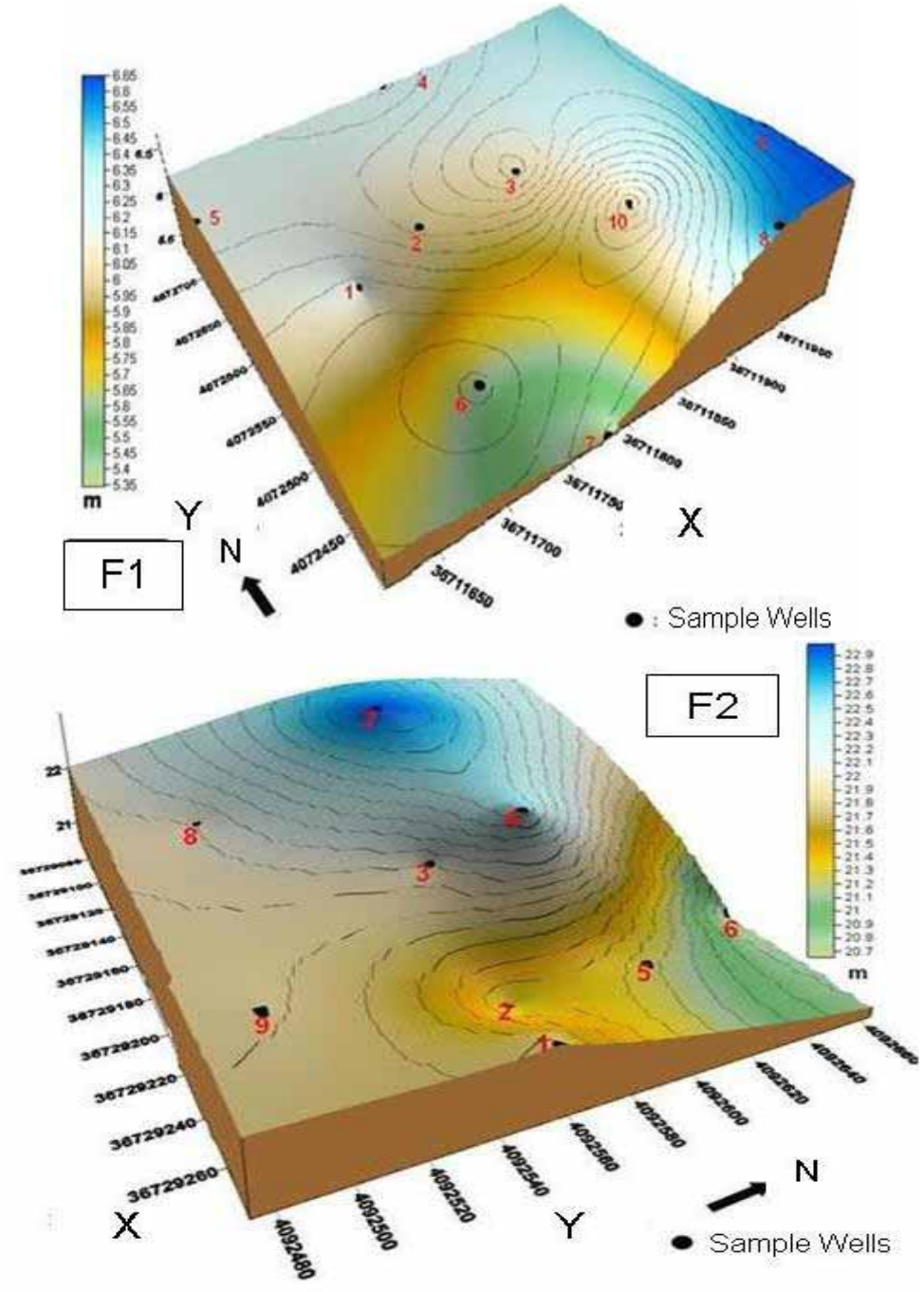

FIGURE 3
Contour Maps Of The Business Facılıtıes

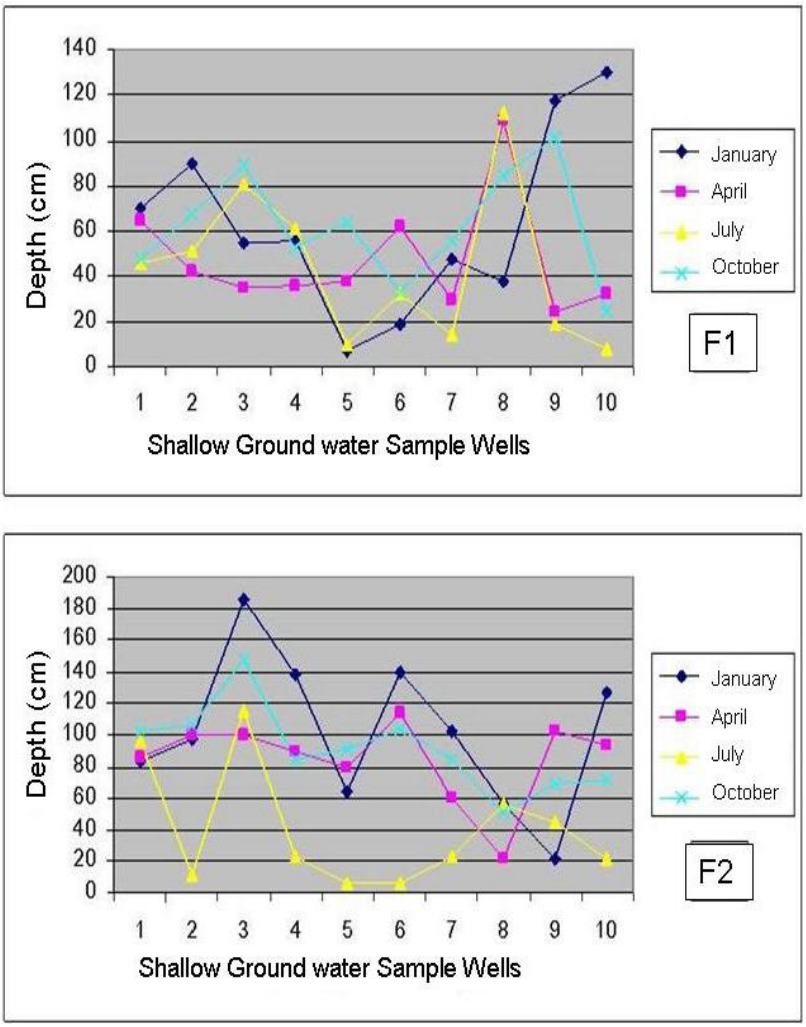

FIGURE 4
The Depths of the Shallow Ground Water

The graphics showing the depth contour of the seasonal static shallow ground water are given as in the shapes in Figure 4.

The depths of the ground water in the farm facilities is influenced by rain and watering in the farm lands around the farm facility. In addition, leaking into the depths due to keeping the waste water of the farm facilities in reserve on the soil show the differences in the levels of the shallow ground water.

Areal distribution maps were made for NO_3 concentrations observed for 4 periods of season in the ground water observation wells in our facilities. It is possible to mention about an inverse proportion between level of shallow ground water and nitrate amount in shallow ground water. High amounts of nitrate will be measured in observation wells with high levels of shallow ground water if there is a case of impact by animal manure.

The lower the levels of shallow ground water are, the less the amount of the nitrate is.

However, the proportion between the levels of shallow ground water and nitrate amount can be different from expected one because of the factors such as the structure of the soil, chemical fertilization and the alteration in the amount of manure kept in reserve on soil.

For F1 in Figure 5, the highest nitrate value in January was measured as 54.63 mg/L in well number 5 and the lowest value was measured as 21.15 mg/L in well number 9. The average nitrate was 41.64 mg/L in January. High nitrate values were measured in the wells nearby the farm land and lower nitrate values were measured in the wells around the animal manure droppings due to the fact that there was less rain in April compared to January. The highest nitrate value was measured as 39.84 mg/L in well number 5 which is nearby the farm land and the lowest value was measured as 8.64 mg/L in well number 8 in April. The average nitrate level was 17.96 mg/L in April (Figure 5).

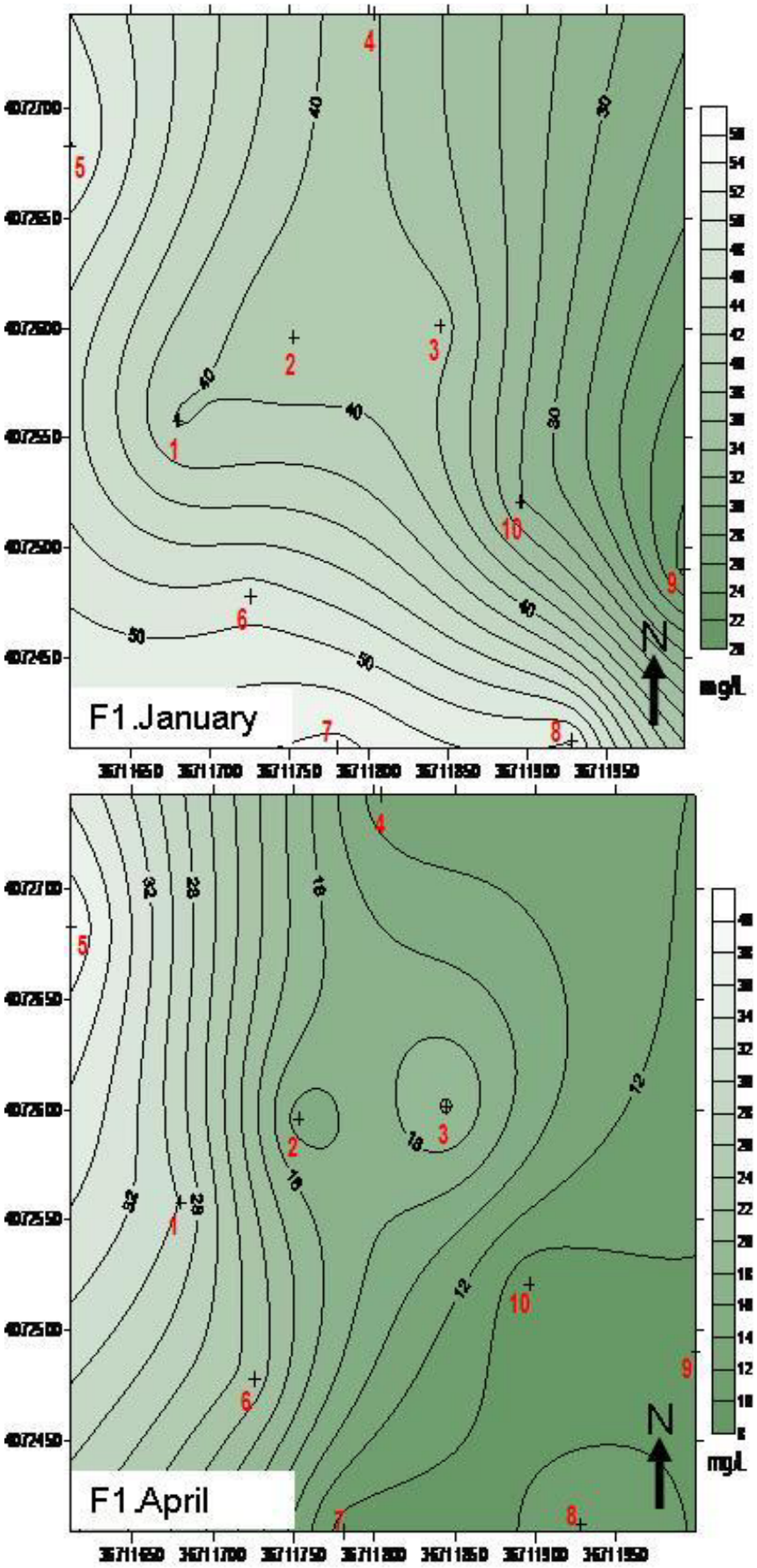

FIGURE 5
F1/January-Aprıl Pın Map Of The Shallow Ground Water Nıtrate Concentration

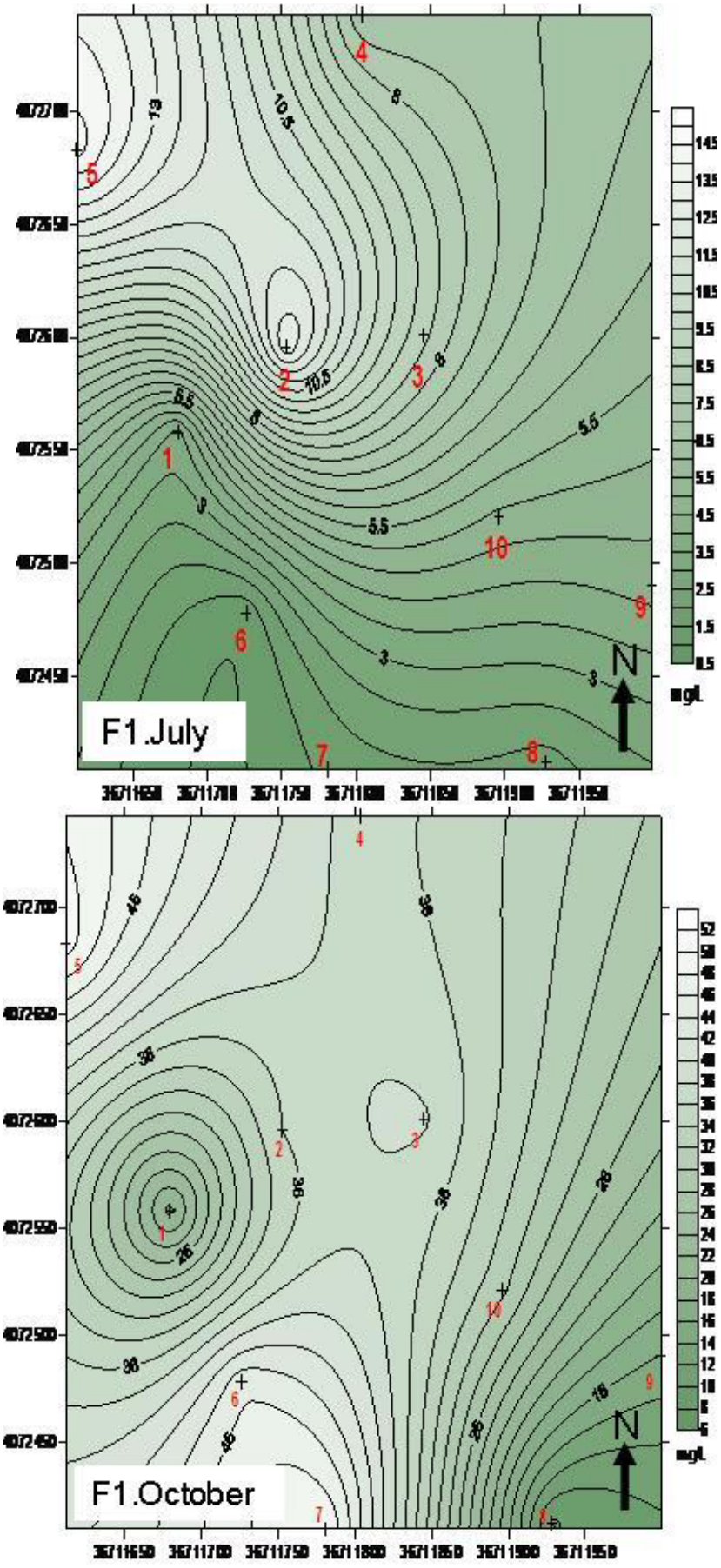

FIGURE 6
F1/July-October Pin Map Of The Shallow Ground Water Nitrate Concentration

For F1 in Figure 6, the lowest nitrate levels were measured in July since July was a dry month. The highest nitrate value in July was measured as 14.74 mg/L in well number 5 in the land where chemical fertilization was applied and lowest value was measured as 1.13 mg/L in well number 8.

The average nitrate was 6.04 mg/L.The nitrate level in October was said to be influenced by the amount of rain that month. The highest nitrate value in October was measured as 51.05 mg/L in well number 7 and lowest value was measured as 7.76 mg/L in well number 8 which has the lowest ground water depth in October. The average nitrate was 33.10 mg/L(Figure 6).

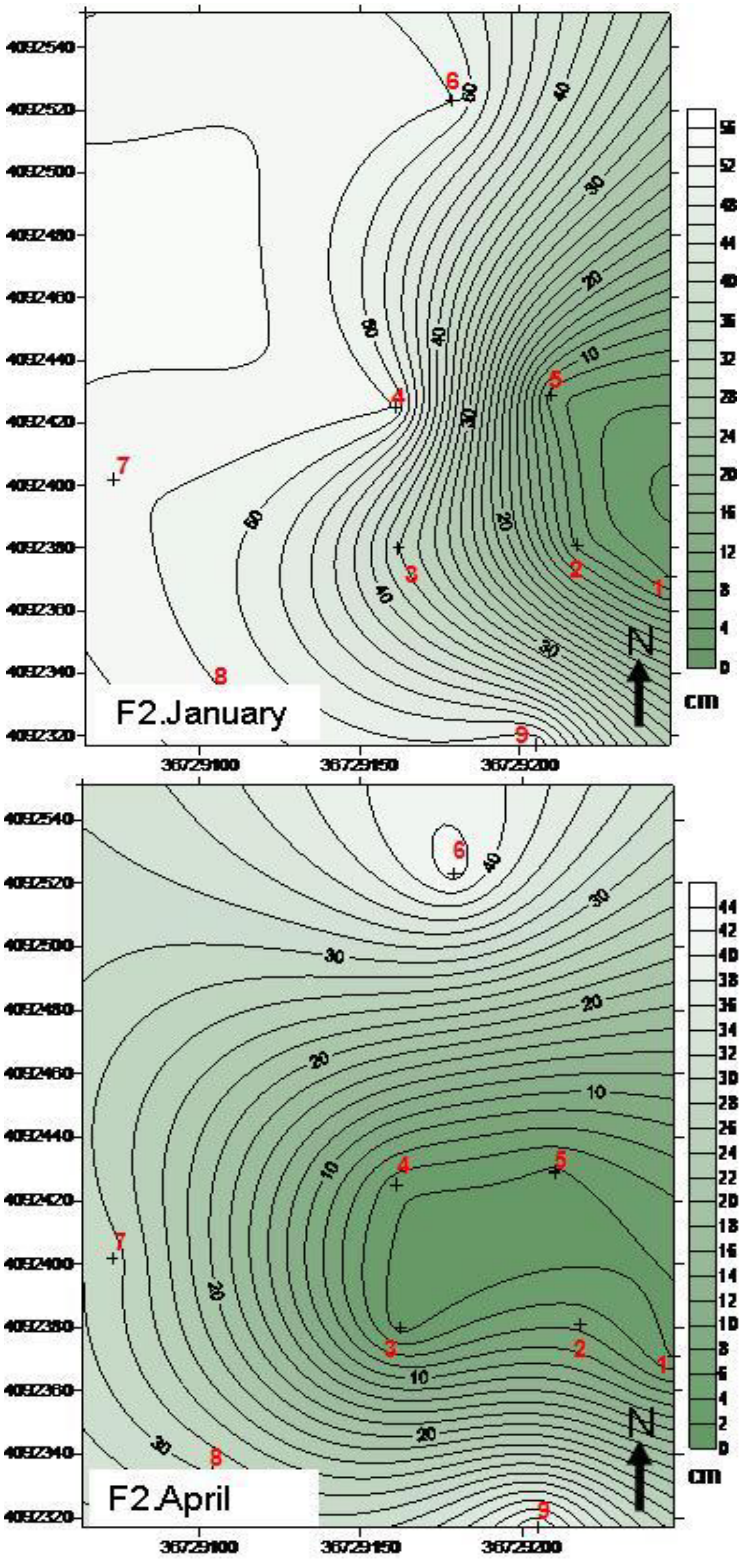

FIGURE 7
F2/ January-April Pin Map Of The Shallow Ground Water Nitrate Concentration

Studying the pin map (Figure 7) of nitrate the highest nitrate value was measured as 52.24 mg/L in well 8 where the manure taken from the barn facility was kept in reserves for short time. The lowest value was measured as 3.77 mg/L in well 1 which had never contacted with manure. The average nitrate value was measured as 34.95 mg/L in January. As it was rainy in January, the highest values among the measurements of ground water nitrate in F2 were obtained in January. When the map of nitrate distribution in April in F2 was studied, the highest nitrate value was measured as 42.85 mg/L, 42.25 mg/L in wells number 6 and 9 digged in spots close to the farm lands. Besides usage of animal manure in farm lands in spring cause the transportation of manure from the business facility. The decrease in the amount of rain influenced the distribution of the nitrate throughout the month. The lowest nitrate value in April was measured as 1.28mg/L in well number 3. The average nitrate value of April was measured as 17.408 mg/L (Figure 7).

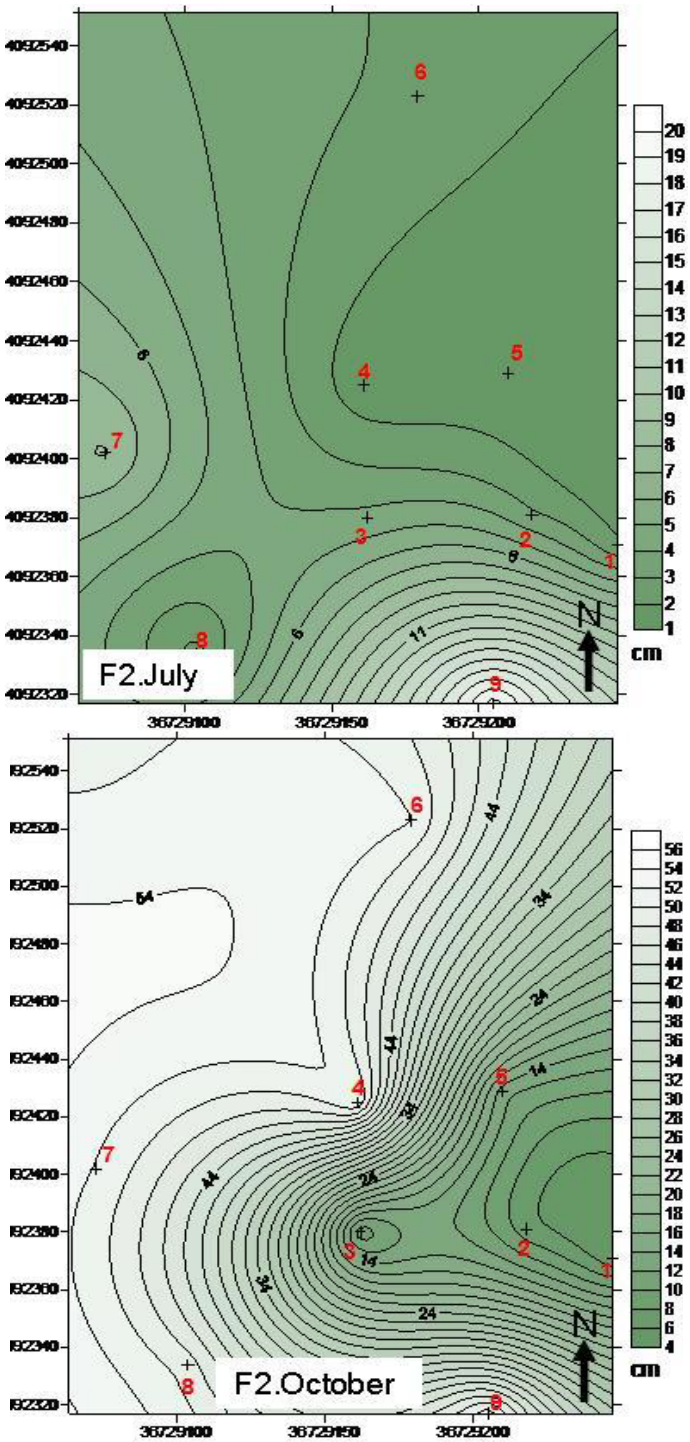

FIGURE 8
F2/July-October Pin Pin Map Of The Shallow Ground Water Nitrate Concentration

When Figure 8 is examined, the lowest nitrate amount was measured as 1.35 mg/L in well number 4 in July. The highest nitrate value was 19.45 mg/L in well number 9. The average value in July was 4.94 mg/L.

The highest nitrate value in October was measured as 52.11 mg/L in well number 4 and the lowest was measured as 4.505 mg/L in well number 1. The average nitrate value in October in F2 is 32.11 mg/L (Figure 8).

The changes of nitrate amounts in shallow ground water in time were considered meaningful according to importance level of $p< 0.01$ for F1 and $p<0.05$ for F2. In Duncan Test results values of July made the first group, values of April made the second group and January and October both made the third. According to these facts values of July were different from the other months and values of April were diffferent from the values of January and October and also the values of January and October are said to be statistically equivalent.

CONCLUSIONS

Nitrate is undissolved and stable in aerobic under ground water circumstances.

Water treatment is requıred for denitrification of nitrate in case of its exceeding the border value of 45 mg NO_3/L stated Turkish Drinking Water Standard TS 266.

Since nitrate denitrification is not preferred in water treatment, prevention of the nitrate contamination in under ground water has become a prior topic [9].

It was declared in the Regulations of Humane Consumption of Water in Turkey and European Unıon that the maxımum nitrate and nitrite amounts in drinking water are supposed to be 50 mg/L and 0.50 mg/L [10],[11].

In Environmental Protection Agengy reports, it was emphasized that drinking water was influenced by fertilization and leakage in the septic tanks and contaminated by nitrate and the maximum nitrate level in drinking water was declared to be 10 mg/L [12].

Waters with nitrate and nitrite must be considered as contaminated by human or animal excrement.

Nitrate value is supposed to be 20-45 mg/L and maximum limit value is declared to be 50 mg/L in the related standards [13]. The NO_3 border value is 10 mg/L for drinking water according to World Health Organizatıon. It is 25 mg/L in Europe, 45 mg/L in the USA. It is 100 mg/L in underdeveloped African Countries [14].

In study [15], in order to determine the impact of the present waste management on water sources, the samples were taken from the surface water and they were found out to have the average nitrate level of 62.9±0.090 mg/L.The value was 21.3± 0.08 mg/L in under ground water. It was emphasized that decharging the liquid wastes from stockbreeding farm facilities in the region into surface water caused the increase in the nitrate and phosphorus concentrations in surface and ground waters. The increase in these concentrations were observed especially after the rainy days.

[16] declared that water and nitrate flew down 0.8 m annually in the soil profile according to leverage flow principle and nitrate mixed up in the under ground water after being washed up 4-6 m because of the heavy rains.

[17] mentioned that clinical methemoglobinemia data is observed in children who drink weel water including high level of nitrate.

When the given standard values are compared with the nitrate data in our wells, the value in some months and wells exceed the maximum value - 50mg/L- in drinking water and 10 mg/L limit value in underground water. The excessiveness of nitrate and amonium values measured in wells show that the nitrogen compounds in the manure leaked into the depths and it srengthen the possibility of these components' merge in the under ground water after being washed up.

Determining the locations to build stock breeding farm facilities and manure storages topography, land structure, the land use properties, present geological and hydrogeological structure, water sources and climate data must be determined meticulously and necessary legal arrangements must be made.

In conclusion, the validity of the laws, regulations and codes of conducts on this topic are required to be evaluated in order to remove the unfavourable conditions in the business facilities and the elimination of the negative environmental effects caused by the manure produced in animal barns must be eliminated.

ACKNOWLEDGEMENTS

This study was produced from Phd thesis and supported by Çukurova University Scientific Research Projects Unit. Phd Project Number: ZF2009D8.

REFERENCES

[1] Yaldız, O. (2004). Biogas Technology. Akdeniz University Number:78, s 184, Antalya.
[2] Anonymous (2001). Nebraska Department of Environmental Quality, Title 130 Rules and Regulations Pertaining to Livestock Waste Control.

[3] Anonymous (2003b) Nebraska Department of Environmental Quality. Guideline for Ground Water Monitoring Plans at Livestock Waste Control Facilities. Environmental Guidance Document 00-002. 6 pp.
[4] Oğur, R., Tekbaş, Ö.F. (2005) Basic Water Analysis Techniques, Aydın Printing House, Ankara (in Turkish).
[5] Bouyoucos, G.D. (1951) A Recalibration of the Hydrometer Method for Making Mechanical Analysis of the Soil. Agronomy Journal. 43, 434-438.
[6] Anonymous (1993) Soil Survey Manual, USDA. Handbook No: 18. Washington D.C.
[7] Richards, L.A Ed. (1954) Diagnosis and Improvement of Saline and Alkali Soils. United States Department of Agriculture Handbook. 60,94.
[8] Bremner, J.M. (1965) Methods of Soil Analysis. Part 2. Chamical and Microbiological Properties. Ed. A.C.A. Black, Amer. Soc. of Argon. Inc. Pub. Agron. Series. No:9, Madison USA.
[9] Polat, R., Elçi, A., Şimşek, C., Gündüz, O. (2007) Seasonal Assessment of The Extent of Nıtrate Contamination in Ground Water Around Nif Mountain in İzmir 7. National Environmental Engineering Congress, Life and Technology. 24-27 October 2007, İzmir.
[10] Anonymous (1998b) Council Directive 98/83/ EC of 3 November 1998 on the Quality of Water Intended for Human Consumption, Official Journal of the European Communities L 330/42.
[11] Anonim (2005b) Regulation on Water for Human Consumption. Official Newspaper, Issue: 25730, Ankara (in Turkish).
[12] Anonymous (2005a) Code of Good Agricultural Practice for the Prevention of Pollution of Water Department of Agriculture and Rural Development. ISBN: 1-85527-577-5, North Ireland.
[13] Anonymous (2006) World Health Organization. Guidelines For Drinking-Water Quality: İncorporating First Addendum. Vol. 1, Recommendations. 3rd ed.
[14] Anonymous (1996) Guidelenes for Drinking Water Quality, 2nd Edition Vol. II, Health Criteria and Other Supporting Information, Genova.
[15] Polat, H.E. (2007) Assesment of Waste Management Systems at Cattle Breeding Enterprises in Ankara Province. Ankara University, Graduate School of Natural and Applied Sciences, Department of Farm Structures and Irrigation, PhD Thesis, Ankara (in Turkish).
[16] Funk, R., Maidl, F.X., Wagner, B., Fıschbeck, G. (1995) Vertical Water and Nitrate Movement in to Deeper Soil Layers on Fields Located in The South of Germany. Z. Pflanzenernahr. Bodenk. 158, 399-406.
[17] Comly (1945) Groups of Dairy Farms. Manure Management Program, Cornell University. Ithaca, NY.

Received: **25.06.2018**
Accepted: **01.03.2019**

CORRESPONDING AUTHOR

Muge Erkan Can
Çukurova University,
Department of Agricultural Structures and Irrigation, Adana, Turkey

e-mail:merkan@cu.edu.tr

© by PSP Volume 28 – No. 5/2019 pages 3617-3625 Fresenius Environmental Bulletin

TRACE ELEMENT SOLUBILITY IN A COMPOST-BIOCHAR RECLAIMED MINE SOIL

Alfonso Rodriguez-Vila[1,*], Ruben Forjan[1], Rafael S Guedes[2], Emma F Covelo[1]

[1] Department of Plant Biology and Soil Science, Faculty of Biology, University of Vigo, Lagoas, Marcosende, 36310 Vigo, Pontevedra, Spain

[2] Institute of Agricultural Sciences, Federal Rural University of Amazonia (ICA-UFRA), 2501, Belém-PA, 66077-830, Brazil

ABSTRACT

Mining activities cause detrimental effects on water quality worldwide. The aim of this study was to assess the effectiveness of a compost-biochar amendment in regulating the solubility of trace elements in a mine soil grown with *Brassica juncea* plants. A 3-month greenhouse experiment was carried out and the mine soil was mixed with different proportions of the compost-biochar amendment (20, 40, 80 and 100%) and planted with *B. juncea*. Trace element concentrations in soil pore water (extracted with Rhizon samplers) and a series of soil characteristics associated with element solubility were analysed. Compost-biochar amendment enhanced soil condition (pH, TC, TN, DOC) and generally reduced the solubility of Al, Co, Cu, Fe, Mg, Mn, Ni and Zn in the mine soil, compared to the unamended controls. In addition, the amendment mixture increased the release of K, P and Na and promoted *B. juncea* plants growth. It was concluded that the combined use of compost-biochar amendment and *B. juncea* plants can be an efficient strategy for increase the immobilization of potential toxic trace elements in a mine soil and reduce the associated environmental risk.

KEYWORDS:
Settling pond, pore water, trace element, organic amendment, remediation

INTRODUCTION

The mining industry produces large volumes of chemically unstable wastes, carrying significant potential to release certain trace elements into aquatic environment, such as toxic metals [1]. These kinds of pollutants are mainly characterized by persistence against chemical or biological degradation, high environmental mobility and strong tendency for bioaccumulation in the food chain [2]. Most of the existing technologies to removal of the pollutants are often ineffective, uneconomical or very technically complicated [2].

Organic materials may be useful for remediation of mine soils because organic amendments, such as compost and biochar, can increase the pH of acidic soils and bind metals [3, 4]. Organic amendments represent a sustainable option, which is environmentally effective, economically affordable and socially acceptable [1]. The use of compost as amendment can improve the physical, chemical and biological properties of degraded soils by supplying organic matter and can be used in soil reclamation [5, 6]. Compost improves soil fertility, provides organic matter, increases aggregate stability, aeration, water infiltration and retention, and decreases soil erosion [7]. Biochar is an organic material produced by burning biomass under conditions of low temperatures and minimal oxygen [8]. The multiple benefits of use biochar as amendment include the improvement of soil properties, the reduction of environmental pollution and the mitigation of climate change [9]. Biochar is reported to increase pH, cation exchange capacity, electrical conductivity, water retention capacity and the retaining of toxic metals in the soil [10].

In the recent years the development of phytoremediation technology is being driven primarily by the high cost of many other soil remediation practices, as well as the desire of use green and sustainable techniques [11]. Nevertheless, the establishment of vegetation in highly contaminated soils or in mining waste, can be inhibited by high concentrations of metals [12]. Other factors that can limit plant growth are macronutrient deficiencies and physical conditions, especially those properties leading to poor water retention capacity, aeration and root penetration [11]. Some plant species have the ability to tolerate high concentration of metals in its above-ground tissues [13]. Indian mustard (*Brassica juncea*) has been reported as a plant species which can be potentially used in phytoremediation due to its rapid growth and high biomass [14].

The objective of the study was to evaluate the effect of a compost-biochar amendment in a mine soil grown with *B. juncea*, especially on the trace element concentrations in soil pore water. With respect to the literature, several studies have evaluated the influence of organic amendments on mine soils [15, 16, 17], but only a few authors studied the concentration of trace elements in pore water [18, 19]. Moreover, there is a lack of understanding over the influence of compost and biochar combination

on pore water trace element concentrations. This study aims to fill this knowledge gap by evaluating the influence of compost-biochar amendment on the solubility of trace metals in a soil from the depleted copper mine of Touro (Spain). It was hypothesized that the application of the organic amendment mixture and the plantation of *Brassica juncea* could reduce the solubility of contaminants in the mine soil.

MATERIALS AND METHODS

Soil sampling. The sampling area was located in the setting pond from the depleted copper mine of Touro (Galicia, Spain) (Lat/Lon (Datum ETRS89): 8°20′12.06″W 42°52′46.18″N). The mine soil used for this study (S) was collected in the settling pond of this depleted copper mine (Figure 1). Copper was extracted for 15 years, from 1973 to 1988. This activity produced a settling pond of 71 ha resulting from the accumulation of waste after the process of concentrating the metal in flotation banks, and it has been completely dry for several years. Once copper extraction ended, the soils were partially reclaimed by planting *Pinus pinaster* Aiton and *Eucalyptus globulus* Labill in some locations. Later, some mine sites were amended using organic wastes, sewage sludge and paper mill residues, among others [20].

The materials used as an amendment for the greenhouse experiment were a mixture of compost supplied by Ecocelta Galicia S.L. (Ponteareas, Pontevedra, Spain) and biochar provided by PROININSO S.A. (Málaga, Spain). The compost (CP) was made from rabbit and horse manure, fruit wastes, pruning residues and seaweeds. The biochar (B) used was made from holm oak wood with a pyrolysis temperature of 400ºC for 8 hours. Selected characteristics of the untreated soil and the two amendments are shown in Table 1.

Greenhouse experiment. The greenhouse experiment was carried out in pots with the settling pond soil amended with the previously described mixture of compost and biochar and vegetated with *Brassica juncea* L. plants. The soil was treated with 20%, 40%, 80% and 100% of amendment: CB20 = 20% amendment; CB40 = 40% amendment; CB80 = 80% amendment and CB100 = 100% amendment.

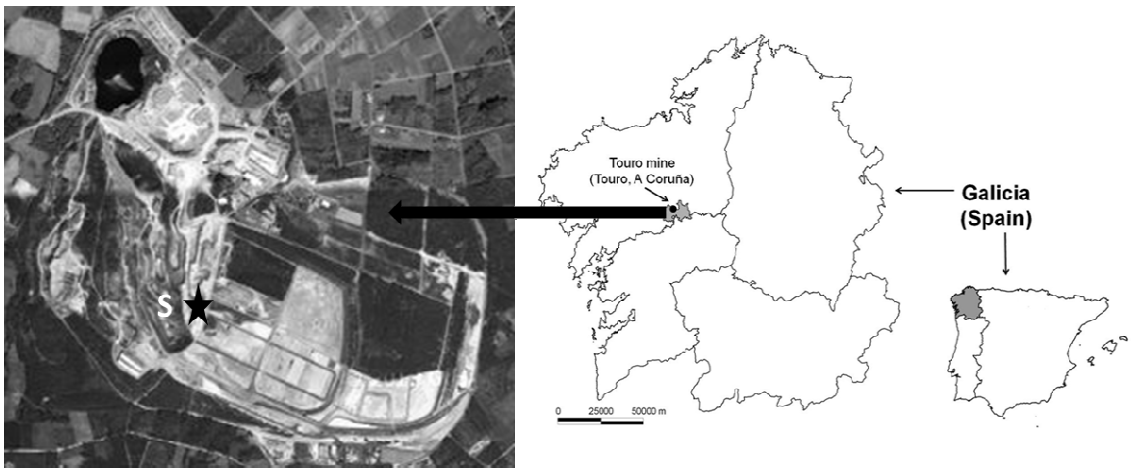

FIGURE 1
Location of the sampled area in Touro mine.

TABLE 1
Selected chemical characteristics in the mine soil (S) and in the two amendments (biochar B and compost CP)

	S	B	CP
pH H_2O	2.96±0.07c	9.93±0.22a	9.03±0.07b
pH KCl	2.73±0.02c	9.64±0.05a	8.82±0.05b
TC (g kg^{-1})	u.l	667±57.22a	214±24.12b
TN (g kg^{-1})	u.l	5.8±0.87b	18.4±1.42a
C/N	-	115a	11b
SOC (g kg^{-1})	u.l	599a	175b
IC (g kg^{-1})	u.l	68.28±9.31a	39.4±5.45b
DOC (g kg^{-1})	u.l	1.59±0.07b	59.8±6.41a

Note: Mean ± CI values (n = 3). Values followed by different letters differ significantly with $P < 0.05$. u.l.: undetectable level; TC: soil total carbon; TN: soil total nitrogen; SOC: soil organic carbon; IC: soil inorganic carbon; DOC: dissolved organic carbon.

Amendment mixture was made of 95% compost and 5% biochar and was mixed with the mine soil before filling the pots with the corresponding soil mixture. Some pots were only filled with mine soil (CB0, with 0% amendment) as the control treatment. The plastic pots were filled with a dry weight of 200 g of the corresponding soil mixture. Control pots were supplemented with drinking straws cut into 1 cm lengths in order to minimize the difference in the substrate volume between the control soil and the amended soils [21]. Six pots were filled with each type of mixture: three were used for planting mustard, and the other three were left unplanted in order to evaluate the effect of the vegetation on soils. The soil samples where plants were planted were labelled with the letter P (e.g., CB20P).

Three seedlings of *B. juncea*, previously germinated from seeds until they grew two fully expanded leaves, were transferred to each pot. After 45 days, the plants were thinned to one per pot following uniform criteria. The plants, with three replicates per treatment, were harvested 90 days after transplanting. The greenhouse was maintained at an average temperature of 15 ± 3 ºC and 75 ± 5 % relative air humidity.

Soil analysis. The soil samples collected from the field (mine soil) and from the pots were air dried, passed through a 2 mm sieve and homogenized in a vibratory homogeniser for solid samples (Fritsch Laborette 27 rotary sampler divider) prior to analysis.

Soil reaction was determined with a pH electrode in 1:2.5 water or KCl to soil extracts [22]. Soil total carbon (TC), inorganic carbon (IC) and total nitrogen (TN) were determined in a LECO CN-2000 module using solid samples. Soil organic carbon (SOC) contents were calculated from the difference TC ─ IC. Dissolved organic carbon (DOC) was extracted with bidistilled H_2O according to [23].

Pore water analysis. One week before harvesting the *B. juncea* plants, a "Rhizon" soil pore water sampler (Eijkelkamp Agrisearch Equipment, The Netherlands) was carefully inserted into the soil of each treatment replicate pot at an angle of approximately 45º. Vacuum tubes (10 mL) were attached through a Luer lock system with hypodermic needles to extract pore water. Pore water samples were analysed for Al, Ca, Co, Cu, Fe, K, Mg, Mn, Na, Ni, P, Pb and Zn concentrations by ICP-AES, carried out in triplicate.

Statistical analysis. All of the analytical determinations were performed in triplicate. The data obtained were statistically treated using the programme SPSS version 19.0 for Windows. Analysis of variance (ANOVA) and a test for homogeneity of variance were carried out. In case of homogeneity, a post-hoc least significant difference (LSD) test was carried out. If there was no homogeneity, Dunnett's T3 test was performed. Correlated bivariate analyses and a principal component analysis (PCA) were also carried out.

RESULTS

Characteristics of the mine soil, compost and biochar. The untreated soil from the settling pond at the mine of Touro (S) showed an extremely acidic pH (2.96) and soil total carbon (TC), soil total nitrogen (TN) and dissolved organic carbon (DOC) contents below the detection limit (Table 1). The compost (CP) and biochar (B) used as soil amendment had high pH values 9.93 and 9.03 and TC contents 214 and 667 g kg^{-1}, respectively (Table 1). Dissolved organic carbon content was 59.8 g kg^{-1} in CP and 1.59 g kg^{-1} in B (Table 1). The amendments also showed TN contents of 18.4 g kg^{-1} in CP and 5.8 g kg^{-1} in the biochar (Table 1). Total carbon content was higher in the biochar and DOC and TN contents were higher in the used compost (Table 1).

Characteristics of the greenhouse soil samples. The pH of the untreated mine soils (CB0 and CB0P) was still extremely acidic according to [24], after 3 months of experiment. The use of compost and biochar as soil amendment promoted an increase on soil pH in the mine soil (Table 2). The pH in the amended soils ranged 7.04 – 9.03, showing significantly higher pH values than the controls without amendment. The TC and TN concentrations were undetectable in the untreated soils. Compost and biochar promoted an increase on TC and TN contents, and it was observed that the higher the proportion of amendment, the higher the concentration of TC and TN in the soil (Table 2). Soil organic carbon and IC concentrations were undetectable in the unamended soils and increased significantly after the addition of amendment (Table 2). Dissolved organic carbon concentrations were also undetectable in the control soils and were also affected by the compost-biochar incorporation. The DOC concentrations ranged 3.64 – 43.76 g kg^{-1} in the amended soils and significantly increased after the addition of amendment and the plantation of *Brassica jun*cea.

The effect of compost-biochar amendment and *B. juncea* plants was evaluated on the concentration of trace elements in soil pore water (Table 3). The application of compost and biochar to the settling pond soil was very effective in reducing Al and Cu concentration in soil pore water, indicating metal immobilization (Table 3). Compost and biochar reduced Al and Cu pore water concentrations from 1406 to 0.07 mg L^{-1} (99.99%) and from 344 mg L^{-1}

to 0.40 (99.88%) mg L^{-1}, respectively (Table 3). The solubility of Co and Ni in soil was clearly reduced after the addition of compost and biochar as soil amendment. The concentration of Co and Ni in pore water decreased from 21.96 to 0.03 (99.86%) mg L^{-1} and from 21.50 to 0.06 (99.95%) mg L^{-1}, respectively (Table 3). Compost and biochar reduced Fe concentration in pore water from 37.25 mg L^{-1} to 0.18 (99.43%) mg L^{-1} (Table 3). Magnesium (Mg) and Mn concentration in pore water significantly decreased from 536 to 72.38 (86.5%) mg L^{-1} and from 41.54 to 0.14 (99.66%) mg L^{-1}, respectively (Table 3). The compost-biochar amendment reduced Zn concentration in pore water from 8.2 to 0.11 (98.66%) mg L^{-1} (Table 3). Nevertheless, Pb concentration in soil pore water was low for all treatments and it did not showed a specific trend after compost-biochar addition, compared to the controls (Table 3). In addition, compost-biochar application to the mine soil increased significantly K, P and Na concentrations in soil pore water (Table 3). Compost and biochar increased pore water concentrations of K (from 4.14 to 6865 mg L^{-1}), P (from values below the detection limit to 94.85 mg L^{-1}) and Na (from 34.86 to 2621 mg L^{-1}), respectively (Table 3). And the highest Ca pore water concentration was in the soil CB20P (Table 3).

Brassica juncea plants did not survive in the untreated settling pond soil (CB0P), with all of them dying one week after being planted in that soil. The biomass produced by mustard plants in the different soil treatments was 0.16 g ± 0.04 (CB20P), 0.14 g ± 0.02 g (CB40P), 0.13 g ± 0.02 (CB80P), 0.16 g ± 0.01 (CB100P). There were no significant differences between the biomass produced in the different soil treatments.

DISCUSSION

Effect of the treatments on soil properties. The amended soils showed a significant increase on soil pH values, compared to the untreated controls (Table 2). The pH of the unamended soils remained extremely acidic according to [24], after three months of greenhouse experiment (Table 2). The application of organic amendment helped to correct the TC and TN deficiencies in the mine soil (Table 2). The TC concentration significantly increased after compost-biochar addition due to their high carbon content (Table 1). The SOC and IC concentrations also increased in the mine soil after being amended (Table 2) and it was observed that higher the proportion of amendment, higher the concentration of SOC in the soil (Table 2). The untreated mine soil had undetectable levels of TN (Table 2) and the TN increased significantly after the application of compost and biochar, probably due to the TN provided by these organic materials (Table 2). These results agree with those found in previous studies by [25, 26]. [25] evaluated the effect of compost application to the soil. Total organic carbon and total nitrogen significantly increased in soils treated with this organic amendment. [26] observed that biochar and compost organic amendments improved soil properties, including significant increases in soil carbon content. [27] reported that soil organic carbon increased after poultry manure-derived biochar application. The soil samples with both treatments (organic amendments and *B. juncea*) had generally higher TC and TN contents and higher C/N than the soils without plants (Table 2). Amendment incorporation into the mine soil significantly increased the DOC, compared to the untreated soils (Table 2). [28] also reported that DOC significantly increased in soils amended with compost and biochar.

Influence of treatments on soil pore water concentrations. The concentration of trace elements in soil pore water was clearly affected by the addition of compost and biochar and the plantation of *B. juncea* in the mine soil. The addition of compost and biochar to the mine soil increased Cu immobilization in soil (Table 3). A previous study [20] reported that the soil from the settling pond at the mine of Touro had high pseudototal concentration of Cu (452 mg kg^{-1}), above the generic reference level (50 mg kg^{-1}) established for Galician soils [29]. The addition of compost and biochar to the mine soil reduced Cu solubility and the associated toxicity risk (Table 3). [30] observed that the combination of compost and biochar was effective for reducing Cu concentrations in pore water in a contaminated soil. [31] reported that green waste compost reduced Cu and Zn solubility in contaminated mine soils. [32] showed that Cu concentration in pore water was significantly reduced after adding compost and biochar as soil amendment. The application of compost and biochar significantly increased Al and Fe immobilization in the mine soil (Table 3). [33] evaluated the addition of organic material (compost, plant residues and biochars differing in feedstock and pyrolysis temperature) to sulfuric soil on Al and Fe mobility. The addition of organic materials reduced leaching of Al and Fe. In amended treatments, the release of Al and Fe was lower than in unamended soil, the decrease was referred to retention. The application of compost and biochar significantly reduced Mn and Zn concentration in pore water (Table 3). [1] studied the immobilization of metals in mine tailings amended with food waste-based compost. The metal immobilization efficiency of compost was evaluated based on collected leachate quality. Results indicated that compost was successful for increasing Al, Fe, Mn and Zn immobilization. Compost-biochar amendment also significantly reduced Co, Ni and Mg concentration in pore water (Table 3). Combined compost and biochar amendment would have as-

sisted reductions in trace metal concentrations in the present study due to both increases in soil organic matter content (Table 1) and increases in soil pH (Table 2). Incorporation of organic matter into the soil can be used to reduce the potential toxic trace element leaching [34,35]. Lead concentration in pore water was low in all treatments and it did not show a specific trend after compost and biochar application (Table 3). Solubility of Pb in soils is usually very restricted [36]. Compost and biochar enhance K, P and Na release from soil (Table 3). [37] observed significantly increasing soil pore water P in a contaminated soil after green waste compost application. [38] reported that application of compost increased the concentrations of P in soil solution. [39] reported an increase on dissolved P and K in a contaminated mine soil amended with compost. [40] reported that K and Na concentration on soil solution was generally higher in soils amended with urban waste compost compared to no-organic amended soil.

TABLE 2
Selected chemical properties in soil samples at 3 months of experiment

Soil sample	pH H_2O	pH KCl	TC (g kg^{-1})	SOC (g kg^{-1})	IC (g kg^{-1})	DOC (g kg^{-1})	TN (g kg^{-1})	C/N
CB0	2.83±0.08g	2.72±0.04g	u.l	u.l	u.l	u.l	u.l	-
CB0P	2.70±0.17h	2.60±0.18h	u.l	u.l	u.l	u.l	u.l	-
CB20	7.04±0.22f	7.02±0.27f	20.23±1.35g	16.36g	3.87±0.52f	3.89±0.47f	1.8±0.18f	11c
CB40	7.79±0.13d	7.74±0.1d	33.8±1.21f	28f	5.8±2.35ef	8.46±0.6e	2.97±0.32e	11c
CB80	8.66±0.1b	8.41±0.03b	117±5.08d	99.97d	17.03±2.28cd	25.56±1.17c	9.57±1.04c	12b
CB100	9.03±0.08a	8.80±0.06a	188±6.41b	151b	37.27±4.04a	43.76±1.82a	15.3±1.76a	12b
CB20P	7.11±0.16e	7.07±0.15f	24.5±0.99fg	19.57g	4.93±2.25ef	3.64±0.81f	2.1±0.07f	11c
CB40P	7.75±0.16d	7.56±0.15e	50.87±1.23e	38.60e	12.27±4.53de	7. 74±0.27e	4.13±0.1d	12b
CB80P	8.27±0.26c	8.09±0.23c	149±3.55c	128c	20.77±2.99bc	23.21±1.05d	11.13±0.35b	13a
CB100P	8.71±0.14b	8.47±0.39b	207±1.68a	180a	27.37±4.39b	39.57±1.6b	15.33±0.52a	13a

Note: Mean ± CI values (n = 9). Values followed by different letters in each column differ significantly with $P < 0.05$. u.l.: undetectable level; TC: soil total carbon; SOC: soil organic carbon; IC: soil inorganic carbon; DOC: dissolved organic carbon; TN: soil total nitrogen.

TABLE 3
Pore water trace element concentrations (mg L^{-1}) in soil samples at 3 months of experiment

	CB0	CB0P	CB20	CB40	CB80	CB100	CB20P	CB40P	CB80P	CB100P
Al (mg L^{-1})	1406±35 7a	874±85.0 4b	0.19±0.0 2c	0.13±0.0 5c	1.43±0.12 c	3.51±0.3 5c	0.07±0. 03c	0.14±0.2 3c	1.71±0. 23c	4.40±0.4 3c
Ca (mg L^{-1})	337±14.5 6c	322±10.0 2c	283±45. 86c	200±33. 13d	105±26.4 6e	85.09±8. 25e	578±88 a	417±26.1 2b	102±32. 86e	101±29.6 3e
Co (mg L^{-1})	21.96±4. 36a	13.14±1. 79b	0.03±0.0 1c	0.03±0.0 1c	0.06±0.02 c	0.08±0.0 2c	0.03±0. 01c	0.04±0.0 1c	0.05±0. 01c	0.04±0.0 1c
Cu (mg L^{-1})	344±95.9 1a	220±9.12 b	0.61±0.2 5c	0.75±0.1 3c	1.49±0.72 c	3.45±0.3 2c	0.40±0. 12c	0.71±0.1 9c	1.32±0. 22c	0.79±0.0 4c
Fe (mg L^{-1})	37.25±8. 35a	31.71±3. 02a	0.50±0.0 2d	0.66±0.0 2d	13.83±3.0 2c	24.99±2. 23b	0.18±0. 07d	0.59±0.0 2d	8.48±4. 02cd	11.80±3. 06c
K (mg L^{-1})	4.14±0.1 9f	5.80±0.9 5f	3220±20 9e	3524±33 2e	6865±157 0b	7424±41 9a	3553±2 44e	5195±25 0d	5828±8 0.68c	6512±33 2b
Mg (mg L^{-1})	536±46.5 9a	331±23.8 1b	251±24. 96c	190±31. 42d	74.95±10. 13e	59.88±2. 46e	517±51. 5a	332±67.1 3b	72.38±1 0.77e	62.87±7. 35e
Mn (mg L^{-1})	41.54±4. 89a	25.48±2. 31b	0.20±0.0 4c	0.14±0.0 6c	0.58±0.13 c	1.03±0.1 c	0.34±0. 04c	0.17±0.0 3c	0.66±0. 18c	1.10±0.1 5c
Na (mg L^{-1})	38.19±1. 17e	34.86±2. 93e	1154±18 4d	1267±14 4d	2621±233 a	2608±23 4a	1355±1 65d	1879±16 6c	2174±1 18b	2270±12 4b
Ni (mg L^{-1})	21.5±3.5 2a	13±1.76b	0.08±0.0 3c	0.08±0.0 2c	0.17±0.04 c	0.25±0.0 5c	0.06±0. 01c	0.06±0.0 1c	0.15±0. 05c	0.15±0.0 2c
P (mg L^{-1})	u.l	u.l	8.94±0.3 g	13.11±0. 22f	53.01±2.0 2d	65.42±2. 27c	35.87±2 .5e	41.57±3. 86e	94.85±9 .81a	76.22±8. 73b
Pb (mg L^{-1})	0.09±0.0 2c	0.07±0.0 1d	0.09±0.0 2c	0.13±0.0 3a	0.05±0.01 ef	0.06±0.0 1e	0.11±0. 02b	0.08±0.0 2cd	0.04±0f g	0.03±0g
Zn (mg L^{-1})	8.2±0.95 a	5.55±0.6 5c	0.16±0.0 2f	0.22±0.0 6f	2.41±0.27 e	6.17±0.7 1b	0.11±0. 03f	0.18±0.0 4f	2.55±0. 22e	3.80±0.3 2d

Note: Mean ± CI values (n = 3). Values followed by different letters in each row differ significantly with $P < 0.05$. u.l.: undetectable level.

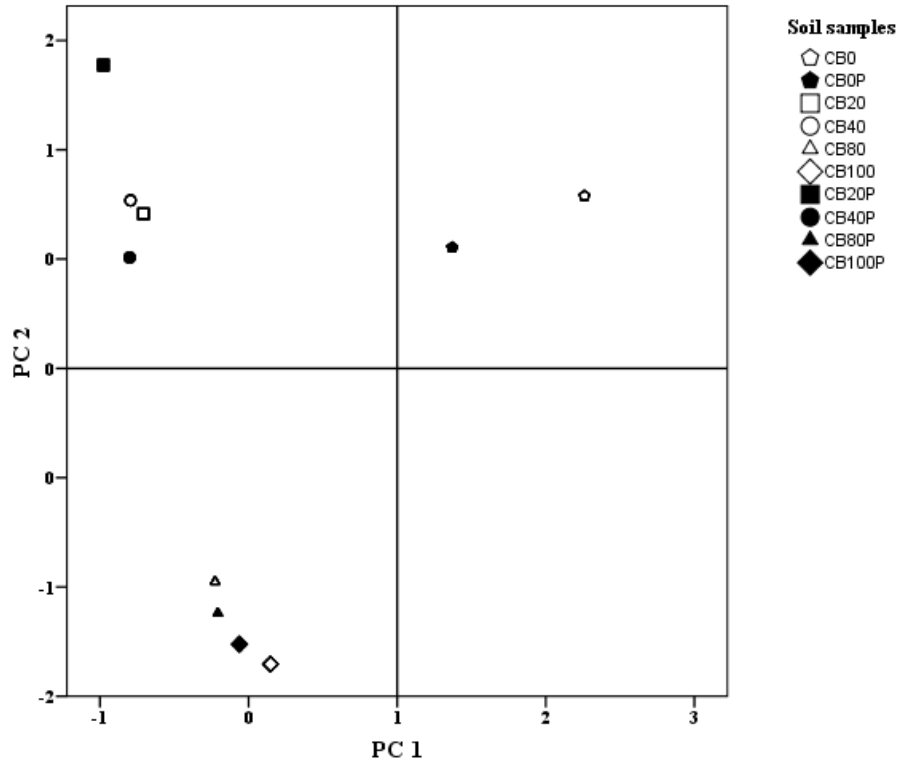

FIGURE 2
Scatter plot with the two principal components obtained in the PCA (PC 1 and PC 2) referred to the soil samples after three months of experiment.

TABLE 4
The component score coefficients matrix from the PCA for the soil samples after 3 months of experiment

Indicators	PC1	PC2
Al	0.94	0.34
Ca	-0.06	0.87
Co	0.94	0.34
Cu	0.94	0.34
Fe	0.95	-0.18
K	-0.59	-0.76
Mg	0.31	0.87
Mn	0.94	0.32
Na	-0.59	-0.75
Ni	0.94	0.33
P	-0.36	-0.81
Pb	-0.18	0.86
Zn	0.92	-0.30

Additional benefits of the application of compost-biochar amendment to the mine soil were observed in the growth of *B. juncea* plants. Mustard plants did not survive in the untreated settling pond soil, probably due to the lack of organic matter and the extremely acidic pH (Table 2). The addition of compost-biochar amendment to the mine soil promoted plant growth, as *B. juncea* plants were capable of grow in all the amended soils. The selection of an adequate plant species is a very important fact to the success of the phytostabilization techniques. Number of plants have been identified with metal accumulating capacity and can be used in the remediation of contaminated soils [41]. Phytoremediation of metals have received significant attention as a non-impact environmentally safe remediation strategy for polluted soils [42]. *Brassica juncea* is a tolerant plant to soil metals, grows fast and can produce large amount of above ground biomass [43].

Principal component analysis (PCA) in the soil samples. The concentrations of the measured trace elements in pore water were selected to perform a principal component analysis (PCA) (Table 4). The two principal components obtained accounted for 91 % of the total variance. According to the position of the soil samples in the scatter plot (Figure 2), the amended soils significantly changed their trace element concentration in comparison to

the control soils (CB0 and CB0P). The component score coefficients matrix obtained (Table 4) showed that CB0 and CB0P were positively influenced by most of the analysed trace elements (Al, Ca, Co, Cu, Fe, Mg, Mn, Ni, Pb and Zn). And there was a negative correlation with K, Na and P (Table 4). The scatter plot showed that the soils CB20, CB20P, CB40 and CB40P were positively influenced by the pore water concentration of Ca, Mg and Pb were negatively influenced by K, Na and P (Table 4). In addition, the soils CB80, CB80P, CB100 and CB100P were not influenced by any of the trace element contents (Table 4, Figure 2).

CONCLUSIONS

This study has demonstrated the capacity of compost-biochar amendment to increase soil pH, TC, TN and DOC content, and generally reduce the concentration of metals, such as Al, Co, Cu, Fe, Mg, Mn, Ni and Zn in soil pore water, compared to the unamended soils. The presence of compost-biochar amendment improved the ability of the mine soils to retain contaminants. In addition, the application of compost-biochar amendment also enhanced the ability of the mine soil to sustain vegetation, as *B. juncea* did not survive in the untreated soil. The combined use of compost-biochar amendment and *B. juncea* plants may be an efficient strategy to increase the immobilization of potential toxic trace elements in mine soils and reduce the associated contamination risk.

REFERENCES

[1] Hwang, T., Neculita, C.M. (2013) In situ immobilization of heavy metals in severely weathered tailings amended with food waste-based compost and zeolite. Water Air Soil Poll. 224, 1388.

[2] Abdolali, A., Guo, W.S., Ngo, H.H., Chen, S.S, Nguyen, N.C., Tung, K.L. (2014) Typical lignocellulosic wastes and by-products for biosorption process in water and wastewater treatment: A critical review. Bioresource Technol. 160, 57–66.

[3] Walker, D.J., Clemente, R., Bernal, M.P. (2004) Contrasting effects of manure and compost on soil pH, heavy metal availability and growth of *Chenopodium album* L. in a soil contaminated by pyritic mine waste. Chemosphere. 57, 215–224.

[4] Rees, F., Simonnot, M.O., Morel, J.L. (2014) Short-term effects of biochar on soil heavy metal mobility are controlled by intra-particle diffusion and soil pH increase. Eur. J. Soil Sci. 65, 149–161.

[5] Iovieno, P., Morra, L., Leone, A., Pagano, L., Alfani, A. (2009) Effect of organic and mineral fertilizers on soil respiration and enzyme activities of two Mediterranean horticultural soils. Biol. Fert. Soils. 45, 555–561.

[6] Almendro-Candel, M.B., Navarro-Pedreño, J., Jordán, M.M., Gómez, I., Meléndez-Pastor, I. (2014) Use of municipal solid waste compost to reclaim limestone quarries mine spoils as soil amendments: Effects on Cd and Ni. J. Geochem. Explor. 144, 363–366.

[7] Naeth, M.A., Wilkinson, S.R. (2013) Can we build better compost? Use of waste drywall to enhance plant growth on reclamation sites. J. Environ. Manage. 129, 503–509.

[8] Beesley, L., Marmiroli, M. (2011) The immobilisation and retention of soluble arsenic, cadmium and zinc by biochar. Environ. Pollut. 159, 474–480.

[9] Lehmann, L. (2007) Bio-energy in the black. Front. Ecol. Environ. 5, 381–387.

[10] Bakshi, S., He, Z.L., Harris, W.G. (2014) Biochar amendment affects leaching potential of copper and nutrient release behavior in contaminated sandy soils. J. Environ. Qual. 43, 1894–1902.

[11] Pulford, I.D., Watson, C. (2003) Phytoremediation of heavy metal-contaminated land by trees–a review. Environ. Int. 29, 529–540.

[12] Dzantor, E.K., Beauchamp, R.G. (2002) Phytoremediation, Part I: Fundamental basis for the use of plants in remediation of organic and metal contamination. Environ. Pract. 4, 77–87.

[13] Wang, Y., Hu, H., Zhu, L.-Y., Li, X.-X. (2012) Response to nickel in the proteome of the metal accumulator plant *Brassica juncea*. J. Plant Interact. 7, 230–237.

[14] Ishikawa, S., Ae, N., Murakami, M., Wagatsuma, T. (2006) Is *Brassica juncea* a suitable plant for phytoremediation of cadmium in soils with moderately low cadmium contamination? - Possibility of using other plant species for Cd-phytoextraction. Soil Sci. Plant Nutr. 52, 32–42.

[15] De Varennes, A., Cunha-Queda, C., Qu, G. (2010) Amendment of an acid mine soil with compost and polyacrylate polymers enhances enzymatic activities but may change the distribution of plant species. Water Air Soil Poll. 208, 91–100.

[16] Melgar-Ramírez, R., González, V., Sánchez, J.A., García, I. (2012) Effects of application of organic and inorganic wastes for restoration of sulphur-mine soil. Water Air Soil Poll. 223, 6123–6131.

[17] Galende, M.A., Becerril, J.M., Gómez-Sagasti, M.T., Barrutia, O., Epelde, L., Garbisu, C., Hernández, A. (2014) Chemical stabilization of metal-contaminated mine soil: Early short-term soil-amendment interactions and their effects on biological and chemical parameters. Water Air Soil Poll. 225, 1863.

[18] Clemente, R., Walker, D.J., Pardo, T., Martínez-Fernández, D., Bernal, M.P. (2012) The use of a halophytic plant species and organic amendments for the remediation of a trace elements-contaminated soil under semi-arid conditions. J. Hazard. Mater. 223-224, 63–71.

[19] Ciadamidaro, L., Puschenreiter, M., Santner, J., Wenzel, W.W, Madejón, P., Madejón, E. (2015) Assessment of trace element phytoavailability in compost amended soils using different methodologies. J. Soils Sediments. 17(5), 1251-1261.

[20] Rodríguez-Vila, A., Asensio, V., Forján, R., Covelo, E.F. (2015) Chemical fractionation of Cu, Ni, Pb and Zn in a mine soil amended with compost and biochar and vegetated with *Brassica juncea* L. J. Geochem. Explor. 158, 74–81.

[21] Puig, C.G., Álvarez-Iglesias, L., Reigosa, M.J., Pedrol, N. (2013) *Eucalyptus globulus* leaves incorporated as green manure for weed control in maize. Weed Sci. 61, 154–161.

[22] Porta, J. (1986) Techniques and experiments in Soil Science. Barcelona: Official College of Agricultural Engineers of Catalonia (in Catalan).

[23] Sanchez-Monedero, M.A., Roig, A., Martínez-Pardo, C., Cegarra, J., Paredes, C. (1996) A microanalysis method for determining total organic carbon in extracts of humic substances. Relationships between total organic carbon and oxidable carbon. Bioresource Technol. 57, 291–295.

[24] USDA Natural Resources Conservation Service (USDA-NRCS) (1998) Soil quality indicators : pH. Soil quality information sheet.

[25] Aranda, V., Macci, C., Peruzzi, E., Masciandaro, G. (2015) Biochemical activity and chemical-structural properties of soil organic matter after 17 years of amendments with olive-mill pomace co-compost. J. Environ. Manage. 147, 278–285.

[26] Bass, A.M., Bird, M.I., Kay, G., Muirhead, B. (2016) Soil properties, greenhouse gas emissions and crop yield under compost, biochar and co-composted biochar in two tropical agronomic systems. Sci. Total Environ. 550, 459–470.

[27] Zolfi-Bavariani, M., Ronaghi, A., Ghasemi-Fasaei, R., Yasrebi, J. (2016) Influence of poultry manure–derived biochars on nutrients bioavailability and chemical properties of a calcareous soil. Arch. Agron. Soil Sci. 62(11), 1578-1591.

[28] Sánchez-García, M., Sánchez-Monedero, M.A., Roig, A., López-Cano, I., Moreno, B., Benitez, E., Cayuela, M.L. (2016) Compost vs biochar amendment: a two-year field study evaluating soil C build-up and N dynamics in an organically managed olive crop. Plant Soil. 408(1-2), 1-14.

[29] Macías, F., Calvo de Anta, R. (2009) Niveles genéricos de referencia de metales pesados y otros elementos traza en los suelos de Galicia. Spain: Xunta de Galicia.

[30] Karami, N., Clemente, R., Moreno-Jiménez, E., Lepp, N.W., Beesley, L. (2011) Efficiency of green waste compost and biochar soil amendments for reducing lead and copper mobility and uptake to ryegrass. J. Hazard. Mater. 191, 41–48.

[31] Sizmur, T., Palumbo-Roe, B., Hodson, M.E. (2011) Impact of earthworms on trace element solubility in contaminated mine soils amended with green waste compost. Environ. Pollut. 159, 1852–1860.

[32] Zeng, G., Wu, H., Liang, J., Guo, S., Huang, L., Xu, P., Liu, Y., Yuan, Y., He, X., He, Y. (2015) Efficiency of biochar and compost (or composting) combined amendments for reducing Cd, Cu, Zn and Pb bioavailability, mobility and ecological risk in wetland soil. RSC Advances. 5, 34541–34548.

[33] Dang, T., Mosley, L.M., Fitzpatrick, R., Marschner, P. (2016) Addition of organic material to sulfuric soil can reduce leaching of protons, iron and aluminium. Geoderma. 271, 63–70.

[34] Ruttens, A., Colpaert, J.V., Mench, M., Boisson, J., Carleer, R., Vangronsveld, J. (2006) Phytostabilization of a metal contaminated sandy soil. II: Influence of compost and/or inorganic metal immobilizing soil amendments on metal leaching. Environ. Pollut. 144, 533–9.

[35] Marchand, L., Mench, M., Marchand, C., Le Coustumer, P., Kolbas, A., Maalouf, J.-P. (2011) Phytotoxicity testing of lysimeter leachates from aided phytostabilized Cu-contaminated soils using duckweed (*Lemna minor* L.). Sci. Total Environ. 410-411, 146–153.

[36] Kabata-Pendias, A. (2004) Soil-plant transfer of trace elements–an environmental issue. Geoderma. 122, 143–149.

[37] Hartley, W., Dickinson, N.M., Riby, P., Leese, E., Morton, J., Lepp, N.W. (2010) Arsenic mobility and speciation in a contaminated urban soil are affected by different methods of green waste compost application. Environ. Pollut. 158, 3560–3570.

[38] Vieira, F.C.B., He, Z.L., Wilson, C., Bayer, C. (2009) Speciation of aluminum in solution of an acidic sandy soil amended with organic composts. Commun. Soil Sci. Plan. 40, 2094–2110.
[39] Pardo, T., Bernal, M.P., Clemente, R. (2014) Efficiency of soil organic and inorganic amendments on the remediation of a contaminated mine soil: I. Effects on trace elements and nutrients solubility and leaching risk. Chemosphere. 107, 121–128.
[40] Cambier, P., Pot, V., Mercier, V., Michaud, A., Benoit, P., Revallier, A., Houot, S. (2014) Impact of long-term organic residue recycling in agriculture on soil solution composition and trace metal leaching in soils. Sci. Total Environ. 499, 560–573.
[41] Tak, H.I. (2015) Modulation of growth, antioxidant system in seedling of mustard under different levels of Nickel in adaptive response to metal resistant bacteria. Front. Biol. 10, 272–278.
[42] Franchi, E., Rolli, E., Marasco, R., Agazzi, G., Borin, S., Cosmina, P., Pedron, F., Rosellini, I., Barbafieri, M., Petruzzelli, G. (2016) Phytoremediation of a multi contaminated soil: mercury and arsenic phytoextraction assisted by mobilizing agent and plant growth promoting bacteria. J. Soils Sediments.
[43] Mourato, M.P., Moreira, I.N., Leitão, I., Pinto, F.R., Sales, J.R., Martins, L.L. (2015) Effect of heavy metals in plants of the genus *Brassica*. Int. J. Mol. Sci. 16, 17975–17998.

Received: **10.01.2017**
Accepted: **18.03.2019**

CORRESPONDING AUTHOR

Alfonso Rodriguez-Vila
Department of Plant Biology and Soil Science,
Faculty of Biology,
University of Vigo, Lagoas, Marcosende,
36310 Vigo, Pontevedra – Spain

e-mail: fonso@uvigo.es

© by PSP Volume 28 – No. 5/2019 pages 3626-3636 Fresenius Environmental Bulletin

SPATIAL AND TEMPORAL VARIATION OF AIR POLLUTION: THE CASE OF THE MARMARA REGION

Serpil Mentese*

Bilecik Seyh Edebali University, Faculty of Arts and Sciences, Bilecik, Turkey

ABSTRACT

Nowadays, air pollutants are still posing a risk in some areas although air pollutant parameters are decreasing. The fact that air pollutants are still posing a risk in some areas is a consequence of spatial differences. For this reason, the spatial distribution and temporal change of air pollutant parameters (SO_2, PM_{10}, NO and NO_2) in the Marmara Region between March 2013-December 2015 were aimed to demonstrate in this study. For this purpose, SO_2, PM_{10}, NO and NO_2 data measured by Marmara Clean Air Center Directorate by means of approximately 39 stations in 11 provinces in the Marmara Region were used. The Ordinary Kriging method was used to create spatial distribution maps in the study. The bivariate correlation analysis was applied by considering the independent variable of time to indicate how air pollutants change in terms of years and months. It has been found that all pollutants being studied are at higher levels in winter although NO_2 is not very obvious. Both in SO_2 and PM_{10}, it was determined that the concentration levels in the southwest (Canakkale and Edirne) of the study area were usually at higher levels. The highest NO concentration levels were observed in Istanbul and Bursa, where the population and traffic were the highest. In NO_2, it was determined that the values were almost at the same level within the study area.

KEYWORDS:
Air Pollution, Marmara Region, GIS, Ordinary Kriging, Correlation Analysis

INTRODUCTION

Nowadays, developments in industry and technology have increased the mankind's pressure on natural resources to higher levels compared to the past. This situation has brought about many environmental problems, as well. One of the most important of these is the change in the natural composition of the air, which is one of the physical environment elements. Rapid population growth, industrialization efforts, rapid and irregular urbanization and traffic have been influential on the change of the natural composition of the air.

The measurement of sulfur dioxide (SO_2) and particulate matter (PM), which are the pollutants that give the feature of polluted air to the air, by changing the natural composition of the air, has been found sufficient to be able to decide on the level of pollution by the World Health Organization, and it has been proposed to measure these two pollutants in all countries. As a result of the deterioration of air quality in cities and increase in the findings indicating its potential effects on public health, pollutants such as NO, NO_2 and CO started to be measured in addition to the pollutant parameters such as PM_{10} and SO_2 in the control of air pollution in urban and industrial areas [1]. The source areas of these pollutant parameters are different from each other. For example, while SO_2 is mixed with air by heating and through the chimneys of some industrial facilities [2]; PM gets into the atmosphere largely from industrial facilities and partially through heating [3]. While nitrogen oxide emissions are pollutants resulting from industrial facilities mostly from transportation [4], NO_2 is a pollutant resulting especially from traffic [5,2].

Air pollution causes negative effects on human health and other living beings, and local and universal problems appear [6]. Thus, the World Health Organization (WHO), European Union (EU), European Environmental Protection Agency (EPA) and Turkish Air Quality Control Regulation (AQCR) have determined the target limit values for pollutants andthe standards defining the level at which air pollution begins [7]. When the target limit values for air pollutants are compared with each other, it is clear that the limit values determined in the Air Pollution Control Regulation in Turkey are higher when compared to the limit values of other countries. Since exposure to these pollutants is the same all over the world, it is required for the target limit values to be of the same standard in each country. Moreover, air quality measurement stations established to identify air quality in cities provide an opinion about the general air quality, and they are established in certain areas. However, when it is considered that there is exposure to much higher pollutant concentrations in microenvironments [8] in which people maintain their daily activities, it is important to establish measurement stations not in specific areas but in

more than one and different areas regarding the spatial differentiation of the area.

In the detection of spatial distribution, the point pattern analysis is used as a powerful tool in the determination of the relationship of a specific case in different locations by benefiting from statistical techniques [9]. Therefore, in this study, it is aimed to reveal the spatial pattern and temporal change of air pollutant parameters in the Marmara Region between March 2013- December 2015 because revealing the spatial pattern and temporal change of air quality parameters is important in terms of sustainable air quality management.

MATERIALS AND METHODS

Study Area. The study area is the region with the lowest average elevation in Turkey. The Samanli Mountains and Uludag in the south and the Yıldız Mountains in Trakya region constitute the most important elevations of the region. It is the most industrialized and most heavily populated region in Turkey. There are 11 provinces in the Marmara Region, being Istanbul, Edirne, Kirklareli, Tekirdag, Canakkale, Kocaeli, Yalova, Sakarya, Bilecik, Bursa and Balikesir (Figure 1).

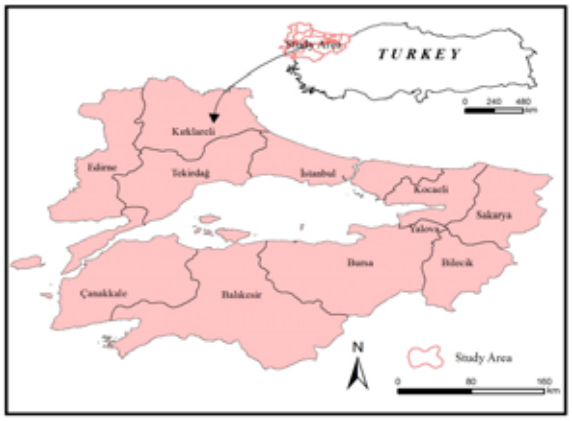

FIGURE 1
Location map of the study area.

There are more than one climatic (Black Sea, the Mediterranean and continental climate) characteristics observed in the study area. The annual average temperatures vary between 14-16 ºC. Prevailing wind direction mostly consist of northern and northeastern. The total population of the provinces in the Marmara Region is approximately more than 24 million as from 2017. Istanbul is in the first place with the population of 14.985.000. With regard to the total population, the populations of the other provinces in the Marmara Region are 2.940.081 in Bursa, 1.871.456 in Kocaeli, 1.201.492 in Balikesir, 997.737 in Tekirdag, 988.888 in Sakarya, 523.258 in Canakkale, 402.147 in Edirne, 352.856 in Kirklareli, 247.841 in Yalova and 219.752 in Bilecik. The provinces with a high population (Istanbul-Bursa-Kocaeli) are also the most developed industrial cities in the region. The region has developed in terms of industry and mining, agriculture and animal husbandry and tourism. Iron and steel, food, weaving, garment industry, automotive, cement, petrochemistry products constitute the primary industrial products of the region.

Material, The data on the air pollutant parameters (SO_2, PM_{10}, NO and NO_2) of the Marmara Region between March 2013-December 2015 were provided by Marmara Clean Air Center Directorate. Marmara Clean Air Center Directorate measures air pollutant parameters by means of approximately 39 stations in 11 provinces in the Marmara Region. These stations are located in Sile, Silivri, Sultangazi, Kagithane, Sultanbeyli, Esenyurt, Basaksehir, Umraniye, Mecidiyekoy, Sirinevler, Uskudar, Kandilli, Izmit, Korfez, Alikahya, Golcuk, Yenikoy, Kandira, Merkez (Tekirdag), Cerkezkoy, Merkez (Sakarya), Ozanlar, Bozuyuk, Altinova, Armutlu, Kulturpark, Beyazit Street, Uludag University, Kestel, Inegol, Bandirma, Erdek, Karaagac, Kesan, Limankoy, Luleburgaz, Lapseki, and Can. The stations were separated into categories such as traffic, rural, semi-rural, industrial, urban, semi-rural-industrial according to their locations.

Method, In the study, the distribution of air pollutant parameters in the area was examined and thus, spatial differentiation was determined. In the determination of spatial distribution, the relationship of a specific case in different locations was determined with the point pattern analysis and the Kriging interpolation method was preferred in the spatial distribution of air pollutant parameters. The Kriging method is the most frequently used method for the interpolation of spatial data [6]. With the Kriging method, surface curves are efficiently obtained from data dispersed in the irregular structure. The Ordinary Kriging method was used in the study to create regional distribution maps. The estimation of values in a non-sampled point in ordinary kriging is made by assuming that the regional variables are stable and their average is constant [10].

Furthermore, the data of the PM_{10}, SO_2, NO and NO_2 pollutants were collected monthly and annually and examined by using statistical techniques. The bivariate correlation analysis was applied by considering the independent variable of time to indicate how air pollutants change in terms of years and months.

RESULTS AND DISCUSSION

Significant differences were observed between summer (July) and winter (december) seasons in

terms of SO_2 levels in the Marmara Region (Figure 2). It was identified that values in winter were significantly higher when compared to summer. Moreover, SO_2 concentration levels were observed to be high throughout the study area in winter. Especially, when the limit value of 150 mg/m^3 determined for SO_2 in Turkey is considered, it stands out that the values in Edirne and Canakkale in 2013 and in Edirne and its surroundings in the years of 2014 and 2015 during the winter months were at a considerable level. It was determined in the study conducted by Ozsahin et al., [11] in Kesan that SO_2 values were significantly higher than the standard limit value. The use of poor quality fuel and climatic and especially topographic factors were indicated as factors causing this condition. Since Canakkale and its surroundings are an area where coal mining and coal-fired thermal power plants are concentrated [12], it is possible that there will be more pollution when compared to other areas.

However, it was also observed that the values were significantly low in summer. In the study conducted by Ozdemir et al. (2018) [13] in summer for all air pollutants, the average values are much lower than in other seasons. It was identified that the values in summer were slightly more than 10 mg/m^3. This situation indicates that SO_2 values during summer in the study area are acceptable in terms of the health of living creatures and do not cause any problem on them.

Changes in SO_2 by years during Mart 2013-December 2015 are indicated in Table 1. When the long-term annual SO_2 change in the study area was examined, it was determined that the pollutant was in the tendency to increase in Lapseki, Kesan, Alikahya, Ozanlar, Cerkezkoy and the center of Tekirdag. This tendency to increase was found to be statistically significant at the confidence level of 99% ($p<0,01$) only in Ozanlar and the center of Tekirdag (Table 1). It was identified in the study conducted by Tagil and Koc [14] in Edirne in 2000 that the SO_2 rate increased during the time studied. Source sites were used as a basis for the establishment of measurement stations in the study area. Some stations are urban, some are rural, and some are traffic-related measurement stations. Among the measurement stations in the study area, Ozanlar where pollution statistically increased at the confidence level of 99% was an urban, Cerkezkoy was a urban/ industrial and the center of Tekirdag was a traffic-related measurement station. SO_2 was in the tendency to decrease in the other places of the study area. This tendency to decrease was found to be statistically significant only in Inegol. It does not express statistical significance in other places.

While SO_2 increases in some areas, it is in the tendency to decrease in some areas. The findings obtained in this study are parallel with the findings of most studies in the literature. For example, it was determined in the studies conducted in different areas by Erbaslar and Tasdemir [15] Beyhun et al., [16], Ibret ve Aydinozu [17], Sezer Turalioglu [18], Ozcan [19] and Tecer and Tagil [1] that there was a statistically significant decrease in SO_2 levels. These tendencies to decrease were connected to the use of natural gas becoming more widespread every year. However, in this study, tendencies to decrease could not be determined throughout the study area, and there was a tendency to increase in SO_2 in some areas.

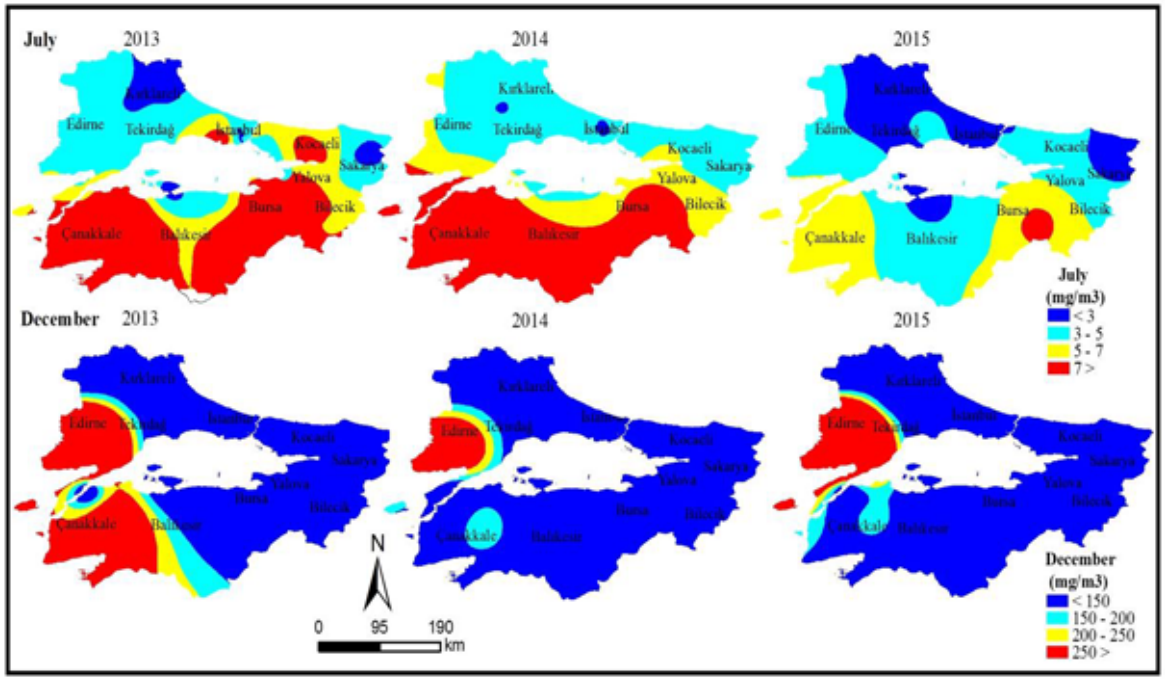

FIGURE 2

Spatial Distribution of SO_2 in the Marmara Region in Summer (July) and Winter (December).

TABLE 1

Correlation Table Showing Monthly and Annual Temporal Change of SO_2 in the Marmara Region.

SO_2		Month	Year			Month	Year			Month	Year
Bandirma-Balikesir	P. C.	-,170	-,121	Karaagac-Edirne	P. C.	-,053	-,074	Limankoy-Kirklareli	P. C.	,127	-,261
	Sig.	,337	,495		Sig.	,765	,677		Sig.	,474	,136
	N	34	34		N	34	34		N	34	34
Erdek-Balikesir	P. C.	-,267	-,323	Kesan-Edirne	P. C.	,073	,079	Luleburgaz-Kirklareli	P. C.	-,251	-,091
	Sig.	,133	,066		Sig.	,683	,656		Sig.	,152	,609
	N	34	34		N	34	34		N	34	34
Bozuyuk-Bilecik	P. C.	-,261	-,230	Basaksehir-İstanbul	P. C.	-,273	-,155	Alikahya-Kocaeli	P. C.	-,209	,061
	Sig.	,136	,190		Sig.	,119	,382		Sig.	,235	,732
	N	34	34		N	34	34		N	34	34
Beyazit Street.-Bursa	P. C.	-,203	-,016	Esenyurt-İstanbul	P. C.	-,359*	-,287	Golcuk-Kocaeli	P. C.	-,027	-,161
	Sig.	,250	,929		Sig.	,037	,100		Sig.	,879	,364
	N	34	34		N	34	34		N	34	34
İnegol-Bursa	P. C.	,095	**-,497****	Kagithane-İstanbul	P. C.	-,461**	-,029	Korfez-Kocaeli	P. C.	-,441*	-,271
	Sig.	,594	,003		Sig.	,006	,873		Sig.	,012	,134
	N	34	34		N	34	34		N	34	34
Kestel-Bursa	P. C.	-,300	-,309	Kandilli-İstanbul	P. C.	-,429*	-,072	Ozanlar-Sakarya	P. C.	-,123	**,707****
	Sig.	,085	,076		Sig.	,011	,687		Sig.	,490	,000
	N	34	34		N	34	34		N	34	34
Kultur Park-Bursa	P. C.	-,082	-,202	Sirinevler-İstanbul	P. C.	-,426*	-,054	Cerkezkoy-Tekirdag	P. C.	-,200	**,758****
	Sig.	,645	,253		Sig.	,012	,762		Sig.	,257	,000
	N	34	34		N	34	34		N	34	34
Uludag Unv.-Bursa	P. C.	-,219	-,304	Sultanbeyli-İstanbul	P. C.	-,162	-,105	Merkez-Tekirdag	P. C.	-,195	**,673****
	Sig.	,213	,081		Sig.	,359	,554		Sig.	,269	,000
	N	34	34		N	34	34		N	34	34
Can-Canakkale	P. C.	-,111	-,160	Sultangazi-İstanbul	P. C.	-,165	-,103	Altinova-Yalova	P. C.	-,136	-,110
	Sig.	,533	,366		Sig.	,359	,568		Sig.	,444	,538
	N	34	34		N	33	33		N	34	34
Lapseki-Canakkale	P. C.	,100	,172	Umraniye-İstanbul	P. C.	-,346*	-,160	Armutlu-Yalova	P. C.	,229	,004
	Sig.	,575	,331		Sig.	,045	,366		Sig.	,192	,980
	N	34	34		N	34	34		N	34	34

*. Correlation is significant at the 0.05 level (2-tailed).

**. Correlation is significant at the 0.01 level (2-tailed).

Significant differences were observed between summer and winter seasons in the PM_{10} concentration levels in the study area, as in SO_2 (Figure 3). While the concentration levels during summer exceeded approximately 50 mg/m^3, they were more than 110 mg/m^3 during December representing the winter season. This finding obtained was proved with the studies in the literature, and it is a known finding. It was revealed in the studies conducted in various areas that PM concentrations increase in winter [20, 21, 17, 22, 23, 24, 25]. The climatic characteristics of winter constitute the parameter effective in the formation of pollution. It was identified in the study conducted by Ozdemir et al. (2010) [26] in five different areas in Istanbul that $PM_{2.5}$ and PM_{10} concentrations were at a low level during summer months. However, their concentration values were higher during cold months.

While PM_{10} levels were 40-45 mg/m^3 almost in the whole of the study area during the summer of 2013, they decreased around Kocaeli, Sakarya, Yalova and Kirklareli in 2014. However, there were increases observed in Balikesir and its surroundings. On the other hand, in 2015, it was determined that the concentration levels exceeded 50 mg/m^3 in Istanbul.

It was determined that the concentration levels in the southwest of the study area (Canakkale, Edirne) were higher (110 mg/m^3 >) during the winter of 2013 (Figure 3). In 2014, the concentration levels were less than 110 mg/m^3 in the whole study area. In 2015, they were more than 110 mg/m^3 only in Edirne. Thus, in the study conducted by Gumus et al. (2015) [27], the highest $PM_{2.5}$ and PM_{10} correlation was determined in Kesan and Cerkezkoy where anthropogenic pollution (depending on heating and industrial) was high. Also this situation, in the study conducted by Kahya et al. (2017) [28] the Kesan (Edirne) station had the highest $PM_{2.5}$ concentrations. It can be assumed that these highest values were originated from pollution caused by fossil fuel heating. Moreover, the topography of the

Kesan was also effective on these obtained results [28].

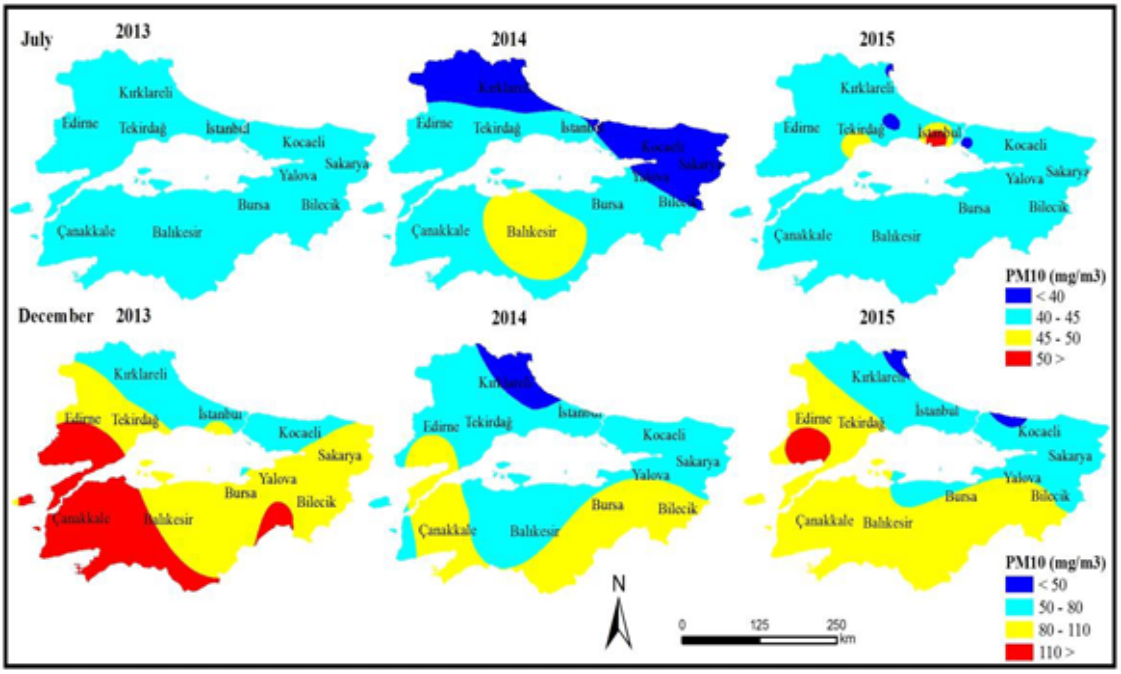

FIGURE 3
Spatial Distribution of PM_{10} in the Marmara Region in Summer (July) and Winter (December).

TABLE 2
Correlation Table Showing Monthly and Annual Temporal Change of PM_{10} in the Marmara Region.

PM_{10}		Month	Year			Month	Year			Month	Year
Bandirma-Balikesir	P. C.	-,231	-,229	Kandilli-Istanbul	P. C.	-,129	-,022	Alikahya-Kocaeli	P. C.	-,062	-,178
	Sig.	,188	,192		Sig.	,468	,900		Sig.	,727	,313
	N	34	34		N	34	34		N	34	34
Bozuyuk-Bilecik	P. C.	,049	-,197	Mecidiyekoy-Istanbul	P. C.	-,092	-,256	İzmit-Kocaeli	P. C.	-,036	-,223
	Sig.	,782	,265		Sig.	,604	,144		Sig.	,839	,204
	N	34	34		N	34	34		N	34	34
Beyazit Street - Bursa	P. C.	-,074	,031	Sile-Istanbul	P. C.	-,311	**-,451****	Kandira-Kocaeli	P. C.	-,152	**,547****
	Sig.	,677	,862		Sig.	,073	,008		Sig.	,392	,001
	N	34	34		N	34	34		N	34	34
İnegol-Bursa	P. C.	,120	-,083	Silivri-Istanbul	P. C.	-,272	-,103	Korfez-Kocaeli	P. C.	-,243	-,199
	Sig.	,499	,640		Sig.	,120	,561		Sig.	,167	,259
	N	34	34		N	34	34		N	34	34
Kestel-Bursa	P. C.	-,058	-,207	Sirinevler-İstanbul	P. C.	-,342*	-,259	Merkez-Sakarya	P. C.	-,064	**,863****
	Sig.	,744	,239		Sig.	,048	,140		Sig.	,717	,000
	N	34	34		N	34	34		N	34	34
Can-Canakkale	P. C.	-,104	-,037	Umraniye-İstanbul	P. C.	-,033	**-,592****	Cerkezkoy-Tekirdag	P. C.	-,210	**,805****
	Sig.	,559	,834		Sig.	,853	,000		Sig.	,233	,000
	N	34	34		N	34	34		N	34	34
Kesan-Edirne	P. C.	-,022	,053	Uskudar-Istanbul	P. C.	-,241	-,237	Merkez-Tekirdag	P. C.	-,120	**,775****
	Sig.	,903	,766		Sig.	,170	,177		Sig.	,499	,000
	N	34	34		N	34	34		N	34	34
Basaksehir-Istanbul	P. C.	-,283	,235	Limankoy-Kirklareli	P. C.	-,238	,217	Armutlu-Yalova	P. C.	-,079	**,355***
	Sig.	,104	,182		Sig.	,176	,218		Sig.	,657	,039
	N	34	34		N	34	34		N	34	34
Esenyurt-Istanbul	P. C.	,125	**,477****	Luleburgaz-Kirklareli	P. C.	-,022	,021				
	Sig.	,481	,004		Sig.	,902	,905				
	N	34	34		N	34	34				

*. Correlation is significant at the 0.05 level (2-tailed).
**. Correlation is significant at the 0.01 level (2-tailed).

Considering the limit value of 150 mg/m3 determined for PM_{10} in the Air Pollution Control Regulation in Turkey, the levels lower than this limit value were observed in the whole study area. This situation makes us think that there was not any risk in terms of PM_{10} during the study throughout the study area. However, when it is considered that the limit values in Turkey are 2 or 3 times more than the limit values in other countries, it is clear that these values (110 mg/m3 >) are at a considerable level. Shortly, although the national legal target values are not exceeded in terms of the study area, on a large scale, it is observed that there are values over the standards determined by the EU, EPA and WHO.

When the long-term annual PM_{10} change in the study area was examined (Table 2), it was determined that the pollutant was in the tendency to increase in Beyazit Street, Kesan, Basaksehir, Esenyurt, Limankoy, Luleburgaz, Kandira, the center of Sakarya, Cerkezkoy and the center of Tekirdag. This tendency to increase was found to be statistically significant at the confidence level of 99% only in Esenyurt, Kandira, center of Sakarya merkez and center of Tekirdag (Table 2). Among the measurement stations in the study area, Esenyurt where pollution statistically increased at the confidence level of 99% was an urban/industrial, center of Sakarya and Tekirdag were a traffic and Kandira was a rural ecology measurement station. PM_{10} correlation indicating a tendency towards increase was observed at stations with significant anthropogenic pollution and indicating urban/industrial and traffic characteristics. However, among these stations, Kandira with different characteristics and indicating rural/ecological characteristics attracts attention. Although Kandira station has a rural/ecological characteristic, pollution indicated a gradual increase during the period of time studied at this station.

PM_{10} was in the tendency to decrease in the other places of the study area. This tendency to decrease was found to be statistically significant only in Sile and Umraniye. A decrease in PM_{10} has been observed throughout Turkey [23, 15, 27].

There are decreases in PM_{10} and SO_2 levels among air pollutant parameters in parallel with the spread of the use of natural gas [29, 15, 30, 31, 19, 26]. This is because SO_2 and PM emissions in natural gas are considerably low. However, nitrogen oxides appear as the most important pollutant emission in this fuel [32, 33, 34]. Due to their effects such as the fact that they react with O_3 concentration at the ground level, affect the health of living creatures negatively and cause acid rains, nitrogen oxides are important in terms of air pollution. Although nitrogen oxides have more than one forms, NO and NO_2 are the most important ones in terms of air pollution [35, 36].

In the study area, while NO levels varied between 4 and 12 mg/m^3 during July representing the summer season, the concentration levels increased in winter, and they were more than 90 mg/m^3 (Figure 4). In other words, significant differences were observed between summer and winter seasons in terms of the concentration levels. Considering the spatial distribution of NO in the study area, the highest concentration was determined in Istanbul, Tekirdag and Bursa in summer.

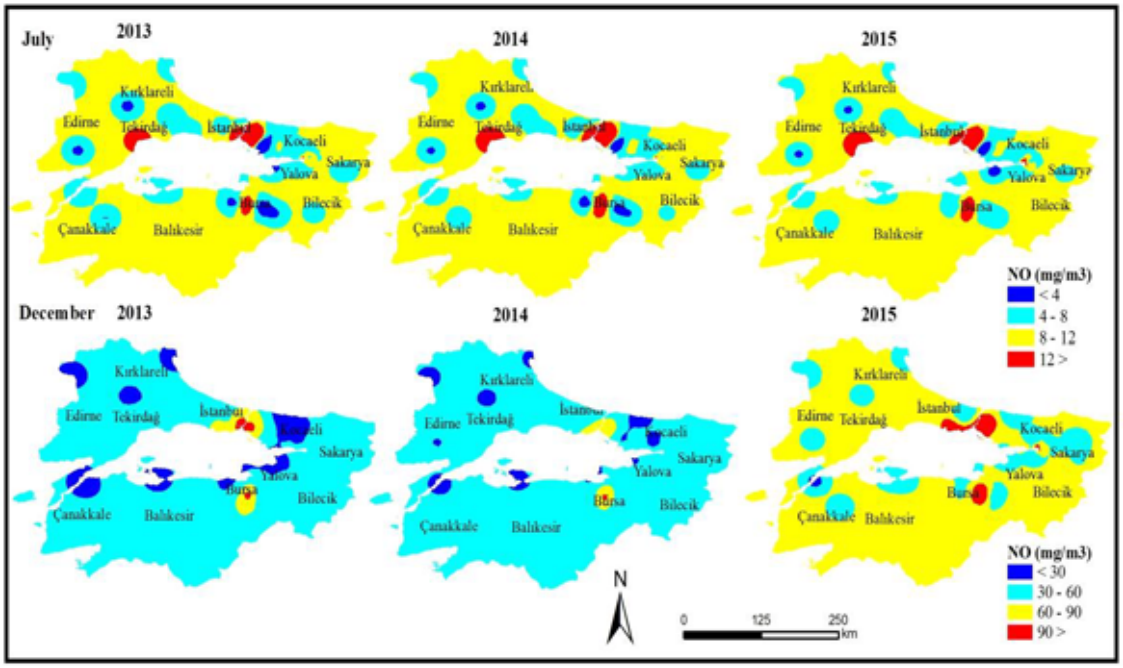

FIGURE 4
Spatial Distribution of NO in the Marmara Region in Summer (July) and Winter (December).

On the other hand, it exhibited differences during the period studied. While the highest concentrations in 2013 were in Istanbul and Bursa, the highest concentrations were also in the same areas in 2014. However, there were decreases determined. It was observed in 2015 that the concentration levels increased throughout the study area. During winter, the highest concentrations were observed around Istanbul and Bursa where the population and traffic were the highest.

It was identified in the study conducted by Saitoa et al., (2012) [37] that the NO_X rate increased in winter season. The long-term limit value identified for NO by the Air Pollution Control Regulation in Turkey is 200 µg/m^3. It was identified that the limit value, which is 200 µg/m^3, was never exceeded in the study area during the period studied. It is possible to say that the NO values in the study area are not at threatening levels in terms of the limit values.

When the long-term annual NO change in the study area was examined (Table 3), it was determined that the pollutant was in the tendency to increase in Bandirma, Erdek, Beyazit Street, Inegol, Kestel, Kulturpark, Uludag University, Can, Lapseki, Karaagac, Kesan, Esenyurt, Kandilli, Mecidiyekoy, Sile, Silivri, Sirinevler, Sultanbeyli, Umraniye, Uskudar, Limankoy, Luleburgaz, Alikahya, Izmit, Kandira, Korfez, center of Sakarya,

TABLE 3
Correlation Table Showing Monthly and Annual Temporal Change of NO in the Marmara Region.

NO		Month	Year			Month	Year			Month	Year
Bandirma-Balıkesir	P. C.	,163	,090	Basaksehir-İstanbul	P. C.	,209	-,092	Limankoy-Kırklareli	P. C.	-,095	**,683****
	Sig.	,357	,613		Sig.	,236	,606		Sig.	,593	,000
	N	34	34		N	34	34		N	34	34
Erdek-Balıkesir	P. C.	,493**	,328	Esenyurt-İstanbul	P. C.	,215	,166	Luleburgaz-Kırklareli	P. C.	,410*	,266
	Sig.	,004	,063		Sig.	,223	,348		Sig.	,016	,129
	N	33	33		N	34	34		N	34	34
Bozuyuk-Bilecik	P. C.	,400*	-,097	Kagithane-İstanbul	P. C.	,145	-,145	Alikahya-Kocaeli	P. C.	,094	,111
	Sig.	,019	,585		Sig.	,414	,414		Sig.	,599	,532
	N	34	34		N	34	34		N	34	34
Beyazit Street.-Bursa	P. C.	,206	,084	Kandilli-İstanbul	P. C.	,039	,066	Golcuk-Kocaeli	P. C.	,083	-,021
	Sig.	,242	,638		Sig.	,826	,710		Sig.	,640	,905
	N	34	34		N	34	34		N	34	34
Inegol-Bursa	P. C.	,281	,064	Mecidiyekoy-İstanbul	P. C.	,267	,143	İzmit-Kocaeli	P. C.	,215	**,978****
	Sig.	,108	,720		Sig.	,126	,420		Sig.	,222	,000
	N	34	34		N	34	34		N	34	34
Kestel-Bursa	P. C.	,267	,152	Sile-İstanbul	P. C.	,487**	**,354***	Kandira-Kocaeli	P. C.	,482**	**,702****
	Sig.	,127	,390		Sig.	,003	,040		Sig.	,004	,000
	N	34	34		N	34	34		N	34	34
Kulturpark-Bursa	P. C.	,300	,082	Silivri-İstanbul	P. C.	,245	,051	Korfez-Kocaeli	P. C.	,210	**,929****
	Sig.	,084	,644		Sig.	,162	,774		Sig.	,234	,000
	N	34	34		N	34	34		N	34	34
Uludag Unv.-Bursa	P. C.	,385*	,081	Sirinevler-İstanbul	P. C.	,069	,040	Merkez-Sakarya	P. C.	,118	**,691****
	Sig.	,024	,651		Sig.	,696	,823		Sig.	,506	,000
	N	34	34		N	34	34		N	34	34
Can-Canakkale	P. C.	,251	,079	Sultanbeyli-İstanbul	P. C.	,352*	,070	Ozanlar-Sakarya	P. C.	,284	,048
	Sig.	,152	,656		Sig.	,041	,695		Sig.	,103	,787
	N	34	34		N	34	34		N	34	34
Lapseki-Canakkale	P. C.	-,255	,145	Sultangazi-İstanbul	P. C.	,240	-,220	Cerkezkoy-Tekirdag	P. C.	,268	,118
	Sig.	,145	,413		Sig.	,171	,212		Sig.	,125	,508
	N	34	34		N	34	34		N	34	34
Karaagac-Edirne	P. C.	,383*	,143	Umraniye-İstanbul	P. C.	,257	,086	Altinova-Yalova	P. C.	,064	,100
	Sig.	,025	,421		Sig.	,142	,629		Sig.	,721	,574
	N	34	34		N	34	34		N	34	34
Kesan-Edirne	P. C.	,193	,151	Uskudar-İstanbul	P. C.	,135	,032	Armutlu-Yalova	P. C.	,190	,108
	Sig.	,274	,393		Sig.	,447	,857		Sig.	,281	,541
	N	34	34		N	34	34		N	34	34

*. Correlation is significant at the 0.05 level (2-tailed).
**. Correlation is significant at the 0.01 level (2-tailed).

Ozanlar, Cerkezkoy, Altinova ve Armutlu. This tendency to increase was found to be statistically significant at the confidence level of 99% only in Sile, Limankoy, Izmit, Kandira, Korfez and center of Sakarya (Table 3). Among the measurement stations in the study area, Sile, Limankoy and Kandira where pollution statistically increased at the confidence level of 99% were a rural, Izmit and center of Sakarya were a traffic and Korfez was an industrial measurement station. NO was in the tendency to decrease in the other places of the study area. It does not express statistical significance in other places.

It is determined that seasonal differences in NO_2 levels are not significant as much as SO_2, PM_{10} and NO levels in the study area (Figure 5). Since NO_2 is a pollutant resulting from transportation [38, 5, 39], it is likely that it will be observed close to each other in all years. However, when Figure 5 is examined again, it is determined that the concentration levels increase during winter. While the levels were between 20 and 30 mg/m^3 throughout the study area in summer, it was observed that they exceeded 30 mg/m^3 in some areas during winter. It was determined that the concentration levels were almost the same during summer when considered in terms of years. However, the levels increased in winter in 2015.

The long-term limit value identified for NO_2 by the Air Pollution Control Regulation in Turkey is 100 µg/m^3. It was identified that the limit value, which is 100 µg/m^3, was never exceeded in the study area during the period studied. According to the air quality limit values of Turkey in effect, the estimated annual average limit value was determined to be 40 µg/m^3 for NO_2 for 2024 [40]. Although the limit values for NO_2 are not exceeded in the study area, it is recorded that there are values above the standards especially during winter in 2024.

When the long-term annual NO_2 change in the study area was examined, it was determined that the pollutant was in the tendency to increase in Kesan, Basaksehir, Sirinevler, Limankoy, Kandira, Korfez, center of Sakarya, Ozanlar and Armutlu (Table 4). This tendency to increase was found to be statistically significant at the confidence level of 99% only in Limankoy, Kandira, Korfez, center of Sakarya and Ozanlar. Among the measurement stations in the study area, Limankoy where pollution statistically increased at the confidence level of 99% was a rural, Kandira was a rural/ecology, Korfez was a industrial, center of Sakarya was a trafic and Ozanlar was an urban measurement station. NO_2 was in the tendency to decrease in the other places of the study area.

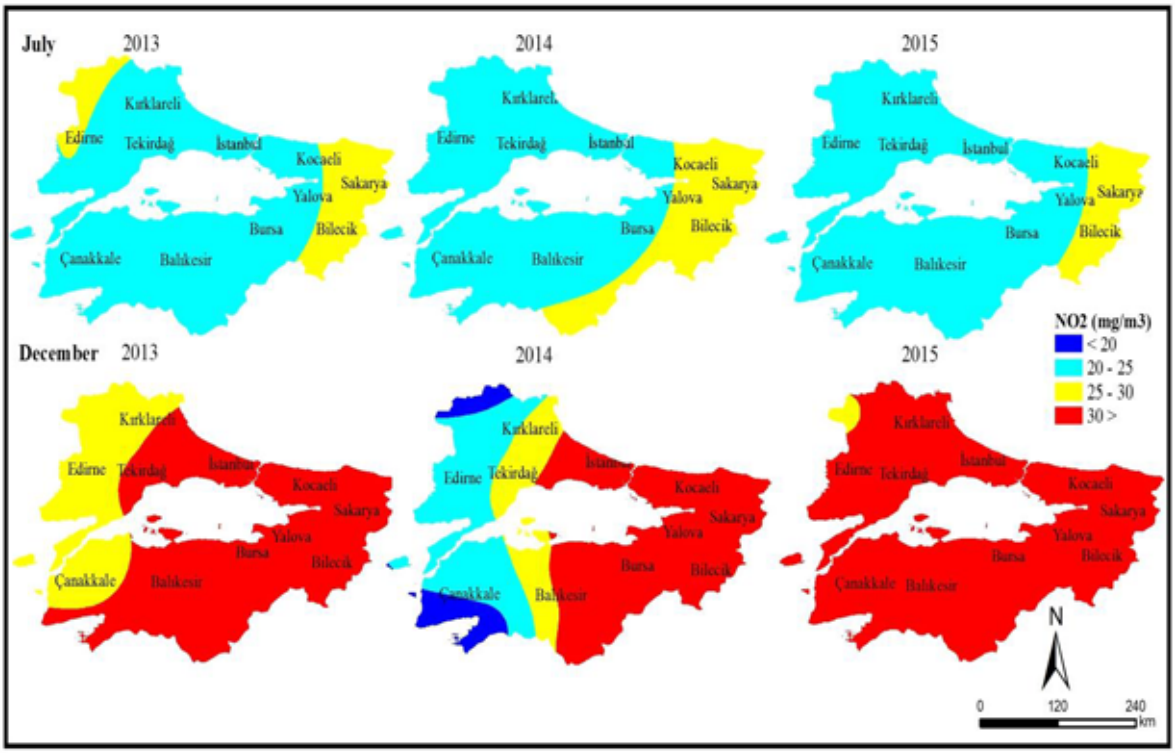

FIGURE 5
Spatial Distribution of NO_2 in the Marmara Region in Summer (July) and Winter (December).

TABLE 4
Correlation Table Showing Monthly and Annual Temporal Change of NO_2 in the Marmara Region.

NO_2		Month	Year			Month	Year			Month	Year
Bandirma-Balıkesir	P. C.	-,097	-,244	Esenyurt-İstanbul	P. C.	-,168	**-,400***	Luleburgaz-Kirklareli	P. C.	,037	-,076
	Sig.	,585	,163		Sig.	,343	,019		Sig.	,834	,670
	N	34	34		N	34	34		N	34	34
Bozuyuk-Bilecik	P. C.	,147	-,173	Kagithane-İstanbul	P. C.	-,189	**-,536****	Alikahya-Kocaeli	P. C.	-,429*	-,013
	Sig.	,406	,328		Sig.	,284	,001		Sig.	,011	,944
	N	34	34		N	34	34		N	34	34
Beyazit Street-Bursa	P. C.	-,144	,021	Kandilli-İstanbul	P. C.	-,526**	-,127	Golcuk-Kocaeli	P. C.	-,123	-,053
	Sig.	,415	,906		Sig.	,001	,475		Sig.	,490	,764
	N	34	34		N	34	34		N	34	34
İnegol-Bursa	P. C.	-,106	,105	Mecidiyekoy-İstanbul	P. C.	-,462**	-,168	İzmit-Kocaeli	P. C.	-,172	-,033
	Sig.	,552	,554		Sig.	,006	,341		Sig.	,330	,854
	N	34	34		N	34	34		N	34	34
Kestel-Bursa	P. C.	-,087	,190	Sile-İstanbul	P. C.	,123	-,179	Kandira-Kocaeli	P. C.	,181	**,902****
	Sig.	,624	,281		Sig.	,487	,311		Sig.	,305	,000
	N	34	34		N	34	34		N	34	34
Kulturpark-Bursa	P. C.	,230	-,080	Silivri-İstanbul	P. C.	-,016	,000	Korfez-Kocaeli	P. C.	-,021	**,549****
	Sig.	,190	,652		Sig.	,928	1,000		Sig.	,905	,001
	N	34	34		N	34	34		N	34	34
Uludag Unv.-Bursa	P. C.	-,075	,038	Sirinevler-İstanbul	P. C.	-,418*	,043	Merkez-Sakarya	P. C.	-,298	**,271****
	Sig.	,673	,831		Sig.	,014	,809		Sig.	,086	,121
	N	34	34		N	34	34		N	34	34
Can-Canakkale	P. C.	-,133	-,061	Sultanbeyli-İstanbul	P. C.	-,079	-,076	Ozanlar-Sakarya	P. C.	-,037	**,946****
	Sig.	,453	,733		Sig.	,657	,668		Sig.	,834	,000
	N	34	34		N	34	34		N	34	34
Lapseki-Canakkale	P. C.	-,319	-,174	Sultangazi-İstanbul	P. C.	-,127	**-,559****	Cerkezkoy-Tekirdag	P. C.	-,088	-,015
	Sig.	,066	,324		Sig.	,476	,001		Sig.	,622	,931
	N	34	34		N	34	34		N	34	34
Karaagac-Edirne	P. C.	,105	**-,341***	Umraniye-İstanbul	P. C.	-,058	-,226	Merkez-Tekirdag	P. C.	-,546**	**-,455****
	Sig.	,553	,048		Sig.	,746	,199		Sig.	,001	,007
	N	34	34		N	34	34		N	34	34
Kesan-Edirne	P. C.	-,016	,134	Uskudar-İstanbul	P. C.	-,446**	**-,363***	Altinova-Yalova	P. C.	-,076	-,139
	Sig.	,931	,449		Sig.	,008	,035		Sig.	,668	,434
	N	34	34		N	34	34		N	34	34
Basaksehir-İstanbul	P. C.	-,164	,033	Limankoy-Kırklareli	P. C.	-,112	**,427***	Armutlu-Yalova	P. C.	-,036	,109
	Sig.	,353	,854		Sig.	,529	,012		Sig.	,839	,540
	N	34	34		N	34	34		N	34	34

*. Correlation is significant at the 0.05 level (2-tailed).
**. Correlation is significant at the 0.01 level (2-tailed).

CONCLUSION

The spatial distribution and temporal change of air pollutant parameters (SO_2, PM_{10}, NO, NO_2) measured in different categories (industrial, urban, semi-rural, trafic etc.) in the Marmara Region between March 2013-December 2015 were revealed in the study.

As a result of the study, it was determined that SO_2 concentration levels were high throughout the study area in winter. However, they were considerably low during summer. Thus, it was observed that SO_2 values, especially around Edirne and Canakkale, were not at an underestimated level in terms of the spatial distribution and limit value. Although PM also exhibited difference during winter in terms of the years studied as SO_2, it was determined that in general, the concentration levels were higher in the southwest of the study area (Canakkale and Edirne). However, considering the limit values, contrary to SO_2, there were levels observed lower than the target limit value in PM_{10}. The highest NO

concentration levels in the study area were identified in Istanbul and Bursa where the population and traffic were the highest. Although seasonal differences were not significant in NO_2 as in the other pollutants, it was determined that the values during summer were between 20 and 30 mg/m^3 and more than 30 mg/m^3 during winter in some areas. It was identified that the limit value determined for both NO and NO_2 was never exceededduring the period studied.

In addition to the spatial differences observed in the study area, temporal differences were also observed. While increases were observed in air pollutant parameters in some areas by years, decreases were determined in some areas. Moreover, the measurement stations measuring air pollutant parameters were established based on different characteristics (industry, rural, traffic, etc.). When the source sites of the measurement stations at which each pollutant parameter exhibited an increase at 95% confidence level were considered, it was identified that the source sites did not have a homogeneous structure. Therefore, they all exhibited different characteristics in terms of the source.

REFERENCES

[1] Tecer, L.H. and Tagil, S. (2013) Spatial-Temporal Variations of Sulphur Dioxide Concentration, Source, and Probability Assessment Using a GIS-Based Geostatistical Approach. Pol. J. Environ. Studies. 22(5), 1491-1498.

[2] Amato, G.D., Cecchi, L., Amato, N.D. and Liccardi, G. (2010) Urban Air Pollution and Climate Change as Environmental Risk Factors of Respiratory Allergy: An Update. J Investig Allergol Clin Immunol. 20(2), 95-102.

[3] Bayram, H. (2005) Air Pollution Problem in Turkey: Causes, Measures Taken and the Current Situation. Turkish Thoracic Journal. 6(2), 159-165.

[4] Tunay, O. and Alp, K. (1996) Air pollution and control. Istanbul Chamber of Commerce Publication. 3, Istanbul.

[5] Itano, Y., Bandow, H., Takenaka, N., Saitoh, Y., Asayama, Y. and Fukuyama, J. (2007) Impact of NOx reduction on long term ozone trends in an urban atmosphere. Science of The Total Environment. 379, 46-55.

[6] Oztaner, Y.B., Guney, B., Kalkan, K., Kahya, C., Bektas Balcik, F. and Cakir, S. (2014) Comparıson of Interpolatıon Techniques to Determine $PM_{2.5}$ Dıstrıbutıon: Marmara Region Case Study. Remote Sensing-Cbs Symposium (UZAL-GIS 2014). 14-17 October 2014, Istanbul.

[7] Dogan, F., Kitapcioglu, G. (2007) Comparing air pollution in Izmir according to years. Ege Journal of Medicine. 46(3), 129-133.

[8] Onat, B. And Alver Sahin, U. (2000) Investigating of the Particulate Matter Size and the Relation of Black Smoke Near Traffic. Ecology. 21(83), 77-83.

[9] Zimeras, S. (2008) Exploratory point pattern analysis for modeling earthquake data. 1st WSEAS International Conference on Environmental and Geological Science and Engineering (EG'08). September 11-13, 112-120, Malta.

[10] Inal, C. and Yigit, C.O. (2003) The usability of Kriging Interpolation Method in Geodetic Applications. Geographic Information Systems and Geodetic Networks Workshop. (24-26 September 2003), Konya.

[11] Ozsahin, E., Eroglu, I. and Pektezel, H. (2016) Air Pollution in Keşan (Edirne). Selcuk University Journal of the Institute of Social Sciences. 36, 83-100.

[12] TEMA (2017) Air Pollution Modeling of Thermal Power Plants: The Peninsula Çanakkale and Biga. Istanbul.

[13] Ozdemir, E.T., Deniz, A., Yavuz, V., Dogan, N. and Akbayir, I. (2018) Investigation of The Fog-Air Quality Relationship in Istanbul. Fresen. Environ. Bull. 26, 30-36.

[14] Tagil, S. and Koc, T. (2000) Air Quality in Edirne, Turkish Geography Society, Past, Present and Future Trakya (Editor: Suna Doganer). 28. Geography Profession Week. Edirne, 10-12 June 1998, 115-131.

[15] Erbaslar, T. and Tasdemir, Y. (2007) The Relationships Among Classic Air Pollutants Measured in the Atmosphere of Bursa. Uludag University Journal of The Faculty of Engineering. 12(2), 9-19.

[16] Beyhun, N.E., Vancelik, S., Acemoglu, H., Kosan, Z. and Guraksin, A. (2008) Ambient air pollution in Erzurum City Center during 2003-2006. TAF Prev Med Bulletin. 7(3), 237-242.

[17] Ibret, B.U. and Aydinozu, D. (2009) A Sample for The Effect of The Wrong Settlement Choice in Urbanization on Air Pollution: The Center of Kastamonu. Istanbul University Journal of Geography. 18, 71-88.

[18] Sezer Turalioglu, F. (2011) The Effect of Urbanization and Usage of Naturalgas in Air Quality of Erzurum. Igdır University Journal of the Institute of Science and Technology. 1(2), 41-45.

[19] Ozcan, H.K. (2012) Long Term Variations of the Atmospheric Air Pollutants in Istanbul City. Int. J. Environ. Res. Public Health. 9, 781-790.

[20] Berktas, M.B. and Bircan, A. (2003) Effects of Atmospheric Sulphur Dioxide and Particulate Matter Concentrations on Emergency Room Admissions Due to Asthma in Ankara. Journal of Tuberkuloz and Toraks. 51(3), 231-238.

[21] Cicek, I., Turkoglu, N. and Gurgen, G. (2004) Statistical Analysis of Air Pollution in Ankara. Fırat University Journal of Social Science. 14(2), 1-18.
[22] Mentese, S. (2011) Relationship Between Air Pollution (PM_{10} & SO_2) And Respiratory Diseases in Zonguldak. Unpublished Master Thesis. Balıkesir University Institute of Social Sciences. Balıkesir.
[23] Mentese, S. and Tagil, S. (2012) The Effect of Climate Elements on Air Pollution in Bilecik. Balıkesir University Journal of Institute of Social Sciences. 15(28), 3-16.
[24] Mayda, A.S. and Yilmaz, M. (2013) Düzce Air Quality Monitoring Station 2007-2011 between Data Evaluation. TAF Preventive Medicine Bulletin. 12(1), 11-18.
[25] Duman-Yuksel, U. (2015) Assessment of The Air Quality in Ankara, Turkey. Fresen. Environ. Bull. 24, 986-996.
[26] Ozdemir, H., Borucu, G., Demir, G., Yigit, S. and Ak, N. (2010) Examining the Particulate Matter ($PM_{2.5}$ ve PM_{10}) Pollution on the Playgrounds in Istanbul. Ecology. 19(77), 72-79.
[27] Gumus, O., Alver Sahin, U., Onat, B., Ozcelik, R., Gedik, E., Solakoglu, I. and Tas, N. (2015) Marmara Region Analysis of Air Quality by Statistical Methods. 6. National Air Pollution and Control Symposium. 7-9 October 2015. Izmir, Turkey.
[28] Kahya, C., Bektas Balcik, F., Oztaner, Y.B., Ozcomak, D. and Seker, D.Z. (2017) Spatio-Temporal Analysis of $PM_{2.5}$ Over Marmara Region, Turkey. Fresen. Environ. Bull. 26, 310-317.
[29] Tayanc, M. (2000) An Assessment of Spatial and Temporal Variation of Sülfür dioxide Levels Over Istanbul, Turkey. Environmental Pollution. 107(1), 61-69.
[30] Nazim, E., Beyhun, S., Vancelik, H., Acemoglu, Z. and Guraksin Kosan, A. (2008) Ambient air pollution in Erzurum City Center during 2003-2006. TAF Prev Med Bulletin. 7(3), 237-242.
[31] Dadaser Celik, F. and Kirmaci, H.K. (2011) Trends in Sulfurdioxide and Particulate Matter Levels in Kayseri (Turkey): 1990-2007. Ecology. 20(79), 83-92.
[32] Arayici, S. (1995) NOx Formation in Natural Gas Combustion. II. Air Pollution, Modeling and Control Symposium, Istanbul Technical University, 116-121.
[33] Sonibare, J.A. and Akeredolu, F.A. (2004) A Theoretical Prediction of Non- methane Gaseous Emissions from Natural Gas Combustion. Energy Policy. 32, 1653–1665.
[34] Kecebas, A., Gedik, E. and Kayfeci, M. (2010) The Effect of Using Geothermal Energy and Natural Gas on Air Pollution Arisen from Using Fossil Fuels: Afyon Example. Electronic Journal of Machine Technologies. 7(3), 23-30.
[35] Erturk, F. (1993) Effects of Air Pollution on Environment. In: Tiris, M., Kalafatoglu, E., Okutan, H. (eds.) Air Pollution Sources and Control, Gebze, MAM, Kocaeli, 15-47.
[36] Cetin, S., Ayberk, S. (2008) Investigation of the Relationship between NOx and CO Emissions in Kocaeli Province Environmental Basin. Environmental Problems Symposium. 14-17 May 2008, 1302-1311.
[37] Saito, S., Nagao, I. and Tanaka, H. (2002) Relationship of NOx and NMHC to photochemical O_3 production in a coastal and metropolitan areas of Japan. Atmospheric Environment. 36, 1277–1286.
[38] Lu, W.Z. and Wang, X.K. (2003) Interaction patterns of major air pollutants in Hong Kong territory. Science of the Total Environment. 324, 247–259.
[39] Republic of Turkey Ministry of Health (2012) Air Quality and Health. https://www.toraks.org.tr/userfiles/file/hava-kalitesi-ve-saglik.pdf
[40] Republic of Turkey, Environment and Urban Ministry (2008) Air Quality Assessment and Management Regulations. Ankara.

Received: **01.11.2017**
Accepted: **21.02.2019**

CORRESPONDING AUTHOR

Serpil Mentese
Bilecik Seyh Edebali University,
Faculty of Arts and Sciences,
Department of Geography,
Gulumbe Campus,
11100, Bilecik – Turkey

e-mail: serpil.mentese@bilecik.edu.tr

© by PSP Volume 28 – No. 5/2019 pages 3637-3648 Fresenius Environmental Bulletin

CADMIUM UPTAKE AND ACCUMULATION, SUBCELLULAR DISTRIBUTION AND CHEMICAL FORMS IN YOUNG SEEDLINGS OF *SALIX BABYLONICA* L.

Jie Ouyang, Binbin Li, Wenxiu Xue, Yi Jiang, Chonghao Li, Xiaoshuo Shang, Jinhua Zou*

Tianjin Key Laboratory of Animal and Plant Resistance, College of Life Sciences, Tianjin Normal University, Tianjin 300387, China

ABSTRACT

To understand the cadmium (Cd) accumulative ability and resistance mechanism of Cd stress by *Salix babylonica* L., Cd uptake and accumulation, subcellular distribution and chemical forms were investigated in *S. babylonica* exposed to 10, 50 and 100 μM Cd for 7 and 14 d. Subcellular localization of Cd on the surface of leaves and mature zone of root tips was investigated by SEM and EDXA. The results indicated that the seedling growth was accelerated by 10 μM Cd, and significantly inhibited by 50 and 100 μM Cd. Root was the main organ to uptake and accumulate Cd, and the contents of Fe and Mn decreased significantly. The order that distributions of Cd among tissue fractions was: cell wall > soluble fraction > cell organelle. The proportion of CdNaCl was the highest, Cd integrated with pectates and proteins in cell walls may be responsible for the adaptation of *S. babylonica* to Cd stress. The results of EDXA indicated that root cell wall play a key role in Cd detoxicity and the vascular bundle have more potential in Cd transportation. The Cd content of leaf main vein was higher than leaf epidermal cells.

KEYWORDS:
Cadmium, *Salix babylonica* L., subcellular distribution, chemical forms, uptake and accumulation, EDXA

INTRODUCTION

Contamination by heavy metal has become a major public-health concern because of its toxicity and long-term effects [1, 2]. Cadmium (Cd) is one of the most significant heavy metals [3], and highly toxic to humans and plants at very low concentrations [4, 5]. Cd can be easily absorbed by plants and transferred to aerial parts where it can accumulate to high levels and thus enter the food chain, becoming detrimental to human health [6]. Excessive Cd can damage the plant cellular processes those resulting in growth inhibition, morphological alterations, plant senescence, or even death [7].

In response to Cd toxicity, plants have developed protective cellular mechanisms to alleviate Cd-induced toxicity: synthesis of phytochelatins and metallothioneins, metal compartmentalization in vacuoles, and the increased activity of antioxidant enzymes. Other indirect alleviating mechanisms such as microelements (iron (Fe), manganese (Mn), zinc (Zn) and selenium (Se)) interfering with Cd uptake may decrease Cd concentration in plants [8].

The uneven subcellular distribution could be responsible for the Cd sensitive of plants [9]. Owing to Cd's high mobility and toxicity at low concentrations, considerable attention has been paid to its toxic effect on plants. There is some evidence that subcellular distribution and chemical forms of heavy metals may be associated with metal tolerance and detoxification in plants [10]. It was reported that NaCl-extractable Cd in plants play an important role in alleviation of Cd toxicity [11, 12]. Heavy metal fixation by pectates and proteins in cell wall and sequestration in vacuole are responsible for its detoxication in plant [13]. Cell walls and vacuoles are considered to have great potential for Cd accumulation [14, 15].

Cd can be found in various tissues after absorbed by roots, and its deposition and distribution in tissue compartments can be gained through energy-dispersive X-ray analyses (EDXA). Evidence on Cd subcellular localization in root tip and leaves of different plants analyzed by EDXA was reported [14, 16-18]. Evidences were provided for the importance of the root cell walls in the adsorption of Cd by willow roots [19]. In higher plants, roots are the first organs with contact to the toxic metal ions, and roots usually accumulate significantly higher amounts of metal than shoots do [20].

There are a variety of plants tolerant to risk elements and the problems associated with low level Cd pollution [21, 22, 15]. Considerable attention in terms of phytoremediation is focused on fast-growing trees, especially willows (*Salix* spp., *Salicaceae* family) [23, 24]. This focus is connected with their characteristics which make them ideal plant species for phytoremediation application, including worldwide spread, easy propagation and cultivation, large biomass, fast growing, deep root system, high transpiration rate, tolerance to hypoxic conditions, and high metal accumulation capability

[25-28]. *S. babylonica*, a popular ornamental tree species of willow native to dry areas of northern China, is planted widely in China for use in bioremediation of contaminated water or soil environments [29]. It was reported that *S. babylonica* could tolerate and accumulate Cd at low concentration (10 μmol/L), and was suitable for potential phytoremediation [30, 31].

Poisoning and environmental contamination are caused by the excessive Cd. Plant roots and leaves are sensitive to the environmental stress. Resistance to Cd stress is associated with avoidance and tolerance, and the study of resistance mechanism of plant is important. Therefore, the present study is aimed at investigating the characteristics of Cd uptake and accumulation, localization, subcellular distribution and chemical forms in *S. babylonica* roots and leaves under Cd stress.

MATERIALS AND METHODS

Plant material and culture conditions. Healthy woody cuttings (20 cm long) from shoots of *S. babylonica* grown in the campus of Tianjin Normal University, Tianjin, China were collected and fully rinsed with distilled water before starting the experiment. They were germinated in distilled water in plastic containers for two weeks. Then the plants were grown in containers with 6 L half-strength Hoagland's solution for a week. The Hoagland's solution (pH 5.5) consisted of 5 mM KNO_3, 5 mM $Ca(NO_3)_2$, 1 mM KH_2PO_4, 50 μM H_3BO_3, 10 μM FeEDTA, 4.5 μM $MnCl_2$, 3.8 μM $ZnSO_4$, 0.3 μM $CuSO_4$, and 0.1 μM $(NH_4)_6Mo_7O_{24}$. The plants were randomly divided into four groups. Control groups were grown in the Hoagland's solution and the other three groups were treated with three different Cd concentrations: 10, 50 and 100 μM $CdCl_2$ solutions for 7 and 14 d. Cd was provided as cadmium chloride ($CdCl_2$). The solutions were continuously aerated with an aquarium air pump every day. The plants were harvested respectively on 7 and 14th d. The root length and shoot length were measured. All experiments were performed in three replicates.

Determination of Cd and other minerals. Plants exposed to 10, 50, and 100 μM Cd solutions for 7 and 14 d and control were harvested respectively based on uniformity of size and color (removing the greatest and the smallest plants and then selected randomly). The plants were washed, thoroughly with running tap water, and then with de-ionized water. After removal of necrotic and putrid tissue, the roots were immersed in 20 mM EDTA-Na_2 for 15 min and rinsed in de-ionized water, to remove traces of nutrients and Cd ions from the root surfaces. The plants were divided into four parts: roots, leaves, new stems and old stems. All dried plant samples were prepared using wet-digestion method [32]. Concentrations of Cd, Mn and Fe were analyzed using atomic absorption spectrometer (PerkinElmer AAnalyst 400, USA).

Tissue fractionation. The fresh roots (4 g) and leaves (4 g) of *S. babylonica* from control group and treated groups (different Cd concentration: 10, 50, 100 μM) were homogenized at 4 ºC in 20 mL cooled extraction buffer of 250 mM sucrose, 50 mM Tris-HCl and 1.0 mM dithiothreitol, pH 7.5, with chilled mortar and pestle. Cells were separated into three fractions (cell wall, organelle-containing, and soluble fractions) according to the method reported by Zhang et al. and Wu et al. [4, 33]. The concentrations of Cd in three fractions were measured by atomic absorption spectrometer (PerkinElmer AAnalyst 400, USA).

Cd chemical forms extraction. The Cd associated with different chemical forms was successively extracted by designated solutions in the following order according to the methods of Zhang et al. and Wu et al. [4, 33].

(1) 80% ethanol, extracting inorganic Cd giving priority to nitrate, chloride, and aminophenol cadmium (CdE);

(2) deionized water, extracting water-soluble Cd with organic acids and Cd $(H_2PO_4)_2$ (CdW);

(3) 1 mol/L NaCl, extracting pectate- and protein-integrated Cd (CdNaCl);

(4) 2% HAc, extracting insoluble $CdHPO_4$, $Cd_3(PO_4)_2$, and other Cd-phosphate complexes (CdHAc);

(5) 0.6 mol/L HCl, extracting oxalic acid bound Cd (CdHCl);

(6) cadmium in residues (CdR).

The roots and leaves of *S. babylonica* exposed to 10, 50, 100 μM Cd for 7 and 14 d were separated. The roots were rinsed clearly with 20 mM EDTA and de-ionized water and the leaves were washed thoroughly with de-ionized water. Two grams of each sample were extracted with 20 mL of the designated solutions mentioned above; the extraction was shaken for 22 h at 25 ºC and centrifuged at 5,000 rpm for 10 min, then the supernatant was collected and stored, the dregs were suspended with another 10 mL of the designed solutions for 2 h at 25 ºC, and the second supernatant was collected after the suspension centrifuged at 5,000 rpm for 10 min. Two supernatant were combined and brought to dryness on an drying oven. The Cd content of the plant material remaining after all of the extractions and all of extracting solution had been conducted was determined by wet-digesting it with HNO_3: $HClO_4$ (4:1, v/v). The content of Cd in different chemical forms was measured by atomic absorption spectrometer (PerkinElmer AAnalyst 400, USA).

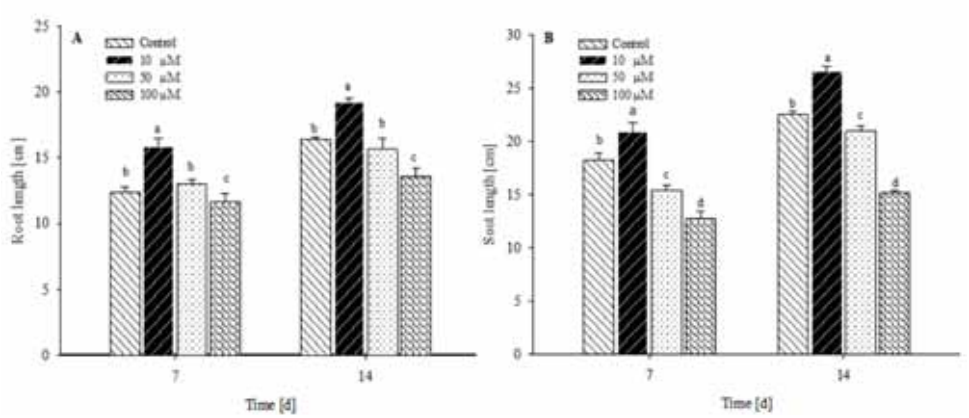

FIGURE 1
Effects of different Cd concentrations on the root and shoot length of Salix babylonica exposed to Cd stress for 7 and 14 d. A: root length, B: shoot length.
Vertical bars denote SE. Values with different letters differ significantly from each other ($P < 0.05$, *t*-test).

Sample preparation for scanning electron microscope. Elemental distribution and composition of experimental plants was determined from samples of freeze-dried root and leaf materials. The samples of 1 cm length were cut from the root tips (young root tissue including the maturation zone) or the base of leaf of *S. babylonica*, exposed to 100 μM Cd for 24 h, and rapidly frozen in liquid nitrogen for 60 min, and then put frozen samples into lyophilizer (Lyophilizer LGJ-10C, Sihuan, Beijing) immediately for 2 days. The cross-sections of the roots and leaves were coated by gold using the sputter/coater (EMITECH K550X, Quorum Group, England). The energy dispersive X-ray microanalytical studies were carried out using a scanning electron microscope (SEM) (FEI Nova NANOSEM 230, Oregon, USA) provided with energy dispersive X-ray spectrum analysis (Genesis Apollo 10, EDXA, USA). The spectra were collected by 30 KeV and X-ray detector equipped with a super ultra-thin window. The collection time was 120 s. The Cd composition in the roots (maturation zone) and leaves were displayed as wt% (weight percent in relation to total elements).

Statistical analysis. Data from this investigation were analyzed with Sigma Plot 13.0 using means ± standard error (SE) and performed with statistical package SPSS (version 17.0). For equality of averages the *t*-test was applied. Figures were processed by Photoshop CS6. Results were considered statistically significant at $P < 0.05$.

RESULTS

Effects of Cd on seedling growth. The effects of Cd on roots and shoots growth of *S. babylonica* varied with the concentration and treatment time (Fig. 1). The root length increased significantly ($P < 0.05$) at 10 μM Cd during the whole experiment in comparison with control and the other treatment groups. 50 and 100 μM Cd showed the significantly inhibitory effect on root growth (Fig. 1A). The same trend as the root growth, 10 μM Cd had a significant role in promoting shoot growth in comparison with control ($P < 0.05$). However, the shoot length exposed to 50 and 100 μM Cd decreased significantly ($P < 0.05$) during the whole experiment time when compared with control (Fig. 1B).

Cadmium accumulation and its effects on other minerals. The accumulation of Cd in *S. babylonica* roots and shoots varied with Cd concentration. The presence of significant correlations between the concentration of Cd and microelements (Fe and Mn) was showed in Tab. 1. The Cd content of the roots and shoots increased with increasing Cd concentration. Root was the main organ accumulating Cd (roots > old stems > new stems > leaves). Cd had obvious inhibitory effects on uptake and accumulation of Fe and Mn. In the presence of Cd, the contents of Fe and Mn in roots and shoots of *S. babylonica* decreased significantly ($P < 0.05$) with increasing Cd concentration.

Chemical forms of Cd. Cd bound to the different chemical forms in the roots and leaves of *S. babylonica* exposed to three Cd concentrations (10, 50 and 100 μM) for 7 and 14 d can be measured with different extracting agents. The Cd content and the percentage of the variety of chemical forms were shown in Tab. 2 and Fig. 2. The different Cd chemical forms including CdE, CdW, CdNaCl, CdHAc, CdHCl, and CdR. The Cd content of the different chemical forms both in roots and leaves all increased significantly ($P < 0.05$) with increasing concentrations of Cd and treatment days (Tab. 2). The proportion of the chemical forms varied with Cd concentrations used and treatment days during the whole experiment (Fig. 2). The proportion of CdNaCl in roots exposed to 10 - 100 μM Cd for 7 d was the highest, follow by CdW, CdHAc, CdE,

CdHCl, and CdR, but, for 14 d, the proportion of CdHAc was larger than CdW (Fig. 2A), and the proportion of Cd chemical form in leaves from high to low was in the order: CdNaCl > CdHAc > CdW > CdHCl > CdE > CdR, respectively (Fig. 2B). During the whole experiment, the proportion of Cd extracted by 2% HAc, and 0.6 M HCl increased with increasing Cd concentrations, while the proportion of Cd extracted by 1 M NaCl, and deionized water decreased (Fig. 2).

TABLE 1
Cd, Fe, Mn concentrations of different organs in *Salix babylonica* exposed to 10, 50, and 100 μM Cd for 7 and 14 days.

		μg/g dry weight ±SE					
Treatment	Element	Cd		Fe		Mn	
(μM)	Days	7	14	7	14	7	14
Control	Roots	2.66±0.03a	3.28±0.03a	796.72±0.29d	854.44±0.24d	279.12±0.12d	292.84±0.03d
10		497.43±0.37b	697.12±0.89b	603.00±0.61c	654.50±1.75c	260.93±0.03c	206.62±0.05c
50		828.03±1.25c	877.37±0.89c	481.50±0.28b	588.18±0.08b	142.15±0.09b	202.96±0.23b
100		893.62±1.51d	929.96±1.30d	459.21±0.61a	558.18±0.69a	137.68±0.13a	183.18±0.28a
Control	Leaves	2.25±0.00a	2.81±0.03a	180.06±0.08d	162.75±0.14d	118.34±0.09d	130.16±0.53d
10		14.06±0.14b	54.43±0.19b	168.53±0.46c	145.31±0.29c	113.25±0.11c	112.56±0.14c
50		39.78±0.10c	58.28±0.07c	138.56±0.03b	131.25±0.08b	96.53±0.22b	87.25±0.05b
100		43.21±0.13d	100.62±0.17d	132.50±0.39a	117.06±0.08a	85.62±0.05a	78.96±0.12a
Control	New stems	2.68±0.03a	2.65±0.03a	153.75±0.51d	127.56±0.51d	21.06±0.06d	17.03±0.03d
10		15.40±0.20b	38.28±1.25b	144.46±0.13c	113.41±0.46c	19.45±0.04c	15.75±0.05c
50		87.28±0.05c	83.21±0.17c	117.93±0.11b	110.87±0.38b	15.12±0.00b	12.12±0.00b
100		115.37±0.37d	155.62±0.46d	115.34±0.12a	105.38±0.19a	15.00±0.00a	11.21±0.03a
Control	Old stems	11.90±0.16a	7.12±0.18a	72.28±0.16d	67.00±0.17d	16.19±0.08d	15.03±0.16d
10		32.37±0.19b	60.93±0.03b	68.13±0.25c	64.63±0.13c	14.00±0.00c	12.34±0.03c
50		166.56±0.29c	163.81±0.11c	65.56±0.06b	60.06±0.58b	10.68±0.06b	8.46±0.03b
100		175.25±0.17d	176.03±0.34d	42.63±0.09a	38.13±0.36a	10.37±0.00a	5.71 ±0.03a

Values followed by different letters differ significantly from each other ($P < 0.05$). Means±SE, n=6.

TABLE 2
Different chemical forms of Cd in *Salix babylonica* exposed to 10, 50, and 100 μM Cd for 7 and 14 days.

Days	Organ	Treatment	Extractable form (μg/g FW)					
		(μM)	CdE	CdW	CdNaCl	CdHAc	CdHCl	CdR
7	Roots	10	3.95±0.01a	16.85±0.018a	32.28±0.30a	11.07±0.03a	1.58±0.03a	0.73±0.01a
		50	4.83±0.00b	42.90±0.02b	58.63±0.17b	24.45±0.09b	2.91±0.00b	1.55±0.03b
		100	12.23±0.02c	61.79±0.07c	80.92±0.32c	45.62±0.06c	6.38±0.02c	2.04±0.01c
14		10	1.70±0.00a	16.55±0.16a	36.69±0.14a	19.23±0.04a	1.59±0.00a	0.64±0.01a
		50	13.00±0.01b	33.85±0.02b	78.86±0.21b	47.28±0.07b	5.80±0.03b	2.00±0.07b
		100	27.42±0.06c	62.05±0.04c	92.34±0.14c	76.53±0.09c	24.12±0.04c	3.22±0.20c
7	Leaves	10	0.03±0.01a	0.45±0.00a	4.89±0.03a	0.20±0.00a	0.38±0.00a	0.17±0.00a
		50	0.07±0.01b	0.73±0.02b	6.07±0.02b	0.50±0.04b	0.47±0.00b	0.21±0.01b
		100	0.12±0.00c	1.32±0.02c	10.85±0.03c	1.21±0.03c	0.94±0.00c	0.31±0.00c
14		10	0.16±0.00a	0.45±0.01a	6.37±0.03a	1.12±0.03a	0.45±0.02a	0.13±0.01a
		50	0.34±0.02b	0.82±0.01b	8.10±0.02b	2.47±0.01b	1.64±0.01b	0.15±0.03b
		100	0.45±0.00c	1.26±0.01c	10.02±0.06c	5.22±0.02c	2.28±0.02c	0.28±0.01c

Values followed by different letters differ significantly from each other ($P < 0.05$, *t*-test). Means±SE, n=6.

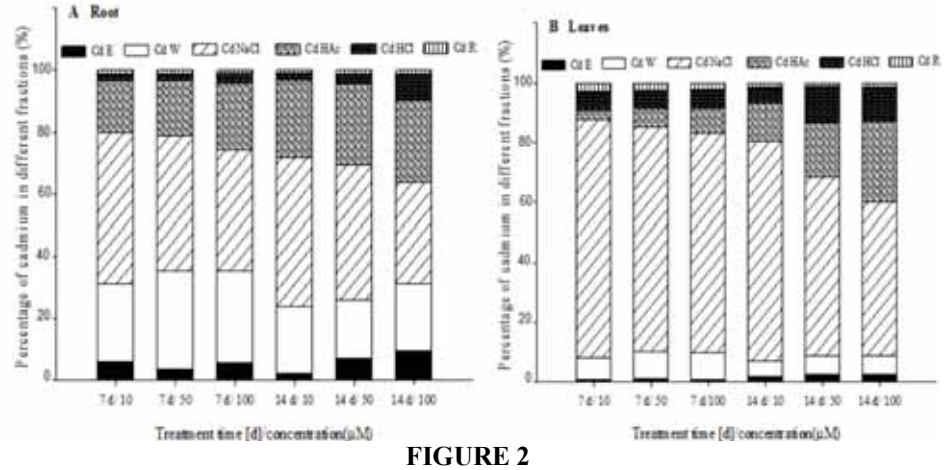

FIGURE 2
Different chemical forms of Cd proportion in *Salix babylonica* exposed to 10, 50, and 100 μM Cd for 7 and 14 days. A: Cd proportion in roots; B: Cd proportion in leaves.

TABLE 3
Cd in subcellular distribution (μg/g FW) in roots and leaves of *Salix babylonica* exposed to 10, 50, and 100 μM Cd for 7 and 14 days.

Treatment (μM)		7 d			14 d		
		Cell wall	Cell organelle	Soluble fraction	Cell wall	Cell organelle	Soluble fraction
10		18.99±0.03a	5.57±0.01a	21.28±0.04a	22.07±0.01a	3.12±0.01a	27.85±0.02a
50	Roots	42.55±0.07b	15.73±0.02b	26.01±0.02b	43.87±0.03b	6.59±0.02b	40.14±0.04b
100		55.27±0.04c	21.56±0.03c	31.37±0.03c	60.23±0.05c	11.47±0.00c	45.29±0.07c
10		0.95±0.02a	0.33±0.01a	0.83±0.01a	1.05±0.01a	0.44±0.02a	0.81±0.01a
50	Leaves	4.22±0.01b	0.65±0.07b	1.99±0.02b	9.96±0.02b	1.44±0.01b	3.23±0.01b
100		8.08±0.01c	1.11±0.02c	3.22±0.01c	10.47±0.03c	2.04±0.04c	3.37±0.00c

Values followed by different letters differ significantly from each other ($P < 0.05$, *t*-test). Means±SE, n=6.

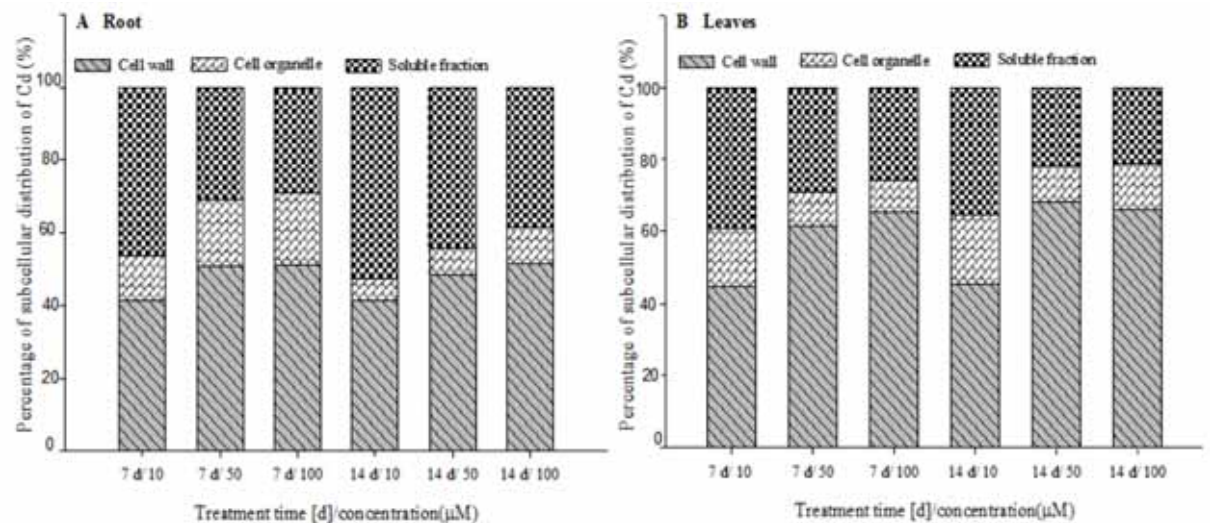

FIGURE 3
Proportional changes of Cd ion contents in cell wall, cell organelle, and soluble fraction in *Salix babylonica* exposed to 10, 50, and 100 μM Cd for 7 and 14 days. A: Cd proportion in roots; B: Cd proportion in leaves.

Subcellular distribution of Cd. The subcellular distribution of Cd in roots and leaves was expressed as Cd content in the different fractions (cell wall, cell organelle, and soluble fraction). Cd subcellular distribution in roots of *S. babylonica* exposed to 10, 50, 100 μM Cd for 7 and 14 d was in the following order: cell wall > soluble fraction > cell organelle as well as in leaves (Tab. 3). The Cd levels increased significantly ($P < 0.05$) with increasing Cd concentrations used and treatment days set. However, the Cd content in cell organelle decreased at 14th d compared with 7th d in roots of *S. babylonia*. 80% Cd of total that absorbed in roots or leaves of *S. babylonica* was located in the parts of cell wall and soluble fraction. With the increasing of Cd concentration, the proportion of Cd in cell wall increased, while the proportion of Cd in soluble fraction decreased (Fig. 3). For instance, the proportion of Cd distributed in the cell wall, soluble fraction and cell organelle when roots exposed to 100 μM Cd for 14 d was 51.48%, 38.71%, 9.80%, respectively, and, the leaves, 65.93%, 21.23%, 12.84%. The evidence indicated that the cell wall was the main accumulation site for Cd.

Subcellular location of Cd. The data from EDXA revealed the subcellular localization of Cd in transverse sections of the mature zone of root tips and leaves in *S. babylonica* exposed to 100 μM Cd for 24 h. Vascular cylinder (V), epidermis (EP) and cortex (C) of the mature zone of root tip can be distinguished (Fig. 4A). The Cd content in different parts of the roots exposed to Cd for 24 h was different, i.e., vascular bundle (15.07 Wt%) > Epidermal cells (2.55 Wt%) (Fig. 4 E, B), and Cell wall (3.29 Wt%) > Cytoplasm (2.18 Wt%) (Fig. 4 D, C). The Cd content in main vein (M) and epidermis (E) of leaf was showed in Fig. 5 (B-C): leaf main vein (0.37 Wt%) > leaf epidermal cells (0.20 Wt%).

DISCUSSION

The present investigation results was in agreement with the findings of Yang and Chen [31] that low Cd concentration (10 μM) accelerated plant growth of *S. babylonica* significantly ($P < 0.05$), and 50 and 100 μM Cd had significantly inhibitory effects ($P < 0.05$). Fig.1 showed that the length of roots and shoots were inhibited by high level Cd.

It has been reported that a few clones of willows have high heavy metal tolerance [34-36]. Data from the present investigation showed that *S. babylonica* had the ability to accumulate Cd, and root was the main organ accumulating Cd. The Cd content of the roots and shoots increased with increasing Cd concentration. This was in accordance with the findings of Dos Santos Utmazian and Wenzel [37], Yang and Chen [31], and Ling et al. [38]. But its accumulating Cd ability was low when compared with *Salix smithiana, Salix dasyclados* and *Salix matsudana* [30, 36, 39]. In the presence of Cd, the contents of Mn and Fe in roots and shoots of *S. babylonica* decreased significantly ($P < 0.05$) with increasing Cd concentration during the whole period treatment. Because these two elements compete with Cd in the active transporters and can minimize Cd transportation into plants, the concentrations of Fe and Mn, and Cd levels in the seedlings showed a negative correlation during the whole experiment. This may explain why concentrations of Fe and Mn gradually declined with increased Cd concentrations in the seedlings. Evidence from Kovács et al.'s work [40] demonstrated that Fe ions might compete with Cd ions for the same membrane binding (transport) sites in plants. Fe deficiency can enhance the accumulation of some metals in shoots of grass species [41]. Adding an adequate Fe ion to plants exposed to Cd can result in increased activity of antioxidative enzymes against oxidative stress [42]. Adding Mn to the solution containing Cd can significantly improve plant growth and reduced the concentrations of Cd in all organs of the plant [43].

Different chemical forms of Cd are associated with the various biological activities of Cd in plants and be reported as the important factors that characteristics of Cd migration, accumulation, and phytotoxicity degree. In the present investigation, the proportion of CdE and CdW was low in leaves, although water-soluble Cd in inorganic form (extracted by 80% ethanol) and organic form (extracted by H_2O) were thought to have more deleterious and induced stunted growth and chlorosis in the plants due to its highest capacity to migrate [44]. However, compared with leaves, roots represented higher proportion of CdE and CdW. During the whole experiment, the proportion of Cd extracted by 2% HAc, and 0.6 M HCl increased with increasing Cd concentrations. CdHAc in leaves and roots at 14th d represent 12.95% (10 μM Cd, leaf), 26.76% (100 μM Cd, leaf), 25.17% (10 μM Cd, root), 26.79% (100 μM Cd, root) of total Cd, and the proportion of CdHCl, 5.26% (10 μM Cd, leaf), 11.71% (100 μM Cd, leaf), 2.08% (10 μM Cd, root), 8.44% (100 μM Cd, root), indicating that the Cd is transformed into a nontoxic or low toxicity complex to protect the cells. CdHCl and CdR have low toxic effects when compared with CdNaCl.

Followed CdE and CdW, pectate- and protein-integrated Cd (NaCl fraction) was thought the next one important deleterious factor. However, in this investigation, the profile of Cd chemical forms in roots and leaves of *S. babylonica* was characterized by the highest proportion of CdNaCl. The results obtained here are consistent with earlier findings [11, 14, 45-47]. After exposed to Cd for 14 d, CdNaCl represent 73.22% (10 μM Cd, leaf), 59.84% (50 μM Cd, leaf), 51.32% (100 μM Cd, leaf), 48.02% (10 μM Cd, root), 43.62% (50 μM Cd, root), 32.32% (100 μM Cd, root) of total Cd. The proportion of CdNaCl of leaves and roots from *S. babylonica* was generally higher in low-Cd cultivars than in high-Cd cultivars. Because Cd has a strong affinity to proteins and pectic or sulfhydryl compounds (-SH) and other side chains, it can easily combine with proteins and disturb the enzyme activity. It was demonstrated that NaCl extractant binds to proteins and pectic acid [9, 48]. One of the effective defense mechanisms to reduce the Cd biological activity was that Cd in plants be bounded by pectate and chelated by peptides, polypeptides or proteins, and the importance of this defense mechanism may vary in accordance with the concentration of Cd supplied, the species involved, and the exposure time [48]. It can be suggested that Cd integrated with pectates and proteins may be responsible for the adaptation of *S. babylonica* to Cd stress.

Different distributions of Cd among tissue fractions can explain the difference in sensitivity to Cd. In different species or genotypes, the subcellular distribution of Cd was considered to be important in influencing the migration, accumu-lation, and phytotoxicity of Cd [49-51]. It was reported that cell wall fraction plays a main role in Cd deposition in rice shoot, which restrains the translocation from shoot to the grain [52]. In this investigation, the roots demonstrated high accumulation capacity of Cd, which was consistent with the results of Zou et al. [36]. For instance, 60.23 μg/g Cd was accumulated in roots of *S. babylonica* when treated at 100 μM Cd for 14 d, however, 10.47 μg/g in leaves. The Cd subcellular distribution was in the order: cell wall > soluble fraction > cell organelle. In addition, the Cd content in the cell wall showed increasing trend with elevated Cd supply. About 65.93% and 51.48% of Cd were accumulated in the cell wall of leaves and roots, respectively, at 100 μM Cd for 14 d. Cell walls acted as important protective barriers against Cd, which was consistent with the result of Wang et al. [51]. The results above indicating that cell wall was the main accumulation site for Cd and Cd binding and/or precipitation in the cell wall may serve as the first barrier to reduce the cytosolic free Cd ions and lessen the damage to the cells.

The high proportion of Cd in the soluble fraction was the next large proportion of Cd in *S. babylonica*, and once the Cd ions are inside the cytosol,

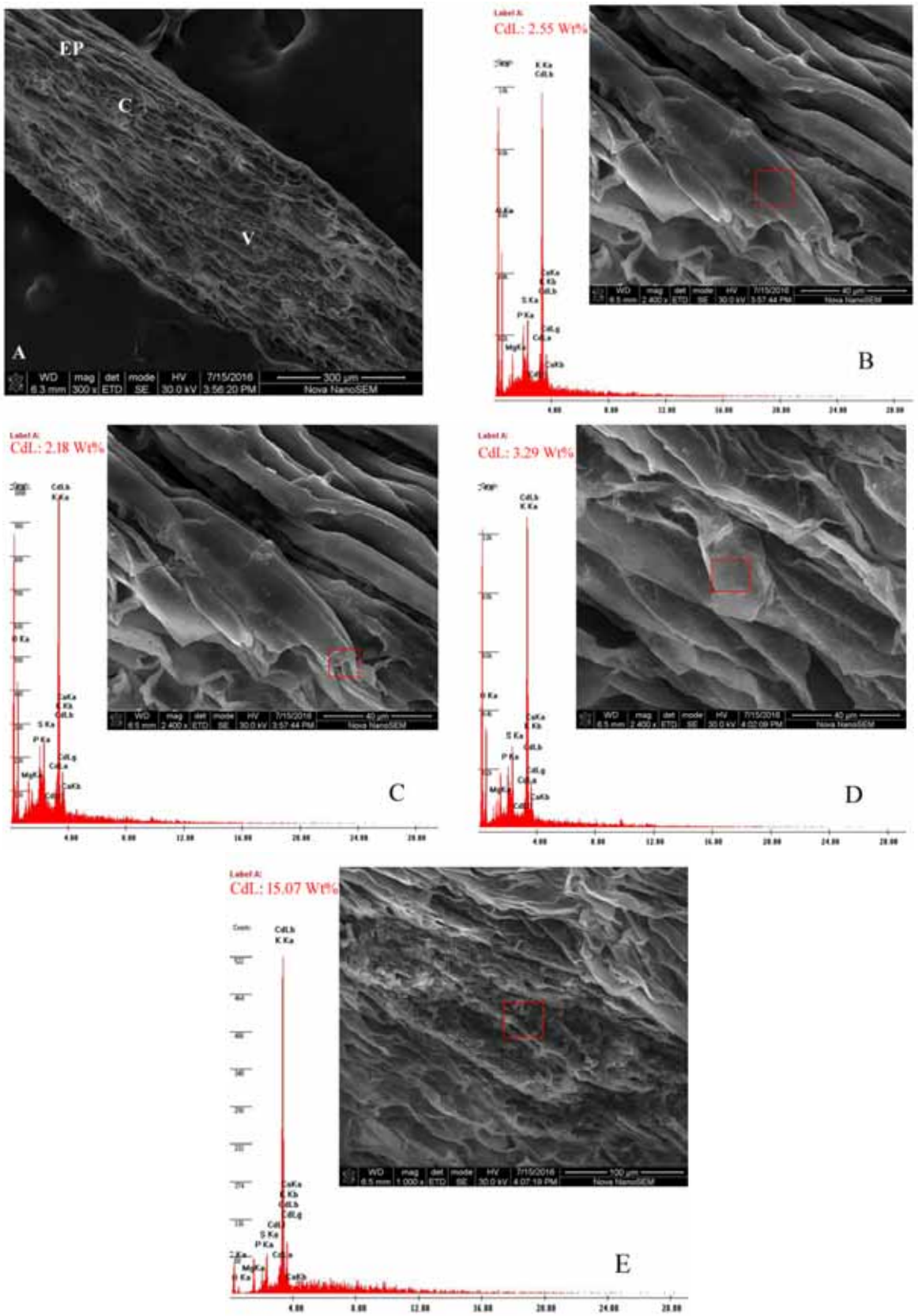

FIGURE 4

EDXA spectra taken from the SEM micrographs, Cd localization in mature zone in root tip cells of Salix babylonica exposed to 100 µM Cd for 24 h. A: Transverse section of mature zone (scale bars = 300 µm); B: Epidermal cells (scale bars = 40 µm); C: Cytoplasm (scale bars = 40 µm); D: Cell wall (scale bars = 40 µm); E: vascular bundle (scale bars = 100 µm). Red box sites of the analysis; x-axis-energy [keV]. V = vascular cylinder; EP = epidermis; C = cortex.

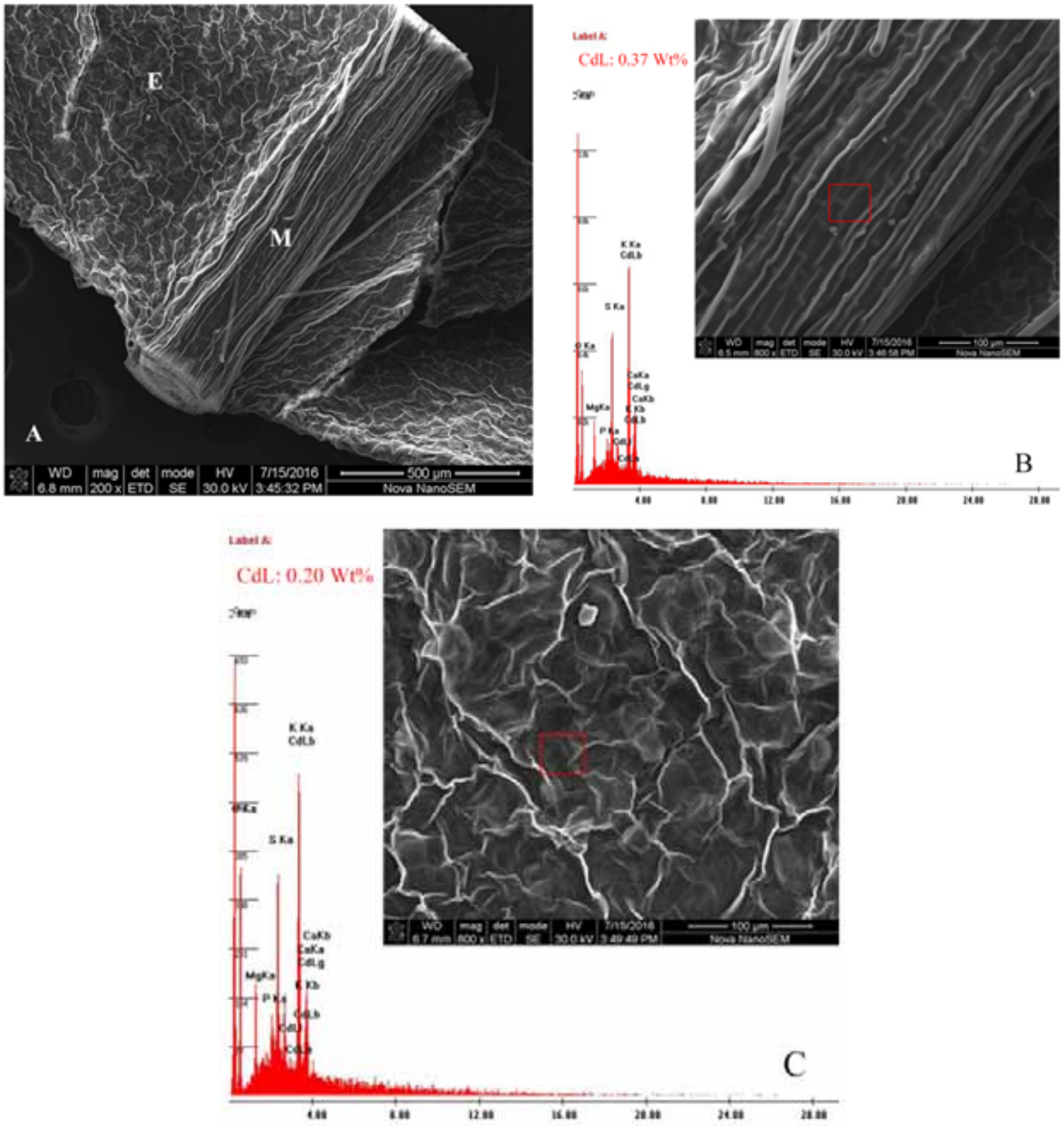

FIGURE 5

EDXA spectra taken from the SEM micrographs, Cd localization in leaf of Salix babylonica exposed to 100 µM Cd for 24 h. A: Transverse section of leaf (scale bars = 500 µm); B: Leaf main vein (scale bars = 100 µm); C: Leaf epidermal cells (scale bars = 100 µm). Red box sites of the analysis; x-axis-energy [keV]. M = main vein; E = epidermis.

plants can avoid Cd stress by forming metal chelates/complexes. The total three fractions of Cd accumulated by roots was higher than that by leaves (Tab. 3), and the high proportion of Cd in the soluble fraction may limit root-to-shoot translocation of Cd, which resulting in low Cd levels in the shoots [53, 54].

The results of EDXA showed subcellular location of Cd on the mature zone of root tip cells and surface of leaves (Fig. 4, Fig. 5). In skew cross-section of the mature zone of root, the Cd level is in the order: vascular bundle > cortical cells > epidermal cells. In cortical cells, Cd ions were observed in cell wall and cytoplasm, Cell wall > Cytoplasm. However, Shi et al. [18] reported that the order of Cd accumulated in mature zone of *Hordeum vulgare* root tip was cortical cells > vascular bundle > epidermal cells.

Root tip of plants is the sensitive organ to environment stresses, and the first plant tissue in direct contact with metal ions in the growth medium and plays a major role in metal tolerance [36]. Cell wall, as the first barrier to prevent metals from entering a cell, is a pivotal site for Cd storage in plants [14]. In the present study, subcellular localization of Cd by SEM and EDXA shows that the

majority of Cd accumulated in root vessel cells, and cell wall accumulated greater amounts of Cd than cytoplasm and epidermal cells. The results may indicate cell wall of root tip is the main Cd storage sites and vessel cells in mature zone of root tip have more potential in Cd uptake. As could be seen from Fig. 5, the Cd level in the leaf main vein was higher than the epidermal cells, which suggesting that the main vein was the main site of leaf to accumulate Cd. The subcellular localization of Cd and the accumulation of Cd have obvious relevance in the leaves exposed to Cd, Shi et al. [17] reported that the level of Cd in stomata and veins in the leaves of *Hordeum vulgare* exposed to Cd were high.

CONCLUSIONS

Based on the information provided in this article, it is concluded that:

(1) Cd could decrease the uptake and accumulation of Fe and Mn in *S. babylonica*.

(2) Root was the main organ to uptake and accumulate Cd compare with shoots.

(3) Cd content in the different fractions: cell wall > soluble fraction > cell organelle. Cell wall was the main accumulation site for Cd, suggesting that the cell wall barrier was crucial for the detoxification of Cd.

(4) The proportion of CdE and CdW was low in leaves. The proportion of CdNaCl in roots and leaves was the highest, and it could be suggested that Cd integrated with pectates and proteins in cell walls, which might be responsible for the adaptation of *S. babylonica* to Cd stress. After exposed to Cd for 14 d, CdNaCl represent 73.22% (10 μM Cd, leaf), 59.84% (50 μM Cd, leaf), 51.32% (100 μM Cd, leaf), 48.02% (10 μM Cd, root), 43.62% (50 μM Cd, root), 32.32% (100 μM Cd, root) of total Cd.

(5) Cd can be mainly absorbed in vascular bundle of mature zone in the root tips and leaf main vein of *S. babylonica* under Cd stress. Cell wall play a key role in Cd detoxicity.

ACKNOWLEDGEMENTS

This project was supported by Natural Science Foundation of Tianjin, China (grant NO. 17JCYBJC22500) and Doctor Foundation of Tianjin Normal University (52XB1914). The authors wish to express their appreciation to the reviewers for their comments and suggestions.

REFERENCES

[1] Lai, H.Y., Lam, C.M., Wang, W.Z. and Ji, Y.J. (2017) Cadmium uptake by cuttings of impatiens walleriana in response to different cadmium concentrations and growth periods. Bull Environ Contam Toxicol. 98, 317-322.

[2] Zeiner, M. and Cindrić, I.J. (2017) Review - trace determination of potentially toxic elements in (medicinal) plant materials. Anal Methods. 9, 1550-1574.

[3] Suvarapu, L.N. and Baek, S.O. (2017) Determination of heavy metals in the ambient atmosphere: A review. Toxicol Ind Health. 33, 79-96.

[4] Zhang, C.L., Zhang, P., Mo, C.R., Yang, W.W., Li, Q.F., Pan, L.P. and Lee, D.K. (2013) Cadmium uptake, chemical forms, subcellular distribution, and accumulation in Echinodorus osiris Rataj. Environ Sci Proc Impacts. 15, 1459-1465.

[5] Shahid, M., Dumat, C., Khalid, S., Niazi, N.K. and Antunes, P.M.C. (2017) Cadmium bioavailability, uptake, toxicity and detoxification in soil-plant system. Rev Environ Contam. T. 241, 73-137.

[6] Hao, X.Q., Li, T.X., Yu, H.Y., Zhang, X.Z., Zheng, Z.C., Chen, G.D., Zhang, S.J., Zhao, L. and Pu, Y. (2015) Cd accumulation and subcellular distribution in two ecotypes of Kyllinga brevifolia Rottb as affected by Cd treatments. Environ Sci Pollut Res. 22, 7461-7469.

[7] Lin, Y.F. and Aarts, M.G.M. (2012) The molecular mechanism of zinc and cadmium stress response in plants. Cell Mol Life Sci. 69, 3187-3206.

[8] Choppala, G., Saifullah, Bolan, N., Bibi, S., Iqbal, M., Rengel, Z., Kunhikrishnan, A., Ashwath, N. and Ok, Y.S. (2014) Cellular mechanisms in higher plants governing tolerance to cadmium toxicity. Crit Rev Plant Sci. 33, 374-391.

[9] He, J.Y., Zhu, C., Ren, Y.F., Yan, Y.P., Cheng, C., Jiang, D.A. and Sun, Z.X. (2008) Uptake, subcellular distribution, and chemical forms of cadmium in wild-type and mutant rice. Pedosphere. 18, 371-377.

[10] Zhao, Y.F., Wu, J.F., Shang, D.R., Ning, J.S., Zhai, Y.X., Sheng, X.F. and Ding, H.Y. (2015) Subcellular distribution and chemical forms of cadmium in the edible seaweed, Porphyra yezoensis. Food Chemistry. 168, 48-54

[11] Yin, A.G., Yang, Z.Y., Ebbs, S., Yuan, J.G., Wang, J.B. and Yang, J.Z. (2016) Effects of phosphorus on chemical forms of Cd in plants of four spinach (Spinacia oleracea L.) cultivars differing in Cd accumulation. Environ Sci Pollut Res. 23, 5753-5762.

[12] Luo, N., Li, X., Chen, A.Y., Zhang, L.J., Zhao, H.M., Xiang, L., Cai, Q.Y., Mo, C.H., Wong, M.H. and Li, H. (2017) Does arbuscular mycorrhizal fungus affect cadmium uptake and chemical forms in rice at different growth stages? Sci Total Environ. 599–600, 1564-1572.

[13] He, S.Y., He, Z.L., Wu, Q.L., Wang, L. and Zhang, X. (2015) Effects of GA(3) on plant physiological properties, extraction, subcellular distribution and chemical forms of Pb in Lolium perenne. Int J Phytoremediat. 17, 1153-1159.

[14] Wu, H.F., Wang, J.Y., Ou, Y.J., Li, B.B., Jiang, W.S., Liu, D.H. and Zou, J.H. (2016) Cadmium uptake and localization in roots of Salix matsudana koidz. Fresen. Environ. Bull. 25, 2700-2706.

[15] Ge, W., Jiao, Y.Q., Sun, B.L., Qin, R., Jiang, W.S. and Liu, D.H. (2012) Cadmium-mediated oxidative stress and ultrastructural changes in root cells of poplar cultivars. S Afr J Bot. 83, 98-108.

[16] Liu, D.H., Kottke, I. and Adam, D. (2007) Localization of cadmium in the root cells of Allium cepa by energy dispersive X-ray analysis. Biol Plant. 51, 363-366.

[17] Shi, Q.Y., Wang, J.R., Zou, JH., Jiang, Z., Wang, J.Y., Wu, H.F., Jiang, W.S. and Liu, D.H. (2015) Cadmium uptake and accumulation and its toxic effects on leaves in Hordeum vulgare. Fresen. Environ. Bull. 24, 4504-4511.

[18] Shi, Q.Y., Wang, J.R., Zou, J.H., Jiang, Z., Wang, J.Y., Wu, H.F., Jiang, W.S. and Liu, D.H. (2016). Cd Subcellular localization in root tips of Hordeum vulgare. Pol J Environ Stud. 25, 903-908.

[19] Chen, G.C., Liu, Y.Q., Wang, R.M., Zhang, J.F. and Owens, G. (2013) Cadmium adsorption by willow root: the role of cell walls and their subfractions. Environ Sci Pollut Res. 20, 5665-5672.

[20] Ekmekci, Y., Tanyolac, D. and Ayhan, B. (2008) Effects of cadmium on antioxidant enzyme and photosynthetic activities in leaves of two maize cultivars. J Plant Physiol. 165, 600-611.

[21] Baker, A.J.M. (1981) Accumulators and excluders—strategies in the response of plants to heavy-metals. J Plant Nutr. 3, 643-654.

[22] Sheoran, V., Sheoran, A.S. and Poonia, P. (2011) Role of hyperaccumulators in phytoextraction of metals from contaminated mining sites: a review. Crit Rev Environ Sci Technol. 41, 168-214.

[23] Pulford, I.D. and Watson, C. (2003) Phytoremediation of heavy metal-contaminated land by trees-a review. Environ Int. 29, 529-540.

[24] Meers, E., Du Laing, G., Unamuno, V., Ruttens, A., Vangronsveld, J., Tack, F.M.G. and Verloo, M.G. (2007) Comparison of cadmium extractability from soils by commonly used single extraction protocols. Geoderma. 141, 247-259.

[25] Dimitriou, I. and Aronsson, P. (2010). Landfill leachate treatment with willows and poplars efficiency and plant response. Waste Manag. 30, 2137-2145.

[26] Abhilash, P.C., Powell, J.R., Singh, H.B. and Singh, B.K. (2012) Plant-microbe interactions: novel applications for exploitation in multipurpose remediation technologies. Trends Biotechnol. 30, 416-420.

[27] Guo, B.H., Dai, S.X., Wang, R.G., Guo, J.K., Ding, Y.Z. and Xu, Y.M. (2015) Combined effects of elevated CO_2 and Cd-contaminated soil on the growth, gas exchange, antioxidant defense, and Cd accumulation of poplars and willows. Environ Exp Bot. 115, 1-10.

[28] Vondráčková, S., Tlustoš, P., Hejcman, M. and Száková, J. (2017) Regulation of macro, micro, and toxic element uptake by Salix × smithiana using liming of heavily contaminated soils. J Soils Sediments. 17, 1279-1290.

[29] Li, H., Zhang, G.C., Xie, H.C., Li, K. and Zhang, S.Y. (2015) The effects of the phenol concentrations on photosynthetic parameters of Salix babylonica L. Photosynthetica. 53, 1-6.

[30] Wang, W.W., Wu, Y.J., Akbar, S., Jia, X.Q., He, Z.H. and Tian, X.J. (2016) Effect of heavy metals combined stress on growth and metals accumulation of three Salix species with different cutting position. Int J Phytoremediat. 18, 761-767.

[31] Yang, W.D. and Chen, Y.T. (2009) Studies on cadmium uptake, accumulation and tolerance in Salix babylonica. J Nanjing Forest Univ. 33, 17-20.

[32] Piper, C.S. (1942) Soil and plant analysis. Waite agricultural research institute, The University of Adelaide, Australia. 56, 263p.

[33] Wu, H.F., Wang, J.Y., Ou, Y.J., Li, B.B., Jiang, W.S., Liu, D.H., Zou, J.H. (2017) Characterisation of early responses to cadmium in roots of Salix matsudana Koidz. Toxico Enviro Chem. 99, 913-925.

[34] Yang, J.L., Li, K., Zheng, W., Zhang, H.Z., Cao, X.D., Lan, Y.X., Yang, C.P. and Li, C.H. (2015) Characterization of early transcriptional responses to cadmium in the root and leaf of Cd-resistant Salix matsudana Koidz. BMC Genomics. 16, 1-15.

[35] Zhao, M.Z., Liu, Z.L., Chen, W. and Cai, S.Y. (2014) Responses of Trifolium repens cv. rivendel seeds to cadmium stress in terms of electrolyte leakage and soluble protein content changes. Adv Mater Res. 955-959, 593-596.

[36] Zou, J.H., Wang, G., Ji, J., Wang, J.Y., Wu, H.F., Ou, Y.J. and Li, B.B. (2017) Transcriptional, physiological and cytological analysis validated the roles of some key genes linked Cd stress in Salix matsudana Koidz. Environ Experi Bot. 134, 116-129.

[37] Dos Santos Utmazian, M.N. and Wenzel, W.W. (2007) Cadmium and zinc accumulation in willow and poplar species grown on polluted soils. J Plant Nutr Soil Sci. 170, 265-272.

[38] Ling, T., Jun, R. and Fangke, Y. (2011) Effect of cadmium supply levels to cadmium accumulation by Salix. Int J Environ Sci Tech. 8, 493-500.

[39] Dos Santos Utmazian, M.N., Wieshamme, G., Vega, R. and Wenzel, W.W. (2007) Hydroponic screening for metal resistance and accumulation of cadmium and zinc in twenty clones of willows and poplars. Environ Pollut. 148, 155-165.

[40] Kovács, K., Kuzmann, E., Vértes, A., Lévai, L., Cseh, E. and Fodor, F. (2010) Effect of cadmium on iron uptake in cucumber roots: A Mössbauer-spectroscopic Study. Plant Soil. 327, 49-56.

[41] Puschenreiter, M., Gruber, B., Wenzel, W.W., Schindlegger, Y., Hann, S., Spangl, B., Schenkeveld, W.D.C., Kraemer, S.M. and Oburger, E. (2017) Phytosiderophore-induced mobilization and uptake of Cd, Cu, Fe, Ni, Pb and Zn by wheat plants grown on metal-enriched soils. Environ Exp Bot .138, 67-76.

[42] Solti, Á., Sárvári, É., Tóth, B., Mészáros, I., Fodor, F. and Szigeti, Z. (2016) Stress hardening under long-term cadmium treatment is correlated with the activation of antioxidative defence and iron acquisition of chloroplasts in Populus. Zeitschrift Für Naturforschung C. 71, 323-334.

[43] Rahman, A., Nahar, K., Hasanuzzaman, M. and Fujita, M. (2016) Manganese- induced cadmium stress tolerance in rice seedlings: Coordinated action of antioxidant defense, glyoxalase system and nutrient homeostasis. CR Biol. 339, 462-474.

[44] Xu, P.X., Wang, Z.L. (2013) Physiological mechanism of hypertolerance of cadmium in Kentucky bluegrass and tall fescue: Chemical forms and tissue distribution. Environ Exp Bot. 96, 35-42.

[45] Zhang, W., Lin, K.F., Zhou, J., Zhang, W., Liu, L.L. and Zhang, Q.Q. (2014) Cadmium accumulation, subcellular distribution and chemical forms in rice seedling in the presence of sulfur. Environ Toxicol Phar. 37, 348-353.

[46] Xue, M., Zhou, Y.H., Yang, Z.Y., Lin, B.Y., Yuan, J.G., Wu, S.S. (2014) Comparisons in subcellular and biochemical behaviors of cadmium between low-Cd and high-Cd accumulation cultivars of pakchoi (Brassica chinensis L.). Front Environ Sci Eng. 8, 226-238.

[47] Yang, W.D., Chen, Y.T. and Qu, M.H. (2009) Subcellular distribution and chemical forms of cadmium in Salix matsudana. Acta Bot Boreal-Occident Sin. 29, 1394-1399.

[48] Toppi, L.S.D. and Gabbrielli, R. (1999) Response to cadmium in higher plants. Envir Exp Bot. 41, 105-130.

[49] Qiu, Q., Wang, Y.T., Yang, Z.Y. and Yuan, J.G. (2011) Effects of phosphorus supplied insoil on subcellular distribution and chemical forms of cadmium in two Chinese flowering cabbage (Brassica parachinensis L.) cultivars differing in cadmium accumulation. Food Chem Toxicol. 49, 2260-2267.

[50] Wang, X., Liu, Y.G., Zeng, G.M., Chai, L.Y., Song, X.C., Min, Z.Y. and Xiao, X. (2008) Subcellular distribution and chemical forms of cadmium in Bechmeria nivea (L.) Gaud. Environ Exp Bot. 62, 389-395.

[51] Wang, Y., Chai, L.Y., Yang, Z.H., Mubarak, H., Xiao, R.Y. and Tang, C.J. (2017) Subcellular distribution and chemical forms of antimony in Ficus tikoua. Int J Phytoremediat. 9, 97-103.

[52] Liu, J.G., Qu, P., Zhang, W., Dong, Y., Li, L. and Wang, M.X. (2014) Variations among rice cultivars in subcellular distribution of Cd: The relationship between translocation and grain accumulation. Environ Exp Bot. 107, 25-31.

[53] Su, Y., Liu, J., Lu, Z., Wang, X., Zhang, Z. and Shi, G. (2014) Effects of iron deficiency on subcellular distribution and chemical forms of cadmium in peanut roots in relation to its translocation. Environ Exp Bot. 97, 40-48.

[54] Lai, H.Y. and Cai, M.C. (2016) Effects of extended growth periods on subcellular distribution, chemical forms, and the translocation of cadmium in Impatiens walleriana. Int J Phytoremediat. 18, 228-234.

Received: **23.11.2017**
Accepted: **27.03.2019**

CORRESPONDING AUTHOR

Jinhua Zou
Tianjin Key Laboratory of Animal and
Plant Resistance,
College of Life Sciences,
Tianjin Normal University,
Tianjin 300387 – China

e-mail: zjhmon@126.com

© by PSP Volume 28 – No. 5/2019 pages 3649-3657 Fresenius Environmental Bulletin

THE USABILITY OF PUMICE CONCRETE PRODUCED BY DIFFERENT KINDS OF CONCRETE MIXING WATER IN CONSTRUCTION OF RIGID PAVEMENTS

Abdulrezzak Bakis[1,*], Ercan Isik[1], Edip Avsar[2]

[1]Bitlis Eren University, Engineering and Architecture Faculty,Department of Civil Engineering,13100, Bitlis, Turkey.
[2]Bitlis Eren University, Engineering and Architecture Faculty, Department of Environmental Engineering, 13100 Bitlis, Turkey

ABSTRACT

This study selected a total of eight types of samples as C30/37 normal-strength control concrete and seven types of Pumice Concrete (PC) for rigid pavement construction. The PC samples were produced in fibrous and non-fibrous forms. In all the samples, city water and lake water were used for concrete mixing water. 7- and 28-day20°C standard water curing was applied on the control sample (C30/37 concrete) and PC samples. At the end of the curing process, compressive and flexural experiments were carried out on all the samples. As a result of the study, the highest compressive strength for C30/37 concrete was found as 37.39 MPa, and the highest flexural strength was found to be 4.51 MPa. The highest compressive strength for the non-fibrous PC produced by city water was found as 80.42 MPa, and the highest flexural strength was found as 10.57 MPa. The highest compressive strength for the non-fibrous PC produced by lake water was found as 65.27 MPa, and the highest flexural strength was 8.94 MPa. The highest compressive strength for fibrous PC produced by city water was found as 86.55 MPa, and the highest flexural strength was 11.12 MPa. The highest compressive strength for fibrous PC produced by lake water was found as 70.98 MPa, and the highest flexural strength was 9.86 MPa. The results of the study demonstrated the usability of pumice concrete produced by city and lake water in rigid pavements.

KEYWORDS:
Lake Van, pumice, concrete, strength, water

INTRODUCTION

The term pomza is expressed as ponce in French and pumice in English. In Turkish, it is called pumice stone, heel stone and callus stone [1]. Pumice formations created as a result of volcanic eruptions that have a spongy structure are found in different regions of the world where there are volcanic activities [2]. Pumice contains many independent pores from macro to micro scales. According to the Mohs scale, its hardness is 5 to 6 [3]. Nowadays, pumice is used in different sectors such as the construction, chemistry and cosmetics sectors [4].

As a pumice grain grows, its specific gravity decreases. As the grain size of pumice increases, the percentage of pores within also increases. The pore percentage of pumice increases as it moves away from a volcanic vent. Due to the excess of pores and its low specific gravity, it is usually used for insulation purposes in the construction sector. As pumice is a volcanic glass, it is easy to grind. It might be in white, yellowish, gray-brown and dull red colors [5,6]. In Turkey, pumice is particularly used in trass cement production [7]. In concrete production sector, pumice aggregate is limitedly used in the production of insulation-purposed walls and similar constructional components. As pumice aggregate has a quite low compressive strength, it cannot be used in concrete production, especially in rigid pavement construction and in the carrier sections of buildings such as beam, column and foundation. It is possible to manufacture concrete with high compressive and flexural strength by decreasing the void ratio through grinding the pumice aggregate and using it in optimum mixing ratio.

This study created seven different types of Pumice Concrete (PC) to obtain high-strength concrete from pumice aggregates. Pumice aggregates were grinded between the sizes of 0 and 1 mm to be used in pumice concrete. Pumice concrete samples were created in fibrous and non-fibrous forms. A fibrous PC mixture contains cement, silica fume, pumice powder, steel fiber, water and super plasticizer. Non-fibrous PC mixtures do not contain steel fiber. It is known that steel fibers have a positive effect on flexural strength in particular.

With the addition of partial macro fibers to the plain concrete, the flexural capacity of the concretes is increased [8, 9, 10]. Silica fume is used in the mixture in order to reach high strength in concrete production [11, 12]. In the formation of pumice concretes, both city and lake waters were used as concrete mixing water. As lake water, the water from the Lake Van situated in the Eastern Anatolia Region of Turkey was used. 7- and 28-day 20°C

standard water curing was applied on the Pc samples that were prepared in different types. At the end of the curing process, compressive and flexural strength experiments were carried out on the PC samples. Additionally, following the compressive and flexural strength experiments, the usability of different PC types in rigid pavement was discussed.

The bitumen that is used in the construction of flexible pavements is oxidized over time as a result of environmental and climatic effects. As a result, the asphalt gets old and needs constant maintenance and repair. There is no such problem in concrete road pavements. When they are compared, the maintenance costs for concrete roads are lower and their service life is longer than asphalt pavements. In the construction of asphalt pavements as flexible pavements, environmental pollution occurs during the process of heating the bitumen material. With the increase in the number of concrete roads, it is aimed to reduce maintenance cost, material requirement and environmental pollution with respect to asphalt pavements.Water is an important raw material in terms of concrete production. Today, the use of alternative water resources in concrete production is of environmental importance when clean water resources are rapidly consumed. In this context, water from the Lake Van, which has high alkalinity and no drinkable characteristics, was used as an alternative raw material in this study.

TABLE 1
Chemical properties of CEM I 42.5R cement [13]

The chemical features (%)	
SiO_2	18.90
$Al2O_3$	5.15
Fe_2O_3	3.36
CaO	63.59
MgO	1.57
SO_3	2.65
Ignition loss	3.59
K_2O	0.77
Na_2O	0.40
Cl	0.02

MATERIALS AND METHODS

This study used the CEM I 42.5 R type cement in all concrete mixture types. As C30/37 concrete aggregate, broken limestone was used in the mixture. For Pumice Concrete(PC) production, acidic pumice powder was used as the aggregate in the mixture. In all sample types, city and lake water were used as the mixing water. In the study, 7 different types Pumice Concrete (PC) were created. In the pumice concretes, pumice aggregates were ground between 0 and 1 mm. The pumice concrete samples were created as fibrous and non-fibrous. Fibrous PC mixture contains cement, silica fume, pumice powder, steel fiber, water and super plasticizer. Non-fibrous PC mixtures do not contain steel fiber. Chemical properties of the CEM I 42.5 R cement are presented in Table 1.

The appearance of silica fume may be seen in Figure 1.

Physical and chemical properties of silica fume that was used in this study are presented in Table 2 [14].

The appearance of acidic pumice may be seen in Figure 2.

FIGURE 1
The appearance of silica fume

TABLE 2
Physical and chemical properties of silica fume.

Physical and chemical properties	
SiO_2 (%)	95.56
Al_2O_3 (%)	0.71
Fe_2O_3 (%)	0.44
CaO (%)	0.68
MgO (%)	1.25
SO_3 (%)	0.58
Ignition loss (%)	0.78
Specific gravity (g/cm^3)	2.25
Specific surface (cm^2/g)	200000

FIGURE 2
The appearance of pumice

The appearance of acidic pumice powder may be seen in Figure 3.

The properties of acidic pumice are presented in Table 3.

FIGURE 3
The appearance of pumice powder

TABLE 3
Chemical analysis of acidic pumice (%) [15]

Ignition loss	3
MgO	0.6
Al_2O_3	14
SiO_2	70
Na_2O+K_2O	9
CaO	0.9
Fe_2O_3	2.5

FIGURE 4
Steel fibers used in the production fibrous PC.

Steel fibers that were used in the production fibrous Pumice Concrete (PC) may be seen in Figure 4.

Steel fibers that would be used in fibrous PC production were at 30 mm length and 0.55 mm diameter. The physical and mechanical properties of the steel fibers are shown in Table 4.

TABLE 4
Technical properties of steel fibers [16].

Fiber Type	Steel Fiber
Diameter (mm)	0.55
Length (mm)	30
Fragility	55
Tensile strength (MPa)	1100
Specific weight	7.85

The properties of super plasticizer are given in Table 5.

TABLE 5
The properties of super plasticizer [14]

Properties	
Form	Liquid
Density	1.1 kg/L
pH	4.00–5.50
Chloride content	< 0.1% (TS EN 480–10)

LAKE VAN WATER QUALITY AND APPLICATION IN TERMS OF CONCRETE MIXING WATER

In order to determine the water quality of Lake Van, water quality sampling analysis and literature survey were carried out. The results that were obtained were compared to the information in the Modification Regulation of Surface Water Quality Classes Regulation (Turkish Official Gazette Date and number: 10.08.2016/29797) Annex 5: Environmental Quality Standards and Usage Purposes for Some Parameters in Surface Waters. The results are presented in Table 6.

When Lake Van water was investigated in terms of water quality, it was determined as class 4 for conductivity, out of class for pH, class 2 for COD and class 1 for TN and NO_3^-. The high pH and conductivity parameters were not due to water pollution, but about the lake's own alkaline character. A higher level of HCO-, CO32-, Cl- and SO42- ions in the water increases the conductivity value. In this case, Lake Van should be evaluated within its own characteristics. It is also understood that the water mass is in an oligotrophic (TN <0.35 mg / L) state.

The mixing water that is used for cement manufacturing must comply with the TS EN 1008 standard (Concrete-mixed water - Determination of the suitability of water as concrete mixed water, including water recovered from sampling, testing and operations in the concrete industry). According to the TS EN 1008 Turkish standard, the waters that may be used in the construction of concrete are classified as follows;

- Drinking waters
- Wastewater recovered from operations in the concrete industry
- Waters from underground sources
- Natural surface waters and industrial wastewater
- Sea water and lake water [19]

The limit values of some harmful substances in concrete mixture water are given in Table 7 [20]. Foreign materials that may be found in waters include clay, silt, moss, sugar, calcium, magnesium,

TABLE 6
LakeVan water quality and comparison to the regulation

Parameter	Unit	Bilgili et al. [17]	Current Study	Water quality classes
pH	-	9.54	9.9	Out of regulation classes
HCO^-		2110.63		
CO_3^{2*}		3412.41		
Cl^-		5320.13		
SO_4^{2-}		2466.36		
Ca^{2+}		6.74		
Mg^{2+}		97.66		
Na^+	mg/L	7673.15		
K^+		524.60		
TOC			11.7	
COD			42.2*	Class 2
TN			<0.05	Class 1
NO_3^-			1.19	Class 1
Br^-			0.95	
Conductivity	µs/cm		29100	Class 4
Orp	mV		154.5	
Turbidity	NTU		1.64	

The *COD value was calculated based on the formula'COD=7.25+2.99*TOC' which was taken from Dubber and Gray[18].

sodium, chloride, sulphate, various kinds of salts, acids and oils. If the ratio of the materials such as clay, silt and stone which may be found in the mixing water is higher than 0.2%, the processing ability of fresh concrete decreases [21]. When the water quality parameters are compared to the limit values, it is seen that the limit values were exceeded in terms of SO_4^{2-}, Cl^-, carbonates and bicarbonates.

TABLE 7
Limit values of harmful substances in concrete mixture water

Harmful substances	Unit	Limit Value
SO_4^{2-}	mg/L	2000
Cl^-	mg/L	5000
NO_3^-	mg/L	500
$Ca(HCO_3)_2$ and $Mg(HCO_3)_2$	mg/L	400
Total organic matter	g/L	50
Na_2CO_3 and K_2CO_3	ppm	1000
pH	-	≥4

In the study, seven types fibrous and 7 types non-fibrous Pumice Concretes were selected for rigid pavement construction. All samples were prepared in dimensions of 15x15x15 cm. The concrete samples were placed by bottling them in the molds. 7-day 20°C standard water curing and 28-day 20°C standard water curing processes were applied on the concrete samples that were removed from the mold 24 hours later. At the end of the curing process, compressive and flexural strength experiments were carried out on the samples. In the compressive strength experiments, TS EN 12390-3: 2010 was used,the flexural strength experiments utilized the TS EN 12390-5: 2010 standard [22, 23].

THE QUANTITIES OF MATERIALS IN THE C30/37 CONCRETE MIXTURE

The quantities in 1 m^3 mixture as kg unit for producing C30/37 concrete are shown in Table 8.

TABLE 8
The quantities of materials in the C30/37 concrete mixture

Materials	Quantity (kg/m^3)
Cement	450
0-4 mm (Crushed limestone)	803
4-8 mm (Crushed limestone)	389
8-16 mm (Crushed limestone)	569
City water	189
TOTAL	2400

THE QUANTITIES OF MATERIALS IN THE NON-FIBROUS PUMICE CONCRETE MIXTURE

Seven types of mixtures were composed as non-fibrous Pumice Concrete (PC-C1) in which city water was used as the concrete mixing water. The quantities in 1 m^3 mixture as kg unit for producing PC-C1 concrete are shown in Table 9.

Seven types of mixtures were created as non-fibrous Pumice Concrete (PC-S1) in which lake water was used as the concrete mixing water. The quantities in 1 m^3 mixture as kg unit for producing PC-S1 concrete are shown in Table 10.

In non-fibrous concrete mixtures, the amount of cement in the mixture no.4 was taken in the manner that would correspond to 450kg per 1 m^3 concrete. The amount of cement in mixture no.3

was prepared to be 25% less than the amount of cement in mixture no.4. The amount of cement in mixture no.2 was prepared to be 50% less than the amount of cement in mixture no.4, and the amount of cement in mixture no.1 was prepared to be 75% less than the amount of cement in mixture no.4. Moreover, the amount of cement in mixture no.5 was prepared to be 25% more than the amount of cement in mixture no.4, the amount of cement in mixture 6 was prepared to be 50% more than the amount of cement in mixture no.6, and the amount of cement in mixture no.7 was prepared to be 75% more than the amount of cement in mixture no.4. Thus, 7 types of non-fibrous Pumice Concrete (PC) mixture were created. In PC production processes, non-fibrous concretes that used city water as the mixing water were displayed as PC-C1. Likewise, non-fibrous concretes that used lake water as the mixing water were displayed as PC-S1. In 7 types of PC-C1 and 7 types of PC-S1 concrete shown in Tables 2.7 and 2.8, the water-binder ratio was taken as 0.28, and the silica fume/cement ratio was taken as 0.25. The amount of super plasticizer was kept on a fixed value that would correspond to 72 kg for 1 m^3 of concrete.

THE QUANTITIES OF MATERIALS IN THE FIBROUS PUMICE CONCRETE MIXTURE

7 types of mixtures were produced as fibrous Pumice Concrete (PC-C2) in which city water was used as the concrete mixing water. The quantities in 1 m^3 mixture as kg unit for producing PC-C2 concrete are shown in Table 11.

TABLE 9
The quantities of materials in the PC-C1 concrete mixture (kg/m^3)

Materials	PC-C1 (1)	PC-C1 (2)	PC-C1 (3)	PC-C1 (4)	PC-C1 (5)	PC-C1 (6)	PC-C1 (7)
Cement	113	225	338	450	563	675	788
Silica Fume	28	56	84	113	141	169	197
Pumice (0-1 mm)	2128	1968	1788	1608	1427	1248	1067
Super plasticizer	72	72	72	72	72	72	72
City water	39	79	118	157	197	236	276
Total	2400	2400	2400	2400	2400	2400	2400

TABLE 10
The quantities of materials in the PC-S1 concrete mixture (kg/m3)

Materials	PC-S1 (1)	PC-S1 (2)	PC-S1 (3)	PC-S1 (4)	PC-S1 (5)	PC-S1 (6)	PC-S1 (7)
Cement	113	225	338	450	563	675	788
Silica Fume	28	56	84	113	141	169	197
Pumice (0-1 mm)	2128	1968	1788	1608	1427	1248	1067
Super plasticizer	72	72	72	72	72	72	72
Lake water	39	79	118	157	197	236	276
Total	2400	2400	2400	2400	2400	2400	2400

TABLE 11
The quantities of materials in the PC-C2 concrete mixture (kg/m^3)

Materials	PC-C2 (1)	PC-C2 (2)	PC-C2 (3)	PC-C2 (4)	PC-C2 (5)	PC-C2 (6)	PC-C2 (7)
Cement	113	225	338	450	563	675	788
Silica Fume	28	56	84	113	141	169	197
Pumice (0-1 mm)	2128	1929	1729	1529	1328	1130	929
Super plasticizer	72	72	72	72	72	72	72
Steel fiber	20	39	59	79	99	118	138
City water	39	79	118	157	197	236	276
Total	2400	2400	2400	2400	2400	2400	2400

TABLE 12
The quantities of materials in the PC-S2 concrete mixture (kg/m^3)

Materials	PC-S2 (1)	PC-S2 (2)	PC-S2 (3)	PC-S2 (4)	PC-S2 (5)	PC-S2 (6)	PC-S2 (7)
Cement	113	225	338	450	563	675	788
Silica Fume	28	56	84	113	141	169	197
Pumice (0-1 mm)	2128	1929	1729	1529	1328	1130	929
Super plasticizer	72	72	72	72	72	72	72
Steel fiber	20	39	59	79	99	118	138
Lake water	39	79	118	157	197	236	276
Total	2400	2400	2400	2400	2400	2400	2400

TABLE 13
Results of compressive and flexural strength tests

Concrete Type	Compressive Strength (MPa)		Flexural Strength (MPa)	
	7-day	28-day	7-day	28-day
C30/37	28.55	37.39	3.75	4.51
PC-C1-1	3.81	5.15	0.49	0.67
PC-C1-2	7.43	9.57	0.99	1.27
PC-C1-3	18.48	23.96	2.49	3.21
PC-C1-4	33.55	43.87	4.63	5.32
PC-C1-5	**61.51**	**80.42**	**8.31**	**10.57**
PC-C1-6	54.33	70.48	7.29	9.53
PC-C1-7	43.61	56.97	5.93	7.25
PC-S1-1	2.94	3.76	0.37	0.48
PC-S1-2	3.97	5.12	0.49	0.67
PC-S1-3	6.60	8.57	0.87	1.12
PC-S1-4	29.49	38.23	3.96	4.97
PC-S1-5	**50.32**	**65.27**	**6.89**	**8.94**
PC-S1-6	45.48	58.97	6.12	7.89
PC-S1-7	37.16	48.24	4.97	6.32
PC-C2-1	3.99	5.19	0.55	0.71
PC-C2-2	7.97	10.35	1.12	1.45
PC-C2-3	19.98	24.19	2.77	3.39
PC-C2-4	36.23	47.32	5.10	6.71
PC-C2-5	**66.34**	**86.55**	**9.17**	**11.12**
PC-C2-6	58.77	76.33	8.15	10.61
PC-C2-7	47.12	61.55	6.53	8.51
PC-S2-1	3.12	3.97	0.45	0.56
PC-S2-2	4.23	5.48	0.59	0.77
PC-S2-3	7.13	9.27	1.10	1.33
PC-S2-4	31.97	41.56	4.43	5.79
PC-S2-5	**54.37**	**70.98**	**7.53**	**9.86**
PC-S2-6	49.33	64.52	6.87	8.95
PC-S2-7	40.24	52.46	5.62	7.34

Seven types of mixtures were produced as fibrous Pumice Concrete (PC-S2) in which lake water was used as the concrete mixing water. The quantities in 1 m^3 mixture as kg unit for producing PC-S2 concrete are shown in Table 12.

In the fibrous concrete mixtures, the quantity of cement in the mixture no.4 was taken in the manner that would correspond to 450kg for 1 m^3 concrete. The amount of cement in mixture no.3 was prepared to be 25% less than the amount of cement in mixture no.4, the amount of cement in mixture no.2 was prepared to be 50% less than the amount of cement in mixture no.4, and the amount of cement in mixture no.1 was prepared to be 75% less than the amount of cement in mixture no.4. Moreover, the amount of cement in mixture no.5 was prepared to be 25% more than the amount of cement in mixture no.4, the amount of cement in mixture 6 was prepared to be 50% more than the amount of cement in mixture no.6, and the amount of cement in mixture no.7 was prepared to be 75% more than the amount of cement in mixture no.4. Thus, 7 types of fibrous Pumice Concrete (PC) mixture were created. In the PC production processes, fibrous concretes that used city water as the mixing water were displayed as PC-C2. Likewise, fibrous concretes that used lake water as the mixing water were displayed as PC-S2. In 7 types of PC-C2 and 7 types of PC-S2 concrete shown in Tables 2.9 and 2.10, the water-binder ratio was taken as 0.28, and the silica fume/cement ratio was taken as 0.25. The amount of super plasticizer was kept on a fixed value that would correspond to 72 kg for 1 m^3 of concrete. In all the fibrous PC-C2 and PC-S2 production processes, steel fibers were taken as 17.5% of the amount of cement inweight.

RESULTS AND DISCUSSION

In the specifications, in order to rate the concrete pavement, one criterion or a few criteria such as 0.40-0.45 maximum water-binder ratio, 28 MPa minimum compressive strength, 4,5 MPa minimum flexural strength and 270-335 kg/m3 minimum amount of cement was/were used as the basis [24]. In all the fibrous and non-fibrous pumice concrete samples, the water-binder ratio was 0.28. The compressive strength of the normal-strength concretes was between 20 and 60 MPa, and the compressive strength of the high-strength concretes was between 60 and 155 MPa [25]. The results of strength tests were given in Table 13.

As seen in Table 13, among the non-fibrous concrete PC-C1 samples that used city water as the mixing water, the highest compressive strength 80.42 MPa and the highest flexural strength 10.57 MPa were obtained from the PC-C1-5 sample. Among the non-fibrous concrete PC-S1 samples

that used lake water as the mixing water, the highest compressive strength 65.27 MPa and the highest flexural strength 8.94 MPa were obtained from the PC-S1-5 sample.

As seen in Table 13, among the fibrous concrete PC-C2 samples that used city water as the mixing water, the highest compressive strength 86.55 MPa and the highest flexural strength 11.12 MPa were obtained from the PC-C2-5 sample. Among fibrous concrete PC-S2 samples that used lake water as the mixing water, the highest compressive strength 70.98 MPa and the highest flexural strength 9.86 MPa were obtained from the PC-S2-5 sample.The maximum compressive strengths of the fibrous and non-fibrous pumice concretes that used city and lake water as the mixing water are shown in Figure 5.

The maximum flexural strengths of the fibrous and non-fibrous pumice concretes that used city and lake water as the mixing water are shown in Figure 6.

As is seen in Figure 5, the highest compressive strength among the concrete types was obtained from the fibrous pumice concrete PC-C2-5 that used city water as the concrete mixing water. In Figure 5, it may be seen that the compressive strength of the PC-C2-5 concrete after 7-day 20°C standard water curing was 66.34 MPa, and the compressive strength of the PC-C2-5 concrete after 28-day 20°C standard water curing was 86.55 MPa. As seen in Figure 6, the highest flexural strength among the concrete types was obtained from the fibrous pumice concrete PC-C2-5that used city water as the concrete mixing water. In Figure 6, it may be seen that the flexural strength of the PC-C2-5 concrete after 7-day 20°C standard water curing was 9.17 MPa, and the flexural strength of the PC-C2-5 concrete after 28-day 20°C standard water curing was 11.12 MPa.

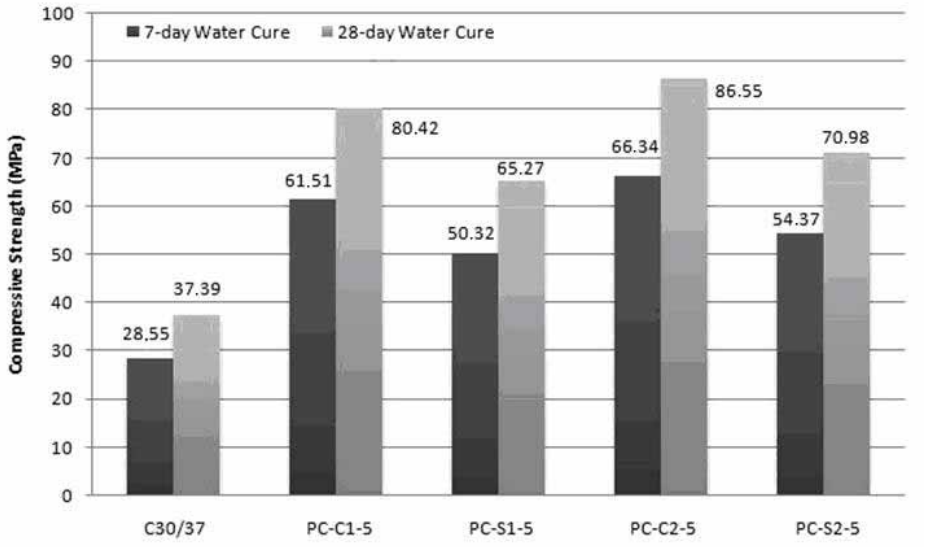

FIGURE 5
Maximum Compressive Strength of the Concretes

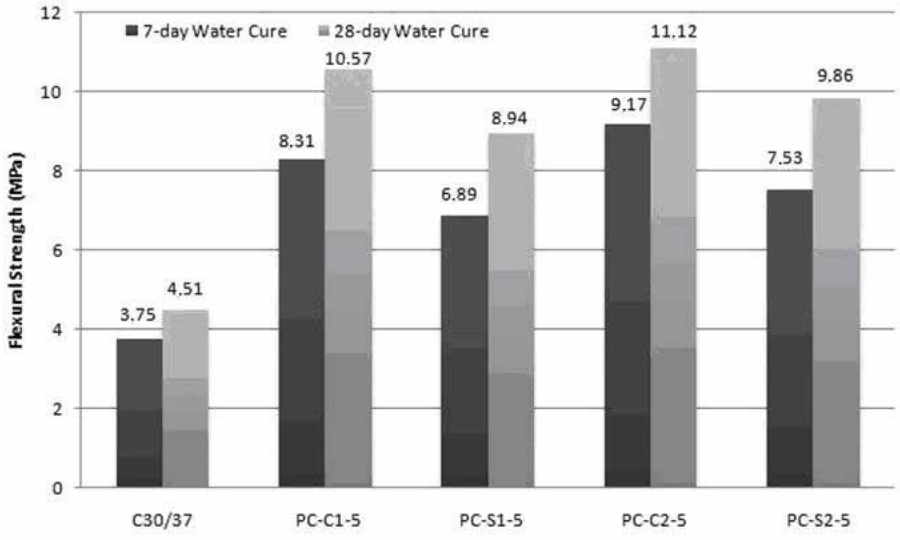

FIGURE 6
Maximum Flexural Strength of the Concretes

CONCLUSIONS

This study investigated the usability of Pumice Concrete (PC) which used city and lake water as the concrete mixing water in rigid pavement construction. Fibrous pumice concretes that used city water as the mixing water in PC productions were expressed as PC-C1. Likewise, non-fibrous pumice concretes that used lake water as the mixing water were expressed as PC-S1. In pumice concrete productions, fibrous pumice concretes that used city water as the mixing water were expressed as PC-C2. Likewise, fibrous pumice concretes that used lake water as the mixing water were expressed as PC-S2. The following results were obtained in the study:

- For rigid superstructure pavement concrete, it is required that the maximum water-binder ratio is be 0.40-0.45, the minimum compressive strength is 28 MPa, the minimum flexural strength is 4.5 MPa, and the minimum amount of cement is 270-335 kg/m^3. In all the fibrous and non-fibrous pumice concrete samples, the water-binder ratio was 0.28. The PC-C1-4, PC-C1-5, PC-C1-6, PC-C1-7, PC-S1-4, PC-S1-5, PC-S1-6, PC-S1-7, PC-C2-4, PC-C2-5, PC-C2-6, PC-C2-7, PC-S2-4, PC-S2-5, PC-S2-6 and PC-S2-7 concretes may be used as rigid pavement materials because they satisfy the rigid pavement criteria.
- The compressive strength of thenormal-strength concretes was between 20 and 60 MPa. The PC-C1-3, PC-C1-4, PC-C1-7, PC-S1-4, PC-S1-6, PC-S1-7, PC-C2-4, PC-S2-4 and PC-S2-7 concretes may be classified as normal-strength concretes.
- The compressive strength of the high-strength concretes was between 60 and 155 MPa. The PC-C1-5, PC-C1-6, PC-S1-5, PC-C2-5, PC-C2-6, PC-C2-7, PC-S2-5 and PC-S2-6 concretes may be classified as high-strength concretes.
- As a result of all types of pumice concrete production, it was observed that the mixture that provided the highest compressive and flexural strength values was the fibrous pumice concrete PC-C2-5 that used city water as the mixing water. Inside this concrete mixture, according to the total amount of the mixture, there was 23.46% cement, 5.88% silica fume, 55.33% pumice powder, 3% plasticizer, 4.13% steel fiber and 8.21% city water. The amount of silica fume corresponded to 25% of the amount of cement. The water-binder ratio of the mixture was 0.28.
- In this study, 7 and 28-day 20°C standard water curing was applied on all the types of pumice concretes that were studied. It is possible to obtain higher compressive and flexural strength from pumice concretes by exposing them to combined curing via heat treatment.

REFERENCES

[1] Özkan, Ş.G. and Tuncer, G. (2001) An overview of pumice mining. 4th Industrial Raw Materials Symposium. İzmir, Turkey, 200-207 (In Turkish).

[2] Gündüz, L., Sarıışık, A., Tozaçan, B., Davraz, M., Uğur, A. and Çankıran, O. (1998) Pumice technology. Volume 1.Isparta, Turkey (In Turkish).

[3] Anonyms (2001) Industrial raw materials subcommission building materials. Special Commission Report of DPT Mining, Industrial Raw Materials Sub-Commission, Building Materials Working Group Report. Ankara, Turkey, 354p. (In Turkish).

[4] Bakış A, Işık E, El A.A. and Ülker, M. (2017) A study on the mixture ratio of pumice powder concrete on the concrete pavement and the construction of building. IOSR. Journal of Mechanical and Civil Engineering. 14(3), 83-90.

[5] Dinçer, İ., Orhan, A. and Çoban, S. (2015) Feasibility report of pumice research and application centre. Nevşehir, Turkey (In Turkish).

[6] Karaman, M.E. and Kibici, Y. (2008) Basic principles of geology. Belen Publishing, Ankara, Turkey, 254p. (In Turkish).

[7] Ünsal, N. (2001) Geology for civil engineers. Alp Publishing, Ankara, Turkey, 187p (In Turkish).

[8] Bakış, A. (2015) Investigation on the usability of reactive powder concrete (RPC) in rigid road superstructure construction. PhD Thesis. Atatürk University, Science Institute, Erzurum, Turkey(In Turkish).

[9] Ji, T., Chen, C.Y. and Zhuang, Y.Z. (2012) Evaluation method for cracking resistant behaviour of reactive powder concrete. Construction and Building Materials.28(1), 45-49.

[10] Zheng, W., Luo, B. and Wang, Y. (2013)Compressive and tensile properties of reactive powder concrete with steel fibres at elevated temperatures. Construction and Building Materials.41, 844-851.

[11] Tohumcu, İ. and Bingöl, A.F. (2013) Fresh concrete properties and compressive strength of self-compacting concretes with silica fume and fly ash. DEU, Journal of Engineering Sciences.15(2), 31-44 (In Turkish).

[12] Gündeşli, U. (2008) A literature review on the use of fly ash, silica fume and blast – furnace slag in concrete and cement as an additive. Master Thesis. Çukurova University, Science Institute, Adana, Turkey (In Turkish).

[13] Anonymous (2017) Çimsa Cement, Chemical properties of CEM I 42.5R cement**.** http://www.cimsa.com.tr.

[14] Anonymous (2017a) İksa Concrete and Construction Chemicals, The properties of super plasticizer. http://www.iksa.com.tr.

[15] Efe, T. (2011) Investigation of applicability of Edremit travertine and pumices outcropping north of Van Lake in cement sector. Master Thesis. Yüzüncü Yıl University, Science Institute, Van, Turkey (In Turkish).
[16] Aral, M. (2006) Mechanical behaviour of cement based composites with hybrid fibres-an optimum design.Master Thesis. İstanbul Technical University, Graduate School of Science Engineering and Technology, İstanbul, Turkey (In Turkish).
[17] Bilgili, A., Sağmanlıgil, H., Çetinkaya, N., Yarsan, E. and Türel, İ. (1995) The natural quality of Van Lake and the levels of some heavy metals in grey mullet (Chalcalburus-tarichi, Pallas 1811) samples taken from this lake. Ankara University Veterinary Faculty Journal. 42, 445-450 (In Turkish).
[18] Dubber, D. and Gray, N.F. (2010) Replacement of chemical oxygen demand (COD) with total organic carbon (TOC) for monitoring wastewater treatment performance to minimize disposal of toxic analytical waste. Journal of Environmental Science and Health Part A. 45(12), 1595-1600.
[19] Avşar, E. and Durmaz Bekmezci, H. (2017) Technical report belonging to Adabağ construction industry joint-stock company Doğanşehir / Malatya ready mixed concrete plant. Bitlis Eren University Engineering and Architecture Faculty Environmental Engineering Dept. (in Turkish).
[20] Anonymous (2017b) Chamber of Civil Engineers (IMO), Concrete mixed water, http://www.imo.org.tr/resimler/dosya_ekler/bf21df6804e955e_ek.pdf.
[21] Anonymous (2017c) Harran University, Water used in concrete. http://eng.harran.edu.tr/moodle/moodledata/55/Beton_icin_Su.pdf.
[22] TS EN 12390-3 (2010) Concrete-hardened concrete tests-section 3: determination of compressive strength of test samples. TSE, Ankara, Turkey (In Turkish).
[23] TS EN 12390-5 (2010) Concrete-hardened concrete tests-section 5: determination of bending strength of test samples. TSE, Ankara, Turkey (In Turkish).
[24] Tunç, A. (2007) Road materials and applications. Nobel Publishing, İstanbul, Turkey (In Turkish).
[25] Taşdemir, M.A., Bayramov, F., Kocatürk, N. and Yerlikaya, M. (2004) New developments in the performance based design of concrete. Concrete 2004 Congress, İstanbul, Turkey (In Turkish).

Received: **23.3.2018**
Accepted: **27.03.2019**

CORRESPONDING AUTHOR

Abdulrezzak Bakiş
Bitlis Eren University
Engineering and Architecture Faculty
Department of Civil Engineering
Rahva Campus
13000 Center Bitlis– Turkey

e-mail: arezzakbakis@gmail.com

© by PSP Volume 28 – No. 5/2019 pages 3658-3666 Fresenius Environmental Bulletin

COMPARISON OF CATIONIC DYES (BASIC ORANGE 2, BASIC YELLOW 2 AND BASIC VIOLET 3) REMOVAL FROM AQUEOUS SOLUTION USING CLAY AS AN ADSORBENT

Burhanettin Farizoglu[1], Baybars Ali Fil[1,*], Onur Sozudogru[2], Erdinc Aladag[3], Sinan Kul[4]

[1]Balikesir University, Engineering Faculty, Department of Environmental Engineering, 10145 Balikesir, Turkey
[2]Ataturk University, Engineering Faculty, Department of Environmental Engineering, 25240 Erzurum, Turkey
[3]Yuzuncu Yil University, Engineering Faculty, Department of Environmental Engineering, 65080 Van, Turkey
[4]Bayburt University, Applied Science Faculty, Department of Emergency Aid and Disaster Management, 69000 Bayburt, Turkey

ABSTRACT

The present work aims to investigate the removal of three cationic dyes (Basic Orange 2, Basic Yellow 2 and Basic Violet 3) from aqueous solutions by montmorillonite under various experimental conditions. Cationic dyes were selected Basic Orange 2 (BO2), Basic Yellow 2 (BY2) and Basic Violet 3 (BV3). The effects of pH, initial dye concentration, adsorbent dose, agitation speed and ionic strength, on the removal of dyes were studied. According to the experiments results, it was shown, that maximum removal was achieved in less than 45 min. The results indicate that the montmorillonite can be used as a low cost alternative according to other adsorbents in the removal of dyes from wastewater. The maximum adsorption efficiency levels attained were as follows: 95.849% BO2, 99.562% BY2 and 99.169% BV3 onto montmorillonite at pH: 5.0, 100 mg/L initial dye concentration, 0.75g/L clay dosage, 300 rpm agitation speed, 0 M NaCl ionic strength and 293 K, reaction time of 45 min.

KEYWORDS:
Adsorption, Dye removal, Montmorillonite, Cationic dye, pH

INTRODUCTION

When dyestuff industry wastewaters is discharged to the receiving environment without treatment in addition to the creation of visual negativity, it can be permanent environment pollution. Because, dyestuff industry wastewater contains toxic organic substances. Therefore, this type of wastewater must be treated as needed to limit before being discharged the receiving environment [1].

In the literature, there are many treatment methods for wastewater to treatment dyestuff wastewater. These treatment methods includes many methods such as adsorption [2], electro-fenton [3], electrocoagulation [4], ozonation [5], electro oxidation [6], chemical coagulation [7] and biosorption [8] etc.

Adsorption of these methods has widespread application. Adsorption method appears as a feasible method in cases where the adsorbent is quite cheap and abundant [9]. The treatment of dyestuff industry wastewater by adsorption method has been used in many adsorbent types. These types of adsorbents can be sorted such as clay [10, 11], activated carbon [12, 13], fly ash [14], chitosan and adsorbents obtained from the evaluation of various industrial wastes [15].

Clays which of these types of adsorbents are silicate type adsorbents and clay are used widely in the treatment of dyestuff wastewater. The most commonly used types of clay can be classified as montmorillonite, sepiolite, illite, vermiculite, zeolite, kaolin and bentonite. Montmorillonite, a member of the smectite family, is 2:1 clay, meaning that it has 2 tetrahedral sheets sandwiching a central octahedral sheet. The particles are plate-shaped with an average diameter of approximately 1 micrometer. Montmorillonite clay minerals are used in many areas such as detergents, ceramics, cosmetics and paper industries [16, 17].

In this study, the treatment of Basic Orange 2 (BO2), Basic Yellow 2 (BY2) and Basic Violet 3 (BV3) dyestuff from synthetic wastewater were investigated using montmorillonite clay with adsorption method. Experimental parameters are selected as initial pH of the wastewater, initial dyestuff concentration, the amount of adsorbent, the agitation speed and ionic strength. The changes between the experimental parameters and wastewater removal efficiency were examined.

MATERIALS AND METHODS

The montmorillonite sample was obtained from Süd-Chemie Processing Plants (Balikesir, Turkey). The chemical composition of the montmorillonite found in Turkey was given in Table 1. The synthetic dye solutions of Basic Orange 2 (BO2),

Basic Yellow 2 (BY2) and Basic Violet 3 (BV3) (analytical grade from Merck Co) were prepared in double-distilled water. The parameters chosen in the experiments were given in Table 2. To remove dyes from aqueous solution was selected a batch system as reaction vessel. Removal time was set as 45 min result of the preliminary tests. The selected dyes was shown in Figure 1. BO2, BY2 and BV3 dye concentrations in the sample solution were determined using a spectrophotometer (Spekol-1100 UV–Vis spectrophotometer) at a wavelength of 433 nm, 455 nm and 584 nm, respectively. Calibration curves were plotted between absorbance and concentration of the dye solution

TABLE 1
Chemical composition of montmorillonite (a) and physicochemical properties of montmorillonite (b)

(a)

Component	Weight, %
SiO_2	49.40
Al_2O_3	19.70
MgO	0.27
CaO	1.50
Fe_2O_3	0.30
Na_2O	1.50
H_2O	25.67

(b)

Parameters	Value
Color	White
Density / g cm^{-3}	2.3 – 3
Transparency	Semi-transparent and opaque
Brightness	Matt
Surface Area / m^2 g^{-1}	95.36
Reflective index	1 – 2

TABLE 2
Experimental parameters

Parameter	Study Ratio
Initial dye concentration mg/L	50, 100 and 200
Adsorbent dosage (g/L)	0.50, 0.75, 1.00 and 1.50
pH	3.0, 5.0, 7.0 and 9.0
Stirring speed (rpm)	100, 200, 300 and 400
Ionic strength (M NaCl)	0, 0.001, 0.010 and 0.100

The percentage of dyes removed were calculated by the following equation:

$$\%\,efficiency = \left(\frac{C_0 - C_t}{C_0}\right) \times 100 \quad (1)$$

The adsorption capacity of dyes were calculated for kinetic studies by the following equation:

$$q_t = \frac{(C_0 - C_t).V}{m} \quad (2)$$

where C_0 (mg/L) and C_t (mg/L) are the dye concentrations at initial and after time t, respectively. V is the volume of the solution (L) and m is the mass (g) of montmorillonite. q_t is the amount of dyes adsorbed at equilibrium, (mg/g).

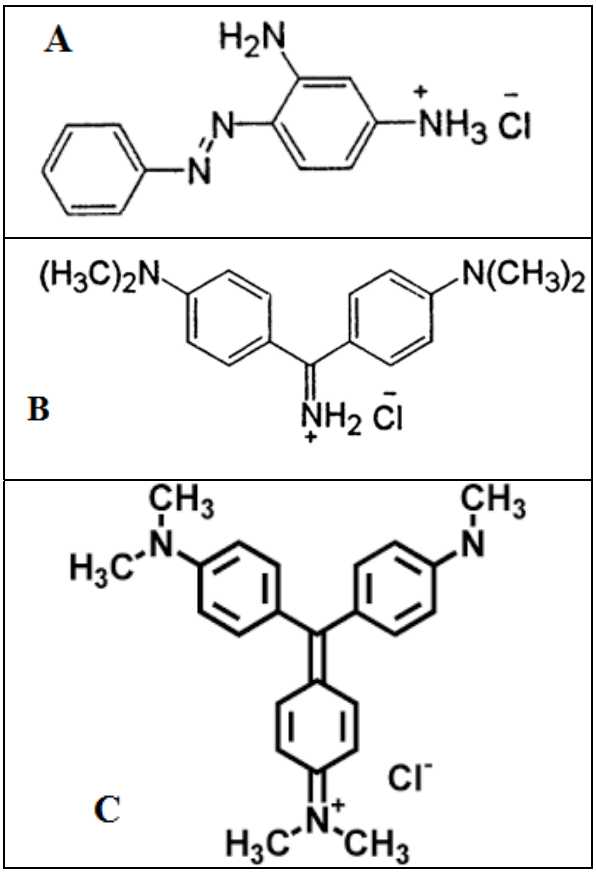

FIGURE 1
The structure of cationic dyes (A: Basic Orange 2, B: Basic Yellow 2, C: Basic Violet 3)

RESULT AND DISCUSSION

Effect of Initial pH. In order to establish the effect of pH on the adsorption of BO2, BY2 and BV3 onto clay, the batch equilibrium studies at different pH values were carried out in the range of 3.0 – 9.0 for a constant adsorbent dosage of 0.75 g/L, 300 rpm agitation speed, ionic strength of 0 M NaCl and initial dye concentrations of 100 mg/L at 293 K (Fig. 2). pH is an important parameter in controlling the adsorption of dye onto adsorbent. The removal efficiency of dye adsorbed increased for BO2, BY2 and BV3 from 95.066% to 96.598%, from 99.534% to 99.684% and from 97.984% to 99.634% by variation in pH from 3.0 to 9.0, respectively. Generally, for cationic dyes, the adsorption capacity have the tendency to increase as initial pH

of the solution increases. When solution pH increases, high OH^- ions accumulate on the adsorbent surface. Therefore, electrostatic interaction between negatively charge adsorbent surface and cationic dye molecule increases the adsorption [2, 18].

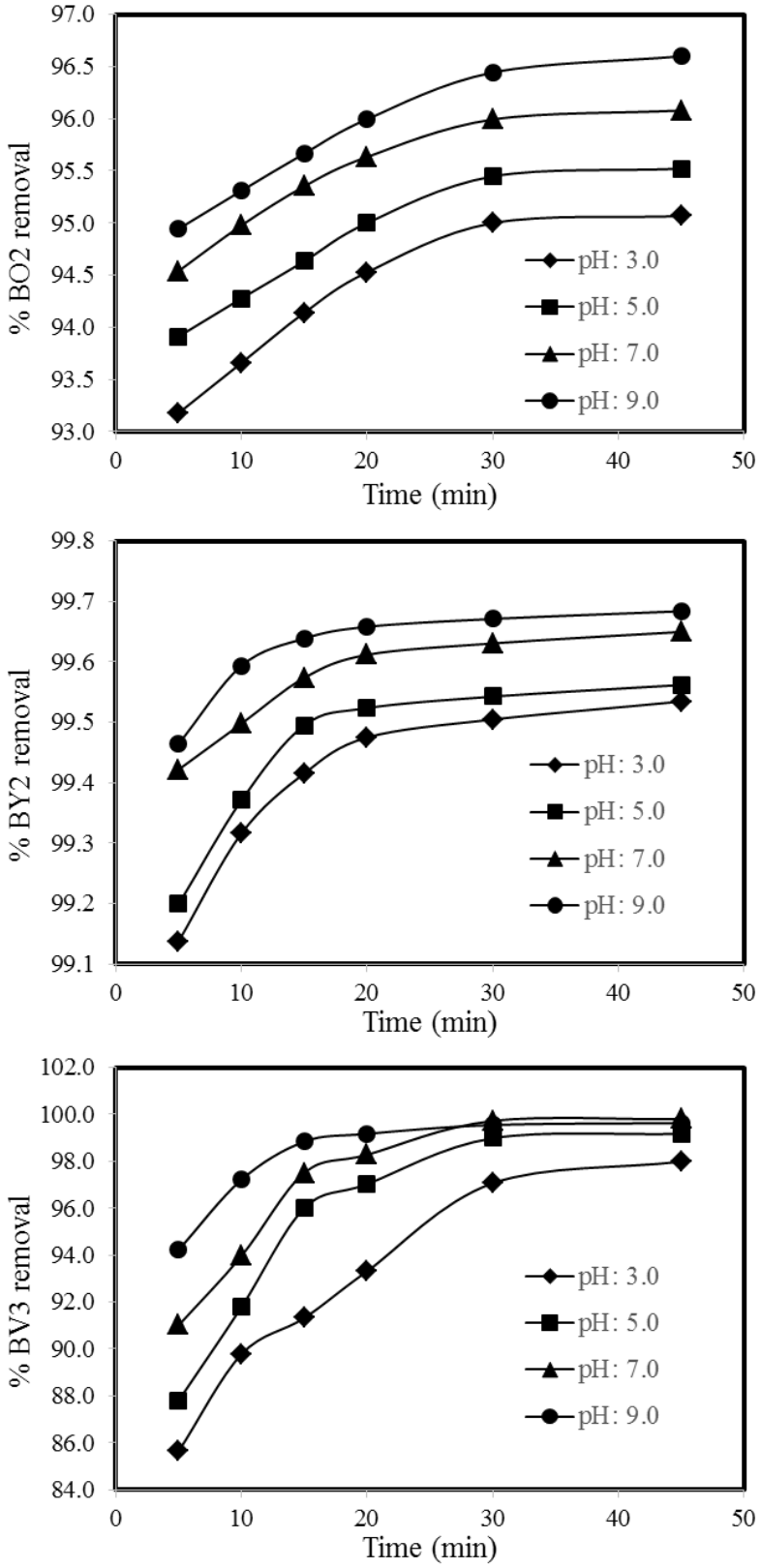

FIGURE 2

Effect of solution pH on dye adsorption on montmorillonite (Conditions: initial dye concentration 100 mg/L, adsorbent dosage 0.75 g/L, temperature 293 K, agitation speed 300 rpm, ionic strength 0 M NaCl)

Effect of initial dye concentration. The effect of initial concentrations on the percentage removal of BO2, BY2 and BV3 was shown in Fig. 3. The experiments were conducted at pH 5.3, 300 rpm agitation speed, 0.75 g/L adsorbent dosage, 0 M NaCl ionic strength and 293 K for three dyes. The concentrations of three dyes were varied for 50, 100 and 200 mg/L. The results showed that the value of percentage removal of BO2 decreases from 95.520% to 83.039%, of BY2 decreases from 99.608% to 88.318% and of BV3 decreases from 99.758% to 80.934% by montmorillonite, respectively. Thus, the percentage removal is a direct function of initial concentrations of dyes. This may probably be due to the limited number of available active sites on the surface of montmorillonite to accommodate higher concentration of dyes. Similar results is available in the literature [19].

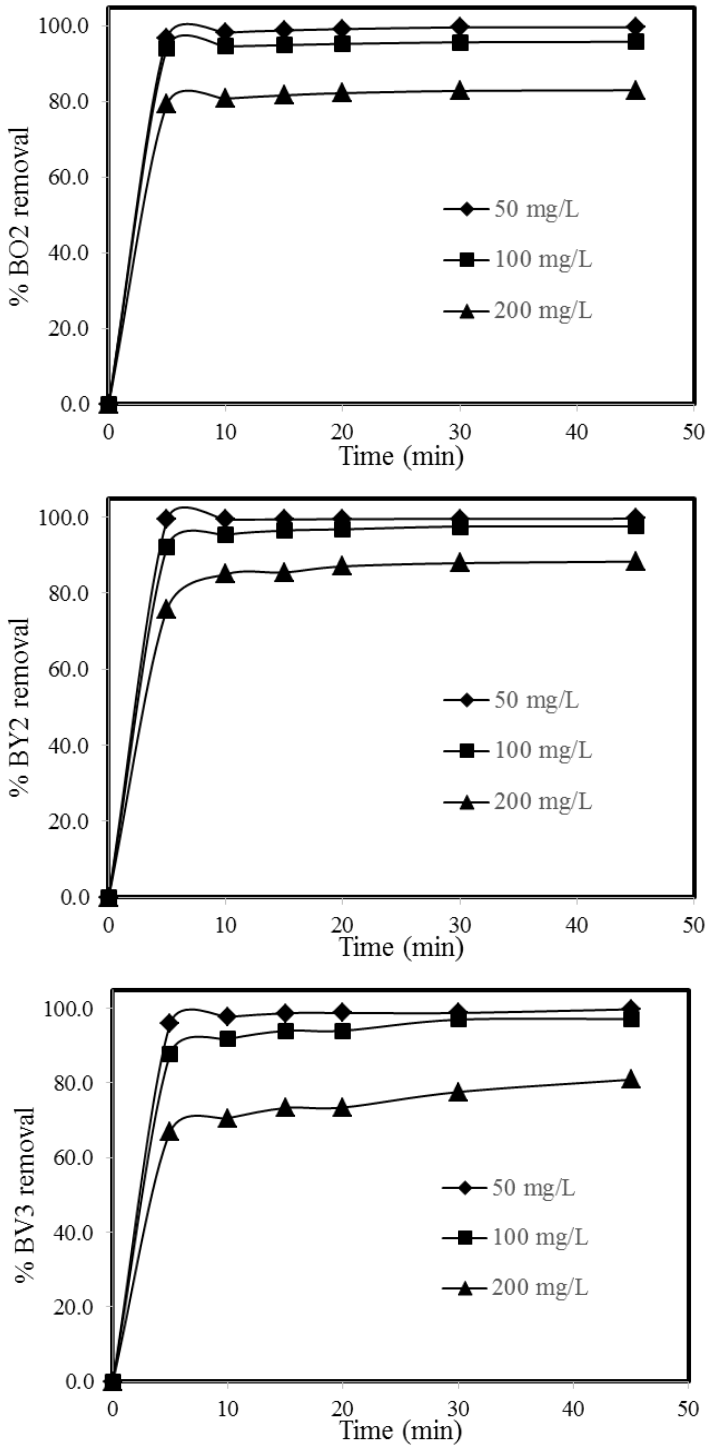

FIGURE 3
Effect of initial dye concentration on dye adsorption on montmorillonite (Conditions: agitation speed 300 rpm, adsorbent dosage 0.75 g/L, temperature 293 K, ionic strength 0 M NaCl, solution pH: 5.0)

Effect of adsorbent dose. The adsorption of cationic dyes were studied by changing the quantity of adsorbent and the parameters were as follows: 0.50, 0.75, 1.00 and 1.50 g/L at 293K temperature, pH: 5.0, 100 mg/L the initial dyestuff concentration, 0 M NaCl and 300 rpm stirring speed. Obtained results were showed in Figure 4. It is obvious as with increasing amount the adsorbent dosage for adsorption of cationic dyes onto montmorillonite increases which results in an increase in removal efficiency. The decrease in adsorption capacity with an increase in the adsorbent concentration could be ascribed to the fact that some of the adsorption sites remained unsaturated during the process [20, 21].

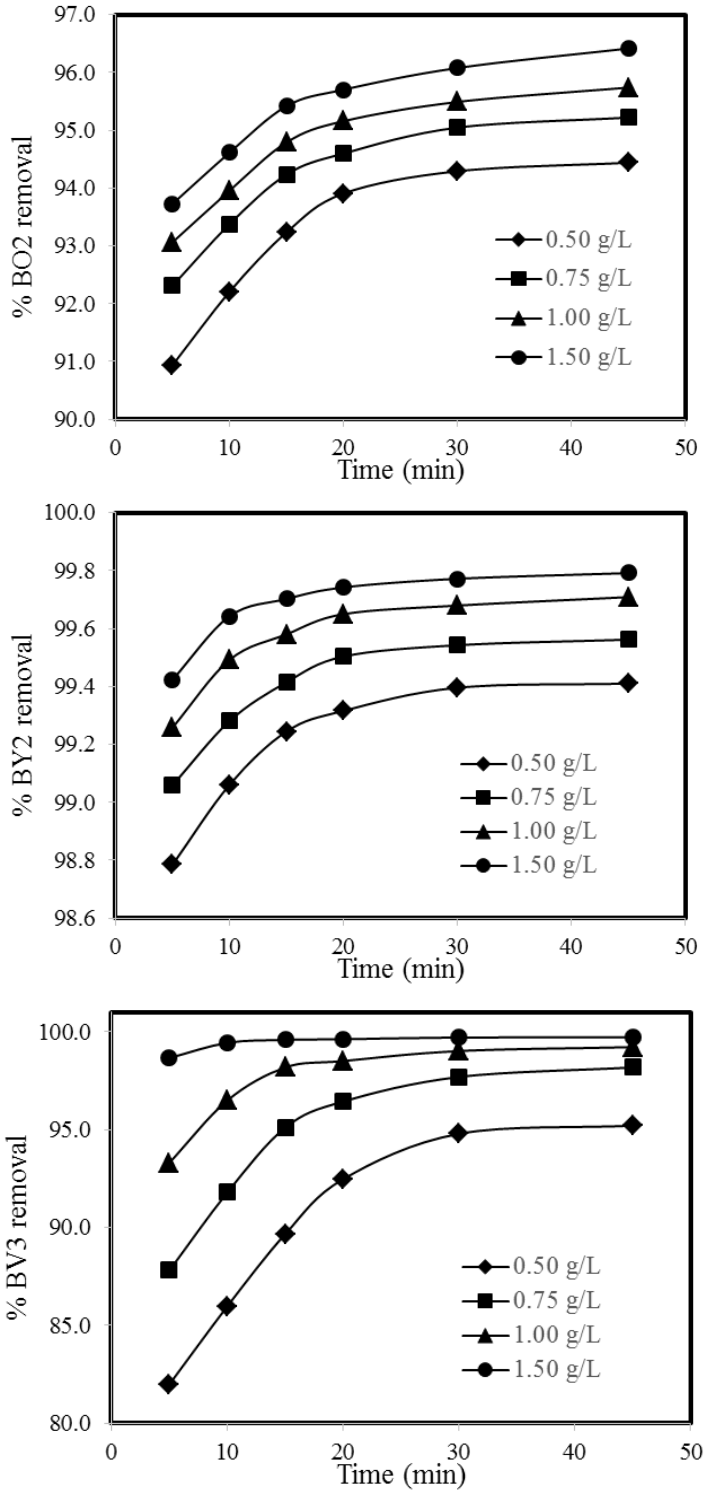

FIGURE 4

Effect of adsorbent dosage on dye adsorption on montmorillonite (Conditions: initial dye concentration 100 mg/L, agitation speed 300 rpm, temperature 293 K, ionic strength 0 M NaCl, solution pH: 5.0)

Effect of agitation speed. 100, 200, 300 and 400 rpm agitation speeds were used in conjunction with initial dye concentrations of 100 mg/L at 45 minutes, adsorbent dose 0.75 g/L, temperature 293K, 0 M NaCl and pH; 5.0 were kept constant. The results were showed in Fig. 5. The sorption is influenced by mass transfer parameters. When the agitation speed is low, the greater contact time is required to attend the equilibrium. With increasing the agitation speed , the rate of diffusion of dye molecules from bulk liquid to the liquid boundary layer surrounding the particle become higher because of an enhancement of turbulence and a decrease of thickness of the liquid boundary layer [22, 23]

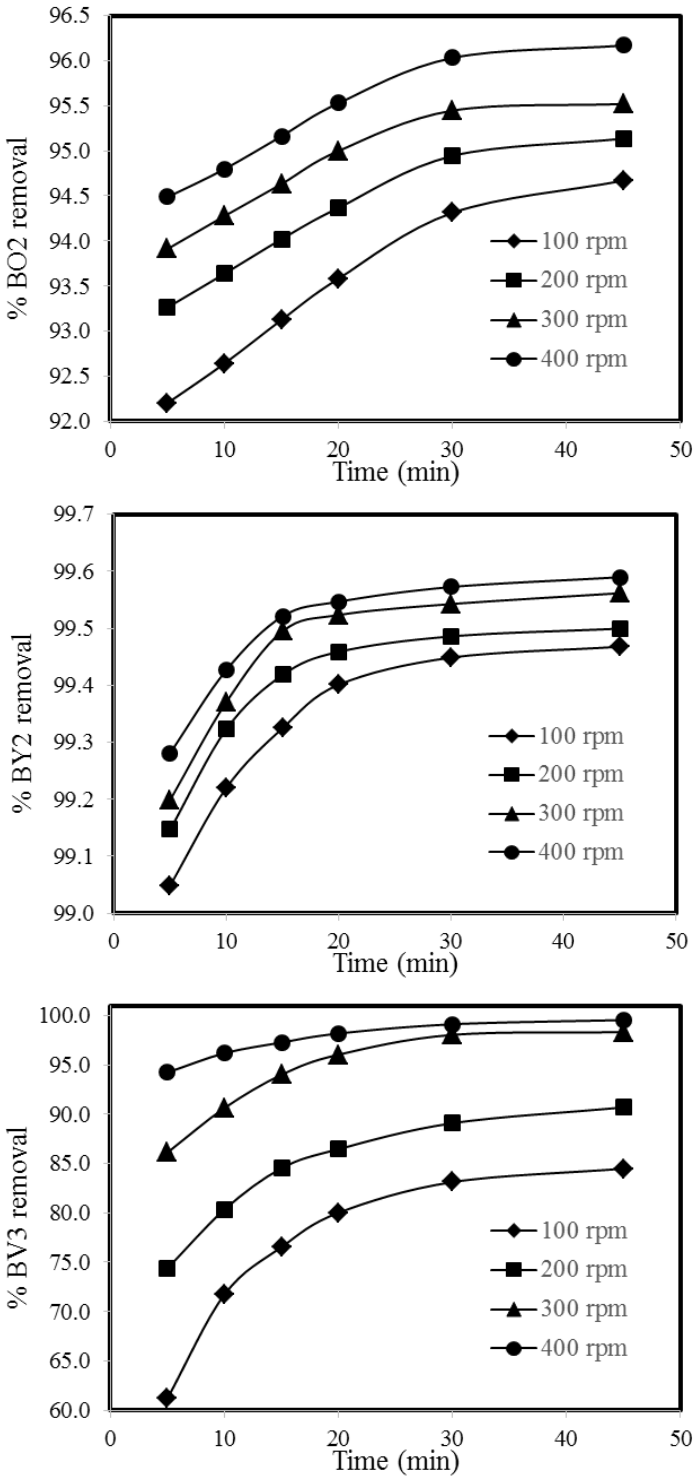

FIGURE 5

Effect of agitation speed on dye adsorption on montmorillonite (Conditions: initial dye concentration 100 mg/L, adsorbent dosage 0.75 g/L, temperature 293 K, ionic strength: 0 M NaCl, solution pH: 5.0)

Effect of ionic strength. The effect of ionic strength on cationic dye removal was shown in Fig. 6. The removal of cationic dye as BO2, BY2 and BV3 increased slightly increasing ionic strength from 0 M NaCl to 0.100 M NaCl at 293 K, 300 rpm agitation speed, 0.75g/L adsorbent dosage, 100 mg/L initial dye concentration and pH: 5.0. It was seen from Fig. 6 that when clay for BO2 was used with an increase in ionic strength from 0 M to 0.100 M NaCl, the removal efficiency increased from 95.520% to 96.196% for the initial dye concentration of 100 mg/L; in the case of BY2 and BV3, the efficiency increased from 99.562% to 99.686% and from 99.169% to 99.568% for the same experimental conditions [24].

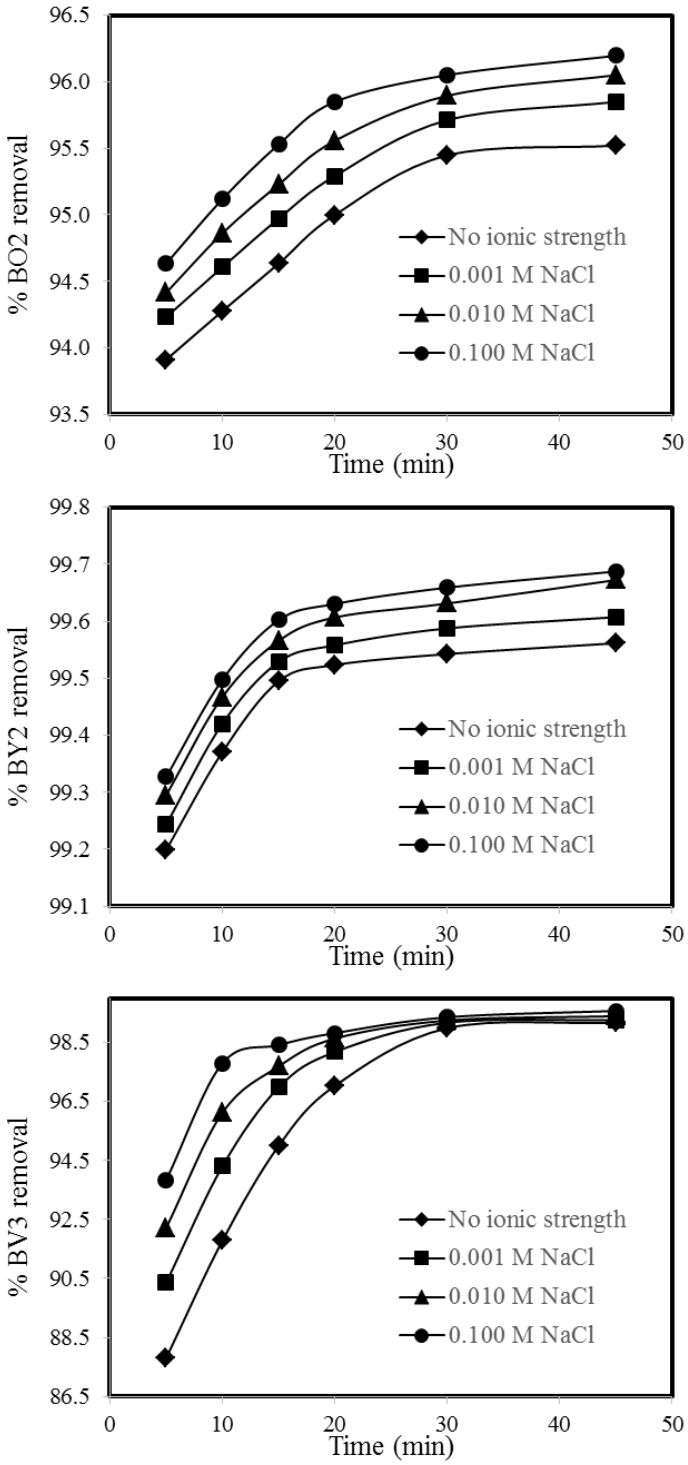

FIGURE 6

Effect of ionic strength on dye adsorption on montmorillonite (Conditions: initial dye concentration 100 mg/L, adsorbent dosage 0.75 g/L, temperature 293 K, agitation speed 300 rpm, solution pH: 5.0)

CONCLUSION

Removal of cationic dye from synthetic aqueous solution was agitation speed, ionic strength, initial pH value and clay dose. With increasing in initial dye concentration decreases removal efficiency but the percent removal decreases with the increase in initial dye concentration. According to experimental results of cationic dyes adsorption using montmorillonite clay, the selectivity sequence could be given as BY2 > BV3 > BO2 at pH: 5.0, 100 mg/L initial dye concentration, 0.75g/L, 300 rpm agitation speed, 0 M NaCl ionic strength and 293 K of synthetic aqueous solutions.

REFERENCES

[1] Kaur, S., Rani, S. and Mahajan, R. K. (2013) Adsorption Kinetics for the Removal of Hazardous Dye Congo Red by Biowaste Materials as Adsorbents. J. Chem. 2013, 12p.

[2] Weng, C.-H. and Pan, Y.-F. (2007) Adsorption of a cationic dye (methylene blue) onto spent activated clay. J. Hazard. Mater. 144, 355-362.

[3] Panizza, M. and Cerisola, G. (2009) Electro-Fenton degradation of synthetic dyes. Water Res. 43, 339-344.

[4] Yilmaz, A.E. (2012) Determination of the optimum conditions in the removal of color from synthetic textile wastewater using electrocoagulation method. Fresen. Environ. Bull. 21, 1052-1059.

[5] Kasiri, M.B., Modirshahla, N. and Mansouri, H. (2013) Decolorization of organic dye solution by ozonation; Optimization with response surface methodology. Int. J. Ind. Chem. 4, 1-10.

[6] Ramírez, C., Saldaña, A., Hernández, B., Acero, R., Guerra, R., Garcia-Segura, S., Brillas, E. and Peralta-Hernández, J.M. (2013) Electrochemical oxidation of methyl orange azo dye at pilot flow plant using BDD technology. J. Ind. Eng. Chem. 19, 571-579.

[7] Rodrigues, C.S.D., Madeira, L.M. and Boaventura, R.A.R. (2012) Treatment of textile dye wastewaters using ferrous sulphate in a chemical coagulation/flocculation process. Environ. Technol. 34, 719-729.

[8] Bagda, E. and Bagda, E. (2012) Removal of Basic Blue and Crystal Violet with a Novel Biosorbent: Oak Galls. J. Environ. Protect. Ecol. 13, 517–531.

[9] Janoš, P., Buchtová, H. and Rýznarová, M. (2003) Sorption of dyes from aqueous solutions onto fly ash. Water Res. 37, 4938-4944.

[10] Guiza, S., Bagane, M., Al-Soudani, A.H. and Amore, H.B. (2004) Adsorption of basic dyes onto natural clay. Adsorp. Sci. Technol. 22, 245-256.

[11] Koumanova, B. and Jitaru, M. (2007) Adsorption on natural materials from Balkan area – alternative methods applied for the environmental protection. J. Environ. Protect. Ecol. 8, 35-42.

[12] Malik, P.K. (2004) Dye removal from wastewater using activated carbon developed from sawdust: adsorption equilibrium and kinetics. J. Hazard. Mater. 113, 81-88.

[13] Secula, M.S., Cretescu, I. and Diaconu, M. (2014) Adsorption of Acid Dye Eriochrome Black T from Aqueous Solutions onto Activated Carbon. Kinetic and Equilibrium Studies. J. Environ. Protect. Ecol. 15, 1583–1593.

[14] Ugurlu, M. and Karaoglu, M.H. (2011) Adsorption of ammonium from an aqueous solution by fly ash and sepiolite: Isotherm, kinetic and thermodynamic analysis. Micropor. Mesopor. Mater. 139, 173-178.

[15] Yilmaz, A.E., Fil, B.A., Bayar, S. and Karcıoğlu Karakaş, Z. (2015) A new adsorbent for fluoride removal: The utilization of sludge waste from electrocoagulation as adsorbent. Global Nest J. 17, 186-197.

[16] Tsai, W.-T., Hsu, H.-C., Su, T.-Y., Lin, K.-Y., Lin, C.-M. and Dai, T.-H. (2007) The adsorption of cationic dye from aqueous solution onto acid-activated andesite. J. Hazard. Mater. 147, 1056-1062.

[17] Rafatullah, M., Sulaiman, O., Hashim, R. and Ahmad, A. (2010) Adsorption of methylene blue on low-cost adsorbents: A review. J. Hazard. Mater. 177, 70-80.

[18] Tahir, S. S. and Rauf, N. (2006) Removal of a cationic dye from aqueous solutions by adsorption onto bentonite clay. Chemosphere. 63, 1842-1848.

[19] Fil, B.A. and Özmetin, C. (2012) Adsorption of Cationic Dye from Aqueous Solution by Clay as an Adsorbent: Thermodynamic and Kinetic Studies. J. Chem. Soc. Pakistan. 34, 896-906.

[20] Patil, S., Deshmukh, V., Renukdas, S. and Patel, N. (2011) Kinetics of adsorption of crystal violet from aqueous solutions using different natural materials. Inter. J. Environ. Sci. 1, 1116-1134.

[21] Fil, B.A., Yilmaz, M.T., Bayar, S. and Elkoca, M.T. (2014) Investigation of adsorption of the dyestuff astrazon red violet 3rn (basic violet 16) on montmorillonite clay. Brazilian J. Chem. Eng. 31, 171-182.

[22] Jadhav, D.N. and Vanjara, A.K. (2004) Adsoprtion of kinetic study: Removal of dyestuff effluent using sawdust, polymerized sawdust and sawdust carbon-II. Indian J. Chem. Techn. 11, 42-50.

[23] Fil, B.A., Karakas, K.Z., Boncukcuoglu, R. and Yilmaz, A.E. (2013) Removal of cationic dye (Basic Red 18) from aqueous solution using natural Turkish clay. Global Nest J. 15, 529-541.
[24] Jirekar, D.B., Pathan, A.A., and Farooqui, M. (2014) Adsorption studies of Methylene blue dye from aqueous solution onto phaseolus aureus biomaterials. Oriental J. Chem. 30, 1263-1269.

Received: **13.01.2018**
Accepted: **01.03.2019**

CORRESPONDING AUTHOR

Baybars Ali Fil
Balikesir University, Engineering Faculty,
Department of Environmental Engineering,
10145 Balikesir – Turkey

e-mail: baybarsalifil2@gmail.com

© by PSP Volume 28 – No. 5/2019 pages 3667-3672 Fresenius Environmental Bulletin

ENVIRONMENTAL IMPACTS AND SUSTAINABILITY OF IRRIGATION SCHEMES IN NORTHERN GHANA: A SURVEY FOR GOLINGA AND BOTANGA COMMUNITIES

Mohammed Alhassan[1], Hakan Buyukcangaz[2,*]

[1]Bursa Uludag University, Institute of Natural Sciences, 16059, Bursa, Turkey
[2]Bursa Uludag University, Faculty of Agriculture, Department of Biosystems Engineering, 16059, Bursa, Turkey

ABSTRACT

Most farmers in sub-Saharan Africa live in areas with relatively abundant water resources. The availability of these water resources, however, is extremely seasonal because of the patterns of the annual rain season(s) and the increasing effects of climate change all over the world. A survey was conducted at Golinga and Botanga irrigation schemes in Northern Ghana where 200 respondents were interviewed. The objectives of this study include: (i) to assess the management and sustainability of irrigation projects, (ii) to find out the impact of the irrigation projects on rural communities' development, (iii) to find out the challenges that hinders farmers from effectively using irrigation water from the perspective of farmers and to find the possible solutions to the challenges.

38 and 40% of respondents from Golinga and Botanga irrigation schemes respectively agreed that cropping areas have moderately expanded due to the presence of irrigation scheme however, 52 and 39% of respondents from both schemes respectively indicated that the presence of the irrigation scheme to them has little impact in helping farmers expand their cropping areas. There was also moderate increase in crop yields in both communities due to the constant water supply to farmers obtained from irrigation projects. The study shows that the major challenge that hinders farmers from using irrigation water is the high cost of renting irrigable land for farming in the irrigation schemes indicated by a response of 47 and 64% amongst farmers in Botanga and Golinga irrigation schemes respectively.

The study suggests that the need for relevant stakeholders to; revise the cost of renting irrigable lands, acquire and adopt the use of simple and affordable technologies (machines), implement reforms and policies to reduce land consolidation and fragmentation, organize and mobilize farmers in farmer cooperatives to promote collective marketing and organize capacity building sessions for farmers regarding the project sustainability.

KEYWORDS:
Northern Ghana, irrigation, Golinga and Botanga communities

INTRODUCTION

Most farmers in Sub-Saharan Africa (SSA) live in areas with relatively abundant water resources. Large areas of the continent receive more than 1,000 mm of rain each year and possess significant groundwater resources with high rates of recharge. The availability of these water resources, however, extremely seasonal because of the patterns of the annual rainy season(s) and the increasing effects of climate change all over the globe, and most areas in SSA experience significant fluctuations not only in rainfall but also in groundwater and surface water availability [1].

Ghana is endowed with sufficient water resources, and estimates of Ghana's irrigation potential range from 0.36 to 2.9 million hectares depending on the degree of water control [2]. However, the country faces significant variability in water resources, both spatially and temporally, such as periodic floods and droughts, and uneven distribution of annual precipitation that, on average, is 283.2 billion m^3/year. The dependence on rainfed agriculture, particularly in the north, means that even though production of the major staple food crops is adequate in most years, seasonal food insecurity is widespread [3]. From the above background, therefore, this study aims at assessing the management and sustainability of irrigation projects, finding out the impact of the irrigation projects on rural communities' development, finding out the challenges that hinder farmers from effectively using irrigation water from the perspective of farmers, and to find the possible solutions to the challenges.

MATERIALS AND METHODS

Description of Study Area. Ghana is located between Ivory Coast to the west and Togo to the east. To the north is Burkina Faso, and the south is the Gulf of Guinea. It is only a few degrees top of the equator. Due to this fact, Ghana climate is usually warm and humid depending on the month. The northern belt is mainly covered by low scrub or bush and grassy plains. This area is normally

known as the Savannah Belt. Golinga and Botanga irrigation schemes are located in Tolon/Kumbungu District of Northern Ghana nearby Tamale (Figure 1). While the major crops cultivated on the Golinga scheme are roselle (*Hibiscus sabdariffa* L.) and vegetable jute (*Corchorus olitorius* L.), rice (*Oryza sativa* L.) is major crop grown in Botanga scheme. Surface irrigation methods are mostly preferred by the farmers in both schemes.

Climate. Table 1 shows the average annual climate in the northern region of Ghana. The table indicates an average minimum and maximum temperatures of 22.4°C and 34.6°C respectively, an average humidity of 47%, and an average wind of 124 km/day.

Field Survey. A well-structured questionnaire comprising open and closed ended questions was used as an instrument for data collection. To have a true representative sample from the two communities, a total of two hundred (200) farmers were selected and interviewed from both Botanga and Golinga, one hundred (100) farmers each from both communities. Since there are 200 farmers at both communities, the number of farmers who attended the survey is 100% of all farmers.

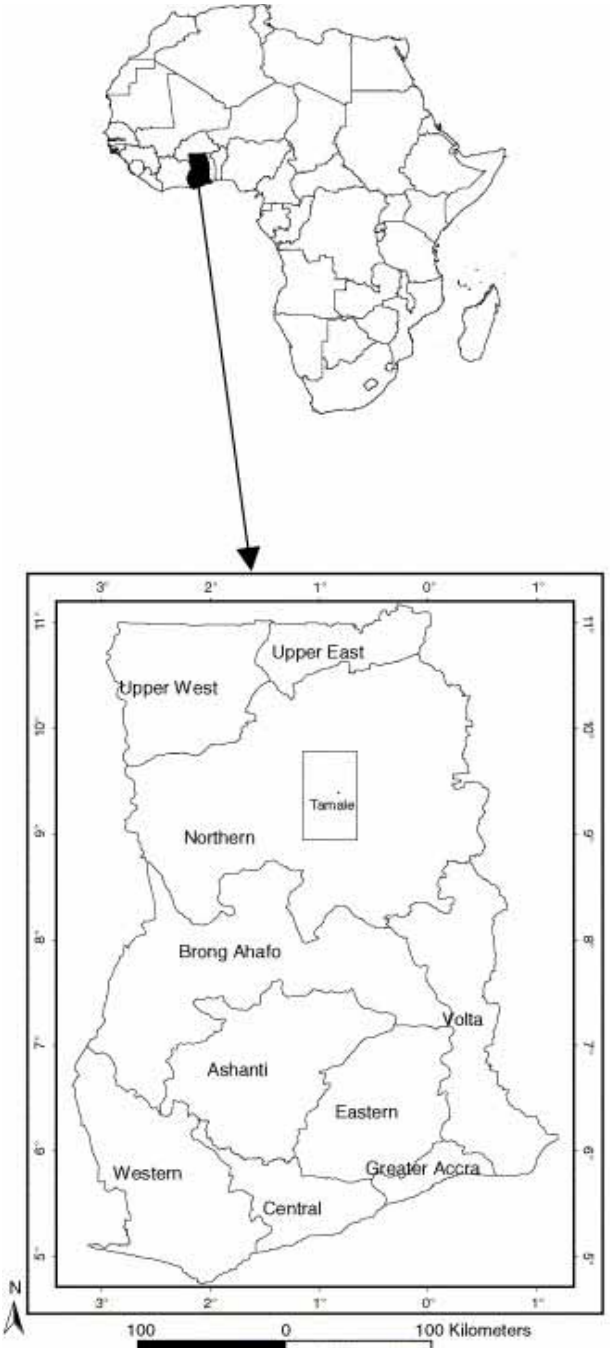

FIGURE 1
Study area in Northern Ghana [4]

TABLE 1
Long-term monthly average meteorological data for Northern Ghana [5]

Month	Min Temp (°C)	Max Temp (°C)	Humidity (%)	Wind (km/day)	Radiation (MJ/m²/day)	ET_o (mm/day)	Rain (mm)
January	20.5	35.9	19	24	20.1	3.25	4.0
February	22.8	37.4	21	168	20.1	6.50	12.0
March	24.6	37.3	31	120	21.7	5.95	48.0
April	24.8	36.2	46	120	20.9	5.65	88.0
May	24.1	34.0	54	144	21.4	5.61	112.0
June	22.6	31.4	63	120	19.2	4.61	146.0
July	22.3	30.0	66	96	17.4	3.90	142.0
August	22.0	39.7	69	96	16.2	4.42	198.0
September	21.9	30.3	69	216	17.2	4.57	231.0
October	22.0	32.6	57	96	21.3	4.71	92.0
November	21.5	35.5	39	72	21.0	4.56	14.0
December	19.9	35.2	27	216	19.5	6.59	3.0
Average	22.4	34.6	47	124	19.7	5.03	90.83

TABLE 2
Expansion of cropping area

Options	Golinga		Botanga	
	Frequency	Percentage (%)	Frequency	Percentage (%)
High	9	9	9	9
Moderately	38	38	40	40
Low	52	52	39	39
Very Low	1	1	12	12
Total	100	100	100	100

Pearson chi2(3) = 11.2161 Pr = 0.011

Statistical Analysis. The data collected from both primary and secondary sources were then collated, synthesized and analyzed to draw inferences and conclusions. Descriptive analysis such as frequency distribution, percentages, means and standard deviations was used interpreted the results by using SPSS Version 20. Chi-square test and Levene test were used, as the test is applied when you have two categorical variables from a single population. Both test were used to determine whether there is a significant association between the two variables. In order to sure about the accuracy of the results, the independent t-test was used. The independent t-test, also called the two sample t-test, independent-samples, is an inferential statistical test that determines whether there is a statistically significant difference between the means in two unrelated groups. For a 95% confidence level (which means that there is only a 5% chance of your sample results differing from the true population average), a good estimate of the margin of error (or confidence interval) is given by $1/\sqrt{N}$, where N is the number of participants or sample size [6]. All statistical analyses were not given in the paper.

RESULTS

Data was collected from beneficiaries who use the irrigation schemes and those who do not. Of the total sampled size at Botanga irrigation scheme, 81% of farmers were found enrolled on the irrigation scheme while 19% were not in the scheme at all due to the cost of renting irrigation facility, lack of technical support from the irrigation authority about irrigation operation, and absence of a ready market for their products whereas, in Golinga irrigation scheme, 77% of the farmers were enrolled on the irrigation dam as against to 23%. Physical, social, environmental and economic impacts of irrigation scheme on both communities and the general well-being of farmers were given in this section.

Impacts of irrigation on food security. Impacts of irrigation scheme on food security in both communities include expansion of cropping area, increase in cropping intensity, increase in crop diversification, and increase crop productivity. 38 and 40% of respondents from Golinga and Botanga irrigation schemes respectively agreed that crop areas have moderately expanded due to the presence of irrigation scheme however, 52 and 39% of respondents from both schemes respectively indicated that the presence of the irrigation scheme to them has little impact in helping farmers expand their cropping areas. Since the P-value (0.011) is less than the significance level (0.05), ($p = 0.011 < 0.05$) we cannot accept the null hypothesis. Thus, we conclude that there is a relationship between increases in crop intensity in both communities. (Table 2).

Based on Levene's test to check the homogeneity of variances, p-value is greater than the significance level ($p= 0.398<0.05$). Therefore, we can accept the null hypothesis, hence we can say with

TABLE 3
Independent-samples T test for expansion in crop area

	Levene's Test for Equality of Variances		t-test for Equality of Means						
	F	Sig.	t	df	Sig. (2-tailed)	Mean Difference	Std. Error Difference	95% Confidence Interval of the Difference	
								Lower	Upper
Equal variances assumed	4.478	.036	.848	198	.398	.09000	.10617	-.11937	.29937
Equal variances not assumed	-	-	.848	190.5	.398	.09000	.10617	-.11942	.29942

TABLE 4
Improved nutrition, health and calorie intake

Options	Golinga		Botanga	
	Frequency	Percentage (%)	Frequency	Percentage (%)
High	3	3	2	2
Moderately	27	27	44	44
Low	56	56	48	48
Very Low	14	14	6	6
Total	100	100	100	100

Pearson chi2(3) = 8.0858 Pr = 0.044

TABLE 5
Loss of soil fertility

Options	Golinga		Botanga	
	Frequency	Percentage (%)	Frequency	Percentage (%)
High	27	27	5	5
Moderately	59	59	54	54
Low	8	8	26	26
Very Low	5	5	15	15
Total	100	100	100	100

Pearson chi2(3) = 29.8714 Pr = 0.000

95% confidence level there is no difference in expansion of cropping area in both communities.

Cropping intensity refers to raising a number of crops from the same field during one agricultural year. Survey results show that 33 and 23% of respondents from Golinga and Botanga irrigation projects respectively agreed that crop intensity have highly increased due to the presence of irrigation scheme. Since the P-value (0.000) is less than the significance level (0.05), ($p< 0.05$) based on Pearson chi-square test, we cannot accept the null hypothesis. Thus, we conclude that there is a relationship crop intensity and irrigation schemes on both communities.

38 and 51% of the respondents from Golinga and Botanga irrigation schemes respectively indicated that there was moderate increase in crop diversification by irrigation schemes. Since the P-value (0.007) is less than the significance level (0.05), ($p<0.05$), we cannot accept the null hypothesis. Thus, we conclude that there is a relationship between irrigation scheme and crop diversification.

Socioeconomic impacts. Socioeconomic problems from irrigation scheme on both communities include employment generation and improved nutrition, health, and calorie intake. Survey results show that 10.5 and 3.5% of respondents from Golinga and Botanga irrigation projects respectively agreed that there has been high increase in employment opportunities in the area due to the presence of irrigation schemes. Based on chi-square test, we conclude that there is a relationship between employment generations and irrigation schemes in both communities. 27 and 44% of respondents from Golinga and Botanga irrigation projects respectively indicated a moderate improvement in nutrition, health and calorie intake due to irrigation schemes. Since the P-value (0.044) is less than the significance level (0.05), ($p<0.05$), we cannot accept the null hypothesis. Thus, we conclude that there is a relationship in both Golinga and Botanga in terms of improved nutrition, health and calorie intake (Table 4).

Environmental impacts of irrigation projects. Environmental problems related to irrigation scheme on both communities include people displaced because of irrigation development, loss of soil fertility, surface water pollution, groundwater pollution, and water borne diseases. 65 and 39% of respondents from Golinga and Botanga communities are believing a moderate rate of displacement of people due to irrigation schemes, respectively. 59 and 54% of respondents from Golinga and Botanga communities respectively indicated a moderate loss in soil fertility as continuous irrigation causes leaching of soil nutrients making the topsoil deficient of soluble minerals as it is given in Table 5. Since the P-value (0.000) is less than the signifi-

cance level (0.05), ($p<0.05$), we conclude that there is a relationship between soil fertility and irrigation schemes in both communities.

13 and 40% of respondents from Golinga and Botanga communities indicated a moderate rate of groundwater pollution due to irrigation scheme, respectively. Groundwater pollution consists of salinity and various chemicals such as fertilizers, pesticides. Since the P-value (0.000) is less than the significance level (0.05), ($p<0.05$), there is relationship between groundwater pollution and irrigation schemes in both communities (Table 6).

Key constraints to adoption of irrigation technologies. The major challenge that hinders farmers from using irrigation water is the high cost of renting irrigable land for farming in the irrigation schemes indicated by a response of 47 and 64% amongst farmers in Botanga and Golinga irrigation schemes, respectively. 24 and 16% of respondents in both schemes respectively indicated that the absence of adequate technical support hinders farmers from using irrigation water. The absence of adequate machines (technology) is major constraint for adoption irrigation based on 19 and 7% of respondents in both schemes. 10 and 13% of respondents in both communities respectively indicated that the absence of a ready market for agriculture produce in the area is a key constraint for farmers in using irrigation water, therefore, appropriate solutions are important to ensure that farmers effectively utilize the irrigation schemes (Figure 2).

DISCUSSION AND CONCLUSION

A field survey was carried out to evaluate the sustainability of Golinga and Botanga irrigation schemes. Irrigation has major impact on food security by expansion of cropping areas, increase in crop productivity, cropping intensity, and crop diversification. The study shows that there is a relationship between increase in crop productivity (P-value $0.000<0.05$), cropping intensity (P-value $0.000<0.05$), crop diversification (P-value $0.007<0.05$), expansion of cropping area (P-value $0.011<0.05$), employment generation (P-value $0.000<0.05$), and improvement in nutrition, health, and calorie intake (P-value $0.044<0.05$), which is due to the presence of irrigation projects which makes crop production possible throughout the year.

Of the gross estimated 1.9 million ha of potentially irrigable area, only less than 2 percent has been developed [2]. The study indicates challenges that hinder farmers from effectively using or benefiting from the irrigation projects which include the high cost of renting irrigable land, inadequate technical support, inadequate machinery, and lack of ready market for their farm products as the major challenges they face.

TABLE 6
Groundwater Pollution

Particulars	Golinga		Botanga	
	Frequency	Percentage (%)	Frequency	Percentage (%)
High	4	2.00	3	1.50
Moderately	13	6.50	40	20.00
Low	38	19.00	32	16.00
Very Low	45	22.50	25	12.50
Total	100	50.00	100	50.00

Pearson chi2(3) = 20.1261 Pr = 0.000

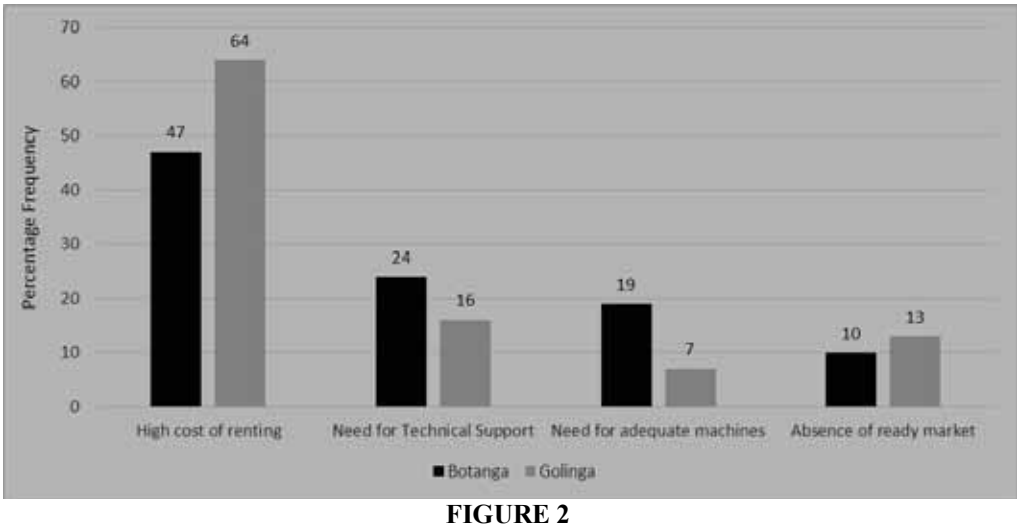

FIGURE 2
Key constraints to adoption of irrigation technologies

There is a need for policymakers and other relevant stakeholders responsible for determining the cost of renting irrigable land to revise the cost this can be done through streamlining provision of incentives to farmers benefiting from the irrigation schemes to ensure that more farmers benefit from the irrigation projects. There is also a need to use simple and affordable machines (technology) necessary for irrigation to ensure efficiency and reduce the cost of maintaining the project. There is a need to organize capacity building for farmers through seminars, conferences, and training aimed at improving farmers' knowledge on selection, management, operation and maintenance of the irrigational structures thereby enhancing its efficiency and effectiveness. There is also a need to sensitize and mobilize farmers into cooperatives to decide on which crops to grow in order to participate in collective marketing that can enable them to access better markets and have a high bargaining power for their crop products and also be in position to practice contract farming which will eventually increase their earning from agriculture and improve their standards of living.

ACKNOWLEDGEMENTS

This study is a part of the M.Sc thesis entitled 'Sustainable irrigation water management in Northern Ghana: Golinga and Botanga irrigation schemes' of Mohammed Alhassan under supervision of Assoc. Prof. Hakan Buyukcangaz at Bursa Uludag University of Turkey.

REFERENCES

[1] International Fund for Agricultural Development (IFAD). (2012) Challenges and opportunities for agricultural water management in West and Central Africa. https://www.ifad.org/documents/10180/65ed0c33-fb96-4115-a05d-24ddd6f70bf6.
[2] Namara, R.E., Horowitz, L., Nyamadi, B., Barry, B. (2011) Irrigation Development in Ghana: Past experiences, emerging opportunities, and future directions. GSSP Working Paper # 27, IFPRI.
[3] International Water Management Institute (IWMI). (2010) Banking on groundwater. Colombo, Sri Lanka.
[4] Braimoh, A.K. (2006) Random and systematic land-cover transitions in northern Ghana, Agriculture, Ecosystems and Environment. 113(1-4), 254-263.
[5] Ghana National Communication on Climate Change (2013) Climate Change Financing and Aid Effectiveness. Ghana Case Study.
[6] Niles, R. (2006) Statistics Every Writer Should Know, Journalism Help. RobertNiles.com.

Received: **09.03.2018**
Accepted: **11.03.2019**

CORRESPONDING AUTHOR

Hakan Buyukcangaz
Bursa Uludag University,
Faculty of Agriculture,
Department of Biosystems Engineering,
16059, Bursa – Turkey

e-mail: cangaz@uludag.edu.tr

© by PSP Volume 28 – No. 5/2019 pages 3673-3685 Fresenius Environmental Bulletin

MULTIVARIATE STATISTICAL ANALYSIS OF THE HEAVY METAL CONTAMINATION IN THE SOILS OF XIONGAN NEW AREA, NORTHEAST CHINA

Chang Li[1], Sanggyun Na[1,*], Kui Cai[2]

[1]College of Business Administration, Wonkwang University, 460 Iksandae-ro, Iksan 54538, Jeonbuk, Korea
[2]Institute of Geological Survey, Hebei GEO University, Shijiazhuang 050031, Hebei, China

ABSTRACT

With rapid industrial growth in China, heavy metal pollution in the soil has become increasingly critical. Thus, evaluating soil pollution is necessary to help the government combat this pollution. Herein, top and deep soil data (pH and concentrations of SiO_2, Al_2O_3, TFe_2O_3, Cu, Pb, Co, Cd, Hg, Mn, and Ni), collected from the Hebei agricultural geology project, were analyzed. The correlation and primary component (PC) analyses suggested the probable presence of natural and anthropogenic sources of metals in the study area. The enrichment factor, geoaccumulation index, and ecological risk index were used to evaluate the level of heavy metal pollution. The result of the analyses indicated that the concentrations of Cu, Pb, Cd, and Hg were higher in deep soils than in top soils in the study area. Ni, Co, and Mn (PC 1) mainly originated from natural sources, referred to as the natural group. Cu, Pb, Cd (PC 2), and Hg (PC 3) mostly originated from anthropogenic influences, referred to as anthropogenic groups. The analysis also indicated that Cu, Pb, and Cd likely originated from the mixed pollution caused by farming and traffic sources, whereas Hg possibly originated from coal-burning exhausts and atmospheric deposition. The results of the geoaccumulation index and ecological risk assessment show that the soils were unpolluted to moderately polluted and had potential ecological risk because of Hg and Cd. The average ecological risk index value (~168) of the heavy metals indicates moderate ecological risk.

KEYWORDS:
Statistical analysis, Heavy metals, Source, Contamination, Xiongan New Area

INTRODUCTION

In recent decades, environmental pollution has attracted much attention. Especially in rapidly developing China [1, 2], environmental problems, such as atmosphere, water, and soil pollution, have become difficult problems that the Chinese government urgently needs to solve. Heavy metal pollution in the soil environment has been characterized in numerous research studies as being of long duration, of wide-ranging sources, and difficult to control [3, 4, 5]. Currently, determining the source of heavy metal pollution, stopping this pollution, and purifying the polluted soil are challenging tasks in the research on heavy metal pollution of soil.

Soil heavy metals originate from natural and anthropogenic sources [5, 6]. Natural sources of heavy metals depend on the parent rock, soil composition, and the physical and chemical properties of the soil, which cause differences in regional background values. Studies have shown that soil pH, organic matter, and clay are important factors controlling the geochemical behavior of heavy metals [6, 7, 8, 9, 10, 11]. On the other hand, the amount of heavy metals released into the soil through human activities overlaps with natural sources and exceeds the natural background value, resulting in regional pollution. The anthropogenic sources of soil heavy metal pollution mainly include irrigation water, chemical fertilizers, solid waste, industrial wastewater, coal, fossil fuel combustion, and tail gas emissions [12, 13]. These anthropogenic factors lead to an increase of heavy metals in the soil, often exceeding the health standards and causing harm to humans through water and crops [14, 15, 16]. Therefore, determining whether the concentration of heavy metals in soil is from natural or anthropogenic inputs is extremely important.

Geostatistical methods are some of the most effective ways to discriminate natural from artificial sources [17, 18]. Geostatistical methods can show the spatial distribution and variation of heavy metals in the soil environment. Among various geostatistical methods, Kriging Interpolation analysis is a

multidimensional method. This method, combined with principal component analysis, had a significant effect on multiscale research. It enables examination of the spatial correlation between various variables at multiple scales and determination of the sources of heavy metals based on the grouping results of the principal component analysis [19, 20, 21].

In April 2017, in order to focus on building non-capitals, the Chinese government, adjusted Beijing by optimizing the urban layout and spatial structure of the Beijing-Tianjin-Hebei region and set up the Xiong'an National New Zone (Anxin, Rongcheng, and Xiongxian and surrounding areas). This new district is another New Area of national significance, following the Shenzhen Special Economic Zone and Shanghai Pudong New Area. One of the goals is to create a beautiful new eco-city. Therefore, management and protection of the new zone's ecological environment is particularly important. At present, most of the industrial enterprises in the New Area are non-ferrous metals, hardware, plastic products, and other enterprises, which are commonly associated with high-pollution areas.

Therefore, the primary objectives of this study were to (1) determine the total concentrations of Cu, Pb, Mn, Ni, Co, Hg, and Cd in the top and deep soils; (2) identify the natural and/or anthropogenic origins of these heavy metals using correlation and principal component analyses; (3) assess the levels of contamination by these heavy metals based on the enrichment factor (EF), geoaccumulation index (Igeo), and ecological risk index (Er); and (4) analyze the spatial distributions of these heavy metals using the Kriging Interpolation method. At present, no study has evaluated soil pollution in the New Area. Present study will provide insight into the pollution levels of heavy metals and will also provide support to the government for solving the problem of soil pollution in the New Area.

MATERIALS AND METHODS

Characteristics of the study area. The study area covers an area of about 1500 km^2 (Anxin 738.6 km^2, Xiongxian 524 km^2, Rongcheng 314 km^2) and is located in the central southern part of Heibei Province in northern China. This region is located at 115°40′–116°20′E and 38°40′–39°10′N. Plains cover the entire study area. Overall, the terrain exhibits a slight tilt from northwest to southeast. The study area has a temperate continental climate and four distinct seasons, with an average annual temperature of 12.2 °C and average annual precipitation of 500–600 mm. Owing to the effect of the Yongding River and Hutuo River alluvial fan, the parent materials of the soil in the new area include residual deposits, slope wash, and alluvium. Fluvoaquic soil is the primary soil type in the study area, with wheat and corn as the main crops.

Data and methods. In this study, a systematic grid sampling design was applied to select 388 top soil sites (2 × 2 km size; 0–20 cm) and 99 deep soil sites (4 × 4 km size; 180–200 cm) in Xiongan. At every sampling site, four to six subsamples in the top soil within a 100 m radius were taken from the upper 20 cm of soil. Visible plant detritus and any fragments were removed from the samples after air-drying at 26 °C. The subsamples were mixed thoroughly to obtain a composite sample (1 kg). First, all collected samples were air-dried, then immediately transported to the laboratory. Figure 1 indicates the locations of the sampling sites.

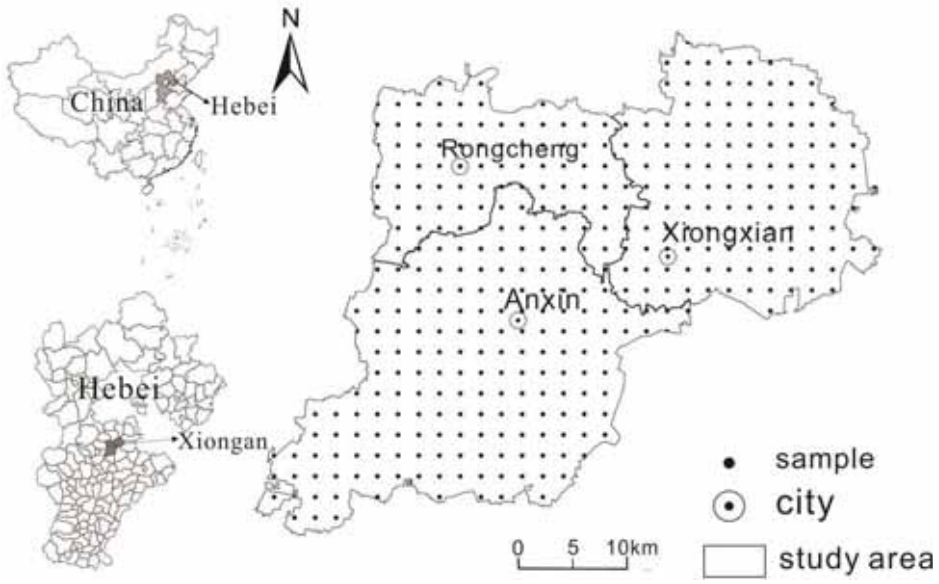

FIGURE 1
Map of the sampling sites

These samples were analyzed for pH, SiO_2, Al_2O_3, TFe_2O_3, Cu, Pb, Co, Cd, Hg, Mn, and Ni. The sample analysis methods and analysis quality control were performed according to the multi-objective geochemical analysis program reported by Ye [22]. Cu, Pb, Cd, Co, and Ni were analyzed using inductively coupled plasma mass spectrometry (ICP-MS); Al_2O_3, TFe_2O_3, SiO_2, and Mn via powder X-ray fluorescence spectrometry (XRF); and Hg using cold vapor atomic fluorescence spectrometry (CVAFS). The potassium dichromate method was used for organic matter determination. The pH was determined by the potentiometric method. The detection limits for the elements were Cu: 1 μg/g, Pb: 2 μg/g, Mn: 6 μg/g, Cd: 0.02 μg/g, Co: 1 μg/g, Ni: 2 μg/g, Hg: 0.0005 μg/g, Al_2O_3: 0.05%, TFe_2O_3: 0.05%, and SiO_2: 0.1%.

Quality assurance and quality control. Degree of accuracy. Four standard substances (GSS2, GSS3, GSS4, GSS6) were analyzed, and the logarithmic difference of the measured value and the standard value was calculated (ΔlgC). Maximum and mean values of Δ lgC were 0.092 and 0.036, respectively. All Δ lgC values were smaller than the multi-target regional geochemical survey specification (1:250,000) [23] allowed limit; the percent of pass of the sample was 100%.

TABLE 1
Descriptive statistics of heavy metal concentrations in the top (n=388) and deep soils (n=99)

		Units	Min	Max	Mean	Median	S. D	CV (%)	Skewness	Kurtosis	Background value [a]	Environmental Quality[b] Standard [b]
Cu	top	mg/kg	15.90	226.10	32.88	27.15	21.2	64.48	5.83	42.71	25.34	35
	deep		15.10	42.70	25.96	25.1	5.54	21.35	0.76	0.55		
Pb	top	mg/kg	16.70	259.80	28.60	25.70	16.16	56.50	9.33	115.7	21.78	35
	deep		16.10	32.50	22.51	22.05	3.32	14.77	0.88	0.757		
Co	top	mg/kg	8.20	20.80	13.86	13.75	2.31	16.67	0.35	-0.29	13.26	-
	deep		9.40	20.10	13.49	13.20	2.14	15.90	0.69	0.29		
Ni	top	mg/kg	20.30	50.20	32.92	31.90	6.10	18.53	0.43	-0.50	31.72	40
	deep		18.20	49.30	31.89	30.40	5.75	18.06	0.35	0.077		
Cd	top	mg/kg	0.090	2.69	0.206	0.17	0.20	97.09	8.33	83.99	0.107	0.2
	deep		0.068	0.20	0.11	0.11	0.03	24.86	1.09	0.83		
Mn	top	mg/kg	372.30	1061.10	663.49	641.05	108.7	16.39	0.96	1.05	654.14	-
	deep		399.20	1027.40	654.15	639.60	114.7	17.55	0.51	0.34		
Hg	top	mg/kg	0.017	0.23	0.039	0.036	0.02	51.28	4.58	40.87	0.018	0.15
	deep		0.01	0.041	0.019	0.018	0.006	32.27	1.09	1.49		
TFe_2O_3	top	mg/kg	3.43	7.41	5.07	4.94	0.80	15.78	0.56	-0.38	4.9	-
	deep		3.41	7.32	4.93	4.72	0.76	15.31	0.60	0.07		
Al_2O_3	top	mg/kg	11.51	16.16	13.29	13.24	0.88	6.62	0.46	-0.28	12.67	-
	deep		11.14	15.66	13.07	12.97	0.87	6.66	0.40	-0.10		
SiO_2	top	mg/kg	45.81	64.22	58.02	58.21	2.65	4.57	-0.35	0.38	60.86	-
	deep		52.25	64.78	58.33	59.02	2.73	4.68	-0.43	-0.56		
pH	top	-	7.65	8.67	8.32	8.33	0.14	1.68	-0.41	1.10	8.32	-
	deep	-	8.03	9.32	8.57	8.56	0.18	2.15	0.42	2.24		

[a] Soil trace element background concentrations of the study area from Hebei agricultural geology project

[b] Environmental Quality Standard for Soils (GB15618-1995)

Degree of precision. The logarithmic deviation of the measured value and the monitoring value was calculated（λ）; the maximum and mean values of Δ lgC were 0.120 and 0.045, respectively. All logarithmic deviations （λ） were smaller than the multi-target regional geochemical survey specification (1:250,000) allowed limit, and the percent of pass of the sample was 100%.

Geostatistical analyses. Statistical analyses were carried out using SPSS 17.0 (SPSS Inc., USA). Principal component analysis (PCA) was carried out to cluster metals that behaved similarly in order to identify potential sources. Varimax rotation with Kaiser normalization was applied because orthogonal rotation minimizes the number of variables with high loading on each component and facilitates the interpretation of results. Kriging interpolation was used to establish the spatial distributions of heavy metals. Before geostatistical analyses , the data were normalized by Box-Cox and logarithm transformation. The normalized data were analyzed by ArcGIS (version 9.3).

RESULTS AND DISCUSSION

Descriptive statistics. The soil data (pH and concentrations of SiO_2, Al_2O_3, TFe_2O_3, Cu, Pb, Co, Cd, Hg, Mn, and Ni) used herein were collected from the Hebei agricultural geology project conducted in 2017. The descriptive statistics results for heavy metal concentrations and pH values in the top and deep soils, as well as background values of the Xiongan New Area and Environmental Quality Standard values of China, are shown in Table 1.

Because deep soil is not affected by human activities, it can reflect the characteristics of the natural environment and represent original background levels [24]. The average elemental contents represent the baseline value of soil elements in the region, whereas the reference value represents the original background levels of the study area and can be used as the background value of the study area. For data processing, first the average value of element X1 and standard deviation S1 in the deep soil samples in the study area was calculated; then, the data of the study area X1 ± 2S1 was removed, and the average value X2 was calculated, which is the reference value of soil elements in the study area [25]

The soil pH ranged from 7.65 to 8.67, indicating that all the soils were alkaline, with 1.03% of the soils having a pH between 7.0 and 8.0, and 98.97% having pH above 8.0. Table 1 shows that the pH values of the top and deep soils did not vary significantly.

Excluding Co, Ni, Mn, SiO_2, Al_2O_3 and TFe_2O_3 (Table 1), the concentrations of all other heavy metals in top soil samples were greater than that of deep soil samples. The average concentration ratios from the top to deep soil for Cu, Pb, Cd, and Hg were 1.26, 1.27, 1.87, and 2.05, which are higher than that of Ni, Co, Mn, SiO_2, Al_2O_3 and TFe_2O_3, respectively. The maximum concentration of Cd in the soil samples was 13 times that of the Environmental Quality Standard value for Cd in China.

The variation (CV= standard deviation /average) was defined as the value of the mean concentration of heavy metals in the soil samples of Xiongan divided by the corresponding background soil value. The CV values for the seven heavy metals in the study ranged from 15.78 to 97.09%. The lowest CV was for SiO_2, and the highest for Cd, showing that Cd had the greatest variability among the heavy metals studied; therefore, it is most likely to be affected by human factors [3,26]. SiO_2, Al_2O_3 and TFe_2O_3 had the lower CV value, 4.57%, 6.62% and 15.78%, suggesting that those compounds have low variation, which can also be seen from its maximum and minimum values (Table 1). SiO_2, Al_2O_3 and TFe_2O_3 is considered a constant element in the soil. The CV values of the seven heavy metals in the soils followed a descending order: Cd > Cu > Pb > Hg > Ni > Co > Mn > TFe_2O_3> Al_2O_3> SiO_2. The CV of the ratio of top soil to deep soil for Cu, Pb, Co, Ni, Cd, Mn, Hg, SiO_2, Al_2O_3 and TFe_2O_3 were 3.02, 3.82, 1.05, 1.03, 3.91, 0.93, 1.59, 0.98, 0.99 and 1.03, respectively. It is obvious that the CV of Cu, Pb, Cd, and Hg were greater for the top soil than for the deep soil, suggesting that the top soil was influenced by human activities.

The average value of Cd, Cu, Pb, and Hg in the sampled soils (Table 1): 0.206, 32.88, 28.60, and 0.039 mg/kg, respectively. The standard deviations of these four metals were greater than those of the other heavy metals. This indicates a wide variation of concentrations in the soil samples. The skewness values for Co, Ni, Mn, SiO_2, Al_2O_3 and TFe_2O_3 were 0.35, 0.43, 0.96, -0.35, 0.46 and 0.56, respectively, which are smaller than 1, suggesting a normal distribution. However, the skewness values for Pb, Cu, Cd, and Hg were 9.33, 5.83, 8.33, and 4.58, respectively, and the kurtosis values were 115.75, 42.71, 83.99, and 40.87. The kurtosis values were very high because most of the samples were clustered together at relatively low values; thus the data were not normally distributed, which indicates the existence of highly contaminated points [27]. The raw dataset of Hg was normally distributed after log-transformation.

The results showed that some elements were more enriched in the top soil than in the deep soil (Table 1). The mean concentrations of Cd and Hg were far higher than their background values, which were based on deep soils in the study area [24] and can be used to assess metal contamination in the soil.

In fact, the mean concentrations of Cd and Hg were, respectively, 1.93 and 2.17 times higher than their corresponding background values. Compared to the enriched elements in the top soil, the mean concentrations of Co, SiO_2, Al_2O_3, TFe_2O_3, Mn, and Ni exhibited generally low levels, close to their local background values. Moreover, these elements displayed low CV values and quite homogeneous distributions across the study area, thus suggesting a major natural source.

Based on the guideline values provided by the Chinese Environmental Quality Standard for Natural Source Soils [28], the levels of Cu and Cd samples (in the present study area), which are 26.28% and 20.62%, respectively, exceeded the standard; this suggests that the soils in several areas are threatened by Cu and Cd. The maximum concentrations of Cu, Pb, Cd, and Hg were 8.92, 11.93, 25.14, and 12.78 times higher than their corresponding background values in the study area. Hence, environmental departments in the government should monitor these heavy metals and adopt appropriate preventive measures against the resulting contamination.

Correlation analysis. Pearson correlation coefficients were calculated among the seven elements and related soil compounds (TFe_2O_3, SiO_2, Al_2O_3), and the results are shown in Table 2.

A significant positive correlation at $P<0.01$ was found between the following pairs: Ni–TFe_2O_3 (0.986), Ni–Co (0.890), Mn–Co (0.671), Cu–Pb (0.853), Cu–Cd (0.831), and Pb–Cd (0.877).

TFe_2O_3, Al_2O_3, Ni, Mn, and Co exhibited positive correlations. TFe_2O_3, Al_2O_3, and SiO_2, which were identified as the main products of rock weathering, were prevalent in the soil. Therefore, the metals Co, Mn, and Ni, which positively correlated with TFe_2O_3 or Al_2O_3, mainly originated from the parent materials of the soil. Cai et al. [12], Hei et al. [29], and Chen et al. [30] also obtained a similar result.

However, Hg had a low correlation with three other heavy metals (Cu, Pb, Cd), indicating that it may have a different pollution source.

Also, relatively poor correlations occurred between the elements Cu, Pb, Cd, and Hg and the major soil components SiO_2, Al_2O_3, and TFe_2O_3 (Table 2). This could be attributed to human activities that disrupt the relationship between SiO_2, Al_2O_3, and TFe_2O_3 and Cu, Pb, Cd, and Hg elements.

Principal component analysis. PCA is widely applied in environmental studies, as it can help to distinguish natural sources from anthropogenic ones, identify possible nonpoint sources of contamination, and group sources into significant groups [31, 32, 33].

Tables 3–4 present the varimax rotation results for the total metal concentration in the soil. The eigenvalues of the first two extraction factors were greater than 1, and the third eigenvalue was greater than 1 when the matrix was rotated (Table 3). Figure 2 is a graphical representation of these three parts that shows the correlation between these metals. The results show that PCA can reduce the initial dimension of the dataset to three components, therefore explaining 89.96% of the data variation. The first principal component (PC1) explains 43.55% of the total variance and loads heavily on TFe_2O_3, Mn, Co, and Ni. The second principal component (PC2), dominated by Cu, Pb, and Cd, accounts for 33.84% of the total variance. The third principal component (PC3) has a high loading (0.974) of Hg, accounting for 12.57% of the total variance.

TABLE 2
Correlation analysis for heavy metal elements and compounds

	SiO_2	Al_2O_3	TFe_2O_3	Mn	Cu	Pb	Co	Ni	Cd
Al_2O_3	-0.587**								
TFe_2O_3	**-0.734****	**0.958****							
Mn	-0.658**	**0.608****	**0.731****						
Cu	-0.405**	0.470**	0.508**	0.432**					
Pb	-0.308**	0.341**	0.375**	0.381**	**0.853****				
Co	-0.657**	**0.835****	**0.895****	0.671**	0.456**	0.339**			
Ni	-0.718**	**0.943****	**0.986****	**0.709****	0.521**	0.390**	**0.890****		
Cd	-0.241**	0.239**	0.278**	0.323**	**0.831****	**0.877****	0.270**	0.290**	
Hg	-0.113*	0.091	0.128*	0.141**	0.317**	0.339**	0.101*	0.141**	0.358**

**$P<0.01$ level of significance
*$P<0.05$ level of significance

TABLE 3
Total Variance Explained

Compo-nent	Initial Eigenvalues			Extraction sums of Squared Loadings			Rotation Sums of Squared Loadings		
	Total	% of Variance	Cumulative%	Total	% of Variance	Cumulative%	Total	% of Variance	Cumula-tive%
1	4.547	56.838	56.838	4.547	56.838	56.838	3.484	43.551	43.551
2	1.843	23.040	79.879	1.843	23.040	79.879	2.707	33.843	77.394
3	0.807	10.085	89.964	0.807	10.085	89.964	1.006	12.570	89.964
4	0.399	4.991	94.955						
5	0.160	1.998	96.954						
6	0.126	1.580	98.534						
7	0.104	1.299	99.832						
8	0.013	0.168	100						

TABLE 4
Rotated component matrix

Heavy metal	PC1	PC2	PC3
TFe2O3	**0.961**	0.182	0.036
Cu	0.350	**0.874**	0.105
Pb	0.208	**0.928**	0.126
Cd	0.110	**0.942**	0.152
Mn	**0.790**	0.224	0.061
Co	**0.923**	0.159	0.013
Ni	**0.951**	0.197	0.047
Hg	0.053	0.220	**0.974**

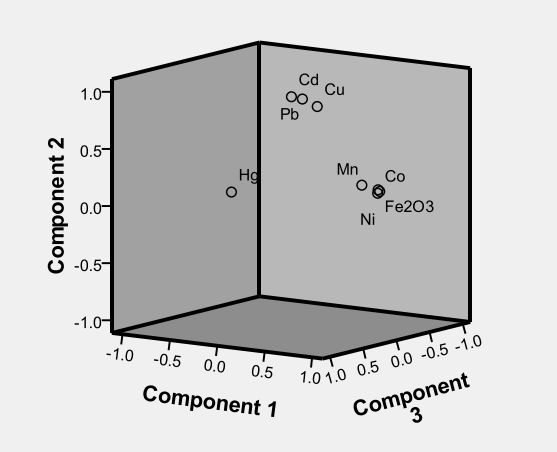

FIGURE 2
The component plot in rotated space

PC1 mainly included Co, Mn, TFe_2O_3, and Ni and could be a lithogenic component, as parent materials control the variabilities of soil Co, Mn, TFe_2O_3, and Ni. The spatial distribution map fully supports this point. Figure 4 shows the Co, Mn, TFe_2O_3, and Ni nonpoint source pollution in the study area and no significant anthropogenic inputs of Co, Mn, TFe_2O_3, and Ni. Researchers demonstrated that TFe2O3, Mn, Co, and Ni are mainly derived from the parent rock and parent materials [8, 11, 12]. In addition, the Co and Ni content in the soil is much higher than the Co and Ni content that is introduced into the soil through chemical fertilizers [31, 34].

PC2 included Cu, Pb, and Cd and could be defined as an anthropogenic source component. Pb is affected by anthropogenic activities such as vehicular and industrial exhausts and wastewater irrigation. Cd and Cu are affected mainly by the use of agrochemicals [31, 35].

Xia et al. [8] suggested that atmospheric deposition was the dominant source for soil heavy metals. The PCA and correlation coefficient analysis results reveal that Cd, Cu, and Pb were derived from similar anthropogenic sources. In addition, Cd has a high concentration in farmyard manure [8, 36].

PC3 is Hg, which can be defined as an anthropogenic component related to industrial and coal burning. The distribution map shows high concentrations of Hg in and around Anxin and Rongcheng. Further, the Hg concentration is remarkably high in urban areas with heavy traffic, coal-burning exhausts, and vehicular exhausts; additionally, atmospheric deposition results in soil with high Hg contaminations [37, 38]. Streets et al. [39] suggested that high Hg concentration in the northern part of China was caused by heavy coal burning in residential and small industrial areas. Therefore, the Hg source in this study can be mainly determined from coal burning and small industries.

Spatial distribution of heavy metals. Figure 4 shows the spatial distribution of the seven heavy metals in the study area. The trends for soil Co, Mn, Ni, and TFe_2O_3 were similar in spatial distribution. The spatial distributions of Mn, Ni, and Co exhibited nonpoint source contamination. The spatial distribution results indicated that the soil parent materials and pedogenic processes are major factors with respect to their amounts and distributions in the study area [32,38].

The hotspots with the highest levels of Cu, Pb, and Cd were located in Lin village, Niu Jiao village, and Xi Lao Dian village, respectively. In southwest Anxin county, there are high risk regions that may be related to local metal product, transportation machinery, and plastic products factories.

However, differences in heavy metal content are observed in the spatial distribution map of this study area. Lv et al. [19] reported that human inputs have altered the natural spatial variations of Cd, Cu, and Pb at the local scale. The findings in this study are in agreement with Lv et al.'s result [19].

The distribution of Hg was different from those of the other heavy metals in high-value areas and was mainly concentrated in the northwest in Wang Gongdi village, in the southwest Niu Jiao village, and across Rongcheng County. This indicated that industrial fumes, coal-burning exhausts, domestic waste, and vehicular exhausts may be the main sources of soil Hg in Xiongan County. Hg can accumulate in soils through atmospheric deposition [13] or long-range transport of Hg in the atmosphere [40]. According to most researchers, Cu, Pb, Cd, and Hg constitute an anthropogenic component related to specific human activities, whereas the remaining elements (Co, Mn, Fe, and Ni) appear to be associated with soil parent materials [6, 8, 9, 12, 19]. In the present study, it also seems reasonable to conclude that Cu, Pb, Cd, and Hg originate from an anthropogenic component related to specific human activities, whereas the remaining elements (Co, Mn, Fe, and Ni) appear to be associated with the soil parent materials, which are mainly from the Taihang Mountains east of the Yongding River and the Hutuo River alluvial fan.

Pollution level assessment. Enrichment factor (EF). The EF is an indicator of natural and anthropogenic sources [12, 25].

The EF is an important index reflecting the disturbance degree of human activities to the natural environment. It is a comparison between the measured values of the elements in the sample and the background content of the elements that is used to determine the status of human influence on the elements in the environment [41]. The following principles must be true when selecting a reference element: the selected reference elements must be stable in natural environment; the element must be a major element in the reference system; and the element must be ubiquitous in the samples. Based on these principles, Fe, Si, Ti, and Al can be used as reference elements [42, 43]. Fe was used as the reference element in the current study. This selection was made by considering the correlation and multivariate statistical analyses; the selection process was not affected by human activities and was not related to major heavy metal pollutants [12, 27].

The EF of each element, which is a normalization of an element of interest against a reference element, was calculated using the following equation:

$$EF = (Ci/Cn)_{sample}/(Ci/Cn)_{background}$$

where Ci represents the concentration of heavy metal elements, and Cn represents the concentration of Fe. The sample values represent the concentrations in the sample collected, and background represents the background values of the elements.

The EF was split into five classes as follows: EF < 2, class 1, deficiency to minimal enrichment; 2 ≤ EF < 5, class 2, moderate enrichment; 5 ≤ EF < 20, class 3, significant enrichment; 20 ≤ EF < 40, class 4, very high enrichment; and EF ≥40, class 5, extremely high enrichment [12]. The EF values for heavy metals are shown in Fig. 3. The EFs of Hg, Cd, Pb, and Cu were higher than 5, whereas the EFs of Ni, Co, and Mn were less than 2. The EF can be an indicator of natural and anthropogenic sources. The EFs of Hg, Cd, Pb, and Cu EFs were much higher than those of Mn, Co, and Ni (Fig. 3), indicating that these elements in the study area mainly originated from anthropogenic sources. The decreasing order of mean EF for all the studied elements was Hg > Cd > Pb > Cu > Mn > Co > Ni, revealing lack of contamination by Co, Ni, and Mn and implying a significant contribution of natural sources towards these elements (Table 5). The ranges of EFs suggest anthropogenic origins for other studied metals, excluding Co, Ni, and Mn. Coal-burning and industrial processes are considered to be the major pollution sources in Xiongan New Area.

Geoaccumulation index (Igeo). The geoaccumulation index method can be used to evaluate the contamination levels of heavy metals in soils [44, 45]. The Igeo is computed using the following equation:

$$I_{geo} = \log_2[Cn/(k \times Bn)]$$

where Cn is the concentration of a metal (n) in the sample, and Bn is the geochemical background concentration of the metal (n). The factor k (1.5) is a background matrix correction factor attributed to lithogenic effects [46].

Igeo is classified into seven levels: unpolluted (Igeo ≤ 0), unpolluted to moderately polluted (0 < Igeo ≤ 1), moderately polluted (1 < Igeo ≤ 2), moderately to strongly polluted (2 < Igeo ≤ 3), strongly

polluted (3 < Igeo ≤ 4), strongly to extremely polluted (4 < Igeo ≤ 5), and extremely polluted (Igeo > 5) [46]. The Igeo values of the surface sediments from the study area decreased in the following order: Hg > Cd > Pb > Cu > Mn > Co > Ni, ranging from -0.20 to 0.92 (average 0.14) for Hg, -0.26 to 1.21 (average 0.04) for Cd, -0.29 to 0.90 (average -0.08) for Pb, -0.38 to -0.77 (average -0.10) for Cu, -0.38 to 0.02 (average -0.16) for Co, -0.37 to 0.02 (average -0.17) for Ni, and -0.41 to 0.045 (average -0.16) for Mn (Table 5). However, the percentage of samples for Hg, Cd, Cu, Pb, Ni, Mn, and Co that had Igeo values above 0 was 85.82, 51.80%, 20.62, 12.63, 0.52, 2.32, and 0.26%, respectively. In other words, the soil of the study area was contaminated (Igeo > 0) by heavy metals such as Hg, Cd, Cu, and Pb (especially Hg and Cd) to some degree (Fig. 3), which probably originated from anthropogenic sources, whereas, Ni, Mn, and Co were not relevant as soil contaminants in the study area and are likely to have natural origin.

Ecological risk (E_r). Igeo represents the "contamination" level, and E_r represents the "pollution" level. To assess the degree of heavy metal pollution in the study area, the risk index (RI) was calculated as follows:

$$RI = \sum_{i=1}^{m} E_r$$

$$E_r = T_r \times \frac{C_i}{C_n}$$

where C_i and C_n are the heavy metal concentrations in a sample and in the background, respectively; E_r is the ecological risk of each element; and RI shows the ecological risk of multiple elements. T_r is the "toxic-response factor" for a given substance and has value of 5, 5, 30, 40, 5, 2, and 1 for Cu, Pb, Cd, Hg, Ni, Mn, and Co, respectively [27, 47]. The following terminologies are used to describe the risk levels: E_r < 40, low potential ecological risk; 40 ≤ E_r < 80, moderate potential ecological risk; 80 ≤ E_r < 160, considerable potential ecological risk; 160 ≤ E_r < 320, high potential ecological risk; E_r ≥ 320, very high ecological risk; RI < 150, low ecological risk; 150 ≤ RI < 300, moderate ecological risk; 300 ≤ RI < 600, considerable ecological risk; and RI ≥ 600, very high ecological risk[27].

The E_r results of the seven metals in Xiongan New Area are shown in Fig. 3. The average E_r values of heavy metals exhibited a decreasing order of Hg > Cd > Pb > Cu > Co > Ni > Mn (Table 4). The results of the mean concentrations of Hg (87.31) and Cd (56.28) indicate considerable potential ecological risk and moderate potential ecological risk, respectively; whereas Pb, Cu, Co, Ni, and Mn pose low potential ecological risk. Based on these results, most sampling locations exhibited low ecological risk (max values of Cu, Pb, Co, Ni, and Mn are 44.61, 59.64, 7.84, 7.91, and 1.67, respectively), implying that these metals may not have harmful effects on the ecosystem. However, the average RI value (168.11) of heavy metals indicates moderate ecological risk.

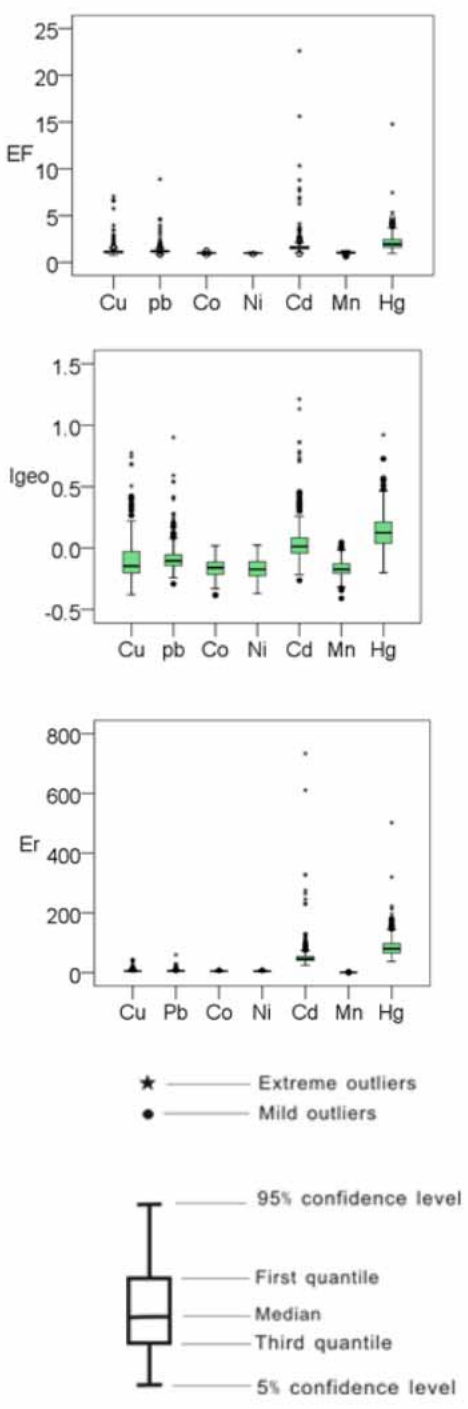

FIGURE 3
Box plot of EF, Igeo, and E_r for heavy metals in the study area

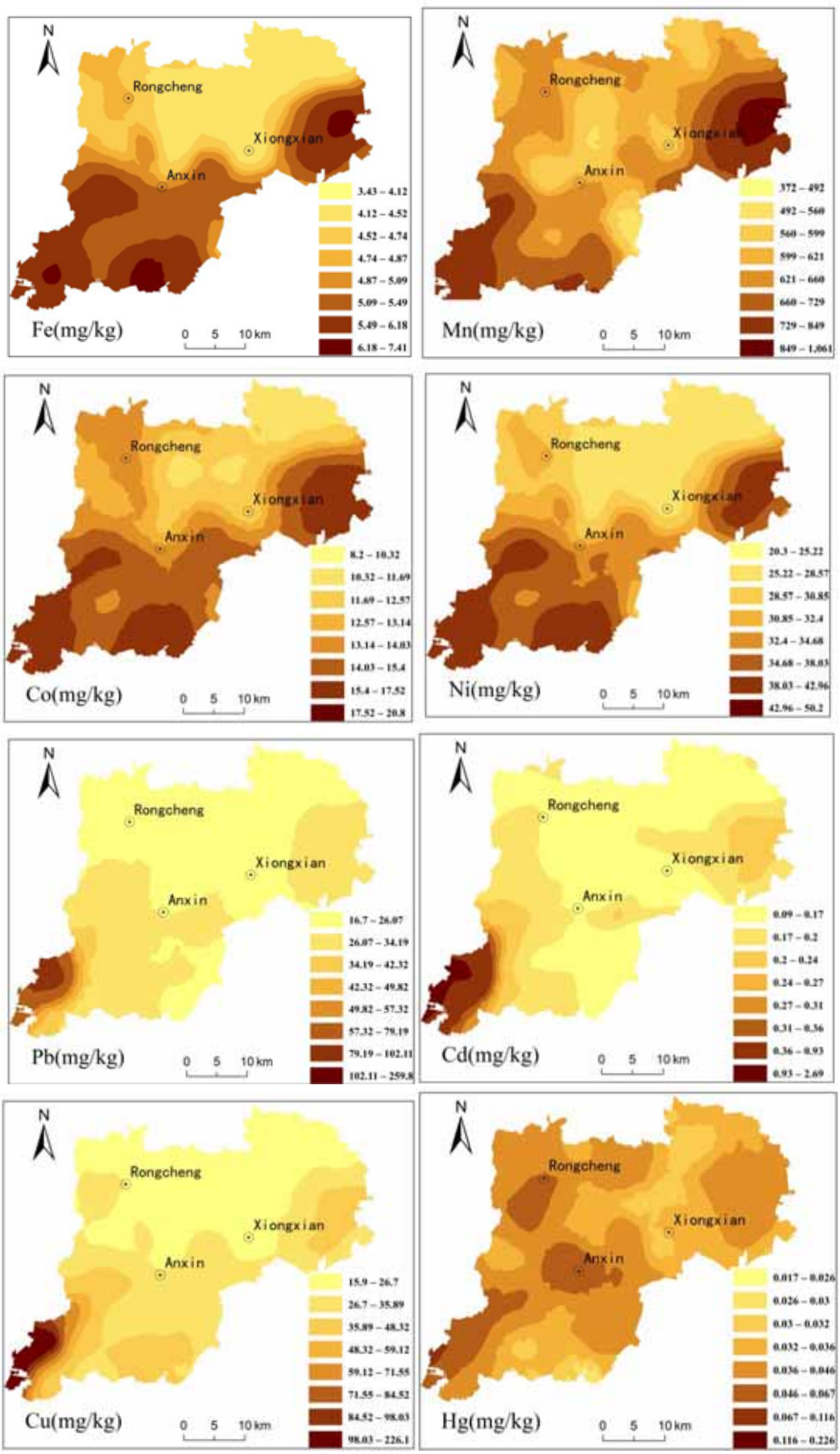

FIGURE 4
Spatial distribution of heavy metals in the top soil of the study area

TABLE 5
Values of enrichment factor (EF), geoaccumulation index (Igeo), and ecological risk (E_r) analysis of the heavy metals

statistic	EF							Igeo							E_r								
	Cu	Pb	Co	Ni	Cd	Hg	Mn	Cu	Pb	Co	Ni	Cd	Hg	Mn	Cu	Pb	Co	Ni	Cd	Hg	Mn	*RI*	Ecological risk
Min	0.7	0.7	0.7	0.8	0.8	0.9	0.5	-	-	-	-	-	-	-	3.14	3.8	3.0	3.2	24.55	37.78	0.5	83.05	low
Max	7.05	8.90	1.27	1.10	22.60	14.78	1.26	0.77	0.90	0.02	0.02	1.21	0.92	0.045	44.61	59.64	7.84	7.91	733.64	502.22	1.67	988.44	very high
Mean	1.22	1.26	1.01	0.10	1.83	2.16	1.01	-0.1	0.0	0.1	0.1	0.04	0.14	-0.1	6.49	6.57	5.23	5.19	56.28	87.31	1.04	168.11	moderate
S. D.	0.63	0.55	0.08	0.04	1.57	1.00	0.11	0.16	0.12	0.07	0.08	0.17	0.15	0.07	4.19	3.71	0.87	0.96	55.88	37.76	0.17	84.58	

CONCLUSIONS

Using the statistical software SPSS 17.0 and ArcGIS 9.3 to analyze the data, the results show that average concentrations of the heavy metals Mo, Ni, and Co are close to the deep soil concentrations and background values. On the contrary, concentrations of the heavy metals Cu, Pb, Cd, and Hg are much higher than the average deep soil concentrations. In particular, the average concentrations of Cd and Hg were 1.93 and 2.17 times their corresponding background concentrations. The correlation and PCAs involved three PCs. The first PC is Mo, Ni, Co, and major soil compounds, i.e., TFe_2O_3 that originate from natural sources. The second PC contains Cu, Pb, and Cd, and the third PC contains Hg. Although both, the second and third PCs, originate from anthropogenic sources, their pollutants may vary. The main sources of the second PC (Cd, Cu, and Pb) originate from the combined pollution caused by farming and vehicle exhaust. The main sources of the third PC (Hg) are coal-burning exhausts and atmospheric deposition. In the study area, the levels of heavy metal pollution of soil were evaluated using the enrichment factor, geoaccumulation index, and ecological risk index. The results of EF, Igeo, and E_r show that Cu, Pb, Cd, and Hg pollution (particularly Cd and Hg) have reached harmful levels. Furthermore, the location of polluted areas were determined using spatial distribution mapping, which will provide a basis for local environmental departments to control the soil pollution caused by heavy metals.

ACKNOWLEDGEMENTS

This paper was supported by Wonkwang University in 2019.

REFERENCES

[1] Liu, R., Wang, M., Chen, W.P. (2018) The influence of urbanization on organic carbon sequestration and cycling in soils of Beijing. Landscape and Urban Planning. 169, 241–249.

[2] Agomuo, E.N., Amadi, P.U. (2017) Accumulation and toxicological risk assessments of heavy metals of top soils from markets in Owerri, Imo state, Nigeria. Environmental Nanotechnology, Monitoring and Management. 8, 121-126.

[3] Chen, T., Liu, X.M., Zhu, M.Z., Zhao, K.L., Wu, J.J., Xu, J.M., Huang, P.M. (2008) Identification of trace element sources and associated risk assessment in vegetable soils of the urban-rural transitional area of Hangzhou, China. Environ. Pollut. 151, 67–78.

[4] Eisa, S., Neda, R., Mahshad. K.G. (2016) A comparative study of metals in roadside soils and urban parks from Hamedan metropolis. Iran. Environmental Nanotechnology Monitoring and Management. 6, 169–175.

[5] Khalid, S., Shadid, M., Niazi, N.K., Murtaza, B., Bibi, I., Dumat, C. (2016) A comparison of technologies for remediation of heavy metal contaminated soils. Journal of Geochemical Exploration. 182, 247-268.

[6] Liu, Y., Wang, H.F., Li, X. T., Li, J.C. (2015) Heavy Metal Contamination of Agricultural Soils in Taiyuan, China. Pedosphere. 25, 901–909.

[7] Tian, K., Huang, B., Xing, Z., Hu, W.Y. (2017) Geochemical baseline establishment and ecological risk evaluation of heavy metals in greenhouse soils from Dongtai, China. Ecological Indicators. 72, 510–520.

[8] Xia, X.Q., Yang, Z.F., Cui, Y.J., Li, Y.S., Hou, Q.Y., Yu, T. (2014) Soil heavy metal concentrations and their typical input and output fluxes on the southern Songnen Plain, Heilongjiang Province. China Journal of Geochemical Exploration. 139, 85–96.

[9] Men, C., Liu, R. M., Xu, F., Wang, Q.R., Guo, L.J., Shen, Z.Y. (2018) Pollution characteristics, risk assessment, and source apportionment of heavy metals in road dust in Beijing. China Science of the Total Environment. 612, 138–147.

[10] Chantigny, M.H. (2003) Dissolved and water-extractable organic matter in soils: a review on the influence of land use and management practices. Geoderma.113, 357–380.

[11] Mehdi, A., Sahand., J., Amaneh, A., Nematollah, J., Amir, H.M., Reza, D.C.S., Hamideh, A., Razegheh, A. (2017) Zoning of heavy metal concentrations including Cd, Pb and As in agricultural soils of Aghili plain, Khuzestan province, Iran. Data in Brief. 14, 20–27.

[12] Cai, L.M., Xu, Z.C., Bao, P. (2015) Multivariate and geostatistical analyses of the spatial distribution and source of arsenic and heavy metals in the agricultural soils in Shunde, Southeast China. Journal of Geochemical Exploration. 148, 189–195.

[13] Katharina, H., Øyvind, M., Torunn, B., Eiliv, S., (2017) The presence of mercury and other trace metals in surface soils in the Norwegian Arctic. Chemosphere. 188, 567–574.

[14] Chen, H.Y., Yuan, X.Y., Li, T.Y., Hu, S., Ji, J.F., Wang, C. (2016) Characteristics of heavy metal transfer and their influencing factors in different soil–crop systems of the industrialization region, China Ecotoxicology and Environmental Safety. 126, 193–201.

[15] Fan, Y., Li, H., Xue, Z.J., Zhang, Q., Cheng, F.Q. (2017) Accumulation characteristics and potential risk of heavy metals in soil vegetable system under greenhouse cultivation condition in Northern China. Ecological Engineering. 102, 367–373.

[16] Huang, B., Wang, M., Yan, L., Sun, W., Zhao, Y., Shi, X., Weindorf, D.C. (2011) Accumulation, transfer and environmental risk of soil mercury in a rapidly industrializing region of the Yangtze River Delta, China. J. Soils Sediments. 11, 607–618.

[17] Pan, L.-B., Ma, J., Wang, X.L., Hou, H. (2016) Heavy metals in soils from a typical county in Shanxi Province, China: Levels, sources and spatial distribution. Chemosphere. 148, 248-254.

[18] Jiang, Y.X., Chao, S.H., Liu, J.W., Yang, Y., Chen, Y.J, Zhang, A.C., Cao, H.B. (2017) Source apportionment and health risk assessment of heavy metals in soil for a township in Jiangsu Province, China. Chemosphere. 168, 1658–1668.

[19] Lv, J.S., Liu, Y., Zhang, Z.L., Dai, B. (2014) Multivariate geostatistical analyses of heavy metals in soils: Spatial multi-scale variations in Wulian, Eastern China. Ecotoxicology and Environmental Safety. 107, 140–147.

[20] Mollon, L.C., Norton, G.J., Trakal, L., Moreno-Jimenez, E., Elouali, F.Z., Hough. R.L., Beesley, L. (2016) Mobility and toxicity of heavy metal(loid)s arising from contaminated wood ash application to a pasture grassland, soil. Environmental Pollution. 218, 419–427.

[21] Meisam, R.M., Behnam, K., Farid, M., Reza, S., Ahmadreza, L., Maryam, K. (2017) Distribution, source identification and health risk assessment of soil heavy metals in urban areas of Isfahan province, Iran. Journal of African Earth Sciences. 132, 16–26.

[22] Ye, J.Y., Jiang, B.L. (2004) Regional geochemical exploration sample analysis. China Geological Press. Beijing (in Chinese).

[23] Ministry of Land and Resources of the People's Republic of China. (2014) Specification of multi-purpose regional geochemical survey (1:250000) (DZ/T 0258-2014). http://g.mlr.gov. cn/ 201701/t20170123_1428726.html

[24] Guo, H.Q., Ma, Z.S., Hao, J.J., Gao, H.Q., Wang, S.M. (2007) Characteristics and Significance of reference values of the geochemical elements in soil samples from eastern Hebei Province. Rock and Mineral analysis. 26, 281–286.

[25] Zhao, S.Z, Liu, L.P., Wang, X.K., Li, S.B., Zhu, S., Zheng, P., Zhang, Q., Zhang, B., Meng, K.W. (2008) Characteristic sand bed mud in the inner Mongolia Stretch of the Yellow River. Geoscience. 22, 304–312.

[26] Qing, X., Zong, Y.T., Lu, S.G. (2015) Assessment of heavy metal pollution and human health risk in urban soils of steel industrial city (Anshan), Liaoning, Northeast China. Ecotoxicology and Environmental Safety. 120, 377-385.

[27] Shahab, A.D., Majid, A., Mahin, K. (2017) Multivariate statistical analysis of heavy metals contamination in atmospheric dust of Kermanshah province, western Iran, during the spring and summer 2013. Journal of Geochemical Exploration. 180, 61–70.

[28] Environmental Protection Administration of China (EPAC) (1995) Environmental Quality Standard for Soils (GB15618-1995). http://kjs.mep.gov.cn/hjbhbz/bzwb/trhj/trhjzlbz/199603/t19960301_82028.htm.

[29] Hei, L., Jin, P.W., Zhu, X.P., Ye, W.C., Yang, Y.T. (2016) The Tenth International Conference on Waste Management and Technology (ICWMT)Characteristics of speciation of heavy metals in municipal sewage sludge of Guangzhou as fertilizer Procedia. Environmental Sciences. 31, 232–240.

[30] Chen, H.Y., Teng, Y.G., Lu, S.J., Wang, Y.Y., Wang, J.S. (2015) Contamination features and health risk of soil heavy metals in China. Science of the Total Environment. 512–513, 143–153.

[31] Liu, P., Zhao, H.J., Wang, L., Liu, Z.H. (2011) Analysis of Heavy Metal Sources for Vegetable Soils from Shandong Province. China Agricultural Sciences in China. 10, 109–119.

[32] Sun, C.Y, Liu, J.S., Wang, Y., Sun, L.Q., Yu, H.W. (2013) Multivariate and geostatistical analyses of the spatial distribution and sources of heavy metals in agricultural soil in Dehui, Northeast China. Chemosphere. 92, 517–523.

[33] Tao, S. (1994) Applied Mathematical Statistic Methods. China Environmental Science Press. Beijing, China, 54–180.

[34] Facchinelli, A., Sacchi, E., Mallen, L. (2001) Multivariate statistical and GIS-based approach to identify heavy metal sources in soils. Environ. Pollut. 114, 313–324.

[35] Abollino, O., Aceto, M., Malandrino, M., Mentasti, E., Sarzanini, C., Petrella, F. (2002) Heavy metals in agricultural soils from Piedmont, Italy: distribution, speciation and chemometric data treatment. Chemosphere. 49, 545–557.

[36] Lee, H.H., Owens, V.N., Park, S.K., Kim, J., Hong, C.O. (2018) Adsorption and precipitation of cadmium affected by chemical form and addition rate of phosphate in soils having different levels of cadmium. Chemosphere. 206, 369-375.

[37] Rodríguez, J.A., Nanos, N., Grau, J.M., Gil, L., López-Arias, M. (2008) Multiscale analysis of heavy metal contents in Spanish agricultural topsoils. Chemosphere. 70, 1085–1096.

[38] Engle, M.A. Gustin, M.S., Lindberg, A.W. Ariya, P.A. (2005) The influence of ozone on atmospheric emissions of gaseous elemental mercury and relative gaseous mercury from substrates. Atmos. Environ. 39, 7506–7517.

[39] Streets, D.G., Hao, J.M., Wu, Y., Jiang, J.K., Chan, M., Tian, H.Z., Feng, X.B. (2005) Anthropogenic mercury emissions in China. Atmos. Environ. 39, 7789–7806.

[40] Lantzy, R.J., Mackenzie, F.T. (1979) Atmospheric trace metals: global cycles and assessment of man's impact. Geochim. Cosmochim. Acta. 43, 511–525.

[41] Buat-Menard, P., Chesselet, P. (1979) Variable influence of the atmospheric flux on the trace metal chemistry of oceanic suspended matter. Earth and Planetary Science Letters. 42, 398-411.

[42] Chao, Y.C., Simpson, R.W., Mctainsh, G.H. (2000) Source apportionment of PM2.5 and PM10 acrosols in Brisbane (Australia) by receptor modelling. Atmospheric Environment. 33, 3251–3268.

[43] Yang, L,P., Chen, F.H., Zhang, C.J. (2002) Chemical characteristics of atmospheric dust in Lanzhou. Journal of Lanzhou University (Natural Sciences). 38, 115–120.

[44] Marrugo-Negrete, J., Pinedo-Hernandez, J., Diez, S. (2017) Assessment of heavy metal pollution, spatial distribution and origin in agricultural soils along the Sinú River Basin. Colombia. Environmental Research. 154, 380–388.

[45] Ryszard, M., Joanna, K., Michał, G.., Paweł, Z., Agnieszka, J., Tomasz, Z., Wojciech, K., Maryla, T., Kalina, O. (2017) Assessment of heavy metals contamination in surface layers of Roztocze National Park forest soils (SE Poland) by indices of pollution. Chemosphere. 168, 839–850.

[46] Müller, G. (1969) Index of geoaccumulation in sediments of the Rhine river. Geojournal. 2, 108.

[47] Hakanson, L. (1980) An ecological risk index for aquatic pollution control. A sedimentological approach. Water Res. 14, 975–1001.

Received: **11.04.2018**
Accepted: **08.03.2019**

CORRESPONDING AUTHOR

Sanggyun Na
College of Business Administration,
Wonkwang University,
No.460, Iksandae-ro, Iksan,
Jeonbuk 54538 – Korea

e-mail: nsghy@wku.ac.kr

© by PSP Volume 28 – No. 5/2019 pages 3686-3695 Fresenius Environmental Bulletin

ASSESSMENT OF SOMACLONAL VARIATION IN SALT-ADAPTED AND NON-ADAPTED REGENERATED DATE PALM (*PHOENIX DACTYLIFERA* L.)

Suliman A Al-Khateeb[1,*], Abdullatif A Al-Khateeb[2], Muhammad Naeem Sattar[1], Akbar S Mohmand[1,3], Hossam S El-Beltagi[2,4]

[1]Environment and Natural Resources Department, College of Agriculture and Food Sciences, King Faisal University, P.O. Box 400, Al-Ahsa 31982, Kingdom of Saudi Arabia.
[2]Agricultural Biotechnology Department, College of Agriculture and Food Sciences, King Faisal University, P.O. Box 420, Alhassa 31982, Kingdom of Saudi Arabia
[3]Research. Innovation and Commercialisation (ORIC), Bacha Khan University Charsadda, KP, Pakistan
[4]Biochemistry Department, Faculty of Agriculture, Cairo University, Giza, Cairo, Egypt

ABSTRACT

Date palm (*Phoenix dactylifera* L.) has been under cultivation as a socio-economic crop primarily in dry lands of North Africa, Middle East and Central America. The production of date palm is severely affected by many abiotic stresses including drought and salt stress. In a broader prospect, soil salinity has gained worldwide concerns, encompassing over 20% of the arable land. In the present study date palm cultivar, 'Sukary' was used to raise somatic embyogenic calli under various salt levels. After eight sub-culturing the calli were subjected step wise (a lap of 50mM increase after every four weeks) to 0, 200 and 400 NaCl treatments. The best performing calli were further subjected to multiplication media to generate the plants, which were assessed for salt tolerance/adaptation. The salt-adapted (SA) and salt non-adapted (SNA) plantlets were assessed for the presence of any inherent somaclonal variation using 30 RAPD primers. The RAPD analysis did not produce any polymorphic bands and thus genetic variation was absent in the SA somaclones. The date palm somaclones thus obtained, have better performance on successive NaCl treatments due to salt adaptation mechanism.

KEYWORDS:
Date palm, Salt tolerance, NaCl, Somaclonal variation, RAPD

INTRODUCTION

Salt stress is among major biotic stresses hindering crop production, worldwide [1-3]. The total area affected by salt stress has been estimated ~80 mha [4, 5]. Salinity has drastic effects on overall plant physiology in many different ways ranging from physiological and metabolic changes, which end up into molecular impairment [6-8]. Apart from extensive research to understand salt tolerance mechanism of crop plants, improving salt tolerance in crop plants remains intangible as compared to resistance against insect, pests and diseases. Palm trees have excellent tolerance towards various adverse environmental hazards and are potential source of economic returns in dry areas [9]. Among palm trees, date palm (*Phoenix dactylifera* L. Family: *Arecaceae*) is a monocotyledonous perennial tree, which has been cultivated as an economical fruit tree in the arid and semi-arid regions. Despite the fact that date palm produces limited number of off-shoots, the major mode of propagation in date palms is vegetative propagation through offshoots to maintain cultivar genetic integrity [10-12]. Therefore, different programs for genetic improvement in date palm include modern agro-biotechnology and in vitro propagation for the production of genetically stable plants on commercial scales. In vitro regeneration of date palm plants using different tissues as source of explants have been well documented by many researchers [13, 14]. Generation of plants through tissue culturing usually undergo somaclonal variations among regenerated plants, most probably due to the stresses imposed during in vitro propagation [15]. These variations include methylated DNA, chromosomal rearrangements and in most cases point mutations [16, 17]. The variability in somaclones occurs mostly due to genetic and/or epigenetic variations during culturing of explants [18]. Occurrence of genetic variability among genotypes is the ultimate goal in plant breeding and modern biotechnological approaches made it quite accessible for plant breeders. Plant regeneration through tissue culturing has been extensively used in plant biotechnology for crop improvement, despite the appearance of somaclonal variations. Although somaclonal variation is undesirable to maintain genetic stability of the regenerated plants, however, it offers a natural source of variation too [19]. The role of biotechnological approaches is important for estimation and conservation of somaclonal variations under in vitro culturing. The most common approach is to employ dif-

ferent molecular markers including biochemical, physiological and DNA-based molecular markers [20]. The DNA-based markers include Restriction Fragment Length Polymorphism (RFLP), Random Amplified Polymorphic DNA (RAPD), Amplified Fragment Length Polymorphism (AFLP), Sequence Characterized Amplified Regions (SCAR), Simple Sequence Repeat (SSR) and Inter Simple Sequence Repeat (ISSR) [21-23].

Isozymes patterns analysis using specific enzymes provides much convenience to detect genetic changes during plant regeneration but is vulnerable to oncogenic variations [24]. However, such approaches are very limited in their applications because these only deal with coding regions of genomic DNA. On the other hands, DNA based molecular markers such as RFLP and AFLP are routinely used to assess the genetic integrity of the regenerated plants, but these require expensive restriction endonuclease enzymes, radiolabeled probes and hence are not suitable for routine lab work [25]. However, PCR based molecular markers such as RAPD and ISSR need small quantities of genomic DNA and hence provide rapid and simpler results. RAPD is very discriminative, useful and reliable technique to detect genetic changes even among closely related organisms [26]. Both RAPD and ISSR techniques are routinely employed for the detection of somaclonal variations of micropropagated date palm plants [27-30].

The micro-propagation of date palm for commercial use is a reliable technique however, the plantlets, thus produced from calli showed genetic variations unlikely from their mother plants [31] due to prolonged sub-culturing period. This makes regenerated plantlets suspicious for the presence of any somaclonal variation [32]. Thus, RAPD has been reported as a reliable and quick molecular tool to detect any somaclonal variations in the regenerated plantlets [33, 34]. In the present study, the main objective was to produce regenerated salt adapted/tolerant plant by subjecting date palm cv. Sukary calli to various salt levels. Another objective was to monitor via RAPD markers, whether or not, the physiological changes in the regenerated date palm plants are due to somaclonal variations.

MATERIALS AND METHODS

Embryogenesis and establishment of date palm plantlets. All the experiments in this study were carried out at Department of Environment and Natural Resources, College of Agriculture and Food Sciences, King Faisal University, Saudi Arabia. The formation of somatic embryogenic calli was achieved successfully from date palm cultivar 'Sukary' as has been described by Al-khateeb and Al-khateeb [35]. The callus culture was transferred in three basal media (MS-media) combinations for plant regeneration [36, 37].

In Vitro Salt Selection. After callus development the embryogenic calli were exposed to two types of NaCl stress protocols. One part was subjected directly to three NaCl treatments, i.e. 0, 200 and 400 mM NaCl added directly to MS-basal medium. The second part of calli were transferred stepwise to 200 and 400 mM NaCl with a 50 mM gradual increment of NaCl after every 4 weeks until the maximum salt level i.e. 400 mM NaCl, respectively. For this purpose the calli from 50 mm NaCl was transferred to 100 mM NaCl for 4 weeks and then gradually subjected to 150 mM NaCl, until 400 mM NaCl and so forth. After eight successive passages, all the calli were cultured on salt-free media to obtain date palm plantlets. All the calli under each salt treatment were routinely assessed for fresh weight addition, initiation of shoot and root, and plantlet regeneration.

Plant regeneration. The best performing calli were selected and further subjected to regeneration media as has been described for plantlet regeneration [38]. The regenerated plantlets, thus obtained, were re-exposed to respective salt stress (i.e. 200 and 400 mM NaCl) for eight weeks for the assessment of salt tolerance/adaptation.

Morphological data collection. The in vitro effect of three salt treatments was determined for root length, shoot length, total plant dry weight and dry root/shoot ratio (Table 1). The plants roots were washed to remove excessive salts and ions with distilled water according to Al-Khateeb et al. [35]. The Na^+ and K^+ contents were determined using the dry-ashing procedure [39]. Further effects of salt treatments was also observed for leaf Na^+ and K^+, leaf K^+/Na^+ ratio, root Na^+ and K^+ concentrations and root K^+/Na^+ ratio. For this purpose, fresh leaves and roots (~500 mg) were homogenized using pestle and mortar and the extractions were carried out in 25 ml volumetric flasks using deionized distilled water at 95ºC for 4h. Moreover, Infra-Red Gas analyzer (IRG) was used to measure photosynthetic rate, stomatal conductance and mesophyll conductance to assess the effect of salt treatments.

Genomic DNA Extraction. Plant leaves (100-150 mg) of micropropagated date palm cultivar 'Sukary' plantlets were harvested for isolation of total genomic DNA under two NaCl treatments i.e. 200 mM and 400 mM including control plants. A modified DNA-extraction protocol was adopted using plant DNA-miniprep modified from Arif et al. [40]. Briefly, the freshly harvested date palm leaves were collected in sterile mortar. After adding 100mg sterile sand and 500 µl of lysis buffer [0.1 M Tris-HCl (pH 8.0), 0.05 M EDTA, 0.5 M NaCl and 0.01M β-mercaptoethanol] the plant material was

finely crushed using pestle and mortar. The crushed leaf material together with the buffer and sand were collected in sterile Eppendorf tubes (1.5 ml) and 1 ml of lysis buffer was added and vortexed, simultaneously. These extracts were then incubated and occasionally mixed at ~65ºC for 25 min. The extracts were cooled at 23ºC for 5 min and centrifuged at 12000 rpm for 5 min. Later, the supernatant (~200 µl) was transferred carefully into a sterile Eppendorf tube with equal volume of chloroform:isoamylalchohol (24:1). The tubes were mixed well with gentle shaking and centrifuged at 12000 rpm for 5 min. The supernatant (200 µl) was transferred to a new tube and the DNA was precipitated with cold isopropanol (500 µl). All the incubation and centrifugation steps were accomplished at room temperature. All the tubes were kept at -80ºC for 30 min followed by centrifugation at 12000 rpm for 10 min. After decanting and washing the DNA pellets with 70% cold ethanol, pellets were air dried at room temperature and the DNA was dissolved in 50 µl MQ water. The DNA was quantified and the quality was analyzed by loading 2 µl of total genomic DNA on 1% agarose gel electrophoresis in 0.5x TAE buffer. The DNA was stored at -20ºC until any downstream application.

RAPD-PCR analysis of isolated DNA. RAPD assay was accomplished in a total reaction volume of 25 µl including DNA-template (~50-100 ng), 2.5 µl of 10 pmol of 10-mer primer (Macrogen, Korea) (Table-4), 2.5 µl of dNTPs (0.4 mM each) DreamTaq DNA polymerase (Thermo Scientific) and 2.5 µl DreamTaq buffer (10x). PCR was carried out in a thermal cycler (BioRad) with initial denaturation at 95 ºC for 5 min, 35 cycles of 95 ºC for 35sec, 36 ºC for 35 sec, 72 ºC for 2 min, and a final extension at 72 ºC for 5 min. The PCR products were separated in 1% agarose gel using 0.5x TAE buffer. The size for all amplicons was confirmed by comparing to 1Kb DNA ladder (Takara).

Statistical analysis. To analyze the data, analysis of variance (ANOVA) was employed in randomized complete block design [41]. To compare the treatment means, the least significant difference (LSD) at 5% level of probability was used. SAS *software package* was used for all the statistical analysis.

RESULTS AND DISCUSSION

The induction of embryogenic callus was accomplished using shoot tips of date palm cultivar 'Sukary' as explant on MS-basal media. The calli were maintained by eight continuous sub-culturing on freshly prepared MS-basal media. Finally, the calli were subjected to regeneration media and the best performing calli were exposed to three NaCl treatments, i.e. 0, 200 and 400 mM NaCl. Two parallel batches of calli were produced as salt non-adapted (SNA) somaclones (those exposed directly to 200 and 400 mM NaCl) and salt-adapted (SA) somaclones (exposed gradually to 200 and 400 mM NaCl) . In this experiment four replicates for each treatment were used for morphological, physiological and biochemical studies. Four plants as negative control were obtained from the embryogenic calli grown under salt-free MS medium.

Morphological and physiological analysis of selected somaclones. The morphological data, including root length, shoot length, total plant dry weight and dry shoot/root ratio was collected. The regenerated plants or somaclones showed significant variation in the physiological parameters when compared to their the negative control (Table 1). The root length and shoot length were significantly increased with increasing salt concentrations in both the SNA and SA. Root length was recorded as 16.7 and 23.6 cm at 200 and 400 mM NaCl, respectively for SNA. Similarly, for SA at 200 and 400 mM the root length was significantly increased from 24.8 to 38.6 cm, respectively (Table 1). However, the root length of SA was higher as compared to the negative control as well as SNA somaclones. A similar pattern was observed in case of shoot length. The shoot length of SNA was 16.7 and 23.6 cm as compared to 24.8 and 38.6 cm in case of SA at 200 and 400 mM NaCl, respectively (Table 1). However, a different pattern was noted for total dry weight and dry leaf/root ratio. In SNA total dry weight was 0.749 and 0.560 gm at 200 and 400 mM NaCl. Whereas, in case of SA it was 0.386 and 0.701 gm, respectively. A similar pattern was observed for dry leaf/shoot ratio in SNA and SA (Table 1). It was observed that the performance of SA was significantly higher or comparable to SNA as well as negative control plants for root and shoot lengths at 200

TABLE 1
In vitro effect of salt stress on growth characters of the somaclones of the date palm cultivar, Sukary.

	Treatments	Root length (cm)	Shoot length (cm)	Total dry weight (gm)	Dry leaf/shoot ratio
Control	0:0	32.5±4.4^{b}	4.1±0.2^{c}	0.749±0.279^{a}	0.701±0.089^{c}
Somaclones Non-adapted (SNA)	0:200	16.7±0.4^{d}	1.2±0.2^{d}	0.749±0.279^{a}	3.078±0.01^{a}
	0:400	23.6±4.3^{c}	5.1±0.4^{a}	0.560±0.103^{b}	0.613±0.001^{c}
Somaclones Adapted (SA)	200:200	24.8±4.4^{c}	4.4±0.3^{c}	0.386±0.068^{c}	0.789±0.003^{c}
	400:400	38.6±4.9^{a}	5.4±0.7^{a}	0.701±0.089^{a}	1.469±0.001^{b}
	LSD at 5%	6.6	1.8	0.235	1.081

and 400 mM NaCl. Total dry weight and dry shoot/root ratio were decreased with increasing salt concentration in SNA, whereas, in case of SA it was vice versa.

The effect of increasing salt concentration was also determined for Na^+, K^+ concentrations and K^+/Na^+ ratio in leaves and roots of regenerated SNA as well SA (Table 2). It was observed that Na^+ accumulation was increased in leaves and roots of both SNA as well as SA somaclones as compared to the control plants. The K^+ concentrations were increased in leaves of both SNA as well as SA somaclones whereas, in roots it showed variable pattern. The K^+ concentrations were decreased in roots of SNA while, it was still increased in the SA somaclones (Table 2). The leaf K^+/Na^+ ratio in SNA somaclones was almost unchanged with increasing Na^+ in the external media. Whereas, K^+/Na^+ ratio in the leaves of SA somaclones was decreased with increasing salt concentration. On the other hand, the root K^+/Na^+ ratio was almost unchanged in case of SA as compared to the SNA somaclones. The reduction in K^+ accumulation in the roots of SA as compared to SNA somaclones at 400 mM NaCl points towards the better salt adaptation in the somaclones exposed under successive salt concentrations. The K^+/Na^+ ratio of leaves was decreased with increasing salt concentration, whereas, the K^+/Na^+ ratio of roots in SA somaclones was unchanged even at higher salt concentrations as compared to negative control (Table 2). This is another clue that SA somaclones has better adaptation than SNA under increased salt stress. There are certain reports indicating that the plants with high K^+ usually pose better tolerance to Na^+ accumulation [42, 43]. However, the ability of plant cells to cope with increased salt stress depends upon cytosolic K^+/Na^+ ratio rather than accumulation of Na^+ and/or K^+ concentrations of shoots and roots [44, 45]. For example, elevation of Na^+ concentrations in salt-tolerant tomato [46] and Na^+ exclusion in salt tolerant bread wheat have no relationship to the salt tolerance [47], respectively. Thus, intracellular K^+/Na^+ ratio is regarded as a major element of salt tolerance in plants. Thereby, plants optimize their cytosolic K^+/Na^+ ratio by either lessening accumulation of Na^+ or preventing the loss of K^+ [48]. In all the somaclones (SNA and SA) during this study, high accumulation of Na^+ was noted, which directed towards ionic toxicity of Na^+ under saline stress through osmotic impairment. However, an increase in K^+ concentrations and lower K^+/Na^+ ratio of SA somaclones showed that these have better osmatic regulation to cope with higher salinity.

Salt tolerance is strongly associated with maintenance of high photosynthetic rate and better stomatal conductance [49]. The effect of salinity on photosynthetic rate, stomatal conductance and mesophyll conductance was also measured in the regenerated date palm plants. It was noted that photosynthetic rate was decreased significantly in SNA somaclones from 4.38 to 4.17 (µmol/m2/s) at 200 and 400 mM NaCl, respectively. Whereas, photosynthetic rate of SA somaclones was measured as 4.93 at 200 mM NaCl and 3.56 (µmol/m2/s) at 400 mM NaCl as compared to control (6.58 µmol/m2/s) (Table 3). The stomatal conductance of SNA somaclones was significantly decreased from 8.88 to 4.55 (mmol/m2/s) whereas, in SA somaclones it decreased from 7.63 to 3.85 (mmol/m2/s) at 200 and 400 mM NaCl, respectively. It was decreased in SNA, while increased with increasing salt concentration in SA. However, in both SNA and SA somaclones the stomatal conductance was significantly decreased than the negative control. The measurement of mesophyll conductance showed a similar trend in both SNA and SA somaclones, i.e. decreased with increasing salt concentrations (Table 3). The mesophyll conductance of SNA and SA somaclones was 18.13 and 20.15 at 200 mM NaCl, while it was 11.73 and 12.10 (mmol/m2/s) at 400 mM NaCl, respectively. Salt tolerance in plants requires better maintenance of photosynthetic rate and stomatal conductance and ultimately a high concentration of chlorophyll in cells [50]. On the other hand, it can be a direct effect of Na^+ as observed in other woody plants such as citrus [51]. Besides, decrease in photosynthetic rate is directly associated to the stomatal closure to help plants to maintain their turgor pressure in the cells [52]. During our study, we found that the photosynthetic rate, stomatal conductance and mesophyll conductance were positively correlated to each other. The stomatal conductance of both SNA and SA somaclones was reduced significantly as compared to the control. However, compared to SNA somaclones the lower photosynthesis and stomatal

TABLE 2
In vitro effect of salt stress on the mineral concentrations (mg/100 g DW) of the somaclones of the date palm cultivar, Sukary.

	Treatments	Leaf			Root		
		Na	K	K^+/Na^+ ratio	Na	K	K^+/Na^+ ratio
Control	0:0	75.2±8.9^{d}	108±11.1^{b}	1.43±0.26^{a}	62.5±7.5^{e}	88.5±6.4^{c}	1.43±0.20^{a}
Somaclones non-adapted (SNA)	0:200	243±11.4^{b}	105.1±3.0^{c}	0.43±0.00^{d}	151±7.1^{d}	105±4.9^{b}	0.70±0.00^{b}
	0:400	709±67.6^{a}	384.7±25^{a}	0.55±0.04^{c}	209±13.9^{b}	91.7±6.1^{c}	0.44±0.00^{d}
Somaclones adapted (SA)	200:200	141.0±3.4^{c}	110±2.7^{b}	0.78±0.00^{b}	159±3.9^{c}	77.6±1.9^{d}	0.49±0.00^{c}
	400:400	234±14.7^{b}	114±7.1^{b}	0.49±0.00^{c}	276±17.3^{a}	123±7.7^{a}	0.45±0.00^{d}
	LSD at 5%	47.6	21.5	0.229	18.4	9.0	0.140

TABLE 3
In vitro effect of salt stress on physiological characters of the somaclones of the date palm cultivar, '*Sukary*'

	Characters/ Treatments	Photosynthesis (umol/m^2/s)	Stomatal conductance (mmol/m^2/s) (gs)	Mesophyll conductance (mmol/m^2/s) (gm)
Control	0:0	6.58±1.07^a	33.50±2.65^a	29.58±4.92^a
Somaclones Non-adapted (SNA)	0:200	4.38±0.20^c	8.88±0.98^b	18.13±3.55^c
	0:400	4.17±0.15^d	4.55±0.92^d	11.73±1.75^d
Somaclones adapted (SA)	200:200	4.93±0.50^b	7.63±0.67^c	20.15±3.64^b
	400:400	3.56±0.42^e	3.85±0.76^d	12.10±1.40^d

TABLE 4
List of RAPD primers used to detect genetic variation in regenerated date palm plants of cultivar 'Sukary'under salinity stress.

No.	Primer Name	Primer Sequence	Band Score			Size range (bp)
			Control	200 mM	400 mM	
1	OPA-03	AGTCAGCCAC	8	8	8	600-3600
2	OPA-05	AGGGGTCTTG	5	5	5	1800-5000
3	OPA-07	GAAACGGGTG	3	3	3	600-4000
4	OPA-10	GTGATCGCAG	5	5	5	1100-4500
5	OPA-15	TTCCGAACCC	1	1	1	4000
6	OPB-10	CTGCTGGGAC	8	8	8	500-4000
7	OPC-02	GTGAGGCGTC	1	1	1	2000
8	OPC-05	GATGACCGCC	4	4	4	1800-4000
9	OPC-08	TGGACCGGTG	0	0	0	No amplification
10	OPC-11	AAAGCTGCGG	0	0	0	No amplification
11	OPD-11	AGCGCCATTG	0	0	0	No amplification
12	OPD-12	CACCGTATCC	0	0	0	No amplification
13	OPD-20	ACCCGGTCAC	2	2	2	1800-2200
14	OPE-01	CCCAAGGTCC	6	6	6	250-2800
15	OPE-18	GGACTGCAGA	4	4	4	1800-3100
16	OPE-19	ACGGCGTATG	6	6	6	600-2800
17	OPF-10	GGAAGCTTGG	2	2	2	1900-3000
18	OPG-18	GGCTCATGTG	0	0	0	No amplification
19	OPH-04	GGAAGTCGCC	2	2	2	3000-3500
20	OPI-02	GGAGGAGAGG	3	3	3	1800-2800
21	OPI-08	TTTGCCCGGT	7	7	7	1100-4000
22	OPM-10	TCTGGCGCAC	5	5	5	1500-3000
23	OPN-13	AGCGTCACTC	5	5	5	1050-4000
24	OPP-08	ACATCGCCCA	0	0	0	No amplification
25	MOH-2	GAGGCGTCGC	2	2	2	2000-3500
26	MOH-3	CCCTACCGAC	0	0	0	No amplification
27	MOH-5	CACCTTTCCC	2	2	2	2100-2900
28	MOH-7	GTTCCGCTCC	8	8	8	500-5000
29	MOH-8	GTGAGGCGTC	9	9	9	500-4000
30	MOH-9	GGACCCAACC	9	9	9	1100-4000

conductance of SA revealed that the SA somaclones have adjusted their turgor pressure under gradual increase in the salt stress and thus have improved their adaptation better than SNA somaclones.

The dominantly highest salt prevails in nature is NaCl, which primarily exerts two major effects on plants i.e. osmotic stress and ionic toxicity. Salt stress exerts drastic effects on overall plant physiology in many different ways ranging from physiological and metabolic changes, which end up into molecular impairment [6, 7]. Such impairments in plant growth are due to drastic changes in osmotic pressure and ionic balance in cells, which ultimately leads to provoke secondary stresses, including oxidative stress and nutritional impairments [53]. The plants growing in salt-free environment usually have higher gradient of water and minerals in the root cells due to high osmotic pressure as compared to the soil solution. Whereas, highly saline environment exerts a negative effect on this gradient and ultimately increase the osmotic pressure in the soil solution, which ultimately leads to inaccessibility of water and indispensable cations, such as K^+ and Ca^{2+} ions, to the plants [54]. As a result, Na^+ and Cl^- ions enter into the cells and exerts cellular toxicity on cell membranes and cytosol [55, 56]. There is always a contest between Na^+ toxicity and K^+ accumulation to activate certain enzymes in plant cells under salt stress. The tolerant/adapted plants always keep a balance between Na^+ and K^+ accumulation. Thus in the SA somaclones the accumulation of K^+ is almost unchanged in leaves at 200 and 400 mM NaCl whereas, it was increased at 400mM NaCl in roots as compared to the SNA somaclones (Table 2). It might result into relative increase in root length of the SA somaclones in comparison to the SNA somaclones in this study (Table 1). The SA somaclones, thereby, has adjusted themselves to the gradual elevation of NaCl.

Molecular analysis of selected somaclones. Leaf samples of date palm cultivar 'Sukary' plants derived from SA calli under the salt treatments 200 and 400 mM NaCl and negative control at 0 mM NaCl were used for RAPD analysis. RAPD fingerprinting was carried out using two sets of PCRs for each sample to assess the presence of any somaclonal variation in the SA somaclones. A control sample from the mother plant was run along with the samples of each treatment. Only those bands were considered for analysis, which were reproducible from the repeated PCR run. In order to examine the genetic fidelity of the selected somaclones against salt stress, 30 RAPD primers were used, out of which 23 primers produced clear and reproducible bands (Table 4). These 23 primers produced 107 amplicons for each treatment ranging between 250-5000 bp in size. These primers produced 1-9 bands with an average of 4.65 bands per RAPD primers. In total 321 bands (Total plants analyzed x Total number of amplicons produced) were generated using RAPD.

The entire RAPD analysis produced only monomorphic pattern among all date palm somaclones and their mother plants while no polymorphism was observed (Fig. 1). This is a comparable analysis as evident from the previous studies with various plant species employing PCR based RAPD analysis [57-59], including date palm [60]. Appearance of somaclonal variations during in vitro culturing relies upon the type of explant used in the experiment and the method of regeneration [17]. Moreover, the use of synthetic type of plant growth regulators also reported to cause somaclonal variations [57]. The plant genome undergoes certain changes associated with ploidy, chromosomal abnormality, appearance of SNPs and epigenetic changes [61].

Thus, during regular in vitro culturing it is of utmost importance to regulate the genetic fidelity of the micropropagated plants. Various molecular techniques are in use for the assessment of genetic stability of these micropagated plants, which involve use of DNA-markers. Among such techniques RAPD has become a robust technique due to its economical applications [57]. RAPD has become a reliable and widely used tool in molecular plant research for the assessment of inter- and intra-specific genetic variability and to study genetic expression patterns in plants [62]. Besides RAPD, other molecular markers also offer a consistent, dominant and rapid tool to be used in analyzing somaclonal variation during in vitro regeneration in higher plants [63-67]. During this study, we could not find any somaclonal variation among different salt treatments endured by date palm cultivar 'Sukary'. Our study is consistent to previously reported studies for the absence of somaclonal variation during in vitro culturing of different tree plants, i.e. oak, Olea, *Juniperus phoenicea* and *Pinus thunbergii* [64, 65, 68]. These results were related to woody plant, indicating that this protocol could not be successful in woody species.

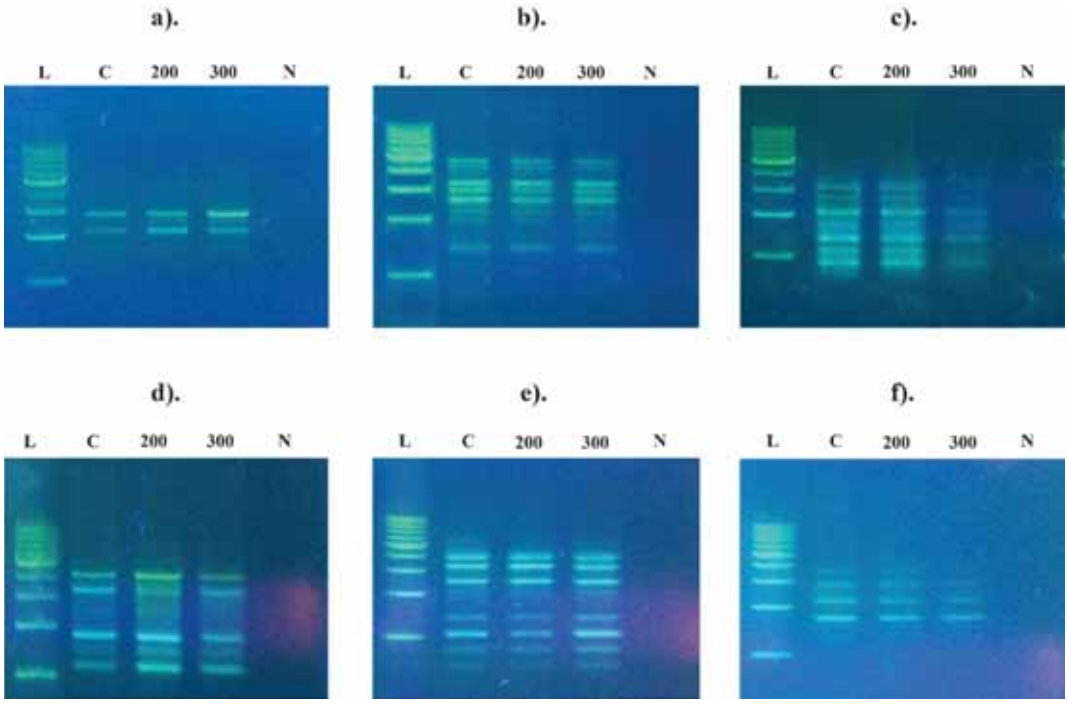

FIGURE 1

RAPD profiling of regenerated date palm (cultivar '*Sukary*') plantlets under three salinity levels i.e. Control, 200 mM NaCl and 300 mM NaCl generated by primer MOH-05 a), MOH-07 b), OPA-03 c), OPA-10 d), OPB-10 e) and OPC-05 f). L-DNA Ladder (1Kb, Takara), C-control plant (0 mM NaCl), 200 mM NaCl, 400 mM NaCl and N-negative control for PCR.

Thus, it is obvious that the variations between SA and SNA somaclones are not inherent rather, these are the results of salt adaptation mechanism of the SA somaclones. Alternatively, the somaclonal variation may also appear due to occurrence of point mutation in the plant genomes, which cannot be detected by marker-assisted techniques. Thus, application of more advanced techniques such as next generation sequencing of the whole genome or exome capture sequencing of the functional region in the genome may give a clear picture of the genetic changes occuring during somaclonal variations [69].

CONCLUSION

During our study, the SA somaclones of date palm showed positive morphological and physiological response to the high salinity levels. Nevertheless, this response was seemed not related to the genetic changes incurred during salt stress. Besides the major changes at chromosomal level or duplication and deletion of specific regions, the abiotic stress tolerance in the somaclones may also arise due to base changes in the respective genes. Further studies to detect such point mutations in stress related genes through exome capture sequencing or whole genome sequencing may provide better insight into the in vitro stress response of somaclones in the future. It may also help to devise better strategies against salt stress in date palm.

ACKNOWLEDGEMENTS

This study was supported by a research grant project “08-BIO14-06” from ‘King Abdulaziz City for Science and Technology’ under National Science, Technology and Innovation Plan (NSTIP), Kingdom of Saudi Arabia.

REFERENCES

[1] El-Beltagi, H.S., Salama, Z.A., El Hariri, D.M. (2008) Some biochemical markers for evaluation of flax cultivars under salt stress conditions. J. Nat. Fibers. 5, 316-330

[2] El-Beltagi, H.S., Mohamed, H.I., Mohammed, A.H.M.A., Zaki, L.M., Mogazy, A.M. (2013) Physiological and biochemical effects of γ-irradiation on cowpea plants (*Vigna sinensis*) under salt stress. Not. Bot. Hort. Agrobot. Cluj 41, 104-114.

[3] Golldack, D., Li, C., Mohan, H., Probst, N. (2014) Tolerance to drought and salt stress in plants, unraveling the signaling networks. Front. Plant Sci. 5, 151.

[4] Zhang, H., Han, B., Wang, T., Chen, S.X., Li, H.Y. (2012) Mechanisms of plant salt response, insights from proteomics. J. Proteome Res. 11, 49-67.

[5] El-Beltagi, H.S., Ahmed, S.H., Namich, A.A.M., Abdel-Sattar, R.R. (2017) Effect of salicylic acid and potassium citrate on cotton plant under salt stress. Fresen. Environ. Bull. 26, 1091-1100.

[6] Wang, W.X., Barak, T., Vinocur, B., Shoseyov, O., Altman, A. (2007) Abiotic resistance and chaperones, possible physiological role of SP1, a stable and stabilizing protein from Populus. In, Vasil, K. Plant Biotechnology 2000 and Beyond. 1st Ed. (Dordrecht, Kluwer), 439-443.

[7] Sobhanian, H., Aghaeib, K., Komatsu, S. (2011) Changes in the plant proteome resulting from salt stress, toward the creation of salt-tolerant crops. J. Proteom. 74, 1323-1337.

[8] Flowers, T.J., Colmer, T.D. (2015) Plant salt tolerance, adaptations in halophytes. Ann. Bot. 115, 327–331.

[9] Hassan, S., Bakhsh, K., Z.A. Gill, Maqbool, A., Ahmad, W. (2006) Economics of growing date palm in Punjab, Pakistan. Int. J. Agri. Biol. 8, 788-792.

[10] Taha, H.S., Bakheet, S.A., EL-Bahr, M.K. (2003) Alternative approach for micropropagation of the date palm c.v. Zaghlool. Arab J. Biotechnol. 6, 103-112.

[11] El-Beltagi, H.S., Ahmed, O.K., El-Desouky, W. (2011) Effect of low doses γ-irradiation on oxidative stress and secondary metabolites production of rosemary (*Rosmarinus officinalis* L.) callus culture. Radiat. Phys. Chem. 80, 968-976.

[12] Mohamed, H.I., Akladious, S.A., El-Beltagi, H.S. (2018) Mitigation the harmful effect of salt stress on physiological, biochemical and anatomical traits by foliar spray with trials on wheat cultivars. Fresen. Environ. Bull. 27, 7054-7065.

[13] Abul-Soad, A.A., Al-Khayri, J.M. (2018) Date palm somatic embryogenesis from inflorescence explant. In, Jain S., Gupta P. (eds) Step Wise Protocols for Somatic Embryogenesis of Important Woody Plants. Forestry Sciences. Vol 85. Springer, Champ. 329-347.

[14] Al-Khayri, J.M. (2018) Somatic Embryogenesis of Date Palm (*Phoenix dactylifera L.*) from Shoot Tip Explants. In, Jain S., Gupta P. (eds) Step Wise Protocols for Somatic Embryogenesis of Important Woody Plants. Forestry Sciences. Vol 85. Springer, Cham. 231-244.

[15] Matthes, M., Singh, R., Cheah, S.C., Karp, A. (2001) Variation in oil palm (*Elaeis guineensis* Jacq.) tissue culturederived regenerants revealed by AFLPs with methylationsensitive enzymes. Theor. Appl. Genet. 102, 971–979.

[16] Afify, A.M.R., El-Beltagi, H.S., Abd El-Salam, S.M., Omran, A.A. (2012) Protein solubility, digestibility and fractionation after germination of sorghum varieties. PLoS ONE. 7, e31154, 1-6.
[17] Krishna, H., Alizadeh, M., Singh, D., Singh, U., Chauhan, N., Eftekhari, M., Sadh, R.K. (2016) Somaclonal variations and their applications in horticultural crops improvement. 3 Biotech. 6, 54.
[18] Bhojwani, S.S., Dantu, P.K. (2013) Plant tissue culture, an introductory text. Springer New Delhi, India.
[19] Hammerschlag, F.A., Garces, S., Koch-Dean, M., Ray, S., Lewers, K., Maas, J., Smith, B.J. (2006) In vitro response of strawberry cultivars and regenerants to *Colletorichum acutatum*. Plant Cell Tissue Org. Cult. 84, 255-261.
[20] Khan, S., Al-Qurainy, F., Mohammad, N. (2012) Biotechnological approaches for conservation and improvement of rare and endangered plants of Saudi Arabia. Saudi J. Biol. Sci. 19, 1-11.
[21] Elshibli, S., Korpelainen, H. (2007) Microsallite markers reveal high genetic diversity in date palm (*Phoenix dactylifera* L.) germplasm from Sudan. Genetica. 134, 251-260.
[22] Ahmad, R., Anjum, M.A., Malik, W. (2018) Characterization and evaluation of mango germplasm through morphological, biochemical, and molecular markers focusing on fruit production, An overview. Mol. Biotechnol. 2018.
[23] Rasheed, A., Xia, X. (2019) From markers to genome-based breeding in wheat. Theor. Appl. Genet. 132(3), 767-784.
[24] Jones, R.C., Steane, D.A., Lavery, M., Vaillancourt, R.E., Potts, B.M. (2013) Multiple evolutionary processes drive the patterns of genetic differentiation in a forest tree species complex. Ecol. Evol. 3(1), 1-17.
[25] Bertaccini, A., Paltrinieri, S., Contaldo, N. (2019) Standard Detection Protocol, PCR and RFLP Analyses Based on 16S rRNA Gene. In: Musetti, R., Pagliari, L. (eds.) Phytoplasmas. Methods in Molecular Biology. vol 1875. Humana Press, New York, NY.
[26] Sudhaa, G.S., Ramesh, P., Sekhar, A.C.., Krishna, T.S., Bramhachari, P.V., Riazunnisa, K. (2019) Genetic diversity analysis of selected Onion (*Allium cepa* L.) germplasm using specific RAPD and ISSR polymorphism markers. Biocat. Agric. Biotech. 17, 110-118.
[27] Venkatachalam, L., Sreedha, R.V., Bhagyalakshmi, N. (2007) Micropropagation in banana using high levels of cytokinins does not involve any genetic changes as revealed by RAPD and ISSR markers. Plant Growth Reg. 51, 193-205.
[28] Santos M.D.M., Buso, G.C.S., Torres, A.C. (2008) Evaluation of genetic variability in micropropagated propagules of ornamental pineapple [*Ananas comosus* var.bracteatus (Lindley) Coppens and Leal] using RAPD markers. Genet. Mol. Res. 7, 1097-1105.
[29] Ahmed, O., Chokri, B., Noureddine, D., Mohamed, M., Mokhtar, T. (2009). Regeneration and molecular analysis of date palm (*Phoenix dactylifera* L.) plantlets using RAPD markers. African J. Biotech. 8, 813-820.
[30] Huang, W.J., Ning, G.G., Liu, G.F., Bao, M.Z. (2009) Determination of genetic stability of long-term micropropagated plantlets of *Platanus acerifolia* using ISSR markers. Biol. Plant. 53, 159-163.
[31] Gantait, S., El-Dawayati, M.M., Panigrahi, J., Labrooy, C., Verma, S.K. (2018) The retrospect and prospect of the applications of biotechnology in *Phoenix dactylifera* L. Appl. Microbiol. Biotechnol. 102, 8229-8259.
[32] Kanita, A., Kothari, S.I. (2002) High efficiency adventitious shoot bud formation and plant regeneration from leaf explants of *Dianthus chinensis* L. Sci. Hort. 96, 205-212.
[33] Trifi. M., Rhouma, A., Marrakchi, M. (2000) Phylogenetic relationships in Tunisian datepalm (*Phoenix dactylifera* L.) germplasm collection using DNA amplification fingerprinting. Agronomie. 20, 665-671.
[34] Kumar, N., Modi, A.R., Singh, A.S., Gajera, B.B., Patel, A.R., Patel, M.P., Subhash, N. (2010) Assessment of genetic fidelity of micropropagated date palm (*Phoenix dactylifera* L.) plants by RAPD and ISSR markers assay. Physiol. Mol. Biol. Plants. 16 , 207-213.
[35] Al-Khateeb, A.A., Al-Khateeb, S.A. (2015) Effect of different combinations of growth hormones and its interaction on callogenesis. Res. J. Biotechnol. 10(11), 83-88.
[36] Al-Khateeb, A.A., Al-Khateeb, S.A. (2016) In vitro role of hormones at multiplication stage of date palm (*Phoenix dactylifera* L.) cvs. Khalas and Sukary. Res. J. Biotech. 11(1), 58-63
[37] Murashige, T., Skoog, F. (1962) A revised medium for rapid growth and bioassays with tobacco tissue cultures. Physiolo. Plant. 13, 473-497.
[38] Al-Khateeb, A.A. (2001) Influence of different carbon sources and concentrations on the root formation of date palm (*Phoenix dactylifera* L.) cv. Khanezi. Zagazig J. Agric. Res. 28, 597-608.
[39] AOAC. (2000) Official Methods of Analysis of the Association of Official Analytical Chemists.17th edn. (edited by Horwitz, W.) Washington, D.C.

[40] Arif, I. A., Bakir, M. A., Khan, H.A., Ahamed, A., Al Farhan, A.H., Al Homaidan, A.A., Al Sadoon, M., Bahkali, A.H., Shobrak, M. (2010) A Simple Method for DNA Extraction from Mature Date Palm Leaves, Impact of Sand Grinding and Composition of Lysis Buffer. Int. J. Mol. Sci. 11, 3149-3157.

[41] Gomez, K.A., Gomez, A. (1984) Statistical Procedure for Agricultural Research—Hand Book. John Wiley and Sons, New York.

[42] Caterina, R., Giuliani, M.M. (2007) Influence of salt stress on seed yield and oil quality of two sunflower hybrids. Ann. Appl. Biol. 151, 145-154.

[43] Liang, W., Ma, X., Wan, P., Liu, L. (2019) Plant salt-tolerance mechanism: A review. Biochem. Biophys. Res. Commun. 495, 286-291.

[44] Shabala, S., Cuin, T.A. (2007) Potassium transport and plant salt tolerance. Physiol. Plant. 133, 651-669.

[45] Almeida, D.M., Oliveira, M.M., Saibo, N.J.M. (2017) Regulation of Na+ and K+ homeostasis in plants: towards improved salt stress tolerance in crop plants. Genetic. Mol. Biol. 40, 326–345.

[46] Egea, I., Pineda, B., Ortíz-Atienza, A., Plasencia, F.A., Drevensek, S., Garcia-Sogo, B., Yuste-Lisbona, F.J., Barrero-Gil, J., Atares, A., Flores, F.B., Barneche, F., Angosto, T., Capel, C., Salinas, J., Vriezen, W., Esch, E., Bowler, C., Bolarin, M.C., Moreno, V., Lozano, R. (2018) The SlCBL10 Calcineurin B-Like Protein Ensures Plant Growth under Salt Stress by Regulating Na^+ and Ca^{2+} Homeostasis. Plant Physiol. 176, 1676-1693.

[47] Genc, Y., McDonald G.K., Tester, M. (2007) Reassessment of tissue Na1 concentration as a criterion for salinity tolerance in bread wheat. Plant Cell Environ. 30(11), 1486-98.

[48] Ganie, S.A., Molla, K.A., Henry, R.J., Bhat, K.V. Mondal, T.K. (2019) Advances in understanding salt tolerance in rice. Theor. Appl. Genet. 132(4), 851-870.

[49] Martinez, V., Nieves-Cordones, M., Lopez-Delacalle, M. (2018) Tolerance to stress combination in tomato plants: new insights in the protective role of melatonin. Molecules. 23(3), 535.

[50] Zanetti, F., Zegada-Lizarazu, W., Lambertini, C., Monti, A. (2019) Salinity effects on germination, seedlings and full-grown plants of upland and lowland switchgrass cultivars. Biomass Bioenerg. 120, 273-280.

[51] Kusumi K., Hirotsuka, S., Kumamaru, T., Iba, K. (2012) Increased leaf photosynthesis caused by elevated stomatal conductance in a rice mutant deficient in SLAC1, a guard cell anion channel protein. J. Exp. Bot. 63, 5635-44.

[52] López-Climent, M.F., Arbona, V., Pérez-Clemente, R.M., Gómez-Cadenas, A. (2008) Relationship between salt tolerance and photosynthetic machinery performance in citrus. Environ. Exp. Bot. 62, 176–184.

[53] Chinnusamy, V., Zhu J., Zhu, J.K. (2006) Gene regulation during cold acclimation in plants. Physiol. Plant. 126, 52-61.

[54] Munns, R., James, R.A., Läuchli, A. (2006) Approaches to increasing the salt tolerance of wheat and other cereals. J. Exp. Bot. 57, 1025-1043.

[55] Hasegawa, P.M., Bressan, R.A., Zhu, J.K., Bohneert, H.J. (2000) Plant cellular and molecular responses to high salinity. Annual Rev. Plant Physiol. Plant Mol. Biol. 51, 463-499.

[56] Zhu, J.K. (2001) Plant salt tolerance. Trend. Plant Sci. 6, 66-71.

[57] Martins, M., Sarmento, D., Oliveira, M.M. (2004) Genetic stability of micropropagated almond plantlets, as assessed by RAPD and ISSR markers. Plant Cell Rep. 23, 492-496.

[58] Joshi, P., Dhavan, V. (2007) Assessment of genetic fidelity of micropropagated Swertia chirayita plantlets by ISSR marker assay. Biol. Plant. 51, 22-26.

[59] Lakshman, V., Venkataramareddy S.R., Neelwarne, B. (2007) Molecular analysis of genetic stability in long-term micropropagated shoots of banana using RAPD and ISSR markers. Electronic J. Biotechnol. 10, 1-8.

[60] Moghaieb. R.E.A., Abdel-Hadi, A., Hadi, A., Ahmed M.R.A. (2011) Genetic stability among date palm plantlets regenerated from petiole explants. African J. Biotechnol. 10, 14311-14318.

[61] Neelakandan, A.K., Wang, K. (2012) Recent progress in the understanding of tissue culture-induced genome level changes in plants and potential applications. Plant Cell Rep. 31, 597-620.

[62] Dabkevicius, Z., Gelvonauskis, B., Leistrumaite, A. (2008) Investigation of genetic resources of cultivated plants in Lithuania. Biologija. 54, 51-55.

[63] Burg, K., Helmersson, A., Bozhkov, P., Arnold S.V. (2007) Developmental and genetic variation in nuclear microsatellite stability during somatic embryogenesis in pine. J. Exp. Bot. 58, 687-698.

[64] Loureiro, J., Capelo, A., Brito, G., Rodriguez, E., Silva, S., Pinto, G., Santos, C. (2007) Micropropagation of *Juniperus phoenicea* from adult plant explants and analysis of ploidy stability using flow cytometry. Biol. Plant. 51, 7-14.

[65] Lopes, T., Capelo, A., Brito, G., Loureiro, J. Santos, C. (2009) Genetic variability analyses of the somatic embryogenesis induction process in *Olea* spp. using nuclear microsatellites. Trees. 23, 29-36.
[66] Munir, F., Naqvi, S.M.S., Mahmood, T. (2011) In vitro culturing and assessment of somaclonal variation of *Solanum tuberosum* var. desiree. Turk. J. Biochem. 36, 296-302.
[67] Pandey, R.N., Singh, S.P., Rastogi, J., Sharma, M.L., Singh, R.K. (2012) Early assessment of genetic fidelity in sugarcane (*Saccharum officinarum*) plantlets regenerated through direct organogenesis with RAPD and SSR markers. Aust. J. Crop Sci. 6, 618-624.
[68] Valladares, S., Sanchez, C., Martinez, M.T., Ballester A., Vieitez, A.M. (2006) Plant regeneration through somatic embryogenesis from tissues of mature oak trees, True-to-type conformity of plantlets by RAPD analysis. Plant Cell Rep. 25, 879-886.
[69] Sattar, M.N., Iqbal, Z., Tahir, M.N., Shahid, M.S., Khurshid, M., Al-Khateeb, A.A., Al-Khateeb, S.A. (2017) CRISPR/Cas9: A practical approach in date palm genome editing. Front Plant Sci. 8, 1-16.

Received: **15.03.2019**
Accepted: **26.03.2019**

CORRESPONDING AUTHOR

Suliman A Al-Khateeb
Environment and Natural Resources Department,
College of Agriculture and Food Sciences,
King Faisal University, P.O. Box 400,
Al-Ahsa 31982 – Kingdom of Saudi Arabia.

e-mail: skhateeb@kfu.edu.sa

© by PSP Volume 28 – No. 5/2019 pages 3696-3703 Fresenius Environmental Bulletin

EVALUATION ON THE STATUS QUO OF WATER ENVIRONMENTAL FOR THE UPPER AND MIDDLE REACHES OF THE YARLUNG ZANGBO RIVER IN THE LOW WATER PERIOD

Haitao Wang[1], Bo Ma[1], Shizhan Tang[1], Zhongxiang Chen[1], Lei Li[1], Jilong Wang[1], Guo Hu[1], Feng Ji[1,*], Junhua Gong[2], Chi Zhang[2]

[1]Heilongjiang River Fisheries Research Institute of Chinese Academy of Fishery Sciences, Harbin, Heilongjiang, China, 150070
[2]River Fisheries Research Institute of Tibet Academy of Agricultural and Animal Husbandry Sciences, Lhasa, Tibet, China, 850000

ABSTRACT

Water samples at 12 sampling sites in the upper and middle reaches of the Yarlung Zangbo River were collected; water quality indexes such as permanganate index, total phosphorus, petroleum, total nitrogen, ammonia nitrogen and heavy metal, etc. were detected; influence factors such as population density and river discharge, etc. in the upper and middle reaches of the Yarlung Zangbo River were combined to analyze the correlation between human activities and runoff rate & water quality. Results showed that sampling sites 6 and 7 close to Lhasa, with the largest density of population in Tibet, had both the highest content of ammonia nitrogen and total nitrogen in the water body of the Yarlung Zangbo River. Heavy metal elements such as Cu, Zn and Cr had a higher content in the densely populated areas. Content of nickel (Ni), zinc (Zn), arsenic (As), aluminum (Al), vanadium (V), manganese (Mn), ferrum (Fe), barium (Ba) and lead (Pb) was greatly affected by river runoff. Organic pollutants such as PCB, PAH, organochlorine pesticide, plasticizer, etc. were not detected at all sampling sites.

KEYWORDS:
Yarlung Zangbo River, low water period, water environment

INTRODUCTION

Originated from Jiema Yangzong glacier in the north of the Himalayas, the Yarlung Zangbo River flows through Shigatse, Nyingchi, etc. of Tibet Autonomous Region, steers away from Namche Barwa Snow Mountain, flows into India and Bangladesh through Motuo, and finally becomes merged in the Indian Ocean. The Yarlung Zangbo River is one of the world famous high mountain rivers. It is mostly located in high mountain areas, with rich mineral resources in mountainous areas along the bank. Most parts of the river have a large fall and suffer serious water and soil loss; such topographic features and climatic conditions cause climate change sensitivity and vulnerability of ecosystem [1-5].

In recent years, the government of China has paid special attention to the development and economic growth of Tibet. From the perspective of agriculture, rice planting industry of Nyingchi Prefecture has already taken shape. From the perspective of transportation, plenty of road and bridge projects have been under construction. From the perspective of industry, water-power enginee-ring construction along the bank of the Yarlung Zangbo River has been intensified. Such human activities have posed a great threat to the vulnerable ecological environment. During the low water period, shrinkage of river runoff causes a "concentration effect" to some pollutants. Since low water period is the most vulnerable period of river environment, great changes in water quality can easily affect aquatic organisms in the Yarlung Zangbo River. Current situation of water quality of the Yarlung Zangbo River has been investigated in this paper, which provides data foundation for evaluation of its environmental changes.

MATERIALS AND METHODS

Research area and sampling site. According to the development situations of industry and agriculture along the bank of the Yarlung Zangbo River as well as the construction situations of water & electricity, roads & bridges, etc., combined with the distribution of spawning ground, feeding ground, etc. of fish, 12 sampling sites from St.1 to St.12 (N 29º15.93" and E 95º11.292-N 30°10.515′ and E 83°06.037) were confirmed (Table 1).

Sampling sites covered the lower reaches of environmentally sensitive areas, as shown in Fig. 1. Water samples were selected from surface layer, middle layer and bottom layer and were mixed evenly; samples of heavy metals and other metallic

elements were stored in a 250mL polyethylene bottle, and samples of petroleum, permanganate index, total phosphorus, total nitrogen and ammonia nitrogen were stored in a glass bottle.

Detection method. Metallic elements were analyzed by using inductively coupled plasma mass spectrometry (ICP-MS) [6-11]; petroleum was analyzed by using infrared spectroscopy (IR); total phosphorus, total nitrogen and ammonia nitrogen were analyzed by using spectrophotometry; PCB, PAH, organochlorine pesticide and plasticizer were analyzed by using gas chromatography.

TABLE 1
Sampling site's longitude and latitude

Sampling site	North latitude (N)	East longitude (E)
St.1	29°15′093"	95°11′292"
St.2	29°30′815"	94°51′109"
St.3	29°11′829"	94°06′238"
St.4	29°04′391"	92°50′719"
St.5	29°16′804"	92°04′009"
St.6	29°16′042"	90°46′026"
St.7	29°20′705"	89°38′741"
St.8	29°21′934"	88°06′687"
St.9	29°06′573"	87°29′980"
St.10	29°19′001"	85°12′010"
St.11	29°42′865"	83°59′028"
St.12	30°10′515"	83°06′037"

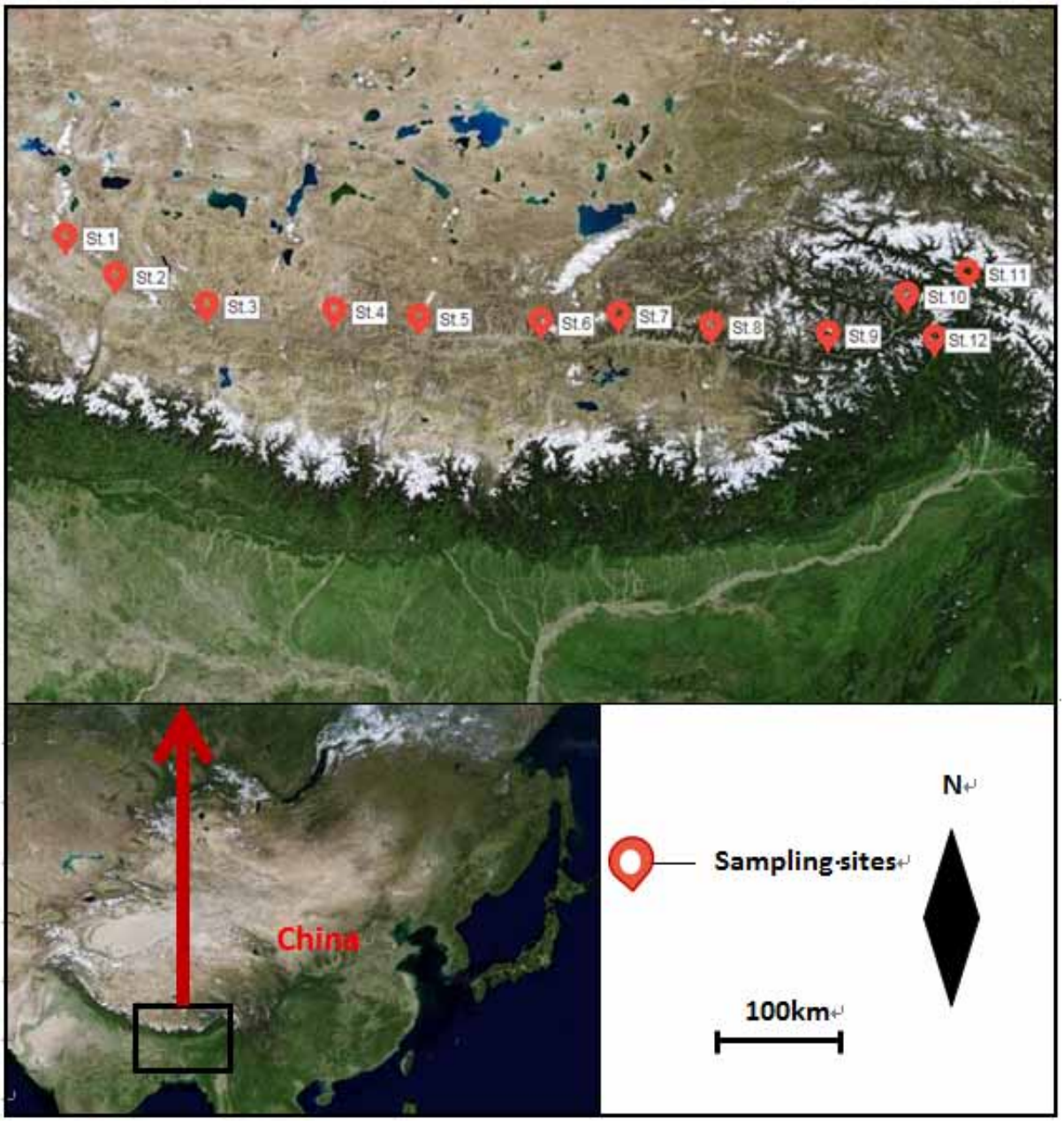

FIGURE 1
Sampling site's location diagram

RESULTS AND CONCLUSIONS

Analysis of total nitrogen and ammonia nitrogen. Total nitrogen (TN) and ammonia nitrogen (NH_4^+-N) are main existing forms of nitrogen in the water ecosystem, and excess nitrogen input may cause side effects such as water acidification, eutrophication, toxicity, etc. and endanger health of the ecological system [12-13]. With the increase of human activities along the bank of the Yarlung Zangbo River year by year and the development of rice planting industry in Nyingchi and other regions, it is of great importance to pay close attention to nitrogen cycle of the Yarlung Zangbo River. Content of TN and NH_4^+-N of the Yarlung Zangbo River is shown in Fig. 2a and 2b. Content of TN is approximate to that of content of TN, and the sampling site 7 (St.7) has the highest content of TN and NH_4^+-N.

Petroleum. Petroleum is a mixture with complicated components, containing many carcinogenic substances difficult for micro-biological degradation. High-concentration petroleum in water can generate micronucleus in the fish body, resulting in structural imbalance of marine ecosystem, decrease of biodiversity index and productivity impairment. Long-term exposure of petroleum will affect ingestion, growth and reproduction of marine animals and cause irreversible tissue damages. Carcinogenic substances contained in petroleum may be concentrated in fat of animals, and then transferred by food chain, affecting the quality of aquatic products, and consequently pose a direct threat to human health. Ocean is the gathering place of petroleum pollutants. With the increase in exploitation, processing and utilization of total petroleum compounds and the increase in total petroleum compounds which enter the sea by all means, marine petroleum pollution has become a key pollutant of offshore areas [14]. Content of petroleum in the water body of the Yarlung Zangbo River is shown in Fig. 2c. Differences in the content of petroleum substances show no obvious rules at 12 sampling sites, sampling site 3 has the highest content of petroleum, while sampling sites 5, 7, 8, 9 and 10 have the lowest content of petroleum.

Total phosphorus. Phosphorus is an indispensable part for growth and reproduction of marine phytoplankton, as well as the foundation for marine primary productivity and food chain. Its input, dispersion and removal is a process combining physical, chemical and biological actions. Thus, change of its concentration is mainly affected by water movement, offshore runoff, biological effect, etc. Moderate nutritive salt in seawater is conducive to growth of phytoplankton, while excess nutritive salt will cause eutrophication of water and even red tide under certain conditions. Marine phosphate is originated from land runoff and atmospheric sedimentation. In the continental shelf, river is the main way for phosphate to enter the sea [15]. Content of total phosphorus in the water body of the Yarlung Zangbo River is shown in Fig. 2d. Content of total phosphorus shows little differences at all sampling sites, while sampling sites 1, 7 and 12 have the highest content of total phosphorus.

Permanganate index. Permanganate index (COD_{Mn}) means the calculation of oxygen consumption under certain conditions according to the permanganate consumed by using organic and inorganic reductive substances contained in permanganate oxidation water samples, which is expressed by oxygen concentration (mg/L). It is an important index used to balance the pollution level of surface water in our country and a compre-hensive reflection of pollution level of water body by organic matters and reductive inorganic matters [16-17]. Content of COD_{Mn} in the water body of the Yarlung Zangbo River is shown in Fig. 2e. Sampling sites 1 and 10 have the highest content of COD_{Mn}, while other sampling sites show little differences.

Metallic elements. Metallic elements contained in water are special substances which will gather in the body of aquatic organisms [18]. Where, heavy metals such as cadmium (Cd), mercury (Hg), arsenic (As), lead (Pb), etc. are harmful elements with different carcinogenic effects. Moderate metallic elements such as copper (Cu), zinc (Zn), etc. are conducive to organisms, while excess of such metallic elements has toxic action on organisms. Some are essential elements for organisms which play an indispensable role in organism's vital movement. For example, Fe is essential for oxygen transportation of organisms. Although biological significance of some metallic elements such as strontium (Sr) has not been identified, they exist in geological background and sediments of rivers, and may migrate between river water and sediments. Content of such elements existing in high mountain rivers such as the Yarlung Zangbo River has also drawn public attention [19]. Content of Co, Se, Hg, Cd, etc. in the water body of the Yarlung Zangbo River is shown in Table 2, and contents of other metallic elements are shown in Fig. 2f-2p. Content of metallic elements shows good rules at all sampling sites, content of nickel (Ni), zinc (Zn), arsenic (As), aluminum (Al), vanadium (V), manganese (Mn), ferrum (Fe), barium (Ba) and lead (Pb) decreases from sampling site 1 to sampling site 12, except individual exceptions.

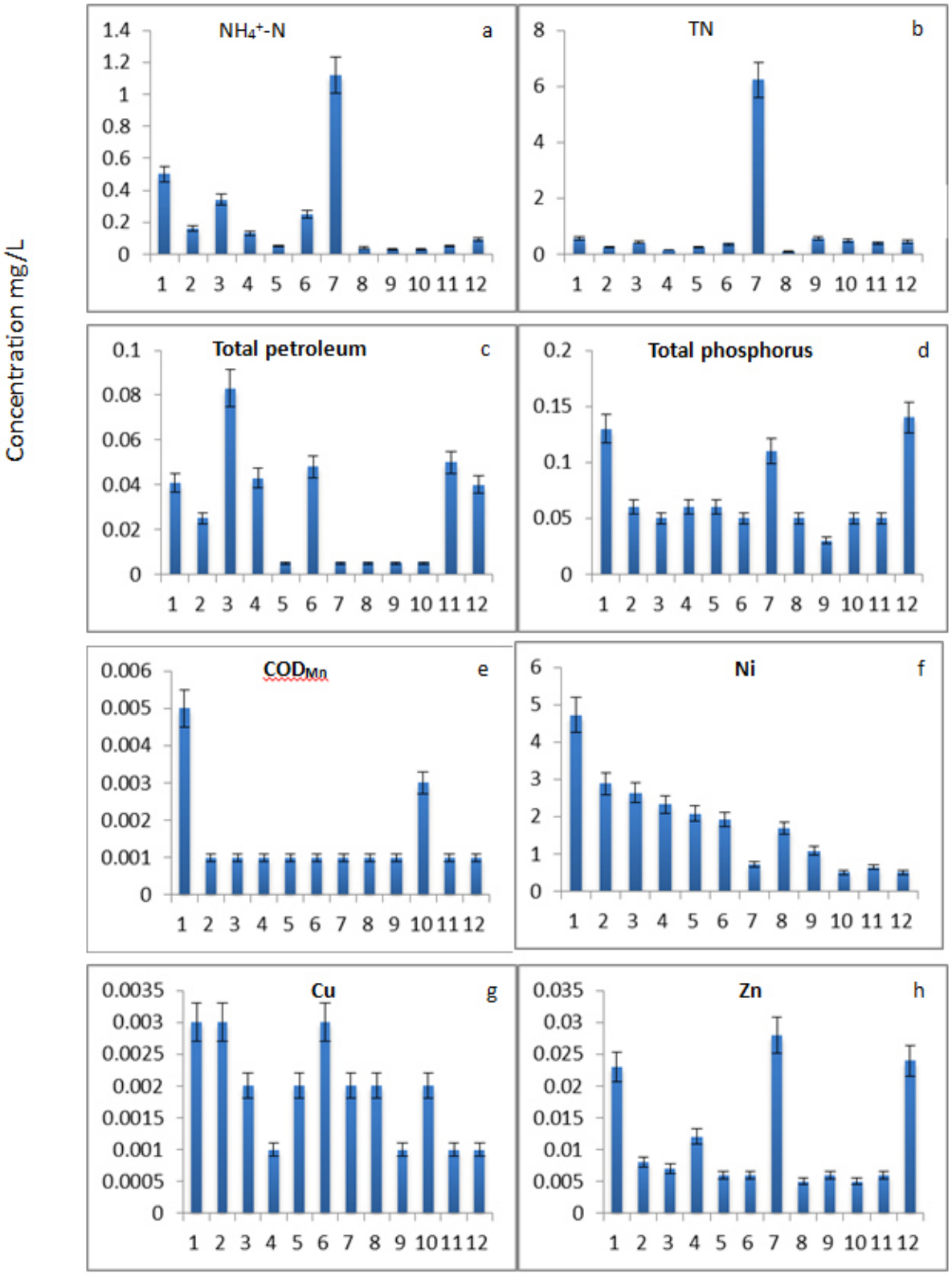

FIGURE 2-CONTINUED

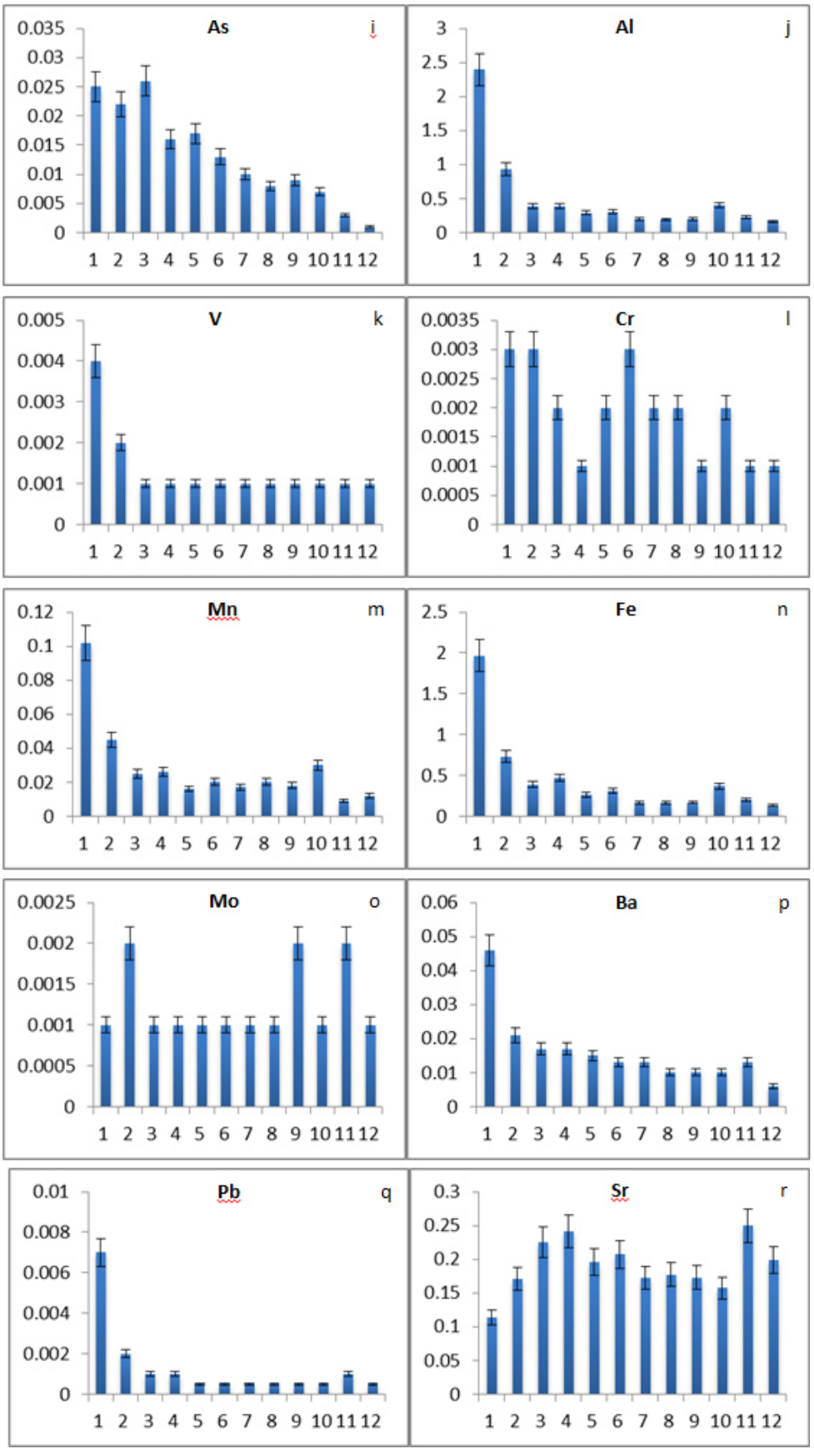

FIGURE 2
Sampling site
Physical and chemical parameters of water quality of Yarlung Zangbo River

TABLE 2
Content of POPs and some metallic elements in water of the Yarlung Zangbo River

Item	Co	Se	Hg	Cd	PCB	PFOS	Plasticizer	Organochlorine pesticide
St.1	N.D	N.D	N.D	N.D	N.D	N.D	N.D	N.D
St.2	N.D	N.D	N.D	N.D	N.D	N.D	N.D	N.D
St.3	N.D	N.D	N.D	N.D	N.D	N.D	N.D	N.D
St.4	N.D	N.D	N.D	N.D	N.D	N.D	N.D	N.D
St.5	N.D	N.D	N.D	N.D	N.D	N.D	N.D	N.D
St.6	N.D	N.D	N.D	N.D	N.D	N.D	N.D	N.D
St.7	N.D	N.D	N.D	N.D	N.D	N.D	N.D	N.D
St.8	N.D	N.D	N.D	N.D	N.D	N.D	N.D	N.D
St.9	N.D	N.D	N.D	N.D	N.D	N.D	N.D	N.D
St.10	0.001	N.D	N.D	N.D	N.D	N.D	N.D	N.D
St.11	N.D	N.D	N.D	N.D	N.D	N.D	N.D	N.D
St.12	N.D	0.001	N.D	N.D	N.D	N.D	N.D	N.D

Persistent organic pollutants (POPs). Pollution arising from organic pollutants such as PCB, PAH, organochlorine pesticide, plasticizer, etc. is featured with durability, bioaccumulation and long-distance mobility, with potential hazards to human health and ecological environment. Such pollutants, featuring strong lipid solubility and easy enrichment of organisms, will undergo trophic level biological amplification in the transfer process of food chain (web); as a result, content of pollutants in the body of organisms at a higher trophic level exceeds the content of pollutants in environmental media, thus consequently threatening human health [20]. Pollutants such as PCB, PAH, organochlorine pesticide, plasticizer, etc. in the water body of the Yarlung Zangbo River are not detected (Table 2).

CONCLUSIONS

Influences of human activities. Human life often imposes great pressure on water environment. After entry of the industrial revolution, human intervention in coastal zones have approached or exceeded natural changes from the perspective of strength, breadth and speed. Human activities have become factors of earth surface system next only to solar energy and internal energy of earth system [21]. Under long-term effect of human activities, river has become the most threatened ecological system. Some countries and regions protect river environment through legislation. For example, EU Water Framework Directive is intended to prevent degeneration of river environment and improve ecological quality of river [22].

Human activities have great effects on output of river ecosystem such as nitrogen, metallic elements and so on. Production and life have changed the cyclic process of such substances, inputted plenty of pollutants into terrestrial ecosystem through fertilizer application, combustion of fossil fuels, metal smelting, etc., promoted the delivery of nitrogen in the terrestrial ecosystem to water body, destroyed the balance between material and energy of the ecological system, and consequently caused water pollution, which have been proved by heavy metal pollution and eutrophication of lakes & reservoirs and offshore areas reported in recent years [12, 18, 23]. Water environment of the Yarlung Zangbo River during the low water period is closely related to population distribution; traditional "Yarlung Zangbo River and its two tributaries" Region (sampling site 4-8, middle reaches of the Yarlung Zangbo River and its main tributaries Lhasa River and Nianchu River basin) is the traditional political and economic center of Tibet with large density of population. According to statistics, population of this region cover 36% of the total population of Tibet [24-25]. Sampling sites 6 and 7 close to Lhasa, with the largest population density in Tibet, have both the highest content of ammonia nitrogen and total nitrogen in the water body of the Yarlung Zangbo River. Sampling site 7 has the highest content of heavy metal elements such as Cu, Zn and Cr, which are closely related to human life.

Influences of environmental background and runoff variation. The Yarlung Zangbo River is a high mountain river with a large river fall. Water body sediments in some reaches become suspended solids and are mixed up with water body under water scouring action; some dissolvable pollutants contained in such suspended solids will be dissolved in the water body under the effect of acid rain, etc. With certain hereditability, content of many heavy metals contained in sediments is approximate to but higher than the background value of soil of Tibet. With little differences in China's crustal abundance, content of many heavy metals contained in sediments is generally lower than the global crustal abundance [26]. Sampling site 1, that is, the first sampling site where glacier water flows into the Yarlung Zangbo River, has the highest content of nickel (Ni), zinc (Zn), arsenic (As), aluminum (Al), vanadium (V), manganese (Mn), ferrum (Fe), barium (Ba) and lead (Pb) in the water

body of the Yarlung Zangbo River.

With the confluence of other rivers, overland runoff of the Yarlung Zangbo River has increased gradually. Jian Liu et al. studied change of annual average runoff of the Yarlung Zangbo River, and obtained the result that the section runoff in the upper reaches in Lhatse County was $56.18\times10^8m^3$, the section runoff in the lower reaches in Nuxia increased to $605.71\times10^8m^3$ and the overall runoff increased by 10.78 times [27]. Considering the dilution effect of runoff, the content of pollutants has decreased slowly with the increase in runoff, and the concentration of pollutants has a good correlation with the surface runoff.

ACKNOWLEDGEMENTS

Thanks to The Central Public-interest Scientific Institution Basal Research Fund, CAFS (NO. 2017HY-ZD0205) and Special Fund for Argo-scientific Research in the Public Interest (201403012) and for supporting the research of this thesis.

REFERENCES

[1] He, W., Jia, Y. (2016) Bioavailability of adsorbed and coprecipitated Cu, Ni, Pb, and Cd on iron and iron/aluminum hydroxide to Phragmites australis. Environmental Science and Pollution Research. 18, 1-9.

[2] Jiang, L., Feng, W., Guo, B. (2014) Analysis of correlation between dynamic monitoring of vegetational cover and precipitation factors of the Yarlung Zangbo River basin in the past 13 years. Resources and Environment of Yangtze River Basin. 23, 1610-1619.

[3] Xu, M., Wang, Z., Pan, B. (2012) Benthonic animal diversity and ecological evaluation in the Yarlung Zangbo River basin. Chinese Journal of Ecology. 32, 2351-2360.

[4] Zhang, Z., Dai, X., Wang, C. (2006) Environmental geochemistry and endemic disease in Yarlung Zangbo Grand Canyon. Geology of China. 33, 1424-1430.

[5] Yao, T., Li, Z., Yang, W. (2010) Glacier distribution and material balance characteristics of the Yarlung Zangbo River basin and influences upon lakes. Chinese Science Bulletin. 55,1750-1756.

[6] Yang, J., Jiang, F., Ma, C., Rui, Y., Rui, M., Adeel, M., Cao, W., Xing, B. (2018) Alteration of Crop Yield and Quality of Wheat upon Exposure to Silver Nanoparticles in a Life Cycle Study. Journal of Agricultural and Food Chemistry. 66(11), 2589-2597.

[7] Konate, A., He, X., Zhang, Z., Ma, Y., Zhang, P., Alugongo, G.M., Rui, Y. (2017) Magnetic (Fe3O4) Nanoparticles Reduce Heavy Metals Uptake and Mitigate Their Toxicity in Wheat Seedling. Sustainability. 9(5), 790.

[8] Ji, Y., Zhou, Y., Ma, C., Feng, Y., Hao, Y., Rui, Y., Wu, W., Gui, X., Van, N.L., Han, Y., Wang, Y., Xing, B., Liu, L., Cao, W. (2017) Jointed toxicity of TiO2 NPs and Cd to rice seedlings: NPs alleviated Cd toxicity and Cd promoted NPs uptake. Plant Physiology and Biochemistry. 110(SI), 82-93.

[9] Rui, M., Ma, C., Hao, Y., Guo, J., Rui, Y., Tang, X., Zhao, Q., Fan, X., Zhang, Z., Hou, T., Zhu, S. (2016) Iron Oxide Nanoparticles as a Potential Iron Fertilizer for Peanut (Arachis hypogaea). Frontiers in Plant Science. 7, 815.

[10] Van, N.L., Rui Y., Gui X., Li X. Liu S., Han Y. (2014) Uptake, transport, distribution and Bio-effects of SiO2 nanoparticles in Bt-transgenic cotton. Journal of Nanobiotechnology. 12, 50.

[11] Li, X.g, Gui, X., Rui, Y., Ji, W., Le, V.N., Yu, Z., Peng, S. (2014) Bt-transgenic cotton is more sensitive to CeO2 nanoparticles than its parental non-transgenic cotton. Journal of Hazardous Materials. 274, 173-180.

[12] Rong, N., Shan, B., Lin, C. (2016) Haihe basin nitrogen pollution characteristics and evolution trend. Journal of Environmental Sciences. 36, 420-427.

[13] Collos, Y., Harrison, P.J. (2014) Acclimation and toxicity of high ammonium concentrations to unicellular algae. Marine Pollution Bulletin. 80, 8-23.

[14] Liu, L., Wang, J., Hu, Y. (2014) Petroleum pollution variation trend in offshore areas of the Bohai Sea. Chinese Journal of Oceanography and Limnology. 45, 88-93.

[15] Zhang, X., Deng, C., Wei, W. (2007) Research on distribution of inorganic phosphorus, organophosphorus and total phosphorus in dissolved form of the Yellow River Estuary and offshore areas. Journal of Environmental Sciences. 27, 660-666.

[16] Xia, L., Jian, W., Jie, C. (2016) Research on determination of permanganate index in drinking water using continuous flow analytical method. Chinese Journal of Health Laboratory Technology. 26, 2754-2755.

[17] Wang, L., Zhang, X. (2015) Research on determination of permanganate index in surface water by using continuous flow analytical method. Analysis Instruments. 4, 41-45.

[18] Wang, H., Mou, Z. (2011) Detection and Comparison of 10 Metals in Brachymystax Lenok from the Genhe River and Ussuri River. Asian Journal of Chemistry. 23, 4515-4516.

[19] Wang, H., Zhan, P. (2011) Determination of Trace Elements in Hucho taimen Pallas from Ganhe River Simultaneously by CRC-ICP-MS. Asian Journal of Chemistry. 23, 1881-1882.
[20] Chen, Q., Zhou, Y., Qiu, Y. (2016) Research progress on fish as a persistent organic pollutant biological indicator. Environmental Science and Technology. 39, 99-110.
[21] Xu, L., Li, J., Li, W. (2014) Research overview on influences of human activities upon resources and environment in the coastal zone. Natural Science Edition of Journal of Nanjing Normal University. 3, 124-131.
[22] Li, Y., Li, Y., Li, K. (2016) Influences of human activities upon characteristics of fish and macrobenthos communities in Huntaihe river basin. Research of Environmental Sciences. 29, 1145-1153.
[23] Zhang, W., Li, X., Su, J. (2014) Research overview on responses of river nitrogen output to net nitrogen input of human activities in the basin. Chinese Journal of Applied Ecology. 25, 272-278.
[24] Tang, W., Zhong, X., Zhou, W. (2011) Dynamic evolution of spatial distribution of population in the "Yarlung Zangbo River and its two tributaries" Region of Tibet. Chinese Population: Resources and Environment. 21, 159-164.
[25] Luo, Y. (2010) Research on population distribution and sustainable development of ecological environment of Tibet. Chengdu University of Technology.
[26] Bo, J., Li, C., Kang, S. (2014) Overlying deposit heavy metal form distribution in the middle of the Yarlung Zangbo River and risk evaluation. Environmental Science. 9, 3346-3351.
[27] Liu, J., Yao, Z., Chen, C. (2007) Runoff variation trend of the Yarlung Zangbo River and reason analysis. Journal of Natural Resources. 22, 471-477.

Received: **28.05.2018**
Accepted: **01.03.2019**

CORRESPONDING AUTHOR

Feng Ji
Heilongjiang River Fisheries Research Institute of Chinese Academy of Fishery Sciences,
Harbin, Heilongjiang, 150070 – China

e-mail: wahata2002@163.com

© by PSP Volume 28 – No. 5/2019 pages 3704-3712 Fresenius Environmental Bulletin

COMPARISON OF THREE DIFFERENT OPTIMIZATION-BASED LAND REALLOCATION MODELS IN LAND CONSOLIDATION: A CASE STUDY IN AYDIN/TURKEY

Ela Ertunc*, Tayfun Cay

Konya Technical University, Faculty of Engineering and Natural Sciences, Department of Geomatics Engineering, 42130, Konya, Turkey

ABSTRACT

Land consolidation (LC) is the primary and most effective land management instrument to address land fragmentation problems, which has been applied in many countries around the world. Land consolidation is not just the reallocation of fragmented parcels, it is in an important instrument of rural development in many countries.

Land consolidation projects consist of various steps. Land reallocation is crucial and challenging stages with many factors playing a role in it. Thus, the usage of computer technology has been essential for fast and efficient progress in projects.

In this case study, three different land reallocation models, Fuzzy Logic (FL) based, Genetic Algorithm (GA) based, and designed Fuzzy Genetic Algorithm (FGA) based land reallocation models, are compared for Land consolidation projects in the reallocation of newly created regular-size parcels to landowners. As a result, the Genetic Algorithm based and Fuzzy Genetic Algorithm based models are more successful than the Fuzzy Logic based model in terms of the average parcel size, the number of parcels, and the average number of parcels per landowner. The benefits derived from both models are much higher compared to conventional models. The proposed models save time and improve the results for future land consolidation projects.

KEYWORDS:
Agriculture, Land consolidation, Land reallocation, Rural area

INTRODUCTION

Agriculture forms the basic economic and social sector necessary to sustain human life. In spite of increases in the human population, the total area of farmland has remained stable. Furthermore, due to land fragmentation, the efficiency of farmland has decreased with each passing day. This situation will get worse unless land consolidation (LC) and urban transformation projects can solve this problem [1].

Land consolidation is the primary and most effective land management instrument to address land fragmentation problems, which has been applied in many countries around the world [2, 3, 4, 5, 6, 7, 8, 9, 10, 11, 12].

Land consolidation is not just the reallocation of fragmented parcels, it is an important instrument of rural development in many countries [3, 13, 14, 15, 16, 17, 18, 19, 20].

Land consolidation traditionally consists of many stages and is a long and laborious process. Land reallocation, the most important process in land consolidation, is split into two sub-processes: land redistribution and land partitioning [21].

Both of these stages are complex, time-consuming and challenging parts of the LC process [22]. In land reallocation, blocks are formed in the project area at the block-planning stage.

However, there are studies which focus on speeding up the reallocation stage of LC. A mathematical model [23], fuzzy logic [24], decision-support machines [25], and genetic algorithms [22] have been used to automate the reallocation stage.

In this study, land reallocation was performed for the same application area according to the Genetic Algorithm (GA) based and Fuzzy Logic (FL) based land reallocation methods available in the literature. Furthermore, a new Fuzzy Genetic Algorithm method or Hybrid method (FGA) was developed using the Genetic Algorithm and Fuzzy Logic methods, and land reallocation was performed according to this method. The results of these three different reallocation methods were compared.

MATERIALS STUDIED

Documents of cadastral parcels, grading maps, interview forms and information on the area, owners and other rights of the parcels were obtained from the Agricultural Reform Regional Directorate (ARRD). The agricultural land classification and gradation mapping of this LC project are performed by the ARRD, according to the Land Reform regarding the rearrangement of land in irrigated

areas (Law No. 3083, date: 1984). Block plans were processed on the cadastral map by the ARRD.

Area descriptions. Boğaziçi (Madrandere) is a neighborhood connected to Koçarlı district of Aydin province. Boğaziçi neighborhood is 17 km away from Aydın province and 15 km away from Koçarlı district and has an altitude of 40 m. The location map of Boğaziçi neighborhood is presented in Figure 1.

The Boğaziçi project area is 92.28 hectares. There are 102 enterprises and 81 cadastral parcels in the project area. The average parcel size is 11,392.41 m². 10 blocks (island) were formed during block planning.

METHODS

How land reallocation was performed according to the FL, GA and FGA methods will be briefly explained in this section.

Fuzzy Logic Based Land Reallocation Model. In the FL based land reallocation method, land reallocation is performed based on the following points considered by farmers during the reallocation stage:

- The location where the farmer has the largest parcel,
- The location where the farmer's parcel density is,
- The location of the farmer's fixed facility,
- The location where the farmer has the second largest parcel

These criteria are the input variables of the fuzzy system. The place where the largest parcel is located was taken as the first input variable, and the other 3 criteria were taken as the second input variable. These criteria need to be in terms of angle and distance since they express location information. An input variable is required to determine which blocks will be given by which of these criteria. Therefore, the fact that parcel areas are smaller or larger than each other was taken into account. Thus, a fuzzy system with 5 inputs and 2 outputs was developed. The general structure of the developed system is presented in Figure 2.

FIGURE 1
The location map of the Boğaziçi (Madrandere) neighborhood

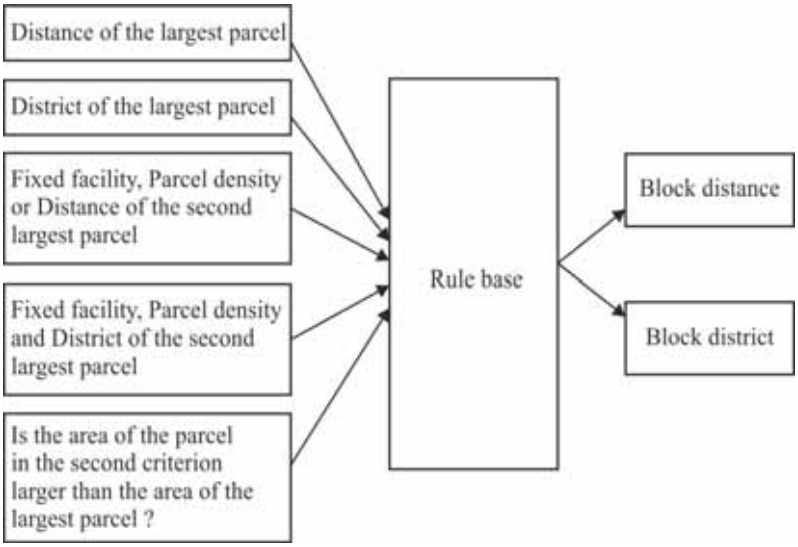

FIGURE 2
General structure of Fuzzy Logic model [24]

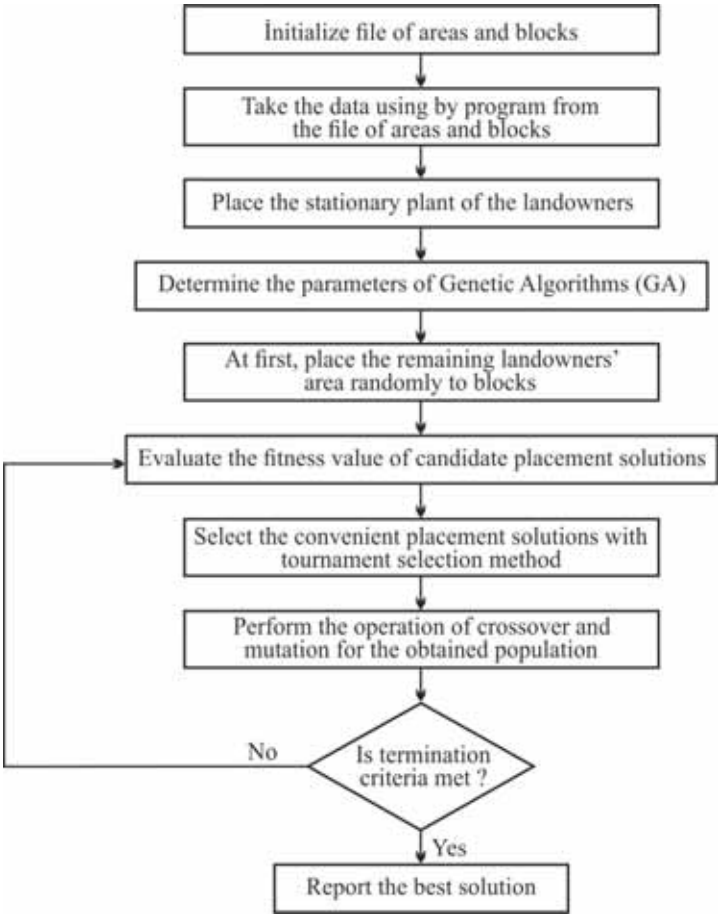

FIGURE 3
Flowchart for automatic reallocation process using Genetic Algorithm [22]

In the fuzzy system, trapezoidal membership functions were used for distance inputs in input and output variables, while triangular and trapezoidal membership functions were used for neighborhood inputs. There are 3 membership functions selected for "near", "far" and "too far" linguistic variables in distance input variables and 4 membership functions for "narrow", "medium", "wide" and "too wide" linguistic variables in neighborhood input variables. Since the input "Is the area of the parcel in the second criterion larger than the area of the largest parcel?" is a query, it takes either the value of "0" or the value

of "1". A total of 288 rules were created based on membership functions. Output values were obtained by using input values for each landholding in the fuzzy system. A reallocation process was performed in this way.

Genetic Algorithm Based Land Reallocation Model. The flowchart for the automatic block reallocation according to the GA is as follows (Figure 3).

In reallocation according to the GA, the population is first created, and the fitness value is calculated for each individual in the population. In land reallocation, the best individual with the minimization problem is an individual with the smallest fitness value. Individuals are ranked from best to worst. According to the rate of elitism, the individual to be transferred to the next population is determined. Other individuals are determined by tournament selection. After the selection process is completed, crossover and mutation operations are employed, and these operators are applied. The inclusion of each block number at least once by every individual should be checked while these operations are performed. Individuals who do not meet this condition are formed again by checking this situation in the program. In the study, the number of population and the number of iterations were set at 100 and 1000, respectively. The rate of elitism and the mutation rate were determined as 0.05 and 0.08, respectively.

Fuzzy Genetic Algorithm Based Land Reallocation Model. Fuzzy genetic algorithms (FGA) basically involve the use of fuzzy logic and genetic algorithms together. In this study, a more developed method was designed using the fuzzy techniques of GA. In the present study, the FL method was used to adjust the parameters of the GA and to adapt the genetic operators (in determining the crossover technique and crossover rate of GA). The fuzzy genetic algorithm structure is presented in Figure 4.

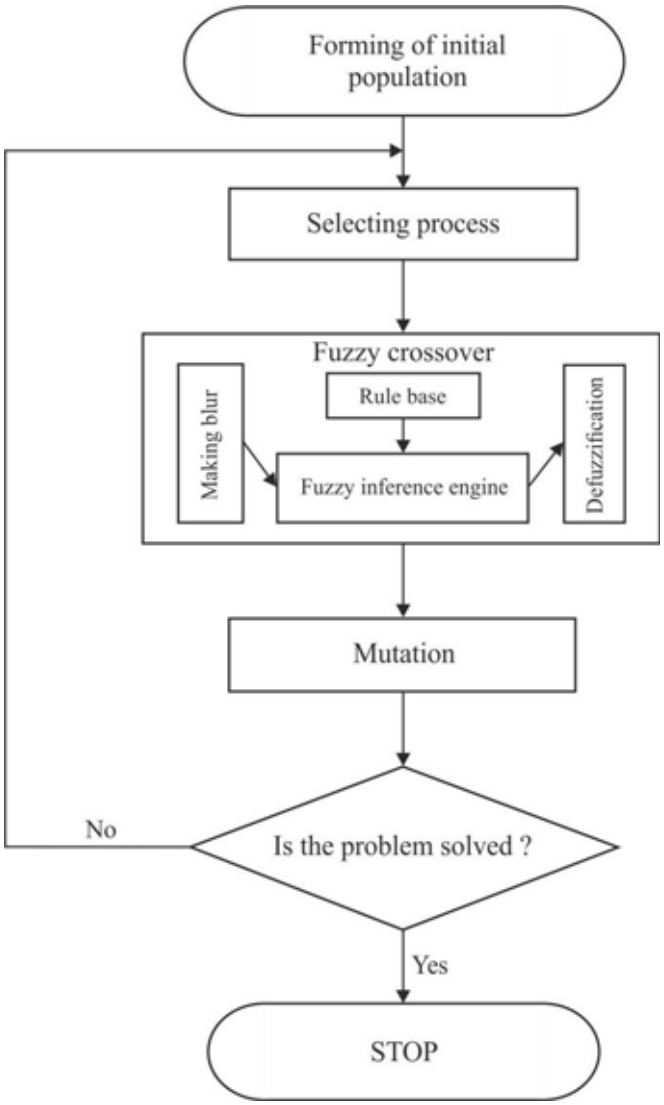

FIGURE 4
Fuzzy Genetic Algorithm [26]

TABLE 1
Crossover techniques according to their levels

Low	Medium	High
1-point	k-point	Segragation
2-point	Uniform	Inversion

With the FGA, not only the level of the crossover technique but also the crossover rate is determined for each iteration by means of fuzzy logic. The crossover rate is evaluated by the fuzzy logic rule set according to the situation of the population, and the crossover ratio obtained by clarification is directly used. The crossover techniques used in the method are presented in Table 1.

In this method, the number of population and the number of iterations were also set as 100 and 1000, respectively. Other individuals are determined by tournament selection. The rate of elitism is 0.05. The crossover rate and the crossover technique to be used are determined by the FL method. The mutation rate was determined as 0.08. The algorithm is over when the number of predefined iterations is reached.

RESULTS

The FGA, GA and FL block reallocation results obtained for Boğaziçi Neighborhood were compared. In the cadastral state and the parceling plan formed by the three different methods of land consolidation project belonging to Boğaziçi Neighborhood, the situations of the enterprises number 8, 10 and 76 taken as example are presented in Figure 5.

FIGURE 5
The situations of the enterprises number 8, 10 and 76 according to the cadastral state (a), according to the parceling plan formed by hybrid method or fuzzy genetic algorithm (FGA) (b), according to the parceling plan formed by genetic algorithm (GA) method (c) and according to the parceling plan formed by fuzzy logic (FL) method (d) in land consolidation project belonging to Boğaziçi Neighborhood

TABLE 2
The number of parcels in the reallocation models

Parcel Size (da)	The Cadastral State	Hybrid Method (FGA)	Genetic Algorithm Method (GA)	Fuzzy Logic Method (FL)
	The Number of Parcels	The Number of Parcels	The Number of Parcels	The Number of Parcels
0-5	24	18	13	25
5-10	25	24	28	29
1320-20	19	20	20	13
20-30	10	2	2	2
30+	3	2	2	3
Total	**81**	**66**	**65**	**72**
Total Rate (%)	**-**	**19**	**20**	**11**

TABLE 3
The average parcel size in the reallocation models

	The Area (m^2)	Increase (%)
The Cadastral State	11,392.41	-
Fuzzy Genetic Algorithm (FGA) Method	13,056.24	15
Genetic Algorithm (GA) Method	13,257.10	16
Fuzzy Logic (FL) Method	11,968.22	5

TABLE 4
The number of parcels per enterprise in the reallocation models

The Number of Parcel	The Cadastral State		Hybrid Method (FGA)		Genetic Algorithm Method (GA)		Fuzzy Logic Method (FL)	
	The Number of Enterprise	The Ratio of Enterprise (%)	The Number of Enterprise	The Ratio of Enterprise (%)	The Number of Enterprise	The Ratio of Enterprise (%)	The Number of Enterprise	The Ratio of Enterprise (%)
1	69	67.6	98	96.1	97	95.1	94	92.2
2	16	15.7	4	3.9	5	4.9	7	6.9
3	5	5.0	-	-	-	-	1	0.9
4	1	0.9	-	-	-	-	-	-
5	2	2.0	-	-	-	-	-	-
6	4	3.9	-	-	--		-	-
7	2	2.0	-	-	-	-	-	-
8	2	2.0	-	-	-	-	-	-
9	1	0.9	-	-	-	-	-	-
Total	**102**	**100**	**102**	**100**	**102**	**100**	**102**	**100**

Analysis of models in terms of the number of parcels. The cadastral parcels in Boğaziçi neighborhood and the analysis of the FGA, GA and FL models in terms of the numbers of parcels are presented in Table 2. According to Table 2, while there were a total of 81 cadastral parcels including 32 jointly owned cadastral parcels before the study in Boğaziçi Land Consolidation project area, 66 parcels, 65 parcels, and 18 parcels were formed by the FGA model, GA method, and FL method, respectively. According to the decrease in the number of parcels and the increase in consolidation rate, the FGA based reallocation model and the GA method gave very close results.

Analysis of models in terms of average parcel sizes. The average parcel sizes and increase percentages of the enterprises in Boğaziçi neighborhood according to the models applied are presented in Table 3.

When the results of different reallocation methods are evaluated in terms of the average parcel size, these rates are 15% in the FGA model, 16% in the GA model and 5% in the FL model. According to the results, the percentage increase in the average parcel size is more in the FGA and GA methods.

Analysis of models in terms of the number of parcels per enterprise. The situation of different reallocation models in Boğaziçi application area in terms of the number of parcels per enterprise is presented in Table 4.

TABLE 5
The number of jointly owned parcels in the reallocation models

The number of Shares in Parcel	The Cadastral State	Hybrid Method (FGA)	Genetic Algorithm Method (GA)	Fuzzy Logic Method (FL)
1	49	43	39	54
2	7	13	16	8
3	9	4	7	4
4	1	5	2	4
5	4	1	1	1
6	2	-	-	1
7	8	-	-	-
11	1	-	-	-
The Number of Jointly Owned Parcels	**32**	**23**	**26**	**18**
The Percent of Jointly Owned Parcels	**39%**	**35%**	**40%**	**25%**
Total	**81**	**66**	**65**	**72**

The ratio of enterprises with a parcel before consolidation in the application area was 67.6%. After consolidation, this ratio was 96.1% in the hybrid model, 95.1% in the genetic algorithm model, and 92.2% in the fuzzy logic model. After consolidation, enterprises were gathered in a parcel as much as possible. The FGA method gave more successful results than the other methods when it is evaluated in terms of gathering enterprises in a parcel.

Analysis of models in terms of the number of jointly owned parcels. The situation of reallocation models in Boğaziçi application area in terms of the number of jointly owned parcels per enterprise is presented in Table 5. According to Table 5, the number of jointly owned parcels before reallocation was 32 (39%). After reallocation, the number of jointly owned parcels was 23 (35%) for the FGA reallocation model, 26 (40%) for the GA model, and 18 (25%) for the FL model. Accordingly, the FL model gave the best result in terms of the number of jointly owned parcels per enterprise compared to other methods.

CONCLUSION

The basic economic activity necessary for a human to maintain his life is agriculture. Despite this importance of agriculture for a human to maintain his existence, soil availability remains the same and is even decreasing gradually against the ever-increasing world population. Since it is not possible to increase the areas where agriculture can be done in parallel with the increase in population, the solution is to find procedures and methods which will enable to obtain more productivity from existing agricultural lands which can be considered as limited. Undoubtedly, this method is land consolidation. By using the optimization methods of land consolidation projects, these projects will be accelerated, the yield obtained from agriculture will increase, and significant contributions will be made both to the enterprise and to the economy of the country. Furthermore, the development of rural areas will be supported by ensuring that agriculture will regain its importance. For these reasons, Land Consolidation projects are used as the most effective land management approach.

Although there are studies on land reallocation in the literature, this problem needs to be developed and improved from many aspects. A newly created hybrid method was used in this study. Three different reallocations were performed for the same application area using two different methods available in the literature. According to the results obtained, the FGA method is more successful than the other methods.

ACKNOWLEDGEMENTS

This paper has been prepared by benefiting from the inventions of the project whose number is 114Y608 which supported by TÜBİTAK (The Scientific and Technological Research Council of Turkey)-Turkey.

REFERENCES

[1] FAO (2003) The Design of Land Consolidation Pilot Projects in Central and Eastern Europe. FAO Land Tenure Studies, Rome.

[2] Akkaya Aslan, S.T., Kirmikil, M., Gündoğdu, K.M. and Arıcı, İ. (2018) Reallocation model for land consolidation based on landowners' requests. Land Use Policy. 70(2018), 463-470.

[3] Crecente, R., Alvarez, C. and Fra, U. (2002) Economic, social and environmental impact of land consolidation in Galicia. Land Use Policy. 19(2), 135–147.
[4] Derlich, F. (2002) Land consolidation: a key for sustainable development French experience. In: Proceedings of the XXII International FIG Congress. 19–26 April, Washington, D.C., USA. Available from. http://www.fig.net/pub/fig_ 2002/Ts7-4/TS7_4_derlich.pdf.
[5] Magel, H. (2003) Land Policy and Land Management in Germany. Public Lecture in Melbourne, 6 February, 2003. Available from. http://www.fig.net/council/council_2003_2006 /magelpapers/magel_melbourne_feb_2003.pdf.
[6] Van Dijk, T. (2003) Dealing with Central European Land Fragmentation. Eburon, Delft.
[7] Thomas, J. (2004) Modern Land Consolidation –recent Trends on Land Consolidation in Germany. Paper from FIG symposium on modern land consolidation? Volvic, France. 5p.
[8] Van Dijk, T. (2007) Complications for traditional land consolidation in Central Europe. Geoforum 38, 505–511.
[9] Sklenicka, P. (2006) Applying evaluation criteria for the land consolidation effect to three contrasting study areas in the Czech Republic. Land Use Policy. 23(4), 502–510.
[10] Thomas, J. (2006) Attempt on systematization of land consolidation approaches in Europe. ZfV –Zeitschrift für Geodäesie. Geoinformation und Land management. 3(2006), 156.
[11] Yaslıoglu, E., Akkaya Aslan, S.T., Kirmikil, M., Gündoğdu, K.S. and Arıcı, I. (2009) Changes in farm management and agricultural activities and their effect on farmers' satisfaction from land consolidation: the case of Bursa-Karacabey-Turkey. Eur. Plann. Stud. 17(2), 327–340.
[12] Arıcı, I. and Akkaya Aslan, S.T. (2014) Planning and projecting of land consolidation. Dora Publications 237, 605–978 ISBN: 978-605-4798-49-0. (in Turkish).
[13] Van Huylenbroeck, G., Coelho, C. and Pinto, P.A. (1996) Evaluation of land consolidation projects (LCPs): A multidisciplinary approach. J. Rural Stud. 12(3), 297–310.
[14] Van den Brink, A. (2004) Land consolidation and the emergence of the metropolitan landscape. In: Proceedings of Symposium on Modern Land Consolidation. 10–11 Sept. Volvic (Clermont-Ferrand), France. Available from. http://www.fig.net/commission7/france_2004/ papers_symp/ts_03_vandenbrink.pdf.
[15] Borec, A. (2000) The significance of land consolidation for the development of farmland in Slovenia then and now. Berichte Uber Landwirtschaft, 78, 320–334.
[16] Semlali, H. (2001) A GIS solution to land consolidation technical problems in Morocco. In: Proceedings of FIG Working Week, New Technology for a New Century. 6-11 May, Seoul, Republic of Korea. Available from. http://www.fig.net/pub/proceedings/korea/full-papers/pdf/ session24/semlali.pdf
[17] González, X.P., Alvarez, C.J. and Crecente, R. (2004) Evaluation of land distributions with joint regard to plot size and shape. Agric. Syst. 82, 31–43.
[18] González, X.P., Marey, M.F. and Alvarez, C.J. (2007) Evaluation of productive rural land patterns with joint regard to the size, shape and dispersion of plots. Agric. Syst. 92, 52–62.
[19] Akkaya Aslan, S.T., Gündoğdu, K.S., Yaslıoğlu, E., Kirmikil, M. and Arıcı, I. (2007) Personal, physical and socioeconomic factors affecting farmers' adoption of land consolidation. Spanish Journal of Agricultural Research. 5(2), 204-213.
[20] Pasakarnis, G. and Maliene, V. (2010) Towards sustainable rural development in central and eastern Europe: applying land consolidation. Land Use Policy. 27, 545–549.
[21] Demetriou, D., Stillwell, J. and See, L. (2012) Land consolidation in Cyprus: why is an integrated planning and decision support system required? Land Use Policy. 2(1), 131–142.
[22] Uyan, M., Çay, T., İnceyol, Y. and Haklı, H. (2015) Comparison of designed different land reallocation models in land consolidation: A case study in Konya/Turkey. Computers and Electronics in Agriculture. 110, 249- 258.
[23] Ayrancı, Y. (2007) Re-allocation aspects in land consolidation: a new model and its application. Asian network for scientific information. J. Agron. 6(2), 270–277.
[24] Çay, T., İşcan, F. (2011) Fuzzy expert system for land reallocation in land consolidation. Expert Syst. Appl. 38, 11055–11071.
[25] Çay, T., Uyan, M. (2013) Evaluation of reallocation criteria in land consolidation studies using the Analytic Hierarchy Process (AHP). Land Use Policy. 30, 541–548.
[26] Varnamkhasti, M.J., Lee, L.S., Bakar, M.R. and Leong, W.J.A. (2012) Genetic Algorithm with Fuzzy Crossover Operator and Probability. Hindawi Publishing Corporation Advances in Operations Research. 16.

Received: **27.06.2018**
Accepted: **18.03.2019**

CORRESPONDING AUTHOR

Ela Ertunc
Department of Geomatics Engineering
Faculty of Engineering and Natural Sciences
Konya Technical University
Konya 42130 – Turkey

e-mail: elaertunc@selcuk.edu.tr

© by PSP Volume 28 – No. 5/2019 pages 3713-3717 Fresenius Environmental Bulletin

THE NOVEL BIOLOGICAL TESTS ON VARIOUS EXTRACTS OF *CERIOPORUS VARIUS*

Mustafa Sevindik*

Akdeniz University, Science Faculty, Biology Department, Antalya, Turkey

ABSTRACT

The present study aimed to determine the total antioxidant status (TAS), total oxidant status (TOS), oxidative stress index (OSI) and antimicrobial activity of *Cerioporus varius* (Pers.) Zmitr. & Kovalenko mushrooms collected in Gaziantep province, Turkey. The TAS, TOS and OSI of the mushroom were analyzed with Rel Assay Diagnostics kits. Antimicrobial activity of the mushroom was tested on 6 bacteria and 3 fungus strains with the modified agar dilution method. It was determined that the TAS of *C. varius* was 2.312±0.137, the TOS was 14.358±0.174 and the OSI was 0.627±0.047. Furthermore, it was determined that EtOH, MeOH and DCM mushroom extracts exhibited antimicrobial activities against the tested bacterial and fungal strains. In conclusion, it was determined that *C. varius* can be used as a natural antioxidant and antimicrobial source.

KEYWORDS:
Cerioporus varius, antioxidant, oxidant, antimicrobial, oxidative stress.

INTRODUCTION

Mushrooms have been served as natural ingredients of nutrients and medicines since early ages. Biological activity studies conducted on fungi, which have pharmacological significance and are believed to include about 140.000 species worldwide, are still very limited [1]. Taking supplemental antioxidants is of great importance in cases where endogenous antioxidants are insufficient in reducing the effects of oxidative stress, a significant cause of several diseases [2, 3]. Furthermore, the increase in the resistant bacteria against synthetic antimicrobial agents led the researchers to search for new natural antimicrobial sources [4]. Previous studies reported antioxidant and antimicrobial activities in mushrooms [5-8]. Thus, mushroom studies are significant for the identification of new natural antioxidant and antimicrobial sources.

In Turkey, approximately 2200 macrofungal species were reported so far [9, 10]. In Turkey with its rich macrofungal biodiversity, several studies were conducted on biological microfungal activities in recent years. *C. varius* is a common fungus species that grow saprophytically on dead broad-leaved tree logs [11]. The present study aimed to determine the antioxidant and antimicrobial capacity of *Cerioporus varius* (Pers.) Zmitr. & Kovalenko (Syn. *Polyporus varius* (Pers.) Fr.), characterized by a steep fruiting body, decurrent tubes and ochraceous stipe with black lower back.

EXPERIMENTAL

Laboratory Studies. The study material was collected during the routine field studies conducted in Gaziantep during 2017 and 2018. Morphological (shape, color, size) and ecological properties of mushroom samples were recorded under the field conditions. Microscopic properties of the samples that were transported to the laboratory under adequate conditions were determined by light microscopy with a 3% KOH solution (Leica DM750). The specimen was identified morphologically with the references by Breitenbach and Kränzlin [12], Bernicchia [11] and Ellis and Ellis [13].

After the identification of the fungal samples, ethanol (EtOH), methanol (MeOH) and dichloromethane (DCM) extracts were obtained with a Soxhlet extractor (Gerhardt EV 14). The extracts were concentrated on a rotary evaporator (Heidolph Laborator 4000 Rotary Evaporator).

Determination of TAS, TOS and OSI. Total antioxidant status (TAS) and total oxidant ststus (TOS) of the mushroom were determined with Rel Assay kits (Assay Kit Rel Diagnostics, Turkey). The TAS of the mushroom was determined using Trolox as the calibrator and the results are presented as mmol Trolox equiv./L [14]. The TOS was determined using hydrogen peroxide as the calibrator and the results are presented as μmol H_2O_2 equiv./L [15]. OSI was determined by dividing the TOS value by the TAS value. When the OSI (arbitrary unit: AU) was calculated, the following formula was used, and the result was indicated as a percentage [15]. In the study, 6 mushroom samples were tested in 5 repeats.

$$\text{OSI (AU)} = \frac{\text{TOS, } \mu\text{mol } H_2O_2\text{equiv./L}}{\text{TAS, mmol Trolox equiv./L X 10}}$$

Antimicrobial Activity Tests. Antimicrobial activity tests were conducted with the agar dilution method recommended by the Clinical and Laboratory Standards Institute (CLSI) and the European Committee on Antimicrobial Susceptibility Testing (EUCAST) on the EtOH, MeOH and DCM extracts of the mushroom samples. Minimal inhibitor concentrations (MIC) was determined against standard bacterial and fungal strains for each extract. Antibacterial activity was determined against *Staphylococcus aureus* ATCC 29213, *Staphylococcus aureus* MRSA ATCC 43300, and *Enterococcus faecalis* ATCC 29212 gram positive bacteria. *Escherichia coli* ATCC 25922, *Pseudomonas aeruginosa* ATCC 27853 and *Acinetobacter baumannii* ATCC 19606 were used as gram negative bacteria. For antifungal activity tests, *Candida albicans* ATCC 10231, *Candida krusei* ATCC 34135 ATCC 13803, and *Candida glabrata* ATCC 90030 fungi obtained from the American culture collections were used. Bacterial strains were pre-cultured in Muller Hinton Broth medium, while fungal strains were pre-cultured in RPMI 1640 Broth medium. To obtain standard inoculum, the bacteria and fungi turbidity was set based on McFarland 0.5 equivalence. All extracts were tested at 800-12.5 µg/mL concentrations and all extracts were diluted with distilled water. Solvents used in extracts were simply tested for antimicrobial activity. Fluconazole and amphotericin B was used as reference drugs for fungi, whereas amikacin, ampicillin and ciprofloxacin were used as reference drugs for the bacteria. The lowest dilution that prevented the propagation of the bacteria and fungi was determined as the minimum inhibitory concentration (MIC) [16-21].

RESULTS AND DISCUSSION

TAS, TOS and OSI Result. It was determined in the study conducted with *C. varius* that the TAS was 2.312±0.137 mmol/L, the TOS was 14.358±0.174 µmol/L and the OSI was 0.627±0.047. There are no previous studies that were conducted to determine the impact of *C. varius* on oxidative stress. In studies that aimed to determine the oxidative stress of different mushroom species, it was determined that TAS of *Helvella leucomelaena* and *Sarcosphaera coronaria* were 2.367 and 1.066, TOS values were 55.346 and 41.662 and OSI values were 2.338 and 3.909, respectively [22]. It was determined that the TAS value of *C. varius*, examined in the present study, was lower when compared to *H. leucomelaena* and higher when compared to *S. coronaria*. Furthermore, it was observed that the TOS and OSI values were lower than those of the previously studied two fungi. In a different study, it was reported that the TAS value of *Trametes versicolor* was 0.820, the TOS value was 17.760, and the OSI value was 2.166 [23]. As determined in the present study, the TAS value of *C. varius* were higher than *T. versicolor*. Also TOS and OSI values of *C. varius* were lower. It was reported that the TAS value of *Ompholatus olearius* was 2.836, the TOS value was 8.262 and the OSI value was 0.291 [24]. When compared to this study, it was determined that the TAS value of *C. varius* were lower and the TOS and OSI values was higher. In another study, it was reported that the TAS values of *Trametes gibbosa, Fomes fomentarius, Fuscoporia torulosa, Daedalea quercina, Inonotus hispidus* and *Trichaptum biforme* were 0.590, 3.270, 4.033, 0.312, 2.922 and 0.802, respectively. TOS values for the same fungi were determined as 3.522, 2.601, 2.969, 6.868, 6.534 and 4.356, respectively. OSI values for the same fungi were reported as 0.597, 0.080, 0.074, 2.201, 0.224 and 0.543, respectively [25]. Compared to this study, TAS value of *C. varius* was lower than *F. fomentarius, F. torulosa* and *I. hispidus* fungi and higher than the other fungi reported in the study by Bal et al. [25]. It was determined that the TOS value of *C. varius* was higher than that of all fungi examined in that study, while the OSI value of *C. varius* was higher than other fungi, but lower than *D. quercina*. It was reported that the TAS value of *Cyclocybe cylindracea* was 4.325, the TOS value was 21.109 and the OSI value was 0.488 [26]. When compared to this study, it was determined that the TAS and TOS values of *C. varius* were lower and the OSI value was higher. In other previous studies, the TAS value of *Pleurotus eryngii* was determined as 1.93 and the TAS value of *Auricularia polytricha* was determined as 0.93 [27,28]. When compared to these studies, it was determined that the TAS value of the *C. varius* mushroom was higher than the fungi scrutinized in these studies. In general terms, it is considered that the differences in TAS, TOS and OSI values between *C. varius* and other mushrooms reported in the literature was due to the stress factors in the fungus habitat, the substrate the fungus uses and the regional differences. In conclusion, it was determined in the study that *C. varius* has antioxidant potential.

Antimicrobial Activity. Despite technological advances, it was not possible to prevent the increase in the number of infectious diseases. Synthetic antibiotics that are currently prescribed against these infectious diseases, which are basically caused by microorganisms, are insufficient. Furthermore, the resistance of bacteria that they developed against these synthetic antibiotics is a serious problem [29, 30]. New antimicrobial sources that could provide remedies to these diseases are quite

TABLE 1
Antimicrobial Activities of *C. varius*

	S. aureus	*S. aureus* MRSA	*E. faecalis*	*E. coli*	*P. aeruginosa*	*A. baumannii*	*C. albicans*	*C. glabrata*	*C. krusei*
EtOH	200	200	100	200	200	200	200	200	200
MeOH	200	200	200	400	400	800	200	200	400
DCM	400	400	200	400	100	400	100	200	100
Ampicillin	1.56	3.12	1.56	3.12	3.12	-	-	-	-
Amikacin	-	-	-	1.56	3.12	3.12	-	-	-
Ciprofloksasin	1.56	3.12	1.56	1.56	3.12	3.12	-	-	-
Flukanazol	-	-	-	-	-	-	3.12	3.12	-
Amfoterisin B	-	-	-	-	-	-	3.12	3.12	3.12

*The MIC values are presented in units of μg/mL

.

important.

Previous studies did not attempt to determine the antimicrobial activity in *C. varius* extracts. However, the antimicrobial activities in *Polyporus* species were investigated in the literature. In these studies, it was reported that *Polyporus grammocephalus* (Current name: *Favolus grammocephalus*) MeOH extracts had antimicrobial activities against *Proteus vulgaris, Escherichia coli* and *Pseudomonas aeruginosa* [31]. It was also reported that *Polyporus arcularius* (Current name: *Lentinus arcularius*) was effective against *Escherichia coli, Salmonella typhimurium, Staphylococcus aureus* and *Bacillus subtilis* [32]. Antimicrobial activity of *Polyporus squamosus* (Current name: *Cerioporus squamosus*) was reported on *Micrococcus flavus, Salmonella typhimurium, Escherichia coli, Enterobacter cloacae, Listeria monocytogenes, Bacillus cereus, Staphylococcus aureus* and *Pseudomonas aeruginosa* [33]. When compared to the above-mentioned studies, it was determined that *C. varius* EtOH, MeOH and DCM extracts were effective on *Staphylococcus aureus, S. aureus MRSA, Enterococcus faecalis, Escherichia coli, Pseudomonas aeruginosa, Acinetobacter baumannii, Candida albicans, C. albicans, C. krusei* and *C. glabrata*. In conclusion, it was determined that *C. varius* might be considered as a natural antimicrobial source against the tested microorganisms.

CONCLUSION

Antioxidant and antimicrobial properties of *C. varius* mushrooms collected in Gaziantep province (Turkey) were determined in the present study. The study findings demonstrated that *C. varius* had high TAS value. Thus, it was determined that the mushroom may be utilized as a natural antioxidant source. Furthermore, it was determined that the mushroom may be used as a natural antimicrobial source against the tested microorganisms. *C. varius*, which is not an edible mushroom due to its hard structure, will be usable in the future through extraction with different methods. Based on the study data, further medical and pharmaceutical studies can be conducted on *C. varius* mushroom.

ACKNOWLEDGEMENTS

We would like to express our gratitude to Dr. Ismail SEN for their contributions to the present study.

Author declare no conflict of interest.

REFERENCES

[1] Reis, F.S., Heleno, S.A., Barros, L., Sousa, M.J., Martins, A., Buelga, C.S., Ferreira, I.C.F.R. (2011) Toward the Antioxidant and Chemical Characterization of Mycorrhizal Mushrooms from Northeast Portugal. Journal of Food Science. 76(6), 824-830.

[2] Sánchez, C. (2017) Reactive oxygen species and antioxidant properties from mushrooms. Synthetic and systems biotechnology. 2(1), 13-22.

[3] Gürgen, A., Yildiz, S., Can, Z., Tabbouche, S., Kiliç, A.O. (2018) Antioxidant, Antimicrobial and Anti-Quorum Sensing Activities of Some Wild and Cultivated Mushroom Species Collected from Trabzon, Turkey. Fresen. Environ. Bull. 27, 4120-4131.

[4] Alves, M.J., Ferreira, I.C., Dias, J., Teixeira, V., Martins, A., Pintado, M. (2012) A review on antimicrobial activity of mushroom (Basidiomycetes) extracts and isolated compounds. Planta medica. 78, 1707-1718.

[5] Kalac, P. (2016) Edible Mushrooms. 1st Edition, Chemical Composition and Nutritional Value. Academic Press. 236p.

[6] Ramesh, C., Pattar, M.G. (2010) Antimicrobial properties, antioxidant activity and bioactive compounds from six wild edible mushrooms of western ghats of Karnataka. India. Pharmacognosy research. 2(2), 107.

[7] Kosanić, M., Ranković, B., Dašić, M. (2012) Mushrooms as possible antioxidant and antimicrobial agents. Iranian Journal of Pharmaceutical Research: IJPR, 11(4), 1095.

[8] Boonsong, S., Klaypradit, W., Wilaipun, P. (2016) Antioxidant activities of extracts from five edible mushrooms using different extractants. Agriculture and Natural Resources. 50(2), 89-97.
[9] Allı, H., Çöl, B., Şen, İ. (2017) Macrofungi Biodiversity of Kütahya (Turkey) Province. Biodicon. 10(1), 133-143.
[10] Bernicchia, A. (2005) Polyporaceae, Fungi Europaei 10. Candusso, Bologna.
[11] Breitenbach, J., Kranzlin, F. (1986) Fungi of Switzerland. Vols. 2. Switzerland: Verlag Mykologia.
[12] Ellis, M.B., Ellis, J.P. (1990) Fungi without gills. London: Chapman and Hall.
[13] Sesli, E., Denchev, C.M. (2008) Checklists of the myxomycetes, larger ascomycetes, and larger basidiomycetes in Turkey. Mycotaxon. 106, 65–67.
[14] Erel, O. (2004) A novel automated direct measurement method for total antioxidant capacity using a new generation, more stable ABTS radical cation. Clinical biochemistry. 37(4), 277-285.
[15] Erel, O. (2005) A new automated colorimetric method for measuring total oxidant status. Clinical biochemistry. 38(12), 1103-1111.
[16] Bauer, W.A., Kirby, W.M., Sherris, J.C., Turck, M. (1966) Antibiotic susceptibility testing by a standardized single disk method. Am J Clin Pathol. 45, 493-496.
[17] Hindler, J., Hochstein, L., Howell, A. (1992) Preparation of routine media and reagents used in antimicrobial susceptibility testing. Part 1. McFarland standards. In: Isenberg, H.D. (ed.) Clinical microbiology procedures handbook, vol. 1. American Society for Microbiology, Washington, D.C. 5.19.1-5.19.6.
[18] CLSI (The Clinical and Laboratory Standards Institute) (2012) Antimicrobial Susceptibility Testing of Anaerobic Bacteria; Approved Standard—Eighth Edition (M11-A8).
[19] EUCAST (European Committee on Antimicrobial Susceptibility Testing) (2014) Breakpoint tables Fungal isolate for interpretation of MICs. 2014; Version 7.0
[20] Matuschek, E., Brown, D.F., Kahlmeter, G. (2014) Development of the EUCAST disk diffusion antimicrobial susceptibility testing method and its implementation in routine microbiology laboratories. Clin Microbiol Infect. 20, 255-266.
[21] EUCAST (European Committee on Antimicrobial Susceptibility Testing) (2015) Breakpoint tables for Bacteria interpretation of MICs and zone diameters. 2015; Version 5.0
[22] Sevindik, M., Akgul, H., Korkmaz, A.İ., Sen, İ. (2018) Antioxidant Potantials of *Helvella leucomelaena* and *Sarcosphaera coronaria*. J Bacteriol Mycol Open Access. 6(2), 00173.
[23] Akgul, H., Sevindik, M., Coban, C., Alli, H., Selamoglu, Z. (2017) New Approaches in Traditional and Complementary Alternative Medicine Practices: *Auricularia auricula* and *Trametes versicolor*. J Tradit Med Clin Natur. 6(239), 2
[24] Sevindik, M., Akgul, H., Bal, C. (2017) Determination of Oxidative Stress Status of *Ompholatus olearius* Gathered from Adana and Antalya Provinces in Turkey. Sakarya University Journal of Graduate School of Natural and Applied Sciences. 21(3), 324-327.
[25] Bal, C., Akgul, H., Sevindik, M., Akata, I., Yumrutas, O. (2017) Determination of the Anti-Oxidative Activities of Six Mushrooms. Fresen. Environ. Bull. 26, 6246-6252.
[26] Sevindik, M., Akgul, H., Bal, C., Selamoglu, Z. (2018) Phenolic Contents, Oxidant/Antioxidant Potential and Heavy Metal Levels in *Cyclocybe cylindracea*. Indian J of Pharmaceutical Education and Research. 52(3), 437- 41.
[27] Yildirim, N.C., Turkoglu, S., Yildirim, N., Kaplan Ince, O. (2010) Antioxidant properties of wild edible mushroom Pleurotus eryngii collected from Tunceli province of Turkey. Digest Journal of Nanomaterials and Biostructures (DJNB). 7(4), 1647-1654.
[28] Avci, E., Cagatay, G., Avci, G.A., Cevher, S.C., Suicmez, M. (2016) An Edible Mushroom with Medicinal Significance; Auricularia polytricha. Hittite Journal of Science and Engineering. 3(2), 111-116.
[29] Peres-Bota, D., Rodriguez, H., Dimopoulos, G., DaRos, A., Mélot, C., Struelens, M.J., Vincent, J.L. (2003) Are infections due to resistant pathogens associated with a worse outcome in critically ill patients? Journal of Infection. 47(4), 307-316.
[30] Lima, V.N., Oliveira-Tintino, C.D., Santos, E.S., Morais, L.P., Tintino, S.R., Freitas, T.S., Geraldo, Y.S., Pereira, R.L., Cruz, R.P., Menezes, I.R., Coutinho, H.D. (2016) Antimicrobial and enhancement of the antibiotic activity by phenolic compounds: Gallic acid, caffeic acid and pyrogallol. Microbial pathogenesis. 99, 56-61.
[31] Giri, S., Biswas, G., Pradhan, P., Mandal, S.C., Acharya, K. (2012) Antimicrobial activities of basidiocarps of wild edible mushrooms of West Bengal, India. International Journal of Pharm. Tech. Research. 4(4), 1554-1560.
[32] Yamaç, M., Bilgili, F. (2006) Antimicrobial activities of fruit bodies and/or mycelial cultures of some mushroom isolates. Pharmaceutical biology. 44(9), 660-667.

[33] Mocan, A., Fernandes, Â., Barros, L., Crişan, G., Smiljković, M., Soković, M., Ferreira, I.C. (2018) Chemical composition and bioactive properties of the wild mushroom Polyporus squamosus (Huds.) Fr: a study with samples from Romania. Food and function. 9(1), 160-170.

Received: **02.07.2018**
Accepted: **10.03.2019**

CORRESPONDING AUTHOR

Mustafa Sevindik
Akdeniz University,
Science Faculty,
Biology Department,
Antalya – Turkey

e-mail: sevindik27@gmail.com

© by PSP Volume 28 – No. 5/2019 pages 3718-3723 Fresenius Environmental Bulletin

ROSA CANINA L. ETHANOLIC EXTRACT INDUCES THE ANTI-PROLIFERATIVE AND APOPTOSIS POTENTIAL IN MCF-7 AND MDA-MB-468 CELL LINES

Mehmet Berkoz[1,*], Ferbal Ozkan-Yilmaz[2], Arzu Ozluer-Hunt[3], Metin Yildirim[4], Oruc Allahverdiyev[5], Ali Aslan[5]

[1]Department of Biochemistry, Faculty of Pharmacy, Van Yuzuncu Yil University, 65080 Van, Turkey
[2]Department of Basic Sciences, Faculty of Fisheries, Mersin University, 33169 Mersin, Turkey
[3]Department of Aquaculture, Faculty of Fisheries, Mersin University, 33169 Mersin, Turkey
[4]Department of Biochemistry, Faculty of Pharmacy, Mersin University, 33169 Mersin, Turkey
[5]Department of Pharmacology, Faculty of Pharmacy, Van Yuzuncu Yil University, 65080 Van, Turkey

ABSTRACT

Rosa canina L. (rose hip) fruits have been used for their diuretic, laxative, anti-gout, anti-rheumatism properties in traditional medicine. Rose hip berries contain a variety of components such as flavonoid. The previous studies showed that flavonoid has anti-cancer properties. Tha aim of this study is to evaluate and screen the effect of apoptosis and the anticancer potential of rose hip ethanolic extract on human breast cancer cell lines; MCF-7 and MDA-MB-468. The anti-proliferative activity of rose hip extract was evaluated using MTT, flowcytometry by annexin V/PI double staining, and caspase-3 activity. The results of MTT showed that the ED_{50} of both human breast cancer cell lines was 25µg/mL of rose hip extract, 48 hours after treatment. Flowcytometry by annexin V/PI showed that rose hip extract induced late apoptosis in MCF-7 and early apoptosis in MDA-MB-468. In addition, the caspase-3 colorimetric method showed that caspase-3 increased in the MDA-MB-468 after treatment with rose hip extract. As a result, the ethanol of rose hip ethanolic extract induced apoptosis in both human breast carcinoma cell lines.

KEYWORDS:
Rosa canina L., rose hip, MCF-7, MDA-MB-468, anti-proliferation, apoptosis

INTRODUCTION

In normal conditions, the body has a balance between cell death and cell proliferation. This balance is known as hemostasis and is necessary for normal cell growth. If this balance is disturbed, it leads to cancer. Cancer is a serious concern all over the world and the most common cause of mortality and morbidity after cardiovascular diseases [1]. Breast cancer is the most common cancer among women; each year nearly 400,000 women suffering from this disease lose their lives, and nearly 234,000 new cases of breast cancer are reported every year [2]. The known causes of breast cancer are not so similar to those of other cancers; however, studies indicate various factors that can increase the risk of getting breast cancer, such as genetic predisposition, obesity, pregnancy after the age of 35, exposure to radiation dangers such as UV, a history of cancer in first-degree relatives, a history of breast cancer in one breast, and continuous use of birth control pills overa long period [1].

Currently, the treatment for breast cancer is dominated by modern medicine, which relies more on surgery, radiotherapy, chemotherapy, hormone therapy, immunotherapy, and so on [1]. Unfortunately, in most cases, treatment is not effective or leads to unpleasant side effects, hence researchers are trying to use compounds with fewer side effects and to induce apoptosis in cancer cells [3]. Natural products can be used as medicines to treat cancer. Since the 1950s, 60% of cancer drugs have been made from natural products or their derivatives. Plants and herbs are low-cost natural products with few side effects that can be used for cancer treatment. In this way, not only are cancer cells controlled, but also healthy cells are not damaged [4].

Rosa canina (rose hip) is the fruit of the rose plant that ranges in color from red to orange; however, there are some species whose color ranges from dark purple to black. Rose hip extracts have been used as chemopreventive agents due to their mechanistic actions on cancer cells [5]. The elevated levels of lycopene found in rose hip extracts are associated with increased apoptosis in prostate cancer. Rose hip fruits have shown potent anti-proliferative activity against colon, breast, and cervical cancer cells in vitro. Rose hip is high in vitamin C causing this pseudo fruit to be rich in ascorbic acid, phenolic components, and carotenoids [6,7]. These high antioxidant contents cause rose hip to have high antioxidant activities. Studies have shown that it is useful in treating arthritis due to its anti-inflammatory and anti-oxidant effects.

Studies have shown that the Vitamin C and flavonoids found in rose hip is responsible for the antioxidant activity associated with rose hip products [5]. However, it is the polyphenols found within this plant that is responsible for the antiproliferative activity. The anti-proliferative effects on cell proliferation in estrogen receptor positive (ER^+) breast cancer cell line (MCF-7) and estrogen receptor negative (ER^-) breast cancer cell line (MDA-MB-468) have not yet been tested. The current study was conducted to evaluate and screen the effect of apoptosis and the anticancer potential of rose hip extract on MCF-7 and MDA-MB-468 cell lines.

METHODS AND MATERIALS

Plant materials. Berries of rose hip was collected from the Bekiralanı village (on Toros Mountains) of Turkey's Mersin province (GPS coordinates 36° 59' 03.6'' N, 34° 31' 24.1'' E). Plant collection was done in May 2017. Prof. Dr. Ali Aslan confirmed the taxonomic determination of *Rosa canina* L.

Preparation of hydroalcoholic extract of rose hip. After the collection, rose hip berries were dried in indirect light and a clean environment. The freeze-dried rose hip berries were grounded to powder and then 70% ethanol solution was extracted using a Soxhlet extractor. The solution was filtered and evaporated under a rotary evaporator in order to obtain a hydroalcoholic extract; the solid extract was stored in a freezer at -20 °C.

Cell culture. Cancer cell lines; MCF-7 and MDA-MB-468 were obtained from from American Type Culture Collection (ATCC). The cell lines were grown adherently as a monolayer in 75 mL plastic flasks in RPMI 1640 medium supplemented with 10% FBS (heat inactivated 30 minutes, 56 °C before use), 100 U/mL penicillin, and 100 µg/mL streptomycin in incubator under standard cultured condition (37 °C and 5% CO_2). For enumeration, 30µL of trypan blue (0.2%) stained the same volume (30 µL) of cell concentration, and neobar lam was used for counting and viability (more than 95% for adhering cell lines before testing) of the cells.

Cell treatments. For treatment with rose hip extract, first rose hip extract as powder was dissolved in DMSO and kept in a freezer at -20 °C. The cell lines were seeded into sterile 6 or 96 well plates; the cell number was almost equal in all the wells for adhering cell lines to button plates. Incubation was done over night. The medium was aspirated, and different concentrations that were prepared with medium and different concentrations of rose hip extract (0-12.5-25-50-100 µg/mL) were added. The number of cell lines in seeding was different in different tests as indicated therein.

Cell viability assay. Cell viability and antiproliferation of rose hip extract were carried out through an MTT reduction assay [6]. The measurement was repeated in triplicate to confirm the results. The results were calculated by dividing the percentage of absorbance in the treated cells by the percentage of absorbance in the untreated (control) cells, defined as the viability percentage. ED_{50} was 50%, the concentration range that inhibits the growth of cell lines.

Apoptosis assay. The apoptotic effect of rose hip extract on the cell lines was analyzed by means of a flowcytometry assay, using an annexin V/Propidium iodide (PI) double staining Kit (Biovision, San Francisco, California, USA), according to the manufacturer's protocol. Partec PAS II flowcytometry was used for analysis of the samples. The results consist of four sections: living cells (were not stained with PI or annexin V), early apoptosis (stained with annexin V connected to phosphatidylserine in outer layer of cell membrane), late apoptosis (stained with both annexin V and PI to fragmented DNA), and necrosis cells (stained with PI) [9].

Caspase-3 activity assay. A colorimetric assay kit (R&D System Co., Minneapolis, Minnesota, USA) was used for measuring caspase-3 activity according to the manufacturer's protocol.

Statistical analysis. The data were analyzed using SPSS 15.0 software package. The values are expressed as mean ± SD. Analysis of variance (ANOVA) was conducted, followed by Tukey correction, to test for differences in mean values between groups. The results were considered significant at $p<0.05$.

RESULTS

The morphology of the MCF-7 cell line changed in a dose- and time-dependent manner; in low concentrations, the cells were deformed, and with increasing dose and time, granulated cellular contents, dropsy, and shrinkage were increased, even, after 48 hours (at a 100 µg/mL concentration) and 72 hours (at 50µg/mL and 100µg/mL concentrations), the rupture of membranes and the release content of cytosol were clearly observed. The MDA-MB-468 cell line had approximately the same condition (Figure 1).

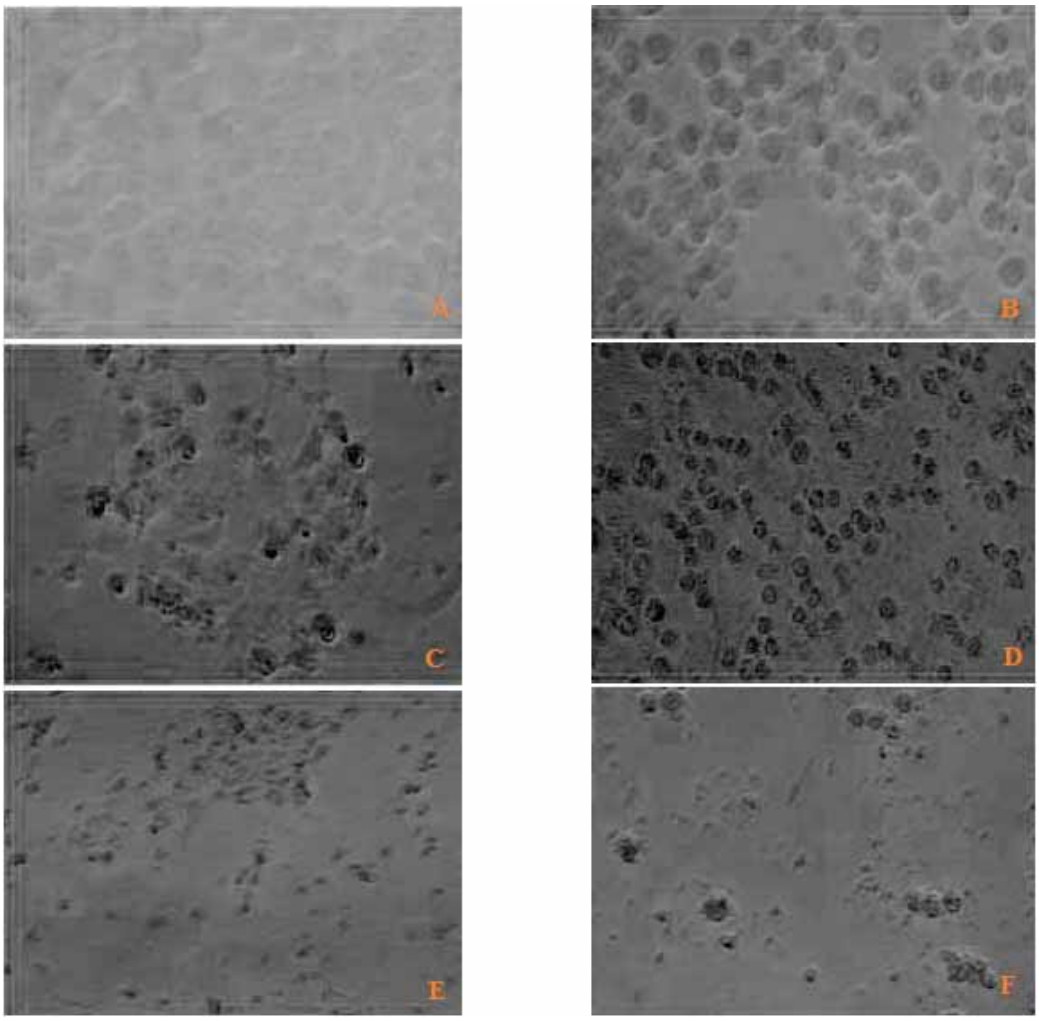

FIGURE 1

Effects of rose hip extract on the morphological alterations of MCF-7 and MDA-MB-468 cells were monitored for 72 hours at two different doses of rose hip extract.

Control MCF-7 cells (Figure 1A) and control MDA-MB-468 cells (Figure 1B) dispersed homogeneously with distinct boundaries after over night incubation. Figure 1C; MCF-7 cells exposed to 50 µg/mL rose hip extract for 72 hours, Figure 1D; MDA-MB-468 cells exposed to 50 µg/mL rose hip extract for 72 hours, Figure 1E; MCF-7 exposed to 100µg/mL rose hip extract for 72 hours, and Figure 1F; MDA-MB-468 exposed to 100µg/mL rose hip extract for 72 hours.

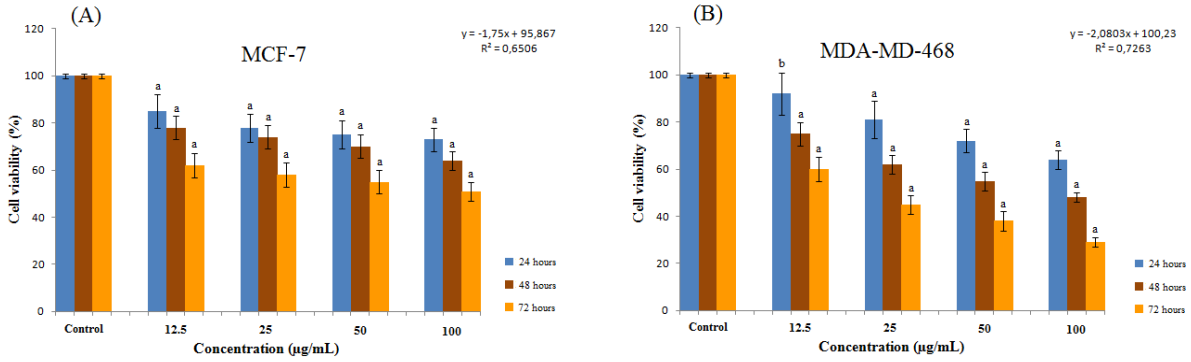

FIGURE 2

Effect of rose hip extract in inhibition of cell growth of the breast cancer MCF-7 (shown in Figure 2A) and MDA-MB-468 (shown in Figure 2B) cell lines.

Cells were treated with different concentrations of rose hip extract for 24, 48 and 72 hours, and proliferation was measured withan MTT assay. Rose hip extract reduced cell proliferation in MCF-7 (25µg/mL) and MDA-MB-468 (25µg/mL) breast cells in a time- and dose-dependent manner. Each value is presented as a mean ± SD of three experiments (each triplicate).[a]p <0.01; [b]p<0.05 compared to untreated control groups.

The effects of rose hip extract on both human breast carcinoma cell lines were examined. The cells were exposed to different concentrations of rose hip extract for 24, 48, and 72 hours. After these periods, the cell lines' viability was measured by an MTT assay. Concentration 25 µg/mL of rose hip extract had significant inhibitory effects on both cell lines: 51.67±1.527 for MCF-7 and 53,48±1.577 for MDA-MB-468 after treatment for 48 hours. Exposed to 25 µg/mL concentration of rose hip extract during 48 hours can inhibit growth by 50% in both cell lines. Figure 2 shows the results of MTT in both cell lines, showing a significant difference in the dose-time manner ($p<0.001$).

The cell lines were stained with annexin V/PI and analyzed using flowcytometry to explore whether rose hip extract shows cytotoxicity through induction of apoptosis. To do so, the cell lines were treated in appropriate doses (0-12.5-25-50-100 µg/mL) for 48 hours. The cell population shifted from viable (annexin V^-/PI^-) to early apoptosis (annexin V^+/PI^-) and late apoptosis (annexin V^+/PI^+) in high doses and in the MDA-MB-468 cell line more towards early apoptosis (annexin V^+/PI^-) through an increase in the dose, based on the results of annexinV/PI double staining also in the MCF-7 cell line through induction of late apoptosis (annexin V^+/PI^+). These shifts were significantly different in both cell lines ($p<0.001$) (Figure 3).

Caspase enzymes play an important role in apoptotic responses; therefore, the effect of rose hip extract in inducing apoptosis in the cell lines was investigated by measuring the activity of caspase-3. The treatment of the MDA-MB-468 cell line of breast cancer in a 25 µg/mL concentration of rose hip extract was observed. Also, a significant increase in caspase-3 activity of MDA-MB-468 was observed after treatment with rose hip extract in ED_{50} (approximately 25 µg/mL) at various times (6, 12, and 24 h), and the amount of caspase-3 differed significantly between treated and untreated cell lines ($p<0.001$); however, there was no such increase in the MCF-7 cell line (Figure 4).

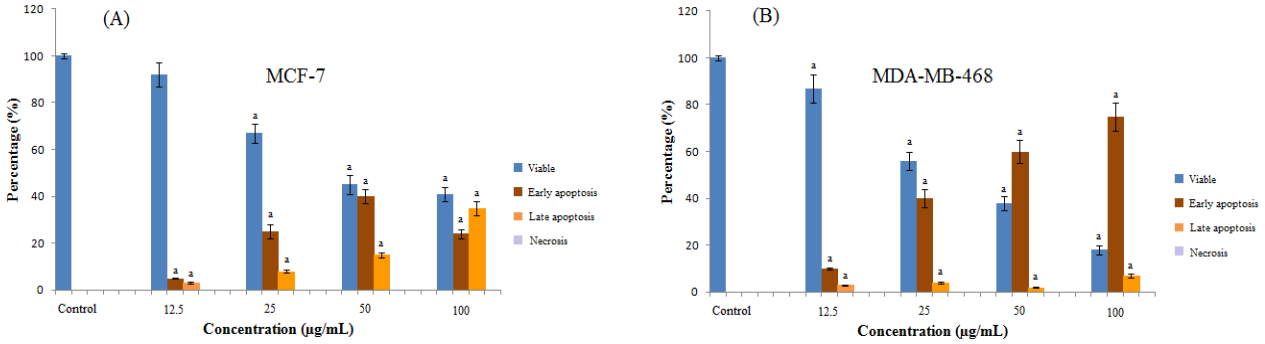

FIGURE 3

Flowcytometric evaluation of apoptosis in MCF-7 cells (Figure 3A) and in MDA-MB-468 cells (Figure 3B) using annexin-V/PI double staining.

After 48 hours treatment, rose hip extract resulted in a significant increase in late apoptotic cells and a moderate increase in early apoptotic cells, in a dose-dependent manner. Results, mean ± SD three independent experiments. [a]$p<0.01$ compared to untreated control groups.

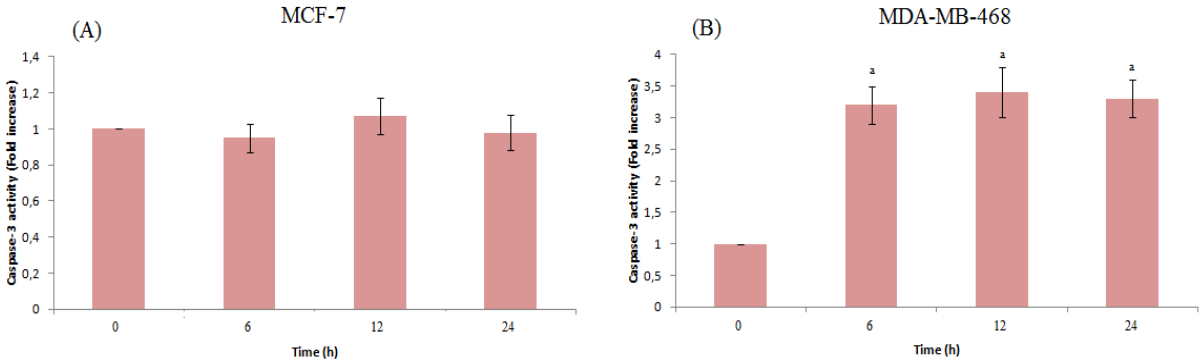

FIGURE 4

The effect of rose hip extract on caspase-3 activity in MCF-7 (Figure 4A) and MDA-MB-468 (Figure 4B) cells.

Cells were incubated to a concentration of rose hip extract (25µg/mL) in a time-dependent manner (6, 12, and 24 hours). [a]$p<0.01$ compared to untreated control groups.

DISCUSSION

Breast cancer has the highest prevalence among women compared to other cancers, and surgery is the main therapy for this disease, with chemotherapy, radiotherapy, hormone therapy, and gene therapy used as minor therapies. However, these therapies have several problems. For example, in surgery, in addition to tumor cells, healthy cells are also removed; the radiation used in minor therapy harms normal cells [10, 11].

Moreover, these treatments are expensive. Thus, many researchers have focused on lowpriced new drugs with a natural origin that induce apoptosis in tumor cells, but not in healthy cells, and are especially prepared using local and traditional medicines [3, 4].

Plants as natural resources have played a vital role as a source of effective agents against cancer [3]. Natural products such as *Ginkgo biloba* have been shown to have anti- proliferative properties in breast cancer cells [12]. Park et al. [13] observed the inhibitory effects of cell proliferation using *Ginkgo biloba* extract in MDA-MB-231 breast cancer cell line. Pomegranate extracts and genistein have been observed to have cytotoxic and anti-proliferative effects in MCF-7 cancer cells [14]. Tanih et al. [15] observed the crude acetone extract of *Sclerocarya birrea* inhibited proliferation of the MCF-7 cell line via an apoptotic programmed cell death. Yang and colleagues [16] observed the anti-migratory and anti-invasion effects of chrysin in MDA-MB-231 and BT-549 cell lines.

Rose hip is commonly known as "*kuşburnu, itburnu, gülburnu, gül elması*" in Turkish herbal medicine. Previous studies have shown that it has antioxidant properties and contains carotenoids, flavonoids, and polyphenolic compounds that are known as anticancer components. Interestingly, Rose hip extract has antioxidant properties [5]. In the current study, the anticancer and apoptotic activities of rose hip extract were investigated. The results showed that rose hip extract exhibited cytotoxicity towards the MCF-7 and MDA-MB-468 human breast cancer cell lines with an ED_{50} of 25 µg/mL for both; this was determined by means of an MTT assay. To determine the type of cell death (apoptosis or necrosis), annexinV/PI double staining was used. The findings showed that rose hip extract induced apoptosis in MCF-7 and MDA-MB-468, while the apoptotic cells of both cancer cell lines were shifting to late apoptosis and early apoptosis, respectively.

Apoptosis is a programmed cell death that regulates normal physiological processes and plays an essential role in the progress and maintenance of tissue homeostasis. Apoptosis has two main pathways, an extrinsic apoptosis pathway (death receptor dependent pathway) and an intrinsic apoptosis pathway (mitochondria-dependent apoptosis) [17]. Briefly, in the extrinsic apoptosis, the interaction between the death ligand and the death receptor leading to caspase-8 activation as a starter caspase, activated caspase-8 then activates caspase-3, while in the intrinsic apoptosis pathway, cytochrome C is released from mitochondria leading to caspase-9 activation as a starter caspase, activated caspase-9 then activates caspase-3 [18]. Thus, in this study, caspase-3 activity was measured; it was found that caspase-3 increased in the MDA-MB-468 cell line in a time dependent manner (25µg/mL of rose hip extract). Caspase activity did not change in a time-dependent manner (25µg/mL of rose hip extract) because the MCF-7 cell line did not express caspase-3 due to deletion (functional 47 bp) inside the exon 3 of capsase-3 gene. Therefore, the induction of apoptosis in the MCF-7 cell line was treated with rose hip extract, probably due to a caspase-independent or a non-caspase-3-dependent mechanism [19].

There is little data regarding the effect of rose hip extract on cell lines. The anti-oncogenic properties of rose hip extracts have been tested in HeLa, Caco-2, and HT-29 cancer cell lines and their effects have been suggested to be related to anti-oxidant and anti-proliferative effects [6, 7]. Rose hip extracts have also been reported to modulate the activity of one or more phases involved in cell cycle regulation. One of the key factors in the development and progression of cancer is the ability of cells to promote cell proliferation and inhibit apoptosis [7]. Therefore, any treatment possessing antiproliferative effects in cancer cells regaining that balance between cell proliferation and cell death are indicative of having potential anti-oncogenic properties [6, 7].

In conclusion, our study demonstrates for the first time the cytotoxic effect of the ethanol extract of rose hip against the MCF-7 and MDA-MB-468 cancer cell line depending on the dose of exposure without affecting the normal cells. We also reported that rose hip ethanol extract display cell lysis by the apoptosis pathway. These findings provide evidence that rose hip has potential as an anti-breast cancer agent.

REFERENCES

[1] Arteaga, C.L. (2013) Progress in breast cancer: overview. Clinical Cancer Research. 19, 6353-6359.

[2] Rastegar, H., Ahmadi Ashtiani, H., Anjarani, S., Bokaee, S., Khaki, A. and Javadi, L. (2013) The role of milk thistle extract in breast carcinoma cell line (MCF-7) apoptosis with doxorubicin. Acta Medica Iranica. 51, 591-598.

[3] Buyel, J.F. (2018) Plants as sources of natural and recombinant anti-cancer agents. Biotechnology Advances. 36, 506-520.

[4] Kapinova, A., Stefanicka, P., Kubatka, P., Zubor, P., Uramova, S., Kello, M., Mojzis, J., Blahutova, D., Qaradakhi, T., Zulli, A., Caprnda, M., Danko, J., Lasabova, Z., Busselberg, D. and Kruzliak, P. (2017) Are plant-based functional foods better choice against cancer than single phytochemicals? A critical review of current breast cancer research. Biomedicine and Pharmacotherapy. 96, 1465-1477.

[5] Chrubasik, C., Roufogalis, B.D., Müller-Ladner, U. and Chrubasik, S. (2008) A systematic review on the Rosa canina effect and efficacy profiles. Phytotherapy Research. 22, 725-733.

[6] Tumbas, V.T., Canadanović-Brunet, J.M., Cetojević-Simin, D.D., Cetković, G.S., Ethilas, S.M. and Gille, L. (2012) Effect of rosehip (*Rosa canina* L.) phytochemicals on stable free radicals and human cancer cells. Journal of the Science of Food and Agriculture. 92, 1273-1281.

[7] Jiménez, S., Gascón, S., Luquin, A., Laguna, M., Ancin-Azpilicueta, C. and Rodríguez-Yoldi, M.J. (2016) *Rosa canina* extracts have antiproliferative and antioxidant effects on Caco-2 human colon cancer. PLoS One. 11, 1-14.

[8] Hashemi, M., Karami-Tehrani, F., Ghavami, S., Maddika, S. and Los, M. (2005) Adenosine and deoxyadenosine induces apoptosis in oestrogen receptor-positive and -negative human breast cancer cells via the intrinsic pathway. Cell Proliferation. 38, 269-285.

[9] Dai, G., Zheng, D., Guo, W., Yang, J. and Cheng, A.Y. (2018) Cinobufagin induces apoptosis in osteosarcoma cells via the mitochondria-mediated apoptotic pathway. Cellular Physiology and Biochemistry. 46, 1134-1147.

[10] Patten, D.K., Sharifi, L.K. and Fazel, M. (2013) New approaches in the management of male breast cancer. Clinical Breast Cancer. 13, 309-314.

[11] Akram, M. and Siddiqui, S.A. (2012) Breast cancer management: past, present and evolving. Indian Journal of Cancer. 49, 277-282.

[12] Zhao, X.D., Dong, N., Man, H.T., Fu, Z.L., Zhang, M.H., Kou, S. and Ma, S.L. (2013) Antiproliferative effect of the Ginkgo biloba extract is associated with the enhancement of cytochrome P450 1B1 expression in estrogen receptor-negative breast cancer cells. Biomedical Reports. 1, 797-801.

[13] Park, Y.J., Kim, M.J., Kim, H.R., Yi, M.S., Chung, K.H. and Oh, S.M. (2013) Chemopreventive effects of Ginkgo biloba extract in estrogen-negative human breast cancer cells. Archives of Pharmacal Research. 36, 102-108.

[14] Jeune, M.A., Kumi-Diaka, J. and Brown, J. (2005) Anticancer activities of pomegranate extracts and genistein in human breast cancer cells. Journal of Medicinal Food. 8, 469-475.

[15] Tanih, N.F. and Ndip, R.N. (2013) The acetone extract of Sclerocarya birrea (Anacardiaceae) possesses antiproliferative and apoptotic potential against human breast cancer cell lines (MCF-7). The Scientific World Journal. 2013, 1-7.

[16] Yang, B., Huang, J., Xiang, T., Yin, X., Luo, X., Huang, J., Luo, F., Li, H., Li, H. and Ren, G. (2014) Chrysin inhibits metastatic potential of human triple-negative breast cancer cells by modulating matrix metalloproteinase-10, epithelial to mesenchymal transition, and PI3K/Akt signaling pathway. Journal of Applied Toxicology. 34, 105-112.

[17] Francis, S.H., Turko, I.V. and Corbin, J.D. (2001) Cyclic nucleotide phosphodiesterases: relating structure and function. Progress in Nucleic Acid Research and Molecular Biology. 65, 1-52.

[18] Lugnier, C. (2006) Cyclic nucleotide phosphodiesterase (PDE) superfamily: a new target for the development of specific therapeutic agents. Pharmacology and Therapeutics. 109, 366-398.

[19] Yu, J.H., Zheng, G.B., Liu, C.Y., Zhang, L.Y., Gao, H.M., Zhang, Y.H., Dai, C.Y., Huang, L., Meng, X.Y., Zhang, W.Y. and Yu, X.F. (2013) Dracorhodin perchlorate induced human breast cancer MCF-7 apoptosis through mitochondrial pathways. International Journal of Medical Sciences. 10, 1149-1156.

Received: **03.07.2018**
Accepted: **19.03.2019**

CORRESPONDING AUTHOR

Mehmet Berkoz
Department of Biochemistry,
Faculty of Pharmacy,
Van Yuzuncu Yil University,
Zeve Campus, 65080 Van – Turkey

e-mail: mehmet_berkoz@yahoo.com

© by PSP Volume 28 – No. 5/2019 pages 3724-3728 Fresenius Environmental Bulletin

PCR BASED MOLECULAR CHARACTERIZATION OF CITRUS BACTERIAL CANKER FROM GRAPEFRUIT (*CITRUS PARADISI*)

Syeda Khola Tazeen[1,*], Khalid Farooq Akbar[1], Arif Muhammad Khan[2], Atifa Masood[1], Amna Fayyaz[3], Umair A Khan[1], Sumaira Arooj[4],

[1]Department of Botany, The University of Lahore, Sargodha Campus, Sargodha, Pakistan
[2]Department of Biotechnology, University of Sargodha, Sargodha, Pakistan
[3]Department of Plant Pathology, University of Agriculture, Faisalabad. Pakistan
[4]Department of Botany, University of Agriculture, Faisalabad, Pakistan

ABSTRACT

Citrus bacterial canker (CBC) occurs due to *Xanthomonas axonopodis* pv. *Citri* (Xac) is a pathogenic bacteria. It was first reported in Japan, USA and many areas of India in 19th century. Synchronized by the spread of the causative agent the diversity of labelled pathogen continues to spread with new strains appearing in many other regions of the world. However, its diagnosis is quite difficult due to its symptoms similarity with other bacterial strains. This piece of study was designed to identify *Xanthomonas axonopodis* using polymerase chain reaction (PCR). PCR is more accurate, precise and fast method which is used for detection and quantification of many bacterial species. Two primers Xac01 *and* Xac02 were used for PCR based CBC detection. These primers were based on *rpf* gene region which give very specific results in *Xac* identification and can separate two much similar bacterial strains. There is another Primer pair designed on the *pthA* gene which act as universal primer and usually used for detection of all varieties of citrus canker bacteria. Leaves sample from different infected *Citrus paradisi* plants were collected for further analysis. Results confirmed that three samples among five have CBC. It is concluded that using PCR we can detect citrus canker disease more specifically which will help in discovering new eradication methods for its control.

KEYWORDS:
Citrus Bacterial Canker, *Xanthomonas axonopodis,* polymerase chain reaction, *pthA, rpf*, primers, *Citrus paradisi*

INTRODUCTION

Grapefruits belongs to the family *Rutaceae* commonly known as citrus family considered as second most important family of fruits after grapes around the world both in production and area. It consists of more than 2000 species across 160 genera having herbs, shrubs and flowering plants [1]. Pakistan is present in the list of top ten citrus fruits cultivar in the world. Some genera of citrus like lemon (*Citrus limon*), orange (*Citrus sinensis*), grapefruit (*Citrus paradisi*), and lime (typically *Citrus aurantifolia*) have great impact on economic earnings of Pakistan [2]. This family also have medicinal and dietetic value due to presence of Vitamin C, potassium, carbohydrates and other micronutrients [3]. But unfortunately from last few decades citrus product rate is decreasing gradually due to many pathogenic and non-pathogenic diseases. Among these diseases, citrus bacterial canker is most damaging and prevalent disease affect citrus production rate in many countries of the world including Pakistan [4, 5].

There are three different types of CBC triggered by different strain types of *Xanthomonas* bacterium e.g *X. axonodopis, X.campestris, X. Citri*. Although each strain has quite similar disease symptoms separated from each other on the basis of host range, cultural physiological characteristics and bacteriophage sensitivity [6]. CBC is mainly a leaf-spotting disease but under acute disease condition leaf defoliation, shoot-die back and fruit drop also occur. Serological technique such as ELISA (enzymes linked immune-sorbent assay), RFLP and PCR are commonly used diagnostic tests for CBC [7].

PCR is one of the best method for accurate identification of bacterium isolate from extract of lesions on infected tissue [8, 9]. PCR primers usually designed using variation in the intergenic spacer (ITS) region of 16s and 23s ribosomal DNA to check all strains and variants of citrus canker [10].

MATERIALS AND METHODS

Sample collection and DNA extraction. Samples of infected leaves of grape fruit plants were collected from the field areas of Sargodha, Pakistan. Four samples C1, C2, C3, and C4 were collected from four different infected grapefruit

plants. Each sample consisted of three leaves per plant. Leaves samples wrapped in a polythene bag and were bought to virology lab, University of Agriculture, Faisalabad. All the samples were washed twice and stored at -20 ^{0}C till extraction of DNA. Asymptomatic leaves from healthy grapefruit plant were taken as controls. Extraction of DNA from leaf samples was done by using CTAB method [11]. Then agarose gel electrophoresis was performed for checking presence and quality of DNA [12].

Polymerase chain reaction (PCR). DNA based amplification was done in 50 µl reaction volume having under study (infectious leaves) DNA extraction product 2µg (5 µl), dNTPs 2 mM (5 µl), PCR Buffer 10X (5 µl), $MgCl_2$ 1.5 mM (3 µl), Primer I 5 µM (1 µl), Primer II 5 µM (1 µl), *Taq* polymerase 1.5U (0.5 µl), d d_3H_2O 29.5 µl. In three repeating cycles of PCR, timing of denaturation (94°C), annealing (50-64°C) and extension (72°C) was optimized according to CBC primers activity; normally thirty seconds, one minute and one minute per 1000 bases to amplify, respectively. Final PCR product was checked and confirms by running on 1% gel electrophoresis along with DNA ladder viewed under ultraviolet trans-illuminator and photographed using the Gel Documentation System (Stratagene).

T/A cloning and restriction Digestion. By using T/A cloning dissimilarity among DNA sample between different plants was observed. PCR products were purified by phenol-chloroform extraction, ligated into pTZ 57RT (fermantas) vector and transformed into *E.coli* top 10 strain .Then white colonies were picked and bacterial DNA was isolated from cells through plasmid isolation. Bacterial DNA was double restricted by two restricted enzymes BamH1 and EcoR1 and fragments were analyzed by agarose gel electrophoresis. Expected fragments of sized 581bp were obtained in all four samples which indicates the presence of desired pathogen [12, 13].

RESULTS AND DISCUSSION

The leaf samples of infected grape fruit plants were collected from the citrus growing areas of Sargodha showing distinctive symptom of disease *i.e.* lesions on the leaves, twigs, and fruits of citrus plants (Figure 1) [14]. There are many other plant diseases caused by other strains of *xanthomonas* bacteria which infect leaves and shows similar symptom therefore precise characterization is very important for proper analysis of this harmful and widespread disease [15]. The accurate characterization of causative bacterial strain is critical because it can be mixed up with related organisms like *alfalfae* subsp. *citrumelonis (*formerly *X. axonopodis* pv. *Citrumelo* [16]. So diagnosis of CBC frequently checked by using standard isolation and characterization methods. Molecular method designed to detect the pathogen are already well-known in the previous writings but some analyses cannot detect and differentiate among most similar bacterial species like *X. fuscans* subsp. *aurantifolii* [17, 18].

TABLE 1
Primer pair used in PCR

Designation	Primer pair (Reference)	Primer sequence	Origin	PCR Product Size(bp)
Xac_{o1}	[14]	CGC CAT CCC CAC CAC CAC CAC GAC	*rpf* gene	581
Xac_{02}	[14]	AAC CGC TCA ATG CCA TCC ACT TCA	*rpf* gene	581

FIGURE 1
Typical symptoms of CBC: Raised corky lesions on the leaves, Leaf defoliation

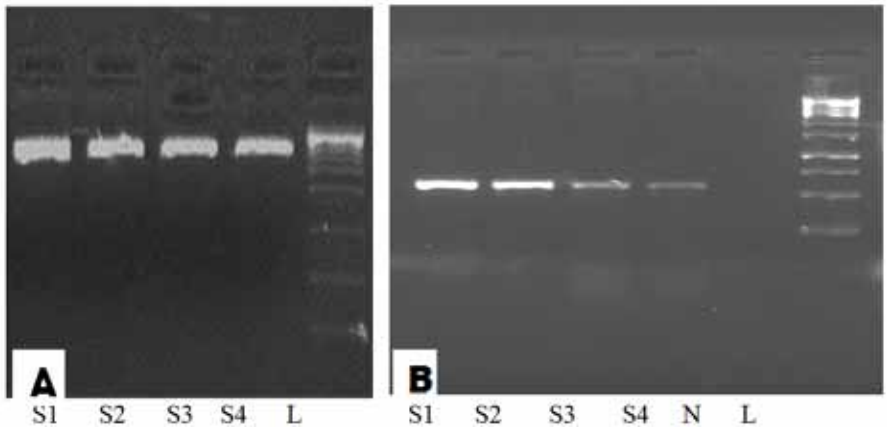

FIGURE 2

(A) Gel picture showing DNA presence in all samples (B) PCR amplification in Lane S1, S2, S3 and S4 showing the presence of citrus canker infection in sample plants. Gel lane N represent negative control. While gel lane L represent 1kb DNA ladder.

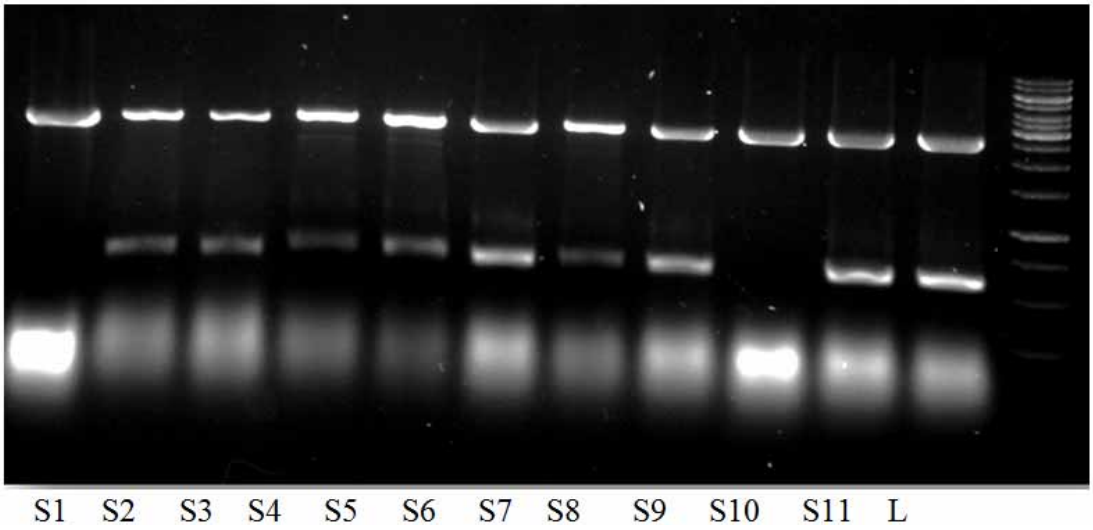

FIGURE 3

Restriction analysis of DNA fragment by *BamH1* and *EcoR1* enzymes. Samples S2 to S8, S10 and S11, restricted with *BamH1* and *EcoR1* enzymes showing clone of 581bp. Sample no. S1 and S9 showing no clone during restriction analysis.

An effective molecular method PCR has been established for rapid documentation of the bacterium. The primer pair which was early used to distinguish and classify citrus canker strains were constructed on a plasmid sequence but these primers were unable to distinguish a variant of strain A i- e A^W, which was recently discovered. Novel universal primers based on *pth* gene which is major virulence element in all canker strain are now available for all the canker strains in the world [19]. These universal primers uses specific sequences intergenic spacer region (ITS) of 16S and 23S ribosomal DNAs. The present research work was designed to identify the causal agent of citrus canker by molecular method that is using PCR primers constructed on the *rpf* gene region. A Xac-specific genomic region was identified inside the *rpf* gene cluster between *rpfB* and *rpfJ* of strain IAPAR 306. Genome bases sequences in *rpf* gene region were used for designing primers labelled Xac_{01} (5´-CGC CAT CCC CAC CAC CAC CAC GAC- 3´) and Xac_{02} (5´ -AAC CGC TCA CTG CCA TCC ACT TCA- 3´).

Four samples S1, S2, S3, and S4 from infected leaves were collected and DNA was isolated using CTAB method. After DNA extraction gel electrophoresis was performed to confirm the presence and quantity of DNA. Then PCR was performed and the results obtained. PCR was positive for all the four samples S1, S2, S3, S4. Expected 581 bp fragments were obtained from amplification of DNA samples. Health leaves of citrus plants were used as negative control. Then the product was purified, cloned and analyzed by restriction analysis. Clones of different size were obtained through double digestion of DNA fragments using restriction enzymes *BamH1* and *EcoR1*. It was concluded that the correct identification of the pathogen is critical because the pathogen is confused with other organisms which cause

mild form of citrus canker. So, PCR is a molecular method for recognition of *xanthomonas axonopodis* pv *.citri* (Xac) is more reliable in commercial citrus fruits, and to expand the controlling of canker disease.

REFERENCES

[1] Fujioka, K., Greenway, F., Shread, J. and Ying, Y. (2006) The effects of grapefruit on weight and insulin resistance: relationship to the metabolic syndrome. J Med Food. 9(1), 49-54.

[2] Frederick, G. and Xulan, H. (1990) The possible role of Yunnan, China, in the origin of contemporary Citrus species (*Rutaceae*). Economic Botany. 44 (2), 267–277.

[3] Guo, K., Xiang, B., Zhao, S. and Wu, C. (2018) Study on identification to pathogens of woods canker, genetic differentiation research to its main species valsa mali and rapid detection to primary infection source of *v. Mali* in Xinjiang. Fresen. Environ. Bull. 27, 2978-2984.

[4] Dadasoglu, F., Kotan, R., Cakir, A., Cakmakci, R., Kordali, S., Ozer, H., Karagoz, K. and Dikbas, N. (2015) Antibacterial activities of essential oils, extracts and some of their major components of *Artemisia spp. L.* Against seedborne plant pathogenic bacteria. Fresen. Environ. Bull. 24, 2715-2724.

[5] Graham, J.H., Johnson, E.G., Myers, M.E., Young, M., Rajasekaran, P., Das, S. and Santra, S. (2016) Potential of Nano-Formulated Zinc Oxide for Control of Citrus Canker on Grapefruit Trees. Trees, Plant Disease. 100(12), 2442-2447.

[6] Graham, J.H., Gottwald, T.R., Cubero, J. and Achor, D. (2004) *Xanthomonas axonopodis pv. citri:* factors affecting successful eradication of citrus canker. Mol Plant Pathol. 5(1), 1-15.

[7] Gottwald, T.R., Hughes, G., Graham, J.H., Sun, X. and Riley, T. (2001) The citrus canker epidemic in Florida: The scientific basis of regulatory eradication policy for an invasive species. Phytopathology. 91(1), 30–34.

[8] Cubero, J., Graham, J.H. and Gottwald, T.R. (2001) Quantitative PCR method for diagnosis of citrus bacterial canker. Appl. Environ. Micro. 67(6), 2849–2852.

[9] Karanfil, A. and Korkmaz, S. (2018) Genetic diversity of Turkish citrus chlorotic dwarf-associated virus isolates based on coat protein gene. Fresen. Environ. Bull. 27, 6403-6407.

[10] Yang, Y. and Gabriel, D.W. (1995) Xanthomonas avirulence/pathogenicity gene family encodes functional plant nuclear targeting signals. Mol. Plant Microbe Interact. 8, 627–63.

[11] Doyle, J.J. and Doyle, J.L. (1990) Isolation of plant DNA from fresh tissue. Focus. 12(1), 13-15.

[12] Schaad, N.W., Jones, J.B. and Chun, W. (2001) Laboratory Guide for Identification of Plant Pathogenic Bacteria. 3nd. Ed. APS Press, St. Paul, MN, USA, 151-174.

[13] Golmohammadi, M., Cubero, J., Peñalver, J., Quesada, J.M., López, M.M. and Llop, P. (2007) Diagnosis of *Xanthomonas axonopodis pv. citri,* causal agent of citrus canker, in commercial fruits by isolation and PCR-based methods. Applied Microbiology. 103(6), 2309-2315.

[14] Cubero, J. and Graham, J.H. (2002) Genetic relationship among worldwide strains of Xanthomonas causing canker in citrus species and design of new primers for their identification by PCR. Appl. Environ. Micro. 68(3), 1257–1264.

[15] Kasikci, E.S., Aksoy, A., Cevreli, B., Gozler, T., Kulaksiz, H. and Midi, A. (2017) The effect of hesperidin on oxidative stress in an experimental obstructive jaundice. Fresen. Environ. Bull. 26, 6760-6764.

[16] Huseyin, B., Gerald, V., Robert, E.S., Jaw-Fen W., Savita, S. and Jeffrey B.J. (2005) Characterization of a Unique Chromosomal Copper Resistance Gene Cluster from *Xanthomonas campestris pv. Vesicatoria.* Applied and Environmental Microbiology. 71(12), 8284–8291.

[17] Gambley, F.C., Miles, K.A., Ramsden, M., Doogan, V., Tomas, E.J., Parmenter, K. and Whittle, L. (2009) The distribution and spread of citrus canker in Emerald, Australia. Australasian Plant Pathology. 38(6), 547-557.

[18] Yacoubi, B.E., Brunings, A.M., Yuan, Q., Shankar, S. and Gabriel, W.D. (2007) In Planta Horizontal Transfer of a Major Pathogenicity Effector Gene. Applied and Environmental Microbiology. 73(5), 1612-1621.

[19] Jones, J.B., Lacy, G.H., Bouzar, H., Stall, R.E. and Schaad, N.W. (2004) Reclassification of the Xanthomonads Associated with Bacterial Spot Disease of Tomato and Pepper. Systematic and Applied Microbiology. 27(6), 755-762.

Received: **30.08.2018**
Accepted: **21.02.2019**

CORRESPONDING AUTHOR

Syeda Khola Tazeen
Department of Botany,
The University of Lahore (Sargodha Campus),
Sargodha – Pakistan

e-mail: kholatazeen02@gmail.com

© by PSP Volume 28 – No. 5/2019 pages 3729-3739 Fresenius Environmental Bulletin

COMPARISON OF TOXIC EFFECTS OF ALKALI SALTS (Na_2CO_3 AND $NaHCO_3$) ON SORGHUM GROWTH PARAMETERS AND SOIL CHEMICAL PROPERTIES

Tanveer Ali Sial[1,2], Inayatullah Rajpar[2], Mehurnisa Memon[2], Muhammad Siddique Lashari[2], Ying Zhao[1,*], Punhoon Khan Korai[3], Farhana Kumbhar[4], Kashif Akthar[5]

[1]College of Natural Resources & Environment, Northwest A&F University, Yangling, Shaanxi, 712100, China
[2]Department of Soil Science, Sindh Agriculture University, Tandojam, Pakistan
[3]Faculty of Agriculture, Lasbela University of Agriculture, Water and Marine Sciences, Uthal, Balochistan, Pakistan
[4]Department of Plant Breeding & Genetics, Sindh Agriculture University, Tandojam, Pakistan
[5]Department of Agronomy, Faculty of Crop Production Sciences, University of Agriculture, Peshawar, Pakistan

ABSTRACT

Soil sodicity is major threat to agriculture at arid and semiarid areas of the world, which increased due to agricultural lands irrigated with low quality of water. The aim of this study is to compare the toxic effects of two alkali salts on growth of sorghum (*Sorghum bicolor* L.), uptake of ion contents in leaves and soil properties. The experiment was treated with two alkali salts (Na_2CO_3 and $NaHCO_3$), each at two concentrations (60 and 120 mM) in addition to a control (no salt amendment) for ten weeks. Results indicated that both salts significantly ($p<0.05$) reduced the plant height (13-37%), dry (18-48%) fodder biomass pot^{-1} (31-64%) and chlorophyll content (31-60%) over control. The content of nitrogen (N), phosphorus (P), potassium (K^+), calcium (Ca^{2+}), magnesium (Mg^{2+}) and K^+:Na^+ (77, 79, 47, 44, 74 and 86%) reduced at higher salt concentration of Na_2CO_3 120 mM. Similarly, soil mineral nitrogen NH_4^+-N (8.3-1.13 mg kg^{-1}), NO_3^- (16.5-1.7 mg kg^{-1}), available P (10.5- 2.2 mg kg^{-1}) K (281-107 mg kg^{-1}), Ca^{2+} + Mg^{2+} (3.5-1.1 mg kg^{-1}), and K^+:Na^+ ratio (17.3-0.8) decreased, while soil pH and Na^+ (17 and 87%) increased for the Na_2CO_3 120 mM. Our results suggested that sorghum plants are moderately tolerance at lower concentration and may not grow at higher concentration, and Na_2CO_3 is toxic than $NaHCO_3$ salt.

KEYWORDS:
Sodicity, Salt concentration, Sorghum growth, Nutrients uptake.

INTRODUCTION

Deterioration of soil fertility status by different salts concentrations (saline and sodic salts) are major problems throughout the world, especially arid and semiarid regions [1, 2]. The total salt affected soils occupied around 3.0% of the global area (836 million hectares has been categorized as saline and sodic soils [1]. Since few decades' crops irrigated with low quality water and widespread agricultural practices which declined soil fertility status and reduced the production and quality of arable crops [3, 4]. Owing to poor water resources and unfavorable irrigation in the countries like Australia, China, Indonesia as well as Pakistan, the salt affected lands are expanding [5, 6, 1]. Farmers in arid and semi-arid regions of the world are compelled to use poor quality groundwater to irrigate the crops due to limited water resources. Approximately 831 million hectares (MH) of salt affected land in the world, about 50.0% is due to salt accumulation of sodium (Na^+) [7]. The higher accumulation of Na^+ decreased the microbial activity, poor aggregation and low soil organic matter [8]. Factually, the damage caused by sodic soil (i.e. sodium carbonate and bicarbonate (Na_2CO_3 and $NaHCO_3$) is potentially destructive compared to the neutral salts such as sodium chloride and sodium sulfate (NaCl and Na_2SO_4) [9]. The Na^+ concentrations disturbed the metabolic process and declined plant growth, root traits and photosynthetic, respiration and induce immature plant leaf senescence [10, 11], but depends on the capability of plant itself to survive under different salt concentrations [12]. In addition to general osmotic stress, high concentrations of Na^+ are toxic to maize and sorghum [13]. Farhangi- Abriz and Nikpour – Rashidabad [14] established that potassium K^+ is antagonistic relationship with Na^+ in plant and reduced the uptake of potassium, calcium and magnesium (K^+, Ca^{2+} and Mg^{2+}) in leaf and root under salt concentration [15]. [17] addressed that crop growth declined due to reduction in soil water availability and osmotic stress, especially lower concentration of macro nutrients such as P K^+, Ca^{2+} and nitrate nitrogen (NO_3^--N) under higher salts accumulations.

Pakistan is basically an agricultural country but most of its productive area falls in the arid and semi-arid climate. The rainfall varies considerably with less than 10 mm per annum in some parts of the country to more than 500 mm in other parts [19]. The

drought and nonstop scarcity of water have affected Pakistan's agricultural economy [20] to an extreme level. The agricultural segments in Pakistan contribute 1/4th of the gross domestic product (GDP), 2/3rd of exports and closely 1/2 of the employment. On the contrary, rain-fed area (20% of the cultivated areas) contributes only 10% towards agriculture [21]. Fodder crops play pivotal role in the agricultural economy of developing countries by providing cheapest source of feed for livestock. Sorghum being a potential crop is locally grown on moderately saline and sodic areas of the Pakistan [22] and yet the common use of saline and sodic irrigation water on these lands can further aggravate the status [23].

Our objectives are: 1) to compare the toxic effects of different salt types (Na_2CO_3 and $NaHCO_3$) on morphological attributes (growth, chlorophyll, root and shoot biomass, 2) to understand the relationship between sodicity levels and uptake of N, P, K^+, K^+:Na^+, Ca^{2+} and Mg^{2+} contents in sorghum leaves, and 3) to determine the negative effect of both salt concentrations (60 and 120 mM) on soil chemical properties.

MATERIALS AND METHODS

Study area. The pot experiment was conducted at Sindh Agriculture University, Department of Soil Science (25.367˚N latitude and 68.367˚E longitude) Tandojam, Sindh province of Pakistan. Surface soil (0-15 cm) in bulk was collected from Latif experimental farm, Sindh Agriculture University, Tandojam. It located at subtropical region and monsoon climate and the average an annual temperature was recorded 35.02 ˚C. The highest temperature (>45˚C) was recorded during May to June and lowest temperature (10-25˚C) was recorded during December to January. The annual average rainfall 178.2mm and relative air humidity 55.8% were recorded. Soil was silty clay in texture and slightly alkaline and non-saline in reaction, basic properties of soil are presented in Table 1.

TABLE 1
Basic properties of soil used in the study

Parameters	Soil
Sand	9.40%
Silt	51.10%
Clay	39.50%
Textural class (Silty clay)	
pH (1:2.5 H_2O)	7. 85 ± 0.3
EC (1:2.5 H_2O) (dS m^{-1})	0. 96 ± 0.03
SOM (%)	0. 95 ± 0.01
Olsen P (mg kg^{-1})	5.12 ± 0.5
K exchangeable (mg kg^{-1})	234.65 ± 5
NO_3^- - N (mg kg^{-1})	1.93 ± 0.01
NH_4^+- N (mg kg^{-1})	2. 96 ± 0.2

Soil collection. For greenhouse study, surface soil (0-15 cm) in bulk was collected from Latif Experimental Farm, Sindh Agriculture University, Tandojam. Soil was silty clay in texture and slightly alkaline in reaction, basic properties of soil are cited in Table 1.

Experiment setup. A 10 kg quantity of air-dried soil (<2mm) was placed in each 12 kg perforated polyethylene pots. Five treatments include application of two levels of Na^+ (60 mM and 120 mM) using two different salts (Na_2CO_3 and $NaHCO_3$) and a control, replicated thrice and were arranged in a randomized completely block design (RCBD) during the Kharif season. Soil in each pot was leveled manually and irrigated with distilled water (1,000 ml). Soil moisture was checked every day and maintained at 70% of water holding capacity (WHC). Nitrogen and phosphorus fertilizers were applied at the rate of (0.75 g N and 0.40 g P_2O_5) each pot in the form of urea and di-ammonium phosphate. All the phosphorus was incorporation into the each pot. Whereas, nitrogen was applied in 3 equal parts; ten seeds of sorghum variety (Red Janpur) were planted in each pot followed by thinning, leaving five seedlings.

Plant and soil analysis. After 10 weeks the aboveground parts (stem and leaves) and underground part (roots) of sorghum were uprooted and all parts were thoroughly washed normal water then by distilled water. Roots were spread on white paper towel to record root length. Both roots and shoots from each treatment were air-dried under the shade for a day, followed by oven drying at 65-68 ˚C till constant weight. Plant height, fresh and dry shoot and root (only dry) weight, number of green and dry leaves, leaf area and root length were recorded.

Soil samples collected from each treatment after the harvest of sorghum were analyzed for EC1:2, pH1:2, soil organic matter (SOM%), mineral nitrogen (NO_3^- and NH_4^+), available P, K^+, Na^+, Ca^{2+} + Mg^{2+}, CO_3^{2-} and HCO_3^-. Soil analysis was carried out by standard methods as given under [24]. For texture determination, soil was dispersed with $(NaPO_3)_{13}$ and Na_2CO_3 using Hydrometer method [25]. Soil pH and electrical conductivity (EC) were measured in 1:2.5 (soil: deionized water) extracts using pH/ EC Meter (2182A, Spectrum Technologies, Inc.). For organic matter determination, soil was oxidized using $K_2Cr_2O_7$ and H_2SO_4 as per details under Walkley-Black method. Mineral-N was determined by extracting the samples with 2M KCl in 1:5 soil: extractant ratio. After extraction, NH_4^+ and NO_3^- - N were determined by steam distillation of NH_3, using heavy MgO for NH_4^+ and Devarda's Alloy for NO_3^- - N [26]. The distillate was collected in saturated H_3BO_3 and titrated to pH 5.0 with dilute H_2SO_4. This method determines dissolved and adsorbed forms of available nitrogen (NH_4^+ and NO_3^- - N) in samples. Available P within the soil was measured using a

TABLE 2
Effects of alkali salts (Na_2CO_3 and $NaHCO_3$) on mean growth attributes of Sorghum (mean ± standard error; n= 3).

Treatments		Plant height (cm)	Fresh plant biomass (g pot^{-1})	Dry plant biomass (g pot^{-1})	No. of green leaves plant^{-1}	No. of dry leaves plant^{-1}	Root dry weight (g pot^{-1})	Root length (cm)	Leaf area index
Control	0 mM	103± 2.8a	43.06±2.11a	20.96±1.8a	7±0a	3±00c	11.97±1.26a	25.21±2.1a	4.2± 0.3a
Na_2CO_3	60 mM	85± 4.2c	30.21±2.13c	15.25±1.5b	5±0c	3±00c	6.96±0.7c	18.97±2.1b	3. 7± 0.5b
	120 mM	65±1.9d	23.75±1.99d	10.94±1.5 c	2±0d	5±00a	4.25±0.95e	16.21±1.5c	3.0± 0.3c
$NaHCO_3$	60 mM	90±2.8b	35.18±2.63b	17.18±2.0b	6±0b	3±00c	8.25±1.01b	19.28±2.0b	3.8±0.2ab
	120 Mm	68±3.7d	27.35±0.91c	12.31±1.3c	4±0c	4±00ab	5.80±0.85d	17.46±1.8bc	3.1±0.2c

Letters indicate significant difference between the treatments, which was analyzed using a LSD test ($p<0.05$).

0.5 M $NaHCO_3$ (pH 8.5) extract followed by visible light spectroscopic analysis of a blue colored complex [27] method. Extractable Na^+ and K^+ were determined by extraction with 1 N NH_4OAc followed by analysis of the extract on flame photometer (PFP7, Jenway UK) as described by [28], while Ca^{2+} and Mg^{2+} were determined by titration with ethylene di-amine tetra-acetic acid (EDTA) [29]. As for CO_3^{2-} and HCO_3^-, titration method [23] was applied using H_2SO_4 and $AgNO_3$ titrant and $C_{20}H_{14}O_4$, $C_{14}H_{14}N_3NaO_3S$ and K_2CrO_4 indicators, respectively.

Total N, P, K^+ and Na^+ contents of sorghum leaves were analyzed by colorimetrically after digestion with (H_2SO_4+$HClO_4$) briefly described by [30] and Ca^{2+} and Mg^{2+} in a similar way using flame photometer and EDTA titration methods as described under soil analysis.

Measurement of chlorophyll content. The chlorophyll SPAD values of sorghum plants were measured by using SPAD meter method. A transferable Minolta chlorophyll meter (SPAD-502, Osaka 590-8551, Japan) was used for the measurement. Randomly selected 3 to 4 fresh leaves of each sorghum plant and measured the chlorophyll from three plants an each pot.

Statistical analysis. Data pertaining to morphological attributes, salt concentration in leaf and in soil after the harvest of sorghum was subjected to one- way analysis of variance using computer software SPSS-12 (IBM). Figures were produced using Origin Pro. 9.0 software. In case of significant ($p<0.05$) parameters, the means were separated using LSD test. CANOCO software was used for redundancy analysis (RDA).

RESULTS

Effect of alkali salts on morphological characteristics of Sorghum. The characteristics recorded were plant height, fresh and dry biomass, green and dry leaves, leaf area index, root length, root dry weight root length ratio presented in (Table 2). Sorghum plants under induced sodicity using alkali salts (Na_2CO_3 and $NaHCO_3$) at 60 and 120 mM of Na^+ was concentration showed significantly ($p<0.05$) reduced growth traits. Plant height, fresh and dry weight were adversely affected. Plant height reduced under both salts concentrations (17.3% and 36.3%) for the Na_2CO_3 treatments and (12.2% and 33.4%) for the $NaHCO_3$ treatments, respectively. Fresh and dry weights reduced from 43 and 20.9 g in control to 23.7 and 10.9 g in 120 mM Na_2CO_3 treatment.

The sodicity exhibited adverse effects on the growth of leaves. Application of alkali salts significantly ($p<0.05$) reduced the production of green leaves, thereby increasing dry leaves per plant. Maximum number of green (7) and minimum dry (3) leaves were recorded for the control treatment (no salt was applied). At higher salt concentration of 120 mM, there was less production of green leaves, thus increase in number of dry leaves. Green leaves reduced from 6 to 5 and 3 and dry leaves increased from 3 to 3 and 4 with 60 and 120 mM $NaHCO_3$ respectively. Similarly, with corresponding concentrations of 60 and 120 mM Na_2CO_3, green leaves reduced from 6 to 4 and 2 and dry leaves increased from 3 to 3 and 6. In case of leaf area index, it decreased from 4.2 to 3.0 under 120 mM $NaHCO_3$ giving maximum percent decrease of 28.3. However, the treatment differences in leaf area index obtained under 120 mM Na_2CO_3 (3.04) and 120 mM $NaHCO_3$ (3.1) were non-significant ($p<0.05$).

The results of the experiment revealed that, both salts at higher concentrations significantly ($p<0.05$) reduced root length and dry weight of sorghum plants. The maximum reduction was recorded under higher levels of sodic stress. The greater root weight and length recorded for the control treatments (11.9 g and 25.2 cm), followed by 60 mM $NaHCO_3$ (8.3 g and 19.3 cm), 60 mM Na_2CO_3 (6.9 g and18.9 cm), 120 mM $NaHCO_3$ (5.8 g and 17.5 cm) and 120 mM Na_2CO_3 (4.3 g and16.2 cm) treatments respectively. Root length ratio was statistically increased with increasing concentrations of both alkali salts, lowest root length ration was recorded for the control

(0.71 cm g^{-1}) t and highest for the 120 mM Na_2CO_3 (1.05 cm g^{-1}).

Impact of alkali salts on chlorophyll contents. Application of both salt concentrations were significantly ($p<0.05$) decreased the chlorophyll contents by sorghum as compared to control (Figure 1). The maximum reduction was (60.4%) for the 120 mM Na_2CO_3 followed by 120 mM $NaHCO_3$ (52.2%), 60 mM Na_2CO_3 (36.4%) and 60 mM $NaHCO_3$ (31.4%) treatments as compared to control.

Effect of alkali salts on chemical attributes of leaves. The data related to N, P, K^+, Na^+, K^+:Na^+ ratio and Ca^{2+} and Mg^{2+} (Table 3) determined in the leaves revealed that application of alkali salts significantly ($p<0.05$) affected the concentration of nutrients. Application of both alkali salts with increased concentration apparently increased the Na^+ content in leaves. Increased Na^+ concentration in turn, reduced the total N, P, and K^+ contents and thereby the K^+:Na^+ ratio in leaves. Similarly, Ca^{2+} and Mg^{2+} content also decreased with the increase in salt concentration of both salts. The Na^+ content increased from (1.6 g kg^{-1}) under control to maximum of (12.5 g kg^{-1}) under 120 mM Na_2CO_3 treatment. High Na^+ concentration resulted in low N, P, K^+, Ca^{2+}, Mg^{2+} and K^+:Na^+ ratio. Maximum reduction of N, P and K contents (77.5%, 79.3% and 47.4%), Ca^{2+} (44.3%), Mg^{2+} (74.3%) and K^+:Na^+ ratio (86.2%) was observed for soil treated with 120 mM Na_2CO_3 over control treatment. In contrast, the lowest reduction in N, P and K^+ (48.4%, 24.5%, and 21.3%), Ca^{2+} (17.4%), Mg^{2+} (41.2%) and K^+:Na^+ ratio (38.3%) was observed for the 60 mM $NaHCO_3$ over control.

Influences of alkali salts on soil chemical properties. The data related to soil properties revealed significant ($p<0.05$) changes in electrical conductivity (EC), pH, Na^+ and K^+:Na^+ (Figure 1), mineral nitrogen (NH_4^+-N and NO_3^--N), available P and K^+ (Figure 2), Ca^{2+}, Mg^{2+}, CO_3^{2-} and HCO_3^- contents of soil (Figure 4). While EC, pH, Na^+, CO_3^{2-} and HCO_3^- increased, $Ca^{2+} + Mg^{2+}$, K^+ and K^+:Na^+ ratio decreased with the increase of salt concentration. The increase in soil EC, pH, Na^+, CO_3^{2-} and HCO_3^- values became much prominent with the increase in salt concentration from 0 to 120 mM of each salt. Nonetheless, use of Na_2CO_3 increased the respective soil parameters to a maximum level, compared to $NaHCO_3$.

TABLE 3

Effects of alkali salts (Na_2CO_3 and $NaHCO_3$) on mineral composition of Sorghum leaves (mean ± standard error; n=3).

Treatments		N	P	K^+	Na^+	K^+:Na^+	Ca^{2+}	Mg^{2+}
		(g kg^{-1})					(g kg^{-1})	
Control	**0 mM**	25.98 ± 1.44a	3.86 ± 0.17a	8.7 ± 1.0a	1.6 ± 0.1e	4.32 ± 0.04a	1.26 ± 0.01 a	2.60 ± 0.3a
Na_2CO_3	**60 mM**	10.39 ± 0.57b	1.88± 0.08c	6.1 ± 0.9c	5.3 ± 0.5c	2.66 ± 0.09ab	0.92 ± 0.01 b	1.24 ± 0.06b
	120 mM	5.84 ± 0.48e	0.82± 0.08e	4.6 ± 0.5e	12.5 ± 1.3a	0.59 ± 0.01b	0.71 ± 0.02 c	0.67 ± 0.01c
$NaHCO_3$	**60 mM**	13.52± 0.97b	2.93± 0.08b	6.9 ± 0.9b	4.3 ± 0.3d	1.25 ± 0.03b	1.04 ± 0.06 ab	1.52 ± 0.08b
	120 mM	8.14± 0.37d	1.24± 0.05d	5.3 ± 0.5d	7.8 ± 1.0b	0.41 ± 0.01 b	0.80 ± 0.01c	0.72 ± .03 c

Letters indicate significant difference between the treatments, which was analyzed using a LSD test ($p<0.05$)

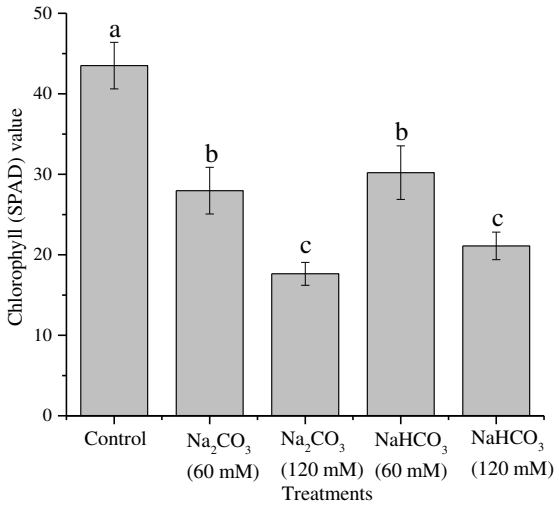

FIGURE 1

The effects of alkali salts (Na_2CO_3 and $NaHCO_3$) on chlorophyll (SPAD) values of sorghum plants.

Error bars represent the standard deviation of the mean (n = 3). Different letters indicate there were significant differences ($p < 0.05$) between the treatment mean.

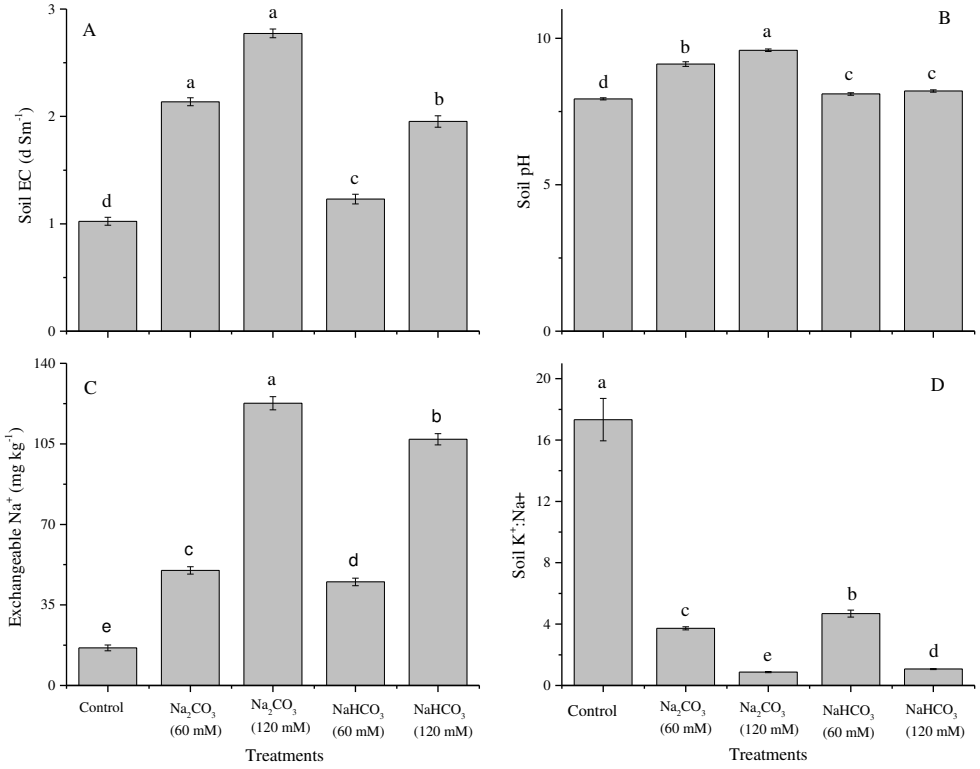

FIGURE 2

The effects of alkali salts (Na_2CO_3 and $NaHCO_3$) on soil EC, pH, Na^+ and K^+: Na^+ after sorghum harvested.

Error bars represent the standard deviation of the mean (n = 3). Different letters indicate there were significant differences ($p < 0.05$) between the treatment mean.

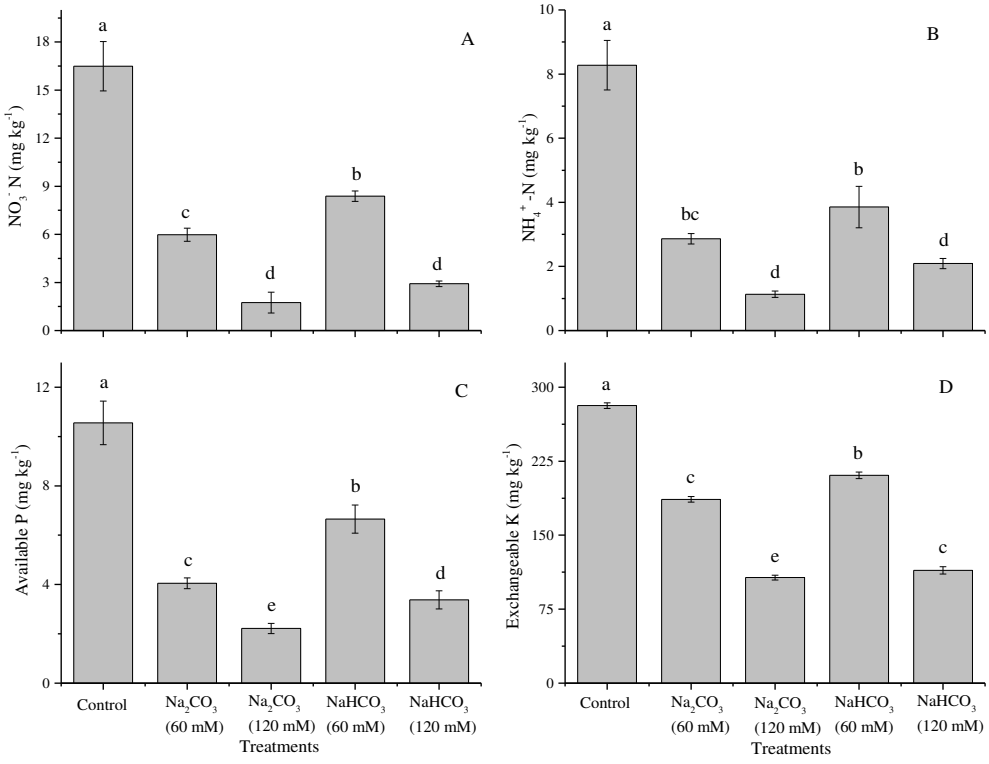

FIGURE 3

The effects of alkali salts (Na_2CO_3 and $NaHCO_3$) on soil NH_4^+-N, NO_3^- - N, available P and K after sorghum harvested.

Error bars represent the standard deviation of the mean (n = 3). Different letters indicate there were significant differences ($p < 0.05$) between the treatment mean.

TABLE 4
The bivariate correlation test between soil physicochemical properties after Sorghum plants harvested.

	EC	pH	NO_3^-	NH_4^+	AP	$Ca^{2+}+Mg^{2+}$	AK	Na^+	K:Na	CO_3^{-2}	HCO_3^-
EC		.912**	-.660**	-.622*	-.554*	-.910**	-.852**	.833**	-.745**	.882**	.914**
pH			-.408	-.377	-.296	-.818**	-.599*	.575*	-.563*	.779**	.870**
NO_3^-				.970**	.975**	.832**	.923**	-.866**	.936**	-.752**	-.640*
NH_4^+					.963**	.815**	.884**	-.803**	.936**	-.760**	-.604*
AP						.768**	.866**	-.809**	.890**	-.682**	-.560*
$Ca^{2+}+Mg^{2+}$							.884**	-.848**	.870**	-.865**	-.872**
AK								-.971**	.908**	-.838**	-.783**
Na^+									-.806**	.731**	.748**
K^+:Na^+										-.880**	-.764**
CO_3^{-2}											.855**
HCO_3^-											

Abbreviations= EC (Electrical conductivity), NO_3^- (Nitrate), NH_4^+ (Ammonium), AP (Olsen phosphorus), $Ca^{2+}+Mg^{2+}$ (Calcium + Magnesium), AK (Available potassium), Na^+ (Sodium), CO_3^- (Carbonate) and HCO_3^- (Bicarbonate).
**. Correlation is significant at the 0.01level (2- tailed).
*. Correlation is significant at the 0.05 level (2- tailed).
Pearson correlation

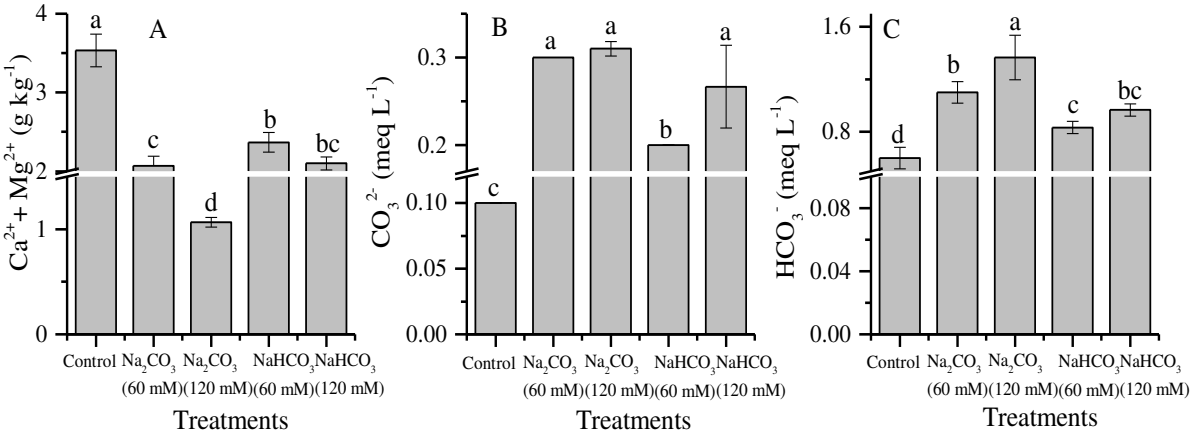

FIGURE4
The effects of alkali salts (Na_2CO_3 and $NaHCO_3$) on soil $Ca^{+2}+Mg^{+2}$, CO_3^{-2} and HCO_3^- contents after sorghum harvested.

Error bars represent the standard deviation of the mean (n = 3). Different letters indicate there were significant differences ($p < 0.05$) between the treatment mean.

The EC values increased from 1.0 dS m^{-1} in control to 2.8 and 2.0 dS m^{-1} and pH from 7.9 in control to 9.6 and 8.2 in 120 mM Na_2CO_3 and $NaHCO_3$ (Figure 2A and 2B). EC values increased by 52.2% and 63.3% with Na_2CO_3 and 17.5% and 48.3% with $NaHCO_3$ at corresponding concentrations of 60 and 120 mM over control. As for pH it increased by 1.19 and 1.66 unit with Na_2CO_3 and by 0.17 and 0.27 unit with $NaHCO_3$ compared to control. Soil Na^+, also exhibited the similar trend under all the treatments (Figure 2C). Sodium content increased from 16 g kg^{-1} in control to a maximum of 123 g kg^{-1} under 120 mM Na_2CO_3. The percent increase in Na^+ contents of soil at 120 mM salt concentration was more or less similar with Na_2CO_3 (87.0%) and $NaHCO_3$ (85.3%). Alkaline salts being a source of CO_3^{2-} and HCO_3^- also enhanced the level of CO_3^{2-} and HCO_3^- in the soil. Na_2CO_3 maintained its superiority over $NaHCO_3$ in increasing both CO_3^{2-} and HCO_3^- (Figure 4-B and C). The soil EC, pH, Na^+, CO_3^{2-} and HCO_3^- values increased following both salts concentration and positively correlated with Na_2CO_3 and $NaHCO_3$ noted in Table 4.

Considering other parameters in soil, there was reduced accumulation of N, P, K^+ (Figure 3 A-3D) $Ca^{2+} + Mg^{2+}$ (Figure 4 A) and K^+:Na^+ ratio in soil with the addition of both alkali salts (Na_2CO_3 and $NaHCO_3$) as compared to control (Figure 2D). Soil mineral nitrogen (NH_4^+ -N and NO_3^- -N), available P and K^+ and $Ca^{2+} + Mg^{2+}$ showed negatively correlation with EC, pH, Na^+, CO_3^{2-} and HCO_3^- because they antagonistic behavior with each other (Table 4). Among two alkali salts, Na_2CO_3 accumulated maximum Na^+ in soil, and was vice versa in case of inorganic nitrogen, available P and K and $Ca^{2+} + Mg^{2+}$. The highest reduction of (NH_4^+ -N and NO_3^- -N), available P and K^+ and $Ca^{2+} + Mg^{2+}$ and K^+:Na^+ ratio were recorded (86.5% and 89.5%, 79.3%, 62.3%, 70.5% and 95.3% for the 120 mM Na_2CO_3 against control.

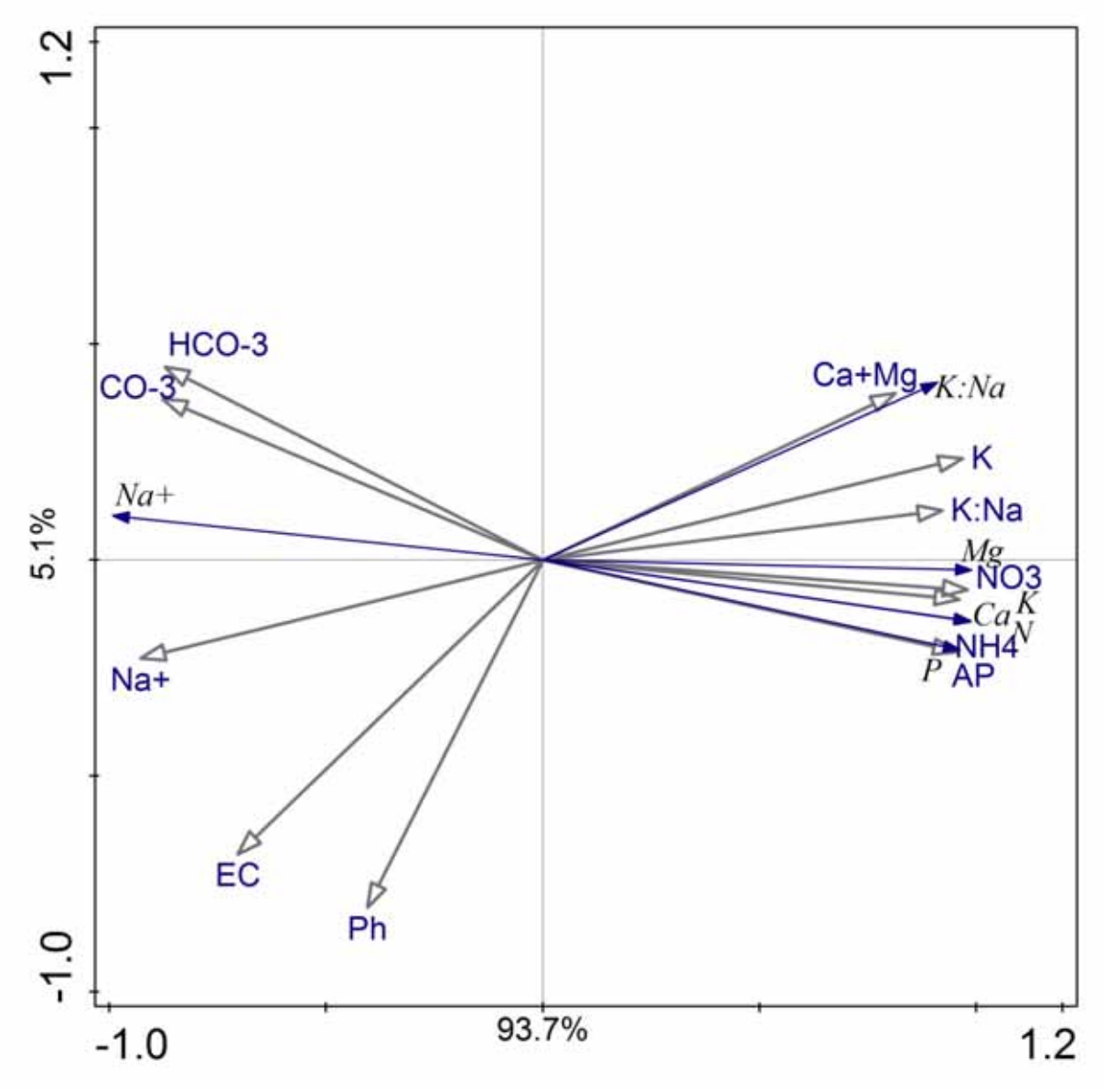

FIGURE 5

Ordination plot of results from redundancy analysis to identify relationships between soil properties, EC (Electrical conductivity), NO_3^- (Nitrate), NH_4^+ (Ammonium), AP (Available phosphorus), Ca^{2+}+Mg^{2+} (Calcium + Magnesium) AK (Available potassium), Na^+ (Sodium), CO_3^- (Carbonate) and HCO_3^- (Bicarbonate) and plant nutrients N (Nitrogen), P (Phosphorus), (K) Potassium, Na^+ (Sodium), K^+ : Na^+ (Potassium : Sodium), Ca^{2+} (Calcium), Mg^{2+} (Magnesium)

DISCUSSION

The plants growth decline by salt stress conditions via different reactions during metabolism process which had been affected by the salt accumulation in shoot [31] and reduced the uptake of macro nutrients under toxicity of Na^+ ions [14, 15]. In normal course, the cations i.e. Ca^{2+}, Mg^{2+}, K^+, H^+ including Na^+ are adsorbed onto clay particles in soil. When Na^+ is adsorbed in excess (>5% of other cations), the soil is termed as sodic. Alkaline soils of semi-arid region generally have accumulation of Na_2CO_3 and $NaHCO_3$ [32, 33]. The research work related to effects of alkali salts on agricultural crops and relevant soils is scanty. Information related to type and concentration of alkali salts on the growth and properties of sorghum is of basic importance and will help grower in formulating the future yield targets along with sodicity status of soil. Through this study, the growth of sorghum and effect on soil properties as a result of (0, 60 and 120 mM) Na_2CO_3 and $NaHCO_3$ has been put on record.

Compare the toxic effects of both alkali salts on sorghum plants growth parameters, root traits and soil fertility. In most cases 120 mM $NaHCO_3$ performed equally with 60 mM Na_2CO_3. Both alkali salts behaved equally with regard to dry plant biomass, number of dry leaves and chlorophyll content. Results indicated that lowest percent decreased in

plant height (12.4%), fresh (18.2%) and dry (18.4%) weights, number of green (16.3%) and dry (4.3%) leaves, chlorophyll content (31.2%), root weight (31.3%) and length (23.2%), and leaf area index (10.3%) over control was observed with 60 mM $NaHCO_3$, while, the highest one (37.7%, 45.2%, 48.3%, 72.4%, 55.5%, 64.2%, 36.3% and 28.4% correspondingly) was achieved with 120 mM Na_2CO_3. Our results are agreed with previous study [14] conducted a pot experiment and addresses that soybean growth parameters (shoot and root dry weight) were declined with increase salt concentrations. Similar trend was established by [34], who observed that cucumber shoot and root growth and chlorophyll contents were reduced by salt stress as soil treated with NaCl concentrations (60 and 120 Mm). The highest reduction of growth and physiological parameters were noted for the (NaCl 120 mM) as compared to 60 mM and control treatments. Another study performed by [35] stated that (*Jatropha curcus* L.) plants growth traits such as plant height, shoot and root growths were significantly reduced under high sodicity stress as compared to low concentrations. The present study shows similar picture, the maximum reductions of sorghum growth parameters under higher concentration of both salts. However, Na_2CO_3 more toxic effects on sorghum growth as compared $NaHCO_3$. It might be due to higher accumulation of Na^+, in sorghum leaves and high soil pH values and toxicity of HCO_3^- in soil were measured in Na_2CO_3 than $NaHCO_3$ treatments. [36, 35] examined that plants growth and root development reduced under sodic soil conditions due to soil redox potential, toxicity of Na^+ and HCO_3^- ions in soil. [37] established that the higher stress on sorghum crop with $NaHCO_3$ compared to NaCl. [38] considered that negative effect of alkali salt ($NaHCO_3$) on *Salsola ferganica* L. at same concentration of germination over NaCl alone or mixed with $NaHCO_3$.

In present study, we observed the greater toxic effects of Na_2CO_3 on sorghum as compared to $NaHCO_3$ treatments. It might be more Na^+ accumulation and lowest uptake of (N, P, K^+, K^+:Na^+, Ca^{2+} and Mg^{2+}) in sorghum leaves were measured for the Na_2CO_3 concentrations. These findings were addressed by [15] that higher concentration of external Na^+ not only interruptions with (K, Ca^{2+} and Mg^{2+}) uptake by root network and declined plant growth. The similar trend was evaluated by [14] that higher concentrations of salt decreased the uptake of K^+, Ca^{2+} and Mg^{2+} and declined the K^+:Na^+ in soybean leaves under pot experiment environment. [39] assessed that soil pH plays an important role in plant growth and great potential to availability of nutrients. In present study, soil pH positively correlated to Na^+ and negatively correlated to plant growth parameters and macronutrients in soil and leaves. Both salts at higher concentration (120 mM) accelerated leaf burn and leaf necrosis which is indicated the chlorophyll content. High Na^+ levels in soil compete with other ions (i.e. NH_4^+, NO_3^- -N, available P and K^+, Ca^{2+}, and Mg^{2+}) by replacing K^+, and in severe conditions Ca^{2+} and Mg^{2+} causing nutritional imbalances in plant cells. These disorders ultimately lead towards nutrient deficiencies and Na^+ toxicity [40,41]. This is in line with the results described by [42] and [43] where enhanced salt levels Na^+, reduced Ca^{2+} in plants. According to previous studies noted the Na^+ interaction with K, Ca^{2+}, and Mg^{2+} and K^+:Na^+ in plants and soils. In present study we have focused on N and P uptake in sorghum leaves, both salt concentrations had negatively effects on N and P uptake as compared to untreated soil.

The chemical changes in soil properties after the harvest of sorghum show a different picture. EC, pH, Na^+, CO_3^- and HCO_3^{2-} increased with the increase in salt concentration, whereas mineral nitrogen, available P and K^+, $Ca^{2+} + Mg^{2+}$ and K^+:Na^+ ratio decreased. Statistically similar, CO_3^{2-}, HCO_3^- and $Ca^{2+} + Mg^{2+}$ contents were recorded for the 120 mM $NaHCO_3$ and 60 mM Na_2CO_3. A minimum percent increase in EC (17.1%), pH (2.1%), Na^+ (64.2%), CO_3^{2-} (50.4%) and HCO_3^- (30.6%) and decrease in NH_4^+-N (53.1%), NO_3^--N (49.2%), available P (36.2%) K^+ (33.2%), K^+:Na^+ ratio (73.4%) and $Ca^{2+} + Mg^{2+}$ (33.2%) was observed with 60 mM $NaHCO_3$, while, greater increase percent (63.2%, 17.5%, 87.3%, 68.2% and 56.4%) and decrease (89.4%, 86.2%,79.3%, 62.5%, 70.4% and 95%, respectively) with 120 mM Na_2CO_3 over control. Similar results were observed by [44] in treatments irrigated with sodic water. These results are similar with [23] reported that application of sodic salts enhance the salt content in cotton-wheat rotation. Soil macronutrients such mineral nitrogen (NH_4^+-N and NO_3^--N) available P and K^+, $Ca^{2+} + Mg^{2+}$ and K^+:Na^+ are negatively correlated to EC, pH, Na^+, CO_3^- and HCO_3^{2-} presented in (Figure 5).

CONCLUSION

It is concluded that growth and productivity of sorghum plants was significantly reduced, and the chemical properties of soil were deteriorated under Na^+ stressed environment. Reduction in plant biomass, chlorophyll and root biomass increased with the increase in concentration of Na_2CO_3 and $NaHCO_3$ salts, as a result of high pH, Na^+:K^+ ratio and excess accumulation of Na^+, CO_3^{2-} and HCO_3^-, respectively. At equal concentrations the *Sorghum bicolor* plants seem to be more sensitive to Na_2CO_3 than $NaHCO_3$ salt. It is suggested that both salts at higher concentration (120 mM) are not suitable for cultivation of sorghum on silty loam soils. The irrigation water with excess Na^+ acts as a source of sodicity and thereafter should be avoided on sorghum crop.

ACKNOWLEDGEMENTS

The authors would like to thank Department of Soil Science, Sindh Agriculture University, Tandojam, Pakistan for providing research facilities for conducting this work.

The authors declare that they have no any competing interests.

REFERENCES

[1] Singh, Y.P., Singh, R., Sharma, D.K., Mishra, V.K. and Arora, S. (2016) Optimizing gypsum levels for amelioration of sodic soils to enhance grain yield and quality of rice. J. Ind. Soci. Soil Sci. 64, 33-40.

[2] Ferreira, A.C.C., Leite, L.F.C., A.S.F. and Araújo, N. (2014) Eisenhauer, Land-use type effects on soil organic carbon and microbial properties in a semi-arid region of northeast Brazil. Land Degra. Develo. 27, 171-178.

[3] Kammann, C.I., Linsel, S., Johannes, W. and Koyro, H.W. (2011) Influence of biochar on drought tolerance of Chenopodium quinoa Willd and on soil plant relations. Plant and Soil. 345, 195-210.

[4] Singh, K., Singh, B. and Tuli, R. (2013b) Sodic soil reclamation potential of *Jatropha curcas*: a long term study. Ecolo. Enginee. 58, 434–440.

[5] Li, X.Y., Wang, Z.M., Song, K.S., Zhang, B., Liu, D.W. and Guo, Z.X. (2007) Assessment for salinized wasteland expansion and land use change using GIS and remote sensing in the west part of Northeast China. Enviro. Monit. Assess. 131, 421-437.

[6] Ahmad, S., Ghafoor, A., Akhtar, M.E. and Khan, M.Z. (2016) Implication of gypsum rates to optimize hydraulic conductivity for variable-texture saline-sodic soils reclamation. Land Degra. and Develo. 27, 550-560.

[7] Gong, B., Wen, D., Bloszies, S., Li, X., Wei, M. and Yang, F.J. (2014) Comparative effects of NaCl and $NaHCO_3$ stresses on respiratory metabolism, antioxidant system, nutritional status, and organic acid metabolism in tomato roots. Acta Physio. Plant. 36, 2167-2181.

[8] Wiesmeier, M., Steffens, M., Mueller, C.W., Kolbl, A., Reszkowska, A., Peth, S., Horn, R. and Kogel-Knabner, I. (2012) Aggregate stability and physical protection of soil organic carbon in semi-arid steppe soils. Euro. J. Soil Sci. 63, 22–31.

[9] Gong, B., Wen, D., Vandenlangenberg, K.M., Wei, M., Yang, F.J., Shi, Q.H. and Wang, X.F. (2013) Comparative effects of NaCl and $NaHCO_3$ stress on photosynthetic parameters, nutrient metabolism, and the antioxidant system in tomato leaves. Sci. Horti. 157, 1-12.

[10] Maser, P. (2002) Altered shoot/root Na^+ distribution and bifurcating salt sensitivity in Arabidopsis by genetic disruption of the Na^+ transporter AtHKT1. FEBS Lett. 531, 157–161.

[11] Farooq, M., Gogoi, N., Hussain, M., Barthakur, S., Paul, S., Bharadwaj, N., Migdadi, H.M., Alghamdi, S.S. and Siddique, K.H. (2017) Effects, tolerance mechanisms and management of salt stress in grain legumes. Plant Physiol. Bioch. 118, 199-217.

[12] Maas, E.V. and Hoffman G.J. (1977) Crop salt tolerance current assessment. J. Irrig. Draine. Divisi. 103, 115-134.

[13] Hasegawa, P.M., Bressan, R.A., Zhu, J.K. and Bohnert, H.J. (2000) Plant cellular and molecular responses to high salinity. Ann. Rev. of Plant Physio. Plant Mole. Biol. 51, 463-499.

[14] Farhangi- Abriz, S. and Nikpour R. N. (2017) Effect of lignite on alleviation of salt toxicity in soyabean (*Glycine max* L.) plants. Plant Physio. Biochem. 120, 187-193.

[15] Silva, E.N., Silveira, J.A.G., Rodrigues, C.R.F. and Viegas, R.A. (2015) Physiological adjustment to salt stress in Jatropha curcas is associated with accumulation of salt ions, transport and selectivity of K^+, osmotic adjustment and K+:Na+ homeostasis. Plant Biol. 17, 1023–1029.

[16] Krishnamurthy, L., Serraj, R., Tom Hash, C., Dakheel, A.J. and Reddy, B.V.S. (2007) Screening sorghum genotypes for salinity tolerant biomass production. Euphyt. 156, 15-24.

[17] Tavakkoli, E., Fatehi, F., Coventry, S., Rengasamy, P.G. and McDonald, K. (2011) Additive effects of Na^+ and Cl^- ions on barley growth under salinity stress. J. Experi. Bot. 62, 2189–2203.

[18] Serrano, R. (1996) Salt tolerance in plants and micro-organisms: toxicity targets and defines responses. Inter. Rev. Cyto. 165, 1-52.

[19] Bhutta, M.N., Chaudhary, M.R. and Hafeez, C.A. (2003) Water quality issues and status in Pakistan. In: Proc. of seminar on strategies to address the present and future water quality issues. Pakistan Council of Research in Water Resources, Islamabad. Publication No. 123.

[20] World Bank (2001) Pakistan Drought Emergency Recovery Assistance Project. Staff Appraisal Report.

[21] Pakistan Ministry of Food, Agriculture and Livestock (2002) Agricultural Statistics of Pakistan 2000-2001. Ministry of Food, Agriculture and Livestock, Islamabad, Pakistan.

[22] Almodares, A. and Sharif, M.E. (2007) Effects of irrigation water qualities on biomass and sugar contents of sugar beet and sweet sorghum cultivars. J. Enviro. Bio. 28(2), 213-218.

[23] Murtaza, G., Ghafoor, A. and Qadir, M. (2006) Irrigation and soil management strategies for using saline-sodic water in a cotton-wheat rotation. Agric. Water Manag. 81, 98-114.
[24] Abenavoli, M.R., Leone, M., Sunseri, F., Bacchi, M. and Sorgona, A. (2016) Root phenotyping for drought tolerance in bean landraces from Calabria (Italy). J. Agro. Crop Sci. 202, 1-12.
[25] Estefan, G., Sommer, R. and Ryan, J. (2013) Methods of Soil, Plant and Water Analysis: A Manual for the West Asia and North Africa Region. 3rdEd. ICARDA, Beirut, Lebanon.
[26] Bouyoucos, G.J. (1962) Hydrometer method improved for making particle-size analysis of soils. Agro. J. 53, 464-465.
[27] Bremner, J.M. and Keeney, D.R. (1965) Steam distillation method for determination of ammonium nitrate and nitrite. Anal. Chem. Acta. 32, 215-163.
[28] Murphy, J. and Riley, J.P. (1962) A modified single solution method for the determination of phosphate in natural waters. Analytica Chimica Acta. 27, 31-36.
[29] Jackson, M.L. (1958) Soil Chemical Analysis. Prentice Hall, London.
[30] Richards, L.A. (1954) Diagnosis and improvement of saline and alkali soils. USDA (Washington) Handbook. No.60:112.
[31] Parkinson, J.A. and Allen, S.E. (1975) A wet oxidation procedure suitable for the determination of nitrogen and mineral nutrients in biological material. Geoch. Et Cosmoch. Acta. 52, 730-733.
[32] Roy, S.J., Negrao. S. and Tester, M. (2014) Salt resistant crop plants. Current Opinion in Biotechno. 26, 115–124.
[33] Shi, D.C. and Sheng, Y.M. (2005) Effect of various salt-alkaline mixed stress conditions on sunflower seedlings and analysis of their stress factors. Enviro. Experi. Bot. 54, 8–21.
[34] Yang, C.W., Xu, H.H., Wang, L.L., Liu, J., Shi, D. and Wang, D.L. (2009) Comparative effects of salt-stress and alkali-stress on the growth, photosynthesis, solute accumulation, and ion balance of barley plants. Photosy. 47, 79-86.
[35] Ahmad, H., Hayat, S., Ali, M., Ghani, M.I. and Zhihui, C. (2017) Regulation of Growth and Physiological traits of Cucumber (*Cucumis sativus* L.) through various levels of 28-Homobrassinolide under salt stress conditions. Can. J. Plant Sci. 98(1), 132-140.
[36] Singh, Y.P., Nayak, A.K., Sharma, D.K., Singh, G., Mishra, V.K. and Singh, D. (2015) Evaluation of *Jatropha curcas* genotypes for rehabilitation of degraded sodic lands. Land Degrad. Develop. 26, 510-520.
[37] Wright, D. and Rajpar, I. (2000) An assessment of the relative effects of adverse physical and chemical properties of sodic soils on the growth and yield of wheat (*Triticum aestivum* L.). Plant Soil. 223, 277-285.
[38] Chen, S., Xing, J. and Lan, H. (2012) Comparative effects of neutral salt and alkaline salt stress on seed germination, early seedling growth and physiological response of a halophyte species *Chenopodium glaucum*. Afri. J. Biotec. 11, 9572-9581.
[39] Wang, X., Geng, S., Ri, Y.J., Cao, D., Liu, J., Shi, D. and Yang, C. (2011) Physiological responses and adaptive strategies of tomato plants to salt and alkali stresses. Sci. Horti. 130, 248-255.
[40] Puga, A.P., Abreu, C.A., Melo, L.C., Paz-Ferreiro, J., Beesley, L. (2015) Cadmium, lead, and zinc mobility and plant uptake in a mine soil amended with sugarcane straw biochar. Environ. Sci. Pollut. Res. 22, 17606–17614.
[41] Qadir, M. and Schubert, S. (2002) Degradation processes and nutrient constraints in sodic soils. Land Degrad. Develop. 13, 275-294.
[42] Turner, N.C., Colmer, T.D., Quealy, J., Pushpavalli, R., Krishnamurthy, L., Kaur, J., Singh, G., Siddique, K.H. and Vadez, V. (2013) Salinity tolerance and ion accumulation in chickpea (*Cicer arietinum* L.) subjected to salt stress. Plant Soil. 365, 347-361.
[43] Ottow, E.A., Brinker, M., Teichmann, T., Fritz, E., Kaiser, W., Brosch, M., Kangasjarvi, J., Jiang, X.N. and Polle, A. (2005) Populus euphratica displays apoplastic sodium accumulation, osmotic adjustment by decreases in calcium and soluble carbohydrates, and develops leaf succulence under salt stress. Plant Physio. 139, 1762-1772.
[44] Safavi, S. and Khajehpour, M.R. (2008) Effects of salinity on Na^+, K^+ and Ca^{+2} contents of borage (*Borago officinalis* L.) and echium (Echium amoenum Fisch. & Mey.). Res. in Pharma. Sci. 2, 23-27.
[45] Ramos, T.B., Simunek, J., Goncalves, M.C., Martins, J.C., Prazeres, A. and Pereira, L.S. (2012) Two-dimensional modeling of water and nitrogen fate from sweet sorghum irrigated with fresh and blended saline waters. Agric. Water Manage. 111, 87-104.

Received: **31.08.2018**
Accepted: **18.02.2019**

CORRESPONDING AUTHOR

Ying Zhao
College of Natural Resources and Environment,
Northwest A&F University,
Yangling, Shaanxi, 712100 – China

e-mail: yzhaosoils@gmail.com

© by PSP Volume 28 – No. 5/2019 pages 3740-3744 Fresenius Environmental Bulletin

THE EFFECTS OF LIQUID WORM FERTILIZER AND LIQUID BAT GUANO FERTILIZER ON PLANT GROWTH AND YIELD IN GRAFTED TOMATO PLANTS (*LYCOPERSICON ESCULENTUM* L).

Garip Yarsi*

Plant and Animal Production Department, Vocational School of Silifke, University of Mersin, Silifke, Mersin, Turkey

ABSTRACT

In this study, tomato plants were planted in pots filled with peat: perlite mixture at a ratio of 2: 1 in the period of 2-3 true leaves liquid worm fertilizer, liquid bat guano fertilizer and a mixture of the both were used as fertilizer and control plants were not applied to these fertilizers. The effect of the fertilizers on the number of leaves, plant height, root length, fresh and dry weight of plant, fresh and dry weight of root, chlorophyll content, rootstock and scion diameter, yield and some quality parameters were investigated. The study was carried out with 4 replications of 12 plants in each repetition. Using organic fertilizers (liquid worm and liquid bat guano fertilizers) positively affected the biomass of the grafted tomato plants. The yield was lowest with 16,42 kg/m^2 for control plants. This was followed by the mixture of liquid worm and bat guano fertilizer 22,12 kg/ m^2 and the liquid bat guano with 21,19 kg/m^2. The highest yield per plant was liquid worm fertilizer with 22,96 kg/m^2. As a result of this study, it was determined that liquid worm fertilizer, liquid bat guano and mixture of both caused a positive increase in plant biomass and yield compared to the control plants.

KEYWORDS:
Worm and Bat fertilizer, tomato, plant growth, yield

INTRODUCTION

Turkey is one of the major producer countries with about 12 million 150 thousand tons of tomato production [1]. Changes in agricultural production systems in the world and in Turkey have caused growers to search for new sources of agricultural inputs. The increase in prices of chemical fertilizers has led both fertilizer producers and farmers to new production materials such as "vermicompost". Vermicompost is used especially in vegetable and fruit growing. Both the use and production of this fertilizer in Turkey has been increasing day by day [2]. Vermicompost significantly increases plant growth in many plant species including horticulture [3]. The positive results of vermicompost result from the ability of groundworms to consume a wide variety of organic wastes [4, 5, 6]. Vermicompost has high microbial activity due to fungus, bacteria and actinomycetes [7].

In some studies, it has been reported that the use of vermicompost positively contributes to plant growth, yield, nutrient content and physical and chemical properties of soil [8, 9, 10, 11, 12, 13, 14]. Orozco [14] reported that the Vermicompost contains various nutrients such as nitrates, phosphates, interchangeable calcium and soluble potassium for plants. Alaboz [12] in a study to determine the effect of irrigation and vermicompost in pepper production reported that vermicompost increased fresh and dry weight of plants. In a study of tomato, use of vermicompost has been reported to increase plant growth and yield [15]. Belliturk [2] reported that the use of vermicompost not only increased P and K amounts in peppers and eggplant but also increased N content, soil organic matter content and beneficial microorganisms in soil positively. Microorganisms, such as bacteria, fungi, yeasts, actinomycetes and algae, can produce plant growth regulators (PGRs) such as auxins, gibberellins, cytokinins, ethylene and abscisic acid [16].

In the studies carried out in pepper and tomato, it is reported that different organic fertilizers and bat guano given from soil and leaf increased fresh and dry weights in tomato and pepper plant [17,18]. Mengistu [19] in a study in tomato reported that, using of vermikompost increased plant growth and yield.

Bat guano fertilizer containing 23.0% to 79.0% of organic matter is one of the basic organic fertilizer sources [20] and this fertilizer provides positive contribution to plant growth [21]. In a study on lettuce, Ünal [22] reported that bat guano fertilizer increased the amount of nutrients in both soil and plant. In a study by Sothearen [23], they reported that bat guano fertilizer was used in 5 plant species which have economic importance and it had positive effects.

Excessive using of pesticides and fertilizers in areas where conventional agriculture is concerned

threatens both environmental health and human health. By using organic fertilizers, agricultural pollution has been reduced. The aim of this study is to investigate the effects of the use of worm and bat guano fertilizers on yield and quality and to make suggestions to farmers. As a result of these fertilizers in tomato cultivation, positive contributions will be made both to environmental health and human health.

MATERIALS AND METHODS

Plant Materials and Experimental design. This study was conducted at the Plant and Animal Production Department of Silifke Vocational School, University of Mersin in 2017-2018. Retinto (Seminis Seed Company) tomato variety was used as a scion and beaufort (Seminis Seed Company) as a rootstock. The grafted seedlings, which was used Slant-Cut Grafting method, were bought from Yonca Seedling Company, Tarsus-Turkey. The experiment was conducted in 4 replications and 12 plants each replication.

On January, tomato plants were planted in pots filled with peat: perlite mixture at a ratio of 2: 1 in the period of 2-3 true leaves and liquid worm fertilizer, liquid bat guano and a mixture of both were used as fertilizer and control plants were not applied to these fertilizers. Polyethylene plastic pots with a diameter of 22,5 cm and a height of 25 cm (8.5 liter) were used. The plants were harvested 40 days after planted for the biomass. For the yield the plants were stayed from January to end of June. The fertilizer was given two different times for plants which were planted for the biomass (first, immediately after planting and second, 20 days later) and four different times for plants which were planted for yield (first, immediately after planting and 20,40,60 days after planting). Liquid worm fertilizer (1 liter fertilizer/ 200 liter water); Liquid bat guano fertilizer (1 liter fertilizer/ 200 liter water); Liquid worm + bat guano (0.5 liter Worm and 0.5 liter bat guano/ 200 liter water).

Biomass and Yield Parameters. Chlorophyll content: Chlorophyll was measured 3 times of same leaves in 5 plants (SPAD 502)

Rootstock diameter (mm): Measured with a digital caliper just below the grafting point

Scion diameter (mm): Measured with a digital caliper just above the grafting point

Root length (cm): Measured with the help of a ruler

Plant height (cm): Measured with the help of a ruler

Number of leaves: Fully developed leaves counted

Fresh weight (g): Weighed with precision scales (0.001)

Dry weight(g): Plants and roots dried at 65 ºC for 48 hours and weighed with scales (0.001)

Yield (kg/m^2): The fruits collected until the end of the harvest are weighed and the yield per square meter is calculated

Average fruit weight (g): Weighed with precision scales (0.001)

Number of cluster in plant: The clusters in plants were counted and the number of average cluster was found.

Number of fruit in cluster: The fruits in cluster were counted and the number of average fruit was found.

Data Analysis. SPSS 13.0 package program was used and the difference between applications was made according to Duncan test (1% and 5%)

RESULTS AND DISCUSSION

In this study, when Table 1 is examined, it is observed that fertilizers formed with liquid worm fertilizer, liquid bat guano and their mixture in equal proportions have no statistical effect on rootstock diameter in grafted tomatoes but important effect on scion diameter. In control plants, the scion diameter had the lowest measurement value with 4.22 mm. In liquid worm fertilizer application, this value was measured as highest with 5.64 mm. The diameter of the scion was measured as 4.58 mm and 5.32 mm in bat guano and mixture of both (liquid worm + liquid bat guano) applications respectively and was statistically in the same group.

TABLE 1
Effect of different organic fertilizer usage on plant growth in grafted tomatoes

Applications	Rootstock diameter (mm)	Scion diameter (mm)	Chloro-phyll (First)	Chlorophyll (Last)	Number of the leaves	Plant height (cm)	Root length (cm)
Control	2,89a	4,22b	43,9a	44,9b	11,0b	31,3b	13,1b
W Fert.*	2,97a	5,64a	44,0a	48,3a	15,7a	54,6a	37,3a
BG Fert.**	3,01a	4,58ab	43,8a	50,1a	17,34a	51,9a	36,4a
W Fert.+ BG Fert.	3,10a	5,32ab	43,9a	50,5a	17,3a	51,2a	33,8a

Mean followed by the same letters do not significantly difference in $p \leq 0.05$
* Worm Fertilizer; ** Bat Guano Fertilizer

When the chlorophyll content was examined, there was no statistical difference in the first measurements, but the difference was statistically significant in the last measurements. While control was the lowest with 44.9, it was determined as 48.3, 50.1 and 50.5 in liquid worm fertilizer, liquid bat guano and mixture of both (Liquid worm + Liquid bat) applications, respectively. A similar situation is seen in the number of leaves, plant height and root length. While the control had the least number of leaves with 11.0 leaves, in Liquid bat guano and mixture of both (liquid worm + liquid bat) fertilizer this value was the highest with 17.3. The effect of the fertilizers used on plant height was also statistically significant. Fertilizer applications were in the same group by taking higher values than control (Table 1). It is observed that the fertilizers used in the root length lead to a positive increase (Table 1). Liquid worm fertilizer has the highest value with 37.3 cm.

Table 2 shows the effect of fertilizers on plant fresh and dry, root fresh and dry weight. Mixture of both (liquid worm + liquid bat) fertilizer application with 15.58 g of plant weight is the highest value. This application was followed by liquid bat fertilizer with 15.31 g and 14.44 g with liquid worm fertilizer. While these three applications were statistically in the same group, the control was in the different group with 8.62 g. Plant dry weight has parallel results with fresh weights. In terms of root fresh weight, the highest value was measured with 3.02 g in liquid bat guano application. This was followed by mixture of both (liquid worm + liquid bat) with 2.68 g, liquid worm with 2.42 g and control with 0.72 g, respectively. While fertilizer applications were in the same group, control application took place in different groups (Table 2). Root dry weights also results in parallel to the root fresh weight. These results are similar with Eswaran and Mariselvi [24] (2016) in tomatoes.

TABLE 2
The effect of different organic fertilizer usage on plant fresh-dry and root fresh-dry weight in grafted tomatoes

Applications	Fresh Root Weight(g)	Dry Root Weight(g)	Fresh Plant Weight(g)	Dry Plant Weight(g)
Control	0,72c	0,11b	8,62b	0,76b
W Fert.*	2,42b	0,26a	14,44a	1,64a
BG Fert.**	3,02a	0,27a	15,31a	1,33a
W Fert.+ BG Fert.	2,68ab	0,26a	15,58a	1,35a

Mean followed by the same letters do not significantly differ in p≤0.05
* Worm Fertilizer; ** Bat Guano Fertilizer

FIGURE 1
Roots of tomato K: Control; S: Worm Fertilizer; Y: Bat Guano S+Y: Worm + Bat Guano

TABLE 3
Effect of organic different fertilizer usage on the yield of grafted tomatoes

Applications	Yield (kg/m^2)	Average Fruit Weight (g)	Number of Cluster (per plant)	Number of fruits in cluster
Control	16,42c	114,03b	7,87b	6,63b
W Fert.*	22,96a	133,53a	8,67a	7,23a
BG Fert.**	22,12ab	135,13a	8,40a	6,93ab
W Fert.+ BG Fert.	21,19b	130,46a	8,30a	7,20a

Mean followed by the same letters do not significantly differ in p≤0.05
* Worm Fertilizer; ** Bat Guano Fertilizer

TABLE 4
Correlations amount some parameters.

		Scion Diameter	Root length	Root dry weight	Yield kg/plant
Scion Diameter	Pearson Correlation	1	,569	,618*	,569
	Sig.(2-tailed)		,053	,032	,054
	N	12	12	12	12
Root length	Pearson Correlation	,569	1	,934**	,967**
	Sig.(2-tailed)	,053		,000	,000
	N	12	12	12	12
Root dry weight	Pearson Correlation	,618*	,934**	1	,914**
	Sig.(2-tailed)	,032	,000		,000
	N	12	12	12	12
Yield kg/m^2	Pearson Correlation	,569	,967**	,914**	1
	Sig.(2-tailed)	,054	,000	,000	
	N	12	12	12	12

*Correlation is significant at the 0,05 level (2-tailed)
**Correlation is significant at the 0,01 level (2-tailed)

The effect of fertilizer applications on yield per plant, average fruit weight, average number of cluster and number of fruits in the cluster was found to be statistically significant (Table 3). The yield was lowest with 16,42 kg/m^2 for control. This was followed by the liquid bat guano with 22,12 kg/m^2 and mixture of both (liquid worm + liquid bat) 21,19 kg/m^2, respectively. The highest yield was liquid worm fertilizer with 22,96 kg/m^2. While the highest value of liquid bat guano was found with 135.35 g of fruit weight, the control had the lowest value with 114.03 g. Liquid worm fertilizer has the highest values with 8.67 clusters and 7,23 clusters of fruits, and these values are the lowest with 7.87 and 6.63 for the control, respectively.

Correlations. Table 4 shows the correlations among some parameters. When Table 4 is examined, it is seen that there is a strong correlation between scion diameter and root dry weight (0.618 *, $p \leq 0.05$); root length with root dry weight (0.934 **, $p \leq 0.01$) and yield (0.967 **, $p \leq 0.01$); between yield and root dry weight (0.914 **, $p \leq 0.01$).

CONCLUSIONS

As a result of the study, it was determined that liquid worm fertilizer and liquid bat guano application had a positive effect on plant growth in grafted tomato plants. These results are similar that was reported by [25, 12]. The application of worm fertilizer and bat guano separately and in mixed form also increased in yield compared to the control application. These results are similar to those of [13, 26]. According to the results of the study, the use of liquid worm fertilizer, liquid bat guano and mixture of both fertilizers in grafted tomato cultivation contributed positively to both plant growth and yield. The use of these fertilizers can be recommended to farmers.

REFERENCES

[1] Anonymous (2018) http://tuik.gov.tr (Date of access: 28.02.2019)
[2] Bellitürk, K., Adiloğlu, S., Solmaz, Y., Zahmacıoğlu, A., Adiloğlu, A. (2017) Effects of İncreasing Doses of Vermicompost Applications on P and K Contents of Pepper (*Capsicum annuum* L.) and Eggplant (*Solanum melongena* L.). Journal of Advanced Agricultural Technologies. 4(4), 372-375.
[3] Hashemimajd, K., Kalbasi, M., Golchin, A., Shariatamadari, H. (2004) Comparison of vermicompost and composts as potting media for growth of tomatoes. J Pl Nutr. 27, 1107-1123.
[4] Chan, P.L.S. and Griffiths, D.A. (1988) The vermicomposting of pre-treated pig manure. Biol Wastes. 24, 57-69.
[5] Hartenstein, R. and Bisesi, M.S. (1989) Use of earthworm biotechnology for the management of effluents from intensively housed livestock. Outlook on Agric. 18, 3-7.
[6] Cavender, N., Atiyeh, R.M. and Knee, M. (2003) Vermicompost stimulates mycorrhizal colonization of roots of Sorghum bicolor at the expense of plant growth. Pedobiol.47, 85-89.
[7] Tomati, U., Grappelli, A. and Galli, E. (1988) The hormone like effect of earthworm casts on plant growth. Biol. Fertil. Soils. 5, 288-294
[8] Küçükyumuk, Z., Gültekin, M., Erdal, İ., (2014) Effects of Vermicompost and Mycorrhiza on Plant Growth and Mineral Nutrition in Pepper. Suleyman Demirel University Journal of the Faculty of Agriculture. 9, 51-58. (in Turkish).
[9] Atiyeh, R.M., Subler, S., Edwards, C.A., Bachman, G., Metzger, J.D., Shuster, W. (2000) Effects of vermicomposts and composts on plant growth in horticultural container media and soil. Pedo Biologia. 44, 579–590.

[10] Kizilkaya, R., Hepsen Turkay, F.S., Turkmen, C., Durmus, M. (2012) Vermicompost effects on wheat yield and nutrient contents in soil and plant. Archives of Agronomy and Soil Science. 58, 175–179.
[11] Azarmi, R., Giglou, M.T., Taleshmikail, R.D. (2008) Influence of vermicompost on soil chemical and physical properties in tomato (Lycopersicum esculentum) field. African J. Biotechnology. 7, 2397-2401.
[12] Alaboz, P., Işıldar, A.A., Müjdeci, M., Şenol, H. (2017) Effects of Different Vermicompost and Soil Moisture Levels on Peper (Capsicum annuum) Grown and Some Soil Properties. Yyü Tar.Bil.Derg. 27(1), 30-36.
[13] Avila-Juarez, L., Rodriguez Gonzalez, A., Rodrigunez Pina, N., Guevara Gonzalez, R.G., Torres Pacheco, I., Ocampo Velazguez, R.V., Moustapha, B. (2015) Vermicompost Leachate as a Supplement to Increase Tomato Fruit Quality. Journal of Soil science Plant Nutrition. 15(1), 46-59.
[14] Orozco, F.H., Cegarra, J., Trujillo, L.M., Roig, A. (1996) Vermicomposting of Coffee Pulp Using the Eartworm Eisenia fetida: Effects on C and N contents and the Availability of Nutrients. Biol. Fert. Soils. 22,162-156.
[15] Vaidyanathan, G., Vijayalakshmi, A. (2017) Effect of Vermicompost on Growth and Yield of Tomato. European Journal of Pharmaceutical and Medical Research. 4(9), 653-656.
[16] Frankenberger Jr., W.T. and Arshad, M. (1995) Phytohormones in Soils: Microbial Production and Function. Marcel and Decker, New York. 503p.
[17] Koç, F. (2008) Effects of Different Organic Fertilizers on Growth and Nutrition of Tomato and Pepper Plants. Master Thesis. Ankara University Graduate School of Natural and Applied Science Department of Soil Science and Plant Nutrition, Ankara. (in Turkish).
[18] Soba, M.R. (2012) The Effects of Bat Guano Applied to the Soil and Leaf on the Nutrition of Tomatoes and Peppers, yield Amount and Some Quality Parameters. Master Thesis. Ankara University Graduate School of Natural and Applied Science Department of Soil Science and Plant Nutrition, Ankara (in Turkish).
[19] Mengistu, T., Gebrekidan, H., Kibret, K., Woldetsadik, K., Shimelis, B., Yadav, H., (2017) The Integrated use of excreta-based Vermicompost and Inorganic NP Fertilizer on Tomato (Solanum Lycopersicum L.) Fruit Yield, Quality and Soil Fertility. Int J Recycl Org Waste Agricult. 6, 63-77
[20] Altıntaş, A., Kontas, T., Yıldız, G., and Erkal, N. (2005) Mineral levels of bat guano. Veterinary Journal of Ankara University. 52, 1–5.
[21] Demirtaş, I., Arı, N., Arpacıoğlu, A., Kaya, H., and Özkan, C. (2007) Different organic fertilizer chemical properties. The effect of spent mushroom compost use on some soil properties and yield in greenhouse tomato cultivation, 220–23. Erzurum: Turkey V. National Horticulture Congress.
[22] Ünal, M., Can, O., Aydın Can, B., Poyraz, K., (2018) The effect of Bat Guano Applied to the Soil in Different Forms and Doses on Some Plant Nutrient Contents. Communications in Soil Science and Plant Analysis. 46(6),708-716.
[23] Sothearen, T., Furey, N.M., Jurgens, J.A. (2014) Effect of bat guano on the growth of five economically important plant species. Journal of Tropical Agriculture. 52, 169-173.
[24] Eswaran, N., Mariselvi, S. (2016) Efficacy of Vermicompost on Growth and Yield Parameters of Lycopersicum esculentum (Tomato). International Journal of Scientific and Research Publications. 6 (1), 95-108.
[25] Pritam, S., Garg, V.K., Kaushik, C.P. (2010) Growth and yield response of Marigold to potting media containing Vermicompost produced from different wastes. Environ. 30, 123-130.
[26] Joshi, R. and Vig, A.P. (2010). Effects of Vermicompost on Growth, Yield and Quality of Tomato (Lycopersicum esculentum L.). African Journal of Basic and Applied Sciences. 2 (3-4),117-123.

Received: **11.02.2019**
Accepted: **11.03.2019**

CORRESPONDING AUTHOR

Garip Yarsi
University of Mersin,
Vocational School of Silifke
Plant and Animal Production Department,
33940 Mersin – Turkey

e-mail: ggyarsi@gmail.com

© by PSP Volume 28 – No. 5/2019 pages 3745-3755 Fresenius Environmental Bulletin

IMPROVEMENT OF SOME ECONOMIC TRAITS IN CANOLA (*BRASSICA NAPUS* L.) USING DIFFERENT SELECTION PROCEDURES

Dora A Said[1], Ismael A Khatab[1], Aboughazala E Mohamed[2], Alaa Eldin M Shaheen[2,*]

[1]Department of Genetics, Faculty of Agriculture, Kafrelsheikh University, 33516, Egypt
[2]Oil Crops Res. Dept., Field Crops Res. Inst., Agric. Res. Center, Egypt

ABSTRACT

Some selection procedures i.e. selection index involving three indices and pedigree line selection for two separately traits (seed yield/plant and seed oil content) were used to improve seed yield and yield components in early segregating generations; F_2, F_3 and F_4 of the canola cross (Line 99 x Serw 4). Mean performances of F_4 generation were higher than those of F_3 for seed yield/plant, oil seed content, 1000 seed weight and plant height. The highest predicted genetic advance from F_3 generation and exceeded 35% of the F_3 mean was obtained with the indices I_{w1}, ped.$_w$ and I_{w123}. These indices maintained the same trend in F_4 generation as the highest realized and predicted advances as values and percentages (more than 23% and 18% of F_4 mean, respectively). Deviations of the realized advance from the predicted of seed yield determined in F_3 to F_4 generation were negative for selection index involving oil seed content and number of racemes/plant and pedigree selection for oil seed content. These results showed that the genetic variations for seed yield in early generations did not be exhausted enough and the improvement of seed yield/plant could be continued in further generations using direct pedigree selection for seed yield/plant and the indices I_{w123} and I_{w1}. High heritability estimates were recorded for all the studied traits with higher values in F_4 generation than those of F_3 generation, except for seed yield/plant, indicating high magnitude of genetic variability and a possible success in the selection of the early generations. The values of phenotypic coefficient of variation (PCV) and genotypic coefficient of variation (GCV) in F_4 were higher than those of F_3 generation for most studied traits, this indicated that the magnitude of the genetic variability continued in these materials was sufficient for providing rather substantial degrees of improvement through the selection of superior progenies. Seed yield/plant showed positive and highly significant phenotypic and genotypic correlations with number of racemes/plant in F_3 generation, positive and significant or highly significant phenotypic correlation with number of racemes/plant and 1000 seed weight in F_4 generation and positive and highly significant genotypic correlation with 1000 seed weight in F_4 generation. The path coefficients of seed yield with its components were changed from F_3 to F_4 generations. This could be due to the efficiency of selection procedures applied in this study.

KEYWORDS:
Brassica napus, Canola, Predicted gain, Realized gain, Segregating generations, Selection procedures.

INTRODUCTION

Canola (*Brassica napus* L) is commonly known as rapeseed or oilseed rape. It belongs to the family Brassicaceae (formerly Cruciferae) which contains about 350 genera and 3500 species with high diverse morphology.

It is one of the most important oil crops in the world [1]. It contains 6% saturated fatty acids and 94% unsaturated fatty acids (high in monounsaturated fatty acids), it has 50% less saturated fat than corn oil [2]. Canola is the third largest source of edible oil after soybean and palm oil [3] providing 14% of the world supply.

Canola seeds contain approximately 43% oil or more and produce meals with 35 to 40% protein.

The total cultivated area of canola all over the world is about 36.59 million hectare produced 72.15 MMT seeds and 28.52 MMT oil [3]. The new promising varieties can produce edible oils able to cover the big oil gap between local production and consumption.

Traits which have high range of genetic variability, heritability and genetic advance would be an effective tool for improving seed yield [4]. Development of high-yielding cultivars required an accurate knowledge of the existing genetic variation for yield and its components. The observed variability is a combined estimate of genetic and environmental causes, of which only the former one is heritable.

Selection in segregating generations has always been a challenge for plant breeder. So, the knowledge of an appropriate multiple selection

TABLE 1
Origins and characteristics of the two canola parental genotypes.

Parents	Origin	FF	50% F	100% F	PH	No. racemes	Yield	1000 SW	Oil%	MAT
Line 99	FAO	86.33	99.33	107.33	171.67	8.00	30.44	3.90	42.32	159.33
Serw4	Egypt	85.33	101.67	107.33	178.83	9.93	34.06	4.21	43.40	161.67

FF = days to first flowering & 50% F = days to 50% flowering & 100% F = days to 100% flowering & PH = plant height (cm) & No. racemes = number of racemes/plant & Yield = seed yield/plant (g) &1000 SW = 1000 seed weight (g) & Oil% = seed oil content (%) & MAT = days to physiological maturity.

criteria based on the selection procedures would be more desirable.

Response to selection is attributed to significant genetic variation and high heritability [5]. Knowledge of heritability is very important as an indicator for the possibility of improvement that can be brought through selection.

However, estimates of heritability alone do not give an idea about the expected gain in the next generation, but have to be considered coupled with values of genetic advance and the change in mean value among successive generations [6]. The traits having high heritability in conjunction with high genetic advance are considered under control of additive genes, whereas with high heritability and low genetic advance are under the control of non-additive (dominant and/or epistatic) genes which limits the possibility of improvement through selection [7].

It is now well known that seed and oil yield in canola are quantitative and complex traits that controlled by many genes and direct selection per se is not effective for improvement. So, indirect selection through traits having higher heritability and correlated strongly with oil and seed yield has more genetic efficiency than direct selection in genetic improvement of these traits [8].

Estimation of phenotypic and genotypic correlations is considered an effective selection tool for selecting the best individual traits which have strong correlation with yield [9]. Using of simple correlation analysis couldn't fully indicate the relation among the traits. So, the path analysis is used to identify the amount of direct and indirect effects of the variables on the dependent one [10]. Hence, correlation in combination with the path coefficient analysis quantifies the direct and indirect contribution of one trait upon another [11].

The main objectives of this work were to determine the predicted and realized gains from different selection procedures for improving seed yield and seed oil content and to determine the correlated response between selected and unselected traits in canola. Also, determination of the best indirect selection criteria for genetic improvement of seed yield in canola and studying the correlation between seed yield per plant and other studied traits was another purpose for this study.

MATERIALS AND METHODS

The present study was carried out at the Experimental Farm of Sakha Agricultural Research Station, Agric. Res. Center during 2014/2015, 2015/2016 and 2016/2017 growing winter seasons.

The materials used were The F_2, F_3 and F_4 generations of canola (*Brassica napus* L.) cross (Line 99 x Serw 4). Serw 4 which was used as a parent is also a commercial variety. Both parents were chosen to represent a wide range of variability for yield and its components.

Sowing date was during October for the three growing seasons. All agronomic practices were applied according to recommendations.

The origins and characteristics for the parents are presented in Table (1).

In the first season 2014/2015 (F_2 generation), F_2 seeds and original parents were grown in no replicated rows, the cross was represented by twenty rows, 4 m long, 60 cm between ridges and each ridge had 25 hills 15 cm apart. Only one plant was left per hill at thinning time. The data was recorded on 500 plants for the cross of the F_2 generation, and then the selection within the cross was practiced on the bases of 50% flowering, agronomic and yield characters (plant height, numbers of racemes/plant, and seed yield/plant) where the best 10% plants were selected and grown in F_3 generation. Fifty superior single plants having the highest performance (direct selection) were selected individually.

In the second season 2015/2016 (F_3 generation), each of the 50 selected plants and parents were grown in a row as a family where a random sample of F_3 seeds of the 50 selected plants (F_3 families) and parents were evaluated in mid-October in a randomized complete block design (RCBD) with three replications. Experimental plot (family) was represented by single row, 4 m long, 60 cm apart and 15 cm between seeds within a row. Only one plant released per hill at thinning time.

The 50 families were ranked using five selection procedures. The five superior families of each selection procedures were selected using 10% selection intensity (the best 10% of the families). The recommended practices for canola production were also applied during this growing season.

Ten random guarded plants in each row from each family were taken to record data (plant height, number of racemes per plant, seed yield per plant,

1000-seed weight and seed oil content). Moreover, the flowering date (first, 50% and 100% flowered plants) was recorded for each plot (row). Equal numbers of seeds for each family were saved and mixed from all families to represent the bulk sample for each population.

In the third season 2016/2017 (F_4 generation), the selected 11 families were grown on the end of October and evaluated in a randomized complete block design in three replications with the original parents. The same procedures of the previous season were followed. Ten guarded plants were randomly taken from each plot to collect data.

Selection procedures were as follows:

I_{w123}= Selection index involving seed yield/plant, seed oil content, plant height and number of racemes/plant.

I_{w1} = Selection index involving seed yield/plant and seed oil content.

I_{13} = Selection index involving seed oil content and number of racemes/plant.

Ped. $_w$= Pedigree selection for seed yield/plant.

Ped.$_1$ = Pedigree selection for seed oil content.

The studied characters were: seed yield (g)/plant (x_w), seed oil content (x_1), plant height (x_2), number of racemes/plant (x_3), 1000-seed weight, days to first flowering, days to 50% flowering, days to 100% flowering and days to physiological maturity.

Seed oil content (%): the oil percentage was determined from three gram seed sample using Soxholet method according to [12].

Statistical and genetic analysis. Heritability in broad sense was calculated according to the following expressions:

$$h_b^2 \text{ (in } F_2 \text{ generation)} = \frac{VF_2 - (VP_1 + VP_2)/2}{VF_2} x100$$

$$h_b^2 \text{ (in } F_3 \text{ and } F_4 \text{ generations)} = \frac{\sigma^2 g}{\sigma^2 p} X100 \text{ [13]}$$

Where:

VF_2= The phenotypic variance of the F_2 generation.

VP_1, VP_2 = The variances of the first and second parents, respectively.

$\sigma^2 g$ = The genotypic variance of the F_3 and F_4 generations.

$\sigma^2 p$ = The phenotypic variance of the F_3 and F_4 generations.

The phenotypic and genotypic coefficients of variation were estimated using the formula developed by [14].

Relative importance or economic values (a_i) was calculated according to [13].

a_w (seed yield/plant) = $\bar{X}_1 . \bar{X}_2 . \bar{X}_3$

a_1 (seed oil content) = $\bar{X}_2 . \bar{X}_3$

a_2 (plant height) = $\bar{X}_1 . \bar{X}_3$

a_3 (number of racemes/plant) = $\bar{X}_1 . \bar{X}_2$

Where: X,s represent the mean values of the studied traits.

The appropriate index weights (b_is) were calculated from the following formula postulated by [15] and [16]:

$(b)=(P)^{-1}.(G).(a)$

Where:

(b)=Vector of relative index coefficients,

$(P)^{-1}$=Inverse phenotypic variance-covariance matrix,

(G)=Genotypic variance-covariance matrix and

(a)=Vector of relative economic values.

The formula suggested by [15] and [16] was used in calculating various selection indices:

$I=b_1x_1+b_2x_2+\ldots\ldots\ldots\ldots+b_nx_n$

Predicted improvement in seed yield on the basis of an index was estimated according to the following expression:

Selection advance (SA)=$SD(\sum b_i.\sigma g_{iw})^{1/2}$ [13]

Where:

SD denotes selection differential in standard units.

b_i denotes index weights for characters considered in an index.

σg_{iw} denotes genotypic covariances of the traits with yield.

Predicted genetic advance in seed yield based on pedigree selection was estimated from the following expression:

(ΔGw) due to selection for $X_i=K.\sigma g_{wi}/\sigma p_i$ [17].

Also, the predicted response in any selected and unselected trait was calculated as suggested by [18] and [13].

The realized gains were calculated as deviation of generation mean for each character from procedure mean of that trait.

RESULTS AND DISCUSSION

Heritability estimates in broad sense (h^2_b), phenotypic (PCV%), genotypic coefficient of variation (PCV%) and mean values for all the studied traits are displayed in Table (2). Heritability estimates in F_4 generation were higher than those of F_3 generation for all the studied traits, except for seed yield/plant. The heritability values obtained in both F_3 and F_4 generations ranged from 65.10 to 97.90 for all the studied traits, indicating high magnitude of genetic variability and a possible success in the selection of the early generations which were evaluated. [19] found high broad sense estimates ranging from 97% to 69% for all the studied traits. Also, similar results were reported by [20-26].

Also, high heritability estimates in conjunction with the slight differences in PCV and GCV values were found for most of the studied traits indicating that these traits were less influenced by environmental factors and controlled mainly by genetic effects, also, selection for them is fairly

easy and may be effective for improving seed yield/plant as selection gain will be high.

The estimates of phenotypic coefficient of variation (PCV) were generally higher than those of genotypic coefficient of variation (GCV) for all the studied traits in F_2, F_3 and F_4 generations. But in many cases, the two values differed only slightly, which reflect to some extent the impact of environment on the expression of these traits. These findings are in agreement with those obtained by [27].

Also, the values of PCV and GCV in F_4 were higher than those of F_3 generation for some studied traits. This indicates that the magnitude of the genetic variability continued in these materials was sufficient for providing reasonable amounts of improvement through the selection of superior progenies. On the other hand, F_4 generation showed reduction in PCV and GCV values for some of the studied traits. This was due to the reduction in genetic variability and heterozygosity as a consequence of applying different selection procedures which exhausted a major part of variability. Similar results were reported by [19].

The highest values of PCV and GCV were recorded for seed yield/plant, number of racemes/plant and 1000 seed weight, which indicates that selection of these traits based on phenotype could be useful for yield improvement. This result is in agreement with those obtained by [21, 24, 25, 28]. Meanwhile, low to moderate estimates of PCV and GCV were recorded for other studied traits. Similar results were obtained by [29, 30]. The lowest values of PCV and GCV were obtained for days to 100% flowering and days to physiological maturity.

Comparing means of F_4 with those of F_3, it is clear that the means of F_4 were higher than those of F_3 generation for seed yield/plant, plant height, seed oil content and 1000 seed weight, whereas, these means were lower than those of F_3 for number of racemes/plant, number of days to first flowering, number of days to 50% flowering, number of days to 100% flowering and days to physiological maturity. It should be noted that the reduction in the means of flowering and physiological maturity traits from F_4 to F_3 generation is desirable as it is considered an indicator for earliness. This was due to the possible accumulation of desirable alleles as a consequence of effectiveness of selection procedures applied in this study. Similar results were obtained by [19].

Phenotypic and genotypic correlation coefficients. Plant breeders must be interested in the total array of economic traits and not only one character. So, the correlation analysis gives us a good indicator to predict the corresponding change which occurs in one trait according to the proportionate change in the others.

The results of phenotypic and genotypic correlation coefficients in F_3 and F_4 generations (Tables 3 and 4) revealed positive and highly significant phenotypic and genotypic correlations between seed yield/plant and number of racemes/plant in F_3 generation, positive and significant or highly significant phenotypic correlation with number of racemes/plant and 1000 seed weight in F_4 generation

TABLE 2
Estimates of broad sense heritability (h^2_b), phenotypic (PCV) and genotypic (GCV) coefficients of variation, means and standard errors ($S\bar{X}$) for the studied traits in F_2, F_3 and F_4 generations.

Trait	Generation	h^2_b	PCV %	GCV %	Mean ± $S\bar{X}$
Plant height (cm)	F_2	90.84	10.00	9.64	145.6 ± 1.54
	F_3	80.61	5.41	4.86	175.40 ± 0.92
	F_4	89.43	4.16	3.94	177.58 ± 1.38
Number of racemes/plant	F_2	92.3	16.62	15.63	7.5 ± 0.16
	F_3	65.10	9.50	7.67	9.7 ± 0.1
	F_4	68.74	10.68	8.85	9.6 ± 0.23
Seed yield/plant (g)	F_2	92.86	30.08	29.55	29.0 ± 0.74
	F_3	97.90	21.25	21.02	36.82 ± 0.65
	F_4	76.58	12.57	11.00	48.12 ± 1.29
Seed oil content (%)	F_3	84.11	4.57	4.26	42.01 ± 0.18
	F_4	84.24	3.72	3.41	44.77 ± 0.32
Days to first flowering	F_3	96.67	5.81	5.71	96.99 ± 0.47
	F_4	97.79	7.07	6.99	88.91 ± 1.08
Days to 50% flowering	F_3	93.50	4.17	4.03	105.24 ± 0.37
	F_4	95.03	3.62	3.53	102.52 ± 0.66
Days to 100% flowering	F_3	95.30	3.96	3.87	111.86 ± 0.37
	F_4	95.87	2.97	2.91	111.03 ± 0.59
1000 seed weight	F_3	86.88	8.34	7.65	3.51 ± 0.03
	F_4	88.41	8.37	7.87	4.04 ± 0.06
Days to physiological maturity	F_3	73.44	1.09	0.93	166.93 ± 0.21
	F_4	93.27	1.57	1.52	161.03 ± 0.46

TABLE 3
Estimates of phenotypic correlation coefficients (r_p) in both F_3 and F_4 generations among all pairs of studied traits.

Trait	Generation	FF	50% F	100% F	PH	No. racemes	Yield	Oil %	1000 SW
50% F	F_3	0.919**							
	F_4	0.937**							
100% F	F_3	0.834**	0.930**						
	F_4	0.726**	0.766**						
PH	F_3	0.301*	0.358*	0.408**					
	F_4	0.096	0.196	0.364*					
No. racemes	F_3	0.199	0.233	0.220	0.097				
	F_4	-0.224	-0.271	-0.212	0.544**				
Yield	F_3	-0.083	-0.072	0.008	0.093	0.416**			
	F_4	-0.437**	-0.405**	-0.528**	0.143	0.344*			
OIL%	F_3	0.133	0.155	0.224	0.450**	-0.006	0.064		
	F_4	-0.312*	-0.193	-0.004	0.052	-0.225	0.269		
1000 SW	F_3	-0.186	-0.136	-0.106	-0.108	-0.323*	-0.063	0.021	
	F_4	-0.290	-0.243	-0.392**	0.409**	0.082	0.366*	0.025	
MAT	F_3	0.133	0.229	0.177	-0.148	-0.206	-0.191	-0.382**	0.244
	F_4	0.558*	0.605**	0.639**	-0.138	-0.296	-0.414**	0.117	-0.764**

*and ** significant at the 0.05 and 0.01 levels of probability, respectively.

TABLE 4
Estimates of genotypic correlation coefficients (r_g) in both F_3 and F_4 generations among all pairs of studied traits.

Trait	Generation	FF	50% F	100% F	PH	No. racemes	Yield	Oil%	1000 SW
50% F	F_3	0.958**							
	F_4	0.954**							
100% F	F_3	0.866**	0.984**						
	F_4	0.747**	0.793**						
PH	F_3	0.345*	0.411**	0.469**					
	F_4	0.255	0.568**	0.969**					
No. racemes	F_3	0.264	0.294	0.292	0.057				
	F_4	-0.254	-0.252	-0.202	0.824**				
Yield	F_3	-0.086	-0.073	0.011	0.107	0.529**			
	F_4	-0.480**	-0.459**	-0.587**	0.143	0.252			
Oil%	F_3	0.142	0.180	0.255	0.534**	-0.037	0.066		
	F_4	-0.349*	-0.196	-0.011	0.098	-0.384**	0.310		
1000 SW	F_3	-0.201	-0.156	-0.105	-0.133	-0.455**	-0.068	0.013	
	F_4	-0.315*	-0.271	-0.415**	0.675**	0.012	0.376**	0.043	
MAT	F_3	0.165	0.244	0.207	-0.196	-0.344*	-0.216	-0.458**	0.260
	F_4	0.581**	0.636**	0.660**	-0.382**	-0.315*	-0.469**	0.118	-0.859**

*and ** significant at the 0.05 and 0.01 levels of probability, respectively.
FF = days to first flowering & 50% F = days to 50% flowering & 100% F = days to 100% flowering & PH = plant height (cm) & No. racemes = number of racemes/plant & Yield = seed yield/plant (g) & 1000-SW = 1000 seed weight (g) & Oil% = seed oil content (%) & MAT = days to physiological maturity.

and positive and highly significant genotypic correlation with 1000 seed weight in F_4 generation. These results are in agreement with those obtained by [31, 32]; whereas highly significant negative correlation with days to first flowering, days to 50% flowering and days to physiological maturity in F_4 generation at phenotypic and genotypic levels. These results are in line with those obtained by [23] who found that all traits showed positive correlation with seed yield/plant at both phenotypic and genotypic levels, except days to 50% flowering and days to maturity. On the contrary, [9] and [33] reported positive and significant correlation between seed yield and days to flowering.

Days to physiological maturity also showed negative significant genotypic correlation coefficient with plant height, number of racemes/plant, seed yield/plant and 1000 seed weight in F_4 generation.

Also, plant height exhibited positive and highly significant correlation with both of number of racemes/plant and 1000 seed weight in F_4 generation at phenotypic and genotypic levels. A strong association for these relationships with high heritability (Table 2) showed that number of racemes/plant and 1000 seed weight should be considered as the most important traits during selection and could play a major role in improving seed

yield/plant in segregated generations, also, plant height in improving number of racemes/plant and 1000 seed weight.

On the other hand, seed oil content was positively and high significantly correlated with plant height in F_3 at phenotypic level and negatively and high significantly correlated with number of racemes/plant in F_4 at genotypic level.

Seed yield/plant showed non-significant positive correlation with plant height and seed oil content in both F_3 and F_4 generations at both phenotypic and genotypic levels. Also, seed oil content exhibited non-significant positive correlation with 1000 seed weight in both F_3 and F_4 generations at the genotypic and phenotypic levels and non-significant negative correlation with number of racemes/plant in F_3 and F_4 at phenotypic level and in F_3 at the genotypic level.

Path coefficient analysis. Association of traits identified by correlation coefficient may not give a clear picture of relative importance of direct and indirect effects of each yield component on seed yield and could not fully explain the relationships among traits. The path coefficient splits the correlation coefficients into direct and indirect through alternative traits or pathways and thus helps to explain the direct and indirect effects on seed yield.

Data from path coefficient analysis presented in Table (5) showed that days to 100% flowering had maximum direct effect on seed yield/plant (0. 481) followed by number of racemes/plant (0.468) in F_3 generation. While, plant height exhibited the highest direct effect on seed yield/plant (0.654) followed by seed oil content (0.354) and days to first flowering (0.255) in F_4 generation.

For days to 100% flowering, data in Table (5) indicated that it had positive indirect effect on seed yield/plant via number of racemes/plant (0.103) followed by plant height (0.033) in F_3 generation and via plant height (0.238) followed by days to first flowering (0.185) and 1000 seed weight (0.157) in F_4 generation.

Days to physiological maturity had positive indirect effect on seed yield/plant in F_3 through days to 100% flowering (0.085) followed by 1000 seed weight (0.017) and via 1000 seed weight (0.305) followed by days to first flowering (0.142) in F_4 generation.

Regarding number of racemes/plant, it had positive indirect effect on seed yield/plant through days to 100% flowering (0.106) in F_3 and via plant height (0.355) followed by days to 100% flowering (0.231) in F_4 generation. The correlation coefficient of number of racemes/plant and seed yield/plant were positive and significant or highly significant at phenotypic level in F_3 and F_4 generations and positive and highly significant at genotypic level in F_3 generation. It is mainly due to the positive direct effect and positive indirect effects of other traits. So, selection would be effective for number of racemes/plant. [20] found that number of racemes/plant in F_3 generation had direct effect on seed yield, so this trait is considered a good criteria for selection in the segregated generations in *Brassica napus* L. breeding program.

Concerning plant height, it had positive indirect effect on seed yield/plant through days to 100% flowering (0.196) followed by number of racemes/plant in F_3 generation (0.045) and via days to physiological maturity (0.033) followed by days to 50% flowering (0.029) and days to first flowering (0.024) in F_4 generation.

TABLE 5
Direct (diagonal) and indirect effects on seed yield/plant through all the studied traits in F_3 and F_4 generations.

Trait	Generation	FF	50% F	100% F	PH	No. racemes	1000-SW	OIL%	MAT	r(Y/P)
FF	F_3	**0.036**	-0.621	0.401	0.024	0.093	-0.013	0.001	-0.004	-0.083
	F_4	**0.255**	0.141	-0.792	0.063	0.023	0.116	-0.111	-0.132	-0.437**
50% F	F_3	0.033	**-0.676**	0.448	0.029	0.109	-0.010	0.001	-0.007	-0.072
	F_4	0.239	**0.150**	-0.835	0.128	0.028	0.097	-0.068	-0.143	-0.405**
100% F	F_3	0.030	-0.629	**0.481**	0.033	0.103	-0.007	0.002	-0.005	0.008
	F_4	0.185	0.115	**-1.091**	0.238	0.022	0.157	-0.001	-0.151	-0.528**
PH	F_3	0.011	-0.242	0.196	**0.081**	0.045	-0.008	0.004	0.005	0.093
	F_4	0.024	0.029	-0.396	**0.654**	-0.056	-0.163	0.018	0.033	0.143
No. racemes	F_3	0.007	-0.158	0.106	0.008	**0.468**	-0.023	0.000	0.006	0.416**
	F_4	-0.057	-0.041	0.231	0.355	**-0.103**	-0.033	-0.080	0.070	0.344*
1000-SW	F_3	-0.007	0.092	-0.051	-0.009	-0.151	**0.070**	0.000	-0.008	-0.063
	F_4	-0.074	-0.036	0.427	0.267	-0.008	**-0.399**	0.009	0.181	0.366*
Oil%	F_3	0.005	-0.105	0.108	0.037	-0.003	0.001	**0.010**	0.012	0.064
	F_4	-0.079	-0.029	0.004	0.034	0.023	-0.010	**0.354**	-0.028	0.269
MAT	F_3	0.005	-0.155	0.085	-0.012	-0.097	0.017	-0.004	**-0.031**	-0.191
	F_4	0.142	0.091	-0.697	-0.090	0.030	0.305	0.041	**-0.237**	-0.414**

FF = days to first flowering & 50% F = days to 50% flowering & 100% F = days to 100% flowering & PH = plant height (cm) &No. racemes = number of racemes/plant &1000 SW = 1000 seed weight (g) & Oil% = seed oil content (%) & MAT = days to physiological maturity.

TABLE 6
Predicted and realized gains from the different selection procedures for improving seed yield (g)/plant in F_3 and F_4 generations.

Selection procedures	Predicted gain F_3			Realized gain F_4			D	Predicted gain F_4		
	i	ii%	iii%	i	ii%	iii%		i	ii%	iii%
I_{W123}	13.94	37.86	93.22	11.31	23.5	100.0	2.63	8.66	18.00	100.0
I_{W1}	14.73	40.01	98.52	11.31	23.5	100.0	3.42	8.66	18.00	100.0
I_{13}	2.14	5.82	14.33	7.84	16.3	69.36	-5.7	6.00	12.47	69.28
Ped. $_W$	14.95	40.61	100.0	11.31	23.5	100.0	3.64	8.66	18.00	100.0
Ped.$_1$	-2.54	-6.90	-16.99	7.84	16.3	69.36	-10.4	6.00	12.47	69.28

$\overline{F}_3 = 36.82$ $\overline{F}_4 = 48.12$
(i) Predicted and realized gains as seed yield (g)/plant.
(ii%) Predicted and realized gains percentage as estimated from generation mean.
(iii%) Predicted and realized gains as a percentage of the response to truncation pedigree selection for seed yield only.
(D) Deviations of realized gains from predicted gains are given as seed yield (g)/plant.

As for seed oil content, it had positive indirect effects on seed yield/plant via plant height (0.034) followed by number of racemes/plant (0.023) in F_4 generation and through days to 100% flowering (0.108) followed by plant height (0.037) in F_3 generation.

In case of 1000 seed weight, it had positive indirect effect on seed yield/plant in F_4 generation through days to 100% flowering (0.427) followed by plant height (0.267) and days to physiological maturity (0.181). Results of path analysis coefficient revealed that selection for number of racemes/plant, plant height, 1000 seed weight and days to 100% flowering would be more effective in improving seed yield/plant in *Brassica napus* L. Similar results were obtained by [31] and [34].

Gain from selection for seed yield/plant. Predicted and realized advances from selection procedures for seed yield alone are summarized in Table (6). The highest predicted genetic advance from F_3 generation and exceeded 35% of the F_3 mean was obtained with the indices ped.$_w$, I_{w1}, and I_{w123}. These indices maintained the same trend in F_4 generation as the highest realized and predicted advances as values and percentages (more than 23% and 18% of F_4 mean, respectively).

Also, means scored and means as percentage for seed yield/plant using five different selection procedures in F_4 (Tables 9 and 10) indicated that all selection procedures increased seed yield/plant over the better parent from 164.3% to 174.4% and the highest predicted genetic advance exhibited the highest mean and means scored by the same highest indices. These results showed that the genetic variations for seed yield in early generations did not be exhausted enough and the improvement of seed yield/plant could be continued in further generations using direct pedigree selection for seed yield/plant and the indices I_{w123} and I_{w1}. The moderate and positive genotypic correlation between seed yield/plant and number of racemes/plant in F_3 and F_4 generation (Table 4) could indicate the direct improvement of seed yield/plant selecting for number of racemes/plant and positive role of this trait included in some indices.

On the other hand, the lowest predicted advance for seed yield/plant was obtained when selection for seed oil content (with ped.$_1$ index) due to negative and low indirect effects on seed yield/plant through the interaction between two traits. These results indicate the importance of direct selection for seed yield. However, direct selection for seed oil content had positive effect on seed yield/plant.

Deviation of the realized advance from the predicted of seed yield/plant using different selection procedures from F_3 to F_4 generations are displayed in Table (6). These deviations were negative for I_{13} and ped.$_1$ indices which illustrate that the realized gain in F_4 exceeded the predicted gain in F_3. This could be due to the high estimates of heritability for most of the studied traits in both generations. These results are in line with the opinion of the possibility to continue improving seed yield/plant in further generations. These results are in agreement with those obtained by [4, 19, 21, 23, 25, 26, 34, 35, 36].

Gain from selection for selected seed oil content, plant height and number of racemes/plant. Regarding to seed oil content (Table 7), the highest predicted genetic advance in in F_3 (more than 6%) and F_4 (more than 3.5%) generation was obtained with the indices I_{13} and ped.$_1$. Also, the high predicted genetic advances in F_4 combined with high mean scored and mean as percentage value over the better parent applying five different selection procedures in F_4 (Tables 9 and 10) indicate the possibility to the continued improvement for this trait in further generations using direct pedigree selection for seed oil content. [37] recorded high genetic advance for seed oil content.

For number of racemes/plant (Table 7), F_4 mean was lower than F_3 mean, also, mean scored and mean as percentage value did not exceeded the better parent using selection index involving seed oil content and number of racemes/plant (I_{13} index) and pedigree selection for seed oil content (ped.$_1$) in

F_4 (Tables 9 and 10). This may be due to the negative and highly significant genotypic correlation between seed oil content and number of raceme/plant in F_4 generation. Predicted genetic advance in F_3 for ped.$_1$ index exhibited negative value. However, in F_4 generation predicted response increased for this index, this increasing combined with relatively higher heritability than F_3 could support the idea of the possibility to improve this trait from F_4 generation using this selection index. Similar results were obtained by [37] and [34].

In respect to plant height (Table 7), predicted genetic advance in F_3 were higher than F_4 using I_{w123}, I_{13} and ped.$_1$ indices, and mean scored and mean as percentage using three different selection procedures in F_4 (Tables 9 and 10) revealed that I_{w123}, I_{w1} and ped.$_w$ selection procedures increased plant height to 102.01%. These results indicate that most of the genetic variations for plant height were exhausted in F_3 generation using these selection procedures, Also, the higher value for F_4 generation mean than F_3 one confirm this result. The I_{w123} index exhibited the highest predicted response in F_3, while I_{w123}, I_{w1} and ped.w in F_4 generation for plant height improvement. These results are in agreement with those obtained by [19, 26, 35, 36].

Gain from selection for unselected traits. Predicted gain for unselected traits from five selection procedures are presented in Table (8). Regarding days to first flowering, days to 50% flowering and days to 100% flowering, selection index involving in seed yield/plant and oil seed content exhibited the highest values of predicted gains for these traits in F_3 generation. Also, I_{13} index and pedigree selection for seed oil content gave the highest values of predicted gain for these traits in F_4 generation. These results could be attributed to the high and negative genotypic correlation between oil seed content and days to first flowering and days to 100% flowering.

TABLE 7
Predicted responses to selection by using five different selection procedures which estimated from F_3 and F_4 means for seed oil content, plant height and number of racemes/plant.

Selection procedures	Seed oil content				Plant height				No. racemes			
	Predicted response F_3		Predicted response F_4		Predicted response F_3		Predicted response F_4		Predicted response F_3		Predicted response F_4	
	i	ii%	i	ii%	i	ii%	i	ii%	i	ii%	i	ii%
I_{W123}	1.12	2.66	0.45	1.00	7.28	4.15	4.32	2.43	0.56	5.77	0.44	4.56
I_{W1}	0.46	1.11	0.45	1.00	2.90	1.65	4.32	2.43	0.46	4.74	0.44	4.56
I_{13}	2.69	6.40	1.61	3.59	5.77	3.29	-4.77	-2.68	0.16	1.69	0.06	0.62
Ped.$_w$	-0.09	-0.21	0.45	1.00	2.72	1.55	4.32	2.43	0.38	3.89	0.44	4.56
Ped.$_1$	2.97	7.07	1.61	3.59	5.95	3.39	-4.77	-2.68	-0.22	-2.31	0.06	0.62
X_0	$\bar{F}_3$ = 42.01		$\bar{F}_4$ = 44.77		$\bar{F}_3$ = 175.4		$\bar{F}_4$ = 177.58		$\bar{F}_3$ = 9.7		$\bar{F}_4$ = 9.6	

TABLE 8
Predicted responses to selection by using five different selection procedures which estimated from F_3 and F_4 means for unselected traits.

Selection procedures	Days to first flowering				Days to 50% flowering				Days to 100% flowering			
	Predicted response F_3		Predicted response F_4		Predicted response F_3		Predicted response F_4		Predicted response F_3		Predicted response F_4	
	i	ii%	i	ii%	i	ii%	i	ii%	i	ii%	i	ii%
I_{W123}	-0.56	-0.58	-1.87	-2.10	-0.40	-0.38	-0.96	-0.94	0.33	0.29	-2.11	-1.90
I_{W1}	-2.11	-2.17	-1.87	-2.10	-1.33	-1.27	-0.96	-0.94	-0.63	-0.56	-2.11	-1.90
I_{13}	1.95	2.01	-8.39	-9.43	0.35	0.33	-5.08	-4.96	0.71	0.63	-4.66	-4.20
Ped.$_w$	-1.91	-1.97	-1.87	-2.10	-1.33	-1.27	-0.96	-0.94	-0.44	-0.39	-2.11	-1.90
Ped.$_1$	3.89	4.01	-8.39	-9.43	1.85	1.76	-5.08	-4.96	1.66	1.48	-4.66	-4.20
X_0	$\bar{F}_3$ = 96.98		$\bar{F}_4$ = 88.91		$\bar{F}_3$ = 105.22		$\bar{F}_4$ = 102.52		$\bar{F}_3$ = 111.86		$\bar{F}_4$ = 111.03	

Selection procedures	1000 seed weight				Days to physiological maturity			
	Predicted response F_3		Predicted response F_4		Predicted response F_3		Predicted response F_4	
	i	ii%	i	ii%	i	ii%	i	ii%
I_{W123}	-0.04	-1.27	0.27	6.76	-1.07	-0.64	-1.58	-0.98
I_{W1}	0.02	0.55	0.27	6.76	-0.53	-0.32	-1.58	-0.98
I_{13}	-0.17	-4.86	0.12	2.99	-2.00	-1.20	-2.05	-1.27
Ped.$_w$	-0.03	-0.74	0.27	6.76	-0.39	-0.23	-1.58	-0.98
Ped.$_1$	0.02	0.45	0.12	2.99	-1.52	-0.91	-2.05	-1.27
X_0	$\bar{F}_3$ = 3.51		$\bar{F}_4$ = 4.04		$\bar{F}_3$ = 166.93		$\bar{F}_4$ = 161.03	

TABLE 9
Means scored by using five different selection procedures for studied traits in F_4 generation.

Trait / Method	FF	50% F	100% F	PH	No. racemes	Yield	1000 SW	Oil %	MAT
I_{W123}	87.00	101.50	108.83	182.42	10.23	59.43	4.35	45.30	159.33
I_{W1}	87.00	101.50	108.83	182.42	10.23	59.43	4.35	45.30	159.33
I_{13}	80.33	97.17	106.17	172.25	9.68	55.96	4.18	46.68	158.83
Ped. $_W$	87.00	101.50	108.83	182.42	10.23	59.43	4.35	45.30	159.33
Ped.$_1$	80.33	97.17	106.17	172.25	9.68	55.96	4.18	46.68	158.83
BP	86.33	101.67	107.33	178.83	9.93	34.06	4.21	43.40	161.67

TABLE 10
Means as a percentage from better parent scored by using five different selection procedures for studied traits in F_4 generation.

Trait / Method	FF	50% F	100% F	PH	No. racemes	Yield	1000 SW	Oil %	MAT
I_{W123}	100.78	99.83	101.40	102.01	103.02	174.49	103.33	104.38	98.55
I_{W1}	100.78	99.83	101.40	102.01	103.02	174.49	103.33	104.38	98.55
I_{13}	93.05	95.57	98.92	96.32	97.48	164.30	99.29	107.56	98.24
Ped. $_W$	100.78	99.83	101.40	102.01	103.02	174.49	103.33	104.38	98.55
Ped.$_1$	93.05	95.57	98.92	96.32	97.48	164.30	99.29	107.56	98.24

FF = days to first flowering & 50% F = days to 50% flowering & 100% F = days to 100% flowering & PH = plant height (cm) & No. racemes = number of racemes/plant & Yield = seed yield/plant (g) &1000 SW = 1000 seed weight (g) & Oil % = seed oil content (%) & MAT = days to physiological maturity.

TABLE 11
Characteristics of the two selected families from F_4 generation for seed yield/plant improvement.

Trait / Family	FF	50% F	100% F	PH	No. racemes	Yield	1000 SW	Oil %	MAT
4	86.33	101.33	108.33	172.67	9.23	62.15	4.09	47.01	160.33
10	87.67	101.67	109.33	192.17	11.23	56.71	4.6	43.6	158.33
BP	86.33	101.67	107.33	178.83	9.93	34.06	4.21	43.40	161.67

Bp = better parent

TABLE 12
Characteristics of the two selected families from F_4 generation for oil seed content improvement.

Trait / Family	FF	50% F	100% F	PH	No. racemes	Yield	1000 SW	Oil %	MAT
4	86.33	101.33	108.33	172.67	9.23	62.15	4.09	47.01	160.33
5	74.33	93.0	104.0	171.83	10.13	49.77	4.26	46.35	157.33
BP	86.33	101.67	107.33	178.83	9.93	34.06	4.21	43.40	161.67

Bp = better parent
FF = days to first flowering & 50% F = days to 50% flowering & 100% F = days to 100% flowering & PH = plant height (cm) & No. racemes = number of racemes/plant & Yield = seed yield/plant (g) &1000 SW = 1000 seed weight (g) & Oil% = seed oil content (%) & MAT = days to physiological maturity.

On the other hand, F_4 means were lower than F_3 means for these traits, also, means scored and means as percentage using two selection procedures in F_4 (Tables 9 and 10) revealed that these two selection procedures decreased number of days to first flowering, days to 50% flowering and days to 100% flowering over the better parent in F_4 generation from 100.78% to 93.05%, from 99.83% to 95.57% and from 101.40% to 98.92%, respectively. It is worth mentioning that the lower values of predicted gain are more desirable than the higher. These results confirm the possibility to improve these traits in further generations using pedigree selection for seed oil content and the index I_{13}.

For 1000-seed weight, selection index involving in seed yield/plant and seed oil content (I_{w1}) exhibited the highest predicted gain in F_3 generation and I_{w123}, I_{w1} and ped.$_w$ in F_4 generation. These results could be attributed to the high and positive genotypic correlation between 1000-seed weight and seed yield/plant and seed oil content (Tables 3 and 4). This means that 1000-seed weight could be improved using direct selection for seed yield/plant and seed oil content. Most of the predicted responses for 1000-seed weight in F_3 were negative, but, were positive in F_4 generation. Also, the high predicted genetic advance in F_4 combined with high mean scored and mean as percentage value over the better parent using the three different selection pro-

cedures (direct pedigree selection for seed yield/plant and the indices I_{w123} and I_{w1}) in F_4 generation (Tables 9 and 10) confirm the possibility to improve this trait in further generations using these indices.

On the other hand, the high heritability estimates for these traits (Table 2) along with high genetic advance (Tables 6, 7 and 8) is more useful in predicting the selection efficiency than heritability alone. These results are in agreement with those obtained by [37] who found high heritability coupled with high genetic advance for seed oil content and number of races/plant, Also, [38] reported high heritability in conjunction with high genetic advance for days to flowering, [21] and [35] observed high heritability associated with high genetic advance for plant height and seed yield/plant, [34] recorded high heritability along with high genetic advance for seed yield/plant, 1000-seed weight and number of racemes/plant, indicating the role and existence of additive gene action in inheritance of these traits and the selection for these traits is expected to be more effective in improvement of these traits in further segregated generations.

Based on selection procedures in F_3 and F_4 generations and the characteristics of the selected families from F_4, presented in Tables (11 and 12), the families number 4 and 10 is considered the best for seed yield improvement and the families 4 and 5 is the best for oil seed content improvement. Data in Tables (11 and 12) confirms that the family 4 is very important for improvement of both seed yield/plant and seed oil content as it includes the best values for seed yield/plant and seed oil content. This study recommends plant breeders with these families for using in breeding programs.

Finally, maximum gains for seed yield/plant were maintained from F_3 generation to F_4 generation when applying of selection indices. However, pedigree selection for seed yield/plant and pedigree selection for oil seed content would appear to be most effective for improvement of seed yield/plant and seed oil content, respectively.

REFERENCES

[1] Bybordi, A. (2010) Effect of salinity on yield and component characters in canola (Brassica napus L.) cultivars. Not. Sci. Biol. 2, 81-83.

[2] Weiss, E.A. (1983) Oil seed crops. Longman Group Limited. 161-215

[3] FAS, USADA (2018) Foreign Agric. Service, United State Dept., Agric. 2018.

[4] Ali, I., Ahmed, H.M. and Shah, S.A. (2013) Evaluation and selection of rapeseed (*Brassica napus* L.) mutant lines for yield performance using augmented design. The Journal of Animal and Plant Sciences. 23(4), 1125-1130.

[5] Singh, R.K. and Chowdhury, B.D. (1985) Biometrical method in quantitative genetic analysis. 2nd Ed. Kalyani Publishers, Ludhiana, New Delhi, India, 54-57.

[6] Shukla, S., Bhargava, A., Chatterjee, A., Srivastava, A. and Singh, S.P. (2006) Genotypic variability in vegetable amaranth (*Amaranthus tricolor* L.) for foliage yield and its contributing traits over successive cuttings and years. Euphytica. 151, 103-110.

[7] Akbar, M., Mahmood, T., Yaqub, M., Anwar, M., Ali, M. and Iqbal, N. (2003) Variability, correlation and path coefficient studies in summer mustard (*Brassica juncea* L.). Asian J. Pl. Sci. 2, 696-698.

[8] Falconer, D.S. (1998) Introduction to quantitative genetics. Ronald Press, New York.

[9] Ali, N., Javidfar, F., Elmira, J.Y. and Mirza, M.Y. (2003) Relationship among yield components and selection criteria for yield improvement in winter rapeseed (*Brassica napus* L.). Pakistan J. Bot. 35(2), 167-174.

[10] Farshadfar, E., Galiba, G., Kozsegi, B. and Sutka, J. (1993) Some aspects of the genetic analysis of drought tolerance in wheat. Cereal Research Communications. 21, 323-330.

[11] Dewey, D.R. and Lu K.H. (1959) A correlation and path coefficient analysis of components of crested wheat grass seed production. Agron. J. 51, 515-518.

[12] A.O.A.C. (1990) Association of Official Agriculture Chemists, Official Methods of Analysis. 13th ed. Washington D.C., USA.

[13] Walker, J.T. (1960) The use of a selection index technique in the analysis of progeny row data. Emp. Cott. Gr. Rev. 37, 81-107.

[14] Burton, G.W. (1952) Quantitative inheritance in grasses. Proc. 6th Internat. Grassland Congr. 1, 277-283.

[15] Smith, H.F. (1936) A discriminant function for plant selection. Ann. Eugenics. 7, 240-250.

[16] Hazel, L.N. (1943) The genetic basis for constructing selection indices. Genetics. 28, 476-490.

[17] Miller, P.A. and Rawlings, J.O. (1967) Selection for increased lint yield and correlated responses in upland cotton, Gossypium hirsutum L. Crop Sci. 7, 637-640.

[18] Robinson, H.F., Comstock, R.E. and Harvey, P.H. (1951) Genetic and phenotypic correlations in corn and their implications in selection. Agron. J. 43, 283-287.

[19] Fahmy, R.M., El-Sharayhi, R.E.A. and Sedeck, F.Sh. (2014) Genetic evaluation and correlation coefficients of yield and yield components for segregating generations in canola. Egypt. J. Plant Breed. 18(3), 467 – 481.

[20] Sadat, H.A., Nematzadeh, G.A., Jelodar, N. B. and Chapi, O.G. (2010) Genetic evaluation of yield and yield components at advanced generations in rapeseed (*Brassica napus* L.). African Journal of Agricultural Research. 5(15), 1958-1964.
[21] Fahmy, R.M., Ahmed, F.H.A. and El-Sharayi, R.E.A. (2013) Genetic Variability, Heritability and Correlation Coefficients of Yield and Yield Components in Canola. Egyptian Journal of Plant Breeding. 17(2), 181-202.
[22] Khan, F.U., Uddin, R., Khalil, I.A., Khalil, I.H. and Ullah, I. (2013) Heritability and Genetic Potential of Brassica Napus Genotypes for Yield and Yield Components. American-Eurasian J. Agric. and Environ. Sci. 13(6), 802-806.
[23] Bind, D., Singh, D. and Dwivedi, V.K. (2014) Genetic variability and character association in Indian mustard [*Brassica Juncea* (L) CZERNS & COSS]. Agric. Sci. Digest. 34(3), 183–188.
[24] Shekhawat, N., Jadeja, G.C. and Singh, J. (2014) Genetic variability for yield and its components in indian mustard (*Brassica juncea* L. Czern & Coss). Electronic Journal of Plant Breeding. 5(1), 117-119.
[25] Akabari, V.R. and Niranjana, M. (2015) Genetic variability and trait association studies in Indian mustard (*Brassica juncea*). International Journal of Agricultural Sciences. 11(1), 35-39.
[26] Bibi, T., Rauf, S., Mahmood, T., Haider, Z. and Salah-ud-Din (2016) Genetic Variability and Heritability Studies in Relation to Seed Yield and its Component Traits in Mustard (*Brassica Juncea* L.). Academia Journal of Agricultural Research. 4(8), 478-482.
[27] Elnenny, E.M.M., Abd EL-Satar, M.A. and Ahmed, F.H.A. (2015) Genetic variability, selection criteria and genetic divergence in some canola genotypes. Egypt. J. Plant Breed. 19(7), 2081– 2097.
[28] Singh, A., Avtar, R., Singh, D., Sangwan, O. and Balyan, P. (2013) Genetic variability, character association and path analysis for seed yield and component traits under two environments in Indian mustard. Journal of Oilseed Brassica. 4(1), 43-48.
[29] Tripathi, N., Kumar, K. and Verma, O.P. (2015) Genetic Variability, Heritability and Genetic Advance in Indian Mustard (*Brassica juncea* L. Czern and Coss.) for Seed yield and it's Contributing Attributes Under Normal and Saline/Alkaline Condition. International Journal of Science and Research. 4(8), 2319-7064.
[30] Yadav, N.P., Kumar, B. and Singh, U.K. (2017) Utilization of Genetic Variability for Yield Improvement in Indian mustard (*Brassica Juncea* L.) Under Medium Land Condition. Chem Sci Rev Lett. 6(23), 2063-2067.
[31] Tahira, Mahmood, T., Tahir, M.S., Saleem, U., Hussain, M. and Saqib, M. (2011) The estimation of heritability, association and selection criteria for yield components in mustard (*Brassica Juncea*). Pak. J. Agri. Sci. 48(4), 251-254.
[32] Tiwari, A.K., Singh, S.K., Tomar, A. and Singh, M. (2017) Heritability, genetic advance and correlation coefficient analysis in Indian mustard (*Brassica Juncea* (L.) Czern & Coss). Journal of Pharmacognosy and Phytochemistry. 6(1), 356-359.
[33] Maurya, N., Singh, A.K. and Singh, S.K. (2012) Inter-relationship analysis of yield and yield components in Indian mustard, *Brassica juncea* L. Indian Journal of Plant Sciences. 1(2-3), 90-92.
[34] Lodhi, B., Thakral, N.K., Avtar, R. and Singh, A. (2014) Genetic variability, association and path analysis in Indian mustard (*Brassica juncea*). Journal of Oilseed Brassica. 5(1), 26-31.
[35] Uzair, M., Shahzadi, I., Jatoi, G.H., Bibi, T., Rauf, S., Mahmood, T. and Salah-ud-Din (2016) Genetic variability and heritability studies in relation to seed yield and its components traits in mustard (*Brassica Juncea* L.). Sci. Int. (Lahore). 28(4), 4267-4270.
[36] Lyngdoh, Y., Kanaujia, S.P. and Shah, P. (2017) Genetic variability, characters association and path coefficient analysis in green mustard (*Brassica juncea* L.) genotypes. International Journal of Recent Scientific Research. 8(8), 19388-19391.
[37] Ghosh, S.K. and Gulati, S.C. (2001) Genetic variability and association of yield components in Indian mustard (*Brassica juncea* L.) Crop Res. Hisar. 21(3), 345-349.
[38] Singh, D., Mishra, V.K. and Singh, R.P. (2003) Studies on heritability and genetic advance of seed yield and its components in yellow sarson (*Brassica campestris* Linn. var. yellow sarson Prain). Agric. Sci. Digest. 23(1), 69 –70.

Received: **02.10.2018**
Accepted: **31.12.2018**

CORRESPONDING AUTHOR

Alaa Eldin Shaheen
Oil Crops Research Department,
Field Crops Research Institute,
Agricultural Research Center.
Cairo – Egypt

e-mail: alaa.shaheen18@yahoo.com

© by PSP Volume 28 – No. 5/2019 pages 3756-3767 Fresenius Environmental Bulletin

THE VISUAL QUALITY EFFECTS OF HISTORICAL BUILDING GARDENS ON URBAN TEXTURE IN THE SUSTAINABLE LANDSCAPE

Kubra Yazici[1,*], Bahriye Gulgun Aslan[2]

[1]Tokat Gaziosmanpasa University, Faculty of Agriculture, Department of Horticulture, 60240, Tokat, Turkey
[2]Ege University, Faculty of Agriculture, Department of Landscape Architecture, 35040, Izmir, Turkey

ABSTRACT

Historical surroundings are places that consist of urban details and building groups which need to be preserved and used due to their physical homogeneity, long history together with cultural, social, economic, archeological and aesthetic values. Places with historical and cultural heritage in rapidly growing and changing cities, lose their unique identities and legibility in time and become a body of undefined locations. Therefore, policies intended to preserve and develop that actively include urban landscape designing in every step, should be planned in historical city centers. The study area was chosen as Sivas (Turkey) due to its rich historical past and urban identity shaped by this history. In this study, 19 historical structures from different periods with various qualities and usages were evaluated. The aim of this study was to preserve the cultural values qualitatively and quantitatively in terms of environment and city, while contributing to tourism. Polls with designated parameters were conducted on specialists; and the contribution of historical surroundings to the urban identity, green areas and city structure were defined. The data gathered from these polls were used in a Q-SORT analysis to evaluate the relationship between historical structures and environment. Another evaluation was done with a SWOT analysis on the contribution of historical structures to the belief and memoir tourism. As a result of this study, differences between study areas in which these 19 historical structures were evaluated and open-green area existence, were identified. Suggestions were given on the preservation and development of the quality and quantity of cultural values with regards to a sustainable environment and urban ecology.

KEYWORDS:
Urban Character, Historical Texture, City Landscaping, Urban Ecology

INTRODUCTION

A city is a place, an establishment where various technical, economic, social, political and cultural subjects exist together [1, 2]. These establishments differ from each other as they are formed by various cultural and social structures. These different characters of cities are defined by notions like "urban identity", "urban profile" or "urban image" [3, 4]. An urban identity shapes up in a long period of time. It forms the city as a mixture of its geographical content, cultural level, architecture, local customs, lifestyle and qualifications [5]. Urban identity is also defined as traits and factors exclusive to that city which help distinguish it from the other ones [6]. Apart from its physical environment, a city's social, cultural, economic and political components also add different qualities to the urban identity [7].

Parts that form the urban identity can be evaluated with the factors derived from the natural and man-made environment. Natural beauties and sceneries, historical and cultural values are significant assets surrounding the humankind. Natural and historical environmental values together with sociological and cultural factors, shape the beginning and limiting conditions of human behavior and make the cities possess unique traits. Identity factors derived from the natural environment are the traits like topographical condition, climate conditions, vegetation and general location of the city [8, 9]. Identity of a city is not only the physical environment. Urban identity is shaped socially. Identity elements derived from the humane environment are formed together with the identity of self and city, natural environment and all the human influence existing in the city [10, 11]. Each element has its unique character and identity. Therefore, all the elements taking part in the formation of the city, shape up the urban identity by affecting it positively or negatively. In this context, all the elements and factors that carried the city from past times to our day, have their own effects on the identity.

The aim of preserving and renovating the historical environment is to establish historical and cultural sustainability, reviving the historical environment in a healthy way while protecting its iden-

tity in accordance with modern living conditions, putting the historical places that are currently idle as building inventory into good use, preserving the city landscaping and protecting the conventional settlement model. Therefore, works aimed at conservation conducted in cultural environments that are going through change and transformations are important in terms of sustaining the physical and social structure. In all of city landscaping or only in some parts of it, historical elements that are located inside the settlement area should thought in accordance with the surrounding open-green areas. The aim of this study is to put forward the contribution of the historical elements located in the city center of Sivas to the urban fabric and open-green spaces.

Within the scope of this study, the aim was to preserve the cultural values qualitatively and quantitatively in terms of environment and city, while contributing to tourism. Many methods can be used to evaluate and historical buildings. In this study, Q sort analysis and SWOT analysis were used to analyze the visual quality and to determine the important criteria of each cultural values and to evaluate ecotourism potential.

Q- Sort analysis or Q factor analysis as it is named in the foreign literature, is a relatively new tool not only as approach but particularly following the quite recent rediscovery of its usefulness in those fields where psychometric knowledge of individuals has thorough implications [12, 13]. Concordantly, Q-Sort analysis was conducted for historical building and environmental protection notions and the relationship between these notions and landscape designing and its criteria. Another SWOT analysis was done for determining and developing existing tourism sources. SWOT analysis; environmental analysis is a critical part of the strategic management planning process. The SWOT (Strengths, Weaknesses, Opportunities and Threats) framework is proposed by many as an analytical tool which should be used to categorize significant environmental factors both internal and external to the organization. SWOT analysis has been praised for its simplicity and practicality. As a framework it has been widely adopted but, generally, its use has been accepted uncritically. It is timely to reappraise its value as a strategic management tool [14].

There were studies showing that areas with architectural aspects compatible with the nature in terms of vegetation, fabric, color and form together with characterizing the aesthetic and visual aspects of water in landscaping; increase the visual quality and are preferable to the users in recreational objectives [15, 16]. According to [17]; visual quality studies should be used as an important leading tool in planning and designing rural and urban areas in terms of the visual data created by the changes in physical environment. They should also be used in forming some of the administrative policies. Criteria for monitoring and defining the landscaping in survey forms used in reviewing the visual landscaping evaluation as published in the Scotland Natural Heritage Environmental Evaluation guidebook [18]: Visible physical components: land form, land cover, utilities on the land, water existence, forest land, coppices, woodlands, agricultural areas, animals, settlements, other usages of the land (like area or city parks), linear features (highways or coastal line) or point features (like castles of monuments

According to [19], the urban landscape is not just an issue of urban design, but also planning and the issue of values, human goals, and recognition of social responsibilities by the whole society are of high importance [20]. In Lynch's opinion, three factors of perceptive, physical and operational ones in urban landscape are significant [21]. He rendered the concept of city's image by publishing a book entitled as « The Image of the City ». Lynch described subjective aspects of the urban landscape in this book; thus, if Cullen emphasized more on the objective aspects, Lynch had an emphatic focus on its subjective aspects [6]. According to [20] the urban landscape is the triple integration of objective landscape, subjective landscape and emotional landscape of the city which is the basis of behavior. In general, urban landscape is the result of the human contact level with the city and in this regard, not only do human beings affect the structure of the visual vista of the city through their activities on the urban landscape, the behavior and subjective perception of citizens are affected by contact with the urban landscape [23].

[24]; Visual Q methodology is particularly suited for the assessment of such perceived impact of photovoltaic systems. A selection (concourse) of landscape images with photovoltaic elements was collected and used during this Q-sort analysis. The final Q sample included 54 images of various photovoltaic plants in urban and rural settings. The P set was composed of 34 participants, including landscape and photovoltaic professionals. This analysis identified three distinctive factors that are representative of the different viewpoints on the integration of photovoltaic systems within the urban and rural landscapes. We conclude with a discussion of the wider land-use policy implications of this analysis.

According to [25]; the remaining 18 landscape scenes formed the last ‘Mixed’ class and used Q-sort analysis. Scores of for each photograph were summed across participants and an average urbanization score was calculated. These means determined to which class of urbanization each photograph was assigned. However, a number of photographs seemed to balance between two categories (scores close to e.g., 1.5, 2.5 etc.) and could therefore not be unequivocally assigned to one class.

[26], the Derak district of Shiraz city was selected as a case study area using Photo grid method and then all high-rise buildings in this area were

identified and analyzed. Aesthetic preferences data were evaluated by Q-SORT method with the psychophysical approach. Eventually, aesthetic factors have been presented in two main categories: 'primary and distinctive'. Findings lead to the development of APPD model which suggests that when the landscape design of a building moves toward distinctive factors, the degree of its aesthetic preferences increases.

According to [27], the significant wetlands in the immediate vicinity of Sivas were used as material with a holistic view. These wetlands are located to the north of Sivas are Hafik Lake (Kochisar Lake), Lota Lakes and Todurge Lake (Demiryurt Lake). The images representing the condition of the study area together with the necessary information and the score card, were submitted to the experts for their evaluation. The aim of this study was to find out wetlands of landscape photographs in terms of potential differences (water property size, plant existence, topographic diversity, neighbors views, natural elements, cultural existence) and was to develop sustainable recreational areas in terms of visual preferences with Q-sort analysis.

Q-Sort analysis method was used for this study and the mentioned historical building in Sivas city (Turkey). They were considered to be important in the close vicinity of Sivas were; Ulu Mosque, Sifaiye Madrasah, Buruciye Madrasah, Cifte Minareli Madrasah, Gok Madrasah, Divrigi Ulu Mosque and Darussifası, Abdulvahap Gazi Shrine, Seyh Hasan Bey Kumbet, Ahi emir Ahmed Shrine, Behram Pasa Han, Kursunlu Baths, Tashan, Ziyabey Library, Government mansion, Gendarmerie Building, Ataturk Congress and Ethnography Museum, İnonu Museum, Gurun (Surp Kevork) Church, Meydan Baths. The aim of this study was to evaluate the visual landscaping quality, ecotourism usage potential, the urban ecology effects of the historical buildings. Therefore, Some parameters were examined (pressure of other buildings in the surroundings, dominance in area (focus center), building restoration, the amount of green area the in historical building, perceptibility, guidance to historical building, accessibility). A second aim of our study, these historical buildings was to bring suggestions to protect in sustainable landscape with SWOT analysis.

MATERIALS AND METHODS

Materials. The material of this study was Sivas historical city center with an area of 500 hectares (ha) which has been the home for many different civilizations in many different eras (Roman, Anatolian Seljuk, Beyliks, Ottoman and Republic periods) and was a religious, governmental, scientific and commercial center in which many different cultures settled. Communities that ruled over Sivas throughout the history in different eras, had given the city different names exclusive to themselves. These are; Sebaste, Sipas, Megapolis, Kabira, Diaspolis, Talaurs, Danishmend City, State of Greeks, State of Sivas and Sivas. Another opinion is that the name of 'Sivas' used today was derived from the previous name 'Sipas'. During the times in which the city was first established, there were three water sources under tall sycamores in the same place where the center of the city is located today.

During the Seljuk Period, Sivas had evolved into one of the most important centers of the era as one of the intersection points of regional and national trade routes. Especially the many commercial structures built around Kayseri, Malatya and Tokat show how vibrant and effective was the Sivas based business life. It appears that with the construction of Sifaiye Madrasa, the housing texture to the south and east of Toprakkale had started to spread to the north. The rules of foundation belonging to Sifaiye Madrasa building was also accepted for other buildings.

This study deals with historical artifacts located in the city center of Sivas and are important and accessible in terms of faith and culture tourism (Table 1*)*. However, Gurun church which is still standing in Gurun, even though it had not been renovated in any way, was also another subject of this study. Data and documents on the artifacts were gathered from [28] and [29]. The reason for choosing the historical buildings that are subject to this study, is that because they are structures easily accessible by tourists and they also contribute to the urban identity.

Methods. 19 works belonging to different periods with different qualifications and applications are reviewed in this study. The contribution of historical environments to urban identity, urban open-green areas and city structure are gathered by surveys conducted by experts using designated parameters.

The data obtained are evaluated with a Q-Sort analysis for the relationship between the historical buildings and the environment. In terms of the contribution to the faith and memoir tourism in the city, a SWOT analysis is used for reviewing the data. As a result of the study, the difference between the study areas in which 19 works are reviewed and the open-green area existence, are detected. Suggestions are put forward on the preservation and development of cultural values both in terms of quality and quantity with regards to sustainable environment and city culture (Figure 1).

TABLE 1
Location and general features of the historic buildings

Name	Location	Current State	Construction Period
Ulu Mosque	in the green area	Mosque	Anatolian Seljuk
Sifaiye Madrasah	in the green area	In repair	Anatolian Seljuk
Buruciye Madrasah	Seljuk park	The Muftis	Anatolian Seljuk
Cifte Minareli Madrasah	in the green area	Depends on the directorate of the foundations	Anatolian Seljuk
Gok Madrasah	in the green area	Restoration	Anatolian Seljuk
Divrigi Ulu Mosque and Darussifası	in the green area	Mosque	Anatolian Seljuk
Abdulvahap Gazi Shrine	in the green area	Cemetery	Ottoman Empire
Seyh Hasan Bey Kumbet	Inside the park	Depends on the directorate of the foundations	Eretna seigniory
Ahi emir Ahmed Shrine	In the middle of the street	Depends on the directorate of the foundations	1333
Behram Pasa Han	in the green area	Relive restoration	Ottoman Empire
Kursunlu Baths	in the green area	Currently baths	Ottoman Empire
Tashan	On the street	Trade	Ottoman Empire
Ziyabey Library	On the street	Library	Ottoman Empire
Government Office	City center	Governorship	Ottoman Empire
Gendarmerie Building	City center	General Command of Gendarmerie	Ottoman Empire
Ataturk Congress and Ethnography Museum	Inside the park	Museum	Ottoman Empire
İnonu Museum	On the road	Museum	Ottoman period
Gurun (Surp Kevork) Church	On the street	İdle build	Ottoman Empire
Meydan Baths	On the street	Baths	Ottoman Empire

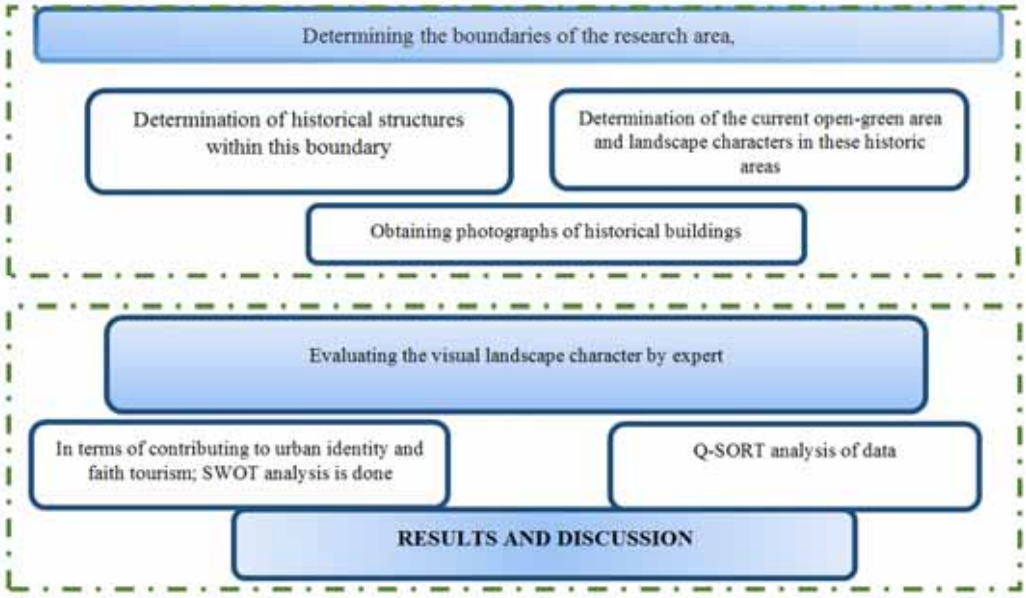

FIGURE 1
Work flow diagram

SWOT analysis is a method used for detecting the advantages and disadvantages of a product against its competitors, determining the opportunities and threats the company may encounter regarding the products and using the data obtained in strategic marketing plans. SWOT analysis also enables us to focus on our strong sides that have the potential to present many great opportunities. This analysis method is used in the strategic planning phase and problem identifying/solution forming phases when quantitative data is inadequate. The word "SWOT" is formed by the initials of four English words; Strengths, Weaknesses, Opportunities and Threats. SWOT analysis can also be used in determining the tourism politics of a country by revealing inner (strong and weak sides) and outer (opportunities and threats) factors of that country's tourism potential [30].

On the other hand, in Q-Sort analysis; the data obtained from questionnaires of every 30 expert for each of the 19 images was recorded and divided for each of the 19 historical buildings, studied, evaluated and pointed numerically (very beautiful +2, beautiful +1, ordinary 0, ugly -1, and very ugly -2) and the results of this study were set in a separate table. The number of experts is obtained by the data of landscape architects living in Sivas according to UCTEA Chamber of Landscape Architects. So, the points every landscape character (pressure of other buildings in the surroundings, dominance in area (focus center), building restoration, the amount of green area the in historical building, perceptibility, guidance to historical building, accessibility) got based on experts' opinions, was calculated (Table 2). High points of every historical building suggest photo's desirability and higher priorities of public preferences. In order to calculate the points for each photograph, the following method was used: Scoring was done for each building according to five-point Likert scale as +2, +1, 0, -1, -2 and the recreationally significant areas are designated by a Q-Sort analysis. While in the analysis the general landscaping integrity of the historical buildings and their contribution to urban identity is pointed, the second phase of the study contains the analysis of landscape character.

TABLE 2
Urban identity used parameters and scoring for determination of historical buildings in Sivas city [33].

Points Criteria	+2	+1	0	-1	-2
pressure of other buildings in the surroundings	No buildings around	Less evident	Evident	Dominant	Very dominant
Dominance in area (focus center)	Very evident	Evident	In the middle	Less evident	Not at all clear
Building restoration	Very well-kept	Well-groomed	In the middle	Less well-groomed	Neglected
The amount of green area the in historical building	Very dominant green area	Dominant green area	Balanced green area and structural elements	Dominant structural elements	Very dominant structural elements
Perceptibility	Very visible	Visible	In the middle visible	Less visible	It's not visible
Guidance to historical building	Very adequate	Enough	Indecisive	Little enough	Inadequate
Accessibility	Very easy	Easy	In the middle	Difficult	Very difficult

TABLE 3
Determination of contribution to city identity of historical buildings and assessment of the "pressure of other buildings in the surroundings" parameter

The number of the photo selectors of different qualities (from 30 experts)-**pressure of other buildings in the surroundings**						
Photo name	Very Beautiful n1	Beautiful n2	Ordinary n3	Ugly n4	Very Ugly n5	Photo points N
Ulu Mosque	5	12	6	7	0	15
Sifaiye Madrasah	8	11	7	4	0	23
Buruciye Madrasah	3	15	8	4	0	17
Cifte Madrasah	1	19	10	0	0	21
Gok Madrasah	0	17	9	4	0	13
Divrigi Ulu Mosque and Darussifası	7	19	5	0	0	33
Abdulvahap Gazi Shrine	15	12	3	0	0	43
Seyh Hasan Bey Kumbet	0	5	12	13	0	-8
Ahi emir Ahmed Shrine	0	6	10	14	0	-8
Behram Pasa Inn	8	12	7	3	0	25
Kursunlu Baths	3	16	7	4	0	18
Tashan	0	3	14	13	0	-10
Ziyabey Library	0	2	15	12	3	-16
Government Office	9	12	7	2	0	28
Gendarmerie Building	10	13	6	1	0	32
Ataturk Congress and Ethnography Museum	7	14	7	2	0	26
İnonu Museum	3	10	10	7	0	9
Gurun (Surp Kevork) Church	0	0	10	13	7	-27
Meydan Baths	0	4	16	10	0	-6

Q-sort formula was used and the resulted findings are listed in Table 3; Table 4; Table 5; Table 6; Table 7; Table8; Table 9;

$$N = \sum_{i=1}^{5} n_i (3 - i)$$

Total points of every photo = N

The number of selectors with the quality of very beautiful = n1

The number of selectors with the quality of beautiful = n2

The number of selectors with the quality of ordinary= n3

The number of selectors with the quality of ugly = n4

The number of selectors with the quality of very ugly = n5 [31].

RESULTS AND DISCUSSION

Following the study conducted, 7 parameters on the visual landscaping character are revealed with a Q-Sort analysis under general expert opinion.

In light of the gathered information; Abdulvahap Mosque turns out to be the structure with least pressure among the other historical buildings around Divrigi Great Mosque and Darussifası. Besides, it is also an important historical building of Sivas in terms of dominating the area (Table 3).

Reviewing the historical buildings, it is seen that the most important problem is the city's pressure. This pressure can be defined as the existence of high-rise buildings with old and neglected exteriors in cities which are constantly getting more crowded. This has a negative effect in terms of visual quality. Surroundings of Ziya Bey Library can be an example of this situation. Historical buildings should be considered in connection with their surroundings in sense of being the focus point of the area. Asides from its topographic structure, the existence of outside pressure to the region is also a defining factor in being the center of focus (Table 4).

In Table 5, area domination of historical buildings is evaluated according to a Q-Sort analysis. When the results are reviewed, it is seen that he highest points belong to the Government Office (52) and Gendarmerie Building (51). Another statement can be made that the historical buildings in the city center of Sivas have a generally positive result in dominance over the region. The lowest points among the positive results are Square Bathhouse (16 points), Inonu Museum (26 points) and Ziya Bey Library (28 points). Gurun Church is not a focus point as it is neglected and located between street alleys.

When the building effect is evaluated in determining their contributions to the historical structures and urban identity, the highest points belong to Government Office (51) and Great Mosque (50). When Table 6 is reviewed, it is seen that all the works evaluated other than Gurun Church have high points in terms of historical artifacts.

TABLE 4
Determination of contribution to city identity of historical buildings and assessment of "focus center" parameter

The number of the photo selectors of different qualities (from 30 experts)-**Dominance in area (focus center)**						
Photo name	Very Beautiful-n1	Beautiful-n2	Ordinary-n3	Ugly-n4	Very Ugly-n5	Photo points N
Ulu Mosque	15	9	6	0	0	39
Sifaiye Madrasah	16	8	5	1	0	39
Buruciye Madrasah	17	13	0	0	0	40
Cifte Madrasah	19	10	1	0	0	48
Gok Madrasah	20	10	0	0	0	50
Divrigi Ulu Mosque and Darussifası	16	12	2	0	0	44
Abdulvahap Gazi Shrine	16	12	2	0	0	44
Seyh Hasan Bey Kumbet	15	13	2	0	0	43
Ahi emir Ahmed Shrine	16	10	4	0	0	42
Behram Pasa Inn	17	12	1	0	0	46
Kursunlu Baths	10	12	8	0	0	32
Tashan	12	11	7	0	0	35
Ziyabey Library	11	8	9	2	0	28
Government Office	22	8	0	0	0	52
Gendarmerie Building	21	9	0	0	0	51
Ataturk Congress and Ethnography Museum	15	3	12	0	0	33
İnonu Museum	5	16	9	0	0	26
Gurun Church	0	0	10	15	5	-25
Meydan Baths	0	15	14	1	0	14

TABLE 5
Determination of contribution to city identity of historical buildings and assessment of "Building restoration" parameter

The number of the photo selectors of different qualities (from 30 experts)- **Building restoration**						
Photo name	Very Beautiful n1	Beautiful n2	Ordinary n3	Ugly n4	Very Ugly n5	Photo pointsN
Ulu Mosque	20	10	0	0	0	50
Sifaiye Madrasah	19	11	0	0	0	49
Buruciye Madrasah	10	14	6	0	0	34
Cifte Madrasah	16	10	4	0	0	42
Gok Madrasah	15	12	3	0	0	42
Divrigi Ulu Mosque and Darussifası	12	13	3	2	0	35
Abdulvahap Gazi Shrine	12	15	3	2	0	37
Seyh Hasan Bey Kumbet	10	16	4	0	0	36
Ahi emir Ahmed Shrine	12	13	5	0	0	37
Behram Pasa Inn	7	12	11	0	0	28
Kursunlu Baths	12	11	7	0	0	35
Tashan	14	15	1	0	0	43
Ziyabey Library	18	10	2	0	0	46
Government Office	21	9	0	0	0	51
Gendarmerie Building	20	10	0	0	0	40
Ataturk Congress and Ethnography Museum	17	12	1	0	0	46
İnonu Museum	19	11	0	0	0	49
Gurun (Surp Kevork) Church	0	0	0	17	13	-44
Meydan Baths	5	11	5	7	0	10

TABLE 6
Determination of contribution to city identity of historic buildings and assessment of "The amount of green area the building" parameter

The number of the photo selectors of different qualities (from 30 experts) **Amount of green area in historical building**						
Photo name	Very Beau-tiful n1	Beautiful n2	Ordinary n3	Ugly n4	Very Ugly n5	Photo points N
Ulu Mosque	13	12	5	0	0	38
Sifaiye Madrasah	10	9	10	1	0	28
Buruciye Madrasah	15	13	7	0	0	43
Cifte Madrasah	0	7	14	9	0	-2
Gok Madrasah	0	0	17	13	2	-25
Divrigi Ulu Mosque and Darussifası	0	0	10	14	6	-28
Abdulvahap Gazi Shrine	6	8	9	7	0	13
Seyh Hasan Bey Kumbet	2	6	12	10	0	0
Ahi emir Ahmed Shrine	2	7	10	11	0	0
Behram Pasa Inn	6	12	8	4	0	20
Kursunlu Baths	0	0	10	12	8	-28
Tashan	0	0	0	14	16	-46
Ziyabey Library	0	0	0	15	15	-45
Government Office	0	2	5	11	12	-33
Gendarmerie Building	0	1	4	14	11	-38
Ataturk Congress and Ethnography Museum	10	6	7	7	0	21
İnonu Museum	7	12	9	2	0	24
Gurun (Surp Kevork) Church	0	0	0	7	23	-53
Meydan Baths	0	0	0	10	20	-50

In designating the historical buildings and their contributions to urban identity, size of the green area the building has, is significant. Amount of green space in urban areas is the most important natural element that increases the visual quality of the historical places. For example; existence of Seljuk Park increases the historical structure feeling of Sifahiye Madrasa which has one of the highest points shown in Table 7. According to other parameters, negative values are present in the evaluation of green areas. The amount of green area of the historical places in the city center are lower. The green area percentage increases in accordance with the distance from the city center. The dominance of the buildings in the city center restricts the existence of green spaces.

When the" perceptibility" parameter is evaluated in designating the historical buildings and their contribution to the urban identity (Table 8); we see that the buildings in Sivas being high-rises with minarets, increases their perceptibility. The buildings with high points in perceptibility are Buruciye Madrasa (56 points), Great Mosque (36 points), Behram Pasha Inn (44 points), Gok Madrasa (45 points), Government Office (49 points) and Gendarmerie Building (46 points) (Table 8). Abdulvahap Gazi Shrine is also among the historical places with high perceptibility (46 points) in accordance with its location.

TABLE 7
Determination of contribution to city identity of historic buildings and assessment of "Perceptibility" parameter

The number of the photo selectors of different qualities (from 30 experts)-Perceptibility						
Photo name	Very Beautiful n1	Beautiful n2	Ordinary n3	Ugly n4	Very Ugly n5	Photo points N
Ulu Mosque	15	6	9	0	0	36
Sifaiye Madrasah	16	4	10	0	0	36
Buruciye Madrasah	17	6	3	4	0	56
Cifte Madrasah	21	7	2	0	0	49
Gok Madrasah	20	6	3	1	0	45
Divrigi Ulu Mosque and Darussifası	10	7	12	1	0	26
Abdulvahap Gazi Shrine	20	6	4	0	0	46
Seyh Hasan Bey Kumbet	5	16	6	3	0	23
Ahi emir Ahmed Shrine	4	16	3	7	0	17
Behram Pasa Inn	17	10	3	0	0	44
Kursunlu Baths	12	10	5	3	0	31
Tashan	15	9	6	0	0	39
Ziyabey Library	10	11	7	2	0	29
Government Office	20	9	1	0	0	49
Gendarmerie Building	17	12	1	0	0	46
Ataturk Congress and Ethnography Museum	16	7	7	0	0	39
İnonu Museum	7	10	12	1	0	23
Gurun (Surp Kevork) Church	1	4	16	3	6	-10
Meydan Baths	6	7	8	9	1	9

TABLE 8
Determination of contribution to city identity of historic buildings and assessment of "guidance to historical building" parameter

The number of the photo selectors of different qualities (from 30 experts)-**Guidance to historical building**						
Photo name	Very Beautiful n1	Beautiful n2	Ordinary n3	Ugly n4	Very Ugly n5	Photo points N
Ulu Mosque	14	13	3	0	0	41
Sifaiye Madrasah	13	15	2	0	0	41
Buruciye Madrasah	10	12	8	0	0	32
Cifte Madrasah	8	11	12	0	0	28
Gok Madrasah	10	7	13	0	0	34
Divrigi Ulu Mosque and Darussifası	4	9	11	6	0	11
Abdulvahap Gazi Shrine	5	12	8	5	0	17
Seyh Hasan Bey Kumbet	9	14	3	4	0	28
Ahi emir Ahmed Shrine	8	13	6	3	0	26
Behram Pasa Inn	9	12	7	2	0	30
Kursunlu Baths	8	10	12	0	0	26
Tashan	11	12	7	0	0	34
Ziyabey Library	16	10	4	0	0	42
Government Office	18	9	3	0	0	45
Gendarmerie Building	17	10	3	0	0	44
Ataturk Congress and Ethnography Museum	15	12	3	0	0	42
İnonu Museum	5	10	12	3	0	17
Gurun (Surp Kevork) Church	0	0	3	14	13	41
Meydan Baths	10	8	7	5	0	23

TABLE 9
Determination of contribution to city identity of historical buildings and assessment of "Accessibility" parameter

The number of the photo selectors of different qualities (from 30 experts)-**Accessibility**						
Photo name	Very Beautiful n1	Beautiful n2	Ordinary n3	Ugly n4	Very Ugly n5	Photo points N
Ulu Mosque	14	14	2	0	0	42
Sifaiye Madrasah	14	15	1	0	0	43
Buruciye Madrasah	15	14	1	0	0	44
Cifte Madrasah	25	4	1	0	0	54
Gok Madrasah	13	10	7	0	0	36
Divrigi Ulu Mosque and Darussifası	5	9	12	4	0	15
Abdulvahap Gazi Shrine	15	12	3	0	0	42
Seyh Hasan Bey Kumbet	14	13	3	0	0	41
Ahi emir Ahmed Shrine	15	14	1	0	0	44
Behram Pasa Inn	17	12	1	0	0	46
Kursunlu Baths	18	12	0	0	0	48
Tashan	15	12	3	0	0	42
Ziyabey Library	14	11	5	0	0	39
Government Office	19	11	0	0	0	49
Gendarmerie Building	16	12	2	0	0	44
Ataturk Congress and Ethnography Museum	19	11	0	0	0	49
İnonu Museum	11	14	5	0	0	36
Gurun (Surp Kevork) Church	2	5	12	11	0	-2
Meydan Baths	13	10	7	0	0	29

"Existing guidance to historical building" parameter is reviewed in Table 9 with regards to historical buildings and their contribution to urban identity. According to the review, the highest points in this parameter belong to Government Office (45 points), Gendarmerie Building (44 points), Sifahiye Madrasa (41 points) and Great Mosque (41 points).

When the "accessibility" parameter is reviewed in designating the historical buildings and their contribution to urban identity, historical places' being in the city center has a positive effect in terms of their accessibility. However, as Gurun Church is left as an abominable building without any security measures, it has a lower point in accessibility.

SWOT Analysis Results.

Strengths.

❖ Being a home for many civilizations throughout the history.

❖ As there are many advantages regarding the geographical location of Sivas, the city had been dominated by different civilizations (Hittites, Romans, Byzantines, Seljuk and Ottomans

❖ Existence of hot springs.

❖ Aside from its local customs, existence of a rich food culture with a wide range of options.

❖ Being a distinct center in the region in terms of handicrafts.

❖ Especially the existence of picnic areas. (Highlands)

❖ Rural areas being suitable for recreational activities.

❖ Existence of suitable rural areas for setting up eco-farms.

❖ Existence of proper ground and area structure for different types of nature tourism.

❖ Having a historically rich past and heritage.

Opportunities.

❖ New employment chances can be created in areas that are thought to have tourism potential.

❖ Religious tourism having potential for the good of Sivas nationwide and internationally.

❖ Rural tourism and ecotourism being alternative income sources for the locals.

❖ Visitors coming for rural tourism also provide local people with chances to socialize, resulting in the advancement of social interactions in the region.

❖ There are many institutions that provide support, incentive and donations for ecotourism investments.

❖ Raising the workforce of the people living in rural areas employed in rural tourism and ecotourism activities, by enlisting them in training programs.

❖ Securing the women's place in families and society with the help of creating job opportunities by the revival of ecotourism and rural tourism.

Weaknesses.

❖ As the hot spring's maintenance is lacking, it is not possible to adequately advertise the existence of a place like this.

❖ Lack of rural tourism and ecotourism awareness.

❖ Lack of planning from local and national administrators on rural tourism.

❖ Not paying attention to the preservation of historical areas.

❖ Inability to bring many historical places to light and open them to visitors because they are not renovated or decorated.

❖ Lack of advertisement for Zab River.

❖ Lack of organizations and initiatives for setting up eco-farms that will help rural tourism and/or ecotourism to develop.

❖ Not organizing adequate fairs and activities in order to promote local products, handicrafts, foods etc.

❖ Immigration of people to other cities in which tourism is more alive.

❖ Inadequate or nonexistent organizations for accommodation or transportation in areas with rural tourism and/or ecotourism potential.

❖ Remote distance of picnic areas from the city center. Thus, difficulty in visiting them especially in winter.

❖ Lack of employment chances for teenagers living in rural areas.

❖ Inadequate rehabilitation works.

❖ Being unaware of the richness in natural resources.

❖ Not benefiting from natural resources enough.

❖ Being unable to prevent immigration from rural areas to the city.

❖ Lack of rural planning.

Threats.

❖ Unplanned urbanization.

❖ Excessive damage to the historical areas as a result of not turning all of them into protected sites.

❖ Areas that have the potential to be used for rural tourism and ecotourism standing idle.

❖ As the immigration rate to the cities rise, it becomes harder to find young people to work in ecotourism activities. This is also a negative effect for landscape observation areas.

❖ Environmental pollution.

❖ High traffic volume.

CONCLUSION AND SUGGESTIONS

When we look at the city development throughout the history; we see that the historical fabric of Sivas was mainly formed during the Anatolian Seljuk's period whereas the planned city order was established in Republic period and afterwards. City of Sivas which has rich historical roots is significant in harboring the remnants of this diversity. Historical structures belonging to Anatolian Seljuk's and Ottoman periods are positioned at the historical city center and they are the elements that give the city its identity and form its silhouette. Spatial development of the city drastically changed with the industrialization movement. The city center had developed around the radial road stems formed by the wide arteries and the connection of the main arteries to the city square resulted in increased traffic volume in the city center [28]. Therefore, many of the places and buildings in the Sivas historical city center fall short in terms of green areas. Physical evolution of the city center on the other hand, continues.

In planning decisions made for the historical cities with urban heritage, it is seen that investments focused on cultural tourism in historical environments, exist both spatially and functionally [33, 34]. Therefore, historical cities together with the cultural heritage they possess, should be handled and reorganized based on the planning strategies focused on cultural tourism and within the scope of existing urban open-green areas and changing spatial privileges [35, 36]. With this regard, historical structures and their surroundings with potential to support urban development in Sivas, will have qualities that will enable cultural and recreational opportunities with urban landscaping design works done properly [31, 32].

Historical buildings that are still standing, made functional and durable again by restoration works. Pressure on the cultural values located at the historical city center caused by the urban development is being tried to be reduced by the applied urban design works. With the help of restoration works applied on the exterior sides of the structures causing visual pollution with no aesthetic values in the historical city center around Gok Madrasa, Ziyabey Library, Sifaiye Madrasa, Buruciye Madrasa, Government Office and Gendarmerie Building, the historical artifacts are highlighted. These historical buildings are also being currently used in order to keep their functionality. Restoration works forming a background for the ancient artifacts in the historical city center will emphasize its texture. However, these structures and structure groups that have both national and international significance should be highlighted by buffer areas formed by active or passive green area applications. They also should be defined in a cultural scale in a way that they will be a part of open-green area and serve for recreational and touristic purposes. Application of landscape designing and achieving the desired result is a time-consuming process, because live materials are used [37]. In this regard, landscape designing is not a solid, closed architectural layout sheet. It is a living, evolving, growing side member of urban designing and it changes color and form according to seasons. There are some goals that are desired in landscape designing, in a nutshell they are [38]:

• Rather than being strict suggestions, the designs should have flexibility that can adapt to changing conditions if necessary. They should generate options.

• They should be in accordance with urban and local high-level decisions.

• They should integrate with their immediate surroundings and historical urban fabric if available. They ought to present solutions to problems about transportation.

• They should support the contributions to creating habitable, high quality surroundings.

• Security should be provided for the existing or new ecosystems in the area.

• Environmental conditions and facts about nature sciences should be taken into account.

• Costs for the design setup process, management, maintenance and administration should be calculated properly, in accordance with the cost-benefit analyses.

In conclusion, attractions of Sivas are tempting visitors to attend city tours rather than stay in the city for some period of time. For this reason, mainly local administrators together with investors and relevant institutions and organizations, should create similar attractions that would inspire people and extend the time of their stay. It is mandatory to combine both product and market-oriented approaches and designate strategies accordingly in order to create tourism demand and provide economic progress in Sivas. According to the results of surveys conducted in many countries worldwide, the new favorites in tourism are natural, historical and cultural attractions.

REFERENCES

[1] Bekci, B., Cengiz, C. and Cengiz, B. (2012) Evaluating urban biodiversity in terms of user preferences urban residential landscapes in Bartın (Turkey). Fresen. Environ. Bull. 21, 1626-1634.

[2] Atabeyoglu, O. (2004) Erzurum The evaluation of the gardens of the institution and public houses in the respect of landscape architecture. Ataturk University, Faculty of Agricultural Erzurum.

[3] Zencirkiran, M., Ender, E., Cetiner, S., Gorur, A., Eraslan, E., Tanriverdi, D.O. and Celik, B.H. (2018) A research on Kocaeli geophytes and their ornamental purposes for sustainable landscape design. Fresen. Environ. Bull. 27, 6042-6052.

[4] Duzenli, T., Yilmaz, S. and Tarakcı, E. (2017) A study on healing effects of hospital gardens. Fresen. Environ. Bull. 26, 7342-7352.

[5] Antrop, M. (2004) Landscape change and the urbanization process in Europe. Landscape and Urban Planning. 67, 9-26.

[6] Lynch, K. (1960) The Image of the city. MIT Press, Massachusetts, Cambridge.

[7] Kollarou, V., Athanasopoulou, Kollaros, A.G. and Lantitsou, K. (2017) Mid-size town's public open spaces and environmental quality. Fresen. Environ. Bull. 26, 1271-1280.

[8] Onem, B. and Kılıncaslan, İ. (2005) Urban identity and environmental perception: a case study for Halic. Journal of ITU Architecture, Planning, Design. 4(1), 115-125.

[9] Yoruk, İ., Gulgun, B., Sayman, M. and Unal Ankaya, F. (2006) Examining the Ege University campus by the concept of ergonomy and anthropometry in the embrace of landscape architecture applications. Ege Journal of Agricultural Research. 43(1), 157-168.

[10] Bekci, B. and Taskan, G. (2013) Evaluation of usage areas of *Lamium purpureum* L. var. in urban landscape of Bartin vicinity (Turkey). Fresen. Environ. Bull. 22, 2880-2887.

[11] Yazici, K., Gulgun Aslan, B. and Ankaya, F. (2017) Examination of landscape scenery areas and activities: a case study in Van Province of Turkey. Karabuk University Journal of Institute of Social Sciences. Special issue. 3, 168-176.

[12] Gobster, P. (1998) Urban parks as green walls or green magnets? Interracial relations in neighborhood boundary parks. Landscape and Urban Planning. 41, 43-55.

[13] Kramer, B., Hegedus, P. and Gravina, V. (2003) Evaluating a dairy herd improvement project in Uruguay to test and explain q methodology. Proceedings of the 19th Annual Conference. Raleigh, North Carolina, USA, 347.

[14] Pickton, D. and Wright, S. (1998) What's SWOT in strategic analysis? Briefings in Entrepreneurial Finance. 7(2), 101-109.

[15] Ozhancı, E. and Yılmaz, H. (2011) Evaluation of recreation areas for visual landscape quality; sample of Erzurum, Turkey. Igdır University Journal of the Institute of Science and Technology. 1(2), 67-76.

[16] Thompson, C.W. (2002) Urban open-space in the 21st century. Landscape and Urban Planning. 60, 59-72.

[17] Ak, M.K. (2010) Determination and improvement of visual quality at a sample of Akcakoca coastline. Ankara University, Faculty of Landscape architecture Ankara.

[18] Scottish Natural Heritage (2013) A hand book on environmental impact assessment guidance for competent authorities, consultees and others involved in the environmental impact assessment process in Scotland. 4th Ed.

[19] Raskin, E. (1974) Architecture and people. Prentice-Hall. 540-558.

[20] Golkar, K. (2003) From the birth to maturity of urban design. Soffeh Journal. 36, 23-28.

[21] Reza Zadeh, R. (2007) Principals and organizing criteria, rules and regulations of urban landscape. Center Studies Architecture and Urban, Tehran.
[22] Stubbs, M. (2004) Heritage-sustainability: developing a methodology for the sustainable appraisal of the historic environment. Planning, Practices and Research. 19(3), 285-305.
[23] Crow, T., Brown, T. and De Young, R. (2006) The riverside and Berwyn experience: contrasts in landscape structure, perceptions of the urban landscape, and their effects on people. Landscape and Urban Planning. 75(4), 282-299.
[24] Naspetti, S., Mandolesi, S. and Zanoli, R. (2016) Using visual q sorting to determine the impact of photovoltaic applications on the landscape. Land Use Policy. 57, 564–573.
[25] Dupont, L., Ooms, K., Duchowski, A.T., Marc Antrop, M., and Eetvelde, V. (2017) The Visual exploration of the rural-urban gradient using eye-tracking. Spatial Cognition and Computation. An Interdisciplinary Journal. 17, 65-88.
[26] Keshtkaran, R., Habibi, A. and Sharif, H. (2017) Aesthetic preferences for visual quality of urban landscape in Derak high-rise buildings (Shiraz). Journal of Sustainable Development. 10(5), 94-106.
[27] Solecki, W. and Welch, J.M. (1995) Urban parks: green spaces or green walls? Landscape and Urban Planning. 32, 93-106.
[28] Anonymous (2017a) Sivas Provincial Directorate of Culture and Tourism. Official web page, Sivas, Turkey.
[29] Anonymous (2017b) Sivas Municipality. Official web page, Sivas, Turkey. Access link Http://www.sivas.bel.tr/.
[30] Ozcan, K. (2008) An Open-Green Space Effective Planning Model for Sustainable Urban Conservation: A Case Study for Konya Urban Conservation Area, Turkey. Journal of Ecology. 68, 43-53.
[31] Golchin, P., Narouie, B., and Masnavi, M.R. (2012) Evaluating visual quality of educational campus based on users preferences (case study: Sistan and Baloochestan University, Iran). Journal of Environmental Studies. 38(62), 43.
[32] Erdogan, A. and Atabeyoglu, O. (2016) The effect of historical buildings on urban fabric: the sample of Kayseri city center. Turkish Journal of Forestry. 17(1), 83-92.
[33] Christopher, M.L. (1992) Urban tourism and its contribution to economic regeneration. Urban Studies. 29(3-4), 599-618.
[34] Mason, D.R. (1997) Managing development at cultural heritage sites: conservation practice and sustainability. Routledge Press, London.
[35] Strange, I. (1997) Planning for change, conserving the past: towards sustainable development policy in historic cities. Cities. 14(4), 227-233.
[36] Steinberg, F. (1996) Conservation and rehabilitation of urban heritage in developing countries. Habitat International. 20(3), 463-475.
[37] Celik, D. and Yazgan M.E. (2007) Mapping of climate index on wood preservation: case of Turkey. Journal of Bartin Faculty of Forestry. 9(11), 26-33.
[38] Yaslica, E., Tanrivermis, E. and Akay, A. (1999) The place of landscape design in urban design process. I. National Urban Design Congress. İstanbul.

Received: **11.10.2018**
Accepted: **26.03.2019**

CORRESPONDING AUTHOR

Kubra Yazici
Tokat Gaziosmanpasa University
Faculty of Agriculture
Department of Horticulture
60240 Tokat – Turkey

e-mail: k-yazici-karaman@hotmail.com

© by PSP Volume 28 – No. 5/2019 pages 3768-3777 Fresenius Environmental Bulletin

DETERMINATION OF ECOLOGICALLY SUITABLE SETTLEMENT AREAS BY USING GIS BASED MULTI-CRITERIA DECISION MAKING ANALYSIS: THE CASE OF NIGDE PROVINCE

Rifat Olgun*, Tahsin Yilmaz

Department of Landscape Architecture, Faculty of Architecture, Akdeniz University, Antalya, Turkey

ABSTRACT

Due to the increase in the world's population, urbanization is swiftly increasing. With the increase in the urbanization, the ecological construction of the cities degenerates over time. In this context, sustainable urban planning methods that use various methods depending on the developing technology in order to preserve the ecological structure of the cities are being developed. One of these approaches is the combination of remote sensing, geographic information systems (GIS), and the analytic hierarchy process (AHP), which is one of the multi-criteria decision-making methods, to identify the settlement areas that are ecologically appropriate. It has been published in many studies that it was possible to obtain healthy results for the determination of ecologically appropriate settlement areas by collectively using these methods.

In this context, the purpose of the study is to evaluate the urban development areas of Niğde city in terms of ecological criteria and to present suggestions for sustainable urban development areas taking ecological criteria into consideration. At the end of the analyzes performed with the use of GIS and AHP methods, it was determined that 9.45% of the research area (745.62 ha) was suitable for the 1st-degree ecological settlement. In conclusion, it is prominent to take into consideration the natural environmental factors of the region when planning new settlements in terms of sustainable and ecological urban planning, based on the urban development.

KEYWORDS
Ecology, settlement suitability, GIS, multi-criteria decision-making, AHP, Niğde.

INTRODUCTION

While the population of the world increased slowly until the industrial revolution, the population increase rate has been accelerated since the industrial development and the population was accumulated in urban areas. In this context, the urbanization was extended based on the industrial development of the developed countries since the end of the 18th century. Cities signify the complex structure within a certain system of integrity that integrates natural, economic, social and ecological environments within a certain period and location [1, 2]. In this complex structure, since the density of structures and unplanned development have been increased significantly due to the industrialization and fast population growth, the relationship between the urban areas and rural areas has been ruptured; the available green areas in the cities and the natural structure of the region deteriorated fast; the life in the city became monotonous; the biodiversity has been damaged and the cities became environments that are insufficient in terms of social, cultural and biological opportunities [3, 4, 5, 6].

Hence, it is necessary to produce new methods for conducting research in cities, to conduct researches in large-scale areas like the cities and to create new evaluation tools depending on the development of technology. In this context, technological developments in Remote sensing (RS) and Geographic Information System (GIS) field facilitated the studies of large-scaled cities [3, 6]. In addition, determination of sustainable urban development areas taking into account ecological criteria requires to adopt a systematic approach and necessitates the use of Geographic Information System together with multi-criteria decision-making techniques. The integration of GIS and AHP considerably facilitates the decision-making process in this context [8, 9, 10].

Sustainable urbanization signifies as a dynamic process, in which various environmental, social, economic and management factors are taken into account [11, 12]. Concordantly, the purpose of the study is to evaluate the urban development areas of Niğde city in terms of ecological criteria and to present the suggestions for determination of sustainable urban development areas taking ecological criteria into consideration. Within this scope, the combined use of Remote Sensing, GIS, and AHP methods are essential assessment tools for taking urban planning decisions based on ecology [13, 14]. Thus, remote sensing, GIS and AHP techniques were used together in this study.

MATERIALS AND METHODS

Niğde is located on the southeast of the Central Anatolia Region, in the Central Taurus Mountains and on the north of the area, where Bolkarlar and Aladağlar head the north [15]. It covers an area of 7.795,22 km² and it has an elevation of 1,229 meters above sea level [16]. 28.8% of the district's territory consists of mountain areas while 41,2% are undulating land and 30% of the land consists of bottom land [17]. The research area consists of a total area of 7.889,83 ha, which is located within the boundaries of the adjacent area of Niğde Municipality (Fig. 1).

The research was carried out in three stages, namely Calculation of Criteria Weights with AHP, Creation of data infrastructure structure with GIS and Weighted overlay analysis.

Calculation of criteria weights with AHP. This section consists of 4 different stages.

1st Stage. Determining factor, sub-factor, and conformity values. In order to evaluate the ecological aspects of urban development areas and to define the optimal settlement areas; ecological evaluation factors, sub-factors, and conformity values for potential settlement areas have been determined by benefiting from the standards set forth in the legislation thanks to the works of researchers [18, 19, 20, 21, 22, 23]. In this context, the following values have been determined as the evaluation factors for the ecology-based suitable settlement areas; land use capability class, slope, aspect, elevation, geological structure, soil depth, drainage, vegetation and hydrology (the proximity to the water). The conformity values of the evaluation sub-factors were determined with the 4-point likert scale from the most important to the lowest (4- very suitable, 3- suitable, 2- less suitable, 1- inappropriate).

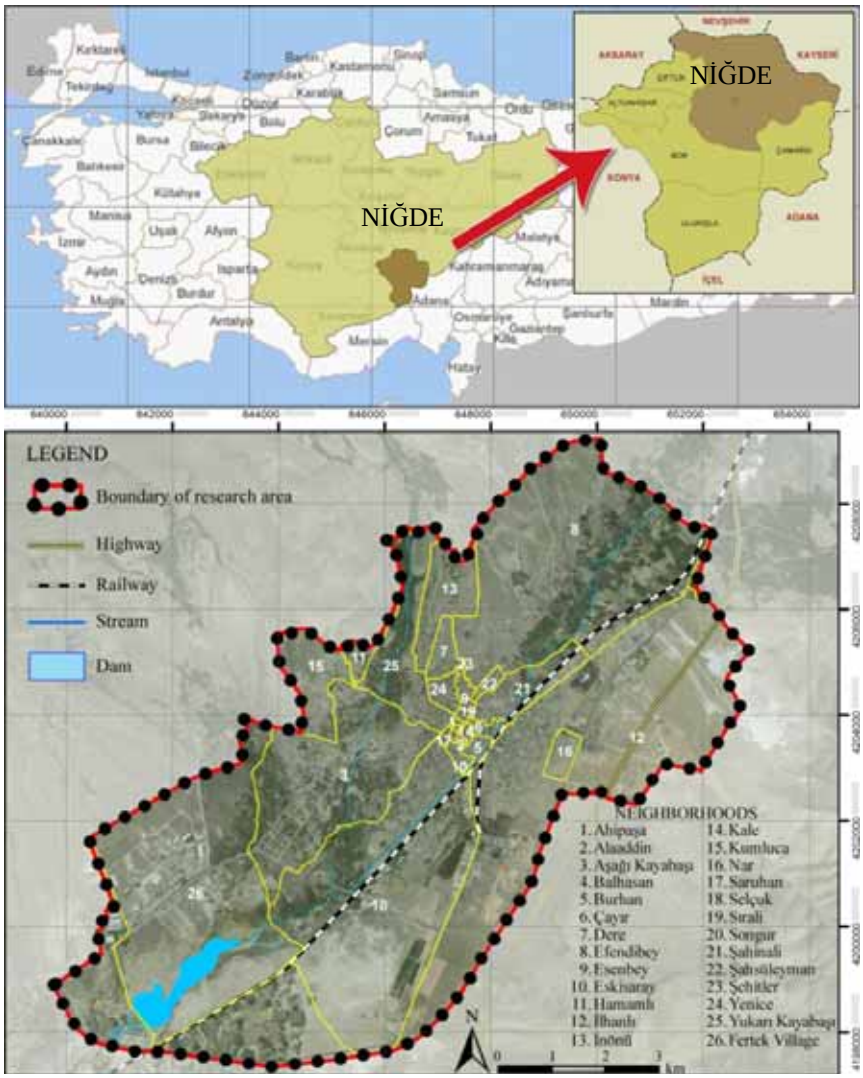

FIGURE 1
Location map of the research area.

2nd Stage. Creating the paired comparison matrix. For determining by the expert groups the conformity values of the factors by taking into account the natural and ecological criteria, a questionnaire form was prepared by including the paired comparison questions among the criteria. The questionnaire was filled by the experts in city and regional planning (5 persons), landscape architecture (7 persons) on the voluntary basis. According to the comparisons made by experts, paired comparison matrices were created. In this context, in order to assign a value to the paired comparison matrices, the level of significance varied from 1 to 9 developed by Saaty was used [24].

3rd Stage. Calculating the priority vector matrix and eigenvalue (λmax). After preparing the paired comparison matrix, the matrix must be normalized. In order to normalize the matrix, the sum of each column in the matrix is calculated and the matrix elements are divided by the sum of the related columns. Then, in the normalized matrix, the sum of the lines created for each alternative or criteria is taken. This value signifies the priority value for criteria or alternatives. The matrix consisting of the priority values is defined as the "priority vector matrix".

For each criterion/alternative in the priority vector matrix, the weighted total matrix is obtained by multiplying the priority value for each criterion/alternative by all the elements that exist in the column in the paired comparison matrix of that criterion/alternative. The values of the sum in the weighted total matrix were divided into priority vector matrix column values and the value of eigenvalue (λmax) was calculated by taking the arithmetic average of the values in the last matrix that was created [25, 26].

4th Stage. Calculating Consistency Index and Consistency Ratio. The following formulas were used to calculate the consistency ratio and consistency index of the generated matrix [25, 27] (1). In this context, if the Consistency Ratio is 10% (0.1) or less, the matrix is considered to be consistent [28, 29]. The consistency ratio is calculated as 0.09 in the study.

$$CR = CI / RI \qquad CI = (\lambda max - n) / (n - 1) \qquad (1)$$

CR: Consistency Ratio **CI:** Consistency Index **RI:** Random Index **λmax:** The largest eigenvalue of the matrix **n:** Number of elements in the matrix

Creation of data infrastructure with GIS. The data on land use capability class, soil depth, vegetation, and drainage were obtained from the Ministry of Agriculture and Forestry in 2018. TIN (Triangulated Irregular Network) model was created in ArcGIS environment by using 1/25000 scaled vector contour line obtained from General Directorate of Mapping (GDM). The digital elevation model was generated from the obtained TIN data. After converting the TIN value to TIN Triangle data, the analysis of the slope and aspect is completed. The data of the geological structure was obtained from the General Directorate of Mineral Research and Exploration. The data on the hydrological structure was generated from the existing plans that were provided from Niğde Municipality.

The data obtained about the evaluation factors determined for the selection of the settlement area in accordance with the ecological criteria were digitized in the shapefile format in the ArcGIS environment for completing the analysis and converted into a raster data format after the pre-treatments. 1/25000 scale maps in raster data format are divided into 10x10 m plan squares.

Weighted overlay analysis. Determined evaluation factors and evaluation sub-factors were grouped within themselves and the conformity values were arranged according to their values on relative importance. The conformity values distributed to the evaluation sub-factors were multiplied with the coefficients that are determined according to the opinions of the experts and hence, the total weight of each of the factors was ascertained (Table 1). By using the "multilayered weighted map overlay technique " (weighted overlay), which is one of the spatial analysis methods within the ArcGIS spatial analyst tools, the obtained data were used to plan the propositions for the settlement areas, taking into consideration the ecological parameters for the urban development.

The conformity values of the sub-factors of the evaluation factors to be used for the determination of ecology-based settlement areas are determined as following; the land use capability is class VII and VIII, the slope is light, the aspect is sunny, the elevation is low, geographic structure except for alluvial areas, shallow and very shallow soil depth, outside the forest regime and the presence of water with a distance of 2000 m and more.

RESULTS

Within the scope of the study, for determining the suitable settlement areas based on the ecology for the city of Niğde and its immediate surroundings; the land was analyzed in terms of the following factors; land use capability class, slope, aspect, elevation, geological structure, soil depth, drainage, vegetation, and hydrology (proximity to the water). In this context, geological structure has the highest weight value for determining the suitable settlement areas based on the ecology, while it is followed by drainage and slope (Table 1).

TABLE 1
The evaluation factors used in the determination of suitable ecological-based settlements

Main Criteria	Sub-criteria	Score	Weight	Percent	Main Criteria	Sub-criteria	Score	Weight	Percent
Land Use Capability Class	VII. and VIII. Class	4	0.113	11.3	Geological Structure	Other geological formations	4	0.303	30.3
	VI. Class	3				Alluvial areas	1		
	V. Class	2			Soil depth (cm)	Shallow and very shallow	4	0.036	3.6
	I., II., III., IV. Class	1				Medium deep and deep	1		
Slope (%)	0-2	4	0.151	15.1	Drainage	Sufficient	4	0.224	22.4
	3-6	3				Insufficient or Damaged	1		
	7-12	2			Vegetation	Outside the forest regime	4	0.071	7.1
	13-20	1				Inside the forest regime	1		
	21≤	1			Hydrology (proximity to the water)	2000≤	4	0.055	5.5
Aspect	S, SE, SW	4	0.026	2.6		1000-2000	3		
	E, W	3				300-1000	2		
	NE, NW	2				0-300	1		
	N	1							
Elevation (m)	1000-1200	4	0.021	2.1	Max. eigenvalue (λmax) = 10.150 n = 9 Consistency index (CI) = (λmax -n)/(n-1) = 0.144 Random index (RI) = 1.45 Consistency ratio (CR) = CI/RI = 0.09				
	1201-1400	3							
	1401-1600	3							
	1601-1800	2							
	1801-2000	2							
	2001≤	1							

The regions which are located in the east and west of the existing urban area and which are used as the agricultural area generally consist of alluvial soils with II land capability class. The following areas consist of VII class land class as land use; the area between the Niğde-Kayseri motorway and Niğde southern highway located within the boundaries of İlhanlı Neighborhood, and the region located in the north of İnönü Neighborhood where the current urban settlement ends, the region located at the border of Kayardı sustainable protection and controlled usage area in Yukarı Kayabaşı Neighborhood and the region where it is planned to build a city park project on an area of approximately 70 thousand square meters, the region where Kumluca Neighborhood is located and the semi-natural area located on the southern section of the Akkaya Damn (Figure 2).

The slope in the area of study which is located between Melendiz Mountain and Aladağlar and Bolkar Mountains, which connects the Bor Plain with the Misli Plain, ranges between 0-6% in the east and west directions, while it is above 21% in the north and south directions. In addition, the current settlement of the city heads the south-south-east with all directions. The elevation difference is not so high in the east-west direction in the research area. However, the land structure rises towards the north and south of the city, since there are high mountainous areas there. The elevation of the research area, which has an elevation difference between 1150 m and 1450 m, increases from the west of the Bor Plan towards the east of the area (Figure 2).

When the geological map prepared according to the data obtained from the data of the earth science data of the General Directorate of Mineral Research and Exploration [30] was determined, the geological formation of the research area was found to be containing the Miocene (pyroclastic rocks), quaternary (alluvial fan, slope debris, moraine, etc.), Pleistocene (unsorted terrestrial debris) and Pliocene (andesite). In terms of soil depth, the research area is generally similar to the land use capability class. On the region where the current urban settlement ends in the northern part of the Inönü Neighborhood and located in Yukarı Kayabaşı Neighborhood is located on the boundary of the Kayardı sustainable protection and controlled use area, is located in the district of Kumluca, the region where Kumluca Neighborhood is located, the area on the north of the organized ındustrial area and on the south of Akkaya Dam, the soil depth is very shallow (0-20 cm). In addition, when the area of research is examined in terms of drainage, it is observed that drainage is sufficient in the remaining areas except for the agricultural areas that are located to the east and west of the existing settlement (Figure 2).

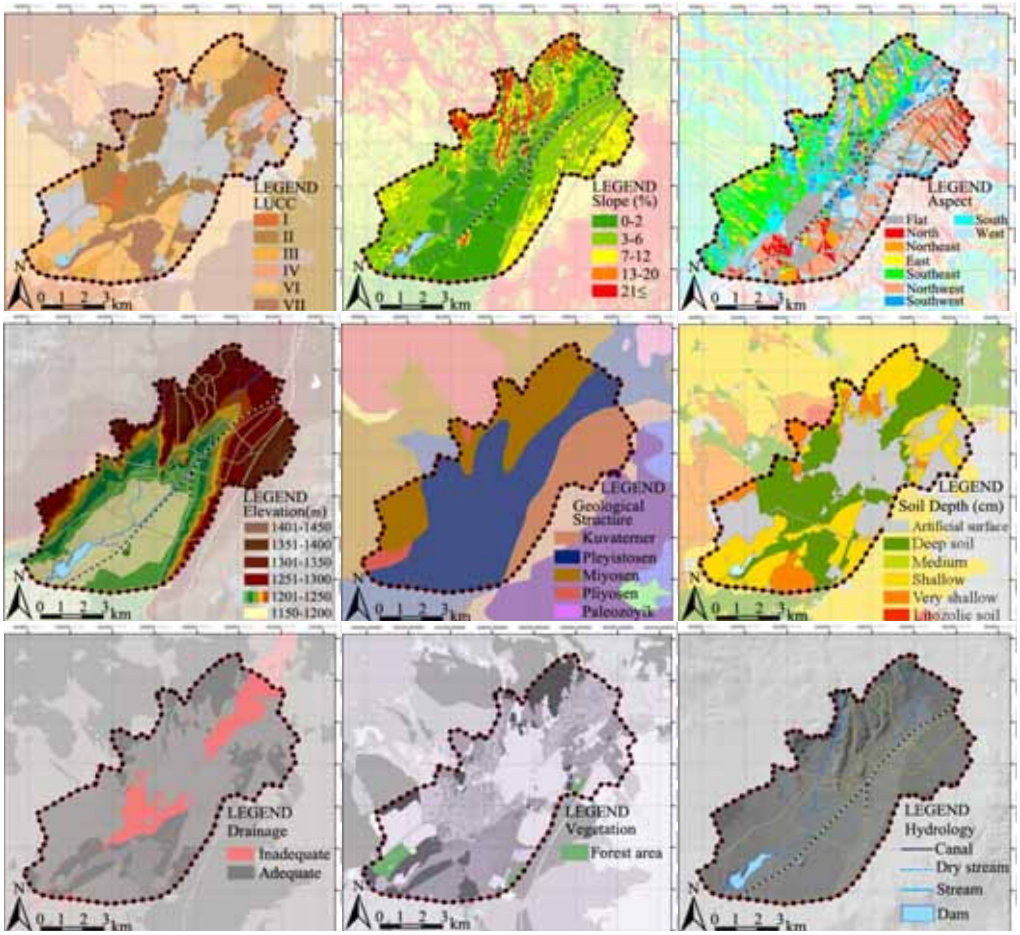

FIGURE 2
Analysis maps for ecologically suitable settlement areas selection

Niğde city, where the forest area is insufficient, there are particularly the memorial forests formed by public or private institutions and organizations, foundations and associations and there is a city forest that was formed by the municipality. Under the influence of continental climate, the rainfall is considerably high during spring in Niğde. Although many small river beds are formed during the rainfall, Zondi Stream and Yukarıyağdan Stream, which are connected to Akkaya Dam through the city and have water in all periods of the year, constitute the main hydrological structure that exists within the boundaries of the research area.

The related analyzes were performed by using "multilayered weighted map overlay technique" (weighted overlay) in ArcGIS software taking into consideration the conformity values that were generated. At the end of the analyzes that were carried out, it was observed that 9.45% (745.62 ha) of the research area was suitable for first degree settlement and 43.28% (3413.48 ha) of the research area was found to be 2nd degree suitable for settlement and 16.07% (1267.74 ha) of 3rd degree suitable for settlement (Figure 3).

As a sustainable urban development area for the development of the city, areas suitable for first-degree settlement are in the northeast of the city center and they are the continuation of the existing neighborhood settlement within the borders of Efendibey Neighborhood. The other region is located in the north of the center and it is within the boundaries of Kumluca Neighborhood, which was included in the urban area of Niğde after the election of the local administration in 2014 when the neighboorhood acquired the status of a quarter. Another area suitable for the settlement is the region behind the Niğde Organized Industrial Zone and within the boundaries of Fertek village. Natural areas and agricultural areas that are not covered by vegetation, particularly in the west of the city, or that have a small amount of vegetation are found to be suitable for 2nd and 3rd-degree settlement. In addition, the area which is not suitable for settlement is located on the edge of Yukarıyağdan Stream in the boundaries of Efendibey Neighborhood, located in the northeast of the city center.

DISCUSSION AND CONCLUSION

It is important to use the AHP method that reduces the subjectivity together with the geographic information systems in the sustainable ecological urban planning stage in order to obtain accurate

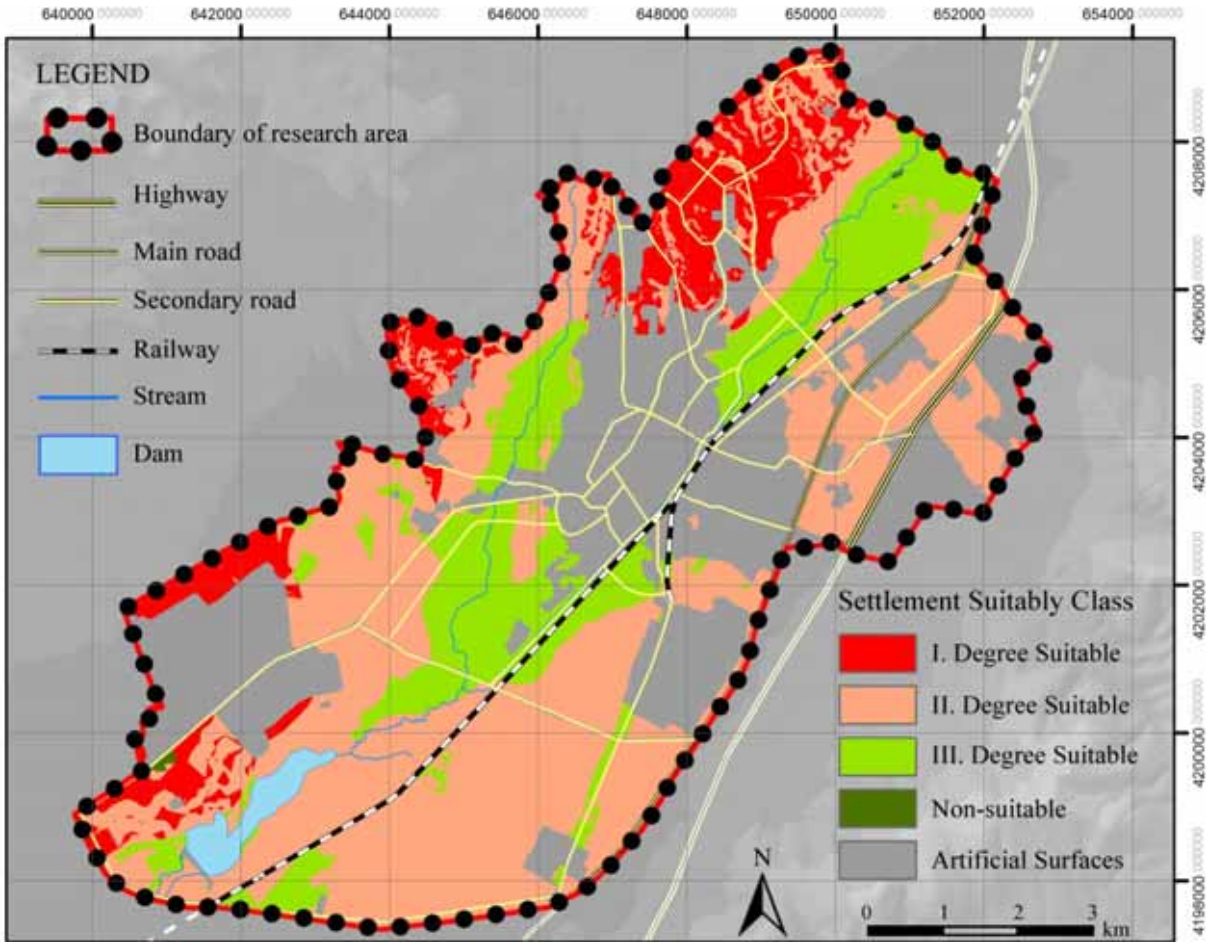

FIGURE 3
Ecologically suitable settlement areas map of research area

results [31]. In this context, the evaluation of decision makers is very significant since the weight of the factors are determined according to the preferences of decision-makers when multi-criteria decision-making analysis are conducted, as Chen et al. [32] and Partigöç et al. [33] mentioned in their works. Shukla et al. [13] and Merugu and Jain [34], in their work, stated that the use of the paired comparison method in determining the weight values of each factor is more appropriate than the direct allocation of the weights by the decision-maker. However, the weight values of the factors are determined subjectively by the researcher in the studies conducted for ecologically appropriate site determination for the settlements. Therefore, in order to exclude the subjective evaluation of the researcher, the weighted values of the factors were determined at the end of a survey that was conducted with 12 experts (landscape architecture and city and regional planning) working in the planning discipline. In the research, the standards set forth in the legislation and the works of researchers [18, 19, 20, 21, 22, 23] have been utilized. When analyzing the potential settlements by taking into account the ecological evaluation factors, results were found to be similar to the results obtained by the researchers in the determination of the settlements, which conform to the ecological criteria.

The distance of the settlement areas to the fault lines is particularly important in determining the suitable areas for settlement as well. Although there is no specific distance in the legislation, Demirtaş [35] and Pektezel [36] suggested that this distance should not be less than 15 meters when planning the residential areas in our country. Thus, since according to the data obtained from the geology data about Duman et al. [37], Emre et al. [38], Akbaş et al. [39], General Directorate of Mineral Research and Exploration [30] there is no active fault line within the region and there is no landslide in the region, this fact did not affect the selection for suitable settlement areas.

In the study of Karakuş and Cerit [40] for the determination of the most suitable areas in terms of a settlement in the city of Sivas and its close surroundings, it was determined that the most suitable areas for settlements are located in the southeast section of the study area although this region is not an area of 1st degree (2nd degree). Karakuş and Cerit [40] stated that the areas not suitable for settlement were concentrated near the city center and the northwest of the study area and that the settlement of Sivas

city center was also classified as the 3rd class settlement area. In addition, the presence of lands that are significant for agriculture and the high level of areas at higher elevations are factors that negatively affect the suitability of the settlement. Hence, the proportion of the areas that are not suitable for settlement increases. In contrary to the study conducted by Karakuş and Cerit [40], there are areas suitable for ecological-based 1st-degree settlement in the north and northeast of the city within the boundaries of the research area. The existing settlement areas within the research area are also located on the 2nd and 3rd-degree settlement areas. In the study conducted by Şahap [41] for Şanlıurfa, it was determined that some of the settlement areas are located on the 1st-degree agricultural areas, which are not suitable for settlement and emphasized that the areas to be opened to the new settlements should not be built on particularly fertile agricultural lands (Harran plains). According to the study conducted by Denizduran et al. [42], the district has received extensive migration from the thermal power plant in Afşin (Kahramanmaraş) district by increasing the city's business potential. With this migration movement, the population of the city increased and the settlement areas started to occupy the first class agricultural lands. Similarly, in the study conducted for the city of Adana, Peker Say et al. [43] stated that urban development in Adana headed towards fertile agricultural lands. In this context, since 41.1% of the research area is located on the fertile agricultural lands between Bor and Misli Plains and this area constitutes I., II. and III. degree agricultural areas, there are fertile agricultural lands in the northeast and southwest of the existing settlements. As shown in other studies conducted for other cities, since the current urbanization heads these directions, there is a pressure on the agricultural areas. In the study conducted by Özşahin ve Kaymaz [44], it was carried out an analysis by using 1/25000 scale thematic maps of the city of Antakya and Analytic Hierarchy Process, which is one of the most criteria decision-making methods. Hence, it was analyzed the suitability of Antakya city natural components for the settlement. The study revealed that more than half of the city consists of less suitable areas for settlement. Similarly, it was concluded that the space suitable for the first-degree settlement area consisted of 745.62 ha in terms of ecological criteria according to the analysis carried out by using the analytical hierarchy process method, which is one of the multi-criteria decision-making methods, by using 1/25000 scale thematic maps in Niğde city.

The population of Niğde has not increased swiftly over the years. Because the population of Niğde tended to migrate to large cities around the city. On the one hand, while the population of the city tends to migrate to other cities, on the other hand, thanks to the increase in the employment opportunities and thanks to the developing industry and investments, the city receives immigration. The migration of the young population from the rural areas, in particular from the rural areas where there is a difficult socio-economic life, causes an increase in the urban population. In addition, thanks to the development of the university and other institutions and organizations, the population of students and civil servants are considerably important in the city. Since the population increases, the urban area is expanding and new settlements are established. This disrupts the ecological structure of the ecosystem such as soil, water, flora, fauna, and natural structure. When we examine the zoning plans prepared according to the projection of 2035 by the local governments, it is comprehended that the settlement areas are planned to develop in the north and northeast of the city, particularly in the boundaries of Dere, İnönü and Efendibey Neighborhoods. In addition, after 2014 local elections, intensive housing planning has been realized in Kumluca Neighborhood, which is included in the boundaries of the urban area. In this context, the planning works have been carried out in Kumluca, Dere and İnönü districts in the north of Efendibey Neighborhood, which is the continuation of the existing settlement, and these studies revealed that these regions are the 1st-degree ecology-bases suitable areas for settlement.

In order to maintain the balance within the ecosystem, central and local administrations, who have a prominent role in the planning of cities, should take into account the ecological parameters of the city in determining the new settlement areas because of the growing and developing urbanization. For achieving a sustainable ecological urban development, it is necessary to use GIS and multi-criteria decision-making mechanisms in the planning of cities, and the landscape plans prepared at different scales should be used as the basis for developing the urban plans as well. In addition, Sedigheh [45] and Çavuş and Koç [46] stated in their studies that it would be more useful to take into account natural environmental factors, as well as the social and technical factors, for determining the suitability of settlements in terms of ecology and thus, the results would be more comprehensive.

ACKNOWLEDGEMENTS

Author has declared that there is no conflict of interests.

REFERENCES

[1] Zarghami, M. and Akbariyeh, S. (2012) System dynamics modeling for complex urban water systems: Application to the city of Tabriz, Iran. Resources Conservation and Recycling. 60, 99-106.

[2] Zhou, D., Xu, J., Wang, L., Lin, Z. (2015) Assessing urbanization quality using structure and function analyses: A case study of the urban agglomeration around Hangzhou Bay (UAHB), China. Habitat International. 49, 165-176.
[3] Das, S., Bhattacharya, A., Mali, S. (2013) Study on urban land suitability assessment using remote sensing and GIS: A case study of Khairagarh, in Chhattisgarh. International Journal of Computer Applications. 74, 20-26.
[4] Karakaya Aytin, B. and Korkut, A.B. (2015) Investigation open and green areas existence in the boundaries of protected area of Edirne city. Journal of Tekirdag Agricultural Faculty. 12, 100-108.
[5] Şalap Ayça, S., Jankowski, P., Clarke, K.C., Kyriakidis, P.C. and Nara, A. (2018) A metamodeling approach for spatio-temporal uncertainty and sensitivity analysis: An application for a cellular automata-based urban growth and land-use change model. International Journal of Geographical Information Science. 32, 637-662.
[6] Cetin, M., Sevik, H., Yigit, N., Ozel, H.B., Aricak, B. and Varol, T. (2018) The variable of leaf micromorphogical characters on grown in distinct climate conditions in some landscape plants. Fresen. Environ. Bull. 27, 3206-3211.
[7] Masser, I. (2001) Managing our urban future: The role of remote sensing and geographic information systems. Habitat International. 25, 503-512.
[8] Mohit, M.A. and Ali, M.M. (2006) Integrating GIS and AHP for land suitability analysis for urban development in a secondary city of Bangladesh. Journal Alam Bina Jilid. 8, 1-20.
[9] Stojkovic, S., Đurdic, S. and Andelkovic, G. (2015) Application of multi-criteria analysis and GIS in ecotourism development (case study: Serbian Danube region). Glasnik Srpskog Geografskog Društva. 95, 51-66.
[10] Serbu, R., Marza, B. and Borza, S. (2016) A spatial analytic hierarchy process for identification of water pollution with GIS software in an eco-economy environment. Sustainability. 8, 1-25.
[11] Mori, K. and Yamashita, T. (2015) Methodological framework of sustainability assessment in city sustainability index (CSI): A concept of constraint and maximisation indicators. Habitat International. 45, 10-14.
[12] Ochoa, J.J., Tan, Y., Qian, Q.K., Shen, L. and Moreno, E.L. (2018) Learning from best practices in sustainable urbanization. Habitat International. 78, 83-95.
[13] Shukla, A., Kumar, V. and Jain, K. (2017) Site suitability evaluation for urban development using remote sensing, GIS and analytic hierarchy process (AHP). In: Proceedings of International Conference on Computer Vision and Image Processing, Springer Science+Business Media, Singapore, 377-388.
[14] Parry, J.A., Ganaie, S.A. and Bhat, M.S. (2018) GIS based land suitability analysis using AHP model for urban services planning in Srinagar and Jammu urban centers of J&K, India. Journal of Urban Management. 7, 46-56.
[15] Iri, R., Inal, M.E. and Türkmen, H.H. (2010) Passed Bor's Market, Drive Donkey to Nigde. Detail Publishing, Ankara, 200.
[16] Altay, O. (2016) Investigation of heavy metal content of soil from Nigde city. MSc Thesis. Erciyes University Graduate School of Applied and Natural Sciences, Kayseri, Turkey.
[17] Governor of Niğde Province (2014) Niğde provincial administration strategic plan. Niğde, 101.
[18] Ortaçeşme, V. (1996) Evaluation of the Mediterranean coastal area of Adana province within the frame work of ecological landscape planning principles and optimal land use proposals. PhD Thesis. Çukurova University Graduate School of Applied and Natural Sciences, Adana, Turkey.
[19] Zengin, M. (2007) Determination of the land-uses in the close proximity of the River of Kura in Ardahan and optimal land use proposals. PhD Thesis. Atatürk University Graduate School of Applied and Natural Sciences, Erzurum, Turkey.
[20] Akten, M. (2008) The research on optimal land use planning in Isparta plain. PhD Thesis. Süleyman Demirel University Graduate School of Applied and Natural Sciences, Isparta, Turkey.
[21] Konaklı, N. (2011) The determination of optimal land use planning in the sample of Altinapa lake dam watershed. PhD Thesis. Çukurova University Graduate School of Applied and Natural Sciences, Adana, Turkey.
[22] Mansuroğlu, S., Kınıklı, P. and Saatci, B. (2012) Ecological assessment of urban development in Antalya and suggestions in the scope of sustainability. Ege University Journal of Agricultural Faculty. 49, 255-264.
[23] Kumar, S. and Bansal, V.K. (2016) A GIS-based methodology for safe site selection of a building in a hilly region. Frontiers of Architectural Research. 5, 39-51.
[24] Vaidya, O.S. and Kumar, S. (2006) Analytic hierarchy process: An overview of applications. European Journal of Operational Research. 169, 1-29.
[25] Gıran Taşcıoğlu, S. (2011) A'wot analysis of tourism planning application: Oymapınar culture and tourism protect and development region. Akdeniz University Journal of Agricultural Faculty. 24, 87-93.

[26] Abdurrahman, S. (2015) Investigation of energy supply security of Macedonia and evaluation with quantitative SWOT analysis. MSc Thesis. İstanbul Technical University Graduate School of Applied and Natural Sciences, İstanbul, Turkey.
[27] Shrestha, R.K., Alavalapati, J.R.R. and Kalmbacher, R.S. (2004) Exploring the potential for silvopasture adoption in south-central Florida: An application of SWOT-AHP method. Agricultural Systems. 81, 185-199.
[28] Wind, Y. and Saaty T.L. (1980) Marketing applications of the analytic hierarchy process. Management Science. 26, 641-658.
[29] Chen, Y., Yu, J. and Khan, S. (2010) Spatial sensitivity analysis of multi-criteria weights in GIS-based land suitability evaluation. Environmental Modelling and Software. 25, 1582-1591.
[30] General Directorate of Mineral Research and Exploration (2018) Geoscience map viewer. http://yerbilimleri.mta.gov.tr/anasayfa.aspx.
[31] Uy, P.D. and Nakagoshi, N. (2007) Analyzing urban green space pattern and eco-network in Hanoi, Vietnam. Landscape and Ecological Engineering. 3, 143-157.
[32] Chen, Y., Yu, J., Shahbaz, K. and Xevi, E. (2009) GIS-based sensitivity analysis of multicriteria weights. In: 18th World Imacs/Modsım Congress, Cairns, Australia, 3137-3143.
[33] Partigöç, N.S., Aydın, C. and Tarhan, Ç. (2017) Land use suitability analysis via multi-criteria decision making analysis and GIS: The case of Izmir city. Academia Journal of Interdisciplinary Scientific Research. 3, 55-70.
[34] Merugu S. and Jain, K. (2014) A review of Some ınformation extraction methods, techniques and their limitations for hyperspectral dataset. International Journal of Advanced Research in Computer Engineering and Technology. 3, 2394-2400.
[35] Demirtaş, R. (2003) How far should be from active fault in terms of settlement and building security? Antakya and Osmaniye Seismicity and Effects on Urbanization. In: UCTEA Series of Conferences, Ankara. 46-67.
[36] Pektezel, H. (2015) The geoecological GIS based planning analysis of Suleymanpasa (Tekirdag). The Journal of Academic Social Science Studies. 35, 163-185.
[37] Duman, T.Y., Çan, T. and Emre, Ö. (2011) 1/1.500.000 landslide inventory map of Turkey. General Directorate of Mineral Research and Exploration Special Publications Series-27, Ankara, Turkey.
[38] Emre, Ö., Duman, T.Y., Özalp, S., Elmacı, H., Olgun, Ş. and Şaroğlu, F. (2013) 1/1.250.000 scale active fault map of Turkey. General Directorate of Mineral Research and Exploration Special Publications Series, Ankara, Turkey.
[39] Akbaş, B., Akdeniz, N., Aksay, A., Altun, İ., Balcı, V., Bilginer, E., Bilgiç, T., Duru, M., Ercan, T., Gedik, İ., Günay, Y., Güven, İ.H., Hakyemez, H.Y., Konak, N., Papak, İ., Pehlvan, Ş., Sevin, M., Şenel, M., Tarhan, N., Turhan, N., Türkecan, A., Ulu, Ü., Uğuz, M.F., Yurtsever, A. (2017) Geological map of Turkey. General Directorate of Mineral Research and Exploration Special Publications, Ankara, Turkey.
[40] Karakuş, C.B. and Cerit, O. (2017) Determination of the most suitable areas in terms of settlement for Sivas city and its surroundings by using GIS. Cumhuriyet University Faculty of Science Science Journal. 38, 131-145.
[41] Şahap, A. (2015) The effects of urban development on land use by means of remote sensing and geographic information system: A case study in Şanlıurfa city. MSc Thesis. Harran University Graduate School of Social Sciences. Şanlıurfa, Turkey.
[42] Denizduran, M., Kızılelma, Y., Acar, Ö. and Bengin, E. (2017) The analysis of the temporal changes with remote sensing in the city, Afşin (Kahramanmaraş) and its surrounding. In: Tufuab IX. Technical Symposium, Afyonkarahisar, Turkey, 125-130.
[43] Peker Say, N., Yücel, M. and Özyurt Ökten, S. (2012) Spatial development of Adana and effect on agricultural lands. KSU J. Nat. Sci. Special Issue, 1-7.
[44] Özşahin, E. and Kaymaz, Ç.K. (2015) The analysis of habitability of urban spaces ın terms of natural environmental components by means of GIS and AHP: The case of Antakya (Hatay). Eastern Geographical Review. 20, 111-134.
[45] Sedigheh, L. Habibi, K. and Koohsari, M.J. (2009) An analysis of urban land development using multi-criteria decision model and geographical information system (a case study of Babolsar City). American Journal of Environmental Sciences. 5, 87-93.
[46] Çavuş, C.Z., Koç, T. (2015) The analysis of the land use suitability for settlement at the east of Gallipoli Strait (Dardanelles). Journal of Geographical Sciences. 13, 41-60.

Received: **11.10.2018**
Accepted: **27.03.2019**

CORRESPONDING AUTHOR

Rifat Olgun
Department of Landscape Architecture
Faculty of Architecture
Akdeniz University
Antalya, Konyaaltı 07070 – Turkey

e-mail: rifatolgun@akdeniz.edu.tr

© by PSP Volume 28 – No. 5/2019 pages 3778-3786 Fresenius Environmental Bulletin

DETERMINATION OF SUITABLE RECREATIONAL AREAS BASED ON EXPERT OPINION WITH Q-SORT ANALYSIS; BORABOY LAKE NATURAL PARK (AMASYA, TURKEY)

Kubra Yazici[1,*], Suheda Basire Akca[2]

[1]Tokat Gaziosmanpasa University, Faculty of Agriculture, Department of Horticulture, 60240, Tokat, Turkey
[2]Bulent Ecevit University, Caycuma Food and Agriculture, Vocational School, 67900, Zonguldak, Turkey

ABSTRACT

As a result of natural environment and places not being handled with a protectionist approach during planning, they are deteriorating and disappearing in time. Especially while using natural locations, it is possible to preserve and develop the sources while ensuring sustainability during the planning phase. In this context, it is important to prefer and preserve the natural sources with regards to sustainable environment. For this reason, it is important to determine how the image of destination is perceived by tourists. The aim of this study is to determine the indices of aesthetic preference for visual quality of Natural Park (Boraboy Lake and Natural Park) which contribute to recreational area design to make better decisions for rural landscape. Boraboy Lake were preferred as a case study area photo grid method in this area were identified and analyzed. The consensus based on expert opinion was measured by the standard deviation (SD) in visual preference judgement within the respondents. One –way Q-sort analysis was used to explore the relationships between landscape characters effect on consensus, and VAQ (Visual aesthetic quality). Eventually, aesthetic factors were presented in two main categories: 'primary and distinctive'. Findings lead to the development of sustainable rural landscape which suggest that the Boraboy Lake natural park of landscape features had a significant influence on the aesthetic preferences.

KEYWORDS:
Visual Quality, Landscape, Landscape Assessment, Expert Opinion, Q-Sort Analysis

INTRODUCTION

The landscape aesthetics value for human well-being has gained significant respect in public perception and also in socio-ecological research [1]. Studies on landscape preference and landscape aesthetics have been carried out since the 1960s [2]. Totally, visual landscape research is an interdisciplinary approach important for architect and urban designer. It includes different type of disciplines such as (landscape) architecture and urban planning and design, (humanistic) geography, psychology and sociology, environmental ethics [3, 4 -5]. (There are many theories, methods, and applications concerning landscape perception and Valuable overviews are given by [6, 7- 8]; as well as the more recent overviews of [9, 10 - 11]. In recent decades, a lot of effort has been put into explaining the components of landscape aesthetics as well as evaluating it. And the issues of evaluation and landscape beauty have been taken into consideration from different aspects.

Environmental protection consists of all the incentives and protective measures that will guarantee the safety of wild animals, plant species and their natural living populations and under natural conditions; landscape and landscape parts [12, 13-14]. According to [15, 16-17], environmental protection areas are the ones that are considered as a whole with the natural and cultural resources in order to protect and sustain the biological diversity [19, 20]. These areas are also protected under the law [21, 22]. Environmental protection contributes to the continuity of plant and animal population, richness of species and the preservation of natural or nearly natural ecosystems. With the elements under its protection, it both helps with the protection and development of genetic diversity and the advancement of scientific studies [23, 24]. Natural parks are considered to be among the most important elements of protection areas and they are the regions aimed to transfer the rich natural and cultural resources of our nation to the next generations undisturbed [25]. According to the natural parks law no. 2873 art. 2/b enacted on 9.8.1983, the description of natural parks is as follows: "Parts of nature that have the characteristics of vegetation and wildlife, have an integrity of landscape and are suitable for the public's recreational use". Tourism regions, areas and centers in places that are included in the scope of this law are subject to the opinion of Ministry of Forestry and Water Affairs when it comes to the planning decisions on tourism investments [26]. According to the 14th article of this law, several protective measures are taken in the places that are included within the scope of this law.

There are currently 41 natural parks in Turkey with a total surface area of 81.425 hectares [25].

Boraboy Lake and Natural Park which are the subjects of this study are declared as protected areas according to the richness and sensitivity of their natural resources. Boraboy Lake is an old lake created as a result of a landslide and it is located in the inner parts of Central Black Sea Region, to the northeast of Amasya (Figure. 1). This lake which is within the borders of Tasova county of Amasya, is located approximately 2 kilometers to the west of Golbeyli (Boraboy) district. The natural environment created by the lake and the rich vegetation surrounding it, is a significant recreation area for the region.

The aim of this study was to establish the administration of the area according to the preservation criteria, carrying out regulations and developing methods that would establish the continuity of biological (flora, fauna) and ecological structure, geomorphological, geological, natural, cultural and recreational landscaping values of the nature park, within the protection-usage balance. The purpose of this study was to extract the indices of Aesthetic preferences for visual quality in Boraboy Lake and Nature Park which contribute to landscape type to make better decisions for designing rural landscape. As the research focuses on landscape feature, the goal of this study was as follows: Important areas according to the recreational use of the Boraboy Lake and Nature Park (which were the subjects of this study) were determined and these areas were evaluated within the scope of sustainable usage.

MATERIALS AND METHODS

The main material of the study was the "Boraboy Lake and Nature Park" located in the Tasova county of Amasya city. With the approval number 1840 on 03 September 2013, this area was declared as a nature park. The area is 255, 36 hectares big and it consists of endemic/endangered species, natural forests and suitable living spaces for wildlife, lake ecosystems and a unique landscape [25]. The area is 65 kilometers far from the city center and 15 kilometers far from Tasova County. It is reached by following the Amasya-Tasova highway for 44 kilometers and then making a left to the Tasova-Samsun highway. After making another left on the 14th kilometer of this road, one can reach the area. The lake is 80 meters wide and 25 meters deep and it is located on an eastward-westward valley. It has a measurement of 900 x 300 meters and is surrounded by beech, Scotch pine, cedar and chestnut trees. This wonder of the nature lake has the color of emerald green Figure 1, [27].

As the method of the study; the first stage was a literature research conducted in order to determine the natural and cultural resource value of the area. All the natural and cultural data, written sources, maps and reports about the area were gathered from official sources. Then they were reviewed and evaluated. In the second stage, areas and observations points with current landscape value were determined by a group of 20 experts coming from different areas of expertise in order to assign a recreational landscape value to the area. This valuation process is done by conducting a poll, carried out by 30 landscape architects. For this purpose, during the designation of the criteria to be discussed by the experts, Philip Lewis' [28], visual analysis method aimed at perceivable landscaping and used in outdoors recreation planning, is utilized. Experts (30 people) according to this method, associated visually significant points to each other, in light of area's existing resource values.

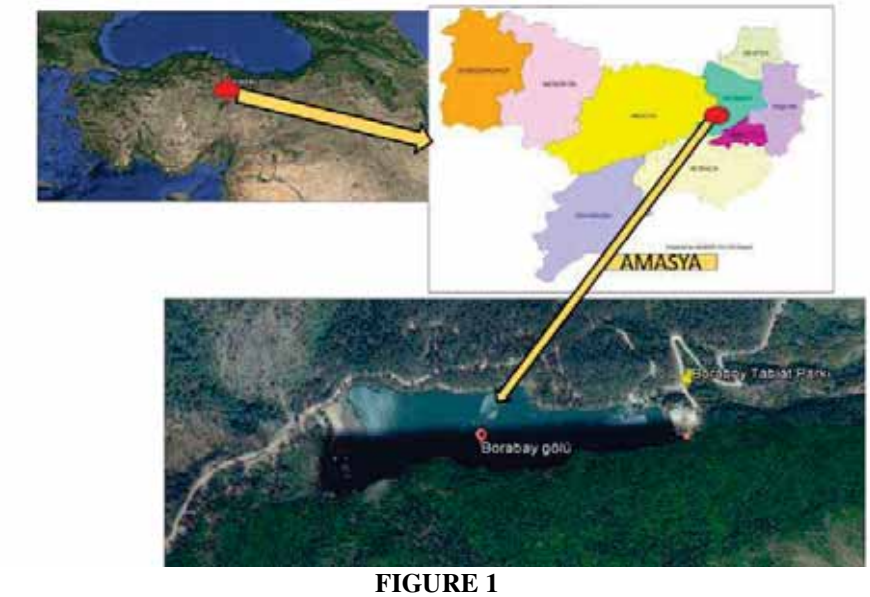

FIGURE 1
Location of Boraboy Lake and Nature Park in the country and region

The criteria on which this study was based; are the "vantage points" with fine and wide viewing opportunities of the field, primarily in accordance with the rich geomorphological structure of the area. As the area was a natural park, firstly some spots with rich visual opportunities in terms of natural resources, were considered as "basic visual landscaping values". Besides, "forests" were also considered to be an important criterion in terms of basic landscaping value as they had a visually significant effect. Woodlands and lake areas occupy large regions and they were constantly advancing in terms of recreational use as a result of their natural and cultural aspects. So, they were accepted as important areas within the scope of visual landscaping value. Another criterion taken into consideration while determining the recreational landscaping value of the areas was "incremental landscaping values". All the other cultural and natural data that are important with regards to recreational potential were evaluated in this context. Visual quality according to [29]; was the assessment of wide-range monitoring conducted on the study area on-vehicle, on foot or by plane. Q sort analysis was used to analyze the visual quality and to determine the important criteria of each wetland. Q- Sort analysis or Q factor analysis as it is named in the foreign literature, is a relatively new tool not only as approach but particularly following the quite recent rediscovery of its usefulness in those fields where psychometric knowledge of individuals has thorough implications [30].

Visual quality evaluation depends on seven basic factors. Of these specified areas, people are asked to make visual choices according to expert opinions (urban and region planners, architects, biologists, ecologists, geologists, environmental engineers, topographical engineers, hydrogeologists, sociologists and historians). 20 photos were shown to the group of experts and they were asked to sort them by grading. Each photograph was graded according to five-point Likert scale as +2, +1, 0, -1, -2 and the recreationally important regions of the area are determined (by Q-sort analysis).

$$N = \sum_{i=1}^{5} n_i (3 - i)$$

Total points of every photo = N

The number of selectors with the quality of very beautiful = n1

The number of selectors with the quality of beautiful = n2

The number of selectors with the quality of ordinary= n3

The number of selectors with the quality of ugly = n4

The number of selectors with the quality of very ugly = n5 [31].

Accordingly, 5 spots in the area with highest points are chosen (Table 1). Criteria discussed here are utilized from [32, 33-34-35];

1. Evaluation of the topographical structure: In this concept; existence of strange rock formations, valleys, hills and prairies were reviewed and evaluated.

2. Vegetation

3. Water; water sources in the area, existence of rivers and wetlands are evaluated.

4. Sociocultural structure of the area, settlement conditions.

5. Neighboring views.

6. Rarity.

TABLE 1
Classification of visual landscape values [14, 35]

Basic Visual Landscape Values				
Class		**Code**	**Source**	
Landscape Scenery Areas		T.1	Landscape Scenery Areas	
Additional Visual Landscape Value				
Class	**Subclass**	**Code**	**Source**	
	Topographic structure	1	Interesting geomorphological formations	**Natural**
		2	Valleys	
		3	Hills	
	Vegetation	1	Forest cover	
		2	Endemic plant	
	Water surface and wetland	1	Lake	
		2	Water supply	
	Socio-cultural items	1	Residential	**Socio-Cultural**
	Recreational items	1	Daily use of area	**Recreational Items**
		2	Tent camping area	
		3	Wood cottage houses	

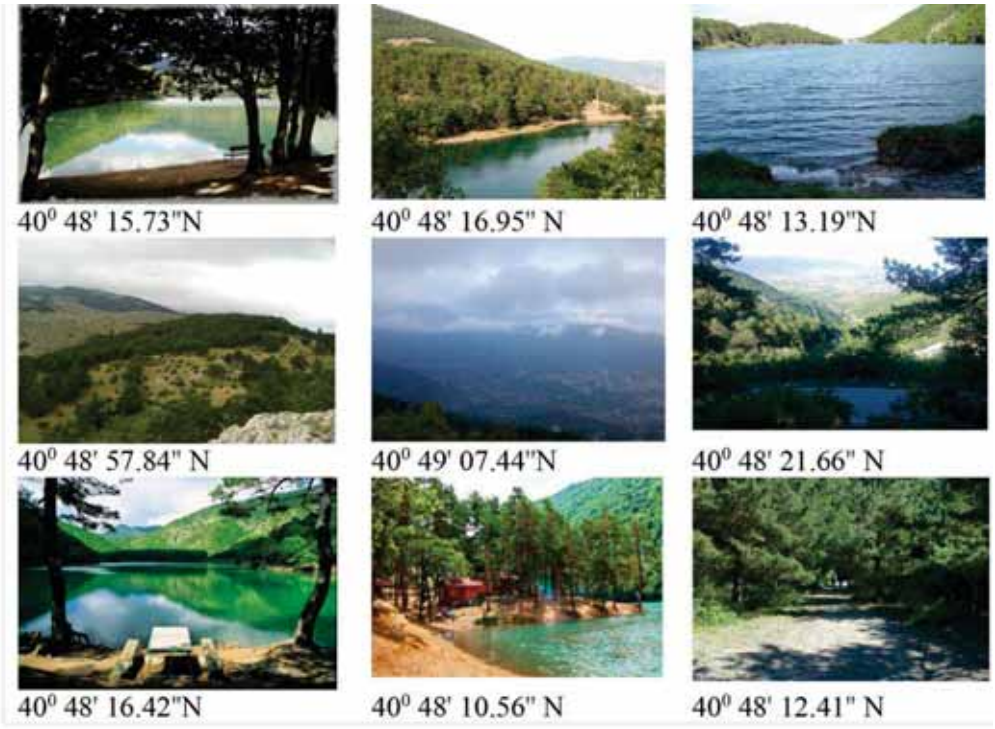

FIGURE 2
Points and coordinates about the visual landscape value of Boraboy Lake and Natural Park

The study area was chosen upon considering the work conducted by [14] and [20] Boraboy Lake's and Nature Park's natural traits and vantage points with a dominant view of the natural landscape were specified as "basic visual landscaping values". Locations in the area with visual landscaping value were determined based upon the data relayed by the expert opinions and then photographed. 10 of the photographs chosen among these are given on Figure 2 with their coordinates.

With the help of [20] study; recreational resource values of Boraboy Lake and Nature Park were determined according to the analysis of the experts on the specified areas with high values of visual landscaping. In scope of these data; there was a "recreational usage analysis" on Table 2, created by the experts for the recreationally significant areas of the region in terms of opportunities (visual preference, spots with wide selection of visual advantages) and limitations (functional and structural). Accordingly, potential usage of the area's recreational resources and limitations were presented.

Considering these data gathered, the natural resource values and the relationship of human utilization were evaluated and the districting of the nature park according to usage was foreseen and planning decisions in this direction were taken. With this districting study; determining the areas with common traits and problems, developing plan decisions for each of the identified regions, increasing the feasibility of the plan and laying the groundwork for an effective administrative organization were aimed. Regional studies carried out in light of these objectives, would make it easier to come up with a healthy, applicable and effective plan.

RESEARCH FINDINGS

Each photograph was graded according to five-point Likert scale and the recreationally important regions of the area are determined by Q-sort analysis. Also the one –way ANOVA analysis showed that there was significant in judgement among all classification of visual landscape values on standard deviation.

Natural sources. 800 meters above the sea level (1050 meters altitude), known as a crater lake; this is a natural landslide lake formed by the clogging of a small lake with the debris coming from the surrounding area. It is 80 meters wide and 25 meters deep, located on an eastward-westward valley. The lake has a measurement of 900 x 300 meters and is surrounded by beech, Scotch pine, cedar and chestnut trees. It is a wonder of the nature and has the color of emerald green. Its south shore is steep. Its north shore can be conveniently used as a picnic area. It is formed by the clogging of the Catagan stream, with the landslide debris coming from the Civili hill located in the foothills of Akdag. It is spread through the bottom of a valley with an altitude of 1050 meters. Water leaking from the bottom of the east end of the lake, regains its rapid flow and forms one of the tributaries of Green River. It has the climatic characteristics of Black Sea climate [25].

Evaluated in terms of fauna; Amasya is one of the important regions in the sense of endemic plants and Boraboy Lake with its surroundings is the most important endemic plant site of Amasya. According to the latest evaluations conducted in Amasya, there are 245 endemic taxa (type-sub type variety) detected within the provincial borders of Amasya and 29 of these endemic types seem to be scattered around Amasya Akdag – Boraboy Lake and their surroundings. In terms of flora richness, surroundings of Boraboy Lake are covered with Scotch pine and oak trees. There are also local name plant of types like *Carpinus* sp*., Ostrya* sp., *Sorbus* sp., *Cornus* sp., *Acer* sp., *Crataegus monogyna, Santalum album*, *Corylus columa*, *Rubus fructicosus* and *Rhododendron sp.,* in this region. Known species in terms of fauna richness in Boraboy Lake, Nature Park area are these: Mammals; deer, rabbit, wolf, fox, wild boar, squirrel, hedgehog, weasel, badger. The area is also a home for many local and migratory bird types. Among these are; quail, coot, jack snipe, turtle dove, pigeon, rock dove, wood pigeon, common blackbird, song thrush, cormorant, grey heron, bittern, stork, black stork, hawk, sparrow hawk, vulture, shaker falcon, eagle-owl, Syrian woodpecker, coal tit, great tit, blue tit, common rose finch, wall creeper and robin redbreast. There are also reptiles; tortoise, terrapin, lizards, snakes, snails; freshwater fish like carp and bullhead inside Boraboy Lake.

Resource values. the main resource value of the field is the Boraboy Lake. Asides from that, there are some significant endemic plants types, fauna and flora on the area and its surroundings.

Cultural values. many of the visitors coming from the surrounding villages, valleys and counties, use the location as a picnic area. During weekdays, most of the visitors are the ones coming from close-range villages, counties and valleys. The visitor population increases considerably with the people coming from neighboring cities like Amasya, Samsun, Tokat and counties connected to them. During weekdays, the visitor population mainly consists of people with lower financial power. However, people visiting on the weekends tend to be a richer and educated crowd in comparison and the area is not only used for picnic purposes but also for recreational activities.

Recreation opportunities. aside from the sloping lands, the Nature Park is also an attraction with its plain and recreationally suitable topography. Landscape openings and the lake located in the middle of the region make a positive effect on the recreational usability of the field. The park is also an attraction point for nature walks on alternative and different roads other than the existing hiking paths, in terms of the many beautiful landscapes that can be viewed on the way. The most commonly practiced tourism activities in the region are the nature walks but there are also touristic options like highland tourism, line fishing, camping, caravan tourism and trekking. The people participating in these tourism activities are mostly day trippers but there also a total of 19 country houses for the lodgers, 10 of which came into operation in 2016, each of them with a 50 m^2 space. Other than these, the findings show that there are many future projects aimed at the development of Boraboy Lake and these projects are backed by OKA (Middle Black Sea Development Agency). Thus, the area is a central place, frequently receiving local and foreign visitors.

The operation rights of Boraboy Lake belong to "Boraboy Education, Culture and Solidarity Association Financial Management and these rights can be obtained by any person of company as long as they win the bidding that is held each year. The tourism types performed in the region show accordance to the [13]. Other than that, there are plans to have organizations in which athletes and teenagers may visit the area in groups and go camping. However, as the area is considered to be a level 1 and level 3 protected area, there are limitations to the applications that are being planned for the region [28].

The experts were asked if there was any place that acts as an example for the operation and quality of the Boraboy Lake; they answered that there is no such place. Besides, they commented that the place is one of a kind and there is not any equivalent place that can be taken as an example. When the features that could bring out Boraboy Lake are reviewed, it is clear that there are possible applications which can be arranged by revealing the natural beauties of the lake and combining them with the opportunities presented by Akdag which is located above the lake. Some of the suggestions put forward in this context are paintball, floating restaurant, ATVs (all-terrain vehicles), horse riding etc.

Landscaping sources determined by field studies within the scope of the method are systematically listed on Table 1. The nature park is rich in landscaping value with its forest texture and geomorphological/topographical structure. Thus, in designating observation points with regards to landscaping values, the viewing spots overseeing the existing natural landscaping were prioritized. In addition to this, other perceivable landscaping values that have a positive effect in terms of visual landscaping, are taken into account while identifying viewing spots. Also, a "problem-possibility analysis" was conducted in light of the study done by [35], in order to review the problems and possible solutions of the area so as to set up guidelines for the planning of Boraboy Lake and the Nature Park. The problems detected about the area, the sources of these problems and the possibilities presented by

the region are listed on Table 2.

Considering the above information; Boraboy Lake is scrutinized by the experts, in terms of recreational usage. A Q-Sort analysis was conducted with 12 parameters related to visual landscaping characters (Table 2).

The parameters reviewed in Boraboy Lake did not yield a negative point. Upon examination in terms of recreational aspects; it is seen that the highest points (49 points) is set for the country houses for the lodgers. The location for the use of day trippers has (43 points) and tent camp area has (36 points). The lake factor which is used in evaluating the water existence, also has a high point of (47 points). The lack of any settlement nearby is an aspect in preventing the environmental pollution. In light of the data obtained, the settlement criterion has a high point of (44 points) (Table 2). Also, standard deviation of obtained surveys see Figure 3.

TABLE 2
Q-sort analysis results of Boraboy Lake and Natural Park

		Very Beautiful n1	Beautiful n2	Ordinary n3	Ugly n4	Very Ugly n5	Photo point N
Landscape Scenery Areas		15	9	6	0	0	39
Topographic structure	Interesting geomorphologic formations	6	10	8	5	1	15
	Valleys	7	12	7	4	1	20
	Hills	14	10	4	2	0	45
Vegetation	Forest cover	16	14	0	0	0	42
	Endemic plant	15	9	6	0	0	39
Water surface and wetland	Lake	18	11	1	0	0	47
	Water supply	13	11	6	0	0	37
Socio-cultural items	Residential	15	14	1	0	0	44
Recreational items	Daily use of area	17	9	4	0	0	43
	Tent camping area	14	8	8	0	0	36
	Wood cottage houses	19	11	0	0	0	49

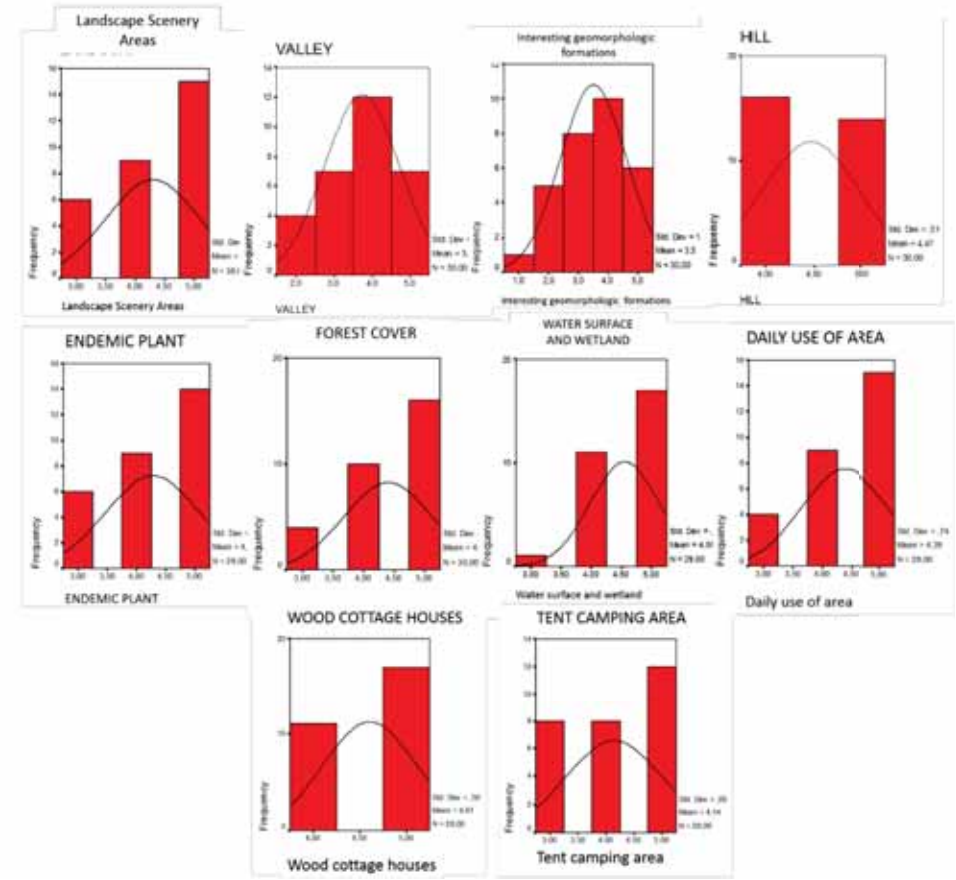

FIGURE 3
Frequency distribution of landscape items in Boraboy Natural Park

When we look at the scoring obtained by the evaluation of the data, it is seen that Boraboy Lake with its water surface and lodging options in its surroundings, is an important nature park. Also, standard deviation of obtained surveys see Figure 3.

RESULTS AND SUGGESTIONS

Nature protection consists of all the encouraging and protective measures that secure the wild animals, plant species, natural habitats for them, the landscaping and the landscaping elements of these habitats [19]. In his study, states that one of the most important tourism types practiced around Boraboy Lake is hiking in nature [13]. He also mentions that there are maps and signboards on the way of these hiking areas. These maps and signs have useful information on them like bird types, tree types and the nature area. On the other hand, it should be mentioned that these maps and signboards should be updated according to the developing aspects and changing situations of the area.

Based on the statement of [5]; "protection, especially aims at the preservation of the recreative and touristic characteristics of an area", existing recreational value of the area is determined, and analyses were conducted in light of the expert opinions.

Accordingly, 7 regions deemed recreationally significant in Boraboy Lake and the Nature Park area are designated with their coordinates and marked on the map of the location. These marked spots are the most visually impressive locations of the nature park and among these spots, there are two open spaces in the forest suitable for camping. These areas present opportunities for landscape viewing, relaxation, visitations, nature walks and camping. However, since the nature park is quite fragile in terms of natural resources, protective measures taken for the usage of these areas must always be in effect. This area is especially rich in forest existence and endemic plant types, so it is crucial that none of the recreational activities should cause any harm to the existing resource values of the area.

As mentioned in the study of [26], landscape planning is a planning approach based on the landscaping ecology. Areas with landscaping value can only be preserved as long as the usage continuity of their natural and cultural sources is established. Landscape evaluation consists of landscape planning and strategy developing for the preservation, administration, improvement and application of the landscape. For this purpose, it is important to set up planning decisions aimed at protection-application during the physical planning of these areas. Concordantly, designation of the development strategies aimed at the protection and recreation of Boraboy Lake and the Nature Park, was conducted based on the recreational usage analysis. The sustainable application of the rich resource value and recreational potential of Boraboy Lake and the Nature Park could only be possible as long as the ecological integrity of the area is intact, and the existing habitat is preserved.

When the findings of the study are reviewed, it is possible to make below suggestions:

- Within the scope of the study area, alternatives for accommodation should be created.
- It should be aimed to increase both the visitor number and the days they choose to stay by presenting more possibilities that would serve as reasons to visit the area.
- There should be an equivalent area specified as an example and based upon the planning of this area, plans should be formed for Boraboy Lake.
- Prominent aspects of the area should be included in the publicity banners.
- Environmental factors that can provide sustainability, should be designated in order to form solutions.
- Troubles about the roads and water system of Boraboy Lake should be addressed.

REFERENCES

[1] Howley, P. (2011) Landscape aesthetics: assessing the general publics' preferences towards rural landscapes. Ecological Economics. 72, 161-169.
[2] Purcell, T., Peron, E. and Berto, R. (2001) Why do preferences differ between scene types? Environment and Behavior. 33(1), 93-106.
[3] Nighties, S., Van Lammeren, R. and Van Der Hoeven, F. (2011) Exploring the visual landscape: advances in physiognomic landscape research in the Netherlands. Research in Urbanism Series 2. Tu Delft.
[4] Keshtkaran, R., Habibie, A. and Shari, H. (2017) Aesthetic preferences for visual quality of urban landscape in Derak high-rise buildings (Shiraz). Journal of Sustainable Development. 10(5), 2017
[5] Dirik, H. (2011) Nature conservation reasons and evaluation. Access link, Http://Www. Paraketa. Net/2011/01.
[6] Arpa Yenilmez, N. and Ceran, Y. (2015) Ecotourism, protected areas and nature conservation. Fresen. Environ. Bull. 24, 250-257.
[7] Daniel, T.C. (2001) Weather scenic beauty? Visual landscape quality assessment in the 21st century. Landscape and Urban Planning. 54(1-4), 267-281.
[8] Zube, E.H., Sell, J.L. and Taylor, J.G. (1982) Landscape perception: research, application and theory. Landscape Planning. 9(1), 1-33.

[9] Arthur, L.M., Daniel, T.C. and Boster, R.S. (1977) Scenic assessment: an overview. Landscape Planning. 4, 109-129.
[10] Lothian, A. (1999) Landscape and the philosophy of aesthetics: is landscape quality inherent in the landscape or in the eye of the beholder. Landscape and Urban Planning. 44(4), 177-198.
[11] Scott, K. and Benson, F. (2002) Public and professional attitudes to landscape: scoping study. Newcastle, University of Newcastle.
[12] Colak, A.H. (2001) Nature conservation national parks and hunting in the forest. Wild life General Directorate Publications. ISBN: 975-8273- 7:354, Ankara.
[13] Dogancilli, S.O. (2016) Alternative tourism in Amasya: evaluation of Boraboy Lake from ecotourism. 1. International academic research congress. 103-110, Antalya.
[14] Erduran F. and Cırık, U. (2011) Determination of recreational landscape values of Gelincik Nature Park. Journal of Agricultural faculty of Ataturk University. 42(1), 63-77, 2011.
[15] Zencirkiran, M., Ender, E., Cetiner, S., Gorur, A., Eraslan, E., Tanriverdi, D.O. and Celik, B., H. (2018) A research on Kocaeli geophytes and their ornamental purposes for sustainable landscape design. Fresen. Environ. Bull. 27, 6042-6052.
[16] Fairweather, R. and Swaffield, S. (2001) Visitor experiences of Kaikoura, New Zealand: an interpretative study using photographs of landscapes and Q method. Tourism Management. 22(3), 219-228.
[17] Turkyılmaz, B., Kurucu. Y., Bolca. M., Altınbas. U., Esetlılı. M.T., Gulgun. B., Ozen. F., Gencer, G., Guney, A., Hepcan, S. and Ozden, N. (2007) A GIS based model for rating natural protection areas according to natural protection priorities. The International Journal of Sustainable Development and World Ecology. 14(3), 278-286.
[18] Sahin S., Dilek F., Cakcı I. and Koylu P. (2005) Akdag Natural park conservation and recreation landscape planning. Rural Environment Yearbook. 60-68, Ankara,
[19] Bolca, M., Turkyilmaz, B., Kurucu, Y., Altinbas, U., Esetlili, M.T. and Gulgun, B. (2007) Determination of impact of urbanization on agricultural land and wetland land use in Balcova Delta by remote sensıng and GIS technique. Environmental Monitoring and Assessment. 131, 409-419.
[20] Aks Planning and Eng. Ltd. St. (2010a) Gelincik Mountain long term development planning report. Ankara.
[21] Demiroglu, D., Yucekaya, M., Gunaydin, A., S. and Tascioglu, S. (2017) Ecological approach to urban parks: the case of urban parks in Kilis, Turkey. Fresen. Environ. Bull. 26, 7142-7149.
[22] Yazici, K., Gulgun Aslan, B. and Ankaya, F. (2017) Examination of landscape scenery areas and activities: a case study in Van Province of Turkey. Karabuk University Journal of Institute of Social Sciences. Special issue. 3, 168-176.
[23] Birisci, T., Mansuroglu, S., Sogut, Z. and Kalayci Onac, A. (2017) Tree, environment and soil. In every sphere of life soil book. E-Isbn: 978-605-4303-80-9, 233-254.
[24] Birisci, T., Mansuroglu, S., Sogut, Z., Kalayci Onac, A.E. and Dag, V. (2017) Nature Friendly Landscape Applications. International Conference on Agriculture, Forest, Food Sciences and Technologies, Cappadocia/Turkey. Abstract E-Book, 1227.
[25] Anonymous. (2017) Amasya Provincial Directorate of Culture and Tourism. Official web page Amasya.
[26] Cetinkaya, G. (2003) Nature conservation areas and biosphere reserve. Rural Environment Yearbook. 32-40, Ankara
[27] Anonymous (2011) Turkish Ministry of Forest (MOF) & General directorate of National Parks, Game and Wildlife (GDNPGW).Official internet site Ankara.
[28] Belknap, R.K. and Furtado, J.G. (1967) Three approaches to environmental resource analysis. The Conservation Faundation. Washington, USA.
[29] Martinez-Falero, E. and Gonzales-Alonso, S. (1995) Techniques in landscape planning. Boca Raton. Lewis Publishers, 1995.
[30] Pitt, D.G. and Zube, E.H. (1979) The Q-sort method: use in landscape assessment research and landscape planning. Proceedings of a Conference on Applied Techniques for Analysis and Management of the Visual Resource, Berkeley.
[31] Golchin, P., Narouie, B., and Masnavi, M. R. (2012) Evaluating visual quality of educational campus based on users preferences (case study: Sistan and Baloochestan University, Iran). Journal of Environmental Studies. 38(62), 43.
[32] Uzun, O. and Muderrisoglu, H. (2011) Visual landscape quality in landscape planning: examples of Kars and Ardahan cities in Turkey. African Journal of Agricultural Research. 6, 1627- 1638.
[33] Scottish Natural Heritage (2013) A hand book on environmental impact assessment guidance for competent authorities, consultees and others involved in the environmental impact assessment process in Scotland. 4th Ed.

[34] Aks Planning and Eng. Ltd. St. (2010b) Gelincik Mountain long term development plan analytical survey report. Ankara.
[35] Cakcı, I. (2007) A research of methodology for visual landscape assessment in landscape planning. Ankara University. Department of Landscape Architecture, Ankara.

Received: **12.10.2018**
Accepted: **26.03.2019**

CORRESPONDING AUTHOR

Kubra Yazici
Tokat Gaziosmanpasa University
Faculty of Agriculture
Department of Horticulture
60240 Tokat – Turkey

e-mail: k-yazici-karaman@hotmail.com

© by PSP Volume 28 – No. 5/2019 pages 3787-3794 Fresenius Environmental Bulletin

A NEW APPROACH FOR THE ESTIMATION OF DEPRECIATION FACTOR AND ENERGY LOSS IN LIGHTING SYSTEM

Mustafa Sahin*

Department of Electrical and Electronic Engineering, Technology Faculty, Afyon Kocatepe University, Afyonkarahisar, Turkey

ABSTRACT

In lighting systems, luminaires, lamps and wall surfaces become dirty in the long run. Besides, the luminous flux in the lighting elements also decreases depending on usage. As a result, the brightness level in interior space decreases gradually. The amount of decrease in the lightness level is determined by the depreciation factor (*df*). For the detection of depreciation factor, measurements should be taken at several different points over the lighting system. By using these measurements, the average brightness levels can be calculated according to the standards which are prepared by the Chartered Institution of Building Services Engineers (CIBSE). The depreciation factor is calculated by using the average brightness values in the next step. This is a process that requires time and effort. In the present study, an ANN model was created as an alternative to all these long and exhaustive measurements and this ANN was trained for estimation of depreciation factor. The correlation coefficient (*r*) of the trained ANN was calculated as 0.99. The fact that the actual and obtained estimated values were close to each other. After 24 months from the first obtained data, the existing lighting system has been improved and so 20% of the electricity energy which does not produce light has been recovered. Thus, energy waste and light loss were prevented. Moreover, the ergonomic comfort conditions of the lighting environments were kept at the desired level.

KEYWORDS:
Energy save, Illumination, ANN, Depreciation factor, Lighting systems lifetime.

INTRODUCTION

Fossil fuel reserves which meet a significant part of energy need today have being running out quickly. This situation has led people to find new alternative sources of energy, and to use existing sources of energy in maximum efficiency and in an economic way [1]. Electrical energy is needed in every step of our daily life [2] (heating, air conditioning, transportation, industry and illumination) [3]. However, when the cost of the methods used in the generation of electrical energy and the difficulties of transmitting it to the consumer are considered, it has been inevitable to carry out studies to employ it more consciously and economically [4-5].

In parallel with the development of industry in recent years, the number of shopping malls and office based public and private sector buildings, administration and management centers have increased. These buildings have large interior spaces including under ground level as well, so these buildings increase the need for artificial lighting [6]. 19% of electrical energy consumed in the world is spent on illumination. The part of electricity spent on illumination except for the industrial organizations is 47%. When this ratio is considered, it is inevitable that electric energy should be used economically for illumination as it should be for all areas of industry and home use. Energy saving is to use the energy in an efficient way without having any decrease in production, comfort and workforce and not to waste it [7].

The main purpose of designing a lighting system is to obtain enough light without increasing energy costs while avoiding extensive lighting. In order to use the energy in an efficient way on lightening, a proper lighting design should be performed during installation process [8]. Installation load of lighting system and the operating time of lighting system should be minimized, and the maintenance and cleanup practices during the operation should be performed regularly on an existing system. Therefore, energy saving in lighting is possible by using lamps with a high efficiency factor and through a right and safe maintenance method [9].

What is important in lighting is to create an order which will provide the proper lighting for the purposes of the practice on current situation. Here, properties such as color and the direction of the light, softness or sharpness of the shadows at the obtained light play significant role [10]. A good lighting has been a must today both to meet the special wishes of individuals and to solve various problems of societies under ordinary or extraordinary circumstances. Otherwise, visual fatigue

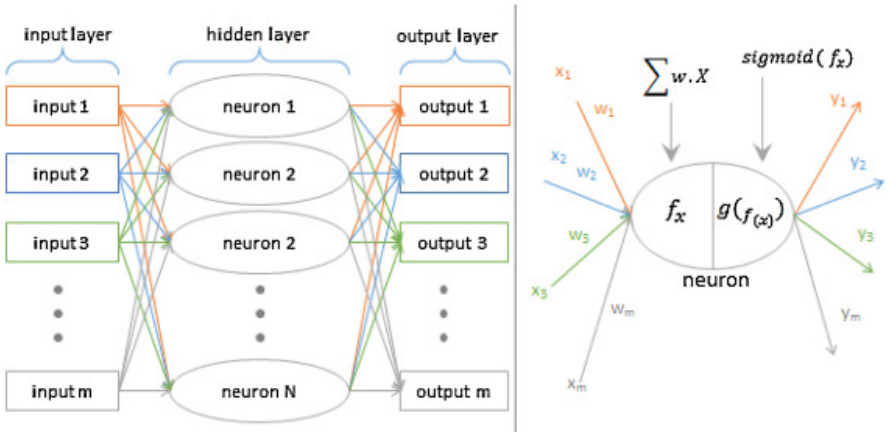

FIGURE 1
Graphical representation of a neural network (left) and artificial neuron (right)

occurs because of unsuitable lighting and it may also cause serious traumas in work places [11]. In a study carried out in a work place, it has been found out that physical fatigue of two out of every three people is due to weak lighting in the work place [12].

The ANNs are generally accepted as computer systems which perform learning function as the basic characteristic of brain to solve complicated problems [13]. The ANNs structurally consist of three sections as input layer, hidden layer and output layer with interconnected process units (Fig.1) [14]. Each neuron consists of two main sections as an activation function and transfer function.

Each connection on process units has a weight value. The information of an ANN is hidden in these weight values and spreads throughout the ANN [15]. Learning practice is performed by using key information samples [16]. Today, computer codes are used for estimation and the used algorithms are based on the solution of complicated mathematical equilibrium [17]. Significant amount of time and powerful computers are needed to reach the right result [18]. Moreover, since the neural networks can process deficient or damaged data, they have the opportunity to minimize the mistakes [19].

Since determination of depreciation amount in lighting systems is difficult, evaluating system performance and determining the maintenance interval are complicated practices. In order to determine maintenance interval, it is necessary to measure illuminance levels at numerous points of work plane in the environment. Based upon these measurements, isolux curves are created based on minimum illumination level, average illumination, smoothness factor and counter illumination level. When such procedures are considered, the determination of the depreciation amount of a lighting system is a tiring process and it takes a considerable time and effort [20].

When these difficulties are taken into account for determining the depreciation amount of a lighting system, it is inevitable to search for a new solution and use different methods to calculate both natural and artificial lighting system parameters [21].

A limited number of studies have been conducted in the literature. In Kocabey's (2014) study, the Finite Element Method (FEM) was used to determine the maintenance interval in lighting systems. In our study, the same procedure has been performed by the ANN method [22]. In the Kazanasmaz's (2009) study, they predicted the daylight brightness level by using an ANN. The ANN method was also used in our study, but unlike Kazanasmaz's study, the *df* was estimated within artificial lighting systems [23].Tran (2014) worked on controlling a sensorless LED lighting system by using the ANN. In our study, a new prediction model was created differently from Tran's work [24]. Şahin (2016) estimated the brightness distribution in the environment with the ANN in order to calculate the *df* in lighting systems. In this study, *df* was directly estimated with ANN.

In this present study, illuminance level measurements were performed on the minimum spot as designated by the suggestions of the International Commission on Illumination CIE [25]. The ANN was created and trained by using these measured data and depreciation factor related to the current lighting system was estimated. In the direction of these estimations, depreciation rate related to the current lighting system was designated. In this way, the determination of whether it was the maintenance time of the system or the system expiration was ensured. Energy loss depending on time of use was responded at the right time and improved and as a result of this, the electric energy which did not transform into light was prevented. In line with these ideas, as a generally accepted method to solve complicated and badly conditioned problems, the ANNs have been used to estimate the depreciation factor of a current lighting system.

MATERIALS AND METHODS

Lighting Systems and the Necessity of Their Maintenance. Illumination is described as "to apply light in order environment and objects to be seen properly" by International Commission on Illumination CIE [26]. The environment and the objects here differ in accordance with the purpose of the lighting application. These differences cause the concept of 'Lighting Technique' to emerge. At first, lighting technique needs to provide visual perception to occur at the best conditions, and thenit should offer the most economic solution in terms of first installation and the cost of use. Moreover, it should be satisfying in terms of aesthetical values and architectural suitability [27]. In this way, illumination becomes an issue aiming not only to meet the physiological need of seeing of people but also to bring visional comfort, labor productivity and architectural properties of surface to the foreground.

No matter how well a lighting system is designed, illuminance level at the beginning decreases depending on time. The reasons of this decrease are:

- The decrease in light flux in lighting equipments
- Failure of lamps
- Becoming dirty of lighting luminaire and lighting equipment
- Becoming dirty or dusty of walls.

Since the decrease of illuminance level in the system is slow and continuous, it cannot be easily recognized. According to researches, it has been found out that eyesight decreases as a result of wrong illumination or decreases of light flux in lighting equipments, occupational accidents increase due to eye pain that occurred in time, productivity and trading size reduce and insufficient illumination does not respond to aesthetical senses and comfort [28]. Besides, physiological and psychological effects of illumination are quite strong. It affects emotional status and motivation level of people [29]. As a part of sensory and perceptual data, illumination and visual perception have an important place. Its effect on emotional status is proved with experimental studies and with other studies [30].

Maintenance is the main factor for a quality of illumination. Periodic maintenance (cleaning, polishing, replacement of lamp and luminaire) can reduce the decrease in the speed of light flux in lighting system. However, this decrease in illumination level, which is called depreciation, cannot be prevented completely and continues throughout the service period (10-20 years) depending on other factors and illuminance level draws a curve as seen in Figure 2 below.

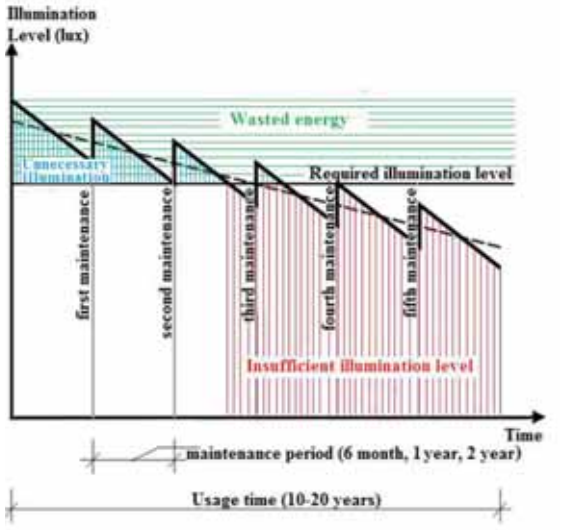

FIGURE 2
Time dependent graphics of illuminance level in an interior space [31]

The rate between the average value in service period and average illuminance level during the initial setup phase in a lighting system is called depreciation factor.

$$df = E_{avg1} / E_{avg2} \qquad (1)$$

Where df is depreciation factor, E_{avg1} is initial mean illuminance and E_{avg2} is mean illuminance at the end of the life cycle [31].

For instance, a depreciation multiplier of 1.5 expresses energy loss at a rate of one-third. Illuminance level obtained in such a situation is higher in the first period of the usage, and it becomes insufficient gradually in the second period. Since this decrease in illuminance level does not have anything to do with consumed electric energy, the cost related to this stays the same during the period of usage. That is to say, the money spent on lighting stays the same, but the illuminance level is imbalanced in the first and second periods. This is an undesired situation in lighting systems.

In order to prevent losses occurred due to depreciation in lighting systems, initial illuminance level can be designed in a way which is more than needed. In this way, although illuminance level is ensured at an adequate level longer than usual, more energy loss occurs. Another solution for depreciation is to use dimmer systems. It necessitates an extra initial investment therefore dimmer systems are not a preferable method in practice. In the light of this information, "Estimation of Depreciation Factor of Lighting System with the ANN" is suggested as a new method.

Illuminance measurements. The purpose of the current study was to estimate the depreciation factor of interior lighting systems by using the ANN and to determine whether it was the mainte-

nance time of the system via obtained data from these estimations. Hence, it is primarily necessary to prepare the data to be used for the training of the ANN therefore related illuminance level values and depreciation factor values were used for the training of ANN.

Necessary measurements were performed at "Circuit Components and Measurement Laboratory", Department of Electric and Electronics Engineering. In order to evaluate lighting systems, illuminance level measurements should be performed in the dark therefore, the measurements started at 10:00 pm. Since the laboratory where the measurements were performed was in the campus and on the third floor, there was no light outside and all the lights were turned off in halls except laboratory. The size of the place where the measurements were performed was 9,8 m wide, 11,7 m long, and 3,5m high and the color of walls in the laboratory was "cream".

The laboratory is lighted with 12 high visibility luminaires in total, which were lined in 3 rows and 4 luminaires for each row. Four TDL 18 Watt Daywhite 1050 lumen fluorescent lamps were used on each luminaire. First, 81(9x9) fixed points were determined and marked on the tables and measurements were made at these points. The distance of a worktable from the floor was 130cm. A LUTRON luxmeter has been used for the measurements.

After all the cleaning and maintenances were performed, necessary initial measurements were made and saved as 9x9 matrixes. The measured data to be used in the AAN training were repeated every month for 12 months period. Since the faculty provides education both day and night, the laboratory was used actively during the time of the measurements. During this period, both lighting equipments and interior walls had worn off, got dusty and dirty to some extend and as a result, illuminance level decreased in the laboratory. When compared to the previous period, an unnoticeable decrease in the values appeared in every measurement period in accordance with the usage, depreciation and pollution. The same measurements were repeated at the end of this usage period and these data were also saved as 9x9 matrixes.

According to the suggestions of the International Commission on Illumination (CIE), real values can be approximated at specific failure rates as a result of illuminance level measurements. However, since the isolux curves are not available, it is not possible to have information about the smoothness of light in the environment. It is necessary to perform measurements at more points but this is a hard and tiring job. In this study, the depreciation factor of lighting system in the laboratory was estimated by using an ANN which was trained with the values obtained from illuminance level measurements performed at the minimum points as possible.

The ANN Model for the Estimation of Depreciation Factor. While evaluating the lighting system, various methods are used to control the efficiency of interior lighting. These are numerical methods such as Maxwell equations, finite elements, and finite difference. Any physical event desired can be modeled using these mathematical methods. Then, this mathematical model can be solved numerically. The solution of partial differential equations emerged as a result of the analysis of these kinds of mathematical models is usually difficult and takes time or can be even impossible to solve. When the solution is impossible, an alternative solution becomes inevitable. Using new methods such as artificial neural networks as alternatives to experimental studies and numerical calculation methods, which are quite costly and inconvenient in terms of both economy and time, would be much more convenient.

Therefore, the artificial neural networks method was used to estimate the depreciation factor in the present study. It was aimed to control the maintenance time of the system and to increase the reliability of it through artificial neural networks. In other words, the estimation of *df* for related to system was aimed when interior lux values are limited in number and on specific points (on two cross diagonal lines) by training an ANN with this limited information. In this way, a more reliable and easier way of determination of maintenance time of lighting system was enabled.

In this study, three different ANN models were established, which were

- Feed-Forward back propagation ANN model,
- Radial Basis Function ANN model,
- Perceptron ANN model.

In this study, each ANN model was trained separately. At the end of each ANN model training, the Perceptron ANN model gave 3.79% error rate, the Radial Basis Function ANN model gave 3.41% error rate and the Feed-Forward back propagation ANN model gave 2.17% error rate. It was observed that the Feed-Forward back propagation ANN model was most successful one among these three models for the prediction of the illuminance level distribution. In this study, the Feed-Forward back propagation ANN model was preferred because of its performance for the prediction of illuminance level distribution with low error rate.

While the ANN model was being constructed, two groups were allocated for training and test purposes. 80% of the monthly measurements were used for the training and remaining 20% of the monthly measurements were used for testing. All measurements lasted 24 months.

The data used in the training of the ANN model consisted of two parts: weight and target data. Weights were applied to the input of the ANN.

Light levels on cross diagonal were used as the weight. Depreciation factor was used as the target. The reason for use of the illumination levels on the cross diagonal was to predict the depreciation factor of the system with fewer measurements. Parameters used for the training of the ANN and minimum and maximum values (range) of these parameters are given in Table 1. 450 (2x9x25) input variables and 25 output variables were used for the training of the ANN.

TABLE 1
The input and output variables used for construction of the model

Code	Input Variable (cross-diagonal illumination values)	Mini-mum	Max-imum
$X_{0,1,...24}$		201.4	260.7
	Target Variable		
Y_1	Depreciation Factor	1	1.294

Values higher or lower than the normal can be observed between input and target data and these can be included in training set by mistake. If these values are different than the normal, this may misdirect the network while calculating net inputs. To scale all training data in a certain range, that is to say, in 0-1 range will help the information from different environment to be reduced to the same scale. In this way, the effect of too high or too low values entering the system by mistake will disappear. This is possible through normalization process. Learning performance of the ANN can be increased through normalization just before the training session. If the input and target data to be used in the training are subjected to certain processes, they could make the training of artificial neural network more productive.

Various normalization methods are available in the practice. Min-Max normalization was used in this study. Minimum describes the lowest value of the data, and maximum describes the highest value of a data. The equation below was used to reduce the data in 0-1 range through the Min-Max method.

$$x' = (x_i - x_{min})/(x_{max} - x_{min}) \qquad (2)$$

Where x' is normalized data, x_i is input value, x_{max} is the biggest input value and x_{min} is the smallest input value.

Normalized input and target data is used for the training of artificial neural network (Table 2). At the end of the process, inverse transformation is applied and transformation to real values is obtained.

TABLE 2
Min. and Max. values of normalized data being used for ANN training

Code	Input Variable (cross-diagonal illumination values)	Mini mum	Maxi mum
$X_{0,1,...24}$		0	1
	Target Variable		
Y_1	Depreciation Factor	0	1

In the last stage, suitable training algorithm for designated Feed-Forward backpropagation network model for the chosen study is determined. In this stage, different training algorithms were used in this study and testing values for three different algorithms with the best results are given in Table 3.

TABLE 3
Testing values for three different algorithms with the best results

Training Algorithm	*r-testing*	*r2-testing*
TRAINLM	0.9941	98.82
TRAINGD	0.9762	95.29
TRAINBG	0.9710	94.28

Correlation coefficient *r* is a measure which is used to determine whether ANN is trained well or not. This is obtained depending on the difference between desired network output and targeted output. Correlation coefficient varies between – 1 and 1. When *r* is equal to 1, it is accepted that there is a perfect similarity between network output and targeted output. When *r* is equal to -1, it is accepted that there is an inverse relationship between output and targeted output. When *r* is equal to 0 there is no similarity between output and targeted output. Levenberg-Marquardt (LM) algorithm was used as training algorithm in this study. Correlation coefficient of this algorithm was $r=0.9941$ and r^2 value (specificity coefficient) obtained as a result of ANN training was 98.82. Parameters related to artificial neural network trained for the study are given in Table 4 below.

TABLE 4
ANN training parameters

Type of ANN	Feed-Forward Backpropagation
Training Algorithm	Levenberg-Marquardt (trainlm)
Learning Function	Trainlm
Performance Function	MSE
Number Of Layers	Between 1 and 10
Number Of Neurons	Between 1 and 20
Activation Function	Tansig, Logsig

RESULTS AND DISCUSSION

Experimental laboratory was subjected to 24 months of usage after the lighting system was installed. Within this time frame, both the lighting fixtures and interior walls in the environment were worn, polluted and got dusty. However, the extent and rate of wear at any point on this time frame or at the end of this period was not known and could not be computed. Making measurements at a lot of spots in the environment is necessary to determine the energy that cannot be transformed into light at the end of that period. This is a time-consuming process.

In this study, a Feed-Forward backpropagation type ANN was used to estimate the depreciation factor. The Levenberg-Marquardt (LM) algorithm was preferred as the network training algorithm. The initial average brightness level of the laboratory was measured as 260.76 lx and the depreciation factor at the beginning was 1.00. The average brightness level decreased in time and depreciation factor increased. The measurements for these values are given in Table 5.

The ANN has been trained with 80% of data was finally tested. The predicted and measured depreciation factor values for the test result are given in table 6.

To obtain true values of *df* in the table, the brightness levels must be measured at many points in the interior space. Using these measured values, the average brightness level in the lighting system was calculated and the *df was* found using an average brightness level. The ANN estimated *df* using a minimum number of light level measurements. This was also a great convenience.

At the end of the 12 months of usage period, the *df* of the lighting system was calculated as 1.132. This value was estimated as 1.141 by the ANN. According to the measurement results, 11.6% of the consumed electricity was not converted into light. The ANN estimated that 12.3% of the consumed electricity was not converted into light. After 12 months of use, 11-12% of electricity energy, which was not converted into light will be prevented by intervening the lighting system.

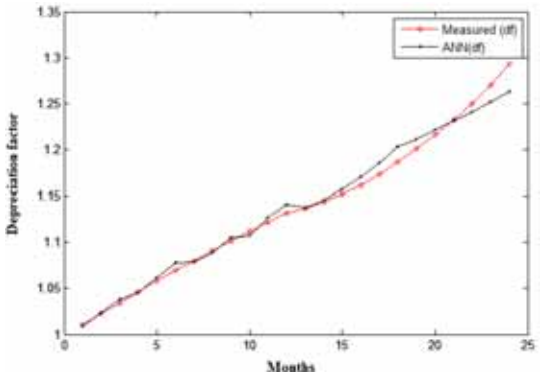

FIGURE 3
Comparison of measurement values and the ANN estimations after 24 month period of use

At the end of the 24 months of usage period, the *df* of the lighting system was calculated as 1.294. This value was estimated as 1.263 by the ANN. According to the measurement results, 22.72% of the consumed electricity was not converted into light. The ANN estimated that 20.82% of the consumed electricity was not converted into light. After 24 months of use, 20-22% of electricity energy, which is not converted to light, will be prevented by intervening the lighting system. A graphical comparison of measured and estimated depreciation factor values for the 24-month period of use is given in Figure 3.

The curve drawn in red color in Figure 6 shows the *df* values obtained as the actual measurement result. The curve drawn in black color shows the *df* values obtained from the ANN estimations. This correlation coefficient of these values was 0.994. This proves the success of the ANN in estimating the *df.*

TABLE 5
Measured average brightness level and depreciation factors

Months	**initial**	**1**	**2**	**3**	**4**	**5**	**6**	**7**	**8**	**9**	**10**	**11**	**12**
Average (*lx*)	260.7	257.8	254.8	252.0	249.1	246.4	243.6	241.3	238.9	236.6	234.4	232.2	230.3
Measured (*df*)	1.00	1.011	1.023	1.034	1.046	1.058	1.07	1.08	1.091	1.101	1.112	1.122	1.132
Months		**13**	**14**	**15**	**16**	**17**	**18**	**19**	**20**	**21**	**22**	**23**	**24**
Average (*lx*)		229.1	227.9	226.3	224.4	222.2	219.5	217.1	214.3	211.5	208.5	205.1	201.4
Measured (*df*)		1.137	1.144	1.152	1.161	1.173	1.187	1.201	1.216	1.232	1.25	1.27	1.294

TABLE 6
Comparison of measured depreciation factor and estimated by ANN

Months	**1**	**2**	**3**	**4**	**5**	**6**	**7**	**8**	**9**	**10**	**11**	**12**
Measured *(df)*	1.011	1.023	1.034	1.046	1.058	1.070	1.080	1.091	1.101	1.112	1.122	1.132
ANN *(df)*	1.009	1.024	1.038	1.045	1.062	1.078	1.079	1.089	1.105	1.107	1.127	1.141
Months	**13**	**14**	**15**	**16**	**17**	**18**	**19**	**20**	**21**	**22**	**23**	**24**
Measured *(df)*	1.137	1.144	1.152	1.161	1.173	1.187	1.201	1.216	1.232	1.250	1.270	1.294
ANN *(df)*	1.138	1.146	1.157	1.170	1.186	1.203	1.211	1.221	1.231	1.241	1.252	1.263

CONCLUSION

A good lighting system can be designed with the help of useful lighting simulation programs. However, it is not possible to calculate the amount of *df* after a certain service time with these programs. Therefore, it is necessary to make individual measurements at many points. Measuring all these individual points is very difficult job and takes a lot of time. For this purpose, an ANN was used to estimate the *df* in this study. The selected lighting system was used for 24 months after its first installation. At this time, the lighting elements and the interior walls of the interior space were worn, polluted and got dirty at a certain rate. During this time, the brightness level measurements were made in this interior region at certain intervals. By using these measurements, actual *df* values were calculated. The same values were also estimated by the trained ANN. At the end of the study, the results predicted by the ANN model were compared with real-time measurement results and estimated values were almost the same as the actual measured values.

At the end of the two-year period of use, the system was intervened and the approximately 20% of electrical energy which was not converted to light was avoided. Moreover, the solution that can be put forward was facilitated by the ANN as a result of long experimental measurements. The suggested possible solution has been unveiled as a result of the long-duration experimental measurements. These processes were simplified with the help of the ANN which is providing great convenience in the determination of insufficiencies resulting because of worn, polluted, dusty lighting fixtures and interior walls in time. It was also easy to the determine maintenance plans by using the ANN. These determinations have contributed to lighting based on energy saving. The use of the ANN can be expanded in the estimation of brightness level distribution in interior spaces. In other words, it is possible to use the ANN to predict *df* of lighting systems with more diverse characteristics by using different variables in the training of ANN. This will allow the estimations to be implemented in various interior lighting systems.

REFERENCES

[1] Lund, H. (2007) Renewable energy strategies for sustainable development. Energy. 32, 6 912–919.

[2] Kralikova, R., Andrejiova, M., Wessely, E. (2015) Energy Saving Techniques and Strategies for Illumination in Industry. Procedia Engineering. 100, 187-195.

[3] Teng, F., Aunedi, M., Strbac, G. (2016) Benefits of flexibility from smart electrified transportation and heating in the future UK electricity system. Applied Energy. 167, 420–431

[4] Liu, J., Zhang, W., Chu, X., Liu, Y. (2016) Fuzzy logic controller for energy savings in a smart LED lighting system considering lighting comfort and daylight. Energy and Buildings. 127, 95-104.

[5] Teke, A., Timur, O., Bayındır, K.Ç. (2016) Development and testing of an energy saving tool – Suitability analysis with case study. International Journal of Electrical Power and Energy Systems. 77, 59-69.

[6] Russell, S. (2012) The Architecture of Light (2nd Edition): A textbook of procedures and practices for the Architect, Interior Designer and Lighting Designer. Conceptnine.

[7] Akella, A.K., Saini, R.P., Sharma, M.P. (2009) Social, economical and environmental impacts of renewable energy systems. Proceedings of Renewable Energy. 34, 390-396.

[8] IEA (2014) Policies for Energy-Efficiency lighting. Energy Efficiency Policy Profiles, International Energy Agency.

[9] Koninklijke Philips Electronics N.V. (2012) The LED Lighting Revolution. A Summary of The Global Savings Potential.

[10] De Graaf, D.T., Dessouky, M., Müller F.O.H. (2014) Sustainable lighting of museum buildings. Renewable Energy. 67, 30–34.

[11] Khosrowshahi, F., Alani, A. (2011) Visualisation of Impact of Time on The Internal Lighting of A Building. Automation in Construction. 20, 145–154.

[12] Soori, K.P., Vishwas, M. (2013) Lighting control strategy for energy efficient office lighting system design. Energy and Buildings. 66, 329–337.

[13] Şahin M., Oguz Y., Buyuktumturk F. (2015) Approximate and Three-Dimensional Modeling of Brightness Levels in Interior Spaces by Using Artificial Neural Networks. Journal of Electrical Engineering and Technology. 10, 1822-1829.

[14] Khayatian, F., Sarto, L. and Dall'O, G. (2016) Application of neural networks for evaluating energy performance certificates of residential buildings. Energy and Buildings. 125, 45–54.

[15] Schmidhuber, J. (2015) Deep learning in neural networks: An overview. Neural Networks. 61, 85–117.

[16] Kalogirou, S.A. (1999) Applications of Artificial Neural Networks in Energy Systems a Review. Energy Conversion and Management. 40, 1073-1087.

[17] Bayata, H.F., Bayrak, O.U., Pehlivan, H. (2018) Characteristics and Estimation of Traffic Accident Counts Using Artificial Neural Network and Multivariate Analysis: A Case Study in Turkey North Transit Interurban. Fresen. Environ. Bull. 27, 2290-2298.
[18] Kalogirou S.A. (2000) Artificial Neural Networks in Renewable Energy Systems Applications: A Review. Renewable and Sustainable Energy Reviews. 5, 373-401.
[19] Rabunal, J.R., Dorado, J. (2006) Artificial Neural Networks Real Life Applications. University of A Coruña, Spain.
[20] Can, E., Sayan, H. (2016) PID and fuzzy controlling three phase asynchronous machine by low level DC source three phase inverter. Tehnički vjesnik. 23, 753-760.
[21] Janjai, S., Plaon, P. (2011) Estimation of sky luminance in the tropics using artificial neural networks: Modeling and performance comparison with the CIE model. Applied Energy. 88, 840-847.
[22] Kocabey, S., Ekren, N. (2014) A new approach for examination of performance of interior lighting systems. Energy and Buildings. 74, 1-7.
[23] Kazanasmaz, T., Günaydın, M., Binol, S., (2009) Artificial neural networks to predict daylight illuminance in office buildings. Building and Environment. 44, 1751-1757.
[24] Tran, D., Tan, Y.K. (2014) Sensorless illumination control of a networked LED-lighting system using feedforward neural network. IEEE transactions on industrial electronics. 61, 2113-2121.
[25] Commission: (2001) Interior Lighting Code. London British Standards Institution. CIBSE.
[26] Commission Internationale de L'Eclairage (2002) The Correlation of Models of Vision and Visual Performance. CIE Publication.
[27] Yang, H.I., Nam, E.J. (2010) Economic analysis of the daylight-linked lighting control system in office buildings. Solar Energy. 84, 1513–1525.
[28] Commission: (2003) Advanced Lighting Guidelines. The New Buildings Institute, USA.
[29] Veitch, J.A., Newsham, G.R. (1998) Lighting quality and energy efficiency effects on task performance, mood, health, satisfaction and comfort. Journal of the Illuminating Engineering Society. 47, 107-129.
[30] Bommel, W.J.M., Beld G.J. (2004) Lighting for work: a review of visual and biological effects. Lighting Res. Technol. 36, 255-269.
[31] Şahin, M., Oğuz, Y., Büyüktümtürk, F. (2016) ANN-based Estimation of Time-dependent Energy Loss in Lighting Systems. Energy and Buildings. 116, 455-467.

Received: **16.10.2018**
Accepted: **27.03.2019**

CORRESPONDING AUTHOR

Mustafa Sahin
Department of Electrical and Electronic Engineering,
Technology Faculty,
Afyon Kocatepe University,
Afyonkarahisar – Turkey

e-mail: mustafasahin@aku.edu.tr

© by PSP Volume 28 – No. 5/2019 pages 3795-3804 Fresenius Environmental Bulletin

SPATIAL DISTRIBUTION PATTERN OF PINUS TABULAEFORMIS CARR. POPULATION ON THE LOESS PLEATEAU, CHINA

Junjun Cui[1], Weizhong Li[1], Shuoxin Zhang[1,2,*]

[1]College of Forestry, Northwest A&F University, 3 Taicheng Road, Yangling, Shaanxi 712100, China
[2]Qinling National Forest Ecosystem Research Station, Huoditang, Ningshan, Shaanxi 716100, China

ABSTRACT

Spatial pattern analysis is an important method to research population biological characteristics, interactions among populations and relationships between population and environment. In this study, two 1-hectare permanent sample plots were established within a natural, secondary *P. tabulaeformis* forest in the Huanglong Mountain region to investigate the spatial distribution patterns of individuals at different growth stages, and the spatial relationships among individuals. Results showed that (1) the diameter structure of *P. tabulaeformis* was complete and the plants were distributed each diameter class in the two plots, individuals in Plot Ⅰ were mainly concentrated at saplings and small trees, fewer number of middle and large trees, belonging to growing population; the individuals in Plot II were mainly concentrated at small and middle trees, fewer number of saplings and large trees, the stable population. (2) The distribution pattern of each growth stage and the spatial scale were closely related, saplings and small trees express as aggregated distribution at small scales, and the aggregated intensity is higher in plot Ⅰ, with the scales increased, individuals tend to be randomly distributed, middle and large trees show random distribution. (3) In terms of the correlation between individuals at different growth stages, there is a significantly positive correlation between saplings and small trees, and saplings and middle trees at small and medium scales, and no significant correlation at large scales; the saplings and large trees are negatively correlated at some scales; there is no significant correlation between small trees and large trees, and between middle trees and large trees.

KEYWORDS:
Point pattern analysis, O-ring Statistic, Spatial Scale, Spatial distribution pattern, Spatial Correlation

INTRODUCTION

Intra- and inter-specific interactions, fundamental to the structure and organization of plant communities [1], are resulted from seed dispersal pattern, self-thinning, regeneration mode and environmental heterogeneity [2-4]. Each of these processes works at a specific spatiotemporal scale. A major focus of ecological research is to understand the nature of these processes. Spatial pattern, an indicator of regeneration and interaction among individuals, provides a good entry point for revealing the nature of forest dynamics. In a forest, the individuals may obey random, aggregated or regular distribution, depending on the location and spatial scale [5, 6].

Located in the upper and middle reaches of the Yellow River, the Loess Plateau is known for severe water shortage and soil erosion [7, 8]. Frequent droughts cause the Loess Plateau to have a sparse vegetation cover. Additionally, strong rainstorms, highly erodible loess soil layers, fragmented landscapes, and forest removal have led to the destruction of the area's ecological system and exacerbated water scarcity and soil erosion [9, 10]. Over the past three decades, the Chinese government has attached great importance to the ecological restoration on the plateau. Considerable manpower, materials and money have been invested in this region to restore the vegetation cover and curb the soil erosion [11]. One of the most effective moves lies in the forest restoration project [12]. The zonal vegetation type in the region is *P. tabulaeformis* forest. *P. tabulaeformis* is a drought-tolerant plant that thrives in poor soil. The forest has the functions of soil and water conservation and environment protection [13]. Recent research has suggested that the spatial distribution of *P. tabulaeformis* is critical to vegetation restoration on the Loess Plateau [14-16]. The existing studies on *P. tabulaeformis* have mainly discussed the community structure, population dynamics, and niche characteristics [17-21].

Focusing on the spatial structure of forest stands on the Loess Plateau, this paper attempts to answer the following questions: what is the spatial distribution of *P. tabulaeformis* and does it change with the spatial scale? Which factors affect the

spatial patterns and correlations of *P. tabulaeformis*?

MATERIALS AND METHODS

Ethics statement. Forestry Bureau of Huanglong County, the governing authority of Huanglong Mountain natural reserve, has given the author the permission to conduct field study in the natural reserve. The author confirms that the field study did not involve endangered or protected species.

Study area. The study area, a typical region of the Loess Plateau, is located in the Huanglong Mountain natural reserve, Shaanxi Province, China (35°28′46″-36°02′01″N, 109°38′49″-110°12′47″E). The mean annual temperature stands at 10.2°C, and the mean monthly temperature changes between -5.7°C (January) and 21.5°C (July). The mean annual precipitation is 611.8mm, with the wettest months being July, August and September. The frost-free period lasts about 126~186 days. The land is predominantly covered by grey-cinnamon soils and the native vegetation is warm temperate broadleaf deciduous forest.

Experimental Design. In 2013~2014, two 1-hectare square plots were established at random locations in the study area. Plot I lies in Hugoumen Forest Farm at an altitude of 1,430~1,488 m above mean sea level (AMSL). The plot is covered by a natural secondary broadleaf coniferous and mixed forest. There is a plurality of tree species, namely, *P. tabulaeformis*, *Quercus liaotanggensis* Koidz, *Betula platyphylla* Suk, *Acer ginnala* Maxim, *Toxicodendron verniciflnum* (Stokes) Barkl., *and Populus simonii* Carr. Plot II, situated in Guanzhuang Forest Farm at an altitude of 1,315~1,371 m AMSL, is also covered by a natural secondary broadleaf coniferous and mixed forest. The common tree species in the forest include *P. tabulaeformis*, *Q. liaotanggensis*, *Populus davidiana*, and *B. platyphylla*.

TABLE 1
Stand structure of trees at the two sample sites

Measurement	Plot	
	I	II
Mean slope (°)	25.09	22.19
Slope aspect (°)	N by W 14	N by W 13
Canopy density (%)	79	62
Species composition[1]	30% *Pine*, 30%*Quercus*, 30% *Betula*, 10% broadleaf trees	80% *Pine*, 10% *Quercus*, 10% broadleaf trees
Density / (trees·ha^{-1})	2467	1103
Tot. basal area / (m^2·ha^{-1})	25.53	21.49
Mean height / (m)	7.01	9.45
Mean diameter / (cm)	11.48	15.78

[1] By volume.

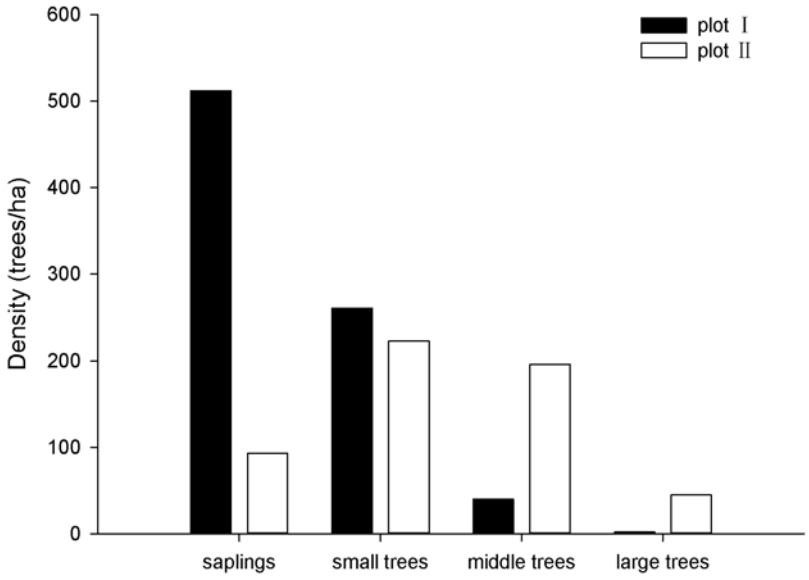

FIGURE 1
Distribution of the different growth stages of *P. tabulaeformis* in plots I and II

The elevation of each plot was determined with a portable GPS. In each plot, the location of all trees with a diameter at breast height (DBH)≥2.5cm was recorded, together with their DBH (cm), height(m), and crown breadth(m^2) (Table 1). Besides, the locations were permanently marked and the tree species were identified. The dynamics of population distribution was analysed by a diameter-class structure [22]. All *P. tabulaeformis* individuals were classified into four growth stages [23, 24] (Figure 1): saplings (2.5cm≤DBH＜10cm), small trees (10cm≤DBH ＜ 20cm), middle trees (20cm≤DBH ＜ 30cm), and large trees (DBH≥30cm).

Data analysis. The second-order characteristics, as the summary statistic of all point-to-point distances in a mapped area, offer the potential to detect different pattern types and scales [25]. Two of the most popular metrics for point pattern analysis are Ripley's K function and O-ring statistic [26,27].

The Ripley's K function describes the occurrence of point patterns in a given area of interest at different scales (distances) and the specific distribution of individuals (e.g. dispersed distribution, clustered distribution, random distribution). The downside is that the results of longer distances are affected by shorter distances, which blurs the spatial correlation at a given scale.

The problem is eliminated by the O-ring statistic, an improved version of Ripley's K function. The circles of the function are replaced with concentric rings. The replacement isolates specific distance classes and permits analysis of spatial patterns at a given distance [28-31]. Moreover, the O-ring statistic includes both univariate and bivariate measures. The univariate O-ring statistic adopts the heterogeneous poisson process if the species distributions are clearly patchy, and complete spatial randomness (CSR) if otherwise. The bivariate O-ring static, however, selects an antecedent condition null model, considering the asymmetric competition among different species [32].

Through the above analysis, the univariate O-ring statistic, O(r) was employed to discuss the spatial distribution patterns of individual P. tabulaeformis population at different growth stages, and the bivariate O-ring statistic, O12(r) was chosen to depict the spatial correlation among individuals.

The generalized O-ring equation is:

$$O(r) = \lambda g(r) \tag{1}$$

$$g(r) = \frac{dk(r)}{dr} / 2\pi r \tag{2}$$

For the CSR, O(r) is equal to λ. If O(r)＞λ, the individuals obey aggregated distribution at distance r; if O(r)＜λ, the individuals obey regular distribution. To remove edge effect, the study area was divided into many small cells. Then, the O-ring statistic is estimated as:

$$O^w(r) = \frac{\sum_{i=1}^{n} \text{Point}[R_i^w(r)]}{\sum_{i=1}^{n} \text{Area}[R_i^w(r)]} \tag{3}$$

$$O_{12}^w(r) = \frac{\frac{1}{n_1}\sum_{i=1}^{n_1} \text{Point}_2[R_{1i}^w(r)]}{\frac{1}{n_1}\sum_{i=1}^{n_1} \text{Area}[R_{1i}^w(r)]} \tag{4}$$

Equations (3) and (4) are respectively the formulas for the univariate and bivariate O-ring statistics. In Equation (4), n_1 is the number of points of object 1; $R_i^w(r)$ is the ring with radius r and width w centring on the i-th point of object 1.

In Equation 5, $\text{points}_2[X]$ is the number of points of object 2 in region X, the area of which is determine by operator Area[X] in Equation 7.

$$\text{Points}_2[R_{1,i}^w(r)] = \sum_{\text{allx}} \sum_{\text{ally}} S(x,y) P_2(x,y) I_i^w(x_i, y_i, x, y) \tag{5}$$

$$\text{Area}[R_{1,i}^w(r)] = z^2 \sum_{\text{allx}} \sum_{\text{ally}} S(x,y) I_i^w(x_i, y_i, x, y) \tag{6}$$

$$I_i^w(x_i, y_i, x, y) = \begin{cases} 1 & \text{if} \quad r - \frac{w}{2} \le \sqrt{(x-x_i)^2 + (y-y_i)^2} \le r + \frac{w}{2} \\ 0 & \text{otherwise} \end{cases} \tag{7}$$

where (x_i, y_i) are the coordinates of the i-th point of object 1; I_i^w is the ring radius r and width w centring on the i-th point with coordinates (x_i, y_i); S(x, y) is a variable that equals 1 if (x, y) are inside the study area and equals 0 if otherwise; $P_2(x, y)$ is the number of points of object 2 in each cell; I_i^w (x_i, y_i, x, y) (Equation 7) is a variable that varies in the circle with radius r centring on the i-th point of object 1; z^2 is the area of one cell. The univariate statistic was calculated under the condition that object 2 equals to object 1.

The calculations were conducted on Programita, a software package for spatial point pattern analysis in ecology [33]. The spatial scale varied from 0 to 50 m at step widths of 1m. Then, the Monte-Carlo simulation was performed 99 times, from which a 95% confidence interval was derived.

RESULTS AND DISCUSSION

Community characteristics and structure of *P. Tabulaeformis*. The *P. tabulaeformis* in Plot II surpass those in Plot Ⅰ in basal area, height and mean diameter, but lagged behind in density (Table 2). In terms of growth stage, saplings account for 63% of the total number of trees in Plot Ⅰ, as compared with 16.7% in Plot II (Figure 1). The proportions of middle and large trees are smaller in Plot Ⅰ than in Plot II. The size distribution is approximately J-shaped in Plot Ⅰ, but close to a normal distribution in Plot II.

TABLE 2
***P. tabulaeformis* metrics from the two plots**

Measurement	Plot	
	I	II
Density / (trees·ha^{-1})	815	557
Basal area / (m^2·ha^{-1})	7.91	17.44
Mean height / (m)	8.22	12.97
Mean diameter / (cm)	11.12	19.97

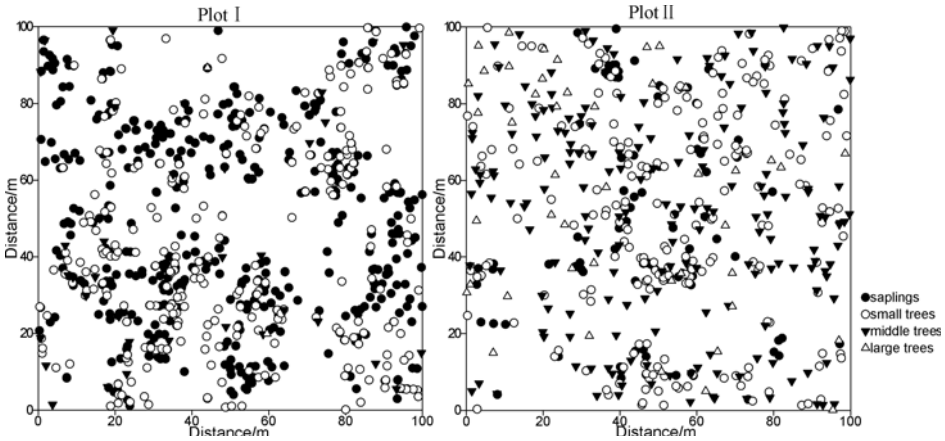

FIGURE 2
Spatial distribution of *P. tabulaeformis* at four growth stages in two 100×100m plots.
Sample sizes are 815 and 557 trees in plots I and II, respectively.

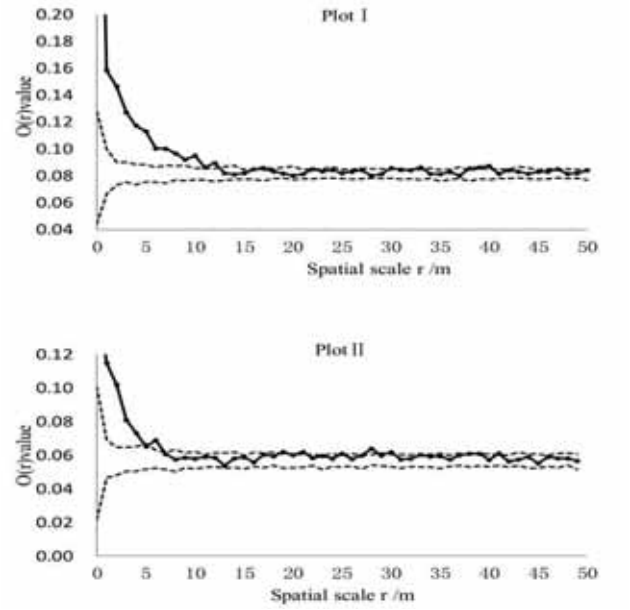

FIGURE 3
Spatial distribution pattern of all *P. tabulaeformis* in plots I and II.
(The solid line is the O(r) value. Dashed lines correspond to the confidence intervals generated from 99 Monte Carlo simulations under the null hypothesis of complete spatial randomness.)

Spatial patterns of the population of *P. tabulaeformis* population. Figure 2 displays the spatial distribution of individual *P. tabulaeformis* individuals in the two plots. The two plots share similar overall patterns of aggregation (Figure 3). The individuals are aggregated at scales<12 m in Plot Ⅰ, and 7 m in Plot II. At larger scales, the individuals are randomly distributed in both plots.

Spatial distribution by growth stage. In Plot Ⅰ, the saplings are aggregated at scales<10m, and are randomly distributed at higher scales (Figure 4-IA); small trees (Figure 4- IB) tend to aggregate at scales<7 m while middle trees (Figure 4- IC) are randomly distributed at all scales; the large trees are too few to exhibit a clear distribution pattern.

In Plot II, the overall pattern is similar to that of Plot I (Figure 4). Specifically, the saplings (Figure 4-IIA) and small trees (Figure 4-IIB) are aggregated only at scales<10 m, while middle (Figure 4-IIC) and large (Figure 4-IID) trees are distributed randomly regardless of scale.

Spatial correlations between different growth stages. There are only minor differences in the correlation between growth stages. In both plots, saplings and small trees are positively aggregated at scales <10 m, and potentially at 3 m distance for small and middle trees (Figures 5, 6). There is no obvious indication of aggregation for any other tree size pairings or distance.

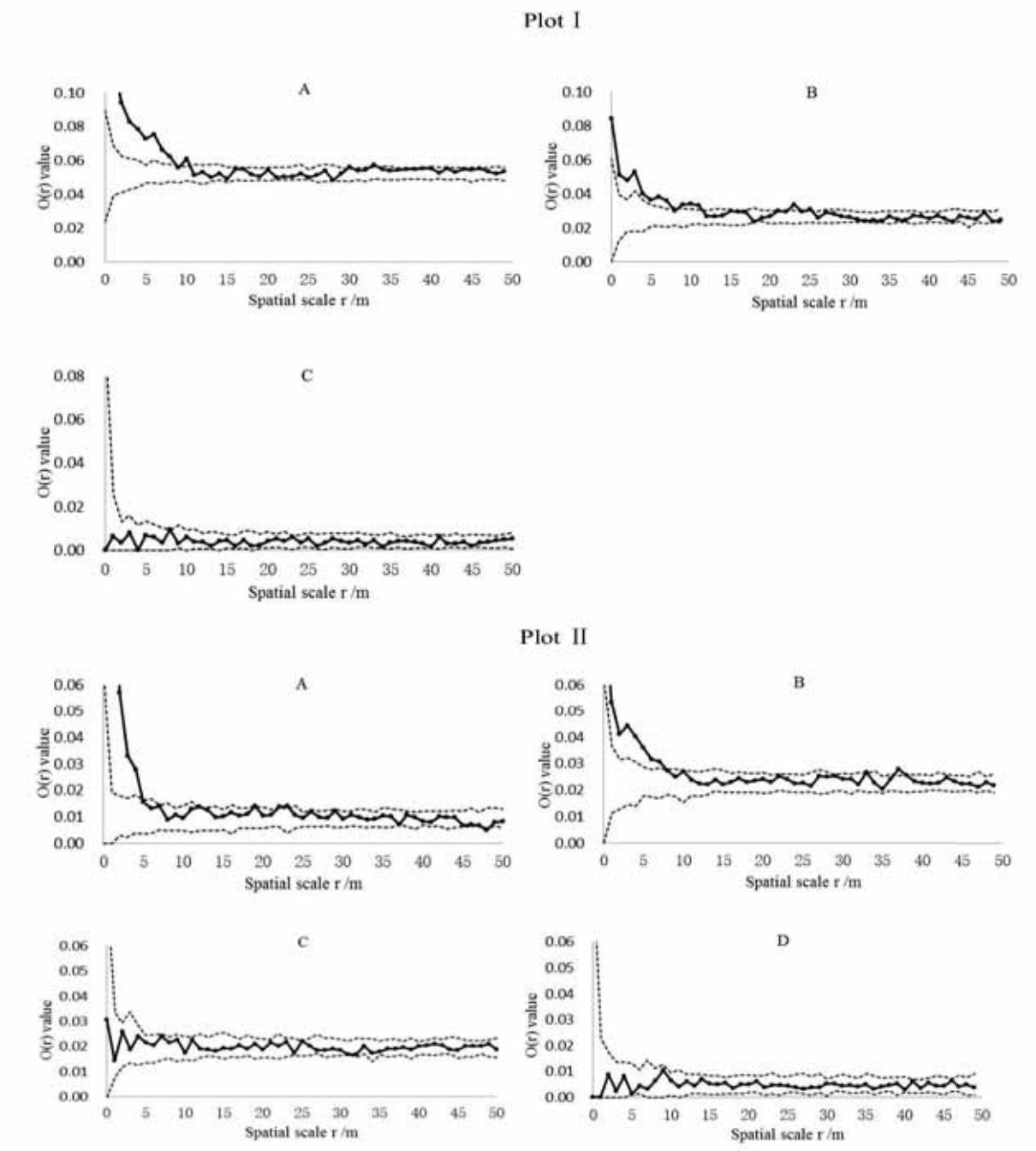

FIGURE 4
Spatial distribution pattern of the different growth stages of *P. tabulaeformis* in plots I and II.
(The solid line is the O(r) value. Dashed lines correspond to the confidence intervals generated from 99 Monte Carlo simulations under a null hypothesis of complete spatial randomness. A saplings, B small trees, C middle trees, D large trees.)

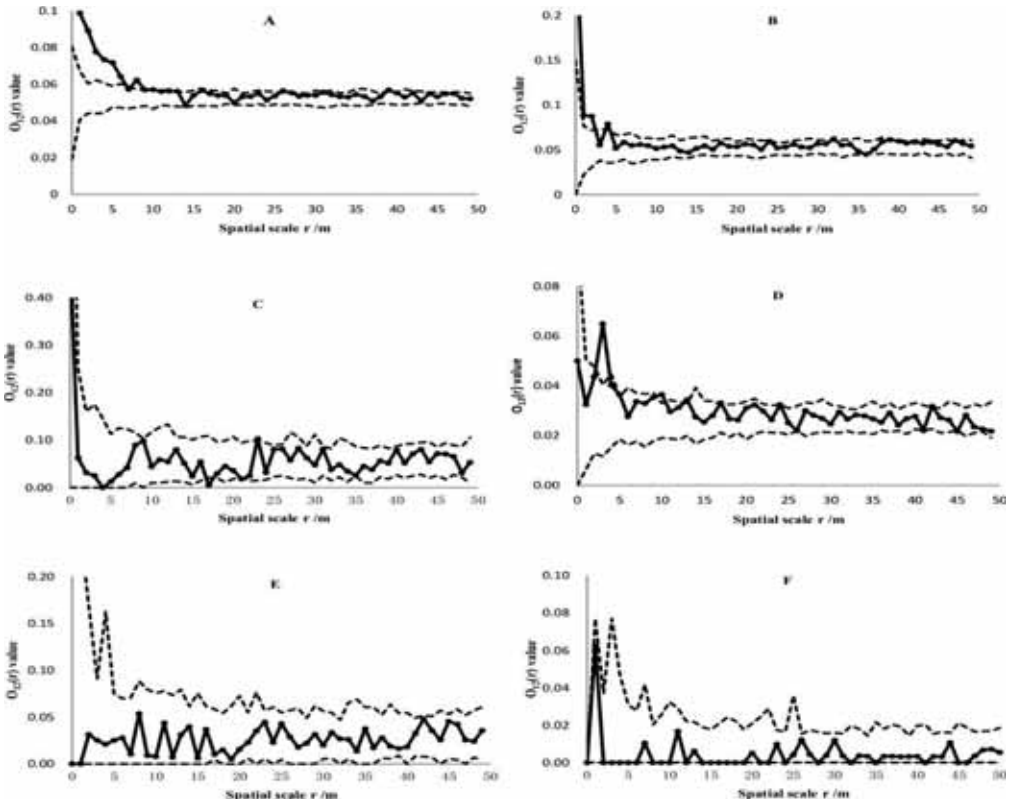

FIGURE 5

Spatial association between different growth stages of *P. tabulaeformis* in plot I.

(The solid line is the O(r) value. Dashed lines correspond to the confidence intervals generated from 99 Monte Carlo simulations under the null hypothesis of complete spatial randomness. A saplings and small trees, B saplings and middle trees, C saplings and large trees, D small trees and middle trees, E small trees and large trees, F middle trees and large trees.)

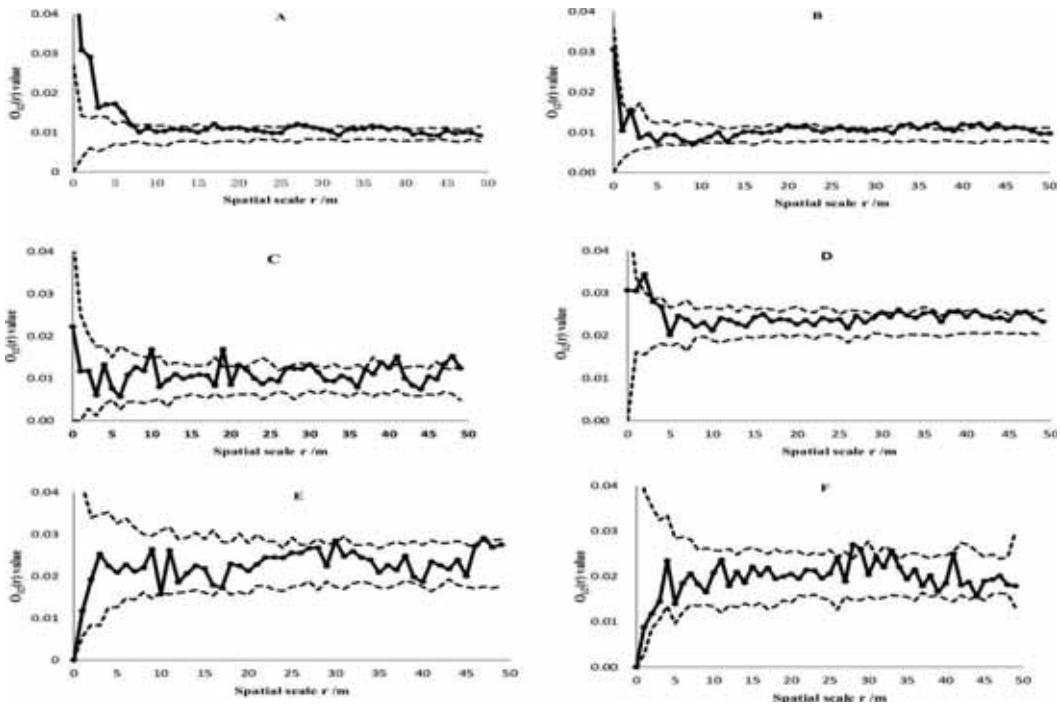

FIGURE 6

Spatial association between different growth stages of *P. tabulaeformis* in plot II.

(The solid line is the O(r) value. Dashed lines correspond to confidence intervals generated from 99 Monte Carlo simulations under the null hypothesis of complete spatial randomness. A saplings and small trees, B saplings and middle trees, C saplings and large trees, D small trees and middle trees, E small trees and large trees, F middle trees and large trees.)

P. tabulaeformis of the two plots differ in DBH distribution. In Plot Ⅰ, the distribution pattern is inverse J-shaped, a signal of the ongoing regeneration within the tree stand. The gradual decline in the number of individuals at DBH>20cm may be attributable to density-dependent mortality. By contrast, Plot II is dominated by small and meddle trees. The relatively few of saplings indicates that little regeneration is taking place in this tree stand. A possible reason lies in the low seed germination rate. Even if the small and middle trees could produce a large number of good quality seeds, the germination rate is still under the constraint of inadequate light. *P. tabulaeformis* is a sun-loving plant. Except for the early stage of individual growth, the plant needs sufficient light, soil nutrient and water throughout its life [34]. Hence, the thick litter layer under the tree stand adds to the difficulty in seed germination. In the only shade-loving growth stage, the plant grows from a seedling into a small tree.

The plant species patterns are under the influence of environmental heterogeneity, intra- and inter-specific competition and life history strategies [35, 36]. Different processes can induce varied spatial patterns. The aggregated distribution pattern, a commonplace in small diameter-class species [37], is often caused by regeneration strategies like limited seed dispersal, vegetative recruitment and effect of nurse trees. As the diameter-class increases, the intra- and inter-specific competition for resources becomes increasingly fierce. The weak aggregation in large diameter-class species verifies the role of herbivores and plant diseases in reducing aggregation. The aggregation has already suppressed by pests on the trees at the diameter of 1cm [38]. The pest effect is not so pronounced on trees with diameter greater than 1cm. The effect is not observed when the tree diameter grows to 10~30 cm. The spatial distribution of *P. tabulaeformis* populations in this study was consistent is consistent with this rule, and the aggregated distribution characteristics echo with the previous research findings [39-41].

The forest spatial patterns are closely related to scales [42]. The spatial distribution of trees may fit one pattern at one interval and another at a different interval [43, 44]. In this research, the spatial pattern of *P. tabulaeformis* is dependent on scale. It is discovered that the tree population obeys aggregated distribution at small scales at some growth stages, but shifts to less aggregated patterns with the increase of scales between individuals. The trend could be explained by the less resource demand of shorter individuals [45]. The aggregated distribution at small scales, e.g. saplings and small trees, can also be attributed to the proximity of fallen seeds to the crown of the mother tree, as well as other environmental factors [46]. As shown in Figure 4, the aggregation is less in the upper DBH class, because adult trees in the class demand more resources (e.g. light, water, nutrient) than younger trees [47-49]. Due to the lack of available resources, self-thinning is likely to happen, thus reducing the aggregation degree [50]. There exists a positive correlation among the previous three growth stages at most scales (Figures 5, 6), indicating that the conspecific trees thrive in these growth stages. The saplings are negatively correlated with large trees at medium scales in Plot Ⅰ (Figure 5). However, the correlation turns positive at some large scales in Plot II (Figure 6). This reveals that the canopies of large trees hinder the growth of saplings. Hence, different growth stages have different requirements on persistence and recruitment, a premise that supports the regeneration niche hypothesis [51]. That the small and middle trees have independent associations with large trees may be explained by the negative effect of forest floor micro-environmental conditions on the survival, establishment, and growth of young trees. To some extent, the finding is consistent with the Janzen-Connell hypothesis, which suggests that high mortality rate is likely to occur to large trees.

CONCLUSIONS

With the aim to facilitate forest management planning, this paper probes into the spatial distributions and correlations of the population of *P. tabulaeformis* in natural secondary forest at different growth stages. The research results reveal the necessity to rationally allocate population density except for cultivating large-diameter timber. The forest of high canopy density should be adjusted timely to allow the regeneration and growth of seedlings under canopy, and promote the stable development of population. In future, the author will create a favourable habitat for seedlings development of *P. tabulaeformis* through low intensity thinning and reducing canopy gaps. The patterns are determined by the biological characteristics and environmental factors of *P. tabulaeformis*, including but not limited to seed dispersal, regeneration mechanism, and micro-environmental conditions of forest floor. In addition, the spatial patterns of species are under the joint action of various factors, such as selective cutting, physiological effect, and disturbance. Thus, the future research should be performed with a large amount of monitoring data.

ACKNOWLEDGEMENTS

This study was funded by National Natural Science Foundation of China (31170587). We are very grateful to Mr Hongjian Deng, Shuo Niu, Duoduo Tan, Huanjie Wang and Yang Wu for their help in field experiments.

REFERENCES

[1] Yilmaz, M., Kir, B. (2018) Effects of different row spacings and different fertilization doses on the seed yield and some yield properties of the tall fescue plant. Fresen. Environ. Bull. 27, 5661-5668.

[2] Kenkel, N.C. (1988) Patten of self-thinning in jack pine: testing the random mortality hypothesis. Ecology. 69(4), 1017-1024.

[3] Dale, M.R.T. (1999) Spatial pattern analysis in plant ecology. Quarterly Review of Biology. 15(1),195-196.

[4] Barot, S., Gignoux, J., Menaut, J.C. (1999) Demography of a savanna palm tree: Predictions from comprehensive spatial pattern analyses. Ecology. 80(6), 1987-2005.

[5] Szwagrzyk, J., Czerwczak, M. (2010) Spatial patterns of trees in natural forests of East-Central Europe. Journal of Vegetation Science. 4(4), 469-476.

[6] Condit, R., Ashton, P.S., Baker, P., Bunyavejchewin, S., Gunatilleke, S., Gunatilleke, N., Hubbell, S.P., Foster, R.B., Itoh, A., LaFrankie, J.V., Lee, H.S., Losos, E., Manokaran, N., Sukumar, R., Yamakura, T. (2000) Spatial patterns in the distribution of tropical tree species. Science. 288(5470), 1414-1418.

[7] Yang, X.M., Wang, F., Bento, C.P.M., Xue, S., Gai, L. (2015) Short-term transport of glyphosate with erosion in Chinese loess soil - a flume experiment. Science of the Total Environment. 512-513, 406-414.

[8] Wang, F., Mu, X., Li, R., Fleskens, L., Stringer, L.C. (2015) Co-evolution of soil and water conservation policy and human - environment linkages in the Yellow River Basin since 1949. Science of the Total Environment. 508, 166-177.

[9] Zhang, B.Q., Wu, P.T., Zhao, X.N., Wang, Y., Gao, X.D. (2013) Changes in vegetation condition in areas with different gradients (1980–2010) on the Loess Plateau, China. Environmental Earth Sciences. 68(8), 2427-2438.

[10] Gao, X.D., Wu, P.T., Zhao, X.N., Wang, J.W., Shi, Y.G. (2014) Effects of land use on soil moisture variations in a semi-arid catchment: implications for land and agricultural water management. Land Degradation and Development. 25(2), 163-172.

[11] Cao, X.C., Wang, Y.B., Wu, P.T., Zhao, X.N., Wang, J. (2015) An evaluation of the water utilization and grain production of irrigated and rain-fed croplands in China. Science of the Total Environ. 529, 10-20.

[12] Zhang, J.T. (2005) Succession analysis of plant communities in abandoned croplands in the eastern Loess Plateau of China. Journal of Arid Environments. 63(2), 458-474.

[13] Zhang, L., Miao, Y.M., Sun, Y.X., Bi, R.C. (2012) Analysis of spatial pattern and spatial association of Pinus tabulaeformis populations at different developmental stages. Bulletin of Botanical Research. 32(1), 91-98.

[14] Zhang, X.B., Wang, R.J., Zhou, T.L., Shangguan, Z.P. (2008) Gap features and renewal dynamics in secondary natural Pinus tabulaeformis forest in hilly loess region. Chinese Journal of Applied Ecology. 19(10), 2103-2108.

[15] Zhang, Y.T., Li, J.M., Chang, S.L., Li, X., Lu, J.J. (2012) Spatial distribution pattern of Picea schrenkiana population in the Middle Tianshan Mountains and the relationship with topographic attributes. Journal of Arid Land. 4(4), 457-468.

[16] Yang, Y.W., Duan, Y.X., Ji, M., Zeng, Y. (2014) Study on population structure and spatial distribution characteristics of Pinus tabulaeformis in the forest region of the Helan Mountains in Inner Mongolia. Forest Resources Management. 2, 87-92.

[17] Zhang, X.B., Guo, X.Q., Shangguan, Z.P., Liu, F.S. (2006) Community characteristics of natural Pinus tabulaeformis forest in Hilly Loess Regions. Bulletin of Botanical Research. 26(2), 169-175.

[18] Hou, L., Lei, R.D., Wang, D.X., Kang, B.W., Chen, S.J. (2006) Niche characteristics of community populations of natural Pinus tabulaeformis forests tended by closing in Huanglongshan Mountain. Acta Botanica Boreal-Occidentalia Sinica. 26(3), 585-591.

[19] Yang, J.L. (2007) Community Characteristics of Pinus tabulaeformis Forests in the Ziwuling Mountains. MA thesis. Gansu Agricultural University, Lanzhou, China.

[20] An, L.J. (2008) The complexity and stability analysis of major communities in Malan forest region of Ziwuling Mountain. MA thesis. Shaanxi Normal University, Xi'an, China.

[21] Cui, C.M., Wang, X.A., Guo, H., Li, W. (2011) Structure and dynamic change of natural Pinus tabulaeformis is populations in the Ziwuling forest area. Arid Zone Research. 28(1), 111-117.

[22] Frost, I., Rydin, H. (2000) Spatial pattern and size distribution of the animal-dispersed tree Quercus robur in two spruce-dominated forests. Ecoscience. 7(1), 38-44.

[23] Miao, Y.M., Liu, R.T., Bi, R.C. (2008) Population structure and dynamics of Pinus tabulaeformis in Huoshan Mountain of Shanxi Province. Journal of Wuhan Botanical Research. 26(3), 288-293.

[24] Guo, W., Shangguan, T.L., Wang, Z.M., Li, R.Q. (2013). Population structure and dynamics of Pinus tabulaeformis in Lingkong Mountain of Shanxi Province Journal of Plant Science. 31(2), 130-135.
[25] Wiegand, T., Moloney, K.A. (2004) Rings, circles, and null-models for point pattern analysis in ecology. Oikos. 104(2), 209-229.
[26] Ripley, B.D. (1981) Spatial Statistics. Hayward Wiley, New York, USA, 252.
[27] Illian, J., Penttinen, A., Stoyan, H., Stoyan, D. (2008) Statistical Analysis and Modelling of Spatial Point Patterns. Technometrics. 47, 516-517.
[28] Fortin, M.J., Dale, M.R.T. (2005) Spatial Analysis [electronic resource]: A Guide for Ecologists, Cambridge University Press, England, 100.
[29] Hao, Z.Q., Zhang, J., Song, B., Ye, J., Li, B. (2007) Vertical structure and spatial associations of dominant tree species in an old-growth temperate forest. Forest Ecology and Management. 252(1-3), 1-11.
[30] Xu, X.M., Harwood, T.D., Pautasso, M., Jeger, M.J. (2009) Spatio-temporal analysis of an invasive plant pathogen (Phytophthora ramorum) in England and Wales. Ecography. 32(3), 504-516.
[31] Zhang, J., Hao, Z.Q., Sun, I.F., Song, B., Ye, J. (2009) Density dependence on tree survival in an old-growth temperate forest in northeastern China. Annals of Forest Science. 66(2), 204-209.
[32] Kang, D., Guo, Y.X., Ren, C.J., Zhao, F.Z., Feng, Y.Z., Han, X.H., Yang, G.H. (2014) Population structure and spatial pattern of main tree species in secondary Betulaplatyhylla Forest in Ziwuling Mountains, China. Scientific Reports. 4, 6873-6875.
[33] Wiegand, T., Kissling, W.D., Cipriotti, P.A., Aguiar, M.R. (2006) Extending point pattern analysis to objects of finite size and irregular shape. Journal of Ecology. 94(4), 825-837.
[34] Wu, T., Zhang, W.H., Lu, Y.C., Fan, S.H. (2006) Effects of Different Forest Practices on Pinus tabulaeformis Population Numbers and Species Diversity in the Forest Region of HuangIongshan Mountain. Acta Botanica Boreali-Occidentalia Sinica. 26(5), 1007-1013.
[35] Takahashi, K., Homma, K., Vetrova, V.P., Florenzev, S., Hara, T. (2001) Stand structure and regeneration in a Kamchatka mixed boreal forest. Journal of Vegetation Science. 12(5), 627-634.
[36] Rozas, V. (2003) Regeneration patterns, dendroecology, and forest-use history in an old-growth beech-oak lowland forest in Northern Spain. Forest Ecology and Management. 182(1-3), 175-194.
[37] Zhu, Y., Bai, F., Liu, H.F., Li, W.C., Li, L. (2011) Population distribution patterns and interspecific spatial associations in warm temperate secondary forests, Beijing. Biodiversity Science. 19(2), 252-259.
[38] Harms, K.E., Wright, S.J., Calderon, O. (2000) Pervasive density-dependent recruitment enhances seeding diversity in a tropical forest. Nature. 404(6777), 493-495.
[39] Lesthwick, J.R., Mitchell, N.D. (1992) Forest pattern, climate and volcanism in central North Island. Journal of Vegetation Science. 3(5), 603-616.
[40] Zhang, J.T., Meng, D.P. (2006) Spatial distribution patterns of dominant tree species in Pinus tabulaeformis-Quercus liaotungeusis forest in Luyashan Mountain, China. Acta Botanica Boreali-Occidentalia Sinica. 26(8), 1682-1685.
[41] Yang, J.L., Wang, H., Wang, B., Sun, D. (2007) Spatial distribution pattern and interspecific association of main tree species in Pinus tabulaeformis forest in Ziwuling Mountains. Acta Botanica Boreali-Occidentalia Sinica. 27(4), 791-796.
[42] Cerrillo, R.M.N., Manzanedo, R.D., Bohorque, J., Sanchez, R., Sanchez, J. (2013) Structure and spatio-temporal dynamics of cedar forests along a management gradient in the Middle Atlas, Morocco. Forest Ecology and Management. 289(2), 341-353.
[43] Wiegand, K., Jeltsch, F., Ward, D. (2000) Do spatial effects play a role in the spatial distribution of desert-dwelling Acacia raddiana. Journal of Vegetation Science. 11(4), 473-484.
[44] Schurr, F.M., Bossdirf, O., Milton, S.J., Schumacher, J. (2004) Spatial pattern formation in semi-arid shrubland: a priori predicted versus observed pattern characteristics. Plant Ecology. 173(2), 271-282.
[45] Zhang, M.T., Kang, X.G. (2015) Distribution patterns and associations of dominant tree species in a mixed coniferous-broadleaf forest in the Changbai Mountains. J. Mountain Sci. 12(3), 659-670.
[46] Boyden, S., Binkley, D., Shepperd, W. (2005) Spatial and temporal patterns in structure, regeneration, and mortality of an old-growth ponderosa pine forest in the Colorado Front Range. Forest Ecology and Management. 219(1), 43-55.
[47] Druckenbrod, D.L., Shugart, H.H., Davies, I. (2005) Spatial pattern and process in forest stands within the Virginia piedmont. Journal of Vegetation Science. 16(1), 37-48.
[48] Quesada, M., Sanchez-Azofeifa, G.A., Alvarez-Anorve, M., Stoner, K.E., Avila-Cabadilla, L. (2009) Succession and management of tropical dry forests in the Americas: Review and new perspectives. Forest Ecology and Management. 258(6), 1014-1024.

[49] Li, L., Huang, Z.L., Ye, W.H., Cao, H.L., Wei, S.G., Wang, Z.G., Lian, J.Y., Sun, I.F., Ma, K.P., He, F.L. (2009) Spatial distributions of tree species in a subtropical forest of China. Oikos. 118(4), 495-502.
[50] Grubb, P.J. (1977) The maintenance of species-richness in plant communities: the importance of the regeneration niche. Biological Reviews. 52(1), 107-145.
[51] Wang, X.G., Ye, J., Li, B.H., Zhang, J., Lin, F. (2010) Spatial distributions of species in an old-growth temperate forest, northeastern China. Canadian Journal of Forest Research. 40(6), 1011-1019.

Received: **17.10.2018**
Accepted: **28.01.2019**

CORRESPONDING AUTHOR

Shuoxin Zhang
College of Forestry,
Northwest A&F University,
3 Taicheng Road, Yangling,
Shaanxi 712100 – China

e-mail: sxzhang@nwsuaf.edu.cn

© by PSP Volume 28 – No. 5/2019 pages 3805-3810 Fresenius Environmental Bulletin

SUSTAINABLE CONSUMPTION AND ORGANIC FARMING: THE CASE OF BURSA, TURKEY

Sule Turhan*

Bursa Uludag University, Faculty of Agriculture, Department of Agricultural Economics, Gorukle, 16059, Bursa, Turkey

ABSTRACT

Organic farming as a key to sustainable agriculture has captured the attention of many countries worldwide. Nowadays, a significant number of conscious consumers are turning every day to the consumption of organic products for healthy living, soil and water. Thus, the concept of sustainable, healthy and natural nutrition, which comes into our daily life with the development of organic agriculture, gradually increases in importance. This research was aimed at determining organic product consumption trends of consumers and examining some marketing features in Turkey in the province of Bursa, where the first organic product market was located. For this purpose, a total of 541 consumers were surveyed in organic product markets in Bursa. According to the results of the analysis, product price and income level were important factors in organic product consumption. In addition, the majority of consumers (71.35%) did not trust organic products. An interesting finding is that the middle-income group (about 30-40%) consumed the most organic products. It is extremely important to increase the consumption of organic products for sustainable consumption in the region. There is a need to improve the quality of organic products and regulation of the market place, and to reduce market margin in favor of the consumer in organic product marketing.

KEYWORDS:
Organic, agriculture, sustainability, consumption

INTRODUCTION

The fact that the increase in the targeted productivity in agriculture does not increase in line with the use of inputs, that the soil is becoming increasingly arid and that problems have emerged that cannot be resolved in terms of human, animal and environmental health have led to a review of agricultural systems and to the development of alternatives. Many of today's food production systems are unsustainable and compromise the capacity of the Earth to produce food in the future. Hence, food systems must undergo radical changes towards greater resource efficiency in order to respond to the food and nutritional needs of an increasingly urbanized planet [1]. In this background, organic consumers represent an important trend in sustainable food consumption [2, 3, 4].

Organic agriculture, which has been developing in different countries and in different degrees especially since the 1930s, gained a commercial dimension in the 1980s, and in 1985-86 this development was reflected onto our country, too. According to the 2016 data, organic production is carried out in approximately 524 thousand ha by 68 thousand producers and the number of organic agriculture product types has increased to 225 [5]. Nowadays, a significant number of conscious consumers are oriented every day towards the consumption of organic products for healthy living, soil and water. This new and modern approach leads consumers to an organic philosophy. People see more and more organic products for their health and environment, and they want to consume quality products that are safe for their families and their healthy lives. Consumers who are concerned about healthy eating and a reliable food supply have a positive attitude towards organic products [6-7]. However, the market for organic products, which cannot reach a sufficient quantity and variety, faces various constraints and problems in terms of marketing. Producers suffer from difficulties in finding markets for the products they produce with great labor and cost, while consumers complain about the high prices of organic products and the inability to obtain the products easily [8, 9, 10].

The fact that the Turkish people are informed about organic products and the demand that will arise as a result of these products will reveal the possibilities of marketing these products in the country and will provide the guiding information for the creation of an internal market for these products. For this reason, in this study, it is aimed to investigate the factors affecting the attitudes and preferences of the consumers who use organic products in organic product marketing. For this purpose, an attempt has been made to determine the attitudes, habits, and factors that affect the consumption of organic products of families living in the province of Bursa by statistical methods.

TABLE 1
Demographic characteristics of surveyed consumers

Personal Characteristics	Frequency	%	Average	Standard Deviation	Standard Error
Gender			**1.45**	**0.56**	**0.02**
Female	281	52			
Male	260	48			
Age	**Frequency**	**%**	**3.24**	**1.32**	**0.06**
Less than 18	25	4.60			
18-29	162	29.95			
30-39	142	26.25			
40-49	108	19.96			
50-59	71	13.13			
60 and above	33	6.11			
Educational Attainment	**Frequency**	**%**	**3.90**	**1.35**	**0.06**
Literate	13	2.40			
Primary school	69	12.75			
Secondary school	61	11.28			
High school	177	32.72			
University	210	38.82			
Graduate and above	11	2.03			
Income	**Frequency**	**%**	**2.56**	**1.39**	**0.06**
0-100 Euros	60	11.09			
101-200 euros	93	17.19			
201-300 euros	240	44.36			
301-400 euros	122	22.55			
401+ euros	26	4.81			

MATERIALS AND METHODS

In the study, a survey was conducted as the data collection tool. In the light of the information obtained after the literature research, questionnaire questions were formed. Some of the survey questions prepared for the research were prepared using various research studies on the subject [11, 12, 13]. Some questions were formed by the researchers considering the purpose of the research, the content of the subject and the characteristics of the population to which the questionnaire would be applied [14].

In the research, the population was composed of consumers using organic products in Bursa. Due to the extremely limited number of organic products consumed in Turkey, it can be said that the audience is limited. For this reason, a survey was conducted on the consumers who consumed organic products in the shops and markets where organic products were sold in the province of Bursa, where the organic product market is intensified, based on the non-probability sampling approach. In the study, a 5% error margin was chosen and sample size was determined as 541 consumers. While the sample size was selected, it was determined by proportional distribution by considering the number of households in 17 districts in Bursa Province. The group to be surveyed was decided by using the optimum sample size formula [15, 16].

$n= Nt^2 pq / d^2 (N-1) + t^2 pq$

Field work was carried out between June and September 2014. Firstly, descriptive statistical values of the obtained data were found [16]. For this purpose, arithmetic mean and standard error and standard deviation values were calculated. The normality of each question was analyzed using the Shapiro-Wilks (W statistic) test [17, 18, 19]. Pearson correlation method was used to determine the correlations of the factors included in the questionnaire. In the study of the relationships between variables, in order to test whether these were statistically significant, chi-square test was used [20, 21, 22].

FINDINGS AND DISCUSSION

In this study, it was aimed to determine organic product consumption trends in Bursa province. For this purpose, 541 consumers were interviewed by mutual interview. The normality test (W test) showed that the data were distributed normally. According to the results of the survey, 52% of the participants who participated in the research were men and 48% of the participants were women. While the majority of the participants were between 40 and under, their levels of education were mostly high school and university. In terms of income, 29% of the people had incomes of 200 euros and under, 44% of them had incomes of 201-300 euros and 27% of them had incomes of 400 euros and more (Table 1).

Table 2 presents the distribution of organic product consumers' preferences according to gender. The fact that the chi-square tests were significant showed that gender was effective in consumption. Organic product consumption is concentrated in the last ten years (72.65%). The proportion of consumers using them for more than ten years is

27.35%. Consumption of female consumers covers older periods than men. There are no significant differences in the lifespan of female and male consumers.

The confidence factor for organic products was not high (28.65%). However, the percentage of those who found it partially reliable was 30.13%. The importance of informing consumers about this issue arises. The reasons for increasing demand for organic products are not analyzed very well for producers and marketers.

There is a need to raise the awareness of society about the reliability of organic products. Packaging type is important in organic product marketing. Consumers' awareness of this issue in recent years also affects the consumption of organic products. Paper packages were most commonly preferred for packaging of organic products (51.80%). The preference of glass packaging for male consumers was higher (36.18%). Plastic packaging and other types of packaging were generally not preferred by consumers. Chi-square (x^2) analysis performed in order to determine whether there was a difference between the organic product consumption frequencies of the consumers in Bursa Province ($x^2 = 33.89$, p 0.001) was found to be significant at 0.1% level. The income level affected the frequency of consumption and the frequency of consumption varied according to the income level. Frequency of consumption of organic products increased as income level increased (Table 3). The frequency of consumption per week was also found in lower income groups, but was as low as 20.09% and 13.70%. The percentage of those who did not consume organic products was higher in lower income groups. The consumer classes that bought the most organic products were in the 101-200 and 201-400 income levels. This group can also be called the middle income class. In the highest group, there was low organic product intake. When the distribution of the consumption of organic products according to gender is examined, the ratio of the female consumers

TABLE 2
Distribution of consumers' organic product consumption characteristics by gender

	Female Number	%	Male Number	%	Total Number	%
Consumption history (years)						
0	73	25.98	42	16.15	115	21.46
1-5	58	20.64	46	17.69	104	19.22
6-10	87	30.96	87	33.46	174	32.16
11-20	53	18.86	69	26.55	122	22.35
21-+	10	3.56	16	6.15	26	4.81
	$x^2 = 31.97$	$p < 0.001$				
Trust in organic products						
Yes	72	25.63	83	31.92	155	28.65
No	130	46.26	93	35.77	223	41.22
Partially	79	28.11	84	32.31	163	30.13
	$x^2 = 16.47$	$p < 0.001$				
Packaging type preference						
Plastic	18	5.88	36	11.84	54	8.85
Paper	168	54.90	148	48.68	316	51.80
Glass	110	35.95	110	36.18	220	36.07
Other	10	3.27	10	3.30	20	3.28
	$x^2 = 11.70$	$p < 0.008$				
Should there be a price difference						
No	218	77.58	182	70.00	400	73.94
Yes	9	3.20	7	2.69	16	2.96
No idea	54	19.22	71	27.31	125	23.10
	$x^2 = 11.76$	$p < 0.002$				
Place of purchase						
Supermarket	146	30.04	148	33.64	294	31.75
Street Market	115	23.66	84	19.03	199	21.49
Greengrocer	155	31.89	136	30.91	291	31.43
Organic product selling point	70	14.41	72	16.36	142	15.33
	$x^2 = 14.18$	$p < 0.003$				
Price difference rate						
10%	127	45.20	104	40.00	231	42.70
20%	116	41.28	120	46.15	236	43.62
50%	37	13.17	35	13.46	72	13.31
100%	1	0.35	1	0.39	2	0.37
	$x^2 = 5.33$	$p < 0.15$				

TABLE 3
Frequency of organic product consumption according to the income level of consumers

Income (Euro)	Never consume		Every week		Once a month		Once a year	
	Score	%	Score	%	Score	%	Score	%
0-100 euros	50	32.46	44	20.09	21	16.67	9	21.43
101-200 euros	37	24.03	30	13.70	20	15.87	7	16.67
201-300 euros	46	29.87	73	33.33	40	31.75	16	38.10
301-400 euros	15	9.74	57	26.03	38	30.16	10	23.80
401+ euros	6	3.90	15	6.85	7	5.55	0	0.000

$X^2 = 33.89$ $p < 0.001$

TABLE 4
Distribution of the days for purchasing organic food

	Monday	Tuesday	Wednesday	Thursday	Friday	Saturday	Sunday
Score	46	32	43	27	70	236	293
%	8.50	5.91	7.95	4.99	12.94	43.62	54.16

who purchased them every week (one or several times) was at the highest level (46.62%). The proportion of those who did not consume any organic products was higher in males (30.77). Men's consumption preferences were close to each other or monthly. According to these results, it is seen that female consumers gave more importance to the consumption of organic products.

It is seen that the days of the weekends are weighted when the purchase days of the consumers buying organic products are examined (Table 4). Many consumers stated that they wanted to shop on more than one day. 43.62% of consumers emphasized that they wanted to shop on Saturdays and 54.16% on Sundays, while approximately one third said they could buy organic products on weekdays. This situation shows that it is not enough to establish organic product markets only on certain days, and that it is necessary to have permanent sales points that sell every day of the week.

TABLE 5
The importance of the factors that consumers considered when buying organic products according to their importance

Factors	(%)
Freshness	90.55
Cheapness	90.17
Taste and flavor	89.01
Hygiene	87.66
Expiration date	86.54
Quality	86.01
Brand	85.33
Type of packaging	82.67

The main quality factors of organic products, the characteristics that consumers cared about and their results according to their importance in terms of consumers are presented in Table 5. Usually freshness (90.55%) and cheapness (90.17%) were preferred in the first place, while all consumers stated that they paid attention to more than one feature. The taste and flavor characteristics of the products are in the third place (89.01%) as an important feature, followed by hygiene with a rate of 87.66%. Considering that a national brand of organic products which is accepted in our country is not yet fully on the market, it is acceptable for consumers to ignore the brand issue. However, attention should be given to the packaging of organic products as necessary and consumers should be made aware of this issue.

66.67% of the respondents reported positive opinions about the price difference between traditional products and organic products. According to this, we can say that organic products are not sold by consumers at higher prices, provided that they bear certain quality characteristics. Female consumers did not accept price differences as much as men (34.31%). The first choices in the shopping places where consumers bought organic products were supermarkets with a rate of 31.75%, and the second preference was groceries with a rate of 31.43%. In addition, neighborhood markets were widely preferred by consumers. Some consumers stated that they could buy from more than one shopping place. There are no major differences between men and women in the ranking. When the information about the identification of the organic products of the consumers is examined, 59.99% of the products without using synthetic drugs and fertilizers, and 63.21% of the products in the form of hormones were not used. Specifically, only 31.42% of the certified products show that consumers did not have accurate and sufficient information about organic products. Equipping consumers with the right information is an urgent need for manufacturers and marketers in terms of market growth. Consumers had preferred options for more frequent consumption of organic products. These are, in order of importance, lower price, more sales points, greater durability, being better-tasting and being more attractive. In this respect, while price level stands out as an important factor, it is seen that consumers also attached importance to other quality

elements. 49.72% of the organic product consumers explained the media and internet as the sources of information they used the most. Some consumers stated that they could not follow the information about the subject and 7.95% stated that they used printed publications. While there is a lack of information about the general public, there is a need for a wide range of information to be presented on public control, which provides accurate information on this subject. The prices of traditional and organic products are an important marketing factor for the consumer. In the province of Bursa, 73.94% of consumers wanted price differences. This is the same for both sexes. Accordingly, we can say that manufacturers and marketers have to pay great attention to the fact that marketing of organic products should be done in the most advanced way and that marketing costs and market margins should be low. It was determined that the difference between the traditional and organic products should not be more than 20%. Consumers do not desire higher price differences. Organic products have to give importance to low price policy in market entry strategies. Correlation analysis was performed to determine the correlation between the factors influencing the marketing of organic products. According to the results of the statistical analysis, the level of knowledge about consumer rights, the type of organic products consumed, the confidence in organic products, the media information, the type of product received, the level of information about the organic product and the place of purchase were high.

An important issue in marketing is the effectiveness of campaigns and promotions. 75.60% of the consumers stated that these activities affected their shopping. In addition, 63.77% of consumers emphasized that they attached importance to branded products. Similarly, the proportion of those who preferred to buy from the producer associations and the agricultural cooperative products is significant at 76.34%. They should be the pioneers and supporters of local governments and state-owned organizations in opening more sales outlets.

CONCLUSION

Sustainable consumption is the use of products and services that have a minimal impact on the environment so future generations can meet their needs. In recent years an important trend in sustainable food consumption is represented by organic consumers. Organic agriculture not only preserves the environment but also improves public health, bringing significant benefits both to the economy as well as to the social cohesion of rural areas. The consumption of organic products is becoming increasingly important as an alternative food source for healthy eating. However, despite the support given, production and consumption amounts show a slow development. The reasons for this are low growth of the market and marketing problems. In this research, it was aimed to examine the main factors affecting consumption in order to shed light on marketing problems. In the research, a questionnaire was applied to the consumers in order to determine the organic product consumption trends in Bursa Province.

Consumers' knowledge about organic products has been found to be incomplete. First of all, consumers should be informed that organic products are certified products. Consumer demands should be taken into account in production diversification. It is important to create special market places for these products. Excessively high prices reduce consumption demand. State subsidies are needed for low production costs. However, there are deficiencies in marketing services, special marketing processes should be developed for organic product marketing and producers and marketers should be informed about this issue.

REFERENCES

[1] Turhan Ş., Vural, H., Ak, I., Erdal, B. (2017) Consumer Trends for Organic Products: The Case of Marmara Region in Turkey. Fresen. Environ. Bull. 26, 8160-8165.

[2] Annunziata, A., Vecchio, R. (2016) Organic Farming and Sustainability in Food Choices: An Analysis of Consumer Preference in Southern Italy, Agriculture and Agricultural Science Procedia 8-2016. ISSN:2210-7843, Published by Elsevier. 93 – 200.

[3] Colucci, F., Menegoni, P., Nocenzi, M., Presenti, O. (2012) Development of Consumption and the Relationship Between Sustainability and Welfare. Review of Studies on Sustainability. ISSN 2239-1959. 2, 47-67.

[4] Gürbüz, İ.B., Manaros, M. (2018) Local Sustainability: Evaluating Visitors' Level of Satisfaction in Cumalıkızık, Turkey, Fresen. Environ. Bull. 27, 3433-3438.

[5] Anonymous (2017) Turkey's Statistic. Turkish Statistical Institute, Ankara, (10) http://www.tuik.gov.tr.(Accessed: 01/06/2017).

[6] Sarıkaya, N. (2007) A Field Study on Factors and Attitudes Affecting Organic Product Consumption. Kocaeli University, Journal of Social Sciences Institute. 14(2), 110-125.

[7] Shears, P., Hillier, D. (2001) Retailing Organic Foods (Case Study). British Food Journal. 103(5), 358-365.

[8] Karabas, S., Gurler, A.Z. (2012) Estimation of Factors Affecting Consumer Behavior on Logit Regression Analysis in Organic Product Preference. Adıyaman University Journal of Social Sciences Institute. ISSN: 1308–9196, 5(10), 129-156.
[9] Canan Ozbag, B., Tipi, T. (2009) A Comparative Study of Certification Process in Organic Agriculture with Turkish Authorities and Some Other Countries, 1. GAP Organic Farming Congress. 17-20 November 2009, Şanlıurfa, 1018-1023.
[10] Turhan Ş., Rehber, E., Erdal, B., Vural, H. (2018) Toward an Integrated Safe and Sustainable Food System. Fresen. Environ. Bull. 27, 3212-3217.
[11] Mclver, H. (2004) Organic Hip: Popular Picks at Health Food Stores. Better Nutrition. 66(2), 58-61.
[12] Crucefix, D. (1998) Organic Agriculture and Sustainable Rural Livelihoods in Developing Countries. Soil Association, June, UK, 40-56.
[13] Akdoğan, Ş.M., Güllü, K., Babayiğit, S. (2005) A Study of Consumers' Perceptions of Supermarkets. Erciyes University Social Sciences Institute Journal. Kayseri. ISSN:1300-1582. (2) 37-70.
[14] Salali, H.E., Atis, E. (2018) Assessing Farmers' and Consumers' Attitudes Toward Local Wheat Varieties: The Case of Aegean Region, Fresen. Environ. Bull. 27, 1928-1934.
[15] Easwaran, S., Singh, S.J. (2006) Marketing Research Concepts, Practices and Cases. Oxford University Press, New Pelh. 605.
[16] Vural, H. (2012) Agriculture and Food Economics Statistics. Uludag University Agricultural Faculty, Lecture Notes N.107, Bursa, 115.
[17] Bollerslev, T. (1987) A Conditionally Heteroskedastic Time Series Model for Speculative Prices and Rates of Return. Review of Economics and Statistics, UK, 69.
[18] Gallant, A.R. (1987) Nonlinear Statistical Models. ISBN:9780470316719. Wiley, New York, 616p.
[19] Dent, J.B., Fawcett, R.H., Thornton, P.K. (1989) Economics of crop protection with reference to weed control. Proc. Brighton Crop Prot. Conf. Weeds. 917–926.
[20] Scheuneman, J. (1979) A New Method for Assessing Bias in Test Items. Journal of Educational Measurement. ISSN:1745-3984. 16, 143-152.
[21] Camilli, G. (1979) A Critique of the Chi-square Method for Assessing Item Bias. Unpublished Paper, Laboratory of Educational Research, University of Colorado.
[22] Gönen, E., Kalınkara, V., Vural, H. (1988) A Research on Consumption Expenditures of Ankara University, Faculty of Agriculture, Department of Home Economics Students, Ankara University Agricultural Faculty, N. 556 Ankara, 47.

Received: **18.10.2018**
Accepted: **18.03.2019**

CORRESPONDING AUTHOR

Sule Turhan
Bursa Uludag University,
Faculty of Agriculture,
Department of Agricultural Economics,
Gorukle, 16059, Bursa – Turkey

e-mail: sbudak@uludag.edu.tr

© by PSP Volume 28 – No. 5/2019 pages 3811-3816 Fresenius Environmental Bulletin

AMINO ACID COMPOSITION ANALYSIS AND NUTRITION EVALUATION FOR GEGEN LEAF PROTEIN CONCENTRATION

Shijie Su, Jinhua Shao*, Qiao Deng, Qian Tan

School of Chemical and Biological Engineering, Hunan University of Science and Engineering, Yongzhou 425199, China

ABSTRACT

The traditional Chinese medicine, Gegen, is the dried roots of leguminous plant Pueraria lobate (Willd) Ohwi, or Pueraria thomsonii Benth. As one of the first batch of plants approved by the Chinese Ministry of Health that could serve as Chinese medicine homologous food, the utilization of wild Gegen resource mainly falls in its roots and flowers, while its leaves are simply discarded as wastes. We want to provide scientific theory basis for comprehensive utilization of Gegen LPC (leaf protein concentration). We carried out analysis for abundance and composition of amino acids in Gegen leaf protein concentration (LPC), via the method of fuzzy recognition and ratio coefficient of amino acid (RCAA), employing whole egg protein as control as recommended by FAO of the United Nations, with the amino acid reference pattern by FAO/WHO as evaluation standard, and performed a comprehensive evaluation for Gegen LPC's nutritional value as well as comparisons with 4 types of food proteins. We found that, there was a variety of amino acids in Gegen LPC, including at least 17 types of amino acids, 33.7% of which was consisted of essential amino acids, and the first restricting amino acid was valine (Val). The SRCAA of Gegen LPC reached 65.00 m, which indicated Gegen LPC as a protein source of great nutritional values. Gegen LPC is a protein source with great nutritional values.

KEYWORDS:
Gegen leaves, Leaf protein concentration (LPC), Amino acid (a.a.), Nutritional evaluation

INTRODUCTION

Plant leaf protein concentration (LPC), also known as green protein concentration, refers to proteins extracted from stems and leaves of plants [1]. Protein generally contributes 30%~60% of LPC contents, which endorses LPC with complete amino acid composition and makes LPC well-balanced in nutrition. LPC is very similar to commonly-seen animal proteins in composition, but superior to the latter in composition, as it contains no animal cholesterols, and therefore it could serve as suitable protein additives in human foods [2-3]. Due to its wide range of sources, high nutritional value and satisfying effective applications, LPC is recognized as a kind of high-quality food by Food and Agriculture Organization (FAO) of the Unites Nations, and a new type of protein resource with high development and utilization potentials [4-5].

The traditional Chinese medicine, Gegen, is the dried roots of leguminous plant Pueraria lobate (Willd) Ohwi, or Pueraria thomsonii Benth, and with a very long history of application which were collected in Benjing, Bielu and other Chinese traditional literatures records. Gegen tastes sweet, spicy and minty, and belongs to Spleen Meridian and Stomach Meridian, with potentials to relieve superficial symptoms, to defervesce, to promote saliva secretion, to release suppressed rashes and to promote body energy to stop diarrhea. Not only has Gegen anti-inflammatory and antipyretic functions, it could also dilate coronary arteries to increase coronary perfusion and lower blood pressure [6, 7]. What's more, Gegen contains polysaccharides and a variety of trace elements [8]. As one of the first batch of plants approved by the Chinese Ministry of Health that could serve as Chinese medicine homologous food, Gegen has been widely applied in the production of health care foods [9]. Currently the utilization of wild Gegen resource mainly falls in its roots and flowers, while its leaves are simply discarded as wastes, resulting in a waste of resource. There is still no report on amino acid composition analysis and nutrition evaluation for Gegen LPC. In this study, we analyzed and discussed the amino acid composition of Gegen LPC via the method of fuzzy recognition and ratio coefficient of amino acid (RCAA), and performed comparison with human essential amino acid reference pattern by FAO/WHO to provide scientific theory basis for comprehensive utilization of Gegen LPC.

MATERIALS AND METHODS

Materials and reagents. Gegen leaves were purchased in Yongzhou, Hunan, China, in November, cleaned by running water, air-dried and then

screened (with 60-mesh sieve) for further use. Sodium chloride, hydrochloric acid, phenyl isothiocyanate, sodium acetate trihydrate are all analytical grade domestic products; acetonitrile and methanol are chromatographic grade. Standard samples of 17 amino acid were all purchased from Sigma-Aldrich.

Equipment and apparatus. YP602N electronical analytical scale was purchased from Shanghai Shunyuping Scientific Apparatus Company. GL21M frozen centrifuge was purchased from Hunan Kaida Industrial Corporation. PHS-802 digital pH meter was purchased from Guiyang Xuetong Instrument Company. Agilent 1260 liquid chromatographic instrument was purchased from Anjielun Science and Technology Company Ltd. LGJ-18A freeze dryer was purchased from Beijng Sihuan Scientific Instrument Company Ltd.

Methods.Extraction of Gegen LPC. Gegen leaf powder (30 g) was well-mixed with 600 ml distilled water (1:20) and processed with ultrasonic cell disrupter for 15 min. Then the mixture was incubated in a 20℃ water-bath for 15 min before getting centrifugated at 5000 rpm at 4℃ for 20 min. After centrifugation the filtrate was collected, and its pH was adjusted to reach 3.0 to obtain precipitation at 75℃ for 15 min. The precipitation was isolated by discarding the supernatant after centrifugation at 12000 rpm for 20 min, and freeze-dried to get Gegen LPC powder.

Determination of protein abundance. The protein abundance in Gegen leaves was determined according to the method described in GB/T 5009.5-2010 Determination of protein in food, from national food safety standard for People's Republic of China.

Determination of amino acid composition. Certain amount of protein sample was dissolved with 16ml 6mol/L HCl in a 20 ml hydrolytic tube, which was later vacuum degassed for 30min and then sealed with nitrogen, for hydrolysis at 110℃. About 22~24 h later the hydrolyzing tube was cooled down and opened, and its content was completely transferred into a 50ml volumetric flask by washing the tube with deionized water, and topped up to 50ml. Then 1ml hydrolysate was transferred into a small vial and the hydrolysate would be firstly deacidified and dried under vacuum and then be rinsed with 1ml water and then dried for twice. The precipitate then would be fully dissolved by 1ml 0.02 mol/L HCl, half of which would be well mixed with 250 μL 1 mol/L triethylamine (dissolved in acetonitrile), 25 μL 0.1 mol/L phenyl isothiocyanate (dissolved in acetonitrile) in a 5ml plastic centrifugation tube and rested at room temperature for 1 hour. Then the mixture would be mixed vigorously with 2 ml hexane and rested for 10min. The lower layer of solution would be filtered through 0.22 μm aqueous phasic filter membrane and then loaded on apparatus for analysis.

Condition for chromatograph. a. Mobile Phase A: 0.1mol/L NaAc solution (pH 6.5) was obtained by dissolving 8.2 g NaAc with 900mL water, which was adjusted to reach 6.5 in pH value and topped up to 1'000mL with acetonitrile (93:7).

b. Mobile Phase B: acetonitrile-water (8:2). Agilent 1260 liquid chromatographic instrument was equipped with DAD detector; the column for chromatograph employed octadecylsilane chemically bonded silica as stuff bulking agent (C18 column); the flow rate was controlled at 10 ml/min; column temperature was set at 40°C; the volume of loaded sample was 10 ul; wave length of 254 nm was chosen.

The gradient for elution is shown as Table 1.

TABLE 1
The gradient for elution

Time (min)	Moving phase A (%)	Moving phase B (%)
0	100	0
14	85	15
29	66	34
30	0	100
37	0	100
37.1	100	0
45	100	0

Evaluation method. Fuzzy recognition. We used Canberra distance [10] to define the closeness between Gegen LPC and the standard protein (FAO whole egg protein) [11] μ (a, u_i), whose calculation method was based on Formula (1).

$$\mu(a, u_i) = 1 - 0.09\sum_{k=1}^{7}\frac{|a_k - u_{ik}|}{a_k + u_{ik}} \quad (1)$$

Herein this formula, a_k (k=1, 2, …, 7) represents the abundance of 7 essential amino acids (EAA) in standard protein, which was virtually egg protein with essential amino acids including isoleucine 50.3 mg/g, leucine 92.5 mg/g, lysine 56.3 mg/g, methionine 34.1 mg/g, phenylalanine 56.3 mg/g, threonine 52.3 mg/g, valine 68.39 mg/g; u_{ik} represented abundance of the k^{th} EAA of the i^{th} evaluation subject (1 stand for alfalfa LPC; 2 stand for ryegrass LPC; 3 stand for soybean LPC; 4 stand for mung bean LPC). Closeness could reflect the similarity between the protein quality of evaluation subject and the standard protein, which means the closer its value was to 1, the higher nutritional value of the corresponding protein should be.

Score of ratio coefficient of amino acid (SRCAA). The nutritional value of protein in food is mainly dependent on the type, quantity and composition ratio of essential amino acids. The closer the essential amino acid composition ratio of the food is to that of human body, the higher quality of the food would be [12-13]. Our experiment was based on the method of SRCAA [14-15], which meant that the composition of Gegen LPC was compared to the human essential amino acid pattern recommended by FAO/WHO in 1973 [15], and ratio of amino acid (RAA), ratio coefficient of amino acid (RCAA) and score of ratio coefficient of amino acid (SRCAA) were calculated following Formula (2), (3) and (4), to evaluate and discuss the nutritional values of Gegen LPC.

$$RAA = \frac{\text{ACTUAL EAA}}{\text{FAO/WHO EAA}} \quad (2)$$

ACTUAL EAA: the abundance of certain essential amino acid in the protein to be evaluated FAO/WHO EAA: the abundance of corresponding amino acid in FAO/WHO pattern

Herein this formula, the abundance of certain essential amino acid in the protein to be evaluated, as well as the abundance of corresponding amino acid in FAO/WHO pattern were determined for each 1g of protein, which meant the unit of amino acid abundance was mg/g pro.

$$RCAA = \frac{RAA}{\overline{RAA}} \quad (3)$$

$$SRCAA = 100 \times \left[1 - \frac{\sqrt{\sum_{i=1}^{n}(RCAA_i - \overline{RCAA})}}{\overline{RCAA}}\right] 2 \quad (4)$$

RESULTS AND DISCUSSION

Protein abundance in Gegen LPC. The rough protein in Gegen leaf was determined for more precise analysis and evaluation for its nutritional value. The result of comparisons between Gegen LPC and protein abundance in some commonly seen foods.

From what was reflected in Table 2, we could find that the rough protein abundance in Gegen leaf was 42.56%, which was higher than that in commonly seen foods like milk powder, fine flower and oats, and comparable to that in soybean protein.

Amino acid composition of Gegen LPC. The amino acid abundances in Gegen LPC determined by amino acid automatic analyzer were shown in Figure 1 and Table 3.

With the aid of amino acid analyzer, we performed compositional analysis for amino acids in Gegen LPC powder, which included determinations for 17 essential amino acids. The result shown in Table III indicated a complete amino acid composition in Gegen LPC, which covered all 17 essential amino acids, including 7 essential amino acids except for tryptophan. The total amino acid abundance in Gegen LPC was 38.1%, and the abundance of essential amino acids contributed 33.7% of total amino acids, with EAA/NEAA (E/N) ratio of 0.507,

TABLE 2
Comparison of protein contents between different foods

Food	Pueraria Leaf	Alfalfa Leaf [16]	Milk powder	Fine flour [17]	Soya bean [18]	Oat [19]
Protein content (%)	42.56	18-24	12-18	12	41	11.35-19.90

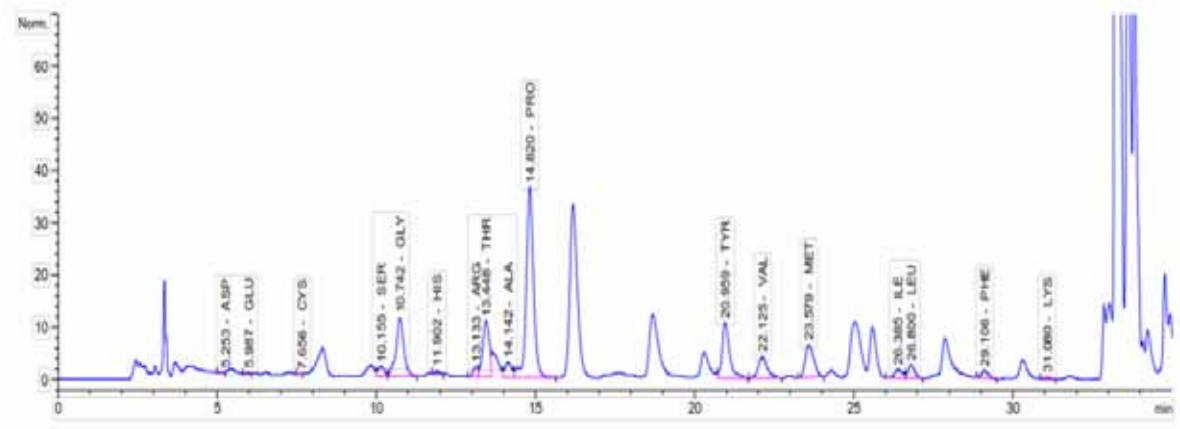

FIGURE 1
The amino acid abundances in Gegen LPC determined by amino acid automatic analyzer

which was a little bit lower than the FAO/WHO standard for essential amino acids (40%) and the E/N value (0.6) [15]. The top two amino acids of the highest abundances were proline and tyrosine, taking up 14.86% and 8.75% of total amino acid, respectively, which were widely applied in medicine, chemistry industry apart from food. Proline would be remarkably accumulated under adverse environments including drought, high or low temperature, high salt-containing soil. Tyrosine is the substrate of monophenolase of tyrosinase, and the major raw material for the final production of pheromone and pheomelanin.

Balance analysis for Gegen LPC. Evaluation outcome of fuzzy recognition. Table 4 shows the closeness to standard protein (whole egg protein) of Gegen LPC, Alfalfa LPC, Ryegrass LPC, soybean protein and Mung protein calculated via fuzzy recognition. The closeness to whole egg protein, the standard protein, of Gegen LPC is 0.637, which is close to that of soybean protein, and this might indicate Gegen LPC is of the highest nutritional value.

Evaluation outcome of SRCAA. If a protein is equipped with a complete composition of amino acids of reasonable ratios closer to the requirements of FAO/WHO amino acid pattern, the protein's nutritional value is higher and could meet the nutritional demands of human body. RAA, RCAA and SRCAA of Gegen LPC, Alfalfa LPC, Ryegrass LPC, soybean protein and mung protein were calculated following in Formula (2) to (4), respectively. The closer RCAA value is to 1, the closer the amino acid composition ratio of corresponding food protein is to the FAO/WHO amino acid pattern of proteins. An essential amino acid with RCAA>1 is relatively in excess, while the situation would be just the way around if the RCAA<1, which might mean the amino acid is relatively inadequate in abundance. The first restricting amino acid is the one with the lowest RCAA value. From Table V we could find the first restricting amino acid is valine. Among all amino acids in Gegen LPC, threonine is of higher abundance than the standard protein and other amino acids are comparable to those of standard protein. Therefore, based on the theory of protein mutual complementation [19] Gegen LPC could be used as food enhancer to make mutual complementation with other proteins to improve the nutritional value of varies of foods.

TABLE 3
Amino acid contents in mulberry leaf proteins and plant proteins from four other species

Amino acid type		Pueraria leaf protein	Alfalfa leaf protein	Ryegrass leaf protein	Soy Protein	Mung bean protein
EAA	Isoleucine	11.06	34.0	21.4	16.5	25.8
	Leucine	26.64	58.6	42.1	27.9	45.1
	Lysine	22.98	38.4	26.6	55.0	27.7
	Methionine	10.24	12.6	8.9	7.4	12.2
	Phenylalanine	14.91	51.3	37.8	24.3	39.1
	Threonine	29.54	29.8	21.3	15.0	22.9
	Valine	12.98	39.2	29.1	18.8	30.5
NEAA	Aspartic acid	28.32	56.1	39.2	44.0	44.0
	Serine	24.71	24.4	18.6	19.7	22.0
	Glycine	27.27	32.5	26.3	26.3	17.0
	Alanine	16.03	38.8	32.2	16.2	28.7
	Glutamate	26.68	57.4	57.4	70.9	61.0
	Cystine	3.70	8.7	7.5	7.2	8.0
	Tyrosine	33.35	34.7	27.3	16.0	28.3
	Histidine	9.38	14.9	9.2	9.8	10.1
	Arginine	26.64	37.0	27.8	28.6	26.6
	Proline	56.63	37.6	25.2	18.6	29.4
	Total amino acid	381.06	606.0	457.9	381.5	487.2
	EAA/TAA	0.337	0.435	0.408	0.349	0.417
	EAA/NEAA	0.507	0.771	0.691	0.538	0.716

Note: Essential amino acids (EAA); Amount of amino acid (TAA); Non-essential amino acids (NEAA).

TABLE 4
Closeness degree of the plant leaf proteins compared with standard proteins

Food protein to be evaluated	Protein code to be evaluated	Closeness degree
Pueraria leaf protein	u1	0.637
Alfalfa leaf protein	U3	0.835
Ryegrass leaf protein	U4	0.740
Soy Protein	U5	0.662
Mung bean protein	U6	0.767

TABLE 5
Comparison of amino acid ratio coefficients of proteins from mulberry leaf and other plants

Protein source	Protein eigen-value	FAO/WHO Recommended amino acid composition							SRCAA
		Isoleu-cine	Leucine	Lysine	Methio-nine	Phenyl-alanine	Threo-nine	Proline	
Pueraria leaf protein	RAA	0.2197	0.288	0.4082	0.3003	0.2648	0.5648	0.1898	65.00
	RCAA	0.6879	0.9017	1.278	0.9402	0.8291	1.7683	0.5942	
Alfalfa leaf protein	RAA	0.85	0.84	0.70	0.61	1.43	0.75	0.85	70.63
	RCAA	1.00	0.98	0.82	0.72	1.69	0.88	1.00	
Ryegrass leaf protein	RAA	0.54	0.60	0.48	0.47	1.09	0.53	0.58	67.70
	RCAA	0.87	0.98	0.79	0.76	1.77	0.87	0.95	
Soy Protein	RAA	0.41	0.40	0.43	0.42	0.67	0.38	0.38	78.03
	RCAA	0.94	0.91	0.98	0.95	1.53	0.85	0.85	
Mung bean protein	RAA	0.25	0.39	0.46	0.38	0.63	0.42	0.26	71.36
	RCAA	0.97	0.96	0.75	0.86	1.68	0.86	0.91	

SRCAA is further calculated based on RCAA value, which could directly indicate the nutritional level of protein (the close it is to 100, the higher its nutritional level is). SRCAA of Gegen LPC is approximately 65, close to the nutritional value of plant proteins like Ryegrass LPC, Alfalfa LPC and Mung protein, as well as animal proteins like pork (74) and beef (76) [20], meaning that Gegen LPC should be of relatively high utilization value.

Based what has been obtained from our study, we can see that there is a variety of amino acid types in Gegen LPC, covering a complete composition of human essential amino acids, and therefore Gegen LPC could be regarded as a perfect protein resource. In Gegen LPC, essential amino acids took up about 38.1% of total amino acids, meaning the E/N ratio was 0.507 which was close to the FAO/WHO standard for essential amino acids (40%) and the E/N value (0.6). The first restricting amino acid for Gegen LPC was valine (Val), and the SRCAA of Gegen LPC was 65.00, which indicated very high nutritional value. By now, people have performed many deep studies on medical and clinical applications of a variety of chemical components in Gegen LPC, and also have profound utilization value in the area of food industry [21]. Gegen LPC's nutritional value is better than those of many different kinds of plant proteins and fruits, and roughly close to that of animal proteins, which could make it a high-quality eatable protein resource with high utilization value. What's more, Gegen could be obtained from a wide spectrum of sources, after processed with water-extraction and acid-precipitation method to be transformed into Gegen LPC that contains 42.56% protein in its contents. The processing method to obtain Gegen LPC is simple and cost-efficient and of a promising prospect of development and application. When Gegen LPC is used a high-quality protein added into human health-care foods, cosmetics, the waste produced after LPC extraction could still be used as feedstuff or others. China possesses the largest resource of Gegen, and if it could be fully developed and utilized in fields like food and medicine, there would be great significance in changing the protein resource structure and improving the nutritionally unbalanced diet of our citizens, increasing agriculture production and income.

CONCLUSIONS

Gegen LPC is a protein source with great nutritional values.

ACKNOWLEDGEMENTS

This work was supported by Hunan Department of Education scientific research project (No.15A083); Hunan University of Science and Technology research project (2017); and Hunan undergraduate research-based learning and innovative experimental plan project (2016).

REFERENCES

[1] Carlsson, R., Hanczakowski, P. (1985) The nutritive value of mixtures of white leaf protein and food proteins. Journal of the Science of Food and Agriculture. 36, 946-950.
[2] Pirie, N.W. (2012) Food protein sources. Cambridge University Press, Cambridge, 133-139.
[3] Stadkilde, L., Damborg, V.K., Jargensen, H., Laerke, H.N., Jensen, S.K. (2018) White clover fractions as protein source for monogastrics: dry matter digestibility and protein digestibility-corrected amino acid scores. J Sci Food Agric. 98, 2557-2563.
[4] Aletor, O., Oshodi, A.A., Ipinmoroti, K. (2002) Chemical composition of common leafy vegetables and functional properties of their leaf protein concentrates. Food Chemistry. 78, 63-68.
[5] Sujak, A., Kotlarz, A., Strobel, W. (2006) Compositional and nutritional evaluation of several lupin seeds. Food Chemistry. 98, 711-719.

[6] Wang, X.L., Jiao, F.R., Yu, M., Lin, L.B., Xiao, J., Zhang, Q., Wang, L., Duan, D.Z., Xie, G. (2017) Constituents with potent α-glucosidase inhibitory activity from Pueraria lobata (Willd.) ohwi. Bioorg Med Chem Lett. 27, 1993-1998.
[7] Mun, S.C., Mun, G.S. (2015) Dynamics of phytoestrogen, isoflavonoids, and its isolation from stems of Pueraria lobata (Willd.) Ohwi growing in Democratic People's Republic of Korea. J Food Drug Anal. 23, 538-544.
[8] Kim, H.S., Shin, B.R., Lee, H.K., Kim, Y.J., Park, M.J., Kim, S.Y., Lee, M.K., Hong, J.T., Kim, Y., Han, S.B. (2013) A polysaccharide isolated from Pueraria lobata enhances maturation of murine dendritic cells. Int J Biol Macromol. 52, 184-191.
[9] Wei, S.Y., Chen, Y., Xu, X.Y. (2014) Progress on the pharmacological research of puerarin: a review. Chin J Nat Med. 12, 407-414.
[10] Qian, A.P., Lin, Q., Yan, S.A., Lin, X.X., Wu, L.Q. (2008) Amino acids in Vacinium bracteatum leaves and their nutritional evaluation. Fujian Journal of Agricultural Sciences. 23, 306-309.
[11] Longvah, T., Deosthale, Y.G. (1998) Compositional and nutritional studies on edible wild mushroom from northeast India. Food Chemistry. 63, 331-334.
[12] Czernicka, M., Zagula, G., Bajcar, M., Saletnik, B., Puchalski, C. (2017) Study of nutritional value of dried tea leaves and infusions of black, green and white teas from Chinese plantations. Rocz Panstw Zakl Hig. 68, 237-245.
[13] Zhang, P., Ma, G., Wang, C., Lu, H., Li, S., Xie, Y., Ma, D., Zhu, Y., Guo, T. (2017) Effect of irrigation and nitrogen application on grain amino acid composition and protein quality in winter wheat. PLoS One. 12, e0178494.
[14] Zhang, L., Li, Q., Chen, C., Li, X., Li, M., Hu, J., Shen, X. (2017) Propioniciclava sinopodophylli sp. nov., isolated from leaves of Sinopodophyllum hexandrum (Royle) Ying. Int J Syst Evol Microbiol. 67, 4111-4115.
[15] Noblet, J., Etienne, M. (1987) Metabolic utilization of energy and maintenance requirements in pregnant sows. Livestock Production Science. 16, 243-257.
[16] Broderick, G.A. (2018) Utilization of protein in red clover and alfalfa silages by lactating dairy cows and growing lambs. J Dairy Sci. 101, 1190-1205.
[17] Giuberti, G., Rocchetti, G., Sigolo, S., Fortunati, P., Lucini, L., Gallo, A. (2018) Exploitation of alfalfa seed (Medicago sativa L.) flour into gluten-free rice cookies: Nutritional, antioxidant and quality characteristics. Food Chem. 239, 679-687.
[18] van den Broeck, H.C., Londono, D.M., Timmer, R., Smulders, M.J., Gilissen, L.J., van der Meer, I.M. (2015) Profiling of Nutritional and Health-Related Compounds in Oat Varieties. Foods. 5, 2-5.
[19] Móricz, Á.M., Ott, P.G., Yüce, I., Darcsi, A., Béni, S., Morlock, G.E. (2018) Effect-directed analysis via hyphenated high-performance thin-layer chromatography for bioanalytical profiling of sunflower leaves. J Chromatogr A. 1533, 213-220.
[20] Afolabi, I.S., Nwachukwu, I.C., Ezeoke, C.S., Woke, R.C., Adegbite, O.A., Olawole, T.D., Martins, O.C. (2018) Production of a New Plant-Based Milk from Adenanthera pavonina Seed and Evaluation of Its Nutritional and Health Benefits. Front Nutr. 5, 9-11.
[21] Jungsukcharoen, J., Dhiani, B.A., Cherdshewasart, W., Vinayavekhin, N., Sangvanich, P., Boonchird, C. (2014) Pueraria mirifica leaves, an alternative potential isoflavonoid source. Biosci Biotechnol Biochem. 78, 917-926.

Received: **20.10.2018**
Accepted: **28.02.2019**

CORRESPONDING AUTHOR

Jinhua Shao
School of Chemical and Biological Engineering,
Hunan University of Science and Engineering,
Yongzhou 425199 – China

e-mail: il0749@163.com

© by PSP Volume 28 – No. 5/2019 pages 3817-3823 Fresenius Environmental Bulletin

STUDY ON MECHANICAL CHARACTERISTIC OF DRILLING RISER IN DEEP WATER OF MARINE

Yu Song*, Jin Yang

China University of Petroleum (Beijing), ChangPing, Beijing, 102249, China

ABSTRACT

A dynamic analysis model considering the actual riser string configuration is established to analyze the mechanical behavior of a drilling riser. Riser lateral displacement, bending moment, and deflection of the deep water well considering actual riser string configuration are simulated. The effects of wind speed, drilling platform drift distance, surface current speed on riser mechanical behavior are discussed. Results indicate that riser string configuration has a significant effect on riser mechanical behavior. Drilling platform should avoid a large drift distance, which may result in the deflection over the flex joint working range.

KEYWORDS:
Drilling riser, Dynamic analysis, Mechanical behavior, deep water

INTRODUCTION

Drilling riser system is the critical connection of subsea wellhead and drilling vessel. With exploration and development of oil and gas moving into deepwater and ultra deepwater, drilling riser system components are more likely to suffer accidents. Complex environmental conditions, operational loads, variable operation modes, and human errors can all contribute to the occurrence of the accidents. Any accident of drilling riser system will lead to discharge of pollutants, drilling downtime, and even can lead to catastrophic consequences [1-3]. From May 2003 to April 2004, several drilling riser accidents caused discharge of 6500 barrels of synthetic-based mud and a large amount of downtime [4]. Since 1983, such major drilling riser accidents, as unplanned disconnect of connector, break of drilling riser column, leakage of choke/kill lines, collapse of drilling riser main pipe, deformation caused by collision, burst of main pipe induced by wear, failure of the auxiliary equipments and grounding of the suspended riser column during typhoon evacuation can all be found throughout the references reviews [5-9].

Azar and Soltveit [10] developed a marine riser analysis model and considered the depth of seawater, density of the drilling fluid, and riser tension. Their studies showed the bending moment decreasing with increased wind speed and water depth. Patel et al. [11] investigated the mechanical behavior of a riser using the time domain method and compared this behavior with that observed through the frequency domain method for displacement and stress. Ahmad and Datta [12] presented a frequency domain iterative procedure method for riser analysis and proved the frequency domain iterative method could be more efficient than the time integration method in riser analysis.

Patel and Seyed [13] comprehensively reviewed riser modeling and analysis techniques. Atadan et al. [14] considered the riser system and drilling platforms as a whole system and analyzed the riser and drilling platform system using the cantilever model. Their research demonstrated that the mass of the platform had an effect on the first resonance of the riser system.

Chucheepsakul et al. [15] introduced a new method to analyze the flexible marine pipes that could also be used in similar types of elastic structures, such as onshore pipes, submerged pipes, marine cables, onshore cables, and strings. Kaewunruen et al. [16] employed Hamilton's principle to analyze the nonlinear free vibration of the riser and demonstrated that the internal flows could reduce the degree of the hardening of the risers. Pham et al. [17] comprehensively reviewed the manufacture, experimental investigations, and numerical analyses of deep-water risers. Athisakul et al., [18] applied the finite element method to investigate the three-dimensional analysis of the extensible marine riser and revealed that the axial extensibility reduced the stability of the riser system. Li et al. [19] analyzed the transverse vibration of the riser and indicated that the largest transverse displacement was found in the upper section of the riser. Major et al. [20] studied the effect of drilling string rotation on the dynamic response of drilling risers and demonstrated that the drill string rotation reduced the natural frequency and increased the amplitude of the vibration of the drilling riser.

This study aims to investigate the mechanical behavior of deep-water drilling riser and the deformation, bending moment, and deflection of the drilling riser under different ocean environments were obtained. Riser mechanical behavior focuses on riser strength, whereas vortex induced vibration focuses on riser fatigue.

EXPERIMENTAL

Analysis model. The riser close to the seabed is connected to the subsea blowout preventer stack through the lower flex joint. The riser near the water surface is connected to a diverter through the upper flex joint. The riser at the top ends can move with the drifting of the drilling platform, as shown in Fig. 1a. Thus, the mechanical model can be regarded as a simply supported beam located in the vertical plane. The simplified riser mechanical model in deep-water drilling can be expressed in Fig. 1b.

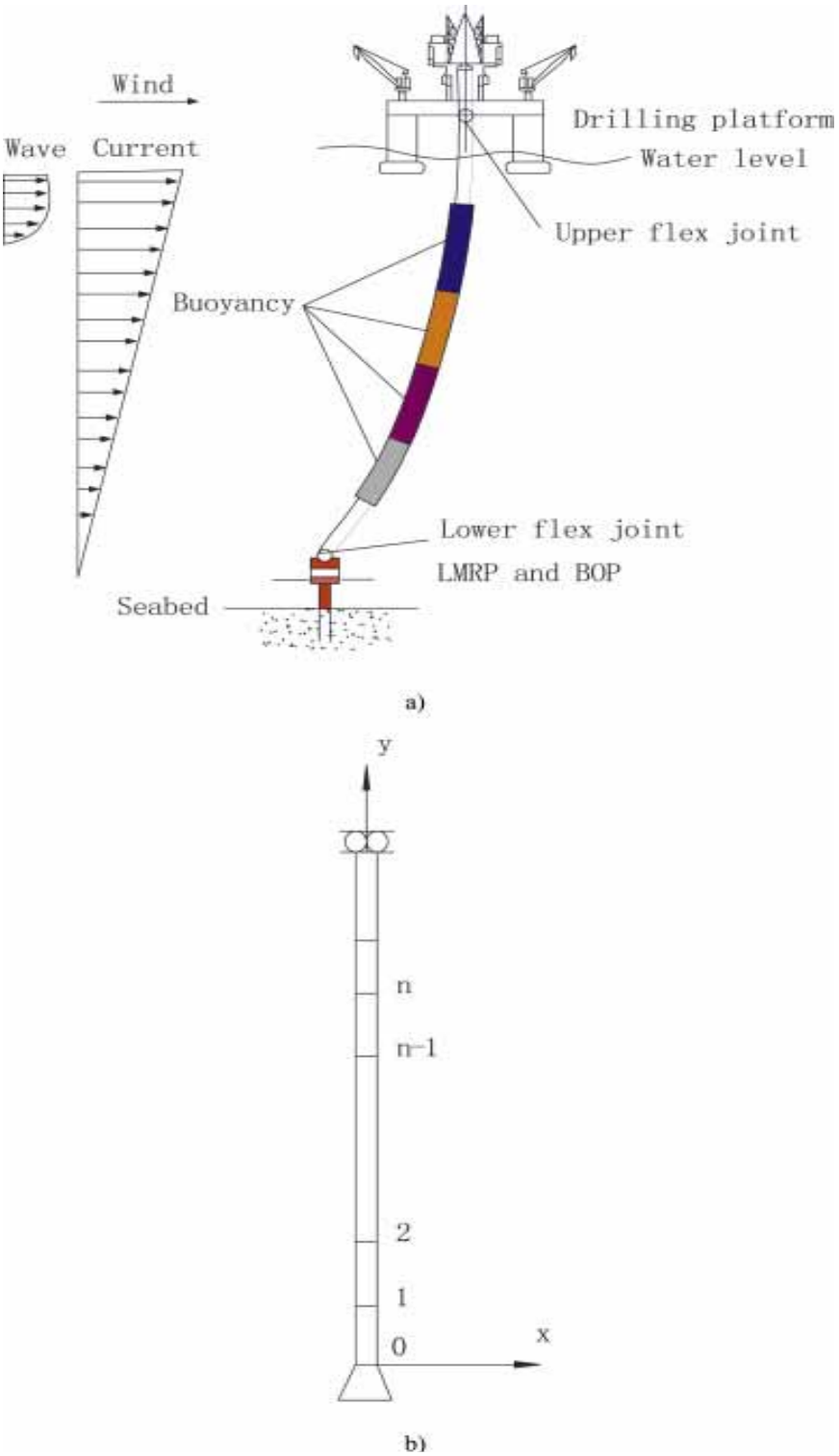

FIGURE 1
The simplified riser mechanical model: a) is the riser schematic diagram under different ocean environment loadings; b) is the drilling riser analysis model.

RESULTS AND DISCUSSION

Effect of drilling platform drift distance on riser mechanical behavior. The drilling platform drift distance must be controlled in a certain range. Otherwise, the riser system must disconnect. A large drilling platform drift distance may destroy the wellhead, blowout preventer, riser, and slip joint. The drilling platform drift distance can be expressed by the percentage of water depth. If the drilling platform drift distance is more than 1% of the water depth, then a yellow alert signals the disconnection of the riser system. The riser system must disconnect if the drilling platform drift distance is close to 2% or more than 3% of the water depth. However, drilling platform drift distance may also considerably affect riser mechanical behavior. Drilling platform drift distances with 0%, 1%, 2%, and 3% of water depth are calculated to discuss the effect of drilling platform drift distance on riser mechanical behavior. The corresponding drilling platform drift distances are 24 m, 46 m, and 69 m.

As shown in Fig. 2 and 3. Thus, the distribution of the riser deflection increases with the increase in drilling platform distance. Moreover, the water surface is the boundary of the ocean environment loads. Risers above the water surface have no direct action from the ocean environment loads, whereas risers below the water surface have direct ocean environment loads. Therefore, the maximum bending moment appeared near the water surface under the drilling platform drifting condition, and the bending moment from 2050 m to the upper flex joint significantly increases with the increase in drilling platform distance. A large drilling platform drift distance may destroy the riser and result in deflection over the flex joint's working range.

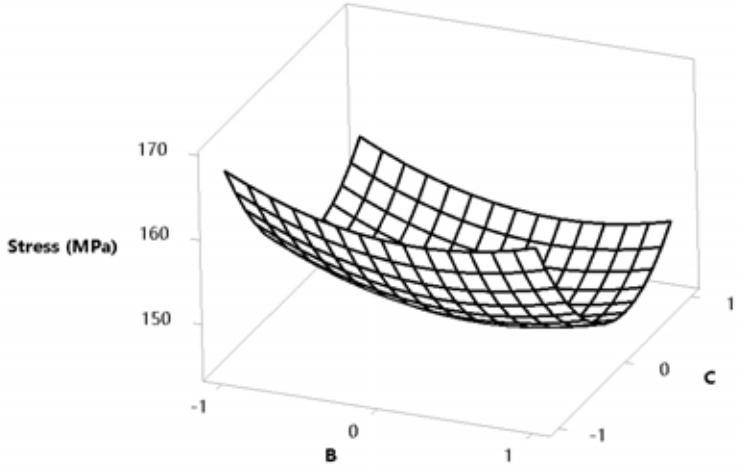

FIGURE 2
Surface Plot of Stress (MPa) vs C, B

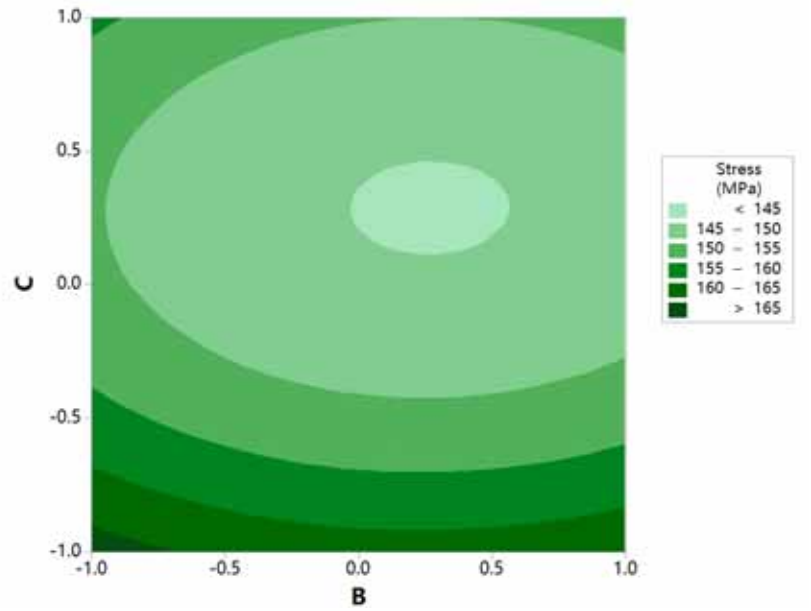

FIGURE 3
Contour Plot of Stress (MPa) vs C, B

Effect of surface current speed on riser mechanical behavior. Fig. 4 and 5 show the effect of the surface current speed on the distribution of the riser lateral displacement. It demonstrates that riser lateral displacement significantly increase with the increase in surface current speed. Ekman drift current theory states that current speed profile along the water depth is determined by surface current speed and the increase in current speed profile with the increase in surface current speed. Consequently, the ocean environment loads increase, thereby resulting in the increase of the riser lateral displacement, bending moment, and deflection. Thus, surface current speed has a considerable effect on ocean environment loadings. Accordingly, surface current is a key parameter in the design of the riser string configuration.

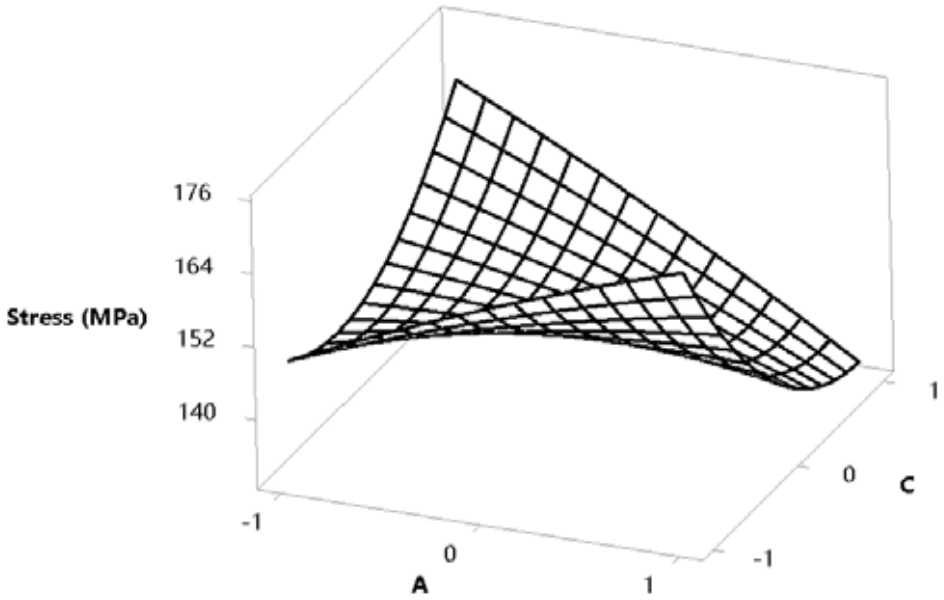

FIGURE 4
Surface Plot of Stress (MPa) vs C, A

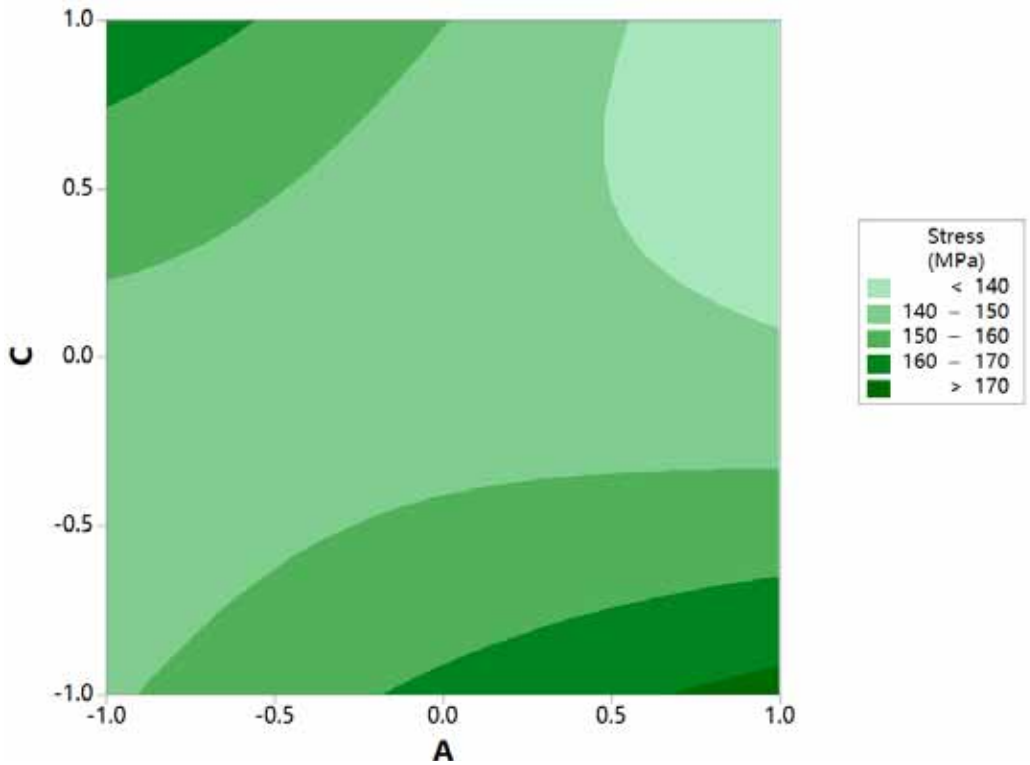

FIGURE 5
Contour Plot of Stress (MPa) vs C, A

Effect of wind speed on riser mechanical behavior. Fig.6 and 7 show the effect of wind speed on the distribution of riser lateral displacement. Riser lateral displacement increase with the increase in wind speed. The increasing trend is more evident in the area closer to the water surface. The increase in wind speed can increase the surface current speed, thereby increasing the loading. However, the action depth from the wind is limited because of the damping effect of seawater. Thus, wind-induced ocean environment loads may be found at the upper side of the riser that is close to the water surface. Therefore, the influence of the variation in wind speed on the distribution of riser lateral displacement is limited, as shown in Fig. 6 and 7. Accordingly, the influence of wind speed on riser mechanical behavior is significantly less compared with the influence of ocean current.

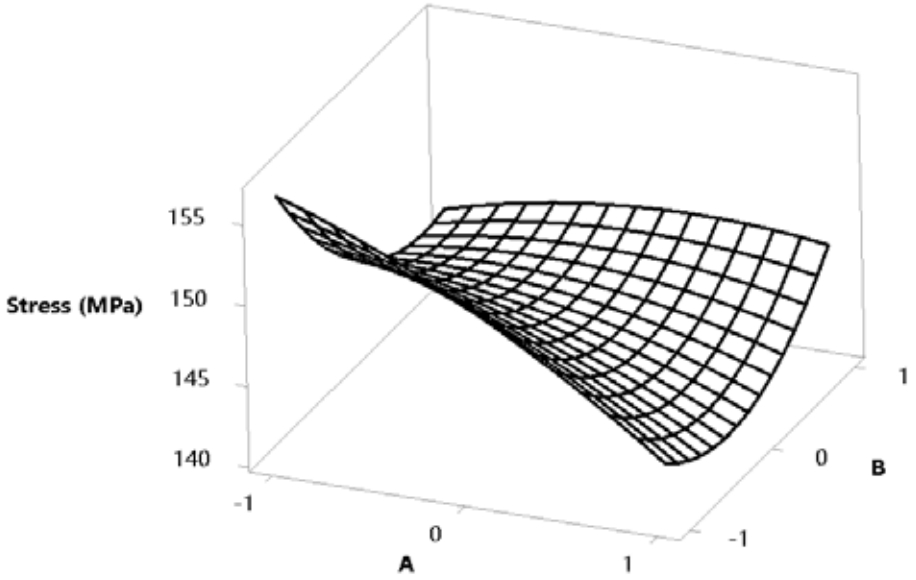

FIGURE 6
Surface Plot of Stress (MPa) vs B, A

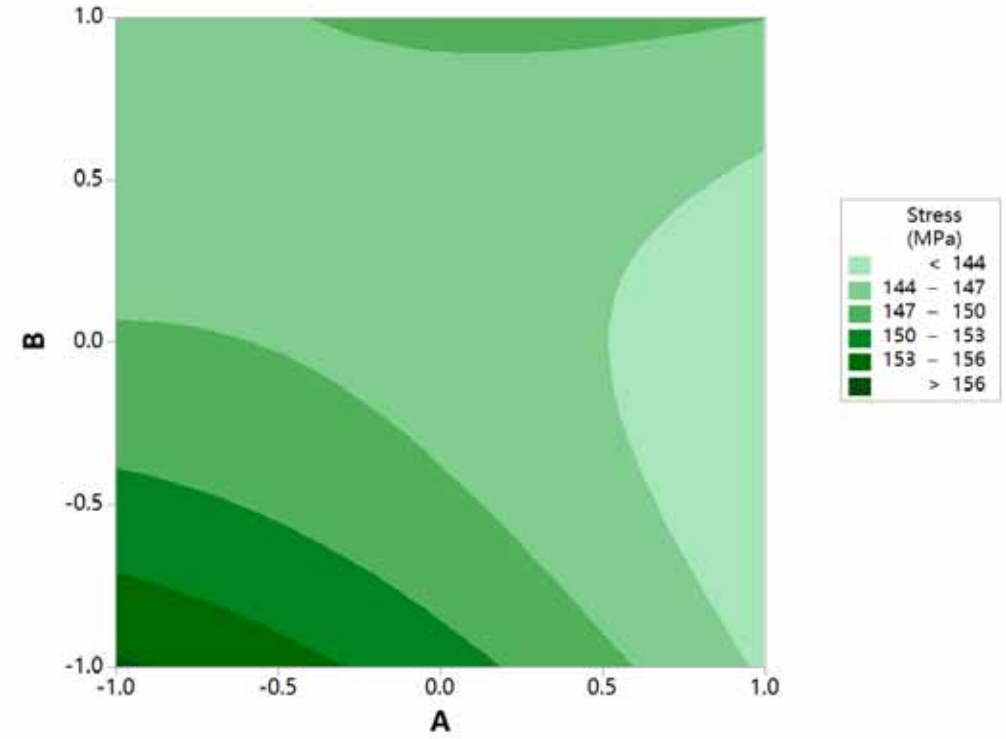

FIGURE 7
Contour Plot of Stress (MPa) vs B, A

CONCLUSIONS

A dynamic analysis model considering the actual riser string configuration is established to analyze the mechanical behavior of a drilling riser. Riser lateral displacement, bending moment, and deflection of the deep water well considering actual riser string configuration are simulated. The effects of wind speed, drilling platform drift distance, surface current speed on riser mechanical behavior are discussed. Results indicate that riser string configuration has a significant effect on riser mechanical behavior. Drilling platform should avoid a large drift distance, which may result in the deflection over the flex joint working range.

ACKNOWLEDGEMENTS

The authors gratefully acknowledge the financial support of National Natural Science Foundation of China (Grant No.51434009) and National Basic Research Program of China (973 Program) (Grant No.2016ZX05033004-006).

REFERENCES

[1] Ni, W., Li, Q., Song, X. (2017) Analysis of Wellbore Stability of Shale Gas Reservoir Drilling. Fresen. Environ. Bull. 26, 510-515.
[2] Li, X., Zhang, Y. (2018) Supercritical Water Oxidation of Waste Drilling Fluid. Fresen. Environ. Bull. 27,1884-1888.
[3] Zhang, X. (2018) Study on Recent Advances of Waste Drilling Fluid Treatment. Fresen. Environ. Bull. 27, 4460-4468.
[4] Yuanjiang, C., Xiangfei, W., Guoming, C., Jihua, Y., Keren, R. (2018) Comprehensive risk assessment of deepwater drilling riser using fuzzy Petri net model. Process Safety and Environmental Protection. 117, 483-497.
[5] Liangjie, M., Qingyou, L., Shouwei, Z., Guorong, W., Qiang, F. (2016) Deep water drilling riser mechanical behavior analysis considering actual riser string configuration. Journal of Natural Gas Science and Engineering. 33, 240-254.
[6] Holand, P. (1991) Subsea blowout-preventer systems: reliability and testing. SPE Dril. Eng. 6, 293-298.
[7] Ju, S., Chen, G., Song, L., Chang, Y. (2011) Accidents investigation and precautionary measure for deepwater drilling riser. China Pet. 37, 83-87.
[8] Chang, Y., Chen, G., Wu, X., Ye, J., Chen, B., Xu, L. (2018) Failure probability analysis for emergency disconnect of deepwater drilling riser using Bayesian network. J. Loss Prev. Process Ind. 51, 42-53.
[9] Liu, X., Chen, G., Chang, Y., Liu, K., Zhang, L., Xu, L. (2013) Analyses and countermeasures of deepwater drilling riser grounding accidents under typhoon conditions. Pet. Explor. Dev. 40, 738-742.
[10] Azar, J.J., Soltveit, R.E. (1978) A Comprehensive Study of Marine Drilling Risers. SPE p. 7200.
[11] Patel, M.H., Sarohia, S., Ng, K.F. (1984) Finite-element analysis of the marine riser. Eng. Struct. 6(3), 175-184.
[12] Ahmad, S., Datta, T.K. (1992) Nonlinear response analysis of marine risers. Comput. Struct. 43 (2), 281-295.
[13] Patel, M.H., Seyed, F.B. (1995) Review of flexible riser modelling and analysis techniques. Eng. Struct. 17(4), 293-304.
[14] Atadan, A.S., Calisal, S.M., Modi, V.J., Guo, Y. (1997) Analytical and numerical analysis of the dynamics of a marine riser connected to a floating platform. Ocean. Eng. 24(2), 111-131.
[15] Chucheepsakul, S., Monprapussorn, T., Huang, T. (2003) Large strain formulations of extensible flexible marine pipes transporting fluid. J. Fluid. Struct. 17 (2), 185-224.
[16] Kaewunruen, S., Chiravatchradej, J., Chucheepsakul, S. (2005) Nonlinear free vibrations of marine risers/pipes transporting fluid. Ocean. Eng. 32(3), 417-440.
[17] Pham, D.C., Sridhar, N., Qian, X., Sobey, A.J., Achintha, M., Shenoi, A. (2016) A review on design, manufacture and mechanics of composite risers. Ocean. Eng. 112, 82-96.
[18] Athisakul, C., Monprapussorn, T., Chucheepsakul, S. (2011) A variational formulation for three-dimensional analysis of extensible marine riser transporting fluid. Ocean. Eng. 38(4), 609-620.
[19] Li, Z., Wang, P., Zhao, M., Li, X. (2015) Transverse vibration analysis of the riser in deep water. Open Pet. Eng. J. 8(1), 38-44.
[20] Major, I.E., Big-Alabo, A., Odi-Owei, S. (2015) Effect of drill string rotation on the dynamic response of drilling risers. Int. J. Appl. Mech. 20(3), 503-516.

Received: **24.10.2018**
Accepted: **14.02.2019**

CORRESPONDING AUTHOR

Yu Song
China University of Petroleum (Beijing),
ChangPing, Beijing, 102249 – China

e-mail: 1783727392@qq.com

© by PSP Volume 28 – No. 5/2019 pages 3824-3828 Fresenius Environmental Bulletin

MORPHOMETRIC COMPARISON BETWEEN *SCARDINIUS ERYTHROPHTHALMUS* (LINNAEUS, 1758) AND *SCARDINIUS ELMALIENSIS* (BOGUTSKAYA, 1997)

Ali Ilhan*

Ege University, Faculty of Fisheries, 35100, Bornova, Izmir, Turkey

ABSTRACT

In this study, some morphometric characters of Rudd, *Scardinius erythrophthalmus* and Elmalı Rudd, *Scardinius elmaliensis* were determined and compared. One *S. erythrophthalmus* samples collected from different locations and 27 *S. elmaliensis* samples collected from Avlan Lake (Elmalı-Antalya) were examined and morphometric characters, were measured at each specimen. In addition, meristic characters including the number of fin rays, the number of lateral line scales and the number of gill rakers were counted. The ratios between the morphometric characters were also calculated. The total length of *S. erythrophthalmus* individuals varied between 5.5 and 22.5 cm while the total length of *S. elmaliensis* individuals varied between 6.8 and 20.1 cm. The maximum body height-standard height, eye diameter-nose length, eye diameter-head length and nose length-head length ratios revealed that the two species were statistically different from each other.

KEYWORDS:
Scardinius, Elmalı Rudd, endemic, morphometry, gill raker

INTRODUCTION

Scardinius genus are include small-middle sized fish that usually live in lakes characterized with submerse plants and wide lowland rivers [1].

Rudd, *Scardinius erythrophthalmus* is characterized with 39-42 lateral line scales, D: III 8-9, A: III 10-13.5, double lined 3.5-5.3 or 2.5-5.2 pharyngeal teeth and 9-12 gill rakers [1, 2]. Its natural distribution includes many streams in Northern Europe, Mediterranean and Black Sea basins and Northern Asia. They live in nutrient-rich slow-flowing rivers, backwaters, ponds and lakes rich with well vegetation. It is known they can live up to 17 years and spawn for the first time at 3-4 years. They predominantly feed on planktons, terrestrial insects and plants. Their conservation status in the IUCN red list is LC (Least Concern= does not qualify for a high risk or insufficient information available to assess the status) [1].

Elmalı Rudd, *Scardinius elmaliensis* was evaluated as a subspecies of *Scardinius erythrophthalmus by* Bogutskaya [3] due to the differences in two diagnostic characters including the fewer number of rays at the anal fin and the higher number of gill rakers. In the following years, Kuru [4] have reported it as a subspecies as *S. erythrophthalmus elmaliensis.* Taxon was first mentioned as a species by Fricke et al. [5]. The descriptive characters of the species are 39-40 lateral line scales, D: III 9, A: III 10, double lined 3.5-5.2 or 3.5-5.3 pharyngeal teeth and 15-16 gill rakers [3]. It is known for its presence in Avlan Lake in Antalya territory and it is endemic for the inland waters in Turkey. Although there is no sufficient information regarding its biology, it will be saying it is similar to *S. erythrophthalmus*. It is classified EN (Endangered B1) in the IUCN red list [6].

Although there are studies conducted on the biological properties [7], growth and reproduction properties [8], digestive system contents [9], length-weight relation and conditions [10], age determination [11] and growth parameters [12, 13] of *Scardinius erythrophthalmus* and length-weight relation of *Scardinius elmaliensis*, there are no studies on the morphometric characters of the two species. Therefore, as this study is the first on this subject, any comparison with other studies could not be carried out.

The aim of this study was to determine and compare some morphometric characters of two different Rudd species (*S. erythrophthalmus* and *S. elmaliensis*) collected from the inland waters in Turkey and, thus, determine the similarities and differences between these two species.

MATERIALS AND METHODS

The samples used as the material of the study were obtained from Ege University Museum of the Faculty of Fisheries (ESFM/PISI). One hundred and seventy-one *S. erythrophthalmus* samples collected from different locations and 27 *S. elmaliensis* samples collected from Avlan Lake (Elmalı-

Antalya) were examined regardless of their sex (Table 1).

The total and standard lengths of the fish were measured using 1 mm precision measurement ruler. The weight values of the fish were determined using 0.01 g precision measurement scale. Morphometric characters including head length, head height, the maximum body height, eye diameter, interorbital distance, nose length, dorsal fin length and height, anal fin length and height, predorsal-postdorsal distances, preanal distance, preventral-postventral distance, pecto-ventral distance, ventra-anal distance, caudal peduncle length and height values were measured using a 0.01 mm precision digital caliper (Figure 1).

The number of fin rays and the number of lateral line scales were determined using 3X magnification lupe while the number of gill rakers were determined using a binocular microscope. In addition, standard length-total length, head length-total length, the maximum body height-total height, eye diameter-head length, nose length-head length, eye diameter-interorbital distance, eye diameter-nose length, head height-the maximum body height, predorsal distance-postdorsal distance and preventral distance-postventral distance ratios were calculated. The obtained ratios were analyzed for significance using the t-test.

TABLE 1
Locations of examined specimens *Scardinius*

Locality	Coordinate	Number
Scardinius erythrophthalmus		
Apolyont Lake, Nilüfer-Bursa	40°10'00" N 28°40'60" E	28
Manyas Lake, Bandırma-Balıkesir	40°13'60" N 28°30'00" E	32
Gelemen D.Ü.Ç., Tekkeköy-Samsun	41°13'42" N 36°29'00" E	2
Kadıköy Stream, Balya-Balıkesir	39°46'47" N 27°36'29" E	10
Yassıgeçit Stream, Keşan-Edirne	40°13'60" N 28°30'00" E	3
Gala Lake, Enez-Edirne	40°45'34" N 26°11'05" E	40
Köy Lake, İpsala-Edirne	40°13'60" N 28°30'00" E	11
Meriç River, Enez-Edirne	40°43'52" N 26°05'09" E	14
Tunca River, Edirne	41°42'04" N 26°32'41" E	10
Gölhisar Lake, Gölhisar-Burdur	37°07'04" N 29°36'09" E	13
Taşkısığı Lake, Adapazarı-Sakarya	40°52'00" N 30°24'04" E	3
Gölbaşı pond, Karasu-Sakarya	41°05'11" N 30°44'44" E	5
Scardinius elmaliensis		
Avlan Lake, Elmalı-Antalya	36°34'15" N 29°57'02" E	27

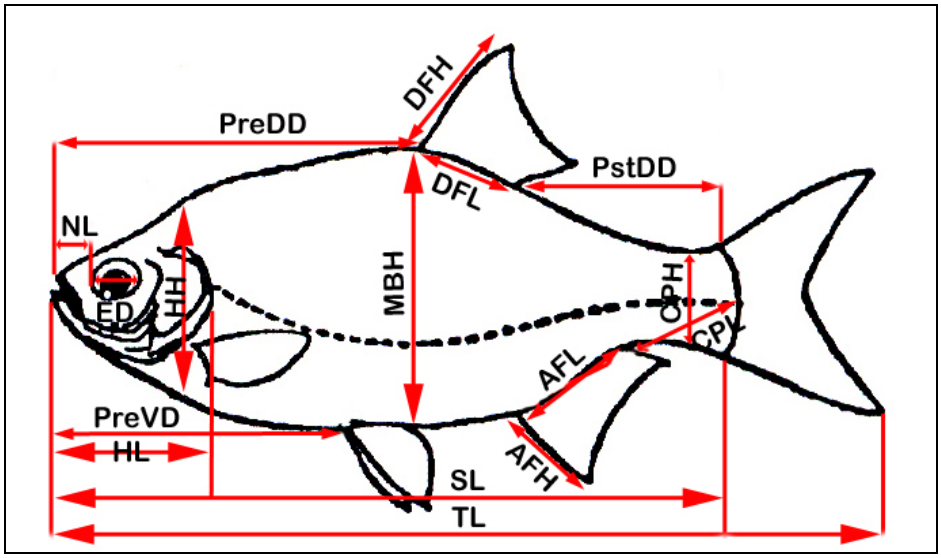

FIGURE 1
Morphometric characters in *Scardinius*

TL: Total length, SL: Standard length, HL: Head length, HH: Head height, MBH: Maximum body height, ED: Eye diameter, NL: Nose length, DFL: Dorsal fin length, DFH: Dorsal fin height, AFL: Anal fin length, AFH: Anal fin height, PreDD: Predorsal distances, PstDD: Postdorsal distances, PreVD: Preventral distance, CPL: Caudal peduncle length, CPH: Caudal peduncle height.

TABLE 2
Some metric characters of *Scardinius erythrophthalmus* and *Scardinius elmaliensis*.

	Scardinius erythrophthalmus (N: 171)			*Scardinius elmaliensis* (N: 27)		
Character	Min-Max.	Meant±CI	SE	Min-Max.	Meant ±CI	SE
TL (cm)	5.5-22.5	12.32±0.567	0.287	6.8-20.1	11.95±1.325	0.643
SL (cm)	4.5-19.1	10.18±0.470	0.238	5.7-17.2	10.20±1.150	0.558
HL (mm)	12.00-41.66	24.59±1.085	0.548	16.52-43.74	26.58±2.674	1.298
HH (mm)	8.30-34.67	19.63±0.935	0.472	12.75-33.98	21.19±2.307	1.120
MBH (mm)	11.77-65.00	33.06±1.891	0.955	16.86-49.18	30.41±3.425	1.662
ED (mm)	3.59-9.23	6.18±0.200	0.101	4.12-8.77	6.18±0.467	0.227
İOD (mm)	4.48-18.44	9.95±0.485	0.245	5.83-15.50	10.18±1.010	0.490
NL (mm)	3.07-13.55	7.35±0.344	0.173	4.22-11.28	7.56±0.735	0.357
CPH (mm)	3.75-20.51	10.71±0.586	0.296	6.21-17.64	11.14±1.230	0.597
CPL (mm)	14.93-61.03	33.34±1.577	0.797	18.90-52.56	31.10±3.504	1.701
DFL (cm)	4.98-30.34	14.40±0.723	0.365	7.02-20.28	12.39±1.305	0.634
DFH (mm)	9.50-44.53	22.13±0.973	0.491	12.56-31.12	19.23±1.794	0.871
AFL (cm)	6.02-25.96	14.06±0.738	0.373	7.52-20.10	12.21±1.341	0.651
AFH (mm)	5.37-46.00	16.56±0.892	0.451	9.84-26.30	15.59±1.632	0.792
PreDD (mm)	24.56-103.44	55.67±2.805	1.417	35.50-97.43	59.34±6.382	3.098
PstDD (mm)	14.89-70.39	34.75±1.618	0.817	17.75-58.39	32.64±4.096	1.989
PreVD (mm)	21.84-87.12	49.37±2.271	1.147	30.93-83.43	51.81±5.206	2.527
PstVD (mm)	21.84-98.30	52.25±2.594	1.310	28.61-79.39	47.93±5.224	2.536
PrePD (mm)	11.48-41.18	24.88±1.075	0.543	17.07-45.39	27.59±2.706	1.314
PreAD (mm)	10.81-133.46	70.92±3.448	1.741	41.56-117.24	72.29±7.712	3.744
P-VD (mm)	10.19-48.40	24.72±1.247	0.630	14.61-38.56	25.94±2.588	1.256
V-AD (mm)	8.13-47.86	23.46±1.252	0.632	12.80-36.47	22.16±2.495	1.211

Min: Minimum, Max: Maximum, Mean : Mean, CI: Confidence Intervals, SE: Standard Error, TL: total length, SL: standard length, HL: head length, HH: head height, MBH: maximum body height, ED: eye diameter, İOD: interorbital distance, NL: nose length, CPH: caudal peduncle height, CPL: caudal peduncle length, DFL: dorsal fin length, DFH: dorsal fin height, AFL: anal fin length, AFH: anal fin height, PreDD: predorsal distance, PstDD: postdorsal distance, PreVD: preventral distance, PstVD: postventral distance, PrePD : prepectoral distance, PreAD: Preanal distance, P-VD: pecto-ventral distance, V-AD: ventra-anal distance.

RESULTS

In this study, 171 *Scardinius erythrophthalmus* samples collected from different locations and 27 *Scardinius elmaliensis* samples collected from Avlan Lake (Elmalı-Antalya) were examined. Total length distribution of *samples* varied between 5.5 and 22.5 cm in *Scardinius erythrophthalmus* individuals and between 6.8 and 20.1 cm in *Scardinius elmaliensis* individuals (Table 2). Considering the average values of examined metric characters, it was seen that both species had almost the same values. For both species, it was seen that head length value was higher than head weight value and lower than the maximum body weight value. Similarly, nose length value was higher than eye diameter and lower than interorbital distance value. In addition, the average dorsal and anal fin lengths were remarkably close to each other (Table 2).

Examining the meristic characters of both species, it was found that the number of dorsal and ventral fin rays were the same in both species whereas the number of anal fin soft rays and the number of gill rakers which are regarded as the reason for the distinction of the species were different (Table 3). Also, although they were not mentioned in the identification of the species, the number of ligne lateral and ligne transversal scales, and the number of pectoral-fin soft rays were different (Table 3).

The ratios between the metric characters determined in both species were calculated and the obtained average values were analyzed using the t-test for significant differences. Accordingly, the ratios of 12 different characters between each other were calculated. The maximum body height-standard height, eye diameter-nose length, eye diameter-head length and nose length-head length ratios revealed that the two species were statistically different from each other (Table 4).

DISCUSSION AND CONCLUSION

Considering the average values of examined metric characters, it was seen that both species had almost the same values. The differences between the number of anal-fin soft rays and the number of gill rakers in these two species which are shown as the reasons for the classification of *S. elmaliensis* first as a subspecies and then as a species separate from of *S. erythrophthalmus* were also determined

in the present study. Also, although it was not mentioned in the previous studies on the distinction of these species, the number of ligne lateral and ligne transversal scales, and the number of pectoral-fin soft rays were also different in the two species.

In addition, as a result of the comparison of the ratios between the metric characters using the t-test, it was determined that the maximum body height-standard length, eye diameter-head length and nose length-head length ratios were different between the two species. The differences in the meristic characters including the number of anal and pectoral-fin soft rays, the number of gill rakers, the number of ligne lateral and ligne transversal scales as well as the differences observed between the ratios of some metric characters are of great importance in terms of the morphological distinction between the species.

In conclusion, it was again revealed that *Scardinius* population in Avlan Lake was different from the other populations in Anatolia and it has a special importance in terms of the inland waters biodiversity in Turkey. It is remarkable that the species sustained its existence despite the fact that Avlan Lake was drained for agricultural reclamation purposes between 1977 and 1997 [14]. This is definitive proof indicating how delicate the situation is for the continuity of the species. According to Fricke et al. [5], threats to the continuity of *S. elmaliensis* are loss of habitat, pollution, weirs and dams on streams and water withdrawal from the system for irrigation purposes. In light of this information, for the continuity of *Scardinius elmaliensis* species, based on the fact that they have a very limited area, it is crucial to protect Avlan Lake from all kinds of negative effects (pollution, exotic species, water usage) in the short term. In prospective studies, the lake can be evaluated as a protected area for *Scardinius elmaliensis*.

TABLE 3
Some meristic characters of *Scardinius erythrophthalmus* and *Scardinius elmaliensis*.

Meristic character	*Scardinius erythrophthalmus* (N: 171)	*Scardinius elmaliensis* (N: 27)
D	III 8-9	III 8-9
A	III 11-13	III 11
P	I 15-16	I 14-15
V	II 9	II 9
L.lat.	40-41	39-40
L.trans.	7/3	6-7/3
GR	10-12	14-15

D: dorsal fin ray, A: anal fin ray, P: pectoral fin ray, V: ventral fin ray, L.lat.: ligne lateral scales, L.tran.: ligne transversal scales row, GR: gill rakers.

TABLE 4
The ratios of morphometric characters of *Scardinius erythrophthalmus* and *Scardinius elmaliensis*.

	Scardinius erythrophthalmus			*Scardinius elmaliensis*			
	Min-Max.	Mean±CI	Se	Min-Max.	Mean±CI	Se	t-test
SL/TL	0.76-0.93	0.83±0.009	0.0017	0.82-0.92	0.85±0.007	0.0036	t= -6.5176, p›0.05
HL/TL	0.17-0.25	0.20±0.005	0.0010	0.20-0.25	0.22±0.005	0.0230	t= -88.9419, p›0.05
HL/SL	0.20-0.29	0.24±0.002	0.0011	0.23-0.29	0.26±0.006	0.0028	t= -6.7608, p›0.05
MBH/TL	0.13-0.33	0.26±0.011	0.0022	0.20-0.29	0.25±0.007	0.0355	t= -64.1496, p›0.05
MBH/SL	0.15-0.40	0.32±0.005	0.0026	0.24-0.34	0.30±0.008	0.0038	t= 4.2305, p‹0.05
ED/HL	0.19-0.35	0.26±0.013	0.0025	0.20-0.28	0.24±0.008	0.0040	t= 4.7153, p‹0.05
HH/HL	0.69-0.94	0.79±0.017	0.0034	0.72-0.98	0.79±0.023	0.0111	t= 0.0015, p›0.05
NL/HL	0.22-0.38	0.30±0.009	0.0019	0.23-0.33	0.29±0.009	0.0046	t= 2.6694, p‹0.05
ED/IOD	0.45-0.87	0.65±0.039	0.0078	0.48-0.74	0.62±0.026	0.0126	t= 1.9620, p›0.05
ED/NL	0.19-0.35	0.26±0.013	0.0025	0.20-0.28	0.24±0.008	0.0040	t= 4.7153, p‹0.05
HH/MBH	0.43-1.24	0.61±0.030	0.0059	0.62-0.81	0.70±0.020	0.0099	t= -7.7172, p›0.05
PrDD/PstDD	1.27-1.99	1.60±0.064	0.0129	1.52-2.00	1.84±0.049	0.0237	t= -9.0465, p›0.05
PreVD/PstVD	0.83-1.10	0.95±0.021	0.0041	1.00-1.18	1.09±0.019	0.0094	t= -13.1506, p›0.05

Min: Minimum, Max: Maximum, Mean: Mean, CI: Confidence Intervals, SE: Standard Error, SL: standard length, TL: total length, HL: head length, MBH: maximum body height, ED: eye diameter, HH: head height, NL: nose length, İOD: interorbital distance, PreDD: predorsal distance, PstDD: postdorsal distance, PreVD: preventral distance, PstVD: postventral distance.

REFERENCES

[1] Kottelat, M. and Freyhof, J. (2007) Handbook of European freshwater fishes. Publications Kottelat, Cornol, Switzerland. 646p.

[2] Geldiay, R. and Balık, S. (2007) Freshwater Fishes of Turkey (V. Press). Publications of Ege University Fisheries Faculty No: 46 Lesson Book Concordance No: 16, İzmir, 1-644. (in Turkish).

[3] Bogutskaya, N.G. (1997) Contribution to the knowledge of leuciscine fishes of Asia Minor. Part. 2. An annotated check-list of leuciscine fishes (Leuciscinae, Cyprinidae) of Turkey with description of a new species and two new subspecies. Mitteilungen aus dem Hamburgischen Zoologischen Museum und Institut. 94, 161-186.

[4] Kuru, M. (2004) Recent Systematic Status of Inland Water Fishes of Turkey. GÜ, Gazi Eğitim Fakültesi Dergisi. 24(3), 1-21. (in Turkish).

[5] Fricke, R., Bilecenoğlu, M. (2007) Annotated checklist of fish and lamprey species (Gnathostomata and Petromyzontomorphi) of Turkey, including a Red List of threatened and declining species. Stuttgarter Beiträge zur Naturkunde, A. 706, 169

[6] Freyhof, J. (2014) *Scardinius elmaliensis*. The IUCN Red List of Threatened Species. Version 2015.1. <www.iucnredlist.org>. Downloaded on 15 June 2015.

[7] Erdem, Ü., Güher, H. And Türeli, C. (1994) Some Biological Properties of *Scardinius erythrophthalmus* L., 1758 and *Carassius carassius* L., 1758 (Pisces) in Hamam Lake (İğneada-Kırklareli). XII. National Biology Congress, 6-8 July 1994, Edirne, IV, 122-126. (in Turkish).

[8] Ustaoğlu, M.R (1997) Investigations on Growth and Reproduction Characteristics of Rudd (*Scardinius erythropthalmus* (L., 1758)) Population in Lake Kuş (Bandırma). IX. National Fisheries Symposium 17-19 September 1997, Eğirdir/Isparta, I, 1-11. (in Turkish).

[9] Polat, N. (2003) Stomach Contents of Rudd (*Scardinius erythrophthalmus* L., 1758) Inhabiting Samsun-Bafra Fish Lakes (Tatlı Lake and Gıcı Lake). Fırat Üniversitesi Fen ve Mühendislik Bilimleri Dergisi. 15(4), 463-471. (in Turkish).

[10] Okgerman, H. (2005) Seasonal Variations in the Length-weight Relationship and Contidion Factor of Rudd (*Scardinius erythrophthalmus* L.) in Sapanca Lake. International Journal of Zoological Research. 1(1), 6-10.

[11] Polat, N. (2007) A Research on Age Determination, Length-Weight Relationship and Condition Factor of Rudd (*Scardinius erythrophthalmus* Linnaeus, 1758) Population in Gölhisar Lake (Burdur). Turkish Journal of Aquatic Life. 3-5(5-8), 99-107. (in Turkish).

[12] Koyuncu, V., Şahin, Y. and Emiroğlu, Ö. (2007) Growth Parameters Research of the Scardinius erythorphthalmus L.1758 in Lake Uluabat. Turkish Journal of Aquatic Life. 3-5(5-8), 288-296. (in Turkish).

[13] Küçükkara, R., Ceylan, M., Çubuk, H., Erol, K.G., Akçimen, U. And Savaşer, S. (2008) Investigation of growth features of Rudd (*Scardinius erythrophthalmus* L., 1758) population in Uluabat Lake. E.U. Journal of Fisheries and Aquatic Sciences. 25(4), 289–293. (in Turkish).

[14] Timur, Ö.B. (2007) A Research on the Effects of Drainage Works on Landscape Values a Case Study: Avlan Lake. Master Thesis. Ankara University Graduate School of Natural and Applied Sciences Department of Landscape Architecture, 100p. (in Turkish).

Received: **30.10.2018**
Accepted: **25.03.2019**

CORRESPONDING AUTHOR

Ali Ilhan
Faculty of Fisheries
Ege University
İzmir, Bornova 35100 – Turkey

e-mail: alilhan73@gmail.com

© by PSP Volume 28 – No. 5/2019 pages 3829-3834 Fresenius Environmental Bulletin

EFFECTS OF CONCRETE ADDITIVES ON VITAL TISSUES OF RAINBOW TROUT (*ONCORHYNCHUS MYKISS*): A HISTOLOGICAL EXAMINATION

Akif Er, Ozgur Oztek, Sevki Kayis*

Aquaculture Department, Faculty of Fisheries Sciences Recep Tayyip Erdogan University, 53100 Rize, Turkey

ABSTRACT

The construction of reinforced concrete structures in aquatic systems and water basins has now become an inevitable need. Concrete structures, both simple and large, such as retaining walls, the design of landscape areas, bridges, hydroelectric power plants, and dams affect water basins. These structures contribute positively to mankind but the negative impact on the aquatic environment is inevitable. The present study determined the toxic effects of various concrete elements, such as cement (C), cement/set accelerating admixture (CS), cement/plasticizer (CP), and all additives (CSP) on rainbow trout (*Oncorhynchus mykiss*) cultivated in freshwater. The negative control group was devoid of additives. The mortality rates reported for these additives were 5, 20, 35, and 45%, respectively. Negative control groups were not associated with mortality. In addition, histological examination revealed severe toxic symptoms and effects on gills, liver, kidney, and spleen of fish.

KEYWORDS:
Cement, set accelerating admixture, plasticizer, trout.

INTRODUCTION

Concrete is one of the oldest and most widely used construction materials owing to its low cost, availability, long-term durability, and ability to protect against extreme weather conditions. It is used in the construction of various structures, such as roads, sidewalks, building scaffoldings, bridges, and dams. Concrete is produced from a mixture of aggregates (75%), cement (7–14%), some additive materials, and water [1]. The chemical additives in the concrete increase the fluidity of the concrete, enhance its strength and modify its physical properties such as making it less permeable and frost resistant as well as changing its freezing time [2]. In this regard, for the construction of dams, hydroelectric power plants, and bridges, which are built on aquatic systems, appropriate additives are necessary to have a minimum negative effect on the aquatic life.

Contamination of the aquatic area by concrete causes serious damage to aquaculture facilities and wild fish fauna. Cement constitutes a major and important substance in concrete; therefore, its negative effects on fish have been investigated by some researchers [3, 4]. For example, an in vitro study analyzed the effects of Portland cement (100 mg/L) on rainbow trout fry (3.6 cm and 0.48 g *Oncorhynchus mykiss*) [3]. Portland cement increased the pH of the water to above 10.5, which was found to be toxic to fish. Another study investigated the toxicity and histopathological effects of Portland cement powder on Nile tilapia (*Oreochromis niloticus*) gills and liver tissues [5]. The most common pathology observed at all exposed doses of cement on fish was gill lamella destruction, epithelial hyperplasia, and epithelial hypertrophy. Hepatic lesions observed in fish exposed to Portland cement were attributed to hepatocyte degeneration, vacuolization of cell cytoplasm, fatty degeneration, and hypertrophy of hepatocytes. The toxic effects of cement on rainbow trout (*O. mykiss*) and Siberian sturgeon (*Acipenser baerii*) were investigated by Kurtoğlu et al. [4]. This study reported severe pathologies, especially in the gills, due to cement-borne toxicity.

Despite the reported toxic effects of various chemicals added to cement on fish, no measures have been implemented to prevent these effects. The present study determined the toxic effects of some concrete additives including cement on rainbow trout.

MATERIALS AND METHODS

A total of 150 fish (*O. mykiss*) (mean weight: 60 ±1.2 g) were used in the study. These were obtained from the aquaculture research unit of the Faculty of Fisheries Sciences in Recep Tayyip Erdoğan University. The water quality parameters used in the experiment included temperature of 12 °C, pH 7.5, dissolved oxygen 11.3 mg/L, ammonia < 0.01 mg/L, nitrite < 0.01 mg/L, nitrate 0.01 mg/L, total hardness 120 mg/L ($CaCO_3$), and carbon dioxide 1.5 mg/L. For the experiment, 15 fiberglass tanks (50 L) with ventilation system installed to provide sufficient oxygen were used in triplicate.

A previously determined LC_{50} value of cement (0.44 g/L for 96 h) on rainbow trout [4] was used as the main value in our study to determine the value of other additives in concrete. The percentages of set accelerating admixture (based on chloride < % 0,1) and plasticizer (based on naphthalene formaldehyde sulfonate) used in our study were 3% and 1.5%, respectively; these were same as those used in a study by Rixom and Mailvaganam [6] and Şimşek et al. [7]. In the present study, negative control (free of additives, NC), positive control cement (C, 0.44 g/L), cement/set accelerating admixture (CS, 0.44/0.132 g/L), cement/plasticizer (CP, 0.44/0.06 g/L), and all additives (CSP, 0.44/0.132/0.06 g/L) were used.

The pH values were measured at the beginning of the experiment. The fish were exposed to various additives and their behavior was recorded during the experiment. The trial was terminated at 24 h to determine the acute effects of the additives on fish.

Histological studies were performed to determine the pathologies on vital tissues of fish. For this, fish were anesthetized with benzocaine before their death; they were then cut off the abdomen and transferred to 10% neutral buffered formalin as a whole. After 24 h, the samples were transferred to 50% ethyl alcohol. The liver, spleen, kidney, and gills of fish were removed, passed through a series of alcohol concentrations followed by treatment with xylose. The tissues were embedded in paraffin and then cut to a thickness of 0.5 μm; these were then stained with hematoxylin and eosin. The stained tissue sections were then fixed using entallan and covered with coverslips [8]. Histopathological changes were examined with a light microscope. The pathologies were reported as follows: none: - (0 lesion), few: + (1-4 lesions), moderate: ++ (5-8 lesions) and high: +++ (≥9 lesions) [9].

RESULTS

The pH values measured at the beginning of the experiment, after addition of the additives to the groups, were NC: 7.5, C: 10.42±0.5, CS: 10.61 ±0.2, CP: 10.77 ±0.3, and CSP: 10.75±0.2. At the end of the trial, different mortality rates were observed in some groups. The highest fish mortality rate of 45% was observed in the group exposed to all additives (CSP). The mortality rates of the other groups were recorded as 5% (C), 20% (CS), and 35% (CP). No deaths were observed in the negative control group (NC).

Table 1 lists the pathologies that occurred in the vital organs of fish. Histopathological findings of the gill structure revealed hyperplasia in all the groups. Significant deformities in the gill structure were among the common findings in the additive group. Unlike all groups, the presence of fatty vacuoles in the gills was a characteristic histological finding in the CSP group. Gill pathologies in all groups are shown in Figure 1. Histopathological findings in the kidney tissue included the presence of dense melanomacrophage centers compared to the control group. This pathology was found more intensely in the CS, CP, and CSP groups. Cell loss (necrotic losses) was another important finding in the kidney (Figure 2). Liver histopathology revealed intense but small diameter fat vacuoles. Another finding in the liver was the formation of melanomacrophage centers. Also, significant tissue loss and intensive melanomacrophage centers were observed in the spleen (Figures 3 and 4).

TABLE 1
The changes in the histopathological parameters due to the toxic effects of cement admixtures in rainbow trout.

Histopathological symptoms	NC	C	CS	CP	ÇPA
Gills					
Hyperplasia	-	+++	++	+++	++
Deformation	-	+	+++	++	++
Thrombose	-	-	-	-	+
Epithelial lifting	-	-	+	+	+++
Fat vacuoles	-	-	-	-	++
Liver					
Space between cells	-	-	++	-	+++
Hypertrophy	-	-	-	-	++
Fat vacuoles	-	++	-	++	-
Tissue loss	-	++	++	++	++
Liver					
Melanomacrophage centers	+	++	++	++	+++
Necrosis	-	-	-	-	+
Kidney					
Melanomacrophage centers	+	++	+++	+++	+++
Tissue loss	-	-	-	++	++
Necrosis	-	-	-	++	+

NC: negative control, C: cement, CS: cement/set accelerating admixture, CP: cement/plasticizer and CSP: all additives, (-): none, (+): few, (++): moderate, (+++): high

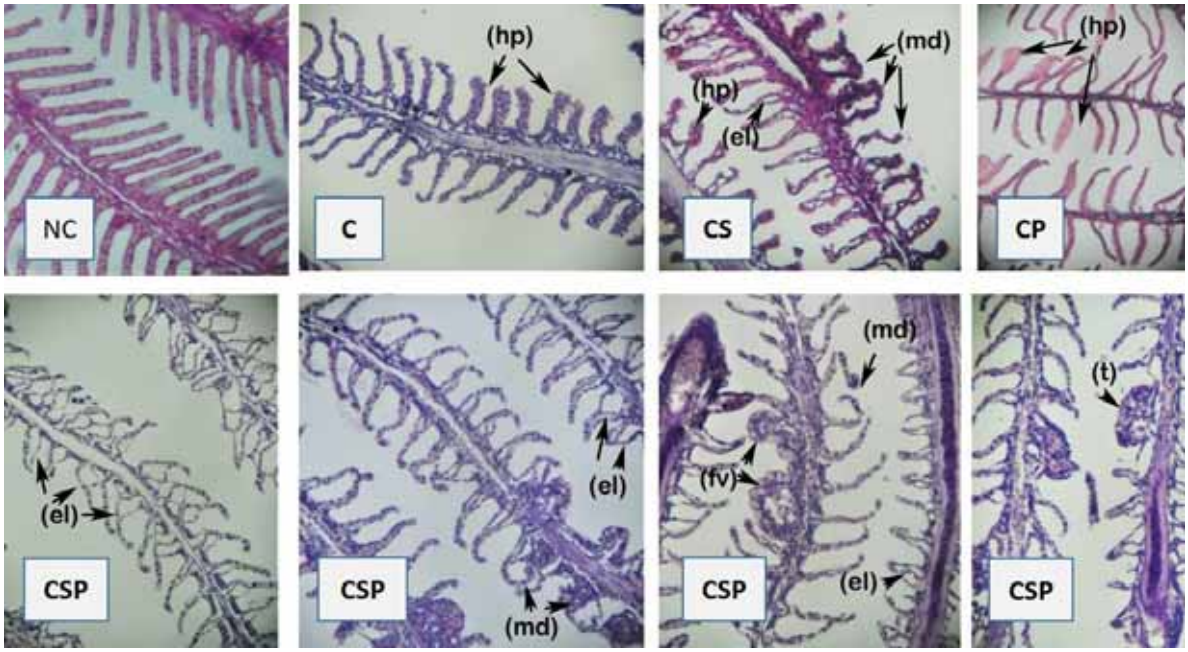

FIGURE 1

The changes in the histopathological parameters due to the toxic effects of cement and other concrete admixtures in the gills in rainbow trout.

(NC): negative control, (C): cement, (hp): hyperplasia, (CS): cement/set accelerating admixture, (hp): hyperplasia, (el): epithelia lifting, (md): multiple deformations, (CP): cement/plasticizer, (hp): hyperplasia, all additives (CSP): (el): epithelia lifting, (md): multiple deformations, (fv): fat vacuoles, (t): thrombose.

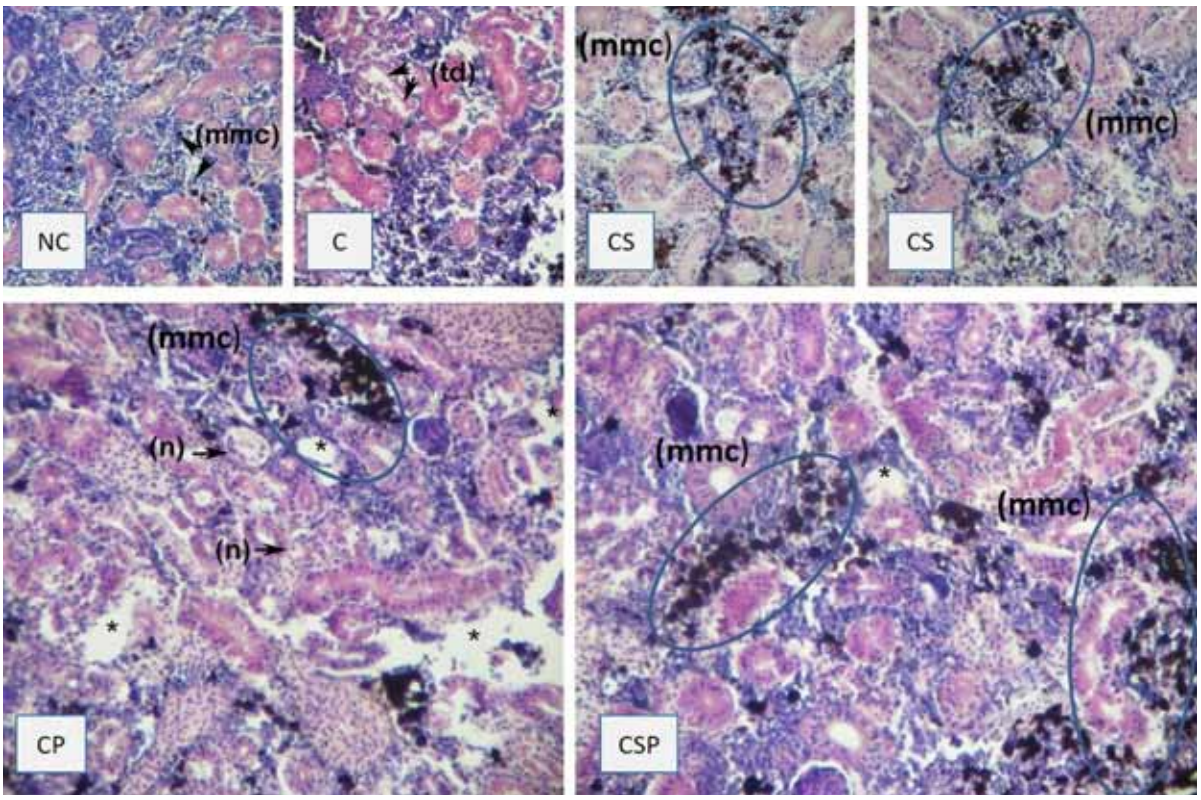

FIGURE 2

Histopathological changes due to the toxic effects of cement and other concrete admixtures in the kidneys in rainbow trout.

(NC): negative control: melanomacrophage centers, (C): cement, (td): tubular degeneration, (CS): cement/set accelerating admixture (CS) (mmc): melanomacrophage centers, (CP): cement/plasticizer, (mmc): melanomacrophage centers (n): necrotic cells, (*): tissue loses, (CSP): all additives, (mmc): melanomacrophage centers, (*): tissue loses.

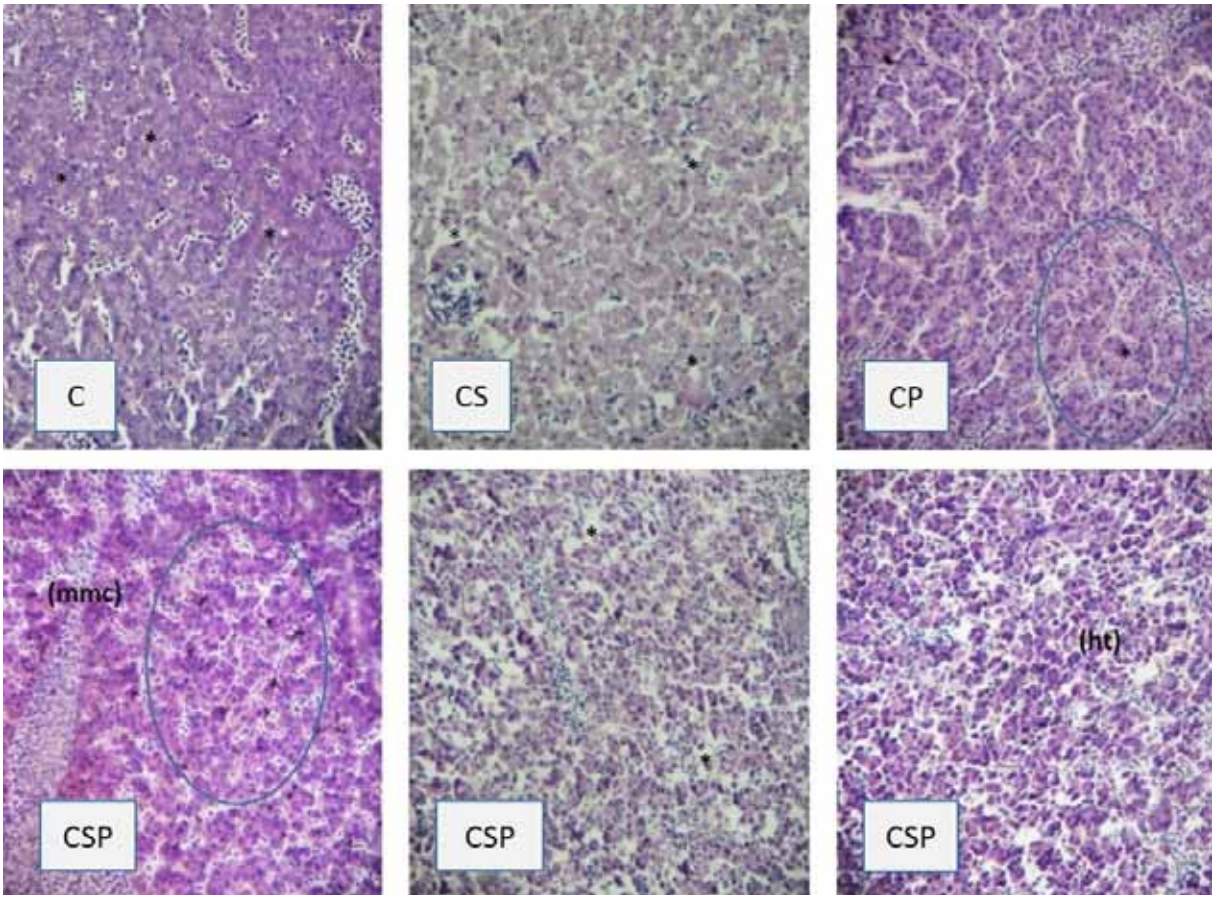

FIGURE 3

Histopathological changes due to the toxic effects of cement and other concrete admixtures in the livers in rainbow trout.

(C): cement, (*): fat vacuoles, (CS): cement/set accelerating admixture, (*): tissue loses, (CP): cement/plasticizer, (*): tissue loses, (CSP): all additives, (mmc): melanomacrophage centers, (*): tissue loses, (ht): hypertrophy.

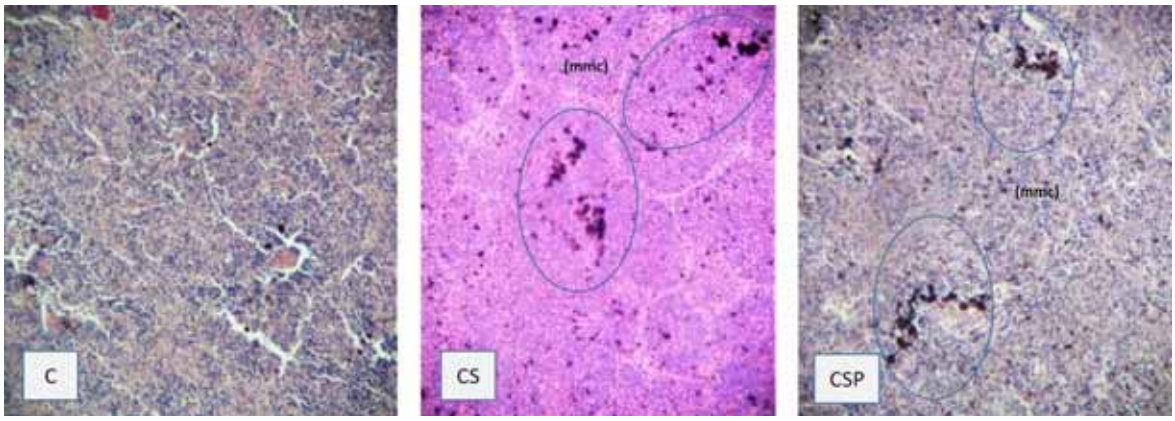

FIGURE 4

Histopathological changes due to the toxic effects of cement and other concrete admixtures in the spleens in rainbow trout.

(C): cement, (*): tissue loses (CS): cement/set accelerating admixture, (mmm): melanomacrophage centres, (CSP): all additives, (mmc): melanomacrophage centres, (*): tissue loses.

DISCUSSION

The problems caused by concrete structures built in aquatic areas are of most importance as these lead to massive fish deaths. Many cases of fish mortality have been reported due to the contamination of aquaculture and natural aquatic areas with concrete water. However, the mechanisms by which this contamination affects water and fish have not been clearly explained. One of the major effects of these additives is the elevation of pH of aquatic areas along with toxic effects on fish. In this

context, Samis [3] published a study on the toxic effects of cement in trout. Similarly, Kurtoğlu et al. [4] conducted a study on the toxic effects of cement on rainbow trout (*O. mykiss*) and Siberian sturgeon (*A. baerii*) and reported LC_{50} values for both genera to be 0.44 g/L and 0.62 g/L (96 h), respectively. They reported severe pathological findings, especially in the gills of fish. In the recent years, to increase the quality of concrete production, additives have been widely used in the production of concrete. However, the toxic effects of these substances on fish have not been examined. In the present study, we evaluated the toxic effects of some concrete additives (set accelerating admixture and plasticizer) on rainbow trout.

Water quality is an important criterion that concerns fish health. Within this criterion, pH is crucial in many aspects because the toxicity of many substances changes with changes in pH values. The optimum pH of water for fish is between 6 and 9 [10]. A study by Kurtoğlu et al. [4] on rainbow trout reported pH of water to be 10.5 in the experimental group with 500 mg/L of cement. In the present study, pH values in the additive groups (10.61–10.75) were higher than in the cement group (10.42), indicating that pH value is adversely affected by concrete additives used to produce cement.

The studies on the toxicity of concrete and its contents in fish are limited. A study by Samis [3] reported a 24-hour cement application (100 mg/L at 15 °C) to cause 60% mortality in rainbow trout. In another study, Kurtoğlu *et al.* [4] reported that application of cement (500 mg/L at 10 ±0.5 °C) for 96 h resulted in the death of 50% of fish (rainbow trout). Unlike these reports, the present study reported 5% mortality in the cement group. This contradiction can be attributed to differences in the time of experiments, length, and weight of fish, and water quality criteria. For instance, the fish used in the study by Samis [3] were fingerling (3.6 g), whereas the fish weight in the current study was 60 g. Similarly, the fish weight and time of experiment in the study by Kurtoğlu et al. [4] was 40 g and 96 h, respectively. However, the duration of the experiment was 24 h in our study.

Studies related to toxic effects of various substances, such as pesticides, fertilizers, and nanoparticles on fish tissues by histopathological methods are quite common [9, 11, 12]. These studies focused especially on gills, liver, spleen, and kidneys of fish and included symptoms such as hyperplasia, epithelial lifting, thrombosis, hypertrophy, and necrosis that are generally reported in the gill tissues. Also, melanomacrophage centers and fat vacuolization are specially mentioned in the kidney, liver, and spleen tissues. In the present study, similar massive hyperplasia was observed in the gills in the cemented group. When the differences among the gills of fish groups were examined, epithelial lifting was intensively observed in the CSP group. However, unlike other groups, the presence of fat vacuoles in the gill lamella in the CSP group was noteworthy. Fat vacuoles in tissues are regarded as a sign of metabolic damage [13]. These findings clearly demonstrate that concrete water has a detrimental effect on gill metabolism in trout at the prevailing dose and duration. The presence of fatty vacuoles, especially of small diameter in the liver, also reveals deterioration of liver metabolism.

Melanomacrophage centers found in the liver, kidney, and spleen are formed when macrophages combine with pigment cells. These structures are known to have a fundamental role in fish, such as the decomposition of toxic materials and cellular degradation products [14]. The most important histopathological finding in the present study was the increase in melanomacrophage centers that were clearly observed in the basic tissues of the immune system such as spleen and kidney.

The findings of the current study demonstrated that concrete additives exert serious toxic effects on the trout. Therefore, necessary precautions should be implemented during application of concrete in aquatic environments.

REFERENCES

[1] Li, Z. (2011) Advanced Concrete Technology. John Wiley and Sons, Inc. USA.

[2] Uysal, M., Yılmaz, K. (2012) The Effect of The Use of Excessive Dosages of Plasticizer on Properties of Concrete. Journal of Engineering and Architecture Faculty of Eskişehir Osman Gazi University. 15(1), 19–35.

[3] Samis, S. (1983) Toxicity of Portland cement to salmonio fish. Report, D. Mcleay & Associates Ltd. West Vancouver, B.C. V7t J.88., Water Quality Unit Habitat Management Division Fisheries and Oceans Canada.

[4] Kurtoğlu, İ.Z., Kayış, Ş., Ak, K., Gençoğlu, S., Düzgün, A., Ulutaş, G. and Er, A. (2016) Histopathology of rainbow trout (*Oncorhynchus mykiss*) and sturgeon (A*cipenser baerii*) exposed to sublethal concentrations of cement. Fresen. Environ. Bull. 25, 2998–3002.

[5] Adamu, K. and Iloba, K. (2008) Effects of sublethal concentrations of Portland cement powder in solution on the aminotransferases of the African catfish (*Clarias gariepinus* (Burchell, 1822)). Acta Zoologica Lituanica. 18(1), 50–54.

[6] Rixom, R. and Mailvaganam, N. (1999) Chemical Admixtures for Concrete. Third Edition. ISBN 0–419–22520. 446p.

[7] Şimşek, O., Aruntaş, H.Y., Demir, İ., (2007) Determination of Type and Ratio of Superplasticizers in Concrete Production Journal of the Faculty of Engineering and Architecture of Gazi University. 22(4), 829–835.
[8] Luna, L.G. (1968) Manual of Histologic Staining Methods of the Armed Forces Institute of Pathology. Blakiston Division. McGraw-Hill Co. New York.
[9] Boran, H., Çapkin, E., Altinok, İ. and Terzi, E. (2012) Assessment of acute toxicity and histopathology of the fungicide captan in rainbow trout. Experimental and Toxicologic Pathology. 64, 175–179.
[10] MacIntyre, C.M.P., Ellis, T.P., North, B.P. and Turnbull, J.F. (2008) The influences of water quality on the welfare of farmed rainbow trout: A review. Chapter 10. In: Branson, E.J. (Ed.) Fish Welfare. Blackwell Publishing, UK.
[11] Çapkin, E., Kayış, S., Boran, M. and Altinok, İ. (2010) Acute toxicity of some agriculture fertilizers to rainbow trout. Turkish Journal of Fisheries and Aquatic Sciences. 10, 19–25.
[12] Çapkin, E., Özçelep, T., Kayış, Ş. and Altinok, İ. (2017) Antimicrobial agents, triclosan, chloroxylenol, methylisothiazolinone and borax, used in cleaning had genotoxic and histopathologic effects on rainbow trout. Chemosphere. 182, 720–729.
[13] Pacheco, M. and Santos, M.A. (2002) Biotransformation, genotoxic and histopathological effects of environmental contaminants in European eel (*Anguilla anguilla* L.). Ecotoxicology and Environmental Safety 53, 331–347.
[14] Dönmez, A.E. (2016) Melanomacrophage centers in fishes. Ege Journal of Fisheries and Aquatic Sciences. 33(1), 81–87.

Received: **31.10.2018**
Accepted: **18.03.2019**

CORRESPONDING AUTHOR

Şevki Kayis
Aquaculture Department
Faculty of Fisheries Sciences
Recep Tayyip Erdoğan University
Rize 53100 – Turkey

e-mail: akif.er@erdogan.edu.tr

© by PSP Volume 28 – No. 5/2019 pages 3835-3842 Fresenius Environmental Bulletin

GENETIC CHARACTERIZATION OF GRAPEVINE GERMPLASM (*VITIS VINIFERA* L.) BY SSR (SIMPLE SEQUENCE REPEATS) IN SANLIURFA PROVINCE, SOUTHEAST TURKEY

Huseyin Karatas[1,*], Eda Karaagac[2], Dilek Karatas[1], Sabit Agaoglu[2]

[1]Dicle University, Agriculture Faculty, Horticulture Department, 21280 Diyarbakir, Turkey
[2]Ankara University, Agriculture Faculty, Horticulture Department, Ankara, Turkey

ABSTRACT

In this study, grape cultivars growing in Şanlıurfa were analyzed and compared using molecular markers. The analysis was performed with 50 genotypes using 7 microsatellite markers. Total number of alleles per locus ranged from 7 (VrZAG62 and VrZAG79) to 9 (VVS2), with a mean number of 7.9 alleles per locus. The expected and observed heterozygosity were 0.7509 and 0.6958, respectively. Clustering analysis was conducted using the UPGMA method (Unweighted Pair-Group Method using Arithmetic means). The analysis of similarity index revealed 6 distinct groups, each of which included several subgroups: Group I included 8, Group II included 4, Group III included 11, Group IV included 9, Group V included 10, and Group VI included 8 subgroups. The two reference genotypes, Cabernet Sauvignon and Merlot, were classified into a separate subgroup within Group V. In conclusion, 17 synonyms and 8 homonyms were identified for the genotypes analyzed in our study.

KEYWORDS:
Grape, Şanlıurfa, molecular markers synonyms, homonyms.

INTRODUCTION

Şanlıurfa Province, due to its rich civilization history, has been home to numerous cultures and societies, where viticulture is widely performed and a large number of grape cultivars grow. Studies have also shown that the geographical features of Şanlıurfa are highly suitable for viticulture, particularly for the grape cultivars used in research studies. However, there is a widespread confusion regarding nomenclature of the grape cultivars growing in this region. This in turn leads to a significant problem regarding the knowledge of grape cultivars growing in the region and this problem could only be solved by performing genetic identification of all the cultivars growing in this region by using molecular markers such as Random Amplified Polymorphic DNA (RAPD), Amplified Fragment Length Polymorphism (AFLP), and Simple Sequence Repeats (SSR).

Microsatellites, a highly powerful type of DNA markers, provide a unique genetic profile for every cultivar, permitting unambiguous identification that is not affected by environment, disease or farming methods [32]. Since the first grape microsatellites were reported by [53], many more microsatellites have been developed for characterization of *Vitis* germplasm [8, 10, 47,16]. Microsatellite markers have been extensively used for genotyping [56, 18, 24, 11], for pedigree analysis [32, 46], and recently for investigating the parentage of cultivars and genome mapping [22, 1]. These markers have also been used for identification of chimaeras of grapes in recent years [19, 41, 23, 4, 57, 30, 51, 50, 17, 6, 37, 15, 5].

The aim of this study was to perform molecular identification of 48 grape cultivars including 39 cultivars growing in Şanlıurfa Province and 9 cultivars that had been previously transplanted to the Tekirdağ National Germplasm Repository Vineyard from this region using the SSR technique, in order to contribute to better characterization of the grape germplasm of both Turkey and the world and also to the determination and protection of the genotypes of diverse plant species around the world.

MATERIALS AND METHODS

The study was performed at Ankara University Agriculture Faculty Horticulture Department. The materials included 39 genotype samples of cultivars that were collected from Şanlıurfa Province and its districts and 9 genotype samples of cultivars that had been transplanted to the Tekirdağ National Germplasm Repository Vineyard several years earlier. Additionally, two genotypes of European origin that are commonly used as reference genotypes around the world, Cabernet Sauvignon and Merlot, were also used in the analysis and the molecular analysis was performed for a total of 50 genotypes

using the SSR technique.

One-year-old seedlings obtained from each genotype were planted in polyethylene tubes and then germinated in greenhouse conditions until green buds were obtained. The fresh leaves of these buds were used for DNA extraction.

DNA extraction was performed using the method described by [27]. The DNA concentration used for polymerase chain reaction (PCR) amplification was diluted to 30 ng/µl.

The analysis was performed with 7 SSR primers including 6 microsatellite loci (VVS2, VVMD5, VVMD7, VVMD27, VrZAG62, and VrZAG79) which were used in a previous GENRES 081 European Union (EU) research project and are commonly accepted as standard loci around the world and one primer, VrZAG47, which has been previously shown to be a polymorphic primer. Forward primers of each primer pair were labeled with fluorescent dyes including Vic (green), Ned (yellow), and Fam (blue).

DNA amplification was conducted using GeneAmp PCR System 9700 with EU-Applied Biosystems, and PCR optimization was performed for each cultivar. PCR amplification was conducted using a reaction volume of 20 µl containing 5 µl of DNA, 2 µl of 10X Buffer, 1.2 µl of $MgCl_2$, 0.6 µl of dNTP, 1 µl of primer 1, 1 µl of primer 2, 0.2 µl of GoldTaq, and 9 of µl distilled water. Touchdown PCR was conducted using the following cycling conditions: 95 °C for 10 min, 94 °C for 30 s, and 52 °C for VVS2, VVMD5, and VVMD7, 58 °C for VVMD27, 55 °C for VrZAG47, and 62 °C for VrZAG62 and VrZAG79 for 30 s each, according to the rate of primer annealing, with a reduction of 0.2 °C/cycle. Following the completion of 25 cycles, additional 15 cycles were conducted with a decrease of 5 °C from the primer annealing temperature, ultimately followed by holding at 72 °C for 40 min.

To monitor the amplification of the fragments in each locus, at least 10 samples representing each locus were loaded on agarose gel. After the amplification, the amplified fragments were subjected to sequencing using ABI Prism 3730 automated DNA sequencer with GeneScan™ 500 LIZ™ dye Size Standard. The resultant data were analyzed, visualized, and processed with GeneMapper v 3.7 software. The number of alleles per locus was calculated as the peak levels.

Genetic similarity between the genotypes was determined using the Microsat software [34] and the genetic parameters (number of alleles per locus, allele frequency, expected heterozygosity, observed heterozygosity, parentage, null allele frequency, and probability of identity) were determined using the IDENTITY 1.0 software [55]. The dendrograms were established and visualized by the NTSys software (version 2.02g, Exeter Software, Setauket, NY). Clustering analysis was conducted using the UPGMA method (Unweighted Pair-Group Method using Arithmetic means).

RESULTS

The data obtained by the GeneMapper v. 3.7 software regarding the molecular analysis of the 50 genotypes characterized by 7 microsatellite markers, including peak levels and the number of alleles and basepair per locus were presented in Table 1.

The results indicated that the total number of alleles per locus ranged from 7 to 10 and the mean number of alleles per locus was 7.9. Of the 7 loci, VVS2 was detected with the highest number of alleles and VrZAG62 and VrZAG79 were detected with the lowest numbers of alleles. The expected and observed heterozygosity were 0.71 and 0.67, respectively. The PI value per locus was greater than the reference value of 0.05 stipulated by [49]. Taken together, these values suggest that the microsatellite markers used in our study are highly polymorphic for genotypic analysis of grapevine.

Genetic similarity between the genotypes was determined using the Microsat software according to the following formula: genetic distance (D), D=1-(proportion of shared alleles) (dissimilarity index). The resultant value was converted to genetic similarity index. The genotypes that showed a value of 1.000, *i.e.* those with the highest similarity index, were accepted as synonym cultivars. The genotypes that showed a value of 0.929 were accepted as genetically similar and the genotypes that had no shared alleles or showed no genetic similarity in any locus were accepted as genetically dissimilar.

The analysis of similarity index revealed 6 distinct groups, each of which included several subgroups: Group I included 8, Group II included 4, Group III included 11, Group IV included 9, Group V included 10, and Group VI included 8 subgroups. The two reference genotypes, Cabernet Sauvignon and Merlot, were classified into a separate subgroup within Group V. The genotypes that showed a value of 1.000 on the dendrogram were accepted as synonym cultivars. The dendrogram also revealed that the genotypes showed no remarkable dissimilarity between each other and had close relationship with each other. Furthermore, several synonyms and homonyms were found among the accessions in the dendrogram (Figure 1).

DISCUSSION AND CONCLUSION

Molecular microsatellite markers have been extensively used and have been shown to be a favorable technique for the identification of cultivars and the determination of synonyms and homonyms [9, 45, 43, 13, 44, 21, 14, 40, 39, 29, 31, 35, 52, 38, 21].

[42] performed a similar study by using microsatellite markers and obtained positive results. In

another study, [36] concluded that microsatellite markers are a useful technique for data sharing among the studies performing genetic analysis of grapevine germplasms. In the current study, a total of 56 alleles were detected in the 50 genotypes characterized by 7 loci. Moreover, the total number of alleles per locus ranged from 7 (VrZAG62 and VrZAG79) to 9 (VVS2), with a mean number of 7.9 alleles per locus. In contrast, the studies in which greater mean numbers of alleles were identified compared to our study were performed with greater numbers of genotypes and those genotypes demonstrated greater variation compared to those in our study. In contrast, the studies by [14, 12, 24, 11] were performed with fewer genotypes and lower mean numbers of alleles were identified in these studies compared to those in our study. However, in the studies conducted by [18, 28], greater mean numbers of alleles were identified compared to those in our study.

TABLE 1
Numbers of alleles per locus (Şanlıurfa genotypes)

No	Genotypes	Microsatellite loci													
		VVS2	**VVS2**	**VVMD5**	**VVMD5**	**VVMD7**	**VVMD7**	**VVMD27**	**VVMD27**	**VrZAG47**	**VrZAG47**	**VrZAG62**	**VrZAG62**	**VrZAG79**	**VrZAG79**
1	*Ş* Hünüsü	141	149	224	228	236	250	179	191	157	169	186	186	254	256
2	*Ş* Şire	133	139	222	234	244	246	177	191	155	169	194	198	246	256
3	*Ş* Sergi karası	133	139	222	234	244	246	177	191	155	169	194	198	246	246
4	*Ş* Cibin	133	139	234	234	244	246	177	191	155	169	194	198	246	246
5	*Ş* Tilgören	141	149	228	228	244	252	179	191	157	169	202	202	236	244
6	*Ş* Çiloreş	131	131	222	222	246	246	191	191	169	169	198	202	240	254
7	*Ş* Çilorut	133	141	230	236	244	250	191	191	169	169	190	190	240	254
8	*Ş* Simore	141	149	224	228	236	250	179	191	157	169	186	194	254	254
9	*Ş* Zeyni	131	133	222	230	244	246	191	191	169	169	190	202	248	254
10	*Ş* Tahannebi	131	155	230	234	244	244	191	191	169	169	190	202	254	254
11	*Ş* Zeynebi	139	141	224	234	236	244	179	191	157	169	186	194	248	256
12	*Ş* Bastıkkabarcığı	131	131	232	232	244	246	177	191	155	169	198	202	246	246
13	*Ş* Kabarcık	131	141	222	222	236	236	191	191	169	169	194	194	240	256
14	*Ş* Külahi	131	149	222	222	244	244	191	191	169	169	194	194	254	256
15	*Ş* Yediveren bag	149	153	222	228	236	248	177	191	155	169	186	202	244	254
16	*Ş* Horoz karası	131	133	222	230	244	246	191	191	155	169	190	202	240	254
17	*Ş* Hatunparmağı beyaz	131	133	222	230	244	246	191	191	169	169	190	202	240	248
18	*Ş* Azezi	131	131	222	222	246	246	191	191	169	169	198	202	240	254
19	*Ş* Kayısı	131	131	222	222	246	246	191	191	169	169	198	202	240	254
20	*Ş* Şarabi	141	149	230	242	230	246	175	191	153	169	202	202	240	244
21	*Ş* Danaburnu	143	149	230	230	236	250	179	191	157	169	186	186	244	256
22	*Ş* Keçiemceği	133	139	222	234	244	246	191	191	155	169	194	198	246	246
23	*Ş* Dımışkı	131	131	222	222	246	246	191	191	169	169	198	202	240	254
24	*Ş* Muhammediye	131	141	222	232	246	246	181	191	159	169	188	202	248	254
25	*Ş* Yediveren Çardak	149	153	222	228	236	248	177	191	155	169	186	202	244	254
26	*Ş* Hatunparmağı siyah	131	149	230	232	230	244	191	191	169	169	194	202	244	254
27	*Ş* Elmaüzümü	133	149	228	230	246	246	191	191	169	169	192	198	248	254
28	*Ş* Karamikeri	131	141	230	234	236	246	177	191	155	169	194	202	244	254
29	*Ş* Köseni	139	149	224	242	236	244	177	191	155	169	190	190	246	254
30	*Ş* Çördüğü	131	133	222	230	244	246	191	191	169	169	190	202	248	254
31	*Ş* Serpenekıran	131	131	230	242	244	250	175	177	153	155	190	202	244	246
32	*Ş* Halebi	137	141	230	242	246	250	175	191	153	169	202	202	240	244
33	*Ş* Avderi	139	149	228	234	244	244	191	191	169	169	190	202	254	254
34	*Ş* Kızılbanki	131	141	222	232	240	246	181	191	159	169	188	188	244	254
35	*Ş* Antepüzümü	139	149	228	234	244	244	191	191	169	169	190	202	254	254
36	*Ş* Dusuzu	131	141	230	230	244	250	177	181	153	159	190	202	244	244
37	*Ş* Siyahüzüm	133	139	222	234	244	246	191	191	155	169	194	198	246	246
38	*Ş* Kızlartahtası	131	131	222	222	246	246	191	191	169	169	198	202	240	254
39	*Ş* Şefafı	131	149	222	230	230	246	191	191	157	169	194	202	244	254
40	*TŞ* Simore	131	133	232	232	240	246	181	181	155	159	186	198	246	246
41	*TŞ* Çilorut	133	141	230	236	244	250	191	191	169	169	190	190	240	254
42	*TŞ* Siverek	131	131	222	232	246	246	191	191	155	169	198	202	240	254
43	*TŞ* Ruhali	133	141	230	236	244	250	177	191	169	169	190	190	240	254
44	*TŞ* Tilgören	131	141	222	242	244	246	181	181	155	169	190	198	240	246
45	*TŞ* Kayısı	131	141	222	230	246	246	177	177	155	159	186	202	254	256
46	*TŞ* Zerik	131	143	228	228	244	246	191	191	155	155	190	202	246	248
47	*TŞ* Çiloreş	131	131	222	222	246	246	191	191	169	169	198	202	240	254
48	*TŞ* Çörtük	133	141	230	236	244	250	191	191	169	169	190	190	240	254
49	**Cabernet Sauvignon**	137	149	228	236	236	236	171	185	151	165	186	192	244	244
50	**Merlot**	137	149	222	232	236	244	185	187	165	167	192	192	256	256

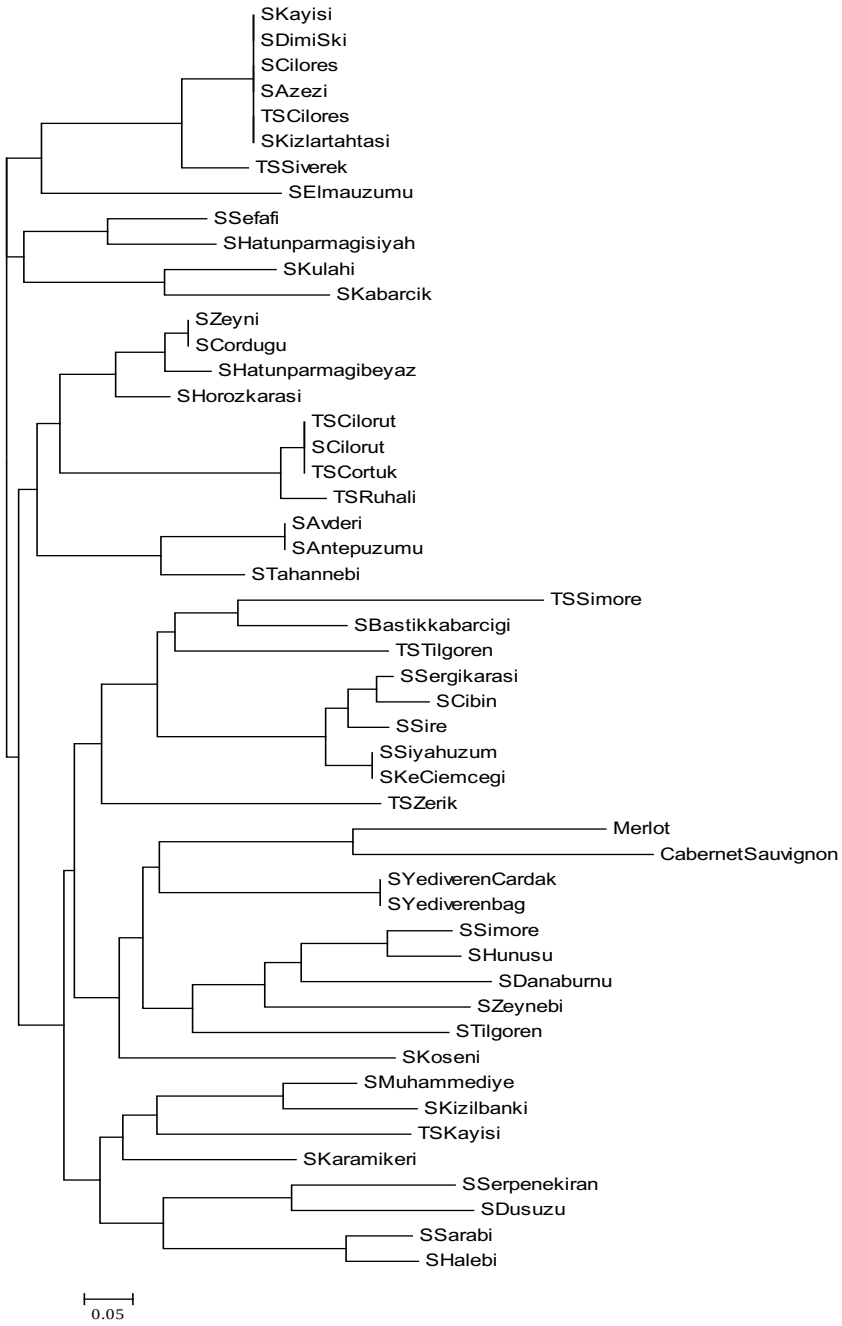

FIGURE 1
Dendogram of 50 grape cultivars based on similarity index from SSR data

TABLE 2
Synonyms and homonyms identified in the 50 genotypes characterized by 7 microsatellite markers

Synonyms
Ş Yediveren bağ, *Ş* Yediveren Çardak
Ş Keçiemceği, *Ş* Siyah üzüm
Ş Çilorut, *TŞ* Çilorut, *TŞ* Çörtük
Ş Avderi, *Ş* Antepüzümü
Ş Çiloreş, *Ş* Azezi, *Ş* Kayısı, *Ş* Dımışkı, *Ş* Kızlartahtası, *TŞ* Çiloreş
Ş Zeyni, *Ş* Çördüğü
Homonyms
Ş Hatunparmağı siyah, *Ş* Hatunparmağı beyaz
Ş Simore, *TŞ* Simore
Ş Tilgören, *TŞ* Tilgören
Ş Kayısı, *TŞ* Kayısı

The expected and observed heterozygosity of our genotypes were 0.7509 and 0.6958, respectively. These findings indicate that the observed heterozygosity was lower than the expected heterozygosity, which could be explained by the presence of null alleles. Nevertheless, the fact that there was no significant difference between these two rates implicates that our cultivars were heterozygous. On the other hand, the observed heterozygosity of our genotypes was lower than those reported in the literature [48, 14, 18, 3, 11, 54].

The PI value per locus for our genotypes was greater than the reference value of 0.05 stipulated by [58], implicating that the microsatellite markers employed in this study are highly polymorphic for the genotypes analyzed. Of these markers, VVMD5 and VVS2, which had the lowest PI values, revealed the greatest differentiation among the genotypes. In the literature, the most informative markers reported by the studies include VVMD5 [28, 26, 25, 29], VVS5 [7], and VVMD14, VVMD28, and VVMD36 [12]. In our study, VVMD27 was the least informative marker.

Of the 7 markers employed in this study, VVS2 had the highest number of alleles (n=9). In a similar way, VVS2 has also been detected with the greatest number of alleles in numerous studies [28, 7, 26, 18, 29, 36], followed by VVMD5, VVMD7, VVMD27, and VrZAG62 (n=8) and VrZAG79 (n=7).

The proportion of shared alleles among the genotypes revealed 17 synonyms and 8 homonyms among the genotypes (Table 2).

For the reference genotypes analyzed in our study, *i.e.* Cabernet Sauvignon and Merlot, we found similar outcomes with the previous studies [10, 52] (with regard to the difference between the two alleles in a single loci for each of the 7 loci.

In conclusion, 17 synonyms and 8 homonyms were identified for the genotypes analyzed in our study. Nevertheless, for the homonyms detected in our study, no clear information was available as to which homonym was the real name of each genotype. On the other hand, a total of 31 distinct grape cultivars were identified among the 50 genotypes analyzed, indicating that the rich gene sources of these cultivars in this region should be protected. Moreover, our findings suggested that the microsatellite markers used in this study are highly appropriate for genetic identification of grape cultivars and for the detection of synonyms and homonyms.

REFERENCES

[1] Adam-Blondon, A.F., Roux, C., Claux, D., Butterlin, G., Merdinoglu, D., This, P. (2004) Mapping 245 SSR markers on the Vitis vinifera genome: a tool for grape genetics. Theoretical and Applied Genetics. 109(5), 1017-1027.

[2] Akkak, A., Boccacci, P., Lacombe, T. and Botta, R. (2005) Relationships and genetic diversity of grapevine (*Vitis vinifera* L.) grown in Algeria and in Mediterranean basin. Electronic Forum on Biotechnology in Food and Agriculture, Conference 13. International Workshop, 5-March 2005, Turin, Italy. (Poster).

[3] Aradhya, M.K., Dangl, G.S., Prins, B.H., Boursiquot, J.M., Walker, M.A., Meredith, C.P. and Simon, C.J. (2003) Genetic structure and differentiation in cultivated grape, *Vitis vinifera* L. Genet. Res. Camb. 81, 179-192.

[4] Arroyo-Garcia, R., Bolling, L., Ruiz-Garcia, L., Ocete, R., Söylemezoğlu, G., Aras, S., Uzun, İ. and Martinez-Zapater, J.M. (2004) Chloroplasts haplotype distribution in *Vitis vinifera* L. along the Mediterranean basin and the pattern of domestication of wine grapevine cultivars. Plant and Animal Genomes XII. Conference. Town and Country Convention Center. San Diego, CA.

[5] Biagini, B., Imazio, S., Scienza, A., Failla, O., De Lorenzis, G. (2016) Renewal of wild grapevine (*Vitis vinifera* L. subsp. *sylvestris* (Gmelin) Hegi) populations through sexual pathway: Some Italian case studies. Flora. 219, 85-93.

[6] Bodor, P., Höhn, M., Pedryc, A., Deák, T., Dücső, I., Uzun, I., Cseke, K., Böhm, É. I., Bisztray, G.D. (2010) Conservation value of the native Hungarian wild grape (*Vitis silvestris* Gmel.) evaluated by microsatellite markers. Vitis 49(1), 23–27.

[7] Borrego, J., Rodriguez, I., Andrés M.T., Martin, J., Chavez, J., Cabello, F. and Ibáñez, J. (2001) Characterization of the most important Spanish grape varieties through isoenzyme and microsatellite analysis. Proc. Int. Symp. on Molecular Markers. Acta Hort. 546, 371-375.

[8] Bowers, J.E. Dangl, G.S., Vignani, R., Meredith, C.P. (1996) Isolation and characterization of new polymorphic simple sequence repeat loci in grape (*Vitis vinifera* L.). Genome. 39, 628-633.

[9] Bowers, J.E. and Meredith, C.P. (1997) The parentage of a classic wine grape, Cabernet Sauvignon. Nat. Genet. 16, 84-87.

[10] Bowers, J. E., Dangl, G.S. and Meredith, C.P. (1999) Development and characterization of additional microsatellite DNA markers for grape. Am. J. Enol. Vitic. 50(3), 243-246.

[11] Costantini, L., Monaco, A., Vouillamoz, J.F., Forlani, M. and Grando, M.S. (2005) Genetic relationships among local *Vitis vinifera* cultivars from Campania (Italy). Vitis 44(1), 25-34.

[12] Crespan, M. and Milani, N. (2001) The Muscats: A molecular analysis of synonyms, homonyms and genetic relationship within a large family of grapevine cultivars. Vitis 40(1), 23-30.

[13] Dalbó, M.A., Ye, G.N., Weeden, N.F., Steinkellner, H., Sefc, K.M. and Reisch, B.I. (2000) A gene controlling sex in grapevines placed on a molecular marker-based genetic map. Genome. 43, 333-340.

[14] Dangl, G.S., Mendum, M.L., Prins, B.H., Walker, A.M., Meredith, C.P. and Simon C.J. (2001) Simple sequence repeat analysis of a clonally propagated species: A tool for managing a grape germplasm collection. Genome. 44, 432-438.

[15] De Andrés, M.T., Benito, A., Pérez-Rivera, G., Ocete, R., Lopez, M.A., Gaforıo, L., Muñoz, G., Cabello, F., Martinez Zapater, J. M., Arroyo-Garcia, R. (2012) Genetic diversity of wild grapevine populations in Spain and their genetic relationships with cultivated grapevines. Molecular Ecology. 21, 800-816.

[16] Di Gaspero, G., Cipriani, G., Marazzo, M.T., Andreetta, D., Castro, M.J.P., Peterlunger, E., Testolin, R. (2005) Isolation of (AC)n-microsatellites in *Vitis vinifera* L. and analysis of genetic background in grapevines under marker assisted selection. Mol. Breed. 15, 11–20.

[17] Di Vecchi Staraz, M., Laucou, V., Bruno, G., Lacombe, T., Gerber, S., Bourse, T., Boselli, M., This, P. (2009) Low Level of Polen-Mediated Gene Flow from Cultivated to Wild Grapevine: Consequences for the Evolution of the Endangered Subspecies *Vitis vinifera L. subsp. silvestris.* Journal of Heredity. 100(1), 66-75.

[18] Fatahi, R., Ebadi, A., Bassil, N., Mehlenbacher, S.A. and Zamani, Z. (2003) Characterization of Iranian grapevine cultivars using microsatellite markers. Vitis. 42(4), 185-192.

[19] Franks, T., Botta, R., Thomas, M.R. (2002) Chimerism in grapevines: implications for cultivar identity, ancestry, and genetic improvement. Theor. Appl. Genet. 104, 192–199.

[20] García-Muñoz, S., Lacombe, T., de Andrés, M.T., Gaforio, L., Muñoz-Organero, G., Laucou, V., This, P., Cabello, F., (2012) Grape varieties (Vitis vinifera L.) from the Balearic Islands: genetic characterization and relationship with Iberian Peninsula and Mediterranean Basin. Genetic resources and crop evolution. 59(4), 589-605.

[21] Grando, M.S., Frisinghelli, C. and Stefanini, M. (2000) Genotyping of local grapevine germplasm. ISHS Acta Horticulturae. 528, VII. International Symposium on Grapevine Genetics and Breeding, May, Montpellier, France.

[22] Grando, M.S., Bellin, D., Edwards, K.J., Pozzi, C., Stefanini, M., Velasco, R. (2003) Molecular linkage maps of *Vitis vinifera* L. and Vitis riparia Mchx. Theoretical and applied genetics. 106(7), 1213-1224.

[23] Hocquigny, S., Pelsy, F., Dumas, V., Kindt, S., Heloir, M.C., Merdinoglu, D. (2004) Diversification within grapevine cultivars goes through chimeric states. Genome. 47(3), 579-589.

[24] Hvarleva, T., Rusanov, K., Lefort, F., Tsvetkov, I., Atanassov, A. and Atanassov, I. (2004) Genotyping of Bulgarian *Vitis vinifera* L. cultivars by microsatellite analysis. Vitis. 43(1), 27-34.

[25] Lefort, F. and Roubelakis-Angelakis, K.A. (2001) Genetic comparison of Greek cultivars of *Vitis vinifera* L. by nuclear microsatellite profiling. American Journal of Enology and Viticulture. 52(2), 101-108.

[26] Lodhi, M.A., Daly, M.J., Ye, G.N., Weeden, N.F. and Reisch, B.I. (1994) A simple and efficient method for DNA extraction from grapevine cultivars and *Vitis* species. Plant Mol. Biol. 12(1), 6-13.

[27] Lópes, M.S., Sefc, K.M., Dias, E.E., Steinkellner, H., Machado, M.L.D. and Machado, A.D. (1999) The use of microsatellites for germplasm management in a Portuguese grapevine collection. Theor. Appl. Genet. 99(3-4), 733-739.

[28] Martin, J.P., Borrego, J., Cabello, F. and Ortiz, J.M. (2003) Characterization of the Spanish diversity grapevine cultivars using sequence-tagged microsatellite site markers. Genome. 46, 1-9.

[29] Martinez L.E., Cavagnaro, P.F., Masuelli, R. W., Zuniga, M. (2006) SSR-based assessment of genetic diversity in South American Vitis vinifera varieties. Plant Science. 170, 1036-1044.

[30] Merdinoglu, D., Wiedeman-Merdinoglu, S., Coste, P., Dumas, V., Haetty, S. and Butterlin, G. (2003) Genetic analysis of downy mildew resistance derived from *Muscadinia rotindifolia*. ISHS Acta: VIII International Conference on Grape Genetics and Breeding. Horticulturae. 603, 451-456.

[31] Meredith, C. Dangl, G.S., Bowers, J.E. (1996) Clarifying the identity of some California winegrapes by DNA profilling. Riv. Vitic. Enol. 49(1), 65-68.

[32] Meredith, C. (2001) Grapevine genetics: probing the past and facing the future. A Agriculturae Conspectus Sientificus. 66, 21–25.

[33] Minch, E., Ruiz-Linares, A., Goldstein, D.B., Feldman, M. and Cavalli-Sforza, L.L. (1995) Microsat (version 1.4d): a computer program for calculating various statistics on microsatellite allele data. Stanford. California, University of Stanford.

[34] Montaner, C., Martin, J. P., Casanova, J., Marti, C., Badia, D., Cabello, F. and Ortiz, J.M. (2004) Aplication of microsatellite markers for the characterization of "Parraleta": an autochthonous Spanish grapevine cultivar. Scientia Horticulturae. 101, 343-347.

[35] Nei, M. (1987) Molecular evolutionary genetics. Columbia University Press, New York. 106-107.
[36] Nuñez, Y., Fresno, J., Torres, V., Ponz, F. and Gallego, F.J. (2004) Practical use of microsatellite markers to manage *Vitis vinifera* germplasm: Molecular identification of grapevine samples collected blindly in D.O. "El Bierzo" (Spain). Journal of Horticultural Science and Biotechnology. 79(3), 437-440.
[37] Ocete, R., Arroya-Garcia, R., Morales, M.L., Cantos, M., Gallardo, A., Perez, M.A., Gomez, I. and Lopez, M.A. (2011) Characterization of Vitis vinifera L. subspecies sylvestris (Gmelin) Hegi in the Ebro river Basin (Spain). Vitis 50(1), 11-16.
[38] Ortiz, J.M., Martín, J.P., Borrego, J., Chávez, J., Rodríguez, I., Muñez, G. and Cabello, F. (2004) Molecular and morphological characterization of a *Vitis* gene bank for the establishment of a base collection. Genetic Resources and Crop Evolution 51, Kluwer Academic Publishers. 403-409.
[39] Reale, S., Pilla, F. and Angiolillo, A. (2002) Molecular characterization of an autochthonous grape cultivar of Central Italy. Proceedings of the XLVI Italian Society of Agricultural Genetics-SIGA Annual Congress Giardini Naxos, Italy, 18-21 September.
[40] Regner, F., Staldbauer, A. and Eisenheld, C. (2001) Molecular markers for genotyping grapevine and for identifying clones of traditional varieties. Proc. Int. Symp. on Molecular Markers. Acta Hort. 546, 331-342.
[41] Riaz, S., Garrison K.E. and Dangl, G.S. (2002) Genetic divergence and chimerism within ancient asexually propagated winegrape cultivars. Journal of the American Society for Horticultural Science. 127(4), 508-514.
[42] Riaz, S., Dangl, G.S., Edwards, K.J. and Meredith, C.P. (2004) A microsatellite marker based framework linkage map of *Vitis vinifera* L. - Theor. Appl. Genet. 108, 864-872.
[43] Sánchez-Escribano, E.M., Martín, J.P., Carreño, J. and Cenis, J.L. (1999) Use of sequence-tagged microsatellite site markers for characterizing table grape cultivars. Genome 42, 87-93.
[44] Scoot, K.D., Eggler, P., Seaton, G., Rosetto, M., Ablett, E.M., Lee, L.S., Henry, R.J. (2000) Analysis of SSRs derived from grape ESTs. Theor. Appl. Genet. 100, 723-726.
[45] Sefc, K.M., Steinkellner, H., Wagner, HW., Glössl, J. and Regner, F. (1997) Application of microsatellite markers to parentage studies in grapevine. Vitis. 36(4), 179-183.
[46] Sefc, K.M., Steinkellner, H., Glössl, J., Kampfer, S., Regner, F. (1998) Reconstruction of a grapevine pedigree by microsatellite analysis. Theoretical and Applied Genetics. 97(1-2), 227-231.
[47] Sefc, K.M., Regner, F., Turetschek, E., Glössl, J., Steinkellner, H. (1999) Identification of microsatellite sequences in *Vitis riparia* and their applicability for genotyping of different *Vitis* species. Genome. 42, 367-373.
[48] Sefc, K.M., Lopes, M.S., Lefort, F., Botta, R., Roubelakis-Angelakis, K.A., Ibañez, J., Pejic, I., Wegner, H.W., Glössl, J. and Steinkellner, H. (2000) Microsatellite variability in grapevine cultivars from different European regions and evaluation of assignment testing to assess the geographic origin of cultivars. Theor. Appl. Genet. 100, 498-505.
[49] Sefc, K.M., Lefort, F., Grando, M.S., Scott, K.D., Steinkellner, H. and Thomas, M.R. (2001) Microsatellite markers for grapevine: A state of the art. In: Roubelakis-Angelakis, K.A. (ed.) Molecular Biology and Biotechnology of the Grapevine. Kluwer Academic Publishers. The Netherlands. 1-29.
[50] Shidfar, M., (2008) SSRs (Simple Sequence Repeats) Based Genetic Characterization of Eskişehir and Kayseri Provinces Grapevine germplasms. Ankara University Graduate School of Natural and Applied Science. Ph.D. Thesis. Ankara. (In Turkish).
[51] Şelli, F., Bakır, M., İnan, G., Aygün, H., Boz, Y., Yaşasın, A.S., Özer, C., Akman. B., Söylemezoğlu, G., Kazan, K., Ergül, A. (2007) Simple sequence repeat-based assessment of genetic diversity in Dimrit and Gemre grapevine accessions from Turkey. Vitis. 46(4), 182-187.
[52] This, P., Jung, A., Boccacci, P., Borrego, J., Botta, R., Constantini, L., Crespan, M., Dangl, G.S., Eisenheld, C., Ferreria-Montteiro, F., Grando, S., Ibáñez, J., Lacombe, T., Laucou, V., Magalhães, R., Meredith, C.P., Milani, N., Peterlunger, E., Regner, F., Zulini, L. and Maul, E. (2004) Development of a standard set of microsatellite reference alleles for identification of grape cultivars. Theor. Appl. Genet. 109, 1448-1458.
[53] Thomas, M.R., Scott, N.S. (1993) Microsatellite repeats in grapevine reveal DNA polymorphisms when analyzed as sequence-tagged sites (STSs). Theoretical and Applied Genetics. 86(8), 985-90.
[54] Vouillamoz, J.F., McGovern, P., Ergül, A., Soylemezoglu, G., Tevzadze, G., Meredith, C.P. and Grando, M.S. (2006) Genetic characterization and relationships of traditional grape cultivars from Transcaucasia and Anatolia. Plant Genetic Resources. 4(2), 144-158.

[55] Wagner, H.W. and Sefc, K.M. (1999) IDENTITY 1.0. Centre for Applied Genetics. University of Agricultural Science, Vienna.
[56] Zullini, L., Russo, M. and Peterlunger, E., (2002) Genotyping wine and table grape cultivars from Apulia (Southern Italy) using microsatellite markers. Vitis. 41(4), 182-187.
[57] Zullini, L., Fabro, E. and Peterlunger, E., (2005) Characterisation of the grapevine cultivar Picolit by means of morphological descriptors and molecular markers. Vitis. 44(1), 35-38.

Received: **05.11.2018**
Accepted: **21.03.2019**

CORRESPONDING AUTHOR

Huseyin Karatas
Dicle University,
Agriculture Faculty,
Horticulture Department,
21280 Diyarbakır – Turkey

e-mail: hkaratas@dicle.edu.tr

© by PSP Volume 28 – No. 5/2019 pages 3843-3853 Fresenius Environmental Bulletin

THE INFLUENCE OF Mn PROMOTER FOR SUPPORTED Ni/TiO_2 CATALYST CO METHANATION

Gangqiang Wu[1,2], Shaoping Xu[1,*], Yuyan Wang[2], Zhongmin Lang[2], Yaxiong Wang[2]

[1]School of Chemical Engineering, Faculty of Chemical, Environmental and Biological Science and Technology, Dalian University of Technology, Dalian Liaoning 116024, China
[2]School of Chemistry and Chemical Engineering of Inner Mongolia University of science and Technology, Baotou 014010, China

ABSTRACT

In recent years, coal and biomass synthetic natural gas have become a hot issue. The traditional natural gas synthesis route is based on the conversion of carbon raw materials, through the catalytic conversion reaction of methanation, to synthesize natural gas. Among all the active components of methanation catalysts, nickel-based catalysts have been widely used for their high reactivity, methane selectivity and low cost. However, nickel-based catalysts are prone to form nickel carbonyl at low temperature (200-300℃) and low hydrogen-carbon ratio, which results in nickel particle sintering. It is possible to produce high molecular carbon at 500 degrees centigrade and decrease in activity at 500 degree Celsius. This may be due to the thermal sintering of the carrier, the formation of carbon deposition, or the growth of nickel crystals due to the migration and reduction of particles. In order to further improve the high temperature stability and sulfur tolerance of the catalyst, a series of xNi/TiO_2 and $20Ni/xMn\text{-}TiO_2$ catalyst were prepared by impregnation method and the effect of Ni and Mn loading on the catalytic performance for CO Methanation was studied respectively. XRD, SEM, TG/DTG and evaluation of activity were used to examine the catalysts. A fixed bed tubular reactor is used as the catalyst evaluation device. The reactor was heated in three stages. The bed temperature was measured by a thermocouple extending into the bed. Spectrometer (Agilent-GC7890B) analysis, thermal conductivity tank detector (TCD) analysis of CH_4, CO_2, CO, H_2. Hydrogen flame ionization detector (FID) was used to analyze other alkanes in the product. The activity of the catalyst was evaluated and characterized by XRD, SEM and TG/DTG. The results show that the activity of $20Ni/TiO_2$ is the highest, up to 99%, in the xNi/TiO_2, while the Ni loading affect xNi/TiO_2 activity is not the main factor; With 20 Ni/TiO_2 catalysts for the further study, add Mn in the xNi/TiO_2 catalyst will improve its CH_4 selectivity and temperature interval. Characterization analysis found that adding Mn will increase the degree of dispersion of active components. The reduction method and temperature test of $20Ni/8Mn\text{-}TiO_2$ shows that the catalyst reduced under 400℃ TPR performance better.

KEYWORDS:
Catalyst, Methanation, Natural gas, Manganese additive, Titanium dioxide

INTRODUCTION

Due to the increasing demand for natural gas and petrochemical resources dries up, synthetic gas of coal and biomass in recent years has become a hot issue [1-3]. Traditional gas synthetic route is based on the conversion of carbon materials through the catalytic conversion of methane synthetic natural gas [4, 5]. Methanation steps is a key step to synthesis gas. Nickel-based catalysts with high reaction activity and selectivity of methane and lower economic costs and widely application in all of the methanation catalyst active component. However, nickel-based catalysts are easy to generate carbonyl nickel in nickel particles sintering [6, 7] under low temperature (200-300℃) and low hydrogen/carbon ratio under and likely to generate polymer carbon Under the 500℃ [3, 8-11]. While the temperature is greater than 500℃ the activity of catalyst is reduced. This may be due to the nickel crystal growth for carrier's thermal sintering, the formation of carbon deposition, or the migration and reduce of particles [12]. Besides Ni based catalyst sulfur resistance is low, trace sulfur elements can lead to catalyst deactivation. Therefore, improve the high temperature stability of the catalyst and the sulfur resistance is imperative.

According to the research of Barrientos [13], different carrier load Ni catalyst generate different carbon amount and variety. The interaction of metal carrier can also affect the formation of carbon amount and variety [13-16]. The condition of Carrier sintering and phase shift also will change with the change of the intermediate [17-20]. Barrientos [13] found that Ni/TiO_2 catalysts showed good resistance to carbon deposition and the sintering performance under low temperature. Besides Ni/TiO_2 catalyst than Ni/SiO_2 catalyst showed better carbonyl nickel resistance [13, 21]. The study of Park and Ouaguenouni [22, 23] showed in methane, carbon dioxide reforming reaction can reduce the formation carbon. Li libo [24] etc. Research results show that Mn additives added to form $MnNi_2O_4$

complexes and it is advantageous to the catalyst reduction, while Mn fertilizer produced by the electronic effect make the methanation catalyst activity. Yao, etc. [25] by the impregnation method introduces Mn fertilizer in Ni/TiO_2 catalyst, the research results show that the introduction of Mn fertilizer can improve the dispersion of active component Ni, reduced the size of the NiO, especially the formation of $NiMn_2O_4$ can prevent the sintering of catalyst, so as to improve the steam reforming of methane catalytic reaction activity and stability.

In this work, the load of active component Ni is examined for Ni/TiO_2 catalyst activity and adding additives Mn to modification the catalysts while the influence of additives content on the properties of catalyst were examined.

EXPERIMENTAL

Instruments and reagents. $Ni(NO)_3 \cdot 6H_2O$ (Sinopharm Chemical Reagent Co., Ltd, AR), TiO_2 (Sinopharm Chemical Reagent Co., Ltd, AR), $(CH_3COO)_2Mn \cdot 4H_2O$ (Sinopharm Chemical Reagent Co., Ltd, AR), BRURER D8 ADVANCE XRD, Zeiss SIGMA 500/VP SEM, STA 2500 Regulus simultaneous thermal analyzer, Agilent 7890B GC gas chromatograph, high temperature muffle furnace, catalyst evaluation experiment device.

The preparation of the catalyst. The TiO_2 support was activated and calcined at 900℃ for 4 h before impregnation. A solution of 0.2, 0.4, 0.6, 0.8, 1 g $(CH_3COO)_2Mn \cdot 4H_2O$ was dissolved in 3 mL of water to give a solution. 10g TiO_2 carrier was placed in the adjuvant solution, stirred and allowed to stand at room temperature for 8h, then dried at 80C for 6 hours and calcined at 500℃ for 4 h. 2g Ni $(NO_3)_2 \cdot 6H_2O$ was dissolved in 3 mL of water to obtain a nickel nitrate solution. The carrier was placed in a solution of nickel nitrate and stirred at room temperature for 8 hours. The mixture was dried at 80℃ for 6 hours and calcined at 500℃ for 4 h. To obtain a catalyst.

Catalyst activity evaluation. Catalyst evaluation device. The catalyst evaluation device is shown in Fig 1.

The catalyst evaluation device is a fixed bed tube reactor, the reactor is heated by three stages, and the bed temperature is measured by a thermocouple extending into the bed. The reaction air volume is RCS 2000A produced by Beijing JinXun Electronics Co., Ltd. (TCD), CH_4, CO_2, CO, and H_2 were analyzed by a gas chromatograph (Agilent-GC7890B). The gas flow rate of the reactor was analyzed by a gas chromatograph (Agilent-GC7890B). The hydrogen flame ion detector (FID) analyzes the other alkanes in the product.

Evaluation of catalyst activity. Catalyst loading: 2ml of quartz sand into the reactor, then 2ml catalyst into the reactor, and then into the 2ml quartz sand, in the reactor to form a constant temperature zone reaction bed.

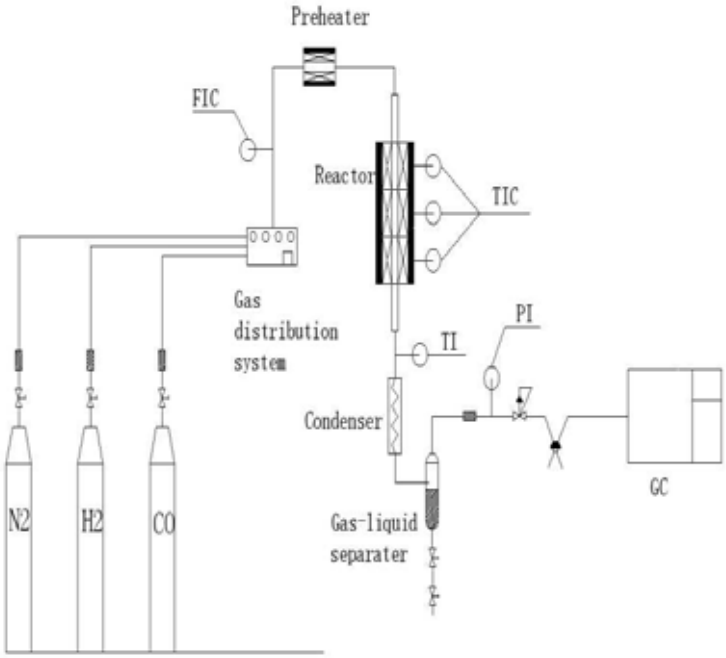

FIGURE 1
Catalyst evaluation experiment device

Reduction of catalyst. The catalyst active component packed into the reactor is NiO, so it needs to be reduced to metal Ni with catalytic activity. The reduction treatment was carried out by continuously flowing pure H_2 (90 mL / min) and N_2 (40000mL/min) at 400℃ for 180 min at constant temperature, and the mixture was cooled to room temperature by heating.

Evaluation of the activity of the catalyst. (1) The temperature inside the reactor was raised from room temperature to 200℃ over 20 min. (2) Starting from 200℃ to 500℃, the activity of the catalyst was tested every 30℃. The temperature of each test point is kept for 20 min. Each time the temperature rise time is 5 min. (Example: 200℃ for 20 min to test its activity, after 20 min after 5 min after heating to 230℃ to keep 20 min, and so on until 500℃ to maintain 20 min after the end of its activity).

Activity calculation. CO conversion rate calculation formula:

$$C_{CO} = \frac{CO_{in} - CO_{out}}{CO_{in}} \times 100\%$$

CH_4 Selective formula:

$$S_{CH_4} = \frac{CH_4}{CO_{in} - CO_{out}} \times 100\%$$

RESULTS AND DISCUSSION

From Fig.2(a), it can be seen that TiO_2 is about 100nm uniform particles, NiO uniformly adsorbed on the TiO_2 carrier. By comparing Fig.2(b) and (c), it was found that the NiO particles became smaller and the dispersion was more uniform after the addition of the additive Mn. Figure.2(c) and (d) show that 20Ni/8Mn-TiO_2 catalyst is more homogeneous and finer than 20Ni/2Mn-TiO_2 particles, which indicates that the addition of Mn promoter is beneficial to improve the dispersibility of 20Ni/TiO_2 more the additive is added, the better the dispersibility.

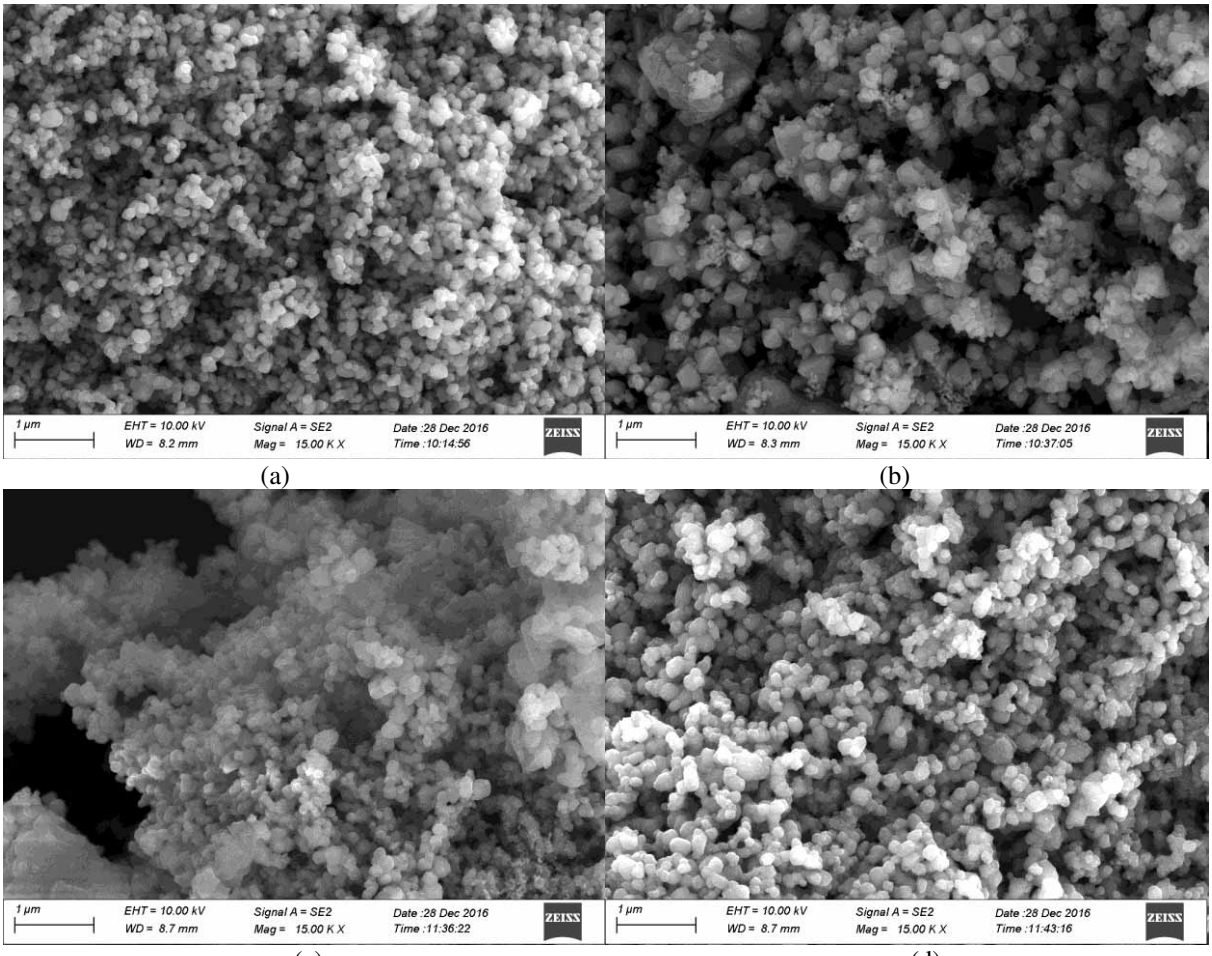

FIGURE 2
SEM image of catalyst TiO_2(a), 20NiTiO_2(b), 20Ni/8Mn-TiO_2(c) and 20Ni/8Mn-TiO_2(d)

TABLE 1
Average crystallite size of xNi/TiO_2 catalyst

Sample	D_{xrd} (nm)
TiO_2(Anatase)	103.4
10Ni/TiO_2	204.0
20Ni/TiO_2	157.5
40Ni/TiO_2	143.5

Effect of Ni loading on Ni/TiO_2 catalyst. As can be seen from Table 1, the anatase grains before firing are relatively small; this may be due to the fact that the sintered TiO_2 sintered at 900℃ leads to a larger grain size, and as the amount of Ni increases. The decrease in grain size may be due to the fact that the NiO grain size is smaller than that of the calcined TiO_2.

In Fig.3, TiO_2 is the XRD pattern before calcination at 900℃. We can see that the crystal form of TiO_2 before calcination is anatase, and the catalyst carrier is calcined at 900℃. Its crystal form is rutile, indicating that the crystal morphology of TiO_2 was changed at 900℃. It can be seen from Fig.3 that there is no obvious NiO peak in the XRD pattern of 10Ni/TiO_2 and 20Ni/TiO_2 catalysts, and the NiO peak appears in the 40Ni/TiO_2 catalyst, which shows that in the 10Ni/TiO_2, 20Ni/TiO_2 catalyst NiO particles are well dispersed in the carrier. In the 40Ni/TiO_2 catalyst, NiO particles accumulate, crystallize and grow, and accumulation on the surface of the carrier may lead to clogging of the pores.

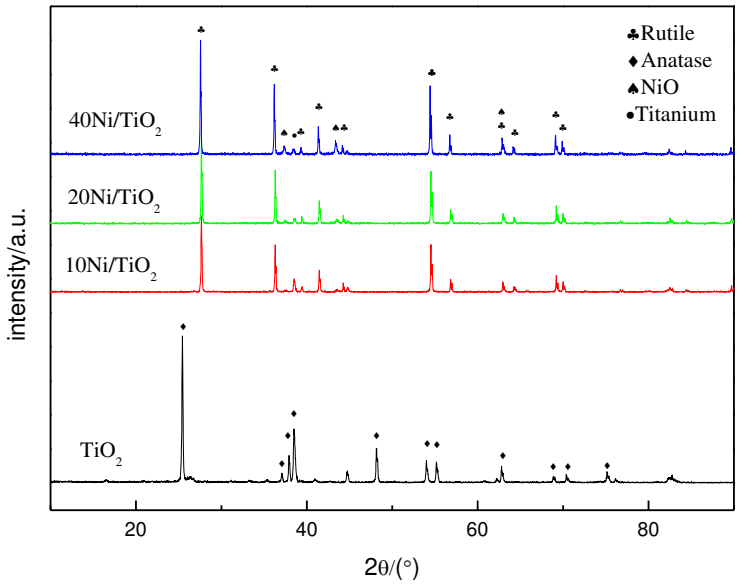

FIGURE 3
XRD patterns of xNi/TiO_2 catalysts

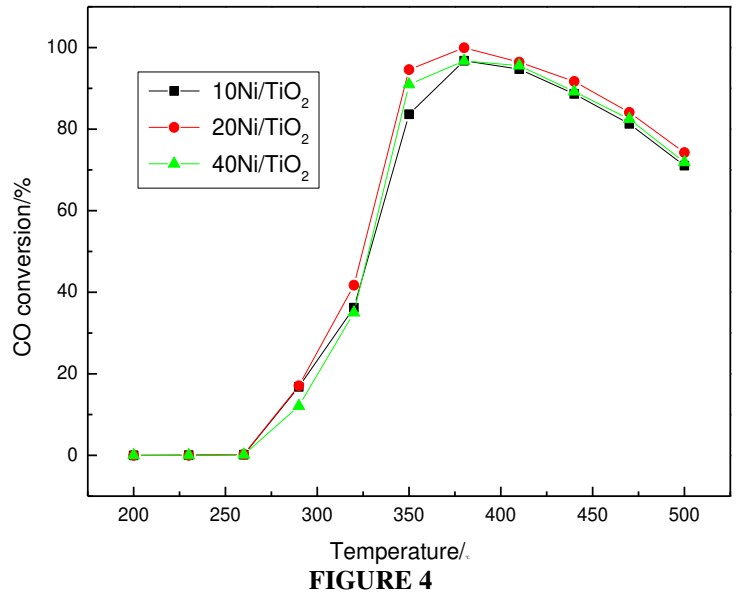

FIGURE 4
The influence of temperature on the CO conversion of xNi/TiO_2 catalyst

As shown in Fig.4, we can see that the activity range of CO methanation reaction of xNi/TiO_2 catalyst is about 350~470℃. The CO conversion of 20Ni/TiO_2 catalyst is higher because 10% Ni. The supported catalyst has a low catalytic activity and a low catalytic activity. The catalyst with 40% Ni loading may be due to the decrease of the active site due to the aggregation of Ni particles, resulting in less than 20Ni/TiO_2 activity.

It can be seen from Figure 5 at low temperature CO conversion rate is low, CH_4 selectivity is high, the reaction of the CO all the basic conversion to CH_4, with the temperature increase in the catalyst selectivity will appear a significant decline , It can be seen from Fig.7 that CO_2 appears to be present at a certain temperature since the main reaction at low temperature is a complete methanation reaction, and a direct methanation reaction takes place after a certain temperature. It can also be seen from Fig. 5 that the 20Ni/TiO_2 catalyst is better than the other two kinds of supported catalysts in the optimum active temperature range.

From Fig.6, we can see that the CH_4 yield of different catalysts is not very different, and the activity temperature of 20Ni/TiO_2 is slightly lower than that of the other two catalysts.

In general, the effect of Ni on the Ni/TiO_2 catalyst is not very large. In comparison, the 20Ni/TiO_2 catalyst is better than the other two catalysts in CO conversion and low temperature activity (Fig.7). Therefore, we further studied the effect of adding 20% Ni loading on the basis of the addition of Mn to modify the TiO_2, and the effect of adding auxiliaries was studied.

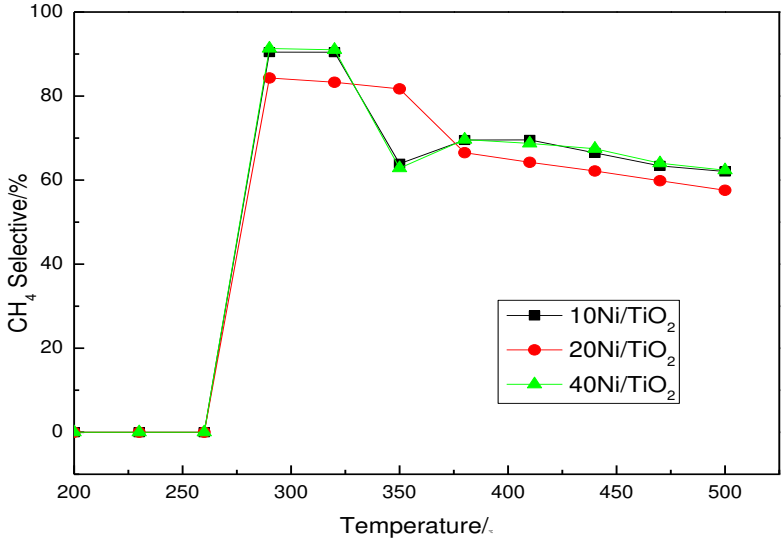

FIGURE 5

The influence of temperature on the CH_4 conversion of xNi/TiO_2 catalyst

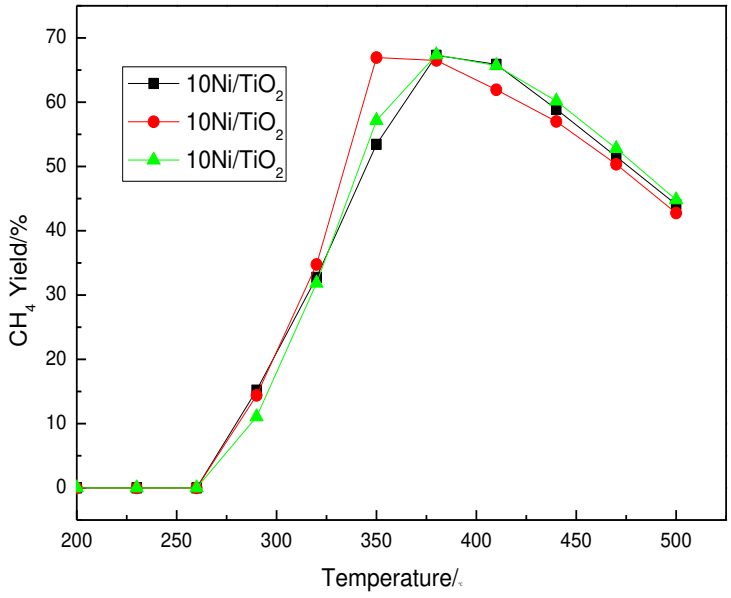

FIGURE 6

The influence of temperature on the CO_2 yield of xNi/TiO_2 catalyst

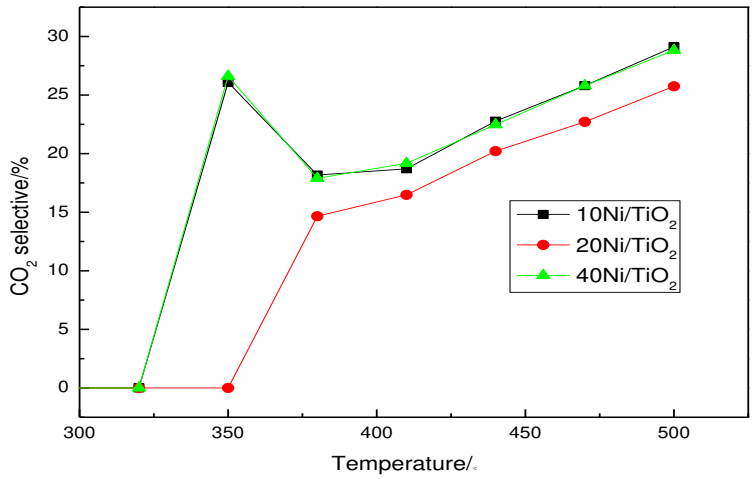

FIGURE 7
The influence of temperature on the CO_2 conversion of xNi/TiO_2 catalyst

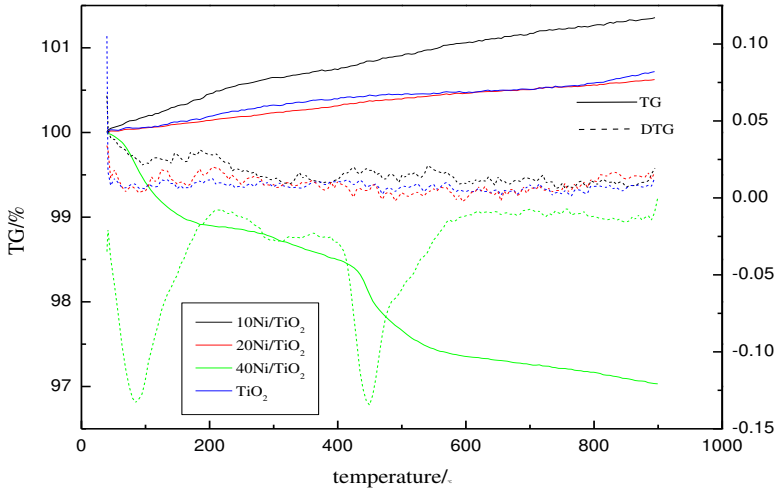

FIGURE 8
TG curve of used xNi/TiO_2 catalyst

Figure 8 shows the TG chart after the activity test of xNi/TiO_2 catalyst. We can see that the three other catalysts except 40Ni/TiO_2 catalyst are constantly absorbing and increasing their weight during the heating process, and no weight loss reaction occurs. less. And 40Ni/TiO_2 catalyst at 450℃ weightlessness indicates the existence of a carbon deposition material.

TABLE 2
Average crystallite size of 20Ni/xMn-TiO_2 catalyst

Sample	D_{xrd} (nm)
TiO_2（Anatase）	103.4
20Ni/TiO_2	157.5
20Ni/2Mn-TiO_2	129.4
20Ni/4Mn-TiO_2	113.3
20Ni/6Mn-TiO_2	107.4
20Ni/8Mn-TiO_2	111.1
20Ni/10Mn-TiO_2	104.5

The effect of Mn addition on catalyst. From Table 2 we can see that the average grain size of the catalyst after the addition of the additive Mn is reduced. This shows that the appropriate amount of additive additives Mn can improve the dispersion of the catalyst.

Figure 9 shows the XRD patterns of the different additions of the additives, which is the main peak of NiO at 43.3°, but it can be seen that the NiO is very well dispersed in the 20Ni/xMn-TiO_2 catalyst.

Figure 10 for the addition of different amounts of Mn additives after the catalyst CO conversion rate diagram, from the overall view of the CO conversion rate is the first increase in the process of decline. From Fig.10, we can see that the activity range of the catalyst after adding Mn promoter increased from 350~470℃ to 320~500℃. In addition, the optimum catalyst temperature is reduced to 350℃. Figure.10 can also be seen in 20Ni/8Mn-TiO_2 compared to several other catalysts have a high conversion rate, while a good thermal stability.

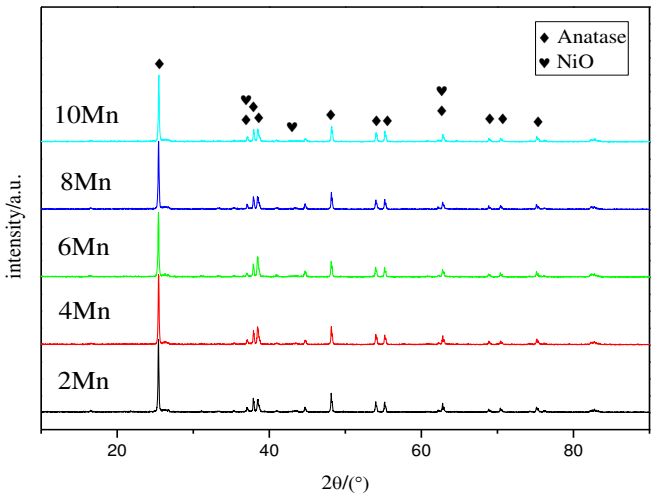

FIGURE 9
XRD patterns of 20Ni/xMn-TiO_2 catalysts

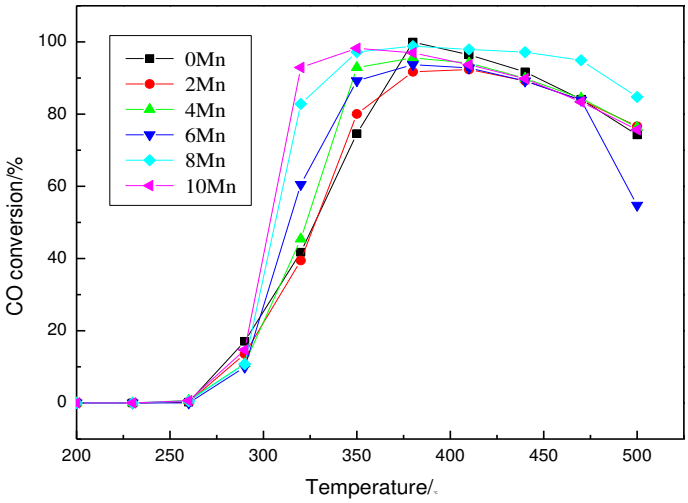

FIGURE 10
The influence of temperature on the CO conversion of 20Ni/xMn-TiO_2 catalyst

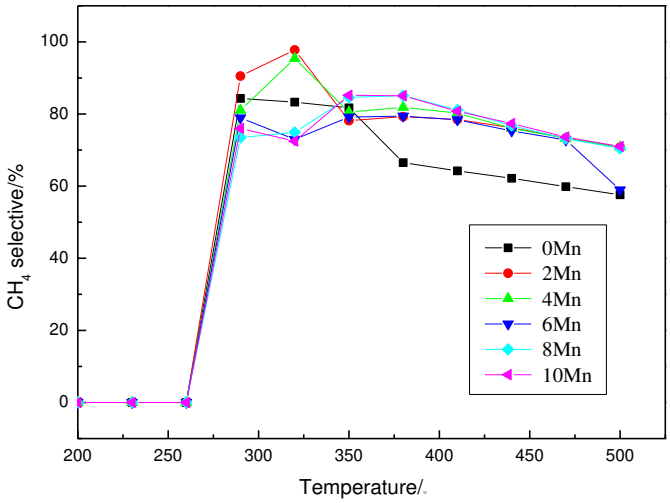

FIGURE 11
The influence of temperature on the CH_4 conversion of xNi/TiO_2 catalyst

It can be seen from Figure 11 that the methane selectivity of the catalyst after the addition of the Mn promoter is significantly increased. With the increase of Mn addition, the methane selectivity at low temperature is slightly decreased. It can be deduced that this is due to the decrease of the activation temperature after the addition of Mn.

It can be seen from Fig.12 that the yield of 20Ni/8Mn-TiO_2 catalyst is better, the maximum yield of CH_4 is above 80% at 350℃, and the addition of other Mn additive is compared with that of 20Ni/TiO_2 catalyst There is a certain upgrade. Therefore, 20Ni/8Mn-TiO_2 catalyst has the best effect from the overall performance.

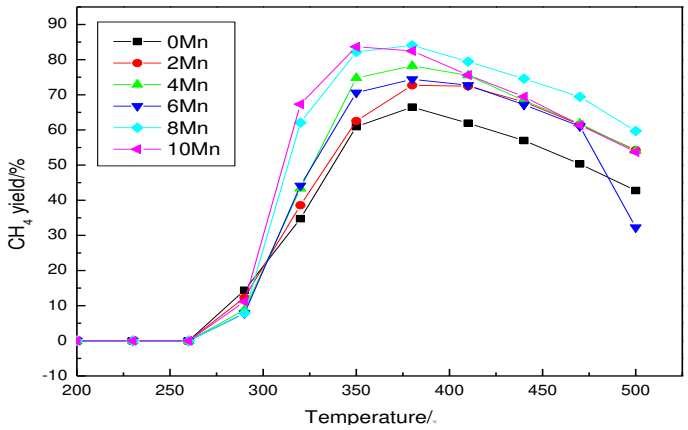

FIGURE 12
The influence of temperature on the CH_4 yield of 20Ni/xMn-TiO_2 catalyst

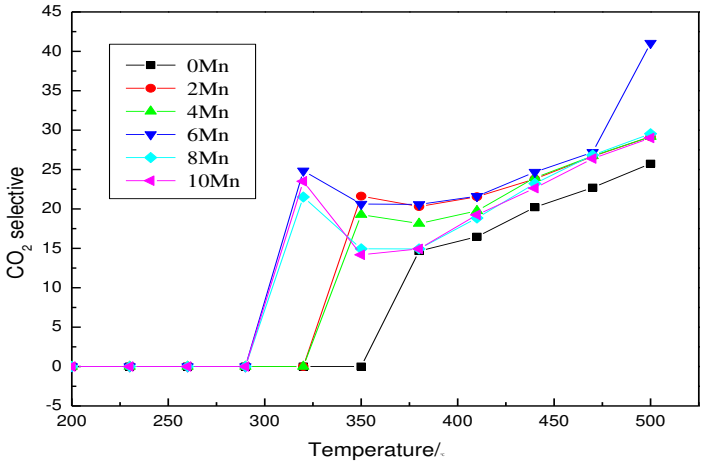

FIGURE 13
The influence of temperature on the CO_2 yield of 20Ni/xMn-TiO_2 catalyst

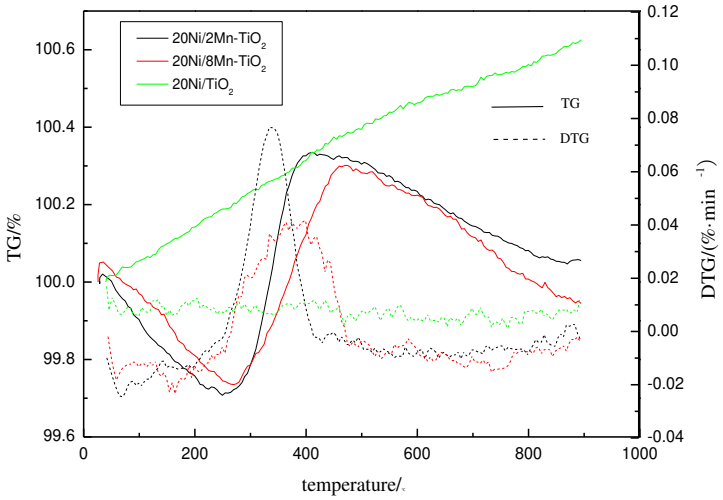

FIGURE 14
TG curve of used 20Ni/xMn-TiO_2 catalyst

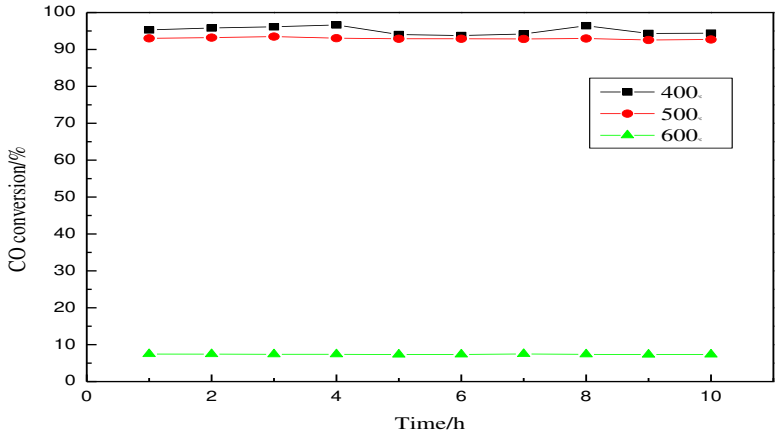

FIGURE 15
The influence of reduction temperature on the CO conversion of 20Ni/8Mn-TiO_2

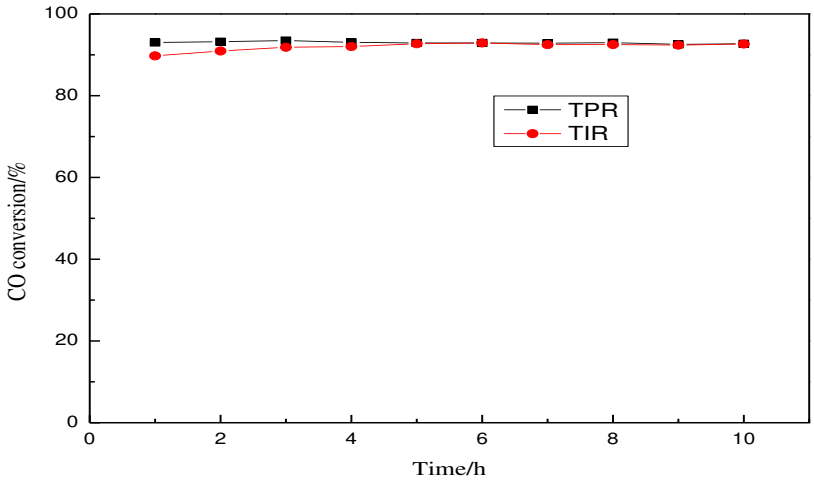

FIGURE 16
The influence of reduction method on the CO conversion of 20Ni/8Mn-TiO_2

It can be seen from Fig.13 that the addition of CH_4 and CO_2 after the addition of the additive Mn increases, whereby it can be deduced that the addition of Mn to inhibit other side reactions is beneficial to the formation of methane.

Figure 14 is 20Ni/xMn-TiO_2 catalyst activity test after the TG diagram, we can see that the catalyst after adding Mn additives with the temperature increase after weight loss weight gain. And the weight loss temperature range of 40~200℃ this range is not the carbon weight loss range, indicating that the increase in reactivity while carbon deposition and no significant increase.

According to the previous study, we selected 20Ni/8Mn-TiO_2 catalyst at different reduction temperature (400, 500, 600℃) and different reduction (TPR, TIR) reduction after its test at 380℃, the results shown in Figure.15, 16 The We found that the 20Ni/8Mn-TiO_2 catalyst reduced at 400℃ had the highest CO conversion and had little activity at 600℃. TPR reduction catalyst was slightly better than TIR, but this effect was very weak.

CONCLUSION

The Ni-based catalyst with TiO_2 as carrier and prepared by impregnation method was found to have a high catalytic activity of 99%. By comparing the different Ni loading catalyst, it was found that the loading had some influence on the catalyst, but not the main factor. Which Ni load of about 20% higher activity. It was found that the additive addition Mn could improve the dispersibility of the catalyst, reduce the grain size of the catalyst, decrease the reaction activation temperature, increase the reactivity interval, improve the CO conversion and CH_4 selection. And the inhibition of other side effects increases the selectivity of CH_4. The results showed that the activity of 20Ni/8Ca-TiO_2 catalyst was better, the conversion rate of CO was 98.8% and the yield of CH_4 was up to 84%. At the same time, the reduction of TPR in 20Ni/8Mn-TiO_2 catalyst is superior to that of 20Ni/8Mn-TiO_2 catalyst at 400℃.

ACKNOWLEDGEMENTS

This study was supported by Inner Mongolia Natural Science Foundation (No.2016MS0514, No.2017MS0219) and National Natural Science Foundation (No.21868022).

REFERENCES

[1] Kopyscinski, J., Schildhauer, T.J., Biollazi, S.M.A. (2010) Production of synthetic natural gas (SNG) from coal and dry biomass-A technology review from 1950 to 2009. Fuel. 89(8), 1763-1783.

[2] Gao, J., Jia, C., Li, J., Zhang, M.,Gu, F., Xu, G., Zhong, Z., Su, F. (2013) Ni/Al_2O_3 catalysts for CO methanation: Effect of Al_2O_3 supports calcined at different temperatures. Energy Chem. 22(6), 919–927.

[3] Nguyen, T.T.M., Wissing, L., Skjøth-Rasmussen, M.S. (2013) High temperature methanation: Catalyst considerations. Catal. Today. 215, 233–238.

[4] Lebarbier, V.M., Dagle, R.A., Kovarik, L., Albrecht, K.O., Li, X.H., Li, L., Taylor, C.E., Bao, X., Wang, Y. (2014) Sorption-enhanced synthetic natural gas (SNG) production from syngas: A novel process combining CO methanation, water-gas shift and CO_2 capture. Appl. Catal. B: Environ. 144, 223–232.

[5] Zwart, R.W.R., Boerrigter, H. (2005) High Efficiency Co-production of Synthetic Natural Gas (SNG) and Fischer−Tropsch (FT) Transportation Fuels from Biomass. Energy Fuels. 19, 591–597.

[6] Shen, W.M., Dumesic, J.A., Hill, C.G. (1981) Criteria for stable Ni particle size under methanation reaction conditions: Nickel transport and particle size growth via nickel carbonyl. Catal. 68, 152–165.

[7] Enger, B.C., Holmen, A. (2012) Nickel and Fischer-Tropsch Synthesis. Catal. Rev. 54, 437–488.

[8] Yan, X..L., Yuan, C., Bao, J.H., Li, S., Qi, D.Z., Wang, Q.Q., Zhao, B.R., Hu, T., Fan, L.M., Fan, B.B., Li, R.F., Tao, F., Pan, Y.X. (2018) A Ni-based catalyst with enhanced Ni-support interaction for highly efficient CO methanation. Catalysis Science and Technology. 8(14), 3474-3483.

[9] Mccarty, J.G., Wise, H. (1979) Hydrogenation of surface carbon on alumina-supported nickel. Journal of Catalysis. 57(3), 406-416.

[10] Bartholomew, C.H. (1982) Carbon Deposition in Steam Reforming and Methanation. Catalysis Reviews. 24(1), 67-112.

[11] Bartholomew, C.H. (2001) Mechanisms of catalyst deactivation. Applied Catalysis A General. 212(1–2), 17-60.

[12] Rostrup-Nielsen, J.R., Pedersen, K., Sehested, J. (2007) High temperature methanation: Sintering and structure sensitivity. Applied Catalysis A General. 330(40), 134-138.

[13] Barrientos, J., Lualdi, M., Boutonnet, M. Jaras, S. (2014) Deactivation of supported nickel catalysts during CO methanation. Applied Catalysis A General. 486,143-149.

[14] Bartholomew, C.H., Strasburg, M.V., Hsieh, H.Y. (1988) Effects of Support on Carbon Formation and Gasification on Nickel during Carbon Monoxide Hydrogenation. Applied Catalysis. 36(00), 147-162.

[15] Mirodatos, C., Praliaud, H., Primet, M. (1987) Deactivation of nickel-based catalysts during CO methanation and disproportionation. Journal of Catalysis. 107(2), 275-287.

[16] Loosdrecht, J.V.D., Kraan, A.M.V.D., Dillen, A.J.V. (1997) Metal-Support Interaction: Titania-Supported and Silica-Supported Nickel Catalysts. Journal of Catalysis. 170(2), 217-226.

[17] Chary, K.V.R., Rao, P.V.R., Rao, V.V. (2008) Catalytic functionalities of nickel supported on different polymorphs of alumina. Catalysis Communications. 9(5), 886-893.

[18] Rynkowski, J., Kaźmierczak, A., Praźmowska-Wilanowska, A., Tadeusz P. (1996) Influence of calcination and lithium promotion on the surface properties of oxide supports. Reaction Kinetics and Catalysis Letters. 58(1), 169-175.

[19] Khalil, T., El-Nour, F.A., El-Gammal, B. (2001) Determination of surface area and porosity of sol–gel derived ceramic powders in the system TiO_2–SiO_2–Al_2O_3. Powder Technology. 114(1–3), 106-111.

[20] Keller, N., Pham-Huu, C., Roy, S. Ledoux, M.J., Estournes, C., Guille, J.(1999) Influence of the preparation conditions on the synthesis of high surface area SiC for use as a heterogeneous catalyst support. Journal of Materials Science. 34(13), 3189-3202.

[21] Vannice, M.A., Garten, R.L. (1979) Metal-support effects on the activity and selectivity of Ni catalysts in, ja:math, synthesis reactions. Journal of Catalysis. 56(2), 236-248.

[22] Park, J.H., Lee, D., Lee, H.C. Park, E.D. (2010) Steam reforming of liquid petroleum gas over Mn-promoted Ni/γ-Al_2O_3 catalysts. Korean Journal of Chemical Engineering. 27(4), 1132-1138.

[23] Ouaguenouni, H.S., Benadda, A., Kiennemann, A. Barama, A. (2009) Preparation and catalytic activity of nickel–manganese oxide catalysts in the reaction of partial oxidation of methane. Comptes Rendus Chimie. 12(6–7), 740-747.

[24] Li, L.B, Wei, S.Q., Xu, G.L. (2004) Influence of Second Metal on Ni-Based Catalysts Prepared by CO-Preciptation Method for Methanation on of Carbon Dioxide. Natural Gas Chemical Industry. 29(1), 27-31.
[25] Yao, L., Zhu, J.Q., Peng, X.X., Tong, D.M., Hu, C.W.(2013) Comparative study on the promotion effect of Mn and Zr on the stability of Ni/SiO_2 catalyst for CO_2, reforming of methane. International Journal of Hydrogen Energy. 38(18), 7268-7279.

Received: **06.11.2018**
Accepted: **19.02.2019**

CORRESPONDING AUTHOR

Shaoping Xu
School of Chemical Engineering,
Faculty of Chemical, Environmental and Biological Science and Technology,
Dalian University of Technology,
Dalian Liaoning 116024 – China

e-mail: 3253490092@qq.com

© by PSP Volume 28 – No. 5/2019 pages 3854-3864 Fresenius Environmental Bulletin

THE INFLUENCE OF URBAN GROWTH ON SURROUNDING MEDITERRANEAN LANDSCAPES WITH PARTICULAR REFERENCE TO DEGRADATION OF OLIVE ORCHARDS

Derya Gulcin*

Department of Landscape Architecture, Faculty of Agriculture, University of Aydin Adnan Menderes, 09010, Aydin, Turkey

ABSTRACT

Monitoring land use/land cover (LULC) changes is important in making effective decisions in landscape planning and management. Quantifying the changing pattern of land helps us to understand how ecological impacts reveal and affect ecosystem services. The changes in landscapes can be assessed in different qualitative and quantitative ways. One of the aims of this study is to classify land cover using object-based image analysis and quantify the changes of landscape patterns by applying landscape metrics in the Efeler district, an urban settlement of Aydin province, during the 25 years from 1986 to 2011. In this context, a combination of satellite imagery, geographic information systems (GIS), and landscape metrics was used. A Spot-1 image dated 1986 and a Worldview Ortoready pan-sharpened satellite image dated 2011 were respectively processed for LULC classification. Six classes of land use including agriculture, bare soil, built environment, forest, main road, and river were identified. According to the overall accuracy assessment of the 2 classified images, the accuracy values were computed as 85.6% (for the LULC map dated 1986) and 89.8% (for the LULC map dated 2011). Change-detection results showed that during the whole study period there was a remarkable increase in the built environment and the main road, while bare soil decreased dramatically. It is also interesting that although urban expansion increased, the total area of agricultural land remained almost the same. The location of the agricultural land changed notably, but the percentage of this area was unchanged. Within the boundary of urban settlement, agricultural areas, and especially olive orchards, were fragmented due to the developmental strategies of Aydin. Within the scope of change-detection analysis, degradation of olive orchards was highlighted. Heterogeneous structure and fragmented patterns of land cover were analyzed using several metrics at different levels.

KEYWORDS:
Land use/land cover, change detection, GIS, olive orchards, landscape metrics

INTRODUCTION

Landscape consists of various patches as spatial components that are modified by ecological processes and human activities [1]. Severe changes of these patches may result in landslides [2], deforestation [3], agricultural expansion and intensification [4, 5], desertification [6], or soil degradation [7], which needs to be evaluated in terms of conservation policies. For these reasons, analyzing the structure of landscapes has become an important issue for environmentalists and researchers in the last decades. Landscape changes due to anthropogenic effects have caused a dramatic loss of natural vegetation, fragmentation, and degradation of land [8], and the composition and structure of landscapes have been changed unprecedentedly over time [9, 10, 11]. Monitoring land use/land cover (LULC) is an effective method to quantify the changing pattern of land at different spatial scales [12, 13, 14, 15]. LULC can be seen as an indispensable part of recent studies, especially for land conservation strategies. Change detection also helps us to understand landscape dynamics during a specific period [16]. As the main factor of landscape change, dispersed urbanization has adverse impacts on LULC. Like other developing countries, Turkey experienced a fast increase in the urban population, causing challenges in the urbanization agenda over the past several decades. According to the National Report of Turkey [17], in 1950, the percentage of Turkey's population residing in urban areas rose to 25%, and then to 44% in 1980, 65% in 2000, and 77% in 2012. Due to this dramatic increase of urbanization, problems such as biodiversity loss, destruction of green and gray infrastructure, and vulnerability against disasters have emerged in most parts of the country. Many studies assessed the effects of urbanization in different parts of Turkey to provide protection of existing natural environments and to promote urban development in qualitative ways [18, 19, 20, 21, 22, 23]. Like other landscape types, agricultural landscapes are under pressure by dispersed urbanization around the world. In this regard, the use of tree crops, and especially the olive tree as a bioclimatic indicator, has been studied recently in environmental research

[24, 25]. Climate-based studies show that olive orchards increase land quality [25]. Besides this ecological value, olive orchards have cultural, socioeconomic, culinary, and aesthetic value. Therefore, their fragmentation due to land degradation should be assessed in geographical areas incorporating olive orchards. In order to respond to this need, studies pointing out the fragmentation of olive orchards have been developed since 2008 in Turkey [26, 22].

Remote sensing (RS) and geographical information system (GIS) techniques play a crucial role for mapping LULC, making spatial analyses, and assessing landscape changes [27, 28, 29, 30, 31, 32, 33, 34]. The advent of modern technologies of satellite imagery and other processes in both RS and GIS enables researchers to conduct consistent LULC analyses with better accuracy and low cost [16, 35]. The integration of GIS with RS by different models such as object-oriented data modeling [36, 37, 38, 39] has been applied many times as an effective tool in detecting LULC. Moreover, landscape metrics may be used to quantify landscape patterns and enrich the results produced by RS-based change analysis [40, 41]. The combined use of RS, GIS, and landscape metrics can be helpful in examining various physical structures of LULC changes in urban areas, such as shape, size, and distribution, which are significant variables in quantifying urban transformation. A great number of spatial metrics have been introduced [42] and applied to measure different spatial characteristics of urban areas, such as fragmentation [43, 44, 45, 46, 47], connectivity [48, 49], heterogeneity [50, 51, 52], and landscape diversity [53]. Multiple measurements have been taken into consideration to analyze the complexity of landscapes that occur with many ecological processes in time [54].

This research primarily uses theory and practice integrated with RS, GIS, and landscape metrics. One of the objectives is to classify LULC using object-based image analysis and quantify the changes of landscape patterns by applying landscape metrics in the Efeler district, an urban settlement of Aydin province, located in western Turkey, during the 25 years from 1986 to 2011. Within the boundary of urban settlement, agricultural areas, and especially olive orchards, were fragmented due to the development strategies of Aydin. Within the scope of change-detection analysis, degradation of olive orchards is highlighted as the second aim of this study. Heterogeneous structure and fragmented patterns of land cover are analyzed using several metrics at different levels.

Research Area. In this research, the transformation of the Efeler district and the urban settlement of Aydin, located in the western part of Turkey, were investigated (Figure 1). Surrounded by fertile plains, arable lands are planted mainly with maize, cotton, wheat, chestnut, olive, and fig. Agriculture has become more significant recently because of the increasing trend of exported products. According to the Environmental Status Report of Aydin, fig, olive, and chestnut rank first in the country's fruit production. Cotton is ranked as the second most cultivated crop throughout all provinces of Turkey [53]. In the province of Aydin, where a Mediterranean climate is dominant, summers are hot and arid while winters are warm and rainy. The annual average temperature is around 26 °C and annual rainfall is between 580 and 1000 mm [55].

In the urban area of Aydin, olive orchards are the most prominent agricultural pattern. They have cultural, ecological, culinary, and aesthetic importance. Dispersed urbanization is considered as a threat to these orchards, resulting in fragmentation over time. Agricultural landscapes are discrete mosaics of different types of patches and corridors. In order to achieve and maintain connectivity, it is necessary to assess the composition and configuration of these elements [56].

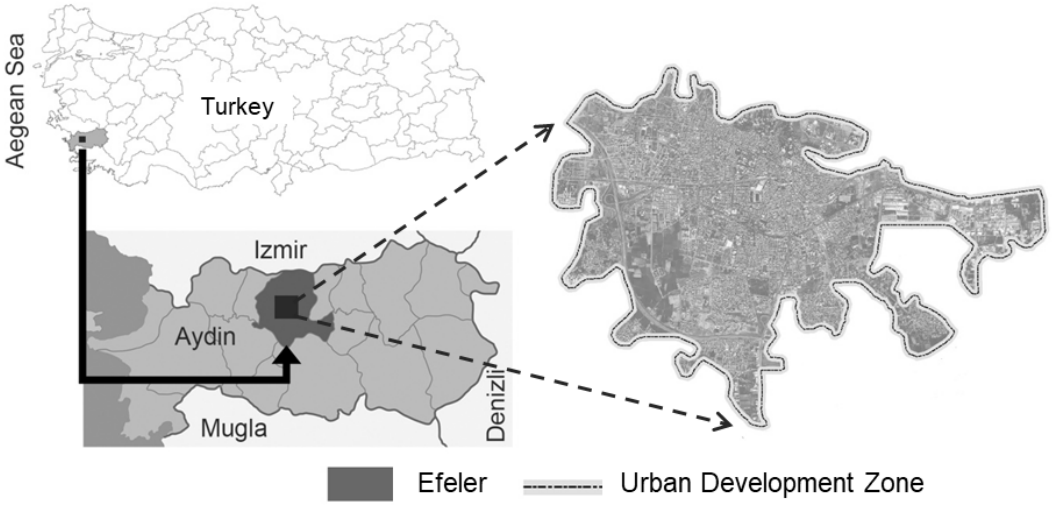

FIGURE 1
Location of the research area

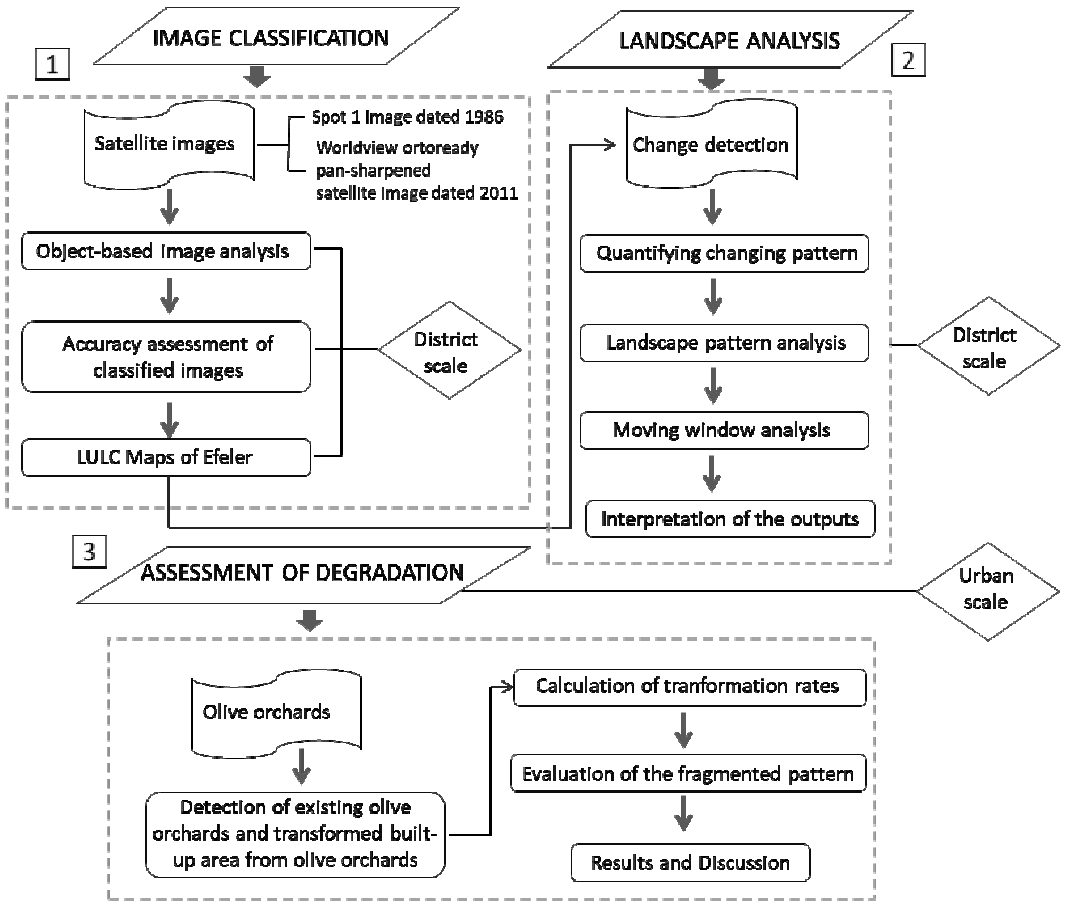

FIGURE 2
Methodological scheme

MATERIALS AND METHODS

High resolution satellite images (a Spot-1 image dated 1986 and a Worldview Ortoready pan-sharpened satellite image dated 2011) were used as the main study materials. Both images were geo-registered to UTM projection with WGS 84 spheroid and datum. In this research, the combination of RS, GIS, and landscape metrics was utilized (Figure 2). Image classification, landscape analysis, and assessment of degradation are the main steps. First of all, both images of the Efeler district were classified by object-based image analysis in eCognition, which has been used as an object-based processing software program since 2000. Next, overall accuracies for classified images were calculated and LULC maps were produced. In the second step, a series of landscape analyses were applied. The main objective of these analyses is to quantify the degradation of olive orchards due to urban transformation between 1986 and 2011 using RS and GIS. Heterogeneous structure and fragmented patterns of land cover were analyzed using 5 metrics (largest patch index - LPI, total edge - TE, edge density - ED, mean patch area - AREA_MN, and mean radius of gyration distribution - GYRATE_MN) at class and landscape scale. Within the scope of landscape pattern analysis, it is difficult to understand the spatial changes that occur over time by calculating standard metrics. Thus, a moving window approach, which is a preferred method for analyzing fractal landscapes, was adopted to describe the areas in the landscape and spatial heterogeneity was interpreted simultaneously. In the analysis, 10-m resolution grid images with diameter of 500 × 500 m and 8-pixel neighborhood rule were used.

In the last step, the degradation of olive orchards due to the development strategies within the boundaries of the urban settlement of Aydin was assessed by change-detection analysis. The calculation of transformation rates was conducted and an evaluation of the fragmented pattern was made. To conclude, the findings are discussed from a comparative perspective in the results section of this research.

Image Classification. One of the main objectives of this research was to classify LULC classes of the Efeler district from 1986 to 2011 by means of high spatial resolution satellite images through object-based classification. eCognition software provides not only spectral information, but also the shape, compactness, and other parameters to extract objects. Accurate segmentation may be seen as a key point in object-oriented classification. During the segmentation process, the subdivision of a satel-

lite image into separate object regions occurs based on certain criteria of homogeneity and heterogeneity in color and shape [39]. Multi-resolution segmentation is a bottom-up region-merging method arranging classes in a semantic hierarchy that integrates scale and compactness parameters. In this research, the classification was done by multi-resolution segmentation using the following parameter values: the scale parameter is equal to 40, shape criterion 0.20, and compactness criterion 0.60. Six classes of land use including agriculture, bare soil, built environment, forest, main road, and river were identified (Figure 3). According to the overall accuracy assessment of the 2 classified images, the accuracy values were computed as 85.6% (for the LULC map dated 1986) and 89.8% (for the LULC map dated 2011) in ArcMap 10.4.1.

Change Detection. The results of change-detection analysis showed that during the whole study period, there was a remarkable increase in the built environment and main road while bare soil decreased dramatically. It is also interesting that although urban expansion increased, the total area of agricultural land remained almost the same. The location of agricultural land changed notably but the percentage of this area was unchanged (Figure 4).

The data presented in Table 1 and Figure 4 reveal that both positive and negative changes occurred in the LULC pattern of the Efeler district. Over 25 years, the agricultural land in the research area increased from 31703.5 ha in 1986 to 37956.1 ha in 2011, which accounts for 10.2% of the total change in the research area. The bare soil area decreased from 12333.3 ha in 1986 to 2154.1 ha in 2011, which accounts for -16.7% of the total change in the research area. The built environment increased from 2140.4 ha in 1986 to 4347.0 ha in 2011, which accounts for 3.6% of the total change. The forest cover increased from 14362.1 in 1986 to 16140.2 in 2011, accounting for 2.9% of total change. The main road and river changed slightly, accounting for 0.3% and -0.4% of the total change in the research area, respectively.

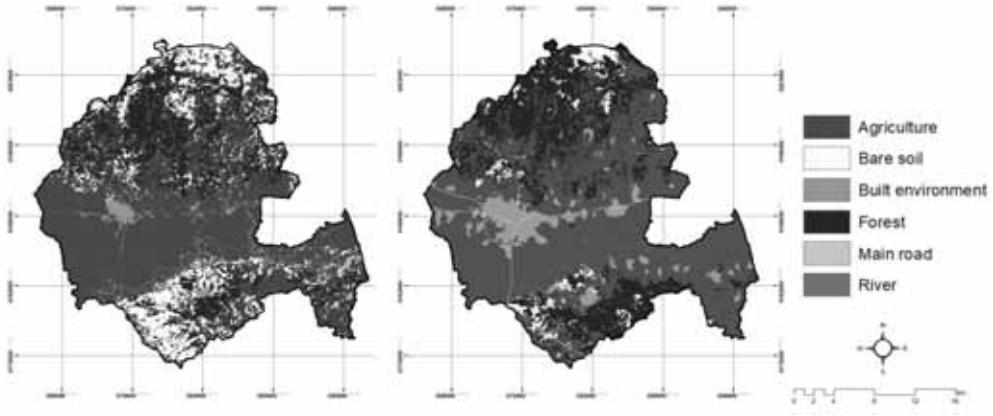

FIGURE 3
LULC maps of Efeler in 1986 and 2011

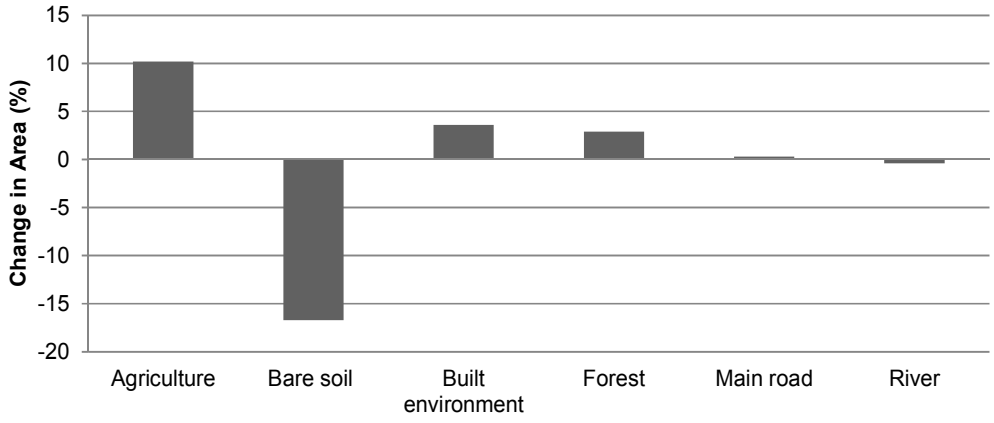

FIGURE 4
LULC change in area (%) over 25 years

TABLE 1
LULC classes and areas in hectares

	1986		2011		Change, 1986-2011	
LULC classes	**Area (ha)**	**%**	**Area (ha)**	**%**	**Area (ha)**	**%**
Agriculture	31703.5	51.9	37956.1	62.2	6252.6	10.2
Bare soil	12333.3	20.2	2154.1	3.5	-10179.2	-16.7
Built environment	2140.4	3.5	4347.0	7.1	2206.6	3.6
Forest	14362.1	23.5	16140.2	26.4	1778.1	2.9
Main road	134.3	0.2	341.3	0.6	207.0	0.3
River	388.7	0.6	123.6	0.2	-265.1	-0.4
Total	61062.3	100.0	61062.3	100.0	0.0	0.0

TABLE 2
Area and edge metrics of LULC in 1986 and 2011 at landscape level

Years	LPI (%)	TE (m)	ED (m/ha)	AREA_MN (ha)	GYRATE_MN (m)
1986	13.6	5216475.0	85.4	15.7	110.6
2011	19.2	3351100.0	54.8	39.9	122.1

TABLE 3
Area and edge metrics of LULC in 1986 and 2011 at class level

LULC classes	LPI (%)	TE (m)	ED (m/ha)	AREA_MN (ha)	GY-RATE_MN (m)	LPI (%)	TE (m)	ED(m/ha)	AREA_MN (ha)	GY-RATE_MN (m)
Agriculture	13.6	4102923.0	67.1	33.7	126.7	19.2	2887870.0	47.2	59.6	115.2
Bare soil	2.9	2814548.0	46.0	46.0	100.2	0.9	487140.0	7.9	11.7	115.3
Built environment	0.6	734822.0	12.0	3.6	81.5	1.2	398060.0	6.5	35.0	197.5
Forest	9.5	2481644.0	40.6	16.0	114.2	13.0	2709520.0	44.3	27.8	96.3
Main road	0.2	161359.0	2.6	134.6	7728.8	0.5	133050.0	2.1	341.5	6049.9
River	0.5	137654.0	0.5	38.8	724.5	0.1	86560.0	1.4	41.1	1906.4

Landscape Pattern Analysis. Area and edge metrics indicate fragmentation and change in landscape structure [57]. These metrics were used to evaluate the landscape pattern of the Efeler district at class and landscape levels. From all area-edge metrics, the largest patch index (LPI), total edge (TE), edge density (ED), mean patch area (AREA_MN), and mean radius of gyration distribution (GYRATE_MN) were computed in FRAGSTATS. The results show that agricultural areas are the dominant landscape type, both in 1986 and 2011, although the LPI value of the built environment has doubled in time (Table 2).

LPI is one of the important metrics showing the fragmentation of landscapes. According to Lavers and Haines-Young [58], larger patches contain more species. From 1986 to 2011, the LPI values of all LULC classes except bare soil and river increased. In this context, when LPI is examined, 13.6% of agricultural area in 1986 and 19.2% in 2011 was covered with a large patch. The decrease of LPI for bare soil and river implies that urban development maintained a dispersed pattern. Moreover, LPI is not dramatically changed for forest, indicating that smaller patches consisting of woody surfaces form in different areas over time. ED and TE are calculated from edge metrics, which are other indicators of landscape fragmentation and habitat quality (Table 3). Edge length and density describe the shape of the patch, showing the distribution of plant and animal species [57]. When all land use classes are examined, TE and ED show a decrease in the 25-year period, excluding forest areas. The increase of ED from 40.6 to 44.3 in forest areas shows that the landscape quality of the forest changed slightly over 25 years.

AREA_MN describes the average mean surface area of patches. Among all LULC classes, there is a decrease only for bare soil, implying its transformation into forest and agricultural areas. GYRATE_MN represents the mean distance between patch centers. A decrease of GYRATE_MN, especially for agricultural and forest areas, may cause fragmentation through the network of these patches. This can be revealed by the changing locations of agricultural areas and smaller patches of woody surfaces that have been formed in the forest. The heterogeneous structure and fragmented patterns of land cover are illustrated in Figure 5 by applying a moving window analysis.

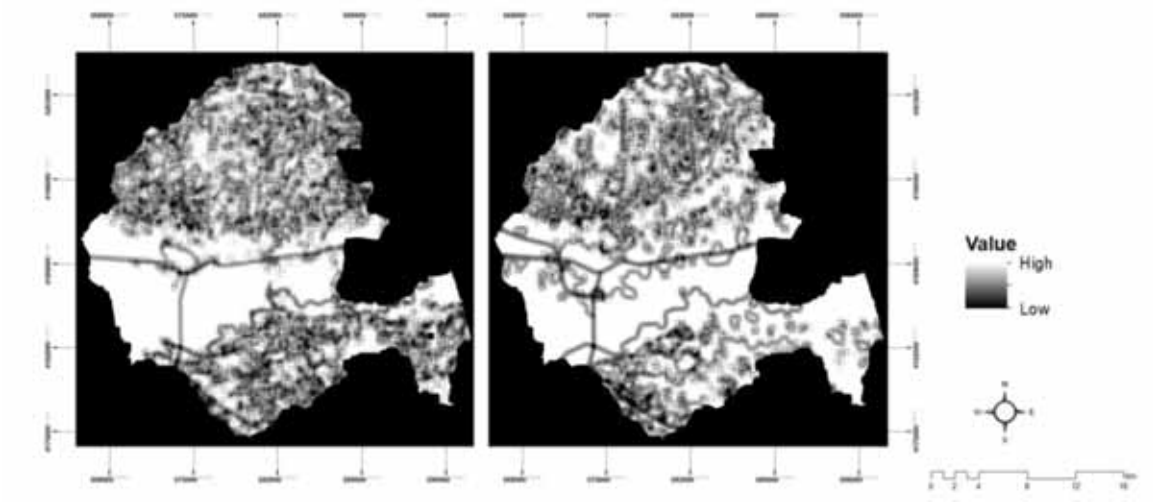

FIGURE 5
Maps obtained by moving window technique using FRAGSTATS based on the mean radius of gyration distribution (GYRATE_MN) metric.

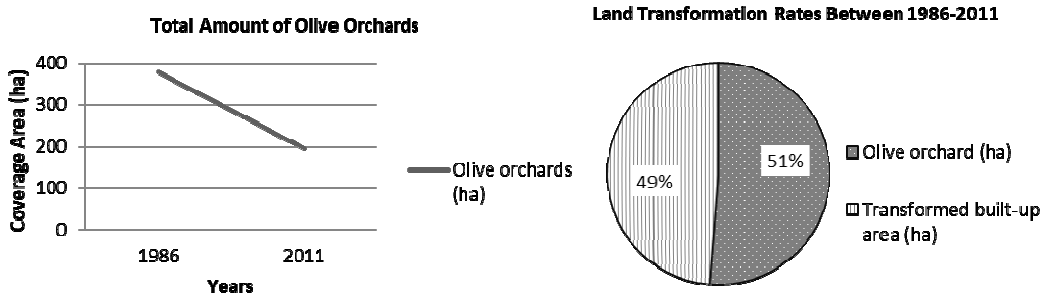

FIGURE 6
Change in the total amount of olive orchards and percentages of land transformation rates

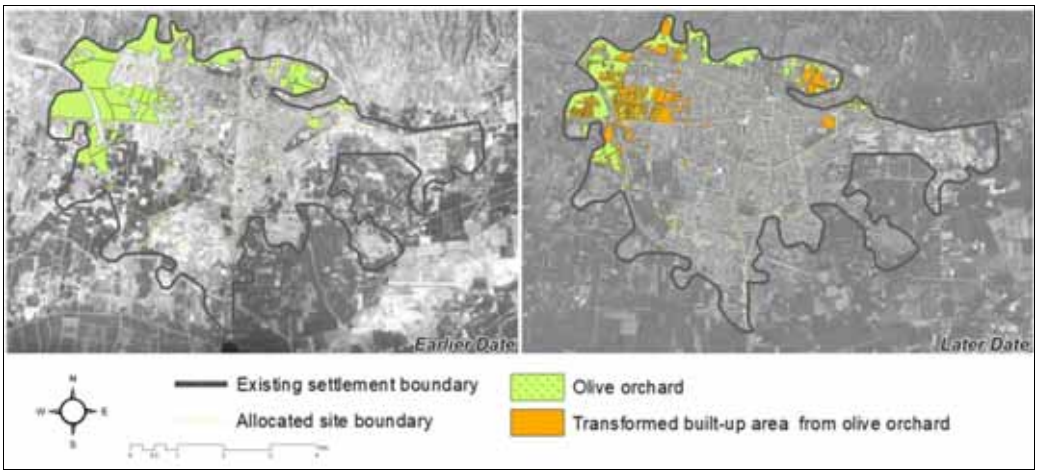

FIGURE 7
Current olive orchards and transformed built-up areas

Degradation of Olive Orchards. Over the last 25 years, the urban area of Aydin has experienced dramatic population growth, which increased from 28,724 in 1985 to 43,295 in 2011 [55]. The land covered by the urban area of Aydin increased to 4347.0 ha from 2140.4 ha. As an inevitable result of dispersed urbanization, the change in urban area has had a particularly adverse impact on olive orchards in Aydin. Due to land encroachment, the amount of olive orchards in the Aydin urban area has been reduced, although there has been little change in the amount of agricultural land. As a result of the change detection, it was determined that the overall amount of olive orchards decreased from 379.3 to 194.5 ha. This means that 48.7% of the total olive orchards have been transformed into

built-up areas. When the data derived from the Turkish Statistical Institute from recent years are examined, it is observed that olive orchards have increased slightly in the last decade, but this insignificant increase seen in recent years is not enough to offset the fragmentation of the olive orchards that have been degraded due to transformation. Figure 6 and Figure 7 highlight that the transformation of the olive orchards in built-up areas provides a better understanding of the fragmentation occurring, especially at the fringes of the urban area.

This research revealed that even though there was a slight increase in agricultural areas over 25 years in the Efeler district of Aydin province, this does not preclude the occurrence of fragmentation and land degradation. The pressure on olive orchards may be seen in Figure 8.

In the next step, fragmentation, which is more common in the urban fringe, was examined at the neighborhood scale and the percentage values of the loss of olive orchards were calculated (Figure 9). In this context, the neighborhoods in which olive orchards have been completely lost are Orta, Kuyulu, Kadikoy, Efeler, Zeybek, and Mesudiye. When the ratio of current olive orchards is examined, the Ilicabasi, Kemer, Isikli, Mimar Sinan, Kalfakoy, Zafer, and Girne neighborhoods are ranked from top to bottom.

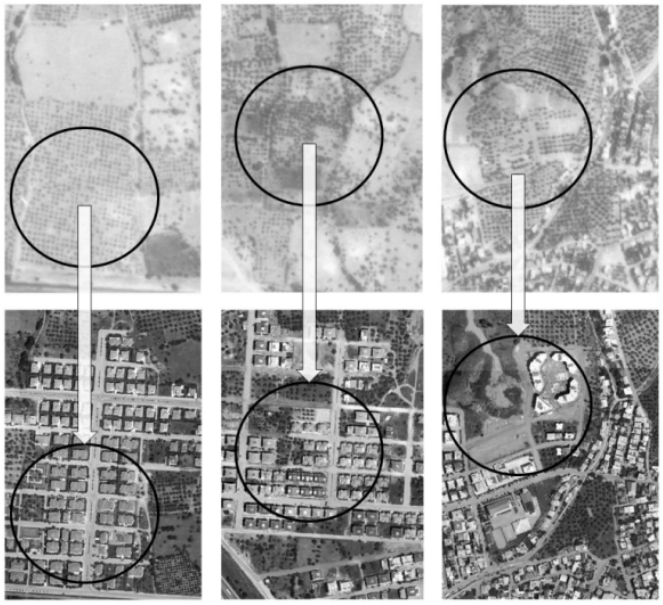

FIGURE 8
Examples of the transformed built-up area from olive orchards

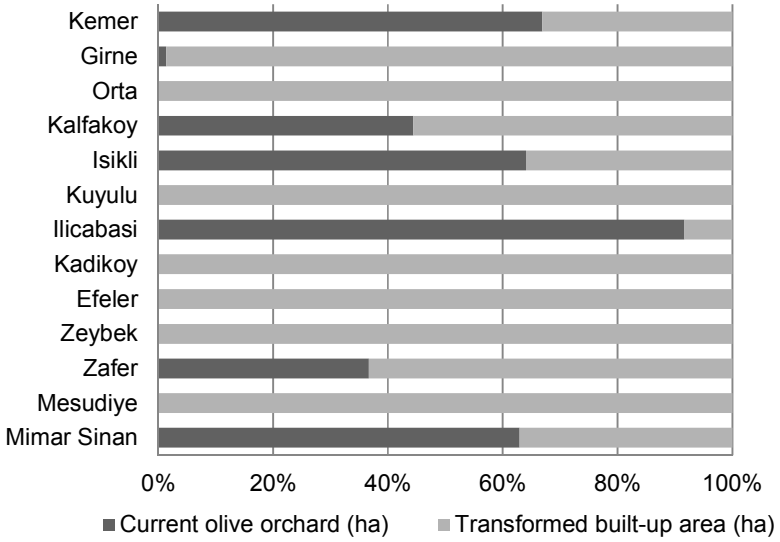

FIGURE 9
The percentage of current olive orchards and transformed built-up areas in 13 neighborhoods of the Aydin urban area

TABLE 4
The amount of current olive orchards and transformed built-up areas from olive orchards in 13 neighborhoods of the Aydin urban area

Neighborhood	Current olive orchards (ha)	Transformed built-up area (ha)	Total area (ha)
Mimar Sinan	99.1	58.3	157.4
Kemer	51.8	25.6	77.4
Isikli	24.6	13.8	38.4
Zafer	11.7	20.2	31.9
Girne	0.4	29.1	29.5
Mesudiye	0	19	19
Kalfakoy	3.6	4.5	8.1
Orta	0	5.5	5.5
Zeybek	0	3.6	3.6
Ilicabasi	3.3	0.3	3.6
Efeler	0	1.74	1.74
Kuyulu	0	1.7	1.7
Kadikoy	0	1.5	1.5

Table 4 shows the amount of current olive orchards and transformed built-up areas from olive orchards in 13 neighborhoods of the Aydin urban area. The highest transformation of olive orchards has occurred in Mimar Sinan, with a loss of 58.3 ha. Following this, 29.1 ha from Girne, 25.6 ha from Kemer, 20.2 ha from Zafer, and 13.8 ha from Isikli have been lost. A total of 184.8 ha out of 379.3 ha has been transformed into built-up area.

CONCLUSIONS

From an ecological perspective, olive orchards contribute to biodiversity, connecting natural elements of landscapes and their functions, and providing food resources. The loss of olive orchards may result in land degradation, harming animal species, especially avian species, and plant species as well [59]. Therefore, further studies should focus on the amount of change in olive orchards in Mediterranean landscapes and reclamation strategies for them to avoid degradation.

In previous studies, it has been shown that agricultural patches were mostly transformed into residential areas in the city of Aydin [60]. It is obvious that not only the Aydin urban area but also many other cities in Turkey face urbanization problems causing degradation of agricultural areas. This pressure, particularly for olive orchards, has been debated for years. From a legal point of view, there are serious challenges for sustainable development that have long been under discussion. "The Olive Law" has protected Turkey's olive trees since the 1930s, but proposed changes to this law may threaten the orchards. According to the proposals of Article 9 of Law No. 3573 in 2017, olive orchards are expected to have no less than 15 trees per decare (1000 square meters, or approximately 0.25 acres). This means that any olive orchard comprising fewer than 15 trees per decare will not be classed as an olive orchard. The Food, Agriculture, and Livestock Ministry may permit industrial construction and mining activities if the intention is for the public good on the condition that an alternative area for the investment cannot be found. The current regulations can put the sustainability of olive orchards at risk. If industrial and mining activities increase around these orchards, the fragmented pattern of olive orchards will increase correspondingly. There is no doubt that Aydin will be among the most adversely affected cities in Turkey as a result of these changes, as olive farming is most dominant in Aydin. Thus, both the local government and stakeholders in Aydin should plan their strategies and coordinate activities by adopting an integrated planning approach in line with the goals of sustainable development plans.

In this research, change-detection analysis in an urban area with particular reference to degradation of olive orchards was performed. With this aim, high resolution satellite images were used to monitor the changes by means of RS and GIS. Monitoring LULC has a significant role in landscape planning studies. In this context, valuable landscape types such as olive orchards should be evaluated by landscape analyses to determine strategies for their conservation and sustainability. Consequently, multi-disciplinary studies, more effective strategies, and multi-dimensional approaches may be adopted to manage landscape transformations incorporating both short-term and long-term targets.

ACKNOWLEDGEMENTS

I would like to thank Assoc. Prof. Dr. Bulent Deniz for sharing the satellite image dated 1986. The other high resolution satellite image was provided by the Municipality of the Metropolitan City of Aydin. I would like to thank the Directorate of the Development and Urban Planning Department

and all data producers of the municipality. I have no conflict of interest to declare.

REFERENCES

[1] Forman, R.T., Godron, M. (1981) Patches and structural components for a landscape ecology. BioScience. 31(10), 733-740.

[2] Persichillo, M.G., Bordoni, M., Meisina, C. (2017) The role of land use changes in the distribution of shallow landslides. Science of the Total Environment. 574, 924-937.

[3] Brandt, C.J., Thornes, J. B. (1996) Mediterranean Desertification and Land Use. John Wiley, Chicester, ISBN 0471942502, 9780471942504.

[4] Alphan, H. (2018) Analysis of road development and associated agricultural land use change. Environmental Monitoring and Assessment. 190(1), 5.

[5] Piquer-Rodríguez, M., Butsic, V., Gärtner, P., Macchi, L., Baumann, M., Pizarro, G.G., Volante, J.N., Gasparri, I.N., Kuemmerle, T. (2018) Drivers of agricultural land-use change in the Argentine Pampas and Chaco regions. Applied Geography. 91, 111-122.

[6] Wijitkosum, S. (2016) The impact of land use and spatial changes on desertification risk in degraded areas in Thailand. Sustainable Environment Research. 26(2), 84-92.

[7] Tolba M.K. (1992) The World Environment 1972–1992: Two Decades of Challenge. London: Chapman and Hall. (An authoritative review edited by Dr M. K. Tolba, previously Executive Director of UNEP, together with a large panel of experts.), 884p.

[8] Green, B.H., Simmons, E.A., Woltjer, I. (1996) Landscape conservation: Some steps towards developing a new conservation dimension. The University of London, Department of Agriculture, Horticulture and Environment.

[9] Baker, W.L. (1989) A review of models of landscape change. Landscape Ecology. 2(2), 111-133.

[10] Lindenmayer, D.B., Fischer, J. (2013) Habitat fragmentation and landscape change: an ecological and conservation synthesis. Island Press, ISBN 159726606X, 9781597266062

[11] Wang, X., Blanchet, F.G., Koper, N. (2014) Measuring habitat fragmentation: an evaluation of landscape pattern metrics. Methods in Ecology and Evolution. 5(7), 634-646.

[12] Lambin, E.F. (1997) Modelling and monitoring land-cover change processes in tropical regions. Progress in Physical Geography. 21(3), 375-393.

[13] Kyrimis, K. (2000) Monitoring land cover change detection with remote sensing methods in Magnesia prefecture in Greece. Fresen. Environ. Bull. 9, 659-666.

[14] López, E., Bocco, G., Mendoza, M., Duhau, E. (2001) Predicting land-cover and land-use change in the urban fringe: a case in Morelia city, Mexico. Landscape and Urban Planning. 55(4), 271-285.

[15] Duran, Z., Musaoglu, N., Seker, D.Z. (2006) Evaluating urban land use change in historical peninsula, Istanbul, by using GIS and remote sensing. Fresen. Environ. Bull. 15, 806-810.

[16] Rawat, J.S., Kumar, M. (2015) Monitoring land use/cover change using remote sensing and GIS techniques: A case study of Hawalbagh block, district Almora, Uttarakhand, India. The Egyptian Journal of Remote Sensing and Space Science. 18(1), 77-84.

[17] Un-Habitat, (2014) Turkey Habitat III National Report. Turkish Ministry of Environment and Urbanization, Ankara.

[18] Alphan, H., Yilmaz, K.T. (2005) Monitoring environmental changes in the Mediterranean coastal landscape: the case of Cukurova, Turkey. Environmental Management. 35(5), 607-619.

[19] Tagil, S. (2006) Change of habitat fragmentation and quality in the Balikesir Plain and its surroundings with landscape pattern metrics (1975–2000). Ecology. 60, 24-36.

[20] Esbah, H. (2007) Land use trends during rapid urbanization of the city of Aydin, Turkey. Environmental Management. 39(4), 443-459.

[21] Onur, I., Maktav, D., Sari, M., Kemal Sonmez, N. (2009) Change detection of land cover and land use using remote sensing and GIS: a case study in Kemer, Turkey. International Journal of Remote Sensing. 30(7), 1749-1757.

[22] Doygun, H. (2009) Effects of urban sprawl on agricultural land: a case study of Kahramanmaras, Turkey. Environmental Monitoring and Assessment. 158(1-4), 471.

[23] Sen, G., Gungor, E., Sevik, H. (2018) Defining the effects of urban expansion on land use/cover change: a case study in Kastamonu, Turkey. Environmental Monitoring and assessment. 190(8), 454.

[24] Moriondo, M., Trombi, G., Ferrise, R., Brandani, G., Dibari, C., Ammann, C.M., Lippi, M., Bindi, M. (2013) Olive trees as bioindicators of climate evolution in the Mediterranean Basin. Global Ecology and Biogeography. 22(7), 818-833.

[25] Cecchini, M., Zambon, I., Pontrandolfi, A., Turco, R., Colantoni, A., Mavrakis, A., Salvati, L. (2018) Urban sprawl and the 'olive' landscape: Sustainable land management for 'crisis' cities. GeoJournal. 1-19.

[26] Kuruku, Y., Kucukyilmaz, C. (2008) Monitoring the impacts of urbanization and industrialization on the agricultural land and environment of the Torbali, Izmir Region, Turkey. Environmental Monitoring and Assessment. 136(1), 289–297.
[27] Cihlar, J. (2000) Land cover mapping of large areas from satellites: status and research priorities. International Journal of Remote Sensing. 21(6-7), 1093-1114.
[28] Yang, X., Lo, C.P. (2002) Using a time series of satellite imagery to detect land use and land cover changes in the Atlanta, Georgia metropolitan area. International Journal of Remote Sensing. 23(9), 1775-1798.
[29] Bartholome, E., Belward, A.S. (2005) GLC2000: A new approach to global land cover mapping from Earth observation data. International Journal of Remote Sensing. 26(9), 1959-1977.
[30] Dogru, O.A., Balcik, F.B., Goksel, C., Ulugtekin, N. (2006) Monitoring coastal dunes by using remote sensing and GIS integration in northwest Turkey: A case study of Kilyos dunes. Fresen. Environ. Bull. 15, 1216.
[31] Kara, F. (2010) Determination of land use/land cover change and urban growth by using remote sensing: a case study of Duzce Province in Turkey. Fresen. Environ. Bull. 19, 1312–1319.
[32] Knorn, J., Rabe, A., Radeloff, V.C., Kuemmerle, T., Kozak, J., Hostert, P. (2009) Land cover mapping of large areas using chain classification of neighboring Landsat satellite images. Remote Sensing of Environment. 113(5), 957-964.
[33] Karakus, C.B., Kavak, K.S., Cerit, O. (2014) Determination of Variations in Land Cover and Land Use by Remote Sensing and Geographic Information Systems Around the City of Sivas (Turkey). Fresen. Environ. Bull. 23, 667-677.
[34] Feurdean, A., Munteanu, C., Kuemmerle, T., Nielsen, A.B., Hutchinson, S.M., Ruprecht, E., Parr, C.L., Perşoiu, A., Hickler, T. (2017) Long-term land-cover/use change in a traditional farming landscape in Romania inferred from pollen data, historical maps and satellite images. Regional Environmental Change. 17(8), 2193-2207.
[35] Blaschke, T. (2010) Object based image analysis for remote sensing. ISPRS Journal of Photogrammetry and Remote Sensing. 65(1), 2-16.
[36] Goodchild, M.F. (1994) Integrating GIS and remote sensing for vegetation analysis and modeling: methodological issues. Journal of Vegetation Science. 5(5), 615-626.
[37] Câmara, G., Souza, R.C.M., Freitas, U.M., Garrido, J. (1996) Spring: Integrating remote sensing and GIS by object-oriented data modelling. Computers and Graphics. 20(3), 395-403.
[38] Blaschke, T., Lang, S., Lorup, E., Strobl, J., Zeil, P. (2000) Object-oriented image processing in an integrated GIS/remote sensing environment and perspectives for environmental applications. Environmental Information for Planning, Politics and the Public. 2, 555-570.
[39] Benz, U.C., Hofmann, P., Willhauck, G., Lingenfelder, I., Heynen, M. (2004) Multi-resolution, object-oriented fuzzy analysis of remote sensing data for GIS-ready information. ISPRS Journal of Photogrammetry and Remote Sensing. 58(3-4), 239-258.
[40] Schneider, A., Friedl, M.A., McIver, D.K., Woodcock, C.E. (2003) Mapping urban areas by fusing multiple sources of coarse resolution remotely sensed data. Photogrammetric Engineering and Remote Sensing. 69(12), 1377-1386.
[41] Liu, T., Yang, X. (2015) Monitoring land changes in an urban area using satellite imagery, GIS and landscape metrics. Applied Geography. 56, 42-54.
[42] McGarigal, K., Marks, B.J. (1995). FRAGSTATS: spatial pattern analysis program for quantifying landscape structure. Gen. Tech. Rep. PNW-GTR-351. Portland, OR: US Department of Agriculture, Forest Service, Pacific Northwest Research Station. 122p, 351.
[43] Southworth, J., Nagendra, H., Tucker, C. (2002) Fragmentation of a landscape: Incorporating landscape metrics into satellite analyses of land-cover change. Landscape Research. 27(3), 253-269.
[44] Nagendra, H., Munroe, D.K., Southworth, J. (2004) From pattern to process: landscape fragmentation and the analysis of land use/land cover change. Agriculture, Ecosystems and Environment. 101(2–3), 111-115.
[45] Seto, K.C., Fragkias, M. (2005) Quantifying spatiotemporal patterns of urban land-use change in four cities of China with time series landscape metrics. Landscape Ecology. 20(7), 871-888.
[46] Ji, W., Ma, J., Twibell, R.W., Underhill, K. (2006) Characterizing urban sprawl using multi-stage remote sensing images and landscape metrics. Computers, Environment and Urban Systems. 30(6), 861-879.
[47] Fan, C, Myint, S. (2014) A comparison of spatial autocorrelation indices and landscape metrics in measuring urban landscape fragmentation. Landscape and Urban Planning. 121, 117-128.

[48] Linehan, J., Gross, M., Finn, J. (1995) Greenway planning: developing a landscape ecological network approach. Landscape Urban Planning. 33(1-3), 179-193.
[49] Zhang, L., Wang, H. (2006) Planning an ecological network of Xiamen Island (China) using landscape metrics and network analysis. Landscape and Urban Planning. 78(4), 449-456.
[50] Wu, J., Jelinski, D.E., Luck, M., Tueller, P.T. (2000) Multiscale analysis of landscape heterogeneity: scale variance and pattern metrics. Geographic Information Sciences. 6(1), 6-19.
[51] Plexida, S.G., Sfougaris, A.I., Ispikoudis, I.P., Papanastasis, V.P. (2014) Selecting landscape metrics as indicators of spatial heterogeneity-A comparison among Greek landscapes. International Journal of Applied Earth Observation and Geoinformation. 26, 26-35.
[52] Tagil, S., Gormus, S., Cengiz, S. (2016) The Relation Among Urban Expansion, Landscape Pattern and Ecological Process Around Denizli (UZAL-CBS 2016), 5-7.
[53] Yazgi, D., Yilmaz, K.T. (2017) The Assessment of Landscape Fragmentation in an Agricultural Environment Degradation or Contribution to Ecosystem Services? Fresen. Environ. Bull. 26, 7941-7950.
[54] Luck, M., Wu, J. (2002) A gradient analysis of urban landscape pattern: a case study from the Phoenix metropolitan region, Arizona, USA. Landscape Ecology. 17(4), 327-339.
[55] TUIK (2013) Selected Indicators for Aydin. ISBN 978-975-19-6064-1. Turkish Statistical Institute, Ankara.
[56] Esbah, H., Cook, E.A., Hepcan, S., Kara, B., Deniz, B. (2012) Ecological networks: potential of agricultural landscapes. The Green Belt as a European Ecological Network–strengths and gaps. 10, 80.
[57] Forman, R.T.T., Godron, M. (1986) Landscape Ecology. John Wiley and Sons, New York, 620p.
[58] Laver, C.J., Haines-Young, R.H. (1993) Equilibrium landscapes and their aftermath: Spatial heterogeneity and the role of the new technology. In: Haines-Young, R., Green, D.R. and Cousins, S. (Eds.) Landscape Ecology and Geographic Information Systems. Taylor and Francis, London, 57-74.
[59] Rey, P.J. (2011) Preserving frugivorous birds in agro-ecosystems: lessons from Spanish olive orchards. Journal of Applied Ecology. 48(1), 228-237.
[60] Deniz, B (2005) Use of landscape structure indices in assessing urban land use transformation and their contribution in urban planning practices: Case of the City of Aydin. In Turkish. Dissertation. Ege University, Izmir, Turkey. 223p.

Received: **09.11.2018**
Accepted: **26.03.2019**

CORRESPONDING AUTHOR

Derya Gulcin
Department of Landscape Architecture,
Faculty of Agriculture,
University of Aydin Adnan Menderes,
09010, Aydin – Turkey

e-mail: derya.yazgi@adu.edu.tr

© by PSP Volume 28 – No. 5/2019 pages 3865-3875 Fresenius Environmental Bulletin

INVESTIGATION OF THE MECHANICAL PROPERTIES OF MARBLE DUST AND SILICA FUME SUBSTITUTED PORTLAND CEMENT SAMPLES UNDER HIGH TEMPERATURE EFFECT

Oguzhan Yavuz Bayraktar[1], Gulsum Saglam Citoglu[2], Cagatay Mehmet Belgin[3], Mehmet Cetin[4,*]

[1]Kastamonu University, Faculty of Engineering and Architecture, Department of Civil Engineering, Kuzeykent, Kastamonu, 37150, Turkey
[2]Kastamonu University, Vocational School of Abana Sabahat Mesut Yilmaz, Department of Civil Engineering, Abana, Kastamonu, 37150, Turkey
[3]Gazi University, Faculty of Engineering, Department of Civil Engineering, Ankara, 06100, Turkey
[4]Kastamonu University, Faculty of Engineering and Architecture, Department of Landscape Architecture, Kuzeykent, Kastamonu, 37150, Turkey

ABSTRACT

The mechanical behaviors that can occur under the influence of high temperature in the mortars produced by silica fume and waste marble dust were investigated in this study. For this purpose, Portland cement (CEM I), waste marble dust (MD) from Afyon Çavdarlar Marble Factory, silica fume (SF) of ETİ electrometallurgy INC. industrial waste, CEN standard sand and water were used in the production of mortar. Mechanical experiments such as high temperature effect and cooling process with some physical experiments were performed on MD, SF and SFMD. Blended cements were obtained by using MD, SF and SFMD at 5.0%, 10.0%, 15.0% and 20.0% ratio with substitution method in Portland cement. Density, Blaine, initial set and final set were performed on the produced mortars and 40x40x160 mm sized mortar prism samples were obtained using these cements. These samples were exposed to five temperature effects as 20, 150, 300, 700 and 900 ° C. The mortar samples kept at 20 ° C were accepted as reference mortar. A total of 1053 samples were studied in two different ways of cooling mortars as air-cooling (spontaneously at 20 ° C ± 2 in laboratory environment) and sprinkling (water spraying). After the mortar samples reached at room temperature, flexional resistance and compressive strength tests were carried out on 7th, 28th and 90th days. According to the test results; it was determined that MD, SF and SFMD can be used as pozzolanic additives in cement mortars both alone and together and can be evaluated in buildings with high probability of fire up to certain temperature values.

KEYWORDS:
Portland cement, Waste marble dust, Silica fume, High temperature, Physical and mechanical properties

INTRODUCTION

People's needs such as living, health food and shelter are increasing at the same rate with the rapid increase in the world population. Environmental pollution also increases at the same rate with the increasing needs. Environmental pollution has become one of the most important problems of today [1, 2]. Environmental pollution occurs in two ways. One of them is the natural pollution, which refers to wastes of the living things except people, and the other one is the pollution that occurs by the wastes of people. The nature can clean the natural pollution by the natural recycle mechanism in a short while. However, human resourced pollutants especially the ones caused by industrial activities can stay in nature for a long time and have negative effects on people [3-5].

The increasing use of natural resources and release of wastes produced by humans to the atmosphere and to the environment caused negative effects on both environment and human health. Especially pollutant sources, such as industrial activities, fossil fuels used for heating and exhaust gas emissions caused by vehicle traffic are the most important pollutants of air, soil and water, which are necessary for the survival of living things. The release of toxic substances into the environment is particularly spreading from industrialized countries. Heavy metals are released into the atmosphere due to the presence of many industrial facilities and heavy traffic. These pollution sources have increased rapidly in the last two decades in parallel with the population growth in the cities. For this reason, a rapid increase in important diseases such as lung diseases and heart diseases has been observed since the 2000s. Particularly heavy metals cause genotoxic effects and cancer, damaging the immune system and the neurological system. The most important reason of the increase in the occurrence of these diseases is the increase of heavy metal pollution in the atmosphere. Monitoring air

pollution in industrial facilities and cities is very important to determine the impact of pollution on past environmental systems. As the most reliable source for determining the increase in heavy metal air pollution, the materials used in the concrete structures should be considered as it is in the examination of the wood from the past to the present. It was observed that the climate potential in the atmosphere was also affected. Therefore, the use of recycled materials in the construction sector is increasing rapidly and prevents the contamination. In particular, the use of recycled materials is aimed at reducing the amount of air pollution required to be reduced [1-12].

Uncontrolled consumption of river sands in coastal areas has led to disruption of ecosystems with unpredictable long-term consequences, such as the destruction of local species. For sustainable concrete structure, long term alternatives of traditional building materials are sought. Developing countries should use environment-friendly materials that are abundant, especially to address sustainability. Concrete is a composite material consisting of fine and coarse aggregates that are embedded in a hard cement mixture, which fills the gap between the aggregate particles and connect all of them together. The fine and coarse aggregates form the skeleton of the concrete and generally constitute 60-75% of its volume. Approximately 1 ton of concrete is produced annually around the world. The increase in the demand for concrete every year puts a lot of pressure on the supply of concrete components to meet the demands. One of the top ten countries that use natural resources for constructions is Turkey. With the rapid decline of resources such as river sand and coarse aggregate, this research focuses on alternative materials for fine and coarse aggregates. Where the performance of the concrete is more important than the strength criteria, this also leads to the use of many locally accessible and marginal materials in concrete. When a reliable design database for concrete produced with marginal material is formed, the replacement of natural fine aggregates by structural and non-structural elements will be economical for developing countries. One of these marginal materials is the laterite, a natural soil that is widely expanded in many parts of the world, especially in tropical and subtropical regions [1-21].

Development of the industry day by day; increasing material consumption causes significant pollution problems in addition to the problem of rapid depletion of natural resources (raw material and energy). Increased production constitutes a significant amount of waste. These wastes cause an increasing environmental damage. Many countries and international organizations are trying to minimize these losses by encouraging re-usage of wastes by new regulations [22]. Nowadays, intensive studies are carried out on recycling of by-products or wastes obtained during the production of various products. There are different applications in obtaining high performance mixtures. Use of various additives, material selection at the top performance value, high quality control, different design methods, current test techniques are among these applications [23].

While developed countries have clear rules on waste management, there is no law on waste in developing countries. Therefore, existing wastes are left out without any processes and they cause various negative effects [24]. According to the international Kyoto protocol agreement which is for fighting against global warming and climate change, that was signed in 1997 and effectuated in 2005; by the directive of " the waste processes of the high energy consuming factories such as cement, iron-steel, lime factories will be re-regulated" the waste products are required to be used in cement production and so it is aimed both to prevent the environmental pollution caused by these wastes and to reduce the cost of cement which is one of the most expensive components used in concrete [25].

The concrete and cement sector is criticized due to consumption of natural resources and energy in high amounts and the high emissions -notably CO_2 caused- by cement production. These criticisms are tried to be overcome with alternative solutions [26]. One of the suggestions for solving the problem is recycling. The developed countries, which see the fact with the rising energy crisis that recycling does not only avoid the waste of resources but also increases life standards, sought and developed methods for the recovery and reuse of waste [27]. Recycling of wastes will not only protect the environment but will also obtain economic benefits. Increasing popularity of environmentally friendly, low-priced, robust construction materials requires new researches. It is necessary to obtain new raw materials, which are in accordance with standards in use and do not harm the environment, by using them alone or mixed with other materials [22]. CO2 emissions can be minimized by the use of industrial wastes with pozzolanic properties such as fly ash, blast furnace slag, silica fume, etc., in cement based systems (such as plaster, mortar, concrete), reducing the need for natural resources and energy [26].

Silica fume; (SF) is one of the most effective waste materials used in cement or concrete due to its pozzolanic properties. Silica fume is an excellent pozzolanic material because it has an amorphous structure, it contains very fine grain and high amount of SiO_2. The fact that silica fume is composed of very fine grains reduces the consistency and workability of fresh concrete and increases the need for water. Therefore, when silica fume is used as an additive for the production of high strength concrete, water-reducing additive is also used. Cement and concrete with silica fume additive is used

in places that require high strength and durability [28].

Marble dust can be defined as the marble particles in colloidal structure, which are formed during the cutting of blocks and slabs in marble processing plants, and most of them are below 1 mm. The studies show that at the results of the chemical analysis of MD, the amount of CaO is at least 40% [29]. During the processing of marble, marble dust is produced as waste material. Reusage of marble dust in different industrial areas will be beneficial for reducing environmental pollution [30]. They can be reused in variable areas. While large-scale wastes can be used as building materials in the construction sector, dust wastes can be used directly in different industrial branches [31].

It is very important to know the behavior of the materials used in buildings in order to determine the precautions to be taken for the protection from fire. The behavior of a building material against fire is determined by performance criteria such as participation to fire, flame formation, flame propagation rate, flame continuity [32]. Combustion is a stable exothermic chain reaction of flammable substances with oxygen or other oxidizing agents under certain conditions. The presence of oxygen and the thermal energy source to provide ignition is required for the start of a combustion reaction, together with the combustible material [33]. Due to the dense structure and high void ratio of the mineral reinforced high strength concretes, the percentages of strength loss under high temperature have been found to be higher than the concrete with no mineral admixture [30].

The reuse of marble dust and silica fume from industrial waste materials in construction was investigated in this study. These two waste materials were added separately and jointly in Portland cement in different proportions and it was aimed to examine both the compressive and tensile strengths under high temperature effect and their effects on the physical properties of cement.

MATERIALS AND METHODS

Materials. Cement. In this study, PC 42.5R (CEM I) cement produced at Limak Ankara Cement Factory was used. Chemical and physical properties of cement are given in Table 1.

Waste Marble Dust and Silica Fume. Marble dust (MD) in the experimental study; the marble pieces were ground to approximately cement fineness. Silica fume (SF) was used as another additive. No action was taken on the SF used in the experiments. The specific surface of the SF was determined via the BET method. Chemical composition and physical properties of silica fume and marble dust are given in Table 2.

TABLE 1
Chemical and physical properties of cement PC 42.5

Oxide	Value	Analysis	Properties	Value
SiO_2	20.41	Physical	Specific surface, cm2/g	3320
Al_2O_3	5.35		Volume expansion, mm	1.2
Fe_2O_3	3.30		Normal consistency water (%)	28.5
CaO	63.50		Initial set, sec	163
MgO	1.65		Final set, sec	240
SO_3	2.93		Density, g/cm^3	3.16
Na_2O	0.16		Remaining more than 40 (μm) (%)	7.9
K_2O	0.71		Remaining more than 90 (μm) (%)	0.6
Total	98.01			

TABLE 2
Chemical composition and physical properties of SF and MD

Oxide (%)	SF	MD	Physical properties	SD	MD
SiO_2	94.62	1,92	Density, g/cm^3	2.36	2,72
Al_2O_3	0.20	0,38	Remaining more than 40 (μm) (%)		51,23
Fe_2O_3	0.20	0,03	Remaining more than 90 (μm) (%)		32,35
CaO	1.40	54,34	Specific surface (blaine) (m^2/kg)	20000	-
MgO	-	0,39			
SO_3	0.21	0,08			
K_2O	-	0,05			
Na_2O	-	0,18			
K.K.	-	42,63			
Total	96.63	100			

Methods. Production of Cements and Cement Experiments. Cement was produced by using SF, MD and SFMD via substitution method in 5%, 10%, 15% and 20% ratio. The mortars were produced in 40x40x160 mm dimensions according to TS EN 196-1 [34,35]. The amount of water required in each group mixture was determined by flow table test according to the flow diameter specified in ASTM C230, C109 and C1437 standards [34]. (TSE, 2002). The produced samples were stored at a temperature of 20^0C $\pm 2^0$C at a relative humidity of 95%.

Production of cement mortars and mortar experiments. The chemical composition and physical properties of PC 42.5, MD and SF that are used in the production of PC 42.5, MD, SF, SFMD blended cements were determined. This was done in accordance with the standard of "TS EN 196-1 Cement Test Methods - Part 1: Resistance" in 40x40x160 mm dimensions by using triple steel mortar molds.

4 types of mortar samples (PC 42.5, MD, SF, and SFMD) prepared with CEN standard sand were subjected to bending and compressive strength tests at three different day ages (7, 28, 90). Mortar samples are produced in the form of mortar prism with dimensions of 40x40x160 mm. Samples removed from the molds after 24 hours of production were kept in a laboratory with 95% relative humidity at 20 ± 2 ° C until the day of experiments on 7, 28 and 90 days. The mixture ratios to be used in the experiments were determined by considering the flow rate values and the mixture calculations were made.

The mortar sample with cement binding was named as PC42.5; the mortar samples with cement and marble dust binding at 5, 10, 15, 20 % ratios were named as MD5, MD,10, MD15, MD20; the mortar samples with cement and silica fume binding at 5, 10, 15, 20 % ratios were named as SF5, SF10, SF15, SF20; the mortar samples bonded with cement and marble dust with silica fume at 5, 10, 15, 20 % ratios were named as SFMD5, SFMD10, SFMD15, SFMD20.

High temperature applications. The application of high temperature was carried out in accordance with the requirements of BS EN 13501-1 standards [36]. After the cure periods of 7, 28 and 90 days, the mortar samples were stored in the oven (105 ± 5° C) (for 24 hours) before exposure to high temperature. The mortar samples that were brought to dry state in the oven were placed in the high temperature oven to determine the high temperature effect. At heat treatment phase the samples were heated at 6 ° C / min according to TS EN 1363-1 [37] in high temperature oven at high temperatures of 150, 300, 700 and 900° C for 2 hours [37]. Reference mortar samples at 20° C were not exposed to high temperature.

Cooling applications. Half of the samples which were kept at 150, 300, 700 and 900° C for 2 hours at high temperature application, were cooled in air (20° C ± 2 in laboratory) and the other half was cooled by sprinkling (water spraying) method. Flexural strength and compressive strength tests were applied to the mortar samples after cooling process. The mortar samples that were cooled in the air were kept in the laboratory between 30-180 min. depending on the cooling speed temperature until they reached at the temperature of 20°C, and the mortar samples that were cooled by the sprinkler method were kept in the laboratory for about 20-80 minutes until they reached at the temperature of 20°C.

Compressive strength and flexional resistance experiment. The pressure and flexural resistance values were determined by taking 3 samples representing each group which were exposed to high temperature one day after leaving them for cooling. Pressure and flexural resistance tests were performed in accordance with TS-EN 196-1 standard [35, 38].

EXPERIMENTAL FINDINGS AND DISCUSSION

Physical Properties of Produced Cement. Density, blaine, initial and final set and fineness tests were performed on the produced cement samples and the results are given in Table 3.

The lowest values of blaine tests of the produced samples were found in MD5; and the highest values were found in SFMD20 and the lowest values of density tests were found in SFMD20 and the highest values were of SF20. The initial set and final set time periods are in the limits given by TS EN 196-3 [39].

Chemical Properties of Produced Cement. According to the ASTM C 618 the sum of $SiO_2+Al_2O_3+Fe_2O_3$ must be at least 70% by weight, and sulfur trioxide (SO_3) must be 5% at most by weight in a pozzolan. As seen on Table 2, the sum of $SiO_2+Al_2O_3+Fe_2O_3$ in SF is 95.02% and the sum of $SiO_2+Al_2O_3+Fe_2O_3$ in MD is 56.67 % and it is higher than the limit value for a C type pozzolan material.

Flexional resistance of SF and MD mixed mortars. Table 4 shows the 7, 28 and 90 day flexional resistance test results of SF, MD and SFMD cement mortar prisms. As a result, the substitution rate of SF and MD in cement was evaluated in accordance with mixing water and the effect of cement mortar on the mechanical properties under high temperature was investigated.

TABLE 3
The physical properties of cement types

Cement type	Density (g/cm^3)	Blaine (cm^2/g)	Initial Set (sec)	Final Set (sec)	Remaining more than 40 (μm) (%)	Remaining more than 90 (μm) (%)
PC 42.5	3.16	2962	140	200	8.3	0.5
SFMD 5.0	3.10	5440	325	353	39.8	16.1
SFMD 10.0	3.04	8660	297	333	41.2	17.9
SFMD 15.0	2.89	10700	230	310	42.7	19.0
SFMD 20.0	2.85	10810	190	300	43.1	20
SF 5.0	3.13	3890	270	340	7.6	0.3
SF 10.0	3.14	3900	330	390	6.4	0.2
SF 15.0	3.15	4200	380	450	5.2	0.1
SF 20.0	3.16	4500	440	500	4.1	0.1
MD 5.0	3.14	2963	333	420	40.5	18
MD 10.0	3.12	3120	345	408	41.9	18.9
MD 15.0	3.11	3395	320	370	43	19.8
MD 20.0	3.10	3690	300	365	43.8	20.2

When the Table 4 is examined for the air cooled samples;

It was determined that flexional resistance values of 7 days old SF5 substituted samples are greater when compared to the 20 (Reference mortar samples) and 150° temperature of PC 42,5 cement; the flexional resistance values of 28 days old SF10, SF15, SFMD5 substituted samples are close to the 20 and 150° temperature of PC 42,5 cement;

the flexional resistance values of 28 days old SF5, SF10 substituted samples are greater when compared to the 20 and 150° temperature of PC 42,5 cement; the flexional resistance values of 28 days old SF15, SFMD5 and SFMD10 substituted samples are close to the 20 and 150° temperature of PC 42,5 cement;

the flexional resistance values of 90 days old SF5, SF10, SF15 substituted samples are greater when compared to the 20 and 150° temperature of PC 42,5 cement; the flexional resistance values of 90 days old SFMD5, SFMD10 and SFMD15 substituted samples are close to the 20 and 150° temperature of PC 42,5 cement.

It has been determined that; there is difference between 7, 28 and 90th days, the increase in temperature values is in the opposite direction with the flexional resistance, there is difference between air and sprinkler method cooling, and that the flexional strength reduces while the temperature increases between 300-900°C interval.

When the flexional resistance of produced mortar samples obtained by 7, 28 and 90 days air-cooling is compared to each other, it has been seen that the highest and lowest resistance were of the mortar samples at 150 and 900°C respectively.

The 7 days old SF5 mortar samples that were produced by sprinkler cooling method at 150, 300, 700 and 900°C, the 28 days SF5 and SF10 mortar samples that were produced by sprinkler cooling method at 150, 300, 700 and 900 °C and the 90 days old SF5, SF10, and SF15 mortar samples that were produced by sprinkler cooling method at 150, 300, 700 and 900 °C obtained the most proximate resistance at 150 °C to the mortar sample produced at 20°C (Reference mortar samples). The flexional resistance values obtained at 900°C by sprinkler cooling method are low.

When the flexional resistance of produced mortar samples obtained by 7, 28 and 90 days cooling by sprinkler method is compared to each other, it has been seen that the highest and lowest resistance were of the mortar samples at 150 and 900°C respectively.

The compressive strength of SF and MD substituted mortars. The results of 7, 28 and 90 days compressive strength test results of SF, MD and SFMD substituted cement mortar prisms are given in Table 5. As a result, the substitution rate of SF and MD in cement was evaluated in accordance with mixing water and the effect of cement mortar on the mechanical properties under high temperature was investigated.

When the Table 5 is examined, about the samples produced by air cooling, it was determined that;

The compressive strength values of 28 days old SF5 samples were higher than 20 and 150° temperature of pure PC 42,5 cement; the compressive strength values of SF10 samples were higher than 20 and 150, 300° temperature of pure PC 42,5 cement; and that the compressive strength values of SFMD5, SFMD15 and MD5 samples are close to the 20 and 150° temperature of pure PC 42,5 cement.

It was determined that the compressive strength values of 90 days old SF5 samples were higher than 20 and 150,300, 900° temperature of pure PC 42,5 cement; the compressive strength values of SF10 samples were higher than 20 and 150 and 900° temperature of pure PC 42,5 cement; the compressive strength values of SF15, SF20, SFMD5 samples were quite close to 20 and 150° temperature of pure PC 42,5 cement.

TABLE 4
Flexional resistance of mortar samples

Conditions	Flexional resistance (MPa)									
	Day		7							
	Cooling application	20 (Reference mortar samples)	In air				In water			
	High temperature application °C		150	300	700	900	150	300	700	900
Mortar type	PC 42.5	6,7	6,5	5,8	2,7	1,4	5,7	4,3	1,3	0,0
	MD5	5,2	5,0	4,2	2,0	1,2	4,6	3,9	1,0	0,0
	MD10	5,1	4,8	4,1	1,8	0,0	4,4	3,6	1,9	0,0
	MD15	4,5	3,9	3,1	1,5	0,0	3,1	2,9	0,0	0,0
	MD20	3,9	3,2	2,9	1,0	0,0	2,9	2,3	0,0	0,0
	SF5	6,9	6,7	5,4	2,3	1,5	5,4	4,1	1,2	0,0
	SF10	6,3	5,9	5,1	3,4	1,4	5,5	3,9	2,8	0,0
	SF15	5,8	5,9	4,3	2,6	0,0	5,1	3,1	2,9	0,0
	SF20	5,1	4,6	3,3	2,2	0,0	3,9	2,6	1,2	0,0
	SFMD5	6,1	5,8	5,3	2,4	1,5	4,7	4,0	2,1	0,0
	SFMD10	5,9	5,2	4,8	3,1	1,4	4,4	3,7	2,4	0,0
	SFMD15	5,8	4,4	4,1	2,2	0,0	3,2	3,0	1,5	0,0
	SFMD20	4,8	3,2	2,0	0,0	0,0	2,2	0,0	0,0	0,0
Conditions	Flexional resistance (MPa)									
	Day		28							
	Cooling application	20 (Reference mortar samples)	In air				In water			
	High temperature application °C		150	300	700	900	150	300	700	900
Mortar type	PC 42.5	8,4	8,6	7,7	3,9	2,6	8,3	6,4	2,9	1,4
	MD5	6,4	6,4	5,6	3,3	1,7	5,9	4,4	2,2	1,5
	MD10	6,3	6,1	5,4	2,9	1,4	4,9	4,2	2,1	0,0
	MD15	5,4	5,1	4,5	3,5	1,3	4,3	3,0	1,9	0,0
	MD20	4,8	4,2	3,3	2,4	1,2	3,8	2,6	1,2	0,0
	SF5	8,7	9,0	6,4	3,8	1,6	8,2	5,2	3,1	2,2
	SF10	9,0	9,4	5,4	3,1	1,8	8,5	5,1	3,0	1,4
	SF15	8,1	8,6	5,2	2,9	1,4	6,8	4,2	2,4	1,2
	SF20	6,4	5,9	4,6	0,0	0,0	5,2	3,9	0,0	0,0
	SFMD5	7,2	7,8	6,5	3,6	2,1	6,3	4,2	2,9	1,2
	SFMD10	7,8	7,9	6,5	3,2	1,8	6,5	4,8	2,8	1,6
	SFMD15	6,8	6,4	5,6	3,6	1,4	4,1	3,6	0,0	0,0
	SFMD20	5,6	4,8	3,4	2,1	0,0	3,4	2,40	0,0	0,0
Conditions	Flexional resistance (MPa)									
	Day		90							
	Cooling application	20 (Reference mortar samples)	In air				In water			
	High temperature application °C		150	300	700	900	150	300	700	900
Mortar type	PC 42.5	9,5	9,7	9,4	6,2	3,4	8,2	7,1	4,9	2,6
	MD5	7,6	7,7	6,8	5,6	2,2	6,1	4,8	2,7	1,2
	MD10	7,5	6,8	5,9	4,4	1,5	5,2	3,6	2,4	1,0
	MD15	6,9	6,3	5,2	3,9	0,0	5,1	3,2	2,3	0,0
	MD20	5,4	4,8	4,1	3,6	0,0	4,1	2,8	2,0	0,0
	SF5	10,1	10,4	9,6	6,1	3,8	8,4	6,8	4,3	2,5
	SF10	10,1	10,4	9,7	5,9	2,9	8,2	6,3	4,1	2,2
	SF15	9,4	9,8	7,7	5,4	2,2	7,6	4,2	3,1	1,8
	SF20	8,9	8,6	6,8	3,4	1,8	6,8	2,6	2,8	1,2
	SFMD5	9,1	9,6	8,4	4,8	3,0	7,8	6,2	3,6	2,2
	SFMD10	8,8	9,4	7,8	4,2	2,4	6,5	4,8	3,2	1,8
	SFMD15	7,2	8,9	6,4	3,8	1,4	4,5	2,5	2,5	0,0
	SFMD20	6,0	5,45	3,2	2,4	0,0	0,0	2,1	0,0	0,0

When the compressive strength of produced mortar samples obtained by 7, 28 and 90 days air-cooling is compared to each other, it has been seen that the highest and lowest resistance were of the mortar samples at 150 and 900°C respectively.

While the most proximate compressive strength of the 28 days old SF5, SF10, SF15, MD5, SFMD5 mortar samples that were produced by sprinkler method cooling at 150, 300, 700 and 900°C to the mortar sample produced at 20 ° C were obtained at 150°C; the most proximate compressive strength of the 90 days old SF5, SF10, SF15, SF20, SFMD5 mortar samples that were produced by sprinkler method cooling at 150, 300, 700 and 900°C to the mortar sample produced at 20° C were obtained at 150 °C. the compressive strength values of SF20 mortar samples produced by sprinkler method cooling at 700 and 900°C and

TABLE 5
The compressive strength of mortar samples

Compressive strength (MPa)										
Conditions	Day		7							
	Cooling App.	20	In air				In water			
	High Temp. App.°C	(Reference mortar samples)	150	300	700	900	150	300	700	900
Mortar type	PC 42.5	38,4	40,5	37,7	20,8	18,4	33,6	31,2	13,5	10,5
	MD5	29,2	28,1	22,1	12,8	10,4	24,4	20,3	8,6	6,2
	MD10	24,9	24,5	21,4	10,5	8,6	22,3	18,5	6,4	4,4
	MD15	19,6	18,3	12,6	9,4	7,8	16,6	10,2	5,6	3,2
	MD20	16,2	12,3	8,4	4,3	2,6	10,2	6,5	3,6	0,0
	SF5	38,2	38,9	32,4	16,1	14,8	24,5	21,2	12,2	10,6
	SF10	37,8	35,4	31,1	14,3	12	23,8	20,5	10,2	7,4
	SF15	35,8	22,4	28,6	12,0	9,6	21,1	18,4	0,0	6,2
	SF20	34,2	18,1	15,4	8,0	7,8	18,2	12,4	0,0	0,0
	SFMD5	31,0	35,4	30,5	14,6	12,8	24,3	20,4	11,4	8,8
	SFMD10	25,9	26,4	22,1	13,2	10,2	22,4	18,5	9,6	7,2
	SFMD15	21,4	20,3	18,4	12,3	9,8	18,5	12,4	6,8	5,2
	SFMD20	18,6	15,6	12,6	8,5	0,0	13,4	11,6	0,0	0,0
Compressive strength (MPa)										
Conditions	Day		28							
	Cooling App.	20	In air				In water			
	High Temp. App.°C	(Reference mortar samples)	150	300	700	900	150	300	700	900
Mortar type	PC 42.5	41,2	43,2	39,6	31,4	28,6	36,6	34,3	16,7	14,8
	MD5	37,2	37,4	29,2	22,2	19,6	30,2	24,2	12,2	10,5
	MD10	33,6	33,8	24,6	18,4	16,2	26,5	20,3	10,8	8,5
	MD15	29,2	29,4	18,3	10,5	8,2	20,4	14,5	7,6	5,8
	MD20	24,2	24,6	16,5	8,5	6,2	15,8	7,6	6,4	4,2
	SF5	43,2	47,5	39,4	24,2	21,3	38,1	30,2	15,6	12,8
	SF10	42,6	48,2	40,5	22,1	18,5	40,4	29,6	14,8	11,5
	SF15	39,4	38,5	32,6	16,2	14,5	35,2	28,2	6,4	0,0
	SF20	37,2	30,0	31,3	0,0	0,0	34,5	25,4	0,0	0,0
	SFMD5	39,0	41,0	34,5	24,8	19,6	37,7	32,5	12,5	10,6
	SFMD10	35,9	34,5	32,3	21,8	16,5	32,3	28,5	10,6	8,5
	SFMD15	31,1	32,4	30,4	18,4	14,2	28,2	24,2	8,5	6,4
	SFMD20	27,1	25,6	18,5	8,4	6,8	16,8	16,8	4,2	2,2
Compressive strength (MPa)										
Conditions	Day		90							
	Cooling App.	20	In air				In water			
	High Temp. App.°C	(Reference mortar samples)	150	300	700	900	150	300	700	900
Mortar type	PC 42.5	51,5	54,3	52,3	38,2	32,2	52,2	44,6	34,0	29,6
	MD5	45,3	44,9	40,5	30,5	26,5	42,8	36,4	24,3	21,6
	MD10	43,2	42,2	38,6	26,8	22,5	34,6	32,2	18,5	15,6
	MD15	39,5	40,8	32,4	21,6	16,5	32,3	19,6	10,2	8,2
	MD20	35,4	28,5	18,5	9,6	8,2	18,6	12,6	8,4	5,8
	SF5	55,7	58,4	54,2	35,4	32,5	52,4	42,6	28,5	25,5
	SF10	54,1	57,3	51,4	36,3	33,5	49,5	38,4	30,2	27,8
	SF15	52,2	52,4	48,2	18,4	15,2	48,2	32,6	13,7	12,3
	SF20	50,1	49,3	39,5	2,8	0,0	35,4	22,1	4,6	0,0
	SFMD5	49,1	52,6	46,8	34,2	29,6	50,5	39,7	28,7	25,8
	SFMD10	46,2	47,0	40,5	33,6	25,3	42,6	36,2	24,5	23,2
	SFMD15	43,2	42,2	38,6	28,4	20,6	38,5	30,5	21,6	18,3
	SFMD20	39,7	35,6	28,2	12,3	9,6	26,6	18,5	12,0	9,2

SF15 mortar samples produced by sprinkler method cooling at 900°C could not been calculated. When the compressive strength of mortar samples obtained by 7, 28 and 90 days sprinkler cooling method is compared to each other, it has been seen that the highest and lowest resistance were of the mortar samples at 150 and 900°C respectively.

RESULTS AND DISCUSSION

As a result of the study, it was determined that the flexional resistance and compressive strength at all temperatures after 150° C decreased on days 7, 28 and 90. This may be due to the fact that mineral additive subjected to this research reduce the amount of pores in mortar samples. In addition, the amount of $Ca(OH)_2$ decreases in the system due to the pozzolanic reaction occurring between the reactive silica (SiO_2) that mineral additives include and $Ca(OH)_2$ in the cement [39]. Mixtures containing a certain proportion of mineral additive, which are substituted in the cement, contain less calcium hydroxide compared to pure PC cement, which may also be the reason of increase of strength up to 150° C.

Since the materials used in the study are waste materials, the use of these materials in the mortar is important in order to prevent the environmental pollution caused by them and to reduce the costs of the samples produced. In this study, as a result of experiments on mortars; it was determined that flexional resistance and compressive strength of all cement mortars that were produced by sprinkling cooling method decreased at all ages, and the densities of blended cements decreased in proportion to the amount of marble dust; the initial and final set periods of SF5 and SF10 samples of SF blended cements were lower than MD5 and MD10 samples of MD blended cements, however the initial and final sets periods of SF15 and SF20 samples were higher than MD15 and MD20 samples; the blended mortars produced by air cooling have reached values close to the control mortar values from the 7th day in terms of compressive strength, and the SF blended cements had higher compressive strengths at all ages compared to the MD blended cements at 7^{th} and 28^{th} days but they exhibited an inverse behavior on 90^{th} day at higher temperatures at 700 and 900°C.

It was determined that the compressive strength of air-cooled 7, 28 and 90 days old SFMD substituted cements were higher than the MD substituted cements at all temperatures. As for the compressive strengths of 90 days air cooled samples, SFMD5 that was produced by substitution of SF and MD in dual use at 5% ratio were found to be close to PC 42.5 mortar produced by air cooling method at 20° (Reference mortar samples) and 150 300, 700, 900° C temperature. In the microstructure of the sections taken from high temperature applied mortar samples, it was seen that aggregate distribution, crack development and pore structure could not be distinguished well up to 300 ° C, but at later temperatures cracks between aggregate grains of binder were growing.

The increase of flexional resistance and compressive strength of the mortar samples between 100-300 ° C and the water vapor formed during the high temperature caused a high pressure in the blended mortar samples [21]. This creates an internal balance. This situation is observed especially in 90-days old samples. According to the former researches, as calcium hydroxide at 500 ºC and calcium silicates at 900ºC are known to be completely decomposed [21], in experimental study, some experimental results belonging to samples at 700 and 900ºC temperatures were too low or no value was obtained.

Studies on the use of different substitutes in cement are very important in terms of both waste disposal and cost reduction. Therefore, many studies have been carried out on this subject.

Kabeer & Vyas [40] used marble dust, a waste product formed during the cutting and shaping of marble blocks, to replace traditional river sand in cement mortars in their study. For this purpose, they examined four different mixture mortars in terms of workability, drying shrinkage, compressive strength, bond and adhesive strength, density, water absorption and dynamic Young modules. The results of their study indicated that the mortars blended with river sand and marble dust at 20% ratio can be used for masonry and processing purposes.

Khodabakhshian et al. [41] added silica fume (0%, 2.5%, 5%, 10%) and waste marble dust (0%, 5%, 10%, 20%) to Portland cement in different proportions and found that the durability and strength of the concrete containing waste marble dust has a tendency to decrease over 10%, but satisfactory results are obtained below this level. With regard to the use of silica fume, they have observed that they improve the strength and durability of the concrete with waste marble dust by preventing the reduction of its properties compared to conventional concrete. In addition to achieving approximately the same results as the traditional concrete mix, partial replacement of cements using 20% waste marble dust and 10% silica fume has resulted in a 30% cement reduction that reduces the harmful effects of the cement industry on the environment.

Yıldız et al. [42], added marble dust at 10%, 20%, 30%, 40% and 50% ratios by volume to the mortar samples containing glass fiber at 0.25 kg/m^3, 0.50 kg/m^3, 0.75 kg/m^3 and 1 kg/m^3 proportions to be replaced with the filing materials in order to investigate the mechanical and physical properties of waste marble dust and glass fiber added cement mortars exposed to sulphate attack. The obtained

mortar samples were subjected to three different curing conditions in 5% Na_2SO_4 solution. Flexural strength, compressive strength and apparent porosity tests were carried out on the samples and their mechanical and physical changes under the effect of sulfate were determined. As a result of the study, it has been concluded that the use of marble dust in glass fiber reinforced mortar samples with the material to be displaced up to 40% by volume in order to increase the tensile strength will provide positive gains in terms of both economy and sulfate resistance.

Kara & Yazıcıoğlu [43] have determined the physical and mechanical changes that occur as a result of carbonation in concrete produced by substituting different amounts of marble dust (MD) waste and 10% silica fume (SF) in their study. During the study, they produced eight different types of C30 class concrete with the same settling value as 5%, 10%, 15% MD substituted, 10% SF substituted, 5% MD + 10% SF, 10% MD + 10% SF, 15% MD + 10% SF substituted and reference (without additive). They performed flexional resistance, carbonation depth, capillary water absorption, ultrasound transition rate, abrasion and compressive strength tests on concrete types. As a result they stated that, as the carbonation depth increases in concrete samples containing different ratios MD, SF and MD + SF; the ultrasound velocity values increased, the capillarity coefficients decreased, the amount of wear decreased and the compressive strength increased.

Kaya & Yazıcıoğlu [33] investigated the effect of high temperature on the mechanical and physical properties of calcined mortar. Cement used in mortars was reduced as 10%, 15% and 20% by weight and it was replaced by calcined bentonite. They examined the compressive strength of the prepared samples at 7, 28 and 56 day curing ages. They also applied high temperature of 250, 500, 750 and 1000 ° C to the samples that completed the 56 day cure age. Ultra sound, water absorption, porosity, weight loss and compressive strength of the samples before and after high temperature were measured and compared with each other. According to the results, the lowest resistance losses before and after high temperature exposure were obtained from the reference sample at 500° C and from 10% bentonite added samples at 750 and 1000° C.

Gökçer et al. [44] added waste marble dust to the mortar samples reinforced with different amounts of glass fiber by displacing the filling material as 10%, 20% and 30% by weight in their study. They examined the effect of high temperature on the mechanical and physical properties of the samples. For this purpose, porosity, capillary water absorption, ultrasound velocity, compressive strength and flexural strength tests were performed on the prepared samples and they observed the changes occurring in the samples at high temperature. The use of waste marble dust in the glass fiber blended mortar samples indicated that a more dense structure was formed and thus less strength loss occurred in high temperature mortar samples.

CONCLUSIONS

As a result of the study, it was determined that marble dust and silica fume can be used separately or together in different proportions in cement production. Due to the fact that these materials are waste materials, it is important to use them in the mortar, to prevent environmental pollution and to reduce the cost of produced samples. At this point, it is important to know how the quality of concrete changes depending on the proportions of the materials used.

In this study it was determined that flexional resistance and compressive strength of all cement mortars at all ages decreases in the samples produced by cooling via sprinkling method, and the densities of blended cements decrease in proportion to the amount of marble dust; and that the initial set and final set times of SF5 and SF10 blended cements are more than the MD5, MD10 blended cements; however the initial and final set times of SF15 and SF20 is less than MD15 and MD20 blended cements. According to these results, in places where the early resistance gain significance and the weather is cold it is more appropriate to use MD15 or MD20 blended cements. The compressive strength of SF blended cements on 7^{th} and 28^{th} days are higher than MD blended cements at all temperatures but an inverse behavior was observed on 90^{th} day at higher temperatures at 700 and 900°C. It would be beneficial to determine the ratios by considering these results in the cements to be produced.

Considering the results of the study in the cements to be produced, it is possible to select and use contribution ratios which do not make significant concessions in cases where high temperature exposure may occur in concrete design. For example; the compressive strength of SFMD5 was very close to the PC 42,5 mortar. It is a strong example of this that while the compressive strength of air cooled for 90 days PC 42.5 cement was 51,5 MPa, at 20°C; 54,3 MPa at 150°C; 52,3 MPa at 300 °C; 38,2 MPa at 700°C and 32,2 MPa at 900°C; the compressive strength of 90 days air cooled SFMD5 was 49,1 MPa at 20°C; 52,6 MPa at 150°C; 46,8 MPa at 300°C; 34,2 MPa at 700°C and 29,6 MPa at 900°C.

The environmental factors should be taken into consideration on a sustainable concrete design. The situations such as fire, explosion, exacerbation etc. which can cause to be exposed to high temperature in reinforced concrete structures should always be considered. The usage of brick dust and silica fume by substitution into cement may minimize the

possible accidents in buildings which can be exposed to high temperature. Thus, environmental, economic and, most importantly, significant benefits for human life can be provided.

REFERENCES

[1] Cetin, M., Sevik, H., Saat. A. (2017) Indoor Air Quality: The Samples of Safranbolu Bulak Mencilis Cave. Fresen. Environ. Bull. 26, 5965-5970.

[2] Cetin, M., Sevik, H., Yigit, N. (2018) Climate type-related changes in the leaf micromorphological characters of certain landscape plants. Environmental Monitoring and Assessment. 190, 404.

[3] Turkyilmaz, A., Sevik, H., Cetin, M., (2018) The use of perennial needles as biomonitors for recently accumulated heavy metals. Landscape and Ecological Engineering. 14(1), 115-120.

[4] Turkyilmaz, A., Sevik, H., Isinkaralar, K., Cetin, M. (2018) Using Acer platanoides annual rings to monitor the amount of heavy metals accumulated in air. Environmental Monitoring and Assessment. 190, 578.

[5] Turkyilmaz, A., Sevik, H., Cetin, M., Ahmaida Saleh, E.A. (2018) Changes in Heavy Metal Accumulation Depending on Traffic Density in Some Landscape Plants. Pol. J. Environ. Stud. 27(5), 2277-2284.

[6] Cetin, M., Sevik, H., Yigit, N., Ozel, H.B., Aricak, B., Varol, T. (2018) The variable of leaf micromorphogical characters on grown in distinct climate conditions in some landscape plants. Fresen. Environ. Bull. 27, 3206-3211.

[7] Cetin, M., Adiguzel, F., Kaya, O., Sahap, A. (2018) Mapping of bioclimatic comfort for potential planning using GIS in Aydin. Environment, Development and Sustainability. 20(1), 361-375.

[8] Cetin, M., Zeren, I., Sevik, H., Cakir, C., Akpinar, H. (2018) A study on the determination of the natural park's sustainable tourism potential. Environmental Monitoring and Assessment. 190(3), 167.

[9] Cetin, M., Sevik, H., Canturk, U., Cakir, C. (2018) Evaluation of the recreational potential of Kutahya Urban Forest. Fresen. Environ. Bull. 27, 2629-2634.

[10] Cetin, M., Sevik, H. (2016) Change of air quality in Kastamonu city in terms of particulate matter and CO2 amount. Oxidation Communications. 39(4-II), 3394–3401.

[11] Cetin, M. (2016) A Change in the Amount of CO2 at the Center of the Examination Halls: Case Study of Turkey. Studies on Ethno-Medicine. 10(2), 146-155.

[12] Cetin, M. (2017) Change in Amount of Chlorophyll in Some Interior Ornamental Plants. Kastamonu University Journal of Engineering and Sciences. 3(1), 11-19.

[13] Bayraktar, O.Y., Saglam-Citoglu, G., Caglar, H., Caglar, A., Arslan, M., Cetin, M. (2018) The mechanical properties of the different cooling requirements of high-temperature plaster. Fresen. Environ. Bull. 27, 5399-5409.

[14] Cetin, M. (2015) Using Recycling Materials for Sustainable Landscape Planning. In: Environment and Ecology at the Beginning of 21st Century. Chapter 55. ST. Kliment Ohridski University Press, Sofia, ISBN:978-954-07-3999-1, 783-788. 821p.

[15] Cetin, M. (2015) Consideration of Permeable Pavement in Landscape Architecture. Journal of Environmental Protection and Ecology. 16(1), 385-392.

[16] Cetin, M. (2013) Landscape Engineering, Protecting Soil, and Runoff Storm Water. In: Advances in Landscape Architecture-Environmental Sciences. Chapter 27. InTech-Open Science-Open Minds, Online July 1st, 2013. ISBN 978-953-51-1167-2, 697-722.

[17] Cetin, M. (2013) Pavement design with porous asphalt. PhD Thesis. Temple University. Philadelphia

[18] Brooks, R., Cetin, M. (2012) Application of construction demolition waste for improving performance of subgrade and subbase layers. Int. J. Res. Rev. Appl. Sci. 12(3), 375-381.

[19] Cetin, M., Brooks, R., Udo-Inyang, P. (2012) An innovative design methodology of pavement design by limiting surface deflection. International Journal of Research and Reviews in Applied Sciences. 13(2),607-610.

[20] Cetin, M., Brooks, R., Udo-Inyang, P. (2012) A comparative study between the results of an innovative design methodology by limiting surface deflection and AASHTO design method. International Journal of Research and Reviews in Applied Sciences. 13(2), 611-616.

[21] Bayraktar, O.Y. (2016) Statistical Comparison of Mechanical Behavior at the Time of Accumulation in Temperature of Mortars Produced with Pozzolanic Additive Materials. PhD Thesis. Gazi University, Institute of Science and Technology. Ankara.

[22] Bilgin, N. (2010) The Use of Marble Powder Wastes in the Production of Construction Materials. M.Sc. Thesis. Metallurgical and Materials Engineering. Yıldız Technical University. İstanbul

[23] Kalay, E. (2010) Application of Pumice, Marble Powder and Lime in Compressed High Plasticity Clay Soil Stabilization. Master Thesis. Süleyman Demirel University Graduate School of Natural and Applied Sciences. Isparta.

[24] Dhanapandiana, S., Manoharana, C., Ramkumarb, T., Gnanavela, B., Sutharsana P., Shanthic M. (2010) Effect of Incorporation of Granite and Marble Rejects in Clay Brick Products. Physico-Mechanical Analysis. Acta Physica Polonica A. 118(4), 688-695.
[25] Sağlam, G. (2012) The Use of Waste Marble Powder and Waste Plaster in Cement Production. M.Sc. Thesis. Gazi University Institute of Science and Technology. Ankara.
[26] Tangüler, M., Gürsel, P., Meral, Ç. (2015) Life Cycle Analysis for Fly Ash Concretes in Turkey. The 9th National Congress of Concrete. 20-23 October, Ankara.
[27] Yıldız, T. (2012) The Effects of Combined Use of Waste Marble Powder and Glass Fiber on Concrete's Mechanical Properties. M.Sc. Thesis. Firat University, Institute of Science and Technology. Diyarbakır.
[28] Özcan, F., Atiş, C.D. (2017) Carbonation and Stretch Properties of Mortars Produced by Silica Fume. Ömer Halisdemir University Journal of Engineering Sciences. 6(2), 634-641.
[29] Demir, İ., Başpınar, M.S., Abadan, S., Kahraman, E., Ünal, O. (2014) Investigation of the use of marble powder as a recycling material in aerated concrete production. ISEM, 20-23 October, Adıyaman.
[30] Kaya, T., Karakurt, C., Dumangöz, M. (2014) The Effect of High Temperature on the Porosity and Compressive Strengths of Mineral Additive Self - Floating Concrete. Bilecik Seyh Edebali University Journal of Science. 1(1), 1-10.
[31] Günaydın, O., Güçlüer, K., Ünal, O. (2016) The Investigation of the Usability of Adiyaman Waste Marble Powders in Aerated Concrete Production. Electronic Journal of Building Technology. 12(1), 21-29.
[32] Kızılkanat, A.B., Yüzer, N., (2008) The Relative Strength/Color Change Relationship of Mortar at High Temperature Effect. IMO Technical Magazine. 289, 4381-4392.
[33] Kaya, T., Yazıcıoğlu, S. (2015) High Temperature Effect on Physical and Mechanical Properties of Calcined Bentonite Additive Mortars. BEU Journal of Science. 4(2), 150-160.
[34] C109/C109M-02 (2002) Standard Test Method for Compressive Strength of Hydraulic Cement Mortars (Using 2-in. or [50-mm] Cube Specimens). American Society For Testing And Materials. (2002).
[35] TS EN 196-1 (2002) Cement Test Methods - Part 1: Determination of Strength, TSE. (2002).
[36] British Standards Institution, BS EN 13501-1, (2007) Fire Classification of Construction Products and Building Elements. Classification Using Data from Reaction to Fire Tests. London: BSI. (2007).
[37] TS EN 1363-1 (2013) Fire Resistance Tests - Part 1: General Rules, TSE. (2013).
[38] Ünal, O., Uygunoğlu, T. (2004) Soma Thermal Power Plant Waste Assessment Fly Ash in the Construction Industry. Turkey 14th Coal Congress Proceedings. Zonguldak, Turkey.
[39] TS EN 196-3, (2002) Cement Test Methods - Part 13: Determination of Expiration Time and Volume Expansion, (2002).
[40] Kabeer, K., Vyas, A.K. (2018) Utilization of marble powder as fine aggregate in mortar mixes. Construction and Building Materials. 165, 321-332.
[41] Khodabakhshian, A., Ghalehnovi, M., De Brito, J., Shamsabadi, E.A. (2018) Durability Performance of Structural Concrete Containing Silica Fume and Marble Industry Waste Powder. Construction and Building Materials. 165, 321, 12p.
[42] Yıldız, S., Alişer, B., Keleştemur, O. (2017) Investigation of Mechanical and Physical Properties of Waste Marble Powder and Glass Fiber Additive Cement Mortars Under Sulphate Effect. Fırat Univ. Journal of Science. 29(2), 23-31.
[43] Kara, C., Yazıcıoğlu, S. (2016) The Effect of Marble Powder Waste and Silica Smoke on Carbonation of Concrete. BEU Journal of Science. 5(2), 191-202.
[44] Gökçer, B., Yıldız, S., Keleştemur, O. (2013) High-Temperature Behavior of Waste Marble Powder and Glass Fiber Coated Mortar Samples SDU International Technologic Science. 5(2), 42-55.

Received: **10.11.2018**
Accepted: **18.03.2019**

CORRESPONDING AUTHOR

Mehmet Cetin
Department of Landscape Architecture
Faculty of Engineering and Architecture
Kastamonu University
Kuzeykent, Kastamonu 37150 – Turkey

e-mail: mcetin@kastamonu.edu.tr

© by PSP Volume 28 – No. 5/2019 pages 3876-3885 Fresenius Environmental Bulletin

EFFECTS OF FERTIGATION STRATEGIES ON NITRATE-NITROGEN LEACHING AND YIELD PARAMETERS OF CUCUMBER GROWN IN GLASSHOUSE

Nilcan Ayan, Dursun Buyuktas*, Cihan Karaca, Ruhi Bastug

Akdeniz University, Faculty of Agriculture, Department of Agricultural Structures and Irrigation, Antalya, Turkey

ABSTRACT

In this study, the amount of nitrate leached from the soil and its effects on yield and quality of cucumber plant grown under greenhouse conditions were determined as a result of different fertigation strategies which was formed by changing the application time of the mixture of fertilizer solution during the irrigation cycle. For this purpose, five different fertigation strategies were applied, i.e. feeding of fertilizer solution during the whole irrigation period (F1), feeding of fertilizer solution during the first half of irrigation period (F2), feeding of fertilizer solution during the second half of irrigation period (F3), feeding of fertilizer solution between 1/4'th and 3/4'th irrigation period (F4) and injection of fertilizer solution immediately upon start of irrigation (F5) The highest and least yield was obtained in F1 (16.66 tons da^{-1}) and F3 (15.05 tons da^{-1}) fertigation strategies respectively. It was determined that fertigation strategies did not affect statistically the yield, fruit length, fruit diameter, plant height and stem diameter. On the other hand, it was found that the effect of fertigation strategies on nitrate-nitrogen (NO_3-N) leaching was statistically significant. The highest NO_3-N leaching was observed in F2 and the least in F4 fertigation strategy. It was concluded that the best fertigation strategy to prevent the pollution of groundwater by minimizing NO_3-N leaching, the most appropriate strategy is F4, i.e. feeding of fertilizer solution between 1/4'th and 3/4'th irrigation period.

KEYWORDS:
Greenhouse, Accumulation, Irrigation, Pan Evaporation, Mediterranean

INTRODUCTION

Greenhouse cultivation developed rapidly in the last 30 years [1] is an agricultural sector which is common in countries with the coast to the Mediterranean. According to the Turkish statistical data [2], 99% of the total greenhouse areas of Turkey (691 707 da) are located on the coasts of the Mediterranean, while 40% are in the province of Antalya because of climatic, technological and logistical advantages. Common crops grown widely in greenhouses located in Antalya, Turkey, are tomato (60%), cucumber (14%), pepper (11%), eggplant (4%) and other vegetables, fruit and ornamental plants (11%) are grown [2]. Therefore, the province of Antalya has an important region among intensive agricultural applications especially intensive irrigation. Fertilization is very important in terms of increasing soil productivity and plant yield to meet plant nutrients which are removed from the soil as a result of intensive agricultural activities. It is an indisputable truth that water and plant nutrients, especially N minerals, are the most important inputs in terms of plant growth, quality and yield.

The application of plant nutrient with irrigation water (fertigation) is the most efficient method to enhance crop production and reduce potential environmental damage in comparison to the conventional method [3]. In fertigation applications, it is aimed to accumulate the fertilizer and water in the root zone. Although the loss of plant nutrients is less in the drip irrigation method than in the other irrigation methods, it can reach a significant level as a total loss in irrigation with short intervals [4]. Because of the incorrect fertigation strategies, excessive fertilizer accumulation in the root zone may negatively affect the development of the plant and increase the cost of the input economically. On the other hand, if the plant nutrients reach out of the root zone, plant nutrient deficiency will occur and more fertilization will be required to increase the yield. As a result of excessive fertigation, nitrate having negatively charged ions will be leached out of the plant root zone and cause groundwater pollution.

The World Health Organization [5] has reported a critical value of 50 mg L^{-1} for nitrate (equivalent to 11 mg/L as nitrate-nitrogen) in drinking water for the protection of the health of the most sensitive subpopulation infants. For this reason, numerous simulations based studies [6, 7, 8, 9, 10, and 11] were conducted to determine the effects of fertigation strategies. Bristow et al. [6] investigated two basic strategies for the mixing time of fertilizer with water during irrigation. In the first strategy, the fertigation starts with irrigation and then only water was given until the end of the irrigation period. In

the second one, the fertigation starts near the end of the irrigation cycle. The authors reported that if the first strategy was applied, the accumulation of fertilizer around the dripper prevented and the loss of fertilizer was reduced even further. Cote et al. [7] reported similar results in their study of simulations for highly permeable coarse-textured soils in subsurface trickle irrigation. Contrary to these studies, Gärdenäs et al. [8] and Hanson et al. [12] reported that nitrate leaching was less and nutrient use efficiency was higher with fertigation application initiated at the end of the irrigation cycle. But Phogat et al. [9] did not find any relation between the time of fertilizer and nitrate leaching.

Published studies showed that there is a dilemma about the time of fertigation in terms of nitrate-nitrogen leaching and yield characteristics. Therefore, the aims of this study are 1) to assess the effects of different fertigation strategies on the nitrate distribution in the plant root zone, 2) to determine the amount of nitrate leached from the root zone, and 3) to examine the effects of different fertigation strategies on yield and yield parameters of cucumber plants grown in the glasshouse.

MATERIALS AND METHODS

This study was conducted in a gable-roofed (60×16 m) glasshouse having an area of 960 m^2 located in the north-south direction between September and December 2012 at the Research and Application Farm of Agricultural Faculty at Akdeniz University. The experimental area is located at coordinates of 36°53'53"N and 30°38'15" E and is 54 m above sea level. Some physical properties of the experimental soil are given in Table 1.

The experimental area has a Mediterranean climate and its summers are hot and dry, winters are warm and rainy. The annual average temperature in Antalya is 18.5 °C and the long-term average total rainfall is 1119 mm. Total evaporation, average minimum and maximum temperature during the experiment were measured as much as 245 mm, 14.2 °C, and 36.3 °C, respectively. The maximum and minimum temperature changes measured in the greenhouse during the experimental period are given in Figure 1.

The salinity and pH of the irrigation water used in the irrigation is 0.68 dS m^{-1} and 7.1, respectively. Cucumber (*Cucumis sativus* L.) which was named Yaren variety widely grown in the region was used as plant material in the experiment. The experimental area was prepared for seedling planting on August 31, 2012. Seedlings were planted after 24 kg 15-15-15 compound fertilizers were applied to the seedling beds on September 5, 2012. The monthly fertilization program (kg 240 m^{-2}) applied two times per month in the greenhouse during the experimental time is given in Table 2.

TABLE 1
Physical characteristics of the soil

Soil depth (cm)	Sand (%)	Clay (%)	Silt (%)	Texture class	Field capacity (%)	Permanent wilting point (%)	Bulk density (g cm^{-3})
0-20	31.61	39.73	28.66	Clay Loam	30.0	22.0	1.28
20-40	36.28	39.80	23.92	Clay Loam	23.0	16.0	1.52

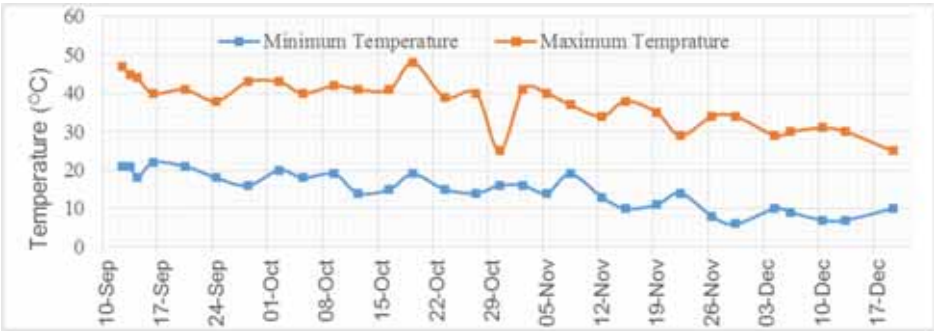

FIGURE 1
Maximum and minimum temperature measured in the greenhouse

TABLE 2
Monthly fertilization program (kg 240 m^{-2})

Month	%33 N Ammonium nitrate	Monoammonium Phosphate	Potassium Nitrate	Magnesium Sulphate	Calcium-Bor (lt)
September	0.36	0.24	0.36	0.24	-
October	0.6	0.48	0.72	0.48	0.5
November	1.44	0.72	1.8	0.48	0.5
December	1.44	0.48	1.44	-	0.5

The study was conducted in 3 replicates, according to randomized block trial design. Cucumber seedling planting was arranged according to the double row planting technique and was performed with 40 cm spacing along the row and 50 cm spacing between the rows and 2 m spacing was left between the treatments. The experimental design is given in Figure 2.

Drip irrigation method is used for irrigating the plots. The amount of water delivered to the plots was measured using a water gauge. One lateral drip line having in-line drippers spaced at 20 cm and discharging 2 L h^{-1} at 100 kPa pressure was laid down along each plant row. In the study, soil water content was monitored with PR2 profile probe (Delta T, USA) which was placed near the dripper and 20 cm away from dripper before and after every irrigation during the growing season in all treatments. The amount of irrigation water was calculated based on the measured amount of evaporation from Class A Pan located in the greenhouse.

Based on the studies conducted by Cemek et al. [13], Ayas and Demirtaş [14] and Wang et al. [15], the amount of irrigation water was determined as much as the amount of evaporation from the Class A Pan in four days. However, from planting (September 2, 2012) until September 16, crops are irrigated 8 times as much as 106 mm without taking pan evaporation into consideration for a homogenous standing. The first and last irrigation based on pan evaporation in the experiment was performed on 20.09.2012 and 19.12.2012 respectively. The plants were irrigated 34 times including the irrigations not based pan evaporation.

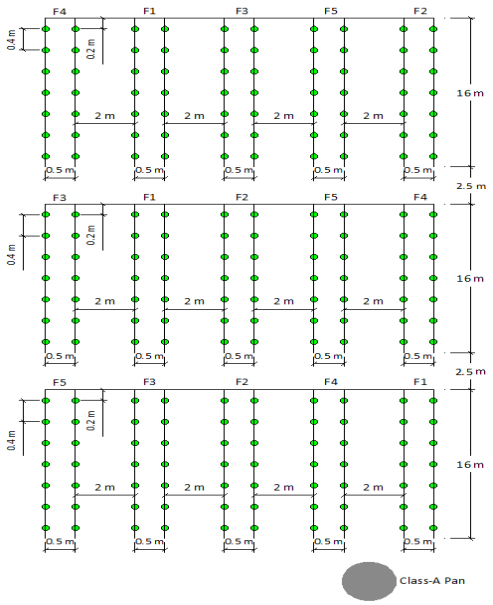

FIGURE 2
The experimental design

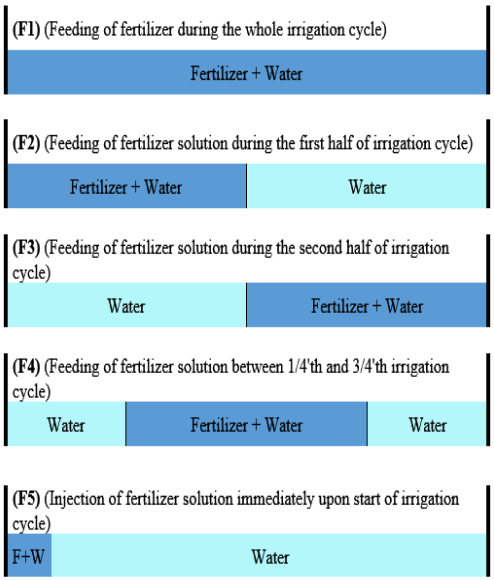

FIGURE 3
Fertigation strategies used in the study

The amount of water use of cucumber was computed based on water budged. The amount of water measured at 45 cm depth was considered deep percolation [16]. Five different fertigation strategies identified, based on changing the timing of feeding in the cycle of irrigation. The strategies are shown in Figure 3.

In order to determine the amount of nitrate-nitrogen (NO_3-N) in the soil, before and after fertigation, soil samples were taken from three different depths (15, 30 and 45) just under the dripper and 20 cm away from the dripper. Previous studies [17] indicated that the root system of the cucumber plant was developed in the upper 30 cm layer of soil and the root density was mostly concentrated at the upper 15 cm depth of the soil. For this reason, the amount of NO_3-N at the depth of 45 cm below the dripper and 20 cm away from the dripper, which was just the edge of wetting front horizontally determined after visual inspection, was considered to be leached.

The amount of NO_3-N was determined using the DR 2800 spectrophotometer (Hach, USA) according to the Cd reduction method [18]. Plant height and plant stem diameter (bottom, middle and top part) were measured every two weeks to determine the response of the cucumber plant to fertilization at different times in the experiment. Four plants were identified from each treatment and a total of 20 plants were used to measure for height and diameter. The plant length was measured by the meter. The stem diameter was measured by digital caliper. Harvesting at the experiment was started on 28 September 2012 after 28 days of planting. Between September 28 and December 20, crops were harvested 21 times. After each harvest, the fruit diameter and length were measured taking samples of 5 fruits from each treatment. The experimental data were analyzed by the General Linear Model (GLM) using Statistical Analysis Software, (SAS/STAT). Duncan's Multiple Range test was used, if necessary, to separate the means of the data at 0.05 level of significance.

RESULTS AND DISCUSSION

Applied Irrigation Water and Crop Water Use. The time course of applied water in each irrigation and cumulative applied irrigation water is shown in Figure 4. As given in materials and methods section, the amount of irrigation was equal to the amount of evaporation in Class A Pan located inside the greenhouse.

The amount of irrigation water declined depending on decreasing evaporation. The amount of evaporation measured in four days was as much as 20 mm in beginning of growing season which is in first half of September while it was measured as much as 5 mm in four days towards to the end of the growing season in the second half of December. The pan evaporation values obtained in the experiment was in agreement with those of Fernández et al. [19] under similar environmental conditions. Pan evaporation values were determined by Fernández et al. [19]. as 2.5 for autumn and 1.1 mm day^{-1} for winter growing season.

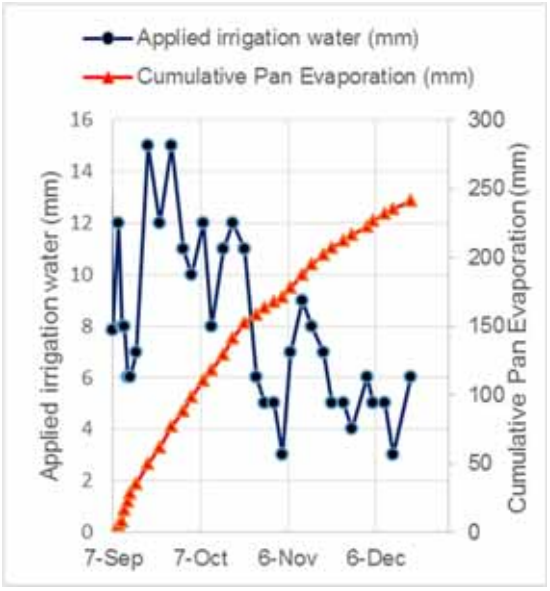

FIGURE 4
Applied irrigation water and cumulative pan evaporation

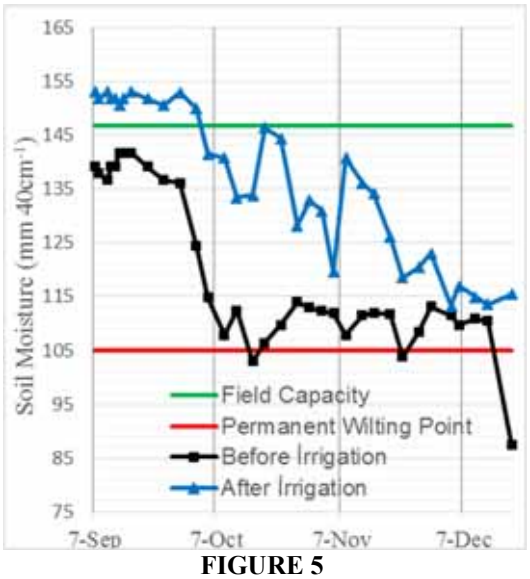

FIGURE 5
Change in soil water content

TABLE 3
Components of water balance during the experiment.

Applied irrigation water (mm)	Soil water depletion (mm)	Deep percolation (mm)	Crop water use (mm)
310	24	64	270

The amount of applied irrigation water, depleted soil water, the amount of percolated water and seasonal water use throughout the experimental period are given in Table 3. The amount of crop water use in the whole growing season which equals 110 days from planting to the time when experiment ended was 270 mm. The average daily water use was equal to 2.45 mm while daily applied water was 2.82 mm. In a study conducted in Cyprus by Nikolaou et al. [20] under greenhouse conditions in spring growing season reported applied water as much as 180 mm in ten week periods which corresponds to daily average applied irrigation water of 2.57 mm.

The change in soil water content at the point 20 cm away from dripper before and after irrigation event during the experiment is presented in Figure 5. The soil water content in the beginning of the experiment when crop is not grown fully was somewhat higher than field capacity resulting percolation of some of the irrigation water. When crop growth is fully completed, soil water content did not reach field capacity after irrigation meaning that the amount of applied water is not enough to meet crop water requirement. In another words, in most of the experimental period, soil water movement occurred under unsaturated conditions which is slower than that of the saturated conditions usually occurred in the beginning of the experimental period.

Yield and Yield Parameters. Cumulative plant height is presented in Figure 6. Year-end plant height, total yield, average fruit diameter, average fruit length, and average stem diameter are statistically analyzed. It was found that the fertigation strategies did not affect statistically all of the parameters mentioned.

The year-end plant height ranged from 359 cm (F1) to 394 cm (F5). The total yield varied between 15.05 ton da^{-1} (F3) and 16.66 ton da^{-1} (F1). Çakir et al. [21] and Alomran et al. [22]) reported cucumber yield of 10.71 and 15.0 ton da^{-1}, respectively, for similar conditions. Fruit diameters ranged from 3.0 (F2) to 3.16 (F3) cm while fruit lengths varied between 16.20 (F2) and 16.67 (F5) cm. In similar environmental conditions and cultural practices, Wang et al. [23] reported for the fruit diameter and the fruit length of 3.23 cm, 20.3 cm, respectively.

Accumulation and Leaching of NO_3-N. The amount of NO_3-N obtained from two different points (under the dripper and 20 cm away from the dripper) and three different soil depths (15, 30, and 45 cm) was given in Table 4. The amount of NO_3-N increased as soil depth increases in soil samples taken from the point under the dripper meaning that NO_3-N moving downwards. In addition, the amount of NO_3-N increased at location 20 cm away from the dripper. This was the result of accumulating the NO_3-N towards the edges of the wetting front. Li et al. [24] reported also that nitrate is accumulated toward the boundary of the wetted volume for different fertigation strategy.

Statistical evaluation of NO_3-N at different depths depending on fertigation strategies is presented in Table 5. It was determined that the effect of different fertigation strategies and the interaction between soil depths and fertigation strategies on average NO_3-N distribution under the dripper is not significant (Table 5a). However, the amount of NO_3-N at different depths was found significant ($P < 0.01$). The highest mean NO_3-N value was determined at 45 cm (4.80 mg kg^{-1}). There was no significant difference in the amount of NO_3-N in other soil depths (15 cm-2.26 mg kg^{-1} and 30 cm 2.80 mg kg^{-1}). The vertical distribution of NO_3-N in F2 and F4 strategies were relatively uniform. However, the amount of NO_3-N at the depth of 45 cm soil layer in F1, F3, and F5 strategies are statistically different. This means that NO_3-N is leaching from those strategies.

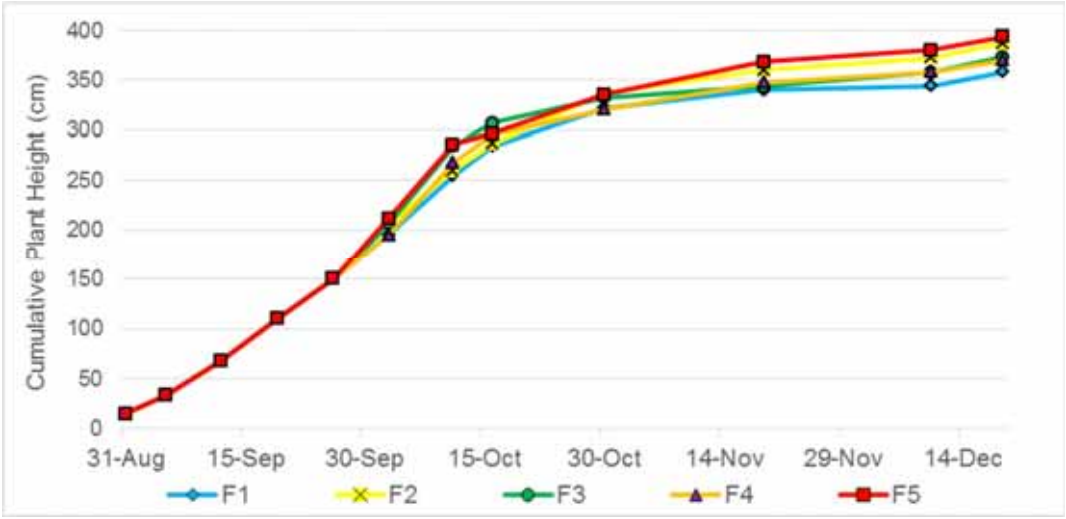

FIGURE 6
Cumulative plant height measured during experiment

TABLE 4
The amount of NO_3-N (mg kg^{-1}) obtained from two different points (under the dripper and 20 cm away from the dripper) and three different soil depths (15, 30, 45 cm)

Date	Depth (cm)	F1		F2		F3		F4		F5	
		Horizontal distance from the dripper (cm)									
		0	20	0	20	0	20	0	20	0	20
	15	0.91	25.17	2.16	16.10	0.91	1.93	1.14	0.91	1.70	12.59
19.09.2012	30	1.59	22.34	1.36	7.94	1.14	4.65	0.57	0.68	1.02	5.11
	45	3.40	16.22	0.91	20.86	2.27	10.21	1.02	1.36	2.16	18.03
	15	0.91	3.06	1.59	20.18	1.36	4.54	0.91	8.73	1.70	6.81
21.09.2012	30	0.23	1.82	1.02	11.11	1.02	3.06	0.91	6.92	0.91	6.92
	45	0.34	1.48	3.40	10.09	3.06	1.93	1.36	8.73	1.70	6.35
	15	1.02	0.68	1.02	1.02	1.14	21.43	0.57	9.98	0.46	4.08
04.10.2012	30	1.48	2.27	1.02	1.14	4.88	15.65	0.91	5.45	0.80	4.65
	45	2.61	3.74	2.04	1.48	14.17	17.46	0.80	11.91	1.59	16.44
	15	1.14	1.14	1.36	2.38	0.80	1.02	2.04	1.59	0.80	1.02
06.10.2012	30	1.14	1.02	1.02	3.06	1.93	1.36	0.80	2.27	0.80	1.25
	45	1.25	1.82	1.48	3.97	1.14	3.74	1.14	4.43	0.80	2.72
	15	0.91	23.70	1.02	26.31	0.80	9.53	4.65	3.74	0.57	6.69
18.10.2012	30	1.36	31.07	1.14	11.79	2.50	4.31	1.02	1.02	0.80	3.29
	45	2.04	22.34	1.14	7.03	4.99	0.80	1.14	6.01	1.02	2.84
	15	0.80	6.81	0.91	10.55	0.91	4.65	1.14	9.98	1.59	15.76
20.10.2012	30	1.02	2.27	1.93	9.64	1.25	1.25	1.36	5.67	2.61	9.98
	45	1.59	4.31	4.65	18.26	1.70	1.82	1.48	13.83	4.88	10.09
	15	0.91	23.81	0.91	13.38	2.50	14.17	0.80	13.15	0.46	3.52
07.11.2012	30	1.02	19.28	3.97	12.25	6.69	15.31	1.48	9.19	1.02	3.40
	45	4.43	20.75	3.18	21.09	18.71	12.47	1.93	10.89	1.93	3.40
	15	3.52	14.86	2.38	29.59	2.95	8.51	8.73	10.43	1.93	23.13
09.11.2012	30	5.67	8.28	2.84	25.17	4.65	4.54	7.15	12.93	2.95	22.90
	45	7.15	7.83	6.01	20.52	10.21	3.97	12.13	10.21	3.63	28.23
	15	1.36	31.63	2.27	2.38	2.04	19.50	0.91	9.19	0.68	1.02
21.11.2012	30	2.27	30.73	3.74	3.86	2.16	16.10	1.70	8.51	0.80	2.84
	45	11.57	22.90	6.01	4.54	2.50	10.43	2.16	6.13	1.02	4.88
	15	6.13	1.93	4.99	8.17	2.27	10.89	4.43	9.07	0.91	22.56
23.11.2012	30	1.82	5.79	4.08	6.47	1.82	12.47	5.33	14.29	2.38	23.24
	45	2.16	1.59	6.24	12.47	2.38	12.93	6.47	10.43	4.43	26.76
	15	2.61	31.07	4.43	13.38	3.52	17.01	1.82	14.06	1.02	13.72
05.12.2012	30	3.52	32.54	4.08	13.04	3.06	17.46	1.25	9.98	2.95	5.11
	45	9.19	23.47	6.47	12.93	20.30	19.16	1.36	18.03	2.27	3.18
	15	2.72	8.39	2.95	21.77	3.29	12.13	3.18	13.04	1.14	5.79
07.12.2012	30	3.86	7.71	4.08	18.94	3.97	8.28	2.72	15.42	1.25	5.11
	45	8.39	6.01	3.29	21.09	2.61	10.32	4.99	16.10	2.16	9.98
	15	4.43	33.22	8.62	31.18	3.18	22.22	1.70	10.89	3.40	20.30
18.12.2012	30	6.13	33.79	7.94	28.23	3.63	23.58	2.72	12.59	3.97	15.31
	45	8.28	24.15	21.32	32.31	3.97	14.06	2.61	9.19	17.80	10.55
	15	5.11	10.55	5.79	21.77	3.74	10.55	5.56	8.85	1.70	11.11
20.12.2012	30	8.51	10.09	12.47	17.35	2.50	9.30	9.87	8.73	4.08	10.89
	45	8.62	8.17	8.28	12.25	2.38	3.74	9.19	9.87	7.26	10.32

Unlike NO_3-N determined under dripper, the effect of different fertigation strategies on NO_3-N distribution at depths 20 cm away from the dripper is statistically significant ($P < 0.01$) (Table 5b). The interaction and vertical distribution of NO_3-N were not significant. However, the mean amount of NO_3-N determined 20 cm away from the dripper is rather higher than that of the values found under the dripper indicating that NO_3-N is moving towards edge of wetting front. The highest NO_3-N was obtained from F1 (14.04 mg kg^{-1}) and F2 (13.98 mg kg^{-1}) strategies.

The amount of NO_3-N leached during the growing season is given in Table 6, while statistical evaluation of total leached NO_3-N at the end of the growing season is presented in Figure 7, and 8, under the dripper and 20 cm away from the dripper, respectively. All of the leached NO_3-N at the depth of 45 cm at the end of the growing season together with the statistical evaluation is depicted in Figure 9. It was found that the effect of fertigation strategies on NO_3-N which was leached is statistically significant. Usually, in the fertigation applications towards the end of the growing season the leaching amount of NO_3-N increased (Table 6). Even between fertigation applications, nitrate continued to move since it is highly mobile.

The highest leached amount of NO_3-N under the dripper was found to be in F3 (fertigation in the second half of irrigation cycle) (Figure 7) while it was in F2 (fertigation in the first half of irrigation cycle) for the point 20 cm away from the dripper (Figure 8). The least leached NO_3-N under the dripper was found to be in F4 (fertigation of fertilizer solution between 1/4'th and 3/4'th irrigation cycle) strategy (Figure 7) while it was in F3 strategy for the point 20 cm away from the dripper (Figure 8). In the F3 strategy, NO_3-N is transported mostly under saturated soil water conditions while in F2, it is

TABLE 5
Statistical evaluation of average NO_3-N (mg kg^{-1}) values obtained during the growing season at different fertigation strategies and depths

(a) Under the dripper

Depth (D) of Sample	Fertigation Strategies (FS)										P > F	Mean of Depths	
	F1		*F2*	*F3*		*F4*	*F5*						
15	*2.32*	*b*	*2.89*	*2.10*	*b*	*2.68*	*1.29*	*b*			**ns**	**2.26**	**b**
30	*2.83*	*b*	*3.62*	*2.94*	*b*	*2.70*	*1.88*	*ab*			**ns**	**2.80**	**b**
45	*5.07*	*a*	*5.32*	*6.46*	*a*	*3.41*	*3.76*	*a*			**ns**	**4.80**	**a**
P > F	*		**ns**	*		**ns**	*						
Mean of FS	**3.41**		**3.94**	**3.83**		**2.93**	**2.31**						
Significance level	**Fertigation Strategies (FS): ns**					**Depth (D): ****					**FS x D: ns**		

(b) 20 cm away the dripper

Depth (D) of Sample	Fertigation Strategies (FS)										P > F	Mean of Depths
	F1		*F2*	*F3*		*F4*	*F5*					
15	*15.43*		*15.58*	*11.29*		*8.83*	*10.58*				**ns**	**12.34**
30	*14.93*		*12.14*	*9.81*		*8.12*	*8.57*				**ns**	**10.71**
45	*11.77*		*15.58*	*8.79*		*9.79*	*10.98*				**ns**	**11.10**
P > F	**ns**		**ns**	**ns**		**ns**	*ns*					
Mean of FS	**14.04**	**A**	**13.98**	**A**	**9.96**	**B**	**8.91**	**B**	**10.05**	**B**		
Significance level	**Fertigation Strategies (FS): ****						**Depth (D): ns**				**FS x D: ns**	

The capital letters show the comparison of the averages given along the horizontal (along the row) at the 5% significance level according to the Duncan test. The small letters are given in vertical (along the column) and the capital letters given in horizontal (along the row) show the comparison of the averages at the 5% significance level according to the Duncan test.
*, **: %5, %1 significance level of probability, respectively. ns: not significant.

TABLE 6
The leaching amount of NO_3-N (mg kg^{-1}) during the growing season

Time	Fertigation Strategies									
	F1		F2		F3		F4		F5	
	Horizontal distance from the dripper (cm)									
	0	20	0	20	0	20	0	20	0	20
19.09.2012	3.4	16.2	0.9	20.9	2.3	10.2	1.0	1.4	2.2	18.0
21.09.2012	0.3	1.5	3.4	10.1	3.1	1.9	1.4	8.7	1.7	6.4
04.10.2012	2.6	3.7	2.0	1.5	14.2	17.5	0.8	11.9	1.6	16.4
06.10.2012	1.3	1.8	1.5	4.0	1.1	3.7	1.1	4.4	0.8	2.7
18.10.2012	2.0	22.3	1.1	7.0	5.0	0.8	1.1	6.0	1.0	2.8
20.10.2012	1.6	4.3	4.7	18.3	1.7	1.8	1.5	13.8	4.9	10.1
07.11.2012	4.4	20.8	3.2	21.1	18.7	12.5	1.9	10.9	1.9	3.4
09.11.2012	7.2	7.8	6.0	20.5	10.2	4.0	12.1	10.2	3.6	28.2
21.11.2012	11.6	22.9	6.0	4.5	2.5	10.4	2.2	6.1	1.0	4.9
23.11.2012	2.2	1.6	6.2	12.5	2.4	12.9	6.5	10.4	4.4	26.8
05.12.2012	9.2	23.5	6.5	12.9	20.3	19.2	1.4	18.0	2.3	3.2
07.12.2012	8.4	6.0	3.3	21.1	2.6	10.3	5.0	16.1	2.2	10.0
18.12.2012	8.3	24.2	21.3	32.3	4.0	14.1	2.6	9.2	17.8	10.6
20.12.2012	8.6	8.2	8.3	12.3	2.4	3.7	9.2	9.9	7.3	10.3
Total	71.0	164.8	74.4	198.9	90.4	123.0	47.8	137.1	52.7	153.8

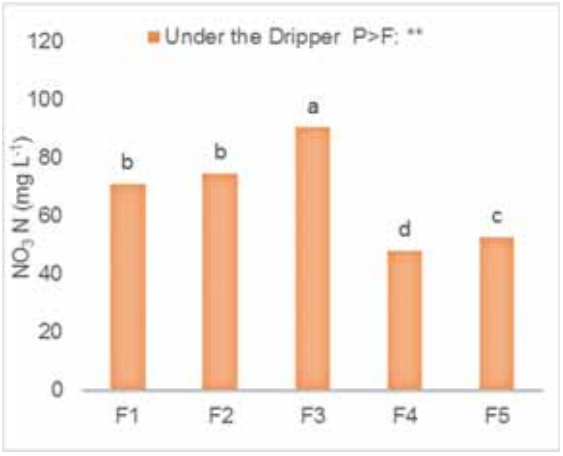

FIGURE 7
Effect of different fertigation strategies on NO_3-N leaching under the dripper

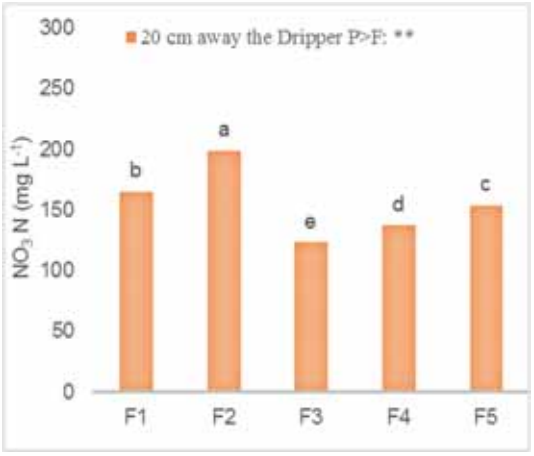

FIGURE 8
Effect of different fertigation strategies on NO_3-N leaching at 20 cm away from the dripper

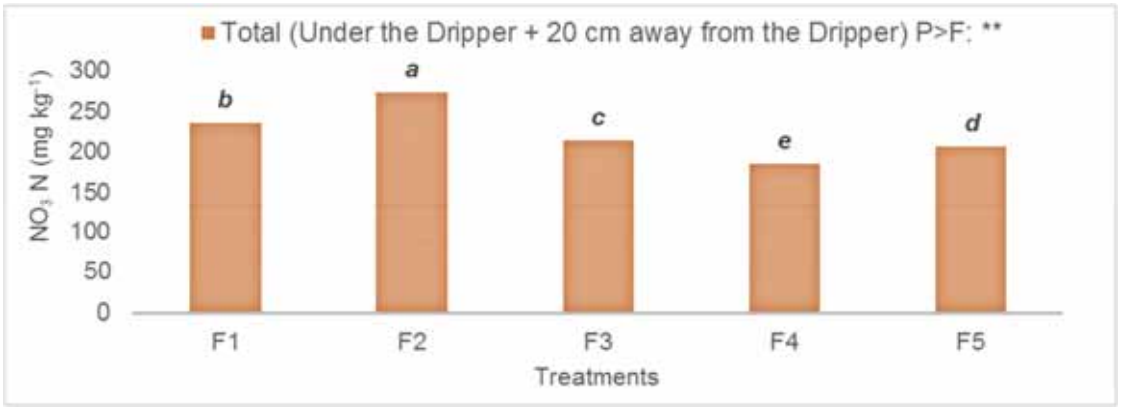

FIGURE 9
Effect of different fertigation strategies on total NO_3-N leaching

conveyed under unsaturated soil water conditions. Since the hydraulic conductivity was high under saturated conditions, the fertilizer carried out by irrigation water very fast and the fertilizer was transported deeper than the targeted root zone.

The total amount of nitrogen leached was significantly affected by the fertigation strategies ($p<0.05$) (Figure 9). The highest amount of leached NO_3-N was observed in F2 strategy while the least was found in F4 strategy. Hanson et al. [25] reported that NO_3-N was more uniformly distributed in the root zone of the plant by fertigation during the irrigation cycle. Also, Hou et al. [26] suggested that fertilizers should be given at the beginning of the irrigation for efficient use of the nitrogen. The results obtained in this study contradicts to the previous studies and shows that fertilizers should be given between 1/4'th and 3/4'th irrigation cycle to obtain relatively more uniform NO_3-N distribution in the root zone to minimize the amount of NO_3-N that was leached.

CONCLUSION

In this study, the amount of NO_3-N leaching in the soil and its effect on yield and yield parameters of cucumber were investigated by differentiating the mixing time of the fertilizer solution in the irrigation cycle under different fertigation strategies under the greenhouse conditions. Five different fertigation strategies, namely feeding of fertilizer solution during the whole irrigation period (F1), feeding of fertilizer solution during the first half of irrigation period (F2), feeding of fertilizer solution during the second half of irrigation period (F3), feeding of fertilizer solution between 1/4'th and 3/4'th irrigation period (F4) and injection of fertilizer solution immediately upon start of irrigation period (F5) were applied. The amount of NO_3-N in the soil was determined by soil samples made in two different zones (under the dripper and 20 cm away from the dripper) and three different depths (15, 30 and 45 cm). In the experiment, it was found that different fertigation strategies did not affect plant yield parameters (cumulative yield, plant height, fruit length, fruit diameter and stem diameter) but it affected the amount of NO_3-N leached from the root zone. The NO_3-N leaching results were determined to be F3> F2=F1= F5> F4, according to analyzes made from soil samples at a depth of 45 cm under the dripper. At the point 20 cm away from the dripper, NO_3-N leaching was determined as F2>F1>F5>F4>F3. When total amount of leached NO_3-N is taken into account, it was found that F2>F1>F3>F5>F4. In order to increase marginal utilization and reduce NO_3-N leaching from cucumber root zone as well as not to cause ground water pollution, fertigation applications should be carried out in the middle of irrigation period (F4 strategy).

ACKNOWLEDGEMENTS

The authors are grateful to the Scientific Research Administration Unit of Akdeniz University, Antalya, Turkey, for financial support of this research (Project No: 2012.02.0121.007).

REFERENCES

[1] Baytorun, N. (2016) Greenhouses, Greenhouse Types, Equipment and Air Conditioning. 1st ed. Nobel Academic Publishing Education Consultancy, Ankara, Turkey. (In Turkish).
[2] TUİK (2017) Plant Production Statistics. Turkish Statistical Institute. (In Turkish). Ankara.
[3] Abbasi, F, Rezaee, H.T., Jolaini, M, Alizadeh, H.A. (2012) Evaluation of fertigation in different soils and furrow irrigation regimes. Irrigation and Drainage. 61, 533–541.

[4] Nachmansohn, J. (2016) Minimized nutrient leaching through fertilizer management - An evaluation of fertilization strategies. Swedish University of Agricultural Sciences.
[5] WHO (2016) Nitrate and Nitrite in Drinking - Water. Background document for development of WHO Guidelines for Drinking-water Quality 33.
[6] Bristow, K.L., Cote, C.M., Thorburn, P.J., Cook, F.J. (2000) Soil Wetting and Solute Transport in Trickle Irrigation Systems. In: Rome, Italy: International Commission on Irrigation and Drainage (ICID), 1–9.
[7] Cote, C.M., Bristow, K.L., Charlesworth. P.B., Cook, F.J., Thorburn, P.J. (2003) Analysis of soil wetting and solute transport in subsurface trickle irrigation. Irrigation Science, 22, 143–156.
[8] Gärdenäs, A., Hopmans, J.W., Hanson. B.R., Šimůnek, J. (2005) Two-dimensional modeling of nitrate leaching for various fertigation scenarios under micro-irrigation. Agricultural Water Management. 74, 219–242.
[9] Phogat, V., Skewes, M.A., Cox, J.W., Alam, J., Grigson, G., Šimůnek, J. (2013) Evaluation of water movement and nitrate dynamics in a lysimeter planted with an orange tree. Agricultural Water Management. 127, 74–84.
[10] Zhang, J.J., Li, J.S., Zhao, B.Q., Li, Y.T. (2015) Simulation of water and nitrogen dynamics as affected by drip fertigation strategies. Journal of Integrative Agriculture. 14, 2434–2445.
[11] Qin, W., Heinen, M., Assinck, F.B.T., Oenema, O. (2016) Exploring optimal fertigation strategies for orange production, using soil-crop modelling. Agriculture, Ecosystems and Environment. 223, 31–40.
[12] Hanson, B., Šimůnek, J., Hopmans, J.W. (2006) Evaluation of urea-ammonium-nitrate fertigation with drip irrigation using numerical modeling. Agricultural Water Management. 86, 102–113.
[13] Cemek, B., Kara, T., Apan, M., Taşan M. (2004) Comparative study on evaporation values obtained from class A pan and small-scale evaporation pans in greenhouse. J. of Faculty of Agriculture of Uludag University. 18, 13–24 (In Turkish).
[14] Ayas, S. and Demirtaş, Ç. (2009) Deficit irrigation effects on cucumber (Cucumis sativus L. Maraton) yield in unheated greenhouse condition. Journal of Food, Agriculture and Environment. 7, 645–649.
[15] Wang, Z., Liu, Z., Zhang, Z., Liu, X. (2009) Subsurface drip irrigation scheduling for cucumber (Cucumis sativus L.) grown in solar greenhouse based on 20 cm standard pan evaporation in Northeast China. Scientia Horticulturae. 123, 51–57.
[16] Allen, R.G., Pereira, L.S., Raes, D, Smith, M. (1998) Crop evapotranspiration: Guidelines for computing crop water requirements. Roma: FAO.
[17] Chartzoulakis, K., Michelakis, N. (1990) Effects of different irrigation systems on root growth and yield of greenhouse cucumber. Acta Hort (ISHS). 278, 237–244.
[18] Kurunc, A., Ersahin, S., Uz, B.Y. (2011) Identification of nitrate leaching hot spots in a large area with contrasting soil texture and management. Agricultural Water Management. 98, 1013–1019.
[19] Fernández, M.D., Bonachela, S., Orgaz, F. (2010) Measurement and estimation of plastic greenhouse reference evapotranspiration in a Mediterranean climate. Irrigation Science. 28, 497–509.
[20] Nikolaou, G., Neocleous, N., Katsoulas, N., Kittas, C. (2017) Effect of irrigation frequency on growth and production of a cucumber crop under soilless culture. Emir. J. Food Agric. 29(11), 863-874.
[21] Çakir, R., Kanburoglu-Çebi, U., Altintas, S., Ozdemir, A. (2017) Irrigation scheduling and water use efficiency of cucumber grown as a spring-summer cycle crop in solar greenhouse. Agricultural Water Management. 180, 78–87.
[22] Alomran, A.M., Louki, I.I., Aly, A.A., Nadeem, M.E. (2013) Impact of deficit irrigation on soil salinity and cucumber yield under greenhouse condition in an arid environment. Journal of Agricultural Science and Technology. 15, 1247–1259.
[23] Wang, Z., Liu, Z., Zhang, Z., Liu, X. (2009) Subsurface drip irrigation scheduling for cucumber (Cucumis sativus L.) grown in solar greenhouse based on 20 cm standard pan evaporation in Northeast China. Scientia Horticulturae. 123, 51–57.
[24] Li, J., Zhang, J., Rao, M. (2004) Wetting patterns and nitrogen distributions as affected by fertigation strategies from a surface point source. Agricultural Water Management. 67, 89-104.
[25] Hanson, B., Hopmans, J.W., Simunek, J., Gardenas, A. (2004) Crop nitrate availability and nitrate leaching under micro-irrigation for different fertigation strategies. In: ASAE Annual International Meeting. 2004
[26] Hou, Z, Li, P, Li, B, Gong, J, Wang, Y. (2007) Effects of fertigation scheme on N uptake and N use efficiency in cotton. Plant and Soil. 290, 115–126.

Received: **13.11.2018**
Accepted: **18.03.2019**

CORRESPONDING AUTHOR

Dursun Buyuktas
Akdeniz University,
Faculty of Agriculture,
Department of Agricultural
Structures and Irrigation
Antalya – Turkey

e-mail: dbuyuktas@akdeniz.edu.tr

© by PSP Volume 28 – No. 5/2019 pages 3886-3892 Fresenius Environmental Bulletin

EFFECT OF ZINC NUTRITION ON BLOOD PARAMETERS OF WUMENG SEMI-FINE WOOL SHEEP IN NATURAL HABITAT

Yongkuan Chi[1], Yongbi Chen[1], Shuzhen Song[1], Xiaoyun Shen[1,2,3,*]

[1]School of Karst Science/ State Engineering Technology Institute for Karst Desertification Control, Guizhou Normal University, Guiyang 550001, China
[2]School of Life Science and Engineering, Southwest University of Science and Technology, Mianyang 621010, China
[3]World Bank Poverty Alleviation Project Office in Guizhou, Southwest China, Guiyang 550004, China

ABSTRACT

The Wumeng semi-fine wool sheep industry is the pillar industry in the Wumeng mountainous area. In order to reduce the impact of overmuch or too little trace element nutrients on the Wumeng semi-fine wool sheep industry, we have carried out research on the effect of zinc on blood parameters of Wumeng semi-fine wool sheep in natural habitat. It was analyzed the contents of mineral nutrients in soil, forage and animal tissues and determined the blood physiological and biochemical parameters of Wumeng semi-fine wool sheep. The results showed that the zinc (Zn) content in the soil of the experimental pasture was significantly lower than that in the control pasture (P<0.01), and the Zn content in the forage of the experimental pasture was significantly lower than that in the control pasture (P<0.01); the Zn content in the blood of the experimental group was significantly lower than that in the control group (P<0.01), but there was no significant difference in other elements (P>0.05); the content of RBC, LY, NE in the blood of the experimental group was significantly lower than that in the control group (P<0.01); the activity of SOD,GSH-Px, CAT, AKP in serum of the experimental group was significantly lower than that in the control group (P<0.01), the content of MDA in serum of the experimental group was significantly higher than that in the control group (P<0.01), but there was no significant difference between the content of Hb, PCV, WBC, BUN and the activity of LDH, AST, ALT, γ-GT activity (P>0.05). So it can be seen that zinc deficiency in natural habitat has a significant effect on blood physiological and biochemical parameters of Wumeng semi-fine wool sheep, furthermore, it has very significant effect on antioxidant enzymes of the body.

KEYWORDS:
Wumeng mountainous area, Wumeng semi-fine wool sheep, natural habitat, zinc deficiency, the activity of antioxidant enzyme

INTRODUCTION

The Wumeng semi-fine wool sheep is mainly distributed in the Wumeng mountainous area at the border of Guizhou, Yunnan and Sichuan provinces, it has the characteristics of high production performance, strong adaptability, gentle temperament and easy management, it is the most important sheep breed in Wumeng mountainous area, so it plays an irreplaceable economic role in the development of local grassland and ecological animal husbandry, it is also the material basis for the survival of local people [1]. Mineral nutrition is the basic nutrient in the food chain, its migration and circulation in the whole ecosystem is realized through soil (water)-plant-animal- human body [2]. The results show that the mineral nutrition content in soil reflects the supply level of mineral nutrition in soil to plant, and the deficiency and overmuch of some mineral nutrition in soil will directly affect the mineral nutrition content in forage or feed, to some extent, it affects the nutrition and health of humans and animals [3].

Zinc is one of the most important elements of 15 trace elements involved in physiological function [4]. Zinc is a component of zinc protein, and it is also an important component of many enzymes in animals [5]. Zinc not only participates in the metabolism of carbohydrates, fats, proteins, nucleic acids, vitamins and trace elements in animals, but also plays an important role in physiological functions such as bone development, fur growth, coagulation and biofilm stability [6]. Zinc is an inherent component of adrenal cortex, which has important physiological significance in maintaining the normal development of sexual organs and sexual function in animals [7]. Zinc is directly involved in the formation, maturation, activation and capacitation of spermatozoa and promotes the normal functioning of reproductive organs and functions [8]. Zinc is also involved in the processes of immune and antioxidant, which affects the immune function of animals by inhibiting the damage of peroxides to cells [9]. The main manifestations of zinc deficiency in animals are slow growth, low feed utilization rate, dermatogeratosis of skin, abnormal bone de-

velopment and reproductive dysfunction [10]. The typical performance of zinc deficiency in sheep is that wool can shed and become brittle, and the symptom of dermatogeratosis of skin can appear [11]. However, when zinc content is overmuch, it will also have a serious impact on livestock production and health, therefore, zinc needs to be used scientifically and reasonably [12].

The purpose of this study is to reveal the relationship between mineral nutrition in habitat and the industry of Wumeng semi-wool sheep, and to elucidate the distribution of zinc nutrition in natural habitat and its effect on blood parameters of the Wumeng semi-fine wool sheep, thereby to provide theoretical reference for healthy breeding of Wumeng semi-fine wool sheep and development of animal husbandry in Wumeng mountainous area.

MATERIALS AND METHODS

Study area. The experimental area is located in the Sheep Farm of Qixingguan District and Hezhang County, Bijie City, Guizhou province, this area belongs to Wumeng mountainous area. It is a subtropical and warm temperate zone warm monsoon climate where is no chilly winter and hot summer, the average altitude is 1 600-2 900 m, the annual average temperature is 11.5-12.8 ℃, the frost-free period is 185-259 days, and the annual average rainfall is 900-1200 mm, and the annual average sunshine duration is 1400-1900 hours. The main plant species are: *Lolium perenne*, *Trifolium repens*, *Festuca ovina*, *Poa annua*, *Carex rigescens*, *Potentilla fulgens* and *Potentilla discolor* [13].

Experimental animals. 20 Wumeng semi-fine wool sheep in the Sheep Farm of Wumeng mountainous area in Hezhang County were randomly selected as the experimental group, the experimental sheep was form 1 to 2 years old with the obvious symptom of loss of appetite, growth retardation, dermatogeratosis of skin, coarse and shedding wool. 20 healthy Wumeng semi-fine wool sheep in the experimental pasture of Qishingguan District in Bijie City were randomly selected as the control group.

Experiment design. The sheep farm of Hezhang County and the experimental pasture of Qishingguan District in Bijie City were used as the experimental group and the control group respectively. It was analyzed the mineral nutrients in soil, forage and animal tissues and the activities of physiological indexes and biochemical enzyme in animals, while it was compared the content of mineral content, physiological and biochemical indexes in blood of Wumeng semi-fine wool sheep in the experimental group and the control group.

Sample collection. Soil sample collection: 10 soil samples were collected from each pasture, the quadrats of 1 m × 1 m was randomly selected for sample, each quadrat interval was 100 m, the surface soil samples of 0-30 cm were collected from each quadrat, each sample was 200 g, marking the sample points prepare for collecting forage samples at the same location.

Forage sample collection: 10 mixed forage sample were collected from each pasture. In order to reduce the effect of different forage varieties on trace element content, the soil sample collection point was taken as the center, select 10 sample points evenly distributed from the center of the circle 250 m (each sample point is 250 m apart), 25g forage was collected at each sample point and then mixed to form a forage sample, and a forage sample was 250g.

Blood and liver sample collection: each animal was collected 20mL blood from jugular vein by using a sterile vacuum blood collection tubes, the blood sample was carried back to the laboratory for treatment within 4 hours at 4-8°C for analysis of blood parameters and determination of trace element content. According to the method of Rockey et al. (2009) to collect liver sample, the liver sample was obtained by using a rapid biopsy gun puncture the liver at a 45° angle to the end of the skin in the right side of the liver and the liver was punctured 6cm, the liver sample was fixed in the specimen bottle after collection, the liver sample was carried back to the laboratory like the blood sample [14].

Sample processing. Soil samples were dried to constant weight at 20 ℃ and crushed, stone particles were removed by 2mm sieve, fine sand was removed by 0.075mm sieve, the soil sample was dissolve by microwave digestion method with the mixture of nitric acid (HNO_3), perchloric acid ($HClO_4$) and hydrofluoric acid (HF) (5:2:5) [15].

The forage sample was washed with tap water and distilled water, dried to constant weight at 20 ℃ and crushed. The forage sample was dissolve by microwave digestion method with the mixture of nitric acid (HNO_3), perchloric acid ($HClO_4$) (4:1) [15].

Animal serum was centrifuged with low temperature centrifuge at 4 ℃ for 3500 R/min, the serum was separated from EP tube and stored at -80 ℃. The blood and liver sample was dissolve by microwave digestion method with the mixture of nitric acid (HNO_3) and perchloric acid ($HClO_4$) (4:1) [15].

Detection indicators. The content of trace elements in soil, forage and animal tissues were determined by inductively coupled plasma atomic emission spectrometry (Inductively Coupled Plasma Atomic Emission Spectroscopy, ICP-AES), the instrument is the inductively coupled plasma emis-

sion spectrometer (HK9600 Type Atomic Emission Spectroscopy, Huaketiancheng Co., Ltd, China), many elements were analyzed that were copper (Cu), iron (Fe), manganese (Mn), zinc (Zn), molybdenum (Mo) and selenium (Se) [16]. Hemoglobin (Hb), red blood cell count (RBC), packed cell volume, white blood cell count (WBC), lymphocytes (LY) and neutrophils (NE)were measured using an animal-specific automatic blood analyzer (SF-3000, Sysmex-Toa Medical Electronics, Kobe, Japan) [16]. The activity of Lactate Dehydrogenase (LDH), Alkaline Phosphatase (AKP), Aspartate Aminotransferase (AST), Alanine Aminotransferase (ALT), Glutamyl Transpeptidase (γ-GT), Superoxide Dismutase (SOD), Glutathione Peroxidase (GSH-Px) and Catalase (CAT) and the content of blood urea nitrogen (BUN) and malondialdehyde (MDA) were detected by an automatic biochemical analyzer (Olympus AU 640, Olympus Optical Co., Tokyo, Japan) [16].

Data analysis. The experimental data were analyzed by SPSS version 20.0 for windows (Chicago, Illinois, USA. The data were expressed as mean ($\overline{x}$) ± standard deviation (S) and its difference was evaluated by independent sample t-test.

RESULTS AND ANALYSIS

Analysis of mineral nutrition content in natural habitat. The Zn content in soil of the experimental pasture was significantly lower than that in the control pasture (P<0.01), and there was no significant difference in other elements (Table 1). The Zn content in forage of the experimental pasture was significantly lower than that in the control pasture (P<0.01), and there was no significant difference in other elements (P>0.05) (Table 1).

The Zn content in blood of Wumeng semi-fine wool sheep in the experimental pasture (zinc deficiency) was significantly lower than that in the control group (P<0.01). There was no significant difference in other elements of Wumeng semi-fine wool sheep in the experimental pasture compared with the control pasture (P>0.05) (Table 2).

TABLE 1
The content of trace element in soil and forage (μg/g)

Element	Soil		Forage	
	Experimental pasture	Control pasture	Experimental pasture	Control pasture
Mn	192.44±17.12	193.45±15.33	67.28±7.23	68.78±7.22
Zn	35.87±3.17a	78.12±3.55b	38.67±7.18a	69.93±5.22b
Cu	10.87±2.27	11.74±2.16	4.68±1.33	4.51±1.29
Fe	4152.33±77.34	4137.24±72.33	522.34±37.21	523.57±35.65
Mo	1.89±0.13	1.86±0.17	0.82±0.12	0.87±0.13
Se	0.13±0.01	0.12±0.01	0.08±0.02	0.09±0.01

The different letters in the same row indicate significantly different (P<0.01), the same below.

TABLE 2
The content of mineral elements in blood of Wumeng semi-fine wool sheep (μg/g)

Mineral Element	Experimental animals	Control animals
Mn	0.27±0.08	0.28±0.07
Zn	3.51±0.12a	7.97±0.13b
Cu	0.54±0.03	0.56±0.02
Fe	459.29±21.33	458.18±21.26
Mo	0.23±0.03	0.22±0.04
Se	0.07±0.01	0.08±0.01

TABLE 3
Blood routine indicators of Wumeng semi-fine wool sheep

Blood routine indicators	Experimental group	Control group
Hb(g/L)	112.69±11.71	112.65±21.15
RBC(10^{12}/ L)	6.87±1.59a	11.60±1.57b
PCV (%)	35.85±2.71	35.87±2.63
WBC(10^9/L)	9.36±1.33	9.33±1.37
LY (%)	33.23±3.33a	57.67±7.32b
NE (%)	27.56±1.36a	45.46±2.35b

TABLE 4
Biochemical parameters in blood of Wumeng semi-fine wool sheep

Biochemical parameters	Experimental group	Control group
LDH (U/L)	3.58±0.34	3.59±0.38
AKP (IU/L)	237.26±19.56a	271.24±12.35b
AST (IU/L)	39.45±4.34	39.58±4.13
ALT (IU/L)	13.67±2.26	13.56±2.68
γ-GT(IU/L)	19.65±2.10	19.87±2.16
BUN (nmol/L)	6.92±1.30	6.52±1.38

TABLE 5
Antioxidant indicators of Wumeng semi-fine wool sheep

Antioxidant indicators	Experimental group	Control group
SOD(U/L)	12.23±1.54a	17.58±1.73b
GSH-Px(U/L)	12.54±2.21a	19.35±1.37b
CAT(U/ml)	1.32±0.15a	1.97±0.17b
MDA (nmol/L)	23.45±1.73a	13.70±1.19b

Analysis of physiological and biochemical indexes in blood of Wumeng semi-fine wool sheep. The RBC, LY and NE in the blood of the Wumeng semi-fine wool sheep in the experimental group were significantly lower than those in the control group (P<0.01). There was no significant difference in Hb, PCV and WBC of Wumeng semi-fine wool sheep in the experimental group compared with the control group (P>0.05) (Table 3).

The AKP activity in blood of the Wumeng semi-fine wool sheep in the experimental group was significantly lower than that in the control group (P<0.01), and there was no significant difference in the other biochemical indicators of Wumeng semi-fine wool sheep in the experimental group compared with the control group (P>0.05) (Table 4).

The activities of SOD, GSH-Px and CAT in blood of Wumeng semi-fine wool sheep in the experimental group were significantly lower than those in the control group (P<0.01), and the MDA content in blood of Wumeng semi-fine wool sheep in the experimental group was significantly higher than that in the control group (P<0.01), and there was no significant difference in other antioxidant indicators of Wumeng semi-fine wool sheep in the experimental group compared with the control group (P>0.05) (Table 5).

DISCUSSION

Animals do not have the ability to store zinc, so it needs to feed from diets to maintain their health and nutrient balance [17]. Plant growth depends on soil, which provides most of the nutrients needed for plant growth [18]. Hezhang County is a typical rocky desertification area in Wumeng mountainous area, the distribution of land resources is unbalanced and grassland degradation is serious in this area [19]. The zinc in the soil is mainly derived from rock weathering, the common range of zinc content in soil in the world is 10-300 μg /g, the average value of zinc content in soil in the world is of 50-100μg /g [20]. The zinc content in the soil of the experimental pasture was obviously lower than the normal average value, which resulted in that the zinc nutrition of forage could not meet the needs of animal growth and development.

Zinc is an essential mineral nutrient for animals [21]. Zinc in animals is mainly obtained from diets, it is digested and absorbed through the digestive system. In the process of absorption, zinc mainly exists in the form of zinc ion. Firstly, zinc in the intestinal lumen enters the cell through the apical membrane (brush border) of the small intestinal mucosa; secondly, zinc enters the cell from the apical membrane of the small intestinal mucosa to the basement membrane, and then enters the blood from the basement membrane; finally, the absorbed zinc binds to hemoglobin in the blood, the digestion and metabolism through blood circulation into the liver, bones and other tissues [22]. Liver is the main place of zinc storage and metabolism [23]. The lower is the content of zinc in liver, the higher is the degree of zinc deficiency [10]. Copper and iron are trace elements that affect the absorption and utilization of zinc in the body [24]. The main absorption sites of iron and zinc are in duodenum, and there is competition in the absorption pathway between them [25]. The interaction between copper and zinc not only occurs in the absorption stage, but also in the blood transport [26]. However, there was no significant difference in copper and iron content in soil and forage between the experimental pasture and the control pasture in our study.

Zinc is an important substance that induces B cells to secrete globulin, it can improve the immune function of animal B cell and enhance the synthesis ability of immunoglobulin, If the animal is deficient in zinc, it will lead to disorder of the secretion of

immunoglobulin, which will lead to decrease the number of lymphoid tissues and lymphocytes, hinder the growth and development of the animal body and have low immune function [27]. Zinc deficiency also reduces the bactericidal ability of neutrophils [28]. Zinc can participate in the synthesis of alkaline phosphatase, lactate deaminase, superoxide dismutase, glutathione peroxidase and other important enzymes [29]. Zinc deficiency can decrease the activity of alkaline phosphatase in the blood, change the calcification of bone, make the proliferation of chondrocytes on the bone growth plate and decrease the bone mineral density [30]. Zinc-deficient sheep stand on the back of the arch, the limbs gather together, and the hind limbs bend with an internal arc [31]. Zinc deficiency also reduces the activity of lactate dehydrogenase, blocks the decomposition and synthesis of lactic acid and the replacement of lactic acid and pyruvate, and causes accumulation of lactic acid and pyruvate, which resulted in edema of limbs, swelling of joints and lameness in animals [32]. Superoxide dismutase and glutathione peroxidase can scavenge free radicals, while zinc is not only one of the components of superoxide dismutase, but also an activator of glutathione peroxidase [33]. Zinc deficiency can lead to the activity of superoxide dismutase and glutathione peroxidase, hinder the scavenging of superoxide anion radicals and induce lipid peroxidation in tissues, which lead that the content of malondialdehyde is increase in the products of lipid peroxidation, thus it is declined the ability of scavenging free radical and seriously affected the function of antioxidant system [34].

According to the results of the experiment, we can find that the low zinc content in natural habitat have a significant effect on the blood index of Wumeng semi-fine wool sheep, which will lead to abnormal antioxidant system function and immune function and affect the growth and development of Wumeng semi-fine wool sheep. Therefore, it is very necessary to supplement zinc for animals or grassland in zinc-deficient pastures, and it is an important way to maintain the healthy and sustainable development of Wumeng semi-fine wool sheep industry.

ACKNOWLEDGEMENTS

This study was supported by Project of National Key Research and Development Program (2016YFC0502601), the National Natural Science Foundation of China (No. 41671041, 41561066). Guizhou Provincial Research Foundation for Basic Research (Qian Ke He Ji Chu [2018]1149). Yongkuan Chi, Yongbi Chen and Shuzhen Song contributed equally to this work.

REFERENCES

[1] Shen, X.Y., Chi, Y.K, Xiong, K.N., Cheng, W.H., Zhang, J.H. (2014) Serum biochemical values and mineral contents of tissues in Guizhou semi-fine wool sheep. Journal of Animals and Veterinary Advance. 12(11), 1078-1080.

[2] Lan, W.C. (2004) The relationship between trace element and ecology environment. Journal of Minzu University of China (Natural Sciences Edition). 13(2), 163-168.

[3] Wu, C.X., Fu, H., Pei, S.F., Qin, Y. (2008) Study on the contents of available trace elements in different grassland soils on the western slope of the Helan mountain. Arid Zone Research. 25(1), 136-144.

[4] Zhang, R.Q. (2003) Research progress on zinc in nutriology. Journal of Domestic Animal Ecology. 4, 66-68.

[5] Chen, J.W., Huang, M.Q., Chen, H. (2015) Research and Application of Zinc in Animal Husbandry. Sichuan Animal and Veterinary Sciences. 42(6), 31-33.

[6] Chai, S.F., Tian, Z.X. (2013) Application of trace element zincum in swine and poultry production. Feed and Husbandry. 10, 10-12.

[7] Wen, Q.N. (2014) Applied research and effect of trace element in ruminant production. Feed Industry. 35(9), 52-55.

[8] Ren, Y.S., Yue, W.B., Zhang, J.X., Lv, L.H. (2005) Relationship between zinc and animal reproduction. Heilongjiang Journal of Animal Reproduction. 2,17-18.

[9] Zhang, J., Zheng, S.M., Gao, L. (2005) Animal zinc deficiency. Chinese Journal of Animal Husbandry and Veterinary Medicine. 5(5), 55.

[10] Li, C.T. (2009) Effects of zinc on livestock and poultry and evaluation of zinc in aircraft. Agricultural Technology and Equipment. 163, 44-45.

[11] Wang, X.Y., Ma, J.X. (2004) Causes and control of zinc deficiency and zinc poisoning in animals. Modern Animal Husbandry Science and Technology. 11, 145.

[12] Wang, Y.D., Zhao, Y.R. (2018) Biological characteristics of zinc and function in weaned piglets. Feed Review. 1, 32-35.

[13] Gao, J.F., Su, X.L., Xiong, K.N., Zhou W. (2011) Grasslands eco-environment and stock-breeding development in the karst areas of Guizhou province. Acta Prataculturae Sinica. 20(4), 279-286.

[14] Rockey, D.C., Caldwell, S.H., Goodman, Z.D., Nelson, R.C., Smith, A.D. (2009) Liver biopsy. Hepatology. 49(3), 1017-1044.

[15] Streeter, R.M., Divers, T.J., Mittel, L., Korn, A.E., Wakshlag, J.J. (2012) Selenium deficiency associations with gender, breed, serum vitamin E and creatine kinase, clinical signs and diagnoses in horses of different age groups: A retrospective examination 1996-2011. Equine Veterinary Journal. 44(S43), 31-35.
[16] Shen, X.Y, Du, G.Z., Chen, Y.M., Fan, B.L. (2006) Copper deficiency in yaks on pasture in western China. The Canadian veterinary journal. 47(9), 902-906.
[17] Zhang, L.F. (2017) Advances in the application of zinc microelement in sheep production. Feed China. 7, 45-47.
[18] Zhang, C.M. (2011) Analysis and evaluation of available Zn, Mn, Cu and Fe contents of topsoil in Gulang irrigation region. Pratacultural Science. 28(6), 1221-1225.
[19] Ding, F. (2013) The Problem of grassland animal husbandry in Wumeng mountain area and its countermeasures-- A case study of Hezhang county, Guizhou province. Gansu, Lanzhou University.
[20] Chi, Y.K., Xiong, K.N., Chen, H., Min X.Y., Xiao H., Liao J.J., Shen X.Y. (2018) Effect of grazing to copper pollution meadow on copper metabolism in Wumeng semi-fine wool sheep. Polish Journal of Environmental Studies. 28(3), 1083-1091.
[21] Pang, Q.H., Zhang, L., Zhang, C.Y., Yang, X.H., Lu, J.Y. (2002) Advances of the zinc research in the health and nutrition of animals. Progress in Veterinary Medicine. 2, 41-43.
[22] Namkung, H., Gong, J., Yu, H., De Lange, C.F.M. (2006) Effect of pharmacological intakes of zinc and copper on growth performance, circulating cytokines and gut microbiota of newly weaned piglets challenged with coliform lipopolysaccharides. Canadian Journal of Animal Science. 86(4), 511-522.
[23] Chi Y.K., Xiong K.N., Xiao H., Chen, H., Huang D.H., Wen Y.Q., Shen X.Y. (2018) A comparative study on meat quality between Guizhou semi-fine wool sheep and a series of semi-fine wool sheep in southwest China. Fresen. Environ. Bull. 27, 4239-4238.
[24] Dietrich, N., Schneider, D.L., Kornfeld, K. (2017) A pathway for low zinc homeostasis that is conserved in animals and acts in parallel to the pathway for high zinc homeostasis. Nucleic Acids Research. 45(20), 11658.
[25] Norum, U., Bondgaard, M., Bjerregaard, P. (2003) Copper and zinc handling during the moult cycle of male and female shore crabs carcinus maenas. Marine Biology. 142(4), 757-769.
[26] Hoadley, J.E., Leinart, A.S., Cousins, R.J. (1988) Relationship of 65zn absorption kinetics to intestinal metallothionein in rats: effects of zinc depletion and fasting. Journal of Nutrition. 118(4), 497-502.
[27] Zhang, X. (2017) Effects of zinc on animal immunological function. Contemporary Animal Husbandry. 17, 20-21.
[28] Inigo-Figueroa, G., Méndez-Estrada, R.O., Quihui-Cota, L., Velásquez-Contreras, C.A., Garibay-Escobar, A., Astiarazan-Garcia, R. (2013) Effects of dietary zinc manipulation on growth performance, zinc status and immune response during *Giardia Lamblia* infection: a study in CD-1 mice. Nutrients. 5(9), 3447-3460.
[29] Crespo-Martínez, C., Sirvent-Ochando, M., Vázquez-Polo, A., Caba-Porras, I., Romero-Jiménez, R., Tejada-González, P. (2017) Survey on the use of zinc sulfate in parenteral nutrition in spanish hospitals. Farm Hosp. 42(2), 68-72.
[30] Park, S.Y., Birkhold, S.G., Kubena, L.F., Nisbet, D.J., Ricke, S.C. (2004) Review on the role of dietary zinc in poultry nutrition, immunity, and reproduction. Biological Trace Element Research. 101(2), 147-163.
[31] Alloway, B.J. (2009) Soil factors associated with zinc deficiency in crops and humans. Environmental Geochemistry and Health. 31(5), 537-548.
[32] Anilkumar, C., Ramana, J.V., Ramaprasad, J., Sudheer, S.D., Reddy, P.S., Shakeela, S. (2012) Dietary supplementation of zinc sulphate and zinc-methionine: changes in levels of mineral composition (copper, zinc, iron and manganese) in various organs of broilers. Journal of Animal Production Advances. 2(9), 409-419.
[33] Romeo, A., Vacchina, V., Legros, S., Doelsch, E. (2014) Zinc fate in animal husbandry systems. Metallomics. 6(11), 1999-2009.
[34] Shaheen, A.A, EL-Fattah A.A.A. (1995) Effect of dietary zinc on lipid peroxidation, glutathione, protein thiols levels and superoxide dismutase activity in tissues. The International Journal of Biochemistry and Cell Biology. 27(1), 89-95.

Received: **23.11.2018**
Accepted: **17.03.2019**

CORRESPONDING AUTHOR

Xiaoyun Shen
School of Karst Science,
Guizhou Normal University,
Guiyang 550001 – China

e-mail: sfdxsxy@163.com

© by PSP Volume 28 – No. 5/2019 pages 3893-3899 Fresenius Environmental Bulletin

ANALYSIS OF BOREHOLE STABILITY FOR INCLINED WELLS IN FRACTURED CARBONATE FORMATION

Yuanwei Sun[1], Yuanfang Cheng[2,*], Yongchao Hao[1], Meng Meng[3], Xiaodong Dai[1], Yanli Wang[1], Shuxin Dong[1], Guowei Peng[1]

[1]College of Oil and Gas Engineering, Shengli College China University of Petroleum, Dongying 257061, China
[2]School of Petroleum Engineering, China University of Petroleum (East China), Qingdao 266580, China
[3]Department of Petroleum Engineering, University of Tulsa, Tulsa 74104, USA

ABSTRACT

Typically, the required mud weight is determined by a wellbore stability analysis in which the rock material is assumed to be linear elastic, homogeneous, and isotropic in mechanics and strength behaviors. This traditional stability analysis, however, may lead to erroneous results particularly for a well drilled into fractured carbonate formation, and ignoring the strength anisotropy associated with planes of weakness such as foliations, or schistosity presented in carbonated rocks. Therefore, based on the porous elastic mechanics model of borehole stability and the single weak-plane strength theory, borehole stability model for inclined wells in fractured carbonate formations is established. Based on those, this paper quantitatively analyzed the effects of attitude of fissures and system researched the hole collapse pressure under different well track along with the change of weak plane occurrence characteristics. The basis for wellbore stability during drilling and production was provided. The results showed that collapse pressure is controlled by weak plane occurrence characteristics. Compared with traditional hole stability analysis model, the method of this article can provide a scientific calculated means and methods for solving the carbonate borehole instability.

KEYWORDS:
Carbonate formations, inclined wells, borehole stability, structural fracture, a single weak plane strength theory

INTRODUCTION

Carbonate reservoir plays an extremely important role in the world oil and gas production, which is of great significance for solving the problem of energy shortage in the world [1-3]. Such reservoirs [4-6] often collapse in open-hole completion formation during drilling and production [7], which severely restricts the development of resource. Only by thoroughly understanding the mechanism of wellbore instability of carbonate reservoir can the wellbore stability be guaranteed during drilling and production. Brudy et al. [8] proposed a series of countermeasures for the wellbore instability of this type of reservoir, mainly including optimizing the borehole structure, scientific selection of large-displacement well trajectory and reasonable selection of drilling fluid density [9-11]. The content of shale in carbonate reservoir is small [12], and mechanical factors are the main reasons for borehole instability. Physical and chemical factors can be ignored in borehole stability analysis. In this type of formation, there is a group of weak surface, which leads to failure before the rock body under low wellbore fluid pressure and unexpected complex situation of drilling [13-18]. Only by considering the influence of weak surface in borehole stability analysis, the drilling problems for practical engineering can be solved. A lot of researches have been carried out at home and abroad on wellbore instability caused by weak surface of reservoirs. Ma Morsy [19], Jung et al. [20] studied the wellbore stability of horizontal Wells in rational shale reservoirs based on the theory of single structural surface. The occurrence of bedding surface is the main factor leading to the collapse and instability of horizontal Wells. Neretnieks [23], Lu et al. [21] selected the weak surface model to study the cause of wellbore collapse in fractured formation at great depth for open and vertical well. Result proves the formation which the fracture dipping angle ranges from 0° to 20° and fracture azimuth tends to be nearly the horizontal minimum in-situ stress are the safest situation for vertical well, followed by the formation which the fracture dipping angle ranges from 60° to 90° and fracture azimuth tends to be nearly the horizontal maximum in-situ stress. Yang [22], He et al. [23] found that after considering the weak surface, there was no well inclination bearing with monotonously increasing or decreasing wellbore collapse pressure, and the danger and safety areas appeared alternately, with complex distribution.

At present, there is a lack of systematic research on the change rule of wellbore collapse pressure for inclined well with weak surface occurrence. Based on the engineering geological characteristics of carbonate reservoirs and the single weak surface criterion, this paper studies the variation rule of the wellbore collapse pressure of vertical wells, horizontal

wells and inclined wells with the weak surface occurrence, providing a basis for the evaluation and design of the wellbore stability of fractured carbonate reservoirs.

FAILURE CONDITION FOR WEAK PLANE

Micro-fractures are developed in complex carbonate formation rocks, and the strength of fractures is obviously lower than the strength of the rock body, which is often referred to as the weak surface. In 1960, Jaeger [3] first proposed the single weak surface strength theory, which described the shear failure of isotropic rock mass with one or a group of parallel weak surfaces, which was a generalization of the Mohr-Coulomb criterion. Therefore, according to the single weak surface strength theory, the failure state of fractured stratum rocks can be divided into two modes, as shown in Figure.1

(1) If the failure doesn't happen along the weak plane, rock mass strength is equal to the strength of the rock body, at this point, the angle of failure surface with σ_1, $\emptyset_0=\pi/4+\varphi_0/2$, i.e. the rock mass strength is:

$$\sigma_1 = \sigma_3 + \frac{2\left(c_0 + \sigma_3 \tan\varphi_0\right)}{\left(1-\tan\varphi_0 \cot\phi_0\right)\sin 2\phi_0} \quad (1)$$

(2) When the rock mass is destroyed along the weak surface, the strength of the rock mass is controlled by the strength of the weak surface, that is, the rock mass strength is:

$$\sigma_1 = \sigma_3 + \frac{2\left(c_w + \sigma_3 \tan\varphi_w\right)}{\left(1-\tan\varphi_w \cot\phi\right)\sin 2\phi} \quad (2)$$

If the failure doesn't happen along the weak plane, the angle between the normal of the fracture plane and the direction of the first principal stress $\emptyset$ meets that, $\emptyset_1 \le \emptyset \le \emptyset_2$. If $\emptyset$ meet this condition, and the stress state meet the type shown in (2), the failure of the rock will cause a slip along the weak plane, the strength of rock mass is controlled by the strength of weak surface. If $\emptyset$ fails to satisfy this condition, the direction of rock failure is along the angle $\emptyset_0=\pi/4+\varphi_0/2$, the strength of rock mass is controlled by the strength of rock matrix. The values of angle $\emptyset_1$ and $\emptyset_2$ can be obtained through the type (3).

$$\phi_1 = \frac{\varphi_w}{2} + \frac{1}{2}\arcsin\left[\frac{(\sigma_1+\sigma_3+2cw\cot\varphi_w)\sin\varphi_w}{\sigma_1-\sigma_3}\right] \quad (3)$$
$$\phi_2 = \frac{\pi}{2} + \varphi_w - \phi_1$$

In the formula: σ_1 is the maximum principal stress, MPa; σ_3 is the minimum principal stress, MPa; c_w is the cohesion of carbonate rock weak plane, MPa; φ_w is the internal friction angle of weak plane, °; c_0 is the cohesion of the rock mass, MPa; φ_0 is the internal friction angle of rock mass, °; $\emptyset$ is the angle of weak plane and the maximum principal stress, °; $\emptyset 0$ is the angle of rock mass failure surface and the maximum principal stress, °.

According to the single weak surface criterion, when c_w=10MPa, φ_w=15°, c_0=20MPa and φ_0=25°, the rock strength under different confining pressure is shown in Figure.2, which indicates that there is severe anisotropy in the fractured formation.

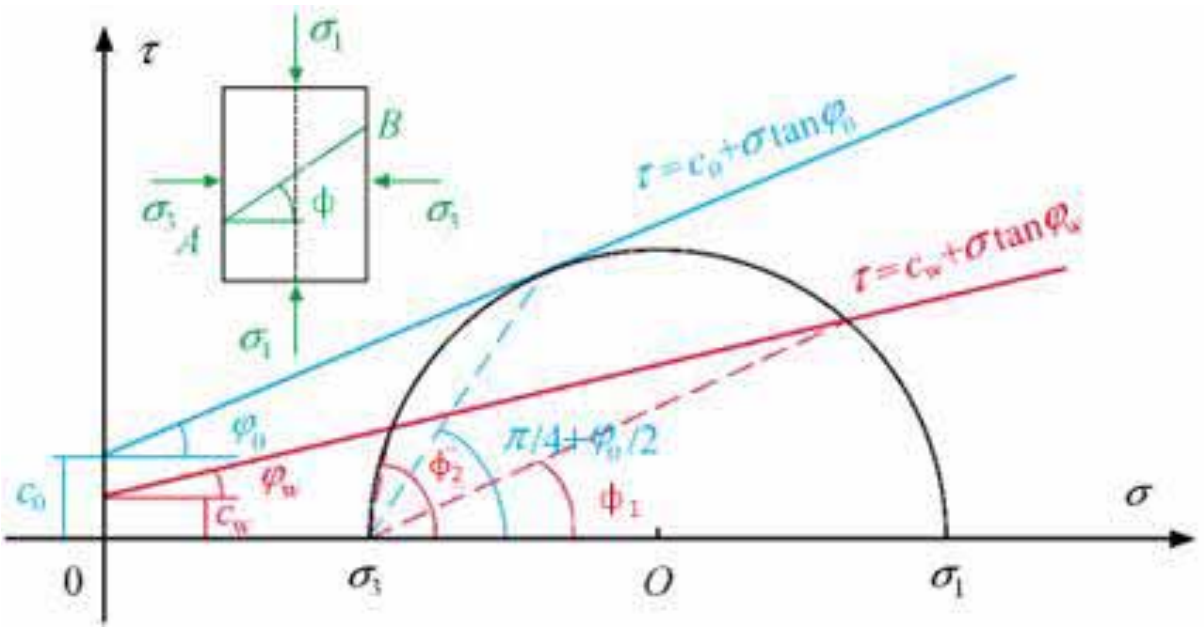

FIGURE 1
The rock strength criterion of single weak-plane carbonate rocks

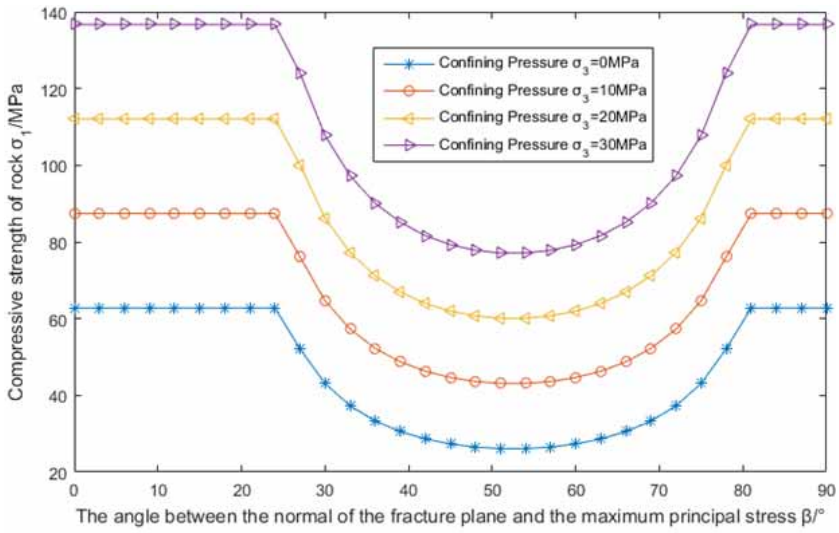

FIGURE 2
Relationship between β and strength of wellbore rock

THE MODEL OF WELLBORE INSTABILITY ANALYSIS IN FRACTURED FORMATION

Wellbore stress distribution of inclined wells. Wellbore stress distribution is the basis of wellbore stability analysis. The rock of deep strata is subject to three main in-situ stresses, wellbore stress distribution is controlled by in-situ stress, angle of well deviation and azimuth [24-29]. Assuming that the formation is an elastic uniform continuous medium with holes, the stress component of inclined Wellbore is [30]:

$$\sigma_r = P_w$$
$$\sigma_\theta = \sigma_x^o + \sigma_y^0 - 2(\sigma_x^o - \sigma_y^0)\cos 2\theta - 4\tau_{xy}^0 \sin 2\theta - P_w$$
$$\sigma_z = \sigma_z^o - \nu[2(\sigma_x^o - \sigma_y^0)\cos 2\theta + 4\tau_{xy}^0 \sin 2\theta]$$
$$\tau_{\theta z} = 2(-\tau_{xz}^o \sin\theta + \tau_{yz}^o \cos\theta)$$
$$\tau_{r\theta} = 0$$
$$\tau_{rz} = 0 \quad (4)$$

In the case of a given inclination and direction, the stress distribution of the wellbore is only a function of θ. It is not hard to obtained that the changes of the σ_θ and σ_z are the same with the change of θ [21]. Therefore, the maximum or minimum value can be obtained at the same position:

$$d\sigma_\theta/d\theta = 0 \quad (5)$$

By solving the above equation, the following formula can be getted:

$$\theta_1 = \frac{1}{2}arctan\left(\frac{2\tau_{xy}}{\sigma_x^o - \sigma_y^o}\right), \quad \theta_1 = \frac{\pi}{2} + \frac{1}{2}arctan\left(\frac{2\tau_{xy}}{\sigma_x^o - \sigma_y^o}\right) \quad (6)$$

The circumferential stress of the wellbore reaches its extreme value at θ_1 or θ_2. After determining the extreme point of wellbore circumferential stress, the calculated stress is compared with the corresponding strength criterion to judge whether the wellbore is stable or not.

Model resolution. Since most of the failure criteria used in borehole stability analysis are expressed as the principal stress, it is necessary to convert the wellbore stresses into the form of principal stress. In a deviated well, the significant difference between inclined wells and vertical wells is that the dipping angle α and the azimuth of well β must be considered by inclined wells. The azimuth angle of horizontal maximum in-situ stress HA, ω=β-HA, β and HA are all expressed by XX degree in the northeast geodetic coordinate system.

$$\sigma_i = p_w - p_p$$
$$\sigma_j = \frac{\sigma_\theta + \sigma_z}{2} + \frac{1}{2}\sqrt{(\sigma_\theta - \sigma_z)^2 + 4\tau_{\theta z}^2} - p_p$$
$$\sigma_k = \frac{\sigma_\theta + \sigma_z}{2} - \frac{1}{2}\sqrt{(\sigma_\theta - \sigma_z)^2 + 4\tau_{\theta z}^2} - p_p \quad (7)$$

The angle between the action surface of the maximum principal stress for wellbore and the axis of the hole is shown below:

$$\gamma = \frac{1}{2}arctan\frac{2\tau_{\theta z}}{\sigma_\theta - \sigma_z} \quad (8)$$

In the formula (8), $\sigma_\theta, \sigma_z, \tau_{\theta z}$ represents the tangential stress, axial stress and shear stress respectively in the cylindrical coordinate system with the inclined well as the axis.

In the geodetic coordinate system (*N,E,Sky*), the azimuth of the weak surface formation is north TR east, the dipping angle is DIP, so the direction vector n of the normal line of the weak surface is:

$$n = ia_1 + ja_2 + ka_3 \quad (9)$$

In the formula (9):

$$a_1 = sin(DIP)\,cos(TR), a_2 = sin(DIP)\,sin(TR), a_3 = cos(DIP) \quad (10)$$

In the rectangular coordinate system, the direction vector n of the maximum principal stress of wellbore σ_1 in the geodetic coordinate system can be expressed as:

$$N = ib_1 + jb_2 + kb_3 \quad (11)$$

In the formula (11):

b_1=cos$\beta\ cos\ \alpha\ sin\ \theta - sin\ \beta\ cos\ \theta + cos\ \beta\ sin\ \alpha\ cos\ \gamma$

b_2=sin$\beta\ cos\ \alpha\ sin\ \theta + cos\ \beta\ cos\ \theta + sin\ \beta\ sin\ \alpha\ cos\ \gamma$

b_3=$-\ sin\ \alpha\ sin\ \theta + cos\ \alpha\ cos\ \gamma$ (12)

The angle between maximum principal stress of wellbore and the normal of weak plane is

Sidewall Angle of maximum principal stress and the fracture plane normal $\emptyset$ is expressed below:

$$cos\phi = \frac{n \cdot N}{|n||N|} = \frac{a_i b_i}{(a_i a_i)^{1/2} + (b_j b_j)^{1/2}} \quad (i,j = 1,2,3) \quad (13)$$

Firstly, the angle between the maximum principal stress of the wellbore and the normal line of the weak plane is determined. If the angle between the maximum principal stress and the normal line of the weak plane obtained by the formula ranges from $\emptyset_1$ to $\emptyset_2$, then the three principal stresses obtained by equation (7) and the angle obtained by equation (8) are substituted into equation (2), the collapse pressure of the borehole, which failure happened along the weak plane can be obtained by solving this nonlinear equation. If the angle calculated by equation (8) is not satisfied $\emptyset_1 \leq \emptyset \leq \emptyset_2$, equation (3) is substituted into equation (1), then this nonlinear equation can be solved to get the collapse pressure of the well without shear failure along the fracture plane [22]. Thereinto, the nonlinear equation is solved by iterative method.

ANALYSIS OF THE INFLUENCE OF WEAK SURFACE OCCURRENCE TO WELLBORE STABILITY

In order to analyze the borehole instability rule of Dengying Formation (Sinian) in the central Sichuan region, the influence of borehole trajectory and fracture surface occurrence on borehole stability was studied with reservoir parameters (as shown in table 1) in this region. The purpose of safe drilling was achieved by optimizing borehole trajectory.

TABLE 1
Comparison table of industrial circulating cooling water and oilfield sewage

Number	Parameters	Value
1	Vertical depth/(m)	4981～5851
2	Vertical stress/(MPa)	114.96
3	Horizontal maximum principal stress/(MPa)	103.96
4	Horizontal minimum principal stress/(MPa)	85.96
5	Formation pressure/(MPa)	57.28
6	Rock mass cohesion/(MPa)	23
7	Internal friction angle of rock mass/(°)	37
8	Weak plane cohesion/(MPa)	0.5
9	Weak plane friction angle/(°)	37
10	Effective stress coefficient	0.75
11	Poisson's ratio	0.26

Model resolution. Assume that the direction of horizontal maximum geostress is due north, the basic parameters of sinian carbonate reservoir were substituted into the fracture formation borehole instability analysis model mentioned above. The influence of weak surface inclination and direction on the wellbore collapse pressure is obtained through numerical calculation. The influence of different fracture orientations and horizontal hole orientations on the bottom hole minimum pressure to maintain the stability of the wellbore is shown in Figure.3, at the case of weak plane dipping angle is 0°、30°、60° and 90°, respectively.

The results prove that, (1) When the weak surface dipping angle is 0°, the collapse pressure is independent of weak surface azimuth. The variation of collapse pressure with borehole orientation is similar to sin function. The minimum value is obtained in the direction of the horizontal maximum ground stress, and the maximum value is obtained in the direction of the horizontal minimum ground stress, which is the direction of the most prone to wellbore instability accidents for horizontal wells. (2) The collapse pressure has no obvious changing with the increasing or decreasing of the weak surface inclination. And its distribution is complex, which should be analyzed by specific weak surface strata occurrence. (3) It can be seen from the analysis of the most stable and volatile area of the wellbore in different fractured reservoirs that, when the weak plane dipping angle is 0 °, the safest position for horizontal well is where the azimuth is 0 °, at this point, the wellbore collapse is 23.26MPa; the most easily collapsed azimuth for horizontal wells is 90 °, at this point, the collapse pressure is 25.50MPa; When the inclination of the weak surface is 30°, and the azimuth of weak plane and well is 60°、120°、240° and 300° respectively, the borehole is the most stable, and the minimum bottom hole pressure to maintain the stability of the borehole wall is 19.78MPa. When the azimuth of weak plane is 60° and well azimuth is 180°, the minimum bottom hole pressure to maintain the stability of wellbore is 33.21MPa; When the dipping angle of weak plane is 60°, the safest situation for horizontal wells is when the azimuth of weak plane is 60° and well azimuth is 270°, the wellbore collapse pressure is 18.88MPa; the most easily collapsed situation for horizontal wells is when the azimuth of weak plane is 90° and well azimuth is 180°, the minimum bottom hole pressure to maintain the stability of wellbore is 33.40MPa; When the dipping angle is 90° and azimuth is 240° for weak plane, the wellbore collapse pressure is 18.88MPa under the condition of well azimuth is 90°, which is the safest azimuth for horizontal wells; When the azimuth of weak plane is 60° and well azimuth is 0°, the well is susceptible to collapse and the wellbore collapse is 33.40MPa. In summary, the horizontal well orientation in fractured carbonate reservoirs should be determined according to the weak-surface occurrence and the optimal well trajectory design scheme.

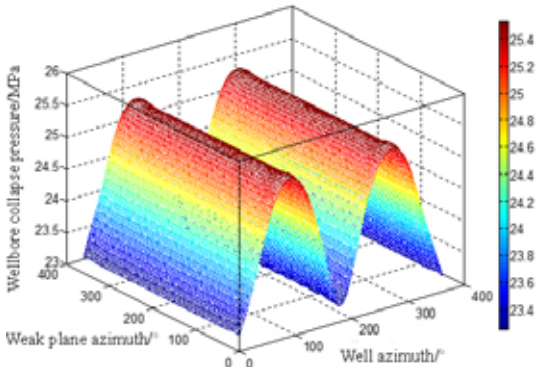

(a) When weak plane dipping angle is 0°

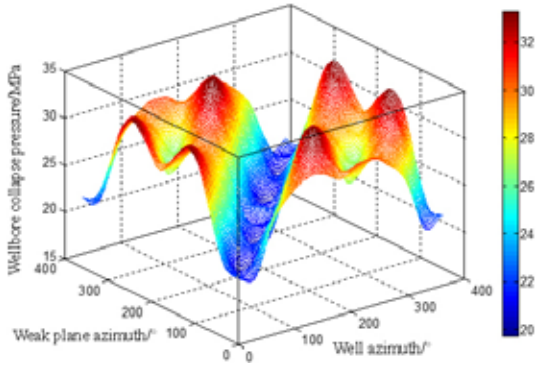

(b) When weak plane dipping angle is 30°

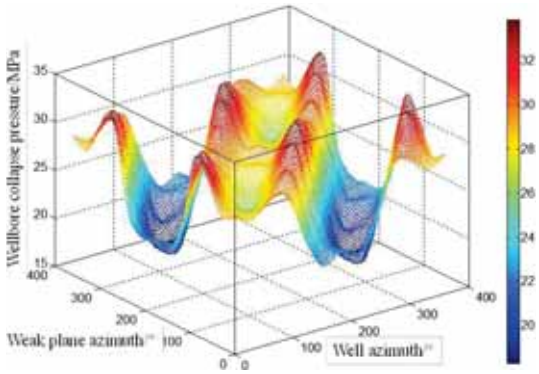

(c) When weak plane dipping angle is 60°

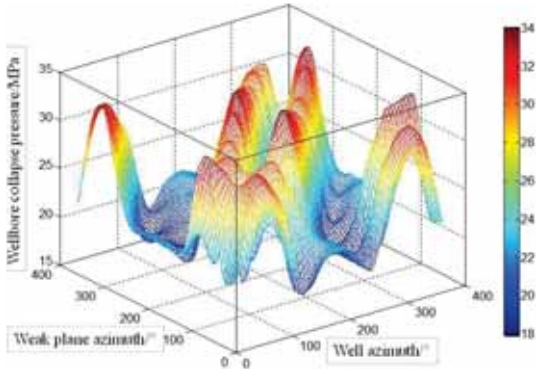

(d) When weak plane dipping angle is 90°

FIGURE 3
Horizontal well collapse pressure changing with the weak plane azimuth and wellbore azimuth

The effect of weak plane to inclined wells. The variation of wellbore collapse pressure for inclined wells with the weak plane inclination angle and azimuth is analyzed. When the hole deviation angle is 30°, the calculation results of wellbore collapse pressure for the hole azimuth is 90° and 180° are shown in Figure.4~5. The analysis mainly draws the following conclusions,

(1) At the case of well azimuth is 90°, wellbore collapse pressure is generally high for different trajectory. When the weak plane dipping angle is 30° and azimuth is 90°, the wellbore collapse pressure gets the minimum value, i.e. 18.30MPa; besides, when the weak plane dipping angle is 50° and azimuth is 30°or the weak plane dipping angle is 90° and azimuth is 270°, the minimum bottom hole pressure maintaining borehole stability is relatively small, i.e. 21.30MPa;

(2) At the case of well azimuth is 180°, when the dipping angle of weak plane is greater than 60°, the wellbore collapse pressure is relatively high, basically above 25MPa. When weak plane dipping angle is less than 60°, the wellbore pressure has large variation range, when the weak plane azimuth is 0°, 180° or 360°, the collapse pressure obtained the minimum value, 17.88MPa; when the weak plane azimuth is 120° or 240°, the collapse pressure obtained the maximum value, 28.84MPa.

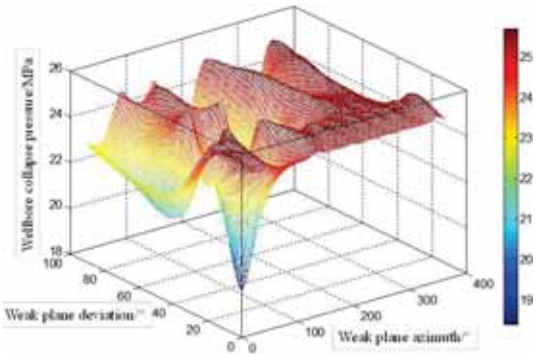

FIGURE 4
Well collapse pressure changing with the weak plane occurrence when α=30° and β=90°

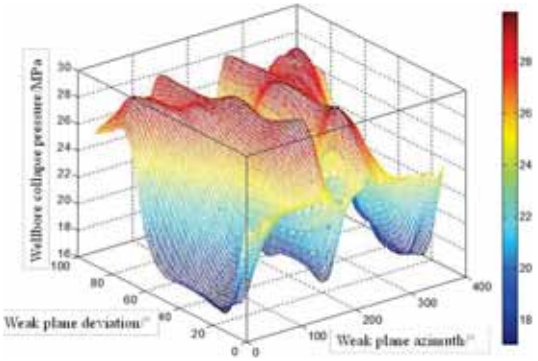

FIGURE 5
Well collapse pressure changing with the weak plane occurrence when α=30° and β=180°

(3) When well azimuth is 90°, the changing of wellbore collapse pressure is complex and irregular. In the case of well azimuth is 180°, when weak plane dipping angle is less than 60°, the changing of wellbore collapse pressure is basically the same, which increases first then decreases with the increase of weak plane azimuth. When weak plane dipping angle is greater than 60°, the collapse pressure changes irregularly with the weak surface inclination and maintains at a high level.

As for inclined wells, the stability of wells for different weak surfaces varies greatly, wellbore stability analysis should be carried out according to the actual calculation results and in combination with specific conditions. Under specific weak surface occurrence and reservoir environment conditions, appropriate changes in borehole trajectory can improve the stability of wellbore, reduce the occurrence of instability accidents, and ensure the safe and efficient drilling.

CONCLUSION AND PROSPECT

(1) For horizontal well, when the weak surface dipping angle is 0°, the collapse pressure is independent of weak surface azimuth. The variation of collapse pressure with borehole orientation is similar to sin function. The collapse pressure has no obvious changing with the increasing or decreasing of the weak surface inclination. And its distribution is complex, which should be analyzed by specific weak surface strata occurrence.

(2) There are great differences in the stability of inclined wells with different weak surface occurrences. The stability analysis of borehole should be based on the actual calculation results and in combination with specific conditions. Under specific weak surface occurrences and reservoir environmental conditions, the stability of borehole walls can be improved by appropriately changing the borehole trajectory.

(3) In the wellbore stability analysis of fractured carbonate reservoirs, the influence of weak plane occurrence is crucial. Appropriate changes in wellbore trajectory can improve the stability of the wellbore. The influence of natural fracture occurrence should be fully considered to prevent the wellbore from collapsing and instability, leading to stuck drilling or well scrapping.

ACKNOWLEGEMENTS

This research was financially supported by the National Natural Science Foundation (NO.51574270), the National Key Basic Research and Development Program (973 program) (NO.2015CB251201), and the National Key Research and Development Program (NO.2016YFC0304005).

REFERENCES

[1] Kidambi, T., Kumar, G.S. (2016) Mechanical earth modeling for a vertical well drilled in a naturally fractured tight carbonate gas reservoir in the Persian Gulf. Journal of Petroleum Science and Engineering. 141, 38-51.

[2] Maleki, S., Gholami, R., Rasouli, V., Moradzadeh, A., Ghavami Riabi, R., Sadaghzadeh, F. (2014) Comparison of different failure criteria in prediction of safe mud weigh window in drilling practice. Earth-Science Reviews. 136(3), 36-58.

[3] Jaeger, J.C. (1960) Shear failure of anistropic rocks. Geological Magazine. 97(1), 65-72.

[4] Olivella, S., Alonso, E.E. (2004) Modelling gas flow through deformable fractured rocks. Elsevier Geo-Engineering Book Series. 2(04), 31-36.

[5] Zhu, H., Zhu, J., Rutter, R., Zhang, J., Zhang, H. Q. (2018) Sand Erosion Model Prediction, Selection and Comparison for Electrical Submersible Pump (ESP) Using CFD Method. In ASME 2018 5th Joint US-European Fluids Engineering Division Summer Meeting. American Society of Mechanical Engineers.

[6] Chen, P., Gao, D., Wang, Z., Huang, W. (2017) Study on aggressively working casing string in extended-reach well. Journal of Petroleum Science and Engineering. 157, 604-616.

[7] Zhang, H., Ou F.J., Yin, G.Q., Yi, J.B., Yuan, F., Xie, B., Li, C., Zhao, W. (2013) Application of research of the relationship between ground stress and fractures in the trajectory optimization of horizontal wells. Advanced Materials Research. 765-767(15), 300-306.

[8] Brudy, M., Zoback, M.D. (1993) Compressive and tensile failure of boreholes arbitrarily-inclined to principal stress axes: application to the KTB boreholes, Germany. Int. j. rock Mech. min. sci. geomech. Abstr. 30(7), 1035-1038.

[9] Lan, K., Xiong, Y.M., Yan, G.Q., Liu, M.G. (2011) Horizontal borehole stability and its influence on well completion optimization in the Northeast Sichuan Basin. Journal of Jilin University. 41(4), 1233-1238.

[10] Lu, Y.H., Chen, M., Jin, Y., Zhang, G.Q. (2012) A mechanical model of borehole stability for weak plane formation under porous flow. Liquid Fuels Technology. 30(15), 10.

[11] Meng, M., Qiu, Z.S. (2018) Experiment study of mechanical properties and microstructures of bituminous coals influenced by supercritical carbon dioxide. Fuel. 219, 223-238.

[12] Wang, Y., Dusseault, M.B. (1994) Stresses around a circular opening in an elastoplastic porous medium subjected to repeated hydraulic loading. International Journal of Rock Mechanics and Mining Sciences and Geomechanics Abstracts. 31(6), 597-616.

[13] Neretnieks, I. (2004) Predicting solute transport in fractured rocks- processes, models and some concerns. Elsevier Geo-Engineering Book Series. 2, 19-30.
[14] Rocha-Lona, L., Alvarez-Reyes, S. E., Eldridge, S., Garza-Reyes, J. A., Kumar, V. (2013) Asphaltene precipitation due to natural depletion of reservoir: determination using a sara fraction based intelligent model. Fluid Phase Equilibria. 354(5), 177-184.
[15] Chen, P., Ma, T., Xia, H. (2015) A collapse pressure prediction model for horizontal shale gas wells with multiple weak planes. Natural Gas Industry B. 2(1), 101-107.
[16] Meng, M., Zamanipour, Z., Miska, S., Yu, M., Ozbayoglu, E.M. (2019) Dynamic stress distribution around the wellbore influenced by surge/swab pressure, Journal of Petroleum Science and Engineering. 172, 1077-1091.
[17] Meng, M., Baldino, S., Miska, S.Z., Takach, N. (2019) Wellbore Stability in Naturally Fractured Formations Featuring Dual-Porosity/Single-Permeability and Finite Radial Fluid Discharge. Journal of Petroleum Science and Engineering. 174, 790-803.
[18] Dong, B., Meng, M., Qiu, Z., Lu, Z., Ye, Z., Zhong, H. (2019) Formation damage prevention using microemulsion in tight sandstone gas reservoir. Journal of Petroleum Science and Engineering. 173, 101-111.
[19] Morsy, S., Hetherington, C.J., Sheng, J.J. (2015) Effect of low-concentration HCL on the mineralogy, physical and mechanical properties, and recovery factors of some shales. Journal of Unconventional Oil and Gas Resources. 9, 94-102.
[20] Jung, H.B., Kabilan, S., Carson, J.P., Kuprat, A.P., Um, W., Martin, P. (2014) Wellbore cement fracture evolution at the cement–basalt caprock interface during geologic carbon sequestration. Applied Geochemistry. 47(8), 1-16.
[21] Lu, D., Ni, H., Li, M., Li, W., Song, W., Xing, G. (2018) Wellbore collapse pressure analysis under supercritical carbon dioxide drilling condition. Journal of Petroleum Science and Engineering. 161, 458-467.
[22] Yang, Z.Z., Yi, L.P., Li, X.G., Chen, Y.T., Sun, J. (2018) Model for calculating the wellbore temperature and pressure during supercritical carbon dioxide fracturing in a coalbed methane well. Journal of CO_2 Utilization. 26, 602-611.
[23] He, S., Zhou, J., Chen, Y., Li, X., Ming, T. (2017) Research on wellbore stress in under-balanced drilling horizontal wells considering anisotropic seepage and thermal effects. Journal of Natural Gas Science and Engineering. 45, 338-357.
[24] Kwiatek, G., Martínezgarzón, P., Plenkers, K., Leonhardt, M., Zang, A., Dresen, G., Bohnhoff, M. (2017) Insight into subdecimeter fracturing processes during hydraulic fracture experiment in Äspö hard rock laboratory, Sweden. Egu General Assembly Conference.
[25] Chaudhuri, R.A. (2018) A nonlinear resonance (eigenvalue) approach for computation of elastic collapse pressures of harmonically imperfect relatively thin rings. Thin-Walled Structures. 127, 344-353.
[26] Holmlund, P., Johansson, E., Qvarlander, S., Wåhlin, A., Ambarki, K., Koskinen, L.O.D., Malm, J., Eklund, A. (2017) Human jugular vein collapse in the upright posture: implications for postural intracranial pressure regulation. Fluids and Barriers of the Cns, 14(1), 17.
[27] Chen, P., Gao, D., Wang, Z., Huang, W. (2015) Study on multi-segment friction factors inversion in extended-reach well based on an enhanced PSO model. Journal of Natural Gas Science and Engineering. 27, 1780-1787.
[28] Lechner, C., Koch, M., Lauterborn, W., Mettin, R. (2017) Pressure and tension waves from bubble collapse near a solid boundary: a numerical approach. Journal of the Acoustical Society of America. 142(6), 36-49.
[29] Zhu, H., Zhu, J., Zhang, J., Zhang, H.Q. (2017) Efficiency and Critical Velocity Analysis of Gravitational Separator Through CFD Simulation. In ASME 2017 International Mechanical Engineering Congress and Exposition. American Society of Mechanical Engineers.
[30] Meng, M., Zamanipour, Z., Miska, S. Yu, M.J., Ozbayoglu, E.M. (2019) Dynamic Wellbore Stability Analysis under Tripping Operations. Rock Mechanics and Rock Engineering. 2019, 1-21.

Received: **06.02.2019**
Accepted: **18.03.2019**

CORRESPONDING AUTHOR

Yuanfang Cheng
School of Petroleum Engineering
China University of Petroleum (East China)
Qingdao 266580 – China

e-mail: sunyw1902@163.com

© by PSP Volume 28 – No. 5/2019 pages 3900-3905 Fresenius Environmental Bulletin

EFFECTS OF DIFFERENT COLORED MULCH POLYETHYLENE COVERS ON SOLARIZATION AND SOIL TEMPERATURE IN GREENHOUSES

Elif Yuksel Turkboylari[1,*], Ahmet Nedim Yuksel[2], Erhan Gezer[2]

[1]Department of Plant and Animal Production, Vocational Collage of Technical Science, Namik Kemal University, Tekirdag, Turkey
[2]Departmant of Biosystem Engineering, Faculty of Agriculture, Namik Kemal University, Tekirdag, Turkey

ABSTRACT

The solarization applications performed by means of sun is effective in disinfection of the soil in greenhouses. A trial was completed in a plastic covered greenhouse for determining the effect of solarization on soil temperature and disinfection. In this trial, temperature values were measured from May to September in parcels covered with 0,15±0,01 mm thick transparent and black polyethylene and soil parcels.

In these months, the surface temperature on the black polyethylene covered parcels was measured between 49.0 ºC and 57.7 ºC. These values are 5.0 ºC to 6.1 ºC higher than the transparent polyethylene covered parcel (44.0 ºC – 51.6 ºC). As for the soil parcel, the maximum soil temperature varied between 44.1 ºC – 46.9 ºC. The temperatures, which were measured as a result of the solarization and exceeded 45 ºC – 50 ºC, are significant values for soil disinfection. It was determined that temperature of surfaces with black cover increased up to 57.7 ºC when the air temperature in the greenhouses exceed 40 ºC. However, the surface temperature of the soil under the black cover was around 43.6 ºC and thus 14.1 ºC lower than the surface temperature of the black polyethylene cover. The difference between the low greenhouse temperatures might be lowered down to 2 ºC – 3 ºC. The temperature of the soils under the polyethylene covers resistant to solar rays is lower than the soils under the transparent polyethylene cover.

The soil surface temperature of the transparent polyethylene covered parcel might be 2 ºC to 3 ºC higher than the polyethylene covered parcel.

The maximum temperatures measured at 10 to 15 cm depth of the soil were between 32.12ºC and 40.7 ºC in the parcel covered with transparent polyethylene and thus 1.1 ºC to 4.9 ºC higher than the parcel with black polyethylene cover. These values varied between 23.2 ºC and 35.2 ºC on the soil parcel and thus were lower than other covered parcels.

KEYWORDS:
Greenhouse, solar energy, solarization, soil temperature, mulch polyethylene cover

INTRODUCTION

Agricultural activities must be sustained to meet food and nutritional requirements of the people and all living creatures in the world. Sustainable agriculture becomes more difficult since the world population increases and the agricultural lands are being misused. These conditions require continuously harvesting more number of products from a unit of agricultural land. The intensive cultivation practices might cause rapid changes on the natural soil characteristics and the organic matter might decrease and its physical, chemical and biological structure might start to deteriorate.

Sustainable production in greenhouses becomes much more crucial considering the special and expensive production conditions in the agriculture and the high efficiency achieved in the greenhouses.

In fall, winter and spring, the air temperatures are low in our country and the production in greenhouses requires heating. Actually, heating highly increases the production costs in the greenhouses and leads to expensive production activities. Thus, sun is used as the source of energy for cultivation activities in the greenhouses [1].

Generally, the greenhouses practicing monoculture cultivates the same plants continuously over and over again and this cultivation increases the plant disease specific for that plant and population of pests in the soil. Besides, the air temperature and humidity in the greenhouse are also high. The hotbeds have insufficient air and the soil moisture is high due to irrigation and this paves the way for rapid increase and spread of all types of diseases and pests in the greenhouse. To do healthy, efficient and quality production in the greenhouses, effects of diseases and pests in the soil must be reduced by a specific level. It is determined that solarization applications are efficient for disinfection of the hotbeds [2].

Solarization Applications in the Greenhouses. Disinfecting hotbeds by using solar energy before planting is an environment friendly method. The basis of solarization with solar energy is to heat the soil up to high temperatures using sun lights. In

Turkey, this method can be used in the greenhouses during very hot July and August when production activities are not performed in the greenhouses. After preparation of the soil and irrigation, the solarization might be practiced by covering the soil with polyethylene cover or another cover. The purpose of solarization applied with covering the hotbed with a polyethylene cover is to increase the soil temperature and to ensure transmission to sub layers [3]. This method has advantages such as low costs and having no negative impact on the environment. However, this must be applied for a long time such as minimum 3 to 4 weeks [4].

The soil temperature is the most important element that control physical, chemical and biological phenomena observed in the soil. It is the hardest soil condition to control. The most significant factor in heating the soil is the infrared lights of the sun that have long wavelengths. The infrared lights coming from the sun heat the atmosphere and soils. Also, the short wavelength sun lights hit the earth and their wavelengths increase and they heat the earth and objects as thermal energy. The energy received by the soil heats the soil if it is more than the energy lost by the soil. The direction of heat transmission in the soil is from high temperature to lower temperature [5].

The soil heating effect of solar radiation might be increased through use of miscellaneous substances and covers on the soil. The polyethylene cover laid on the soil surface does not only reduce the heat loss of the soil but also prevents water loss of soil through evaporation. It is stated that water drops and water vapor on the inner surface of the polyethylene cover laid on the soil surface block long wavelength lights and create the "greenhouse effect" as well as heating the soil more [6].

The effectiveness of solarization depends on causes of disease in the soil, sensitivity of harmful microorganisms and nematodes to high soil temperatures.

Most of the causes of diseases and nematodes harming the cultivated plants are present in the soil. Controlling soil based causes seen in the hotbeds is possible through physical and chemical methods. The physical disinfection is performed through increasing the heat of hotbeds with a number of methods and solarization. For chemical disinfection, some extremely toxic chemical substances (pesticides) are applied to the soil. This method is highly dangerous for the environment and human health and adversely affects the natural balance. The producers prefer agrochemicals due to advantages such as easy application and being effective in a short period of time. Today, conscious and controlled use of agrochemicals must be guaranteed for sustainable agricultural production and protection of environmental health. Excessive use of chemicals increases the production costs and causes expensive production activities. Residues on fruits and vegetables emerge as a problem during marketing and exportation operations. This is why healthy food production must be guaranteed through a sustainable agricultural system and limited use of chemical substances [7,8]. Otherwise, these excessive toxic substances might come back to the humans and other living creatures through the food chain [9-11]. Furthermore, these chemical substances have several adverse effects such as diseases and harmful organisms as well as resistance of weeds [12].

Different researchers used a variety of different substances for solarization. In Nigeria, permeable polyethylene film and organic mulch was used for solarization during onion production in the arid season [13]. Solarization provided better results than other organic mulches (peanut shells, corn shells, sawdust). MeBr and soil solarization applications were compared on the greenhouses cultivating tomatoes. *Fusarium spp.* population was significantly reduced with both methods and yield increased significantly. This study presented that soil solarization can be used in the greenhouses cultivating tomatoes, as an alternative to MeBr fumigation [14].

0.25 mm transparent, black and 0.75 mm black polyethylene covers were used for the soil solarization study done in India. The highest soil temperature was 52.2 °C at 12 cm depth under 0.25 mm transparent polyethylene covers and wet conditions. This value was measured as 50.1 °C under dry conditions. The highest soil temperature was 39.6 °C in the area with no solarization [15].

This study focused on a different use of sun, one of the renewable energy resources, in the greenhouses. Majority of the causes of disease and nematodes, which damage the cultivated plants grown in the greenhouses, is present in the soil. To control these, the physical control method, which heats the soil up to a certain temperature, was preferred instead of chemical control method that has negative impact on the environment and people. The greenhouses do not have any production activities during the hot summer months and the study focused on increasing the soil temperature through the polyethylene cover and solarization applications in the hotbeds and disinfecting effect of this process during these months.

MATERIALS AND METHODS

General Characteristics of the Research Area. The research area is the Thrace Region, located on the northwest of Turkey, and the city center of Tekirdağ province. The Thrace Region is located on the European continent of Turkey and between 26º-29º Eastern longitudes and 40º-42º northern latitudes. Tekirdağ Province, namely the location of research area, is located between 26º-

41′-28°10′ Eastern longitudes and 40°35′-41°35′ northern latitudes. The area is around 62188 hectares. Tekirdağ has a slightly rough terrain and rather young geological structure. The city achieved its current view during the time IV. Tekirdağ is categorized under sub-humid climate type [16].

Characteristics of the Polyethylene Cover. Soil parcels and parcels covered with transparent and black polyethylene covers were used as material in the plastic covered greenhouse. During solarization, we worked on determining the effect of 0.15±0.01 mm thick transparent and black colored polyethylene covers on the soil temperature and disinfection of the parcels.

Method. The process followed as a method measured cover surface and under cover soil surface temperatures on the transparent and black polyethylene covered parcels and soil temperatures at 10-15 cm depth at 14:00 o'clock on the day of testing. The surface temperature and soil temperature at 10-15 cm depth were measured on the soil parcel.

Furthermore, interior and exterior air temperatures of the greenhouse and moisture values were determined. The interior temperature of the greenhouse varied significantly from the exterior air temperature. The major factors of this temperature difference were related to sunny weather and ventilation windows and open or closed doors.

RESULTS AND DISCUSSION

Testing parcels were created on the plastic covered greenhouse for determining the effect of solarization through sun lights on the soil temperature and, indirectly, on the soil disinfection. In this test, temperatures were measured on the transparent and black polyethylene covered parcels and the soil parcels. The temperature measurements took place daily on the polyethylene covers and soil surface as well as at 10-15 cm depth of the soil. The albedo value (reflection capacity) of the dark colored, black polyethylene cover used for solarization is low. Thus, it traps more number of sun lights when compared to other covers. The surface temperature is higher than the transparent polyethylene cover [3]. However, this surface temperature cannot manifest itself in the soil. In other words, non-transparent covers trap the heat but they cannot transmit it to the sub soil layers. The fact that sun lights cannot go through the cover is a factor in this process.

In the parcel covered with the transparent polyethylene cover, the soil surface temperature was measured 1.5 °C to 2.3 °C higher than the plastic cover surface temperature. It is determined that degrees exceeding 45 °C - 50 °C, which are achieved as a result of the solarization, are important for disinfection [17, 18]. The soil surface temperature under the transparent polyethylene cover is higher than the black polyethylene covered parcel [15]. In the summer months, the maximum soil surface temperature varied between 44.1 °C - 46.9 °C on the soil parcel.

The temperature measurements related to the solarization in the parcels were examined between May and September. The solarization works took place during these months because the greenhouses do not have production activities in these months and the air temperature is high. In these months, the surface temperature on the black covered parcel varied between 49.0 °C and 57.7 °C. These values were measured between 44.0 °C and 51.6 °C on the parcel covered with the transparent plastic covered parcel (Figure 1). The surface temperature of the black polyethylene cover was 5.0 °C to 6.1 °C higher than the transparent polyethylene cover.

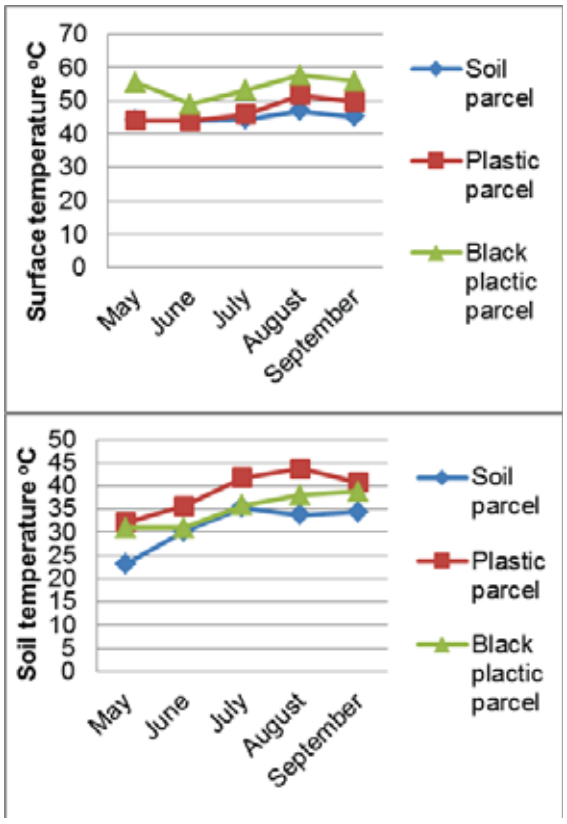

FIGURE 1
Maximum temperature changes on the parcel surface and soil at 10-15 cm depths

In this test, it is determined that the black polyethylene cover does not transmit the sun lights adequately. Thus, the surface temperature of the black polyethylene is higher than the surface temperature of the soil under it. The measurements revealed that cover surface temperature increased up to 57.7 °C on the black polyethylene covered parcels when the air temperature exceeded 30 °C and interior temperature of the greenhouse exceed-

ed 40 °C. However, the surface temperature of the soil under the cover increased up to 43.6 °C and it was nearly 14.1°C lower than the black plastic cover. The correlation between the surface temperature of the black polyethylene cover and surface temperature of the soil under the cover is shown on Figure 1. When the interior temperature of the greenhouse increased, the difference between the surface temperature of the black polyethylene cover and surface temperature of the soil under it increased. The difference might decrease down to 2 ^{o}C – 3 ^{o}C in case of lower exterior air temperatures and in winter (Figure 2).

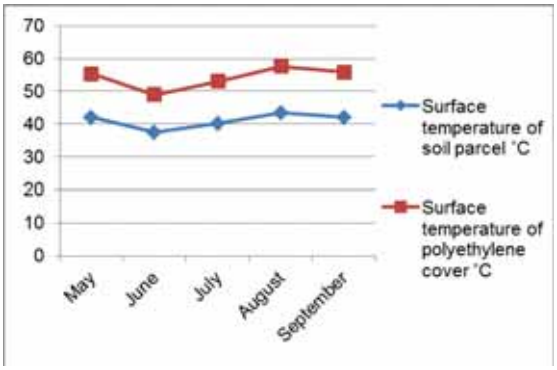

FIGURE 2
Maximum temperatures of the black polyethylene cover surface and soil parcel surface

As is seen, there are differences between the transparent and black polythene covered parcels in terms of the temperatures measured at 10-15 cm depth of soil.

The black polyethylene cover used for the solarization does not transmit the sun lights and the soil cannot be heated adequately. Also, the organic solarization material that does not transmit the sun lights cannot adequately heat the sub soil layers.

The maximum soil temperatures at the 10-15 cm depth of the soil were higher on the transparent plastic covered parcel when compared to the black covered parcel. From May to September, these values varied between 32.1^{o}C (May) and 43.7 ^{o}C (August) on the transparent covered parcel. In the same period, the maximum soil temperatures measured at the 10-15 cm depth of the parcel covered with black polyethylene cover varied between 31.0 ^{o}C (May) and 38.8 ^{o}C (August). The soil temperature of the transparent covered parcel was 1.1 ^{o}C to 4.9 ^{o}C higher than the black covered parcel.

These values varied between 23.2 ^{o}C and 35.2 ^{o}C on the soil parcel and this is rather lower in comparison to the other two parcels.

If the minimum soil temperatures on the parcels are compared; this value was between 18.8 ^{o}C and 22.4 ^{o}C on the black covered parcel and lower, namely between 17.7 ^{o}C and 20.8 ^{o}C, on the transparent covered parcel. This suggests that the black plastic cover does not transmit the sun light and also that it transmits and protects heat at a lower ratio. The minimum soil temperatures on the soil parcel were between12.0 ^{o}C and 20.3 ^{o}C. The values that are low in May catch up with the values of transparent covered parcel in July and August. The sub soil layers are heated less because the movement of soil temperature is in less and small in the vertical direction [5, 19].

CONCLUSION

The tests were done to determine the effect of solarization through sun lights in the plastic covered greenhouse on the soil disinfection. The purpose of the test was to determine the effect of 0.15±0.01 mm thick transparent and black polyethylene on the soil temperature.

The albedo (reflection) value of the dark colored, black polythene cover is low and it traps sunlight more than other covers [3]. The surface temperature is higher when compared to the transparent polyethylene cover. However, this surface temperature cannot manifest itself in the soil. It is confirmed the surface temperature of the black cover increased up to 57.7 °C on the days with high air temperature. However, the surface temperature of the soil under the cover increased up to 43.6 °C. The soil surface temperature was 14.1°C lower than the black cover.

It is determined that the surface temperature of the transparent plastic cover increased up to 51.6 °C and the soil surface temperature was 2.3 °C higher and marked 53.9 °C. It is confirmed that the soil surface temperature under the polyethylene cover was higher than the black polyethylene covered parcel. The temperature value connected with the transparent polyethylene cover was also studied by other researchers [15]. It is stated that the soil temperature that was measured as a result of solarization and exceeded 45 ^{o}C-50 ^{o}C is an important level of temperature for disinfection [17, 18].

The difference observed in terms of soil surface temperatures under the transparent and black polyethylene covers was also observed at the maximum temperatures at 10-15 cm depth of soil. The maximum temperatures at 10-15 cm depth of soil on the plastic covered parcel varied between 32.1°C and 43.7 °C from May to September. These values are 1.1 °C to 4.9 °C higher than the black polyethylene covered parcel. These values varied between 23.2 °C and 35.2 °C in the soil parcel and thus were lower than the other parcels.

When the minimum temperatures of the parcels are compared, it is seen that these values were between 18.8 °C and 22.4 °C on the black covered parcel but they were lower, namely between 17.7 °C and 20.8 °C, on the transparent covered parcel. This suggests that black plastic cover does not transmit sunlight and also transmits heat less and

preserves it. The maximum soil temperature measured in the transparent plastic covered parcels is higher than that of the black plastic covered parcel, which, in turn, means this type of cover is more transparent for the sun rays. However, at the same time, it was concluded this type of cover did not keep the heat well because the measured minimum soil temperatures were lower.

ACKNOWLEDGEMENTS

This study was supported by Namik Kemal University Scientific Research Projects Coordination Unit (Project Number: NKUBAP.03.GA.16. 062)

REFERENCES

[1] Yüksel, A.N. and Yüksel, E. (2012) Greenhouse construction technique. Hasad Publishing, İstanbul, 272p. (in Turkish).
[2] Katan, J. (1987) Soil solarization. In: Chet, I. (ed.) Innovative approaches to plant disease control. Wiley and Sons, New York. 77-105.
[3] Yücel, S., Yıldız, H.H., Aksoy, E., Çetinkaya-Yıldız, R., Çolak-Ateş, A., Özarslandan, A. and Dinçer, D. (2016) Soil solarization. Ministry of Food, Agriculture and Livestock, General Directorate of Agricultural Studies and Policies, Ankara:13-19. (in Turkish).
[4] Doğan, M.N. and Erkılıç, E. (1998) Soil solarization and fields of application. Ç.U. Agriculture Faculty Journal. 13(2), 91-100. (in Turkish).
[5] Bahtiyar, M. (1996) Soil Physics. T.U. Tekirdağ Agriculture Faculty Publishment No: 260, 302-319. (in Turkish).
[6] Mahrer, Y. (1979) Prediction of soil temperature regime under transparent polyethylene. J. Appl. Metorol. 18, 12-63.
[7] Özkan, B.H., Vuruş-Akçagöz, H. and Karadeniz, C.F. (2003) Producer attitudes and behaviors towards use of agricultural pesticides for growing citrus in Antalya province. Anadolu J. of AARI, 13(2), 103-106, Mara. (in Turkish).
[8] Delen, N., Durmuşoğlu, E., Güncan, A., Turgut, C. and Burçak, A. (2005) Use of pesticides in Turkey, issue of residues and loss of sensitivity in organisms. 6th Technical Congress of Turkish Chamber of Agricultural Engineers, 3-7 January 2005, 629-648. (in Turkish).
[9] Saber, M.S.M. (2001) Clean biotechnology for sustainable farming. Engineering in Life Sciences. 1(6), 217-223.
[10] Çakmakçı, R., Dönmez, M.F., Canpolat, M. and Şahin F. (2005) Effect of bacteria encouraging plant development on plant development and soil characteristics in greenhouse and different cropland conditions. VIth Turkish Field Crops Congress, Antalya. (in Turkish).
[11] Kitiş, Y.E. (2012) What is solarization? How is it applied? Journal of Agricultural. 10, 1-4. (in Turkish).
[12] Fennimore, S.A. and Doohan, D.J. (2008) The challenges of specialty crow weed control. Weed Technology. 22, 364-372.
[13] Adetunji, I.A. (1994) Response of onion to soil solarization and organic mulching in semi-arid tropics. Scientia Holticulturae. 60(1-2),161-166.
[14] Ioannou, N. (2000) Soil solarization as a substitute for methyl-bromide fumigation in greenhouse tomato production in Cyprus. Phytoparasitica. 28(3), 248-256.
[15] Raj, M. and Kapoor I.J. (1993) Soil solarization for the control of tomato wilt pathogen (*Fusarium oxysporum schl*.). Zeitschrift für Pflanzenkrankheiten und Pflanzen Schutz. 100(6), 651-652.
[16] Anonymous (2007) Use and Management of Water Resources in Tekirdağ Province. Tekirdağ Governorship Publications, Tekirdağ. (in Turkish).
[17] Herald, C.M. and Robinson, A.F. (1987) Effects of soil solarization on rotylenchulus reniformis in the lower Rio Grande Valley of Texas. Journal of Nematology. 19, 93-103.
[18] Pullman, G.S., Davey, E. and Garber, R.H. (1981) Soil solarization and thermal death: A logarithmic relationship between time and temperature for four soilborne plant pathogens. Phytopathology. 71, 959-964.
[19] Altındişli-Atağ, G., Sarıyev, A., Elekçioğlu, İ.H., Gök, M., Pamiralan, H. and Akça, H. (2017) Investigation of the effects of basaltic Tuff and Farm manure applications on soil Solarization in greenhouse conditions and mathematical modeling of soil temperature. Ministry of Food, Agriculture and Livestock, Research and Development Program, 94p. (in Turkish).

Received: **28.11.2018**
Accepted: **27.03.2019**

CORRESPONDING AUTHOR

Elif Yuksel Turkboylari
Department of Plant and Animal Production,
Vocational Collage of Technical Science,
Namik Kemal University,
Tekirdag – Turkey

e-mail: eyuksel@nku.edu.tr

© by PSP Volume 28 – No. 5/2019 pages 3906-3916 Fresenius Environmental Bulletin

EVALUATION ON THE ECOTOURISM RESOURCES OF TRADITIONAL VILLAGES FROM THE PERSPECTIVE OF ARTIFICIAL NEURAL NETWORK: A CASE STUDY IN HUNAN PROVINCE, CHINA

Chengjun Tang[1], Shaoyao He[1,*], Wei Zhang[1], Wenjuan Liu[2], Mengmiao Zhang[1]

[1]School of Architecture, Hunan University, Changsha 410082, China
[2]Hunan Institute of Science and Technology, College of Civil Engineering & Architecture, Yueyang 414000, China

ABSTRACT

Evaluation on the ecotourism resources of traditional villages can promote the sustainable development of rural tourism. Taking 10 typical traditional villages in the western part of Hunan area as research subjects, 1 decision layer, 3 criterion layers and 22 indicator layers have been established. Simulation training is conducted by adopting the rapidity and dynamics of artificial neural network in Clementine 12.0 and RBF evaluating model. In the meantime, quantitative comprehensive evaluation on the ecotourism resources of sample villages is also carried out on the basis of dynamic approach model in combined with fuzzy comprehensive evaluation approach. The result indicates that the credibility of the dynamic model in artificial neural network is higher than that of other 2 models; the overall situation of the ecotourism resources of sample villages is above the average, yet in need of further development and utilization. It is suggested to deeply explore the historical and cultural connotation implied by the ecological resources of traditional villages, improve the transportation convenience, promote infrastructure construction; strengthen propaganda as well as to systemically integrate the regional resources, so as to further upgrade the availability of the ecotourism resources of traditional villages, take control of the reasonable degree of protection and development of the ecotourism resources in the western Hunan area, and boost the economic sustainable development.

KEYWORDS:
Ecotourism resources, artificial neural network, clementine data-mining, evaluating indicator, traditional village, sustainable development

INTRODUCTION

Referring to the earlier-shaped villages in possession with abundant cultural and natural resources, as well as certain historical, cultural, scientific, artistic, economic and social values, traditional villages boast the greatest heritage inherited from Chinese agricultural and farming civilization. The villages inherited in the western part of Hunan (hereinafter referred to as the western Hunan) area are mainly traditional villages shaped during Ming and Qing dynasties and ever before. These villages still retain rich historical memory and cultural roots, which enables them to be significant sacred lands for tourists both abroad and at home. Therefore, how to protect and inherit the culture of traditional villages; how to scientifically categorize, effectively evaluate, protect and make use of ecotourism resource; as well as how to attract even more tourists to come to rural traditional villages for visits, have become important subjects in urgent need of addressing by rural ecotourism developments [1, 2].

From 2012 to 2016, 4 batches with 4157 directories of Chinese traditional villages have been published by the Ministry of Housing and Urban-Rural Development, the Ministry of Culture, and the Ministry of Finance. Altogether 257 villages in Hunan have been enlisted, taking up 6.2% of the nation's total. Currently, there are few research materials for the evaluation on the ecotourism resources of traditional villages, and most of the literature is concentrated on such aspects as tourism resources value, tourism environment, tourism service, and etc. of the traditional villages which cannot systemically reflect and historical, scientific and cultural values of the tourism resources of traditional villages, or can hardly embody the important status of ecotourism resource in the development and protection of traditional villages [3-7]. From the perspective of evaluating methods, relevant literature mainly adopts quantitative evaluating methods [8-10], for example, analytical hierarchy process, and the combination of analytical hierarchy process and fuzzy comprehensive evaluation, as well as GIS evaluation; whereas less artificial neural network to evaluate the ecotourism resources of traditional villages. This research conducts comprehensive evaluation on the tourism resources of 10 representative traditional villages in the western Hunan area by adopting the nodes of artificial neural network in Clementine12.0, data-mining software [11-14]. On this basis, suggestions of sustainable utilization of the ecotourism resources of traditional villages in the western Hunan area are

TABLE 1
The Division of Ecotourism Resources of the Traditional Villages in Western Hunan

Major category	Sub category	Basic category	Village characteristics
Natural landscape resources	Earthscape	Topography	Deben Village is located in the alpine and gorge region with winding mountains surrounded and terrains drastically rugged; Lao Siyan Village has karsts landform;
		Terrace	Yan Paixi Village is surrounded by peripheral terraces, with shallow hilly tier upon tier as if done by the spirits; 9 ancient aqueducts are just like 9 dragons coming down from the heaven, and irrigating thousands of mu of fertile farmland;
		Famous woods and ancient trees	In the front of Yan Paixi Village tower 3 ancient maple trees, whose metaphor is that Guanyin, a Bodhisattva ignites and inserts "3 incenses". This is implied with ancient "Fengshui" study;
	Forests and rivers	Forests	Shu Jiatang Village has cedar, pine, cypress, cedrela, cryptomeria fortune, camphor and other timberland;
		Rivers	Zhonghuang Village has Qiabi River; Lao Sicheng Village has Lingxi River;
	Relics landscape	Traditional residential	Shu Jiatang Village and Lahao Village use stone to build, and Tujia ethnic group uses wood to build hanging houses, and Deben Village is the one of Miao ethnic group;
		Characteristic blocks	Lahao Village has characteristic blocks; and Zhonghuang Village has streets and lanes with the Republic of China features;
Settlement landscape resources	Mono-landscape	Ancestral halls	Lao Sicheng Village has the Hall of Patriarch;
		Stockade gates	Lahao Village has Baojia Building; and Shuangfeng Village has Shuangfeng Stockade Gate;
		Bridges	Laohao Village has Fengyu Bridge; and Liuhe Village has Sangong Bridge;
		Relic Sites	Lao Sicheng Village has Tu Sicheng Relic Sites;
		Architectural sketches	Shuangfeng Village has Guyou Mill; Lao Sicheng Village as Guyou Mill; Shu Jiatang Village has "Southern Great Wall"; Lao Siyan Village has the original location of ancient dock; Liuhe Village has Longdong Mansion, Xianren Cave and Xima Cave;
Folk culture resources	Social folks	Mastaba folks	Shu Jiatang Village has stone tablet; Lahao Village has ancient tombs; and Tusi has Dezheng Stele
		Festival folks	Shu Jiatang Village has "Baishou Festival", Tiaoma Festival, 8 April, 6 June, and Mid-July all in Chinese lunar calendar;
		Folk arts and crafts	Lahao Village has weaving, embroidery, processing of silver ornaments, traditional printing and dyeing of Miao ethnic group; and Laoche Village has brocade of Tujia ethnic group;
	Spiritual folks	Sacrifice folks	Laoche Village offers sacrifices to the land, the mountain deity, worships the Dragon King, and has the Dragon Lantern Dance;
		Folklores	Yan Paixi Village has Songfu Legend;
		Folk dramas	Yan Paixi Village has Zuotan Opera;
		Songs and dances	Laoche Village has Baishou Dance, folk songs of Tujia ethnic group, Tima Song; and Lao Sicheng Village has Kujia Song;

proposed, which is useful for the sustainable development of the traditional villages tourism and the implementation of rural revitalization strategy in this area.

EXPERIMENTAL

Choosing the subjects. There are altogether 82 villages from Xiangxi Tujia and Miao Autonomous Prefecture enlisted into *the Directory of Chinese Traditional Village.* These villages have abundant material cultural heritages and intangible cultural heritages, which mainly formed during Ming and Qing Dynasties, with the earliest village dated back to Warring States Period. This research selects 10 representative villages, whose historical sites are well-preserved with plenty of cultural relics, providing rich resources to develop rural tourism. Combined with the status quo of the ecotourism resources of sample villages, the author divides ecotourism resources into 3 major categories, 6 sub ones, and 19 basic ones, as specifically indicated by Table 1.

RESEARCH METHODS

Characteristics of BP and RBF neural network. Back-Propagation (BP) network model belongs to a multi-layer feed forward neural network that is one-way transmitted. It has one input layer, one output layer, one or several hidden layers. Each layer has several nodes, every of which stands for a neuron. Each and every node in the same layer is not connected with one another, yet in the neighboring layer, is fully connected. Information is one-way transmitted among every layer starting from the input layer, and passes every hidden layer in succession, and finally arrives the output layer [15, 16]. Both hidden nodes and output nodes of BP neural network adopt the same adder and Sigmoid activation function. The adder equation is, $U_j = \sum_{i=1}^{n} W_{ij} X_i + \theta_j$, among which, U_j is the adder of the node *j*, W_{ij} is the link weight between the node *i* of the upper layer and the node *j* of this layer,

Xi is the output value of the node i of the upper layer, and θ_j is the deviation of the nodes. BP neural network adopts (0,1) type of Sigmoid activation function, and its function equation is $f(U_j) = \frac{1}{1+e^{-U_j}}$.

Radial Basis Function (RBF) neural network is a feed forward network with sound performances [17], such as the optimal approximation, concise training, fast learning convergence speed, as well as surmounting of local minimum problem. Currently, it has been proved that RBF can approximate arbitrary functions in succession with arbitrary precision, and therefore it is widely applied to model identification, non-linear control, image processing and other fields. This neural network is composed of input layer, hidden layer and output layer, three layers of network [18]. The weight from input layer to hidden one is fixed as 1. Neuron in the hidden layer is the input as the activation function of this neuron after the multiplication of the vector distance between W_i, the weight vector and X_i, the output vector of this layer and the deviation b_i. The transferring function of the hidden layer unit adopts the RBF of Gaussian kernel function, and the equation is $\ker(\|x-x_c\|) = e^{-\frac{\|x-x_c\|^2}{2\sigma^2 h}}$, x is the input variable, x_c is the center of the kernel function, σ is the width of kernel function, and h is radial covering length.

Construction of evaluating system and data collection and processing. Construction of evaluating system. According to the resources categorization standards and expert opinions of *Categorization, Investigation and Evaluation of Tourism Resources* (GB/T18972-2003), ecotourism resources evaluation indicator of traditional villages in western Hunan is primarily set-up [19,20]. On this basis, ecotourism resources evaluation indicator system of traditional villages in western Hunan is finally established after soliciting opinions from 30 experts, adjusting, adding and deleting the indicator system in accordance with such principles as the natures of objective, systematic, dynamic beneficial, and etc. of ecotourism resources evaluation [21, 22]. This system includes three layers, namely, decision layer (A), criterion layer (B_1、B_2、B_3) and indicator layer (AB_1C_1~AB_3C_8) (Table 2).

Data collection and processing. Since artificial neural network is to predict the evaluating results on the basis of the simulation results of training sample set, evaluating data need to be divided into 3 parts for processing, namely, training sample set, testing sample set and predicting sample set. For the former two sets, 22 evaluating indicators are set(AB_1C_1~AB_3C_8), with 5 evaluating rates, “1.00”(poor)、“0.75”(average)、“0.50”(moderate)、“0.25”(good)、“0”(excellent); meanwhile, expectation value (output value) is realized by 5 categorical variables, with “0” indicating poor evaluating result, “0.25”, average; “0.50”, moderate; “0.75”, good; and “1.00”, excellent. In Clementine, the above mentioned data is sample-partitioned according to the proportion of 70% of training sample set, and 30% of testing sample set. Sample set is tested and model deviation is calculated by making use of training model of training sample set. Drawing support of the investigation and survey period of editing *the Interpretation and Inheritance of Traditional Chinese Architecture Hunan Volume*, the research team investigated the sample villages during March and July in 2016 [23, 24]. Predictive sample

TABLE 2
Evaluation A on the ecotourism resources of traditional villages in western Hunan

Evaluation A on the tourism resources of traditional villages in western Hunan	Resources factor value B_1	Functionality AB_1C_1 Ecology AB_1C_2 Sociability AB_1C_3 Economy AB_1C_4 Ornamentality AB_1C_5 Uniqueness AB_1C_6
	Historical, cultural and artistic value B_2	Completeness AB_2C_1 Historicity AB_2C_2 Regionality AB_2C_3 Plurality AB_2C_4 Science popularity AB_2C_5 Continuity AB_2C_6 Inclusiveness AB_2C_7 Faith AB_2C_8
	Tourism environmental ambience B_3	Regional combination AB_3C_1 Environmental capacity AB_3C_2 Traffic condition AB_3C_3 Infrastructure AB_3C_4 tourist source market AB_3C_5 Tourism advertising AB_3C_6 Development degree AB_3C_7 Environmental protection AB_3C_8

TABLE 3
The Setting of Structure Model Parameter

Neural network calculating method		Quick analytical method	Dynamic analytical method	RBF
Network structure		22; 7; 5	22; 3; 4; 5	22; 5; 5
Pattern model		Expert	Simple	Expert
Number of training cycles (data passing times)		200	Automatic settings by the system	200
Training parameter	(Alpha) Impulse	0.9	—	0.9
	(Eta) Learning rate	Initial Eta=0.3; high Eta=0.1; Eta declining=30; low Eta=0.01	Automatic settings by the system	Initial Eta=0.4; Eta automatic calculation; RBF clustering number =20; RBF radical covering length =1
Precision of training simulation		100%	100%	100%

data were obtained by means of on-site questionnaire for tourists, and by adopting Likert 5-point Scale for the data statistics [25]. 100 sheets of questionnaire were handed out in every village, with 90~ 95 valid and the data were entered into SPSS software for data evaluation [26]. Since the range of the variable input by artificial neural network was usually valued 0~1, $\bar{x}_i = \dfrac{\bar{x}_i - x_{\min}}{x_{\max} - x_{\min}}$ was adopted ($\bar{x}_i$ is the average of the evaluating indicator of i, x_{max}, x_{min} are the maximum and minimum respectively of the indicator data of i) to conduct standardized transformation and processing of the data. Finally, the above mentioned data were introduced to the neural network model in Clementine12.0, data-mining software to realize the evaluation on ecotourism resources [27, 28].

RESULTS AND DISCUSSION

Parameter setting. Three-layer (input layer, hidden layer and output layer) neural network design is adopted. Network's input layer is the evaluating indicator of the ecotourism resources of traditional villages; output layer consists of 5 categorized neurons; whereas there is yet determined criterion with authority for the composition of hidden layer. The optimal network is opted by adopting trail-and-error method, and comparing among the network structure of the dynamic method, quick method and RBF of BP neural network nodes in the Clementine, simulation training cycle, parameter setting, training precision (Table 3), and the confidence degree of simulation results [29, 30]. The precision of training simulation refers to the prediction precision of estimation, and is based on the calculation of training sample set. For categorical output variable, prediction precision means the proportion taken up by correctly predicted sample of the entire sample. The learning rate setting strategy in Clementine is to make it change automatically in its process of model training, and the automatic change equation is $Eta(t) = Eta(t-1) \times \exp\left(\log\left(\dfrac{Eta_{low}}{Eta_{high}}\right)/d\right)$. Etalow and Etahigh indicate the maximum and minimum in respective of the change range of learning rate, and d is attenuation [31].

By setting the parameter of Table 3, 22 evaluating indicators are analyzed for simulation, and the result is as Table 4. From Table 4, it can be known that the actual output value of three methods totally conforms to the expected one, but the confidence degree in prediction being calculated is different, high to low in succession is BP neural network dynamic method, RBF model, BP neural network quick method. This indicates that BP neural network dynamic method is higher in the success rate of prediction with the best evaluating effects.

Evaluation on the ecotourism resources of traditional villages. Adopting the above mentioned well-trained network model to evaluate the ecotourism resources of the sample villages, and the results can be shown as Table 5. From Table 5, it can be known that the confidence degree in prediction of the tree evaluating method models is different. Overall speaking, the confidence degree of quick method model evaluation is the lowest, next is that of RBF model evaluation [32]; yet that of dynamic method model evaluation is relatively higher, which indicates that evaluation result of dynamic method model is higher. This conforms to the result of the confidence degree in prediction of the training sample in Table 2, and therefore, the evaluation result of dynamic method model is adopted.

Importance analysis indicates the degree of correlation between evaluating indicator and output nodes [33]. The higher the value is, the more important this evaluating indicator is to output nodes, and also to other indicators. The importance of 22 evaluating indicators (AB_1C_1~AB_3C_8) is calculated by adopting the model calculating method of BP neural network dynamic method and Tchaban algorithms based on neural network weight with the calculating equation $Q_{ik} = \dfrac{x_i(t)}{Y_K(t)} \sum_{j=1}^{L} W_{ij}(t) V_{jk}(t)$. In the

TABLE 4
Training Results and Confidence Degree

Evaluating indicator	Excellent	Good	Moderate	Average	Poor
AB_1C_1	0	0.25	0.5	0.75	1.0
AB_1C_2	0	0.25	0.5	0.75	1.0
AB_1C_3	0	0.25	0.5	0.75	1.0
AB_1C_4	0	0.25	0.5	0.75	1.0
AB_1C_5	0	0.25	0.5	0.75	1.0
AB_1C_6	0	0.25	0.5	0.75	1.0
AB_2C_1	0	0.25	0.5	0.75	1.0
AB_2C_2	0	0.25	0.5	0.75	1.0
AB_2C_3	0	0.25	0.5	0.75	1.0
AB_2C_4	0	0.25	0.5	0.75	1.0
AB_2C_5	0	0.25	0.5	0.75	1.0
AB_2C_6	0	0.25	0.5	0.75	1.0
AB_2C_7	0	0.25	0.5	0.75	1.0
AB_2C_8	0	0.25	0.5	0.75	1.0
AB_3C_1	0	0.25	0.5	0.75	1.0
AB_3C_2	0	0.25	0.5	0.75	1.0
AB_3C_3	0	0.25	0.5	0.75	1.0
AB_3C_4	0	0.25	0.5	0.75	1.0
AB_3C_5	0	0.25	0.5	0.75	1.0
AB_3C_6	0	0.25	0.5	0.75	1.0
AB_3C_7	0	0.25	0.5	0.75	1.0
AB_3C_8	0	0.25	0.5	0.75	1.0
Expected value	1.00	0.75	0.5	0.25	0
Output value of quick method	1.00	0.75	0.5	0.25	0
Confidence degree of quick method	0.77	0.02	0.11	0	0.21
Output value of dynamic method	1.00	0.75	0.5	0.25	0
Confidence degree of dynamic method	0.97	0.97	0.97	0.97	0.97
RBF output value	1.00	0.75	0.5	0.25	0
RBF model confidence degree	0.41	0.56	0.48	0.68	0.31

equation, t refers to time; $x_i(t)$, the evaluating indicator value of the moment t; $Y_K(t)$, output node value of the moment t; W_{ij}(t), the network weight between the input node of i, and hidden node of j of the moment t; V_{jk}(t), the network weight between the hidden node of j, and the output node of k of the moment t [34]. According to the importance of evaluating indicator, $Z_m = \frac{Q_{ik}}{\sum_{n=1}^{3} Q_{nm}}$, normalization equation can be utilized to calculate the importance of the indicator in every criterion layer, which is illustrated as Table 6 [35].

Every criterion layer (resources factor value, historical, cultural and artistic value, and tourism environment ambience) adopts fuzzy comprehensive evaluation method to conduct secondary comprehensive evaluation. Every weight distribution of indicator layer against criterion layer is defined as Z_m, and R_m is the factor set for every criterion layer (this factor evaluating value stands for frequency value) shown as Table 7. The comprehensive evaluating result of resources factor value is $B_1 = Z_1 \times R_1 =$ (0.023,0.065,0.233,0.388,0.291); historical, cultural and artistic value, $B_2 = Z_2 \times R_2 =$ (0.031,0.073,0.180,0.345,0.371); and ecotourism environment ambience, $B_3 = Z_3 \times R_3 =$ (0.031,0.083,0.235,0.408,0.243). According to the principle of maximum membership, sample villages' resources result of resources factor value, historical, cultural and artistic value, and tourism environment ambience is "good", "excellent" and "good" in respective. While according to the principle of weighted average, equation $u = \sum_{n=1}^{n} B \times S_i / \sum_{i=1}^{n} S_i$ is based, among which, B is comprehensive evaluating value; S_i, grading of comment set {excellent, good, moderate, average, poor} as (5, 4, 3, 2, 1) in respective. By calculating the result of resources factor value, historical, cultural and artistic value, and tourism environment ambience as 3.849, 3.913, 3.739 in respective, the value of the ecotourism resources of 10 traditional villages ranges from high to low is historical, cultural and artistic value, resources factor value, and tourism environment ambience.

According to the evaluation results of neural network dynamic method (Table 5) [36], the evaluating results of ecotourism resources of western Hunan's traditional villages; the comprehensive evaluating result of Lahao Village of Fenghaung County, Deben Village of Jishou City, Lao Sicheng Village of Yongshun County, and Shuangfeng Village of Yongshun County is"good"; Shu Jiatang Village of Fenghuang County, Zhonghuang Village of Jishou City, Yan Paixi Village and Lao Siyan Village of Guzhang County, Laoche Village of Longshan County, and Liuhe Village of Longshan County, "moderate". The results indicate that the ecotourism resources situation of these 10 traditional villages is above the average as a whole, and therefore, resources are still in need of further development and utilization. From the perspective of the importance of evaluating indicator in Table 6, infrastructure (AB_3C_4), transport condition (AB_3C_3), tourist source

TABLE 5
Evaluations on the Ecotourism Resources of Sample Villages

Evaluating indicator	Fenghuang County		Jishou County		Guzhang County		Yongshun Country		Longshan County	
	Shu Jiatang Village	Lahao Village	Deben Village	Zhong-huang Village	Paixi Village	Lao Siyan Village	Lao Sicheng Village	Shuang feng Village	Laoche Village	Liuhe Village
AB_1C_1	0.42	0.22	0.26	0.36	0.39	0.21	0.36	0.27	0.33	0.37
AB_1C_2	0.32	0.26	0.20	0.33	0.31	0.34	0.25	0.19	0.38	0.33
AB_1C_3	0.35	0.32	0.27	0.32	0.32	0.34	0.30	0.28	0.34	0.34
AB_1C_4	0.34	0.31	0.23	0.24	0.33	0.30	0.20	0.25	0.33	0.31
AB_1C_5	0.33	0.24	0.27	0.24	0.29	0.23	0.15	0.21	0.26	0.25
AB_1C_6	0.32	0.27	0.25	0.31	0.28	0.21	0.24	0.26	0.29	0.27
AB_2C_1	0.23	0.21	0.20	0.29	0.27	0.24	0.19	0.23	0.28	0.30
AB_2C_2	0.33	0.22	0.21	0.31	0.34	0.28	0.28	0.25	0.34	0.31
AB_2C_3	0.21	0.27	0.24	0.27	0.25	0.18	0.18	0.27	0.26	0.27
AB_2C_4	0.29	0.24	0.23	0.27	0.28	0.29	0.28	0.24	0.26	0.26
AB_2C_5	0.42	0.32	0.25	0.35	0.35	0.31	0.31	0.31	0.38	0.34
AB_2C_6	0.24	0.25	0.21	0.24	0.26	0.25	0.15	0.23	0.31	0.27
AB_2C_7	0.47	0.35	0.30	0.38	0.35	0.29	0.25	0.32	0.37	0.32
AB_2C_8	0.46	0.33	0.27	0.37	0.33	0.32	0.34	0.32	0.33	0.32
AB_3C_1	0.49	0.33	0.23	0.39	0.37	0.33	0.31	0.24	0.35	0.33
AB_3C_2	0.21	0.27	0.25	0.23	0.27	0.27	0.22	0.28	0.21	0.23
AB_3C_3	0.37	0.23	0.23	0.32	0.34	0.29	0.23	0.22	0.26	0.31
AB_3C_4	0.29	0.27	0.26	0.30	0.27	0.26	0.28	0.24	0.33	0.28
AB_3C_5	0.39	0.35	0.36	0.30	0.33	0.31	0.37	0.35	0.36	0.34
AB_3C_6	0.37	0.20	0.22	0.22	0.33	0.28	0.21	0.24	0.25	0.32
AB_3C_7	0.29	0.31	0.30	0.28	0.26	0.29	0.24	0.27	0.30	0.34
AB_3C_8	0.27	0.23	0.25	0.22	0.31	0.27	0.20	0.26	0.25	0.33
Quick method evaluation	0.50	0.75	0.75	0.75	0.50	0.75	0.75	0.75	0.50	0.50
Confidence degree of quick method evaluation	0.03	0.02	0.04	0.01	0.01	0.02	0.03	0.03	0.01	0.01
Dynamic method evaluation	0.50	0.75	0.75	0.50	0.50	0.50	0.75	0.75	0.50	0.50
Confidence degree of dynamic method evaluation	0.97	0.25	0.95	0.93	0.96	0.18	0.98	0.94	0.95	0.92
RBF evaluation	0.75	0.75	0.75	0.75	0.75	0.75	0.75	0.75	0.75	0.75
Confidence degree of RBF model evaluation	0.23	0.48	0.59	0.38	0.33	0.47	0.54	0.53	0.34	0.37

market (AB_3C_5), and regionality (AB_2C_3) of traditional villages exert more influence on the evaluation on the folk ecotourism resources of ancient villages, and therefore, are more important than other evaluating indicators; next come the tourism advertising (AB_3C_6), historicity (AB_2C_2), regional combination (AB_3C_1), functionality (AB_1C_1), sociability (AB_1C_3), and ornamentality (AB_1C_5) of the tourism resources of traditional villages; thirdly are economy (AB_1C_4), ecology (AB_1C_2), environmental capacity (AB_3C_2), completeness (AB_2C_1), science popularity (AB_2C_5), plurality (AB_2C_4), continuity (AB_2C_6), and inclusiveness (AB_2C_7) of the tourism resources of traditional villages. However, the faithfulness (AB_2C_8), uniqueness (AB_1C_6), environmental protection (AB_3C_8), and development degree (AB_3C_7) of villages' historical, cultural and artistic value are relatively of the least importance. Viewing from the importance of 22 indicators, infrastructure, transport condition, tourist source market, and historical and cultural regionality, and etc. of ecotourism resources exert huge influence on tourist resources evaluation; and the proportion of these 4 indicators evaluated as "good" is 60.5%, 63.1%, 57.6%, and 74.4% (Table 7) in respective. This indicates that there is still great room for these 4 evaluating indicators to improve, particularly, traditional villages' supporting facilities, conditions for transport convenience and tourist source market [37]. Given that western Hunan's traditional villages are located in the mountainous areas, and farther away from urban core zones, though it is advantageous to protect the completeness of village culture, it still leads to poor transport convenience, low service level, as well as weaker infrastructure in comparison with mature tourism villages [38].

Therefore, the transport convenience should be upgraded; and the construction of the supporting facilities should be strengthened for traditional villages, so as to improve the quality of experience and degree of satisfaction for tourists [39]. Furthermore, as for the folk culture characteristic of Xiangxi Autonomous Prefecture, the influence of folk-featuring products can be expanded through newspapers, TV, broadcast and other media or by holding the press conference. Meanwhile, screen culture works, including scenery documentaries, folk custom documentaries, or forms such as Shen Congwen Writers' Union, Huang Yongyu Art Exhibition can also be made use of to enable many more people not only to know about, but more to desire for Xiangxi Autonomous Prefecture [40].

TABLE 6
Analyses into the Importance of Evaluating Indicator

Criterion layer	Evaluating indicator	Importance of criterion layer indicator (Z_m)	Importance of the overall evaluating indicator (Q_{ik})
Resources factor value B_1	AB_1C_1	0.1917	0.0589
	AB_1C_2	0.1625	0.0507
	AB_1C_3	0.1405	0.0545
	AB_1C_4	0.1344	0.0521
	AB_1C_5	0.1981	0.0525
	AB_1C_6	0.1031	0.0414
Historical, cultural and artistic value B_2	AB_2C_1	0.1679	0.0495
	AB_2C_2	0.1553	0.0621
	AB_2C_3	0.2492	0.0659
	AB_2C_4	0.1639	0.0485
	AB_2C_5	0.1631	0.0490
	AB_2C_6	0.1827	0.0474
	AB_2C_7	0.1168	0.0431
	AB_2C_8	0.1071	0.0412
Tourism environment ambience B_3	AB_3C_1	0.2311	0.0613
	AB_3C_2	0.1871	0.0494
	AB_3C_3	0.1797	0.0689
	AB_3C_4	0.1736	0.0697
	AB_3C_5	0.1714	0.0675
	AB_3C_6	0.2121	0.0649
	AB_3C_7	0.1308	0.0397
	AB_3C_8	0.1619	0.0401

TABLE 7
Fuzzy Comprehensive Evaluation Result

Criterion layer	Evaluating indicator	Poor	Average	Moderate	Good	Excellent
Resources factor value	AB_1C_1	0.023	0.089	0.196	0.425	0.267
	AB_1C_2	0.027	0.058	0.231	0.367	0.317
	AB_1C_3	0.031	0.043	0.167	0.372	0.387
	AB_1C_4	0.022	0.042	0.236	0.355	0.345
	AB_1C_5	0.032	0.067	0.344	0.366	0.191
	AB_1C_6	0.031	0.187	0.229	0.306	0.247
	Fuzzy evaluation result	0.023	0.065	0.233	0.388	0.291
Historical, cultural and artistic value	AB_2C_1	0.067	0.112	0.223	0.351	0.247
	AB_2C_2	0.028	0.059	0.176	0.369	0.368
	AB_2C_3	0.037	0.068	0.151	0.223	0.521
	AB_2C_4	0.031	0.112	0.225	0.415	0.217
	AB_2C_5	0.033	0.049	0.209	0.368	0.343
	AB_2C_6	0.035	0.068	0.238	0.345	0.311
	AB_2C_7	0.018	0.084	0.129	0.414	0.355
	AB_2C_8	0.029	0.036	0.235	0.337	0.363
	Fuzzy evaluation result	0.031	0.073	0.180	0.345	0.371
Tourism environment ambience	AB_3C_1	0.035	0.058	0.187	0.426	0.294
	AB_3C_2	0.019	0.046	0.187	0.392	0.356
	AB_3C_3	0.024	0.056	0.289	0.434	0.197
	AB_3C_4	0.029	0.118	0.248	0.423	0.182
	AB_3C_5	0.037	0.098	0.289	0.379	0.197
	AB_3C_6	0.015	0.113	0.207	0.376	0.289
	AB_3C_7	0.023	0.031	0.309	0.396	0.241
	AB_3C_8	0.027	0.046	0.207	0.326	0.394
	Fuzzy evaluation result	0.031	0.083	0.235	0.408	0.243

Note: Evaluating value in the table represents frequency value, for instance, the proportion of tourists choosing "excellent" in AB_1C_1 is 26.7% as well as others.

It can be known from the fuzzy comprehensive evaluation on criterion layer that the evaluating result of historical, cultural and artistic value is "excellent", which demonstrates the characteristics of the tourism resources of western Hunan's traditional villages, such as Laoche Village's Baishou Dance, Tujia ethnic group's folk songs, Tima Song, and Yan Paixi Village's Zuotan Opera, as well as other folk culture resources, all of which are in possession with unique regionality, historicity, originality and artistry. Miao ethnic group's embroidery, and traditional printing and dyeing are intangible cultural heritage of Hunan Province. All of these become a great attraction for tourists. In addition, the evaluating result of resources factor value is "good", which indicates that the tasting value and involvement are still in need of further upgrading for traditional villages' resources. Both the connotation and implication of the resources should be dug out. Therefore, resources factor value and artistic characteristics of traditional villages' resources should be utilized to deeply explore the historical and cultural connotations implied, and traditional villages' features should be fully concentrated, with folk etiquette and custom, folk handicrafts, folk songs and dances as well as some unique activity forms characterized by local features being documented. At the same time, with the assistance of folk tourism activities, such as Shu Jiatang Village's "Baishou Festival", Tiaoma Festival, 8 April, 6 June, and Mid-July all in Chinese lunar calendar, and etc., folk traditional festivals, folk handicraft, arts and entertainment skills are fully demonstrated. Monotonous folk song and dance performances in the past can be adjusted according to tourists' needs [41]. From the perspectives of religion, society, economy, sporting economy, daily life and others to actively develop ethnic customs, folk customs, celebration and ancient lyrics, folk skills, humanistic architectures, cultural activities, historical and cultural sites in possession with ethnic features [42]; open up places for performing ethnic songs and dances, ethnic costume performances as well as exhibition halls, so as to provide a wide range of tourists with personalized products and tourism services of high quality and great pleasure. Meanwhile, series of festival activities are conducted regularly. Developing festival culture, and forming brand festival culture are to attract tourists' involvement, satisfy their psychological demands, and develop plural and integrated tourism economy [43]. The unique culture of Xiangxi Autonomous Prefecture is embodied with depth, and the culture brand strategy is well implemented through certain forms of expression, which enables tourists to better profoundly and comprehensively understand and experience the Xiangxi Autonomous Prefecture's folk culture. Moreover, Xiangxi Autonomous Prefecture's folk commodities are varied and rich in ethnic features, local colors as well as thick in cultural implication, thus with commodious room for development Practical and effective measures should be adopted to protect, and fully explore such traditional handicraft as wax printing, silver making, brocading, embroidering, root carving, stone sculpturing, paper cutting and etc. [44]. Local people are trained to research and develop ethnic commodities [45]; exhibition hall can be set up for ethnically featured commodities, meanwhile opening up traditional manual workshops, as well as increasing commodities' values of appreciation and culture, so that tourists can be involved in experiencing the manufacturing process for themselves, and eventually increase the commodities' attractiveness [46].

From the perspective of planning and developing, ecotourism resources of western Hunan's traditional villages are precisely categorized, evaluated and reasonably partitioned to realize the advantages complement among villages. Based on this, it has been a key direction for the future planning and development of rural ecotourism resources to combine with other villages or scenic spot ecotourism resources so as to realize the sharing between resources and tourist sources. Only by relying on tourist scenic spots well-known both inside and outside around for joint development, which complement multiple resources within the region, can rural tourism meet the personalized tourists' demands, expand tourist source market, realize resources sharing, as well as enhance the popularity and branding of traditional villages' scenic areas. For instance, by making use of the influence of western Hunan's Fenghuang County (national AAAA scenic area), a historically and culturally famous county at the national level, a tourism route from Fenghuang County, to Shu Jiatang Village, and till Lahao Village takes shape. Along this route, there are such sightseeing as ancient buildings, Chen Dounan House, Tuojiang River Hanging House, old slab-stone street, Wanming Tower, Qifeng Mountain, stone-built complex, southern Great Wall, and etc. After touring the scenic areas, tourists can also live in the ancient houses built in Ming and Qing Dynasties to experience rural traditional residential as well as historical folk culture. Folk resources of these 2 traditional villages, both with their own features, complement each other with their own advantages, plus being well-known traditional villages both inside and outside around western Hunan, the popularity and branding of the folk culture scenic area are thus being promoted [47]. In addition, relying on the resources advantages of traditional villages, according to the leading principles of integrating regional resources, constructing tourism network, and cultivating interbank market to actively promote inter-regional cooperation on ecotourism resources of traditional villages, and strengthen advantages complement as well as Internet operation [48]. In the meantime, the Wuling Mountain Tourism Circle", which stretches about 3000 km from Zhang Jiajie, to Taohua Yuan, Jishou, Fenghuang, Huaihua, Tongren, Fanjing Moutain, Three Gorges, Enshi, Yongshun and Zhang Jiajie, is

also integrated to undertake the tourist source from Changsha-Zhuzhou-Xiangtan City Cluster, Wuhan-centered City Circle, and Chengdu-Chongqing City Cluster.

CONCLUSION

It is suggested to deeply explore the historical and cultural connotation implied by the ecological resources of traditional villages, improve the transportation convenience, promote infrastructure construction; strengthen propaganda as well as to systemically integrate the regional resources, so as to further upgrade the availability of the ecotourism resources of traditional villages, take control of the reasonable degree of protection and development of the ecotourism resources in the western Hunan area, and boost the economic sustainable development.

ACKNOWLEDGEMENTS

This work was supported by research project of graduate students in Hunan (CX2017B092) and natural science foundation of Hunan Province (2016JJ4017).

REFERENCES

[1] Gordon, J.S., Gruver, J.B., Flint, C.G., Luloff, A.E. (2013) Perceptions of wildfire and landscape change in the Kenai Peninsula, Alaska. Environmental Management. 4, 807-820.

[2] Westling, E.L., Surridge, B.W.J., Sharp, L., Lerner, D.N. (2014) Making sense of landscape change: Long-term perceptions among local residents following river restoration. Journal of Hydrology. 519, 2613-2623.

[3] Powell, R.B., Ham, S.H. (2008) Can ecotourism interpretation really lead to pro-conservation knowledge, attitudes and behaviour? Evidence from the Galapagos Islands. Journal of Sustainable Tourism. 4, 467-489.

[4] Brown, G., Brabyn, L. (2012) The extrapolation of social landscape values to a national level in New Zealand using landscape character classification. Applied Geography. 1, 84-94.

[5] Stefańska, I., Witkowski, L., Rzewuska, M., Dzieciątkowski, T. (2016) Development and evaluation of the internal-controlled real-time PCR assay for *Rhodococcus equidetection* in various clinical specimens. Journal of Veterinary Medical Science. 4, 543-549.

[6] Moschino, V., Schintu, M., Marrucci, A., Marras, B., Nesto, N., Da Ros, L. (2017) An ecotoxicological approach to evaluate the effects of tourism impacts in the Marine Protected Area of La Maddalena (Sardinia, Italy). Marine Pollution Bulletin. 1(2), 306-315.

[7] Duan, X.J, Ruan, Q., Gan, Q.Q., Song, X.Q., Fang, S.A., Zhang, X.R., Zhang, J.B. (2018) Radiosynthesis and evaluation of novel 99mTc(CO)3-labelled thymidine dithiocarbamate derivatives for tumor imaging with SPECT. Journal of Organometallic Chemistry. 8, 154-163.

[8] Roberts, J.A., Bacon, D.R. (1997) Exploring the subtle relationships between environmental concern and ecologically conscious consumer behavior. Journal of Business Research. 1, 79-89.

[9] Lee, T.H., Jan, F.H., Yang, C.C. (2013) Conceptualizing and measuring environmentally responsible behaviors from the perspective of community-based tourists. Tourism Management. 3, 454-468.

[10] Gao, J., Hong, W.Y., Li, W.M. (2009) Visitors' environmental attitude & behavior in natural reserve—The case of Poyang Lake Natural Reserve. Economic Geography. 1, 1931-1936.

[11] Lu, L., Bao, J., Huang, J.F., Zhu, Q.J., Mu, C.L., Chu, X.L., Xu, Y., Zha, X.L. (2016) Recent research progress and prospects. in tourism geography of China. Journal of Geographical Sciences. 8, 1197-1222.

[12] Sujarwo, W., Arinasa, I.B.K., Salomone, F., Caneva, G., Fattorini. S. (2014) Cultural Erosion of Balinese Indigenous Knowledge of Food and Nutraceutical Plants. Economic Botany. 4, 426-437.

[13] Santos, L.C.M., Gasalla, M.A., Dahdouh-Guebas, F., Bitencourt, M.D. (2017) Socio-ecological assessment for environmental planning in coastal fishery areas: A case study in Brazilian mangrove. Ocean and Coastal Management. 138, 60-69.

[14] Wang, D.L. (2017) Empirical Analysis and Market Potential Evaluation Model Construction of Cultural Tourism Resources from Sustainable Perspective. Boletín Técnico. 20,74-81.

[15] Banda, E., Folly, K.A. (2012) Short Term Load Forecasting Using Artificial Neural Network. Lecture Notes in Engineering and Computer Science. 1, 108-112.

[16] Ali, J.B., Fnaiech, N, Saidi, L., Chebel-Morello, B., Fnaiech, F. (2015) Application of empirical mode decomposition and artificial neural network for automatic bearing fault diagnosis based on vibration signals. Applied Acoustics. 3, 16-27.

[17] Witekkrowiak, A., Chojnacka, K., Podstawczyk, D., Dawiec, A., Pokomeda, K. (2014) Application of response surface methodology and artificial neural network methods in modelling and optimization of biosorption process. Bioresource Technology. 5, 150-160.
[18] Hodo, E., Bellekens, X., Hamilton, A., Dubouilh, P.L, Iorkyase, E., Tachtatzis, C., Atkinson, R. (2017) Threat analysis of IoT networks Using Artificial Neural Network Intrusion Detection System. Tetrahedron Letters. 39, 6865-6867.
[19] Xiang, Q.C., Liu, L. F., Liu, T. Z., Liu, P. L., Deng, Y. Y. (2013) On Evaluation and In-Depth Development of Tourism Resources. in Miaoqian Town, Hunan Province. Journal of Hengyang Normal University. 6, 56-60.
[20] Zhu, H., Liu, J.M., Tao, H., Zhang, J. (2015) Evaluation and Spatial Analysis of Tourism Resources Attraction in Beijing Based on the Internet Information. Journal of Natural Resources. 12, 2081-2094.
[21] Lu, W. (2017) Research on the Performance and Countermeasures of Business Participation in Tourism-aided Poverty Alleviation from the Perspective of Multiple Cases. Journal of Sichuan Tourism University. 6, 51-55.
[22] Dou, Y.D., Fu, H.Q., Li, B.H., Liu, P.L. (2018) Study on Evaluation of Tourism Development Potential of Traditional Villages. A Case Study of Yongzhou City. Resource Development and Market. 9, 1309+1321-1326.
[23] Lew, A.A. (1987) A framework of tourist attraction research. Annals of Tourism Research. 14, 553-575.
[24] Powell, R.B., Brownlee, M.T.J., Kellert, S.R., Ham, S.H. (2012) From awe to satisfaction: Immediate affective responses to the Antarctic tourism experience. Polar Record. 2, 145-156.
[25] Hong, X.T., Zhang, H.M., Zhang, Y.C., (2018) Influence of Tourism Experience on Environmental Attitude and Behavior: A Longitudinal Tracking Study. Journal of Natural Resources. 9, 1642-1656.
[26] Jia, R., Zhao T., Sun, H., Yan X. (2015) Microseismic signal denoising method based on empirical mode decomposition and independent component analysis. Chinese Journal of Geophysics Chinese Edition. 58, 1013-1023.
[27] Smith, L., Broad, S., Weiller, B. (2008) A closer examination of the impact of zoo visits on visitor behaviour. Journal of Sustainable Tourism. 5, 544-562.
[28] Ballantyne, R., Packer, J., Falk, J. (2011) Visitors' learning for environmental sustainability: Testing short and long-term impacts of wildlife tourism experiences using structural equation modelling. Tourism Management. 6, 1243-1252.
[29] Hinds, J., Sparks, P. (2008) Engaging with the natural environment: The role of affective connection and identity. Journal of Environmental Psychology. 2, 109-120.
[30] Xu, F., Hu, B., Dou, Y., Song, Z., Liu, X. (2018) Prehistoric heavy metal pollution on the continental shelf off Hainan Island, South China Sea: From natural to anthropogenic impacts around 4.0 kyr BP. Holocene. 28, 455-463.
[31] Ibanez, L., Moureau, N., Roussel, S. (2017) How do incidental emotions impact pro-environmental behavior? Evidence from the dictator game. Journal of Behavioral and Experimental Economics. 66, 150-155.
[32] Panapakidis, I.P., Dagouma, A.S. (2016) Day-ahead electricity price forecasting via the application of artificial neural network based models. Applied Energy. 172, 132-151.
[33] Choi, S.I., Kang, H.M., Kim, H., Chang, H.L., Chong, K.L. (2016) A measure for the promotion of mountain ecological villages in South Korea: focus on the national mountain ecological village investigation of 2014. Springerplus. 1, 1-13.
[34] Robledano-Aymerich, F., Asunción Romero-Díaz, F., Belmonte-Serrato, V., Zapata-Pérez, M., Martínez-Hernández, C., Martínez-López, V. (2014) Ecogeomorphological consequences of land abandonment in semiarid Mediterranean areas: Integrated assessment of physical evolution and biodiversity. Agriculture Ecosystems and Environment. 4, 222-242.
[35] Caneva, G., Traversetti, L., Sujarwo, W., V Zuccarello, V. (2017) Sharing Ethnobotanical Knowledge in Traditional Villages: Evidence of Food and Nutraceutical "Core Groups" in Bali, Indonesia. Economic Botany. 4, 303-313.
[36] Qin, K.R., Wang, H.Y., Yu, Z.H., Wang, H. (2017) Plant Resources Investigation and Evaluation Based on the Development of Rural Ecological Tourism: A Case Study of the Surrounding Villages in the Baima Mountain Nature Reserve. Hubei Agricultural Sciences. 8, 1445-1449.
[37] Hou, Q., Mou, C., Wang, Q., Tan, Z. (2018) Provenance and tectonic setting of the Early and Middle Devonian Xueshan Formation, the North Qilian Belt, China. Geological Journal. 53, 1404-1422.
[38] Kil, N., Holland, S.M., Stein, T.V. (2014) Structural relationships between environmental attitudes, recreation motivations, and environmentally responsible behaviors. Journal of Outdoor Recreation and Tourism. 7, 16-25.
[39] Yu, H., Huang, Y., Ning, J., Zhu, B., Cheng, Y. (2014) Effect of cation exchange capacity of soil on stabilized soil strength. Soils and Foundations. 54, 1236-1240.

[40] Rattan, J., Eagles, P.F.J., Mair, H.L. (2012) Volunteer tourism: Its role in creating conservation awareness. Journal of Ecotourism. 1, 1-15.
[41] Liu, R.F. (2010) Selective marketing for sustainable development of tourism based on the analysis of environmental behavior: A case study of Jiuzhaigou. Human Geography. 6, 114-119.
[42] Jia, Y., Lin, D. (2016) Tourists' perception of urban service, place attachment and loyal behaviors: A case study of Xiamen. Geographical Research. 2, 390-400.
[43] Kong, H. (2014) Are tour guide in China ready for ecotourism? An importance-performance analysis of perceptions and performance. Asia Pacific. Journal of Tourism Research. 1, 17-34.
[44] Hunt, C.A., Durham, W.H., Driscoll, L., Honey, M. (2015) Can Ecotourism deliver real economic, social, and environmental benefits? A study of the Osa Peninsula, Costa Rica. Journal of Sustainable Tourism. 3, 339-357.
[45] Tynan, C., McKechnie, S. (2009) Experience marketing: A review and reassessment. Journal of Marketing Management. 25, 501-517.
[46] Liu, J., Yan, J.M., Qiu, H. (2013) Study on classification system of ecotourism land. China Land Sciences. 9, 71-77.
[47] Ryan, R.L. (2011) The social landscape of planning: Integrating social and perceptual research with spatial planning information. Landscape and Urban Planning. 4, 361-363.
[48] Chu, Y., Zhao, Z., Zhang, C., Chen, C., Chen, Y. (2016) Spatial features of preference difference and conflict potential among multi-groups in tourism community: A case of Tangyu town in Xi'an. Acta Geographica Sinica. 6, 1045-1058.

Received: **29.11.2018**
Accepted: **25.03.2019**

CORRESPONDING AUTHOR

Shaoyao He
School of Architecture
Hunan University
Changsha 410082 – China

e-mail: 2099780005@qq.com

© by PSP Volume 28 – No. 5/2019 pages 3917-3927 Fresenius Environmental Bulletin

ASSESSMENT OF PLANT RESIDUES (DICHONDRA REPENS) AND NUTRIENTS AMENDMENTS FOR THE REMEDIATION OF COPPER-PHENANTHRENE CO-CONTAMINATED SOIL

Guihong Lan[1,2,*], Qianxia Xu[1], Dianjun Fang[3], Jiao Du[1], Lei Jian[4], Ruifeng Li[1]

[1]College of Chemistry and Chemical Engineering, Southwest Petroleum University, 610500 Chengdu, P.R. China
[2]College of Architecture and Environment, Sichuan University, 610065 Chengdu, P.R. China.
[3]Jilin oilfield company oil production technology research institute, 138000 Songyuan, P.R. China.
[4]Sichuan Academy of Environmental Sciences, 610041 Chengdu, P.R. China

ABSTRACT

The clean-up of soils co-contaminated with heavy metals and organic compounds is a contemporary issue of remediation efforts. In this study, the purpose is to investigate the effect of plant residues and nutrients on soil enzymatic activity, number of hydrocarbon degrading bacteria and microbial community through pyrosequencing of 16S rRNA gene amplicons, to enhance the simultaneous removal of phenanthrene and copper from the co-contaminated soil. The experiment was divided into five groups (S0-S4) by adding various nutrients and 0, 1, 3, 5, 7% of plant residue (dichondra repens) for the survival of microorganisms. The results showed that the degradation rate of phenanthrene in the simulated soil reached 32.69%, 65.25%, 78.89%, 81.59%, 92.84% and the conversion rate of soluble copper reached 13.31%, 44.72%, 50.33%, 55.95%, 60.11% in S0 to S4, respectively. The enzyme activities of dehydrogenase and urease were transiently promoted by the presence of additive after 15 days, subsequently the number of hydrocarbon-degrading bacteria also increased, but the shift became weaker or disappeared as the exposure time increased to 61 days. Then we selected S4 which has the best degradation effect for sequencing analysis and it produced a change of species richness, the original bacterial flora of that was *Actinobacteria* (40.4%), then it gradually left a community dominated by members of *Proteobacteria* (50.4%) and *Bacteroidetes* (45.5%), with *Arachidicoccus* and *Sphingobium* as the most abundant genus. The results indicated that more plant residues and nutrients has potential for clean-up of heavy metals and polycyclic aromatic hydrocarbons (PAHs) from co-contaminated soils.

KEYWORDS:
Plant residues, Phenanthrene, Copper, Co-contaminated soil, Microbial remediation

INTRODUCTION

Soils contaminated with both heavy metals and polycyclic aromatic hydrocarbons (PAHs) have been a common environmental problem [1]. Some researchers found that the combined effect of heavy metals and PAHs on ecological systems and human health was synergistic [2, 3]. Soil contaminated with polycyclic aromatic hydrocarbons (PAHs) and heavy metals display high levels of multi-contamination, both them persisted in the environment due to their low availability and low degradability [4, 5]. Therefore, the clean-up of combined contaminants in soils, such as PAHs and heavy metals, is an urgent task.

Among them, phenanthrene is one of 16 types of PAHs that have the least molecular weight in areas associated with PAHs carcinogenicity [6] under Environmental Protection Agency (EPA) priority control. Compared with high molecular weight polycyclic aromatic hydrocarbons, low molecular weight polycyclic aromatic hydrocarbons is more water-soluble and volatile and easily used by organisms. Therefore, many scientific researchers use the phenanthrene as a reference to study the toxicity and degradation pathways of PAHs, as well as various environmental factors affecting the degradation rate and bioavailability of PAHs [7]. PAH contamination of soil is often associated with the presence of high levels of potentially toxic metals [8]. There are many research methods to repair soil contaminated by metals and polycyclic aromatic hydrocarbons. Zhao. B et al [9] researched nonionic surfactant and organic acid solutions to enhance the simultaneous removal 99.9% of phenanthrene and 85.7% of copper (II) from the co-contaminated soil by column flushing. But they are complex and costly. Sneath. H.E. et al. [10] used 1% of biochar and 5% of iron filing enhancing phenanthrene degradation by 44-65% and reducing Cu and As leaching, but it negatively impacted soil structure and released high levels of Fe causing sunflower plant mortality. However, Hlerema. I.N. et al. [11] used

maize and pineapple residue reducing Cd concentration from 3.3 mg/kg to 0.15 mg/kg (a safe level) in soil. Li. S. et al. [12] applied strain mixed with plant residue to increase 15% of Cu and 30.3% of Zn accumulation by wheat seedlings in soil. This study offers a safe strategy for the post-treatment of plant residue. Although many studies employed soil amendments in order to reduce metal toxicity and increase PAHs degradation rate on microorganism [10, 13], the impact of toxic metals and PAHs on soil amended with plant residues has not received much attention so far [14]. So adding plant residues to amend co-contaminated soil seems to have more potential for in situ clean-up of heavy metals and polycyclic aromatic hydrocarbons (PAHs). It appears to be more green, economical and pollution-free.

Dichondr repens as plant residue added into the soil can improves soil structure and provides essential nutrients when it is decomposed [15]. Consequently it reduces soil dependence on fertilizers [16]. However, the effect of its amount on copper and phenanthrene co-contaminated soil modification is unknown, especially for soil microbial community and few literatures have studied it. To better predict the effect of plant residues on the soil, dichondra repens as plant residues was proposed to evaluate the impact on different treatment soil in this study. In this paper, phenanthrene and typical heavy metal copper are used as representative pollutants, and nutrients and plant residue are used as additives to microbial remediation of phenanthrene-copper complex contaminated soil. By comparing different amounts of fresh horseshoe gold added in soil, the purpose is to explore its impact on hydrocarbon-degrading bacteria, soil enzyme activity and soil microbial community structure, and to study the degradation effect of phenanthrene in soil and different forms of copper conversion process.

MATERIALS AND METHODS

Preparation of tested soil. In this experiment, the soil we used was simulated. The original soil was collected from agricultural topsoil (0-15cm) of the third stage of southwest petroleum university which is located in Chengdu, Sichuan Province. After removing the debris such as stones and roots, the soil was dried in the shade and screened with 2mm sieve. The combined pollution soil of phenanthrene and copper was prepared by homogeneous mixture method as experimental soil: a certain amount of phenanthrene was dissolved in dichloromethane, and the solution was sprayed evenly in the air-dried soil, and the mixture was even. Then, a certain amount of $CuSO_4 \cdot 5H_2O$ was dissolved in pure water and added to the above soil so that the soil was mixed evenly and the phenanthrene and copper contaminated soil was prepared. The tested soil contained 145mg/kg phenanthrene and 500mg/kg copper.

Experimental design. Add 5.5kg of test soil to each pot. Add the nutrients, sawdust and fresh dichondra repens according to the five microbial repair methods in Table 1. Corn starch, ammonium nitrate, monopotassium phosphate is added to provide sufficient carbon, nitrogen and phosphorus sources for microorganisms in the soil. The dichondra repens is the fresh dichondra repens that the garden workers just harvested. And chopped into a pot. The experiment consisted of 5 groups, 2 sample in each group. Turn the soil and water it every day to keep the water content at about 20% of the maximum water holding capacity of the soil. Samples were taken every 7 days for the first 3 weeks of the repair process and every 10 days after 3 weeks until the end of the experiment. The soil of the compost should be thoroughly mixed before each sampling, the diagonal sampling method was used for sampling. The experiment was carried out for 61 days.

The number of soil hydrocarbon-degrading bacteria. The number of hydrocarbon-degrading bacteria is an important index to measure the degradation effect of petroleum hydrocarbon in soil. Therefore, it is used to measure the degradation effect of phenanthrene in simulated soil. The fresh soil samples collected were weighed at 4g in a 50mL centrifuge tube. 20mL of aseptic water was added to the tube, and the soil suspension was obtained by oscillating on a vortex oscillator for 5min.The suspension of 1mL soil sample was taken with a syringe in the culture medium of hydrocarbon-degrading bacteria, and the dilution gradient was successively 10-9 times, and the suspension was parallel for 3 times. The medium

TABLE 1
Treatment of soil sample

Group	Corn starch/%	Ammonium nitrate/%	Monopotassium phosphate/%	Sawdust/%	Fresh dichondra repens/%	Sample
0	0	0	0	0	0	Blank S0
1	2	0.23	0.035	3	1	Group S1
2	2	0.23	0.035	3	3	Group S2
3	2	0.23	0.035	3	5	Group S3
4	2	0.23	0.035	3	7	Group S4

was placed in a 35℃ incubator for 2 weeks. 0.1mL 3g/L ionitrotetrazol purple color solution was added, and the growth of hydrocarbon-degrading bacteria was recorded according to MPN method [17] after culture it for another one day.

Soil dehydrogenase and urease activity. The activity of urease in soil samples was determined by colorimetry. Samples after dry, apply 5 g in the soil under 50 ml conical flask, add 1 ml toluene, 15 min after add 10 ml of 10% urea liquid and 20 ml of citrate buffer pH 6.7, at 37 ℃ thermostatic cultivation in 24 h, with 0.45 um filter membrane filtration, take 3 ml of filtrate to 50 ml of volumetric flask, according to determine the color of standard curve method for determination of absorbance, blank contrast experiment at the same time.

The activity of dehydrogenase in soil samples was determined by triphenyl tetrazolium chloride (TTC) method [18]. 3g dry soil was weighed and put in 10mL centrifuge tube. 2mL pure water was added and 0.03g $CaCO_3$ and 2mL 1%TTC solution were added. The mixture was thoroughly mixed. Culture 24h in a 30℃incubator.5mL toluene was added to oscillate on the vortex oscillator for 5min and centrifuged at 4000 r/min. The absorbance of supernatant was measured at OD485 of the visible spectrophotometer and compared with the standard curve.

Copper and phenanthrene content in different soil forms. The contents of soluble copper, reducible copper, oxidizable copper and residual copper in soil samples were determined by BCR extraction [19, 20] and total digestion.

The soil sample of 5g drying and screening was placed in a 50mL colorimetric tube, 10mL dichloromethane was added, and the supernatant was extracted for 30min in an ultrasonic cleaner (temperature is controlled at 20±2℃). The supernatant was then poured out after standing [21], and then 10mL dichloromethane was added for repeated extraction for 3-4 times. The supernatant was collected for filtration, and the phenanthrene content was determined by using an ultraviolet spectrophotometer.

16S rDNA genes library preparation and sequencing. The soil samples of S4 (day 1, day 15, day 31, day 41 and day 61) with the best microbial repair effect were selected for total DNA extraction and HiSeq sequencing and their microbial flora structure was analyzed. DNA was extracted from the soil samples using the E.Z.N.A. Soil DNA kit (OMEGA Bio-Tek) and detected by gradient gel electrophoresis. A genetic-diversity analysis of the bacterial communities in the soil microcosms was performed by the PCR amplification of bacterial 16S ribosomal-DNA (rDNA) fragments followed by DGGE. The PCR products were analyzed by electrophoresis on a 1.2% (w/w) agarose gel. After extracting the total DNA of the sample, primers were designed based on the V3 and V4 region, and sequencing adapters were added to the ends of the primers for PCR amplification.

RESULTS AND METHODS

Effect of the treatments on the hydrocarbon degrading bacterial-population density and enzymatic activities of the soil. The influence of the number of hydrocarbon degrading bacteria in soil by the different amount of dichondra repens is shown in Fig. 1. A dramatic increase of about two and three orders of magnitude was observed in the hydrocarbon degradation bacteria population originally in S0 after treatment of the S1 to S4 microcosms during 20 days. In contrast, a significant decrease in the population of bacteria occurred after 20th day (Fig. 1). The addition of dichondra repens significantly increased the number of hydrocarbon-degrading bacteria even at 1% of a low addition of dichondra repens. Most increase in hydrocarbon degrading bacteria occurred in the first 21 days of cultivation, in which most soil urease and dehydrogenase activity increased higher than the blank control group (Figs 2 and 3). However, the activity of soil urease and dehydrogenase increased rapidly on the 15th day, and after a few days, the growth of hydrocarbon-degrading bacteria was promoted.

In the first 21 days of the experiment, in the early stage of the experiment, the nutrient-rich nutrient ratio was more balanced, which helped to increase the number of hydrocarbon-degrading bacteria. The number of hydrocarbon degrading bacteria in the soil of the four experimental groups showed a rapid growth trend and reached the maximum at 21d. At this time, the highest number of hydrocarbon degrading bacteria in experimental group S4 was about 9.58×10^8 cfu/g. From 21d to 61d, the number of hydrocarbon degrading bacteria in the experimental group decreased rapidly until the dynamic balance was reached. The number of hydrocarbon degrading bacteria in the blank group S0 was about 5.77×10^6 cfu/g. In the later stage of the experiment, with the progress of microbial remediation, nutrients were gradually consumed, and the proportion of nutrients such as C, N, and P was unbalanced, which reduced the number of hydrocarbon degrading bacteria.

In microbial remediation, the lack of nutrients is one of the limiting factors for the restoration of petroleum hydrocarbon contaminated soil. Pascault et al. [22] added various plant residues to modifications of the diversity of soil microbial communities induced, the dynamics and the identity of the bacterial groups stimulated depended on the residue added and degradability. Esmaeil Shahsavari et al. [23] investigated the effect of 4 types of plant resi-

dues on the bioremediation of aliphatic hydrocarbons, confirming that adding plant materials significantly enhanced both hydrocarbonoclastic and general microbial soil activities. The results showed that the addition of nutrient additives can significantly improve the degradation rate of petroleum hydrocarbons and the number of microorganisms in soil, microbial diversity and dehydrogenase activity. In this experiment, microbial remediation of phenanthrene-copper contaminated soil was carried out by adding different proportions of fresh dichondra repens. During the 61d repair process, the number of hydrocarbon degrading bacteria added to the 7% dichondra repens experimental group was the largest at the same time, which was beneficial to the soil. Degradation of hydrocarbon contaminants. The addition of fresh dichondra repens not only brings nutrients to microbial remediation, but also further improves the soil environment. The experimental results can show that within a certain range, the larger the amount of organic waste is, the more abundant the nutrients are, the larger the growth of indigenous microorganisms in the soil, and the faster the number of hydrocarbon degrading bacteria increases.

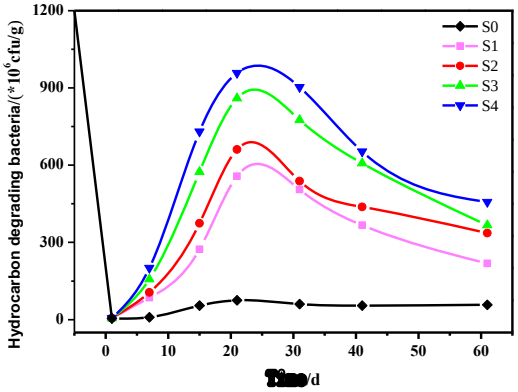

FIGURE 1

Variation trend of soil hydrocarbon degradation bacteria content during microbial remediation

Fig. 2 and 3 shows the effect of the different treatments on the soil enzyme activity. After adding dichondra repens, the soil urease and dehydrogenase activity significantly increased. In both enzymes, they underwent a rapid increase firstly before 15 days, the enhanced enzyme activity promotes the increase of hydrocarbon degrading bacteria, then there's a slight downward trend to 21 days and maintained stably thereafter during 21 to 31 days in S1 to S4. Whereas the enzymes activity declined greatly to an all-time low after 61 days. Hydrocarbon-degrading bacteria also decrease with the trend (Fig 1). In contrast, the enzymatic activity was not affected in blank group, while all the enzymatic activities gradually became diminished after 20 days. The reduction of enzyme activity was attributed to the reduction of bacteria, which can produces urease and dehydrogenase, because of the short of nutrients (Figs 1, 2 and 3). Urease activity was significantly correlated with soil fertility. The addition of fresh dichondra repens improved soil nutrient structure, and the more it was added, the higher soil urease activity was.

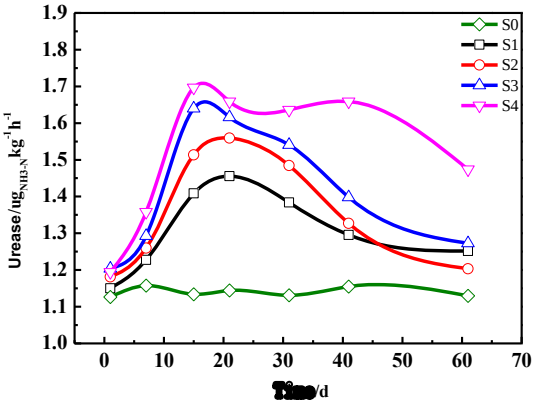

FIGURE 2

Trend of soil urease activity during microbial remediation

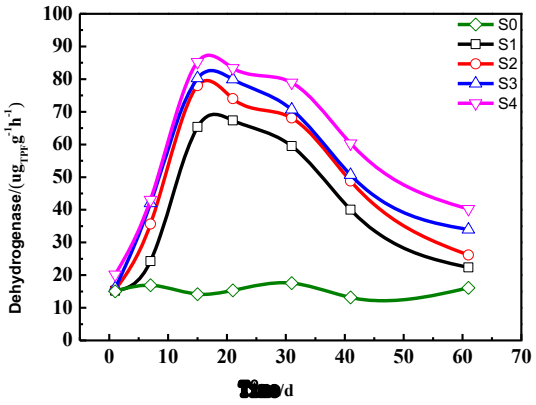

FIGURE 3

Trend of soil dehydrogenase activity during microbial remediation

Effect of the treatments on the copper conversion of the soil and on phenanthrene elimination. As compared to blank group S0, a dramatic change in in the status of Cu was observed in other experimental group. After adding plant residues and nutrients, the conversion of soluble copper to other forms of copper was significantly promoted. The conversion rate of soluble copper reached 60.11% (from 176.64 to 70.46 mg/kg) in S4 after 61 days, while only 13.31% decrease for S0 (Table 2 and Fig 4A).

The results in Fig. 4 B and Table 2 showed that the increasing rate of reducible copper was only 8.46% (from 200.17 to 215.88 mg/kg) in S0 after 61 days, whereas this percent for S1 to S4 was 19.32%, 14.76%, 14.70%, 7.83% within the same period. We can see S1 increase to the greatest extent and excessive plant residues limit the increas-

ing rate of reducible copper in comparison with S0. Addition of 1% dichondra repens maximizes the conversion process of soluble copper to reducible copper.

In Fig 4 C and D, while the content of reducible copper and residual copper had significant positive correlation with addition of horseshoe gold, the content of reducible copper and residual copper is increasing with the increase of the amount of dichondra repens. In S4, 27.98% and 24.31% of soluble copper were converted to reduced copper and residual copper after 61 days, respectively, while only 4.46% and 0.39% of conversion rate in the blank group S0.

From the present study, it is concluded that integrated application of plant residues and nutrients significantly higher promoted copper conversion rate compared to blank group alone. It produced relatively more content of low toxic form of copper over microbial remediation. Oxidizable and residual copper was the most dominant form of copper [24]. The highest contribution rate can be achieved about 86.98% of soluble copper conversion rate. The content of highly toxic soluble copper decreases during microbial remediation,

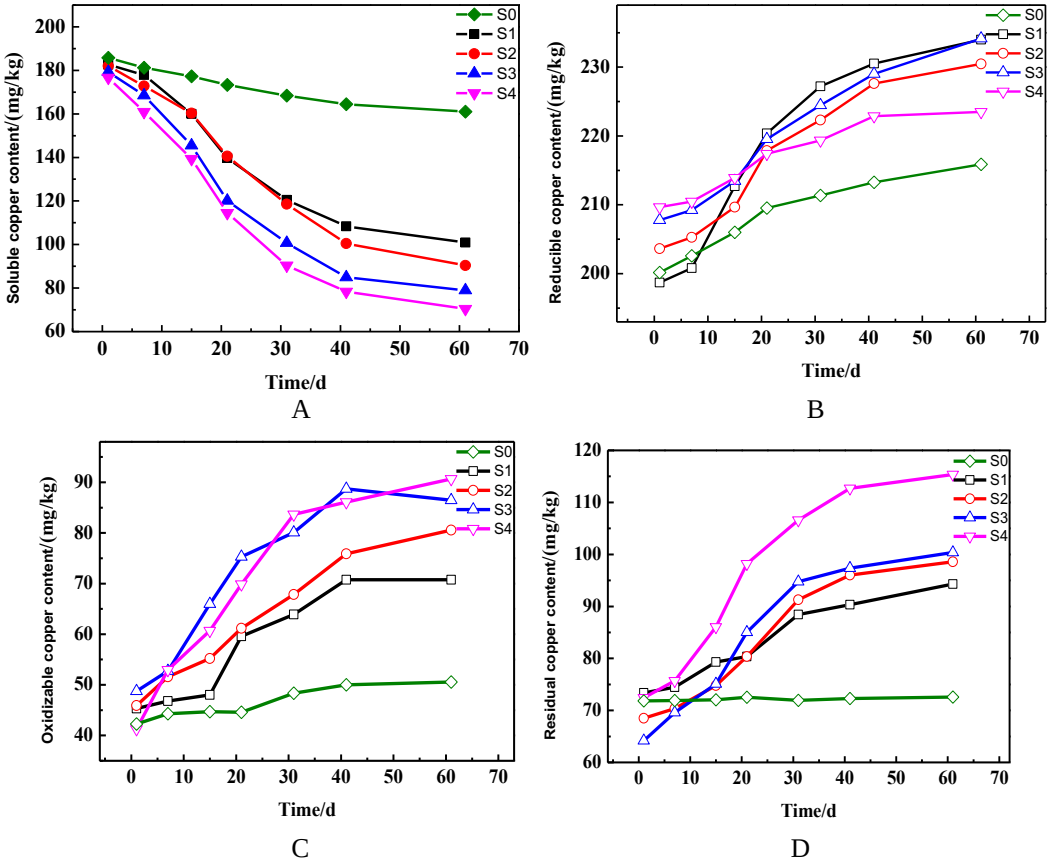

FIGURE 4
Trend chart of different forms of copper content in different soil during microbial remediation (A represents the residual amount of soluble copper after conversion to other forms of copper. B, C and D represent the contents of reducible copper, oxidizable copper and residual copper respectively)

TABLE 2
Conversion rate of different copper forms and degradation rate of phenanthrene

Sample	Soluble copper%	Reducible copper%	Oxidizable copper%	Residual copper%	Phenanthrene%
S0	13.31[a]	8.46[b]	4.46[b]	0.39[b]	32.69[b]
S1	44.72[a]	19.32[b]	13.93[b]	11.47[b]	65.25[b]
S2	50.33[a]	14.76[b]	19.06[b]	16.52[b]	78.89[b]
S3	55.95[a]	14.70[b]	21.05[b]	20.20[b]	81.59[b]
S4	60.11[a]	7.83[b]	27.98[b]	24.31[b]	92.84[b]

The " a " represents decrease, " b " represents increase.

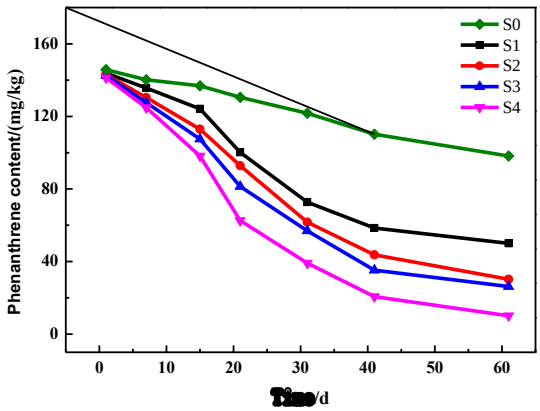

FIGURE 5
Variation trend of phenanthrene content in soil during microbial remediation bacterial community.

while the content of low toxicity reductive copper, oxidizable copper and residual copper increases, indicating that the microorganism can convert the higher toxic soluble copper ions into less toxic copper forms, and then reduced the inhibition of copper on soil enzyme activity, which is beneficial to the survival of microorganisms in the soil and the reuse of soil. With the soil enzyme activity, microbial population and community diversity increasing, it can also promote the conversion of heavy metals in the soil to low toxicity forms in turn. Many studies have shown that the organic amendments have a bearing on the transformation of micronutrients in soil [25, 26].

Residual phenanthrene pollutants of the bioremediation process performed are shown in Fig 5 continuous decrease of phenanthrene was observed, as it shown, which suggested that phenanthrene can be degraded by indigenous microbes. The initial addition of 7% dichondra repens and nutrients resulted in a high rate of TPH degradation (92.84%), whereas the value is about three times of S0 (145.81 to 98.14 mg/kg). It's degraded to the greatest extent in S4 after 61 days, while the addition of 0, 1, 3, or 5% dichondra repens only resulted in degradation rates of 32.69%, 65.25%, 78.89% and 81.59%, respectively (Table 2). As it shown in Fig 1, the hydrocarbon-degrading bacteria increases to the maximum by the presence of additive after 20 days, which make it maximized the degradation of the phenanthrene. But the shift became weaker or disappeared as the exposure time increased to 61 days. In the present study, the higher value we obtained also suggests that elevated the amount of plant residues and the presence of nutrients play important roles in the extent of the phenanthrene removal that was achieved and the associated rates of degradation during bioremediation. These observations are consistent with those reported by Ordonez-Fernandez, R. et al. [27].

Effect of the treatments on the soil. Bacterial composition: General analysis of the pyrosequencing data set. The taxonomic composition and diversity of the bacterial communities of the microcosm S0 and S4 after 15, 31, and 61 days of subsequent bioremediation were profiled by pyrosequencing. The pyrosequencing-based analysis and subsequent statistical inference provided 20690 prokaryotic sequences (at an average length of 417 bp) after the data trimming.

The coverage in all the samples was over 99.32%. The rarefaction curves corresponding to samples from S4 taken at 41 and 61 days did not approach saturation, indicating that their microbial communities were highly complex (Fig.6 A). These rarefaction curves estimating the OTU richness confirmed the difference between the soil samples from the S0, and experimental microcosms after the various treatments (Table 3), where S4 (at 31 and 41 days) were predicted to have a higher degree of microbial-species richness than the other soil samples. A low species richness (ACE and Chao1) was observed in the S0 microcosms. The new community contained an uneven assemblage (reciprocal Simpson) with less species diversity (Shannon). This pattern was improved as a result of the subsequent bioremediation over the first 41 days. Although the diversity (Shannon) and equitability (reciprocal Simpson) indices declined

TABLE 3
Pyrosequencing-based analysis of the different communities studied

Sample	OTU	ACE	Chao1	Simpson(reciprocal)	Shannon	Coverage[%]
S0	469	542.10	538.60	4.89	3.20	99.32
S4(15d)	487	561.88	596.20	7.91	3.21	99.49
S4(31d)	494	572.71	605.91	21.19	4.05	99.40
S4(41d)	500	539.04	552.98	31.85	4.30	99.50
S4(61d)	504	574.55	584.56	32.47	4.39	99.45

The number of total sequences, observed OTUs clustered at a 99.32%-similarity level, coverage (i.e., Hill numbers), ACE and Chao1 (species richness), Shannon (the exponential of the Shannon diversity) and Simpson (the reciprocal of Simpson's index) for the different communities studied, were calculated through the use of a randomly selected subset of sequences per sample. The bioremediation of the original soil (S0) was taken as control treatment.

in the soil community after the 61th day of bioremediation, it is always higher than S0 (Table 3). We can see that after 61 days of cultivating in S4, Simpson and Shannon index are increasing, indicating that the species diversity are increasing. But ACE and Chao1 were increasing in S4 (at 15 and 31 days) and decreasing in S4 (at 41 and 61 days), indicating that the species richness was increasing for the first 31 days while decreasing at 41 days to 61 days. This may be due to some dominant bacteria from scratch or bacteria from less to more, the competition between the communities, inhibiting the disadvantages, the growth of strains and strains adapted to the environment become the main flora in this environment with the reduction of nutrients and growth and metabolism process. Compared with S0, the soil species richness and diversity of S4 is higher, indicating that the flora structure is more complex, the microorganisms are rich and diverse. The diversity and richness estimators described by Hill [28] in the soil community from the S4 microcosms suggested that the bioremediation treatment had resulted in after a few month the selection of a less rich community with a similar, though somewhat lower, species diversity.

Effect of the treatments on bacterial diversity. In the figure, the rarefaction curves for the S0 and S4 microcosms are plotted. The rarefaction curves corresponding to samples from S0 and S4 taken at 15, 31, 41 and 61 days did not approach saturation, indicating that their microbial communities were highly complex (Fig.6 A). As the number of sequencing increases, the curve of S0 to S4 (at 15, 31, 41 and 61 days) shows a sharp rise in order, it indicates that more and more species are found in the community. These rarefaction curves estimating the OTU richness confirmed the difference between the soil samples from S0 and S4, where S4 (61d) was predicted to have a higher degree of microbial species richness than the other soil samples, S0 was just the opposite. After 61 days of cultivating, the microorganisms had better adaptability in S4 soil and worse in S0 soil.

The microorganism in soil is a dynamic change process and successional changes in the soil's resident community occurred during the course of the microbial remediation. All the sequences were found to be classified with in the domain Bacteria. Fig. 6B summarizes the relative abundance of the different orders identified in each microcosm.

In phylum, the main bacterial flora of *Actinobacteria* was gradually transformed into the *Proteobacteria* and *Bacteroidetes* with the addition of additives. Members of the phylum *Actinobacteria* (40.4%), *Proteobacteria* (25.5%) and *Bacteroidetes* (10.2%) represented the bacterial community of S0, with *Sphingomonas* and *Arachidicoccus* being the most representative genera. After 61 days in S4, *Proteobacteria* and *Bacteroidetes* produced an increase to 52.3% and 35.5%, while *Actinobacteria* produced a low to 7.9%. 15 days after adding nutrients, Comparing with S0, the soil of S4 produced a change of species richness leaving a community dominated by members of *Proteobacteria* (50.4%) and *Bacteroidetes* (45.5%), with *Arachidicoccus* and *Sphingobium* as the most abundant genus. Other nine phyla (*Verrucomicrobia, Chloroflexi, Firmicutes, Acidobacteria, Nitrospirae, Planctomycetes, Gemmatimonadetes, Saccharibacteria, Chlamydiae*) respectively represented less than 1% of the total reads. Then, the relative proportion of *Proteobacteria* and *Bacteroidetes* increased to 61 days.

However, in genus of soil, the microbe species are abundant and the proportion of each microbe is very low. The microbial communities was predominated by the phylum *Sphingomonas* (6.5%) and *Arachidicoccus* (1.0%) in S0 but Others reached 90.5%, while adding plant residues and nutrients, the community structure has changed dramatically. The *Arachidicoccus*, *Sphingobium*, *Rhodanobacter* and *Chitinophaga* became members of a major community ranging from 37.7% to 12.1%, 13.1% to 8.8%, 4.2% to 11.0% and 3.1% to 12.3% of the total reads during 61 days. The proportion of *Others* is reduced to 15.1% in 15 days, then goes back up to 27.1% in the end. The addition of plant residues seems to significantly alter the community structure of microorganisms in contaminated soil, the initial population of that was dominated by *Others* and the later dominant bacteria also contain *Arachidicoccus*.

Overall it was possible to observe that Proteobacteria and Bacteroidetes dominate the studied soils, which suggest that its members may play major functions in petroleum hydrocarbon polluted soil. The principal component analysis correlated the most abundant families with the most efficiently-degraded PAHs. However we cannot prove that the most abundant bacteria were responsible for the phenanthrene degradation, since we only sequenced the 16S rRNA gene fragment. Nevertheless, our results suggest possible relationships between the degradation processes and microbial community. Although it is decreasing on 61 days, *Arachidicoccus* appears to be the dominant community in genus of S4. It's a novel plant growth-promoting bacteria isolated from rhizosphere soils [29]. That may be caused by the addition of dichondra repens to the soil. Then it was the genus *Sphingobium* (belonging to the phylum *Proteobacteria*). It is a rich new type of microbial resource that can be used for biodegradation of aromatic compounds, because *Sphingobium* has a very extensive metabolic capacity for aromatic compounds, and it is able to synthesize valuable extracellular biopolymers [30], the specific effects of *Sphingobium sp* on complex structures of hard-to-degrade aromatics make it abundant in

petroleum hydrocarbon-contaminated soils and seems to play an important role on biormediation processes. Researches [31] showed that soil organic amendment may be the key factors in shaping the soil bacterial community structure. Numerous studies have suggested that dichondra repens releases nutrients and in so doing provides a new environment for the adaptable microbial community. Liang. X. et al. [32] proved adding maize residues input to soils affect the magnitude and direction of priming effect and alter the composition and structure of soil microbial community.

The analysis based on the relative abundance of orders was made with the STAMP software (v 2.1.3). Fig.7 represents the PCA from the bacterial community at the taxonomic level of order of S0 and S4 along with the sampling time during the subsequent bioremediation treatment in the last of those microcosms. An explained variance of 74.15% was obtained. The figure indicates that the S4 (15 and 31-day) microcosms shifted to the right of the PC1 axis, thus implying the abundance of members of *Proteobacteria* and *Bacteroidetes* phylum. The presence of members of the order *Actinobacteria* mainly pointed out the difference between the bacterial communities from S4 up to the 31th day (constituting the early changes) from those incubated after 31 days until the end of the bioremediation treatment, including S0 (consisting in the later changes) on the PC2 axis [33].

STATISTICAL ANALYSIS

Statistical analysis of the results was performed with SPSS 11.0 for Windows (SPSS Inc.). Means were compared using a t-test. The least significant difference of means at a 5% confidence level ($P < 0.05$) in the microbial communities was applied to assess significant differences.

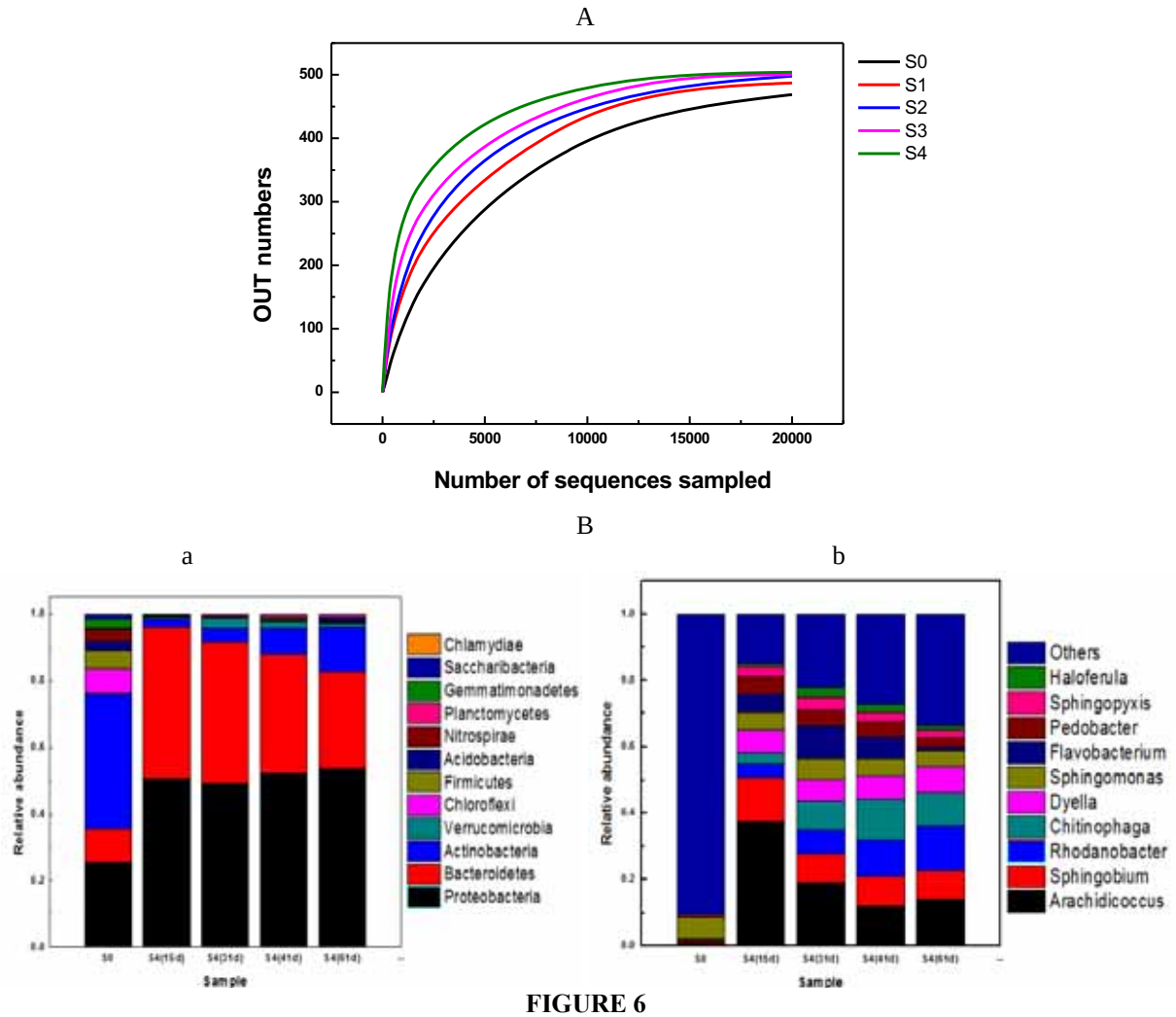

FIGURE 6

A. Rarefaction analysis constructed by means of the Mothur v.1.34.0 software. B. Stack column diagrams illustrating the relative phylotype frequency at the level of order as revealed by pyrosequencing (a represents the levels of phylum, b represents the levels of genus).

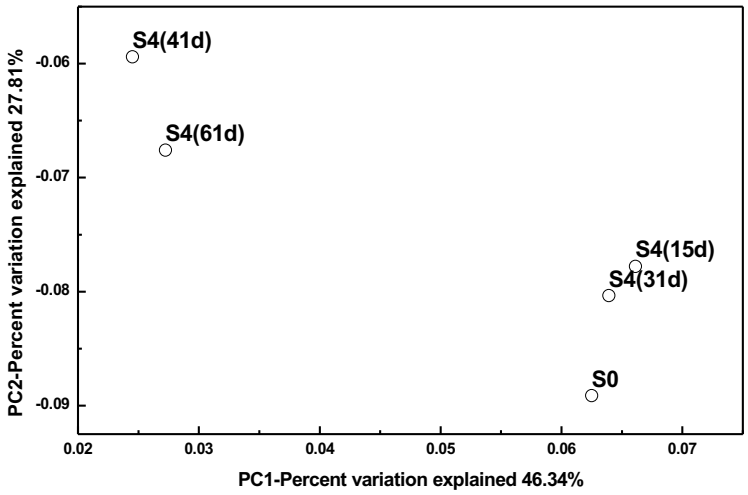

FIGURE 7
Principal-component-analysis (PCA) plot. Comparison of the bacterial-community taxonomic profiles from each microcosm at the level of order, including those of the microcosms of S0 and S4 (at 15, 31, 41 and 61 days).

CONCLUSION

Adding nutrients and plant residues to the soil significantly promotes the growth of microorganisms in the soil, which may increase the predictability of nutrient release from organic amendments and lead to a more sustained nutrient supply to soil microbe and increase the activity of dehydrogenase and urease in soil, then increase the number of hydrocarbon-degrading bacteria which is helpful to improve the degradation rate of phenanthrene and the conversion rate of copper to low toxicity. The highest degradation rate of phenanthrene in the simulated soil reached 92.84% and the conversion rate of soluble copper reached 60.11% with addition of 7% dichondra repens, including 27.98% and 24.31% of high-toxic soluble copper were converted to low-toxic reduced copper and residual copper after 61 days, respectively. Comparing with blank group S0, adding various nutrients and plant residue significantly changed the microbial community structure and increased soil microbial community richness and diversity, and the soil of experimental group S4 produced a change of species richness leaving a community dominated by members of *Proteobacteria* (50.4%) and *Bacteroidetes* (45.5%), with *Arachidicoccus* and *Sphingobium* as the most abundant genu.

ACKNOWLEDGEMENTS

We would like to thank Sichuan province science and technology key research and development projects “Integrated research, development and demonstration of standard technology for stable waste water treatment in typical industrial clusters” for their support of this study (the Project Number: 18ZDYF0051).

REFERENCES

[1] Zhu, Z.Q., Yang, X.E., Wang, K., Huang, H.G., Zhang, X., Fang, H., Li, T.Q., Alva, A.K. and He, Z.L. (2012) Bioremediation of Cd-DDT co-contaminated soil using the Cd-hyperaccumulator Sedum alfredii and DDT-degrading microbes. J Hazard Mater. 235, 144-51.

[2] Soltani, N., Keshavarzi B., Moore, F., Tavakol, T., Lahijanzadeh, A.R., Jaafarzadeh, N. and Kermani, M. (2015) Ecological and human health hazards of heavy metals and polycyclic aromatic hydrocarbons (PAHs) in road dust of Isfahan metropolis, Iran. Science of The Total Environment. 505, 712-723.

[3] Shen, G., Lu, Y. and Hong, J. (2006) Combined effect of heavy metals and polycyclic aromatic hydrocarbons on urease activity in soil. Ecotoxicology and Environmental Safety. 63, 474-480.

[4] Sandrin, T.R. and Maier, R.M. (2003) Impact of metals on the biodegradation of organic pollutants. Environ Health Perspect. 111, 1093-1101.

[5] Bourceret, A., Cébron, A., Tisserant, E., Poupin, P., Bauda, P., Beguiristain, T. and Leyval, C. (2016) The bacterial and fungal diversity of an aged PAH- and heavy metal-contaminated soil is affected by plant cover and edaphic parameters. Microbial Ecology. 71, 711-724.

[6] Mallick, S., Chakraborty, J. and Dutta, T.K. (2010) Role of oxygenases in guiding diverse metabolic pathways in the bacterial degradation of low-molecular-weight polycyclic aromatic hydrocarbons: A review. Critical Reviews in Microbiology. 37, 64-90.
[7] Schwarz, A., Adetutu, E.M., Juhasz, A.L., Aburto-Medina, A., Ball, A.S. and Shahsavari, E. (2018) Microbial degradation of phenanthrene in pristine and contaminated sandy soils. Microbial Ecology. 75, 888-902.
[8] Thavamani, P., Megharaj, M., Krishnamurti, G.S.R., McFarland, R. and Naidu, R. (2011) Finger printing of mixed contaminants from former manufactured gas plant (MGP) site soils: Implications to bioremediation. Environment International. 37, 184-189.
[9] Zhao, B., Che, H., Wang, H. and Xu, J. (2016) Column Flushing of Phenanthrene and Copper (II) Co-Contaminants from Sandy Soil Using Tween 80 and Citric Acid. Soil and Sediment Contamination: An International Journal. 25, 50 - 63.
[10] Sneath, H.E., Hutchings, T.R. and de Leij, F.A.A.M. (2013) Assessment of biochar and iron filing amendments for the remediation of a metal, arsenic and phenanthrene co-contaminated spoil. Environmental Pollution. 178, 361-366.
[11] Hlerema, I.N., Eiasu, B.K. and Koch, S.H. (2017) Pineapple (Ananas comusus) Plant Material as Supplement for Maize Residue-based Oyster Mushroom Substrate and Reduction of Cadmium Soil Contamination. HortScience. 4, 667-671.
[12] Li, S., Wang, J., Gao, N., Liu, L. and Chen, Y. (2017) The effects of Pantoea sp. Strain Y4-4 on alfalfa in the remediation of heavy-metal-contaminated soil, and auxiliary impacts of plant residues on the remediation of saline-alkali soils. Can J Microbiol. 63, 278-286.
[13] Mandal, A., Biswas, B., Sarkar, B., Patra, A.K. and Naidu, R. (2016) Surface tailored organo-bentonite enhances bacterial proliferation and phenanthrene biodegradation under cadmium co-contamination. Science of the Total Environment. 550, 611 - 618.
[14] Thavamani, P., Megharaj, M., Krishnamurti, G.S., McFarland, R. and Naidu, R. (2011) Finger printing of mixed contaminants from former manufactured gas plant (MGP) site soils: Implications to bioremediation. Environ Int. 37, 184-9.
[15] Kong, L. (2014) Maize residues, soil quality, and wheat growth in China. A review. Agronomy for Sustainable Development. 34, 405-416.
[16] Abera, G., Wolde-meskel, E. and Bakken, L.R. (2013) Effect of organic residue amendments and soil moisture on N mineralization, maize (Zea mays L.) dry biomass and nutrient concentration. Archives of Agronomy and Soil Science. 59, 1263 - 1277.
[17] Jia, J., Zong, S., Hu, L., Shi, S., Zhai, X., Wang, B., Li, G. and Zhang, D. (2017) The dynamic change of microbial communities in crude oil-contaminated soils from oilfields in China. Journal of Soil Contamination. 26, 171-183.
[18] Tan, X., Liu, Y., Yan, K., Wang, Z., Lu, G., He, Y. and He, W. (2017) Differences in the response of soil dehydrogenase activity to Cd contamination are determined by the different substrates used for its determination. Chemosphere. 169, 324-332.
[19] Rao, C.R.M., Sahuquillo, A. and Lopez Sanchez, J.F. (2008) A review of the different methods applied in environmental geochemistry for single and sequential extraction of trace elements in soils and related materials. Water, Air, and Soil Pollution. 189, 291-333.
[20] Ignatowicz, K. (2017) The impact of sewage sludge treatment on the content of selected heavy metals and their fractions. Environmental Research. 156, 19-22.
[21] Song, M., Yang, Y., Jiang, L., Hong, Q., Zhang, D., Shen, Z., Yin, H. and Luo, C. (2017) Characterisation of the phenanthrene degradation-related genes and degrading ability of a newly isolated copper-tolerant bacterium. Environmental Pollution. 220, 1059-1067.
[22] Pascault, N., Ranjard, L., Kaisermann, A., Bachar, D., Christen, R., Terrat, S., Mathieu, O., Lévêque, J., Mougel, C., Henault, C., Lemanceau, P., Péan, M., Boiry, S., Fontaine, S. and Maron, P. (2013) Stimulation of different functional groups of bacteria by various plant residues as a driver of soil priming effect. Ecosystems. 16, 810-822.
[23] Shahsavari, E., Adetutu, E.M., Anderson, P.A. and A.S. Ball. (2013) Plant residues—a low cost, effective bioremediation treatment for petrogenic hydrocarbon-contaminated soil. Science of The Total Environment. 443, 766-774.
[24] Sharma, U. and Subehia, S.K. (2016) Fractions of copper in soil and their contribution to copper availability in Rice-Wheat cropping system under Long-Term integrated nutrient management in an acid alfisol. Communications in Soil Science and Plant Analysis. 47, 980 - 988.

[25] Hoang, T.C., Schuler, L.J., Rogevich, E.C., Bachman, P.M., Rand, G.M. and Frakes, R.A. (2009) Copper release, speciation, and toxicity following multiple floodings of copper enriched agriculture soils: Implications in everglades restoration. Water, Air, and Soil Pollution. 199, 79-93.
[26] Rupa, T.R., Tripathi, A.K., Rao, C.S., Singh, K.N. and Rao, A.S. (2001) Distribution and plant availability of soil copper fractions following copper sulphate and farmyard manure applications. Journal of Plant Nutrition and Soil Science. 164, 451.
[27] Ordonez-Fernandez, R., Repullo-Ruiberriz De Torres, M.A., Roman-Vazquez, J., Gonzalez-Fernandez, P. and Carbonell-Bojollo, R. (2015) Macronutrients released during the decomposition of pruning residues used as plant cover and their effect on soil fertility. The Journal of Agricultural Science. 153, 615-630.
[28] Hill, M.O. (1973) Diversity and evenness: A unifying notation and its consequences. Ecology. 54(2), 427-432.
[29] Madhaiyan, M., Poonguzhali, S., Senthilkumar, M., Pragatheswari, D., Lee, J.S. and Lee, K.C. (2015) Arachidicoccus rhizosphaerae gen. Nov., Sp. Nov., A novel plant growth-promoting bacteria in the family Chitinophagaceae isolated from rhizosphere soils. International Journal of Systematic and Evolutionary Microbiology. 65, 578-586.
[30] Zhao, Q., Yue, S., Bilal, M., Hu, H., Wang, W. and Zhang, X. (2017) Comparative genomic analysis of 26 Sphingomonas and Sphingobium strains: Dissemination of bioremediation capabilities, biodegradation potential and horizontal gene transfer. Science of The Total Environment. 609, 1238-1247.
[31] Sun, D., Li, K., Bi, Q., Zhu, J., Zhang, Q., Jin, C., Lu, L. and Lin, X. (2017) Effects of organic amendment on soil aggregation and microbial community composition during drying-rewetting alternation. Science of The Total Environment. 574, 735-743.
[32] Liang, X., Yuan, J., Yang, E. and Meng, J. (2017) Responses of soil organic carbon decomposition and microbial community to the addition of plant residues with different C:N ratio. European Journal of Soil Biology. 82, 50-55.
[33] Medina, R., David Gara, P.M., Fernández-González, A.J., Rosso, J.A. and Del Panno, M.T. (2018) Remediation of a soil chronically contaminated with hydrocarbons through persulfate oxidation and bioremediation. Science of The Total Environment. 618, 518-530.

Received: **02.12.2018**
Accepted: **24.02.2019**

CORRESPONDING AUTHOR

Guihong Lan
College of Chemistry and Chemical Engineering,
Southwest Petroleum University,
610500 Chengdu – China

e-mail: guihonglan416@sina.com

© by PSP Volume 28 – No. 5/2019 pages 3928-3932 Fresenius Environmental Bulletin

INVESTIGATION OF CAUSATIVE AGENTS IN COMMUNITY-ACQUIRED ATYPICAL PNEUMONIA CASES

Emel Caliskan[1,*], Sukru Oksuz[1], Cihadiye Elif Ozturk[1], Idris Sahin[1], Ozge Kilincel[2], Nida Akar[3], Ege Gulec Balbay[4], Fatif Alasan[5]

[1]Duzce University Faculty of Medicine, Department of Medical Microbiology, Duzce, Turkey.
[2]Duzce Ataturk State Hospital, Microbiology Laboratory, Duzce, Turkey.
[3]Hacettepe University Faculty of Medicine, Department of Medical Mycology, Ankara, Turkey.
[4]Duzce University Faculty of Medicine, Department of Chest Disease, Duzce, Turkey.
[5]Afyonkarahisar State Hospital, Department of Chest Disease, Afyonkarahisar, Turkey.

ABSTRACT

To investigate the causative agents involved in atypical community-acquired pneumonia (CAP) patients with lower respiratory tract infections. This prospective study (October 2014–August 2016) included 92 adult patients with pre-existing CAP. Serum samples were analyzed for IgG and IgM antibodies using the indirect immunofluorescence antibody (IFA) method. Causative agents associated with typical pneumonia were evaluated in simultaneously obtained sputum cultures. The IgM antibodies and/or the cultures of typical agents exhibited positivity for atypical CAP causative agents in 26 (28%) of the patients. Positive IgM antibodies were found for influenza B virus in five patients, parainfluenza serotype 2 virus in four, echovirus in four, parainfluenza serotype 1 virus in two, parainfluenza serotype 3 virus in two, influenza A (H1N1) virus in two, *C. pneumoniae* in two and *H. influenzae* in one. Thirteen (50%) of these patients had typical bacterial growth, while more than one agent was detected in five (20%). The rate of atypical causative agents other than *L. pneumophila* was quite high. Viruses were the main agents in the atypical CAP patients. The high incidence of typical pneumonia agents found in these patients indicates the necessity of determining the etiologic agents prior to initiation of treatment.

KEYWORDS:
Atypical pneumonia, indirect immunofluorescence antibody, influenza virus, elderly patient.

INTRODUCTION

Depending on the causative microorganisms, clinical picture and treatment choice, community-acquired pneumonia (CAP) is classified as either typical or atypical pneumonia. Community-acquired pneumonia is an infectious disease with a high mortality and morbidity, thus, especially for elderly patients, it is very important to identify the causative agents quickly and start appropriate treatment as soon as possible [1-3]. Typical pneumonia causes can be identified in any number of laboratories, and effect-oriented treatment can be started, whereas atypical pneumonia is usually treated empirically without identifying the causative agent. Many microorganisms, including *Mycoplasma pneumoniae, Chlamydophila pneumoniae, Legionella pneumophila* and respiratory tract viruses, can affect atypical pneumonia [4]. Although each requires very different treatments, the clinical manifestations are not always distinctive in the definition of typical and atypical pneumonia. In addition, markers such as blood leukocyte count and procalcitonin level may be insufficient to distinguish bacterial/viral infection. In particular, infections in which bacteria and viruses are co-causative can lead to incorrect treatment [5]. For this reason, microbiological tests with high specificity and sensitivity should be used in the diagnosis. Indirect methods such as enzyme immunoassay (EIA), indirect immunofluorescence antibody (IFA), or polymerase chain reaction (PCR) are used in the diagnosis, since isolation of atypical pneumonia agents can be difficult or dangerous [6,7].

This study aimed to investigate serum samples of patients pre-diagnosed with atypical CAP for atypical pneumonia causative agents via IFA, and to investigate bacterial cultures for agents associated with typical pneumonia.

MATERIALS AND METHODS

Patients included in the study were among those with a preliminary diagnosis of atypical pneumonia who presented to the Chest Diseases Polyclinic with lower respiratory tract infections between October 2014 and August 2016 and who, according to the *Turkish Thoracic Society Consensus Report on the Diagnosis and Treatment of Community-acquired Pneumonia in Adults (2009),* did not meet typical pneumonia criteria (acute onset and noisy breathing, fever with chills, pleuritic chest pain, purulent sputum, leukocytosis, neutrophil dominance, con-

solidation findings upon physical examination and/or lobar involvement on chest radiograph).

The causative agents of atypical pneumonia were investigated in serum, and the agents associated with typical pneumonia were investigated in samples of sputum taken simultaneously. In the serum samples, antibodies were determined via the IFA method using the "Respiratory Tract Profile 1 IgM and IgG" commercial kit (Euroimun, Germany). Using this kit, the presence of IgM and IgG antibodies was examined to detect respiratory syncytial virus (RSV), adenovirus, influenza A virus (H1N1, H3N2), influenza B virus, parainfluenza virus serotypes 1, 2, 3 and 4, *Bordetella pertussis*, *Bordetella parapertussis*, *Mycoplasma pneumoniae*, coxsackie virus serotypes B1 and A7, echovirus, *Chlamydophila pneumoniae*, *Haemophilus influenzae* and *Legionella pneumophila* serotypes 1 and 12. The assessments were carried out in accordance with the instructions of the manufacturing firm.

Sputum samples were incubated at 37 °C for 18-24 h on 5% sheep blood agar, eosin methylene blue (EMB) agar and chocolate agar (Oxoid, UK). After incubation, the VITEK 2 Compact System (BioMérieux, France) automated identification system was used to identify the bacteria that had reproduced.

For the statistical evaluations of the study, descriptive statistics were calculated using the SPSS v.22 packet program. Continuous data were summarized as mean ± standard deviation, categorical frequency and percentage.

RESULTS

The 92 adult cases of pre-diagnosed community-acquired atypical pneumonia included 47 (52%) males and 45 (49%) females with a mean age of 70.6 ± 13. In 26 (28%) of the patients, typical pneumonia bacterial reproduction was detected and/or IgM antibodies against atypical agents were found. The distribution of these agents is shown in Table 1 and Figure 1. It was determined that 14 (88%) of the patients with IgM positivity were over 65 years of age and empirical antibiotic treatment was started for all of the participating patients.

Among the causative agents, IgM antibodies were found to be negative for parainfluenza virus serotype 4, H3N2, RSV, adenovirus, coxsackie virus serotypes B1 and A7*, B. pertussis, B. parapertussis*, *M. pneumoniae* and *L. pneumophila* serotypes 1 and 12.

TABLE 1
Distribution of agents in patients with acute CAP

Microorganism	Acute CAP positivity	
	n	%
The agents in the CAPs formed by the single agent		
İnfluenza B virus*	3	11,5
İnfluenza A virus (H1N1)*	2	7,5
Parainfluenza serotype 2 virus*	2	7,5
Echovirus*	2	7,5
*C. pneumonia**	1	4
*H. influenzae**	1	4
Klebsiella pneumoniae **	4	15
*Enterobacter aerogenes***	2	7,5
*Escherichia coli***	2	7,5
*Staphylococcus aureus***	1	4
*Streptococcus pneumoniae***	1	4
The agents in the CAPs formed by the two agents		
Parainfluenza serotype 1* ve serotype 2 virus*	1	4
Parainfluenza serotype 1 virus* ve echovirus*	1	4
*Escherichia coli***ve influenza B virus*	1	4
The agents in the CAPs formed by the three agents		
*Klebsiella oxytoca***+parainfluenza serotype 3 virus**+C. pneumonia**	1	4
The agents in the CAPs formed by the five agents		
İnfluenza B virus*+ echovirus*+parainfluenza serotype 2* ve serotype 3 virus**+ *E. aerogenes***	1	4
Total	26	100

CAP: Community-acquired pneumonia, *: IgA antibody positivity in serum by IFA method, **: Bacteria detected in sputum culture

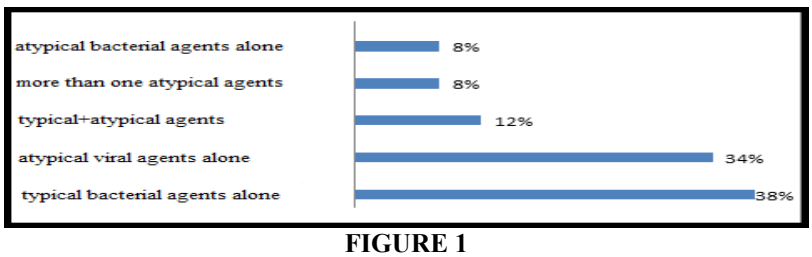

FIGURE 1
Grouping of acute CAP agents

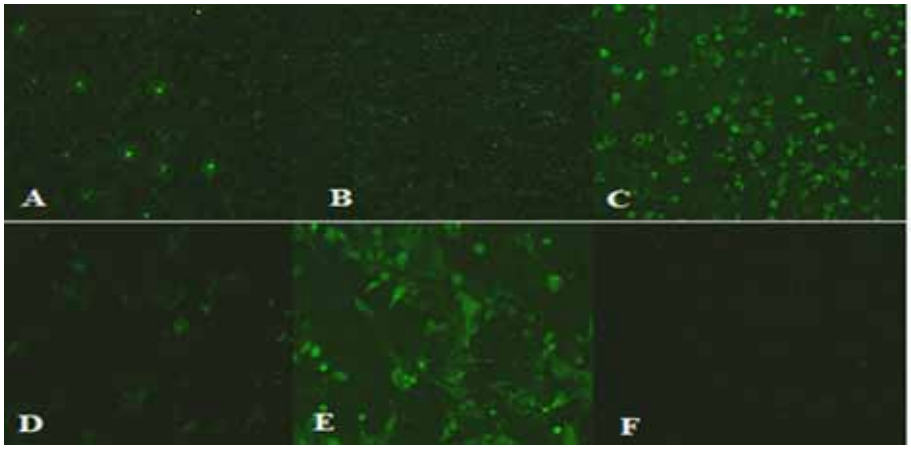

FIGURE 2
Fluorescence microscopy images of some of the IgG- and IgM-positive samples
(A: *M. pneumoniae* IgG, B: *H. influenzae* IgG, C: *C. pneumoniae* IgG, D: İnfluenza virus serotype B IgM, E: RSV IgG, F: *L. pneumophila* serotype 12 IgG)

TABLE 2
The IgG positivity rates for the atypical pneumonia agents (%)

Microorganism	IgG positivity %
İnfluenza B virus	79
Parainfluenza virus serotype 1	75
Parainfluenza virus serotype 2	86
Parainfluenza virus serotype 3	87
Parainfluenza virus serotype 4	75
Echovirus	86
H1N1	84
H3N2	83
Respiratuar sinsityal virüs	**99**
Adenovirus	90
Coxsackie virus serotype B1	86
Coxsackie virus serotype A7	76
C. pneumoniae	82
H. influenzae	79
B. pertussis	82
B. parapertussis	**65**
M. pneumoniae	85
L. pneumophila serotype 1	**7**
L. pneumophila serotype 12	**17**

The IgG positivity was found to be highest for RSV (99%) and lowest for *L. pneumophila* serotype 1 (7%). In terms of the causative agents, the IgG positivity was found to be statistically significant (p <0.05). This difference was attributed to the low positivity for *L. pneumophila* serotype 1, *L. pneumophila* serotype 12 and *B. parapertussis* (Table 2). In addition, in our study, viral agents were encountered at a higher rate than atypical bacterial agents (p <0.05). The IgG positivity rates for the atypical pneumonia agents are presented in Table 2; Fluorescence microscopy images of some of the IgG- and IgM-positive samples are shown in Figure 2.

DISCUSSION

The inability to treat atypical pneumonia causative agents with beta-lactam antibiotics differentiates atypical from typical pneumonia. In addition, distinguishing whether the atypical pneumonia agent is viral or bacterial is important for proper administration of antibiotics and prevention of resistance. Erdem et al. reported that atypical pneumonia accounts for 29% of all pneumonia in Turkey [8]. Koksal et al., in a multicenter study conducted on CAP patients, found typical pathogens in 35.8%, atypical bacteria in 20.2% and viruses in 20.6%, and no etiologic agents in the remaining CAP patients. They also reported that 56.9% of the patients were under 65 years of age [9]. In our study, among the determinants, the frequency of viral agents alone, especially the influenza B virus, was 34%, the frequency of typical bacterial agents alone was 38%, and the frequency of atypical bacterial agents alone was 8%. The variation in distribution among the agents in our study was attributed to the inclusion of CAP patients who were considered to have atypical pneumonia, to the climatic conditions of our region and to the fact that the majority of the patient group consisted of elderly patients. However, despite the high frequency of viral agents, the application of empirical antibiotic therapy was carried out. This finding is important for our hospital in terms of avoiding inappropriate use of antibiotics and the high rate of antibiotic resistance that can develop accordingly.

When we examined the IgG positivities detected in the patients, we found that the rate of viral agents, especially RSV, in our region was very high, while the rates of *L. pneumophila* serotypes 1 and 12 and *B. parapertussis* were lower. *Legionella* bacteria can be found in nature in various water resources and climate systems, and factors such as suitable temperature, low water flow and the presence of sediment facilitate its growth [10]. Various studies around the world have shown that the seroprevalence of *L. pneumophila* varies between 1.6% and 17.1% [11-13]. In our study, *L. pneumophila* serotype 1 positivity was found to be 7% and serotype 12 positivity to be 17%. Although there are few epidemiological studies on *B. parapertussis*, it

has been reported to affect children, to have no seasonal characteristics, and to cause epidemics [14]. Studies have also shown that *B. pertussis* vaccination is inadequate in the prevention of *B. parapertussis* infection [15]. In our study, *B. parapertussis* seropositivity was found to be 65%. *B. pertussis* vaccination was started in Turkey in 1968 and it was assumed that since the infection was usually encountered in childhood, the IgG positivity in the majority of our patients was compatible with a childhood infection. *M. pneumoniae* and *C. pneumoniae* are the most common bacterial agents of atypical pneumonia. A multicenter study involving Asian countries reported that these bacteria account for 25% of all CAP in adult patients[2]. Since the rates of these two agents in our study were 85% and 82%, respectively, it is felt that, as these bacteria are so frequently encountered in our region, they should be kept in mind during diagnosis and treatment.

Nowadays, lower respiratory tract infections with bacteria and viruses together as the causative agents are being more frequently encountered [16]. Juven et al. reported that bacteria and viruses were co-causative in 30% of children with CAP [17]. In their study, Koksal et al. found that 50.9% of CAP patients had a single pathogen and 11.9% had multiple pathogens, and they recommended combination treatments in empirical therapy [9]. In our study, more than one cause was found in five patients (20%), and at least three of them (12%) were positive for both atypical and typical causative agents. Correct application of diagnostic methods is seen as a guide to the treatment. In addition, isolation of typical pneumonia agents in 13 (14%) of the patients considered to have atypical pneumonia in our study showed that diagnosing only with clinical findings may lead to errors in treatment. For this reason, with the possibility that the clinical presentation may vary, it is necessary to plan treatment by defining both typical and atypical etiologic agents together.

In elderly patients, CAP may be more severe than in younger patients and may be fatal when treatment is delayed. The atypical view of your clinic and underlying diseases may delay the diagnosis, especially in the elderly [18]. In addition, some factors that may lead to treatment failure include living in a care facility, the presence of multi lobular involvement on chest X-rays, being female and the presence of accompanying cerebrovascular disease [19]. Studies of the influenza A virus (H1N1, H3N2) and influenza B virus, which are common causes of atypical pneumonia, have shown that recurrent annual vaccination, particularly in elderly patients, has the effect of lessening the severity of the disease and reducing mortality [20,21]. In our study, it was determined that the majority of the patients were elderly and that 19 out of a total of 22 atypical pneumonia agents were viruses. Five of the viruses were influenza B virus, and two of them were influenza A virus (H1N1), indicating that influenza vaccination is important for our region.

In conclusion, when we investigated the seropositivity of a large number of viruses and bacteria in the CAP patients in our study, we found that the rate of encountering atypical agents other than *L. pneumophila* was very high. Viruses were found to be the major cause of atypical CAP cases. Furthermore, the coexistence of both typical and atypical pneumonia agents seen in atypical CAP also indicates the need to determine the etiologic agents prior to initiation of treatment. These findings will contribute to the epidemiological data of our region and will serve as a guide in vaccination and treatment planning, especially for elderly patients.

ACKNOWLEDGEMENT

The study was supported by the Düzce University Medical Faculty Scientific Research Projects (DUBAP) and was approved by the Düzce University Faculty of Medicine Ethics Committee (No. 2014/53).

REFERENCES

[1] Sharma, L, Losier, A, Tolbert, T, Charles, S. Cruz, D, Marion, CR. (2017) Pneumonia Updates on Legionella, Chlamydophila, and Mycoplasma pneumonia. Clin Chest Med. 38(1), 45-8. (in English)

[2] Song, J.H., Oha, W.S., Kanga, C.I., Song, J.H., Oh, W.S., Kang, C.I., Chung, D.R., Peck, K.R., Ko, K.S., Yeom, J.S., Kim, C.K., Kim, S.W., Chang, H.H., Kim, Y.S., Jung, S.I., Tong, Z., Wang, Q., Huang, S.G., Liu, J.W., Lalitha, M.K., Tan, B.H., Van, P.H., Carlos, C.C., So, T., Asian Network for Surveillance of Resistant Pathogens Study Group. (2008) Epidemiology and clinical outcomes of community-acquired pneumonia in adult patients in Asian countries: a prospective study by the Asian network for surveillance of resistant pathogens. International Journal of Antimicrobial Agents. 31, 107-14. (in English)

[3] Umut, S. and Saryal, S.B. (2009) Turkish thoracic society adult pneumoniae diagnosis and treatment reconciliation report. Turkish Thoracic Journal. 10 (supp 9), 1-16. (in Turkish)

[4] Ellison, R.T., Donowitz, G.R. (2015). Acute Pneumonia, In: Mandell GL, Bennett JE, Dolin R (eds), Mandell, Douglas and Bennett's Principles and Practice of Infectious Diseases., 8thed. Churchill Livingstone, Philadelphia, 823-46. (in English)

[5] Waterer, G.W. (2017) Diagnosing viral and atypical pathogens in the setting of community-acquired pneumonia. Clin Chest Med. 38(1), 21-8. (in English)
[6] Somer, A. (2012) Atypical pneumonias in pediatrics. ANKEM. 26(supp 2), 234-40. (in Turkish)
[7] Cunha, B.A. (2006) The atypical pneumonias: clinical diagnosis and importance. Clin Microbiol Infect. 12 (Ek 3), 12-24. (in English)
[8] Erdem, H., Artuk, C., Coskun, O. (2009) Infectious etiology of hospitalized community-acquired pneumonia patients in Turkey. FLORA. 14(2), 53-7. (in Turkish)
[9] Koksal, I., Ozlu, T., Bayraktar, O., Yılmaz, G., Bülbül, Y., Oztuna, F., Caylan, R., Aydın, K., Sucu, N. and TUCAP Study Group. (2010) Etiological agents of community-acquired pneumonia in adult patients in Turkey; a multicentric, cross-sectional study. Tüberküloz ve Toraks Dergisi. 58(2), 119-27. (in English)
[10] Babaoglu, G., Aydin, D., Arseven, O., Berkiten, R. (2003) Investigation of Legionella pneumophila in patients with atypical pneumonia by direct and indirect microbiological methods. Türk Mikrobiyol Cem Derg. 33, 35-8. (in Turkish)
[11] Valcin, O., Pule, D., Lucenko, I., Krastiņa, D., Steingolde, Z., Krumiņa, A. and Berziņs, A. (2015) Legionella pneumophila seropositivity-associated factors in Latvian blood donors. Int. J. Environ. Res. Public Health. 13(58), 2-8. (in English)
[12] Rahimiana, M. and Hosseini, B.M. (2017) Serological study of Bordetella pertussis, Mycoplasma pneumonia and Chlamydia pneumonia in Iranian hajjpilgrims with prolonged cough illnesses: A follow-up study. Respiratory Medicine. 132, 122-31. (in English)
[13] Kurutepe, S., Ecemiş, T, Özgen, A., Biçmen, C., Çelik, P., Aktoğu Özkan, S. and Sürücüoğlu, S. (2012) Investigation of bacterial etiology with conventional and multiplex PCR methods in adult patients with community-acquired pneumonia. Mikrobiyol Bul. 46(4), 523-31. (in Turkish)
[14] Karalius, V.P., Rucinski, S.L., Mandrekar, J.N. and Patel, R. (2017) Bordetella parapertussis outbreak in Southeastern Minnesota and the United States, 2014. Medicine (Baltimore). 96(20), e6730. (in English)
[15] Botteroa, D., Gaillarda, M.E., Erreab, A., Moreno, G., Zurita, E., Pianciola, L., Rumbo, M. and Hozbor, D. (2013) Outer membrane vesicles derived from Bordetella parapertussis as an acellular vaccine against Bordetella parapertussis and Bordetella pertussis infection. Vaccine. (31), 5262-8. (in English)
[16] Zaki, M.S. and Goda, T. (2009) Clinico-pathological study of atypical pathogens in community-acquired pneumonia: a prospective study. J Infect Developing Countries. 3(3), 199-205. (in English)
[17] Juven, T., Mertsola, J., Waris, M., Leinonen, M., Meurman, O., Roivainen, M., Eskola, J., Saikku, P. and Ruuskanen, O. (2000) Etiology of community-acquired pneumonia in 254 hospitalized children. Pediatr Infect Dis J. 19(4), 293-8. (in English)
[18] Takada, T., Yamamoto, Y., Terada, K., Ohta, M., Mikami, W., Yokota, H., Hayashi, M., Miyashita, J., Azuma, T., Fukuma, S. and Fukuhara, S. (2017) Diagnostic utility of appetite loss in addition to existing prediction models for community-acquired pneumonia in the elderly: a prospective diagnostic study in acute care hospitals in Japan. BMJ Open. 7(11), e019155. (in English)
[19] Dogan, C., Cetin, Ö., Kiral, N., Sarac, G. and Salepci, B. (2014) Analysis of advanced age pneumonia cases and factors effective on treatment success. Eurasian J Pulmonol. 16, 94-8. (in Turkish)
[20] Casado, I., Dominguez, A., Toledo, D., Chamorro, J., Astray, J., Egurrola, M., Fernandez-Sierra, M.A., Martin, V., Morales-Suarez-Varela, M., Godoy, P., Castilla, J. and Project PI12/02079 Working Group. (2018) Repeated influenza vaccination for preventing severe and fatal influenza infection in older adults: a multicentre case-control study. CMAJ. 190(1), E3-E12. (in English)
[21] Shim, E., Smith, K.J., Nowalk, M.P., Raviotta, J.M., Brown, S.T., DePasse, J. and Zimmerman, R.K. (2018) Impact of seasonal influenza vaccination in the presence of vaccine interference. Vaccine. 36,853-8. (in English)

Received: **04.10.2018**
Accepted: **08.04.2019**

CORRESPONDING AUTHOR

Emel Caliskan
Duzce University Faculty of Medicine,
Department of Medical Microbiology,
Duzce, Turkey.

e-mail: emelcaliskan81@yahoo.com.tr

© by PSP Volume 28 – No. 5/2019 pages 3933-3938 Fresenius Environmental Bulletin

STUDY ON THE IMPACT OF LAND USE CHANGE ON RUNOFF AND WATER ENVIRONMENT

Jun Cai, Xiaoqian Ma*

College of Economics and Management, Anhui Agricultural University, Hefei, 230036, China

ABSTRACT

Runoff has changed significantly in most regions in China over the past decades. Climate variability and land-use changes are considered to be the two main factors contributing to runoff variation. Investigating the mechanism of runoff variation is of great significance for the sustainable utilization of water resources. In this study, the sensitivities of runoff were estimated with regard to these two factors in central China during the study period from 1980 to 2000. The objectives of this study therefore are to (1) investigate the tendencies and change points of annual runoff in the area of Hefei of Anhui from 1980 to 2000; (2) the relative impacts of land-use changes on the decrease of runoff; (3) analyze the impact of Land Use Change on Water Environment. The findings of this study will be very helpful for future water resources planning and land-use improvement strategies. The results revealed a significant decreasing trend in annual runoff and indicated that land-use changes had a greater effect on runoff than climate variability since 1980. Forests have the most effective impact on runoff reduction, followed by grassland or farmland. The green water holding capacity of the covered green land is stronger than that of the bare green land, and the reduction of chemical pollutants such as COD is stronger than that of bare land, and its ability to reduce COD is most prominent. In the area of 486.61 km^2 in the central urban area, the pollution caused by rainfall runoff is about 800,000 tons, and the pollution caused by runoff increases at an average annual rate. If the annual rainfall is too large, the pollution situation will be more serious.

KEYWORDS:
Land-use changes, Runoff variation, Sensitivity analysis, Water Environment

INTRODUCTION

Land use and land-cover (LULC) change is widely recognized as one of the most important components of global environmental change. Land use and land-cover and climate change are the two foremost drivers of hydrologic processes, influencing the available water resources and flow regimes in a river basin around the world [1-5]. Changes in LULC, primarily ascribed to anthropogenic activities, including alterations in types of vegetation, modification in land use practices and their spatial patterns is supposed to have substantial influence on the hydrologic characteristic of a river basin. Alterations in LULC impacts the water resources availability and hydrological cycle [6-10]. Translation of land-cover for urban and agricultural uses often effects integrity of soil, nutrient fluxes, and assemblies of inherent species. Such changes can disturb watershed hydrology by altering canopy interception, soil properties, infiltration, surface roughness, albedo and evapotranspiration. Therefore, interactions among these factors at basin scale can have a confounding effect that might result in variations in the timing and volumes of surface runoff [11-13].

Land use change can affect not only river flow, but also other compartments of the water cycle, such as groundwater, which can decline during the dry season as a consequence of reduced infiltration volume. This affects groundwater recharge and soil water content more in general, thus contributing to reduce evapotranspiration (ET) [14]. ET may also decrease because of higher surface albedo, lower surface aerodynamic roughness, lower leaf area and shallower rooting depth caused by changing land use from forest to pasture [15]. In areas where precipitation recycling is large and strongly depends on ET, this may ultimately affect also microclimate. Therefore, comprehending the hydrologic response of a catchment to LU changes formulates a pivotal step towards water resources planning and management. Moreover, with rise in scarcity of available water wealth, hydrologic impacts due to change in LU have drawn substantial attention from the hydrologic community.

Assessing impacts of LULC changes on hydrology is the essential for watershed management and ecological restoration. Quantification of the impact due to changes in land use on dynamics of streamflow in river basins has been the area of interest for hydrologists in recent years. In the past 30 years, land use changes associated with rapid urbanization and deforestation have greatly altered a large proportion of regions [16]. The effect of alteration in LULC on available water resources and hydrological processes has been one of the most popular focus of research during the past dec-

ades [17]. For example, change in land use can lead to variation in flood frequency, base flow, severity, and annual mean discharge [18]. Several studies have revealed that the removal of vegetation can lead to increase in the base flows if infiltration properties of soil remain unperturbed. However, if removal of vegetation is followed by land use practices, which compact soils and make them vulnerable to erosion, then it can lead to decrease in percolation to groundwater. Lin and Wei [19] in their study reported a trend of increased flooding with decreasing forest cover. Moreover, Bradshaw et al. [20] revealed that deforestation is largely correlated with occurrence of flood and its severity. Urbanization has been the most frequently witnessed driver to change in LULC, and has been extensively explored in recent years. Increase in impervious areas through urbanization results into decrease in the volume of water, which infiltrates into the soil.

Different model concepts exist (empirical, conceptual and physically based models) among which physically based spatially distributed models are considered suitable for the analyses of LULC impacts on erosion at smaller scales as a certain complexity is necessary for the predictions of the changing LULC conditions. The parameter values of these model types have a physical meaning and therefore can be better estimated, which increases the quality of the simulated output. The hydrological and soil erosion model SHETRAN has been successfully applied to simulate effects of changing LULC and climate. SHETRAN studies used several approaches to investigate the impacts of a changing LULC. On the one hand, hypothetical scenarios derived from a simple change of vegetation properties are used and on the other hand the analyses of observed land use in different catchments were compared to reflect changed LULC.

The objectives of this study therefore are to (1) investigate the tendencies and change points of annual runoff in the area of Hefei of Anhui from 1980 to 2000; (2) the relative impacts of land-use changes on the decrease of runoff; (3) analyze the impact of Land Use Change on Water Environment. The findings of this study will be very helpful for future water resources planning and land-use improvement strategies.

EXPERIMENTAL

The land area of Hefei City is 704,701.37 hectares. Among them, 549,526.57 hectares of agricultural land, accounting for 77.98% of the total land area; 114,858.75 hectares of construction land, accounting for 16.30% of the total land area; 40,316.05 hectares of unused land, accounting for 5.72% of the total land area. In the agricultural land, the cultivated land is 377,564.63 hectares, the garden is 2292.25 hectares, the forest land is 34531.16 hectares, the grassland is 36.26 hectares, and the other agricultural land is 135102.27 hectares. In the construction land, the residential area and industrial and mining land are 90058.60 hectares, the transportation land is 5,78.73 hectares, and the water conservancy facilities are 18,821.42 hectares. In the unused land, the unused land is 5714.42 hectares and the other land is 34601.63 hectares.

RESULTS AND DISCUSSION

Land-use changes. Land-use can be divided into six categories in the study area, including forest, grassland, farmland, water bodies, built-up land and unused land. Significant variations in land-use types occurred between 1980 and 2000, forest, grassland and farmland were the major types of land-use, occupying more than 90% of the total study area. Changes in land-use types were most significant from 1990 to 1995. Forest represented the largest area, increasing from 31.94% to 37.01% during this period, due to the afforestation project advocated by the Chinese government. Grassland, which covered 30.14%, was also one of the main types of land-use, but decreased by 1.23%. Although farmland covered 28.41% of the study area, it decreased in total area by 3.80% from 1990 to 1995. Water bodies, built-up land and unused land showed minimal changes, these land-use types are estimated to cover approximately 4.44% of the study area. By 2000, the coverage rates of forest, grassland and farmland recovered to the levels of 1990, covering 31.41%, 32.82% and 32.06%, respectively. A significant land-use transition was found between forest and farmland from 1980 to 2000.

The impact of land-use changes on runoff. A significant decreasing trend in runoff was found, despite the lack of an obvious decreasing trend in precipitation in the study region. This clearly indicates that the runoff decline is influenced by other factors. Fig. 1 shows that the influence of climate weakened after 1979, and land-use changes could be seen as the main cause of runoff variation. This confirmed findings of previous studies that land-use changes are the primary factors influencing runoff reduction. As the major types of land-use, forest, grassland and farmland changed considerably during the study period. In the 1980s, the total farmland area reached 57×10^3 km^2 due to land reform policies, accounting for 31.71% of the total land area. In the early 1990s, the coverage of forest and grassland greatly increased under the Grain for Green policy, representing more than two-thirds of the total area.

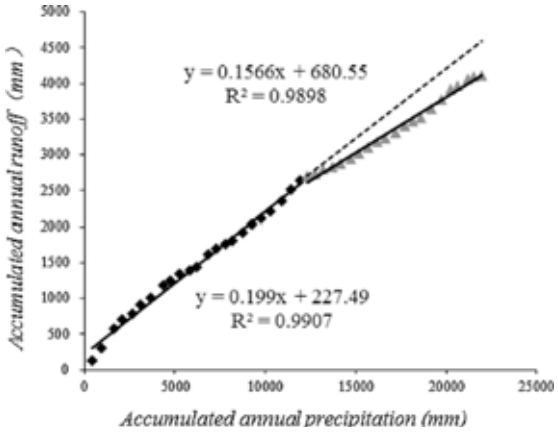

FIGURE 1
Double cumulative curve of accumulated annual precipitation and accumulated annual runoff in the Heifei area

Most studies demonstrated that vegetation can decrease runoff, but the extent of the reduction has not been quantified. The forest, grassland and farmland of this study were simulated by the model to estimate the impacts on runoff. The results show that the average reduction of runoff in forest, grassland and farmland in the study area was 57.53, 38.33 and 35.62 mm, respectively. This indicates that the effect of farmland and grassland on runoff in the study area is far less than that of forest.

The reserves of forest, grassland and farmland of different watersheds differed due to their different areas. To compare the effects of forest, grassland and farmland on runoff, the relationship between the influence of these three vegetation types on runoff in 66 watersheds and their coverages are shown in Fig. 2. There is a significant positive correlation between runoff and its coverage in forest, grassland and farmland in different watersheds, the sensitivities of runoff to forest (ε_{forest}), grassland (ε_{grass}), and farmland ($\varepsilon_{farmland}$) were 0.79–2.04, 0.7–1.67 and 0.61–1.60, respectively, with means of 1.46, 1.21 and 1.18, respectively. These results imply that with a 10% increase in forest, grassland and farmland coverage, runoff will decrease by 1.46, 1.21 and 1.18 mm, respectively. According to the perspective of water balance, reduced runoff should be stored as soil water or returned to the atmosphere as ET. Forests have a more efficient impact on reducing runoff, mainly because of the intrinsic properties of forests. They can intercept rainfall, alter soil micro-topography and increase soil porosity to store more water to infiltrate into the soil. In contrast, agricultural activities destroy the natural structure of the soil and reduce the infiltration rate of the water. Furthermore, previous studies showed that afforestation can increase the annual average ET by 2.7–11.1%, while conversion of forest to farmland will decrease the annual average ET by 3.1–22.2%.

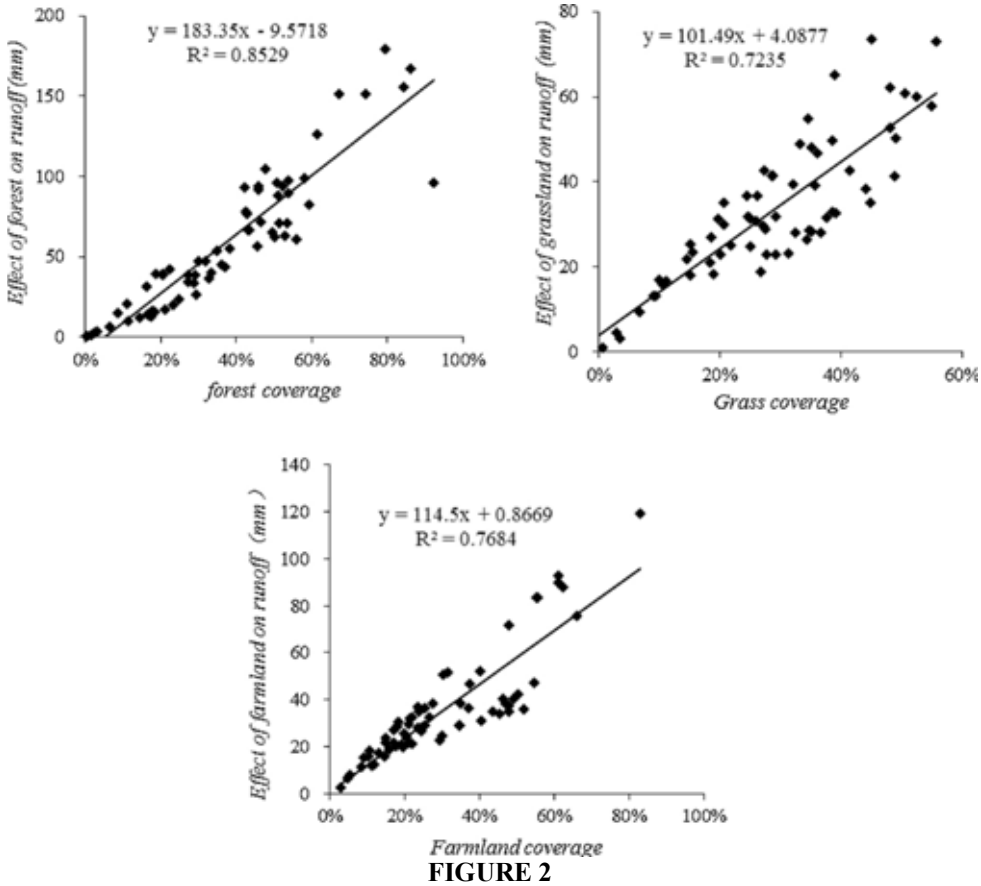

FIGURE 2
Relationship between effects of forest, grassland, and farmland on runoff and their coverage

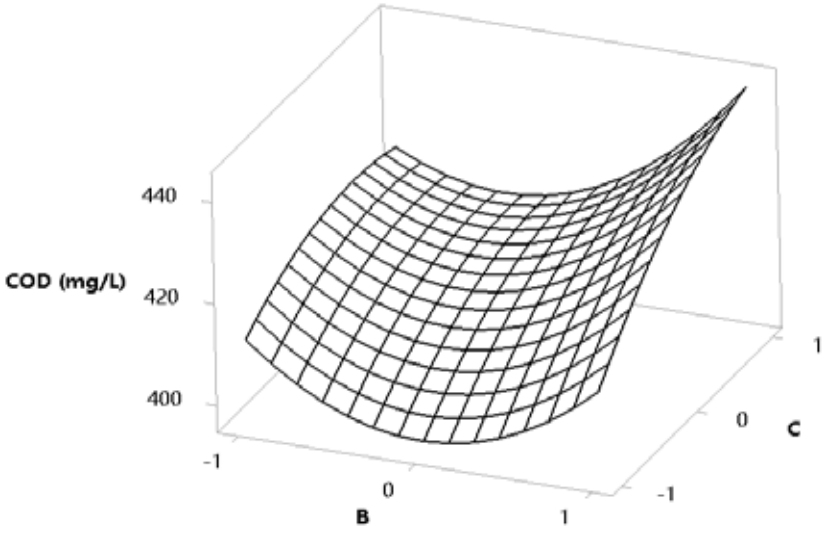

FIGURE 3
Surface Plot of COD (mg/L) vs C, B

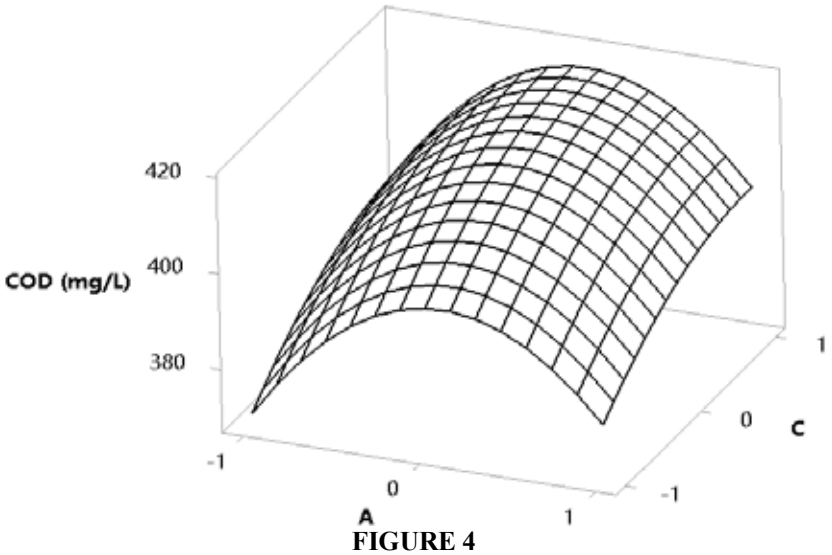

FIGURE 4
Surface Plot of COD (mg/L) vs C, A

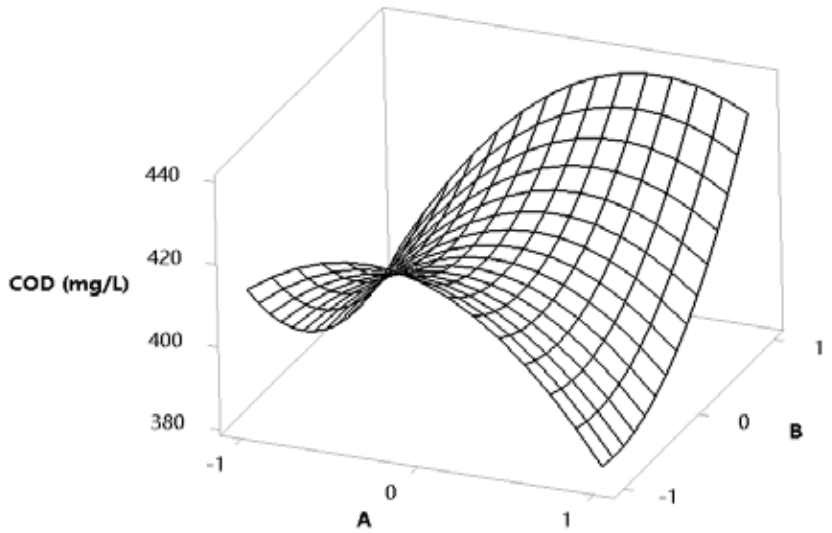

FIGURE 5
Surface Plot of COD (mg/L) vs B, A

Simulation experiment of Water Environment Effect of green ground thickness, green area and green rate on COD is studied (Fig.3-5). The green water holding capacity of the covered green land is stronger than that of the bare green land, and the reduction of chemical pollutants such as COD is stronger than that of bare land, and its ability to reduce COD is most prominent. In the area of 486.61 km^2 in the central urban area, the pollution caused by rainfall runoff is about 800,000 tons, and the pollution caused by runoff increases at an average annual rate. If the annual rainfall is too large, the pollution situation will be more serious.

CONCLUSION

In this study, the sensitivities of runoff were estimated with regard to these two factors in north China during the study period from 1980 to 2000. The objectives of this study therefore are to (1) investigate the tendencies and change points of annual runoff in the area of Hefei of Anhui from 1980 to 2000; (2) the relative impacts of land-use changes on the decrease of runoff; (3) analyze the impact of Land Use Change on Water Environment. The findings of this study will be very helpful for future water resources planning and land-use improvement strategies. The results revealed a significant decreasing trend in annual runoff and indicated that land-use changes had a greater effect on runoff than climate variability since 1980. Forests have the most effective impact on runoff reduction, followed by grassland or farmland. The green water holding capacity of the covered green land is stronger than that of the bare green land, and the reduction of chemical pollutants such as COD is stronger than that of bare land, and its ability to reduce COD is most prominent. In the area of 486.61 km^2 in the central urban area, the pollution caused by rainfall runoff is about 800,000 tons, and the pollution caused by runoff increases at an average annual rate. If the annual rainfall is too large, the pollution situation will be more serious.

ACKNOWLEDGEMENTS

This project in humanities and social sciences is funded with support from the Bureau of Education in Anhui for colleges and universities (SK2017a0563).

REFERENCES

[1] Sun, L. Guo, J., Sun, K. (2017) Influence of The Urban Water Environment From Human Activities: A Case Study With Identification And Quantification. Fresen. Environ. Bull. 26, 5377-5382.

[2] Liu, X. (2018) Application of Electronic Tongue Technology and Multivariate Statistical Analysis in Water Environment. Fresen. Environ. Bull. 27, 5107-5112.

[3] Gashaw, T., Tulu, T., Argaw, M., Worqlul, A.W. (2018) Modeling the hydrological impacts of land use/land cover changes in the Andassa watershed, Blue Nile Basin, Ethiopia. Sci. Total Environ. 619–620, 1394-1408.

[4] Serpa, D., Nunes, J.P., Santos, J., Sampaio, E., Jacinto, R., Veiga, S., Lima, J.C., Moreira, M., Corte-Real, J., Keizer, J.J., Abrantes, N. (2015) Impacts of climate and land use changes on the hydrological and erosion processes of two contrasting Mediterranean catchments. Sci. Total Environ. 538, 64-77.

[5] Wang, R., Kalin, L., Kuang, W., Tian, H. (2014) Individual and combined effects of land use/cover and climate change on Wolf Bay watershed streamflow in southern Alabama. Hydrol. Process. 28, 5530-5546.

[6] Brown, A.E., Zhang, L., McMahon, T.A., Western, A.W., Vertessy, R.A. (2005) A review of paired catchment studies for determining changes in water yield resulting from alterations in vegetation. J. Hydrol. 310, 28-61.

[7] Yu, H., Huang, Y., Ning, J., Zhu, B., Cheng, Y. (2014) Effect of cation exchange capacity of soil on stabilized soil strength. Soils and Foundations. 54, 1236-1240.

[8] Kindu, M., Schneider, T., Döllerer, M., Teketay, D., Knoke, T. (2018) Scenario modelling of land use/land cover changes in Munessa-Shashemene landscape of the Ethiopian highlands. Sci. Total Environ. 622–623, 534-546.

[9] Wilson, C.O., Weng, Q. (2011) Simulating the impacts of future land use and climate changes on surface water quality in the Des Plaines River watershed, Chicago Metropolitan Statistical Area, Illinois. Sci. Total Environ. 409, 4387-4405.

[10] Romanowicz. R.J., Booij, M.J. (2011) Impact of land use and water management on hydrological processes under varying climatic conditions. Phys. Chem. Earth. 36, 613-614,

[11] Li, Z., Liu, W., Zhang, X., Zheng, F. (2009) Impacts of land use change and climate variability on hydrology in an agricultural catchment on the Loess Plateau of China. J. Hydrol. 377, 35-42.

[12] Shrestha, M.K., Recknagel, F., Frizenschaf, J., Meyer, W. (2017) Future climate and land uses effects on flow and nutrient loads of a Mediterranean catchment in South Australia. Sci. Total Environ. 590–591, 186-193.
[13] Zhang, Y., Guan, D., Jin, C., Wang, A., Wu, J., Yuan, F. (2011) Analysis of impacts of climate variability and human activity on streamflow for a river basin in Northeast China. J. Hydrol. 410, 239-247.
[14] Xu, F., Hu, B., Dou, Y., Song, Z., Liu, X. (2018) Prehistoric heavy metal pollution on the continental shelf off Hainan Island, South China Sea: From natural to anthropogenic impacts around 4.0 kyr BP. Holocene. 28, 455-463.
[15] Wagner, P.D., Kumar, S., Schneider, K. (2013) An assessment of land use change impacts on the water resources of the Mula and Mutha Rivers catchment upstream of Pune, India. Hydrol. Earth Syst. Sci. 17, 2233-2246.
[16] Wu, J., Miao, C., Zhang, X., Yang, T., Duan, Q. (2017) Detecting the quantitative hydrological response to changes in climate and human activities. Sci. Total Environ. 586, 328-337.
[17] Zeiger, S.J., Hubbart, J.A. (2016) A SWAT model validation of nested-scale contemporaneous stream flow, suspended sediment and nutrients from a multiple-land-use watershed of the Central USA. Sci. Total Environ. 572, 232-243.
[18] Li, J., Li, G., Zhou, S., Chen, F. (2016) Quantifying the effects of land surface change on annual runoff considering precipitation variability by SWAT. Water Resour. Manag. 30, 1071-1084.
[19] Lin, Y., Wei, X. (2008) The impact of large-scale forest harvesting on hydrology in the Willow watershed of Central British Columbia. J. Hydrol. 359, 141-149
[20] Bradshaw, C.J.A., Sodhi, N.S., Peh, K.S.H., Brook, B.W. (2007) Global evidence that deforestation amplifies flood risk and severity in the developing world. Glob. Chang. Biol. 13, 2379-2395.

Received: **06.12.2018**
Accepted: **19.03.2019**

CORRESPONDING AUTHOR

Ma Xiaoqian
College of Economics and Management,
Anhui Agricultural University,
Hefei, 230036 – China

e-mail: 1467947594@qq.com

© by PSP Volume 28 – No. 5/2019 pages 3939-3945 Fresenius Environmental Bulletin

PREVALENCE CHARACTERISTICS OF PNEUMOCONIOSIS IN A CHINESE CITY: A SYSTEMATIC ANALYSIS OF 1980–2017 STUDIES

Li-jiang Zhang, Yao-qin Lu, Hao-feng Yang, Hui-min Yu, Bao-ling Rui*

Section for Occupational Disease Prevention, Center of Prevention and Control for Diseases in Urumqi, Urumqi, 830002, China

ABSTRACT

Nowadays, pneumoconiosis is a chronic occupational lung disease in China among coal, manufacture, building and other industries. However, information on the exact prevalence and characteristic of the disease is not available. Therefore, the aims of our investigation were to provide the significant original information and analyze the characteristics by conducting a systematic analysis in a city of China from 1980 to 2017.

Based on predetermined inclusion and exclusion criteria, 4797cases were selected and association analysis was further conducted. The prevalence was analyzed according to gender, age, nationality, industries, stages, disease type, age of diagnosis and time of dust exposure, etc.

As a result, silicosis and coal workers' pneumoconiosis is the major type of pneumoconiosis in a Chinese city. It also showed a clear industry distribution and the age of diagnosis is large in recent decades.

There conclusions suggested that occupational health monitoring and primary prevention should be strengthened. On the other hand, these results may provide a deeper understanding of the pneumoconiosis and government in China need to step up their efforts on implementing more rigorous policies to protect people from dust pollution.

KEYWORDS:
Pneumoconiosis, Characteristics, Industry, Silicosis, Coal, Prevalence

INTRODUCTION

The first case report on pneumoconiosis from coal workers' was reported by Gregory in 1831 [1]. Pneumoconiosis is the main occupational lung disease, which followed inflammation of the alveoli and irreversible lung damage [2]. Owing to increasing demand for heavy physical labor workers around the world, more and more of works are at risk for pneumoconiosis. Furthermore, without effective protection for workers, pneumoconiosis is a preventable but difficultly curable occupational lung disease [3].

In China, some process on pneumoconiosis has been made in the last two decades. In 1992, the national Chinese pneumoconiosis epidemiological survey showed that the overall prevalence of coal workers' pneumoconiosis (CWP) was 6.49% among Chinese Coal miners, which is from a survey of millions people [2]. Meanwhile, CWP accounts for about 48% among the total number of cases of pneumoconiosis, and the number of patients with CWP among patients with occupational disease remains the highest. Some individual regional studies also reveal the prevalence of CWP and pneumoconiosis is very serious in China [4, 5]. On the other hand, environmental factors and genetic variations contribute to coal workers' pneumoconiosis (CWP). In 2017, Liu et al. demonstrated that LRBA SNPs were associated with CWP susceptibility among 703 CWP cases and 705 controls in a Chinese population [6]. Wang et al. also identified 4 new CWP associated loci among 703 CWP cases and 705 exposed controls in Han Chinese man, which may advance our understanding of the susceptibility to CWP in 2018 [7]. These may provide a deeper understanding of the genetic predisposition of CWP. Therefore, pneumoconiosis still belongs to legal serious occupational disease and is not effectively controlled in China [8].

In this study, the 1980–2017 studies regarding the prevalence of pneumoconiosis in a Chinese city was conducted. 4797 pneumoconiosis cases were collected and analyzed to grasp pneumoconiosis characteristic and furthermore control pneumoconiosis occurrence. From the big data, the differences among the gender, age, nationality, time of dust exposure, stages of pneumoconiosis, industry types of pneumoconiosis, etc. were analyzed to provide a scientific basis for the prevalence and prevention of pneumoconiosis.

MATERIALS AND METHODS

Data source. A total of 4797 pneumoconiosis cases from 1980 to 2017 were recruited in this study. The case data of 1980 to 2005 was from registration information of occupational disease diagnosis institutions in a city. The case data of 2006 to 2017 was from pneumoconiosis report data in occupational disease and occupational health information monitoring system, Chinese disease prevention and control information system. The quality of identified reports was evaluated using strictly inclusion and exclusion criteria and all cases had complete information. The basic information, stage, diagnosis age and work type of pneumoconiosis cases were analyzed.

Statistical analysis. Data were expressed as means ± 25th and 75th percentiles., and the differences between groups were evaluated using SPSS version 21.0; Kruskal-Wallis H Test for multiple groups comparison and Nemenyi Test and Dunnet-t Test for two groups comparison. Statistical significance was set at $P < 0.05$ and extremely significance was set at $P < 0.01$.

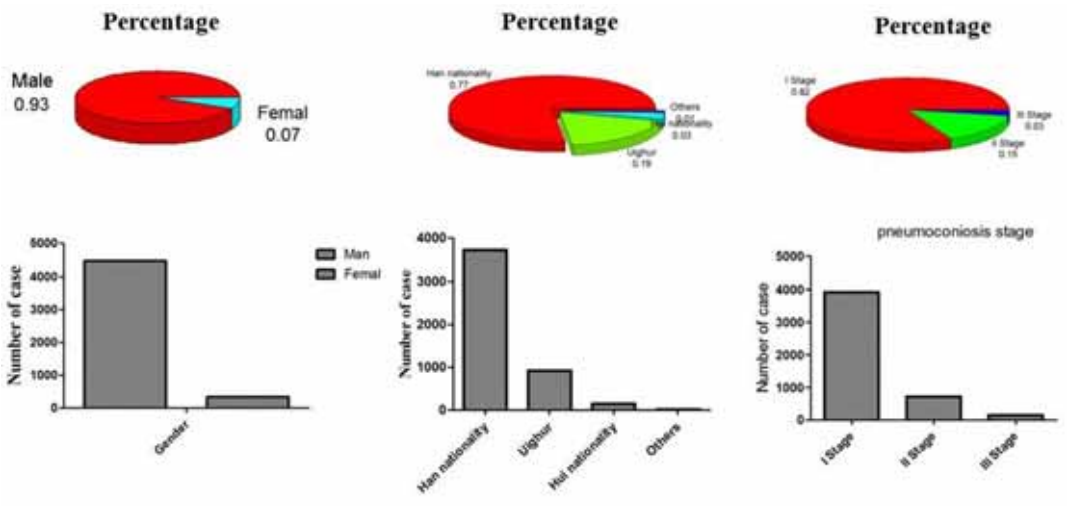

FIGURE 1
Gender, nationality and stage of all pneumoconiosis in pie chart and histogram.

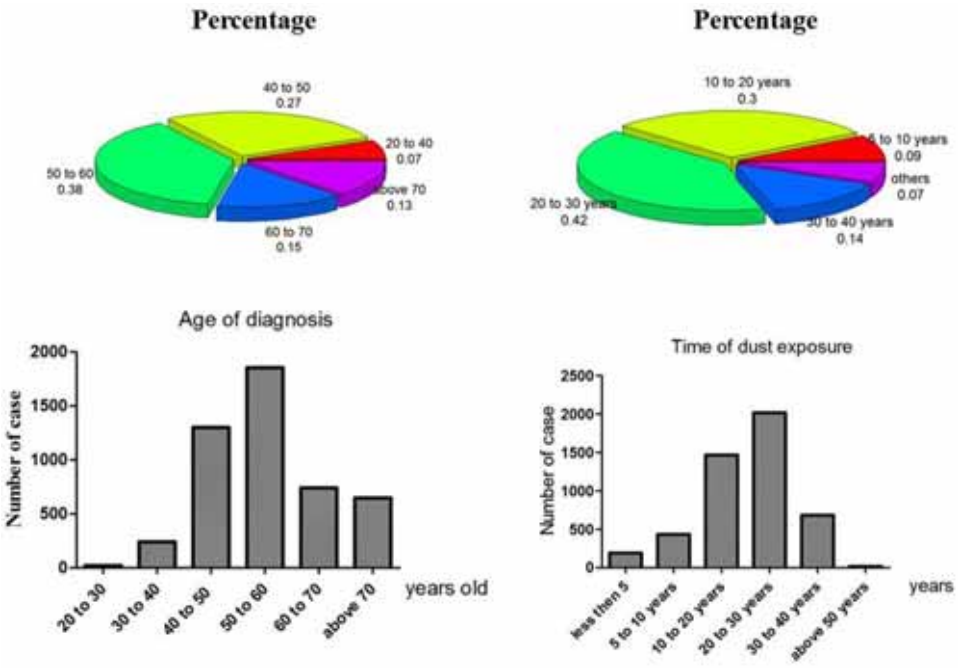

FIGURE 2
Diagnosis age and dust exposure time of all pneumoconiosis in pie chart and histogram

RESULTS

Baseline characteristics. The number of pneumoconiosis was 4974 from 1980 year to 2017 year, including 4460 male and 337 female. Meanwhile, Han and Uighur were the two main ethnic among all pneumoconiosis patients and their account for proportion was 77% and 19%, respectively. Among them, I, II and III stage of pneumoconiosis was 3925, 716 and 156 respectively (Figure 1).

The media age of diagnosis was 53 year old and their 25th and 75th percentiles was 48 and 61, respectively. It mainly distributed in 50~60 years old group, which accounted for 38%. On the other hand, the media time of dust exposure was 21 years, their 25th and 75th percentiles was 14 and 27, respectively. It mainly distributed in 20~30 years old group, which accounted for 42% (Figure2). The occurrence of disease involved 12 industries, which was mainly distributed in four industries: coal (1441 cases), manufacture (974 cases), building (716 cases), electricity (688 cases). Their rate was 30%, 20%, 15% and 14%, respectively. Pneumoconiosis types consisted of silicosis (2603 cases, 54%), coal worker pneumoconiosis (1753 cases, 37%), welders pneumoconiosis (300 cases, 6%) and other pneumoconiosis types (141 cases, 3%) (Figure 3).

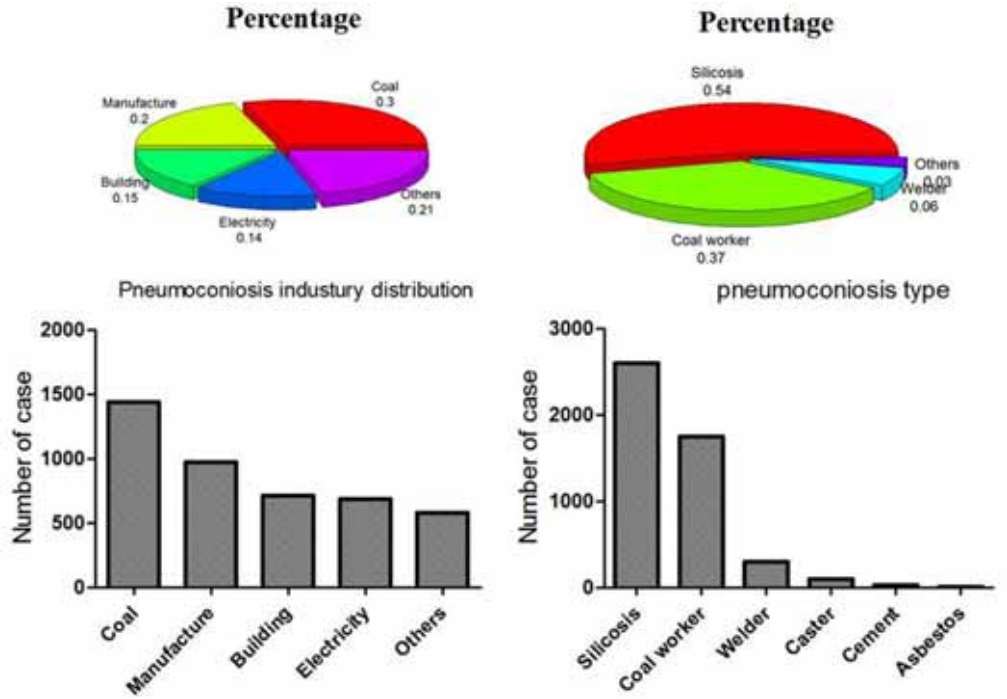

FIGURE 3
Industry distribution and types of all pneumoconiosis in pie chart and histogram

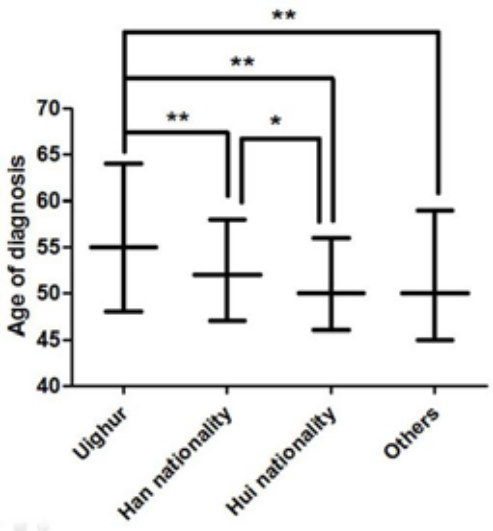

FIGURE 4
Difference analysis between diagnosis age and nationality among all pneumoconiosis

Statistical analysis and difference comparison for pneumoconiosis. Pneumoconiosis patients' diagnosis age existed significance difference ($P < 0.01$) with their nationality and the maximum age was Uighur among different ethnic patients (Figure 4). Patients' diagnosis age had also significance difference ($P < 0.01$) among their stages and the highest stage was II stage (Figure 5). Significance difference ($P < 0.01$) also existed in different between pneumoconiosis type and the contact time of pollution source. Among them, welder worker' working age was the highest and the asbestos was the lowest (Figure 6).

In addition, diagnosis age and dust exposure time of pneumoconiosis were also shown in the Table 1 and we found that diagnosis age and time of pneumoconiosis had strong correlation (R^2=0.965) through their regression analysis (Figure 7). The pooled rate of the new pneumoconiosis patients combined with tuberculosis was 6.4%. The pooled rate of the new pneumoconiosis patients combined with emphysema, pleural adhesions and lung bulla was 1%. Among them, coal workers' pneumoconiosis was the highest and their rate was 54.40%; the second was silicosis and their rate was 43.97% (Figure 8).

TABLE 1
Diagnosis age and dust exposure time of pneumoconiosis

Time	Case number	Percent (%)	Diagnosis age [$M(P_{25},P_{75})$, year old]	Time of dust exposure [$M(P_{25},P_{75})$, year]
1980~	2400	50.03	50(46,55)	20(14,25)
1990~	937	19.53	53(48,57)	25(18,30)
2000~	939	19.57	56(47,74)	21(13,27)
2010~	521	10.86	62(50,78)	19(10,27)
Total	4797	100.00	52(47,59)	21(14,26)

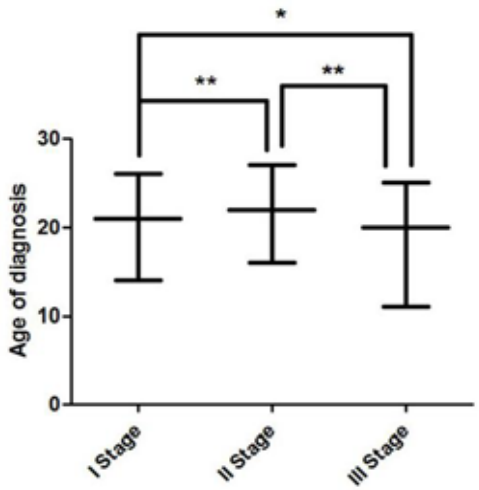

FIGURE 5
Difference analysis between diagnosis age and stage among all pneumoconiosis

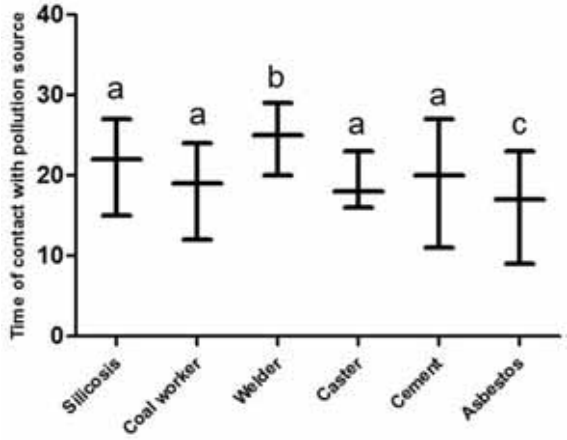

FIGURE 6
Difference analysis between dust exposure time and types among all pneumoconiosis

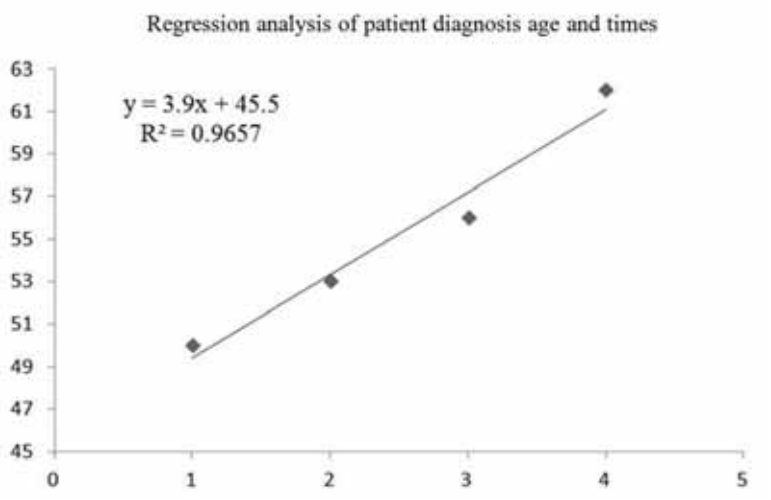

FIGURE 7
Regression analysis of patient diagnosis age and times among all pneumoconiosis

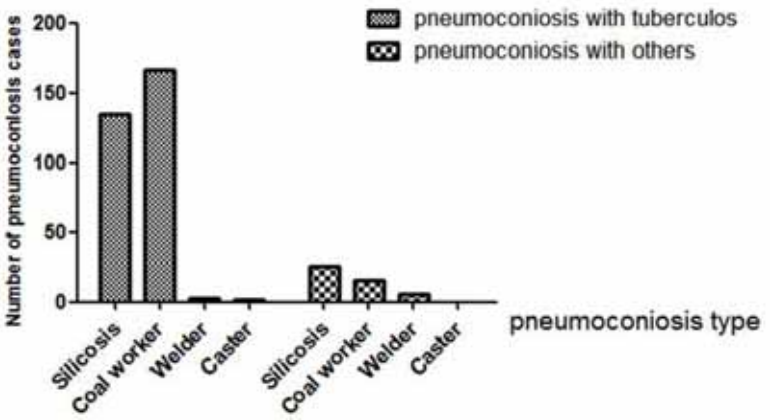

FIGURE 8
The distribution of tuberculosis and other diseases among all pneumoconiosis

DISCUSSION

Pneumoconiosis is a occupational, progressive and irreversible lung disease, which caused by continuous exposure and inhalation of dusts. The direct economic losses amount to 8 billion CNY each year, and the indirect economic losses amount to 20 billion RMB each year in China. The current situation of pneumoconiosis in China is may be more serious [9].

In the recent 40 years, males accounted for 93.03% among the new cases of pneumoconiosis in a city. There suggested that most of the dust operations were heavy physical labor and male-dominated related. In the stage of disease, I stage of occupational pneumoconiosis is 81.82% and it is lower than other reports, which is about 90% (Figure 1). This result suggested that some patients were directly diagnosed as II stage and III stage pneumoconiosis in their first occupational health examination. To further prevent the damage of pneumoconiosis, we should strengthen physical examination and expand their scope at the same time.

In the present study, the diagnosis age was mainly distributed in 40 to 60 years old (about 66%), followed by over 60.0 years old (15.39%), and the median age of diagnosis was 53.0 years old among 4994 pneumoconiosis cases. The time of dust exposure was mainly concentrated in 10.0 to 29 years (72.53%), followed by patients over 30 years (14.18%), and the median age of dust exposure was 21 years (Figure 2). With the development of time in recent decades, we also found that the age of diagnosis has increased in recent years. These phenomena suggest government's work in prevention and control of pneumoconiosis has achieved good results and workers' health rights have been effectively protected. A further systematic analysis of the age of diagnosis and working age of dust exposure showed that the median age of new pneumoconiosis cases in Uighur was 55 years, which was higher than that of the Han nationality

and other ethnic groups. There may be owing to language barriers, and lacking of communication, education, knowledge and awareness of occupational health care. Therefore, a lot of work needed to do to prevent and treat pneumoconiosis [10].

In the type of disease, the major types of pneumoconiosis were silicosis (54%) and coal worker pneumoconiosis (37%), which was consist with the trends of other reports (Figure 3). Among different type pneumoconiosis, silicosis was mainly distributed in the industries of building, manufacturing and electricity, and most coal workers' pneumoconiosis was distributed in the coal industry. This distribution of lung diseases and the type of pneumoconiosis show a concentrated trend and consistency. On the other hand, some difference still existed in the pneumoconiosis industry distribution. Our study showed that pneumoconiosis distributed in coal, manufacturing and electricity, and other reports were in coal, building, non-ferrous metals and metallurgical industries. These results may be caused by the difference of regional industry distribution and it is important to focus the unique characteristic of industry distribution for preventing the pneumoconiosis.

Owing to no obvious clinical manifestations and no specific characteristic in early tuberculosis test by X-ray chest tuberculosis [11], pneumoconiosis patients are often misdiagnosed clinically. This may cause the all pneumoconiosis patients, which combined with tuberculosis, were mainly coal worker pneumoconiosis and silicosis. Therefore, early diagnosis and correct diagnosis of pneumoconiosis have important practical significance for protecting pneumoconiosis patients.

CONCLUSIONS

The increased new pneumoconiosis may contribute to lack of attention to occupational health, inefficient surveillance, and weak occupational health services. According to the incidence and characteristics of pneumoconiosis, we recommended expanding the coverage of occupational health monitoring, which could carry out occupational health examinations for workers and publicize knowledge of preventing occupational disease prevention. Our aim was to detect early, diagnose early and treat early in future.

REFERENCES

[1] Gregory. J.C. (1831) Case of particular black infiltration of the whole lungs resembling melanosis. John Stark. 36, 389-394.

[2] Mo, J., Wang, L., Au, W., Su, M. (2014) Prevalence of coal workers' pneumoconiosis in China: A systematic analysis of 2001–2011 studies. International Journal of Hygiene and Environmental Health. 217(1), 46-51.

[3] Liu, H., Tang, Z., Yang, Y., Weng, D., Sun, G., Duan, Z., Chen, J. (2009) Identification and classification of high risk groups for Coal Workers' Pneumoconiosis using an artificial neural network based on occupational histories: a retrospective cohort study. BMC Public Health. 9(1), 366.

[4] Han, L., Han, R., Ji, X., Wang, T., Yang, J., Yuan, J., Wu, Q., Zhu, B., Zhang, H., Ding, B., Ni, C. (2015) Prevalence Characteristics of Coal Workers' Pneumoconiosis (CWP) in a State-Owned Mine in Eastern China. International Journal of Environmental Research and Public Health. 12(7),7856.

[5] Han, L., Gao, Q., Yang, J., Wu, Q., Zhu, B., Zhang, H., Ding, B., Ni, C. (2017) Survival Analysis of Coal Workers' Pneumoconiosis (CWP) Patients in a State-Owned Mine in the East of China from 1963 to 2014. International Journal of Environmental Research and Public Health. 14(5), 489.

[6] Liu, Y., Yang, J., Wu, Q., Han, R., Yan, W., Yuan, J., Ji, X., Li, Y., Yao, W., Ni, C. (2017) LRBA Gene Polymorphisms and Risk of Coal Workers' Pneumoconiosis: A Case–Control Study from China. International Journal of Environmental Research and Public Health. 14(10),1138.

[7] Wang, T., Li, Y., Zhu, M., Yao, W., Wu, H., Ji, X., Hu, Z., Shen, H., Fan, X., Ni, C. (2018) Association analysis identifies new risk loci for coal workers' pneumoconiosis in Han Chinese men. Toxicol Sci. kfy017.

[8] Kales, S.N., Christiani, D.C. (2004) Acute Chemical Emergencies. New England Journal of Medicine. 350(8), 800-808.

[9] Xia, Y., Liu, J., Shi, T., Xiang, H., Bi, Y. (2014) Prevalence of Pneumoconiosis in Hubei, China from 2008 to 2013. International Journal of Environmental Research and Public Health. 11(9), 8612.

[10] Ayaaba, E., Liu, Y., Li, Y., Han, L., Quansah, D., Yedu, C.N. (2017) Measures to Control the Prevalence of Pneumoconiosis in Coal Mining: A Review of the Literature. Control of CWP in Coal Mines. 4-13p.

[11] Halldin, C.N., Hale, J.M., Blackley, D.J., Laney, A.S. (2017) Radiographic features of importance in the National Institute for Occupational Safety and Health-administered Coal Workers' Health Surveillance Program: characterising the use of the 'other symbols'. BMJ Open. 7(8), e015876.

Received: **07.12.2018**
Accepted: **12.03.2019**

CORRESPONDING AUTHOR

Bao-ling Rui
Section for Occupational Disease Prevention,
Center of Prevention and Control for Diseases in
Urumqi, Urumqi, 830002 – China

e-mail: ruibaoling@163.com

© by PSP Volume 28 – No. 5/2019 pages 3946-3962 Fresenius Environmental Bulletin

RELATIONSHIP BETWEEN ORIGIN AND DISTRIBUTION OF DOLOMITES IN LOWER PALEOZOIC, JIZHONG DEPRESSION, NORTH CHINA

Wei Yan[1,*], Zhenkui Jin[1], Mengzhu Yao[1], Wenlong Zhao[2]

[1]China University of Petroleum-Beijing, College of Geosciences, Changping, Beijing China
[2]Exploration and Development Research Institute, PetroChina Huabei Oilfield Company, Renqiu, P.R China

ABSTRACT

The origin and distribution of the Lower Paleozoic dolomites in the Jizhong Depression, North China, are related and affect the distribution of the reservoir. The Lower Paleozoic dolomites can be divided into four types: Type-A is gypsiferous mud-silt-sized crystalline dolomites; Type-B is non-gypsiferous mud-silt-sized crystalline dolomites; Type-C is silt-fine-sized crystalline dolomites; Type-D is medium-coarse-sized crystalline dolomites. Type-A dolomites contains gypsum, with stratiform stromatolites, bird's eye structures and brecciated structures. The ordering of dolomites averages 0.56. $\delta^{13}C$ averages -0.155‰ (PDB) and $\delta^{18}O$ averages -5.669‰ (PDB). Type-B dolomites are gypsum-free and not associated with gypsum bed. $\delta^{13}C$ averages -2.114‰ (PDB). The rest of the characteristic are similar to type A. Type-C dolomites are subhedral and euhedral. Metasomatic relict structure are common. The ordering of dolomites averages 0.75. $\delta^{13}C$ averages -0.693‰ (PDB) and $\delta^{18}O$ averages -6.079‰ (PDB). Cathodoluminescence is orange and represents zonal structure. Type-D dolomites are subhedral or anhedral. Mosaic structure, recrystallization and residual porphyritic features are common. The ordering of dolomites averages 0.86. $\delta^{13}C$ averages -1.433‰ (PDB) and $\delta^{18}O$ averages -0.149‰ (PDB). The homogenization temperature of inclusions ranges between 90-330°C. Cathodoluminescence is dark brown. Type-A dolomites and Type-B dolomites are thin, with a small horizontal distribution, but the number of dolomite layer is more. Type-C dolomites have large thickness and large horizontal distribution. It is generally distributed under Type-A and Type-B dolomites. Type-D dolomites have a massive distribution with a large vertical thickness. The range of horizontal distribution is relatively small. These characteristics can be used to analyze the original rock of dolomite, dolomitization temperature, stratigraphic burial history, the occurrence time of dolomitization, and the source of magnesium ions. It is indicated that Type-A and Type-B dolomites are formed in tidal flat environment. Type-A dolomites are formed as a result of evaporative pumping. The origin of Type-B dolomites are similar to that of dolomite in Andros Island, Bahamas. Type-C dolomites are formed as a result of seepage reflex dolomitization, and have a sandwich structure. Type-D dolomites are formed as a result of burial hydrothermal dolomitization, closely related to the deep faults of the Himalayan Movement and Cenozoic magmatic rocks. These dolomitizations result in different patterns of dolomite distribution. Type-A, Type-B and Type-D dolomites underwent dissolution during the formation process, and could form good reservoirs for oil and gas.

KEYWORDS:
North China Platform, Jizhong Depression, Lower Paleozoic, Dolomite, Seepage reflux dolomitization, Hydrothermal dolomitization.

INTRODUCTION

The Lower Paleozoic strata in the Jizhong Depression are dominated by carbonate rocks, especially dolomites. Dolomites as important reservoir rocks face two challenges in exploration and development. First, it is not sure exactly where dolomite is developed before drilling. Secondly, dolomites in different positions vary greatly in physical properties. These two challenges are widespread in the oil and gas fields that are in the exploration stage, making it difficult to predict and analyze dolomite reservoirs. Research on the origin and distribution of dolomite may help resolve these two challenges. There are few studies on the types and origins of dolomites in the Jizhong Depression. Previous studies mostly focused on the dolomites of North China Platform. Feng [1, 2] and Jin [3] discussed the origin of the Lower Paleozoic dolomites of North China Platform and clarified that the Lower Ordovician "Sanshanzi Dolostones" are multi-genetic and diachronous dolomites. There are also many studies on adjacent basins and depressions on the North China Platform [4-7]. These studies suggest that the origin of Ordovician dolomites include evaporative pumping penecontemporaneous dolomitization, seepage reflux dolomitization, mixed-water dolomitization and

deep burial dolomitization, which provide important reference and inspiration for this study.

Mixed-water dolomitization of previous studies is problematic in North China Platform, because no dolomite has been found in Modern mixing-zones [8-11]. Thus, the main origins of the dolomite on the North China platform, especially the unique "Sanshanzi Dolostones", need to be restudied. Moreover, Buried hydrothermal dolomite has many hydrothermal sources and genetic mechanisms [12-16], but there is no relevant research on Jizhong Depression and North China Platform. The study of the hydrothermal dolomite in Jizhong Depression can provide a research example for hydrothermal dolomite in other sedimentary basins. More importantly, the type and distribution of dolomite in sedimentary basins are different. How to judge the dolomite reservoir effectively in the exploration process requires the study of origin and distribution of dolomite.

This paper drew lessons from previous studies [17, 18], classified dolomite according to crystalline size, inclusions and tectonic features. The geochemical characteristics and distribution of these types of dolomites were described and the orgin of dolomites were studied. The relationship between the origin and distribution of dolomite is discussed, so as to predict the distribution of dolomite and dolomite reservoir.

Dolomite is mainly formed in the low-latitude marine environment with high salinity and hot temperature. The study of dolomite characteristics formed during this period is of great significance for understanding the evolution process of the environment at that time and thereafter.

MATERIALS AND METHODS

Geological setting. Jizhong Depression, located in the middle of North China Platform (Fig. 1A), with an area of about 32,000 km^2. The whole depression takes the form of northeast-southwest, bordering on the Cangzhou uplift in the east and Taihang uplift in the west. It is a Meso-Cenozoic sedimentary depression developed on the basis of North China Platform [19]. The formation of depression generally goes through four stages of development: the formation stage of Mesozoic platform crystalline basement, Mesoproterozoic and Late Paleozoic platform development stage, Mesozoic folding-fault depression development stage and Cenozoic fault rift-depression development stage [20].

Due to the tectonic uplift at the end of the Caledonian Movement, the Silurian and Devonian were entirely missing. The Lower Paleozoic is only the Cambrian and Ordovician, and it is missing in the west of Jizhong Depression (Fig. 1B).

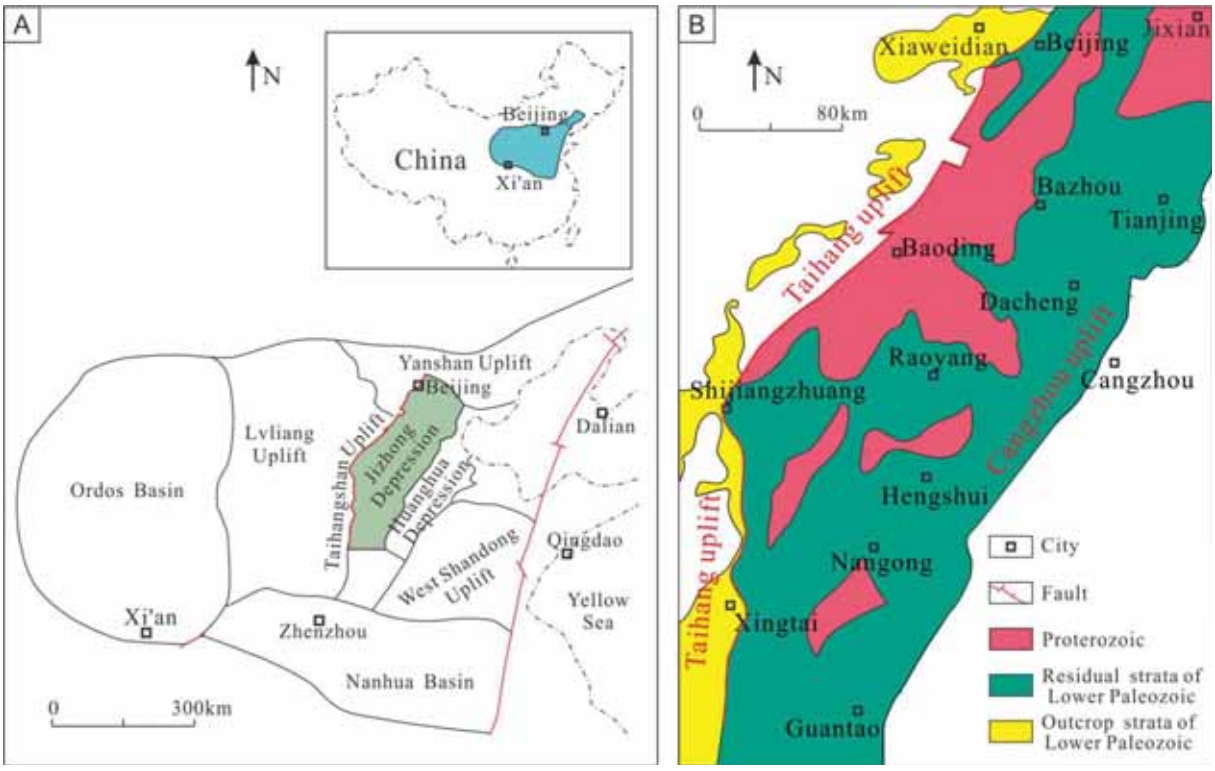

FIGURE 1
[A] Simplified geological map of North China Platform. Jizhong Depression is developed on the basis of North China Platform. [B] The Lower Paleozoic strata distribution of the residual strata in the Jizhong Depression and the outcrop strata of the Taihang uplift.

TABLE 1
$\delta^{13}C$ and $\delta^{18}O$ values for the Lower Paleozoic dolomites in the Jizhong Depression

Sample	Rock types	$\delta^{13}C_{PDB}$	$\delta^{18}O_{PDB}$	Z	Sample	Rock types	$\delta^{13}C_{PDB}$	$\delta^{18}O_{PDB}$	Z
1	Type-A	0.413	-4.788	125.76	32	Type-C	-1.773	-6.098	120.63
2	Type-A	2.302	-5.977	129.04	33	Type-C	-2.008	-8.023	119.19
3	Type-A	-0.054	-5.217	122.05	34	Type-C	-1.608	-4.108	121.96
4	Type-A	3.508	-4.568	129.66	35	Type-C	-1.089	-5.478	122.34
5	Type-D	0.366	-7.538	124.30	36	Type-A	-1.236	-3.956	120.25
6	Type-A	0.716	-6.798	122.83	37	Type-C	-1.182	-5.963	121.91
7	Type-A	-1.226	-3.701	120.40	38	Type-C	-1.017	-7.384	121.54
8	Type-B	-3.489	-7.752	116.29	39	Type-C	-1.113	-8.504	120.78
9	Type-B	-5.175	-5.232	114.10	40	Type-C	-0.710	-4.885	123.41
10	Type-B	-4.669	-4.581	115.46	41	Type-C	-0.911	-6.277	122.31
11	Type-A	2.067	-6.070	125.96	42	Type-C	-0.739	-8.479	121.56
12	Type-D	-0.853	-7.783	121.68	43	Type-C	0.323	-5.833	125.06
13	Type-A	-0.482	-6.07	120.74	44	Type-C	0.890	-5.277	126.49
15	Type-B	-3.765	-6.094	116.55	45	Type-C	0.686	-4.849	126.29
17	Type-B	-2.192	-6.161	119.74	46	Type-C	-1.969	-5.571	120.49
18	Type-B	-2.086	-6.285	119.90	47	Type-C	0.730	-6.441	125.59
19	Type-B	-2.012	-7.197	119.59	48	Type-C	1.204	-4.889	127.33
20	Type-B	-1.280	-5.674	121.85	49	Type-D	0.473	-8.248	124.16
21	Type-A	-0.304	-7.369	120.46	50	Type-D	0.998	-8.479	125.12
22	Type-A	1.071	-6.893	123.51	51	Type-D	-1.223	-8.344	120.64
23	Type-B	-1.171	-6.045	121.89	52	Type-C	0.752	-6.202	125.75
24	Type-B	-1.162	-6.394	121.74	53	Type-D	-4.669	-7.671	113.92
25	Type-B	-1.224	-8.170	120.72	54	Type-D	-4.277	-7.309	114.90
26	Type-B	-0.664	-6.296	122.80	55	Type-D	-2.039	-9.289	118.50
27	Type-B	-0.431	-4.963	123.95	56	Type-C	-0.248	-5.385	124.11
28	Type-B	-0.274	-5.679	123.91	57	Type-D	-1.983	-8.583	118.96
29	Type-C	-2.101	-5.799	120.11	58	Type-D	-1.123	-8.245	120.89
31	Type-C	-2.205	-5.832	119.88	60	Type-C	-0.456	-6.370	123.19
					61	Type-A	1.362	-6.623	124.25

According to the lithofacies palaeogeography of the Lower Paleozoic, the seawater in the Early Cambrian Epoch 2 invaded from the northeast, and formed a restricted sea environment in Beijing. At the end of the Fujunshan Age, there was exposure, resulting in an unconformity. In Mantou Age and Maozhuang Age, tidal flat sediments were developed in the whole depression, and the lithology were purple-red mudstones and mud-silt-sized crystalline dolomites. At the beginning of the Xuzhuang Age, seawater became deeper, and the sea water reached its highest level during the Zhangxia Age. This period was dominated by Oolitic bank. In the early Gushan Age, the tidal flat reappeared, and coexisted with bamboo leaf-shaped gravel bank.

Until the end of the Liangjiashan Age the North China Platform was exposed due to the rise of the Huaiyuan Movement. At the same time, a parallel unconformity was formed. Transgression began again in the Middle Ordovician, and three large transgressions and regressions took place. The tidal flat sediments were formed in Majiagou I Formation, Majiagou III Formation and Majiagou V Formation, and the open sea sediments were formed in Majiagou II Formation, Majiagou IV Formation and Majiagou VI Formation [21].

The data of this study came from outcrop section and drilling analysis. Based on the observation of five outcrop sections, more than 160 dolomite samples were collected, and two of outcrop sections were selected for detailed measurement. The two sections are respectively located in Xiaweidian Village (39°59'N，116°01'E), west mountain of Beijing, and in Nanwang Village (37°56' N，114°09' E), west of Shijiazhuang city. Mud logging data, well logging data and 36 dolomite samples were collected in drilling data.

Thin sections were fabricated for all samples, and the half area of the thin sections was stained with Alizarin Red S. According to the observation of thin sections under a polarizing microscope, the size of the dolomite crystals of each sample was measured. Based on these statistical results, 68 samples were selected for carbon and oxygen isotope analysis, 54 samples for X-ray diffraction analysis, 36 samples for fluid inclusion analysis and 38 samples for cathodoluminescence analysis.

Whole-rock carbon and oxygen isotope analysis was performed by the State Key Laboratory of Nanjing Institute of Geology and Palaeontology, Chinese Academy of Sciences. The instrument was a MAT-253 isotope mass spectrometer, and the sample preparation system was a vacuum pre-treatment series, with the laboratory control temperature of 22°C ± 10°C and humidity of 50% RH ± 5%. The results of the analysis used the PDB standard, with $\delta^{13}C$ and $\delta^{18}O$ testing accuracy of 0.030 and 0.080 respectively. Analytical data are shown in Table 1.

Cathodoluminescence was done on a CL8200MK5-2 cathodoluminescence system and all samples were tested with a beam voltage of 17 kV and a beam current of 500 μA. X-ray diffraction was used to analyze the ordering of dolomite and the molar content of $CaCO_3$ and performed on a Bruker D2 Phaser X-ray diffractometer, operating at 30 kV and 10 mA, a CuKα radiation wavelength was used for measurement, and 2θ angular scanning range of 4.5°-50° was selected. Analytical data are shown in Table 2. The instrument for fluid inclusions was Linkam-350 cooling-heating stage, with temperature range from -196°C to 350°C, temperature accuracy of 0.1°C and maximum heating / cooling rate of 30°C/min. The temperature control rate set in the heating and freezing process was generally 40°C/min, and rate near phase transformation point was 4°C/min. Analytical data are shown in Table 3. These analyses were completed at the State Key Laboratory of Petroleum Resources and Prospecting, China University of Petroleum (Beijing).

TABLE 2
Ordering and molar concentration of $CaCO_3$ values for the Lower Paleozoic dolomites in the Jizhong Depression

Sample	Rock types	Ordering	d (104)	$NCaCO_3$/%	Sample	Rock types	Ordering	d (104)	$NCaCO_3$/%
3	Type-A	0.537	2.891	51.66703	71	Type-B	0.632	2.889	51.00037
4	Type-A	0.601	2.888	50.66704	72	Type-B	0.574	2.891	51.66703
5	Type-D	0.877	2.886	50.00038	73	Type-B	0.531	2.89	51.3337
6	Type-A	0.523	2.891	51.66703	74	Type-A	0.546	2.89	51.3337
7	Type-A	0.635	2.887	50.33371	75	Type-A	0.659	2.889	51.00037
11	Type-A	0.481	2.891	51.66703	76	Type-A	0.636	2.893	52.33369
12	Type-D	0.854	2.886	50.00038	77	Type-A	0.548	2.888	50.66704
13	Type-A	0.514	2.886	50.00038	78	Type-A	0.606	2.887	50.33371
16	Type-C	0.819	2.886	50.00038	79	Type-A	0.623	2.887	50.33371
21	Type-A	0.594	2.886	50.00038	80	Type-A	0.651	2.889	51.00037
30	Type-B	0.601	2.891	51.66703	81	Type-A	0.505	2.891	51.66703
31	Type-C	0.834	2.886	50.00038	82	Type-A	0.509	2.892	52.00036
32	Type-C	0.857	2.887	50.33371	83	Type-A	0.489	2.892	52.00036
46	Type-C	0.703	2.886	50.00038	84	Type-C	0.681	2.892	52.00036
50	Type-D	0.737	2.887	50.33371	85	Type-C	0.730	2.889	51.00037
51	Type-D	0.836	2.886	50.00038	86	Type-C	0.757	2.886	50.00038
52	Type-C	0.755	2.888	50.66704	87	Type-C	0.653	2.886	50.00038
59	Type-B	0.615	2.887	50.33371	88	Type-C	0.792	2.886	50.00038
62	Type-B	0.586	2.89	51.3337	89	Type-C	0.621	2.89	51.3337
63	Type-B	0.452	2.892	52.00036	90	Type-C	0.838	2.888	50.66704
64	Type-B	0.623	2.887	50.33371	91	Type-C	0.796	2.887	50.33371
65	Type-B	0.583	2.886	50.00038	92	Type-C	0.633	2.892	52.00036
66	Type-B	0.576	2.891	51.66703	93	Type-C	0.861	2.886	50.00038
67	Type-B	0.564	2.887	50.33371	94	Type-D	0.957	2.894	52.66702
68	Type-B	0.613	2.888	50.66704	95	Type-D	0.855	2.885	49.66705
69	Type-B	0.574	2.888	50.66704	96	Type-D	0.916	2.886	50.00038
70	Type-B	0.576	2.89	51.3337	97	Type-D	0.894	2.886	50.00038

TABLE 3
Homogenization temperature data of fluid inclusions from Lower Paleozoic dolomites in Jizhong Depression

Sample	Rock types	Temperature	Sample	Rock types	Temperature
5	Type-D	291	105	Type-D	193
12	Type-D	289	106	Type-D	204
50	Type-D	98	107	Type-D	186
51	Type-D	165	108	Type-D	235
49	Type-D	104	109	Type-D	221
98	Type-D	126	110	Type-D	216
99	Type-D	136	111	Type-D	223
100	Type-D	142	112	Type-D	253
101	Type-D	170	113	Type-D	268
102	Type-D	158	114	Type-D	287
103	Type-D	169	115	Type-D	313
104	Type-D	171			

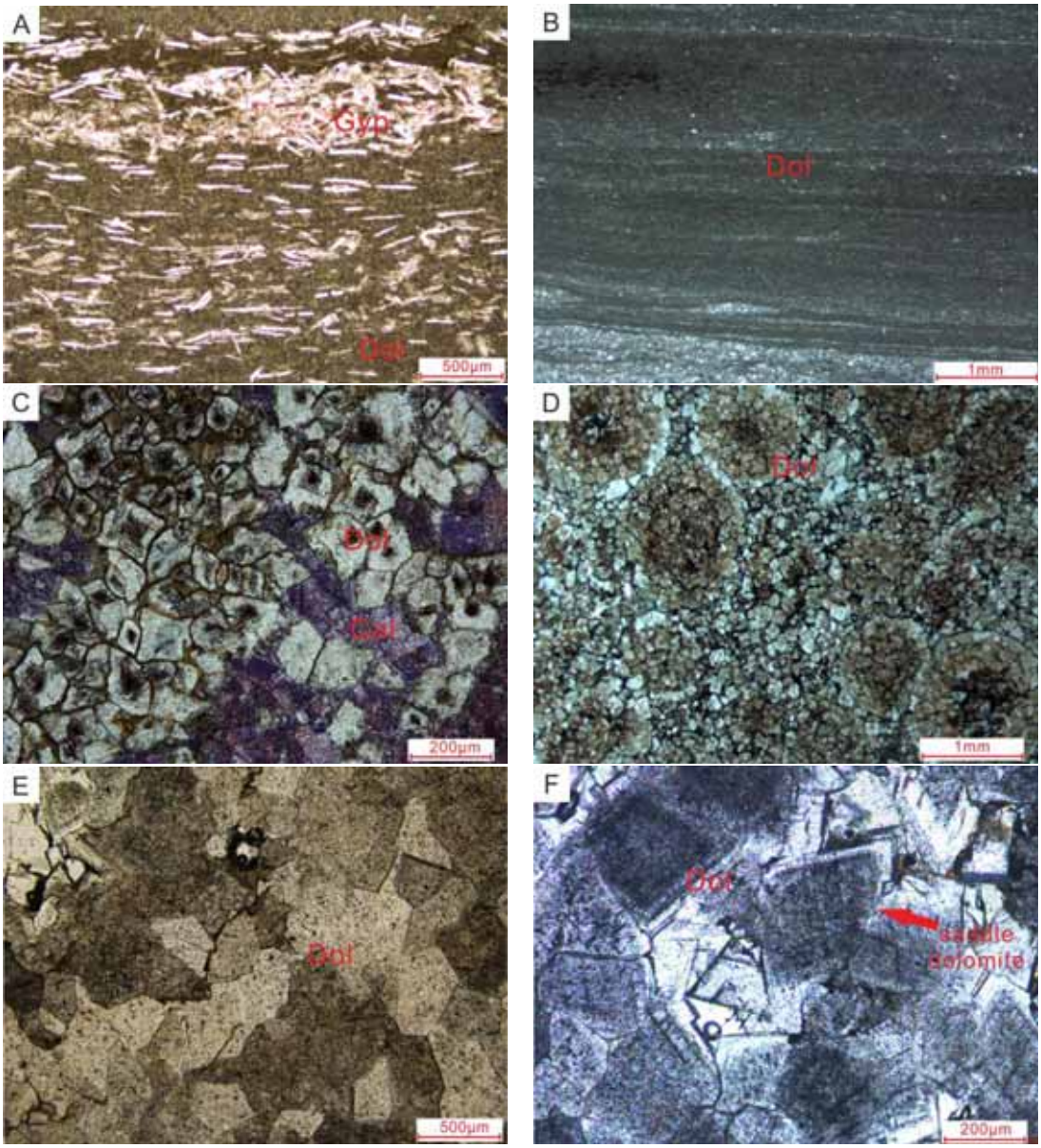

FIGURE 2

Photomicrographs of Lower Palaeozoic, Jizhong Depression. [A] Type-A dolomites (Dol), lath-shaped pseudomorphs after gypsum (Gyp) is of oriented arrangement. [B] Type-B dolomites (Dol) with stromatolite structure. [C] Type-C dolomites contains calcite cements (Cal). Dolomites (Dol) are characterized by dirty interiors and bright margins. [D] Type-C dolomites have the residual oolitic structure. [E] Type-D dolomite. Dolomites are irregular in shape and inlay contact with each other. [F] Type-D dolomites contains saddle dolomite.

The data of CaO, MgO and Sr contents are from Huabei Oilfield Company, and the samples are all drill cores. MgO and CaO contents were measured on FEI Quanta 200F field emission scanning electron microscope, using an accelerating voltage of 200 kV and a maximum angle of ± 40°. The abundances of Sr were measured on an ICPS-1000IV inductively coupled plasma atomic emission spectrometry (ICP-AES), according to the SY/T6404-1999 of the People's Republic of China for determination of metallic elements in sedimentary rocks.

RESULTS AND DISCUSSION

Dolomite type. Dolomites of different crystalline sizes often differ in color, beds and sedimentary structure. Many studies in recent years have shown that dolomite of a different crystalline often corresponds to a different origin. For example, mud-sized crystalline dolomites are often formed in tidal flat environment [22,23]; the medium-coarse-sized crystalline dolomites are often dolomitized by allosource fluid at high burial temperatures [24]. The do-

lomites in the Jizhong Depression are different obviously and easy to be distinguished in crystalline size, color, bed, sedimentary structure and whether to contain gypsum. Therefore, based on these characteristics, this paper divides these dolomites into four types: Type-A is gypsiferous mud-silt-sized crystalline dolomites; Type-B is non-gypsiferous mud-silt-sized crystalline dolomites; Type-C is silt-fine-sized crystalline dolomites; Type-D is medium-coarse-sized crystalline dolomites.

The characteristics of Type-A. Type-A dolomites are less than 0.1mm, thin in layer, and gray or yellowish brown in color, often having bird's eye structure and horizontally-laminated bed. Brecciated structure formed by erosion collapse is common. Drusy and nodular gypsum associated minerals are mostly contained. Under a microscopic observation of thin sections, lath-shaped pseudomorphs after gypsum is of oriented arrangement (Fig. 2A). X-ray diffraction analysis shows that the ordering of these dolomites is relatively low, ranging from 0.48 to 0.65 (Fig. 3A), averaging 0.56. The molar concentration of $CaCO_3$ range from 50.00038% to 52.33369%, averaging 51.09840%. Carbon and oxygen isotopes are commonly positive (Fig. 3B). The average$\delta^{13}C$ is -0.155 ‰ (PDB), with a range of -2.236 to 2.508 ‰ (PDB). The average $\delta^{18}O$ is -5.669 ‰ (PDB), with a range of -7.369 to -3.701 ‰ (PDB). The content of MgO and CaO are low and have a positive correlation (Fig. 3C). The Sr content (p. p. m) are also low (Fig. 3D). The cathodoluminescence of the dolomites is uniformly dark brown (Fig. 4B). In combination with log analysis, the curves of GR (Gamma Ray Log) value were high, and the curves of resistivity value were low in the context of high resistance.

The characteristics of Type-B. Type-B dolomites are often seen in bird's eye and stromatolite structure. They sometimes represent psammitic and psephitic shape. $\delta^{13}C$ overall is more negative than Type-A dolomites, with an average of -2.114 ‰ (PDB), ranging from -5.175 to 0.274 ‰ (PDB). It is similar to the Type-A dolomites in oxygen isotopes, dolomite ordering and molar concentration of $CaCO_3$. The most obvious difference between the two is that it neither contains gypsum nor coexists with the gypsum layer (Fig. 2B).

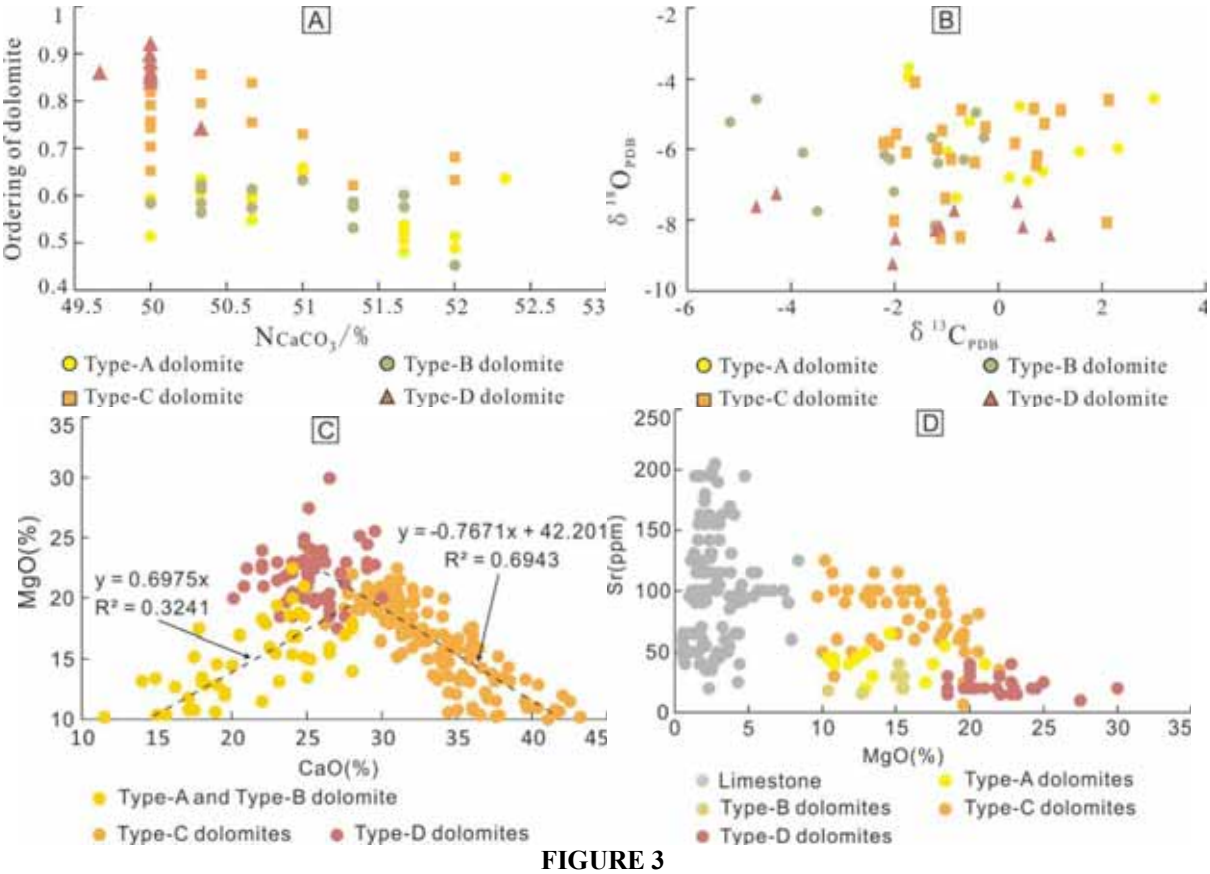

FIGURE 3

Cross plot of geochemical data in the dolomite of Lower Paleozoic in Jizhong Depression. [A] Cross plot of the ordering of dolomite and the molar concentration of $CaCO_3$. [B] Cross-plot of $\delta^{13}C$ and $\delta^{18}O$ values. [C] Cross-plot of CaO(%) and MgO(%) contents. [D] Cross-plot of MgO (%) and Sr content (%)

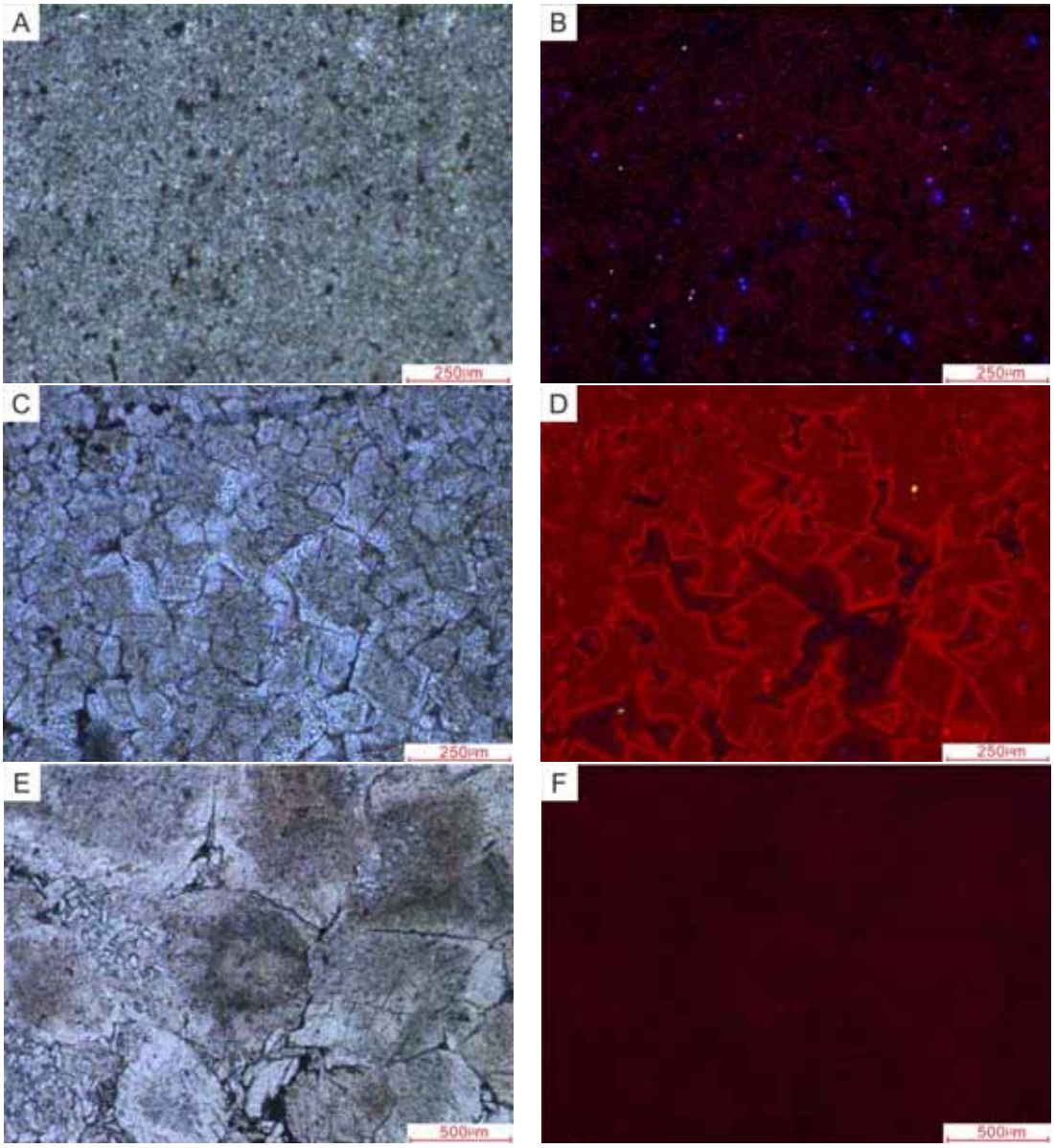

FIGURE 4
Thin section photomicrographs and cathodoluminescence images of Lower Paleozoic dolomites, Jizhong depression.
[A] Mud-sized crystalline dolosmites, with uniform structure. [B] Same view as A, but taken under cathodoluminescence. The dolomites are uniformly dark brown in colour. [C] Fine-sized crystalline dolomites. The dolomites are subhedral to euhedral. [D] Same view as C, but taken under cathodoluminescence. The cathodoluminescence of the dolomite crystals is orange to orange yellow, showing the characteristics of the zonal structure. [E] Medium-coarse-sized crystalline dolomites. Dolomite crystals are big, and are anhedral. [F] Same view as C, but taken under cathodoluminescence. Dolomite crystals are dull brownish red.

The characteristics of Type-C. The crystalline of such dolomite ranges between 0.05 and 0.25 mm, and the color is light gray and gray. When dolomitization is not complete, the dolomites are mainly subhedral to euhedral, with dirty interiors and bright margins (Fig. 2C). When dolomitization is complete, anhedral dolomite is visible. There is very little clay mineral, and no gypsum is contained. In the Type-C dolomites, many kinds of metasomatic relict structures are developed, such as relict oolitic structure (Fig. 2D), relict bamboo leaf-shaped psephitic structure, relict psammitic structure and relict bioclastic structure. The ordering of such dolomite is higher than Type-A and Type-B dolomites, averaging 0.75 (Fig. 3A). The average molar concentration of $CaCO_3$ is 50.556%. The value of carbon and oxygen isotope is lower than Type-A and Type-B dolomites (Fig. 3B). The $\delta^{13}C$ values range from -2.205 to 1.205 ‰ (PDB), averaging -0.693 ‰ (PDB). The $\delta^{18}O$ values range from -8.504 to -4.108‰ (PDB), averaging -6.079 ‰ (PDB). Some dissolved pores

are filled with sparry calcite, which contains fluid inclusions. Their homogenization temperature ranges from 43ºC to 75ºC. The content of MgO and CaO have a negatively correlation (Fig. 3C). The Sr content (p. p. m) are high (Fig. 3D). The cathodoluminescence of the dolomite crystals is orange to orange yellow (Fig. 4D), showing zonal structure. In logging response, the GR value is shown as a relatively flat low value, obviously lower than Type-A and Type-B dolomites; the resistivity shows a lower value.

The characteristics of Type-D. The crystalline size of such dolomite ranges between 0.2-2.00 mm, the color is dark-gray to light-gray. It is mostly distributed in massive form in space, and composed of subhedral or anhedral dolomites. Dolomite crystalline mostly appear to be of inlaid structure, and recrystallization is obvious (Fig. 2E). Saddle dolomite can be seen (Fig. 2F), crystal surface is bent, and wavy extinction is visible under orthogonal light. In addition, some relict porphyritic features can also be seen. The porphyritic form is irregular, and the boundaries are not obvious and cut by dolomite crystals. The size of the dolomite crystals varies greatly, mainly being xenomorphic. Type-D dolomite has a high ordering, averaging 0.86; the molar concentration of $CaCO_3$ is 50.3337% on average (Fig. 3A). The $\delta^{13}C$ value is high (Fig. 3B), ranging from -4.669 to 0.998 ‰ (PDB), averaging -1.433 ‰ PDB. The $\delta^{18}O$ value is low with a distribution range from -9.289 to -7.309 ‰ (PDB), averaging -8.149 ‰ (PDB). The content of MgO and CaO are relatively high (Fig. 3C). But the Sr content (p. p. m) are low (Fig. 3D). The cathodoluminescence of the dolomite crystals is dull brownish red (Fig. 4F). There are two phase gas-liquid fluid inclusions in these dolomites (Fig. 5). The homogenization temperature of fluid inclusions is between 90-330°C. Type-D dolomites have similar electrical characteristics to Type-C dolomites, with relatively flat low GR values and low resistivity values.

Distribution. Type-A dolomites are mainly distributed in Mantou Formation and Maozhuang Formation of Cambrian, Majiagou I Formation, Majiagou III Formation and Majiagou V Formation of Ordovician. Type-B dolomites are mainly found in the Lower Ordovician and the lower part of Fujunshan Formation of Cambrian.

Type-C dolomites are mainly distributed in the Liangjiashan Formation and the Yeli Formation of Ordovician, and Fujunshan Formation and Fengshan Formation of Cambrian. These dolomites are usually developed under Type-A and Type-B dolomites. There are two sets of the largest dolomite masses in the Lower Paleozoic in North China Platform, which main lithology are Type-C dolomites. The one is the "Sanshanzi Dolostones" over the North China Platform (Fig. 6A), which is distributed in the Lower Ordovician and part of the Upper Cambrian, with a thickness of 100-300 m, area greater than 200000 km^2, and featured by being thick in the south and thin the north. The other is the Fujunshan Formation dolomites of Cambrian, with a thickness of 10-20 m, and area greater than 200000 km^2. In both sets of dolomites, from top to bottom, dolomitization weakened and dolomite content decreased. The lithology also shows regular changes. Porphyritic fine-sized crystalline dolomites, porphyritic lime dolomites, dolomitic limestones, and limestones are distributed in turn.

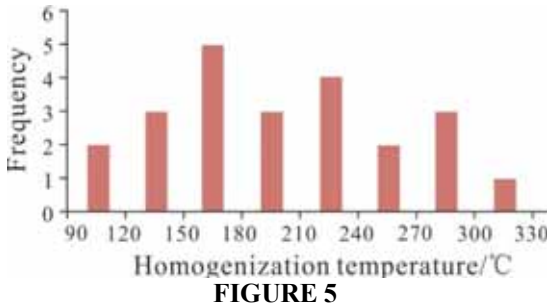

FIGURE 5
Homogenization temperature histogram of fluid inclusions from Lower Paleozoic dolomites in Jizhong Depression.
The samples are medium-coarse-sized crystalline dolomites. The homogenization temperature indicate that the dolomitizing water was hot, up to 300°C.

Type-D dolomites are distributed in thick massive way within the limitations. For example, the dolomites in the T17 Well Majiagou V Formation, Majiagou IV Fromation (Fig. 6A), and Zhangxia Formation (Fig. 6B) are characterized by a limited distribution range in the plane. It is only distributed near the fault with a large thickness.

The analysis of the sedimentary structure and geochemistry of the Lower Paleozoic dolomites, the forming environment of original rock, dolomitization temperature, stratigraphic burial history, the occurrence time of dolomitization, and the source of magnesium ions can be inferred. Comparing with the evaporative pumping model of Persian Gulf tidal flat [25], multi-cause dolomitization of Bahamian Platform [26-28], seepage reflux model [29,30] and burial hydrothermal model, the origin of dolomite in this study area is identified. Analyzing the origin of dolomite not only provides us with the possibility to judge the type and origin of dolomite in sedimentary basins through the macroscopic distribution pattern, but also helps us to find dolomite reservoirs.

Origin of Type-A dolomites. The Type-A dolomites often have bird's eye structure, which is an environmental symbol of supratidal zone. In addition, stratiform stromatolites and lamellar structure also indicate the original rocks are formed in supratidal environment. It is considered the original rock is thin-layered lime mudstone. Dolomite is formed in

low-temperature rapidly crystallized surface environment since its ordering is low and cathodoluminescence is dark brown. Moreover, dolomite has high $\delta^{18}O$ value and contains gypsum, indicating it is formed in salted seawater with high concentration. These features make it comparable to the evaporative pumping dolomites in modern Persian Gulf. In the sabkha environment of Persian Gulf, aragonite is replaced and occurs dolomitization as a result of xerothermic climate and intense evaporation. At the same time, gypsum is generated. Recent studies show that microorganisms play an important role in dolomitization process. With the participation of microorganisms, stromatolite is prone to occur dolomitization and supratidal dolomites are often symbiotic with stromatolite.

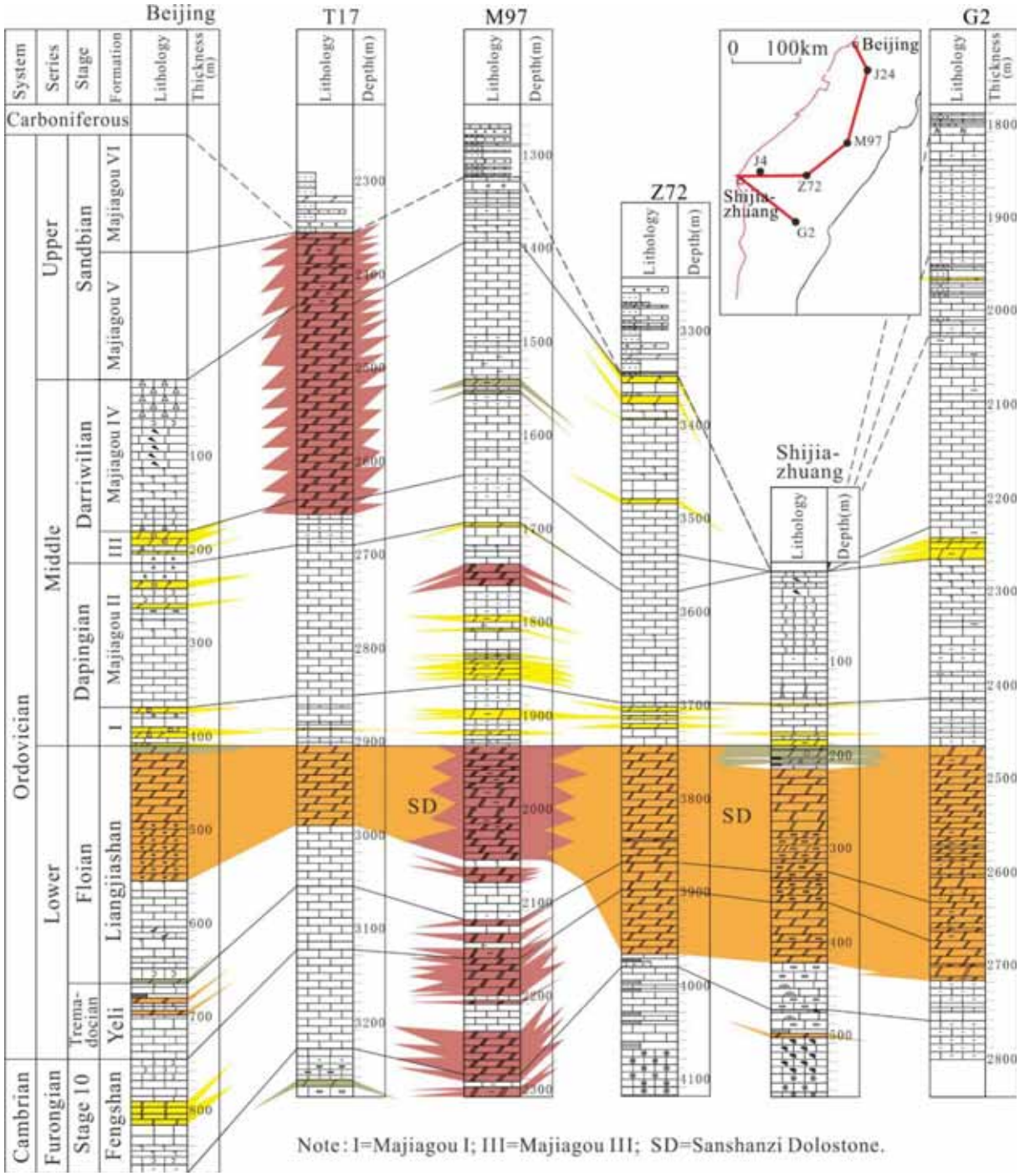

(A)

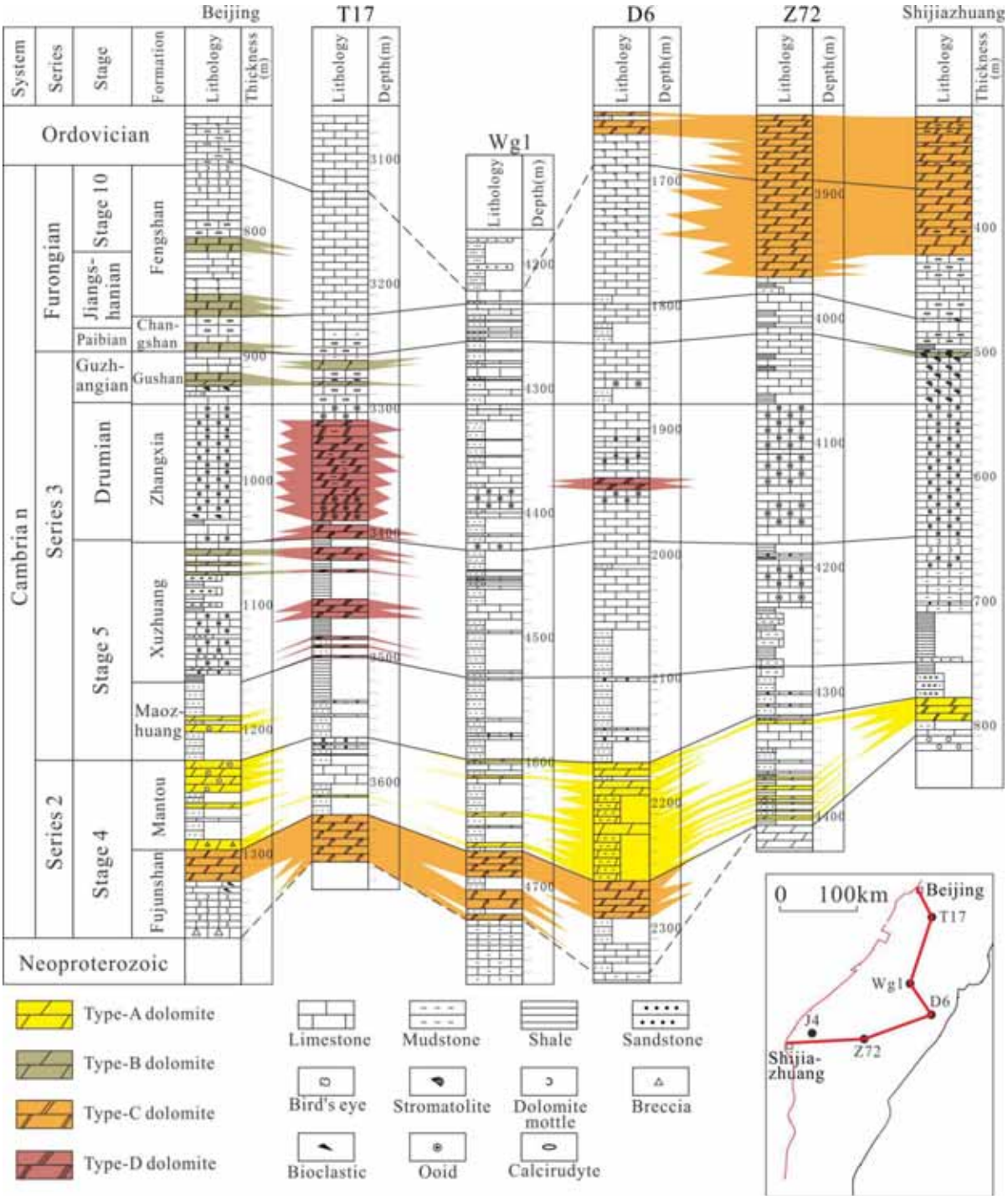

(B)

FIGURE 6

The distribution of dolomites in the Lower Paleozoic in the Jizhong Depression.

[A] The distribution of Ordovician dolomites. Type-A dolomites and Type-B dolomites are lamellar distribution; "Sanshanzi Dolostone" (mainly Type-C dolomites) is very thick layer distribution; some wells (T17, D6) containing Type-D dolomites. [B] The distribution of Cambrian dolomites. The dolomites are mainly distributed in Fujunshan formation (Type-C dolomites), Mantou formation (Type-A dolomites), Fengshan formation (Type-B dolomites and Type-C dolomites). The T17 well developed Type-D dolomites in the Zhangxia formation.

Origin of Type-B dolomites. Type-B dolomites often have bird's eye structure and stratiform stromatolites, which indicate the original rock is thin-layered lime mudstone and formed in tidal flat environment. Some dolomites represent psammitic and psephitic shape, indicating that sometimes it is broken by stormy waves in the early stages of diagenesis. In relatively humid environment, gypsum may not form or be dissolved away after formation, so gypsum doesn't occur. Based on the formula of

Keith and Weber [31], the paleo-salinity (Z value) of dolomites was calculated using $\delta^{18}O$ and $\delta^{13}C$ value. The results showed that the Z values of Type-B dolomites were generally less than 120, but the Z values of Type-A dolomites were more than 120 (Table 1). The obvious difference indicates when Type-B dolomites are formed, the salinity is relatively low. These characteristics indicate that Type-B dolomites are similar with the supratidal penecontemporaneous dolomites in Bahamas Platform. Due to the humid climate in the Bahamas, gypsum is not easily formed or preserved in supratidal zone, and thus gypsum is absent in dolomites. For the Bahamian platform dolomite formation mechanism, some people believe that it is evaporative pumping dolomitization, some people think that it is formation of mixed-water dolomitization [32, 33], and some people think that it is a combination of multiple mechanisms.

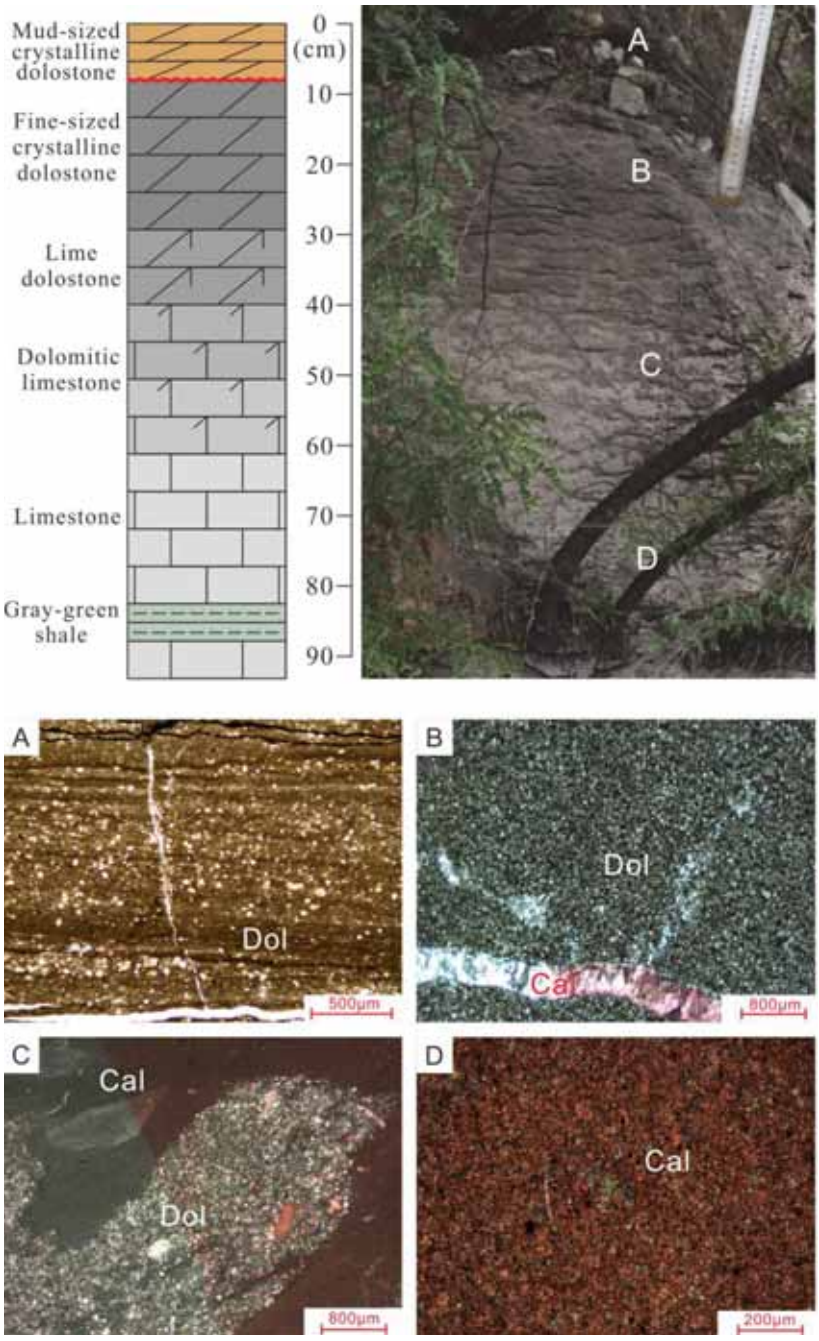

FIGURE 7

The dolomitization weakens from top to bottom, Ordovician, Baoduzhai of Shijiazhuang, Hebei, China. The upper section is composed of Type-A dolomites with terrigenous muddy debris (A), while the lower section is composed of Type-C dolomites and limestone, between which, an unconformities is existed. The dolomitization intensity gradually decreases below the unconformities. The dolomites transit from dark gray fine-sized crystalline dolomites (B) to porphyritic limy dolomites (C), dolomitic limestone and lime mudstone (D).

Origin of Type-C dolomites. The Type-C dolomites have an extremely small amount of clay minerals, so their GR curves are low and flat, indicating their original rock contain a small amount of mud and are formed in open sea or restricted sea environment. The cathodeluminescence is bright and represents zonation, suggesting the dolomites are formed in shallow burial reducing environment. The homogenization temperature ranges from 43ºC to 75ºC, indicating the dolomites are formed in low temperature. Most dolomites have metasomatic relict structure, indicating they are formed as a result of metasomasis at late diagenetic stage. The ordering of dolomite is relatively high and the molar concentration of $CaCO_3$ is closed to 50%, indicating crystallization occurs in low temperature and at slow speed. The negative $\delta^{18}O$ value indicates the diagenesis of dolomites is affected by freshwater fluids.

In addition, the dolomites of this type have some obvious features. Taking the dolomites with a thickness of 1m in the Baoduzhai Outcrop of Shijiazhuang as an example (Fig. 7), the following features are shown: (1) There are two lithologic sections. The upper section is composed of mud-silt-sized crystalline dolomites with terrigenous muddy debris (Fig. 7a), while the lower section is composed of silt-fine-sized crystalline dolomites and limestone, between which, an unconformities is existed; (2) The dolomitization intensity gradually decreases below the unconformities. The dolomites transit from dark gray fine-sized crystalline dolomites (Fig. 7b) to porphyritic limy dolomites (Fig. 7c), dolomatic limestone and lime mudstone (Fig. 7d). Mud-silt-sized crystalline dolomites (Fig. 7b) have an ordering of 0.77, heavy $\delta^{18}O$ value (-5.832 ‰ (PDB)) and single-phase fluid inclusions, indicating their formation mechanism is seepage reflux dolomitization. That is, dolomitization takes place due to the downward seepage of evaporated brine.

The high-density brine of seepage reflux dolomitization is generally formed in supratidal flat and sabkha environment [34]. In the Jizhong Depression, seepage reflux dolomites are often associated with the sediments of supratidal flat and unconformities. For example, “Sanshanzi Dolostones” occur below Majiagou I Formation that is composed of the sediments of tidal flat. Between Majiagou I Formation and “Sanshanzi Dolostones”, there is an unconformities formed in response to Huaiyuan Movement [35].

The dolomite crystals of “Sanshanzi Dolostones” are mainly composed of silt-fine-sized crystals, in which, bamboo leaf-shaped psephitic and oolitic relict structure are common. The carbonate rocks with bamboo leaf-shaped psephitic and oolitic relict structure are generally formed in turbulent shallow-water marine environment and dolomitization generally occurs after burial diagenesis. Lamellar silt-fine-sized crystalline dolomites are argillaceous, indicating the original rocks are formed in tidal flat environment. Part of dolomite is varying in crystalline sizes, indicating it is formed as a result of secondary dolomitization. In addition, the dolomitization in the lower part of shale weakens obviously, indicating that shale hinders the downward seepage of the dolomitized fluids in the upper part. These characteristics indicate “Sanshanzi Dolostones” are formed as a result of seepage reflux dolomitization. The tectonic movement of Huaiyuan Period is intense in the south but weak in the north. Therefore, dolomites are better developed in the south than in the north due to sufficient high-magnesium water supply and the promotion of unconformities in the downward seepage of fluids.

A similar set of dolomites is developed in the upper part of Cambrian Fujunshan Formation and their characteristics are as follows: (1) The Mantou Formation is composed gypsiferous purplish red shale and mud-silt-sized crystalline dolomites, indicating the depositional environment is sabkha environment; (2) There is an unconformities between Mantou Formation and Fujunshan Formation; (3) Below the unconformity, dolomitization gradually weakened and dolomite content decreased.

Origin of Type-D dolomites. The spatial distribution of Type-D dolomites is distinctly different from that of other three types. Such as in T17 Well, Upper Ordovician strata are composed of 300 m thick dolomites (Fig. 2A). In the strata 200 m below Zhangxia Formation, limestone is completely dolomitized. Similarly there is the Ji4 well, which contains at least 570 m of continuous dolomite formations. Coring samples showed that the lithology was mainly Type-D dolomites. Their common features are that the dolomite body cuts through the horizon, has a large vertical distribution, and has a small horizontal distribution. It is difficult to be tracked between wells (5 km well space). The dolomites are closed to fault zone and have no genetic markers of supratidal environment. According to these characteristics, it is concluded that the formation of dolomites is not under the control of depositional environment and the original rocks are various types of carbonate rocks.

Type-D dolomites mainly occur in the vicinity of deep faults (Fig. 9). These faults are extensional and strike-slip faults formed since the Jurassic period, closed to which, magmatic rocks of Himalayan Period are distributed [36], indicating dolomitization is closely related to the Himalaya tectonic movement. The present buried depth of Lower Paleozoic strata is more than 2000 m. Taking T17 Well as example, the present buried depth of Ordovician strata is about 3000m. Several times of large-scaled subsidence occurred in geological history, especially in Paleogene. The burial depth of the Lower Paleozoic is about 4000m in this period. According to geothermal gradient, the formation temperature is calculated as about 110°C (Fig. 8). However, many homogenization temperature of fluid inclusions obtained from

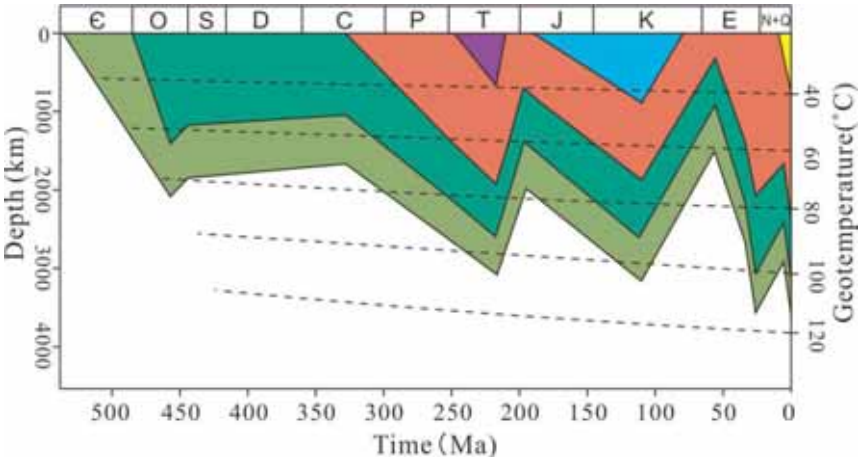

FIGURE 8

Burial history of T17 well, Jizhong Depression, China.

The deepest buried depth of the Lower Paleozoic is about 4000m. According to the geothermal gradient, the maximum geotemperature is about 110°C.

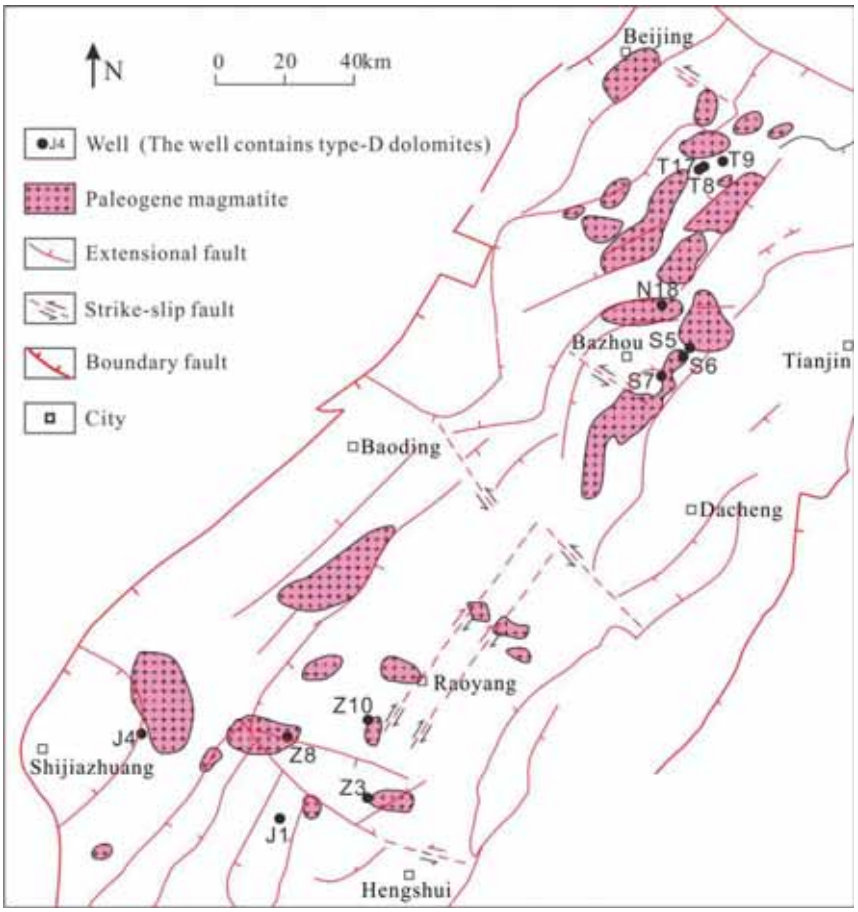

FIGURE 9

Sketch maps showing the distribution of Paleogene magmatic rocks and deep faults.

Modified from Peng [36]. The wells in figure all containing Type-D dolomites.

Type-D dolomites exceeds 200°C, which is much higher than normal formation temperature, indicating Type-D dolomites are formed as a result of hydrothermal dolomitization. In addition, the saddle dolomites are often considered as a sign of hydrothermal activity [37-39].

The dolomites formed in a buried and high-temperature environment (>60°C) have medium to coarse sized crystalline structure [40]. When the dolomites are concentrated in morphology and formed at a higher temperature, it may be the hydrothermal dolomites. At present, although there is no report of hydrothermal dolomites in Lower Paleozoic in North

China Platform, a large number of hydrothermal dolomites are discovered in many oil and gas fields in the world. These hydrothermal dolomites are mainly distributed in the vicinity of extensional fault [41], strike-slip fault [42] and overthrust fault [43,44], indicating their formation is closely related to faulting activities. Under the impact of tectonic movements, a large number of open fracture-cave systems are formed within rock mass and the geothermal gradient becomes anomalous, which provide pathway and driving force for the circulation of thermal fluids. The hydrothermal dolomites in North America covers an area from a few square kilometers to tens of square kilometers, with a thickness from a few meters to tens of meters. Since the temperature is high and crystallization process is slow during buried hydrothermal dolomitization, the dolomites have high ordering and crystals are medium-coarse-sized. The hydrothermal dolomites with negative $\delta^{18}O$ value contain two-phase gas-liquid fluid inclusions [45]. Since Fe and Mn are rich during dolomitization, cathodeluminescence is weak. The Type-D dolomites have above characteristics.

In summary, the Type-D dolomites are affected by tectonic movement and formed in the early Himalayan movement, Paleogene. In the deep burial stage, dolomitization occurs due to the enrichment of magnesium ions. Magnesium ions originate from hydrothermal fluid, which derived from the mantle in Paleogene. Hydrothermal fluid is driven by tectonic movements and move along deep faults. It can be mixed with formation water during its movement. Dolomitization occurs when it enters permeable limestone strata. The farther the limestone is from the fault zone, the harder the hydrothermal fluid is to enter it, and the weaker the effect of dolomitization.

Implication of dolomitization and its distribution. Type-A dolomites and Type-B dolomites are formed in tide flat environment. They are distributed in thin layers and are controlled by sedimentary facies. Their dolomitization occurs at early diagenetic stage, so the dolomites retain primary sedimentary structures and have the sedimentary characteristics of supratidal flat and sabkha. Atmospheric fresh water dissolves gypsum to form solution vug in the syngenetic phase. For the tide flat dolomite of non-gypsum, it tends to be dense. Therefore, in the dolomites developed on the tidal flats, only the gypsiferous mud-silt-sized crystalline dolomites (Type-A) can form a good reservoir.

Type-C dolomites are formed in seepage reflux dolomitization. It is closely related to unconformities and supratidal flat facies and characterized by sandwich structure. The upper part is evaporative tidal flat sediments, the middle part is an unconformities, and the lower part is secondary replacement dolomites. The upper evaporative tidal flat sediments provides the sources of high-magnesium water, and often form cap rock. Therefore, the lower dolomites are distributed below the evaporative tidal flat and its periphery, and the degree of dolomitization gradually weakens downwards. The formation period of unconformities is also the leaching period of atmospheric freshwater to the lower rock formation during the epigenetic period. After leaching, high-magnesium water and atmospheric freshwater can easily enter the underlying rock formation. So it was that many pores are formed in dolomite, such as vugs, caverns and channels. As of the "Sanshanzi Dolostones", the upper evaporative tidal flat of Majiagou I Formation can form a good cap rock, the development of vugs and caverns can form a good reservoirs. With proper oil and gas configuration, good oil and gas reservoirs can be formed.

Burial hydrothermal dolomites are distributed in the vicinity deep faults and Himalayan magmatic rocks. The farther away from fault zone, the weaker the effect of dolomitization. The geometry and developmental position of burial hydrothermal dolomites are distinctly different from those of other genetic types. It's have small distribution range, with a thickness from tens of meters to hundreds of meters and an area from a few hundred square meters to several square kilometers. Burial hydrothermal dolomitization may occur in any carbonate strata near deep fault. Type-A, Type-B and Type-C dolomites can undergo recrystallization and secondary dolomitization under hydrothermal conditions to form Type-D dolomites. Therefore, in the practice of production, the developmental position of burial hydrothermal dolomites can be predicted by the position of deep faults and Cenozoic magmatic rocks in oil and gas reservoir exploration. In ddition, it can also be judged from the geometry of dolomites.

Hydrothermal dolomites are widely distributed in the world and recognized as an important exploration target. Studies have shown that hydrothermal dolomization and hydrothermal dissolution occur simultaneously [46]. Dolomite formed by hydrothermal dolomization is in mosaic contact and does not develop intercrystalline pores. The hydrothermal dissolution will expand the vugs and channels of the original rock [47]. At the edge of the hydrothermal channel, cementation is greater than dissolution [48]. In the vicinity of the dominant hydrothermal channel, the hydrothermal fluid flows quickly, the quantity is large, and the dissolution is strong [49, 50]. Therefore, for the hydrothermal dolomite, its high quality reservoir is located near the dominant hydrothermal channel near the deep faults.

CONCLUSIONS

The four types of dolomite have different origins in the Lower Paleozoic of Jizhong Depression, North China. Type-A dolomites are formed in sabkha environment as a result of evaporative pumping. Type-B dolomites genesis are similar to the dolomite

genesis of Andros Island, Bahamas. These two types of dolomites are formed on the tidal flat. Type-C dolomites are formed as a result of seepage reflex dolomitization. Type-D dolomites are formed as a result of burial hydrothermal dolomitization.

There are many potential connections between the origin and distribution of dolomite. Type-A dolomites and Type-B dolomites are formed in tidal flat environment, controlled by the distribution of tidal flat facies, and are distributed in thin-layered. Type-C dolomites has a sandwich-like structure of "supratidal flat sediment- unconformities-seepage reflux dolomites". The dolomites in the upper part of the Fujunshan Formation and "Sanshanzi Dolostones", which are the two largest sets of dolomites in North China Platform, are mainly formed as a result of seepage reflux dolomitization. Due to the control of hydrothermal fluid, the Type-D dolomites have a small distribution range. Its spatial form is concentrated and distributed in the vicinity of deep faults and Cenozoic magmatic rocks. These correlations can be applied to the exploration of dolomite reservoirs.

Different dolomite distribution patterns and dolomitization have important influence on the reservoir. Type-A dolomites can form good reservoirs based on its containing dissolved pores. The distribution of Type-C dolomites is controlled by the evaporative tidal flat. Type-C dolomites can form good reservoirs within a wide range due to the effect of freshwater leaching during the epigenetic period. Type-D dolomites are affected by the hydrothermal fluid and forms a good reservoir near the dominant hydrothermal channel.

ACKNOWLEDGEMENTS

Grateful acknowledgement is made to my supervisor, Professor Zhenkui Jin, for his considerable help by means of suggestion. Financial and digital supported by North China Oil Field is gratefully acknowledged. The authors also would like to express our gratitude to all those who have helped us during the writing of this thesis. This work was supported by the National Science and Technology Major Project [grant numbers 2016ZX05006-005].

REFERENCES

[1] Feng, Z.Z. (1979) A preliminary discussion on the Lower Ordovician litho-facies and paleogeography in north China. Chinese Journal of Geology. 4, 302-313.

[2] Feng, Z.Z., Zhang, Y.S., Jin, Z.J. (1998) Type, origin, and reservoir characteristics of dolostones of the Ordovician Majiagou Group, Ordos, North China Platform. Sedimentary Geology. 118, 127-140.

[3] Jing, Z.K., Feng, Z.Z. (1993) Types and reservoiring performance of dolostones of the Lower Paleozoic in the eastern North China Platform. Acta Sedimentologica Sinica. 11, 11-18.

[4] Yang, S., Jiao, Y.Q., Wu, L.Q., Lin, H.X., Liu, H., Zhang, S.P., Li, J.Y. (2007) Dolomite reservoirs analysis and prediction of the yeli and liangjiashan formations in the eastern part of north China. Geological Science and Technology Information. 26, 61-67.

[5] Bai, X.L., Zhang, S.N., Huang, Q.Y., Ding, X.Q., Zhang, S.Y. (2016) Origin of dolomite in the Middle Ordovician peritidal platform carbonates in the northern Ordos Basin, western China. Petroleum Science. 13, 434-449.

[6] Li, F.J., Du, L.C., Zhao, J.X., Li, Y.G., Xiang, F., Li, F.P. (2016) Dolomite genesis in Member Ma55 of Majiagou Formation, Sudong area, Ordos Basin. Acta Petrolei Sinica. 37, 328-338.

[7] Yang, H., Shi, K., Liu, J.W. (2016) The characteristics of Ordovician Dolomite petrography and its composition of Carbon and Oxygen stable isotope in Ordos Basin. Journal of Northwest University (Natural Science Edition). 46, 415-422.

[8] Meng, Y., Xu, Z., Gao, C., Xu, Y., Li, R. (2018). The identification of the Eocene magmatism and tectonic significance in the middle Gangdese magmatic belt, southern Tibet. Acta Petrologica Sinica. 34, 513-546.

[9] Yang, T., Cao, Y., Friis, H., Liu, K., Wang, Y. (2018) Origin and evolution processes of hybrid event beds in the Lower Cretaceous of the Lingshan Island, Eastern China. Australian Journal of Earth Sciences. 65, 517-534.

[10] Song, Y., Stepashko, A., Liu, K., He, Q., Shen, C. (2018) Post-rift Tectonic History of the Songliao Basin, NE China: Cooling Events and Post-rift Unconformities Driven by Orogenic Pulses From Plate Boundaries. Journal of Geophysical Research Solid Earth. 123, 2363-2395.

[11] Luczaj, J.A. (2006) Evidence against the Dorag (mixing-zone) model for dolomitization along the Wisconsin arch-A case for hydrothermal diagenesis. AAPG Bulletin. 90, 1719-1738.

[12] Davies, G.R., Smith Jr, L.B. (2006) Structurally controlled hydrothermal dolomite reservoir facies: An overview. AAPG Bulletin. 90, 1641-1690.

[13] Beckert, J., Vandeginste, V., John, C.M. (2016) Relationship between karstification and burial dolomitization in permian platform carbonates (Lower Khuff - Oman). Sedimentary Geology. 342, 165-179.

[14] Hips, K., Haas, J., Győri, O. (2016) Hydrothermal dolomitization of basinal deposits controlled by a synsedimentary fault system in Triassic extensional setting, Hungary. International Journal of Earth Sciences. 105, 1215-1231.

[15] Jiang, L., Cai, C., Worden, R.H., Crowley, S.F., Jia, L., Zhang, K., Duncan, I.J. (2016) Multiphase dolomitization of deeply buried Cambrian petroleum reservoirs, Tarim Basin, north-west China. Sedimentology. 63, 2130-2157.

[16] Rustichelli, A., Iannace, A., Tondi, E., Celma, C.D., Cilona, A., Giorgioni, M., Parente, M., Girundo, M., Invernizzi, C. (2017) Fault-controlled dolomite bodies as palaeotectonic indicators and geofluid reservoirs: New insights from Gargano Promontory outcrops. Sedimentology. 64, 1871-1900.

[17] Meng, F., Gao, S., Song, Z., Niu, Y., Li, X. (2018) Mesozoic high-Mg andesites from the Daohugou area, Inner Mongolia: Upper-crustal fractional crystallization of parental melt derived from metasomatized lithospheric mantle wedge. Lithos. 302, 535-548.

[18] Ren, Y., Zhong, D.K., Gao, C.L., Sun, H.T., Peng, H., Zheng, X.W., Qiu, C. (2017) Origin of dolomite of the lower Cambrian Longwangmiao Formation, eastern Sichuan Basin, China. Carbonates and Evaporites. 5, 1-20.

[19] Yi, S.W., Zhao, S.F., Fan, B.D., Liu, J.W., Yang, N.R., Xie, H.X. (2010) Development characteristics of buried hill and reservoir forming pattern in central faulted structural belt of Jizhong Depression. Acta Petrolei Sinica. 31, 361-368.

[20] Zhai, M.G. (2011) Cratonization and the Ancient North China Continent: A summary and review. Science China Earth Sciences. 54, 1110-1114.

[21] Chi, X.Y., Sun, W.F. (2010) Ordovician sequence paleogeography and reservoir quality in Jizhong Depression. Marine Geology Frontiers. 27, 11-16.

[22] Warren, J. (2000) Dolomite: occurrence, evolution and economically important associations. Earth-Science Reviews. 52, 1-81.

[23] Bazargani-Guilani, K., Faramarzi, M., Tak, M.A.N. (2010) Multistage dolomitization in the cretaceous carbonates of the east Shahmirzad area, north Semnan, central Alborz, Iran. Carbonates and Evaporites. 25, 177-191.

[24] Wierzbicki, R., Dravis, J.J., Alaasm, I., Harland, N. (2006) Burial dolomitization and dissolution of upper Jurassic Abenaki platform carbonates, Deep Panuke reservoir, Nova Scotia, Canada. AAPG Bulletin. 90, 1843-1861.

[25] Bontognali, T.R., Vasconcelos, C., Warthmann, R.J., Bernasconi, S.M., Dupraz, C., Strohmenger, C.J., McKenzie, J.A. (2010) Dolomite formation within microbial mats in the coastal sabkha of Abu Dhabi (United Arab Emirates). Sedimentology. 57, 824-844.

[26] Shinn, E.A., Ginsburg, R.N., Lloyd, R.M. (1965) Recent supratidal dolomite from Andros Island, Bahamas. Dolomitization and Limestone Diagenesis. 13, 112-123.

[27] Shinn, E.A., Lloyd, R.M., Ginsburg, R.N. (1969) Anatomy of a modern carbonate tidal-flat, Andros Island, Bahamas. Journal of Sedimentary Research. 39, 1202-1228.

[28] Murray, S.T., Swart, P.K. (2017) Evaluating Formation Fluid Models and Calibrations Using Clumped Isotope Paleothermometry on Bahamian Dolomites. Geochimica et Cosmochimica Acta. 206, 73-93.

[29] Xu, F., Hu, B., Dou, Y., Song, Z., Liu, X., (2018) Prehistoric heavy metal pollution on the continental shelf off Hainan Island, South China Sea: From natural to anthropogenic impacts around 4.0 kyr BP. Holocene. 28, 455-463.

[30] Hou, Q., Mou, C., Wang, Q., Tan, Z. (2018) Provenance and tectonic setting of the Early and Middle Devonian Xueshan Formation, the North Qilian Belt, China. Geological Journal. 53, 1404-1422.

[31] Yang, R., Van Loon, A.J. (2016) Early Cretaceous slumps and turbidites with peculiar soft-sediment deformation structures on Lingshan Island (Qingdao, China) indicating a tensional tectonic regime. Journal of Asian Earth Sciences. 129, 206-219.

[32] Vahrenkamp, V.C., Swart, P.K., Ruiz, J. (1991) Episodic dolomitization of late Cenozoic carbonates in the Bahamas: Evidence from strontium isotopes. Journal of Sedimentary Research. 61, 1002-1014.

[33] Vahrenkamp, V.C., Swart, P.K. (1994) Late Cenozoic dolomite of the Bahamas: metastable analogues for the genesis of ancient platform dolomites. In: Purser, B., Tucker, M., Zenger, D. (Eds.) Dolomites: a volume in Honour of Dolomieu. Blackwell Scientific, International Association of Sedimentologists Special Publication, Oxford, 133–153.

[34] Vinci, F., Iannace, A., Parente, M., Pirmez, C., Torrieri, S., Giorgioni, M. (2017) Early dolomitization in the lower cretaceous shallow-water carbonates of southern apennines (Italy): clues about palaeoclimatic fluctuations in western tethys. Sedimentary Geology. 362, 17-36.

[35] Feng, Z.Z. (1990) Lithofacies paleogeography of Early Paleozoic of North China platform. Geological Publishing House, Beijing.

[36] Peng, N., Cui, X.M., Cui, Z.Q., Li, X., Liu, N., Dong, X.Y. (2010) Tertiary volcanic lithofacies characteristics and oil-gas reservoir accumulation model, Jizhong depression. Petroleum Geology and Recovery Efficiency. 17, 17-20.

[37] Ni, J., Xi, B., Jun, J., Yang, H., Xia, Z. (2016) Early Cretaceous exhumation of the Sulu orogenic belt as a consequence of the eastern Eurasian tectonic extension: insights from the newly discovered Wulian metamorphic core complex, eastern China. Journal of The Geological Society. 173, 531-549.

[38] Machel, H.G., Lonnee, J. (2002) Hydrothermal dolomite—a product of poor definition and imagination. Sedimentary Geology. 152, 163-171.
[39] Mansurbeg, H., Morad, D., Othman, R., Morad, S., Ceriani, A., Al-Aasm, I., Kolo, K., Spirov, P., Proust, J.N., Preat, A., Koyi, H. (2016) Hydrothermal dolomitization of the Bekhme formation (Upper Cretaceous), Zagros Basin, Kurdistan Region of Iraq: Record of oil migration and degradation. Sedimentary Geology. 341, 147-162.
[40] Gregg, J.M. (2004) Basin fluid flow, base-metal sulphide mineralization and the development of dolomite petroleum reservoirs. Geological Society, London, Special Publications. 235, 157-175.
[41] Jacquemyn, C., Desouky, H.E., Hunt, D., Casini, G., Swennen, R. (2014) Dolomitization of the latemar platform: fluid flow and dolomite evolution. Marine and Petroleum Geology. 55, 43-67.
[42] Berger, Z., Davies, G. (1999) The development of linear hydrothermal dolomite (HTD) reservoir facies along wrench or strike slip fault systems in the Western Canada Sedimentary Basin. Canadian Society of Petroleum Geologists Reservoir. 26, 34-38.
[43] López-Horgue, M.A., Iriarte, E., Schröeder, S., Fernández-Mendiola, P.A., Caline, B., Corneyllie, H., Frémont, J., Sudrie, M., Zerti, S. (2010) Structurally controlled hydrothermal dolomites in Albian carbonates of the Asón valley, Basque Cantabrian Basin, Northern Spain. Marine and Petroleum Geology. 27, 1069-1092.
[44] Lapponi, F., Bechstaedt, T., Boni, M., Banks, D.A., Schneider, J. (2014) Hydrothermal dolomitization in a complex geodynamic setting (Lower Palaeozoic, northern Spain). Sedimentology. 61, 411-443.
[45] Azmy, K.A., Lavoie, D.L., Knight, I.K., Chi, G.C. (2008) Dolomitization of the lower Ordovician aguathuna formation carbonates. Canadian Journal of Earth Sciences. 45, 795-813.
[46] Davies, G.R., Wendte, J. (2005) Major dolostone reservoir types, outcrop and subsurface analogues, western Canada: Distinct types or continuum? In: American Association of Petroleum Geologists–Canadian Society of Petroleum Geologists, Joint Convention, Field Trip Guidebook, Calgary, 1-84.
[47] Zhao, W.Z., Shen, A.J., Zheng, J.F., Wang, X.F., Lu, J.M. (2014) The porosity origin of dolostone reservoirs in the Tarim, Sichuan and Ordos basins and its implication to reservoir prediction. Science China: Earth Sciences. 44, 1925-1939.
[48] Chen, D.Z. (2008) Structure-controlled hydrothermal dolomitization and hydrothermal dolomite reservoirs. Oil and Gas Geology. 29, 614-622.
[49] Qian, Y.X., Chen, D.Z., You, D.H., Qin, R.H., He, Z.L., Dong, S.F., Ma, Y.F., Jiao, C.L., Tian, M. (2012) Types of dolostones and pore evolution of the Middle and Upper Cambrian in Kuruk Tag area of northeastern Tarim Basin. Journal of Palaeogeography. 14, 461-476.
[50] Hu, Z.W., Li, Y., Han, X., Huang, S.J., Li, B.K. (2015) Reviews on the Hydrothermal Alteration of Carbonate Reservoirs. Geological Science and Technology Information. 34, 58-65.

Received: **13.12.2018**
Accepted: **20.03.2019**

CORRESPONDING AUTHOR

Wei Yan
China University of Petroleum-Beijing,
College of Geosciences,
Changping, Beijing – China

e-mail: 1738959751@qq.com

© by PSP Volume 28 – No. 5/2019 pages 3963-3980 Fresenius Environmental Bulletin

THE EFFECT OF DENSITY GRADIENT ON SPATIAL DISTRIBUTION AND GROWTH DYNAMICS OF NATURAL *PINUS SYLVESTRIS* L. VAR. *MONGOLICA* LITV. PURE FOREST IN NORTHEAST CHINA

SeMyung Kwon[1], Leilei Pan[2], Alamgir Khan[1], Kebin Zhang[1,*]

[1]School of Soil and Water Conservation, Beijing Forestry University, Beijing, 100083, China
[2]Institute of Desertification Studies, Chinese Academy of Forestry, Beijing, 100091, China

ABSTRACT

Stand structure indices were examined in this study to clarify stand structure and interaction among individual trees. This analysis provides a greater understanding of density-dependent interactions among intraspecific trees with different vitality using a point pattern analysis method. This study was undertaken in Hulunbuir Sandland, Inner Mongolia, China, in natural *Pinus sylvestris* L. var. *mongolica* Litv. stands which have different densities and relatively little human interference Results for Regeneration seedlings (R-seedlings) (31.07% ±15.5), Suppressed trees (S-trees) (55.0% ±13.3) and Dominant trees (D-trees) (13.3% ±2.6) indicated that this forest was under a period of renewal and growth. Apart for R-seedlings, growth dynamics differed depending on the density gradient in all plots, and obvious significant differences were recorded between S-trees growth and density gradient. The spatial distribution of S-trees was also found to have a significant impact on germination and growth of R-seedlings in these forests. However, D-trees did not directly affect germination and survival of R-seedlings. Findings from this study will provide a reference for afforestation, reforestation and plantation management in close-to-nature forests.

KEYWORDS:
Pinus sylvestris L. var. *mongolica* Litv., Spatial distribution, Growth dynamics, SIAFOR program, Programita software

INTRODUCTION

Desertification in arid, semi-arid and dry subhumid areas is a major global environmental issue which has serious implications in China [1, 2]. This issue not only effects local populations [3], it also has major influences on atmospheric processes, resulting in frequent sandstorms in neighboring countries [4, 5]. To effectively control desertification in China, the Chinese government has implemented regeneration programs over the last 70 years to revegetate degraded land in dryland areas [6, 7]. Since the late 1950s, Mongolian Scots Pine (*Pinus sylvestris* var. *mongolica*) has been introduced into Horqin Sandy Land from Hulun Buir Sandy Land and planted in the majority of drylands of China [9]. This species is a needle leaved tree characterized by a high tolerance to cold environments, drought conditions and infertile soils, and it has been recorded to have good growth in sandy soils [8]. In 1978 when the "Three-North Shelter Forest Program" was implemented, Mongolian Scots Pine was the main evergreen species used for afforestation and reforestation [10]. However, in recent years large areas of Mongolian Scots Pine plantations have become degraded [11-13]. This degradation has resulted in a reduction of their protective functions and a reduction in other ecosystem services, such as carbon fixation capacity and timber production [14-16].

It was projected that unexpected climate change, such as reduced precipitation and an increase in temperature, will result in nutrient imbalance [17, 18], an extension of pest survival time [19, 20] and other factors such as the rotation age of trees in forests etc. It is expected that forest plantations will gradually decline, thus close-to-nature silviculture [21-23] is expected to be the best solution to restore degraded forests. In general, close-to-nature plantation management can be achieved by controlling stand density and inducing natural regeneration [21, 24]. For degraded Mongolian Scots Pine plantations, close-to-nature forest management techniques seem to be an alternative solution for restoration. Therefore, examining changes in natural Mongolian Scots pine forests is important to gain a better understanding of potential density changes and spatial pattern distributions [25-27].

In this study, five secondary natural Mongolian Scots pine forests with different stand densities and relatively little human interference were studied in Hulunbuir Sandland, Inner Mongolia. The aims of this study were: (1) to clarify stand structure and the interrelationships among individual trees using stand

structure indices, and (2) to increase our understanding of density-dependent interactions among intraspecific trees with different vitality using a point pattern analysis method. Results from this study will provide a baseline for afforestation, reforestation and plantation management for close-to-nature forests established using the Three-North Shelter Forest Program to combat desertification in north China.

MATERIALS AND METHODS

Description of the study area and sample plot selection. This study was undertaken in Hulun Buir Sandland, Inner Mongolia, northeastern China, between 47°38'N and 47°39'N latitude and 119°11'E and 119°12'E longitude (Table 1). The study site is located in the border areas of China and Mongolia between Da Xing'anling Mountains and the Mongolian Plateau, characterized by hills consisting of Quaternary sand covering a large area. The climate of the research area is typical continental semiarid with a mean annual temperature of -1.5°C, and a mean annual precipitation of 344 mm, mainly occurring between July and August. Elevation of the study sites ranged from 700-1100 m a.s.l. The main forest stand is natural pure forest of *Pinus sylvestris* L. var. *mongolica* Litv. grouped with several other woody species (e.g., *Malus baccata* (L.) Borkh, *Armeniaca sibirica* (L.) Lamarck, *Crataegus dahurica* Koehne ex C.K. Schneider) in an understory vegetation which has very little human interference.

We selected five 50×50 m sample plots in natural pure *Pinus sylvestris* L. var. *mongolica* Litv. stands which had highly similar physical characteristics and different stand densities. In each sample plot, parameters such as tree position (X and Y coordinates), DBH (basal diameter was measured for trees less than 2 m in height), height, crown radius and length, and tree age of all trees were measured (Table 1). Tree age was determined by either counting the total number of branches (smaller trees) or using the annual ring counting method (larger trees). Tree data were classified into three groups following the IUFRO classification for tree vitality: Dominant trees (D-trees), middle layer or Suppressed trees (S-trees), and the lowest layer or Regeneration seedlings (R-Seedlings) [28]. Duncan's multiple range test was used to compare growth characteristics (mean height, DBH, crown radius: four directions from the main bole with magnetic north to the vertically projected edge of the crown, crown length: vertical length of a living branch, and age of each trees) of the three groups within the five plots.

Stand structure and the relationship between neighboring trees. SIAFOR 1.0 (Structural Index Assessment in Forest stands) program was used to analyze stand structure of the five plots [29]. Four nearest-neighbor indices, spatial point pattern index 'CE' [30, 31], relative mingling index 'S' [32], mingling index 'DM' and differentiation index 'T' [33] were analyzed. The permutation test for DM and T [34] generated 1000 permutations, it randomly reassigning species or size values to tree coordinates, and it indicated whether the index value was significantly different from that under random conditions [29]. CE, DM and T were separately calculated for each species and calculated together for all species; S was calculated for each pair of species [29].

Instead of tree species, tree classification was used to analyze stand structure of the five plots. The description of the main characteristics and statistical tests for these indices is listed in Table 2 [29].

Spatial point pattern analysis. Current spatial point pattern analysis methods [35-37] were used to analyze the spatial patterns found at the five study plots. Univariate $g(r)$ and bivariate $g_{12}(r)$ pair correlation functions were used to quantify observed spatial patterns [35-39]. $g(r)$ and $g_{12}(r)$ were initially calculated using Ripley's $K(r)$ function, an accumulation distribution, whereby the existence of the accumulation effect may affect the accuracy of the results [39, 40], as:

$$\widehat{K}(r) = \frac{A}{n^2}\sum_{i=1}^{n}\sum_{\substack{j=1 \\ j\neq i}}^{n} {w_{ij}}^{-1} I_r(u_{ij}) \qquad (1)$$

where, A is the plot area; uij is the distance between i and j at two points; $Ir(u_{ij})$ is the indicator function; and w_{ij} is a weight value for edge correction. When u_{ij} is less than or equal to r, $Ir(u_{ij})=1$; when $u_{ij} > r$, $Ir(u_{ij})=0$. For homogeneous patterns, $g(r)$ can be defined as the expected density of points in a ring of radius r and width dw centered in an arbitrary point, divided by intensity l of the pattern [35]. We compared the univariate spatial patterns to the null models of complete spatial randomness (CSR) or to a Thomas process that describes clustering [41,42]. Using the Thomas process, we were able to identify additional characteristics of clustering [42]. For $g(r)$, its relationship with $K(r)$ can be described as:

$$g(r) = (2\pi r)^{-1} dK(r)/dr \qquad (2)$$

where, $dK(r)$ is the differentiation of the $K(r)$ function; and dr is the differentiation of radius r. $g(r) > 1$ indicates spatial aggregation, $g(r) < 1$ indicates regularity, and $g(r) = 1$ indicates randomness. The bivariate $g_{12}(r)$ function describes the spatial relationship between two patterns (pattern 1 and pattern 2), as:

$$g_{12}(r) = (2\pi r)^{-1} dK_{12}(r)/dr \qquad (3)$$

Equation (3) calculates the number of related species (or pattern 2) in a ring area with an associated species (or pattern 1) as the center of the circle using a radius of r. The $g_{12}(r)$ function can be defined as the expected density of type 2 points in a ring of radius r with width dw centered in an arbitrary type 1 point, divided by the intensity l2 of the pattern of type 2 points [39]. To investigate the relationship between R-seedlings, S-trees and D-trees, a toroidal shift null model was used [39, 43]. This method provided a non-parametric way to test independence

between two patterns. This null model treats the study plot as a torus and involves random shifts of complete pattern 2 relative to pattern 1 (which is kept fixed) [44]. If $g_{12}(r)$ function values are above or below the simulation envelopes, the two patterns indicate attraction or repulsion, respectively.

All analyses were carried out using Programita software for point spatial pattern analysis [39] using a cell size of 0.5 × 0.5 m. This spatial resolution was fine enough to respond to our objectives. For estimation of the pair-correlation functions, a ring width of 1 m was used. Details on the estimators of the pair-correlation function and edge correction can be found in Wiegand and Moloney (2004) [39]. Spatial patterns were analyzed by separating all tree stands (survival and mortality trees) with surviving trees to understand the effect of spatial distribution of trees on sustainable growth.

RESULTS

Stand Structure. The age of trees classified by IUFRO was: R-seedlings - 14.96 ±4.78 years; S-trees - 24.47 ±3.08 years; and D-trees - 33.57 ±3.78 years. DBH distribution results (Figure 2) for each plot approximately appeared as a reversed-J shape for R-seedlings (31.07% ±15.5), S-trees (55.0% ±13.3) and D-trees (13.3% ±2.6). This result indicates that all plots were not considered as mature stands, reflecting that small trees and seedlings had a greater distribution pattern than those of older trees. In addition, tree age of R-seedlings, S-trees and D-trees in all plots also indicated that this forest was under a period of vegetation renewal (Figure 2). For the three groups, the Mean survival rate of R-seedlings (16.5% ±9.0) was the lowest compared to S-trees (90.7% ±3.5) and D-trees (100%). In addition, with an increase in stand density, mortality rates increased (Figure 2f).

The number of R-seedlings ranged from 93 to 971 trees per plot, with the lowest survival rate recorded in P3 (mid-density, 5.3 %) and the highest rate in P2 (high density, 27.6 %) (Figure 2f). Survival rates for S-trees ranged from 332 (P3; mid-density; 85.0 %) to 564 trees per plot (P2; high density; 94.2 %) (Figure 2f). Survival rates for D-trees ranged from 73 (P5; lowest density; 100%) to 153 trees per plot (P2; high density; 100%) (Figure 2f).

TABLE 1
Stand parameters of the five sample plots

Plot	Density (tree/ha)	No. tree (R/S/D)*	Altitude (m)	Gradient (°)	Slope aspect	Understory cover	Latitude	Longitude
P1	3,340	971/564/149	900	10	ES	40%	47°38'N	119°11'E
P2	2,908	322/515/153	900	10	E	20%	47°38'N	119°11'E
P3	2,476	263/559/130	900	6	S	20%	47°39'N	119°11'E
P4	1,968	142/412/89	900	2	WS	60%	47°39'N	119°12'E
P5	1,544	93/332/73	890	1	S	50%	47°39'N	119°12'E

* R: Regeneration seedlings, S: Suppressed trees, D: Dominant trees.

TABLE 2
Characteristics and statistical test of the nearest-neighbour indices implemented in SIAFOR.

Index	Equation*	Range	Description	Statistical test
CE	$\frac{1/N\sum_{i=1}^{N} r_i}{0.5\left(A/N\right)^{1/2} + 0.0514\left(P/N\right) + 0.041\left(P/N^{3/2}\right)}$	0-2.15	Spatial point pattern of trees within a plot: clustered (<1), random (=1) or regular (>1)	z test H0:CE=1; H1:CE≠1
S(s1, s2)	$1 - \frac{n(b+c)}{(a+c)(c+d)+(b+d)(a+b)}$	-1-1	Relative mingling of species s1 and s2 within a plot: aggregated-associated (<0), neutral (=0) or segregated-separated (>0)	χ^2 test H0:S=0; H1:S≠0
DM	$\sum_{i-1}^{N}\left(\frac{1}{3}\times\sum_{j=1}^{3} V_{ij}\right)$	0-1	Mingling within a plot: degree of dissimilarity of species between neighbouring trees	Permutation test H0:DM=DM_{ran}; H1:DM≠DM_{ran}
T	$\sum_{i=1}^{N}\left(\frac{1}{3}\times\sum_{j=1}^{3}\left[1-\frac{\mathrm{MIN}(S_i,S_j)}{\mathrm{MAX}(S_i,S_j)}\right]\right)$	0-1	Differentiation within a plot: degree of dissimilarity of size between neighbouring trees	Permutation test H0:T=T_{ran}; H1:T≠T_{ran}

* r_i is the distance between tree i and its nearest neighbour; N total number of trees;
A the plot area; P the plot perimeter; a and d number of trees of s1 and s2 in the plot with a nearest neighbor of the same species; b and c number of trees of s1 and s2 in the plot with a nearest neighbor of the other species; n sum of trees of s1 and s2;
V_{ij} equals 1 if tree i and neighbour j are of a different species, otherwise it is 0;
Si and S_j is the size of tree i and neighbor j, S can be diameter (TD), height (TH), crown length (TCl) and crown radius (TCr).

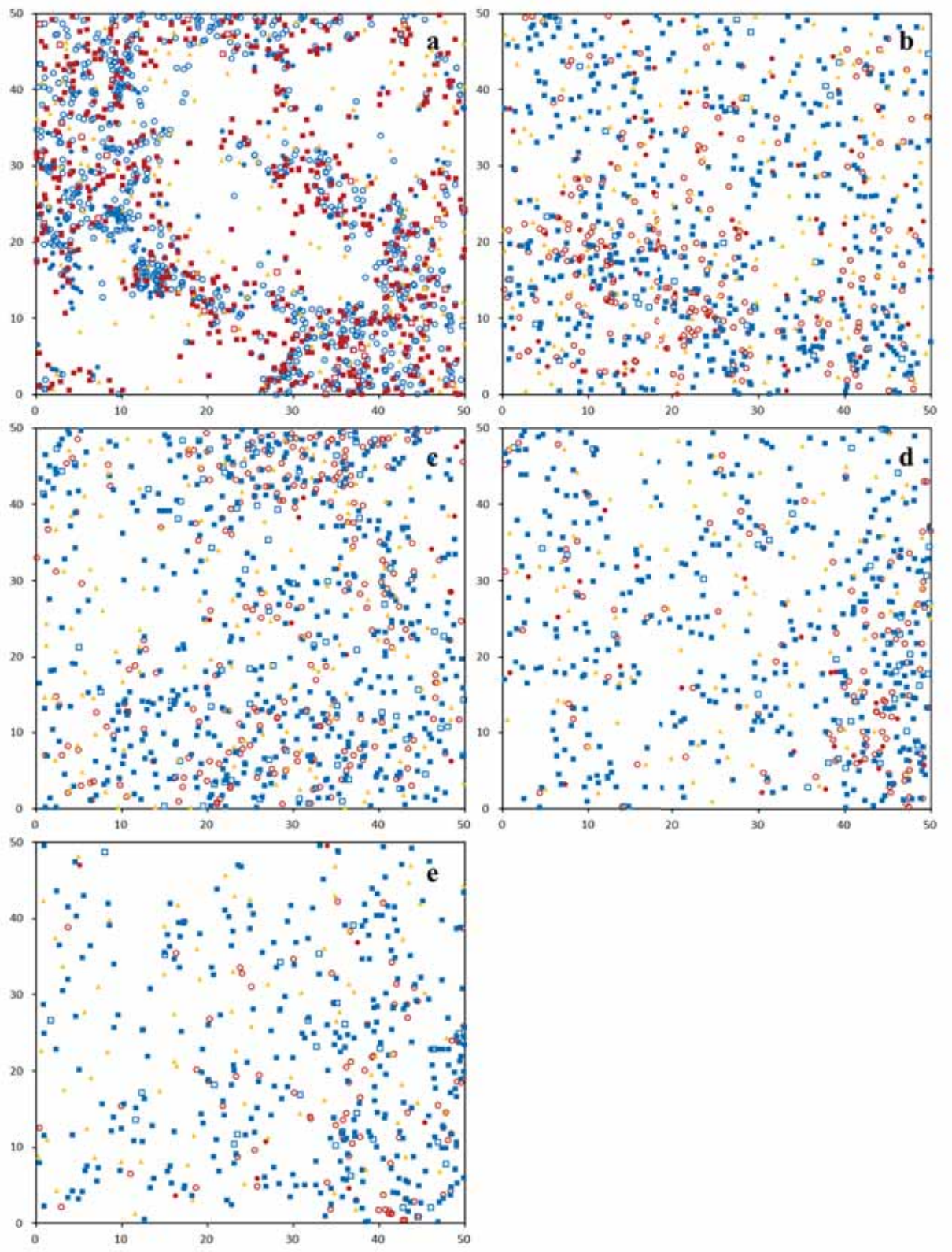

FIGURE 1
Spatial distribution of individual trees within the five plots
(a: plot 1, b: plot 2, c: plot 3, d: plot 4, e: plot 5). ● Survival regeneration seedlings, ○ Mortality regeneration seedlings, ■ Survival suppressed trees, □ Mortality suppressed trees, ▲ Survival dominant trees, △ Mortality dominant trees

The basal area of R-seedlings, S-trees and D-trees in each plot was analyzed using surviving trees. The number of surviving trees of R-seedlings, S-trees and D-trees increased with an increase in stand density. For basal area of R-seedlings and D-trees, density was greatest in the high density plot (P1), resulting in the highest basal area (1.0 m^2/ha and 20.9 m^2/ha, respectively). Basal area of S-trees were the

highest in the middle-density stand (P3; 40.3 m^2/ha), followed by low density stands (P4 and P5) and high density stands (P2 and P1). Basal area of R-seedlings were the lowest in P1 and P2 (high density stands), followed by S-trees and D-trees (Table 3).

Growth dynamics. The effect of density gradient changes due to tree height, DBH, crown radius and length are shown in Figure 3. Results for each classification indicate:

Height: For R-seedlings, as stand density increased no corresponding trend in tree growth characteristics within the five plots were recorded. Mean height of R-seedlings were in the order of P1 (5.24 ±1.44 m) > P2 (5.10 ±1.45 m) > P4 (4.91 ±0.90 m) > P5 (4.83 ±1.35 m) > P3 (4.22 ±0.93 m). Mean height results for S-trees were 8.89 (±1.80 m) P1, 9.78 (±1.93 m) P2, 9.39 (±1.78 m) P3, 9.34 (±2.02 m) P4 and 10.09 (±2.07 m) for P5. Mean heights for D-trees were P3 (11.56 ±0.94 m), P1 (12.07 ±1.67 m), P2 (12.21 ±1.05 m), P4 (12.45 ±1.01 m) and P5 (12.51 ±1.15 m). Although trend changes for tree height and density were not significant for S-trees and D-trees, the lowest level of tree growth of all groups was recorded in P3.

DBH: Mean DBH results for R-seedlings recorded no significant differences between each plot. R-seedlings with a middle density and DBH (3.80 ±0.65 cm; P3) recorded the lowest values, followed by P5 (4.12 ±1.03 cm). P4 recorded the highest mean DBH results (4.37 ±0.82 cm), followed by P1 (4.30 ±0.96 cm) and P2 (4.17 ±0.98 cm). Mean DBH results for S-trees recorded a changing characteristic with a change in plot density: lower density plots recorded higher mean DBH. The lowest DBH was recorded in the most dense plot (P1; 9.39 ±2.82 cm) with P2-P5 having values of 10.67 ±3.12 cm, 12.00 ±3.22 cm, 12.60 ±4.16 cm, and 13.71 ±4.77 cm, respectively (Figure 3b). A similar trend was recorded for D-trees, however the level of change was not as obvious as that for S-trees. The highest mean DBH value for D-trees was recorded in the most dense plot (P1; 19.76 ±7.56 cm), followed by P2-P5 (19.93 ±3.56 cm, 20.30 ±3.15 cm, 23.12 ±4.53 cm and 23.06 ±2.63 cm, respectively; Figure 3b).

Crown Radius and Length: R-seedlings results for crown radius and length (Figure 3c and d) indicate a change with stand density; results for crown length however did not record a significant change with density. Crown radius results were lowest in the densest plot (P1; 0.59 ±0.13 m), followed by P2, P5, P4 and P3 (0.62 ±0.12 m, 0.66 ±0.13 m, 0.67 ±0.13 m and 0.71 ±0.19 m, respectively). The lowest crown mean length was recorded in P3 (mid-density; 1.54 ±0.62 m), followed by P5, P2, P1 and P4 (1.62 ±0.58 m, 1.73 ±0.81 m, 1.90 ±0.94 m and 2.00 ±0.85 m, respectively).

Results for crown radius and length for S-trees indicated that stand density had an obvious influence compared to R-seedlings (Figure 3c and d). The mean value of crown radius and length increased with a decrease in stand density (P1-P5 values were 0.79 ±0.22 m and 3.43 ±1.54 m; 0.81 ±0.21 m and 4.08 ±1.46 m; 0.87 ±0.20 m and 3.90 ±1.49 m; 1.01 ±0.26 m and 4.44 ±1.81 m; and 1.13 ±0.35 m and 4.54 ±1.81 m, respectively). The influence of stand density on crown radius and length was also recorded for D-trees. The highest crown radius and length values were recorded in P5 (1.86 ±0.37 m and 7.39 ±1.58 m, respectively). Results for P4, P1, P2 and P3 were 1.64 ±0.41 m and 6.99 ±1.79 m; 1.55 ±0.85 m and 6.49 ±2.44 m; 1.43 ±0.44 m and 6.39 ±1.56 m; and 1.35 ±0.31 m and 5.84 ±1.21 m, respectively.

The relationship between neighbouring trees. CE Index. Although CE index results for R-seedlings in P3, P4 and P5 only had a few individuals, individuals in P1 and P2 recorded a significant clustered distribution. Results for S-trees recorded a significant clustered pattern in P1, an insignificant clustered pattern in P2 and P4, and an insignificant regular pattern in P3 and P5. Results for D-trees indicated a significant regular pattern in P2, P4 and P3, and an insignificant regular distribution in P1 and P5 (Table 3).

DM index. DM index results for the degree of dissimilarity between neighbouring trees was dependent on the relative frequency and spatial pattern of a certain classification within a stand. Our results reveal that P3 (middle-density stand) had the highest (0.981) DM index for R-seedlings, followed by P5, P4 and P2 (0.979, 0.945 and 0.880). P1, having the highest stand density, recorded the lowest DM value (0.806). DM results for S-trees recorded the opposite pattern to that of R-seedlings (higher density stands had higher the DM values). P1 recorded the highest value (0.376), followed by P2, P4, P3 and P5 (0.335, 0.242, 0.234 and 0.216, respectively). The highest DM value for D-trees (0.824) was recorded in P1, followed P4, P5, P2 and P3 (0.820, 0.813, 0.719 and 0.719, respectively). The DM value in P4 was found to be significant (Table 3).

T (n) index. The differentiation index T (n) is the degree of dissimilarity of size of parameters (diameter, TD; height, TH; crown length, TCl; and crown radius, TCr) between neighboring trees. The T (n) index ranges from 0 to 1 indicating the degree of differentiation. TD, TH and TCr indices results for R-seedlings recorded only a few individuals in P3-P5 for analysis (Table 3). T (n) results for S-trees recorded the lowest and highest values (TH, TCl and TCr) in P3 (mid-density stand) and P5 (lowest density stand), respectively. Similarly, results for D-trees recorded the highest TH value in P1 (highest density) and the lowest TD and TCr values in P5. These results had no significant difference and P3 recorded the lowest TH and TCl values (Table 3).

S index. S index indicates the relative association of R-seedlings, S-trees and D-trees within each plot. In P1, our test results indicated that R-seedling and S-trees had significant segregated association; in P3 a significant aggregated association distribution was recorded. Similarly, segregated association was shown between D-trees with S-trees in P1 and R-seedlings with S-trees in P2; R-seedling with D-trees showed an aggregated association in P2, indicating that there was no significant difference with other groups (Table 3).

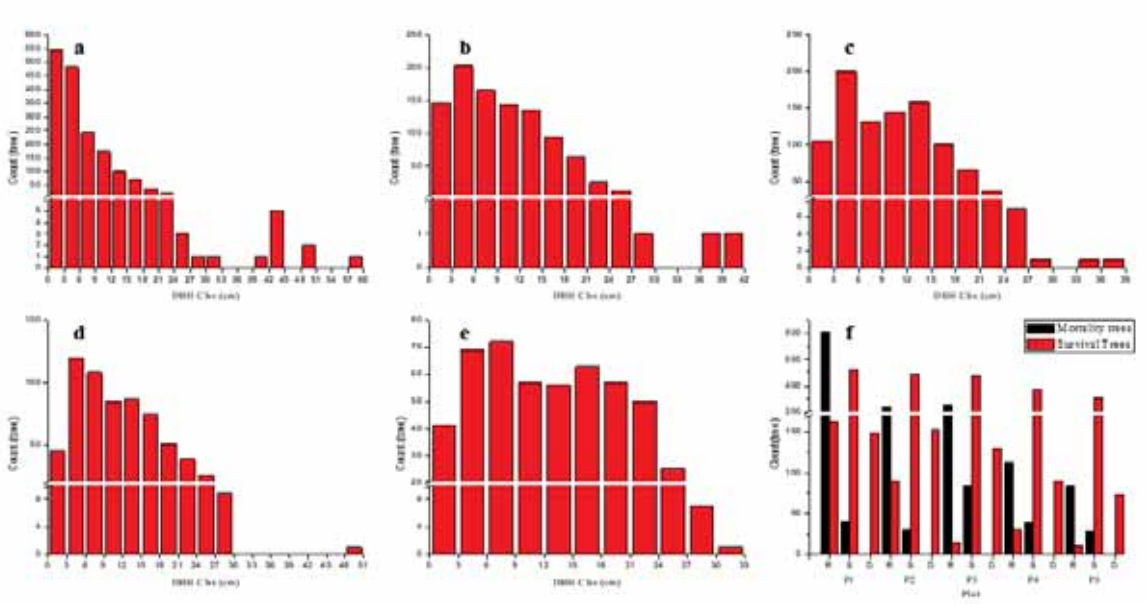

FIGURE 2
DBH distribution (a: P1, b: P2, c: P3, d: P4, e: P5), survival and mortality trees (f) in P1-P5. R: Regeneration seedlings, S: Suppressed trees, D: Dominant trees

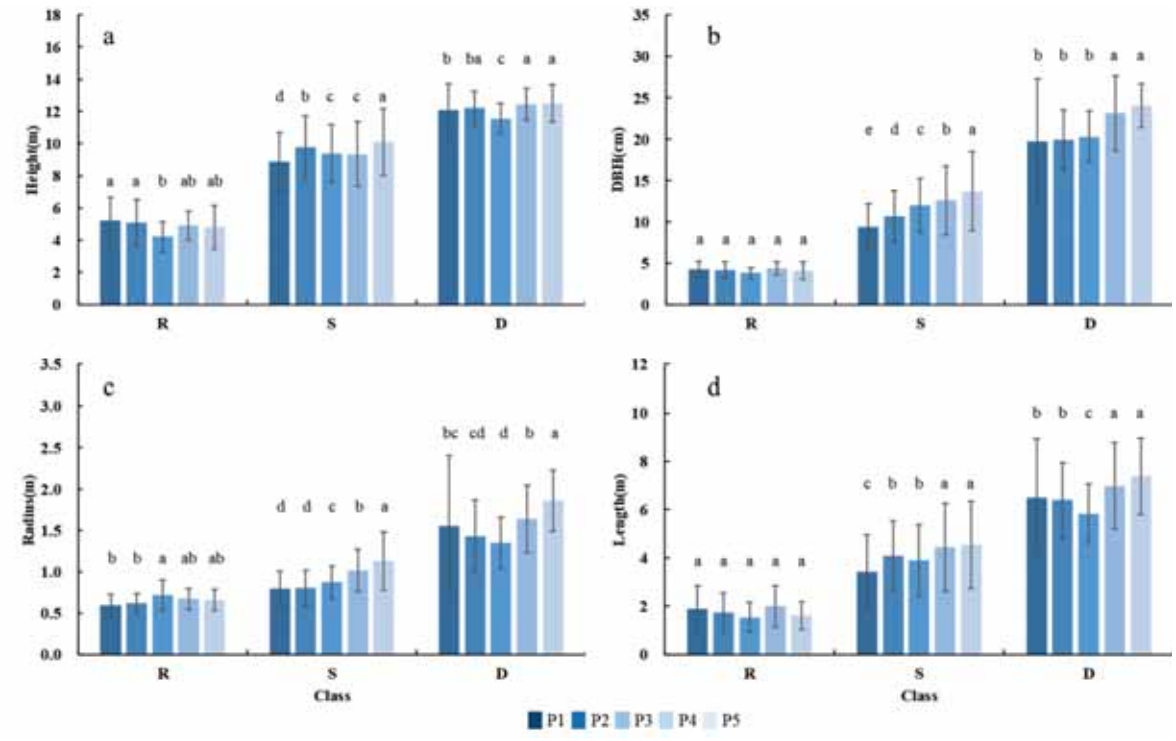

FIGURE 3
Duncan's multiple range tests comparing growth characteristics
(Mean height: a, DBH: b, crown radius and length: c and d) of each plot. Different letters above the bars indicate significant differences ($p<0.05$), R: Regeneration seedlings, S: Suppressed trees, D: Dominant trees

Spatial patterns. The spatial distribution of R-seedlings, S-trees, and D-trees in each plot was analyzed using total trees (survival and mortality trees) and surviving trees separately (Figure 4). For total R-seedlings, it was significantly clustered on the 1-14 m scale in each plot. R-seedlings of P1 were clustered at the 0-10 m scale with a mean $g(r)$ of 1.39 ±0.41 and it tended to have a regular distribution at the 12-25 m scale with a mean $g(r)$ of 0.90 ±0.03 (Figure 4a). R-seedlings in P2 were clustered at the 0-19 m scale with a mean $g(r)$ of 1.27 ±0.22, and they tended to have a random distribution at the 19-25 m scale (Figure 4c). R-seedlings in P3 were clustered at the 0-9 m scale with a mean $g(r)$ of 1.38 ±0.17, and they tended to have a regular and random distribution (Figure 4e). R-seedlings in P4 were clustered at the 0-14 m scale with a mean $g(r)$ of 1.74 ±0.46, tending to have a regular and random distribution (Figure 4g). R-seedlings in P5 were clustered at the 0-20 m scale with a mean $g(r)$ of 1.76 ±0.73, having a random distribution (Figure 4i). In addition, although the survival results for R-seedlings had a low level of significance for all plots (due to a small number of reasons), the general trend was a clustered distribution on some scales (Figure 4b, d, f, h and j).

Results for S-trees recorded a clustered distribution on the small scale (0-8 m) in each plot. Results for total trees and surviving trees recorded some differences in the distributed scale total trees and surviving trees, however there was no difference in the trend at all scales. S-tree in all plots clustered at the different scale had a respective mean $g(r)$ value. Results for P1-P5 were P1, 0-6 m scale (mean $g(r)$: 1.26 ±0.12; Figure 5a); P2, 0-6 m scale (mean $g(r)$: 1.10 ±0.05; Figure 5c); P3, 0-10 m scale (mean $g(r)$: 1.09±0.05; Figure 5e); P4, 0-9 m scale (mean $g(r)$: 1.13 ±0.08; Figure 5g); and P5, 0-20 m scale (mean $g(r)$: 1.15±0.10; Figure 5i). Moreover, S-tree results tended to have random distributions with a fluctuation around the upper and lower envelope line at some scales. Results for surviving S-trees were clustered at the 0-10 m scale for P1 (mean $g(r)$: 0.90±0.02; Figure 5b), at the 0-6 m scale for P2 (mean $g(r)$: 1.10±0.07; Figure 5d), at the 0-8 m scale for P3 (mean $g(r)$: 1.08±0.03; Figure 5f), at the 0-5 m scale for P4 (mean $g(r)$: 1.14±0.06; Figure 5h), and at the 0-21 m scale for P5 (mean $g(r)$: 1.14±0.09; Figure 5j).

Spatial pattern results for D-trees recorded a random distribution at the 2-25 m scale. Results on a small scale (0-2 m) for each plot recorded a regular distribution. As dead trees were not dominant in all plots, there was no difference between total trees and surviving trees for D-trees (Figure 6).

Spatial associations. Spatial associations between R-seedlings, S-trees and D-trees in each plot analyzed by total trees and surviving trees are shown in Figures 7, 8 and 9.

Spatial associations for S-trees and R-seedlings in terms of total trees recorded significant positive associations for all plots. Results for P1-P5 were: 0-6 m scale (mean $g_{12}(r)$: 1.39±0.20; Figure 7a), 0-8 m scale (mean $g_{12}(r)$: 1.18±0.03; Figure 7c), 0-5 m scale (mean $g_{12}(r)$: 1.29±0.17; Figure 7e), 0-4 m scale (mean $g_{12}(r)$: 1.49±0.18; Figure 7g) and 0-4 m scale (mean $g_{12}(r)$: 1.61±0.33; Figure 7i), respectively. For scales greater than 8 m, there was a tendency for independent associations with a fluctuation around the upper envelope line. Due to the high mortality of R-seedlings, no association with a fluctuation around the upper envelope line was recorded between surviving S-trees and R-seedlings. However, results for P1 recorded a positive association at the 0-1 m scale (Figure 7b).

Spatial associations between D-trees and R-seedlings total trees in all plots were predominantly not positively associated at most scales (random distribution). However, some associations were positively associated at the 1-2 m scale (P3, mean $g_{12}(r)$: 1.20±0.01; Figure 8e) whilst surviving trees of D-trees and R-seedlings were found to be in a negative association at the 4 m scale (P5, mean $g_{12}(r)$: 0.13; Figure 8j).

Spatial associations between D-trees and S-trees of total trees at all plots also recorded a negative association at the 0 m scale (P1, mean $g_{12}(r)$: 0.79; Figure 9a), the 0-1 m scale (P2, mean $g_{12}(r)$: 0.73±0.13; Figure 9c), the at the 0 m scale for P3-P5 (mean $g_{12}(r)$: 0.73, Figure 9e; mean $g_{12}(r)$: 0.64, Figure 9g; and mean $g_{12}(r)$: 0.58, Figure 9i, respectively). Between surviving D-trees and S-trees, results indicated that total trees were almost similar to the spatial associations. The spatial associations for surviving D-trees and S-trees also recorded a negative association at a small scale in all plots (Figure 9).

DISCUSSION

Density gradient and the forest structure relationship. In general, greater tree growth is recorded in areas with lower tree density [45, 46] as stand density affects both the properties of single trees and the whole stand [47]. In high-density forests, the lack of natural resources and competition between trees in the stand has led to a decline in tree growth, especially in average DBH [47, 48].

Results from our study also showed that all mean growth values (height, DBH, crown length, crown radius) in low density plots tended to have high growth for S-trees and D-trees; this growth was not recorded for R-seedlings. Environmental conditions such as more water availability, higher soil nutrients and suitable shading may have resulted in the higher density in P1 and P2. Furthermore, a fixed crown can provide a favorable environment for seed germination and survival, thus leading to more active germination of R-seedlings [49]. However, due to

strong competition among all tree groups, this resulted in low tree growth (Figure 2). Results for P3 (a stand with a mid-density pattern) indicated that survival rate and crown growth values of R-seedlings and S-trees were lower than those in the other plots, however P3 recorded the highest basal area values. P4 and P5 (low stand densities) recorded high growth rates compared to other plots with the same density. In high-density forest, tree growth was relatively low due to limited resources and strong competition among trees for these resources. However, mid-density forest recorded higher growth rates due to relatively moderate density competition. However, due to the effects of existing trees in that forest, there are limitations to germination. On the other hand, low-density forest recorded the highest growth rates, this being due to more resources and less trees. The relatively small level of germination in these stands is disadvantageous compared to other densities. Results from previous studies [50-52] indicated that natural regeneration in natural forests has less impact on density (Table 3). Results in our study also show that there was no significant difference between R-seedling growth values of each plot associated with a change in density gradient (Figure 3).

Characteristic of spatial distribution in relation with regeneration. A number of different ecological processes led to aggregation distribution of trees; this space distribution pattern is scale dependent on a theoretical basis [42]. Generally, small trees prefer to have a cluster distribution pattern rather than a random distribution [53]. When tree species are in a cluster distribution, they can best resist adverse environmental conditions and can adjust with environmental conditions by promoting a stable population [54].

CE index and univariate point pattern analysis results indicated that D-trees in natural forest have the advantage of relatively abundant sunshine, water and soil nutrient resources, thus resulting in relatively less competition [55]. Results in Table 3 and Figure 6 recorded the same pattern for D-trees in our study. As larger trees consume the majority of resources in a community, R-seedlings are therefore forced to prefer less compatible areas with fewer resources [56-58]. Overall, P1 and P5, having high and low densities, respectively, recorded more clustered patterns compared to P2-P4 (Table 3 and Figure 4). Our results indicate that other factors such as soil texture, nutrient availability, precipitation, seed diffusion, habitat variation and aspect are also important ecological factors that result in tree species having a cluster distribution in a forest [38, 59-62]. Results for S-trees indicated the same pattern as for R-seedlings, they had a relatively less clustered distribution than R-seedlings and a more random distribution as density increased (Table 3 and Figure 5).

The relationship between tree and tree is an important factor influencing the distribution pattern [63]. S index and bivariate point pattern analysis results showed that mutual promotion relationships between S-trees and R-seedlings existed in all plots. Both S-seedling and R-seedlings showed a significant impact on each other in terms of germination. In addition, the cluster distribution of R-seedlings was relatively low in plots with a low density of S-trees, a finding which confirms that the distribution of S-trees will have a significant impact on the distribution of R-seedlings. Moreover, DM index of S-trees have the lowest degree of dissimilarity of species between neighboring trees compared with other groups (Table 3), a finding that also indicated that S-trees have a significant impact on the distribution of R-seedlings [33]. The spatial pattern distribution of D-trees and S-trees were roughly divided into separated and isolated spatial distributions. Findings from our study also indicate that D-trees have stronger competition between themselves, thus other trees recorded a distribution away from this group.

TABLE 3
Stand structure and interaction of the five plots for R, S and D.

Plot	Group	Survival tree	Basal area (m^2/ha)	Index						S index with		
				CE	DM	TD	TH	TCl	TCr	R	S	D
P1	R	163	1.0	0.758**	0.806**	0.222^{-}	0.256*	0.416^{-}	0.204^{-}			
	S	523	15.8	0.838**	0.376^{-}	0.268*	0.202**	0.379**	0.241**	0.153**		
	D	149	20.9	1.063^{-}	0.824^{-}	0.222^{-}	0.132*	0.301^{-}	0.298^{-}	0.109^{-}	0.105*	
P2	R	89	0.5	0.867*	0.880^{-}	0.233^{-}	0.261^{-}	0.390^{-}	0.191^{-}			
	S	485	18.8	0.951^{-}	0.335*	0.276^{-}	0.195^{-}	0.326^{-}	0.238*	0.103*		
	D	153	19.7	1.180*	0.791^{-}	0.141^{-}	0.089^{-}	0.233^{-}	0.230^{-}	-0.193*	-0.054^{-}	
P3	R	14	0.1		0.981^{-}							
	S	475	23.0	1.012^{-}	0.234^{-}	0.258^{-}	0.190**	0.350**	0.220**	-0.028^{-}		
	D	130	17.2	1.167**	0.791^{-}	0.136*	0.087^{-}	0.196^{-}	0.199^{-}	0.079^{-}	-0.139**	
P4	R	30	0.2		0.945^{-}							
	S	373	20.6	0.979^{-}	0.242^{-}	0.303^{-}	0.215^{-}	0.360^{-}	0.235*	0.122^{-}		
	D	89	15.5	1.205*	0.820*	0.162^{-}	0.087^{-}	0.246^{-}	0.209*	0.088^{-}	-0.063^{-}	
P5	R	10	0.1		0.979^{-}							
	S	303	20.1	1.005^{-}	0.216^{-}	0.322**	0.203**	0.362**	0.288**	-0.015^{-}		
	D	73	13.4	1.106^{-}	0.813^{-}	0.110^{-}	0.096^{-}	0.201^{-}	0.185^{-}	-0.156^{-}	-0.035^{-}	

Statistical testing results are represented by the percentage of replications resulting in the acceptance of the null hypothesis (-), and those resulting in its rejecting at the 0.05 (*) and 0.01 (**) significance level.

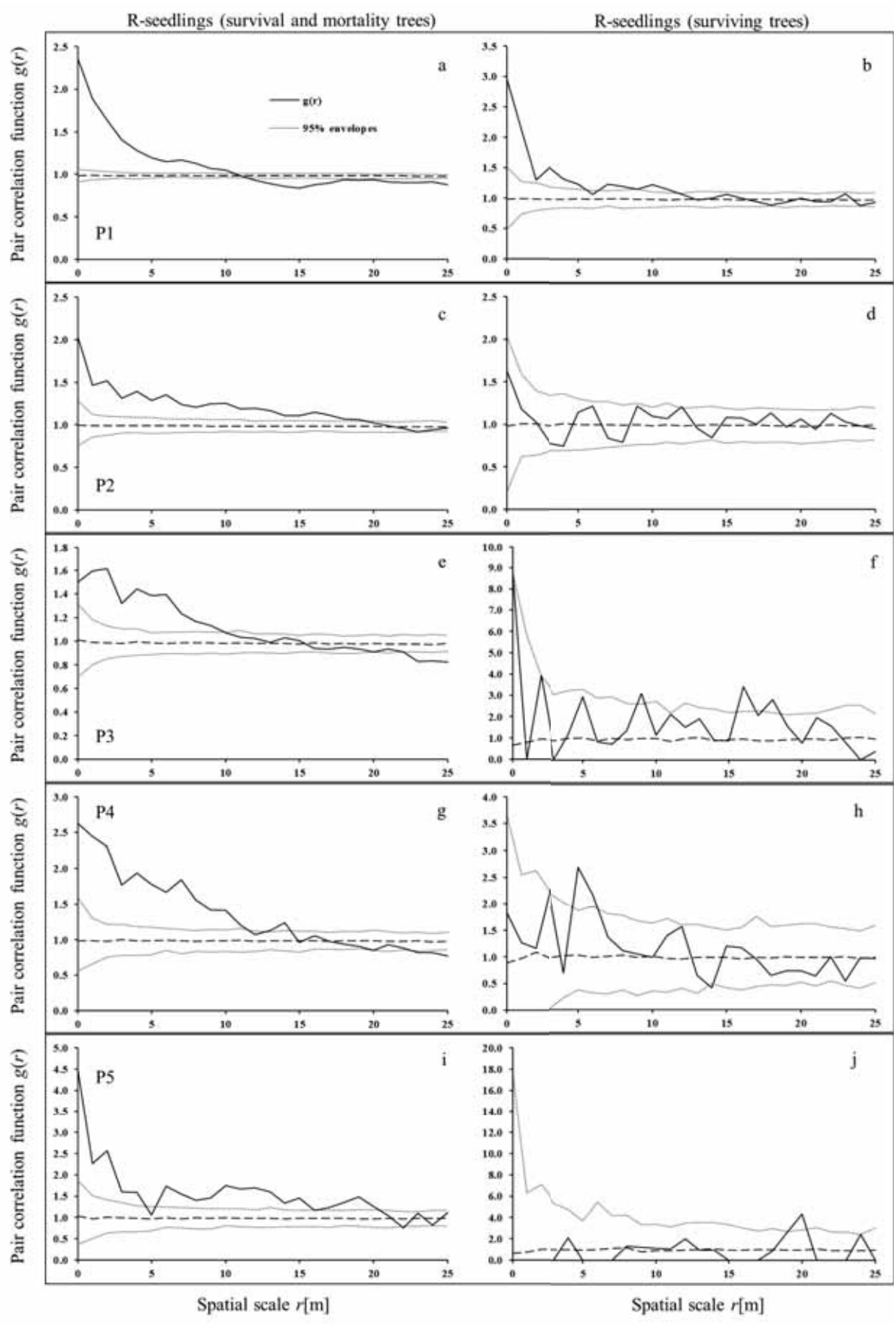

FIGURE 4
Spatial patterns of R-seedlings in the five plots analyzed by the univariate function *g*(*r*) with the null model of CSR.

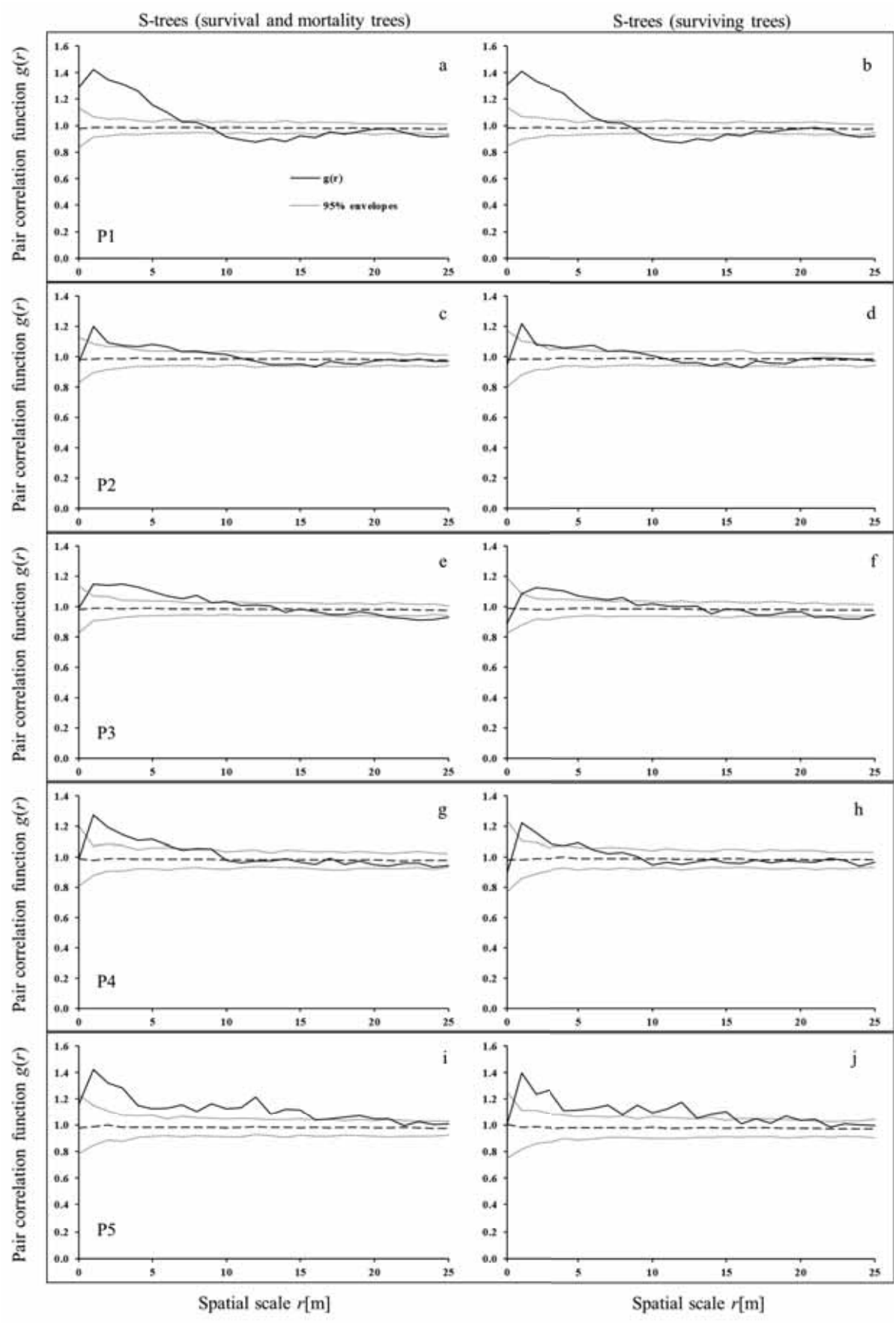

FIGURE 5
Spatial patterns of S-trees in the five plots analyzed by the univariate function *g*(*r*) with the null model of CSR.

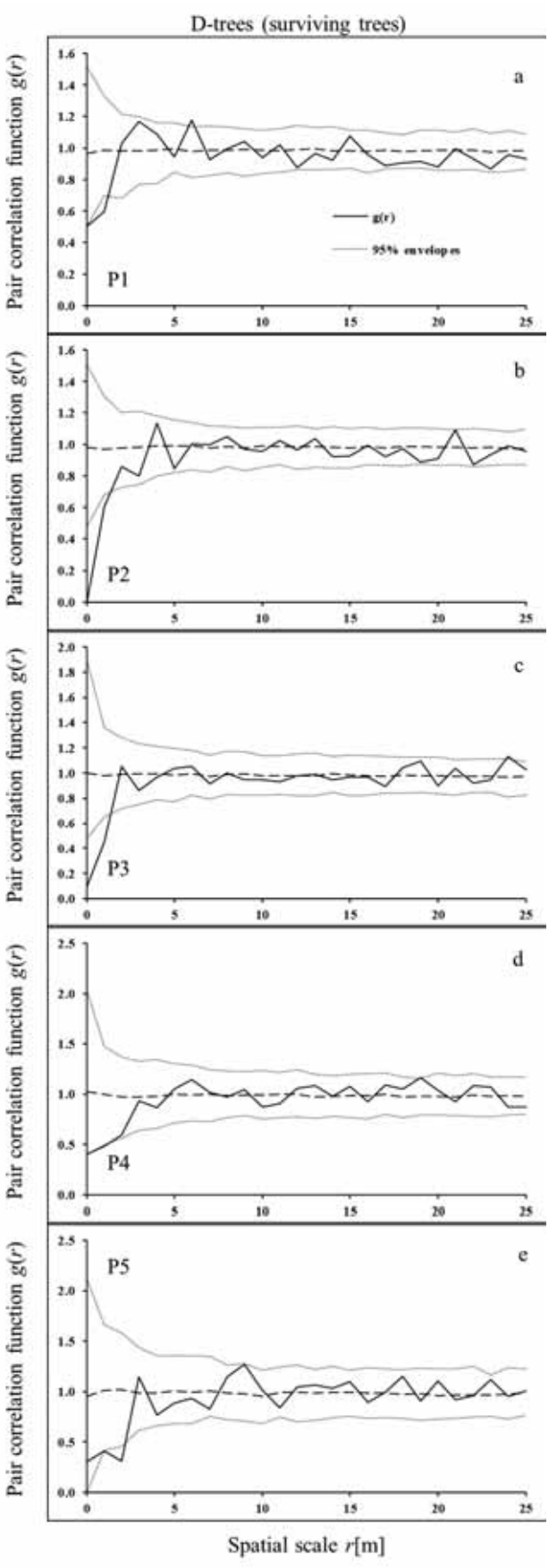

FIGURE 6
Spatial patterns of D-trees in the five plots analyzed by the univariate function *g*(*r*) with the null model of CSR.

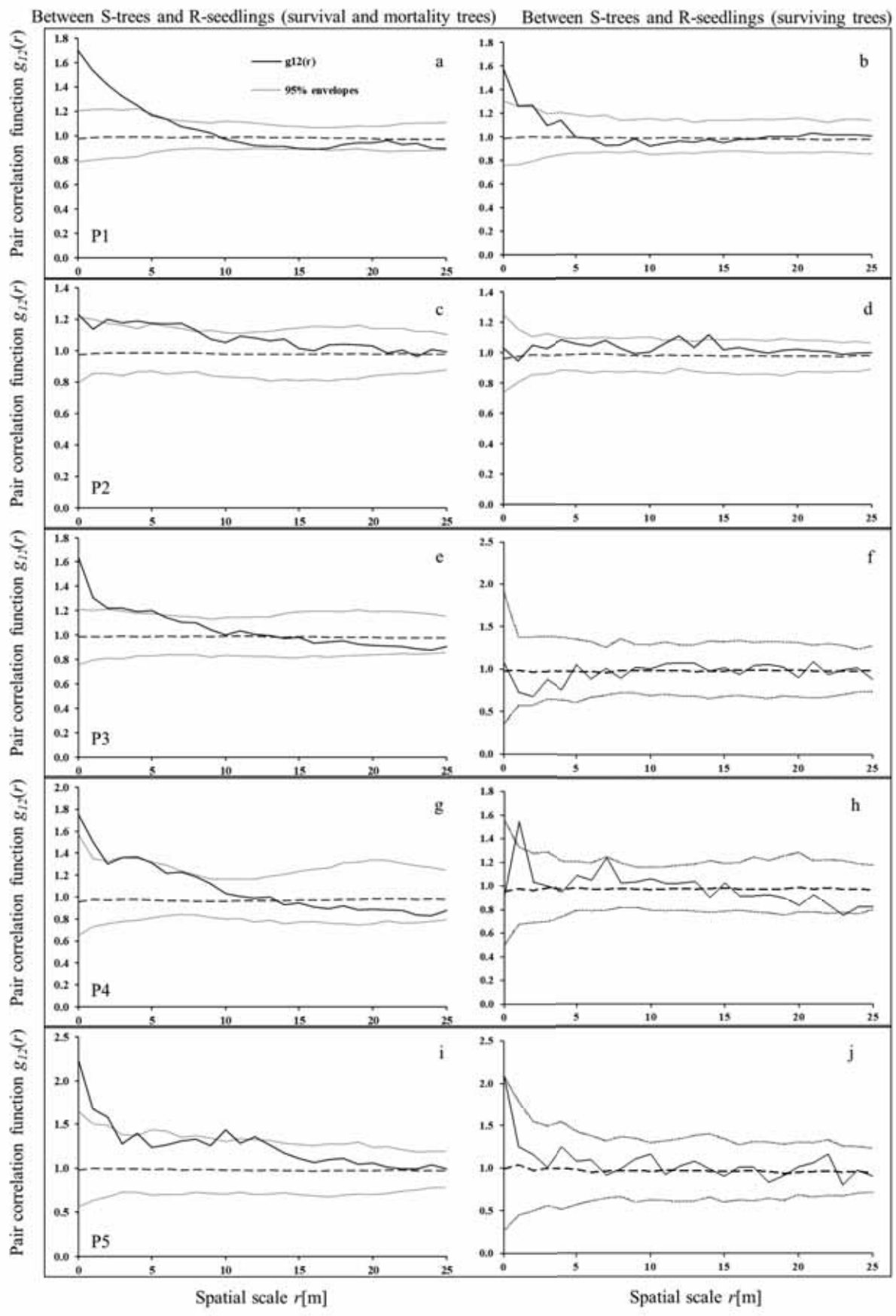

FIGURE 7
Spatial association between S-trees and R-seedlings in all plots with the null model of independence.

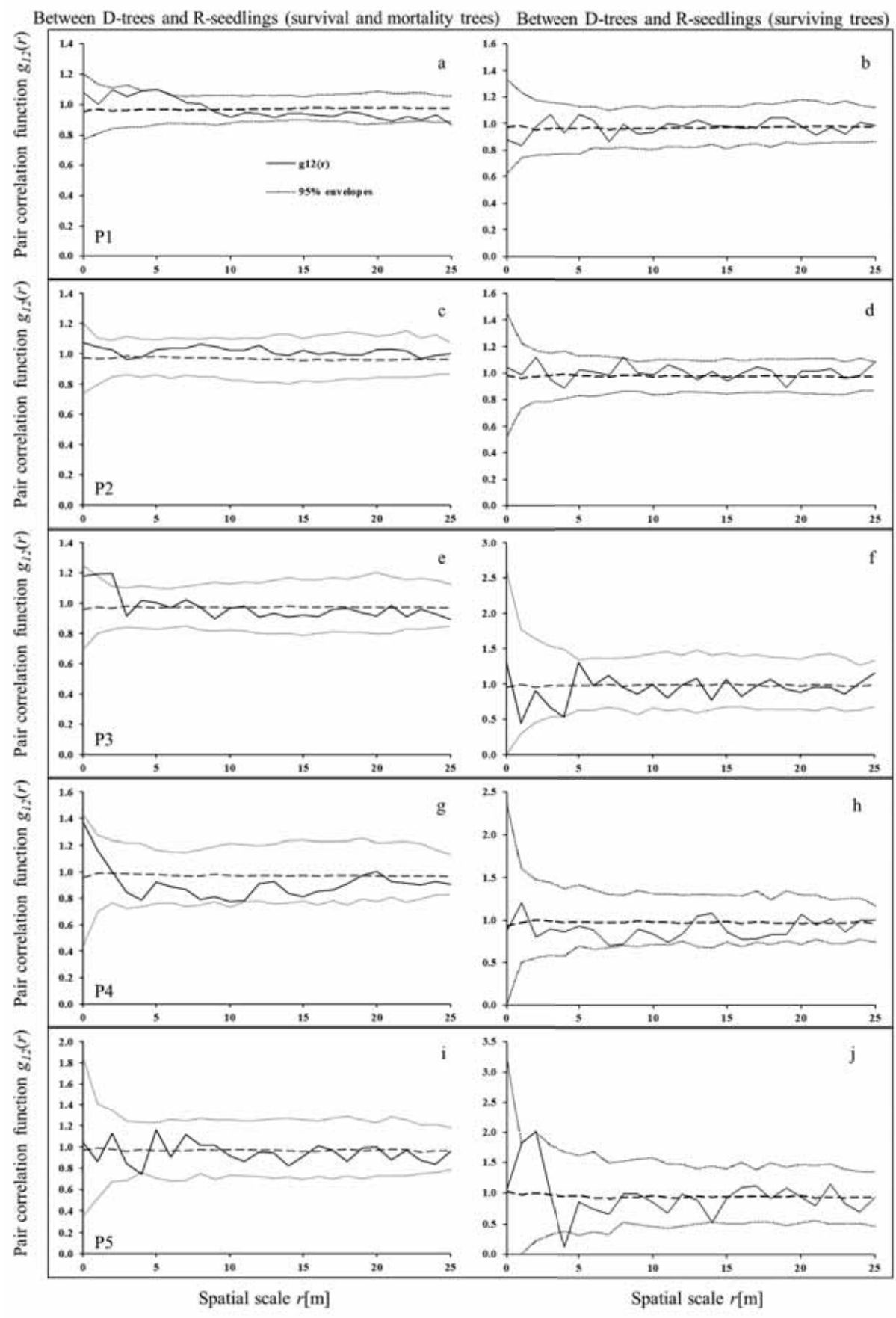

FIGURE 8
Spatial association between D-trees and R-seedlings in all plots with the null model of independence.

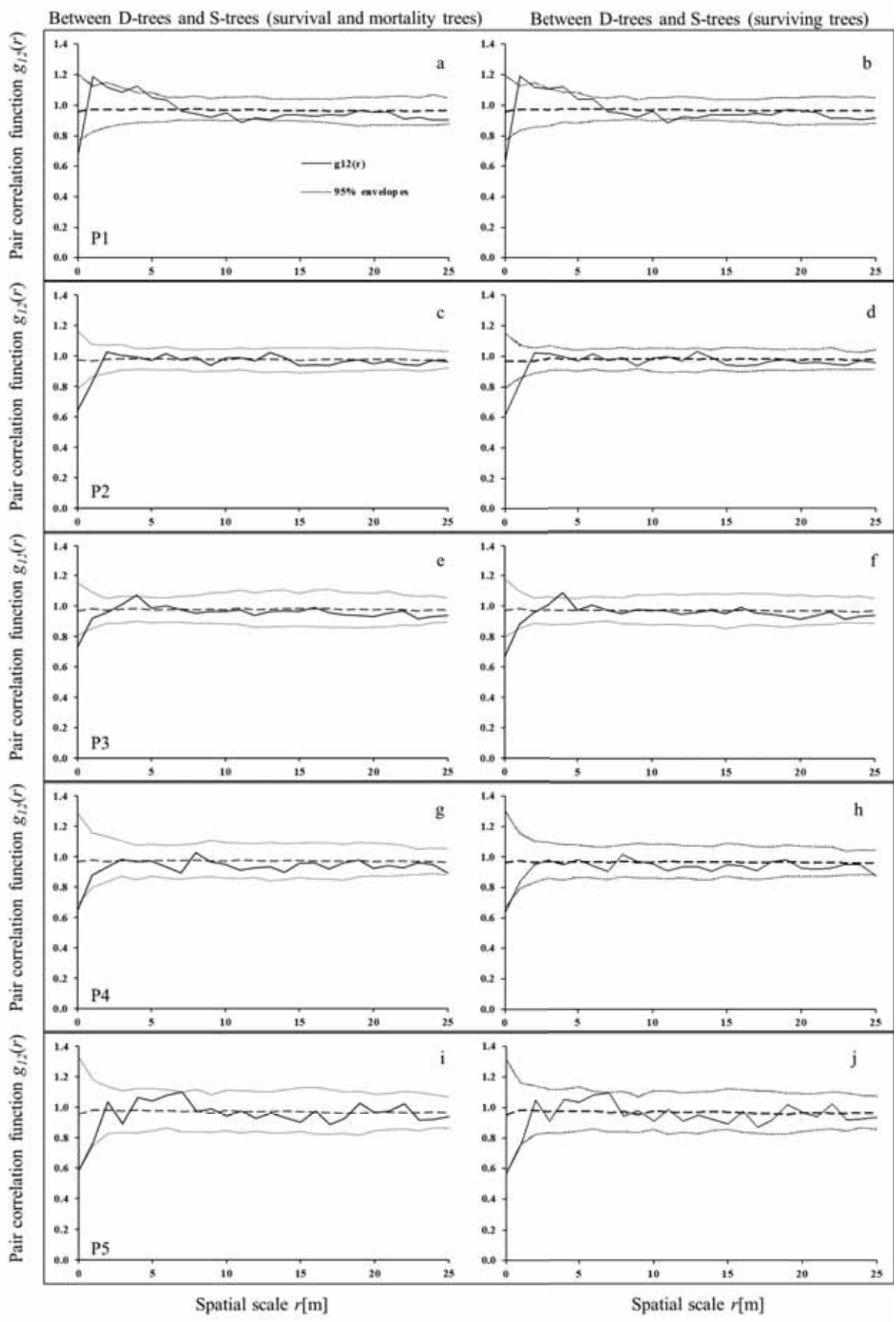

FIGURE 9
Spatial association between S-trees and D-trees in all plots with the null model of independence.

However, survival and tree mortality spatial pattern analysis indicated that the mutual promotion relationship between R-seedlings and S-trees could be confirmed in plot 1, thus having a certain effect on survival. For low density stands, S index cloud bivariate point pattern analysis was used to identify the survival rate of these trees. Therefore, S-trees showed an aggregated-associated distribution. On the contrary, in high density stands, it was confirmed that competition intensity between S-trees was too high, thus the distribution of trees was neutral or had segregated-separated distribution.

Afforestation and management recommendations. Afforestation and reforestation are key methods for the restoration of degraded land, and these practices can contribute to increasing resources for mitigating atmospheric CO_2 [64]. However, although large areas of Mongolian Pine plantations have been degraded in recent years [11-13], close-to-nature plantation management is expected to be the best solution to restore degraded forest [21-23]. This restoration can be achieved by controlling stand density and inducing natural regeneration [21, 24]. In addition to controlling forest density, controlling the spatial distribution of trees will enable continuous forest formation by increasing biomass and extending the growth period of trees [47, 48].

Our results confirmed previously published results [45, 46]. A decline in forest density results in an increase in tree growth in natural Mongolian Scots Pine, and regeneration is greatly affected by tree spatial patterns. In particular, the spatial distribution pattern of S-trees has a significant influence on germination and growth of R-seedlings. Results from our study provide a baseline for future investigations to fully understand current forest scenarios.

ACKNOWLEDGEMENTS

This research was supported by the National Key Research and Development Program of China (2016YFC0500908), and the National Natural Science Foundation of China (31670715; 41471029; 41701249).

REFERENCES

[1] Ci, L.J., Yang, X.H. and Chen, Z.X. (2002) The potential impacts of climate change scenarios on desertification in China. Earth Science Frontiers. Earth Science Frontiers. 9(2), 287-294.

[2] Reynolds, J.F., Smith, D.M.S., Lambin, E.F., Turner, B.L., Mortimore, M., Batterbury, S.P., Downing, T.E., Dowlatabadi, H., Fernández, R.J., Herrick, J.E. (2007) Global desertification: building a science for dryland development. Science. 316(5826), 847-851.

[3] Chen, Y. and Tang, H. (2010) Desertification in north china: background, anthropogenic impacts and failures in combating it. Land Degradation and Development. 16(4), 367-376.

[4] Ma, C.J., Tohno, S., Kasahara, M., and Hayakawa, S. (2004) Properties of the size-resolved and individual cloud droplets collected in Western Japan during the Asian dust storm event. Atmospheric Environment. 38(27), 4519-4529.

[5] Geng, H., Hwang, H., Liu, X., Dong, S., Ro, C.U. (2014) Investigation of aged aerosols in size-resolved Asian dust storm particles transported from Beijing, China, to Incheon, Korea, using low-z particle epma. Atmospheric Chemistry and Physics. 14(7), 3307-3323.

[6] Wang, X., Chen, F., Hasi, E. and Li, J. (2008) Desertification in China: an assessment. Earth-Science Reviews. 88(3-4), 188-206.

[7] Wang, F., Pan, X., Wang, D., Shen, C., Lu, Q. (2013) Combating desertification in China: Past, present and future. Land Use Policy. 31, 311-313.

[8] Zhu, J.J., Kang, H.Z. and Zhi hui, L.I. (2006) Comparison of different types of drought stresses affecting photosynthesis of Mongolian pine seedlings on sandy soils. Journal of Beijing Forestry University.

[9] Zheng, X., Zhu, J.J., Yan, Q.L., and Song, L.N. (2012) Effects of land use changes on the groundwater table and the decline of pinus sylvestris var. mongolica plantations in southern horqin sandy land, northeast china. Agricultural Water Management, 109, 0-106.

[10] Jiang, F.Q., Yu, Z.Y., Zeng, D.H., and Zhu, J.J. (2009) Effects of climate change on the three-north shelter forest program and corresponding strategies. Chinese Journal of Ecology. 28(9), 1702–1705 (in Chinese with English abstract).

[11] Shuren, J. (2001) Report on the causes of the early decline of pinus slyvestris var.mongolica shelterbelt and its preventative and control measures in Zhang Gutai of Liaoning Province. Scientia Silvae Sinicae. 369(s1–3), 393-402.

[12] Gossner, M.M., Lachat, T., Brunet, J., Isacsson, G., Bouget, C., Brustel, H., Brandl, R., Weisser W.W., and Muller J. (2013) Current near-to-nature forest management effects on functional trait composition of saproxylic beetles in beech forests. Conservation Biology. 27(3), 605-614.

[13] Shi, Z., Xu, L., Dong, L., Gao, J., Yang, X., Lu, S., Feng, C., Shang, J., Song, A., Guo, H., and Zhang, X. (2015) Growth-climate response and drought reconstruction from tree-ring of Mongolian Pine in Hulunbuir, Northeast China. Journal of Plant Ecology. 9(1), 51-60.

[14] Wu, X.Y., Jiang, F.Q., Li, X.D., and Qiu, S.F. (2004) Major features of decline of pinus sylvestris var. mongolica plantation on sandy land. Chinese Journal of Applied Ecology. 15(12), 2221.
[15] Zhu, J., Kang, H., Xu, M., Wu, X., Wang, W. (2007) Effects of ectomycorrhizal fungi on alleviating the decline of Pinus sylvestris var.mongolica plantations on Keerqin sandy land. Chinese Journal of Applied Ecology.18, 2693-2698.
[16] Sun, S.J., Li, C.Y., He, C.X., Zhang, J.S., Meng, P. (2017) Retrospective analysis of the poplar plantation degradation based on stable carbon isotope of tree rings in Zhangbei County, Hebei, China. Chinese Journal of Applied Ecology. 28(7), 2119-2127.
[17] Eastaugh, C.S., Pötzelsberger, E., Hasenauer, H. (2011) Assessing the impacts of climate change and nitrogen deposition on Norway spruce (Picea abies L. Karst) growth in Austria with BIOME-BGC. Tree Physiology. 31(3), 262-274.
[18] Seidl, R., Schelhaas, M.J., Lexer, M.J. (2011) Unraveling the drivers of intensifying forest disturbance regimes in Europe. Global Change Biology. 17(9), 2842-2852.
[19] Garnas, J.R., Ayres, M.P., Liebhold, A.M., Evans, C. (2015) Subcontinental impacts of an invasive tree disease on forest structure and dynamics. Journal of Ecology. 99(2), 532-541.
[20] Ayres, M.P., Hicke, J.A., Kerns, B.K., Mckenzie, D., Littell, J.S., Band, L.E., Luce, C.H., Weed, A.S., Raymond, C.L. (2014) Disturbance Regimes and Stressors. 57, 55-92.
[21] O'Hara, K.L. (2016) What is close-to-nature silviculture in a changing world? Forestry. 89(1), 1-6.
[22] Brang, P., Spathelf, P., Larsen, J.B., Bauhus, J., Boncina, A., Chauvin, C., Drossler, L., Garcia-Guemes, C., Heiri, C., Kerr, G., Lexer, M.H., Mason, B., Mohren, F., Muhlethaler, U., Nocentini, S. and Svoboda, M. (2014) Suitability of close-to-nature silviculture for adapting temperate European forests to climate change. Forestry. 87(4), 492-503.
[23] Bässler, C., Ernst, R., Cadotte, M., Heibl, C., Müller, J., Barlow, J. (2014) Near-to-nature logging influences fungal community assembly processes in a temperate forest. Journal of Applied Ecology. 51(4), 939-948.
[24] Lv, X. (2012) Close-to-Nature Shelterbelt Establishment in Jinshan, Shanghai. Journal of Chinese Urban Forestry. 2, 11.
[25] Medugu, N.I., Majid, M.R., Johar, F., Choji, I.D. (2010) The role of afforestation programme in combating desertification in Nigeria. International Journal of Climate Change Strategies and Management. 2(1), 35-47.
[26] Hanberry, B.B., Fraver, S., He, H.S., Jian, Y., Dan, C.D. and Palik, B.J. (2011) Spatial pattern corrections and sample sizes for forest density estimates of historical tree surveys. Landscape Ecology. 26(1), 59-68.
[27] Gossum, P.V., Luyssaert, S., Serbruyns, I. and Mortier, F. (2005) Forest groups as support to private forest owners in developing close-to-nature management. Forest Policy and Economics. 7(4), 589-601.
[28] Chirici, G., Winter, S., Mcroberts, R.E. (2011) National Forest Inventories: Contributions to Forest Biodiversity Assessments, Springer Netherlands. 141, 104-112.
[29] Kint, V., De Wulf, R., Lust, N. (2004) Evaluation of sampling methods for the estimation of structural indices in forest stands. Ecological Modelling. 180(4), 461-476.
[30] Clark, P.J., Evans, F.C. (1954) Distance to Nearest Neighbor as a Measure of Spatial Relationships in Populations. Ecology. 35(4), 445-453.
[31] Donnelly, K.P. (1978) Simulations to Determine the Variance and Edge Effect of Total Nearest-Neighbor Distance. Simulation methods in archeology. Cambridge University Press, London, 91-95.
[32] Pielou, E.C. (1977) Mathematical Ecology. Journal of Animal Ecology. 47(3), 1-385.
[33] Gadow, K.V., Hui, G. (1999) Modelling Forest Development. Forestry Sciences. 57, 26-59.
[34] Lewandowski, A., Pommerening, A. (1997) On the description of forest structure - Expected and observed mingling of species. Forstwissenschaftliches Centralblatt. 116(1-6), 129-139. (in German with English abstract).
[35] Stoyan, D., Stoyan, H. (1994) Fractals, random shapes and point fields: methods of geometrical statistics. Journal of the Royal Statistical Society. 159, 1-194.
[36] Illian, J., Burslem, D. (2007) Contributions of spatial point process modelling to biodiversity theory. Journal de la Société Française de Statistique and Revue de Statistique Appliquée. 148(1), 9-30.
[37] Yu, H., Wiegand, T., Yang, X., Ci, L. (2009) The impact of fire and density-dependent mortality on the spatial patterns of a pine forest in the Hulun Buir sandland, Inner Mongolia, China. Forest Ecology and Management. 257(10), 2098-2107.
[38] Condit, R., Ashton, P.S., Baker, P., Bunyavejchewin, S., Gunatilleke, S., Gunatilleke, N., Hubbell, S.P., Foster, R.B., Itoh, A., Lafrankie, J.V. (2000) Spatial Patterns in the Distribution of Tropical Tree Species. Science. 288, 1414-1418.

[39] Wiegand, T., Moloney, K.A. (2004) Rings, circles, and null-models for point pattern analysis in ecology. Oikos. 104(2), 209-229.
[40] Ripley, B.D. (1977) Modelling Spatial Patterns. Journal of the Royal Statistical Society. 39(2), 172-212.
[41] Thomas, M. (1949) A generalization of Poisson's binomial limit for use in ecology. Biometrika. 36(1-2), 18-25.
[42] Wiegand, T., Gunatilleke, S., Gunatilleke, N., Okuda, T. (2007) Analyzing the spatial structure of a Sri Lankan tree species with multiple scales of clustering. Ecology. 88(12), 3088-3102.
[43] Goreaud, F., Pélissier, R. (2003) Avoiding Misinterpretation of Biotic Interactions with the Intertype K12-Function: Population Independence vs. Random Labelling Hypotheses. Journal of Vegetation Science. 14, 681–692.
[44] Dixon, D.P.M. (2006) Ripley's K Function. John Wiley and Sons.
[45] Dobrowolska, D. (2008) Effect of stand density on oak regeneration in flood plain forests in Lower Silesia, Poland. Forestry. 81(4), 511-523.
[46] Demirezen, D., Aksoy, A., Uruc, K. (2007) Effect of population density on growth, biomass and nickel accumulation capacity of Lemna gibba (Lemnaceae). Chemosphere. 66(3), 553-557.
[47] Guner, S., Yagci, V., Tilki, F., Celik, N. (2010) The effects of initial planting density on above- and below-ground biomass in a 25-year-old Fagus orientalis Lipsky plantation in Hopa, Turkey. Scientific Research and Essays. 5(14), 1856-1860.
[48] Comeau, P., Heineman, J., Newsome, T. (2006) Evaluation of relationships between understory light and aspen basal area in the British Columbia central interior. Forest Ecology and Management. 226(1-3), 80-87.
[49] Dean, W.R.J., Milton, S.J., Jeltsch, F. (1999) Large trees, fertile islands, and birds in arid savanna. Journal of Arid Environments. 41(1), 61-78.
[50] Lundqvist, L., Fridman, E. (1996) Influence of local stand basal area on density and growth of regeneration in uneven-aged Picea abiesstands. Scandinavian Journal of Forest Research. 11(1-4), 364-369.
[51] P.P.Du T. Deetlefs B.Sc., M.F., D.F. (1954) The relationships between stand density, crown size and basal area growth in stands of Pinus Taeda L. in the native habitat of this species. Journal of the South African Forestry Association. 24(1), 1-28.
[52] Nilson, K., Lundqvist, L. (2001) Effect of stand structure and density on development of natural regeneration in two picea abies stands in Sweden. Scandinavian Journal of Forest Research. 16(3), 253-259.
[53] Chu, G., Wang, M., Zhang, S. (2014) Spatial patterns and associations of dominant woody species in desert–oasis ecotone of South Junggar Basin, NW China. Journal of Plant Interactions. 9(1), 738-744.
[54] Mei, W., Zhang, S., Chu, G. (2014) Point Pattern Analysis of Different Life Stages of Haloxylon ammodendron in Desert-oasis Ecotone of South Junggar Basin. Polish Journal of Environmental Studies. 23(6), 367-373.
[55] Zhang, J., Hao, Z.Q., Song, B., Ye, J., Li, B.H., Yao, X.L. (2007) Spatial distribution patterns and associations of Pinus koraiensis and Tilia amurensis in broad-leaved Korean pine mixed forest in Changbai Mountains. Chinese Journal of Applied Ecology. 18(8), 1681-1687.
[56] Zhang, J., Meng, D. (2004) Spatial pattern analysis of individuals in different age-classes of Larix principis-rupprechtii in Luya mountain reserve, Shanxi, China. Acta Ecologica Sinica. 24(1), 35-40.
[57] Flores, J., Jurado, E. (2010) Are nurse-protégé interactions more common among plants from arid environments? Journal of Vegetation Science. 14(6), 911-916.
[58] Silvertown, J.W. (1984) Introduction to plant population ecology. Vegetatio. 56(2), 86-86.
[59] Frelich, L.E., Sugita, S., Reich, P.B., Davis, M.B., Friedman, S.K. (2010) Neighbourhood Effects in Forests: Implications for within-Stand Patch Structure. Journal of Ecology. 86(1), 149-161.
[60] Schurr, F.M., Bossdorf, O., Milton, S.J., Schumacher, J. (2004) Spatial pattern formation in semi-arid shrubland: a priori predicted versus observed pattern characteristics. Plant Ecology. 173(2), 271-282.
[61] Fraver, S., D'Amato, A.W., Bradford, J.B., Jonsson, B.G., Jönsson, M., Esseen, P.A. (2014) Tree growth and competition in an old-growth Picea abies forest of boreal Sweden: influence of tree spatial patterning. Journal of Vegetation Science. 25(2), 374-385.
[62] Larson, A.J., Churchill, D. (2012) Tree spatial patterns in fire-frequent forests of western North America, including mechanisms of pattern formation and implications for designing fuel reduction and restoration treatments. Forest Ecology and Management. 267(3), 74-92.
[63] Miriti, M.N. (2006) Ontogenetic shift from facilitation to competition in a desert shrub. Journal of Ecology. 94(5), 973-979.
[64] Smink, C. (2011) Forest and recreation – New functions of afforestation as seen in Denmark. New Perspectives on People and Forests. Springer Netherlands.

Received: **20.12.2018**
Accepted: **23.02.2019**

CORRESPONDING AUTHOR

Kebin Zhang
School of Soil and Water Conservation
Beijing Forestry University
Beijing 100083 – China

e-mail: ctccd@126.com

© by PSP Volume 28 – No. 5/2019 pages 3981-3990 Fresenius Environmental Bulletin

COMBINED EFFECT OF CHILLING AND LIGHT STRESS ON THE METABOLIC PROFILE OF *ORIGANUM VULGARE* L. IN THE JUVENILE STAGE

Maciej Szczalba[1], Katarina Kaffkova[2], Andrzej Kalisz[1], Tomas Kopta[3], Robert Pokluda[3], Agnieszka Sekara[1,*]

[1]University of Agriculture in Krakow, Poland, Faculty of Biotechnology and Horticulture, Department of Vegetable and Medicinal Plants, Krakow, Poland
[2]Crop Research Institute, Division of Crop Genetics and Breeding, Team of Genetic Resources of Vegetables and Specialty Crops, Olomouc, Czech Republic
[3]Mendel University in Brno, Faculty of Horticulture, Department of Vegetable Growing and Floriculture, Lednice, Czech Republic

ABSTRACT

Wild marjoram is the most widely distributed species among the genus *Origanum* L. and is valued as an aromatic and medicinal crop. It is commonly marketed as a fresh herb in pots for culinary purposes. Combined stress factors affecting plants within the producer–consumer chain can significantly change their chemical composition. The aim of the study was to evaluate the effects of chilling and light stress applied to young plants of wild marjoram (*Origanum vulgare* L.) on selected bioactive compounds. Potted plants meeting market standards were subjected to temperature and light regimes: (a) 5 °C, light irradiance of 0, 100 and 250 μmol m^2 s^{-1} and (b) 18 °C, light irradiance of 0, 100, and 250 μmol m^2 s^{-1} for 7 days, in phytotron chambers. Analyses proved a significant influence of the stress factors applied on dry matter, soluble sugars, photosynthetic pigments and compounds associated with stress acclimation. The general effect observed was an increase in most bioactive compounds, with the exception of pigments, in potted wild marjoram plants subjected to chilling in conditions of limited light irradiance (100 μmol m^2 s^{-1}). In chilling conditions, a lack of light and irradiance at the level of 250 μmol m^2 s^{-1} mitigated the stress response but simultaneously decreased the biological quality of plants. The combined application of specified chilling and light levels may increase, by initiating mild stress, the health-promoting value of potted wild marjoram dedicated as a product for the fresh market.

KEYWORDS:
Wild marjoram, multiple stresses, stress 'cross-talk', antioxidant defence

INTRODUCTION

The genus *Origanum* (Lamiaceae family) is a herb native to the Mediterranean, Iran-Siberian and Euro-Siberian regions, and contains 38 species recognised across the world. Most of them are used as culinary herbs for their aromatic properties [1, 2]. With respect to biodiversity preservation, plants of this genus are valued for their attractiveness to beneficial insects [3]. Wild marjoram (*Origanum vulgare* L.) is the most widely distributed species among the genus and has been valued as a medicine and spice since ancient times [4]. Its foliage contains essential oil, with thymol and carvacrol considered as the major terpene components [5]. Wild marjoram herb is characterised by the highest total antioxidant capacity and phenolic content compared with other Lamiaceae including thyme, sage, rosemary, mint and sweet basil [6, 7]. The volatile oil as well as several other antioxidants may contribute to the antimicrobial, anti-inflammatory, cardioprotective, blood sugar- and lipids-modulating action [8]. Wild marjoram is also valuable for the food industry; dried aerial parts are included in many spice mixtures, and the essential oil is useful for its capability to preserve food [9].

The wide spectrum of wild marjoram's applications and long traditions of its culinary usage gave rise to a continuous supply of potted herb used in households as a spice due to its flavour and taste [10]. Optimal growing conditions applied during plant development at the production stage are often substituted by light and/or temperature stress during transport, storage and shelf-life [11]. The phenomenon of acclimation enables plants to stay in good condition even when sequential stress factors change their type or action. Over the past decade, investigations into the molecular mechanisms underlying stress tolerance in plants have emphasised individual stresses. However, plants are often simultaneously challenged by combined stresses involving different mechanisms of tolerance [12]. Acclimation strategies of plants to combined stress

depend largely on the age of the plant, genetically based stress-resistant or susceptible characteristics, and the severity of the two stresses involved [13]. They include genetic, biochemical and physiological responses evoked by both stresses, constituting a stress combination in which a dominant stressor can appear. Chinnusamy et al. [14] determined that drought, salinity and chilling induce plant response in the form of enhanced synthesis of osmoprotectants. Munns [15] showed changes in the transport and compartmentation of ions in plants under heat and salt stress. The interaction between two stresses can either be additive or antagonistic, but simultaneously applied stresses affect plant development more severely than the individual ones [16]. Light and chilling stress interactions have been investigated mainly for tropical species with respect to limiting the distribution of chilling-sensitive plants to higher latitudes [17, 18]. A model chilling-sensitive plant, cucumber, was chilled (5 °C) in the light (1000 μmol m^{-2} s^{-1}) and exhibited a considerable decrease in antioxidants and leaf pigments and a high level of lipid peroxidation [19]. There are few results on the effect of limited light irradiance, below 250 μmol m^2 s^{-1}, applied together with chilling stress on the plant metabolome involved in stress-mediated response focused on chilling-sensitive plants [20, 21]. A common effect of combined stressor action is overproduction of reactive oxygen species (ROS) which are active, as signalling molecules, in mediating important signal transduction pathways that coordinate an astonishing range of diverse plant processes under stress conditions [22, 23]. To overcome oxidative stress, plants upregulate the synthesis of enzymatic antioxidants like superoxide dismutase (SOD), catalase (CAT) and peroxidase (POX) as well as non-enzymatic ones (L-ascorbic acid, phenols and carotenoids) which are also information-rich redox buffers and important components of redox signalling that interact with biomembrane-related compartments [24].

There are a few studies regarding *Origanum* L. focused on the application of different stressors and analysis of their consequences, e.g. relationships between water stress and essential oil content [25], nutrient stress and phenolic content [26] or morphological changes due to reduced irradiance of light [27]. However, stress action cannot be perceived as a clearly negative factor, because there is evidence that moderate abiotic stress can increase the content of pro-health compounds [28]. As shown, research has so far been limited to responses to individual stresses. The understanding of adaptation to combined stresses is limited mainly to salt and drought interactions, or biotic and abiotic stresses, acting during field crop production [29]. Light and temperature stress 'cross-talk', commonly applied during the post-harvesting producer–consumer marketing of many species of potted herbs and spices, may significantly modify plants' chemical composition and overall quality.

On the basis of the references studied, we hypothesised that (i) both low temperature and light irradiance can affect the metabolic profile of young wild marjoram plants conferred by priming stress-response chemicals, (ii) the effect of the combined application of these stressors could be different from that of applying individual stressors, and (iii) the activation of ROS defence mechanisms can affect the chemical composition of the herb, improving its biological quality.

MATERIALS AND METHODS

Plant material and experiment design. The experiment was conducted in a greenhouse and growing chambers of the Department of Vegetable and Medicinal Plants, University of Agriculture in Krakow, Poland. Seeds of wild marjoram (*Origanum vulgare* L.) were purchased from W. Legutko Company, Poland. On 17 March 2015, wild marjoram seeds were sown into 12 nursery plant trays (96 cells, cell volume 53 cm^3) in a greenhouse. Plant trays were pre-filled with peat substrate (Klassman TS2, Klasmann-Deilmann GmbH, Germany). The temperature in the greenhouse was 24 ± 2 °C during germination and 20/18 °C (day/night) during growth; plants were irrigated according to ruling standards. Fertilisation was performed with Kristalon Green liquid fertiliser (Yara International ASA, Poland) (18% N, 18% P_2O_5, 18% K_2O, 3% MgO and 2% S) at a dose of 10 g dm^{-3} water 5 weeks after sowing. On 27 May, 10-week-old plants at the stage of market standard requirements were transferred to phytotron chambers. The different temperatures in the chambers, 5 °C (chilling treatment) and 18 °C (control), provided the first experimental factor. Light irradiance at canopy level (second experimental factor) was 0, 100 and 250 μmol m^2 s^{-1}, respectively (Philips Master Tl-d 90 Graphica 36W/950sl lamps, Philips Lighting Holding B.V., The Netherlands); the photoperiod was 12/12 h (day/night). Each experimental treatment consisted of three replications, with 60 cells × one plant per cell per replication. Aboveground parts of plants (herb) were harvested on 4 June and subjected to laboratory analyses. Samples were analysed in the laboratory of the Department of Vegetable and Medicinal Plants, University of Agriculture in Krakow, Poland. Before analyses, plant material was washed and milled.

Stress biomarkers and antioxidant analysis. Dry weight (DW) was determined according to the standard gravimetric method as described by Kalisz et al. [30]. Samples were weighed with a Sartorius A120S balance (Sartorius AG, Germany) and dried at 65 °C until constant weight was achieved; then,

the loss of weight was calculated and expressed as FW percentage.

Soluble carbohydrates (SC) were analysed by the anthrone method described by Yemm and Willis [31]. Plant material (1 g) was extracted with 50 cm^3 of 80% ethanol for 30 min at 100 °C, then cooled to 20 °C. After addition of anthrone (4 cm^3), the SC was determined spectrophotometrically at λ = 625 nm.

L-ascorbic acid (L-AA) was determined by modified Tillman's titration method [32]. Fresh plant material (25 g) and 100 cm^3 of 1% oxalic acid were homogenised; the solution was kept in darkness for 30 min, then filtrated and titrated by 2,6-dichlorophenolindophenol until a light pink colour was observed.

Chlorophyll *a* and *b* and carotenoids (Chl. *a*, Chl. *b* and Cars, respectively) were determined by the colourimetric method [33]. Fresh plant material (0.1 g) was ground with $MgCO_3$ (3 mg), then 25 cm^3 of 80% aqueous acetone was added. The solution was kept in the dark for 30 min at 20 °C, filtrated, and absorbance was measured at λ = 470, 646 and 663 nm (respectively for Cars, Chl. *a* and Chl. *b*).

Hydrogen peroxide (H_2O_2) was determined by extraction with 0.1% trichloroacetic acid (TCA). The reaction mixture contained the supernatant, potassium phosphate buffer (pH 7.6) and potassium iodide. After addition of the colour reagent, the sample was stirred thoroughly and then incubated in dark for 60 min at 20 °C. The intensity of the resulting yellow colour was measured at λ = 390 nm. The H_2O_2 concentration was read from a calibration curve [34].

Total antioxidant activity (TAA) was evaluated on the basis of DPPH radical scavenging with the use of 2,2-diphenyl-1-picrylhydrazyl (DPPH reagent). A mixture of fresh plant material (2.5 g) ground with 80% methanol was centrifuged (10 min, 4 °C, 3492 *g*). The test tubes, containing 0.1 cm^3 of supernatant and 4.9 cm^3 of 0.1 mM DPPH dissolved with 80% methanol, were incubated in the dark (15 min, 20 °C), then absorbance was measured at λ = 517 nm. The TAA was expressed as DPPH [%] = [(A0 − A1)/A0] × 100; A0 and A1 are the absorbance of the reference and test solutions, respectively [35].

The Folin–Ciocalteu colourimetric method was used for determination of total phenolics content (TPC) [36]. Fresh plant material (2.5 g) was mixed with 10 cm^3 of 80% methanol, then samples were centrifuged (15 min, 4 °C, 3492 *g*). The supernatant (0.1 cm^3) and sodium carbonate (2 cm^3) were mixed; after 5 min, 0.1 cm^3 of Folin–Ciocalteu reagent mixed with deionised water at a 1:1 ratio was added. After 45 min, absorbance was measured at λ = 750 nm against a reference solution. The results were shown as gallic acid equivalents (GAE), mg GAE per 100 g FW.

Malondialdehyde (MDA) activity was measured by the thiobarbituric acid method [37]. MDA was extracted from plant cells with 0.1% TCA. The reaction mixture consisted of supernatant, K-phosphate buffer (pH 7.6) and 0.5% thiobarbituric acid dissolved in 20% TCA. The MDA and thiobarbituric acid reaction showed orange colouration at 95 °C. The MDA content was calculated from the difference in absorbance measured at λ = 532 and 600 nm, using a molar absorbance coefficient. TCA (0.1%) was used as a blank.

CAT activity was measured by the method of Aebi [38]. Plant material (2.5 g) was ground in an ice bath, mixed with 20 cm^3 of 0.05 M potassium phosphate buffer and centrifuged for 15 min (4 °C, 3492 *g*). Then 1.8 cm^3 of 0.05 M potassium phosphate buffer was mixed with 1.0 cm^3 of 0.15% H_2O_2 solution in 0.05 M phosphate buffer (pH 7.0). The supernatant (0.2 cm^3) was added every minute for 5 min, and the decrease in absorbance at λ = 240 nm was measured. A mixture of 2.0 cm^3 of 0.05% M phosphate buffer and 1.0 cm^3 of 0.15% H_2O_2 in phosphate buffer was used as a blind sample. CAT activity was defined as 1 mmol of H_2O_2 decomposed during 1 min per g FW.

POD activity was determined as described by Cullen [39] with p-phenylenediamine and H_2O_2. Plant material (2.5 g) was ground in an ice bath with 10 cm^3 of 0.05 M phosphate buffer and centrifuged (15 min, 4 °C, 3492 *g*). The mixture analysed was composed of 2 cm^3 of the diluted supernatant, 2 cm^3 of 0.05 M potassium phosphate buffer, 0.2 cm^3 *p*-phenylenediamine and 0.2 cm^3 H_2O_2. Absorbance was measured at λ = 485 nm at 60-s intervals, for 2 min. POD activity was expressed in units (U) per gram FW whereby one unit was defined as an increase in the absorbance by 0.1 per minute.

Statistical analysis. All values were expressed as means of three replicates ± SD. Results were processed by two-way ANOVA using STATISTICA 13.0 (Dell Inc., USA). Significance levels were reported as significant at $p \leq 0.05$, and non-significant according to Tukey's honest significant difference (HSD) test. Equations to predict H_2O_2 as well as TAA as a function of independent variables (priming stress-response chemicals: CAT, POD, TPC, L-AA, Chl. *a*, Chl. *b*, Cars and MDA) were developed by a stepwise regression procedure with backward elimination to remove the least significant variables. The coefficient of determination (R^2) was calculated, and simple regression equations were developed to assess the significance (N = 24, $p \leq 0.05$) of interrelationships between the parameters investigated; the most evident relationships were shown.

TABLE 1
Dry weight, soluble carbohydrate and L-ascorbic acid content in wild marjoram fresh herb depending on application of temperature and light stress.

Temperature (°C)	Light irradiance (μmol m^2 s^{-1})	Dry weight (g 100 g^{-1} FW)	Soluble carbohydrates (g 100 g^{-1} FW)	L-ascorbic acid (mg 100 g^{-1} FW)
5	0	22.16 ± 0.11 bc*	2.40 ± 0.12 d	32.73 ± 0.86 c
	100	24.93 ± 0.16 d	3.74 ± 0.25 f	36.97 ± 0.35 d
	250	22.58 ± 0.17 c	3.46 ± 0.21 e	13.03 ± 0.30 a
18	0	15.81 ± 0.10 a	1.18 ± 0.10 a	23.03 ± 0.50 b
	100	20.09 ± 0.09 b	1.69 ± 0.07 b	20.61 ± 0.50 b
	250	21.69 ± 0.170 b	1.95 ± 0.05 c	38.79 ± 1.34 d
Mean for temperature				
5		23.22 ± 0.38 B	3.20 ± 0.18 B	27.58 ± 3.16 A
18		19.20 ± 0.75 A	1.60 ± 0.10 A	27.47 ± 2.48 A
Mean for light irradiance				
0		18.98 ± 1.20 A	1.79 ± 0.23 A	27.88 ± 1.89 B
100		22.51 ± 0.97 C	2.71 ± 0.39 B	28.79 ± 3.11 B
250		22.14 ± 0.20 B	2.70 ± 0.29 B	25.91 ± 4.91 A

* Means of three replicates ± SD; data were subjected to two-way ANOVA; means within a column followed by different letters (capital letters for main effects and lowercase letters for interaction effects) are significantly different at $p \leq 0.05$ according to Tukey's HSD test.

RESULTS AND DISCUSSION

According to studies focused on investigation of chilling-sensitive species, chilling injury can be induced in complete darkness but is more marked under weak light [20]. In the present experiment, the interaction between the two stress factors, light irradiance and temperature, had a significant influence on DW content in wild marjoram foliage (Table 1). The highest level of DW was recorded in plants treated with 5 °C and light irradiance of 100 μmol m^2 s^{-1} while the lowest level of DW was noted in plants grown at 18 °C without light. Lack of light caused a decline in DW especially in control plants, where the result of higher temperature was increased respiration and organic matter decomposition. According to Kudoh and Sonoike [20], chilling injury in the light is regarded as a kind of irreversible photoinhibition, damaging photosynthesis gradually over several days. We did not observe visible symptoms of chilling-light 'cross-talk' on wild marjoram leaves, but the effect of this treatment was reflected firstly in DW content as well as in the other biochemical parameters described below.

The SC content in plant material ranged from 1.18% to 3.74% FW. The combined effect of both stress factors had a significant influence on the SC content in the herb of wild marjoram. However, SC content was two times higher in chilled plants than in the control regardless of light irradiance, pointing to light as the dominant factor in chilling and light stress 'cross-talk'. The highest level of SC was recorded in wild marjoram treated with 5 °C and 100 μmol m^2 s^{-1}, while the lowest was recorded for the treatment at 18 °C and 0 μmol m^2 s^{-1}. Additionally, we determined a positive correlation between SC and H_2O_2 content ($r = 0.68$, $p \leq 0.001$), suggesting that increased H_2O_2 may indicate a significant role of SC as osmoprotectants targeted to protect cytoplasm integrity against possible H_2O_2 injury. Also, reference data show that plants' acclimation to low temperatures includes accumulation of SC [40] because they play a crucial role in cell osmotic adjustment and maintaining membrane integrity [23, 41].

Light irradiance plays a key role in producing L-AA in plants. According to Verkerke et al. [42], the best way to enhance the content of this vitamin is applying a light with low irradiance for a longer period (20 h) rather than applying light with higher intensity for a shorter period (14 h). Analysis of the interaction between experimental factors indicated significant differences in L-AA content in wild marjoram herb. Plants cultivated under light irradiance of 250 μmol m^2 s^{-1} were characterised by the lowest (at 5 °C) as well as the highest (at 18 °C) L-AA content. Among chilling treatments, the most favourable light irradiance for L-AA synthesis was 100 μmol m^2 s^{-1}. In cold stress conditions, plants accumulate metabolites which have antioxidative functions [43], for example, L-AA [44]. These results prove an important role of L-AA in detoxifying O_2^- and H_2O_2 in plant cells.

Chilling stress limits photosynthetic activity and causes a decrease in the concentration of photosynthetic pigments [45]. In this study, it was observed that Chl. *a*, Chl. *b* and Cars concentration changed depending on temperature and light irradiance (Fig. 1). Generally, in chilled plants, the concentration of pigments was lower regardless of light irradiance; this phenomenon was also confirmed by Kudoh and Sonoike [20]. In the case of wild marjoram treated at 5 °C, the content of Chl. *a*, Chl. *b* and Cars was highest with light irradiance of 250 μmol m^2 s^{-1}. In contrast, for plants cultivated at 18 °C, the effect was different: the highest content of pigments was observed for light irradiance of 100

µmol m^2 s^{-1}, but there were no differences between 0 and 250 µmol m^2 s^{-1}. According to Ahmed et al. [46], combined drought and salt stress results in enhanced reduction of Chl. *b* as compared to that observed under individual stresses in barley. The present experiment showed similar plant reactions against chilling and light stress involving Chl. *a*, Chl. *b* and Cars; the most disruptive combination was 5 °C and 250 µmol m^2 s^{-1}. Carotenoids play an important role in protection against damage caused by excessive light irradiance [47], which could explain the increase in Cars content in the treatment with low temperature and high light irradiance.

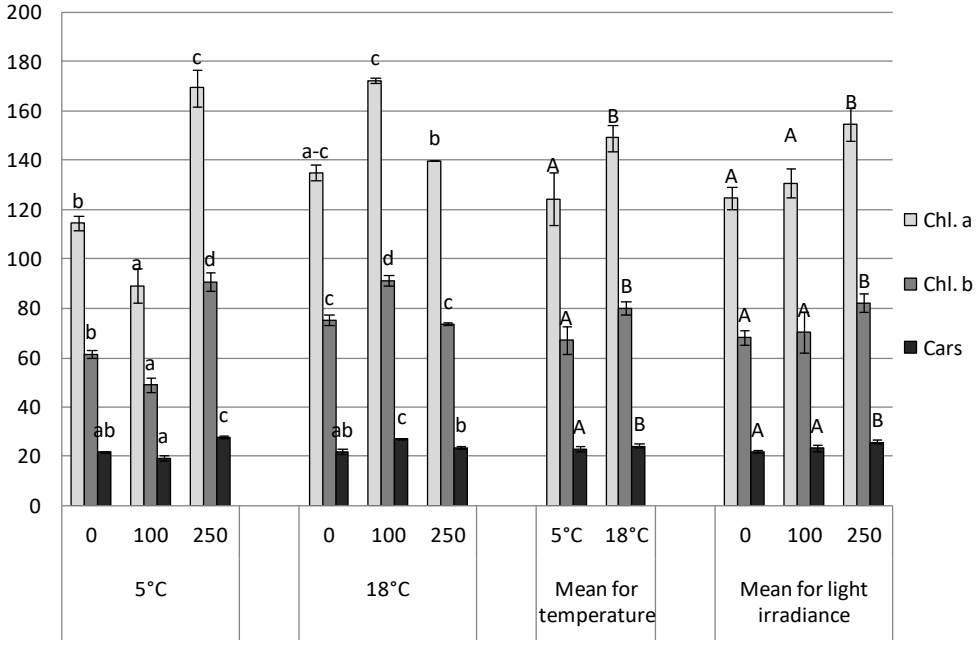

FIGURE 1

Chlorophyll *a* (Chl. *a*), chlorophyll *b* (Chl. *b*) and carotenoids (Cars) (mg 100 g^{-1} FW) in wild marjoram as affected by chilling and light stress

Means followed by different lowercase letters for interaction and capital letters for the main effect of temperature (5 and 18 °C) and light irradiance (0, 100, 250 µmol m^2 s^{-1}) are significantly different at $p \leq 0.05$ according to Tukey's HSD test; bars represent standard deviations (± SD).

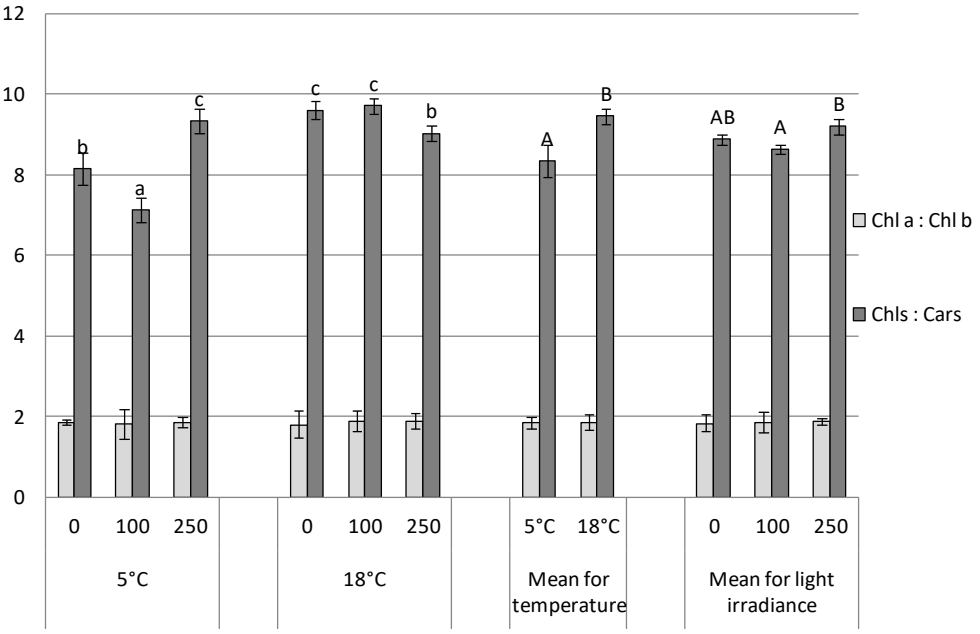

FIGURE 2

Chlorophyll *a*:chlorophyll *b* ratio (Chl. *a*:Chl. *b*) and chlorophylls:carotenoids (Chls:Car) ratio in wild marjoram as affected by chilling and light stress;

for abbreviations, see Fig. 1.

The highest Chl. *a* to *b* ratio was observed in wild marjoram treated with 5 °C and 250 μmol m^2 s^{-1} as well as 18 °C and light irradiance of 0 and 100 μmol m^2 s^{-1}. No significant differences were observed regarding the Chls:Cars ratio (Fig. 2). The investigations performed on chilling-sensitive species assumed that the decrease in the amount of chlorophyll could be due to degradation of the PSI reaction-centre complex, which has a high Chl. *a*:Chl. *b* ratio [20]; this could explain the lowest value observed at 5 °C and 100 μmol m^2 s^{-1} in the present experiment.

Chilling stress causes an increase in ROS due to modifications of plant physiology that can damage cellular organelles [48]. The highest accumulation of H_2O_2 was observed as a combined effect of 5 °C treatment together with 100 μmol m^2 s^{-1} light irradiance (Table 2). Plants have developed a defence system against ROS which includes an increase in the synthesis of CAT, POX and phenolic compounds [49, 50]. The wild marjoram plants treated at 5 °C were characterised by TPC as well as TAC differentiated to a high degree, from the lowest value in darkness to the highest value in light irradiance of 100 μmol m^2 s^{-1} for both parameters described. In the 18 °C treatment, TPC decreased with an increase of light irradiance; however, in the case of TAA, differences between 100 and 250 μmol m^2 s^{-1} treatments were not statistically significant. As mentioned above, although the highest TPC and TAA were observed in chilled plants at light irradiance of 100 μmol m^2 s^{-1}, the overall level of phenols and antioxidant activity were lower in chilled plants in comparison with the control. Most studies report an increase of phenolic compounds content [44, 51]; nonetheless, some studies have shown a decrease in phenols content in low temperature-treated plants [52].

To precisely describe H_2O_2 production and scavenging in the conditions of the present experiment, we performed a stepwise regression procedure with backward elimination to remove the least significant variables affecting H_2O_2 as well as TAA. The base equation for the model was: H_2O_2 = B0 + B1 × L-AA + B2 × Chl. *a* + B3 × Chl. *b* + B4 × Cars + B5 × TAA + B6 × TPC + B7 × MDA + B8 × CAT + B9 × POX, where B0 is a constant and B1–9 are regression coefficients. The simplified equations for the wild marjoram herb H_2O_2 and TAA are as follows:

H_2O_2 (mol g^{-1} FW) = 0.248 − 0.011 × TAA (% DPPH) + 0.004 × TPC (mg GAE 100 g^{-1} FW) + 0.09 × CAT (μmol H_2O_2 min^{-1} g^{-1} FW) + 0.023 × POX (U min^{-1} 100 g^{-1} FW)

TAA (% DPPH) = B + B1 × TPC (mg GAE 100 g^{-1} FW) + B2 × POX (U min^{-1} 100 g^{-1} FW) + B3 × H_2O_2 (mol g^{-1} FW)

The R^2 values showed that the regression prediction fitted the data: 88% for the H_2O_2 model, corresponding with TAA, TPC, CAT and POX. For TAA it was equal to 0.91%; that model involved TPC, POX and H_2O_2. Additionally, we showed that TAA is strongly correlated with TPC ($r = 0.92$, $p \leq 0.001$), pointing to phenolic compounds as important antioxidants in the wild marjoram stress defence system.

The highest MDA content was observed in plants under light irradiance of 0 and 100 μmol m^2 s^{-1} at a temperature of 5 °C (Table 2), indicating significantly increased lipid peroxidation of which the final product is MDA, as reported previously by Oliviera et al. [53] and Sharma et al. [54]. However, the present results showed also the protective effect of high light irradiance in chilling conditions on cell membrane permeability, reflected by a lower MDA content for the treatment under light irradiance of 250 μmol m^2 s^{-1} at a temperature of 5 °C. Simultaneous occurrence of light and chilling stresses resulted in a high degree of complexity in wild marjoram plant responses. The combined stresses are largely controlled by different, and sometimes opposing, signalling pathways that may interact with and inhibit each other.

TABLE 2
H_2O_2, total phenolics and malondialdehyde content and antioxidant activity in wild marjoram fresh herb depending on application of temperature and light stress.

Temperature (°C)	Light irradiance (μmol m^2 s^{-1})	H_2O_2 (mol g^{-1} FW)	Antioxidant activity (% DPPH)	Total phenolics (mg GAE 100 g^{-1} FW)	Malondialdehyde (μmol g^{-1} FW)
5	0	0.966 ± 0.07 ab*	19.48 ± 0.89 a	133.6 ± 0.59 a	26.63 ± 0.28 c
	100	1.345 ± 0.03 c	49.23 ± 1.67 d	229.1 ± 1.95 f	26.63 ± 0.24 c
	250	1.129 ± 0.10 b	26.50 ± 0.82 b	157.7 ± 1.46 b	11.32 ± 1.04 a
18	0	1.008 ± 0.17 ab	48.68 ± 1.22 d	213.0 ± 6.41 e	20.44 ± 1.13 b
	100	1.035 ± 0.02 ab	31.80 ± 0.92 c	200.3 ± 0.26 d	17.79 ± 0.42 b
	250	0.928 ± 0.02 a	34.72 ± 1.08 c	186.5 ± 0.27 c	10.45 ± 0.40 a
Mean for temperature					
5		1.146 ± 0.17 B	31.74 ± 3.88 A	173.5 ± 2.26 A	21.53 ± 2.20 B
18		0.990 ± 0.10 A	38.40 ± 2.29 B	199.9 ± 3.80 B	16.23 ± 1.33 A
Mean for light irradiance					
0		0.987 ± 0.12 A	34.08 ± 5.56 B	173.3 ± 5.30 A	23.54 ± 1.29 B
100		1.190 ± 0.17 B	40.52 ± 3.41 C	214.7 ± 5.53 B	22.21 ± 1.69 B
250		1.029 ± 0.13 A	30.61 ± 1.68 A	172.1 ± 5.49 A	10.88 ± 0.54 A

*For abbreviations, see Table 1.

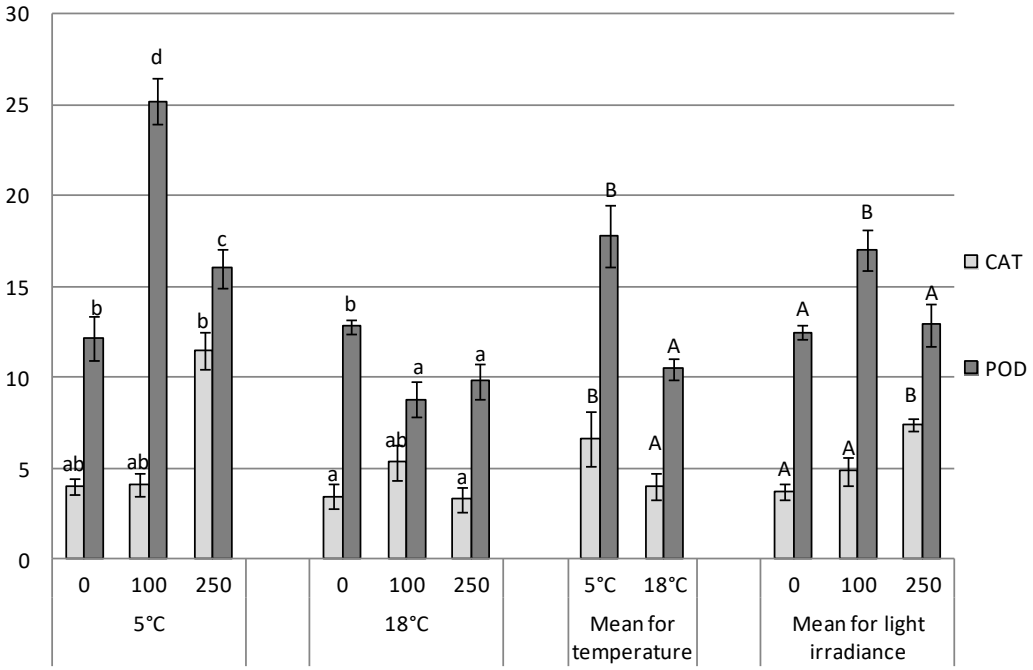

FIGURE 3
Catalase (CAT; µmol H_2O_2 min^{-1} g^{-1} FW) and peroxidase (POX; U min^{-1} 100 g^{-1} FW) activity in wild marjoram as affected by chilling and light stress; for abbreviations. see Fig. 1.

Increased CAT and POX activity and MDA content in plants cultivated in stress conditions have been confirmed for *Avena nuda* L. by Liu et al. [55]. Cold acclimation is attributed to enhanced activity, including that of POX [56]. CAT is more involved in detoxification of H_2O_2 than in regulation as a signalling molecule in plants [57]. Although Wang et al. [58] showed a correlation between elevated CAT activity and tolerance to dark chilling stress, we did not observe a significant increase of CAT in plants chilled in darkness (Fig. 3). CAT is present in different isoforms in cellular organelles where H_2O_2-generating enzymes are found. According to Dat et al. [59], CAT isoforms exhibit differential thermal extremes. As reported by Apel and Hirt [60], the changing balance of scavenging enzymes induces compensatory mechanisms; for example, POX can be up-regulated when CAT activity is reduced in plants. In the conditions of the present experiment, we did not show a correlation between CAT and POX activity ($r = 0.14$, $p = 0.51$), so future investigations on the action of CAT as well as POX isoforms could contribute to the precise highlighting of cold acclimation of plants in conditions of light and chilling stress.

CONCLUSIONS

The response of wild marjoram plants to combined light and chilling stress cannot be directly extrapolated from the reaction to individual stress factors. Chilling and light stress applied simultaneously affected Chl. *a*, Chl. *b* and carotenoid synthesis; the most disruptive combination was 5 °C and 250 µmol m^2 s^{-1}. SC, acting probably as osmoprotectants, were noted in the highest amount in wild marjoram treated with chilling stress combined with light irradiance of 100 and 250 µmol m^2 s^{-1}. Low light irradiance interacted with chilling temperature with respect to an increase in L-AA content, as well as to antioxidant activity and total phenolics in wild marjoram herb. The response of the metabolome of the species investigated to low temperature and light stress was significant but did not induce long-term destructive changes mitigating adaptation abilities. The increasing demand for healthy food has necessitated the intensification of investigations into stress combinations affecting plant composition as well as those including storage, transport and shelf-life. The development of precise stress applications for particular crops in subsequent steps of production and marketing could maintain or even improve their biological quality. The fact that a combination of stresses shows unpredictable action is an important challenge for intensive studies to understand plants' response to multiple stresses.

ACKNOWLEDGEMENTS

No potential conflict of interest is reported by the authors.

This study was supported by the Ministry of Science and Higher Education of the Republic of Poland.

REFERENCES

[1] Aligiannis, N., Kalpoutzakis, E., Mitaku, S. and Chinou, I.B. (2001) Composition and antimicrobial activity of the essential oils of two *Origanum* species. J Agric Food Chem. 49(9), 4168-4170.

[2] Sahin, F., Gulluce, M., Daferera, D., Sokmen, A., Polissiou, M., Agar, G. and Özer, H. (2004) Biological activities of the essential oils and methanol extract of *Origanum vulgare* ssp. *vulgare* in the Eastern Anatolia region of Turkey. Food Control. 15, 549-557.

[3] Wojciechowicz-Żytko, E. and Jankowska, B. (2017) Herbs as a source of nutrition for flower-visiting hoverflies (Diptera, Syrphidae). Folia Hort. 29(2), 135-141.

[4] Singletary, K. (2010) Oregano: overview of the literature on health benefits. Nutr Today. 45(3), 129-138.

[5] Figueredo, F., Cabassu, P., Chalchat, J and Pasquier, B. (2006) Studies of Mediterranean oregano populations. VIII - Chemical composition of essential oils of oregano of various origins. Flav Frag J. 21, 134-139.

[6] Shan. B., Cai, B., Sun, M. and Corke, H. (2005) Antioxidant capacity of 26 spice extracts and characterization of their phenolic constituents. J Agric Food Chem. 53, 7749-7759.

[7] Radušienė, J., Ivanauskas, L., Janulis, V. and Jakštas, V. (2008) Composition and variability of phenolic compounds in *Origanum vulgare* from Lithuania. Biologia. 54(1), 45-49.

[8] Arcila-Lozano, C., Loarca-Pina, G., Lecona-Uribe, S. and Gonzalez-deMejia, E. (2004) Oregano: properties, composition and biological activity. Arch Latinoam Nutr. 54, 100-111.

[9] Morshedloo, M.R., Craker, L.E., Salami, A., Nazeri, V., Sang, H. and Maggi, F. (2017) Effect of prolonged water stress on essential oil content, compositions and gene expression patterns of mono- and sesquiterpene synthesis in two oregano (*Origanum vulgare* L.) subspecies. Plant Physiol Biochem. 111, 119-128.

[10] Singletary, K. (2010) Oregano: overview of the literature on health benefits. Nutrition Today. 45(3), 129-138.

[11] Tibaldi, G., Fontana, E. and Nicola, S. (2011) Growing conditions and postharvest management can affect the essential oil of *Origanum vulgare* L. ssp. *hirtum* (Link) Ietswaart. Ind Crops Prod. 34(3), 1516-1522.

[12] Pandey, P., Ramegowda, V. and Senthil-Kumar, M. (2015) Shared and unique responses of plants to multiple individual stresses and stress combinations: physiological and molecular mechanisms. Front Plant Sci. 6, 723.

[13] Mittler, R. (2006) Abiotic stress, the field environment and stress combination. Trends Plant Sci. 11, 15-19.

[14] Chinnusamy, V., Schumaker, K. and Zhu, J.K. (2004) Molecular genetic perspectives on cross-talk and specificity in abiotic stress signalling in plants. J Exp Bot. 55, 225-236.

[15] Munns, R. (2002) Comparative physiology of salt and water stress. Plant Cell Environ. 25, 239-250.

[16] Karami, L., Ghaderighaderi, N. and Javadi, T. (2017) Morphological and physiological responses of grapevine (*Vitis vinifera* L.) to drought stress and dust pollution. Folia Hort. 29(2), 231-240.

[17] Zhou, J., Lan, Q-J., Tang, J-H. and Lu, Y-C. (2008) Survey of chilling injury to tropical and subtropical plant germplasm resources in Guangxi. Guangxi Trop Agric (China). 117, 25-29.

[18] Huang, W., Zhang, S.B. and Cao, K.F. (2010) The different effects of chilling stress under moderate light intensity on photosystem II compared with photosystem I and subsequent recovery in tropical tree species. Photosynth Res. 103, 175-182.

[19] Wise, R.R. (1995) Chilling-enhanced photooxidation: the production, action and study of reactive oxygen species produced during chilling in the light. Photosynth Res. 45, 79-97.

[20] Kudoh, H. and Sonoike, K. (2002) Irreversible damage to photosystem I by chilling in the light: cause of the degradation of chlorophyll after returning to normal growth temperature. Planta. 215, 541-548.

[21] Wang, W.B., Kim, Y.H., Lee, H.S., Deng, X.P. and Kwak, S.S. (2009) Differential antioxidation activities in two alfalfa cultivars under chilling stress. Plant Biotechnol Rep. 3, 301-307.

[22] Shao, H.B., Chu, L.Y., Lu, Z.H. and Kang, C.M. (2008) Primary antioxidant free radical scavenging and redox signaling pathways in higher plant cells. Int J Biol Sci. 4, 8-14.

[23] Shao, H.B., Guo, Q.J., Chu, L.Y., Zhao, X.N., Su, Z.L., Hu, Y.C. and Cheng, J.F. (2007) Understanding molecular mechanism of higher plant plasticity under abiotic stress. Colloids Surf B. 54, 37-45.

[24] Awasthi, R., Kalpna, B. and Harsh, N. (2015) Temperature stress and redox homeostasis in agricultural crops. Front Environ Sci. 3, 11.

[25] Morshedloo, M.R., Mumivand, H., Craker, L.E. and Maggi, F. (2018) Chemical composition and antioxidant activity of essential oils in *Origanum vulgare* subsp. *gracile* at different phenological stages and plant parts. J Food Process Preserv. 42(2), e13516.

[26] Lattanzio, V., Cardinali, A., Ruta, C., Fortunato, I., Linsalata, V. and Cicco, N. (2009) Relationship of secondary metabolism to growth in oregano (*Origanum vulgare* L.) shoot cultures under nutritional stress. Environ Exp Bot. 65(1), 54-62.

[27] Shafiee-Hajiabad, M., Novak, J. and Honermeier, B. (2015) Characterization of glandular trichomes in four *Origanum vulgare* L. accessions influenced by light reduction. J Appl Bot Food Qual. 88, 300-307.

[28] Świeca, M. (2015) Elicitation with abiotic stresses improves pro-health constituents, antioxidant potential and nutritional quality of lentil sprouts. Saudi J Biol Sci. 22(4), 409-416.

[29] Ramegowda, V. and Senthil-Kumar, M. (2015) The interactive effects of simultaneous biotic and abiotic stresses on plants: mechanistic understanding from drought and pathogen combination. J Plant Physiol. 176, 47-54.

[30] Kalisz, A., Sękara, A., Grabowska, A., Cebula, S. and Kunicki, E. (2015) The effect of chilling stress at transplant stage on broccoli development and yield with elements of modeling. J. Plant Growth Reg. 34(3), 532-544.

[31] Yemm, E.W. and Willis, A.J. (1954) The estimation of carbohydrates in plant extracts by anthrone. Biochem J. 57, 508-514.

[32] Kostecka, M., Szot, I., Czernecki, T. and Szot, P. (2017) Vitamin C content of new ecotypes of Cornelian cherry (*Cornus mas* L.) determined by various analytical methods. Acta Sci. Pol. Hortorum Cultus. 16(4), 53-61.

[33] Sumanta, N., Haque, C.I., Nishika, J. and Suprakash, R. (2014) Spectrophotometric analysis of chlorophylls and carotenoids from commonly grown fern species by using various extracting solvents. Res J Chem Sci. 2231, 606X.

[34] Junglee, S., Urban, L., Sallanon, H. and Lopez-Lauri, F. (2014) Optimized assay for hydrogen peroxide determination in plant tissue using potassium iodide. Am J Anal Chem. 5, 730-736.

[35] Molyneux, P. (2004) The use of the stable free radical diphenylpicrylhydrazyl (DPPH) for estimating antioxidant activity. Songklanakarin J Sci Technol. 26(2), 211-219.

[36] Djeridane, A., Yousfi, M., Nadjemi, B., Boutassouna, D., Stocker, P. and Vidal, N. (2006) Antioxidant activity of some Algerian medicinal plants extracts containing phenolic compounds. Food Chem. 97, 654-660.

[37] Giera, M., Lingeman, H. and Niessen, W.M.A. (2012) Recent advancements in the LC- and GC-based analysis of malondialdehyde (MDA): A brief overview. Chromatographia. 75, 433.

[38] Aebi, H. (1984) Catalase *in vitro*. Methods Enzymol. 105, 121-126.

[39] Cullen, P.J., Pankaj, S.K. and Misra, N.N. (2013) Kinetics of tomato peroxidase inactivation by atmospheric pressure cold plasma based on dielectric barrier discharge. Innov. Food Sci Emerg Technol. 19, 153-157.

[40] Wanner, L.A. and Junttila, O. (1999) Cold-induced freezing tolerance in *Arabidopsis*. Plant Physiol. 120, 391-400.

[41] Chen, Z., Cuin, T.A., Zhou, M., Twomey, A., Naidu, B.P. and Shabala, S. (2007) Compatible solute accumulation and stress-mitigating effects in barley genotypes contrasting in their salt tolerance. J Exp Bot. 58, 4245-4255.

[42] Verkerke, W., Labrie, C. and Dueck, T. (2015) The effect of light irradiance and duration on vitamin C concentration in tomato fruits. Acta Hortic. 1106, 49-54.

[43] Pospíšil, P. (2012) Molecular mechanisms of production and scavenging of reactive oxygen species by photosystem II. Biochim Biophys Acta. 1817, 218-231.

[44] Sivaci, A., Kaya, A. and Duman, S. (2014) Effects of ascorbic acid on some physiological changes of pepino (*Solanum muricatum* Ait.) under chilling stress. Acta Biol Hung. 65, 305-318.

[45] Yadegari, L.Z., Heidari, R. and Carapetian, J. (2008) The influence of cold acclimation on proline, malondialdehyde (MDA), total protein and pigments contents in soybean (*Glycine max*) seedlings. Res J Biol Sci. 3(1), 74-77.

[46] Ahmed, I.M., Dai, H., Zheng, W., Cao, F., Zhang, G., Sun, D. and Wu, F. (2013) Genotypic differences in physiological characteristics in the tolerance to drought and salinity combined stress between Tibetan wild and cultivated barley. Plant Physiol Biochem. 63, 49-60.

[47] Giannakoula, A., Papastergiou, I.I. and Hatzigaidas, A. (2006) The effects of development at chilling temperatures on the function of the photosynthetic apparatus under high and low irradiance in leaves of lettuce (*Lactuca sativa* L.). In: Mastorakis, N., Cecchi, A., WSEAS, (eds.) Proceedings of the 5th WSEAS International Conference on Environment, Ecosystems and Development. Nov 20-22; Venice, Italy. WSEAS. 396-401.

[48] Karabal, E., Yucel, M. and Oktem, H.A. (2003) Antioxidant responses of tolerant and sensitive barley cultivars to boron toxicity. Plant Sci. 164, 925-933.

[49] Foyer, C.H. and Noctor, G. (2005) Redox homeostasis and antioxidant signaling: a metabolic interface between stress perception and physiological responses. Plant Cell. 17, 1866-1875.

[50] Mehr, Z.S., Khajeh, H., Bahabadi, S.E. and Sabbagh, S.K. (2012) Changes on proline, phenolic compounds and activity of antioxidant enzymes in *Anethum graveolens* L. under salt stress. Int J Agron Plant Prod. 3, 710-715.
[51] Rivero, R.M., Ruiz, J.M., García, P.C., López-Lefebre, L.R., Sánchez, E. and Romero, R. (2001) Resistance to cold and heat stress: accumulation of phenolic compounds in tomato and watermelon plants. Plant Sci. 160, 315-321.
[52] Amarowicz, R., Weidner, S., Wojtowicz, I., Karamać, M., Kosińska, A. and Rybarczyk, A. (2010) Influence of low-temperature stress on changes in the composition of grapevine leaf phenolic compounds and their antioxidant properties. Funct Plant Sci Biotechnol. 4, 90-96.
[53] Oliveira, J.G., Alves, P.L.C.A. and Magalhães, A.C.N. (2002) The effect of chilling on the photosynthetic activity in coffee (*Coffea arabica* L.) seedlings. The protective action of chloroplastid pigments. Braz J Plant Physiol. 14, 95-104.
[54] Sharma, P., Jha, A.B., Dubey, R.S. and Pessarakli, M. (2012) Reactive oxygen species, oxidative damage, and antioxidative defense mechanism in plants under stressful conditions. J Bot. 2102, 217037.
[55] Liu, W., Yu, K., He, T., Li, F., Zhang, D. and Liu, J. (2013) The low temperature induced physiological responses of *Avena nuda* L., a cold-tolerant plant species. Sci World J. 2013, 658793.
[56] Turan, O. and Ekmekci, Y. (2011) Activities of photosystem II and antioxidant enzymes in chickpea (*Cicer arietinum* L.) cultivars exposed to chilling temperatures. Acta Physiol Plant. 33, 67-78.
[57] Sofo, A., Scopa, A., Nuzzaci, M. and Vitti, A. (2015) Ascorbate peroxidase and catalase activities and their genetic regulation in plants subjected to drought and salinity stresses. Int J Mol Sci. 16(6), 13561-13578.
[58] Wang, L.J., Jiang, W.B. and Huang, B.J. (2004) Promotion of 5-aminolevulinic acid on photosynthesis of melon (*Cucumis melo*) seedlings under low light and chilling stress conditions. Physiol Plant. 121, 258-264.
[59] Dat, J., Vandenabeele, S., Vranova, E., Van Montagu, M., Inze, D. and Van Breusegem, F. (2000) Dual action of the active oxygen species during plant stress responses. Cell Mol Life Sci. 57, 779-795.
[60] Apel, K. and Hirt, H. (2004) Reactive oxygen species: metabolism, oxidative stress, and signal transduction. Annu Rev Plant Biol. 55, 373-399.

Received: **20.12.2018**
Accepted: **07.03.2019**

CORRESPONDING AUTHOR

Agnieszka Sękara
University of Agriculture in Krakow, Poland,
Faculty of Biotechnology and Horticulture,
Department of Vegetable and Medicinal Plants,
29-Listopada 54, 31-420 Krakow – Poland

e-mail: agnieszka.sekara@urk.edu.pl

© by PSP Volume 28 – No. 5/2019 pages 3991-4000 Fresenius Environmental Bulletin

ANTI-ACETYLCHOLINESTERASE, ANTIPROTOZOAL AND CYTOTOXIC ACTIVITIES OF SOME TURKISH MARINE ALGAE

Esin Cinar[1], Ergun Taskin[1,*], Deniz Tasdemir[2], Evrim Ozkale[1], Ulrike Grienke[3], Darya Firsova[3]

[1]Manisa Celal Bayar University, Faculty of Arts & Sciences, Department of Biology, 45140, Manisa, Turkey
[2]GEOMAR Centre for Marine Biotechnology, Research Unit Marine Natural Products Chemistry, GEOMAR Helmholtz Centre for Ocean Research Kiel, Germany
[3]National University of Ireland Galway School of Chemistry, Galway, Ireland

ABSTRACT

The crude (MeOH:$CHCl_3$) and *n*-hexane-soluble extracts from four brown algae (Phaeophyceae) [*Petalonia fascia, Cystoseira crinita, Cystoseira foeniculacea,* and *Halopteris scoparia*], one red alga (Rhodophyta) [*Jania rubens*] and three green algae (Chlorophyta) [*Chaetomorpha aerea, Codium fragile* subsp. *fragile,* and *Ulva compressa*] from Turkish coasts (Izmir Bay, Ayvalık and Çanakkale) were assessed *in vitro* for their acetylcholinesterase (AChE) inhibitory activities at 200, 150, 50, 20 µg/mL test concentration with Ellman's method. The crude extract of *P. fascia* possessed the highest inhibition (IC_{50} value of 19,22±10,47 µg/mL) against AChE. Galanthamine HBr was used as standard drug that gave against AChE enzyme IC_{50} of 3.44±1.14 µM. In the second stage, the crude, hexane-soluble, chloroform-soluble and water-methanol soluble extracts of the marine algae were observed *in vitro* against parasitic protozoa (*Plasmodium falciparum, Trypanosoma brucei brucei, Trypanosoma cruzi* ve *Leishmania infantum*). According to results, the most potent protozoal activities were shown by the Khex of *C. crinita* (IC_{50} value of 10,62 µg/ml), followed by the Khex of *C. fragile* subsp. *fragile* (IC_{50} value of 11,89 µg/ml). The hekzan-soluble (Khex) and chloroform-soluble (KCH) extracts gave the best results. The marine algae were also tested on MRC-5 cells (human fibroblasts) for by controlling tamoxifen. The extracts of *H. scoparia*, *C. aerea* ve *C. fragile* subsp. *fragile* showed toxicity.

KEYWORDS:
Marine algae, Acethylcholinesterase, *Plasmodium, Trypanosom, Leishmania,* cytotoxicity.

INTRODUCTION

Dementia is a syndrome due to disease of the brain, usually chronic, characterised by a progressive, worldwide deterioration in intellect including memory, learning, orientation, language, comprehension and judgement. While dementia mainly affects older people approximately after age of 65, there is growing awareness of cases that start before the age of 65 years [1]. Extend the life of aging as a result of human societies, dementia creates a major health problem [2]. Dementia syndrome is linked to a large number of underlying brain pathologies [1]. More than one hundred diseases have been reported to cause dementia [2]. Common type of dementia are Alzheimer's disease (AD), vascular dementia (VaD), dementia with Lewy bodies (DLB) and frontotemporal dementia (FTD). AD is the most common type of dementia (50-75 %) and one of the fourth leading causes of death in developed nations (after heart disease, cancer and strokes) [1,3]. It's estimated that occure 4.6 million new AD cases every year. In AD, determined senil amiloid plaques, neurofibriller tangles, sinaps-neuron loss and marked atrophy in brain as histopathologyc signs [4]. The definitive diagnosis of AD, it is not possible while patiens are living. Because of this reason, it is required pathological examination with autopsy [5]. Accepted risk factors for AD are age, family story and apoliprotein E (Apo E) gene e4 allele [6]. Acetylcholinesterase (AChE) inhibitors are widely used for treatment of AD to increase levels of acetylcholine (ACh) in the brain for cholinergic neurotransmission [7]. Some synthetic AChE inhibitors such as donepezil, takrin, rivastigmin have been used for the treatment of AD. Because of bioavailability problems and side effects like hepatotoxicity and gastrointestinal disorder researcher is trying to find better ChE inhibitors from natural sources [3].

Parasitic protozoans are eucaryotic and single-celled organisms that give rise to toxic, nervous, inflammatory, mechanical, traumatic and exploitative effects living on the host [8]. These effects occur a result of protozoal parazitic diseases and the largest cause of death in tropical and subtropical regions.

Malaria, African trypanosomiasis (Sleeping sickness), American trypanosomiasis (Chagas disease) and Leishmaniasis are among the major parasitic diseases distributed throughout the world [9-10]. Malaria, caused by *Plasmodium (P.) falciparum*, is transmitted to humans by female *Anopheles* mosquitoes and the third leading cause of death among infectious diseases [11]. Leishmaniasis, is caused by *Leishmania (L.) infantum* and transmitted bt the sandfly, is recognized one of the most important of the six infectious diseases by WHO. African trypanosomiasis, is caused by *Trypanosoma (T.) brucei brucei*, transmitted by the tsetse fly. American trypanosomiasis is a potentially life-threatening illness caused by the *T. cruzi*, is mostly transmitted to humans by the faeces of triatomine bugs [12]. Chemotherapy is implemented for the treatment of parasitic disease. But chemotherapeutic agents are inadequate in chronic phases disease because of severe side effects also parasites that are resistant to these agents today [13-15]. The most effective treatment is needed to daily parenteral administration but a number of reasons, such as parasites tent to be chronic, not create enough immun response in host and have complex circle, make difficult development of vaccines [11]. Therefore there is a need for new, effective, natural agents.

Marine algae are base of the aquatic food chain and their essential roles in nitrogen and phosphorus cycling are critical to aquatic ecosystems (16). They produce secondary metabolites due to developed an extensive chemical defense system, e.g. herbivory, pathogens and intense competition. These bioactive secondary compounds such as carotenoids, dietary fibre, protein, essential fatty acids, vitamins, and minerals that possess a broad spectrum of biological. Studies of marine algae have shown their extensive biological activity, including AChE [3, 17- 22] and antiprotozoal activity [23- 28].

The objectives of the present study were to evaluate extracts from 8 species of seaweeds from Turkey marine algae against acetylcholinesterase (AChE) enzyme with Ellman's method and cultured protozoa responsible for human malaria, leishmaniasis, African trypanosomiasis and American trypanosomiasis. Also the extracts of these algae were evaluated for their cytotoxic potentials.

MATERIALS AND METHODS

Sample collection and Identification. Fresh samples of marine algae were collected by hand or scuba diving from various locations from the the Dardanelles and the Aegean coast of Turkey (Figure 1, Table 1), and identified by Prof. Dr. Ergün TAŞKIN (Manisa Celal Bayar University, Faculty of Arts and Sciences, Biology Department, Manisa, Turkey).

Preparation of algal extracts. Algae samples were washed with tap water and twice with distilled water to remove the adhering salts and other epiphytes then air-dried on a blotting paper. Dried samples were pulverized in blender and soaked in aqueous methanol for 7 days at room temperature and filtered using Whatman No. 1 filter paper. The crude extract was concentrated in a rotary evaporator at low temperature (45°C). Solvent-solvent partitioning was performed by using Kupchan and Tsou (1973) method [29, 30]. The crude extract was dissolved with methanol. The prepared solution was then fractionated using solvents of increasing polarity (water-methanol-soluble, chloroform-soluble, hexane-soluble subextract).

***In vitro* Acetylcholinesterase (AChE) Inhibitory Activity Assay.** The inhibition of AChE was measured using a 96-well microplate assay based on Ellman's method [31] as previously described [32, 33]. The absorbance was quantitatively measured at 405 nm by a BioTek EL 808 microplate reader after 0, 15, 30, and 45 min after adding 0.22 U/mL AChE. Data were collected by the software programme Gen5 (version 1.11).

The self-absorbance of all ingredients of the assay were corrected by subtracting the absorbance at time zero from the subsequent absorbance values. For the microplate assay, samples and the positive control galanthamine HBr (GNT; IC_{50} 3.2±1.0 µM) were dissolved in DMSO to stock solutions and diluted with buffer A at 1:100. The final concentration of DMSO in the microplate assay was 1%.

The percentage of the enzyme inhibition was calculated by comparing the rates for the sample to the blank (containing 1% DMSO; n=4). The IC_{50} values were determined with Probit analysis. For statistical processing PASW Statistics 18 was used.

Reagents. AChE (EC 3.1.1.7) from *Electrophorus electricus* (electric eel), acetylthiocholine iodide (ATCI), 5,5'-dithiobis-(2-nitrobenzoic acid) (DTNB, Ellman's reagent), and the positive control galanthamine-HBr were purchased from Sigma-Aldrich Co. LLC.

***In vitro* Antiprotozoal Activity Assay. Against *Plasmodium falciparum*.** *P. falciparum* GHA strain and the standard drug chloroquine were used for the assay. The strain was maintained in RPMI-1640 medium supplemented with 0.37 mM hypoxanthine, 25 mM Hepes, 25 mM $NaHCO_3$, and 10% O^+ human serum together with 2-4% washed human O^+ erythrocytes. Compound stock solutions were prepared in 100% DMSO at 20 mM or mg/ml. Assay were performed in 96-well microtiter plates, each well containing 10 µl of the watery compound dilutions together with 190 µl of the malaria parasite inoculum (1% parasitaemia, 2% HCT). After 72h incubation at 37°C, plates were frozen at -20°C. After

thawing, 20 µl of each well is transferred into another plate together with 100 µl Malstat™ reagent and 20 µl of a 1/1 mixture of PES (phenazine ethosulfat, 0.1 mg/ml) and NBT (Nitro Blue Tetrazolium Grade III, 2 mg/ml). The plates were kept out of light for 2 hours and change in colour was measured spectrophotometrically at 655 nm. The results were expressed as % reduction in parasitaemia compared to control wells and IC_{50} values were calculated [34].

TABLE 1
Collection times and sites of the Turkish marine algae

Algae	Family	Collection site	Collection time
Phaeophyceae (Brown algae)			
Petalonia fascia (O.F.Müll.) Kuntze	Scytosiphonaceae	Izmir Bay	March 2012
Halopteris scoparia (L.) Sauv.	Stypocaulaceae	Ayvalık	July 2011
Cystoseira crinita Duby	Cystoseiraceae	Çanakkale	April 2011
Cystoseira foeniculacea (L.) Grev.		Ayvalık	July 2011
Rhodophyta (Red algae)			
Jania rubens (L.) J.V.Lamour.	Corallinaceae	Izmir Bay	October 2011
Chlorophyta (Green algae)			
Ulva compressa L.	Ulvaceae	Izmir Bay	March 2011
Chaetomorpha aerea (Dillwyn) Kütz.	Cladophoraceae	Çanakkale	April 2011
Codium fragile subsp. *fragile* (Suringar) Hariot	Codiaceae	Çanakkale	April 2011

FIGURE 1
Map of Turkey showing sampling sites.

Against *Trypanosoma brucei brucei*. *T. brucei brucei* Squib 427 strain and the standard drug suramin were used in this study. The strain was maintained in Hirumi (HMI-9) medium, supplemented with 10% inactivated fetal calf serum. Compound stock solutions were prepared in 100% DMSO at 20 mM or mg/ml. Assays were performed in sterile 96-well microtiter plates, each well containing 10 µl of the compound dilutions together with 190 µl of the parasite suspension (1.5×10^4 parasites/well). After 3 days incubation, parasite growth was assessed fluorimetrically after additon of 50 µl resazurin per well. After 24h at 37°C, fluorescence is measured (λ_{ex} 550nm, λ_{em} 590 nm). The results were expressed as % reduction in parasite growth/viability compared to control wells and IC_{50} is calculated [34].

Against *Trypanosoma cruzi*. *T. cruzi* Tulahuen CL2, β galactosidase strain and the standard drug benznidazole were used. The strain was maintained on MRC-5_{SV2} cells in MEM medium, supplemented with 200 mM L-glutamine, 16.5 mM $NaHCO_3$, and 5% inactivated fetal calf serum. Compound stock solutions were prepared in 100% DMSO at 20 mM or mg/ml. Assays were performed in sterile 96-well microtiter plates, each well containing 10 µl of the watery compound dilutions together with 190 µl of MRC-5 cell/parasite inoculum (4×10^3 cell/well + 4×10^4 parasites/well). Parasite growth controlled after 7 days incubation at 37°C and 5% CO_2. Parasite burdens were assessed after adding the substrate CPRG (chlorophenolred β-d-galactopyranoside): 50 µl/well of a stock solution containing 15.2 mg CPRG + 250 µl Nonidet in 100 ml PBS. The change in color was measured spectrophotometrically at 540 nm after 4h incubation at 37°C. The results were expressed as % reduction in parasite burdens compared to control wells and IC_{50} was calculated [34].

Against *Leishmania infantum*. *L. infantum* MHOM/MA(BE)/67 strain and the standard drug miltefosine were used. The strain was maintained in the Golden Hamster (*Mesocricetus auratus*). Compound stock solutions were prepared in 100% DMSO at 20 mM or mg/ml. Assays were performed in 96-well microtiter plates, each well containing 10 µl of the compound dilutions together with 190 µl of macrophage/parasites inoculum (3×10^4 cells + $4{,}5\times10^3$ parasites/well). The inoculum was prepared in RPMI-1640 medium, supplemented with 200 mM L-glutamine, 16.5 mM $NaHCO_3$, and 5% inactivated fetal calf serum. After 5 days incubation, parasite burdens (mean number of amastigotes/macrophage) were microscopically assessed after staining the cells with a 10% Giemsa solution. The results are expressed as % reduction in parasite burden compared to untreated control wells and a IC_{50} was calculated [34].

***In vitro* cytotoxicity evaluation on human fibroblasts (MRC-5 cell line).** MRC-5_{SV2} cells were cultured in MEM + Earl's salts-medium, supplemented with L-glutamine, $NaHCO_3$ and 5% inactivated fetal calf serum. Compound stock solutions were prepared in 100% DMSO at 20 mM or mg/ml. Assays were performed in sterile 96-well microtiter plates, each well containing 10 µl of the watery compound dilutions together with 190 µl of MRC-5_{SV2} inoculum (3×10^4 cells/ml). after 3 days incubation, cell viability was assessed fluorimetrically after addition of 50 µl resazurin per well. After 4 hours at 37°C, fluorescence was measured (λ_{ex} 550 nm, λ_{em} 590 nm). The results were expressed as % reduction in cell growth/viability compared to control wells and IC_{50} was determined [34].

RESULTS

In the present study, marine algae (*Petalonia fascia, Cystoseira crinita, Cystoseira foeniculacea, Halopteris scoparia, Jania rubens, Chaetomorpha aerea, Codium fragile* subsp. *fragile, Ulva compressa*) from three different localities [İzmir Bay and Ayvalık (Aegean coast of Turkey), and Çanakkale (Dardanelles, Sea of Marmara) of Turkey were screened for their *in vitro* diverse biological activities against some test agents.

AChE inhibitory activity. The AChE inhibitory properties of the crude (CR) and hexane-soluble (Khex) extracts of the marine algae observed at concentrations between 20-200 µg/mL. The results, expressed as IC_{50} values, are summarised in Table 2 and Figure 2. The best AChE inhibitory activity was demonstrated by the CR of *P. fascia* (19,22±10,47 µg/mL), followed by the Khex of *C. aerea* (28,68±12,84). The remaining 4/13 algae extracts showed good inhibition of AChE with IC_{50} values ranging between 54.78± 6.08 µg/mL and 105.34±11.39 µg/mL, while remaining 6/13 extracts showed low AChE inhibitory activity with IC_{50} values ranging between 197.8±87.10 µg/mL and 425.91±298.55 µg/mL. The lowest AChE inhibitions were showed by *H. scoparia* and *C. fragile* subsp. *fragile* extracts. The Khex of *C. foeniculacea, J. rubens* and *C. fragile* gave no significant result against AChE. Also the positive control galanthamine HBr gave IC_{50} of 3.44±1.14 µM.

TABLE 2
Acetylcholinesterase inhibitory activity of marine algal extracts

S. No	Algae / Type of extract		IC_{50} value [µg/mL]	Standart deviation [µg/mL]
	Phaeophyceae			
1	***P. fascia***	**CR**	**19,22**	10,47
		KHex	205,55	38,56
2	***H. scoparia***	**CR**	425,91	298,55
		KHex	242,16	125,40
3	***C. crinita***	**CR**	**51,66**	28,42
		KHex	**105,34**	11,39
4	***C. foeniculacea***	**CR**	197,83	87,10
	Rhodophyta			
5	***J. rubens***	**CR**	**63,69**	15,78
	Chlorophyta			
6	***U. compressa***	**CR**	**56,90**	26,45
		KHex	**54,78**	6,08
7	***C. aerea***	**CR**	197,09	85,22
		KHex	**28,68**	12,84
8	***C. fragile subsp. fragile***	**CR**	243,37	122,98
	Standard			
	Galanthamine HBr		3.44 µM	1.14 µM

[**S. No:** Species extract number, **CR:** Crude (MeOH:$CHCl_3$), **Khex:** Hexane-soluble subextract, **KCH:** Chloroform-soluble subextract, **KAqM:** Water-methanol-soluble subextract].

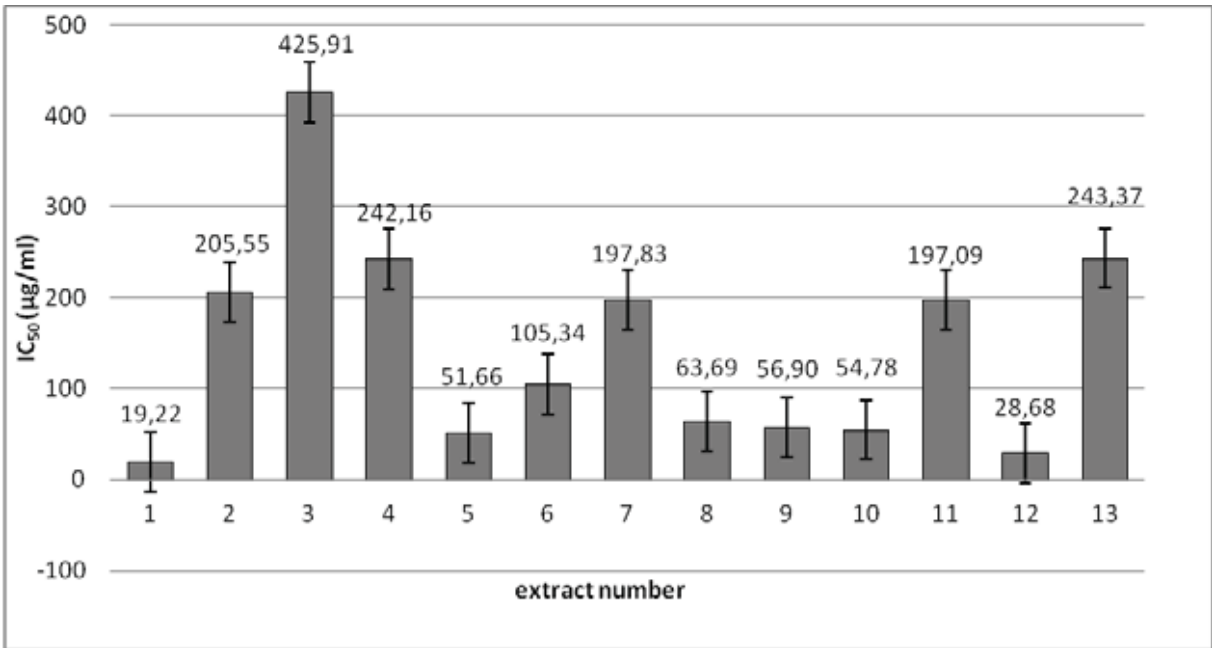

FIGURE 2
IC_{50} values of algal extracts
(**1:** The CR of *P. fascia*, **2:** The Khex of *P. fascia*, **3:** The CR of *H. scoparia*, **4:** The Khex of *H. scoparia*, **5:** The CR of *C. crinita*, **6:** The Khex of *C. crinita*, **7:** The CR of *C. foeniculacea*, **8:** The CR of *J. rubens*, **9:** The CR of *U. compressa*, **10:** The Khex of *U. compressa*, **11:** The CR of *C. aerea*, **12:** The Khex of *C. aerea*, **13:** The CR of *C. fragile* subsp. *fragile*).

Antiprotozoal activity. The *in vitro* inhibitory activity of the crude (CR), hexane-soluble (Khex), chloroform-soluble (KCH) and water-methanol-soluble (KAqM) extracts of the marine algae (total 32 extracts) were evaluated against four parasitic protozoa (*P. falciparum, L. infantum, T. brucei brucei* and *T. cruzi*). Table 3 displays the IC_{50} values determined for each extract as well as standard compounds (suramin, benznidazole, miltefosine, chloroquine). According to results, the most potent

protozoal activities were shown by the Khex of *C. crinita* (IC_{50} value of 10,62 µg/ml), followed by the Khex of *C. fragile* subsp. *fragile* (IC_{50} value of 11,89 µg/ml). At least one extract of each species showed test parasites except for *L. infantum*. The 15 algal extracts gave IC_{50} values ranging from 16.12 to 23.24 µg/ml against *T. brucei brucei*. Due to 20/32 extracts effected against *T. cruzi,* as this pathogen was found to be the most sensitive parasite (IC_{50} values ranging from 10.62 to 30.91 µg/ml). Against *L. infantum* was showed activity by only the KCH of *J. rubens* and the Khex of *C. fragile* subsp. *fragile* (IC_{50} values of 16 µg/ml and 25.40 µg/ml, respectively). The 16 algal extracts showed antimalarial activity with IC_{50} values ranging from 11.89 to 21.85 µg/ml. None of the KAqM extracts displayed activity against all test parasites. The Khex and KCH extracts gave the best results.

Toxicity test. The toxicity of the crude (CR), hexane-soluble (Khex), chloroform-soluble (KCH) and water-methanol-soluble (KAqM) extracts of the marine algae were also tested on human fibroblasts (MRC-5 cells) for by controlling tamoxifen (Table 3). When tested for toxicity, four extracts, the CR and Khex of *H. scoparia*, the Khex of *C. aerea* and *C. fragile* subsp. *fragile*, appeared to be associated with some toxicity.

TABLE 3
Antiprotozoal activity of marine algal extracts

S. No	Algae / Type of Extract		Test parasites (IC_{50} values, µg/ml) *Tbb*	*Tc*	*Li*	*Pf*	MRC-5 Line
	Phaeophyceae						
1	***C. crinita***	**CR**	> 32	> 32	> 32	> 32	> 32
		Khex	> 32	10,62	> 32	> 32	> 32
		KCH	16,35	22.19	> 32	18,47	> 32
		KAqM	> 32	> 32	> 32	> 32	> 32
2	***C. foeniculacea***	**CR**	> 32	25,17	> 32	> 32	> 32
		Khex	16,23	15,84	> 32	21,77	> 32
		KCH	> 32	21,97	> 32	21,19	> 32
		KAqM	> 32	> 32	> 32	> 32	> 32
3	***P. fascia***	**CR**	> 32	23,35	> 32	20,16	> 32
		Khex	16,35	16,78	> 32	> 32	> 32
		KCH	16,35	19,12	> 32	14,55	> 32
		KAqM	> 32	> 32	> 32	> 32	> 32
4	***H. scoparia***	**CR**	> 32	22,17	> 32	18,78	16,23
		Khex	16,23	16,45	> 32	20,95	14,66
		KCH	17,59	22,80	> 32	15,46	> 32
		KAqM	> 32	> 32	> 32	> 32	> 32
	Rhodophyta						
5	***J. rubens***	**CR**	16,23	17.62	> 32	21,85	> 32
		Khex	16,99	20,96	> 32	> 32	> 32
		KCH	16,23	14,93	16	16	> 32
		KAqM	> 32	> 32	> 32	> 32	> 32
	Chlorophyta						
6	***C. aerea***	**CR**	> 32	> 32	> 32	> 32	> 32
		Khex	16,23	13,79	> 32	> 32	14,72
		KCH	> 32	> 32	> 32	25,85	> 32
		KAqM	> 32	> 32	> 32	> 32	> 32
7	***C. fragile* subsp. *fragile***	**CR**	17,28	> 32	> 32	> 32	> 32
		Khex	23,24	19,23	25,40	11,89	17,59
		KCH	16,12	30,91	> 32	12,36	> 32
		KAqM	> 32	> 32	> 32	> 32	> 32
8	***Ulva compressa***	**CR**	17,91	14	> 32	> 32	> 32
		Khex	16,35	14,81	> 32	> 32	> 32
		KCH	> 32	> 32	> 32	17,08	> 32
		KAqM	> 32	> 32	> 32	> 32	> 32
	Standard compounds		0,023[a]	3,33[b]	6,1[c]	0,36[d]	8,2[e]

[**CR:** Crude (MeOH:$CHCl_3$), **Khex:** Hexane-soluble subextract, **KCH:** Chloroform-soluble subextract, **KAqM:** Water-methanol-soluble subextract, ***Tbb***: *Trypanosoma brucei brucei,* ***Tc****: Trypanosoma cruzi,* ***Lf:*** *Leishmania infantum,* ***Pf****: Plasmodium falciparum,* **MRC-5 Line:** Human Fetal Lung Fibroblats Cells, Standard compounds: [a]Suramin, [b]Benznidazole, [c]Miltefosine, [d]Chloroquine, [e]Tamoxifen].

DISCUSSION

Acetylcholine (ACh) is a neurotransmitter at cholinergic synapses in the nervous systems and hydrolyzed mainly by the enzyme acetylcholinesterase (AChE). Increasing AChE concentrations to inhibit the rate of hydrolysis of ACh is considered the most effective treatment against AD [35]. Synthetic drugs (donepezil, takrin, rivastigmin) and natural drugs (physostigmine and galanthamine) for AD treatment can't answer the purpose because of possessing adverse effect and changing or altering the underlying cause of this terminal disease [36]. Researchers have previously attempted to develop ChE inhibitors on synthetically or plants and fungi used in drugs trials, but now started to work with marine algae [37].

Researchers have focused on marine environments due to marine organisms have ability to produce secondary metabolites. To date, many bioactive chemically unique compounds have isolated from such as algae, sponges, corals, ascidians and fungi, and marine algae, which is one of the largest producers in marine ecosystem, has been extensively investigated the last 20 years [38]. Marine algae are among the richest sources of known and novel bioactive compounds [39, 40]. These metabolites has just started to be explored the last few decades of which sterols, phlorotannins, alkaloids, terpenoids have showed AChE inhibitory activity [41, 42]. Since most of the acetylcholinesterase inhibitors, such as alkaloids, are known to contain nitrogen, the higher activity of these extracts may be due to their rich alkaloidal content [35]. Alkaloids can inhibit AChE activity mainly due to their rich alkaloid content [35, 40, 43].

In the present study, the highest extract concentration tested was 200 mg/mL, with IC_{50} results ranging from 19,22±10,47 to 425,91±298,55. Among the solvent extracts derived from the CR of a brown alga *Petalonia fascia* crude and the Khex of a green alga *Chaetomorpha aerea* extracts possessed the highest acetylcholinesterase inhibitory activities under *in vitro* condition. Kontath et al. [44] have reported that the alkaloid extracts of two species of *Lycopodium* (*L. clavatum* and *L. thyoides*) significantly inhibited the AChE activity *in vitro*. AChE activity was found to be inhibited in the rat cortex, hippocampus and striatum homogenates incubated *in vitro.* An ethanolic extract of fresh-water algae *Spirogyra gratiana* possessed the highest inhibition as 42.5± 2.28% at 2.0 mg/mL against AChE [45].

The presence of clerodene or similar diterpenes has been offered as the responsible for the AChE activity of the organic extracts of the roots of *C. mimosoides* by the Adewusi et al. [46]. AChE Activity of this species has been reported as the highest as IC_{50} 0.03 ± 0.08 mg/ml.

Japanese and Chinese cultures have used seaweed decoctions since ancient times for the treatment of parasitic diseases, as well as other diseases [15, 47]. As a result of some related studies, various seconder metabolites of seaweeds, such as terpenes, sulfated fucans, kainic acid, oxylipin, galactan sulfate, derived from marine algae showed antiprotozoal activity [48-52]. Polysaccharides, polyketides and polysaccharide derivates (prumycin) also have potential antiplasmoidal activity [53]. In the present study, the *in vitro* inhibitory activities of the CR, Khex, KCH and KAqM extracts of 8 marine algae (total 32 extracts) were evaluated against four parasitic protozoa (*P. falciparum, L. infantum, T. b. brucei* and *T. cruzi*). According to results, the most potent protozoal activities were shown by the Khex of *C. crinita* (IC_{50} value of 10,62 µg/ml), followed by the Khex of *C. fragile* subsp. *fragile* (IC_{50} value of 11,89 µg/ml). The hekzan-soluble (Khex) and chloroform-soluble (KCH) extracts gave the best results (Table 2). The active antiprotozoal compounds were relatively apolar [28].

Algal extracts tested for toxicities and four algal extracts that are the CR and Khex of *H. scoparia*, the Khex of *C. aerea* and *C. fragile* subsp. *fragile*, appeared to be associated with some toxicity. But these extracts showed no effect all test parasites. For this reason, it is considered that the marine algae extracts possess selective biological effects.

CONCLUSION

This study was performed to screen biological activities of marine algae collected from different localities from Turkey. The results of the present study indicated that solvent extracts derived from the CR of a brown alga *Petalonia fascia* and the Khex of a green alga *Chaetomorpha aerea* extracts possessed the highest acetylcholinesterase inhibitory activities under *in vitro* condition. The significance of natural AChE inhibitory activity from these two algae will further be characterized, and they will be evaluated for their bioavailabilities and potential toxicities *in vivo*. According to antiprotozoal assay results, the brown alga *Cystoseira crinita* and the green alga *Codium fragile* subsp. *fragile* were found as having most potent protozoal activities. Seasonal changes in activities of the extracts could be related the synthesis of different compounds during the different growth conditions [19]. For standardization of extracts of the inhibitory activities, identification of the compounds or compound groups responsible for the related activity is important.

ACKNOWLEDGEMENTS

This study was supported by Manisa Celal Bayar University (FBE BAP 2010/066).

REFERENCES

[1] Alzheimer's Disease International. World Alzheimer Report (2009): 1–93. http://www.alz.co.uk/research/files/WorldAlzheimerReport.pdf.

[2] Hanağası, H.A. and Emre, M. (2009) The concept of dementia and approach to the patient. Türkiye Klinikleri Dergisi-Nöroloji. 1(Special issue), 1–4.

[3] Natarajan, S., Shanmugiahthevar, K.P., Kasi, P.D. (2009) Cholinesterase inhibitors from Sargassum and Gracilaria gracilis: Seaweeds inhabiting South Indian coastal areas (Hare Island, Gulf of Mannar). Natural Product Research. 23, 355–369.

[4] Öztürk, G.B., Karan, M.A. (2009) Pathophysiology of Alzheimer's disease. Klinik Gelişim. 22, 36–45.

[5] Yazıcı, T.G., Şahin, H.A. (2010) Alzheimer's disease. Klinik Gelişim. 23, 48–52.

[6] Selekler, K. and Topçuoğlu, E.S. (1998) Alzheimer's disease. Turkish Journal of Geriatrics. 1, 63–67.

[7] Wszelaki, N., Kuciun, A. and Kiss, A. (2010) Screening of traditional European herbal medicines for acetylcholinesterase and butyrylcholinesterase inhibitory activity. Acta Pharmaceut. 60, 119–128.

[8] Omurtag, C. (1975) Medical Protozoology. Ankara University, Faculty of Pharmacy Publications, Textbook. No:34.

[9] Orhan, I., Şener, B., Atıcı, T., Brun, R., Perozzo, R. and Taşdemir, D. (2006) Turkish freshwater and marine macrophyte extracts show in vitro antiprotozoal activity and inhibit FabI, a key enzyme of *Plasmodium falciparum* fatty acid biosynthesis. Phytomedicine. 13, 388–393.

[10] World Health Organization (WHO) (2010) Working to Overcome the Global Impact of Neglected Tropical Diseases. First WHO report on neglected tropical diseases.

[11] Tezer, H. and Devrim, İ. (2008) Antiprotozoal vaccines in developing. Magazine Child Infections 2. 2(Special Issue 2), 76–82.

[12] World Health Organization (WHO) (2010) Working to Overcome the Global Impact of Neglected Tropical Diseases. First WHO report on neglected tropical diseases. 12 October 2010. http://www.who.int/neglected_diseases/2010report/NTD_2010report_web.pdf (accesses on 20 June 2013).

[13] Barrett, M.P., Boykin, D.W., Brun, R. and Tidwell, R.R. (2007) Human African trypanosomiasis: Pharmacological re-engagement with a neglected disease. Br J Pharmacol. 152, 1155–1171.

[14] Nwaka, S., Ramirez, B., Brun, R., Maes, L., Douglas, F. and Ridley, R. (2009) Advancing drug innovation for neglected diseases-criteria for lead progression. Plos Negl Trop Dis. 3, e440.

[15] Spavieri, J., Allmendinger, A., Kaiser, M., Casey, R., Hingley-Wilson, S., Lalvani, A., Guiry, M.D., Blunden, G. and Taşdemir, D. (2010) Antimycobacterial, Antiprotozoal and Cytotoxic Potential of Twenty-one Brown Algae (Phaeophyceae) from British and Irish Waters. Phytotherapy Research. 24, 1724–1729.

[16] Chanda, S., Dave, R., Kaneria, M. and Nagani, K. (2010) Seaweeds: A novel, untapped source of drugs from sea to combat Infectious diseases. In: Mendez-Vilas, A. (ed.) Current Research, Technology and Education Topics in Applied Microbiology and Microbial Biotechnology. FORMATEX Research Center, Badajoz, Spain, 473–480.

[17] Gupta, A., Vijayaraghavan, M.R. and Gupta, R. (1998) The presence of cholinesterase in marine algae. Phytochemistry. 49, 1875–1877.

[18] Jin, D.Q., Lim, C.S., Sung, J.Y., Choi, H.G., Ha I. and Han, J.S. (2006) *Ulva conglobata*, a marine algae, has neuroprotective and anti-inflammatory effects in murine hippocampal and microglial cells. Neuroscience Letters. 402, 154–158.

[19] Stirk, W.A., Reinecke, D.L. and Staden, J.V. (2007) Seasonal variation in antifungal, antibacterial and acetylcholinesterase activity in seven South African seaweeds. J. Appl. Phycol. 19, 271–276.

[20] Choi, B.W., Rhu, G., Park, S.H., Kim, E.S., Shin, J., Rohn, S.S., Shin, H.C. and Lee, B.H. (2007) Anticholinesterase activity of plastoquinones from *Sargassum sagamianum*: Lead compounds for Alzheimer's disease theraphy. Phytotherapy Research. 21, 423–426.

[21] Yoon, N.Y., Eom, T.K., Kim, M.M. and Kim, S.K. (2009) Inhibitory effect of phlorotannins isolated from *Ecklonia cava* on mushroom tyrosinase activity and melanin formation in mouse B16F10 melanoma cells. J. Agric. Food. Chem. 57, 4124–4129.

[22] Nguyen, H. and Kim, S.M. (2012) Antioxidative, anticholinesterase and antityrosinase activities of the red alga *Grateloupia lancifolia* extracts. African Journal of Biotechnology. 11(39), 9457–9467.

[23] Navarro, M.C., Montilla, M.P., Cabo, M.M., Galisteo, M., Caceres, A., Morales, C. and Berger, I. (2003) Antibacterial, Antiprotozoal and Antioxidant Activity of Five Plants Used in Izabal for Infectious Diseases. Phytother. Res. 17, 325–329.

[24] Truiti, M.C.T., Ferreira, I.C.P., Zamuner, M.L.M., Nakamura, C.V., Sarragiotto, M.H. and Souza, M.C. (2005) Antiprotozoal and molluscicidal activities of five Brazilian plants. Brazilian Journal of Medical and Biological Research. 38, 1873–1878.

[25] Allmendinger, A., Spavieri, J., Kaiser, M., Casey, R., Hingler-Wilson, S., Lalvani, A., Guiry, M., Bhadury, P. and Wright, P.C. (2010) Exploitation of marine algae: biogenic compounds for potential antifouling applications. Planta. 219, 561–578.

[26] Süzgeç-Selçuk, S., Meriçli, A.H., Güven, K.C., Kaiser, M., Casey, R., Hingley-Wilson, S., Lalvani, A. and Taşdemir, D. (2011) Evaluation of Turkish Seaweeds for Antiprotozoal, Antimycobacterial and Cytotoxic Activities. Phytotherapy Research. 25(5), 778–783.

[27] Ravikumar, S., Inbaneson, A.J., Suganthi, P., Gokulakrishnan, R. and Venkatesan, M. (2011) In vitro antiplasmodial activity of ethanolic extracts of seaweed macroalgae against *Plasmodium falciparum.* Parasitol Res. 108(6), 1411–1416.

[28] Vonthron-Sénécheau, C., Kaiser, M., Devambez, I., Vastel, A., Mussio, I. and Rusig, A.M. (2011) Antiprotozoal Activities of Organic Extracts from French Marine Seaweeds. Mar. Drugs. 9, 992–933.

[29] Kupchan, S.M. and Tsou, G. (1973) Tumor inhibitors. A new antileukemic simaroubolide from *Brucea antidysenterica*. J. Org. Chem. 38, 178–179.

[30] Muhit, M.A., Tareq, S.M., Apu, A.S., Basak, D. and Islam, M.S. (2010) Isolation and Identification of Compounds from the Leaf Extract of *Dillenia indica* Linn. Bangladesh Pharmaceutical Journal. 13(1), 49–53.

[31] Ellman, G.L., Courtney, K.D., Andres, V.J. and Featherstone, R.M. (1961) A new and rapid colorimetric determination of acetylcholinesterase activity. Biochem. Pharmacol. 7, 88–95.

[32] Rollinger, J.M., Hornick, A., Langer, T., Stuppner, H. and Prast, H. (2004) Acetylcholinesterase inhibitory activity of scopolin and scopoletin discovered by virtual screening of natural products. J. Med. Chem. 47, 6248–6254.

[33] Schuster, D., Kern, L., Hristozov, D.P., Terfloth, L., Bienfait, B., Laggner, C., Kirchmair, J., Grienke, U., Wolber, G., Langer, T., Stuppner, H., Gasteiger, J. and Rollinger, J.M. (2010) Applications of integrated data mining methods to exploring natural product space for acetylcholinesterase inhibitors. Comb. Chem. HTS 13, 54–66.

[34] Maes, L. (2007) Standard procedures used for the TDR in vitro screening against Malaria, Sleeping sickness, Chagas disease, Leishmaniasis, Cytotoxicity. Antwerp University, Laboratory of Microbiology, Parasitology and Hygiene, Belgium.

[35] Orhan, I., Şener, B., Choudhary, M.I. and Khalid, A. (2004) Acetylcholinesterase and butyrylcholinesterase inhibitory activity of some Turkish medicinal plants. J. Ethnopharma. 91, 57–60.

[36] Kannan, R.R.R., Aderogba, M.A., Ndhlala, A.R., Stirk, W.A. and Staden, J.V. (2013) Acetylcholinesterase inhibitory activity of phlorotannins isolated from the brown alga, *Ecklonia maxima* (Osbeck) Papenfuss. Food Research International. 54, 1250–1254.

[37] Syad, A.N., Shunmugiah, K.P. and Kasi, P.D. (2012) Assessment of anticholinesterase activity of *Gelidiella acerosa*: Implications for its therapeutic potential against Alzheimer's Disease. Evidence-Based Complementary and Alternative Medicine. 2012, Article ID 497242, 8p.

[38] Taşkın, E., Çakı, Z., Öztürk, M. and Taşkın, E. (2010) Assessment of in vitro antitumoral and antimicrobial activities of marine algae harvested from the eastern Mediterranean Sea. African Journal of Biotechnology. 9(27), 4272–4277.

[39] Faulkner, D.J. (2002) Marine natural products. Nat. Prod. Rep. 19, 1–49.

[40] Blunt, J.W., Copp, B.R., Munro, M.H.G., Northcote, P.T. and Prinsep, M.R. (2006) Marine natural products. Nat. Prod. Rep. 23, 26–78.

[41] Stirk, W.A., Reinecke, D.L. and Staden, J.V. (2007) Seasonal variation in antifungal, antibacterial and acetylcholinesterase activity in seven South African seaweeds. J Appl Phycol. 19, 271–276.

[42] Yoon, N.Y., Chung, H.Y., Kim, H.R. and Choi, J.S. (2008) Acetyl- and butyrylcholinesterase inhibitory activities of sterols and phlorotannins from *Ecklonia stolonifera.* Fisheries Science. 74, 200–207.

[43] Elgorashi, E.E., Stafford, G. and van Staden, J. (2004) Acetylcholinesterase enzyme inhibitory effects of Amaryllidaceae alkaloids. Planta Med. 70, 260–262.

[44] Konrath, E.L., Neves, B.M., Lunardi, P.S., Passos, C.S., Simões-Pires, A., Ortega, M.G., Gonçalves, C.A., Cabrera, J.L., Moreira, J.C.F. and Henriques, A.T. (2012) Investigation of the in vitro and ex vivo acetylcholinesterase and antioxidant activities of traditionally used Lycopodium species from South America on alkaloid extracts. Journal of Ethnopharmacology. 139, 58–67.

[45] Kartal, M., Orhan, I., Abu-Asaker, M., Atıcı, T. and Şener, B. (2009) Antioxidant and Anticholinesterase Assets and Liquid Chromatography-Mass Spectrometry Preface of Various Fresh-Water and Marine Macroalgae. Phcog. Mag. 5(20), 291–297.
[46] Adewusi, E.A., Moodley, N. and Steenkamp, V. (2011) Antioxidant and acetylcholinesterase inhibitory activity of selected southern African medicinal plants. South African Journal of Botany. 77, 638–644.
[47] Moo-Puc, R., Robledo, D. and Freile-Pelegrin, Y. (2008) Evaluation of selected tropical seaweeds for in vitro anti-trichomonal activity. J. Ethnopharmacol. 120, 92–97.
[48] Numata, A., Kanbara, S., Takahashi, C., Fujiki, R., Yoneda, M., Fujita, E. and Nabeshima, Y. (1991) Cytotoxic activity of marine algae and a cytotoxic principle of the brown alga *Sargassum tortile*. Chemical and Pharmaceutical Bulletin. 39, 2129–2131.
[49] Itoh, H., Noda, H., Amano, H., Zhuaug, C. and Mizuno, T. (1993) Antitumor activity and immunological properties of marine algal polysaccharides, especially fucoidan, prepared from *Sargassum thunbergii* of Phaeophyceae. Anticancer Research. 13, 2045–2052.
[50] Mazumder, S., Ghosal, P.K., Pujol, C.A., Carlucci, M.J., Damonte, E.B. and Ray, B. (2002) Isolation, chemical investigation and antiviral activity of polysaccharides from *Gracilaria corticata* (Gracilariaceae, Rhodophyta). International Journal of Biological Macromolecules. 31, 87–95.
[51] Topcu, G., Anydoqmus, Z., Imre, S., Goren, A.C., Pezzuto, J.M., Clement, J.A. and Kingston, D.G. (2003) Brominated sesquiterpenes from the red alga *Laurencia obtusa*. Journal of Natural Products. 66, 1505–1508.
[52] Barbosa, J.P., Pereira, R.C., Abrantes, J.L., dos Santos, C.C., Rebello, M.A., Frugulhetti, P.P. and Teixeira, V.L. (2004) In vitro antiviral diterpenes from the Brazilian Brown alga *Dictyota pfaffii*. Planta Medica. 70, 856–860.
[53] Otoguro, K., Ishiyama, A., Kobayashi, M., Sekiguchi, H., Izuhara, T., Sunazuka, T., Tomoda, H., Yamada, H. and Omura, S. (2004) *In vitro* and *in vivo* antimalarial activities of a carbohydrate antibiotic, prumycin against drug resistant strains of Plasmodia. J Antibio. 57(6), 400–402.

Received: **21.12.2018**
Accepted: **18.03.2019**

CORRESPONDING AUTHOR

Ergun Taskin
Department of Biology
Faculty of Arts & Sciences
Manisa Celal Bayar University
Muradiye, Manisa 45140 – Turkey

e-mail: ergun.taskin@cbu.edu.tr

© by PSP Volume 28 – No. 5/2019 pages 4001-4006 Fresenius Environmental Bulletin

ANTI-PROLIFERATIVE AND APOPTOTIC EFFECTS OF VINCRISTINE AND VINBLASTINE ON MULTIPLE MYELOMA

Ela Nur Simsek Sezer*, Tuna Uysal

Selçuk University, Science Faculty Biology Department, Konya, Turkey

ABSTRACT

Vinca alkaloids are usually included in a combination of chemotherapy applications for curative therapies. The best known are vincristine (VCR) and vinblastine (VBL), which are derived from *Catharanthus roseus* (Apocynaceae). The purpose of this study was to demonstrate the anti-proliferative and apoptotic effects of VCR and VBL on multiple myeloma (MM) cells. Toward this aim, the WST-1 assay was performed for cell proliferation analyses and the expression levels of the apoptotic gene regions were determined using quantitative RT-PCR. According to the WST-1 results, 2 *Vinca* alkaloids had an anti-proliferative effect on each of the MM cell lines. The WST-1 results showed that at the applied concentrations, VBL was more effective than VCR on the studied MM cells. On the other hand, the RT-PCR results indicated that alkaloids have a positive effect on a significant number of apoptotic gene regions at the molecular level. These results show that VCR and VBL have variable positive effects over the apoptotic genes in terms of gene expressions. From our findings, it was deduced that VBL is more effective than VCR with regards to the inhibition of cell proliferation and it has the potential to be used instead of VCR in clinical approaches. Consequently, this study promotes further studies of the *Vinca* alkaloids and their mechanism of actions.

KEYWORDS:
Vinca alkaloids, WST-1, multiple myeloma.

INTRODUCTION

Cancer is the second leading cause of death worldwide. Although significant progress has been made in the control and treatment of cancer, there are still prominent deficiencies [1]. Multiple myeloma (MM) is the second most common haematological cancer, characterized by uncontrolled proliferation of monoclonal plasma cells in the bone marrow [2]. The lifetime risk for MM is around 1 in 143 and the causes of MM have not been clearly identified to date. Research suggests that it is related to a decline in immune functions, some occupations, and exposure to chemicals and radiation [3]. Despite the occurrence of new therapies and agents, MM remains a difficult cancer to treat.

Over the last decade, herbal medicine has become an essential alternative for world health. Herbal medicines play a considerable role in the prevention and treatment of cancer, and they are comparatively economical [4].

Medicinal plants continue to play a pivotal role in the health system for a large amount of the world's population [5, 6]. Moreover, plants and plant-derived compounds have a long history of application in cancer therapies [7]. Alkaloids are a class of organic compounds made up of oxygen, nitrogen, hydrogen, and carbon, and they are derived from several plant species. Many alkaloids have toxic characteristics as well as physiological effects that make them useful as a drug [8]. The first *Vinca* alkaloids to progress into clinical use were vincristine (VCR) and vinblastine (VBL), from the *Catharanthus roseus* G. Don. (Madagascar periwinkle) (Apocynaceae) [9].

This plant is endemic to Madagascar Island and has long been considered to have a wide range of medicinal properties, ranging from the treatment of diabetes to wound healing [10]. The alkaloids of *Vinca* have been part of standard care for more than 30 years [10]. There have been at least 86 alkaloids extracted from plants in the genus *Vinca* [11]. *Vinca* alkaloids execute their anticancer activity via binding to the tubulin and arresting the cell division of the cancerous cells [12]. *Vinca* alkaloids also inhibit angiogenesis, the growth and spread of cancer cells, and promote apoptosis [13, 14]. The alkaloids of *Vinca* have generally been included in combination chemotherapies for medicinal treatments. VBL has been widely used for the treatment of breast cancer, both non-Hodgkin's and Hodgkin's lymphoma, leukaemia, Ewing's sarcoma, testicular carcinoma nephroblastoma, small-cell lung cancer, and germ cell tumours. VCR was approved to treat, lymphoblastic leukaemia, metastatic melanoma, oestrogen-receptor neuroblastoma, negative breast cancer, colorectal cancer, glioma, B-cell lymphoma, MM, both non-Hodgkin's lymphoma Hodgkin's lymphoma, and rhabdomyosarcoma [15].

The aim of this study was to reveal the

comparative antiproliferative and apoptotic effects of the 2 best known *Vinca* alkaloids on MM and shed light on new approaches to cancer therapy.

MATERIALS AND METHODS

Cell line. The ARH-77 and RPMI-8226 MM cell lines were obtained from the ATCC via the Gülhane Military Medical Academy. The cells were grown in an atmosphere containing 5% CO_2 at 37 ºC. For the VCR and VBL, a stock solution of 1 mg/mL was purchased, and the desired concentrations were prepared using that.

Cell viability assay. Cell viability was measured using a colorimetric assay for 96-well plates with the WST-1 cell proliferation reagent. The ARH-77 and RPMI-8226 cells were counted and transferred to 96-well plates for the cytotoxicity assay, and the plates were incubated for 24 h. After the *Vinca* alkaloids were applied at various concentrations (1–100 µM), the treated cells were then incubated for 24–48 h. Following incubation, WST-1 was added, and the optical densities of the plates were measured using an Elisa microplate reader at 420–480 nm. Each experiment was performed in triplicate and the graphs were generated using the mean of the 3 experiments.

Molecular studies. In order to determine the apoptotic effects of the alkaloids, the total RNA extraction was performed using an Axygen RNA isolation kit according to the manufacturer's instructions, and 0, 5–1 µg RNA was reverse-transcribed to cDNA via a cDNA synthesis kit (Fermentas). The gene expression analysis was performed with real-time polymerase chain reaction reactions (RT-PCR). The B-actin gene was used as a housekeeping gene. Apoptotic gen regions and β-actin mRNA expression levels were measured by quantitative real-time RT-PCR. The data were analysed via the comparative CT method, and the fold change was calculated by $2^{-\Delta\Delta CT}$.

Statistical Analysis. For the statistical analysis of data, multiple comparisons were performed using 1-way analysis of variance (ANOVA) followed by the Dunnett's test for post hoc analysis.

RESULTS

Effects on cell proliferation. Our data indicated that 2 *Vinca* alkaloids, both VBL and VCR, were cytotoxic to the MM cell lines ARH-77 and RPMI-8226.

After treatment with the alkaloids for 24 and 48 h, the WST-1 assay revealed a dramatic decrease in mitochondrial dehydrogenase activity, an indicator of cell viability [16], in the MM cells in a dose- and time-dependent manner. The responses of the MM cells against increasing concentrations of the *Vinca* alkaloids are shown in Figs. 1 and 2.

When the anti-proliferative effects of the alkaloids were evaluated, it was observed that VBL was more effective than VCR in both cell lines.

Real-Time PCR results. In order to determine the expression level of the pro-apoptotic and anti-apoptotic genes in the treated MM cells, the mRNA levels of Bak, Bax/Bcl-2, Apaf, p53, GADD45A, HRK, caspase-8, and caspase-3 were evaluated via qRT-PCR. The relative expression graphs of studied gene regions are given in Fig. 3.

After 24 h treatment with IC_{50} concentrations of the alkaloids, Bax/Bcl-2, Apaf, p53 HRK, BAK, and caspase-3 expressions were induced in the MM cells. Extract treatment up-regulated pro-apoptotic proteins such as Bax, Apaf, p53 HRK, BAK, DFFA, and caspase-3, and down-regulated anti-apoptotic proteins like Bcl-2.

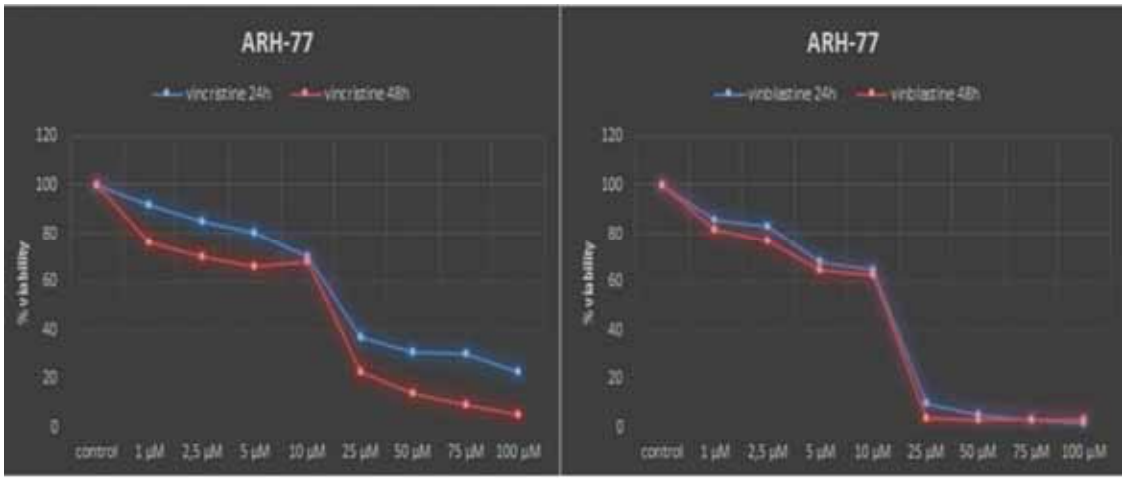

FIGURE 1
Anti-proliferative effects of VCR and VBL on the ARH-77 cell line.

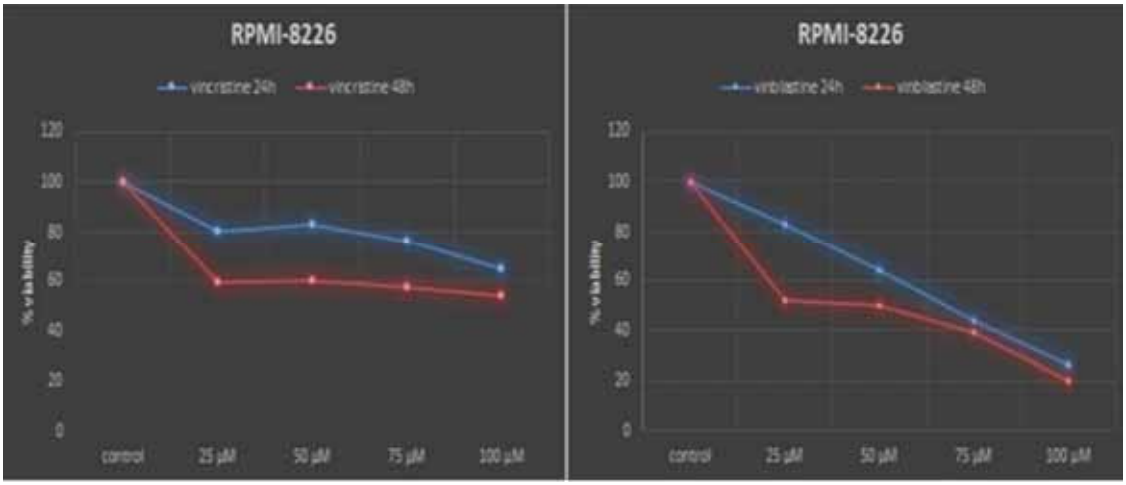

FIGURE 2
Anti-proliferative effects of VCR and VBL on the RPMI-8226 cell line.

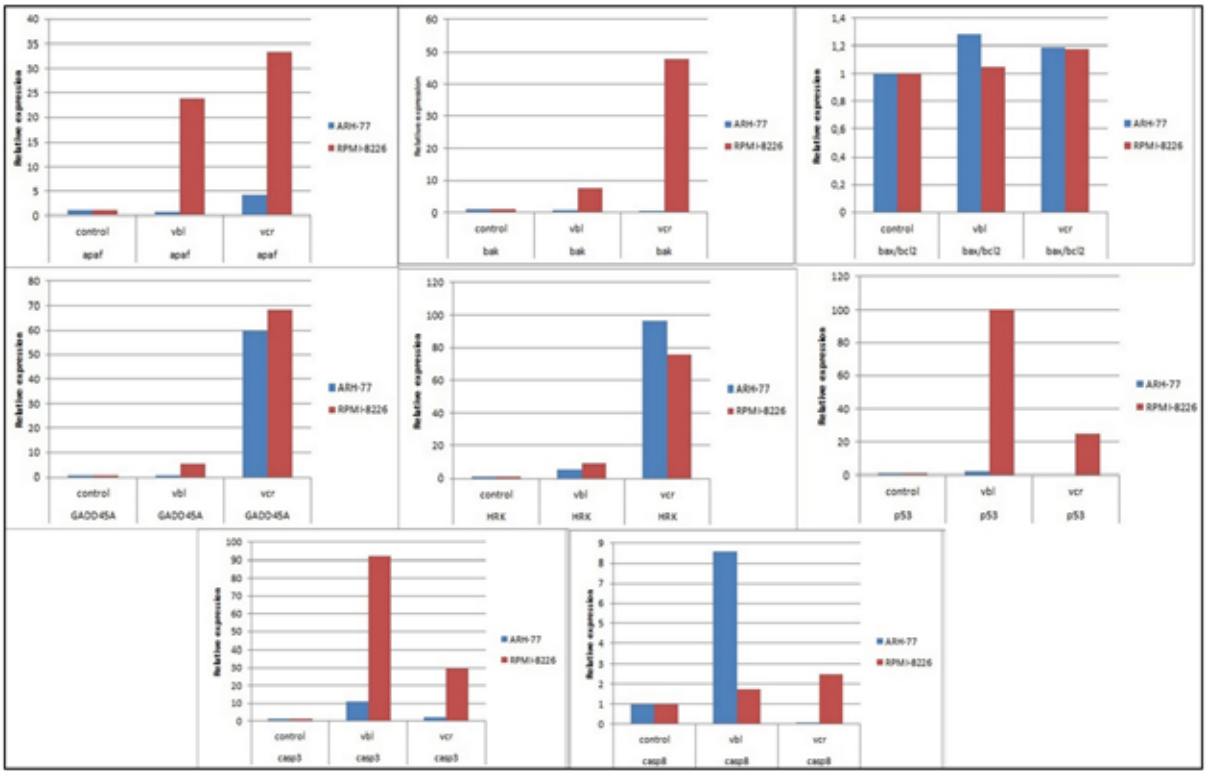

FIGURE 3
Relative expression levels of apoptosis-related genes in the VCR and VBL treated MM cells.

In the ARH cell line, VCR more effectively up-regulated the APAF, GADD45A, and HRK gene regions, while VBL was more effective with BAK, BAX/BCL-2, p53, Casp3, and Casp8. In the other cell line, RPMI-8226, this situation changed for the BAK, BAX/BCL-2, and Casp8 gene regions. Real-time PCR results indicated that alkaloids act on different apoptotic gene regions at the molecular level. These results showed that VCR and VBL have different, but mostly apoptosis-inducing, effects in terms of gene expressions.

DISCUSSION

VCR and VBL have been previously reported to inhibit the cell proliferation of various types of cancer cells, including leukaemia, melanoma, mouse neuroblastoma, mouse leukaemia L1210, mouse lymphoma S49, HeLa, and human promyelocytic leukaemia HL-60 [17]. According to the literature, although there are some studies on the apoptotic effects of *Vinca* alkaloids in different cell lines, there is no data on the MM cell lines studied herein. The previous studies examining the effects

of *Vinca* alkaloids on cell proliferation are summarised as follows: It was reported that 4 alkaloids inhibited B16 melanoma cell proliferation, the order of effectiveness when compared at a single concentration, was VBL > vindesine (VDS) > VCR > vinepidine [18]. In another study, it was reported that the relative inhibition of L1210 leukaemia cell proliferation was VDS > VBL > VCR [19], and in yet another study, VDS was reported to be more effective than VBL and VCR in prolonging the life of mice bearing B16 melanoma tumours [20]. In agreement with these reports, VCR and VBL had a strong inhibitory effect over both the resistant and sensitive MM cell lines, and they prevented the proliferation of each one within the critical time intervals. More specifically, our results indicated that VBL was more effective than VCR in terms of the inhibition of the proliferation of the 2 studied MM cell lines. Moreover, no different side effects were observed when compared to the others. As a general contribution, it can be said that various alkaloids could display slightly different effects on several kinds of cancer depending on their chemical structure and action mechanism. More specifically, due to it exhibiting an excellent result in our comparisons, we believe that VBL should be used as a preferable chemotherapy drug for clinical approaches of MM.

While the disruption of the mitotic process is a critical feature of the *Vinca* alkaloids, the final effect of this metaphase arrest is the death of the cell through activation of apoptotic pathways [21, 22]. BAX, BCL-2, and p53 are the most critical gene regions that have the ability to regulate the apoptosis of tumour cells [23] and the ratio of BAX to BCL-2 also determines the susceptibility of a cell to apoptosis [24]. In a previous study, consistent with our results, it was reported that treatment of BT-20 cells with VCR and VBL up-regulated P53 expression [25]. It was also reported that VCR up-regulated the expression of Bax, Bak, PUMA, Noxa, p53, and p21 proteins, and down-regulated and/or phosphorylated the Bcl-2 protein in melanoma cell lines [26]. The present study showed the effects of *Vinca* alkaloids on 8 apoptotic gene expressions that play an important role in the process of apoptosis in MM cell lines. The applied alkaloids had similar, but variable, apoptotic effects on MM. In our study, both VCR and VBL up-regulated the BAX/BCL-2 ratio and p53 gene expressions. One of the most remarkable observations was the application of VBL in the RPMI-8226 cell line increased the p53 expression 5 times more than the VCR did. This means that VBL was more effective on the p53 pathway. On the other hand, VCR was very effective in regulating the GADD45A and HRK gene regions, which regulate growth arrest and apoptosis, respectively. With regards to the other gene regions, the alkaloids caused similar gene expressions over each of the MM cell lines, and no significant changes were observed between them.

Caspase-3 is the most widely investigated member of the pro-apoptotic gene family. Recent studies have suggested that proteolytic cleavage and the activation of caspase-3 may be functionally important in the induction of apoptosis. Various anticancer drugs have been reported to induce caspase-3 activation in the pathway leading to apoptosis [27–29]. One of these drugs, VBL, induces apoptosis, resulting in Bcl-2 inactivation, and the activation of caspase-3 in human small-cell lung carcinoma Ms-1 cells [30]. Furthermore, it has been reported that VCR induces apoptosis in SH-SY5Y (neuroblastoma) cells through the activation of caspase-3 and -9 [31]. In our study, both the VBL and VCR applications up-regulated the caspase-3 expression, and VBL was more effective than VCR in the 2 studied cell lines. Therefore, when the apoptotic effects of alkaloids are considered in general, it is very important that VBL up-regulates both p53, as the main junction point of apoptosis, and caspase-3, as the last scavenger of apoptosis.

In conclusion, this study is the first to declare that the *Vinca* alkaloids applied, VCR and VBL, have variable but positive effects over the apoptotic genes in terms of gene expressions. Moreover, VBL was more effective than VCR with regards to the anti-proliferation of MM cells, and it could potentially be a primary drug to been used instead of VCR in clinical approaches. Therefore, this work encourages future studies with regards to *Vinca* alkaloids, cancer prevention, phytotherapy, and drug development.

ACKNOWLEDGEMENTS

We are grateful to Prof. Dr Ferit AVCU (Memorial Hospital, Turkey) and Prof. Dr Güner Hayri ÖZSAN (9 Eylül University, Turkey) for providing the cell material and their helpful contributions. We also would like to thank the BAP (Scientific Researching Projects) Foundation of Selçuk University for their financial support (Project number 15101005).

REFERENCES

[1] Desai, A.G., Qazi, G.N., Ganju, R.K., El-Tamer, M., Singh, J., Saxena, A.K., Bedi, Y.S., Taneja, S.C., Bhat, H.K. (2008) Medicinal plants and cancer chemoprevention. Current drug metabolism. 9(7), 581-591.

[2] Collins, C.D. (2010) Multiple myeloma. Cancer imaging: the official publication of the International Cancer Imaging Society. 10(1), 20-31.

[3] Multiple Myeloma Research Foundation (MMRF). (2018) https:// themmrf.org.

[4] Nigam, S.K. (2015) What do drug transporters really do? Nature reviews Drug discovery. 14(1), 29.
[5] Cox, P.A. (1994) The ethnobotanical approach to drug discovery: strengths and limitations. In Ethnobotany and the search for new drugs. 185, 25-41.
[6] Cox, P.A., Balick, M.J. (1994) The ethnobotanical approach to drug discovery. Scientific American. 270(6), 82-87.
[7] Hartwell, J.L. (1982) Plants Used Against Cancer. Quarterman publications, Lawrence, MA.
[8] Sahelian R. (2011) Alkaloid substances in plants, information on vinca, ergot and ephedra alkaloid compounds.
[9] Cragg, G.M., Newman, D.J. (2005) Plants as a source of anti-cancer agents. Journal of ethnopharmacology. 100(1-2), 72-79.
[10] Coufal, N., Farnaes, L. (2011) The *Vinca* Alkaloids. In Cancer Management in Man: Chemotherapy, Biological Therapy, Hyperthermia and Supporting Measures. Springer, Dordrecht. 25-37.
[11] Hesse, M. (2002) Alkaloids: nature's curse or blessing?. John Wiley and Sons.
[12] Moudi, M., Go, R., Yien, C.Y.S., Nazre, M. (2013) *Vinca* alkaloids. International journal of preventive medicine. 4(11), 1231.
[13] Pandey, G., Madhuri, S. (2008) Some anti-cancer agents from plant origin. Pl. Arch. 8(2), 527-532.
[14] Madhuri, S., Pandey, G. (2009) Some anti-cancer medicinal plants of foreign origin. Current science. 96, 779-783.
[15] Emanuela, M., Giuseppe, C., Sonia, C., Edoardo, C., Serena, P., Francesca, P., Rui, M., Angela, M.S., Simona, C. (2018) *Vinca* alkaloids and analogues as anti-cancer agents: Looking back, peering ahead. Bioorganic and medicinal chemistry letters. 28(17), 2816-2826.
[16] Mosmann, T. (1983) Rapid colorimetric assay for cellular growth and survival: application to proliferation and cytotoxicity assays. Journal of immunological methods. 65(1-2), 55-63.
[17] Ferguson, P.J., Phillips, J.R., Selner, M., Cass, C.E. (1984) Differential activity of vincristine and vinblastine against cultured cells. Cancer research. 44(8), 3307-3312.
[18] Jordan, M.A., Himes, R.H., Wilson, L. (1985) Comparison of the effects of vinblastine, vincristine, vindesine, and vinepidine on microtubule dynamics and cell proliferation in vitro. Cancer research. 45(6), 2741-2747.
[19] Howard, S.M., Theologides, A., Dziubinski, J., Sheppard, J.R. (1980) Vinca alkaloids and the hormonal response of l1210 cells. Cancer Res. 40(8 Pt 1), 2695-700.
[20] Sweeney, M.J., Boder, G.B., Cullinan, G.J., Culp, H.W., Daniels, W.D., Dyke, R.W., Gerzon, K., McMahon, R.E., Nelson, R.L., Poore, G.A. & Todd, G.C. (1978) Antitumor activity of deacetyl vinblastine amide sulfate (vindesine) in rodents and mitotic accumulation studies in culture. Cancer research. 38(9), 2886-2891.
[21] Harmon, B.V., Takano, Y.S., Winterford, C.M., Potten, C.S. (1992) Cell death induced by vincristine in the intestinal crypts of mice and in a human Burkitt's lymphoma cell line. Cell Prolif. 25(6), 523–536.
[22] Tsukidate, K., Yamamoto, K., Snyder, J.W., Farber, J.L. (1993) Microtubule antagonists activate programmed cell death (apoptosis) in cultured rat hepatocytes. Am J Pathol. 143(3), 918–925.
[23] Song, G., Mao, Y., Cai, Q., Yao, L., Ouyang, G., Bao, S. (2005) Curcumin induces human HT-29 colon adenocarcinoma cell apoptosis by activating p53 and regulating apoptosis-related protein expression. Brazilian Journal of Medical and Biological Research. 38(12), 1791-1798.
[24] Salakou, S., Kardamakis, D., Tsamandas, A. C., Zolota, V., Apostolakis, E., Tzelepi, V., Papathanasopoulos, P., Bonikos, D.S., Papapetropoulos, T., Petsas, T., Dougenis, D. (2007) Increased Bax/Bcl-2 ratio up-regulates caspase-3 and increases apoptosis in the thymus of patients with myasthenia gravis. In vivo. 21(1), 123-132.
[25] Mavrogiannis, A.V., Kokkinopoulou, I., Kontos, C.K. and Sideris, D.C. (2018) Effect of *Vinca* Alkaloids on the Expression Levels of microRNAs Targeting Apoptosis-related Genes in Breast Cancer Cell Lines. Current Pharmaceutical Biotechnology. 19(13), 1076-1086.
[26] Zhu, B.K., Wang, P., Zhang, X.D., Jiang, C.C., Chen, L.H., Avery-Kiejda, K.A., Watts, R., Hersey, P. (2008) Activation of Jun N-terminal kinase is a mediator of vincristine-induced apoptosis of melanoma cells. Anti-cancer drugs. 19(2), 189-200.
[27] Ibrado, A.M., Huang, Y., Fang, G. and Bhalla, K. (1996a) Bcl-xL overexpression inhibits taxol-induced Yama protease activity and apoptosis. Cell Growth Differ. 7, 1087–1094.
[28] Ibrado, A.M., Huang, Y., Fang, G., Liu, L. and Bhalla, K. (1996b) Overexpression of Bcl-2 or Bcl-xL inhibits Ara-C-induced CPP32/Yama protease activity and apoptosis of human acute myelogenous leukemia HL-60 cells. Cancer Res. 56, 4743–4748
[29] Erhardt, P. and Cooper, G.M. (1996) Activation of the CPP32 apoptotic protease by distinct signaling pathways with differential sensitivity to Bcl-xL. J. Biol. Chem. 271, 17601–17604.

[30] Tashiro, E., Simizu, S., Takada, M., Umezawa, K., Imoto, M. (1998) Caspase-3 Activation Is Not Responsible for Vinblastine-induced Bcl-2 Phosphorylation and G2/M Arrest in Human Small Cell Lung Carcinoma Ms-1 Cells. Japanese Journal of Cancer Research. 89(9), 940-946.

[31] Tu, Y., Cheng, S., Zhang, S., Sun, H., Xu, Z. (2013) Vincristine induces cell cycle arrest and apoptosis in SH-SY5Y human neuroblastoma cells. International Journal of Molecular Medicine. 31(1), 113-119.

Received: **24.12.2018**
Accepted: **27.03.2019**

CORRESPONDING AUTHOR

Ela Nur Simsek Sezer
Selçuk University,
Science Faculty Biology Department,
Konya – Turkey

e-mail: elasimsek@selcuk.edu.tr

© by PSP Volume 28 – No. 5/2019 pages 4007-4012 Fresenius Environmental Bulletin

STUDY ON COORDINATION DEVELOPMENT OF ECOLOGICAL-ENVIRONMENT AND ECONOMY BASED ON COUPLING MODEL: A CASE STUDY OF WUHAN CITY

Zhentang Ke*, Qingli Xia

Huanggang Normal College, Huanggang, Hubei, 438000, China

ABSTRACT

The environmental issues that accompany rapid economic growth have attracted the attention of the government and the public. Multiple non-linear and complicated interactions exist between the economy and environment subsystem. Accordingly, understanding the operating mechanism of the economy–environment system and evaluating its coordination level are of immense significance for sustainable urban development. This study uses system dynamics (SD) to build a dynamic model of the economy–environment system. Furthermore, a coupling coordination degree model (CCDM) that focuses on the coordination of the economy–environment system is established using data from 2000 to 2013 for Wuhan City, China. Coordination assessment results based on the CCDM show that the coordination of the economy scenario performs the worst, the environment scenario performs best in the short term.

KEYWORDS:
Ecological environment, economic development, Wuhan, Coordination assessment, CCDM

INTRODUCTION

The sustainable development of ecological environment and social economy has always been the focus of attention in the world [1-4]. The coordinated development of ecological environment and social economy was the common responsibility and pursuit of the international community. China, as the largest developing country in the world, has created the "miracle of China" at an average annual rate of 9.8% over 30 years of reform and opening up, but at the same time, "high investment, high pollution and high emissions" model has also led to a series of environmental problems. Environment pollution and ecological destroy gradually evolved into constraints of China's economic and social sustainable development of the outstanding obstacles.

At present, the economic growth continues at the same time the environment is worsening, the ecological damage is becoming more and more serious. Comprehensive evaluation of the environmental economy has been widespread concern in academia [5, 6]. Scholars have studied from the perspective of coordinated development on social economy and ecological environment, ecological security warning, economic growth and environmental pollution, ecological economy [7, 8]. But on the whole, there were few studies on qualify the relationship between social economic development with ecological quality and environmental quality at home and abroad, and lacked of macroeconomic research on the development stage and path of regional environmental economy. Some developed countries mainly focus on the study of micro-scale, such as atmospheric environment [9], water environment [10] and other aspects of pollution characteristics, pollution on biological and human health [11] and macro-scale focuses on pollution emissions and economic growth, cross-border pollution and regional environmental quality [12, 13] and so on.

Single study cannot guide the overall regional environmental governance; other issues had increasingly arisen in the process of solving some problems [14, 15]. At present, there are several methods used in regional environmental assessment, such as ecological footprint, coordination degree, matter element analysis [16] and ecological health risk analysis. Although these methods have their own advantages, but they cannot fully objective evaluate the region's comprehensive socio-economic development level, the development stage and the main contradictions.

It is urgent to develop clear information evaluation models to simulate the relationship between ecological environment and social economic development for management and decision-making basis. Three-dimensional model has been gradually applied to the evaluation field, such as the city's environmental quality [17], eco-city planning [18], and the natural capital utilization [19]. Few coupled model has been studied, such as Niccolucci et al., 2009 [20], Niccolucci et al., 2011 [21] proposed the concept of "three-dimensional ecological footprint" for natural capital accounting. Application of three-dimensional model on simulation the relationship between ecological environment and social economic development, especially on carrying capacity

of regional ecological environment to social economic development was less reported. Therefore, a three-dimensional evaluation model for the carrying capacity of regional ecological environment to social economic development has been established to evaluate the comprehensive level of regional integrated system. It can clarify the main contradiction between social development stage and sustainable development, and can provide management and decision-making basis to achieve economic and environmental coordination, sustainable development.

In summary, this study presents a CCDM method to model the dynamic interactions and future development of the urban system. Comparisons with existing results and policy recommendations are provided in this paper.

MATERIALS AND METHODS

Study area. This study takes Wuhan City (113°41'-115°05'E, 29°58'-31°22'N) as a case study. This city is the capital of Hubei Province in China and located in the middle reaches of the Yangtze River. Wuhan covers an area of 8498.41km^2, thereby accounting for 4.62% of the total area of Hubei Province. With a population of 10.89 million and a gross domestic product (GDP) of 1341.03 billion Yuan in 2017, Wuhan has been the most economically dynamic region in Central China since the launch of the economic reform and opening-up policy in 1978.

Evaluation of the coupling coordination degree. Assessment indicator system for the economy–environment system. We constructed an indicator system based on previous case studies and the structure of our established SD model [22] to synthetically analyse the development level of each subsystem and the coupling relationships of the economy–environment system. Table 1 shows the structure of the indicator system, which contains 9 indicators. The indicator system synthetically reflects economic production and industrial structure in the economy subsystem and environmental pollution and environmental governance in the environment subsystem.

Data pre-processing. To render the results comparable and eliminate the impact of dimension, we use the following two formulas to standardise the indicators:

Positive indicator:

$$r_{ij}=(X_{ij}-\min X_j)/(\max X_j-\min X_j) \quad (1)$$

Negative indicator:

$$r_{ij}=(\max X_j-X_{ij})/(\max X_j-\min X_j) \quad (2)$$

Where maxXj and minXj is the maximum and minimum, respectively, of indicator j in all years; Xij and rij are the original and standardised values of indicator j in year i. A positive indicator means that the greater the value is, the better the implication for the development of the system and vice versa.

Evaluation of the economy, resource and environment subsystems. The weights of each indicator in Table 1 are determined by the entropy method (EM) in this work. The 'entropy' concept originates from thermodynamics, whilst Shannon [23] introduced this concept to describe the uncertainty of an information source. In information theory, 'entropy' is a measure of the degree of disorder in a system that can be used to measure the amount of information and the weight of the known data. That is, the more useful information an indicator provides, the greater the weight it will play in decision-making. EM is an objective weight determination method that has been widely used in comprehensive evaluation. The detailed steps of calculating the weights by EM are as follows:

TABLE 1
Indicator system used to assess CCD of the economy–environment system

Subsystem	Indicator	Direction	Unit	Weight
Economy subsystem	Per capita GDP	+	Yuan/capita	0.3562
	Per capita built-up area	+	Km^2/capita	0.2474
	Proportion of the secondary industry	+	%	0.2717
	Proportion of the tertiary industry	+	%	
Environment subsystem	Discharge of COD	–	Tons/capita	0.0745
	Discharge of SO_2	–	Tons/capita	0.2122
	Discharge of solid waste	–	Tons/capita	0.2528
	Environmental protection investment	+	Yuan/capita	0.2201
	Pollution Index	–	Dimensionless	0.2404

Notes: '+' and '–' represent the positive and negative indicators, respectively.

TABLE 2
Division of the development stages of the economy–environment system

Value of D	0≤D<0.25	0.25≤D<0.5	0.5≤D<0.75	0.75≤D≤1
Development stages	Seriously unbalanced	Slightly unbalanced	Barely balanced	With superior balance

Proportion (P) of the indicator j in year i:

$$P_{ij} = r_{ij} / \sum_{i=1}^{m} r_{ij} \quad (3)$$

Information entropy (e) of each indicator j:

$$e_j = -\frac{1}{\ln m} / \sum_{i=1}^{m} (P_{ij} \bullet \ln P_{ij}) \ (0 \le e_j \le 1) \quad (4)$$

Entropy redundancy (e) of each indicator j:

$$d_j = 1 - e_j \quad (5)$$

Weight (W) of each indicator j:

$$W_j = d_j / \sum_{j=1}^{n} d_j \quad (6)$$

Evaluation of the level (L) of indicator j in year i:

$$L_{ij} = W_j \times r_{ij} \quad (7)$$

Comprehensive level (CL) of the subsystem in year i:

$$CL_i = \sum_{j=1}^{n} S_{ij} \quad (8)$$

Where n is the number of indicators in a subsystem, m denotes the number of years and rij is calculated by Formulas (1) or (2). According to Formulas (3)–(6), we obtained the weights of each indicator in Table 1. The comprehensive level of each subsystem are calculated through Formulas (7)–(8).

Coupling coordination degree model. Coupling, which originates from the physical science, is a phenomenon in which two or more systems influence each other through various interactions. In recent years, this concept is often used in studies of eco-environment and urbanisation. For example, CCDM has been used for the compound system of the eco-environment–urbanisation system, the socio-economy–carbon emission system and the low-carbon development–urbanisation system. However, CCDM is often used in situations with two subsystems and this method is rarely applied to the case of multi-subsystems coupling. Jiang et al. [24] provided a detailed proof of the multi-subsystem coupling formula. The general form indicates that CCDM of the three subsystems is provided in Formula (9):

$$C = \left\{ \frac{f(X) \bullet g(Y) \bullet h(Z)}{\left[\frac{f(X) + g(Y) + h(Z)}{3} \right]^3} \right\}^{\frac{1}{3}}, \quad D = \sqrt{C \bullet T} \quad \text{and}$$

$$T = \alpha f(X) + \beta g(Y) + \gamma h(Z) \quad (9)$$

Where C is the coupling degree, whilst f(X), g(Y) and h(Z) are the comprehensive levels of the economy, resource and environment subsystems, respectively. Here, the value of f(X), g(Y) and h(Z) is determined by Si as indicated in Formula (8). D is the CCD and T reflects the overall development level of the economy–environment system. α, β and γ represent the contribution of each subsystem. This study assumes that each subsystem is equally important to the coordinated development of the economy–environment system. Thus, α=β=γ=13.

After calculating the CCD, scholars often divide CCD into several levels in a subjective manner. The current study applies the quartile method to divide CCD. Accordingly, this method may be more objective for measuring the CCD level. Table 2 shows the division of CCD.

RESULTS AND DISCUSSION

Coordinated relationship between ecological environment and economy. Through the calculation and analysis of the statistical data of Wuhan from 2000 to 2013, the eco-environment comprehensive index, the economic comprehensive index and the coupling development degree are respectively obtained. It can be seen from Table 3 that the coupling development degree of Wuhan ecological environment and economic system is fluctuating continuously. Changes have occurred, and the trend of decline has risen first, and the degree of coupling development has been coordinated from development, low-level development, mild imbalance development, low-level coordinated development, and then back to coordinated development. From 2000 to 2002, Wuhan ecological environment and economic system are coupled. The degree of development showed coordinated development. From 2003 to 2009, the coupling development degree of Wuhan's ecological environment and economic system changed from low level to slight change, and the coupling development degree reached the minimum in 2004. Wuhan's ecological environment and economy from 2010 to 2013 The degree of system coupling development has once again transitioned to coordinated development. The change in coupling development degree shows that people are gradually aware of the importance of protecting the ecological environment and have begun to work on the simultaneous development of the industrial ecological environment and the agricultural economy.

TABLE 3
Coordination between Ecological Environment and Economy in Wuhan City

Year	Ecological environment comprehensive index (G)	Economic index (F)	D	Classification of coupling development level	G/F	Basic type
2000	0.6358	0.4609	0.7315	Coordinated development	0.7228	Coordinated development of ecologically dominant
2001	0.6473	0.1564	0.7580	Coordinated development	0.7979	Coordinated development of ecologically dominant
2002	0.6218	0.4794	0.7538	Coordinated development	0.7710	Coordinated development of ecologically dominant
2003	0.3808	0.4178	0.6312	Low level development	1.0974	Low level coordinated development
2004	0.2953	0.3695	0.5730	Mild imbalance development	1.2522	Mild imbalance development ecological profit and loss type
2005	0.3436	0.3415	0.5853	Mild imbalance development	0.9939	Run-in type of Mild imbalance development
2006	0.3719	0.3386	0.5954	Mild imbalance development	0.9107	Run-in type of Mild imbalance development
2007	0.3754	0.4049	0.6242	Low level development	1.0790	Low level coordinated development
2008	0.3736	0.4435	0.6367	Low level development	1.1873	Low level coordinated development
2009	0.3491	0.5142	0.6448	Low level development	1.4732	Low level coordinated development ecological lag
2010	0.5676	0.4873	0.7242	Coordinated development	0.8586	Synchronous type of coordinated development
2011	0.4996	0.4854	0.7017	Coordinated development	0.9716	Synchronous type of coordinated development
2012	0.5118	0.4964	0.7098	Coordinated development	0.9698	Synchronous type of coordinated development
2013	0.5230	0.5627	0.7363	Coordinated development	1.0760	Synchronous type of coordinated development

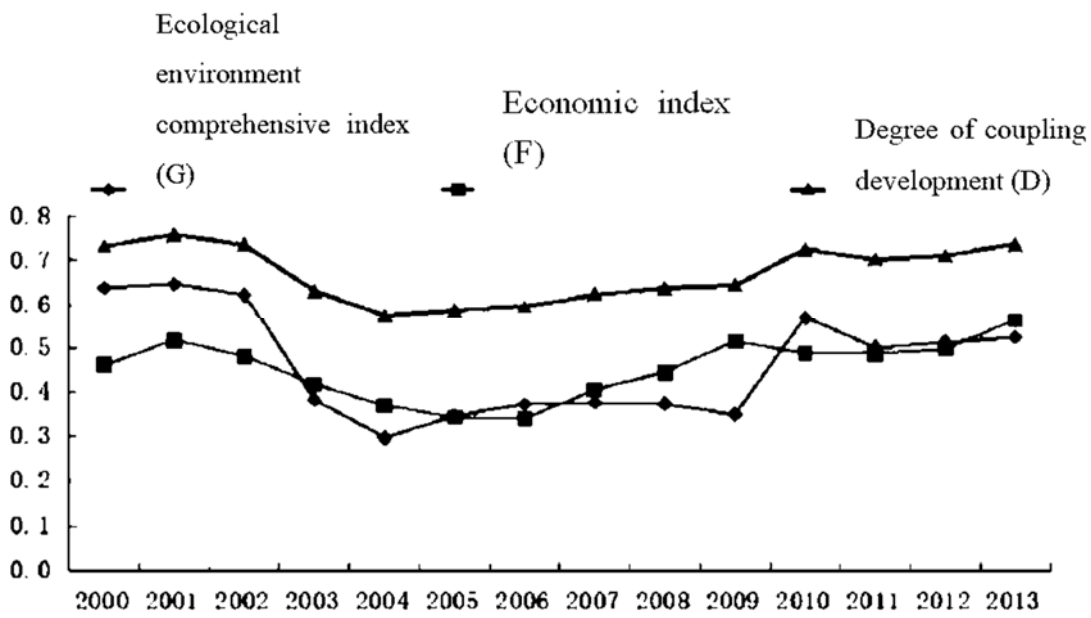

FIGURE 1
Coupling development degree of Wuhan eco-economic system

Coordinated development of ecological environment and economy. Wuhan Ecological Environment and Economic System. Wuhan's ecological environment and economic system as a whole are in a state of volatility, as shown in Figure 1. In the past 14 years, the coupling degree of ecological environment and economic system in Wuhan has fluctuated, which makes it possible for the population of Wuhan to continue to increase and the industrial structure to adjust continuously. With the introduction of ecological environment and economic friendly sustainable development strategy, returning farmland to forests, afforestation and other attempts to improve the ecological environment, but the deterioration of ecological environment is slow, and its benefits are difficult to appear in the short term. The ecological environment fitting curve can reflect out, the time series shows fluctuations, and the overall ecological environment is gradually improving.

CONCLUSIONS

This study combines the method and theory of SD and CCDM to analyse and assess the simulated results of the economy–environment system in Wuhan City.

Our results presents the following findings. (1) The SD model developed in this study can effectively simulate the dynamic and interactive relationships in the economy–environment system. (2) Different scenarios emphasises on different aspects. Compared with the current scenario, the economy scenario is good for economic growth but unfavourable for the environment. By contrast, the environment scenarios are conducive to energy conservation and emission reduction, respectively, but both would hinder economic development.

Our analysis provides several recommendations for Wuhan and other developing cities. Firstly, the development of Wuhan relies heavily on resource consumption. Future policies should attach importance to energy utilisation and resource conservation. Thereafter, exerting efforts toward improving the energy structure and natural environment may be a good choice for sustainable urban development.

ACKNOWLEDGEMENTS

The authors acknowledge the financial support from Science and Technology Planning Project of Hubei Province (No. 2018ADD171, No.2017AD C082) and Scientific research project of Educational Commission of Hubei Province (No. 03201717602).

REFERENCES

[1] Zhang, W.L., Liu, H.J., Wu, C., Sun, J. (2018) Marine biological quality assessment and ecological environment survey in the Bohai bay, China. Fresen. Environ. Bull. 27, 820-830.
[2] Garry, S., Peter, N. (2016) The evolution of sustainable remediation in Australia and New Zealand: A storyline. J. Environ. Manage. 184(15), 27-35.

[3] Broman, G.I., Robèrt, K.H. (2017) A framework for strategic sustainable development. J. Cleaner Prod. 140, 17-31.
[4] Jia, X., Foo, D.C.Y., Tan, R.R., Li, Z. (2017) Sustainable development paths for resource-constrained process industries. Resour. Conserv. Recycl. 119, 1-3.
[5] Siva, V., Gremyr, I., Bergquist, B., Garvare, R., Zobel, T., Isaksson, R. (2016) The support of quality management to sustainable development: a literature review. J. Cleaner Prod. 138, 148-157.
[6] Boggia, A., Rocchi, L., Paolotti, L., Musotti, F., Greco, S. (2014) Assessing rural sustainable development potentialities using a dominance-based rough set approach. J. Environ. Manage. 144(1), 160-167.
[7] Yuan, B., Ren, S., Chen., X. (2017) Can environmental regulation promote the coordinated development of economy and environment in China's manufacturing industry?–A panel data analysis of 28 sub-sectors. J. Cleaner Prod. 1491, 1-24.
[8] Wang, Q., Yuan, X., Cheng X., Mu, R., Zuo, J. (2014) Coordinated development of energy, economy and environment subsystems—a case study. Ecol. Indic. 46(6), 514-523.
[9] Yang, Z. Jing, S. Feng, D., Yu, L., Li, H. (2016) Vulnerability assessment of atmospheric environment driven by human impacts. Sci. Total Environ. 571(15), 778-790.
[10] Liu, L., Silva, E.A., Wu, C., Wang, H. (2017) A machine learning-based method for the large-scale evaluation of the qualities of the urban environment. Comput. Environ. Urban Syst. 65, 113-125.
[11] Xu, B., Hao, J. (2017) Air quality inside subway metro indoor environment worldwide: a review. Environ. Int. 107, 33-46.
[12] Almeida, T.A.D.N., Cruz, L., Barata, E., García-Sánchez, I.M. (2017) Economic growth and environmental impacts: an analysis based on a composite index of environmental damage. Ecol. Indic. 76(2017), 119-130.
[13] Özokcu, S., Özdemir, Ö. (2017) Economic growth, energy, and environmental kuznets curve. Renewable Sustainable Energy Rev. 72, 639-647.
[14] Boggia, A., Rocchi, L., Paolotti, L., Musotti, F., Greco, S. (2014) Assessing rural sustainable development potentialities using a dominance-based rough set approach. J. Environ. Manage. 144(1), 160-167.
[15] Miao, C.L., Sun, L.Y, Yang, L. (2016) The studies of ecological environmental quality assessment in Anhui province based on ecological footprint. Ecol. Indic. 60, 879-883.
[16] Deng, X., Xu, Y., Han, L., Yu, Z. Yang, M., Pan, G. (2015) Assessment of river health based on an improved entropy-based fuzzy matter-element model in the Taihu plain China. Ecol. Indic. 57, 85-95.
[17] Fan, X.G., Mi, W.B., Ma., Z.N. (2015) Construction and application of economy-pollution-environment three-dimensional evaluation model for district. Environ. Sci. 36(2), 751-758.
[18] Ren, H., Du, Y., Chen, Y., Ren, P., Dong, H. (2016) Study on the 3d evaluation model of eco-city planning under the distance measure perspective. Sci. Technol. Prog. Policy. 33(16), 81-85.
[19] Fang, K. (2015) Assessing the natural capital use of eleven nations: an application of a revised three-dimensional model of ecological footprint. Acta Ecol. Sin. 35(11), 3766-3777.
[20] Niccolucci, V., Bastianoni, S., Tiezzi, E.B.P., Wackernagel, M., Marchettini, N. (2009) How deep is the footprint? A 3d representation. Ecol. Model. 220(20), 2819-2823.
[21] Niccolucci, V., Galli, A., Reed, A, Neri, E., Wackernagel, M., Bastianoni, S. (2011) Towards a 3d national ecological footprint geography. Ecol. Model. 222(16), 2939-2944.
[22] Guan, D.J., Gao, WJ., Su, W.C., Li, H.F., Hokao, K. (2011) Modeling and dynamic assessment of urban economy-resource-environment system with a coupled system dynamics-geographic information system model. Ecol. Indicat. 11(5), 1333-1344.
[23] Shannon, C.E. (1948) A mathematical theory of communications. Bell Syst. Technical J. 27(4), 379-423.
[24] Jiang, L., Bai, L., Wu, Y. (2017) Coupling and coordinating degrees of provincial economy, resources and environment in China. J. Nat. Resour. 32(5), 788-799.

Received: **27.12.2018**
Accepted: **23.03.2019**

CORRESPONDING AUTHOR

Zhentang Ke
Huanggang Normal College
Huanggang Hubei 438000 – China

e-mail: 3391864568@qq.com

© by PSP Volume 28 – No. 5/2019 pages 4013-4020 Fresenius Environmental Bulletin

EFFECTS OF WATER AND FERTILIZER AND BIOCHAR REGULATING MODELS ON THE COMPREHENSIVE WARMING POTENTIAL OF GREENHOUSE GAS IN PADDY FIELDS IN NORTHEAST CHINA

Yanyu Lin[1,2], Shujuan Yi[1,2,*], Zhongxue Zhang[3], Mengxue Wang[4], Tangzhe Nie[3]

[1]College of Engineering, Heilongjiang Bayi Agricultural University, Daqing 163319, China
[2]Quality Supervision, Inspection and Testing Center for Agricultural Products Processing, Ministry of Agriculture (Daqing), Daqing 163319, China
[3] Key Laboratory of Efficient Use of Agricultural Water Resources, Ministry of Agriculture, Harbin 150030, China
[4]College of Agricultural, Heilongjiang Bayi Agricultural University, Daqing 163319, China

ABSTRACT

Taking the Chernozem Land of northeastern China as the research object, this paper adopts the three-factor secondary saturated D311 optimal design scheme to analyze the comprehensive warming potential of greenhouse gases in paddy fields in northeastern cold Chernozem Land by static black box-gas chromatography. The static black box-gas chromatography helps to analyze the effects of water, nitrogen fertilizer, and straw biochar on the comprehensive warming potential of greenhouse gases in paddy fields of northeastern China. The results show that the three factors have a comprehensive warming potential for greenhouse gases: biochar > nitrogen fertilizer > water. The increased irrigation amount has an increased effect on the comprehensive warming potential greenhouse gases firstly, and then the effect has decreased. The increase of nitrogen fertilizer and biochar can reduce the comprehensive warming potential of greenhouse gases; the interaction of the two factors can reduce greenhouse gas synthesis. The potential of warming effect is as follows: water + biochar > nitrogen fertilizer + biochar > water + nitrogen fertilizer. In this paper, combined with the output, when the greenhouse gas comprehensive warming potential reduction target is controlled at 20% to 40% of normal emissions, the integrated water and biochar optimization schemes are as follows, irrigation volume is at 4591~5420kg/hm2, nitrogen application rate is at 100.11~ 112.54kg/hm2, the amount of biochar is 21.29~22.14t/hm2.

KEYWORDS:
Northeast cold rice paddy, water and fertilizer and biochar, greenhouse gases, comprehensive warming potential

INTRODUCTION

Scientific research and observational data show that global climate is undergoing changes by warming, and large amounts of greenhouse gases are the main factors of current global climate change [1]. Rice is the main source of greenhouse gases, and CH4 and N2O are the most important trace greenhouse gases, which emitted by rice. The contribution rate of CH4to greenhouse effect is at 15%~ 30%, and the contribution rate of N2O to greenhouse effect is at 80%~ 90% respectively [2, 3]. Therefore, the research of the comprehensive warming potential greenhouse gases in paddy fields of the northeastern China has a positive significance for mitigating greenhouse gas emissions, which is proposing emission reduction measures.

There are many factors affecting greenhouse gas emissions in Paddy Fields, and the irrigation pattern of Paddy Fields has a significant effect on the emission of greenhouse gas. Studies have shown that compared with submerged irrigation, CH4 emissions from paddy fields are significantly reduced under inadequate irrigation conditions [4, 5], while N2O emissions increase, especially in the case of soil dry-wet alternating [6, 7]. Similarly, fertilization measures have an important impact on greenhouse gas emissions from Paddy Fields. Researches have shown that the application of nitrogen fertilizers will increase the concentration of NH4+-N and inhibit the growth of CH4 oxidizing bacteria, which is resulting in lower CH4 emissions in paddy fields and N2O emissions. The amount is increased [8- 10]. Studies have pointed out that the application of nitrogen fertilizer is the main factor for N2O emissions from farmland mineral soil [11]. According to the EIA survey, 78% of N2O emitted from agricultural soils in the United States is derived from the application of nitrogen fertilizer [12]. Wang et al. [13] showed that half reduced when the amount of chemical fertilizer applied, emissions of soil N2O have greatly reduced, which is accounting for 22%. When the amount of chemical fertilizer

not applied, emissions of soil N2O have greatly reduced to 41% of current emissions, respectively. Because of its strong nitrogen and carbon-fixing capacity, Biochar can play an important role in the global carbon geochemical cycle, climate change, and environmental systems, Biochar has become a hot research in the field of atmospheric science and environmental science [14]. Studies have shown that the application of biochar to the soil will significantly improve the quality and permeability of soil. Shenbagavalli et al. [15] found that biochar could inhibit the release of greenhouse gases, of which CO2 and N2O are most effective.

At present, although many scholars have conducted in-depth research on the emission laws of greenhouse gas in Paddy Fields in the management of water, fertilizer, and biochar [16- 18], they have studied by single factors, and most of them have concentrated in the southern Paddy Fields. In the region, the impact of its integrated management on the emission laws of greenhouse gas in Paddy Fields (factor coupling effects) has rarely reported. The purpose of this experiment is to study the influence of the interaction between water, nitrogen fertilizer, and biochar on the comprehensive warming potential gas emissions of rice greenhouse, and combine the growth season emission of reduction targets in Paddy Field to find the optimal water, fertilizer, and biochar. The project has planned to provide field management techniques for the reduction of paddy field in the northeast cold land.

MATERIALS AND METHODS

Overview of the test site. The experiment has carried out from May to October 2018 in the Rice Irrigation Test Center Station (125°44' E, 45°63' N) in Heping Town, Qing'an County of Heilongjiang Province, which is a typical cold Chernozem Land. The average annual temperature is at 2.5 °C, the average annual precipitation is at 550 mm, and the average annual water surface evaporation is at 750 mm. The crop period of water heat growth is 156 days to 171 days, and the annual frost-free period is 128 days. The climate has characterized by a cold temperate continental monsoon climate. The soil type is soil type of white paddy soil with a bulk density of 1.01 g/cm3 and a porosity of 61.8%. Basic physical and chemical properties of soil include organic matter mass ratio is at 41.4 g / kg, pH value is 6.40, and total nitrogen mass ratio is 15. 06g / kg, total phosphorus mass ratio is 15.23g / kg, total potassium mass ratio is 20.11g / kg, alkali nitrogen mass ratio is at 154.36mg/kg, the effective phosphorus mass ratio is at 25.33 mg/ kg, and the available potassium mass ratio is at 157.25 mg/kg [19].

Test design. The experiment used saturated D311 optimal design [20] to study the effects of irrigation, nitrogen, and biochar on the CH4 emission during the growing season. The water and fertilizer were applied to the local farmers' standard, specifically the irrigation amount is at 5000~ 10000 kg/hm2, nitrogen fertilizer (pure nitrogen) is at 50 ~ 150kg / hm2, biochar is at 0 ~ 40t / hm2. The specific design scheme is shown in Table 1.

This experiment consisted of 11 treatments, 3 repetitions, and random blocks. The area of each plot was 10 m × 10 m = 100 m2. The rice also planted around the plot to add protection. The technical measures included rice breeding, transplanting, plant protection and drug use, and the same field management conditions. In order to reduce the impact of lateral infiltration on the test, the cell and the community treated with an isolation treatment, that is, the plastic plate and cement concrete are used as the seepage in the surrounding area. The material is buried 40cm deep below the surface of the field. The irrigation method adopts pipeline water supply, and each pipeline is equipped with a water meter to control the irrigation amount. The nitrogen fertilizer has applied according to the ratio of base fertilizer, manure fertilizer and panicle fertilizer to 5:3:2, and P-fertilizer has applied as base

TABLE 1
Saturated D-311 optimal design of processing table

NO.	Coded value			Actual value			GWP
	X_1	X_2	X_3	W（m^3/hm^2）	N(kg/hm^2)	BC(t/hm^2)	（kg/hm^2）
1	0	0	2	5000	100	40	3450.11
2	0	0	-2	5000	100	0	5955.66
3	-1.414	-1.414	1	3200	65	30	5119.64
4	1.414	-1.414	1	6800	65	30	5098.78
5	-1.414	1.414	1	3200	135	30	4593.49
6	1.414	1.414	1	6800	135	30	4377.51
7	2	0	-1	7500	100	10	4731.18
8	-2	0	-1	2500	100	10	4269.39
9	0	2	-1	5000	150	10	4782.40
10	0	-2	-1	5000	50	10	5087.59
11	0	0	0	5000	100	20	4133.44

fertilizer once, and the application amount is at 45kg/hm2. K-fertilizer base fertilizer at 8.5 leaf age (spot differentiation stage) have applied twice, the ratio was 1:1 before and after, the application amount is at 80kg/hm2, biochar has applied to the soil surface, and the charcoal and the plough layer are used by the rotary tiller. The soil is evenly mixed. The tested fertilizers were urea (including N 46%), diammonium phosphate (N is at 18%, P2O5 is at 46%), potassium fertilizer (K2O content 40%), and the tested biochar was straw biochar products of Liaoning Jinhefu Agricultural Development Co., Ltd.

The tested rice variety was the local main plant variety Longqingdao No.3, the planting density was 4 per hole, the base fertilizer was applied on May 6, the transplanting was carried out on May 17, and the manure was applied on May 31, and the application was carried out on July 19. Spike fertilizer, harvested on September 20th. The growth period of rice is 127 days, which is divided into the regreening period is from May 17th to May 30th. The tillering period is from May 31st to July 7th, and the jointing and booting stage is from July 8th to July 25th, heading flowering period is from July 26th to August 4, milk ripening period is from August 5th to August 24th, and yellow ripening period is from August 25th to September 20th.

Gas collection and determination. Gas sampling has chosen on a sunny day. This article uses static black box-gas chromatography. The box body is a rectangular parallelepiped with a length of 18 cm on the side of the cross section. It is made of Plexiglas material, and the outer surface of the box is covered with a heat insulating material (sponge and aluminum foil) to reduce the temperature change of the gas in the tank due to solar radiation during sampling. The box height was 90cm in the early stage of rice growth, and the box height increased to 130cm after the heading period. A three-port valve air hole is provided at a side of the box 30 cm from the top for connecting the three-port valve for collecting gas. There is a built-in fan at the top of the sampling box, which is used to mix the gas in the tank during sampling. Before the transplanting, the wooden base has placed in the sampling basin, and the base is flush with the mud surface. When sampling, the sampling box has lightly placed on the base of the return frame, and the water in the base water tank ensures the gas isolates from inside to outside. The rice has transplanted for 1 week and the detection time was from 10:00 to 12:00 [21-22], and each treatment was repeated three times in parallel, once a week, until one week before harvest. At the time of sampling, about 100 mL of gas has extracted from the tank by a syringe. The samples have collected once at 0 min, 5 min, 10 min, and 15 min, respectively, then the gas in the syringe has immediately transferred to the aluminum foil sampling bag, and the sampling bag has taken back to the laboratory in time.

The gas concentration has measured by Shimadzu GC-14B gas chromatograph. The detectors are the ion detector of hydrogen flame FID and thermal conductivity detector TCD. The temperature was 200 ° C and 100 ° C. The separation materials include GDX-502 and Porapak Q. The column temperatures are 100 ° C and 55 ° C, respectively, and the standard gas has supplied by the National Standards Center.

Calculation methods and data analysis. Calculation formula for greenhouse gas emission flux in Paddy Fields [23]: $F = \rho \cdot h \cdot dc / dt \cdot 273 / (273 + T)$.

Where: F is the gas discharge flux (mg·m-2·h-1), ρ is the gas density under standard conditions (kg·m-3), h is the box height (m), and dc/dt is within the sampling box. The gas concentration change rate (mL·m-3·h-1), 273 is the gas equation constant, and T is the average temperature (°C) in the sampling tank during the sampling process. In this paper, the gas emission flux has calculated according to the curve of the concentration of gas sample and time. The growth season is the product of the average flux value of each growth period, the total length of the growth period, then accumulating and obtaining [24].

The test data was statistically analyzed using Excel2003, SPSS 17.0, and MATLAB 7.0.

RESULTS AND ANALYSIS

Greenhouse gas comprehensive warming potential effect function. The comprehensive warming potential (GWP) converts the warming potential of various greenhouse gases into CO2 emission equivalents. The comprehensive warming effect of the 100 a time scale is calculated [24].

$GWP=295E_{C\text{-}N2O}+28E_{C\text{-}CH4}$

Seasonal cumulative emissions of $E_{C\text{-}N2O}$-N_2O, kg/hm2

Seasonal cumulative emissions of $E_{C\text{-}CH4}$-CH_4, kg/hm2

The X1(W), X2(N), and X3(C) code values are independent variables. The warming potential Y of the greenhouse gas in Table 1 is the quadratic polynomial regression analysis of the dependent variable, and the greenhouse gas warming potential has obtained. Equation with irrigation amount, nitrogen fertilizer, and biochar is shown as follows.

$Y=4583.31+36.79X_1-148.42X_2-291.81X_3-24.39X_1X_2-84.38X_1X_3-72.08X_2X_3-141.04X_1^2-28.40X_2^2-16.74X_3^2$

The F test is performed on the regression equation: F = 144.48> (F0.01 (10, 20)) = 3.37). The

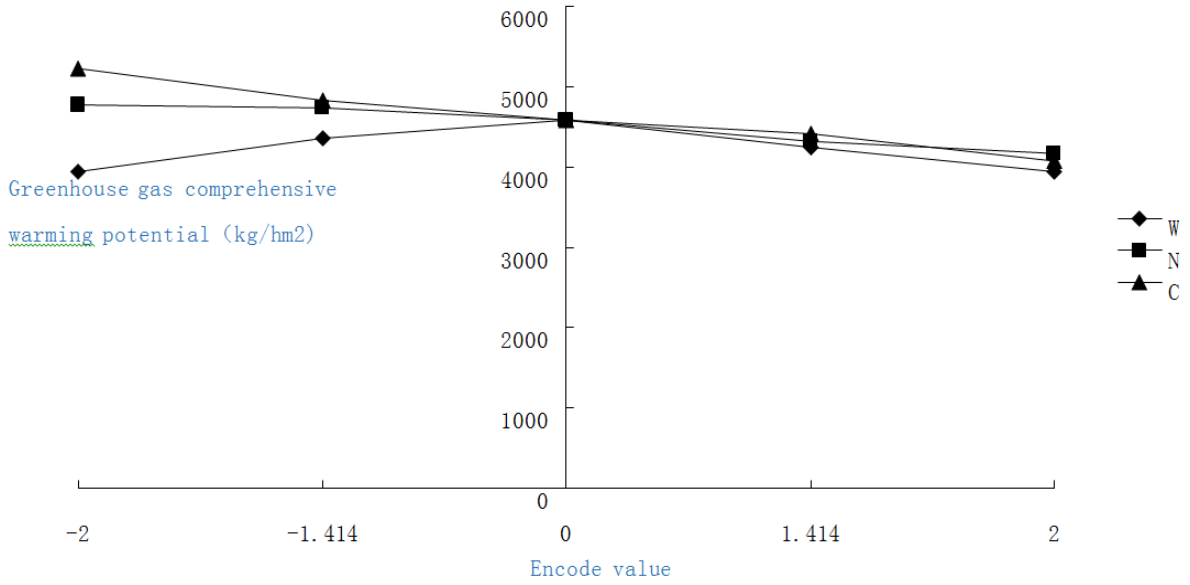

FIGURE 1
Single factor effect curve

relationship among the regression equations is extremely significant, that is, the equation can reflect the comprehensive warming potential of greenhouse gases and irrigation amount. The absolute value of the primary coefficient is the regression equation, which is the basis for judging the influence of various factors on the comprehensive warming potential of greenhouse gases. Therefore, the equation can be seen that the degree of influence on CH4 emissions is from large to small, which include biochar, nitrogen fertilizer, and water.

Single factor effect analysis. The above-mentioned main effect model adopts the "dimension reduction method", and another two factors are set at zero code value, and the effect of single factor on CH4 growth season emissions is obtained. The single factor effect equation is obtained and the single factor effect curve is drawn in Figure 1.

$Y_1=4583.31+36.79X_1-141.04X_1^2$

$Y2=4583.31-148.42X_2-28.40X_2^2$

$Y3=4583.31-291.81X_3+16.74X_3^2$

It can be seen from Fig. 1 that within the range of coded values, the effect of irrigation amount on CH4 emissions is firstly promoted and then suppressed, and the increase of nitrogen fertilizer and biochar can significantly inhibit CH4 emissions.

It can be seen from Fig. 1 that in the range of coded values, the increase of irrigation amount has an effect on the warming potential of greenhouse gases, which is first to promote post-inhibition, while the increase of nitrogen fertilizer and biochar can significantly inhibit the warming potential of greenhouse gases.

Factor interaction of effect analysis. Set any one factor to zero code value to get the interaction effect equation of the other two factors. The equation is as follows:

$Y_{12}=4583.31+36.79X_1-148.42X_2-24.39X_1X_2-141.04X_1^2-28.40X_2^2$

$Y_{13}=4583.31+36.79X_1-291.81X_3-84.38X_1X_3-141.04X_1^2-16.74X_3^2$

$Y_{23}=4583.31-148.42X_2-291.81X_3-72.08X_2X_3-28.40X_2^2-16.74X_3^2$

This two-factor cross-effect equation is plotted (Figure 2). It can be seen from Fig. 2 that the 2-factor interaction has an inhibitory effect on the warming potential of greenhouse gases, and the degree of influence from large to small is as follows, water + biochar, nitrogen fertilizer + biochar, water + nitrogen fertilizer. It can be seen from the figure (a) and figure (b) that when the irrigation amount is fixed at a certain level, the comprehensive warming potential of greenhouse gases decreases with the increasing nitrogen fertilizer and biochar application, as can be seen from figure (c). When nitrogen fertilizer or biochar is fixed at a certain level, the increase of irrigation amount will increase, or the comprehensive warming potential of greenhouse gases will decrease, and the emission reduction effect is not very obvious.

Analysis of water and fertilizer, and biochar management optimization plan. The frequency effect analysis method is used to optimize the main effect model, and the coded values are divided into five levels (-2, -1.414, 0, 1.414, 2) within the experimental design range, which constitute T=53 = 125 processing combinations, the output will control the greenhouse gas comprehensive warming

potential reduction target within the range of 20% to 40%. Because the factors of the treatment 11 in this test are all at zero level, it is considered normal treatment, that is, the normal comprehensive increase is selected. The frequency potential analysis was carried out by frequency analysis of 60%-80% (2480.07～ 3306.75kg/hm2), and 50 optimization results of water and fertilizer, and biochar management simulation equations have obtained. The frequency analysis is shown in Table 2.

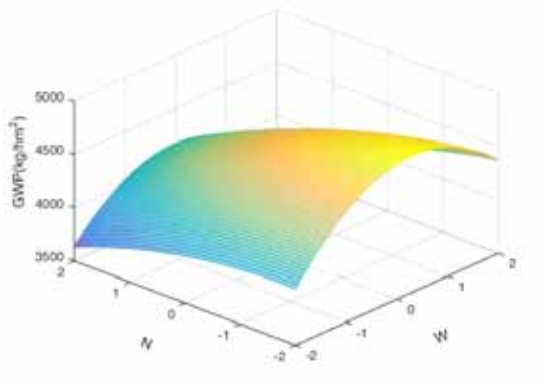

(a): Surface diagram of irrigation amount and nitrogen fertilizer interaction effect

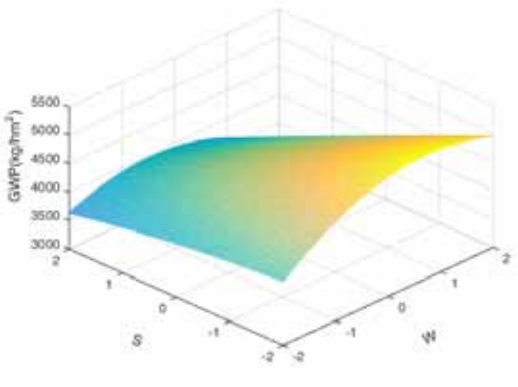

(b): Irrigation amount, biochar interaction effect of surface diagram

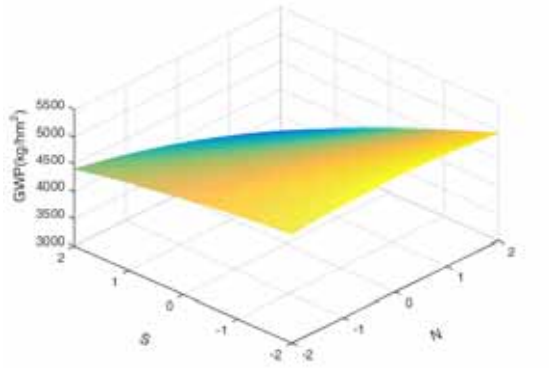

(c): Surface diagram of nitrogen and biochar interactions

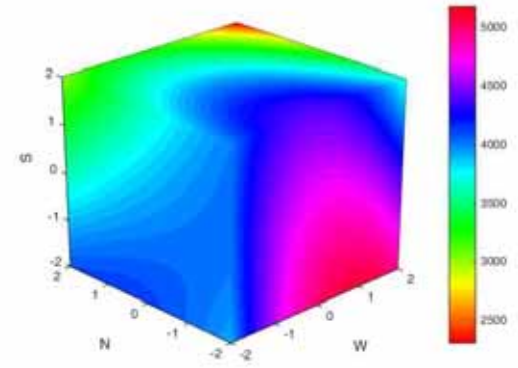

(d): Four-dimensional map of irrigation, nitrogen, and biochar interactions

FIGURE 2
Analysis of the effect of factor interaction on greenhouse gas warming potential

TABLE 2
Water and fertilizer, and biochar allocation schemes for greenhouse gas comprehensive warming potential between 2480.07 and 3306.75kg/hm2

Coded value	Irrigation amount		Nitrogen fertilizer		bio-charcoal	
	NO.	Frequency /%	NO.	Frequency /%	NO.	Frequency /%
-2	10	18	9	16	5	12
-1.414	10	18	11	30	14	25
0	10	18	10	18	20	40
1.414	7	20	8	12	6	13
2	13	26	12	24	5	10
MEAN	0.076		0.244		0.047	
Standard error	0.164		0.126		0.154	
Confidence interval（95%）	-0.3272～0.3365		0.0045～0.5017		0.2579～0.4272	
Optimization（kg/hm²）	4591～5420		100.11～112.54		21.29～22.14	

DISCUSSION

The amount of irrigation has an important impact on the emissions of greenhouse gas in paddy fields. Studies have shown that when the amount of irrigation is relatively small, it will promote gas exchange between soil and atmosphere, the anaerobic conditions of the soil has destroyed; the activity of producing CH4 has inhibit. Sexual promotion has promoted the direct discharge of CH4 into the atmosphere to some extent. When the amount of water is sufficient, the paddy field will maintain a deeper water layer for a long time. The atmosphere and soil will have blocked by the water layer, which may close some of the pores and reduce the emission of CH4 through the plant body [25, 26], while O2 diffuses into the soil. To the limit, it also affects the movement, distribution, and release of denitrifying gas in the soil. As N2O stays in the soil for a longer period of time, the possibility of further reduction to N2 increases, resulting in a decrease in N2O emissions [27]. Therefore, the impact on the comprehensive warming potential of greenhouse gases has increased or decreased, which is consistent with the results of this experimental study.

The application of nitrogen fertilizer will increase the N2O emissions in paddy fields, and the promotion of high nitrogen levels is more significant. This is consistent with the results of the current literature review. The impact on CH4 emissions from Paddy Fields remains to have further studied. Shangguan Xingjian [28] and others believe that urea can reduce the emission of CH4 in paddy fields. However, Wang et al. [29] believe that urea has a different effect on CH4 release (promotion or inhibition), probably because it can increase the soil pH. The pH value of soil in most acidic soils becomes favorable for the formation of CH4, while the Chernozem Land is mostly neutral and alkaline. The application of urea in neutral or alkaline soil inhibits the formation of CH4 due to the increase of pH. The results of this study are more inclined to Shangguan Xingjian, the application of nitrogen fertilizer will inhibit the production of CH4, thereby reducing the overall warming potential of greenhouse gases.

This experiment shows that biochar application can effectively reduce CH4 and N2O emissions in paddy fields. The reason may be that biochar input effectively improves soil aeration, and the carbon content of soil water-soluble organic reduces, thereby improving soil fertility. In addition, biochar input as a carbon source can provide sufficient matrix for CH4 oxidizing bacteria to reduce CH4 emissions through oxidation [30], and the C/N value of biochar itself inhibits the transformation and denitrification of nitrogen microbes is higher [31]. Therefore, the reduction of soil N2O emissions has ultimately achieved. Thereby it is reducing the overall warming potential of greenhouse gases.

In recent years, in order to pursue rice production, apply nitrogen fertilizer blindly, and neglect the impact on the environment, this study attempts to add biochar to the soil, and cooperate with water and fertilizer, which helps to establish a comprehensive warming potential of greenhouse gases in paddy fields. The mathematical model of water, nitrogen fertilizer and biochar, the model can reflect the relationship between the comprehensive warming potential of paddy field, water-fertilizer, and biochar through the significance test, which makes the quantitative study of water and fertilizer, and biochar more convenient. The relationship has a good Application prospects. However, the influence of the coupling effect of water, fertilizer, and biochar on greenhouse gas emissions is only preliminary, and no qualitative research has conducted. In the course of further in-depth research, it is also necessary to accumulate emission data of greenhouse gas for different growth period of rice, which makes the model perfect and has practical guiding significance.

CONCLUSION

(1) Water, nitrogen fertilizer, and biochar have different effects on the comprehensive warming potential of greenhouse gases in Paddy Fields. The analysis results show that the three factors affect the performance: biochar>nitrogen fertilizer>water. the effect of the increasing irrigation amount on the comprehensive warming potential of greenhouse gases is firstly increased and then decreased, and the increase of nitrogen fertilizer and biochar can be obvious. The comprehensive warming potential of greenhouse gases has reduce in Paddy Fields.

(2) The interaction between the two factors will reduce the greenhouse warming potential of Paddy Fields. The analysis results show that the effect of interaction is as follows: water + biochar > nitrogen fertilizer + biochar > water + nitrogen fertilizer. When the irrigation amount has fixed at a certain level, the comprehensive warming potential increases have the application of nitrogen fertilizer and biochar. In addition, when the nitrogen fertilizer or biochar is fixed at a certain level, the irrigation amount has an increase or decrease in its comprehensive warming potential, and the emission reduction effect is not very obvious.

(3) Combining the output, the greenhouse gas of Paddy Field has comprehensive warming potential emission reduction target, which has controlled within the range of 20% to 40%, and the main effect model has optimized by the frequency analysis method. The optimized water and fertilizer and biochar-blending scheme is as follows. The irrigation amount is at 4591~ 5420 kg/hm2, the nitrogen application rate is at 100.11~ 112.54kg/hm2, and

the biochar content is at 21.29~ 22.14t/hm2.

ACKNOWLEDGEMENTS

This work is funded by the Heilongjiang Bayi Agricultural University Talents Plan Program (XYB201801), Heilongjiang Provincial Postdoctoral General Funding Program, Heilongjiang Bayi Agricultural University Support Program for San Heng San Zong (TDJH201803), Key Laboratory of Efficient Use of Agricultural Water Resources, Ministry of Agriculture, PRChina (2017004). The Ministry of Agriculture's Agricultural Products Quality Supervision, Inspection and Testing Center (Daqing) postdoctoral workstation also supports this research.

REFERENCES

[1] National Development and Reform Commission (2014) National Climate Change Plan (2014-2020).

[2] Wang, M. (2001) China's rice field methane emissions. Beijing: Science Press. 85-87.

[3] Bouwman, A.F., Boumans, L.J.M., Batjes, N.H. (2002) Emissions of N2Oand NO from fertilized fields: Summary of available measurement data. Global Biogeochemical Cycles. 16(4), 1058-1070.

[4] Peng, S., Yang, S., Xu, J. (2010) Effects of controlled irrigation on CH4 and N2O emissions and greenhouse effect in paddy fields. Water Scientific Progress. 21(2), 235-240.

[5] Li, D., Peng, S., Xu, J., Ding, J., He, Y, Yu, J. (2005) Ecological and environmental effects of paddy fields under water-saving irrigation conditions. Journal of Hohai University (Natural Science Edition). 33(6), 629-633.

[6] Xu, H., Cai, Z., Li, X. (2000) Effects of land management on seasonal changes of CH4 and N2O emissions in paddy soil during winter crop season. Journal of Applied Ecology. 11(2), 215-218.

[7] Sheng, Z., Song, X., Yan, X. (2013) Research progress on low carbon production in rice. Chinese Rice Science. 27(2), 213-222.

[8] Zou, J.W., Huang, Y., Jiang, J.Y., Zheng, X.H., Sass, R.L. (2005) A 3-year field measurement of methane and nitrous oxide emissions from rice paddies in China: Effects of water regime, crop residues, and fertilizer application. Global Biogeochemical Cycles. 19(2), 20-21.

[9] Cai, Z.C., Xing, G.X., Yan, X.Y., Xu, H., Tsuruta, H., Yagi, K., Minami, K. (1997) Methane and nitrous oxide emissions from rice paddy fields as affected by nitrogen fertilizers and water management. Plant and Soil. 196(1), 7-14.

[10] Ma, J., Li, X.L., Xu, H., Han, Y., Cai, Z.C., Yagi, K. (2007) Effects of nitrogen fertilizer and wheat Straw application on CH4 and N2O emissions from a paddy rice field. Australian Journal of Soil Research. 45(5), 359-367.

[11] Meng, L., Ding, W.X., Cai, Z.C. (2005) Long term application of organic manure and nitrogen fertilizer on N2O emissions, soil quality and crop production in a sandy loam soil. Soil Biol Biochem. 37, 2037-2045.

[12] EIA-Energy Information Administration (2006). Emissions of greenhouse gas in the United States 2005. DOE/EIA-0573, Washington D.C., 48.

[13] Wang, X., Li, C., Ouyang, Z. (2003) Greenhouse gas emissions and China's grain production. Ecological Environment. 12(4), 379-383.

[14] Liu, Y. (2011) Effects of biomass carbon input on soil nitrogen loss and greenhouse gas emission characteristics. Hangzhou: Zhejiang University.

[15] Shenbagavalli, S., Mahimairaja, S. (2012) Characterization and effect of biochar on nitrogen and carbon dynamics in soil. International Journal of Advanced Biological Research. 2(2), 249-255.

[16] Shi, S., Li, Y, Wan, Y., Qin, X., Gao, Q. (2011) CH4 and N2O emissions from double-season rice fields with different nitrogen and phosphorus fertilizers. Environmental Science. 32(7), 1899-1907.

[17] Yuan, W., Cao, Z., Cheng, J., Xie, N. (2008) Evaluation of CH4 and N2O emissions from rice fields and greenhouse effect under intermittent irrigation mode. Chinese Agricultural Sciences. 41(12), 4294-4300.

[18] Shi, S., Li, Y., Wan, Y., Qin, X., Gao, Q. (2011) CH4 and N2O emissions from double-season rice fields with different nitrogen and phosphorus fertilizers. Environmental Science. 32(7), 1899-1907.

[19] Wang, M., Zhang, Z. (2015) Suitable water-saving irrigation mode inhibits N2O emission in cold rice fields and increases rice yield. Journal of Agricultural Engineering. 31(15), 72-79.

[20] Xu, Z. (1997) Regression analysis and experimental design. Beijing: China Agricultural Press. 102-143.

[21] Li, J., Wang, M., Chen, D. (1998) Selection of sampling time in discontinuous measurement of methane emission in paddy fields. Journal of the Graduate School of the Chinese Academy of Sciences. 15(1), 24-29.

[22] Epstein, H.E., Burke, L.C. (1998) Plant functional type effects on trace gas fluxes in the short grass steppe. Biogeochemistry. 42(1-2), 145-168.

[23] Zheng, X.H., Wang, M.X., Wang, Y.S., Shen, R.X., Li, J., Heyer, J., Kogge, M., Li, L.T., Jin, J.S. (1998) Comparison of manual and automatic methods for measurement of methane emission from rice paddy fields. Advances Atmospheres Science. 15(4), 569-579.
[24] Yan, G. (2012) Effects of application of bio-black carbon on soil properties, maize growth and greenhouse gas emissions in rain-fed dryland under different fertilization modes. Nanjing: Nanjing Agricultural University.
[25] Ding, Y. (1997) The main scientific achievements and problems of the IPCC Second Climate Change Science Assessment Report. Advances in Earth Science 12(2), 158-163.
[26] National Development and Reform Commission (2004). Initial National Information Circular on Climate Change in the People's Republic of China. China Planning Press, Beijing, 1-110.
[27] Zhang, Y., Hu, C., Zhang, J., Dong, W., Wang, Y., Song, L. (2011) Research progress on source/sink intensity and greenhouse effect of main greenhouse gases (CO2, CH4, N2O) in farmland soil. Chinese Journal of Eco-Agriculture. 29(4), 966-975.
[28] Shangguan, X., Wang, M. (1996) Transmission of rice field CH4 [M]. Beijing: China Environmental Science Press.
[29] Liang, B.C., Wang, X.L., Ma, B.L. (2002) Maize root-induced change in soil organic carbon pools. Soil Science Society of America Journal. 66(13), 845-847.
[30] Mizuta, K., Matsumoto, T., Hatate, Y., Nishihara, K., Nakanishi, T. (2004) Removal of nitrate-nitrogen from drinking water using bamboo powder charcoal Bioresource Technology. 95(3), 255-257.
[31] Hua, L., Tang, Z., Jie, J. (2013) The effect of biochar on greenhouse gas emissions from farmland and its influencing factors. Journal of Eco-Environment. 22(6), 1068-1073.

Received: **28.12.2018**
Accepted: **31.03.2019**

CORRESPONDING AUTHOR

Shujuan Yi
College of Engineering,
Heilongjiang Bayi Agricultural University,
Daqing 163319 – China

email: yishujuan_2005@yeah.net

© by PSP Volume 28 – No. 5/2019 pages 4021-4027 Fresenius Environmental Bulletin

STUDY ON SEWAGE TREATMENT VIA A LOW TEMPERATURE PROCESS

Wanyong Xiong*, Huang Jian, Luo Xin, Xiaole Wen

Department of Environment and Resources, Fuzhou University, Fuzhou, China

ABSTRACT

With the enhancing of people's environmental awareness in recent years, especially after the stressing of the sustainable development, the treatment of sludge water and sludge in the waterworks is increasingly at a premium, and the environmental departments have also raised higher and higher requirements on the emission and treatment of production waste in the waterworks. Many of Chinese newly built large-scale water-works and expansion and reconstruction projects of water works have also begun to think about the problem of sludge water and sludge treatment, with different process flows adopted. The major purpose of this paper is to treat the sewage via low temperature process. Effect of DO, internal reflux ratio r, external reflux ratio R, sludge age SRT, sewage temperature and pH on COD removal is studied. The result shows that the best COD removal was 95.8% and TP removal is 90.7%.

KEYWORDS:
Sewage treatment, Industrial park, Process optimization, Low temperature

INTRODUCTION

The high-speed of development of Chinese society and economy has also induced a good many environmental problems in recent years, such as severe insufficiency of water resources, increasingly severe water pollution, etc [1-4]. In 2013, the Ministry of Water Resources monitored the environment of water in an about 2.08×10^5km reach in China, finding that the length of I-type water accounts for 4.8% of the evaluated length, 42.5% for II-type water, 21.3% for III-type water, 10.8% for IV-type water, 5.7% for V-type water, 14.9% for IV-type water. In the same year, the discharged industrial, agricultural and domestic waste water and sewage in China reached 7.68 billion m^3. Not only the complicated pollutants in the waste water and sewage result in severe pollution of the aquatic environment, but also substantive nutrient substances such as nitrogen and phosphorus, etc. entered the water, becoming the major reason of water ultrophication. In order to comprehensively treat the urban waste water and sewage and ameliorate the water environment, Chinese environmental protection department suggested the means of controlling the gross and making emphatic treatment, and required that the sewage treatment rate should not have been lower than 50% by 2010 in the cities with established cities and designated towns. By June 2015, 3,802 sewage treatment plants have been finished, whose daily processing capacity of sewage reached $1.61x10^8m^3$ [5]. In the meanwhile, to further efficiently remove the high-concentration pollutants and nutrient substances like nitrogen and phosphorus in the sewage, the government raised the requirements of upgrading and rebuilding the existing sewage treatment plants, and manifold advanced treatment technologies, including the membrane separation technology, active carbon absorption technology, enhanced coagulation technology, advanced oxygenation technology and enhanced denitrification and dephosphorization, etc. have received more and more attention [6]. In the meanwhile, via monitoring and evaluation of the overall process of sewage treatment, it has been found that the pollutants are transferred into the sludge in the sewage treatment, and if the sludge is not treatment, the pollutants will be dissolved out for the second time and continue to pollute the water, so the sludge treatment is also a key factor guaranteeing the stable operation of the sewage treatment plant [7].

The statistics show that 1,427 counties in China had constructed sewage treatment plants in China by June 2015, accounting for 88.4070% of the total of counties, while the construction of the sewage treatment plants in the villages and towns has just started, built-up rate being low [8]. In 2012, the Heilongjiang Department of Housing and Urban-Rural Development investigated and examined the finished small-scale sewage treatment plants in the province according to the requirements of the Ministry of Housing and Urban-Rural Development, finding the need for a complete, stable, and reliable optimization operation scheme to raise the operating efficiency of sewage treatment plants in the small cold cities and towns in northeast China. After nearly two years of investigation, comparison and optimization, the A2O process is determined as having significant advantages in stable operation and simplicity of operation, so it was deeply re-

searched [9-11]. In June 2015, the "Bulletin of National Construction and Operation of Condition of Town Sewage Treatment Facilities Construction in the Second Quarter of 2015" issued by the Ministry of Construction shows that the information reporting condition of the sewage treatment plants in the small towns was temporarily not included in the examined content, which indirectly indicates that to study the optimized operation mode of sewage treatment plants in Chinese medium and small towns in China counts for much, and to provide systematic technological countermeasures for stable operation of sewage treatment plant in the medium and small towns cannot only avoid the possible environmental pollution due to excessive emission by the already constructed town-level sewage treatment plants, but also is favorable for providing technical support for the about-to-be-constructed sewage plants in villages and towns in China in future several years [12-15].

MATERIALS AND METHODS

Depollution principle of sewage treatment process and influencing factors for operation. Depollution principle of the process. The anaerobic-aerobic method, oxygen-biological nitrogen phosphorus removal process (A2O process in brief) is a simultaneous denitrification and dephosphorization sewage treatment process developed by America in 1970s, whose basic principle is based on the principle of biological denitrification and biological dephosphorization. The common process flow is as shown in Fig.1. The well operating A20 process can perfectly denitrify and dephosphorize the waster water. Its denitrification and dephosphorization principle is as described below.

Principle of biological denitrification. The sewage biological denitrogenation is an effective method of removing the nitrogenous organic compounds in the waste water and sewage, whose basic principle is in two aspects: The first is that the microbes utilize the nitrogenous substances in the sewage to synthesize the living matters like protein, etc. via the assimilation, for their own growth and reproduction. Generally the nitrogen removed by the assimilation accounts for 4%-5% in the total nitrogen (TN) of the raw waste water. The second is the process of ammoniation, nitration and denitrification, which is the major mode of nitrogen removal in the sewage. The schematic diagram of biological denitrification is as shown in Fig.1-2.

The ammoniation. The ammonifiers decompose the nitrogen compound and translate it into ammonia nitrogen in the oxygen-free or aerobic condition, causing the ammoniation reaction, as shown in Fig.2.

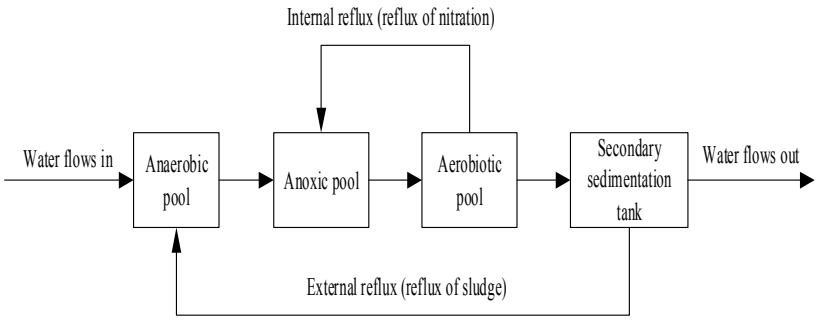

FIGURE 1
Schematic diagram of process flow

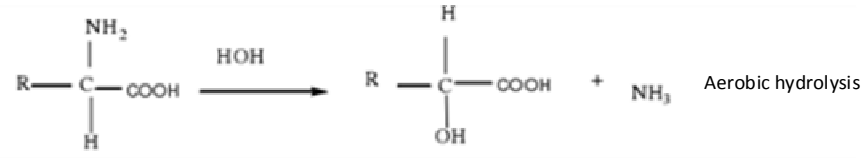

(a) Aerobiotic hydrolization

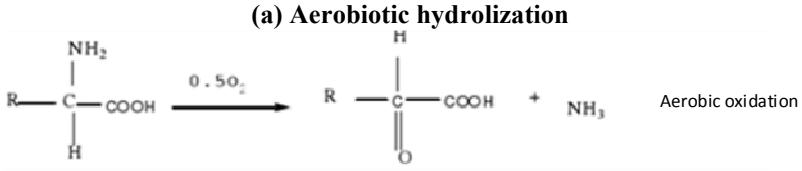

(b) Aerobiotic oxygenation
FIGURE 2
Decomposition of organonitrogen compound

Nitrification. In the aerobiotic reactor, as the nitrifier is a kind of chemoautotroph, and the physiological activity of obligate aerobes needs no organic nutrient substance, but obtains energy from inorganic carbonization or oxidation reaction of NO_2. Under the action of nitrococcus, with synthesizing agent as the carbon source, NH4+ ammonia nitrogen (NH4+) is translated into hydroxylamine NHZOH, nitre phthalidyl NOH and nitrite nitrogen NO_2. Then, the action of the nitromonas makes NO_2 further translated into nitrate nitrogen NO_3.

This shows that the biological denitrification can thoroughly remove the ammonia in the waste water without secondary pollution, and is applicable to treatment of waste water with NH_3-N concentration not exceeding 200 mg/L. Yet the process is largely influenced by the temperature, as the denitrification efficiency is low at low temperature.

According to the principle of biological denitrification, a series of new processes were proposed.

(1) Short-cut nitrification denitrification. In recent years, the researchers have gone deeper into the research and developed the short-cut nitrification denitrification technology which is a new biological denitrification technology designed to reduce the dosed alkali, shorten the nitration time and reduce the volume of reactor accordingly. The technology controls the nitration to be in the NO_2 phase, and directly takes NO_2 as the final receptor of electrons, to prevent the NO_2 from being further oxygenated into NO_3. The research shows that the short-cut nitrification and denitrification can save the oxygen supply by about 25% and reduce the energy dissipation and environmental cost, can save the carbon source by 40% and raise the removal rate of total nitrogen, also can reduce the formed sludge by up to 50%.

(2) Moderate temperature nitrosification. The core of SHARON process is to utilize the nitrococcus to effectively remove the nitrogen in the waste water and sewage. The moderate temperature nitrosation technology mainly requires to be conducted at high temperature (30-35°C). As the nitrococcus has rate of growth higher than that of nitrifier, to control the hydraulic retention time to be within the smallest retention time of the nitrifier and the nitrococcus can naturally eliminate the nitrifier, thereby maintaining stable accumulation of HNO_2. However, the SHARON process also has some drawbacks. For example, the operating conditions (high temperature and high ammonia nitrogen mass concentration) restrict the development and application of the process.

(3) The oxygen-free ammoxidation process: In this process, the microbes directly oxygenate the ammonia nitrogen into N_2O with nitrate as the electron acceptor in the anaerobic condition. It is featured with advantages of simple and convenient operation, good removal effect and low capital cost, etc.

(4) Simultaneous nitrification denitrification: This process was developed to decrease the dosed alkali and reduce the volume of reactor. The simultaneous nitrification denitrification is featured with stable pH in the reactor, low capital cost, and low energy dissipation.

(5) Aerobic denitrification and heterotrophic nitrification: The aerobic denitrifier was discovered in 1980s, which belongs to a kind of heterotrophic nitrification bacteria. Thus the denitrification does not always require strictly controlling the anaerobic condition, but can realize biological oxidation of the organic nitrogen and inorganic nitrogen compound from the reduced state in the aerobic condition, thereby removing the nitrogen.

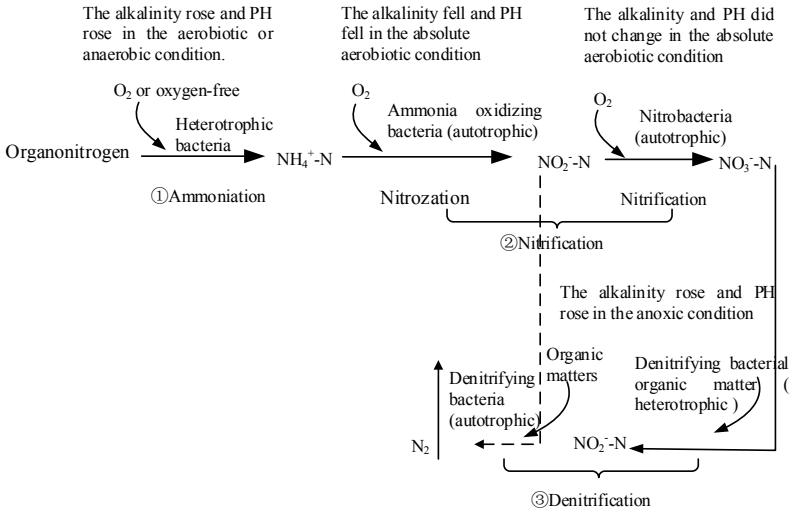

FIGURE 3
The schematic diagram of biological denitrification

Testing system and devices. Small-scale device of sewage treatment system and process flow. The experimental A2O sewage treatment system was made from the lucite. The reactor had five cells with size of L×D×H=100mm×200 mm×300 mm. Wherein, the two front cells were respectively the anaerobic zone and acoxic zone, and the three rear cells were respectively the aerobic zones. The secondary sedimentation tank adopted the vertical sedimentation basin with dischargeable capacity of 20L. The schematic diagram of the reactor is as shown in Fig.4. The total effective volume of the reactor was 30L, total hydraulic retention time was 10h, and the actual extra height was 10cm. In the operational process of the reactor, stirring paddle was arranged in the anaerobic zone and anoxic zone to guarantee the sludge can be mixed evenly. In the aerobic zone, the aeration device was used for oxygen supply and valve was set to control the aeration amount.

To make the sewage sludge reflow in the reactor, water inlet and external reflux port were arranged on the bottom of the anaerobic section of the reactor, and internal reflux port was arranged on the top of anoxic section, while the water outlet (The center was flush with the water surface) was arranged on the top of the third cell in the aerobic section of the reactor. In this experiment, the volume of sediment zone and sludge zone of the secondary sedimentation tank was respectively 15.0 L and 5.0 L. In the research on chemical-aided denitrification and dephosphorization, polyaluminium chloride and complex polymeric molysite were added into the first cell (added to the front end) and the third cell (added to the terminal end) of the aerobic section respectively. The volume ratio of anaerobic, anoxic and aerobic sections for the reactor was 1:1:3. Between the sections was separated by the partition. The flow modes are upward, downward, upward, downward, and upward. The mutual matching of devices was repetitively considered in the operational process of reactor, to guarantee the efficient operation of the reactor.

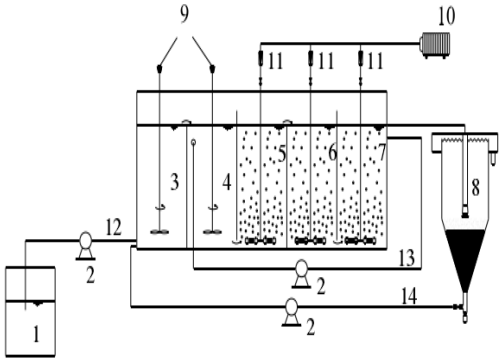

FIGURE 4
Schematic diagram of small-scale device of sewage treatment

RESULTS AND DISCUSSION

Experiment of packing addition. As the removal rate of NH_4-N and TP by the A2O system at low temperature declines obviously, to raise the removal efficiency of nitrogen and phosphorous for the small towns' sewage at low temperature, the packing was attempted to be added in the second cell of the aerobic section of the A2O system. The packing adopted the fluidized packing. The initial packing rate in the second cell of the aerobic section was 30% (V/V), and the testing water temperature was 5-12°C. The running parameters of the experiment were: water inflow of 72 L/d, internal reflux ratio of 200%, external reflux ratio of 100%, and the dissolved oxygen of below 0.2 mg/L in the anaerobic section of the reactor, dissolved oxygen of 0.2-0.5 mg/L in the anoxic section, the dissolved oxygen concentration of up to above 5 mg/L in the second cell of the aerobic section. The SRT was 7~10 d in the process of experiment. The major reason for raising the concentration of dissolved oxygen in the second cell of the aerobiotic section was to enable the packing to suspend in the pool to fully contact the active sludge. In this condition, the microbes can proliferate rapidly, and generate biomembrane within a short time. After the biomembrane grew for 40 d, the denitrification and dephosphorization effect of the system was determined.

Test of solidified sludge compaction. The unconfined compressive strength (UCS) is an important index reflecting the rate of hydration reaction of solidified sludge. The determination of unconfined compressive strength of sludge solidified by different curing agents adopted the YYW-2 strain control-type unconfined pressure gauge produced by Nanjing Soil Instrument Factory. The concrete experimental method is in the Laboratory Manual for Soil Engineering SL237-020-1999. The test was repeated on each sample for three times to control the data quality.

The US EPA Test Method 1311-TCLP was adopted to systematically evaluate the leaching toxicity of heavy metal of the solidified sludge sample, with concrete steps as shown below: before determination, extracted the solidified sludge sample by the solid to liquid ratio of 200 g/L using the acetic acid solution with PH of 4.93, then made the extract pass 0.45gm filter membrane, determined the concentration of Zn, Pb, Cd, Ni, Cr, Cu,Hg and As in the extracting solution using ICP. Three duplicate samples were set.

Influence on removal of phosphorus. The A20 treatment process with mean concentration of inflow TP of 7.1 mg/L, 7.6 mg/L, 7.8 mg/L was run in conditions I, II, and III. The influence of cellular oxygen supply in the aerobic section on the TP

removal is as shown in Fig.3. The test result shows that the concentration change of inflow TP was the largest when the aerobic section of A20 system runs in condition I, with average removal rate being only 45%, which is mainly because the too high concentration of dissolved oxygen in the A2O system in this condition influenced the progress of denitrification reaction, resulting in raised concentration of nitrate nitrogen reflowing to the aerobic section, thereby influencing the normal progress of anaerobic phosphorus release. Compared with the anaerobic released phosphorus amount of 10 ~ 14 mg/L in the condition I, the release phosphorus amount in condition II and III will reach 25-30 mg/L and 20~25mg/L respectively. The research also found that in condition I, the dissolved oxygen carried in by the reflowing of sludge destroyed the anoxic condition of the anoxic section of the A2O system, which largely reduced the phosphorus uptake of phosphorus-accumulating bacteria in the anoxic section. Besides, the mean concentration (0.71 mg/L) of TP in the water outflow in the condition II was significantly lower than the mean concentration (2.36 mg/L) of TP in the outflow in condition III, and the corresponding TP removal rates were respectively 90.7% and 69.7%, which speaks volume for the obvious influence of dissolved oxygen in the reactor on the aerobiotic phosphorus uptake of phosphorus-accumulating bacteria. Related studies show that to fully achieve the purpose of aerobiotic phosphorus uptake, the A2O system should guarantee the dissolved oxygen in the aerobic section is adequate, and hydraulic retention time should be 3-4hs. Thus, to realize a satisfactory dephosphorization effect, the working parameters of the condition III can be taken as the optimum parameters.

To explore the influence of the cellular oxygen supply in the aerobic section of A2O system on the phosphorous uptake and release by the phosphorus-accumulating bacteria, the experiment detected the PHA changes in the running process of A2O system, with result as shown in Fig.6.

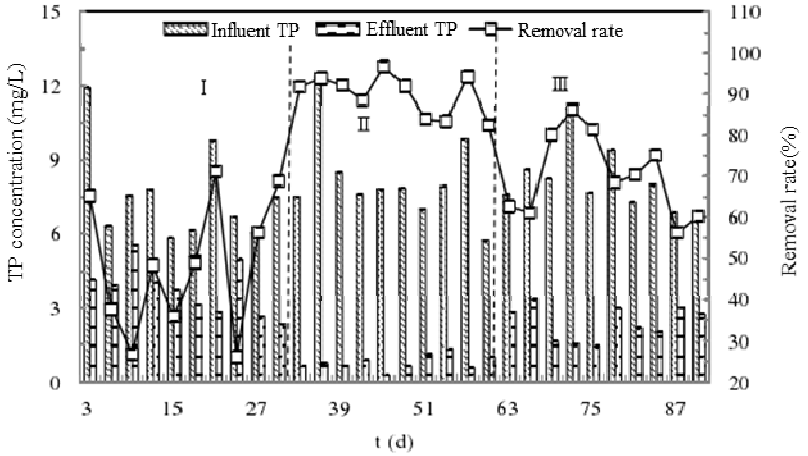

FIGURE 5
The TP removal effect in the condition of cellular oxygen supply in the aerobic section of A2O system

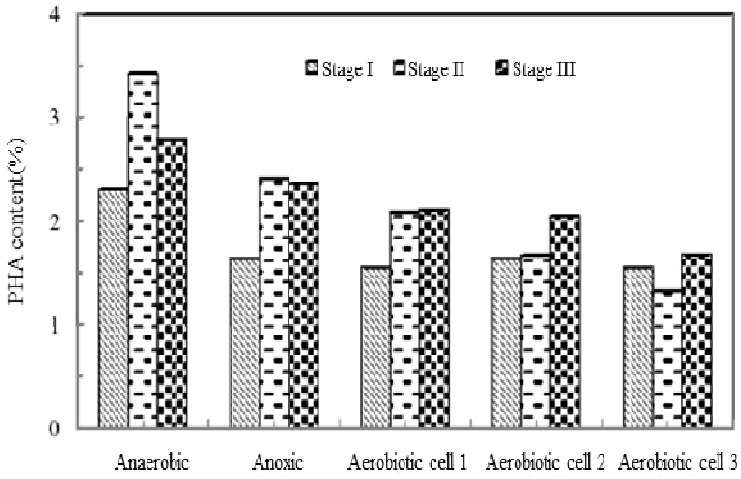

FIGURE 6
The PHA change in the system in the condition of cellular oxygen supply in the aerobic section of A2O system

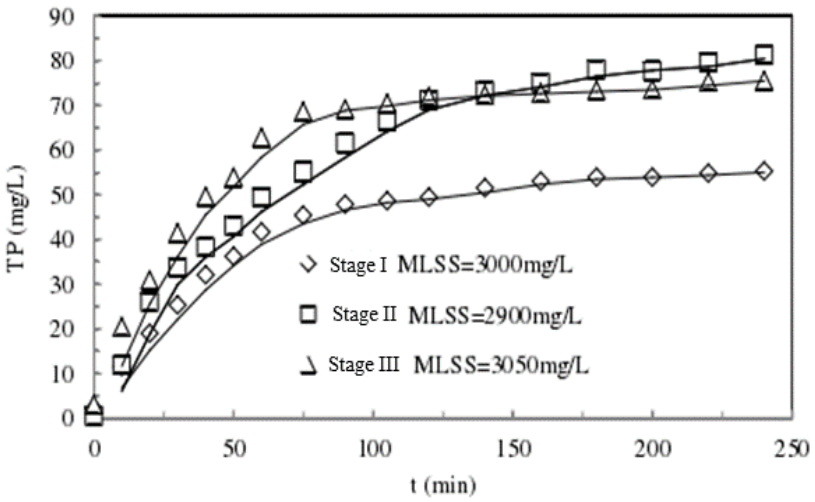

FIGURE 7
TP content in supernatant sample for the anaerobic section in the system in condition of cellur oxygen supply in aerobic section of A2O system

It is observed that in the whole process flow of A2O system, the PHA content was decreasing gradually, which mainly occurred between the anaerobic section and anoxic section. With the increase of dissolved oxygen concentration in the third cell in the aerobic section, the PHA content synthesized in the anaerobic section increased markedly. To be concrete, the synthesized amount of PHA in the anaerobic section in stage I was the least, being 2.1%, and PHA did not decompose obviously in three consecutive cells in the aerobic section; the PHA content increased slightly in the anaerobic section in stage I, being up to 3.3%, and the PHA decomposed obviously in the three consecutive cells in the aerobic section; in stage III, the PHA content in the third cell of aerobic section significantly lowered. This is consistent with the experimental result of phosphorus uptake of 1.5 mg/L in the third cell of aerobic section in condition III.

It is observed from Fig.7 that the phosphorus release rate of the system in different oxygen supply conditions in the aerobic section presents a trend of condition III>condition II>condition I. The high released phosphorus amount in condition III is mainly caused by low concentration of dissolved oxygen and nitrate nitrogen concentration in the sludge reflux. The maximum phosphorus amount in the operation process of condition I, II, III appeared for different time periods too: condition II (140min) > condition I (90min) > condition III (75min). The rate of anaerobic phosphorus release usually rests with the activity of the phosphorus-accumulating bacteria (the maximum capacity of phosphorus storage) and the content of available organic matters. In the experiment, the substrate concentration in the A2O was the same, and the condition II had larger released phosphorus amount, which is closely related to its higher phosphorus release ability and longer phosphorus release time, thereby indirectly proving that the reaction conditions of condition II are favorable for the A2O system to fully remove the phosphorous.

CONCLUSION

The major purpose of this paper is to treat the sewage via low temperature process. Effect of DO, internal reflux ratio r, external reflux ratio R, sludge age SRT, sewage temperature and pH on COD removal is studied. The result shows that the best COD removal was 95.8% and TP removal is 90.7%.

REFERENCES

[1] Sushanta, S., Bholanath, S., Sajal, P. (2018) Phytoavailability of heavy metals in relation to soil chemical properties and health risk assessment through major exposure pathways in a long-term sewage contaminated areas of kolkata, India. Fresen. Environ. Bull. 27, 7559-7571.

[2] Hu, Z.R., Wentzel, M.C., Ekama, G.A. (2002) Anoxic growth of phosphate-accumulating organisms (PAOs) in biological nutrient removal activated sludge systems. Water Research. 36(19), 4927-4937.

[3] Zhu, G., Peng, Y., Li, B., Guo, J., Yang, Q., Wang, S. (2008) Biological Removal of Nitrogen from Wastewater. Reviews of Environmental Contamination and Toxicology. 192, 159-195.

[4] And, S.M., Mataalvarez, J. (2002) Utilization of SBR Technology for Wastewater Treatment: An Overview. Ind. Eng. Chem. Res. 41(23), 5539-5553.
[5] Guo, J., Peng, Y., Huang, H., Wang, S., Ge, S., Zhang, J., Wang, Z. (2010) Short- and long-term effects of temperature on partial nitrification in a sequencing batch reactor treating domestic wastewater. Journal of Hazardous Materials. 179(1), 471-479.
[6] Li, H., Li, Z., Li, Z., Yu, J., Liu, B. (2015) Evaluation of ecosystem services: A case study in the middle reach of the Heihe River Basin, Northwest China. Physics and Chemistry of The Earth. 89-90, 40-45.
[7] Liu, Y.Q., Moy, B., Kong, Y.H. (2010) Formation, physical characteristics and microbial community structure of aerobic granules in a pilot-scale sequencing batch reactor for real wastewater treatment. Enzyme and Microbial Technology. 46(6), 520-525.
[8] Yu, H., Huang, Y., Ning, J., Zhu, B., Cheng, Y. (2014) Effect of cation exchange capacity of soil on stabilized soil strength. Soils and Foundations. 54, 1236-1240.
[9] Andreottola, G., Foladori, P., Ragazzi, M. (2001) On-line control of a SBR system for nitrogen removal from industrial wastewater. Water Science and Technology. 43(3), 93-100.
[10] Hu, B.L., Zheng, P., Tang, C.J., Chen, J.W., van der Biezen, E., Zhang, L., Ni, B., Jetten, M.S., Yan, J., Yu, H.Q., Kartal, B. (2010) Identification and quantification of anammox bacteria in eight nitrogen removal reactors. Water Research. 44(17), 5014-5020.
[11] Bodík, I., Herdová, B., Drtil, M. (2002) The use of upflow anaerobic filter and AnSBR for wastewater treatment at ambient temperature. Water Research. 36(4), 1084-1088.
[12] Mohan, S.V., Mohanakrishna, G., Raghavulu, S.V., Sarma, P.N. (2007) Enhancing biohydrogen production from chemical wastewater treatment in anaerobic sequencing batch biofilm reactor (AnSBBR) by bioaugmenting with selectively enriched kanamycin resistant anaerobic mixed consortia. International Journal of Hydrogen Energy. 32(15), 3284-3292.
[13] Torres, P., Foresti, E. (2001) Domestic sewage treatment in a pilot system composed of UASB and SBR reactors. Water Science and Technology A Journal of the International Association on Water Pollution Research. 44(4), 247.
[14] Bassin, J.P., Dezotti, M., Sant'Anna Jr., G.L. (2011) Nitrification of industrial and domestic saline wastewaters in moving bed biofilm reactor and sequencing batch reactor. Journal of Hazardous Materials. 185(1), 242-248.
[15] Tabatabaei, M., Rahim, R.A., Abdullah, N., Wright, A.D.G., Shirai, Y., Sakai, K., Sulaiman, A., Hassan, M.A. (2010) Importance of the methanogenic archaea populations in anaerobic wastewater treatments. Process Biochemistry. 45(8), 1214-1225.

Received: **28.12.2018**
Accepted: **22.03.2019**

CORRESPONDING AUTHOR

Wanyong Xiong
Department of Environment and Resources,
Fuzhou University,
Fuzhou – China

e-mail: 1708949755@qq.com

© by PSP Volume 28 – No. 5/2019 pages 4028-4034 Fresenius Environmental Bulletin

STUDY ON FEATURE OF LATE PALEOZOIC SEDIMENTARY IN THE ORDOS BASIN

Qingan Zhou[1], Qiqi Lyu[2,3,*], Shicai Zhong[4], Shunshe Luo[2], Yulong Guan[1]

[1]School of Geoscience, Yangtze University, Wuhan, Hubei, 430100, China
[2]Hubei Cooperative Innovation Center of Unconventional Oil and Gas (Yangtze University), Wuhan, Hubei, 430100, China
[3]Petro China Research Institute of Petroleum Exploration & Development, Beijing, 100083, China
[4]Research Institute of Petroleum Exploration & Development, Changqing Oilfield Company, China National petroleum Corporation, Xian, Shanxi, 710018, China

ABSTRACT

Geochemical markers are the most important indicators of the sedimentary environment. The trace element characteristics in mudstone can reflect the medium environment well. Among the seawater and freshwater environment, the commonly used trace elements are: Sr, Ba, B, Ga, Rb and so on. In order to further demonstrate the sea-land transitional environment of the Late Paleozoic Ordos Basin, this study carried out mineralogical and geochemical analysis tests on mudstone samples in the drilling core and field sections of the eastern, southern and northwestern basins. The geochemical base profiles of the east-west and north-south directions in the basin were established respectively, and the test results of different horizons in different regions were compared and analyzed.

KEYWORDS:
Late Paleozoic sedimentary, rocks, Ordos Basin, Geochemical markers

INTRODUCTION

The Ordos Basin is a typical intracratonic basin with a basin fill gently dipping (<2°) to the west [1-4]. As one of the main petroliferous basins in China [5-7], several Ordovician and lower-middle Permian gas fields, including the Changqing, Jinbian, Sulige, and Yulin gas fields, have been discovered in the north and central parts of basin since gas exploration in the Ordos Basin began in the 1980s [8-12]. Recent exploratory wells in the northern Ordos Basin (i.e., the Hangjinqi area) found significant volumes of gas in upper Paleozoic sandstones [13-15]. Gas systems in this area are characterised by upper Carboniferous (Taiyuan Formation) and lower Permian (Shanxi Formation) deltaic and swamp coal source rocks, upper Carboniferous to middle Permian fluvial and deltaic sandstone reservoirs, and upper Permian deltaic and fluvial mudstone cap rocks [16-20].

The results of the third resource evaluation indicate that there are 1.5 trillion m3 of natural gas resources in the Paleozoic in the southern Ordos Basin [11-25]. The exploration prospects are very large, but the exploration level is very low. There were only 30 exploration wells in the Paleozoic (some wells showed good gas in the Upper Paleozoic and obtained low-yield airflow). Deepening the understanding of natural gas geology in the southern part of the basin is an important basic research work to accelerate the pace of exploration in the region. This paper focuses on the sedimentary characteristics of the Upper Paleozoic in the southern part of the Ordos Basin, with a view to helping to understand the geological conditions of natural gas in the area.

EXPERIMENTAL

After petrographic examination and the removal of altered surfaces, whole-rock samples were crushed and powdered in an agate mill to ~200 mesh. Chemical analyses were conducted at the laboratory. Major element compositions were analyzed by X-ray fluorescence (XRF; PW2404) using fused glass disks. Trace element compositions were determined using an Agilent 7500a inductively coupled plasma mass spectrometer (ICP-MS) after acid digestion of samples in Teflon bombs. The analytical results for the US Geological Survey basalt and andesite standards (BHVO-1, BCR-2, AGV-1) indicated that the analytical precision was better than 5% for major elements and 10% for trace and rare earth elements [26].

RESULTS AND DISCUSSION

According to the ancient salinity of more than 35 ‰ is super salty water, 25 ‰ -35 ‰ is salt water, 10 ‰-25 ‰ is brackish water, less than 10 ‰ is the standard of brackish water and fresh water. The calculation results show that (Fig. 1), the water in the entire Shanxi Basin is dominated by mixed water. Among them, the Taiyuan group at the bot-

tom of the stone box group, the ancient salinity value has a significantly reduced trend, and there are two distinct cycles of cyclical changes. The first paleo-salt cycle is the Taiyuan Formation-Mountain 21 sub-segment. The second paleo-salt cycle is a sub-segment of the 13th section of the mountain 13 sub-segment, while the bottom of the lower stone box group and the underlying strata have an ancient salinity mutation surface. This trend indicates the late Paleozoic in the background of the retreat, the intermittent transgression in the Shanxi period, and the accompanying sea-lake communication events, as well as the continental deposition of the Lower Shihezi Formation.

Combined with the normal salinity of modern seawater 35 ‰ as a reference. The ancient salinity value of Taiyuan group is 5.787-44.605‰, with an average of 24.179‰; the mountain 23 sub-section is 8.321-39.783‰o, with an average of 18.452‰. Taking the normal seawater salinity of 35‰ as the reference, the maximum value of 44.605‰ in the Taiyuan Formation and the maximum value of 39.783‰ in the Shan 23 subsection indicate that there is an indisputable fact about the marine evidence in these two periods. In the whole mountain section 2, the ancient salinity value of the mountain 22 sub-section is 4.519-15.001‰, with an average of 9.738‰; the mountain 21 sub-section is 2.405-12.921‰, with an average of 9.461‰. Compared with the 23rd section of the mountain, the overall change trend of the paleo-salinity is reduced, which indicates that the mountain 2 is out of a large-scale transgression-sea retreat; the entire salinity of the whole mountain 1 and the mountain 13 sub-segment It is 6.390-30.803‰, with an average of 10.628‰; the mountain 12 subsection is 5.788-27.644‰, with an average of 10.296‰; the mountain 11 subsection is 6.580-14.219‰, The average is 9.517 baht. Among them, the high value appeared in the mountain 12 subsection (27.644‰), and its ancient salinity still showed an overall decreasing trend, indicating that there was a new round of transgression from the Shan 1 period, but the scale was higher. All the previous periods were reduced, and the end of the 11th phase ended. From the beginning of the lower stone box period, the ancient salinity value is 6.427-10.355‰, with an average of 7.854‰. The range and average value of the paleo-salinity values are lower than any previous period, indicating that it is in the sea. In the late Paleozoic era, the seawater in this period completely withdrew from the Ordos Basin at the western end of the North China Platform.

According to the analysis trend of different salinity of different layers in different regions. The entire Shanxi group of the basin, from south to north (Fig. 2), shows the following characteristics: the small layers of the mountain 23~Mountain 12 show a trend of decreasing the paleo-salinity from south to north, starting from the mountain 11 It is not obvious, and the ancient salinity value is relatively uniform. This is because the main material margin area of the entire Shanxi Basin is located in the northern Yinshan ancient land, and the north-south-developed river-sea-continental transitional delta-shore shallow sea (tidal flat) sedimentary environment Controlling most areas of the basin, the range of influence of seawater to the north is limited; from west to east (Fig. 3), the following characteristics are shown: the entire small layer of the entire Shanxi period shows a trend of decreasing the paleo-salt value from west to east. The Late Carboniferous began the interaction and

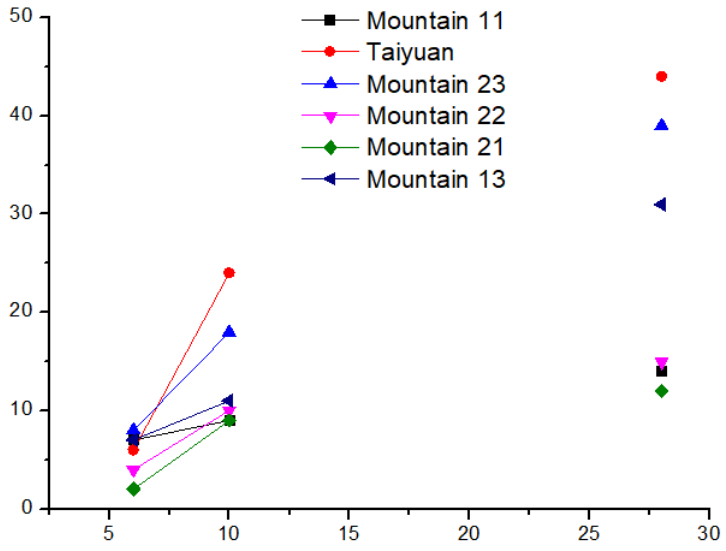

FIGURE 1
The paleo-salinity content of the bottom of the Taiyuan Formation-Lower Shihezi Formation in the Ordos Basin

control of the Ordos Basin in the western Qilian Sea and the eastern North China Sea, and a large-scale retreat began in the Shanxi period. The difference between the above-mentioned paleo-salt values indicates that the impact of Qilian Sea on the southwestern part of the basin is always stronger than that of the North China Sea to the southeastern part of the basin during the intermittent transgression and retreat of the Shanxi period. The trend of this kind of change is most obvious in the early stage of the mountain 2, and with the continuous retreat in the later period, the difference between the east and the west gradually decreases and is not obvious in the late Shanxi. In summary, the intermittent transgression of the entire Shanxi Basin is caused by the joint influence of the Qilian Sea in the western part of the basin and the North China Sea in the eastern part of the basin, and the impact of the Qilian Sea on the southwestern part of the basin is stronger than that of the North China Sea to the southeast of the basin. The degree of influence of the ministry.

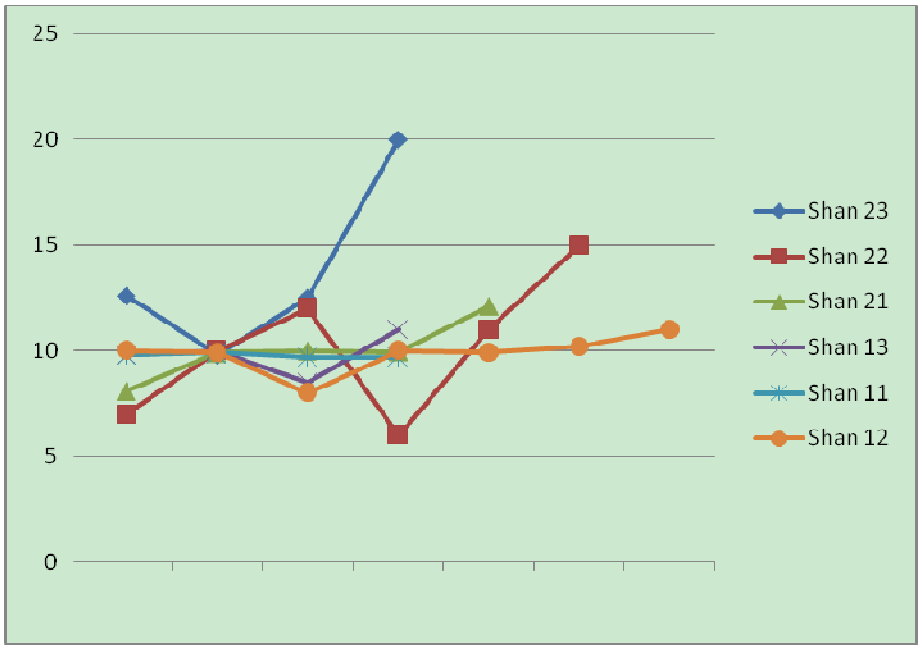

FIGURE 2
Trends of paleo-salinity of small layers in the Shanxi Formation in the eastern part of the basin (from north to south)

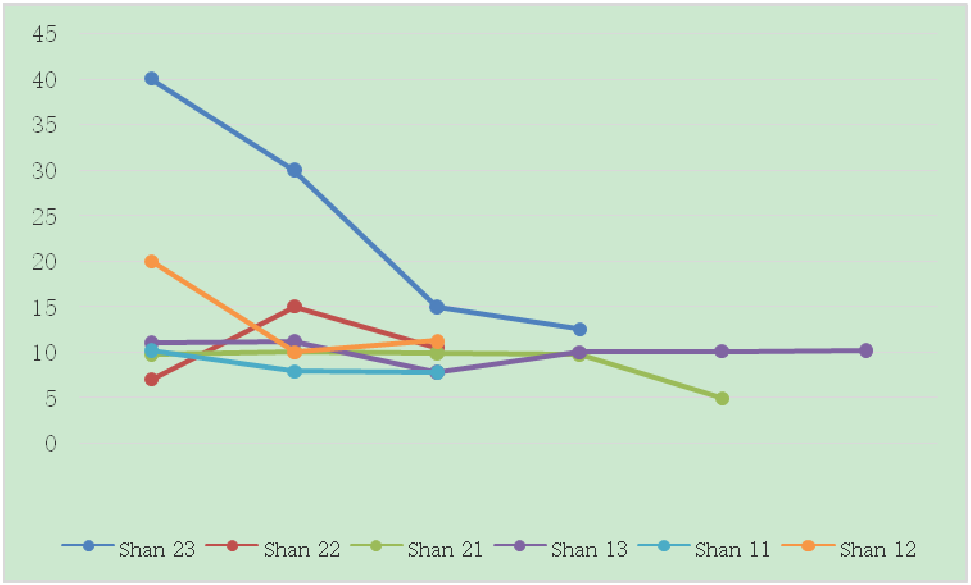

FIGURE 3
Trends of paleo-salinity in small layers of the Shanxi Formation in the southern part of the basin (from west to east)

During the process of transporting terrigenous clastic sediments from rivers to the oceans, the geochemical behaviors of sputum and sputum that are transported in a free state have been different due to changes in the geochemical environment, especially in the estuary where sea-land interactions occur. Firstly, on the one hand, due to its small solubility product, when fresh water and seawater are mixed, Ba^{2+} in fresh water combines with SO_4^{2-} in seawater, which is easier to form Ba S04 precipitate. On the other hand, the ionic radius of strontium is higher. Large, with a smaller hydration energy than Sr, easy to be adsorbed by clay minerals, colloids, organic matter, etc., so that the strontium content in the continental and marine-continental transitional sediments is higher, so that less strontium enters the ocean, and the strontium content in the seawater is far. It is lower than Sr; secondly, Sr has a larger activity than Ba, and it is not easy to form chemical precipitation during transportation. Compared with strontium, it is also adsorbed by clay minerals, colloids, organic matter, etc. It is weak, so most of the free cockroaches are transported into the sea, so that the strontium in the seawater is much larger than the strontium. On the other hand, because the ionic radius of the strontium is too large, it is difficult to enter the aragonite or the six-time coordination of the nine-time coordination. In the calcite biocrust, the strontium in the marine biocapsule is much larger than the strontium, so the strontium content in the marine sediment is higher than that in the strontium deposit, which makes the continental sediment relatively rich in S-sl and marine sediments. Sr-rich relatively poor Ba, from Lu Xianghai, Sr / Ba gradually increases. Sr / Ba value gradually increases as the distance from the coast, according to which ratio may reflect the qualitative paleosalinity.

The results of seabed samples in China show that the Sr/Ba in mudstone is 0.8-1, and the study of the Mesozoic continental strata in Ordos found that the Sr/Ba of most mudstone samples is 0.54, which is divided by Sr/Ba. The common standards of sedimentary environment, combined with this study, determine the sedimentary environment determination criteria in the study area: greater than 0.8 for seawater, 0.5-0.8 for mixed water, and less than 0.5 for fresh water. Through the analysis of trace elements in the mudstone samples at the bottom of the Shanxi group and the Xiashi box group in the study area, the analytical data were put on the Sr/Ba content relationship map. It can be seen that the Sr/Ba content data points of the Shanxi group samples in the study area are located in the marine phase. The sedimentary area, while the data points at the bottom of the lower stone box group are completely distributed in the continental deposition area. The above characteristics indicate that the entire Erdos Basin in Shanxi has obvious traces of seawater influence, while the seawater has completely withdrawn from the lower Shihezi period, and the basin enters the evolution stage of the inland depression lake basin, showing the mountain 2 segment-mountain segment-1 At the bottom of the stone box group, the whole phase gradually transitions from the marine phase to the transition phase of the continental phase.

According to the variation trend of different levels of Sr/Ba in different regions. The entire Shanxi group of the basin, from south to north (Fig. 4), shows the following characteristics: the small layers of the mountain 23-mountain 12 show a trend of decreasing Sr/Ba from south to north, and this trend changes from the mountain 11 stage. It is not obvious that Sr/Ba is relatively uniform; from west to east (Fig. 5), the following characteristics are shown: the entire small layer of the entire Shanxi period from west to east also shows a decreasing trend of Sr/Ba. The above trend is the same as the trend of paleo-salt.

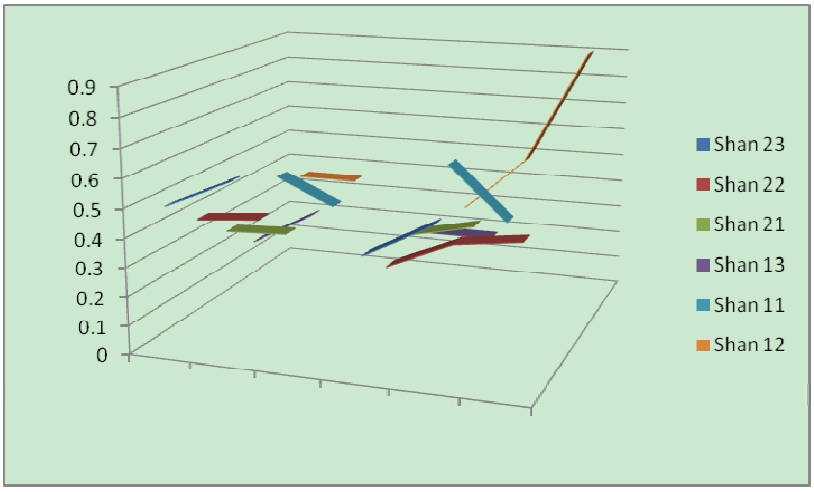

FIGURE 4
Trends of Sr/Ba in small layers of the Shanxi Formation in the eastern part of the basin (from north to south)

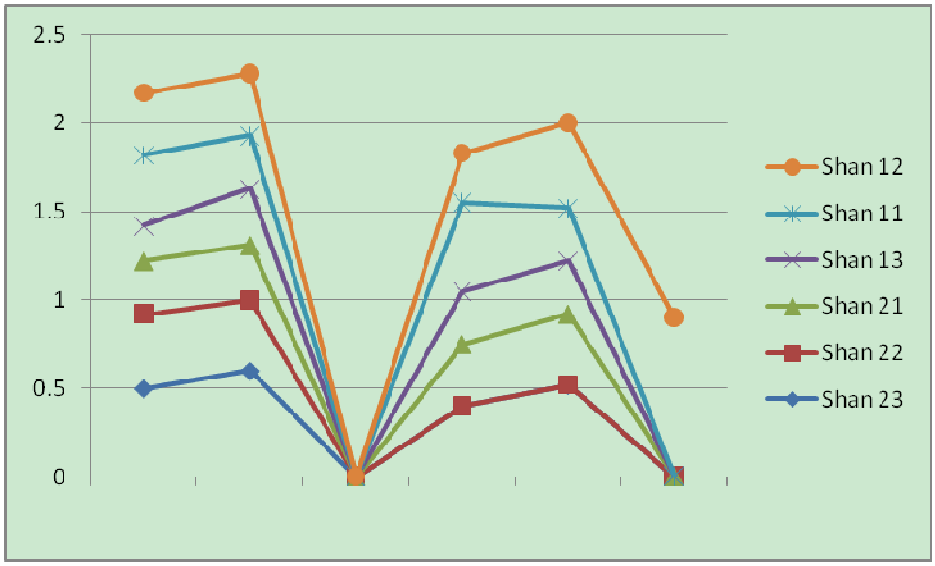

FIGURE 5
Trends of Sr/Ba in small layers of the Shanxi Formation in the southern part of the basin (from west to east)

It should be pointed out that the variation trend of the internal small layer Sr/Ba is slightly different with the control and influence of the sedimentary environment and the paleogeographic evolution of the Shanxi Formation. As far as the data of the small layers of the 2nd section of the mountain are concerned, the Sr/Ba performance gradually increases from the 23rd stage of the mountain, and the data of the 22nd stage of the mountain is the highest, until the data of the mountain 2l period begins to decrease again; likewise, in the 1st section of the mountain The data of each small layer also showed the above change law, that is, Sr/Ba showed a gradual increase from the 13th stage of the mountain, and the data of the 12th stage of the mountain was the highest, and the data of the mountain 11th stage began to decrease again. The appearance of this feature and sub-level transgression. The change of the regressive sedimentary cycle is related to the fact that both the mountain 2 and the largest sea (lake) in the mountain phase appear in the middle and late stages of each period.

The three elements of B, Ga, and Rb in the crystal framework of clay minerals vary regularly from the freshwater area to the seawater area with the depositional environment. Based on this, Shimada et al. made an environmental map indicating the relationship between the three elements. Yan Qinshang (1979) and others from Tongji University [27] have also used the sample analysis results of known phases to vote. It is found that the conclusions drawn by this method are consistent with the actual ones, so it is reliable to use this method as the basis for environmental analysis. The results of the analysis of mudstone samples in the eastern and southern basins were investigated. It was found that all the data points in the Shanxi Formation were located in the marine sedimentary area, indicating that the entire Erdos Basin in Shanxi has obvious signs of being affected by seawater.

With the control and influence of sedimentary environment changes and paleogeographic evolution, the bottom of the 2nd Member-Mountain 1 and the Lower Shihezi Formation, the whole shows the transition from the marine phase to the transition phase, and finally evolves into the continental phase. The specific performance is as follows: In terms of the data of each small layer of the 2nd section of the mountain, the data of the mountain 23-mountain 22-mountain 21 marine phase is gradually decreasing, while the data of the transitional phase and the continental phase are gradually increasing, showing the sea to the land. The obvious evolutionary characteristics; as far as the Shan 1 is concerned, the data of the marine phase is generally less than that of the mountain 2, indicating that the scale of the retreat in this period has increased from the previous period, and most of the basin is the continental and transitional environment. The data of each small layer still shows that the data of the mountain 13-mountain 12-mountain 11 marine area is gradually decreasing, while the data of the transition phase and the land phase are gradually increasing. It shows that the period has been transformed into an obvious continental environment, and some of the points in the transitional phase may be due to the dryness of the climate, resulting in a large partial salinization of the shallow lake facies.

CONCLUSION

Based on the sedimentary geochemical indicators, the geochemical test results of different layers in different areas of the basin were analyzed and compared. It is believed that the key period of land-sea transition in the Late Paleozoic Ordos Basin is the end of Shanxi (Mountain 1). Among them, the marine characteristics of the early Shanxi (Mountain 2) basin are obvious, and the intermittent transgression is frequent and the tidal effect is strong, which is the residual land surface filling stage; while the late Shanxi (Mountain 1) basin is persistent. The background of the sea receding, the tidal action tends to be weak, and it is the filling stage of the offshore lake basin: among them, the difference between the geochemical indicators is generally decreasing from west to east, while the difference between north and south is generally decreasing from south to north.

ACKNOWLEDGEMENTS

This research was financially supported by the Foundation of State Key Laboratory of Petroleum Resources and Prospecting, China University of Petroleum, Beijing (Grant No. PRP/open-1804) and the Science and Technology Research Project of Hubei Provincial Department of Education of China (No. Q20181308).

REFERENCES

[1] Darby, B.J., Ritts, B.D. (2002) Mesozoic contractional deformation in the middle of the Asia tectonic collage: the intraplate western Ordos fold–thrust belt, China. Earth Planet Sci. Lett. 205, 13-24.

[2] Meng, F., Gao, S., Song, Z., Niu, Y., Li, X. (2018) Mesozoic high-Mg andesites from the Daohugou area, Inner Mongolia: Upper-crustal fractional crystallization of parental melt derived from metasomatized lithospheric mantle wedge. Lithos. 302, 535-548.

[3] Xie, X., Heller, P.L. (2013) U–Pb detrital zircon geochronology and its implications: the early Late Triassic Yanchang Formation, south Ordos Basin, China. J. Asian Earth Sci. 64, 86-98.

[4] Xu, F., Hu, B., Dou, Y., Song, Z., Liu, X. (2018) Prehistoric heavy metal pollution on the continental shelf off Hainan Island, South China Sea: From natural to anthropogenic impacts around 4.0 kyr BP. Holocene. 28, 455-463.

[5] Yin, S., Xie, R., Wu, Z., Liu, J., Ding, W. (2019) In situ stress heterogeneity in a highly developed strike-slip fault zone and its effect on the distribution of tight gases: A 3D finite element simulation study. Marine and Petroleum Geology. 81(1), 1-17.

[6] Zhang, W., Li, S., Wei, J., Zhang, Q., Liu, R. (2018) Grouting rock fractures with cement and sodium silicate grout. Carbonates and Evaporites. 33, 211-222.

[7] Yang, Y., Li, W., Ma, L. (2005) Tectonic and stratigraphic controls of hydrocarbon systems in the Ordos basin: a multicycle cratonic basin in central China. AAPG Bull. 89, 255-269.

[8] Wang, X., Zhang, X., Gao, J., Li, J., Jiang, T. (2018) A slab break-off model for the submarine volcanic-hosted iron mineralization in the Chinese Western Tianshan: Insights from Paleozoic subduction-related to post-collisional magmatism. Ore Geology Reviews. 92, 144-160.

[9] Tang, X., Zhang, J., Shan, Y., Xiong, J. (2012) Upper Paleozoic coal measures and unconventional natural gas systems of the Ordos Basin, China. Geosci. Front. 3, 863-873.

[10] Zou, C.N., Zhu, R.K., Wu, S.T., Yang, Z., Tao, S.Z., Yuan, X.J., Hou, L.H., Yang, H., Xu, C.C., Li, D.H., Bai, B., Wang, L. (2012) Types, characteristics, genesis and prospects of conventional and unconventional hydrocarbon accumulations: taking tight oil and tight gas in China as an instance. Acta Petrolei Sinica. 33, 173-187.

[11] Cao Y., Liu, L., Chen D., Wang, C., Yang W., Kang L., Zhu X. (2017) Partial melting during exhumation of Paleozoic retrograde eclogite in North Qaidam, western China. Journal of Asian Earth Sciences. 148, 223-240.

[12] Yang, M.H., Li, L., Zhou, J., Jia, H.C., Sun, X., Gong, T., Ding, C. (2015) Structural evolution and hydrocarbon potential of the upper paleozoic northern Ordos Basin, north China. Acta Geologica Sinica (English Edition). 89, 1636-1648.

[13] Wang, M.J., He, D.F., Bao, H.P., Lu, R.Q., Gui, B.L. (2011) Upper palaeozoic gas accumulations of the Yimeng uplift, Ordos Basin. Petrol. Explor. Dev. 38, 30-39.

[14] Zhang, S.C., Mi, J.K., Liu, L.H., Tao, S.Z. (2009) Geological features and formation of coal-formed tight sandstone gas pools in China: cases from Upper Paleozoic gas pools, Ordos basin and Xujiahe formation gas pools, Sichuan Basin. Petrol. Explor. Dev. 36, 320-330.

[15] Yin, S., Lv, D., Ding, W. (2018) New method for assessing microfracture stress sensitivity in tight sandstone reservoirs based on acoustic experiments. International Journal of Geomechanics. 18(4), 1-16.

[16] Ni, W., Li, Q., Song, X. (2017) Analysis of wellbore stability of shale gas reservoir drilling. Fresen. Environ. Bull. 26, 510-515.
[17] Qiu, X., Liu, C., Mao, G., Deng, Y., Wang, F., Wang, J. (2014) Late triassic tuff intervals in the Ordos Basin, Central China: Their depositional, petrographic, geochemical characteristics and regional implications. Journal of Asian Earth Sciences. 80, 148-160.
[18] Ji, W.M., Li, W.L., Liu, Z., Lei, T. (2013) Research on the upper paleozoic gas source of the Hangjinqi block in the norhtern Ordos Basin. Nat. Gas Geosci. 24, 905-914.
[19] Wang, G., Chang, X., Yin, W., Li, Y., Song, T. (2017) Impact of diagenesis on reservoir quality and heterogeneity of the Upper Triassic Chang 8 tight oil sandstones in the Zhenjing area, Ordos Basin, China. Marine and Petroleum Geology. 83, 84-96.
[20] Yang, R., He, Z., Qiu, G., Jin, Z., Sun, D., Jin, X. (2014) A Late Triassic gravity flow depositional system in the southern Ordos Basin. Petroleum Exploration and Development. 41(6), 724-733.
[21] Qiu, X., Liu, C., Wang, F., Deng, Y., Mao, G. (2015) Trace and rare earth element geochemistry of the Upper Triassic mudstones in the southern Ordos Basin, Central China. Geological Journal. 50(4), 399-413.
[22] Sun, J., Dong, Y. (2019) Middle–Late Triassic sedimentation in the Helanshan tectonic belt: Constrain on the tectono-sedimentary evolution of the Ordos Basin, North China. Geoscience Frontiers. 10, 213-227.
[23] Xu, Q., Shi, W., Xie, X., Busbey, A.B., Liu, K. (2018) Inversion and propagation of the Late Paleozoic Porjianghaizi fault (North Ordos Basin, China): Controls on sedimentation and gas accumulations. Marine and Petroleum Geology. 91, 706-722.
[24] Jin, R., Yu, R.-A., Yang, J., Zhou, X., Zhang, T. (2019) Paleo-environmental constraints on uranium mineralization in the Ordos Basin: Evidence from the color zoning of U-bearing rock series. Ore Geology Reviews. 104, 175-189.
[25] Guo, P., Liu, C., Wang, J., Deng, Y., Wang, W. (2018) Detrital-zircon geochronology of the Jurassic coal-bearing strata in the western Ordos Basin, North China: Evidences for multi-cycle sedimentation. Geoscience Frontiers. 9, 1725-1743.
[26] Liu, X. S., Ning, J. G., Tan, Y. L., Gu, Q. H. (2016) Damage constitutive model based on energy dissipation for intact rock subjected to cyclic loading. International Journal of Rock Mechanics and Mining Sciences. 85, 27-32.
[27] Yan, Q.S., Zhang, G.D., Xiang, L.S., Wang, H.Z., Wu, B.Y., Dong, R.X., Wang, Y.Y., Guo, W.Y. (1979) Marine inundation and related sedimentary environment of Funing Group (Lower Paleogene), in Jinhu Depression, North Jiangsu Plain. Acta geologica Sinica. (1), 74-83.

Received: **03.01.2019**
Accepted: **18.03.2019**

CORRESPONDING AUTHOR

Qiqi Lyu
Hubei Cooperative Innovation Center of Unconventional Oil and Gas
(Yangtze University),
Wuhan, Hubei, 430100 – China

e-mail: 201673021@yangtzeu.edu.cn

© by PSP Volume 28 – No. 5/2019 pages 4035-4043 Fresenius Environmental Bulletin

LC-MS/MS DETECTION AND ANALYSIS OF FURAN METABOLITE RESIDUES IN PROPOLIS

Rui Wang[1], Gang Wei[2,*]

[1]School of Perfume and Aroma Technology, Shanghai Institute of Technology, Shanghai, 201418, China
[2]Shanghai Key Laboratory of Diabetes, Shanghai Institute for Diabetes, Shanghai Jiao-Tong University Affiliated Sixth People's Hospital, Shanghai 200233, China

ABSTRACT

In this paper, the high-sensitivity and high-selective fluorescence-derived reagents were used for pre-column derivatization and high-performance liquid chromatography to detect the metabolites of nitrofuran antibiotics. The method of liquid chromatography-tandem mass spectrometry for the determination of nitrofuran metabolites in bee pollen was established. The sample was acidified by perchloric acid, purified by solid phase extraction, derivatized, extracted with ethyl acetate, and analyzed by tandem mass spectrometry. At the three levels of 1.0, 2.0, 5.0 μg/kg, the average recovery of nitrofuran metabolites ranged from 93.7% to 97.2%, the intra-day relative standard deviation was less than 10%, and the relative standard deviation during the day was less than 13.5%. It has good linearity in the range of 0.5-20 ng/mL (r>0.99 detection limit is 0.25μg/kg, and the limit of quantification is 1.0μg/kg. The detection method is simple, the selectivity is good, the anti-interference ability is strong, and it is suitable for bee pollen. Analysis of the nitrofuran metabolites was confirmed.

KEYWORDS:
LC-MS/MS detection and analysis, Nitrofuran metabolites, Tandem mass spectrometry, Extraction purification, Ethyl acetate

INTRODUCTION

Nitrofuran antibiotics, the picture is a synthetic broad-spectrum antibacterial drug with a basic structure of 5-nitrofuran. These antibiotics are common to most Gram-positive and Gram-negative bacteria, and some fungi [1]. Inhibition, has been widely used in the prevention and treatment of animal infectious diseases such as poultry, livestock, aquatic products, bees, etc., but the side effects of nitrofuran drugs have attracted people's attention [2-4]. Fish, shrimp, poultry, rabbit meat and casings exported from China have been detected to contain oxazolone and nitrofurazone, especially in fish and poultry, which has seriously restricted the export of animal food in China [5]. Due to the serious harm of nitrofuran drugs, many countries have strict inspection and quarantine requirements and regulations for such drugs. For example, the European Union stipulates that nitrofuran drugs should not be detected in animal-derived foods [6]. Determination of oxazolone by high performance liquid chromatography, the detection limit is US regulations, the use of furazolidone and clozapine in food animals is prohibited [7, 8]; the Korean version of the "Food Code" stipulates that furazolidone should not be detected in pork. In fact, the establishment of China's national standards is to a greater extent in order to achieve the goal of connecting with the international community as soon as possible [9].

However, since the standard method is actually a standard for the minimum amount that can be detected by existing instruments and detection methods, technical obstacles and extremely expensive instruments make analysis methods difficult to popularize. At present, only a few laboratories in Switzerland, the United Kingdom, and so on have been able to detect the limited amount of nitrofuran residue. With the improvement of the performance of instruments and equipment and the continuous improvement of detection methods, the detection standards will develop in a lower direction [10-12]. Therefore, it is imperative to establish a method for detecting nitrofuran metabolites that is accurate, sensitive, specific, convenient, efficient, and easy to promote.

For the above purposes, high-sensitivity, high-selective fluorescence-derived reagents for pre-column derivatization and high-performance liquid chromatography for the determination of metabolites of nitrofuran antibiotics were established to establish a difurther-like antibiotic metabolites in animal-derived foods. HPLC method for the detection of light and liquid tandem mass spectrometry. By optimizing the pretreatment conditions of the sample, the liquid chromatographic separation conditions and the measurement conditions of the derivative, a new method for detecting metabolites of nitrofuran antibiotics was established, and the actual sample was studied to realize the determination method. universality. This paper focuses on animal-derived foods and aquatic products, carries out research on safety testing technology,

and formulates corresponding testing methods. It has certain significance for promoting industrialization by standardization and promoting the safe production of agricultural products and food.

Nitrofurans, including oxazolone, furanone, valproxil, and nitrofurazone, belong to a class of synthetic broad-spectrum antibiotics that all contain a 5-nitrofuran ring structure [13]. Nitro-methane drugs are commonly used as feed additives to promote growth and are mainly used in livestock (ie poultry, pigs and cattle, aquaculture (such as fish and shrimp) and bee colonies to prevent and treat infections of bacteria and Pathogens caused by Escherichia coli and Salmonella such as gastritis, enteritis, poultry cholera and blackhead coccidiosis. In 1995, nitrofurans used in livestock production in the European Union have been completely banned due to concerns about drug residues [14].

Carcinogenicity and its potential harm to human health. Under the EU regulations, the testing of food produced by EU member states is also applicable to this regulation [15]. Therefore, the trade of food in these regions is exempt from the detection of nitrofuran among EU member states. Residual drugs. On the contrary, this puts higher requirements on the residue detection of nitrofurans in animal-derived foods exported to the EU. In some countries, such as Australia, the United States, the Philippines, Thailand and Brazil. Confirmed virgins for livestock are also banned. Although nitrofurans are completely banned during livestock production, this is completely banned. These drugs are effective for livestock and human treatment: nitrofurazone is used in local burn infections and skin infections; oxazolone is effective in the treatment of cholera, bacterial ventral bay and giardiasis; Used to treat urinary tract infections.

Nitro-purine drugs, metabolites, metabolite molecules and metabolic derivatives and their related structures are shown in Figure 1. These compounds are rapidly converted into metabolic molecules that bind to tissues after ingestion. Due to the instability of the drug, it has been very difficult to effectively monitor the illegal use of nitrofuran drugs. This is due to the rapid metabolism of nitrofurans in the blood and tissues, resulting in a short half-life of the parent drug in the body. However, in the weeks following administration, the metabolic molecules formed by metabolism in the body bind to the tissue proteins. Therefore, only the metabolites labeled with nitrofurans can be used to detect the residual amount of the parent drug. Although the nitrofuranium metabolism process has not been reported in the literature, this potential mechanism is by cleavage of the nitrofuran ring, and the specific structure remaining is bonded to the protein in the tissue. In vivo, these metabolic molecules are naturally decomposed by gastric acid, and the hydrolyzed metabolic molecules become targets for residual analysis.

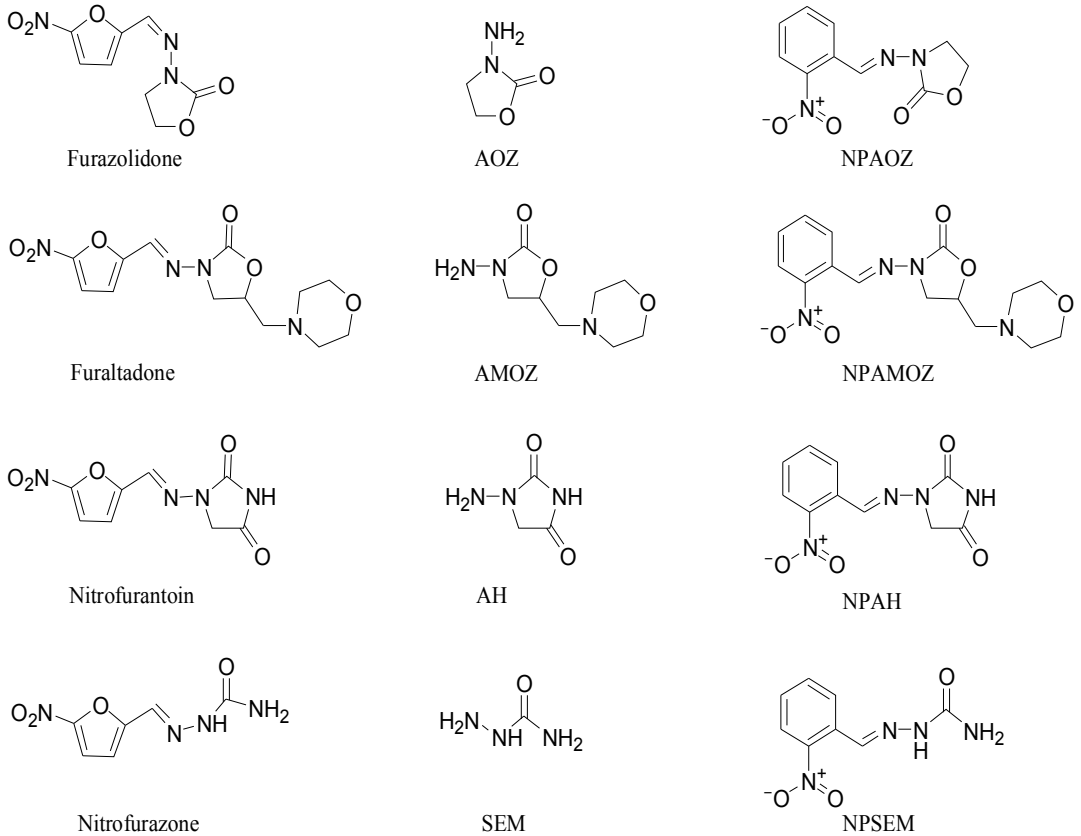

FIGURE 1
Nitro-purine drugs, metabolites, metabolite molecules, and metabolic derivatives

Studies on the bioavailability of nitrofuran metabolites have shown that this residue can be transferred to another species. When mice are fed a radioactive isotope-labeled whee-sucking pig tissue, the total amount is absorbed by the mouse, and bioavailability occurs by eating contaminated meat and animal products (such as fresh eggs, or even the consumption of contaminated cooked foods, as well as the residues of nitrofurans, will be transmitted through the chicken's biological chain, and more importantly, there is a potential risk to people's health.

MATERIALS AND METHODS

Nitrofuran metabolite sample preparation. Propolis concept. Propolis is a natural resinous substance collected by bees from plant shoots, buds and exudates, and mixed with beeswax and other secretions to form a viscous substance. Bees use propolis as a sealant for beehives, and more importantly, bees use propolis as a preservative for animal carcasses, which are left after the animals invading the hive are killed by bee crabs. Propolis is a lipophilic substance that is characterized by being hard and brittle at low temperatures, softening at soft temperatures, softening, and very viscous, so it is called propolis [16].

There are no national or industry standards for the detection of nitrofuran metabolite residues in bee pollen and propolis, and there are few reports in the literature[17]. The existing national standards and industry standards for the detection of nitrofuran metabolite residues are only applicable to products such as animal-derived foods, honey and royal jelly. The main components in honey are fructose and glucose, and the main components in royal jelly are water and protein. The matrix of bee pollen and peak gum is much more complicated than royal jelly, mainly amino acids, proteins, vitamins and flavonoids. Experiments have shown that the use of the national standard method for the determination of nitrofuran metabolite residues in royal jelly to treat bee pollen and propolis is prone to emulsification during the experiment, which seriously affects the experimental results. The nitrofurantoin metabolite (AHD) and nitrofurazone metabolite (SEM) have many interference peaks around the qualitative and quantitative ion peaks, which cannot be quasi-deterministic and quantitative [18]. This will not meet the current maximum residue limit (MRPL) of 1.0 mg/kg in China, Europe, America and Japan. Therefore, it is urgent to establish a method for detecting the residual amount of nitrofuran metabolites in bee pollen and propolis.

Based on the national standard method for the determination of nitrofuran metabolite residues in royal jelly, this paper optimizes the method according to the characteristics of bee pollen and propolis matrix, in order to establish a simple, rapid, accurate and reliable determination of bee pollen, propolis in nitro A method of furan metabolites.

High performance liquid chromatography. High performance liquid chromatography (HPLC) is a highly efficient and sensitive method for the quantitative analysis and detection of mixture components formed by the combination of chromatographic separation technology and signal detection technology [19]. High performance liquid chromatography (HPLC) is a continuous exchange process of solute between a stationary phase and a mobile phase under high pressure conditions. The solute causes an exclusion effect due to the partition coefficient, affinity, adsorption force or molecular size between the two phases. The difference is that different solutes are separated. The commonly used detectors for high performance liquid chromatography include ultraviolet detectors, fluorescence detectors, refractive index detectors and electrochemical detectors [20]. UV detectors and electrochemical detectors are used for the detection of nitrofurans and metabolites. Have been reported.

Liquid chromatography is widely used in the separation and analysis of multi-component mixtures, especially the separation of difficult-to-volatile compounds, but conventional detectors are difficult to characterize analytical components. Mass spectrometry is based on the structural information of organic compounds and provides a single-component chemical structure characteristic mass spectrum. It is a highly sensitive and highly specific detection technology. The combination of chromatographic separation technology and mass spectrometry technology can complement each other in qualitative and quantitative analysis of mixture components, providing new ideas for related detection techniques, and is of great significance for the qualitative and quantitative analysis of trace or trace components in mixtures.

Sample preparation. Various sample preparation methods have been reported to have been analyzed; the sample matrix is such as animal feed animal tissue, eggs and aquatic products (such as fish and shrimp honey and milk. In these matrices (such as carrageen and algae) The presence of flour and salt semicarbazide is not associated with the nitrofuran drug overdose.

The metabolic molecules of nitrofurans that bind to tissue proteins are small molecular products. These small molecular weight metabolic molecules are usually derivatized with o-nitrobenzoic acid and metabolites to increase molecular mass and improve detection sensitivity. Metabolic molecules that bind to tissue proteins are released under acidic conditions prior to derivatization. Based on this method, sample preparation obtains the total

amount of nitrofuran-like metabolic molecules in the tissue (including free and bonding. Then, using various extraction methods, the metabolic molecules of the respective characteristics are separated from the sample matrix. The nitrofuran drug, the tissue-bound metabolite, metabolite and metabolic derivative are shown in Figure 2.

In general, sample preparation includes hydrolysis, derivatization, extraction and purification (solvent extraction is a commonly used method for the purification of nitrofurans. The extraction of nitrobenzene derivatives is to use a neutral organic solvent. (such as ethyl acetate, and further purification with a non-polar solvent (such as cyclohexane) when needed, in order to remove fat before sample detection. It has been studied to use solvent extraction to detect furazolidone metabolites in egg sample preparation, The egg sample was acid-hydrolyzed and derivatized simultaneously, then adjusted with sodium chlorate (or dipotassium hydrogen phosphate) and extracted with ethyl acetate. The ethyl acetate layer was then dried with nitrogen and reconstituted with acetonitrile before detection. The residue was detected by liquid chromatography tandem mass spectrometry.

Solvent extraction (for sample preparation, usually depends on the nature of the sample matrix and analyte. Some samples need to be pretreated before extraction, such as meat tissue is generally pulverized into fine powder or homogenized, and then stored At low temperatures, fresh tissue samples (such as liver, kidney, and muscle) are pretreated with cold methanol and ethanol, which is usually an effective method for defatting and removing free metabolites. Instead of using sample preparation, multiple extractions with ethyl acetate are used to ensure the most residual residue from the tissue. Although solvent extraction is effective, the cost of a large number of high quality solvents is expensive.

Solid phase extraction (as an effective solvent extraction method. The analyte can be separated and concentrated before detection. Although solid phase extraction is time consuming and requires pretreatment of the column during sample preparation, it greatly reduces the organic solvent. The column contains octadecyl bonded silica, which is often used for reversed phase extraction of non-polar, moderately polar compounds, such as antibiotics, and the like, using solid phase extraction liquid chromatography mass spectrometry to detect semicarbazide in egg tissue. In addition, et al. used a solid phase extraction method to detect pig liver. In this study, in order to eliminate excess o-nitrobenzene from the sample, two different solid phase extractions were used to remove excess.

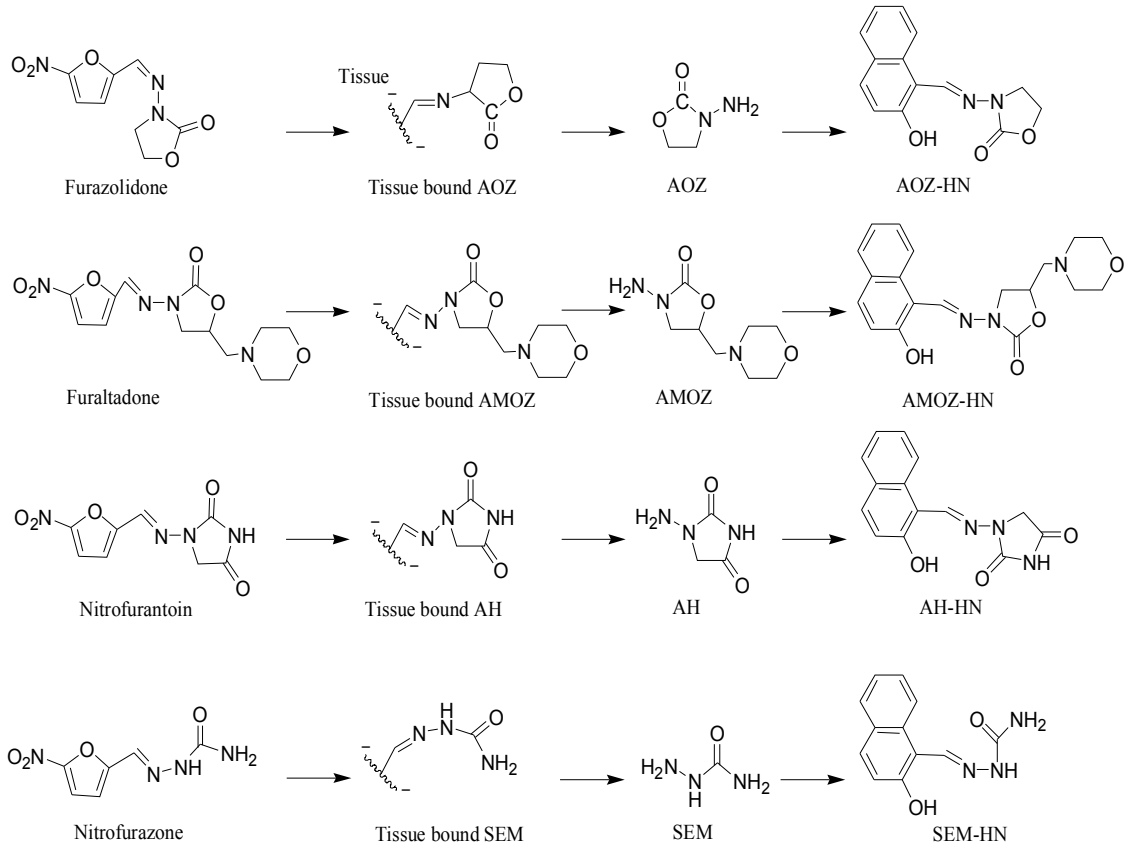

FIGURE 2
Nitrofuran drug, tissue-bonded metabolites, metabolites and metabolic derivatives

Selection of purification methods. In order to reduce the interference of the co-extracts on the metabolite determination, the sample needs to be purified. The liquid-liquid extraction (and the effect of solid-phase extraction) were compared. Experiments showed that the column-to-pork and shrimp samples were easy to automate solid phase extraction, but the extraction effect of the four metabolic derivatives did not have a good purification effect. The experiment used extracting pork and shrimp samples, and further studied the effects of the extracts of four metabolic derivatives on the extraction of ethyl acetate. The results showed that the optimal extraction effect can be achieved without adjustment, and the operation is simple. The results are stable and easy to trace.

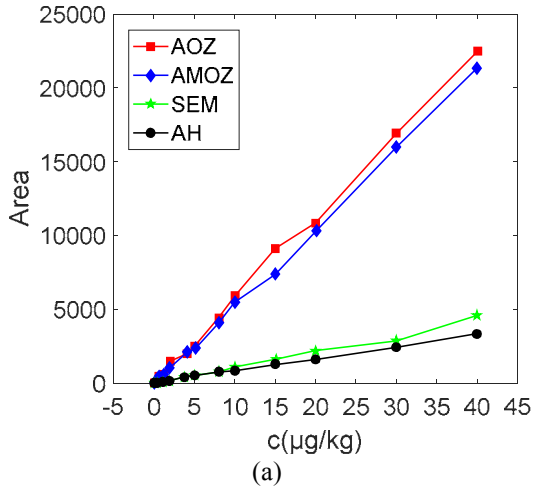

FIGURE 3
Nitrofuran drug originals, tissue-bonded metabolites, metabolites and metabolic derivatives

The chromatographic conditions are optimized according to GB/T 21311-2007 liquid chromatography conditions, with acetonitrile and 0.1% formic acid (containing 0.5mmol/L ammonium formate) as gradient eluent, column temperature: 40°, flow rate: $0.3\text{mL}\cdot\text{min}^{-1}$, the separation of the four metabolic derivatives is the best, and the relative phosgene deviation of the qualitative ion pair and the quantitative ion pair of each metabolite does not exceed the relative ion abundance in the qualitative determination in GB/T 21311-2007 The maximum allowable deviation table is specified in the table.

Transfer different volumes of mixed standard working solution (added to the methanolic mixed solution of hydrochloric acid to make the solution concentration 0.25, 0.50, 1.0, 2.0, 2.5, 4.0, 5.0, 7.5, 10, 15 and 20.0 ng/mL, respectively. The test was carried out according to the sample step, and the residue dissolved in the final acetonitrile aqueous solution was determined by high performance liquid chromatography tandem mass spectrometry, and a standard working curve was drawn, and the four metabolites were quantitatively analyzed by an external standard method. The correlation coefficient of the four components in the sample (the working curve is shown in Fig. 3. At the same time, under the selected conditions of this experiment, the parallel treatment of pork and shrimp tissue samples is added with $25\mu L$ and $0.2ng/\mu L$ mixed standard working fluids for experiments and then respectively. 10 times the standard deviation calculation to determine $LOD < 0.5\mu g/kg$; $LOQ < 1.0\mu g/kg$ of the method.

RESULTS AND DISCUSSION

Detection and analysis. Sample preparation method. Acid solution screening and condition optimization. Since the nitrofuran metabolites can only be released under appropriate acidic conditions, and the bee pollen sample matrix is complex, the appropriate acid solution is selected and the appropriate concentration is determined to extract the nitrofuran metabolites from the bee pollen to It is important. This experiment investigated three different concentrations of acid solution: hydrochloric acid: 0.1, 0.5, 1.0 mol / L; trichloroacetic acid (mass fraction): 5%, 10%, 15%, 20%; perchloric acid (volume Score): 0.1%, 0.5%, 1.0%, 2.0%, 3.0%, 4.0%, 5.0%. (Reagent 1. 0.1 mol / L HCl; reagent 2. 0.5 mol / L HCl; reagent 3. 1.0 mol / L HCl; reagent 4. 5% trichloroacetic acid; reagent 5. 10% trichloroacetic acid; reagent 6. 15 %%perchloric acid; Reagents 7. 20% trichloroacetic acid; reagent 8. 0.1% perchloric acid; reagent 9. 0.5% perchloric acid; reagent 10.1% perchloric acid; reagent 11. 2% perchloric acid; Reagent 12.3% perchloric acid; reagent 13. 4% perchloric acid; reagent 14. 5% perchloric acid.) These three acids to four nitrofuran metabolites (SEM, AOZ, AHD, AMOZ) The effect of recovery is shown in Figure 4. 1.0% perchloric acid has the highest recovery rate for the four nitrofuran metabolites.

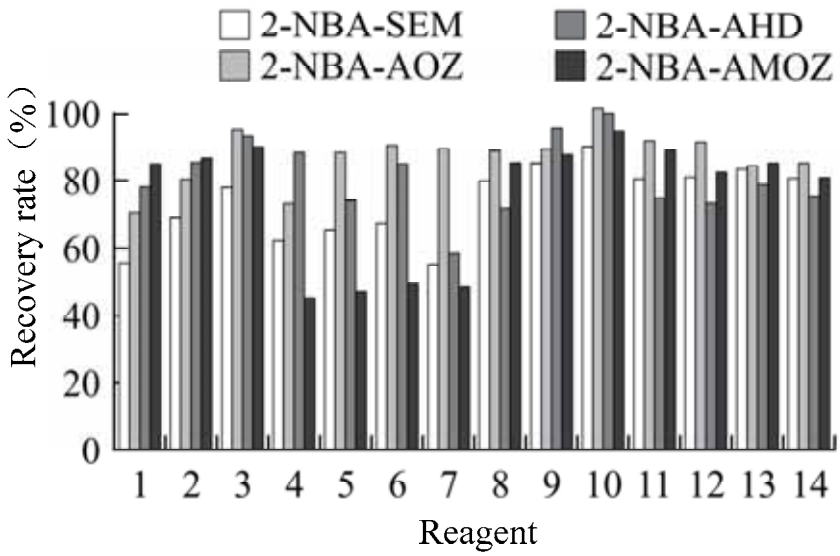

FIGURE 4
Effect of acid solution and concentration on recovery

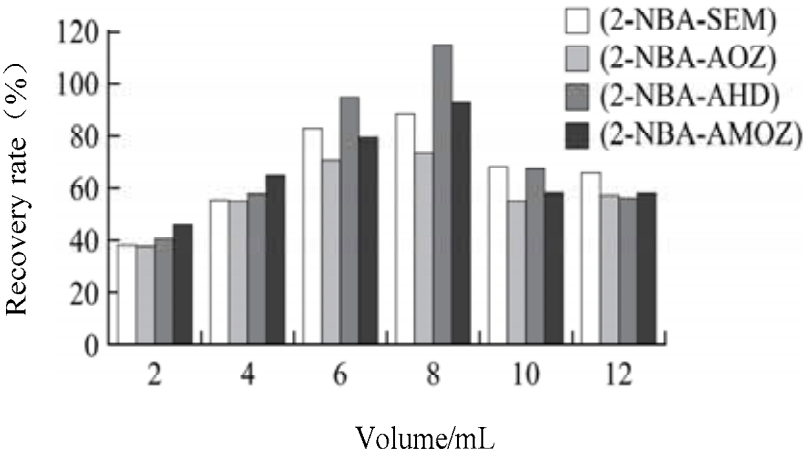

FIGURE 5
Effect of perchloric acid addition volume on recovery

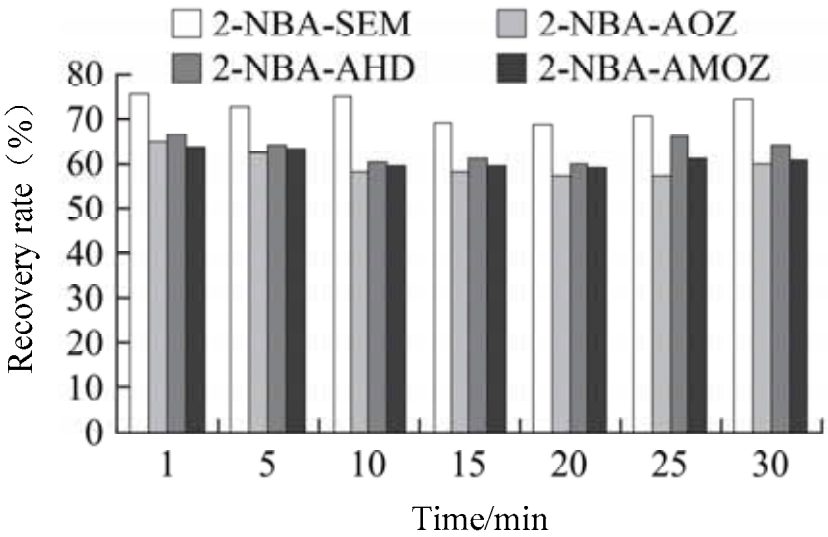

FIGURE 6
Effect of ultrasonic time on recovery

After determining the appropriate acid solution, the standard value of 2%g/kg was added to the bee pollen, and the different addition amount of 1.0% perchloric acid (2, 4, 6, 8, 10, 12 mL) was determined. The effect of the rate, the results are shown in Figure 5. 1.0% perchloric acid has an optimal volume for the recovery of four nitrofuran metabolites, too large and too small will reduce the recovery of metabolites, 8mL 1.0% high Chloric acid has a high recovery rate for the four nitrofuran metabolites, so 8mL of 1.0% perchloric acid was chosen for acid hydrolysis.

Effect of ultrasonic time on acid hydrolysis. In order to maximize the dissolution of the nitrofuran metabolites in bee pollen, ultrasonic treatment is used to increase the recovery rate. After adding 8 mL of 1% perchloric acid, the ultrasonic vibration was set for 1, 5, 10, 15, 20, 25 min and 30 min respectively, and the recovery was determined by the standard addition method, the standard value was 2 μg/kg. It can be seen from Fig. 6 that the ultrasonic time of 1 to 30 min has no significant effect on the recovery rate. Considering the need of batch detection, 1 min is selected as the final ultrasonic acid hydrolysis reaction time.

Comparison and selection of solid phase extraction (SPE) purification methods. Since bee pollen contains various components such as amino acids, proteins, vitamins, flavonoids, and fatty acids, it can be directly used for liquid-liquid extraction method. 186 2013, Vol.34, No.16 Food science analysis and detection cause emulsification, which affects extraction efficiency. Therefore, in this experiment, a solid phase extraction cartridge was selected for purification to improve the recovery rate.

It has been reported that the purification of nitrofuran metabolites can be carried out by first derivatization and re-solid phase extraction. Therefore, in this study, the sample liquid after derivatization is adjusted to a neutral value after passing through the HLB column, ethyl acetate. Elute and receive the sample and eluent. It was found that no matter what kind of loading system (acidic/neutral), there was no target in the received sample solution, only the 2-NBA-AMOZ internal standard peak had some peaks and the peak shape was poor.

Among the eluents received, there were only 2-NBA-AOZ and 2-NBA-AMOZ in the four nitrofuran metabolites, and there were interference peaks. The 2-NBA-SEM interference peaks were many, while 2-NBA- AHD could not see the spiked peak shape. It can be seen that the solid phase extraction purification is carried out after the derivatization, and the internal standard and the spiked peak of the four nitrofuran metabolites cannot be clearly seen through the enrichment, which seriously affects the detection quality. This may be because the bee pollen composition is complex, and the derivatized product may chemically react with certain components in the sample, causing the nitrofuran metabolite to be destroyed or degraded, and the interferent is more, so the target is not received. Therefore, the most suitable method is to use a solid phase extraction to purify and then definitize.

The existing S P E cartridges for purifying nitrofuran metabolites are mainly Oasis® MCX (60 mg, 3 mL Waters), Oasis® HLB (60 mg, 3 mL Waters), C18 (500 mg, 3 mL, Supelclean). Therefore, these three kinds of small columns were selected for the solid phase extraction experiment, which was carried out before the derivatization step. As can be seen from Figure 7, Oasis® HLB cartridges and C-18 cartridges can provide high recovery rates for the four metabolites. Oasis® MCX is relatively low, but the C-18 cartridges are more stringent. The liquid cannot be drained in the middle of the column, so the Oasis® HLB cartridge was used as the purification cartridge for this study.

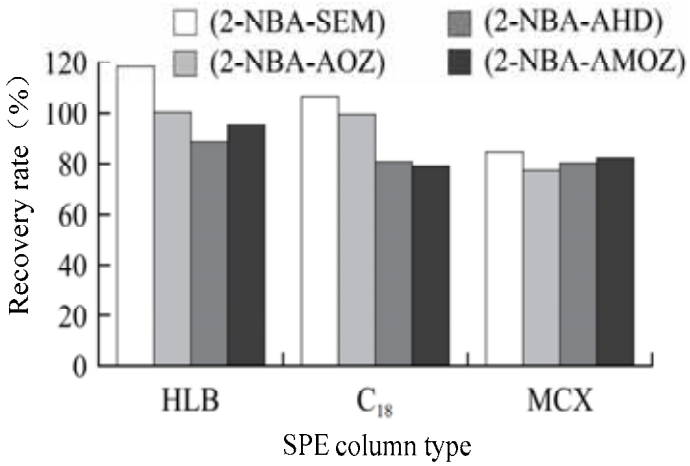

FIGURE 7
Effect of solid phase extraction cartridge on recovery

TABLE 1
Average recovery and precision of 3 levels of propolis added

Derivative name	Add concentration (μg/kg)	Propolis		
		The average recovery rate (%)	Intraday precision (%)	Daytime precision (%)
2-NBA-SEM	1.0	96.2	6.4	13.5
	2.0	95.2	6.1	9.6
	5.0	96.5	5.4	11.2
2-NBA-AOZ	1.0	97.2	5.7	12.4
	2.0	93.2	7.9	10.5
	5.0	95.1	4.9	12.5
2-NBA-AHD	1.0	94.2	5.8	10.6
	2.0	95.2	5.6	9.8
	5.0	94.8	4.9	9.7
2-NBA-AMOZ	1.0	96.5	6.5	10.4
	2.0	95.3	6.4	11.0
	5.0	93.7	6.8	8.9

Linear range, limit of quantitation, recovery and precision. The sample was pretreated according to the optimized method, and the standard working curve was drawn. The results showed that the four nitrofuran metabolites showed a good linear relationship at 0.5-20 ng/mL, and the detection limit (LOD) was 0.251 μg/kg. (LOQ) was 1.0 μg/kg. 1.0 g of the propolis sample was weighed and treated according to the experimental method. Three addition levels were 1.0, 2.0, 5.01 μg/kg, and 6 parallel samples per level were repeated for 3 days. The recovery rate, intraday precision and daytime precision are shown in Table 1. It can be seen from Table 1 that the average recovery of the method is stable between 93.7% and 97.2%, the intra-day precision is less than 10.0%, and the daytime precision is less than 13.5% at the three addition levels of 1, 2 and 5 μg/kg.

CONCLUSION

In this study, a high-performance liquid chromatography-tandem mass spectrometry (HPLC-MS/MS) method for the determination of nitrofuran metabolites in bee pollen was established, and it was applied in actual detection, and good detection results were obtained. Aiming at the complex matrix of bee pollen samples, the sample pretreatment method was optimized, including the type and concentration of acid solution, acid hydrolysis time, solid phase extraction purification and extraction conditions optimization and selection, and the optimal pretreatment conditions were obtained. In view of the complex matrix of bee pollen and propolis sample, it is firstly purified by solid phase extraction, decontaminated after removing impurities, and then extracted with ethyl acetate. This is a simple liquid-liquid extraction method for the detection of metabolites of nitro-furans. The method or solid phase extraction method is different. The two extraction methods are used to obtain better purification effect, which can meet the requirements of daily testing and detection limit (1.01μg/kg).

REFERENCES

[1] Ueland, G.Å., Methlie, P., Øksnes, M. (2018) The short cosyntropintest revisited - new normal reference range using LCMSMS. Journal of Clinical Endocrinology and Metabolism. 103(4), 1696-1703.

[2] Masika, L.S., Zhao, Z., Soldin, S.J. (2016) Is measurement of TT3 by immunoassay reliable at low concentrations? A comparison of the Roche Cobas 6000 vs. LC-MSMS. Clinical Biochemistry. 49(12), 846-849.

[3] Souillot, M., Rigaud, C., Ruet, S. (2016) Development of a new panel of 9 steroids in amniotic fluid in LC–MSMS. Annales Dendocrinologie. 77(2), 177-177.

[4] Lee, G.O., Kosek, P., Lima, A.A.M. (2014) Lactulose: Mannitol Diagnostic Test by HPLC and LC-MSMS Platforms: Considerations for Field Studies of Intestinal Barrier Function and Environmental Enteropathy. Journal of Pediatric Gastroenterology and Nutrition. 59(4), 544-50.

[5] Wang, S.H., Wang, T.F., Wu, C.H. (2014) In-Depth Comparative Characterization of Hemoglobin Glycation in Normal and Diabetic Bloods by LC-MSMS. J Am Soc Mass Spectrom. 25(5), 758-766.

[6] Saito, T., Umebachi, R., Namera, A. (2015) Identification and Quantification of Aconitines and Colchicine in Serum, Urine, and Plants using MonoSpin C 18 and LC-MSMS. Chromatographia. 78(15-16), 1041-1048.

[7] Zhou, S., Hu, Y., Desantos-Garcia, J.L. (2015) Quantitation of permethylated N-glycans through multiple-reaction monitoring (MRM) LC-MS/MS. Journal of the American Society for Mass Spectrometry. 26(4), 596-603.
[8] Loedige, I., Stotz, M., Qamar, S. (2014) The NHL domain of BRAT is an RNA-binding domain that directly contacts the hunchback mRNA for regulation. Genes Dev. 28(7), 749-764.
[9] Elliott, J.E., Hindmarch, S., Albert, C.A. (2014) Exposure pathways of anticoagulant rodenticides to nontarget wildlife. Environmental Monitoring and Assessment. 186(2), 895-906.
[10] Westin, A.A., Mjønes, G., Burchardt, O. (2014) Can Physical Exercise or Food Deprivation Cause Release of Fat-Stored Cannabinoids? Basic and Clinical Pharmacology and Toxicology. 115(5), 467-471.
[11] Witters, E., Vanhoutte, K., Dewitte, W. (2015) Analysis of cyclic nucleotides and cytokinins in minute plant samples using phase-system switching capillary electrospray–liquid chromatography–tandem mass spectrometry. Phytochemical Analysis. 10(3), 143-151.
[12] Melsom, T., Fuskevåg, O.M., Mathisen, U.D. (2015) Estimated GFR is biased by non-traditional cardiovascular risk factors. American Journal of Nephrology. 41(1), 7-15.
[13] Vanstraelen, K., Wauters, J., Vercammen, I. (2014) Impact of Hypoalbuminemia on Voriconazole Pharmacokinetics in Critically Ill Adult Patients. Antimicrobial Agents and Chemotherapy. 58(11), 6782-9.
[14] Zhu, Z., Go, E.P., Desaire, H. (2014) Absolute Quantitation of Glycosylation Site Occupancy Using Isotopically Labeled Standards and LC-MS. Journal of the American Society for Mass Spectrometry. 25(6), 1012-1017.
[15] Ibáñez, A.B., Bauer, S. (2014) Analytical method for the determination of organic acids in dilute acid pretreated biomass hydrolysate by liquid chromatography-time-of-flight mass spectrometry. Biotechnology for Biofuels. 7(1), 1-9.
[16] Gelderman, M.P., Baek, J.H., Yalamanoglu, A. (2015) Reversal of hemochromatosis by apotransferrin in non-transfused and transfused Hbbth3/+ (heterozygous B1/B2 globin gene deletion) mice. Haematologica. 100(5), 611-22.
[17] Liu, X.G., Dong, F.S., Jun, X.U. (2014) Dissipation and Adsorption Behavior of the Insecticide Ethiprole on Various Cultivated Soils in China. Journal of Integrative Agriculture. 13(11), 2471-2478.
[18] Ma, Y., Sun, Z., De, M. (2014) Towards an animal model of ovarian cancer: cataloging chicken blood proteins using combinatorial peptide ligand libraries coupled with shotgun proteomic analysis for translational research. Omics-a Journal of Integrative Biology. 18(5), 280-297.
[19] Taylor, A.M., Cabrices, O.G., Lee, L.A. (2015) Automated sample hydrolysis for a forensic toxicology urine screening LC-MS/MS method. Toxicologie Analytique Et Clinique. 27(2), S53-S54.
[20] Rumpler, M.J., Colahan, P., Sams, R.A. (2014) The pharmacokinetics of methocarbamol and guaifenesin after single intravenous and multiple-dose oral administration of methocarbamol in the horse. Journal of Veterinary Pharmacology and Therapeutics. 37(1), 25-34.

Received: **03.01.2019**
Accepted: **27.03.2019**

CORRESPONDING AUTHOR

Gang Wei
Shanghai Key Laboratory of Diabetes,
Shanghai Institute for Diabetes,
Shanghai Jiao-Tong University Affiliated Sixth People's Hospital,
Shanghai 200233 – China

e-mail: weigang888a@163.com

© by PSP Volume 28 – No. 5/2019 pages 4044-4048 Fresenius Environmental Bulletin

PREDICTION METHOD OF PORE PRESSURE OF SHALE IN SONGLIAO BASIN

Guoxin Li[1], Ying Guo[2,*], Weiliang Liu[3], Jie Cui[4]

[1]College of Engineering and Technology, Chengdu University of Technology, Leshan 61400, China
[2]Institute of Geology and Paleontology, Linyi University, Linyi 276000, China
[3]School of Ocean Sciences, Sun Yat-sen University, Guangzhou 510275, China
[4]Exploration & Development Research Institute of Liaohe Oilfield Company, Panjin 124010, China

ABSTRACT

Serious wellbore instability frequently occurs during drilling operations in shale formations. Selection of safe mud parameters to alleviate shale instability problems during drilling operations can benefit from predictive models. Only a few experimental measurements and analysis of model predictions are available. In this paper, pore pressure transmission test on shale is conducted and pore pressure changes in the shale sample under hydraulic and chemical loading is measured. Comparison with experimental data shows that the simulation results are in good agreement with the actual pressure measurements in the test. This result provides further validation for the theoretical model.

KEYWORDS:
Shale instability, Pore pressure, shale, Songliao basin

INTRODUCTION

Wellbore instability problems that often occur in shale bedding planes rich in clay minerals is one of the most significant difficulties in exploration and production phases of shale oil and gas industry [1, 2]. These problems are caused by the stress in the near wellbore region exceeding the shale strength during drilling. In addition to poroelastic effects, shale-drilling fluid chemical interactions strongly affect the borehole instability [3-7]. As the water-based fluids come into contact with the shale, water and ions penetrate into the rock due to differences in chemical and hydraulic potentials of pore and drilling fluids. This interaction induces pore pressure and effective stress state alterations near the wellbore wall. On the other hand, as the monomolecular layers of water are incorporated into the crystalline structure of the clay minerals in the shale, swelling phenomena is occurred and consequently decreases the strength of the formation. These chemo-mechanical processes may lead to wellbore failure. Although, oil-based muds have been successfully used in the past to overcome the problem of wellbore instability in shale formations, their high cost and environmental concerns restrict their use worldwide [8].

In order to efficiently manage the problem of shale instability using water-based muds, it is important to consider the mechanisms of water-based mud interaction with shale. These chemo-mechanical processes are greatly affected by the low permeability characteristic and presence of negatively charged clay platelets in the shale. It is well established that these characteristics of the shale lead to some semi-permeable membrane behaviors [9-11]. As a result, fluid transport into the formation is dominantly controlled by osmosis driven by chemical potential rather than hydraulic gradient [12-14]. However, since shales perform as leaky or non-ideal membranes, solutes can also penetrate into the formation [15-18]. Solute diffusion into low permeability shales results in chemical osmosis being a time dependent process and thereby time dependent nature of the problem of wellbore instability in shales [19, 20].

Attempts have been made to incorporate the chemical effects into the poroelastic model for better analyzing shale deformation while drilling. Sherwood [21] modified the Biot's linear poroelastic theory to include the chemical potential of the species within the pore fluid. However, he assumed that shale acts as an ideal ion exclusion membrane and neglected the movement of ions into the shale. The partially coupled chemo-poroelastic model failed to correctly describe the behavior of the shale during some experiments, since the effect of ion transport into the shale was not considered [22].

Based on arguments from non-equilibrium thermodynamics, Heidug and Wong [13] developed the first comprehensive coupled chemo-poroelastic model of hydration swelling for water-absorbing rocks under isothermal conditions. This continuum model is based on the extension of poroelasticity equations [17] and Darcy's flow law that incorporates the effects of chemical osmosis and swelling phenomena. A diffusion equation is also used for the transport of solute in the porous media. Solute transport due to advection in low permeability shales is neglected in this study. The feature that sets this model apart from many related works is its consistency with the second law of thermodynamics. Heidug and Wong [13] also used the finite

element solution of this theory to analyze an experiment on the linear flow of a salt solution through a shale sample. Results obtained from the model were in a good qualitative agreement with the observations from the experiment. This theory was subjected to some extensions later by incorporating the effects of thermal loading, electrical interactions [19], transversely isotropic behavior of shale and elasto-plastic behavior of shale [20].

Based on the aforementioned theory, Ghassemi and Diek [3] developed a robust linear physicochemical theory by expressing the chemical potential as a linear function of the solute mass fraction. Moreover, in contrast to the case of an incompressible fluid considered by Heidug and Wong [13], they proposed linearized version for compressible constituents. The main advantage of the linear model is that allows analytical treatment of the equations which is most useful for rapid field applications. Huang and Ghassemi [22] used the analytical solution to the linearized chemo-poroelastic equations for analyzing pore pressure and solute concentration distributions in a pressure transmission test and showed that there exists good agreement in the trends of the evolution of the fields of interest.

In this paper, pore pressure transmission test on shale is conducted and pore pressure changes in the shale sample under hydraulic and chemical loading is measured. Comparison with experimental data shows that the simulation results are in good agreement with the actual pressure measurements in the test. This result provides further validation for the theoretical model.

EXPERIMENTAL

The study block is a block in the northern part of the Songliao Basin. Its lithology is dominated by mud shale and is mainly controlled by western provenance. The distribution of wells in the work area is extremely uneven. The drilling in the northwest is close to the source area, while the drilling in the southeast is less. The block is fully covered by 3D seismic and has undergone high-precision processing. The measured formation pressure data shows that the target layer is from top to bottom, from northwest to southeast, the formation pressure is gradually increased, and the overpressure is gradually increased. The pressure coefficient is mainly 1.15 to 1.38, and the highest is up to 1.5. Mainly due to the hydrocarbon generation of source rocks. Using the measured pressure data, well logging data and the high-resolution seismic velocity body obtained from the pre-stack AVA inversion, the pore structure and the pressure coefficient body are predicted by the combination of well-seismic layers.

RESULTS AND DISCUSSION

With the rapid development of unconventional oil and gas exploration, theoretical understanding and exploration and development technologies have been increasingly advanced, and unconventional oil and gas has become an important replacement energy source for future oil and gas resources.

In the process of unconventional oil and gas exploration and development, it is recognized that abnormal high pressure is not only conducive to the preservation of oil and gas reservoirs, but also the pore pressure of the formation is directly related to the production of oil and gas layers. In general, the higher the pore pressure, the larger the yield; when the pressure value is small, not only the yield is low, but also a certain external force is applied during the mining process, which increases the development cost. In addition, accurate pore pressure prediction helps to drill safely and economically, and can effectively prevent drilling accidents.

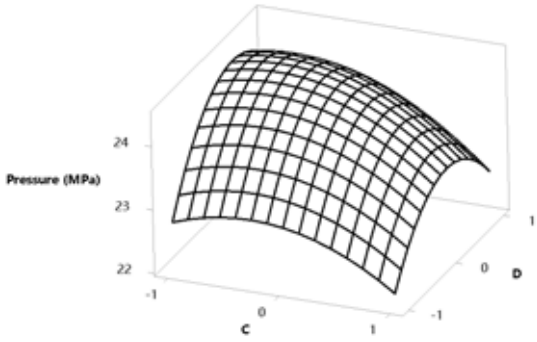

FIGURE 1
Surface Plot of Pressure (MPa) vs D, C

In the Bowers method, the relationship between sediment loading and sedimentation unloading is considered in the relationship model between effective stress and velocity. The formation pore pressure prediction model suitable for under compaction and fluid expansion is established. For Fig.1-2, effect of acoustic wave velocity, effective stress at unloading point on pore pressure is studied. It can be seen that the formation pore pressure obtained by the equivalent depth method does not agree well with the measured pressure data, and the average relative error of the three points is 17.33%. The formation pore pressure obtained by Bowers method agrees well with the measured pressure data, with an average error of 3.15%. It is also determined that the calculation of formation pore pressure model for Songliao Basin is Bowers method. This is mainly due to the fact that the overpressure of the target layer in the study block is mainly "hydrocarbon generation boost", and the Bowers method is suitable for the mixed genetic mechanism of under compaction and hydrocarbon generation pressurization. Therefore, it is finally determined that the Bowers method is used to calculate the formation pore pressure.

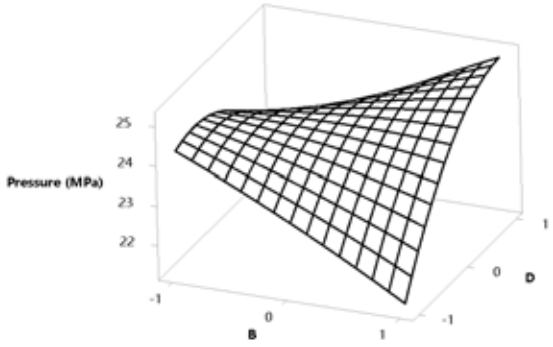

FIGURE 2
Surface Plot of Pressure (MPa) vs D, B

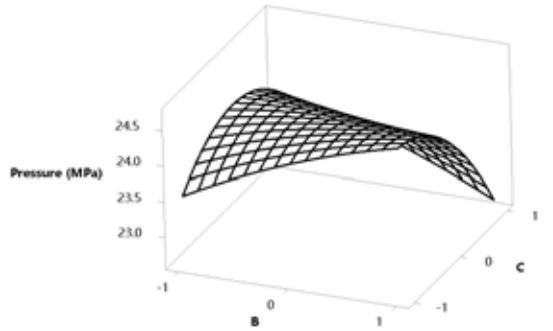

FIGURE 3
Surface Plot of Pressure (MPa) vs C, B

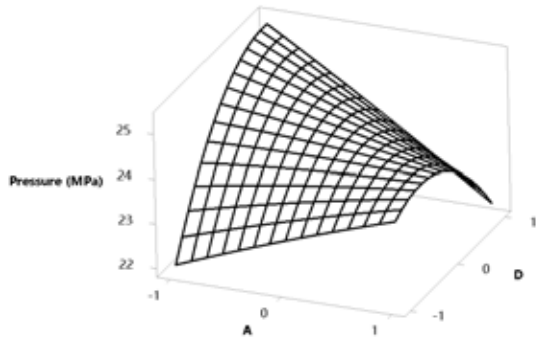

FIGURE 4
Surface Plot of Pressure (MPa) vs D, A

Fig. 3-6 shows the induced pore pressure profile caused by chemical loading in the sample corresponding to different times. The induced pore pressure in response to chemical osmotic flow is zero at upstream end and negative inside the sample. The peak value of pore pressure decreases with time and moves toward the no-flow boundary of the sample till the peak value at the downstream end of the sample is reached and then increases. Therefore, the maximum magnitude of the induced osmotic pore pressure is occurred at the downstream end of the sample.

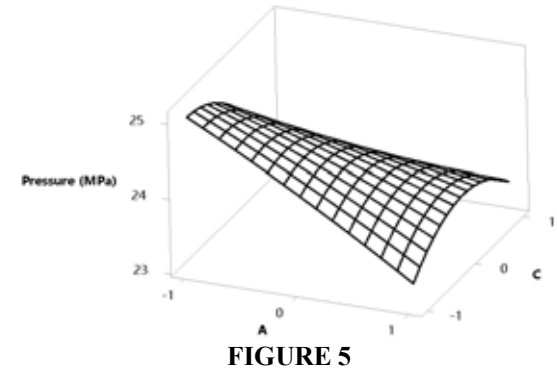

FIGURE 5
Surface Plot of Pressure (MPa) vs C, A

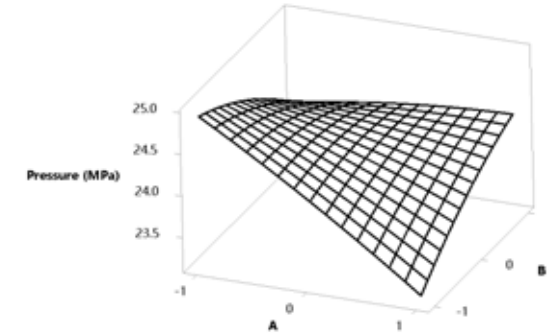

FIGURE 6
Surface Plot of Pressure (MPa) vs B, A

CONCLUSION

Results indicate that, as expected, if the drilling mud is more saline than the sample according to the industry-wide practice to avoid wellbore instability, osmosis reduces the pore pressure inside the sample. Comparison between the numerical solution of the model for the test and experimental results shows good agreement. This further verifies the accuracy of the applied theory in a quantitative manner and enables using the proposed model for simulating wellbore stability.

ACKNOWLEDGEMENTS

This research was financially supported by the National Natural Science Foundation of China (No.41502277, NO.41472054, and NO.41688103).

REFERENCES

[1] Ni, W.J., Li, Q., Song, X.M. (2017) Analysis of wellbore stability of shale gas reservoir drilling. Fresen. Environ. Bull. 26, 510-515.
[2] Kivi, I.R., Ameri, M.J., Ghassemi, A. (2016) Experimental and numerical study of membrane properties and pore pressure transmission of Ghom shale. Measurement. 91, 93-100.

[3] Li, J., Liu, S., Zhang, J., Fan, Z., Sun, Z., Zhang, M., Yuan, Y., Zhang, P. (2015) Architecture and facies model in a non-marine to shallow-marine setting with continuous base-level rise: an example from the Cretaceous Denglouku Formation in the Changling Depression, Songliao Basin, China. Marine and Petroleum Geology. 68, 381-393.

[4] Song, Y., Stepashko, A., Liu, K., He, Q., Shen, C., Shi, B., Ren, J. (2017) POST-RIFT tectonic History of the Songliao Basin, NE China: cooling events and post-rift unconformities driven by orogenic pulses from Plate Boundaries. Journal of Geophysical Research: Solid Earth. 123(3), 2363-2395.

[5] Ghassemi, A., Diek, A. (2003) Linear chemo-poroelasticity for swelling shales: theory and application. J. Petrol. Sci. Eng. 38, 199-212.

[6] Sarout, J., Detournay, E. (2011) Chemoporoelastic analysis and experimental validation of the pore pressure transmission test for reactive shales. Int. J. Rock Mech. Min. Sci. 48, 759-772.

[7] Lomba, R.F.T., Chenevert, M.E., Sharma, M.M. (2000) The role of osmotic effects in fluid flow through shales. J. Petrol. Sci. Eng. 25, 25-35.

[8] Lv, D., Li, Z., Liu, H., Li, Y., Feng, T., Wang, D., Wang P., Li S. (2015) The characteristics of coal and oil shale in the coastal sea areas of Huangxian Coalfield, Eastern China. Oil Shale. 32(3), 204-217.

[9] Qiu, X., Liu, C., Mao, G., Deng, Y., Wang, F., Wang, J. (2015) Major, trace and platinum-group element geochemistry of the Upper Triassic nonmarine hot shales in the Ordos Basin, Central China. Applied Geochemistry. 53, 42-52.

[10] Al-Bazali, T., Zhang, J., Chenevert, M.E., Sharma, M.M. (2008) Factors controlling the compressive strength and acoustic properties of shales when interacting with water-based fluids. Rock Mech. Rock Eng. 45, 729-738.

[11] Lomba, R.F.T, Chenevert, M.E., Sharma, M.M. (2000) The ion-selective membrane behavior of native shales. J. Petrol. Sci. Eng. 25, 9-23.

[12] Zhou, X., Ghassemi, A. (2009) Finite element analysis of coupled chemo-poro-thermo-mechanical effects around a wellbore in swelling shale. Int. J. Rock Mech. Min. Sci. 46, 769-778.

[13] Heidug, W., Wong, S.W. (1996) Hydration swelling of water-absorbing Rocks: a constitutive model. Int. J. Numer. Anal. Meth. Geomech. 20, 403-430.

[14] Wang, D., Shao, L., Li, Z., Li, M., Lv, D., Liu, H. (2016) Hydrocarbon generation characteristics, reserving performance and preservation conditions of continental coal measure shale gas: A case study of Mid-Jurassic shale gas in the Yan'an Formation, Ordos Basin. Journal of Petroleum Science and Engineering. 145, 609-628.

[15] Pang, H., Pang, X. Q., Dong, L., Zhao, X. (2018) Factors impacting on oil retention in lacustrine shale: Permian Lucaogou Formation in Jimusaer Depression, Junggar Basin. Journal of Petroleum Science and Engineering. 163, 79-90.

[16] Yu, M., Chenevert, M.E., Sharma, M.M. (2003) Chemical–mechanical wellbore instability model for shales: accounting for solute diffusion. J. Petrol. Sci. Eng. 38, 131-143.

[17] Sherwood, J.D. (1993) Biot poroelasticity of a chemically active shale. Proc. R. Soc. Lond. 440, 365-377.

[18] Sherwood, J.D., Bailey, L. (1994) Swelling of shale around a cylindrical well-bore. Proc. R. Soc. Lond. 444, 161-184.

[19] Biot, M.A. (1941) General theory of three-dimensional consolidation. J. Appl. Phys. 12, 155-164.

[20] Roshan, H., Aghighi, M.A. (2012) Analysis of pore pressure distribution in shale formations under hydraulic, chemical, thermal and electrical interactions. Trans. Porous Med. 92, 61-81.

[21] Roshan, R., Rahman, S.S. (2011) Analysis of pore pressure and stress distribution around a wellbore drilled in chemically active elastoplastic formations. Rock Mech. Rock Eng. 44, 541-552.

[22] Huang, J., Ghassemi, A. (2010) A chemo-poroelastic solution for pore pressure transmission test considering solute diffusion. The 44th US Rock Mechanics Symposium (USRMS), UT.

Received: **04.01.2019**
Accepted: **18.03.2019**

CORRESPONDING AUTHOR

Ying Guo
Institute of Geology and Paleontology,
Linyi University,
Linyi 276000 – China

e-mail: guoying@lyu.edu.cn

© by PSP Volume 28 – No. 5/2019 pages 4049-4053 Fresenius Environmental Bulletin

EVALUATION AND ANALYSIS OF COORDINATED DEVELOPMENT OF ECOLOGICAL ENVIRONMENT AND ECONOMY

Zangen Lin*, Liming Zhao

Tianjin University, College of Management and Economics, Tourism Management, No.92 Weijin Road, Nankai District, Tianjin, China

ABSTRACT

Using the coupling coordination model, 26 indexes of ecological environment system and economic system were selected to evaluate the ecological environment and economic coupling of Tianjin from 2003 to 2017. The results show that the overall ecological environment and economic coupling of Tianjin are relatively low, but overall goes to the good direction. We successfully developed a model that could be used for evaluating the carrying capacity of regional ecological environment to social economic development and that could be generalized to other regions. The model can simulate the relationship between socioeconomic and ecological environment, and made the results more intuitive, spatial, and visual. Taking Tianjin as the research area, the results of the evaluation were consistent with the analysis results of the original data characteristics, including the indexes: forest cover, per capita GDP and industrial wastewater discharged. It is consistent with the actual situation in the model.

KEYWORDS:
Coupling evaluation model, Carrying capacity, Ecological environment, Economic development

INTRODUCTION

The sustainable development of ecological environment and social economy has always been the focus of attention in the world [1-4]. The coordinated development of ecological environment and social economy was the common responsibility and pursuit of the international community. China, as the largest developing country in the world, has created the "miracle of China" at an average annual rate of 9.8% over 30 years of reform and opening up, but at the same time, "high investment, high pollution and high emissions" model has also led to a series of environmental problems. Environment pollution and ecological destroy gradually evolved into constraints of China's economic and social sustainable development of the outstanding obstacles.

At present, the economic growth continues at the same time the environment is worsening, the ecological damage is becoming more and more serious. Comprehensive evaluation of the environmental economy has been widespread concern in academia [5, 6]. Scholars have studied from the perspective of coordinated development on social economy and ecological environment, ecological security warning, economic growth and environmental pollution, ecological economy [7, 8]. But on the whole, there were few studies on qualify the relationship between social economic development with ecological quality and environmental quality at home and abroad, and lacked of macroeconomic research on the development stage and path of regional environmental economy. Some developed countries mainly focus on the study of micro-scale, such as atmospheric environment [9], water environment and other aspects of pollution characteristics, pollution on biological and human health [10, 11] and macro-scale focuses on pollution emissions and economic growth, cross-border pollution and regional environmental quality [12, 13] and so on.

Single study cannot guide the overall regional environmental governance; other issues had increasingly arisen in the process of solving some problems [14, 15]. At present, there are several methods used in regional environmental assessment, such as ecological footprint, coordination degree, matter element analysis [16] and ecological health risk analysis. Although these methods have their own advantages, but they cannot fully objective evaluate the region's comprehensive socio-economic development level, the development stage and the main contradictions.

It is urgent to develop clear information evaluation models to simulate the relationship between ecological environment and social economic development for management and decision-making basis. Application of the coordinated model on simulation the relationship between ecological environment and social economic development, especially on carrying capacity of regional ecological environment to social economic development was less reported.

TABLE 1
Indicator system used to assess CCD of the economy–environment system

Subsystem	Indicator	Direction	Unit	Weight
Economy subsystem	Per capita GDP	+	Yuan/capita	0.3562
	Per capita built-up area	+	Km^2/capita	0.2474
	Proportion of the secondary industry	+	%	0.2717
	Proportion of the tertiary industry	+	%	0.1247
Environment subsystem	Discharge of COD	–	Tons/capita	0.0745
	Discharge of SO_2	–	Tons/capita	0.2122
	Discharge of solid waste	–	Tons/capita	0.2528
	Environmental protection investment	+	Yuan/capita	0.2201
	Pollution Index	–	Dimensionless	0.2404

Notes: '+' and '−' represent the positive and negative indicators, respectively.

EXPERIMENTAL

Evaluation of the coupling coordination degree. Assessment indicator system for the economy–environment system. We constructed an indicator system based on previous case studies and the structure of our established SD model to synthetically analyse the development level of each subsystem and the coupling relationships of the economy–environment system. Table 1 shows the structure of the indicator system, which contains 9 indicators. The indicator system synthetically reflects economic production and industrial structure in the economy subsystem and environmental pollution and environmental governance in the environment subsystem.

Data pre-processing. To render the results comparable and eliminate the impact of dimension, we use the following two formulas to standardise the indicators:

Positive indicator:

$$r_{ij}=(X_{ij}-\min X_j)/(\max X_j-\min X_j), \quad (1)$$

Negative indicator:

$$r_{ij}=(\max X_j-X_{ij})/(\max X_j-\min X_j), \quad (2)$$

Where maxXj and minXj is the maximum and minimum, respectively, of indicator j in all years; Xij and rij are the original and standardised values of indicator j in year i. A positive indicator means that the greater the value is, the better the implication for the development of the system and vice versa.

Evaluation of the economy, resource and environment subsystems. The weights of each indicator in Table 1 are determined by the entropy method (EM) in this work. In 'entropy' theory, 'entropy' is a measure of the degree of disorder in a system that can be used to measure the amount of information and the weight of the known data. That is, the more useful information an indicator provides, the greater the weight it will play in decision-making. EM is an objective weight determination method that has been widely used in comprehensive evaluation. The detailed steps of calculating the weights by EM are as follows:

Proportion (P) of the indicator j in year i:

$$P_{ij}=r_{ij}/\sum_{i=1}^{m} r_{ij}, \quad (3)$$

Information entropy (e) of each indicator j:

$$e_j=-\frac{1}{\ln m}/\sum_{i=1}^{m}(P_{ij}\bullet \ln P_{ij})\ (0\le e_j\le 1), \quad (4)$$

Entropy redundancy (e) of each indicator j:

$$d_j=1-e_j, \quad (5)$$

Weight (W) of each indicator j:

$$W_j=d_j/\sum_{j=1}^{n} d_j, \quad (6)$$

Evaluation of the level (L) of indicator j in year i:

$$L_{ij}=W_j\times r_{ij}, \quad (7)$$

Comprehensive level (CL) of the subsystem in year i:

$$CL_i=\sum_{j=1}^{n} S_{ij}, \quad (8)$$

Where n is the number of indicators in a subsystem, m denotes the number of years and rij is calculated by Formulas (1) or (2). According to Formulas (3)–(6), we obtained the weights of each indicator in Table 1. The comprehensive level of each subsystem are calculated through Formulas (7)–(8).

Coupling coordination degree model. Coupling, which originates from the physical science, is a phenomenon in which two or more systems influence each other through various interactions. In recent years, this concept is often used in studies of eco-environment and urbanisation. For example, CCDM has been used for the compound system of the eco-environment–urbanisation system, the socio-economy–carbon emission system and the low-carbon development–urbanisation system. However, CCDM is often used in situations with two subsystems and this method is rarely applied to the case of multi-subsystems coupling. The general form indicates that CCDM of the three subsystems is provided in Formula (9):

$$C = \left\{ \frac{f(X) \bullet g(Y) \bullet h(Z)}{\left[\frac{f(X) + g(Y) + h(Z)}{3} \right]^3} \right\}^{\frac{1}{3}},$$

$D = \sqrt{C \bullet T}$ and $T=\alpha f(X)+\beta g(Y)+\gamma h(Z)$ (9)

Where C is the coupling degree, whilst f(X), g(Y) and h(Z) are the comprehensive levels of the economy, resource and environment subsystems, respectively. Here, the value of f(X), g(Y) and h(Z) is determined by Si as indicated in Formula (8). D is the CCD and T reflects the overall development level of the economy–environment system. α, β and γ represent the contribution of each subsystem. This study assumes that each subsystem is equally important to the coordinated development of the economy–environment system. Thus, α=β=γ=13.

After calculating the CCD, scholars often divide CCD into several levels in a subjective manner. The current study applies the quartile method to divide CCD. Accordingly, this method may be more objective for measuring the CCD level. Table 2 shows the division of CCD.

RESULTS AND DISCUSSION

Table 3, Figure 1, and Figure 2 show that Tianjin's annual economic comprehensive benefits and environmental comprehensive benefits have increased in 2003-2017, and the annual gap between the two is not much different; in addition, economic and environmental development The degree of coordination is above 0.9, compared with the criteria given in Table 3, are all in the category of quality coordination.

TABLE 2
Division of the development stages of the economy–environment system

Value of D	0≤D<0.25	0.25≤D<0.5	0.5≤D<0.75	0.75≤D≤1
Development stages	Seriously unbalanced	Slightly unbalanced	Barely balanced	With superior balance

TABLE 3
Economic and Environmental Comprehensive Benefit Index and Its Coordination Degree of Tianjin

Year	Comprehensive economic benefits	Comprehensive environmental benefits	Coordination	Type
2017	0.9912	0.9787	0.9578	Quality coordination
2016	0.9846	0.9431	0.8893	Quality coordination
2015	0.9624	0.9221	0.8501	Quality coordination
2014	0.9444	0.8975	0.8051	Quality coordination
2013	0.9156	0.8893	0.7909	Quality coordination
2012	0.8757	0.8698	0.7564	Quality coordination
2011	0.8407	0.8249	0.6805	Quality coordination
2010	0.8325	0.7998	0.6391	Quality coordination
2009	0.7705	0.7355	0.5396	Quality coordination
2008	0.7405	0.6631	0.4385	Quality coordination
2007	0.6818	0.6241	0.3895	Quality coordination
2006	0.6242	0.5836	0.3406	Quality coordination
2005	0.5135	0.5579	0.3112	Quality coordination
2004	0.5012	0.5152	0.2655	Quality coordination
2003	0.4497	0.4706	0.2216	Quality coordination

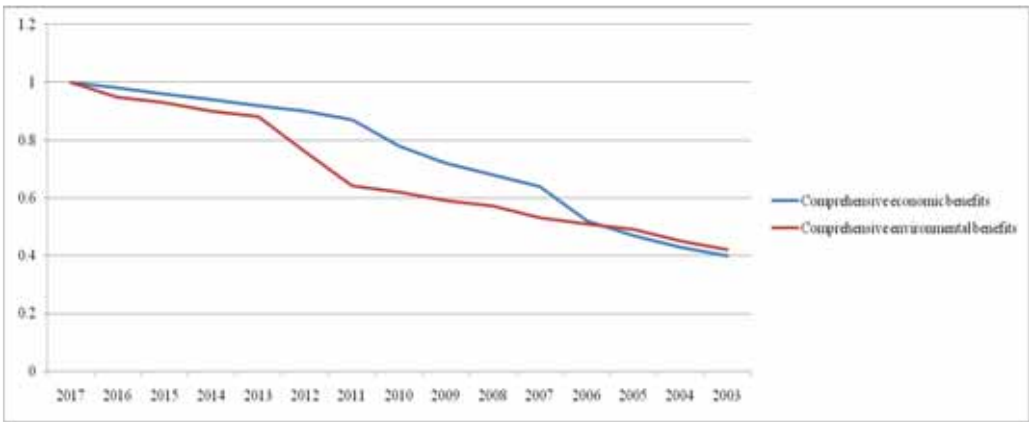

FIGURE 1
Economic and Environmental Comprehensive Benefit of Tianjin

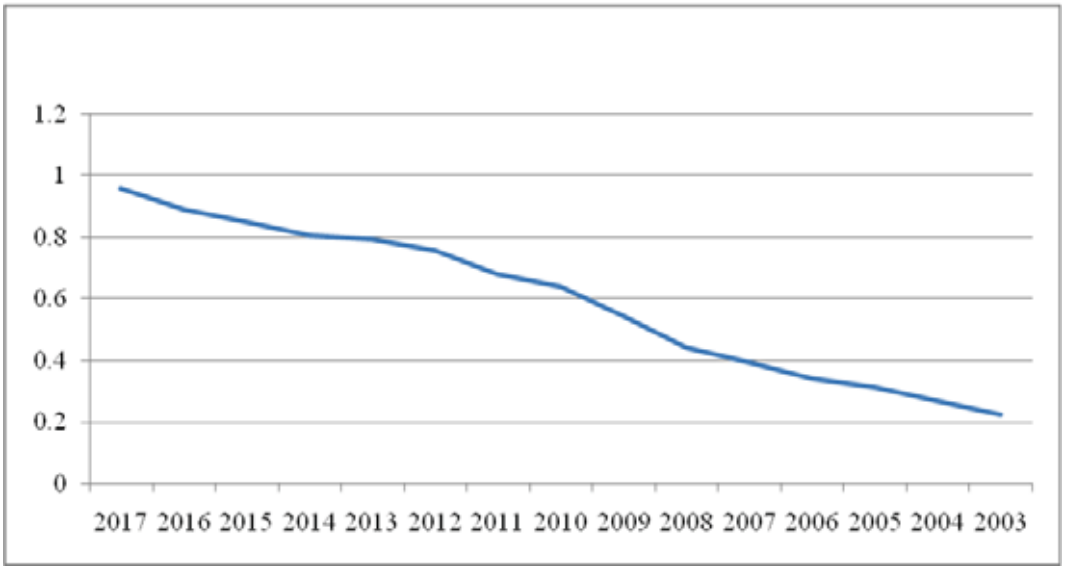

FIGURE 2
Environmental System and Economic System Coordination of Tianjin

TABLE 4
The coordinated development degree and type of environment and economy in Tianjin

Year	Degree of coordination development	f(x), g(y) comparison	Type
2017	0.9871	f(x) > g(y)	High quality coordinated development environment lag
2016	0.9824	f(x) > g(y)	High quality coordinated development environment lag
2015	0.9724	f(x) > g(y)	High quality coordinated development environment lag
2014	0.9544	f(x) > g(y)	High quality coordinated development environment lag
2013	0.9456	f(x) > g(y)	High quality coordinated development environment lag
2012	0.9427	f(x) > g(y)	High quality coordinated development environment lag
2011	0.9107	f(x) > g(y)	High quality coordinated development environment lag
2010	0.9005	f(x) > g(y)	High quality coordinated development environment lag
2009	0.8625	f(x) > g(y)	Good coordination development environment lag
2008	0.8105	f(x) > g(y)	Good coordination development environment lag
2007	0.7918	f(x) > g(y)	Intermediate coordination development environment lag
2006	0.7642	f(x) > g(y)	Intermediate coordination development environment lag
2005	0.7305	f(x) < g(y)	Intermediate coordination development environment lag
2004	0.7112	f(x) < g(y)	Intermediate coordination development environment lag
2003	0.6747	f(x) < g(y)	Primary coordinated development environment lag

It can be seen from Table 4 that the coordinated development of environmental and economic development in Tianjin during the 15 years from 2003 to 2017 shows an overall upward trend, indicating that there are some unstable situations in Tianjin while developing social exhibitions, but the environment and economy the overall level of coordination is rising.

Finally, the dynamic trend index of the overall coordinated development degree of Tianjin in 2017 is calculated to be >1, which indicates that Tianjin has an upward trend in the coordinated development of environment and economy during the period from 2003 to 2017. Although the upward trend is not obvious, it also reflects the easing of the contradiction between Tianjin's economic development and the ecological environment.

CONCLUSIONS

(1) We successfully developed a model that could be used for evaluating the carrying capacity of regional ecological environment to social economic development and that could be generalized to other regions. The model can simulate the relationship between socioeconomic and ecological environment, and made the results more intuitive, spatial, and visual.

(2) Taking Tianjin as the research area, the results of the evaluation were consistent with the analysis results of the original data characteristics, including the indexes: forest cover, per capita GDP and industrial wastewater discharged. It is consistent with the actual situation in the model.

REFERENCES

[1] Smith, G., Nadebaum, P. (2016) The evolution of sustainable remediation in Australia and New Zealand: A storyline. J. Environ. Manage. 184(15), 27-35.

[2] Broman, G.I., Robèrt, K.H. (2017) A framework for strategic sustainable development. J. Cleaner Prod. 140, 17-31.

[3] Jia, X., Foo, D.C.Y., Tan, R.R., Li, Z. (2017) Sustainable development paths for resource-constrained process industries. Resour. Conserv. Recycl. 119, 1-3.

[4] He, J., Wan, Y., Feng, L., Ai, J., Wang, Y. (2016) An integrated data envelopment analysis and emergy-based ecological footprint methodology in evaluating sustainable development, a case study of Jiangsu Province China. Ecol. Indic. 70, 23-34.

[5] Boggia, A., Rocchi, L., Paolotti, L., Musotti, F., Greco, S. (2014) Assessing rural sustainable development potentialities using a dominance-based rough set approach. J. Environ. Manage. 144(1), 160-167.

[6] Siva, V., Gremyr, I., Bergquist, B., Garvare, R., Zobel, T., Isaksson, R. (2016) The support of quality management to sustainable development: a literature review. J. Cleaner Prod. 138, 148-157.

[7] Yuan, B., Ren, S., Chen, X. (2017) Can environmental regulation promote the coordinated development of economy and environment in china's manufacturing industry?– a panel data analysis of 28 sub-sectors. J. Cleaner Prod. 149, 11-24.

[8] Wang, Q., Yuan, X., Cheng, X., Mu, R., Zuo, J. (2014) Coordinated development of energy, economy and environment subsystems—a case study. Ecol. Indic. 46 6), 514-523.

[9] Yu, H., Huang, Y., Ning, J., Zhu, B., Cheng, Y. (2014) Effect of cation exchange capacity of soil on stabilized soil strength. Soils and Foundations. 54, 1236-1240.

[10] Liu, L., Silva, E.A., Wu, C., Wang, H. (2017) A machine learning-based method for the large-scale evaluation of the qualities of the urban environment. Comput. Environ. Urban Syst. 65, 113-125.

[11] Xu, B., Hao, J. (2017) Air quality inside subway metro indoor environment worldwide: a review. Environ. Int. 107, 33-46.

[12] Das Neves Almeida, T.A., Cruz, L., Barata, E., García-Sánchez, I.M. (2017) Economic growth and environmental impacts: an analysis based on a composite index of environmental damage. Ecol. Indic. 76, 119-130.

[13] Özokcu, S., Özdemir, Ö. (2017) Economic growth, energy, and environmental kuznets curve. Renewable Sustainable Energy Rev. 72, 639-647.

[14] Boggia, A., Rocchi, L., Paolotti, L., Musotti, M., Greco, S. (2014) Assessing rural sustainable development potentialities using a dominance-based rough set approach. J. Environ. Manage. 144(1), 160-167.

[15] Miao, C.L., Sun, L.Y., Yang L. (2016) The studies of ecological environmental quality assessment in Anhui province based on ecological footprint. Ecol. Indic. 60, 879-883.

[16] Deng, X., Xu, Y., Han, L., Yu, Z., Yang, M., Pan, G. (2015) Assessment of river health based on an improved entropy-based fuzzy matter-element model in the Taihu plain China. Ecol. Indic. 57, 85-95.

Received: **06.01.2019**
Accepted: **21.03.2019**

CORRESPONDING AUTHOR

Zangen Lin
Tourism Management
College of Management and Economics
Tianjin University
Tianjin – China

e-mail: 160403504@qq.com

© by PSP Volume 28 – No. 5/2019 pages 4054-4071 Fresenius Environmental Bulletin

MYCOFLORA ASSOCIATED WITH GRAM POD BORER AFFECTED CHICKPEA

Hafeez-U-Rahman Jamro[1], M Ibrahim Khaskheli[1,*], Jan M Mari[1], Maqsood A Rustamani[2]

[1]Department of Plant Protection, Sindh Agriculture University, Tando Jam, Pakistan
[2]Department of Entomology, Sindh Agriculture University, Tando Jam, Pakistan

ABSTRACT

The association of gram pod borer (GPB), *Helicoverpa armigera* Hübner with chickpeas disease causing fungi has not been reported. Thus, present studies were conducted during the year 2015 and 2016 at Sindh Agriculture University, Tandojam, Pakistan. The results pertaining to GPB affected seeds and seed shells, larva and adults moth of *H. armigera* revealed the association of 65 different fungal strains belonging to 17 different genera**.** The specific genera and species were confirmed through molecular characterization using ITS region of rDNA of fungi blasted in NCBI database. Out of 65 strains; 20 strains found associated with GPB affected seed, 07 with seed shell, 09 with live larva; whereas 16 with dead larva, and 13 with moth. Significantly (P <0.05 = 0.0000) highest frequency was recorded for *A. alternata* (64.20 and 19.40%) followed by *Chaetomium* sp. (38.20 and 0.00%), *A. tenuissima* (36.70 and 0.00%), *C. lunata* (32.70%), *Drechslera* sp. (31.70 and 0.00%) and *L. theobroae* (31.20 and 9.40%) and *F. oxysporum* (0.00 and 6.90%) from GPB affected seed of 2015 and 2016. In case of seed shell highest frequency percent was recorded for *A. niger* (55.90 and 30.70%) followed by *A. flavus* (52.80 and 11.90%) and *A. alternata* (35.90 and 21.90%), when isolated through agar plate and blotter paper method, respectively. Significantly higher frequency was recorded for *A. flavus* (20.40%) followed by *A. niger* (9.40%), *A. alternata* (8.40) and *Penicillium* sp. (7.40%) from un-treated larvae. Whereas, from treated larvae *Fusarium* sp. (10.40%) followed *C. lunata* (5.40%). In case of dead larvae (un-sterilized), higher frequency was recorded for *A. alterna* (25.40%) followed by *A. fumigatus* (15.40%) and *A. niger* (14.40%). Whereas, from surface sterilized larvae, *A. alterna* (13.40%) followed by *Fusarium* sp. (12.20%) and *B. bassiana* (6.40%) were isolated with higher frequency. From adult moth (un-sterilized), higher frequency was recorded for *A. alternata* (43.20%) followed by *Paecilomycete* (36.20%) and *A. niger* (34.20%) and *T. virens* (13.20). Whereas, the frequency of other fungi associated with adult moth (Surface sterilized) was lower that ranged from 0 to 11.50%. These results indicate the relationship of these pathogens with chickpea diseases and GPB. In addition, the influence of GPB in dissemination and/or providing possible entry to these pathogenic fungi for complex disease development cannot be ignored.

KEYWORDS:
Fungal strains, *Helicoverpa armigera*, association, chickpea diseases

INTRODUCTION

Chickpea, *Cicer arietinum* L. is an important legume crop belongs to the family Fabaceae (subfamily Faboideae) and ranked 3rd among the legume crops [1, 2]. Generally, chickpea prefers relatively well drained soils and is well adapted to diverse climates such as arid, cool semi-arid regions of the tropics, sub-tropics as well as the temperate areas [1]. Worldwide, chickpea is widely distributed crop and is cultivated in more than 50 countries with lion share (approximately 83%) contributed by south Asian countries including India, Pakistan, Nepal, and Bangladesh [3-7].

Pakistan being a 5th major producer of Chickpea in world, however, its production is very low as compared to other chickpea producing countries [7]. In Pakistan, it is mostly cultivated in rainfed areas of Punjab and Khyber Pakhtunkhwa; whereas on residual moisture after harvesting of rice crop in Sindh and Baluchistan provinces [8]. It is believed that chickpea is a great source of biomolecules such as proteins, carbohydrates, dietary fiber, minerals and vitamins and its use has been increased for reducing risk of human diseases [9]. Despite the fact that the chickpea has great economic and nutritional value, the production of chickpea is far below than other countries where chickpea is commonly cultivated, which likely due to several biotic and abiotic factors. Chickpea plant is highly susceptible to various insect pests at different critical growth stages from seedling stage to maturity. Around 60 species of insect pests belonging to orders Lepidoptera, Hemiptera, Diptera and Thysanoptera are commonly found in chickpea crop [10-11]. However, Gram pod borer (*Helicoverpa armigera* Hübner) [12-13] is considered as major pest of this crop.

Apart from insect pests, around 50 pathogens of economic significance have been reported in literature to affect the chickpea plant and causing severe diseases. Among them most important diseases caused by these pathogen include: wilt (*Fusanum oxysporum* Schlecht emend.), several root and stem rots (*Rhizoctonia bataticola* Taub.; *Fusarium solani* Mart.; *Operculella padwickii* Kheswalla, *Sclerotinia sclerotiorum* Lib.), blights (*Ascochyta rabiei* Pass.; Labrousse; *Stemphylium sarciniforme* Cav.), grey mold *(Botrytis cineria* Pers. ex Fr.), rust *(Uromyces ciceris-arietini* Grogn.), and viral diseases such as stunt caused by pea leaf roll virus. Datta and Lal [14] reported that pathogens in chickpeas are the main cause for yield loss (up to 90%). Jendoubi et al. [15] reported that chickpea Fusarium wilt is key soil-borne fungus which limit chickpeas production and under optimum environmental conditions. Iruela et al. [16] and Mulwa et al. [17] indicated that chickpea yield can be limited by the ascochyta blight and Fusarium wilt. It has also been reported by Baite and Dubey [18] that rainfall period can reduce the growth of chickpea severely since rainfall events can increase the disease infection and spread. However, the associations of gram pod borer with Chickpea disease causing fungi have not been reported before in the literature.

Based on aforementioned facts it was planned to determine the association of gram pod borer with chickpea disease causing fungi. To cater the need, present studies were conducted on the association of mycoflora with gram pod borer infested chickpea.

MATERIALS AND METHODS

The present studies were conducted during the year 2015 and 2016 at post graduate laboratory, Department of Plant Protection, Faculty of Crop Protection, Sindh Agriculture University, Tandojam, Pakistan. Samples were collected from agro-ecological zones of Sindh, Pakistan i. e Upper Zone (Dokri, Larkana) and Lower zone (Tandojam) from the crops season of 2015 and 2016.

Isolation of Fungi. Isolation of fungi was conducted from gram pod borer affected seeds, seed shell of chickpeas, larvae (field dead and live) and adult of gram pod borer, *Helicoverpa armigera* through standard isolation techniques. The specimen for isolation of fungus was collected from gram pod borer sensitive (Choola) variety. To fulfill the objective of current study, series of following different experiments were conducted:

1. Isolation of fungi from gram pod borer affected seeds (fresh & one year old).
2. Isolation of fungi from gram pod borer affected seed shells (fresh & one year old).
3. Isolation fungi from field live collected larvae of *H. armigera* (Surface sterilized and Unsterilized).
4. Isolation fungi from field dead collected larvae of *H. armigera* (Surface sterilized and Unsterilized).
5. Isolation fungi from field adult collected larvae of *H. armigera* (Surface sterilized and Unsterilized).

Isolation fungi from seed and seed shell. Isolation of fungi from gram pod borer affected seeds and seed shells were conducted by using isolation techniques describe (Figure 1) by International Rules for Seed Testing Association [19] such as: Standard blotter method (SBM); and Standard Agar-plate method (SAM).

Standard blotter method (SBM). Seed and seed shell samples of 2015 and 2016 crop seasons were used for the isolation of associated mycoflora. Three layers of blotter papers circular in shape and 150 mm diameter according to size of Petri dishes were cut with the help a scissor. The blotters were dipped and moistened with sterilized distilled water and excess water was removed from the petrdishes. The moistened blotter papers were transferred to sterilized petridish with the help of sterilized forceps. Randomly collected seed samples were thoroughly washed with tap water and the dried. These seeds and seed shells were surface sterilized in 0.1 per cent mercuric chloride solution ($HgCl_2$) for 30 seconds followed by three washing with sterilized distilled water in beakers under aseptic conditions using laminar air flow. All seeds were then completely dried by placing on sterilized blotting paper. A total of 10 randomly collected seeds and seed shells were placed in such a manner that 09 were in outer circle and one in the centre. The inoculated plates were then incubated in incubator at 25± 2˚C for 7 days under 12 hrs alternating cycles of light and darkness. All plates were examined on 3rd days, 5th days and 07th days after incubation (DAI). The experiment was conducted on 07-04-2016 with complete randomized design (RCD) with 10 replications. After seven days all fungi developing on samples were examined and purified through single spore isolation technique on Potato Dextrose Agar (PDA) medium freshly prepared with the help of sterilized needle for purification. All the isolates were given initially different laboratory codes based on the colony characteristics and then were identified (Figure 1).

Standard agar plate method. In standard agar plate method, randomly collected seeds and seed shells were thoroughly washed with tap water and then dried. These seeds were surface sterilized in 0.1 per cent mercuric chloride solution ($HgCl_2$) for 30 seconds followed by three washing with ster-

ilized distilled water in beakers under aseptic conditions using laminar air flow. All seeds and seed shells were then completely dried by placing on sterilized blotting paper. Five seeds and seed shells of each were transferred aseptically to the 90 mm diameter petriplates containing sterile PDA medium amended with an antibacterial agent and filled up to quarter strength in manner that 4 seeds were kept at outer circle and 01 seed at the centre of petridish. The inoculated plates were incubated at 25±20ºC (Figure 1). All the plates were monitored regularly and growing colonies were subjected to different laboratory codes for further analysis. The culture, thus, obtained was subjected to purification. A single spore culture technique was used to purify the isolates. Sub-culturing of isolates were made time to time to maintain the fresh culture for further analysis until the end of experiments.

The frequency of the fungi in the collected specimens of both years was recorded by using the following formula:

$$\text{Frequency (\%)} = \frac{Number\ of\ Pieces\ colonized}{Total\ Number\ of\ Pieces\ studied} \text{X100}$$

Isolation of fungi from different life stage of *H. amigera*. Series of experiments for the isolation of fungi from different life stage such as larvae, and adult moth of *H. amigera* were designed to confirm the association mycoflora. Surface sterilized and un-sterilized samples were used in each experiment. Samples were first washed with sterilized distilled water and then were surface sterilized with 0.1% mercuric chloride ($HgCl_2$) for 2-3 minutes. All treated samples were twice washed in sterilized distilled water for 2 minutes. Treated samples were completely dried before inoculation. In addition, un-surface sterilized samples were also used for the isolation of fungi. One surface sterilized live larvae per plate (after sterilization became dead) were placed on PDA medium; whereas, one unsterilized live larva were released in PDA medium. Similarly, the adult of *H. amigera* (Surface sterilized and un-sterilized) were placed in PDA medium (Figure 1).

All inoculated plates were incubated at 25±20ºC and were monitored regularly. The growing colonies were subjected to different laboratory codes as explained earlier and frequency percentage was determined. The culture, thus, obtained was subjected to purification as explained earlier for further analysis. The frequency percent of fungi was determined by following the formula as mentioned above.

Identification of fungal genera. Morphological and cultural characters. Temporary slides of fungal isolates from pure cultures were made and observed under light microscope. Morphological and cultural characters of isolated fungi were recorded and compared with standard keys for establishing their identity [20-24]. In addition, internet databases were also used to compare the morphological characteristics of isolates. Moreover, identification of all isolates were further confirmed through molecular characterization (Figure 1).

Molecular characterization. DNA Extraction. Five samples from each isolate of fungi were selected for DNA extraction. Fungal genomic DNA was purified (Figure 2) using GentraPuregene Yeast Kit by following the protocol described in the kit:

The DNA Extraction Protocol followed as under:

1. Pure 5mm disc from purified fungal cultures were inoculated in YM broth and incubated for 72hours with continuous shaking at 130rpm at room temperature (25°C-30-C°). The growing mycelium in the form of round balls were harvested and twice washed with sterilized distilled water in sterile Petri plates.
2. To isolate DNA from the mycelium was crushed in sterilized pestle and mortar using liquid nitrogen.
3. A small amount of mycelium was picked up with the help of sterile needle and mixed with 1.5ml autoclaved distilled water in 1.5ml Eppendorf tube and centrifuged for 3 minutes.
4. Supernatant was discarded carefully and 1ml sterile water was added to the pelleted cells and vortexed.
5. The suspension was centrifuged and the supernatant was discarded again.
6. 300µl of cell suspension solution was added in the pellet cells and pipetted up and down for almost 20 times.
7. 1.5µl of lytic enzyme solution was also added in the middle of tube and was mixed by inverting 25 times.
8. Samples were incubated for 45mins in incubator at 37°C.
9. After incubation, samples were centrifuged for 3min at high speed (13000 x g) and supernatant was discarded carefully.
10. 300µl of lysis solution was added into the pellet samples and pipetted up and down about 20 times.
11. 100µl of protein precipitate solution was added and samples were vortexed for 20 seconds at high speed.
12. Samples were centrifuged for 5min at high speed (13000 x g). At this stage tight pellet of protein was appeared.
13. Supernatant was transferred in a clean microcentrifuge tube containing 300µl of isopropanol.
14. Samples with isopropanol were gently mixed by inverting 50 times and centrifuged for 3 min at 13000 x g.
15. DNA was visible in a small white pellet.
16. Supernatant was discarded and the tubes were drained on a clean piece of absorbent paper carefully, so that the pellet was remain in the tube.

17. 300µl of 70% ethanol was added and tubes were inverted several times to wash the DNA pellet.

18. Samples were centrifuged for 3min at 13000 x g. supernatant was discarded, tubes were drain on a clean piece of absorbent paper and allowed to air dry for 5min.

19. 100µl of DNA Hydration Solution was added, samples were briefly vortexed for 5sec at medium speed.

20. 1.5µl of RNase A solution was added and samples were mixed by vortexing for 1sec. To collect the DNA, tubes were pulse spin and incubated at 37°C for 1hr in incubator.

21. After the completion of incubation period samples were incubated in pre heated water bath on 65°C for 1hr to dissolve the DNA.

22. After incubation samples were incubated at room temperature on gentle shaking.

23. Purified DNA was stored at -20°C.

PCR amplification. Amplification of conserved regions of fungal genomic DNA was performed by universal primers ITS1 (forward) and ITS4 (reverse). The sequences of ITS1 and ITS4 were 5´-TCCGTAGGTGAACCTGCGG-3´ and 5´-TCCTCCGCTTATTGATATGC-3´respectively. Primers were in a concentration of 100nm/µl designed by integrated DNA technologies (IDT). Primers working solutions were prepared in 100µl nuclease free water with a concentration of 1nM/µl (1000picomoles). 25µl of PCR reaction mix was prepared with the following components: 1.0 µl (10pico moles) of each ITS1 and ITS4 primers, 2µl template DNA, 12.5µl Master mix (contained75 mM of tris-HCl pH 8.8, 0.625 units/µl of *Taq* DNA polymerase, 20 mM of $(NH_4)_2SO_4$, 1.5mM of $MgCl_2$ and 0.2mM each of dNTP) and 8.5 nuclease free water (PCR water). Reaction was performed in THERMO HYBRID PCR Express Thermal cycler. PCR protocol consisted 40 cycles with 5 minutes initial denaturation temperature at 95°C. PCR conditions were; denaturation at 95°C for 30 sec, annealing at 58°C for 30 sec, extension at 72°C for 1 min and final extension at 72°C for 5 min. After PCR amplification temperature was maintained at 4°C until samples were removed from thermal cycler.

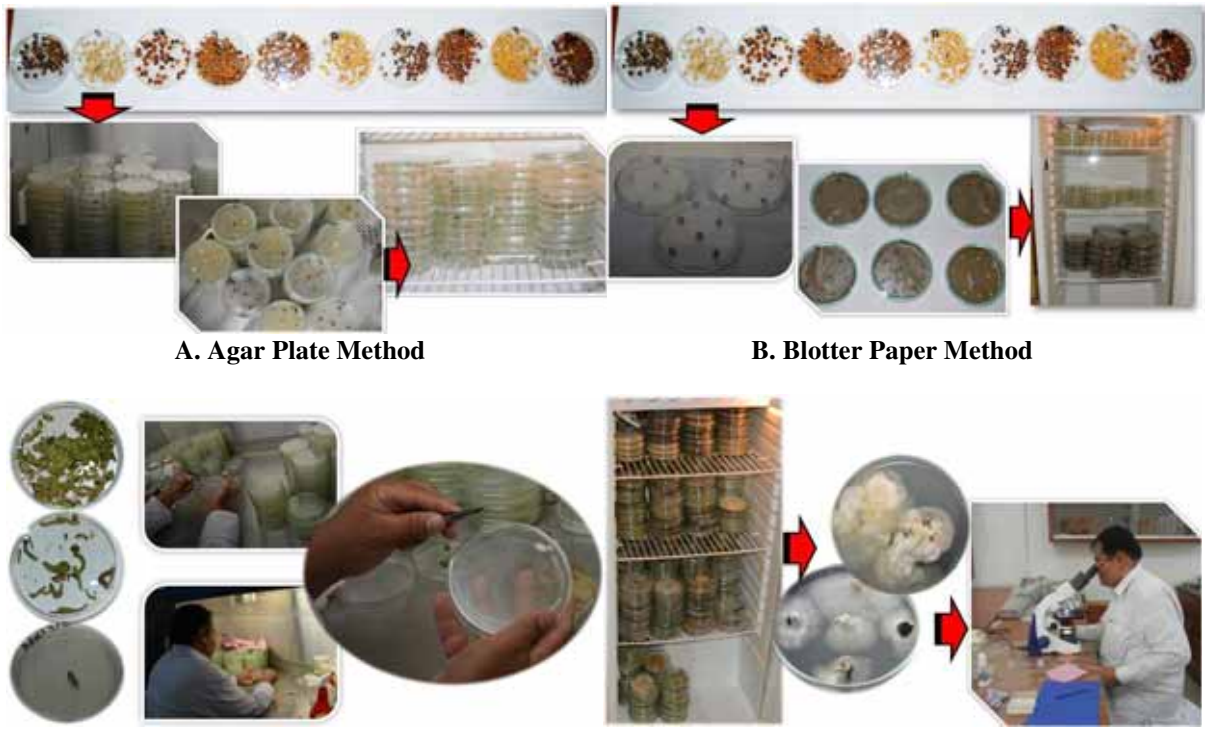

A. Agar Plate Method **B. Blotter Paper Method**

C. Isolation from different life stage **D. Identification**

FIGURE 1

Isolation fungi from gram pod affected seeds, seed shell and different life stages of gram pod borer (Live and dead larva; adult) collected from chickpea field during the study periods

Note: A) Isolation through agar plate; B) Isolation through blotter paper methods; C) Isolation from different life stages of gram pod borer (Live and dead larva; adult); D) Identification through morphological characteristics.

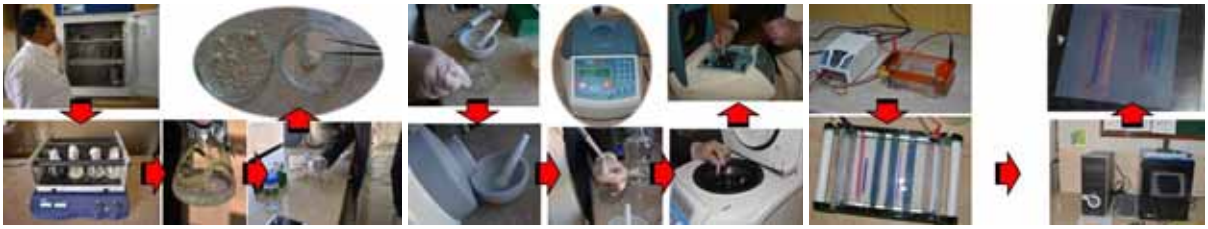

FIGURE 2
Different steps followed during molecular characterization of fungal isolates.

Gel Electrophoresis for Genomic DNA Visualization. Gel electrophoresis was performed to check the quality of DNA. 1.5% gel was prepared by adding 1.12gm of agarose into 75ml of 1X TBE buffer [Tris-Borate EDTA (Ethylenediaminetetraacetic acid)] with 8.5pH and heated in microwave oven till the gel was completely dissolved. 5µl ethidium bromide was added and the molten gel was poured into the gel caster pre fitted with 8 or 16 well comb. The comb was removed when gel completely solidified and the gel caster along with gel was placed in the gel electrophoresis tank prefilled with 1X TBE buffer.

5µl genomic DNA of each sample was mix with 2µl of ThermoScientific 6X loading dye by pipetting and loaded in the gel. The dye contained 10mM Tris-HCl (pH 7.6), 0.03% xylene cyanol FF, 0.03% bromophenol blue, 60% glycerol 60mM EDTA. Gel was run on 120V for 45 min. For the conformation of DNA gel was placed on UVP Benchtop transilluminator (302nm) to observe bands (Figure 2).

Sequence analysis. The PCR product was sent to the company for sequencing of DNA of each sample. The nucleotide sequence of each sample was blasted by using nucleotide internet database of National Center for Biotechnology Information Database (NCBI).

Phylogenetic analysis of different isolates. The Phylogenetic tree was constructed through Neighbor-Joining method associated taxa clustered (bootstrap 1000 replicates). The Nucleotide sequence obtained from the National Center for Biotechnology Information Database (NCBI). The obtained sequences were analyzed with Clustalx 1.83, and the Phylogenetic tree was constructed through MEGA (version 3.1). The circled isolate denotes the member cultured in present study.

Statistical analysis. The data obtained in present were statistically analyzed by using the standard procedures for analysis of variance, ANOVA (linear model), and mean separation (least significant difference, LSD) of frequency (%) of fungi from each experiment was analysed by using the computer software Statistix 8.1 [25]. All differences described in the text were significant at the 5% level of probability.

RESULTS

The associations of fungi with gram pod borer affected seeds, seed shells and different life stages of gram pod borer have not been reported before in the literature. In our study we determined the association of gram pod borer with chickpea disease causing fungi. The results pertaining to gram pod affected seeds and seed shells, larva and adult moth of *H. armigera* revealed the association of several fungal genera in current studies (Figure 3 and 4). On overall basis from all specimens of current study, a total of sixty five different fungal strains belonging to seventeen different genera (*Alternaria, Aspergillus, Curvularia, Chaetomium, Colletotrichum, Drechslera, Fusarium, Lasiodiplodia, Macrophomina, Paecilomyces, Penicillium, Pleospora, Rhizoctonia, Sordariomycetes*, *Stemphylium, Beauveria* and *Trichoderma*) were identified. It was further observed that a total of twenty different fungal strains were identified from the seeds and seven from seed shells of 2015 and 2016 chickpeas crop. There were twenty different fungal strains found associated with gram pod borer affected seed and seven with seed shell of both years isolated through agar plate and blotter paper method. Moreover, nine different fungal strains found associated with field live collected larva (surface sterilized and un-sterilized); whereas from field dead collected larva, sixteen fungal strains were confirmed. When adult of gram pod bore was placed on PDA medium, 13 different fungal strains were identified from surface sterilized and un-sterilized moth. All the fungal strains were tentatively identified through their cultural and morphological characteristics and thereafter were confirmed through molecular characterization (Table 1).

Morphological characterization. The cultural and morphological characteristics of most frequently associated fungal strains such as: *Alternaria alternata* (Fr.) Keissler, *Alternaria solani* Sorauer, *Alternaria tenuissima*, *Aspergillus flavus, Aspergillus fumigatus* Fresenius, *Aspergillus niger* van Tiegh, *Aspergillus terreus, Beauveria bassiana*, *Chaetomium* sp., *Colletotrichum* sp., *Curvularia lunata* (Wakker) Boedijn, *Cercospora* sp., *Drechslera* sp. Synonym: *Biporalis australiensis (*M. B. Ellis), *Fusarium equiseti* (Corda) Sacc., *Fusarium oxysporum* (Schl.) Snyder & Hansen,

Fusarium solani (Mart.) Sacc., *Lasiodiplodia theobromae, Macrophomina phaseolina* (Tassi) Goid., *Paecilomyces* sp., *Penecilium* sp., *Rhizoctonia solani* (Kohn), *Rhizopus stolonifer, Stemphylium* Wallr. and *Trichoderma viride* are documented in Figure 5.

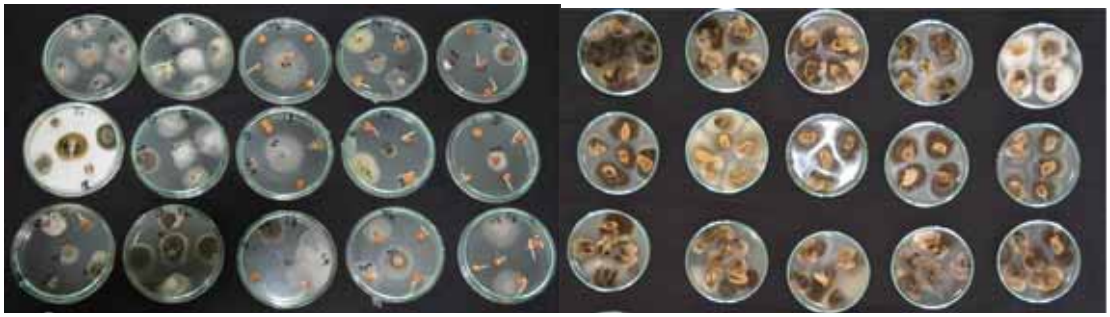

Chickpea Seeds **Seed shells**

FIGURE 3
Association of different fungal strains with seeds and seed shell infested with gram pod borer

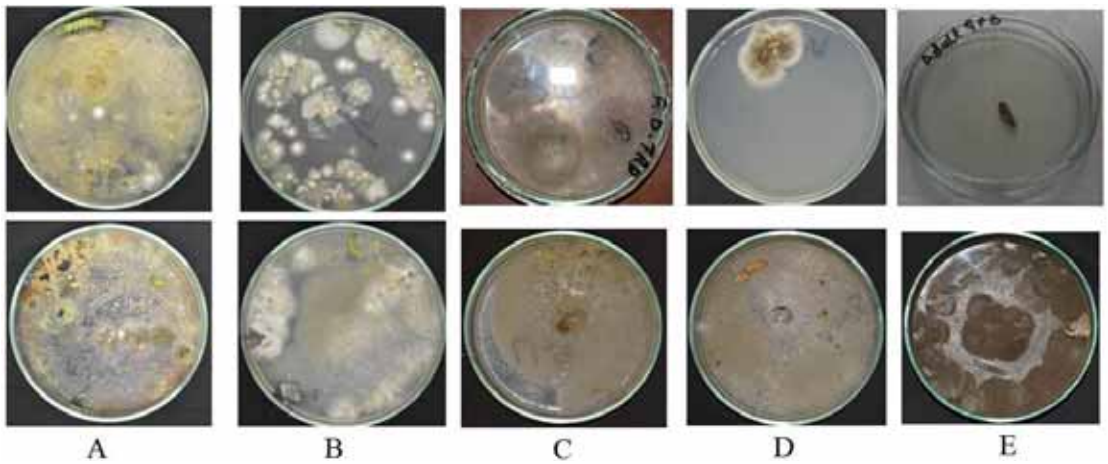

FIGURE 4
Association of different fungal strains with the larva (Field-Lab live and dead) and adult moth of gram pod borer

Note: A) Field Live larvae; B) Lab. Live Larvae; C) Field Dead Larvae; D) Lab. Dead; E) Adult Moth

TABLE 1
Fungal isolates associated with gram pod borer affected seeds, seed shell and different life stages of *H. armigera*

S. No.	Seeds	Seed Shells	Live Larva	Dead Larva	Adult
1	*Acremonium sclerotigenum*	*A. alternate*	*A. alternate*	*A. alternate*	*A. alternate*
2	*Alternaria alternate*	*A. flavus*	*A. solani*	*A. flavus*	*A. flavus*
3	*A. solani*	*A. fumigatus*	*A. flavus*	*A. fumigatus*	*A. fumigatus*
4	*A. tenuis*	*A. niger*	*A. niger*	*A. niger*	*A. niger*
5	*A. tenuissima*	*C. lunata*	*Chaetomium* sp.	*Beauveria bassiana*	*Chaetomium* sp.
6	*Aspergillus flavus*	*Penicillium* spp.	*C. lunata*	*Chaetomium* sp.	*C. lunata*
7	*A. fumigatus*	*R. stolonifer*	*Drechslera* sp.	*C. lunata*	*Fusarium* spp.
8	*A. niger*	-	*Fusarium sp*	*Fusarium* spp.	*Paecilomyces* sp.
9	*Chaetomium* sp.	-	*Penicillium* spp.	*Paecilomyces* sp.	*Penicillium* spp.
10	*Colletotrichum truncatum*	-	-	*Penicillium spp*	*Pleospora herbarum*
11	*Curvularia lunata*	-	-	*Pleospora herbarum*	*R. stolonifer*
12	*Drechslera* sp.	-	-	*Rhizoctonia bataticola*	*Sordariomycetes* sp.
13	*Fusarium equiseti*	-	-	*R. stolonifer*	*T. virens*
14	*Fusarium oxysporum*	-	-	*Sordariomycetes* sp.	-
15	*Macrophomina phaseolina*	-	-	*Stemphylium* spp.	-
16	*Penicillium spp.*	-	-	*Trichoderma virens*	-
17	*Rhizopus stolonifer*	-	-	-	-
18	*Stemphylium* spp.	-	-	-	-
19	*Lasiodiplodia theobromae*	-	-	-	-
20	*A. terreus*	-	-	-	-
Total	**20**	**7**	**9**	**16**	**13**

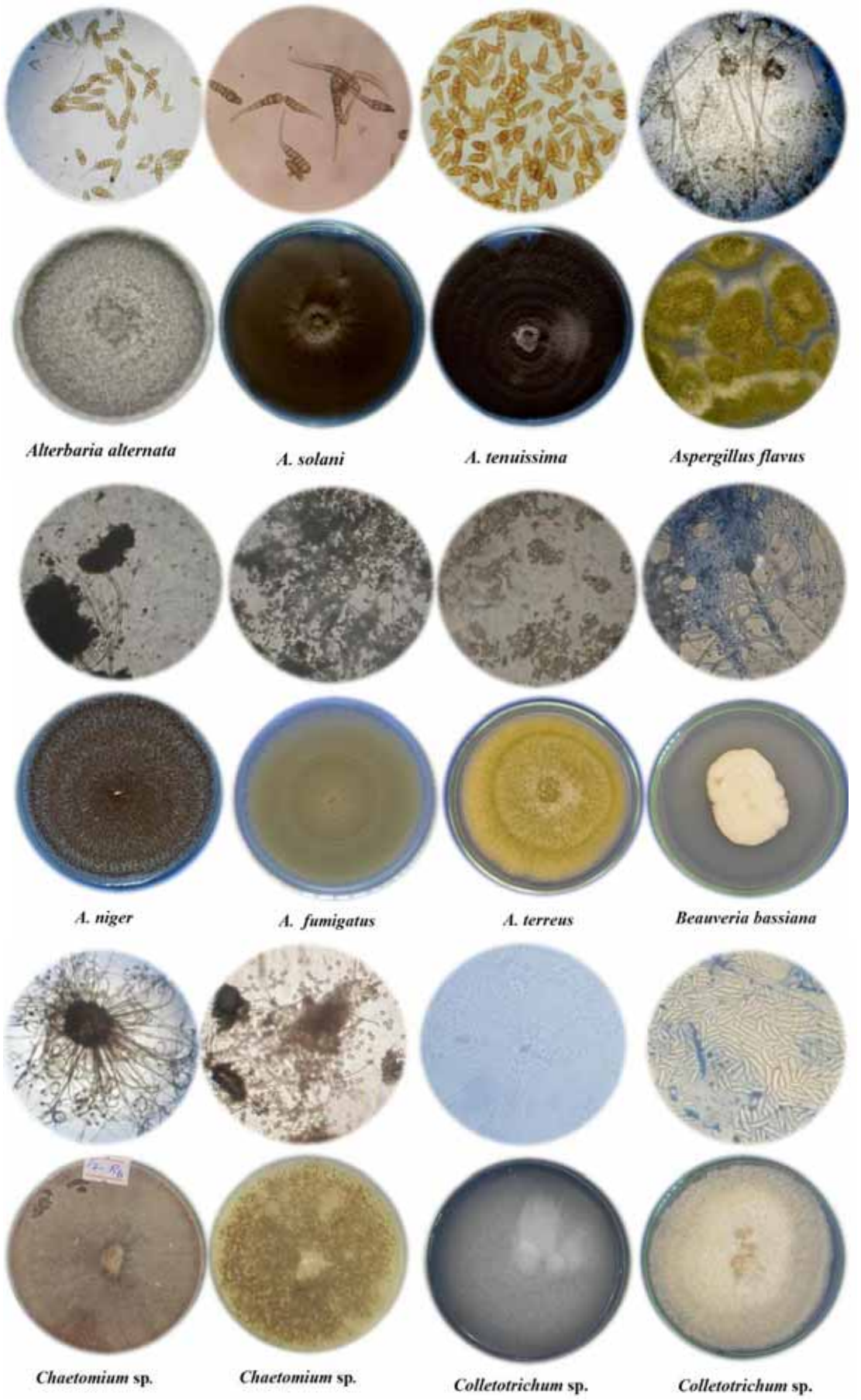
Alterbaria alternata
A. solani
A. tenuissima
Aspergillus flavus
A. niger
A. fumigatus
A. terreus
Beauveria bassiana
Chaetomium sp.
Chaetomium sp.
Colletotrichum sp.
Colletotrichum sp.

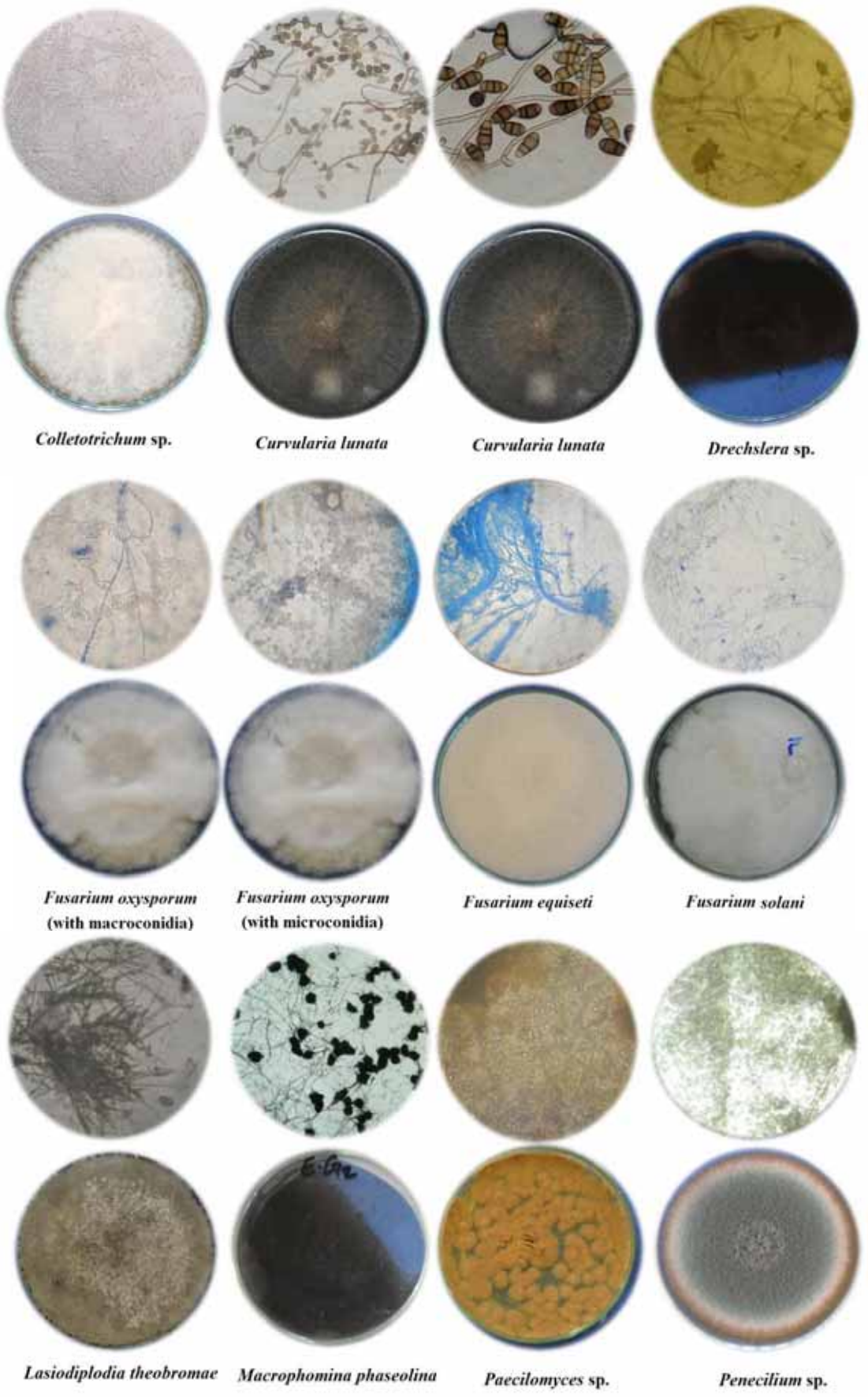
Colletotrichum sp.
Curvularia lunata
Curvularia lunata
Drechslera sp.
Fusarium oxysporum (with macroconidia)
Fusarium oxysporum (with microconidia)
Fusarium equiseti
Fusarium solani
Lasiodiplodia theobromae
Macrophomina phaseolina
Paecilomyces sp.
Penecilium sp.

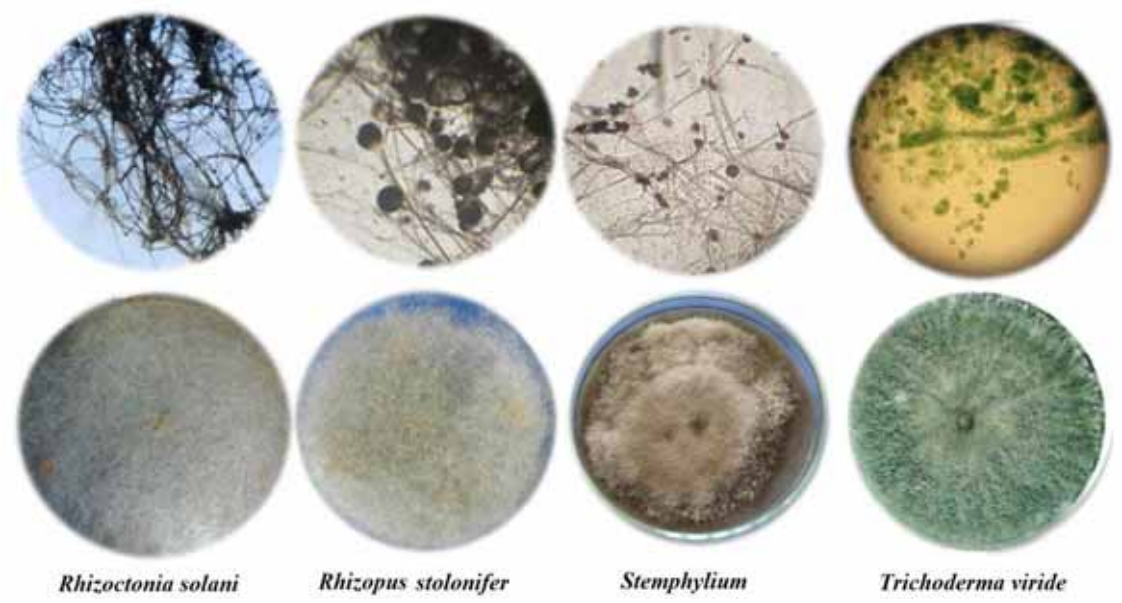

FIGURE 5
Cultural and morphological characteristics of different fungal strains isolated in current study

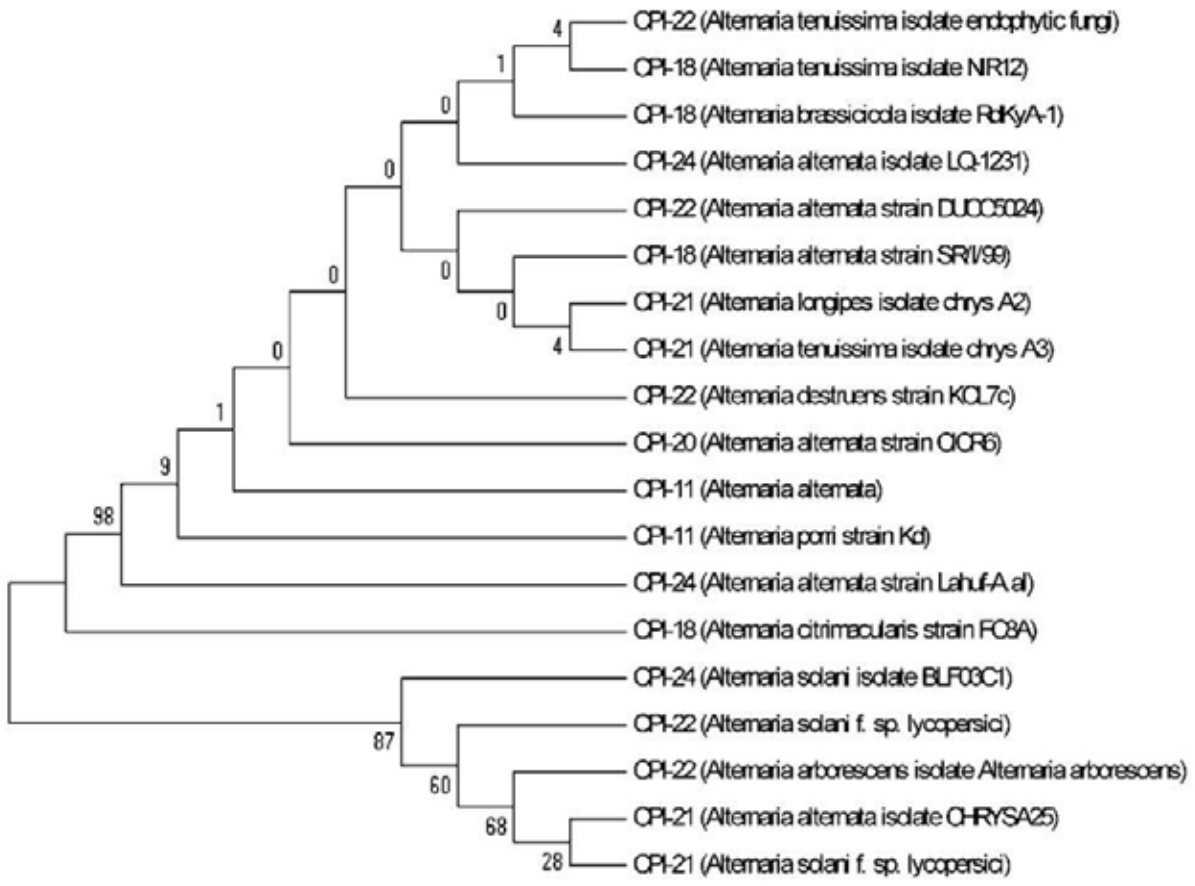

FIGURE 6
Phylogenetic analysis of genus *Alternaria* associated isolates.

Note: The Phylogenetic tree was constructed through Neighbor-Joining method associated taxa clustered (bootstrap 1000 replicates). The Nucleotide sequence obtained from the National Center for Biotechnology Information Database (NCBI). The obtained sequences were analyzed with Clustalx 1.83, and the Phylogenetic tree was constructed through MEGA (version 3.1). The circled isolates denote the member culture in present study.

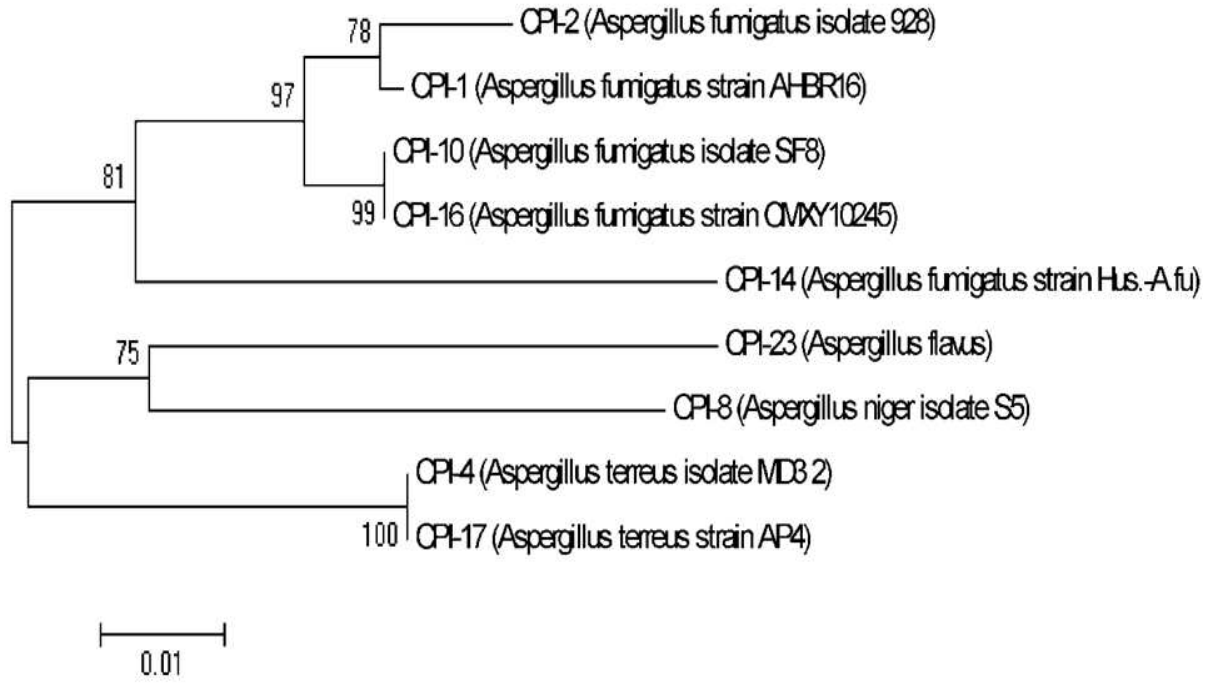

FIGURE 7

Phylogenetic analysis of genus *Aspergillus* associated isolates.

Note: The Phylogenetic tree was constructed through Neighbor-Joining method associated taxa clustered (bootstrap 1000 replicates). The Nucleotide sequence obtained from the National Center for Biotechnology Information Database (NCBI). The obtained sequences were analyzed with Clustalx 1.83, and the Phylogenetic tree was constructed through MEGA (version 3.1). The circled isolates denote the member culture in present study.

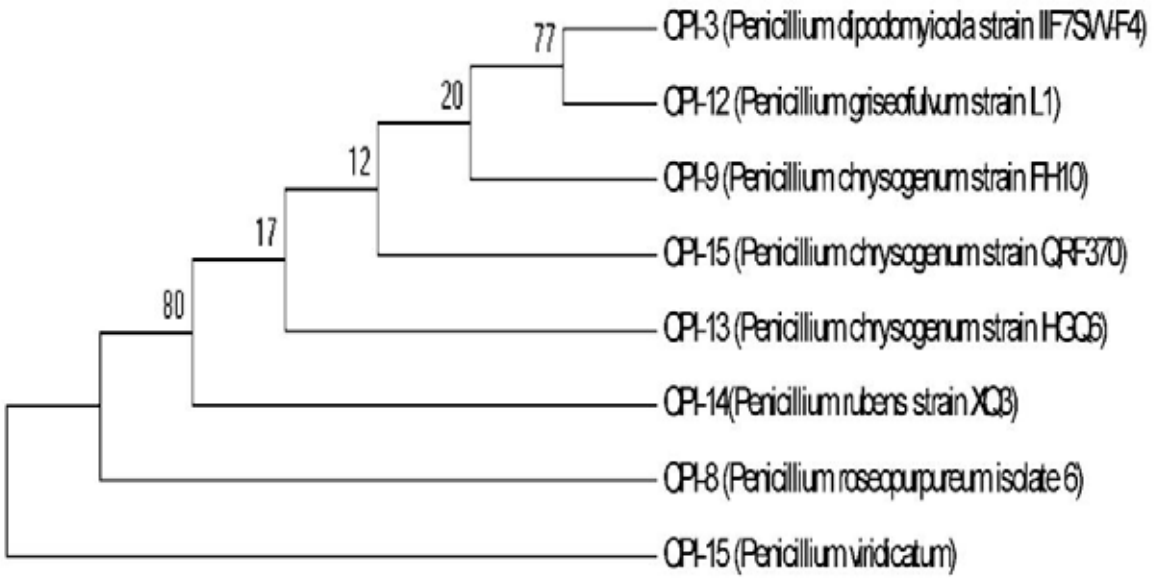

FIGURE 8

Phylogenetic analysis of genus Penicillium associated isolates.

Note: The Phylogenetic tree was constructed through Neighbor-Joining method associated taxa clustered (bootstrap 1000 replicates). The Nucleotide sequence obtained from the National Center for Biotechnology Information Database (NCBI). The obtained sequences were analyzed with Clustalx 1.83, and the Phylogenetic tree was constructed through MEGA (version 3.1). The circled isolates denote the member culture in present study.

TABLE 2
Different fungal strains gen bank accession and GI isolated from gram pod borer affected seeds, seed shells and different life stages of *H. armigera*

S. No	Lab Code	Isolate	Gen Bank Accession	Gen Bank GI
1	CPI-7	*Acremonium sclerotigenum* isolate A1	MG980070.1	1347826466
2	CPI-11	*Alternaria alternata*	JQ080319.1	380447312
3	CPI-21	*A. alternata* isolate CHRYSA25	KX156938.1	1043111902
4	CPI-24	*A. alternata isolate* LQ-1231	MF141011.1	1279122625
5	CPI-20	*A. alternata strain* CICR6	KF747365.1	560207868
6	CPI-22	*A. alternata strain* DUCC5024	KJ728679.1	664818462
7	CPI-24	*A. alternata strain* Lahuf-A.al	MF099865.1	1191949177
8	CPI-18	*A. alternata strain* SR/I/99	KJ728834.1	659225145
9	CPI-22	*A. arborescens isolate* A674	KX463046.1	1139416976
10	CPI-18	*A. brassicicola isolate* RdKyA-1	MF167583.1	1198370140
11	CPI-24	*A. citrimacularis* strain FC8A	KP863716.1	906541939
12	CPI-22	*A. destruens* strain KCL7c	MG182675.1	1253806173
13	CPI-21	*A. longipes* isolate chrys A2	KU639594.1	1028336416
14	CPI-11	*A. porri* strain Kd	KT447157.1	984697830
15	CPI-20	*A. solani* f. sp. *lycopersici*	KX452728.1	1050550885
16	CPI-21	*A. solani* f. sp. *lycopersici*	KX430179.1	1050550884
17	CPI-24	*A. solani* isolate BLF03C1	MH312016.1	1387845362
18	CPI-21	*A. tenuissima* isolate chrys A3	KU639595.1	1028336417
19	CPI-22	*A. tenuissima* isolate endophytic fungi	MG561951.1	1279695442
20	CPI-18	*A. tenuissima* isolate NIR12	MG786766.1	1328374884
21	CPI-23	*Aspergillus flavus*	HQ340103.1	330897167
22	CPI-2	*A. fumigatus* isolate 928	KU936230.1	1092191070
23	CPI-10	*A. fumigatus* isolate SF8	KX011021.1	1025824576
24	CPI-1	*A. fumigatus* strain AHBR16	KF305755.1	527851622
25	CPI-16	*A. fumigatus* strain CMXY10245	MG991603.1	1349758520
26	CPI-14	*A. fumigatus* strain Hus.-A.fu	MF163444.1	1198318131
27	CPI-9	*A. fumigatus* strain Hus.-A.fu	MF163444.1	1198318131
28	CPI-8	*A. niger* isolate S5	KX897146.1	1148880127
29	CPI-4	*A. terreus* isolate MD3_2	JQ697515.1	387860691
30	CPI-17	*A. terreus* strain AP4	KF860883.1	584013156
31	CPI-13	*Beauveria bassiana* isolate FAFU-BSF2	MH715012.1	1442531291
32	CPI-28	*Cercospora* sp. PG2	HQ232415.1	310750932
33	CPI-19	*Chaetomium* sp. 15003	EU750691.1	190645817
34	CPI-19	*C. uniseriatum* strain LC3756	KP336751.1	940676158
35	CPI-7	*Colletotrichum gloeosporioides* isolate LSC-31	KU097221.1	1021765884
36	CPI-21	*Corynespora* sp. isolate OLS1	KU898065.1	1074969396
37	CPI-27	*Curvularia lunata*	-	-
38	CPI-34	*Drechslera* sp.	-	-
39	CPI-38	*Fusarium equiseti* isolate XSD-80	EU326202.1	162285925
40	CPI-40	*F. oxysporum isolate* FO-12 18S	AY928419.1	60593128
41	CPI-38	*F. solani*	EU029589.1	157824570
42	CPI-6	*Lasiodiplodia theobromae* isolate Lt-A2	KX270362.2	1393545685
43	CPI-35	*Macrophomina phaseolina* isolate MP-018	MH371315.1	1390642155
44	CPI-35	*M. phaseolina* isolate SMPMb28F	KC513786.1	459649108
45	CPI-37	*Paecilomyces* sp.	HM626196.1	307563850
46	CPI-23	*Paradendryphiella salina* strain CF-285749	MG065798.1	1253224937
47	CPI-9	*Penicillium chrysogenum* strain FH10	EU409812.1	166203656
48	CPI-12	*P. chrysogenum* strain HGQ6	JF834167.1	334854872
49	CPI-3	*P. chrysogenum* strain HGQ6	JF834167.1	334854872
50	CPI-15	*P. chrysogenum* strain QRF370	KP278201.1	817011885
51	CPI-3	*P. dipodomyicola* strain IIF7SW-F4	KY218703.1	1104561771
52	CPI-12	*P. griseofulvum* strain L1	MF034654.1	1189013873
53	CPI-8	*P. roseopurpureum* isolate 6	MH481292.1	1402357422
54	CPI-14	*P. rubens* strain XQ3	KU216705.1	1004525512
55	CPI-15	*P. rubens* strain XQ3	KU216705.1	1004525512
56	CPI-9	*P. rubens* strain XQ3	KU216705.1	1004525512
57	CPI-9	*P. viridicatum*	HG326300.1	530445851
58	CPI-23	*Pleospora herbarum* strain MFLUCC 14-0920	KY659560.1	1213948660
59	CPI-18	*Rhizoctonia bataticola* clone RB50	HQ392798.1	311062962
60	CPI-6	*R. bataticola* isolate VRF 25/07	EF446282.1	133711976
61	CPI-8	*Sordariomycetes* sp. TC204	JX174135.1	403314319
62	CPI-23	*Stemphylium lycii* CBS 125241	NR_154932.1	1360449954
63	CPI-23	*S. solani* strain FE30	KU743971.1	1060717068
64	CPI-23	*Stemphylium* sp. isolate CCTU1067	KY077541.1	1173132660
65	CPI-33	*Trichoderma virens*	AF099007.1	4323321

Note: Gen Bank Accession and GI were obtained from NCBI BLASTn database

Molecular characterization. The isolates associated with gram pod borer affected seeds, seed shell, and its different life stages (larva and adult) were isolated and initially identified based on morphological characteristics. However, the specific genera and species of all isolates were confirmed through molecular characterization using ITS region of rDNA of fungi. The sequences of all strains except *Curvularia lunata* and *Drechslera* sp. were blasted in NCBI BLASTn data based and Gen Bank Accession number and Gen Bank GI were obtained (Table 2).

Sequence alignment and Phylogenetic analysis. The phylogenetic analyses of different isolates were conducted based on internal transcribed spacer (ITS) regions. In present study, we determined the morphological taxonomy of twenty four (24) fungal isolates, and the domain consisting of protein sequences obtained from various sources are aligned by using redundant entries. A combined rooted neighbor-joining (NJ) tree (1000 replicates) was generated through MEGA 4.5 by following the default parameters; poisson correction, pairwise deletion, and bootstrap. Conserved motifs protein sequences of all sorted member were identified using a motif based sequence analysis tool. The BLAST search for the resulting motifs in NCBI and MS-Homology databases was carried out to determine their significance. In order to understand the putative role of fungal isolates, we analyzed the deduced amino acid sequence by BLASTn and searched in NCBI database indicated as inquiry aligned with isolated strains. Comparison of the amino acid sequence and phylogenetic analysis of isolates was also performed which revealed that sequences belong to different groups/species.

A total of sixty five fungal isolates belonging to seventeen genera were classified into six different group species, the most common of which were *Alternaria, Aspergillus* and *Penicillium.* Isolates were identified to species level based on similarities with known sequences in NCBI (GenBank) database and a large proportion of the fungi were belonging to *Alternaria* (98%) followed *Aspergillus* (75-81%) and *Penicillium* (80%) species.

Frequency percent of fungi. The results pertaining to the frequency percent of fungi associated with gram pod affected seeds and seed shells, larva and adults moth of *H. armigera* revealed the significant difference among each other.

Frequency percent of fungi from Seeds. Significantly highest frequency percent was recorded for *A.alternata* (64.20%) followed by *Chaetomium* sp. (38.20%), *L. theobromae* (20.30%), *A. tenuissima* (36.70%), *C. lunata* (32.70%), *Drechslera* sp. (31.70%) and *L. theobroae* (31.20%) when isolated through agar plate method. The frequency of other fungi associated with seed was lower that ranged from (3.0 to 30.70%) (Figure 9). The association of these fungi further revealed that older seeds had higher frequency compared to fresh seeds. On overall basis all fungal strains significantly produced higher frequency in the seeds of 2015 compared to 2016 when isolation mad through agar plate method (Figure 9). Moreover, when isolation of fungi was made through blotter paper method had lower frequency compared to agar plate method. Significantly higher frequency was recorded for *A. alternata* (19.40%) followed by *A. niger* (11.40%), *L.theobromae* (9.40%) and *F.oxysporum* (6.90%). However, the frequency of other fungi was ranged from 0.3 to 5.50% (Figure 9). Similar to agar plate method, the association of these fungi further revealed that older seeds had higher frequency compared to fresh seeds. On overall basis all fungal strains significantly produced higher frequency in the seeds of 2015 compared to 2016 when isolation mad through blotter paper method (Figure 9).

It is also obvious from the results that obtained through combined analysis of agar plate and blotter methods; the overall frequency of fungi in blotter paper method was much lower than agar plate method. All the fungi significantly produced higher frequency on agar plate method (Figure 9).

Frequency percent of fungi from Seed shell. In case of seed shell a total of seven twenty different fungal strains (*A. alternata, A. flavus, A. fumigatus, A. niger, C. lunata, Penicillium* sp., and *R. stolonifer*) were identified. Significantly highest frequency percent was recorded for *A. niger* (55.90%) followed by *A. flavus* (52.80%) and *A. alternata* (35.90%) from seed shells of 2015 and 2016 when isolated through agar plate method. The frequency of other fungi associated with seed shell was lower that ranged from 0.30 to 21.4% (Figure 10). The association of these fungi further revealed that older seed shells had higher frequency compared to fresh seed shell. On overall basis all fungal strains significantly produced higher frequency in the seed shell of 2015 compared to 2016 when isolation made through agar plate method (Figure 10).

Moreover, when isolation of fungi from seed shell was made through blotter paper method had lower frequency compared to agar plate method. Significantly higher frequency was recorded for *A. niger* (30.70%) followed by *A. alternata* (21.90%) and *A. flavus* (11.90%). However, the frequency of other fungi was ranged from 0.40 to 4.70% (Figure 10). Similar to agar plate method, the association of these fungi further revealed that older seed shell had higher frequency compared to fresh seeds. On overall basis all fungal strains significantly produced higher frequency in the seed shells of 2015 compared to 2016 when isolation made through blotter paper method (Figure 10).

It is also obvious from the results that obtained through combined analysis of agar plate and blotter methods; the overall frequency of fungi from seed shell isolated through blotter paper method was much lower than agar plate method. All the fungi significantly produced higher frequency on agar plate method (Figure 10).

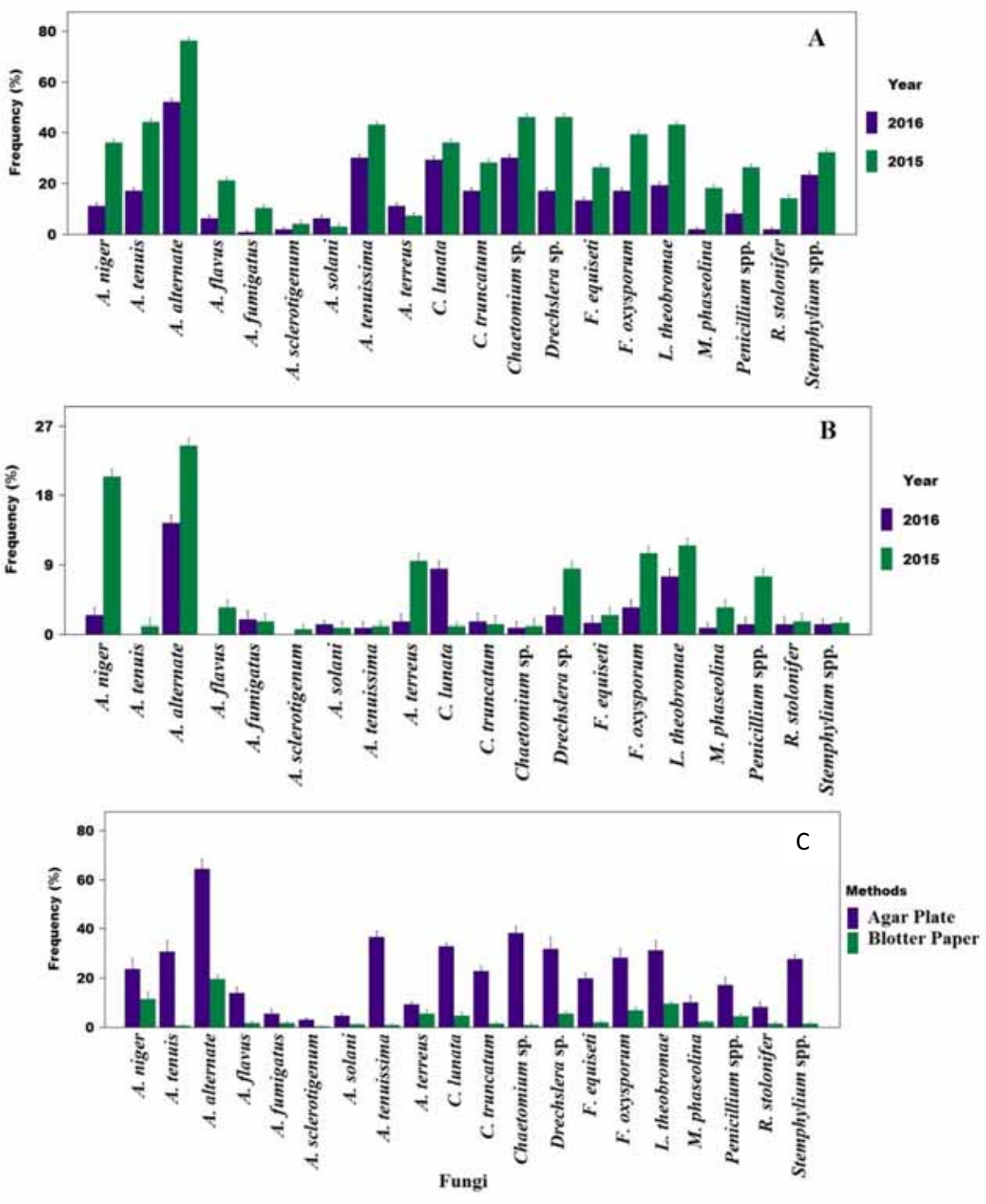

	A. Agar Plate Method	B. Blotter Paper Methods	C. Combined
SE =	0.6997	1.1381	0.7931
LSD =	1.3821	2.2481	1.5603

FIGURE 9

Frequency percent of different fungal strains isolated from gram pod borer affected seeds chickpea.

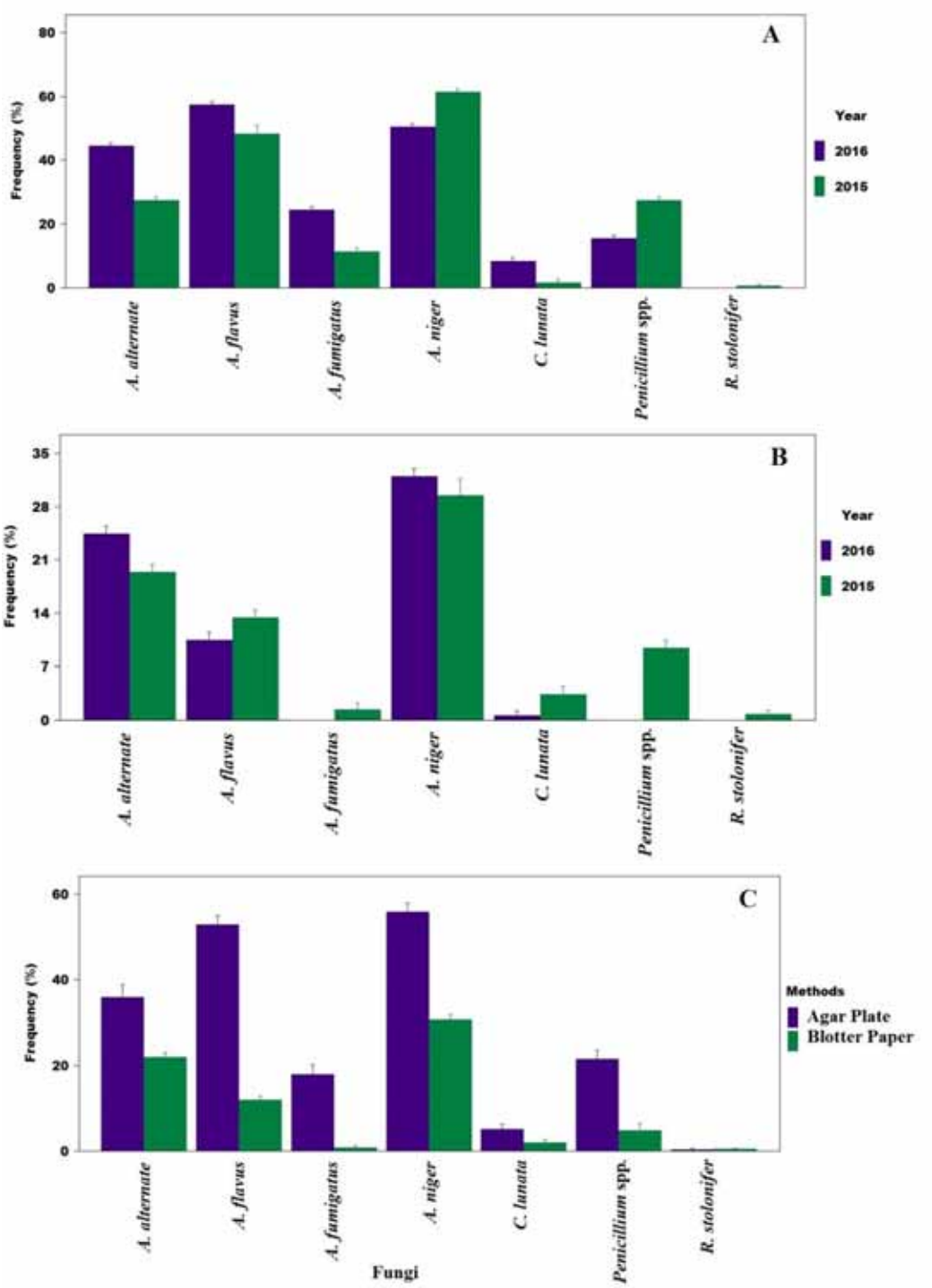

A. Agar Plate Method		B. Blotter Paper Methods	C. Combined
SE	= 0.9004	1.1900	0.7931
LSD	= 1.8068	2.3879	1.5603

FIGURE 10

Frequency percent of different fungal strains isolated from gram pod borer affected seed shells of chickpea.

Frequency percent of fungi from different life stages. There were nine different fungal strains found associated with field live collected larva (surface sterilized and un-sterilized). The fungal strains associated with live larva were *A. alternate, A. solani, A. flavus, A. niger, Chaetomium* sp., *C. lunata, Drechslera* sp., *Fusarium* sp., and *Penicillium* sp. There was significant different among the all isolated fungi for frequency percent. Significantly higher frequency was recorded for *A. flavus* (20.40%) followed by *A. niger* (9.40%), *A. alternata* (8.40) and *Penicillium* sp. (7.40%) from

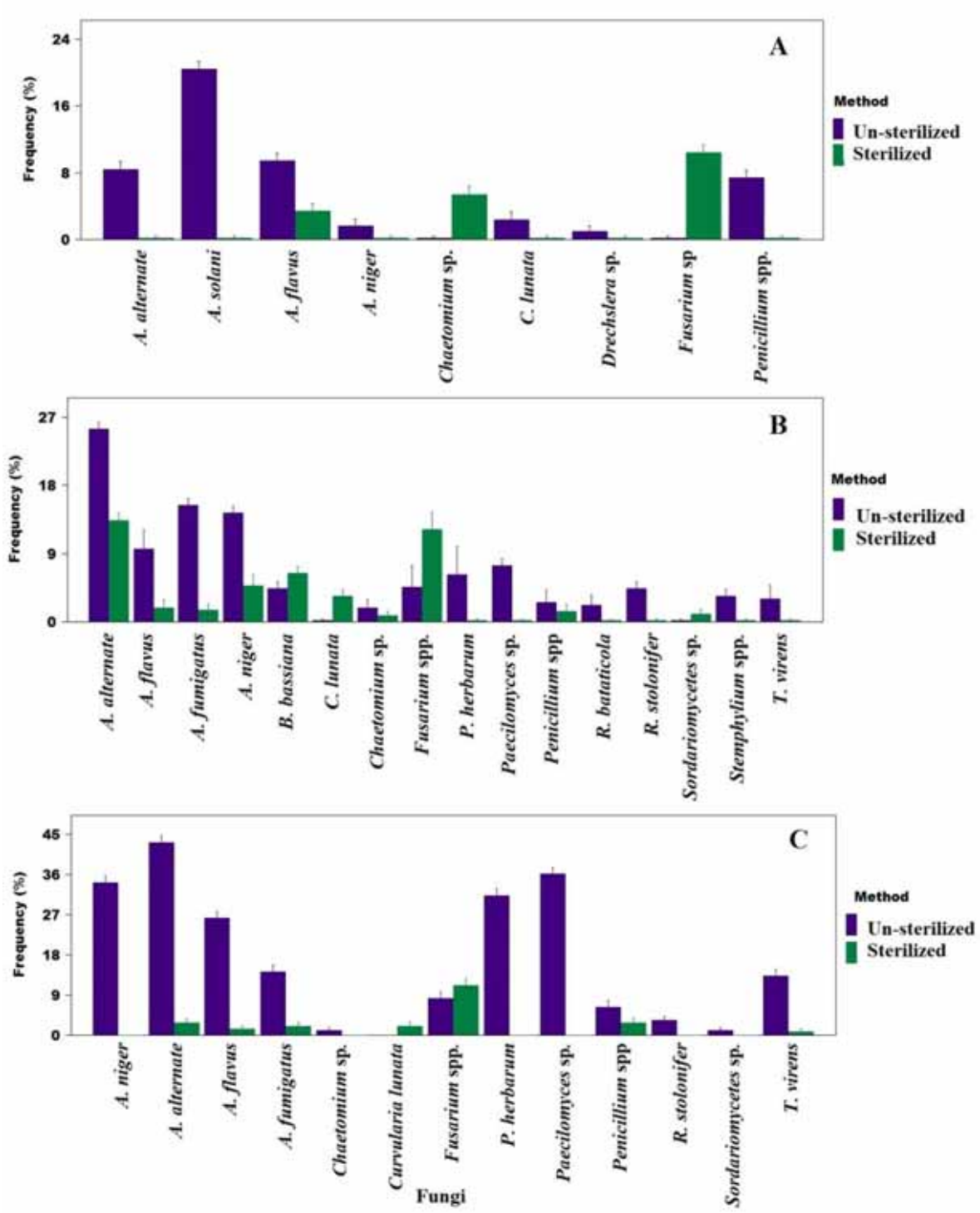

	A. Live Collected Larvae	B. Dead Collected Larvae	C. Adult Moth
SE =	0.5614	2.0731	1.0321
LSD =	1.1202	4.1032	2.0477

FIGURE 11

Frequency percent of different fungal strains isolated from different life stages of gram pod borer collected from chickpea field.

un-treated larvae. Whereas, from treated larvae *Fusarium* sp. (10.40%) followed *C. lunata* (5.40%). The frequency of other fungi associated with live larva was lower that ranged from 0.20 to 3.40% (Figure 11).

Moreover, there were sixteen different fungal strains found associated with field dead collected larva (surface sterilized and un-sterilized). The fungal strains associated with dead larva were *A. alternata, A. flavus, A. fumigates, A. niger, Beauveria bassiana, Chaetomium* sp., *C. lunata, Fusarium* sp.,

Paecilomyces sp., *Penicillium* sp., *Pleospora herbarum, Rhizoctonia bataticola, R. stolonifer, Sordariomycetes* sp., *Stemphylium* sp., and *Trichoderma virens.* There was significant different among the all isolated fungi for frequency percent. Significantly higher frequency was recorded for *A. alterna* (25.40%) followed by *A. fumigatus* (15.40%), *A. niger* (14.40%), *A. flavus* (9.60%), and *Paecilomycetes* (7.40%) and *P. herbarum* (6.20%) from un-treated dead larvae. Whereas, from treated dead larvae *A. alterna* (13.40%) followed by *Fusarium* sp. (12.20%) and *B. bassiana* (6.40%) were isolated with higher frequency. The frequency of other fungi associated with dead larva was lower that ranged from 0.20 to 4.80% (Figure 11).

There were thirteen different fungal strains found associated with adult moth (surface sterilized and un-sterilized). The fungal strains associated with adult moth were *A. alternate, A. flavus, A. fumigates, A. niger, Chaetomium* sp., *C. lunata, Fusarium* sp*., Paecilomyces* sp., *Penicillium* sp., *Pleospora herbarum, R. stolonifer* and *Sordariomycetes* sp. There was significant different among the all isolated fungi for frequency percent. Significantly higher frequency was recorded for *A. alternata* (43.20%) followed by *Paecilomycete* (36.20%), *A. niger* (34.20%), *P. herbarum* (31.20%), *A. flavus* (26.20%), *A. fumigatus* (14.20%) and *T. virens* (13.20) from un-treated adult moth. Whereas, the frequency of other fungi associated with adult moth was lower that ranged from 0 to 11.50% (Figure 11).

DISCUSSION

Association of fungi with gram pods borer. There are several pathogenic diseases have been reported to cause economic losses in chickpea crop. It was also mentioned in the literature that around 50 pathogens of economic significance are affecting the chickpea plant and causing severe diseases. However, the associations of gram pod borer with Chickpea diseases have not been reported before in the literature. In our study we determined the association of gram pod borer with chickpea disease causing fungi. The results pertaining to gram pod affected seeds and seed shells, larva and adults moth of *H. armigera* revealed the association of several fungal genera in current studies. It was noticed that several pathogenic fungal genera were found associated with seeds, seed shells, larva (live and dead) and moth such as *Alternaria, Aspergillus, Curvularia, Chaetomium, Colletotrichum, Drechslera, Fusarium, Lasiodiplodia, Macrophomina, Paecilomyces, Penicillium, Pleospora, Rhizoctonia, Sordariomycetes* and *Stemphylium.* However, two entomopathogenic fungi such as *Beauveria* and *Trichoderma* were also found associated with field dead moth of *H. armigera*. On overall basis from all specimens of current study, we isolated a total of sixty five different fungal strains belonging to seventeen different genera. All the isolates were initially identified based on morphological characteristics. The specific genera and species of all isolates were then confirmed through molecular characterization using ITS region of rDNA of fungi. The sequences of all strains except *Curvularia lunata* and *Drechslera* sp. were blasted in NCBI BLASTn data based and Gen Bank Accession number and Gen Bank GI were obtained. Isolates were identified to species level based on similarities with known sequences in NCBI (GenBank) database and a large proportion of the fungi were found associated with *Alternaria* followed *Aspergillus* and *Penicillium* species that maybe due to their frequent occurrence and availability in the environment.

The frequency percent of fungi associated with gram pod affected seeds and seed shells, larva and adults moth of *H. armigera* were also significantly varied. *A. alternata* followed by *Chaetomium* sp., *L. theobromae*, *A. tenuissima*, *C. lunata*, *Drechslera* sp. and *L. theobroae* were remained dominant when isolated through agar plate method. The association of these fungi further revealed that older seeds had higher frequency compared to fresh seeds. It was observed that overall frequency of fungi in blotter paper method was much lower than agar plate method. All the fungi significantly produced higher frequency on agar plate method. In case of seed shell, significantly highest frequency percent was recorded for *A. niger* followed by *A. flavus* and *A. alternata* from seed shells of 2015 and 2016, when isolated through agar plate method. Similar to agar plate method, the association of these fungi further revealed that older seed shell had higher frequency compared to fresh seeds. In the recent past, Shamsi and Khatun [26] found the association of nine species of fungi with seeds of nine varieties of chickpea. The isolated fungi were *Alternaria alternata*, *Aspergillus flavus*, *A. niger, A. fumigatus, A. nidulans, Curvularia lunata, Penicillium* sp., *Rhizopus stolonifer* and *Trichoderma viride*. However, in our study we observed a total of twenty different fungal strains from the seeds and seven from seed shells of 2015 and 2016 chickpeas crop. Shamsi and Khatun [26] further revealed that the fungal association varied with duration of storage period. Species of *Aspergillus, Penicillium* and *Rhizopus* become predominating fungi with increase of the storage period. In our study we also found that older seeds had higher frequency compared to fresh seeds.

Moreover, no any literature available with regards to the association of fungal strains with different life stages of gram pod borer. In our study, we inoculated field collected live and dead larvae and adult moths in order to determine the associa-

tion of different diseases fungal causing strains that might the serving as vector from one plant to another plants or may also help in providing the primary infection site to those fungal strains cause complex disease problem in chickpea crops. In our study *A. flavus* followed by *A. niger*, *A. alternata* and *Penicillium* sp. produced significantly higher frequency when isolated from un-treated larvae. Whereas, from treated larvae *Fusarium* sp. followed *C. lunata*. The frequency of other fungi associated with live larva was lower. The fungal strains associated with dead larva revealed significantly higher frequency for *A. alterna* followed by *A. fumigatus*, *A. niger*, *A. flavus*, and *Paecilomycetes* and *P. herbarum* from un-treated dead larvae. Whereas, from treated dead larvae *A. alterna* followed by *Fusarium* sp. and *B. bassiana* were isolated with higher frequency. The fungal strains associated with adult moth produced significantly higher frequency for *A. alternata* followed by *Paecilomycete*, *A. niger*, *P. herbarum*, *A. flavus*, *A. fumigatus* and *T. virens* from un-treated adult moth. In the literature, it has been reported that around 50 pathogens of economic significance affects the chickpea plant. Among them most important include: wilt (*Fusanum oxysporum* Schlecht emend.), several root and stem rots (*Rhizoctonia bataticola* Taub.; *Fusarium solani* Mart.; *Operculella padwickii* Kheswalla, *Sclerotinia sclerotiorum* Lib.) blights (*Ascochyta rabiei* Pass.; Labrousse; *Stemphylium sarciniforme* Cav.) grey mold *(Botrytis cineria* Pers. ex Fr.), rust *(Uromyces ciceris-arietini* Grogn.), and viral diseases such as stunt caused by pea leaf roll virus. However, the associations of gram pod borer with chickpea disease causing fungi have not been reported before in the literature. It has also been mentioned by Datta and Lal [14] that pathogens in chickpeas are the main cause for yield loss (up to 90%) particularly fungus *Fusarium oxysporum f.sp. ciceris* which often found in pulse crops. In our study, we found the association of *Fusarium oxysporum* with gram pod borer affected seed, and different other *Fusarium* spp with seed, seed shell, live and dead larvae, and adult moth of gram pod borer. *Rhizoctonia bataticola* and *C. lunata* were isolated from dead larva and moth, respectively; while *Lasiodiplodia theobromae* isolated from gram pod borer affected seeds. However, *Alternaria alternate* and other species of *Alternaria* genus, they may cause several foliar, fruit and root diseases, have also been isolated from all samples (seeds, seed shell, larva and adult) used in current study. These results indicate the relationship of these pathogens with chickpea disease and gram pod borer. The influence of gram pod borer in dissemination and/or providing possible entry to these pathogenic fungi for complex disease development cannot be ignored.

REFERENCES

[1] Joshi, P.K., Parthasarathym Rao, P., Gowda, C.L.L., Jones, R.B., Silim, S.N., Saxena, K.B. and Kumar, J. (2001) The world chickpea and pigeon pea Economies: Facts, Trends, and Outlook. Patancheru 502 324, Andhra Pardesh, India: International Crops Research Institute for the Semi-Arid Tropics. ISBN 92- 9066-443-6. Order code BOE 030. 68p.

[2] FAO (2015) FAOSTAT. Food and Agriculture Organization of the United Nations. Rome: Available online at: http://faostat.fao.org

[3] Saxena, M.P., Goldworthy, R. and Righer, N. M. (2001) Chickpea. The Physiology of Tropical Field Crops. John Willey and Sons. 419-452.

[4] Varshney, R.K., Song, C., Saxena, R.K., Azam, S., Yu, S., Sharpe, A.G. Cannon, S., Baek, J., Rosen, B.D., Tar'an, B., Millan, T., Zhang, X., Ramsay, L.D., Iwata, A., Wang, Y., Nelson, W., Farmer, A.D., Gaur, P.M., Soderlund, C., Penmetsa, R.V., Xu, C., Bharti, A.K., He, W., Winter, P., Zhao, S., Hane, J.K., Carrasquilla-Garcia, N., Condie, J.A., Upadhyaya, H.D., Luo, M.C., Thudi, M., Gowda, C.L., Singh, N.P., Lichtenzveig, J., Gali, K.K., Rubio, J., Nadarajan, N., Dolezel, J., Bansal, K.C., Xu, X., Edwards, D., Zhang, G., Kahl, G., Gil, J., Singh, K.B., Datta, S.K., Jackson, S.A., Wang, J. and Cook, D.R. (2013) Draft genome sequence of chickpea (*Cicer arietinum*) provides a resource for trait improvement. Nature Biotechnol. 31, 240-248.

[5] ARS (2014) *Cicer arietinum,* Germplasm Resources Information Network (GRIN). Agricultural Research Service (ARS), United States Department of Agriculture (USDA).

[6] ICARDA (2019) Chickpea. The International Center for Agricultural Research in the Dry Areas (ICARDA). Source: https://www.icarda.org/crop/chickpeas, Accessed on: 10-01-2019.

[7] FAO (2018) FAOSTAT. Food and Agriculture Organization of the United Nations. Rome: Available online at: http://faostat.fao.org

[8] Hussain, N., Aslam, M., Ghaffar, A., Irshad, M. and Naeem-ud-Din. (2015) Chickpea genotypes evaluation for morpho-yield traits under water stress conditions. The Journal of Animal and Plant Sciences. 25(1), 206-211.

[9] Shuro, A.R. (2017) Quality traits, measurements and possible breeding methods to improve the quality traits of Kabuli type chickpea (*Cicer arietinum* L.). International Journal of Agricultural Research and Review. 5(4), 628-635.

[10] Fichetti, P., Avalos, S., Mazzuferi, V., Carreras, C. (2009) Lepidoptera associated with the cultivation of chickpea (*Cicer arietinum* L.) in Córdoba, Argentina. Bol Sanid Veget "Plagues". 35, 49-58. (in Spanish).
[11] Avalos, S., Mazzuferi, V., Fichetti, P., Berta, C., Carreras, J. (2010) Entomofauna associated with chickpea in the northwest of Córdoba (Argentina). Hortic Argent. 29, 5-11 (in Spanish).
[12] Ahmed, K. and Awan, M.S. (2013) Integrated management of insect pests of chickpea *Cicer arietinum* (L. Walp.) in south Asian countries: Present status and future strategies- A Review. Pakistan Journal of Zoology. 45(4), 1125-1145.
[13] Sharma, H., Shukla, A., Bhowmick A.K. and Sharma, A.K. (2018) Evaluation of chickpea (*Cicer arietinum* L.) genotypes against gram pod borer (*Helicoverpa armigera*, Hubner) under field conditions. Journal of Entomology and Zoology Studies. 6(5), 597-602.
[14] Datta, J. and Lal, N. (2012) Genetic diversity of Fusarium wilt races of Pigeonpea in major regions of India. African Crop Science Journal. 21(3), 201-211.
[15] Jendoubi, W., Bouhadidam, M., Boukteb, A., Béji, M. and Kharrat, M. (2017) Fusarium Wilt Affecting Chickpea Crop. Agriculture. 7(3), 23.
[16] Iruela, M., Castro, P., Rubio, J., Cubero, J.I., Jacinto, C., Millán, T. and Gil, J. (2007) Validation of a QTL for resistance to Ascochyta blight linked to resistance to Fusarium wilt race 5 in chickpea (*Cicer arietinum* L.). Eur. J. Plant Pathol. 119, 29–37.
[17] Mulwa, R.M.S., Kimurto, P.K. and Towett, B.K. (2010) Evaluation and selection of drought and pod borer (*Helicoverpa armigera*) tolerant chickpea genotypes for introduction in semi-arid areas of Kenya. Second RUFORUM Biennial Meeting 20 - 24 September 2010, Entebbe, Uganda.
[18] Baite, M.S. and Dubey, S.C. (2018) Pathogenic variability of *Ascochyta rabiei* causing blight of chickpea in India. Physiological and Molecular Plant Pathology. 102, 122-127.
[19] ISTA (2015) International Rules for Seed Testing 2015. International Seed Testing Association, Bassersdorf, Switzerland.
[20] Barnett, H.L. and Hunter B. (1972) Illustrated genra of imperfect fungi. Burgress publishing company Minneapolis.
[21] Burgess, L.W., Nelson, P.E., Tousson T.A. and Marasas, W.F.O. (1985) *Fusarium scirpi*: amended description and notes on geographic distribution. Mycologia. 77, 212-218.
[22] Booth, C. and Sutton, B. C. (1984) *Fusarium pallidoroseum*, the correct name for *F. semitectum*. Transactions of British Mycological Society. 23(4), 702-704.
[23] Brayford, D. (1993) The identification of *Fusarium* species. International Mycological Institute, Kew, Surrey, England, 27p.
[24] Nelson, P.E., Toussoun T.A. and Marasas, W.F.O. (1983) *Fusarium* species. An illustrated manual of identification. The State Univ. Press, University Park, Pennsylvania.
[25] Analytical Software (2005) Statistix 8.1 user's manual. Tallahassee, FL.
[26] Shamsi, S. and Khatun, A. (2016) Prevalence of fungi in different varieties of chickpea (*Cicer arietinum* L.) seeds in storage. J. Bangladesh Acad. Sci. 40(1), 37-44.

Received: **16.01.2019**
Accepted: **18.03.2019**

CORRESPONDING AUTHOR

M Ibrahim Khaskheli
Department of Plant Protection,
Sindh Agriculture University,
Tando Jam – Pakistan

e-mail: mikhaskheli@sau.edu.pk

© by PSP Volume 28 – No. 5/2019 pages 4072-4079 Fresenius Environmental Bulletin

COMPARATIVE ANATOMICAL STUDIES ON SOME SPECIES OF *CARTHAMUS* L. IN TURKEY

Canan Yagci-Tuzun[1], Burcu Tarikahya Hacioglu[2], Ali Savas Bulbul[3,*], Yusuf Arslan[4], Ilhan Subasi[5]

[1]Ministry of Agriculture and Forestry, Mediterranean Fisheries Research, Production and Training Institute, Yeşilbayır Mahallesi Akdeniz Bulvarı, No:2, 07190, Döşemealtı, Antalya, Turkey
[2]Hacettepe University, Faculty of Science, Department of Biology, 06800 Beytepe Campus, Ankara, Turkey
[3]Kahramanmaraş Sütçü İmam University, Faculty of Arts and Sciences, Department of Biology, Kahramanmaraş, Turkey
[4]Bolu Abant Izzet Baysal University, Faculty of Agricultural and Natural Science, Department of Field Crops, Bolu, Turkey
[5]Ministry of Agriculture and Forestry, Central Research Institute for Field Crops, Ankara, Turkey

ABSTRACT

Carthamus L. (Asteraceae) has been used in many secto rssuch as food, dye, cosmetic, biofuel industry and also used to cure many disease in traditional medicine. Within this study, it was aimed to present detailed anatomical characterization of five wild species of *Carthamus* grown in Anatolia, namely, *C.dentatus* Vahl., *C.glaucus* Bieb., *C.lanatus* L., *C.persicus* Willd. and *C.tenuis* (Boisand Balansa) Bornm. And to contribute to botanical and agricultural studies. Free-hand sections were taken from root, stem and leaf of each taxa. Sections were examined with light microscope and photographed by digital camera. Various measurements were taken on microscopic images. Variations on collenchyma to us cells in cortex, arrangements of scelerenchyma to us cells in vascular bundles, type of vascular bundles and state of the piths in stem; cuticular ornamentation, leaf types based on their adaxial-abaxial and crystal lines tructures in leaves were observed. Furthermore, an identification key was given based on anatomical features. Although anatomical features were generally similar, some of the characters varied among the species. According to the anatomical properties, *C. persicus* and *C. glaucus* were closely related to *C. dentatus* and *C.tenuis*, respectively, whereas *C. lanatus* was quite different from the others.

KEYWORDS:
Anatomy, *Carthamus*, Asteraceae, identification key, industrial crop, oil-bearing crop.

INTRODUCTION

Asteraceae is a very large cosmopolitan family, which is highly advanced and well recognized with worldwide distribution [1]. Asteraceae contains more than 1500 genera and 22,000 species ranging from annual herbs to woody shrubs [2]. *Carthamus* L. is an annual plant that is a member of the family Asteraceae (Compositae), tribe Cardueae (thistles) and subtribe Centaureinae [3]. Turkey is among rich countries in flora because is located in the intersection of Irano-Turanian, Mediterranean and Euro-Siberian floristic regions. Asteraceae is represented by 140 genera and 1,186 species in the Flora of Turkey and the East Aegean Islands [4], [5]. The *Carthamus* L. species have the following species in the Anatolian flora; *C.lanatus* L., *C. dentatus* Vahl., *C. persicus* Willd (syn. *C. flavescens* Spreng), *C. glaucus* Bieb. subsp. *glaucus*, *C. tenuis* (Bois and Balansa) Bornm. *tenuis* and *C. tenuis* (Bois and Balansa) Bornm. subsp. *gracillimus* [4] There are several studies performed with *Carthamus* species of Turkey by our working group; consisting molecular phylogeny [6], [7], micromorphology [8], [9] and seed fatty acid compositions [10].

The genus *Carthamus*, especially *C. tinctorius,* has been cultivated for centuries to obtain linoleic acid-rich edible oil. These species have been also used as colorant in food, clothes, dyes and cosmetic preparations. *C. tinctorius* has been used as colorant, additive as well as used both traditionally and modern medicines to treatment of cough, fever, throat and rheumatic problems, neural and cardiovascular disorders thanks to its bioactive compounds [11], [12], [13] *Carthamus lanatus* has anti-inflammatory and analgesic [14], [15]; sedative, antitumor and interferon-inducing [16], antibacterial [17], [18], [19]; clastogenic effect [20], antioxidant and cytotoxic activity [21], [22]. Isolated fucopyranosides from *C. glaucus* showsan anti inflammatory effect [23].

Nowadays, the genus *Carthamus* have an increasing interest owing to breeding studiesamong wild types and other varieties that have in good quality that have been conducted in order to increase oil yield. It is obviously known that comprehensive identification of the material is crucial to get success in breeding studies as well as contribute taxonomy. There are various anatomical studies on the genus especially *C. tinctorius* such as achene [24]; stem, anther and achene (in normal and mutant varieties) [25]; stem, leaf and root (combining with stress conditions) [26]; leaf and stem anatomy

[27], [28]. However, there is no detailed study about anatomy of wild species of *Carthamus*. It was aimed that present comparative anatomical features of root, stem and leaf of five species of *Carthamus* L., namely *C. dentatus* Vahl., *C. glaucus* Bieb., *C. lanatus* L., *C. persicus* Willd (syn. *C. flavescens* Spreng) and *C. tenuis* (Bois and Balansa) Bornm. grown in Turkey and establish the taxonomic relationships among taxa within this study.

MATERIALS AND METHODS

The material of this study consisted of 5 species of *Carthamus*, namely *Carthamus dentatus*, *C. glaucus, C. lanatus, C. persicus*, and *C. tenuis*. The collection sites were given in Table 1. Plant materials collected from their habitats and immediately put into 70% ethyl alcohol for fixation and kept until the anatomical studies started. Free-hand sections were taken from root, stem and leaf of each taxa. Safranin O (Sigma-Aldrich S2255) and Toluidine Blue O (Sigma-Aldrich T3260) were used to distinguish tissues and cells [29], [30], [31], [32]. Sections were examined with Leica DM 1000 light microscope and photographed by Leica DFC 295 digital camera. Leica Application Suite (LASv4.2) with measurement module was used to analyse microscopic images.

TABLE 1
The collection sites of the material

Species	City	Locality	Altitude (m)	Voucher number
Carthamus dentatus	Antalya	Serik, Yukarıkocayatak	14	B.Tarıkahya 2692 & Y.Arslan
Carthamus glaucus	Hatay	Erzin-Gökdere road	165	B.Tarıkahya 2662 & Y.Arslan
Carthamus lanatus	Ankara	Kalecik, Çandır	940	B.Tarıkahya 2729 & Y.Arslan, İ.Subaşı
Carthamus persicus	Ankara	İkizce village	1067	B.Tarıkahya 2767 & Y.Arslan
Carthamus tenuis	Mersin	Erdemli, 37 km to Silivri	32	B.Tarıkahya 2660 & Y.Arslan

TABLE 2
Summary of anatomical features of *Carthamus* species

	C. dentatus	*C. glaucus*	*C. lanatus*	*C. persicus*	*C. tenuis*
ROOT					
Secondary growth	+	+	+	+	+
Adventitious root	-	-	-	-	-
Epidermis	Partially crushed	Partially crushed	Partially crushed	Partially crushed	Completely crushed
Periderm	+	+ (in some plants periderm is inchoate)	+ (in some plants periderm is inchoate)	+	+
Resin ducts	+	+	+	+	+
Pith filled with	Xylem	Xylem	Xylem	Xylem	Xylem
STEM					
Trichomes	Multicellular non-glandular-unbranched and multicellular glandular	Multicellular non-glandular-unbranched and multicellular glandular	Multicellular non-glandular-unbranched and multicellular glandular	Multicellular non-glandular-unbranched and multicellular glandular	Multicellular non-glandular-unbranched and multicellular glandular
Epidermal structure	Papillae	Papillae	Papillae	Papillae	Papillae
Epidermis	Uniseriate	Uniseriate	Uniseriate	Uniseriate	Uniseriate
Collenchymatous cells	-	-	-	Angular	-
Resin ducts	+	+	+	+	+
Arrangements of sclerenchymatous cells in vascular bundles	Like a ring	Bunch	Bunch	A few cells	Bunch
Type of vascular bundles	Bicollateral	Collateral	Collateral	Bicollateral	Collateral
Pith	Filled with parenchymatous tissue	Rounded hollow	Filled with parenchymatous tissue	Filled with parenchymatous tissue	Filled with parenchymatous tissue
LEAF					
Cuticular ornamentation	Fingerprint-like	Fingerprint-like	Fingerprint-like	No ornamentation	Fingerprint-like
Epidermal cells (in surface sections)	Wavy anticlinal walls	Wavy anticlinal walls	Wavy anticlinal walls	Wavy anticlinal walls	Wavy anticlinal walls
Leaf types based on their adaxial-abaxial structure	Unifacial	Unifacial	Bifacial	Unifacial	Unifacial
Stomata	Amphistomatic	Amphistomatic	Amphistomatic	Amphistomatic	Amphistomatic
Stomata type based on subsidiary cells	Anomocytic (Ranunculaceae)	Anomocytic (Ranunculaceae)	Anomocytic (Ranunculaceae)	Anomocytic (Ranunculaceae)	Anomocytic (Ranunculaceae)
Number of subsidiary cells	3-4 cells	3-4 cells	3-4 cells	3-4 cells	3-4 cells
Trichomes in both adaxial and abaxial surface	Multicellular non-glandular-unbranched and multicellular glandular	Multicellular non-glandular-unbranched and multicellular glandular	Multicellular non-glandular-unbranched and multicellular glandular	Multicellular non-glandular-unbranched and multicellular glandular	Multicellular non-glandular-unbranched and multicellular glandular
Crystalline structure	Styloids	-	-	-	-
Resin ducts	+	+	+	+	+

RESULTS

Root. Adventitous root formation was not observed. Most part of epidermis was crushed and had single-layered cells in *C. dentatus*, *C. glaucus*, *C. lanatus* and *C. persicus* (Fig 1. A, B, C, D, respectively) whereas epidermis was completely crushed in *C. tenuis* (Fig 1. E). Periderm consisted of multi-layered cells. It was observed in some sections that periderm formation was inchoate in *C. glaucus* and *C. lanatus*. Cortex consisted of multi-layered cells. It was observed in all taxa that 8-9 layer cortex cells which were between epidermis and 5-7 layered cells closer to vascular cylinder were crushed. 10-12 layered cortex cells which states upper part of phloem towards to periderm were lignified in *C. tenuis* (Fig 1. E). There were many orderly arranged resin ducts and sclerenchyma bundles in cortex. Endodermis was not well defined. Phloem and xylem components were clearly observed in vascular cylinder. Vascular cambium consisted of single layer cells. There were 1-3 layered ray cells in xylem. Xylem components presented in pith. The root characteristics of the species and measurements were given briefly in Table 2 and 3, respectively.

TABLE 3
Measurements of anatomical features of *Carthamus* species

	C. dentatus	*C. glaucus*	*C. lanatus*	*C. persicus*	*C. tenuis*
ROOT					
Cuticle Thickness (µm)	10.80 ± 1.539	6.31 ± 2.310	5.20 ± 0.959	4.70 ± 0.703	-
Width of epidermal cells (µm)[a]	44.22 ± 7.426	54.55 ± 7.895	22.61 ± 6.169	54.93 ± 13.306	-
Length of epidermal cells (µm)[b]	53.27 ± 8.981	29.47 ± 6.212	20.84 ± 3.249	17.09 ± 5.648	-
STEM					
Cuticle Thickness (µm)	6.27 ± 1.16	5.4 ± 1.046	6.57 ± 0835	6.42 ± 0.655	4.07 ± 0.518
Width of epidermal cells (µm)[a]	15.53 ± 2.048	17.73 ± 7.124	22.16 ± 5.319	15.42 ± 1.988	22.60 ± 4.233
Length of epidermal cells (µm)[b]	11.28 ± 1.640	13.97 ± 4.990	12.71 ± 3.717	8.11 ± 1.423	9.98 ± 2.017
LEAF					
Abaxial cuticle thickness (µm)	6.18 ± 1.070	6.86 ± 1.575	6.08 ± 0.952	5.69 ± 0.934	5.60 ± 0.800
Width of abaxial (lower) epidermal cells (µm)[a]	14.92 ± 4.578	21.85 ± 5.518	23.60 ± 10.479	19.59 ± 6.509	16.88 ± 6.392
Length of abaxial epidermal cells (µm)[a]	9.30 ± 1.838	12.19 ± 2.865	16.95 ± 5.120	10.36 ± 2.774	11.46 ± 2.595
Stomatal density of abaxial surface (mm^2)	243.36 ± 45.39	312.64 ± 54.83	129.88 ± 11.82	335.59 ± 35.55	300.60 ± 57.37
Adaxial cuticle thickness (µm)	7.86 ± 1.868	7.28 ± 0.951	5.44 ± 0.745	6.51 ± 1.081	5.74 ± 0.880
Width of adaxial (upper) epidermal cells (µm)[a]	18.75 ± 6.454	19.72 ± 5.670	33.93 ± 13.642	20.24 ± 8.955	23.05 ± 6.727
Length of adaxial epidermal cells (µm)[a]	12.45 ± 2.374	10.49 ± 1.940	15.19 ± 4.447	13.67 ± 3.587	11.97 ± 2.016
Stomatal density of adaxial surface (mm^2)	323.98 ± 37.99	233.43 ± 36.99	129.75 ± 21.16	191.38 ± 36.20	293.96 ± 46.10

[a] Width of two epidermal cells (between periclinal walls)
[b] Length of epidermal cells between cuticle and cortex cells (between anticlinal wall

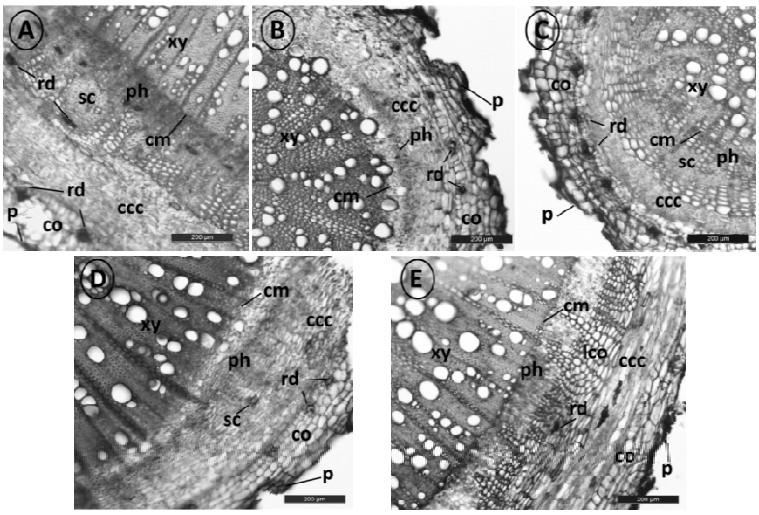

FIGURE 1
Cross sections of root A. *C. dentatus*, B. *C. glaucus*, C. *C. lanatus*, D. *C. persicus*, E. *C. tenuis*. p. Periderm, co. Cortex, rd. Resin duct, ccc. Crushed cortex cells, sc. Sclerenchymatous cells, ph. Phloem, cm. Cambium, xy. Xylem, lco. Lignified cortex cells (bar 200 µm)

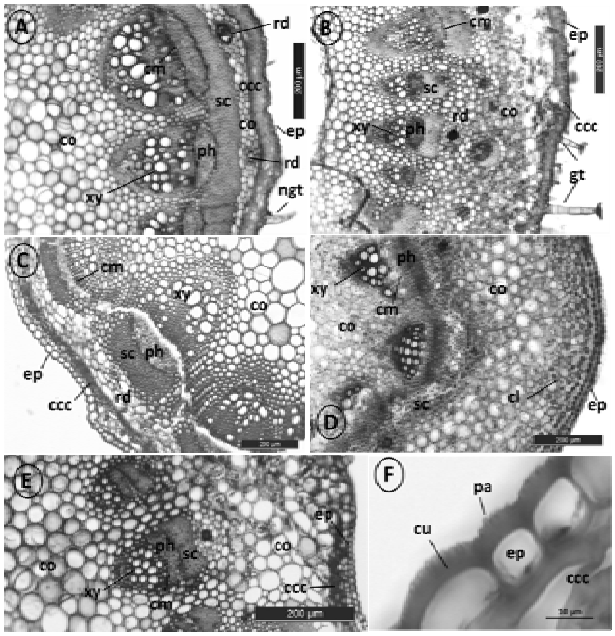

FIGURE 2

Cross sections of stem A. *C. dentatus*, B. *C. glaucus*, C. *C. lanatus*, D. *C. persicus*, E. *C. tenuis*. ep. Epidermis, ngt. Non-glandular trichome, gt. Glandular trichome, co. Cortex, rd. Resin duct, ccc. Crushed cortex cells, sc. Sclerenchymatous cells, ph. Phloem, cm. Cambium, xy. Xylem, lco. Lignified cortex cells, cl. Chlorenchymatous cells, pa. Papillae, cu. Cuticle (bar 200 µm in A-E, 10 µm in F)

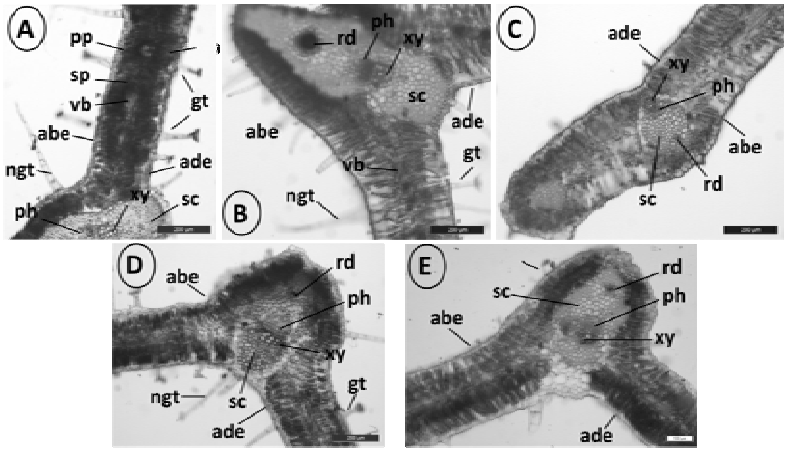

FIGURE 3

Cross sections of leaf A. *C. dentatus*, B. *C. glaucus*, C. *C. lanatus*, D. *C. persicus*, E. *C. tenuis*. abe. Abaxial epidermis, ade. Adaxial epidermis, ngt. Non-glandular trichome, gt. Glandular trichome, sp. Spongy parenchyma, pp. Palisade parenchyma, vb. Vascular bundle, rd. Resin duct,, sc. Sclerenchymatous cells, ph. Phloem, xy. Xylem (bar 200 µm)

Stem. Although multicellular, non-glandular, unbranched and multicellular glandular trichomes were observed in all taxa, *C. glaucus* (Fig 2. B) had more dense trichome. Cuticleswere thick and there were papillae on epicuticular area in all the taxa. Epidermis was uniseriate. Cortex cells which were closer to epidermis were crushed in *C. dentatus, C. glaucus, C. lanatus* and *C. tenuis* (Fig 2. A, B, C, E, respectively) despite *C. persicus* (Fig 2. D) had angular collenchymatous cells instead of crushed cortex cells. Resin ducts presented in cortex. Sclerencyma fibres presented in both phloem and xylem in vascular bundles. These sclerencymatous-cells arranged like a ring between cortex and vascular bundles in *C. dentatus* (Fig 2. A) whereas *C. persicus* (Fig 2. D) had only a few sclerancymatous cells towards to phloem. Vascular bundles were bicollateral typein *C. dentatus* and *C. persicus* (Fig 2. A and D) and collateral type in *C. glaucus*, *C. lanatus* and *C. tenuis* (Fig 2. B, C and E). Cambium consisted of 1-3 layer cells. Rounded hollow pith was observed in *C. glaucus* (Fig 2. B) whereas pith was filled with parencymatous tissue in other taxa. The stem characteristics of the species and measurements were given briefly in Table 2 and 3, respectively.

Leaf. In cross sections of the leaf, it was observed that *C. lanatus* (Fig 3. C) had bifacial (dorsiventral) leaf although all other taxa had unifacial (isobilateral) leaf (Fig 3. A, B, D and E, respectively). All the taxa hadamphistomatic stoma type. Multicellular glandular and multicellular non-glandular unbranched trichomes were presented in both abaxial and adaxial surface. Prismatic crystals observed in *C. dentatus*. Vascular bundles which were main veins were surrounded by sclerencymatous cells. There were resin ducts that were also surrounded by sclerencymatous cells in abaxial side of midrib. Vascular bundles were collateral type.

In surface sections, it was observed that stomata were anomocytic (Ranunculaceae) type for all the taxa. Stomata had 3-4 subsidiary cells. Fingerprint-like ornamentation was observed in cuticular layer of both adaxial and abaxial surfaces in *C. dentatus*, *C. glaucus*, *C. lanatus* and *C. tenuis* (Fig 4. A) except *C. persicus* (Fig 4. B). The leaf characteristics of the species and measurements were given briefly in Table 2 and 3, respectively.

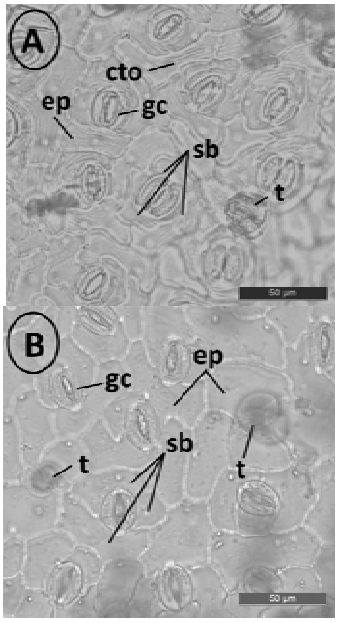

FIGURE 4
Surface sections of leaf A. *C. glaucus*, B. *C. persicus.* ep. Epidermis, cto. Cuticular ornamentation, gc. Guard cell, sb. Subsidiary cells, t. Silhouette of trichome (bar 50 µm)

DISCUSSION

Anatomical characters of stem, root and leaf of the five *Carthamus* species naturally grow in Turkey were investigated in the presented study. According to our results, root anatomy were similar among species. Some other characters revealed differences such as collenchymatous cells in cortex, arrangements of scelerenchymatous cells in vascular bundles, type of vascular bundles and state of the piths in stem; cuticular ornamentation, leaftypes based on their adaxial-abaxial and crystalline structures in leaves. Due to the family has a wide variety of plants, anatomical characters are also various. Recent studies focused on to find out physiological adaptations, for instance reactions of the tissues of stress conditions [26], [27] or mutations [24], using the anatomical investigations on a species and its varieties. However, studies on comparative anatomical investigations among species have limited. Bibi [33] briefly gave morphological and anatomical descriptions of *C. oxycantha* where grown in Karak District in Pakistan. “Anatomy of the Dicotyledones” Metcalfe and Chalk [34], gives general and main information about the family basis on anatomical features.

Metcalfe and Chalk [34] stated that resin ducts (canals) which are common in this family could be observed in the cortex or in the region of endodermis in some genus including *Carthamus*. They also emphasized that resin ducts observed in phloem in the root of *Carthamus*. Both types of resin ducts were observedin the root of all investigated taxa. Bibi [33] indicated that there was ground tissue in the pith of root in *C. oxycantha* which was quite different from our findings (Fig 1, Table 2).

Metcalfe and Chalk [34] noted that 2-4 layers of lignified or suberized cells could be present immediately below the epidermis in the stem. Collenchymatous and/or chlorenchymatous cells could be observed in outer part of cortex. 4-9 layers of crushed and lignified cells were observed in this study. *C. persicus* has angular collenchymatous cells. It was reported that numbers of collateral vascular bundles were present in herbaceous species of Asteraceae. *C. dentatus* and *C. persicus* had bicollateral bundles whereas other taxa had collateral bundles in this study. Some species like *Taraxacum officinale* had hollow scape as *C. glaucus*. It was pointed out in Anatomy of the Dicotyledones [34] there could be medullary vascular bundles as well as cortical bundles in the stem. Only cortical bundles were observed in the stem of all investigated taxa. It was pointed out that there were cuticle layer, epidermis, parenchymatous cortex, endodermis and numerous vascular bundles from outer to inner side of the stem in *C. oxycantha* [33].

Glandular and non-glandular trichomes could be observed in this family. Although there was no information about non-glandular trichomes in *Carthamus*, uniseriate trichomes consist of uniform cells were observed cross sections of stem and leaf of all investigated taxa. Uniseriate multicellular glandular trichomes were observed in this study as in previous studies [28], [34]. There was no information about trichomes in *C. oxycantha* [33].

It was noticed that stomata in Asteraceae were various however mostly Ranunculaceous and mesophyll was very variable [34]. Anomocytic (Ranunculaceous) type stomata presented in this study. *C.*

lanatus had bifacial and all other taxa had unifacial leaf types based on their adaxial-abaxial structure in cross sections. Observing the amphistomatic stomata type in all the taxa was compatible with the results of previous study [28]. It was recorded that crystals in Asteraceae had rare and presented variable form. Raphides, prismatic and styloidic crystals had been reported in some genus [28], [34], [35]. Kartal [35] was aimed to observe crsytalline structure of some taxa from Asteraceae and revealed that both prismatic and styloid crystals were presented in stem, leaf, corolla, anther, filament, style and ovary of *C. dentatus* and *C. lanatus*. Special methods was not used to screen crystals and this might be why we observedstyloids only in the leaf of *C. dentatus* in our study.

It was obviously clear that *C. persicus* and *C. glaucus* were closely related to *C. dentatus* and *C. tenuis*, respectively, whereas *C. lanatus* was quite different from the others. Previous studies on *C. tinctorius*, well known and the most studied species, indicated that varieties could show different anatomical characteristics and reactions against stress such as salinity and Zn [26], [27], [28].

Agricultural studies combining with anatomical, physiological and morphological studies may give better results especially in breeding. Results of this study may be used to contribute for determining the compatibility of the taxa in the agricultural sector, especially in breeding studies as well as to serve the systematic botanical studies. New anatomical-physiological studies should be studied to evaluate of the possible agronomic potential of the wild type of *Carthamus*species in the light of the findings in this study.

Identification Key. According to the anatomical properties, an identification key for the wild *Carthamus* species of Turkey was presented below:

1a.Leafdorsiventral...*C. lanatus*

1b.Leaf isobilateral…..2

2a. Vascular bundles of stem bicollateral.....3

3a. Scelerenchymatous cells in vascular bundles arranged like a ring……*C. persicus*

3b. There are a few scelerenchymatous cells in vascular bundles…….....*C. dentatus*

2b. Vascular bundles of stem collateral……4

4a. Stem pith rounded and hollow….*C. glaucus*

4b. Stem pith filled with parenchymatous tissue……..*C. tenuis*

ACKNOWLEDGEMENTS

This study was financially supported by The General Directorate of Agricultural Research and Policies, Republic of Turkey, Ministry of Agriculture and Forestry with the Project number TAGEM/TA/11/06/01/12.

REFERENCES

[1] Nielsen, M.S. (1965) Introduction to the Flowering plants of West Africa. University of London Press Ltd., London.

[2] Griffee, P. (2001) Ecoport - *Carthamus tinctorius* L., Food and Agricultural Organisation (FAO) of the UN (search entity for *Carthamus tinctorius*). http://ecoport.org/ep?Plant=2514. Accessed 16 July 2018.

[3] Berville, A., Breton, C., Cinliffe, K., Darmency, H., Good, A.G., Gressel, J., Hall, L.M., McPherson, M.A., Medail, F., Pinatel, C., Vaughan, D.A. and Warwick, S.I. (2005) Issues of ferality or potential for ferality in oats, olives, the *Vigna* group, ryegrass species, safflower and sugarcane. In: Gressel, J. (ed.) Crop Ferality and Volunteerism. CRC Press, Boca Raton, Florida, 231-255.

[4] Kupicha, F.K. (1975) *Carthamus*. In: Davis, P.H. (ed.) Flora of Turkey and the East Aegean Islands. vol 5. Edinburgh University Press, Edinburgh, 590-594.

[5] Erik, S., Tarıkahya, B. (2004) About Flora of Turkey. Kebikeç. 17, 139-163. (In Turkish).

[6] Tarıkahya, H.B., Karacaoğlu, Ç., Özüdoğru, B. (2014) The Speciation History and Systematics of *Carthamus* (Asteraceae) with Special Emphasis on Turkish Species by Integrating Phylogenetic and Ecological Niche Modelling Data. Plant Systematics and Evolution. 300(6), 1349-1359.

[7] Yaman. H., Tarıkahya, H.B., Arslan, Y., Subaşı, İ. (2014) Molecular characterization of the wild relatives of safflower (*Carthamus tinctorius* L.) in Turkey as revealed by ISSRs. Genetic Resources and Crop Evolution. 61, 595–602.

[8] Tarıkahya, H.B., Arslan, Y., Subaşı, İ., Katar, D., Bülbül, A.S., Çeter, T. (2012) Achene Morphology of Turkish *Carthamus* Species. Australian Journal of Crop Science. 6, 1260-1264.

[9] Bülbül, A.S., Tarıkahya, H.B., Arslan, Y., Subaşı, İ. (2013) Pollen Morphology of *Carthamus* L. Species in Anatolian Flora. Plant. Syst. Evol. 299, 683-689.

[10] Arslan, Y., Tarıkahya H.B. (2018) Seed fatty acid compositions and chemotaxonomy of wild safflower (*Carthamus* L.-Asteraceae) species of Turkey. Turk. J. Agric. For. 42, 45-54.

[11] Weiss, E.A. (1971) Castor, Sesame and Safflower. Barnes and Noble, Inc. New York, 529-744.
[12] Dajue, L., Mündel, H. (1996) Safflower. *Carthamus tinctorius* L. In: Heller, J., Engels, J., Hammer, K. (eds) Promoting the conservation and use of underutilized and neglected crops 7. Institute of Plant Genetics and Crop Plant Research, Gatersleben/International Plant Genetic Resources Institute, Rome, Italy
[13] Khalil, H.E., Al-Ahmed, A. (2017) Phytochemical Analysis and Free Radical Scavenging Activity of *Carthamus oxyacantha* Growing in Saudi Arabia: A Comparative Study. Int. J. Pharm. Sci. Rev. Res. 45(1), 51-55.
[14] Bocheva, A., Mikhova, B., Taskova, R., Mitova, M., Duddeck, H. (2003) Antiinflammatory and analgesic effects of *Carthamus lanatus* aerial parts. Fitoterapia. 74, 559-563.
[15] Jalil, S., Taskova, R., Mitova, M., Duddeck, H., Choudhary, M., Atta-ur-Rahman, I. (2003) In vitro Anti-inflammatory Effect of *Carthamus lanatus* L. Z. Naturforsch. 58, 830-832.
[16] Ivancheva, S., Nikolova, M., Tsvetkova, R. (2006) Pharmacological activities and biologically active compounds of Bulgarian medicinal plants. In: Phytochemistry: Advances in Research. Editor: Imperato, F. Research Signpost 37/661 (2), Fort P.O., Trivandrum-695 023, Kerala, India, 87-103.
[17] Taskova, R., Mitova, M., Najdenski, H., Tzvetkova, I., Duddeck, H. (2002) Antimicrobial activity and cytotoxicity of *Carthamus lanatus*. Fitoterapia. 73, 540-543.
[18] Abou-Zeid, H.M., Bidak, L.M., Gohar, Y.M. (2014) Phytochemical Screening and Antimicrobial Activities of Some Wild Medicinal Plants of The Western Mediterranean Coastal Region, Egypt. International Journal of Pharmaceutical Sciences and Research. 5, 3072-3080.
[19] Feroz, S., Ali, J. (2016) Preliminary phytochemical analysis, antioxidant, and antimicrobial evaluation of *Carthamus lanatus.* Innovare Journal of Science. 4, 1-3.
[20] Topashka-Ancheva, M., Taskova, R., Handjieva, N., Mikhova, B., Duddeck, H. (2003) Clastogenic Effect of *Carthamus lanatus* L. (Asteraceae). Z. Naturforsch. 58c, 833-836.
[21] Mitova, M., Taskova, R., Popov, S., Berger, R., Krings, U., Handjieva, N. (2003) Bioactive Phenolics from *Carthamus lanatus* L. Z. Naturforsch. 58c, 704-707.
[22] Stefanov, K., Taskova, R., Mitova, M., Topashka, M., Seizova, K., Duddeck, H. (2003) Analysis and Biological Activity of the Lipid Extract of *Carthamus lanatus* L. Comptes rendus de l'Academie bulgare des Sciences. 56(9), 13-18.
[23] Taglialatela-Scafati, O., Pollastro, F., Cicione, L., Chianese, G., Bellido, M.L., Munoz, E., Özen, H.Ç., Toker, Z., Appendino, G. (2012) STAT-3inhibitorybisabolanes from *Carthamusglaucus*. J Nat Prod. 75(3), 453-458.
[24] Lockwood, T.E. (1966) A comparative anatomical study on the effects of mutant genes on the pericarp and seed coat of safflower (*Carthamus tinctorius* L.). MS Thesis. University of Arizona
[25] Ebert, W.W., Knowles, P.F. (1968) Developmental and anatomical characteristics of thin-hull mutants of *Carthamus tinctorius* Compositae. Am. J. Bot. 55,421-430.
[26] Gadallah, M.A.A., Ramadan, T. (1997) Effects of zinc and salinity on growth and anatomical structure of *Carthamus tinctorius* L. Biol. Plantarum. 39, 411-418.
[27] Gao, W., Sha, T., Liu, L., Deng, C., Lu, L. (2012) Study on vegetative organs anatomical structure and pollen feature of different Safflower varieties. Guihaia. 1, 46-52.
[28] Najmaddin, C., Mahmood, B.J. (2016) Anatomically and Palynologically Studies of Some *Carthamus tinctorius* Genotypes.International Journal of Biological Sciences. 3(1), 1-13.
[29] Sass, J.E. (1940) Elements of botanical microtechnique. McGraw-Hill, New York
[30] Johansen, D.A. (1940) Plant microtechnique. McCraw-Hill, New York.
[31] Algan, G. (1981) Bitkisel dokular için mikroteknik (Microtechniques for botanical tissues). Fırat University Science Faculty Press, Elazığ, Turkey
[32] Parker, A.J., Haskins, E.F., Deyrup-Olsen, I. (1982) Toluidine Blue: A Simple, Effective Stain for Plant Tissues. The American Biology Teacher. 44(8), 487-489.
[33] Bibi, H., Afzal, M., Muhammad, A., Kamal, M., Sohail, UllahI., Khan. W. **(**2014**)** Morphological and anatomical studies on selected dicot xerophytes of district Karak. American-Eurasian J. Agric. Environ. Sci. Pakistan. 14, 1201-1212.
[34] Metcalfe, C.R., Chalk, L. (1950) Anatomy of the Dicotyledons. vol 2. Clarendon Press, Oxford, 782-804
[35] Kartal, Ç. (2016) Calcium Oxalate Crystals in Some Species of the Tribe Cardueae (Asteraceae). Botanical Sciences. 94(1), 107-119.

Received: **16.01.2019**
Accepted: **18.03.2019**

CORRESPONDING AUTHOR

Ali Savas Bulbul
Kahramanmaraş Sütçü İmam University,
Faculty of Arts and Sciences,
Department of Biology,46030 Kahramanmaraş-Turkey
e-mail: asavasbulbul@gmail.com

© by PSP Volume 28 – No. 5/2019 pages 4080-4092 Fresenius Environmental Bulletin

SUITABILITY EVALUATION OF HUMAN SETTLEMENTS IN RAPID URBANIZATION PLATEAU BASED ON GIS: A CASE STUDY OF CHENGGONG NEW DISTRICT IN KUNMING

Linlin Song[1,2], Lei Yuan[1,2,*], Kun Yang[1,2], Tiantian Zhao[1], Jie Wang[1]

[1]School of Information Science and Technology, Yunnan Normal University, Kunming, China
[2]Engineering Research Centre of Ministry of Education on Geography Information Technology of Western Resource Environment, Kunming, China

ABSTRACT

In recent years, with the rapid development of China's economic construction and urbanization, the large-scale agglomeration of industry and population has caused a series of problems, such as urban environmental pollution, ecological damage and so on. Creating a good human settlements environment is the inevitable requirement of solving ecological environmental problems and the general trend of socially sustainable development. Therefore, how to enhance the living environment in the context of rapid urbanization has become a hot topic of concern to the entire society. This paper takes the Chenggong New District of Kunming City, Yunnan Province, which has developed rapidly in recent years as an example, by combining GIS spatial analysis method, analytic hierarchy process and human settlements environment model, scientific evaluation of the suitability of human settlements in Chenggong New District by selecting natural factor indicators such as terrain fluctuation, climate suitability, hydrological conditions, land cover, and human factors indicators such as transportation, medical facilities and educational facilities. The results show that: ① Taking into account the geographical environment, humanities and other influencing factors, the suitability of human settlements in Chenggong New District is characterized by widespread suitable areas and more suitable areas. The suitability of human settlements is generally increasing from mountain to hill to then plain. The areas where the habitat environment is apter include Longcheng Street, Dounan Street, Wujiaying Street, and Yuhua Street. Generally suitable areas mainly include Luoyang Street, Luolong Street, Wulong Street, and Qidian Street. ② Natural factors are the most basic elements affecting the quality of human settlements, and they are also the most closely related elements of mortal habitation, production, and life. The natural factors affecting the suitability of human settlements in Chenggong New District are biological factors including topography, climate, hydrology, and land cover. Human factors such as education, transportation, and medical care have less impact on the suitability of human settlements. Under the background of rapid urbanization, the evaluation of the suitability of urban human settlements can quantitatively analyze the living environment of various areas in Chenggong New District, and provide suggestions and countermeasures for improving the living environment. At the same time, the improvement of the human settlements environment will enhance the urban living environment and the business service activity environment, improve the gathering and radiation ability of many elements such as talents, technology, and funds needed for urban development, and promote the sustainable development of the city.

KEYWORDS:
GIS, Suitability of Human Settlement Environment, Analytic Hierarchy Process, Rapid urbanization

INTRODUCTION

Human settlements environment is a multi-level, multi-disciplinary and intersecting space system, which is the general term of the social, economic, cultural and natural environment of human living. It is closely related to human living together [1-5]. Human settlement environment is the main place where human beings use and transform nature, and also the result of combining natural conditions with human subjective initiative, which is the geospatial basis for production and life. Its main purpose is to meet the needs of human survival and development [6-9]. The rapid development of urbanization and industrialization has resulted in a series of problems, such as transitional exploitation of resources, deterioration of ecological environment and continuous compression of living space. At the same time, the sharp increase in the population has led to an increase in the demand for resources and the ecological environment, making the contradiction between human settlements and urban construction increasingly prominent [10-15]. Therefore, how to improve

the living environment in the context of rapid urbanization, build a livable urban efficient form, and explore the sustainable development model of society has become a hot issue in the current urban economic construction process. At present, research on human settlements has become a hot topic of common concern in the world. Research at home and abroad is mainly reflected in two aspects: the first is to study the suitability of urban human settlements by integrating natural factors, comprehensive factors, and transportation factors. The second is the study of the impact of human factors on single elements or certain elements of natural systems [16-19]. Foreign scholars environment of human settlements from the beginning of the 1930s, through the interaction of a variety of disciplines to permeation of thought, research methods currently use the relationship between human and land to study the interaction between human living space structure and geographical environment. Compared with foreign research, China's research on the suitability of human settlements started late, but it developed rapidly. At present, domestic scholars mainly conduct research on natural, climate, population distribution and other factors through natural perspectives. However, the current research objects are mainly concentrated in coastal large and medium-sized cities and arid plains in the inland plains, and the research on human settlements in the plateau areas with the perspective of rapid urbanization using GIS technology is still lacking. Because the ecological environment of the plateau region is quite different from the ecological environment of other inland regions, the vulnerability and limited nature of natural resources leads to the study of urban human settlements in the plateau. Therefore, this paper analyzes the spatial pattern distribution of urban human settlements in the plateau area by taking the GIS spatial analysis technique as an example. The main purpose is to provide scientific basis for the future urban planning and economic construction of Chenggong New Area by evaluating the current situation of suitability of human settlements environment. At the same time, it also has important theoretical and practical significance for maintaining the harmony, stable and sustainable development of human settlements and environment in the plateau region.

RESEARCH AREA OVERVIEW AND DATA SOURCES

Research area overview. Chenggong New District is the resident center of Kunming City. It is located at 102°45′~103°00′ east longitude and 24°42′~25°00′ north latitude. The terrain is high in the east and low in the west, with an altitude of 1775-820 meters. The highest peak in Liangwang mountain in the territory is 2820 meters above sea level. Chenggong New District is a representative area of rapid urbanization in typical plateau areas. Chenggong New District has a good climate with an average annual temperature of 14.7 degrees Celsius. The illumination time is sufficient, and the annual sunshine number is 2,200 hours, which have great advantages for crop growth. The average annual rainfall is 800 mm and the forest coverage rate is 46%. The Chenggong New district is a typical low latitude plateau area and the climate belongs to the low latitude plateau monsoon climate. It includes 10 subdistrict offices, including 65 community neighborhood committees and 155 natural villages. With the "One Belt, One Road" strategic plan positioning Yunnan as a radiation center for South Asia and Southeast Asia, Chenggong New District is becoming the core area of Yunnan's "One Belt, One Road" strategy.

Data Selection Sources. The data required for this article are derived from the Chenggong Yearbook, and digital elevation model (DEM) data at 90 meters resolution is mainly used to extract terrain relief, and land use change data and standardized vegetation index maps in Chenggong District are mainly used for calculation of land/vegetation cover index. Monthly observation data of years of average temperature and relative humidity in Chenggong District, mainly used for climate suitability evaluation. The multi-year average precipitation tax bureau and water system distribution vector data in Chenggong District are used for hydrological density calculation.

RESEARCH METHOD

Relief Degree of Land Surface. Relief Degree of Land Surface, also known as surface relief, is a comprehensive representation of regional elevation and surface cutting degree. Terrain conditions directly or indirectly affect the choice and development of human settlements and the advantages and disadvantages of land use methods and quality [20-22]. Referring to the research methods of terrain fluctuations by various scholars at home and abroad [23-24], this paper defines the terrain relief as follows：

$$R_{DLS} = A_{LT} / 1000 + \{[Max(H) - Min(H)] \times [1 - P(A) / A]\} / 500 \quad (1)$$

In the formula: R_{DLS} is the terrain relief index; A_{LT} is the average altitude in a certain area (m); *Max(H)* is the highest altitude in the region; *Min(H)* is the lowest altitude in the region, the unit is m; *P(A)* is the flat area (km^2) in the study area; A is the total area of the study area (km^2).

Climate index model. The climatic conditions have a great impact on people's comfort. When people choose their living environment, the mild and appropriate climatic environment has a greater impact

on the living environment. The index of "temperature and humidity index" is used as the criterion for evaluating the climate suitability of human settlements in Chenggong New Area [25-26]. The calculation formula is as follows:

$$T_{HI} = 1.8t - 0.55(1-f)(1.8t - 26) \quad (2)$$

In the formula: t is the annual average temperature (°C) in Chenggong New Area; f is the annual average air relative humidity (%).

Hydrological index model. Water is one of the essential material conditions for human survival. According to domestic and international research methods on the suitability of regional water resources in human settlements, the corresponding indicators of water resources used in this study include rainfall and water area. The first factor is the precipitation, which reflects the natural water supply capacity of the study area; the second factor is the water area, which reflects the strength of the water collection and catchment capacity of the study area; The proportion of precipitation and water area is used to indicate the abundance of water resources in the study area. The specific calculation formula is:

$$W_{RI} = \alpha P + \beta Wa \quad (3)$$

In the formula, WRI is the hydrological index, P and Wa are the precipitation and water area of the study area, α and β are the weights of the ratio of precipitation to the water area.

Land Use/Land Cover Index Model. The state of vegetation to a certain extent can be said to be an indicator of the quality of human settlements, which are crucial in the evaluation of the suitability of human settlements. With reference to relevant research methods at home and abroad. This paper expresses the coverage of surface vegetation by constructing the representation of the ground cover index in different areas of Chenggong New District.

$$I_{LC} = I_{NDV} \times i_{LT} \quad (4)$$

Among them, I_{LC} is the land use/land cover index; I_{NDV} is the land use/land cover index standardized by the evaluation unit; i_{LT} is the weight of various types of land use.

Human factor index model. The human factor index of this paper mainly includes indicators such as urban transportation, medical resources, and educational resources. The traffic road network was extracted from the land use map of Chenggong New District, and the coordinate of the hospital and school in Chenggong New District was obtained by using the coordinate picker in Baidu API. Buffer analysis and grid analysis in ArcGIS have made buffers for different impacts of traffic, hospitals, and schools. According to the size of each street buffer, the corresponding traffic index, medical index, and education index are given. The human factor index table is shown in Table 1.

ESTABLISHMENT AND EVALUATION OF THE SUITABILITY EVALUATION MODEL OF HUMAN SETTLEMENTS IN CHENGGONG NEW DISTRICT

Determination of the weight of human settlements indicators. Considering the difference in the degree of influence of each evaluation factor on the evaluation target, this paper uses the Analytic Hierarchy Process (AHP) algorithm to determine the weight of each evaluation index [27]. After the operation of establishing the hierarchical structure model, constructing the judgment matrix, hierarchical single sorting, consistency test, and hierarchical total sorting, the weight of the evaluation factors in the regional human settlement environment suitability evaluation model is calculated. As shown in Table 2 below:

Establishment of Evaluation Model of Human Settlements in Chenggong New District. The index model of human settlements environment can provide some guidance for the quality of human settlements environment, economic development and sustainable development of resources [28]. Therefore, considering the particularity of the environment in the study area. This paper uses the I_{HE} model to characterize the suitability of the human settlements in Chenggong District. The formula is as follows:

$$I_{HE} = \alpha_i \times D_{NRLS} + \beta_i \times I_{NTH} + \chi_i \times I_{NER} + \delta_i \times I_{NLC} + \varepsilon_i \times I_{JT} + \phi_i \times I_{YL} + \varphi_i \times I_{JY} \quad (5)$$

TABLE 1
Human factor index table

Name	Traffic index	Medical Index	Education index
Longcheng Street	100	90	90
Dounan Street	100	90	90
Luolong Street	90	80	85
Wulong Street	100	80	85
Wujiaying Street	80	90	90
Yuhua Street	90	90	90
Qidian Street	70	70	80
Luoyang Street	90	70	80
Majinpu Street	80	70	80
Dayu Street	90	65	75

TABLE 2
Weight table of human settlements environmental adaptability index

	Relief Degree of Land Surface	Climate suitability	Hydrological index	Land cover index	traffic	Medical	education	Weights	Eigenvector value
Relief Degree of Land Surface	1	1/2	2	2	1/2	1/2	1/2	0.1139	0.2852
Climate suitability	2	1	2	1/2	1/2	1/2	1/2	0.1139	0.2852
Hydrological index	1/2	1/2	1	1/2	1/2	1/2	1/2	0.0729	0.1827
Land cover index	1/2	2	2	1	1/2	1/2	1/2	0.1139	0.2852
traffic	2	2	2	2	1	3/2	2/3	0.1943	0.4867
Medical	2	2	2	2	2/3	1	2/3	0.1737	0.4351
education	2	2	2	2	3/2	3/2	1	0.2174	0.5445

TABLE 3
Topographic relief index table

Name	Average Altitude (m)	Highest altitude (m)	Minimum altitude (m)	Flat area (km^2)	Total area (km2)	Relief Degree of Land Surface
Longcheng Street	1906.6	1936	1900	7.58	9.47	19.21
Dounan Street	1893.1	2100	1886.5	10.143	11.27	19.345
Luolong Street	1900	2111	1880	7.104	17.76	20.948
Wulong Street	1904.04	1948	1980	14.728	18.41	19.172
Wujiaying Street	1926	2125	1940.03	34.712	86.78	21.476
Yuhua Street	1920	2033	1911	9.097	16.54	20.298
Qidian Street	2200	2450	2000	37.8	126	28.3
Luoyang Street	1900	2245	1880	46.578	77.63	21.92
Majinpu Street	2092	2820	1900	52.41	104.82	30.12
Dayu Street	1913	2110	1888	17.99	25.7	20.462

The model can calculate the Habitat Environment Index of the study area, and then partition and evaluate each street in Chenggong New Area according to the Habitat Environment Index. Among them, I_{HE} is the regional human settlement environment index, the value is 0-100; D_{NRLS} is the standardized terrain relief index; I_{NTH} is the standardized temperature and humidity index; I_{NER} is the standardized hydrological index; I_{NLC} is the standardized land use/land cover index; I_{JT} is the traffic index and I_{YL} is the medical index. I_{JY} is the education index; The αi, βi, γi, δi, εi, φi and ψi before the relevant sub-index are the weight corresponding to the respective indices.

RESULT ANALYSIS

The quality of human settlements directly affects the quality of life of residents. Therefore, the corresponding evaluation of the suitability of human settlements can help to analyze the current quality of life in the city and the development direction of the next stage [29-31]. Natural factors are the most basic elements affecting the quality of human settlements, and they are also the elements most closely related to human habitation, production, and life. In this paper, considering the natural environment and human factors of Chenggong New District, the suitability evaluation of terrain relief, climate suitability, hydrological index, land cover index, transportation convenience, hospital facilities, and educational facilities was selected.

Single factor evaluation of natural suitability of human settlements in Chenggong New District. Appropriate evaluation of relief degree of land surface. The terrain is the most basic element of natural factors, and it directly affects the living environment. At the same time, it also indirectly affects the living environment by affecting solar radiation, water and heat balance, soil distribution, and vegetation growth. The street terrain relief index table (Table 3) can be calculated from the human settlement environment evaluation model. The spatial distribution map of topographic relief obtained by GIS processing (Fig. 1) can be analyzed and concluded that among the 10 streets in Chenggong New District, Qidian Street, and Majinpu Street have large elevation difference, and the topographic relief is relatively large, which belongs to the inappropriate living area; Luoyang Street, Luolong Street, Wujiaying Street and Dayu Street belong to the terrain with little fluctuation, but there is a certain fluctuation, so this area is generally suitable area; Longcheng Street, Dounan Street, Wulong Street, and Yuhua Street are relatively flat, and are the most suitable areas for living. The three-dimensional climate is remarkable, and it is more suitable for population distribution.

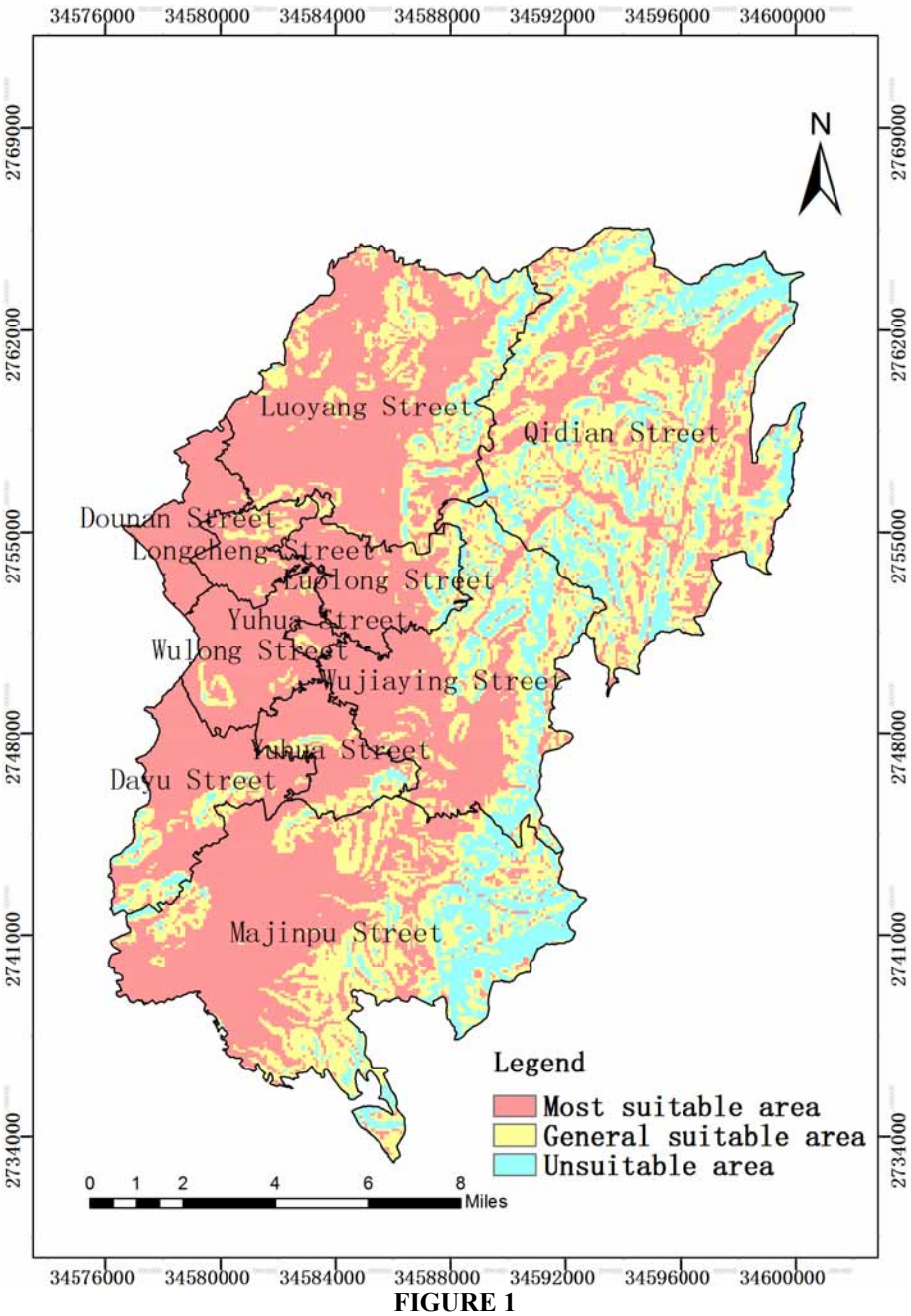

FIGURE 1
Topographic relief map

TABLE 4
Climate suitability index

Name	Annual average temperature °C	Annual average humidity%	Climate suitability
Longcheng Street	16	75	28.451
Dounan Street	15.5	80	27.691
Luolong Street	14	80	25.288
Wulong Street	18	70	34.038
Wujiaying Street	14.7	68	26.541
Yuhua Street	16	80	29.108
Qidian Street	17.8	81	32.671
Luoyang Street	14.7	80	26.51
Majinpu Street	14	78	25.297
Dayu Street	16.7	70	30.729

Climate suitability evaluation. Climate is an important factor in determining the quality of living environment, and it is also an indispensable standard in the evaluation of habitat suitability. This study evaluates the climate suitability of Chenggong New District by using the temperature and humidity index reflecting the climate suitability of human settlements. The climate suitability indicator of each street can be calculated from the human settlement environment evaluation model (Table 4). The spatial distribution map of climate suitability (Figure 2) obtained by GIS analysis shows that Wulong Street and Qidian Street are the most suitable areas for climate; Longcheng Street, Dounan Street, Dayu Street, and Yuhua Street are generally suitable for residential areas; Luoyang Street, Luolong Street, Wujiaying Street, and Majinpu Street are among the unsuitable areas for climate.

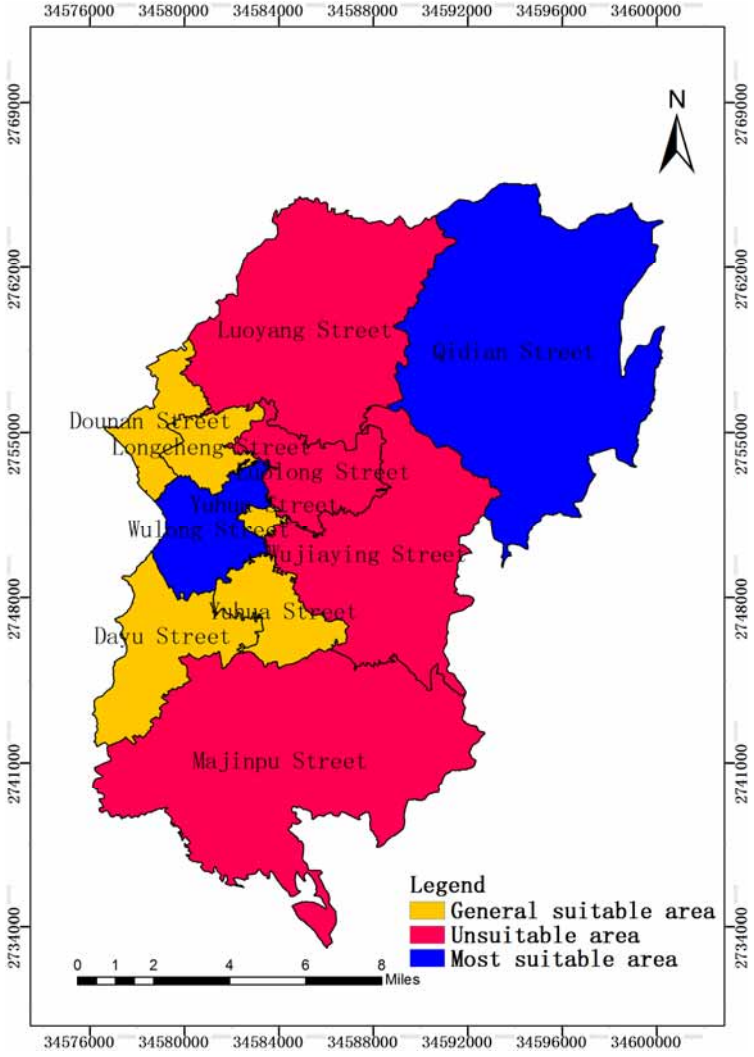

FIGURE 2
Climate Fitness Map

TABLE 5
Hydrological index table

Name	Average annual rainfall (ml)	Water area	Hydrological index
Longcheng Street	968	1	9.744
Dounan Street	950	1	9.6
Luolong Street	800	2.53	11.46
Wulong Street	950	1	9.6
Wujiaying Street	786	6.95	20.188
Yuhua Street	789.6	2.63	11.5768
Qidian Street	1049	7.91	24.212
Luoyang Street	800	9.97	26.34
Majinpu Street	958	8.11	23.884
Dayu Street	1004.4	1	10.0352

Hydrological suitability evaluation. As one of the most important factors for human survival, hydrological conditions are affected and restricted by factors such as topography, climate, vegetation, etc., making them have large spatial differences in different regions [20]. The hydrological indicator table of each street can be calculated from the human settlement environment evaluation model (Table 5). The spatial distribution map of hydrological suitability obtained by GIS processing (Figure 3) shows that Luoyang Street, Majinpu Street, and Qidian Street belong to the most suitable hydrological habitable area. There are abundant water resources and relatively large rainfall in the area, so it is suitable to develop planting industry; Wujiaying street belongs to the habitable area of hydrology, while the remaining streets belong to the area where water resources are relatively scarce. Water resources planning should be paid attention to in the future development.

Suitability evaluation of land cover index. The land is an indispensable substance in the process of human development, and the growth of plants cannot be separated from the land. The individual land cover indicator table can be calculated from the human settlement environment evaluation model (Table 6). The spatial distribution map of land cover suitability (Figure 4) obtained by GIS analysis shows that the vegetation coverage of Qidian street, Luoyang Street, Luolong Street, Wujiaying Street, and Majinpu Street is relatively large. However, the presence of more vegetation indicates that it is more likely to be in a mountainous area, so the area is not suitable for living. The remaining streets of Longcheng and Dounan are relatively less green and less dense, and the land is in a gentle zone. It is suitable for living from the land cover index, but the economy of the region is relatively fast, and landscaping should be paid attention to in the future development.

TABLE 6
Land cover index table

Name	Land cover index
Longcheng Street	47
Dounan Street	38.2
Luolong Street	50.6
Wulong Street	33.3
Wujiaying Street	65.2
Yuhua Street	53
Qidian Street	53.6
Luoyang Street	52.7
Majinpu Street	49.9
Dayu Street	41.5

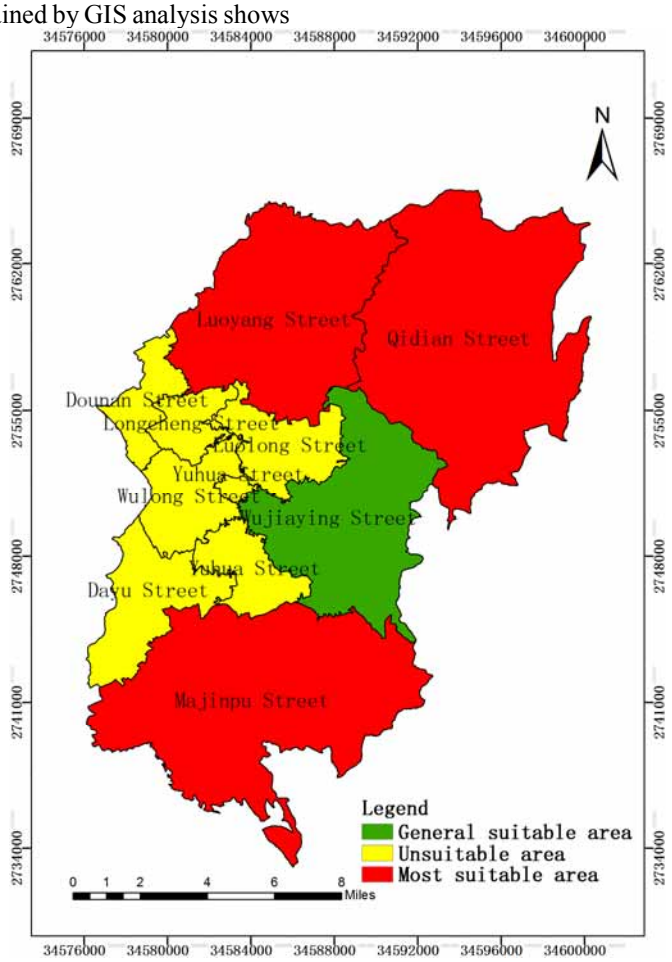

FIGURE 3
Hydrological suitability map

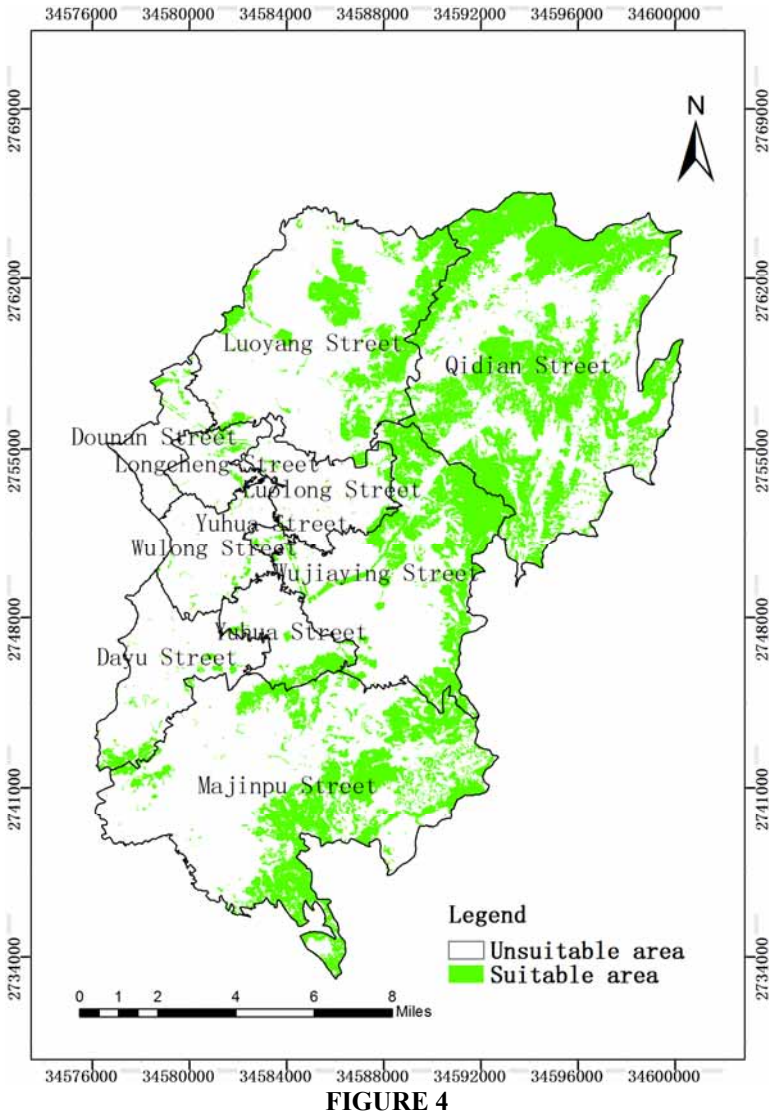

FIGURE 4
Land cover index suitability map

Human suitability evaluation. The spatial distribution map analysis of traffic, medical care and education obtained by GIS analysis leads to the following conclusions : In terms of transportation, some areas of Qidian Street, Wujiaying Street, and Majinpu have not yet reached full coverage of traffic network, and future traffic development can extend to these areas; The remaining streets of Longcheng, Dounan, Luolong and Yuhua basically achieved the full coverage of the traffic network, which is the best traffic area. In terms of medical care: the medical facilities in Qidian, Luoyang, Majinpu and Dayu Street are relatively small, therefore, in terms of medical facilities, this part of the area is an uninhabitable area, and the subsequent development focus should be shifted to these areas. The remaining streets of Longcheng, Dounan, Wujiaying, and Yuhua are relatively fast, and the distribution of medical facilities is relatively more concentrated. It is a suitable living area at this stage. In terms of education: the core areas of Chenggong New District such as Long Street, Dounan, Wujiaying, Yuhua, and Luolong Street Schools are more distributed, so the area is a more suitable residential area; The remaining streets of Qidian, Majinpu and Dayu are relatively few, and the development of educational facilities in the future should be tilted towards the region.

Comprehensive Evaluation of Natural Suitability of Human Settlements in Chenggong New District. According to the terrain relief, climate suitability, hydrological index, and land use/land cover index and human factors, the street habitat index was obtained (Table 7). From the evaluation results, the areas where the living environment is more suitable are the core areas of the main city, including Longcheng Street, Dounan Street, Wujiaying Street, and Yuhua Street; The general residential area is suitable for the current development of areas such as Luolong Street, Luoyang Street, Qidian Street, and Wulong Street; The unsuitable area of human settlements is the focus of the next development, as most of its areas have not been developed, such as Majinpu and Dayu Street.

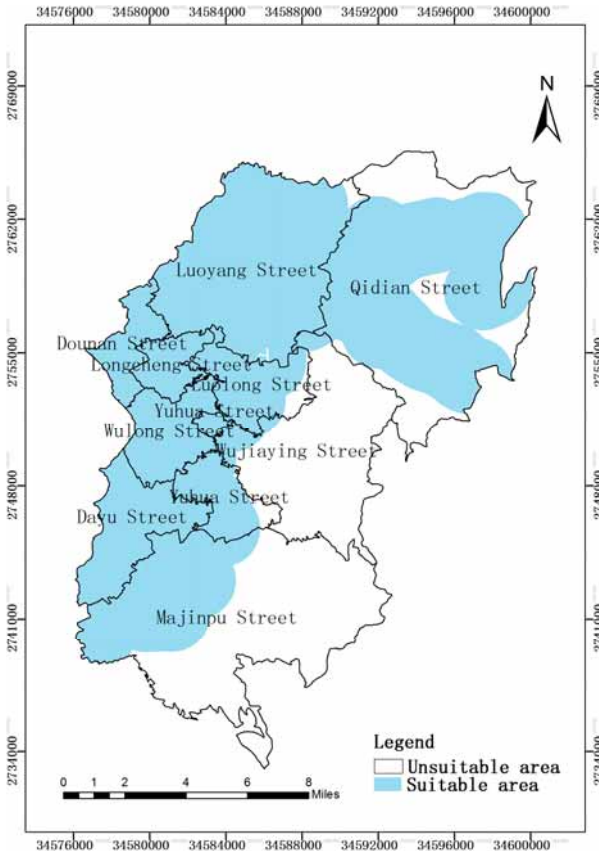

FIGURE 5
Traffic Suitability Chart

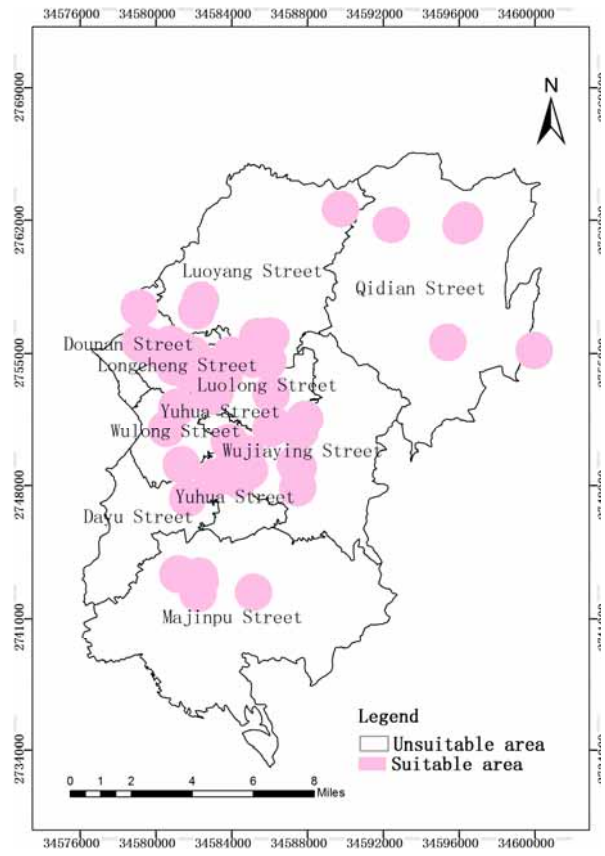

FIGURE 6
Medical Suitability Chart

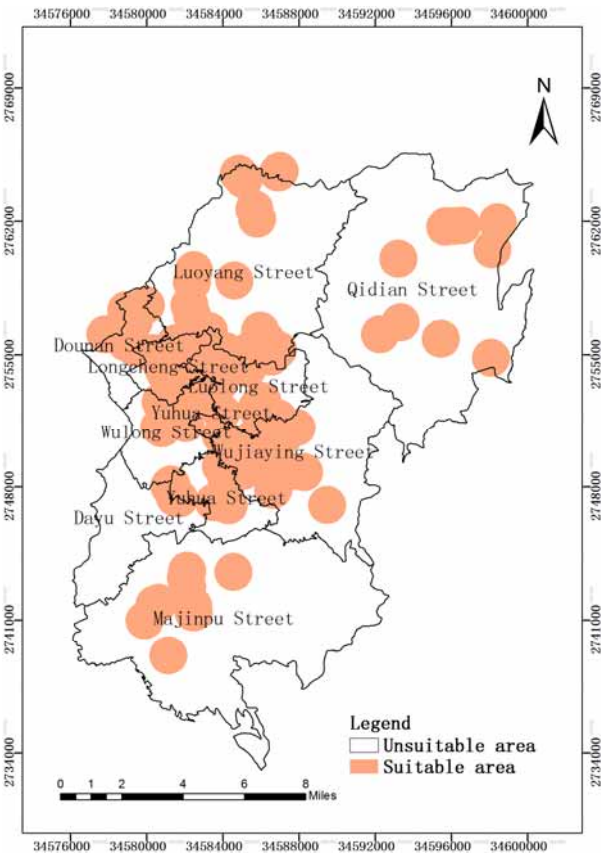

FIGURE 7
Education suitability map

TABLE 7
Suitability index of human settlements

Name	Habitat environment index	Type area
Longcheng Street	65.16	Suitable area
Dounan Street	64.04	Suitable area
Yuhua Street	63.98	Suitable area
Wujiaying Street	63.63	Suitable area
Wulong Street	61.46	General suitable area
Luolong Street	60.37	General suitable area
Luoyang Street	58.9	Marginal suitable area
Qidian Street	55.41	Marginal suitable area
Majinpu Street	55.4	Unsuitable area
Dayu Street	55.12	Unsuitable area

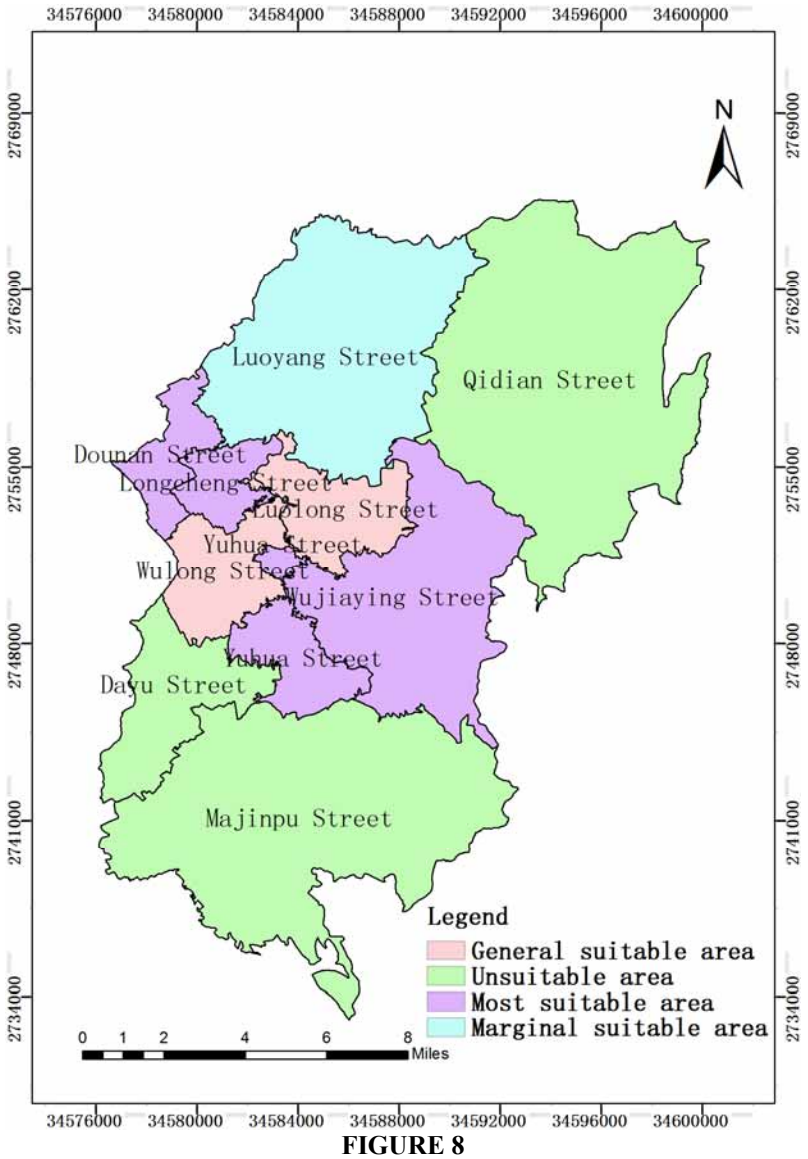

FIGURE 8
Zoning map of human settlement environment suitability evaluation

The development of Chenggong New District has been getting better and better in recent years, and each street has its corresponding functional division. According to the analysis, the Chenggong New Area Suitability Zoning Map (Figure 8) shows: Longcheng Street, Dounan Street, Wujiaying Street, and Yuhua Street are relatively suitable areas for living, but the area is now basically in a state of develop-

ment saturation, and its economy, transportation, education and medical facilities are relatively complete and suitable for living. Wulong Street and Luolong Street are generally suitable areas. The terrain is flat and the climate is mild, which is suitable for the next development area; The remaining Luoyang Street, Qidian Street, Majinpu Street, and Dayu Street are rich in good climate water resources, but because of the large terrain, there is a certain distance from the main city of Chenggong, and the medical education facilities are not perfect. Therefore, it is temporarily unfit for living area, however, in the next development of Chenggong New District, the center should transfer to this area, which is the scope of the next plan for Chenggong.

CONCLUSION

This paper uses GIS technology to study the characteristics and spatial differences of the suitability of human settlements in the context of rapid urbanization and provides decision-making basis for the optimization of human settlements in the plateau and land science planning. Using a combination of GIS spatial analysis method, analytic hierarchy process, and human settlement environment model, Choosing natural and human factors, this paper takes Chenggong District as the research object to construct a human settlements environment evaluation model and quantitatively evaluate the suitability and limitation of human settlements environment in Chenggong District. The results show that: (1) According to the classification of environmental suitability modeling and evaluation in Chenggong District, it is found that: The suitability of human settlements in Chenggong District showed a trend of decreasing from the northeast and southwest to the central and western regions. The more suitable areas were mainly distributed in Longcheng, Dounan, Yuhua and Wujiaying streets. Generally, suitable areas are mainly distributed in Wulong Street and Luolong Street, and the marginally suitable areas and unsuitable areas are mainly distributed in Luoyang, Qidian, Majinpu and Dayu Street. (2) Natural factors are the most basic elements affecting the quality of human settlements, and they are also the most closely related elements of human living, production, and life. According to the single factor suitability evaluation of the human settlement environment in Chenggong District, the hydrological conditions have the greatest impact on the human settlement environment, and the climatic conditions are second. In terms of human factors, since the Chenggong District is in the period of rapid urbanization development, the economic development of each region is extremely unbalanced, so the living environment is greatly affected by traffic indicators, and the impact of medical conditions is second. (3) The natural suitability evaluation model of human settlements constructed in this paper is in line with the existing economic development and ecological environment in Chenggong District, and provides a way of thinking about the suitability of human settlements in the plateau. At the same time, given that Chenggong District is in the stage of rapid urbanization development, Chenggong District is an important gateway for regional economic development and opening up in southwest China. It should vigorously protect water and soil resources, strengthen ecological civilization construction, and gradually improve transportation, medical care, and education systems. In order to improve the overall suitability of the human settlement environment in the Chenggong District, efforts should be made to coordinate economic construction and promote coordinated development of population resources.

REFERENCES

[1] Guo, X.N., Su, W.C., Li, Q., Pan, Z.Z. (2016) Evaluation of natural adaptability of human settlements in karst area of southern Guizhou based on GIS and RS. Karst of China. 35(2).

[2] Xiao, W., Xu, J.F., Yang, K., Li, S.C., Lu, J.C., Tang, Z.W. (2017) Evaluation of soil erosion in Chaohu Lake basin based on GIS and USLE model. Science and Technology and Engineering. 17(16), 35-43.

[3] Shen, F., Huang, Y.P., Wang, F., Ma, J.J., Chen, M.X. (2018) Natural suitability assessment of human settlements in Anhui Province based on GIS and raster data. Resources and environment in the Yangtze River Basin. 27(3).

[4] Wu, M., Yang, C., Lin, N. (2017) Application of High Resolution Remote Sensing Images in Land Cover Change Monitoring. Science and Technology and Engineering. 17(22), 100-106.

[5] Xin, S., Chaoyang, S., Mo, L. (2017) Comparative study on the optimization strategies of the human settlement environment of the rural settlements in Asia. IOP Conference Series: Earth and Environmental Science.

[6] Hao, Y., Tulson, H., Yang, J. (2015) Evaluation of Urban Habitat Environment Suitability in the Environment of Drought Environment—Taking Bazhou, Xinjiang as an Example. Journal of Sichuan Normal University (Natural Science). 38(3), 466-474.

[7] Ma, L., Lei, T., Zhang, W., Li, J. (2018) Evaluation of Suitability of Human Settlements in Shaanxi Province. Henan Science. 2018(4).

[8] An, M., Ma Li, H., Nasman, N. (2017) Evaluation of Suitability of Human Settlements in Kaikong River Basin Based on 3S Technology. Transactions of the Chinese Society of Agricultural Engineering. 2017(09), 276-283.

[9] Luo, J., Zhou, T., Du, P., Xu, Z.G. (2018) Spatial-temporal variations of natural suitability of human settlement environment in the Three Gorges Reservoir Area—A case study in Fengjie County, China. Frontiers of Earth Science. 2018(2), 1-17.
[10] Qing, F., Xia, X., Jiang, Z. (2018) Evaluation of Suitability of Human Settlements in Xindu District of Chengdu Based on RS and GIS. Journal of Qiqihar University (Natural Science Edition). 2018(2).
[11] Chai, Z., Xiao, H., Zhang, L., Liu, Y.J. (2017) Research on Suitability Evaluation of Habitat Environment in Changji Prefecture. Geospatial Information. 2017(12), 45-47.
[12] Long, Y., Lang, W. (2016) Human Settlement Study of China in the New Data Environment. Journal of Urban and Regional Planning, 2016.
[13] Yuan, J., Huang, J., Zhang, R., Zhou, C.L., Lan, D., Li, L., Yu, M.Y. (2017) Evaluation of climate comfort of human settlements in Qujing City. Journal of Yunnan University: Natural Science Edition. 2017(S1), 77-82.
[14] Li, Y.C., Liu, C.X., Zhang, H., Gao, X. (2011) Evaluation on the human settlements environment suitability in the Three Gorges Reservoir Area of Chongqing based on RS and GIS. Journal of Geographical Sciences. 21(2), 346-358.
[15] He, P., Tong, L.Q., Guo, Z.Z., Liu, C.L., Tu, J.N., Wang, S.S., Xu, J.M. (2016) Evaluation of landslide hazard susceptibility in Zanda area, Tibet based on analytic hierarchy process. Science Technology and Engineering. 16(25), 193-200.
[16] Zhang, Y., Zhou, L., Yu, W. (2016) Construction of Ecological Suitability Evaluation Factor System of Tibetan Barley Based on GIS. Anhui Agricultural Sciences. 44(13), 119-121.
[17] Deng, S., Zhang, Q. (2014) GIS-Based Evaluation of Natural Suitability of Human Settlement Environment in Guangdong Province. Acta Scientiarum Naturalium Universitatis Sunyatseni, 2014.
[18] Yu, C., Dang, X. (2017) Study on the Sustainability Zoning Method of Human Settlements in the Loess Plateau from the Perspective of Watershed: Taking Jinghe River Basin as an Example. Journal of Architecture. 2017(s1), 143-147.
[19] Guan, J., Wahaf, H., Li, X.H., Cheng, Y. (2018) Spatial and temporal evolution of human settlements suitability in Keriya Oasis in recent 20 years. Journal of Ecology and Rural Environment. 34(6), 512-520.
[20] Cao, W., Wang, S. (2017) Climate comfort assessment of urban human settlements in Beijing, Tianjin and Hebei. Glacier permafrost. 39(2), 435-442.
[21] Li, X.M., Jin P.Y. (2012) Characteristics and Spatial-temporal Differences of Urban Human Settlement Environment in China. Scientia Geographica Sinica. 2012.
[22] Chen, C., Zhang, W., Zhan, D.S., Li, X.L. (2017) Assessment of urban human settlements quality and its influencing factors in Bohai Rim region. Progress in Geographic Science. 36(12), 1562-1570.
[23] Liu, J., Zhan, R., Sun, W. (2016) Land suitability evaluation of Tianjin Binhai New Area based on GIS. Land and Resources Remote Sensing. 28(3), 160-165.
[24] Eddudóttir, S.D., Erlendsson, E., Tinganelli, L., Gísladóttir, G. (2016) Climate change and human impact in a sensitive ecosystem: the Holocene environment of the Northwest Icelandic highland margin. Boreas. 45(4), 715-728.
[25] Wang, Y., Zhang, Z. and Yang, B. (2016) Suitability evaluation of Stevia rebaudiana planting in Liangzhou District of Wuwei City based on GIS. China Sugar. 38(1), 40-42.
[26] Yang, Q., Chen, J., Li, B.H., Zhu, Y.Y. (2018) Study on the Evolution and Driving Force of Urban Habitat Environment in Urban Agglomerations in the Middle Reaches of the Yangtze River. Geographical Science. 38(2).
[27] Gao, J., Li, X., Chen, D.C., Zhang, Y.J. (2017) Study on the Equity of Urban Greenbelt in Shahekou District of Dalian City Based on GIS - From the Perspective of Sustainable Human Settlement Environment. Surveying and Mapping Bulletin. 2017(6), 40-44.
[28] Bratic, G., Brovelli, M.A., Molinari, M.E. (2018) A Free and Open Source Tool to Assess the Accuracy of Land Cover Maps: Implementation and Application to Lombardy Region (Italy). ISPRS - International Archives of the Photogrammetry, Remote Sensing and Spatial Information Sciences. XLII(3), 87-92.
[29] You, X., Dai, Q., Guo, C. (2017) Rural Human Settlement Environment Assessment in Southern Hilly Areas Based on Entropy Weight TOPSIS Model: A Case Study of Ganzhou. Journal of Mountainous Areas. 2017(6).
[30] Jia, H., Li, Y. (2017) Distribution characteristics and spatial pattern optimization of residential areas in tropical counties based on GIS --- Taking Lingshui Li Autonomous County of Hainan Province as an example. Science of Soil and Water Conservation in China. 15(5), 78-85.
[31] Qin, K., Liu, Y. (2016) Evaluation of suitability of urban construction land development based on GIS - Taking Jintan District of Changzhou City as an example. Mapping and spatial geographic information. 2016(11), 102-107.

Received: **17.01.2019**
Accepted: **17.03.2019**

CORRESPONDING AUTHOR

Lei Yuan
School of Information Science and Technology,
Yunnan Normal University,
Kunming – China

e-mail: v_ict@163.com

© by PSP Volume 28 – No. 5/2019 pages 4093-4100 Fresenius Environmental Bulletin

ANALYSIS OF GENETIC VARIABILITY AND HERITABILITY FOR SEEDCOTTON YIELD IN A SINGLE SEED DECENT POPULATION

Adem Bardak[1,*], Khezir Hayat[2], Halil Tekerek[1], Donay Parlak[1], Sadettin Celik[3], Rao Sohail Ahmad Khan[4], Ali Can Sever[1], Ridvan Ucar[5], Ramazan Sadet Guvercin[6], Remzi Ekinci[7]

[1]Department of Agricultural Biotechnology, Faculty of Agriculture, Kahramanmaras Sutcu Imam University, Kahramanmaras, Turkey
[2]Central Cotton Research Institute, Multan, Pakistan
[3]Department of Agricultural Biotechnology, Faculty of Agriculture, Bingol University, Bingol, Turkey
[4]Centre of Agricultural Biochemistry and Biotechnology (CABB), University of Agriculture, Faisalabad, Pakistan
[5]Department of Field Crops, Faculty of Agriculture, Bingol University, Bingol, Turkey
[6]Turkoglu Vocational School of Higher Education, Department of Medical and Aromatic Plants, Kahramanmaras Sutcu Imam University, Kahramanmaraş, Turkey
[7]Department of Field Crops, Faculty of Agriculture, Dicle University, Diyarbakir, Turkey

ABSTRACT

Variation is very important for the plant breeders and selection is effective when magnitude of variability in the breeding population is adequate. Genetic variability and heritability were observed among $F_{2:4}$ populations of cotton for three seasons. Parents, including *G. barbadense* (Askabat-100), *G. hirsutum* (Nazilli84S, Giza45, Albania-6172 and IS-4), and their $F_{2:4}$ populations were grown in a randomized complete block design with three replications during 2015. Statistical analysis revealed highly significant differences for all the traits. On average basis, the $F_{2:4}$ populations showed better performance than parental cultivars for yield and yield components. Additionally, from moderately high to high heritability (broad sense) values (0.61-0.95) were calculated for all parameters in the populations. Yield contributing components specially number of bolls per plant and boll weight directly affected the seed cotton yield in all populations among which Albania6172 x Giza 45 exhibited the highest boll weight. In general, our results revealed that $F_{2:4}$ populations developed by single seed descent method held not only a larger genetic potential but also a positive association between yield and yield contributing traits. As a whole, it might be interpreted that moderate to high heritability could be used a selective parameter for plant improvement in segregating populations.

KEYWORDS:
Genetic variability, Seedcotton yield, heritability, genetic advance, segregating generations

INTRODUCTION

Cotton is a crop of global importance as an ultimate source of natural fiber all over the world. It is also known as "white gold" owing to its major share in textile. Moreover, cotton is grown in tropical and sub-tropical regions of the world as its by-products are used for dietary purpose and for animals as a seedcake.

Genetic variability is compulsory among germplasm entries for the development of cultivars having high seedcotton yield and other economical traits [1]. The extent of variation among filial generations is vital for selection purposes. Hereditary behavior and mode of gene action of the economic traits play a significant role for the development of breeding methodology in plant sciences [2].

The concept of early generation was used in self-pollinated plants as a mean to select the best hybridized plants among populations with success in number of species [3]. Through this concept, the useful entries in breeding program are selected, and resources and duration needed for the process are reduced [4]. For development of any breeding strategy, breeders consider the number of the parents to be used for hybridization, the magnitude of proceeding filial generations, the filial stage to be considered for selection and the morphological characters to be screened. The use of filial stage in morphological screening of cotton for selection purposes has been studied for a long time [5] and it has been found to be beneficial for evaluation of genotypes which were introduced anciently [6].

The genetic pattern of different polygenic traits is determined through relationship of heritability and selection response [7]. Thanks to it, a number of alternative early generation screening has been practiced. Bulking, for instance, was applied in F_2 for selection of improved barley [8] while advanced progenies were selected using $F_{2:3}$ progenies in soybean [9]. Selection as single seed descent and progeny row play a vital role for minimizing errors during the conduction of replicated trials. In any breeding program, selection of plants on advance stages contributes to the increase in

selection efficiency. [10] observed genetic advance for ascertaining selection in two crosses of cotton and revealed that absolute and expected genetic advance were equal in one cross while these were not related in the second.

Since the final output in cotton variety development is to produce high lint yield with fine fiber, all economical traits are considered jointly in the selection process as well as the other factors by which these traits might be influenced such as environment and management practices. The researchers have recognized the existence of desirable or undesirable relations among yield and fiber quality improvement. When yield is improved, usually there is a hindrance for refinement of fiber traits [11]. [12] screened cotton genotypes for the assessment of relationship between yield and fiber attributes. They postulated that information about the kind and the extent of genetic variation is crucial in order to carry a reliable selection in cotton.

Additionally, it has been demonstrated that ginning outturn (GOT %) is an important yield component which is directly connected with lint production and therefore, it can be used for the evaluation of other yield components [13]. Therefore, it is of immense value to evaluate different breeding materials for ascertaining the expected and absolute variations for selection related to yield components and GOT (%) [4]. The outcome of any crop improvement depends upon the precise screening of multi-dimensional breeding materials and transgressive segregation is expected to be high among populations having desirable traits.

In our study, to develop more targeted breeding strategies to combine high yield with good ginning outturn, three separate populations that would be advanced for variety development were generated by using elite parents in terms of yield and fiber quality. Single seed plant descent was applied as the method of breeding for this purpose. Once all generations were obtained, we used our selection criteria including lint yield, GOT, fiber quality and seed cotton yield to determine the usefulness of the method.

MATERIALS AND METHODS

Plant material and trial layout. The present study was conducted at the experimental farm of Kahramamaras Sutcu Imam University at East Mediterranean Transitional Zone Agricultural Research Institute Kahramanmaras during the growing seasons from 2013 to 2015. The genetic materials used in this study included three populations belonging to *Gossypium hirsutum* L. and *G. barbadense* L. The first population derived from the cross between Nazilli84S x Askabat-100, second from Albania6172 x Giza-45 and the third was developed using Nazilli84S x IS-4. During 2013, F_2 generations of the three populations were sown on May the 13th in spaced plants; rows 70 cm apart and 20 cm between plants. Three weeks after planting, the plants were thinned to one plant. At the end of the season, two picks were done on single plant basis. After ginning, seeds were delinted. In 2014; $F_{2:3}$ generations, randomly selected single plant seeds from pop I, pop II and pop III, were sown on May the 15th. The plot size was 4 m long, 70 cm apart and 20 cm between plants within a row for each population. After full emergence, seedlings were thinned to one plant per hole. At maturity; the best plants were randomly selected from the families for seedcotton yield from each population. In season 2015, $F_{2:4}$ generations were sown on the 27th of April 2015 in randomized complete block design having three replications along with the parents with same plot size. Thinning was performed after two weeks of germination to ensure single plant per hole. In three growing seasons, the recommended cultural practices for cotton production were adopted similarly, other cultural practices including hoeing, irrigation, fertilizer and insecticide applications were carried out in accordance with the region's requirements. Picking was done manually on an individual plant basis during the month of October for calculating the data on various variables.

Traits measurement and statistical analysis. Data were recorded for bolls, boll weight and seedcotton yield per plant from guarded plants in each population. Then ginning was done using roller gin at Agriculture Faculty, Kahramanmaras Sutcu Imam University, Kahramanmaras Turkey. Ginning outturn (GOT %) calculated using the following formula:

$$GOT\ (\%) = \frac{Lint}{Seedcotton} \times 100$$

Analysis of variance was determined using SAS ($p < 0.01$) [14]. Frequency distribution of genotypes was calculated. Genotypic (GCV) and phenotypic coefficients of variance (PCV), and heritability (broad sense) were computed according to [15]. The genetic advance in percentage of mean was calculated by using the method described by [16].

RESULTS AND DISCUSSIONS

Relative values for means, range, and coefficient of variation (CV %) for different characters contributing to seedcotton yield between all populations (Nazilli84S x Askabat-100), (Albania6172 x Giza45) and (Nazilli84S x IS-4) are shown in (Table-1). Analysis of variance showed highly significant differences ($P \geq 0.01$) in all populations for seedcotton yield, yield components and ginning outturn (GOT %). The variability was ranged from

3.48 to 46.43 in $F_{2:4}$ populations. While Albania6172 x Giza 45 produced the highest CV (%) for seedcotton yield, the lowest value (3.48) was found for GOT (%) among individuals of Nazilli84S x IS-4, which depicted that broad variation is present among populations. Based on overall mean and variability performance of genotypes, Giza45, Albania6172 and Nazilli84S though performed well for couple of traits, yet none of the genotypes was superior for all the traits simultaneously. [17-18] evaluated upland cotton cultivars for determining valuable traits and observed highly significant differences for yield and yield components.

In our study, by using frequency distribution, we were able to observe that intra and interspecific populations had diverse traits in-contrast to parents and we thought it could be helpful for developing a new variant with more desirable characteristics (Fig. 1-3). Frequency distribution can be used for the detection of variation in a given population. Transgressive segregants can also be developed and genetic effects can be evaluated with such information [19].

TABLE 1
Descriptive statistics and analysis of variance of different characters for $F_{2:4}$ populations

Source of Variation	Populations	Max.	Min.	Mean	S.D	CV (%)	Mean Square		F Value
							Genotype (DF=115)	Error (DF=226)	
Seedcotton Yield* (g)	Nazilli84S x Askabat100	30.01	3.14	10.07	5.51	34.24	104.1	11.89	8.75**
	Albania6172 x Giza 45	40.32	3.14	17.27	9.21	46.43	254.35	64.27	3.96**
	Nazilli84S x IS-4	47.55	6.55	17.85	7.59	25.85	198.68	21.28	9.33**
Boll number*	Nazilli84S x Askabat100	16.33	2.33	5.17	2.08	31.06	15.59	2.57	6.05**
	Albania6172 x Giza 45	11.33	1.67	4.97	1.95	30.37	11.99	2.28	5.26**
	Nazilli84S x IS-4	18.33	2.33	7.03	3.33	24.09	36.72	2.87	12.79**
Boll weight (g)*	Nazilli84S x Askabat100	3.92	0.96	1.89	0.66	15,44	1.35	0.085	15.92**
	Albania6172 x Giza 45	6.39	1.02	3.34	1.09	22.7	3.6	0.57	6.27**
	Nazilli84S x IS-4	5.07	1.32	2.66	0.74	10.75	1.62	0.08	19.86**
G.O.T (%)*	Nazilli84S x Askabat100	45.72	36.12	39.37	1.93	5.32	11.28	4.39	2.57**
	Albania6172 x Giza 45	48.08	35.81	41.15	2.71	5.34	21.98	4.82	4.55**
	Nazilli84S x IS-4	48.78	40.62	45.22	1.89	3.48	20.84	2.48	8.40**

** = Highly significant 0.01
* = Per plant,
CV (%) = Coefficient of variation
S.D = Standard deviation
GOT (%) = Ginning outturn

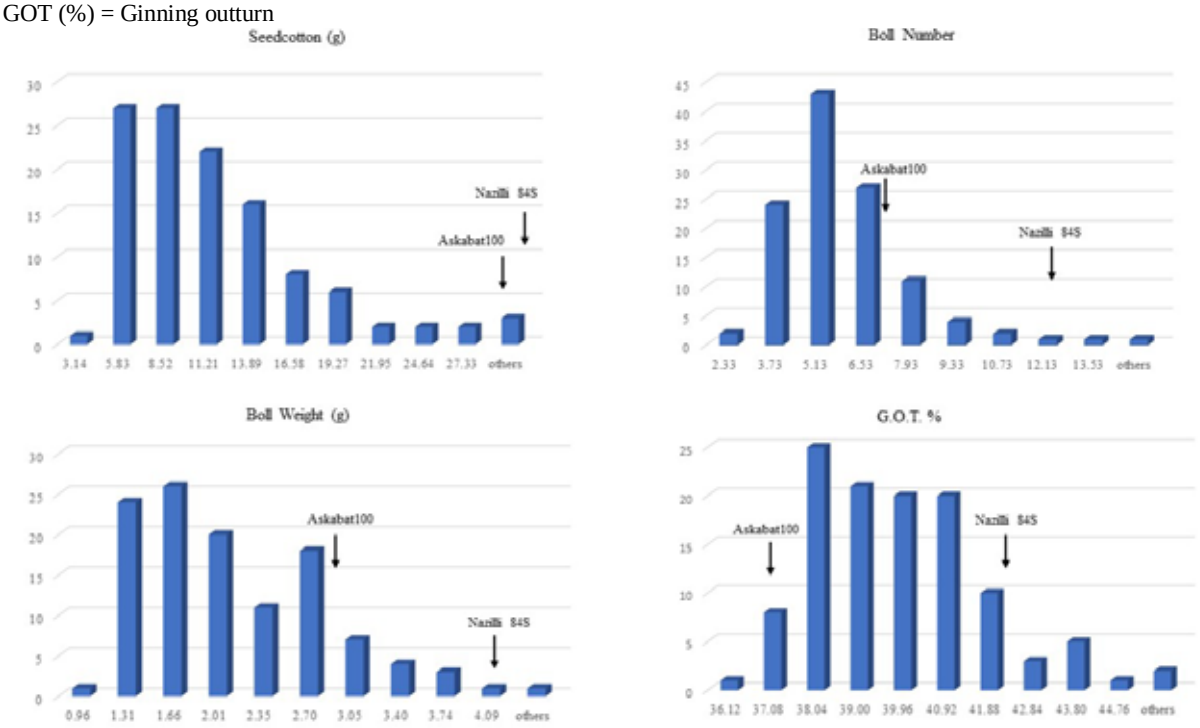

FIGURE 1
Frequency distribution for Nazilli84S x Askabat100 derived $F_{2:4}$ population

Plant yield showed wider ranges (3.14 - 48.78g) in all populations and maximum yield (48.78g per plant) was produced in Nazilli84S x IS-4 in-contrast to the parents (Fig. 1-3). Seedcotton yield per plant has genotypic variance ranged from 0.42 to 63.36 with highest found in Albania6172 x Giza 45 while genotypic coefficient of variance (GCV) ranged from 3.85 to 55.06. The maximum GCV (55.06%) was observed for seedcotton yield in the population developed from Nazilli84S x Askabat-100 (Table 2). On the other hand, phenotypic coefficient varied from 45.2 to 58.5% among all populations with maximum PCV (58.5) observed for seedcotton yield in Nazilli84S x Askabat100 followed with 53.32 in Albania6172 x Giza 45. The researchers usually observe decrease in genetic variability during variety development, which is a big hindrance for selection of parents for hybridization program. In order to keep breeding procedure on continuous scale via traditional ways, it is compulsory to have uniform genetic variation. In current research, we demonstrated that seedcotton yield is directly connected to yield components. Environmental coefficient of variation also revealed significant variation as it ranged between 25.84 and 46.42%. Our findings are in accordance with a number of previous studies [20, 1].

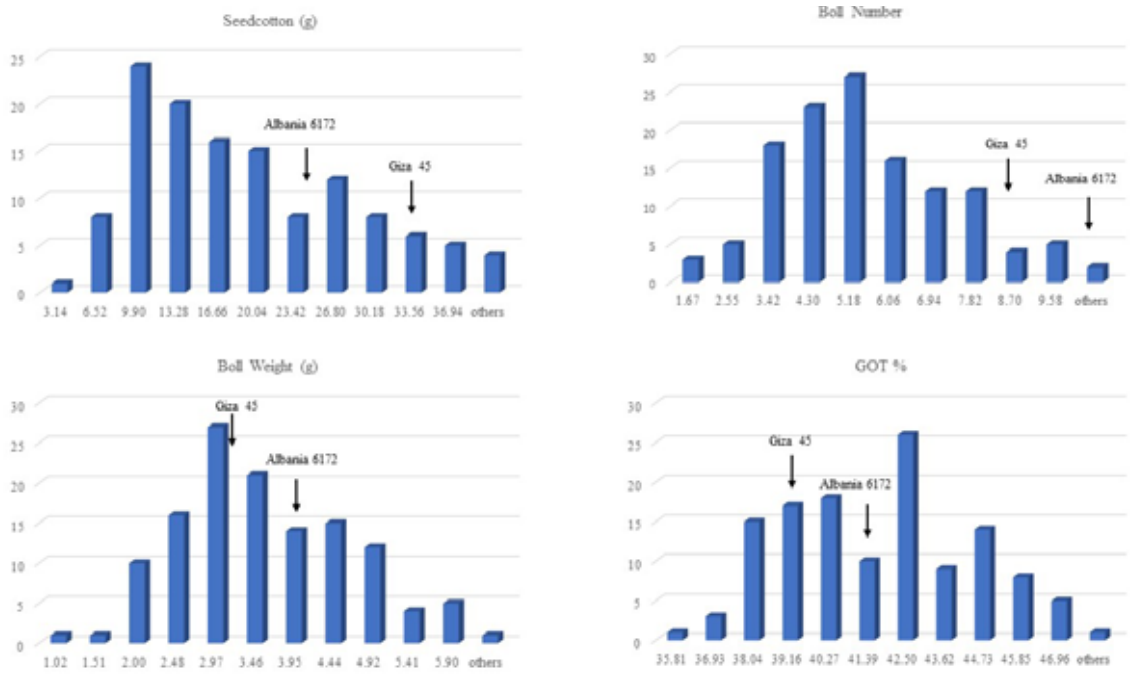

FIGURE 2
Frequency distribution for Albania6172 x Giza 45 derived $F_{2:4}$ population

TABLE 2
Genetic, environmental and phenotypic variances with heritability for various yield traits in $F_{2:4}$ populations

Parameters	Populations	Vg	GCV %	Vp	PCV %	ECV %	H^2	GA	GA %
Seedcotton yield* (g)	Nazilli84S x Askabat100	30.74	55.06	34.7	58.5	34.24	0.89	7.3	72.54
	Albania6172 x Giza 45	63.36	46.09	84.78	53.32	46.42	0.75	9.63	55.78
	Nazilli84S x IS-4	59.13	43.08	65.08	45.2	25.84	0.91	10.26	57.49
Boll number*	Nazilli84S x Askabat100	4.34	40.3	5.2	44.09	31.01	0.84	2.67	51.55
	Albania6172 x Giza 45	3.24	36.2	4.0	40.22	30.38	0.81	2.27	45.61
	Nazilli84S x IS-4	11.28	47.78	13.63	52.51	24.1	0.83	4.28	60.87
Boll weight*	Nazilli84S x Askabat100	0.42	34.36	0.45	35.49	15.43	0.94	0.88	46.56
	Albania6172 x Giza 45	1.01	30.09	1.20	32.8	22.6	0.84	1.29	38.65
	Nazilli84S x IS-4	0.51	26.94	0.54	27.63	10.63	0.95	0.98	36.77
G.O.T (%)*	Nazilli84S x Askabat100	2.3	3.85	3.76	4.93	5.32	0.61	1.66	4.21
	Albania6172 x Giza 45	5.72	5.81	7.33	6.58	5.34	0.78	2.96	7.19
	Nazilli84S x IS-4	6.12	5.47	6.95	5.83	3.48	0.88	3.25	7.19

* = plant, Vg = Genetic variance, Vp = Phonotypic variance, GCV = Genotypic coefficient of variation,
PCV = Phenotypic coefficient of variation, H^2 = Heritability (broad sense), GA = Genetic advance,
GA % = Genetic advance on mean basis,
GOT % = Ginning outturn

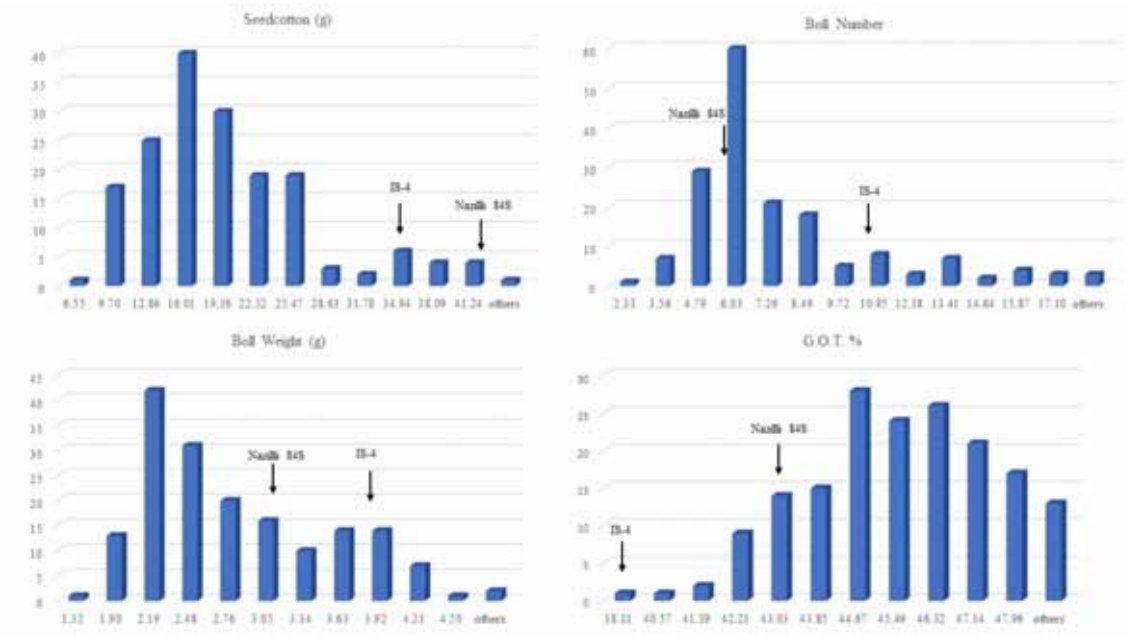

FIGURE 3
Frequency distribution for Nazilli84S x IS-4 derived $F_{2:4}$ population

Number of bolls ranged from 1.67 to 18.33 with a mean of 5.17, 4.97 and 7.03 between the populations as most bolls per plant found in Nazilli84S x IS-4. It was also observed from frequency distribution that the individuals in the $F_{2:4}$ populations were having more bolls per plant as compared to the parents (Fig. 1-3). Genotypic variances were calculated to be in the range of 3.24 to 11.28 and GCV was found to vary between 36.2 and 47.78 for number of bolls per plant while highest GCV (47.78%) was found in Nazilli84S x IS-4. Phenotypic coefficient of variation fluctuated from 40.22 to 52.51 and maximum 52.51% was in Nazilli84S x IS-4. It has been observed that environment has also influence upon this trait as its value was found to vary from 24.1 to 31.01%.

Boll weight was observed in the range of 0.96 to 6.39g with means of 1.89, 3.34 and 2.66 for all populations and Albania6172 x Giza 45 has the highest 6.39g boll weight. Moreover, the parents were having less boll weight as compared to $F_{2:4}$ populations. Genotypic coefficient of variation ranged from 26.94 to 34.36 and highest GCV (34.36%) was found in Nazilli84S x Askabat100 followed by Albania6172 x Giza 45 with 30.09. Our results showed that this character is highly heritable as values for heritability were between 0.84 and 0.95 for all populations with the highest (0.95) observed in Nazilli84S x IS-4. Genetic advance on mean basis was to be scaled from 36.77 to 46.56. The highest (46.56) value for this trait was detected in Nazilli84S x Askabat100. The ultimate goal of seedcotton yield production relies on number of bolls per plant and boll weight. In current research, we demonstrated that seedcotton yield is directly connected to yield components. We also found that Albania6172 x Giza-45 produced the highest genotypic and phenotypic variance for seedcotton (63.36 and 84.78 respectively). Genotypic and phenotypic variation for number of bolls per plant and boll weight were observed from 11.28 & 13.63 and 30.09 & 32.8 respectively (Table 2). Our findings are in accordance with a number of previous studies [20-22].

Ginning outturn percentage had its maximum (48.78) and minimum (35.81) values in filial populations (Fig. 1-3). The two populations having the highest GOT % (48.78 and 48.08) originated from Nazilli84S x IS-4 and Albania6172 x Giza 45, respectively, with the mean values of 45.22 and 41.15. GCV were calculated to vary between 3.85 and 5.81 and PCVs ranged from 4.93 to 6.58 among all populations. The ultimate outcome after ginning of seedcotton is presented as ginning outturn percentage, and it is expected to be high since it is an important attribute of fiber quality. Earlier findings which screened cotton genotypes for yield and yield components showed that this trait has a negative impact on seedcotton yield [23-24]. However, in our findings, we realized that some plants among $F_{2:4}$ populations developed from Nazilli84S x IS-4 had high GOT (%) and they can be used for developing breeding strategies for improving multiple characters at the same time. Overall, our observations in GOT were in accordance with the results of many previous studies such as [25-27]. Improvement in lint percentage and fiber yield could be the results of high selection intensity, genotypic coefficient of variance and heritability. These factors play a major role in genetic advances we encountered in two populations derived from Nazilli84S x Askabat100 and Albania6172 x Giza 45. Similar

results were obtained by [10, 27].

In the present study, there was a close correspondence between genotypic and phenotypic coefficient of variation for most recorded traits, which evidenced that these characters were barely influenced by the environment. Seedcotton yield on plant basis exhibited that environmental factors strongly affected the trait and it must be included for conduction of any breeding program.

Heritability allows the analysis of traits governed by many genes in genetic studies and highlights phenotypic coefficient variation role for breeding [28-29] Appropriate selection strategies can be developed using heritability estimated values for refinement of economic characters. Phenological selection allows steady estimation of genetic advance with GCV as well as heritability. In our study, seedcotton yield per plant, number of bolls per plant and boll weight produced moderately high to highly heritable values as they ranged from 0.75 to 0.91 (75 - 91%), 0.81 to 0.84 (81 - 84%), 0.84 to 0.95 (84 - 95%), respectively. In a population, variation is observed due to both genetics and environmental factors. However, only genetic variability is heritable from generation to the next generation. Since heritability alone does not give an idea about the expected gain in the next generation as environmental factors may vary, it has to be considered in conjunction with the genetic advance. Genetic advance on mean basis, on the other hand, was found to vary from 55.78 to 72.54, 45.61 to 60.87 and 36.77 to 46.56 in $F_{2:4}$ populations derived from Nazilli84S x Askabat100, Albania6172 x Giza 45 and Nazilli84S x IS-4 with respect to their order. [30-31] postulated that yield determination is more difficult than the determination of other phenological traits in cotton since it is also affected by other factors. Similarly to the researchers in the past, who calculated moderate to high heritability for bolls per plant, boll weight and seed cotton yield in upland cotton and concluded that these characters can be improved in advance generations of cotton [32-34], we also observed moderately high heritability for plant yield basis 0.75 with 55.78 genetic advance on mean basis in one of the crosses, namely Albania6172 x Giza 45.

CONCLUSION

It is interpreted that moderately high to very high heritability and moderate to high genetic advance observed among all characters which clearly showed the predominance of heritability and indicated the fact that they can be used for variety development. Albania6172 x Giza 45 population is really extreme population and different than others because Giza 45 is a late cultivar, Albania6172 is verticillium sensitive and tend to open bolls early in contrast to Giza. Other parents are tended to be closer to each other. This is why phenotypic variation is high.

REFERENCES

[1] Ahsan, M.Z., Majidano, M.S., Bhutto, H., Soomro, A.W., Panhwar, F.H., Channa, A.R. and Sial, B.K. (2015) Genetic variability, coefficient of variance, heritability and genetic advance of some *Gossypium hirsutum* L. Accessions. J. of Agri. Sci. 7, 147-151.

[2] Vineela, N., Murthy, S., Ramakumar, P.V. and Ratna, K.S. (2013) Variability studies for physio-morphological and yield components traits in american cotton (*Gossypium hirsutum* L.). J. of Agri. and Vet. Sci. 4, 7-10.

[3] Immer, F.R. (1941) Relation between yielding ability and homozygosis in barley crosses. J. of Amer. Soc. of Agro. 33, 200-206.

[4] El-Yazied, M.A., Soliman, Y.A.M. and El-Mansy, Y.M. (2014) Effectiveness of recurrent selection for improvement of some economic characters in Egyptian cotton. Egy. J. of Agri. Res. 1, 135-150.

[5] Jensen, N.F. (1988) Plant Breeding Methodology. Wiley Inter science, New York, NY.

[6] Richmond, T.R. (1951) Procedures and methods of cotton breeding with special reference to American cultivated species. Adv. Genetics. 4, 213–245.

[7] Tabasum, A., Aziz, I., Asghar, M.J. and Iqbal, M.Z. (2012) Inheritance of seed cotton yield and related traits in cotton (*G. hirsutum* L.). Pak. J. of Bot. 44, 2027-2031.

[8] Harlan, H.V., Martini, M.L., and Stevens, H. (1940) A study of methods in barley breeding. USDA Tech. Bull. 720. U.S Gov. Print. Office, Washington D.C.

[9] Weiss, M.G., Weber, C.R. and Kalton, R.R. (1947) Early generation testing in soybeans. J. of the Ameri. Soci. of Agro. 39, 791-811.

[10] Ahmed, M.F., Esmail, A.M., El-Marakby, A.M. and Rashed, M.A. (2003) Actual versus predicted genetic selection gains for some agronomic traits and identifying molecular markers assistant to selection for earliness in cotton crosses. Egy. J. of Plant Breed. 7, 419-438.

[11] Campbell, B.T., Chee, P.W., Lubbers, E., Bowman, D.T., Meredith, W.R., Johnson, J., Fraser, D., Bridges, W. and Jones, D.C. (2012). Dissecting genotype × environment interactions and trait correlations present in the Pee Dee cotton germplasm collection following seventy years of plant breeding. Crop Sci. 52, 690-699.

[12] Farooq, J., Anwar, M., Riaz, M., Farooq, A., Mahmood, A. and Shahid, M. (2014) Correlation and path coefficient analysis of earliness, fiber quality and yield contributing traits in cotton (*Gossypium hirsutum* L.). J. of Ani. and Pla. Sci. 24, 781-790.
[13] Coyle, G.G. and Smith, C.W. (1997) Combining ability for within-boll yield components in cotton *Gossypium hirsutum* L. Crop Sci. 37, 1118–1122.
[14] SAS. (1987) Statistical Analysis Systems. Procedures Guide for Personal Computers. SAS Institute Inc., Cary, North Carolina, USA.
[15] Johnson, H.W., Robinson, H.F. and Comstock, R.E. (1955) Genotypic and phenotypic correlation in soybean and their implications in selection. Agro. J. 47, 477-483.
[16] Falconer, D.S. (1989) Introduction to Quantitative Genetics. 3rd ed. Longman Scientific and Technical, Longman House, Burnt Mill, Harlow, Essex, England.
[17] Islam, M.K., Akhteruzzaman, M. and Sharmin, D. (2013) Multivariate and genetic component analysis of new cotton (*Gossypium hirsutum* L.) genotypes. Bangladesh J. Prog. Sci. Techno. 11, 185-190.
[18] Farooq, J., Anwar, M., Riaz, M., Mahmood, A., Farooq, A. and Iqbal, M.S. (2013) Association and path analysis of earliness yield and fibre related traits under cotton leaf curl virus (CLCuV) intensive conditions in *G. hirsutum* L. Plant Knowledge J. 2, 43-50.
[19] Preetha, S. and Raveendran, T.S. (2007) Genetic variability and association analysis in three different morphological groups of cotton (*Gossypium hirsutum* L.). Asian J. of Plant Sci. 6, 122-128.
[20] Abbas, H.G., Mahmood, A. and Ali, Q. (2013) Genetic variability, heritability, genetic advance and correlation studies in cotton (*Gossypium hirsutum* L.). International Res. J. of Microbio. 4, 156-161.
[21] Rao, P.J.M. and Gopinath, M. (2013) Association analysis of yield and fibre quality characters in upland cotton (*Gossypium hirsutum* L.). Aust. J. Basic Appl. Sci. 7, 787-790.
[22] Raza, H., Khan, N.U., Khan, S.A., Gul, S., Latif, A., Khan, J.H., Raza, S. and Baloch, M. (2016) Genetic Variability and Correlation Studies in F4 Populations of Upland Cotton. The J. of Animal and Plant Sci. 26, 1048-1055.
[23] Arshad, M., Afzal, M, Khan, M.I. and Mahmood, R. (2003) Performances of newly developed cotton strains for economic and fiber traits in national coordinated varietal trials. Pak. J. of Sci. and Ind. Res. 46, 373-375.
[24] Iqbal, M., Chang, M.A., Iqbal, M.Z., Hassan, M.U., Nasir, A. and Islam, N. (2003) Correlation and path coefficient analysis of earliness and agronomic characters of upland cotton in Multan. Pak. J. of Agro. 2, 160-168.
[25] Lioyd, M.O. and Bridges, B.C. (1995) Breeding cotton for conventional and late planted production system. Crop Sci. 35, 132-136.
[26] Khan, N.U., Basal, H. and Hassan, G. (2010) Cottonseed oil and yield assessment via economic heterosis and heritability in intraspecific cotton populations. Afri. J. of Biotech. 9, 7418-7428.
[27] El-Lawendey, M.M., El-Mansy, Y.M. and Soliman, Y.A. (2008) Multivariate analysis of economic characters in cotton (*Gossypium barbadense* L.). Min. J. of Agri. Res. 33, 955-972.
[28] Dabholkar, A.R. (1992) Elements of biometrical genetics. Concept Publishing Company, New Delhi, India.
[29] Falconar, D.S. and Mackay, T.F. (1996) Introduction of quantitative genetics. 4th ed. Longman, Essex. England. 464p.
[30] Ahmed, A.E., Abdalla, A.H. and Fadlalla, A.S. (2006) A note on the stability of five medium staple cotton (*G. hirsutum* L.) varieties for some fiber properties in the Gezira scheme of the Sudan. Univ. of Khartoum J. of Agri. Sci. 14, 313-319.
[31] Magadum, S., Banerjee, U., Ravikesavan, R., Gangapur, D. and Boopathi, N.M. (2012) Variability and heritability analysis of yield and quality traits in interspecific population of cotton (*Gossypium Spp.*). Bioinfol. 9, 484-487.
[32] Batool, S., Khan, N.U., Makhdoom, K., Bibi, Z., Hassan, G., Marwat, K.B., Ullah, F., Raziuddin, K.B. and Khan, I.A. (2010) Heritability and genetic potential of upland cotton genotypes for morpho-yield traits. Pak. J. of. Bot. 42, 1057-1064.
[33] Ahmad, M., Khan, N.U., Mohammad, F., Khan, S.A., Munir, I., Bibi, Z. and Shaheen, S. (2011) Genetic potential and heritability studies for some polygenic traits in cotton (*G. hirsutum* L.). Pak. J. of. Bot. 43, 1713-1718.
[34] Khan, F.K., Rehman, S., Abid, M.A., Malik, W., Hanif, M., Bilal, M., Qanmber, G., Latif, A., Ashraf, J. and Farhan, U. (2015) Exploitation of Germplasm for Plant Yield Improvement in Cotton (*Gossypium hirsutum* L.). Green Physio. Genet. Gen. 1, 1-10.

Received: **25.09.2017**
Accepted: **18.03.2019**

CORRESPONDING AUTHOR

Adem Bardak
Department of Agricultural Biotechnology,
Faculty of Agriculture,
Kahramanmaras Sutcu Imam University,
46100 Kahramanmaras – Turkey

e-mail: adembardak@ksu.edu.tr

© by PSP Volume 28 – No. 5/2019 pages 4101-4105 Fresenius Environmental Bulletin

EFFECTS OF ZEOLITE, GYPSUM AND SULFURIC ACID APPLICATIONS ON AMMONIA VOLATILIZATION FROM CHICKEN FRESH MANURE

Ilknur Gumus*

Department of Soil Science and Plant Nutrition, Faculty of Agriculture, University of Selcuk, 42031 Konya, Turkey

ABSTRACT

Volatile ammonia, which emanate from chicken fresh manure significantly contributes to the atmospheric nitrogen pollution, adversely poultry performance and decreasing of manure's fertilizer value. Nowadays, the proliferation of organic wastes is attributed to the scaling up of poultry farms, and these organic wastes generate a plethora of ammonia losses, which in turn jeopardize atmospheric quality. These organic residues with regard to their use as nutrient source and soil conditioners in agricultural areas is considered one of their recycling ways and their fertility value is contingent on the extent of plant nutrients which lies in organic fertilizers obtained from these organic wastes. Therefore, the aim of this study was to investigate the effects of zeolite, sulfuric acid and gypsum applications on nitrogen losses as ammonia gas (NH_3) from chicken fresh manure. The experiment was carried out in a closed system under laboratory condition whereby two different concentrations (1 and 2%) of zeolite, gypsum and sulfuric acid were separately applied to 250g of chicken fresh manure based on oven dry weight. The prepared samples were left to the incubation for 6 days and then daily and total nitrogen losses as NH_3 were measured by vacuuming at certain intervals. The experimental results showed that the addition of zeolite, gypsum and sulfuric acid at the rate of 1% substantially decreased the nitrogen losses in gas form by 32%, 53.31% and 52.29% respectively, while the application of zeolite, gypsum and sulfuric acid at the rate of 2% significantly reduced losses by 54.23%, 58.87% and 62.09% respectively.

KEYWORDS:
Ammonia volatilization, chicken manure, gypsum, sulfuric acid, zeolite

INTRODUCTION

Currently, intensive production of poultry and livestock has raised a serious environmental concern with the public. Specifically, ammonia is considered the most harmful gas in the broiler houses and can not only induce environmental problems, but also be detrimental to the health and performance of birds [1]. The applications of chicken manure to agricultural land are the significant source of ammonia (NH_3) emissions to the atmosphere, which in turn has a deleterious effect on the environment. Additionally, this emission also induces the loss of available N for crop uptake [2]. The volatilization of ammonia during manure handling and storage noticeably decreases the agronomic value of the product and occasions a significant contribution to the environmental pollution [3].

The poultry industry progress in Turkey is expected to continue in the incoming years and also the poultry sector is rapidly developing at large. Chickens are often grown in the production houses at densities of 13.5–21.2 bird m^{-2}. There are 323 million poultry in Turkey according to the last agricultural census [4]. The amount of wet waste of these animals is about 5,923,571 t y^{-1} and these wastes could be largely a problem for businesses if it is not properly used [5]. The poultry produce daily feces of 3 to 4% by body weight. On the average, the rate of one bird excretion into the poultry house is estimated as 22 kg/year. Despite of the increasing significance of poultry in recent years, there is an insufficient effort for properly removal of chicken wastes. The produced wastes are collected into the open storage pits which are around the plant and then transported to another area from the plant. It was revealed that approximately 7 million tons of poultry feces lead to the environmental problems in Turkey [6]. Additionally, in the poultry houses, ammonia (NH_3) volatilization from poultry litter impairs bird health, decreases the fertilizer value of litter, and adversely impacts the environmental quality [7]. The reduction of ammonia volatilization through combining of poultry manure and chemical amendment has been found to increase agricultural productivity.

The objective of this research was to study the effects of the additives zeolite, sulfuric acid and gypsum on NH_3 volatilization from chicken fresh manure within the short period of time.

MATERIALS AND METHODS

The experiment was carried out under laboratory conditions during the incubation of 6 days by employing of chicken fresh manure, which was supplied from a poultry farm. The natural Turkish zeolite (Gördes town of Manisa) used as adsorbent in this study was a commercial sample supplied from Rota A.Ş Mining Company, İstanbul, Turkey. The natural zeolite samples were crushed in a mortar and sieved through 250 µm sieve. The crushed samples were dried in an oven at 105 ºC for 24h before being used in the experiment. The experiment was carried out using a randomized complete plot design with four replications. The treatments per kg of chicken manure were: 250g of chicken manure based on oven dry weight, two different concentrations of zeolite, gypsum and sulfuric acid (1-2%) that were applied to each unit.

Ammonia volatilization from soil was measured by a closed airflow system with modifications [8]. The system consisted of an exchange chamber (2.5 L glass bottle), a trap (500 ml glass bottle) and stopper fitted with both an inlet and outlet. The inlet of the chamber was connected to an air pump and the outlet was connected by polyethylene pipe to trap containing boric acid solution (%1.5). Chicken manure (250 g) was placed in the glass bottle. The treatments were mixed homogeneously, before being applied to the chicken fresh manure. The prepared samples were left to incubation for 6 days at 22 ± 3 °C, after being arranged, water was added to bring moisture content to 50% and then daily and total nitrogen losses as NH_3 were measured by vacuuming with certain intervals. Air passed through 2.30 L min^{-1} and released NH_3 was captured in the trapping solution containing 100 ml boric acid with bromocresol green and methyl red indicator. The incubation glass bottle was maintained at room temperature. Boric acid- indicator was replaced every day and back titrated with 0.002 N H_2SO_4, to estimate released NH_3.

Statistical analysis of data. The collected data from the experiment were analyzed using analysis of variance tests based on randomized plot design (using F-LSD at $P < 0.05$) according to the procedures outlined by [9]. All statistical results were calculated using the one-way Analysis of Variance procedure on MINITAB statistic software package [10].

RESULTS AND DISCUSSIONS

Some characteristics of the chicken fresh manure prior to the start of the experiment are presented in Table 1. Fresh manure from chickens if the feces are collected and stored on a regular basis significantly losses occurs. It was evidenced that the reduction of fertilizer value of the feces is the main reason of causing nitrogen loss in ammonia (NH_3) form [11]. As it is presented in table 1, the pH of the chicken fresh manure used during the experiment is higher. Research indicated that ammonia volatilization increased pH, moisture content, wind speed, NH_3 concentration and temperature [12]. Additionally, it is believed that pH increases with increasing of the NH_3 to NH_4^+ ratio, thereby resulting in increased volatilization rates [13]. Moore et al. [14] revealed that NH_3 volatilization from poultry litter dramatically increased once the pH rose above 7.0.

TABLE 1
Some properties of the chicken fresh manure (CFM) used in the study

Properties	CFM
pH in water (1:5)	8,62
EC in water (1:5)(dS cm-1)	9,54
Organic matter (%)	73,17
$CaCO_3$ (%)	4,36
C (%)	39,46
N (%)	3.60
C/N	10,96

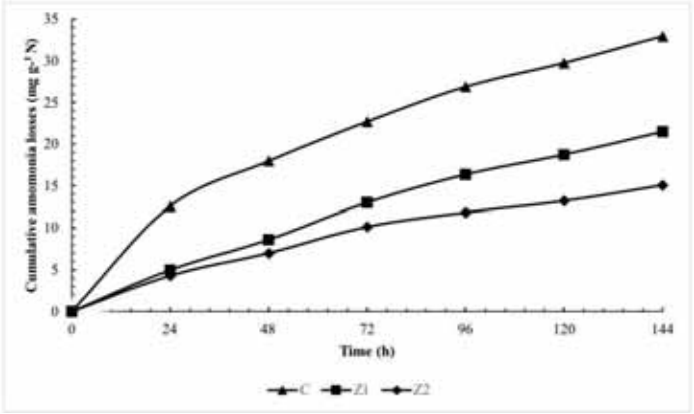

FIGURE 1
The effects of zeolite on nitrogen losses in the form of ammonia gas (NH_3) from chicken fresh manure

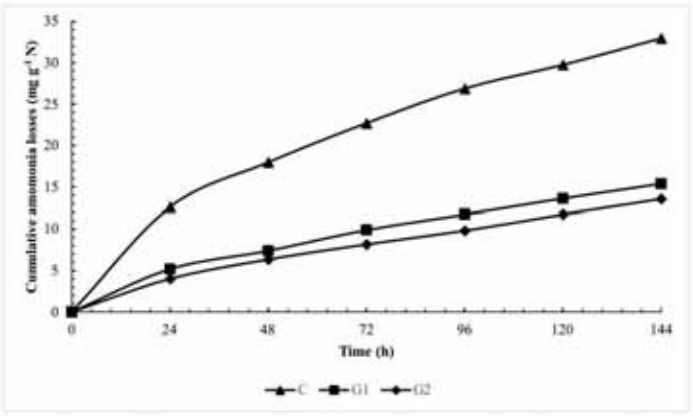

FIGURE 2
The effects of gypsum on nitrogen losses in the form of ammonia gas (NH_3) from chicken fresh manure

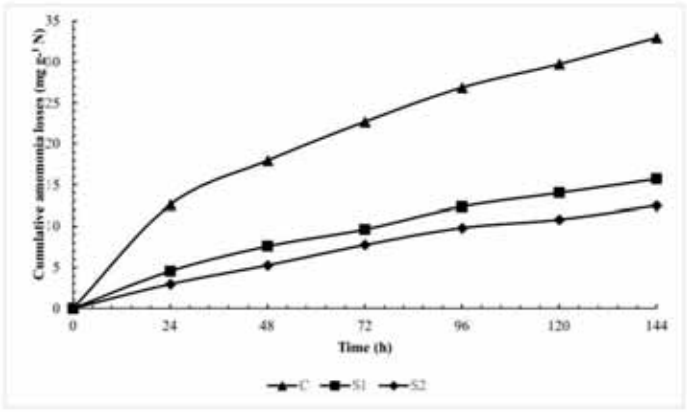

FIGURE 3
The effects of sulfuric acid on nitrogen losses in the form of ammonia gas (NH_3) from chicken manure

Ammonia volatilization from the chicken fresh manure was initially high but decreased with time. As it is shown in Figure 1, experimental results showed that the average cumulative ammonia volatilization from the untreated chicken fresh manure (control) during the incubation period of 144 hours was 32.95 mg N. The effects of zeolite on nitrogen losses in the form of ammonia gas (NH_3) from chicken manure were given in Figure 1. The results of the study revealed that the average cumulative ammonia volatilization of 1 and 2% of zeolite application during the incubation period of 144 hours were 22.32 and 15.08 mg N respectively. From the observation of Figure 1, application of 1 and 2 % of zeolite application to chicken manure compared to the control resulted in reducing of NH_3 volatilization by 32 and 54.23 % respectively. It was evidenced that Zeolites are naturally occurring alumino silicate minerals with a high cation exchange capacities [15]. Zeolite is characterized by a rigid three- dimensional lattice with tunnels that are 10^{-9} m in size containing internal exchange sites that have an affinity for NH_4^+. The small sizes of the tunnels physically protect NH_4^+ from nitrification by microbes and may reduce ammonia volatilization [16, 17]. Kithome et al. [18] stated that the zeolite and chemical amendments are proposed to be the most suitable for reducing NH_3 losses during composting of poultry manure. Gümüş and Şeker [19] reported that zeolite applications decreased the nitrogen losses in gas form during two years of trials under field condition.

As it is shown in Figure 2, the experimental results indicated that the average cumulative ammonia volatilization by applying of 1 and 2% of gypsum during the incubation period of 144hours were 15.38 and 13.55 mg N respectively. The application of 1 and 2 % gypsum to chicken fresh manure compared to the control, decreased NH_3 volatilization by 53.31 and 58.87 % respectively. Furthermore, the addition of sulphate salts fertilizers and manures reduced NH_3 volatilization. Similar study done by Zia et al. [20] found that gypsum application reduced NH_3 volatilization from a range of ammonium-based fertilizers. Additionally, mineral amendments such as gypsum, rock phosphate, superphosphate, $CaCl_2$ and bentonite were used to reduce NH_3 volatilization from cattle and chicken manure. It was evidenced that the reduction of NH_3 volatilization is apparently attributed to the decrease of pH of the manure due to amendments [21]. The evidenced study indicated that gypsum

application was an effective amendment encountered in reducing ammonia volatilization in poultry manure [19]. The aforementioned results were also validated by Zia et al. [20] whereby hydrated calcium sulfate (gypsum) application reduced NH_3 volatilization from a range of ammonium-based fertilizers.

From the observation of Figure 3, the results of the study revealed that the average cumulative ammonia volatilization through 1 and 2% of sulfuric acid application during the incubation period of 144 hours was 15.72 and 12.49 mg N respectively and the application of 1 and 2 % sulfuric acid to chicken fresh manure compared to the control significantly decreased NH_3 volatilization by 52.29 and 62.09 % respectively. Moreover, the addition of chemical amendments reduced NH_3 losses and various acids are used to reduce nitrogen which is lost as ammonia gas from fertilizers. It is perceived that the chemical amendments namely phosphoric acid or aluminum sulphate ($Al_2(SO_4)_3.14H_2O$) decreased NH_3 volatilization. It was evidenced that poultry litter treated with H_3PO_4 decreased NH_3 volatilization by 44%, while the poultry manure treated with aluminum sulphate scaled down NH_3 volatilization by 62% [3]. Additionally, Sulfuric acid and aluminum sulphate applications significantly reduced NH_3 emissions, and the greatest decrease relative to raw slurry were obtained with H_2SO_4 (75% in pig and 81% in dairy slurry) and aluminum sulphate (69% in pig and 87% in dairy slurry) [22].

CONCLUSIONS

Reducing NH_3 volatilization during in-house composting at high level, caged layer facilities cost, effectiveness at reducing atmospheric NH_3 concentrations below critical levels for poultry and human health, and impacts on the composting process and end product quality has to be considered. Results from this study indicate that zeolite, gypsum and sulfuric acid are the most efficacious in reducing ammonia volatilization from chicken fresh manure of the tested compounds. Experimental result revealed that zeolite, gypsum and sulfuric acid (2%) applications significantly reduced the losses of ammonia volatilization. Additionally, gypsum and sulfuric acid are used to increase the acidity of manure while reducing losses of ammonia volatilization. The selectivity of the natural zeolites for a particular ion, such as NH_4^+, is very much contingent on its origin as well as the type of ions already present in the structure. Since the high NH_3 levels in chicken houses induce the major economic losses to producers, the use of zeolite, gypsum and sulfuric acid as a chemical amendment play a significant role in increasing poultry productivity, while decreasing the negative environmental impact.

ACKNOWLEDGEMENTS

The author would like to thanks Prof. Dr. Cevdet Şeker and Phd student Noel Manirakiza for his helpful comments and Hamza Negiş for his helpful laboratory analysis, which were conducted under the auspices of the Department of Soil Science and Plant Nutrition, Faculty of Agriculture, University of Selçuk.

REFERENCES

[1] Moore Jr, P.A., Daniel, T.C., Edwards, D.R., and Miller, D.M. (1995) Effect of Chemical Amendments on Ammonia Volatilization from Poultry Litter. Journal of Environmental Quality. 24(2), 293-300.

[2] Misselbrook, T.H., Nicholson, F.A., and Chambers, B.J. (2005) Predicting ammonia losses following the application of livestock manure to land. Bioresource Technology. 96, 159–168.

[3] Witter, E., and Kirchmann, H. (1989) Effects of addition of calcium and magnesium salts on ammonia volatilization during manure decomposition. Plant and Soil. 115, 53-58.

[4] TUIK (2016) www.tuik.gov.tr/doi: 21871

[5] Avcioglu, A.O., Colak, A., Turker, U. (2013) Turkey's Chicken Waste Biogas Potential. Journal of Tekirdag Agricultural Faculty. 10(1), 21-28.

[6] Eleroglu, H., Yildiz, S. and Yildirim, A. (2013) The Applied Methods for Removal of Poultry Feces That Creates Environmental Problem. Gaziosmanpasa Journal of Scientific Research. 2, 14-24.

[7] Burt, C.D. (2015) Gypsum Effect on Broiler Litter. getd.libs.uga.edu. https://getd.libs.uga.edu/pdfs/burt_christopher_d_201512_phd.pdf.

[8] Siva, K.B., Aminuddin, H., Husni, M.H.A., and Manas, A.R. (1999) Ammonia Volatilization from Urea as Affected by Tropical- based Palm Oil Palm Effluent (pome) and Peat. Communications in Soil Science Society of America Journal. 48, 921-926.

[9] Snedecor, G.W. and Cochron, W.G. (1980) Statistical Methods. 7th Edition. Iowa State. University Press. Ames Iowa.

[10] Minitab (1995) Minitab Reference Manuel (Release 7.1). Minitab Inc. State Coll. PA. 16801. USA.

[11] Taban, S., Turan, M.A., Katkat, A.V. (2013) Agriculture Organic Matter and Chicken Manure. Journal of Poultry Research. 10, 9-13.

[12] Reddy, K.R., Khaleel, R., Overcash, M.R. and Westerman, P.W. (1979) A non-point source model for land areas receiving animal wastes: II. Ammonia volatilization. Trans. ASAE. 22, 1398–1405.

[13] DeLaune, P.B., Moore Jr., P.A., Daniel, T.C. and Lemunyon, J.L. (2004) Effect of Chemical and Microbial Amendments on Ammonia Volatilization from Composting Poultry Litter. J. Environment Quality. 33, 728-734.
[14] Moore Jr., P.A., Huff, W.E., Daniel, T.C., Edwards D.R. and Sauer T.C. (1997) Effect of aluminum sulfate on ammonia fluxes from poultry litter in commercial broiler houses. In Proc. 5th Int. Symp. on Livestock Environ., Bloomington, MN. 29–31 May 1997. Vol. 2. Am. Soc. Agric. Eng., St. Joseph, MI. 883–891.
[15] McCrory, D.F. and Hobbs, P.J. (2001) Additives to Reduce Ammonia and Odor Emissions from Livestock Wastes: A Review. J. Environmental Quality. 30, 345-355.
[16] Ferguson, G.A. and Pepper, I.L. (1987) Ammonium Retention in Sand Amended with Clinoptilolite. Soil Science of America Journal. 51, 231-234.
[17] Guisnet, M. and Gilson, J.P. (2002) Introduction to Zeolite Science and Technology. Zeolites for Cleaner Technologies. Elvesier. https://doi. org/10.1142/9781860949555_0001. 1-28.
[18] Kithome, M., Paul, J.W. and Bomke, A.A. (1999) Reducing Nitrogen Losses during Simulated Composting of Poultry Manure using Adsorbents or Chemical Amendments. J. Environmental Quality. 28, 194-201.
[19] Gumus, I. and Seker, C. (2010) Effects of Zeolite Application on Nitrogen Losses From an Fresh and Composted Poultry Manure in Corn Farming. International Scientific Conference Devoted to The 65-Th Anniversary of The U.U. Uspanov Institute of Soil Science And Agrichemistry. Current Condition of Soil Surface, Conservation and Reproduction of Soil Fertility. 13-17 September 2010 Kazakistan Almaata.
[20] Zia, M.S., Aslam, M., Arshad, M. and Ahmed, T. (1999) Ammonia Volatilization from Nitrogen Fertilizers with and without Gypsum. Soil Use Management. 15, 133-135.
[21] Termeer, W.C. and Warman, P.R. (1993) Use of Mineral Amendments to Reduce Ammonia Losses from Dairy- Cattle and Chicken Manure Slurries. Bioresource Technology. 44, 217-222.
[22] Regueiro, I., Coutinho, J. and Fangueiro, D. (2016) Alternatives to Sulfuric Acid for Slurry Acidification: Impact on Slurry Composition and Ammonia Emissions during Storage. J. Clean Prod. 131, 296-307.

Received: **02.01.2018**
Accepted: **14.03.2019**

CORRESPONDING AUTHOR

Ilknur Gumus
Selçuk University
Faculty of Agriculture
Department of Soil Science and Plant Nutrition
42100 Konya – Turkey

e-mail: ersoy@selcuk.edu.tr

© by PSP Volume 28 – No. 5/2019 pages 4106-4113 Fresenius Environmental Bulletin

COMPARATIVE STUDY OF OXIDATIVE DEGRADATION OF TETRACYCLINE IN AQUEOUS SOLUTION BY $Fe^{2+}/Na_2S_2O_8$ AND $Fe^0/Na_2S_2O_8$ PROCESS

Liangbo Zhang*

National Engineering Laboratory for Wheat & Corn Further Processing, College of Chemistry, Chemical and Environmental Engineering, Henan University of Technology, Zhengzhou 450001, China

ABSTRACT

Comparative experimental studies were conducted to investigate the oxidative degradation of tetracycline (TC), one of the most frequently detected pharmaceuticals in waters, by $Fe^{2+}/Na_2S_2O_8$ and $Fe^0/Na_2S_2O_8$ process. Results showed that the removal efficiencies of TC in $Fe^0/Na_2S_2O_8$ system were higher than those in $Fe^{2+}/Na_2S_2O_8$ system in certain adding dosage of activator, concentration of persulfate (PS), temperature, pH and initial concentration of TC. The TC removal increased with the increments of PS concentration, temperature and the initial concentration of TC in the two systems. However, the rise of pH caused a negative effect on the performance of TC degradation. In addition, TC removal increased and then decreased with the increment of initial activator (Fe^{2+} and Fe^0) dosages. Results showed that 0.1 mmol·L^{-1} was the best amount of Fe^{2+} and Fe^0, where the removals of TC could reach to 87.6% and 91.8% respectively. When the concentration of PS was 2.0 mmol·L^{-1}, the removals of TC in $Fe^{2+}/Na_2S_2O_8$ and $Fe^0/Na_2S_2O_8$ system could reach 59.0% and 77.7%, respectively. The TC degradation followed a first-order kinetics pattern and acidic circumstance favored the degradation of TC in the two systems. For $Fe^0/Na_2S_2O_8$ system, the removals of TC were high, increased from 75.3% to 79.9% corresponding of TC initial concentrations from 30 to 100 mg·L^{-1}. However, for $Fe^{2+}/Na_2S_2O_8$ system, the removals of TC increased from 25.7% to 52.7% under same reaction conditions.

KEYWORDS:
Tetracycline, Zero valent iron, Advanced oxidation processes (AOPs), Sulfate radicals, Degradation

INTRODUCTION

The presence of antibiotics in water environment is a serious threat to the public health and living condition. Tetracyclines (TCs) are a group of antibiotics that have been widely used in human and veterinary applications as either medication or growth enhancing substances [1]. The widespread overuse of TCs, especially in the industry of livestock feeding, results to the pollution of surface and underground water at many sites around the world [2, 3]. Furthermore, this may cause environmental risks and human health problems through the food chain enrichment seriously. Compared to conventional biological treatment (i.e. activated sludge process) or physical treatment, Advanced oxidation processes (AOPs) have been proposed as one kind of effective alternatives for treating antibiotics. And these technologies have been successfully used to deal with the recalcitrant compounds which have relative high solubility and stability at room temperature [4-6]. Reactive oxygen species, such as hydroxyl radicals (·OH) can be produced during AOPs, which are effective in the degradation of many kinds of non-biodegradable pollutants.

But recently, the sulfate radicals ($SO_4^{\bullet-}$) has been applied to degrade organic contaminants widely [7-10]. Sulfate radicals can be generated from the decomposition of persulfate ions ($S_2O_8^{2-}$) by using heat [11], light [12], transition metals [13], as shown in the following reaction (Eq. (1)) [14].

$$S_2O_8^{2-} + \text{heat/UV} \rightarrow 2SO_4^{\bullet-} \quad (1)$$

Owing to the advantages of cost effectiveness, high activity and the environmentally friendly nature, Fe^{2+} has been commonly selected as the activator of persulfate (PS) to generate $SO_4^{\bullet-}$ in practical application [15]. The corresponding reaction equations are as follows.

$$S_2O_8^{2-} + Fe^{2+} \rightarrow SO_4^{\bullet-} + SO_4^{2-} + Fe^{3+} \quad (2)$$

$$SO_4^{\bullet-} + Fe^{2+} \rightarrow SO_4^{2-} + Fe^{3+} \quad (3)$$

However, the activation method has some disadvantages, such as Fe^{2+} can be oxidized into Fe^{3+}, in addition, the excessive Fe^{2+} can act as a scavenger of $SO_4^{\bullet-}$ and iron sludge produced in the reaction process is not reusable effectively [16].

Zero valent iron (Fe^0) due its non-toxic, cheap, high reactivity, is now considered useful for removing organic contaminants [17]. The Fe^0-Fenton oxidation integrates Fe^0 reduction and Fenton oxidation is regarded as an effective process for degrading organic contaminants, where it is usually preceded by Fe^0 reduction process [18]. The use of Fe^0 overcomes the disadvantage of Fe^{2+} and has the advantage of avoiding the addition of other anions by

ferrous salts [19]. Fe^0 can produce Fe^{2+} by the following reactions:

$$Fe^0 \rightarrow Fe^{2+} + 2e \quad (4)$$

$$Fe^0 + 2H_2O \rightarrow Fe^{2+} + 2OH^- + H_2 \quad (5)$$

$$Fe^0 + 2Fe^{3+} \rightarrow 3Fe^{2+} \quad (6)$$

To data, $Fe^0/Na_2S_2O_8$ system has been reported to remove many non-biodegraded organic pollutants such as *p*-nitrophenol [20], dyes [21] and bisphenol A [22]. However, to the best of our knowledge, very limited information is available on the oxidation of TC in water by $Fe^0/Na_2S_2O_8$ process.

The object of this study was to compare the degradation performances of TC between $Fe^{2+}/Na_2S_2O_8$ and $Fe^0/Na_2S_2O_8$ process. Then, several key influencing factors were evaluated, including the initial activator dosage (Fe^{2+} and Fe^0), the concentration of PS, temperature, pH and the initial concentration of TC.

MATERIALS AND METHODS

Materials. The commercial tetracycline hydrochloride [$C_{22}H_{25}N_2O_8Cl$] (USP grade, 99%) was used in this study. Its characteristic information was shown in Table 1. Sodium persulfate ($Na_2S_2O_8$, 98%) and $FeSO_4 \cdot 7H_2O$ was purchased from Kimiou Chemical Reagent Co. Ltd. (Tianjin, China). Ethanol (EtOH), sodium hydroxide (NaOH) and sulfuric acid (H_2SO_4) were obtained from Luoyang Reagent Co. Ltd. (Henan, China). Sample solutions were prepared using deionized water.

Procedure. A stock solution of tetracycline was prepared fresh with deionized water before each experiment and the initial concentration was fixed at 50 $mg \cdot L^{-1}$ except for the experiment investigating the influence of initial TC concentration on the removal rate. Then $FeSO_4 \cdot 7H_2O$ or Fe^0 were added into 50 mL of tetracycline solution with constant stirring by using a thermostatic water bath oscillator (ZWY-110×30, China) and stirred for a certain time, the agitation speed was 150 $r \cdot min^{-1}$, the temperature could be regulated by thermostatic water bath oscillator. Finally, $Na_2S_2O_8$ was added to start the reaction. When the reaction completed, the water sample from the supernatant after filtered by 0.22 μm filter membrane was send to be measured by high performance liquid chromatography (HPLC).

Concentrations of TC were determined based on the calibration curves and accordingly the removal efficiency (*R*%) of TC was calculated using the following equation:

$$R\% = \frac{C_0 - C_t}{C_0} \times 100\% \quad (7)$$

where *R*% represented the TC removal efficiency, C_0 ($mg \cdot L^{-1}$) was the initial concentration of TC in the solution, and C_0 ($mg \cdot L^{-1}$) expressed the concentration of TC at *t* min.

Analysis methods. TC samples were quantified with HPLC (Thermo Fisher UltiMate 3000, USA) equipped with an HYPERSIL. C18 analytical HPLC 5-μm (4.6 mm×250 mm) reversed phase column and UV detector (DIONEX UltiMate 3000) with the detection wavelength of 359 nm. The column temperature was 30°C and the injection volume was 20 μL. The mobile phase was a mixture of acetonitrile and oxalic acid (0.1 $mol \cdot L^{-1}$) at a ratio of 31:69 (v/v). The flow rate was 1.0 $mL \cdot min^{-1}$.

RESULTS AND DISCUSSION

Effect of initial activator dosage. In this study, two different forms of iron sources (Fe^{2+} and Fe^0) were used to test the formation of $SO_4^{\bullet-}$. The TC removals in different adding amounts of two iron sources were shown in Fig. 1.

According to Fig. 1, the removal of TC in $Fe^0/Na_2S_2O_8$ system was higher than that in $Fe^{2+}/Na_2S_2O_8$ system in certain adding dosage of activator. Moreover, the degradation regularity of TC in $Fe^0/Na_2S_2O_8$ system was consistent with that in $Fe^{2+}/Na_2S_2O_8$ system. The TC removal increased and then decreased with the increment of adding amounts.

TABLE 1
Characteristics of tetracycline hydrochloride

Chemical structures	Molecular mass ($g \cdot mol^{-1}$)	Molecular formula	Ionization constant pK_a
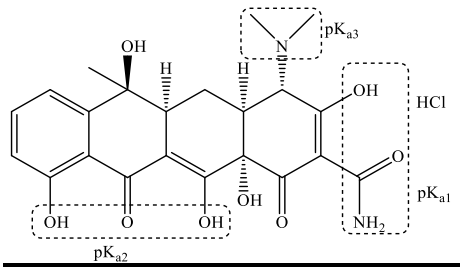	480.9	$C_{22}H_{24}N_2O_8 \cdot HCl$	pK_{a1}=3.3 pK_{a2}=7.3 pK_{a3}=9.7

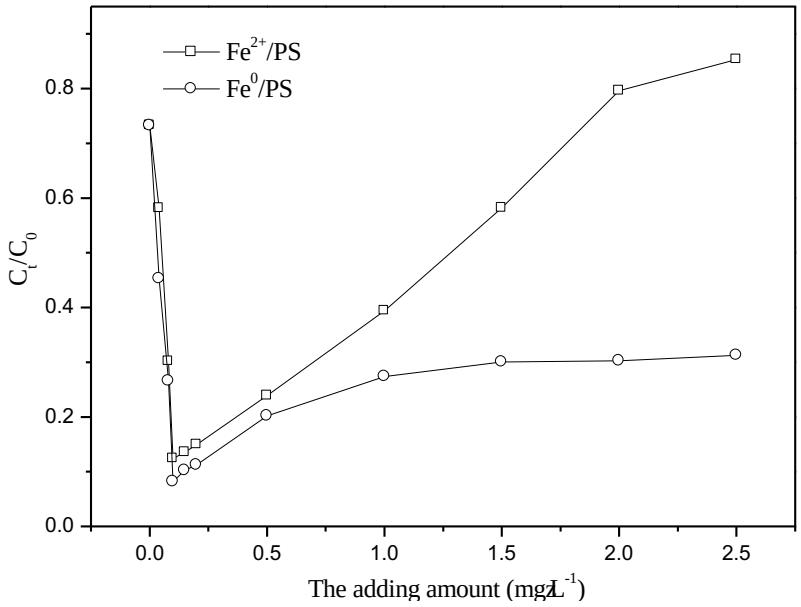

FIGURE 1
TC removals in different adding amounts of Fe^{2+} and Fe^0 in $Fe^{2+}/Na_2S_2O_8$ and $Fe^0/Na_2S_2O_8$ system

When the adding amounts of Fe^{2+} or Fe^0 were zero, namely without activator to activate $Na_2S_2O_8$, the removal rate of TC was 26.7%. Moreover, when the adding amounts of Fe^{2+} and Fe^0 reached 0.1 mmol·L^{-1}, the removals of TC were 87.6% and 91.8% respectively. But when adding amounts of Fe^{2+} and Fe^0 increased from 0.1 to 2.5 mmol·L^{-1}, the corresponding removals of TC decreased from 87.6% and 91.8% to 14.7% and 68.7% respectively. Results showed that moderate Fe^{2+} and Fe^0 can promote the degradation of TC, but the inhibitory action may appear when the adding amounts of Fe^{2+} and Fe^0 increase to a certain value. This is probably expressed by equations (2) and (3), caused by such reasons.

For Fe^{2+}, when the concentration of Fe^{2+} is high, $SO_4^{\bullet-}$ produced by equation (2) can react with Fe^{2+} lied in solution (see Eq. (3)), which inhabiting the degradation of TC. In addition, the ferrous ion could also decompose persulfate anion according to reaction (8). Thus, excess amount of Fe^{2+} would lead to the declination of TC removal efficiency. Similar tread was also observed by Chen et al. [23], who reported the removal of MTBE decreased with excessive Fe^{2+} because of the reaction between Fe^{2+} and $SO_4^{\bullet-}$. Peng et al. drew the similar conclusion that a 0.5/1 M ratio of Fe^{2+}/PS was observed to be best [24].

$$S_2O_8^{2-} + 2Fe^{2+} \rightarrow 2SO_4^{2-} + 2Fe^{3+} \quad (8)$$

For Fe^0, excess the Fe^0 dosage likely provided too much Fe^{2+} which could scavenge $SO_4^{\bullet-}$ produced in the $Fe^0/Na_2S_2O_8$ system (Eq. (3)), leading to reduce the overall degradation efficiency. Wang et al. drew the similar conclusion that the optimum Fe^0 to $Na_2S_2O_8$ molar ratio was 2:1 and the oxidation was complete almost in 60 min [25].

According to Fig. 1, Fe^0 has higher ability than Fe^{2+} to activate PS oxidizing TC. Since Fe^{2+} quickly activate PS to generate $SO_4^{\bullet-}$, it is evident the degradation of TC decreases when any excess Fe^{2+} content. A higher degradation of TC was obtained using Fe^0 as a source of dissolved Fe^{2+}, where Fe^0 can serve as a slow-releasing source of dissolved Fe^{2+} to improve generated sulfate radicals [26].

Effect of the concentration of PS. PS concentration is a critical parameter as the source of sulfate radicals in $Fe^{2+}/Na_2S_2O_8$ and $Fe^0/Na_2S_2O_8$ system. The TC removals in different concentrations of PS in two systems were shown in Fig. 2. It was indicated that the removal efficiency of TC in $Fe^0/Na_2S_2O_8$ system was higher than that in $Fe^{2+}/Na_2S_2O_8$ system in certain concentration of PS. Moreover, the degradation regularity of TC in $Fe^0/Na_2S_2O_8$ system was consistent with that in $Fe^{2+}/Na_2S_2O_8$ system, the TC removal increased with the increasing of PS concentration.

When the concentration of PS increased from 0.5 to 5.0 mmol·L^{-1}, the removals of TC in $Fe^{2+}/Na_2S_2O_8$ and $Fe^0/Na_2S_2O_8$ system increased from 25.6% and 64.5% to 70.3% and 82.0% respectively. When the concentrations of PS in the two systems were zero, the removal of TC were around 13.0%, indicating low oxidation efficiency. According to Fig. 2, when the concentration of PS was above 2.0 mmol·L^{-1}, the removals of TC in $Fe^{2+}/Na_2S_2O_8$ and $Fe^0/Na_2S_2O_8$ system had no obvious variations, ranged from 59.0% and 77.7% to 70.3% and 82.0% respectively, which indicated the degradation efficiency of TC had no notable increase when the concentration of PS reached a certain degree.

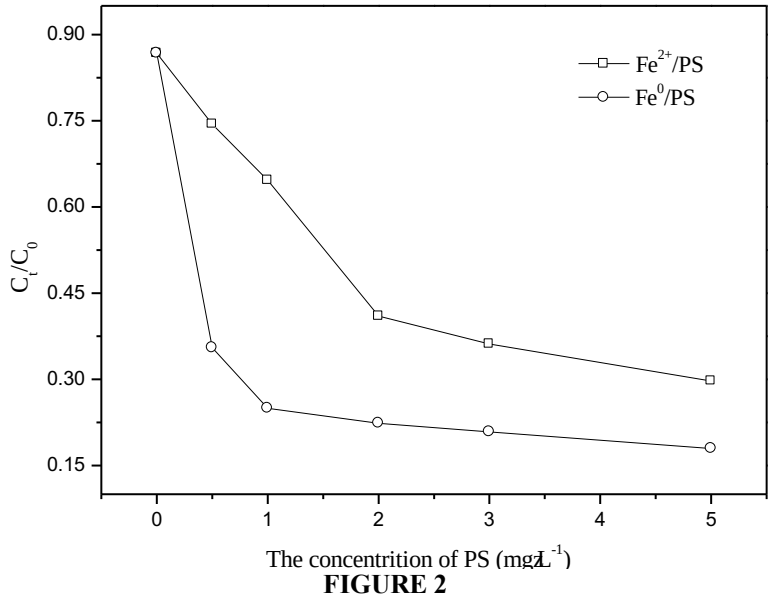

FIGURE 2
TC removals in different concentrations of PS in $Fe^{2+}/Na_2S_2O_8$ and $Fe^0/Na_2S_2O_8$ system

It should be noted that, as for $Fe^{2+}/Na_2S_2O_8$ and $Fe^0/Na_2S_2O_8$ process, when the PS concentration is low, increasing the concentration of oxidant is essential for generating a higher level of $SO_4^{\bullet-}$ to overcome the competition of other organic materials and inorganic ions [27]. However, at higher persulfate concentrations, more $SO_4^{\bullet-}$ would be generated, correspondingly. But excessive $SO_4^{\bullet-}$ could be decomposed according to the following Eqs. (9) and (10).

$$SO_4^{\bullet-} + S_2O_8^{2-} \rightarrow SO_4^{2-} + S_2O_8^{\bullet-} \quad (9)$$

$$SO_4^{\bullet-} + SO_4^{\bullet-} \rightarrow S_2O_8^{2-} \quad (10)$$

As for $Fe^0/Na_2S_2O_8$ process, with the increasing concentration of PS, more PS molecules can reach the surface of Fe^0 and react with Fe^0 and Fe^{2+}. In addition, with the increment of PS, the fixed dosage of Fe^0 limits the available amount of $SO_4^{\bullet-}$.

In all, based on the effects of TC oxidation and the dosage of oxidant, the optimal PS concentration was ultimately considered as 2.0 mmol·L^{-1} as the initial concentration in this study.

In $Fe^0/Na_2S_2O_8$ system, a higher degradation of TC was obtained using Fe^0 as a source of dissolved Fe^{2+} and the higher activity of Fe^0 than that of Fe^{2+}. In addition, the curve of degradation of $Fe^{2+}/Na_2S_2O_8$ process was milder than that of $Fe^0/Na_2S_2O_8$ process. It is probably that Fe^{2+} in liquid phase can react with $Na_2S_2O_8$ to produce $SO_4^{\bullet-}$ with the increase of PS steadily. Nevertheless, as solid phase in $Fe^0/Na_2S_2O_8$ system, the strong activity of Fe^0 results in the removal of TC increased rapidly with the low dosage of PS, however, more PS molecules can reach the surface of Fe^0 and occupy the active site of Fe^0 surface with the increasing of PS, which lead to the gently removal of TC.

Effect of temperature. Temperature affects the rate of chemical reaction. In general, the higher temperature is favorable for the reaction. The effects of temperature on TC degradation in $Fe^{2+}/Na_2S_2O_8$ and $Fe^0/Na_2S_2O_8$ system at 30, 50, 70 and 90°C were shown in Fig. 3. It was indicated that the removal efficiency of TC in $Fe^0/Na_2S_2O_8$ system was higher than that in $Fe^{2+}/Na_2S_2O_8$ system in certain temperature. Moreover, the degradation regularity of TC in $Fe^0/Na_2S_2O_8$ system was consistent with that in $Fe^{2+}/Na_2S_2O_8$ system, the TC removal increased with the increment of temperature.

According to Fig. 3, when the temperature increased from 30 to 90°C, the removals of TC in $Fe^{2+}/Na_2S_2O_8$ system and $Fe^0/Na_2S_2O_8$ system ranged from 58.9% and 77.0% to 70.4% and 93.8%, respectively. Result showed that the absorbed energy of TC increases when the temperature rises, which increasing the concentration of $SO_4^{\bullet-}$. Moreover, the reaction rate constant also increases with the increase of temperature. The degradation process followed the first-order kinetics pattern in the two systems. The reaction rate constants of different temperature were listed in Table 2. It also indicated more $SO_4^{\bullet-}$ were generated in the $Fe^{2+}/Na_2S_2O_8$ and $Fe^0/Na_2S_2O_8$ system due to the activation of persulfate by heat and more Fe^{2+} with the increase of temperature, and the rate constant (k) increased from 0.0043, 0.0073 to 0.0060, 0.0104 min^{-1} with the temperature ranged from 30 to 90°C respectively.

According to the apparent kinetic rate constants at different temperatures, the activation energy for TC degradation by the two systems was calculated by the Arrhenius equation (Eq. (11)) [28].

$$\ln k = -\frac{E_a}{RT} + \ln A_0 \quad (11)$$

where A_0 is the Arrhenius factor, E_a is the Arrhenius activation energy (kJ·mol^{-1}), R is the gas constant (8.314 J·(mol·K)$^{-1}$) and T is the solution temperature (K). As shown in Fig. 4, a linear

relationship was obtained in the Arrhenius plot of ln$k$ versus $1 \cdot T^{-1}$. The activation energy (E_a) calculated through the slope were 5.173 and 5.223 kJ·mol^{-1} in $Fe^{2+}/Na_2S_2O_8$ and $Fe^0/Na_2S_2O_8$ system respectively, suggesting that degradation of TC in the two systems could be easily achieved.

Effect of pH. According to Fig. 5, when pH increased from 3.0 to 12.0, the removals of TC in $Fe^{2+}/Na_2S_2O_8$ and $Fe^0/Na_2S_2O_8$ system ranged from 56.6% and 80.9% to 30.4% and 60.7% respectively. The removal rate of TC decreased with the increase of pH. It could be seen that acidic circumstance favored the degradation of TC. The reason might be ascribed to the increase of the formation rate of Fe^{2+} or Fe^0 (Eq. (12)), which could generate more $SO_4^{\bullet-}$ in the two systems under the condition of acidic circumstance.

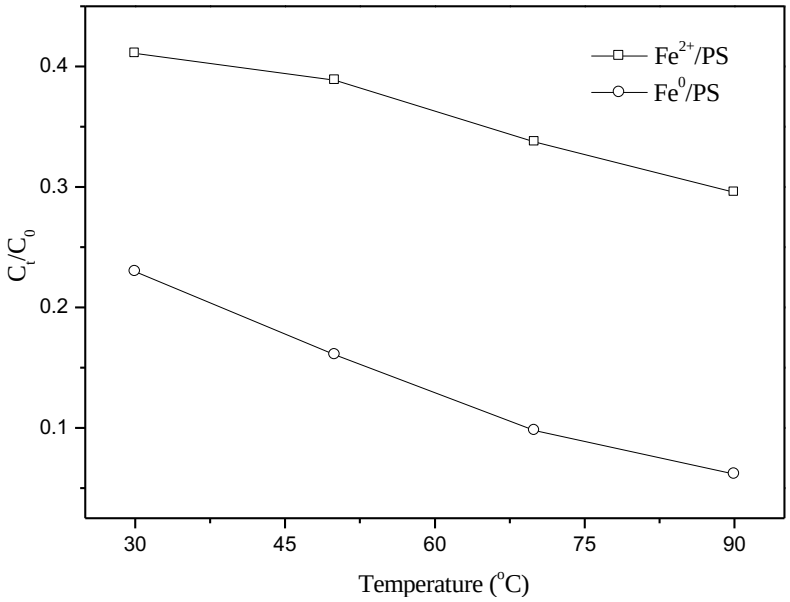

FIGURE 3
TC removals in different temperature in $Fe^{2+}/Na_2S_2O_8$ and $Fe^0/Na_2S_2O_8$ system

TABLE 2
Kinetics parameters of different temperatures in $Fe^{2+}/Na_2S_2O_8$ and $Fe^0/Na_2S_2O_8$ system

Temperature (°C)	Reaction rate constant (min^{-1})		Correlation coefficient (R^2)	
	$Fe^{2+}/Na_2S_2O_8$ process	$Fe^0/Na_2S_2O_8$ process	$Fe^{2+}/Na_2S_2O_8$ process	$Fe^0/Na_2S_2O_8$ process
30	0.0043	0.0073	0.9693	0.9742
50	0.0046	0.0085	0.9826	0.9673
70	0.0053	0.0092	0.9961	0.9816
90	0.0060	0.0104	0.9819	0.9757

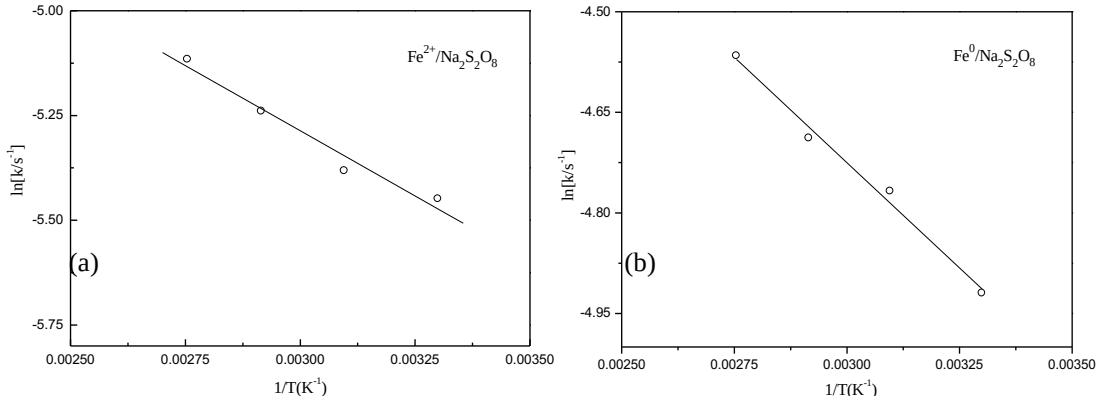

FIGURE 4
The relationship between observation constants and temperature.
(a)$Fe^{2+}/Na_2S_2O_8$ process; (b) $Fe^0/Na_2S_2O_8$ process

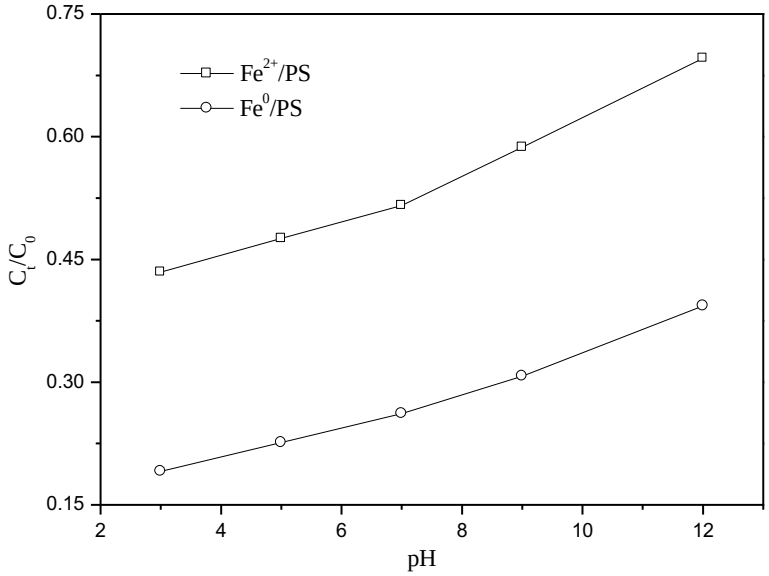

FIGURE 5
TC removals in different pH in $Fe^{2+}/Na_2S_2O_8$ and $Fe^0/Na_2S_2O_8$ system

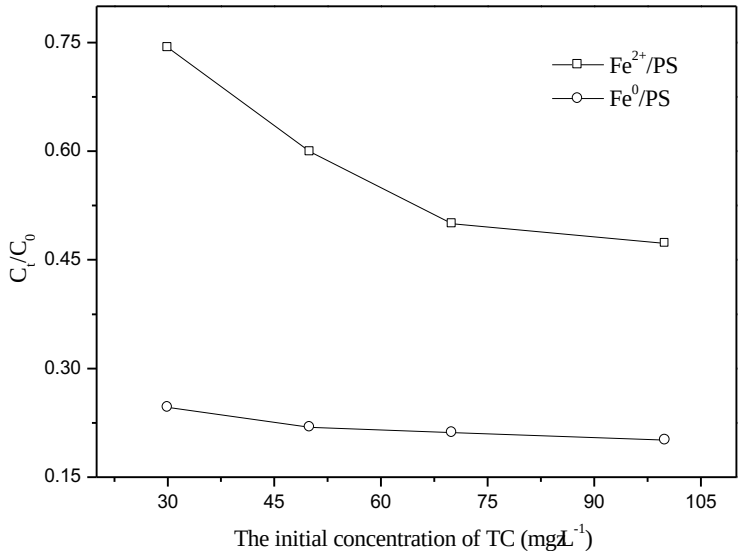

FIGURE 6
TC removals in different initial concentration of TC in $Fe^{2+}/Na_2S_2O_8$ and $Fe^0/Na_2S_2O_8$ system

$$Fe^0 + 2H^+ \rightarrow Fe^{2+} + H_2 \quad (12)$$

Moreover, it was indicated that the removal efficiency of TC in $Fe^0/Na_2S_2O_8$ system was higher than that in $Fe^{2+}/Na_2S_2O_8$ system in certain pH.

In acidic surrounding, the O–O bond in PS brakes into $SO_4^{\bullet-}$ and HSO_4^- asymmetrically (Eq. (13)).

$$S_2O_8^{2-} + H^+ \rightarrow SO_4^{\bullet-} + HSO_4^- \quad (13)$$

The activity energy of uncatalyzed reaction of $S_2O_8^{2-}$ is 140 kJ·mol^{-1}, but that of catalyzed reaction is 108.8 kJ·mol^{-1} [29], thus acidic condition is favorable to degrade TC. Alkaline condition remarkably inhibits the degradation, the removal rate decreases with the increment of pH. Because Fe^{2+} and Fe^{3+} are almost insoluble at a high pH, the iron ions turn into iron hydroxides and participate in bottom of the reactor. Furthermore, $SO_4^{\bullet-}$ can turn into ·OH in alkaline condition (Eq. (14)). Despite the low oxidation-reduction potential, $SO_4^{\bullet-}$ can be purged by ·OH under the condition of high pH (Eq. (15)) [30].

$$SO_4^{\bullet-} + OH^- \rightarrow SO_4^{2-} + \cdot OH \quad (14)$$

$$2SO_4^{\bullet-} + 2\cdot OH \rightarrow 2HSO_4^- + O_2 \quad (15)$$

In addition, the $Fe^0/Na_2S_2O_8$ system was effective for TC degradation, the reason might be ascribed to the increase of the formation rate of Fe^{2+} (Eq. (8)), which could generate more $SO_4^{\bullet-}$ in this system steadily.

Effect of initial concentration of TC. Since the concentration of target pollutant influenced on activity of the catalyst which impacted the generation and utilization efficiency of $SO_4^{\bullet-}$, the effects of initial TC (30, 50, 70, 100 mg·L^{-1}) in $Fe^{2+}/Na_2S_2O_8$

and $Fe^0/Na_2S_2O_8$ system were investigated (see Fig. 6).

According to Fig. 6, it was indicated that the removal efficiency of TC in $Fe^0/Na_2S_2O_8$ system were higher than that in $Fe^{2+}/Na_2S_2O_8$ system in certain initial concentration of TC. Moreover, the degradation regularity of TC in $Fe^0/Na_2S_2O_8$ system was consistent with that in $Fe^{2+}/Na_2S_2O_8$ system, the TC removal increased with the increment of its initial concentration.

For $Fe^{2+}/Na_2S_2O_8$ process, the removals of TC increased from 25.7% to 50.0% when the initial concentration of TC increased from 30 to 70 $mg \cdot L^{-1}$, indicating an obvious variation. When the initial concentration of TC was over 70 $mg \cdot L^{-1}$, the removal efficiency of TC varied insignificant. However, for $Fe^0/Na_2S_2O_8$ process, the removals of TC increased from 75.3% to 79.9% when the initial concentration of TC increased from 30 to 100 $mg \cdot L^{-1}$, indicating an inconspicuous variation.

The reason might be ascribed that the increasing initial TC concentration leads to increasing the probability of reaction between TC and the sulfate radical. Consequently, many more TC molecules improved the utilization efficiency of $SO_4^{\bullet-}$ and this led to more TC being degraded.

CONCLUSIONS

The removal efficiencies of TC in $Fe^0/Na_2S_2O_8$ system were higher than those in $Fe^{2+}/Na_2S_2O_8$ system in certain adding dosage of activator, concentration of persulfate (PS), temperature, pH and initial concentration of TC. Moreover, the degradation regularities of TC in $Fe^0/Na_2S_2O_8$ system were consistent with those in $Fe^{2+}/Na_2S_2O_8$ system under several different influence factors investigated in this study.

The TC removal increased with the increments of PS concentration, temperature and the initial concentration of TC in the two systems. However, the rise of pH caused a negative effect on the performance of TC degradation. In addition, TC removal increased and then decreased with the increment of initial activator dosages. 0.1 $mmol \cdot L^{-1}$ was determined as the best adding amounts of Fe^{2+} and Fe^0. In this study, the optimal PS concentration was ultimately considered as 2.0 $mmol \cdot L^{-1}$. Results showed that the TC degradation followed first-order kinetics pattern in the two systems. Acidic circumstance favored the degradation of TC. In conclusion, $Fe^0/Na_2S_2O_8$ process can be as a potential technology for purifying tetracycline polluted water.

ACKNOWLEDGEMENTS

The authors acknowledge the financial support from National Engineering Laboratory for Wheat & Corn Further Processing, Henan University of Technology (Grant No. NL2018010). We also thank the anonymous reviewers for their careful review and valuable suggestions on the manuscript.

REFERENCES

[1] Ji, Y., Shi, Y., Dong, W., Wen, X., Jiang, M. and Lu, J. (2016) Thermo-activated persulfate oxidation system for tetracycline antibiotics degradation in aqueous solution. Chem. Eng. J. 298, 225-233.

[2] Wan, Y., Jia, A., Zhu, Z. and Hu, J. (2013) Transformation of tetracycline during chloramination: kinetics, products and pathways. Chemosphere. 90(4), 1427-1434.

[3] Mboula, V.M., Hequet, V., Gru, Y., Colin, R. and Andrces, Y. (2012) Assessment of the efficiency of photocatalysis on tetracycline biodegradation. J. Hazard. Mater. 209-210(4), 355-364.

[4] Xin, Y.J., Liu, H.L, Han, L. and Zhou, Y.B. (2011) Comparative study of photocatalytic and photoelectrocatalytic properties of alachlor using different morphology TiO_2/Ti photoelectrodes. J. Hazard. Mater. 192, 1812-1818.

[5] Zhao, Q., Ge, Y., Zuo, P., Shi, D. and Jia, S. (2016) Degradation of Thiamethoxam in aqueous solution by ozonation: Influencing factors, intermediates, degradation mechanism and toxicity assessment. Chemosphere. 146, 105-112.

[6] Antoniou, M.G., de la Cruz, A.A. and Dionysiou, D.D. (2010) Degradation of microcystin-LR using sulfate radicals generated through photolysis, thermolysis and e-transfer mechanisms. Appl. Catal. B Environ. 96, 290-298.

[7] Guan, Y.H., Ma, J., Ren, Y.M., Liu, Y.L., Xiao, J.Y., Lin, L.Q. and Zhang, C. (2013) Efficient degradation of atrazine by magnetic porous copper ferrite catalyzed peroxymonosulfate oxidation via the formation of hydroxyl and sulfate radicals. Water Res. 47(14), 5431-5438.

[8] Ye, T.T., Wei, Z.S., Spinney, R., Tang, C.J., Luo, S., Xiao, R.Y. and Dionysiou, D.D. (2017) Chemical structure-based predictive model for the oxidation of trace organic contaminants by sulfate radical. Water Res. 116, 106-115.

[9] Frontistis, Z., Mestres, E.M., Konstantinou, I. and Mantzavinos, D. (2016) Removal of cibacron black commercial dye with heat- or iron-activated persulfate: statistical evaluation of key operating parameters on decolorization and degradation by-products. Desalin. Water Treat. 57, 2616-2625.

[10] Xiao, R.Y., Ye, T.T., Wei, Z.S., Luo, S., Yang, Z.H. and Spinney, R. (2015) Quantitative Structure Activity Relationship (QSAR) for the Oxidation of Trace Organic Contaminants by Sulfate Radical. Environ. Sci. Technol. 49(22), 13394-13402.
[11] Kordkandi, S.A. and Forouzesh, M. (2014) Application of full factorial design for methylene blue dye removal using heat-activated persulfate oxidation. J. Taiwan Inst. Chem. E. 45, 2597-2604.
[12] Shih, Y.J., Li, Y.C. and Huang, Y.H. (2013) Application of UV/persulfate oxidation process for mineralization of 2,2,3,3-tetrafluoro-1-propanol. J. Taiwan Inst. Chem. E. 44, 287-290.
[13] Ding, Y., Zhu, L., Wang, N. and Tang, H. (2013) Sulfate radicals induced degradation of tetrabromobisphenol A with nanoscaled magnetic $CuFe_2O_4$ as a heterogeneous catalyst of peroxymonosulfate. Appl. Catal. B Environ. 129, 153-162.
[14] House, D.A. (1962) Kinetics and mechanism of oxidations by peroxydisulfate. Chem. Rev. 62, 185-203.
[15] Rastogi, A., Al Abed, S.R. and Dionysiou, D.D. (2009) Effect of inorganic, synthetic and naturally occurring chelating agents on Fe(II) mediated advanced oxidation of chlorophenols. Water Res. 43, 684-694.
[16] Nidheesh, P.V. and Gandhimathi, R. (2012) Trends in electro-Fenton process for water and wastewater treatment: An overview. Desalination. 299, 1-15.
[17] Cheng, R., Wang, J.L. and Zhang, W.X. (2007) Comparison of reductive dechlorination of *p*-chlorophenol using Fe^0 and nanosized Fe^0. J. Hazard. Mater. 144(1-2), 334-339.
[18] Xu, L. and Wang, J. (2011) A heterogeneous Fenton-like system with nanoparticulate zerovalent iron for removal of 4-chloro-3-methyl phenol. J. Hazard. Mater. 186, 256-264.
[19] Li, H., Wan, J., Ma, Y., Wang, Y. and Huang, M. (2014) Influence of particle size of zero-valent iron and dissolved silica on the reactivity of activated persulfate for degradation of acid orange 7. Chem. Eng. J. 237, 487-496.
[20] Lai, B., Zhang, Y.H., Li, R., Zhou, Y.X. and Wang, J. (2014) Influence of operating temperature on the reduction of high concentration *p*-nitrophenol (PNP) by zero valent iron (ZVI). Chem. Eng. J. 249, 143-152.
[21] He, C., Yang, J.N., Zhu, L.F., Zhang, Q., Liao, W.C., Liu, S.K., Liao, Y., Asi, M.A. and Shu, D. (2013) pH-dependent degradation of acid orange II by zero-valent iron in presence of oxygen. Sep. Purif. Technol. 117, 59-68.
[22] Xi, Y., Sun, Z., Hreid, T., Ayoko, G.A. and Frost, R.L. (2014) Bisphenol A degradation enhanced by air bubbles via advanced oxidation using in situ generated ferrous ions from nano zero-valent iron/palygorskite composite materials. Chem. Eng. J. 247, 66-74.
[23] Chen, K.F. and Liang, S.H. (2009) Methyl tert-butyl ether (MTBE) degradation by ferrous ion-activated persulfate oxidation: feasibility and kinetics studies. Water Environ. Res. 81, 687-694.
[24] Peng, H.J., Zhang, W., Liu, L. and Lin, K.F. (2017) Degradation performance and mechanism of decabromodiphenyl ether (BDE209) by ferrous-activated persulfate in spiked soil. Chem. Eng. J. 307, 750-755.
[25] Wang, Q.F., Shao, Y.S., Gao, N.Y., Chu, W.H., Deng, J., Shen, X., Lu, X., Zhu, Y.P. and Wei, X.Y. (2016) Degradation of alachlor with zero-valent iron activating persulfate oxidation. J. Taiwan Inst. Chem. E. 63, 379-385.
[26] Oh, S.Y., Kang, S.G. and Chiu, P.C. (2010) Degradation of 2,4-dinitrotoluene by persulfate activated with zero-valent iron. Sci. Total Environ. 408, 3464-3468.
[27] Tsitonaki, A., Petri, B., Crimi, M., Mosbæk, H., Siegrist, R.L. and Bjerg, P.L. (2010) In situ chemical oxidation of contaminated soil and groundwater using persulfate: a review. Environ. Sci. Technol. 40, 55-91.
[28] Xu, X.R. and Li, X.Z. (2010) Degradation of azo dye Orange G in aqueous solutions by persulfate with ferrous ion. Sep. Purif. Technol. 72, 105-111.
[29] Kolthoff, I.M. and Miller, I.K. (1951) The chemistry of persulfate. I. The kinetics and mechanism of the decomposition of the persulfate ion in aqueous medium. J. Am. Chem. Soc. 73(7), 3055-3059.
[30] Criquet, J. and Leitner, N.K.V. (2009) Degradation of acetic acid with sulfate radical generated by persulfate ions photolysis. Chemosphere. 77, 194-200.

Received: **27.02.2018**
Accepted: **28.03.2019**

CORRESPONDING AUTHOR

Liangbo Zhang
National Engineering Laboratory for Wheat & Corn Further Processing, College of Chemistry, Chemical and Environmental Engineering, Henan University of Technology, Zhengzhou 450001 – China

e-mail: zlb@haut.edu.cn

© by PSP Volume 28 – No. 5/2019 pages 4114-4122 Fresenius Environmental Bulletin

PHYSIOLOGICAL RESPONSES OF ALFALFA SEEDLINGS TO FREEZE-THAW CYCLES AND ALKALINE SALT STRESS

Guozhang Bao[1,*], Mengyu Zhang[1], Yanfang Li[1], Yixin Chang[1], Wenyi Tang[1], Saning Zhu[1], Cunxin Fan[2], Xuemei Ding[3]

[1]College of New Energy and Environment, Jilin University, Key Laboratory of Groundwater Resources and Environment of the Ministry of Education, Changchun, 130012, China
[2]The Administration of Jingyu Water Conservation, Jingyu, Jilin Province, 135200 China
[3]College of Animal Science, Jilin University, Changchun, 130062 China

ABSTRACT

Sodium carbonate and sodium bicarbonate are the two main salts that cause grassland salinization in northeast China. In spring, the plants often bear the double stress of saline and alkaline conditions. In this paper, *Medicago sativa CV. Dongme-1* seedlings were used to study the effects of freeze-thaw (FT) and alkaline salt stress on the content of osmotic adjustment substances, biological membrane permeability, and antioxidant enzyme activity. The results showed that under the stress of FT+$NaHCO_3$ and FT+Na_2CO_3, the protein content in seedlings decreased by 1.39~7.97% and 3.93~12.29%, respectively; MDA content increased by 10.67~46.99% and 3.74~46.41%, respectively; free proline increased by 11.07~45.32% and 43.67~73.73%, respectively; and the activity of SOD and POD increased. During the FT cycle, both proline and MDA content initially increased and then decreased. Under alkaline salt and FT stress, a large amount of superoxide anion was produced in seedlings. The content of MDA increased, inhibiting seedling growth, and the contents of protein, soluble sugar and free proline in plants increased significantly. Meanwhile, the defense mechanism of seedlings induces the activity of SOD and POD to resist stress injury; the damage to seedlings under combined stress (alkaline salt and FT stress) was higher than that under a single stress (alkaline salt stress or FT stress). Moreover, Na_2CO_3 stress was more harmful to the seedlings than $NaHCO_3$ stress. The results of this study prove the adaptable changes in the alfalfa seedlings, reflecting their abilities of saline-alkaline tolerance and cold resistance.

KEYWORDS
Medicago sativa L., Freeze-thaw action, Alkaline salt stress, Chilling resistance, Saline-alkaline tolerance

INTRODUCTION

China is a country in which salinization has become rather serious and saline soil has grown to 33 million hm^2, especially in the cold northeast, where the herbages are mainly limited by the important environmental factor of freeze-thaw actions in winter. Stress from low temperatures decreases the photosynthesis of plants and enhances respiration; thus, the synthesis of energy and material is blocked, which causes the plants to starve. This seriously affects the growth of plants and can even lead to death [1].

The area of saline land in northeastern China is ranked in the world top three areas for commodity grain and animal husbandry, and soil salinity seriously restricts regional agricultural and economic development [2]. In western Jilin Province, the area of saline land is rather large and the phenomenon of bare patches due to sodic and saline soils is also serious. According to a plant survey, *Medicago sativa L.* is one of the most common saline planting herbages in western Jilin Province [3] and even in northeastern China and the circumpolar latitude regions. *Medicago sativa L.*, characterized by great cold resistance and saline-alkaline tolerance, is usually used for improvements to saline land in northeastern China. It is also a common experimental material for plant chilling resistance and saline-alkaline tolerance tests.

Medicago sativa L. (alfalfa) is a perennial legume with strong stress resistance and a wide range of adaptations that can live in many types of climate and soil environments [4]. *Medicago sativa L.* is adaptable to neutral to slightly alkaline soils as well as conditions where the soluble salt of soil is below 0.3%, but is not suitable for acidic or alkaline soil. The optimum pH value for *Medicago sativa L.* is 7 ~ 8. *Medicago sativa L.* has high yield, longevity, regeneration, strong palatability, nutrition and other features and is an important source of protein feed for animal husbandry [5].

Currently, studies on the physiological response mechanism of *Medicago sativa L.* seedlings

under freeze-thaw and alkaline salt stress mainly focus on single-factor stress, for instance, neutral salt and mixed salt alkaline stress [6], salt effects of stress on the growth of *Medicago sativa L.* and expression of salt resistance genes [7, 8], soil temperature and saline-alkaline component synergistic reaction to salt resistance of seed germination and growth period and so on [9]. In cold saline alkali land areas, the rational development and utilization of feed resources in the region has become the primary problem [10].

In the early spring and autumn period of the northeast cold area, freeze-thaw events and saline-alkaline stress phenomena are common [11], mainly saline alkali stress [12]. Therefore, *Medicago sativa L.* seedlings were selected as experimental materials in this experiment, which studied the changes in seedlings protein, MDA, and free proline content, and the activities of POD and SOD under freeze-thaw and $NaHCO_3$ or Na_2CO_3 stress to explore chilling resistance and saline-alkaline tolerance in the seedlings and provide a scientific basis for the agricultural use of cold saline-alkaline areas.

MATERIALS AND METHODS

Materials. *Medicago sativa L.* Breeding. In this study, the indoor petri dish culture experimental method was used; seedlings were used for experiments after 7 days of cultivation.

Cultivation of *Medicago sativa L.* Full seeds disinfected with 0.1% $KMNO_4$ solution were cultured in 100 mm diameter petri dishes. Each dish was put into two layers of moistened filter paper, 100 seeds were evenly placed into the dish with water, then covered for cultivation [13]. The seedlings were placed into a light incubator for pregermination and germination without light. When cultured to germination, 12 h of illumination was set, and the temperature during the full illumination period was 25°C. The temperature during the dark period was 15°C. During the germination period, 4 ml of water was dropped on the seedlings every day at morning, noon and evening. When the seedlings produced the third cotyledons, plants with similar growth were selected for further experiments.

Method. Treatment of Materials. The treatment solvents were selected as $NaHCO_3$ and Na_2CO_3 solutions, for which the concentration was 0 mmol/L and 100 mmol/L. Each treatment cycle lasted two days and was performed once.

The two experimental groups were placed into the freeze-thaw cycle test after treatment with alkaline salt ($NaHCO_3$ only and Na_2CO_3 only). The temperature was set to 10, 5, 0, -3, 0, 5 and 10°C, and each temperature lasted for 2 h of treatment; thus, the seedlings experienced freeze and thaw. The seedlings were divided into 6 groups: control groups (group1 and group4) with no treatment; test groups (group2 and group5) with freeze-thaw treatment only; alkaline salt groups (group3 was $NaHCO_3$ with freeze-thaw treatment; group6 was Na_2CO_3 with freeze-thaw treatment). According to the sample volume required for the testing indicators, the experimental groups and the control groups were sampled at each temperature. Three sets of parallel samples were taken from each group was taken, placed on ice bags and quickly analyzed. The lowest temperature of cold resistance for *Medicago sativa L.* seedlings was -3°C.

Physiological Index Determination. Coomassie blue staining for the determination of soluble protein content [14]; thiobarbituric acid for the determination of the content of MDA [14]; acidic ninhydrin colorimetric method determination of free proline content [14] and SOD and POD kits for the determination of activity were used.

Data Processing. In data processing, Microsoft Excel 2007 and SPSS19.0 software were used for statistics and analysis. The significance level was at 0.05, and all of the results are presented as mean(±)SE. The mean values along with the standard error (±) are shown as bars in the figures by using Origin 8.0 software.

RESULTS AND ANALYSIS

Change in Osmotic Adjustment. Changes of Protein content. Fig.1 indicates that under freeze-thaw stress, the protein content of group3 and group6 compared with that of group2 and group5 decreased by 1.39~7.97% and 3.93~12.29%, respectively, and Na_2CO_3 had a greater impact on protein content than $NaHCO_3$. After the treatment with alkaline salt, the seedlings were stressed, resulting in blockage of protein synthesis in the body or an increase in protein decomposition enzyme activity, leading to a decrease in protein content, which was proven in Mao Gui et al.'s [15] research.

In the freeze-thaw cycle, group3 and group6 showed roughly the same trend.

At the freezing stage, from T1 to T3, group1 was significantly different from the treatment groups. At T2, the alkaline salt groups (group3 and group 6) peaked at 8.67 $mg \cdot g^{-1}$ and 7.93 mg·g-1; group2, group3, group5 and group6 were significantly different ($P < 0.05$) at this temperature. As the temperature dropped, the content of protein increased. When the temperature reached 0°C, group3 and group6 increased by 13.84% and 25.35%, respectively, and these two groups were not significantly different from each other. At T4, the protein content decreased as the stress increased, and group

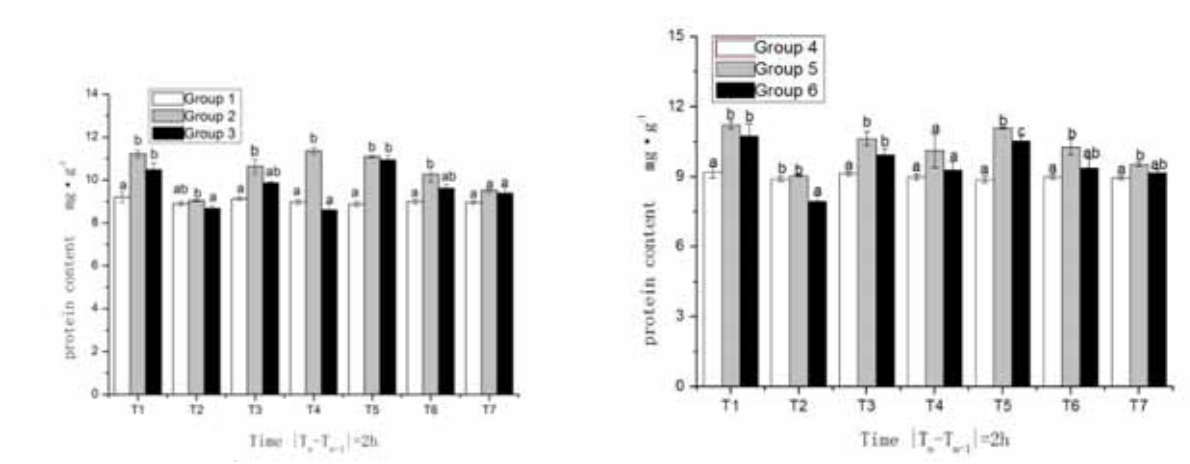

FIGURE 1
Protein content under different stresses

The left chart is $NaHCO_3$ treatment; the right chart is Na_2CO_3 treatment; T1-T7 represents 2-14 h after different temperature treatments corresponding to 10, 5, 0, -3, 0, 5 and 10°C. Group1 and group4 are no treatment, group2 and group5 are freeze-thaw stress only, and group3 and group6 are freeze-thaw stress and alkaline salt stress, respectively. The different letters indicate significant differences among treatments ($P<0.05$). Values expressed are the means ± SEs of three replicates.

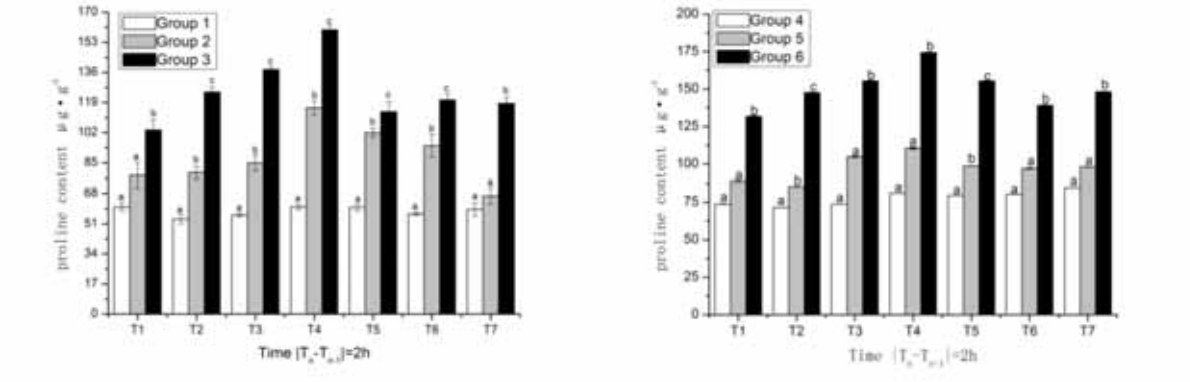

FIGURE 2
Proline content under different stresses

The left chart is $NaHCO_3$ treatment; the right chart is Na_2CO_3 treatment; T1-T7 represents 2-14 h after different temperature treatments corresponding to 10, 5, 0, -3, 0, 5 and 10°C Group1 and group4 are no treatment, group2 and group5 are freeze-thaw stress only, and group3 and group6 are freeze-thaw stress and alkaline salt stress, respectively. The different letters indicate significant differences among treatments ($P<0.05$). Values expressed are the means ± SEs of three replicates.

2 showed significant differences from group 3 ($P < 0.05$).

At the thawing stage, the content of free proline in the seedlings initially increased and then decreased. With the rise in temperature, seedlings continued to be stressed by the low temperature, but not as much; thus, the protein content increased and peaked at 0°C and group5 which showed a significant difference ($P < 0.05$) compared with group6 at T5. When the temperature rose above zero, the protein content in the seedlings decreased slightly since the seedlings had been stressed under constant low temperatures for a long period.

After treatment with a freeze-thaw cycle, the protein content in the alkaline salt groups (group2 and group5) was higher than that of the control groups (group1 and group4). The results were consistent with the findings of Lin S.Z. et al. [16], Fleck, R. A. et al. [17] and Guy C.L. et al. [18] on the mechanism of plant adaption to low-temperature stress. For the plant varieties with chilling resistance, proper stress could stimulate them to generate protective substances more effectively, hence, the content of protein increased and relieved the harm to the plants caused by stress.

Changes in the proline content. In Fig. 2, under freeze-thaw stress, after $NaHCO_3$ (group3) and Na_2CO_3 (group6) treatment, the free proline content in seedlings compared with group1 and group4 increased by 11.07~45.32% and 43.67~73.73%, respectively; group3 and group6 compared with group2 and group5 were significantly different over the whole cycle. ($P <0.05$); Na_2CO_3 had an even more obvious effect. This showed that *Medicago sativa L.* seedlings showed a resistance reaction under

alkaline salt stress, which led to an increase in the proline content, and alkaline salt stress was more serious than neutral salt stress. This was consistent with Wang B.P. et al.'s [19] study on response mechanisms in alfalfa seedlings. With increasing salt concentration, the proline content increased, and alkaline salt had a stronger effect than neutral salt.

In the freeze-thaw cycle, the free proline content in the seedlings showed a trend of initially increasing and then decreasing. At the freezing stage, both the testing group (left) and alkaline salt group (right) increased as the temperature decreased; when it was -3 °C, they peaked at 116.03 $\mu g \cdot g^{-1}$ and 163.01 $\mu g \cdot g^{-1}$, 110.36 $\mu g \cdot g^{-1}$ and 174.25 $\mu g \cdot g^{-1}$, respectively, which showed significant differences at 10℃, 5℃ and 0℃($P<0.05$)(not reflected in the diagram).

At the thawing stage, the proline content first dropped and then stabilized. The result was consistent with Zhang W.H. et al.'s [20] research. With the drop in temperature in a certain range, the content of free proline first increased and then decreased.

Changes in Biological Membrane Permeability. Changes in MDA content. From Fig. 3, it can be seen that under freeze-thaw stress, after treatment with $NaHCO_3$ and Na_2CO_3 (group3 and group6), MDA content in seedlings compared with freeze-thaw groups (group1 and group4) increased by 10.83~46.99% and 3.74~46.41%. Under freeze-thaw stress, the seedlings were stressed by alkaline salt, so the MDA content increased. The data also showed that Na_2CO_3 had a greater impact than $NaHCO_3$, which was consistent with the findings of Gao et al. [21] that under alkaline salt stress, the MDA content inside wheatgrass seedlings was proportional to the concentration of alkaline salt; in a certain range of concentrations, plant cells could prevent damage through a series of regulatory mechanisms.

In the freeze-thaw cycle, the changes in MDA content between the two alkaline salt groups were similar; as the temperature dropped, MDA content in both increased and vice versa. During the whole process, the MDA content of both the testing groups (group2 and group5) and the alkaline salt groups (group3 and group6) were higher than that of the control groups (group1 and group4), and MDA content peaked at 20.96 $\mu mol \cdot L^{-1}$, 25.76 $\mu mol \cdot L^{-1}$, 32.70 $\mu mol \cdot L^{-1}$ and 37.76 $\mu mol \cdot L^{-1}$ at -3°C. From T2 to T7, group5 was significantly different from group6 ($P < 0.05$); at T4~T6, group2 and group3 were significantly different from each other.

After continuous cold stress, the MDA content was still high, although it slightly decreased. On the whole, it could be seen that the lower the temperature was, the higher the MDA content in plants would be. This was consistent with Shao et al.'s [22] study on the mechanism of physiological and biochemical responses in seedling adaptation to low temperature. Under extended low temperature stress, the MDA content in the seedlings increased.

Changes in Enzyme Activity. Changes in SOD Activity. Fig. 4 indicates that after treatment with $NaHCO_3$ (left) and Na_2CO_3 (right), the activity of SOD in group3 and group6 was higher than that in group2 and group4; group3 and group6 respectively increased their SOD activity by 3.21~11.01% and 3.33~9.70%, respectively. The activity of SOD strengthened in order to resist harm caused by alkaline salt. This was consistent with the study of Liu et al. [23]. In a certain concentration range, the activity of SOD increased with increasing alkaline concentration.

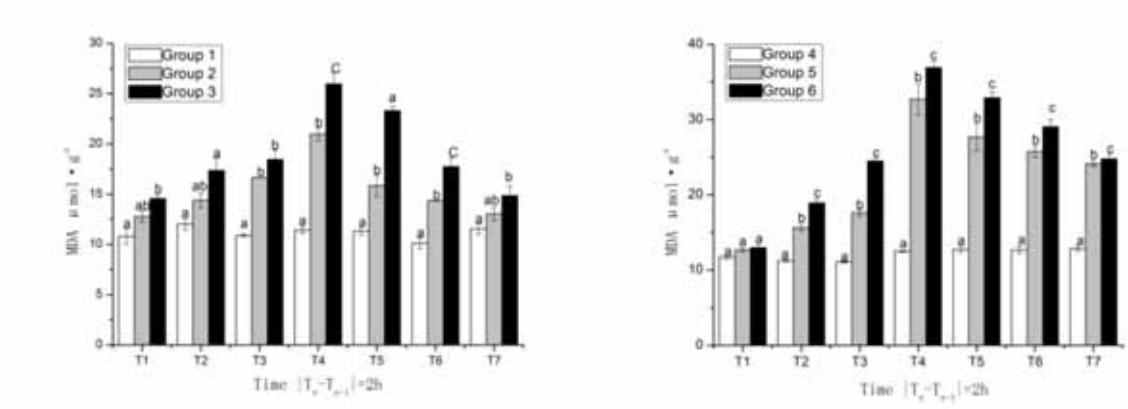

FIGURE 3
MDA content under different stresses

The left chart is $NaHCO_3$ treatment; the right chart is Na_2CO_3 treatment; T1-T7 represents 2-14 h after different temperature treatments corresponding to 10, 5, 0, -3, 0, 5 and 10℃. Group1 and group 4 are no treatment, group2 and group5 are freeze-thaw stress only, and group 3 and group 6 are freeze-thaw stress and alkaline salt stress, respectively. The different letters indicate significant differences among treatments ($P<0.05$). Values expressed are the means ± SEs of three replicates.

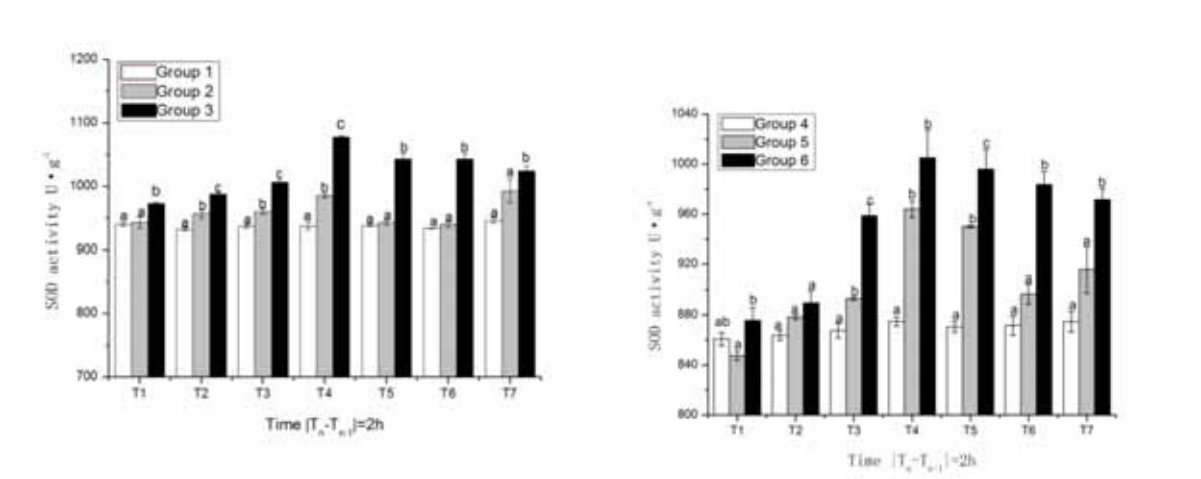

FIGURE 4
SOD activity under different stresses

The left chart is $NaHCO_3$ treatment; the right chart is Na_2CO_3 treatment; T1-T7 represents 2-14 h after different temperature treatments corresponding to 10, 5, 0, -3, 0, 5 and 10°C. Group1 and group4 are no treatment, group2 and group5 are freeze-thaw stress only, and group3 and group 6 are freeze-thaw stress and alkaline salt stress, respectively. The different letters indicate significant differences among treatments ($P<0.05$). Values expressed are the means ± SEs of three replicates.

In the freeze-thaw cycle, group3 and group6 showed a pattern of SOD activity that initially increased and finally stabilized, and the SOD activity of treated groups was higher than that of the control groups. Group2 and group3 showed obvious differences throughout the whole cycle ($P<0.05$); at T3 and T5, group5 showed significant differences from group6. At -3°C, the SOD activity was significantly different from that at 10°C, 5°C and 0°C ($P< 0.05$) (Not reflected in the picture). This revealed that the seedlings were the most sensitive at -3°C. Below 0°C, the activity of SOD increased sharply as the damage to the seedlings became more serious.

At the thawing stage, SOD activity dropped slightly and then stabilized, but the value was still high, which showed that the seedlings were still stressed seriously after continuous placement at low temperature. This was consistent with the study of He et al. [24]. Under the freeze-thaw stress, the SOD activity inside the seedlings significantly increased to overcome the low-temperature stress to maintain normal growth.

Changes in POD Activity. Fig. 5 shows that the POD activity of alkaline salt treatment groups (group3 and group6) increased by 0.48~6.35% and 0.61~14.34% compared with that of the control groups (group1 and group4) under freeze-thaw stress. Both of the alkaline salt groups (group3 and group6) showed an upward trend, though group6 showed a more obvious increase. This was similar to the results of a study in which alfalfa seedlings promoted their oxidation resistance to eliminate active oxygen free radicals [25].

In the freeze-thaw cycle, both the test groups (group2 and group5) and alkaline salt treatment groups (group3 and group6) showed higher POD activity than the control groups (group1 and group4), showing a trend of initially increasing, then dropping and finally stabilizing. The seedlings were sensitive at T4, in which group2 and group3 peaked at 7.89U · $mgprol^{-1}$ and 8.33 U · $mgprol^{-1}$; at T5, their POD values were 6.92 U · $mgprol^{-1}$ and 7.91 U · $mgprol^{-1}$, respectively, showing a significant difference between -3°Cand 0°C ($P<0.05$) (not shown in the figure). At T2 and T4, there was a significant difference between the POD values of group5 and group6 ($P<0.05$).

When the temperature increased to 5°C, the POD activity stabilized. The results showed that low temperatures could strengthen POD activity. This was consistent with the research in [26] and [27].

Effects of $NaHCO_3$ and Na_2CO_3 on Alfalfa Seedling Physiological Indexes. According to Table 1, MDA, soluble sugar, free proline content, SOD and POD activities all showed an upward trend after alkaline salt treatment, but the protein content decreased. The $NaHCO_3$ group MDA content, soluble sugar content, free proline content, SOD activity and POD activity increased by 7.97%, 5.56%, 30.48%, 1.74%, 6.79%, respectively, and the protein content was reduced by 4.22% compared with the control group. The Na_2CO_3 treatment group MDA content, soluble sugar content, free proline content, SOD activity and POD activity increased by 8.86%, 8.47%, 56.83%, 2.46%, 20.35%, respectively, compared with the control group; the protein content decreased by 9.89% compared with the control group. From the table, the increase in physiological index values in the $NaHCO_3$ group was higher than that in the Na_2CO_3 treatment group.

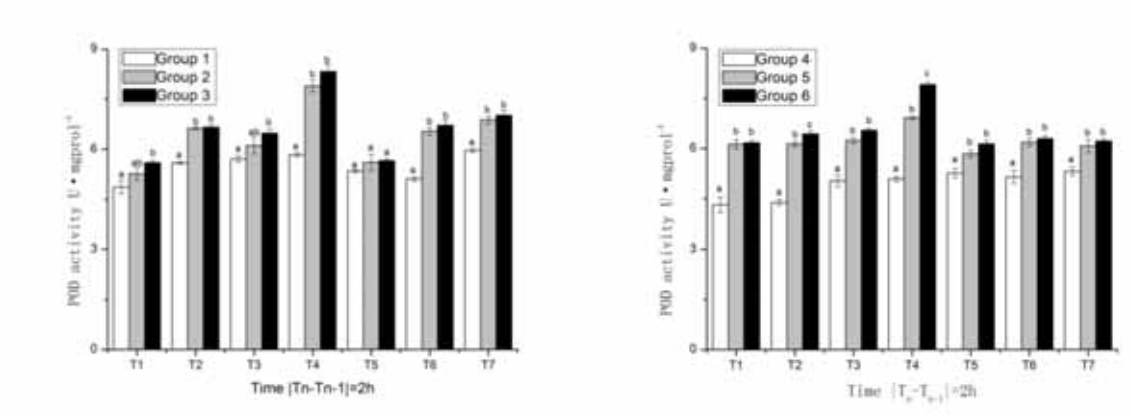

FIGURE 5
POD activity under different stresses

The left chart is $NaHCO_3$ treatment; the right chart is Na_2CO_3 treatment; T1-T7 represents 2-14 h after different temperature treatments corresponding to 10, 5, 0, -3, 0, 5 and 10 ℃. Group1 and group4 are no treatment, group2 and group5 are freeze-thaw stress only, and group3 and group6 are freeze-thaw stress and alkaline salt stress, respectively. The different letters indicate significant differences among treatments ($P<0.05$). Values expressed are the means ± SEs of three replicates.

TABLE 1
Comparison of the increase in six physiological indexes in the alkaline salt treatment group

	MDA	Protein	Soluble Sugar	Proline	SOD activity	POD activity
$NaHCO_3$	7.97%	-4.22%	5.56%	30.48%	1.74%	6.79%
Na_2CO_3	8.86%	-9.89%	8.47%	56.83%	2.46%	20.35%

ANALYSIS AND DISCUSSION

Changes in Osmotic Adjustment Substances. Proline is an important osmosis-regulating substance used by plants to maintain the balance of internal osmotic potential [28]. Under normal conditions, the content of proline in plants is very low, but in the case of drought and low temperature stress, the free proline in the plant would accumulate to a large amount, and the cumulative index is related to the stress resistance of the plant [29]. The results of this study generally confirmed that the proline content of seedlings was used to balance the osmotic potential. The proline content under combined stresses was much higher than that under single-factor stress, which showed that combined freeze-thaw and alkaline salt stress induce greater harm to the seedlings. This is due to the *Medicago sativa L.* seedlings under combined stress not only being dominated by free proline osmotic adjustment but also forced to resist chilling injuries [30]. The stress of seedlings was aggravated, and the growth of seedlings was restrained. The alkaline salt stress of Na_2CO_3 was more significant than that caused by $NaHCO_3$.

Protein is the most abundant biological macromolecule in plant cells and is one of the most important basic substances for organism structure and function. As the main component of enzymes, it can be involved in the chemical reactions of the cell [31]. This experiment showed that under combined stress, the protein content was lower than under a single stress factor, and the variation in protein content was as follows: test groups (freeze-thaw only) > alkaline salt groups (combined stress). This might be because the growth of seedlings was restrained, the protein synthesis was blocked, or protein synthesis enzymes were decomposed under combined stress [32]. This may also be because the protein synthesis rate became lower than the protein decomposition rate. Under freeze-thaw stress, the protein content increased because the low temperature caused anti-freeze gene expression and then synthesis of the anti-freeze protein. According to the results, the effect of Na_2CO_3 on seedlings was significantly higher than that of $NaHCO_3$. During the freeze-thaw cycle, the protein content decreased with decreasing temperature, possibly because under low-temperature stress, the seedlings were continuously stressed and showed resistance actions; thus, the protein content increased. At -3°C, the temperature was very low, so the seedlings were injured by freezing and the protein content dropped. With increasing temperature, the stress was relieved, and the protein content increased and then stabilized with the assistance of resistance capacity. The study of Wang et al. [32] supported this view and noted that low temperature could lead to an increase in protein.

Changes in Membrane Permeability. When plant organs are in senescence or under stress, membrane lipid peroxidation usually occurs; malondialdehyde (MDA) is one of the products [33]. The accumulation of MDA is usually regarded as an index for membrane lipid peroxidation to indicate the intensity of cell membrane lipid peroxidation and the

resistance actions [34]. Under freeze-thaw and alkaline salt stress, the balance of intracellular activated oxygen metabolism was destroyed, resulting in the peroxidation of membrane lipids and the degradation of unsaturated fatty acids and producing MDA, which causes damage to the plasma membrane and enzymes, causing the membrane structure and physiological function to be destroyed [35]. This experiment confirmed that a decrease in temperature and aggravated stress resulted in an increase in MDA content; as the temperature increased, MDA content declined but remained high. This may be caused by the continuous low temperature in the thaw process; the stress on the seedlings was still serious, thus, the cells showed severe membrane lipid peroxidation. The results were previously confirmed [36] that under stress, the MDA content was proportional to the level of stress, which directly revealed the injury intensity of freeze-thaw and alkaline salt stress.

Changes to the Protective Enzyme System. When plants are under alkaline salt and freeze-thaw stress, the reactive oxygen of the cell accumulates intracellularly and, when it exceeds the normal level, causes oxidative damage [37]. Under these conditions, by enhancing the antioxidant enzyme activity and eliminating reactive oxygen species, plants protect themselves against the damage of active oxygen [38].

SOD is the first line of defense in protecting plant cells against reactive oxygen [39]; it transforms the superoxide anion radical into H_2O_2 to protect plants against hydroxyl free radical damage, and its activity can directly reflect the plant's capacity of tolerance for active oxygen [40]. This experiment showed that the variation of SOD was as follows: control groups>test groups (freeze-thaw only)>alkaline salt groups (combined stress). According to the results, the test group was hurt the most, and the stress caused by Na_2CO_3 on seedlings was significantly higher than that caused by $NaHCO_3$. Under combined stress, the seedlings were sensitive at -3°C, and the difference between the two groups was significant. This revealed that the seedlings were damaged during the freeze-thaw cycle and that the content of activated oxygen was too high. As a result, plants enhanced the SOD activity to reduce the damage [41]. This was noted in Gong et al.'s study [42]. At low temperatures, SOD increased slowly.

POD is able to protect cells from H_2O_2 damage and is regarded as a major enzyme that protects cells [43]. The experimental proof is that, under freeze-thaw and alkaline salt stress, the POD activity of *Medicago sativa L.* seedlings was enhanced, and was higher than that in the control group at every temperature. Both treatment groups showed a trend of initially increasing and then dropping and finally stabilizing. At -3□, the activity of POD reached its peak. This may be because the seedlings were stressed the most at this time, which led to the rise in POD activity, and redundant H_2O_2 was eliminated to maintain the normal growth of the seedlings [44].

CONCLUSIONS

The experiments indicated that seedling chilling resistance and saline-alkaline resistance could be reflected by 5 indexes (the content of protein, MDA, and free proline and the activity of SOD and POD). By stabilizing the biological membrane permeability and increasing the content of osmotic adjustment substances, the removal of activated oxygen to resist combined stress could be carried out in a timely manner. Under combined stress, the MDA content inside the seedlings increased; thus, peroxidation of membrane lipids enhanced and activated oxygen increased, causing cell membrane system damage. The seedlings enhanced the activity of POD and SOD to eliminate activated oxygen and protect *Medicago sativa L.* from damage from superoxide anion free radicals. Under combined stress, the free proline and protein contents of the Na_2CO_3 treatment groups were higher than those of the $NaHCO_3$ groups. This result was the same as for the changes in POD activity, but the SOD and MDA contents tended to show the opposite result. During a short-term freeze-thaw process, the *Medicago sativa L.* seedlings showed a series of changes. Whether this short-term physiological mechanism is adaptable for further research and whether the changes could promote seedling adaptation to the environment remains to be studied.

ACKNOWLEDGEMENTS

This work was sponsored by the National Natural Science Foundation of China (grant number 31772669).

REFERENCES

[1] Guo, Y.W., Li, X., Li. and Gao, D.S. (2014) Advance in the Mechanism of Biochemistry and Molecular Biology in Response to Cold Stress of Plant. College of Horticulture, Shandong Agricultural University, Tai'an, China. 12(2), 54-57. (in Chinese).

[2] Wang, C.Y., Wu, Z.J., Shi, Y.L. and Wang, R.G. (2012) The Resource of Saline Soil in the Northeast China. Institute of Applied Ecology, CAS, Shenyang, China. 12, 643-647. (in Chinese).

[3] Bai, L.Y., Zhou, S.Z. and Zhang, W. (2012) Experimental Study on Cultivating Alfalfa in the West of Jilin Province. Agriculture and Technology. 32(02), 83. (in Chinese).

[4] Bicakci, T., Aksu, E. and Arslan, M. (2018) Effect of Seed Coating on Germination, Emergence and Early Seedling Growth in Alfalfa (Medicago Sativa L.) Under Salinity Conditions. Fresen. Environ. Bull. 27, 6978-6984.

[5] Wang, X.S. and Han, J.G. (2009) Changes of free proline content, activity, and active isoforms of antioxidative enzymes in two alfalfa cultivars under salt stress. Agricultural Sciences in China. 8(4), 431-440. (in Chinese).

[6] Bao, A.K., Wang, S.M. and Wu, G.Q. (2009) Over expression of the Arabidopsis H^+-PPase enhanced resistance to salt and drought stress in transgenic alfalfa (*Medicago sativa* L.). Plant Science. 176(2), 232-240.

[7] Al-Khateeb, S.A. (2006) Effect of salinity and temperature on germination, growth and ion relations of Panicum turgidum Forssk. Bioresource Technology. 97, 292-298.

[8] Temel, S., Keskin, B., Simsek, U. and Yilmaz, I. H. (2016) The Effect of Soils Having Different Salt Content on Mineral Accumulations of Some Forage Legume Species. Fresen. Environ. Bull. 25, 1038-1050.

[9] El Shaer, H.M. (2006) Halophytes as cash crops for animal feeds in arid and semi-arid regions. In: Öztürk, M., Waisel, Y., Khan, M.A., Görk, K. (eds.) Biosaline Agriculture and Salinity Tolerance in Plants. Birkhauser, Basel, Verlag, 117-128.

[10] Zhang, S.W., Yang, J.C. and Li, Y. (2010) Changes of Saline-alkali Land in Northeast China and Its Causes since the Mid-1950s. Journal of Natural Resources. 25(3), 435-442.

[11] Yao, R.J., Yang, J.S. and Liu, G.M. (2006) Characteristics and Agro-Biological Management of Saline-Alkalized Land in Northeast China. Soils. 38(3), 256-262.

[12] Yuan, Z.X. (2010) Analysis of Saline-Alkali Characteristics and Nutrient Status of Soil in Western Jilin Province. Northeast Normal University, Changchun, China. (in Chinese).

[13] Mertoglu, K., Ileri, O. and Altay, Y. (2018) Aqueous Leaf Extracts Effect of Some Apple Cultivars on Growth Characteristics of The Green Manure Legumes Via Allelopathy. Fresen. Environ. Bull. 27, 4052-4060.

[14] Wang, X.K. (2010) Principles and techniques of plant physiology and biochemistry experiment. 2nd edition. Beijing China Higher Education Press. 190-281. (in Chinese).

[15] Mao, G.L. and Xu, X. (2005) Studies on In Vivo Selection of Salt-tolerant Mutant of *Lycium barbarum L.* and Its Physiological and Biochemical Characteristics. Acta Botanica Boreali-occidentalia Sinica. 25(2), 275-280.

[16] Lin, S.Z., Li, X.P. and Zhang, Z.Y. (2002) The effects of cold acclimation on the freezing resistance and total soluble protein in populus tomentosa seedlings. Scientia Silvae Sinicae. 18(6), 137-141.

[17] Fleck, R.A., Day, J.G., Clarke, K.J. and Benson, E.E. (1990) Elucidation of the metabolic and structural basis for the cryopreservation recalcitrance of Vaucheria sessilis. Cryo-Letters. 20(5), 271-282.

[18] Guy, C.L. (2003) Freezing tolerance of plants: Current understanding and selected emerging concepts. Canadian Journal of Botany. 81(18), 1216-1223.

[19] Wang, B.P., Dong, X.Y. and Dong, K.H. (2013) Effects of Saline-alkali Stress on the Physiological Characteristics of Alfalfa Seedlings. Acta Agrestia Sinica. 21(6), 1124-1129. (in Chinese).

[20] Zhang, W.H. and Hu, T.M. (2002) Effect of Low Temperature Stress on Physiological Process of Warm Season Turfgrass Dichondra repens Forst. Journal of Jilin Agricultural University. 24(5), 39-41. (in Chinese).

[21] Gao, W.J., Xu, J. and Xie, K.Y. (2011) Physiological responses of Agropyron cristatumunder Na_2CO_3 and $NaHCO_3$ stress. Acta Prataculturae Sinica. 20(4), 299-304. (in Chinese).

[22] Shao, Y.R., Xu, J.X. and Xue, L. (2013) Effects of low temperature stress on physiological-biochemical indexes and photosynthetic characteristics of seedlings of four plant species. Acta Ecologica Sinica. 33(14), 4237-4247.

[23] Liu, B.S., Kang, C.L. and Wang, X. (2014) Physiological and biochemical response characteristics of *Leymus chinensis* to saline-alkali stress. Transactions of the Chinese Society of Agricultural Engineering. 30(23), 166-173. (in Chinese).

[24] He, Y.J., Xue, L. and Ren, X.R. (2008) Effects of low temperature stress on physiological characteristics of six tree species seedlings. Chinese Journal of Ecology. 27(4), 524-531. (in Chinese).

[25] Hu, Z.Y. (2014) The effects of different saline-alkaline stress on seed germination of Elymus dahuricus and *Medicago sativa*. Jilin Agricultural University, Changchun, China (in Chinese).

[26] Zhang, Z.H. (2012) Effect of low temperature stress on 4 kinds of physiological and biochemical indexes of cold plateau native grasses. Heilongjiang Animal Science and Veterinary Medicine. 21(11), 79-82. (in Chinese).

[27] Wang, R.Y., Ren, Y.S. and Yue, W.B. (2006) Effect of Low Temperature Stress on the Survival and Physiological and Biochemical Indexes of Alfalfa Seedlings. Acta Laser Biology Sinica. 15(4), 342-348. (in Chinese).

[28] Ashraf, M. and Foolad, M.R. (2007) Roles of glycine betaine and proline in improving plant abiotic stress resistance. Environmental and Experimental Botany. 59(2), 206–216.
[29] Bao, G.Z., Ao, Q., Li, Q.q., Bao, Y.S. and Zheng, Y. (2017) Physiological Characteristics of Medicago sativa L. in Response to Acid Deposition and Freeze-Thaw Stress. Water, Air, and Soil Pollution. 228, 376.
[30] Dierking, R.M., Young, C.A. and Kallenbach, R.L. (2012) Mediterranean and continental tall fescue: I. effects of endophyte status on leaf extension, proline, mono- and disaccharides, fructan, and freezing survivability. Crop Science. 52(1), 451-459.
[31] Bian, W., Bao, G., Qian, H., Song, Z., Qi, Z., Zhang, M. Chen, W. and Dong, W. (2018) Physiological Response Characteristics in Medicago sativa Under Freeze-Thaw and Deicing Salt Stress. Water Air and Soil Pollution. 229(6).
[32] Wang, H.L., He, H.P. and Gong, L.Z. (2011) Research Progress on the Cold Resistance of Plant. Hubei Agricultural Sciences. 06, 1091-1094+ 1100. (in Chinese).
[33] Jaleel, C.A., Gopi, R., Sankar, B., Manivannan, P., Kishorekumar, A., Sridharan, R., Panneerselvam, R. (2007) Studies on germination, seedling vigour, lipid peroxidation and proline metabolism in *Catharanthus roseus* seedlings under salt stress. South African Journal of Botany. 73(2), 190-195.
[34] Dhindsa, R.S., Plumb-Dhindsa, P.L. and Reid, D.M. (1982) Leaf sensecence and lipid peroxidation: Effect of some phytohormones, and scavengers office radicals and singlet oxygen. Physiol Plant. 56, 453-457.
[35] Yu, D.J., Hwang, J.Y., Chung, S.W., Oh, H.D., Yun, S.K. and Lee, H.J. (2017) Changes in cold hardiness and carbohydrate content in peach (Prunus persica) trunk bark and wood tissues during cold acclimation and deacclimation. Scientia Horticulturae. 219, 45-52.
[36] Chen, G.Y. (2011) Comparative Study on the resistance of Suaede salsa L. and Puccinellia tenuiflora under different concentrations of NaCl and Na_2CO_3 stress. Shandong Normal University, Jinan. (in Chinese).
[37] Chen, Y.H., Shen, Z.G. and Liu, Y.L. (2000) Effects of Chilling and High pH Stresses on the ATPase Activities of Plasma Membrane and Tonoplast Vesicles Isolated from Rice (*Oryzasativa L.*) Roots. Plant Physiology Journal. 05, 407-412. (in Chinese).
[38] Liu, Z., Deng, J. and Tang, Q.Z. (2006) Advances in plant resistance to cold. Guangxi Agricultural Sciences. 37(6), 667-670. (in Chinese).
[39] Bowler, C., Montagu, M.V. and Inze, D. (1992) Superoxide dismutase and stress tolerance. Annual Review of Plant Physiology and Plant Molecular Biology. 43, 83-86.
[40] Yusefi, M., Asl, V.N. and Moharramnejad, S. (2017) Response of Oxidative Defense System to Salt-Treat in Alfalfa (*Medicago Sativa L.*). Fresen. Environ. Bull. 26, 5219-5224.
[41] Song, T.T., Song, T.T., Xu, H.H., Sun, N., Jiang, L., Tian, P., Yong, Y.Y., Yang, W.W., Cai, H. and Cui, G.W. (2017) Metabolomic Analysis of Alfalfa *(Medicago sativa L.)* Root-Symbiotic Rhizobia Responses under Alkali Stress. Frontiers in Plant Science. 8, 15.
[42] Mckersie, B.D., Chen, Y.R., de Beus, M., Bowley, S.R., Bowler, C., Inze, D., D'Halluin, K., Botterman J. (1993) Superoxide dismutase enhances tolerance of freezing stress in transgenic alfalfa (*Medicago sativa L.*). Plant Physiol. 103, 1155–1163
[43] Min, K., Chen, K.T. and Arora, R. (2014) Effect of short-term versus prolonged freezing on freeze–thaw injury and post-thaw recovery in spinach: Importance in laboratory freeze–thaw protocols. Environmental and Experimental Botany. 106, 124-131.
[44] Ximenez-Embun, M.G., Glas, J.J., Ortego, F., Alba, J.M., Castanera, P. and Kant, M.R. (2017) Drought stress promotes the colonization success of a herbivorous mite that manipulates plant defenses. Exp. Appl. Acarol. 73(3-4), 297-315.

Received: **01.03.2018**
Accepted: **27.03.2019**

CORRESPONDING AUTHOR

Guozhang Bao,
College of New Energy and Environment,
Jilin University,
Changchun, 130012 – China

e-mail: baogz@jlu.edu.cn

© by PSP Volume 28 – No. 5/2019 pages 4123-4130 Fresenius Environmental Bulletin

INVESTIGATION OF THE EFFECT OF PRESS COMPACTION AND THE USE OF ZEOLITE ON MECHANICAL PROPERTIES IN THE PRODUCTION OF LOW STRENGTH REACTIVE POWDER CONCRETE (RPC)

Selcuk Memis[1,*], Sirri Sahin[2]

[1]Kastamonu University, Department of Civil Enginineering, 37100, Kastamonu, Turkey
[2]Department of Agricultural Buildings and Irrigation, Atatürk University, 25140, Erzurum, Turkey

ABSTRACT

In this study, reaktive powder concrete (RPC) samples obtained from ground zeolite mixed with cement, gypsum and lime were produced by using a press compacting processes and steam-curing. The compressive strength, density and water absorption properties of the samples were determined. According to experimental results, while dry unit weight is varied between 1477 and 1677 kg m^{-3}, compressive strength of 28 days specimens ranged from 7.3 to 25.3 MPa and water absorption changed approximately between 19% and 9%. Building materials produced from addition of low-rate cement, gypsum and lime to ground zeolite using the pressure method had generally better physical and mechanical properties as compared to the traditional building materials.

KEYWORDS:
Reaktive powder concrete (RPC), Zeolite, Cement, Gypsum, Lime, Press compaction

INTRODUCTION

Concrete is a building material that plays an important role with the strength and durability of our modern world infrastructure (H). In other words; concrete is the most man-made building material with the necessary mechanical and durability properties together with the low cost of the desired shape and size. And also the cement is one of the greatest complement of this concrete [1, 2]. In most cases the properties of the concrete are based on the Portland cement (PC), which is still used today and is the main hydraulic binder [1, 3, 4]. However, the biggest polluter of CO_2 emissions from the production of Portland cement that the main component of concrete, has been the main problem for the last 20 years [1, 5]. Statistical data show that total emission of PC's will reach 3.5 billion tons per year by 2025 [5].

There are many types of concrete that can be produced in many types, which are named with different names according to their production forms, materials and methods. Reactive powder concrete (RPC) that was originally developed in Parish Bouygues' company laboratory in early 1990s, is a type of concrete and RPC has advantages over concretes produced by conventional concrete technology, too [6, 7].

Reactive powdered concrete is a name given to building materials prepared by adding a mixture of pozzolanic binder (such as silica füme has maximum size of 600μm) and a fine aggregate (such as crushed quartz sand) to a new generation of superplasticizers and has a water/binder ratio of <0.18 [8, 9, 10]. The RPC has some advantages over conventional counterparts when compared to cement based materials. At the beginning of these, because of the use of materials of dimensions of 100-600μm instead of coarse aggregate, the homogeneity is obtained at a density and compactness [6 ,7, 8, 11]. Secondly, compressive strengths can be improved by using superplasticizer in low water cement ratios. The use of materials such as silica fume having a high surface area due to fineness in the mixture causes decrease in the proportion of voids formed in the material and increase in reactivity. This increase is due to the reaction of fine materials with $Ca(OH)_2$ and the formation of additional calcium silicate hydrate (C-S-H) chains. In addition, the properties of the steel fiber to be added to these blends can be improved or the RPC mixture can be developed by various methods such as compression and autoclaving, steam curing, hot curing. Compared to these conventional concrete, RPCs with different advantages can be obtained and are available in strengths of up to 150 MPa and even 800 MPa [6, 9, 11]. Topçu ve Karakurt (2005) has applied 2.5 MPA pre-setting pressure in RPC blends and achieved 253.2 MPa strength after 7 days 250 ºC steam curing and after 7 days water curing [12].

Among the most common natural pozzolanic materials such as fly ash and silica fume, zeolite is also widely used in some parts of the world due to its low cost and accessibility [3, 13, 14]. The term zeolite was the named (from Greek zeo to boiling) and litos (stone) by the Swedish mine researcher

Alex Fredrik Cronstedt in 1756 [15]. Zeolite, which have two general types of natural and artifical, a type of pozzolan also exhibits this behaviour and it can used as partial replacement with Portland cement [1, 16, 17, 18].

Zeolites are crystalline alumina silicates with uniform pores, channels and cavities. They possess special properties such as ionexchange, molecular sieves, a large surface area and catalyticactivity, which makes them a preferable material for tremendous industrial applications [19]. About 40 natural zeolites have been identified during the past 200 years; the most common ones are analcime, chabazite, clinoptilolite, mordenite and philipsite. Worldwide production of natural zeolite was estimated at about 3–4 M ton on the basis of recorded production and production estimates [20]. Rather than the known application areas, a considerable amount of research concerning the use of natural zeolite, especially clinoptilolite in concrete applications as pozzolanic cement, lightweight aggregates and dimension stone has been conducted in recent years. Turkey has 50 billion tons of natural zeolite, mainly clinoptilolite reserve [3, 18].

Natural zeolite, which has been widely used since ancient times, is an aluminosilicate hydrated from alkali and alkaline earth cations with a three-dimensional framework structure, [1, 13]. One of the most promising types of natural high-quality pozzolans is the group of natural zeolites [5, 21, 22].

The ability to absorb or lose water up to 30% of the weight of natural zeolite is due to the presence of electron imbalance in the Al-O tetrahedroids found in the chemical structure, which is due to the tendency of the unreacted cations to form chemical bonds to the micropores of the surrounding cations [13]. However, Poon et. Al reported that zeolite has a higher pozzolanic activity than silica, much lower than silica fly [1, 13]. Generally, natural zeolite contains large quantities of reactive SiO_2 and Al_2O_3 [15] [16]. This is due to the presence of large quantities of reactive SiO_2 and Al_2O_3 in the natural zeolite which reacts with $Ca(OH)_2$ to form more calcium silicate and calcium aluminosilicate, which allows it to have pozzolanic activity [23]. In other words, these elements combine with $Ca(OH)_2$, a by-product of cement hydration to form further calcium silicate. This reaction called pozzolanic reaction is responsible for increasing the long term strength and refining the pore structure of blended concrete [18, 23, 24]. It has been reported that the durability of this material increased with chemical reaction between lime compounds and light weight aggregate due to the effect of steam curing [25]. Lime–pozzolanic reactions can be accelerated by the process of steam curing for a short period of 10–12 h at 80–90 °C [26]. They are widely used as an additive in cement in which portlandite is a major hydration product. Their widespread use can be explained both by their beneficial effect on the properties of concrete [27].

Pozzolanic materials were ground to very fine powder, they could gain a certain cementitious properties. At the same time, when they mix with a certain amount of cement and lime, their binding property increases. Improvement of concrete strength and durability by incorporation of pozzolans in mixes has been of interest to researchers in the field of construction materials for ages. There is an increasing trend towards the application of natural zeolite in cement and concrete industries [1]. There is an increasing trend towards the application of natural zeolite in cement and concrete industries. In most cases, use of pozzolans in concrete results in reduction of early strength and increment in late strength when used within optimal proportions. The optimal proportions always require high replacement contents of pozzolans [28, 29, 30].

Sabet et al. [13] and Ahmadi and Shekarchi [31] reported that the use of natural zeolite as a mineral additive in the concrete enhances the durability properties. They have also reported that even though natural zeolite reduces sedimentation in fresh concrete, bleeding and segregation can be prevented. By using natural zeolite in hardened concrete, zeolite increases the pressure resistance due to its pozzolanic property. It also increases the durability of conventional concrete by reducing the permeability of concrete and particularly improving resistance to alkali-aggregate reaction [32].

The cement sector, which produces the greatest CO_2 emissions in energy excellence, is an environmental threat. Therefore, as a complement to cement, pozzolanic materials must be used in the production of sustainable materials [2]. Extending the service life of cement and concrete composites through the reduction of PC consumption and increasing the mechanical and durability properties is also of great importance in today's work. Numerous studies have been conducted to investigate the effect of natural zeolite incorporation on the mechanical and durability properties of PC composites and the effect on the strength of natural zeolite is higher in the paste with lower water-cement ratio [33].

In this study, it is aimed to investigate the manufacturability of an RPC concrete which can be produced by compression without using a plasticizer and the properties of existing materials with lower strength, lower cement and water / binder ratio than RPC. Therefore, lower cost buildings materials can be produced using the binding characteristics of zeolite. Wall-building materials, having beter physical and mechanical properties, can be obtained by adding a small proportion of cement, gypsum and lime to ground zeolite by applying steam curing and pressure methods.

MATERIALS AND METHODS

Materials. The material used consisted of ground zeolite, lime, cement, gypsum and water. The zeolite was ground to ultra-fine powder to pass through a 250 µm sieve. In this research the CEM II 42.5 Portland cement (PC) conforming the TS EN 197-1 [34] standard requirements from the Askale Cement Fabrication in Erzurum, Turkey was used. Zeolite used in this experimental study was supplied from the Anka Nanoteknoloji Ltd. Şti in Erzurum Region, East of Turkey. The chemical compositions and physical properties of the used cement and zeolite are given in Table 1.

Mix proportions and Test procedures. The experimental programme was planned to determinethe effects of press compacting processes and steam curing applications upon the physical and mechanical properties of samples produced by mixing cement, lime and gypsum with ground zeolite. Different proportions of cement, lime and gypsum (0%,10%, 20% and 30%) were used as weight quantity in the replacement of ultra-fine compound powder of zeolite.

The ground zeolite, lime and gypsum based on weight were mixed thoroughly in dry state. From each mixture a wet powder has been produced using 10% water of dry mix weight [35]. Mixtures were prepared in a laboratory portable mortar mixer for a total of 5 min. All mix proportions of specimens were shown in Table 2.

TABLE 1
The chemical composition, physical and mechanical properties of the cement and zeolite.

	PC	*Zeolite*
Chemical composition (%)		
CaO	59.00	4.21
SiO_2	18.63	52.05
Al_2O_3	4.48	11.62
Fe_2O_3	3.41	2.41
MgO	2.72	2.09
Na_2O	0.18	2.29
K_2O	0.52	1.14
SO_3	2.37	0.03
CI	0.009	-
LOI	8.11	15.9
Free CaO	0.41	
Physical and mechanical properties of cement		
Comp. str. 2 days (MPa)	17.9	
Comp. str. 7 days (MPa)	31.7	
Comp. str. 28 days (MPa)	45.9	
Specific gravity	2.94	
Initial setting time (min.)	177	
Final setting time (min.)	233	
Volume stability (mm)	1	
Blaine value (m^2/kg)	4191	
90 µm passing (%)	98.8	
32 µm passing (%)	88.5	

TABLE 2
The mix proportions, water absorption, density and compressive strength of specimens

No.	Series	Constituent materials (%)		Water absorption (%)	Density (kg m^{-3})	28 days Comp. Strength (MPa)
		Zeolite	***Cement***			
1	**Reference**	100	-	-	1489	7.3
2		90	10	15	1610	15.7
3	**I**	80	20	11	1653	20.8
4		70	30	9	1677	25.3
		Zeolite	***Gypsum***			
5		90	10	-	1512	8.3
6	**II**	80	20	18	1558	10.7
7		70	30	17	1565	13.6
		Zeolite	***Lime***			
8		90	10	19	1477	9.7
9	**III**	80	20	16	1505	13.1
10		70	30	15	1567	17.6

The corresponding standard cylindrical specimens witha height-diameter ratio of 2 is difficult to produce by the press compacting processes. According to Coppola et al. [35] and Sahin et al. [36], the compressive strength values of cylindrical specimens with a height-diameter ratio of 0.5 (diameter 80 mm, height 40 mm (Figure. 1)) could be used for comparative purposes to study the influence of the different parameters (composition, forming pressure, steam curing, etc.) on the performances of the material. Therefore, specimens were cast in metal moulds in the form of cylinders (80/40 mm) at a pressure of 20 t for 10–15 s the wet powder with mix proportions shown in Table 2. The preparation of specimens and flow chart of the test procedure were given in Figure. 2.

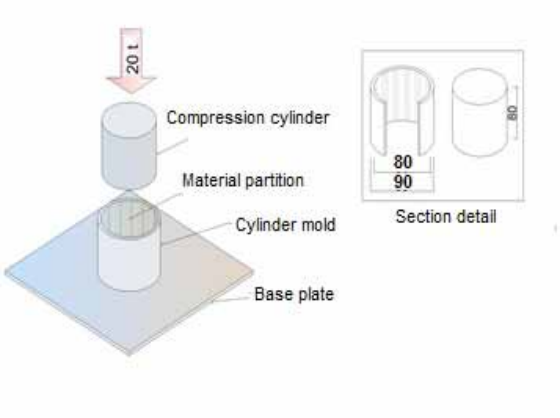

FIGURE 1
Mold plan used in the experimental process

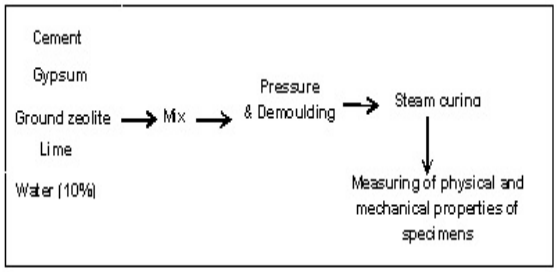

FIGURE 2
Experiment design

After demoulding, specimens were steam-cured for 24 hat 80 °C. Heat treatment cycle had a total duration of 24 h. The heating duration, the treatment duration and the cooling duration were 3, 9 and 12 h, respectively. The humidityin the steam-curing box was above 90%. Then the specimens were taken out from the steam curing and cured inair with RH of 65% at 20 °C as illustrated in Figure. 3. The samples were centrally placed in a compression testing machine and load was applied at a rate of 150 kN/min. Cylinder specimens were tested using an automatic compression testing machine with a maximum capacity of 3000 kN, density and water absorption were conducted at 28 days.

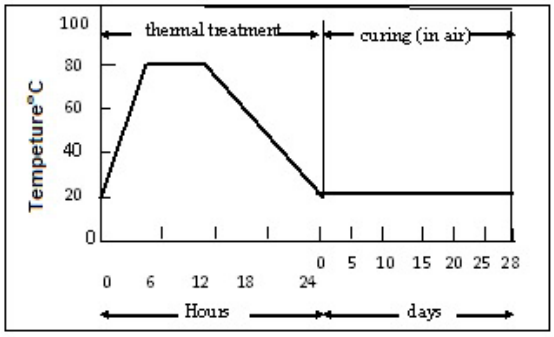

FIGURE 3
Steam curing at 80 °C and then curing at 20 °C (in air).

The compressive strength values, which are indicative of the cementitious properties of pozzolanic material, are determined in terms of the average compressive strength of three samples from each specimen using the testing procedure recommended in Turkish codes at 28 days (TS EN 12390-3) [37]. At the same time, the standard methods recommended in Turkish codes (TS EN 12390-7) [38] are used to determine the density and water absorption.

RESULTS AND DISCUSSION

The experimental results were presented in Figure. 4 as well as in Table 2. The compressive strength values of specimens with cement as partial replacement of ground zeolite were determined to be between 15.7 MPa and 25.3 MPa (Figure. 4). The dry density values of the same specimens varied from 1610 kg m^{-3} to 1677 kg m^{-3} (Table 2). The water absorption values of these specimens were decreased from 15% to 9% depending upon the increase in cement dosage.

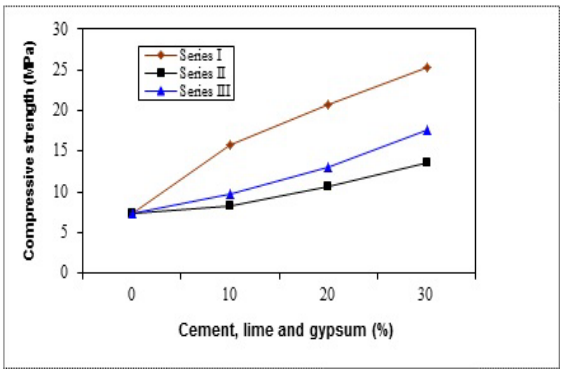

FIGURE 4
The compressive strength of all specimens

The compressive strength values of specimens produced by adding lime and gypsum separately as partial replacement of ground zeolite were found between 9.7–17.6 MPa for specimens including lime and 8.3–13.6 MPa for specimens including

gypsum (Figure 4). Dry density values of specimens were changed between 1477–1567 kg.m^{-3} for specimens including lime and 1512–1565 kg m^{-3} for specimens including gypsum. The water absorption values of lime and gypsum added specimens were observed between 19–15% and 18–17%, respectively. The compressive strength, density and water absorption values of specimens with only ground zeolite were determined 7.3 MPa, 1489 kg m^{-3} and -% (Water absorption values of the samples could not be measured, because scattered in the water), respectively.

In general, the highest compressive strength value of specimens was found as 25.3 MPa in the mix including 30% of cement (Figure. 5). The values of specimens consisting of lime and followed above value, respectively. Dry density of all specimens was found between 1477 kg m^{-3} and 1677 kg m^{-3}. The lowest dry density value was determined for the mixture consisting of 10% of lime (apart from only ground zeolite) and specimens including gypsum and cement followed this value, respectively.

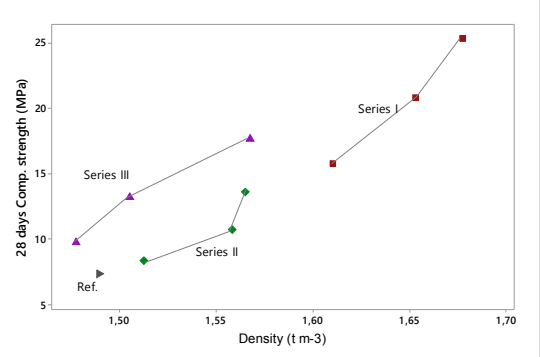

FIGURE 5
Change between compressive strength and density

The water absorption ratios of produced specimens decreased from 19% to 9% depending upon the increase of binding materials (Figure 6). When the binding materials were used as 30% in the mixtures, the lowest water absorption value was found in specimens including cement (Table 2, Figure 6). The production of specimens by using the press compacting processes process andmixing cement, gypsum and lime separately to ground zeolite increased their compressive strengths. The properties of specimens used in the present study and some building materials used in wall construction are shown in Table 3.The compressive strength values obtained from specimens by applying the press compacting processes were found higher than those of some traditional building materials such as clinker bricks, hollow concrete blocks and gas concrete reported by Sahin et al. [24] and Ikeda & Tomisaka [28] have reported that the building materials manufactured through press compacting processes were sounder and stronger than those produced by a slip casting process based on a similar thermal treatment. The high compressive strength values obtained from the present study seem to be in agreement with the previous finding reported by other researchers [23]. These improvements in strength are considered to be responsible of the press compacting processes and the steam curing treatment.

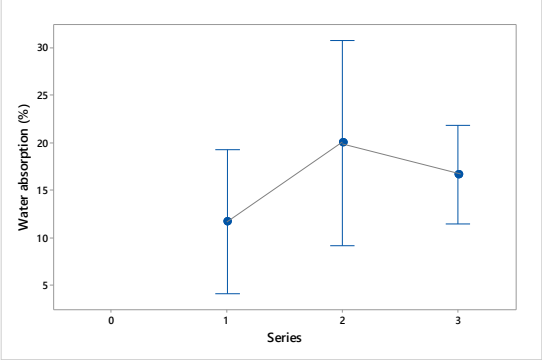

FIGURE 6
Change of water absorption

Curing conditions affect the early strength and physical properties of lightweight concretes [39]. It was reported that the process of steam curing application, at an appropriate temperature increased the pozzolanic property offine material and the strength of the samples produced byusing binding materials such as lime and gypsum [35]. In this study, the use of zeolite ground to ultrafine, together with binding materials, such as cement, lime and gypsum, increased the strength of specimens produced by applying the press compacting processes and steam-curing methods.

TABLE 3
The properties of some building materials used in wall making and specimens produced applying the pressure process

Material	Compressive strength (MPa)	Density (kg.m^{-3})	Water absorption (%)
Specimens produced	*7.3-25.3*	*1489-1677*	*9-19*
Hollow concrete block	2-12.5	500-2200	25-35
Clinker bricks	16	800-1800	18
Gas concrete	2-3.5	800-1400	25-35
Lightweight concrete	17	400-2000	24-50

CONCLUSIONS

In this study, physical and mechanical properties of building materials which were produced from pozzolanic property of ground zeolite and binders such as cement, gypsum and lime were determined. The building materials having sufficient compressive strength as wall blocks were produced using pressure forming (press compacting) processes and steam-curing methods applied to mixtures consisted of various proportions of binders with ground zeolite.

Based on observations and trends determined from this investigation, the following conclusions could be drawn:

- The compressive strength values of specimens produced were determined to be between 7.3 MPa and 25.3 MPa at 28 days. The strengths of samples increase with increased contents of binders. Addition of binders in all three series led to an increase in the strength. The maximum increase in strength value is obtained when there is 30% binder's addition.
- Unit weight changed between 1477 and 1677 kg m^{-3} for specimens aged for 28 days. Addition of binders to zeolite increases the unit weight of produced samples, but the unit weights of all specimens are between the values given by the traditional building materials (apart from gas concrete).
- Water absorption changed between approximately 19% and 9% for specimens aged for 28 days. The specimens had lower water absorption values when compared to lower limit of water absorption values of the other wall building materials.

The results obtained from the present study indicated that specimens produced by applying press compacting processes and steam-curing had generally higher compressive strength as compared to the other wall building materials. Additionally, unit weight values (expect gas concrete) of specimens are in the range of the other wall bulding materials. To obtain desired strengths in wall materials, it is not necessary to increase the quantity of binding material because these specimens can be produced using low-rate cement, gypsum and lime and applying press compacting processes and steam curing methods.

REFERENCES

[1] Najimi, M., Sobhani, J., Ahmadi, B., and Shekarchi, M. (2012) An experimental study on durability properties of concrete containing zeolite as a highly reactive natural pozzolan. Constr. Build. Mater. 35, 1023–1033.

[2] Eskandari, H., Vaghefi, M. and Kowsari, K. (2015) Investigation of Mechanical and Durability Properties of Concrete Influenced by Hybrid Nano Silica and Micro Zeolite. Procedia Mater. Sci. 11, 594–599.

[3] Markiv, T., Sobol, K., Franus, M. and Franus, W. (2016) Mechanical and durability properties of concretes incorporating natural zeolite. Arch. Civ. Mech. Eng. 16(4), 554–562.

[4] Kocak, Y., Tasci, E. and Kaya, U. (2013) The effect of using natural zeolite on the properties and hydration characteristics of blended cements. Constr. Build. Mater. 47, 720–727.

[5] Ramezanianpour, A.A., Mousavi, R., Kalhori, M., Sobhani, J. and Najimi, M. (2015) Micro and macro level properties of natural zeolite contained concretes. Constr. Build. Mater. 101, 347–358.

[6] Ipek, M., Yilmaz, K. and Uysal, M. (2012) The effect of pre-setting pressure applied flexural strength and fracture toughness of reactive powder concrete during the setting phase. Constr. Build. Mater. 26(1), 459–465.

[7] Ipek, M., Yilmaz, K., Sümer, M. and Saribiyik, M. (2011) Effect of pre-setting pressure applied to mechanical behaviours of reactive powder concrete during setting phase. Constr. Build. Mater. 25(1), 61–68.

[8] Yigiter, H., Aydin, S., Yazici, H. and Yardimci, M.Y. (2012) Mechanical performance of low cement reactive powder concrete (LCRPC). Compos. Part B Eng. 43(8), 2907–2914.

[9] Mostofinejad, D., Nikoo, M.R., and Hosseini, S.A. (2016) Determination of optimized mix design and curing conditions of reactive powder concrete (RPC). Constr. Build. Mater. 123, 754–767.

[10] HelmiM., Hall, M.R., Stevens, L.A., and Rigby, S.P. (2016) Effects of high-pressure/temperature curing on reactive powder concrete microstructure formation. Constr. Build. Mater. 105, 554–562.

[11] Yazici, H., Deniz, E. and Baradan, B. (2013) The effect of autoclave pressure, temperature and duration time on mechanical properties of reactive powder concrete. Constr. Build. Mater. 42, 53–63.

[12] Topçu, I.B. and Karakurt, C. (2005) Reactive Powder Concrete. TMH-Turkish Engineering News. 437(3), 25–30.

[13] Sabet, F.A., Libre, N.A. and Shekarchi, M. (2013) Mechanical and durability properties of self consolidating high performance concrete incorporating natural zeolite, silica fume and fly ash. Constr. Build. Mater. 44, 175–184.

[14] Cejka, J., Bekkum Van, H., Corma, A. and Schüth, F. (2007) Studies in Surface Science and Catalysis 168: Introduction to Zeolite science and practice. Studies in Surface Science and Catalysis. 168, 455.
[15] Nagrockiene, D. and Girskas, G. (2016) Research into the properties of concrete modified with natural zeolite addition. Constr. Build. Mater. 113, 964–969.
[16] Poon, C., Lam, L., Kou, S. and Lin, Z. (1999) A study on the hydration rate of natural zeolite blended cement pastes. Constr. Build. Mater. 13(8), 427–432.
[17] Canpolat, F., Yilmaz, K., Köse, M.M., Sümer, M., and Yurdusev, M.A. (2004) Use of zeolite, coal bottom ash and fly ash as replacement materials in cement production. Cem. Concr. Res. 34(5), 731–735.
[18] Quanlin, N. and Naiqian, F. (2005) Effect of modified zeolite on the expansion of alkaline silica reaction. Cem. Concr. Res. 35(9), 1784–1788.
[19] Karakurt, C., Kurama, H. and Topçu, I.B. (2010) Utilization of natural zeolite in aerated concrete production. Cem. Concr. Compos. 32(1), 1–8.
[20] Virta, R.L., (2000). Zeolites, U.S. Geological Survey Minerals Yearbook. https://minerals.usgs.gov/minerals/pubs/commodity/zeolites/zeomyb00.pdf
[21] Colella, C., de' Gennaro, M. and Aiello, R. (2001) Use of Zeolitic Tuff in The Building Industry. Rev. Mineral. Geochemistry. 45(1), 551–587.
[22] Ghourchian, S., Wyrzykowski, M., Lura, P., Shekarchi, M. and Ahmadi, B. (2013) An investigation on the use of zeolite aggregates for internal curing of concrete. Constr. Build. Mater. 40, 135–144.
[23] Nagrockiene, D. and Girskas, G. (2016) Research into the properties of concrete modified with natural zeolite addition. Constr. Build. Mater. 113, 964–969.
[24] Vaičiukynienė, D., Kantautas, A., Rudžionis, Ž., Vaitkevičius, V. and Šukutis, M. (2017) Application of zeolitized glass powder in cement-based materials. Rev. Rom. Mater. Rom. J. Mater. 47(1).
[25] Kumar, S. (2003) Fly ash-lime-phosphogympsum hollow blocks for walls and partitions. Build. Environ. 38(2), 291–295.
[26] Reddy, B.V.V. and Lokras, S.S. (1998) Steam-cured stabilised soil blocks for masonry construction. Energy Build. 29(1), 29–33.
[27] Mehta, P.K. (1987) 'Natural Pozzolans', in Supplementary Cementing Materials for Concrete. 1–33.
[28] Papadakis, V.G. (2000) Effect of fly ash on Portland cement systems. Part II. High-calcium fly ash. Cem. Concr. Res. 30(10), 1647–1654.
[29] Targan, C., Olgun, A., Erdogan, Y. and Sevinc, V. (2002) Effects of supplementary cementing materials on the properties of cement and concrete. Cem. Concr. Res. 32(10), 1551–1558.
[30] Toutanji, H., Delatte, N., Aggoun, S., Duval, R. and Danson, A. (2004) Effect of supplementary cementitious materials on the compressive strength and durability of short-term cured concrete. Cem. Concr. Res. 34(2), 311–319.
[31] Najimi, M., Sobhani, J., Ahmadi, B. and Shekarchi, M. (2012) An experimental study on durability properties of concrete containing zeolite as a highly reactive natural pozzolan. Constr. Build. Mater. 35, 1023–1033.
[32] Sabet, F.A., Libre, N.A. and Shekarchi, M. (2013) Mechanical and durability properties of self consolidating high performance concrete incorporating natural zeolite, silica fume and fly ash. Constr. Build. Mater. 44, 175–184.
[33] Ramezanianpour, A.A., Mousavi, R., Kalhori, M., Sobhani, J. and Najimi, M. (2015) Micro and macro level properties of natural zeolite contained concretes. Construction and Building Materials. 101, 347–358.
[34] TS EN 197-1, (2012). Cemeny -Part I: Composition, spesification and conformity for common cements. Ankara, Turkey.
[35] Gas, F. (1996) Prefabricated building elements based on FGD gypsum and ashes from coal-fired electric generating plants. Mater. Struct. 29(6), 305–311.
[36] Sahin, S., Orung, I., Okuroglu, M. and Karadutlu, Y. (2008) Properties of prefabricated building materials produced from ground pumice aggregate and binders. Constr. Build. Mater. 22(5), 989–992.
[37] TS EN 12390-3 (2010). Testing hardened concrete- Part 3: Compressive strenght of test specimens. Ankara, Turkey.
[38] TS EN 12390-7 (2010).Testing hardened concrete - Part 7: Density of hardened concrete. Ankara, Turkey.
[39] Al-Khaiat, H. and Haque, M.N. (1998) Effect of initial curing on early strength and physical properties of a lightweight concrete. Cem. Concr. Res. 28(6), 859–866.

Received: **08.05.2018**
Accepted: **01.03.2019**

CORRESPONDING AUTHOR

Selcuk Memis
Kastamonu University,
Department of Civil Enginineering,
37100, Kastamonu – Turkey

e-mail: smemis@kastamonu.edu.tr

© by PSP Volume 28 – No. 5/2019 pages 4131-4140 Fresenius Environmental Bulletin

WATER AND SEDIMENT QUALITY ASSESSMENT OF THE LIFEBLOOD OF THRACE REGION (TURKEY): MERIC RIVER BASIN

Cem Tokatli*

Department of Laboratory Technology, Ipsala Vocational School, Trakya University, 22400, Ipsala, Edirne, Turkey

ABSTRACT

Meriç River, which is the longest river in Balkans, is one of the most important aquatic ecosystems in Thrace Region of Turkey. But as many aquatic ecosystems, Meriç River Basin is known to be exposed to an intensive organic and inorganic pollution by means of agricultural and industrial pressure on the system. The aim of this study was to determine the water and sediment quality of Meriç River Basin by using some statistical techniques. For this purpose, water and sediment samples were collected in spring (rainy) season of 2017 from 24 stations selected on the basin. Total of 19 water quality parameters (temperature, dissolved oxygen, % oxygen saturation, pH, EC, TDS, salinity, turbidity, nitrate, nitrite, ammonium, phosphate, sulphate, floride, chloride, ORP, COD, BOD and fecal coliform) were investigated in water samples and also total of 9 inorganic pollution parameters (Cd, Pb, As, B, Cu, Zn, Cr, Ni and Se) were investigated in water and sediment samples. Cluster Analysis (CA) and Factor Analysis (FA) were applied to the results in order to evaluate the detected data effectively. According to detected data, pollution levels of the investigated rivers and lakes as follows; Ergene River > Meriç River > Tunca River > Lakes of Meriç Delta in general. It was also determined that organic contamination levels in water and toxic element levels in sediment of the Meriç River Basin have reached to critical levels and the system is under effect of agricultural and industrial pressure.

KEYWORDS:
Meriç River Basin, Water quality, Sediment quality, Factor Analysis, Cluster Analysis

INTRODUCTION

Pollution of freshwater resources is a matter of serious global concern. Lotic ecosystems are among the most vulnerable freshwater bodies to contamination due to their roles in carrying off point pollution sources (like municipal and industrial wastewater) and non-point pollution sources (like run-off from agricultural lands) in their vast drainage basins [1, 2].

Meriç River, which is known as the lifeblood of Thrace Region of Turkey, is the longest river ecosystem of the Balkans. Ergene and Tunca Rivers are two of the significant branches of Meriç River and they are known to be exposed to an intensive pollution. The Meriç River Delta is formed on about 45,000 ha area at the mouth of Meriç River and it is listed in Class A of International Wetlands. Gala Lake National Park and Sığırcı Lake are significant parts of Meriç River Delta and these lakes are also known to be exposed to an intensive agricultural pressure [3 – 5].

The aim of this study was to evaluate the water and sediment quality of Meriç River Basin by determining some physical, chemical and biological parameters; and classify the basin components according to water – sediment quality characteristics by using the Cluster Analysis; and specify the effective contamination factors according to correlated variables by using the Factor Analysis.

MATERIALS AND METHODS

Study area and collection of samples. Water and sediment samples were collected by using sediment dipper, ekman grab and suitable containers in spring (rainy) season of 2017, when the precipitation and surface runoff have increased significantly in the region. 24 Stations were selected on the Meriç River Basin (2 of them were on the Tunca River, 3 of them were on the Ergene River, 7 of them were on the Meriç River, 2 of them were on the Sazlıdere Stream, 5 of them were on the Gala Lake and 5 of them were on the Sığırcı Lake) by considering the main basin components and pollution sources. Coordinate informations are given in Table 1 and map of study area is given in Figure 1.

Physicochemical analysis. Temperature, dissolved oxygen, % oxygen saturation, pH, EC (electrical conductivity), ORP (oxidation-reduction potential), TDS (total dissolved solids) and salinity parameters were determined by using "Hach Lange HQ40D Multiparameter" device during the field studies; turbidity parameter was determined by

TABLE 1
Coordinate informatiof of selected stations

Stations		North	East	Stations		North	East
Gala Lake	GL1	40.78189	26.21059	Meriç River	M1	41.66233	26.55130
	GL2	40.78089	26.19306		M2	41.63857	26.57971
	GL3	70.77093	26.18911		M3	41.40480	26.63160
	GL4	40.76386	26.16486		M4	41.13640	26.48129
	GL5	40.75516	26.17714		M5	40.94286	26.33319
Sığırcı Lake	SL1	40.84322	26.32872		M6	40.86219	26.23841
	SL2	40.84114	26.34372		M7	40.73987	26.11582
	SL3	40.82173	26.32836	Sazlıdere Stream	SD1	41.61810	26.67925
	SL4	40.82173	26.30954		SD2	41.45525	26.61781
	SL5	40.81802	26.32438	Ergene River	E1	41.28431	26.69829
Tunca River	T1	41.83295	26.58769		E2	41.13641	26.48129
	T2	41.66759	26.55344		E3	41.06200	26.36463

FIGURE 1
Topographic map of Meriç River Basin and selected stations

using "Hach Lange 2100Q Portable Turbiditymeter" device during the field studies; nitrate, nitrite, ammonium, phosphate, sulphate, floride, chloride and COD (chemical oxygen demand) parameters were determined by using "Hach Lange DR3900 Spectrophotometer" device during the laboratory studies; BOD (biological oxygen demand) parameter was determined by using "Hach Lange BOD Trak II" device during the laboratory studies.

Microbiological analysis. Microbiological analysis were carried out using membrane filtration technique. All water samples were filtered with membrane filtration technique and the membrane filter was placed in coliform chromogenic m-FC Agar. All growth mediums were left to incubate for 24 hours at 44.5 ± 0.2 ^{0}C and counted by automatic colony counter.

Chemical analysis. For determination of element levels in water, water samples of one liter were adjusted to pH 2 by adding 2 ml of HNO_3 into each. Afterwards, all the samples were filtered (cellulose nitrate, 0.45 µm) in such a way as to make their volumes to 50 ml with ultra-pure water. For determination of element levels in sediment, sediment samples were dried for 3 h at 105^{o}C. Samples were placed (0.25 g of each sample) in Pyrex reactors of a CEM Mars Xpress 5 microwave digestion unit. $HClO_4$:HNO_3 acids of 1:3 proportions were inserted in the reactors respectively. Samples were mineralized at 200^{o}C for thirty minutes. Afterwards, the samples were filtered in such a way as to make their volumes to 100 ml with ultra-pure distilled water. The element levels in water samples were determined by using the "Agilent 7700 xx" branded Inductively Coupled Plasma – Mass Spectrometer (ICP-MS) device in Trakya University Technology Research and Development Application and Research Center (TÜTAGEM). The center has an international accreditation certificate within the scope of TS EN / ISO IEC 17025 issued by TÜRKAK (representative of the World Accreditation Authority in Turkey). The element analyses were recorded as means triplicate measurements [6 – 8].

Statistical analysis. Cluster Analysis was applied to the results by using the "PAST" package statistical program. Factor Analysis was applied to the results by using the "SPSS 17" package statistical program.

RESULTS

Water and sediment quality. The detected water and sediment quality data in Meriç River Basin are given in Figure 2 and 3. Mean values recorded in water of basin components with some national – international limit values are given in Table 2.

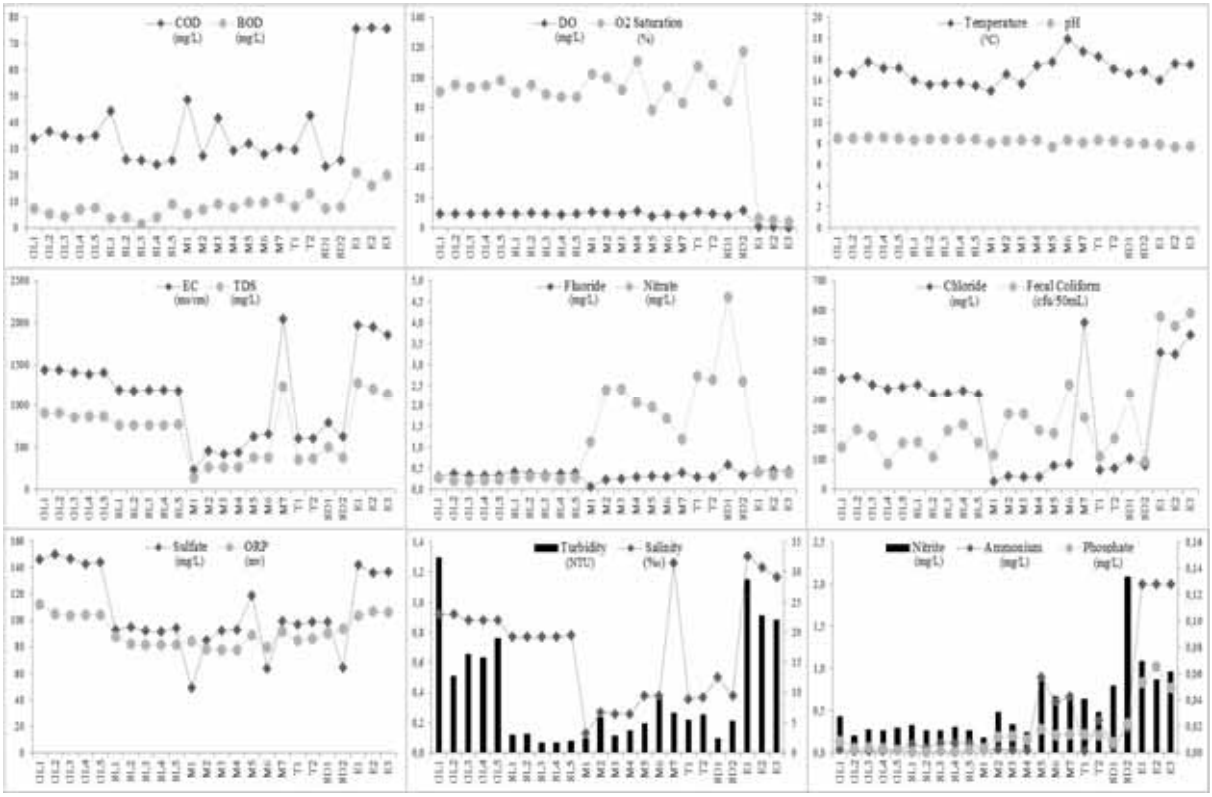

FIGURE 2
Water quality parameters

TABLE 2
Water Quality Criteria, Drinking Water Standards and mean values in the basin

Parameter	Surface Water Standards				Drinking Water Standards			Meriç River Basin* (mean)					
	[a]Water Quality Classes												
	I (clean)	II (slightly polluted)	III (polluted)	IV (highly polluted)	TS266 (2005)	EC (2007)	WHO (2011)	Gala Lake	Sığırcı Lake	Meriç River	Tunca River	Sazlıdere Stream	Ergene River
Temp. (°C)	25	25	30	> 30	-	-	-	15.14 I. Class	13.72 I. Class	15.31 I. Class	15.70 I. Class	14.80 I. Class	15.03 I. Class
pH	6.5-8.5	6.5-8.5	6.0-9.0	Out of 6.0-9.0	6.5-9.5	6.5-9.5	-	8.546 I. Class	8.416 I. Class	8.1657 I. Class	8.32 I. Class	8.06 I. Class	7.77 I. Class
EC (mS/cm)	400	1000	3000	> 3000	2500	2500	-	**1418 III. Class**	**1194 III. Class**	697 II. Class	609 II. Class	707 II. Class	**1925 III. Class**
[b]TDS (mg/L)	500	1500	5000	> 5000	-	-	-	883 II. Class	765 II. Class	417 I. Class	363 I. Class	440 I. Class	1216 II. Class
O_2 sat. (%)	90	70	40	< 40	-	-	-	94.36 I. Class	89.58 II. Class	94.32 I. Class	101.40 I. Class	100.55 I. Class	**5.16 IV. Class**
DO (mg/L)	8	6	3	< 3	-	-	-	9.59 I. Class	9.42 I. Class	9.56 I. Class	10.14 I. Class	10.30 I. Class	**0.53 IV. Class**
COD (mg/L)	25	50	70	> 70	-	-	-	35.00 II. Class	29.18 II. Class	33.97 II. Class	36.35 II. Class	24.50 I. Class	**75.76 IV. Class**
BOD (mg/L)	4	8	20	> 20	-	-	-	6.42 II. Class	4.52 II. Class	**8.62 III. Class**	**10.50 III. Class**	7.80 II. Class	**19.00 III. Class**
NH_4 (mg/L)	0.2	1	2	> 2	0.5	0.3	-	0.0304 I. Class	0.1066 I. Class	0.3310 II. Class	0.2060 II. Class	0.1855 I. Class	**> 2.000 IV. Class**
NO_3 (mg/L)	5	10	20	> 20	50	50	50	0.221 I. Class	0.273 I. Class	1.837 I. Class	2.685 I. Class	3.610 I. Class	0.375 I. Class
NO_2 (mg/L)	0.01	0.06	0.12	> 0.3	0.5	0.5	0.2	0.0190 II. Class	0.0184 II. Class	0.0321 II. Class	0.0360 II. Class	**0.0925 III. Class**	**0.0627 III. Class**
[b]SO_4 (mg/L)	200	200	400	> 400	250	250	-	146 I. Class	93 I. Class	86 I. Class	97 I. Class	81 I. Class	138 I. Class
[c]PO_4 (mg/L)	0.02	0.16	0.65	> 0.65	-	-	-	0.0688 II. Class	0.0208 II. Class	**0.1886 III. Class**	**0.2150 III. Class**	**0.2340 III. Class**	**0.8743 IV. Class**
F (mg/L)	1	1.5	2	> 2	1.5	1.5	1.5	0.342 I. Class	0.388 I. Class	0.268 I. Class	0.299 I. Class	0.463 I. Class	0.445 I. Class
[b]Cl (mg/L)	25	200	400	> 400	250	250	-	**359 III. Class**	**330 III. Class**	125 II. Class	68 II. Class	90 II. Class	**479 IV. Class**
FC (cfu/100mL)	10	200	2000	> 2000	-	-	-	**302 III. Class**	**334 III. Class**	**454 III. Class**	**280 III. Class**	**414 III. Class**	**1148 III. Class**
Tur. (NTU)	-	-	-	-	5	-	-	19.32	2.312	5.14	5.92	3.89	24.6
As (ppb)	20	50	100	> 100	10	10	10	32.738 II. Class	33.261 II. Class	28.192 II. Class	20.709 II. Class	20.392 II. Class	38.355 II. Class
Cu (ppb)	20	50	200	> 200	2000	2000	2000	31.777 II. Class	15.982 I. Class	15.672 I. Class	18.547 I. Class	9.783 I. Class	44.574 II. Class
B (ppb)	1000	1000	1000	> 1000	1000	1000	500	292 I. Class	262 I. Class	237 I. Class	180 I. Class	445 I. Class	354 I. Class
Zn (ppb)	200	500	2000	> 2000	-	-	-	**18513 IV. Class**	**1186 III. Class**	260 II. Class	224 II. Class	**4239 IV. Class**	200 II. Class
Cd (ppb)	2	5	7	> 7	5	5	3	1.488 I. Class	1.918 I. Class	0.737 I. Class	0.643 I. Class	0.574 I. Class	0.923 I. Class
Cr (ppb)	20	50	200	> 200	50	50	50	18.18 I. Class	14.95 I. Class	17.31 I. Class	16.17 I. Class	18.95 I. Class	41.52 II. Class
Pb (ppb)	10	20	50	> 50	10	10	10	10.965 II. Class	7.744 I. Class	2.830 I. Class	2.394 I. Class	2.673 I. Class	4.774 I. Class
Ni (ppb)	20	50	200	> 200	20	20	70	**567.2 IV. Class**	**326.1 IV. Class**	**121.2 III. Class**	**146.1 III. Class**	**173.0 III. Class**	**284.9 IV. Class**
Se (ppb)	10	10	20	> 20	10	10	10	**138.9 IV. Class**	**128.2 IV. Class**	**156.5 IV. Class**	**147.9 IV. Class**	**145.5 IV. Class**	**139.0 IV. Class**

TS266 – Turkish Standards Institute [9]; EC – European Communities [10]; WHO – World Health Organization [11]
[a]Turkish Regulations, 2015 [16]; [b]Turkish Regulations, 2004 [15]; [c]Uslu and Türkman, 1987 [18]
*III. – IV. Class water qualities are given in bold

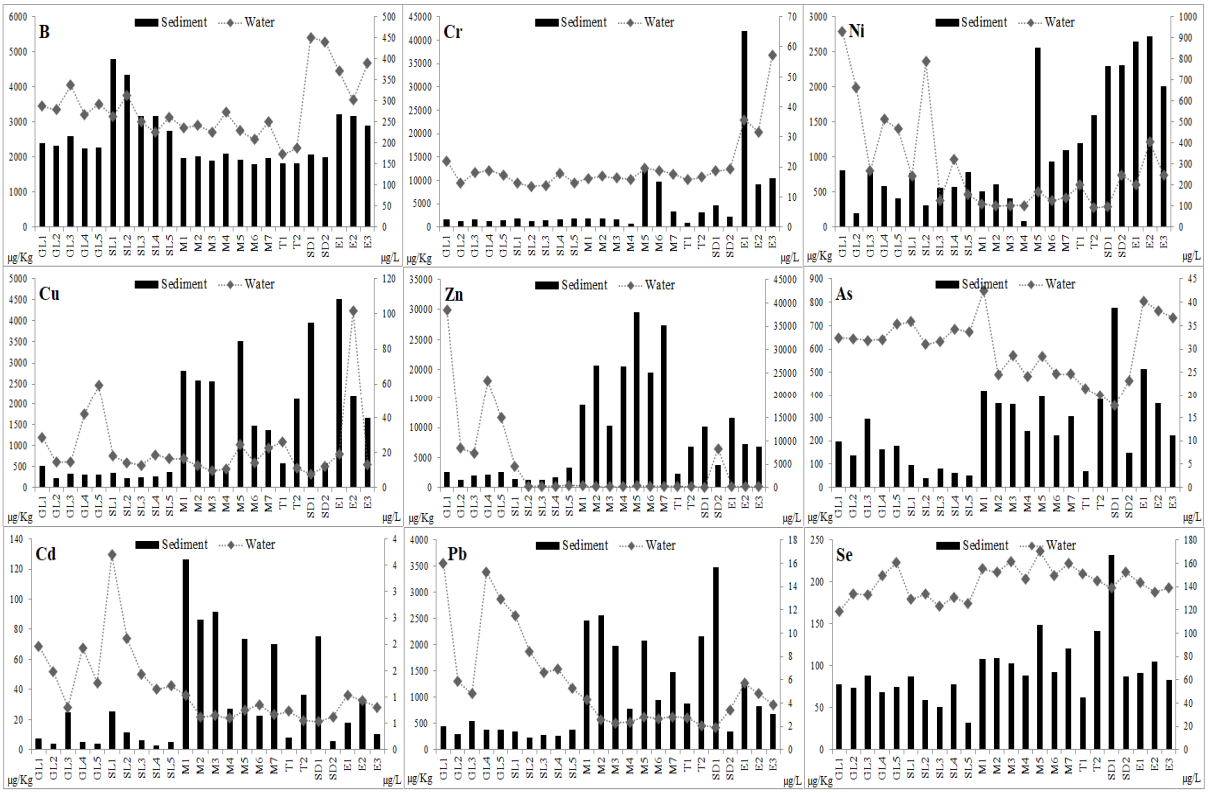

FIGURE 3
Element concentrations

TABLE 3
Total variances explained in FA

Habitat	Compo-nent	Initial Eigenvalues			Extraction Sums of Squared Loadings			Rotation Sums of Squared Loadings		
		Total	% of Variance	Cumulative %	Total	% of Variance	Cumulative %	Total	% of Variance	Cumulative %
Water	1	9.992	52.591	52.591	9.992	52.591	52.591	7.289	38.364	38.364
	2	4.935	25.973	78.565	4.935	25.973	78.565	4.754	25.023	63.387
	3	1.622	8.536	87.100	1.622	8.536	87.100	4.506	23.713	**87.100**
Sediment	1	4.936	61.705	61.705	4.936	61.705	61.705	4.200	52.496	52.496
	2	1.576	19.699	81.405	1.576	19.699	81.405	2.313	28.909	**81.405**

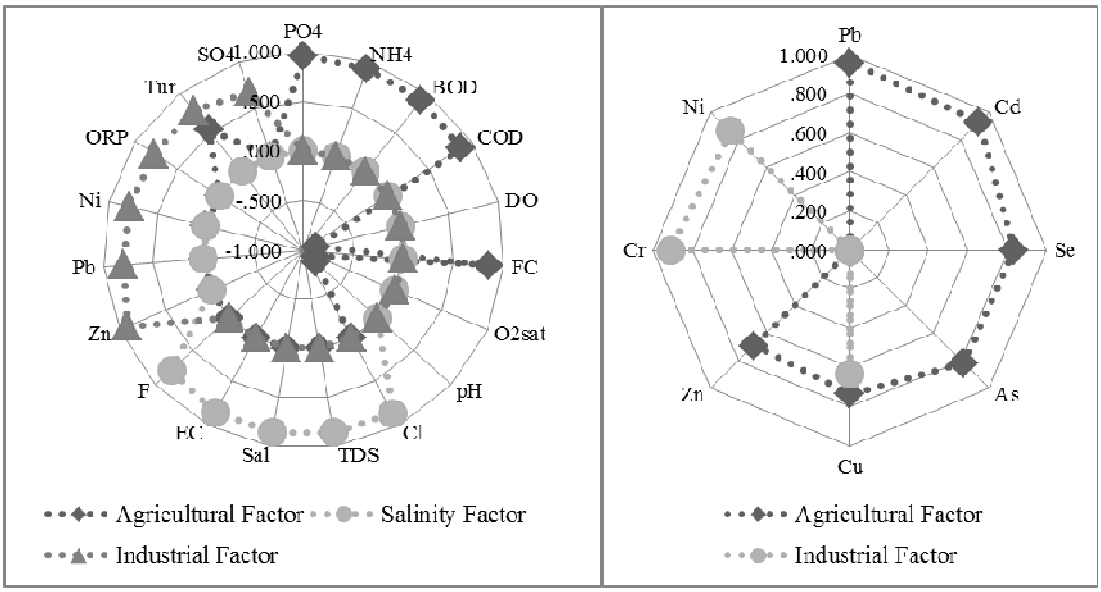

FIGURE 4
Component matrix after rotation for water (left) and sediment (right)

Factor Analysis. Multivariate statistical techniques have been used to assess the quality of many ecosystems. Factor Analysis (FA), which is being used to determine the effective factors on the environment, is a quite powerful and most widely used statistical technique to evaluate the aquatic conditions [12, 13]. FA was used to obtain the effective varifactors on water and sediment of Meriç River Delta by using correlated variables (n = 24 for all parameters). Result of KMO (Kaiser-Meyer-Olkin) measure of sampling adequacy test were 0.712 for water and 0.628 for sediment and these mean that the sampling adequacy were in enough level (>0.5) [14]. Eigenvalues higher than one were taken as criterion for evaluate the principal components required to explain the sources of variance in the data set. According to rotated cumulative percentage variance, 3 factors explained 87.1% of the total variance for water and 2 factors explained 81.4 % of the total variance for sediment (Table 3). The factor loadings are classified according to loading values as "strong (>0.75)", "moderate (0.75 – 0.50)" and "weak (0.50 – 0.30)" [14]. The parameter loadings after rotation higher than 0.5 for the components detected in FA for water and sediment are given in Figure 4.

According to the results of FA for water, first factor, named as "Agricultural Factor" explained 38.3% of total variance and it was related to the variables of PO_4, NH_4, BOD, COD, dissolved oxygen (DO), fecal coliform (FC), oxygen saturation (O2sat), pH and turbidity (Tur) parameters. PO_4, NH_4, BOD and COD parameters were strong and turbidity parameter was moderate positively; dissolved oxygen, fecal coliform, oxygen saturation and pH parameters were strong negatively loaded with this factor. Second factor, named as "Salinity Factor" explained 25.0% of total variance and it was related to the variables of Cl, TDS, salinity (Sal), EC and F parameters. All the parameters were strong positively loaded with this factor. Third factor, named as "Industrial Factor" explained 23.7% of total variance and it was related to the variables of Zn, Pb, Ni, ORP, turbidity (Tur) and SO_4 parameters. Zn, Pb, Ni, ORP and turbidity parameters were strong and SO_4 parameter was moderate positively loaded with this factor (Figure 5, left).

According to the results of FA for sediment, first factor, named as "Agricultural Factor" explained 52.4% of total variance and it was related to the variables of Pb, Cd, Se, As, Cu and Zn parameters. Pb, Cd, Se and As parameters were strong and Cu and Zn parameters were moderate positively loaded with this factor. Second factor, named as "Industrial Factor" explained 28.9% of total variance and it was related to the variables of Cr, Ni and Cu parameters. Cr and Ni parameters were strong and Cu parameter was moderate positively loaded with this factor (Figure 5, right).

Cluster Analysis. Cluster Analysis (CA), which enables to classify the objects according to similar characteristics, is one of the most widely used multivariate statistical techniques to evaluate the water and sediment quality [12, 13]. CA was used to obtain the similarity groups among the investigated basin components according to water and sediment quality characteristics. The diagram of CA calculated by using water and sediment quality parameters in water and sediment of Meriç River Basin are given in Figure 5.

According to the results of CA for water, 3 statistically significant clusters were formed. Cluster 1 corresponded to the stations of Ergene River (E1, E2 and E3) that were high contaminated zones of the basin; Cluster 2 corresponded to the stations of Meriç River (M1, M2, M3, M4, M5, M6 and M7), Tunca River (T1 and T2) and Sazlıdere Stream (SD1 and SD2) that were moderate contaminated zones of the basin; Cluster 3 corresponded to the station of Gala Lake (G1, G2, G3, G4 and G5) and Sığırcı Lake (S1, S2, S3, S4 and S5) that were low contaminated zones of the basin.

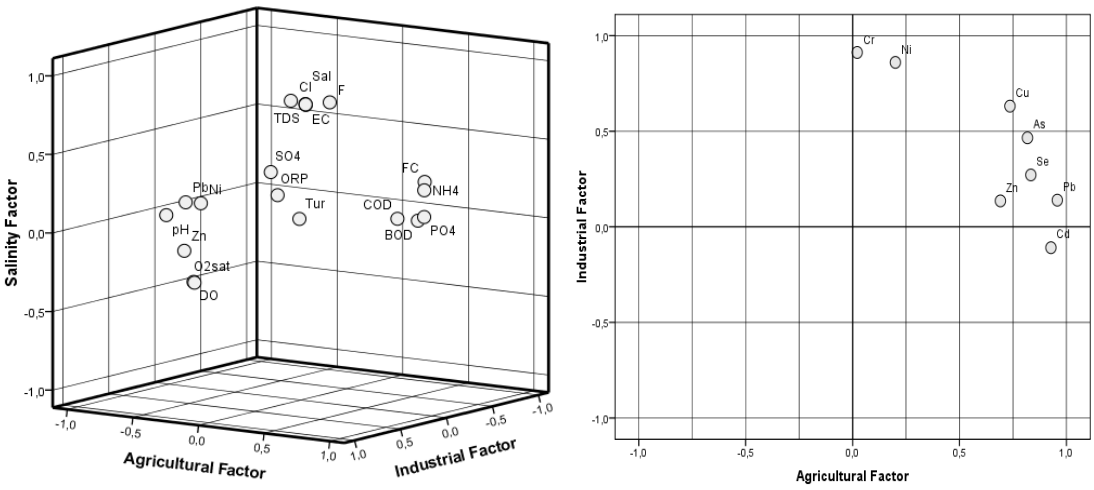

FIGURE 5
Component plot in rotated space for water (left) and sediment (right)

According to the results of CA for sediment, 2 statistically significant clusters were formed. Cluster 1 corresponded to the stations of Ergene River (E1, E2 and E3), Meriç River (M1, M2, M3, M4, M5, M6 and M7) and SD1 and T2 stations that were high contaminated zones of the basin; Cluster 2 corresponded to the stations of Gala Lake (G1, G2, G3, G4 and G5), Sığırcı Lake (S1, S2, S3, S4 and S5) and T1 and SD2 stations that were moderate contaminated zones of the basin.

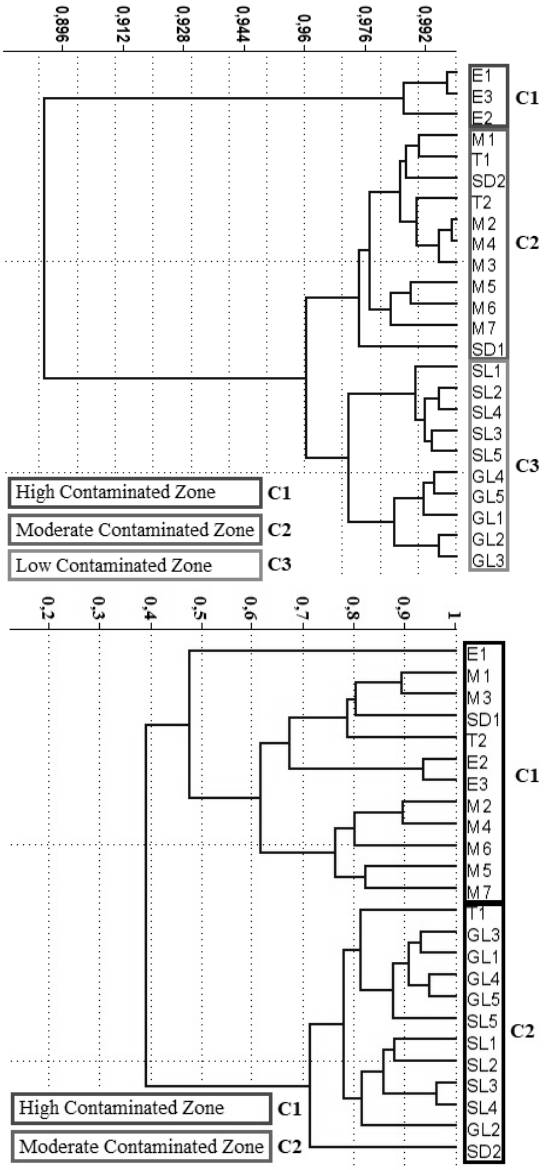

FIGURE 6
Tree diagram of CA for water (left) and sediment (right)

DISCUSSION

According to the Water Pollution Control Regulation criteria in Turkey [15, 16], all the investigated lotic and lentic components of Meriç River Basin have I. – II. Class water quality in terms of temperature, pH, total dissolved solids, nitrate, sulphate, fluoride, arsenic, copper, boron, cadmium, chromium lead accumulations. The basin has also I. – II. Class water quality in terms of dissolved oxygen, oxygen saturation, chemical oxygen demad and ammonium levels except Ergene River (IV. Class) and it has II. Class water quality in terms of nitrite levels except Ergene River and Sazlıdere Stream (III. Class). According to the EC directive specified by European Union Commission for the protection of fish health in freshwater, the dissolved oxygen level in the water for Cyprinid species should not fall below 4 mg/L [17]. The detected dissolved oxygen levels in Ergene River are well below the mandatory value and the average concentrations are around 0.5 mg/L. Except for a few europriaeberios invertebrates and algae species, which have a very wide and very durable ecological valence, this adverse situation makes it impossible to live survive for organisms like fishes or any other vertebrate in Ergene River.

The most critical parameters on the water quality of the system were recorded as phosphate, biological oxygen demand, fecal coliform, nickel and selenium. Because the basin has III. – IV. Class water quality in terms of these parameters in general [16, 18]. Organic and inorganic fertilizers used in agricultural activities increase the level of nitrogen and phosphorus compounds directly in soil and indirectly in water [19, 20]. Although they may occur naturally in some of surface water, the main sources of nitrogen and phosphorus compounds in water are anthropogenic activities including mainly use of intens fertilizers, animal feedlots and municipal wastewater, sludge and septic tanks [21, 22]. According to the results of FA for water, first factor (Agricultural Factor), which was related to the variables of PO_4, NH_4, BOD, COD and fecal coliform, was the most effective factor on the surface water quality in Meriç River Basin. Rice and sunflower are the two main crops produced in the basin and Edirne City is the most important pprovince on rice production in Turkey. It is known that the water leached through paddy fields is contaminated by pesticides and fertilizers and reaches to the system [23].

The water of lentic parts of the system (Gala and Sığırcı Lakes) and Ergene River were determined as salty. These ecosystems have III. Class water quality according to Turkish Regulations [16] and have II. Class water quality (C2: mesohaline) according to irrigation water standards [24] in terms of EC parameter. They have also III. – IV. Class water quality in terms of chlorine parameter [16]. Therefore, especially the use of Gala and Sığırcı Lakes for irrigation may be a problem for the cultivation of stenohaline plants in Meriç Delta, where very fertile agricultural lands are located. EC is a measure of ability of water to pass an electrical current and it is affected by the presence of dis-

solved solids. TDS depends mainly on the solubility of rocks and soils and it is defined as the quantity of dissolved material in water. Salinity is also defined as the total of all salts dissolved in water. These parameters in water environment are closely related and may indicate general water quality. Contaminations to surface water may change the levels of these parameters. It was indicated that sewage water and especially irrigation practices are known as significantly enhancing factors on them [19, 20]. In the present study, according to the results of FA for water, second factor (Salinity Factor), which was related to the variables of EC, TDS, salinity, F and Cl was an effective factor on the surface water quality in Meriç River Basin. The main reason of the recorded quite high values of EC, TDS, salinity and Cl may be unconscious and irregular irrigation practices around the basin and the filtration from septic tanks located in the villages.

Toxic metals are the significant contaminants for the aquatic ecosystems and have hazardous effects on the ecological balance of environment. They can be strongly accumulated and biomagnified along water, sediment and aquatic food chain [25, 26] Meriç, Tunca and Ergene Rivers have II. Class, Sığırcı Lake and Sazlıdere Stream have III. Class and Gala Lake has IV. Class water quality in terms of zinc parameter [16]. Even, the zinc concentrations detected in the water of the Gala Lake were found to be about 70 times higher than the concentrations found in the Meriç and Tunca Rivers. As it is known that fertilizers have an important effect on zinc transfer to the soil, and rains can accelerate these zinc particules migration from soil to the water [27]. This result reflects that even though the agricultural activities in the basin are very intense but Gala Lake, which is exposed to an intensive organic pollution loads carried by many irrigation – drenage channels, is more affected by agricultural activities than the other aquatic environmnets of the basin.

Sediment may act as a sink of various contaminants and pose a risk to water quality through complicated biogeochemical exchanges. Many indices and guidelines have been developed to evaluate the environmental risks of heavy metals in surface sediments. TEL (threshold effects level), which was proved to be an effective sediment quality guideline, is a popular method in evaluating the ecological risk posed by heavy metals in sediments [28 – 30]. Copper, zinc, arsenic, chromium, nickel, cadmium and lead concentrations in sediments of Meriç and Ergene Rivers were considerably higher than deteced in the other lotic and lentic ecosystems in general. According to the sediment quality criteria specified by MacDonald [31], although the detected element accumulations in sediment of Meriç River Basin Cr levels of sediment have not reached the critical levels in general, chromium accumulations recorded in sediment of Ergene River has exceeded the threshold effect level (TEL, 37300 µg/Kg) in especially E1 station. Chromium and nickel occur naturally in the Earth's crust and may enter to the environment a result of natural processes, but the main source of these elements in the environment is antropogenic activities. The most significant anthropogenic point sources of chromium and nickel in surface waters and sediments are the wastewater from electroplating operations, leather tanning industries and textile manufacturing [32 – 34]. In the present study, according to the results of FA for sediment, chromium and nickel elements were found to be as the significant components of second facto (Industrial Factor) with strong parameter loadings. It was indicated that there are more than 1000 industrial enterprises on the catchmet area of Ergene River [35] and the main reason of the recorded quite high concentrations of Cr and Ni in water and sediment may be the wastewater of these industrial enterprises located on the Ergene River Basin.

CONCLUSION

In the present study, current contamination status of the most significant aquatic ecosystem in Thrace Region of Turkey was evaluated from a statistical perspective by using Factor and Cluster Analysis. In this context, water and sediment qualities of Gala and Sığırcı Lakes, which are the most important lentic components of the basin, and Meriç, Ergene and Tunca Rivers, which are the most important lotic components of the basin, have been investigated.

According to detected data observed, the pressure of especially Ergene Rivers on the system was clearly presented and the contamination levels of the investigated aquatic habitats were recorded as; Ergene River > Meriç River > Tunca River > Lakes of Meriç Delta in general.

As a result of this study, phosphate, biological oxygen demand and fecal coliform parameters were recorded as the most critical parameters on the water quality of the system, which were thought to be sourced from mainly agricultural activities conducted intensively almost all around the basin. Chromium and nickel were recorded as the most critical parameters on the sediment quality of the system, which were thought to be sourced from mainly industrial activities conducted intensively around the Ergene River Basin.

According to the results of FA, 3 statistically effective factors named as "Agricultural Factor" “Salinity Factor” and "Industrial Factor" on the water quality of the system; and 2 statistically effective factors named as "Agricultural Factor" and "Industrial Factor" on the sediment quality of the system were identified by using a large number of organic and inorganic quality data.

CA was grouped 24 different sections detected on the basin into 3 clusters of similar water quality characteristic named as "High Contaminated Zone", "Moderate Contaminated Zone" and "Low Contaminated Zone"; and 2 clusters of similar sediment quality characteristic named as "High Contaminated Zone" and "Moderate Contaminated Zone".

The data of the present study clearly reveals that agricultural runoff caused from intensive pesticide and fertilizer applications and industrial runoff caused from Ergene River were the main pollution sources for the Meriç River Basin.

ACKNOWLEDGEMENTS

The author would like to thank for the financial and technical supports supplied by Trakya University, Turkey. This investigation has been supported by the project numbered as 2016/247 accepted by Trakya University, Commission of Scientific Research Projects.

REFERENCES

[1] Köse, E., Tokatlı, C., Çiçek, A. (2014) Monitoring Stream Water Quality: A Statistical Evaluation. Polish Journal of Environmental Studies. 23(5), 1637-1647.

[2] Tokatlı, C., Köse, E., Arslan, N., Çiçek, A., Emiroğlu, Ö., Dayıoğlu, H. (2016) Ecosystem Quality Assessment of an Aquatic Habitat in a Globally Important Boron Reserve: Emet Stream Basin (Turkey). International Journal of Environment and Pollution. 59(2/3/4), 116-141.

[3] Tokatlı, C. (2015) Assessment of the Water Quality in the Meriç River: As an Element of the Ecosystem in the Thrace Region of Turkey. Polish Journal of Environmental Studies. 24(5), 2205-2211.

[4] Tokatlı, C., Baştatlı, Y. (2016) Trace and Toxic Element Levels in River Sediments. Polish Journal of Environmental Studies. 25(4), 1715-1720.

[5] Öterler, B. (2017) Community Structure, Temporal and Spatial Changes of Epiphytic Algae on Three Different Submerged Macrophytes in a Shallow Lake. Polish Journal of Environmental Studies. 26(5), 2147-2158.

[6] APHA (American Public Health Association) (1992) Standard methods for the examination of water and wastewater. In Greenberg, A.E., Clesceri, L.S. and Eato, A.D. (eds.) American Public Health Association. 18th ed., Washington, U.S.A.

[7] EPA (Environmental Protection Agency) METHOD 3051. (1998) Microwave Assisted Acid Digestion of Sediments, Sludges, Soils, and Oils.

[8] EPA (Environmental Protection Agency) METHOD 200.7. (2001) Determination Of Metals And Trace Elements In Water And Wastes by Inductively Coupled Plasma-Atomic Emission Spectrometry.

[9] TS 266 (Turkish Standards) (2005) Waters – Waters Intended for Human Consumption. Turkish Standardization Institute. ICS 13.060.20 (In Turkish).

[10] EC (European Communities) (2007) European Communities (drinking water) (no. 2), Regulations 2007, S.I. No. 278 of 2007.

[11] WHO (World Health Organization) (2011) Guidelines for Drinking-water Quality. World Health Organization Library Cataloguing-in-Publication Data. NLM classification: WA 675.

[12] Köse, E., Emiroğlu, Ö., Çiçek, A., Tokatlı, C., Başkurt, S., Aksu, S. (2018) Sediment Quality Assessment in Porsuk Stream Basin (Turkey) from a Multi-Statistical Perspective. Polish Journal of Environmental Studies. 27(2), 747-752.

[13] Mutlu, E., Uncumusaoglu, A.A. (2018) Analysis of Spatial and Temporal Water Pollution Patterns in Terzi Pond (Kastamonu/Turkey) by Using Multivariate Statistical Methods. Fresen. Environ. Bull. 27, 2900-2912.

[14] Liu, C.W., Lin, K.H., Kuo, Y.M. (2003) Application of Factor Analysis in the Assessment of Groundwater Quality in a Blackfoot Disease Area in Taiwan. Science of the Total Environment. 313, 77–89.

[15] Turkish Regulations (2004) Regulation on Surface Water Quality Management. Official Gazette Dated December 31, 2004. Number: 25687, http://suyonetimiormansu.gov.tr (In Turkish).

[16] Turkish Regulations (2015) Regulation on Surface Water Quality Management. Official Gazette Dated April 15, 2015. Number: 29327, http://suyonetimiormansu.gov.tr (In Turkish).

[17] EC (European Communities) (2006) EC of the European Parliament and of the council of 6 September 2006 on the quality of fresh waters needing protection or improvement in order to support fish life. Directive 2006/44.

[18] Uslu, O., Türkman, A. (1987) Water Pollution and Control. T.C. Prime Ministry Directorate General of Environment Publications, Training Series I, Ankara, Turkey (In Turkish).

[19] Wetzel, R.G. (2001) Limnology: Lake and River Ecosystems. Elsevier Academic Press. 1006p.

[20] Manahan, S.E. (2011) Water Chemistry: Green Science and Technology of Nature's Most Renewable Resource. Taylor and Francis Group. CRC Press, 398p.

[21] Self, J.R., Waskom, R.M. (2013) Nitrates in Drinking Water. Colorado State University Extension. 7/95. Revised 11/13.

[22] Tokatlı, C. (2014) Drinking Water Quality of a Rice Land in Turkey by a Statistical and GIS Perspective: İpsala District. Polish Journal of Environmental Studies. 23(6), 2247-2258.
[23] Tokatli, C., Köse, E., Uğurluoğlu, A., Çiçek, A., Emiroğlu, Ö. (2014) Use of Geographic Information System (GIS) to Evaluate the Water Quality of Gala Lake (Edirne). Sigma Journal of Engineering and Natural Sciences. 32, 490-501 (In Turkish).
[24] Todd, D.K. (1980) Groundwater Hydrology. 2nd edition. John Wiley and Sons, New York. 535p.
[25] Yu, G.B., Liu, Y., Yua, S., Wuc, S.C., Leung A.O.W., Luo, X.S., Xua, B., Li, H.B., Wongc, M.H. (2011) Inconsistency and Comprehensiveness of Risk Assessments for Heavy Metals in Urban Surface Sediments. Chemosphere. 85, 1080–1087.
[26] Eken, M.D., Akman, B. (2017) Evaluation of Pollution From Rivers in Northeastern Mediterranean Region: Heavy Metals. Fresen. Environ. Bull. 26, 4845-4850.
[27] ATSDR (Agency for Toxic Substances and Disease Registry) (2005) Toxicological profile for Zinc. U.S. Department of Health and Human Services.
[28] Keskin, Ş. (2017) Heavy Metal Contamination and Ecological Risk Assessment in the Sediments of Melen River, Duzce, Turkey. Fresen. Environ. Bull. 26, 4357-4366.
[29] Wen, J., Zhang, M., Liu, X., Ciu, X., Yan, X., Wu, B., Chen, B. (2018) Geographical Distribution, Chemical Speciation and Risk Assessment of Heavy Metals in Ting River: The Influence of Heap Bioleaching Plant on The Nearby River. Fresen. Environ. Bull. 27, 2844-2852.
[30] Song, Y., Li, J., Mao, C., Li, T., Feng, Y. (2018) The Estimation of Heavy Metals in Rivers Sediments in Changjiang River Delta by Visible/Near Infrared (Vis/Nir) Spectroscopy. Fresen. Environ. Bull. 27, 6184-6194.
[31] MacDonald, D.D., Ingersoll, C.G., Berger, T.A. (2000) Development and Evaluation of Consensus-Based Sediment Quality Guidelines for Freshwater Ecosystems. Arch. Environ. Contam. Toxicol. 39, 20–31.
[32] ATSDR (Agency for Toxic Substances and Disease Registry) (2000) Toxicological profile for Chromium. U.S. Department of Health and Human Services.
[33] Tokatlı, C., Çiçek, A., Emiroğlu, Ö., Arslan, N., Köse, E., Dayıoğlu, H. (2014) Statistical Approaches to Evaluate the Aquatic Ecosystem Qualities of a Significant Mining Area: Emet Stream Basin (Turkey). Environmental Earth Sciences. 71(5), 2185-2197.
[34] Tokatlı, C. (2017) Bio – Ecological and Statistical Risk Assessment of Toxic Metals in Sediments of a Worldwide Important Wetland: Gala Lake National Park (Turkey). Archives of Environmental Protection. 43(1), 34-47.
[35] DSI (State Water Works) (1997) Pollution Assesment Report of Ergene River. General Directorate of State Water Works of Turkey, Ankara, Turkey (In Turkish).

Received: **05.06.2018**
Accepted: **26.03.2019**

CORRESPONDING AUTHOR

Cem Tokatli
Department of Laboratory Technology,
İpsala Vocational School,
Trakya University,
22400, İpsala, Edirne – Turkey

e-mail: tokatlicem@gmail.com

© by PSP Volume 28 – No. 5/2019 pages 4141-4147 Fresenius Environmental Bulletin

OPTIMIZATION OF ULTRASONIC EXTRACTION OF TOTAL FLAVONOIDS FROM *NICANDRA PHYSALODES*

Yun Zhuang*, Dong Chen, Yao Ma

Jilin Agricultural Science and Technology University, Jilin City, Jilin Province, 132109, China

ABSTRACT

In this research, the total flavonoids were extracted by ultrasonic extraction from the stem of *Nicandra physalodes*. Firstly, single factor analysis was used to optimize the effects of processing parameters including temperature, ultrasonic time, ethanol concentration, ultrasonic power and solid-liquid ratio on the total flavonoids yields. Based on single factor analysis, orthogonal experiment of $L_{18}(3^5)$ was then designed and performed. Through statistical analysis, ratio of liquid to solid had significant effect on the yield of total flavonoids from *Nicandra physalodes*. In addition, the ethanol concentration, extraction time and temperature also played a role on the yields. Thus, the optimum extraction conditions were determined as follows: ratio of liquid to solid 1:20, extraction temperature 60 □, extraction time 40 min, ethanol concentration 40 % (v/v), ultrasonic power 150 w. Under these conditions, we obtained 2.80% extraction rate of total flavonoids.

KEYWORDS:
Nicandra physalodes, flavonoids, ultrasonic extraction

INTRODUCTION

Nicandra Physalodesis is an annual herb of Solanaceae. It is used for medicinal or appreciative cultivation in north and south of China. Early in 1981, researchers had extracted and separated anticancer agents from *Nicandra Physalodesis* [1]. Currently, there has been an upsurge of interest in the therapeutic potential of medicinal plants which might be due to their phenolic compounds, especially flavonoids [2, 3]. *Nicandra Physalodesis* is rich in flavonoids, such as nicandrenone, ferulic acid ketone and other flavonoids [4]. It has been reported that flavonoids have activities of antioxidation [5], antibacterium [6], antiinflammatory [7], anticancer [8] as well as hepatoprotecting [9].

Traditional methods, including heating, boiling and refluxing, have been used to the extraction of flavonoids. However, the disadvantages of these methods are not only wasting long extraction time but also the loss of flavonoids due to hydrolysis, oxidation and impurity substance during extraction [10]. In the past decades, ultrasonic treatment has been employed for preparing flavonoids from different plant materials [11, 12] and showed good extraction efficiency, proved to be a simple, inexpensive and efficient alternative to conventional extraction techniques [13].

To our knowledge, although the medicinal efficacy and application of flavonoids has been reported extensively, there is no research about ultrasonic extraction of total flavonoids from *Nicandra physalodes* so far. Thus, we aimed to study extraction process of total flavonoids from *Nicandra Physalodesis* to obtain optimization conditions which will provide a theoretical basis for the development and utilization of chemical constituents from *Nicandra Physalodesis.*

MATERIALS AND METHODS

The whole plant material of *Nicandra physalodes* used in this study was collected from medicinal plant base of Jilin institute of agricultural science and technology. The rutin standard was bought from China Institute for the Control of Pharmaceutical and Biological Products (Lot Number: 100080-200707). Chemical reagents we used including methanol, ethanol, alchlor, glacial acetic acid and natrium aceticum were analytical grade. Ultraviolet spectrometer (752#) was bought from Shanghai Aubelle instrument Co., Ltd. Ultrasonic cleaner (KQ3200DB) was bought from Kunshan Ultrasonic Instrument Co., Ltd. Thermostat water bath was bought from Jiangsu Jintan Jincheng Guosheng Experimental instrument Factory.

Preparation of standard curve. Rutin was used as the standard sample and dried at 120 ℃ to constant weight. Then weighed precisely 5.5 mg and dissolve in 50 ml methanol to make 0.11 mg/ml standard solution of rutin. Precisely absorb of rutin standard solution (0.11mg/ml) 0.5, 1, 2, 3, 4, 5 ml to capacity bottles and add 2 ml alchlor solution (0.1M), 1 ml NaAc-HAc buffer solution and last quantify total volume of 10 ml, respectively. Put the bottles into a 40 ℃ thermostatic water bath for 10 min and cool it out, then absorbance value was measured and the reagent blank was used as the control. The standard curve was shown in Fig 1. The regression equation was y=10.714x+0.0424, R^2=0.9993.

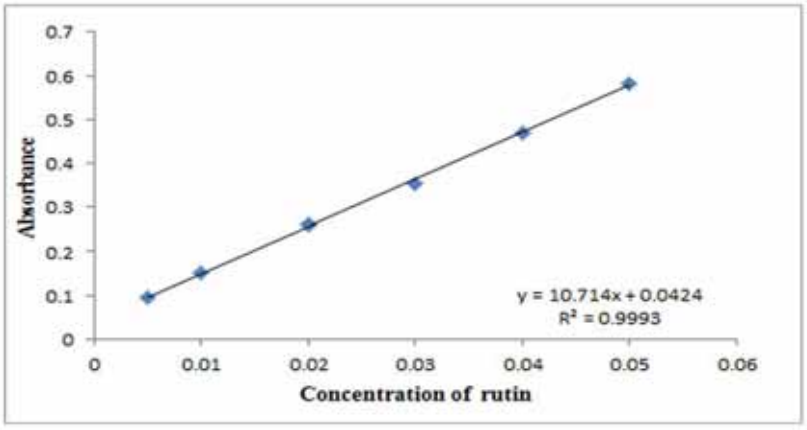

FIGURE 1
The standard curve

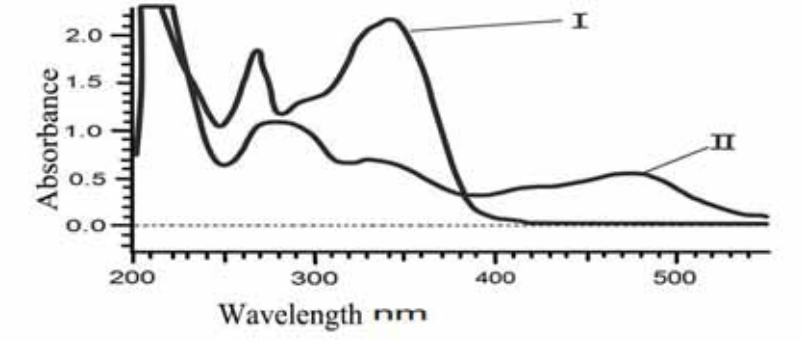

FIGURE 2
The UV–Vis spectra of rutin (I) and sample (II) solution

Preparation of coloring reagent. Precisely weigh alchlor ($AlCl_3$) 1.34 g and dissolve in methanol to quantify total volume of 100 ml (0.1 M). Precisely weigh anhydrous sodium acetate 1.76 g and dissolve in distilled water to quantify total volume of 100 ml (0.2 M). Dilute 1.15 ml glacial acetic acid with 100ml distilled water to make 0.2 M acetum solution and then mixed with 0.2 M sodium acetate solution above to obtain NaAc-HAc buffer solution (pH 5.2).

Wavelength selection. The standard solution of 1ml rutin was taken and placed in the volumetric flask, then added 2 ml $AlCl_3$ solution (0.1 M) and 1 ml NaAc-HAc buffer solution and filled with methanol to quantify total volume of 10 ml. Then put the flask into the water bath at 40 ℃ for 10 min. The absorptions were determined by UV spectrophotometer.

Extraction of total flavonoids. Powders of the samples (1.0 g) were accurately weighed and placed in a conical bottle by adding 20 mL of different concentrations (v/v) of ethanol accurately. After weighing, the conical bottle was placed into the ultrasonic cleaner at indicant temperatures for a series of periods. The ultrasonic power was kept at 50-300W. After extracted solution was cool, fill in the reduced weight and filter out the filtrate (sample solution).

Determination of flavonoids. 1 mL of the sample solution was accurately removed into a volumetric flask (10 mL) by adding 2 mL of $AlCl_3$ (0.1M) solution and NaAc-HAc buffer solution (pH5.2), and filled with methanol to quantify total volume of 10 ml. Then put the flask into the water bath at 40 ℃ for 10 min. The absorptions were determined by UV spectrophotometer.

RESULTS

Selection of detective wavelength. Ultraviolet scanning (presented in Fig. 2) was performed to determine the detective wavelength. We can see rutin had the largest absorption at 323nm, and there was no interference in the blank. So we selected absorption at 323nm for detection.

Single Factor Test. There were many factors affecting the extraction of flavonoids from *Nicandra physalodes.* We worked out the optimum levels of each factor by the single factor test. Single factor

test was performed by one factor varied with different levels while other factors fixed.

(a) Effect of temperature on extraction rate. The effect of different temperatures on extraction rate was investigated. Other conditions were kept the same (40% ethanol(v/v), solid to liquid ratio was 1: 20, ultrasonic power was 150 w, ultrasonic time was 30 min) As shown in Fig. 3A, the extraction rate of flavonoids did not change much when temperature was between 30-50℃. However, there was a significant rise when the temperature was above 50℃ and reached its highest point at 60℃. After 60 ℃, although the temperature was increasing, the extraction rate of flavonoids was decreased gradually probably influenced by impurities.

(b) Effect of time on extraction rate. We controlled the time of ultrasonic process by 10, 20, 30, 40, 50, 60 min and other conditions were kept the same (40 % (v/v) ethanol, solid to liquid ratio was 1: 20, ultrasonic power was 150 w, ultrasonic temperature was 50 ℃) and the curve of extraction rate was just like S-shape. As we can see in fig.3B, the extraction rate of flavonoids increased from 1.34% to 1.62% between 20 and 30 min and reached a maximum at 40 min and then dropped down. As ultrasonic time continued to prolong, the extraction rate was no longer increased.

(c) Effect of ethanol concentration on extraction rate. Ethanol was used as the extraction solvent in our study and different concentrations were set in each group while other factors fixed (solid to liquid ratio was 1: 20, ultrasonic power was 150 w, temperature was 50 ℃, ultrasonic time was 30 min). The result showed that the extraction rate of flavonoids was increasing and reached its crest value of 1.61% when ethanol concentration was 30 % (v/v). After that, with the increase of ethanol concentration, the extraction rate was a slight downward trend. When concentration was 60%, the extraction rate of flavonoids decreased sharply from 1.49% to 1.22% (Fig. 3C).

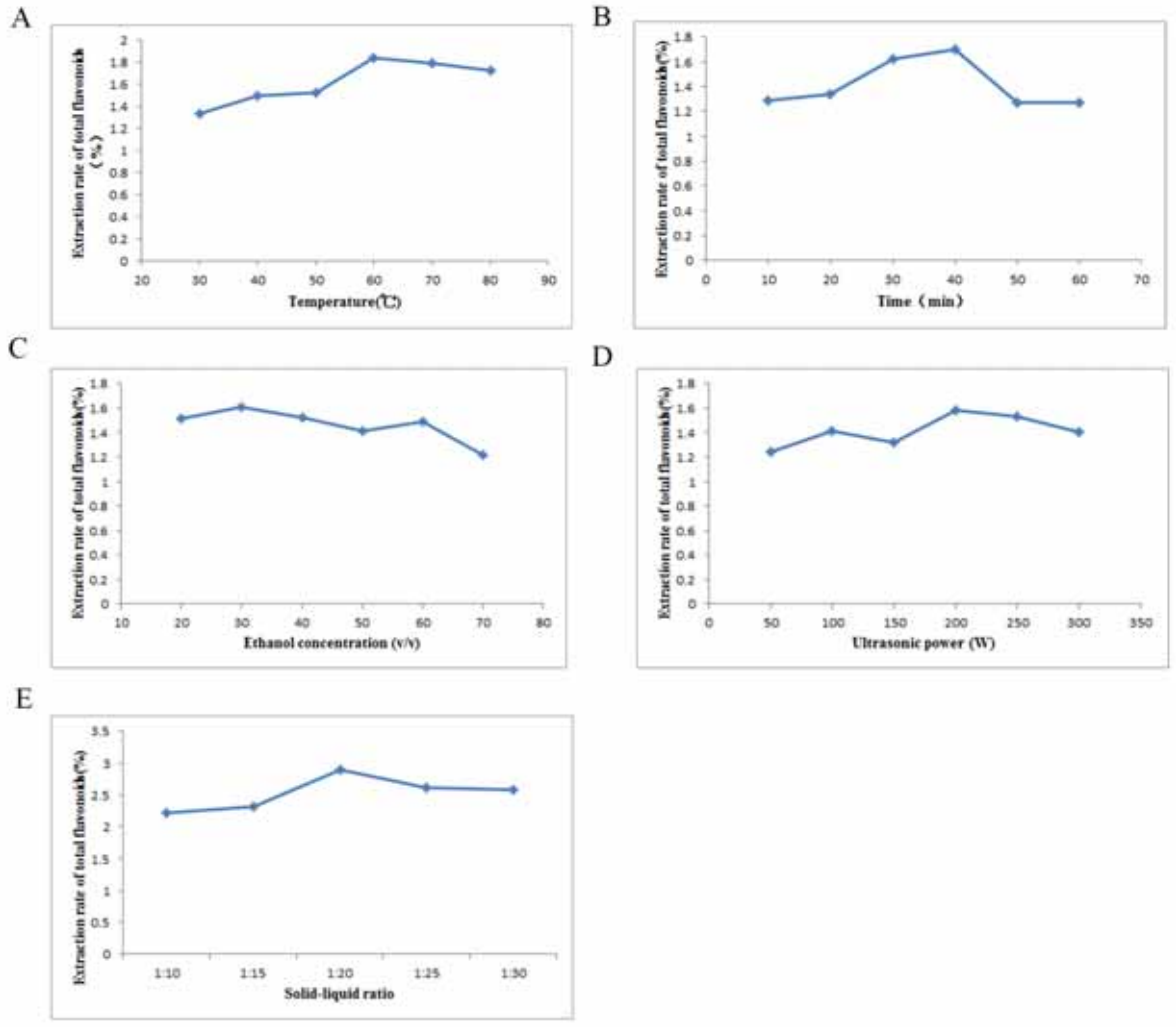

FIGURE 3
The effect of single factor. A Effect of temperature on extraction rate B Effect of time on extraction rate C Effect of ethanol concentration on extraction rate D Effect of ultrasonic power on extraction rate E Effect of solid-liquid ratio on extraction rate

(d) Effect of ultrasonic power on extraction rate. In order to study the influence of ultrasonic power on extraction rate, we set the single factor variable of ultrasonic power from 50 to 300 W while other factors fixed (40% ethanol(v/v), solid to liquid ratio was 1: 20, ultrasonic temperature was 50 ℃, ultrasonic time was 30 min). The result indicated that at 100 w or so, the extraction rate of flavonoids changed little with the increase of power. After 150 w, the extraction rate of flavonoids obviously augmented with the increase of power and appeared a peak at 200 w (Fig. 3D).

(e) Effect of solid-liquid ratio on extraction rate. Solid-liquid ratio was also an important factor affecting the extraction rate. The extraction by solid to liquid ratio 1:10 (g/mL), 1:15, 1:20, 1:30, 1:40 and 1:50 was investigated, other conditions were kept same (40 % ethanol(v/v), ultrasonic power was 150 w, ultrasonic temperature was 50 ℃, ultrasonic time was 30 min). As we can see in fig.3E, the best result of extraction rate could be achieved at 1:20 of material to liquid ratio. In the range of 1: 25-1: 30, the extraction rate of flavonoids remained basically unchanged.

Orthogonal design experiment. Orthogonal experiment of five factors and three levels were adopted to optimize the conditions of extraction L_{18} (3^5). Basis on Table1, eighteen experimental groups were designed with these five factors (Table 2). It indicated that the maximum difference of factor A was the most important factor affecting the extraction effect, and the order of influence degree was A > C > E > B > D. The optimum conditions of ultrasonic extraction were as follows: the ratio of solid to liquid was 1: 20, the concentration of ethanol was 40 %(v/v), the ultrasonic time was 40 min, the temperature was 60 ℃ and the power was 150 w.

TABLE 1
Factors and levels of orthogonal experiment

Level	Factors				
	A Solid to liquid ratio	B Temperature (℃)	C Ethanol concentration (v/v, %)	D Extraction power (w)	E Time (min)
1	1:15	50	20	150	30
2	1:20	60	30	200	40
3	1:25	70	40	250	50

TABLE 2
The results of orthogonal design and range analysis

Number	Factors					Absorbance	Extraction rate (%)
	A	B	C	D	E		
1	1	1	1	1	1	0.154	1.04
2	1	2	2	2	2	0.215	1.61
3	1	3	3	3	3	0.232	1.77
4	2	1	1	2	2	0.170	1.19
5	2	2	2	3	3	0.282	2.24
6	2	3	3	1	1	0.153	1.03
7	3	1	2	1	3	0.145	0.96
8	3	2	3	2	1	0.160	1.09
9	3	3	1	3	2	0.102	0.56
10	1	1	3	3	2	0.174	1.23
11	1	2	1	1	3	0.132	0.84
12	1	3	2	2	1	0.145	0.96
13	2	1	2	3	1	0.158	1.08
14	2	2	3	1	2	0.342	2.80
15	2	3	1	2	3	0.216	1.62
16	3	1	3	2	3	0.148	0.99
17	3	2	1	3	1	0.123	0.75
18	3	3	2	1	2	0.194	1.42
Mean I	1.242	1.082	1.00	1.348	0.992		
Mean II	1.66	1.555	1.378	1.243	1.468		
Mean III	0.962	1.227	1.485	1.272	1.403		
R	0.698	0.473	0.485	0.105	0.476		

TABLE 3
Variance analysis

Variance source	deviation quadratic sum	degree of freedom	variance	F value	P value
A	4.47	2	2.235	7.45	**
B	2.12	2	1.06	3.5	*
C	2.39	2	1.195	3.98	*
D	0.1	2	0.05	0.17	
E	2.33	2	1.165	3.88	*
SS	12.84	43	0.30		

TABLE 4
The results of precision test

Number	1	2	3	4	5	6	x	RSD (%)
A	0.127	0.126	0.122	0.125	0.126	0.125	0.125	1.26

TABLE 5
The results of stability test

Time(min)	10	20	30	40	50	60	x	RSD (%)
A	0.124	0.122	0.126	0.126	0.127	0.128	0.1255	1.58

TABLE 6
The results of repeatability test

Number	1	2	3	4	5	x	RSD (%)
A	0.124	0.121	0.126	0.123	0.127	0.1242	1.72

TABLE7
The results of recovery studies

Number	Content(mg)	Added(mg)	Found(mg)	Recovery (%)	Mean recovery(%)	RSD (%)
1	0.35	0.055	0.39	96.30		
2	0.35	0.11	0.46	102.17		
3	0.35	0.165	0.51	99.03	98.92	1.75
4	0.35	0.22	0.56	98.25		
5	0.35	0.275	0.62	99.20		
6	0.35	0.33	0.65	98.59		

Through variance analysis in Table 3, the ratio of solid to liquid (A) played a very significant role in the extraction of flavonoids. Meanwhile, the temperature (B), ethanol concentration(C) and extraction time (E) all played a role in the extraction except the extraction power (D) which had almost no effect on the extraction yield.

Methodology Studies. (a) Precision test of the apparatus. Apparatus precision was evaluated by the analysis of a solution of the sample for six consecutive times by ultraviolet spectrophotometer. Relative standard deviation (RSD) obtained was 1.26%, which showed that the precision of the apparatus was satisfactory (Table 4).

(b) Stability test of color rendering. Stability was evaluated by analysis a solution of the sample to color render in a water bath of 40℃ for 10, 20, 30, 40, 50 and 60 min. RSD obtained was 1.58%, which indicated that the stability of the solution had excellent stability in 1 h (Table 5).

(c) Repeatability of analytical method. To assess the repeatability of the method, six solutions made by ultrasonic extraction were determined. RSD obtained was 1.72%, which showed acceptable repeatability (Table 6).

(d) Recovery studies. Recovery studies were performed by adding series of rutin to 1ml of sample solution, determined by ultraviolet spectrophotometer detector after ultrasonic extraction. The results were shown in Table 4. We can see from the table that the mean recovery for flavonoids from *Nicandra physalodes* extracted by ultrasonic extraction was 98.92% with 1.75% of RSD, which indicated good effectiveness of the method (Table7).

DISCUSSION

Flavonoids consist of a large group of polyphenolic compounds which have a benzo-r-pyrone structure and occur virtually in most plant parts [14]. Flavonoids had been extracted by several methods from plants. For example, Li YR extracted and purified of total flavonoids from Aconitum tanguticum by using XAD-16 macroporous resin, which the average content of total flavonoids was raised from 4.39% to 46.19% [15]. Lu J performed enzyme extraction technology to extract total flavonoids from Cryptotaenia japonica with the average extraction rate of 4.76% [16]. In our study, the effect of single factor such as temperature, time, ethanol concentration, ultrasonic power or ratio of liquid to solid was not constant to the rate of total flavonoids. They all played the role of promoting the yield under certain conditions. When they exceed the corresponding point, the yield would decrease, which may be due to the influence of the solubility of flavonoids and the production of impurities (Fig. 3). For example, when ultrasonic treatment time was increased from 40 min to 50 min, the extraction rate of flavonoids decreased from 1.70% to 1.27%, which probably due to the excessive ultrasonic treatment time resulting in more impurities (Fig. 3B).

Because of the interaction among the factors, the combination effects of the optimum levels of each factor may not be the optimum extraction conditions. The orthogonal test is a scientific method of arranging multi-factors [17]. Based on the single factor test, the optimal extraction conditions can be worked out by orthogonal test. In our orthogonal design experiment, the mean and p value were calculated and list (Table 2). The results indicated that the ratio of solid to liquid had the greatest influence on the extraction rate and we could obtain the highest extraction yield of flavonoids with 2.8% under the following conditions: the ratio of material to liquid was 1: 20, the concentration of ethanol was 40 %, the ultrasonic time was 40 min, the temperature was 60 ℃ and the power was 150 w. To further verify the suitable of the method, the analytical method was performed. It showed that the method we used was convenient, rapid and reliable in the extraction and determination of total flavonoids.

In the present study, the ultrasonic extraction had been established to extract flavonoids from *Nicandra physalodes* and quantification was performed by means of ultraviolet spectrometer. The extraction yield of flavonoids was 2.8%. According to our knowledge, there is no special component in *Nicandra physalodes* that has ever been reported. Flavonoids are major functional components of *Nicandra physalodes*, and flavonoids from *Nicandra physalodes* had many effective roles in healthy and medical function. Therefore, the rapid and practical method established in our work to extract and determine flavonoids from *Nicandra physalodes* has great significance for studying the active ingredients of *Nicandra physalodes* and for its application.

ACKNOWLEDGEMENTS

This work was supported by grants from the Key Scientific and Technology program of Jilin Province (NO.20140204067YY) and Fund of Jilin Agricultural Technology College (2017312).

REFERENCES

[1] Gunasekera, S.P., Cordell, G.A. and Farnsworth, N.R. (1981) Plant anticancer agents XX. Constituents of Nicandra physalodes. Planta Med. 43, 389-391.

[2] Ghasemi Pirbalouti, A., Siahpoosh, A., Setayesh, M. and Craker, L. (2014) Antioxidant activity, total phenolic and flavonoid contents of some medicinal and aromatic plants used as herbal teas and condiments in Iran. J Med Food. 17, 1151-1157.

[3] Subedi, L., Timalsena, S., Duwadi, P., Thapa, R., Paudel, A. and Parajuli, K. (2014) Antioxidant activity and phenol and flavonoid contents of eight medicinal plants from Western Nepal. J Tradit Chin Med. 34, 584-590.

[4] Jonas, P.F. and Cordell, G.A. (2009) Molecular modeling, NOESY NMR, and the structure of nicandrenone isolated from Nicandra physalodes (Solanaceae). Nat Prod Commun. 4, 783-788.

[5] Heim, K.E., Tagliaferro, A.R. and Bobilya, D.J. (2002) Flavonoid antioxidants: chemistry, metabolism and structure-activity relationships. J Nutr Biochem. 13, 572-584.

[6] Edziri, H., Mastouri, M., Mahjoub, M.A., Mighri, Z., Mahjoub, A. and Verschaeve, L. (2012) Antibacterial, antifungal and cytotoxic activities of two flavonoids from Retama raetam flowers. Molecules. 17, 7284-7293.

[7] Middleton, E., Jr. and Kandaswami, C. (1992) Effects of flavonoids on immune and inflammatory cell functions. Biochem Pharmacol. 43, 1167-1179.

[8] Ferry, D.R., Smith, A., Malkhandi, J., Fyfe, D.W., deTakats, P.G., Anderson, D., Baker, J. and Kerr, D.J. (1996) Phase I clinical trial of the flavonoid quercetin: pharmacokinetics and evidence for in vivo tyrosine kinase inhibition. Clin Cancer Res. 2, 659-668.

[9] Zhu, W., Jia, Q., Wang, Y., Zhang, Y. and Xia, M. (2012) The anthocyanin cyanidin- 3- O-beta-glucoside, a flavonoid, increases hepatic glutathione synthesis and protects hepatocytes against reactive oxygen species during hyperglycemia: Involvement of a cAMP-PKA- dependent signaling pathway. Free Radic Biol Med. 52, 314-327.
[10] Li, H., Chen, B. and Yao, S. (2005) Application of ultrasonic technique for extracting chlorogenic acid from Eucommia ulmodies Oliv. (E. ulmodies). Ultrason Sonochem. 12, 295-300.
[11] Huang, W., Xue, A., Niu, H., Jia, Z. and Wang, J. (2009) Optimised ultrasonic-assisted extraction of flavonoids from Folium eucommiae and evaluation of antioxidant activity in multi-test systems in vitro. Food Chemistry. 114, 1147-1154.
[12] Velickovic D, Nikolova M, Ivancheva S, Stojanovic J and Veljkovic V (2007) Extraction of flavonoids from garden (Salvia officinalis L.) and glutinous (Salvia glutinosa L.) sage by ultrasonic and classical maceration. Journal of the Serbian Chemical Society. 72, 73-80.
[13] Wang, J., Sun, B., Cao, Y., Tian, Y. and Li, X. (2008) Optimisation of ultrasound-assisted extraction of phenolic compounds from wheat bran. Food Chemistry. 106, 482-488.
[14] Kumar, S. and Pandey, A.K. (2013) Chemistry and biological activities of flavonoids: an overview. Scientific World Journal 2013: 162750.
[15] Li, Y.R., Yan, L.X., Feng, W.H., Li, C. and Wang, Z.M. (2014) Extraction and purification technologies of total flavonoids from Aconitum tanguticum. Zhong Yao Cai. 37, 670-674.
[16] Lu, J., Xu, Y.Y., Rong, O., Li, S.B., Zhou, C. and Li, Z.H. (2013) Study on enzyme extraction technology of total flavonoids from Cryptotaenia japonica. Zhong Yao Cai 36. 1158-1162.
[17] Zhu, H., Wang, Y., Liu, Y., Xia, Y. and Tang, T. (2009) Analysis of Flavonoids in Portulaca oleracea L. by UV–Vis Spectrophotometry with Comparative Study on Different Extraction Technologies. Food Analytical Methods. 3, 90-97.

Received: **14.06.2018**
Accepted: **06.01.2019**

CORRESPONDING AUTHOR

Yun Zhuang
Jilin Agricultural Science and
Technology University, No. 1 Xuefu Road,
Zuo Jia town, Changyi District,
Jilin City, Jilin Province, 132109 – China

e-mail: zhuangyun2018@sina.com

© by PSP Volume 28 – No. 5/2019 pages 4148-4158 Fresenius Environmental Bulletin

THE INFLUENCE OF DIFFERENT ENVIRONMENTAL CONDITIONS ON THE PHYSICAL AND CHEMICAL PROPERTIES OF *STYRAX OFFICINALIS* L. SEED OIL

Cuneyt Cesur*

Department of Field Crops, Faculty of Agriculture, Bozok University, 66200 Yozgat, Turkey

ABSTRACT

In this study, the effects of the different environmental conditions on the physical and chemical properties of *Styrax officinalis* L. seed were investigated. Furthermore, the physical and chemical properties of*Styrax officinalis* L. seed crude oil obtained by using screw-press machine were measured with standard methods and compared with the other raw materials. As a result of this experimental study, the oil content of the *Styrax officinalis* L. seeds were found between 44.3 and 60.3%. When the fatty acid compositions of this crude oil were evaluated, the most dominant fatty acids were determined as oleic (45.50±1.4608 wt.%), and linoleic (37.74±1.5560 wt.%) acids. The density (at 15ºC), acid value, free fatty acid content, pH, saponification number, iodine value, cetane number, flash point, calorific value, and water content of *Styrax officinalis* L. seed crude oil were found to be at 939 kg/m3, 3 mg KOH/g, 1.5 wt. %, 200.89, 122.4 g iodine/100g, 45.92, 228ºC, 38.652 MJ/kg and 554.50 ppm, respectively. It is concluded that *Styrax officinalis* L. seed crude oil can be evaluated as a new feedstock in order to produce an alternative fuel such as biodiesel.

KEYWORDS:
Styrax officinalis L., environmental conditions, physical and chemical properties, fatty acid composition, renewable energy source

INTRODUCTION

Biodiversity is an important wealth for the sustainability of human life. The inability to know the value of this wealth is also the cause of many environmental disasters. Since people think completely their own profitability in their agricultural activities, they have not taken it seriously about damaged to nature for many years [1, 2].

People have taken into account the cultivation of plants which have been produced entirely in their agricultural activities and they have ignored the continuity of the lives of other plants and living things that grow in the environment.Therefore, the vitality and diversity of biological have quite decreased in the large areas [3–5].

The irresponsible behaviors of people have caused to continue increasing of the environmental irregularities. As the welfare level of society increases in all over the world, both the quantity and the quality of nutrition also gains importance.

Food is not only used for nutrition purposes but also it has been evaluated with the aim of protecting the health and preventing the diseases [6, 7]. The biomass is not only efficient in the studies of breeding but also the higher quality of the compounds has begun to be preferred. The researches have been accelerated to improve these quality features. Furthermore, it is emphasized that the fatty acids are very important for human life in the scientific researches. Fatty acids have important functions in order to protect the foods because of their antioxidant and antimicrobial properties [8, 9]. It has been reported that oleic acid prevent increasing in cholesterol, regulate blood sugar and has a protective effect against cardiovascular diseases [10–12]. It is notedin many studies that there are more than 900 phytochemicals in plants except vitamins and these phytochemicals decrease the risk of many chronic diseases, especially cancers [7]. Almost all of the physical and chemical properties of oils are determined by the proportions and types of fatty acids [13]. There are two main factors in the formation of these characteristics: Environment and Genetics. The productivity and quality of crops are significantly influenced by cultivationtechniques but the environment in which the plant grows is also very important. Figueiredo et al., 2008 [14] indicated that especially the secondary metabolites are affected by several factors such as physical changes, environmental conditions, geographical changes, genetic, and evolutionary events. In many studies, it is stated that these conditions influence the plant production and chemical properties of the oils [15, 16, 17, 18, 19].

Styrax officinalis L. belongs to Styracaceae family is perennial shrub formsand its seeds have approximately 50% oil content [20]. This plant can grow in the arid areas and resistant to adverse conditions [21, 22]. Therefore, the cost of Styrax *officinalis* L. productionis going to be lower than the other

field crops when it is entired in agricultural production. The usage of oil in the seeds as an energy source in the industrial field can reduce the demand pressure on edible oils.At the same time, it can contribute to supply the food security in all over the world [23, 24, 25, 26, 27, 28,]. Furthermore, the resins obtained from different parts of *Styrax officinalis* L.have been used in the perfumery sectors, cosmetic industries, traditional medicine and medical treatment procedures [29–32].

Most of the regions of Turkey, mainly the Inner Aegean, Central Anatolia, Eastern Anatolia and South East Anatolia, are defined as semi-arid climate zones because the level of annual rainfall is very low [33]. Therefore, the number of plants used in the agricultural production pattern is limited. For this reason, generally cereals have been cultivated in very large areas.This situation leads to the degradation of the soil structure of agricultural land in terms of both physical and chemical properties [34]. Also, it causes irregular the biological activities of the soil. The degradation of soil biological activity destroys crop productivity and finally agricultural production is not profitable [35]. This unfavorable status causing the lack of water resources is not only valid in Turkey, but alsoinall over the world. This is a vicious cycle. The way to get rid of this vicious circle is to increase the biodiversity and to protect it. The investigation of alternative crop cultivations that can be produced in arid climates is important for overcoming the vicious cycle. It can be a source of many economic and social improvements besides benefits from the development and protection of biodiversity.

In the literature survey, no researhes were found on the physical and chemical properties of *Styrax officinalis* L. seed oil to the best knowledge of the authors. This study can open a new idea about the renewable and sustainable energy sources. For this reason, the main objective of this study is to investigate the effects of different environmental conditions and altitudes on the physical and chemical properties of the crude oil obtained from *Styrax officinalis* L. seeds.

MATERIALS AND METHODS

Plant material. *Styrax officinalis* L. seeds used in the study were collected from nature in five different regions and altitudes where wereMersin, Hatay and Kahramanmaraş provinces in the Eastern Mediterranean of Turkey (Figure 1). The altitude and coordinates of the locationswere presented in Table 1.

TABLE 1
The altitudes and coordinates of locations

Location	Latitude & Longitude and Altitude
Pazarcık/Kahramanmaraş	37° 29'25.76" 37° 20'49.63" 865 m
Cennet/Mersin	36° 27'09.34" 34° 06'22.84" 138 m
Cehennem/Mersin	36° 27'14.61" 34° 06'22.84" 137 m
Sertavul/Mersin	36° 46'58.33" 33° 20'54.65" 963 m
Kurtbağı/Hatay	36° 24'35.09" 36° 01'25.22" 520 m

The seeds of *Styrax officinalis* L. that have come to harvest time on the plant were shown in the Figure 2. The seeds were collected in the first week of September in 2016.

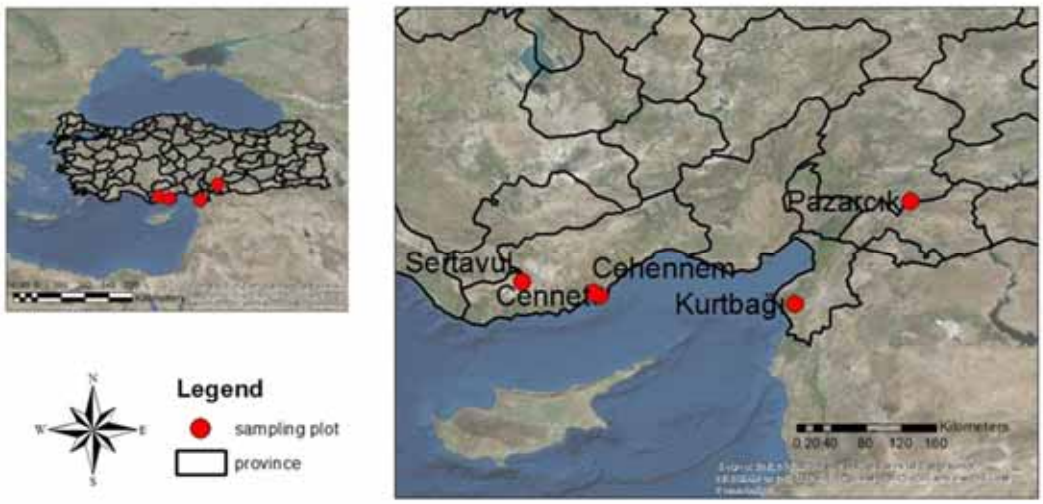

FIGURE 1
Location of collected samples

FIGURE 2
***Styrax officinalis* L. fruits**

Reagents. Fatty acid methyl ester standards were purchased from Sigma-Aldrich Chemical Company (Steinheim, Germany). Ethanol, Petroleum benzine, potassium hydroxide, dietghyl ether, phenolphthalein indicator were purchased from Merck.

Method. Physical characteristics such as 100 seeds weight, inner weight, husk weight, inner-husk ratio, husk length, husk width, inner length, inner width, and crude oil ratio of the *Styrax officinalis* L. seeds were determined in the Faculty of Agriculture, Bozok University, Yozgat, Turkey. The fatty acid compositions were found in the Department of Food Engineering, AbantİzzetBaysal University, Bolu, Turkey.

The oil content and fatty acid composition analysis. The seeds of *Styrax officinalis* L. were finely grounded with using steel mixer. The crude oil of the seeds was extracted by using n-hexane in a Soxhlet apparatus for 4 h. After the solvent was removed using rotary evaporator, the extract was dried under nitrogen. The extracted oils were kept in the sealed glass brown bottles, flushed with nitrogen and stored at the temperature of -18 °C prior to the analysis of the fatty acid compositions.

Fatty acid methyl esters (FAME) were prepared according to the AOAC method. FAMEs were identified by Shimadzu (Kyoto, Japan) gas chromatography equipped with Rtx-2330 capillary column (60 m x 0.25 mm i.d., 0.20 µm film thickness) and FID (flame ionization detector). The temperature for the injector was 250 °C and the temperature for the detector was 260 °C. The oven temperature was held at 140 °C for 5 min, and then increased to 240 °C at 4 °C/min and held at 240 °C for 20 min. Helium at a flow rate of 1.0 mL/min was used as a carrier gas. A sample of 1 µL was injected by the autosampler with a split mode (split ratio of 1:100). The fatty acid methyl esters were identified by comparison with standards and were quantified by the area percentage of each fatty acid methyl ester.

Physicochemical properties of the crude oil. The total concentration of saturated fatty acids (∑SFA, wt.%), the amount of monounsaturated fatty acids (∑MUFA, wt.%), the amount of polyunsaturated fatty acids (∑PUFA, wt.%), the ratio of unsaturated/saturated fatty acids (∑UFA/∑SFA), and the ∑PUFA/(∑SFA + ∑MUFA) ratio were calculated according to Gornas and Rudzinska, (2014) [36]. Acid value was measured with the simple titrimetric method using potassium hydroxide and phenolphthalein indicator.

SN (Saponification number) and IV (Iodine value) of SOME (Seed Oil Metly Ester) were calculated from the fatty acid compositions with the help of Eqs. (1) and (2), respectively [37].

$$SN = \sum (560 \times Ai) / MWi \quad (1)$$

$$IV = \sum (254 \times D \times Ai) / MWi \quad (2)$$

where Ai is the percentage of each component, D is the number of double bonds and MWi molecular mass of each component.

Cetane number of SOME was calculated from Eq. 3 [36]

$$CN = 46.3 + 5458/SN - 0{,}225 \times IV \quad (3)$$

Environmental factors. The climate data of the locationswereobtained from Ministry of Forestry and Water Affairs General Directorate of Meteorology (Turkey).

Climatic variables consisted of perennial average, minimum and maximum temperatures, perennial average rainy days, perennial average precipitation, and perennial mean sunshine duration. The average climatic data of 1926-2016 years for the locations were shown in Table 2.

TABLE 2
Environmental factors at each the sample collection locations (1926 – 2016)

Location	Average Temperature (°C)	Maximum Temperature (°C)	Minimum Temperature (°C)	Average Sunshine Duration (h)	Average Rainy Days	YearlyTotal Rainfall Average (mm)
Kahramanmaraş	16.9	22.9	11.3	81.2	79.8	727.7
Hatay	18.2	23.1	14.0	87.7	93.5	1126.6
Mersin	19.1	23.3	14.7	89.3	65.1	592.3

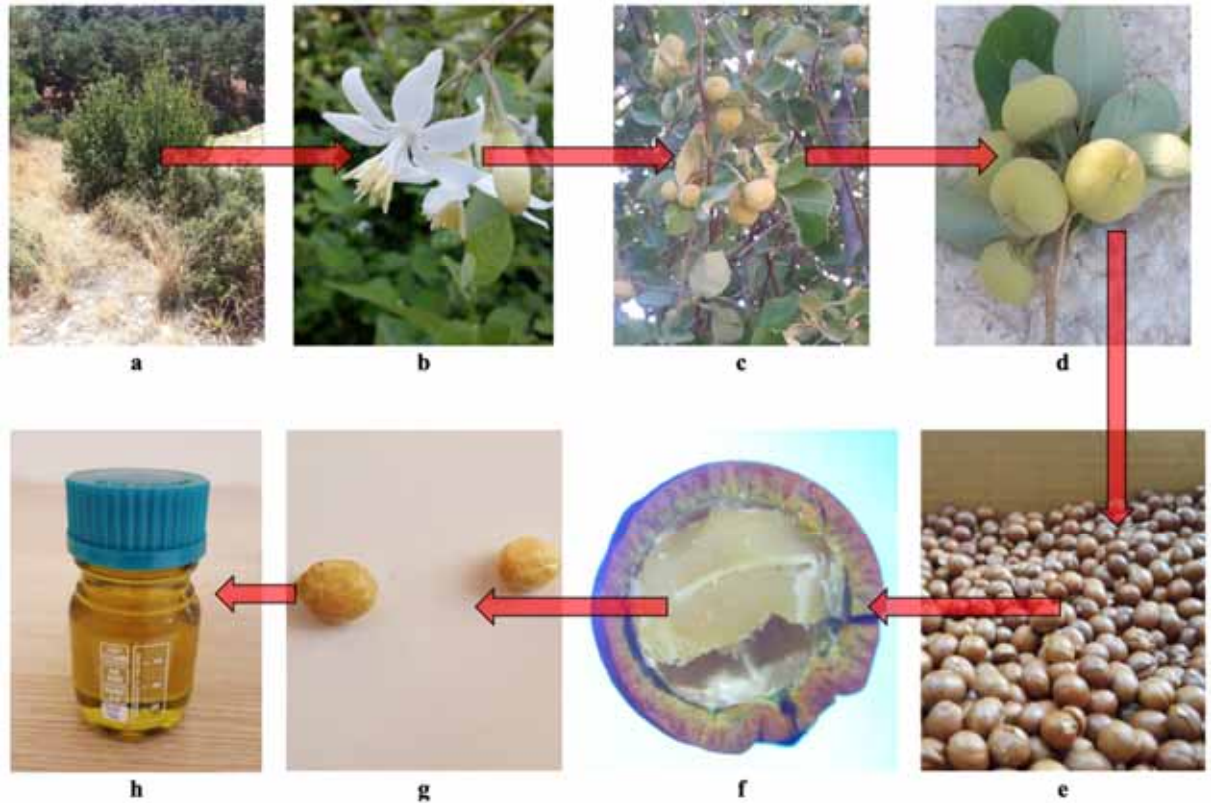

FIGURE 3
***Styrax officinalis* L. (a: Plant, b: Flower, c-d: Fruits, e-f-g: Seeds, and h: Oil)**

TABLE 3
The crude oil ratios and some physical properties of *Styrax officinalis* L. seeds collected from different locations

No	Location	*crude oil ratio	*100 seed weight	*inner weight	*husk weight	*inner-husk ratio	*husk length	*husk width	*inner length	*inner width
		%	g	g	g	%	mm	mm	mm	mm
1	Cennet	60.363 ^{a}	31.950 ^{b}	9.510 ^{b}	22.570 ^{b}	29.767 ^{a}	8.233 ^{b}	8.997 ^{ab}	6.230 ^{bc}	6.230 ^{bc}
2	Cehennem	44.337 ^{c}	34.493 ^{b}	9.857^{b}	23.493 ^{b}	28.560 ^{a}	7.820 ^{b}	9.487 ^{ab}	7.920 ^{a}	7.920 ^{a}
3	Sertavul	50.377 ^{b}	28.380 ^{b}	6.013 ^{c}	21.363 ^{b}	21.210 ^{b}	8.010 ^{b}	8.943 ^{b}	7.317 ^{ab}	7.317 ^{ab}
4	Pazarcık	59.993 ^{a}	46.690 ^{a}	13.347 ^{a}	32.733 ^{a}	28.580 ^{a}	9.223 ^{a}	11.540 ^{a}	9.150 ^{a}	4.917 ^{c}
5	Kurtbağı	45.547 ^{c}	45.783 ^{a}	13.283 ^{a}	32.303 ^{a}	28.990 ^{a}	10.077 ^{a}	8.943 ^{b}	8.880 ^{a}	5.050 ^{c}
MSE**		1.496	4.637	0.350	2.660	1.001	0.040	0.609	0.358	0.193

*1% significant, grouping based on Duncan test
**Mean square error

Statistical analysis. The analysis were conducted by using the statistical software program of SPSS 24. As a result of the applied factor analysis, each data is read by the program and the relations between the examined factors and the properties are calculated. The differences were compared with the Duncan's multiple range test ($P<0.05$). Mean and standard deviation (S.D.) of each of the fatty acids were calculated. A principal component analysis (PCA) was performed to examine the correlations between fatty acid composition and some physical properties. Then, these are revealed in a component diagram [38].

RESULT AND DISCUSSION

Physical properties of *Styrax officinalis* L. seeds. Styrax family include 8 genus and 120 species. It is represented 1 genus and 1 species in Turkey [39]. The pictures of *Styrax officinalis* L. plant, flower, fruits, seeds, and oil were given in Figure 3. These seeds were collected from the East Mediterranean region of Turkey. The crude oil ratio and some physical properties of *Styrax officinalis* L. seeds were presented in Table 3. As can be seen from Table 3, the highest values were obtained from Pazarcik location according to the averages, excluding

the inner width. When the values of Kurtbagi location was examined, it wasfound that all the other values except to the crude oil ratio and inner width values were located in the highest group. It was determined that Kurtbagi and Pazarcik locations are in the same group when considering the crude oil ratio, 100 seed weight and inner weightvalues which are considered to be the most important parameters in terms of the economic efficiency of the plants.

It can be said that annual rainfall and temperature averages are the main factors that cause above mentioned cases. An efficient plant cultivation is not only dependent on environmental conditions but also genetic characteristics of the plants Tardieu (2013) [40] pointed out that all the characteristics of plant production were revealed by the interaction of environment and the genetics. It is not enough to have a seed with superior properties for optimum yield as well as the soil properties and irrigation possibilities for agricultural production, climate characteristics such as average temperature, maximum and minimum temperature, sunshine duration and annual precipitation should be within the plant growth potential [41, 42]. Environmental factors are very important for biomass formation of plants. Also, they have significant implications for the formation of fatty acids and secondary metabolites in the biomass contents [43, 44]. It was reported that the yield of sunflower seeds, oil ratio and oil quality could be changed significantly according to the region, number of irrigation, rainfall condition and cultivar [45]. The amount of oleic acid in the soybean oil increase with the increasing of ambient temperature, meanwhile the amounts of linoleic and linolenic acids decrease. In other study, high temperatures were found to increase the amounts of oleic, palmitic and stearic acids in the soybean oil [25]. Many plants including soybean, peanut, sunflower and rapeseedwere detected to have a positive relationship between temperatures and the amount of oleic acid, whereas it was found to be a negative correlation between temperature andthe amount of linoleic acid [46].

The correlation analysis of the properties examined with the locations waspresented in Table 4. When Table 4 was examined, it was seen that the obtained data were in accordance with the literature [47–53].

The data obtained from area and laboratory measurements were evaluated using Principal Component Analysis and results were shown in Figure 4. Styrax populations differ in terms of the characteristics examined, and represent 53.950% of Component 1 total variation, while Component 2 is 21.673%. Principal Component Analysis is based on correlation analysis. It is possible to say that the locations were positive correlation with 100 seed weight, inner weight, husk weight, husk width, inner lenght. However, the fatty acids of palmitoleic ($C_{16:1}$), margoleic ($C_{17:1}$), linoleic ($C_{18:2}$) were negative correlation with all other properties (Figure 4).

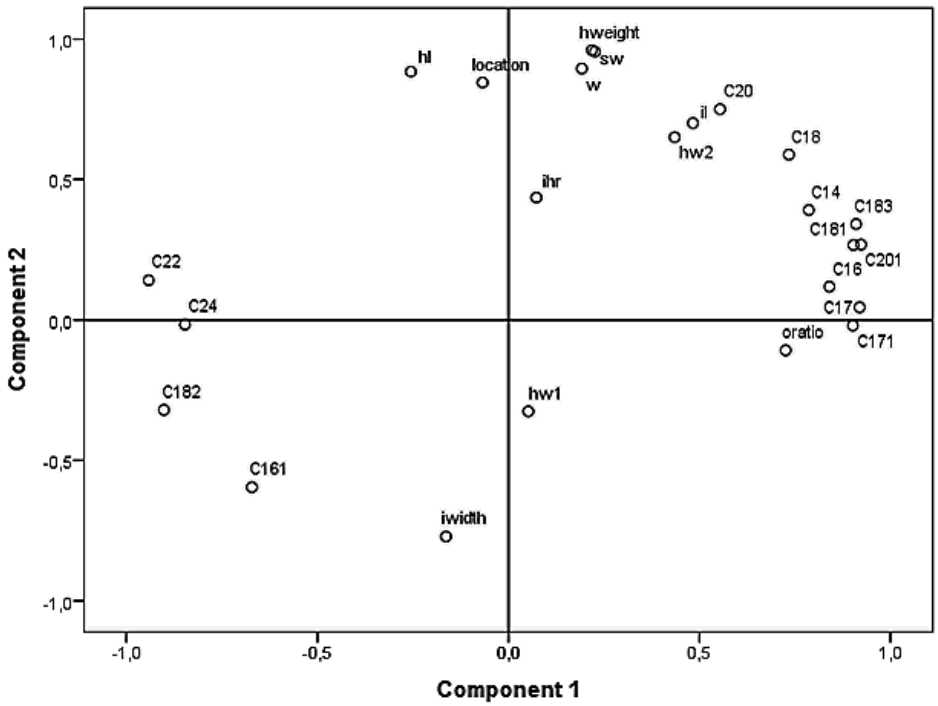

FIGURE 4

The results of Principle Component Analysis

hl: Husk length (mm) sw: 100 seed weight (g) hw1: Husk width 1(mm) oratio: Oil ratio(%)
hweight: Husk weight (g) w: Inner weight (g) hw2: Husk width 2 (mm) iwidth: Inner width(mm)
il: Inner length (mm) ihr: Inner- husk ratio (%)

TABLE 4
Correlation analysis

No	Property	Unit	1	2	3	4	5	6	7	8	9	10
1	Location	-	1.000									
2	100 seed weight	g	0.739**	1.000								
3	Inner weight	g	0.555*	0.953**	1.000							
4	Husk weight	g	0.791**	0.985**	0.909**	1.000						
5	Inner-husk ratio	%	-0.065ns	0.507ns	0.744**	0.413ns	1.000					
6	Husk length	mm	0.827**	0.811**	0.747**	0.836**	0.331ns	1.000				
7	Husk width	mm	0.751**	0.876**	0.808**	0.885**	0.375ns	0.783**	1.000			
8	Inner length	mm	0.768**	0.919**	0.867**	0.925**	0.439ns	0.875**	0.911**	1.000		
9	Inner width	mm	-0.612*	-0.785**	-0.753**	-0.833**	-0.407ns	-0.827**	-0.726**	-0.863**	1.000	
10	Oil ratio	%	-0.284ns	0.054ns	0.109ns	0.069ns	0.199ns	-0.025ns	0.009ns	0.154ns	-0.421ns	1.000

ns: not significant
*: $P < 0.05$
**: $P < 0.01$

When the locations wereevaluated according to the geographical conditions, it can be said that Pazarcık population settles at the Mediterranean climate ends and the South East Anatolia climate begins. Mediterranean climate is dominant from the other locations. However, 100 seed weight was obtained from this population as the highest value. Considering the development and yield of crops, it can be said that annual precipitation is very important, but it is not only determining factor in yield according to the obtained results. It is understood from this example that the genetic material of the plant is important besides the environmental conditions when considering the productivity from the agricultural point of view.

Fatty acid composition of *Styrax officinalis* L. seed oil. The fatty acid contents of *Styrax officinalis* L. seeds collected from five different locations wereanalyzedand given in Table 5. Also, the fatty acid compositions of *Styrax officinalis* L. seed oil were compared with the other edible adn non-edible oils (Table 6). According to the obtained data, there are changes in data at all locations and true appearance of fatty acid distributions resemble each other. Mono and polyunsaturated fatty acids have formed macro ratios in all locations. Other acid ratios can also be defined as minor values.

The linoleic ($C_{18:2}$) acid contents of the *Styraxofficinali*L. seeds collected from the Sertavul and Kurtbagi populations were determined as 38.52% in the Sertavul population and 39.96% in the Kurtagi population. Although the altitudes of the Kurtbagi and Sertavul populations are different from each other, the common feature of both locations are available in an open position in the Mediterranean. Moisture evaporated from the sea brings rain and moisture to Kurtbağı and Sertavul locations as it moves towards the mountains. It can be said that this affects the fatty acid composition. While the height of the Kurtbagi location was determined as 520m from the sea, this height was determined as 963m in the Sertavul location. The altitude of the Cennet and Cehennem populations are almost identical. The altitude of the Cennet location is determined as 138m, and the altitude of the Cehennem location is determined as 137m. Linoleic acid content was determined 36.32% in the Cennet population and 37.64% in the Cehennem population. Comparing the ratios of linoleic acid in these four different locations, it can be said that the Cennet and Cehennem populations with the same altitude form one group and the Kurtbagi and Sertavul populations with the higher altitude form another group. The Pazarcik population has been identified as representing another feature.

Pazarcık population was collected from the location where the Mediterranean region ends and the Southeast Anatolian region begins. Geographical location is relatively different from other populations. While the other four populations are in the Mediterranean climate and overlooking the sea, Pazarcik population is both remote from the sea and at the behind of Toros mountains where the summers are in an arid, hot and low humidity region. The percentage of linoleic acid in Pazarcik population is 36.28. It is seen that this ratio is close to Cennet and Cehennem populations. According to this data, it can be said that the rates of linoleic acid have affected from various factors. Nas, 2001 [13] reported that the cold climates were more suitable for the development of plants having abundant amounts of linoleic acid. $C_{18:1}$ is highly susceptible to environmental interference. Sun et al. (2017) [25] presented that the oleic acid was not affected from environmental

TABLE 5
The fatty acid compositions of *Styrax officinalis* L. seed oils collected from five different locations

Fatty acid composition	Pazarcik	Sertavul	Cennet	Cehennem	Kurtbagi
Saturated fatty acids					
$C_{14:0}$Miristic	0.07	0.08	0.06	0.05	0.06
$C_{16:0}$ Palmitic	9.51	8.33	8.76	8.97	8.98
$C_{17:0}$ Margaric	0.11	0.14	0.10	0.12	0.12
$C_{18:0}$ Stearic	2.49	2.28	2.66	2.21	2.40
$C_{20:0}$ Arachidic	0.17	0.15	0.17	0.16	0.18
$C_{22:0}$Beheric	0.06	0.06	0.05	0.05	0.06
$C_{24:0}$Lignoseric	0.05	0.05	0.06	0.05	0.06
Mono-unsaturated fatty acids					
$C_{16:1}$ Palmitoleic	0.03	0.03	0.03	0.04	0.03
$C_{17:1}$Margoleic	0.06	0.11	0.07	0.09	0.08
$C_{18:1}$ Oleic	46.02	45.15	47.18	45.91	43.23
$C_{20:1}$ Gadoleic	0.25	0.25	0.28	0.28	0.26
Poly-unsaturated fatty acids					
$C_{18:2}$ Linoleic	36.28	38.52	36.32	37.64	39.96
$C_{18:3}$ Linolenic	4.90	4.87	4.27	4.44	4.59
Total	100	100	100	100	100

TABLE 6
The comparison of the fatty acid compositions of *Styrax officinalis* L. seed oil with the other oils

No	Fatty acid composition	Molecular weight	Structure	Systematic name	Formula	This study (SyO)	SO^1	SuO^2	CO^3	SoO^1	PO^2	SeO^4
1	Myristic	228	14:0	Tetradecanoic	$C_{14}H_{28}O_2$	0.06±0.0114	0.05	0.2	0	0	0	0
2	Palmitic	256	16:0	Hexadecanoic	$C_{16}H_{32}O_2$	8.91±0.4264	5.28	4.8	3.49	28.33	40.3	8.5
3	Margaric	270	17:0	heptadecanoic	$C_{17}H_{33}O_2$	0.12±0.0148	-	-	-	-	-	-
4	Steraic	284	18:0	Octadecanoic	$C_{18}H_{36}O_2$	2.41±0.1773	1.79	5.7	0.85	0.89	3.1	3.1
5	Arachidic	312	20:0	Eicosanoic	$C_{20}H_{40}O_2$	0.17±0.0114	0.40	0.4	0	0	0	1.0
6	Behenic	340	22:0	Docosanoic	$C_{22}H_{44}O_2$	0.06±0.0054	0	0	0	0.1	0	0
7	Lig-noseric	367	24.0	cis-15-Tetra-cosenoic	$C_{24}H_{46}O_2$	0.05±0.0054	0	0	0	0	0	0
8	Pal-mitoleic	254	16:1	Hexadec-9-enoic	$C_{16}H_{30}O_2$	0.03±0.0044	0.05	0.8	0	0	0	0
9	Margo-leic	268	17:1	Cis-10-heptade-cenoic	C17H32O2	0.08±0.0192	-	-	-	-	-	-
10	Oleic	282	18:1	cis-9-Octadecenoic	$C_{18}H_{34}O_2$	45,50±1.4608	29.88	20.6	64.4	13.27	43.4	38.8
11	Gadoleic	310	20:1	11-Eicosenoic	$C_{20}H_{38}O_2$	0.27±0.0151	0.14	0	0	0	0	0
12	Linoleic	280	18:2	cis-9-cis-12 Octa-decadienoic	$C_{18}H_{32}O_2$	37.74±1.556	62.29	66.2	22.3	57.51	13.2	46.3
13	Linolenic	278	18:3	cis-9-cis-12 Octa-decatrienoic	$C_{18}H_{30}O_2$	4.61±0.2722	0.08	0.8	8.23	0	0	0
				Saturated fatty acids		11.78±0.6521	7.52	11.6	4.34	15.5	43.4	14.9
				Monounsaturated fatty acids		45.87±1.4995	29.88	20.06	64.4	13.27	43.4	38.8
				Polyunsaturated fatty acids		42.35±1.8282	62.37	67.0	30.53	61.0	13.2	46.3
				Total		100±3.9798	99.96	100	99.27	100	100	100

SyO: Styraxofficinalis, SO: Safflower oil, SuO: Sunflower oil, CO: Canola oil, SoO: Soybean oil, Seo: Sesamum oil, PO: Peanut oil
[1][55] [2][56] [3][57] [4][58]

conditions, however the environmental conditions significantly influenced $C_{20:1}$, $C_{18:2}$, $C_{20:0}$ and $C_{16:0}$ acids. Different studies have shown that the fatty acids are not stable and they illustrate different variation based on the several factors, mainly genetic and ecological characteristics [54, 55]. The fatty acids such as linoleic, linolenic, arachidonic, eicosapentaenoic and docosahexaenoic are the most important polyunsaturated fatty acids in order to feed.

As can be seen in Table 5, the sum of $C_{18:1}$, $C_{18:2}$ and $C_{18:3}$ is high in all populations. These three unsaturated fatty acids, which were the most dominant fatty acids, were found to be at 87.2% in Pazarcik, 88.54% in Sertavul, 87.77% in Cennet, 87.99% in Cehennem and 87.78% in Kurtbagi populations.

The comparison of the fatty acid compositions of *Styrax officinalis* L. seed oil with the other oils were given in Table 6. The average amount of oleic acid in the *Styrax officinalis* L. seed crude oil was calculated as 45.498%. When this ratio compared to the amounts of oleic acids in the other oils, the maximum ratio was found to be at the canola oil following *Styrax officinalis* L. seed crude oil. Researches and applications showed that the oils including long, and one pair of branched fatty acids bond in the chemical structure are suitable for the alternative fuel and the increasing the degree of unsaturation has

a negative effect on the cetane number was also detected [56]. Secondly dominant fatty acid in the *Styrax officinalis* L. seed crude oil was linoleic acid with the ratio of 37.744% which is higher than the amounts of the oleic acids in the canola and peanut oils.

The physical and chemical properties of *Styrax officinalis* L. seed oil. The physical and chemical properties of *Styrax officinalis* L. seed oil were presented in Table 7. As can be seen in Table 7, the calorific value and water content of the crude oil were found to be at 38.652 MJ/kg and 554.50 ppm. When this crude oil used as an alternative energy source, the calorific value was satify the necessary of technological development. The ∑PUFA/(∑SFA+ ∑MUFA) ratio is a potential indicator of the chemical properties of the oils. The ratio close to or less than 1 may indicate that the oil show excellent global properties for biodiesel [39]. Furthermore, *Styrax officinalis* L. seed oil has higher contents of ∑MUFA and ∑PUFA. Therefore, this oil can be evaluated in the production of biodiesel. Because, the researches and applications have shown that the oils, which have higher content of oleic acid, has preffered in the biodiesel production. Also, linoleic and linolenic acids have influence of the low temperature properties of the produced biodiesel. In *Styrax officinalis* L. seed oil, these ratio were measured to be at between 40.59 and 44.55 wt. %. For this reason, the low temperature properties such as cold filter plugging point, poour point, etc. can show excellent values compared with the other feedstocks used in the biodiesel production. Moreover, the free fatty acid content of the crude oil was found as 1.5 wt. % which is one of the most important parameter for determining the step numbers of the production of biodiesel. It is desirable that the free fatty acid content of the oils is less than 2 in order to prefer single-step transesterification process.

CONCLUSION

In the present study, the effects of different environments and altitudes on the physical and chemical properties of *Styrax officinalis* L. seeds collected from different locations in Mersin, Hatay and Kahramanmaraş provinces of Turkey were investigated and compared. Also, the physical and chemical properties of the oils obtained from *Styrax officinalis* L. seeds were measured and compared with the other oils. The following findings were given in the below.

- It was observed that the highest values of seed inner weight, husk length, husk width and 100 seed weight were obtained from the location of Pazarcik. These values were found to be at 14.06 g, 9.23 mm, 11.73 mm and 46.41 g, respectively.
- The oil content of the *Styrax officinalis* L. seeds were found to be at between 44.337 and 60.363%. For this reason, *Styrax officinalis* L. seed oils can be used as a renewable energy feedstock.
- CCA analysis showed that the environmental factors explained 10.60% of the total variation in the fatty acid composition. According to the chemical properties, 13 fatty acids were identified like mirystic ($C_{14:0}$), palmitic ($C_{16:0}$), stearic ($C_{18:0}$), arachidic ($C_{20:0}$), beheric ($C_{22:0}$), lignoseric ($C_{24:0}$), palmitoleic ($C_{16:1}$), margaric ($C_{17:0}$), oleic ($C_{18:1}$), gadoleic ($C_{20:1}$), linoleic ($C_{18:2}$), margoleic ($C_{17:1}$), and linolenic ($C_{18:3}$) acids. The most dominant fatty acids in the oils were determined as $C_{18:0}$, $C_{18:2}$ and $C_{18:3}$ acids.

TABLE 7
Physicochemical properties of *Styrax officinalis* L. seed oil

Property	Units	Styrax officinalis	Mustard	Castor Oil	Poppy
Density at 15ºC	kg/m^3	939	916[1]	963[3]	922,85[5]
Colour	-	Yellower weaker darker	Yellower[1] Stronger Lighter	-	Greener Stronger Lighter
Acid value	mg KOH/g	3	1.5[1]	3[3]	-
Free fatty acid content	wt.%	1.5	0.73[1]	1.21[4]	1[6]
pH	-	6	7[1]	-	3.7[6]
Saponification number	-	200.89	194.43[2]	185[3]	199.5[6]
Iodine value	g iodine/100 g	122.4	107[2]	88[3]	127[6]
Cetane number	-	45,92	50.30[2]	-	-
Flash point	ºC	228	219[1]	294[4]	-
Calorific value	MJ/kg	38.652	39,91[1]	29.60[4]	-
Water content	ppm	554,50	593,78[1]	-	-
∑ SFA	wt.%	11.09-12.46	10.76[1]	2.53[4]	11.72[5]
∑MUFA	wt.%	43.60-47.56	50.34[1]	92.53[4]	13.16[5]
∑PUFA	wt.%	40.59-44.55	38.82[1]	0.42[4]	75.07[5]
UFA/SFA	wt.%	7.03-8.02	8.29[1]	36.74[4]	7.53[5]
PUFA/(SFA+MUFA)	wt.%	0.68-0.80	0.64[1]	0.004[4]	3.02[5]

[1]Cesur, [60];[2]Fadhil et al., [61]**;** [3]Ogunniyi, [62]; [4]Okullo et al., [63]; [5]Bozan and Temelli, [64]; [6]Musa Özcan and Atalay, [65]

- The fatty acids of $C_{18:1}$ and $C_{18:2}$ showed environmental sensitivity, whereas $C_{18:3}$ was less sensitive to the environmental variation compared with the other fatty acids due to genotypic effects.
- The highest rates of macro-fatty acids ($C_{18:1}$, $C_{18:2}$, and $C_{18:3}$) were determined as 88.54% inSertavul, 87.99% in Cehennem, 87.78% in Kurtbag, 87.77% in Cennet and 87.20% in Pazarcık.
- When the physical and chemical properties of the *Styrax officinalis* L. seed oil were evaluated, it can be used in the biodiesel production applications.
- In future study, *Styrax officinalis* L. seed oil biodiesel should be produced and fuel properties should be measured and compared with biodiesel standards such as EN 14214 and ASTM D6751. Moreover, the engine performance and exhaust emission characteristics should be carried out in order to sustainable environment applications.

ACKNOWLEDGEMENTS

This study was financially supported by Scientific Research Projects Fund (Project No. BAP-6602c ZF/16-22), Bozok University, Turkey.

REFERENCES

[1] Gardi, C., Jeffery, S., Saltelli, A. (2013) An estimate of potential threats levels to soil biodiversity in EU. Glob. Chang. Biol. 19, 1538–1548.
[2] Orgiazzi, A., Panagos, P., Yigini, Y., Dunbar, M.B., Gardi, C., Montanarella, L., Ballabio, C. (2016) A knowledge-based approach to estimating the magnitude and spatial patterns of potential threats to soil biodiversity. Sci. Total Environ. 545–546, 11–20.
[3] Jones, R.J.A., Houšková, B., Bullock, P., Montanarella, L. (2005) Soil Resources of Europe. Second edition. 420.
[4] Zhang, J., Ye, Q., Gao, P., Yao, X. (2012) Genetic footprints of habitat fragmentation in the extant populations of Sinojackia (Styracaceae): implications for conservation. Bot. J. Linn. Soc. 170, 232–242.
[5] Tonin, S., Lucaroni, G. (2017) Understanding social knowledge, attitudes and perceptions towards marine biodiversity: The case of tegnùe in Italy. Ocean Coast. Manag. 140, 68–78.
[6] Berner, L.A., O'Donnell, J.A. (1998) Functional foods and health claims legislation: Applications to dairy foods. Int. Dairy J. 8, 355–362.
[7] İşleroğlu, H., Yıldırım, Z., Yıldırım, M. (2005) Flax Seed as a Functional Food.GOÜ. Journal of Agricultural Faculty. 22, 23–30. (in Turkish)
[8] Cafarchia, C., De Laurentis, N., Milillo, M.A., Losacco, V., Puccini, V. (1999) Antifungal activity of Apulia region propolis. Parassitologia. 41, 587–90.
[9] Çoşkun, F. (2006) Natural Preservatives in Foods. Journal of Food Technologies. 2, 27–33. (in Turkish)
[10] Esen, E., Sizmaz, S., Demir, T., Demirkiran, M., Unal, I., Demircan, N. (2015) Evaluation of Choroidal Vascular Changes in Patients with Multiple Sclerosis Using Enhanced Depth Imaging Optical Coherence Tomography. Ophthalmologica. 235, 65–71.
[11] Bail, S., Stuebiger, G., Unterweger, H., Buchbauer, G., Krist, S. (2009) Characterization of volatile compounds and triacylglycerol profiles of nut oils using SPME-GC-MS and MALDI-TOF-MS. Eur. J. Lipid Sci. Technol. 111, 170–182.
[12] Montoya, C., Cochard, B., Flori, A., Cros, D., Lopes, R., Cuellar, T., Espeout, S., Syaputra, I., Villeneuve, P., Pina, M., Ritter, E., Leroy, T., Billotte, N. (2014) Genetic Architecture of Palm Oil Fatty Acid Composition in Cultivated Oil Palm (Elaeis guineensis Jacq.) Compared to Its Wild Relative E. oleifera (H.B.K) Cortés. PLoS One. 9, e95412.
[13] Nas, S. (2001) Vegetable oil technology.3th edition. Pamukkale University Engineering Faculty (in Turkish).
[14] Figueiredo, A.C., Barroso, J.G., Pedro, L.G., Scheffer, J.J.C. (2008) Factors affecting secondary metabolite production in plants: volatile components and essential oils. Flavour Fragr. J. 23, 213–226.
[15] Salgueiro, L.R., Vila, R., Tomàs, X., Cañigueral, S., da Cunha, A.P., Adzet, T. (1997) Composition and variability of the essential oils of Thymus species from section Mastichina from Portugal. Biochem. Syst. Ecol. 25, 659–672.
[16] Miguel, M.G., Duarte, F.L., Venâncio, F., Tavares, R. (2004) Comparison of the Main Components of the Essential Oils from Flowers and Leaves of Thymus mastichina (L.) L. ssp. mastichina Collected at Different Regions of Portugal. J. Essent. Oil Res. 16, 323–327.
[17] Alaoui Jamali, C., Kasrati, A., Bekkouche, K., Hassani, L., Wohlmuth, H., Leach, D., Abbad, A. (2014) Cultivation and the application of inorganic fertilizer modifies essential oil composition in two Moroccan species of Thymus. Ind. Crops Prod. 62, 113–118.
[18] Méndez-Tovar, I., Novak, J., Sponza, S., Herrero, B., Asensio-S-Manzanera, M.C. (2016) Variability in essential oil composition of wild populations of Labiatae species collected in Spain. Ind. Crops Prod. 79, 18–28.
[19] Baydar, H. (2000) The importance of oil production, quality and quality improvement in plants. Ekin Derg. 11, 50–57. (in Turkish).

[20] Cesur, C., Coşge Şenkal, B., Uskutoğlu, T., Doğan, H. (2017) Alternative Oil Plant: Styrax (Styrax Officinalis L.). In: III. Int. Conf. Eng. Nat. Sci., Budapest, 890 – 895.
[21] Sugden, E.A. (1986) Anthecology and Pollinator Efficacy of Styrax Officinale Subsp. Redivivum (Styracaceae). Am. J. Bot. 73, 919.
[22] Wang, Y., Nie, X., Liu, Z. (2015) Biodiesel Synthesis from Styrax confusus Hemsl Catalyzed by S2O8 2−/ZrO2-TiO2-Fe3O4. J. Am. Oil Chem. Soc. 92, 813–820.
[23] Anıl, H. (1980) Four benzofuran glycosides from Styrax officinalis. Phytochemistry. 19, 2784–2786.
[24] Lee, H.-J., Park, S.Y., Lee, O.-K., Jo, H.-J., Kang, H.-Y., Choi, D.-H., Paik, K.-H., Khan, M. (2008) Benzofurans and sterol from the seeds of styrax obassia. Chem. Nat. Compd. 44, 435–439.
[25] Sun, C., Jia, L., Xi, B., Wang, L., Weng, X. (2017) Natural variation in fatty acid composition of Sapindus spp. seed oils. Ind. Crops Prod. 102, 97–104.
[26] Demiray, H., Eşiz Dereboylu, A., Yazici, Z.I., Karabey, F. (2013) Identification of benzoin obtained from calli of Styrax officinalis by HPLC. Turk. J. Botany. 37, 956–963.
[27] Selim, M.Y.E., Ghannam, M.T., Al Awad, A.S., Al Sabek, M.S. (2017) Combustion and exhaust emissions of a direct-injection diesel engine burning jojoba ethyl ester and mixtures with ethanol. Biofuels. 2017, 1–7.
[28] Rozina, Asif, S., Ahmad, M., Zafar, M., Ali, N. (2017) Prospects and potential of fatty acid methyl esters of some non-edible seed oils for use as biodiesel in Pakistan. Renew. Sustain. Energy Rev. 74, 687–702.
[29] Steinner, K., Leifer, W. (1949) Investigation of contact-type dermatitis due to compound tincture of benzoin. J. Invest. Dermatol. 13, 351–9.
[30] Cao, T.Q., Tran, M.H., Kim, J.A., Tran, P.T., Lee, J.-H., Woo, M.H., Lee, H.-K., Min, B.S. (2015) Inhibitory effects of compounds from Styrax obassia on NO production. Bioorg. Med. Chem. Lett. 25, 5087–5091.
[31] Hjorth, N. (1961) Eczematous allergy to balsams, allied perfumes and flavouring agents, with special reference to balsam of Peru. Acta Derm. Venereol. Suppl. (Stockh). 41(1961).
[32] Lovell, C.R. (1993) Plants and the Skin. Blackwell Scientific Publications.
[33] Kapluhan, E. (2013) The effect of drought on agriculture and drought in Turkey. Marmara Coğrafya Derg. 2013. (in Turkish).
[34] Karadoğan, S., Özgen, N. (2006) Analysis of the Nature, Change and Distribution of Agricultural Production in the Southeast Anatolia Region in GIS Environment. In: 4th Geographic Information System. Informatics Days. İstanbul/Turkey. (in Turkish).
[35] Elmastaş, N. (2008) Agricultural Land Use in Ahlat District. GAUN-JSS. 7, 479–501. (in Turkish).
[36] Gornas, P., Rudzinska, M., Seglina, D. (2014) Lipophilic composition of eleven apple seed oils: A promising source of unconventional oil from industry by-products. Ind. Crops. Prod. 60, 86-91.
[37] Atabani, A.E., Badruddin, I.A., Masjuki, H.H., Chong, W.T., Lee, K.T. (2015) Pangium edule Reinw: A Promising Non-edible Oil Feedstock for Biodiesel Production. Arab. J. Sci. Eng. 40, 583–594.
[38] Kalaycı, Ş. (2016) SPSS applied multivariate statistical techniques. Palme Kitapevi, Ankara. (in Turkish).
[39] Cesur, C., Doğan, H., Uskutoğlu, T., Şenkal, B.C. (2017) An alternative oil plant: Styrax (Styrax officinalis L.). In: Curr. Trends Sci. Landsc. Manag. 2017, 209–215.
[40] Tardieu, F.F. (2013) Plant response to environmental conditions: assessing potential production, water demand, and negative effects of water deficit. Front. Physiol. 4, 17.
[41] Mohammadi, K., Heidari, G., Javaheri, M., Rokhzadi, A., Nezhad, M.T.K., Sohrabi, Y., Talebi, R. (2013) Fertilization affects the agronomic traits of high oleic sunflower hybrid in different tillage systems. Ind. Crops Prod. 44, 446–451.
[42] King, A.J., Montes, L.R., Clarke, J.G., Itzep, J., Perez, C.A.A., Jongschaap, R.E.E., Visser, R.G.F., van Loo, E.N., Graham, I.A. (2015) Identification of QTL markers contributing to plant growth, oil yield and fatty acid composition in the oilseed crop Jatropha curcas L. Biotechnol. Biofuels. 8, 160.
[43] Ghebretinsae, A.G., Graham, S.A., Camilo, G.R., Barber, J.C. (2008) Natural infraspecific variation in fatty acid composition of Cuphea (Lythraceae) seed oils. Ind. Crops Prod. 27, 279–287.
[44] Niether, W., Schneidewind, U., Armengot, L., Adamtey, N., Schneider, M., Gerold, G. (2017) Spatial-temporal soil moisture dynamics under different cocoa production systems. Catena. 158, 340–349.
[45] Öztürk, E., Albayrak, Ş.N. (2015) Effects of different nitrogenous fertilizer forms applied on sowing times on yield and agricultural characteristics of oil sunflower. In: 11th Field Crops Congress. Çanakkale, Turkey, 466–470. (in Turkish).
[46] Geleta, M., Stymne, S., Bryngelsson, T. (2011) Variation and inheritance of oil content and fatty acid composition in niger (Guizotia abyssinica). J. Food Compos. Anal. 24, 995–1003.

[47] Okcu, M., Tozlu, E., Dizikısa, T., Kumlay, A.M., Pehluvan, M., Kaya, C. (2010) Determination of Agricultural Properties of Some Safflower (Carthamustinctorius L.) Varieties. Journal of Agricultural Faculty of Atatürk University. 41(1), 1-6. (in Turkish)
[48] Başbağ, S. (2008) Heterotic Effects and Analyses of Correlation Relating to Some Characters on Cotton. Tarim Bilimleri Dergisi. 14, 143–147. (in Turkish)
[49] Pereyra-Irujo, G.A., Aguirrezábal, L.A.N. (2007) Sunflower yield and oil quality interactions and variability: Analysis through a simple simulation model. Agric. For. Meteorol. 143, 252–265.
[50] Kaya, Y., Atakisi, İ. (2003) Path and Correlation Analysis in Different Yield Characters in Sunflower (Helianthus annuus L.). Anadolu J. AARI. 13, 31–45.
[51] Kotoky, R., Rabha, A., Gogoi, A., Chandra, S. (2015) Correlation studies in seed traits, moisture and oil content and effect of hormones on flowering of Jatropha curcas L. Brazilian J. Biol. Sci. 2, 79–84.
[52] Maurya, R., Kumar, U., Katiyar, R., Yadav, H.K. (2015) Correlation and path coefficient analysis in Jatropha curcas L. Genetika. 47, 63–70.
[53] Anand, K., Sharma, R.P., Mehta, P.S. (2011) A comprehensive approach for estimating thermophysical properties of biodiesel fuels. Appl. Therm. Eng. 31, 235–242.
[54] Lajara, J.R., Diaz, U., Quidiello, R.D. (1990) Definite influence of location and climatic conditions on the fatty acid composition of sunflower seed oil? J. Am. Oil Chem. Soc. 67, 618–623.
[55] Salera, E., Baldini, M. (1998) Performance of high and low oleic acid hybridsof sunflower under different environmental conditions. Helia. 21, 55–68.
[56] Eryilmaz, T., Yesilyurt, M.K. (2016) Influence of blending ratio on the physicochemical properties of safflower oil methyl ester-safflower oil, safflower oil methyl ester-diesel and safflower oil-diesel, Renew. Energy. 95, 233–247.
[57] Koh, M.Y., Ghazi, T.I.M. (2011) A review of biodiesel production from Jatropha curcas L. oil, Renew. Sustain. Energy Rev. 15, 2240–2251.
[58] Anand, K., Sharma, R.P., Mehta, P.S. (2011) A comprehensive approach for estimating thermophysical properties of biodiesel fuels. Appl. Therm. Eng. 31, 235–242.
[59] Yaakob, Z., Narayanan, B.N., Padikkaparambil, S., Surya Unni, K., Akbar P.M. (2014) A review on the oxidation stability of biodiesel. Renew. Sustain. Energy Rev. 35, 136–153.
[60] Cesur, C. (2017) The Investigation of Yield and Yield Components, Fatty Acid Composition and Biodiesel Fuel Properties of Wild Mustard (Sinapis L.) Cultivars Grown in Yozgat Ecological Conditions. BAP Project Report, Yozgat.
[61] Fadhil, A.B., Al-Tikrity, E.T.B., Albadree, M.A. (2017) Biodiesel production from mixed non-edible oils, castor seed oil and waste fish oil. Fuel. 210, 721–728.
[62] Ogunniyi, D.S. (2006) Castor oil: A vital industrial raw material. 97, 1086–1091.
[63] Okullo, A.A., Temu, K., Ogwok, P., Ntalikwa, J.W. (2012) Physico-chemical properties of biodiesel from jatropha and castor oils. Int. J. Renew. Energy Res. 2, 47–52.
[64] Bozan, B., Temelli, F. (2008) Chemical composition and oxidative stability of flax, safflower and poppy seed and seed oils. Bioresour. Technol. 99, 6354–6359.
[65] Özcan, M.M., Atalay, Ç. (2007) Determination of seed and oil properties of some poppy (Papaver somniferum L.) varieties. Grasas Y Aceites. 57, 169–174.

Received: **28.06.2018**
Accepted: **25.03.2019**

CORRESPONDING AUTHOR

Cuneyt Cesur
Department of Field Crops,
Faculty of Agriculture,
Bozok University,
66200 Yozgat – Turkey

e-mail: cuneyt.cesur@bozok.edu.tr

© by PSP Volume 28 – No. 5/2019 pages 4159-4164 Fresenius Environmental Bulletin

USE OF HOT WATER OBTAINED FROM SOLAR COLLECTORS IN THE DISINFECTION OF HOTBEDS

Elif Yuksel Turkboylari[1,*], Ahmet Nedim Yuksel[2], Erhan Gezer[2]

[1]Department of Plant and Animal Production, Vocational Collage of Technical Science, Namik Kemal University, Tekirdag, Turkey
[2]Departmant of Biosystem Engineering, Faculty of Agriculture, Namik Kemal University, Tekirdag, Turkey

ABSTRACT

The worldwide restrictions imposed on agro-chemicals (pesticides) used in the disinfection of hotbeds have led researchers and employees to benefit from the sun, which is one of the renewable energy sources in agriculture, for this issue. In this study, the usage possibility of solar collectors and solar energy in the disinfection of hotbeds was investigated in Tekirdag Province in Thrace region of Turkey. Hot water obtained from solar collector with an area of 3 m^2 was transported to the hotbeds by using pipes which were laid into the greenhouse and connected in series. Hot water pipes were placed into the soil with the intervals of 50-55 cm. The effect of the hot water in the system on the temperature of soil surface was measured by infra-red thermometer and significant differences were observed.

The soil surface temperature measured in the greenhouse was measured as 62 ^oC in the parcel where plastic covered and hot water passed. This value was determined as 15.1 ^oC more then what it was in the soil parcel and 10.4 ^oC more then what it was in the plastic covered parcel.

The temperature of the hotbed at 10-15 cm depth was measured by digital soil thermometers having probe. Significant differences between the parcels were identified as a result of measurements of soil temperature conducted in plastic covered parcel in which hot water passed and in plastic covered soil parcel. In the plastic covered parcel with hot water, the soil temperature was measured as 50.2 ^oC. The soil temperature in hot water parcel was determined as 15 ^oC more than the soil temperature in soil parcel and as 6.5 ^oC more than what it was in plastic covered parcel. The temperature of the soil at 20-25 cm depth was measured by the soil temperature sensors. In the hot water parcels, the maximum temperature of the soil at this depth was 27.03 ^oC and it was measured to be 2.13 ^oC more than the temperature in plastic covered parcels.

In the parcel heated by water coming from the solar collector and the water temperature increased up to 78-79 ^oC in summer, the soil temperature could not be raised to the desired extent. This is because the thermal conductivity of soil is very low. Placing of hot water pipes with more frequent intervals (such as 20-25 cm) can increase the soil temperature more. This may also provide opportunity to achieve the soil disinfection in a shorter period.

KEYWORDS:
Greenhouse, hotbed disinfection, solar collector, soil temperature, solarization

INTRODUCTION

An important portion of the energy resources used in the world are fossil energy resources, such as natural gas and oil and they cause environmental problems. Instead of fossil fuels that introduce problems like greenhouse gases in the atmosphere and whose reserves also decrease, the use of environmentally friendly renewable energy sources is becoming widespread.

The sun is the world's leading and, at the same time, an endless source of energy. Comparing with the renewable energy sources on the world, solar energy is too much [1]. What makes solar energy valuable compared to other renewable energy sources is that it is ready to be used in all over the world.

Solarization and Disinfection Applications in Greenhouses. The disinfection of greenhouse soil from harmful organisms by using solar energy is an environmentally friendly practice. The heating of the soil by using the sun rays forms the basis of disinfection with solar energy. This method can be applied in July and August, in which it is very hot in Turkey. In the greenhouse, after soil preparation and irrigation, the soil should be covered with polyethylene cover for solarization application. In the disinfection of the hotbed from pests, it was determined that solarization applications were effective [2]. The solarization application providing heat accumulation in the soil increases the effect of disinfection.

Many of the nematodes and important disease factors causing damages on cultivated plants are soil-borne. Fighting with these soil-based factors in hotbeds can be achieved through physical and

chemical means. In physical disinfection method, the hotbed is warmed up to a certain temperature by various methods. However, in chemical disinfection, some highly toxic chemicals (pesticides) are applied to the soil. The residues and deposits in the products caused by using more chemicals in agriculture emerge as a problem for consumers and exportation of vegetables. Therefore, by limiting the use of chemical materials in agriculture, healthy and safe food production should be ensured. Thus, these toxic substances should be prevented from returning to the people and other living things through nutritional chain [3-6]. It also has many undesirable effects, such as increase in resistance against disease pests and weeds [7]. For this reason, in order to ensure protection of environment, human health, and sustainable agricultural production, the pesticides should be used in accordance with the recommendations [8, 9].

The chemicals suggested for soil fumigation vary depending on many factors such as pests, product, region, time, and soil type. According to Montreal Protocol, production and use of MeBr, which is the most widely used fumigant in the soil, is prohibited worldwide. As a result, in combating with soil pests, some alternatives have been sought. Today, for soil disinfection, some techniques such as solarization, steam application, soilless agriculture, and hot water emerge as the most common alternative applications [10]. The important thing in physical disinfection is to identify what the disease and pests in the soil are and to increase the soil temperature accordingly. Generally, the temperature level of 71-77 ^{o}C are the most widely used levels in the disinfection of hotbeds. The maximum temperature is 82 ^{o}C; at the temperatures above this value, there is a possibility that useful soil bacteria should be in the soil may also lose their liveliness [11].

Solarization is usually applied by using the solar energy in order to heat the soil in the summer months, when the exterior temperature is high and the greenhouse is empty. This method has some advantages such as low-cost and not having a negative impact on the environment. However, it has to be applied 3-4 weeks [12].

If the daily global solar intensity value of 1281.2 kWh m^{-2} year^{-1} (daily average total 3.51 kWh m^{-2} day^{-1}) in Tekirdag Province is taken into consideration, soil disinfection can be more effective with the use of solar collector system in the region [13].

In this study, it was aimed to use hot water obtained from solar collectors for soil disinfection in greenhouses. By increasing the soil temperature via passing the hot water obtained from collectors through hot water pipes placed into the soil, It was aimed to increase the effect of disinfection and consequently to decrease the disinfection time.

MATERIALS AND METHODS

General Characteristics of the Research Area. Tekirdag Province, which is the research area, is in Thrace Region. Thrace Region is on the European continent of Turkey and located between 26^{o}-29^{o} Eastern longitudes and 40^{o}-42^{o} northern latitudes. Tekirdag Province, where the research was conducted, is located between 26^{o}40′-28^{o}10′ eastern longitudes and 40^{o}35′-41^{o}35′ northern latitudes, and the area of it is 621 788 ha. The city, whose geological structure is quite young, gained its today's view in IV. time [14].

The Solar Collector System. The hot water systems with solar collectors used for the disinfection of the hotbeds consist of a tank that contains hot water, planer collectors that collects the solar power and insulated pipes that provide the connection between these two parts. The solar collector used in the experiment was a solar energy heating system with a surface area of 2,5*2,5 m^{2}, 30 vacuum tubes, 200 l hot water and 50 l cold water boiler. Solar collector was used for heating the root zone of the hotbeds in autumn, winter and spring months and for disinfecting it in summer months (Figure 1).

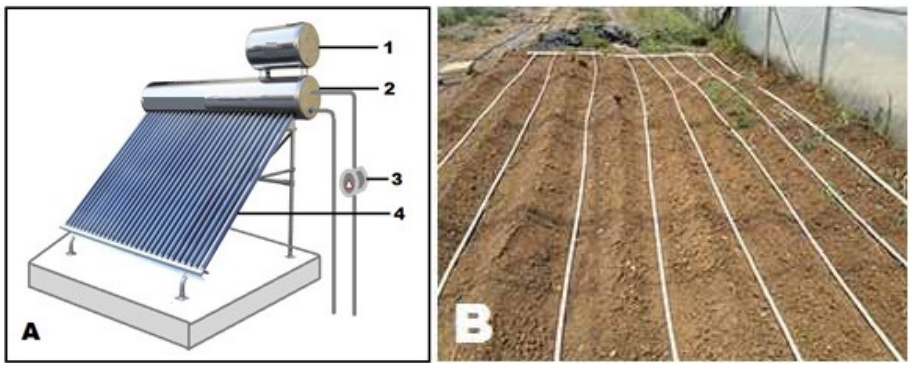

FIGURE 1

The Soil Disinfection System with Solar Collectors. A.Solar collector outside the greenhouse, 1.cold water tank, 2.hot water tank, 3.circulation pump, 4.vacuum tube water heaters, B.soil heating pipes in the greenhouse

Method Used in the Experiment. For the disinfection of hotbeds, hot water obtained from solar collector were circulated in the hotbeds by using pipes. Hot water pipes were placed under 10-15 cm of the soil and with about 50-55 cm intervals. In order to accelerate the movement of water in the pipes and allow it to give the heat energy to the soil easily, a 0.1 kW circulation pump is placed in the system.

Measured Meteorological Values. In this study, anemometer, digital soil thermometer, infrared thermometer, soil temperature sensor and data collection device were used to obtain meteorological data and soil temperatures.

During the experiment, three times a day (at 11:00, 14:00 and 16:00), temperature and humidity values were determined in the greenhouse and also temperature, humidity, wind speed and direction were determined outside the greenhouse.

The greenhouse temperature were showing considerably differences from outside air temperature. The fact that the weather was sunny or cloudy, the wind condition, ventilation windows and the fact that the doors were open or closed had been more effective on the temperature difference.

In the experiment, the temperatures of the soil was measured in plastic covered parcels having hot water pipes and in plastic covered soil parcels. In the parcels, soil surface temperature and the temperature at 10-15 cm and 20-25 cm depth of the soil were measured.

Measurement of Temperature in the Soil. Digital soil thermometer with probe that can measure instant temperature and record daily minimum and maximum temperatures has been used at 10-15 cm depth of soil. Every day, measurement was done by this thermometer at 14:00, and the values were recorded.

The surface temperatures of the parcels were measured by infrared thermal thermometer in three separate points and their average was recorded.

In order to determine the soil temperature changes in the parcels, soil temperature sensors having data recorder device were placed on the parcels. The measurement values of the sensors were automatically transferred to the computer.

Measurement of Hot Water in the Solar Collectors. The temperature of the water in the solar collectors was also measured daily by the thermometers placed in the system. There was only a few degrees of difference between the temperatures of water that was sent to the parcel and returned from the parcel.

RESULTS AND DISCUSSION

Values of the Soil Temperature. For the soil temperatures in the parcels, the values in the period from May, when the production in the greenhouses was almost done, to the end of September, when the production started, were used. The high air temperature was also an important factor in selecting this period.

Soil surface temperatures in parcels were measured by infrared thermometer. The highest soil surface temperatures were obtained in July, August and September. This value was measured between 44.5 ºC and 46.9 ºC in soil parcel, between 45.8 ºC and 51.6 ºC in plastic covered parcel, and between 52.8 ºC and 62.0 ºC in plastic covered and hot water tubular parcel. The highest surface temperature value measured in plastic covered hot water parcels was 15.1 ºC more than what it was in soil parcel and 10.4 ºC more than what it was in plastic covered parcel (Figure 2).

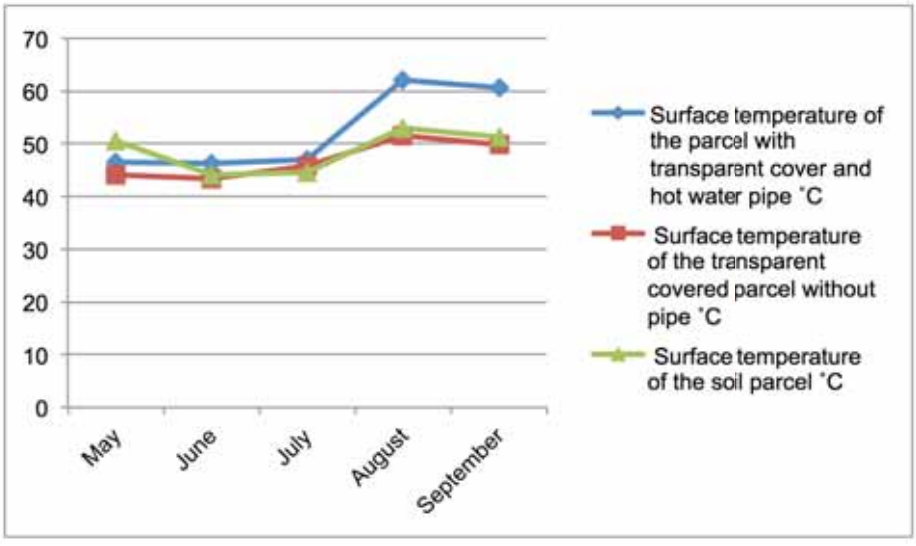

FIGURE 2
The maximum soil surface temperature in the parcels

The minimum and maximum soil temperatures at 10-15 cm depth were also measured by digital soil thermometers. The minimum soil temperatures measured in all parcels were between 17.7 ºC and 23.8 ºC, and no significant difference was found. The reason for this was that, in order the solar collector system to operate it is required to wait some time after sunrise and the temperature of the water in the system to reach at least 35-40 ºC. Therefore, at night, when the outside air temperature decreased, the minimum temperatures measured in the soil did not reveal a significant difference.

It was identified that the maximum soil temperature at 10-15 cm depth of the soil increased up to 50.2 ºC in the plastic covered hot-water parcel. It was also identified that this inside-soil temperature was important in terms of solarization [15]. It was determined that this soil temperature value was 15 ºC more than what it was in soil parcel and 6.5 ºC more than what it was in plastic covered parcel (Figure 3a). Since the movement of soil temperature is minor and slow in the vertical direction, sub soil layers warm less [16]. This effect can be observed with the temperatures measured at 20 to 25 cm depth of soil (Figure 3b). The temperatures measured at these depths of soil are below readings of top soil layers. In the months (May-June-September), when the exterior temperature is lower, the temperature difference increases in the plastic covered parcel having hot water pipes in comparison to the plastic covered parcel. This difference was 4.6° C, 4.8°C and 5.9°C more in the parcel having hot water pipes, respectively in May, June and September. This temperature difference decreases in August since the exterior temperature at 20 to 25 cm depths of soil is at highest level (42.4°C) in this month. The difference between two parcels decreased in this month and recorded as 2.2°C.

In August, the highest value in the minimum temperatures measured by soil temperature sensors at 20-25 cm depth of soil during summer months was 27.03 ºC in plastic covered parcel having hot water pipes. This value was 2.13 ºC more than what it was in plastic covered parcel. In the summer months other than August, the temperature differences were between 0.31 ºC and 3.65 ºC.

The highest indoor air temperatures in the greenhouses were measured at 14:00 and 16:00 in July, August and September. The highest temperature was identified as 43.2 ºC at 16:00 in August. During this time, the outdoor temperature was 35 ºC.

Effect of Solar Collector on Soil Temperature. The hot water obtained from the solar collector used in the experiment was sent to the parcel in the greenhouse through pipes. The effect of this hot water on the surface temperature of the soil and on the temperatures at depths of 10-15 cm clearly observed. Due to the effect of hot water obtained from the collector, the soil surface temperature increased up to 62.0 ºC in the parcel having hot water pipe. This value was 15.1 ºC more than the soil parcel and 10.4 ºC more than the plastic covered parcel. The highest temperature identified at 10-15 cm depth of soil was measured as 50.2 ºC in the plastic covered parcel with hot water pipe. This value was 15 ºC and 6.5 ºC more than the other parcels.

In July and August, the temperature of the water in the solar collector system increased up to 78 ºC and 79 ºC. In the parcel with hot water obtained from the collector system, soil temperatures increased, but they did not reach the expected values.

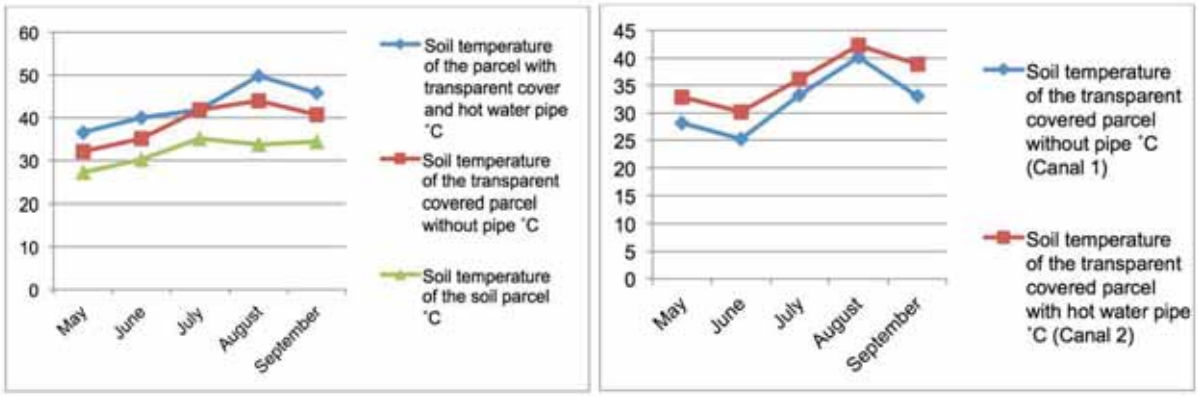

(a) (b)

FIGURE 3
The maximum temperatures of parcels at 10-15 cm (a) and 20-25 cm (b) depth

CONCLUSION

Generally, in the greenhouses where monoculture is applied and is not heated, all kinds of diseases and pests rapidly reproduce and spread due to high humidity and soil moisture in the greenhouses. This situation can cause great economic loss [16]. In order to achieve a healthy, efficient and quality agriculture in greenhouses, the effects of diseases and pests in the soil should be reduced to a certain extent. Disinfection, which is the method of combating with disease agents and nematodes in hotbeds, can be carried out in physical and chemical ways.

Chemical disinfection is carried out by application of some highly toxic chemicals (pesticides) into the soil. This method is highly dangerous for human health and environment, and it affects the natural balance negatively. Through nutritional chain, this substances may return to human and other living beings [6]. It is also stated that the solarization, which is a temperature application into the soil, is an effective way for purifying the soil from pests [2]. In the solarization process, after covering the soil surface with plastic cover, the temperature of the soil under the cover is increased by sun rays.

In this study, both solarization and hot water obtained from solar collector were used in order for disinfection of the soil. In this project, for the soil parcel, for the parcel where the solarization was applied and for the parcel where both solarization was applied and the hot water obtained from solar collector was circulated by pipes, the measurement was done every day at 14:00. Every day, the minimum, maximum and instant temperature levels were determined on the soil surface and at 10-15 cm depth of it. In addition, the temperature change at 20-25 cm depth of soil was examined by the temperature sensors in the plastic covered parcel and also in the plastic covered parcel having hot water pipes.

As a result of the measurements, the highest soil surface temperature was measured as 62 ^{o}C in polyethylene covered parcel having hot water. This value was 10.4^{o}C more than polyethylene covered parcel and 15.1^{o}C more than the soil parcel. The surface temperature in the polyethylene covered hot-water parcel was quite more than the other parcels. This significant difference in the soil temperature levels shows the effect of the solar collector. The soil temperature at 10-15 cm depth was measured, again, significant differences between the parcels were observed. The value measured as 50.2 ^{o}C in polyethylene covered parcel with hot water was 15 ^{o}C more than what it was in soil parcel and 6.5 ^{o}C more than what it was in polyethylene covered parcel. The soil temperature obtained as 50.2 ^{o}C is important in terms of disinfection, because many soil-based pathogens and diseases can survive for several hours at temperatures of 45 ^{o}C and above [17]. The rise of temperature of water in the solar collector to 78 ^{o}C and 79 ^{o}C, the highest surface temperature measured in the soil being 62 ^{o}C, the the highest temperature measured at 10-15 cm depth being 50.2 ^{o}C and the temperature at 20-25 cm depth being 42.4 ^{o}C showed that the soil temperature had not reached to the expected level. This was due to the fact that the soil had a three-phase structure (liquid, solid and gas) and the heat transfer was very slow [18]. In the literature it is also stated that the movement of the heat in the upper zone of the soil to the lower zone of it is difficult [16].

Increasing of the efficiency of the solar collector system on disinfection may be possible by placing the hot water pipes into the soil with more frequent intervals. In the experiment, the hot water pipes were placed with 55 cm intervals. Decreasing this intervals to 20-25 cm may provide the heat to be transfered even further. Through this way, the efficiency of the collector system can be increased.

Because in our country, in the south regions (Mediterranean) where the air temperature and solarization are high, high level of water temperature can be obtained by solar collectors, the soil disinfection can be achieved more effectively and faster.

The solar collector can be used to increase soil temperature in order to increase yield in the fall, winter and spring months, which are production seasons in greenhouses. In the cold seasons, warming of the soil facilitates the continuation of biological and chemical events in the soil and makes it easier for plants to obtain water and nutrients from the soil [19, 20].

ACKNOWLEDGEMENTS

This study was supported by Namık Kemal University Scientific Research Projects Coordination Unit (Project Number: NKUBAP.03.GA.16. 062)

REFERENCES

[1] Kamat, P.V. (2007) Meeting the clean energy demand: Nanostructure architectures for solar energy conversion. The Journal of Physical Chemistry. C. 111(7), 2834-2860.

[2] Katan, J. (1987) Soil Solarization. In: Chet, I. (ed.) Innovative approaches to plant disease control. Wiley and Sons, New York. 77-105.

[3] Saber, M.S.M. (2001) Clean biotechnology for sustainable farming. Engineering in Life Sciences. 1(6), 217-223.

[4] Broun, A.L. and Supkoff, D.M. (1994) Options to methyl bromide for the control of soil-borne diseases and pests in California with reference to the Netherlands. Pest Management Analysis and Planning Program. State of California, Environmental Monitoring and Pest Management Branch, California. 52p.
[5] Çakmakçı, R., Dönmez, M.F. Canpolat, M. and Şahin, F. (2005) In Greenhouse and different field conditions, the effect of the plant-growth-promoting bacteria on plant growth and soil properties. VIth Turkish Field Crops Congress, Antalya. 45-50 (in Turkish).
[6] Kitiş, Y.E. (2012) What is solarization? How is it applied? Journal of Agricultural. 10, 1-4. (in Turkish).
[7] Fennimore, S.A. and Doohan, D.J. (2008) The challenges of specialty crow weed control. Weed Technology. 22, 364-372.
[8] Özkan, B., Vuruş Akçagöz, H. and Karadeniz, C.F. (2003) Producer attitudes and behaviours towards pesticide use in citrus production in Antalya Province. Anadolu Journal of AARI. 13(2), 103-116. (in Turkish).
[9] Delen, N., Durmuşoğlu, E. Güncan, A., Turgut, C. and Burçak, A. (2005) Problems of pesticide use in Turkey, reduction of susceptibility in residues and organisms. 6th Technical Congress of Turkish Chamber of Agricultural Engineers, 3-7 January 2005. 629-648 (in Turkish).
[10] Porter, I.J. and Mattner, S.W. (2002) Non-Chemical Alternatives to Methylbromide for Soil Treatment in Strawberry Production. In: Proceedings of International Conference on Alternatives to Methyl Bromide the Remaining Challenges. 5-8 March 2002. Sevilla, Spain. 39-48
[11] Sevgican, A. (1999) Greenhouse Vegetables. Volume I. Publication No:528. ISBN 975-483-384-2. 302p. (in Turkish).
[12] Doğan, M.N. and Erkılıç, E. (1998) Soil solarization and application areas. Ç.U. Agriculture Faculty Journal. 13(2), 91-100. (in Turkish).
[13] Yüksel A.N. and Yüksel Türkboyları, E. (2017) Use of Solar Panels in Greenhouse Soil Disinfection. International Advanced Researches and Engineering Congress-2017 (IAREC'17). 16-18 November, Osmaniye-Turkey. 2319-2323.
[14] Anonymous (2007) Use and Management of Water Resources in Tekirdag Province. Tekirdag Governorship Publications, Tekirdag. (in Turkish).
[15] Herald, C.M. and Robinson, A.F. (1987) Effects of Soil Solarization on Rotylenchulus Reniformis in the Lower Rio Grande Valley of Texas. Journal of Nematology. 19, 93-103.
[16] Altındişli-Atağ, G., Sarıyev, A., Elekçioğlu, İ.H., Gök, M., Doğan, K., Pamiralan, H. and Akça, H. (2017) Investigation of the effects of basaltic Tuff and Farm manure applications on soil Solarization in greenhouse conditions and Mathematical Modeling of soil temperature. Ministry of Food, Agriculture and Livestock, Research and Development Program Project Report, 94p. (in Turkish).
[17] Pullman, G.S., Davey J.E. and Garber, R.H. (1981) Soil Solarization and Thermal Death: A Logarithmic Relationship Between Time and Temperature for Four Soilborne Plant Pathogens. Phytopathology. 71, 959-964.
[18] Bahtiyar, M. (1996) Soil Physics. T.U. Tekirdağ Agriculture Faculty Publishment No: 260, 302-319. (in Turkish)
[19] Angers, D.A. and Carter, M.R. (1996) Aggregation and organic matter storage in cool, humid agricultural soils. In: Carter, M.R., Stewart, B.A. (eds.) Structure and organic matter storage in Agricultural soils. CRC Press:193-211.
[20] Pepin, S., Dordis, M. Gruyer, N. and Menard, C. (2008) Changes in mineral content and CO_2 release from organic greenhouse soils incubated under two different temperatures and moistre conditions. 16th IFOAM Organic World Congress, Modena, Italy, June 16-20.

Received: **27.07.2018**
Accepted: **25.03.2019**

CORRESPONDING AUTHOR

Elif Yuksel Turkboylari
Department of Plant and Animal Production,
Vocational Collage of Technical Science,
Namik Kemal University,
Tekirdag – Turkey

e-mail: eyuksel@nku.edu.tr

© by PSP Volume 28 – No. 5/2019 pages 4165-4170 Fresenius Environmental Bulletin

THE EFFECTS OF PHOSPHORUS FERTILIZATION AND HARVESTING STAGES ON FORAGE YIELD AND QUALITY OF PEA (*PISUM SATIVUM* L.)

Osman Yuksel[1,*], Mevlut Turk[2]

[1]Usak University, Faculty of Agriculture and Natural Sciences, Department of Field Crops, Usak, Turkey
[2]Isparta University of Applied Sciences, Faculty of Agricultural Sciences and Technologies, Department of Field Crops, Isparta, Turkey

ABSTRACT

The aim of this study was to determine the effects of five phosphorus rates (0, 30, 60, 90 and 120 kg ha^{-1}) and three harvesting stages (beginning of flowering, full flowering, and seed filling) on forage yield and quality of pea (*Pisum sativum* L.). Dry matter (DM) yield, CP ratio, CP yield, acid detergent fiber (ADF), neutral detergent fiber (NDF), total digestible nutrients (TDN), and relative feed value (RFV) were determined. Phosphorus rates and harvesting stages significantly affected most of the components determined for pea. According to two-year averages, phosphorus treatments increased DM yield, CP ratio, CP yield, TDN and RFV values but decreased ADF and NDF ratios. Harvesting at the late stages impaired the forage quality. While the contents of CP, TDN and RFV decreased with advancing growth, DM yield, CP yield, ADF and NDF contents increased. It has been concluded that it is more suitable to harvest forage peas in the seed filling stage and 60 kg ha^{-1} phosphorus rate is sufficient for the high dry matter and crude protein yield in Usak and similar regions.

KEYWORDS:
Pisum sativum, crude protein, dry matter yield, ADF, total digestible nutrients.

INTRODUCTION

Atmospheric nitrogen is a renewable resource for legume crops owing to the biological nitrogen fixation with *Rhizobium* sp bacteria. In 1975, nearly half of the nitrogen needed in agriculture (44 to 66 million tons annually) was provided through legume-rhizobial symbiosis [1]. Since biological N fixation presents economic, environmental, and agronomic benefits, it could be used to a larger degree as an alternative to synthetic fertilizers every year [2].

Legumes are grown worldwide as a source of high-quality protein in human and animal feeding. Being a legume crop, peas are widely grown for hay, pasturage or silage production either alone or mixed with cereals [3]. Field pea has a benefit over many other crops since it has the ability to fix its own nitrogen. This makes it useful not only as an alternative crop but also adds rotational benefits.

As a forage crop, pea hay and seed are rich in crude protein content and most of mineral elements [4-5]. In recent years in Turkey, important developments have been recorded in the cultivation area of forage peas due to the developed winter-resistant varieties. In the future, forage peas may be replaced by hungarian vetches in hard-winter regions by the winter-resistant varieties because of their high dry matter yield and qualities.

Many factors affect the rate of change in nutrient composition with advancing plant development and maturity stages. These factors may include any one or a combination of the following: plant type, climate, season, weather, soil type and fertility, soil moisture, leaf/stem ratio, physiological and morphological characteristics, and others, and may vary with annuals versus perennials, grasses versus legumes, etc. By themselves, nutrient composition levels are not necessarily the only criterion in evaluating the nutritive value of plants [6]. Most plants show a similarity in declining nutrient composition with advancing development towards maturation [7, 8, 9, 10].

Fertilization may not only improve dry matter yield but also affect the chemical content of the produced hay. In general, phosphorus treatment causes an increase in crude protein content due to enhancing nitrogen uptake by plants [11]. Phosphorus fertilization affects dry matter yield and chemical composition of forage crops [12, 13, 14, 15]. Turk et al. [16] reported that P fertilization increased dry matter yield and N, P, K, Ca and Mg contents, but decreased K, tetany ration (K: (Ca + Mg)), acid detergent fiber and neutral detergent fiber and had no effect on Mn, Cu, and Zn.

The main objective of this study was to evaluate the effect of harvesting stages and phosphorus fertilization on dry matter yield and forage quality of pea.

MATERIALS AND METHODS

The field experiments were conducted in Usak located in the Aegean Region of Turkey during 2015-16 and 2016-17 growing seasons. Total precipitation was 418.8 mm in 2015-16 (October–May) and 417.1 mm in 2016-17 growing season. The long-term average precipitation was 468.5 mm. The average temperature was 9.7 ºC in 2015-16 growing season (October–May) and 8.3 ºC in 2016-17 growing season. The long-term average temperature was 8.0 ºC (Table 1).

The experiments were carried out in a randomized complete block design with three replications between November of 2015 and 2016. Five phosphorus rates (0, 30, 60, 90 and 120 kg P ha^{-1} per annum) and three harvesting stages (beginning of flowering in early May, full flowering in mid-May and seed filling in early June) were applied in this study. Töre cultivar was used in this study. The seeding rate was 140 kg ha^{-1}. The individual plot size was 1.8×5m = 9m^2. Phosphorus was administered as triple superphosphate (46% P_2O_5) during sowing in November. The experiment was repeated on an adjacent site in the second year.

The plots were harvested by hand. Dry matter (DM) yield, CP ratio, CP yield, acid detergent fiber (ADF), neutral detergent fiber (NDF), total digestible nutrients (TDN), and relative feed value (RFV) of the samples taken from quadrats (1 m^2) were investigated. The samples taken from each plot were dried at room temperature and then in an oven at 65°C until they reached a constant weight. Following the cooling and weighing processes, the samples were ground for analyses. Nitrogen content was calculated by using the Kjeldahl method [18]. Crude protein content (N×6.25) and then crude protein yields were calculated. Total digestible nutrients (TDN), dry matter intake (DMI), digestible dry matter (DDM), and relative feed value (RFV) were estimated according to the following equations adapted from [19].

TDN = (-1.291 x ADF) + 101.35
DMI = 120/NDF % dry matter basis
DDM = 88.9-(0.779 x ADF % dry matter basis)
RFV = DDM% x DMI% x 0.775

The ANKOM Fiber Analyzer was used for NDF and ADF analysis. Ankom F57 filter bags were used for ADF and NDF analysis in this study [20]. The data of 2016 and 2017 were analyzed together using the Proc GLM [21]. The means were separated by LSD at the significance level of 5%.

TABLE 1
The climate data of the study area [17].

Months	Average temperature (ºC)			Precipitation (mm)		
	2015-2016	2016-2017	1950-2017	2015-2016	2016-2017	1950-2017
October	15.2	14.6	13.3	29.6	26.8	40.2
November	10.0	9.4	8.0	52.3	45.2	58.4
December	4.2	4.1	4.2	75.6	77.2	78.2
January	1.5	-0.1	2.4	69.8	110.2	72.2
February	8.2	4.2	3.1	8.0	22.0	64.4
March	7.9	8.3	6.2	39.4	55.2	55.6
April	14.6	11.0	10.8	63.1	32.0	52.2
May	16.2	15.1	15.7	81.0	48.5	47.3
Mean	9.7	8.3	8.0	-	-	-
Total	-	-	-	418.8	417.1	468.5

TABLE 2
Results of analysis of variance traits determined.

Sources of Variation	D.F.	DM Yield	CP Content	CP Yield	NDF	ADF	TDN	RFV
				Mean Square				
Year (Y)	1	4345.6	0.29	55.52	0.01	0.93	1.54	0.41
Block (year)	4	14775.8	0.24	479.48	1.83	2.78	4.63	78.15
Harvesting Stage	2	548103.4**	21.50**	10182.36**	136.98**	38.73**	64.57**	3995.59***
HS x Y int.	2	889.8	0.55	3.50	1.60	3.95	6.57	91.51
Phosphorus	4	93721.8**	17.66**	7097.02**	14.80*	20.34**	33.90**	615.19**
P x Y int.	4	1213.0	0.37	31.72	0.16	0.34	0.57	6.66
HS x P int.	8	1019.2	0.31	43.01	0.77	1.02	1.70	16.65
HS x P x Y int.	8	3031.6	0.36	172.05	0.15	0.22	0.37	3.50
CV (%)		11.48	3.91	12.12	4.14	3.45	7.11	8.23

D.F, degrees of freedom; * : P ≤ 0.05, ** : P ≤ 0.01.

RESULTS AND DISCUSSION

As shown in Table 2, harvesting stages and phosphorus treatments had significant effects on DM yield, CP ratio, CP yield, ADF, NDF, TDN, and RFV values. Dry matter yield of pea increased significantly as a result of the phosphorus treatments. While the highest DM yield was obtained from 60, 90, and 120 kg ha^{-1} P rates (7.61, 7.64 and 7.65 t ha^{-1}), the lowest DM yield (6.07 t ha^{-1}) was obtained from the control plot (Table 3). Kavut et al. [22] reported that the dry matter yields of the forage pea varieties varied between 7.27 and 8.90 t ha^{-1} in 20 cm row spacing in the Aegean region. The results of the present study confirm those of the studies [12, 13, 22, 23]. The DM yield significantly increased with advanced harvest stages. As plants begin to concentrate DM in pods and seeds, an enhanced forage yield with advancing maturity is consistent with results of several researchers [24-25].

Increasing phosphorus rates resulted in an increase in CP contents. The highest CP (18.68, 19.05, 19.04%) ratio was obtained from 60, 90, and 120 kg ha^{-1} P treatment; on the other hand, the lowest CP ratio (16.84%) was obtained from the control plot (Table 3). These results confirm the results of other researchers [16-23]. Crude protein ratios decreased with advancing stages from 19.05 to 17.36%. Maturity stage at harvest is the most important factor determining forage quality. Besides N and hence protein also decline with advancing plant development; on the other hand, carbohydrate synthesis and storage increased [26]. Buxton [27], reported that the decrease in CP concentration with advancing maturity occurred due to the fact that the protein of leaves and stems decrease and because stems, with their lower protein concentration, made up a larger portion of the herbage in more mature forage. The crude protein content results obtained from the study are similar to those studies [10, 16, 28].

The CP yields showed a similar trend with DM yields. The highest CP yield was obtained from 60, 90 and 120 kg ha^{-1} P rates (1.42, 1.45 and 1.45 t ha^{-1}); whereas, the lowest CP yield (1.01 t ha^{-1}) was obtained from control plot. The effects of harvesting stages were significant for CP yield in two-year averages. While the highest CP yield (1.50 t ha^{-1}) was obtained at seed filling stages, the lowest CP yield (1.13 t ha^{-1}) was obtained at beginning of flowering stages. These results are compatible with the results reported by those researchers [29, 30, 31].

Increasing phosphorus rates resulted in a decrease in ADF and NDF contents. While the highest ADF and NDF ratios were obtained from 0 and 30 kg ha^{-1} P rates, the lowest values were obtained from 90 and 120 kg ha^{-1} P rates. The effects of harvesting stages were significant for ADF and NDF ratios. The NDF ratios increased from 35.80 to 39.98% and the ADF ratios increased from 27.00 to 29.20% with advancing maturity (Table 3). Thorvaldsson [32], noted that with the advancing maturity on forages, ADF and NDF contents increased but the digestibility decreased. Acid detergent fiber and NDF content increased with advancing plant growth. This could be explained by the decrease in the proportion of leaves and increase of the proportion of stems with advanced maturity. The trend in ADF and NDF contents with increasing maturity is normally the reverse of protein [8]. Young plant cells have the primary cell wall, but also the secondary cell wall occurs with maturing. This causes mature plants to be the more fibrous [33].

TABLE 3
Dry matter yield and forage quality measured in different harvesting stages and phosphorus doses in the average of 2016 and 2017 years.

Harvesting Stages	DM Yield (t ha^{-1})	CP (%)	CP Yield (t ha^{-1})	NDF (%)	ADF (%)	TDN	RFV
BF	5.91 c	19.05 a	1.13 c	35.80 c	27.00 c	66,49 a	176,30 a
FF	6.88 b	18.29 b	1.26 b	38.63 b	28.59 b	64,44 b	160,40 b
SF	8.58 a	17.36 c	1.50 a	39.98 a	29.20 a	63,65 c	153,88 c
Mean	7.12	18.23	1.30	38.14	28.26	64.86	163.53
$LSD_{0.05}$	0.42	0.37	8.13	0.68	0.61	0.55	6.11
Phosphorus Doses (kg ha^{-1})							
0	6.08 c	16.84 c	1.01 c	39.25 a	29.66 a	63,06 b	155,90 c
30	6.66 b	17.56 b	1.16 b	38.79 a	28.94 a	63,99 b	159,09 b
60	7.61 a	18.68 a	1.42 a	38.14 ab	28.19 ab	63,76 b	161,46 b
90	7.64 a	19.05 a	1.45 a	37.37 b	27.42 b	65,95 a	168,08 a
120	7.65 a	19.04 a	1.45 a	37.12 b	27.08 b	66,39 a	169,88 a
Mean	7.13	18.23	1.30	38.13	28.26	64.63	162.88
$LSD_{0.05}$	0.55	0.48	10.50	1.25	1.48	1.42	3.1

BF, beginning of flowering; FF, full flowering; SF, seed filling stage

The TDN refers to the nutrients that are available for livestock and are related to the ADF concentration of the forage [28]. As ADF increases, there is a decline in TDN which means that animals are not able to utilize the nutrients that are present in the forage [19]. Harvesting at the late stages causes a reduction in TDN values. While the highest TDN value (66.49) was determined at beginning of the flowering stage, the lowest value (63.65) was determined at the seed filling stage. The TDN values increased with increasing P rates. While the highest TDN values (65.95 and 66.39) were obtained from 90 and 120 kg ha^{-1} P rates, the lowest TDN values (63.06, 63.99 and 63.76) were obtained from 0, 30 and 60 kg ha^{-1} P rates. Similar results were reported by those researchers [28-34].

The RFV is an index that is used to predict the intake and energy value of forages. This index is derived from the digestible dry matter (DDM) and dry matter intake (DMI). Forages with a RFV value of >151, 150-125, 124-103, 102-87, 86-75, and < 75 are categorized as prime, premium, good, fair, poor and rejected, respectively [35]. Harvesting stages had significant effects on RFV values. The RFV values decreased from 176.30 to 153.88 with advancing stages. Phosphorus treatments increased RFV values. While the lowest RFV value (155.90) was determined at control plot, the highest RFV values (166.08 and 169.88) were determined at 90 and 120 kg ha^{-1} P treatments (Table 3). The relative feed value is not a direct measure of the nutritional content of forage, but it is important for estimating the value of forage [36].

CONCLUSION

The results from the different phosphorus rates and harvesting stages applied in pea in Aegean conditions of Turkey can be summarized as follows;

In average of two years, phosphorus rates and harvesting stages significantly affected most of the components determined in pea. Phosphorus treatments increased dry matter yield, crude protein ratio, crude protein yield, TDN, and RFV values and decreased the ADF and NDF ratios. Harvesting at the late stages impaired forage quality. Crude protein content, TDN, and RFV decreased with advancing growth. Dry matter, crude protein yield, ADF and NDF contents increased with advancing maturity.

When the obtained results were evaluated together, it has been concluded that it is more suitable to harvest forage peas in seed filling stage and 60 kg ha^{-1} phosphorus rate is sufficient for high dry matter and crude protein yield in Usak and similar regions.

REFERENCES

[1] Burns, R.C., Hardy, R.W. (1975) Nitrogen fixation in bacteria and higher plants. Springer, New York.

[2] NifTAL Center for BNF Technologies (2000) Biological nitrogen fixation. Nature's partnership for sustainable Agricultural Production. In: Silva, J.A., Uchida, R. (eds.) Plant Nutrient Management in Hawaii's Soil, Approaches for Tropical and Subtropical Agriculture. College of Tropical Agriculture and Human Resources. University of Hawai'i at Manoa. Honolulu. 121-126. Available at: http://www.ctahr.hawaii.edu/oc/freepubs/pdf/pnm.

[3] McKenzie, D.B. Spaner, D. (1999) White lupin: an alternative to pea in oat-legume forage mixtures grown in New Foundland. Can. J. Plant Sci. 79, 43–47.

[4] Acikgoz, E., Katkat, V., Omeroglu, S., Okan, B. (1985) Mineral elements and amino acid concentrations in field pea and common vetch herbages and seeds. J. Agron. Crop Sci. 55, 179–185.

[5] Gurel, F., Gosterit, A. (2009) Importance of honeybee and bumblebee pollination in Turkey. 19th Eucarpia Conference. 26-29 May, Ljubljana, Slovenia.

[6] Cook, C.W., Harris, L.E. (1979) Nutritive value of seasonal ranges. Utah Agricultural Experimental Station Bulletin. 72, 1–55.

[7] Tan, M., Temel, S., Yolcu, H. (2003) Effects of harvest management on the mineral composition of common vetch. Proceedings of the 12th Symposium of the European Grassland Federation, Pleven, Bulgaria. 423–425.

[8] Rebole, A., Alzueta, C., Ortiz, L.T., Barro, C., Rodriguez, M.L., Caballero, R. (2004) Yields and chemical composition of different parts of the common vetch at flowering and at two seed filling stages. Spanish Journal of Agricultural Research. 2(4), 550–557.

[9] Cecen, S., Gosterit, A., Gurel, F. (2007) Pollination effects of the bumblebee and honey bee on white clover (*Trifolium repens* L.) seed production. Journal of Apicultural Research. 46(2), 69-72.

[10] Uzun, A., Gun, H., Acikgoz, E. (2012) Yield and quality characteristics of some pea (*Pisum sativum* L.) varieties harvested at different growing stages. Journal of Agricultural Faculty of Uludag University. 26(1), 27-38.

[11] Benedycka, Z., Benedycki, S., Grzegorczyk, S. (1992) Phosphorus utilization in the dependence on nitrogen fertilization by greensward. Fourth International Imphos Conference, Phosphorus, Life and Environment, Gand, Belgium.

[12] Bell, C.A., Korte, C.J., Heazlewood, C., Castleman, G.H., Matassa, V.J. (2001) Narbon bean response to fertilizer nutrients in the Victorian Mallee. 10th Australian Agronomy Conference, "Science and Technology: Delivering Results for Agriculture?" Hobart January 2001.
[13] Turk, M.A. (2001) Effects of phosphorus on narbon vetch and barley under open and controlled conditions. Agriculture Mediterranean. 131, 112-117.
[14] Dasci, M., Gullap, M.K., Erkovan, H.I., Koc, A. (2010) Effects of phosphorus fertilizer and phosphorus solubilizing bacteria applications on clover dominant meadow: II. Chemical composition. Turkish Journal of Field Crops. 15(1), 18-24.
[15] Koc, A. (2013) Effect of phosphorus doses and application time on the yield and quality of hay and botanical composition of clover dominant meadow in highlands of Turkey. Turkish Journal of Field Crops. 18(2), 205-210.
[16] Turk, M., Albayrak, S., Yuksel, O. (2007) Effects of phosphorus fertilization and harvesting stages on forage yield and quality of narbon vetch. New Zealand Journal of Agricultural Research. 50, 457-462.
[17] Anonymous (2018) Usak climatic datas. Turkish State Meteorological Service. Ankara, Turkey.
[18] Kacar, B. (1972) Chemical Analysis of Plant and Soil. II. Plant Analysis. Ankara University Agriculture Faculty Publication. 453p.
[19] Aydin, N., Mut, Z., Mut, H., Ayan, I. (2010) Effect of autumn and spring sowing dates on hay yield and quality of oat (*Avena sativa* L.) genotypes. Journal of Animal and Veterinary Advances. 9(10), 1539-1545.
[20] Anonymous. (2010) Ankom, Technology, Neutral Detergent Fibre and Acid Detergent Fibre Analyses. http://www.ankom.com/09_ procedures/ procedures.shtml
[21] SAS Institute. (1998) SAS users guide. Version 8. SAS Inst. Cary, NC.
[22] Kavut, Y.T., Celen, A.E., Cibik, E.S., Urtekin, M.A. (2016) A research on the yield and some yield characteristics of some field pea (*Pisum arvense* L.) varieties grown in different row spacings in Aegean region conditions. Journal of Central Research Institute For Field Crops. 25(2), 225-229.
[23] Yuksel, O. (2016) Determination of yield and some quality parameters of forage pea (*Pisum sativum* L.) cultivars in Usak conditions. International Academic Research Congress (INES). 3-5 Nov., Antalya, Turkey, 2266-2270.
[24] Hintz, R.W., Albrecht, K.A., Oplinger, E.S. (1992) Yield and quality of soybean forage as affected by cultivar and management practices. Agronomy Journal. 84, 795–798.
[25] Osborne, S.L., Riedell, W.E. (2006) Soybean growth response to low rates of nitrogen applied at plantings in the Northern Great Plains. Journal of Plant Nutrition. 29, 985–1002.
[26] Koc, A., Gokkus, A. (1996) Annual variation of above ground biomass, vegetation height and crude protein yield on the natural rngelands of Erzurum. Tr. J. Agric. and Forest. 20, 305-308.
[27] Buxton, D.R. (1996) Quality related characteristics of forages as influenced by plant environment and agronomic factors. Animal Feed Science Technology. 59, 37-49.
[28] Surmen, M., Yavuz, T., Cankaya, N. (2011) Effects of phosphorus fertilization and harvesting stages on forage yield and quality of common vetch. International Journal of Food, Agriculture and Environment – JFAE 9(1), 353-355.
[29] Turk, M., Albayrak, S., Yuksel, O. (2011) Effects of seeding rate on the forage yields and quality in pea cultivars of different leaf types. Turkish Journal of Field Crops. 16(2), 137-141.
[30] Shekara, B.G., Sowmyalatha, B.S., Baratkumar, C. (2012) Effect of phosphorus levels on forage yield of fodder cowpea. Journal of Horticulture Letters. 2(1), 12-13.
[31] Uzun, A., Asik, B.B., Acikgoz, E. (2017) Effects of different seeding rates on forage yield and quality components in pea. Turkish Journal of Field Crops. 22(1), 126-133.
[32] Thorvaldsson, G. (2006) Digestibility of Timothy, Timothy Productivity and Forage Quality Possibilities and Limitations. NJF Seminar 384, Agricultural University of Iceland, Akureyri, Iceland, 85-88.
[33] Arzani, H., Zohdi, M., Fish, E., Zahedi Amiri, G.H., Nikkhah, A., Wester, D. (2004) Phenological effects on forage quality of five grass species. J Range Manage. 57, 624 –629.
[34] Yildiz, F., Turk, M. (2015) Effects of Phosphorus fertilization on forage yield and quality of common vetch (*Vicia sativa* Roth.). YYU J Agr Sci. 25(2), 134-139.
[35] Lithourgidis, A.S., Vasilakoglou, I.B., Dhima, K.V., Dordas, C.A., Yiakoulaki, M.D. (2006) Forage yield and quality of common vetch mixtures with oat and triticale in two seeding ratios. Field Crops Research. 99,106-113.
[36] Van Soest, PJ. (1982) Nutritional ecology of the ruminant: Ruminant metabolism, nutritional strategies, the cellulolytic fermentation and the chemistry of forages and plant fibers. O and B Books Publisher, Corvallis, OR., USA.

Received: **15.08.2018**
Accepted: **27.03.2019**

CORRESPONDING AUTHOR

Osman Yuksel
Usak University,
Faculty of Agriculture and Natural Sciences,
Department of Field Crops,
Usak – Turkey

e-mail: osman.yuksel@usak.edu.tr

© by PSP Volume 28 – No. 5/2019 pages 4171-4184 Fresenius Environmental Bulletin

COMBINATION EFFECTS OF BIOCHAR AND EFFECTIVE MICROORGANISMS ON GROWTH AND PHOTOSYNTHETIC INDEXES OF FLUE-CURED TOBACCO

Xu Yang[1,2], Xiaohou Shao[1,2,*], Xinyu Mao[1,2], Maomao Hou[3], Fuzhang Ding[4], Youbo Yuan[4], Xiankun Su[4], Minhui Li[1,2]

[1]Key Laboratory of Efficient Irrigation-Drainage and Agricultural Soil-Water Environment in Southern China (Hohai University), Ministry of Education, Nanjing 210098, China
[2]College of Agricultural Engineering, Hohai University, Nanjing 210098, China
[3]College of Horticulture, Fujian Agriculture and Forestry University, Fuzhou 350000, China
[4]Institute of Tobacco Science in Guizhou Province, Guiyang 550081, China

ABSTRACT

Due to long-term continuous cropping and over use of chemical fertilizers, it has restricted the growth of flue-cured tobacco seriously, and which caused the decreasing yield and quality of tobacco leaves. Different biochar combined with effective microorganisms (EM) treatments were designed to explore the influences on the growth of flue-cured tobacco in the pot experiment. The results showed that the leaf area index (*LAI*) of B1E1 (1.5% biochar combined with 1.5% EM) was the largest (3.89), which increased 28.53% more than that of CK. The biochar and EM application have significantly increased net photosynthetic rate (*Pn*), stomatal conductance (*Gs*) and intercellular CO_2 concentration (*Ci*), and decreased transpiration rate (*Tr)*. The yield of B1E1 was the highest (2546.61 $kg \cdot hm^{-2}$), which have a significant difference with other treatments ($P<0.05$), and it has increased more than 33.6% and 25.83% compared with B2E2 (2.5% biochar combined with 2.5% EM) and CK. Therefore, appropriate amount of biochar combined with EM application have a significantly effect on the growth of flue-cured tobacco, but the excessive biochar and EM will inhibit it, B1E1 is the best coupling treatments, and the results could provide theoretical and practical guidance for the growth of crop.

KEYWORDS:
Biochar, Effective microorganisms, Tobacco, Physiological indexes, Growth indexes

INTRODUCTION

Flue-cured tobacco is the dominant economic crop in China, the production of tobacco leaf plays a very important role in the development of agriculture and national economy in China [1, 2]. Because of the long-term continuous cropping and over use of chemical fertilizers, the soil environment used for tobacco planting was gradually deteriorated [3], such as soil nutrient loss, soil porosity decreased, soil acidification harden, and other issues. All of those situations caused slow spreading of tobacco leaves at the early growth stage and continuous released N in soil at late growth stage, thus resulting in excessively thick leaves, nicotine and nitrogen-containing compounds increased, sugar and aroma of the leaves decreased, also its industrial availability reduced. Good soil conditions are required to produce high quality tobacco leaves. Some early studies used organic manure plus balanced fertilization with N, P and K have promoted soil activity and enhanced crop growth, but the production is not significant. And other studies used biological and chemical modification techniques have still not achieved a good repair effect. Therefore, it is very important to utilize some new soil amendments in tobacco-planting areas to solve the problem of the decreasing yield and quality of flue-cured tobacco.

Biochar is a product of thermal decomposition of organic matter during the pyrolysis process with limited oxygen access in the temperature range of 300-1000℃ [4], and its potential to improve soil fertility and mitigate climate change has been recognized globally [5]. Biochar, rich in nutrients, is constitutionally stable and can persist in soil for thousands of years [6, 7]. The main purposes of using biochar are to improve the soil structure and contribute to C sequestration by the soil, and biochar also has unique properties to improve soil productivity [8]. Biochar is recognized as a good soil amendment, aimed to reduce nutrient loss, provide greater nutrient availability in soil, and improve the efficiency of nutrient utilization in crops [9]. Biochar has a large specific surface area, porous microstructure, and abundant surface functional groups, which can provide favorable soil conditions for microbes [10, 11]. Furthermore, the high porosity of biochar may also be very beneficial for improving soil structure as well as water holding capacity and mitigating the ever-increasing drought stress in dryland agriculture

due to climate change [12, 13]. Biochar amendment to cropland may have effects on reducing N demand by crop production through enhanced N use efficiency which in turn may reduce the emission of GHGs from N fertilizer industry [14]. The porous physical structure of biochar induces a greater sorption capacity to conserve soil moisture and nutrients [13, 15]. Biochar amendments could significantly improve soil fertility by increasing the CEC and consequently the retention and availability of nutrients for plants [16].

In recent years, effective microorganisms (EM) are used in numerous fields associated with agriculture. It is a mixture of beneficial microorganisms containing 80 different species of micro-organisms that are considered as mutually compatible and coexistent in a liquid culture [17, 18]. Positive effects of EM application to enhance the growth, yield and quality of crops have been reported. Hou et al. [19] have researched on EM water-retention agent application in flue-cured tobacco, demonstrating that it can increase net photosynthetic rate (*Pn*) and decrease transpiration rate (*Tr*), which could regulate photosynthetic effects of tobacco leaves at growth stages. Javaid et al. [20] indicated that EM could significantly enhance nitrogen, phosphorus and potassium nutrition of the test plant in farmyard manure amendment both at flowering stage and maturity. Talaat et al. [21] had clearly demonstrated that EM application could increase plant salt tolerance, which mainly contributed to the enhancement in nutrients acquisition and the improvement in osmotic adjustment by compatible solutes accumulation. Moreover, greater osmotic adjustment would reduce oxidative damage and alleviate the cell membrane damages. Hu et al. [22] revealed that long-term application of EM compost gave the highest values for the measured parameters but the lowest values in the control plot. The application of EM in combination with compost significantly increased wheat straw biomass, grain yields, straw and grain nutrition compared with traditional compost and control treatment. The foliar application of effective microorganisms can improve nodulation and yield in pea, with a grain yield increase of 126% for NPK amendment and of 145% for green manure amendment [23]. Compared to chemical fertilizer, EM bokashi fertilizer significantly increased both the nodule numbers per plant and fresh weight per nodule. The peanut plants fertilized with EM bokashi also showed higher photosynthetic rate, transpiration rate and mesophyll conductance [24]. The application of EM-5 Sutociu could simultaneously increase bean plant growth and reduce R. solani disease [25].

At present, there have been some researches on biochar and EM technologies on soil remediation, but most of them focus on single-factor experiments, such as straw returning, EM bacteria, and biochar. There are few studies about biochar and EM combined application effect on soil remediation, especially the effect mechanism is not clear, which greatly restricts the large-scale application of biochar and EM in agricultural production [26]. It is well known that biochar has a large specific surface area and abundant surface functional groups, if biochar combined with the EM is used, it can provide a large specific surface area for the microbes, when both of them persist in soil, the nutrients and effective microorganisms may be released slowly, thereby achieving the purpose of reducing nutrient loss, promoting the soil microbial biomass, activity and diversity, and enhancing the growth, yield and quality of crops. Moreover, it is estimated that the annual output of agricultural straws in China is about 0.7 billion tons and up to 50% of the straw is burned, the release of CO_2, CH_4 and NO_2 by burning occupies by 6.13%, 0.68% and 3.63% of China's emissions in 2000 [27]. And most straw resources are directly burned in the field, abandoned at the edge of the field, or combusted as cooking and heating fuels that cause serious air pollution and resource waste. While turning straw into biochar under low temperatures and limited oxygen conditions is a promising approach for the utilization of waste resources [28]. In order to solve the problem of the poor growth, yield and quality of flue-cured tobacco. Different biochar and EM treatments were designed to investigate the response mechanisms of agronomic traits, dry matter, photosynthetic characteristics and yield of flue-cured tobacco, and the results could provide theoretical and practical guidance for the physiological growth of flue-cured tobacco and the development of agriculture in China.

MATERIALS AND METHODS

Experimental site and the soil properties. The experiment was initiated in a plastic sheet covered greenhouse in the Vegetables and Flowers Institute of Hohai University test base (latitude 31°43'N, longitude 118°46′E), Nanjing, China. The average annual rainfall is about 1106.5 mm. The average yearly temperature is approximately 15.7 ℃ and average humidity is about 81%. Besides, the maximum wind speed is 19.8 m/s and the frost-free period is 237d. The waterproof insulation canopy is installed above the lysimeter to cut off natural rain's effect on the test results. The specimen collected from the experimental site was yellow brown soil, and its physico-chemical properties were shown in Table 1.

Biochar and EM characteristics. The tested biochar applied to soil was obtained from a commercial manufacturer and was produced by pyrolysis where the feedstock was thermochemically decomposed at a temperature of 500 ℃ in an oxygen-poor atmosphere. Biochar was produced from rice straw

and was provided by Jiangsu Huafeng Agricultural Biological Engineering Co., Ltd. Its main properties were as follows: pH of 10.32, total nitrogen content of 2.16 g·kg^{-1}, total phosphorus of 6.85 g·kg^{-1}, total potassium of 7.42 g·kg^{-1}, organic carbon of 545.26 g·kg^{-1}, ash content of 30.26%, CEC of 45.3 cmol·kg^{-1}, H/C of 0.03, O/C of 0.50, and (O+N)/C of 0.51. In addition, it contained more micro-pores, and the pore sizes of the tested biochar were mainly below 4.75 nm.

Members of 5 main groups of microorganisms are used in the source material of EM including lactic acid bacteria (*Lactobacillus plantarum, L. casei, and Streptoccus lactis*), photosynthetic bacteria (*Rhodopseudomonas palustrus and Rhodobacter spaeroides*), yeasts (*Saccharomyces cerevisiae and Candida utilis*), actinomycetes (*Streptomyces albus, S. griseus*) and fermenting fungi (*Aspergillus oryzae, Penicillium sp. and Mucor hiemalis*) [29, 30]. The tested EM is a yellow-brown liquid with pH 3.8, sweet-sour taste and the smell of kvass or fermenting fruit juice. The EM was provided by Corporation EM Research Institute China subsidiary (Aiyile Environmental Biotechnology (Nanjing) Co., Ltd).

Experimental design. The experiment was carried out by plastic pots, which the upper diameter is 38 cm, the bottom diameter is 30 cm and the height is 40.5 cm. The growth periods of flue-cured tobacco were divided into three stages, start-up stage (35 days after transplanted), growth stage (36 to 65 days after transplanted) and maturity stage (66 to ending of harvested), respectively. The study was designed with five levels of biochar application rate and five levels of EM application rate, that is, 0%, 1.5%, 2.5%, 3% and 5% were selected in this experiments respectively, there were 7 different combined treatments in all, each treatment with three replicates (Table 2).

The young plants of flue-cured tobacco K326 were elaborately cultivated in made-in-order seedling trays, they would be transplanted into the pot when it has six expanded leaves. Irrigation water amount of start-up stage, growth stage and maturity stage accounts respectively 30%, 40% and 30% for the total irrigation water. The biochar and EM application rates were calculated as a percentage of soil weight in pots. Inorganic fertilizer was applied according to a proportion of basal fertilizer: additional fertilizer = 7:3 (provided by Tobacco Institute of Science in Guizhou Province, N: P_2O_5: K_2O =1: 2: 3). The amount of nitrogen fertilizer for each treatment is 89.99 kg·hm^{-2} and the amount of P_2O_5 and K_2O for each treatment is converted into 59.99 and 149.99 kg·hm^{-2} respectively. What's more, the basal fertilizer was applied in hole patterns and the latency time of additional fertilizer application was 26 days after transplanting.

Main tested indexes and methods. Agronomic characters and leaf area index of flue-cured tobacco: each treatment chooses 3 strains to determine the plant height, stem circumference, the largest leaf length and width of flue-cured tobacco [31].

Flue-cured tobacco leaf area per plant calculation method [31] is as following:

$$A_s = \sum_{i=1}^{n} (L_i \times W_i \times 0.6345) \quad (1)$$

Where, A_s is the flue-cured tobacco leaf area per plant, n is flue-cured tobacco leaf number, L_i is the largest leaf length, W_i is the maximum blade width.

Flue cured tobacco leaf area index according to the following formula:

$$LAI = A_s / S \quad (2)$$

Where, S is the covered area of flue-cured tobacco per plant.

TABLE 1
Physico-chemical properties of the soil at the experiment site

Property	pH	Organic matter (g·kg^{-1})	Total N (mg·kg^{-1})	Available P (mg·kg^{-1})	Available K (mg·kg^{-1})	Bulk density (g·cm^{-3})	Field capacity (%)
Values	5.87	14.21	129.90	27.20	229.90	1.35	28.0

TABLE 2
Experimental design

Treatment	Biochar (%)	EM (%)	Nitrogen fertilizer (kg·hm^{-2})	Irrigation amount (mm)		
				Start-up stage	Growth stage	Maturity stage
CK	0	0	89.99	180	240	180
B1E0	3	0	89.99	180	240	180
B0E1	0	3	89.99	180	240	180
B1E1	1.50	1.50	89.99	180	240	180
B2E0	5	0	89.99	180	240	180
B0E2	0	5	89.99	180	240	180
B2E2	2.50	2.50	89.99	180	240	180

Photosynthetic characteristics. Photosynthetic characteristics in growth stage and maturity stage of flue-cured tobacco were measured using the LI-6400 portable photosynthetic apparatus produced by American company LI-COR during 8:30~11:30 am. The measured leaf was the most recent fully expanded. Measurement characteristics included the net photosynthetic rate (*Pn*), stomatal conductance (*Gs*), intercellular CO_2 concentration (*Ci*), and transpiration rate (*Tr*) when light intensity was controlled around 800 $\mu mol \cdot m^{-2} \cdot s^{-1}$. LI-6400 was widely used in *LAI* estimation to get rid of the trouble of manual measurement [32], making the *LAI* metering much more convenient.

Dry matter, yield and root-shoot ratio. When the tobacco leaves were matured, they were separated by roots, stems and leaves, then kept in an incubator at 105 ℃ for 8 hours and then dried at 75 ℃ to constant weight, respectively. The dry matter accumulation could be obtained and the root-shoot ratio and the yield could be calculated.

Data Analysis. The data were compared statistically in SPSS software Version 17.0.

RESULTS AND DISCUSSION

Leaf area and *LAI*. The change of per plant leaf area along with the planting time under different biochar and EM treatments is shown in Table 3. It is well-known that leaf area directly affects the yield of flue-cured tobacco and is an important factor in the value of flue-cured tobacco. As can be seen from the table, the growth of tobacco leaf area could divide into three stages: slow growth period, rapid growth period and relatively stable period. It also can be seen from the table that the flue-cured tobacco leaf area per plant of B2E0 treatment was the largest after transplanting 22d, attained 3943.57 cm^2; followed by B1E0, attained 2869.96 cm^2; B0E2 was the lowest, which only attained 1682.9 cm^2. From that B0E2 treatment had significantly lower leaf area than other treatments, which indicated that the single biochar treatment promoted the growth at the start-up stage more obviously, however, because the EM preparation is acidic, the treatment with EM alone might be lack of alkaline biochar neutralization, higher acidity leads to slower growth.

After transplanting 36~76d, leaf area increased significantly due to tobacco gradually into the rapid growth stage. While after transplanting 36d, the effect of biochar and EM treatments on leaf area growth was extremely significant. After transplanting 68d, the leaf area of each treatments becomes consistent, but B1E1 treatment had the largest flue-cured tobacco leaf area per plant, attained 17329.34 cm^2; followed by B0E1, attained 15605.85 cm^2; and B2E2 was the lowest, only attained 12013.83 cm^2. It can be seen that B1E1 treatment was significantly higher than other treatments. The results indicated that the amount of biochar and EM affected the leaf area of flue-cured tobacco significantly and appropriate amount of biochar and EM have more conducive to the growth of flue-cured tobacco.

After transplanting 68~85d, tobacco entered into the maturity stage, and the leaf area of flue-cured tobacco was still a certain increasing and tends to be stable. After transplanting 85d, the leaf area of flue-cured tobacco treated with biochar and EM was relatively higher, among them, B1E1 treatment was also the largest, attained 23609.79 cm^2; followed by B0E1, attained 23053.25 cm^2; B2E2 was also the lowest, only attained 13657.53 cm^2. This indicated that the appropriate amount of biochar combined with appropriate amount of EM was more conducive to leaf area of flue-cured tobacco growth. With regard to the single factor of flue-cured tobacco leaf area per plant, 1.5% biochar combined with 1.5% EM is the best coupling treatments.

The dynamic changes of *LAI* of flue-cured tobacco along with the planting time is shown in Fig 1. As can be seen from the figure, the *LAI* of flue-cured tobacco can be divided into two stages: after transplanting 22~85d, the tobacco leaf area index has been growing; 76-107d after transplanting, with the picking of tobacco and the lower leaves, tobacco leaf area index also decline gradually. After transplanting 85d, flue-cured tobacco *LAI* of each treatment reached its peak, *LAI* of B1E1 was the largest, attained 3.89; followed by B0E1, attained 3.80; B2E2 was the lowest, only attained 2.25. The reason is mainly that B2E2 has applied excessive biochar and EM, leading to a smaller leaf area. In general, the different application of biochar and EM could affect the *LAI* of flue-cured tobacco to a certain extent. Therefore the appropriate amount of biochar combined with EM is more conducive to leaf area of flue-cured tobacco growth.

Net photosynthetic rate. The photosynthetic characteristics of flue-cured tobacco was measured in growth stage and maturity stage. Effects of different biochar and EM treatments on net photosynthetic rate of flue-cured tobacco are shown in Fig 2. It can be seen from the figure that the *Pn* value of flue-cured tobacco leaves in growth stage is higher than that of the maturity stage. It also can be seen from the figure that *Pn* values was in the highest level of B2E2 in growth stage, attained 17.34 $\mu mol \cdot m^{-2} \cdot s^{-1}$, followed by the B1E1, attained 17.25 $\mu mol \cdot m^{-2} \cdot s^{-1}$, CK was the lowest, only attained 14.71 $\mu mol \cdot m^{-2} \cdot s^{-1}$. Compared with the growth stage, the *Pn* value was almost decreased in maturity stage, but B2E2 also was the highest, attained 15.31 $\mu mol \cdot m^{-2} \cdot s^{-1}$, CK was the lowest, only attained 12.64 $\mu mol \cdot m^{-2} \cdot s^{-1}$. It also can be seen from Fig 2, in the growth stage, the EM application was significantly

TABLE 3
The effects of different treatments on per plant leaf area

Treatment	The per plant leaf area of Flue-cured tobacco (cm^2)						
	22d	36d	46d	57d	68d	76d	85d
CK	1778.20 d	5678.36 c	6876.41 c	10912.43 d	11995.64 d	13401.16 d	16836.54 d
B1E0	2869.96 b	5465.52 d	7534.98 b	12349.45 c	14068.00 c	16432.34 c	19609.68 c
B0E1	2826.78 c	8054.46 a	7573.33 b	14606.37 a	15605.85 b	17705.31 b	23053.25 b
B1E1	2850.84 bc	8035.70 a	8857.59 a	14595.89 a	17329.34 a	19451.55 a	23609.79 a
B2E0	3943.57 a	5669.19 c	6937.14 c	12709.90 b	14050.25 c	16411.39 c	19599.64 c
B0E2	1682.90 e	6707.27 b	7545.50 b	12752.13 b	15588.43 b	16446.99 c	19582.46 c
B2E2	1793.34 d	4565.42 e	5321.44 d	9846.05 e	12013.83 d	13373.21 d	13657.53 e

Different letters in the same column indicate significant differences at $P< 0.05$.

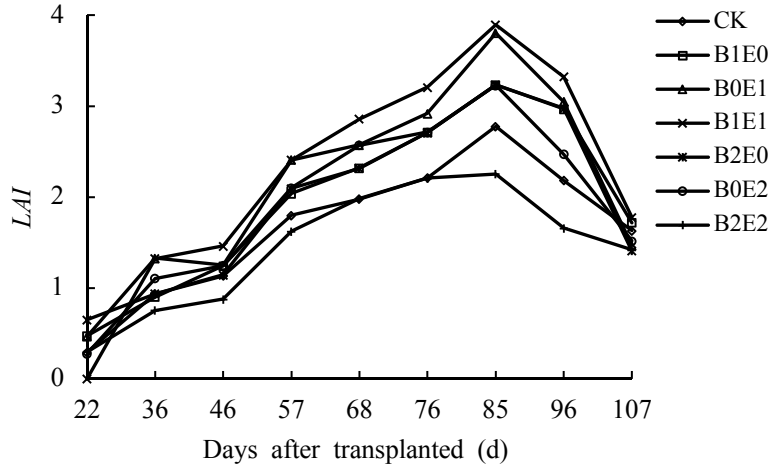

FIGURE 1
Dynamic changes of leaf area index

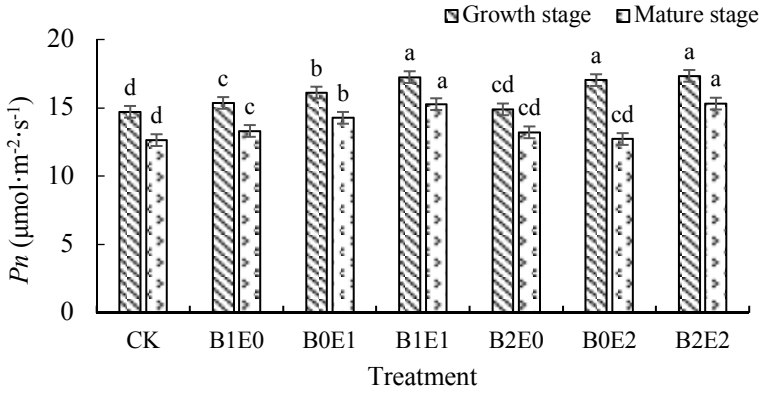

FIGURE 2
Effect of different treatments on net photosynthetic rate

larger than that without EM treatment of the *Pn* value, and there is little relation with the amount of biochar applied at this time. *Pn* was relatively smaller for the B0E2 treatment (high EM and no biochar application), this may be because the tobacco grew slowly in maturity stage, and high EM application had little effect on *Pn*, which also suggested that under the same field management, the *Pn* of combined biochar and EM treatment was significantly greater than that of single application or CK treatment, and the difference is significant ($P<0.05$), which further verify that combined biochar and EM application is more conducive to the growth of tobacco.

Stomatal conductance. Effects of different biochar and EM treatments on stomatal conductance (*Gs*) of flue-cured tobacco are shown in Fig 3. The *Gs* value of flue-cured tobacco leaf at different growth stages was the largest in growth stage, and maturity stage was significantly lower than the growth stage. The results showed that the treatments of different combined biochar and EM had a significant effect on the *Gs* value of flue-cured tobacco leaves. It also can be seen from the figure that *Gs* values was in the highest level of B1E0 in growth stage, attained 0.55 $mol \cdot m^{-2} \cdot s^{-1}$, followed by the B2E0, attained 0.53 $mol \cdot m^{-2} \cdot s^{-1}$, B0E2 was the lowest, only attained 0.40 $mol \cdot m^{-2} \cdot s^{-1}$. This indicated

that the single application of biochar treatment is greater than the single application of EM treatment, but in the case of excessive application of biochar, the value of *Gs* in leaves of flue-cured tobacco is relatively low, this also indicated that excessive EM and biochar is not conducive to the increase of leaf *Gs* value. While compared with the growth stage, the B2E0 was the highest, attained 0.35 mol·m^{-2}·s^{-1}, followed by B2E2, B0E1 was the lowest, only attained 0.22 mol·m^{-2}·s^{-1}. In general, different treatments of biochar and EM during maturity stage had a certain effect on the *Gs* of tobacco leaves, and there has a significant difference between the application of biochar and EM or CK treatments ($P<0.05$).

Intercellular CO_2 concentration. Effects of different biochar and EM treatments on intercellular CO_2 concentration (*Ci*) of flue-cured tobacco are shown in Fig 4. It can be seen from the figure that the *Ci* of flue-cured tobacco leaves in growth stage is higher than that of the maturity stage. The photosynthetic characteristics of flue-cured tobacco reached a higher level at the time of budding, and the closer to the harvest in the later period, the faster of each photosynthetic characteristics decreased.

It can be seen that the treatment of different biochar and EM also had a significant effect on the *Ci*. The *Ci* values was in the highest level of B1E1 in growth stage, attained 309.34 μmol·mol^{-1}, followed by the B1E0, B0E2 was the lowest, only attained 255.11 μmol·mol^{-1}, this indicated that different combinations of biochar and EM treatment can promoted the *Ci* value. It also can be seen from the figure that there is no significant difference between different biochar and EM treatments, this may be in the growth stages, the growth of tobacco was relatively strong, so the different combinations of biochar and EM treatments have little effect on the intercellular CO_2 concentration. Compared with the growth stage, the *Ci* was almost significant decreased in maturity stage, the B1E0 was the highest of the *Ci* value of different treatments in maturity stage, attained 205.32 μmol·mol^{-1}, followed by B0E1, attained 200.78 μmol·mol^{-1}, B0E2 was the lowest, only attained 171.29 μmol·mol^{-1}. Except for B0E2, there was no significant difference in other *Ci* values of flue-cured tobacco ($P<0.05$). In general, the *Ci* values of different biochar and EM treatment was significantly better than the single biochar and EM treatment, this may be due to the reduction of flue-cured tobacco *Gs* by the combined application, when the concentration of CO_2 in the intercellular space was constant, there was a slight surplus of CO_2 in the intercellular space of flue-cured tobacco.

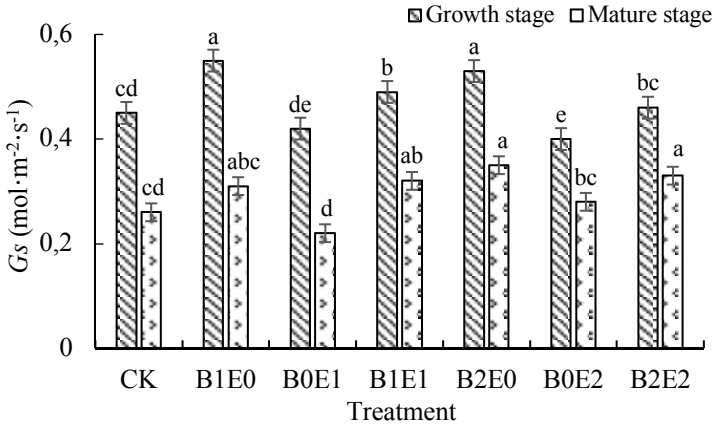

FIGURE 3
Effect of different treatments on stomatal conductance

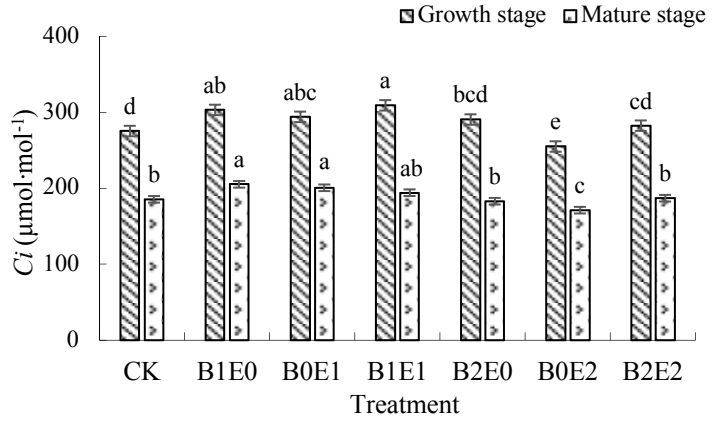

FIGURE 4
Effect of different treatments on intercellular CO_2 concentration

Transpiration rate. Effects of different biochar and EM treatments on transpiration rate (*Tr*) of flue-cured tobacco are shown in Fig 5. It can be seen from the figure that the *Tr* of flue-cured tobacco leaves in growth stages is higher than that of the maturity stage. The *Tr* values was in the highest level of B0E2 in growth stage, attained 3.41 $mmol \cdot m^{-2} \cdot s^{-1}$, followed by CK, attained 3.32 $mmol \cdot m^{-2} \cdot s^{-1}$, B1E0 was the lowest, only attained 2.82 $mmol \cdot m^{-2} \cdot s^{-1}$. Compared with the growth stage, the *Tr* was almost significant decreased in maturity stage, the CK was the highest of the *Ci* value of different treatments in maturity stage, attained 2.27 $mmol \cdot m^{-2} \cdot s^{-1}$, followed by B0E2, attained 2.19 $mmol \cdot m^{-2} \cdot s^{-1}$, B1E0 was the lowest, only attained 1.79 $mmol \cdot m^{-2} \cdot s^{-1}$. The results showed that the higher application rates of biochar and EM did not play a role to reduce the *Tr* value of flue-cured tobacco leaves. This may be due to the higher application rates of biochar and EM accumulated with water in the fixed space under pot control conditions, that detrimental to the growth of flue-cured tobacco.

As shown in Table 4 and Table 5, the results indicated that the related analysis of the main photosynthetic characteristics, biochar and EM application in growth and maturity stage. It can be seen that the *Gs* was significantly positive correlated with biochar application in growth stage, the correlation coefficients was 0.834, the *Ci* was positive correlated with biochar application, the correlation coefficients was 0.415, and the *Pn* and *Tr* were negative correlated with biochar application, the correlation coefficients were 0.266 and 0.360 respectively. While the *Pn* and *Tr* were positive correlated with EM application, the correlation coefficients were 0.735 and 0.439 respectively, the *Gs* was significantly negative correlated with EM application, the correlation coefficients was 0.809, and the *Ci* was negative correlated with EM application, the correlation coefficients was 0.565. In addition, it can be seen from the Table 5 that the *Gs* was significantly positive correlated with biochar in maturity stage, the correlation coefficients was 0.845, the *Pn* and *Ci* was positive correlated with biochar application, the correlation coefficients were 0.103 and 0.113 respectively, and the *Tr* was negative correlated with biochar application, the correlation coefficients was 0.462. While the *Pn* and *Tr* were positive correlated with EM application, the correlation coefficients were 0.135 and 0.293 respectively, the *Gs* and *Ci* were negative correlated with EM application, the correlation coefficients were 0.355 and 0.437 respectively.

In this study, it was found that the application of appropriate amount of biochar and EM could significantly increase the contents of *Pn*, *Gs* and *Ci*, and decrease *Tr*, while the *Pn*, *Gs*, *Ci*, and *Tr* of the treated tobacco both have some fluctuations with the increased of biochar and EM application, it indicated that the effect of biochar and EM application on tobacco photosynthetic characteristics was obvious, it could improve tobacco photosynthetic capacity, but over usage would be bad for improving tobacco photosynthetic characteristics. This also confirms and supplements Chen and Hou's Researchings [19, 33]. Similar study by Wang et al. [34] biochar application at 2400 $kg \cdot hm^{-2}$ increased net photosynthetic rate 77.32%, and biochar could effectively promote the growth and development of root of flue-cured tobacco, optimize root physiological parameters, and improve leaf photosynthetic physiological. The peanut plants fertilized with EM also showed higher photosynthetic rate, transpiration rate and mesophyll conductance [24]. However, Liu et al. [35] indicated that the application of biochar had no obvious effect on tobacco photosynthesis, but the application of biochar combined with AM fungi (*G. intraradices or G. mosseae*) significantly increased net photosynthetic rate, stomatal conductance, transpiration rate and water use efficiency, while significantly decreased intercellular CO_2 concentration, which indicated that the photosynthesis of tobacco leaves was promoted.

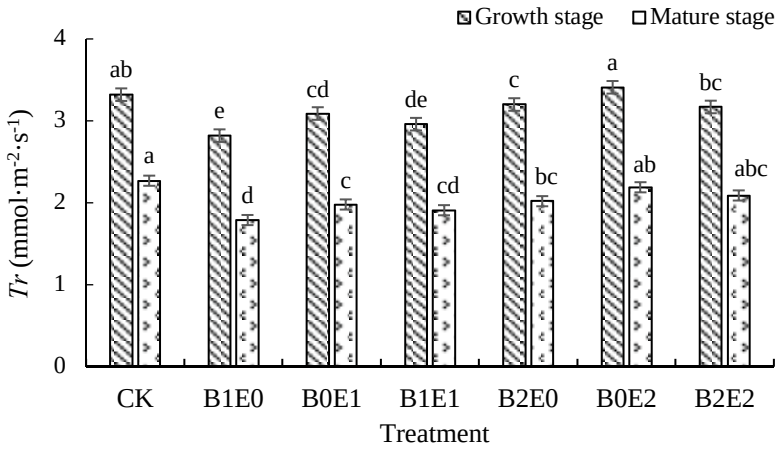

FIGURE 5
Effect of different treatments on transpiration rate

TABLE 4
The related analysis of main photosynthetic characteristics, biochar and EM application in growth stage

Parameter	Biochar	EM	*Pn*	*Gs*	*Ci*	*Tr*
Biochar	1	-0.550	-0.266	0.834*	0.415	-0.36
EM		1	0.735	-0.809*	-0.565	0.439
Pn			1	-0.426	-0.079	-0.004
Gs				1	0.681	-0.683
Ci					1	-0.908**
Tr						1

**and * indicate significant correlation of 0.05 and extremely significant correlation of 0.01 respectively.

TABLE 5
The related analysis of main photosynthetic characteristics, biochar and EM application in maturity stage.

Parameter	Biochar	EM	*Pn*	*Gs*	*Ci*	*Tr*
Biochar	1	-0.550	0.103	0.845*	0.113	-0.462
EM		1	0.135	-0.355	-0.437	0.293
Pn			1	0.232	0.368	-0.391
Gs				1	-0.166	-0.274
Ci					1	-0785*
Tr						1

*indicate significant correlation of 0.05.

Dry matter accumulation and distribution in various parts of flue-cured tobacco. Effects of different biochar and EM treatments on the dry matter accumulation of flue-cured tobacco organs are shown in Table 6. It can be seen that the highest root dry weight of different treatments was the B2E0, attained 57.29 g·plant^{-1}, significantly higher than other treatments, followed by B2E2, attained 52.65 g·plant^{-1}, B0E2 was the lowest, only attained 43.13 g·plant^{-1}, significantly lower than other treatments. Overall, with the increase of biochar application can help increase the root dry weight of tobacco. The highest dry weight of stems was B1E1, attained 64.76 g·plant^{-1}. The lowest dry weight of stems was B2E2, only attained 46.61 g·plant^{-1}. The dry weight of tobacco leaves in each treatment ranged from 102.48~154.34 g·plant^{-1}, as the B1E1 treatment was the highest, attained 154.34 g·plant^{-1}, followed by B0E1, attained 133.76 g·plant^{-1}, and the lowest was B2E2, only attained 102.48 g·plant^{-1}. From the analysis of the above results, we can seen that the accumulation of dry matter in different parts was greatly affected by the different ratios. Dry matter accumulation of roots and stems, accumulation of whole plant dry matter and leaf dry matter accumulation were not necessarily related, the dry weight of roots or stems or leaves may not necessarily be large. An organ may account for the dry weight of the whole plant, and the proportion of other organs to total plant dry weight was not necessarily large. It can be seen from Table 6, there is a certain difference in the dry matter accumulation of roots, stems and leaves among all the treatments. Among them, the highest of tobacco stems and leaves was B1E1 (1.5% biochar combined with 1.5% EM), which attained 64.76 g and 154.34 g, respectively, while the lowest of the dry matter accumulation of tobacco stems and leaves was B2E2 (2.5% biochar combined with 2.5% EM), only attained 46.61 g and 102.48 g, respectively, and there have a significant difference between the maximum and the minimum value.

It also can be seen from Table 6, the dry matter accumulation in stems and leaves reduced with the increasing of biochar and EM application, among them, as B1E1 treatment was the highest, and B2E2 was lowest, compared with B2E2, the dry matter accumulation in stems and leaves increased by 28.03% and 33.6%, respectively, compared with CK, the dry matter accumulation in stems and leaves increased by 18.78% and 25.83%, respectively. Furthermore, CK compared with B2E2, the dry matter accumulation in stems and leaves increased by 11.39% and 10.47%, respectively. It indicated that the dry matter accumulation increased with the increasing of the biochar and EM application in a certain range, but excessive application would reduced the dry matter accumulation, such as B2E2, the root dry matter accumulation decreased with the increasing of biochar and EM application rate, which suggested that biochar and EM application could contribute to the growth of aerial parts of flue-cured tobacco.

It can be seen from Fig 6, the order of the distribution of dry matter in roots, stems and leaves is leaf> stem> root, the dry matter of the whole tobacco plant was mainly distributed in leaves, with leaves accounting for about 50% of total plant dry weight, followed by the stem, accounting for 22.60~24.60% of total plant dry weight, the lowest was the root, accounting for 19.11~26.10% of total plant dry weight. The increase of the biochar application rate could increase the proportion of root in the whole plant dry weight, and the proportion of leaf to total weight decreased relatively, this may be because the biochar application is beneficial to root growth (Fig 6).

TABLE 6
Effect of different treatments on dry matter accumulation in various parts of flue-cured tobacco

Treatment	Root (g plant^{-1})	Stem (g plant^{-1})	Leaf (g plant^{-1})	Total dry matter (g plant^{-1})	Root-shoot ratio	Economic coefficient
CK	46.75 d	52.60 c	114.47 d	213.82 d	0.278	0.535
B1E0	51.21 c	57.54 b	129.85 bc	238.59 b	0.273	0.544
B0E1	46.71 d	57.76 b	133.76 b	238.23 b	0.244	0.561
B1E1	51.75 c	64.76 a	154.34 a	270.85 a	0.236	0.569
B2E0	57.29 a	53.16 c	124.72 c	235.17 b	0.322	0.530
B0E2	43.13 e	52.53 c	124.44 c	220.10 c	0.244	0.565
B2E2	52.65 b	46.61 d	102.48 e	201.74 e	0.353	0.507

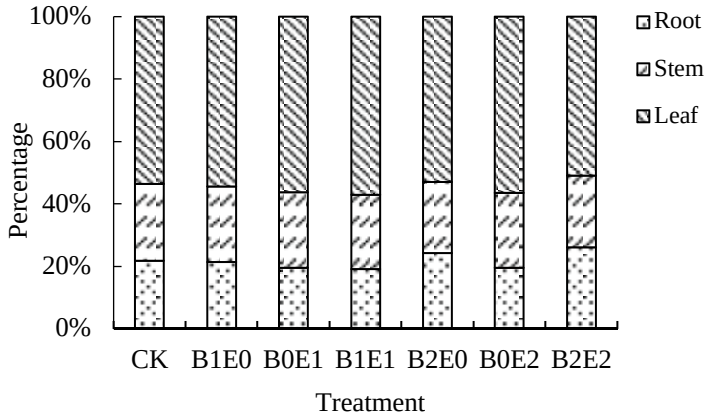

FIGURE 6
The proportion of different dry weight to total dry weight organs of flue-cured tobacco

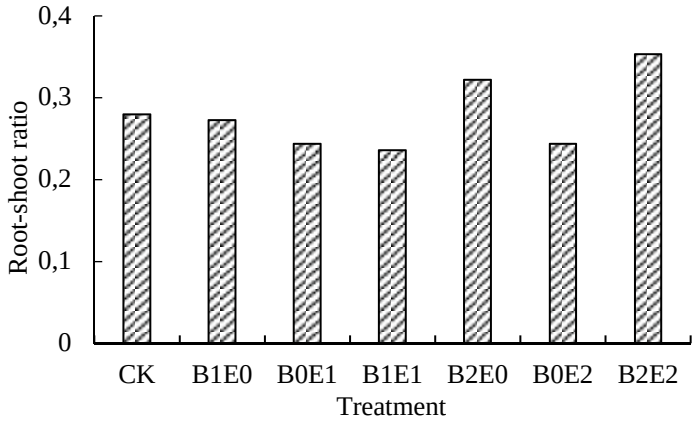

FIGURE 7
The root-shoot ratio of flue-cured tobacco

The root-shoot ratio of flue-cured tobacco varied among different treatments are shown in Fig 7. The root-shoot ratio of flue-cured tobacco increased overall with the increase of biochar application, and did not show a certain relationship with EM. Among them, the B2E2 treatment was the highest, attained 0.353, followed by B2E0, attained 0.322, the B1E1 was the lowest, only attained 0.236, compared with CK treatment, there was no regularity change, but only a positive correlation with the application of biochar content. This may be due to the fact that the increase in the amount of biochar applied to the growth of roots and shoots caused by the proliferation of different effects, manifested as the increase in the amount of biochar application of root growth to promote greater than the above-ground. In the case of the same irrigation, the reason for the lowest root-shoot ratio of B1E1 may be due to the better effect of B1E1 on water retention and drought resistance, more water stored in the soil than other treatments, the development of the root system was inhibited, and the growth of the above-ground part was promoted to be better. The root to crown ratio becomes smaller. When the soil was deficient in water, the water absorbed by the roots is rarely transported upwards, the impact on the growth of flue-cured tobacco was relatively small, the growth of the above-ground parts was inhibited, and the ratio of root to

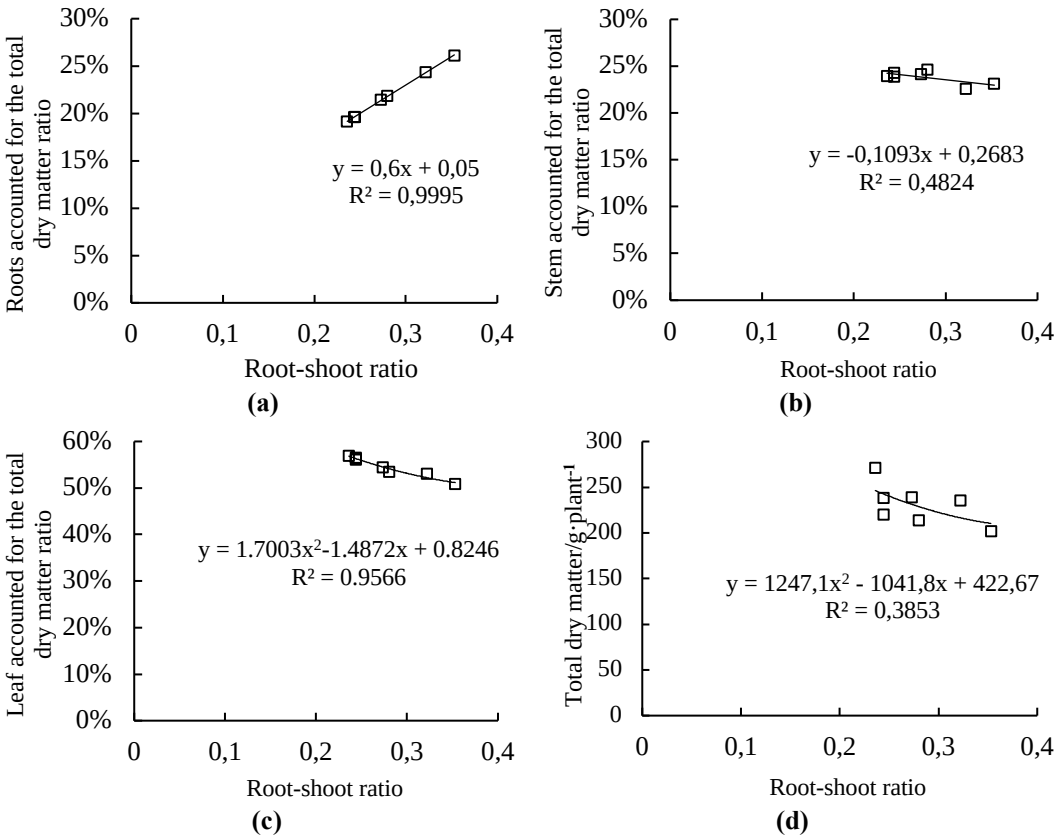

FIGURE 8
The ratio of root (a), stem (b), leaf (c) to total dry matter and root-shoot ratio, and relationship between total dry matter and root-shoot ratio (d)

crown increases. Therefore, the B1E1 treatment has better water retention performance, and enhanced the ability of the plant to resist drought at the later stage, which promoted the growth of flue-cured tobacco.

Fig 8 was the ratio of dry weight, dry weight of stems and dry weight of leaves to total dry matter, and relationship of the root-shoot ratio, total dry matter to root-shoot ratio under different biochar and EM treatments. It can be seen from the figures, the total dry matter showed a slight downward trend with the increasing of the root-shoot ratio; The ratio of the dry weight of tobacco leaves to the total dry weight decreased with the increasing of root-shoot ratio; The proportion of stem dry weight to total dry weight decreased inconspicuous with the increasing of root-shoot ratio. With the increase of root-shoot ratio, the proportion of dry matter distributed in the roots is increasing, and the two of them have a very significant linear positive correlation. From the above analysis, under the same irrigation conditions, the increase of biochar application can promote the growth of underground roots within a certain rang, and the promotion of tobacco leaves is not very obvious. This indicated that excess biochar and EM application will inhibit the growth of flue-cured tobacco leaves, but the appropriate amount of biochar and EM treatment can effectively promote the growth of tobacco leaves, and can play a better effect of water retention and drought resistance, and it also indicated that the biochar and EM can regulate soil moisture and play a role in regulating fertilizer with water.

Effect of different treatments on yield. Effects of different biochar and EM treatments on yield of flue-cured tobacco are shown in Fig 9. It can be seen from the figure that the yield of different biochar and EM treatments have a significant difference ($P<0.05$). Among them, the B1E1 have got the highest yield, attained 2546.61 kg·hm^{-2}, which have a significant difference with other treatments ($P<0.05$), followed by the B0E1, attained 2207.04 kg·hm^{-2}, B2E2 was the lowest, only attained 1690.92 kg·hm^{-2}, compared with B2E2 and CK, the yield of B1E1 have increased more than 33.6% and 25.83%, respectively. It also can be seen from Fig 9, both biochar and EM could increase the yield of flue-cured tobacco to a certain extent, but excessive will play an inhibitory role, such as B2E2, which combined 2.5% biochar and 2.5% EM, so this indicated that the appropriate amount of biochar combined with appropriate amount of EM is more conducive to improve the yield of flue-cured tobacco. With regard to increase the yield of flue-cured tobacco, 1.5% biochar combined with 1.5% EM is the best coupling treatments.

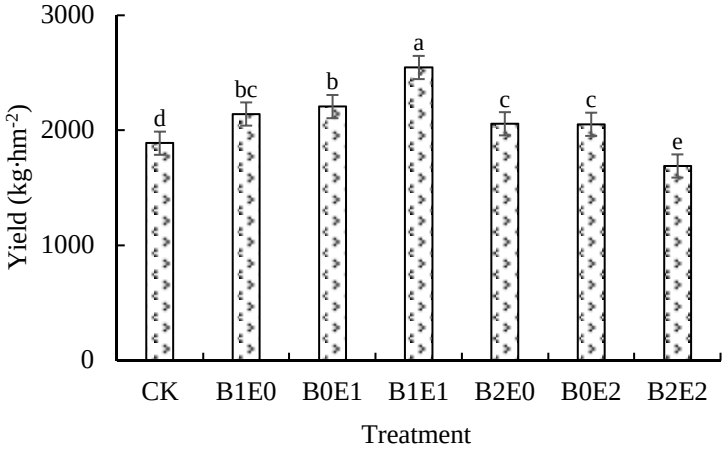

FIGURE 9
Effect of different treatments on yield

In our study, the application of biochar and EM could promoted *LAI*, photosynthesis characteristics, dry matter, and yield. Early study by Zhang and Abbott et al. [36-37] were showed that single biochar or EM application could promoted the growth of tobacco. While we founded that the promotion effect of combined biochar and EM was obviously better than the single biochar or EM treatment for the leaf area, photosynthesis, dry matter and yield of flue-cured tobacco. This may be because of the biochar is rich in mineral nutrient content, and it has a distinct physical structure, which can improve soil nutrient absorption and availability and promote crop growth [38-40], as well as EM is rich in photosynthetic bacteria, lactobacilli, yeasts, and actinomycetes or other beneficial bacteria. So this microorganisms in EM improve crop health and yield by increasing photosynthesis, producing bioactive substances such as hormones and enzymes, accelerating decomposition of organic materials and controlling soil-borne diseases. Some studies had reported that crop growth and yield were increased due to the application of EM [20, 29]. Hussain et al. [41] also reported that EM could increase the yields of rice and wheat. In this study, we showed that biochar combined with EM application have a significantly effect on leaf area, dry matter and yield. Therefore, when biochar combined with EM application, the porous nature and adsorption properties of biochar provide a favorable environment for the growth and reproduction of soil microorganisms, and under double effect of the external environment improvement and root induction hormones, the root structure have significant improvement, and then promoted the growth and yield of flue-cured tobacco.

In recent years, there are many reports on the methods of combined biochar and EM application in crop cultivation [19, 28], and the research on the use of biochar and EM technology and methods needs to be strengthened, and the application of biochar and EM should be as the main direction of "high yield, good quality, water-saving potential, and environmentally friendly" [19]. The results of this study can provide some support for the use of biochar and EM technologies, as well as theoretical methods such as water-saving, drought protection and soil remediation. In addition, due to the high cost of EM, it was usually necessary to carried out expansion culture before application, while in the course of cultivation, how to solve the problem of coordination and symbiosis of the microbial flora in the process of expanding cultivation is also the key to research. Because of the plant areas were widely distributed in China, soil types were diverse, and soil fertility and water holding characteristics were difference, therefore, in the application of biochar and EM, the appropriate application amount should be selected according to the actual conditions in consideration of local conditions. Such as in our study we founded that the excessive biochar and EM will inhibit the physiological growth, photosynthesis and yield of flue-cured tobacco. Therefore, reasonable and appropriate application of biochar and EM should be applied to promote the physiological growth and yield of tobacco or other crops.

CONCLUSIONS

It could be concluded from the results of these experiments that appropriate amount of biochar combined with EM application have a significantly effect on leaf area, dry matter and yield. The leaf area and *LAI* of B1E1 treatment was the largest, compared with CK, the leaf area and *LAI* of B1E1 have increased more than 28.69% and 28.53%, respectively. Furthermore, the biochar and EM application have significantly increased the contents of *Pn*, *Gs* and *Ci*, and decreased *Tr*, have promoted the growth of flue-cured tobacco effectively. On the other hand, compared with CK, the dry matter accumulation of B1E1 treatment in stems and leaves were increased by 18.78% and 25.83%, respectively. And for the yield of flue-cured tobacco, the B1E1 also was the

highest, attained 2546.61 kg·hm^{-2}, which have a significant difference with other treatments, B2E2 was the lowest, only attained 1690.92 kg·hm^{-2}, and followed by CK, attained 1888.755 kg·hm^{-2}, compared with B2E2 and CK, the yield of B1E1 treatment have increased more than 33.60% and 25.83%, respectively. Comprehensive consideration of the physiological and growth indexes of flue-cured tobacco, 1.5% biochar combined with 1.5% EM is the best coupling treatments, the excessive or small amount of application is not conducive to the growth of flue-cured tobacco. Therefore, biochar combined with EM has a positive effect on soil nutrients and the microbial community structure in tobacco fields, and the used of biochar and EM as an amendment to improve soil fertility and microbial environment has favorable application prospects in the tobacco fields, also the results of this study could provide theoretical and practical guidance for the physiological growth of flue-cured tobacco and the development of agriculture in China.

ACKNOWLEGEMENTS

This work was financially supported by Postgraduate Research & Practice Innovation Program of Jiangsu Province (SJKY19_0520), the Fundamental Research Funds for the Central Universities (2019B68214, 2017B755X14, 2017B11014), the Science and Technology project by Guizhou tobacco of China National Tobacco Corporation (201709)/

REFERENCES

[1] Shao, X.H., Wang, Y., Bi, L.D., Yuan, Y.B., Su, X.K., Mo, J.G. (2009) Study on soil water characteristics of tobacco fields based on canonical correlation analysis. Water Science and Engineering. 2, 79-86.

[2] Sun, J.G., He, J.W., Wu, F.G., Tu, S.X., Tan, T.J., Si, H., Xie, H. (2011) Comparative analysis on chemical components and sensory quality of aging flue-cured tobacco from four main tobacco areas of China. Agricultural Sciences in China. 10, 1222-1231.

[3] Zhang, Y.T., He, X.H., Liang, H., Zhao, J., Zhang, Y.Q., Chen, X., Shi, X.J. (2016) Long-term tobacco plantation induces soil acidification and soil base cation loss. Environmental Science and Pollution Research. 23, 5442-5450.

[4] Gul, S., Whalen, J.K., Thomas, B.W., Sachdeva, V., Deng, H.Y. (2015) Physico-chemical properties and microbial responses in biochar-amended soils: mechanisms and future directions. Agriculture, Ecosystems and Environment. 206, 46-59.

[5] Woolf, D., Amonette, J.E., Street-Perrott, F.A., Lehmann, J., Joseph, S. (2010) Sustainable biochar to mitigate global climate change. Nature Communications. 1, 56-64.

[6] Ouyang, L., Wang, F., Tang, J., Yu, L., Zhang, R. (2013) Effects of biochar amendment on soil aggregates and hydraulic properties. Journal of Soil Science and Plant Nutrition. 13, 991-1002.

[7] Amin, F.R., Huang, Y., He, Y.F., Zhang, R.H., Liu, G.Q., Chen, C. (2016) Biochar applications and modern techniques for characterization. Clean Technologies and Environmental Policy. 18, 1457-1473.

[8] Smernik, R.J. (2009) Biochar and sorption of organic compounds. Earthscan: United Kingdom, London. 289-296.

[9] Widowati, W., Asnah, A. (2014) Biochar can enhance potassium fertilization efficiency and economic feasibility of maize cultivation. Journal of Agricultural Science. 6, 24-32.

[10] Farrell, M., Kuhn, T.K., Macdonald, L.M., Maddern, T.M., Murphy, D.V., Hall, P.A., Singh, B.P., Baumann, K., Krull, E.S., Baldock, J.A. (2013) Microbial utilization of biochar-derived carbon. Science of the Total Environment. 465, 288-297.

[11] Milla, O.V., Rivera, E.B., Huang, W.J., Chien, C.C., Wang, Y.M. (2013) Agronomic properties and characterization of rice husk and wood biochars and their effect on the growth of water spinach in a field test. Journal of Soil Science and Plant Nutrition. 13, 251-266.

[12] Karhu, K., Mattilab, T., Bergströma, I., Reginac, K. (2011) Biochar addition to agricultural soil increased CH_4 uptake and water holding capacity-Results from a short-term pilot field study. Agriculture Ecosystems and Environment. 140, 309-313.

[13] Zhang, A.F., Liu, Y.M., Pan, G.X., Hussain, Q., Li, L.Q., Zheng, J.W., Zhang, X.H. (2012) Effect of biochar amendment on maize yield and greenhouse gas emissions from a soil organic carbon poor calcareous loamy soil from Central China Plain. Plant and Soil. 351, 263-275.

[14] Gaunt, J.L., Lehmann, J. (2008) Energy balance and emissions associated with biochar sequestration and pyrolysis bioenergy production. Environmental Science and Technology. 42, 4152-4158.

[15] Novak, J.M., Busscher, W.J., Watts, D.W., Amonette, J.E., Ippolito, J.A., Lima, I.M., Gaskin, J., Das, K.C., Steiner, C., Ahmedna, M., Rehrah, D., Schomberg, H. (2012) Biochars impact on soil-moisture storage in an ultisol and two aridisols. Soil Science. 177, 310-320.

[16] Deenik, J.L., Cooney, M.J. (2016) The potential benefits and limitations of corn cob and sewage sludge biochars in an infertile Oxisol. Sustainability. 8, 131.

[17] Higa, T., Parr, J.F. (1994) Beneficial and effective micro-organisms for a sustainable agriculture and environment. International Nature Farming Research Centre, Japan.
[18] Higa, T. (1998) Effective micro-organisms for sustainable agriculture and healthy environment. Jan van Arkel, Utrecht, the Netherlands. 191. (In Dutch).
[19] Hou, M.M., Shao, X.H., Chen, J.N., Zhai, Y.M., Zhao, T.C., Wang, G. (2016) Optimization of EM water-retention agent application in flue-cured tobacco. Chinese Journal of Eco-Agriculture. 24, 628-636.
[20] Javaid, A., Bajwa, R. (2011) Field evaluation of effective microorganisms (EM) application for growth, nodulation, and nutrition of mung bean. Turkish Journal of Agriculture and Forestry. 35, 443-452.
[21] Talaat, N.B., Ghoniem, A.E., Abdelhamid, M.T., Shawky, B.T. (2015) Effective microorganisms improve growth performance, alter nutrient acquisition and induce compatible solutes accumulation in common bean (Phaseolus vulgaris L.) plants subjected to salinity stress. Plant Growth Regulation. 75, 281-295.
[22] Hu, C., Qi, Y.C. (2013) Long-term effective microorganisms application promote growth and increase yields and nutrition of wheat in China. European Journal of Agronomy. 46, 63-67.
[23] Javaid, A. (2007) Foliar application of effective microorganisms on pea as an alternative fertilizer. Agronomy for Sustainable Development. 26, 257-262.
[24] Yan, P.S., Xu, H.L. (2002) Influence of EM Bokashi on nodulation, physiological characters and yield of peanut in nature farming fields. Journal of Sustainable Agriculture. 19, 105-112.
[25] Roberti, R., Bergonzoni, F., Finestrelli, A., Leonardi, P. (2015) Biocontrol of Rhizoctonia solani disease and biostimulant effect by microbial products on bean plants. Micologia Italiana. 44, 49-61.
[26] Anderson, C.R., Condron, L.M., Clough, T.J., Fiers, M., Stewarta, A., Hil, R.A., Sherlock, R.R. (2011) Biochar induced soil microbial community change: Implications for biogeochemical cycling of carbon, nitrogen and phosphorus. Pedobiologia-International Journal of Soil Biology. 54, 309-320.
[27] Cao, G.L., Zhang, X.Y., Wang, Y.Q., Zheng, F.C. (2007) Estimation of open incineration emission of farmland straw in China. Chinese Science Bulletin. 52, 1826-1831.
[28] Gao, L., Wang, R., Shen, G.M., Zhang, J.X., Meng, G.X., Zhang, J.G. (2017) Effects of biochar on nutrients and the microbial community structure of tobacco-planting soils. Journal of Soil Science and Plant Nutrition. 17, 884-896.
[29] Khaliq, A., Abbasi, M.K., Hussain, T. (2006) Effect of integrated use of organic and inorganic nutrient sources with effective microorganisms (EM) on seed cotton yield in Pakistan. Bioresource Technology. 97, 967-972.
[30] Shin, K., van Diepen, G., Blok, W., van Bruggen, A.H.C. (2017) Variability of effective micro-organisms (EM) in bokashi and soil and effects on soil-borne plant pathogens. Crop Protection. 99, 168-176.
[31] Hou, M.M., Shao, X.H., Chen, J.N., Wang, Y.F., Yuan, Y.B., Ding, F.Z., Wang, X. (2013) A simple method to estimate tobacco LAI and soil evaporation. Journal of Food, Agriculture and Environment. 11, 1216-1220.
[32] Yang, Q.Y., Qiao, J.F. (2009) The application of Li-6400 portable photosynthesis system in rice and analysis of common problems. Research and Exploration in Laboratory. 28, 52-55.
[33] Chen, F.Q., Shao, H.F., Jia, G.T., Xu, Z.C., Huang, W.X., Fan, Y.K., Du, X.Z., Zhang, M.M., Zhao, R.R. (2016) Effect of water retaining agent on photosynthetic characteristics and Chlorophyll Fluorescence Parameters of tobacco. Journal of Agricultural Science and Technology. 18, 157-164.
[34] Wang, H.H., Ren, T.B., Zhang, Z.H., Yuan, Y., Wang, B., Kuang, G., Liu, D.Y., Liu, G.S. (2017) Effects of biochar on root development and leaf photosynthetic characteristics of flue-cured tobacco in the vigorous growing period. Journal of Soil and Water Conservation. 31, 287-292.
[35] Liu, X.L., Zhang, C., Deng, M., Yao, J., Wang, X.B., Cheng, R.T., Guo, T. (2017) Effects of biochar and AM fungi on root morphology, physiological characteristics and chemical constituents of flue-cured tobacco. Tobacco Science and Technology. 50, 30-36.
[36] Zhang, C., Zhao, H.C., Guo, T., Liu, X.L. (2015) Influences of biochar application rate on tobacco seedling growth. Tobacco Science and Technology. 48, 9-12.
[37] Abbott, L.K., Robson, A.D. (1991) Factors influencing the occurrence of vesicular mycorrhizas. Agriculture Ecosystems and Environment. 35, 121-150.
[38] Ahmed, A., Kurian, J., Raghavan, V. (2016) Biochar influences on agricultural soils, crop production, and the environment: A review. Environmental Reviews. 24, 495-502.
[39] Braida, W.J., Pignatello, J.J., Lu, Y.F., Ravikovitch, J.J., Neimark, A.V., Xing, B.S. (2003) Sorption hysteresis of benzene in charcoal particles. Environmental Science and Technology. 37, 409-417.

[40] Oguntunde, P.G., Abiodun, B.J., Ajayi, A.E., Glesen, N.D. (2008) Effects of charcoal production on soil physical properties in Ghana. Journal of Plant Nutrition and Soil Science. 171, 591-596.
[41] Hussain, T., Jilani, G., Javaid, T., Tahir, S.H. (1995) Nature farming with EM technology for sustainable crops production in Pakistan. In: Proceedings of the fourth international conference on Kyusei nature farming. France. 71-78.

Received: **14.9.2018**
Accepted: **28.03.2019**

CORRESPONDING AUTHOR

Xiaohou Shao
Key Laboratory of Efficient Irrigation-Drainage and Agricultural Soil-Water Environment
Southern China (Hohai University)
Ministry of Education
Nanjing 210098 – China

e-mail: shaoxiaohou@163.com

© by PSP Volume 28 – No. 5/2019 pages 4185-4192 Fresenius Environmental Bulletin

RESEARCH AND APPLICATION OF DUST POLLUTION RULE OF MATERIAL PIT AND FOG REDUCTION TECHNOLOGY OF FOGGER

Shaocheng Ge[1,2], Zhihui Huang[1,2,*], Deji Jing[1,2]

[1]College of Safety Science and Engineering, Liaoning Technical University, Fuxin 123000 China
[2]Key Laboratory of Mine Thermodynamic disasters and Control of Ministry of Education, Fuxin 123000 China

ABSTRACT

In order to effectively control the dust pollution caused by the receiving pit in the receiving process, this paper takes the receiving pit of the Harwusu open-pit coal preparation plant as the research object, and through the field test, observation analysis and three-dimensional numerical simulation, the dust pollution of the receiving pit is obtained. law. According to the law of dust pollution, a dust removal scheme for setting the fogger at the edge of the receiving pit is proposed. The computational fluid dynamics simulation software was used to simulate the dust pollution changes at different times during the truck unloading process, and the optimal working parameters of the aerosolizer were determined. Through the three-dimensional numerical simulation of the dust concentration distribution of the receiving pit and the field application test of the Harwusu open-pit coal mine, the dust-reducing effect of the fogger on the dust pollution of the receiving pit is analyzed and verified. The results show that when the remote fogger is installed in the pit, the dust reduction efficiency is up to 93% when the inlet wind speed is 30 m/s. The dust removal scheme provides theoretical and practical basis for the dust control of the pit of the coal handling system.

KEYWORDS:
Receiving pit, fogger, atomization mechanism, pollution law, numerical simulation

INTRODUCTION

With the development of social economy, people gradually realize the importance of high-quality work environment, but the coal handling system of coal preparation plant inevitably produces a large amount of dust [1-4], which seriously endangers the health of workers and damages the surrounding environment. Therefore, research on coal dust control in coal handling systems has become a hot research direction. At present, the research on the prevention and control of dust in the receiving pit is not enough. The research results on dust control are very limited [5-7]. This paper takes the Harwusu Open-pit Coal Mine of Shenhua Zhungeer Co., Ltd. as the research object. The field data test and observation of the pit were carried out to study the law of coal dust emission in the pit. The remote fogger dust suppression scheme was proposed. Combined with numerical simulation and field test application, the feasibility of the scheme was verified. The research in this paper is other coal mines. Theoretical and practical data are provided for dust control of the pit in the coal handling system.

MATERIALS AND METHODS

Survey of the pit and determination of the basic characteristics of dust. The Harwusu Open-pit Coal Mine Coal Preparation Plant is responsible for the processing and washing of raw coal and product coal. The installation and design of the material receiving pit dust removal equipment are not perfect, which not only threatens the safety production, but also seriously endangers the health of the staff and management personnel. In this paper, through the determination of the mass concentration and dispersion of the dust generated during the operation of the pit, the distribution law of the dust concentration of the material receiving pit is grasped, the movement law of the dust particles is understood, and the relevant parameters of the theoretical boundary conditions are collected.

The dust concentration measurement results in Table 1 show that the dust concentration range near the receiving pit is concentrated at 610-690 mg/m^3, which is 152-172 times the safety standard, and the respiratory dust concentration is 32 mg/m^3 to 36.5 mg/m^3. The work site allows 9.6 to 10.8 times the concentration standard, both of which far exceed national standards.

Mathematical model of dust migration. Mathematical model. When the material of the pit is unloaded, the dust movement is a typical gas-solid two-phase flow composed of gas and particles. During the material drop process, the vehicle

enters the air carrier and diffuses the dust. The process of micro-fog in the air from broken atomization to dust capture conforms to the typical gas-liquid-solid multi-phase flow model. Therefore, the multi-phase flow model is used to provide a basis for the selection of the material dedusting equipment and the determination of the control scheme. The gas phase momentum equation follows the N-S equation [8-9] as follows.

$$m_{\mathrm{pi}}\frac{\mathrm{d}u_{\mathrm{pi}}}{\mathrm{d}t}=F_{\mathrm{D}}(u_{\mathrm{g}}-u_{\mathrm{pi}})+F_{\mathrm{A}}+F_{\mathrm{B}} \quad (1)$$

$$F_{\mathrm{D}}=m_{\mathrm{pi}}\frac{18\mu}{\rho_{\mathrm{pi}}d_{\mathrm{pi}}^{2}}\frac{C_{\mathrm{D}}Re}{24} \quad (2)$$

$$Re=\frac{\rho_{\mathrm{g}}d_{\mathrm{pi}}\left|u_{\mathrm{g}}-u_{\mathrm{pi}}\right|}{\mu}; \quad (3)$$

$$F_{\mathrm{A}}=\rho_{\mathrm{g}}gV_{\mathrm{pi}}\ ; \quad (4)$$

$$F_{\mathrm{B}}=\rho_{\mathrm{pi}}gV_{\mathrm{pi}}\ , \quad (5)$$

Where mpi is the mass of a single particle, kg; upi is the particle phase velocity, m•s^{-1}; FD is the specific drag force, kg•s^{-1}; ug is the air velocity, m•s^{-1}; FA is buoyancy, Kg•m•s^{-2}; FB is gravity, kg•m•s^{-2}; μ is aerodynamic viscosity, kg•m^{-1}•s^{-1}; ρpi is particle phase density, kg•m^{-3}; dpi is Particle phase diameter, m; CD is the drag coefficient [10-13]; Re is the particle Reynolds number; ρg is the air density, kg•m^{-3}; Vpi is the single particle volume, m^{3}.

The pneumatic atomization model based on the TAB breaking principle [14] is

$$C_{\mathrm{F}}\frac{\rho_{\mathrm{g}}(u_{\mathrm{g}}-u_{\mathrm{pl}})^{2}}{\rho_{\mathrm{pl}}r}\frac{k}{m_{\mathrm{pl}}}=C_{\mathrm{K}}\frac{\sigma}{\rho_{\mathrm{pl}}r^{3}}\frac{d_{\mathrm{pl}}}{m_{\mathrm{pl}}}, \quad (6)$$

In the formula, CF and Ck are dimensionless numbers, and CF=1/3 and Ck=8 are obtained through experiments; ρpl is the droplet density, kg•m^{-3}; k is the turbulent flow energy, kg•m•s^{-2};

r is the droplet radius, m; mpl is the mass of a single droplet, kg; σ is the surface tension of the liquid, kg•m^{-1}•s^{-2}; dpl is the diameter of the droplet, m.

The Stokes number collision model is

$$S_{\mathrm{tk}}=\frac{\rho_{\mathrm{pi}}d_{\mathrm{pi}}^{2}}{18\rho_{\mathrm{g}}\mu(\nu/\varepsilon)^{1/2}}=\frac{\rho_{\mathrm{pi}}}{18\rho_{\mathrm{g}}}\left(\frac{d_{\mathrm{pi}}}{(\nu^{3}/\varepsilon)^{1/4}}\right)^{2} \quad (7)$$

$$\eta=\left(\frac{S_{\mathrm{tk}}}{S_{\mathrm{tk}}+a}\right)^{b}, \quad (8)$$

Where Stk is Stokes number, is dimensionless; ν is air motion viscosity, m^{-2}•s^{-1}; ε is turbulent dissipation rate, dimensionless; η is collision efficiency; a, b is the parameter related to Reynolds number When Re<1, a=0.65, b=3.7.

TABLE 1
Dust concentration of Haerwusu coal preparation the material pit

No.	Test location	Dust concentration (mg/m^{3})	Respiratory dust concentration/(mg/m^{3})	testing time
1	Receiving pit	612	132.1	10th
2	Receiving pit	690	156.4	11th
3	Receiving pit	655	133.3	12th

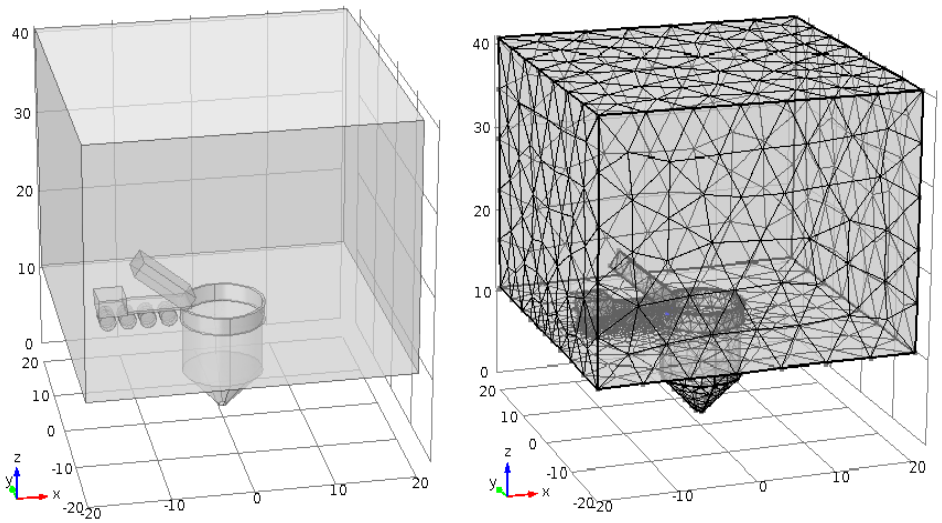

FIGURE 1
Unloading pit 3d model

Geometric model. According to the actual situation of the working space of the receiving pit, the model is built, and a working area of length × width × height = 40 m × 40 m × 30 m is constructed by the pre-processing software to simplify the receiving pit into a conical shape, and the truck is located in the conical shape. On the left side of the pit, the geometric model is shown in Figure 1. The geometric model is hexahedral meshed by Map. The Interval size is 0.6, and a total of 1424665 grid cells are obtained. The mesh model is shown in Figure 1.

FIGURE 2
Dust float during discharging

Dust pollution mechanism and escape law of material receiving pit. Pollution status of material pit in Anjialing Coal Preparation Plant. Dust pollution in the unloading process is an environmental pollution problem that cannot be avoided and must be taken seriously. The whole process of unloading goods by mining trucks is the main cause of pollution. During the process of detachment of the material from the truck compartment, the dust-containing material generates a large amount of induced airflow under the friction of the air. The material is mixed with a large amount of powder and the dust generated by the collision of the materials during the unloading process, and flies freely under the strong induced airflow, and quickly rushes into the free space; the materials squeeze each other during the falling process to further accelerate the dust flying, receiving The dust at the mouth is seriously polluted. Due to the height difference between the truck and the receiving pit, the material carrying high kinetic energy has a great impact force on the receiving pit, and the strong induced gas induces secondary dust. Based on these factors, the dust is very serious during the discharging process, and the dust is very dusty. The spread is severe and the pollution range is large. That is, it seriously affects the normal work of workers and poses a great threat to the health of workers and nearby residents. It is shown in Figure 2.

According to the above reasons, the dust pollution of the material receiving pit is quite serious, and the dust concentration reaches 650 mg/m^3 or more.

Numerical Simulation of Dust Emission Law in Feeding Pit Operation. In order to study the law of dust dissipation during the unloading process, based on the theory of particle gas-solid two-phase flow, according to the actual situation of the site, the starting time of unloading is taken as the starting point, and the dust emission law and pollution mechanism of the material receiving pit are simulated dynamically. 3 is the dynamic change of the dust concentration of the receiving pit in the windless state at each moment.

It can be seen from Fig. 3 that the dust escapes during the unloading process, the mining truck is at the moment of unloading (t=1 s), the dust concentration reaches 650 mg/m^3, and the pollution height is relative to the plane of the mining truck. Above m, at t=30, due to the decrease of dust of large particles, the highest dust concentration drops to 495 mg/m^3, the average concentration reaches 350 mg/m^3 or more, and at t=90 s, the vertical pollution height reaches 10m or more, dust The concentration is 450 mg/m^3, the average concentration is 317 mg/m^3. At t=150 s, the vertical pollution height is above 21 m, the highest dust concentration is 279 mg/m^3, and the average concentration is 203 mg/m^3. The natural sedimentation rate is slow at this stage, and no effective dust reduction is taken. In the case of measures, the dust stays in the air for a long time and spreads to a wide range.

Determination and field application of fog control dust control scheme. Remote fogger proposal and installation plan. The original material receiving pit is equipped with a simple spray pipe system and a dust suppression net. The high-pressure spray realizes watering and dust removal. The original system has the following problems: 1 The fog kinetic energy is small, and the dust cannot be effectively captured. 2 The atomization effect is poor, resulting in waste of water source. The decline of coal quality, 3 effective range can not cover the entire dust source and other reasons, can not effectively control dust pollution. Based on the above analysis of dust pollution and the shortage of the original spray system [15-16], combined with the law of dust dissipation, a remote sprayer with a swing function was proposed to control the dust pollution on the site, and the pendulum was set according to the pollution of the site dust. The head angle increases the atomization effect while in-

creasing the range of water mist, and forms a "mist pool" in the entire receiving pit to firmly control the dust particles in the receiving pit so that it cannot escape at random. It meets the following two advantages:

1) Large coverage, long range, small droplet size and fast speed, can quickly capture dust in the air, form a humid mist pool in the contaminated area to prevent dust from spreading;

2) High operating efficiency, fast atomization speed, strong penetrating power against dust and fog adhesion, which can effectively save water and reduce environmental pollution;

The dust control scheme of the remote sprayer is shown in Figure 4 in the implementation scheme of the receiving pit in the coal preparation plant of Harwusu Open-pit Coal Mine.

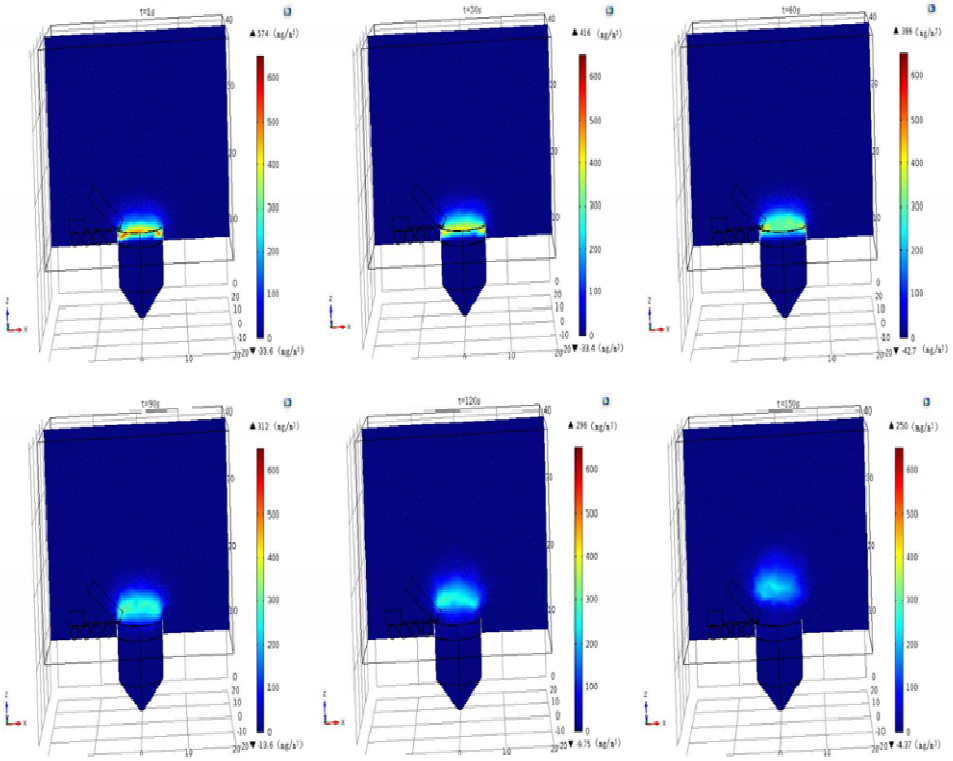

FIGURE 3
Dust migration law of unloading pit

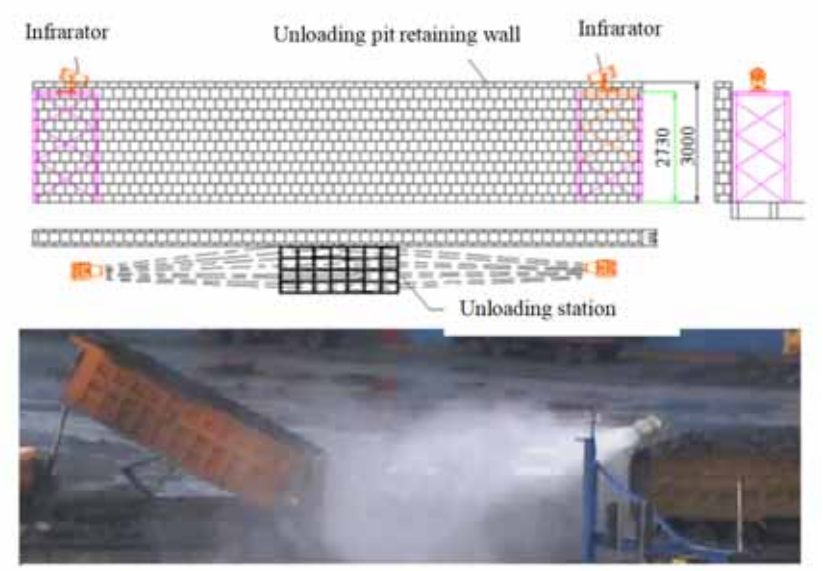

FIGURE 4
Dust control scheme

The coverage of the fogger and the particle size of the water mist are the key factors affecting the dust control effect.

Effective range. The effective range in the atomization field is an important parameter to evaluate the atomization characteristics. It is found that during the spray of the sprayer, the jet at the nozzle exit does not instantaneously diffuse, but keeps the flow state in the nozzle continuing along the axis. After a certain distance, the liquid film gradually breaks into droplets, and Figure 5 shows the relationship between the exit wind speed of the sprayer and the effective range.

It can be seen from Fig. 5 that the overall variation trend of the effective range of the aerosolizer is gradually increased as the exit wind speed increases. When the outlet wind speed is less than 30 m/s, the effective range increases faster, and when the exit is faster. When the wind speed is greater than 30 m/s, the effective range increase is not obvious, and the effective range gradually becomes constant.

Atomization particle size. The average diameter of the Souter's average diameter of the sprayer is plotted as shown in Fig. 6. As can be seen from Fig. 6, the average diameter of the Soder of the sprayer is inversely proportional to the exit wind speed, and the average diameter of the Souter is the largest. The diameter of the droplet corresponding to the value was reduced from 188.2 μm to 59.3 μm. This is because as the wind speed of the outlet increases, the aerodynamic force of the droplets with larger particle size is relatively larger, and it is easier to break into fine droplets during the migration process. However, the outlet wind speed is larger. The higher the load on the fan is, the higher the energy consumption is.

In summary, this paper selects a wind speed of 30 m/s. At this wind speed, the spray of the sprayer is farther away, and the coverage area is extremely large. It has complete inhibition ability for dust below 200 μm, and the surface moisture content of the material increases by only 0.3%.

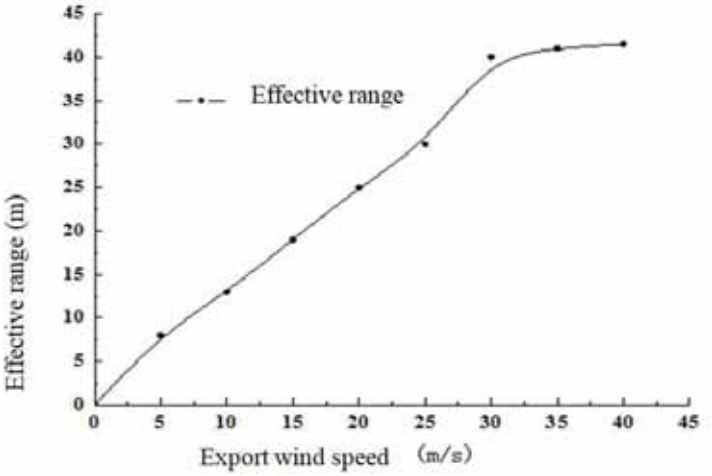

FIGURE 5
Exit velocity and the change of the effective range

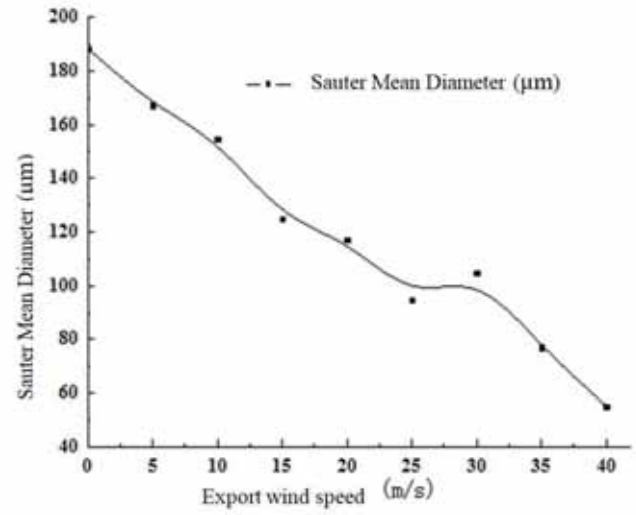

FIGURE 6
Export wind speed and the change of the average diameter

Numerical simulation of atomization effect. The fogger has a swinging function. The spray angle of the sprayer varies at different times. In order to more clearly describe the spray of the sprayer in the swing state, this paper performs numerical simulation according to the actual situation. The following Figure shows the fog sprayer has different atomization effects at different angles of 0.1s, 0.4s, 0.8s, 1.2s, and 1.6s. In the figure, it can be found that the fog sprays have different distributions at different swing angles. The best effect can be achieved by changing the angle of the sprayer nozzle. The angle of the nose of the sprayer is between -40° and 40° of the central axis, as shown in Figure 7.

Injector dust control program effect test Numerical simulation of dust suppression by fogger. After the remote ejector system was installed in the receiving pit, the dynamic numerical simulation of the unloading period of the mining truck was carried out (as shown in Fig. 8). From the time of the unloading t=1s to the t=180s, the area near the receiving pit was in the fog. The diffusion process of dust under the influence of the chemical field is shown in the figure. At t=1s, it is the dust concentration map of the pit area at the initial moment. Due to the large drop, the coal material is dry and the falling speed is fast, causing the coal dust to fly seriously and receiving. The concentration of the pit discharge is greater than 600 mg/m^3; the atomization field formed by the atomizer has completely covered the section of the receiving pit, and the dust is controlled by a high momentum water mist in a certain area, because the large particle size dust is relatively fast, and small The particle size dust and fine dust particles always float on the receiving pit, and they continuously collide with the droplet particles with high kinetic energy, coagulate and kinetics, and the dust particles captured by the droplet particles wet the dust due to its own density. Increase, gradually decrease to achieve the effect of dust reduction, and finally make the dust of the receiving pit completely disappear.

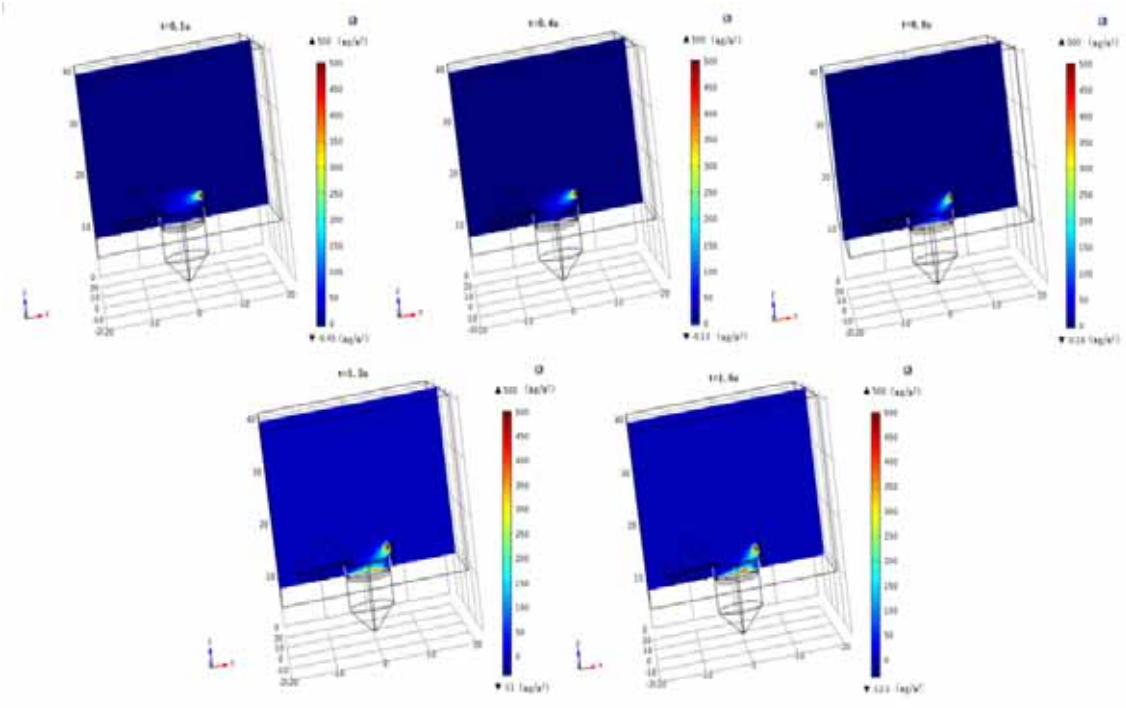

FIGURE 7
Dust migration law of unloading pit

TABLE 3
Dust concentration by field test

Distance to the receiving pit (m)	Before governance (mg/m^3)	After governance (mg/m^3)	Dust reduction rate (%)
	650.4	40.2	93.8
5	524.4	32.6	93.8
7.5	419.9	25.4	94.0
10	312.2	14.1	95.5
12.5	202.0	9.7	95.2

15	96.4	4.5	95.3

TABLE 4
Dust concentration by simulation

Distance to the receiving pit (m)	Before governance (mg/m^3)	After governance (mg/m^3)	Dust reduction rate (%)
0	643.9	41.2	93.6
5	518.2	30.5	94.1
7.5	413.1	26.1	93.7
10	333.8	18.2	94.5
12.5	202.0	9.5	95.3
15	91.1	3.9	95.7

Field experiment effect of material pit dedusting. Dust concentration measuring points were set at six points from the receiving pits of 0m, 5m, 7.5m, 10m, 12.5m and 15m. The test was averaged three times and recorded in the table below. The dust concentration was averaged after the pit area was treated. For the 32mg/m3, the dust concentration before treatment was 640mg/m3, and the total dust concentration was reduced by 93%. The comparison and comparison of the dust removal project after construction confirmed the rationality and effectiveness of the fogger dust removal scheme.

CONCLUSION

Through the combination of theoretical analysis, numerical simulation and field application, this paper systematically studies the dust migration law and control technology of the material receiving pit. The main research results are as follows:

(1) Using the computational fluid dynamics software to carry out numerical simulation study on the dust diffusion during the unloading process of mining trucks, and obtain the migration law of dust particles at different times. Under the windless state, the dust concentration of the receiving pit reaches 620 mg/ m^3.

(2) Aiming at the dust pollution problem of the material receiving pit, a remote sprayer treatment technology is proposed. According to the basic equations of multiphase flow, jet breaking theory and atomization dust reduction theory, the atomization process of the atomizer is simulated and obtained. The effective range of the sprayer and the quantitative relationship between the average dust particle size of the Souter and the exit wind speed were determined, and the wind speed of 30m/s was finally determined.

(3) The remote fogger dust suppression technology was applied at the pit site of the coal preparation plant of Harwusu Open-pit Mine, and the adjustment test was carried out according to the research results. The average dustfall rate of each measuring point of the receiving pit reached over 93%, and a good dust removal effect was obtained, which proved the practicability of the remote fogger dust suppression technology.

REFERENCES

[1] Wang, X.H., Luo, Q., Qin, L., Wang, H.B., Yang, F.M. (2018) Study on the characteristics of water - soluble ion pollution in PM2.5 in fuling district. Fresen Environ Bull. 27, 1138-1144.

[2] Ni, P.Y., Bai, L., Wang, X.L., Jin, H.C., Xi, G.N. (2018) Effect of window ventilation and air cleaner purification on indoor PM2.5 emission and air exchange rate under haze weather. Fresen Environ Bull. 27, 210-214.

[3] Huang, L.K., Wang, G.Z., Mu, D.Y., Wang, J.Y., Wang, W., Guan, H.A. (2017) Monthly variations and chemical compositions of PM1 and PM2.5 during the heating period in Harbin, China. Fresen Environ Bull. 26, 1998-2007.

[4] Ge, S.C., Ge, F., Zhang, Z.W. (2015) Analysis of sealed negative-pressure bag-type dust removing mechanism at a material-receiving point. Journal of Liaoning Technical University (Natural Science). 34, 344-347.

[5] Ge, S.C., Fan, W.T., Zhang, Z.W. (2015) Dust pollution and air-driving shooting-fog dust control of coal conveyer belt tailpiece. Journal of Liaoning Technical University (Natural Science). 34, 459-463.

[6] Yu, H., Huang, Y., Ning, J., Zhu, B., Cheng, Y. (2014) Effect of cation exchange capacity of soil on stabilized soil strength. Soils and Foundations. 54, 1236-1240.

[7] Guan, J. (2010) Optimal choice of the technical parameter of the bag-type dust collector system in mu gua-jie coal preparation plant. Fuxin: Graduate College of Liaoning Engineering Technology University.

[8] Xu, F., Hu, B., Dou, Y., Song, Z., Liu, X. (2018) Prehistoric heavy metal pollution on the continental shelf off Hainan Island, South China Sea: From natural to anthropogenic impacts around 4.0 kyr BP. Holocene. 28, 455-463.

[9] Yang, S.L. (2001) Numerical simulation of 3-Dimensional dust distribution on long wall coal faces. China Safety Science Journal. 4, 61-64.

[10] Jing, D.J. (2013) Study on theory of dust control based on gas-sol-id two-phase flow and its applications in coal preparation plant. Fuxin:

Doctor Dissertation of Liaoning Engineering Technology University.
[11] Zhai, L., Li, S., Zou, B., Sang, H., Fang, X. (2018) An improved geographically weighted regression model for PM2.5 concentration estimation in large areas. Atmospheric Environment. 181, 145-154.
[12] Che, D.F., Li, H.X. (2007) Multiphase Flow and its application. Xi'an: Xi'an Jiaotong University Press.
[13] Yuan, Z.L., Zhu, L.P., Geng, F. (2013) Numerical Analysis of the Gas-Solid Two-Phase. Najing: Southeast University Press.
[14] Chen, X., Ge, S.C., Zhang, Z.W. (2014) Numerical simulation and analysis of multi-ozzle interference base on Fluent. Chinese Journal of Environmental Engineering. 8, 2503-2508.
[15] Ge, S.C., Jing, D.J., Huang, Y.P. (2012) Numerical simulation determination of the production mechanism and technical parameters of high-pressure micro-fog system. Journal of Technical University (Natural Science). 31, 17-20.
[16] Jing, D.J., Ge, S.C., Liu, J. (2012) Study on control technology of dust at coal drop tower based on Eulerian-Eulerian Model. China Safety Science Journal. 22, 26-132.

Received: **24.09.2018**
Accepted: **28.01.2019**

CORRESPONDING AUTHOR

Zhihui Huang
College of Safety Science and Engineering,
Liaoning Technical University,
Fuxin 123000 – China

e-mail: 1114164704@qq.com

© by PSP Volume 28 – No. 5/2019 pages 4193-4198 Fresenius Environmental Bulletin

MUSSEL-INSPIRED MODIFIED NATURAL SPONGE FOR OIL–WATER SEPARATION

Heng Chang[1], Rongxin Su[1,2,*], Renliang Huang[3], Wei Qi[1,2], Zhimin He[1]

[1]State Key Laboratory of Chemical Engineering, Tianjin Key Laboratory of Membrane Science and Desalination Technology, School of Chemical Engineering and Technology, Tianjin University, Tianjin 300350, China
[2]Collaborative Innovation Center of Chemical Science and Engineering (Tianjin), Tianjin 300072, China
[3]School of Environmental Science and Engineering, Tianjin University, Tianjin 300072, China

ABSTRACT

It has become a worldwide challenge to solve oil spill accidents and the increasing amount of industrial organic pollutants. Oil sorbents have become one of the effective approaches for oil spill cleaning. A superhydrophobic natural sponge exhibits excellent performance in oil absorption to remove oils from water was fabricated through mussel-inspired one-step copolymerization approach. Dopamine and n-dodecanethiol were copolymerized in an alkaline aqueous solution to modify the surface of the natural sponges. Then, the superhydrophobic sponge was fabricated and its static contact angel with water can achieve 163.24(±1.98) °. Because of the highly porous structure, the modified sponge exhibited desirable absorption capability of oils/organic solvents, suggesting promising sorbents for the removal of oils from water. After 30 absorption cycles of n-hexane, the superhydrophobic natural sponge still showed good absorption capability. All these merits make the modified natural sponge a competitive candidate for oil sorbent when compared to the conventional absorbents.

KEYWORDS:
Natural sponge, oil-water separation, dopamine, n-dodecanethiol

INTRODUCTION

With the development of industry, oil spills and organic solvent leakages frequently occur and have caused severe environmental and ecological damage [1]. These pollutions have great harm to marine environment and are difficult to be cleaned [2, 3]. And these pollutions also have great harm to organism and human. Once the oil leak into the water body, it starts to spread, cause injure to the organism itself, and eventually the toxicity of oils enriches and causes severe harm to human body through the food chain [4]. It is necessary to develop various methods for oil spill response because of their impacts on the ecosystem.

Nowadays, there are several strategies to treat oily wastewater including chemical methods, biological methods, and physical/mechanical methods [5, 6]. As a common chemical method, in-situ burning is cost efficiency but generates many particulates and carbon dioxide in the environment [7]. Chemical methods usually use dispersants sprayed on the oil spill to break it up into small droplets. For example, In the Deepwater Horizon oil spill, two dispersants (Corexit 9527 and Corexit 9500A) were extensively used to treat oily wastewater [8]. Biological methods include biodegradation of the spilled oil using microbes. Physical/mechanical methods can be categorized as air floatation [9], gravity separation [10], membrane separation [11] and sorbent materials treatment [12].

Nowadays, oil sorbents have become one of the more effective approaches for oil spill cleaning [12]. As a kind of cheap three-dimensional porous material with larger surface area, sponge is an ideal substrate for oil-water separation. Polyurethane (PU) [13], polydimethylsiloxane sponge (PDMS) [14]and melamine sponge (MS) [15] are all modified to developed superhydrophibic surface and used to treat oily wastewater. For example, Zhu et al. [16] fabricated robust superhydrophobic polyurethane sponge through a one-step solution immersion method, which involved the hydrolysis of reactive methyltrichlorosilane on the surface of the sponge in a hexane solution. Tran et al. [17] have developed a porous, robust 3-D eco-friendly PDMS–graphene sponge by embedding 2-D graphene sheets in an elastomeric PDMS structure and this modified sponge can be successfully used for efficient and cost-effective oil spill clean-ups and water purification for environmental applications. But all these sponges are synthetic and may cause environmental pollution. Natural sponge is a marine organism with three-dimensional porous structure and are ideal material for oil spill cleaning. To our best knowledge, no one has used natural sponge to treat with oils spill.

Recently, the mussel-inspired catechol-based chemistry prevails due to its sustainability, easy implementation, and bio-benignancy and super adhesion to any surfaces. Polydopamine (PDA),

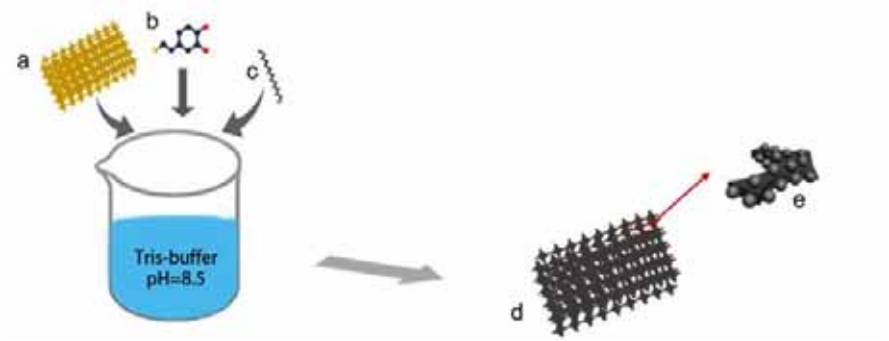

SCHEME 1
Illustration for the synthesis process of the superhydrophobic natural Sponge: a. the pristine natural sponge; b. DOPA; c. n-dodecanethiol; d. superhydrophobic (or the modified) sponge; e. enlarged region of the modified sponge.

one representative of catechol-based chemistry has been widely used to modify various surfaces and served as the versatile platform for a diversity of secondary reactions [18]. The surface coating with PDA is conventionally carried out in a mildly alkaline environment (dopamine/Tris-HCl buffer aqueous solution) in the presence of oxygen under room temperature. As a result, a smooth PDA layer is homogeneously covered on the target surfaces and secondary reactions can happen on these surfaces.

Herein a superhydrophobic natural sponge exhibits excellent performance in oil absorption was developed through mussel-inspired one-step copolymerization approach (Scheme 1). The superhydrophobic sponge was fabricated and its static contact angel with water can achieve 164.2°. The modified sponge exhibited desirable absorption capability of oils/organic solvents and has good recyclability. All these merits make the sponge a competitive candidate when compared to the conventional absorbents.

MATERIALS AND METHODS

Materials. Natural sponge was obtained from local supermarket (China). Dopamine hydrochloride and n-dodecanethiol were purchased from Sigma-Aldrich Co. Ltd. Tris (hydroxymethyl) aminomethane, anhydrous ethanol and other reagents were of analytical grade and used as received without further purification. The oils and organic reagents were used as commercially received. Ultrapure water was used throughout all experiments.

Preparation of Superhydrophobic natural sponge. Initially, a piece natural sponge (2cm×2cm×0.5cm) was washed ultrasonically with ultrapure water and ethanol in turn for three times to remove surface stains and residue. Then the sponge was immersed into 120mL mixture of dopamine solution (4 mg/mL, pH =8.5) and anhydrous ethanol (2:1/v:v). After added n-dodecanethiol (9.88mmol/L) into the mixture, the natural sponge was modified with dodecanethiol at room temperature for 12 hours via dip-coating. The modified sponge was washed with ultrapure water and ethanol in turn for three times and kept in an oven at 60℃ for 24h. Then the superhydrophobic sponge was obtained.

Characterization. Scanning electron microscopy (SEM) images were obtained through a field-emission SEM (HITACHI, s-4800). The surface wettability of the sponge was measured by conducting the static contact angle measurement through a contact angle goniometer (JC2000C, Shanghai, China). More than five contact angles at different locations on one surface were averaged to obtain a reliable value.

Absorption of Oils/Organic Solvents by Using the Superhydrophobic Natural Sponge. Typically, a piece of superhydrophobic natural sponge was immersed to a kind of oils/organic solvents for 30 minutes until it was filled with the oils/organic solvents. Subsequently, the superhydrophobic natural sponge loaded with the oil/organic solvent was taken out for weight measurement. The weight of the super- hydrophobic natural sponge (one piece) before and after absorption was recorded for calculating the weight gain, as illustrated as eq (1).

$$\text{weight gain} = (M_{after} - M_{before}) / M_{before} \times 100\% \quad (1)$$

where M_{before} was the weight of the superhydrophobic natural sponge before adsorption (mg) and M_{after} was the weight was the weight of the superhydrophobic natural sponge after adsorption (mg).

The recyclability of Superhydrophobic Natural Sponge. N-hexane was selected to study the recyclability of the superhydrophobic natural sponge. The weight gain of the superhydrophobic natural sponges was measured and calculated by the method mentioned before. Then the sponge was squeezed and washed ultrasonically with ultrapure water and ethanol in turn for three times to remove n-hexane and dried at 65 °C. The weight gain of the

same sponge was measured and calculated for 30 times.

RESULTS AND DISCUSSION

The surface wettability of the sponge is demonstrated by using the water contact angle measurement. When the superhydrophobic sponge is immersed in water by an external force, it would instantaneously float on the water surface after the force is released. Besides, the presence of silver mirror-like reflection for the immersed superhydrophobic sponge (Figure 1a) should be ascribed to the existence of air layer trapped between the superhydrophobic sponge surfaces and water. Subsequently, as shown in Figure 1b and 1c, the water droplet is supported by the superhydrophobic sponge, which displays a water contact angle can reach to 163.24(±1.98) °, thus confirming the superhydrophobicity of the sponge. The water contact of the prime natural sponge is about 90°. After dropping water droplet on the sponge functionalized with only PDA nanoaggregates, the water contact angle is only ~40°, suggesting the crucial role of the n-dodecylthiol motifs.

The surface superhydrophobicity as demonstrated above may be as a result of the combination of the macroporous structure of the sponge, the micro/nanotextured structure of PDA nanoaggregates, and the hydrophobic chemical property of the n-dodecylthiol motifs on the sponge skeletons. Then, SEM is used for clarifying the morphological evolution of the sponge before and after functionalization with the PDA nanoaggregates and n-dodecylthiol motifs. As illustrated in Figure 2a, the sponge exhibited a three-dimensional hierarchical porous structure with pore size ranging from 20 to 200 μm. After coated with the PDA nanoaggregates with the n-dodecylthiol motifs, the interconnected porous structure of the resultant sponges is maintained (Figure 2b), indicating the simple functionalization process cannot influence the original structure of the pristine sponge. Furthermore, the micro/nanotextured structure of the coated PDA nanoaggregates on the sponge skeletons could be found under higher magnification by using SEM. Clearly, the surface of the skeletons for the pristine sponge is quite smooth (Figure 2c), which becomes rather rougher as a result of the existence of numerous nanoaggregates on the skeletons after the coating process (Figure 2d).

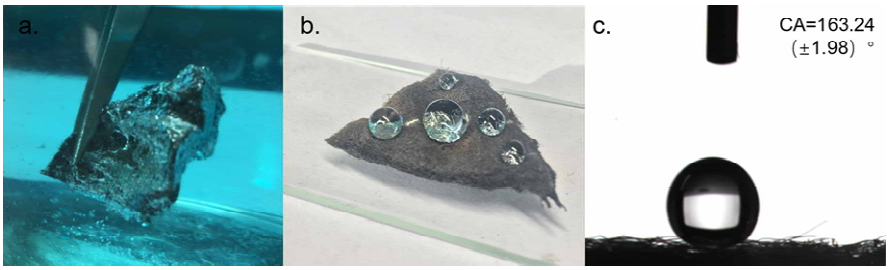

FIGURE 1
Photograph of a modified sponge under water (a), modified sponge with water drops on the surface (b) and static WCA measurements for the modified sponge (c)

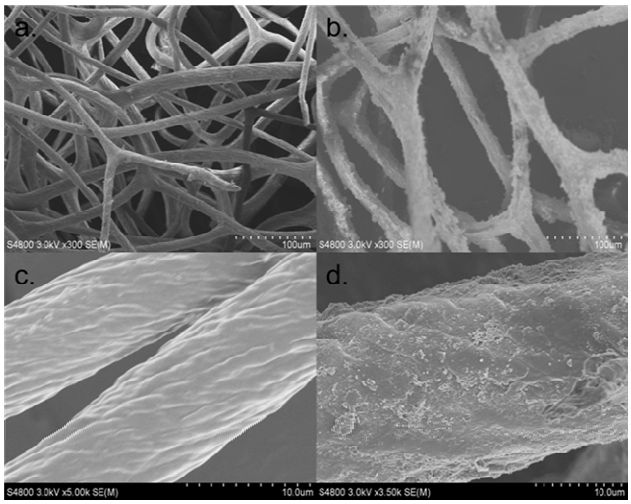

FIGURE 2
SEM images of unmodified sponge (a and c) and modified sponge (b and d)

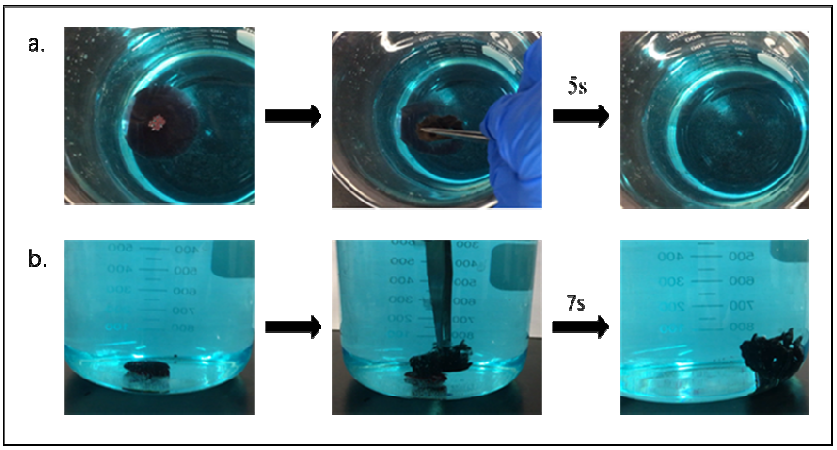

FIGURE 3
Photographs of the removal of n-dodecane (a) and carbon tetrachloride(b) by modified sponge

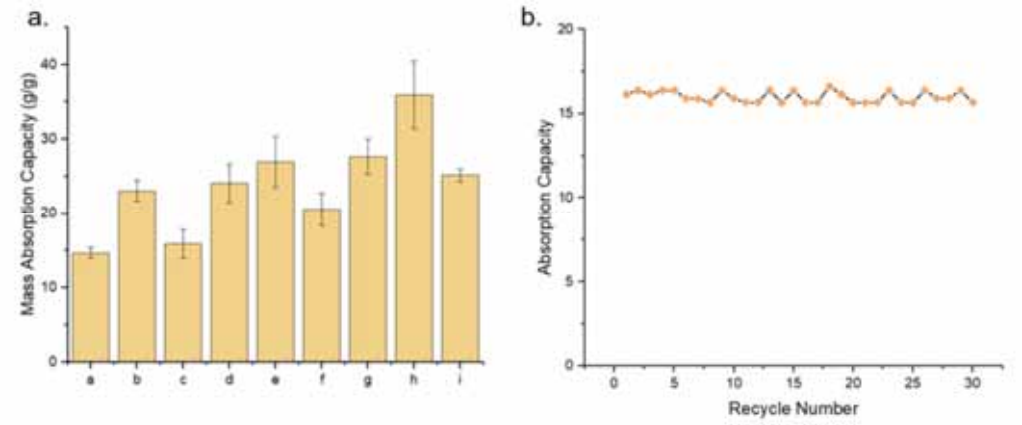

FIGURE 4
Absorption capacity of the modified sponge for various organic oils (a. n-hexane; b. methyl benzene; c. carbon tetrachloride; d. dimethazone; e. corn coil; f. n-dodecane; g. isopropyl alcohol; h. cyclohexanone; i. Petroleum ether) (a) and the recycled absorption of the modified sponge for n-hexane (b)

The high porosity, superhydrophobicity, and strong mechanical stability make the superhydrophobic sponge a promising candidate for the efficient removal of various oils/organic solvents. More specifically, organic/water separation and absorption capacities of the superhydrophobic sponge are measured to investigate the efficiency of the absorbents. In Figure 3a, when a piece of superhydrophobic sponge is forced to contact with a layer of the hexane (stained with oil red O) on the water surface, it would fully absorb the oil within 5s, Meanwhile, other organic solvent such as n-hexadecane stained with oil red O can also be quickly adsorbed by this superhydrophobic sponge. Similarly, when the superhydrophobic sponge is held to contact with chloroform under water, the chloroform droplet can be rapidly sucked up by the sponge (Figure 3b).

In typical absorption measurements, the superhydrophobic sponge is placed on the surface of various oils and organic solvents (Figure 4a), then left briefly for saturated absorption, and finally weighed instantaneously to avoid evaporation of oils/organic solvents. The superhydrophobic sponge exhibits the weight gains ranging from1517% to 3757% for the 9 kinds of oils/organic solvents. The changes in absorption capacity could be because of the difference in density of the oils/organic solvents. The recyclability of a sorbent is also proven to be an important role in oils/organic solvents clean up applications. In this study, n-hexane was used to test the recyclability of the superhydrophobic sponge. As is illustrated in Figure 4b, little changes in thirty absorption capability of the superhydrophobic sponges could be observed after absorption cycles. The excellent mechanical stabilities could confer the superhydrophobic sponge highly efficient recyclability, thus promoting a great potential of this material in removing oils/organic solvent.

CONCLUSIONS

In conclusion, a superhydrophobic natural sponge exhibits excellent performance in oil absorption and oil/water separation was fabricated through mussel-inspired one-step copolymerization approach. The modified sponge exhibited desirable

absorption capability of oils/organic solvents and perfect recyclability, suggesting a promising sorbent for the removal of oily pollutants from water.

ACKNOWLEDGEMENTS

This work was supported by the National Natural Science Foundation of China (grant No. 51473115), the Natural Science Foundation of Tianjin (grant No. 16JCZDJC37900) and Wuqing S&T Commission (WQKJ201726).

REFERENCES

[1] Farrington, J.W. (2013) Oil Pollution in the Marine Environment Inputs, Big Spills, Small Spills, and Dribbles. Environment. 55(6), 3-13.
[2] Can, S., Celik, F., Yilmaz, H., Bak, O.A. (2007) Oil spill simulation: A case study in the strait of Istanbul. Fresen. Environ. Bull. 16, 1517-1522.
[3] Zengel, S., Bernik, B.M., Rutherford, N., Nixon, Z., Michel, J. (2015) Heavily Oiled Salt Marsh following the Deepwater Horizon Oil Spill, Ecological Comparisons of Shoreline Cleanup Treatments and Recovery. PLoS One. 10(7), 27.
[4] Yu, L.H., Yang, H.F., Wang, Y.J., Jiang, W. (2017) Magnetically Enhanced Superhydrophobic Functionalized Polystyrene Foam for the High Efficient Cleaning of Oil Spillage. Powder Technol. 311, 257-264.
[5] Viraraghavan, T., Moazed, H. (2003) Removal of oil from water by bentonite. Fresen. Environ. Bull. 12, 1092-1097.
[6] Doshi, B., Sillanpaa, M., Kalliola, S. (2018) A review of bio-based materials for oil spill treatment. Water Res. 135, 262-277.
[7] Mullin, J.V. (2003) In situ burning of spilled oil at sea: Research and development needs. Spill Sci. Technol. Bull. 8(4), 399-400.
[8] Kujawinski, E.B., Soule, M.C.K., Valentine, D.L., Boysen, A.K., Longnecker, K., Redmond, M.C. (2011) Fate of Dispersants Associated with the Deepwater Horizon Oil Spill. Environ. Sci. Technol. 45(4), 1298-1306.
[9] Saththasivam, J., Loganathan, K., Sarp, S. (2016) An overview of oil-water separation using gas flotation systems. Chemosphere. 144, 671-680.
[10] Chen, L.Q., Wu, S.J., Lu, H.F., Huang, K., Zhao, L.J. (2015) Numerical Simulation and Structural Optimization of the Inclined Oil/ Water Separator. PLoS One. 10(4), 15.
[11] Padaki, M., Murali, R.S., Abdullah, M.S., Misdan, N., Moslehyani, A., Kassim, M.A., Hilal, N., Ismail, A.F. (2015) Membrane technology enhancement in oil-water separation. A review. Desalination. 357, 197-207.
[12] Cortez, J.S.A., Kharisov, B.I., Quezada, T.E.S., Garcia, T.C.H. (2017) Micro- and nanoporous materials capable of absorbing solvents and oils reversibly: the state of the art. Pet. Sci. 14(1), 84-104.
[13] Liu, Y., Ma, J.K., Wu, T., Wang, X.R., Huang, G.B., Liu, Y., Qiu, H.X., Li, Y., Wang, W., Gao, J.P. (2013) Cost-Effective Reduced Graphene Oxide-Coated Polyurethane Sponge As a Highly Efficient and Reusable Oil-Absorbent. ACS Appl. Mater. Interfaces. 5(20), 10018-10026.
[14] Choi, S.J., Kwon, T.H., Im, H., Moon, D.I., Baek, D.J., Seol, M.L., Duarte, J.P., Choi, Y.K. (2011) A Polydimethylsiloxane (PDMS) Sponge for the Selective Absorption of Oil from Water. ACS Appl. Mater. Interfaces. 3(12), 4552-4556.
[15] Wang, C.F., Huang, H.C., Chen, L.T. (2015) Protonated Melamine Sponge for Effective Oil/ Water Separation. Sci. Rep. 5, 14294.
[16] Zhu, Q., Chu, Y., Wang, Z., Chen, N., Lin, L., Liu, F., Pan, Q. (2013) Robust superhydrophobic polyurethane sponge as a highly reusable oil-absorption material. J. Mater. Chem. A. 1(17), 5386-5393.
[17] Tran, D.N.H., Kabiri, S., Sim, T.R., Losic, D. (2015) Selective adsorption of oil-water mixtures using polydimethylsiloxane (PDMS)-graphene sponges. Environ. Sci.-Wat. Res. Technol. 1(3), 298-305.
[18] Lee, H., Dellatore, S.M., Miller, W.M., Messersmith, P.B. (2007) Mussel-inspired surface chemistry for multifunctional coatings. Science. 318(5849), 426-430.

Received: **24.09.2018**
Accepted: **28.02.2019**

CORRESPONDING AUTHOR

Rongxin Su
State Key Laboratory of Chemical Engineering,
Tianjin Key Laboratory of Membrane Science and Desalination Technology,
School of Chemical Engineering and Technology,
Tianjin University,
Tianjin 300350 – P.R. China

e-mail: surx@tju.edu.cn

© by PSP Volume 28 – No. 5/2019 pages 4199-4217 Fresenius Environmental Bulletin

ASSESSMENT OF SALINITY TOLERANCE BREAD WHEAT GENOTYPES: USING STRESS TOLERANCE INDICES

Mohamed Yassin[1], Sahar A Fara[2], Akbar Hossain[3], Hirofumi Saneoka[4], Ayman El Sabagh[5,*]

[1]Wheat Research Department, Field crops research Institute, ARC, Egypt
[2]Central Laboratory for Design & Statistical Analysis Research, ARC, Egypt
[3]Bangladesh Wheat and Maize Research Institute, Dinajpur-5200, Bangladesh
[4]Plant Nutritional Physiology Lab., Graduate School of Biosphere Science, Hiroshima University, Japan
[5]Department of Agronomy, Faculty of Agriculture, Kafrelsheikh University, 33516 Kafr El-Sheikh, Egypt

ABSTRACT

In the context, two field experiments were conducted at the Sakha Agriculture Research Station Farm in consecutive two years (2015-16 and 2016-17) under the normal and salinity stress conditions to find out the genotypes those are tolerance to salinity stress. Treatments were 24 bread wheat genotypes grown under the normal and salinity stress conditions. Among the genotypes 'Misr 2' vice versa in most conditions were recorded the maximum values of grain, straw and biological yields in both seasons. Results showed large values of broad sense heritability (h_b^2) were coupled with high values of genetic advance as a percent of mean (GA %) at 10% selection intensity for grain filling rate, spikes/m^2 and biological yield in both normal and salinity stress conditions. Already, the tested wheat genotypes exhibited different responses for stress (salinity) tolerance indices (STI). Near perfect and positive correlation coefficients (r =1) were found between three pairs of indices (STI and GMP), (YI and YS), (CVI and SSI) indicating that the two STI of each pair are identical for scatting genotypes for saline tolerance and they could be interchangeably used as a substitute for each other. The cluster analysis classified the tested genotypes into five main groups (clusters), where each group contained the genotypes that showed similar yield potential its components. The fifth cluster contained two promising genotypes namely 'lines 16' and 'Misr 2' that were characterized by high grain yield in each of the normal and salt soils, and also recorded the highest values of number of days to heading and maturity, plant height and spikes/m^2. Accordingly, Phenological variation as well as stress tolerance indices of these two wheat cultivars were found the favourable both under normal and salinity stress. Therefore, these two genotypes may be recommended to cultivate under the saline condition of Egypt and also may be used in the future breeding program to develop salinity tolerant wheat cultivars.

KEYWORDS:
Wheat, salinity, tolerance index, cluster analysis.

INTRODUCTION

Wheat (*Triticum aestivum* L.) is a main cereal crop in many parts of the world and it is commonly known as a king of cereals. Wheat as a strategic crop and plays a great role in terms of economy, production, food and nutrition in worldwide [1, 2, 3]. It is the major widely grown species across the globe and feeds more than one - third of the global population [4]. While, food production is limited by saline soils in arid and semi-arid regions of the world [5]. It is the staple food for a large part of world population including Egypt.

In 2017, wheat cultivated estimate area in Egypt was 2.1 million feddan and production was 8.8 million tons [6]. Increasing wheat productivity is a national target in Egypt to fill the gap between wheat consumption and production. Wheat plays a great role in the diet of the Egyptian people. However, the production of wheat is influenced by various biotic or abiotic stresses, which led to changes in growth and yield of plants [7]. Among the abiotic stress, salinity is one of the major abiotic stresses that adversely affect crop productivity and quality of plants including wheat in worldwide [8, 9]. According to the FAO land and plant nutrition management service [6], much of the world's land is not cultivated, due to significant proportion of cultivated land is under salinity [6].

Adverse effects of salinity on plant growth may be due to osmotic stress and ion cytotoxicity. Soil salinity is a pioneer dilemma spread especially in arid and semiarid areas like Egypt, Turkey etc. The soil salinity level in future may be increased because the climatic changes, low of annual rainfall, rising of sea water, water irrigation scarcity, excessive use of fertilizers and absence of a good drainage system, which retarded the aimed sustainable crop production, especially in the north delta of Egypt [10]. Egypt is one of the country that severely suffered due to salinity problems [11]. For example, 33% of the land in Egypt under cultivated, where 3% of total arable land is already salinized [12].

Knowledge on heritability and genetic advance is a basic step to identify the characters amenable to genetic improvement through selection. [13, 14, 15], emphasized that, without considering genetic advance,

the heritability values (h^2) would not be practically useful in breeding program depending on visual selection. Improvement of a complex and low heritable character like grain yield may be more successful and fast using selection through its more heritable components which showed significant positive association with it.

Assessment the influence of salinity stress on wheat, it is now realized that sustainability as well as productivity could be essential for wheat breeding. Stress tolerance indices could be also useful to identify stress-tolerant genotypes [16]. Stress tolerance indices (STI) was defined as a useful tools for determining high yield and stress tolerance potential of genotypes [17]. [18], described stress tolerance (TOL) as the variances in yield between stress and irrigated conditions and also mean productivity (MP) as the average yield of genotypes under stress and non-stress environments. [19], used SSI to assess stress tolerance in wheat genotypes and found year-to-year difference in SSI for genotypes and could rank their pattern. In spring wheat cultivars, [20], using SSI, suggested that SSI more than one indicated above-average susceptibility to drought stress. There are several reports in the literature on the utility of these indices for identifying genotypes with more stable yield under moisture-limited conditions [21, 22]. Cluster analysis is a valuable biometrical tool aimed to quantify the degree of genetic divergence among tested genotypes based on their performance and their contributing characters [23, 24].

Therefore, development of new stress tolerant wheat genotypes with good grain quality are crucial to meet the food demand of increasing population in the world, under future changing climate such as heat and drought stress condition [25, 26]. However, a thorough understanding of physiological responses of plants to stress environment, mechanisms of stress tolerance and possible strategies for improving crop stress-tolerance is imperative [27]. Considering the important issue, the present study was under taken to fulfill the following objectives: to assess the effect of soil salinity on grain yield and its components of wheat genotypes, to identify saline tolerant wheat genotypes based on salinity tolerance indices (STI) and to classify the tested wheat genotypes using cluster analysis depending on the high yield and its attributes for future breeding programme.

MATERIALS AND METHODS

Experimental site. This study was conducted at the Experimental Farm of Sakha Agricultural Research Station, Kafr El-Sheikh, Egypt (31° 5' 12" North, 30° 56' 49" East) to evaluate the influence of salinity soil stress on grain yield and its components of wheat genotypes, as well as identify saline tolerant wheat genotypes based on salinity tolerance indices (STI) and 3- classify the tested wheat genotypes using cluster analysis depending on the high yield and its attributes. The preceding crop was rice in the two seasons.

Before soil preparation for cultivation, some physical and chemical analyses of the experimental site were applied where a composite surface soil sample (0-30 cm depth) was collected during the two study seasons and analyzed in laboratory. Details of soil properties belong to each research site are given in Table 1. The meteorological data were recorded for the two winter growing seasons from Sakha meteorological station (Table 2).

Experimental design and treatments, Plant materials and their source. Treatments were: 24 bread wheat genotypes (Table 3) were grown under normal and salinity stress conditions and were arranged in a randomized complete block design with three replicates. In both the years seeds of all genotypes were sown on 28 November 2015-16 and 2016-17. The plot area (3 m2) consisted of five rows, 3m long and 20 cm apart. Grains were manually drilled in the rows at the rate of 300 seeds m-2. The tested wheat genotypes contained 20 lines that were selected as promising lines from local breeding program and in addition four existing wheat cultivars were used as cheeks. Seeds of all genotypes were collected from 'National Wheat Research Program', Field Crops Research Institute, ARC, Egypt.

Experimental procedure. In each season, the aimed entries were evaluated in two experiments represent two different conditions (normal and saline soils) using flood method of irrigation. The first condition included the normal soil site (Normal, N) while the second one represents the saline soils (stress conditions, S). The recommended cultural practices for wheat cultivation in old land in Egypt were applied at the proper time.

Data collections. Data on days to Heading (DH), Days to Maturity (DM), Grain Filling Period (days) (GFP), Grain Filling Rate (gm) (GFR), Plant Height (cm)(PH), No. of spikes/m2 (s/m2), No. of kernels per spike (KS), 1000-kernel weight (g) (1000KW), Straw yield (kg/m2), Biological yield kg/m2 (BY), Harvest index (%) (HI) and Grain yield (kg/m2) (GY) were recorded.

Statistical analysis. Data were subjected to individual and combined analysis of variance of randomized complete block design with three replications over the two cultivated sites (normal and salt) for each season [28], was run prior to the combined analysis to confirm the homogeneity of individual error terms. Least significant difference (LSD) test was used to detect the significant differences among the items at probability level (0.05). The plot area (3 m^2) consisted of five rows, 3m

TABLE 1
Mechanical and chemical soil analyses of normal and salt-affected soils during two growing seasons.

Location	Sample depth	Soil structure	PH	Anion mEq/l					Cation mEq/l			
				EC dsm^{-1}	$CO3^{--}$	$HCO3^{--}$	CL^{-}	$SO4^{--}$	Ca^{++}	Mg^{++}	Na^{+}	K^{+}
2015/2016												
Normal soil	0 - 30	Clay	8.61	2.33	-	2.5	10	43.32	10.6	6.1	12.38	0.29
	30 - 60	Clay	8.7	2.1	-	2.25	12.5	48.69	6.6	4.9	8	0.33
Saline soil	0 - 30	Clay	8.5	10.1	-	3	85	103.11	87.1	99.21	60.12	1.58
	30 - 60	Clay	8.4	8.9	-	2.8	105	101.98	70.35	56.36	71.32	1.49
2016/2017												
Normal soil	0 - 30	Clay	8.06	2.01	_	3	8.11	9.11	5.6	3.91	10.34	0.31
	30 - 60	Clay	7.9	1.5	_	2.5	4.8	7.16	3.23	2.33	8.42	0.29
Saline soil	0 - 30	Clay	8.51	12.5	_	4	45	41.35	35.64	25.61	41.23	0.45
	30 - 60	Clay	7.6	11	_	3	35.8	45.78	30.69	31.25	49.32	0.33

TABLE 2
Monthly mean of air temperature (AT ^{O}C), relative humidity (RH %) and rainfed (mm/month) in winter seasons 2015-16 and 2016-17 at Sakha site.

Month	Temperature				RH%		Rainfall (mm)	
	2015-16		2016-17					
	Max.	Min.	Max.	Min.	2015-16	2016-17	2015-16	2016-17
Nov.	24.75	14.42	24.9	17.9	75.62	70.1	12.15	-
Dec.	20.36	8.33	19.3	10.8	78.27	69.8	25.0	7.1
Jan.	18.40	6.30	18.2	5.7	74.1	72.3	42.70	4.7
Feb.	23.53	6.70	19.7	10.2	70.00	68.1	-	4.8
Mar.	23.67	11.61	21.7	17.9	69.76	65.3	13.20	-
Apr.	30.03	14.22	26.5	21.6	61.72	60.4	-	5.3
May.	31.15	19.0	32.2	20.1	58.33	61.3	-	-

* Max = maximum temperature, ** Min = minimum temperature.

TABLE 3
Name and pedigree of the studied wheat genotypes*.

Genotype	Pedigree/Cross Name
Line 1	SERI*3 // RL6010 / 4*YR /3/ PASTOR /4/ BAV92 /5/ KAUZ // BOW / NKT
Line 2	SERI*3 // RL6010 / 4*YR /3/ PASTOR /4/ BAV92 /5/ KAUZ // BOW / NKT
Line 3	WEAVER/4/NAC/TH.AC//3*PVN/3/MIRLO/BUC /5/ SAKHA 93
Line 4	SW89.5193/KAUZ // HAAMA-11
Line 5	SW89.5193/KAUZ /3/ KAUZ // BOW / NKT
Line 6	BUC // 7C / ALD /5/ MAYA74 / ON // 1160.147 /3 BB / GLL /4/CHAH"S" /6/ MAYA / VUL // CMH74A.630 /4*SX /7/ SW 89.3064 *2 / BORL 95
Line 7	SAKHA 94 /6/ GIZA 158 /5/ CFN /CNO "S" // RON /3/ BB / NOR 67 /4/ TL /3/ FN / TH // NAR 59*2
Line 8	SAKHA 94 /6/ GIZA 158 /5/ CFN /CNO "S" // RON /3/ BB / NOR 67 /4/ TL /3/ FN / TH // NAR 59*2
Line 9	SAKHA 94 /6/ GIZA 158 /5/ CFN /CNO "S" // RON /3/ BB / NOR 67 /4/ TL /3/ FN / TH // NAR 59*2
Line 10	ATTILA*2/PBW65 /4/ CHEN/AEGILOPS SQUARROSA (TAUS) // BCN /3/ 2*KAUZ
Line 11	ATTILA*2/PBW65 /4/ CHEN/AEGILOPS SQUARROSA (TAUS) // BCN /3/ 2*KAUZ
Line 12	DVERD 2 / AE - SQUARROSA (214)// 2* BCN /3/ PFAU / MILAN
Line 13	CHEN / AEGILOPS SQUARROSA (TAUS) // BCN /3/ 2*KAUZ /4/ HAAMA-11
Line 14	CHEN / AEGILOPS SQUARROSA (TAUS) // BCN /3/ 2*KAUZ /4/ HAAMA-11
Line 15	CHEN / AEGILOPS SQUARROSA (TAUS) // BCN /3/ 2*KAUZ /4/ HAAMA-11
Line 16	CHEN / AEGILOPS SQUARROSA (TAUS) // BCN /3/ 2*KAUZ /4/ HAAMA-11
Line 17	CHEN / AEGILOPS SQUARROSA (TAUS) // BCN /3/ 2*KAUZ /4/ HAAMA-11
Line 18	CHEN / AEGILOPS SQUARROSA (TAUS) // BCN /3/ 2*KAUZ /4/GEN*2 // BUC / FLK /3/ BUCHIN
Line 19	BUC / MN72253 // PASTOR /3/ GIZA 168
Line 20	VEE/PJN//2*TUI/3/GALVEZ/WEAVER /7/ BUC // 7C / ALD /5/ MAYA74 / ON // 1160.147 /3/ BB / GLL /4/CHAH"S" /6/ MAYA / VUL // CMH74A.630 /4*SX
Sids 12	BUC//7C/ALD/5/MAYA74/ON//II60.147/3/BB/GLL/4/CHAT"S"/6/MAYA/VUL//CMH74A.630/4*SX.
Misr 1	OASIS/SKAUZ//4*BCN/3/2*PASTOR.
Giza 171	SAKHA 93 / GEMMEIZA 9.
Misr 2	SKAUZ/BAV92.

*Source: Wheat Res. Depr., FCRI, ARC, Egypt.

TABLE 4
The name, equation and reference of 11 saline tolerance indices.

No.	Index name	Formula	Reference
	% Reduction	**$(Y_n-Y_s)*100/Y_n$**	
The high values of these indices indicated to saline stress tolerance			
1	Mean Productivity (MP)	$(Y_n+Y_s)/2$	[18]
2	Harmonic Mean (HM)	$(2*Y_n*Y_s)/(Y_n+Y_s)$	[31]
3	Geometric Mean Productivity (GMP)	$(Y_n*Y_s)^{0.5}$	[17]
4	Stress Tolerance Index (STI)	$(Y_n \times Y_s)/(\overline{Y}_n)^2$	[17]
5	Yield Index (YI)	$Y_s/\overline{Y}_s$	[32]
6	Yield Stability Index (YSI)	Y_s/Y_p	[32]
7	Modified Stress Tolerance Index (MSTI)	$(YI)^2*STI$	[33]
The low values of these indices indicated to saline stress tolerance			
8	Tolerance Index (TOL)	Y_n-Y_s	[18]
9	Stress Susceptibility Percentage Index (SSPI)	$Tol*100/(2*\overline{Y}_n)$	[35]
10	Stress Susceptibility Index (SSI)	$[1-(Y_s/Y_n)]/[1-(\overline{Y}_s/\overline{Y}_n)]$	[36]
11	Coefficient of variation (CV)	SD/Mean of Y_n and Y_s	[37]

- Y_n and Y_s indicate to average grain yield of each genotype under normal and stress conditions.
- $\overline{Y}_n$ and $\overline{Y}_s$ indicate to average grain yield overall genotypes under normal and stress conditions.

long and 20 cm apart. Grains were manually drilled in the rows at the rate of 300 seeds m^{-2}.

The studied traits were: number of days to heading (DH) and maturity (DM), grain filling period (GFP, the number of days from heading to maturity) and grain filling ratio (GFR, gm m^{-2} $days^{-1}$ and equal to GY divided by GFP), plant height (PH, cm), number of spikes/m^{-2} (S/m^2), number of kernels per spike (KS), 1000-kernel weight (1000 KW, gm) and grain yield (GY, kg /m^2).

Based on the combined analysis of each cultivated site over the two seasons, the genotypic and phenotypic variances and their corresponding coefficient of variations (GCV *and* PCV) were estimated using the proper variance components according to the method suggested by [29]. Broad sense heritability (h_b^2) and genetic advance (GA %) in terms of percentage of mean (with 5 % selection intensity) were estimated according to [30].

For each genotype, eleven stress tolerance indices were calculated based on average grain yield under normal (Y_n) and stress (Y_s) sites over the two seasons. The names, equations and references of the stress tolerance indices are shown in Table 4.

The name, equation and reference of 11 saline tolerance indices. - Y_n and Y_s indicate to average grain yield of each genotype under normal and stress conditions.

- $\overline{Y}_n$ and $\overline{Y}_s$ indicate to average grain yield overall genotypes under normal and stress conditions.

To give overall picture emerges the interrelationships and overlapping among the eleven stress tolerance indices, Spearman rank correlation coefficients between all pairs of these indices were calculated. To classify the tested genotypes for salinity stress tolerance, the model of agglomerate hierarchical cluster analysis was worked out on genotype using the average grain yield and its attributes. A dendrogram was constructed based on Euclidean distance procedure. Genotypes were clustered using un-weighted pair group method using arithmetic average as outlined by [38].

RESULTS AND DISCUSSION

Mean squares (MS) of the studied characters under normal and salinity soils in each season are shown in Table 5. The effect of soil type was highly significant for all traits, except for grain filling periods and 1000 kernels weight in the first season. The current findings are supported by [39], there were variation for each trait at soil type and the performance, phenotypic and genotypic variability, heritability and predicted genetic advance for the traits of the salt affected location to another location. Also, there highly significant differences among the aimed wheat genotypes for all studies traits in the two seasons. Interactions between genotypes and soil type were significant or highly significant for all characters except grain filling ratio and plant height in the 1st season and grain filling period in the 2nd season as produced in Table 5. The significance of the interactions is a result of the different abilities of the cultivars to adjust their traits to the environment, suggesting the importance of genotype assessment under different environments to identify the best ones for a particular environment. In general, these results are in harmony with those reported by [11, 40].

Mean performance. The results of Levene test [40], proved the homogeneity of separate error variances for all studied traits that permits to apply combined analysis. The experimental sites were chosen to represent the agricultural environments of production areas in north delta. Moreover, the experiments were repeated across two seasons to give greater reliability to the results. The mean values of grain yield and its related characters for the 24 wheat genotypes evaluated in two locations (normal and saline soil conditions) in each growing season of 2015-16 and 2016-17 are shown in (Table 6). The means of all genotypes decreased significantly under the saline soil for all characters in the two seasons, except for grain filling period (GFP) and 1000 kernel weight and in first season. This indicated differential response of genotypes to salinity for yield attributes.

Results are present in Table 6 showed that 'Line13' and 'Sids 12' were the earliest genotypes for days to heading in the first and second seasons with value 84.17 and 88.5 days respectively, while Line 10 in the first season and 'Sids 12' in the second season were the earliest genotypes for days to maturity under the two conditions recorded (131.0 and 135.33 days), respectively. While 'Line 8' (94.0 and 99.0 days) and 'Misr 2' (96.17 and 98.83 days) were the latest for days to heading in the both seasons while Line 16 (152.83 days) in the first season and 'Misr 2' (140.83 days) in the second season were lately matured.

The longest GFP was reached in 'Misr 1' (52.0 days) and 'Line 16' (59.17 days), while Line 5 (43.33 days) and Line 10 (41.83 days) had the shortest GFP under the two conditions the first and second season, respectively (Table 6). The highest GFR was observed by Misr2 (40.67 and 34.07 $g/m^{-1}/day^{-1}$) in the two seasons while Line 7 (27.29 $g/m^{-1}/day^{-1}$ and Line 9 (27.47 $g/m^{-1}/day^{-1}$) in the first season and Line 9, and Sids 12 (17.30 $g/m^{-1}/day^{-1}$ and 16.95 $g/m^{-1}/day^{-1}$) in the second season recorded the slowest GFR.The tallest genotypes were Line 8 and Misr 2 (104.0 cm) in first season and Line 9 (112 cm) in the second season while Line 13 (86 cm) and Line 6 (94.17 cm) and Sids 12 (93.33 cm) had the shortest plants in the first and second season, respectively (Table 6).

TABLE 5
Mean squares (MS) of the studied characters under normal and salinity soils in each season of 2015-16 and 2016-17.

S.O.V.	df	Seasons	DH	DM	GFP	GFR	PH	S/m²
Soil (S)	1	2015/2016	4085.34**	3173.44**	57.51^{ns}	24209.24**	10591.84**	1214616.36**
		2017/2018	680.34**	2916.00**	779.34**	12799.95**	19951.56**	2511168.44**
Rep./ Soil	4	2015/2016	23.32	10.74	11.88	23.568	128.30	1431.56
		2017/2018	3.90	5.85	5.29	14.33	44.27	991.28
Genotypes (G)	23	2015/2016	56.55**	45.52**	31.83**	49.26**	110.32**	8698.42**
		2017/2018	43.78**	105.60**	66.72**	112.62**	115.87**	13699.64**
G x S	23	2015/2016	9.96**	15.43**	15.19*	18.10^{ns}	34.96^{ns}	3615.19**
		2017/2018	8.49*	11.74**	11.65 ns	60.90**	31.64**	6145.05**
Error	92	2015/2016	4.67	5.14	7.780	14.685	22.32	1470.23
		2017/2018	4.48	3.94	7.26	15.76	15.10	1903.52
S.O.V.	**df**	**Seasons**	**KS/m²**	**1000KW**	**SY**	**BY**	**HI**	**GY**
Soil (S)	1	2015/2016	9525.62**	67.66 ns	57.12**	214.26**	2087.97**	50.12**
		2017/2018	1708.69**	566.95**	47.28**	172.16**	2576.28**	39.00**
Rep./ Soil	4	2015/2016	34.20	9.455	0.40	0.41	36.62	0.01
		2017/2018	16.42	13.13	0.18	0.31	22.08	0.06
Genotypes (G)	23	2015/2016	103.62**	83.97**	0.40**	0.77**	24.23*	0.11**
		2017/2018	92.86**	77.42**	0.44**	1.12**	59.72**	0.26**
G x S	23	2015/2016	36.13ns	23.62*	0.44**	0.60**	32.62**	0.03 ns
		2017/2018	122.38**	35.42**	0.41**	0.66**	70.86**	0.13**
Error	92	2015/2016	39.21	14.19	0.12	0.18	12.39	0.03
		2017/2018	35.48	12.34	0.15	0.20	19.37	0.03

*, ** = Significant and highly significant at 0.05 and 0.01 levels of probability, respectively.
Mean Productivity (MP), Harmonic Mean (HM), Geometric Mean Productivity (GMP), Stress Tolerance Index (STI), Yield Index (YI), Yield Stability Index (YSI), Modified Stress Tolerance Index (MSTI), Tolerance Index (TOL), Stress Susceptibility Percentage Index (SSPI), Stress Susceptibility Index (SSI) , Coefficient of variation (CV), Days to Heading (DH), Days to Maturity (DM) ,Grain Filling Period (days) (GFP), Grain Filling Rate (gm) (GFR), Plant Height (cm)(PH), No. of spikes/m2 (s/m2), No. of kernels per spike (KS), 1000-kernel weight (g) (1000KW), Straw yield (kg/m2), Biological yield kg/m2 (BY), Harvest index (%) (HI) and Grain yield (kg/m2) (GY).

TABLE 6

Mean values of the studied characteristics for 24 wheat genotypes combined over normal and salinity conditions and the significant of the mean squares of the salinity treatment during 2015-16 and 2016-17 seasons.

Genotype	Days to Heading (DH)					
	2015 -16			2016-17		
	N	S	Comb.	N	S	Comb.
Line 1	95.00	81.67	88.33	93.67	86.00	89.83
Line 2	98.00	88.00	93.00	96.33	90.00	93.17
Line 3	94.67	83.00	88.83	96.67	92.00	94.33
Line 4	97.33	85.00	91.17	95.33	91.33	93.33
Line 5	96.33	85.33	90.83	96.00	89.00	92.50
Line 6	97.00	89.33	93.17	95.67	92.00	93.83
Line 7	95.33	84.00	89.67	97.33	94.33	95.83
Line 8	99.33	88.67	94.00	103.33	94.67	99.00
Line 9	92.00	76.67	84.33	97.33	94.67	96.00
Line 10	88.67	83.00	85.83	97.33	94.00	95.67
Line 11	93.33	81.67	87.50	94.33	88.00	91.17
Line 12	92.67	83.67	88.17	95.67	94.33	95.00
Line 13	89.00	79.33	84.17	96.33	91.33	93.83
Line 14	94.67	84.00	89.33	93.00	88.67	90.83
Line 15	93.67	81.33	87.50	95.67	90.67	93.17
Line16	98.33	85.67	92.00	95.33	92.00	93.67
Line 17	91.00	83.33	87.17	91.67	91.67	91.67
Line 18	95.67	79.33	87.50	95.33	95.33	95.33
Line 19	92.00	81.00	86.50	99.67	95.33	97.50
Line 20	92.67	84.00	88.33	95.00	90.33	92.67
Sids 12	94.67	83.67	89.17	89.00	88.00	88.50
Misr 1	88.00	82.33	85.17	98.67	92.67	95.67
Giza 171	96.00	84.67	90.33	99.67	96.00	97.83
Misr 2	100.67	91.67	96.17	103.00	94.67	98.83
Mean	94.42	83.76	89.09	96.31	91.96	94.13
CV			2.42			2.25
LSD $_{0.05}$ G			2.48			2.43
LSD $_{0.05}$ S			**			**
LSD $_{0.05}$ S × G			3.50			3.43

Genotype	Days to Maturity (DM)					
	2015 -16			2016-17		
	N	S	Comb.	N	S	Comb.
Line 1	139.33	131.33	135.33	142.00	135.00	138.50
Line 2	145.67	132.00	138.83	149.67	135.67	142.67
Line 3	142.33	132.33	137.33	147.00	136.00	141.50
Line 4	147.67	133.00	140.33	149.67	139.33	144.50
Line 5	137.67	130.67	134.17	144.67	131.67	138.17
Line 6	142.33	132.33	137.33	147.33	139.00	143.17
Line 7	143.67	133.33	138.50	149.00	142.00	145.50
Line 8	144.67	134.00	139.33	152.33	139.67	146.00
Line 9	140.67	130.33	135.50	153.67	149.67	151.67
Line 10	133.00	129.00	131.00	142.00	133.00	137.50
Line 11	141.33	132.00	136.67	146.33	136.67	141.50
Line 12	140.00	129.00	134.50	149.00	140.33	144.67
Line 13	135.33	130.00	132.67	145.00	137.33	141.17
Line 14	137.33	132.00	134.67	145.33	136.67	141.00
Line 15	141.67	133.67	137.67	148.67	139.67	144.17
Line16	148.33	134.00	141.17	157.33	148.33	152.83
Line 17	135.00	131.00	133.00	147.33	139.00	143.17
Line 18	143.67	130.00	136.83	151.33	140.00	145.67
Line 19	134.33	129.67	132.00	154.67	142.67	148.67
Line 20	139.67	129.00	134.33	148.67	138.67	143.67
Sids 12	139.00	131.33	135.17	136.33	134.33	135.33
Misr 1	141.67	132.67	137.17	151.00	143.67	147.33
Giza 171	143.33	130.67	137.00	147.67	142.33	145.00
Misr 2	146.33	135.33	140.83	152.67	142.00	147.33
Mean	141.00	131.61	136.31	148.28	139.28	143.78
CV			1.66			1.38
LSD $_{0.05}$ G			2.60			2.28
LSD $_{0.05}$ S			**			**
LSD $_{0.05}$ S × G			3.68			3.22

Genotype	Grain Filling Period (days) (GFP)					
	2015 -16			2016-17		
	N	S	Comb.	N	S	Comb.
Line 1	**44.33**	49.67	47.00	48.33	49.00	48.67
Line 2	**47.67**	44.00	45.83	53.33	45.67	49.50
Line 3	**47.67**	49.33	48.50	50.33	44.00	47.17
Line 4	**50.33**	48.00	49.17	54.33	48.00	51.17
Line 5	**41.33**	45.33	43.33	48.67	42.67	45.67
Line 6	**45.33**	43.00	44.17	51.67	47.00	49.33
Line 7	**48.33**	49.33	48.83	51.67	47.67	49.67
Line 8	**45.33**	45.33	45.33	49.00	45.00	47.00
Line 9	**48.67**	53.67	51.17	56.33	55.00	55.67
Line 10	**44.33**	46.00	45.17	44.67	39.00	41.83
Line 11	**48.00**	50.33	49.17	52.00	48.67	50.33
Line 12	**47.33**	45.33	46.33	53.33	46.00	49.67
Line 13	**46.33**	50.67	48.50	48.67	46.00	47.33
Line 14	**42.67**	48.00	45.33	52.33	48.00	50.17
Line 15	**48.00**	52.33	50.17	53.00	49.00	51.00
Line16	**50.00**	48.33	49.17	62.00	56.33	59.17
Line 17	**44.00**	47.67	45.83	55.67	47.33	51.50
Line 18	**48.00**	50.67	49.33	56.00	44.67	50.33
Line 19	**42.33**	48.67	45.50	55.00	47.33	51.17
Line 20	**47.00**	45.00	46.00	53.67	48.33	51.00
Sids 12	**44.33**	47.67	46.00	47.33	46.33	46.83
Misr 1	**53.67**	50.33	52.00	52.33	51.00	51.67
Giza 171	**47.33**	46.00	46.67	48.00	46.33	47.17
Misr 2	**45.67**	43.67	44.67	49.67	47.33	48.50
Mean	**46.58**	47.85	47.22	51.97	47.32	49.65
CV			5.91			5.43
LSD $_{0.05}$ G	**2.42**		3.20			3.09
LSD $_{0.05}$ S			ns			**
LSD $_{0.05}$ S × G			4.52			ns

Genotype	Grain Filling Rate (gm) (GFR)					
	2015 -16			2016-17		
	N	S	Comb.	N	S	Comb.
Line 1	48.60	17.84	33.22	41.25	33.56	27.66
Line 2	43.37	18.81	31.09	31.92	17.00	24.46
Line 3	42.31	16.22	29.27	34.37	13.13	23.75
Line 4	46.78	20.68	33.73	38.69	17.84	28.26
Line 5	46.73	16.77	31.75	31.37	20.49	25.93
Line 6	42.52	17.20	29.86	36.63	12.98	24.81
Line 7	40.08	14.50	27.29	24.98	11.42	18.20
Line 8	44.67	22.53	33.60	39.19	14.95	27.07
Line 9	38.30	16.64	27.47	22.71	11.89	17.30
Line 10	45.94	17.21	31.58	46.29	14.70	30.50
Line 11	45.93	17.06	31.50	41.19	17.28	29.23
Line 12	45.46	16.46	30.96	29.25	15.66	22.46
Line 13	47.58	14.89	31.24	36.68	11.30	23.99
Line 14	44.17	18.42	31.29	33.96	16.16	25.06
Line 15	37.89	18.64	28.26	28.81	14.16	21.49
Line16	42.34	18.65	30.49	31.19	13.24	22.22
Line 17	49.42	21.59	35.51	36.54	15.69	26.11
Line 18	43.02	20.58	31.80	31.36	18.50	24.93
Line 19	47.24	18.45	32.85	39.21	13.45	26.33
Line 20	41.25	17.00	29.12	24.14	15.19	19.67
Sids 12	40.92	15.82	28.37	21.85	12.04	16.95
Misr 1	42.60	23.58	33.09	38.65	24.93	31.79
Giza 171	44.01	15.59	29.80	38.65	13.38	26.01
Misr 2	53.86	27.48	40.67	45.64	22.50	34.07
Mean	44.37	18.44	31.41	34.35	15.50	24.93
CV			12.20			15.93
LSD $_{0.05}$ G			4.39		4.55	
LSD $_{0.05}$ S			**		**	
LSD $_{0.05}$ S × G			ns		6.44	

Genotype	Plant Height (cm)(PH)					
	2015 -16			2016-17		
	N	S	Comb.	N	S	Comb.
Line 1	101.67	86.67	94.17	106.67	88.33	97.50
Line 2	108.33	93.33	100.83	110.00	85.00	97.50
Line 3	103.33	86.67	95.00	108.33	88.33	98.33
Line 4	101.67	91.67	96.67	108.33	86.67	97.50
Line 5	106.67	85.00	95.83	108.33	85.00	96.67
Line 6	105.00	86.67	95.83	108.33	80.00	94.17
Line 7	105.00	85.00	95.00	110.00	88.33	99.17
Line 8	111.67	96.67	104.17	105.00	88.33	96.67
Line 9	105.00	90.00	97.50	121.67	101.67	111.67
Line 10	106.67	91.67	99.17	111.67	88.33	100.00
Line 11	108.33	86.67	97.50	113.33	91.67	102.50
Line 12	96.67	86.67	91.67	108.33	83.33	95.83
Line 13	91.67	81.67	86.67	103.33	86.67	95.00
Line 14	105.00	88.33	96.67	113.33	86.67	100.00
Line 15	106.67	93.33	100.00	111.67	85.00	98.33
Line16	116.67	91.67	104.17	118.33	96.67	107.50
Line 17	113.33	90.00	101.67	113.33	90.00	101.67
Line 18	105.00	91.67	98.33	116.67	91.67	104.17
Line 19	105.00	88.33	96.67	111.67	88.33	100.00
Line 20	106.67	93.33	100.00	108.33	91.67	100.00
Sids 12	103.33	88.33	95.83	106.67	80.00	93.33
Misr 1	113.33	93.33	103.33	113.33	85.00	99.17
Giza 171	116.67	90.00	103.33	116.67	80.00	98.33
Misr 2	116.67	91.67	104.17	121.67	93.33	107.50
Mean	106.67	89.51	98.09	111.46	87.92	99.69
CV			4.82			3.90
LSD $_{0.05}$ G			5.42			4.46
LSD $_{0.05}$ S			**			**
LSD $_{0.05}$ S × G			ns			6.30

Genotype	No. of spikes/m^2 (s/m^2)					
	2015 -16			2016-17		
	N	S	Comb.	N	S	Comb.
Line 1	287.00	166.44	226.72	387.78	250.00	318.89
Line 2	376.67	192.21	284.44	541.56	218.11	379.83
Line 3	365.83	170.86	268.35	452.33	183.33	317.83
Line 4	439.67	207.01	323.34	519.00	235.44	377.22
Line 5	396.00	244.28	320.14	489.11	266.89	378.00
Line 6	485.67	252.00	368.83	536.67	306.11	421.39
Line 7	393.33	171.54	282.44	429.00	132.22	280.61
Line 8	435.17	251.91	343.54	510.33	241.11	375.72
Line 9	254.17	187.67	220.92	374.44	186.67	280.56
Line 10	369.17	192.73	280.95	483.33	210.00	346.67
Line 11	402.00	205.48	303.74	525.56	271.22	398.39
Line 12	435.83	150.61	293.22	558.89	215.78	387.33
Line 13	377.67	257.56	317.61	477.78	245.56	361.67
Line 14	442.00	217.15	329.58	517.78	231.89	374.83
Line 15	444.00	207.33	325.67	592.11	246.67	419.39
Line16	394.67	248.67	321.67	532.22	285.67	408.94
Line 17	375.33	225.69	300.51	499.67	242.22	370.94
Line 18	378.33	210.00	294.17	627.78	210.00	418.89
Line 19	382.00	192.97	287.49	544.44	244.44	394.44
Line 20	313.33	186.29	249.81	543.33	233.33	388.33
Sids 12	346.53	123.77	235.15	330.00	192.22	261.11
Misr 1	420.33	184.91	302.62	433.33	242.22	337.78
Giza 171	423.33	269.33	346.33	553.33	317.67	435.50
Misr 2	422.67	235.91	329.29	560.00	272.33	416.17
Mean	390.03	206.35	298.19	500.82	236.71	368.77
CV			12.86			11.83
LSD $_{0.05}$ G	2.42		43.97			50.03
LSD $_{0.05}$ S			**			**
LSD $_{0.05}$ S × G			62.18			70.75

Genotype	No. of kernels per spike (KS)					
	2015 -16			2016-17		
	N	S	Comb.	N	S	Comb.
Line 1	70.67	52.90	61.79	59.97	54.03	57.00
Line 2	62.47	46.57	54.52	55.50	48.00	51.75
Line 3	58.40	45.00	51.70	55.00	49.49	52.25
Line 4	55.20	45.24	50.22	54.30	46.00	50.15
Line 5	58.71	37.62	48.16	58.87	44.80	51.83
Line 6	64.53	44.95	54.74	55.10	41.70	48.40
Line 7	67.43	47.95	57.69	60.87	48.00	54.43
Line 8	61.00	39.00	50.00	54.47	39.33	46.90
Line 9	69.83	48.43	59.13	66.11	45.89	56.00
Line 10	63.10	40.43	51.76	63.00	52.20	57.60
Line 11	62.83	48.29	55.56	56.43	47.90	52.17
Line 12	57.80	41.19	49.50	45.27	67.00	56.13
Line 13	54.63	33.67	44.15	52.93	39.54	46.24
Line 14	57.33	41.62	49.48	54.33	42.33	48.33
Line 15	69.33	48.38	58.86	53.93	50.77	52.35
Line16	62.93	52.00	57.47	59.00	51.67	55.33
Line 17	56.97	46.95	51.96	53.50	50.53	52.02
Line 18	57.53	43.19	50.36	61.70	45.07	53.38
Line 19	60.20	56.86	58.53	54.50	53.13	53.82
Line 20	63.63	48.38	56.01	57.63	43.67	50.65
Sids 12	63.13	49.10	56.11	64.50	62.27	63.38
Misr 1	58.47	48.00	53.23	56.23	52.57	54.40
Giza 171	62.77	44.48	53.62	42.07	51.47	46.77
Misr 2	65.30	43.62	54.46	52.17	54.67	53.42
Mean	61.84	45.58	53.71	56.14	49.25	52.70
CV			11.66			11.30
LSD $_{0.05}$ G			7.18			6.83
LSD $_{0.05}$ S			**			**
LSD $_{0.05}$ S × G			ns			9.66

Genotype	1000-kernel weight (g) (1000KW)					
	2015 -16			2016-17		
	N	S	Comb.	N	S	Comb.
Line 1	44.19	45.22	44.70	39.33	39.59	39.46
Line 2	38.85	44.91	41.88	37.49	36.94	37.22
Line 3	42.92	43.32	43.12	44.56	40.07	42.31
Line 4	37.81	40.77	39.29	39.40	34.70	37.05
Line 5	45.23	43.77	44.50	43.35	39.50	41.43
Line 6	38.61	40.24	39.42	39.99	37.04	38.51
Line 7	44.83	47.77	46.30	39.42	36.64	38.03
Line 8	42.66	44.36	43.51	39.64	34.67	37.16
Line 9	46.26	45.75	46.01	46.67	41.46	44.06
Line 10	42.18	48.21	45.20	42.96	45.19	44.08
Line 11	45.15	46.82	45.98	43.63	41.04	42.33
Line 12	38.25	43.59	40.92	30.56	39.03	34.79
Line 13	39.54	37.28	38.41	40.19	25.18	32.68
Line 14	37.70	42.08	39.89	47.91	42.16	45.03
Line 15	37.28	40.58	38.93	34.84	31.47	33.16
Line16	47.96	49.14	48.55	42.89	38.07	40.48
Line 17	41.14	41.14	41.14	50.67	34.83	42.75
Line 18	45.34	44.60	44.97	43.61	38.80	41.20
Line 19	39.53	35.84	37.68	42.56	35.27	38.92
Line 20	39.58	39.74	39.66	43.33	37.55	40.44
Sids 12	58.93	46.84	52.89	50.30	43.51	46.91
Misr 1	36.73	42.08	39.40	42.39	39.02	40.70
Giza 171	38.74	41.82	40.28	39.46	38.92	39.19
Misr 2	36.35	42.78	39.56	43.10	42.40	42.75
Mean	41.91	43.28	42.59	42.01	38.04	40.03
CV			8.84			8.78
LSD $_{0.05}$ G			4.32			4.03
LSD $_{0.05}$ S			ns			**
LSD $_{0.05}$ S × G			6.11			5.70

Genotype	Straw yield (kg/m²)					
	2015 -16			2016-17		
	N	S	Comb.	N	S	Comb.
Line 1	3.29	1.88	2.58	2.27	1.51	1.89
Line 2	2.90	1.73	2.32	3.17	1.56	2.36
Line 3	3.62	1.66	2.64	3.54	1.62	2.58
Line 4	3.52	1.64	2.58	3.73	1.48	2.60
Line 5	2.90	1.58	2.24	2.21	1.66	1.94
Line 6	2.54	2.43	2.48	2.45	1.82	2.13
Line 7	2.65	1.42	2.03	2.31	2.02	2.16
Line 8	2.86	1.87	2.36	3.02	1.76	2.39
Line 9	2.87	2.52	2.70	3.21	1.88	2.54
Line 10	2.86	1.51	2.19	3.14	1.77	2.45
Line 11	3.80	1.62	2.71	2.90	1.86	2.38
Line 12	3.56	1.29	2.42	3.01	1.48	2.25
Line 13	3.24	1.45	2.34	2.28	1.91	2.10
Line 14	3.29	1.92	2.60	2.83	2.02	2.42
Line 15	3.15	1.84	2.49	2.71	1.51	2.11
Line16	3.22	2.10	2.66	3.23	1.79	2.51
Line 17	3.16	1.98	2.57	3.34	1.79	2.57
Line 18	3.20	2.03	2.62	2.88	1.31	2.09
Line 19	2.66	2.04	2.35	2.87	1.80	2.33
Line 20	3.13	2.30	2.71	2.44	1.86	2.15
Sids 12	2.43	1.95	2.19	1.96	1.41	1.69
Misr 1	3.69	2.17	2.93	3.31	1.90	2.61
Giza 171	3.56	2.05	2.80	2.37	1.71	2.04
Misr 2	3.74	2.63	3.18	3.70	1.93	2.82
Mean	3.16	1.90	2.53	2.87	1.72	2.30
CV			13.48			16.73
LSD $_{0.05}$ G			0.39			0.44
LSD $_{0.05}$ S			**			**
LSD $_{0.05}$ S × G			0.55			0.62

Genotype	Biological yield kg/m² (BY)					
	2015 -16			2016-17		
	N	S	Comb.	N	S	Comb.
Line 1	3.02	1.54	2.28	2.37	1.22	1.79
Line 2	2.76	1.43	2.09	2.71	1.29	2.00
Line 3	3.13	1.37	2.25	2.93	1.22	2.07
Line 4	3.26	1.46	2.36	3.24	1.29	2.27
Line 5	2.68	1.29	1.99	2.07	1.41	1.74
Line 6	2.48	1.76	2.12	2.41	1.35	1.88
Line 7	2.54	1.18	1.86	2.00	1.43	1.71
Line 8	2.71	1.61	2.16	2.74	1.35	2.04
Line 9	2.63	1.90	2.27	2.49	1.41	1.95
Line 10	2.72	1.28	2.00	2.89	1.29	2.09
Line 11	3.33	1.37	2.35	2.79	1.50	2.15
Line 12	3.17	1.13	2.15	2.54	1.22	1.88
Line 13	3.02	1.22	2.12	2.26	1.35	1.81
Line 14	2.87	1.56	2.21	2.56	1.56	2.06
Line 15	2.76	1.56	2.16	2.35	1.22	1.79
Line16	2.96	1.67	2.32	2.87	1.41	2.14
Line 17	2.96	1.67	2.32	2.98	1.41	2.19
Line 18	2.93	1.71	2.32	2.57	1.18	1.88
Line 19	2.59	1.63	2.11	2.78	1.35	2.07
Line 20	2.82	1.71	2.26	2.07	1.44	1.76
Sids 12	2.35	1.50	1.93	1.67	1.09	1.38
Misr 1	3.32	1.85	2.58	2.96	1.76	2.36
Giza 171	3.13	1.54	2.33	2.33	1.29	1.82
Misr 2	3.44	2.13	2.79	3.32	1.67	2.49
Mean	2.90	1.54	2.22	2.58	1.37	1.97
CV			10.70			12.62
LSD $_{0.05}$ G	2.42		0.27			0.28
LSD $_{0.05}$ S			**			**
LSD $_{0.05}$ S × G			0.53			0.91

Genotype	Harvest index (%) (HI)					
	2015 -16			2016-17		
	N	S	Comb.	N	S	Comb.
Line 1	39.81	31.96	35.89	46.75	31.26	39.00
Line 2	41.65	32.16	36.91	34.93	34.04	34.48
Line 3	36.37	33.48	34.92	32.44	26.35	29.39
Line 4	40.08	38.64	39.36	36.34	36.49	36.42
Line 5	40.13	32.60	36.36	41.31	34.55	37.93
Line 6	43.28	23.54	33.41	43.45	25.19	34.32
Line 7	42.08	33.19	37.63	36.01	21.22	28.62
Line 8	41.34	35.35	38.34	39.37	27.74	33.55
Line 9	39.39	25.76	32.58	28.43	25.64	27.04
Line 10	41.56	34.85	38.20	39.90	24.42	32.16
Line 11	36.74	34.39	35.57	43.04	31.20	37.12
Line 12	37.53	36.71	37.12	34.24	32.93	33.59
Line 13	40.36	34.35	37.35	44.10	21.45	32.78
Line 14	36.27	31.47	33.87	38.52	28.04	33.28
Line 15	36.73	34.79	35.76	35.91	32.52	34.21
Line16	39.75	30.73	35.24	37.52	30.20	33.86
Line 17	40.86	34.20	37.53	37.83	29.36	33.60
Line 18	39.31	33.99	36.65	37.84	38.69	38.26
Line 19	42.61	30.61	36.61	42.67	26.32	34.49
Line 20	38.39	25.52	31.95	34.55	28.47	31.51
Sids 12	42.73	28.20	35.46	34.74	28.14	31.44
Misr 1	38.24	34.92	36.58	38.25	40.16	39.20
Giza 171	36.88	26.23	31.55	43.79	26.86	35.32
Misr 2	39.75	31.43	35.59	38.01	35.68	36.85
Mean	39.66	32.04	35.85	38.33	29.87	34.10
CV			9.82			12.91
LSD $_{0.05}$ G	2.42		4.04			5.05
LSD $_{0.05}$ S			**			**
LSD $_{0.05}$ S × G			5.56			7.14

Genotype	Grain yield (kg/m^2) (GY)					
	2015 -16			2016-17		
	N	S	Comb.	N	S	Comb.
Line 1	1.19	0.49	0.84	1.11	0.38	0.74
Line 2	1.15	0.46	0.81	0.94	0.43	0.69
Line 3	1.12	0.44	0.78	0.96	0.32	0.64
Line 4	1.31	0.56	0.93	1.17	0.48	0.82
Line 5	1.07	0.42	0.74	0.84	0.49	0.67
Line 6	1.07	0.41	0.74	1.05	0.34	0.69
Line 7	1.07	0.40	0.73	0.72	0.31	0.51
Line 8	1.12	0.57	0.84	1.06	0.37	0.72
Line 9	1.03	0.50	0.77	0.71	0.36	0.53
Line 10	1.13	0.44	0.79	1.14	0.32	0.73
Line 11	1.22	0.47	0.85	1.18	0.47	0.83
Line 12	1.19	0.42	0.80	0.87	0.40	0.63
Line 13	1.22	0.42	0.82	0.99	0.29	0.64
Line 14	1.04	0.49	0.77	0.99	0.43	0.71
Line 15	1.01	0.54	0.77	0.85	0.38	0.62
Line16	1.18	0.50	0.84	1.07	0.42	0.74
Line 17	1.21	0.57	0.89	1.13	0.41	0.77
Line 18	1.14	0.58	0.86	0.98	0.46	0.72
Line 19	1.11	0.50	0.81	1.18	0.36	0.77
Line 20	1.08	0.42	0.75	0.72	0.41	0.57
Sids 12	1.01	0.42	0.71	0.58	0.31	0.44
Misr 1	1.27	0.65	0.96	1.12	0.71	0.91
Giza 171	1.16	0.40	0.78	1.02	0.34	0.68
Misr 2	1.37	0.67	1.02	1.26	0.59	0.93
Mean	2.06	0.88	1.47	1.77	0.73	1.25
CV			11.22			14.29
LSD $_{0.05}$ G	2.42		0.19			0.21
LSD $_{0.05}$ S			**			**
LSD $_{0.05}$ S × G			ns			0.29

TABLE 7
Genetic Parameters of Grain Yield and its Related Characters Computed from 24 Wheat Genotypes Evaluated Under Normal and Salt Sites Over the Two Seasons.

Characteristics	Genetic parameters									
	Grand mean		PCV		GCV		h_b^2		EGA (10 %)	
	Normal	Salt	Normal	Salt	Normal	Salt	Normal	Salt	Normal	Salt
DH	95.36	87.86	3.89	6.23	3.28	5.64	71	82	4.85	8.98
DM	144.64	135.44	4.12	3.93	3.80	3.64	85	86	6.16	5.92
GFP	49.28	47.58	9.63	8.26	8.03	5.67	70	47	11.79	6.85
GFR	39.37	16.97	21.25	24.78	17.41	18.51	67	56	25.11	24.34
PH	109.06	88.72	6.02	6.91	5.11	3.56	72	27	7.64	3.24
N/m²	445.42	221.54	20.63	22.24	17.56	16.58	72	56	26.31	21.76
NKS	4.93	2.62	16.17	19.45	12.69	12.17	62	39	17.52	13.42
1000 GW	3.02	1.81	19.05	22.10	13.31	12.54	49	32	16.37	12.52
GY	39.00	30.96	11.90	18.40	6.61	12.39	31	45	6.46	14.68
SY	58.99	47.41	12.99	16.30	7.49	10.70	33	43	7.59	12.37
HI	41.96	40.66	13.09	13.50	10.06	9.98	59	55	13.60	12.99
BY	1.92	0.81	17.52	25.16	13.88	18.87	63	56	19.35	24.91

The highest values of number of spikes/m2 were found by Line 6 and Giza 171 (369 and 436) in first and second season, respectively. On the other hand, the lowest values of number of spikes /m^2 were obtained by Line 9 and Sids 12 (221 and 261) respectively under most conditions (Table 6).

Line 1 and Sids 12 give the highest values of number of kernels per spike (61.79 and 63.38) in first and second seasons, respectively. Line 13 recorded the lowest values of number of kernels per spike with values (44.15 and 46.24) in the two seasons, respectively (Table 6).

The highest 1000-kernels weight resulted from Sids 12 in the two seasons (52.89 and 46.91 g), while the lowest values were belonged to Line 19 in the first season (37.68 g) and in the second season (32.68 g) (Table 6).

The results revealed that the maximum harvest index values were obtained by Line 4 and Misr 1 recording 39.36 % and 39.20 % while the minimum harvest index values being 31.55 % and 27.04 % were obtained by Giza 171 and line 9 in the first and second season, respectively (Table 6).

Generally, genotype Misr 2 recorded the highest values in the two seasons for each of biological yield (2.79 and 2.49 kg/m^2), straw yield (3.18 and 2.82 kg/m^2) and grain yield (1.02 and 0.93 kg/m^2), results were presented in Table 6. The lowest values were recorded by Sids 12 for grain yield (0.71 and 0.44 kg/m^2) in two seasons, while Line 7 had the minimum values for both of biological and straw yield (1.86 and 2.03 kg/m^2) in the first season and Sids 12 (1.38 and 1.69 kg/m^2) in the second season, respectively.

The current results are similar to the findings obtained by several investigations, [42], reported that the decrease in grain yield might be caused by the salinity, which induced reduction of photosynthetic capacity leading to less starch synthesis and accumulation in the grain. The means of days to heading reduced under salinity conditions [43].as well as, under salinity conditions caused a significant reduction in the number of kernels/panicle. The evaluation of potential yield losses by salinity is estimated that 20% [44]. The influence of salinity on the number of tillers and number kernels/spike, which both initiate during early growth stages, has a greater impact on final grain yield than on yield components in the last stages [10].

Genetic parameters. Estimates of genetic variability, phenotypic (PCV) and genotypic (GCV) coefficients of variation, broad sense heritability (h_b^2), and genetic advance as a percent of the mean (GA %) for the studied traits under the two sites (normal and soils) are presented in Table 7.

High heritability estimates associated with high genetic advance for major quantitative traits in wheat offer better scope of selection of genotypes in early segregating generations [45], reported that salinity also affected the heritability of wheat genotypes. Low heritability under stressed environments and high heritability under non-stressed environment was previously reported by many investigators [11, 39].

Generally, the values of (PCV) were slightly higher than their corresponding values of (GCV) for all studied traits indicating that the variations among tested genotypes were mostly returned to genetic makeup rather than environmental effect at the two sites. The highest estimates of phenotypic (PCV) and genotypic (GCV) coefficients of variation were obtained by grain filling ratio (21.25 and 17.41) followed by number of spikes/m^2 (20.63 and 17.56) in normal soil while the highest estimates of phenotypic (PCV) and genotypic (GCV) coefficients of variation in salt soil sites were recorded by biological yield (25.16 and 18.87) and grain filling ratio, (24.78 and 18.51) reflecting a wide pattern of genotypic variation among tested genotypes considering the two previous characters. In accordance, the selection among the tested genotypes would be effective to improve these traits. On the other hand, days to heading recorded low estimates of PCV and

TABLE 8
Estimates of Salt Tolerance Indices (STI) and their respective ranks of 24 bread wheat genotypes based on grain yield under adequate and salt sites over the two seasons

Geno-types	Grain yield (Kg/m^2)		Salt tolerance indices (STI)											
	Y_n	Y_s	MP[1]	H M[1]	GMP[1]	STI[1]	YI[1]	TOL[2]	SSPI[2]	YSI[1]	MSTI[1]	Red %	SSI[2]	CV[2]
Line 1	1.15	0.44	1.43	1.14	1.28	0.44	0.98	1.28	33.47	0.38	0.43	61.94	1.07	63.44
Line 2	1.04	0.44	1.34	1.13	1.23	0.41	1.00	1.08	28.18	0.43	0.41	57.34	0.99	56.84
Line 3	1.04	0.38	1.28	1.01	1.14	0.35	0.86	1.18	30.79	0.37	0.26	63.09	1.09	65.17
Line 4	1.24	0.52	1.58	1.31	1.44	0.56	1.15	1.30	33.96	0.42	0.74	58.43	1.01	58.37
Line 5	0.96	0.46	1.27	1.11	1.19	0.38	1.01	0.91	23.72	0.47	0.39	52.68	0.91	50.56
Line 6	1.06	0.38	1.29	1.00	1.13	0.35	0.84	1.23	32.14	0.35	0.25	64.60	1.11	67.47
Line 7	0.89	0.35	1.12	0.91	1.01	0.28	0.79	0.97	25.38	0.39	0.17	60.59	1.05	61.46
Line 8	1.09	0.47	1.40	1.18	1.29	0.45	1.05	1.11	29.00	0.43	0.50	56.70	0.98	55.95
Line 9	0.87	0.43	1.17	1.04	1.10	0.33	0.96	0.80	20.76	0.49	0.30	50.70	0.87	48.02
Line 10	1.14	0.38	1.37	1.02	1.18	0.38	0.84	1.37	35.72	0.33	0.27	66.79	1.15	70.90
Line 11	1.21	0.47	1.51	1.22	1.35	0.50	1.05	1.32	34.54	0.39	0.55	61.03	1.05	62.11
Line 12	1.03	0.41	1.29	1.05	1.16	0.37	0.91	1.11	29.08	0.40	0.31	60.29	1.04	61.03
Line 13	1.11	0.36	1.31	0.96	1.13	0.35	0.79	1.35	35.31	0.32	0.22	68.01	1.17	72.86
Line 14	1.02	0.46	1.33	1.14	1.23	0.41	1.03	1.00	26.00	0.45	0.44	54.56	0.94	53.06
Line 15	0.93	0.46	1.25	1.11	1.18	0.38	1.03	0.85	22.05	0.50	0.40	50.47	0.87	47.74
Line16	1.12	0.46	1.42	1.17	1.29	0.45	1.02	1.20	31.33	0.41	0.47	59.32	1.02	59.64
Line 17	1.17	0.49	1.49	1.24	1.36	0.50	1.09	1.22	31.78	0.42	0.60	58.01	1.00	57.78
Line 18	1.06	0.52	1.42	1.25	1.33	0.48	1.16	0.98	25.52	0.49	0.65	51.21	0.88	48.67
Line 19	1.15	0.43	1.42	1.12	1.26	0.43	0.95	1.30	33.99	0.37	0.39	62.97	1.09	64.99
Line 20	0.90	0.42	1.19	1.03	1.10	0.33	0.93	0.87	22.60	0.46	0.29	53.53	0.92	51.68
Sids 12	0.79	0.36	1.04	0.90	0.96	0.25	0.81	0.77	20.02	0.46	0.17	53.99	0.93	52.29
Misr 1	1.19	0.68	1.68	1.55	1.62	0.71	1.51	0.93	24.38	0.57	1.62	43.43	0.75	39.23
Giza 171	1.09	0.37	1.31	1.00	1.14	0.36	0.83	1.28	33.52	0.34	0.25	65.71	1.13	69.20
Misr 2	1.32	0.63	1.75	1.53	1.64	0.73	1.41	1.23	32.16	0.48	1.44	52.10	0.90	49.81
	Corresponding ranks													
Line 1	6	13	6	9	9	9	13	18	18	18	10	18	18	18
Line 2	15	12	12	11	12	12	12	10	10	11	11	11	11	11
Line 3	16	18	18	19	18	18	18	13	13	20	19	20	20	20
Line 4	2	4	3	3	3	3	4	20	20	13	3	13	13	13
Line 5	19	11	19	14	13	13	11	5	5	6	13	6	6	6
Line 6	14	20	17	21	19	19	20	16	16	21	21	21	21	21
Line 7	22	24	23	23	23	23	24	7	7	16	23	16	16	16
Line 8	11	6	10	7	8	8	6	11	11	10	7	10	10	10
Line 9	23	14	22	16	22	22	14	2	2	3	16	3	3	3
Line 10	8	19	11	18	14	14	19	24	24	23	18	23	23	23
Line 11	3	7	4	6	5	5	7	22	22	17	6	17	17	17
Line 12	17	17	16	15	16	16	17	12	12	15	15	15	15	15
Line 13	10	23	14	22	20	20	23	23	23	24	22	24	24	24
Line 14	18	8	13	10	11	11	8	9	9	9	9	9	9	9
Line 15	20	9	20	13	15	15	9	3	3	2	12	2	2	2
Line16	9	10	7	8	7	7	10	14	14	14	8	14	14	14
Line 17	5	5	5	5	4	4	5	15	15	12	5	12	12	12
Line 18	13	3	8	4	6	6	3	8	8	4	4	4	4	4
Line 19	7	15	9	12	10	10	15	21	21	19	14	19	19	19
Line 20	21	16	21	17	21	21	16	4	4	7	17	7	7	7
Sids 12	24	22	24	24	24	24	22	1	1	8	24	8	8	8
Misr 1	4	1	2	1	2	2	1	6	6	1	1	1	1	1
Giza 171	12	21	15	20	17	17	21	19	19	22	20	22	22	22
Misr 2	1	2	1	2	1	1	2	17	17	5	2	5	5	5

GCV in normal soil (3.89 and 3.28) and days to maturity (3.93 and 3.64) recorded low estimates of PCV and GCV in the salt soil sites. Similar results were reported by [13].

It is important to emphasize that, without considering genetic advance (GA), the heritability values (h_b^2) would not be practically valuable in the selection depends on phenotypic appearance. [29], confirmed that heritability estimates in conjunction with genetic advance would give more reliable index of selection value. In the present study, the broad sense heritability values (h_b^2) ranged from 31 for grain yield kg/m^2 to 85 for days to maturity in normal conditions while it ranged from 27 for plant height to 86 days to maturity in salt site. The values of genetic advance (GA based on 10 % selection intensity) ranged from 4.85 for days to heading to 26.31 for number of spikes/m^2 in normal site whereas it ranged from 3.24 for plant height to 24.91 for biological yield in salt site. Maximum values of broad sense heritability (hb^2) coupled with their corresponding genetic advance (GA) values at 10% selection intensity were obtained by grain filling rate (67 and 25.11), number of spikes/m^2 (72 and 26.31) and biological yield (63 and 19.35) in the adequate site, respectively. Regarding the salt site, the maximum values were recorded by the same traits; the grain filling ratio (56 and 24.34), number of spikes/m^2 (56 and 21.76) and biological yield (56 and 24.91), respectively. This result indicated the importance of the additive gene effects, so, the selection in early generations would be effective to develop these traits.

However, days to maturity recorded the highest heritability values (85 and 86), but it accompanied with low genetic advance value (6.16 and 5.92 at 10% selection intensity) in adequate and salt sites, respectively. Days to heading (71 and 4.85) and days to maturity (85 and 6.16) in the normal soil site exhibited the same behavior of broad sense heritability (h_b^2) and genetic advance values, respectively. From the above results, it is obvious the limited scope for improvement of these traits among the tested genotypes. The current conclusions are supported by [11, 39]. [15], confirmed that plant breeders can safely make their selection when they take in consideration high values of heritability and genetic advance. The sufficient variability at both phenotypic and genotypic levels coupled with the high estimates of h2b and GA under all studied salinity levels would allow us to conclude that selection for high GYPP, NTPP, NSPP, SYPP and BYPP even under the elevated levels of salinity would result in a great progress in such traits and thus improving wheat salinity tolerance [11, 39]. Such changes in genetic variation (increase or decrease), would seem likely to arise with increased stress, because different genes may contribute to similar character under diverse environments [47].

Salt tolerance indices. According to grain yield (kg/m^2) in non-stress (Y_p), under water stress conditions (Y_S) twenty quantitative stress tolerant indices and their respective ranks were calculated and presented in Table 8 across seasons. For SSI, the higher value refers to more susceptible to salinity as well as, salt tolerant with high STI and yield under nonstress and stress conditions. While, YI can be used as a selection criterion, although it only ranks cultivars on the basis of Ys.

According to [17, 18] stated that selection based on TOL index leads to selection of genotypes which their yields in non-stress condition are low and have lower MP. Based on a principal component analysis, Geometric Mean Productivity (GMP), Mean Productivity (MP) and Stress Tolerance Index (STI) were considered to be the best parameters for selection of drought-tolerant genotypes [48, 21], reported that lowest SSI values were associated with greater stress tolerance. [49], also indicated that a larger TOL value showed more sensitivity to stress in wheat crop; thus, a smaller value is favored [48]. [50], showed YSI to be a more useful index to discriminate drought-resistant from drought susceptible genotypes; therefore, breeders should select this parameter for selection of stress-tolerant genotypes [48]. A high STI value indicates higher stress tolerance and high yield potential [48].

Under non-stress condition, the grain yield varied from 0.79 for genotype sids 12 to 1.32 (kg/m^2) corresponding to genotype Misr 2, by average of 1.07 (kg/m^2) while, mean grain yield of genotypes under salt stress site ranged from 0.35 kg/m^2 for line 7 to 0.68 kg/m^2 that obtained by the genotype Misr 1), by average grain yield equal 0.45 (kg/m^2). Mean grain yield in salt stress conditions was 57.81 % lower than its respective yield under normal conditions. There were crucial differences among tested genotypes in respect to grain yield under non-stress and salt stress sites which demonstrates high genetic diversity among them that enabled us to screen salt tolerant genotypes.

It is noted that the two indices of GMP and STI give similar ranks for salt tolerance where the three genotypes namely line 11, line 17, genotype Misr 1, Line 4 and genotype Misr 2 identified as salt tolerant genotypes. These genotypes had greater values of GMP and STI while Line 7, Line 9, Line 20 and genotype sids 12 were identified as susceptible genotypes, because of their low values for GMP and STI. In the same context, the two indices *i.e.* TOL and SSPI ranked the tested genotypes, for salt tolerance, in the similar order. Using these two indices, genotypes; Line 10, Line 11 and Line 13 were more tolerant for salinity while Line 9, Line 15 and genotype sids 12 were more sensitive compared to the others. As well as, similar ranking pattern of tolerant/susceptible genotypes were obtained by the three indices of YSI, SSI and CV.

Accordingly, Line 9, Line 15, Line 18 and genotype Misr 1 were preferred to cultivate in the salt site while Line 6, Line 10, Line 13 and genotype Giza 171 were more susceptible for salinity. The similarity among pairs or three indices in ranking genotypes for salt tolerance may be attributed to that these indices are function of each other as shown in Table 8. However, the three indices of MP, HM and MSTI gave a different arrangement of genotypes for their tolerance to salinity. A similar trend of results was found by [24, 51, 52, 53, 54].

Correlation analysis among salinity tolerance indices. To clarify the most suitable salinity tolerant criteria, the correlation coefficients between Yp, Ys, and other quantitative indices of salinity tolerance were considered. The correlation analysis Spearman's rank correlation coefficients between the salinity tolerant indices and mean yield under stress and non-stress conditions are given in Table 9. Results from analysis of correlation revealed that grain yield normal conditions had positive and highly significant correlation with grain yield under stress conditions (r =0.527**).

An appropriate index must have a significant correlation with grain yield under both conditions. Yield in both stress (Ys) and non-stress (Yp) condition were high significantly and positively correlated with salinity tolerant indices MP, HM, GMP, STI, YI, and MSTI. Yield in non-stress (Yp) condition was high significantly and positively correlated

with salt tolerance indices TOL and SSPI and high significantly but negative correlated with YSI. However, yield in stress (Ys) condition was high significantly and positively correlated with YSI and high significantly but negative correlated with two salt tolerance indices SSI and CV. These results indicating that these criteria were more effective in identifying high yielding cultivars under different stress conditions. [54], recorded that the findings under both stress environments indicated positive and significant correlations between YP with TOL, MP, GMP, STI, SSI and HM selection indices. As well as, the correlations between YS with GMP, STI, and HM indicated that selection based on these indices may increase yield in stress and non-stress conditions. The most appropriate index to identify stress-tolerant cultivars is an index which has partly high correlation with seed yield under stress and non-stress conditions [34]. [20], using SSI criterion in spring wheat, recommended that more than 1 unit of SSI value several indicate above-average susceptibility for drought stress and less than 1 unit has below-average susceptibility.

Concerning the relationships among stress tolerance indices, the results appeared that there were highly significant and positive associations between each pair indices of MP, HM, GMP, STI, YI and MSTI. Highly significant and negative correlation coefficients were observed between YSI and each of TOL and SSPI. Also, YI was negatively and significantly associated with each of SSI and CVI. Perfect and positive correlation coefficient (r close to be one) were found between five pairs of indices (YI and YS), (HM and MSTI), (GMP and STI), (TOL and SSPI) and negative correlation coefficient with (YSI and SSI and CV) values were recorded that (r= 0.999**, r= 0.998**, r= 0.998** r= 0.999**, r= 0.999** and r= - 0.999**), respectively.

According to [56,48], who reported that if a significant correlation between MP and GMP exists, then GMP can reflect performance under stress a little better than MP. MP, STI, GMP and YI were highly correlated with grain yield under both conditions, suggesting that these indices were the most suitable to screen drought-tolerant genotypes [48]. The best indices are those which have high correlation with dry matter yield in both nonstress and stress conditions and would be able to identify potential upper yielding and salt tolerant genotypes [57].

Cluster analysis. The improvement of Germplasm and genetic diversity is the key to reliable and sustainable production of the food crops [24]. For significant assessment and utilization of germplasm, measure of extent of available genetic diversity is of utmost importance [58]. The cluster analysis based on squared Euclidean distance was performed to classify the genotypes on the basis of yield and its components across the two locations. The genetic diversity among the tested genotypes is the key to get reliable and sustainable production of crops. The cluster analysis hierarchical classified genotypes into clusters which exhibit high homogeneity within a cluster and high heterogeneity between clusters. Within group genotypes show minimum variance and genetic distance, while between-group genotypes are dissimilar with maximum genetic distance. In the present work, the similarity levels of the 24 wheat genotypes were estimated based on grain yield and its related characters. The genotypes were classified into two main groups (clusters) where the first main cluster contained two sub clusters while the second main cluster consists of three sub clusters. The clustering pattern of these genotypes is tabulated in Table 10 and diagrammatically displayed as dendrogram graph in Figure 1.

Results showed that the 1st sub cluster included 3 genotypes (lines; 1, 10 and 21) that had the highest mean values for each of number of kernels/spike and weight of 1000 grains recorded that 57.95 and 45.54 gm, respectively, while their plants had the lowest values of number of spike/m^2 (287.200) and were the shortest (96.67 cm) and the earliest in heading and maturity (98.56 and 135.47 days, respectively). Four genotypes (lines; 3, 20, 7 and 9) were found among the 2nd sub cluster that had the lowest grain yield (1.189 kg/m^2). Nine genotypes (lines; 2, 19, 15, 6, 12, 4, 22, 8 and 23 Located in the 3th sub cluster had the lightest weigh of 1000 grains (38.78 g). The 4th cluster included seven genotypes (5, 14, 11, 17, 18 and 13) that gave the minimum values of number of kernels/spike (50.300). Two promising genotypes namely; lines 16 and 24 formed the 5th sub cluster that aggregated the genotypes that had the tallest plants (105.830 cm) and attained maximum values of number of spike/m^2 (369.020) and grain yield (1.587 kg/m^2). While their plants were latest heading and maturity (95.170 and 145.540 cm), respectively. In the light of previous results that exhibited the presence of considerable genetic diversity among the tested genotypes, it gave a good chance to achieve sufficient scope for genotypic improvement of wheat through the hybridization among genotypes taken from divergent clusters [59,37]. The cluster analysis sequestrates genotypes into clusters which exhibit high homogeneity within a cluster and high heterogeneity between clusters [60]. The application of cluster analysis using Wards algorithm and squared Euclidean distances and assigned 94 bread wheat inbred lines into three groups [61].

TABLE 9
Spearman rank correlation coefficients among grain yield (under adequate and salt sites), and their corresponding salt tolerance indices.

Indices	Y_n	Y_s	MP	H M	GMP	STI	YI	TOL	SSPI	YSI	MSTI	SSI	CV
Y_n	1												
Y_s	.53**	1											
MP	.95**	.717**	1										
H M	.672**	.967**	.844**	1									
GMP	.821**	.891**	.934**	.956**	1								
STI	.832**	.884**	.934**	.952**	.998**	1							
YI	.522**	.999**	.711**	.965**	.888**	.881**	1						
TOL	.751**	-.061	.579**	.116	.335	.354	-.069	1					
SSPI	.749**	-.066	.576**	.111	.333	.352	-.074	.999**	1				
YSI	-.234**	.625**	-.010	.467*	0.256	0.245	.630**	-.774**	-.773**	1			
MSTI	.649**	.978**	.825**	.998**	0.949**	.946**	.976**	.086	.081	.497*	1		
SSI	.238	-.623**	.016	-.464*	-0.248	-.237	-0.627**	.777**	.776**	-.999**	-.494*	1	
CV	.241	-.618**	.019	-.460*	-0.246	-0.236	-0.623**	.779**	.778**	-.999**	-.490*	.999**	1

*, ** = Significant at 0.05 and 0.01 levels of probability, respectively.

TABLE 10
Summary of cluster analysis showed the included genotypes, similarity level and cluster means of the 24 wheat genotypes using the studied yield characters.

Cluster no.	distance	Included genotypes	Cluster average						
			DH	DM	PH	S/m^2	K/S	1000 GW	GY
1	4.04	1, 10, 21	89.556	135.470	96.670	278.200	57.940	45.540	1.277
2	3.77	3,20,7,9	91.250	141.000	99.580	286.100	54.730	42.490	1.189
3	4.35	2, 19, 15, 6, 12, 4, 22, 8, 23	92.639	141.130	98.333	355.780	52.438	38.779	1.397
4	5.46	5, 14, 11, 17, 18, 13	90.153	138.220	98.060	347.370	50.300	41.690	1.388
5	3.29	16, 24	95.170	145.540	105.830	369.020	55.170	42.840	1.587

- Abbreviations: DH: days to heading, DM: days to maturity, PH: plant height, NK/S: no. kernels/spike, NS/m^2: no. spikes/m^2, 1000 GW: weight 1000 grains, GW: Grain yield.

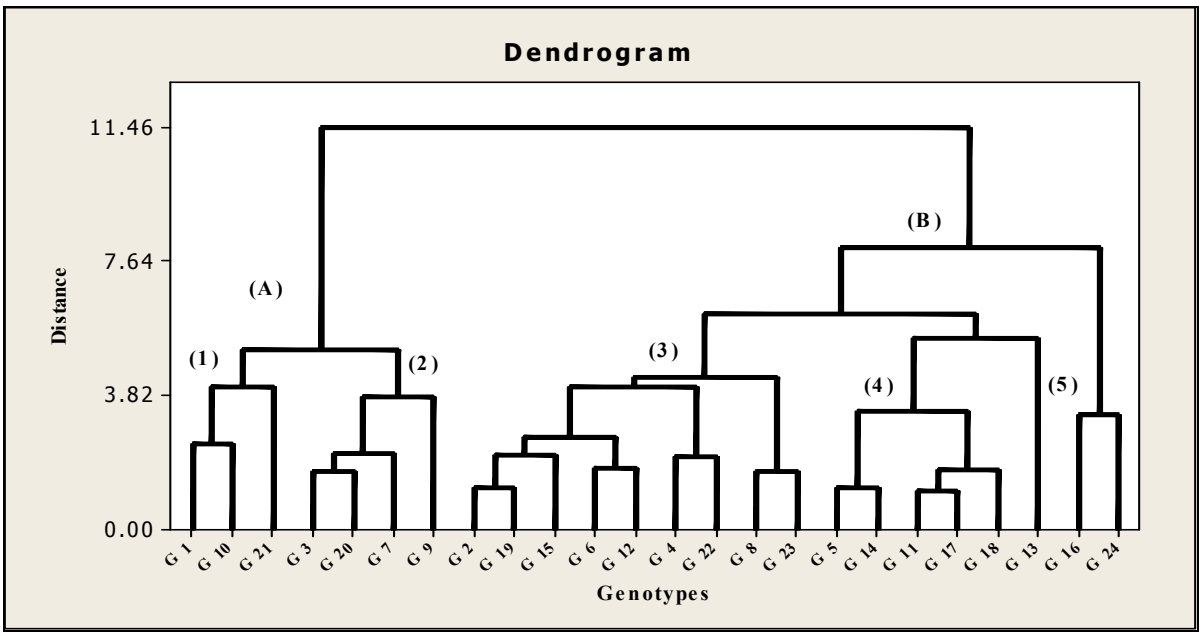

FIGURE 1
Dendrogram showing the similarity among 24 wheat genotypes based on grain yield and salt tolerance indices.

CONCLUSION

Our findings revealed that, among the genotypes, two promising genotypes namely 'Line 16' and 'Misr 2' that were characterized by high grain yield in each of the normal and saline soils, and also recorded the highest values of number of days to heading and maturity, plant height and spikes m-2. Accordingly, these findings indicated that these agronomical and genotypic traits could be useful tools to identify several genotypes in a short time, and provide significant information about salinity stress tolerance, which might be useful to wheat breeders to identify and improving salt-tolerant genotypes. Therefore, these two genotypes may be recommended to cultivate under the saline condition of Egypt and also may be used in the future breeding program to develop salinity tolerant wheat cultivars.

REFERENCES

[1] Jahan, M.A.H.S., Hossain, A., Teixeira da Silva, J.A, EL Sabagh A., Rashid, M.H., Barutçular, C. (2019). Effect of Naphthaleneacetic Acid on Root and Plant Growth and Yield of Ten Irrigated Wheat Genotypes. Pak. J. Bot., 51(2): 451- 459.

[2] Barutcular, C., EL Sabagh, A., Koç, M., Ratnasekera, D. (2017) Relationships between grain yield and physiological traits of durum wheat varieties under drought and high temperature stress in Mediterranean conditions. Fresen. Environ. Bull. 26, 4282- 4291.

[3] Darwish, M.A.H., Farhat, W.Z.E., EL Sabagh, A. (2018) Inheritance of some agronomic characters and rusts resistance in fifteen f2 wheat populations. Revista Cercetari Agronomice. 1(173), 5-28.

[4] Shahzad, A., Iqbal, M., Asif, M., Hirani, A.H., Goyal, A. (2013) Growing wheat on saline lands: Can a dream come true? Australian Journal of Crop Science. 7, 515–524.

[5] Rengasamy, P. (2010) Soil processes affecting crop production in salt affected soils. Functional Plant Biology. 37, 255–263.

[6] FAO/LPNWS (Land and Plant Nutrition Management Service). (2018) The Environmental and Physiological Nature of Salinity. http://plantstress.com/Articles/salinity_i/salinity_i.htm. (Accessed on 24 August 2018).

[7] Abdelaal, A.A.K., Reda, O.I., Yaser, H.M., Esmail, S.M., EL Sabagh, A. (2018) Anatomical, Biochemical and Physiological Changes in Some Egyptian Wheat Cultivars Inoculated with *Puccinia gramini* f. sp. *tritici* f. sp. *tritici* f. sp. *tritici.* Fresen. Environ. Bull. 27, 296-305.

[8] Chinnusamy, V., Jagendorf, A., Zhu, J.K. (2005) Understanding and improving salt tolerance in plants. Crop Sci. 45(2), 437-448.

[9] Borlu, H.O, Celiktas, V., Duzenli, S., Hossain, A., EL Sabagh, A. (2018) Germination and early seedling growth of five durum wheat cultivars (*Triticum durum* desf.) is affected by different levels of salinity. Fresen. Environ. Bull. 27, 7746- 7757.

[10] El-Hendawy, S.E., Hu, Y., Yakout, G.M., Awad, A.M., Hafiz, S.E., Schmidhalter, U. (2005) Evaluating salt tolerance of wheat genotypes using multiple parameters. Eur. J. Agron. 22, 243–253.

[11] Al-Naggar, A.M.M., Sabry, S.R.S., Atta, M.M.M., Abd El-Aleem, O.M. (2015a) Effects of salinity on performance, heritability, selection gain and correlations in wheat (*Triticum aestivum* L.) Doubled Haploids. Sci. Agri. 10(2), 70-83.

[12] Ghassemi, F., Jakeman, A.J., Nix, H.A. (1995) Salinization of land and water resources. University of New South Wales Press Ltd, Canberra, Australia.

[13] Abd El- Mohsen, A.A., Abo Hegazy, S.R., Taha M.H. (2012) Genotypic and phenotypic interrelationships among yield and yield components in Egyptian bread wheat genotypes. J of Plant Breeding and Crop Sci. 4(1), 9-16.

[14] Baloch, M.J., Baloch, E., Jatoi, W.A., Veesar, N.F. (2013) Correlations and heritability estimates of yield and yield attributing traits in wheat (Triticum aestivum L.). Pak. J. Agri. Eng. Vet. Sci. 29(2), 96-105.

[15] Hassan, Wafaa, A., Fares, W.M., Afiah, S.A. (2015) Selecting diverse bread wheat genotypes under saline stress conditions 2- using path analysis. Egypt. J. Plant Breed. 19(5), 373-390.

[16] Mitra, J. (2001) Genetics and genetic improvement of drought resistance in crop plants. Curr. Sci. 80, 758-762.

[17] Fernandez, G.C.J. (1992) Effective selection criteria for assessing stress tolerance. In: Kuo, C.G. (Ed.) Proceedings of the International Symposium on Adaptation of Vegetables and Other Food Crops in Temperature and Water Stress. Publication, Tainan, Taiwan.

[18] Rosielle, A.A., Hamblin, J. (1981) Theoretical aspects of selection for yield in stress and non-stress environments. Crop Sci. 21(6), 943-946.

[19] Clarke, J.M., DePauw, R.M., Townley-Smith, T.F. (1992) Evaluation of methods for quantification of drought tolerance in wheat. Crop Sci. 32, 728-7232.

[20] Guttieri, M.J., Stark, J.C., Brien, K.O., Souza, E. (2001) Relative sensitivity of spring wheat grain yield and quality parameters to moisture deficit. Crop Sci. 41, 327-335.

[21] Golabadi, M., Arzani, A., Maibody, S.A.M.M. (2006) Assessment of drought tolerance in segregating populations in durum wheat. Afric. J. Agric Res. 1, 162-171.
[22] Sharafi, S., Hassemi-Golezani, K., Mohammadi, S. Lak, S. and Sorkhy, B. (2011) Evaluation of drought tolerance and yield potential in winter barley (Hordeum vulgare) genotypes. J. Food, Agric. Environ. 9(2), 419-422.
[23] Abd El-Mohsen, A.A., Abd El-Shafi, M.A., Gheith, E.M.S., Suleiman, H.S. (2015) Using different statistical procedures for evaluating drought tolerance indices of bread wheat genotypes. Adv. Agric. Biol. 4(1), 19-30.
[24] Singh, S., Sengar, R.S., Kulshreshta, N. (2015) Differential response of selected bread wheat (Triticum aestivum L.) genotypes for salt tolerance by using multiple parameters. J. of Wheat Res. 8(1), 19-24.
[25] Hossain, A., Teixeira da Silva, J.A. (2013) Wheat production in Bangladesh: its future in the light of global warming. AoB PLANTS. 5(1), pls042.
[26] Yıldırım, M., Barutcular, C., Hossain, A., Koç M, Dizlek, H., Akinci, C., Toptaş, I., Basdemir, F., Islam, M.S., EL Sabagh, A. (2018) Assessment of The Grain Quality of Wheat Genotypes Grown Under Multiple Environments Using GGE Biplot Analysis. Fresen. Environ. Bull. 27, 4830-4837.
[27] Hossain, M.M., Hossain, A., Alam, M.A., EL Sabagh, A., Murad, K.F.I., Haque, M.M., Muriruzzaman, M., Islam, M.Z., Das S. (2018) Evaluation of Fifty Spring Wheat Genotypes Grown Under Heat Stress Condition in Multiple Environments of Bangladesh. Fresen. Environ. Bull. 27, 5993-6004.
[28] Gomez, K.A., Gomez, A.A. (1984) Statistical Procedures for Agriculture Research. 2nd Ed. John Wiley and Sons Inc., New York, USA., 72, 203-206.
[29] Johnson, H.W., Robinson, H.F., Comstock, R.E. (1955) Estimation of genetic and environmental variability in soybean. Agron. J. 47, 314-318.
[30] Allard, R.W. (1999) Principals of Plant Breeding. 2nd Ed. John Wiley and Sons, New York, USA.
[31] Jafari, M., Bourouni, A., Amiri, R.H. (2009). A new framework for selection of the best performance appraisal method. Eur. J. Soc. Sci. 7(3), 92- 100.
[32] Gavuzzi, P., Rizza, F., Palumbo, M., Campanile, R.G., Ricciardi, G.L., Borghi, B. (1997) Evaluation of field and laboratory predictors of drought and heat tolerance in winter cereals. Canadian Journal of Plant Science. 77, 523-531.
[33] Bouslama, M., Schapaugh, W.T. (1984) Stress tolerance in soybean. Part. 1: Evaluation of three screening techniques for heat and drought tolerance. Crop Sci. 24, 933-937.
[34] Farshadfar, E., Sutka, J. (2002) Screening drought tolerance criteria in maize. Acta Agron. Hung. 50(4), 411–416.
[35] Moosavi, S.S., Yazdi-Samadi, B., Naghavi, M.R., Zali, A.A., Dashti, H., Pourshahbazi, A. (2008) Introduction of new indices to identify relative drought tolerance and resistance in wheat genotypes. Desert. 12(2), 165-178.
[36] Fischer, R.A., Maurer, R. (1978) Drought resistance in spring wheat cultivars. I. Grain responses. Aust. J. Agric. Res. 29, 897-912.
[37] Darwish, M.A.H., Fares, W.M., Eman, Hussein, M.A. (2017) Evaluation of some bread wheat genotypes under saline soil conditions using tolerance indices and multivariate analysis. J. plant production, Mansoura Univ. 8(12), 1383-1394.
[38] Kovach, W.I (1995) A multivariate statistics package for IBM Pc and compatibles, Kovach Computing Service, 85 Nant–Y– Felin, Pentreaeth, Anglesely LL 758 UY Wales, U.K.
[39] Al-Naggar, A.M.M., Sabry, S.R.S., Atta, M.M.M., El-Aleem, O.M.A. (2015b) Field screening of wheat (*Triticum aestivum* L.) genotypes for salinity tolerance at three locations in Egypt. J. Agric. Ecology Res. Intern. (JAERI). 4(3), 88-104.
[40] Ragab, Kh. E., Taha, N.I. (2016) Evaluation of nine Egyptian bread wheat cultivars for salt tolerance at seedling and adult-plant stage. J. Plant Prod., Mansoura Univ. 7(2), 147-159.
[41] Levene, H. (1960) Robust tests for equality of variances. In Ingram Olkin, Harold Hotel ling, Italia, Stanford, Univ. Press, 278- 292.
[42] Turki, N, Harrabi, M, Okuno, K. (2012) Effect of salinity on grain yield and quality of wheat and genetic relationships among durum and common wheat. J Arid Land Studies. 22, 311–314.
[43] Oraby, H.F., Ransom, C.B., Kravchenko, A.N., Sticklen, M.B. (2005) Barley HVA1 gene confers salt tolerance in R3 transgenic oat. Crop Sci. 45, 2218–2227.
[44] Ashraf, M., Harris, P.J.C. (2005) Abiotic Stresses: Plant Resistance through Breeding and Molecular Approaches. Food Products Press, an imprint of The Haworth Press, Inc., Binghamton, New York, USA, 3–15.
[45] Memon, S.M., Ansari, B.A., Balouch, M.Z. (2005) Estimation of genetic variation for agro-economic traits in spring wheat (*Triticum aestivum* L.). Ind. J. Plant. Sci. 4, 171-175.

[46] Munir, A., Shahzad, A., Iqbal, M., Asif, M., Hirani, A.H. (2013) Morphological and molecular genetic variation in wheat for salinity tolerance at germination and early seedling stage. Australian Journal of Crop Science. 7(1), 66-74.
[47] Rumbaugh, M.D., Asay, K.H., Johnson, D.A. (1984) Influence of drought stress on genetic variance of alfalfa and wheat grass seedling. Crop Sci. 24, 297–303.
[48] Khokhar, M.I., Teixeira da Silva, J.A. (2012) Evaluation of barley genotypes for high yield and drought tolerance under normal and water-stressed conditions. Pak. J. Agric. Sci. 49(3), 303-313.
[49] Khayatnezhad, M., Gholamin, R., Jamaati-e-Somarin, S., Zabihi-e-Mahmoodabad, R.H. (2010) Investigation and selection drought indexes stress for corn genotypes. Amer. Euras. J. Agri. Environ. Sci. 9, 22-26.
[50] Mohammadi, R., Armion, M., Kahrizi, D., Amri, A. (2010) Efficiency of screening techniques for evaluating durum wheat genotypes under mild drought conditions. J. Plant Prod. 4, 11-24.
[51] Ali, M.B., El-Sadek, A.N. (2016) Evaluation of drought tolerance indices for wheat (Triticum aestivum L.) under irrigated and rainfed conditions. Communications in Biometry and Crop Science. 11(1), 77–89.
[52] Gadallah, M.A., Milad, S.N., Mabrook, Y.M., Abo Yossef, A.Y., Gouda, M.A. (2017) Evaluation of some Egyptian bread wheat (Triticum aestivum) cultivars under salinity stress. Alex. Sci. Exchange J. 38(2), 259-270.
[53] El Sabagh, A., Barutcular, C., Saneoka, H. (2015) Assessment of Drought Tolerance Maize Hybrids at Grain Growth Stage in Mediterranean Area. International Scholarly and Scientific Research and Innovation. 9(9), 917-920.
[54] Barutcular, C., EL Sabagh, A., Konuskan, O., Saneoka, H. (2016) Evaluation of maize hybrids to terminal drought stress tolerance by defining drought indices. Journal of Experimental Biology and Agricultural Sciences. 4, 610-616.
[55] Majidi, M., Tavakoli, V., Mirlohi, A., Sabzalian, M.R. (2011) Wild safflower species (*Carthamus oxyacanthus* Bieb.): A possible source of drought tolerance for arid environments. Aust. J. Crop Sci. 5(8), 1055-1063.
[56] Narouie Rad, M.R., Ghasemi, A., Arjemandinejad, A.R. (2009) Study of limit irrigation on yield of lentil (*Lens culinaris*) genotypes of national plant gene bank of Iran by drought resistance indices. American-Eurasian J. Agric. and Environ. Sci. 6, 352-355.
[57] Talebi, R., Fayaz, F., Jelodar, N.B. (2007) Correlation and path coefficient analysis of yield and yield components of chickpea (Cicer arietinum L.) under dry land condition in the west of Iran. Asian Journal of Plant Sciences. 6, 1151-1154.
[58] Zubair, M., Ajmal, S.U., Anwar, M., Haqqani, M. (2007) Multivariate analysis for quantitative traits in mungbean [*Vigna radiate* (L.) Wilczek]. Pakistan Journal of Botany. 39, 103-113.
[59] Sheykhi, A., Pirdashti, H., Abbasian, A., Niknejhad, Y. (2014) Segregation of some wheat (Triticum aestivum L.) genotypes using cluster analysis procedure. Int. J. Farm. Alli. Sci. 3, 225-229.
[60] Jaynes, D.B., Kaspar, T.C., Colvin, T.S., James, D.E. (2003) Cluster analysis of spatio-temporal corn yield pattern in an Iowa field. Agron J. 95, 574-586.
[61] Aharizad, S., Sabzi, M., Mohammadi, S.A., Khodadadi, E. (2012) Multivariate analysis of genetic diversity in wheat (Titicum aestivum L.) recombinant inbred lines using agronomic traits. Annals Biol. Res. 3(5), 2118-2126.

Received: **09.10.2018**
Accepted: **13.02.2019**

CORRESPONDING AUTHOR

Ayman El Sabagh
Department of Agronomy,
Faculty of Agriculture,
Kafrelsheikh University,
33516 Kafr El-Sheikh – Egypt

e-mail: ayman.elsabagh@agr.kfs.edu.eg

© by PSP Volume 28 – No. 5/2019 pages 4218-4225 Fresenius Environmental Bulletin

STUDY ON WET SOLIDIFICATION PROCESS OF WATERBORNE SYNTHETIC LEATHER

Qiaobin Liu[1,2,*], Chengzhi Chuai[1], Jinpeng Sun[2], Meiqi Mou[2]

[1]Tianjin University of Science & Technology, Tianjin 300457, P.R. China
[2]North China Institute of Aerospace Engineering, Langfang 065000, P.R. China

ABSTRACT

Waterborne synthetic leather was fabricated by wet solidification process. Effect of polyurethane impregnating solution concentration, concentration of lanthanum acetate, coagulation bath temperature and solidification time on tear strength and average aperture are examined. The results show that concentration of lanthanum acetate and the solidification time are the main influencing factors. Through research, the low temperature differential temperature solidification method has a good effect on pore formation. The optimized wet solidification process has a lanthanum acetate concentration of 10%, a solidification temperature of 21°C, a solidification time of 9 min, and a polyurethane impregnating solution concentration of 12%. These surfaces are expected to be of interest in wide variety of applications.

KEYWORDS:
Waterborne polyurethane, Tear strength, Synthetic leather, wet solidification process

INTRODUCTION

Leather has been an important material since the beginning of the human race [1-3]. Before the development of woven textiles, leather was the only available material to use for clothing. Due to its desirable traits, including high tensile strength, flexibility, resistance to tearing, puncturing, and abrasion, and permeability to air and water, it has applications in footwear, furnishings, automotive industry, clothing, bookbinders, gloves, sports gears, bags, and cases [4].

Genuine or natural leather is expensive and can be challenging to work with it. Therefore, in order to reduce cost and tailor flexibility, there has been a growing demand for synthetic leather [5]. Commercially, two types of synthetic leather are primarily used based on—polyurethane (PU) and polyvinyl chloride (PVC) [6]. A general manufacturing process of synthetic leather is typically a four-step process. In the first step, a polymer solution is laid on a paper layer and pressed between heated rollers, creating a thin layer of synthetic leather. The polymer solution is a mixture of about 55% PU/PVC polymer, about 40% plasticizer, about 1% stabilizers, and the balance fillers [6]. In the second step, the polymer solution, mixed with a riser, is laid on the previous layer. This is passed through an oven, which forms a second, thick, foamy leather layer. The third step includes the simultaneous addition of a cotton-polyester layer and peeling off the paper layer, while the structure is being cured in an oven. The fourth step is laying a resin layer and the setup being passed through textured rollers [7].

Polyurethanes (PUs) are the most versatile class of polymers [8] owing to their diverse applications such as coatings, elastomers, foams, adhesive-based products, textile finishing, thermal insulation etc. [9]. The uniqueness of PUs is reflected in their properties and can be ascribed to the definite micro level construction of linear PUs based on hard and soft segments [10]. The hard segments of PU block derived from isocyanate and soft segments of PU derived from polyols [11]. Mostly, aliphatic diisocyanates combined with polyols are used to synthesis PUs as compared to aromatic diisocyanate. The preference for aliphatic diisocyanate is because they are more reactive to form pre-polymer and color stable PU coating or elastomers, chemically resistant, resistance to yellowing and chalking and resistance to abrasion etc., that can significantly enhance a product's appearance, and length its lifespan [12]. The wide range applications of polyurethane are due to their unique mechanical, chemical and morphological properties [13].

Due to increasing concerns about human health and environmental-friendliness, most of the organic solvent-based coatings have limited their applications as they release large amounts of volatile organic compounds (VOCs) [14]. In contrast, eco-friendly coatings are preferred as a potential substitute of conventional organic solvent-borne coatings, such as waterborne emulsions, radiation

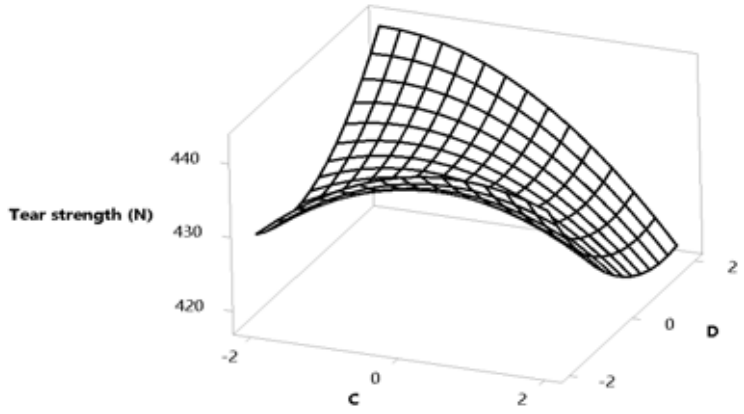

FIGURE 1
Surface Plot of Tear strength (N) vs D, C

curable coatings, powder coatings, high solid content coatings, etc. [15]. Waterborne polyurethane coatings have proven potential industrial coatings owing to their exceptional adhesive strength, ease in tailoring desirable mechanical, thermal and chemical properties, superior weather resistance, excellent solvent resistance, pH stability, less or zero VOCs, durable flexibility even at low temperature and water resistance properties. Waterborne polyurethane (WPU) is being rapidly developed and applied to leather and textile finishing [16], adhesives, pressure sensitive adhesives, floor coverings, and so on [17]. Binary colloidal system of waterborne PUs serves as a continuous emulsion medium for PU particles. The basic building components of water dispersible polyurethane include aromatic or cyclic diisocyanates, long chain polyesters, polyether or polycaprolactone polyols, low molecular weight bis-hydroxyl carboxylic acid, diamine and/or glycol as a chain extender and a neutralizing base [18]. By defaults, conventional PUs having hydrophobic diisocyanate, do not dissolve but this can be converted to water dispersible materials by incorporation of non-ionic or ionic hydrophilic groups in the polymer chain [19]. In WPU, the base neutralizes the pendant −COOH groups forming water dispersible pre-polymer with salt groups. WPU has become more important due to its exceptional properties such as quick drying time, curing at room temperature, gloss temperature, and flexibility impact resistance, transparency, non- flammable, abrasion resistance, low contents of VOCs, adhesion on many substrates, hardness and easy cleaning with water. Moreover, WPU can be injected, molded, extruded and recycled easily.

In this paper, waterborne synthetic leather was fabricated, which will bring some guidance and reference to the synthetic leather process. These surfaces are expected to be of interest in wide variety of applications.

EXPERIMENTAL

Synthetic leather consists of grooved surface to simulate leather feel. A nanocomposite layer of hydrophobic silica nanoparticles and waterborne polyurethane emulsion was used to achieve hierarchical structure. The nanocomposite layer was deposited using spray coating technique because it provides the desired surface as compared to other techniques. The nanocomposite layer was later coated with low energy fluorinated materials, because they are known to provide repellency to low surface tension liquids such as oils. Fluorinated materials are commonly used because fluorine is very electronegative and has a low polarizability.

Polyurethane wet solidification process:
(1) Base fabric after PVA pre-shrinking treatment;
(2) Main solidification tank (21°C);
(3) Secondary solidification tank (17°C);
(4) Hot water wash off PVA;

RESULTS AND DISCUSSION

With the increase of the concentration of polyurethane immersion liquid, the density of polyurethane membrane also increases, the fiber consolidation is not easy to slip, and the tear strength is reduced, but the polyurethane film also bears part of the stress, although the nonwoven substrate reaches The maximum strength, and the polyurethane film does not reach the maximum strength, so its tear strength increases with the increase of the concentration of polyurethane cool impregnation solution.

Fig.1 and 2 indicate that the tear strength changes with the concentration of the polyurethane immersion liquid. The tear strength first increases with the concentration of the polyurethane cool impregnation liquid, and then decreases. When the

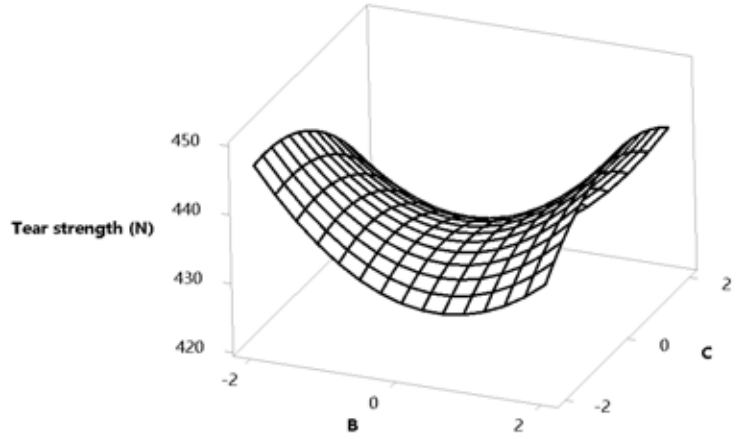

FIGURE 2
Surface Plot of Tear strength (N) vs C, B

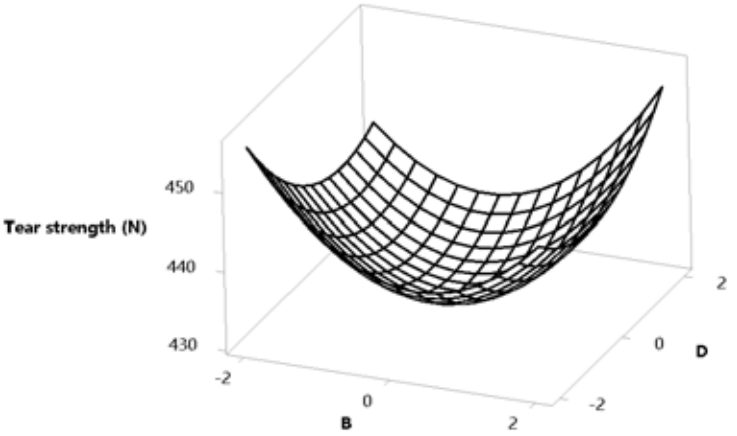

FIGURE 3
Surface Plot of Tear strength (N) vs D, B

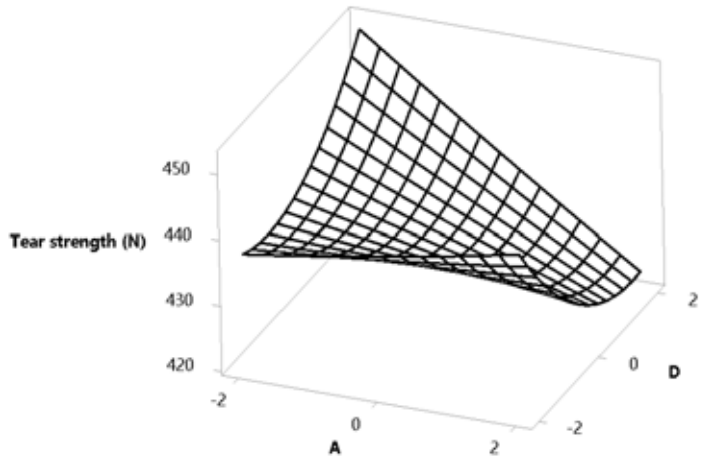

FIGURE 4
Surface Plot of Tear strength (N) vs D, A

concentration of the polyurethane immersion liquid is between, tear strength reaches a peak.

The velocity of the film moving toward the coagulation bath is fast before it enters the coagulation bath, and then the velocity is gradually reduced. As the concentration in the coagulation bath increases, the tear strength decreases. This is because as the solidification time increases, the solidification rate becomes slower, the pore diameter of the membrane becomes smaller, and the drilling force

between the polyurethane membrane and the fiber increases, restricting the movement deformation of the fiber and the yarn, so during the tearing process, the friction between the fibers and between the yarns is reduced, resulting in a reduction in the tear strength of the product. It can be seen from Fig. 3 and 4 that the tear strength is relatively high at 8-16 min of solidification, and the pore size is moderate between 8-12 min.

For Fig.5, it is seen that the concentration of lanthanum acetate in the coagulation tank increases, and the tear strength tends to decrease. In order to obtain a relatively fine and uniform pore size of the bass, and also to meet the high concentration requirements during recovery, the concentration of the coagulation tank is preferably between 10% and 20%.

Fig.6 shows that the relationship between the temperature of the solidification tank and the tear strength indicates that the tear strength has a certain relationship with the solidification temperature.

Since the hydrolysis temperature is 25°C, the solidification temperature must be lower than this temperature. Fig.7 and 8 show that the temperature is low, the diffusion speed of lanthanum acetate is slow; when the temperature is high, the diffusion speed is fast, and the dense surface is formed on the surface of the film, which affects the uniform diffusion of the internal lanthanum acetate, and the pore diameter is small and uneven.

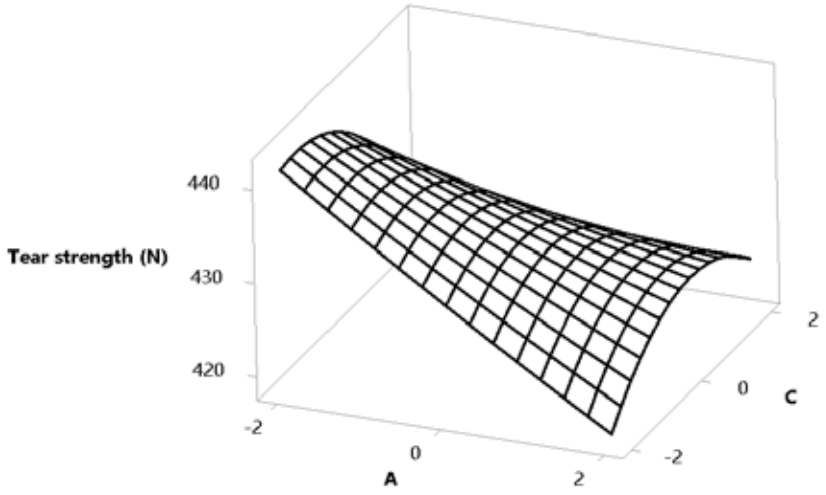

FIGURE 5
Surface Plot of Tear strength (N) vs C, A

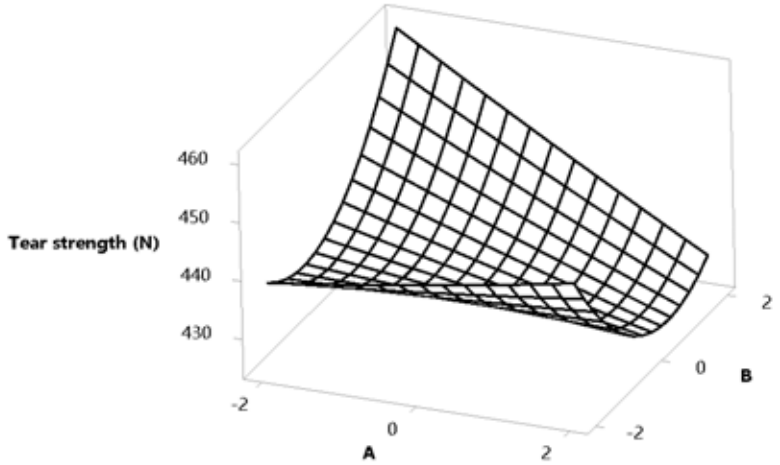

FIGURE 6
Surface Plot of Tear strength (N) vs B, A

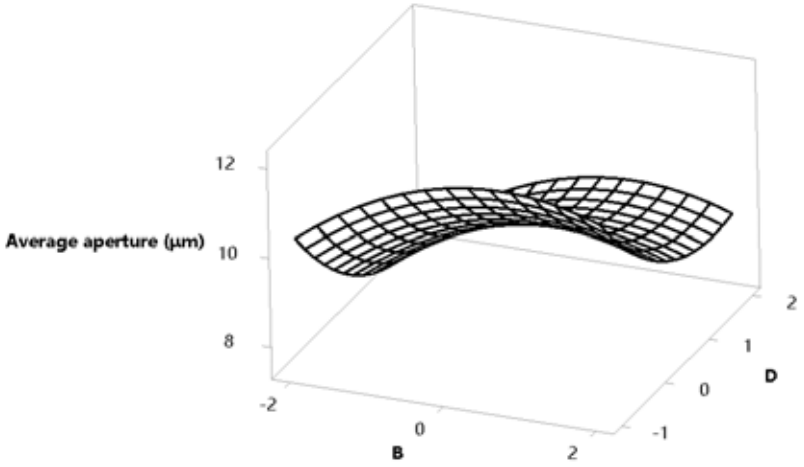

FIGURE 7
Surface Plot of Average aperture (µm) vs D, B

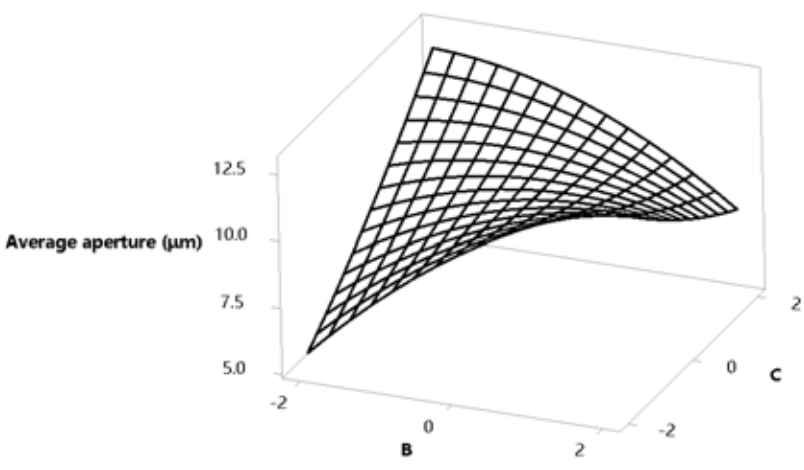

FIGURE 8
Surface Plot of Average aperture (µm) vs C, B

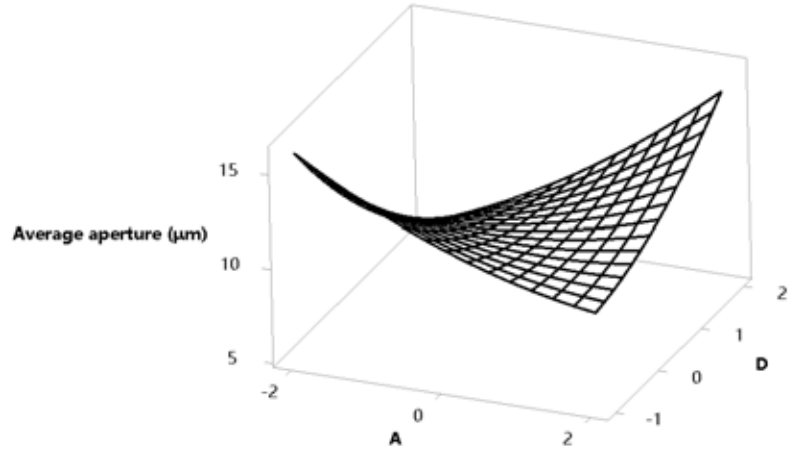

FIGURE 9
Surface Plot of Average aperture (µm) vs D, A

The concentration of lanthanum acetate in the coagulation bath is an important process parameter affecting the solidification rate and microporous structure.

Fig.9 and 10 show that the lower the concentration in the coagulation bath, the typical finger structure in the membrane, the large pore size is high, the solidification rate is slow, and the pore

diameter in the membrane is fine. As the concentration in the coagulation bath increases, the tear strength decreases. This is because as the concentration in the coagulation bath increases, the solidification rate becomes slower, and the adhesion between the polyurethane film and the fiber increases, restricting the movement deformation of the fiber and the yarn, so during the tearing process, between the fibers and the friction between the yarns is reduced, resulting in a reduction in the tear strength of the product.

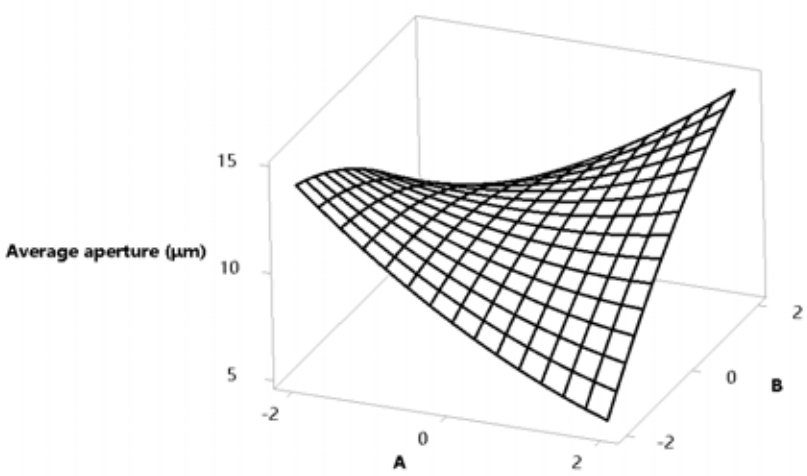

FIGURE 10
Surface Plot of Average aperture (µm) vs B, A

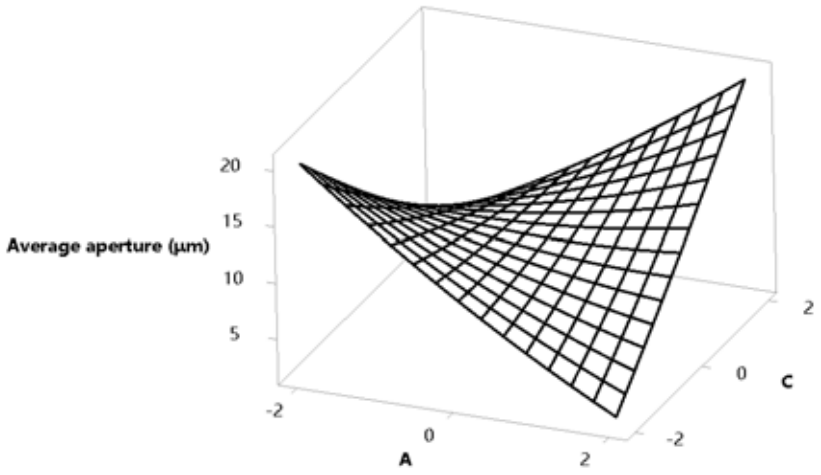

FIGURE 11
Surface Plot of Average aperture (µm) vs C, A

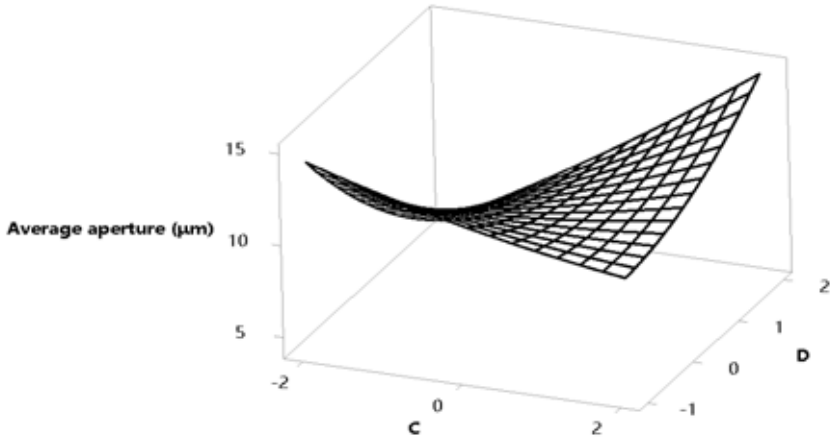

FIGURE 12
Surface Plot of Average aperture (µm) vs D, C

Fig.11 indicates that the average pore size of the product varies with the concentration of polyurethane impregnating solution. When the concentration of polyurethane impregnating solution is between 15% and 20%, the average pore size of the sample is relatively stable and the pore size is moderate. The water droplets have an average diameter of 100 μm and the water vapor molecules have an average diameter of 0.0005 μm. Therefore, it can prevent water droplets, but allows water vapor molecules to pass through, thereby obtaining waterproof and breathable properties.

Fig.12 indicates that the velocity of the film moving toward the coagulation bath is fast before it enters the coagulation bath, and then the velocity is gradually reduced. As the concentration in the coagulation bath increases, the tear strength decreases. This is because as the solidification time increases, the solidification rate becomes slower, the pore diameter of the membrane becomes smaller, and the drilling force between the polyurethane membrane and the fiber increases, restricting the movement deformation of the fiber and the yarn, so during the tearing process. The friction between the fibers and between the yarns is reduced, resulting in a reduction in the tear strength of the product.

CONCLUSIONS

Waterborne synthetic leather was fabricated by wet solidification process. We studied the effect of polyurethane impregnating solution concentration, coagulation bath temperature and solidification time on tear strength, concentration of lanthanum acetate, and average aperture. The results show that concentration of lanthanum acetate and the solidification time are the main influencing factors. Through research, the low temperature differential temperature solidification method has a good effect on pore formation. The optimized wet solidification process has a lanthanum acetate concentration of 16%, a solidification temperature of 21□, a solidification time of 9 min, and a polyurethane impregnating solution concentration of 12%. These surfaces are expected to be of interest in wide variety of applications.

ACKNOWLEDGEMENTS

This paper is supported by Study on the Wet solidification of Ecological Synthesis leather Base, Hebei Science and Technology Department (17274017).

REFERENCES

[1] Adiguzel-Zengin, A.C., Zengin, G. Kilicarislan-Ozkan, C. (2017) Characterization and application of acacia nilotica l. as an alternative vegetable tanning agent for leather processing. Fresen. Environ. Bull. 26, 7319-7326.

[2] Gurler, D.K. (2016) Tannin content of pomegranate rind extract and its potential use in leather production. Fresen. Environ. Bull. 25, 5924-5928.

[3] Dev, G., Bharat, B. (2018) Fabrication of bioinspired superliquiphobic synthetic leather with self-cleaning and low adhesion. Colloids and Surfaces A: Physicochemical and Engineering Aspects. 545, 130-137.

[4] Shazia, M., Ijaz, A.B., Mohammad, Z., Haq, N. B., Muhammad, S. (2016) Synthesis, characterization and efficiency evaluation of chitosan-polyurethane based textile finishes. International Journal of Biological Macromolecules. 93, Part A, 145-155.

[5] Kan, C.W., Kwong, C.H., Ng, S.P. (2015) Surface modification of polyester synthetic leather with tetramethylsilane by atmospheric pressure plasma. Applied Surface Science. 346, 270-277.

[6] Özsin, G., Pütün Eren, A. (2018) A comparative study on co-pyrolysis of lignocellulosic biomass with polyethylene terephthalate, polystyrene, and polyvinyl chloride: Synergistic effects and product characteristics. Journal of Cleaner Production. 205, 1127-1138.

[7] Kim, C., Hsieh, Y.-L. (2001) Wetting and absorbency of nonionic surfactant solutions on cotton fabrics. Colloids Surf. A Physicochem. Eng. Asp. 187–188, 385-397.

[8] Uscátegui, Y.L., Arévalo, F.R., Díaz, L.E., Cobo, M.I., Valero, M.F. (2016) Microbial degradation, cytotoxicity and antibacterial activity of polyurethanes based on modified castor oil and polycaprolactone. Journal of Biomaterials Science Polymer Edition. 27(18), 1860-1879.

[9] Brinkman, E., Vandevoorde, P. (1998) Waterborne two-pack isocyanate-free systems for industrial coatings. Progress in Organic Coatings. 34, 21-25.

[10] Zia, K.M., Bhatti, I.A., Barikani, M., Zuber, M., Islam ud., D. (2008) Surface characteristics of UV-irradiated polyurethane elastomers extended with α, ω-alkane diols. Applied Surface Science. 254, 6754-6761.

[11] Mumtaz, F., Zuber, M., Zia, K.M., Jamil, T., Hussain, R. (2013) Synthesis and properties of aqueous polyurethane dispersions: Influence of molecular weight of polyethylene glycol. The Korean Journal of Chemical Engineering. 30, 2259-2263.

[12] Malik, M., Kaur, R. (2018) Influence of aliphatic and aromatic isocyanates on the properties of poly (ether ester) polyol based PU adhesive system. Polymer Engineering and Science. 58(1), 112-117.
[13] Fiori, D.E. (1997) Two-component water reducible polyurethane coatings. Progress in Organic Coatings. 32(1), 65-71.
[14] Madbouly, S.A., Otaigbe, J.U. (2009) Recent advances in synthesis, characterization and rheological properties of polyurethanes and POSS/polyurethane nanocomposites dispersions and films. Progress in Polymer Science. 34, 1283-1332.
[15] Kim, B., Kim, T., Jeong, H. (1994) Aqueous dispersion of polyurethane anionomers from H12MDI/ IPDI, PCL, BD, and DMPA. Journal of Applied Polymer Science. 53, 371-378.
[16] Wicks, Z.W., Wicks, D.A., Rosthauser, J.W. (2002) Two package waterborne urethane systems. Progress in Organic Coatings. 44, 161-183.
[17] Lin, Y., Hsieh, F. (1997) Water-blown flexible polyurethane foam extended with biomass materials. Journal of Applied Polymer Science. 65, 695-703.
[18] Jang, J.Y., Jhon, Y.K., Cheong, I.W., Kim, J.H. (2002) Effect of process variables on molecular weight and mechanical properties of water-based polyurethane dispersion. Colloids and Surfaces A, Physicochemical and Engineering Aspects. 196, 135-143.
[19] Duecoffre, V., Diener, W., Flosbach, C., Schubert, W. (1998) Emulsifiers with high chemical resistance: A key to high performance waterborne coatings. Progress in Organic Coatings. 34, 200-205.

Received: **25.10.2018**
Accepted: **16.03.2019**

CORRESPONDING AUTHOR

Qiaobin Liu
Tianjin University of Science & Technology
Tianjin 300457 – P.R. China

e-mail: 2284889622@qq.com

© by PSP Volume 28 – No. 5/2019 pages 4226-4231 Fresenius Environmental Bulletin

DETERMINATION OF SOME PHYSICAL AND CHEMICAL CHARACTERISTICS OF GIANT MISCANTHUS (*MISCANTHUS X GIGANTEUS*) SILAGES HARVESTED AT DIFFERENT DEVELOPMENT STAGES

Osman Yuksel*

Usak University, Faculty of Agricultural and Natural Sciences, Department of Field Crops, Usak, Turkey

ABSTRACT

The aim of this study is to determine some physical and chemical characteristics of giant miscanthus silages harvested and ensiled in different development stages. In the study, giant miscanthus (*Miscanthus x giganteus*) was harvested and ensiled without using any additives at the early booting, booting and flowering stages in 2017 year. According to the results of the study, statistically significant differences were determined related to dry matter contents, silage loses, physical observation values, pH, fleig scores and relative feed values of the silages in terms of cutting stages. The crude protein contents of the silages varied between 4.07% and 5.20%, NDF values varied between 71.46% and 77.06% and ADF rates varied between 49.66% and 52.02%. According to the results of the study, late cutting stage increased the silage fermentation performance, however, it decreased the silage quality. At the end of the study, it was found out that it is more suitable to harvest the giant miscanthus in early booting stage for a high quality silage.

KEYWORDS:
Giant miscanthus, *Miscanthus giganteus*, silage, pH, NDF, crude protein

INTRODUCTION

Meeting the quality roughage need is among the most important problems to be solved in order to improve the livestock in Turkey. Low production costs of quality roughages such as hay, green grass, and silage feeds increase the profitability of livestock enterprises [1-2]. It is known that about 70% of the production costs in dairy production or feeder cattle enterprises are feed inputs [3]. Roughages are important as they improve the animal performance by means of protein, fat, cellulose, mineral, and vitamins. They also prevent many metabolic diseases based on feeding and they provide high-need animal products [4]. When the quality roughage demand of the livestock sector is met, the yield per animal will increase as a result of the decrease in the use of the unqualified roughage such as straw and fodder. These roughages have low feed value and high cellulose in feeding animals.

The silage is an important feed source used for the economic, balanced and adequate feeding for ruminants, primarily feeder and dairy cattle, in the countries developed in husbandry [5]. Silage can be made from almost all of the green fodder. However, the dry matter ratio of the green forage that will be used in silage (25-30%) and readily soluble carbohydrate (2.5% and higher) are two important factors. In silage production, only the plants grown for this purpose can be used, and various production residues can also be used for silage.

The giant miscanthus (*Miscanthus x giganteus*) is a perennial, warm-season Asian grass with the C4 photosynthetic pathway. The triploid *Miscanthus x giganteus* with 57 chromosomes breeding by natural hybridization of the tetraploid *Miscanthus sacchariflorus* with 76 chromosomes and diploid *Miscanthus sinensis* with 36 chromosomes (the giant miscanthus) is a sterile plant [6]. Although the giant miscanthus, originated in Japan, is sterile and does not give seed, it can be grown easily with the strong rhizomes [7]. Lewandowski et al. [8], have reported that *M. giganteus* can adapt in a very wide area from the Mediterranean coast to southern Scandinavia. The researchers have reported that *M. giganteus* contain enough sugar in order to be ensiled. Its silage pH is about 4.2 and the silage dry matter is about 40% and the fermentation can be completed after two weeks its ensiling. Burner et al. [9], reported that the giant miscanthus stems are richer than their leaves in terms of nonstructural carbohydrates. In the study conducted by Geren et al. [10] in Izmir, it was stated that the green herbage yield of the giant miscanthus was 11618 kg/da, the crude protein ratio was 5.62% and the silage pH was 3.79 and it can be easily ensilaged due to the high amount of carbohydrate it includes. Whittaker et al. [11], determined the dry matter ratio in the giant miscanthus silages as 35.7%, the silage pH as 5.5,

and the NDF value of the silage as 70.1 in their study conducted with *M. giganteus*, *M sacchariflorus* and corn silages. In the same study, the pH of the corn silage was determined as 5.6.

The giant miscanthus has become the center of interest for high biomass yield it produces from unit area and for its high adaptation capabilty in many countries, especially in Europe. Miscanthus' beneficial environmental profile is mainly due to its perennial nature and because soil organic carbon tends to increase when arable land is converted to its cultivation [12]. It is a very resource and land-use efficient crop with efficient nutrient-recycling mechanisms and high net energy yields per unit area [13, 14]. For this reason, miscanthus is very useful crop both producers and environment.

The previous studies have been mostly about the plant's use in the bioenergy area. However, there is a limited number of studies conducted to determine the potential of the giant miscanthus used as a roughage source for animal feeding. This study was conducted to determine some physical and chemical characteristics of giant miscanthus silages harvested and ensiled at different development stages.

MATERIALS AND METHODS

The study was conducted at Agriculture and Natural Sciences Faculty in Usak University, in 2017. The giant miscanthus (*Miscanthus x giganteus*) plants aged two years were used in the trial field as the material. According to the treatments in the study, the giant miscanthus, harvested in three development periods, (early booting, booting and flowering) was chopped in the laboratory-type by a grinding machine. The samples of each cutting were filled and compressed in the 1 liter plastic jars without any additives and then ensiled without letting the air in as much as possible. After the ensiled jars were closed tightly without letting any air inside, they were wrapped with stretch film and left for fermentation [15]. At the end of a 90-day fermentation period, silo jars were opened.

The physical characteristics of the silages such as colour, smell and structure were determined according to the average scores given by four people who are experienced on silages, according to the scale determined by DLG [16]. In order to determine the dry matter rate, the samples taken from each jar were kept at the drying oven set at 105 ºC until it reached to its constant weight and then the dry matter rates were determined by being proportioned to their wet weights. To determine the silage pH, 2.5 ml of distilled water was added to 1 g of silage sample. After stirring in an agitator for 5 minutes, pH of the silage was determined by digital pH meter [16]. The Fleig scores were calculated based on the formula presented by Denek et al. [17], (Flieg Score = 220 + (2 x % dry matter - 15) - 40 x pH). For the quality analyses, the values obtained from performing nitrogen analysis on the grounded samples of each silage based on the method of Kjeldahl [18] were multiplied by the coefficient of 6.25 and then the crude protein ratios of the samples were determined. The NDF and ADF analyses of silage samples were performed according to the fundamentals reported by ANKOM Technology [19]. Relative feed value (RFV) was calculated according to the formula (RFV = % DDM x % DMI x 0.775) reported by Horrocs and Vallentine [20].

The data obtained from the study were subject to variance analysis in accordance with the randomized parcels experimental designs with three replicatons in the JMP 5.0.1 statistical packaged software. As a result of the analysis of variance, least significant difference (LSD) (5%, 1%) tests were used to determine the significance levels of the differences between the mean values.

RESULTS AND DISCUSSION

Table 1 shows the values related to some physical properties of the giant miscanthus silages ensiled in different development periods. According to the table, the effect of harvest times on the dry matter rates of silages was found to be statistically significant at the level of 0.05. The dry matter rates of silages, according to harvesting stages, varied between 36.69% and 47.62%. The highest dry matter content was determined as 47.62% in the silages harvested the flowering period. Kristensen [21], reported that the dry matter rate of *Miscanthus* was 41% and Lewandowski et al. [8], stated that the dry matter rate in the silages of *Miscanthus* was about 40%. Moreover some researchers reported that the advancing of harvest stage, increased the dry matter content of silages [22-23]. In this context, the study indicated that as the harvest time progressed, the structural carbohydrate amount in the plant tissues increased and this led to an increase in the dry matter rates of the silages.

The effect of the harvest times on the silage loss caused statistically significant differences at the level of 0.05 and the highest silage loss was observed in the silages as 2.66% in the early booting period. The lowest silage loss was determined as 2.27% in the silages in the flowering period (Table 1). This period also corresponded to the period with the highest dry matter rate. This situation was remarkable as it demonstrated that the silage loss also decreased together with the increase in the dry matter rate. The losses in silage production may be caused by mechanical respiration, fermentation and washing [24]. In the present study, the silage loss mainly based on

fermentation and respiration. It has been reported by some researchers that the silage loss may be between 3-30% [24]. In this respect, the silage loss values determined in the present study were found to be quite reasonable.

A decrease which is parallel to the advances of the maturity in the plant was observed in the physical observation values and then it was calculated by summing the scores of the physical parameters like color, smell and structure. The highest physical observation value was determined in the silages of the early booting and booting periods and the lowest values were determined in the flowering period (Table 1). According to the silage quality classification, that can be determined by sense organs, by German Agricultural Organization (DLG), the silages are divided into 5 groups according to their sum of the smell, structure, and color scores based on silage qualification classification (20-18: Very Good, 17-14: Good, 13-10: Average, 9-5 : Low, 4-0: Impaired) [17]. According to the results determined in the study, the silages were in a "very good quality" group in each of three periods.

The effect of harvest stages on silage pH values was found to be statistically significant at the level of 0.01. Accordingly, the silage pH decreased depending on advances of the harvest stage. The lowest pH was determined as 4.71 in flowering and the highest silage pH was determined as 5.09 in the silages produced in the early booting stage (Table 2). McDonald et al. [25], reports that the pH of the silage may increase due to the badly performed silo compaction process. However, in terms of both the Fleig scores and physical quality class, there was no problem related to compression in the present study. In their study, Geren et al. [10], reported the pH of the giant miscanthus silage as 3.79. These values were lower than the results of the present study. Whittaker et al. [11], reported the silage pH in the giant miscanthus as 5.5. The values of the researchers are higher than the values of the present study. Kaiser et al. [26], reported that the high dry matter rate in the silage may cause a buffering effect in the silage pH. In the present study, it was observed that the advances of the maturity affected the silage performance positively as an increase in stem ratio of plants and in the sugar ratio of silages.

The Fleig score is a quality parameter calculated with the dry matter rate and pH in silage. Besides, this value is expected in a high amounth in the quality silages. When the score is calculated by putting the dry matter and pH values data into their places in the Flieg Score= 220+(2x % Dry Matter-15)-40 x pH equation, the silage quality increases according to the quality class order (100-81:Very Good, 80-61:Good, 60-41:Satisfying, 40-21:Average, 20-0:Bad) of the obtained score [25]. In the study, the effect of the ensilage period on the Fleig score was found to be statistically significant at the level of 0.01. The Fleig score values increased as the giant miscanthus became mature. The highest Fleig score (111.58) was determined in flowering period and the lowest values were determined in the early booting period (Table 2). In the study, all three ensilage periods, the silages were among the "very good quality class" in terms of the Fleig scores.

TABLE 1
Dry matter contents, silage losses and physical observations of giant miscanthus silages at different harvesting stages.

Harvesting Stages	Dry Matter (%)	Silage Loss (%)	Physical Observation
Early booting	36.69 b^{+}	2.66 a	19.00 ab
Booting	42.06 ab	2.38 ab	19.67 a
Flowering	47.62 a	2.27 b	18.33 b
$LSD_{0.05}$	6.06*	0.32*	0.94*
CV (%)	7.19	6.52	2.48

$^{+}$: The differences between the averages indicated by the same letters are statistically insignificant.
*: Significant at the level of 0.05.

TABLE 2
pH, fleig score and crude protein contents of giant miscanthus silages.

Harvesting Stages	pH	Fleig Score	Crude Protein (%)
Early booting	5.09 a^{+}	74.91 c	5.20 a
Booting	4.85 b	95.25 b	4.63 b
Flowering	4.71 c	111.58 a	4.07 c
$LSD_{0.05}$	0.08**	10.66**	1.39**
CV (%)	0.84	5.68	3.01

$^{+}$: The differences between the averages indicated by the same letters are statistically insignificant.
**: Significant at the level 0.01.

TABLE 3
The values of NDF, ADF and RFV in giant miscanthus silages at different devolopment stages.

Harvesting Stages	NDF (%)	ADF (%)	RFV (%)
Early booting	71.46 b	49.66	65.35 a
Booting	76.26 a	50.93	60.04 b
Flowering	77.06 a	52.02	58.34 b
$LSD_{0.05}$	0.74**	ns	12.98**
CV (%)	0.05	3.13	2.80

+: The differences between the mean scores indicated by the same letters are statistically insignificant.
**: Significant at the level 0.01. ns: not significant.

The crude protein ratios of the silages produced from the giant miscanthus varied between 4.07% and 5.20%. The highest crude protein content was determined in the early booting stage and the lowest crude protein content was determined in the flowering stage (Table 2). As the harvest time was delayed the crude protein contents decreased. By the way, the harvest times caused significant differences in the crude protein content at the level of 0.01. Naidu et al. [27] and Huyen et al. [28], reported that the crude protein content in giant miscanthus varied between 3-6%. Geren et al. [10], stated that the crude protein contents of giant miscanthus varied from 5.29% to 5.82%. Da Borso et al. [29], reported that there was a sudden decrease in the crude protein rate of the giant miscanthus together with the delay of the harvest period, the crude protein ratios varied between 4.01% and 5.47% in the early harvest and this ratio varied between 2.06% and 2.87% in the late harvest. The crude protein contents determined in the present study are similar to those reported by the previous researchers. In the study, the advancing harvest period caused a decrease in the leaf/stem ratio in the plants and this caused a decrease in the crude protein content.

The NDF value, which is one of the important quality parameters of the forage crops, may give an opinion about the digestibility of the forage. In the study, the NDF rates of the giant miscanthus harvested in different devolopment periods varied between 71.46% and 77.06%. In the silages, the lowest NDF value was determined in the early booting. The NDF values of the silages produced in the booting and flowering periods were found not to be statistically different and the effect of the ensilage period on NDF was statistically significant at the level of 0.01 (Table 3). Norman and Murphy [30], stated that the NDF rate in the giant miscanthus (*Miscanthus x giganteus*) varied between 72.2% and 79.1% and its average value was 77.5%. The values reported by the researcher were similar to the results of the present study. However, there were not enough studies on the digestibility characteristics of the giant miscanthus. On the one hand, the NDF values in silages of plants such as maize and sorghum were reported between 65.82% (maize) and 66.45% (sorghum) [17]. On the other hand, the NDF values we have determined in the giant miscanthus are higher than the NDF values determined in maize and sorghum silages. This showed that the giant miscanthus was richer than maize and sorghum in terms of the cell wall components and also the plant's silage digestibility was lower than those of the plants mentioned.

It was determined that the harvest periods did not have a statistically significant effect on the ADF ratios of the giant miscanthus silages and ADF rates of the silages varied between 49.66% and 52.02%. Burner et al. [9], reported that the ADF values of the giant miscanthus were 52.28% and 40.43% in the leaves and stems respectively. Besides, the giant miscanthus stems were richer than the leaves in terms of nonstructural carbohydrates (organic acid and sugar). Norman and Murphy [30], determined that the ADF rates in the giant miscanthus varied between 43.1%-59.0% and Whittaker et al. [11], determined these rates as 47%. The difference between NDF and ADF rates is mainly due to hemicellulose which is basically one of the cell wall components. In other words, the harvest periods included in the study were effective mainly on the hemicellulose content of the plant and it may be asserted that it did not have a significant effect on the cellulose and lignin contents.

The relative feed values (RFV) of the silages varied between 65.35% and 58.34%. As the harvest period advanced for the silage, decreases in the RFV values of the silages were observed and the analyses of variance showed that these decreases were statistically significant at the level of 0.01 (Table 3). With the delay in the harvest period, the structural carbohydrate amount (hemicellulose, cellulose and lignin) in the cell wall components increased and also the NDF and ADF values of the plant increased. And as the RVF value was calculated mainly through the equation derived from the NDF and ADF rates, the increasing NDF and ADF rates caused a decrease in the RFV value in inverse proportion. In the classification performed by Linn and Martin [31], related to the relative feed values, it was reported that if its RFV value is higher than 151 and the feed has superior quality; if the RFV value is between 125-151, it has high quality; if the RFV value is between 103 -124, it has good quality; it the RFV value is between 87-102, it has average quality; if it the RFV value is

between 75-86, it has poor quality and if this value is lower than 75, it has bad quality. According to the scale reported by the researcher above, the giant miscanthus silages had bad-quality RFV values. In the study conducted on Giant King Grass (*Pennisetum hybridum)* by Geren and Kavut [32], it was reported that RFV values as 95 in average. The RFV values of the giant miscanthus in the present study are lower than the values reported by Geren and Kavut [32].

CONCLUSION

According to the results of this study conducted to determine some physical and quality characteristics of the giant miscanthus silages harvested in different development periods; it was determined that the dry matter rate of the plant was enough for silage production. The values of the silage losses were within the reasonable limits. The silages were involved in the good-quality silage group in all the three cutting stages in terms of the physical quality characteristics and the fleig scores. The advancing harvest period affected the silage performance positively because it increased the sugar-rich stem rate in the forage. However, the advances of the harvest period affected NDF, ADF and RFV values negatively, the crude protein content of the silages particularly.

When the obtained results were evaluated together, it was concluded that it was more suitable to harvest the giant miscanthus in the early booting period for the quality of silage in terms of the crude protein content and the digestibility characteristics.

The giant miscanthus is a high-yielding C4 plant that has high adaptability and is easily harvested and ensilaged. However, the chemical composition of the plant, especially the low crude protein ratio and cell wall components at high levels reduce the roughage quality of the plant significantly. In order to eliminate these problems, some agronomic studies as well as the other studies for improving the quality characteristics of silages, such as the addition of various additives will pave the way for the plant to be used as quality roughage.

REFERENCES

[1] Alcicek, A. (1995) Silo Feed; Factors Affecting Importance and Quality. E.U.A.F. Agricultural Application and Research Center, Publication No. 22, Izmir.

[2] Bilgen, H., Alcicek, A., Sungur, N., Eichhorn, H., Walz, O.P. (1996) Research on harvesting techniques and feed value of some silage roughage forage crops in Aegean region conditions. Animal Husbandry -96 National Congress. 1, 781-789.

[3] Alcicek, A. (2002) Basic Principles of Dairy Cattle Ration. Aegean Agricultural Research Institute Publications. 106, 124-135.

[4] Alcicek, A., Karaayvaz, K. (2003) Use of corn silage in beef cattle. Animalia. 203, 68-76.

[5] Tumer, S. (2001) Silage. Aegean Agricultural Research Institute Publications. 104, Izmir.

[6] Greef, J.M., Deuter, M. (1993) Syntaxonomy of *Miscanthus* x *giganteus*. Angewandte Botanik. 67 (3/4), 87-90.

[7] Jones, M.B., Walsh, M. (2007) Miscanthus, for energy and fibre. Earthscan UK, 192p.

[8] Lewandowski, I., Clifton-Brown, J.C., Scurlock, J.M.O., Huisman, W. (2000) *Miscanthus*: European experience with a novel energy crop. Biomass and Bioenergy. 19, 209-227.

[9] Burner, D.M., Ashworth, A.J., Pote, D.H., Kiniry, J.R., Belesky, D.P., Houx, III, J.H., Carver, P., Fritschi, F.B. (2017) Dual-use bioenergy-livestock feed potential of giant miscanthus, giant reed, and miscane. Agricultural Sciences. 8, 97-112.

[10] Geren, H., Kavut, Y.T., Avcioglu, R. (2011) A preliminary study on ensilability characteristics and yield and other related traits of elephant grass (*Miscanthus x giganteus*) under Mediterranean climatic conditions. Ege Journal of Agric. Res. 48(3), 203-209.

[11] Whittaker, C., Hunt, J., Misselbrook, T., Shield, I. (2016) How well does miscanthus ensile for use in an anaerobic digestion plant? Biomass and Bioenergy. 88, 24-34.

[12] McCalmont, J.P., Hastings, A., McNamara, N.P., Richter, G.M., Robson, P., Donnison, I.S., Clifton-Brown, J. (2015) Environmental costs and benefits of growing Miscanthus for bioenergy in the UK. GCB Bioenergy.

[13] Lewandowski, I., Schmidt, U. (2006) Nitrogen, energy and land use efficiencies of miscanthus, reed canary grass and triticale as determined by the boundary line approach. Agric. Ecosyst. Environ. 112, 335–346.

[14] Cadoux, S., Riche, A.B., Yates, N.E., Machet, J.M. (2012) Nutrient requirements of Miscanthus x giganteus: Conclusions from a review of published studies. Biomass Bioenergy. 38, 14–22.

[15] Siesfers, M.K., Bolsen, K.K. (1997) Agronomic and silage quality traits of forage sorghum cultivars in 1995. Türkiye 1. Silaj Kongresi, 16-19 Eylül, Bursa.

[16] DLG, (1987) Bewertung von Grünfutter, Silage und Heu. DLG-Merkblatt, 224p.

[17] Denek, N., Can, A., Tufenk, S. (2004) Effect of different additives on corn, sorghum and sunflower herbage silages on the quality and in-vitro dry matter digestion. J.Agric Fac. HR. U. 8(2), 1-10.

[18] Kacar, B., Inal, A. (2008) Plant Analysis. Nobel Press, Ankara, 1241, 892p.

[19] Yuksel, O., Albayrak, S., Turk, M., Balabanli, C. (2010) Utilization possibilities of carnation by-products as an alternative roughage source. Turkish Journal of Field Crops. 15(1), 65-68.
[20] Horrocks, R.D., Vallentine, J.F. (1999) Harvested Forages. Academic Press, San Diego, CA, 384p.
[21] Kristensen, E.F. (1995) Miscanthus. Harvesting technique and combustion of *Miscanthus sinensis* "Giganteus" in farm heating plants. In: Chartier, P., Beenackers, A.A.C.M., Grassi, G., (Eds.) Biomass for energy, environment, agriculture and industry. (Proceedings of the Eighth European Biomass Conference, 3-5 October 1994., Vienna, Austria) Pergamon, Oxford, 546-555.
[22] Celen, A.E., Akdemir, H. (1998) Effects of cutting time and nitogen fertilization of forage yield and quality of a sorghum-sudangrass hybrid. Turkish Journal of Field Crops. 3(1), 25-29.
[23] Geren, H. (2001) Effect of sowing dates on silage characteristics of different maize cultivars grown as second crop under Bornova conditions. Ege Journal of Agric. Res. 38(2-3), 47-54.
[24] Kilic, A. (2010) Silo Feed. Hasad Publishing Co., Izmir, 350p.
[25] McDonald, P., Henderson, A.R., Heron, S.J.E. (1991) The Biochemistry of Silage. II. Edition. Chalcombe Publications, Printed in Great Britian by Cambrian Printers Ltd., AberystwFyth, ISBN: 0-948617-22-5, 327p.
[26] Kaiser, A.L., Piltz, J.W., Burns, H.M., Griffiths, N.W. (2004) Successful Silage. Second Edition, Australia, 420p.
[27] Naidu, S.L., Moose, S.P., Al-Shoaibi, A.K., Raines, C.A., Long, S.P. (2003) Cold tolerance of C4 photosynthesis in *Miscanthus giganteus*: adaptation in amounts and sequence of C4 photosynthetic enzymes. Plant Physiology. 132, 1688–1697.
[28] Huyen, T.L.N., Rémond, C., Dheilly, R.M., Chabbert, B. (2010) Effect of harvesting date on the composition and saccharification of *Miscanthus x giganteus*. Bioresource Technology. 101, 8224–8231.
[29] Da Borso, F., Di Marzo, C., Zuliani, F., Danuso, F., Baldini, M. (2018) Harvest time and ensilage suitability of giant reed and miscanthus for bio-methane production and characterzation of digestate for agronomic use. Agronomy Research. 16(X), 444-ccc.
[30] Norman, A.C., Murphy, M.R. (2005). Feed value and in situ dry matter digestibility of *Miscanthus x giganteus* and corn stover. Illinois Livestock Trail, University of Illinois Extension, USA.
[31] Linn, J.G., Martin, N.P. (1989) Forage quality tests and interpretations. http://www.extension.umn.edu/distribution/livestocksystems/DI2637.html.
[32] Geren, H., Kavut, Y.T. (2015) Effect of diffrent plant densities on the yield and some silage quality characteristics of giant king grass (*Pennisetum hybridum*) under mediterranean climatic conditions. Turkish Journal of Field Crops. 20(1), 85-91.

Received: **31.10.2018**
Accepted: **27.03.2019**

CORRESPONDING AUTHOR

Osman Yuksel
Usak University,
Faculty of Agricultural and Natural Sciences,
Department of Field Crops,
Usak – Turkey

e-mail: osman.yuksel@usak.edu.tr

© by PSP Volume 28 – No. 5/2019 pages 4232-4237 Fresenius Environmental Bulletin

DETERMINATION OF PROXIMATE COMPOSITION AND HISTOLOGICAL EVALUATION OF FROZEN AND DRIED OF SEA CUCUMBERS (HOLOTHURIA POLII AND HOLOTHURIA TUBULOSA)

Mustafa Unlusayin[1], Ali Capar[1], Beytullah Ahmet Balci[2,*]

[1]Department of Fish Processing Technology, Faculty of Fisheries, Akdeniz University, Dumlupinar Bulvari Kampus, Antalya, Turkey
[2]Department of Aquaculture, Faculty of Fisheries, Akdeniz University, Dumlupinar Bulvari Kampus, Antalya, Turkey

ABSTRACT

This study was investigated the proximate composition and histological evaluation of frozen and dried of sea cucumbers. Approximately100 of *Holothuria polii* (HP) and *Holothuria tubulosa* (HT) samples from Aegean Sea in İzmir (Turkey) were used in this study. All of the sea cucumbers were frozen and dried. Their water, ash, protein, and fat contents were measured prior to and after processing. The obtained results showed that the values of protein, fat and ash of the freeze and dry samples of HP and HT significantly ($P<0.05$). Also the values of moisture, fat and ash of the HP wet samples and HT wet samples varied significantly ($P<0.05$). The highest values of protein (19.17%) HT frozen samples, (66.32%) HT dried samples and fat (6.31%) HT dried samples and ash (7.78%) HP frozen samples, (22.57%) HP dried samples were investigated. According to the histological evaluation, HP frozen samples; the cell size was smaller than the fresh sample, larger than the dried sample, the connective tissue was irregular and the intercellular space was more found. Therefore, sea cucumbers would be a good basis for frozen utilization of food industries as low cost resource.

KEYWORDS:
Freezing, drying, proximate composition, histological structure, sea cucumber

INTRODUCTION

Sea cucumbers are generally marketed as frozen, cooked-dried, cooked-salted and cooked-salted-dried products. In Turkey, sea cucumbers are not well known and they are not consumed as food, although they have been consumed in many countries such as India, Fiji, Papua New Guinea, China, and Japan of years. Exporting sea cucumbers are annually exported approximately 150 tons. Total amount of 40 tons of dried sea cucumbers are exported to EU Countries and China, Japan, South Korea in 2014.

Thirty seven species of *Holothuroidae* in Mediterranean Sea has found and commercial sea cucumber species are also reported in Turkey in the Aegean, Mediterranean and Marmara Seas [1]. However they are totally exported as they are not consumed domestically. Among commercial sea cucumber species found in Turkey, *Holothuria polii*, *Holothuria tubulosa* and *Holothuria mammata* are known as the most commonly exported species.

The sea cucumbers have high nutritional values with a high quality protein and low fat levels. They are also traditional tonic and widely consumed in East Asian countries sea cucumber can be evaluated as a dietetic food in terms of nutrition [2]. Also it has high rate of Polyunsaturated Fatty Acids (PUFA) and rich in Eicosapentaenoic Acid (EPA) and Docosahexaenoic Acid (DHA) [3]. East Asian markets after being processed by different ways. Products of sea cucumber are highly demanded not only by consumers for their nutritional value, but also by companies for pharmacology medicine and cosmetic purposes [4, 5].

Traditional techniques, which involve salting, repeated boiling and exposure to solar radiation, are long processes that lead to the loss of many active ingredients. Air drying is the simplest method, but it leads to significant changes in quality of the products [2-6].

In this respect, the most determinant factors to avoid the deterioration of the final product are freezing, drying forms and their histological structure of sea cucumbers; *Holothuria tubulosa* and *Holothuria polii*. Therefore, these parameters must be optimized for a better quality of the freeze and dried sea cucumber products.

MATERIALS AND METHODS

Materials. *Holothuria polii* and *Holothuria tubulosa* samples from Aegean Sea were purchased as alive from the commercial firm in İzmir (Turkey). Approximately100 samples each species were

used for experiments. These species were transported to laboratory in seawater with air.

Drying Process. The body of each specimen was cut from the anus nearly to the oral organ, and then their viscera were removed and washed with cold water, weighed and measured. This process were realized according to the method of [1] both species samples were put into boiling water and boiled for 30 min. Then they were allowed to drip dry at environment temperature (+27 °C for 72 h) and placed on grill for sun drying in Antalya (at Faculty of Fisheries Campus).

Freezing Process. Both species fresh sea cucumber in rapidly frozen to minus 35 degrees, the main purpose is to make the sea cucumber body water freezing. Frozen samples were stored minus 18 degrees until analysed (Approx. 72 hours).

Proximate Analysis. Sea cucumber muscles of wet, dry and freeze were homogenized (Heidolph, Hei-Torque Value 100, Germany) by food processor, and moisture content of 3 g of homogenized sample was determined by drying the sample in oven at 105° C (Nüve, FN500, Turkey) until a constant mass was obtained [8]. Ash was determined by using the Lovell method [9] by heating (Elektro-mag, N1813, Turkey) the samples in the furnace at 550 °C for 3–5 h. Total protein was determined by using (Gerhardt Vapodest, VAP 30, Germany) Kjeldahl method [10]. A conversion factor of 6.25 was used to convert total nitrogen to crude protein for all seafood. Total lipids of all sea cucumber species were extracted (Behr Labor-Technik, AK5, Germany) according to the Bligh and Dyer method [11]. Each sample was analysed three times.

Histological Analysis. According to the histochemical techniques, the tissues removed from the sea cucumber of wet, dry and freeze samples were kept in 10% neutral formaldehyde solution for at least 24-48 hours. The tissues were detected in the neutral formaldehyde. They were washed for one hour in order to eliminate the effect of the detection fluid. The tissues kept in different concentrations of alcohol for a certain period after the detection process were subjected to xylol and paraffin baths and blocked and made ready for cutting with rotary microtome (Leica RM2135, Germany). Sections of 5 µ thickness cut from the tissues blocked for normal histology were kept in an oven at 40 °C overnight. They were stained according to the Harris's hematoxylin-eosin (H+E) staining procedures for the general histological diagnosis. The slides stained and mounted in Canada balsam were examined under a binocular research microscope and their microphotographs (Nikon Ci-LTrinoculer and Imaging Source DFK72, Japan) were taken for evaluation in order to identify the histological details [12, 13, 14].

Statistical Analysis. All samples were analysed in three independent replications (n = 3). The means and standard deviations were calculated from the measurements using Excel (Microsoft, Redmond, VA, USA). IBM SPSS Statistics Program (IBM SPSS Statistics for Windows, Version 21.0, and Armonk, NY) was used for non-parametric Mann Whitney-U test range test at 0.05 significance level.

RESULTS AND DISCUSSION

Proximate Composition. The average and standard deviation of *Holothuria polii* (HP) and *Holothuria tubulosa* (HT) were given Table 1. The average weights of wet HP 77.53 g and wet HT 81.88 g were found in this study. Aydın et al. [1] reported that wet HP 59.25 g and wet HT 78.62 g average weights. Especially wet weights of these species were observed similar. Average gutted weights (means after taken out internal organs of fresh sea cucumbers) HP 54.68 g and HT 65.07 g were found in our study. Aydın et al. [1] was found mean gutted weights HP 26.19 g and HT 47.64 g. In our study, average gutted weights of HP and HT values were higher than their study results.

TABLE 1
The average and standard deviation of *Holothuria polii* and *Holothuria tubulosa*

Type of samples*	*Holothuria polii* (HP)		*Holothuria tubulosa* (HT)	
	Length (cm)	Weight (g)	Length (cm)	Weight (g)
Wet	18.83±1.82	77.53±12.22	18.58±3.09	81.88±20.38
Freeze	6.90±0.51	11.73±2.38	6.83±0.60	11.33±2.46
Dry	5.66±0.50	6.36±1.55	6.19±0,80	8.44±2.11
Gutted	-	54.68±6.89	-	65.07±17.47

*30 samples were used in each type (n-30), Gutted; Average gutted weight means after taken out internal organs of fresh sea cucumbers.

Table 2 represents % proximate composition of *Holothuria polii* (HP) and *Holothuria tubulosa* (HT) in this study. The values of moisture, fat and ash of the HPW and HTW varied significantly (P<0.05). The highest value of moisture (87.11%) HTW and fat (1.70%) HTW and ash (8.10%) HPW were observed. No significant difference was found in protein content between HPW and HTW. After freezing process and drying process samples proximate composition were determined. The values of protein, fat and ash of the freeze and dry samples of HP and HT significantly (P<0.05). The highest values of protein (19.17%) HTF, (66.32%) HTD and fat (6.31%) HTD and ash (7.78%) HPF, (22.57%) HPD were investigated. Moisture contents of freeze and dry samples of HP, HT and freeze samples of HP, HT were found insignificant in this study.

Aydın et al. [1] reported that moisture, protein, fat and ash contents of the species ranged between 81.24% and 85.24%, 7.88% and 8.82%, 0.09% and 0.18%, and 5.13% and 7.85%, respectively, with a significant changes among species (P<0.05) with some exceptions. In our study moisture of HPW and HTW ranged 85.73% and 87.11%, and 4.84% and 5.05%, and 1.33% and 1.70%, and 6.14% and 8.10% respectively. Also the values of moisture, fat and ash of the HPW and HTW varied significantly (P<0.05). The protein contents of HPW and HTW was found low in our study. These values may be subjected to seasonal variation [7-15]. Özer et al. [16] reported the moisture content of fresh sea cucumber dropped from 85% to 6.5% after dried process.

One study was carried out by [7] on food quality of Mediterranean Sea cucumbers *Holothuria tubulosa* and *Holothuria polii* in Southern Adriatic Sea. They observed proximate composition was similar in both species: crude protein HT (44.58%), HP (36.99%) and ash HT (46.43%), HP (48.22). On the other hand, low fat content resulted in HT (0.71%) and HP (0.55%) in dry samples. Our results were observed slightly higher crude protein content and fat content, and lower ash content for relating species.

Telahigue et al. [2] also emphasised that the proximate composition of sea cucumbers fresh *H. forskali* body wall while total fats do not exceed 0.4%. Sicuro et al. [7] demonstrated that fat content of HP and HT are very low. Wen et al. [15] reported that sea cucumbers are seafood with high protein and low fat levels. The high protein, low fat and antioxidant content [17] make sea cucumber a potential protein source for consumers. Our results (Fig.1) were close to proximate composition data with their reports.

TABLE 2
Proximate composition (%) of *Holothuria polii* and *Holothuria tubulosa*

Type of samples	Moisture (%)	Protein (%)	Fat (%)	Ash (%)
HPW	85.73±0.51^{b}	4.84±0.05	1.33±0.04^{b}	8.10±0.26^{a}
HTW	87.11±0.25^{a}	5.05±0.44	1.70±0.02^{a}	6.14±0.15^{b}
HPF	68.53±0.58	18.58±0.12^{b}	5.11±0.08	7.78±0.42^{a}
HTF	69.61±0.40	19.17±0.18^{a}	5.09±0.05	6.13±0.08^{b}
HPD	7.70±0.43	63.72±0.21^{b}	6.01±0.07^{b}	22.57±0.29^{a}
HTD	8.50±0.41	66.32±0.39^{a}	6.31±0.03^{a}	18.87±0.43^{b}

HP; *Holothuria polii,* HT*; Holothuria tubulosa,* W; Wet, F; Freeze, D; Dry
Values are shown as mean ± standard deviation of replicate measurements for two independent and parallel experiments.
Different superscript letters in the same column indicate significant differences among the type of samples (P<0.05)

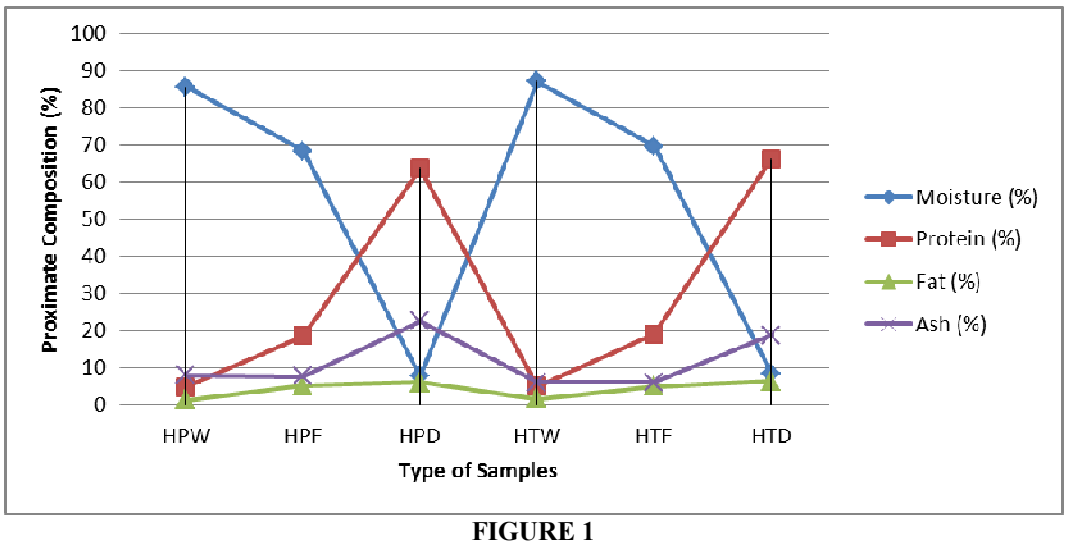

FIGURE 1
Proximate composition (%) of *Holothuria polii* and *Holothuria tubulosa* fresh, dry and freeze samples.
HP; *Holothuria polii,* HT*; Holothuria tubulosa,* W; Wet, F; Freeze, D; Dry

Histological Evaluation. The tissues removed from the sea cucumber of wet, dry and freeze samples were prepared by histochemical techniques. The study results of wet samples of HP and HT tissues were given Figure 2 (A) and (B).

In Figure 2 (A) about HPW; muscle cells were larger, connective tissue was regular, and compact intercellular space was less found in this study. Figure 2 (B) on HTW: Muscle cells were larger, connective tissue was regular, and compact intercellular space was less observed too. On the study, Freeze samples of HP and HT tissues were given Figure 2 (C) and (D).

In Figure 2 (C) about HPF; the cell size was smaller than the fresh sample, larger than the dried sample, the connective tissue was irregular and the intercellular space was more found. Figure 2 (D) on HTF; the cell size was smaller, the connective tissue was irregular and the intercellular space was more found too. Dried samples of HP and HT tissues were given Figure 2 (E) and (F).

In Figure 2 (E) about HPD; muscle cell sizes were smaller, connective tissue was irregular and intercellular space was more observed. Figure 2 (F) on HTD; muscle cell sizes were smaller, connective tissue was irregular and intercellular space was more found in this study.

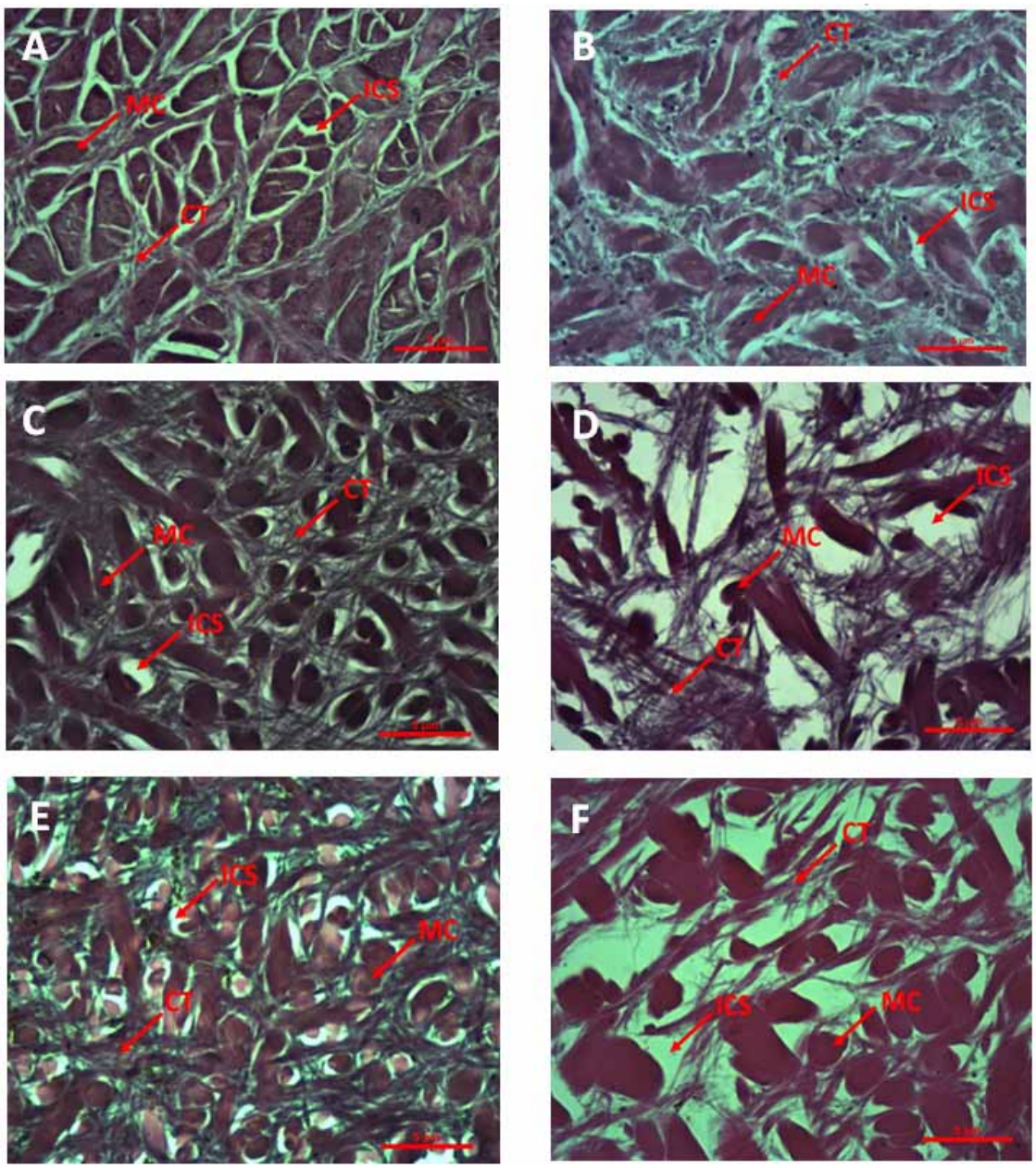

FIGURE 2

Histological Evaluation of *Holothuria polii* and *Holothuria tubulosa* fresh, dry and freeze samples (H+E).

A: HPW tissue, B: HTW tissue, C: HPF tissue, D: HTF tissue, E: HPD tissue, F: HTD tissue, HP; *Holothuria polii,* HT*; Holothuria tubulosa,* W;Wet, F;Freeze D;Dry, CT; Connective tissue, MC; Muscle cell, ICS; Intercellular space

TABLE 3
Quantitative scores in histological measures of *Holothuria polii* and *Holothuria tubulosa* fresh, dry and freeze samples

Type of samples	Muscle Cell (μm)	Connective tissue (μm)	Intercellular Space (μm)
HPW	315.56±88.89 [a]	100.08±47.13 [b]	39.99±9.47 [a]
HTW	351.92±106.74 [a]	113.51±24.25 [b]	48.07±15.09 [a]
HPF	213.01±73.49 [b]	121.45±50.91 [ab]	51.54±25.13 [b]
HTF	207.84±66.70 [b]	274.67±163.61 [a]	98.00±65.50 [b]
HPD	151.12±55.79 [b]	153.01±60.71 [ab]	44.00±9.90 [a]
HTD	225.25±50.22 [b]	109.49±46.38 [b]	142.07±66.86 [b]

HP; *Holothuria polii.* HT*; Holothuria tubulosa.* W; Wet, F; Freeze, D; Dry
Values are shown as mean ± standard deviation of replicate measurements for two independent and parallel experiments. Different superscript letters in the same column indicate significant differences among the type of samples (P<0.05)

Sea cucumbers, as other echinoderms, are characterized by the presence of internal endoskeleton made by microscopic ossicles. These ossicles are embedded in the sea cucumber body [18]. Osmotic dehydration (OD) is one of most important complementary treatment and food preservation technique in the processing of dehydrated foods [19]. Not only has the value of dried sea cucumber depended on its own species, but, the size of the product and the quality in terms of drying process, this is also part of dehydrating the sea cucumbers prior to drying process [20]. In our study was observed, among the histological measures HTD samples of intercellular space (142.07 μm) was found very high (Table 3).

This may be relevant by dehydrating of the sea cucumbers. The three considered parameters have been compared for the 6 experimental groups. Considering muscle cell, connective tissue, intercellular space (Table 3) indicate HPW and HTW for muscle cell, HPF and HTF with HPD and HTD for connective tissue and HPD and HTD for intercellular space were found statistically significant (P<0.05).

CONCLUSIONS

The obtained results showed that all proximate composition and histological evaluation of frozen and dried of sea cucumbers (HP and HT) are valuable for sea cucumbers processing technology. Especially, HTF samples are consisted better results than HPF samples. Sea cucumbers such as HP and HT in this moment are commercially available. Since sea cucumbers are consumed as a food by a very small segment of the population outside East Asia, most people do not have access to its beneficial components. Our study represented sea cucumbers are a good basis for frozen and dried utilization of food industries as low cost resource.

REFERENCES

[1] Aydın, M., Sevgili, H., Tufan, B., Emre, Y. and Köse, S. (2011) Proximate composition and fatty acid profile of three different fresh and dried commercial sea cucumbers from Turkey. Int J Food Sci Tech. 46, 500-508.

[2] Telahigue, K., Hajji, T., Imen, R., Sahbi, O. and El Cafsi, M. (2014) Effects of drying methods on the chemical composition of the sea cucumber *Holothuria forskali*. Open Food Sci. J. 8, 1-8.

[3] Bilgin, Ş. and İzci, L. (2016) The Effects of Drying & Boling Process on Nutritional Components of *Halothuria forskali* (Delle Chiaje, 1823). J Food Health Sci. 2(1), 1-8 (article in Turkish with an English abstract).

[4] Chen, J.X. (2004) Present status and prospects of sea cucumber industry in China. Advances in Sea Cucumber Aquaculture and Management (ASCAM). FAO, Rome, Italy, 25-38.

[5] Chen J. (2003) Overview of sea cucumber farming and ranching practices in China. Beche-de-mer Information Bulletin. 18, 18-23.

[6] Lovatelli, A. (2004) Advances in Sea Cucumber Aquaculture and Management. In: FAO Fisheries Technical Paper, Com. / ed. Conand, C., Purcell, S., Uthicke, S, Hamel, J.F., Mercier, A. (eds.) FAO Rome: Italy, 425p.

[7] Sicuro, B., Piccinno, M., Gai, F., Abeta, M.C., Danieli, A., Dapra, F., Mioletti, S., Vilella, S. (2012) Food quality and Safety of Mediterranean Sea Cucumbers *Holothuria tubulosa* and *Holothuria polii* in Southern Adriatic Sea. Asian J Anim Vet Adv. 7(9), 851-859.

[8] AOAC. (1990) Official Methods of Analysis Association of Official Analytical Chemists International, AOAC: Rockville.

[9] Lovell, R.T. (1981) Laboratory manual for fish feed analysis and fish nutrition studies, Department of Fisheries and Allied Aquaculture. Auburn University.

[10] AOAC. (2000) Official Methods of Analysis Association of Official Analytical Chemists International. 17th ed. AOAC: Rockville.

[11] Bligh, E.G. and Dyer, W.J. (1959) A rapid method for total lipid extraction and purification. Can. J. Biochem. Physiol. 37, 913-917.
[12] Luna, G.L. (1982) Manual of histologic staining methods. American Registry of Pathology. Mc Graw-Hill Co. New York.
[13] Bancroft, J.D. and Stevens, A. (1996) Theory and Practice of Histological Techniques. 4th Edition. Churchill Livingstone, New York.
[14] Presnell, J.K. and Schreibman, MP. (1997) Humason's Animal Tissue Techniques, Fifth Edition. The Johns Hopkins University Press, Baltimore-London.
[15] Wen, J., Hua, C. and Fan, S. (2010) Chemical composition and nutritional quality of sea cucumbers. J Sci Food Agric. 90, 2469-2474.
[16] Özer, N.P., Mol, S. and Varlık, C. (2004) Effect of the handling procedures on the chemical composition of sea cucumber. Turk J Fish Aquat Sci. 4, 71-74.
[17] Zhong, Y., Ahmad Khan, M. and Shahidi, F. (2007). Compositional characteristics and antioxidant properties of fresh and processed sea cucumber (*Cucumaria frondosa*). J Agric Food Chem. 55, 1188-1192.
[18] Daprà, F., Sicuro, B., Cabiale, K., Falzone, M., Visentin, V. and Galloni, M. (2015) The histological evaluation of sea cucumber meal as a potential ingredient in Rainbow Trout diet. Turk J Fish Aquat Sci. 15, 333-340.
[19] Khan, M. (2012) Osmotic dehydration technique for fruits preservation-A review. PAK. J Food Sci. 22(2), 71 –85.
[20] Chong, N.V.W., Pindi, W., Chye, F.Y., Shaarani, S.M. and Lee, J.S. (2015) Effects of Drying Methods on the Quality of Dried Sea Cucumbers from Sabah – A Review. Int J Novel Res in Life Sci. 2(4), 49-64.

Received: **15.11.2018**
Accepted: **17.03.2019**

CORRESPONDING AUTHOR

Beytullah Ahmet Balci
Department of Aquaculture,
Faculty of Fisheries,
Akdeniz University,
Dumlupınar Bulvarı Kampus, Antalya - Turkey

e-mail: abalci@akdeniz.edu.tr

© by PSP Volume 28 – No. 5/2019 pages 4238-4246 Fresenius Environmental Bulletin

ANALYSIS OF EXTRACTION OF GRAPEFRUIT SEED OIL, FATTY ACIDS COMPOSITION AND PHYSICAL AND CHEMICAL PROPERTIES

Jinhua Shao*, Xiaoxia Liu, Hao Zhou, Junyang Liu

School of Chemical and Biological Engineering, Hunan University of Science and Engineering, Yongzhou 425199, China

ABSTRACT

With n-hexane as extractant, the optimal process of ultrasonic-assisted extraction of grapefruit seed oil was optimized by response surface methodology. The fatty acid composition and physical and chemical properties of the obtained grapefruit seed oil were analyzed. The results showed that the best extraction process of grapefruit seed oil was liquid-solid ratio (mL/g) of 12, ultrasonic time of 31 min, ultrasonic power of 191 W, and ultrasonic temperature of 60 °C. Under this condition, grape seed oil extraction rate was 35.67. %. Four kinds of fatty acids were detected by GC-MS, which were palmitic acid (12.74%), linoleic acid (47.73%), oleic acid (32.37%), stearic acid (7.16%), unsaturated fatty acids. The content reaches 80.1%; the grapefruit seed oil is a pale yellow, clear and transparent oily liquid with the characteristic smell and taste of grapefruit seeds. The relative density (d2020) and refractive index (nd20) of grapefruit seed oil were 0.9025 and 1.4745, moisture and volatile matter 0.02%, insoluble impurities 0.03%, iodine value (I2) 95.256 g /100 g, saponification value (KOH) 189.56 mg / g, unsaponifiable 2.46 g / kg, acid value (KOH) and peroxide value were 1.08 mg / g and 2.935 mmol / kg, respectively, smoke point 192°C. All physical and chemical indicators can reach the Chinese edible vegetable oil standard.

KEYWORDS:
Grapefruit seed oil, Fatty acids composition, Physical and chemical properties, Analysis

INTRODUCTION

As an important edible oil source and industrial raw material for human beings, vegetable oils and fats are closely related to people's daily life and national grain and oil security [1]. China's edible oil self-sufficiency rate is obviously insufficient, and it needs a large amount of imports every year and the gap is increasing year by year [2, 3]. The contradiction between limited oil production and sharply increased consumption requires people to explore and develop new plant fat resources.

Citrus (C. grandis Osbecko) is a Citrus plant of the Rutaceae family, which is widely cultivated in the provinces south of the Yangtze River in China, and the yield is increasing year by year [4]. Grapefruit has the functions of strengthening the spleen and stomach, moistening the lungs, enriching the blood, clearing the intestines, facilitating the digestion and helping digestion. It can promote wound healing and has a good therapeutic effect on sepsis [5]. The use of grapefruit has always been mainly for fresh food and food processing, but the attention and application of grapefruit seeds for grapefruit residues are rare, mainly for germplasm preservation and seedling [6]. Like most other plants, grapefruit seeds accumulate and enrich oil during ripening and are a potential plant oil resource. At present, relevant research reports on grapefruit seed oil are almost blank.

Extracting and obtaining plant seed oil is a prerequisite for its development and utilization, so it is of great significance to explore the establishment of a highly efficient and feasible extraction process for specific plant seed oil [7]. The commonly used methods for extracting vegetable oils include pressing method, extraction method, supercritical extraction method, and water enzymatic method [8, 9]. In recent years, ultrasonic waves have been widely used in the extraction of plant active substances because of their good penetration and cell disruption effects, simple operation, low extraction temperature, and no damage to the structure of the material. Previous studies have shown that ultrasound can indeed exert significant positive effects in the extraction of plant seed oil [10, 11]. Based on this, this study optimized the process of ultrasonic-assisted extraction of grapefruit seed oil. It should be pointed out that the extraction of the obtained plant seed oil requires a series of tests to determine its composition and nutritional value, so as to measure and evaluate its development potential as a new edible oil resource, wherein the composition and physical and chemical properties can be very high. It reflects its nutritional value and health benefits. Therefore, based on the ultrasonic assisted extraction process of grapefruit

seed oil, the fatty acid composition and physicochemical properties of the extracted grapefruit seed oil were tested to provide a theoretical basis for the development and utilization of grapefruit seed oil.

MATERIALS AND METHODS

Materials. The grapefruit seeds were picked from Qiyang County, China, and the dried grapefruit seeds were pulverized into powders by a pulverizer for use. All reagents were of analytical grade.

Grapefruit seed oil extraction. Weigh 10.00 g grapefruit seed powder, add a certain volume of n-hexane and stir well, then dilute the mixture for 12 h, then assist the extraction of the grapefruit seed powder solution under certain ultrasonic power, ultrasonic time and ultrasonic temperature. The extract is vacuum filtered to obtain a clear liquid, and the filtered supernatant is subjected to rotary evaporation to collect the oil. Finally, the collected oil is placed in a vacuum oven at 60°C for 2 h to remove residual solvent, and the dried grease is cooled to room temperature. Weighed and calculated the extraction rate. The extraction rate of grapefruit seed oil is calculated according to formula (1):

Extraction rate (%) = (fruit quality of grape seed oil / quality of raw materials) × 100% (1)

Single factor experiment and response surface optimization experiment. The effects of ultrasonic time, ultrasonic power, ratio of material to liquid and ultrasonic temperature on the yield of grape seed oil were investigated. The single factor experiment set liquid-solid ratio (mL/g) 6:1, 8:1, 10:1, 12:1, 14:1, ultrasonic time 20, 25, 30, 35, 40 min, ultrasonic power 100, 150, 200, 250, 300 W, ultrasonic temperature 20, 30, 40, 50, 60°C each 5 gradient levels. When performing a certain factor experiment, the values of the other three factors remained fixed, which were 1:10 ratio of material to liquid, 30 min of ultrasonic time, 150 W of ultrasonic power, and 50 °C of ultrasonic temperature. On the basis of single factor experiment, the design principle of Box-Behnken center was applied. The ratio of material to liquid, time, ultrasonic power and ultrasonic temperature were taken as the object of investigation. The extraction rate was the response value, and the ultrasonic assisted extraction process conditions of grapefruit seed oil were optimized.

GC-MS Analysis of Fatty Acid Composition of Grapefruit Seed Oil. Methylation of the sample. Accurately measure 6.0 mL of grapefruit seed oil in a 25 mL round bottom flask, then add 10.0 mL of a mixture of n-hexane-diethyl ether (2:1), shake it to mix well, and then add 0.5 mol/L KOH - 6.0 mL of methanol solution, refluxed in a constant temperature water bath at 60°C for 20 min. After the reaction is completed, add distilled water to 25 mL, shake evenly, then let stand, and use a plastic pipette to pipette the upper transparent fatty acid methyl ester liquid, and dry it with anhydrous sodium sulfate. Gas chromatography analysis is made [12, 13].

GC-MS analysis conditions. Gas chromatographic conditions: elastic quartz capillary column (30 m × 0.25 mm × 0.255 m); carrier gas is high purity He, purity ≥ 699.999%; column initial temperature 130°C, column temperature: 130-240°C, for 1 min, Warm up to 230°C at 20 °C/min for 5 min, then increase to 240°C at 20 °C/min for 6.5 min for a total of 18.00 min, inlet temperature 250°C, pre-column pressure 84.6 kPa, column flow 1.00 mL /min, split ratio 1:30; 1.0 uL [14] was injected using a microinjector.

Mass spectrometry conditions: EI ion source, ion source temperature 200°C, GC-MS interface temperature 200 ° C, electron energy 70 eV, electron multiplier voltage 0.97 kV, mass scan range 29-450 m / z, solvent peak cut-off time 1.6 min, The mass spectrometry detection start time was 1.7 min [14].

RESULTS AND DISCUSSION

Analysis of physical and chemical properties of grapefruit seed oil. For relative density determination, refer to GB/T 5526-1985 «Measurement method for plant oil and fat test»; Reference index for determination of refractive index GB / T 5527-2010 «Determination of refractive index of animal and vegetable oils»; Determination of saponification value reference GB / T 5535.2-2008 « Determination of saponification value of animal and vegetable oils»; Determination of unsaponifiable matter reference GB / T5535.2-2008 «Determination of unsaponifiable matter of animal and vegetable oils»; Determination of acid value by reference GB / T 5530-2005 «Determination of acid value and acidity of animal and vegetable oils »; Iodine value determination GB / T 5532-2008 «Determination of iodine value of animal and vegetable oils»; Determination of peroxide value reference GB / T 5538-2005 «Determination of peroxide value of animal and vegetable oils»; Determination of moisture and volatile matter reference GB / 5528-2008 «Determination of moisture and volatile matter in animal and vegetable oils»; Determination of insoluble impurities GB/T 5529-1985 «Ingredient testing of vegetable oils - Determination of impurities»; Determination of smoke points GB / T 20795-2006 «Tobacco oil smoke Point determination»; Freezing test reference GB / T 17756-1999 «General technical conditions for salad oil».

Data processing. All experiments were repeated 3 times, and the data were collated, analyzed

and mapped by Excel2003, SPSS19.0, Sigmaplot10.0 and Design-Expert 8.06.

Grapefruit seed oil extraction process. It can be seen from Fig. 1 that the liquid-solid ratio, ultrasonic time, ultrasonic power and ultrasonic temperature all have significant effects on the yield of grapefruit seed oil, but the yields of each factor vary. Under ultrasound-assisted conditions, the yield of mint seed oil increased with the increase of liquid-solid ratio, ultrasonic time and ultrasonic power, and reached a maximum at a liquid-solid ratio of 10:1, an ultrasonic time of 30 min, and an ultrasonic power of 200 W. After that, the stability of the grapefruit seed oil also increased gradually with the increase of the ultrasonic temperature. After reaching the maximum value at 50 °C, it remained stable and decreased sharply after 60 °C. Based on the consideration of yield and cost, determine the liquid-solid ratio (mL/g) 8:1, 10:1, 12:1, ultrasonic time 30, 35, 40 min, ultrasonic power 150, 200, 250 W, ultrasound Response surface experiments were performed at temperatures of 40, 50, and 60°C.

Based on the above single factor test, the Box-Behnken test was used to investigate the four main factors affecting the oil extraction process of grapefruit seed, namely liquid-solid ratio (A), ultrasonic time (B), ultrasonic power (C) and ultrasonic temperature. (D) Design a four-factor three-level response surface optimization test. The response rate of grapefruit seed oil extraction rate was optimized by Design-Expert 8.06. The test plan and results are shown in Table 1. The analysis of variance is shown in Table 2. The results of each response surface are shown in Figure 2.

The regression equation obtained by fitting the response surface analysis results to each factor is:
Y=33.02+2.63A-1.93B+0.30C+2.01D-2.52AB-0.44AC+1.76AD-0.28BC+0.18BD-1.54CD-2.31A2-2.74B2-3.89C2-2.07D2

It can be seen from Table 2 that the regression equation is used to describe the relationship between each factor and the seed oil extraction rate (R2=0.9625). Known by the significance and F value, the main factors influencing the extraction rate of grapefruit seed oil are liquid-solid ratio>ultrasonic temperature>ultrasonic time>ultrasonic power. The gradient of response surface curve reflects the influence of various factors on the extraction rate of seed oil. The steeper the curve, the more

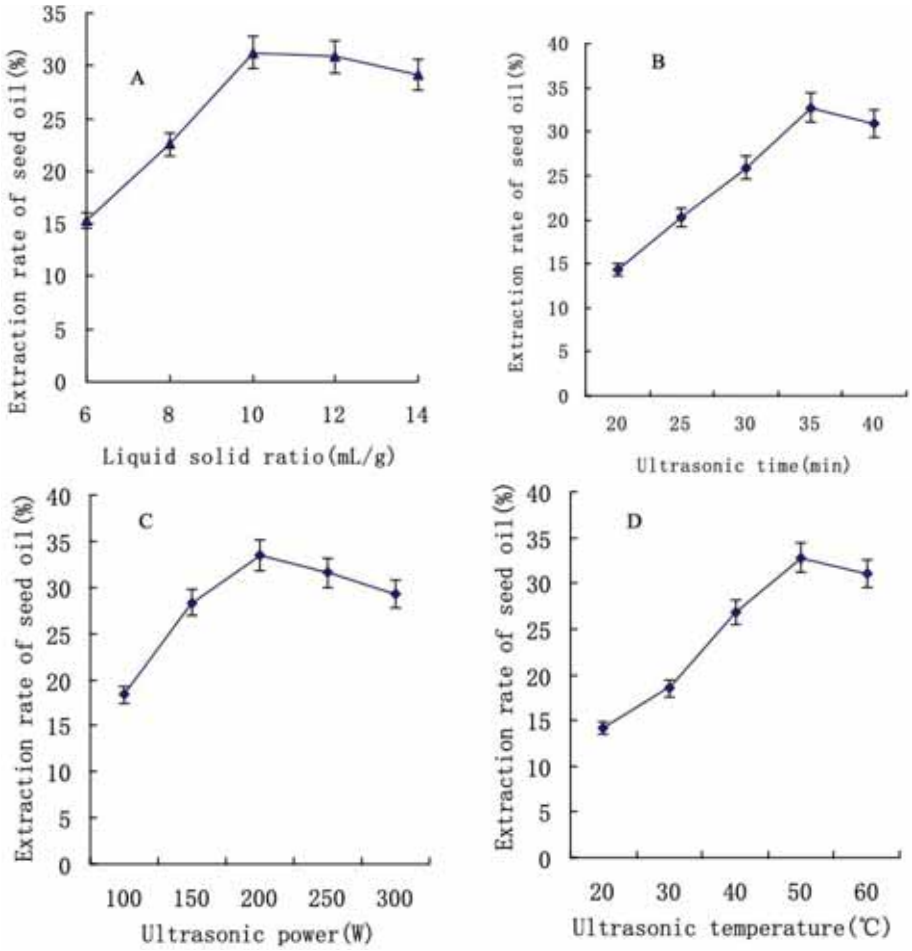

FIGURE 1

Effect of liquid solid ratio (A), ultrasonic time (B), ultrasonic power (C), ultrasonic temperature (D) on extraction rate of seed oil of C. grandis Osbecko.

Values are means ±SD (n =3).SD =standard deviation.

TABLE 1
Box-Behnken test plan and results

No.	Factor				Seed oil extraction rate (%)
	A (mL/g)	B /min	C /W	D /°C	
1	-1 (8)	1	1 (250)	1	18.69
2	1	-1 (30)	1	-1 (40)	25.69
3	-1	0	0	0	19.98
4	0 (10)	0	0 (200)	0 (50)	33.68
5	-1	-1	1	1	15.89
6	0	0 (35)	1	0	19.36
7	0	0	0	0	32.69
8	-1	1 (40)	1	-1	21.63
9	1 (12)	-1	-1 (150)	1 (60)	31.36
10	0	0	0	1	31.32
11	1	1	-1	1	26.69
12	0	0	0	0	34.36
13	1	-1	1	1	32.36
14	1	1	1	-1	17.98
15	0	0	0	-1	19.95
16	1	1	-1	-1	14.96
17	1	0	0	0	29.36
18	0	1	0	0	18.63
19	-1	1	-1	1	20.36
20	1	-1	-1	-1	25.32
21	1	1	1	1	20.36
22	-1	-1	1	-1	21.58
23	0	-1	0	0	27.23
24	-1	-1	-1	-1	15.38
25	-1	1	-1	-1	17.36
26	-1	-1	-1	1	19.63
27	0	0	0	0	21.58
28	0	0	0	0	32.79
29	0	0	-1	0	17.36

TABLE 2
Analysis of Variance of Response Value of Grapefruit Seed Oil Extraction Rate

Source	df	Sum of Squares	Mean Square	F Value	p-value
A	1	165.38	165.38	53.51	< 0.0001
B	1	89.47	89.47	28.95	< 0.0001
C	1	2.11	2.11	0.68	0.4223
D	1	96.88	96.88	31.35	< 0.0001
AB	1	101.71	101.71	32.91	< 0.0001
AC	1	3.06	3.06	0.99	0.3364
AD	1	49.56	49.56	16.04	0.0013
BC	1	1.29	1.29	0.42	0.5290
BD	1	0.51	0.51	0.17	0.6904
CD	1	37.82	37.82	12.24	0.0035
A2	1	138.23	138.23	44.73	< 0.0001
B2	1	195.24	195.24	63.18	< 0.0001
C2	1	391.73	391.73	126.76	< 0.0001
D2	1	110.814	110.84	35.87	< 0.0001
Model	14	1111.28	79.38	25.69	< 0.0001
Residual	14	43.27	3.09		
Lack of Fit 38.80	10	38.80	3.88	3.47	0.1207
Pure Error	4	4.47	1.12		
Cor Total	28	1154.55			

obvious the influence of this factor on the extraction rate of seed oil. It can be seen from Fig. 2 that the liquid-solid ratio has the greatest influence on the extraction rate of seed oil, and there is a certain interaction between factors except AC, BC and BD. The interaction of AB, AD and CD has significant influence ($P<0.05$). This is consistent with the results of the regression analysis in Table 3. The design conditions of the grapefruit seed oil extraction process were optimized by Design-Expert software. The optimum conditions were as follows: liquid-solid ratio (mL/g) was 12, ultrasonic time was 31.14 min, ultrasonic power was 191.18 W, and ultrasonic temperature was 59.42. °C, the grape seed oil extraction rate was predicted to be 36.84%. In order to facilitate the actual operation, the optimum process was corrected to a liquid-solid ratio (mL/g) of 12, an ultrasonic time of 31 min, an ultrasonic power of 191 W, and an ultrasonic temperature of 60.00 °C. Under the modified conditions, the extraction rate of grapefruit seed oil was 35.67%, which was consistent with the theoretical value.

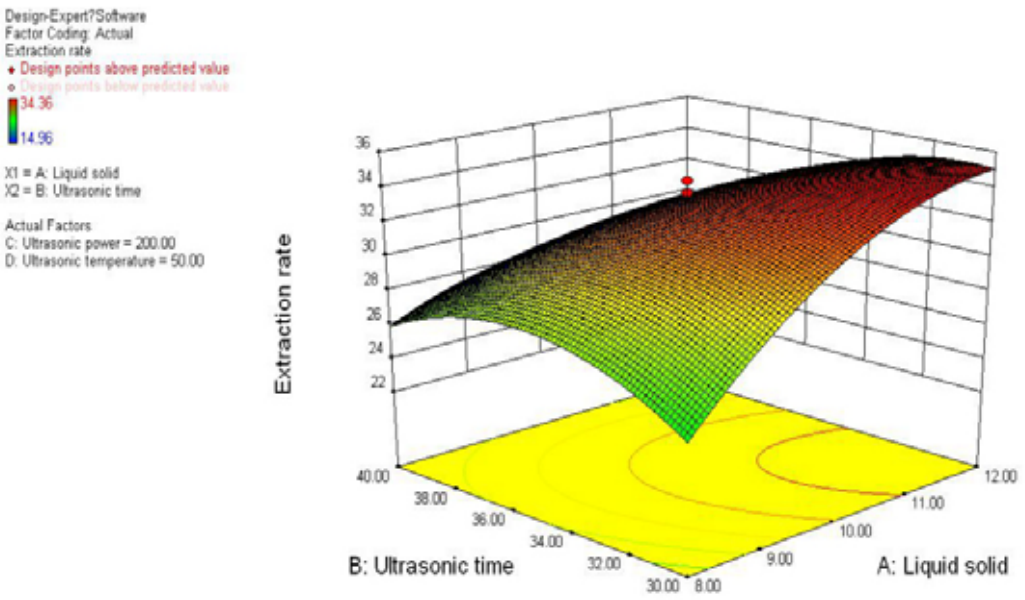
Design-Expert?Software
Factor Coding: Actual
Extraction rate
Design points above predicted value
Design points below predicted value
34.36
14.96
X1 = A: Liquid solid
X2 = B: Ultrasonic time
Actual Factors
C: Ultrasonic power = 200.00
D: Ultrasonic temperature = 50.00
Extraction rate
36
34
32
30
28
26
24
22
40.00
38.00
36.00
34.00
32.00
30.00
B: Ultrasonic time
8.00
9.00
10.00
11.00
12.00
A: Liquid solid

(a)

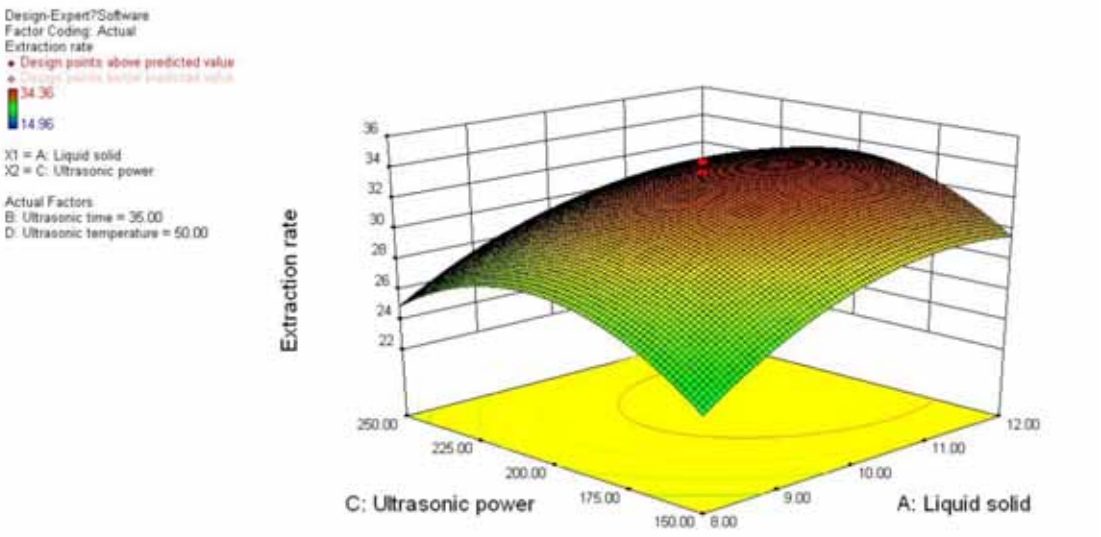
Design-Expert?Software
Factor Coding: Actual
Extraction rate
Design points above predicted value
34.36
14.96
X1 = A: Liquid solid
X2 = C: Ultrasonic power
Actual Factors
B: Ultrasonic time = 35.00
D: Ultrasonic temperature = 50.00
Extraction rate
36
34
32
30
28
26
24
22
250.00
225.00
200.00
175.00
150.00
C: Ultrasonic power
8.00
9.00
10.00
11.00
12.00
A: Liquid solid

(b)

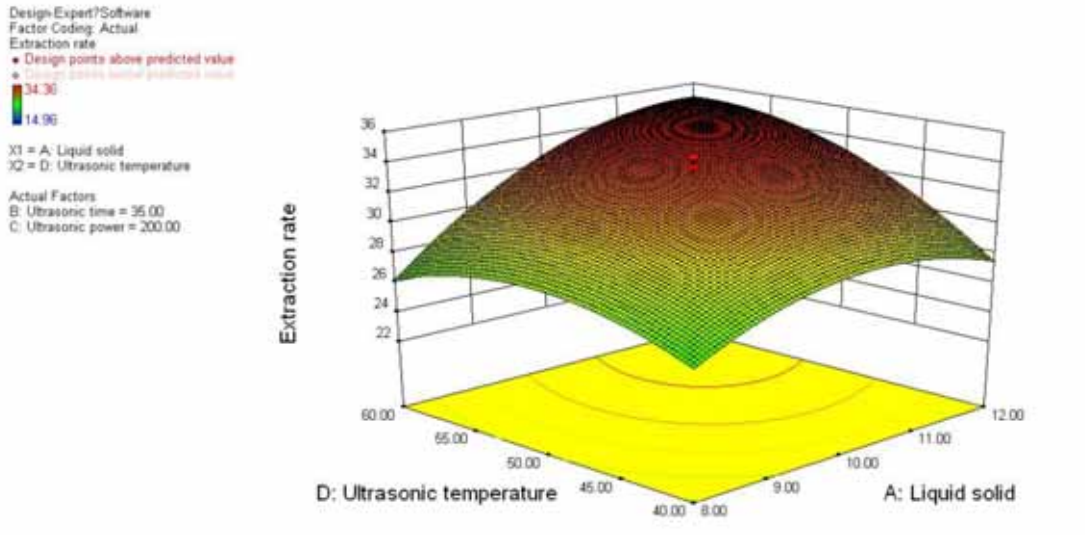
Design-Expert?Software
Factor Coding: Actual
Extraction rate
Design points above predicted value
34.36
14.96
X1 = A: Liquid solid
X2 = D: Ultrasonic temperature
Actual Factors
B: Ultrasonic time = 35.00
C: Ultrasonic power = 200.00
Extraction rate
36
34
32
30
28
26
24
22
60.00
55.00
50.00
45.00
40.00
D: Ultrasonic temperature
8.00
9.00
10.00
11.00
12.00
A: Liquid solid

(c)

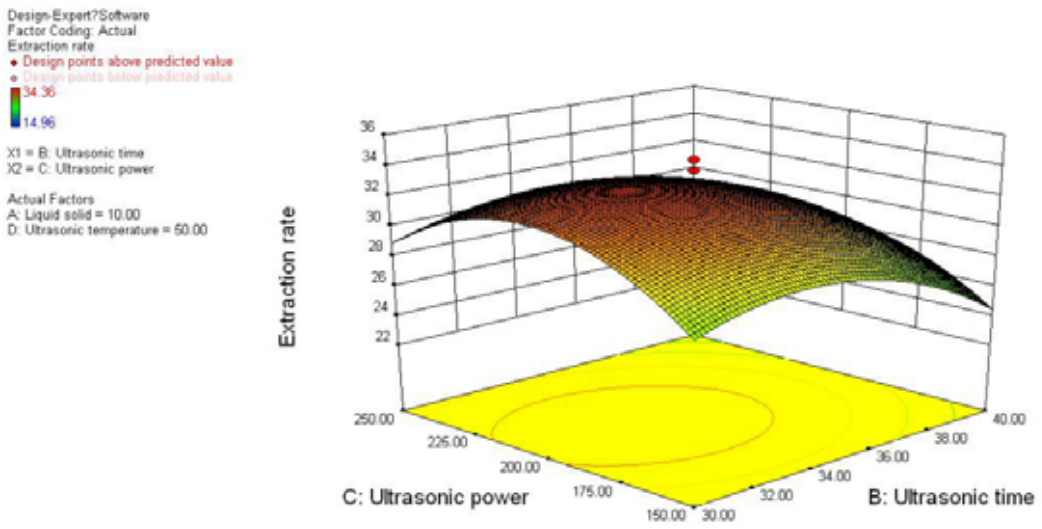

(d)

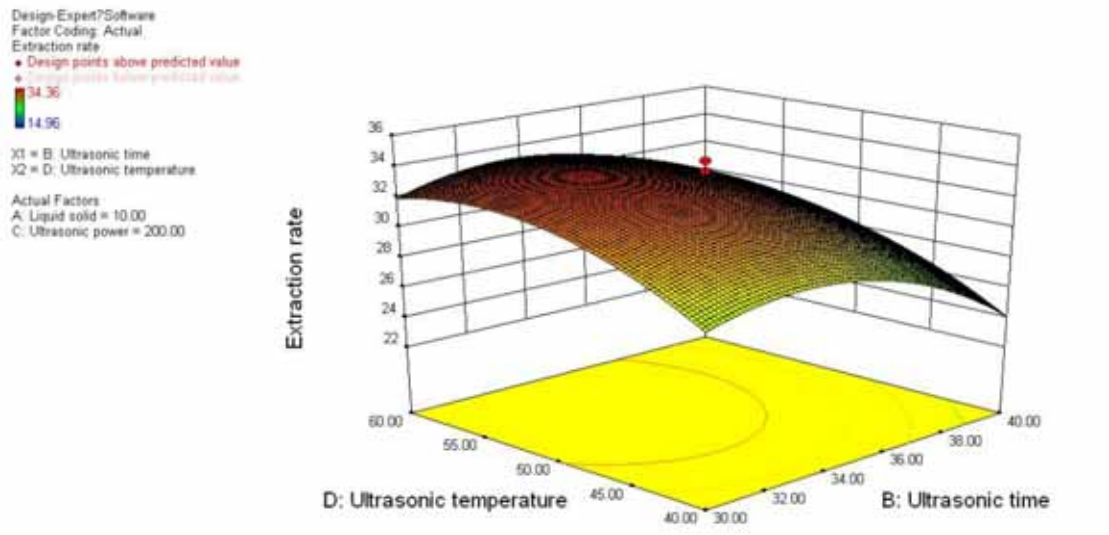

(e)

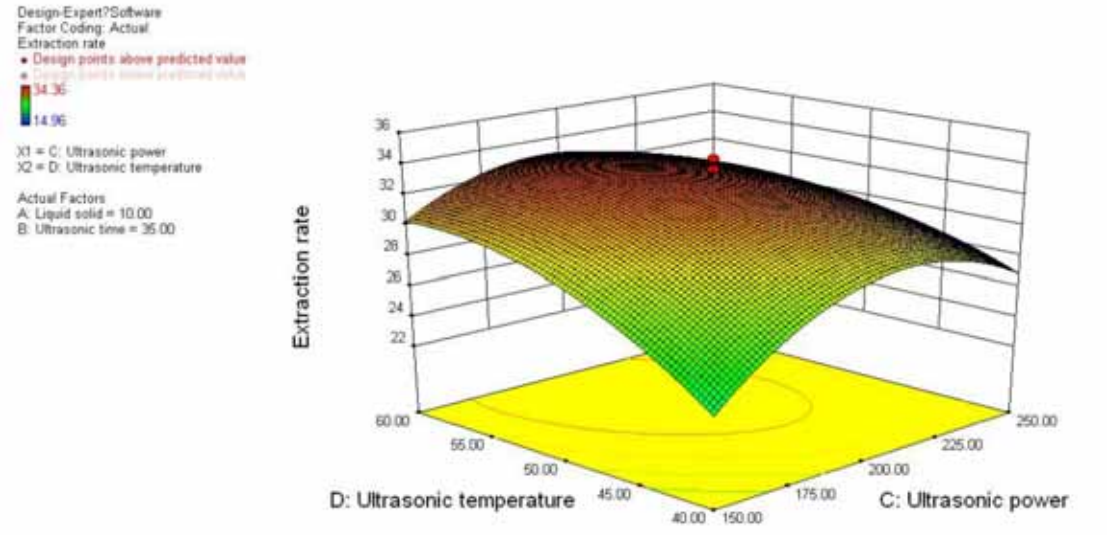

(f)

FIGURE 2
Response surface figures with seed oil extraction rate

TABLE 3
Fatty acid composition and relative content of grapefruit seed oil

No.	Retention time (min)	Fatty acid	Molecular formula	Molecular weight	Relative content (%)
1	13.175	Palmitic acid	C16 H32O2	256	12.74
2	14.463	Linoleic acid	C18 H32O2	280	47.73
3	14.528	Oleic acid	C18 H34O2	282	32.37
4	14.639	Stearic acid	C18 H30O2	278	7.16

TABLE 4
Grapefruit seed oil physical and chemical index value
(Values are means ±SD (n =3).SD =standard deviation)

Measured index	Results
Relative density (d2020)	0.9205±0.033
Refractive index (nd20)	1.4745±0.031
Saponification value (KOH)/(mg/g)	189.56±0.019
Acid value (KOH) /(mg/g)	1.08±0.021
Unsaponifiable material /(g/kg)	2.46±0.024
Iodine value (I2) /(g/100 g)	95.256±0.017
Peroxide value /(mmol/kg)	2.935±0.026
Moisture and volatiles /%	0.02±0.018
Insoluble impurities /%	0.03±0.027
Smoke point /°C	192±0.023
Freezing test (0°CStorage for 5.5 h)	Clarified and transparent

Grapefruit seed oil fatty acid composition. The NMS05 mass spectrometry database was used to perform computer search and artificial spectrum analysis on the spectra. The main components were identified and the components were determined by peak area normalization. The relative amounts in the seed oil, the results are shown in Table 3. As can be seen from Table 3, the main components detected by grapefruit seed oil are palmitic acid (12.74%), linoleic acid (47.73%), oleic acid (32.37 %), stearic acid (7.16%), among which unsaturated fatty acid content It reached 80.1%. In recent years, studies have shown that unsaturated fatty acids can relieve excess cholesterol in the blood, enhance cell membrane permeability, and prevent myocardial tissue and Arteriosclerosis [15]. The highest content of fatty acids in grapefruit seed oil is linoleic acid (47.73%), which is higher in traditional oil crops in China. Linoleic acid is an essential fatty acid in the body and is essential for the synthesis of phospholipids, the formation of cellular structures, and the maintenance of the normal function of all tissues [16, 17]. Oleic acid replaces saturated fatty acids in the diet and has the effect of lowering low-density lipoprotein (LDL) cholesterol [18]. Oleic acid has higher oxidative stability than polyvalent unsaturated fatty acid, can improve the body's antioxidant capacity, protect the cardiovascular system, has better physiological activity, and is considered to be a kind of health-promoting fatty acid [19]. Saturated fatty acids such as palmitic acid and stearic acid can be used as industrial raw materials for the production of lubricants, softeners, water repellents, release agents and polishes [20, 21].

Physicochemical properties of grapefruit seed oil. The measured values of physical and chemical indicators of grapefruit seed oil are summarized in Table 4. As can be seen from Table 4, the relative density (d2020) and refractive index (nd20) of grapefruit seed oil are 0.9205 and 1.4745, respectively. The color is clear and transparent, the taste is fresh and pleasant, and the aroma of grapefruit seed oil is unique, and the moisture and volatile matter and insoluble impurities are less; The iodine value (I2) of grapefruit seed oil is higher, 95.256 g /100 g, which is a kind of dry oil, indicating that the grapefruit seed oil has higher unsaturated fatty acid content; the saponification value (KOH) is 189.56 mg/g, which is more common. The saponification value (KOH) (200 mg/g) of edible oil is small [22]; the unsaponifiable content is 2.46 g/kg, which is similar to the unsaponifiable content of common edible oil; acid value (KOH) and peroxide value are respectively It is 1.08 mg/g and 2.935 mmol / kg, which are lower than the acid value (KOH) of edible vegetable oil specified in GB 2716-2005 "Sanitary Standard for Edible Vegetable Oils" of 3 mg / g or less and the peroxide value is less than or equal to 9.85 mmol / Kg. The above data show that the directly extracted grapefruit seed oil does not need to be refined, and the physical and chemical indicators can reach the Chinese edible vegetable oil standard.

CONCLUSIONS

This study provides a simple and efficient extraction process of grapefruit seed oil. The oil is good, light yellow, no odor, clear and transparent, and the extraction rate is 35.67%. The fatty acid composition was analyzed by GC-MS, and the grapefruit seed oil mainly contained palmitic acid, oleic acid, linoleic acid and stearic acid, and the content of unsaturated fatty acid reached 80.1%.

The measured relative density (d2020) and refractive index (nd20) of grapefruit seed oil were 0.9025 and 1.4745, moisture and volatile matter 0.02%, insoluble impurities 0.03%, iodine value (I2) 95.256 g /100 g, saponification value (KOH) 189.56 mg / g, unsaponifiable 2.46 g / kg, acid value (KOH) and peroxide value are 1.08mg / g and 2.935mmol / kg, respectively, smoke point 192 ° C, all physical and chemical indicators can reach Chinese edible vegetable oil standard. The results of this study provide a high-quality source of edible oil and industrial raw materials for the health food industry and the pharmaceutical industry.

ACKNOWLEDGEMENTS

We greatly acknowledge the financial supports from the Key project of Hunan Provincial Education Department (16A083). Funding Support for applied characteristic disciplines of school level. We also appreciate professor Ma Yongqiang from Harbin University of Commerce for the experimental technology support.

REFERENCES

[1] Kizil, S., Toncer, O., Sogut, T. (2018) Mineral contents and fatty acid compositions of wild and cultivated rose hip (Rosa Canina L.) Fresen Environ Bull. 27, 744-748.

[2] Kaya, M., Kan, A., Yilmaz, A., Karaman, R., Sener, A. (2018) The fatty acid and mineral compositions of different chickpea cultivars cultivated. Fresen Environ Bull. 27, 1240-1247.

[3] Kaplan, M., Kokten, K., Temizgul, R., Beyzi, S.B. (2017) Assessment of oil content and fatty acid composition of Turkish sorghum landrace through GGT biplot analysis. Fresen Environ Bull. 26, 1925-1932.

[4] Tumen, I., Hafizoglu, H., Pranovich, A., Reunanen, M. (2010) Chemical constituents of cones and leaves of cypress (Cupressus sempervirens L.) grown in Turkey. Fresen Environ Bull. 19, 2268-2276.

[5] Huang, Y., Peng, J., Huang, X. (2018) One-pot preparation of magnetic carbon adsorbent derived from pomelo peel for magnetic solid-phase extraction of pollutants in environmental waters. J Chromatogr A. 1546, 28-35.

[6] Liu, Y., Liu, A., Ibrahim, S.A., Yang, H., Huang, W. (2018) Isolation and characterization of microcrystalline cellulose from pomelo peel. Int J Biol Macromol. 111, 717-721.

[7] Dou, K.N., Bai, C.Q. (2018) Extraction Process Optimization and Fatty Acid Composition Analysis of Glycyrrhiza Oil. Journal of the Chinese Cereals and Oils Association. 33, 102-106.

[8] Chi, C., Yang, X.D., Wang, P., Wang, J.L. (2018) Physicochemical Properties and Fatty Acid Compositions Analysis of Red Raspberry Seed Oil from Five Cultivars. Journal of the Chinese Cereals and Oils Association. 33, 36-43.

[9] Hong, Q.Y., Zhang, Y. (2018) Optimization of ultrasonic-assisted extraction of peony seed oil and its fatty acid composition. Food and Fermentation Industries. 44, 159-164.

[10] Zhang, D., Song, M.Y., Li, G.L., Yi, C.X. (2018) Optimization of extraction of physalis seed oil by response surface method and the quality evaluation. Cereals and Oils. 31, 56-59.

[11] Wang, X.N., Hao, J., Liu, Z.C., Yan, M.R., Zhang, C.L. (2018) Study on the ultrasonic-assisted extraction process of Fructus Schizandrae oil and the hepatic protection effect. Food and Machinery. 34, 135-139.

[12] Yan, R.L., Mao, L.Y., Liao, Y., Huang, G.W., Xie, Z.Z., He, X.Y. (2017) Microwave Assisted Extraction of Seed oil and Root Saponin from Phytolacca americana and Their Physicochemical Properties as well as Insecticidal Activity. Natural Product Research and Development. 7, 1218-1223.

[13] Yan, R.L., Mao, L.Y., Liao, Y., Tang, X.M., Fu, J.M., He, F.L. (2018) Ultrasound-assisted extraction of seed oil from Mentha haplocalyx and its fatty acid composition, physicochemical properties and acute toxicity analysis. China Oils and Fats. 43, 16-20.

[14] Wu, F., Han, Q., Yu, Y.J., Ni, S. (2014) GC-MS Analysis of Fatty Acids from Torreya grandis and Camellia oleifera Seed. Chinese Wild Plant Resources. 33, 36-39.

[15] Nicol, M., Alexandre, S., Luizet, J.B., Skogman, M., Jouenne, T., Salcedo, S.P., Dé, E. (2018) Unsaturated Fatty Acids Affect Quorum Sensing Communication System and Inhibit Motility and Biofilm Formation of Acinetobacter baumannii. Int J Mol Sci. 19, 1-6.

[16] Zhuang, P., Shou, Q., Wang, W., He, L., Wang, J., Chen, J., Zhang, Y., Jiao, J. (2018) Essential Fatty Acids Linoleic Acid and A-Linolenic Acid Sex-Dependently Regulate Glucose Homeostasis in Obesity. Mol Nutr Food Res. 62, e1800448.

[17] Rom, O., Jeries, H., Hayek, T., Aviram, M. (2017) Supplementation with linoleic acid-rich soybean oil stimulates macrophage foam cell formation via increased oxidative stress and diacylglycerol acyltransferase1-mediated triglyceride biosynthesis. Biofactors. 43, 100-116.

[18] Li, S., Zhou, T., Li, C., Dai, Z., Che, D., Yao, Y., Li, L., Ma, J., Yang, X., Gao, G. (2014) High metastaticgastric and breast cancer cells consume oleic acid in an AMPK dependent manner. PLoS One. 9, e97330.

[19] Sekar, S., Muller, J.G., Karthikeyan, J., Murugan, P., Lakshminarasimhan, N. (2018) Unveiling the multifunctional roles of hitherto known capping ligand oleic acid as blue emitter and sensitizer in tuning the emission colour to white in red-emitting phosphors. Phys Chem Chem Phys. 20, 19087-19097.
[20] Yamashita, S., Hirashima, A., Lin, I.C., Bae, J., Nakahara, K., Murata, M., Yamada, S., Kumazoe, M., Yoshitomi, R., Kadomatsu, M., Sato, Y., Nezu, A., Hikida, A., Fujino, K., Murata, K., Maeda-Yamamoto, M., Tachibana, H. (2018) Saturated fatty acid attenuates anti-obesity effect of green tea. Sci Rep. 8, 10023.
[21] Nakamura, S., Ishii, N., Nakashima, N., Sakamoto, T., Yuasa, H. (2017) Evaluation of Sucrose Fatty Acid Esters as Lubricants in Tablet Manufacturing. Chem Pharm Bull (Tokyo). 65, 432-441.
[22] Li, G.H., Qian, X.M., Bi, Y.L. (2006) Oil and fat inspection and analysis. Beijing: Chemical Industry Press.

Received: **18.11.2018**
Accepted: **26.02.2019**

CORRESPONDING AUTHOR

Jinhua Shao
School of Chemical and Biological Engineering,
Hunan University of Science and Engineering,
Yongzhou 425199 – China

e-mail: 2217824197@qq.com

© by PSP Volume 28 – No. 5/2019 pages 4247-4255 Fresenius Environmental Bulletin

PROBLEMS AND COUNTERMEASURES OF AGRICULTURAL DEVELOPMENT IN THE KARST AREA OF SOUTHWEST CHINA

Qiang Wu[1], Hua Xiao[2], Shuzhen Song[2], Qian Li[3], Ri Li[2], Hao Zhang[4], Guofu Zhou[1], Hu Chen[2,*]

[1]School of Geography and Environmental Science, Guizhou Normal University, Guiyang 550001, China
[2]School of Karst Science/State Engineering Technology Institute for Karst Desertfication Control, Guizhou Normal University, Guiyang 550001, China
[3]Guizhou Water Invertmengt Group CO., LTD, Guiyang 550081, China
[4]Meteorological Administrative of Qingzhen City, Qingzhen 550014, China

ABSTRACT

The karst area in southwest China is a typical fragile area of ecological environment, and the coordination relationship between agricultural development and environmental protection has great challenges. Based on the fragile background of agricultural development in the karst region of southwest China, such as the vulnerability of land itself, the vulnerability of agricultural water, the fragility of agricultural ecological vegetation, and the fragility of farmers' ideological and cultural environment, this paper discussed the restrictive factors of agricultural development in the karst region of southwest China and put forward the direction of agricultural development in the karst area in the future.

KEYWORDS:
Karst, agriculture, development, problem, direction

INTRODUCTION

The karst area in southwest China is located in the humid climate region of subtropical southeast monsoon, rain hot during the same period, the precipitation is abundant, and the hydrothermal conditions can meet the growth of agricultural crops, the combination advantage of hydrothermal condition for agricultural production is more obvious. But there are many problems in the ecosystem of agricultural arable land in the karst mountain area, such as big difference in topography, "engineering shortage of soil and water", frequent flood and drought disasters, which has a great hindrance to the development of agricultural modernization.

The karst area in southwest China is a typical fragile area of ecological environment, however, it is one of the main producing areas of corn and potato that are traditional major food crops in China. The land for major food crops need to be ploughed and sown every year, so the soil disturbance is strong, and the soil erosion is more serious because of the heavy rainfall in summer and autumn season. In addition, the existing farming ideas and farming patterns have seriously affected the development process of modern agriculture, farmers have high production capital investment and low efficiency, which has become the main constraint factor for the development of the region. How to develop ecological and efficient modern agriculture in karst areas, especially in rocky desertification areas, is a research hotspot of karst-related scholars today. In recent years, many scholars have carried out research on the influencing factors of karst agriculture from many aspects, such as agricultural biomass energy, agricultural landscape pattern, service value of agro-ecosystem, grassland agriculture, eco-agriculture and poverty alleviation tourism, comprehensive development of ecological agriculture, vulnerability assessment of agricultural drought, climate change and agricultural development models of foreign karst [1-13], but there is still a lack of systematic analysis of the problems and countermeasures of agricultural development in the karst area of southwest China. Therefore, based on the background of fragile ecological environment in the karst agricultural development, this paper discussed the existence of problem in the karst agricultural development and put forward corresponding solutions to provide theoretical support for agricultural development in the karst region of southwest China.

THE FRAGILE BACKGROUND OF AGRICULTURAL DEVELOPMENT IN THE KARST REGION OF SOUTHWEST CHINA

The vulnerability of the land itself. Land is not only the material basis and material carrier of agricultural development, but also one of the predominant factors affecting the karst agro-ecosystem.

The soil matrix of karst was mainly composed of soluble minerals and a small amount of acidic insoluble matter, the acid insoluble matter was lower than 10% of the total content of carbonate rock, which was much lower than the content of soluble minerals, the acid insoluble matter accumulated after being weathered and dissolved to form residual soil, the rate of soil formation was extremely slow, and it taken at least 40,000a to form 1cm thick soil layer [14], which is about 10-80 times slower than that in non-karst area [15-16]. The land suitable for karst agricultural development is mostly distributed in the negative geomorphic units, such as peak cluster, depression, intermontane basin and valley, and the soil thickness is different. In addition, because of the low content of acidic insoluble matter in the soil, the soil is generally alkaline, it is easy to cause the lack of trace elements such as Fe, B, Cu and Zn, so it hinders the growth of microbes and bacteria in the roots of crops, which is not conducive to the formation of microenvironment. The organic matter of karst agricultural tillage soil is concentrated in the surface layer, it is disturbed excessively by human being, once the topsoil is lost, the soil fertility decreases rapidly, which seriously affects the agricultural benefit. The vulnerability of karst land itself is the inherent shortage of agricultural development in this region, and it is also the background and fundamental cause of the fragility for agricultural ecosystems in this region.

The vulnerability of agricultural water. The special dual structure of surface and underground in the karst area of southwest China has caused the engineering water shortage in this area and seriously changed the systematic pattern of soil and water spatial separation, which has determined the fragile feature of water environment for karst agricultural development. The agricultural land in the karst area is affected by the dual hydrological structure of surface and underground, it is easy to cause drought and water shortage because the precipitation difficult to be used for a long time, at the same time, there is a great difference in the patency of underground pipeline network in the karst area, in case of heavy rain, depression and intermontane basin are easily blocked that can cause local waterlogging [17]. Because there are many closed depressions and dissolution basins in the karst mountainous area, it is lack of complete surface drainage network, rainfall collected in the depression and dissolution basin, and then entered the karst water-bearing system from the doline, so that it makes the unevenness of temporal distribution for water become more prominent in the karst system in the monsoon area. But beyond that, the underground structure of the karst mountainous area is complex, and the accuracy of drilling wells is very complicated, which makes the structure of water use for agricultural development more complicated and difficult.

The fragility of agricultural ecological vegetation. Forest and grass vegetation plays a key role in the stability of karst agro-ecosystems. The type and coverage of vegetation near the farmland is an important factor to determine the integrity of the farmland system, it is directly determined the strength of income and expenditure for agro-ecosystem. The special environment background of karst area determines that karst agricultural crops should adapt to the characteristics of karst soil (such as saxicole, xeromorphic and calciphilous), which determines the vulnerability of karst crop planting itself. When the intensity of human intervention is increased, the type of vegetation cover outside the farmland system will change, which will inevitably decrease the stability of agro-ecosystem. When native vegetation is destroyed, plantation and secondary vegetation have simple structure, poor biodiversity, low primary productivity and poor function of soil and water conservation [14,16], it will seriously affect the agricultural ecosystem.

The fragility of farmers' ideological and cultural environment. The karst mountainous area of southwest China is one of the most important place that minority nations living together in China. The karst area was influenced by the northern farming culture in history, and the ethnic minorities combined with the foreign farming civilization, the traditional agriculture has gradually become the dominant agricultural mode in this region. Affected by harsh natural, historical, social and economic factors, karst mountain areas, especially rural areas of karst area, are in a closed environment where transportation is inconvenient for a long time, the advanced agricultural culture, technology and information are difficult to enter, as a result, the society is closed and conservative for a long time, the development is slow, which forms the culture characteristic of typical mountainous agriculture [18-19]. The long-term unreasonable farming activities have aggravated the fragile karst ecological environment [20], and the agricultural development is easily affected by all kinds of adverse factors.

The comprehensive action of the four major karst agricultural vulnerability factors fundamentally determine the fragility nature of the development of karst agricultural ecosystem in southwest China, coupled with the long-term unreasonable agricultural intervention and the disturbance of natural factors, the environment of karst agricultural development in southwest China is faced with a series of severe problems.

THE RESTRICTIVE FACTORS OF AGRICULTURAL DEVELOPMENT IN THE KARST AREA OF SOUTHWEST CHINA

Because of the large number of population and scarce land resources, the agricultural population is under great pressure. The karst area of southwest China is main ethnic minority area in China, there are 48 minorities live in this area, the population is about 1.0×10^8, of which about 0.12×10^8 are minorities, it is concentrated nearly 50% of the poor population and one of the most concentrated areas of poverty in China. The karst rocky desertification area in southwest China is the key and difficult point to build a well-off society in China. Furthermore, there are widespread some problems that the population pressure is high and human-land conflict is sharp in the karst area of southwest China. According to the previous report, the population capacity in the peak cluster-depression area is 50 persons per km^2, in the mountain and basin of the karst areas is 1-10 persons per km^2, in the peak forest plain area is 200-300 person per km^2, in the dissolution plain of eastern Yunnan and in hill and plain of central Guizhou are 150-200 people per km^2 [21]. Taking Guizhou as an example, the fifth census data showed that the population density of Guizhou province in 2000 exceeded 200 people per km^2, which exceeded 68% of the national average and even far exceeded the maximum population capacity of the ecological environment [22], of which about 80% were agricultural population. From 1982 to 2000, the annual growth rate of population in Guizhou was 1.53%, it was 25% higher than the national average, and the illiteracy rate increased from 1.31 times of the national average in 1982 to 2.07 times in 2000, and the speed of population quality improvement was falling behind the national average speed, with the increasing serious of population pressure in China, the population pressure in the karst areas was more prominent [23]. The agricultural population is under great pressure, the quality of science and culture is low, the number of poor people is large, and the contradiction between people and land is sharp, which seriously restricts the sustainable development of karst agriculture.

The cultivated area is gradually decrease, the cultivated land quality is degraded. As human activities and exploitation intensity continue to increase, the property of agricultural land is gradually change, the unreasonable development and utilization of agricultural land and the backward agricultural development mode has been deteriorating the land environment day by day, a large amount of cultivated area are decreasing. At present, the cultivated area in China is only about 1.22×10^8 hm^2, which is decreased 8.2×10^6 hm^2 compared with 1997, the per capita cultivated area is decreased from 0.105 hm^2 to 0.092 hm^2 compared with 10 years ago, it is only 40% of the world average [24]. The situation of cultivated land is even more serious in the karst areas of southwest China, the decreased rate of the per capita cultivated area is above 50%in some typical karst countries and cities, such as Zunyi County (75%), Qinglong County (61.8%), Qingzhen County (60.5%), Pu'an County (58.3%) and Xifeng County (57.5%). Bijie in Guizhou province is not only the starting point of the western China development, but also the big population city, the cultivated area in this area decreased from 430.26 km^2 to 364.69 km^2 during1978 to 2008 [25]. As the population continues to increase, the per capita cultivated land will continue to decrease, the contradiction between man and land become more prominent.

The cultivated area in the karst area of southwest China is decreased, at the same time, the cultivated land quality is also degraded. Taking Hunan as an example, the quality problems of cultivated land can be summarized as follows: soil pollution, soil acidification, serious soil erosion, nutrition imbalance, decline of soil fertility, decrease of high yield area and poor quality of replacement farmland [26]. Lime soil that is mainly formed by carbonate rock, It is the main agricultural soil in karst area of southwest China, but its gravel content is high, and its nutrient content is low. It is easy to lose mineral nutrient elements and organic matter with water because of the influence of precipitation, thereby the quality of agricultural land can be affected. The continuous increase of population, the decrease of cultivated land area and the degradation of quality have affected the yield and quality of agricultural crops and seriously threatened the sustainable development of agriculture and the security of food self-sufficiency in China.

Food crops are grown in traditional ways resulting in serious soil and water loss. In the karst mountainous area, the natural environment capacity is small and the land carrying capacity is lower than that of non-karst area. As a result of the rapid increase in population, the problem of food shortage became more and more prominent. In order to survive, people had to destroy a lot of forests and grasslands, assart land in different places, cultivate on steep slopes and carry out predatory managements to solve the problem of feeding, thus the vicious circle of " the more population they give birth to, the poorer they are; the poorer they are, the more land they assart; the more land they assart, the poorer they are " was formed [27], and soil erosion

is becoming more and more serious. Soil is the object of erosion and the main body of soil and water conservation. Cultivation of slope land without soil and water conservation measure is the main cause of karst rocky desertification. The problem of soil and water loss in slop land is the most outstanding problem for soil erosion, the topsoil loss of slope land in the world is 2.5 billion ton per year. In China, slope land accounts for 50% of the total cultivated land, and its loss accounts for 50%-80% of the total loss [27]. Slope land (the gradient is greater than 5 °) in the karst area in Guizhou province accounts for 87% of the total area of dry cultivated land, and its loss accounts for 90% of the total loss. According to the investigation, the soil erosion modulus of maize planted on the slope land with lime soil (of lime soil is from 15° to 20 °) can be reached 5852-7726t/(km^2·a), the density of new ravine can be reached 0.32-1.60km/km^2, the ravine area rate was 12. 80%～20. 00% [28], soil and water loss reached medium and intensity grade. By the long-term field monitoring of the Huajiang demonstration area in Guizhou province, we found that most of slope land have appeared medium and intensity rocky desertification which was assart in the 1950s and 1960s, what's more, some of the agricultural land functions have been completely lost. Agricultural farming without soil and water conservation measures is the main factor leading to the decline of agricultural land function and inducing soil erosion and rocky desertification.

The loss of agricultural land is serious, and the problem of rocky desertification is prominent. Karst rocky desertification referred to a process in which soil was eroded seriously or even thoroughly under the background of fragile karst environment in the tropical and subtropical, so that bedrock was exposed widespread, carrying capacity of land declines seriously, and at last, landscape appeared similar to desert affected by human unreasonable disturbance and natural factors [29]. With the rapid increase of population, human activities are becoming more and more frequent, the development and utilization of land especially the production breadth and depth of traditional agriculture are constantly strengthened, the agricultural ecosystem is deteriorating day by day, the soil and water loss is becoming more and more serious, and the area of rocky desertification continues to expand. According to the State Statistics Department, the total area of rocky desertification land in the karst areas was about $1.2\times 10^5 km^2$ by the end of 2011, accounting for 26.5% of the land area of karst, accounting for 11.2% of the national territorial area, involving in 455 counties and 5575 townships of Guizhou province, Yunnan province, Guangxi province, Sichuan province, Chongqing province, Hubei province, Hunan province, Guangdong province and other 8 provinces (Districts or Cities) (Table 1) [30]. Rocky desertification is the most serious ecological environmental challenge faced by the karst agro-ecosystem in southwest China, it not only seriously affects the production of agriculture, forestry and animal husbandry, but also causes the mankind lose basic living conditions, it will greatly constrain the sustainable development of social economy and the improvement of people's living standards.

Drought and flood caused by man-made and natural factors have seriously affected the agriculture development. After entering the 21st century, the seasonal drought and flood disasters occur frequently in the karst areas of southwest China affected by global climate change and extreme climate, which not only causes harm to agricultural production, but also seriously threatens the safety of drinking water, it has become one of the

TABLE 1
Statistics on land area of rocky desertification in various provinces (districts, cities) of karst areas in southwest China

Province (municipality, autonomous region)	Land area/$10^4 km^2$	Land area of rocky desertification/$10^4 km^2$	The land area of rocky desertification accounts for the national territorial area/%	The area of rocky desertification accounts for the land area of rocky desertification in China/%
Guizhou	18.98	3.02	15.93	25.2
Yunnan	38.43	2.84	7.39	23.7
Guangxi	23.64	1.93	8.15	16
Hunan	21.15	1.43	6.77	11.9
Hubei	18.56	1.09	5.88	9.1
Chongqing	8.17	0.90	10.95	7.5
Sichuan	48.11	0.73	1.52	6.1
Guangdong	17.65	0.06	0.03	0.5
In total	194.69	12.00	11.2	100

important natural disasters that restrict economic and social development and destabilize ecosystems [31]. From the fall of 2009 to the beginning of 2010, a major historical drought occurred in the karst area of southwest China, resulting in 6.73×10^6 hm^2 farmland and 5.27×10^6 hm^2 crops were affected by drought, the farmland of 1.47×10^6 hm^2 were lack of water and moisture, 2.09×10^7 people and 1.37×10^7 head livestock have difficulty drinking water in the five provinces (cities, districts) including Guangxi, Chongqing, Sichuan, Guizhou and Yunnan [32]. There were 6.04×10^6 person affected by drought in 2000 in Yunnan province, 1.48×10^6 person and 9.72×10^5head livestock have difficulty drinking water, the covered disaster area of crop was 8.15×10^5 hm^2, the area of crop failure was 9.3×10^4 hm^2. In the process of drought, the farmland ecosystem is seriously damaged, a large number of crop areas are withered or failure to harvest, natural vegetation is significantly affected by drought, vegetation growth is significantly inhibited, and biodiversity is seriously threatened [33], the entire agricultural system is under unprecedented threat.

Flood disaster not only is meteorological disasters in the mountainous karst areas, but also is mountainous geological disasters. Heavy rain continued longer and dolines were narrow, which can cause flood to submerge farmland, housing and related engineering facilities in depression, valley and intermontane basin, so it can be formed flood and geological disasters [34]. Frequent drought and flood disasters in the karst area of southwest China have a great impact on agricultural production in rural areas, and it is also an important cause of poverty and backwardness in the karst region.

Geological disasters occur frequent that affect agricultural infrastructure. Heavy rainfall lasted long time that is the main reason for geological disasters, such as debris flow, landslide and flood disaster. Guizhou is located in slope zone of the Yunnan-Guizhou Plateau to low mountains and hills in Guangxi, the karst development is strong, the karst area account for more than 72% of the national territorial area, where the rainfall is abundant, heavy rain is concentrated, mountains are high, slopes are steep and ecological environment is fragile, landslide has brought great harm to the social economy, so that the losses have accumulated over 100 million yuan. There are 290 cases of debris flow recorded in western Guizhou, of which 2.32% are oversized, 2.33% are large, 31.4% are medium and 63.9% are small [35]. From 1993 to 2002 in western Guizhou, 73 person are injured and death, 378 hectares of cultivated land were destroyed, and economic losses were in the millions [36]. In addition, the ground subsidence and collapse are also serious threated to people's lives and property safety and affect the use of agricultural infrastructure in the karst mountainous area.

Agricultural infrastructure is backward, so the phenomenon of rain-dependent is widespread. Water is an important basis and guarantee for agricultural development, and it is the foundation of agricultural development. The concentrated distribution area of farmland and water in the karst area of southwest China have small amount of water resources, accounting for only about 5% of the total water resources, which reduces the stability of water source security. The water storage capacity of irrigation and water conservancy facilities is seriously insufficient, the construction of farmland and water conservancy mainly consists of water cabinets and water cellars, the water collection area is small and the storage capacity is limited, which can not meet the water demand of severe drought disasters and lead to “engineering water shortage”. At the same time, because of the heavy rainfall and humid climate in southwest China, the consciousness of “not afraid of drought, fear of flood disaster” and “rain-dependent” are deeply rooted, and the consciousness of drought resistance and water saving is insufficient, which increases the instability of agricultural development.

THE ORIENTATION OF AGRICULTURAL DEVELOPMENT IN THE KARST AREA IN THE FUTURE

Sparing no effort to improve farmers' professional skills and transfer surplus labor. In the current situation, professional technology is the most important factor for farmers to improve the level of agricultural planting and increase their income. Under the national policy of precision poverty alleviation and overall poverty alleviation, agricultural competent departments and scientific and technological personnel should guide farmers to actively and independently study specialized scientific and cultural knowledge, change the traditional and backward concept of agricultural planting, improve the cognitive level of new things and new technologies, strengthen all kinds of professional technical training, and encourage farmers to go out to visit and learn advanced agricultural development mode and technology.

Farmers should be encouraged to participate in various out-of work training to guide them to obtain employment and reduce environmental pressure in rural areas. The karst area is rich in population resources, the famer with the better condition can be encouraged to get employment in the vicinity or to work in developed areas, or to work on advanced

farms to study and learn advanced agricultural techniques, and then they can return to their hometowns to promote the development of local farmers.

Developing modern agriculture according to local conditions. Making use of the advantages of regional and climatic environment in the karst region of southwest China develop modern agricultural crops with high standards and high added value, such as flue-cured tobacco, vegetables, flowers, tea, sugar crops and subtropical fine fruits. They are better condition in karst plain area, valley area and intermontane basin area, we can select the area with flatten terrain to develop the above-mentioned advantageous agriculture that can significantly improve the agricultural level and farmers' income according to the type of local characteristics. It is reported that tobacco, flowers, vegetables, potatoes, sugar cane and tea of local characteristics have been grown on a large scale in karst areas of Yunnan province, 3.6 million farmers are connected to more than 2000 leading enterprises, and agricultural development has achieved certain results.

The area with distinct positive and negative landforms, such as the peak cluster and depression, it can be developed characteristic agroforestry. According to the regional characteristics, the grain crops should be developed at the bottom and mild slope of the depression under the condition that soil and water are not eroded. In steep slopes greater than 15 °, it is strictly prohibited to develop crops that are often cultivated to reduce disturbance of land and develop suitable forest and grass industry and herbivorous animal husbandry as far as possible (Table 2) [20].

Changing the concept of "taking grain as the key link" develop the grassland agriculture and agroforestry to control rocky desertification. Soil in the karst area is easy to occurring water and soil loss after disturbance, and then formed rocky desertification. By developing artificial grassland and integrating feed resources to develop herbivorous animal husbandry, it can significantly prolong the chain of food transformation and improve ecological environment and land efficiency. To develop grassland agriculture and agroforestry according to

TABLE 2
Classification of karst rocky desertification intensity

Classification of rocky desertification		The rate of outcrop rock of 0.2 km^2 polygon (%)	The rate of vegetation and regolith coverage of 0.2 km^2 polygon (%)	Reference index
Non-rocky desertification		＜20	＞80	Non-ladder soil of dry slop land, flatland and construction land with the slope≤15°, good ecological environment, dense forest and shrubs, no soil erosion or soil erosion is not obvious; suitable for farming, forest and pasture.
Potential rocky desertification		20~30	80~70	Non-ladder soil of dry slop land, grassland with the slope＞15°, sparse forest and shrubs, soil conditions are good but soil erosion is obvious; there is a tendency to expose rocks.
Rocky desertification	Mild rocky desertification	31~50	69~50	The rock began to expose, soil erosion is obvious, the vegetation structure of polygon is low, dominated by sparse shrubs or artificial dryland and vegetation.
	Moderate rocky desertification	51~70	49~30	Rocky desertification intensified, soil erosion is serious, shallow soil, most are rocky slope cropland, sparse shrub and grass slope.
	Intense rocky desertification	71~90	29~10	Rocky desertification is strong, there is no soil flow basically, most land are difficult to use and no agricultural value.
	Extremely intense rocky desertification	＞90	＜10	Complete rocky desertification，there is no soil flow, agricultural value is lose, becoming a typical land that is difficult to use,
Non-karst		Do not consider the problem of rocky desertification in the non-karst areas.		

local conditions in the karst areas can adopt ecological farming model to improve the social and economic benefits and ecological benefits of grassland agriculture and agroforestry, such as "grain-grass-livestock" mode, "livestock-marsh-grain" mode, "forest-grass-livestock" mode, "fungus-grass-livestock" mode and "forest-herb-grass-livestock" mode. The combination of ecological agriculture construction, characteristic forestry-grass- livestock industry and farmers' income increase will improve rocky desertification, control rocky desertification and promote the sustainable development of karst agro-ecosystem.

Strengthening agricultural infrastructure enhance the capacity of disaster early warning. To develop modern agriculture in the karst area, it is necessary to strengthen the top-level design, strengthen the investment in water conservancy and water resources, build small-scale water conservancy and water conservation facilities that meet the needs of agriculture and scientifically dispatch agricultural water according to the demand for agricultural water to ensure the safety of agricultural water and completely change the status quo of rain-dependent.

The karst area of southwest China is the hardest-hit area of natural disaster every year, which has a serious impact on agricultural development and production. At present, Guizhou Province has carried out the risk regionalization of drought disaster, rainstorm and flood disaster, wind and hail risk, and low temperature frost risk, which has greatly improved the level of disaster prediction, but there is still a need to improve early warning control in crops and to prevent extreme abnormal disasters such as El Nino and La Nina.

ACKNOWLEDGEMENTS

This study was supported by Project of National Key Research and Development Program (2016YFC0502601), the National Natural Science Foundation of China (31760243) and Qian Ke He Ji Chu [2018]1112. Qiang Wu, Hua Xiao and Shuzhen Song contributed equally to this work.

REFERENCES

[1] Song, S.Z., Xiong, K.N., Chi, Y.K, Shen, X.Y., Guo, T., Lu, Nana. (2018) Research Progress and Prospect of Grassland Planting and Ecological Animal Husbandry in the Karst Rocky Desertification Area. Fresen. Environ. Bull. 27, 7017-7030.

[2] Shi, S.N., Li, X.Q., Xie, B.G., Hu, B.Q., Tang, C.Y., Yan, Y. (2018) Change and comparison of agricultural landscape patterns and ecological service values in karst and non-karst areas: a case study of Quanzhou County. Tropical Geography. 38(4), 487-497.

[3] Shen, X.Y., Chi, Y.K, Huo, B., Wu, T., Xiong, K.N. (2018) Effect of fertilization on ryegrass quality and mineral metabolism in grazing the Wumeng semi-fine wool sheep. Fresen. Environ. Bull. 27, 6824-6830.

[4] Jiang, B., Li, J.C., Hong, J., Zhu, S.L., Lu, Lan. (2018) Convergence development study on the zoology agriculture and pro-poor tourism based on GIS in karst area. Journal of Green Science and Technology. 6, 234-239.

[5] Yue, K.Q., Gu, Z.K. (2017) Discussion on sustainable development of karst rocky desertification area from the perspective of comprehensive development of ecological agriculture—taking the City of Xingyi in Guizhou province technical practice as an example. Journal of Anhui Agricultural Sciences. 45(35), 229-231.

[6] Song, S.Z., Xiong, K.N., Chi, Y.K, Liu Z.Q. (2017) Study on interannual variation of photosynthetic characteristics of cichorium intybus in karst rocky desertification areas. Chinese Journal of Grassland. 39(2), 65-70.

[7] Song, X.j., Liu, S.J., Xun R., Wang, K.L. (2017) Primary research "forage grasses—livestock" ecological product mode, the karst region of Zhougu Village in northwest Guangxi. Hunan Agricultural Sciences. 6, 66-69.

[8] Zhao, J.X., Zhang, Q. (2017) Correlation between soil erosion and agricultural development in karst areas: a case study on Dafang, Guizhou. Guizhou Science. 35(2), 27-32.

[9] Jin, G.M., Yuan, F. (2016) Analysis on the landscape pattern and ecological design of the leisure agriculture in the karst landform unit. Yunnan Geographic Environment Research. 28(5), 49-53.

[10] Lang, Y.X. (2016) Suggestions on the development of ecological agriculture in karst mountain. Anhui Agricultural Science Bulletin. 22(15),17-18.

[11] Wang, Y.C., Jiao, S.L., Huang, F.G. (2016) Evaluation researches on agricultural drought vulnerability in Karst areas in southwest China. Journal of Guizhou Normal University (Natural Sciences). 34(3),13-17.

[12] Wu, Y.D. (2016) Discussion on modern agriculture development pattern in Guizhou karst mountainous area based on ecotope. Guizhou Agricultural Sciences. 2013, 41(8), 246-249.

[13] Ao, X.H. (2016) Impact and adaptive strategies of climate change on agriculture in karst areas—a case study of Liupanshui City in western Guizhou. 11(1), 58-62.
[14] Chi, Y.K., Xiong, K.N., Zhang, Z.Z. (2016) Research on photosynthetic interannual dynamics of gramineous forage in the karst rocky desertification regions of South China. Oxidation Communications. 39(3), 2476-2496.
[15] Guan, D.J., Su, W.C., (2006) Wang, H.J. On eco-environment vulnerability assessment of karst regions in Chongqing. Research of Agricultural Modernization. 18(1), 77-79.
[16] Zeng, X.Y., Mou, R.F., Xu S.G. (2006) The research of karst ecological fragibility. Environmental Science and Management. 31(1), 86-88.
[17] Wang, S.J., Li, Y.b., Li, R.L. (2003) Karst rocky desertification: formation background, evolving and comprehensive taming. Quaternary Sciences. 23(6), 657-666.
[18] Liao, H.X., Ji, Y.L., Peng, S.L. (2016) Resource and environment carrying capacity and sustainable development. 25(7), 1253-1258.
[19] Bao, W.K., Chen, Q.H. (1999) Discussion on several problems of restoring and rehabilitating degraded mountain ecosystem. Journal of Mountain Science. 17(1), 22-27.
[20] Xiong, K.N., Chi, Y.K. (2015) The problems in southern china karst ecosystem in southern of china and its countermeasures. Ecological Economy. 31(1), 23-30.
[21] Hu, L., Xiong, K.N., Xiao, S.Z., Zhu, H.B. (2014) Man-land relationship and its control in Guizhou karst area, Journal of Guizhou University (Natural Science). 31(6), 117-121.
[22] Wan, J. (2003) Land degradation and ecological rehabilitation in karst areas of Guizhou Province, southweastern China. Advance in Earth Sciences. 18(3), 447-453.
[23] Tan, Z.K. (2006) Remote sensing on the influence of the implementation of converting land to forest on controlling desertification in karst region. Research of Soil and Water Conservation. 13(1), 35-37.
[24] Zhao, Q.G., Huang, G.Q., Ma, Y.Q. (2013) The problems in red soil ecosystem in southern of China and its countermeasures. Acta Ecologica Sinica. 33(24),7615-7622.
[25] Chi, Y.K., Xiong, K.N., Xiao, H., Huang, D.H., Wen, Y.Q., Shen, X.Y. (2018) A comparative study on meat quality between Guizhou semi-fine wool sheep and a series of semi-fine wool sheep in southwest China. Fresen. Environ. Bull. 27, 4239-4238.
[26] Zhong, W.Y. (2009) Problems of cultivated land quality and innovation in administrative legislation in Hunan. Soils. 41(3), 356-359.
[27] Xiong, K.N., Chi, Y.K., Shen, X.Y. (2017) Research on Photosynthetic Leguminous Forage in the Karst Rocky Desertification Regions of Southwestern China. Polish Journal of Environmental Studies. 26(5), 2319-2329.
[28] Zhuang, D.C. (2006) Studies on the soil and water loss and strategies of prevention and cure—a case stuely of qiabi small watershed. Journal of Jishou University (Natural Science Edition). 27(4), 80-83.
[29] Zheng, J., Zhang, J.Y., Deng G.S. (2013) Sustainable development model of rural area in Guizhou karst mountainous area. 40(19), 222-224.
[30] Yu, S. (2012) Distribution status quo and characteristics of China's stone desertification area. 22(2), 53-55.
[31] Peng, S.Z., Wu, J.Y., Jun, Q. (????) The causes and countermeasures of seasonal drought in south china. China Rural Water and Hydropower. 3, 149-151.
[32] Gao, J.F., Xiong, K.N., Qin, H.X. (2015) Water resources optimal allocation mode for extremely arid mountains and valleys on karst plateau a case study of the south bank of Huajiang Canyon and Chaoying small watershed of Bijie city, Guizhou Province. Water Saving Irrigation. 10, 57-62.
[33] Wang, W. (2010) Remote sensing analysis of impacts of extreme drought weather on ecosystems in southwest region of china based on normalized difference vegetation index. Research of Environmental Sciences. 12(23), 1447-1455.
[34] Hua, R., An, Y.L., Yang, G.B. (2013) Spatial-temporal variance of agricultural natural disasters and its impact on social environment during 11th five-year period in Guizhou. Guizhou Agricultural Sciences. 41(4), 59-62.
[35] Lv, G. (2016) Analyses of important geodisasters distribution rules and influence factors of Guizhou. Guizhou Geology. 33(2), 108-112.
[36] Zhang, D.F., Zou, Y.L. (2002) The contributory factors and environmental setting of karst geohazards -a typical example in Guizhou province. Bulletin of Mineralogy, Petrology and Geochemistry. 21(1), 39-42.
[37] Dan, W.H., Peng, S.T., Wang, L. (2010) Problems and countermeasures of agriculture large-scale development in southwest karst regions. Guizhou Agricultural Sciences. 38(7), 192-195.

Received: **21.11.2018**
Accepted: **19.02.2019**

CORRESPONDING AUTHOR

Hu Chen
School of Karst Science,
Guizhou Normal University,
Guiyang 550001 – China

e-mail: gy_chenhu@163.com

© by PSP Volume 28 – No. 5/2019 pages 4256-4266 Fresenius Environmental Bulletin

COMPARATIVE ANALYSIS OF MATURE AND PREPROPROTEIN FORM OF THIONINS IN SOME PLANT SPECIES; BIOINFORMATICS APPROACHES

Ibrahim Ilker Ozyigit[1,2,*], Ertugrul Filiz[3], Ibrahim Adnan Saracoglu[4], Bahattin Yalcin[4]

[1]Department of Biology, Faculty of Science and Arts, Marmara University, 34722, Goztepe, Istanbul, Turkey
[2]Department of Biology, Faculty of Science, Kyrgyz-Turkish Manas University, 720038, Bishkek, Kyrgyzstan
[3]Department of Crop and Animal Production, Cilimli Vocational School, Duzce University, 81750, Cilimli, Duzce, Turkey
[4]Department of Chemistry, Faculty of Science and Arts, Marmara University, 34722, Goztepe, Istanbul, Turkey

ABSTRACT

Thionins are one of the most important antimicrobial peptides in broad-range plant defense. A number of studies are present regarding the structural and biological role of mature thionins but preproprotein forms of these molecules have not been extensively studied. Thus, this study aimed to comparatively analyze a total of 56 thionin preproprotein sequences from 14 different plant species. Analyses of primary, secondary and tertiary structures of these forms revealed that preproproteins with "gamma-thionin domain" were relatively shorter and more basic than proteins with "thionin domain" structure. In addition, members of "thionin domain" were more similar to each other than that of "gamma-thionin domain" forms. Sub-cellular localizations of these forms were predicted as extracellular. Structural superposition of precursor and mature thionins showed that a large portion of precursor sequences are cleaved to form a functional protein. Although precursor forms demonstrated the significant structural divergence in modelled species, functional mature forms showed a structural pattern in α-helices; two α-helix proteins included the "thionin domain" family while one α-helix proteins contained the "gamma-thionin domain" family. Results of this study will become valuable theoretical knowledge and provide insight in terms of further understanding the formation of mature functional thionins thereby their biological roles.

KEYWORDS:
α/β-thionins, *γ*-thionins, disulfide bridges, 3D modeling, plant defense

INTRODUCTION

Plants produce a variety of biologically active compounds under biotic and abiotic stress conditions [1]. Proteins such as chitinases, defensins, endoproteinases, glucanases, glycine-rich peptides, hevein-like peptides, homologs of MBP-1, knottin-like peptides, peroxidases, proteinase inhibitors, lipid transfer proteins (LTPs), puroindolines, snakins, osmotins, *α/β*-and *γ*-thionins are constitutively or temporally induced by pathogen invasion [2, 3]. Among these proteins, thionins are the well characterized antimicrobial peptides in many plant species. They are synthesized as preproproteins with an N-terminal signal peptide and a long C-terminal acidic peptide, which later co-and post-translationally processed to yield mature functional thionins [4]. Thionins are small (45-48 residues) and basic peptides (*pI* >8) with a low molecular weight (~5 kDa). They are rich in basic and sulfur-containing residues such as arginine, lysine and cysteine [2, 5]. Two small α-helices and two anti-parallel β sheets with 3-4 disulfide bridges form the thionin structure [4, 6]. The name "thionin" is usually used for two well characterized distinct groups such as *α/β*-thionins and *γ*-thionins [6]. *α/β*-thionins have five different classes, namely class I-V [5]. Type I thionins are 45 residues long, highly basic proteins containing four disulfide bonds. They were found in endosperm of grains such as wheat (*α-, β*-purothionins) and barley (hordothionins) [6, 7]. Type II thionins are 46-47 residues long, less basic proteins with four disulfide bonds. They were isolated from the leaves and nuts of parasitic plant *Pyrularia pubera*, and from the leaves of barley [8, 9]. Type III thionins are 45-46 residues long slightly basic proteins with three disulfide bonds. They were isolated from the leaves and stems of *Viscum album* [10], *Phoradendron tomentosum and Phoradendron liga* [11] and *Dendrophthora clavata* [12]. Type IV thionins are 46 residues long neutral proteins with three disulfide bonds. They were extracted from the seeds of *Abyssinian cabbage* [13]. Type V thionins are the truncated, non-toxic forms of thionins identified in some grains like wheat [13]. *γ*-thionins are another distinct group of thionins. They are 45-47 residues long basic peptides with 4-8 cysteine residues. They have been classified into four main groups according to their primary and S–S bond structure, and biological function. Types I and II were reported to be toxic to bacteria and fungi while types III and IV for the

mammalian cell lines [14]. C-terminus of γ-thionins and basic amino acids such as lysine and arginine were also reported to be an important determinant on antifungal activities [15]. The primary structure analyses demonstrated that α- and β-thionins are more similar between themselves than that of γ-thionins [13]. Studies have reported that wheat thionins accumulated in cell walls of *Fusarium*-inoculated plants may block pathogen infection through cell walls [9]. Thionin genes were reported to be upregulated in wheat genome upon exposure to *F. graminearum* [16]. A barley thionin gene introduced in sweet potato was found to have resistance against black rot disease [17]. Transgenic potato with thionin genes was indicated to develop resistance to gray mold [18]. Rice thionin genes were reported to involve in defense responses against two root pathogens of root-knot nematode *Meloidogyne graminicola* and oomycete *Pythium graminicola* [19]. Plant thionins are excellent candidate proteins for crop protection because they act on pathogens by membrane permeabilization, thereby; there is less likelihood for intruders to develop resistance towards these peptides [20]. A number of studies are present regarding the structural and biological role of mature thionins but preproprotein forms of these proteins have not been extensively studied. Therefore, this study aims to perform a comparative *in silico* analysis of thionin preproproteins in 14 higher plant species.

MATERIALS AND METHODS

Sequence retrieval and domain analysis. 14 plant species, including *Arabidopsis thaliana, Brachypodium distachyon, Brassica rapa, Eucalyptus grandis, Glycine max, Medicago truncatula, Oryza sativa, Phaseolus vulgaris, Populus trichocarpa, Prunus persica, Solanum lycopersicum, Sorghum bicolor, Vitis vinifera and Zea mays* (Table 1) were selected for this study. Then, reference thionin preproprotein sequences with AAC41678.1, XP_003557586.1, BAH03381.1, KCW62396.1, ACU14316.1, AAQ91287.1, BAB93111.1, ADR30066.1, EEE80030.1, EMJ00373.1, NP_001234872.1, AAB33969.1, XP_002263380.2 and ACG24883.1 accession numbers were retrieved from NCBI protein database [21]. These sequences were used as queries in proteome dataset of each species in Phytozome, with an e^{-10} threshold value. Domain analysis of retrieved sequences was performed by using Pfam 27.0 server [22, 23].

Physico-chemical and conserved motif analysis. Sequence length, molecular weight and theoretical isoelectric point (*pI*) of thionin preproproteins were analyzed by Expasy's ProtParam server [24, 25]. Conserved motif analysis was performed by using MEME tool with following parameters: maximum number of motifs to find 5; minimum width of motif, 6 and maximum width of motif, 50 [26, 27]. Sub-cellular localizations of proteins were predicted by CELLO server [28, 29].

Phylogenetic and gene structure analysis. Protein sequences were aligned by ClustalW [30] and phylogenetic tree was constructed by MEGA5 [31] using maximum likelihood (ML) method with follow-ing parameters: Poisson correction, pairwise deletion, and 1000 replicates bootstrap value. Exon/intron organizations of thionin preproprotein genes were analyzed by using GSDS 2.0 server [32, 33].

3D modeling of thionin preproproteins. Most diverged six thionin preproproteins, including *A. thaliana, B. distachyon, O. sativa, P. trichocarpa, B. rapa* and *S. lycopersicum* were selected for 3D modeling. 3D structures were constructed by using Phyre[2] server [34, 35] and visualized by using Swiss Pdb Viewer [36] and PyMol [37]. Model quality was checked by Ramachandran plot analysis [38].

RESULTS AND DISCUSSION

Sequence analysis of thionin preproproteins. We have retrieved 56 thionin preproprotein genes from 14 plant species in Phytozome database based on blastp search. These included; 4 genes from *A. thaliana*; 8 genes from *B. distachyon;* 11 genes from *B. rapa*; 1 gene from *E. grandis*; 4 genes from *G. max*; 3 genes from *M. truncatula*; 9 genes from *O. sativa*; 2 genes from *P. vulgaris*; 1 gene from *P. trichocarpa*; 2 genes from *P. persica*; 5 genes from *S. lycopersicum*; 1 gene from *S. bicolor*; 2 genes from *V. vinifera* and 3 genes from *Z. mays*. Domain analysis showed that thionin preproproteins have either thionin (PF00321) or gamma-thionin (PF00304) domain structure. Preproproteins with gamma-thionin domain ranged from 72 to 120 amino acid residues with a *pI* value of 5.45-9.38 while preproproteins with thionin domain ranged from 109 to 148 residues with 5.23-7.91 *pI* values. This showed that preproproteins with gamma-thionin domains were relatively shorter and more basic than that of preproproteins with thionin domain. In alignment analysis of precursor thionins, an N-terminal signal sequence, a C-terminal region and mature thionin portion, consisting of 40-50 residues with six highly conserved cysteine residues, have been also identified (Figure 1). Spelbrink et al. [15] reported that C-terminus domain and basic amino acids such as lysine and arginine in γ-thionins are an important determinant on antifungal activities. Thus, it could be proposed that high ratio of basic amino acids of lysine and arginine in preproproteins with gamma-thionin domain may be connected with their antifungal activities. Sub-

cellular localization of precursor thionins were predicted as extracellular (Table 1), suggesting that mature thionins could be secreted through the plasma membrane during a pathogenic attack.

TABLE 1
Some gene and protein features of thionin preproproteins in 14 different plant species.

Species name	Plant Group	Access. No. (Phytozome)	Exon number	Protein length (aa)	Molecular weight (kDa)	*pI*	Pfam domain[a]	Predicted location (CELLO server)
Arabidopsis thaliana	Dicot	AT2G15010.1	3	135	14.2594	6.22	Thionin	Extracellular
		AT5G36910.1	3	134	14.1783	6.18	Thionin	Extracellular
		AT1G66100.1	3	134	14.1471	4.39	Thionin	Extracellular
		AT1G72260.1	3	134	14.3506	8.48	Thionin	Extracellular
Brachypodium distachyon	Monocot	Bradi0149s00100.1.p	3	109	11.5864	8.23	Thionin	Extracellular
		Bradi1g57400.1.p	3	139	14.7838	5.61	Thionin	Extracellular
		Bradi1g57302.1.p	3	138	14.5218	6.53	Thionin	Extracellular
		Bradi1g57296.1.p	3	135	14.3875	6.26	Thionin	Extracellular
		Bradi1g57291.1.p	3	126	13.2061	5.23	Thionin	Extracellular
		Bradi1g57285.1.p	3	135	14.3704	5.88	Thionin	Extracellular
		Bradi1g57280.1.p	3	135	14.2123	6.25	Thionin	Extracellular
		Bradi1g57337.1.p	3	139	14.7231	6.67	Thionin	Extracellular
Brassica rapa	Dicot	Brara.G03382.1.p	2	80	8.9565	8.47	Gamma-thionin	Extracellular
		Brara.B02210.1.p	2	82	9.2400	9.24	Gamma-thionin	Extracellular
		Brara.B02211.1.p	2	80	8.9185	9.00	Gamma-thionin	Extracellular
		Brara.G02204.1.p	2	79	8.6231	8.48	Gamma-thionin	Extracellular
		Brara.G03383.1.p	2	80	8.8303	8.70	Gamma-thionin	Extracellular
		Brara.H02365.1.p	2	77	8.7572	8.85	Gamma-thionin	Extracellular
		Brara.G03384.1.p	2	79	8.5670	8.15	Gamma-thionin	Extracellular
		Brara.F03084.1.p	2	80	9.2882	9.41	Gamma-thionin	Extracellular
		Brara.G02203.1.p	2	80	8.8204	8.70	Gamma-thionin	Extracellular
		Brara.E02038.1.p	2	79	8.6538	5.45	Gamma-thionin	Extracellular
		Brara.B02209.1.p	2	80	8.6842	8.47	Gamma-thionin	Extracellular
Eucalyptus grandis		Eucgr.H05052.1						Extracellular
Glycine max		Glyma.08G005300.1.p	2	73	8.1095	9.04	Gamma-thionin	Extracellular
	Dicot	Glyma.06G160300.1.p	2	84	9.4781	9.20	Gamma-thionin	Extracellular
	Dicot	Glyma.05G198000.1.p	2	76	8.6521	8.88	Gamma-thionin	Extracellular
		Glyma.08G268000.1.p	2	74	8.4269	9.49	Gamma-thionin	Extracellular
Medicago truncatula		Medtr6g075430.1	1	127	14.2451	6.08	Gamma-thionin	Extracellular
		Medtr2g079440.1	2	85	9.8365	8.39	Gamma-thionin	Extracellular
	Dicot	Medtr2g079430.1	2	72	8.1204	7.48	Gamma-thionin	Extracellular
Oryza sativa		LOC_Os06g31280.1	2	73	8.1163	6.01	Gamma-thionin	Extracellular
		LOC_Os06g31800.1	3	135	14.7348	6.04	Thionin	Extracellular
	Monocot	LOC_Os06g31890.1	3	135	14.6217	5.77	Thionin	Extracellular
		LOC_Os06g31930.1	3	135	14.6588	6.07	Thionin	Extracellular
		LOC_Os06g32160.1	3	135	14.6448	6.07	Thionin	Extracellular
		LOC_Os06g32350.1	3	135	14.6307	5.79	Thionin	Extracellular
		LOC_Os06g32370.1	3	132	14.2201	5.74	Thionin	Extracellular
		LOC_Os06g32550.1	1	148	16.0983	7.91	Thionin	Extracellular
		LOC_Os06g32600.1	3	140	15.5451	6.79	Thionin	Extracellular
		Phvul.005G071300.1	3	135	14.7200	6.91	Thionin	Extracellular
Phaseolus vulgaris		Phvul.005G071400.1	2	75	8.5879	7.50	Gamma-thionin	Extracellular
	Dicot	Potri.002G033200.1	2	75	8.6590	7.49	Gamma-thionin	Extracellular
		ppb024748m	2	73	8.3056	9.30	Gamma-thionin	Extracellular
Populus trichocarpa	Dicot	ppa021404m	2	84	9.5511	8.93	Gamma-thionin	Extracellular/Mitoch./Nucl.
Prunus persica	Dicot	Solyc07g007760.2.1	1	70	7900.3	9.48	Gamma-thionin	
		Solyc07g007710.2.1	2	78	8.7993	9.14	Gamma-thionin	Extracellular
		Solyc07g007730.2.1	2	76	8.3485	8.98	Gamma-thionin	Extracellular
		Solyc07g007750.2.1	1	79	8.7120	8.77	Gamma-thionin	Extracellular
Solanum lycopersicum		Solyc04g008470.2.1	2	76	8.4459	8.96	Gamma-thionin	Extracellular
		Sobic.002G089500.1.p	1	73	8.2377	9.54	Gamma-thionin	Extracellular
		GSVIVT01036750001	2	78	8.5741	9.38	Gamma-thionin	Extracellular
	Monocot	GSVIVT01000230001	1	55	6.3962	9.00	Gamma-thionin	Nuclear/ Extracellular
	Dicot	GRMZM2G179248_P01	2	75	8.4259	8.72	Gamma-thionin	Extracellular
			2	115	12.2941	8.11	Gamma-thionin	Extracellular
Sorghum bicolor	Monocot	AC208126.3_FGP001	2	101	10.1426	7.53	Gamma-thionin	Extracellular
Vitis vinifera		GRMZM2G010097_P01	2	129	13.8617	6.40	Gamma-thionin	Extracellular
Zea mays								Extracellular

[a] Retrieved precursor thionin sequences belonged to either gamma-thionin (PF00304) or thionin (PF00321) domain family.

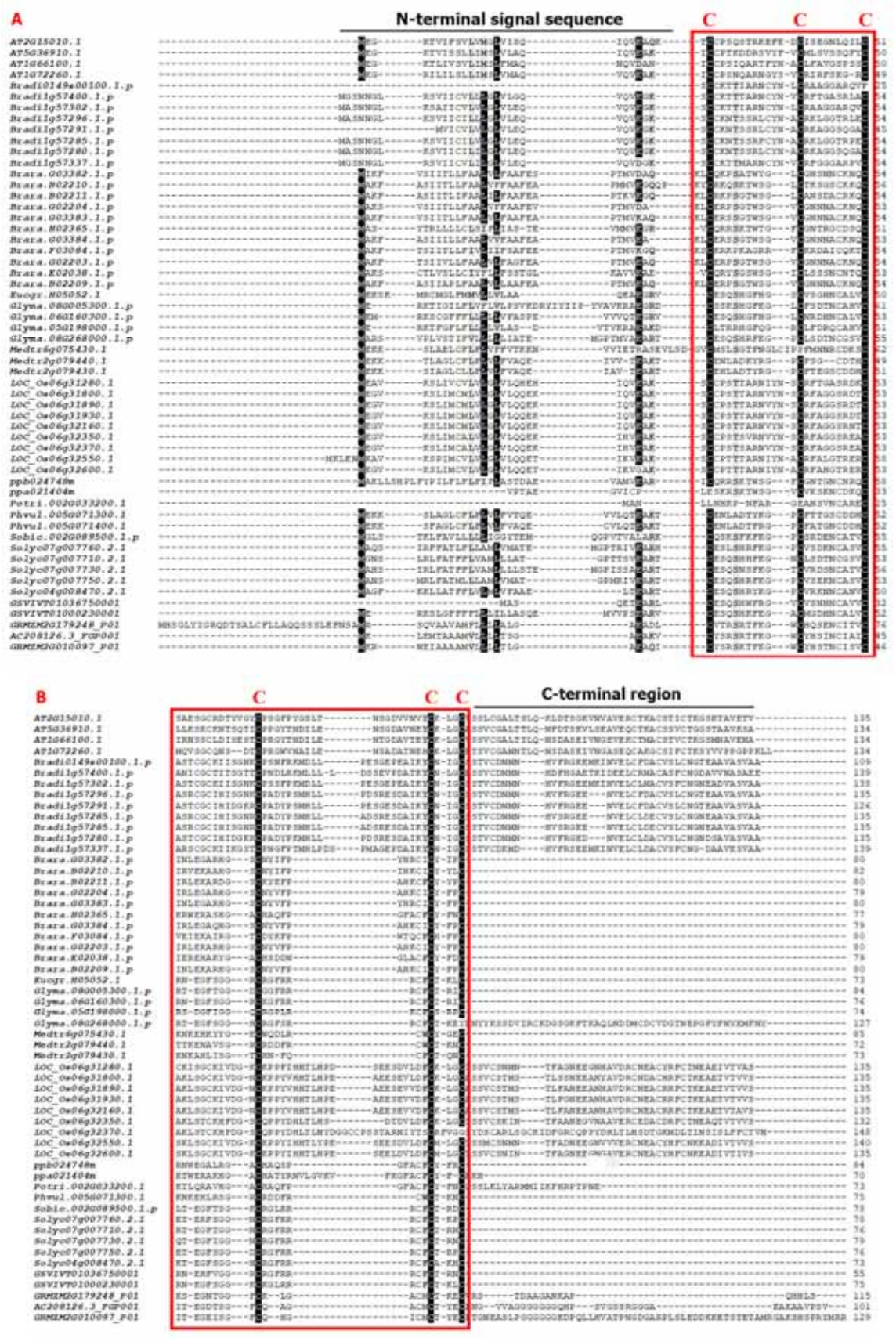

FIGURE 1 A-B

Alignment of 56 precursor thionin sequences from 14 different plant species.

Precursor thionins consisted of an N-terminal signal region, thionin itself and a C-terminal site. Red encircled area approximately corresponds to mature thionin portion, including six highly conserved cysteine residues. These cysteine residues were indicated as red above sequences.

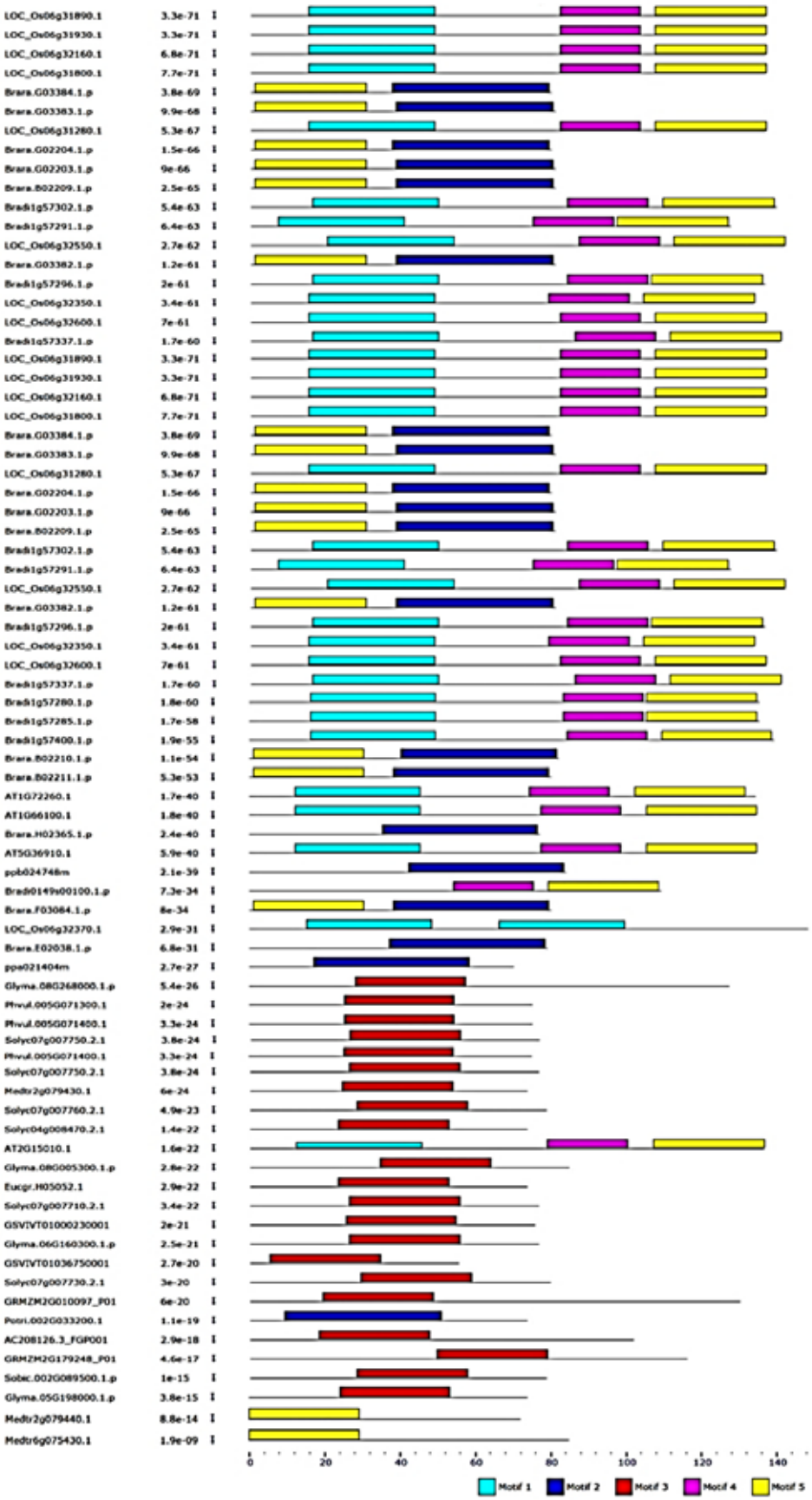

FIGURE 2

Schematic diagram of conserved motifs in thionin preproprotein sequences.

Each motif was represented with different color box such as motif 1, cyan; motif 2, blue; motif 3, red; motif 4, pink; and motif 5, yellow.

TABLE 2
The most conserved five motif sequences of thionin preproproteins in 14 different plant species.

Motif	Width	Sequence	Pfam Domain
1	33	LVLQQEQIQVEAKSCCPSTTARNVYNACRFAGG	Thionin (PF00321)
2	41	TWSGVCGNNNNCKNQCIRWEKARHGSCHYQFPWHKCICYFP	Gamma-thionin (PF00304)
3	29	AEARTCESQSHWFKGWCYSDHNCAHVCRT	Gamma-thionin (PF00304)
4	21	PDVIDYCKIGCSSSVCDNMNH	Not found
5	29	EEFNHIVELCFDACVRFCTKEAPTMVEVQ	Not found

Conserved motif analysis. Motif analysis was performed for the most conserved five motif types (Figure 2). Motif 1 was related with thionin (PF00321) domain structure while motif 2 and 3 associated with gamma-thionin (PF00304) domain. However, motif 4 and 5 did not relate any domain structure (Table 2). Motif 1 was observed in 4 of 14 species; motif 2 in 3 of 14 species; motif 3 in 7 of 14 species; motif 4 in 3 of 14 species and motif 5 in 5 of 14 species. A unique motif pattern, comprising all species was not detected. These motif variations could be related with different classes of thionins in various plant species. Primary structure analysis also demonstrated that preproproteins with thionin domain are more similar between themselves than that of the preproproteins with gamma-thionin domain. These our findings are also supported by previous studies. It has been reported that primary sequence analysis of γ-thionins are not sufficient to determinate their biological function since most residues extremely vary [14]. In addition, α- and β-thionins are more similar between themselves than that of γ-thionins [13]. Therefore, we may propose that preproproteins with thionin domain could belong to α- and β-thionin family since they less vary between themselves and well separated from preproproteins with gamma-thionin domain structure.

Exon/intron structure analysis. Genes encoding preproproteins with thionin domain structure mainly included three exons with an exception of *O. sativa*, while genes encoding preproproteins with gamma-domain had two exons, except for *G. max, P. persica, S. lycopersicum* and *V. vinifera* (Table 1). Notably, *Oryza* (LOC_Os06g32370.1), *Glycine* (Glyma.08G268000.1.p), *Prunus* (ppa021404m), *Solanum* (Solyc07g007730.2.1 and Solyc04g 008470.2.1) and *Vitis* (GSVIVT01036750001) genes only contained one exon. These intron/exon losses may be related with functional diversities of *thionin* and *gamma-thionin* families. In addition, plant thionin genes like other *PRs* are differentially expressed in pathogen specific way [39] thereby their expression are also regulated by other factors such as heavy metals, phytohormones, transcription factors (TFs) *etc.* [19, 40]. Thus, response of thionins to various stresses could differ as a consequence of genetic regulation in molecular specification obtained during phylogenetic development.

Phylogenetic analysis of thionin preproproteins. Sequence alignment of preproproteins was done by ClustalW and phylogenetic tree was constructed using MEGA5 with maximum likelihood (ML) method for 1000 bootstraps (Figure 3). Phylogenetic tree was arbitrarily divided into two main groups, namely A and B, based on domain families. All preproproteins with gamma-thionin domain were clustered in group A while all preproproteins with thionin domain were in group B with a 99% bootstrap value. Then, we further subdivided group A and B into subgroups such as A1 and A2, and B1 and B2, respectively based on the phylogenetic clustering/divergence. Group B1 only contained dicot *A. thaliana* members while group B2 only had monocot *B. distachyon* and *O. sativa* sequences. The molecular variations in preproprotein genes may cause this separation between monocots and dicots. The remaining species were distributed in group A1 and A2. Group A1 included monocot-dicot species, without separation, with gamma-thionin domain, while group A2 only had dicots with gamma-thionin domain. Thus, group A may be related with gamma-thionin family due to its high variability. In contrast, group B may belong to either α- or β-thionin family because of its homogenous distribution. In addition, previous studies mentioned that plant defensin-like peptides may develop specific functions during plant reproduction [41]. For example, a number of defensin-like peptides, including thionins have been indicated to be expressed in the cells of female gametophyte of *Arabidopsis* [42, 43] and maize [44]. Therefore, different thionin genes in various plant species may have been emerged as a result of these molecular specifications to improve the plant defense.

3D structure prediction of thionin preproproteins. Putative 3D models of precursor (Figure 4) and mature (Figure 5) thionin sequences were predicted by using Phyre^2 server at intensive mode for selected six species. Three of modelled species, including *A. thaliana, B. distachyon* and *O. sativa* were selected thionin domain family while remaining three, including *P. trichocarpa, B. rapa* and *S. lycopersicum* were from gamma-thionin domain family. The following templates with PDB IDs of 1OKH in *A. thaliana, B. distachyon* and *O. sativa*; 1BK8 in *P. trichocarpa*; 1AYJ in *B. rapa*; and 1GPS in *S. lycopersicum* were used in prediction of both precursor and mature 3D structures of thionin

sequences. Model validation was performed by Ramachandran plot analysis. In modelled species of both precursor and mature thionins, more than 90% of residues were in allowed regions. This indicated that predicted models were fairly in good quality. To better understand the cleavage of preproprotein thionin sequences into functionally active mature form at structural level, we superposed the predicted 3D models of precursor and mature thionins, and visualized them with PyMol (Figure 4). A large portion of precursor thionin sequences was found to be cleaved to form a functional protein. In precursor sequences of modelled species, a varying of 1-30 amino acid residues beginning from N-terminal region high possibly formed the signal sequences (Figure 4a-f). Furthermore, overall alignment analysis of identified 56 precursor protein sequences

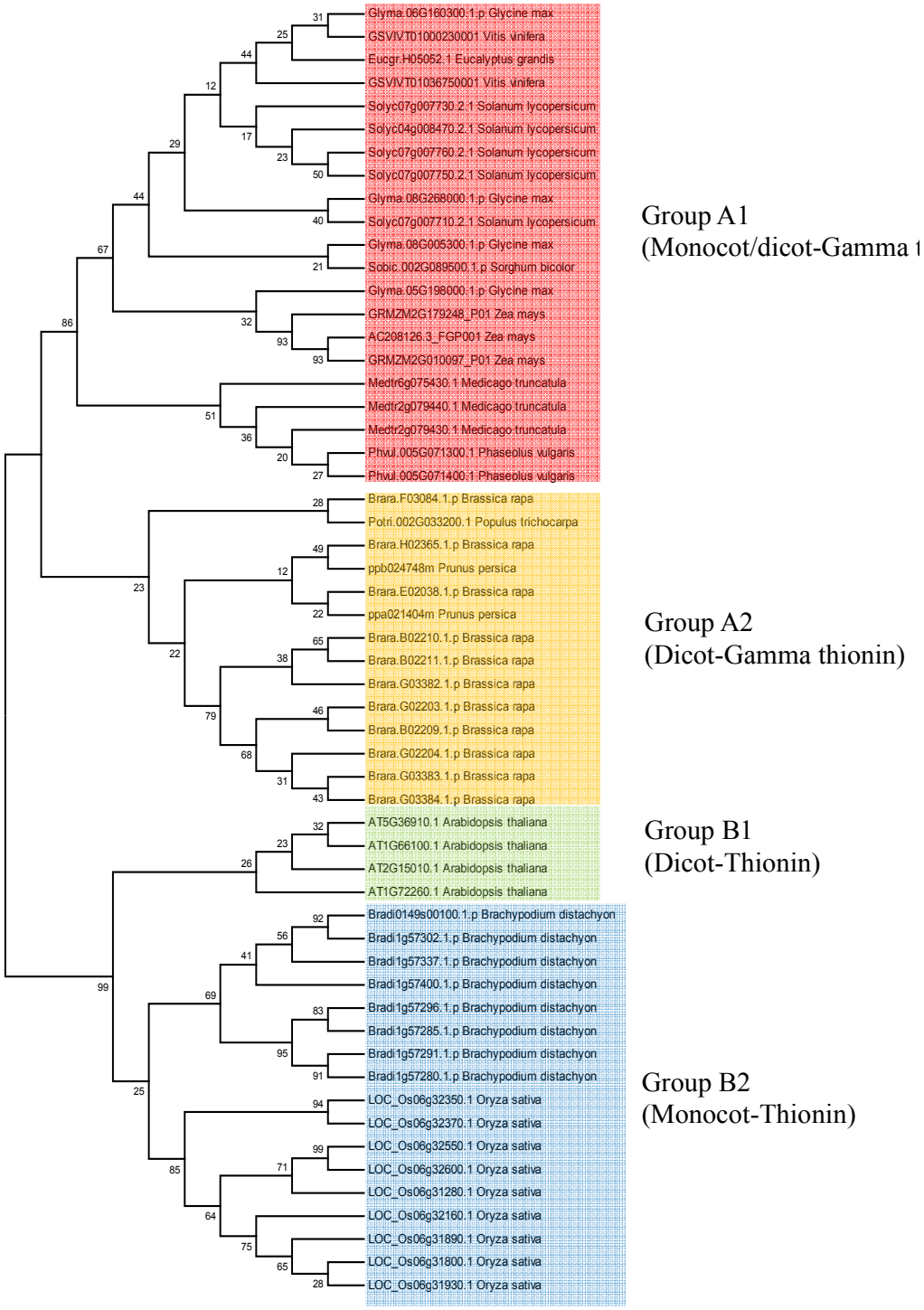

FIGURE 3
Phylogenetic distribution of thionin preproproteins in 14 different plant species.

from 14 species in this study demonstrated the similar alignment results, with first 1-30 amino acids from N-terminal region as being signal sequences (Figure 1). The cloning of different cDNAs and genomic sequences also showed that all precursor thionins consist of an N-terminus signal sequence, a C-terminus acidic domain and thionin itself [4] also reported that precursor thionins and acidic domain peptides have not been isolated from any plant species due to their quick processing upon synthesis. Moreover, amino acid composition analysis showed that thionin preproproteins are mainly rich in cysteine (10.2%), serine (8.2%), alanine (7.9%), leucine (7.7%) and glycine (7.3%). Especially, cysteine residues are very important because of their involvement in protein folding by forming disulfide bridges [4, 6]. Overall, synthesis of thionins in precursor form and then cleavage of large proportion of sequences, including N-terminus signal and C-terminus acidic domains could implicitly indicate that these cleaved sequences may play a role in formation/localization of stress-specific thionin proteins.

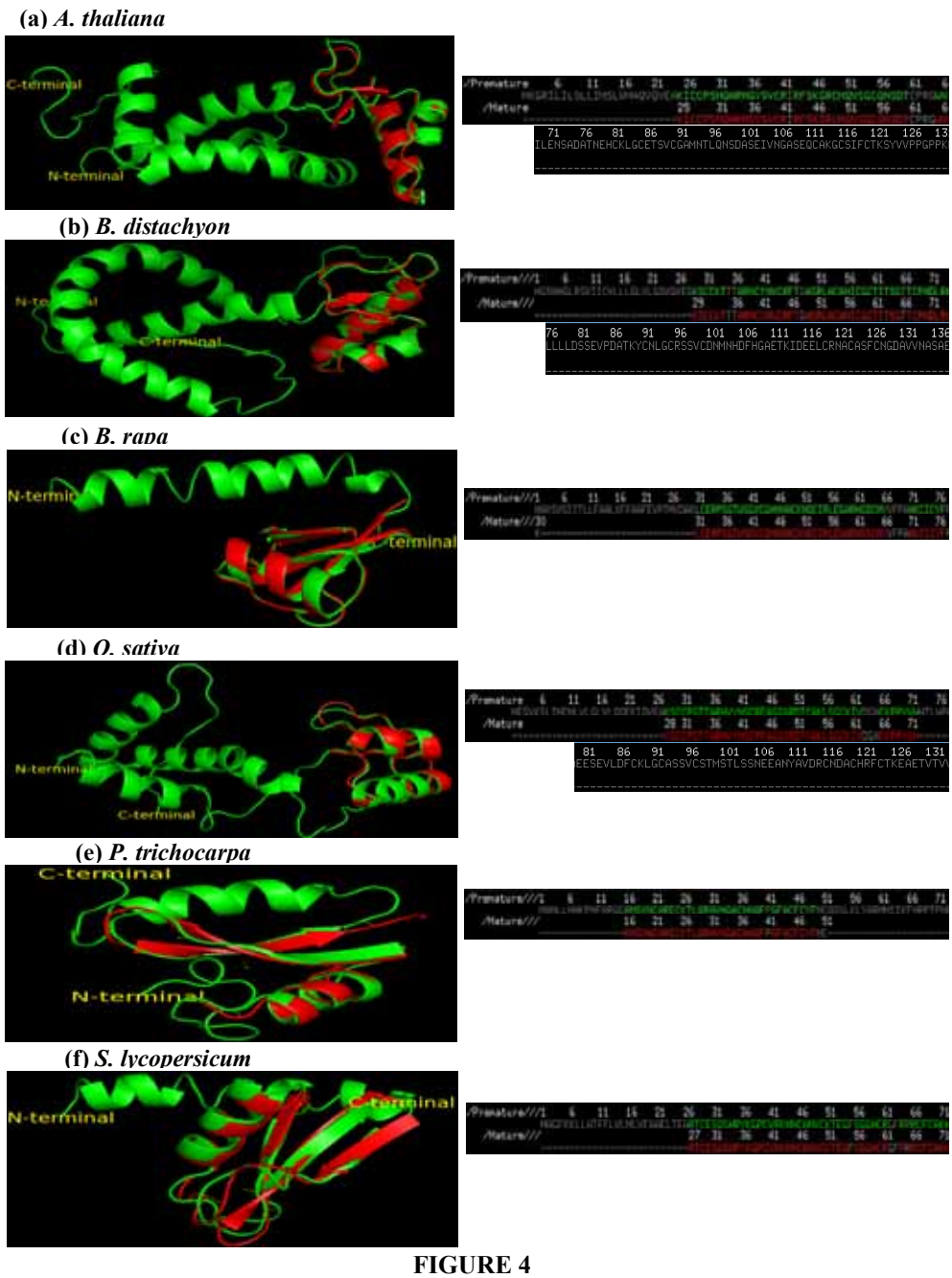

FIGURE 4

Superposition of predicted 3D thionin preproproteins with their mature forms in selected six species, including (a) *A. thaliana*, (b) *B. distachyon*, (c) *B. rapa*, (d) *O. sativa*, (e) *P. trichocarpa* and (f) *S. lycopersicum*. Premature (green colored) and mature (red colored) form of thionin proteins were superposed and visualized by PyMol along with their sequence alignments.

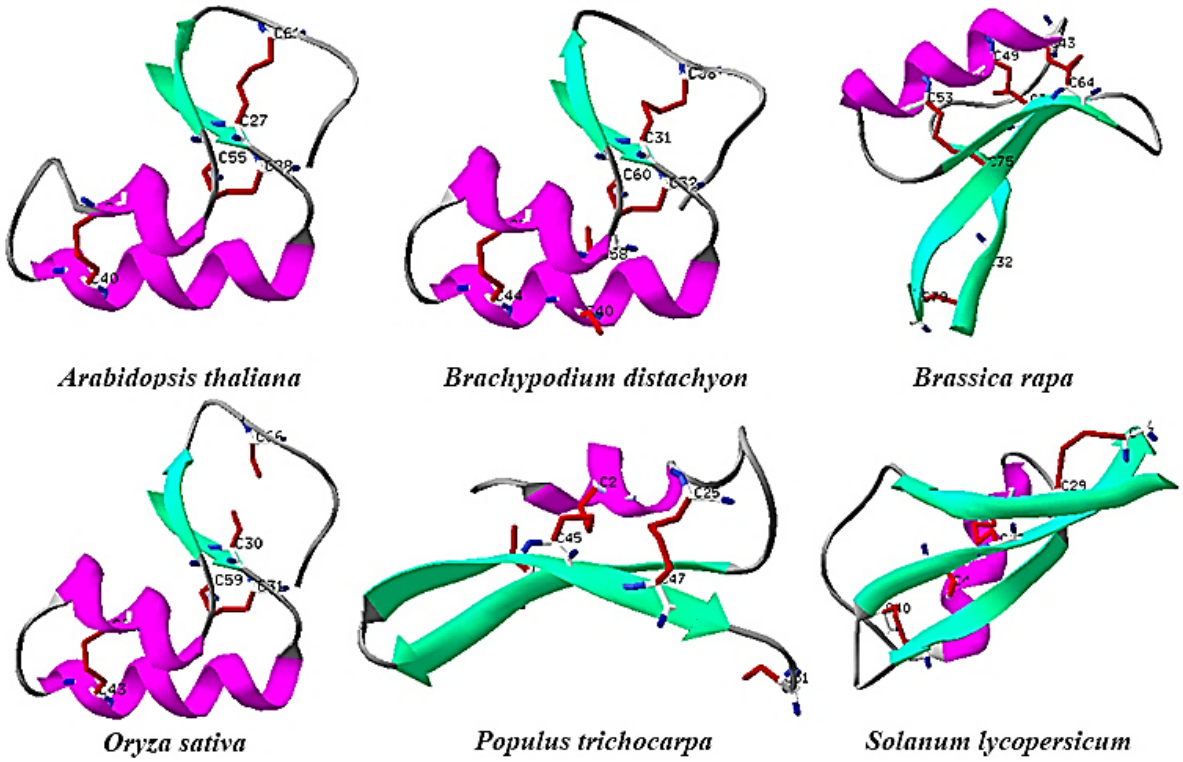

FIGURE 5
Predicted 3D structure of mature thionins in *A. thaliana, B. distachyon, B. rapa, O. sativa, P. trichocarpa* and *S. lycopersicum*.
Magenta and cyan colors indicate the α-helices and β-strands, respectively, and disulfide bridges are shown with red color.

In modelled mature thionins (Figure 5), proteins with thionin domain had two α-helices and two β-strands, while proteins with gamma-thionin domain included two β-strands in *P. trichocarpa,* and three β-strands in *B. rapa* and *S. lycopersicum* with only one α-helix. We also identified a varying of 2-4 disulfide bridges in mature thionins, including Cys27-Cys28-Cys40-Cys49-Cys55-Cys61 (forming three disulfide bridges) in *A. thaliana*; Cys31-Cys32-Cys40-Cys44-Cys54-Cys58-Cys60-Cys68 (forming three disulfide bridges) in *B. distachyon*; Cys32-Cys43-Cys49-Cys53-Cys64-Cys73-Cys75-Cys79 (forming four disulfide bridges) in *B. rapa*; Cys30-Cys31-Cys43-Cys53-Cys59-Cys66 (forming two disulfide bridges) in O. *sativa*; Cys21-Cys25-Cys36-Cys45-Cys47-Cys51 (forming two disulfide bridges) in *P. trichocarpa* and Cys29-Cys40-Cys46-Cys50-Cys60-Cys67-Cys69-Cys73 (forming four disulfide bridges) in *S. lycopersicum*. Although nonfunctional precursor form of thionins have been observed to show significant structural divergence in modelled species, functional mature forms demonstrated a structural pattern in α-helices; two α-helix proteins represented the thionin domain family while one α-helix showed the gamma-thionin domain family (Figure 5). Thus, mature thionin proteins were to have been well conserved during their evolutionary history depending on their roles in plant defense.

CONCLUSION

We have performed *in silico* comparative analysis of thionin preproproteins in 14 higher plant species. In this context, primary, secondary and tertiary structures of precursor and mature thionins were analyzed; exon/intron organizations were determined; motif and domain analysis were performed and phylogenetic tree was constructed. Although we have identified some degree of similarities and divergences between precursor and mature thionin forms at sequence and structural levels, the overall molecular mechanism is too beyond the simplicity to explain with comparisons due to many other biotic factors such as intracellular metal ion distribution, TFs, phytohormones *etc.* are involved in regulation of thionin genes. However, we believe that results of this study will become valuable theoretical knowledge and provide insights to further understand the mature thionins in various plant species.

ACKNOWLEDGEMENTS

No potential conflict of interest was reported by the authors.

REFERENCES

[1] Ferreira, R.B., Monteiro, S.A.R.A., Freitas, R., Santos, C.N., Chen, Z., Batista, L.M. and Teixeira, A.R. (2007) The role of plant defence proteins in fungal pathogenesis. Molecular Plant Pathology. 8(5), 677-700.

[2] Castro, M.S. and Fontes, W. (2005) Plant defense and antimicrobial peptides. Protein and Peptide Letters. 12(1), 11-16.

[3] Jain, S., Kumar, D., Jain, M., Chaudhary, P., Deswal, R. and Sarin, N.B. (2012) Ectopic overexpression of a salt stress-induced pathogenesis-related class 10 protein (PR10) gene from peanut (*Arachis hypogaea* L.) affords broad spectrum abiotic stress tolerance in transgenic tobacco. Plant Cell, Tissue and Organ Culture (PCTOC). 109(1), 19-31.

[4] Abbas, A., Plattner, S., Shah, K.H. and Bohlmann, H. (2013) Comparison of periplasmic and intracellular expression of *Arabidopsis* thionin proproteins in *E. coli*. Biotechnology Letters. 35(7), 1085-1091.

[5] Hussain, S., Güzel, Y., Schönbichler, S.A., Rainer, M., Huck, C.W. and Bonn, G.K. (2013) Solid-phase extraction method for the isolation of plant thionins from European mistletoe, wheat and barley using zirconium silicate embedded in poly (styrene-co-divinylbenzene) hollow-monoliths. Analytical and Bioanalytical Chemistry. 405(23), 7509-7521.

[6] Stec, B. (2006) Plant thionins-the structural perspective. Cellular and Molecular Life Sciences CMLS. 63(12), 1370-1385.

[7] Egorov, T.A., Odintsova, T.I., Pukhalsky, V.A. and Grishin, E.V. (2005) Diversity of wheat anti-microbial peptides. Peptides. 26(11), 2064-2073.

[8] Vernon, L.P. (1992) *Pyrularia* thionin: physical properties, biological responses and comparison to other thionins and cardiotoxin. Journal of Toxicology: Toxin Reviews. 11(3), 169-191.

[9] Asano, T., Miwa, A., Maeda, K., Kimura, M. and Nishiuchi, T. (2013) The secreted antifungal protein thionin 2.4 in *Arabidopsis thaliana* suppresses the toxicity of a fungal fruit body lectin from *Fusarium graminearum*. PLoS Pathogens. 9(8), e1003581.

[10] Amer, B., Juvik, O.J., Dupont, F., Francis, G. W. and Fossen, T. (2012) Novel aminoalkaloids from European mistletoe (*Viscum album* L.). Phytochemistry Letters. 5(3), 677-681.

[11] Guzmán-Rodríguez, J.J., Ochoa-Zarzosa, A., López-Gómez, R. and López-Meza, J.E. (2015) Plant antimicrobial peptides as potential anticancer agents. BioMed Research International. 2015:735087.

[12] Bhave, M. and Methuku, D.R. (2011) Small cysteine-rich proteins from plants: a rich resource of antimicrobial agents. In: Méndez-Vilas, A. (Ed.) Science Against Microbial Pathogens: Communicating Current Research and Technological Advances. 1074-1083.

[13] Nawrot, R., Barylski, J., Nowicki, G., Broniarczyk, J., Buchwald, W. and Goździcka-Józefiak, A. (2014) Plant antimicrobial peptides. Folia Microbiologica. 59(3), 181-196.

[14] Selitrennikoff, C.P. (2001) Antifungal proteins. Applied and Environmental Microbiology. 67(7), 2883-2894.

[15] Spelbrink, R.G., Dilmac, N., Allen, A., Smith, T.J., Shah, D.M. and Hockerman, G.H. (2004) Differential antifungal and calcium channel-blocking activity among structurally related plant defensins. Plant Physiology. 135(4), 2055-2067.

[16] Kosaka, A., Manickavelu, A., Kajihara, D., Nakagawa, H. and Ban, T. (2015) Altered gene expression profiles of wheat genotypes against *Fusarium* head blight. Toxins. 7(2), 604-620.

[17] Muramoto, N., Tanaka, T., Shimamura, T., Mitsukawa, N., Hori, E., Koda, K. and Imaeda, T. (2012) Transgenic sweet potato expressing thionin from barley gives resistance to black rot disease caused by *Ceratocystis fimbriata* in leaves and storage roots. Plant Cell Reports. 31(6), 987-997.

[18] Hoshikawa, K., Ishihara, G., Takahashi, H. and Nakamura, I. (2012) Enhanced resistance to gray mold (*Botrytis cinerea*) in transgenic potato plants expressing thionin genes isolated from Brassicaceae species. Plant Biotechnology. 29(1), 87-93.

[19] Ji, H., Gheysen, G., Ullah, C., Verbeek, R., Shang, C., De Vleesschauwer, D. and Kyndt, T. (2015) The role of thionins in rice defence against root pathogens. Molecular plant pathology. 16(8), 870-881.

[20] Hao, G., Stover, E. and Gupta, G. (2016) Overexpression of a modified plant thionin enhances disease resistance to citrus canker and huanglongbing (HLB). Frontiers in Plant Science. 7, 1078.

[21] The National Center for Biotechnology Information. (2018) Available from: https://www.ncbi.nlm.nih.gov/protein

[22] European Bioinformatics Institute - Sequence Database. (2018) Available from: https://pfam.xfam.org/

[23] Finn, R.D., Bateman, A., Clements, J., Coggill, P., Eberhardt, R.Y., Eddy, S.R. and Sonnhammer, E.L. (2013) Pfam: the protein families database. Nucleic Acids Research. 42(D1), D222-D230.

[24] ExPASy - SIB Bioinformatics Resource Portal. (2018) Available from: https://web.expasy.org/protparam/

[25] Gasteiger, E., Hoogland, C., Gattiker, A., Wilkins, M.R., Appel, R.D. and Bairoch, A. (2005) Protein identification and analysis tools on the ExPASy server. In: The Proteomics Protocols Handbook. Humana Press. 571-607.
[26] National Biomedical Computation Resource. (2018) Available from:http://meme-suite.org/
[27] Bailey, T.L., Boden, M., Buske, F.A., Frith, M., Grant, C.E., Clementi, L. and Noble, W.S. (2009) MEME SUITE: tools for motif discovery and searching. Nucleic Acids Research. 37(suppl_2), W202-W208.
[28] Subcellular Localization Predictive System. (2018) Available from: http://cello.life.nctu.edu.tw/
[29] Yu, C.S., Chen, Y. C., Lu, C.H. and Hwang, J. K. (2006) Prediction of protein subcellular localization. Proteins: Structure, Function, and Bioinformatics. 64(3), 643-651.
[30] Thompson, J.D., Higgins, D.G. and Gibson, T.J. (1994) CLUSTAL W: improving the sensitivity of progressive multiple sequence alignment through sequence weighting, position-specific gap penalties and weight matrix choice. Nucleic Acids Research. 22(22), 4673-4680.
[31] Tamura, K., Peterson, D., Peterson, N., Stecher, G., Nei, M. and Kumar, S. (2011) MEGA5: molecular evolutionary genetics analysis using maximum likelihood, evolutionary distance, and maximum parsimony methods. Molecular Biology and Evolution. 28(10), 2731-2739.
[32] Gene Structure Display Server. (2018) Available from:http://gsds.cbi.pku.edu.cn/
[33] Guo, A.Y., Zhu, Q. H., Chen, X., and Luo, J.C. (2007) GSDS: a gene structure display server. Yi chuan= Hereditas. 29(8), 1023-1026.
[34] Structural Bioinformatics Group - Imperial College London. (2018) Available from: http://www.sbg.bio.ic.ac.uk
[35] Kelley, L.A. and Sternberg, M.J. (2009) Protein structure prediction on the Web: a case study using the Phyre server. Nature Protocols. 4(3), 363.
[36] Johansson, M.U., Zoete, V., Michielin, O. and Guex, N. (2012) Defining and searching for structural motifs using DeepView/Swiss-PdbViewer. BMC Bioinformatics. 13(1), 173.
[37] DeLano, W.L. (2002) The PyMOL molecular graphics system. (2018) Available from: https://pymol.org/pymol.html?
[38] Lovell, S.C., Davis, I.W., Arendall III, W.B., De Bakker, P.I., Word, J.M., Prisant, M.G. and Richardson, D.C. (2003) Structure validation by Cα geometry: ϕ, ψ and Cβ deviation. Proteins: Structure, Function, and Bioinformatics. 50(3), 437-450.
[39] Chen, X. and Ronald, P.C. (2011) Innate immunity in rice. Trends in Plant Science. 16(8), 451-459.
[40] Tian, Z., He, Q., Wang, H., Liu, Y., Zhang, Y., Shao, F. and Xie, C. (2015) The potato ERF transcription factor StERF3 negatively regulates resistance to *Phytophthora infestans* and salt tolerance in potato. Plant and Cell Physiology. 56(5), 992-1005.
[41] De Coninck, B., Cammue, B.P. and Thevissen, K. (2013) Modes of antifungal action and in planta functions of plant defensins and defensin-like peptides. Fungal Biology Reviews. 26(4), 109-120.
[42] Punwani, J.A., Rabiger, D.S. and Drews, G.N. (2007) MYB98 positively regulates a battery of synergid-expressed genes encoding filiform apparatus-localized proteins. The Plant Cell. 19(8), 2557-2568.
[43] Wuest, S.E., Vijverberg, K., Schmidt, A., Weiss, M., Gheyselinck, J., Lohr, M. and Grossniklaus, U. (2010) *Arabidopsis* female gametophyte gene expression map reveals similarities between plant and animal gametes. Current Biology. 20(6), 506-512.
[44] Amien, S., Kliwer, I., Márton, M.L., Debener, T., Geiger, D., Becker, D. and Dresselhaus, T. (2010) Defensin-like ZmES4 mediates pollen tube burst in maize via opening of the potassium channel KZM1. PLoS Biology. 8(6), e1000388.

Received: **27.11.2018**
Accepted: **05.02.2019**

CORRESPONDING AUTHOR

Ibrahim Ilker Ozyigit
Department of Biology,
Faculty of Science and Arts,
Marmara University,
34722, Goztepe, Istanbul – Turkey

e-mail: ilkozyigit@marmara.edu.tr

© by PSP Volume 28 – No. 5/2019 pages 4267-4276 Fresenius Environmental Bulletin

RISK ASSESSMENT OF SOIL HEAVY METAL POLLUTION IN A TYPICAL COAL MINE AREA IN CENTRAL CHINA AND ITS EFFECTS ON ENZYME ACTIVITIES

Yuewei Yang, Meizhen Tang*, Junfeng Chen, Xiaoyu Duan

College of Life Sciences, Qufu Normal University, Shandong, Qufu 273165, People's Republic of China

ABSTRACT

In order to study heavy metal pollution in a coal mine area in Central China, and the effects of heavy metal pollution on soil enzyme activity, soil samples were collected at various distances from the mine entrance. The heavy metal content (Cr, Mn, Cu, Zn, Cd, Pb) in the collected soil samples was evaluated against the baseline value of Central China soil using four methods: single factor pollution index, comprehensive pollution index, geoaccumulation index, and potential ecological risk index. Results showed that the average content of Cr, Mn, Cu, Zn, Cd, and Pb in the uranium tailing area was 16.86, 141.95, 38.81, 100.06, 1.23, and 58.72 mg•kg^{-1}, respectively, of which the highest Cd content was 4.12 times that of the baseline value. The geoaccumulation index for Zn and Pb ranged from 0 to 1, indicating light pollution. The geoaccumulation index for Cd was between 2 and 3, indicating moderate pollution. Evaluation using the potential ecological risk index shows that heavy metal pollution in the surrounding soil of the coal mine area is generally at a high ecological risk level, and that the pollutant with the highest potential ecological risk index is Cd. The results of principal component analysis show that the sources of Mn, Cu and Cd may be associated with the uranium mining process, reflecting the local uranium mining and smelting activities. Soil urease, sucrase, dehydrogenase, and catalase showed 38.34%, 50.53%, 55.06%, and 73.43% reduced activities levels, respectively. Multiple regression analysis showed that, in the presence of heavy metal soil pollution, the inhibitory effect of Cr, Mn, Cu, Zn, Cd, and Pb on the activity of four soil enzymes could be ranked as Cd > Cu > Mn > Zn > Pb > Cr.

KEYWORDS:
coal mine area, heavy metal pollution, ecological risk, enzyme activities

INTRODUCTION

Frequent mining activities have led to varying degrees of soil pollution, especially heavy metal pollution, leading to damage to the function and structure of the ecosystem surrounding the mining area [1]. The 2014 National Communiqué on Soil Pollution Survey indicated that soil pollution in some regions of China is quite serious, and that there are outstanding problems with soil quality in arable lands and in abandoned industrial and mining areas. Of these, when non-ferrous metal mining areas are included, sites with heavy polluting enterprises accounted for 36.3% of the above-limit levels of pollution. Heavy metals such as Pb, Cd, Cu, As, and Cr were all present at different levels. Heavy metal pollution in regional soils caused by mining activities and the resulting ecological environmental risks have been hot topics in the field of environmental studies [2-4]. Domestic and foreign researchers have conducted preliminary analyses on the sources of heavy metals in soil, their distribution characteristics, and soil pollution levels [5-6]. Since Hakanson *et al.* [7] proposed the potential ecological risk index in 1980, some scholars have applied the potential ecological risk index method to the study of soil heavy metals around different types of industrial areas [8-10]. However, there are very few studies on the heavy metal content, sources, and pollution of the soil surrounding mining and smelting waste residue (arsenic alkali residue and slag). The mine of interest in Central China produced a large amount of solid waste in the process of ore smelting - coal mine. Heavy metals in coal mine may be spread by dust, water seepage, ecological migration, or human factors (such as misuse of tailings, irrigation using seepage water), etc., leading to soil and water pollution in nearby areas. In addition, these waste rock and tailings sand contain a large amount of radioactive substances and heavy metals, which are easily transferred and spread by rainwater, flash flooding, and weathering. With lax oversight, area residents sometimes use these waste rocks as construction materials for housing, road paving, etc., allowing the entry of harmful substances into areas of human habitation.

Long-term exposure to environmental radioactivity may damage the liver, kidney, reproductive system, endocrine system, and can lead to the development of cancer [11]. Due to the long-term illogical development and use of the mineral resources in the area of study, the soil surrounding the mine of interest may carry fairly significant ecological risks.

In order to understand the impact of the tailings area on the environment and to further explore the environmental issues generated by historical resource exploitation, the soil around a coal mine area in Central China was studied, and the pollution characteristics and potential risk to the surrounding ecosystem were determined using the single-factor pollution index method, geoaccumulation index method, and potential ecological risk index method. Principal component analysis was used to analyze the main sources of heavy metals in the soil around the coal mine area to reveal the impact of mining activities on soil pollution and to provide a scientific basis for the prevention and control of soil heavy metal pollution in the region.

Heavy metal pollution in tailings areas has become a prominent issue in modern soil ecological protection. In recent years, Chinese and foreign scholars have studied the soil conditions of mining areas, and the focus has mainly been on heavy metal content [12], soil morphology [13], area vegetation, soil microorganism community activity [14-17], ecological restoration [18], etc. in the mining areas (Lead-zinc-silver tailings, copper tailings area, coal mines). However, studies on soil enzyme activities in response to heavy metal pollution in tailings areas are rare. Soil enzymes are some of the important components of soil and participate in numerous metabolic processes. Soil enzyme activity is a reflection of soil biological activity. It can be a comprehensive characteristic of soil fertility and soil nutrient conversion processes. It is sensitive to heavy metal pollution and is often used as a means to determine the potential toxicity of pollutants to organisms [19]. The level of soil enzyme activity can be used to evaluate biological activity and productivity of soil. The level of heavy metal in the soil affects the activity of soil enzymes and conversely, soil enzyme activity can reflect soil contamination to a certain extent [20]. By studying the status of heavy metal pollution in soil near coal mine, the influence of soil heavy metals on soil enzyme activity in the tailings area was evaluated. Multiple linear regression analysis was used to evaluate the effects of soil heavy metal pollution on urease, sucrose, dehydrogenase, and catalase in soil.

MATERIALS AND METHODS

Overview of the Study Area. The coal mine are located in Central China at coordinates 26°46′30″-27°25′42″ north latitude and 113°09′30″-113°52′07″ east longitude. The destructive effect of mining and impact on the surrounding environment are relatively serious. They mainly include destruction of land resources, impact on and destruction of water resources, and geological mining disasters.

Sample Collection and Processing. Soil samples used in this experiment were taken from a coal mine mining area in Central China in August 2016. Twelve sampling units were placed at increasing distances from the mine entrance at the decommissioned uranium mine. Each sampling unit was spaced 5 km from an adjacent unit and covered approximately 1000 m^2 of farmland. In each sampling unit, 10 sampling points were arranged according to a club-shaped layout. Approximately 1 kg of topsoil soil (0 - 20 cm) was collected, mixed, and divided to take about 1 kg of mixed soil as the final sample. In this study, a total of 120 farmland soil samples were collected, which were logical and representative samples of the selected study area that fully reflect the basic properties of farmland soil in the area. The final mixed soil samples were packed into a sealed plastic bags and immediately brought to the laboratory. A portion of the fresh soil was ground and passed through a 2 mm sieve and stored at 0 – 4 °C for the determination of soil enzyme activity. Another portion of the soil was air-dried and was used to determine the basic physical and chemical properties of the soil and its heavy metal content. Determination of heavy metal content: The soil sample was pretreated with water and appropriately diluted. The total amount of Zn, Pb, Mn, Cu, Cd, and Cr was measured using an atomic absorption spectrophotometer (Shimadzu AA-7000) [21]. Soil enzyme determination: determination of urease: indole phenol colorimetric method [22]. Sucrase enzyme assay method: determination using phosphomolybdic acid colorimetry [22]. Dehydrogenase assay method: determination by TTC spectrophotometry [23]. Determination of catalase in soil: $KMnO_4$ titration [24].

RESULTS AND ANALYSIS

Status of Heavy Metal Pollution in Soil. We determined the soil heavy metal content using 12 samples from the coal mine mining area (Table 1). Our results showed that the content of heavy metals in the soil surrounding the coal mine could be ranked as Mn > Zn > Pb > Cu > Cr > Cd. The average soil content of Cr, Mn, Cu, Zn, Cd, and Pb were 16.86, 141.95, 58.72, 100.06, 1.23, and 38.81 $mg \cdot kg^{-1}$, respectively. The contents of Zn, Pb, Cu, and Cd were higher than the baseline value of soil heavy metal levels in Central China and in China.

Figure 1 shows the trend of soil heavy metal variation based on location from the coal mine area. It can be concluded that, as the distance from the coal mine area becomes smaller, the soil heavy metal content increases and the more severe the heavy metal pollution becomes. Table 1 shows that the Pb and Cd levels in the tailings accumulation area are very high. The Pb content was found to be between 44.45 and 79.17 mg•kg^{-1}, while the Cd content was between 0.97 and 1.77 mg•kg^{-1}. These levels are 1.98 and 9.80 times that of the background value of Central China soil and 2.02 and 18.99 times that of the background value of Chinese soil. Compared with China's level two Standards for Soil Environmental Quality (GB15618-1995, p H < 6.5) (Mn level not specified), the average Mn, Zn, Pb, Cu, and Cr contents of the coal mine soil did not exceed the limits. The Cd content exceeds the limit and is 4.12 times that of the level two limit. At present, the national soil environmental quality standards have not yet provided an acceptable level for Mn, but related studies have shown that the appropriate standard for Mn in soil is 170 - 1200 mg•kg^{-1}. The 12 samples taken from this coal mine slag accumulation area did not show Mn content that exceeded this limit. In summary, Cd is the main pollutant in coal mine soil.

Evaluation of Heavy Metal Pollution in Soil. Comprehensive Pollution Index Method. According to the level two standards of the "Standards for Soil Environmental Quality" (GB15618-1995), the single factor pollution index of five metallic elements in the soil around the coal mine area in Central China was calculated. The results are shown in Table 2. The single factor pollution index of Cr, Zn, and Pb in all soil samples was between 0 and 1, indicating that these three metal elements did not heavily pollute the soil, while the single factor pollution index ranges of Cu and Cd were : 0.51 - 1.61 and 3.27 - 5.37 respectively. In terms of pollution, in the two nearest sampling units from the coal mine entrance, Cu is a light pollutant, while in the other sampling units, Cu pollution is negligible. However, Cd is a heavy pollutant in all soils. The comprehensive pollution index can reflect the overall pollution status of the five heavy metal elements. The PN range is 2.41 to 3.97. The comprehensive pollution index shows that soils from sampling units 1, 2, 3, 5, and 8 are heavily polluted, while other sampling units showed moderately polluted soil. This may be closely related to the fact that there was once uranium production at this location.

TABLE 1
Statistical description of heavy metals in uranium tailing of a Central China mine

Element	Maximum values	Minimum values	Average value	Standard deviation	Coefficient of variation	Fold over standard	Background value in Central China soil	Background values in Chinese soil	Soil environmentalquality secondary standard pH<6.5
Cr	22.95	8.71	16.86	3.49	0.21	0.27	71.4	62.6	250
Mn	226.66	78.56	141.95	47.94	0.34	0.32	459.00	440.00	NA
Cu	58.42	25.32	38.81	15.46	0.40	1.59	27.30	24.40	50.00
Zn	124.89	77.47	100.06	11.41	0.11	1.25	94.4	80.01	200
Cd	1.57	0.97	1.23	0.19	0.15	18.96	0.126	0.065	0.30
Pb	79.17	44.45	58.72	7.95	0.14	2.02	29.7	29.1	80

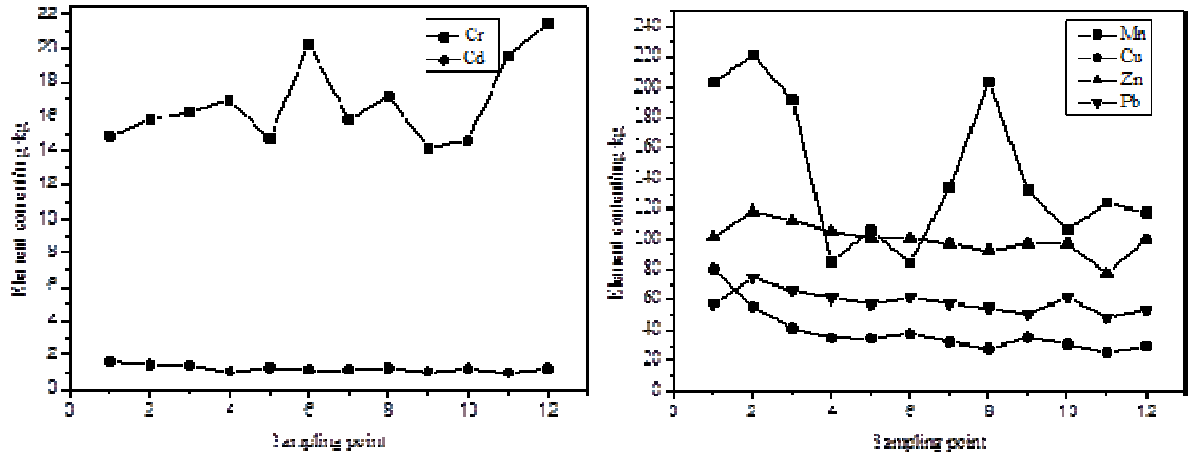

FIGURE 1
Spatial distribution of heavy metals in soils from uranium tailing area in Central China

TABLE 2
Pollution indexes and classification of heavy metals in soils from uranium tailing area in Central China

Sampling	Cr Pi	Pollution level	Cu Pi	Pollution level	Zn Pi	Pollution level	Cd Pi	Pollution level	Pb Pi	Pollution level	Synthetic pollution index	Pollution level
1	0.059	clean	1.61	mild pollution	0.51	clean	5.37	heavy pollution	0.71	clean	3.97	heavy pollution
2	0.063	clean	1.11	mild pollution	0.59	clean	4.80	heavy pollution	0.94	clean	3.56	heavy pollution
3	0.065	clean	0.83	clean	0.56	clean	4.73	heavy pollution	0.83	clean	3.49	heavy pollution
4	0.068	clean	0.70	clean	0.53	clean	3.43	heavy pollution	0.77	clean	2.55	medium pollution
5	0.059	clean	0.69	clean	0.50	clean	4.27	heavy pollution	0.71	clean	3.15	heavy pollution
6	0.081	clean	0.76	clean	0.50	clean	3.80	heavy pollution	0.77	clean	2.81	medium pollution
7	0.063	clean	0.65	clean	0.48	clean	3.83	heavy pollution	0.72	clean	2.83	medium pollution
8	0.069	clean	0.55	clean	0.46	clean	4.17	heavy pollution	0.68	clean	3.07	heavy pollution
9	0.057	clean	0.70	clean	0.49	clean	3.37	heavy pollution	0.63	clean	2.50	medium pollution
10	0.058	clean	0.62	clean	0.48	clean	4.03	heavy pollution	0.77	clean	3.00	medium pollution
11	0.078	clean	0.51	clean	0.39	clean	3.27	heavy pollution	0.61	clean	2.41	medium pollution
12	0.086	clean	0.59	clean	0.50	clean	4.07	heavy pollution	0.67	clean	3.00	medium pollution

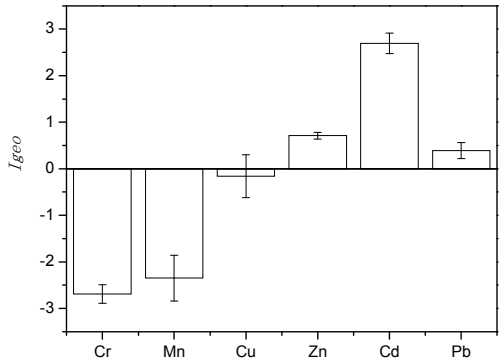

FIGURE 2
Plot of average values of geoaccumulation index of heavy metals in soils from uranium tailing area in Central China

Geoaccumulation Index Method. Geoaccumulation index is commonly used to evaluate the pollution level of heavy metals in sediment and in soil. In this paper, using the background value of Central China soil, the average geoaccumulation index of different sampling units can be calculated according to a formula. As shown in Fig. 2, the Cr and Mn in the soil around the tailings area all show less than 0 in terms of geoaccumulation index, indicating that they are at levels considered to be clean. Zn and Pb geoaccumulation index are both between 0 and 1, falling under the light pollution category. The geoaccumlation range of Cu is -0.69 - 0.97, and while sampling units 1, 2 and 3 fall under the clean category, the other sampling units fall under the light pollution category. The Cd geoaccumulation index is between 2 and 3, belonging in the category of moderate pollution. In this paper, using geoaccumulation index to evaluate the pollution level of Cd in the 12 sampling units around the coal mine area showed results that are essentially consistent with the single factor index evaluation, indicating that Cd contamination of the soil around the tailings area is very serious.

Potential Ecological Risk Index Method. Using the soil background value of Central China as a benchmark for comparison can capture the heterogeneity of specific regions. The potential ecological risk index (Ei value) and comprehensive potential risk index (RI value) of the six heavy metal elements in the uranium deposit area were calculated (Table 3). The results showed that the Ei range of the six heavy metal elements were Ei(Mn) 0.37 - 0.96, Ei(Zn) 0.82 - 1.25, Ei(Pb) 8.16 - 12.61, Ei(Cu) 4.64 - 14.73, Ei(Cr) 0.41 - 0.60, and Ei(Cd) 233.33 - 383.33. The corresponding potential ecological risk indicates that Cr, Mn, Cu, Zn, and Pb all present slight ecological risks, while Cd is a strong ecological risk, and its Ei value is higher than the critical value to indicate strong ecological risk, which is 160. Using the comprehensive potential ecological hazard index (RI value), the RI values of sampling points 1 and 2 in the coal mine mining area are all greater than 360, which indicate a very strong ecological risk, while the RI values of the remaining 10 sampling points were all between 180 and 360, indicating a strong ecological risk, which is mainly due to the large potential ecological risk index of Cd. Therefore, Cd is the main contributor to the potential ecological damage in the coal mine area, followed by Pb. The RI value

of the soil in the coal mine area calculated based on the average content of each element is 313.18, indicating that the soil in the coal mine area in Central China fall under the category of highly harmful.

Comparison and Analysis of Results. In order to ensure the scientific rationale and accuracy of the results, multiple methods were used to conduct a comparative evaluation of heavy metal pollution in our study area. Both the geoaccumulation index method and the potential ecological risk index method compared the heavy metal content around the coal mine area with the background value, but both methods emphasize different aspects. The geoaccumulation index method mainly reflects the enrichment of exogenous heavy metals, and the potential ecological risk index method focuses on the biological toxicity of different heavy metals. In this study, the comprehensive pollution index method, geoaccumulation index method and potential ecological risk index method were used to systematically evaluate the heavy metal pollution and ecological risk in the soil around 12 sampling units around the coal mine site. The results showed that the degree of heavy metal pollution and ecological damage were more or less consistent. Cd showd the largest single factor pollution index, the highest geoaccumulation index, and the highest potential ecological risk coefficient. It contributes the mostto the comprehensive index of potential ecological hazards is the most serious polluter.

Multivariate Statistical Analysis of Heavy Metal Elements. Correlation Analysis of Heavy Metal Elements. The correlation analysis of various heavy metals in the soil of coal mine shows that there is no correlation between Cr and Mn, Cu, Zn, Cd, or Pb (Table 4), indicating that the main source of origin Cr is different from that of the other heavy metals. Mn and Pb are not correlated, but there is a weak correlation between Mn and Zn. There is a significant correlation between Mn and Cu, as well as between Mn and Cd at the 0.01 level. The remaining heavy metals (Cu, Cd, Pb) each show significant correlation with one another, indicating that the three heavy metals may share the same source and similar migration pathways.

Principal Component Analysis of Heavy Metal Elements. Based on the correlation between the different heavy metal elements, Bartlett's sphericity test shows a companion probability of 0.00, which is less than the significance level of 0.05, and the KMO test statistic is 0.711. Factor analysis of six heavy metals was performed using SPSS19.0 software, as shown in Table 5. The six heavy metals can be summarized as two principal components with an eigenvalue of 4.56 (3.31+1.25=4.56 variables). Of the total variance, 76.08% can be explained by the fact that the first two principal components summarize most of the variance. The contribution of the first principal component (PC1) was 55.30%. Mn, Cu, and Cd all had higher positive contributions to PC1 (Fig. 3), and the load values were all greater than 0.8, and were 0.801, 0.858, and 0.905, respectively. In the relationship analysis, there was a significant correlation between the three heavy metals, and the average level of Cd exceeded the background value. Therefore, PC1 is mainly controlled by human activities and is considered to be an “exogenous factor”. Therefore, the Mn, Cu and Cd in the soil characterized in this study are likely to be associated with the uranium mining process, which is related to the local uranium mining activities. The second principal component (PC2) contributes 20.78%, and the highest contributor is Cr, which has a load value of 0.764. At the same time, Zn and Pb also contribute to PC2. As such, PC2 explains the main source of Cr, and also partially dominates the source of Zn and Pb. These elements (Cr, Zn, Pb) are controlled by the local geological background and may be related to the local soil background values. Therefore, PC2 is considered as a “natural source factor”.

TABLE 3
The potential ecological risk index of heavy metal of the soils collected from experimental zones

Sampling	Heavy metal						RI
	Cr	Mn	Cu	Zn	Cd	Pb	
Range	0.41~.0.60	0.37~0.96	4.64~14.73	0.82~1.25	240.48~383.33	8.16~12.61	248.04~410.01
Average index	0.47 (Slight)	0.62 (Slight)	7.10 (Slight)	1.06 (Slight)	294.05 (very strong)	9.88 (Slight)	313.18 (Strong)

TABLE 4
Correlation coefficients among heavy metals in soils from uranium tailing area in Central China

Heavy metal	Cr	Mn	Cu	Zn	Cd	Pb
Cr	1.000					
Mn	-0.123	1.000			*	
Cu	-0.103	0.542**	1.000			
Zn	0.158	0.334*	0.527**	1.000		
Cd	0.001	0.684**	0.794**	0.633**	1.000	
Pb	0.148	0.328	0.432**	0.884**	0.578**	1.000

Note: ** Significant correlation at 0.01 level (both sides); * Significant correlation at 0.05 level (both sides); n=36.

TABLE 5
Principal component analysis (PCA) of heavy metals in soils from uranium tailing area in Central China

Project	PC1	PC2
Eigenvalue	3.31	1.25
Contribution rate (%)	55.30	20.78
Accumulated contribution rate (%)	55.30	76.08
Cd	0.905	0.198
Cu	0.858	0.050
Mn	0.801	-0.128
Zn	0.634	0.668
Pb	0.586	0.678
Cr	-0.276	0.764

TABLE 6
The variations of enzyme activities in different test soil samples

Sampling site	Soil urease	Soil sucrase	Soil dehydrogenase	Soil catalase
1	38.99±1.28b	74.42±1.95ef	3.36±0.12b	1.87±0.03g
2	27.04±0.39b	77.33±2.14def	3.11±0.09b	3.25±0.08f
3	33.06±2.54b	67.23±2.63f	3.72±0.24ab	6.25±0.46c
4	46.68±5.15b	116.53±3.28bc	3.44±0.37b	6.44±0.28c
5	32.62±1.08b	128.53±1.87ab	4.47±0.16ab	6.12±0.16c
6	36.95±1.59b	95.27±2.52cde	4.47±0.28ab	6.36±0.22c
7	52.26±3.48ab	129.33±2.67ab	4.33±0.05ab	7.34±0.37a
8	36.95±1.04b	89.61±4.02def	4.22±0.11ab	4.85±0.08e
9	37.39±2.83b	101.87±4.59cd	4.49±0.25ab	5.48±0.15d
10	45.71±2.16b	150.46±5.18a	4.880.18ab	6.94±0.56b
11	63.23±1.23ab	117.33±2.15bc	4.33±0.37ab	6.88±0.37b
12	69.24±3.77a	131.47±3.51ab	6.92±0.29a	7.04±0.42ab

Annotations: Soil urease (mg NH_4^+-N·g^{-1}·d^{-1}); Soil sucrose (mg glucose·g^{-1}·d^{-1}; Soil dehydrogenase (μg TPF·g^{-1}dry soil·$6h^{-1}$) ; Soil catalase (ml $KMnO_4$·g^{-1}dry soil). Different letters in the same column means a significant difference at 0.05 level。

Changes in Soil Enzyme Activity. The changes in soil enzyme activities at different distances from the coal mine are shown in Table 6. In Table 6, it can be seen that the soil urease, sucrase, dehydrogenase, and catalase activities have different degrees of inhibition under combined pollution from Cr, Mn, Cu, Zn, Cd, and Pb. There was a significant difference in enzyme activity values between soil samples. The lowest enzyme activity was found in the closest soil sample from the coal mine entrance, ie, the enzyme activity in the soil from the No. 1 sampling unit was the lowest. With increasing distance from the coal mine, the soil enzyme activity increased. The urease activity in the coal mine mining area was decreased by 38.34% when compared with the farthest sampling point (No. 12 sampling unit), soil sucrease activity was decreased by 50.53% when compared with the farthest sampling point (No. 12 sampling unit), soil dehydrogenase activity was decreased by 55.06% when compared to the farthest sampling point (No. 12 sampling unit), and the soil dehydrogenase activity was decreased by 73.43% when compared with the farthest sampling point (No. 12 sampling unit). Figure 4 is a box diagram of soil enzyme activity in the coal mine area. The results show that the activities of sucrase in the soil around the tailings area had the most significant difference. The activity of urease showed the second largest difference, the activity of dehydrogenase showed little change, and the activity of catalase showed the smallest change.

The Relationship between Heavy Metal Pollution and Soil Enzyme Activities in Coal Mine Area. The effect of heavy metal elements on soil enzyme activity varies with the type and concentration of heavy metals and the type of soil enzyme. There may be synergistic or antagonistic effects between different metal elements. At present, multiple regression analysis is often used as a research method to reveal the relationship between heavy metal complex pollution and enzyme activity [25-26]. The relationship between soil enzyme activity and soil heavy metal content under heavy metal combined pollution was simulated by multiple regression analysis. The results are shown in Table 7.

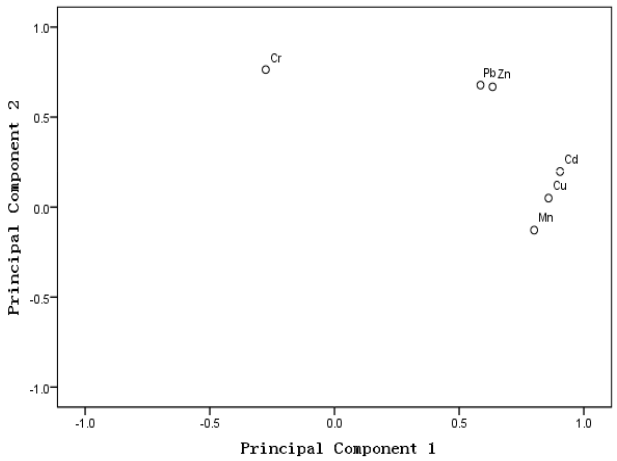

FIGURE 3
Heavy metals in the space defined by two components

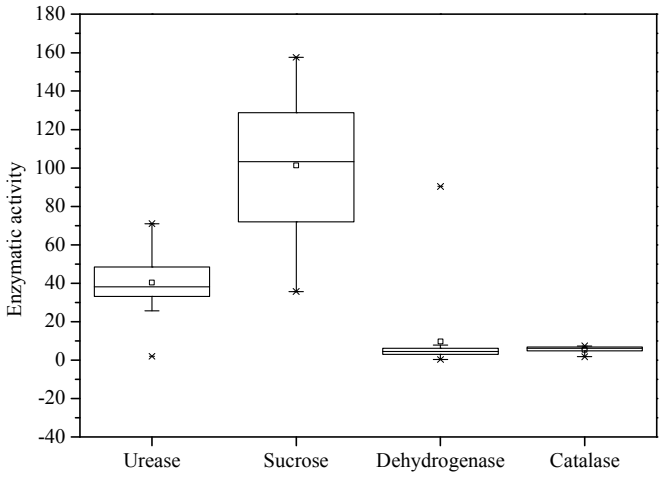

FIGURE 4
Whisker-box plots for the enzymatic activity of soil samples from uranium tailing area in Central China

TABLE 7
The multivariate regression analysis between contents of soil heavy metals (Cr、Mn、Cu、Zn、Cd、Pb) and soil enzyme activities

Dependent variable	Multivariate regression equation	multiple correlation coefficient F and significance	Coefficient of partial correlation F and significance
Soil urease	y=0.397x_1-0.196x_2-0.027x_3-0.295x_4+0.045x_5-0.283x_6	r=0.431 F=5.410**	F_{Cr}=0.637 F_{Mn}= 2.503 F_{Cu}=29.393** F_{Zn}=2.841* F_{Cd}=1.040 F_{Pb}=3.210**
Soil sucrase	y=-0.030x_1-0.692x_2-0.397x_3-0.185x_4-0.419x_5+0.109x_6	r=0.378 F=4.541**	F_{Cr}=1.403 F_{Mn}= 2.108 F_{Cu}=7.425** F_{Zn}=3.236* F_{Cd}=10.888**F_{Pb}=1.384
Soil dehydrogenase	y=0.152x_1-0.119x_2-0.287x_3+0.310x_4-0.156x_5-0.524x_6	r=0.034 F=1.207	F_{Cr}=1.236 F_{Mn}=1.931 F_{Cu}=0.395 F_{Zn}=2.985* F_{Cd}=1.2.12** F_{Pb}=1.276
Soil catalase	y=0.068x_1-0.454x_2-0.770x_3+0.038x_4-0.164x_5+0.108x_6	r=0.799 F=24.181**	F_{Cr}=1.751 F_{Mn}= 2.457 F_{Cu}=112.38**F_{Zn}=4.796** F_{Cd}=8.282** F_{Pb}=6.378**

Annotations: x_1, x_2, x_3, x_4, x_5, x_6 represent the total amount of Cr, Mn, Cu, Zn, Cd, Pb respectively, y represents enzyme activity。

Table 7 shows that, under the combined pollution of Cr, Mn, Cu, Zn, Cd, and Pb, with the increase of Mn, Cu, Zn, and Pb contents, the soil urease activity decreased. Of these, Cu and Pb had a significant inhibitory effect, Zn had an inhibitory effect, and Mn had no apparent effect. With the increase of Cd, Mn, Cu, Zn, and Cd content, the activity of soil invertase was significantly decreased. With the increase of Pb content, the invertase enzyme activity showed a certain

activation, while Cu and Cd showed extremely significant inhibitory effect. The inhibitory effect of Zn was significant. With the increase of Mn, Cu, Cd, and Pb contents, the activity of soil dehydrogenase decreased, and the inhibitory effect of Cd was extremely significant. The inhibitory effects of Cr, Mn, Cu, and Pb were not obvious, but with the increase of Zn content, there was a significant activating effect on dehydrogenase. With the increase of Mn, Cu, and Cd content, the catalase activity decreased, and the inhibitory effects of Cu and Cd were extremely significant, while Cr, Zn, and Pb showed a certain activation effect on soil catalase. Therefore, Table 7 shows that Cr, Mn, Cu, Zn, Cd, and Pb have different effects on the activity of the four soil enzymes, and all four enzymes show extremely significant inhibition under the influence of Cd. Cu showed extremely significant inhibitory effects on soil urease, sucrase and catalase, but no significant effect on soil dehydrogenase. Mn had no obvious inhibitory effect on all four enzyme activities. Pb had extremely significant inhibition on soil urease, and showed significant activation of catalase, with no significant impact on the other enzymes. Zn has a significant inhibition of soil urease, sucrase, very significant activation of soil catalase showed and significant activation of dehydrogenase. Cr showed different effects on four enzymes, and the effect was not significant. Therefore, the inhibitory effect of compound pollution on soil enzyme activities could be ranked as Cd > Cu > Mn > Zn > Pb > Cr. It can be seen that the effect of heavy metal pollution on soil enzyme activity is mostly inhibitory, and the inhibition mechanism may be due to the combination of the active site thiol group in the enzyme molecule and the imidazole-containing ligand to form a more stable complex, resulting in competitive inhibition with the substrate; or it may be due to the inhibition of the growth and reproduction of soil microorganisms by heavy metals, reducing the enzyme synthesis and secretion in vivo, and ultimately leading to a decrease in soil enzyme activity.

CONCLUSIONS

(1) The average content of heavy metal Cr, Mn, Cu, Zn, Cd, and Pb in the soil around the coal mine area in Central China was 16.86, 141.95, 38.81, 100.06, 1.23, and 58.72 mg•kg-1. Based on the "Soil Environmental Quality Standard" level two standards as a benchmark, the results showed that the heavy metal that most seriously exceeded the limit level is Cd, which is 4.12 times higher than the highest standard. Relatively speaking, the degree of pollution from the six kinds of heavy metals is: Cd > Pb > Cu > Zn > Mn > Cr.

(2) The heavy metal geoaccumulation index shows that Zn and Pb geoaccumulation index ranges from 0 to 1, which indicates mild pollution. Cd has a geoaccumulation index between 2 and 3, which indicates moderate pollution. Comprehensive potential ecological risk index evaluation showed that the heavy metal pollution in the soil around the coal mine area of was generally at a high ecological risk level. The potential ecological risk indices of the six heavy metals from high to low were: Cd > Pb > Cu > Zn > Mn > Cr, where the influence of Cd dominates.

(3) Principal component analysis shows the six heavy metals in the soil around the coal mine can be identified as two main components, PC1 is a man-made factor, Mn, Cu, and Cd have a greater load on PC1, and Mn, Cu, and Cd are highly likely to be associated with the uranium mining process, which is related to the local uranium mining smelting activities that once took place at this mine. PC2 is a natural factor, Cr, Zn, Pb, place a large load on PC2. Cr, Zn and Pb are controlled by the local geological background and may be related to the local soil background values. Therefore, PC2 is considered as the natural factor.

(4) The overall change in soil enzyme activities in the coal mine area is in accordance with actual heavy metal pollution. Soil enzyme activity increases with increasing distance from coal mine, and soil enzyme activity is higher in soil with relatively lighter heavy metal pollution soils. With the increase of pollution, the activities of urease, sucrase, dehydrogenase and catalase in soil all showed a decreasing trend.

(5) In term of composite impact, the inhibitory effect of Cr, Mn, Cu, Zn, Cd, and Pb on the four soil enzyme activities is ranked Cd > Cu > Mn > Zn > Pb > Cr. It is clear that the total enzyme activity of the soil can reflect the heavy metal pollution status of the soil in a specific habitat similar to the tailings area, and it can also be used as a biological indicator for evaluating the environmental quality of heavy metal-contaminated soil.

ACKNOWLEDGEMENTS

This research was supported by the National Natural Science Fund of China (NO. 31700433 and NO. 31672314).

REFERENCES

[1] Acosta, J.A., Faz, A., Martínez-Martínez, S., Zornoza, R., Carmona, D.M., Kabas, S. (2011). Multivariate statistical and gis-based approach to evaluate heavy metals behavior in mine sites for future reclamation. J. Geochem. Explor. 109(1–3), 8-17.

[2] Chen, J., Liu, S., Yan, J., Wen, J., Hu, Y., Zhang, W. (2017) Intensive removal efficiency and mechanisms of carbon and ammonium in municipal wastewater treatment plant tail water by ozone oyster shells fix-bed bioreactor – membrane bioreactor combined system. Eco. Eng. 101, 75–83.
[3] Wahsha, M., Bini, C., Argese, E., Minello, F., Fontana, S., Wahsheh, H. (2012) Heavy metals accumulation in willows growing on spolic technosols from the abandoned imperina valley mine in italy. J. Geochem. Explor. 123(12), 19-24.
[4] Yan, Z., Chen, J., Liu, Y., Shao, J., Shu, P., Wen, S. (2017) Effects oxytetracycline on bacterial diversity in livestock wastewater. Environ. Eng. Sci. 34(4), 265-271.
[5] Gao, X., Chen, C.T.A. (2012 Heavy metal pollution status in surface sediments of the coastal Bohai Bay. Water Res. 46(6), 1901-1911.
[6] Islam, M.S., Ahmed, M.K., Raknuzzaman, M., Habibullah-Al-Mamun, M., Islam, M.K. (2015) Heavy metal pollution in surface water and sediment: a preliminary assessment of an urban river in a developing country. Eco. Indic. 48, 282-291.
[7] Hakanson, L. (1980) An ecological risk index for aquatic pollution control: Asedimento-logical approach. Water Res. 14 (8), 975-1001.
[8] Tang, M., Li, Z., Yang ,Y., Jiang, J. (2018) Effects of the inclusion of a mixed Psychrotrophic bacteria strain for sewage treatment in constructed wetland in winter seasons. Roy. Soc. Open Sci. 5(4), 172360.
[9] Sun, Y., Zhou, Q., Xie, X., Liu, R. (2010) Spatial, sources and risk assessment of heavy metal contamination of urban soils in typical regions of Shenyang, China. J. Hazard. Mater. 174(1-3), 455-462.
[10] Liu, S., Chen, J., Yan, J., Hu, Y., Zhou, D. (2017) Conversion Mechanisms of Carbon, Nitrogen, and Phosphorus in Ozone-Fixed-Bed and Membrane Bioreactors for Deep Treatment of Municipal Tail Water. Environ. Eng. Sci. 34(8),562-568.
[11] Fucic, A., Gamulin, M., Ferencic, Z., Katic, J., von Krauss, M.K., Bartonova, A., Merlo, D.F. (2012) Environmental exposure to xenoestrogens and oestrogen related cancers: reproductive system, breast, lung, kidney, pancreas, and brain. Environ. Heal. 11(1), S8.
[12] Bhuiyan, M.A.H., Parvez, L., Islam, M.A., Dampare, S.B., Suzuki, S. (2010) Heavy metal pollution of coal mine-affected agricultural soils in the northern part of Bangladesh. J. Hazard. Mater. 173(1-3), 384-392.
[13] Dang, Z., Liu, C., Haighc, M.J. (2002) Mobility of heavy metals associated with the natural weathering of coal mine spoils. Environ. Pollut. 118(3), 419-426.
[14] Chen, J., Zhang, L., Hu, Y., Huang, W., Niu, Z., Sun, J. (2017) Bacterial community shift and improved performance induced by in situ preparing dual graphene modified bioelectrode in microbial fuel cell. Bioresour. Technol. 241, 220-227.
[15] Chen, J., Hu, Y., Zhang, L., Huan, W., Sun, J. (2017) Bacterial community shift and improved performance induced by in situ preparing dual graphene modified bioelectrode in microbial fuel cell. Bioresour. Technol. 238, 273–280.
[16] Chen, J., Hu, Y., Tan, X., Zhang, L., Huang, W., Sun, J. (2017) Enhanced performance of microbial fuel cell with in situ preparing dual graphene modified bioelectrode. Bioresour. Technol. 241, 735-742.
[17] Chen, J., Hu, Y., Huang, W., Zhang, L. (2017) Enhanced electricity generation for biocathode microbial fuel cell by in situ microbial-induced reduction of graphene oxide and polarity reversion. Int. J. Hydrogen Energy. 42, 12 574–12 582.
[18] Bradshaw, A. (1997) Restoration of mined lands—using natural processes. Eco. Eng. 8(4), 255-269.
[19] Valavanidis, A., Vlahogianni, T., Dassenakis, M., Scoullos, M. (2006) Molecular biomarkers of oxidative stress in aquatic organisms in relation to toxic environmental pollutants. Ecotox. Environ. Safe. 64(2), 178-189.
[20] Gianfreda, L., Rao, M.A., Piotrowska, A., Palumbo, G., Colombo, C. (2005) Soil enzyme activities as affected by anthropogenic alterations: intensive agricultural practices and organic pollution. Sci. Total Environ. 341(1-3), 265-279.
[21] Li, Q., Chen, Y., Fu, H., Cui, Z., Shi, L., Wang, L., Liu, Z. (2012) Health risk of heavy metals in food crops grown on reclaimed tidal flat soil in the Pearl River Estuary, China. J. Hazard. Mater. 227, 148-154.
[22] Neal, C., Neal, M., Wickham, H. (2000) Phosphate measurement in natural waters: two examples of analytical problems associated with silica interference using phosphomolybdic acid methodologies. Sci. Total Environ. 251, 511-522.
[23] Stojnova, K.T., Divarov, V.V., Racheva, P.V., Lekova, V.D. (2015) Extraction-Spectrophotometric Method for Determination of Gallium (III) in the Form of Ion Associate with a Monotetrazolium Salt. J. Appl. Spectrosc. 82(5), 853-856.

[24] Zhan, X., Wu, W., Zhou, L., Liang, J., Jiang, T. (2010) Interactive effect of dissolved organic matter and phenanthrene on soil enzymatic activities. J. Environ. Sci. 22(4), 607-614.
[25] Chen, J., Yang, Y., Liu, Y., Tang, M., Wang, R., Zhang, C., Jiang, J., Jia, C. (2019) Bacterial community shift in response to a deep municipal tail wastewater treatment system. Bioresour. Technol. 281,195-201.
[26] Chen, J., Yang, Y., Liu, Y., Tang, M., Wang, R., Tian, Y., Jia, C. (2019) Bacterial community shift and antibiotics resistant genes analysis in response to biodegradation of oxytetracycline in dual graphene modified bioelectrode microbial fuel cell. Bioresour. Technol. 276, 236-243.

Received: **11.12.2018**
Accepted: **28.03.2019**

CORRESPONDING AUTHOR

Meizhen Tang
College of Life Sciences,
Qufu Normal University,
Shandong, Qufu 273165,
People's Republic of China

e-mail: qsd_tmzh@mail.qfnu.edu.cn

© by PSP Volume 28 – No. 5/2019 pages 4277-4282 Fresenius Environmental Bulletin

THE KINETIC STUDIES ON PHOTOCHEMICAL OF PHOTOPOLYMER COMMONLY SENSITIZED BY VB2 AND AZURE I

Jianbin Xu*

Tendering Office, Henan University, Kaifeng, Henan, 475004, China

ABSTRACT

A photopolymer material was fabricated Sensitized by VB2 and Azure I, the photopolymers' experimental values of transmittance in different film thickness sensitized by VB2 and Azure I were tested, and the experimental values were fitted by curve. Through the fitting curves, the photopolymers' values of the molar absorption coefficient ε, the quantum yield ϕ, the photobleaching coefficient k_p and the scattering loss correlation coefficient T_{sf} in different film thickness sensitized by VB_2 and Azure I were tested, and the change rules were discussed and demonstrated.

KEYWORDS:
VB2, Azure I, Photopolymer, photochemical kinetics

INTRODUCTION

Photopolymer materials have many advantages, such as high diffraction efficiency, high sensitivity, high refractive index modulation, low cost and simple fabrication, which makes them be the focus and hotspot in the field of optical holographic storage materials [1-2]. At the same time, photopolymer materials are considered to be the most promising and first used as holographic storage media. It is the best choice for optical holographic storage materials [3-4]. In the preparation of photopolymer, photosensitizer (dye) is an important component. In order to improve the performance of photopolymer, the choice of dyes is very important [5-6]. In this paper, the photopolymer materials sensitized by VB2 [7] and Azure I [8] were prepared by using VB2 and Azure I as photosensitizers. The experimental values of transmittance of photopolymer sensitized by VB2 and Azure I at different film thickness were tested, and the experimental values were fitted by curve. The specific values of photobleaching rate constant k_p, molar absorption coefficient ε, quantum yield, scattering loss correlation coefficient T_{sf} of photopolymer sensitized by VB2 and Azure I under different film thickness were calculated by fitting curve.

EXPERIMENTAL

Reagents. The photopolymer sample prepared in this experiment is a photopolymerization system with polyvinyl alcohol (PVA) as binder, acrylamide (AA) and N, N'-methylene bisacrylamide (BAA) as common monomer, vitamin B2 (VB2) and azure I as photosensitizer (dye), triethanolamine (TEA) as initiator [9-12].

Experimental instruments. The main instruments and equipment needed in the experiment are as follows:

Laser: argon krypton ion laser, produced by Coherent, USA, model Innova 70C Spectrum. The output wavelengths are mainly 647 nm, 568 nm, 531 nm, 521 nm, 515 nm, 488 nm, 477 nm, 458 nm.

Absorptiometer: ultraviolet visible near infrared spectrophotometer, produced by Varian company of America, model Cary5000.

Ultrasound cleaner, electronic analytical balance, collector constant temperature magnetic stirrer, vacuum drying box, 6.7 cm x 6.7 cm x 1mm optical glass substrate, beaker and dropper, etc.

The main instruments needed for sample preparation are ultrasonic cleaner, magnetic stirrer, electronic analytical balance, 6.0CM x 6.0CM optical glass substrate, beaker, dropper, spiral micrometer, etc.

In addition, there are laser power meter, galvanometer, Fourier lens, spectroscope, beam expander, computer, gas floating platform and other equipment.

SAMPLE PREPARATION

The preparation method is shown in document [13-14].

(1) When the temperature is 20-25ºC and the relative humidity is 40%~60%, the PVA powder of 1.6g is weighed by an electronic balance and put into a beaker. The powder is stirred and heated to 90ºC. After it is completely dissolved, a colorless transparent solution of 8% mass fraction is obtained.

(2) Take appropriate amount of BAA powder and add a certain amount of deionized water, stir and heat it to 70oC to dissolve it fully, then add a certain

amount of AA powder, continue stirring for about 3 hours to make it completely dissolve.

(3) At room temperature, the mixture of BAA and AA was added to the transparent aqueous solution of PVA in the first step, and a proper amount of TEA was added to mix well.

(4) Under darkroom, a suitable amount of dye solution (VB2 and Azure I solution) was added to the above mixed solution by dropper and stirred evenly.

The concentration of each component is shown in Table 1.

(5) In a darkroom with a temperature of 20~25 °C and a relative humidity of 40-60%, a certain amount of the above-mentioned mixed solution is dripped onto a clean optical glass substrate and dried naturally in the darkroom for 36~48 hours so as to forming a photopolymer film with a certain thickness. In the experiment, the thickness of the film can be adjusted by controlling the amount of the drip coating.

Photochemical reaction kinetic parameters of photopolymerization process. According to the principle of photochemical reaction in photopolymer polymerization, the variation of dye concentration in polymer with time can be described as follows:

$$\frac{d[D](t)}{dt} = -\frac{\varphi I_a(t)}{d} \quad (1)$$

In formula [D] (t) is the relationship between dye concentration and time, I_a (t) is the light intensity absorbed at a certain time, I0 is the exposure intensity, D is the thickness of the sample, and t is the time.

In photopolymer, dyes absorb photons in the sensitive spectral range, and their absorption intensity can be expressed by Lambert-Beer law formula as follows:

$$I_a(t) = I_0(1 - e^{-\varepsilon d[D](t)}) \quad (2)$$

The molar absorption coefficient of the dye at the exposure wavelength reflects the ability of the dye to absorb light at that wavelength.

The initial conditions [D](t) = [D](0) = $[D]_0$ is applied, that is the initial concentration of dye in dry film. Because the intensity of incident light remains unchanged throughout the exposure time, the exposure intensity I(t)= I(0)= I_0, the relationship between dye concentration and time is obtained by simultaneous (1) and formula (2).

$$D(t) = \frac{l_n[1 + (e^{\varepsilon d[D]_0} - 1)e^{-\varepsilon\varphi I_0 t}]}{\varepsilon d} \quad (3)$$

In the formula Φ is quantum efficiency, which indicates the yield of light from the initial product to the product. It is defined as: Φ= the number of moles (or molecules)/Einstein number (or photons) = the rate of production of the product/the intensity of the absorbed radiation. The quantum yield can be greater than 1 or less than 1.

The formula (3) for substitution (2) can be used to obtain the relationship between absorption intensity and time.

$$I_a(t) = \frac{I_0(e^{\varepsilon d[D]_0} - 1)e^{-\varepsilon\varphi I_0 t}}{1 + (e^{\varepsilon d[D]_0} - 1)e^{-\varepsilon\varphi I_0 t}} \quad (4)$$

When exposed, the absorbed part of the beam will be $I_a(t)$, and the transmitted part will be $I_T(t)$. The expression of the incident light intensity can be obtained:

$$I_0 = I_a(t) + I_T(t) \quad (5)$$

The transmittance of a sample is defined as the ratio of the light intensity through the sample to the incident light intensity. From the above formulas, the relationship between the transmittance and time can be obtained [15]:

$$T(t) = \frac{I_T(t)}{I_0} = \frac{I_T(t)}{I_a(t) + I_T(t)} = \frac{T_{sf}}{1 + (e^{\varepsilon d[D]_0} - 1)e^{-\varepsilon\varphi I_0 t}} \quad (6)$$

In the upper formula, T_{sf} is a parameter related to scattering and reflection.

In the experiment, the transmittance of the photopolymer can be measured with time. According to formula (6), T_{sf}, molar absorption coefficient ε and quantum efficiency Φ can be defined as parameters respectively, and (6) can be used as the basic fitting formula. The exposure intensity of laser beam, the initial concentration of different dyes used in the experiment, and the thickness of photopolymer film were substituted into (6). The time-dependent transmission curve (discrete points) of the material was obtained by using origin mapping software. If the change curve was fitted by Levenberg-Marquardt algorithm [16], the result could be obtained. The kinetic parameters such as quantum efficiency Φ, molar extinction coefficient ε and T_{sf} of homopolymer [17~18], and the photobleaching rate constant k_p can be calculated from formula $k = \varepsilon\phi I_0$.

RESULTS AND DISCUSSION

Absorption spectra of samples. The absorption spectra of photopolymer sensitized by different dyes by ultraviolet-visible-near infrared spectrophotometer is shown in Fig. 1. It can be seen from Fig. 1 that when VB2 and Azure I are mixed as dyes, the sample has a wide range of photosensitive spectra, and has strong absorption ability in the ultraviolet, violet, blue, blue and red regions. The corresponding absorption peaks are 223 nm, 268 nm, 373 nm, 446 nm and 611 nm, respectively.

According to the absorption spectrum of Fig. 1, a 647 nm laser at the wavelength of Ar^+Kr^+ laser output is used as the exposure source, the exposure intensity is 59.7 mW•cm^{-2}. The experimental data of the transmittance of photopolymer samples with film thickness of 105, 150, 170 and 250 microns are measured respectively. As shown in Fig. 2, the point

in the figure is the experimental data and the real line is the real line. Fitting curve. From Figure 2, it can be concluded that the maximum transmittance of the photopolymer sample decreases with the increase of the thickness of the sample film. This is because the thicker the sample film is, the more dye molecules absorb sensitive light and the more light is absorbed, so the transmittance decreases. When the exposure intensity remains unchanged, the transmittance can be determined by the definition of transmittance. The smaller the rate.

Based on the measured experimental data, the original advanced non-linear fitting tool can be used to fit the experimental data of transmittance under different film thickness, and the corresponding parameters of sample photochemical reaction can be obtained. From Figure 2, it can be seen that the measured experimental values are in good agreement with the fitting curve. The fitting coefficients of the four groups of experimental data are shown in Table 2. The closer the fitting coefficients are to 1, the better the fitting is.

TABLE 1
Concentration of sample components

Component	PVA	AA	BAA	TEA	VB2+ Azure I
Concentration mol/L	8wt%	0.25	0.0324	0.27	8×10^{-4}

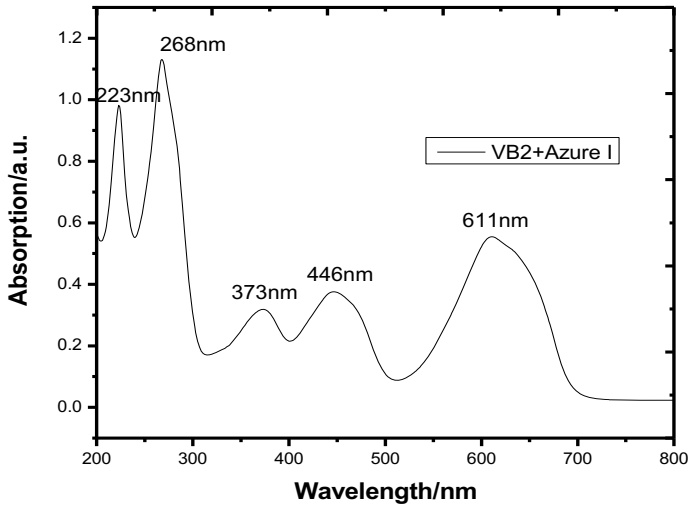

FIGURE 1
Absorption spectra of photopolymers sensitized by VB2 and Azure I

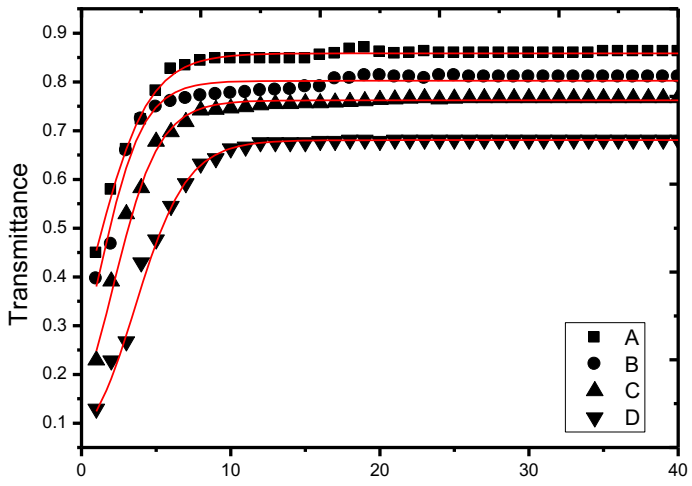

FIGURE 2
Experimental data and fitting curves of transmittance of samples with different film thickness (A) 105 micron; (B) 150 micron; (C) 170 micron; (D) 250 micron

According to the fitting curve of transmittance in Fig. 2, the T_{sf}、ε、ϕ, epsilon and deuterium are defined as parameters by the function model of transmittance (6). The relationship between the molar absorption coefficient ε, the quantum yield ϕ, the scattering loss correlation coefficient T_{sf} and the photobleaching rate constant k_p with the film thickness can be obtained, as shown in Fig. 3 and Fig. 4, respectively.

Fig. 3 shows that the quantum yield increases first and then decreases with the increase of the film thickness. When the film thickness is 150 um, the quantum yield reaches its maximum. This is because with the increase of film thickness, exposure photosensitizer will absorb more photons and transfer more energy to the initiator in the relaxation process, which makes the initiator produce more amino radicals, that is, the higher the quantum yield. However, when the thickness of the film is further increased, the dye molecules cannot be completely bleached, and the energy transferred to the initiator will be reduced. In addition, the increase of the dye molecules will also cause the formation of dimers between dye molecules, which will affect the formation of amino radicals, so the quantum yield will be reduced. Compared with the quantum yield, the change of molar absorption coefficient affected by concentration is smaller (slowly decreasing and then slowly increasing), which may be due to the relationship between the absorption coefficient and the material properties of sample components.

TABLE 2
Fitting coefficient of sample permeability under different film thickness

film thickness (μm)	105	150	170	250
Fitting coefficient	0.9886	0.9787	0.9757	0.9753

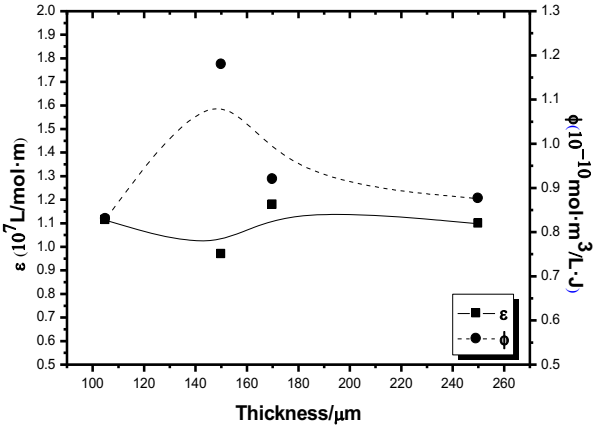

FIGURE 3
The molar absorption coefficient ε and quantum yield ϕ at different film thickness

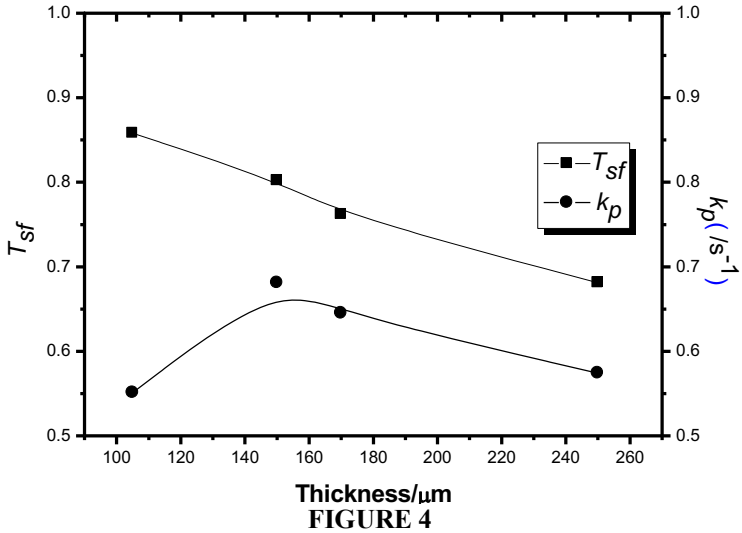

FIGURE 4
Photobleaching rate kp and scattering loss correlation coefficient T_{sf} under different film thickness

TABLE 3
Photochemical reaction parameters of samples with different film thickness

film thickness (μm)	105	150	170	250
Molar absorption coefficient ε ($\times 10^7$L• mol^{-1}•m^{-1})	1.113	0.968	1.177	1.098
quantum yield ϕ($\times 10^{-10}$mol•m^3•L^{-1}•J^{-1})	0.829	1.179	0.919	0.876
Correlation coefficient of scattering loss T_{sf}	0.858	0.802	0.762	0.681
Photochemical bleaching rate constant k_p(S^{-1})	0.551	0.681	0.645	0.574

From Fig. 4, it can be seen that T_{sf} increases first and then decreases with the increase of film thickness. This is because with the increase of film thickness, the number of dye molecules absorbed light will increase, and then the number of free radicals produced by initiators will increase, resulting in faster monomer polymerization. Therefore, the rate constant of polymerization will increase, but when the film thickness increases, the number of free radicals produced by initiators will increase. Too much, the quantum yield will be reduced, affecting monomer polymerization, so the polymerization rate will decline. When the film thickness is 150 um, the maximum value of T_{sf} is obtained. The photobleaching rate indicates the speed of photopolymer polymerization. The larger the value, the faster the polymerization process is. In addition, as can be seen from Figure 3, the quantum yield is also the largest at this time, so the film thickness has an optimal value, and the thickness of the film must be controlled well in the experiment. Fig. 4 shows that T_{sf} decreases with the increase of film thickness. The fitting curve shows that T_{sf} value is related to saturated transmittance of the sample. The larger the saturated transmittance of the sample, the larger the value of T_{sf}. The various parameters of the photochemical reaction of the sample are shown in Table 3.

CONCLUSION

The photobleaching rate constant of photopolymer sensitized by VB 2 and Azure I at different film thickness is calculated by fitting curve of photopolymer samples. The specific values of photobleaching rate constant k_p, molar absorption coefficient ε, quantum yield ϕ and scattering loss correlation coefficient T_{sf} are obtained. It is found that the quantum yield ϕ and photobleaching rate constant k_p depend on film thickness. The increase first increases and then decreases. When the film thickness is 150 um, the values of quantum yield and photobleaching rate are the largest. The change of molar absorption coefficient ε is small, and the T_{sf} decreases with the increase of film thickness. It is found that the T_{sf} value is related to the maximum transmittance of the sample. The larger the maximum transmittance value of the sample under different exposure intensity, the greater the value of T_{sf} is.

REFERENCES

[1] Shelkovnikov, V.V., Vasil'Ev, E.V., Russkikh, V.V. (2016) Monochrome and two-color holograms in layered photopolymer materials. Optoelectronics Instrumentation and Data Processing. 52(4), 404-412.
[2] Pen, E.F., Zarubin, I.A., Shelkovnikov, V.V., (2016) Method for determining the shrinkage parameters of holographic photopolymer materials. Optoelectronics Instrumentation and Data Processing. 52(1), 49-56.
[3] Retailleau, M., Ibrahim, A., Croutxébarghorn, C. (2016) New design of highly homogeneous photopolymer networks for shape memory materials. RSC Advances. 6(52), 47130-47133.
[4] Jiang, T. (2006) A New Field of Information Storage - Holographic Storage and Its Materials. Information Recording Materials. 7(6), 32-35.
[5] Wang, X. (2005) Research status and future development of ultra-large volume holographic storage. Guangxi Physics. 26(4), 24-27.
[6] Duan, X., Zhu, J., Wei, T (2009) Formulation optimization and holographic storage properties of photopolymer in green-sensitive polyvinyl alcohol/acrylamide system. China Laser. 36(4), 983-988.
[7] Mertdinç, S., Tekoğlu, E., Gökçe, H. (2017) Synthesis and Characterization Investigations of Laboratory-Synthesized VB-VB2-V3B4 Reinforced Al-7wt.% Si Composites via Mechanical Alloying and Pressureless Sintering. Solid State Phenomena. 263, 189-194.
[8] Zhang, Y., Liu, Y., He, J. (2013) Electrochemical behavior of graphene/Nafion/Azure I/Au nanoparticles composites modified glass carbon electrode and its application as nonenzymatic hydrogen peroxide sensor. Electrochimica Acta. 90(5), 550-555.
[9] Huang, M. (2001) Summary of high density digital holographic storage characteristics of photopolymer. Physics. 30(12), 768-770.
[10] Huang, M.J., Yao, H.W., Chen, Z.Y., Hou, L.S. Gan, F.X. (2002) Dependence of the high-density holographic recording parameters of photopolymer on sample thickness. Optik. 113(5), 198-199.

[11] Xu, J., Cheng, J. (2010) Holographic storage characteristics of red-sensitive photopolymer sensitized by Azure II. Chinese Journal of Lasers. 7851(5), 34-40.
[12] Malinauskas, M., Farsari, M., Piskarskas, A (2013) Ultrafast laser nanostructuring of photopolymers: A decade of advances. Physics Reports. 533(1), 1-31.
[13] Yu, X., Yu, X.m., Hu, Z.y (2013) Efficiency enhancement of polymer solar cells by post-additional annealing treatment. Optoelectronics Letters. 9(4), 274-277.
[14] Li, C., Li, X., Xue, X (2014) Holographic properties of Fe3O4 nanoparticle-doped organic–inorganic hybrid photopolymer. Optik - International Journal for Light and Electron Optics. 125(21), 6509-6512.
[15] Schwörer, M., Wirz, J. (2015) Photochemical Reaction Mechanisms of 2-Nitrobenzyl Compounds in Solution, I. 2-Nitrotoluene: Thermodynamic and Kinetic Parameters of the aci-Nitro Tautomer. Helvetica Chimica Acta. 84(6), 1441-1458.
[16] Fusco, R., Sansone, M., Petrillo, A. (2016) The Use of the Levenberg–Marquardt and Variable Projection Curve-Fitting Algorithm in Intravoxel Incoherent Motion Method for DW-MRI Data Analysis. Applied Magnetic Resonance. 46(5), 551-558.
[17] Rozentsvet, V.A., Kozlov, V.G., Stotskaya, O.A (2017) Kinetic parameters of cationic polymerization of 1,3-dienes. Russian Chemical Bulletin. 66(6), 1088-1093.
[18] Kuzmin, V.A., Golovina, G.V., Kostyukov, A.A (2016) Spectral and kinetic parameters of photoexcited complexes of albumin and indotricarbocyanine dye with phosphonate substituents. High Energy Chemistry. 50(4), 315-316.

Received: **29.11.2018**
Accepted: **19.03.2019**

CORRESPONDING AUTHOR

Jianbin Xu
Tendering Office
Henan University
Kaifeng, Henan 475004 – China

e-mail: 1825473084@qq.com

© by PSP Volume 28 – No. 5/2019 pages 4283-4292 Fresenius Environmental Bulletin

ANTIBACTERIAL AND ANTI-ADHESIVE PROPERTIES OF BIOSURFACTANTS PRODUCED BY YEASTS FROM FOOD WASTE

Ozge Akgul[1], Zerrin Erginkaya[1], Gozde Konuray[1], Emel Unal Turhan[2,*]

[1]Department of Food Engineering, Faculty of Agricultural, University of Cukurova, Adana, Turkey
[2]Department of Food Technology, Kadirli Applied Sciences School, University of Osmaniye Korkut Ata, Osmaniye, Turkey

ABSTRACT

The aim of this study is to produce biosurfactants by *Yarrowia lipolytica*, *Saccharomyces cerevisiae* and *Rhodotorula glutinis* in different growth mediums and to evaluate antimicrobial and anti-adhesive potential of these biosurfactants. Inhibition effect of biosurfactants were tested on *Escherichia coli*, *Staphylococcus aureus* and *Pseudomonas aeruginosa*. This study achieved the biosurfactant production at different amounts with a low-cost fermentative medium (frying oil waste and corn maceration liquid) by yeast species. The biosurfactant production yield and inhibitory effect of these biosurfactants were found dependent on composition of growth medium, species of yeast and pathogenic bacteria. The most biomass yield was obtained by *Y. lipolytica* in medium containing food waste. All biosurfactants had a certain inhibitory activity against pathogens at concentrations of 5 mg/mL and 10 mg/mL. Additionally, biosurfactants (10 mg/mL) indicated antiadhesion effect against *S. aureus* and *P. aeruginosa*, except *E. coli*. Despite the several advantages of biosurfactants, there is a few reports related to their use on food products and food processing. Biosurfactants from this study have economically the potential to be used as antibacterial substances in food industry for the purpose of cleaning of solid surfaces, tool and equipment, process media etc.

KEYWORDS:
Biosurfactant, yeast, waste oil, corn maceration liquid, antiadhesion

INTRODUCTION

The industrial transformation of renewable substrates into beneficial compounds has taken an attention due to increasing environmental concern. Bioconversation materials consisting of oil, starch, sugar, cellulose and lignocellulose from plants and a variety of organic wastes were provided the synthesis of novel products for various industry field [1, 2, 3]. Most of the oils and fats used in the food industry created great amounts of wastes. Recently, researchers interested in beneficial solutions for waste disposal. Especially, novel products such as biosurfactants from food waste were detected by microbial conversion [4, 5]. Biosurfactants are beneficial microbial amphiphilic compounds with their surface active properties for several industries and processes [6, 7]. Nowadays, this microbiologically produced surfactants prefer to chemically produced surfactants because of their several advantages including their structural diversity (glycolipids, lipopeptides, fatty acids etc.), low toxicity, biodegradability, ecologically safe properties, production from renewable and economic substrates, strong biological solubility and much broader effect [8, 9, 10, 11, 12]. Glycolipids consisting of rhamnolipids, trehalolipids, sophorolipids and mannosylerythritol are the most studied biosurfactants by microbial conversion. Nowadays, the most promising biosurfactants are the sophorolipids produced by yeast species, mainly *Candia* species [2, 7, 13].

Biosurfactants have been utilized in various fields such as cleaning applications, microbial inactivation, biofilm prevention and disruption, biocidal activity, wound healing, environmental applications, pharmaceutical, cosmetic, mining, metallurgical, agrochemical, paper and other industries etc. [13, 14]. Applications of biosurfactant in food industry were mainly listed as food emulsifier, antioxidant agents and antiadhesives as a result of an increasing demand to the use of biosurfactants [14]. In particular, biosurfactants are novel and highly effective compounds to prevent colonizing pathogenic microorganisms from solid surfaces such as stainless steel, glass, paper, high density polyethylene (HDPE), polycarbonate, polyurethane and polytetrafluoroethylene (PTFE, Teflon) which interact with food [15, 16, 17]. Pathogenic bacteria transit from food equipments or solid surfaces in food processing to the raw materials could cause the outbreak of foodborne diseases. As a matter of fact, the use of biosurfactant as a safety disinfectant was recently applied for good hygiene practices in food plant [15]. The biosurfactants obtained from bacteria are commonly emphasized both in the literature and in the market [11, 18, 19]. For example, rhamnolipids from *Pseudomonas aeruginosa* are commercially marketing by Jeneil Biosurfac-

tant, USA, for agricultural objectives and enhancement of bioremediation activities [7].

Biosurfactants are generally produced by aerobic microorganisms in broth medium from a carbon source feedstock including carbohydrates, hydrocarbons, fats, oils or mixtures [14]. The achievement of biosurfactant production is affiliated with the improvement of cheaper processes and the use of low cost raw material [4]. Thus, inexpensive medium components and effective biosynthesis make possible the production of biosurfactant in reducing costs. For this aim, renewable substrates or waste (by product) from food plant could economically be evaluated for the production of the microbiologically-based surfactants [20]. The promising application strategies such as the use of inexpensive substrates, optimized and efficient bioprocesses and the selection of microbial strains with higher production yield make the biosurfactant production process economically attractive [10]. Biosurfactants induced the cell for the uptake of hydrophobic substrates into the cell. Renewable sources or food waste mainly used in biosurfactant as economical were vegetable oils, corn oils, soybean oils and corn maceration liquid etc. [8, 9].

In previous researches, there are mainly knowledge about the biosurfactant production by bacteria in broth medium. Additionally, studies over bacterial biosurfactants mostly focused on medical field or health and there is the lack of the literature related to yeast biosurfactants from food waste for the benefit of food industry. However, the present paper gives applicable information regarding utilization of renewable sources for food waste disposal and antiadhesive properties of biosurfactants. Briefly, this study aimed to determine antimicrobial and anti-adhesive properties of biosurfactants produced by yeast from food waste.

MATERIALS AND METHODS

Microorganisms, medium and food waste. *Yarrowia lipolytica* ZU 110 (Instute of Cell Biology, NAS of Ukrain), *Saccharomyces cerevisiae* NCYC38, *Rhodotorula glutinis* H28 (Hohenheim University, Germany) were used for biosurfactant production. *Escherichia coli* K12, *Staphylococcus aureus* ATCC 6538 and *Pseudomonas aeruginosa* (Department of Biology, Cukurova University) were used as indicator (target) microorganisms to determine the antimicrobial and antiadhesive properties of biosurfactants. Yeast malt broth (YMB) and agar (Sigma-Aldrich) was used for growth and stock solutions of yeasts. Indicator microorganisms were growth in Trypticase Soy Broth (TSB)(Sigma-Aldrich) and stored at -20 °C in TSB supplemented with 20% (v/v) glycerol (Merck-Germany) [21]. Mueller-Hinton Broth/Agar (Merck-Germany) was used in the MIC (Minimum Inhibitory Concentration) test to determine antimicrobial properties of biosurfactants.

Two different substrates were used in the production of biosurfactants by yeasts. Waste fried oil as carbon source and corn maceration liquid (21-45% protein, 20-26% lactic acid, 8% ash, 3% sugar and trace amount of oil) as nitrogen source were supplied from BESLER CATERING firm (Adana) and from SUNAR Corn Integrated Facilities (Adana), respectively.

The growth of yeasts from stock cultures. *Y. lipolytica* and *S. cerevisiae* were incubated for 48 h at 25 °C and *R. glutinis* at 30 °C for 48 h by inoculating into 5 mL YMB medium. Then the yeast was transferred to the flasks containing 50 mL YMB and incubated at the above temperatures for 48 h at 150 rpm. Pathogenic bacteria was growth in Trypticase Soy Broth (TSB) medium enriched with 6 g/L yeast extract from the stock culture at 35 °C for 24 h. Afterward, pathogen bacteria and yeast concentration were adjusted to 10^9 cfu/mL and 10^4 cfu/mL using McFarland device [21].

Determination of optimal growth medium for biosurfactant production. The culture medium (250 mL) containing waste fried oil and corn maceration liquid was prepared in three different concentrations as M1 (250 mL YMB containing 3.75% waste oil and 3.75% corn maceration liquid), M2 (250 mL YMB containing 5% waste oil + 2.5% corn maceration liquid), M3 (250 mL YMB containing 2.5% waste oil + 5% corn maceration liquid). In addition to these medium, 250 mL of YMB (M4) was also used as control sample. pH of M1, M2, M3 and M4 mediums were adjusted to pH 7 (1 M NaOH, Merck-Germany) for the growth of *Y. lipolytica* and *S.cerevisiae* and to pH 4 (1 M HCl, Merck-Germany) for *R. glutinis*. After pH adjustment, these mediums were autoclaved at 121 °C, 20 minutes. Then, 1% (v/v) each yeast (10^4 cfu/mL) was added to each sterile medium. This mixure were incubated at 30 °C, 150 rpm during 7 day for the growth of *R. glutinis a*nd at 25 °C, 150 rpm during 7 day for the growth of *Y. lipolytica* and *S. cerevisiae*. 10 mL of samples from medium was taken every day throughout 7 days of incubation (1th, 2nd, 3rd, 4th, 5th, 6th and 7nd day). After incubation, cooled distilled water was added and centrifuged at 5000 rpm for 20 minutes. Pellet obtained from centrifugation was dried at 105°C for 1 day and then weighed. Dried pellet amounts were recorded as g/L and the medium with the highest biomass was selected for production of biosurfactant [22]. As a result, biomass measurement from yeast provided the detection of the most suitable media.

The production of biosurfactant with the optimal growth medium. For biosurfactant extrac-

tion, ethyl acetate precipitation method was used. After incubation for 7 day, the cells were removed by centrifugation at 5000 rpm for 30 minutes. Supernatant obtained at the end of the centrifugation was adjusted to pH 2.0 with 6 M HCl and transferred into a separatory funnel with the adding of an equal amount of ethyl acetate. The mixture was shaken for the phase separation with three replications. After phase separation, collected organic phase were treated with anhydrous sodium sulphate to remove water and then concentrated on a rotary evaporator at 40 °C to obtain biosurfactant extract. The level of biosurfactant production by yeast was evaluated by measuring this biosurfactant extract as g/L [22, 23].

The detection of biosurfactant presence by oil spreading technique. 10 µL of crude oil (Mersin ATAŞ Petroleum Refinery) were dropped into the center of petri dish (diameter 9 cm) containing 25 mL of pure water. Then, 10 µL of yeast supernatant from incubation for 7 day was added into the middle of the crude oil and the diameter of the zone from supernatant was measured in cm. These zone diameters are compared with zone diameters from tween-80 as a positive control sample. The diameter of the transparent zone (cm) is evaluated as "+" for 0.5-0.9 cm, "++" for 1-1.5 cm, "+++" for 1.5-2.1 cm and "++++" for 2.1 cm. [24, 25, 26].

The measurement of emulsification index and surface tension. The biosurfactant emulsification index assay was performed with a slight modification according to Ramnani et al. [27]. Water, xylene and cell-free supernatant were mixed in the ratio of 20:30:10 in a tape measure and the height of the solvent layer in the tape measure was saved. Then, an emulsion was obtained by vortexing the mixture. The measurement of the height of the emulsion layer was done after 1h, 24 h and 1week. The following equation was used for calculation of emulsification index.

EI (%)= [(height of emulsion layer) / (height of oil + emulsion layer)] × 100.

The surface tension of the cell-free culture supernatants was measured according to the ring method by a tensiometer-"TD1C-LAUDA" [23].

Antibacterial activity of biosurfactant. The antimicrobial effects of biosurfactants from the yeast were determined by MIC Tests. In the MIC method, biosurfactant extract was diluted to 2-10 fold with MHB. Then 0.1 mL of active pathogen culture was transferred into this MHB and incubated at 37 °C for 24-48 hours. Pathogenic bacteria growth in the tubes was visually evaluated according to presence of turbidity. The final dilution in which no bacterial growth is observed was accepted as the MIC value. 0.1 mL of the final dilution with no bacterial growth was added into 10 mL of MHB and incubated at 37 °C for 24-48 hours [28].

Antiadhesive activity of biosurfactant. A 96-well microtiter plate was filled with 200 µL (2.5 mg/mL, 5 mg/mL, 10 mg/mL) of the biosurfactant extract and 200 µL of the control samples with distilled water and incubated at room temperature for 24 hours to provide attachment of biosurfactant extract. Then, the cells were carefully washed 3 times with 200 µL of distilled water. The microtiter plate previously coated with biosurfactant was filled with 180 µL of TSA and incubated at 35°C for 10 days by adding of 200 µL of pathogenic bacteria (10^9 cfu/mL) At the end of the incubation, the microtiter plate wells were washed with distilled water, then were kept with a solution of 200 µL methanol for 15 minutes, and followed by 15 minutes with crystal violet (1% g/L). Then it was filled with 33% (v/v) 200 µL acetic acid. Finally, the optical density was measured at 600 nm by using the ELISA microtiter plate reader and percent of microbial inhibition (%) was calculated from these absorbance values. Microbial inhibition (%) = [1 - (Ac / Ao)] × 100; Ac: The absorbance value of biosurfactant cells; Ao: The absorbance value of control cells [21, 29].

Statistical analysis. Statistical analyses were performed using the "Windows SPSS 15.0 software" statistical package program (SPSS Inc., Chiago, IL, USA). One-way analysis of variance (ANOVA) was used to compare differences in significance among the trials and Duncan's multiple comparison test was used to compare differences between groups ($p<0.05$) [30].

RESULTS

Biomass values from yeast in different mediums provided the selection of medium to be used biosurfactant production. Then, yeast was grown in the medium gave the highest biomass, namely yeast-specific medium. According to results from Section 3.1., M2 medium for *Y. lipolytica* and M1 medium for *S. cerevisiae* and *R. glutinis* were used in other analysis. Thus, mediums containing food waste (M2 and M1) were compared with control sample (M4). Additionally, yeast types were compared with regard to antimicrobial, antiadhesive and biosurfactant productivity.

Biomass values from yeasts in different mediums. To find biomass values from yeast in different growth mediums, samples were taken from all medium throughout 7 days (every day from 1st day to 7nd) and aimed to obtain the highest biomass values. The highest cell mass was reached on 7nd day for each medium. Then, comparison of yeast type and culture media were carried out according

to values obtained from 7nd day, namely the highest values in terms of biomass yield.

As seen in Table 1, optimal growth medium was found as M2 for *Y. lipolytica* and as M1 for *S. cerevisiae* and *R. glutinis*. Yeasts were growth more in the waste oil medium enriched with corn maceration liquid than in M4 (control medium). M2 medium led to the highest growth of *Y. lipolytica*, while M1 provided the highest growth of both *S. cerevisiae* and *R. glutinis*. The cell growth of *S. cerevisiae* and *R. glutinis* in M2 medium were found less than M1 and M3, whereas the cell growth of *Y. lipolytica* in M3 medium was less than M1 and M2. This situation supported that growth medium was strain-specific. As seen our results, YMB medium containing food waste (M1, M2 and M3) induced the growth of yeasts.

Extraction of biosurfactant from optimal yeast growth medium. The amounts of biosurfactants from *Y. lipolytica*, *S. cerevisiae* and *R. glutinis* with their optimal growth medium were presented in Table 2. The highest biosurfactant amount was obtained by *Y. lipolytica*, while *R. glutinis* caused at the least of biosurfatant production. Biosurfactant production of *Y. lipolytica* and *S. cerevisiae* was found statistically different from *R. glutinis*. Additionally, medium containing the food waste created more concentration of biosurfactant. These results detected that medium with food waste was more effective for the production of biosurfactant.

The presence of biosurfactant by oil spreading technique. According to the average zone diameters from yeast biosurfactant (Table 3), medium containing food waste caused "++++" with regard to biosurfactant productivity, whereas M4 medium (YMB=control) had value "+++" for *S. cerevisiae*, "++" for *Y. lipolytica* and *R. glutinis*. These results demonstrated the presence of biosurfactant from yeasts. In accordance with the results based on biosurfactant extraction of the present study, oil spreading activities of biosurfactants from yeast supernatant in medium containing food waste were found more than control medium. However, *S. cerevisiae* had the highest zone diameter unlike the results of biosurfactant extraction. In terms of efficiency of biosurfactant production by yeast species, correlation could not be established between test results from biosurfactant extraction and biosurfactant presence by oil spreading technique.

TABLE 1
Biomass evaluation of yeast growth media (as g/L)

Mediums	*Y. lipolytica*	*S. cerevisiae*	*R. glutinis*
M1	16.75 ± 6.18^{aA}	9.00 ± 0.00^{bA}	18 ± 3.46^{cA}
M2	22.75 ± 2.98^{aB}	5.00 ± 0.00^{bBC}	9 ± 0.00^{cBC}
M3	14.50 ± 2.51^{aBC}	6.75 ± 0.50^{bB}	9.5 ± 0.10^{cB}
M4	4 ± 0.81^{aC}	3.50 ± 0.57^{bC}	6.5 ± 0.57^{cC}

a,b,c: The averages shown in the same line with different exponents are significantly different ($p<0.05$). A, B: The averages shown on the same column with different exponents are significantly different.

TABLE 2
The average amounts of biosurfactants from yeasts (g/L)

Medium	*Y. lipolytica*	*S. cerevisiae*	*R. glutinis*
Medium with food waste (M1 or M2)	13.85 ± 4.11^{cB}	12.44 ± 2.96^{Ba}	7.83 ± 1.10^{bA}
Control (M4)	8.19 ± 0.72^{aB}	2.30 ± 1.27^{aA}	2.78 ± 0.58^{aA}

a,b,c: The averages shown in the same column with different exponents are significantly different ($p<0.05$).
A, B: The averages shown on the same line with different exponents are significantly different

TABLE 3
The average zone diameters from biosurfactant presence by oil spreading technique (as cm)

Medium	*Y. lipolytica*	*S. cerevisiae*	*R. glutinis*
Medium with food waste (M1 or M2)	4.12 ± 2.49^{bA}	6.5 ± 0.40^{Bb}	4.87 ± 2.01^{AB}
YME	1.25 ± 0.64^{aA}	2.25 ± 0.28^{Ab}	1.87 ± 0.47^{aAB}

a,b,c: The averages shown in the same column with different exponents are significantly different($p<0.05$).
A,B: The averages shown on the same line with different exponents are significantly different.

TABLE 4
Emulsification index values of cell free supernatant from yeasts (%)

Hours	*Y. lipolytica* in M2	*Y. lipolytica* in M4	*S. cerevisiae* in M1	*S. cerevisiae* in M4	*R. glutinis* in M1	*R. glutinis* in M4
1	52.05 ± 4.98^{A}	27.90 ± 4.58^{a}	$30.37\pm3,45^{a}$	14.95 ± 1.90^{a}	8.33 ± 3.33^{a}	37.45 ± 24.07^{a}
24	15.37 ± 1.57^{B}	14.56 ± 0.67^{b}	0.00 ± 0.00^{b}	0.00 ± 0.00^{b}	1.66 ± 3.33^{b}	4.99 ± 3.33^{b}
168	0.00 ± 0.00^{C}	3.74 ± 2.84^{c}	0.00 ± 0.00^{b}	0.00 ± 0.00^{b}	0.00 ± 0.00^{b}	0.00 ± 0.00^{b}

a,b,c: The averages shown in the same column with different exponents are significantly different($p<0.05$). A,B: The averages shown on the same line with different exponents are significantly different.

Emulsification index and surface tension. Emulsification index values from different yeast species were compared at different cultivation conditions. As seen in Table 4, after first hour, emulsification index for all yeast species reduced. In general, *Y. lipolytica* showed highest resistance because of its time-dependent stability. Emulsification index from food waste (M1 and M2) were found higher than YMB (M4=control), except for results from *R. glutinis*. As similar to the results from average amounts of biosurfactant extraction, the highest emulsification index value was obtained from *Y. lipolytica*, and that followed *S. cerevisiae* and *R. glutinis*.

In this study, before yeast inoculation, surface tension of YMB medium (control=M4) and waste oil medium was measured as 65 mN/m and 60 mN/m, respectively. After yeast inoculation to YMB and food waste medium, surface tension is expected to decrease. As a matter of fact, surface tension by yeasts were reduced to minimum 38.35 mN/m and to maximum 58.63 mN/m (Table 5). Surface tension values by yeasts used in this study were mostly found similar. Except for *Y. lipolytica*, there are not significant difference among surface tension values in terms of yeast species and growth medium. Namely, there are not significant differences among samples in terms of surface tension except *Y. lipolytica* in YMB medium. For this reason, correlation could not be established between biosurfactant extraction amounts and surface tension. Surface tension value obtained from *S. cerevisiae* in M4 medium (control) (38.35 mN/m) was found close to which corresponded to the surface tension obtained at the critical micelle concentration of glycolipids. Additionally, biosurfactants produced by *S. cerevisiae* were more effective at reducing surface tension.

Antimicrobial properties of biosurfactants. Biosurfactants from yeasts exhibited inactivation effect on pathogens and their MIC values ranged from 5 and to >10 mg/mL (Table 6). The most effective biosurfactant for inhibition of *E. coli* and *S. aureus* were obtained from *S. cerevisiae* due to the least MIC value (5 mg/mL). All biosurfactant showed the same effect on the inhibition of *P. aeruginosa* with regard to MIC value. Biosurfactants produced by *Y. lipolytica* and *R. glutinis* in food waste medium were found less effective against *E. coli* and *S. aureus* than in M4 medium (control sample). As a matter of fact, higher MIC values (>10 mg/mL) of biosurfactants from *Y. lipolytica* and *R. glutinis* in food waste medium were required for inactivation of *E. coli* and *S. aureus* than in M4 medium (control).

TABLE 5
Surface tension values by different yeast species (mN/m)

Growth medium	*Y. lipolytica*	*S. cerevisiae*	*R. glutinis*
Medium with food waste (M1 or M2)	53.11±10.60[a]	40.49±8.08[b]	52.67±4.11[b]
M4 (control)	54.82±4.45[b]	38.35±12.90[b]	58.63±3.85[b]

a,b,c: The averages shown with different exponents are significantly different($p<0.05$).

TABLE 6
MIC values of biosurfactant produced by yeast in different mediums (mg/mL)

Medium	MIC against *E. coli*	MIC against *S. aureus*	MIC against *P. aeruginosa*
Y. lipolytica in M2	>10	>10	10
Y. lipolytica in M4	10	10	10
R. glutinis in M1	>10	>10	10
R. glutinis in M4	10	10	10
S. cerevisiae in M1	5	5	10
S. cerevisiae in M4	5	5	10

TABLE 7
Microbial inhibition from biosurfactants having the antiadhesion effect against pathogens (%)

Biosurfactants	Inhibition of *S. aureus*	Inhibition of *P. aeruginosa*
Y. lipolytica in M2 (10 mg/mL)	3.5±1.73[b]	-
Y. lipolytica in M4 (10 mg/mL)	12±4.08[b]	-
S. cerevisiae in M1 (5 mg/mL)	-	17.5±2.08[b]
S. cerevisiae in M1 (10 mg/mL)	-	34.25±3.09[c]
S. cerevisiae in M4 (10 mg/mL)	-	16.25±3.20[b]
R. glutinis in M4 (10 mg/mL)	-	27.75±10.01[b]

a,b,c: The averages shown with different exponents are significantly different ($p<0.05$).

The antiadhesion effect of biosurfactants against pathogens. In the present study, antiadhesion effects of biosurfactants at level of 2.5 mg/mL, 5 mg/mL and 10 mg/mL were tested. Table 7 represented the values of microbial inhibition from biosurfactants having the antiadhesion effect against pathogens. According to results, antiadhesion effect of biosurfactants was observed mostly at 10 mg/mL of concentrations against *S. aureus* and *P. aeruginosa*. The most antiadhesion potential of biosurfactants was detected against *P. aeruginosa*. There are not any antiadhesion effect at level of 2.5 mg/mL of biosurfactant, while 5 mg/ml of biosurfactant produced by *S. cerevisiae* in M1 medium caused antiadhesion against only *P. aeruginosa*. Additionally, none of the biosurfactants were prevent adhesion of *E. coli*. The highest antiadhesion effect was observed against *P. aeruginosa*. As regards antiadhesion effect, biosurfactant from M4 medium (control samples) mostly caused more inhibition except biosurfactant from *S. cerevisiae* in medium with food waste. Inhibition of *S. aureus* was carried out by biosurfactant from *Y. lipolytica* (10 mg/mL). Biosurfactants from *S. cerevisiae* (5 and 10 mg/mL) and *R. glutinis* (10 mg/mL) led to antiadhesion against *P. aeruginosa*. Briefly, these results showed that antiadhesion effect was dependent on yeast species from which biosurfactants were obtained.

DISCUSSION

Biosurfactants will have the potential to be used more and more every day in many areas of the food industry due to their several advantages. They could be evaluated as multipurpose additives providing emulsification, antiadhesion and microbial inhibition etc. [14]. However, there are some factors that limit the use of biosurfactants. The most important is related to the cost of biosurfactant production. Waste materials or renewable sources may economically be available for production of biosurfactant. The other limitation about biosurfactant production is toxicity. The microorganisms used biosurfactant production should not have any toxic effects [6, 31, 32]. As a matter of fact, this research aimed biosurfactant production by yeasts from food waste and then detected antibacterial and antiadhesive properties of biosurfactants.

Yarrowia (*Candida*) *lipolytica* was the most known biosurfactant producer yeast (liposan) and researchers mainly concentrated on this yeast for biosurfactant studies [6, 33]. However, the other yeast species such as *Saccaromyces cerevisia* and *Rhodotorula glutinis* also have capability to produce biosurfactants [33, 34, 35]. Yeast strains produce biosurfactants in different biomass yield depending on growth medium (pH, compositions, salt etc.), incubation period and conditions (temperature, aeration, agitation etc.) [3, 36, 37, 38]. In the present study, yeast growth with the highest cell concentrations was observed on 7nd day of incubation period. Similarly, Gusmao et al. [39] and Rufino et al. [36] reported that yeasts were exposure to 7 days incubation for experimental analysis due to high biomass yield. Luna et al. [40] stated that the highest biomass production (17.0 g/L) occurred after 120 h of yeast growth.

In recent years, the cultivation medium of yeast generally supplemented with oil waste for the synthesis of biosurfactants. Enrichment of medium with the oil waste or other food industry waste resulted in approximately 7-8 fold higher biomass yield in comparison to the medium without the addition of food waste [20]. A combination of food waste (mostly vegetable oil waste and corn maceration liquids) for the production of biosurfactants from the yeast was found more effective in comparison to medium with single constituents [9]. For example, *C. lipolytica* in medium containing 6% soybean oil refinery residue and 1 % glutamic acid reached the highest biomass concentration after 50 hours [37]. Similarly, in our study, biosurfactant productivity in mixed medium with food waste was more than single M4 medium (control). The yield of biosurfactant from food waste by yeast was changed from 7.83 to 13.85 g/L after 7 day of cultivation, which is in agreement with the results of previous studies [18, 40, 41, 42].

As known from our results, extraction of biosurfactants from waste oil medium enriched with corn maceration liquid was found more efficient than YMB medium (control=M4). In accordance with this, Bednarski et al. [20] reported that the yeast growth medium with oil waste caused greater concentration of glycolipids (7.3-13.4 g/L) than obtained in the medium without addition of oil refinery. Rufino et al. [37] was found 8 g/L of biosurfactant yield by *C. lipolytica* from industrial refinery residue after 72 hours. However, biosurfactant yield by *Y. lipolytica* in the present study was found more because of more incubation period (7 days). Alcantara et al. [33] reported that biomass yield from *Yarrowia lipolytica* and *S. cerevisiae* in waste cooking oil was maximum 20 g/L and 10 g/L, respectively as similar to our results. As known from literature, the synthesis method of biosurfactant was also effective on biomass yield. Batch fermentation by yeast in a fermentor and the fermentor using this pure fatty acid produced the highest biosurfactant yield of 34 g/L and 42 g/L according to the study of Shah et al. [43].

The oil spreading test without specialized equipment and with a small volume of sample is a rapid and easy [11]. *Y. lipolytica*, *R. glutinis* and *S. cerevisiae* from yeast species had capability of oil spreading which demonstrate the presence of biosurfactant [34, 42]. In this study, oil spreading activities of all yeast strains were revealed as positive

and the maximum oil spreading activity were exhibited by *S. cerevisiae* and followed by *R. glutinis* and *Y. lipolytica*. Differently, Fontes et al. [42] stated that the highest value of oil spreading caused by *Yarrowia lipolytica* from sustainable sources was found as approximately 1.1 cm after 72 hours.

An emulsion is fluid system in which liquid microscopic droplets are dispersed in a liquid phase. Biosurfactants may ensure an adequate emulsification by stabilizing the microscopic droplets. However, stability and activity of biosurfactants should be maintained in order to benefit from their emulsification capabilities [40]. The emulsification activity could be affected from cultivation conditions such as growth medium compositions, incubation period, microbial strains, media temperature etc. Especially, emulsification index decreased over time [41]. Our results was also in accordance with this. The optimum temperature for emulsification activity was room temperature [36]. This temperature was selected for the measurement of emulsification index in this study. Emulsification activity could also change according to the hydrocarbon used in related analyses [11, 36]. In this study, emulsification index values were obtained from xylen, but in the next studies, different hydrocarbon substrates should be tested for establishment of better correlations. Rufino et al. [36] found that after 7 days incubation, emulsification index values from *C. lipolytica* were approximately 95% by motor oil, 40% by hexadecane, diesel and 20% by hexane and corn oil, respectively. In general, *Y. lipolytica* in optimal growth medium caused emulsification index around 40% [42, 44]. In previous studies, *R. glutinis* and *S. cerevisiae* indicated emulsification index as 35% and 57%, respectively. Emulsification index from *Yarrowia lipolytica* and *S. cer*evisiae in waste cooking oil were maximum 55% and 65% [33]. Emulsification index values of the present study were less than these literature results.

According to Ring method, surface tension was determined by evaluating the surface tension of pure water (72 mN/m). An effective biosurfactant should decrease this value to 30 mN/m [4, 20]. Biosurfactant or surface-active compounds have the ability to reduce surface tension of water [8]. Various factors such as pH, salinity and temperature etc. which are effective on biosurfactant activity also affect the surface tension properties of the biosurfactant. As the efficiency of biosurfactant increases, surface tension reduces [39]. Previous studies highlighted that the effectiveness of biosurfactants from bacteria on reducing the surface tension is greater than yeasts. For instance, *Pseudomonas aeruginosa* which is the most studied strain for the production of biosurfactants decreases the surface tension to 27.28 mN/m. Recently, yeasts were able to reduce this value as much as bacteria [20, 37]. In general, biosurfactants from yeast reduced the surface tension to values around 35.0 mN/m by yeast (*Yarrowia lipolytica, Candida sphaerica* and *C. glabrata* etc.) but recently this value reached 25 mN/m by *Candida sphaerica* [40]. Gusmao et al. [39] found that surface tension by yeast used vegetable fat waste varied from 36.9 to 28.3 mN/m and reported that properties of surface tension could be affected from growth medium content of yeast. In another study, surface tension values were decreased from 50.0 mN/m to 25.0 mN/m by means of the biosurfactant from *C. lipolytica* in growth medium with industrial refinery residue [18]. In general, *Y. lipolytica* in optimal growth medium caused surface tension between approximately 40 and 45 mN/m [42, 44] Yeast species and growth medium used in this study were appeared as the cause of the higher surface tensions. For the less surface tensions, different microbial species, growth medium and cultivation conditions were tested by the next studies.

As known from previous studies, biosurfactants have inhibitory effect on various pathogen bacteria. As the amounts of biosurfactants increase, more inhibition is observed [18]. The determination of antimicrobial properties was based on MIC value which is the lowest concentration of antibacterial substances inhibiting visible bacterial growth [8]. The present paper detected that the biosurfactants had antimicrobial effects against various pathogens. Inhibitory activities of biosurfactant could show difference according to substrates or sources and microbial species used in their production and also species of the target pathogenic bacteria [45]. The present study supported this hypothesis. Rufino et al. [18] reported that 12 mg/L of biosurfactants from yeast caused 5%, %16.5 and %15.1 inhibition effect *on E. coli*, *Pseudomonas aeruginosa* and *Staphylococcus aureus*, respectively. This situation considered that there is a necessity to more amount biosurfactant for 100% inhibition. Similarly, in our study more biosurfactants than 10 mg/mL were needed for *E. coli* and S. aureus inhibition by *Y. lipolytica* in M2 and *R. glutinis* in M1, with complete cell death. Csutak et al. [34] reported that biosurfactants produced by *R. glutinis* had an inactivation effect on pathogenic yeasts.

Adsorption of biosurfactants to solid surfaces provides several advantages for not only in the medical field, but also in food plant by preventing microbial adhesion and frightening with bacterial colonization [18]. Bacterial biofilms are more resistant to disinfectants than their planktonic form. Therefore, when novel antimicrobials were evaluated for the use of industry, their effects on biofilms or antiadhesive potential were taken into consideration [35]. Most literature on biosurfactants revealed their antiadhesive activities against attachments of *Listeria monocytogenes, Staphylococcus aureus, Micrococcus luteus, Pseudomonas* spp. and *Bacillus* spp. [14, 35]. The biosurfactants from the present study exhibited antiadhesive activity against

only *S. aureus* and *P. aeruginosa*, however the values of anti-adhesive effect were found different depending on the growth medium used in the biosurfactants production and pathogens tested. The anti-adhesive property was proportional to the concentration of the biosurfactant [18]. In accordance with this information, the present paper detected that 10 mg/mL of biosurfactant from *S. cerevisiae* in M1 medium led to more anti-adhesion than its 5 mg/mL for *P. aeruginosa* inhibition.

In conclusion, the present study encourages the industry to the use of food wastes as substrates for the microbiologically production of biosurfactants. Biosurfactants from microorganisms have the potential to compete with chemical surfactants, but need to be developed for the detection of an available and inexpensive substrate with the increased volumetric productivity. The high cost of production limits the commercial applications of biosurfactants. However, optimized cultivation conditions with more economical renewable substrates and microorganism species could provide more profitable and economically feasible production of biosurfactants [7]. The cultivation conditions should be optimized for the aim of higher production yield [4]. Thus biosurfactants were safely and commercially applied as antibacterial agents in food industry due to their antimicrobial and antiadhesive activities [8, 9]. As a result, previous and the next studies give the useful data based on biosurfactants from renewable substrates to industry for economic growth. These data include the selection of the proper microbial strains, use of cheap by product or waste, optimization of process parameters and ensuring productivity. Thus, possibilities related with commercially applicability of biosurfactants will be collected from literature studies.

ACKNOWLEDGEMENTS

We would like to thank the Scientific and Technological Research Council of Turkey (TÜBİTAK, Project No: 215O062) and the Çukurova University Research Fund (Project No: FYL-2015-4362) for their financial support.

REFERENCES

[1] Morita, T., Konishi, M., Fukuoka, T., Imura, T., Kitamoto, D. (2007) Microbial conversion of glycerol into glycolipid biosurfactants, mannosylerythritol lipids, by a basidiomycete yeast, *Pseudozyma antarctica* JCM 10317. Biosci Bioeng. 104, 78-81.

[2] Nitschke, M., Costa, S.G.V.A.O. (2007) Biosurfactants in food industry. Trends in Food Sci Technol. 18, 252-259.

[3] Saharan, B.S., Sahu, R.K., Sharma, D. (2011) A review on biosurfactants: fermentation, current developments and perspectives. GEBJ. 29, 1-39.

[4] Haba, E., Espuny, M.J., Busquets, M., Manresa, A. (2000) Screening and production of rhamnolipids by *Pseudomonas aeruginosa* 47T2 NCIB 40044 from waste frying oils. Appl Microbiol. 88, 379-387.

[5] Sidal, U., Kolankaya, N., Kurtonur, C. (2000) Obtaining biosurfactant from olive oil mill effluent (OOME) using *Pseudomonas* sp. Turk Biol. 24, 611-625. (in Turkish).

[6] Shekhar, S., Sundaramanickam, A., Balasubramanian, T. (2014) Biosurfactant producing microbes and their potential applications: a review. Crit Rev Env Sci Tec. 45, 1522-1554.

[7] Banat, I.M., Franzetti, A., Gandolfi, I., Bestetti, G., Mortinotti, M.G., Fracchia, L., Smyth, T.J., Marchant, R. (2010) Microbial biosurfactants production, applications and future potential. Appl Microbiol Biotechnol. 87, 427-444.

[8] Abolas, A., Pinazo, A., Infante, R., Casals, M., Garcia, F., Manresa, A. (2001) Physicochemical and antimicrobial properties of new rhamnolipids produced by P*seudomonas aeruginosa* at10 from soybean oil refinery wastes. Langmuir. 17, 1367-1371.

[9] Makkar, R.S., Cameotra, S.S., Banat, I.M. (2011) Advances in utilization of renewable substrates for biosurfactant production. AMB Express. 1, 1-19.

[10] Mukherjee, S., Das, P., Sen, R. (2006) Towards commercial production of microbial surfactants. Trends in Biotechnol. 24, 509-515.

[11] Shoeb, E., Ahmed, N., Akhter, J., Badar, U., Siddiqui, K., Ansari, F.A., Waqar, M., Imtiaz, S., Akhtar, N., Shaikh, Q.A., Baig, R., Butt, S., Khan, S., Khan, S., Hussain, S., Ahmed, B., Ansari, M.A. (2015) Screening and characterization of biosurfactant -producing bacteria isolated from the Arabian Sea coast of Karachi. Turk Biol. 39, 210-216.

[12] Velioğlu, Z., Öztürk, R.Ü. (2015) Biosurfactant production by *Pleurotus ostreatus* in submerged and solid-state fermentation systems. Turk Biol. 39, 160-166.

[13] Marchant, R., Banat, I.M. (2012) Microbial biosurfactants: challenges and opportunities for future exploitation. Trends in Biotechnol. 30, 558-565.

[14] Campos, J.M., Stamford, T.L.M., Sarubbo, L.A., Luna, J.M., Rufino, R.D., Banat, I.M. (2013) Microbial biosurfactants as additives for food industries. Biotechnol Prog. 29, 1097-1108.

[15] Oh, I.K., Perez, K., Kahli, N., Kara, V., Li, J., Min, Y., Castillo, A., Taylor, M., Jayaraman, A., Cisneros, Z.L., Akbulut, M. (2015) Hydrophobically-modified silica aerogels: Novel food contact surfaces with bacterial anti-adhesion properties. Food Control. 52, 132-141.

[16] Meylheuc, T., Van, O.C.J., Bellon, F.M.N. (2001) Adsorption of biosurfactant on solid surfaces and consequences regarding the bioadhesion of *Listeria monocytogenes* LO28. J Appl Microbiol. 91, 822-832

[17] Mireles, J.R., Toguchi, A., Harshey, R.M. (2001) *Salmonella enterica* serovar Typhimurium swarming mutants with altered biofilm-forming abilities: Surfactin inhibits biofilm formation. Bacteriol. 183, 5848-5854.

[18] Rufino, R.D., Luna, J.M., Sarubbo, L.A., Rodrigues, L.R.M., Teixeira, J.A.C., Campos Takaki, G.M. (2011) Antimicrobial and anti-adhesive potential of a biosurfactant Rufisan produced by *Candida lipolytica* UCP 0988. Colloid Surface B. 84, 1-5.

[19] Kaya, T., Aslım, B., Kariptaş, E. (2014) Production of biosurfactant by *Pseudomonas* spp. isolated from industrial waste in Turkey. Turk Biol. 38, 307-317.

[20] Bednarski, W., Adamczak, M., Tomasik, J., Płaszczyk, M. (2004) Application of oil refinery waste in the biosynthesis of glycolipids by yeast. Bioresource Technol. 95, 15-18.

[21] Gomes, M.Z., Nitschke, M. (2012) Evaluation of rhamnolipid and surfactin to reduce the adhesion and remove biofilms of individual and mixed cultures of food pathogenic bacteria. Food Control. 25, 441-447.

[22] Sobrinho, H.B.S., Rufino, R.D., Luna, J.M., Salgueiro, A.A., Campos-Takaki, G.M., Leite, L.F.C., Sarubbo, L.A. (2008) Utilization of two agro industrial by-products for the production of a surfactant by *Candida sphaerica* UCP0995. Process Biochem. 43, 912-917.

[23] Accorsini, F.R., Muttan, M.J.R., Lemas, E.G.M., Benincasa, M. (2012) Biosurfactant production by yeasts using soybean oil and glycerol as low cost substrate. Braz Microbiol. 43, 116-125.

[24] Youssef, N.H., Duncan, K.E., Nagle, D.P., Savage, K.N., Knapp, R.M., Mcinerney, M.J. (2004) Comparison of methods to detect biosurfactant production by diverse microorganisms. Microbiol Meth. 56, 339-347.

[25] Karthik, L., Kumar, G., Rao, K.V.B. (2010) Comparison of methods and screening of biosurfactant producing marine *Actinobacteria* isolated from nicobar marine sediment. The IIOAB Journal. 1, 34-38.

[26] Sarin, S., Khamsri, B., Sarin, C. (2011) Isolation of biosurfactant-producing bacteria with antimicrobial activity against bacterial pathogens. Environment Asia. 4, 1-5.

[27] Ramnani, P., Kumar, S.S., Gupta, R. (2005) Concomitant production and downstream processing of alkaline protease and biosurfactant from *Bacillus licheniformis* RG1: bioformulation as detergent additive. Process Biochem. 40, 3352-3359.

[28] Koçan, D. (2007) Minimum inhibition concentration for determining of *Listeria monocytogenes*. PhD Thesis. University of Ankara, Graduate School of Natural and Applied Sciences, Ankara, Turkey. (in Turkish).

[29] Mehdi, H., Giti, E. (2008) Investigation of alkane biodegradation using the microtiter plate method and correlation between biofilm formation, biosurfactant production and crude oil biodegradation. Int Biodeter Biodegr. 62, 170-178.

[30] Bek, Y., Efe, E. (1988) Research and testing methods. University of Cukurova, Agricultural Faculty Textbook, Adana, Turkey, 368p. (in Turkish).

[31] Bankar, A.V., Kumar, A.R., Zinjarde, S.S. (2009) Environmental and industrial applications of *Yarrowia lipolytica*. Appl Microbiol Biotechnol. 84, 847-865.

[32] Gakpe, E., Rahman, P.K.S.M., Hatha, A.A.M. (2007) Microbial Biosurfactants – Review. Mar Atmos Res. 3, 1-17.

[33] Alcantara, V.A., Pajares, I.G., Simbahan, J.F., Rubio, M.L.D. (2012) Substrate dependent production and isolation of an extracellular biosurfactant from *Saccharomyces cerevisiae* 2031. Philippine J. of Sci. 141, 13-24.

[34] Csutak, O., Stoica, A., Vassu, T. (2012) Evaluation of production, stability and activity of biosurfactants from yeasts with application in bioremediation of oil-polluted environment. Rev Chim. 63, 973-977.

[35] Johny, J.M. (2013) Inhibitory effect of biosurfactant purified from probiotic yeast against biofilm producers. OSR-JESTFT. 6, 51-55.

[36] Rufino, R.D., Sarubbo, L.A., Campos Takaki, G.M. (2007) Enhancement of stability of biosurfactant produced by *Candida lipolytica* using industrial residue as substrate. World Microbiol Biotechnol. 23, 729-734.

[37] Rufino, R.D., Luna, J.M., Campos Takaki, G.M., Sarubbo, L.A. (2014) Characterization and properties of the biosurfactant produced by *Candida lipolytica* UCP 0988 Electron J Biotechn. 17, 34-38.

[38] Varjani, S.J., Upasani, V.N. (2017) Critical review on biosurfactant analysis, purification and characterization using rhamnolipid as a model biosurfactant. Bioresource Technol. 232, 389-397.

[39] Gusmao, C.A.B., Rufino, R.D., Sarubbo, L.A. (2010) Laboratory production and characterization of a new biosurfactant from *Candida glabrata* UCP1002 cultivated in vegetable fat waste applied to the removal of hydrophobic contaminant. World Microbiol Biotechnol. 26, 1683-1692.
[40] Luna, J.M., Rufino, R.D., Sarubbo, L.A., Campos, G.M.T. (2013) Characterization surface properties and biological activity of biosurfactant produces from industrial waste by *Candida spherica* UCP0995 for application in the petroleum industry. Colloid Surface B. 102, 202-209.
[41] Sarubbo, L.A., Farias, C.B.B., Campos-Takaki, G.M. (2007) Co-utilization of canola oil and glucose on the production of a surfactant by *Candida lipolytica*. Curr Microbiol. 54, 68-73.
[42] Fontes, G.C., Amaral, P.F.F., Nele, M., Coelho, M.A.Z. (2010) Factorial Design to Optimize Biosurfactant Production by *Yarrowia lipolytica*. Biomed BioTech. 1-8.
[43] Shah, V., Jurjavic, M., Badia, D. (2007) Utilization of restaurant waste oil as a precursor for sophorolipid production. Biotechnol Prog. 23, 512-515.
[44] Fontes, G.C., Ramos, N.M., Amaral, P.F.F., Nele, M., Coelho, M.A.Z. (2012) Renewable resources for biosurfactant production by *Yarrowia lipolytica*. Braz Chem Eng. 29, 483-493.
[45] Yalçın, E., Ergene, A. (2009) Screening the antimicrobial activity of biosurfactants produced by microorganisms isolated from refinery wastewaters. JABS. 3, 163-168.

Received: **02.12.2018**
Accepted: **01.04.2019**

CORRESPONDING AUTHOR

Emel Unal Turhan
Department of Food Technology,
Kadirli Applied Sciences School,
University of Osmaniye Korkut Ata,
Osmaniye – Turkey

e-mail: emelunalturhan@gmail.com

© by PSP Volume 28 – No. 5/2019 pages 4293-4296 Fresenius Environmental Bulletin

STUDY ON THE ENVIRONMENTAL CAPACITY OF ECOTOURISM BASED ON THEORY OF SUSTAINABLE DEVELOPMENT

Rui Zhou*

School of Management, Chongqing College of Electronic Engineering, Chongqing, 401331, China

ABSTRACT

The paper presents the results of the research for prioritization strategies of sustainable development of ecotourism in China. This paper will combine the tourism life cycle theory and the balance between demand capacity and supply capacity affecting the tourism environment capacity, and construct the state model of the tourism environment demand capacity and the dynamic development model of the supply capacity for the tourist attractions at different stages of the life cycle. The development law is analyzed, and the short-term logistic curve type and long-term composite logistic curve development mode of tourism environment capacity are proposed.

KEYWORDS:
Sustainable development, ecotourism, environmental capacity, logistic curve type

INTRODUCTION

Ecotourism is a new type of tourism that is not a consumable resource, it is for educational and adventurous character, focused on undeveloped and sparsely visited natural, cultural and historical sites [1-4]. The purpose of such movement in tourism is understanding and appreciation of the natural and social culture of certain destination [5]. The development objective of ecotourism is to protect natural areas through the provision of income, environmental protection, education and involvement of the local population [6, 7]. It is based on the idea that eco-environment is a local resource that creates economic value of attracting tourists [8-10]. Ecotourism is defined as: "Environmentally responsible travel and visitation to relatively undisturbed natural areas, in order to enjoy and appreciate nature (and any accompanying cultural features both past and present) that promotes conservation, has low negative visitor impacts, and provides for beneficially active socioeconomic involvement of local people" [11, 12].

Implementation of ecotourism has numerous positive impacts. Many authors have stated that ecotourism contributes to the conservation of endangered species [13] and cultural heritage in the world [14]. Also, ecotourism represents a reliable tool for improving the local economy, particularly in underdeveloped regions. In remote and pristine areas ecotourism is responsible for generating revenue for the protection of the environment [15].

At present, many scholars have discussed the concept of environmental capacity in tourist attractions. However, so far, there is no consistent view on the concept and concept system of tourism environmental capacity at home and abroad. This paper will combine the tourism life cycle theory and the balance between demand capacity and supply capacity affecting the tourism environment capacity, and construct the state model of the tourism environment demand capacity and the dynamic development model of the supply capacity for the tourist attractions at different stages of the life cycle. The development law is analyzed, and the short-term logistic curve type and long-term composite logistic curve development mode of tourism environment capacity are proposed.

EXPERIMENTAL

Environmental capacity calculation model. According to the structure of the conceptual system of the environmental capacity of the tourist scenic spot and the coupling relationship between its various components, follow the general equation of self-organization theory, and establish the following two-component models:

$$\frac{dE_i}{dt} = r_i E_i \left(1 - \frac{E_i}{k_i}\right) \quad (1)$$

Where E_i (i=1, 2,...,12) is the development value of each secondary component; r_i is the development rate of each secondary component, which is determined by the sustainable capacity under each secondary component or by tourism The authorities determine the rate of development according to the planning of the tourist attractions; k_i indicates the saturation capacity of each secondary component. The formula (1) is integrated:

$$E_i = \frac{k_i}{1 + ce^{-r_i t}} \quad (2)$$

Where: c is the integral constant, $c = \frac{k_i - E_{i0}}{E_{i0}} \rangle 0$ and $k > E_{i0} \rangle 0$; E_{i0} represents the initial capacity of each secondary component.

Since the negative impacts of tourism on the environment are basically caused by tourists and their activities, and the amount directly affects the economic output of tourism, it is possible to attribute the relevant attributes of various parameters reflecting the scale of capacity. The unified number of tourists to bear is up. It usually appears as a "threshold" beyond which the "functioning" function of the travel activity system will be affected. Therefore, the visual performance of the tourist area's environmental capacity is the number of tourists in the tourist destination. We use the amount of tourists as a quantitative indicator of the environmental capacity of tourist attractions, and reflect the evolution of environmental capacity sustainable development with changes in the amount of tourists.

In the TECC concept group, the environmental capacity of the tourist attraction is the value describing the supply quantity, and the actual visitor quantity (AVQ) is the value describing the demand quantity. The environmental capacity system is an open and complex giant system. The interaction of various subsystems within the giant system is to maintain the coordinated development of each subsystem. In view of the characteristics of the system of sustainable development of the environmental capacity system, the logistic equation can be used to describe the evolution mechanism of the system (as Figure 1 shows).

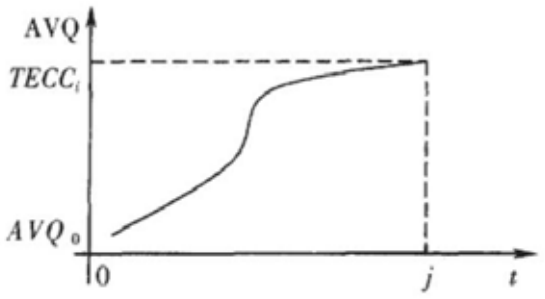

FIGURE 1
Logistic equation

Using AVQ(t) to indicate the development process of the system, the system development speed is $\frac{dAVQ}{dt}$, and the relative development speed is the environmental capacity required by AVQ due to the sustainable development of tourist attractions. The volume and resource capacity are limited, and the faster the development speed, the more prominent the resource scarcity, so that the relative development speed d $\frac{dAVQ}{dt} / dAVQ$ is the linear decreasing function of AVQ, that is, the following formula holds:

$$\frac{1}{AVQ} \times \frac{dAVQ}{dt} = R(t) - \frac{R(t)}{TECC} \times AVQ \quad (3)$$

The above formula is the general form of the Logistic model. Rewrite the above formula as:

$$\frac{dAVQ}{dt} = R(t) AVQ \left(1 - \frac{AVQ}{TECC_i(t)}\right) \quad (4)$$

Integrate the above formula:

$$AVQ(t) = \frac{TECC_j}{1 + c \times e^{-Rt}} \quad (5)$$

Where j = 1, 2, ..., t, represents the jth stage of the evolution of the environmental capacity system, R(t), $TECC_j$ respectively represent the growth rate required for development and the saturation capacity of the development factors. c is the integral constant. $c = \frac{TECC_j - AVQ_0}{AVQ_0} \langle 0$ and $TECC_j \rangle AVQ_0 \rangle 0$.

Where $TECC_j = \min(E_1, E_2, E_3, E_4, E_5, E_6, E_7, E_8, E_9, E_{10}, E_{11}, E_{12}) = \min(E_i)_1^{12} = \min\left(\frac{k_i}{1 + ce^{-r_i t}}\right)_1^{12}$, j=1, 2 , ..., t, i=1, 2,..., 12.

RESULTS AND DISCUSSION

Demand capacity state model based on sustainable bearer. According to formula (5) we can get:

$$ECCR_j = \frac{AVQ}{TECC_j} = \frac{1}{1 + c \times e^{-Rt}} \quad (6)$$

In the formula, the ECCR (Environment Continuble Capacity Rate) indicates the sustainable carrying rate.

In the short term, we assume that $TECC_j$ and R are fixed. According to formula (6) When the demand capacity AVQ in the tourist area increases to $TECC_j$ at this stage, the continued increase of tourists will pose a huge threat to the tourism environment. In order to achieve sustainable carrying of ECCR<1, we can maintain the tourist's aesthetic perception by adjusting the number of tourists, AVQ, to maintain a certain level of TECC for a certain period of time.

Development model based on sustainable bearer supply capacity. In the long run, TECC is dynamically adjusted with the change of period T. The values of TECC are different at different stages of development in the tourist area (as shown in Figure 2). The sustainable carrying dynamics of the tourist area can be achieved through the adjustment of the TECC.

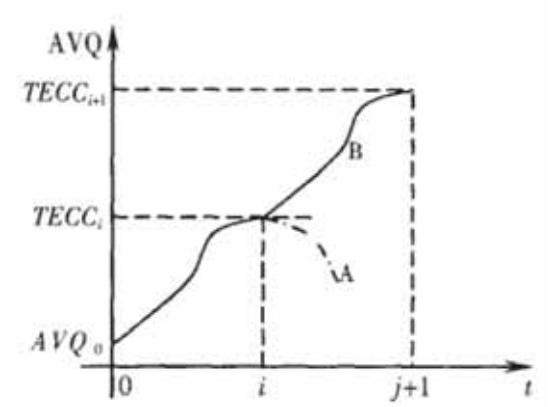

FIGURE 2
Different values of TECC at different stages of development in the tourist area

From Figure 2, we can see that when the AVQ in the tourist area increases to the TECC at this stage, ie AVQ=TECC and there is a trend greater than the current TECC, we must adjust the environmental capacity to achieve sustainable bearing of the scenic spot. From the formula $TECC_j = \min\left(\frac{k_i}{1+ce^{-r_i t}}\right)_1^{12}$, we know that the stage of the sustainable development period is positively correlated with the development speed of the minimum secondary component. In order to increase the environmental capacity of the tourist scenic spot, it is necessary to increase the development of the minimum secondary component. Speed, we can improve the supply capacity of environmental capacity through sustainable capacity, thereby increasing the development speed of the minimum secondary component, and making the environmental capacity jump from one level to the next, forming a composite logistic curve type sustainable development mode. Re-achieve the balance of supply and demand of environmental capacity, then ECCR ≤ 1, thus achieving sustainable carrying of environmental capacity.

CONCLUSION

This paper introduces the concept of sustainable development, perfects the evaluation index system of tourism environment capacity, analyzes the development law of each impact factor of tourism environmental capacity, establishes the state model of environmental demand capacity and the sustainable development dynamic model of supply capacity for demand capacity. . It should be pointed out that on the basis of the scholars' research on the previous environmental capacity concept system, the main limiting factors affecting the environmental capacity are comprehensively considered, and the model is associated with the “life cycle”, and the environmental capacity is in the tourist destination. Planning, construction and management have more theoretical guiding significance, and portray and promote the life cycle evolution of tourist attractions by the development of environmental capacity of tourist attractions, thus abandoning the traditional ideas of limiting tourism attractions to certain life cycle models. There is a certain practical significance.

REFERENCES

[1] Kiper, T., Uzun, O., Topal, T.U. (2016) A method approach for identifying thematic footpaths in ecotourism: Kiyikoy Pabucdere and Kazandere Basins. Fresen. Environ. Bull. 25, 6139-6150.
[2] Mayaka, M.A., Prasad, H. (2012) Tourism in Kenya: an analysis of strategic issues and challenges. Tour Manag Perspect. 1, 48-56.
[3] Liu, C., Li, J., Pechacek, P. (2013) Current trends of ecotourism in China's nature reserves: a review of the Chinese literature. Tour. Manag. Perspect. 7, 16-24.
[4] Lenao, M., Basupi, B. (2016) Ecotourism development and female empowerment in Botswana: a review. Tour. Manag. Perspect. 18, 51-58.
[5] Yu, H., Huang, Y., Ning, J., Zhu, B., Cheng, Y. (2014) Effect of cation exchange capacity of soil on stabilized soil strength. Soils and Foundations. 54, 1236-1240.
[6] Xu, F., Hu, B., Dou, Y., Song, Z., Liu, X. (2018) Prehistoric heavy metal pollution on the continental shelf off Hainan Island, South China Sea: From natural to anthropogenic impacts around 4.0 kyr BP. Holocene. 28, 455-463.
[7] Das, M., Chatterjee, B. (2015) Ecotourism: a panacea or a predicament? Tour. Manag. Perspect. 14, 3-16.
[8] Zhai, L., Li, S., Zou, B., Sang, H., Fang, X. (2018) An improved geographically weighted regression model for PM2.5 concentration estimation in large areas. Atmospheric Environment. 181, 145-154.
[9] Chiu, Y.-T.H., Lee, W.-I., Chen, T.-H. (2014) Environmentally responsible behavior in ecotourism: antecedents and implications. Tour. Manag. 40, 321-329.
[10] Cobbinah, P.B. (2015) Contextualizing the meaning of ecotourism. Tour. Manag. Perspect. 16, 179-189.
[11] Sayyed, M.R.G., Mansoori, M.S., Jaybhaye, R.G. (2013) SWOT analysis of Tandooreh National Park (NE Iran) for sustainable ecotourism. Proc. Int. Aca. Ecol. Environ. Sci. 3 (4), 296-305.

[12] Ghorbani, A., Raufirad, V., Rafiani, P., Azadi, H. (2015) Ecotourism sustainable develoipment strategies using SWOT and QSPM model: A case study of Kaji Namakzar Wetland, South Khorsan Province, Iran. Tour. Manag. Perspect. 16, 290-297.
[13] Santarem, F., Silva, R., Santos, P. (2015) Assessing ecotourism potential of hiking trails: a framework to incorporate ecological and cultural textures and seasonality. Tourism Manage Persp. 190-206.
[14] Nepal, S.K. (2004) Indigenous ecotourism in Central British Columbia: the potential for building capacity in the Tl'azt'en Nations Territories. J. Ecotourism. 3(3), 173-194.
[15] Santarem, F., Silva, R., Santos, P. (2015) Assessing ecotourism potential of hiking trails: a framework to incorporate ecological and cultural textures and seasonality. Tourism Manage Persp. 190-206.

Received: **04.12.2018**
Accepted: **13.03.2019**

CORRESPONDING AUTHOR

Rui Zhou
School of Management,
Chongqing College of Electronic Engineering,
Chongqing, 401331 – China

e-mail: 246604557@qq.com

© by PSP Volume 28 – No. 5/2019 pages 4297-4303 Fresenius Environmental Bulletin

FORMATION OF TRICHLORONITROMETHANE FROM ASPARTIC ACID DURING UV/CHLORINE DISINFECTION

Lin Deng[1,*], Beibei Liu[1], Xueying Liao[1], Wenquan Chen[2], Chaoqun Tan[1]

[1]Department of Municipal Engineering, Southeast University, Nanjing 210096, China
[2]Nanjing Hydrology and Water Resources Survey Bureau of Jiangsu Province, Nanjing 210008, China

ABSTRACT

The formation of trichloronitromethane (TCNM) was investigated during the chlorination of aspartic acid under low pressure (LP) UV irradiation (λ=254nm). LP UV/chlorine disinfection enhanced the formation of TCNM for the first instance, furthermore the concentration of TCNM increased by 10 times in 5 mins. Then, an obvious decrease was observed in the formation of TCNM, and TCNM was nearly undetectable after 22 min. The effects of light intensity, initial concentration of aspartic acid, pH value, free chlorine concentration and the addition of tertbutanol (TBA) on the formation of TCNM were also investigated under UV/chlorine condition. The formation of TCNM increases with the increase of pH value, UV light intensity, initial concentration of aspartic acid, free chlorine concentration. TBA has a minor effect on formation of TCNM in the solution containing aspartic acid under UV/chlorine condition. So hydroxyl radical doesn`t play a most important role in TCNM formation from aspartic acid under UV/chlorine. A possible integrated pathway of TCNM formation from aspartic acid is proposed under UV/chlorine. The new information obtained in this study will reduce the risk of TCNM formation during the treatment of drinking water and waste water. It will helpful for the control of TCNM formation in drinking water and sewage treatment and the development of new disinfection process.

KEYWORDS:
Trichloronitromethane, Formation, UV/chlorine Disinfection, Aspartic Acid

INTRODUCTION

With the wide use of chlorination or chloramination disinfection, more than 600 disinfection by-products (DBPs) have been identified in drinking water and sewage [1-2]. Among these DBPs, more attentions have been paid to nitrogenous disinfection by-products (N-DBPs) due to their wide distribution, high toxicity and potential risks to the safety of human health [3]. N-DBPs include haloacetonitriles (HANs), halonitromethanes (HNMs), and other unregulated DBPs such as haloacetamides (HAcAms) [3-5]. HNMs is a kind of highly toxic N-DBPs, which are stronger than the other controlled DBPs at present especially in cytogenetic toxicity and mutagenicity [2].

Trichloronitromethane (TCNM) is the earliest discovered HNMs as a typical representative of N-DBPs, which is the most common and dominant, being formed in disinfected waters [6]. TCNM is produced when free chlorine reacts with dissolved organic matter (DOM) in water [7]. In addition, TCNM increase significantly in drinking water when preozonation is followed by chlorination or chloramination. Moreover, TCNM formation will be promoted for the increase of bromine and pH value [8]. Dissolved organic nitrogen (DON) in drinking water increase with the increase of algal activity and sewage discharge, which can lead to the increase of TCNM [9]. Therefore, this study of TCNM is significant for understanding HNMs. However, the formation mechanism of TCNM is not very clear in drinking water containing aspartic acid [10].

In recent years, some researchers have investigated the TCNM formation potential when different precursors exist, and the influence of pH, chlorination ratio, nitrite concentration on TCNM formation were studied during the chlorination of phenolic compounds or humic substances and nitrites [11-13]. Some hypotheses of mechanism were put forward to explain the generation path of TCNM formation from Methylamine [13].

Due to increasingly stringent environmental regulations over DBPs and the chlorine resistant pathogen (e.g., *Cryptosporidium parvum*), the application of UV light for disinfection has accelerated in the United States. The number of using UV for primary disinfection has been raised significantly in drinking water plants, from only one in 1987 to more than 28 in 2010 [14-15]. UV lamps can control DNA repair and result in pathogen inactivation due to its polychromatic germicidal light in the range of 200 to 400 nm [16]. It is now clear that UV treatment will play a key action to meet new US regulations because the treatment is highly effective at inactivating pathogen and reducing chlorine doses. Because the use of UV disinfection in drinking water is a relatively recent trend, comparatively few studies have

been conducted to investigate the treatment's effect on DBPs formation either directly by UV irradiation or from subsequent chlorination or chloramination [17]. Some researchers found that UV treatment did not significantly affect THM and HAA formation from subsequent chlorination or chloramination [18-19], but a latter study by Lieu and colleagues [20] reported the increase of trihalomethanes (THMs) and haloacetic acids (HAAs), especially when MP UV was used. It was reported that the formation of TCNM could been enhanced by 550% in drinking waters containing nitrate when MP UV irradiation was followed by chlorination, but it did not affect haloacetonitriles formation [17]. Regardless of the effects on precursors for regulated DBPs, there are clear indications that UV can alter the structure and reactivity of NOM in measurable ways (e.g., formation of aldehydes and acids).

Amino acids are the most common (for about75%) nitrogen compounds in natural water [21]. Few studies focus on the formation and photodegradation of TCNM from amino acids under UV/chlorine. Aspartic acids was widely used in industry because it shows excellent performances including scale inhibition, corrosion inhibition, and biological degradation [27].In this paper, aspartic acid was used as a precursor to deeply analyze the influencing factors of the formation and degradation of TCNM in the process of UV/chlorine disinfection, and the formation and degradation characteristics of TCNM were discussed according to the related theories. It was expected that this study can provide an effective reference for industrial drinking water and sewage treatment process.

MATERIALS AND METHODS

Chemicals and reagents. The reagents used in this experiment were analytical reagent. All solutions were prepared by ultra pure water. The solution was controlled for pH 6–8 by 2 mM phosphate buffer during the reaction time. TCNM (CCl_3NO_2, 99%) and aspartic acid (99%) were purchased from Sigma-Aldrich. NaCl, TBA, NaOH and methy tert-butyl ether (MTBE) were purchased from the Xilong Chemical Company Limited. $Na_2O_3S_2$, Na_2HPO_4, NaH_2PO_4 and KNO_3 were purchased from Tianjin KeMiou Chemical Reagent Company Limited. TCNM was dissolved in MTBE for storage (at 2-8°*C*).

Experimental equipment and UV irradiation procedure. The irradiation experiments were carried out in a reaction equipment (20.0 cm length, 10.0 cm diameter, 1.0 cm wall thickness) with a UV lamp (2.0-10.0 Einstein·L^{-1}·s^{-1}, λ=254 nm, Changzhou Shangzi Lamp Co. Ltd, China) (see Figure 1). The reaction equipment was placed in cooling trap for maintaining a constant temperature (25±2**°*C***) by water circulation.

The reaction solution required for the experiment was prepared in a 500 mL brown flask and then poured reactive solution into the reactor under different experimental conditions. The reactive solution was rapid mixed by a magnetic stirrer. The UV lamp was stabilized about 30 min prior to its use for irradiation. The actual radiation intensity of the reaction equipment was measured by using potassium ferrioxalate as chemical actinometer. The actual UV radiation intensity was 2.88×10^{-6}, 5.92×10^{-6} and 9.62×10^{-6} Einstein·L^{-1}·s^{-1}, respectively when the radiated power of UV lamp was 5 W, 10 W and 15 W LPUV irradiation.

Analytical methods. In the experiments, the concentrations of TCNM were detected according to the USEPA 551.1 [22]. 5 mL samples were taken from the reaction equipment (Figure 1) at proper intervals (e.g. 1, 2, 5, 9, 15, 22 min). The first sample was taken out from reaction solution without LP UV irradiation after free chlorine was added into the solution containing aspartic acid for 1 min. Before analysis, excess sodium thiosulfate has been loaded to inhibit free chlorine. The samples were extracted with 2 mL MTBE for 10 min with a rocking bed. For TCNM analyses, the samples were taken 1 mL MTBE to the vial from the extracted solution, and analyzed using gas chromatography/electron capture detection (Agilent GC). 1mL sample was injected onto a HB-1 column (30 m×0.32 mm i.d. ×5 mm) via an on-column injector with an AS2000 liquid autosampler. The GC temperature program consisted of an initial temperature of 50 °*C* for 5min, followed by ramping up to 140 °*C* in 10°*C*/min, then ramping up to 280 °*C* in 20 °*C*/min. The injection port temperature was 235°*C* and the temperature of detector was 280°*C*. The injection volume carried a high purity nitrogen gas with 1.0 mL/min. The calibration curve equation for TCNM was Y_{Area}= 2.29E6+ 179729.50 C_{TCNM}, R = 0.9995 (n=6), where C_{TCNM} was the concentration of TCNM in the range of 0.0–300 μg/L. The standard error of analyses methods was 2.37 μg/L.

All vitreous apparatuses were dipped in water/HNO_3 (1:1) overnight and washed with distilled water, and then put them into a drying oven at 80 °*C*. All the experiments were triplicate. The experimental data were the mean values with an overall error less than 5%.

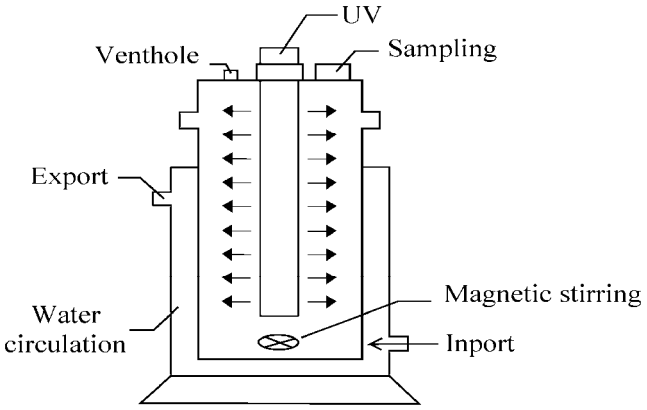

FIGURE 1
The reaction equipment of irradiation experiments

RESULTS AND DISCUSSION

Effects of UV light intensity on TCNM formation from aspartic acid under UV/ chlorine. To evaluate the effects of UV light intensity on TCNM formation from aspartic acid, a set of comparative experiments were conducted under UV/chlorine. The solution contained 1.5 mmol/L aspartic acid and 60mg/L free chlorine at pH 7.0 and 25 °*C* under 2.88×10^{-6} Einstein$L^{-1}s^{-1}$, 5.92×10^{-6} Einstein$L^{-1}s^{-1}$ and 9.62×10^{-6} Einstein$L^{-1}s^{-1}$ irradiation respectively. As shown in Figure 2, the concentration of TCNM remained only a minor increase from 2.3 to 4.0 μg/L in 22 minutes under chlorine alone. In contrast, under 2.88×10^{-6} Einstein$L^{-1}s^{-1}$, 5.92×10^{-6} Einstein$L^{-1}s^{-1}$ and 9.62×10^{-6} Einstein $L^{-1}s^{-1}$ irradiation and free chlorine, TCNM formation rose quickly to the maximum (61.3μg/L, 64.9 μg/L and 69 μg/L) at around 5 min, and then decreased gradually to finally reach a low level (<10 μg/L). Compared to the reaction without LP UV irradiation, TCNM formation from aspartic acid was produced more under UV/chlorine. The results showed that UV/chlorine could promote the production of TCNM from aspartic acid at the beginning, and when the TCNM formation was increased, the photodegradation of TCNM would occur simultaneously. At the same time, it showed that different light intensities have different effects on the formation of TCNM. The possible reason could be that the hydroxyl functional group on the aspartic acid side chain has high reactivity. In addition, the carboxyl functional group was prone to decarboxylation fracture during the reaction, and then reacted with chlorine to form TCNM.

From Figure 2, an interest phenomenon was found to have an obvious increasing trend in the formation of TCNM for the first instance, but the concentration of TCNM was nearly undetectable after 22 min. When the experiment was put under dark condition, the formation of TCNM was just a small amount. To evaluate the photodegradation of TCNM under UV irradiation, the experiments were carried out with four kinds of TCNM solutions with concentration of 50 μg/L, 100 μg/L, 200 μg/L and 300 μg/L under the conditions of pH=7, t=25 °*C*, 9.62×10^{-6} Einstein $L^{-1}s^{-1}$ irradiation. The experimental results were shown in Figure 3. When the concentration of TCNM was 50 μg/L, 100 μg/L, 200 μg/L and 300 μg/L, the degradation rate of TCNM was 80.58%, 75.33%, 72.14% and 69.89% after 60min respectively. When reaction solution containing 50.0 μg/L TCNM, the degradation rate of TCNM was 12.3% without LP UV irradiation after 60 min. From the experiment results the photodegradation rate of TCNM decreased with the increase of the initial concentration and increased with the increase of irradiation time.

Effect of aspartic acid initial concentration on the formation of TCNM under UV/chlorine. The experiments were carried out to investigate the effect of aspartic acid initial concentration on TCNM formation in an aqueous solution containing 60 mg/L free chlorine under the condition of pH=7, 25 °*C* and 9.62×10^{-6} Einstein L^{-1} s^{-1} irradiation. 1.0, 1.5 and 2.0 mmol/L aspartic acid were selected for the experiments. The results were shown in Figure 4. When 1.0 mmol/L aspartic acid was added into the solution under UV/chlorine, the concentration of formed TCNM rose from 2.67 to 52.93 μg/L in 5 min, and then dropped to 4.55 μg/L from 5 to 22 min; When 1.5 mmol/L aspartic acid was added into the solution under UV/chlorine, the concentration of forming TCNM rose from 3.27 to 69.02 μg/L in 5 min, and then dropped to 5.63 μg/L from 5 to 22 min; When 2.0 mmol/L aspartic acid was added into the solution under UV/chlorine, the concentration of forming TCNM rose from 1.05 to 77.51 μg/L in 5 min, and then dropped to 7.25 μg/L from 5 to 22 min. The experimental results showed that the formation of TCNM increased the increase of aspartic acid initial concentration under UV/chlorine.

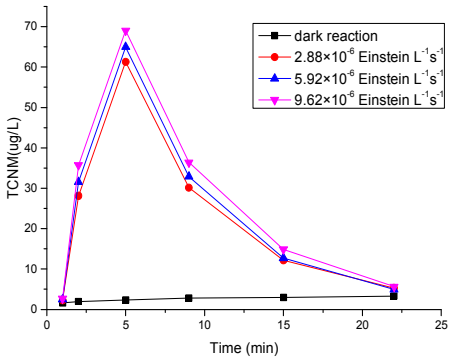

FIGURE 2
Effects of UV light intensity on the formation of TCNM

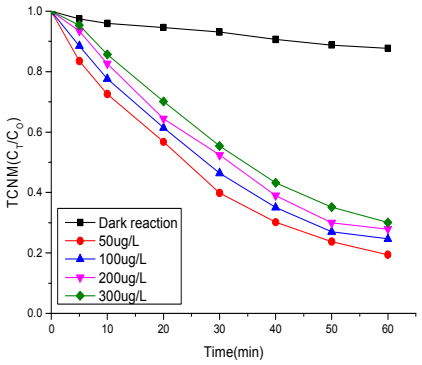

FIGURE 3
Degradation of TCNM in initial concentration under LP UV irradiation

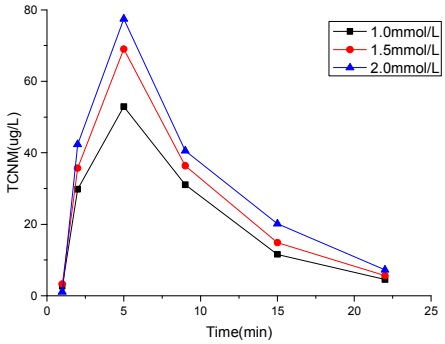

FIGURE 4
Effect of aspartic acid initial concentration on the formation of TCNM under UV/chlorine

Effect of pH on the formation of TCNM under UV/chlorine. The formation of TCNM can change on the influence of pH value which plays an important role in the actual water treatment process. Three pH value (pH=6.0, 7.0, 8.0) that closed to the natural water were selected to evaluate the effect pH on the formation of TCNM. The experiment was carried out in aqueous solution contained 1.5 mmol/L aspartic acid and 60mg/L free chlorine under 25 °*C* and 9.62×10^{-6} Einstein $L^{-1}s^{-1}$ UV irradiation. The experimental results were shown in Figure 5, the concentration of TCNM formation increased with the increase of pH. According to the results, the concentration of TCNM was highest at pH=8 and the peak value was 98.9 μg/L at the fifth minute. There are three reasons for this phenomenon. Firstly, nitro compounds are easier to produce halogenation reaction under alkaline conditions thus promoting the formation of TCNM [13]. Secondly, the presence of hypochlorite is different in different pH conditions in the process of chlorination. Because the pKa of HOCl is 7.52, HOCl existed mainly in acidic conditions while OCl^- mainly existed mainly in alkaline conditions. The oxidation ability and reaction characteristics of HOCl and OCl^- are different, which affect the TCNM formation from aspartic acid to a certain extent [23]. The OCl^- has a stronger oxidizing property so that the formation of TCNM produced more in alkaline conditions than in acidic conditions. Finally, because aspartic acid is acidic, the acidic functional side chains under alkaline conditions is much more active than under acidic or neutral conditions.

Effect of Free chlorine concentration on the formation of TCNM under UV/chlorine. Under UV/chlorine, free chlorine has a great influence on the formation of TCNM as oxidizing agent. In order to investigate the effects of free chlorine on the formation of TCNM, 15 mg/L, 30 mg/L, 45 mg/L, 60 mg/L and 75 mg/L free chlorine solution were selected to carry out the experiment under the condition of pH=7, t=25°*C* and 9.62×10^{-6} Einstein $L^{-1}s^{-1}$ irradiation. The experimental results were shown in Figure 6. When free chlorine was 15~30 mg/L, the concentration of TCNM was very little, almost could not be detected. When free chlorine were 45~75 mg/L, the concentration of TCNM rose very rapidly in the first instance. When free chlorine was 45 mg/L, 60 mg/L and 75 mg/L respectively, the concentration of TCNM reached the maximum in five minutes and the amounts of TCNM were 37.5 μg/L, 69 μg/L and 108.3 μg/L respectively. According to Hu's report, the formation of TCNM was a multi-step reaction [2].

When the concentration of free chlorine was low, free chlorine preferred reaction with amino acid and produced the organic chloramines. When the free chlorine was sufficient, the reaction would proceed to produce TCNM. So, when the free chlorine concentration was 15-30 mg/L, the formation concentration of TCNM was very little and could hardly be detected.

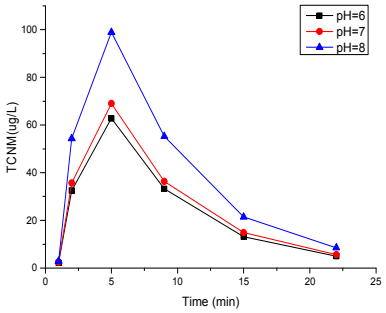

FIGURE 5
Effect of pH on the formation of TCNM under UV/chlorine

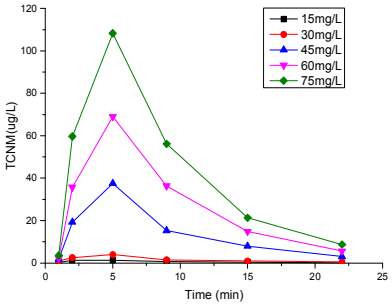

FIGURE 6
Effect of free chlorine concentration on the formation of TCNM under UV/chlorine

Effect of hydroxyl radical on the formation of TCNM under UV/ chlorine. To investigate the effect of hydroxyl radicals on the formation of TCNM under UV/ chlorine, the experiment was carried out with 1.5 mmol/L aspartic acid solution and free chlorine of 60mg/L (pH=7, t=25 °*C*). 2.0 g/L tert-butanol (TBA) was added into the reactive solution to evaluate the effect of hydroxyl free radical on the formation of TCNM. The experimental results were shown in Figure 7. Under the condition of 9.62×10^{-6} $EinsteinL^{-1}s^{-1}$ irradiation, TBA had a minor effect on the formation of TCNM. Without adding TBA, the maximum concentration of TCNM formation was raised to 69 μg/L in 5 min. After adding TBA, the maximum concentration of TCNM formation was only raised to 57.4 μg/L in 5 min and decreased by 11.4%. Therefore, it can be concluded that TBA inhibited hydroxyl radical, meanwhile indicating that hydroxyl radical did not play a dominant role in the formation of TCNM.

Proposed reactive pathways of TCNM formation from aspartic acid under UV/ chlorine. A proposed reactive pathway of TCNM formation from aspartic acid under UV/chlorine is shown in Figure 8. There are two possible pathways to explain the TCNM formation from aspartic acid under UV/chlorine. In the first pathway, the formation of TCNM mainly goes through HOOC-CH=NHCl, HOOC-CH=NCl_2 and CH_3-NO_2. The degradation of organic chloramines could lead to the formation of N-DBPs for the composition of -NHCl or -NCl_2 functional groups [24, 25]. Based on the formation of similar functional groups (-NHCl and -NCl_2) with or without UV irradiation, it was deduced that UV irradiation only changed the sidegroups (R) structure of aspartic acid. When the functional groups of aspartic acid are stripped of sidegroups (R), the suitable organic imines (HOOC-CH=NH_2 and -NH_2) were left in the reactive solution, especially -NH_2. And then those organic imines reacted with chlorine to form organic chloramines (HOOC-CH=NHCl and HOOC-CH=NCl_2). Those organic chloramines could further be oxidized to produce the group of -NO_2 and then lead to the formation of chloronitromethane (CNM), dichloronitromethane (DCNM) and TCNM and the other N-DBPs under UV/chlorine [13, 26]. In the second pathway, the formation of TCNM mainly goes through HOOC-CH=NH_2 and CH_3=NH_2. After UV irradiation, aspartic acid would produce imines (HOOC-CH=NH_2 and CH_3=NH_2) and then further be oxidized by free chlorine to form CNM, DCNM and TCNM [13, 24-26].

CONCLUSIONS

Amino acids are the most common containing DON in water, which have been proved to be the precursors of TCNM. In this study, aspartic acid was selected as the precursor to investigate the effects of pH value, free chlorine concentration, UV light intensity, free radical, TBA on the formation of TCNM. Firstly, under UV irradiation, the photodegradation rate of TCNM increased with the increase of exposure time and decreased the increase of TCNM initial concentration. Secondly, the concentration of TCNM formation increased with the increase of pH, aspartic acid initial concentration, free chlorine concentration and UV light intensity. It can be concluded that hydroxyl radical doesn't play a most important role in the formation of TCNM, because the addition of TBA has a minor effect on formation of TCNM from aspartic acid under UV/chlorine. Finally, a possible integrated pathway of TCNM formation from aspartic acid under UV/chlorine is proposed. The new information obtained in this study can contribute to the development of new source control strategies to reduce the risk of TCNM formation during the treatment of drinking water and wastewater.

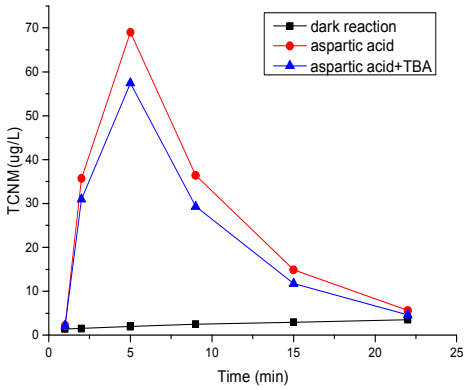

FIGURE 7
Effect of TBA on the formation of TCNM under UV/chlorine

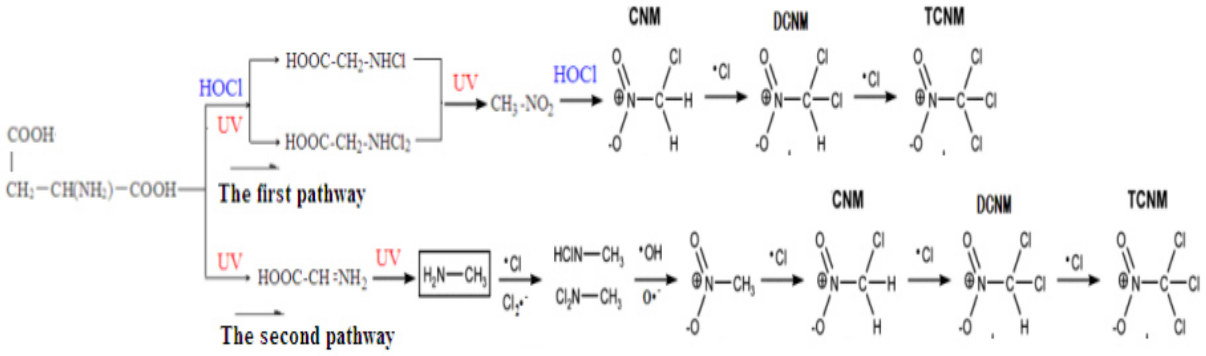

FIGURE 8
Proposed pathways of TCNM formation from aspartic acid under UV/chlorine.

However, the highest concentration of TCNM during UV/chlorine process would most likely happen within 5 min (at the beginning). The treatment measures of drinking water and wastewater were adjusted during UV/chlorine process. Reducing solution pH will help to cut down the formation of TCNM from aspartic acid. Treatment plants employing advanced oxidation processes, such as UV/chlorine, could also be at increased risk of TCNM formation due to generation of intermediates, but sufficient irradiation time was kept to minimize TCNM formation risk at during UV/chlorine process. At the same time TCNM precursors needed to be removed such as aspartic acid and algae organic matter as much as possible before the oxidation step.

ACKNOWLEDGEMENTS

This work was financially supported by the National Natural Science Foundation of China (No.21677032 and No.51608109) and the Natural Science Foundation of Jiangsu Province (BK20151401). Authors gratefully acknowledge the anonymous reviewers of this article.

REFERENCES

[1] Rook, J.J. (2002) Formation of haloforms during chlorination of natural water. Acta Polytechnica. 42(2), 234-243.

[2] Hu, J., Song, H., Addison, J.W., Karanfil, T. (2010) Halonitromethane formation potentials in drinking waters. Water Research. 44(1), 105-114.

[3] Weng, S.C., Blatchley, E.R. (2013) Ultraviolet-induced effects on chloramine and cyanogen chloride formation from chlorination of amino acids. Environment Science and Technology. 47(9), 4269-4276.

[4] Lee, W., Westerhoff, P. (2006) Dissolved organic nitrogen removal during water treatment by aluminum sulfate and cationic polymer coagulation. Water Research. 40(20), 3767-3774.

[5] Chu, W.H., Gao, N.Y., Deng, Y., Krasner, S.W. (2010) Precursors of dichloroacetamide, an emerging nitrogenous DBP formed during chlorination or chloramination. Environment Science and Technology. 44(10), 3908-3912.

[6] Merlet, N., Thibaud, H., Dore, M. (2015) Chloropicrin formation during oxidative treatments in the preparation of drinking water. Environment Science, Technology. 47, 223-228.

[7] Chu, W., Gao, N. (2008) Progress on research of nitrogenous disinfection by-products (Halonitromethanes) in drinking water. Water and Wastewater Engineering. 34(7), 34-46.
[8] Hu, J., Song, H., Karanfil, T. (2010) Comparative analysis of halonitromethane and trihalomethane formation and speciation in drinking water: the effects of disinfectants, pH, bromide, and nitrite. Environment Science and Technology. 44(2), 794-799.
[9] Dotson, A., Westerhoff, P., Krasner, S.W. (2009) Nitrogen enriched dissolved organic matter (DOM) isolates and their affinity to form emerging disinfection by-products. Water Science and Technology. 60(1), 135-143.
[10] Lu, J.F., Liu, F.C., Zhang, Z.F., Jin, C., Liu, X.C. (2015) Study on formation potential of typical nitrogenous disinfection byproducts TCNM in surface raw water. Journal of Water Resources and Water Engineering. 1, 8-11.
[11] Thibaud, H., Laat, J.D., Merlet, N., Dore, M. (1987) Chloropicrin formation in aqueous solution: effect of nitrites on precursors formation during the oxidation of organic compounds. Water Research. 21(7), 813-821.
[12] Thibaud, H., Laat, J.D., Dore, M. (1988) Effects of bromide concentration on the production of chloropicrin during chlorination of surface waters. Water Research. 22(3), 381-390.
[13] Joo, S.H., Mitch, W.A. (2007) Nitrile aldehyde and halonitroalkane formation during chlorination/chloramination of primary amines. Water Science and Technology. 41(4), 1288-1296.
[14] Hargy, T. (2002) Status of UV disinfection of municipal drinking water systems in North America. Water Conditioning and Purification Magazine. 44, 30–34.
[15] Dotson, A., Rodriguez, C.E., Linden, K.G. (2012) UV Disinfection implementation status in US water treatment plants. Journal American Water Works Association. 104(5), 77-78.
[16] Oguma, K., Katayama, H., Ohgaki, S. (2002) Photoreactivation of Escherichia coli after low- or medium-pressure UV disinfection determined by an endonuclease sensitive site assay. Applied and Environmental Microbiology. 68, 6029–6035.
[17] Reckhow, D.A., Linden, K.G., Kim, J., Shemer, H., Makdissy, G. (2010) Effect of UV treatment on DBP formation. Journal American Water Works Association. 102, 100–113.
[18] Liu, W., Andrews, S.A., Sharpless, C., Stefan, M., Linden, K.G., Bolton, J.R. (2002) Comparison of DBP formation from different UV technologies at bench scale. Water Science and Technology: Water Supply. 2(5/6), 515-521.
[19] Malley, J.P., Shaw, J.P. and Ropp, J.R. (1995) Evaluation of by-products produced by treatments in Ground waters with ultraviolet irradiation. AWWA RF and AWWA, Denver.
[20] Liu, W., Cheung, L.M., Yang, X., Shang, C. (2006) THM, HAA and CNCl formation from UV irradiation and chlor(am)ination of selected organic waters. Water Research. 40(10), 2033-2043.
[21] Hagedorn, F., Schleppi, P., Waldner, P., Flühler, H. (2002) Export of dissolved organic carbon and nitrogen from Gleysol dominated catchments - the significance of water flow paths. Biogeochemistry. 50(2), 137-161.
[22] USEPA (2006) National primary drinking water regulations: stage 2 disinfectants and disinfection byproducts rule; Final rule. Federal Register. 71-388.
[23] Shah, A.D., Mitch, W.A. (2011) Halonitroalkanes, halonitriles, haloamides and N-nitrosamines: a critical review of nitrogenous disinfection by-product formation pathways. Water Science and Technology. 46(1), 119-131.
[24] Morris, J.C. (1976) Kinetics of reactions between aqueous chlorine and nitrogen compounds. In: Faust, S.D., Hunter, J.V. (Eds.) Principles and Applications of Water Chemistry. John Wiley and Sons, New York. 23-53.
[25] Fang, J.Y., Yang, X., Ma, J., Shang, C., Zhao, Q.A. (2010) Characterization of algae organic matter and formation of DBPs from chlor(am)ination. Water Research. 44(20), 5897-5906.
[26] Yoon, J., Jensen, J.N. (1993) Distribution of aqueous chlorine with nitrogenous compounds: chlorine transfer from organic chloramines to ammonia. Water Science and Technology. 27(2), 403-409.
[27] Xu, Y., Zhang, B., Zhao, L.L., Cui, Y.C. (2013) Synthesis of polyaspartic acid/5-aminoorotic acid graft copolymer and evaluation of its scale inhibition and corrosion inhibition performance. Desalination. 311(1), 156–161.

Received: **10.12.2018**
Accepted: **27.03.2019**

CORRESPONDING AUTHOR

Lin Deng
School of Civil Engineering
Southeast University
Nanjing 210096 – China

e-mail: dlwhu@163.com

© by PSP Volume 28 – No. 5/2019 pages 4304-4310 Fresenius Environmental Bulletin

LEVELS OF MERCURY IN THREE SPECIES OF TUNA (*KATSUWONUS PELAMIS, AUXIS THAZARD* AND *EUTHYNNUS AFFINIS*) COLLECTED FROM THE JORDANIAN COAST OF THE GULF OF AQABA, RED SEA

Tariq Al-Najjar[1,*], Nashat Dahiyat[3], Nida Sharari[2], Mohammad Wahsha[2], Maroof Khalaf[1]

[1]Department of Marine Biology, The University of Jordan, Aqaba Branch, 77110, P.O. Box 263, Jordan
[2]Marine Science Station, The University of Jordan and Yarmouk University, 77110, P. O. Box 195 Aqaba, Jordan
[3]BenHayyan Aqaba International Laboratories, Aqaba Special Economic Zone Authority (ASEZA), 77110, P.O. Box 2565, Aqaba, Jordan

ABSTRACT

Level of mercury (Hg) heavy metal concentrations were investigated using Direct Mercury Analyzer (DMA) in muscles, liver, gills, gonads and kidney of three fish species (*Katsuwonus pelamis, Auxis thazard* and *Euthynnus affinis*) that were collected from the Jordanian coast of the Gulf of Aqaba, Red Sea during May to December 2015. Heavy metals accumulation varied significantly between organs, generally, the highest Hg concentrations were found in muscles of *K.pelamis, A.thazard* and *E.affinis* with an average 0.500, 0.354 and 0.244 µg/g respectively and the lowest concentrations were found in gills of *K.pelamis* with an average 0.113 µg/g and gonads of *A.thazard* and *E.affinis* with an average 0.140 µg/g and 0.110 µg/g respectively. The accumulation of heavy metals concentrations in the muscles than other organs is an indicator for clean, pollution-free environment. Strong positive correlations have been found between fish length and Hg concentrations. Levels of Hg in tuna fish muscles were within the acceptable limits for human consumption.

KEYWORDS:
Heavy metals, Fishes, Mercury, Aqaba, Red Sea

INTRODUCTION

Fish is widely consumed around the world by many people because it is a good source of protein, Omega-3 and unsaturated fatty acids [1, 2]. Fishes are rich in essential vitamins such as A, B3, B6, B12, and D, and the minerals such as calcium, iron, selenium, and zinc [1, 3, 4].

Fishes are the most significant source of mercury in human diets, and mercury levels in humans have been closely related to fish consumption [5]. Fish are often at the top of the aquatic food chain and may concentrate large amounts of some metals from water and food, therefore, metals bioaccumulate and biomagnified in different fish organs [6, 7, 8, 9].

Contamination of aquatic systems by heavy metals has become a global issue. Heavy metals may enter aquatic systems from different natural and anthropogenic (human activities) sources, including industrial or domestic wastewater, application of pesticides and inorganic fertilizers, storm runoff, leaching from landfills, shipping and harbor activities, geological weathering of the earth crust and atmospheric deposition [10, 11]. Many studies discover a vulnerability of the Gulf of Aqaba to metals pollution; these studies mention that the Gulf of Aqaba has a great probability to get polluted with heavy metals carried by air currents [12].

Several studies have been reported on the heavy metals in marine fish species collected from the Gulf of Aqaba [9, 13, 14, 15, 16, 17, 18, 19]. However, the levels of Hg in the fishes of the family Scombridae were not investigated previously. This study aims to provide knowledge and establish baseline data for the level of mercury in three common species belonging to the family Scombridae; *Katsuwonus pelamis*, *Auxis thazard* and *Euthynnus affinis* that are extensively consuming by locals.

MATERIALS AND METHODS

Study area. The study area lies within the Jordanian portion of the Gulf of Aqaba (Figure 1). It is a partially enclosed water body that constitutes the eastern segment of V-shaped situated at the northern tip of the Gulf and extends south for about 27 km to the Saudi Arabia border. It is located in a sub-tropical arid area between longitude 34° 25' to 35° 00' E and latitude 28°00' to 29°33' N. The Gulf of Aqaba is 180 km long and has a maximum width of 25 km, which decreases at the northern tip to about 5 km. The Gulf biodiversity is unique and some species are endemic to the area due to its semi-enclosed nature. It is connected to the Red Sea through the Straits of Tiran. It is more than 1,800 m deep (averaging 650 meters) [20, 21, 22].

Fish sampling and preparation. The total of 36 samples, twelve fish samples from each of the following species: *Katsuwonus pelamis, Auxis thazard* and *Euthynnus affinis* were collected from local fishermen during May to December 2015. Collected samples were immediately transported to the laboratory in ice boxes and allowed thawing and rinsed with distilled water. Muscle, liver, kidney, gonads and gills were taken out then five gram of each tissue were kept in deep freezer.

Samples Analysis. Samples were analyzed for Hg according to [23] method 7473 (SW-846). using Direct Mercury Analyzer (DMI) (Milestone - DMA-80, Italy).

Sample of 0.1 g dry weight from each organ were homogenized and weighted in sample boat (nickel boats was cleaned using a Muffle furnace at 600°C for 20 minutes). Duplicates, spiked samples, and check standards were analyzed with each patch of samples.

Samples from previous step were analyzed by located the sample boat in auto sampler tray of Direct Mercury Analyzer (DMI) instrument. Controlled heating in an oxygenated decomposition furnace was used to liberate mercury from samples in the instrument. Each sample was dried and then thermally and chemically decomposed within the decomposition furnace. The decomposition compounds were carried by flowing oxygen. Oxidation was completed and halogens and nitrogen/sulfur oxides were trapped. The remaining decomposition compounds were then carried to an amalgamator that selectively traps mercury. The amalgamator was rapidly heated, releasing mercury vapor. Flowing oxygen carried the mercury vapor through absorbance cells positioned in the light path of a single wavelength atomic absorption spectrophotometer. Absorbance (peak height or peak area) was measured at 253.7 nm as a function of mercury concentration.

Statistical Analysis. A non-parametric test (Kruskal Wallis test) was performed to examine significant differences for Hg among species and organs.

RESULTS

Heavy metals concentration among Scombridae fish species. The mean values of Mercury concentrations in muscles of different fish species (*K.pelamis, A.thazard* and *E.affinis*) showed significant differences ($p = 0.0002$). The highest Hg concentration was found in *K.pelamis* with mean value of (0.318 µg/g), followed by *A.thazard* (0.240 µg/g) and *E.affinis* (0.169 µg/g), (table 1) showed the mean + SE of Hg concentration in muscles of three fish species.

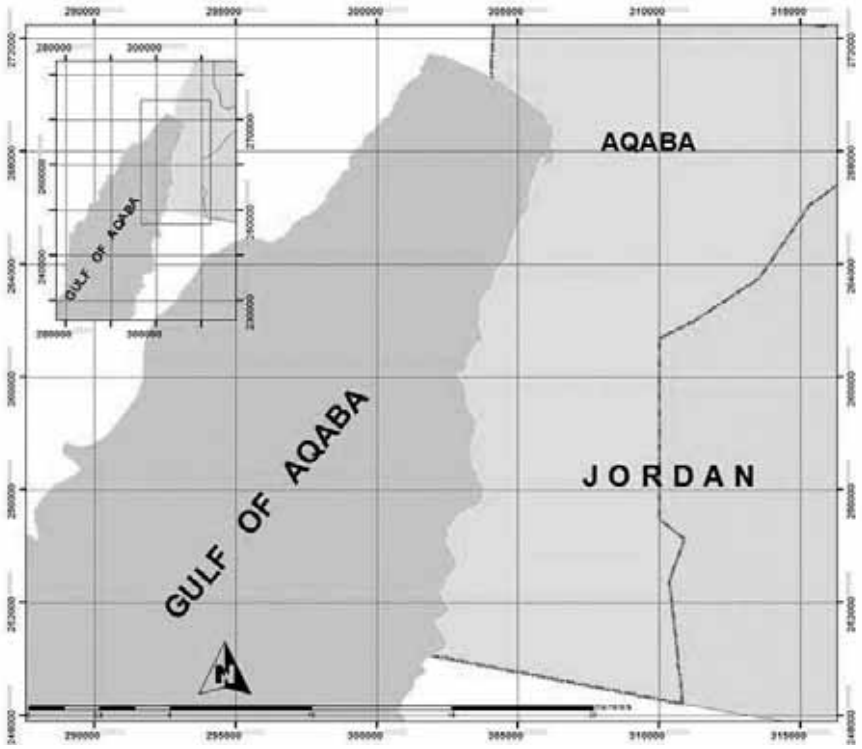

FIGURE 1
Study area in the northern Gulf of Aqaba

TABLE 1
Mean ± SE of Hg concentrations in the muscles for *K.pelamis*, *A.thazard* and *E.affinis* collected from the Jordanian coast of the Gulf of Aqaba, Red Sea

Fish species	Mean (µg/g) ± SE
K.pelamis	0.318 ± 0.026
A.thazard	0. 240 ± 0.015
E.affinis	0.169 ± 0.009

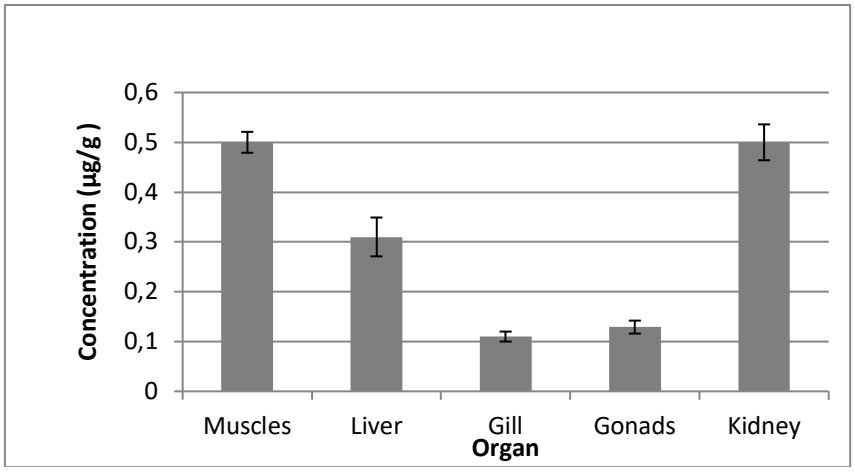

FIGURE 2
Mean concentration µg/g ± SE of Hg in different organs of *K pelamis*

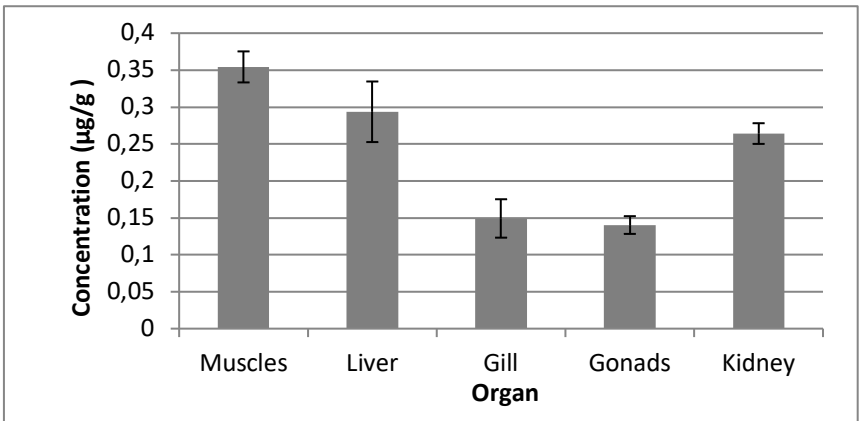

FIGURE 3
Mean concentration µg/g ± SE of Hg in different organs of *A. thazard*

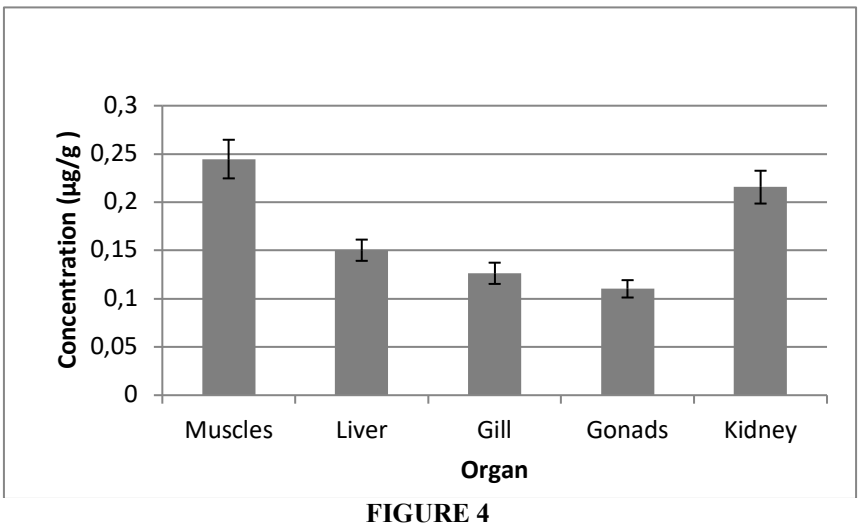

FIGURE 4
Mean concentration µg/g ± SE of Hg in different organs of *E. affinis*

TABLE 2
The correlation coefficient (R^2) and Probability test (P-value) between fish length of *K. pelamis*, *A. thazard* and *E. affinis* and final metal concentrations

	K. pelamis	*A. thazard*	*E. affinis*
R^2	0.058	0.8711	0.8551
P-value	0.4506	< 0.0001	< 0.0001

Mercury concentration among different fish organs of fish species. Results of Hg concentrations (µg/g) between different organs of *K. pelamis* were significantly different ($P < 0.0001$). Muscles and kidney showed the highest mean concentration with mean value of 0.500 µg/g each, among all organs, while the gills had the lowest mean value with 0.113 µg/g (dw) as shown in Figure 2.

Results of Hg concentrations (µg/g) between different organs of *A. thazard* was significantly different ($P < 0.0001$). Muscles had the highest mean concentration among all organs with 0.354 µg/g (dw), followed by liver with 0.293 µg/g (dw), while the gonads had the lowest concentration with 0.140 µg/g (dw) as shown in Figure 3.

Results of Hg concentrations (µg/g) between different organs of *E. affinis* was significantly different ($P < 0.0001$), muscles had the highest mean concentration among all organs with 0.244 µg/g (dw), followed by kidney with 0.215 µg/g (dw), while the gonads had the lowest concentration value with 0.110 µg/g (dw) as shown in Figure 4.

Effect of fish length on Hg concentrations. The results showed that there was a strong positive correlation between Hg and the body length of *A. thazard* and *E. affinis* with $R^2 = 0.8711$ and 0.8551 respectively, whereas, weak correlation for *K.pelamis*. The correlation coefficient (R^2) and P-value between fish length and Hg concentrations.

DISCUSSION

The results of this study showed that there were significant differences between the three fish species *K. pelamis, A. thazard* and *E. affinis* for Hg concentration, this difference could be related to differences in each species physiology, feeding rate, growth rate, life pan, migratory patterns, foraging habits and/or diet [24]. Similar pattern was reported on toxic metals in Italian fresh and canned tuna [25, 26].

The results of this study revealed that Hg concentrations in muscles of *K pelamis*, *A thazard* and *E affinis* fishes were higher than other organs such as liver, gills, gonads and kidney. Similar results were found on comparison and bio-monitoring of Hg heavy metal concentrations in fishes from uncontaminated and contaminated localities [27], they found that Hg concentration in muscles was higher than internal organs in uncontaminated localities, the Hg concentrations were found in the following pattern: muscle > kidney > liver > gonads, this could be because methyl-mercury in adult fishes is more than 90% of total mercury which is primarily found in the fish muscles tissue bound to protein molecules [4, 28, 29], in addition to the distribution of heavy metals in fish organs depends on the degree of contamination of the environment. In Hg-polluted locations, Hg concentrations in internal organs are usually significantly higher than Hg concentrations in muscles, whereas Hg concentration in muscles of fishes captured from uncontaminated localities is usually higher than that found in their internal organs [27], and this finding show clearly proofed that Aqaba marine water is clean and uncontaminated.

Results of this study showed clearly that muscles accumulate more Hg than other organs, this may be due to the long migrations made by these species and to their feeding habits as they are the top predators and occupy the highest level in the food chain. [30] showed that the predatory fish belonging to the higher trophic levels accumulate more Hg than the benthic and planktonophagous species because it is known that the accumulation of Hg is dependent on the length of the food chain. The highest values of Hg in muscles of piscivorous species, and the lowest concentration in muscle tissue of fish feeding invertebrate were observed by [31]. [32] studied Hg concentration in the muscles of pelagic fish species from the Bay of Bengal, and found that Hg concentration for these tuna species are in the following order *K. pelamis* > *A. thazard* > *E. affinis*. Similar pattern for Hg concentration was found in the present study. During the present study, muscles of *K. pelamis* contained Hg above the maximum allowable concentration set by Jordanian standards [33], Australian and New Zealand standards [34] and below the maximum allowable concentration in Canada [35], Finland [34] standards (Table 3). None of the muscles samples of *A. thazard* and *E. affinis* fishes contained Hg above the maximum allowable concentration of the above mentioned standards. Similar and even higher concentrations of Hg were estimated by [36, 37, 38, 39] who found that the concentration of Hg in muscles of tuna is higher than other organs.

The results of this study showed a strong positive correlation between Hg and the fish length of *A. thazard* and *E. affinis*, whereas there was a weak positive correlation between Hg and length of *K. pelamis*. This is in accordance with the studies of [42, 43] in which they found a correlation between Hg heavy metal concentration and fish length. This could be attributed to the specific bio-affinity for

organic matter of CH_3Hg with a high biological half-life, which generally constitutes the dominant pool of the total Hg in the fish muscle. The results of this study was in disagreement with the investigations of [44, 45].

TABLE 3
Hg heavy metal Standards in different countries in fishes (ppm)

Standards	Hg (ppm)	Reference
Jordan	0.5	[33]
Canada	1.0	[35]
EC	1.0	[40]
Australia	0.5	[41]
Finland	1.0	[34]
New Zealand	0.5	[34]
FDA	1.0	[34]

CONCLUSIONS

Results show that heavy metals concentrations were higher in muscles of the studied species than other internal organs. Hg concentration was higher in the muscles of *K. pelamis, A.thazard* and *E.affinis*, and this is an indicator for clean, pollution-free environment. Positive correlations were found between body length and Hg metal concentration for all studied fishes. Levels of Hg heavy metals in tuna fish muscles were within the acceptable limits for human consumption set by Jordanian, Canadian, European, Australian, New Zealand and Finland standards.

AKNOWLEDGEMENTS

The authors would like to thank Dr. Montaser Al-Mansi, Dr. Abdulmajid Al-Ajlouni, Khaldon Alkhudari, Mohammad Abu-ghregeneh for their great help in sample collection. Special thanks for Jordan Food and Drug Administration (JFDA) for their co-operation during analysis, particularly Eng. Mahmoud Mustafa and Mrs. Jumana. We would like to thank the UNDP for funding this research.

REFERENCES

[1] U.S. Department of Agriculture and U.S. Department of Health and Human Services. (2010) Dietary Guidelines for Americans 2010. Washington, D.C.: US Government Printing Office. 7th Edition.

[2] Krauss, R.M., Eckel, R.H., Howard, B., Appel, L.J., Daniels, S.R., Deckelbaum, R.J., Erdman, J.W., Kris-Etherton, P., Goldberg, I.J., Kotchen, T.A., Lichtenstein, A.H., Mitch, W.E., Mullis, R., Robinson, K., Wylie-Rosett, J., Jeor, S., Suttie, J., Tribble, D.L., Bazzarre, T.L. (2000) AHA dietary guidelines revision 2000: a statement for healthcare professionals from the Nutrition Committee of the American Heart Association. Circulation. 102(18), 2284-2299.

[3] Ikem, A. and Egiebor, N.O. (2005) Assessment of trace elements in canned fishes (Mackerel, Tuna, Salmon, Sardines and Herrings) marketed in Georgia and Alabama (United States of America). Journal of Food Composition and analysis. 18, 771-787.

[4] EPA- United States Environmental Protection Agency. (2001) Mercury Update: Impact on Fish Advisories. EPA-823-F-01-011. Office of Water, Washington, D.C.

[5] Yamashita, Y., Omura, Y., Okazaki, E. (2005) Total mercury and methylmercury levels in commercially important fishes in Japan. Fisheries Science. 71(5), 1029-1035.

[6] Mansour, S.A. and Sidky, M.N. (2002) Eco toxicological studies.3. Heavy metals contaminating water and fish from Fayoum Governorate. Egypt. Food Chemistry. 78, 15-22.

[7] Burger, J., Gaines, K.F., Shane Boring, C., Stephens, W.L., Snodgrass, J., Dixon, C. (2000) Metal levels in fish from the Savannah river: Potential hazards to fish and other receptors. Environmental Research. 89, 85-97.

[8] Hadson, P.V. (1988) The effect of metabolism on uptake, deposition and toxicity in fish. Aquatic Toxicology. 11, 3-18.

[9] Wahbeh, M.I. (1985) Levels of zinc, iron, magnesium and cadmium in the tissue of fish from Aqaba, Jordan. Dirasat. 12, 35-42.

[10] Yilmaz, F. (2009) The Comparison of Heavy Metal Concentrations (Cd, Cu, Mn, Pb, and Zn) in Tissues of Three Economically Important Fish (*Anguilla anguilla*, *Mugil cephalus* and *Oreochromis nilo*ticus) Inhabiting Köycegiz Lake-Mugla (Turkey). Turkish Journal of Science and Technology. 4(1), 7-15.

[11] Freedman, B., Hutchinson, T.C. (1981) Sources of metal and elemental contamination of terrestrial environments. In: Effect of heavy metal pollution on plants. Springer Netherlands. 35-94.

[12] Chen, Y., Paytan, A., Chase, Z., Measures, C., Beck, A., Sergio, A., Wilhelmy, S., Post, F. (2008) Sources and fluxes of atmospheric trace elements to the Gulf of Aqaba, Red Sea. Journal of Geophysical Research. 113, 1-13.

[13] Abu-Hilal, A., Badran, M., de Vaugelas, J. (1988) Distribution of trace elements in *Callichirus laurae* burrows and nearby sediments in the Gulf of Aqaba, Jordan (Red Sea). Marine Environmental Research. 25(4), 233-248.

[14] Abu-Hilal, A.H., Badran, M.M. (1990) Effect of pollution sources on metal concentration in sediment cores from the Gulf of Aqaba (Red Sea). Marine Pollution Bulletin. 21(4), 190-197.

[15] Khalaf, M.A., Al-Najjar, T., Alawi, M. and Disi, A.A (2012) Levels of trace metals in three fish species *Decapterus marac*ellus, *Decapterus macrosoms* and *Decapterus russelli* of the family carangidae from the Gulf of Aqaba, Red Sea, Jordan. Natural Science. 4(6), 362-367.

[16] Khalaf, M.A., Alawi, M., Al-Zgool, A., Al-Najjar, T. (2013) Levels of trace metals in the bigeye hound deep sea shark *Iago omanensis* from the Gulf of Aqaba, Red Sea. Fresen. Environmen. Bull. 22, 3534-3540.

[17] Al-Najjar, T., Abu Khadra, K., Rawashdeh, O.Y., Khalaf, M. and Wahsha, M. (2015) Levels of Trace Metals in (*Euthynnus affinis*) Fish from the Gulf of Aqaba, Jordan. Fresen. Environ. Bull. 24, 2995-3000.

[18] Al-Najjar, T., Al-Momani, R., Khalaf, M., Wahsha, M., Sbaihat, M., Khalaf, N., Khadra, K., Magames, H. (2016) Levels of Heavy Metals in Fishes (*Cheilinus trilobatus*) from the Gulf of Aqaba, Jordan. Natural Science. 8, 256-263.

[19] Wahbeh, M.I. and Mahasneh, D. (1987) Concentrations of metals in the tissues of six species of fish from Aqaba, Jordan. Dirasat. 14, 316-326.

[20] ISPAN Irrigation Support Project for Asia and Near East, prepared for US Agency for international development, October (1992) Gulf of Aqaba Environmental Data Survey.

[21] UNEP/IUCN (1988) Coral reefs of the world. UNEP Regional Sea Directories and Bibliographies. IUCN, Gland, Switzerland and Cambridge, UK/UNEP, Nairobi, Kenya.

[22] Hulings, N.C. (1989) A review of the marine science research in the Gulf of Aqaba. Publication of the Marine Science Station, Aqaba-Jordan.

[23] EPA- United States Environmental Protection Agency. (2007) Mercury in Solids and Solutions By Thermal Decomposition, Amalgamation, and Atomic Absorption Spectrophotometry. Method 7473 (sw-846). Available online: https://www.epa.gov/sites/production/files/2015-07/documents/epa-7473.pdf

[24] Kojadinovic, J., Potier, M., Le Corre, M., Cosson, R.P., Bustamante, P. (2006) Mercury content in commercial pelagic fish and its risk assessment in the Western Indian Ocean. Science of the Total Environment. 366(2), 688-700.

[25] Storelli, M.M., Barone, G., Cuttone, G., Giungato, D., Garofalo, R. (2010) Occurrence of toxic metals (Hg, Cd and Pb) in fresh and canned tuna: public health implications. Food and chemical toxicology. 48(11), 3167-3170.

[26] Abolghait, S.K., Garbaj, A.M. (2015) Determination of cadmium, lead and mercury residual levels in meat of canned light tuna (*Katsuwonus pelamis* and *Thunnus albacares*) and fresh little tunny (*Euthynnus alletteratus*) in Libya. Open veterinary journal. 5(2), 130-137.

[27] Havelková, M., Dušek, L., Némethová, D., Poleszczuk, G., Svobodová, Z. (2008) Comparison of mercury distribution between liver and muscle–a biomonitoring of fish from lightly and heavily contaminated localities. Sensors. 8(7), 4095-4109.

[28] Bloom, N.S. (1992) On the chemical form of mercury in edible fish and marine invertebrate tissue. Canadian Journal of Fisheries and Aquatic Sciences. 49(5), 1010-1017.

[29] Kim, J.P. (1995) Methylmercury in rainbow trout (Oncorhynchus mykiss) from Lakes Okareka, Okaro, Rotomahana, Rotorua and Tarawera, North Island, New Zealand. Science of the Total Environment. 164(3), 209-219.

[30] Luczynska, J., Brucka-Jastrzębska, E. (2006) Determination of heavy metals in the muscles of some fish species from lakes of the north-eastern Poland. Pol. J. Food Nutr. Sci. 15(2), 141-146.

[31] Amundsen, P.A., Staldvik, F.J., Lukin, A.A., Kashulin, N.A., Popova, O.A., Reshetnikov, Y.S. (1997) Heavy metal contamination in freshwater fish from the border region between Norway and Russia. Science of the Total Environment. 201(3), 211-224

[32] Penjai, S., Jinnathum, H., Somjet, S., Montri, S., Rankiri, K.J (2008) An assessment of mercury concentration in fish tissues caught from three compartments of Bay of Bengal. Thailand. The ecosystem based fishery management in the Bay of Bengal. Available online: http://map.seafdec.org/downloads/BIMSTEC/020-Mercury-Penjai.pdf

[33] Jordan Institution for Standards and Metrology. (2002) Fish and fish products - Fresh chilled fish. Number 1481/2002. Available online: http://www.jsmo.gov.jo/en/Pages/New-Standards-Technical-Regulations.aspx

[34] FAO- Food and Agriculture Organization. (1983) Compilation of legal limits for hazardous substances in fish and fishery Products. Available online: http://www.fao.org/docrep/014/q5114e/q5114e.pdf (Accessed 28 May 2013).

[35] CFIA - Canada Food Inspection Agency. (2014) Canadian Guidelines for Chemical Contaminants and Toxins in Fish and Fish Products. Available online: http://www.inspection.gc.ca/food/archived-food-guidance/fish-and-seafood/manuals/standards-and-methods/eng/1348608971859/1348609209602?chap=7.
[36] Licata, P., Trombetta, D., Cristani, M., Naccari, C., Martino, D., Caló, M., Naccari, F. (2005) Heavy metals in liver and muscle of bluefin tuna (*Thunnus thynnus*) caught in the straits of Messina (Sicily, Italy). Environmental monitoring and assessment. 107(1-3), 239-248.
[37] Barak, N.E., Mason, C.F. (1990) Mercury, cadmium and lead concentrations in five species of freshwater fish from eastern England. Science of the Total Environment. 92, 257-263.
[38] Goldstein, R.M., Brigham, M.E., Stauffer, J.C. (1996) Comparison of mercury concentrations in liver, muscle, whole bodies, and composites of fish from the Red River of the North. Canadian Journal of Fisheries and Aquatic Sciences. 53(2), 244-252.
[39] Srebocan, E., Pompe-Gotal, J., Prevendar-Crnic, A., Ofner, E. (2007) Mercury concentrations of captive Atlantic blue-fin tuna (*Thunnus thynnus*) farmed in the Adriatic Sea. Veterinarni Medicina-Praha. 2(4), 175.
[40] Commission Regulation (EC) No 629/2008 of 2 July 2008 amending Regulation (EC) No 1881/2006 setting maximum levels for certain contaminants in foodstuffs. Official Journal of the European Union. Available online: https://www.fsai.ie/uploadedFiles/Commission_Regulation_EC_No_629_2008.pdf.
[41] Australia New Zealand Food Standards Code, (2011) Standard 1.4.1 Contaminants and Natural Toxicants. Available online: http://www.inspection.gc.ca/DAM/DAM-food-aliments/STAGING/texttexte/fish_man_standardsmethods_appendix3_1406403090196_eng.pdf.
[42] Szefer, P., Domagała-Wieloszewska, M., Warzocha, J., Garbacik-Wesołowska, A., Ciesielski, T. (2003) Distribution and relationships of mercury, lead, cadmium, copper and zinc in perch (*Perca fluviatilis*) from the Pomeranian Bay and Szczecin Lagoon, southern Baltic. Food Chemistry. 81(1), 73-83.
[43] Kumar, M., Aalbersberg, W.G., Mosley, L. (2004) Mercury levels in Fijian seafood and potential health implications. Report for World Health Organisation. Technical Report No. 2004/03. Suva, Fiji: Institute of Applied Science. 2004, 1-33.
[44] Endo, T., Hisamichi, Y., Haraguchi, K., Kato, Y., Ohta, C., Koga, N. (2008) Hg, Zn and Cu levels in the muscle and liver of tiger sharks (Galeocerdo cuvier) from the coast of Ishigaki Island, Japan: relationship between metal concentrations and body length. Marine Pollution Bulletin. 56(10), 1774-1780.
[45] Gaspic, Z.K., Zvonarić, T., Vrgoč, N., Odžak, N., Barić, A. (2002) Cadmium and lead in selected tissues of two commercially important fish species from the Adriatic Sea. Water Research. 36(20), 5023-5028.

Received: **18.12.2018**
Accepted: **18.03.2019**

CORRESPONDING AUTHOR

Tariq Al-Najjar
Department of Marine Biology,
The University of Jordan,
77110, P.O. Box 263
Aqaba Branch – Jordan

e-mail: t.najjar@ju.edu.jo

© by PSP Volume 28 – No. 5/2019 pages 4311-4319 Fresenius Environmental Bulletin

CHARACTERISTICS OF NITROGEN CHANGES IN HYDROLOGICAL PROCESSES OF *PINUS DENSATA* FOREST IN SEJILA MOUNTAIN

Jie Lu[1,2,*], Xiaoqin Tang[2,3], Jiangrong Li[1,2], Jiangping Fang[1,2], Weilie Zheng[1,2]

[1]Res. Institute of Tibet Plateau Ecology, Tibet Agriculture & Animal Husbandry University, 860000 Nyingchi, Tibet
[2]Key Laboratory of Forest Ecology in Tibet Plateau (Tibet Agriculture & Animal Husbandry University), Ministry of Education, 860000 Nyingchi, Tibet
[3]Plant Sciences College, Tibet Agriculture & Animal Husbandry University, 860000 Nyingchi, Tibet

ABSTRACT

Observations and sampling of atmospheric rainfall, through fall, and trunk stem-flow in the *Pinus densata* forests of Sejila Mountain were conducted. Samples of different forms of N and their contents and inputs were measured and analyzed. The results showed that from April to October, the total amount of atmospheric rainfall was 725.8 mm, the total through fall was 533 mm, and the total trunk stem-flow was 34.8 mm. The variation with the month showed a single-peak type. The relationship between trunk stem-flow and atmospheric rainfall was $y=1.7103x^{0.7869}$ ($R^2=0.9674$), and the relationship between through fall and atmospheric rainfall was: $y=0.413x^{1.121}$ ($R^2=0.9901$). Monthly average concentrations of atmospheric rainfall were 0.4023 mg/L (NO_3^--N), 1.8779 mg/L (TN), 1.2141 mg/L (TON), and 0.2615 mg/L (NH_4^+-N), respectively. The monthly mean concentrations in the through fall were 0.2367 mg/L (NH_4^+-N), 0.4185 mg/L (NO_3^--N), 1.1891 mg/L (TON), and 1.8443 mg/L (TN), respectively. The mean monthly concentrations in trunk stem-flow were 0.2724 mg/L (NH_4^+-N), 0.4173 mg/L (NO_3^--N), 1.2617 mg/L (TON), and 1.9514 mg/L (TN), respectively. Fitting analysis found that atmospheric rainfall had good correlation with the four N component concentrations, and the correlation between through fall and NH_4^+-N was not obvious, and correlated well with the other three, trunk stem flow and concentration of four components the relationship between them was not obvious. In various forms of rain, the correlation between pH value and TN concentration was significant. From April to October, the TN input amount of atmospheric rainfall was 12.3098 kg/hm^2, among which the input amount was more TON, which was 7.9710 kg/hm^2, which accounted for 64.75%. The input amounts of NO_3^--N and NH_4^+-N were 2.5475 kg/hm^2, 1.7914 kg/hm^2, respectively. Accounting for 20.69% and 14.55%, respectively. The input amount of nutrient through fall was 9.5050 kg/hm^2, and the input amount of TON, NO_3^--N and NH_4^+-N accounted for 64.57%, 21.99% and 13.46%, respectively. Trunk stem flow input amount was relatively low, 0.5966 kg/hm^2, and the three inputs accounted for 64.83%, 20.14%, and 15.03%, respectively. After the atmospheric rainfall passing through the canopy and trunk of the *P. densata* forest, the net TN leaching amount was -2.2082 kg/hm^2.

KEYWORDS:
Pinus densata forest, Hydrological process, Nitrogen element, Variation characteristics, Sejila Mountain

INTRODUCTION

Atmospheric nitrogen settlement is an important source of nitrogen in natural ecosystems [1]. The increase in settlement will inevitably affect the biogeochemical cycle of natural ecosystems [2]. N-elements, as a large number of essential elements for plant growth, which are essential for the material circulation process in the ecosystem. Atmospheric rainfall is an important medium in the N-element recycling process. The amount of precipitation, precipitation frequency, and precipitation intensity have a direct effect on the amount and degree of trunk stem flow [3]. Through fall and trunk stem-flow are the precipitation of atmospheric rainfall through the forest canopy, which is an important factor in the nutrient balance of the forest ecosystem, and directly affect the water distribution and nutrient recycling of the forest soil [4-6]. Therefore, the quantitative assessment of nitrogen settlement fluxes in through fall and trunk stem flow is the key to studying the forest ecosystems' acceptance of atmospheric nitrogen settlement, and it is the prerequisite for understanding the feedback mechanism of forest ecosystems to atmospheric nitrogen settlement [7]. At present, there have been relevant reports on the changes characteristics of nitrogen concentration in atmospheric rainfall, through fall, and trunk stem-flow in different forest areas [8-14]. However, due to the differences in space-time and research objects, the research results are varied.

Pinus densata is a pine plant and endemic to China. Distributed in Yunnan, Sichuan, Tibet,

Qinghai, and other places, it grows in river valleys, hillsides, forests, valleys, and sunny slopes at altitudes of 1500 to 4500 m. It has been artificially introduced and cultivated [15]. So far, researches on *P. densata* mainly focus on the development and utilization of *P. densata* resources and turpentine[16], the distribution pattern of *P. densata* [17-18], the development and research of *P. densata* cauliflower industry[19], and natural regeneration characteristics of *P. densata* forests [20-22], investigation and analysis of understory combustible resources [23], natural vegetation restoration process in burned areas of *P. densata* forests [24], and climate and molecular ecology [25-29]. However, there are relatively few researches on the hydrological ecological benefits and ecological environment of *P. densata*. In addition, the characteristics of N-variation in the hydrological processes of the Sejila Mountain pine forest in Tibet studied in this paper are rarely reported [30-31]. It can be said that the study is in its infancy. Tibet is located on the "roof of the world" and has a unique geographic unit and climate zone. The ecological environment is inherently fragile. The forests of the Tibetan Plateau are mainly dominated by virgin forests, and the forests are distributed in the alpine valleys. These forests play an important role in conserving water sources, maintaining water and soil, preventing flooding, and purifying water quality [15]. In this paper, the characteristics of nitrogen changes in the hydrological process of *P. densata* forest were studied in order to provide a theoretical basis for the protection and management of *P. densata* water conservation forest, and lay the foundation for further exploration of the hydrological process of *P. densata* forest.

EXPERIMENTAL

Research Area Situation. The research area is located in Tibet's Sejila Mountain, where the national field scientific observation and research station of the Nyingchi Alpine Forest Ecosystem in Tibet. It is the center of the forest in the southeast of Tibet and is also a region with extremely special and diverse natural environments. This area is a typical sub-humidity semi-humid climate zone, with warm winter and cool summer, and distinct wet and dry seasons. The annual average temperature is -0.73°C, the average temperature of highest month (July) is 9.23°C, the average temperature of lowest month (January) is -13.98°C, the extreme minimum temperature is -31.6°C, and the extreme maximum temperature is 24.0°C. The annual average sunshine duration is 1150.6 h, the sunshine percentage is 26.1%, the highest sunshine month is December (151.7 h), and the sunshine percentage is 40%. The annual average relative humidity is 78.83%, the average annual rainfall is 1134.1 mm, the evaporation is 544.0 mm, which accounts for 48.0% of the average annual precipitation, and the rainy season is from June to September, accounting for 75% to 82% of the annual precipitation, of which the most rainfall is August. At most, the average is 294 mm, accounting for 30% of the annual precipitation. The soil is mainly dominated by brown soils and acid brown soils, with a pH of 4-6. The soil layer is thick and the humiliation process is obvious [32]. The zonal vegetation in this area belongs to subtropical vegetation. Affected by the southwest monsoon and the complex topography, the differences in hydrothermal conditions between the east slope and the west slope have obvious responses in the vegetation community, and the vertical zone changes is significant. There are 1091 kinds of seed plants in this area, belonging to 475 genera of 103 families, of which gymnosperms belong to 2 families, 7 genera, 13 species, and angiosperm has 101 families, 468 genera, and 1078 species, including 91 tropical genus species, 309 genera in temperate zones, 8 endemic genera, and endemic species is as high as 12.4%. A typical *P. densata* forest plot is set up in the study area. The sample plot tree layer is a natural *P. densata* forest. The shrub layers include *Quercus aquifolioides*, *Piptanthus concolor*, *Lonicera lanceolata*, and *Leptodermis potaninii* var. *glauca, Hypericum hookerianum*, *Caragana franchetiana*, *Cotoneaster microphyllus*, etc., with a coverage of about 30%. Herbs mainly contain *Anaphalis spodiophylla*, *Andropogon munroi*, *Vicia tibetica*, *Oryzopsis tibetica*, *Codonopsis convolvulacea*, *PoJygonum nepalense Polygonatum cirrhifolium*, *Anemone rivularis*, *Poa* sp., etc. Cover about 35%.

Research Methods. Water Sample Collection. From April to October of 2015, monitoring and sampling of through fall and trunk stem-flow from the atmospheric rainfall and rainfall within and outside the plot were performed. The specific method is based on the long-term positioning observation method of the Chinese forest ecosystem [33]. The "V" type collectors made of PVC material with a width of 30 cm, a depth of 20 cm, a length of 200 cm, and a horizontal area of 0.6 m^2, were continuously soaked in 3% hydrochloric acid for more than 24 h and washed with distilled water three times or more (others appliances are treated the same). Five collectors were placed diagonally in the plot and supported by a wooden frame to keep the collector about 50 cm above the ground to eliminate the effects of herbaceous plants and shrubs on through fall. Keep the collector at a small angle to the ground. Open a small opening at the lower end of the collector. Connect a clean plastic bucket. Clean the litter in the collector regularly to avoid the impact of litter on the measurement results. Finally, the mean value of five collectors was used as through fall, and the mixed elements were used

to determine the concentration of nutrient elements. A self-reported rain gauge was placed in an open space about 80 m away from the forest to monitor atmospheric rainfall. A collector was placed at the same time as a monitoring control and sampling for determination of nutrient element content. In the sample plot, according to the distribution of *P. densata* diameter, 10 standard wood species with different diameters were selected. Each plant was used with a polyethylene plastic pipe with a diameter of 2 cm and a section of which was cut along the middle seam. The spiral was wound from 2 m upwards. In a circle around the tree trunk, fix the plastic tube with a small nail and seal the joints with glass glue. Place a clean plastic barrel at the bottom of the plastic tube to collect and monitor trunk stem-flow, and take a mixed sample to determine the nutrient element content. Each month, 3 to 5 water samples were collected from atmospheric rainfall, through fall and trunk stem-flow, and a total of 27 and 81 samples were collected.

Test Methods. For the collected water samples, the pH was immediately measured with a pH meter. It was then stored by filtration which used to determine the concentration of N. In this study, nitrate-nitrogen (NO_3^--N), ammonia-nitrogen (NH_4^+-N), and total nitrogen were determined. Nitrate nitrogen determination method [34]: Draw 10ml of the filtered water sample, placed in a 50 ml beaker, add 1 drop of 3% potassium hydroxide solution to make it alkaline, evaporated, add phenol disulfonic acid reagent 2 ml Stir and make full contact with the residue. Add 15 ml of distilled water, add ammonium hydroxide after cooling to make it alkaline, until the yellow no longer deepens. Then, the contents of the beaker were pour into a 100 ml volumetric flask, and the volume was adjusted to the mark with distilled water and shaken. Colorimetry was performed on a spectrophotometer with a wavelength of 430 nm, and the nitrate content (ug) was determined from the standard curve. If the color of the test solution is too dark, a small amount can be taken directly from the colored solution and diluted to perform colorimetry. Ammonia nitrogen determination method [34]: Draw 20 ml of the filtered water sample into a 25 ml volumetric flask, add 1 ml of 40% sodium potassium tartrate solution, add 0.5 ml Na's reagent solution, and dilute to volume with distilled water, then In the spectrophotometer with 430 nm wavelength for colorimetry, the optical density of the water sample to be measured, determine the ammonium content from the standard curve (ug). The total nitrogen is determined by alkaline potassium persulfate digestion and ultraviolet spectrophotometry. For specific operating methods can depend on "National Environmental Protection Standards of the People's Republic of China" (HJ636-2012). The relevant calculation formula is [34]: NO_3^-(mg/L) = $(A\times10^{-3})$/water sample volume × 1000, nitrate nitrogen (mg/L) = NO_3^-(mg/L) × 0.2259; NH_4^+ (mg/L) = $(A \times 10^{-3})$/water sample volume × 1000, ammoniacal nitrogen (mg/L) = NH_4^+ (mg/L) × 0.7765. In the formula: A - check the quality of the nitrate (ammonium ion) from the standard curve, ug - convert ug into mg; 1000 - convert into the content per liter of water; 0.2259 - convert into Nitrate nitrogen content in water samples; 0.7765 - converted to ammonia nitrogen content in water samples.

Data Analysis. The mean, standard deviation, standard error, coefficient of variation, etc. of the nutrient concentrations measured in each of the atmospheric rainfall, through fall and trunk stem-flow were calculated, respectively. Canopy leaching content = through fall nutrient content - atmospheric rainfall nutrient content, canopy leaching coefficient = through fall nutrient content / atmospheric rainfall nutrient content, amount of atmospheric rainfall nutrient input = atmospheric rainfall nutrient concentration × atmospheric rainfall amount / 100, amount of through fall nutrient input = through fall nutrient concentration × through fall amount / 100, net leaching amount = amount of through fall nutrient input + nutrient input amount of trunk stem flow nutrient - atmospheric rainfall input amount of nutrient, total organic nitrogen (TON) = Total nitrogen (TN) - nitrate nitrogen (NO_3^--N)-ammonia nitrogen (NH_4^+-N) [34-35]. Data processing and analysis were performed in Excel 2010 and SPSS 19.0.

RESULTS AND DISCUSSION

Rainfall and Distribution Pattern. From April to October, the total amount of atmospheric rainfall is 725.8 mm. It changes a single-peak type with monthly changes (Fig 1). In July, the maximum amount of rainfall is 159.7 mm, accounting for 22% of the total rainfall. The trend of through fall variation is similar to that of precipitation. The total rainfall from April to October is 533 mm, and the same maximum amount of through fall in July is 118.3 mm, accounting for a total of 22.2%. The change trend of trunk stem flow rate is similar to the change trend of precipitation. From April to October, the total trunk stem flow amount is 34.8 mm, which accounted for 4.80% of the total precipitation. In August, trunk stem flow amount is the largest, which is 7.5 mm, accounting for 21.56% of the total. After fitting, the relationship between trunk stem flow and atmospheric rainfall is: $y=1.7103x^{0.7869}$ (R^2 = 0.9674), where x is the atmospheric rainfall (mm) and y is the trunk stem flow (mm). The relation between through fall and atmospheric rainfall is: $y = 0.413x^{1.121}$ (R^2 = 0.9901), where x is the atmospheric rainfall (mm)

and y is through fall (mm).

N Concentration Characteristics in Atmospheric Rainfall. At different times in the same area, the variation of N content in atmospheric rainfall is very random, resulting in a large difference in the concentration of N elements in each month (Fig 2). As can be seen from Fig 2, in the precipitation from April to October, the monthly concentration of N element changes greatly. The concentration of NO_3^--N changed the most, the maximum concentration is 0.7733 mg/L, the minimum concentration is 0.2203 mg/L, and the maximum concentration value is 3.51 times the minimum concentration value, even if the content of NH_4^+-N is relatively minimal, its maximum concentration value (0.3848 mg/L) is still 1.83 times the minimum concentration (0.2097 mg/L). The order of the maximum and minimum difference in the monthly concentration of the same component is: NO_3^--N>TN>TON>NH_4^+-N. The concentrations of the four components in October are the highest, being 0.7733 mg/L, 3.2454 mg/L, 2.0873 mg/L, and 0.3848 mg/L, respectively. The minimum values are 0.2203 mg/L (July) and 1.3808 mg/L, (July), 0.9302 mg/L (July), and 0.2709 mg/L (August), respectively. The 7-month average concentrations are 0.4023 mg/L (NO_3^--N), 1.8779 mg/L (TN), 1.2141 mg/L (TON), and 0.2615 mg/L (NH_4^+-N).

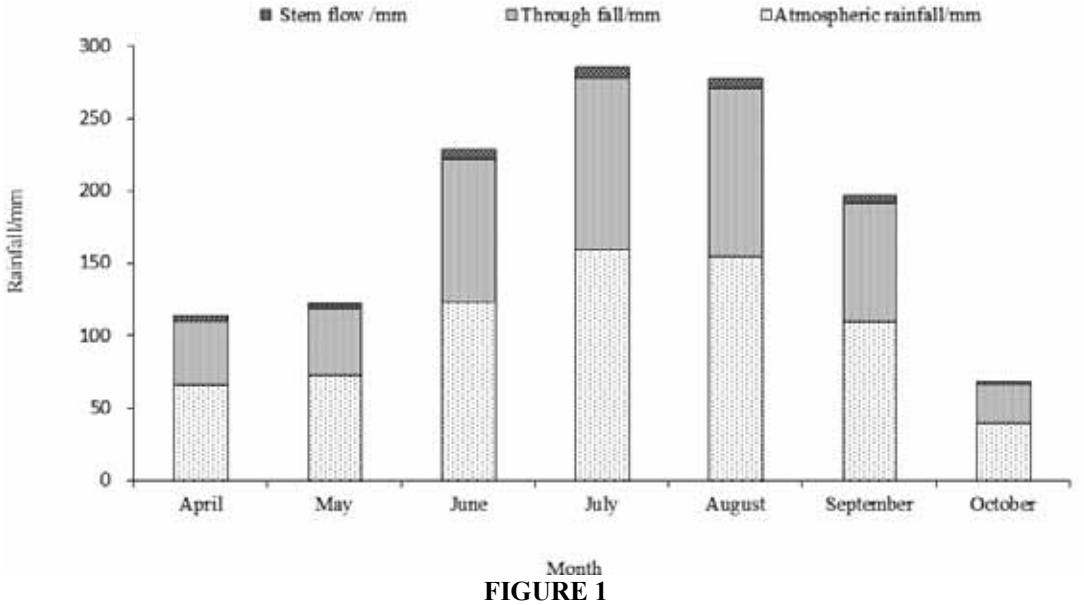

FIGURE 1
Precipitation and distribution of *P. densata* forest

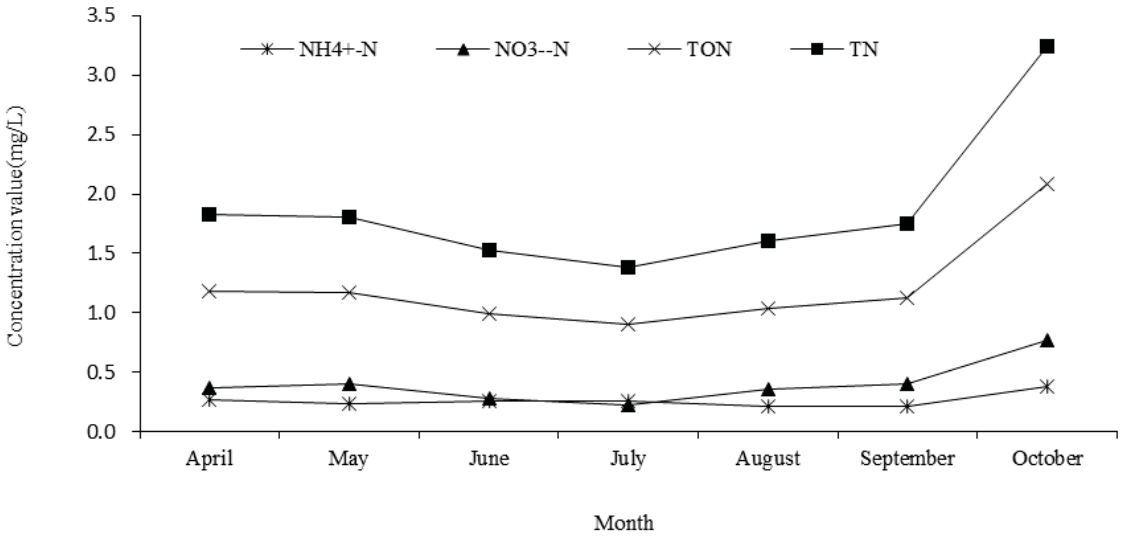

FIGURE 2
Monthly variation of N concentration in atmospheric rainfall

N Concentration Characteristics in Through Fall. Atmospheric rainfall passes through the canopy and forms through fall, and the nutrient concentration also changes (Fig 3). From Fig 3, we can see that in through fall of *P. densata* forest from April to October, TN concentration is relatively high and NH_4^+-N concentration is relatively low. Among the 7 months, the highest concentration is 2.7403 mg/L for TN (October), and the lowest is for NH_4^+-N, which is 0.1049 mg/L (May). The difference between the highest and lowest is 26.12 times. The ratio of the maximum concentration of the same component to the minimum concentration is: NH_4^+-N>NO_3^--N>TON>TN. The highest concentration of NH_4^+-N is 0.3660 mg/L (October), the lowest concentration is 0.1049 mg/L (May), and the phase difference is 2.49, while the NO_3^--N ranked second is 1.43 times worse. The seven months average concentrations are 0.2367 mg/L (NH_4^+-N), 0.4185 mg/L (NO_3^--N), 1.1891 mg/L (TON), and 1.8443 mg/L (TN).

N Concentration Characteristics in Stem flow. Atmospheric rainfall flows along the trunk to the forest land to form trunk stem flow, and the concentration of nutrient elements also changes (Fig 4). From Fig 4, it can be seen that in trunk stem flow of *P. densata* forest from April to October, the concentration of TN is relatively high, and the concentration of NH_4^+-N is relatively low. Among the 7 months, the highest concentrations are TN, 4.0610 mg/L (October), and the lowest concentrations is 0.2185 mg/L, NH_4^+-N (April). The difference between the highest and the lowest is 18.59 times. The ratio of the maximum concentration to the minimum concentration of the same component is ranked as follows: NO_3^--N>TN>TON>NH_4^+-N. The highest concentration of the four components is in October, and the NO_3^--N, TON, and NH_4^+-N are 1.0255 mg/ L, 2.6038 mg/L and 0.4317 mg/L, respectively. The minimum concentrations of NO_3^--N, TN, and TON are 0.2603 mg/L (July), 1.4500 mg/L (August), and 0.9404 mg/L (August), respectively. The 7-month average concentrations are 0.2724 mg/L (NH_4^+-N), 0.4173 mg/L (NO_3^--N), 1.2617 mg/L (TON), and 1.9514 mg/L (TN), respectively.

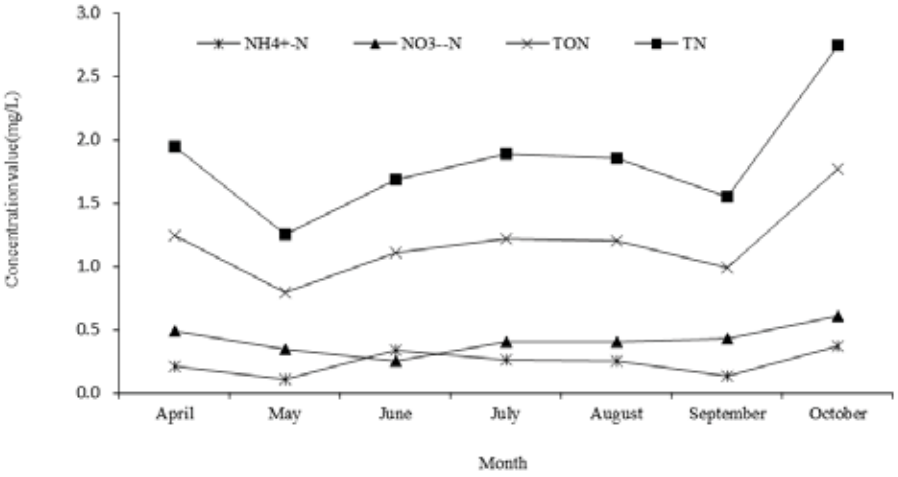

FIGURE 3
Monthly variation of N concentration in through rain after *P. densata* forest

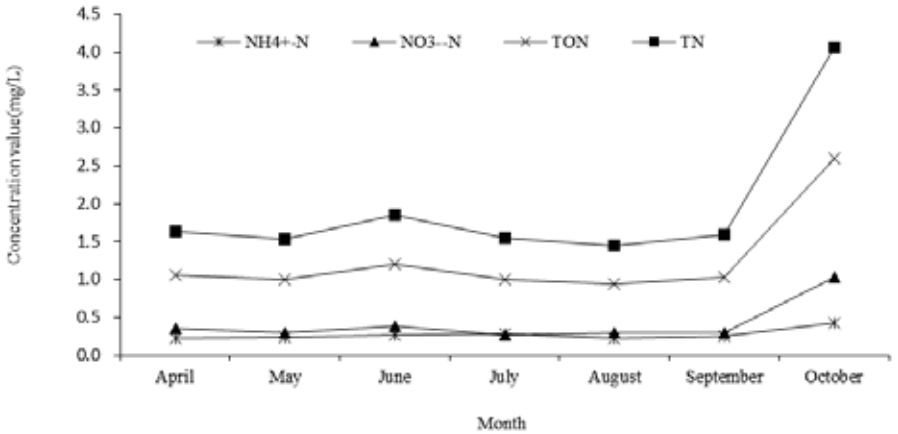

FIGURE 4
Monthly variation of N concentration in trunk stemflow in *P. densata* forest

TABLE 1
Relationship between different forms of rainfall and N-concentration in *P. densata* forest

Types	N	Relationship	R^2
Atmospheric rainfall	NO_3^--N	$y = -0.227\ln(x) + 0.679$	0.7708
	NH_4^+-N	$y = 0.0103x^2 - 0.1x + 0.4551$	0.8494
	TON	$y = 1.836x^{-0.369}$	0.8601
	TN	$y = 2.854x^{-0.374}$	0.8581
Through fall	NO_3^--N	$y = 0.0185x^2 - 0.1784x + 0.7628$	0.7442
	NH_4^+-N	$y = 0.0155x^2 - 0.1244x + 0.4235$	0.3628
	TON	$y = 0.0631x^2 - 0.556x + 2.1508$	0.7505
	TN	$y = 0.0971x^2 - 0.8587x + 3.3371$	0.7639
Stem flow	NO_3^--N	$y = 0.0395x^2 - 0.399x + 1.2233$	0.7328
	NH_4^+-N	$y = 0.0086x^2 - 0.0859x + 0.4449$	0.4495
	TON	$y = 0.0834x^2 - 0.8417x + 2.9597$	0.6700
	TN	$y = 0.1315x^2 - 1.3266x + 4.6278$	0.6740

TABLE 2
N-element input of rainfall in *P. densata* forest from April to October (kg/hm^2)

Types	NH_4^+-N	NO_3^--N	TON	TN
Atmospheric rainfall input amount	1.7914	2.5475	7.9710	12.3098
Through fall input amount	1.2775	2.0898	6.1377	9.5050
Stem flow input amount	0.0897	0.1202	0.3868	0.5966
Net leaching amount	-0.4242	-0.3375	-1.4465	-2.2082

Correlation Analysis. There is a certain correlation between different forms of rainfall and different concentrations of N components. After fitting by exponential, linear, logarithmic, binomial, and power functions, the relational formula with the highest correlation coefficient is taken. The results are shown in Table 1. As can be seen from Table 1, the correlation between atmospheric rainfall and the four N component concentrations is good, and the correlation coefficient is above 0.77. The correlation between through fall and NH_4^+-N is not obvious, and the correlation with the other three is better. Because trunk stem flow is influenced by many factors, such as rainfall intensity, rainfall duration, rainfall interval, tree stem, and canopy, the relationship between stem flux and concentration value is not obvious.

After fitting, it is found that in various forms of rain, the correlation between pH value and TN concentration is significant. The relationship between pH and TN concentration in atmospheric rainfall is: $y = 0.1086x^2 - 0.8899x + 3.228$ ($R^2 = 0.9514$). The equation for the relationship between pH and TN concentration in through fall is: $y = 0.3897x^2 - 4.9577x + 17.119$ ($R^2 = 0.9000$). The relationship between pH and TN concentration in trunk Stem flow is: $y = 11.336x^2 - 97.111x + 209.4$ ($R^2 = 0.9439$).

N-input Features. Nutrients leached from the canopy and tree trunks are water-soluble and can be directly absorbed by plants without complicated decomposition processes, which is beneficial to plant growth and nutrient cycling. Atmospheric rainfall had a large change in N concentration when it flowed through *P. densata* forests, and there is also a large change in the nutrient content of the input forest (Table 2). From Table 2, we can see that the TN input amount during the period from April to October is 12.3098 kg/hm^2, and the more input amount is TON, which is 7.9710 kg/hm^2, accounting for 64.75%. The input amounts of NO_3^--N and NH_4^+-N are 2.5475 kg/hm^2 and 1.7914 kg/hm^2, accounting for 20.69% and 14.55%, respectively. From April to October, the input amount of nutrient penetration is 9.5050 kg/hm^2, and the input amount of TON, NO_3^--N and NH_4^+-N accounted for 64.57%, 21.99% and 13.46%, respectively. The trunk stem flow input amount from April to October is relatively low, which is 0.5966 kg/hm^2. The amount of the three inputs accounted for 64.83%, 20.14% and 15.03%, respectively. After the atmospheric rainfall passes through the canopy and trunk of *P. densata* forest, the net leaching amount of TN is -2.2082 kg/hm^2, and the net leaching of N element is negative, indicating that part of it is absorbed or adsorbed by the canopy and trunk.

CONCLUSION

The concentration and input characteristics of N elements in the hydrological processes from April to October in *P. densata* forest of Sejila Mountain were studied. The main results were as follows:

Rainfall and distribution pattern: From April to October, the total atmospheric rainfall was 725.8

mm, the total through fall was 533 mm, and the total trunk stem flow was 34.8 mm. It changes a single-peak type with monthly changes. In July, the amount of atmospheric rainfall, through fall, and trunk stem flow were the largest, which were 159.7 mm, 118.3 mm, and 7.5 mm, accounting for 22%, 22.2%, and 21.56% of the total, respectively. The relationship between trunk stem flow and atmospheric rainfall was $y=1.7103x^{0.7869}$ ($R^2=0.9674$), and the relationship between through fall and atmospheric rainfall was: $y=0.413x^{1.121}$ ($R^2=0.9901$).

Concentration characteristics of atmospheric rainfall: The order of the maximum and minimum phase difference times of the monthly concentration of the same component is: NO_3^--N>TN>TON>NH_4^+-N. The concentrations of the four components in October were the highest, being 0.7733 mg/L, 3.2454 mg/L, 2.0873 mg/L, and 0.3848 mg/L, respectively. The minimum values were 0.2203 mg/L (July) and 1.3808 mg/L (July), 0.9302 mg/L (July), and 0.2709 mg/L (August), respectively. The seven months average concentrations were 0.4023 mg/L (NO_3^--N), 1.8779 mg/L (TN), 1.2141 mg/L (TON), and 0.2615 mg/L (NH_4^+-N), respectively.

Concentration characteristics in through rain: The ratio of the maximum concentration to the minimum concentration of the same component is: NH_4^+-N>NO_3^-N>TON>TN. The highest concentration of NH_4^+-N was 0.3660 mg/L (October), the lowest concentration was 0.1049 mg/L (May), and the phase difference was 2.49 times, while the NO_3^--N ranked second was 1.43 times worse. The 7-month average concentrations were 0.2367 mg/L (NH_4^+-N), 0.4185 mg/L (NO_3^--N), 1.1891 mg/L (TON), and 1.8443 mg/L (TN), respectively.

Concentration characteristics of trunk stem flow: The ratio of the maximum concentration to the minimum concentration of the same ingredient was ranked as follows: NO_3^--N>TN>TON>NH_4^+-N. The highest concentrations of the 4 components were all in October, NO_3^--N, TON and NH_4^+-N were 1.0255 mg/L, 2.6038 mg/L, and 0.4317 mg/L, respectively. The minimum concentrations of NO_3^--N, TN, and TON were 0.2603 mg/L (July), 1.4500 mg/L (August), and 0.9404 mg/L (August), respectively. The 7-month average concentrations were 0.2724 mg/L (NH_4^+-N), 0.4173 mg/L (NO_3^--N), 1.2617 mg/L (TON), and 1.9514 mg/L (TN), respectively.

Correlation: The correlation between atmospheric rainfall and four kinds of N component concentration values was good, and the correlation coefficients were all above 0.77. The correlation between through fall and NH_4^+-N was not obvious, but it had a good correlation with the other three. The relationship between trunk stem flow and the concentration of four components was not obvious. Fitting found that in various forms of rain, the correlation between pH value and TN concentration was significant.

Input: The TN input amount of atmospheric rainfall during April to October was 12.3098 kg/hm^2, among which the more input amount was TON, which was 7.9710 kg/hm^2, accounting for 64.75%. The input amounts of NO_3^--N and NH_4^+-N were 2.5475 kg/hm^2 and 1.7914 kg/hm^2, accounting for 20.69% and 14.55%, respectively. The input amount of nutrient through the rain was 9.5050 kg/hm^2, and the input amount of TON, NO_3^--N and NH_4^+-N accounted for 64.57%, 21.99% and 13.46%, respectively. Trunk stem flow input amount was relatively low, 0.5966 kg/hm^2, and the three inputs accounted for 64.83%, 20.14%, and 15.03%, respectively. After the atmospheric rainfall passing through the canopy and trunk of the *P. densata* forest, the net TN leaching amount was -2.2082 kg/hm^2.

ACKNOWLEDGEMENTS

The study was financially supported by national science and technology support plan of China (Grand No. 2013BAC04B01). This paper was also supported by CFERN & GENE Award Funds on Ecological Paper.

REFERENCES

[1] Pearson, J., Stewart, G.R. (1993) The Deposition of Atmospheric Ammonia and Its Effects on Plants. New Phytologist. 125(2), 283-305.

[2] Vitousek, P.M., Aber, J.D., Howarth, R.W., Likens, G.E., Matson, P.A., Schindler, D.W., Schlesinger, W.H., Tilman, D.G. (1997) Human Alteration of the Global Nitrogen Cycle: Sources and Consequences. Ecological Application. 7(3), 737-750.

[3] Wang, J., You, W.H., Shi, J., Yu, Y.L. (2008) Nitrate Nitrogen of Stem Flow of Evergreen Broad-leaved Forest in Tiantong. Journal of Inner Mongolia University. 39(4), 440-445.

[4] Guo, Z., Shao, M. (2003) Precipitation, Soilwater and Soilwater Carrying Capacity of Vegetation. Journal of Natural Resources. 18(5), 522-528.

[5] Marin, C.T., Bouten, W., Sevink, J. (2000) Gross Rainfall and Its Partitioning into Throughfall Stemflow and Evaporation of Intercepted Water in Four Forest Ecosystems in Western Amazonia. Journal of Hydrology. 237, 40-57.

[6] Carlyle-Moses, D.E. (2004) Throughfall Stemflow, and Canopy Interception Loss Fluxes in a Semi-arid Sierra Madre Oriental Matorral Community. Journal of Arid Environments. 58(2), 181-202.

[7] Thimonier, A. (1998) Measurement of Atmospheric Deposition under Forest Cano-pies: Some Recommendations for Equipment and Sampling Design. Environmental Monitoring and Assessment. 52(3), 353-387.
[8] Sheng, W.P., Yu, G.R., Fang, H.J., Liu, Y.F., Hu, Z.M. (2010) Determination of Nitrogen Deposition in Through Fall using Ion-exchange Resins: A Field Test in Planted Coniferous Forest Ecosystem at Qianyanzhou. Acta Ecologica Sinica. 30(24), 6872-6880.
[9] Gong, H.D., Wang, K.Y., Yang, W.Q. (2005) Nutrient Characteristics of Through Fall and Stemflow in Three Forests at the Subalpine of Western Sichuan. Scientia Silvae Sinicae. 41(5), 14-20.
[10] Zhang, N., Qiao, Y.N., Liu, X.Z., Chu, G.W., Zhang D.J., Yan J.H. (2010) Nutrient Characteristics in Incident Rainfall, Through fall, and Stem-flow in Monsoon Evergreen Broad-leaved Forest at Dinghushan. Journal of Tropical and Subtropical Botany. 18(5), 502-510.
[11] Fan, H.B., Su, B.Q., Lin, D.X., Chen, S.P. (2000) Biogeochemical Cycle Within Ecosystem of Chinese Fir Plantations II: Dynamics of Nitrogen Deposition. Chinese Journal of Applied and Environmental Biology. 6(2), 133-137.
[12] Xiao, H.L. (2001) Effects of Atmospheric Nitrogen Deposition on Forest Soil Acidification. Scientia Silvae Sinicae. 37(4), 111-116.
[13] Sha, L.Q., Zheng, Z., Feng, Z.L., Liu, Y.H., Liu, W.J., Meng, Y., Li, M.R. (2002) Biogeochemical Cycling of Nitrogen at Atropical Seasonal Rain Forest in Xishuangbanna, SW China. Acta Phytoecologica Sinica. 26(6), 689-694.
[14] Fang, Y.T., Mo, J.M., Gundersen, P., Zhou, G.Y., Li, D.J. (2004) Nitrogen Transformations in Forest Soils and Its Responses to Atmospheric Nitrogen Deposition: A Review. Acta Ecologica Sinica. 24(7), 1523-1531.
[15] Li, W.H. (1985) Tibet Forest. Beijing: Science Press.
[16] Xu, F.X. (1992) Development and Utilization of Pinus Densata Resources and Pine Resin in Tibet. Journal of Plant Resources and Environment. 1(4), 34-38.
[17] Lu, S.H., Pan, C.H. (2008) The Distribution Pattern of Pinus Densata Population in Southeastern Tibet. Journal of Northeast Forestry University. 36(11), 22-24.
[18] Lu, J., Guo, Q.Q., Zheng, W.L., Xu, A.S. (2013) Population Structure and Dynamic Characteristics of Pinus Densata in Southeast Tibet. Scientia Silvae Sinicae. 49(8), 154-160.
[19] Xu, L.H., Chen, L.H., Yang, G., Cao, S.Y. (2014) Analysis and Safety Evaluation of Nutritional Quality of Pinus Densata Dried Flowers. Zhejiang Agricultural Sciences. 6, 897-899, 902.
[20] Yang, D. (2005) Pinus Densata Natural Regeneration. Forestry Science and Technology. 30(6), 15-17.
[21] Chen, D. (1991) On Natural Regeneration Pinus Densata Gengzhang Gully, izang. Scientia Silvae Sinicae. 27(4), 465-469.
[22] Zhang, K.L., Zhong, R.J. (2000) Effects of Topographic Conditions on Natural Regeneration and Growth of Pinus Densata. Forestry Science and Technology. 25(1), 22-23.
[23] Zou, L.H., Zhou, J., Chen, Q.Y. (2005) Investigation and Analysis on Combustible Resources under Pinus Densata Forest in Nyingchi County, Tibet. Forest Inventory and Planning. 30(1), 73-75.
[24] Wang, Y.T., Hou, G.W., Ma, Q.Y. (2011) Studies on Natural Regeneration of Pinus Densata in Burned Forestlands in Western Sichuan Province. Journal of Anhui Agricultural Sciences. 39(13), 7757-7760.
[25] Mao, J.F., Li, Y., Wang, X.R. (2009) Empirical Assessment of the Reproductive Fitness Components of the Hybrid pine Pinus Densata on the Tibetan Plateau. Evol Ecol. 23(3), 447-465.
[26] Song, B.H., Wang, X.Q., Wang, X.R., Ding, K.Y., Hong, D.Y. (2003) Cytoplasmic Composition in Pinus Densata and Population Establishment of the Diploid Hybrid Pine. Molecular Ecology. 12, 2995-3001.
[27] Wu, P., Wang, L.L., Shao, X.M. (2008) Reconstruction of Summer Temperature Variation Form Maximum Density of Alpine Pine During 1917-2002 for West Sichuan Plateau, China. Journal of Geographical Sciences. 18, 201-210.
[28] Liu, X.H., Shao, X.M., Wang, L.L., Zhao, L.J., Wu, P., Chen, T., Qin, D.H., Ren, J.W. (2007) Climatic Significance of the Stable Carbon Isotope Composition of Tree-ring Cellulose: Comparison of Chinese Hemlock (Tsuga chinensis Pritz) and Alpine Pine (Pinus densata Mast) in a Temperate-moist Region of China. Sci China Ser D-Earth Sci. 50(7), 1076-1085.
[29] Ma, X.F., Szmidt, A.E., Wang, X.R. (2006) Genetic Structure and Evolutionary History of a Diploid Hybrid Pine Pinus Densata Inferred from the Nucleotide Variation at Seven Gene Loci. Molecular Biology and Evolution. 23(4), 807-816.
[30] Wujin, D.Z., Zheng, W.L., Zhang, K.L., Lu, J. (2013) The Re-distribution Pattern of Pinus Densata Forest Precipitation in Tibet Sejila Mountains. Forest Resources Management. 6, 133-136, 167.

[31] Li, J., Lu, J. (2014) Water-holding Characteristics of Coniferous Forest Litter in the Sejila Mount. Forest Resources Management. 4, 98-102.
[32] Zheng, W.L. (1995) A Preliminary Study on Wild Flower Resources in Sejila Mountain, Tibet. See: Xu Fengxiang. Study on Tibetan Plateau Ecological Forest. Shenyang: Liaoning University Press. 101-110.
[33] State Forestry Administration. (2011) Forest Industry Standards of the People's Republic of China (LY/T 1952-2011). Beijing: China Standard Press.
[34] Tian, D.L. (2004) The Research Method of the Ecological System of Chinese Fir Plantation. Beijing: Scientific Press. 227-251.
[35] Wang, D.L., Nie, L.S., Li, J.Y. (2006) Transfer Characteristics of Nutrient Elements Through Hydrological Process of Pinus Tabulaeformis Stand in Beijing Xishan area. Acta Ecologica Sinica. 26(7), 2101-2107.

Received: **26.12.2018**
Accepted: **27.03.2019**

CORRESPONDING AUTHOR

Jie Lu
Res. Institute of Tibet Plateau Ecology,
Tibet Agriculture & Animal Husbandry University,
860000 Nyingchi – Tibet

e-mail: tibetlj@163.com

© by PSP Volume 28 – No. 5/2019 pages 4320-4328 Fresenius Environmental Bulletin

GGE BIPLOT ANALYSIS TO EVALUATE YIELD AND QUALITY OF SOME OAT (*AVENA SATIVA* L.) GENOTYPE, ENVIRONMENT AND THEIR INTERACTIONS IN MULTI LOCATION

Fikret Budak*

Duzce University, Faculty of Agriculture & Natural Sciences, Department of Field Crops, Duzce, Turkey

ABSTRACT

Three field location experiments were carried out to determine yield and yield components of different genotype of oat (Checota, Saia6, Seydişehir04, Yeşilköy 1779 and Albatros) in different environmental condition using methodology during 2016 and 2017 seasons that were combined in GGE-biplot analysis. The environmental locations were Balıkesir, Bursa and Manisa. The experiments were arranged in the randomized complete block design (RCBD) with four replicates in each experiment. The purpose of the study was to determinate environmental interaction with forage yield and quality and grain yield of oat (*Avena sativa* L.) genotypes. In the research, herbage yield, dry matter (hay) yield, crude protein, crude fat, ADF and NDF contents were investigated. As a result of the research the highest avarage herbage yield (4638 kg da^{-1}) was observed in Saia 6 and the lowest avarage herbage yield 4028 kg da^{-1} in Yeşilköy 1779, and also the highest and the lowest Average hay yield was obtained by 1359 kg da^{-1} from Saia 6 and 1219 kg da^{-1} from Yeşilköy1779 genotypes. In terms of average yield and dry matter (hay) yield, there were highly significant differences. Concerning average crude protein, crude fat, ADF content also there were significant differences statistically among genotypes. Likewise inpoint of locations the differences among genotypes were highly significant. Also Genotype x environment interaction except NDF and seed yield was highly significant statistically. Considering the average yield, hay yield and crude protein the hightest value were obtained from Manisa location, considering the average yield, hay yield the lowest value was obtained from Balıkesir location.

KEYWORDS:
Oat, GGE biplot, yield, quality, environment

INTRODUCTION

Oat (*Avena sativa* L.) is an important cereal crop because of the fact that the adequate nutritious regular fodder availability is a basic requirement for livestock production to meet the demand of milk, butter and other by products and also grown all over the world for human food. [1, 2]. In proportion to other cereal crops, oat is considered to be better suitable for production under marginal environments, including cool-wet region and soils with low fertility [3, 4, 5]. Oats grow on a wide range of soils at temperatures ranging from 5 to 26°C, and in regions with rainfall over 500 mm. Total production of oat was 250.000 tons in Turkey, 2017 [6].

Oats have many uses as food cereal, feed grain, and green or conserved forage, and also in tropical skin care products. An advantage in using oats in cattle is that they require little or no processing before being fed [7]. Because they often do not require processing, oats may be less susceptible to spoiling [8]. Oat is cultivated in irrigated and rainfed conditions. It contains large amount of digestible crude protein, total digestible nutrients (TDN), vitamin B1, minerals and fat. It is favorite feed of animals and its straw is soft and superior to wheat and barley. The oat grain is valuable feed for dairy cows, horses, poultry and young breeding animals [9]. Generally fodder become available for livestock feeding in late April as a result of which both milk and meat production has been reduced. Winter forage plants can be growth in cool subtropical environment for increased fodder availability during traditional fodder deficit period [10]. Oat has severed advantages are other fodder species because of its high yield potential, nutrition and high regeneration capacity particularly during early winter month. Oat is predominantly grown in American and European countries, mainly Russia, Canada and United States of America. It is used mostly for animal feeding and to some extent as human food. Unlike wheat, which is consumed mainly as refined flour, oats are typically used as a whole grain or a bran enriched product.

The use of oat as animal feed has declined steadily owing to emerging use and interest in oats as human health food. Oat beta-D-glucan is a

valuable functional ingredient having numerous industrial, nutritional and health benefits [11]. Oat has a well-balanced nutritional composition. It is a good source of carbohydrates and quality protein with good amino acid balance. Oat contains high percentage of oat lipids especially unsaturated fatty acid, minerals, vitamins and phytochemicals [12]. Intake of oat β-glucan at daily doses of at least 3 g may reduce plasma total and low-density lipoprotein (LDL) cholesterol levels by 5–10% in normocholesterolemic or hyper-cholesterolemic subjects. Studies have shown that, on average, oat consumption is associated with 5% and 7% reductions in total and LDL cholesterol levels, respectively [13] and every 1% decrease in serum cholesterol would provide a 2-3% reduction in the observed rate of cardiovascular disease [14]. The nutritional benefits of oat have attracted attention from researchers worldwide and have resulted in the increased interest of food industry in using oats as food ingredient in various food products including infant foods [15], bread [16], oat milk [17], beverages [18], breakfast cereals [19] and biscuits [20]. Compared with other cereals, oats have several nutritional advantages. Several physiological responses have been linked to the intake of oat products [21]. The oat trade is very dynamic with new cultivars releasing every year. Grain features of these varieties may have effect in animal performance as well as human health. Then, once oat grain is harvested, its chemical attributes are the main interest according to intended consumption [22]. Oats are grown for both grain and forage for livestock feeding over a long time in many parts of the world [23].

The objective of our study was to analyze GEI data by the GGE- Biplot technique to evaluate the efficacy of the test site and determine the performance of different oat genotypes in order to compare yield and some important quality traits in the different locations of Turkey.

MATERIALS AND METHODS

The field experiment was conducted to study the forage, grain yield, quality of some oat genotypes and GxE interactions were investigated under three different environmental (Balıkesir, Bursa and Manisa) conditions of Turkey during 2016-2017 growing season. The experiment was laid out in randomized complete block design (RCBD) with four replications. Each genotype was sown in 12 m^2 (2.4 by 5.0 m) plots consisting of 12 rows with 20 cm row spacing. Physical and chemical properties of experiment soils texture were loamy in all location, and pH = 7.4, available phosphorus 3.6 ppm, available potassium 123 ppm, and organic matter 0.53 % in Bursa location. In Balıkesir location properties of soil; pH = 6.8, available phosphorus 2.4 ppm, available potassium 156 ppm, and organic matter 0.71 %. pH = 7.0, available phosphorus 4.2 ppm, available potassium 152 ppm, and organic matter 0.49 % in Manisa. The experiments were carried out in rainfed conditions.

Total annual rainfall was 583.0 mm, annual average the lowest and hightest temprature were 9 ºC - 24 ºC respectively in Balıkesir. In Manisa location annual total rainfall was 727.8 mm, annual average the lowest and hightest temprature were 10.9 ºC-22.8 ºC respectively. Total annual rainfall was 706.9 mm, and average the lowest temperature was 9 ºC, and the the hightest temperature 23 ºC.

DATA COLLECTION

Herbage yield (kg da^{-1}). At 50 % flowering stage, all treatments of each replications were harvested and weighed to get fresh fodder yield (HY). The yields obtained were converted into kg da^{-1}.

Dry Matter (%). For dry matter determination, firstly aluminium containers were oven dried and weighed by electric balance. 10 g of plant sample was weighed in each container and placed in an oven at 105 °C till constant weight was attained. Dry matter percentage was calculated by the following formula.

$$\text{Dry Matter (\%)} = \frac{\text{Wt. of oven dry sample}}{\text{Wt. of sample before drying}} \times 100$$

Dry matter yield (kg da^{-1}). Dry fodder yield (DMY) was calculated by applying this formula.

$$\text{DMY (kg } da^{-1}) = \frac{\text{HY x DM (\%)}}{100}$$

Rows were clipped at 5 cm above the ground level to determine the biomass yield. Weight of the total fresh biomass yield was recorded from each plot in the field and the estimated 500 g sample was taken from each plot to the laboratory. The sample taken from each plot was weighed to know the total sample fresh weight using sensitive table balance and oven dried for 24 hours at a temperature of 105ºC for herbage DM yield determination.

Chemical Analysis. The dried samples then ground to pass a 1 mm sieve and used for laboratory analysis. The analysis was made for ash, CP, CF NDF and ADF. Nitrogen (N) content was determined following the micro-Kjeldahl digestion, distillation and content procedures [24] and the crude protein (CP) content was estimated by multiplying the N content by 6.25. Fat was extracted by the Soxhlet method. The structural plant constituents (NDF) and (ADF) were compared according to methods reported by [25]. Neutral Detergent Fiber

(NDF) and Acid Detergent Fiber (ADF) contents were analyzed using an ANKOM 200 Fiber Analyzer (ANKOM Technology Corp. Fairport, NY, USA) according to the methods reported by [26]. Metabolic energy value ME (MJ / t KM) and relative feed value were determined by the method developed by [27]. Digestible Dry Matter (% DDM) was first calculated using the ADF value to calculate the relative feed value. Analysis procedures described [24] were followed for the determination of crude protein, crude fibre, ether extractable fat and total ash percentage. The data thus recorded were subjected to statistical analysis under Complete Randomized Block Design through analysis of variance technique. The differences among treatment Averages were tested by applying Duncan's Multiple Range Test [28]. MSTAT-C and SPSS16 package program were used for average variance, Average Duncan and Biplot analyzes respectively.

RESULTS AND DISCUSSION

Analysis of variance revealed that all the genotypes possessed highly significant genetic variability for all the traits. Average square due to environments were significant for all the traits revealing influence of environment on their expression (except ADF and NDF). The Average square due to environment + genotype x environment were significant for all the characters revealing variable response of genotypes for all the traits in the changing environment. The GxE interaction component was also significant for all the traits revealing that these traits were not stable over the environments. Oat forage, grain yield and quality are determined by multiple variable factors such as genotype and environment. It was indicated that the variability of chemical quality properties in oat was affected by the environment factors. For this reason it is very important to determine the yield, quality traits and the relationships between yield and quality traits of oat genotypes cultivated in various environments. Plant breeders may take advantage of it to develop high yield and quality varieties the best for their location.

Herbage yield (kg da^{-1}). The analysis of variance showed that environment (locations) and genotypes interactions were highly significant differences by a level of significance of P<0.01 (Table 1). The herbage yield of genotypes varied from genotypes to another across different environmental conditions. While the highest herbage yield (5.085 kg da^{-1}) was determined the genotype of Saia 6 in Bursa, the lowest (3.640 kg da^{-1}) was determined Yeşilköy1779 in Balıkesir. Considering the Average yield of genotypes in all locations, varied between 4.028 kg ha^{-1}–4.638 kg da^{-1}. The differences among genotypes were highly significant. The highest herbage yield (4.638 kg da) was obtained from Saia 6, while the lowest yield (4.028 kg da) was obtained from Yeşilköy 1.779. Albatros, Seydişehir and Checota were at the same group and the differences among genotypes were not significant statistically. Considering the average yield of all locations, varied between 4.096 kg da^{-1}- 4.646 kg da^{-1}, maximum herbage yield (4.646 kg da) was determined in Manisa, while the minimum (4.096 kg da^{-1}) in Balıkesir, and the differences among them were significant statistically (Table 1). The variation in hay yield of genotypes may be attributed to genetic characteristics and adaptability of these varieties to different environmental conditions.

Dry matter (hay) yield (kg da^{-1}). The analysis of variance showed that environment (locations) and genotypes interactions were highly significant differences by a level of significance of P<0.01 (Table 2). The DM yield of genotypes varied from genotypes to another across different environmental conditions. While the highest DM yields (1.506 kg da^{-1}) was obtained from the genotype of Saia 6 in Bursa, the lowest (1.138 kg da^{-1}) from Yeşilköy1779 in Balıkesir location. Considering the average DM yield of genotypes in all locations, varied between 1.219 kg ha^{-1}–1.359 kg da^{-1}. The differences among genotypes were highly significant. Genotype of Saia 6 has the highest DM yield (4.638 kg da), while Yeşilköy 1779 has the lowest yield (4028 kg da). Seydişehir Yeşilköy1779 and Albatros were at the same group and the differences among genotypes were not significant statistically. Checota was among others. Considering the average DM yield of all locations, varied between 1.225 kg da^{-1}-1.348 kg da^{-1}, maximum DM yield was determined in Manisa, while the minimum (4.096 kg da^{-1}) in Balıkesir, and the differences among them were significant statistically (Table 2). Buerstmayr et al. [4] reported that the influences of genotype and climate conditions are significant parameters affecting yield and quality of oat. The significant variations among oat genotypes for DM (hay) yield reported in studies conducted by many researchers [29, 30, 31, 32, 33].

Crude protein contents (CP %). Protein content is one of the most important factors influencing forage quality. The data presented in Table 3 indicates that crude protein contents in oat were influenced significantly by different location. The analysis of variance showed that environment (locations) and genotypes interactions were significant differences by a level of significance of P<0.05. The CP content of genotypes varied from genotypes to another across different environmental conditions. While the highest CP content (12.17 %) was obtained from the genotype of Albatros in Manisa, the lowest (9.95 %) from Checota in Bursa. Considering the average CP content of genotypes in all locations, varied between 10.55%–11.29%. The differences among genotypes were significant. Considering the

average CP contents of genotypes there were insignificant among genotypes statically. Protein content is one of the important quality traits for oat. In our study, protein content varied from genotypes to another across different environmental conditions. The variation in CP of genotypes may be attributed to genetic characteristics and adaptability of these varieties to different environment. The influences of genotype and climate conditions are significant parameters affecting yield and quality of oat [4]. Peterson et al. [1] and Yanming et al. [34] reported that genetic variation was important for protein content, Biel et al. [35] indicated hulless oats had higher protein content than hulled oats. Also Welch et al. [36] reported groat protein content varied within oat species. In addition, Doehlert et al. [37] reported that protein content was equally influenced by both genetics and environmental factors.

Crude fat contents (CF %). The analysis of variance showed that environment and genotypes interactions were significant differences by a level of significance of $P<0.05$. The CF content of genotypes varied from genotypes to another across different environmental conditions. While the highest CF content (1.66 %) was obtained from the genotype of Saia 6 in Balıkesir location and Yeşilköy1779 in Bursa, the lowest (1.30 %) from Yeşilköy1779 in Balıkesir. Considering the average CF content of genotypes in all locations, varied between 1.42-1.51percent. The differences among genotypes were significant. Considering the average CF contents of genotypes there were insignificant among genotypes statically (Table 4). The differences in CF of genotypes may be resulted from genetics and environmental factors. Doehlert et al. [37] reported that CF content could be

TABLE 1
Average herbage yield (kg da^{-1}) for different location

	Checota	Saia 6	Seydisehir04	Yeşilköy1779	Albatros	
Balıkesir	4.080 de	4.366 b-d	4.290 cd	3.640 f	4.102 de	4.096 C
Bursa	4.289 cd	5.085 a	4.323 b-d	3.711 ef	4.270 cd	4.336 B
Manisa	4.681 a-c	4.462 b-d	4.615 bc	4.734 ab	4.737 ab	4.646 A
Average	4350 B	4638 A	4410 B	4028 C	4370 B	
LSD%1	Genotype 217.5			Interaction 376.8		Location185

TABLE 2
Average dry matter yield (kg da^{-1}) for different location

	Checota	Saia 6	Seydisehir04	Yeşilköy1779	Albatros	
Balıkesir	1.234 c-e	1.301b-d	1.260 b-e	1.138 e	1.191 de	1.225 B
Bursa	1.267b-e	1.506 a	1.256 b-e	1.148 e	1.234 c-e	1.282 AB
Manisa	1.377 b	1.270b-e	1.331 bc	1.371 bc	1.390 ab	1.348 A
Average	1293 AB	1359 A	1282 B	1219 B	1.271 B	
LSD%1	Genotype 69.98		Interaction 121.2			Location68.92

TABLE 3
Average crude protein of DM (%) for different location

	Checota	Saia 6	Seydisehir04	Yeşilköy1779	Albatros	
Balıkesir	11.42 a-c	10.58 bc	11.68 ab	11.27 a-c	10.27 bc	11.04 A
Bursa	9.95 c	10.58 bc	11.04 a-c	10.57 bc	10.63 bc	10.55 B
Manisa	11.43 a-c	10.87a-c	10.64 bc	11.34 a-c	12.17 a	11.29 A
Average	10.93 ns	10.68 ns	11.12 ns	11.06 ns	11.02 ns	
LSD%5			Interaction 1.325			location 0.4550

TABLE 4
Average crude fat of DM (%) for different location

	Checota	Saia 6	Seydisehir04	Yeşilköy1779	Albatros	
Balıkesir	1.38 a-c	1.66 a	1.32 c	1.30 c	1.44 a-c	1.42 B
Bursa	1.44 a-c	1.36 bc	1.61 ab	1.66 a	1.43 a-c	1.51 A
Manisa	1.45 a-c	1.36 bc	1.45 a-c	1.45 a-c	1.42 a-c	1.43 B
Average	1.43 ns	1.46 ns	1.46 ns	1.47 ns	1.43 ns	
LSD% 5	Interaction 0.2484					Location0.0678

TABLE 5
Average ADF (%) for different location

	Checota	Saia 6	Seydisehir04	Yeşilköy1779	Albatros	
Balıkesir	36.11 ab	35.02 ab	36.10 ab	34.85 ab	36.29 ab	35.67 ^{ns}
Bursa	36.38 ab	37.40 a	36.17 ab	33.90 b	36.53 ab	36.07 ^{ns}
Manisa	34.56 b	33.95 b	35.02 ab	36.34 ab	36.43 ab	35.26 ^{ns}
Average	35.68 ^{ns}	35.45 ^{ns}	35.77 ^{ns}	35.03 ^{ns}	36.42 ^{ns}	
LSD % 1				Interaction 2.307		

TABLE 6
Average NDF (%) for different location

	Checota	Saia 6	Seydisehir04	Yeşilköy1779	Albatros	
Bursa	57.02	56.75	55.87	55.87	56.70	56.439 ns
Balıkesir	55.65	56.44	56.40	56.50	56.51	56.299 ns
Manisa	55.75	55.96	58.07	58.012	56.46	56.852 ns
Average	56.14 ns	56.38 ns	56.78 ns	56.79 ns	56.56 ns	

LSD %5

TABLE 7
Average seed yield (kg/da^{-1}) for different location

Location	Checota	Saia 6	Seydisehir04	Yeşilköy1779	Albatros	**Average**
Bursa	278.5 c-f	255.5 f	265.8 d-f	308.2 a-c	294.0a-d	280.4AB
Balıkesir	321.47a	266.38 d-f	289.88 b-e	266.94 d-f	314.34 ab	291.8 A
Manisa	258.60 ef	270.00 d-f	272.04 d-f	259.28 ef	276.32 d-f	267.2 B
Average	286.19AB	263.96 C	275.91 BC	278.13A-C	294.88 A	

LSD% 5 Genotype 16.56 Interaction 28.68 Location 68.92

attributed to the environment, and that genotypic effects accounted for most of the variation. Also Buerstmayr et al. [4] reported that the influences of genotype and climate conditions are significant parameters affecting yield and quality of oat.

Acid detergent fiber (ADF %) content. Acid detergent fiber contains the poorly digestible cell wall components, namely, cellulose, lignin, and other very resistant substances. Due to its nature, ADF is often used to predict energy content of feeds. Like NDF, ADF is a good indicator of feed quality; higher values within a feed suggest lower-quality feed. The analysis of variance showed that environment x genotypes interactions were high significant differences by a level of significance of P<0.01 (Table 5). The ADF content of genotypes varied from genotypes to another across different environmental conditions. While the highest ADF content (37.40 %) was obtained from the genotype of Saia 6 in Balıkesir location and, the lowest (33.90 %) from Yeşilköy1779 in Bursa. Considering the average ADF content of genotypes in all locations, varied between 35.26-36.07 percent. But the differences among genotypes were insignificant. Considering the average of ADF content differences among genotypes were insignificant statically (Table 5).

Neutral detergent fiber (NDF) of DM (%). The detergent feed analysis system is used to characterize fiber or total cell wall content of a forage or feed. That portion of a forage or feed sample insoluble in neutral detergent which contains the primary components of the plant cell wall, namely, hemicellulose, cellulose, and lignin. As cell wall production increases, as occurs in advancing plant maturity, NDF content will increase. As NDF content of a feed increases, dry matter intake will decrease and chewing activity will increase. The analysis of variance showed that the differences among genotypes, genotypes x environment interactions were insignificant. (Table 6). Also environment was not effective on genotypes.

Seed yield (SY) (kg/da^{-1}). The analysis of variance showed that genotypes and environment x genotypes interactions were significant differences by a level of significance of P<0.05 for seed yield (Table 7). The average SY of genotypes varied from genotypes to another across different environmental conditions. Concerning the average of SY of genotypes in all locations, varied between 267.20 kg da^{1}-291.80 kg da^{1}. The hightest SY was observed in Balıkesir, the lowest SY in Manisa location. The effect of environment on genotypes was significant. (Table 7). The change in seed yield of genotypes may be related to genetic structures and adaptability of these genotypes to different environments. The genotypes, yield and quality traits are also greatly influenced by environmental factors [4, 38]. Yan et al. [39] reported that significant impacts of genotype and environment on grain yields.

A Principal Components Analysis Biplot-PCA) Method. The method has been widely used recently. The GGE biplot analysis is based on a strictly fixed effects model with (additive) main effects for genotypes and environments and multiplicative effects for the interaction all being fixed. The discussion from recent works suggests, however, that either genotypic or environmental effects (or thus interaction effects) should be random [40, 41]. In plant breeding, adaptation of crop cultivars represents a trait of interest with respect to a given environment [42, 43], which multienvironment trials (MET) is carried out for most crops throughout the agricultural world.

In multienvironment trials (MET), a great number of cultivars are assessed in different environments represented by a genotype × environment interaction (GEI) that is represented as an important aspect in plant breeding programs which are adapted as a major objective of plant breeders, geneticists and physiologists in selecting superior genotypes in crop performance trials [44] to develop those cultivars. Furthermore, sorting of crop evaluation in environment and understanding these conditions

TABLE 8
Combined analyses of variance for genotypes of oat yield and quality

V.O.S	DF	Herbage Yield		Dry Matter		Crude Protein		Crude Fat	
		MS	F value	MS	F value	MS	F value	MS	F value
Location	2	1521926.26	46.97**	75784.46	16.85**	2.78	14.23**	0.043	4.60*
Error(R/G)	9	32401.08		4497.33		0.196		0.009	
Genotype	4	569926.20	14.84**	30032.50	7.55**	0.354	0.746^{ns}	0.005	0.154^{ns}
L× Gen.	8	379932.80	9.89**	33236.84	8.36**	1.52	3.21**	0.075	2.53*
Error	36	38393.45		3972.58		0.475		0.03	
CV%		4.49		4.91		6.29		11.87	

V.O.S	DF	ADF		NDF		Seed yield	
		MS	F value	MS	F value	MS	F value
Location	2	3.31	3.13^{ns}	1.65	2.66^{ns}	3020.37	7.45*
Error(R/G)	9	1.05		0.622		405.03	
Genotype	4	3.07	2.13^{ns}	0.928	0.624^{ns}	1612.34	7.24**
L× Gen.	8	5.19	3.61**	2.88	1.92^{ns}	1544.18	6.94**
Error	36	1.43		1.49		222.44	
CV%		3.36		2.16		5.33	

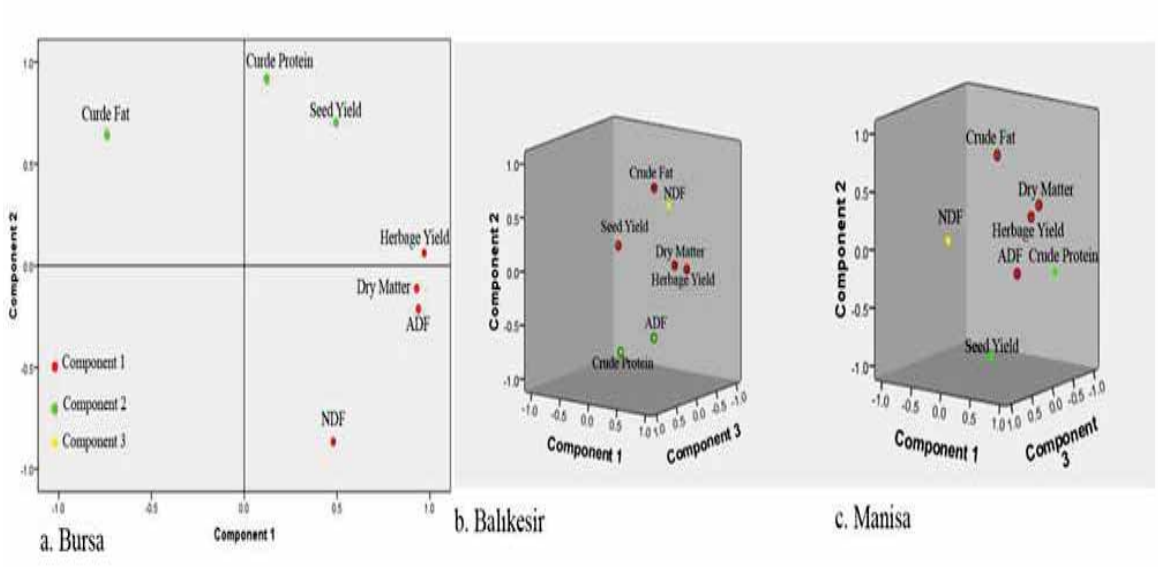

FIGURE 1
Grouping of Oat genotypes characteristic with GGE biplot analysis method and their relation ship with the average values of the examined properties

perfectly could increase heritability of measured traits, raise these lection, strengthen the potential of competitiveness for seed production and maximize grain yields for farmers [45]. In terms of the point above, there have been many attempts to analyze GEI for recording cultivars of crops under different environment interactions using various methods that have been proposed and developed for statistical analysis of GEI, to predict the phenotypic response to shifting in the environment, and to evaluate the performance of genotypes in those environments [46, 47].

Figure 1 shows that the classification of the properties examined according to the locations and the change of the properties. In the study, a basic component analysis was carried out in order to determine the importance of the characteristics. We have had 3 location. According to the results, the characteristics were divided into 2, 3 and 3 basic components in different location. (Figure 1). The characteristics in the first component had the highest significance, and this significance decreased gradually.

CONCLUSION

Consequently it is very important to determine the yield, quality traits and the relationships between yield and quality traits of oat genotypes cultivated in various environments. This may help breeders to develop high yield and quality varieties suitable for their region. In our study showed that oat forage and grain yield and quality were determined by numerous variable factors such as genotype, environment. Genetic variation and environment factors for forage yield, quality were highly significant and also environment factors for grain yield traits was significant

in oat genotypes. The highest forage and hay yield obtained from Saia 6 in Manisa. Concerning quality the hightest value was obtained from Albatros in Manisa. Environment factors for seed yield were highly significant. Also the hightest seed yield was determined in Albatros. There were significant differences in grain yield, protein content, fat concentration, acid detergent fiber, neutral detergent fiber among different oat genotypes used in this study. According to all data Saia 6and Albatross may be recommended to plant breeder.

REFERENCES

[1] Peterson, D.M., Wesenberg, D.M., Burrup, D.E., Erickson, C.A. (2005) Relationships among agronomic traits and grain composition in oat genotypes grown in different environments. Crop Sci. 45, 1249-1255.

[2] Achleitner, A., Tinker, N.A., Zechner, E., Buerstmayr, H. (2008) Genetic diversity among oat varieties of worldwide origin and associations of AFLP markers with quantitative. Theor. Appl. Genet. 117, 1041-1053.

[3] Ren, C.Z., Ma, B.L., Burrows, V., Zhou, J., Hu, Y.G., Guo, L., Wei, L., Sda, L., Deng, L. (2007) Evaluation of early mature naked oat varieties as a summer-seeded crop in dryland Northern climate regions. Field Crop Res. 103, 248-254.

[4] Buerstmayr, H., Krenn, N., Stepdan, U., Grausgruber, H., Zechner, E. (2007) Agronomic performance and quality of oat (*Avena sativa* L.) genotypes of worldwide origin produced under Central European growing conditions. Field Crops Res. 101, 343-351.

[5] Hoffmann, L.A. (1995) World production and use of oats. In: Welch, R.W. (eds.) The Oat Crop-Production and Utilization. Chapman and Dall, London, 34-61.

[6] The Food and Agriculture Organization of the United Nations. http://www.fao.org/faostat/en/#data/QC. (Accessed 2018).

[7] Blair, R. (2011) Nutrition and feeding of organic cattle. CAB Books, CABI.

[8] Pavia, A., Gentry-Running, K. (2011) Horse health and nutrition for dummies. Wiley Publishing, 388p.

[9] Zaman, Q., Hussain, M.N., Aziz, A. and Hayat, K. (2006) Performance of High Yielding Oat Cultivars under Agro-Ecological Conditions of D. I. Khan. Journal of Agricultural Research. 44, 29-35.

[10] Jehangir, I.A., Khan, H.U., Khan, M H., Ur-Rasool, F., Bhat, R.A., Mubarak, T., Bhat, M.A. and Rasool, S. (2013) Effect of sowing dates, fertility levels and cutting managements on growth, yield and quality of oats (*Avena sativa* L.). African J. Agri. Res. 8, 648-51.

[11] Ahmad, A., Anjum, F.M., Zahoor, T., Nawaz, H., Ahmed, Z. (2010) Extraction and characterization of β-glucan from oat for industrial utilization. Int J Biol. Macromol. 46, 304–309.

[12] Head, D.S., Cenkowski, S., Arntfield, S., Henderson, K. (2010) Superheated steam processing of oat groats. LWT - Food Sci Technol. 43, 690–694.

[13] Othman, R.A., Moghadaisan, M.H., Jones, P.J., (2011) Cholesterol-lowering effects of oat β-glucan. Nutrition Reviews. 69(6), 299–309.

[14] Chen, J., Raymond, K. (2008) Beta-glucans in the treatment of diabetes and associated cardiovascular risks. Vasc Health Risk Manag. 4(6), 1265-1272.

[15] Del Valle, F.R., Villanueva, H., Reyes-Govea, J., Escobedo, M., Bourges, H., Ponce, J., Munoz, M.J. (1981) Development, evaluation and industrial production of a powdered soy-oats infant formula using a low-cost extruder. J Food Sci. 46(1), 192–197.

[16] Zdang, D.C., Moore, W.R., Doehlert, D.C. (1998) Effects of oat grain hydro- thermal treatments on wheat–oat flour dough properties and bread baking quality. Cereal Chem. 75, 602–605.

[17] Onning, G., Wallmark, A., Persson, M., Akesson, B., Elmstahl, S., Oste, R. (1999) Consumption of oat milk for 5 weeks lower serum cholesterol and LDL cholesterol in free living men with moderate hypercholesterolemia. Ann Nutr Metab. 43, 301–309.

[18] Gupta, S., Cox, S., Abu-Gdannam, N. (2010) Process optimization for the development of a functional beverage based on lactic acid fermentation of oats. Biochem Eng. J. 52, 199–204.

[19] Ryan, L., Thondre, P.S., Henry, C.J.K. (2011) Oat-based breakfast cereals are a rich source of polyphenols and high in antioxidant potential. J Food Compos Anal. 24, 929–934.

[20] Ballabio, C., Uberti, F., Manferdelli, S., Vacca, E, Boggini, G., Redaelli R, Catassi, C., Lionetti, E, Penas, E. (2011) Restani P. Molecular cdaracterisation of 36 oat varieties and *in vitro* assessment of their suitability for celiac's diet. J Cereal Sci. 54, 110–115.

[21] Wood, P.J. (2007) Cereal β-glucans in diet and health. J. Cereal Sci. 46(3), 230-238.

[22] Martinez, M.F., Arelovish, H.M., Wehrdahne, L.N. (2010) Grain yield, nutrient content and lipid profile of oat genotypes grown in a semi arid environment. Field Crops Research. 116, 92–100.

[23] Stevenson, D.G., Eller, F.J., Radosavljevic, M., Jane, J.L., Inglett, G.E. (2007) Characterisation of oat bran products with and without supercritical carbon dioxide extraction. Int J Food Sci Technol. 42(12), 1489–1496.

[24] AOAC (1995) Official Methods of Analysis.16th ed. Association of Official Analytical Chemists, Arlington, VA.
[25] Van Soest, P.J., Robertson, J.D. and Lewis, B.A. (1991) Methods for dietary fibre, neutral detergent fibre and non-starch polysaccharides in relation to animal Nutrition. Journal of Dairy Science. 74, 3583-3597.
[26] Van Soest, P.J. (1994) Nutritional Ecology of the Ruminant. 2nd Ed. Cornell University Press. Ithaca, N.Y. 528p
[27] Van Dyke, N.J. and Anderson, P.M. (2000) Interpreting a forage analysis. Alabama cooperative extension. Circular ANR-890.
[28] Steel, R.G.D., Torrie, J.H. and Dicky, D.C. (1997) Principle and procedures of statistics. A Biometrical Approach. 2nd Ed. Me-Graw-Hill Book Co. New York.
[29] Aydın, N., Mut, Z., Mut, H., Ayan, I. (2010) Effect of autumn and spring sowing dates on hay yield and quality of oat (Avena sativa L.) genotypes. J. Anim. Vet. Adv. 9(10), 1539-1545.
[30] Gill, K.S., Omokanye, A.T., Pettyjohn, J.P., Elsen, M. (2013) Agronomic performance and beef cattle nutrition suitability of forage oat varieties grown in the Peace Region of Alberta, Canada. J. Agric. Sci. 5 (7), 128-145.
[31] Hussain, A., Khan, S., Bashir, M., Hassan, Z. (2005) Influence of environment on yield related traits of exotic oats cultivars. Sarhad J. Agric. 21, 209-213.
[32] Kim, J.D., Kim, S.G., Abuel, S.J., Kwon, C.H., Shin, C.N., Ko, K.H., Park, B.G. (2006) Effect of location, season and variety on yield and quality of forage oat. Asian-Aust. J. Anim. Sci. 19(7), 970-977.
[33] Chapko, L.B., Brinkman, M.A., Albrecht, K.A. (1991) Genetic variation for forage yield and quality among grain oat genotypes harvested at early heading. Crop Sci. 31, 874-878.
[34] Ma, Y.M., Liu, Z.Y., Bai, Y.T., Wang, W., Wang, H. (2006) Study on diversity of oats varieties in Xinjiang. Xinjiang Agricultural Sciences. 43(6), 510-513.
[35] Biel, W., Bobko, K., Maciorowski, R. (2009) Chemical composition and nutritive value of husked and naked oats grain. Journal of Cereal Science. 49, 413-418.
[36] Welch, R.W., Brown, J.C.W., Leggett, M. (2000) Interspecific and Intraspecific Variation in Grain and Groat Characteristics of Wild Oat (*Avena*) Species: Very High Groat (1→3),(1→4)-β- D glucan in an *Avena atlantica* Genotype. Journal of Cereal Science. 31, 273-279.
[37] Doehlert, D.C., McMullen, M.S., Dammond, J.J. (2001) Genotypic and environmental effects on grain yield and quality of oat grown in North Dakota. Crop Sci. 41, 1066-1072.
[38] Mehraj, U., Abidi, I., Ahmad, M., Gul-Zaffar, Z.A., Dar Rather, M.A., Lone, A.A. (2017) Stability analysis for physiological traits, grain yield and its attributing parameters in oats (*Avena sativa* L.) in the Kashmir Valley. Electronic Journal of Plant Breed. 8, 59-62.
[39] Yan, W., Frégeau-Reid, J., Pageau, D., Martin, R. (2016) Genotype-by-environment interaction and trait associations in two genetic populations of oat. Crop Sci. 56, 1136-1145.
[40] Yang, R.-C. (2007) Mixed model analysis of crossover genotypeenvironment interactions. Crop Sci. 47, 1051–1062.
[41] Smith, A.B., Cullis, B.R. and Thompson, R. (2005) The analysis of crop cultivar breeding and evaluation trials: An overview of current mixed model approaches. J. Agric. Sci. 143, 1–14.
[42] Annicchiarico, P. (2002) Genotype X environment interaction: Challenges and opportunities for plant breeding and cultivar recommendations.FAO Plant Production and Protection Paper 174. FAO.
[43] Van Eeuwijk, F.A., Malosetti, M., Yin, X.Y., Struik, P.C. and Stam, P. (2005) Statistical models for genotype by environment data: from conventional ANOVA models to ecophysiological QTL models. Australian J. Agric. Res. 56, 883-894.
[44] Mohammadi, R., Haghparast, R., Amri, A., Ceccarelli, S. and Buck, H.T. (2010) Yield stability of rainfed durum wheat and GGE biplot analysis of multi-environment trials. Crop Pasture Sci. 61, 92-101.
[45] Badu-Apraku, B., Akinwale, R.O., Menkir, A., Obeng- Antwi, K., Osuman, A.S., Coulibaly, N., Onyibe, J.E., Yallou, G.C., Abdullai, M.S. and Didjera, A. (2011) Use of GGE-biplot fortargeting early maturating maize cultivars tomega-environment in West Africa. African-Crop Sci. J. 19, 79-96.
[46] Akcura, M., Taner, S. and Kaya, Y. (2011) Evaluation of bread wheat genotypes under irrigated multi-environment conditions using GGE biplot analyses. Zemdirbyste-Agriculture. 98, 35-40.
[47] Shojaei, S.H., Mostafavi, K., Khodarahmi, M. and Zabet, M. (2011) Response study of canola (*Brassica napus* L.) cultivars to multi environments using genotype plus genotype environment interaction (GGE) biplot method in Iran. African J. Biotechnol. 10, 10877-10881.

Received: **27.12.2018**
Accepted: **18.03.2019**

CORRESPONDING AUTHOR

Fikret Budak
Düzce University,
Faculty of Agriculture & Natural Sciences,
Department of Field Crops,
Düzce – Turkey

e-mail: fikretbudak@rocketmail.com

© by PSP Volume 28 – No. 5/2019 pages 4329-4339 Fresenius Environmental Bulletin

SHORELINE CHANGE MONITORING IN ATIKHISAR RESERVOIR BY USING REMOTE SENSING AND GEOGRAPHIC INFORMATION SYSTEM (GIS)

Semih Kale[1,*], Deniz Acarli[2]

[1]Faculty of Marine Sciences and Technology, Canakkale Onsekiz Mart University, 17020, Canakkale, Turkey
[2]Gokceada School of Applied Sciences, Canakkale Onsekiz Mart University, 17760, Canakkale, Turkey

ABSTRACT

The main purpose of this study is to monitor shoreline changes of Atikhisar Reservoir in Çanakkale, Turkey. Geographic information system (GIS) and remotely sensed multispectral Landsat satellite images for the period of 1975-2017 were used to determine the shorelines. Satellite imageries were processed and analysed by remote sensing and GIS software. Then satellite images were imported into GIS software and the shorelines were manually digitized by using visual interpretation techniques for evaluating temporal changes in the shorelines. As a result, total length of the perimeter was calculated 18.8km in 1975 while 23.1km in 2017. The shoreline has reached the minimum perimeter in 1985 and the maximum perimeter in 1998. Shoreline has fluctuated during monitoring period and maximum decrease has been observed in 1985 with 35.3% decline while maximum increase has been observed in 2009 with 55.6% increase. The shoreline presents a trend that has complex non-sinusoidal waveform between the periods 1995-2000, 2002-2007, and 2009-2014. In the monitoring period, the shoreline has reached the negative peak in 1985, 1986, 2001, 2008, and 2014. It can be concluded that the shoreline has a trend that 6-yearly circle to reach positive and negative peaks. In conclusion, significant variations were detected in the shoreline. These variations could be affected by climate change, anthropogenic/agricultural activities, and sediment transportation. This paper provides the first knowledge and the most temporally rich assessment of shoreline changes in Atikhisar Reservoir. Therefore, continuous monitoring is vital for taking due precautions to support sustainable management of water resources in the future.

KEYWORDS:
Atikhisar Reservoir, GIS, Remote Sensing, Shoreline Change, Monitoring

INTRODUCTION

Shoreline is defined in an idealistic way as the physical interface of water and land [1]. It is one of the most dynamic processes in the coastal environments. Spatial and temporal changes including geomorphologic, tectonic, hydrodynamic, climatic, seismic, and sedimentation/erosional events can be occurred in shoreline gradually [2] or rapidly [3]. Shoreline change caused by anthropogenic and natural processes has a great importance for the environment. Therefore, monitoring shoreline changes is important for water resources management, urban and coastal planning, and determination of sediment deposit and erosion.

Shoreline extraction is time consuming and difficult while using traditional ground survey techniques [4]. Evaluation of shoreline changes has previously been done using aerial photographs and satellite images. Remote sensing has a significant role in acquisition of the spatial data. Satellite images can be obtained and interpreted easily by remote sensing techniques. Current progresses in geographic information system (GIS) and remote sensing are getting over the difficulties in shoreline extraction. Remotely sensed imageries are commonly used for long-term shoreline changes assessment since their advantages comparing to the traditional methods such as cost efficiency, higher resolution, and capability of broadly viewing [5]. Moreover, as it stated by Alesheikh et al. [6], water absorbs infrared wavelength region while vegetation and soil have strong reflectance. Hence, satellite images could be used for mapping the spatial distribution of water and land. Therefore, remotely sensed satellite images are widely used for coastline mapping.

Investigations on water resources mostly target to estimate changes and to determine and extract water bodies [7]. Management and protection of water resources require comprehensive information about the aquatic ecosystem with the aim of making appropriate action plans to maintain development of water resources in a sustainable way [8]. Landsat satellite imageries provide space-based land remote sensing data that the longest incessantly obtained collection in the world [9].

Shoreline change monitoring studies were performed for different coastal areas of Turkey in different periods by numerous authors [10-26]. Unfortunately, there are few studies on the shoreline change monitoring of lakes in Turkey. Shoreline changes were only analysed for Uluabat Lake [27], Salt Lake [28], Lake Sapanca [29], Lake Burdur [30-31], Lake Acıgöl [32], Meke Lake [33], Lake Seyfe [9], Terkos Lake [34], Akşehir Lake and Eber Lake [35-38], Yamula Dam Lake [39] and Kozan Dam Lake [40]. However, there is no published paper on the monitoring shoreline changes of Atikhisar Reservoir. Therefore, the aim of present study is to monitor shoreline changes of Atikhisar Reservoir by using remotely sensed Landsat satellite images and GIS.

MATERIALS AND METHODS

Çanakkale is located in the northern west of Turkey and divides Europe and Asia continents with a strait titled with its own name Çanakkale Strait. It has typical transition climate type that cold and rainy in winter, and hot and dry in summer [41]. Atikhisar Reservoir (Figure 1) was constructed on Sarıçay Stream which arises from Ida Mountains and flows into Çanakkale Strait [42]. Reservoir get started to storage water in June 1975. Atikhisar Reservoir is the only drinking water source for more than 130 thousand inhabitants. It supplies water for drinking and irrigation to the city centre of Çanakkale and it also serves for preventing floods. Its normal water level was described as 61 m by The General Directorate of State Hydraulic Works (SHW). Surface area was defined as 3 km^2 for normal water level while reservoir volume was determined as 40 hm^3 by SHW. The reservoir is under pressure of agricultural activities and wastes discharged from rural areas [43-44]. The climate of the region is generally defined as transition climate [45] and the basin of Atikhisar Reservoir presents the characteristic of mountainside that is mainly formed with Eosen-Oligosen andesite, dacite, and tuffs [46].

Possible data sources for researches on the shoreline were identified by Boak and Turner [47] as in situ observations, beach surveys, coastal charts and maps, historical photographs, aerial photography, and digital elevation or image data achieved from remote sensing technologies. Many techniques have been developed for the extraction of shorelines from the optical imageries. Remote sensing and GIS technologies are commonly used to determine the changes in shoreline of the lakes. The most common satellites used to explore the Earth are Landsat satellites. Landsat provides the longest perpetually attained assemblage of space-based moderate-resolution land remote sensing data. Therefore, remotely sensed Landsat Multispectral Scanner (MSS), Thematic Mapper (TM), Enhanced Thematic Mapper Plus (ETM+), and Operational Land Imager (OLI) and Thermal Infrared Sensor

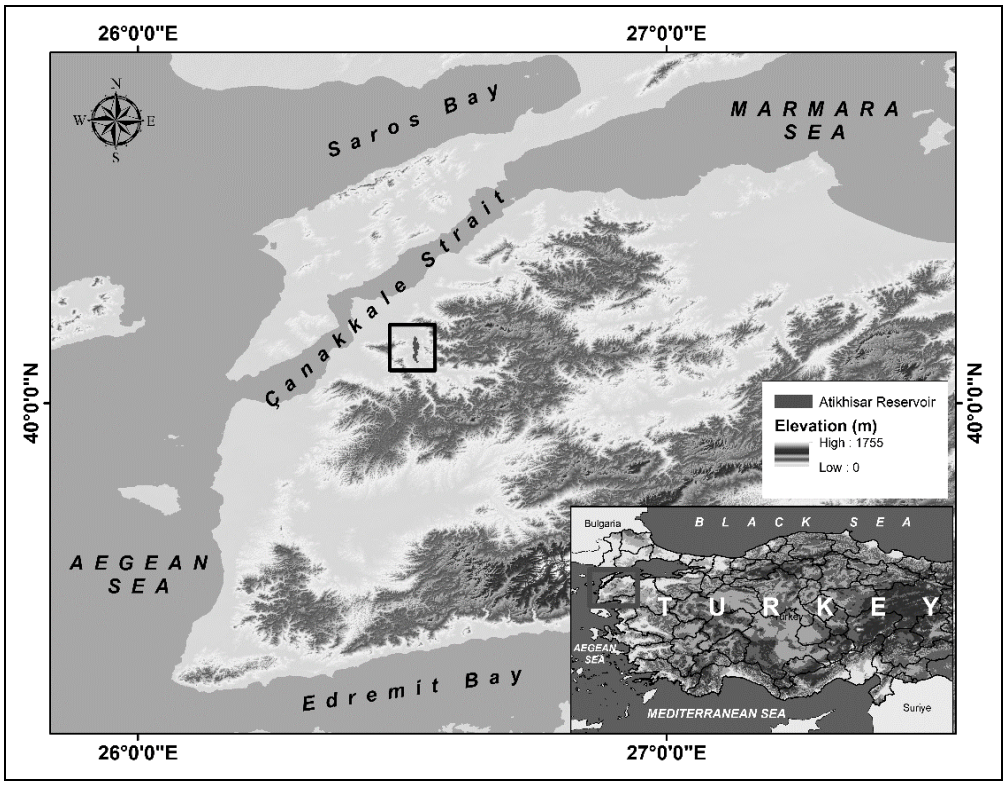

FIGURE 1
The location of Atikhisar Reservoir

(TIRS) imageries were used for monitoring shoreline changes of Atikhisar Reservoir. Spatial resolution for MSS is 60 m and it is 30 m for TM, ETM+, and OLI/TIRS while panchromatic band (band 8) has 15 m spatial resolution for both ETM+ and OLI/TIRS. Satellite images cover the period between 1975 and 2017. Almost all satellite images were used at annual intervals which has available images for the month of June since the reservoir get started to storage water on June 1975 to avoid possible variabilities between different months in the intra-annual variation of shoreline characteristics. Satellite images were acquired from the website of the United States Geological Survey (USGS) (https://earthexplorer.usgs.gov).

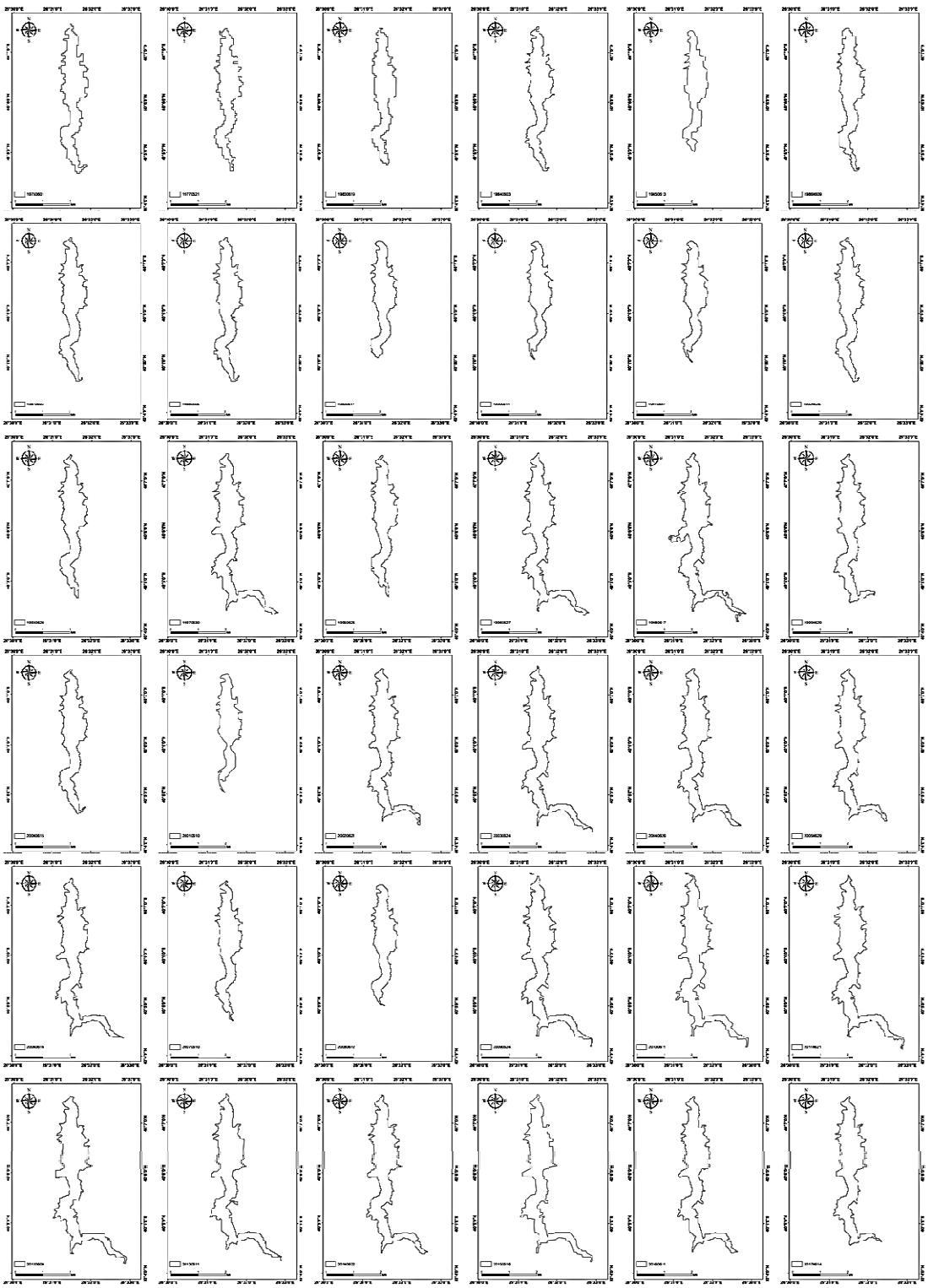

FIGURE 2
Spatial and temporal changes of shoreline from 1975 to 2017

A digital database was firstly produced in GIS environment to perform image processing techniques. The satellite images were imported into GIS software and satellite images were processed by using ERDAS Imagine 2014, ArcMap 10.3, and ENVI 5.2 software. Geometric and radiometric corrections were performed. Images were rectified using geographical projection with World Geodetic System 1984 (WGS84) datum. Shape files were created in ArcGIS for each imageries in order to extract the shorelines. Then, satellite images were manually digitized by using visual interpretation techniques for evaluating temporal changes in the shorelines of Atikhisar Reservoir. Several methods were used for shoreline detection and extraction from satellite imagery [48-55]. The reflectance of water is closely equivalent to zero and less than land in reflective infrared bands. Darker appearance of the water bodies makes easier to extract the shorelines [4]. Therefore, shoreline can easily be extracted and detected from a single band image. Moreover, USGS declared that band 4 for TM, ETM+, band 5 for OLI/TIRS and band 7 for MSS sensors were useful for mapping shorelines. Therefore, these bands were used for the distinction between water and land to digitize shoreline with a high accuracy as it stated by the USGS.

RESULTS

The evaluation of shoreline change was conducted for entire shore of Atikhisar Reservoir. The shorelines were extracted from multi temporal satellite imageries for the period between 1975 and 2017 by visual interpretation (Figure 2). Total length of the perimeter was calculated 18.8 km in 1975 while 23.1 km in 2017. The length of perimeter varied from 12.187 km to 31.7 km, the minimum perimeter was observed in 1985 while the maximum perimeter was recorded in 1998 (Figure 3). Also, almost minimum length in the shoreline was determined in 1986 and 2001 with 12.2 km and 12.411 km, respectively. A maximum decrease in the shoreline has been observed in 1985 with 35.3% decline while maximum increase has been observed in 2009 with 55.6% increase in the length.

Long term analysis of shoreline changes was conducted for 43 years from 1975 to 2017. Moreover, short term analysis of shoreline changes was carried out for four periods at 10 yearly intervals between 1975-1985, 1986-1995, 1996-2005, 2006-2015, and afterward 2015. Short term analyses revealed that 35.3% of shoreline was decreased for the period 1975-1985. Then, the perimeter of shoreline was extremely increased 50% for the period 1986-1995. However, the perimeter of shoreline was dramatically decreased 10.7% and 14.9% for the periods 1986-1995 and 1996-2015, respectively (Figure 4). Likewise, there were fluctuations on the perimeter of the shoreline from 1975 to 2017. Shoreline perimeter has decreased until 1986 and then increased to the initial length in 1987. It showed decreases and increases between 1988 and 1995. Then the shoreline presents a trend that has complex non-sinusoidal waveform between the periods 1995-2000, 2002-2007, 2009-2014. In the period after 1995, the shoreline has reached the negative peak in 2001, 2008, and 2014, respectively. Figure 4 illustrates the change rates of the shoreline compared with the initial length.

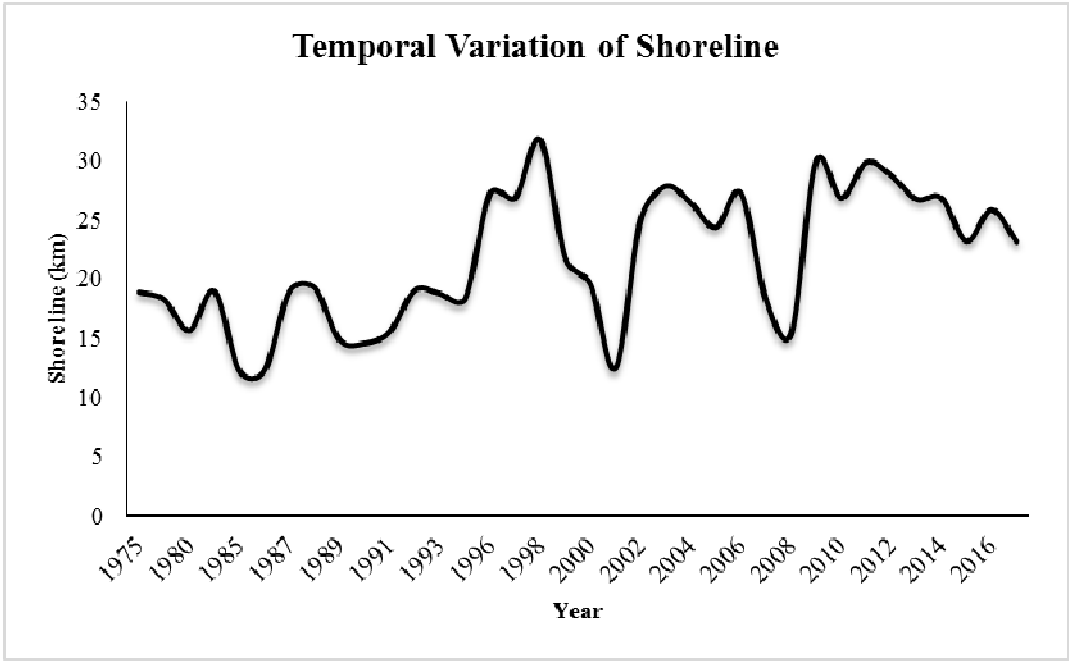

FIGURE 3
Temporal variation of shoreline from 1975 to 2017

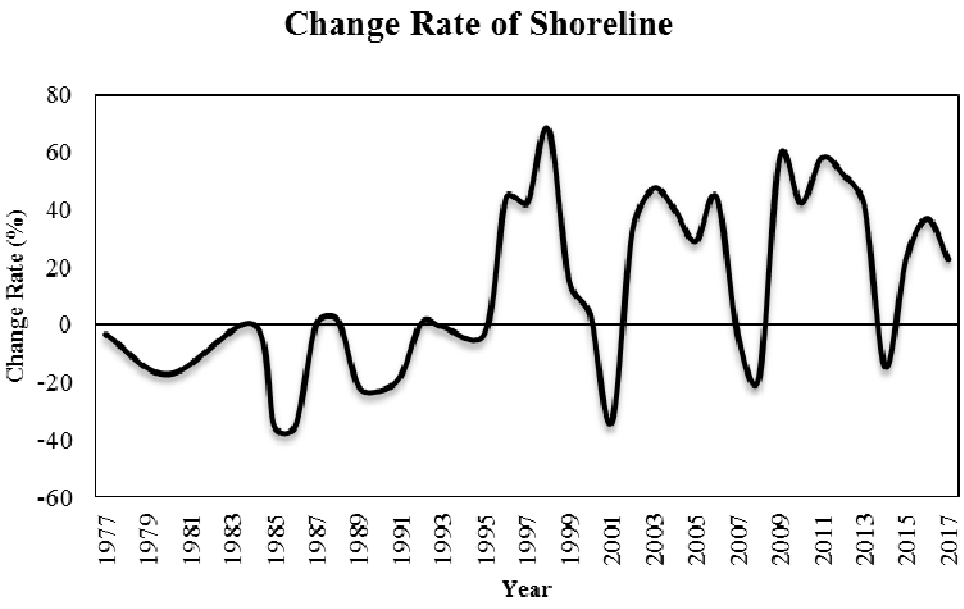

FIGURE 4
Change rate of shoreline from 1975 to 2017

DISCUSSION AND CONCLUSION

Shoreline is a phenomenon depending on the time that temporarily illustrates considerable variability [56]. It is a dynamic feature and an important structure for coastal monitoring, mapping, and resource management. Therefore, the management of environmental resources needs the information about shoreline positions and the variations in the shoreline. Shoreline monitoring is crucial for planning, identifying the vulnerable zones, estimating erosion and sediment transportation [34]. GIS allows to the arrangement of huge dataset with analysing and combining many layers of geospatial data comprising observations from the environment and supports remote sensing technologies [57]. Remote sensing and GIS provides novel techniques and technologies in coastal monitoring researches. Satellite imagery is a unique source to extract shorelines, and satellite images from both radar and multispectral sensors are freely available. Particularly, Landsat images provide priceless important data for monitoring studies. The application of remote sensing and GIS techniques in hydrologic and coastal practises is advantageous for shoreline change monitoring. Erener and Yakar [33] pointed out that remote sensing was a cost-effective approach to trail the dynamics of lake and they claimed that remote sensing and GIS technology is fundamental tool for acquiring and monitoring spatial and temporal data.

Dynamics of shoreline can vary spatially and temporally, and both natural and anthropogenic activities influence the shoreline dynamics. Boak and Turner [47] reviewed numerous published papers and notified that the most common technique for shoreline detection was manual visual interpretation. On the other hand, several methods have been technologically advanced for shoreline extraction from satellite images. Moreover, shoreline can even be extracted from imagery that has a single band because of the reflectivity of land is greater than water, and water has low pixel values in reflective infrared bands that is approximately equivalent to zero [6]. USGS declared that band 4 for TM, ETM+, band 5 for OLI/TIRS and band 7 for MSS sensors were useful for mapping shorelines. Kelley et al. [59] pointed out that the best band is band 5 for extracting the boundary between water and land. Braud and Feng [51] claimed that the most reliably option was band 5 for detecting and delineating the shoreline. Frazier and Page [52] also indicated that band 5 achieved successful accuracy (96.9%) for delineation and detection of water body. Band 5 shows a strong contrast between water and land because of the fact that land has a strong reflectance and water has highly absorption of mid-infrared energy. According to the three infrared bands of TM, band 5 reliably involves the best spectral equilibrium of water to land [6]. Likewise, Shrestha and Di [59] noted that band 5 was relatively the most appropriate for delineation of land and water. Alternatively, band 4 was suggested by Horning [60] and Güney [61] since water absorbs almost all light at the wavelength of band 4 (0.76-0.90 μm, near infrared) and water bodies act very dark. White and El Asmar [62] used band 7 in the Nile Delta region. Manavalan et al. [63] effectively determined the water body of rivers and lakes by applying band 4. Therefore, these suggested bands for different Landsat sensors were used in this study to clearly distinguish water and land for digitizing shoreline with a high accuracy.

Shoreline changes were analysed in many

studies and possible reasons of changes were indicated by many scientists. For instance, Ekercin [10] investigated shoreline changes in Meriç River (it defines the boundary between Turkey and Greece) and reported a soil loss due to the change in shoreline from 1988 to 1993. Tağıl and Cürebal [64] documented both positive and negative changes in the shoreline of Altınova coasts. Sesli et al. [12] determined shoreline changes in the coast of Trabzon and reported a recession with 12.2 ha area due to the erosion, sand dredging activities while a total of 161 ha area was gained by filling the sea. Lipakis [65] reported a 50 m shift in the shoreline of Georgioupolis from 1998 to 2005. Açıkgöz [13] pointed out a change in the coasts of Yumurtalık Wetland with 25% decrease and the author claimed that sediment transportation, sand dredging, and evaporation cause the shoreline change. Kuleli [16] stated a remarkable change in the shoreline of Çukurova coastal zone from 1972 to 2002. Özdemir [14] indicated that the shoreline of Kızılırmak River Delta has moved to the land side and 1.5 km^2 area has lost by the shoreline change. Author argued that this change in the shoreline was primarily affected by anthropogenic effects including the dam building, sand dredging, building coastal structures. Yılmaz [15] notified that shoreline of Kozlu coasts was changed due to the constructing of coastal structures. Kuleli et al. [17] detected significant changes in the shoreline of five Ramsar wetlands in Turkey caused by accretion and erosion for the period of 1975 and 2009. Olgun [19] notified positive and negative shoreline changes in Göksu Delta (Turkey) from 1980 to 2008 and found a relationship between the sediment transportation and the shoreline change. Ceylan [18] highlighted both positive and negative changes in the shoreline of İzmit Bay from 1984 to 2008. Aydın and Uysal [20] documented a decrease in the shoreline of Karasu coasts from 1987 to 2013 caused by erosion, dam building, sand dredging, and mussel harvesting. Güney and Polat [21] pointed out a change in the shorelines of Çandarlı and Aliağa coasts mainly caused by human impacts. Ozturk and Sesli [22] revealed that total length of the shoreline of Kızılırmak Lagoon series was decreased. Özpolat [23] mentioned both positive and negative shoreline changes in Seyhan Delta and the author underlined those changes were mainly caused by human interventions and erosion. Uçar [24] determined a decrease in total length of the shoreline of Küçük Menderes Delta from 1975 to 2016 while both positive and negative changes occurred during the monitoring period. On the contrary, Hussain et al. [66] reported that the total area of eastern part of Meghna Estuary has increased about 120 km^2 from 2007 to 2013 by the changes in shoreline. Al-Mansoori and Al-Marzouqi [67] have also revealed an increase in the shoreline of Dubai coasts by human-induced coastal changes from 2009 to 2015.

In this paper, it was determined that the shoreline has fluctuated between monitoring period and it showed decrease and increase in the length. It presents a trend that has complex non-sinusoidal waveform between the periods 1995-2000, 2002-2007, 2009-2014. In the monitoring period, the shoreline has reached the negative peak in 1985, 1986, 2001, 2008, and 2014, respectively. It can be concluded that the shoreline has a trend that 6-yearly circle to reach positive and negative peaks. Shorelines could be affected by numerous anthropogenic and natural factors since uncontrolled variations in shoreline may adversely influence the aquatic and terrestrial ecosystem. Major changes in shorelines are attributed to agricultural irrigation and the climate change for the study area. In 2001, there was a drought in Çanakkale. Therefore, the shoreline perimeter was declined to almost minimum length with 12.411 km. Similarly, Koç [46] reported a decrease for this period and documented that the water level had its least level. Özelkan and Karaman [68] revealed that water level of Atikhisar Dam Lake decreased in the transition from rainy period to dry period, however it was observed that it increased in the transition from the dry period to the rainy period. Also, authors indicated that the increase in the precipitation increased the water level while the increase in the evaporation decreased the water level of Atikhisar Dam Lake. Therewithal, Tağıl [27] noted that the water surface and depth of Uluabat Lake had decreased from 1975 to 2000. Ormeci and Ekercin [28] indicated a significantly decrease in the water reserve of Salt Lake due to drought and abandoned usage of water between 1990 and 2005. Sener et al. [35] claimed that changes in shoreline of Eber Lake and Akşehir Lake were directly related to surface flow and precipitation. Erener and Yakar [33] stated that both positive and negative changes were appeared in Meke Lake shoreline from 1987 to 2006. Temiz and Durduran [32] called attention to a significant decline in the shoreline of Acıgöl Lake from 1985 to 2015 caused by drought, extremely consumption of water for agricultural and industrial activities. Sarp and Ozcelik [31] revealed a strong decline in the surface area of Lake Burdur. Kesikoglu et al. [39] reported that both increase and decrease in the shoreline of Yamula Dam Lake were associated with the variations in the precipitation and temperature. Arkoç and Özşahin [69] indicated that there was a decrease in the coastline of Gala Lake primarily caused by the variations in precipitation and evaporation. Kaynak et al. [40] investigated shoreline changes in Kozan Dam Lake and reported an increase in the shoreline because of the climatic conditions and the agricultural irrigation.

Shoreline may move to the seaward or landward by several causes. To understand and detect the change in shoreline, the period of occurred variations should be differentiated. Gibeaut et al. [70]

identified the period of variations as short-term, long-term, and episodic changes. Episodic changes were described as a reaction to a single storm. However, short-term changes occur in 5–10 years on the contrary of long-term changes mention the changes occurring in 10–1000 years. Long-term changes could affect all the coast while short-term changes could only influence the coast at the same location with the movements to the seaward or landward. In this paper, occurred changes could be considered as a short-term change. Tağıl and Cürebal [64] declared that natural processes and anthropogenic activities are main factors on the short-term changes. Human interferences could lead to variation in natural characteristics and processes of the shoreline in addition to erosion, sediment transportation, and extremely usage of water for irrigation and consumption. On the other hand, abrupt changes in the climate with rising temperature, decreasing precipitation, increasing evaporation have crucial impact on the shoreline change of Atikhisar Reservoir. For instance, there was a drought in 2001 and the shoreline had almost minimum length during the monitoring period. Therefore, this decline in the perimeter of the shoreline clearly demonstrates the impact of the climate change on the shoreline. Similarly, Özelkan and Karaman [68] noted that the water level of Atikhisar Dam Lake was affected by variations in the precipitation and evaporation. Correspondingly, Arkoç and Özşahin [69] revealed that shoreline changes in Gala Lake were primarily controlled by evaporation and precipitation. Moreover numerous scientists also reported that changes in shoreline of the lakes were detected due to the climatic changes [28, 32, 35, 39-40]. Furthermore, Ejder et al. [42] reported that decrease in streamflow of Sarıçay Stream was attributed to the climatic changes such as increasing temperature and evaporation with decreasing precipitation. Lately, Kale [41] highlighted that there was an increasing trend in the evaporation and Kale [71] emphasized an increasing trend in the temperature for Çanakkale province. Similarly, increasing trend in the temperature and evaporation with decreasing trend in the precipitation were also reported for Çanakkale province by several scientists [72-75]. Authors warned about those trends will keep to continue and the city is thought be affected by the climate change in the future periods. Therefore, the shoreline of Atikhisar Reservoir might be affected and declined in the future periods due to possible impacts of the climate change.

In conclusion, Atikhisar Reservoir is the only water resource that supply drinking water to the city centre of Çanakkale. Therefore, shoreline change monitoring of Atikhisar Reservoir is of great importance. In this paper, shoreline changes were monitored using remote sensing and GIS techniques from the establishment of the reservoir to the present. There is no published paper on the monitoring shoreline changes of this reservoir. Therefore, this paper provides the first knowledge and valuable information on the monitoring temporal variations in shoreline of Atikhisar Reservoir. Also, this paper provides the most temporally rich assessment of shoreline changes in Atikhisar Reservoir. Remotely sensed satellite imageries cover a 43-year period showing extensive temporal and spatial change in the position of shorelines. The results demonstrate that significant shoreline changes were detected in Atikhisar Reservoir. This variation in shoreline could be affected by the climate change, sediment transport, agricultural activities and anthropogenic interventions around the reservoir. As it seen both natural and anthropogenic processes can alter the shoreline, continuous monitoring is essential for taking due precautions to support the sustainable management of water resources in the future. One of the most important aim of water resource management is planning and arrangement of water demands after determining present and future available amounts of surface and groundwater resources [76]. Continuously monitoring of shoreline changes is crucial to the best understanding of the changes in Atikhisar Reservoir. Moreover, investigations on the relationships between land use/land cover patterns, seasonal changes in the shoreline, anthropogenic activities and other processes are suggested for future studies. Shoreline change monitoring in reservoirs is of great importance for decision-makers in water resources to take precautions before the water level declined below the critical level to water supply. The outcomes of this study are vital for decision-makers, managers and stakeholders of reservoir for the development of water sharing policy, planning, management strategy, and decision-making processes by providing valuable assessment of the shoreline change in Atikhisar Reservoir from the first construction time to the present. This paper clearly shows that the integration of GIS and remote sensing technologies is much beneficial for monitoring long term changes in shoreline.

ACKNOWLEDGEMENTS

This study is a part of PhD thesis of the first author. An earlier version of this paper was presented at International Symposium on GIS Applications in Geography and Geosciences (ISGGG-2017) in Çanakkale, Turkey. The authors also would like to thank the US Geological Survey.

REFERENCES

[1] Dolan, R., Hayden, B.P., May, P. and May, S. (1980) Reliability of shoreline change measurements from aerial photographs. Shore and Beach. 48, 22–29.

[2] Thom, B.G. and Cowell, P.J. (2005) Coastal changes, gradual. In: Schwartz, M.L. (Ed.) Encyclopedia of coastal science. Springer, Dordrecht. 251–253.

[3] Scott, D.B. (2005) Coastal changes, rapid. In: Schwartz, M.L. (Ed.) Encyclopedia of coastal science. Springer, Dordrecht. 253–255.

[4] Aedla, R., Dwarakish, G.S. and Venkat Reddy, D. (2015) Automatic shoreline detection and change detection analysis of Netravati-Gurpur rivermouth using histogram equalization and adaptive thresholding techniques. Aquat. Pr. 4, 563–570.

[5] Mahapatra, M., Ratheesh, S. and Rajawat, A.S. (2013) Shoreline change monitoring along the south Gujarat coast using remote sensing and GIS techniques. Int. J. Geol. Agric. Environ. Sci. 3, 115–120.

[6] Alesheikh, A.A., Ghorbanali, A. and Nouri, N. (2007) Coastline change detection using remote sensing. Int. J. Environ. Sci. Tech. 4, 61–66.

[7] Castañeda, C., Herrero, J. and Casterad, M.A. (2005) Landsat monitoring of playa-lakes in the Spanish Monegros Desert. J. Arid Environ. 63, 497–516.

[8] Voutilainen, A., Pyhalahti, T., Kallio, K.Y., Pulliainen, J., Haario, H. and Kaipio, J.P. (2007) A filtering approach for estimating lake water quality from remote sensing data. Int. J. Appl. Earth. Obs. Geoinf. 9, 50–64.

[9] Reis, S. and Yilmaz, H.M. (2008) Temporal monitoring of water level changes in Seyfe Lake using remote sensing. Hydrol Process. 22, 4448-4454.

[10] Ekercin, S. (2000) Analysis of the Meriç River shoreline and its delta by using remotely sensed image. MSc Thesis. İstanbul Technical University, İstanbul, Turkey. 101p.

[11] Al Saleh, F. (2004) Numerical modeling of shoreline changes around Manavgat River mouth. PhD Thesis. Middle East Technical University, Ankara, Turkey. 172p.

[12] Sesli, F.A., Karsli, F., Colkesen, I. and Akyol, N. (2009) Monitoring the changing position of coastlines using aerial and satellite image data: An example from the eastern coast of Trabzon, Turkey. Environ. Monit. Assess. 153, 391–403.

[13] Açıkgöz, G. (2010) Determination of coastal change in Yumurtalık wetland system by using remote sensing data and geographic information systems. MSc Thesis. Çukurova University, Adana, Turkey. 69p.

[14] Ozdemir, S. (2010) Actual coastline changes in Kızılırmak Delta and its results. MSc Thesis. Ondokuz Mayıs University, Samsun, Turkey. 61p.

[15] Yılmaz, N. (2010) Analysis of shoreline change in Zonguldak Kozlu coastal zone. MSc Thesis. Zonguldak Karaelmas University, Zonguldak, Turkey. 107p.

[16] Kuleli, T. (2010) Quantitative analysis of shoreline changes at the Mediterranean coast in Turkey. Environ. Monit. Assess. 167, 387–397.

[17] Kuleli, T., Guneroglu, A., Karsli, F. and Dihkan, M. (2011) Automatic detection of shoreline change on coastal Ramsar wetlands of Turkey. Ocean Eng. 38, 1141–1149.

[18] Ceylan, M. (2012) Coastline change detection with remote sensing and GIS: Izmit Gulf case study. MSc Thesis. National Defense University, Air Force Academy, İstanbul, Turkey. 99p.

[19] Olgun, A. (2012) Monitoring of coastline changes of the Göksu delta by means of remote sensing and geographic information systems. MSc Thesis. İstanbul Technical University, İstanbul, Turkey. 61p.

[20] Aydın, M. and Uysal, M. (2013) Monitoring of coastline change with satellite images: Sakarya-Karasu. Harita Teknolojileri Elek. Der. 5, 24–32.

[21] Güney, Y. and Polat, S. (2015) Coastline change detection using remote sensing data: The case of Aliağa and Çandarlı. J. Aeronaut. Space Tech. 8, 11–17.

[22] Ozturk, D. and Sesli, F.A. (2015) Shoreline change analysis of the Kizilirmak Lagoon Series. Ocean Coast. Manage. 118, 290–308.

[23] Özpolat, E. (2016) Coastline changes in Seyhan Delta (1950 – 2013). MSc Thesis. Harran University, Şanlıurfa, Turkey. 101p.

[24] Uçar, E. (2016) Investigation of Küçük Menderes Delta's shoreline changes. MSc Thesis. Dokuz Eylül University, İzmir, Turkey. 119 p.

[25] Kocababa, S. (2017) Coastline change and risk analysis based on satellite image in Konyaaltı. MSc Thesis. Afyon Kocatepe University, Afyonkarahisar, Turkey. 75p.

[26] Kılar, H. and Çiçek, İ. (2018) Shoreline change analysis in Göksu Delta by using DSAS. Cograf. Bilim. Derg. 16, 89–104.

[27] Tağıl, Ş. (2007) Quantifying the change detection of the Uluabat Wetland, Turkey, by use of Landsat images. Ekoloji, 16, 9–20.

[28] Ormeci, C. and Ekercin, S. (2007) An assessment of water reserve changes in Salt Lake, Turkey, through multi-temporal Landsat imagery and real-time ground surveys. Hydrol. Process. 21, 1424–1435.

[29] Duru, U. (2017) Shoreline change assessment using multi-temporal satellite images: A case study of Lake Sapanca, NW Turkey. Environ. Monit. Assess. 189, 385.

[30] Ataol, M. (2010) The water level changings in Burdur Lake. Cograf. Bilim. Derg. 8, 77–92.
[31] Sarp, G. and Ozcelik, M. (2017) Water body extraction and change detection using time series: A case study of Lake Burdur, Turkey. J. Taibah Univ. Sci. 11, 381–391.
[32] Temiz, F. and Durduran, S.S. (2016) Monitoring coastline change using remote sensing and GIS technology: A case study of Acıgöl Lake, Turkey. IOP Conf. Ser.: Earth Environ. Sci. 44, 042033.
[33] Erener, A. and Yakar, M. (2012) Monitoring coastline change using remote sensing and GIS technologies. Lect. Notes Inf. Technol. 30, 310–314.
[34] Bayram, B., Seker, D.Z., Acar, U., Yuksel, Y., Guner, H.A.A. and Cetin, I. (2013) An integrated approach to temporal monitoring of the shoreline and basin of Terkos Lake. J. Coastal Res. 29, 1427–1435.
[35] Sener, E., Davraz, A. and Sener, S. (2010) Investigation of Aksehir and Eber Lakes (SW Turkey) coastline change with multitemporal satellite images. Water Resour. Manage. 24, 727–745.
[36] Yıldırım, Ü., Erdoğan, S. and Uysal, M. (2011) Changes in the coastline and water level of the Akşehir and Eber Lakes between 1975 and 2009. Water Resour. Manage. 25, 941–962.
[37] Köle, M.M., Ataol, M. and Erkal, T. (2016) Spatial changes of Eber and Akşehir lakes between 1990 and 2016. In: Proceedings of International Geography Symposium. Ankara, Turkey. 859–872.
[38] Kale, M.M. (2018) Historical shoreline change assessment using DSAS: A case study of Lake Akşehir, SW Turkey. In: Doğan, A. and Gönüllü, G. (Eds.) Current Debates in sustainable architecture, urban design and environmental studies. IJOPEC, London, 187–196.
[39] Kesikoglu, M.H., Cicekli, S.Y., Kaynak, T. and Ozkan, C. (2017) The determination of coastline changes using artificial neural networks in Yamula Dam Lake, Turkey. In: Proceedings of the 8th International Conference on Information Technology. Jordan. 737–740.
[40] Kaynak, T., Çiçekli, S.Y. and Kesikoğlu, M.H. (2018) Determination of coastline changes at Kozan Dam Lake by using artificial neural networks method. In: Proceedings of International Conference on Advanced Technologies, Computer Engineering and Science. Turkey. 587–591.
[41] Kale, S. (2017) Climatic trends in the temperature of Çanakkale City, Turkey. Nat. Eng. Sci. 2, 14–27.
[42] Ejder, T., Kale, S., Acar, S., Hisar, O. and Mutlu, F. (2016) Restricted effects of climate change on annual streamflow of Sarıçay Stream (Çanakkale, Turkey). Mar. Sci. Tech. Bull. 5, 7–11.
[43] Akbulut, M., Kaya, H., Çelik, E.Ş., Odabaşı, D.A., Sağır Odabaşı, S. and Selvi, K. (2010) Assessment of surface water quality in the Atikhisar Reservoir and Sarıçay Creek (Çanakkale, Turkey). Ekoloji. 19, 139–149.
[44] Selvi, K. and Kaya, H. (2013) Determination of certain metals in tissues of pike (*Esox lucius* L, 1758) caught from Atikhisar Reservoir, Çanakkale. Alınteri J. Agric. Sci. 25, 23–28.
[45] Koç, T. (2001) Climate and condition in northwest Anatolian: With dimensions of synoptic, statistic and application. Çantay, İstanbul, 372p.
[46] Koç, T. (2007) Sustainable usage problems of Atikhisar Dam Basin (Çanakkale). In: Proceedings of International Congress on River Basin Management. Antalya, Turkey. 815–827.
[47] Boak, E.H. and Turner, I.L. (2005) Shoreline definition and detection: A review. J. Coastal Res. 21, 688–703.
[48] Dolan, R., Fenster, M.S. and Holme, S.J. (1991) Temporal analysis of shoreline recession and accretion. J. Coastal Res. 7, 723–744.
[49] Gao, B.C. (1996) NDWI–A normalized difference water index for remote sensing of vegetation liquid water from space. Remote Sens. Environ. 58, 257–266.
[50] McFeeters, S.K. (1996) The use of the normalized difference water index (NDWI) in the delineation of open water features. Int. J. Remote Sens. 17, 1425–1432.
[51] Braud, D.H. and Feng, W. (1998) Semi-automated construction of the Louisiana coastline digital land/water boundary using Landsat Thematic Mapper satellite imagery – Louisiana Applied Oil Spill Research and Development Program, OSRAPD Technical Report Series, Report No 97-002.
[52] Frazier, P.S. and Page, K.J. (2000) Water body detection and delineation with Landsat TM data. Photogramm. Eng. Remote Sensing. 66, 147–167.
[53] Xu, H. (2006) Modification of normalised difference water index (NDWI) to enhance open water features in remotely sensed imagery. Int. J. Remote Sens. 27, 3025–3033.
[54] Shen, L. and Li, C. (2010) Water body extraction from Landsat ETM+ imagery using adaboost algorithm. In: Proceedings of 18th International Conference on Geoinformatics. Beijing, China. 1–4.

[55] Feyisa, G.L., Meilby, H., Fensholt, R. and Proud, S.R. (2014) Automated water extraction index: A new technique for surface water mapping using Landsat imagery. Remote Sens. Environ. 140, 23–35.
[56] Morton, R.A. (1991) Accurate shoreline mapping: past, present, and future. In: Proceedings of a specialty conference on quantitative approaches to coastal sediment processes. Seattle, Washington, USA. 997–1010.
[57] Kale, S. and Acarlı, D. (2018) Potential application of geographic information system (GIS) in reservoir fisheries. Int. J. Oceanogr. Aquac. 2, 000149.
[58] Kelley, G.W., Hobgood, J.S., Bedford, K.W. and Schwab, D.J. (1998) Generation of three-dimensional lake model forecasts for Lake Erie. J. Weat. For. 13, 305–315.
[59] Shrestha, R. and Di, L.P. (2013) Land/water detection and delineation with Landsat data using Matlab/ENVI. In: Proceedings of Second International Conference on Agro-Geoinformatics. IEEE, Fairfax, VA, USA. 211–214.
[60] Horning, N. (2004) Selecting the appropriate band combination for an RGB image using Landsat imagery Version 1.0. American Museum of Natural History, Center for Biodiversity and Conservation – Available from http://biodiversityinformatics.amnh.org. (Accessed on September 23, 2017).
[61] Güney, Y. (2012) Geomorphology of the coastal region between Çandarlı-Aliağa and coastline changes. MSc Thesis. Uşak University, Uşak, Turkey. 158p.
[62] White, K. and El Asmar, H.M. (1999) Monitoring changing position of coastlines using Thematic Mapper imagery, an example from the Nile Delta. Geomorphology. 29, 93–105.
[63] Manavalan, P., Sathyanath, P. and Raiegowda, G.L. (1993) Digital image analysis techniques to estimate waterspread for capacity evaluations of reservoirs. Photogramm. Eng. Remote Sensing. 59, 1389–1395.
[64] Tağıl, Ş. and Cürebal, İ. (2005) Remote sensing and GIS monitoring of coastline change in Altınova coast, Turkey. Fırat University Journal of Social Science. 15, 51–68.
[65] Lipakis, M. Chrysoulakis, N. and Kamarianakis, Y. (2008) Shoreline extraction using satellite imagery. In: Pranzini, E. and Wetzel, L. (Eds.) Beach erosion monitoring results from BEACHMED-e/OpTIMAL Project. Nuova Grafica Fiorentina, Florence, 87–95.
[66] Hussain, M.A., Tajima, Y., Gunasekara, K., Rana, S. and Hasan, R. (2014) Recent coastline changes at the eastern part of the Meghna Estuary using PALSAR and Landsat images. IOP Conf. Ser. Earth Environ. Sci. 20, 012047.
[67] Al-Mansoori, S. and Al-Marzouqi, F. (2016) Coastline Extraction using Satellite Imagery and Image Processing Techniques. Int. J. Curr. Eng. Technol. 6, 1245–1251.
[68] Özelkan, E. and Karaman, M. (2018) The analysis of the effect of meteorological and hydrological drought on dam lake via multitemporal satellite images: A case study in Atikhisar Dam Lake (Çanakkale). OHU J. Eng. Sci. 7, 1023–1037.
[69] Arkoç, O. and Özşahin, B. (2018) Assessment of coastline change of lakes of Gala Lake National Park (NW Turkey) with multi-temporal satellite images. Kırklareli Univ. J. Eng. Sci. 4, 12–29.
[70] Gibeaut, J.C., Hepner, T., Waldinger, R., Andrews, J., Gutierrez, R., Tremblay, T.A., Smyth, R. and Xu, L. (2001) Changes in gulf shoreline position, Mustang, and North Padre Islands, Texas: A report of the Texas Coastal Coordination Council pursuant to National Oceanic and Atmospheric Administration Award no. NA97OZ0179, GLO Contract Number 00-002R. 30p.
[71] Kale, S. (2017) Analysis of climatic trends in evaporation for Çanakkale (Turkey). Middle East J. Sci. 3, 69–82.
[72] Kale, S., Ejder, T., Hisar, O. and Mutlu, F. (2016) Climate change impacts on streamflow of Karamenderes River (Çanakkale, Turkey). Mar. Sci. Tech. Bull. 5, 1–6.
[73] Kale, S., Ejder, T., Hisar, O. and Mutlu, F. (2016) Effect of climate change on annual streamflow of Bakırçay River. Adıyaman University J. Sci. 5, 1–6.
[74] Ejder, T., Kale, S., Acar, S., Hisar, O. and Mutlu, F. (2016) Effects of climate change on annual streamflow of Kocabaş Stream (Çanakkale, Turkey). J. Sci. Res. Rep. 11, 1–11.
[75] Kale, S., Hisar, O., Sönmez, A.Y., Mutlu, F. and Filho, W.L. (2018) An assessment of the effects of climate change on annual streamflow in rivers in western Turkey. Int. J. Global Warm. 15, 190–211.
[76] Hisar, O., Kale, S. and Özen, Ö. (2015) Sustainability of Effective Use of Water Sources in Turkey. In: Filho, W.L. and Sümer, V. (Eds.) Sustainable Water Use and Management: Examples of New Approaches and Perspectives. Springer, Cham, Switzerland, 205-227.

Received: **02.01.2019**
Accepted: **18.03.2019**

CORRESPONDING AUTHOR

Semih Kale
Çanakkale Onsekiz Mart University
Faculty of Marine Sciences and Technology
17020, Merkez, Çanakkale – Turkey

e-mail: semihkale@comu.edu.tr

© by PSP Volume 28 – No. 5/2019 pages 4340-4352 Fresenius Environmental Bulletin

PHYSICAL AND MECHANICAL PROPERTIES AND INFLUENCE OF DRYING TECHNIQUES ON DRYING CHARACTERISTICS AND SOME QUALITY PARAMETERS OF MALABAR SPINACH (*BASELLA ALBA* L.)

Fusun Hasturk Sahin[1,*], Funda Eryilmaz Acikgoz[2], Merve Eremkere[3], Turkan Aktas[3]

[1]Tekirdag Namik Kemal University, Vocational School of Hayrabolu, Department of Agricultural Machinery, Tekirdag Turkey
[2]Tekirdag Namik Kemal University, Vocational School of Technical Sciences, Department of Plant and Animal Production, Tekirdag Turkey
[3]Tekirdag Namik Kemal University, Faculty of Agriculture, Department of Biosystem Engineering, Tekirdag Turkey

ABSTRACT

The aims of this research were to measure of some physical and mechanical properties and investigate the influence of drying methods on changing of drying kinetics as well some quality properties of Malabar spinach (*Basella alba* L.). For these purposes, Malabar spinach (*Basella alba* L.) was grown in climate-controlled laboratory conditions. Then, the leaves of plant were dried either microwave method or convective hot air drying method. For hot air drying process, three drying temperatures (40, 50 and 60°C) were applied. Three power levels (180, 360 and 600W) were applied for microwave drying process. Mechanical (laceration force, puncture force) and physical properties (leaf lenght, leaf area, stalk thickness, leaf thickness, and initial weight) of fresh Malabar spinach plant samples were measured. Some analyzes such as color (L*, a*, b*), water activity of fresh and dried plant were made to determine quality changes with drying processes. The mean leaf laceration force was determined as 0.0435 kgf while the puncture force value was determined as 0.0144 kgf for fresh leaf samples. Hot air drying process lasted 31, 17 and 6.5 hours for 40, 50 and 60°C drying temperatures, respectively. Microwave drying process took 7.5, 5.5 and 4 minutes for 180, 360 and 600W power levels, respectively. L* and a* values of the samples increased while b* values decreased after all drying applications. Final moisture content values of all dried products were determined between 10.9% and 16%. a_w values of all dried samples were determined lower than the critic level that allows mold growth (a_w <0.6).

KEYWORDS:
Malabar spinach (*Basella alba* L.), hot air drying, microvawe drying, mechanical properties

INTRODUCTION

Fresh vegetables are important as dietary antioxidants and have plenty of bioactive nutrients [1]. They are qualified by high biological quality because of their elevated context of antioxidative components, vitamins and essential minerals [2]. They are playing a significant role in human diet [3].

Basella alba L. or *Basella rubra* Roxb. -Malabar spinach- belongs to the *Basellaceae* family [4, 5]. Malabar Spinach is known as several prevalent nouns, namely Indian spinach, Ceylon spinach and vine spinach. It is cultivated widely in many parts of the world. Its leaves and stems are consumed as food and used in medicine [6]. The pH level of this vegetable (5.3-5.4) is good for skin [5]. Leaves and stems of Malabar spinach have been used since long time as an Ayurvedic cure for some skin illnesses [7] and for inflammation remedy in Thai conventional medicine [8]. Roots and leaves of this vegetable have been used for the elimination of after birth for stomach pains and increasing milk production [9]. Malabar spinach plays an important role in human health because of its chemical composition and properties such as antibacterial, antiviral, antiulser, antioxidant, vitamin [10, 11].

According to Eryilmaz Acikgoz and Adiloglu [11], the true spinach is generally consumed in winter season while Malabar spinach is preferred in warmer climate. Drying process can make that Malabar spinach can be consumed just like true spinach during summer season when true spinach can be found rarely on the market. For Turkey, especially in the summer production of Malabar spinach can be substituted with real spinach *Spinacia oleracea* L.

As it is known, almost all vegetables have quick deterioration feature. For this reason, using of different drying methods or drying systems can be used to dry to increase the shelf-life and ensure seasonal consumption of these vegetables in addition to their fresh consumption.

FIGURE 1
Fresh Malabar spinach leaves

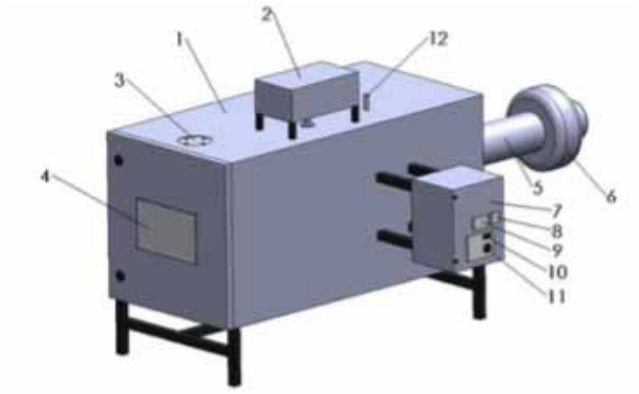

FIGURE 2
Convective hot air dryer
(1: Drying chamber, 2: Scales, 3: Exhaust air outlet, 4: Product entry and exit door, 5: Heater, 6: Fan; 7: Control panel, 8: Heater control switch, 9: Temperature control unit, 10: Power switch, 11: Speed switch, 12: Temperature sensor) [15].

In recent years, dried vegetables have become more important because the food industry directly consume these in place of fresh foods [12]. Longer shelf life makes dried fruits and vegetables more popular, increase product variety and reduced product volume. This can lead to improvements in product quality in food processing applications [13].

The Malabar spinach provides additional benefits over human physiology and metabolic functions beyond the need for essential nutrients to the body. For this reason, it is an important functional food which is defined as foods or food components that are effective in protecting against diseases and reaching a healthier life. In this study, it is aimed to ensure that Malabar spinach used as a functional food which is effective in protection of diseases and to achieve a healthier life is found as a dried product in a season when it is not fresh in the market. This plant has not been dried before. This makes the research original. As in the case of Malabar spinach, vegetables used for drying are no longer just for feeding and for creating meals it is also consumed as a purifying and therapeutic, protective against diseases. For these reasons, in this research, influences of microwave drying and hot air-drying on drying characteristics and some quality parameters of plant were examined in addition to some mechanical and physical properties of Malabar spinach.

MATERIALS AND METHODS

Obtaining of Malabar Spinach. Growing of standard type green Malabar spinach (*Basella alba* L.) samples were carried out in climate-controlled laboratory conditions. Average ambient temperature and humidity values were adjusted as 25ºC and 80%, respective in the climate-controlled lab [11]. Obtained Malabar spinach leaves were shown in Figure 1.

Convective Hot Air Dryer. For hot air-drying applications, convective hot air dryer was used. Dimensions of this drying cabin are 50 cm x 100 cm. Two electrical heaters that were positioned inside heating canal were used to supply hot drying air (Figure 2). The air heating canal that is 50 cm lenght was manufactured from galvanized plates in the form of a cylinder. A centrifuge ventilating fan (Demsan-DYK 18/150) was used to speed up drying air in dryer. This fan can be worked at different speeds by 5-stage speed switch (SCNR5 model). An analogue heat control unit with digital indicator (ARM 396 model) was used to regulate drying air

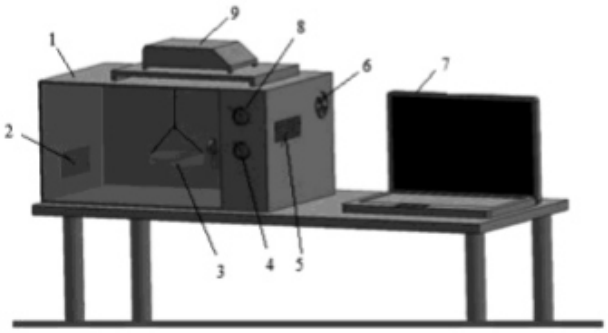

FIGURE 3
Microwave dryer
(1: Microwave oven; 2: Ventilation holes; 3: Tray; 4: Timer; 5: Magnetron; 6: Fan; 7: Computer; 8: Power switch; 9: Scales) [16].

temperature. Drying cabin and air heating cabin were insulated using 30 mm glass wool and aluminium foil to avoid heat losses. Samples were placed on perforated tray to supply the sufficient ventilation to samples [14]. A weighing system includes an electronic scales and sample tray. The scales (AND brand balance) was setted outside the drying cabinet and connected to a PC. Sample tray was connected to electronic scales. Thus, samples were weighed automatically and weights were recorded to the computer periodically.

Microwave Dryer. Microwave drying applications were carried out using a microwave oven (with Beko brand, 2450 MHz frequency, maximum 800 W power and 19 lt capacity) as seen in Fig. 3 [16]. Electronic balance (AND brand) was used to measure the weight losses during microwave drying, continuously using interface programs similar to hot air drying experiments.

Determination of Physical Properties. The movable area measurement device (LI-COR brand LI-3000A) was used to measure of the leaf length and leaf area of Malabar spinach plants. Leaf thickness, stalk thickness and mass of plants were determined according to Hasturk Sahin et al. [17].

Determination of Mechanical Properties (Laceration and Puncture Force). It is important that to identify mechanical properties such as laceration, puncture force etc. which are significant characteristics with regard to post-harvest operations and shelf life. These characteristics of Malabar spinach plants were determined according to Hasturk Sahin et al. [17]. Measurements on mechanical properties were performed as 3 repeat with 3 leaves from 8 plants that were randomly selected.

Determination of Dry Matter. Dry matter amounts were determined by oven drying method using 105°C temperature [18].

Color Analysis. Color measurements of fresh and dried leaf samples were performed using Hunter-Lab tristimulus colorimeter (D25LT Model). CIE L*a*b* color characteristics were measured from 10 points of every sample batch just after drying processes. In addition to changes in L*, a* and b* values (ΔL*, Δa*, Δb*); ΔE*, ΔL*, ΔC* and ΔH* were also calculated using the equations as given below [19].

$$\Delta L^* = L^*_{sample} - L^*_{standard} \qquad \Delta E^* = \sqrt{\Delta L^{*2} + \Delta a^{*2} + \Delta b^{*2}}$$

$$\Delta a^* = a^*_{sample} - a^*_{standard} \qquad \Delta C^* = C^*_{sample} - C^*_{standard}$$

$$\Delta b^* = b^*_{sample} - b^*_{standard} \qquad \Delta H^* = \sqrt{\Delta E^{*2} + \Delta L^{*2} + \Delta C^{*2}}$$

Water Activity Measurements. Water activity values of fresh and dried spinach samples were measured using a water activity measurement equipment by combining Testo 650 data logger. During the measurements, sample was placed in a small chamber. Then, the water in the air is measured after it equilibrates with the sample. Reached equilibrium moisture value was directly measured by a probe which placed into the chamber [20].

Statistical Analysis. All statistical analyses were carried out using PASW Statistics 18 program.

RESULTS AND DISCUSSION

Properties of Fresh Malabar Spinach Leaves. The computation physical and mechanical properties of leaf samples were given in Table 1 with their standard deviations. The physical properties such as leaf lenght, leaf area, stalk thickness, leaf thickness, initial weight and mechanical properties such as laceration force and puncture force were found by various measurement and calculation methods. The mean leaf laceration force was determined as 0.0435 kgf while the puncture force value was determined as 0.0144 kgf for leaf samples.

TABLE 1
Descriptive values for physical, color and mechanical properties of fresh samples

	Minimum value	Maximum value	Mean value	Std. Error	Std. Deviation
Physical properties					
Leaf lenght	5.60	12.00	8.3347	0.18918	1.60529
Leaf area	22.21	102.45	52.1022	2.53031	21.47043
Stalk thickness	1.90	5.20	3.4250	0.11344	0.96261
Leaf thickness	0.25	0.64	.4468	0.01125	0.09544
Initial weight	0.65	4.47	1.9602	0.11739	0.99610
Color properties					
a	-30.04	-19.29	-24.8150	0.25954	2.20223
b	41.44	87.54	64.9099	1.15800	9.82597
L	29.70	45.96	38.2243	0.45495	3.86038
C	39.34	90.59	69.1408	1.21344	10.29642
H	104.90	119.82	111.1075	.27699	2.35037
Mechanical properties					
Laceration force	0.02	0.07	0.0435	0.00124	0.01050
Puncture force	0.00	0.02	0.0144	0.00071	0.00603

TABLE 2
Anova analysis results for physical, color and mechanical properties of fresh samples

		Sum of Squares	df	Mean Square	F	Sig.
Leaf lenght	Between Groups	20.192	7	2.885	1.134	0.353
	Within Groups	162.771	64	2.543		
	Total	182.963	71			
Leaf area	Between Groups	4887.440	7	698.206	1.605	0.150
	Within Groups	27842.100	64	435.033		
	Total	32729.539	71			
Stalk thickness	Between Groups	18.495	7	2.642	3.575	0.003
	Within Groups	47.295	64	0.739		
	Total	65.790	71			
Leaf thickness	Between Groups	0.205	7	0.029	4.248	0.001
	Within Groups	0.442	64	0.007		
	Total	0.647	71			
Initial weight	Between Groups	7.626	7	1.089	1.110	0.368
	Within Groups	62.822	64	0.982		
	Total	70.448	71			
a	Between Groups	166.294	7	23.756	8.539	0.000
	Within Groups	178.044	64	2.782		
	Total	344.337	71			
b	Between Groups	2434.978	7	347.854	5.037	0.000
	Within Groups	4420.049	64	69.063		
	Total	6855.027	71			
L	Between Groups	668.360	7	95.480	15.680	0.000
	Within Groups	389.722	64	6.089		
	Total	1058.083	71			
C	Between Groups	2695.128	7	385.018	5.100	0.000
	Within Groups	4832.022	64	75.500		
	Total	7527.150	71			
H	Between Groups	145.689	7	20.813	5.403	0.000
	Within Groups	246.532	64	3.852		
	Total	392.221	71			
Laceration force	Between Groups	0.002	7	0.000	2.324	0.035
	Within Groups	0.006	64	0.000		
	Total	0.008	71			
Puncture force	Between Groups	0.000	7	0.000	1.679	0.130
	Within Groups	0.002	64	0.000		
	Total	0.003	71			

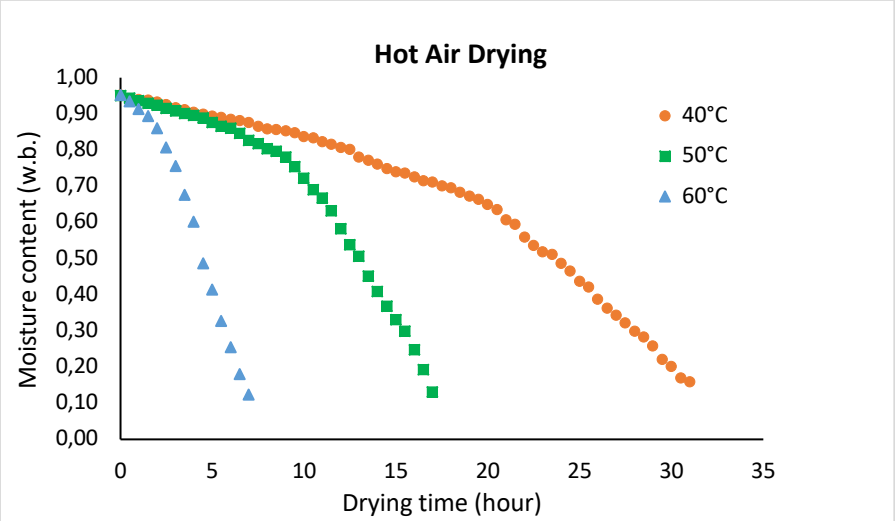

FIGURE 4
Hot air-drying curves for Malabar spinach

Statistical analyzes of these measurements revealed that differences between the mean values calculated for leaf thickness, stalk thickness, laceration force and all color characteristics of the leaves for 8 different spinach plants were found statistically significant ($P < 0.05$) (Table 2).

Hot air-drying kinetics. Relationship between moisture content and drying time during hot air drying of Malabar spinach was given in Figure 4. As seen in this figure, a decrease in drying time occured with the increasing drying temperature. Final moisture content of hot air-dried plant samples were found as 16%, 13.2% and 12.5% for 40°C, 50°C and 60°C drying temperature, respectively.

Doymaz [21] investigated that thin-layer drying of spinach leaves in a convective dryer. Spinach samples were dried using a constant air velocity of 1.2 m/s and four drying air temperatures of 50, 60, 70 and 80°C. Drying rate increased with the increase in drying temperature. Accordingly, the drying time reduced. The drying time reduced from 495 to 165 min when the air temperature was increased from 50 to 80°C. Doymaz [22] researched that thin layer drying behaviour of mint leaves for 35, 45, 55 and 60°C drying temperatures. According to Doymaz [22], the drying periods to reduce moisture content of meant leaves from the 84.7% to 10% at 35, 45, 55 and 60°C temperatures were found as 600, 285, 180 and 105 min, respectively. According to this research results; drying rate increased with the increase of drying air temperature. Results obtained with our research were found parallel to the findings of these researches results.

Drying processes performed using hot air dryer lasted about 31, 17 and 6.5 hours for 40, 50 and 60°C drying temperature, respectively. The moisture content decreased as the drying time increased. Similar results were obtained by Watanabe et al. [23].

Microwave drying kinetics. Microwave drying at 180 W power level lasted 7.5 minutes and final moisture content of spinach sample was determined as 11.5%. At the end of drying, total moisture loss of sample was found as 83.71%. 360W power level applications took 5.5 minutes, moisture content of sample was determined as 11.6% and total moisture loss of samples was 83.61%. Final moisture content of sample was determined as 10.9% at the end of 4 minutes drying time for 600W power level application in microwave drying. This final moisture content value was regarded as the lowest moisture content achieved in all drying applications including with hot air-drying applications. Finally, this period, total moisture loss of leaf samples was found as 84.31%. These changes were shown in Figure 5.

Many researchers found similar results with our results for different type of leafy vegetables. Soysal [24] investigated the microwave drying characteristics of parsley. In that research, seven different microwave output powers (360, 450, 540, 630, 720, 810 and 900W) were tested. Depending on the tested power levels, the microwave drying processes lasted between 3.5-9.75 minutes.

Alibas Ozkan et al. [25] determined that microwave drying characteristics of spinach using 8 different microwave power levels (90, 160, 350, 500, 650, 750, 850 and 1000W). Microwave drying periods were accomplished among 290 and 4005 seconds.

Karaaslan and Tuncer [26] researched that improvement of a drying model for combined microwave-fan-assisted convection drying process of spinach. The drying periods for 180, 360, 540, 720 and 900W microwave powers were determined as 10, 5, 4, 3 and 2.5 minutes, respectively. Researchers indicated that the moisture ratio decreases more quickly while the microwave power is increased.

Namely, the increase in the drying microwave power resulted in a decrease in drying time.

Dadali et al. [27] researched that the influence of microwave output power levels and sample amount on drying kinetics of spinach leave samples. For this purpose, they applied five different power levels (180, 360, 540, 720 and 900W). The microwave drying process took 3.5–18 minutes depending on microwave output power levels. It was found that application of 900W power instead of 180W power shorted the drying time by 80.55%.

As seen in these researches, the drying time of samples was considerably decreased with increasing of the microwave power level. Similar results were also reported by several authors for various foods dried using microwave drying [24, 28, 29, 30, 31, 32].

Changing of color parameters. All dried leaves were shown in Figure 6. It was seen that all of the dried leaves retained their green color tone. On the other hand, some burns occurred on the leaves during microwave drying. In addition to this, rather thin and tender structure spinach leaves samples at the end of microwave drying processeswere obtained compare to hot air dried leaves samples.

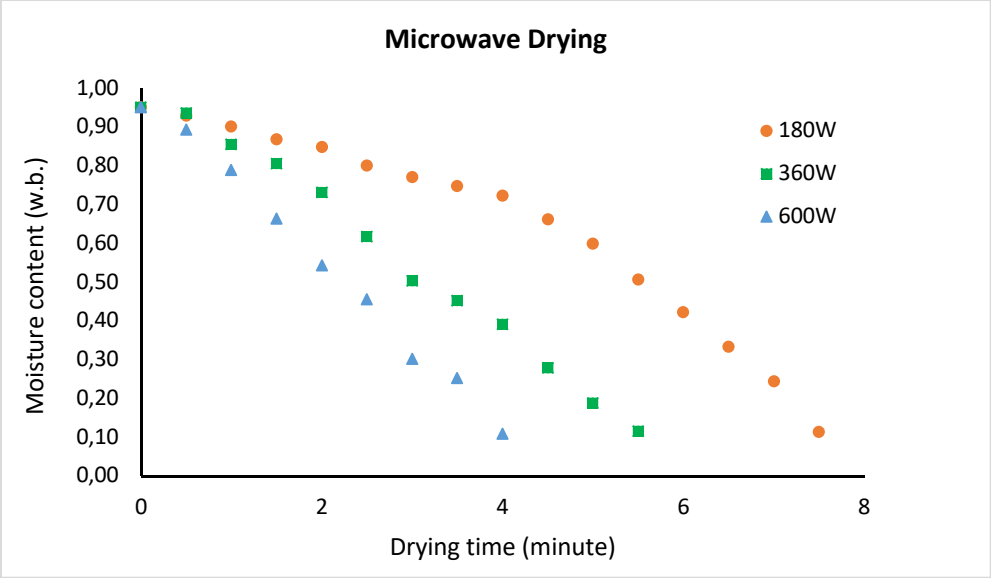

FIGURE 5
Microwave drying curves of Malabar spinach.

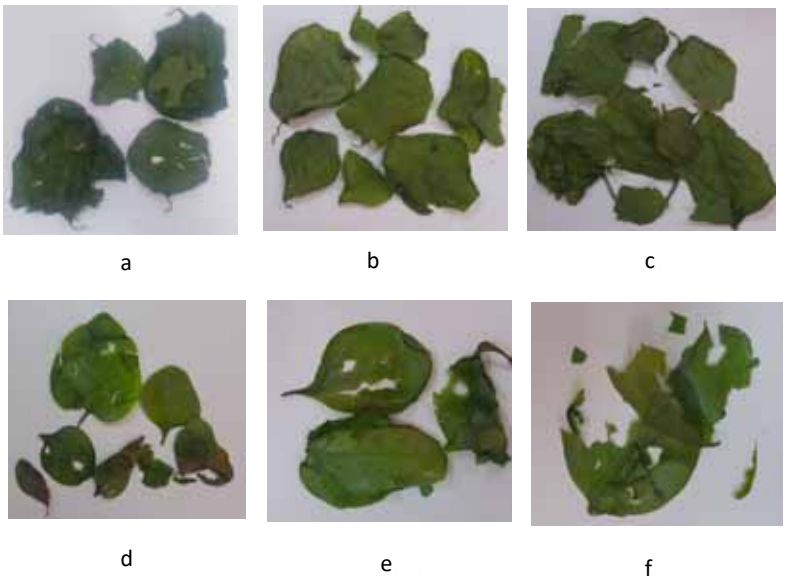

FIGURE 6
Dried leaves (a.40°C, b.50°C, c.60°C, d.180W, e.360W, f.600W applications)

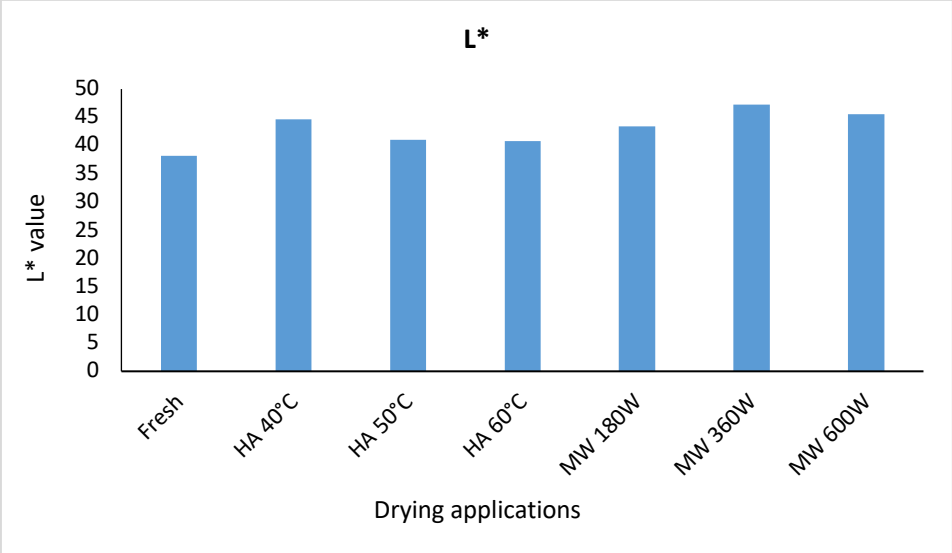

FIGURE 7
Changes of L* values of dried Malabar spinach

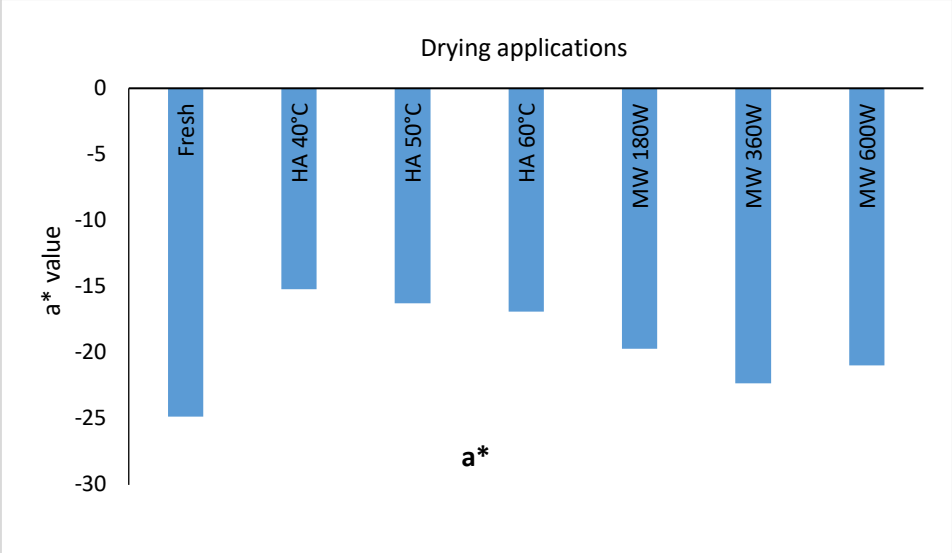

FIGURE 8
Changes of a* values of dried Malabar spinach

The values of L*, a*, b*, C and H are presented in Figs. 7-11. L* values of dried Malabar spinach samples increased compared to that value of fresh sample (Figure 7). This result shows that the brightness of dried samples is higher than fresh ones. It was determined that minimum and maximum L* values were found in the samples that were dried microwave drying at 360W power level (47.19) and hot air drying at 60ºC temperature (40.76), respectively. L* value of fresh sample was determined as 38.22. Alibas Ozkan et al. [25] indicated that L* value losses occured in the dried spinach leaves compared the fresh ones. Dadalı et al. [31] reported that the L value decreased with microwave drying time.

The negative a* value of all dried samples was an expected result because of green color of the leaf samples. a* value of fresh leaf sample was determined as -24.82. a* values of the samples increased with drying applications (Figure 8). This result shows that drying processes decreased green color of plant samples due to negative influences of heat. The a* values of hot air-dried samples were higher than the a* values of microwave dried samples. Karaaslan and Tuncer [26] stated that samples dried by the fan drying method were browner than the samples dried by microwave drying and fan-microwave drying method. According to researchers, the increase of –a* values of samples that were dried fan drying method supported this result. Dadali et al. [31] reported that microwave drying caused more brown compounds.

As seen in Figure 9, b* values decreased after all drying applications. This result shows that the

yellow color tone decreased after all drying processes of leaf samples. b* value of fresh sample was determined as 64.91. b* values of all microwave dried leaf samples were found higher than hot air-dried ones. As a result of hot air-drying applications, b* values of dried samples increased with the rising of drying temperature. It was determined that minimum and maximum b* values were found for the hot air-dried samples that were dried at 40ºC temperature (35.07) and microwave dried samples that were dried at 360W power level (51.18), respectively.

Changing of color parameters were calculated using of L*, a* and b* values of fresh and dried samples as given in Table 3. As seen in Table 3, ΔL* and Δa* values of all samples were found positive while Δb* values of all samples were found negative. It means that dried samples are brighter, more red and more blue compare to fresh sample. Larger ΔE* denotes greater colour change than the reference material namely fresh material [33]. In this case, as seen in Table 3, minimum and maximum color change (ΔE*) occured in microwave dried samples that were dried at 360W power level and hot air-dried samples that were dried at 40ºC temperature, respectively. The ΔC* is the difference in chroma between the sample and standard as identified in a polar coordinate system. The ΔH* is the difference in hue angle between the sample and standard as described in a polar coordinate system [19]. It was determined that minimum and maximum C values were found for the hot air-dried samples that were dried at 40ºC temperature (38.25) and microwave dried samples that were dried at 360W power level (55.86), respectively (Figure 10). C value of samples that were dried using hot air drying at 50 and 60 ºC temperatures and microwave drying at 180 and 600W power levels were found in the same group according to statistically evaluation. Statistically, H values of all dried samples were found in the same group and there was no significant decrease in H values of dried samples compared to color of fresh samples (Figure 11).

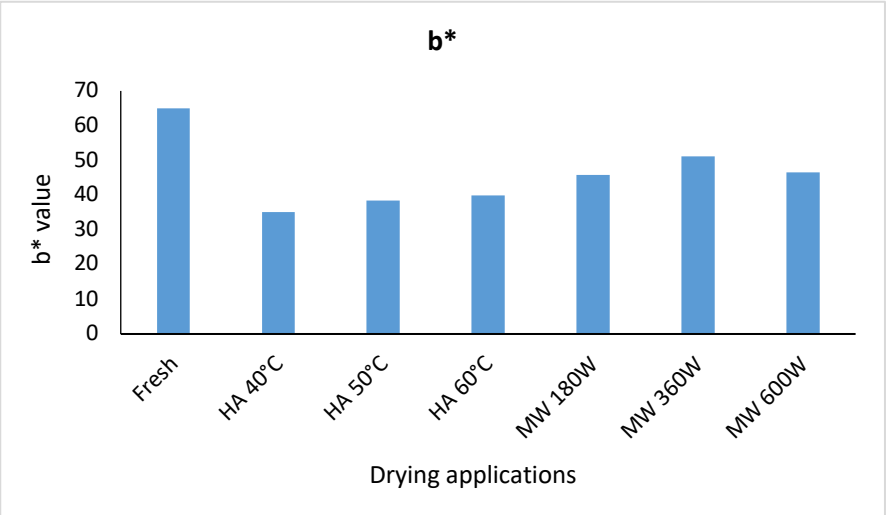

FIGURE 9
Changes of b* values of dried Malabar spinach

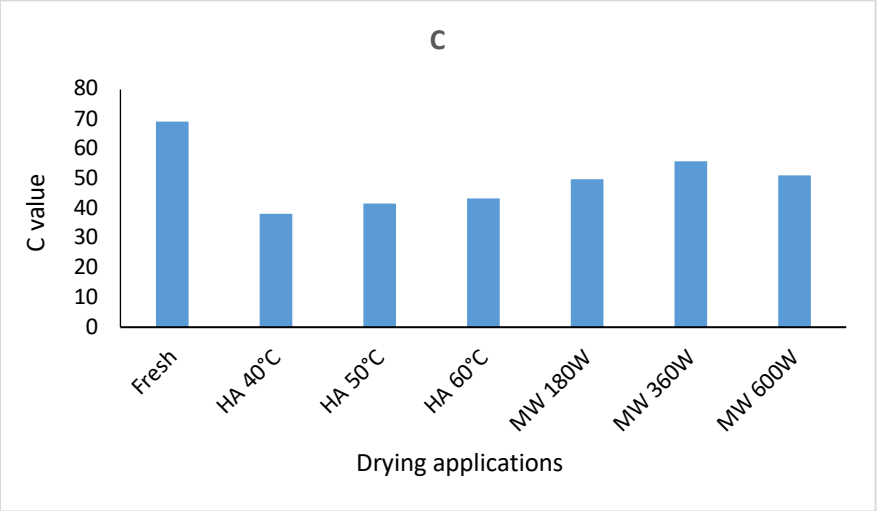

FIGURE 10
Changes of C values of dried Malabar spinach

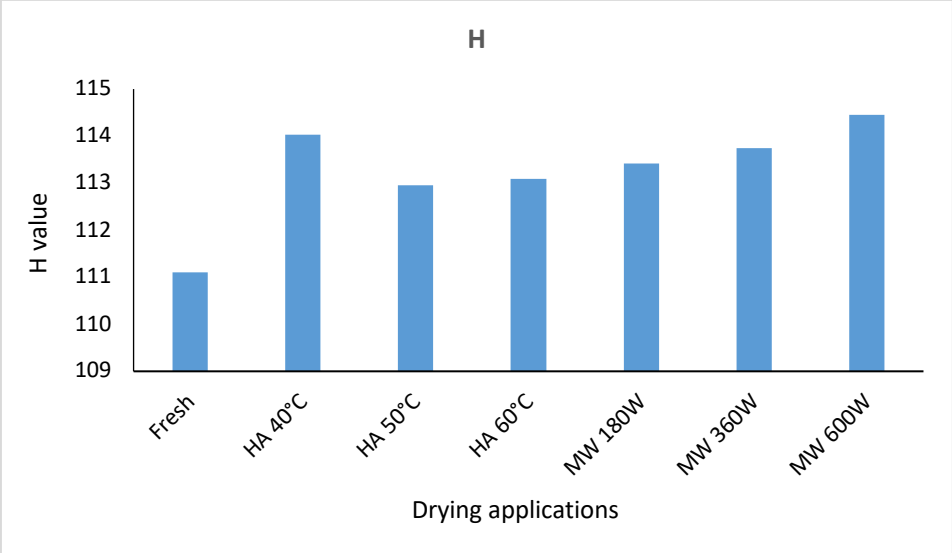

FIGURE 11
Changes of H values of dried Malabar spinach

TABLE 3
Changes the color quality of dried Malabar spinach

Applications	ΔL*	Δa*	Δb*	ΔE*	ΔC*	ΔH*
HAD 40ºC	6.39	9.62	-29.84	32.00	-19.39	37.95
HAD 50ºC	2.82	8.58	-26.53	28.03	-15.94	32.36
HAD 60ºC	2.54	7.93	-24.95	26.30	-14.23	30.01
MWD 180W	5.14	5.12	-19.1	20.43	-7.74	22.45
MWD 360W	8.97	2.49	-13.73	16.59	-1.77	18.94
MWD 600W	7.28	3.86	-18.32	20.09	-6.52	22.34

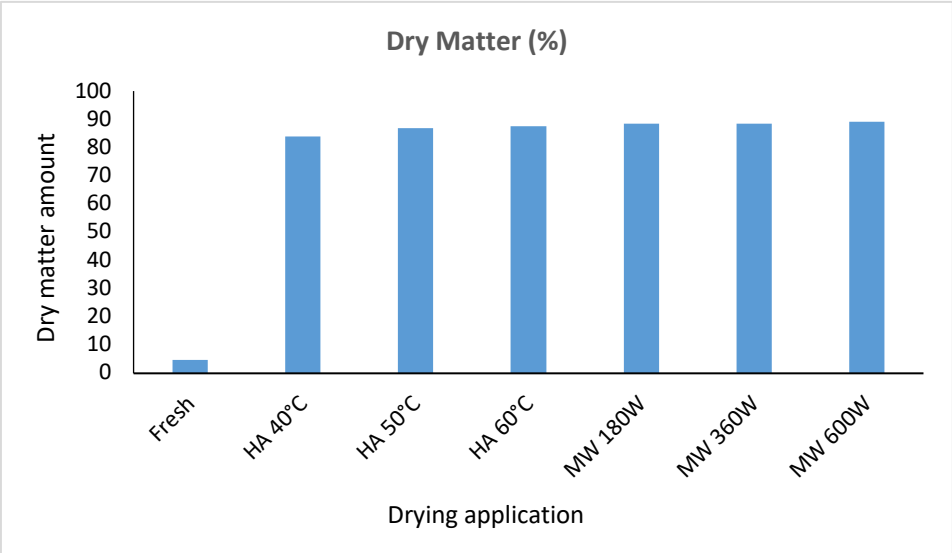

FIGURE 12
Dry matter amounts of Malabar spinach

Changing of dry matter. Changes of dry matter amounts of fresh and dried Malabar spinach leaf samples were shown in Figure 12. Dry matter value of fresh leaf was determined as 4.79% while initial moisture ingredient of plant samples was found to be 95.21% (wet basis). Karaaslan and Tuncer [26] dried the spinach leaves in an oven and they determined initial moisture content of samples as 85%. It was defined that maximum and minimum dry matter amount were found in the samples that were dried microwave method with 600W power level application (89.10%) and hot air drying that was performed at 40ºC temperature (84%), respectively. Moisture contents of these dried products were determined as

10.9% and 16%, respectively and these moisture content values were obtained after 7 minutes and 25.5 hours. Oladele and Aborisade [34] researched that the impact of different storage and drying methods on the quality of *Basella rubra* L. The leaves were dried to roughly 4% moisture content before storage. Lefsrud et al. [35] investigated that stability of carotenoids and dry matter ingredient in spinach and cole during drying. Plants were dried by using oven drying, vacuum drying and freeze-drying methods. Plant samples were dried 120 hours. The moisture content of the samples didn't change considerable in the first 100 h of drying when match the latest 20 h.

Changing of water activity. According to Calıskan Koc and Dirim [36] water activity is an important parameter for dried products because it generally affects the shelf life of the product. Water activity is dissimilar from moisture content as it measures the availability of free water in a food system that is responsible for any biochemical reactions, whereas the moisture content represents the water composition in a food system. High water activity states more free water available for biochemical reactions and therefore, shorter shelf life [37]. Microorganisms can keep their vitality irrespective of the water activity, but for growth bacteria needs a_w >0.8 and yeasts and molds a_w >0.6 [38].

As seen in Figure 13, a_w value decreased for all dried samples. a_w value of fresh leaf samples was determined as 0.975. While minimum a_w value (0.391) was found for 50ºC hot air applications, maximum a_w value (0.529) was found for 600W microwave drying application. a_w values of all dried samples were determined at levels that will not allow mold growth.

The variance analysis results for the samples obtained after drying methods are given in Table 4. Results showed that difference among the mean values of color value of a*, dry matter and water activity of dried samples were found statistically significant ($P<0.05$) while difference among mean values for other properties were found insignificant ($P>0.05$). Duncan test showed that the dissimilar groups as in Table 5 given for mean values.

CONCLUSION

In this research, the mean leaf laceration force was determined as 0.0435 kgf and the puncture force value was determined as 0.0144 kgf for fresh leaf samples as mechanical properties. In all drying methods, the longest drying process lasted 31 hours in hot air drying performed using 40ºC temperature and the shortest drying process took 4 minutes in microwave drying performed using 600W power level application. In this research, dried Malabar spinach leaves were examined in terms of important color criteria, such as L*, a* and b*. According the results, the brightness of dried samples is higher than fresh ones. a* rates of hot air-dried leaves were higher than a* rates of microwave dried leaves. b* rates decreased after all drying applications. This result shows that the yellow color tone decreased after all drying processes of leaf samples. Moisture ingredients and water activity rates of all dried plants ranged from 10.9% to 16% and 0.391 to 0.529, respectively. a_w rates of all dried samples were determined at levels that will not allow mold growth.

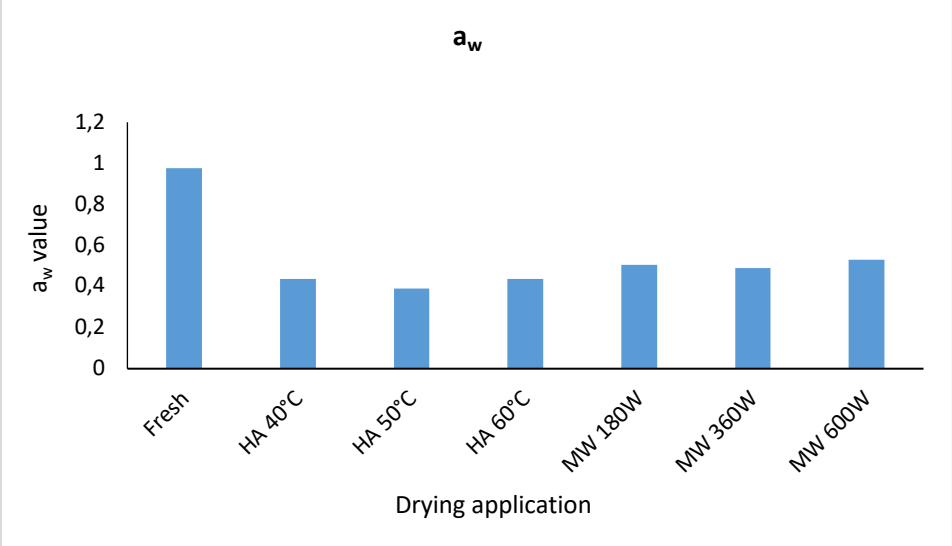

FIGURE 13
Water activity values of Malabar spinach

TABLE 4
Anova analysis result for color, dry matter and water activity properties of dried samples

		Sum of Squares	df	Mean Square	F	Sig.
Replicaton	Between Groups	0.000	5	0.000	0.000	1.000
	Within Groups	12.000	12	1.000		
	Total	12.000	17			
a	Between Groups	122.205	5	24.441	5.781	0.006
	Within Groups	50.735	12	4.228		
	Total	172.941	17			
b	Between Groups	543.110	5	108.622	1.682	0.213
	Within Groups	774.974	12	64.581		
	Total	1318.084	17			
c	Between Groups	662.833	5	132.567	2.010	0.149
	Within Groups	791.591	12	65.966		
	Total	1454.424	17			
L	Between Groups	96.119	5	19.224	2.581	0.083
	Within Groups	89.370	12	7.447		
	Total	185.489	17			
H	Between Groups	4.936	5	.987	0.224	0.945
	Within Groups	52.854	12	4.405		
	Total	57.791	17			
Dry matter	Between Groups	51.085	5	10.217	13.545	0.000
	Within Groups	9.052	12	.754		
	Total	60.137	17			
Water activity	Between Groups	0.040	5	.008	69.404	0.000
	Within Groups	0.001	12	.000		
	Total	0.041	17			

TABLE 5
Mean color, dry matter and water activity values for dried samples

	Color parameters						
Drying Methods	L	a	b	C	H	Dry matter (%)	Water activity
HAD 40°C	$44,61^{ab}$	$-15,20^{a}$	$35,07^{b}$	$38,25^{b}$	$114,03^{a}$	$84,00^{c}$	$0,44^{c}$
HAD 50°C	$41,04^{b}$	$-16,24^{ab}$	$38,38^{ab}$	$41,68^{ab}$	$112,95^{a}$	$86,80^{b}$	$0,39^{d}$
HAD 60°C	$40,76^{b}$	$-16,89^{ab}$	$39,96^{ab}$	$43,41^{ab}$	$113,09^{a}$	$87,50^{ab}$	$0,44^{c}$
MWD 180W	$43,36^{ab}$	$-19,70^{bc}$	$45,81^{ab}$	$49,89^{ab}$	$113,42^{a}$	$88,50^{a}$	$0,51^{b}$
MWD 360W	$47,19^{a}$	$-22,33^{c}$	$51,18^{a}$	$55,86^{a}$	$113,75^{a}$	$88,40^{ab}$	$0,49^{b}$
MWD 600W	$45,50^{ab}$	$-20,96^{c}$	$46,59^{ab}$	$51,11^{ab}$	$114,45^{a}$	$89,10^{a}$	$0,53^{a}$

Dry matter and water activity values for fresh samples are 4.79% and 0.975, respectively
Different letters in the same column shows that average values are statistically important ($p<0.05$)

REFERENCES

[1] Qiu, J., Chen, G., Xu, J., Luo, E., Liu, Y., Wang, F., Zhou, H., Liu, Y., Zhu, F., Ouyang, G. (2016) In vivo tracing of organochloride and organophosphorus pesticides in different organs of hydroponically grown Malabar spinach (*Basella alba* L.). Journal of Hazardous Materials. 316, 52-59.

[2] Lisiewska, Z., Gebczynski, P., Bernas, E., Kmiecik, W. (2009) Retention of mineral constituents in frozen leafy vegetables prepared for consumption. Journal of Food Composition and Analysis. 22, 218-223.

[3] Pinto, E., Petisca, C., Amaro, L.F., Pinho, O., Ferreira, I.M.P.L.V.O. (2010) Influence of different extraction conditions and sample pretreatments on quantification of nitrate and nitrite in spinach and lettuce. Journal of Liquid Chromatography and Related Technologies. 33(5), 591-602.

[4] Deshmukh, S.A., Gaikwad, D.K. (2014) A review of the taxonomy, ethno botany, photochemistry and pharmacology of *Basella alba* (*Basellaceae*). J. Appl. Pharm. Sci. 40, 153-165.

[5] Adhikari, R., Naveen Kumar, H.N., Shruthi, S.D. (2012) A review on medicinal importance of *Basella alba* L. International Journal of Pharmaceutical Sciences and Drug Research. 4(2), 110-114.

[6] Aboshi, T., Ishiguri, S., Shiono, Y., Murayama, T. (2018) Flavonoid glycosides in Malabar spinach *Basella alba* inhibit the growth of Spodoptera litura larvae. Bioscience, Biotechnology and Biochemistry. 82(1), 9-14.
[7] Reddy, M.T., Begum, H., Sunil, N., Rao, P.S., Sivaraj, N., Kumar, S. (2014) Preliminary characterization and evaluation of landraces of Indian spinach (*Basella spp.* L.) for agro-economic and quality traits. Plant Breed. Biotech. 2(1), 48-63.
[8] Lourith, N., Kanlayavattanakul, M. (2017) Ceylon spinach: A promising crop for skin hydrating products. Industrial Crops and Products. 105, 24-28.
[9] Pascaline, J., Charles, M., George, O., Lukhoba, C., Nyamaka Ruth, L., Manani Solomon, D. (2010) Ethnobotanical survey and propagation of some endangered medicinal plants from south Nandi district of Kenya. Journal of Animal and Plant Sciences. 8(3), 1016-1043.
[10] Siriwatanametanon, N., Fiebich, B.L., Efferth, T., Prieto, J.M., Heinrich, M. (2010) Traditionally used Thai medicinal plants: In vitro anti-inflammatory, anticancer and antioxidant activities. J. Ethnopharmacol. 130(2), 196-207.
[11] Eryilmaz Acikgoz, F., Adiloglu, S. (2018) A review on a new exotic vegetable for Turkey: Malabar spinach (*Basella alba* L. or *Basella rubra* L.). Journal of Horticulture. 5(3).
[12] Aktas, T., Hasturk Sahin, F., Fujii, S., Yamamoto, S. (2010) Adsorption isotherms of freeze-dried vegetables. 17th International Drying Symposium (IDS 2010). Magdeburg, Germany, 3-6 October.
[13] Parakash, S., Jha, S.K., Datta, N. (2004) Performance evaluation of blanched carrots dried by three different driers. Journal of Food Engineering. 62(3), 305-313.
[14] Hasturk Sahin, F., Aktas, T., Orak, H.H., Ulger, P. (2011) Influence of pretreatments and different drying methods on color parameters and lycopene content of dried tomato. Bulgarian Journal of Agricultural Science. 17(6), 867-881.
[15] Hasturk Sahin, F., Aktas, T., Altan, D.D., Eryilmaz Acikgoz, F. (2017) Effects of different drying techniques on drying characteristics and some quality attributes of sorrel (*Rumex acetosa* L.). Oxidation Communications. 40(I-II), 345-358.
[16] Celen, S., Aktas, T., Karabeyoglu, S.S., Akyildiz, A. (2016) Drying behavior of prina (crude olive cake) using different type of dryers. Drying Technology. 34(7), 843-853.
[17] Hasturk Sahin, F., Aktas, T., Eryilmaz Acikgoz, F., Akcay, T. (2016) Some technical and mechanical properties of mibuna (*Brassica rapa var. nipposinica*) and mizuna (*Brassica rapa var. Japonica*). PeerJ. 2016, 23p.
[18] Cemeroglu, B. (2007) Food Analysis. The Association of Food Technology Publications. No: 34. Bizim Buro Press, Ankara, 535p. (In Turkish).
[19] Anonymous (1996) CIE L*a*b* Color Scale. Applications Note-Insight on Color, Henter-Lab. 8, 1-4.
[20] Aktas, T., Polat, R. (2007) Changes in the drying characteristics and water activity values of selected pistachio cultivars during hot air drying. Journal of Food Process Engineering. 30(5), 607-624.
[21] Doymaz, I. (2009) Thin-layer drying of spinach leaves in a convective dryer. Journal of Food Process Engineering. 32, 112-125.
[22] Doymaz, I. (2006) Thin-layer drying behaviour of mint leaves. Journal of Food Engineering. 74, 370-375.
[23] Watanabe, T., Orikasa, T., Shono, H., Koide, S., Ando, Y., Shiina, T., Tagawa, A. (2016) The influence of inhibit avoid water defect responses by heat pretreatment on hot air-drying rate of spinach. Journal of Food Engineering. 168, 113-118.
[24] Soysal, Y. (2004) Microwave drying characteristics of parsley. Biosystems Engineering. 89(2), 167-173.
[25] Alibas Ozkan, I., Akbudak, B., Akbudak, N. (2007) Microwave drying characteristics of spinach. Journal of Food Engineering. 78, 577-583.
[26] Karaaslan, S.N., Tuncer, I.K. (2008) Development of a drying model for combined microwave-fan-assisted convection drying of spinach. Biosystems Engineering. 100, 44-52.
[27] Dadali, G., Demirhan, E., Ozbek, B. (2007a) Microwave heat treatment of spinach: drying kinetics and effective moisture diffusivity. Drying Technology. 25(10), 1703-1712.
[28] Dadalı, G., Kılıc Apar, D., Ozbek, B. (2007b) Microwave drying kinetics of okra. Drying Technology. 25(5), 917-924.
[29] Wang, J., Xiong, Y.S., Yu, Y. (2004) Microwave drying characteristics of potato and the effect of different microwave powers on the dried quality of potato. Eur. Food Res. Technol. 219, 500-506.
[30] Alibas, I. (2009) Microwave, vacuum and air-drying characteristics of collard leaves. Drying Technology. 27(11), 1266-1273.
[31] Dadali, G., Demirhan, E., Ozbek, B. (2007c) Color change kinetics of spinach undergoing microwave drying. Drying Technology. 25(10), 1713-1723.
[32] Prabhanjan, D.G., Ramaswamyb, H.S., Raghavan, G.S.V. (1995) Microwave-assisted convective air drying of thin layer carrots. Journal of Food Engineering. 25, 283-293.

[33] Maskan, M. (2000) Microwave/air and microwave finish drying of banana. Journal of Food Engineering. 44(2), 71-78.
[34] Oladele, O.O., Aborisade, A.T. (2009) Influence of different drying methods and storage on the quality of Indian spinach (*Basella rubra* L.). American Journal of Food Technology. 4(2), 66-70.
[35] Lefsrud, M., Kopsell, D., Sams, C., Wills, J., Both, A.J. (2008) Dry matter content and stability of carotenoids in kale and spinach during drying. Hortscience. 43(6), 1731-1736.
[36] Calıskan Koc, G., Dirim, S.N. (2018) Spray dried spinach juice: powder properties. Journal of Food Measurement and Characterization. 12(3), 1654-1668.
[37] Quek, S.Y., Chok, N.K., Swedlund, P. (2007) The physicochemical properties of spray dried watermelon powders. Chemical Engineering and Processing. 46, 386-392.
[38] Vesterlund, S., Salminen, K., Salminen, S. (2012) Water activity in dry foods containing live probiotic bacteria should be carefully considered: A case study with *Lactobacillus rhamnosus* GG in flaxseed. International Journal of Food Microbiology. 157(2), 319-321.

Received: **08.01.2019**
Accepted: **26.03.2019**

CORRESPONDING AUTHOR

Fusun Hasturk Sahin
Tekirdag Namik Kemal University,
Vocational School of Hayrabolu,
Department of Agricultural Machinery,
Tekirdag – Turkey

e-mail: fhasturk@nku.edu.tr

© by PSP Volume 28 – No. 5/2019 pages 4353-4356 Fresenius Environmental Bulletin

STUDY ON INFLUENCING FACTORS ON POLLEN CALLUS AND ADVENTITIOUS BUD INDUCTION IN ANTHER CULTURE OF POPULUS SIMONII×POPULUS NIGRA

Zhilu Zhang*, Zhonghua Liu

Pingdingshan University, Southern Section of Weilai Road, Xinhua District, Pingdingshan City, Henan Province, 467000, China

ABSTRACT

An efficient in vitro pollen callus induction and adventitious bud differentiation system was established in Populus simonii×Populus nigra. Factors influencing culture efficiency, including plant growth regulators, source of callus, temperature, light conditions, and low temperature storage period of anthers were investigated. The relationship between each other is studied. The results show that successive dark and 25°C were best for promoting pollen callus induction (87.4%), bud differentiation frequency of pollen callus was highest (72.5%).

KEYWORDS:
Influencing factors, Populus simonii×Populus nigra, Pollen Callus, Anther Culture

INTRODUCTION

Poplar, as a model forest tree, has been widely used in biotechnology and genetic studies [1-5]. Because poplar is dioecious and undergoes cross-pollination, its genome is characterized by a high level of heterozygosity, which has posed a significant obstacle in poplar breeding and genetic research [6]. Haploid techniques are a valuable tool for the rapid production of homozygous transgenic plants, thereby accelerating cultivar improvement and enabling a timely response to changing market requirements.

In the 1950s, haploid culture was used for tree species, but remained at the callus induction stage. Among the various haploid culture methods, anther culture has been the most conducive to recovering homozygous inbred lines and for generating haploid plants of poplar species and other forest trees [7]. Although many studies have reported the production of haploid poplar, the results of anther culture of poplars have been disappointing and negligible compared with most of the results for herbaceous crops [8], and transgenic haploid poplar plants have not yet been generated.

Success of the procedure depends on the culture medium composition [9, 10], culture conditions [11], pretreatment [12], microspore developmental stages [13], callus formation and plantlet regeneration [14]. Low culture efficiency, early spontaneous chromosome doubling and somatic regeneration from the anther wall tissue are the main obstacles to obtaining pollen plants [15].

In this paper, the effects of different culture conditions on callus induction and adventitious bud formation of Populus euphratica were studied, and the ways to optimize culture conditions and improve culture efficiency were obtained, which provided a convenient and feasible technical method for Populus simonii×Populus nigra single sports species.

MATERIALS AND METHODS

Plant materials and flower induction. Branches of male Populus simonii×Populus nigra were collected from Pingdingshan City in February 2017. The materials were transported to the greenhouse and stored in a cellar at 0°C for 1 week, then grown hydroponically at room temperature (16–20°C) to induce flowering.

Isolation and culture of anthers. Anthers were isolated and developmental stages observed micorscopically from February to April. Mid- and late-uninucleate anthers were agitated in 75% ethanol for 1 min, surface-sterilized using 30% hydrogen peroxide for 10 min, and then rinsed five times with sterile distilled water. Isolated anthers were cultured on MS medium containing 30 g/L sugar supplemented with 2.0 mg/L 2,4-dichlorophenoxyacetic acid (2,4-D) and 0.5 mg/L kinetin (KN) for callus induction. Materials were cultured at 25°C under illumination at 45 μmol/m^{2}s with white light, 25°C in the dark, or 21°C under red light with the same wavelength for 20–70 days.

Adventitious bud induction. After 4 weeks of callus induction, the callus was cultured in MS medium supplemented with different concentrations of 6-benzylaminopurine (6-BA), a-naphthaleneacetic acid (NAA) and thidiazuron

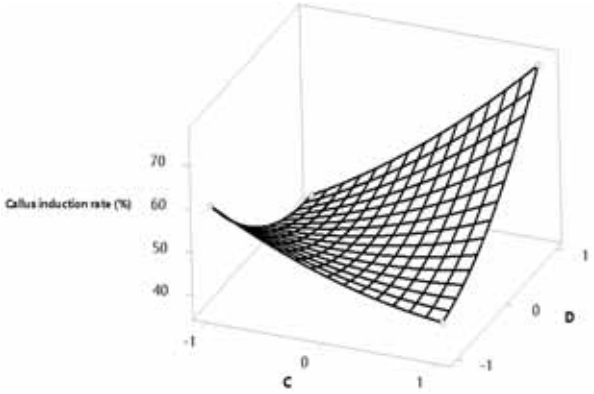

FIGURE 1
Surface Plot of Callus induction (%) vs D, C

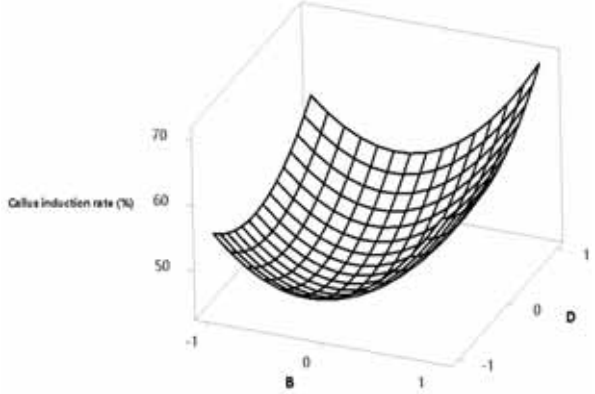

FIGURE 2
Surface Plot of Callus induction rate (%) vs D, B

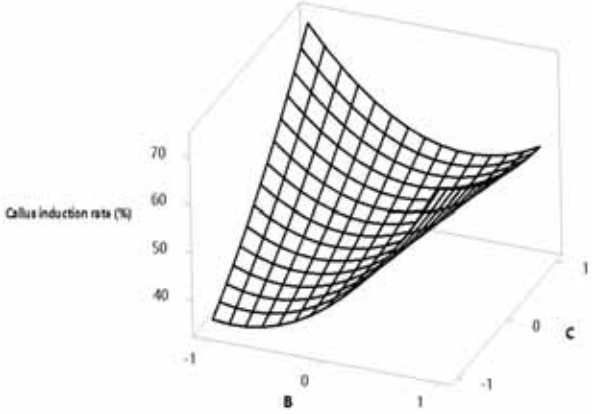

FIGURE 3
Surface Plot of Callus induction rate (%) vs C, B

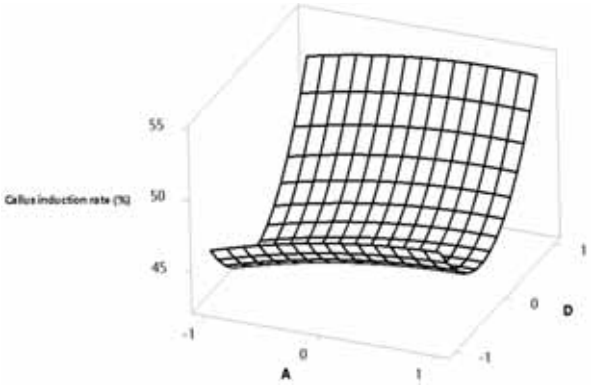

FIGURE 4
Surface Plot of Callus induction rate (%) vs D, A

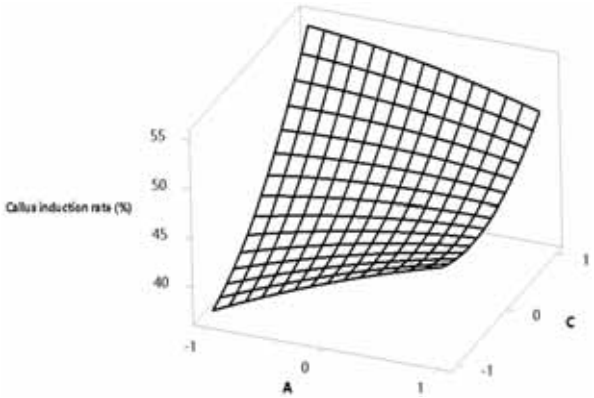

FIGURE 5
Surface Plot of Callus induction rate (%) vs C, A

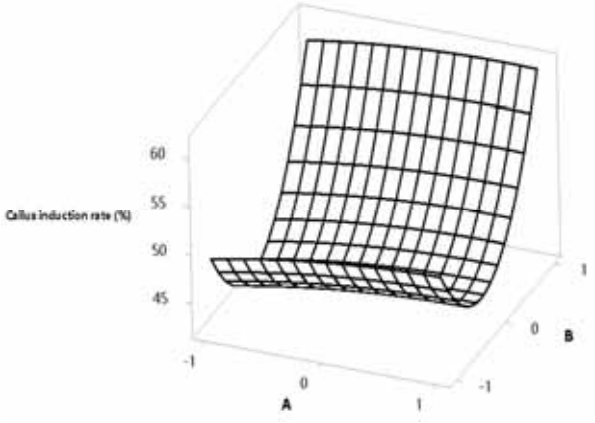

FIGURE 6
Surface Plot of Callus induction rate (%) vs B, A

(TDZ). The cultures were incubated under a 16 h light/8 h dark photoperiod at 25°C under illumination at 45 μmol/m^2s with cool fluorescent lights. After 4 weeks, the induction frequency (%) was calculated to determine the optimal culture conditions for adventitious buds induction.

RESULTS AND DISCUSSION

After one week of preservation of the anthers, from the fourth day of culture, some of the anther wounds began to expand. The texture is tight and the growth is slow. Microscopic observation showed that the two callus had been adhered together from the induction period, but the two basically maintained their original shape during the proliferation process, and it was easier to distinguish after transferring to the adventitious bud induction medium. Pollen callus appeared most on the 20 th to 40 th day of culture, and a small amount was produced after 50 days. The callus induction time lasted for 10 weeks. There was no significant difference in the callus induction rate of pollen grains induced by different methods 20 days before culture. From the 30 th day, the callus induc-

tion rate induced under different temperature and light conditions was very significant. Among them, for 25°C dark culture, the difference between the induction rate and other places was extremely significant; the induction rate was up to 87.4% after 70 days of culture (Figure 1-3). The general trend is that the culture temperature is 25°C and the dark medium culture is more suitable for the induction of pollen callus of Populus euphratica than 22°C and light culture.

The effect of red light on callus induction was not obvious. The anthers stored at low temperature for 7 weeks, 2 weeks after inoculation, a large number of anthers browned and died, resulting in a significant decrease in callus induction rate of anthers. The callus induction rate was significantly different under different temperature and light conditions, and the trend was the same as that of the anther stored at 1 week, that is, the induction rate in the dark culture at 25 °C was up to 23.8%, but the induction rate was only 1 week. 33.3% of the time (Fig.4-6).

The low induction rate of pollen callus is one of the main problems affecting the efficiency of poplar anther culture. The induction rate of pollen callus of Populus euphratica was relatively low, only 9.92%, 6.09%. The culture system established in this paper can significantly increase the induction rate of pollen callus, up to 87.4%. It is thought that the closer to the natural flowering period, the higher the pollen callus induction rate. However, the results of this paper indicate that the anthers of the early harvesting in early February can also obtain high pollen callus induction rate. Therefore, we believe that the time of picking is not the root cause of pollen callus induction ability. As long as the culture conditions are appropriate, the anthers in the dormant period still have considerable pollen callus induction ability. However, the time spent on the flowering branches at low temperatures should not be too long, which is consistent with our previous results.

Induction of adventitious buds. After 30 days of cryopreservation for 1 week, the induced pollen callus was transferred to medium supplemented with 1.0 mglL 6-BA, cultured under different temperature and light conditions, and gradually changed to green at about 1 week, 4 weeks. After subculture with the same medium once, a cluster of adventitious buds emerged from the green callus. The induction rate of adventitious buds under different temperature and light conditions was significantly different. The general trend was that the induction rate of culture temperature was higher than 22°C at 25°C, and the culture under light was higher than that in dark culture. The adventitious bud induction rate was the highest (72.5%) at 25°C. The effect of red light on the induction of adventitious buds was not obvious. The anther wall callus continued to proliferate throughout the culture process, and no adventitious buds were observed. In addition, when the pollen callus formed during the 3070 d anther culture was transferred to a medium containing different plant growth regulators, the adventitious bud induction rate was significantly lower than that of the callus formed 30 days before the culture. Callus in the first 30 days is more likely to induce budding. The effect of TDZ alone treatment is not obvious, but it can increase the induction rate of adventitious buds when mixed with other plant growth regulators.

It is generally believed that when the indica is induced to dedifferentiate, the inoculum should be cultured at 20-28°C, while the adventitious bud induction can be under light (8-16 h/d) and variable temperature (15-20°C). to cultivate. However, there is still no systematic study on the influence of culture environment on the culture of anthers of Populus nigra. In this paper, the pollen callus and adventitious bud induction of the small black poplar are consistent with the temperature requirement, that is, the culture at 25°C is better than 22°C. However, the requirements for light are different. Dark culture is more conducive to pollen callus induction, while adventitious bud induction rate in light culture is significantly higher than dark culture.

CONCLUSIONS

An efficient in vitro pollen callus induction and adventitious bud differentiation system was established in Populus simonii×Populus nigra. Factors influencing culture efficiency, including plant growth regulators, source of callus, temperature, light conditions, and low temperature storage period of anthers were investigated. The relationship between each other is studied. The results show that successive dark and 25°C were best for promoting pollen callus induction (87.4%), bud differentiation frequency of pollen callus was highest (72.5%).

ACKNOWLEDGEMENTS

This paper is supported by National Science Fund for Young Scholars (No. 31600527).

REFERENCES

[1] Demiral, H. (2016) Activated carbons prepared from poplar wood: characterisation and phenol adsorption. Fresen Environ Bull. 25, 4669-4679.

[2] Mao, R., Zeng, D.H. (2013) Effect of land-use change from cropland to poplar-based agroforestry on soil properties in a semiarid region of northeast China. Fresen Environ Bull. 22, 1077-1084.
[3] Taylor, G. (2002) Populus: Arabidopsis for forestry. Do we need a model tree? Ann Bot. 90, 681–689.
[4] Wullschleger, S.D., Jansson, S., Taylor, G. (2002) Genomics and forest biology: Populus emerges as the perennial favorite. Plant Cell. 14, 2651–2655.
[5] Zhao, H., Wang, S., Chen, S., Jiang, J., Liu, G.F. (2015) Phylogenetic and stress-responsive expression analysis of 20 WRKY genes in Populus simonii×Populus nigra. Gene. 565, 130-139.
[6] Deutscha, F., Kumlehnb, J., Ziegenhagenc, B., Fladunga, M. (2004) Stable haploid poplar callus lines from immature pollen culture. Physiol Plant. 120, 613–622.
[7] Kuhn, A., Ballach, H.J., Wittig, R. (1998) Seasonal variation of the distribution of polycyclic aromatic hydrocarbons in poplar leaves. Fresen. Environ. Bull. 7, 164-169.
[8] Yang, J.L., Li, K., Li, C.Y., Li, J.X., Zhao, B., Zheng, W., Gao, Y.C., Li, C.G. (2018) In vitro anther culture and Agrobacterium-mediated transformation of the AP1 gene from Salix integra Linn. in haploid poplar (Populus simonii × P. nigra). Journal of Forestry Research. 29, 321–330.
[9] Newcombe, G. (2003) Native Venturia inopina sp. nov., specific to Populus trichocarpa and its hybrids. Mycological Research. 107, 108-116.
[10] Asaduzzaman, M., Bari, M.A., Rahman, M.H., Khatun, N., Islam, M.A., Rahman, M. (2003) In vitro plant regeneration through anther culture of five rice varieties. J Biol Sci. 3, 167–171.
[11] Raina, S.K., Ifran, S.T. (1998) High-frequency embryogenesis and plantlet regeneration from isolated microspores of indica rice. Plant Cell Rep. 17, 957–962.
[12] Trejo-Tapia, G., Amaya, U.M., Morales, G.S., Sanchez, A.D.J., Bonfil, B.M., Rodriguez-Monroy, M., Jimenez-Aparicio, A. (2002) The effects of cold-pretreatment, auxins and carbon source on anther culture of rice. Plant Cell Tissue Organ Cult. 71, 41–46.
[13] Afza, R., Shen, M., Zapata-Arias, F.J., Xie, J., Fundi, H.K., Lee, K.S., Bobadilla-Mucino, E., Kodym, A. (2000) Effect of spikelet position on rice anther culture efficiency. Plant Sci. 153, 155–159.
[14] Orshinsky, B.R., Sadasivaiah, R.S. (1997) Effect of plant growth conditions, plating density and genotype on the anther culture response of soft white spring wheat hybrids. Plant Cell Rep. 16, 758–762.
[15] Stober, A., Hess, D. (1997) Spike pretreatments, anther culture conditions and anther culture response of seventeen German varieties of spring wheat (Triticum aestivum L.). Plant Breed. 116, 443–447.

Received: **25.01.2019**
Accepted: **29.03.2019**

CORRESPONDING AUTHOR

Zhilu Zhang
Pingdingshan University
Pingdingshan City,
Henan Province 467000 – China

e-mail: zhangzhilu9998a@hotmail.com

© by PSP Volume 28 – No. 5/2019 pages 4357-4362 Fresenius Environmental Bulletin

SCREENING OF ADSORBENTS IN THE PHYTOREMEDIATION OF MERCURY-CONTAMINATED SOIL

Zhongchuang Liu[1,2,*], Boning Chen[3], Li-ao Wang[4,5], Xiang Li[6]

[1]Green Intelligence Environmental School, Yangtze Normal University, 16 Juxian Rd. Lidu, Fuling District of Chongqing, China
[2]Chongqing Multiple-source Technology Engineering Research Center for Ecological Environment Monitoring, Yangtze Normal University, 16 Juxian Rd. Lidu, Fuling District of Chongqing, China
[3] Fuling Environmental Monitoring Center, 3 Taibai Rd. Fuling New District of Chongqing, China
[4]State Key Laboratory of Coal Mine Disaster Dynamics and Control, Chongqing University, 174 Shazheng Street, Shapingba District, Chongqing, China
[5]College of Resources and Environmental Science, Chongqing University, 174 Shazheng Street, Shapingba District, Chongqing, China
[6]International Policy, Faculty of Law and Economics, Chiba University, 1-33, Yayoi-cho, Inage-ku, Chiba-shi, Chiba, 263-8522, Japan

ABSTRACT

In this study, activated carbon, cation exchange resin and zinc powder were selected to adsorb volatile mercury. The specific surface area of cation exchange resin was smaller than that of activated carbon and zinc powder. Among the three adsorbents, activated carbon demonstrated the best adsorption effect on mercury, followed by cation exchange resin, and then zinc powder which exhibited a poor adsorption effect. The best adsorption effect was observed when the weight of adsorbents was 4 g. Since the weight of adsorbents as well as the distance between adsorbent and mercury source had little influence on the effect of adsorbents in capturing the volatile mercury, the best adsorbent was found to be activated carbon.

KEYWORDS:
Adsorbent, Volatile mercury, Secondary pollution

INTRODUCTION

Elemental mercury (Hg^0) and organic mercury ($(CH_3)_2Hg$ have higher vapor pressure and hence a strong volatility. In mercury-contaminated areas, Hg^0 and $(CH_3)_2Hg$ in the soil vaporise into air. Relevant research results show that soil can become a huge mercury pool under certain conditions [1, 2]. One of the main sources of mercury in the atmosphere is the release of large amounts of mercury from soil through diffusion [1, 2]. Hg^0 in the soil can be obtained by the transformation of Hg^{2+} under abiotic or microbial actions [3, 4]. Under sunlight active mercury (mainly Hg^{2+}) in the soil can easily be reduced to Hg^0. Humic acid and fulvic acid in the soil can convert Hg^{2+} to Hg^0 [5]. In the presence of sunlight abiotic process accelerates the transformation thereby enhancing the volatility of mercury [5]. Some bacteria can convert Hg^{2+} into Hg^0 by means of mercury reductase (MerA) [6]. Kim et al. [7] found that the larger the difference between the concentration of mercury in soil-air and that in air near soil, the faster the release of mercury. Generally, the higher the solubility of mercury in the soil, the greater the amount of mercury release. Based on the study of Pedron et al. [8] the addition of chelating agents to mercury-contaminated soils could promote the absorption of mercury by plants, but the chelating agents could also promote the volatilization of mercury. Few studies have reported that a part of mercury could be released into the atmosphere during the growth of plants [9, 10]. During the growth of maple, spruce, poplar and white oak, the average amount of mercury released from leaves was 5.5 $ng/m^2 \cdot h$, 1.7 $ng/m^2 \cdot h$, 2.7 $ng/m^2 \cdot h$ and 5.3 $ng/m^2 \cdot h$, respectively [11]. The leaves of vine, avocado and leucaena also found to release gaseous mercury at room temperature [1, 12, 13]. According to the study by Kozuchowski and Johnson [14], reed also released mercury during its growth and the maximum amount of mercury released into air was 14.3 ng/h. In addition, the amount of gaseous mercury released from the leaves of transgenic poplar was 10 times higher than that of non-transgenic poplar [15]. Therefore, when applying phytoremediation technology to the remediation of mercury-contaminated soil, it is necessary to consider the secondary pollution of atmosphere caused by mercury released from plant leaves. If this problem is not given proper attention, mercury released from plant leaves will not only pollute the atmosphere, but will also pollute the surface water and soil along with rain and snow. Preventing the release of mercury from plant leaves into the atmosphere is an important step in the practical application of phytoremediation, which is also a follow-up problem in the application of phytoremediation of mercury-contaminated soil [16, 17]. However, not many studies have been conducted in measuring the prevention of mercury volatilization from soil or plant

into the atmosphere. On this context, this study aims to explore a route to prevent mercury volatilization from soil or plants to the atmosphere and thereby reducing mercury pollution to the atmosphere.

Controlled environment agriculture (CEA), such as crop production in plastic film and greenhouse environment, is becoming very popular because of its high output [18]. Related to plastic film and greenhouse that are commonly used in crops [18], this study attempts to select several types of adsorbents to fill the adsorption film to compare their adsorption effect on volatile mercury, as well as finding out the best filling material of adsorption film to adsorb gaseous mercury released from soil or plant leaves.

MATERIALS AND METHODS

Activated carbon, cation exchange resin and zinc powder were selected in this study. Activated carbon is a black powder or granular amorphous carbon which can effectively adsorb formaldehyde, xylene and other waste gases in the air [19]. Cation exchange resin is a type of resin which can exchange cations in the liquid phase. It demonstrates good adsorption performance and hence widely used in water treatment, medicine, chemical industry and other fields [20]. Zinc powder is a dark gray powder which is often used to make anti-rust paint, zinc amalgam and as a strong reducing agent [21]. Before adsorption experiments, the surface morphology of activated carbon, cation exchange resin and zinc powder was observed. The microstructure was observed using a positive metallographic microscope (XJZ-1A, Mac Photoelectric Instruments Co. Ltd., Chongqing, China) at a magnification of 800. The capability of adsorbents towards volatile mercury is related to the type, number, and the distance from mercury sources [22]. Therefore, three-factor and three-level experiments were designed. Orthogonal experiments on the weight of adsorbent and the distance between adsorbent and mercury source were designed by single factor pre-experiment. Adsorbents were kept in the packages made of non-woven fabrics and placed into self-made testing experimental device in layers. The device was placed outside shelter from rain with an average diurnal temperature of 10-15 ℃. Factor levels and the adsorption experimental device are shown in Table 1 and Fig. 1, respectively. The volatilization process of mercury in soil is usually very slow [23, 24, 25] and to speed up its volatilization a mercury source of 1000 mL solution (containing 100 μg mercury) was used. The mercury solution was poured into the open foam box of the volatile liquid in the lower part of the device and was volatilized under natural conditions. The mercury content in the adsorbent was determined by cold vapor atomic absorption spectrometry (CVAAS, AA-6300, P/N 206–51800, Shimadzu Corporation, Kyoto, Japan) after 7 days. Digestion of the activated carbon and cation exchange resin samples was accomplished by sulfuric acid, nitric acid and potassium permanganate, whereas the digestion of zinc powder samples was accomplished using dilute sulphuric acid.

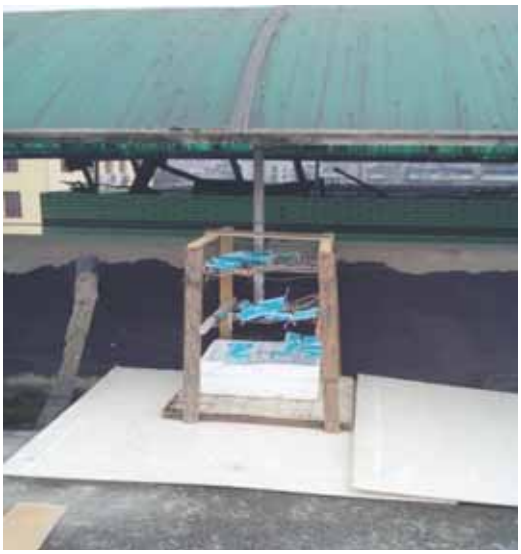

FIGURE 1
The experimental device used in the study of adsorption.

The analysis of mercury in the adsorbents is reported as the mean±SD of triplicate determinations from three adsorbents. The data were analysed by ANOVA test, and the comparison of mean was performed using Tukey tests. All statistical analyses were conducted using SPSS statistical package (SPSS 16.0; IBM, USA).

TABLE 1
Factor levels

Factor / Level	A	Types of Adsorbents	B	Adsorption material quality	C	Distance between Adsorbent and Mercury Source
1	A1	Activated carbon	B1	2g	C1	5cm
2	A2	Cation exchange resin	B2	4g	C2	15cm
3	A3	Zinc powder	B3	6g	C3	25cm

RESULTS AND DISCUSSION

Activated carbon is black, cation exchange resin is yellow and zinc powder is gray-black as shown in Fig. 2. Activated carbon and zinc are in the powder form with a large specific surface area (Fig. 2). However, cation exchange resin is in granular form and its specific surface area is smaller compared to activated carbon and zinc powder (Fig. 2). The surface of activated carbon has a porous structure (Fig. 2) and the micro-graph of cation exchange resin is not obvious (Fig. 2). Also, there is no porous structure on the surface of zinc powder, which shows a relatively flat structure (Fig. 2).

Nine groups of results obtained in orthogonal experiments are shown in Table 2. The amount of mercury adsorbed was the largest when 4 g of activated carbon and the distance between it and the mercury source was 15 cm. However, the amount of mercury adsorbed was the least when 2 g zinc powder and the distance between it and the mercury source was 25 cm. Range (R) analysis was considered for the results of the amount of mercury adsorbed using Eq. (1) and (2) [26, 27]. The trends of three factors are shown in Table 3. The mercury content of the adsorbents at first increased and then decreased with an increase in the weight of adsorbents. In addition, it decreased with an increase in the distance from the mercury source. It has been shown that the effect of adsorption of activated carbon on mercury was the best (Table 3). When the weight of adsorbent was 4 g, the effect of adsorption was better (Table 3). The farther the adsorbents were from the mercury source, the worst the adsorption effect (Table 3). The range of adsorbent species was 0.351, the range of adsorbent weight was 0.148, and the range of distance between adsorbent and mercury source was 0.079 (Table 3). Variance analysis was also considered using Eq. (3)-(9) [28]. F value of the adsorbents was 3.577, F value of the weight of adsorbents was 0.635, and the F value of the distance between adsorbents and mercury source was 0.173 (Table 4). According to the range (R) and variance analyses, the influence of type of adsorbent was greater compared to its weight, whereas the influence of weight of adsorbents was greater compared to the distance between adsorbents and mercury source. It indicates that the type of adsorbents exhibits a great influence on the capture of volatile mercury ($F_{0.25}(2, 2)<F_A=3.577<F_{0.1}(2, 2)$). Also, it shows that the weight of adsorbents has a little effect on the capture of volatile mercury ($F_B<F_{0.25}(2, 2)$). Besides, the distance between adsorbent and mercury source has an insignificant effect on the capture of volatile mercury ($F_C<F_{0.25}(2, 2)$).

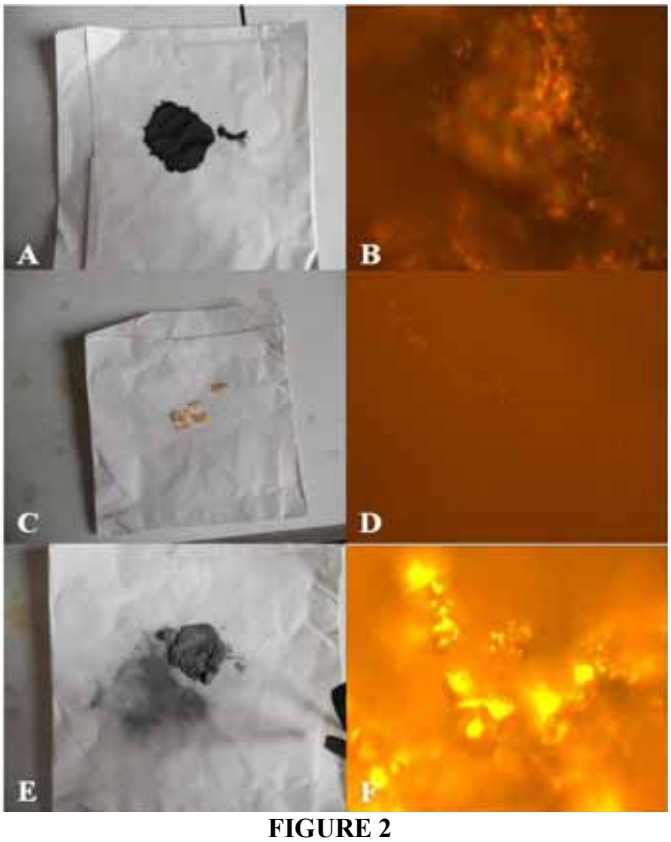

FIGURE 2
Appearance and the microstructure of adsorbents. (A) appearance of activated carbon; (B) microstructure of activated carbon; (C) appearance of cation exchange resin; (D) microstructure of cation exchange resin; (E) appearance of zinc powder; (F) microstructure of zinc powder.

TABLE 2
The design and results of orthogonal experiments.

Group	A	B	C	Mercury content in adsorbent materials (μg)
1	1	1	1	0.504±0.031
2	1	2	2	0.516±0.142
3	1	3	3	0.180±0.005
4	2	1	2	0.170±0.013
5	2	2	3	0.364±0.007
6	2	3	1	0.246±0.024
7	3	1	3	0.026±0.001
8	3	2	1	0.056±0.003
9	3	3	2	0.066±0.010

Mean±standard deviation; n=3; $p<0.05$.

$$K_r=\sum(r)/3 \quad (1)$$

$$R=\max(K_r)-\min(K_r) \quad (2)$$

$$Q=3\left[\left(K1-\bar{x}\right)^2+\left(K2-\bar{x}\right)^2+\left(K3-\bar{x}\right)^2\right] \quad (3)$$

$$Q_T=\sum_{i=1}^{3}\sum_{j=1}^{3}\left(x_{ij}-\bar{x}\right)^2 \quad (4)$$

$$Q_T=Q_A+Q_B+Q_C+Q_e \quad (5)$$

$$Q_e=Q_T-Q_A-Q_B-Q_C \quad (6)$$

$$\bar{Q}=Q/f \quad (7)$$

$$\bar{Q}_e=Q_e/f_e \quad (8)$$

$$F=\bar{Q}/\bar{Q}_e \quad (9)$$

$\sum(r)$ - The sum of results of a factor at the same level; $f_A=f_B=f_C=3-1=2$; $f_T=9-1=8$; $f_e=f_T-f_A-f_B-f_C=8-6=2$.

TABLE 3
Range analysis of orthogonal experimental results.

	A	B	C
K1	0.400	0.233	0.269
K2	0.260	0.312	0.251
K3	0.049	0.164	0.190
R	0.351	0.148	0.079

TABLE 4
Variance analysis of orthogonal experimental results.

	A	B	C
K1	0.400	0.233	0.269
K2	0.260	0.312	0.251
K3	0.049	0.164	0.190
Q	0.186	0.033	0.009
f	2	2	2
F	3.577	0.635	0.173

CONCLUSION

The effect of adsorption of several adsorbents on volatile mercury has been studied. The specific surface area of cation exchange resin is smaller compared to activated carbon and zinc powder. Among the three adsorbents, activated carbon showed the best adsorption effect on mercury, followed by cation exchange resin, and then zinc powder which exhibited the poorest adsorption. When the weight of adsorbents was 4 g, the effect of adsorption was the best. As the weight of adsorbents and the distance between them and mercury source have little influence on the effect of adsorption of volatile mercury, the best adsorbent is the activated carbon. Irrespective of these observed outcomes, there is still a certain gap in terms of considering for practical applications. Thus, it is suggested that in the next stage the adsorbents should be applied in the phytoremediation of mercury-contaminated soil directly to prevent releasing of mercury from soil or plant leaves to the atmosphere.

ACKNOWLEDGEMENTS

The work was supported by Research Project of Yangtze Normal University (No. 2016KYQD28). We are grateful to Lu Wang, Ming Li and Zhenyuan Li at the State Key Laboratory of Coal Mine Disaster Dynamics and Control Chongqing University, for their help with the laboratory assistance.

REFERENCES

[1] Li, X.Y., Li, Z.G., Wu, T.T., Chen, J., Fu, C.C., Zhang, L.M., Feng, X.B., Fu, X.W., Tang, L., Wang, Z.K., Wang, Z.B. (2019) Atmospheric mercury emissions from two precalciner cement plants in Southwest China. Atmospheric Environment. 199, 177-188.

[2] Zhu, W., Li, Z.G., Li, P., Yu, B., Lin, C.J., Sommar, J., Feng, X.B. (2018) Re-emission of legacy mercury from soil adjacent to closed point sources of Hg emission. Environmental Pollution. 242, 718-727.

[3] Figueiredo, N.L., Canário, J., O'Driscoll, N.J., Duarte, A., Carvalho, C. (2016) Aerobic Mercury-resistant bacteria alter Mercury speciation and retention in the Tagus Estuary (Portugal). Ecotoxicology and Environmental Safety. 124, 60-67.

[4] Liu, Z.C., Wang, L.A., Ding, S.M., Xiao, H.Y. (2018) Enhancer assisted-phytoremediation of mercury-contaminated soils by *Oxalis corniculata* L., and rhizosphere microorganism distribution of *Oxalis corniculata* L.. Ecotoxicology and Environmental Safety. 160, 171-177.

[5] Xiao, Z.F., Stromberg, D., Lindqvist, O. (1995) Influence of humic substances on photolysis of divalent mercury in aqueous-solution. Water Air and Soil Pollution. 80(1-4), 789-798.

[6] Giovanella, P., Cabral, L., Costa, A.P., Camargo, F.A.D.O., Gianello, C., Bento, F.M. (2017) Metal resistance mechanisms in Gram-negative bacteria and their potential to remove Hg in the presence of other metals. Ecotoxicology and Environmental Safety. 140, 162-169.
[7] Kim, K.H., Lindberg, S.E., Meyers, T.P. (1995) Micrometeorological measurements of mercury vapor fluxes over background forest soils in eastern Tennessee. Atmospheric Environment. 29(2), 267-282.
[8] Pedron, F., Petruzzelli, G., Barbafieri, M., Tassi, E. (2013) Remediation of a Mercury-Contaminated Industrial Soil Using Bioavailable Contaminant Stripping. Pedosphere. 23(1), 104-110.
[9] Prete, D., Davis, M., Lu, J. (2018) Factors affecting the concentration and distribution of gaseous elemental mercury in the urban atmosphere of downtown Toronto. Atmospheric Environment. 192, 24-34.
[10] Sorkhoh, N.A., Ali, N., Al-Awadhi, H., Dashti, N., Al-Mailem, D.M., Eliyas, M., Radwan, S.S. (2010) Phytoremediation of mercury in pristine and crude oil contaminated soils: Contributions of rhizobacteria and their host plants to mercury removal. Ecotoxicology and Environmental Safety. 73, 1998-2003.
[11] Hanson, P.J., Lindberg, S.E., Tabberer, T.A., Owens, J.G., Kim, K.H. (1995) Foliar exchange of mercury vapor: evidence for a compensation point. Water, Air and Soil Pollution. 80, 373-382.
[12] Haynes, K.M., Kane, E.S., Potvin, L., Lilleskov, E.A., Kolka, R.K., Mitchell, C.P.J. (2017) Gaseous mercury fluxes in peatlands and the potential influence of climate change. Atmospheric Environment. 154, 247-259.
[13] Esbrí, J.M., Cacovean, H., Higueras, P. (2018) Usage Proposal of a common urban decorative tree (*Salix alba* L.) to monitor the dispersion of gaseous mercury: A case study from Turda (Romania). Chemosphere. 193, 74-81.
[14] Kozuchowski, J., Johnson, D.L. (1978) Gaseous emissions of mercury from an aquatic vascular plant. Nature. 274, 468-469.
[15] Gomes, M.A.D.C., Hauser-Davis, R.A., de Souza, A.N., Vitória, A.P. (2016) Metal phytoremediation: General strategies, genetically modified plants and applications in metal nanoparticle contamination. Ecotoxicology and Environmental Safety. 134, 133-147.
[16] Budnik, L.T., Casteleyn, L. (2019) Mercury pollution in modern times and its socio-medical consequences. Science of the Total Environment. 654, 720-734.
[17] Liu, Z.C., Wang, L.A., Ding, S.M. (2018) The Absorption Condition of Mercury in Mercury-Contaminated Soils by *Opuntia Stricta*. Fresen. Environ. Bull. 27, 3439-3443.
[18] Ahamed, M.S., Guo, H.Q., Tanino, K. (2019) Energy saving techniques for reducing the heating cost of conventional greenhouses. Biosystems Engineering. 178, 9-33.
[19] Wang, H.Y., Wang, B.D., Li, J.H., Zhu, T.L. (2019) Adsorption equilibrium and thermodynamics of acetaldehyde/acetone on activated carbon. Separation and Purification Technology. Separation and Purification Technology. 209, 535-541.
[20] Beita-Sandí, W., Selbes, M., Kim, D., Karanfil, T. (2018) Removal of N-nitrosodimethylamine precursors by cation exchange resin: The effects of pH and calcium. Chemosphere. 211, 1091-1097.
[21] Owais, A., Gepreel, M.A.H., Ahmed, E. (2015) Production of electrolytic zinc powder from zinc anode casing of spent dry cell batteries. Hydrometallurgy. 157, 60-71.
[22] Wilcox, J., Rupp, E., Ying, S.C., Lim, D.H., Negreira, A.S., Kirchofer, A., Feng, F., Lee, K. (2012) Mercury adsorption and oxidation in coal combustion and gasification processes. International Journal of Coal Geology. 90-91, 4-20.
[23] Windmöller, C.C., Júnior, W.A.D., Oliveira, A.D., Valle, C.M.D. (2015) The redox processes in Hg-contaminated soils from Descoberto (Minas Gerais, Brazil): Implications for the mercury cycle. Ecotoxicology and Environmental Safety. 112, 201-211.
[24] Lin, X.J., Nishio, K., Konno, T., Ishihara, K. (2012) The effect of the encapsulation of bacteria in redox phospholipid polymer hydrogels on electron transfer efficiency in living cell-based devices. Biomaterials. 33(33), 8221-8227.
[25] Zhou X., Li, Y.X., Zhao, Y. (2014) Removal characteristics of organics and nitrogen in a novel four-stage biofilm integrated system for enhanced treatment of coking wastewater under different HRTs. RSC Advances. 4, 15620-15629.
[26] Li, L., Flora, J.R.V., Caicedo, J.M., Berge, N.D. (2015) Investigating the role of feedstock properties and process conditions on products formed during the hydrothermal carbonization of organics using regression techniques. Bioresource Technology. 187, 263-274.
[27] Wszola, L.S., Simonsen, V.L., Corral, L., Chizinski, C.J., Fontaine, J.J. (2019) Simulating detection-censored movement records for home range analysis planning. Ecological Modelling. 392, 268-278.
[28] Aamery, N.A., Fox, J.F., Snyder, M., Chandramouli, C.V. (2018) Variance analysis of forecasted streamflow maxima in a wet temperate climate. Journal of Hydrology. 560, 364-381.

Received: **28.01.2019**
Accepted: **01.04.2019**

CORRESPONDING AUTHOR

Zhongchuang Liu
Green Intelligence Environmental School,
Yangtze Normal University,
16 Juxian Rd. Lidu,
Fuling District of Chongqing – China

e-mail: liuzhongchuang@yznu.cn.

© by PSP Volume 28 – No. 5/2019 pages 4363-4369 Fresenius Environmental Bulletin

EFFECT OF STRONG DENUDATION ON COALBED METHANE ENRICHMENT IN A STRONGLY DEFORMED ZONE: A CASE STUDY IN SOUTHERN QINSHUI BASIN, CHINA

Yang Tian[1], Chuang Lei[2,*], Baolin Yang[3], Meng Chen[4], Modong Duan[3], Yiming Liu[3]

[1]Hubei Cooperative Innovation Center of Unconventional Oil and Gas, Yangtze University, Wuhan 430100, China
[2]College of Mining Engineering, North China University of Science and Technology, Tangshan 063210, China
[3]Key Laboratory of Tectonics and Petroleum Resources of Ministry of Education, China University of Geosciences, Wuhan 430074, China
[4]Hubei Xinjie Natural Gas Co., Ltd, Wuhan 430040, China

ABSTRACT

The Upper Paleozoic strata in the southern Qinshui Basin was strongly deformed, and the prediction of CBM sweet spots in this area is difficult. Stress is an important factor affecting the permeability of coal reservoirs. Therefore, the influence of strong denudation on coalbed methane enrichment was studied in this paper. The results show that stress unloading, reduction of formation temperature, and tensile strain, all can lead to the reduction of the minimum principal stress in the erosion process. The cumulative reduction of minimum horiaontal stress for the No. 3 coal is generally less than 10 MPa. For the strongly deformed target layer, the fracture and fault systems are extremely developed. Therefore, in the region with a large erosion thickness, the degree of stress reduction is large, and the storage conditions are poor, so the productivity of the coalbed methane well is low. However, the storage conditions are better in regions with a small erosion thickness, therefore the coalbed methane was easily preserved. According to the research in this paper, the preservation effect is an important control factor for the accumulation of coalbed methane in the strongly deformed zone. For the No. 3 coal in the study area, the area with a denudation thickness of less than 2 000 m should be the sweet spots for the exploration of coalbed methane.

KEYWORDS:
Qinshui Basin, coalbed methane, stress, erosion, sweet spot

INTRODUCTION

The world's petroleum industry is entering unconventional oil and gas industry stage. With the gradual depletion of conventional oil and gas resources, the importance of unconventional oil and gas resources is becoming more and more significant [1-2]. Effective exploitation of unconventional oil and gas can protect country's natural gas supply and demand balance, while enhancing the country's international energy decision-making capacity [3-4]. As a whole gas-bearing system, coal measure strata contains a variety of natural gas resources, including coalbed methane (CBM), tight sandstone gas, shale gas and limestone gas [5]. Due to the the high gas content of coal reservoir, CBM is the most exploitable natural gas resource in coal measure strata. However, the CBM reservoir has strong heterogeneity, and the efficient prediction of its sweet spots is still a difficult problem for people.

Coal measure strata are widely distributed in the Upper Paleozoic (Carboniferous - Permian) of China, and have good gas-bearing properties [5]. The distribution of the Paleozoic coal seam is stable, and its thickness is usually in the range of 5-10 m, and the gas content is mainly distributed in 1-40 m^3/t. The coal measure strata have undergone deep burial, multi-stage tectonic evolution and strong uplift and denudation in the geological history period. The enrichment degree of the coalbed methane is extremely uneven.

The target layer studied in this paper is the Lower Permian Shanxi Formation coal in the southern Qinshui Basin. The area is a strongly deformed area, and after the Yanshanian period, strong uplift and erosion occurred, and the maximum denudation thickness exceeded 4 000 m. The commercial development of coalbed methane is importantly influenced by permeability, however, the stress environment is an important factor affecting permeability. Therefore, this paper attempts to explore the effect of strong denudation on coalbed methane enrichment.

GEOLOGICAL BACKGROUND

Location of study area. The Qinshui Basin is located in the southern part of Shanxi Province, China, and is a large-scale composit anticline basin

with the north-south strike. The Qinshui Basin is located on the east side of the largest "mountain-shaped structure" (Consists of Qilan Mountain, Helan Mountain and Lvliang Mountain) in China [6]. "Mountain-shaped structure" is a twisted structure [7]. The activity of the Qilan-Lvliang-Helan mountain-shaped structure began in the late Paleozoic, the embryonic form is formed in the Mesozoic, and the final shape is formed in the new generation.

The study area is situated in a well block of coalbed methane in the southern area of the Qinshui Basin, including the Zhengzhuang block and the Fanzhuang block. The elevation of the terrain is high in in the southeast and low in the northwest.

Deposition system. From the bottom to the top, the Precambrian, Cambrian, Ordovician Fengfeng Formation, Carboniferous Benxi Formation and Taiyuan Formation, Permian Shanxi Formation, Xiashihezi Formation, Shangshihezi Formation and Shiqianfeng Formation, Triassic and Quaternary strata were developed in the southern part of the Qinshui Basin [7]. The main coal-bearing strata are the Carboniferous Upper Taiyuan Formation and the Lower Permian Shanxi Formation. The target layer of the study is the No. 3 coal seam in the Shanxi Formation, and its buried depth is mainly distributed between 400 m and 1 200 m, and its average thickness is 6 m. The No. 3 coal seam is a high rank coal (anthracite) with a R_o (vitrinite reflectance) greater than 3.5%.

STRESS CHANGES IN THE EROSION PROCESS

The Upper Paleozoic strata in the southern Qinshui Basin experienced a complex tectonic evolution process. The burial history of the JS1 well in the area (Fig. 1) indicates that the Upper Paleozoic strata reached the maximum depth at the end of the Triassic period, and then experienced a strong denudation [8-9]. During the erosion process, the stress load of the formation gradually decreases; at the same time, the decrease of the formation temperature and the occurrence of tensile strain both will cause the stress to decrease.

The stress system of underground rock can be simplified to the maximum horizontal principal stress, the minimum horizontal principal stress and the vertical stress [10]. The minimum horizontal principal stress is generally closely related to the fracture system or permeability inside the rock [10]. Therefore, this paper mainly discusses the influence of formation temperature and tensile strain on the minimum horizontal principal stress during the erosion process.

Effect of temperature decrease on stress during denudation. When the sedimentary basin is in a strong denudation process, the stress of the formation itself will decrease, and the “stress relaxation” phenomenon will reopen the originally closed fractures [10-11]. At the same time, in the erosion process, the temperature of the deep formation will continue to decrease. Then, the formation stress will be greatly reduced due to the temperature drop, and the mechanism is “heat shrinkage” [10].

In the erosion process of sedimentary basins, the change of the minimum horizontal principal stress of formation rocks caused by temperature changes can be expressed as:

$$\Delta S_h = \frac{E}{1-\nu}\alpha_T \Delta T \quad (1)$$

Where α_T is the coefficient of thermal expansion. α_T of quartz mineral is 10^{-5}°C^{-1}, while α_T of the other types of sedimentary rock minerals is generally 10^{-6}°C^{-1} [13]; E is Young's modulus, GPa ; ΔT is the amount of temperature change, °C.

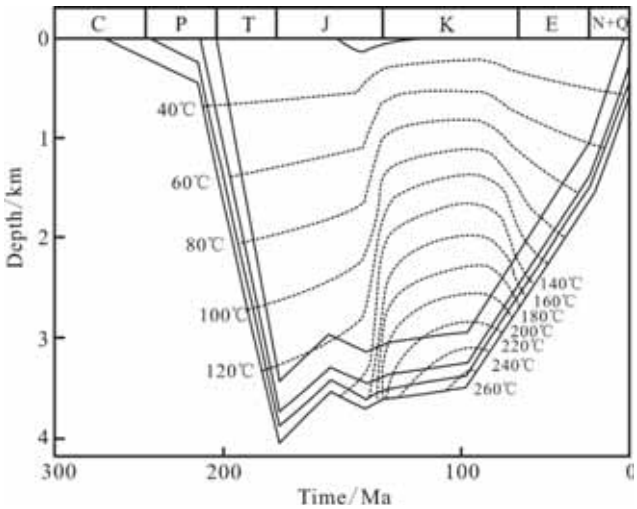

FIGURE 1
The burial and thermal history of the JS1 well in the southern Qinshui Basin [9].

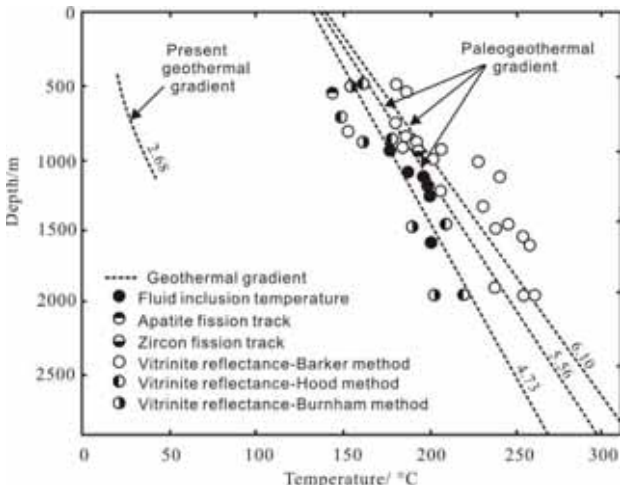

FIGURE 2
Paleotemperature distribution of the QS1 well in the late Mesozoic [12].

TABLE 1
The assignment of thermal and mechanical parameters of the target coal seam in the study area.

Lithology	Geothermal gradient (°C /100 m)	α_T(°C^{-1})	E(GPa)	v
Coal	2.50-6.00	1×10^{-6}	15.0	0.35

Notes: α_T is thermal expansion coefficient; E is Young's modulus; v is Poisson's ratio.

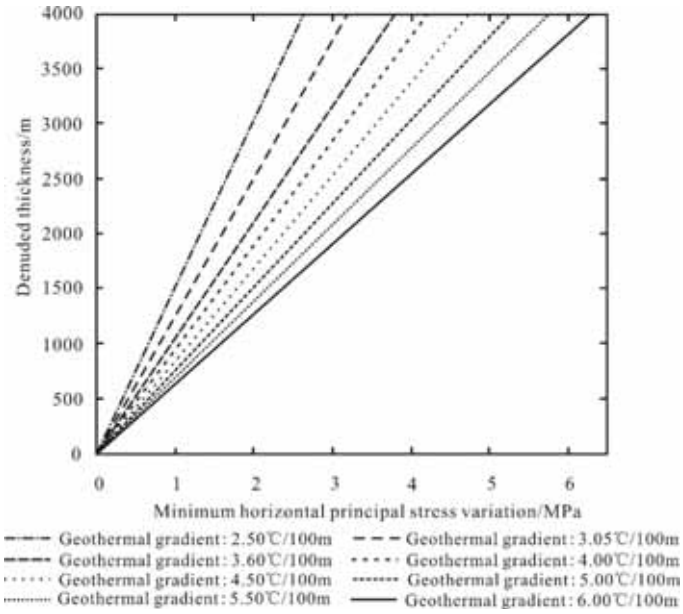

FIGURE 3
Relationship between erosion thickness and minimum horizontal stress variation of the target layer.

According to the results of inclusions, apatite fission tracks and zircon tests [12], the Shanxi Formation strata in the study area reached the maximum depth in the early Yanshanian, and had anomalous thermal events [12]. The geothermal gradient was large, distributed at 2.5-6.0 °C / 100 m range (Fig. 2). The geothermal gradient at the north and south ends of the Qinshui Basin was up to 8.0 °C / 100 m [12]. According to the thermal characteristics of the No. 3 coal in the Shanxi Formation of the study area and the results of rock mechanics tests, we assigned the rock properties of the No. 3 coal (Table 1).

In this paper, the relationship between the amount of denudation of the target coal and the minimum horizontal principal stress was established (Fig. 3). It considered eight cases, where the formation gradients were 2.50, 3.05, 3.60, 4.00, 4.50, 5.00, 5.50, and 6.00 °C/100 m, respectively, which represented the change from the normal geothermal gradient to the abnormally high geothermal gradient.

It can be seen from Fig. 3 that as the geothermal gradient increases, the influence of the erosion or temperature change on the minimum horizontal principal stress of the formation gradually increases. Under the same denudation thickness, the variation of the minimum horizontal principal stress of the

formation gradually increases with the increase of the geothermal gradient. As the thickness of the erosion of the formation increases, the formation temperature gradually decreases, and the minimum horizontal principal stress of the formation decreases (Fig. 3).

The cumulative denudation thickness of the overlying strata of the Shanxi Formation in the southern Qinshui Basin is mostly in the range of 1 000 m - 3 000 m. For the coal rocks of the target layer, the minimum horizontal principal stress was reduced by 1-5 MPa, during the denudation process. During the reduction process of the minimum horizontal principal stress, part of the strongly compacted layers will gradually transform into weakly compacted layers, while the weakly compacted layers may be transformed into a tensile stress environment [14]. Under such high stress conditions, the originally closed fractures are easy to re-open, and at the same time, some new fractures are easily formed in the formation.

Using the above formula and the rock mechanics parameters of No. 3 coal, the relationships between the minimum horizontal principal stress and the buried depth of the stratum in the process of sedimentation and erosion under the influence of temperature were established (Fig. 4). It can be seen that during the deposition process, the change of minimum horizontal principal stress of the rock increases with the increase of temperature. The higher the geothermal gradient, the greater the change in the minimum horizontal principal stress (Fig. 4).

For the erosion process, it is significantly different from the aforementioned deposition process. During the erosion process, the petrophysical properties and mechanical parameters of the sedimentary strata will not change in the reverse direction, or the change is very small which can be neglected [15-16]. Therefore, in the process of formation erosion, as the temperature decreases, the variation of the minimum horizontal principal stress of the formation will not change along the original sedimentary curve; instead, it will change along the tangential direction at the maximum buried depth curve (Fig. 4b).

It can be seen from Fig. 4b that during the erosion process, the deposited formation will produce an additional stress tensor in the direction of the minimum horizontal principal stress, which due to the temperature drop. The larger the ancient maximum buried depth, the greater the additional stress tensor generated by the temperature decrease during the erosion process. These additional stress tensors can further increase the porosity and permeability of the No. 3 coal reservoir in Shanxi Formation.

The starting point of the denudation curve is assumed to be a maximum buried depth of 3000 m.

Effect of horizontal tensile strain on stress during denudation. During the erosion process, due to stress relaxation or stress unloading, the formation rock will produce horizontal tensile strains [17-19]. In the process of stratum erosion, the influence of the horizontal strain on the minimum horizontal principal stress of the formation can be expressed as:

$$\Delta S_h = \frac{E}{1-\nu^2}\Delta\varepsilon_h + \frac{\nu E}{1-\nu^2}\Delta\varepsilon_H \quad (2)$$

It can be seen from the above formula that during the deposition process, the horizontal direction strain is compressive. Then, as the rock E increases and ν decreases, the strain will make the minimum horizontal principal stress of the formation increase. However, in the process of erosion, the change of E and ν of the formation rock can be neglected, but the strain in the horizontal direction is in a tensile state, and thus, the minimum horizontal principal stress of the formation will decrease.

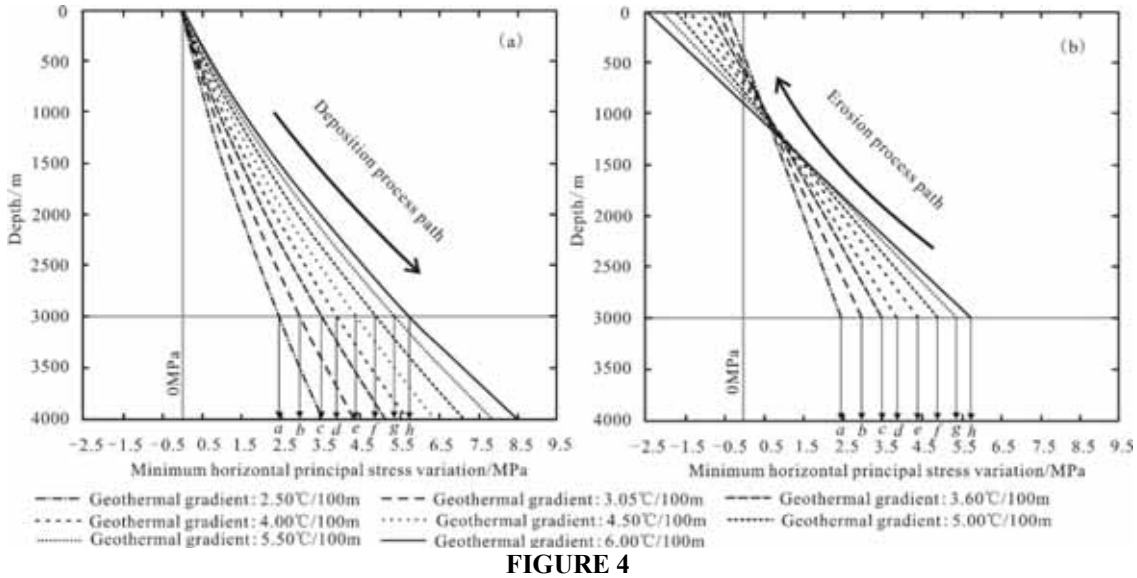

FIGURE 4
Relationship between minimum horizontal principal stress and buried depth of the target layer under influence of temperature during deposition and erosion.

The sedimentary rock mass is continuously compressed during the deposition process, and the sedimentary rock mass on the surface of the earth's crust can be assumed to be a small arc along the ellipsoidal earth [20-21]. Therefore, the transverse strain rate ($\Delta\varepsilon$) of the sedimentary rock mass is related to the radius of the Earth. The radius of the Earth is 6371 km. Assuming that the maximum horizontal strain ($\Delta\varepsilon_H$) of the sedimentary rock mass is equal to the strain ($\Delta\varepsilon_h$) of the minimum horizontal principal stress direction, then, $\Delta\varepsilon=\Delta\varepsilon_H=\Delta\varepsilon_h=1/6371$ km=0.00016/km.

According to the strain law, the change of the minimum horizontal principal stress of the coal rock stratum during the erosion process can be obtained under the condition of the tensile strain (Fig. 5).

It can be seen from Fig. 5 that, as the amount of denudation increases, the reduction of the minimum horizontal principal stress of the formation gradually increases due to the influence of the horizontal strain of the formation rock. This factor has a relatively weaker effect on the minimum horizontal principal stress of the formation rock than the aforementioned temperature factor, but it can also generate a stress tensor environment, which makes the rock prone to rupture or the closed fractures reopen [22-24].

INFLUENCE OF DENUDATION THICKNESS ON PRODUCTIVITY OF COLLBED METHANE WELLS

The unconformity of the target layer is located in the interface between the top surface of the Permian and the bottom surface of the Quaternary, which is a superimposed unconformity. The cumulative erosion amount of each single well was calculated by the acoustic wave time difference method, and the calculation result is shown in Fig. 6. The denudation thickness is mainly distributed between 200 m and 3000 m. The strong erosion centers in the study area are mostly distributed along the NE-SW direction, while the erosion amounts in the northwest areas are relatively small (Fig. 6). The denudation trend on the plane of the study area is unevenly, and it has several strong erosion centers.

Coalbed methane wells were divided into high-yield wells, middle-yield wells and low-yield wells. The daily production capacity of high-yield wells is greater than 2 000 m^3; the daily production capacity of middle-yield wells is between 1000-2000 m^3; and the daily production capacity of low-yield wells is less than 1 000 m^3, which does not reach commercial capacity. It can be observed that high-yield wells are generally distributed in areas with a denudation thickness of less than 2 000 m; and middle-yield wells are generally distributed in areas with a denudation thickness of less than 2500 m; while low-yield wells are generally distributed in areas with a denudation thickness greater than 2000 m.

According to the analysis, the reason for this phenomenon is that, the target layer of the study area is strongly deformed, and the fractures and faults in the No. 3 coal seam and its upper cover layers are extremely developed. In the areas with large erosion thickness, the stress of coal reservoir and its caprock is significantly reduced, and the fluid drainage ability of fractures is strong, so the preservation condition is poor, which leads to the loss of coalbed methane. However, the storage conditions of the regions with a small erosion thickness are better, and the coalbed methane is easy being stored. According to the research in this paper, the preservation effect is an important control factor for the accumulation of coalbed methane in the strong deformed zone. For the No. 3 coal in the study area, the areas with a denudation thickness of less than 2 000 m should be the sweet spots for the exploration of coalbed methane.

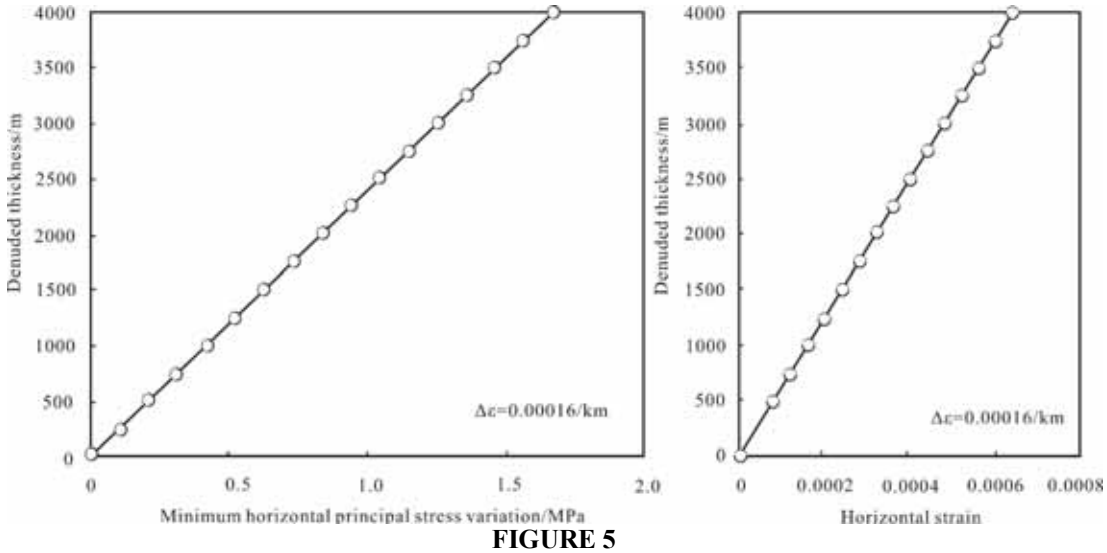

FIGURE 5
Influence of tensile strain on the minimum horizontal principal stress of the target layer during erosion process.

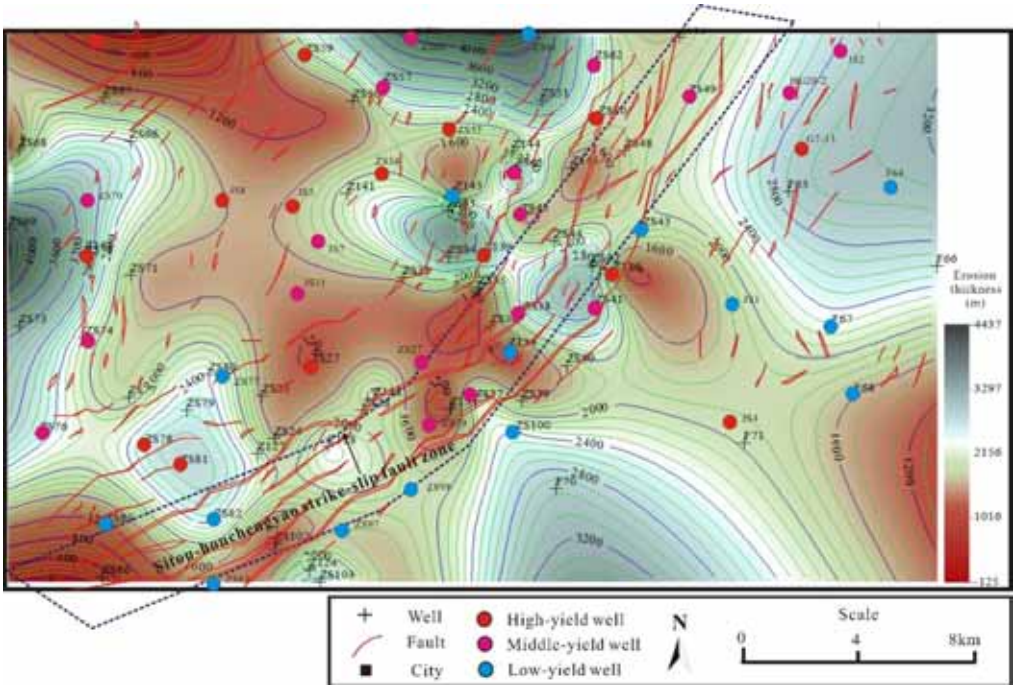

FIGURE 6
Relationship between denudation thickness and productivity of coalbed methane wells.

CONCLUSIONS

(1) Stress unloading, reduction of formation temperature, and tensile strain, all can lead to the reduction of the minimum principal stress in the erosion process. The cumulative minimum horizontal stress reduction for the No. 3 coal is generally less than 10 MPa.

(2) For the strongly deformed target layer, the fracture and fault systems are extremely developed. Therefore, in the region with a large erosion thickness, the degree of stress reduction is large, and the storage conditions are poor, so the productivity of the coalbed methane well is low. However, the storage conditions are better in regions with a small erosion thickness, therefore the coalbed methane was easily preserved.

(3) Preservation effect is an important control factor for the accumulation of coalbed methane in the strongly deformed zone. For the No. 3 coal in the study area, the areas with a denudation thickness of less than 2 000 m should be the sweet spots for the exploration of coalbed methane.

ACKNOWLEDGEMENTS

This work was financially supported by the Open Fund of State Key Laboratory of Oil and Gas Reservoir Geology and Development Engineering, China (No. PLC20180503) and the Subjects of Major National Science and Technology Projects of China (No. 2016ZX05024-002-003, No. 201605027 -001-005).

REFERENCES

[1] Farrell, N.J.C., Healy, D., Taylor, C.W. (2014) Anisotropy of permeability in faulted porous sandstones. Journal of Structural Geology. 63, 50- 67.

[2] Li, Y., Tang, D.Z., Xu, H., Elsworth, D., Meng, Y.J. (2015) Geological and hydrological controls on water coproduced with coalbed methane in Liulin, eastern Ordos basin, China. AAPG Bulletin. 99(2), 207- 229.

[3] Bocora, J. (2012) Global prospects for the development of unconventional gas. Procedia Social and Behavioral Sciences. 65, 436- 442.

[4] Weijermars, R. (2013) Economic appraisal of shale gas plays in continental Europe. Applied Energy. 106, 100-115.

[5] Dai, J.X., Ni, Y.Y., Huang, S.P., Liao, F.R., Yu, C., Gong, D.Y., Wu, W. (2014) Significant function of coal-derived gas study for natural gas industry development in China. Natural Gas Geoscience. 25(1), 1-17 (in Chinese with English abstract).

[6] Liang, J.S., Wang, C.W., Liu, Y.H., Gao, Y.J., Du, J.F., Feng, R.Y., Zhu, X.S., Yu, J. (2014) Study on the tight gas accumulation conditions and exploration potential in the Qinshui Basin. Natural Gas Geoscience. 25(10), 1509- 1517 (in Chinese with English abstract).

[7] Yin, S., Xie, R.C., Wu, Z.H., Liu, J., Ding, W.L. (2019) In situ stress heterogeneity in a highly developed strike-slip fault zone and its effect on the distribution of tight gases: A 3D finite element simulation study. Marine and Petroleum Geology. 81(1), 1-17.
[8] Milliken, K.L., Curtis, M.E. (2016) Imaging pores in sedimentary rocks: Foundation of porosity prediction. Marine and Petroleum Geology. 73, 590- 608.
[9] Su, X.B., Lin, X.Y., Zhao, M.J., Song, Y., Liu, S.B. (2005) The upper Paleozoic coalbed methane system in the Qinshui Basin, China. AAPG Bulletin. 89(1), 81- 100.
[10] Shao, L.Y., Yang, Z.Y., Shang, X.X. (2015) Lithofacies palaeogeography of the Carboniferous and Permian in the Qinshui Basin, Shanxi Province, China. Journal of Palaeogeography. 4(4), 384–412.
[11] Xue, Q., Leung, H., Huang, L., Zhang, R., Liu, B., Wang, J., Li, L. (2019) Modeling of torsional oscillation of drillstring dynamics. Nonlinear Dynamics. 1-17.
[12] Ren, Z.L., Xiao, H., Liu, L., Zhang, S., Qin, Y., Wei, C.T. (2005) Apatite fission track evidence of tectonics and thermal evolution history of Qinshui basin. Chinese Science Bulletin. 50(Supp I), 87-92 (in Chinese with English abstract).
[13] Zoback, M.D. (2007) Reservoir geomechanics. Cambridge, United Kingdom, Cambridge University Press. 25, 448-449.
[14] Yin, S., Lv, D.W., Ding, W.L. (2018) New method for assessing microfracture stress sensitivity in tight sandstone reservoirs based on acoustic experiments. International Journal of Geomechanics. 18(4), 1-16.
[15] Bergbauer, S., Martel, S.J., Hieronymus, C.F. (1998) Thermal stress evolution in cooling pluton environments of different geometries. Geophysical Research Letters. 25(5), 707- 710.
[16] Zhao, D., Guo, Y., Chong, X., Li, G., Wang, Y. (2018) Nuclear magnetic response experiment analysis of tight gas sandstone reservoir. Fresen. Environ. Bull. 27, 1-6.
[17] Thiercelin, M.J., Roegiers, J.C. (2000) Formation characterization: Rock mechanics. In: Economides, M.J. and Nolte, K.G. (eds.) Reservoir Stimulation. New York: Wiley Press. 34p.
[18] Meng, M., Qiu, Z.S. (2018) Experiment study of mechanical properties and microstructures of bituminous coals influenced by supercritical carbon dioxide. Fuel. 219, 223-238.
[19] Meng, M., Zamanipour, Z., Miska, S., Yu, M., Ozbayoglu, E.M. (2018) Dynamic stress distribution around the wellbore influenced by surge/swab pressure. Journal of Petroleum Science and Engineering. 172, 1077-1091.
[20] Zhu, G., Jiang, Z.D., Zhang, B.L., Chen, Y. (2012) Destruction of the eastern North China craton in a backarc setting: evidence from crustal deformation kinematics. Gondwana Research. 22(1), 86-103.
[21] Shiozawa, S., Mcclure, M. (2016) Simulation of proppant transport with gravitational settling and fracture closure in a three-dimensional hydraulic fracturing simulator. Journal of Petroleum Science and Engineering. 138(3), 298- 314.
[22] Price, N.J. (1966) Fault and joint development in brittle and semibrittle rock. United Kingdom: Pergamon Press.
[23] Cundall, P.A., Hart, R.D. (1985) Development of generalized 2-D and 3-D distinct element programs for modeling jointed rock. Miscellaneous Paper SL-85-1. Itasca Consulting Group, US Army Corps of Engineers.
[24] Cook, J.E., Goodwin, L.B., Boutt, D.F., Tobin, H.J. (2015) The effect of systematic diagenetic changes on the mechanical behavior of a quartz cemented sandstone. Geophysics. 80(2), 145-160.

Received: **22.02.2019**
Accepted: **30.03.2019**

CORRESPONDING AUTHOR

Chuang Lei
College of Mining Engineering
North China University of Science and Technology
Tangshan 063210 – China

e-mail: chuanglei2019@126.com.

© by PSP Volume 28 – No. 5/2019 pages 4370-4374 Fresenius Environmental Bulletin

MAGNETIC SUSCEPTIBILITY MEASUREMENTS FOR THE MONITORING OF HEAVY METALS IN THE INDUSTRIAL AREA OF TITO SCALO. COMPARISON WITH THE RESULTS OBTAINED IN DIFFERENT INDUSTRIAL AREAS OF BASILICATA REGION (SOUTHERN ITALY)

presented in the 19th International MESAEP Symposium, Rome-Italy from October 04-06, 2017

Mariagrazia D'Emilio[1,*], Rosa Coluzzi[1], Vito Imbrenda[1], Maria Macchiato[2], Maria Ragosta[3]

[1]Institute of Methodologies for Environmental Research – CNR, 85050 Tito Scalo (PZ), Italy
[2]Department of Physics "E. Pancini", University "Federico II", Napoli, 80131, Italy
[3]School of Engineering, University of Basilicata, Potenza, 85100 Italy

ABSTRACT

Magnetic susceptibility may be very variable in soil both because of natural causes as pedogenesis and because of anthropogenic causes as air and soil pollution. For this peculiarity, magnetic susceptibility measurements are used for monitoring the presence of heavy metals in soil, dust and sediment; however, an accurate data analysis is fundamental for the interpretation of the results.

Here, we present a field survey carried out in a large industrial area of Basilicata Region (Southern Italy), surrounded by areas devoted to agricultural activities, woods, and protected sites (e.g., the WWF natural oasis of "Lago Pantano"). We measured magnetic susceptibility in situ and collected soil samples along a georeferenced grid of about 70 sampling points. These points are representative of both industrial soils and natural and agricultural areas. The results of the field survey are then compared with the results we obtained in other industrial areas of Basilicata by adopting the same time-saving and low-cost technique to get an overall picture of heavy metals distribution at a regional scale.

KEYWORDS:
Soil pollution, Heavy metals, Soil Magnetic Susceptibility

INTRODUCTION

Soils have physical characteristics that depend essentially on their formation process. In particular, the magnetic properties of soil depend on their mineralogical composition, structure and texture [1]. The magnetic minerals present in soils can have both lithogenic, pedogenic and anthropogenic origin [2-4]. In fact, all volatile ashes of industrial origin contain a significant fraction of ferromagnetic particles that are produced during the combustion processes of fossil fuels. Other sources of magnetic particles of anthropogenic origin in the soils are the processing of iron, steel and cement, heating systems and car traffic.

Magnetic susceptibility is used as a proxy variable in monitoring soil pollution by heavy metals [5-6]. The knowledge of magnetic grain dimension can be helpful to distinguish natural and anthropogenic contribution to the increase of magnetic susceptibility in soils. The objective of this study is to assess the contamination level of heavy metals in industrial soils by means of magnetic susceptibility measurements.

In this paper, we present the results of a field survey carried out in a large industrial area of Basilicata Region (Southern Italy). We discuss both in situ and laboratory measurements and compare these results with the values found in other similar industrial areas of the Basilicata.

THE STUDY AREA AND THE SAMPLING GRID

The industrial area of Tito Scalo is located 10 km from Potenza, the chief town of the Basilicata Region and it is considered the real industrial area of this town. The area is characterized by the presence of some large mechanical, steel, and iron industrial plants.

It is located at 800 m above sea level and is surrounded by mountains reaching 1300 m and by springs and streams. In the vicinity there are areas of great naturalistic interest such as the oasis of the WWF "Pantano di Pignola". The geology of the area is rather uniform with a clear prevalence of alluvial deposits.

TABLE 1
Explorative statistical analysis of the magnetic susceptibility values measured in situ by means of MS2D, MS2F, and dual frequencies probes in the Tito industrial area :

K ($\times10^{-5}$ SI)	n	mean	SD	CV%	range
K_D	70	94	93	99	11-366
K_F	70	77	92	120	9-499
K_{BH}	70	139	142	102	12-659
K_{BL}	70	142	146	103	13-661

K_D magnetic susceptibility values measured with MS2D probe ($\times10^{-5}$ SI), K_F magnetic susceptibility values measured with MS2F ($\times10^{-5}$ SI) probe, K_{BH} magnetic susceptibility values at high frequencies ($\times10^{-5}$ SI), K_{BL} magnetic susceptibility values at low frequencies ($\times10^{-5}$ SI), *n* = sample number; *mean* = mean value; *SD* = standard deviation; *CV%* = percentage coefficient of variation; *range* = range of variability.

TABLE 2
Explorative statistical analysis of the magnetic susceptibility values measured in situ by means of MS2D probe in different industrial areas of the Basilicata Region (Tito, Potenza, Melfi, Viggiano)

K ($\times10^{-5}$ SI)	*mean*	*SD*	*CV%*	*range*
K_{TITO}	94	93	99	10-366
$K_{VIGGIANO}$	53	32	60	16-106
$K_{POTENZA}$	72	78	108	8-636
K_{MELFI}	167	98	60	41-607

K_{TITO} magnetic susceptibility values measured with MS2D probe at Tito ($\times10^{-5}$ SI), $K_{POTENZA}$ magnetic susceptibility values measured with MS2D probe at Potenza ($\times10^{-5}$ SI), K_{MELFI} magnetic susceptibility values measured with MS2D at Melfi ($\times10^{-5}$ SI), $K_{VIGGIANO}$ magnetic susceptibility values measured with MS2D at Viggiano ($\times10^{-5}$ SI); *mean* = mean value; *SD* = standard deviation; *CV%* = percentage coefficient of variation; *range* = range of variability.

The sampling grid covers all the industrial area of Tito Scalo. Moreover, we collected additional sampling points in the surrounding natural areas that could be used as blank samples.

The sampling grid included 70 georeferenced sampling points covering an area of 90 km^2.

MATERIALS AND METHODS

Magnetic susceptibility measurements were performed using a Bartington MS2 meter with two field survey in situ probes MS2D (penetration depth of about 10 cm) and MS2F (effective penetration depth of about 1 cm) and with MS2B laboratory dual frequency sensor. The probes measure the volume magnetic susceptibility, expressed as a dimensionless value $\times10^{-5}$ SI and the accuracy of measurements is 5%. The sampling procedure presented by D'Emilio et al. [7-8] was used.

Regarding laboratory measurements, for each sampling point, we selected a small square area (1m ×1m), located at least 5 m from the roadside. At the angles of the square, we collected four soil samples at a deep of about 5 cm. The four samples were mixed in a polyethene bag. The samples were dried in an oven at a temperature of 50 °C. Then they were grounded and sieved with a 2 mm sieve.

After this pre-treatment the samples were analyzed by means of MS2B laboratory dual frequency sensor. All measurements were conducted at the 1.0 sensitivity setting. Each measure was repeated three times with an air reading before both each series and measurement of the standard samples were performed after the measurements of five samples for preventing drift effects. In the following equation we indicate with K_{BH} high-frequency magnetic susceptibility soil measurements and with K_{BL} low-frequency magnetic susceptibility soil measurements. We calculated also the percentage loss of Susceptibility (K_{FD}%), see [9] as:

$$K_{FD} = \frac{(K_{BH} - K_{BL})}{K_{BH}} * 100$$

RESULTS AND DISCUSSION

Magnetic susceptibility soil measurements carried out in situ by means of MS2D probe, MS2F probe and double frequencies probe are shown in Figure 1 (MS2D probe), Figure 2 (MS2F probe), Figure 3 (high frequencies), and Figure 4 (low frequencies). Statistics of the measurements are shown in Table 1. For MS2D magnetic susceptibility K_D ranges from 11 $\times10^{-5}$ SI to 366 $\times10^{-5}$ SI, with a mean value of 94 $\times10^{-5}$ SI, a standard deviation of 93 $\times10^{-5}$ SI and a coefficient of variation of 99%.

K_F ranges from 9 $\times10^{-5}$ SI to 499 $\times10^{-5}$ SI, with a mean value of 77 $\times10^{-5}$ SI, a standard deviation of 92 $\times10^{-5}$ SI and a coefficient of variation of 120%.

High frequency magnetic susceptibility K_{BH} ranges from 12 $\times10^{-5}$ SI to 659 $\times10^{-5}$ SI, with a mean value of 139 $\times10^{-5}$ SI, a standard deviation of 142 $\times10^{-5}$ SI and a coefficient of variation of 102%.

K_{BL} ranges from 13 $\times 10^{-5}$ SI to 661 $\times 10^{-5}$ SI, with a mean value of 142 $\times 10^{-5}$ SI, a standard deviation of 146 $\times 10^{-5}$ SI and a coefficient of variation of 103%. The susceptibility values of superficial soil are very variable. In spite of the overall uniformity of the geology of the investigated area, the coefficient of variation ranges from 99% for MS2D probe to 120 % for MS2F probe. We measure very high values of superficial soil magnetic susceptibility close to the industrial settlements and low values in areas far from industrial settlements that can be considered as not impacted areas (Figures 1-2-3-4).

We may say that the sample points close to industrial areas have ferromagnetic characteristics and contain heavy metal ions probably due to the influence of the anthropogenic activities of the area.

The comparison of superficial soil magnetic susceptibility mean values measured in the industrial area of Tito Scalo with values measured in other industrial area of Basilicata Region, Viggiano Potenza, Melfi, suggests that Tito Scalo industrial area suffers of heavy metals soil contamination [8,10-11]. In fact, in this site magnetic susceptibility mean values are higher than those measured in the other industrial areas of Basilicata except for the Melfi industrial area. In Melfi industrial area a large automotive plant and a cogeneration power plant are operative and both of them produce heavy metals soil pollution. Moreover, in this area the geology is very variable [8] and vulcanic soils are also present. This kind of soils naturally shows high values of magnetic susceptibility. All these characteristics of Melfi industrial areas contribute to increase soil magnetic susceptibility values.

FIGURE 1
Magnetic susceptibility measurements performed with MS2D probe (Tito Scalo industrial area).

FIGURE 2
Magnetic susceptibility measurements performed with MS2F probe (Tito Scalo industrial area).

FIGURE 3
Magnetic susceptibility measurements performed with high frequencies probe (Tito Scalo industrial area).

FIGURE 4
Magnetic susceptibility measurements performed with low frequencies probe (Tito Scalo industrial area).

CONCLUSION

The superficial soil magnetic susceptibility values measured in situ and in the laboratory in this field survey suggest that the examined industrial area of Tito Scalo suffers of heavy metals contamination due to the presence of many industrial settlements operating in the mechanical, steel, and iron sector. The low values of magnetic susceptibility measured far from the industrial area confirm this statement. The comparison of these findings with what observed in other industrial areas of Basilicata by adopting the same time-saving and low-cost technique indicates that the Tito Scalo site is affected by heavy metals soil contamination.

The findings that we obtained with our time-saving and low-cost procedure, would certainly motivate the further use of well-assessed chemical techniques for obtaining heavy metal soil concentrations (i.e., inductively coupled plasma optic emission spectrometer - ICP-OES) in order to better characterize the affected area and identify the most damaged zones.

REFERENCES

[1] Rachwał, M., Kardel, K., Magiera, T., Bens, O. (2017) Application of magnetic susceptibility in assessment of heavy metal contamination of Saxonian soil (Germany) caused by industrial dust deposition. Geoderma. 295, 10–21.

[2] Goebel, M.O., Krueger, J., Fleige, H., Igel, J., Horn R., Bachmann, J. (2017) Frequency dependence of magnetic susceptibility as a proxy for fine-grained iron minerals and aggregate stability of south Chilean volcanic ash soils. Catena. 158, 46–54.

[3] Magiera, T., Mendakiewicz, M., Szuszkiewicz, M., Jabłońska, M., Chróst, L. (2016) Technogenic magnetic particles in soils as evidence of historical mining and smelting activity: A case of the Brynica River Valley. Poland Science of the Total Environment. 566–567, 536–551.

[4] Magiera, T., Parzentny, H., Róg, L., Chybiorz, R., Wawer, M. (2015) Spatial variation of soil magnetic susceptibility in relation to different emission sources in southern Poland. Geoderma. 255–256, 94–103.

[5] Bourliva, A., Papadopoulou, L., Aidona, E., Giouri, K. (2017) Magnetic signature, geochemistry, and oral bioaccessibility of "technogenic" metals in contaminated industrial soils from Sindos Industrial Area, Northern Greece. Environ Sci Pollut Res. (2017)24, 17041-17055.
[6] Kucer, N., Sabikoglu, I., Can, N. (2012) Measurements of environmental pollution in industrial area using magnetic susceptibility method. Acta Physica Polonica A. 121(1), 20–22.
[7] D'Emilio, M., Chianese, D., Coppola, R., Macchiato, M., Ragosta, M. (2007) Magnetic susceptibility measurements as proxy method to monitor soil pollution: development of experimental protocols for field surveys, Environ Monit Assess. 125, 137–146.
[8] D'Emilio, M., Caggiano, R., Coppola, R., Macchiato, M., Ragosta, M. (2010) Magnetic susceptibility measurements as proxy method to monitor soil pollution: the case study of S. Nicola di Melfi. Environ Monit Assess. 169, 619–630.
[9] Grison, H., Petrovsky, E., Kapicka, A., Hanzlikova, H. (2017) Detection of the pedogenic magnetic fraction in volcanic soils developed on basalts using frequency-dependent magnetic susceptibility: comparison of two instruments. Geophys J Int. 209, 654–660.
[10] D'Emilio, M., Macchiato, M., Coppola, R., Loperte, A., Ragosta, M. (2006) Pollution levels in the industrial area of Potenza (Southern Italy). Fresen. Environ. Bull. 15, 36-42.
[11] D'Emilio, M., Coluzzi, R., Macchiato, M., Imbrenda, V., Ragosta, M., Sabia, S., Simoniello, T. (2018) Satellite data and soil magnetic susceptibility measurements for heavy metals monitoring: findings from Agri valley (Southern Italy). Environmental Earth Sciences. 77, 63.

Received: **10.09.2018**
Accepted: **15.11.2018**

CORRESPONDING AUTHOR

Mariagrazia D'Emilio
Institute of Methodologies for
Environmental Research – CNR,
85050 Tito Scalo (PZ) – Italy

e-mail: demilio@imaa.cnr.it

© by PSP Volume 28 – No. 5/2019 pages 4375-4379 Fresenius Environmental Bulletin

RADIUM CONCENTRATION AND MAGNETIC SUSCEPTIBILITY MEASUREMENTS FOR CHARACTERIZING SOILS DEVOTED TO CEREAL CULTIVATION

Mariagrazia D'Emilio[1,*], Rosa Coluzzi[1], Vito Imbrenda[1], Maria Quarto[2]

[1] Institute of Methodologies for Environmental Research – CNR, 85050 Tito Scalo (PZ)
[2] Department of Advanced Biomedical Sciences, University "Federico II", Napoli, 80131, Italy

ABSTRACT

In order to characterize soil samples collected in two different agricultural areas of Potenza suburbs (Southern Italy) devoted to durum wheat cultivation, we used the combination of two techniques: magnetic susceptibility measurements and effective radium concentration obtained from radon emanation. Magnetic susceptibility measurements are generally used as a proxy method for monitoring heavy metals in soil. Radium concentration and radon exhalation rate from soil are used for characterizing different soils. First results suggest that effective radium concentrations in soils can be helpful for the interpretation of magnetic susceptibility field surveys.

KEYWORDS:
Soil Monitoring, Effective Radium Concentration, Soil Magnetic Susceptibility

INTRODUCTION

Protection and conservation of soil are priority tasks for sustainable management, environment protection, and rural areas development [1].

Measurements of soil magnetic susceptibility are widely used to monitor heavy metals in polluted soils because heavy metals and magnetic particles (e.g., magnetite) are emitted from similar sources such as combustion processes or steel industries and have similar transport pathways into the environment [2].

Soils, even in areas very close to each other, can have very heterogeneous features due to soil-forming factors, meteorological parameters, and biological characteristics. This heterogeneity makes complex the control of soil processes and pollutants distribution particularly if proxy variables are used for monitoring large areas [3].

In order to support data interpretation, very often magnetic susceptibility measurements are coupled with chemical analyses of the single heavy metal concentration. These measurements are very expensive and time consuming [4].

In this paper, we evaluated if the effective radium concentration measurements used in conjunction with magnetic susceptibility measurements may be helpful in the characterization of agricultural soils with different paedogenesis to discriminate anthropogenic magnetic particles from those naturally present in soils.

THE SAMPLING TEST SITES

For this study, we carried out in situ measures and we collected soil samples measurements from Venosa and Lavello test sites. These areas are located in the northern part of Basilicata region, Southern Italy. From a geographical point of view, they are parts of the Vulture basin, a valley placed along the Ofanto River. The area is surrounded by low hills varying from 137 to 508 m a.s.l.. This is a rather unpolluted zone where the main land use is agriculture, being wheat the most spread cultivation, and where milk-cow farming is prevalent. The meteorological features of the area are typical of Mediterranean flat areas. The annual average temperature is 13 °C, the rainfalls are more frequent in winter and the prevailing wind direction is N-NW.

MATERIALS AND METHODS

For each sampling point, we selected a small square area (1m ×1 m), located at least 5 m from the roadside. At the angles of the square, we collected four soil samples at a deep of about 5 cm. The four samples were mixed in a polyethene bag. The samples were dried in an oven at a temperature of 50°C. Then they were grounded and sieved with a 2 mm sieve.

Magnetic measurements. Soil magnetic susceptibility measurements were performed using a Bartington MS2 meter with MS2B laboratory dual

frequency sensor. The probes measure volume magnetic susceptibility, expressed as dimensionless value $\times 10^{-5}$ SI.

All measurements were conducted at the 1.0 sensitivity setting. Each measure was repeated three times with an air reading before both each series and measurement of the standard samples after the measurements of five samples for preventing drift effects. In the following, we indicate with K_{BH} high frequency soil measurements and with K_{BL} low frequency magnetic susceptibility soil measurements. We calculated also the percentage loss of Susceptibility (K_{FD}%, see [5]) as:

$$K_{FD} = \frac{(K_{BH} - K_{BL})}{K_{BH}} * 100$$

Effective radium concentrations. Six soil samples collected at the test sites of Lavello (3 samples) and Venosa (3 samples) were analyzed to determine radium concentration by using the CAN Technique. A 100 g mass was inserted in a glass jar with a volume of 5000 ml closed with a stopper and sealed with a polyethylene sheet for 30 days. In each jar, one LR-115 detector was attached below the stopper at distance of 11 cm from the surface of the sample (figure 1). After the exposure, the LR-115 detectors were chemically etched, using a solution of 2.5 N NaOH at 60 °C for 110 min. The track density was determined by acquiring the image of the detector by means of a scanner with double lighting and by using a suitable software for image processing (Image J software: Image Processing and Analysis in Java, version 1.46r, National Institutes of Health, USA). The radium concentration was determined by using the formula:

$$C_{Ra} = \frac{V_a \times C_{Rn}}{m \times (1 - e^{-\lambda t})}$$

where V_a is the free volume of the jar, C_{Rn} is the radon concentration (Bq/m^3), m is the sample mass (kg), λ is the radon decay constant.

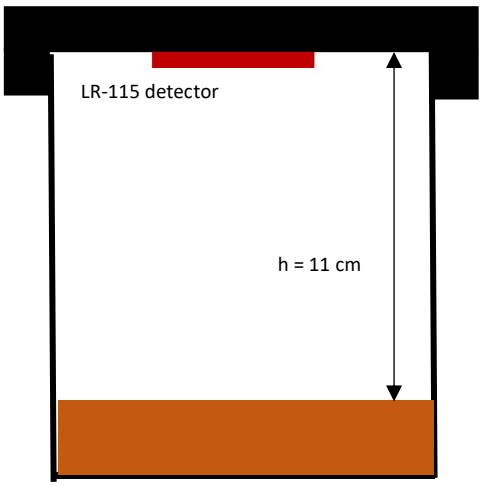

FIGURE 1
Experimental disposal for measuring effective radium concentrations.

TABLE 1
Explorative statistical analysis of magnetic susceptibility values measured by means of dual frequency probe in Lavello legend: K_{BH} magnetic susceptibility values at high frequencies ($\times 10^{-5}$ SI), K_{BL} magnetic susceptibility values at low frequencies ($\times 10^{-5}$ SI), K_{FD} percentage loss of susceptibility, n = sample number; m = mean value; sd = standard deviation; CV% = percentage variation coefficient; r = range of variability.

variable	n	m	sd	CV%	r
K_{BH} ($\times 10^{-5}$ SI)	12	119.4	36.4	30	80.0-206.7
K_{BL}($\times 10^{-5}$ SI)	12	121.8	36.7	30	82.0-210.4
K_{FD}	12	2.0	0.8	39	0.5-2.9

TABLE 2
Explorative statistical analysis of magnetic susceptibility values measured by means of dual frequency probe in Venosa legend: K_{BH} magnetic susceptibility values at high frequencies ($\times 10^{-5}$ SI), K_{BL} magnetic susceptibility values at low frequencies ($\times 10^{-5}$ SI), K_{FD} percentage percentage loss of susceptibility, n = sample number; m = mean value; sd = standard deviation; CV% = percentage variation coefficient; r = range of variability.

variable	n	m	sd	CV%	r
K_{BH} ($\times 10^{-5}$ SI)	12	96.2	28.5	30	60.3-144.5
K_{BL}($\times 10^{-5}$ SI)	12	100.3	29.4	29	64.3-149.0
K_{FD}	12	4.1	1.0	24	3.0-6.2

TABLE 3
Results of radium concentration estimation in soil samples.

Location	Radium Concentration (Bq/kg)
Lavello	12.1 ± 0.6
Lavello	12.2 ± 0.6
Lavello	9.4 ± 0.3
Venosa	15.1 ± 1.1
Venosa	16.6 + 1.5
Venosa	16.0 ± 1.2

RESULTS AND DISCUSSION

Figure 2 (Lavello site) and figure 3 (Venosa site) show magnetic susceptibility measurements carried out in laboratory on the samples collected in the two test sites.

Statistics of the measurements are shown in Table 1 and Table 2. For measurements performed at the Lavello site high frequency magnetic susceptibility K_{BH} ranges from 80.0 $\times 10^{-5}$ SI to 206.7 $\times 10^{-5}$ SI with a mean value of 119.4 $\times 10^{-5}$ SI, a standard deviation of 36.4 $\times 10^{-5}$ SI and a coefficient of variability of 30%.

Moreover. K_{BL} ranges from 82.0 $\times 10^{-5}$ SI to 210.4 $\times 10^{-5}$ SI with a mean value of 121.8 $\times 10^{-5}$ SI, a standard deviation of 36.7 $\times 10^{-5}$ SI and a coefficient of variability of 30%.

For measurements performed at the Venosa site high frequency magnetic susceptibility K_{BH} ranges from 60.3. $\times 10^{-5}$ SI to 144.5 $\times 10^{-5}$ SI with a mean value of 96.2 $\times 10^{-5}$ SI, a standard deviation of 28.5 $\times 10^{-5}$ SI and a coefficient of variability of 30%.

K_{BL} ranges from 64.3 $\times 10^{-5}$ SI to 149.0 $\times 10^{-5}$ SI with a mean value of 96.5 $\times 10^{-5}$ SI, a standard deviation of 29.4 $\times 10^{-5}$ SI and a coefficient of variability of 29%.

We can conclude that we measure higher values of magnetic susceptibility in Lavello. This enhancement in magnetic susceptibility for the Lavello test site can be ascribable to anthropogenic input of magnetic material or to predisposing factors such as differences in geology and soil forming processes (paedogenesis, [6.7]).

Figure 4 and figure 5 show respectively correlations between K_{BH} and K_{BL} in Lavello and Venosa test sites. Both the plots show a linear relationship between K_{BH} and K_{BL} and a high correlation coefficient. This behavior indicates homogeneity in the magnetic size of magnetic grains of examined soils.

Double frequency magnetic susceptibility probe is generally used for evaluating the characteristics of magnetic grains in soil samples. For discussing our results, we adopt the model proposed by Dearing [8].

As shown in Table 1 and Table 2 K_{FD} mean value in Lavello is 2%, whereas K_{FD} mean value in Venosa is 4%. In particular. 5 of the 12 samples collected in Venosa show a K_{FD} value < 2%. Following the Dearing model these soils are defined as "Virtually no Super Paramagnetic (SP) grains". The remaining samples and all the samples collected in Venosa are in the range 2%<K_{FD} < 10%.

These soils are defined as "Admixture of SP and coarser non-SP grains or SP grains < 0.005μm".

In addition, this difference between the two soils can be ascribable both to anthropogenic and natural causes.

For helping the interpretation of the results we measured radium concentration estimation in soil samples [9] that is a characteristic of soil indipendent from anthropogenic influence.

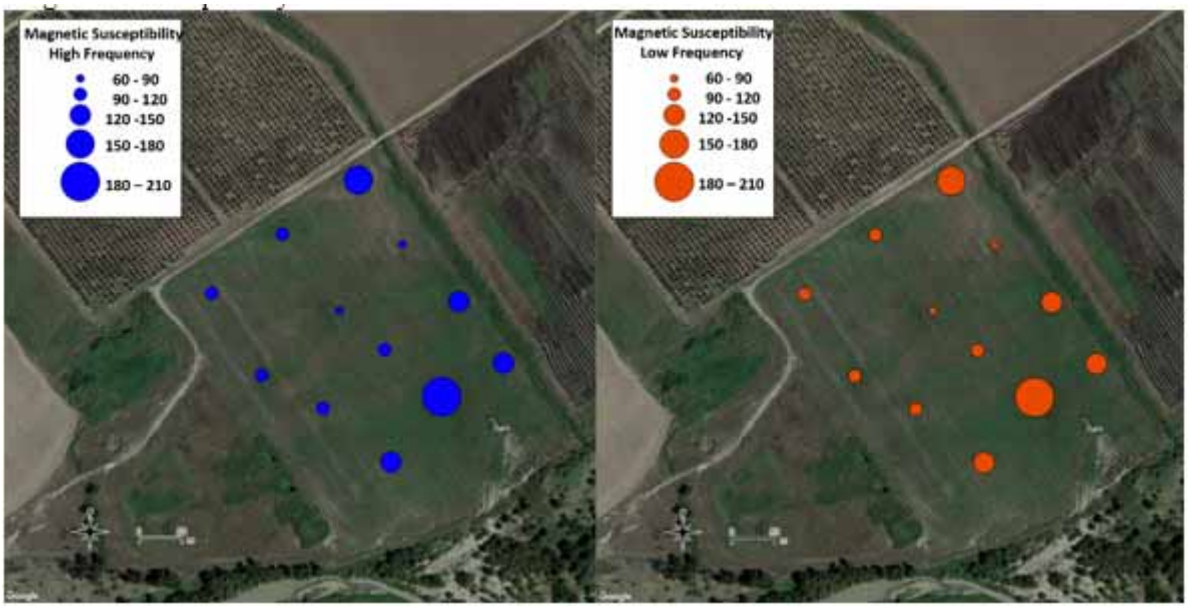

FIGURE 2
Magnetic susceptibility measurements carried out with double frequency probe at Lavello.

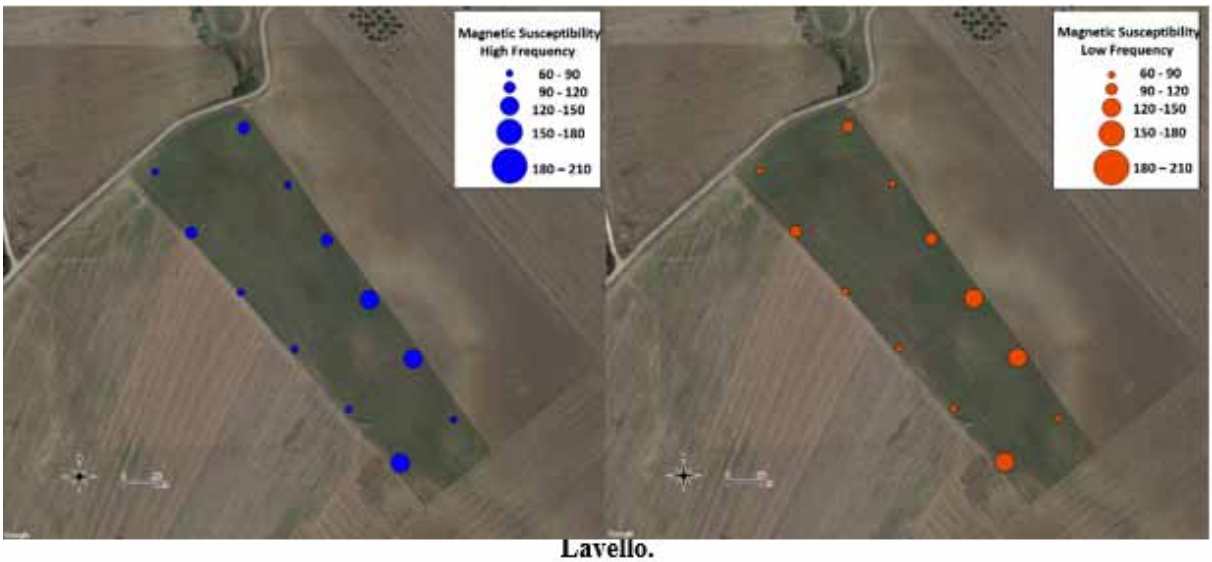

Lavello.

FIGURE 3
Magnetic susceptibility measurements carried out with double frequency probe at Venosa

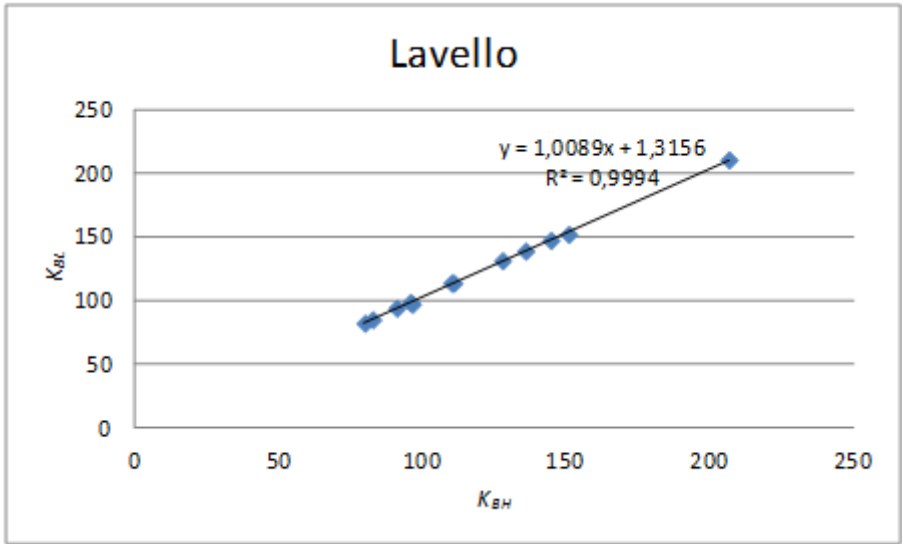

FIGURE 4
Magnetic susceptibility measurements carried out with double frequencies probe at Lavello

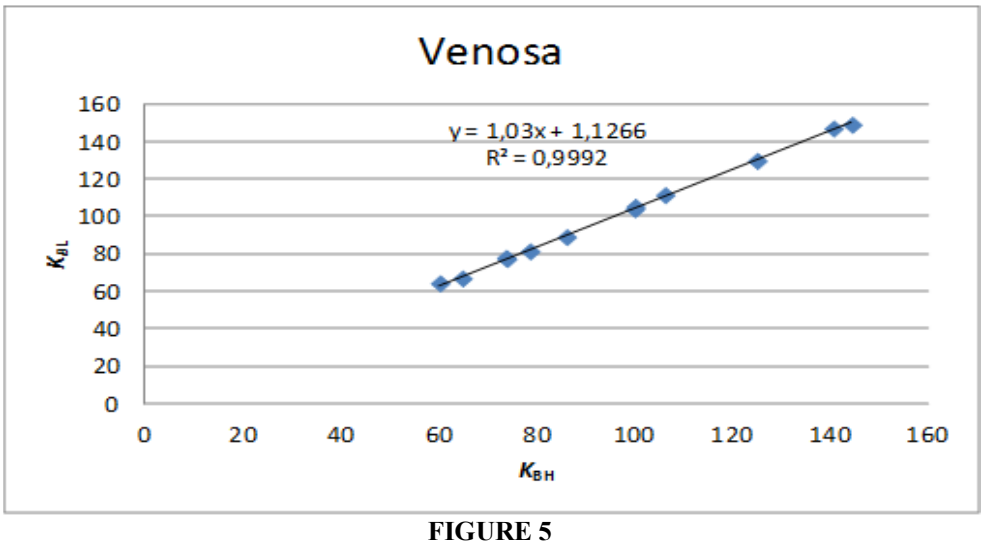

FIGURE 5
Magnetic susceptibility measurements carried out with double frequency probe at Venosa

In Table 3 results of radium concentration estimation are shown. In the two test sites we measured different concentrations of radium. This result suggests us that we are examining soils with different paedogenesis so higher levels of magnetic susceptibility measured in Lavello are probably ascribable to natural processes and anthropogenic causes can be excluded.

CONCLUSION

We measured soil magnetic susceptibility values by means of a double frequency probe on soils sampled in two close agricultural areas of the Basilicata Region (Southern Italy) devoted to cereal production.

Magnetic susceptibility measurements show a good homogeneity of the samples for both the test sites but we measure higher magnetic susceptibility values in Lavello. K_{FD} analysis confirms that the soils of two test sites are different for the presence of different magnetic grains. This difference can be ascribable both to soil forming processes and to anthropogenic influence. We measured radium concentration estimation for helping us to ascertain if the observed differences are due to natural processes. Measurements confirm this hypotesis.

This work is a first attempt to use radium concentration estimation for helping the interpretation of magnetic susceptiblity measurements. We are working for increasing radium measurements and for a best definition of protocols.

ACKNOWLEDGEMENTS

These activities are carried out in the framework of REACT project (Reinterpretation and validation of traditional knowledge for soil conservation in areas of Basilicata devoted to cereal cultivation) – Measure 124 of the Rural Development Programme of Basilicata 2007-2013.

REFERENCES

[1] Baderna, D., Lomazzi, E., Pogliaghi, A., Ciaccia, G., Lodi, M., Benfenat, E. (2015) Acute phytotoxicity of seven metals alone and in mixture: Are Italian soil threshold concentrations suitable for plant protection? Environmental Research. 140, 102–111.

[2] Rachwał, M., Kardel, K., Magiera, T., Bens, O. (2017) Application of magnetic susceptibility in assessment of heavy metal contamination of Saxonian soil (Germany) caused by industrial dust deposition. Geoderma. 295, 10–21.

[3] Blundell, A., Dearing, J.A., Boyle, J.F., Hannam, J.A. (2009) Controlling factors for the spatial variability of soil magnetic susceptibility across England and Wales Earth-Science Reviews. 95, 158–188.

[4] Naimi, S., Ayoubi, S. (2013) Vertical and horizontal distribution of magnetic susceptibility and metal contents in an industrial district of central Iran. Journal of Applied Geophysics. 96, 55–66.

[5] Grison, H., Petrovsky, E., Kapicka, A., Hanzlikova, H. (2017) Detection of the pedogenic magnetic fraction in volcanic soils developed on basalts using frequency-dependent magnetic susceptibility: comparison of two instruments. Geophys. J. Int. 209, 654–660.

[6] D'Emilio, M., Caggiano, R., Coppola, R., Macchiato, M., Ragosta, M. (2010) Magnetic susceptibility measurements as proxy method to monitor soil pollution: the case study of S. Nicola di Melfi. Environ. Monit. Assess. 169, 619–630.

[7] Kanu, M.O., Meludu, O.C., Oniku, S.A. (2014) Comparative study of top soil magnetic susceptibility variation based on some human activities. Geofísica Internacional. 53(4), 411-423

[8] Dearing, J.A. (1999) Environmental Magnetic Susceptibility, Using the Bartington MS2 System. Second edition, England: Chi Publishing.

[9] Girault, F., Poitou, C., Perrier, F., Koirala, B.P., and Bhattarai, M. (2011) Soil characterization using patterns of magnetic susceptibility versus effective radium concentration. Nat. Hazards Earth Syst. Sci. 11, 2285–2293.

Received: **10.09.2018**
Accepted: **15.11.2018**

CORRESPONDING AUTHOR

Mariagrazia D'Emilio
Institute of Methodologies for
Environmental Research – CNR,
85050 Tito Scalo (PZ) – Italy

e-mail: demilio@imaa.cnr.it

© by PSP Volume 28 – No. 5/2019 pages 4380-4391 Fresenius Environmental Bulletin

TEMPERATURE DISPERSION OF COOLING WATER DISCHARGE INTO OLIGOTROPHIC SEAWATER

Riyad Manasrah[1,3,*], Mousa Al-Badaineh[1], Mohammad Rasheed[2], L Kellie Dixon[3]

[1]Faculty of Marine Sciences, The University of Jordan/Aqaba, PO Box 2595, Aqaba 77110, Jordan
[2]Faculty of Sciences, The University of Jordan Amman 11942 Jordan
[3]Mote Marine Laboratory, 1600 Ken Thompson Parkway, Sarasota, FL 34236, USA

ABSTRACT

In order to study temperature dispersion of cooling water discharged into seawater, temperature values were recorded monthly for different transects during the study period (April-August 2015) in front of Aqaba Thermal Power Station (ATPS). A simple conservative model was developed to estimate the dispersion of temperature after discharge from the cooling system into oligotrophic seawater of the Gulf of Aqaba, Red Sea. Temperatures along transects exhibited a clear gradual decrease from the discharge point with distance, ending with little difference from the intake source. The model exhibited very strong correlation with observed temperature ($r > 0.9$), and can be used as a tool for prediction the dispersion of temperature for any cooling system with the same conditions. The study showed that the thermal influence of the outflow decreased significantly at 100m from the discharge point. The maximum difference between either the intake or ambient seawater and a station 100m from the discharge was 1.2 °C. This difference can be considered within the limits determined by Aqaba Special Zone Authority (ASEZA), World Bank and some international standards.

KEYWORDS:
Cooling water, Dispersion model, Gulf of Aqaba, Temperature standards

INTRODUCTION

The Cooling Water System (CWS) is the most efficient method to remove heat from component and industrial equipment [1]. A once-through system that uses a large water volume is the most economical way for cooling power plants located in coastal area [2]. Cooling water effluent is discharged into seawater with temperatures 3-6 °C above ambient seawater [3] However, some systems may discharge water with temperatures as high as 15 °C [4], 8-10 °C [5], 7.5 °C [6] and 6.8 °C [7] above ambient. The temperature of the discharge may change due to the differences in local climates, plant efficiencies, or volumes of water required for cooling [8].

The warm effluent water may cause thermal pollution in the receiving water body [4, 9]. Temperature is a key factor in marine life and any change in temperature may cause stress or even death to aquatic organisms [4]. Change in temperature may impact productivity [10], growth [11], development [12], as well as metabolic and physiological processes [13, 14].

Tropical and subtropical latitudes, like those of the Gulf of Aqaba, generally have little temperature fluctuation, due to the large ocean surfaces and absence of a cold season. For example, the Gulf of Aqaba sea surface temperature fluctuates only 4 to 6 °C seasonally, and 1 °C diurnally [15]. Accordingly, temperature variation of only a few degrees may be considered a proportionally large change for organisms that are adapted to this relatively stable thermal environment [16]. As a consequence, small changes in temperature could have a disproportionately greater impact on the larval development of tropical organisms than on the larvae of temperate systems which naturally experience large temperature variations [17].

Coral reef species live within a relatively narrow temperature margin, and anomalously low and high sea temperatures can induce coral bleaching (e.g. [18]) which has previously affected Red Sea reefs in 1998 and 2002/2003 [19, 20, 21]. Photosynthetic and calcification activities of coral in the Gulf of Aqaba were impacted by higher temperatures [22].

Elevation of seawater temperature may also decrease gas solubility in seawater which may decrease O_2 level while increasing respiration rates (possibly increasing CO_2 levels). This could impact marine organisms, community composition, and biogeochemical cycling of key elements such as carbon, nitrogen, and phosphorus [23, 24].

Studies used different models to estimate the dispersion of warm water from cooling water discharge to open shore. For example, a hydrodynamic model was used to estimate the thermal impact of power plant on tropical coastal lagoon [25], finding that the main thermal impact was restricted to the surface layers and distributed along the shoreline within 100 m of the discharge point.

Power generation and fertilizer industries are currently the primary sources of the relatively warm effluents into coastal marine water along the Jordanian coast of the Gulf of Aqaba. Thermal Power Station (ATPS) discharges approximately 90,000 m^3 hr^{-1}, and represents 90% of all thermal effluents into the Jordanian Gulf of Aqaba.

Aqaba Special Economic Zone Authority (ASEZA) developed guidelines for thermal discharges [26]. Based on these, maximum allowable difference between cooling water discharge and ambient seawater should not be more than 10°C and should be 3°C or less at 100 m distance from the discharge point. According to the World Bank guidelines, the increase in temperature of the receiving water should not be more than 3 °C at the edge of a mixing zone or 100 m from the discharge point [27]. The aim of this study was to predict the dispersion of the effluent discharged from the cooling system of the ATPS. This was achieved using both observation and a simple conservative model that estimated the thermal dispersion of discharge. This study also evaluated the compliance of the thermal discharge with ASEZA, World Bank, and some international guidelines.

MATERIALS AND METHODS

Description of the Study Site. The study was carried out in front of the ATPS outfall, which is located at the industrial area of Jordanian coast, approximately 27 km to the south of Aqaba city (Fig. 1).

The study area was divided into horizontal transects; five transects at sea surface and another five at bottom (T1-T5). Each surface transect extended from the discharge point (DP) with five sampling stations at 5, 20, 50, 100 and 150 m (Fig. 2). Each of the bottom transects had two sampling stations at 30 m and 60 m (Fig. 3), except Transect 4 which had an additional station at 90 m to be used as a control.

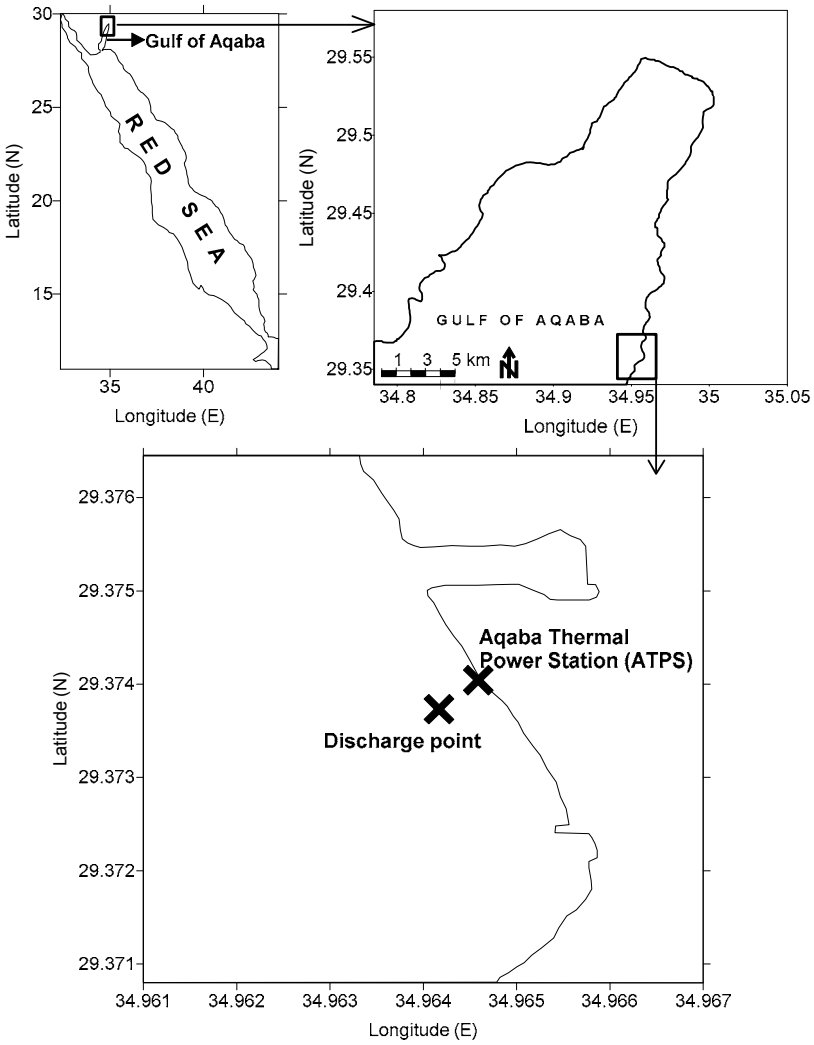

FIGURE 1
Map of the study site in front of Aqaba Thermal Power Station (ATPS) in the northern Gulf of Aqaba, Red Sea.

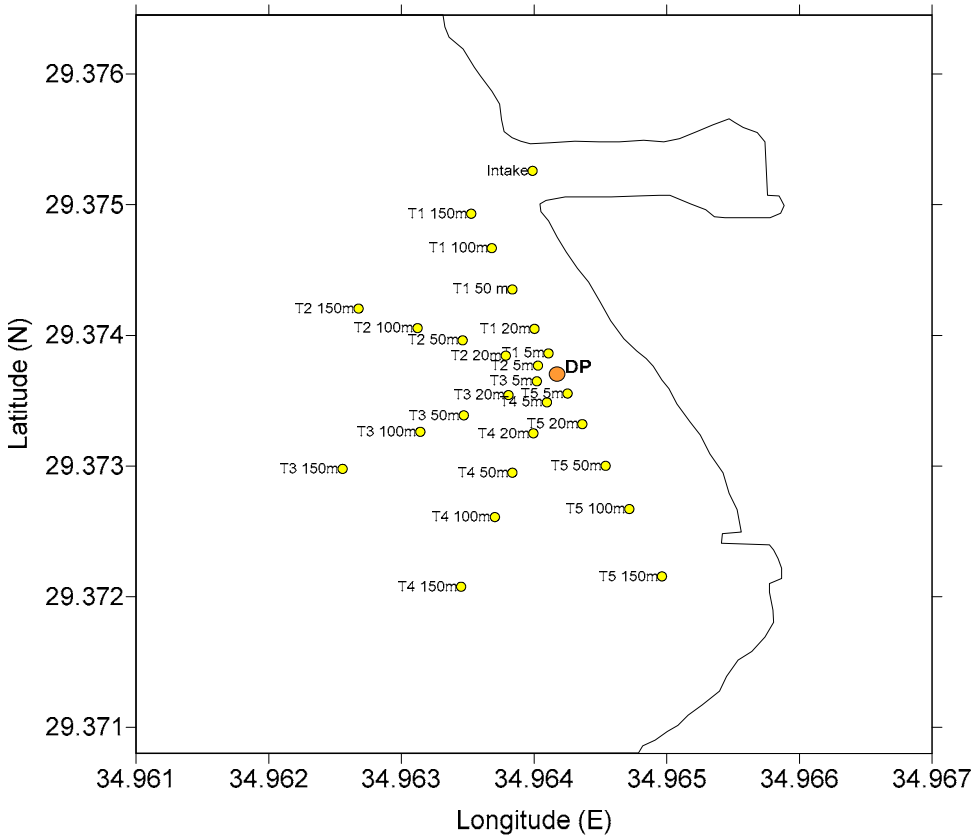

FIGURE 2

Sites of surface temperature measurements within the discharge point (DP) in front of Aqaba Thermal Power Station (ATPS) in the northern Gulf of Aqaba, Red Sea.

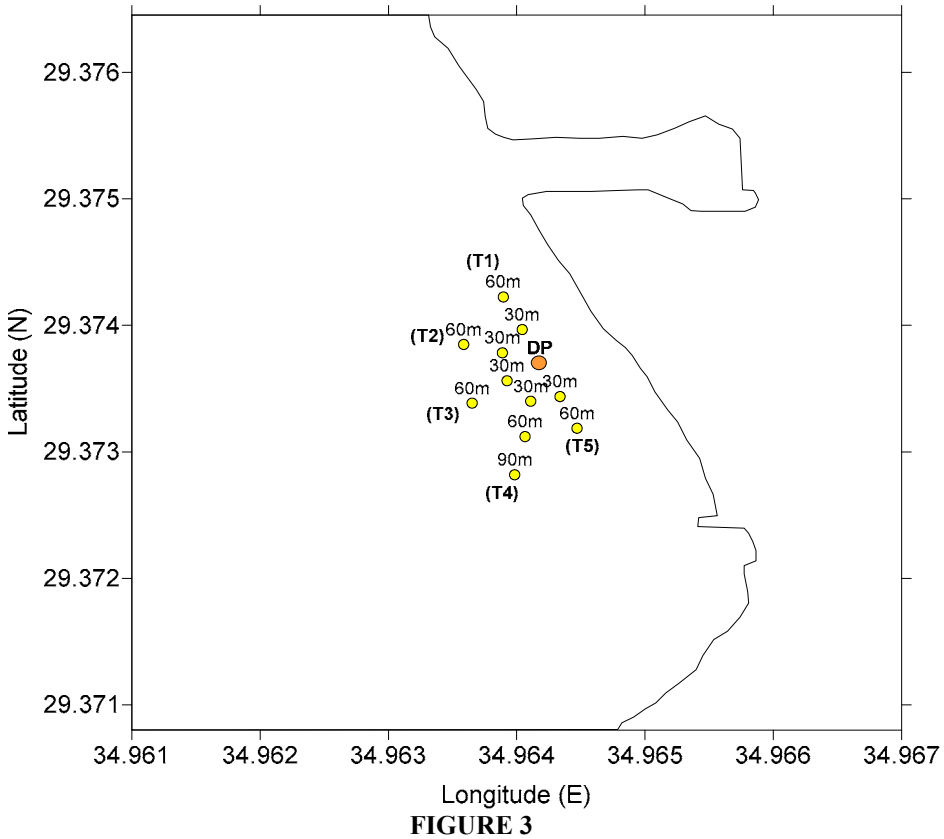

FIGURE 3

Sites of bottom temperature measurements within the discharge point (DP) in front of Aqaba Thermal Power Station (ATPS) in the northern Gulf of Aqaba, Red Sea.

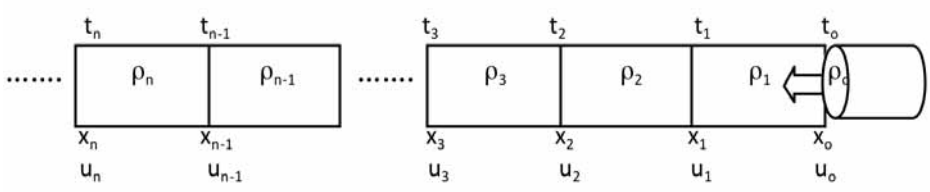

FIGURE 4
Diagram showing a distribution of discharge water flows (u_i) and densities (ρ_i) with respect to different times (t_i) and distances (x_i) through a sequence of water segments.

Temperature Measurement. Surface seawater temperatures were measured monthly during the period April-August 2015 using a bucket thermometer graduated to 0.1 °C (Ama-Digit 15th, Germany). Bottom temperatures were measured using temperature loggers (TR 1060, Canada, accuracy of ±0.002 ºC) that were deployed by divers. Loggers recorded in situ temperature every 30 minutes from April 20th to August 20th, 2015. Seawater temperature was also measured monthly at the intake point that was used as a control and was considered to represent ambient conditions.

Mathematical principles of model. A conservative model was created and used to estimate the dispersion of water temperature after discharge into seawater based on specific conditions in the area. All mathematical calculations were based on basic thermodynamic principles with some simplifying assumptions. These assumptions can be summarized as:

- The ambient water flow is negligible compared to flow of discharge water.
- The initial direction of discharge water flow is parallel to the x-axis of the model.
- The density of ambient water is homogeneous in summer in the upper 40 m of the water column.
- The density of ambient water is homogeneous in spring in the upper 40 m of the water column.
- The horizontal displacement of the discharge water with respect to time remains parallel to x-axis.
- The zero reference of horizontal displacement of discharge water is at the discharge point.
- The volume of the ambient water that will gain heat while the discharge water is passing through it represents 1% of the discharge water, representing a friction factor of 0.01. This value is considered based on seawater viscosity, which is defined as, essentially, fluid friction. Viscosity value for properties similar to Gulf of Aqaba is about 0.01 cm^2s^{-1}, i.e. friction factor is assumed to be 0.01 (e.g. [28]).
- The zero reference of vertical displacement of discharge water is at the sea level.
- A damping of the initial discharge flow speed with respect to time is considered as $u(t) = u_o e^{-2a\Delta t}$, where (a) is the friction factor with a typical value of 0.01.
- The vertical flow speed ($w = u_o e^{-1}\Delta t$) is added to the vertical displacement, which is based on the principle of continuity by inducing a vertical current due to the sinking of horizontal flow of the discharge water.

As Figure 4 shows, assuming that the discharged water started to flow with initial speed (u_o) and density (ρ_o) at time (t_o), where after time interval Δt (t_1-t_o) the water displaced a distance Δx (x_1-x_o). Therefore, the density anomaly in the n^{th} segment of this sequence will be:

$$\Delta\rho_n(t) = \rho_{n-1}(t) - \rho = \frac{\rho_{n-1}\varphi + \rho V\Delta t}{\varphi + V\Delta t} - \rho \qquad (1)$$

Where $\rho_{n-1}(t)$ is the density of the $(n-1)^{th}$ segment after mixing the discharge water and ambient water at time t, V is the volume of ambient water that will be mixed with the discharge water, φ is the volume of discharge water in the n^{th} segment, ρ is the density of the ambient water, which is (as assumed earlier) horizontally and vertically homogeneous in both spring and summer.

The volumes of discharge water of any segment (Fig. 4) and ambient water that will be mixed and exchange heat together are not equaled. This is due to the fact that the ambient water will gain heat only by direct conducting and mixing with the external surface boundaries of the water mass of moving discharge water. Therefore, it can be considered that the volume of ambient water that will exchange heat with the volume of discharge water at any segment (Fig. 4) represents 1% of the volume of discharge water. This ratio represents the friction value due to resistance of high discharge flow, which typically equals 0.01. Therefore the equation (1) becomes:

$$\Delta\rho_n(t) = \rho_{n-1}(t) - \rho = \frac{\rho_{n-1} + 0.01\rho\Delta t}{1 + 0.01\Delta t} - \rho \qquad (2)$$

The same can be considered for temperature anomalies in the n^{th} segment (Fig. 4) with respect to time as:

$$\Delta T_n(t) = T_{n-1}(t) - T = \frac{T_{n-1} + 0.01T\Delta t}{1 + 0.01\Delta t} - T \qquad (3)$$

Where T_n is the water temperature of the discharge water in the (n-1)th segment; T is the temperature of the ambient water.

The horizontal and vertical displacement of the discharge water with respect to time in the nth segment (Fig. 4) and based on the buoyancy force and equation of motion principles can be written as:

$$z_n(t) = z_{n-1} + u_{n-1}\Delta t e^{-0.02\Delta t} e^{-1} + \frac{g}{2\rho}\frac{\rho_{n-1}-\rho}{1+0.01\Delta t}\Delta t^2 \quad (4)$$

$$x_n(t) = x_{n-1} + u_{n-1}\Delta t e^{-0.02\Delta t} + \frac{g}{2\rho}\frac{\rho_{n-1}-\rho}{1+0.01\Delta t}\Delta t^2 \quad (5)$$

The discharge water has horizontal and vertical displacement components, where the term $u_{n-1}e^{-1}$ in equation (4) represents the shared flow speed by the horizontal component to the vertical downward flow. The term $e^{-0.02\Delta t}$ in both equations (4 and 5) represents the damped factor of both horizontal and vertical flow due to the friction loss of initial horizontal discharge water flow with respect to time and space.

RESULTS

Spatial and temporal variations in surface waters temperature. The monthly records of sea surface temperature at all sites in the vicinity of the cooling water discharge for ATPS during April-August followed the normal pattern of the Gulf of Aqaba with a gradual increase from April to August. The maximum and minimum sea surface temperature values were recorded in July (27.9 °C) and April (23.4 °C), respectively.

The results of sea surface temperature at all sites along the transects (T1-T5) and at the intake and discharge points (Fig. 5) showed that the difference between the discharge point and intake (ambient) was near 3 °C. Temperature values along all transects showed a clear gradual decrease from the discharge point.

Temperature variations in bottom waters. Bottom seawater temperature recorded by loggers at each site along the different transects (not shown) revealed a regular increase with respect to time from spring to summer for all transects with very slight differences among all transects.

The maximum monthly average of all stations was 26.69 ºC in August and a minimum of 21.84 ºC was recorded in April. During the period when all stations were reporting data, the median temperature at the discharge point was 24.00 ºC, while the median temperature value at 90 m distance (T4) was 23.75ºC, or 0.25 ºC cooler than at the discharge. The coolest station overall was T3 at 60 m with a median value of 23.73ºC.

Modeled Results. Summer temperature. The temperature in the effluent of the ATPS is assumed to be 29 °C compared to a homogeneous ambient water temperature of 26 °C. The temperature anomaly (ΔT) with distance, computed using equation (3) between discharge and ambient water in summer, are shown in Figure 6. It is obvious that ΔT decreased slower in the first 90 m (1 °C) of horizontal displacement than after the next 90 m (2 °C). ΔT reached a value of 3 °C at (x, z) displacements of (178m, 0m) for flow speed of 3.536 ms^{-1}, which represented the actual speed of discharged cooling water.

The pumped waters from the pipe, which is located at a depth of 8 m, dispersed vertically (using equations 4 and 5) from this depth to reach the surface at about 22 m of horizontal displacement (Fig. 7).

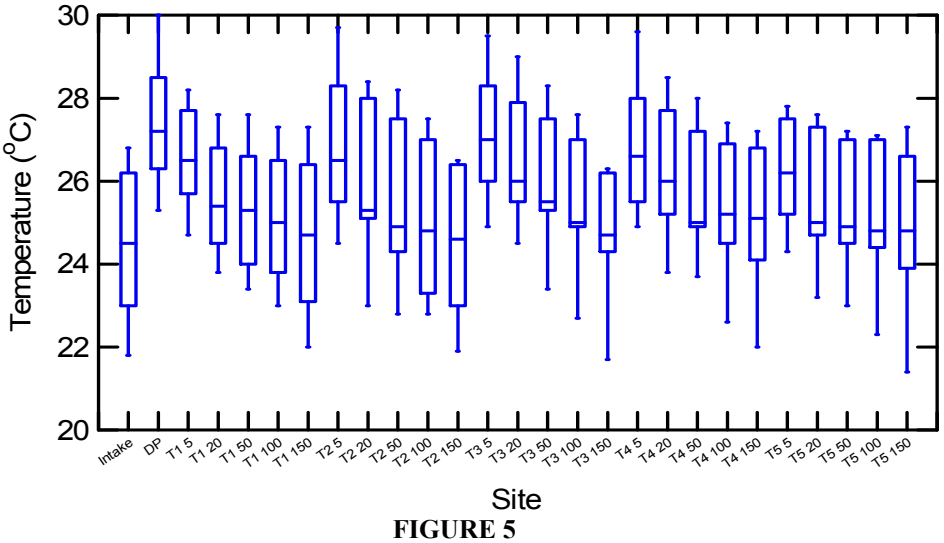

FIGURE 5

Surface seawater temperature (°C) for all transects during the period April-August 2015.
(Box plots indicate median values, first and third quartiles).

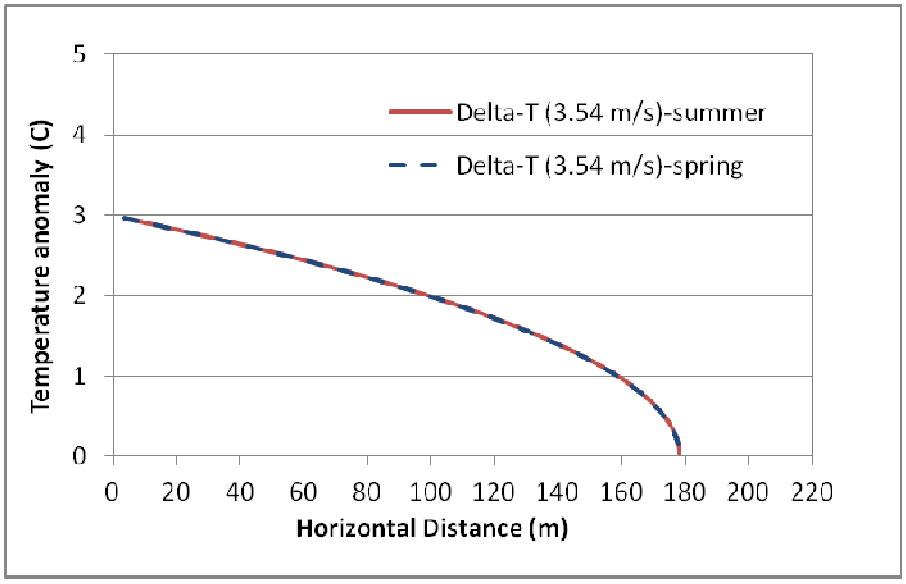

FIGURE 6
Horizontal distribution of temperature anomaly (°C) of discharged water in the ATPS compared to the ambient water in summer and spring seasons calculted by a conservatinve model (Equation 3).

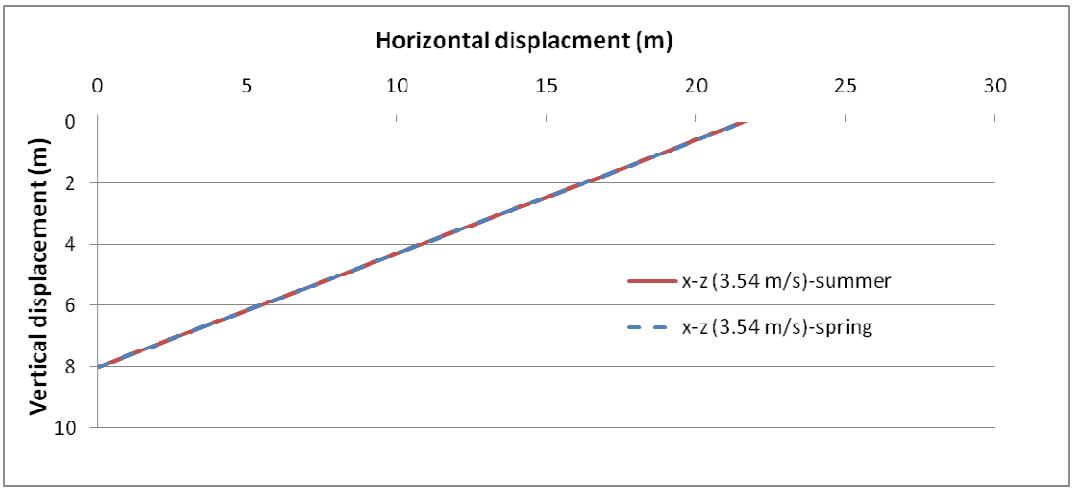

FIGURE 7
Vertical displacement vs. horizontal displacement of discharged water in the ATPS in summer and spring seasons calculted by a conservatinve model (Equation 4 and 5).

Spring temperature. In spring, the temperature in the effluent of the ATPS is assumed to be 25 °C compared to a homogeneous ambient water temperature of 22 °C. The results of temperature (ΔT) anomaly between discharge and ambient water in spring flows using equation (3) are shown in (Fig. 6). The result of spring was similar to summer with very minor differences. As in summer, it was obvious that ΔT for spring decreased slower in the first few tens meters of horizontal displacement than after. Also in spring, discharged water using equations (4) and (5) was again dispersed vertically from 8 m depth and reached the surface at about 22 m horizontal displacement (Fig. 7).

Statistical analyses. A nonparametric comparison test (Kruskal Wailles test) was performed at 95% confidence level to test the differences of temperature among months and locations. The analysis showed that there were significant differences among months for both surface and bottom waters (p<0.0001). These differences are clearly due to the normal seasonal thermal variations of the Gulf of Aqaba (e.g. [15]), which are somewhat larger than the observed thermal increases of the discharge over ambient temperatures.

To examine the influence of the discharge in the absence of seasonal trends, surface temperatures were differenced from the intake (ambient) as the site temperature less the intake for each given month (Fig. 8). The maximum temperature differential observed at the discharge point was 3.5ºC. Median temperature differentials by distance were 0.2, 0.7, 1.2, 1.5, 2.5, and 3.2ºC for 150 m, 100 m, 50 m, 20 m, 5 m, and the discharge point, respectively.

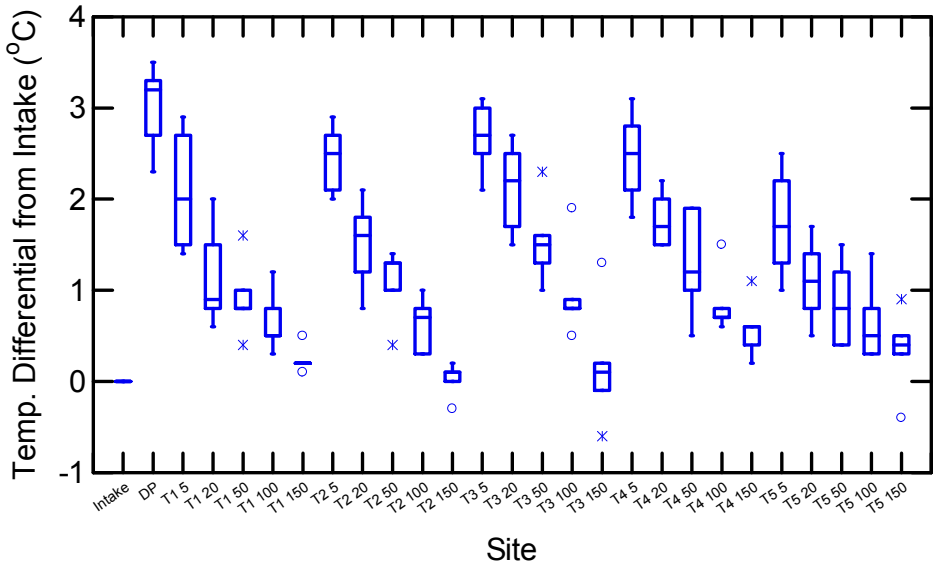

FIGURE 8

Distribution of temperature differentials from monthly intake values for all transects during the period April-August 2015.

(Box plots indicate median values, first and third quartiles).

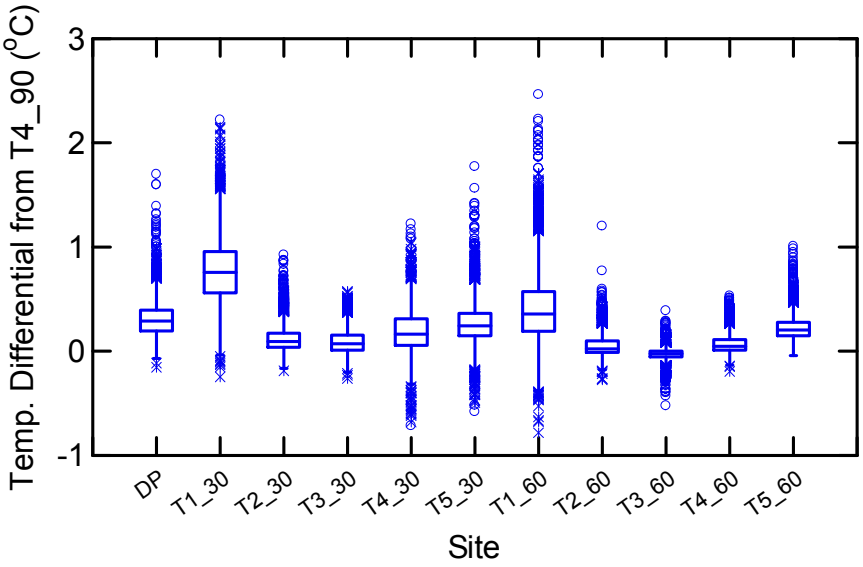

FIGURE 9

Distribution of bottom temperature differentials from ambient (Site T4, 90 m) for all Sites during the period April-August 2015.

(Box plots indicate median values, first and third quartiles).

The distributions of site temperature differentials were evaluated by Kolmorgorov-Smirnov two sample procedures with significance established at $p<0.05$ (Systat Ver. 11.00.01). Within each distance group of sites, there were no significant differences between transects implying a relatively uniform dispersal of water from the discharge point. At 150 m, three of the five sites were not significantly different from the intake. T1 and T4 were significantly different but median differences were 0.2 and 0.6ºC, respectively, with a maximum of 1.1ºC at T4. At 100 m, all sites were significantly different from the intake, but median differences by site were all less than 0.8ºC with a maximum of 1.9ºC reported for T3.

For bottom data, the most distant station, T4 90 m, was used as a representative of ambient temperatures, and temperature differentials were again calculated (Fig. 9). The differential by site indicated that the buoyant plume was generally not as evident at the precise discharge point as it was along Transect 1 at both 30 and 60 m. The median temperature differential of all sites, including the discharge point, was 0.15ºC, and the medians of individual sites were all less than 1ºC. The highest median differentials were 0.76ºC and 0.36ºC at site T1 30

m and 60 m, respectively. In all cases, temperature differentials relative to T4 90 m were less than 3ºC. The somewhat lower variances at Sites T2 and T3 at 30 m and at T2, T3, T4, and T5 at 60 m also indicate that the plume influence, in addition to being modest (median differentials between -0.02 and 0.20ºC), is relatively stable at these sites. The higher variances of T1 at 30 and 60 m indicate that these sites are periodically exposed to the modest influence of the thermal plume.

Bottom temperature differentials were limited to the period when all sites were reporting data (April 20 to July 25, 2015), and subsampled to noon values (the diurnal time of approximate maximum thermal impact) on every fifth day. Subsampling was to reduce autocorrelation in data to non-significant levels and reduce data points per site to prevent inflated Type I error [29, 30] with Kolmogorov-Smirnov two sample testing. There were multiple site-to-site significant differences of thermal differentials (44 out of 55 comparisons), but in all cases, the scale of the difference was small. Differences in all bottom temperature from ambient conditions were comparable in scale to the differences observed for the surface when 150 m from the discharge point.

DISCUSSION

Seawater temperature. Seawater temperatures at the intake of Aqaba Thermal Power Station (ATPS) were almost equivalent to ambient seawater with a maximum temperature of 26.8 °C in July and a minimum of 21.8 °C in April following the normal seasonal pattern in the Gulf of Aqaba. The results are in agreement with some previous studies along the Jordanian coast of Aqaba Gulf [15, 31, 32, 33].

The maximum and minimum differences between the intake and the effluent during the study period were 3.5 °C and 2.3 °C respectively. The technology used for cooling in ATPS is a once-through system, where seawater passes through heat exchangers only one time and large volumes of water are used to minimize thermal increases in effluents. Effluent temperatures of once-through systems are typically 3-6 ºC more than ambient seawater [3]. All differences between intake and discharge for this study were within the typical ranges of once-through systems. Similar ranges in thermal increases were also found in other countries [7, 34, 35].

A mixing zone is defined as the area where an effluent discharge undergoes initial dilution and is extended to cover the secondary mixing in the ambient water body [36]. If we assume that the average percent of temperature increase at the discharge point is 100% then the temperature decreases gradually with distance along all transects to reach approximately 33% of the increase at 100 m This percent indicated that the thermal influence of the discharge had clearly decreased at 100 m from the discharge point. This is in agreement with [36] that recommended that the mixing zone should not exceed 100 m [36].

In regards to bottom water, the temperature values were only minimally impacted by the effluent with a temperature range of 21.5-28.7 °C which is almost the same as the temperature of the Gulf during the same period [15]. As warmer water has lower density compared with colder water, the discharge tends to float immediately to the water surface, thus minimizing thermal increases at bottom.

Aqaba Special Economic Zone [26] defined National Standards for seawater that is used for cooling purposes. The allowable difference in temperature between the intake and discharged waters should not be more than 3ºC at 100 m distance of the discharge point. In the present study, the maximum difference between the intake or ambient seawater and at 100 m distance of the discharge was 1.9 °C with a median difference of 0.7ºC, well within the limit determined by ASEZA. The effluent at discharge and at 100 m also compared favorably with the limits of several international standards oCas shown in Table (1).

Tropical organisms are highly sensitive to small variations in water temperature [37]. Previous studies [22, 34, 35, 38] reported a negative impact of temperature rise on tropical organisms due to changing gas solubility, changes in photosynthesis and respiration rates, etc. However, the increase of temperature found in this study was less than most of the impact levels reported worldwide (Table 2).

TABLE 1
Temperature difference for this study compared to ASEZA and some other international standards for allowable temperature difference between 100 m of the discharge point and the ambient seawater.

Authorities	ΔT (ºC) at discharge	ΔT (ºC) at 100m
ASEZA, Jordan [26]	15 °C	3 °C
RCER[1], KSA [39]	10 °C	2.2 °C
World Bank [27]	-	3 °C
Ministry of Regional Municipalities-Muscat [40]	10 °C	-
Customs and Free Zone Corporation, Dubai, UAE [41]	-	2 °C[2]
This study (maximum, median)	3.5 °C, 3.2 °C	1.9 °C, 0.7 °C

1: RCER: Royal Commission Environmental Regulations.
2: The difference between the ambient sweater temperature and the intake source should be less than 2 °C.

TABLE 2

Temperature difference for this study compared to some previous studies that demonstrated the adverse impact of temperature elevation on some marine organisms in tropical and subtropical regions worldwide.

Location	Organism	ΔT (°C) or maximum allowable	Reference
South California	Corals	1 °C	[42]
Gulf of Panama	Corals	3-4 °C above maximum	[43]
Gulf of Aqaba	Corals	5 °C above maximum	[22]
Hawaii	Corals	3-4 °C	[44]
Australia	Seagrass	Up to 42 °C	[45]
Puerto Rico	Macrobenthos	5-10 °C	[46]
South Florida	Mangroves	5 °C	[47]
Tampa Bay	Algae	3 °C	[48]
This study at discharge (maximum, median)	NA	3.5 °C, 3.2 °C	
This study at 100 m (maximum, median)	NA	1.9 °C, 0.7 °C	
This study at 150 m (maximum, median)	NA	1.3 °C, 0.2 °C	

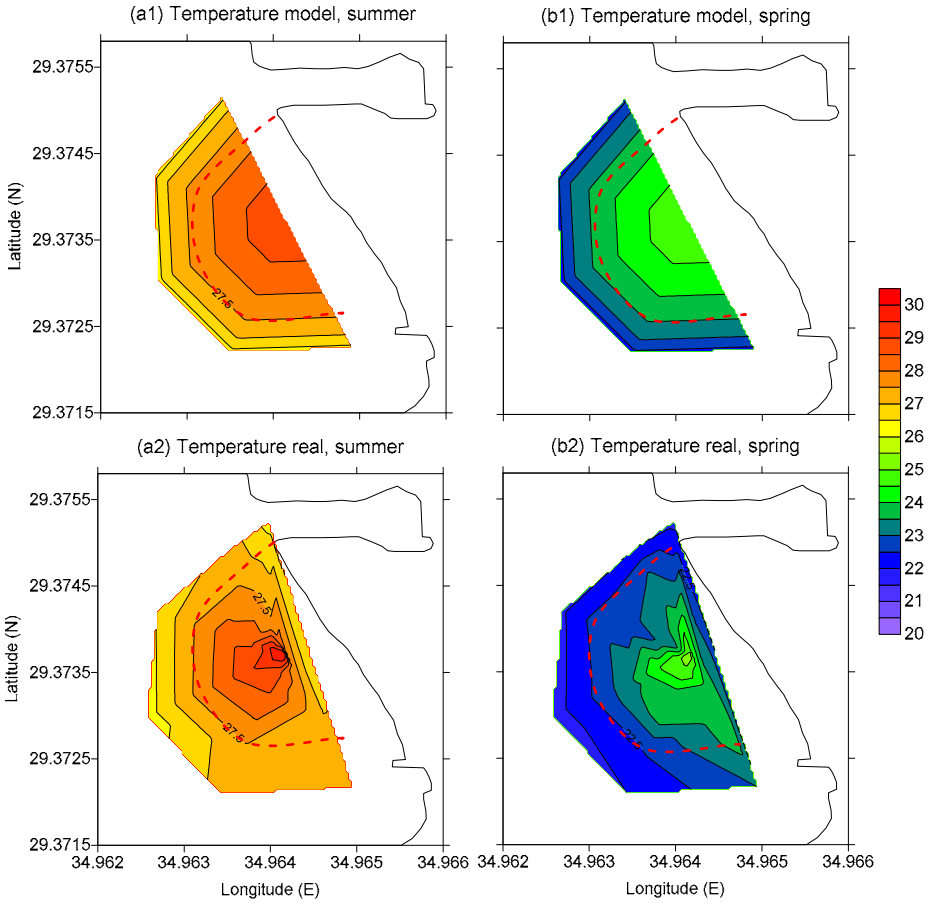

FIGURE 10

Contours of the seawater temperature (°C) dispersion of the real and model of ATPS outfall, for summer and spring (dashed color represents the 100m distance from DP).

Comparison between real data and model results. The comparison between the real measurements and the predicted model results of seawater temperature were performed for summer (July) and spring (April) seasons (Fig. 10).

In summer, the modeled and observed contour results (Fig. 10a1 and a2) revealed similar dispersion around the discharge point with 29°C at discharge point and approximately 27.5°C at100m.

In spring, modeled outcomes (Fig. 10b1) showed that the dispersion of temperature around the discharge point was also quite similar to the observed measurements (Fig. 10b2). The temperature values were 25°C at the discharge point and decreased smoothly to reach about 24°C and 23°C at 100 m distance in the model and the real results, respectively. Nevertheless, there are very slight differences between modeled and observed results including a spatial orientation to thermal dispersion

in observed results that is likely the product of the axis of discharge flow.

A correlation test of seawater temperature at selected locations in both spring and summer seasons was performed to examine the coherence and agreement between modeled and observed results. The test revealed a significant positive relationship between the model and the real measurement in summer (coefficient of determination $R^2 = 0.98$; $p < 0.0001$), and spring ($R^2 = 0.94$; $p < 0.0001$). The strong correlation between model and real results in spring and summer validated the model tool for prediction of dispersion of seawater temperature at any horizontal distance of cooling water discharge in ambient water. The decision not to include other factors such as water current and water direction seem to have no impact on the results due to the general weak current compared to the flow speed of discharge cooling water. Manasrah et. al. [49] found that the range and mean of the current speed in the upper 300 m in the northern Gulf of Aqaba were 0–0.30 ms^{-1} and 0.06 ms^{-1}, respectively, i.e. the maximum current speed of the region represents only about 8% of the speed of discharge cooling water of this study.

CONCLUSIONS

Temperature values showed a clear gradual decrease with distance from the discharge point. At 150m, the surface temperatures differed from ambient by 0.6ºC or less. In general, the temporal temperature variation followed the normal seasonal pattern in the Gulf of Aqaba. The increase of temperature levels due to the discharge of cooling water found in this study was less than most of the impact levels reported worldwide and well within the limit determined by Aqaba Special Zone Authority (ASEZA). The model produced the theoretical dispersion of temperature with distance from discharge and there was high correlation between modeled and observed results. The model can be used as tool for prediction the dispersion of temperature for any cooling system based on the same conditions of this study.

ACKNOWLEDGEMENTS

The Authors would like to express their thankful for staff of the Marine Science Station/Aqaba and Mote Marine Laboratory/Sarasota-Florida for their help and support to accomplish this work. This work was written and analyzed while a Sabbatical Fellow from The University of Jordan/Aqaba Branch to Riyad Manasrah to be spent at the Mote Marine Laboratory in Florida USA. Fulbright scholarship was also awarded to Riyad Manasrah during this period.

REFERENCES

[1] Bejan, A. (2013) Convection heat transfer. 4th edition. John Wiley and sons. Online ISBN: 9781118671627.

[2] Macknick, J., Newmark, R., Heath, G. and Hallett, K.C. (2012) Operational water consumption and withdrawal factors for electricity generating technologies: a review of existing literature. Environ. Res. Lett. 7(4), 1-10.

[3] Majewski, W. and Miller, D.C. (Eds.) (1977) Predicting effects of power plant once- through cooling on aquatic systems. Contribution to the International Hydrobiological Programme, No. 20, UNESCO, Paris.

[4] Langford, T.E. (2001) Thermal discharges and pollution. Encyclopedia of Oceanic Sciences. New York: Academic, 2933–2940.

[5] Ma, S.W.Y., Kueh, C.S.W. Chiu, G.W.L., Wild, S.R. and Yip, J.Y. (1998) Environmental management of coastal cooling water discharges in Hong Kong. Water Science and Technology. 38(8), 267-274.

[6] Altayaran, A.M. and Madany, I.M. (1992) Impact of a desalination plant on the physical and chemical properties of seawater, Bahrain. Water Research. 26(4), 435-441.

[7] Abdul-Wahab, S.A. (2007) Characterization of water discharges from two thermal power/desalination plants in Oman. Environmental Engineering Science. 24(3), 321-337.

[8] Dutton, J.A. (2010) Weather, climate, and the energy industry: a story of sunlight-some old, some new. In: Troccoli, A. (Ed.) Management of weather and climate risk in the energy industry. Springer, Netherland, 13-19.

[9] Hester, E.T. and Doyle M.W. (2011) Human impacts to river temperature and their effects on biological processes: a quantitative synthesis. J. Am. Water Resources Assoc. 47, 571–87.

[10] Fox, J.L. and Moyer, M.S. (1975) Effect of power plant chlorination on estuarine productivity. Chesapeake Science. 16, 66–68.

[11] Nicieza, A.G. and Metcalfe N.B. (1997) Growth compensation in juvenile Atlantic salmon: responses to depressed temperature and food availability. Ecology. 78, 2385-2400.

[12] Koumoundouros, G., Divanach, P., Anezaki, L. and Kentouri, M. (2001) Temperature-induced ontogenetic plasticity in sea bass (Dicentrarchuslabrax). Mar. Biol. 139, 817– 830.

[13] Rombough, P.J. (1997) The effects of temperature on embryonic and larval development. In: Wood, C.M., McDonald, D.G. (eds.) Global warming. implications for freshwater and marine fish. Cambridge University Press, Cambridge, United Kingdom, 177– 223.

[14] Bear, E.A. and McMahon, T.E. (2007) Comparative thermal requirements of westslope cutthroat trout and rainbow trout: implications for species interactions and development of thermal protection standards. Transactions of the American Fisheries Society. 136, 1113–1121.
[15] Manasrah, R., Rasheed, M. and Badran, M. (2006a) Relationships between water temperature, nutrients and dissolved oxygen in the northern Gulf of Aqaba, Red Sea. Oceanologia. 48(2), 237-253.
[16] Relyea, R.A. (2002) Competitor-induced plasticity in tadpoles: consequences, cues, and connections to predator-induced plasticity. Ecology. 72, 523–540.
[17] Pörtner, H. (2010) Oxygen-and capacity-limitation of thermal tolerance: a matrix for integrating climate-related stressor effects in marine ecosystems. J. Exp. Biol. 213, 881–893.
[18] Hoegh- Guldeberg, O., Mumby, P.J., Hooten, A.J., Steneck, R.S., Greenfield, P., Gomez, E., Harvell, C.D., Sale, P.F., Edwards, A.J., Caldeira, K., Knowlton, N., Eakin, C.M., Iglesias-Prieto, R., Muthiga, N., Bradbury, R.H., Dubi, A. and Hatziolos, M.E. (2007) Coral reefs under rapid climate change and ocean acidification. Science. 318(5857), 1737-42.
[19] Antonius, A. (1988) Distribution and dynamics of coral diseases in the Eastern Red Sea. Proc 6th Int Coral Reef Symp. 2, 293–298
[20] Loya, Y. (2004) The coral reefs of Eilat – past, present and future: three decades of coral community structure Studies. In: Rosenberg, E. and Loya Y. (eds.) Coral Health and Disease. Springer-Verlag, Heidelberg, 1-34.
[21] Mohamed, A.R., Ali, A.A.M. and Abdel-Salam, H.A. (2012) Status of coral reef health in the northern Red Sea, Egypt. Proceedings of the 12th International Coral Reef Symposium, Cairns, Australia, 9-13 July 2012, 9A Coral bleaching and climate change. P. 5.
[22] Al-Horani, F. (2005) Effects of changing seawater temperature on photosynthesis and calcification in the scleractinian coral Galaxeafascicularis, measured with O2, Ca+2 and pH microsensors. Scientia Marina. 69(3), 347-354.
[23] U.S. EPA (2008) EPA's Report on the Environment (ROE) (2008 Final Report). U.S. Environmental Protection Agency, Washington, D.C., EPA/600/R-07/045F (NTIS PB2008-112484).
[24] Langford, T.E. (1990) Ecological effects of thermal discharges. Elsevier Applied Science Publishers Ltd. England, 28–103.
[25] Cardoso-Mohedano, J.G., Bernardello, R., Sanchez-Cabeza, J.A., Ruiz-Fernández, A.C., Alonso-Rodriguez, R. and Cruzado, A. (2015) Thermal impact from a thermoelectric power plant on a tropical coastal lagoon. Water, Air, and Soil Pollution. 226(1), 1-11.
[26] ASEZA, Aqaba Special Economic Zone Authority (2013) Standards for using seawater in cooling and discharge to sea. 1-3.
[27] World Bank (1999) Pollution Prevention and Abatement Handbook 1998 – Towards Cleaner Production. World Bank, United Nation Environment Program, WHO, 457p.
[28] Stanley, M. and Batten, R.C. (1969) Viscosity of seawater at moderate temperatures and pressures. J. Geophysical Research. 74(13), 3415–3420.
[29] Weiss, M.S. (1978) Modification of the Kolmogorov-Smirnov Statistic for Use with Correlated Data. Journal of the American Statistical Assoc. 73(364), 872-875.
[30] Durilleul, P. and Legendre, P. (1992) Lack of robustness in two tests of normality against autocorrelation in sample data. Journal of Statistical Computation and Simulation. 42(1-2), 79-91.
[31] Paldor, N. and Anati, D.A. (1979) Seasonal variations of temperature and salinity in the Gulf of Eilat (Aqaba). Deep-Sea Research. 26, 661-672.
[32] Manasrah, R., Badran, M., Lass, H.U. and Fennel, W. (2004) Circulation and winter deepwater formation in the northern Red Sea. Oceanologia. 46(1), 5-23.
[33] Badran, M., Rasheed, M., Manasrah, R. and Al-Najjar, T. (2005) Nutrient flux, fuel of the summer primary productivity in the oligotrophic waters of the Gulf of Aqaba, Red Sea. Oceanologia. 47(1), 47-60.
[34] Nour El-din, N.M. (2004) Impact of cooling water discharge on the benthic and planktonic pelagic fauna along the coastal waters of Qatar, Arabian Gulf. Egyptian Journal of Aquatic Research. 30, 150-159.
[35] Bath, A., Shackleton, B. and Botica, C. (2004) Development of temperature criteria for marine discharge from a large industrial seawater supplies project in Western Australia. Water South Africa. 30(5), 648-654.
[36] SEPA, Scottish Environmental Protection Agency (2006) Supporting guidance (WAT-SG-11) Modelling coastal and transitional discharges. Available from: http://www.sepa.org.uk/pdf/wfd/guidance/pointsource/sg11.pdf.
[37] Nilsson, G.E., Crawley, N., Lunde, I.G. and Munday, P.L. (2009) Elevated temperature reduces the respiratory scope of coral reef fishes. Global Change Biology. 15(6), 1405-1412.
[38] Kushmarol, A., Rosenberg, E., Fine, M., Ben Haim, Y. and Loya, Y. (1998) Effect of temperature on bleaching of the coral Oculina pataqonica by Vibrio AK-1. Marine Ecology Progress Series. 171, 131-137.

[39] RCER (2004) Royal Commission Environmental Regulations. Saudi Arabia Royal Commission for Jubail and Yanbu, Environmental Control Department, Vol I.
[40] Ministry of Regional Municipalities-Muscat (2005) Promulgating the bylaws to discharge liquid waste in the marine environment.
[41] Customs and Free Zone Corporation (2013) Harbor water quality. Dubai, UAE.
[42] Campbell, R., Jones, A. (2005) Appropriate disposal of effluent from coastal desalination facilities. Desalination. 182, 365-372.
[43] Glynn, P.W. and D'Croz, L. (1990) Experimental evidence for high temperature stress as the cause of El Nino-coincident coral mortality. Coral Reefs. 8, 181–191.
[44] Jokiel, P.L. and Coles, S.L. (1974) Effects of heated effluent on hermatypic corals at Kahe Point, Oahu. Pacif. Sci. 28, 1-18.
[45] Kerr, E.A. and Strother, S. (1985) Effects of irradiance, temperature and salinity on photosynthesis of Zostera muelleri. Aquat. Bot. 23, 177–183.
[46] Kolehmainen, S.E., Martin, F.D. and Schroeder, P.B. (1975) Thermal studies on tropical marine ecosystems in Puerto Rico. In: Environmental effects of cooling systems at nuclear power plants. International Atomic Energy Agency, Vienna. 409-421.
[47] Miller, H.G., Cooper, J.M. and Miller, J.D. (1976) Effect of nitrogen supply on nutrients in litter fall and crown leaching in a stand of Corsican pine. Journal of Applied Ecology. 13, 238-248.
[48] Blake, N.J., Doyle, L.J. and Pyle, T.E. (1976) The macrobenthic community of a thermally altered area of Tampa Bay, Florida. In: Esch, G.W. and McFarlane, R.W. (Eds.) Thermal Ecology. II, 296-301.
[49] Manasrah, R., Lass, U. and Fennel, W. (2006b) Circulation in the Gulf of Aqaba (Red Sea) during winter-spring. Journal of Oceanography. 62(2), 219-225.

Received: **28.11.2018**
Accepted: **06.03.2019**

CORRESPONDING AUTHOR

Riyad Manasrah
Faculty of Marine Sciences,
The University of Jordan/Aqaba,
PO Box 2595,
Aqaba 77110 – Jordan

e-mail: r.manasrah@ju.edu.jo

AUTHOR INDEX

SUBJECT INDEX

FEB – GUIDE FOR AUTHORS

General

FEB accepts original papers, review articles, short communications, research abstracts from the entire sphere of environmental-chemistry,-biology,-microbiology,- technology, -biotechnology and-management, furthermore, about residue analysis/ and ecotoxicology of contaminants.

Acceptance or no acceptance of a contribution will be decided, as in the case of other scientific journals, by a board of reviewers. Papers are processed with the understanding that they have not been published before (except in form of an abstract or as a part of a published lecture, review or thesis);that they are not under consideration for publication elsewhere; that their publication has been approved by all co-authors, if any, as well as-tacitly or explicitly- by the responsible authorities at the institute where the work has been carried out and that, if accepted, it will not be published elsewhere in the same form, in either the same or another language, without the consent of the copyright holders.

Language

Papers must be written in English. Spelling may either follow American (Webster) or British (Oxford) usage but must be consistent. Authors who are less familiar with the English language should seek assistance from proficient colleagues in order to produce manuscripts that are grammatically and linguistically correct.

Size of manuscript

Review articles should not exceed 30 typewritten pages. In addition up to 5 figures may be included.

Original papers must not exceed 14 typewritten pages. In addition up to 5 figures may be included.

Short-Communications should be limited to 4 typewritten pages plus not more than 1 illustration.

Short descriptions of the authors, presentation of their groups and their research activities (with photo) should together not exceed I typewritten page. Short research abstracts should report in a few brief sentences (one-fourth to one page) particularly significant findings. Short articles by relative newcomers to the chemical innovation arena highlight the key elements of their Master and PhD-works in about I page.

Book Reviews are normally written in-house, but suggestions for books to review are welcome.

Preparation of manuscript

Dear authors,

FEB is available both as printed journal and as online journal on the web. You can now e-mail your manuscripts with an attached file. Save both time and money. To avoid any problems handling your text please follow the instructions given below:

When preparing your manuscripts have the formula K/SS (Keep It Simple and Stupid) in mind. Most word processing programs such as MS-Word offer a lot of features. Some of them can do serious harm to our layout. So please do not insert hyperlinks and/or automatic cross-references, tables of contents, references, footnotes, etc.

1. Please use the standard format features of your word processor (such as standard.dot for MS Word).
2. Please do not insert automatisms or secret link-ups between your text and your figures or tables. These features will drive our graphic department sometimes mad.
3. Please only use two fonts for text or tables "Times New Roman" and for graphical presentations "Arial".
4. Stylesheets, text, tables and graphics in shade of grey
5. Turn on the automatic language detection in English (American or British)
6. Please - check your files for viruses before you send them to us!!

Manuscripts should send to:parlar@wzw.tum.de
or:parlar@prt-parlar.de

Thank you very much!

STRUCTURE OF THE MANUSCRIPT

Title page: The first page of the manuscript should contain the following items in the sequence given: A concise title of the paper (no abbreviations). The names of all authors with at least one first name spelled out for every author. The names of Universities with Faculty, City and Country of all authors.

Abstracts: The second page of the manuscript should start with an abstract that summarizes briefly the contents of the paper (except short communications). Its length should not exceed 150-200 words. The abstract should be as informative as possible. An extended repetition of the paper's title is not considered to be an abstract.

Keywords: Below the Summary up to 6 key words have to be provided which will assist indexers in cross-indexing your article.

Introduction: This should define the problem and, if possible, the frame of existing knowledge. Please ensure that people not working in that particular field will be able to understand the intention. The word length of the introduction should be 150 to 300 words.

Materials and methods:
Please be as precise as possible to enable other scientists to repeat the work.

Results: Only material pertinent to the subject must be included. Data must not be repeated in figures and tables.

Acknowledgements: Acknowledgements of financial support, advice or other kind of assistance should be given at the end of the text under the heading "Acknowledgements". The names of funding organisations should be written in full.

References: Responsibility for the accuracy of references rests with the authors. References are to be limited in number to those absolutely necessary. References should appear in numerical order in brackets and in order of their citation in the text. They should be grouped at the end of the paper in numerical order of appearance. Abbreviated titles of periodicals are to be used according to Chemical or Biological Abstracts, but names of lesser known journals should be typed in full. References should be styled and punctuated according to the following examples:

ORIGINALPAPERS:
l. Author, N.N. and Author, N.N. (Year) Full title of the article. Journal and Volume, first and last page.
BOOK OR PROCEEDING:
2. Author, N.N. and Author, N.N. (Year) Title of the contribution. In: Title of the book or proceeding. Volume (Edition of klitor-s, ed-s) Publisher, City, first and last page

DOCTORAL THESIS:
3. Author, N.N. (Year) Title of the thesis, University and Faculty, City

UNPUBLISHED WORK:
Papers that are unpublished but have been submitted to a journal may be cited with the journal's name followed by "in press". However, this practice is acceptable only if the author has at least received galley proofs of his paper. In all other cases reference must be made to “unpublished work" or "personal communication".

Discussion and Conclusion: This part should interpret the results in reference to the problem outlined in the introduction and of related observations by the author/s or others. Implications for further studies or application may be discussed. A conclusion should be added if results and discussion are combined.

Corresponding author: The name of the corresponding author with complete postal address

Reprints:
1 - 4 pp.: 200,- EURO + postage/handling
5 - 8 pp.: 250,- EURO + postage/ handling
More than 8pp: 350,- EURO +postage/ handling.
The prices are based upon the number of pages in our journal layout (not on the page numbers of the submitted manuscript).
Postage/ Handling: The current freight rate is Germany 10 €, Europe 18 €, International 30 €.
VAT: In certain circumstances (if no VAT registration number exists) we may be obliged to charge 7% VAT on sales to other EU member countries.MESAEP and SECOTOX members get a further discountof 20% (postage/ handling full).